VERTEBRATE SKELETAL HISTOLOGY AND PALEOHISTOLOGY

EDITED BY
VIVIAN DE BUFFRÉNIL
ARMAND J. DE RICQLÈS, LOUISE ZYLBERBERG
AND KEVIN PADIAN

Associate Editors: Michel Laurin and Alexandra Quilhac

CRC Press
Taylor & Francis Group

VetBooks.ir

www.VetBooks.ir

VetBooks.ir

Vertebrate Skeletal Histology and Paleohistology

www.VetBooks.ir

VetBooks.ir



Taylor & Francis
Taylor & Francis Group
http://taylorandfrancis.com

VetBooks.ir

Vertebrate Skeletal Histology and Paleohistology

Edited by

Vivian de Buffrénil, Armand J. de Ricqlès,
Louise Zylberberg, and Kevin Padian

Associate editors:

Michel Laurin and Alexandra Quilhac

www.VetBooks.ir

CRC Press
Taylor & Francis Group
Boca Raton London New York

CRC Press is an imprint of the
Taylor & Francis Group, an **informa** business

VetBooks.ir

CRC Press
Boca Raton and London
First edition published 2021
by CRC Press
6000 Broken Sound Parkway NW, Suite 300, Boca Raton, FL 33487-2742

and by Taylor & Francis Group
2 Park Square, Milton Park, Abingdon, Oxon, OX14 4RN

© 2021 Taylor & Francis Group, LLC
CRC Press is an imprint of Taylor & Francis Group, LLC

Reasonable efforts have been made to publish reliable data and information, but the author and publisher cannot assume responsibility for the validity of all materials or the consequences of their use. The authors and publishers have attempted to trace the copyright holders of all material reproduced in this publication and apologize to copyright holders if permission to publish in this form has not been obtained. If any copyright material has not been acknowledged please write and let us know so we may rectify in any future reprint.

Except as permitted under U.S. Copyright Law, no part of this book may be reprinted, reproduced, transmitted, or utilized in any form by any electronic, mechanical, or other means, now known or hereafter invented, including photocopying, microfilming, and recording, or in any information storage or retrieval system, without written permission from the publishers.

For permission to photocopy or use material electronically from this work, access www.copyright.com or contact the Copyright Clearance Center, Inc. (CCC), 222 Rosewood Drive, Danvers, MA 01923, 978-750-8400. For works that are not available on CCC please contact mpkbookspermissions@tandf.co.uk

Trademark Notice: Product or corporate names may be trademarks or registered trademarks and are used only for identification and explanation without intent to infringe.

ISBN: 9780815392880 (hbk)
ISBN: 9780367700867 (pbk)
ISBN: 9781351189590 (ebk)

Typeset in Times
by KnowledgeWorks Global Ltd.

Contents

Foreword viii
Contributors x

Section I Introduction

1. **Paleohistology: An Historical – Bibliographical Introduction** 3
Armand J. de Ricqlès

Section II Morphology and Histology of the Skeleton

2. **An Overview of the Embryonic Development of the Bony Skeleton** 29
Vivian de Buffrénil and Alexandra Quilhac

3. **The Vertebrate Skeleton: A Brief Introduction** 39
Michel Laurin, Alexandra Quilhac and Vivian de Buffrénil

Methodological Focus A: The New Scalpel: Basic Aspects of CT-Scan Imaging 55
Damien Germain and Sandrine Ladevèze

4. **Microanatomical Features of Bones and Their Basic Measurement** 59
Vivian de Buffrénil, Eli Amson, Alexandra Quilhac, Dennis F. A. E. Voeten and Michel Laurin

Methodological Focus B: Basic Aspects of 3D Histomorphometry 81
Eli Amson and Damien Germain

5. **Bone Cells and Organic Matrix** 85
Louise Zylberberg

6. **Current Concepts of the Mineralization of Type I Collagen in Vertebrate Tissues** 109
William J. Landis, Tengteng Tang and Robin DiFeo Childs

7. **An Overview of Cartilage Histology** 123
Alexandra Quilhac

Methodological Focus C: Virtual (Paleo-)Histology Through Synchrotron Imaging 139
Sophie Sanchez, Dennis F. A. E. Voeten, Damien Germain and Vincent Fernandez

8. **Bone Tissue Types: A Brief Account of Currently Used Categories** 147
Vivian de Buffrénil and Alexandra Quilhac

Methodological Focus D: FIB-SEM Dual-Beam Microscopy for Three-Dimensional Ultrastructural Imaging of Skeletal Tissues 183
Natalie Reznikov and Katya Rechav

Section III Dynamic Processes in Osseous Formations

9. **Basic Processes in Bone Growth** 193
Vivian de Buffrénil and Alexandra Quilhac

10. **Accretion Rate and Histological Features of Bone** 221
Vivian de Buffrénil, Alexandra Quilhac and Jorge Cubo

11. Bone Remodeling 229
Vivian de Buffrénil and Alexandra Quilhac

12. Remarks on Metaplastic Processes in the Skeleton 247
Vivian de Buffrénil and Louise Zylberberg

Section IV Teeth

13. Histology of Dental Hard Tissues 259
Alan Boyde and Timothy G. Bromage

Section V Phylogenetic Diversity of Skeletal Tissues

14. Introduction 291
Michel Laurin

15. Finned Vertebrates 294
Jorge Mondéjar-Fernández and Philippe Janvier

16. Early Tetrapodomorphs 325
Sophie Sanchez, François Clarac, Michel Laurin and Armand de Ricqlès

17. Lissamphibia 345
Vivian de Buffrénil and Michel Laurin

18. Early Amniotes and Their Close Relatives 363
Aurore Canoville, Michel Laurin and Armand de Ricqlès

19. Testudines 385
Torsten M. Scheyer and Ignacio A. Cerda

20. Lepidosauria 399
Vivian de Buffrénil and Alexandra Houssaye

21. Sauropterygia: Placodontia 425
Torsten M. Scheyer and Nicole Klein

22. Sauropterygia: Nothosauria and Pachypleurosauria 435
Torsten M. Scheyer, Alexandra Houssaye and Nicole Klein

23. Sauropterygia: Histology of Plesiosauria 444
P. Martin Sander and Tanja Wintrich

24. Ichthyosauria 458
P. Martin Sander

25. Archosauromorpha: From Early Diapsids to Archosaurs 467
Armand de Ricqlès, Vivian de Buffrénil and Michel Laurin

26. Archosauromorpha: The Crocodylomorpha 486
Vivian de Buffrénil, Michel Laurin and Stéphane Jouve

27. Archosauromorpha: Avemetatarsalia – Dinosaurs and Their Relatives 511
Kevin Padian and Holly N. Woodward

VetBooks.ir

28. Nonmammalian Synapsids 550
Jennifer Botha and Adam Huttenlocker

29. Diversity of Bone Microstructure in Mammals 564
Vivian de Buffrénil, Christian de Muizon, Maïténa Dumont, Michel Laurin and Olivier Lambert

Section VI Integrative Questions

30. Phylogenetic Signal in Bone Histology 617
Jorge Cubo, Lucas J. Legendre and Michel Laurin

31. Cyclical Growth and Skeletochronology 626
Vivian de Buffrénil, Alexandra Quilhac and Jacques Castanet

32. Aging and Senescence Processes in the Skeleton 645
Catherine Bergot and Vivian de Buffrénil

33. Basic Principles and Methodologies in Measuring Bone Biomechanics 668
Russell P. Main

34. Interpreting Mechanical Function in Extant and Fossil Long Bones 688
Russell P. Main, Erin L.R. Simons and Andrew H. Lee

35. Bone Microanatomy and Lifestyle in Tetrapods 724
Aurore Canoville, Vivian de Buffrénil and Michel Laurin

36. Bone Histology and the Adaptation to Aquatic Life in Tetrapods 744
Alexandra Houssaye and Vivian de Buffrénil

37. Bone Histology and Thermal Physiology 757
Jorge Cubo, Adam Huttenlocker, Lucas J. Legendre, Chloé Olivier and Armand de Ricqlès

38. Bone Ornamentation: Deciphering the Functional Meaning of an Enigmatic Feature 774
François Clarac

39. The Histology of Skeletal Tissues as a Tool in Paleoanthropological and Archaeological Investigations 781
Ariane Burke and Michelle S. M. Drapeau

40. A Methodological Renaissance to Advance Perennial Issues in Vertebrate Paleohistology 793
Alexandra Houssaye, Donald Davesne and Aurore Canoville

Extended Table of Contents 799

VetBooks.ir

Foreword

Every year, students new to our discipline make an important discovery: fossils are not only avatars of gross external anatomical forms, but they can also preserve the fine inner structures of ancient organisms. Under the microscope it is possible to study these hard tissue structures in plants and animals that lived millions and millions of years ago with a level of precision comparable to what we can obtain from living organisms. What an exciting research program!

Although the preservation of fine microscopical structures in fossils was recognized as early as the dawn of the 19th century, for a long time it left little impression on the development of paleontology and biology. Since the first discoveries of fossil microstructures (circa 1815), about a century elapsed before the term *paleohistology* was created (1913), helping to recognize this sub-discipline. The word derives from *palaios* (ancient), as in paleontology, and from *histology*, the study of biological structures at the tissue level of integration, based on the use of the compound microscope. Despite these modest beginnings, paleohistology played an increasingly important role in the development of paleontology. Starting in the 1850s, knowledge of the fine structures of fossil sponges, corals, mollusk shells, fish scales, teeth and especially wood increasingly influenced the general importance given to fossils, and it informed issues of classification, development and growth of organisms of the remote past. Paleohistology thus progressively brought into paleontology a paleobiological flavor, able to enrich the strict gross anatomical and biostratigraphic points of view that too often dominated the discipline.

Paleohistological studies of vertebrate hard tissues were for a long time focused on early aquatic vertebrates ("Agnathans" and other extinct Paleozoic clades), often with the aim of taxonomically identifying fragmentary remains that were mysterious to the morphologists working with gross anatomical characters. Although highly relevant to several important issues in systematics, developmental biology and evolution, such research, mainly conducted in museums by a very small number of highly specialized scientists, long failed to attract the attention of the general scientific community, to say nothing of the public.

Relationships between paleohistology and the various biological fields specializing in the study of skeletal hard tissues (enamel, dentine, bone, cartilage) in extant vertebrates grew progressively over the decades and slowly built an integrated understanding of the long history of hard tissues that found its place in the general evolutionary synthesis of vertebrate evolution. By the middle of the 20th century, the great syntheses of vertebrate paleontological evolution, such as Romer's *Vertebrate Paleontology* and Piveteau's *Traité de Paléontologie,* all included some paleohistological input, particularly on the often very unusual tissues of early Paleozoic aquatic forms. Nevertheless, it was only with the development of the paleohistology of bone, especially of tetrapods, that the field really emerged from the woods. The microscopical structures of the bones and teeth of famous fossil vertebrates such as ichthyosaurs, plesiosaurs, pterosaurs and, above all, dinosaurs began to be described during the late 19th century, mainly with the aim of using these tissues to determine the systematic affiliation of their bearers. But these works, although valuable, did not bring many new paleobiological insights at first.

In the meantime, biologists working on the histology of extant vertebrates made important discoveries about the meaning and implications of various bone tissue types, as well as their relationships to biological factors such as shape development, biomechanical loading, body size, ecology, rate and cyclicity of growth and longevity. All these factors were strongly linked to physiology and life history traits of organisms. These breakthroughs spanned several decades, roughly from 1910 to 1960. It thus became possible, starting in the 1960s, to apply *mutatis mutandis* functional interpretations of bone tissue variability and diversity to fossil vertebrates, within a general evolutionary perspective. This change of focus from mainly taxonomic/systematic issues to functional biological questions in the 1970s enormously contributed to the development of paleohistology and its recognition as a meaningful component of evolutionary biology. Since the beginning of the 21st century, things have developed even further, to the point that paleohistological studies are now often recognized as one of the "cutting edges" of paleontological research. Data and insights have greatly accumulated during the last few decades, new methodologies and techniques are burgeoning and the pace of new research increases steadily.

A synthetic review of the field is timely, as far as vertebrates are concerned. The present book aims to offer such a synthesis, taking into account its various structural, functional, evolutionary-phylogenetic, technological and historical aspects. It is subdivided into six parts.

The first part is a general introduction (Section I) offering a historical coverage of paleohistology. The second main part (Section II) deals with the structural aspects of vertebrate hard tissues, broadly speaking, and taken from the points of view of description and classification, developmental biology and levels of structural integration. We have not tried to duplicate here much of the subject matter of a recent book on paleohistology, *Bone Histology of Fossil Tetrapods*, edited by K. Padian and E.-Th. Lamm (University of California Press, 2013) that, among other things, covers many of the current technical and curatorial aspects of paleohistology, with focus on thin sections from the practical points of view of the researcher, the technician and the collection manager. Instead, we offer here a series of short methodological focuses on various current and novel techniques that offer complementary approaches to the study of hard tissue biology and paleobiology.

The next part of the book (Section III) deals with some basic functional aspects of hard tissues (especially bone): growth,

VetBooks.ir

shape modeling, remodeling and metaplastic transformations. Other important functional aspects are reported in later sections. Section IV is relative to the structure and development of teeth, mainly considered in tetrapods. Then comes a major section of the book, Section V, which offers a detailed view of vertebrate paleohistological diversity, set in current phylogenetic understanding. It is the first effort at a complete comparative analysis of skeletal histodiversity across the vertebrate spectrum since Enlow and Brown (1956–1958), to which it invites interesting historical comparisons. Section VI takes into account the fundamental information and comparative data given in all previous parts in extended perspectives: the role of phylogenetic legacy, ontogenetic constraints, biomechanical functions and adaptations to various environmental conditions are analyzed to decipher the meaning and importance of hard tissue diversity. Finally, in the conclusion of the book, considerations of various integrative approaches, perennial questions and future prospects are succinctly presented.

The editors of this book are convinced that beyond hard results and data, science is an important cultural endeavor and that the history of science is very much a part of science itself. This is why, in a time when any reference older than 5 years is easily neglected in what passes for scholarly Internet research, most chapters here provide deep historical bibliographies as a way to understand how the current "state of the art" was reached. This is all the more striking, perhaps, because this book was planned and written by almost three successive generations of scientists from many countries who learned to build progressively and together what is now a vital field in paleobiology. To them, and to all our younger and future colleagues, we dedicate our efforts.

The Editors

VetBooks.ir

Contributors

Eli Amson
Museum für Naturkunde
Berlin, Germany
Museum für Naturkunde
Stuttgart, Germany

Catherine Bergot
Laboratoire de Radiologie Expérimentale
Université Paris VII
Paris, France

Jennifer Botha
Department of Karoo Palaeontology
National Museum of Bloemfontein
Department of Zoology and Entomology
University of the Free State
Bloemfontein, South Africa

Alan Boyde
Dental Institute
Barts and The London School of Medicine and Dentistry
Queen Mary University of London
London, United Kingdom

Timothy G. Bromage
Department of Molecular Pathobiology
New York University College of Dentistry
New York, New York

Vivian de Buffrénil
Muséum National d'Histoire Naturelle
Paris, France

Ariane Burke
Département d'anthropologie
Université de Montréal
Montréal, Canada

Aurore Canoville
North Carolina Museum of Natural Sciences
Raleigh, NC, USA

Jacques Castanet
Muséum National d'Histoire Naturelle
Paris, France

Ignacio A. Cerda
Instituto de Investigación en Paleobiología y Geología
Museo Carlos Ameghino
Universidad Nacional de Río Negro
Río Negro, Argentina

François Clarac
Department of Organismal Biology
Upsala University
Uppsala, Sweden

Jorge Cubo
Sorbonne Universitié - Muséum National d'Histoire Naturelle, Paris, France
Paris, France

Donald Davesne
Department of Earth Sciences
University of Oxford
Oxford, United Kingdom

Robin DiFeo Childs
Department of Polymer Science
University of Akron
Akron, Ohio

Michelle S. M. Drapeau
Département d'Anthropologie
Université de Montréal
Montréal, Canada

Maïténa Dumont
Koret School of Veterinary Medicine
The Robert H. Smith Faculty of Agriculture, Food and Environmental Sciences
The Hebrew University of Jerusalem
Rehovot, Israel

Vincent Fernandez
Imaging and Analysis Centre
Natural History Museum
London, United Kingdom

Damien Germain
Muséum National d'Histoire Naturelle
Paris, France

Alexandra Houssaye
Muséum National d'Histoire Naturelle
Paris, France

Adam K. Huttenlocker
Department of Integrative Anatomical Sciences
University of Southern California
Los Angeles, California

Philippe Janvier
Muséum National d'Histoire Naturelle
Paris, France

VetBooks.ir

Stéphane Jouve
Sorbonne Université
Paris, France.

Nicole Klein
Steinmann-Institut für Geologie,
Mineralogie und Paläontologie
Universität Bonn
Bonn, Germany

Sandrine Ladevèze
Muséum National d'Histoire Naturelle
Paris, France

Olivier Lambert
Royal Belgian Institute of Natural Sciences
Brussels, Belgium

William J. Landis
Department of Preventive and Restorative Dental Sciences
University of San Francisco
San Francisco, California

Michel Laurin
Muséum National d'Histoire Naturelle
Paris, France

Andrew H. Lee
Arizona College of Osteopathic Medicine and College of
Veterinary Medicine
Midwestern University
Glendale, Arizona

Lucas J. Legendre
Jackson School of Geosciences
The University of Texas at Austin
Austin, Texas

Russell P. Main
College of Veterinary Medicine and Weldon School of
Biomedical Engineering
Purdue University
West Lafayette, Indiana

Jorge Mondéjar-Fernández
Muséum National d'Histoire Naturelle
Paris, France

Christian de Muizon
Muséum National d'Histoire Naturelle
Paris, France

Chloé Olivier
Muséum National d'Histoire Naturelle
Paris, France

Kevin Padian
Museum of Paleontology
University of California
Berkeley, California

Alexandra Quilhac
Sorbonne Université - Muséum National d'Histoire Naturelle
Paris, France

Katya Rechav
Electron Microscopy Unit
The Weizmann Institute of Science
Rehovot, Israel

Natalie Reznikov
Object Research Systems, Inc.
Montréal, Canada

Armand J. de Ricqlès
Collège de France
and
Muséum National d'Histoire Naturelle
Paris, France

Sophie Sanchez
Department of Organismal Biology
Upsala University
Uppsala, Sweden

P. Martin Sander
Institute of Geosciences
University of Bonn
Bonn, Germany

Torsten M. Scheyer
Universität Zürich
Paläontologisches Institut und Museum
Zürich, Switzerland

Erin L. R. Simons
Arizona College of Osteopathic Medicine and College of
Veterinary Medicine
Midwestern University
Glendale, Arizona

Tengteng Tang
Max Planck Institute of Colloids and Interfaces
Potsdam, Germany

Dennis F. A. E. Voeten
Evolutionary Biology Centre
University of Sweden
Uppsala, Sweden

Tanja Wintrich
Institute of Geosciences
University of Bonn
Bonn, Germany

Holly N. Woodward
Oklahoma State University Center for Health Sciences
Tulsa, Oklahoma

Louise Zylberberg
Muséum National d'Histoire Naturelle
Paris, France

VetBooks.ir



Taylor & Francis
Taylor & Francis Group
http://taylorandfrancis.com

VetBooks.ir

Section I

Introduction

VetBooks.ir



Taylor & Francis
Taylor & Francis Group
http://taylorandfrancis.com

VetBooks.ir

1

Paleohistology: An Historical – Bibliographical Introduction

Armand J. de Ricqlès

CONTENTS

Introduction 3
Early Microscopical Investigators 4
The "Early Vertebrates" Tradition 6
Tetrapods: Systematics or Functions – or Both? 9
Epiphyses and Endochondral Ossification 14
Concluding Remarks 16
Acknowledgments 16
References 16

Introduction

Consideration of the vertebrate skeleton and of the bones and teeth that form it is as old as mankind and very likely goes back to other species in the genus *Homo* (Soressi et al. 2013; Zilhão 2012) and perhaps far beyond early hominids. This is suggested by data from prehistoric archaeology and human paleontology, ethnography, and even ethology of primates (Anderson 2004; Asfaw et al. 1999).

As the only part of the vertebrate – and human – body that usually resists rapid decay after death, the skeleton and its components have always carried a strong symbolic burden for humans. But the skeleton has also provided a precious source for raw materials used for food, tools, weapons, and ornaments in our species as well as in others.

From classical Antiquity, through the Middle Ages, and up to Modern times, there are many written records of the knowledge and use of skeletal elements that can hardly be considered "scientific," at least compared to our current understanding of what scientific knowledge is. These records provide data on various topics, from medical and veterinary care to technological use, often mixed with anatomical, artistic, alchemical, religious, and even magical points of view. This early history of the study of skeletons, bones, and teeth has been recorded in detail in various contexts (Desse 1984; Enlow 1963; Halstead and Middleton 1972) and need not be repeated here. It will be enough to recall some landmarks that have preceded – or concurred with – early microscopical investigations and made breakthroughs in the scientific understanding of vertebrate hard tissues as important biological components of the living body.

Andreas Vesalius (Andries van Wesel, 1514–1564) and the *anatomical approach*. A proper description and understanding of the anatomical aspect of the human skeleton can be found in Andreas Vesalius' famous book *De humani corporis fabrica* (Vesalius 1543), generally considered the starting point of precise scientific anatomy. From the same period of the Renaissance comes the famous comparison of human and bird skeletons in the *Histoire naturelle des oiseaux* by Belon du Mans (1555), foreshadowing the later development of comparative anatomy and of the philosophical questions it raises, notably homology and evolution.

Galileo (1564–1642) and the *functional/biomechanical approach*. Galileo Galilei recognized the relationship between bone shape and cross-sectional width with the mechanical function of weight-bearing (Galileo 1638). His concept of a link between the structure of bones and the mechanical demands imposed on them met great success during the engineering-oriented nineteenth century (Wolff 1892). This perennial biomechanical perspective (e.g., Currey 1984; Evans 1957; Frost 1964, 1988; Kummer 1972; Murray 1936) still flourishes today with the development of biomechanics and biophysics.

Hérissant (1714–1773) and the *biochemical approach*. The basic issue of the chemical nature of bone was successfully addressed during the eighteenth century when François David Hérissant, in experiments "using fire and acids," clearly demonstrated the dual nature of bone, simultaneously organic and mineral (Hérissant 1758). This set the trend toward the later enormous development of hard tissue biochemistry, organic/mineral phase relationships, and biomineralization processes (di Masi and Gower 2016). Initially, an issue of major practical concern was to decide if the "gelatin" extracted from bone could be safely used as food (Payen and Rossignon 1843).

Duhamel (1700–1782) and the *growth approach*. The astounding fact of the growth of the hard tissues of bones during early life has remained a mystery for centuries. Following earlier developments on the coloring effect of madder on living bone (Belchier 1736), the renowned experiments of Duhamel

VetBooks.ir

du Monceau (1739, 1743) shed new light on the issue. By feeding various mammals and birds madder and using metal rings and nails as landmarks in growing bones, he deciphered processes of longitudinal and radial growth. However, Duhamel relied on his experience with tree growth to interpret some issues about bone, which led to erroneous interpretations and long-lasting controversies in bone histology (Enlow 1963). Modern experiments on multilabeling of growing tissues with fluorochromes and radioactive isotopes (Ponlot 1960) extended this approach.

It is interesting that the major research fields mentioned above, namely anatomy, the relationship between structure and mechanical functions, chemical nature, and growth are still active domains of research today. They can investigate various "levels of integration" of skeletal structures and processes. Actually, depending on the context, the term "bone" can connote different concepts, such as an anatomical organ (a femur, for instance), a tissue (the bone tissues that form every bone), or chemicals (bone-specific organic and mineral molecules). To clarify this issue, successive levels of integration of bone have been defined (Petersen 1930) and, with some emendations, they have been generally followed by later scientists (Castanet et al. 2003; Glimcher 1981). These levels, both structural and functional, are used as a framework for the organization of this book.

During the last 60 years or so, progress in electronic microscopy, biochemistry, genetics, and molecular biology have shifted the emphasis of research on bone, and hard tissues in general, far from the more traditional morphological-comparative-systematic approaches familiar to the paleontologist. Further current progress in molecular genetics and epigenetics may ultimately create a more synthetic understanding of the vertebrate skeletal biology and evolution at all integrative levels (Shahar and Wiener 2017).

A word of warning may be in order here about the relevance of this chapter's bibliography. The actual number of published research papers on vertebrate skeletal elements, at all levels of integration, ranges into the tens of thousands, spread over several centuries. They are especially numerous in fields such as anatomy, paleontology, physiology, biochemistry, biophysics, mechanobiology, cell biology, biomineralization, growth, metabolism, endocrinology, and various experimental research, often more or less directly linked to biomedical prospects.

No effort at an exhaustive bibliographic approach to those diverse, important, and extensive domains of hard tissue biology can be meaningful. Only a few major or "classical" references are quoted here when deemed relevant. Over the years, hundreds of books, often multiauthored, have offered syntheses of lasting interest on one or several research subjects noted above. We offer below a tiny selection of general literature that may be useful to the more biologically oriented paleontologists and zoologists working on hard tissues.

On general matters of structure, histology, biochemistry, and genetics of extant vertebrate mineralized tissues and mechanisms of mineralization, one may suggest the surveys by Bloom and Fawcett (1968), Bourne (1972), Courvoisier et al. (1978), di Masi and Gower (2016), Francillon-Vieillot et al. (1990), Frost (1964), Glimcher (1976), Glimcher and Lian (1989), Gould and Ramachandran (1968), Hall (2005), Hancox (1972), Johnson (1986), Miles (1967), Noda (1993), Peck (1987), Serafini-Fracassini and Smith (1974), Simkiss (1975), Sognnaes (1960), Stockwell (1979), Veis (1981), and Zipkin (1973).

In this chapter we concentrate on the descriptive-comparative aspects of vertebrate hard *tissues* (histology: Rodahl et al. 1960), with emphasis on twentieth-century paleohistological papers set in their historical contexts. Even in this much more restricted field, no exhaustive bibliographical treatment can be attempted. References in parentheses should be considered only examples. For an example of a more complete bibliographical treatment of restricted subjects, see Castanet et al. (2003) and Ricqlès (1995b) on the skeletal histology of amphibians. Current research papers will be found in each relevant chapter.

Early Microscopical Investigators

It seems that the microscopical observation of hard but recent objects, such as dry bone, goes back to the origins of microscopy itself, considering the observations of Havers (1691), who gave his name to the famous "canals" and "systems" of compact bone (Enlow 1963). Actually, Van Leeuwenhoek (1674, 1693; Figure 1.1) also observed and described similar



FIGURE 1.1 Antonie van Leuwenhoeck. (Leiden, the Netherlands, 1632–1723.) Generally considered the "father" of microscopy and microbiology, Leeuwenhoek started as a draper and, wanting to better check the quality of threads, became interested in magnifying lenses and their uses. He devised a crude one-lens "microscope" of which he built several tens of copies. The lens offered magnifications of about ×270 or more, which allowed him to discover, explore, and describe the new microscopic world. His works are known thanks to the 190 letters he sent to the Royal Society, of which he became a member in 1680. Some of his descriptions of bone structures, later known as Haversian systems and canals, precede Clopton Havers' (1657–1702) *Osteologia Nova* (Havers 1691).

VetBooks.ir

structures (di Masi and Gower 2016). The study of fossil and mineral objects under the microscope came later: the historical origins of paleohistology are rooted in the early nineteenth century (Morrison-Low and Nuttall 2003). Observation of fossils by optical transmission microscopy requires mastery of the production of *thin sections* of very hard, mineralized but often brittle or fragile materials, which is a relatively complex technique (see e.g., Lamm 2013). Some of the technical requirements of thin sections are actually as old as the great civilizations of Antiquity: the art of sawing stones and polishing them flat was mastered for building as well as for jewelry, and those techniques, as well as glass and mirror production, reached new heights among lapidaries and other craftsmen, starting with the Italian Renaissance.

Who first devised thin section techniques? According to Higham (1963), they were invented and initially refined by several investigators, including William Nicol (1766–1851), Anders Retzius (1796–1860), and Richard Owen (1804–1892; Figure 1.2), who observed thin sections of various materials such as fossil wood, bone, teeth, agates, and so forth, in the years 1820–1840. Initially the materials available for holding and consolidating the fossils were restricted to plaster, cement, and various glues. Gluing and mounting media were restricted to Canada balsam, cooked to required values. The use of those products, especially the last one, required real technical knowhow and was difficult to master. Although this technique may be performed under simple, even rudimentary conditions, it generally allows the production of only very small preparations of a few square millimeters at the most (Thomasset 1930).



FIGURE 1.2 Richard Owen. (Great Britain, 1804–1892.) A major comparative anatomist and paleontologist, Richard Owen, built a kind of pre-Darwinian biology that reconciled Cuvierian functionalism and Geoffroy Saint-Hilaire's structuralism. Father of the concept of dinosaurs (Owen 1842b), he was largely responsible for the creation and development of the British Museum of Natural History (now the Natural History Museum, London). He pioneered thin sections of dinosaurs and pterosaurs. His *Odontography* (Owen 1840–1845) is the first large-scale comparative histological study of vertebrate hard tissues.

Actually, the real "father" of thin-section techniques appears to be William Nicol, who successfully prepared and observed thin sections of fossil wood in 1815. His technique was published 16 years later by Witham (1831), but he published his own observations of fossil wood in the same year and later (Nicol 1831, 1834, 1835; see Morrrison-Low and Nuttall 2003). Hence thin section techniques appear to be linked to the study of fossil material (especially fossil wood) from the very beginning, although Nicol also used it to study crystallized minerals and the fluids they contain (Nicol 1828). In the wake of Nicol's research on early plants, the technique was soon used by Miller for vertebrate hard tissues, notably to study the structure of the dermal plates of the placoderm *Asterolepis* (Janvier 2003c).

Accordingly, the paleohistology of fossils and the microscopic petrography and crystallography of minerals developed almost simultaneously, originally using the same techniques, but at different paces and scales. Later, the use of polarized light became important for the optical analysis of organic material (Valentin 1861). Although fossilization implies more or less extensive chemical and mineral changes (Paine 1937) in bone, and to a lesser extent in dentine and especially in enamel, the actual histological details are often rather well preserved and can be precisely deciphered among fossil remains.

On the petrographic microscopy side, the early developments appear to have been especially linked to Henry Clifton Sorby (1826–1908), who processed his first thin section in 1849 and published on it in 1851 (Dawson 1992; Higham 1963). This was followed by the immense development of microscopic petrography and crystallography in geology.

On the paleontological microscopy side, thin sections appear to have been developed a little bit earlier, as demonstrated by Richard Owen's famous *Odontography* (Owen 1840–1845) in two volumes that may be considered the first large attempt at comparative hard tissue histology, as evidenced by the complete title of the book (*Odontography, or a treatise on the comparative anatomy of the teeth, their physiological relations, mode of development and microscopic structure in the vertebrate animals*).

In 1849 John Quekett (1815–1861; Figure 1.3) published two papers of lasting importance because they focused on the great value of bone histological structures "to assess affinities of minute fragments of organic remains" (Quekett 1849a,b), an implicit research program that has stimulated paleohistological research up to this day. Published in two volumes in 1855, Quekett's *Descriptive and illustrated catalogue of the histological series contained in the Museum of the Royal College of Surgeons of England* (Quekett 1855) depicted thin sections of pterosaur and dinosaur bones. The origin of the histological collection was much older, however, going back to the gift of his collection (about 13,000 specimens) to the Royal College

VetBooks.ir



FIGURE 1.3 John Quekett. (Great Britain, 1815–1861.) A microscopist, histologist, and cofounder of the Royal Microscopical Society, Quekett became curator of the Hunterian Museum after Richard Owen left this position to move to the British Museum in 1856. One of his best known works is the *Descriptive and illustrated catalog of the histological series...in the Museum of the Royal College of Surgeons* (Quekett 1855), but perhaps the most influential works have been the two papers (Quekett 1849a,b) that have worked as a kind of agenda for paleohistology.

of Surgeons by the famous anatomist John Hunter (1728–1793) (Padian 2004; Sloan 1992). Thus, the *Pterodactylus* thin sections (Steel 2003) figured in the catalog may well have been processed by Owen himself, who at the same time would have made thin sections of the first recognized representatives (*Iguanodon*) of the new reptilian group for which he coined the name Dinosauria (1842b. Owen also pioneered the early studies of the peculiar structures of the "labyrinthodont teeth" of early stegocephalians (Owen 1842a), together with several other early investigators (see Castanet et al. 2003). Later, Owen figured thin sections of the dermal scutes of the dinosaur *Scelidosaurus* when he described the animal in 1861 (Owen 1861).

From the same period, William Williamson (1816–1895) published in 1849 and 1851 his masterful, well-illustrated studies on the microscopical structure and development of bone, scales, and dermal teeth of early vertebrates (Williamson 1846, 1951). These studies set a distinct trend and style of paleohistological studies among "early" or "lower" vertebrates, as discussed below. Before Williamson, Louis Agassiz (1807–1873: Figure 1.4) had published his pioneering *Recherches sur les poissons fossiles* (Agassiz 1833–1843) and his monograph on the fishes of the Old Red Sandstone (Agassiz 1844–1845), with several plates showing sections of fossil vertebrates and histological details of teeth and other structures. However, it may be that he used polished surfaces observed with the dissecting microscope (reflected light) rather than thin sections (transmitted light), and the same issue may be raised about Pander's (1856–1860) paleohistological observations.

The "Early Vertebrates" Tradition

Starting with Agassiz and Williamson, the histological study of "early vertebrates" (Janvier 1996) has been a noninterrupted – if poorly publicized – field of research, practiced to this day by a small community of specialized paleontologists, mostly in the world's great natural history museums.

The dermal (superficial) skeleton of fossil "agnathans," acanthodians, placoderms, chondrichthyans, actinopterygians, and finned sarcopterygians probably expresses the largest diversity of phosphatic hard tissues that ever evolved. This histodiversity is evident in the scales, spines, dermal rays, teeth, and flat bones of all extinct and extant finned vertebrates (Sire et al. 2009; Zylberberg et al. 1992). These elements are often composed of osseous tissues closely associated with dental tissues. Because the tissues (microstructures), but also their patterns of associations (so-called "mesostructures"), often seem to be highly specific to some systematic groups, hopefully monophyletic, it is understandable that their study has been intensely involved to sort out systematic/phylogenetic issues, as well as formal determination of scrappy material, thus fulfilling Quekett's (1849a,b) implicit program.

Important contributions to the field were provided by Christian Pander (1794–1865). He discovered and named the conodonts (Pander 1856–1860), which have recently been interpreted by some authors as vertebrates (or close to them), while others dispute this, and whose histology and its significance still remain contentious (Blieck et al. 2010; Donoghue 2001; Janvier 2013; Murdoch et al. 2013; Sansom 1996; Sansom et al. 1992, 1994; Schultze 1996; Turner et al. 2010).

The noted comparative anatomist Edwin S. Goodrich (1868–1946) provided important data on the structures of fin-rays (Goodrich 1904) and scales (Goodrich 1907) and was apparently the first author to use the term paleohistology (Goodrich 1913). Later, the field was augmented by the studies of Aldinger (1937) on "ganoid" Permian actinopterygians, by Bryant (1936) on the then oldest known vertebrates, *Astraspis* and *Eryptichius* from the Ordovician of Colorado, and by Denison (1967) on the same material and other contributions (Denison 1963), notably on dipnoan teeth (Denison 1974).

Following Pander's (1856–1860) pioneering works (see Schmitt 2005), the histology of the dermal skeleton among early jawless vertebrates (then called "Ostracoderms") and jawed placoderms and acanthodians, from the Devonian of the Baltic region, was meticulously described by Walter Gross (1903–1974; Figure 1.5) in several important works (Gross 1930, 1935, 1967, 1971). He also published extensively on the dermal skeleton of finned sarcopterygians and jawless Osteostraci (Gross 1956, 1961) with three-dimensional (3D)

VetBooks.ir



FIGURE 1.4 Louis Agassiz. (Swiss-American, 1807–1873.) A great naturalist who worked in geology, botany, zoology, and paleontology, Agassiz was responsible for the establishment of the Museum of Comparative Zoology at Harvard University (1859). With the publication of his *Recherches sur les poissons fossiles* (Agassiz 1833–1843) and his *Monography of fossil fishes from the Old Red Sandstone (or Devonian) of Great Britain and Russia* (Agassiz 1844–1845) he is regarded as the founder of paleoichthyology. His comparative research on the structure, nomenclature, and classification of fish bones, teeth, and scales is a direct antecedent of the paleohistological studies of early finned vertebrates by Christian Pander (1794–1865) and William Williamson (1816–1895).

reconstructions of the complex "pore canal systems" and early descriptions of the "twisted plywood" (Giraud et al. 1978; Meunier 1981, 1984) in the deeper components of the dermal skeleton. Beverly Halstead-Tarlo (1933–1991) provided a massive study of histology among the Heterostraci (Halstead-Tarlo 1964–1965, 1973), as well as several other interesting contributions on the origin and early evolution of the mineralized vertebrate skeleton (Halstead-Tarlo 1963, 1969, 1973).

In the Soviet Union, Alexeï Bystrow (1899–1959) conducted an important and original series of morphological-histological works on bone and dental tissues, mostly of early tetrapods (Bystrow 1935, 1938a,b, 1944, 1947), but also of early finned vertebrates (Bystrow 1939, 1941, 1942, 1957b, 1959), as well as in his stunning opus (Bystrow 1957a) on the heterochronic future of man.

Perhaps the most important contributor to paleohistological studies on early vertebrates remains Professor Tor Ørvig (1916–1994: Figure 1.6), a member of the once famous "Stockholm school" of paleontology at the Swedish Museum of Natural History, under the leadership of Professors Eric Stensiö (1891–1984) and Eric Jarvik (1907–1998). Although this school was finally doomed by its forceful reluctance to accept modern phylogenetic analysis, it provided massive amounts of useful anatomical and histological data on early vertebrates (Schultze 2009). Ørvig's contributions include general reviews of lasting interest on various aspects of the early evolution of skeletal tissues (Ørvig 1965, 1966, 1967, 1968, 1977), as well as more descriptive monographs on early Actinopterygian histological structures and growth (Ørvig 1978a–c). However, his most impressive work probably remains the histological study of the endoskeleton of Placoderms and fossil Chondrichthyans (Ørvig 1951), which actually covers several other topics and offers an almost complete bibliography of a century of research on paleohistology and comparative histology of the vertebrate skeleton.

More recently, Moya M. Smith published detailed studies on the hard tissues of Paleozoic vertebrates, using sophisticated techniques, notably on lungfish denticles and tooth plates (Smith 1984, 1988; Smith and Campbell 1987; Smith et al. 1987). She stirred a revival of research on the histodiversity of the earliest (Cambrian and Ordovician) vertebrates (Donoghue and Sansom 2002; Märss 2006; Ricqlès 1995a; Samson 1996; Sansom and Elliott 2002; Sansom et al. 1992; Wang et al. 2005) and on the problems of the significance of conodont hard tissues relative to early vertebrate phylogeny (Blieck et al. 2010; Donoghue 2001; Sansom et al. 1994).

Some groups, such as cladistians (polypterids), have been thoroughly studied (Gayet and Meunier 1992; Geraudie 1988) because their anatomical and histological peculiarities have, for a long time, made any assessments of their proper phyletic relationships very difficult. Regarding dipnoans, for example, special "links" with chondrichthyans were advocated for a long time. The structure, growth, and significance of the denticles and especially the dentary plates of dipnoans, compared to chimaerid chondrichthyans, have received conflicting interpretations over the years (Denison 1974; Lison 1941; Ørvig 1967, 1968; Peyer 1968; Poole 1967; Schmidt and Kiel 1971; Smith 1984, 1988; Smith and Campbell 1987; Smith et al. 1987).

The fin-rays of finned vertebrates (e.g., actinotrichia, ceratotrichia, lepidotrichia, camptotrichia, etc.) show a great diversity in their ontogeny and fine structure, and in their relationships with other elements of the dermal skeleton: denticles, scales, oral teeth, and bone. They offer a great deal of relevance for phylogenetic studies (Bertin 1958; Geraudie 1988; Geraudie and Meunier 1980, 1982; Goodrich 1904; Jing Lu et al. 2016; Moss 1972; Schaeffer 1977; Zylberberg et al. 1992).

The scales of extinct and extant aquatic vertebrates offer a histological diversity and complexity that has promoted an exceptionally high quantity of research, combining various systematic-phylogenetic, developmental, and functional concerns. Agassiz's (1833–1843) early terminology of ganoid, placoid, cycloid, and ctenoid scales, once used to characterize taxonomic groups during the nineteenth century, was the foundation of much later research that played an important role in deciphering early vertebrate phylogeny (Janvier 1996).

Scale structures among what we now understand as sarcopterygians has been the subject of many studies, often dealing with the significance, function(s), and evolution of cosmine (Agassiz 1844–1845; Bertin 1958; Giraud et al. 1978;

VetBooks.ir



FIGURE 1.5 Walter Gross. (German, 1903–1974.) A specialist in the early Paleozoic of the Baltic area, Gross built an impressive paleohistological knowledge of highly diverse early vertebrates, including jawless and jawed groups, with some 3D reconstructions of complex microanatomical details of the dermal skeleton. He should be recognized as one of the first paleontologists for whom paleohistology took a prevalent role. His only work on tetrapod histology has been very influential. The building of the Berlin Wall in 1961 prevented him from continuing his work in his former laboratory and he spent the rest of his career in Tübingen.

Goodrich 1907; Gross 1956; Meinke 1984; Meinke and Thomson 1983; Meunier and François 1980; Schaeffer 1977; Schultze 1966, 1977, 2016; Thomson 1975; Zylberberg 1988). See Jing Lu et al. (2016) for new developments on the issue.

Again, teeth and tooth-like structures among finned vertebrates offer an astounding histological diversity because, apart from the more "typical" oral teeth and denticles, similar tissues can spread throughout the dermal skeleton. Their various conditions offer a multitude of character states from the points of view of phylogenetic, developmental, and functional biology (Agassiz 1833–1843, 1844–1845; Butler and Joysey 1978; Carlson 1990; Denison 1974; di Masi and Gower 2016; Donoghue 2001; Donoghue et al. 2006; Foote 1928; Gayet and Meunier 1986; Geraudie 1988; Gross 1961, 1971; Hertwig 1874a; Kemp 2002; Lison 1941; Meunier 2011; Miles 1967; Mongera and Nüsslein-Volhard 2013; Moss 1977; Ørvig 1967, 1977; Owen 1840–1845; Peyer 1968; Poole 1967; Reif 1982; Sansom et al. 1994; Schaeffer 1977; Schmidt and Kiel 1971; Schultze 1969, 2016; Sire and Huysseune 2003; Smith 1984, 1988; Smith and Campbell 1987; Smith and Coates 1998; Thomasset 1930; Tomes 1878, 1898; Williamson 1849, 1851).

Some current paleohistological research on the dermal skeleton is directly inspired by the above-mentioned works (Zylberberg et al. 2010). Others deal with more general questions. What is the oldest vertebrate hard tissue? Did dental tissues precede bone evolutionarily? Did the dermal skeleton precede the endoskeleton? Was aspidin (noncellular bone) a "predecessor" of "regular" (osteocytic) bone? Did mineralized tissues all appear together, as "modulations" of a common system when the basic controls of cell-induced phosphatic mineralization of various extracellular matrices, notably collagens, became available (Denison 1963; Donoghue and Sansom 2002; Donoghue et al. 2005, 2006; Hall 1975, 1978, 2005; Halstead-Tarlo 1963, 1969, 1973; Lubosch 1927; Maisey 1988; Moss 1963, 1964, 1968, 1972; Ørvig 1965, 1966, 1967, 1968, 1977; Patterson 1977; Piveteau 1934; Poole 1967; Reif 1982; Romer 1963, 1964; Roumiantsiev 1958; Schaeffer 1977; Schultze 2016; Vaillant 1902; Zhu et al. 2006)? Are the hard tissues of conodonts really homologous to the those of vertebrates (Blieck et al. 2010; Janvier 2013; Murdoch et al. 2013; Sansom et al. 1992, 1994; Schultze 1996)?

As recently described Ordovician and even Cambrian vertebrates or even perhaps early chordate-like fossils become available for study (Sansom 1996; Shu et al. 2003; Wang et al. 2005; Young et al. 1996; Zhu et al. 2006), those classical questions regress toward more and more remote times (Donoghue et al. 2005; Janvier and Arsenault 2002; Janvier 2003a,b). Comparative molecular studies can shed light on the origin of some genes involved in biomineralization (Delgado et al. 2001), suggesting distinct pre-Cambrian origins.

In parallel with paleohistological investigations, histological studies of extant finned vertebrates (chondrichthyans, finned osteichthyans) have always provided a much needed comparative background to interpret conditions among fossils. Important historical contributors include Kölliker (1859), notably on the intriguing issue of acellular (anosteocytic) bone among "advanced" teleosts, and Klaatsch (1890) and Hertwig (1876–1882) on the structure of "fish" (including selachian) teeth and bones. On the structures of scales, Baudelot (1873), Kerr (1952), Mandl (1839), and Tretjakoff and Chinkus (1927, 1930) offered interesting comparative studies, supplemented by numerous more recent works (Meunier 1981, 1984, 1987; Meunier and François 1980; Schönbörner et al. 1981).

The origin and evolution of the superficial (integumentary) skeleton in finned vertebrates has been recently surveyed (Meunier 2011; Sire et al. 2009). A more recent survey of the general matter of the evolution of scales was provided by Schultze (1996, 2016). Those recent surveys cover the massive bibliographic expansion of the field during the last 40 or so years. The new approaches use descriptive-comparative data as a starting point in systematics (Gayet and Meunier 1986) and for ontogenetic (developmental), phylogenetic (evolutionary), biological (ecological), and sometimes even paleobiogeographic issues (Gayet and Meunier 1992). For example, the problem of the origin of the cells that produce the superficial hard tissues, mesodermal or neural crests, or both has recently been revisited (McGonnel and Graham 2002; Mongera and Nüsslein-Volhard 2013).

VetBooks.ir



FIGURE 1.6 Tor Ørvig. (Norwegian-Sweden, 1916–1994.) A member of the well-known Stockholm school active at the Swedish Museum of Natural History under the initial leadership of Eric Stensiö, Ørvig was almost a full-time paleohistologist and specialized in early (Paleozoic) finned vertebrates, although he did some work on more recent tetrapods. His works include the discovery and description of many histological characteristics in various clades of early vertebrates and general considerations on the evolution of vertebrate hard tissues.

Apart from the dermal skeleton, the histology of the endoskeleton of early vertebrates also raises fundamental issues. Did nonmineralized cartilaginous endoskeletons precede the origin of calcified cartilage by millions of years? The origin, diversity, phylogeny, and functional significance of the various patterns of calcified cartilage (and bone) in the endoskeleton of early vertebrates is also a matter of great interest.

The issue is especially important for elasmobranchiomorphs, e.g., the significance of prismatic and areolar cartilages among chondrichthyans, such as selachians, holocephalians, and related extinct groups (Bordat 1987; Dean and Summers 2006; Denison 1963; Kemp and Westrin 1979; Lubosch 1927; Maisey 1988; Moss 1977; Ørvig 1951; Patterson 1977; Wurmbach 1932). This question relates to the issue of the significance of "globular" structures in several hard tissues of early vertebrates, perhaps a "primitive" form of biomineralization, called "spheritic," compared to the "inotropic" mineralization of typical bony tissues, as suggested by Ørvig (1965, 1968). Another problem deals with the monophyletic or polyphyletic origin of endochondral ossification in vertebrates (Wang et al. 2005). In addition to Ørvig's (1951) work, one may mention here the comparative histological studies by Wurmbach (1932) on selachians and the work of Stephan (1900), Blanc (1953), and especially of Haines (1934, 1937) on osteichthyans. This field of study was pursued by Amprino and Godina (1956), Baud and Morgenthaler (1953), Francillon (1974, 1977), Kemp and Westrin (1979), Bordat (1987), and Meunier (1987), and a great deal of additional research is required to decipher various issues, for example, the significance of the peculiar "polyosteonal systems" in the rostrum of swordfishes (Poplin et al. 1976).

Tetrapods: Systematics or Functions – or Both?

The historical development of comparative hard tissue histology and paleohistology in tetrapods has followed an historical pathway rather different from that of "lower" or early finned vertebrates for several reasons (Ricqlès 1993).

First, following Georges Cuvier's (1769–1832) approach, research on the bony and dental components of the tetrapod skeleton was first mostly restricted to comparative anatomy. Gross comparative skeletal morphology offered such a host of meaningful information for systematics as well as for functional biologists. Vertebrate paleontology developed into a science as an extension of comparative anatomy to the study of fossils. After the generalization of the cell theory, it took some time for comparative histology of skeletal tissues of bone and teeth to mature into the mainstream of biological studies, and later to interact with evolutionary issues. During the nineteenth and early twentieth centuries, studies of bone histology and bone biology in general were dominated by, and largely restricted to, medical and veterinary approaches to mammals, mostly humans, and some "model" laboratory animals. Accordingly, hundreds of publications built the "vulgate" of hard tissue histology, summarized in numerous treatises, without much consideration for comparative-evolutionary aspects.

Second, regarding dental tissues *sensu lato*, their almost total restriction among tetrapods to oral teeth has long set their study apart from that of bone histology, contrary to the situation among early vertebrates where extraoral dental tissues are widespread on the dermal skeleton. In spite of Owen's (1840–1845) pioneering synthesis, the all-important issues of the comparative morphology, histology, and functions of mammalian teeth, with their high systematic-phylogenetic, functional, and practical implications for paleontologists, biologists, and odontologists (Butler and Joysey 1978; Lester and von Koenigswald 1989; Tomes 1897), may have somewhat overshadowed the biological-comparative histological studies of teeth among nonmammalian tetrapods, and vertebrates in general (Carlson 1990; Chibon and de Ricqlès 1995; Miles 1967; Peyer 1931, 1968; Poole 1967; Reif 1982; Sander 1997a,b; Schmidt and Kiel 1971; Tomes 1875).

Nevertheless, an exceptionally high number of descriptive-comparative works was developed, over the years on the histology of teeth and tooth-associated tissues in vertebrates and especially tetrapods. As an example, the "plicidentine" of various osteichthyans, early tetrapods ("labyrinthodonts"), and various amniotes has received extensive coverage (Bystrow 1938b; Caldwell et al. 2003; Hertwig 1874b; Schultze 1969); see Castanet et al. (2003) and Chibon and de Ricqlès (1995) for an

VetBooks.ir

extensive review of plicidentine and other tooth tissues among extant lissamphibians and extinct early tetrapods. The wealth of comparative data on the structures, functions, and evolutionary trends in enamel, dentine, and adjacent tissues (cementum) of tetrapods has produced a very active research initiative.

Although the dermoskeleton of tetrapods lacks classical dental tissues, comparative histological studies of scales, scutes, and osteoderms among various tetrapod clades have demonstrated the occurrence of different mineralized tissues that can hardly be considered typical bone (Moss 1972; Vickaryous and Sire 2009). Such occurrences have been described in temnospondyls and other early tetrapods (Bystrow 1944; Colbert 1955; Credner 1893; Findlay 1968), gymnophionans (Zylberberg and Wake 1990; Zylberberg et al. 1980), and anuran amphibians (Ruibal and Shoemaker 1984), early reptiles (Findlay 1970), squamates, (e.g., Buffrénil et al. 2011; Levrat-Calviac and Zylberberg 1986; Zylberberg and Castanet 1985), archosaurs (Owen 1861; Ricqlès et al. 2001c), and early synapsids (Tchudinov 1970). In each case, issues of homologies and developmental biology are raised, and this field currently remains an active domain of research (Vickaryous and Sire 2009).

A peculiarity of the tetrapod dermoskeleton is the fact that the external surface of dermal bones (below the skin) is often "ornamented" by various systems of ridges and furrows, pits, and so forth, especially among early tetrapods *sensu lato* and early amniotes (Bystrow 1935, 1938a, 1944, 1947). The significance of this ornamentation has received numerous, often conflicting explanations.

Following the pathways set by Quekett's (1855) catalogue, comparative descriptions of compact bone histology, mainly derived from the study of cross sections of long bone shafts, progressively developed among extant and extinct amphibians, reptiles, birds, and mammals, understood as the great classical (precladistic) vertebrate classes. Naturally, histological differences recorded among taxa were *a priori* expected to express systematic affinities, either from a purely static-descriptive point of view or, later, within various phylogenetic-evolutionary perspectives.

Paul Gervais (1816–1879; Figure 1.7) started an extensive comparative histological collection of fossil and extant hard tissues (bone, scales, and teeth) and eggshells at the National Museum of Natural History (Paris) during the 1870s (Meunier and Herbin 2014; Ricqlès et al. 2009). However, he only wrote one publication, on the specialized subject of "hyperostoses" (Gervais 1875).

Kiprijanoff (1881–1883) published a massive, pioneering study on the histology of the Mesozoic reptiles of Russia, exquisitely illustrated by high-quality drawings that still deserve attention. Mostly dealing with marine reptiles, the work suffers from the poorly defined anatomical and taxonomic origins of the samples, which is a problem that plagued most early comparative paleohistological studies (Padian 2011). In Austria, Von Ebner (1875) and Schaffer (1889) also dealt with the study of early tetrapod histology, but a real breakthrough came in 1907 with the monograph of Seitz (1907) on the comparative histological study of bone in fossil and recent reptiles. Microscopic photography was extensively used to illustrate precise descriptions and, although there are reservations about the actual origin of some of the material, the work remains a milestone, still deserving consideration.

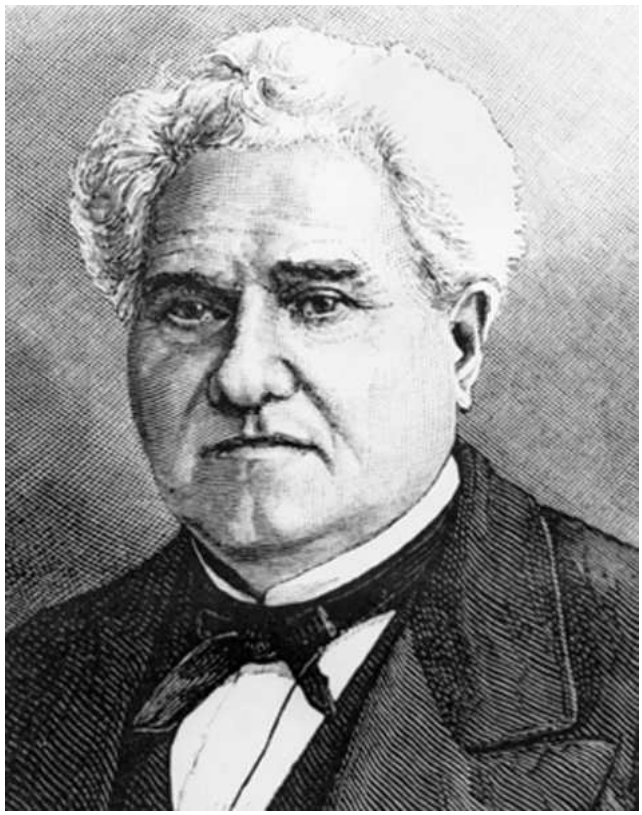


FIGURE 1.7 Paul Gervais. (France, 1816–1879.) Zoologist and comparative anatomist, Gervais published extensively on various aspects of vertebrate zoology and paleontology, notably on fossil mammals, especially from South America. His career culminated as the Chair Professor of Comparative Anatomy at the Paris Museum (1868), where he developed his interest in histology and paleohistology, assembling an important collection of thin sections that are still preserved. Among them are the first eggshells and bone thin sections of dinosaurs discovered in France.

During the1930s, several paleohistological works on compact bone significantly added to the progress made by biologists in assessing the significance of tissue diversity discovered among tetrapods. Gross (1934) published the most important comparative study on stegocephalian, dinosaur and pterosaur bone histology, based on the then current comparative and functional understanding of compact bone provided by the studies of Gebhardt (1901–1906, 1910), Petersen (1930), Weidenreich (1930; Figure 1.8) and others, also summarized by von Eggeling (1938). Gross clearly illustrated, following Seitz (1907), the fundamental distinction between primary and secondary osteons in compact bone.

The concept of the "Haversian system" had been analyzed by Tomes and de Morgan (1853) as expressing a physiological phenomenon of local erosion followed by redeposition within compact bone. Thus this concept precisely matches the concept of "secondary osteons" (Biederman 1913) or "substitution osteons" (Lacroix 1971; Ponlot 1960). Nevertheless, the term Haversian system has long remained loosely used to describe

VetBooks.ir

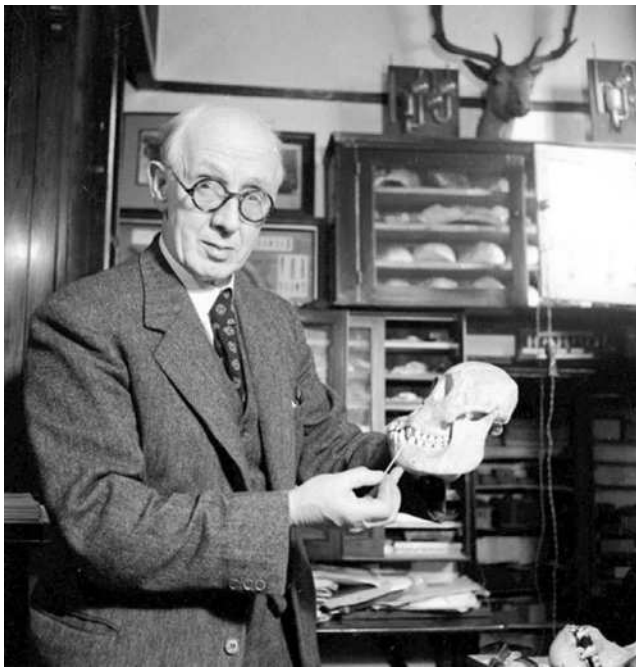


FIGURE 1.8 Frantz Weidenreich. (German, 1873–1948.) Well known and remembered as a paleoanthropologist for his work in China on the "Peking (Beijing) man" (or "*Sinanthropus,*" now *Homo erectus*) with P. Teilhard de Chardin and for other paleoanthropological research, this was Weidenreich's second career, after he had to leave Germany. Far less popular apart for the histologists, are his masterworks published during the 1920s, when he built a powerful synthesis on bone histology. His *Knochenstudien* were influential on the works of Gross and Amprino (quod vide) and far beyond. Weidenreich is a striking example of two successive successful careers in two separate (although related) fields, histology and paleoanthropology, imposed on a gifted man by the vagaries of history.

any situation in compact bone where bone lamellae appear to have been laid down around a vascular canal. This situation is sometimes described as "proto- or pseudo-Haversian systems" often with a "qualitative" or phylogenetic connotation (Crawford 1940; Foote 1913, 1916). Actually, the bone lamellae laid down around a vascular canal without previous erosion of the locally preexisting bone are "primary osteons" (Biederman 1913) or "addition osteons" (Lacroix 1971; Ponlot 1960). The clear distinction between primary and secondary osteons is valuable not only for comparative tissue descriptions (Castanet et al. 2003; Ricqlès 1976) but also for its histophysiological significance (Amprino 1948, 1967; Bourne 1972; Castanet et al. 1986–1987; Frost 1964; Glimcher 1976; Hancox 1972; Murray 1936).

Franz von Nopcsa (1877–1933; Figure 1.9), the eccentric Hungarian paleobiologist (Weishampel and Reif 1984), published several thought-provoking studies on the histological peculiarities of Mesozoic marine reptiles (Nopcsa 1923a,b; Nopcsa and Heidsieck 1934), a field of comparative research that later expanded considerably (Buffrénil 1982; Buffrénil and Mazin 1990; Buffrénil et al. 1987, 1990; Zangerl 1935). Nopcsa also pioneered issues of ontogenetic versus systematic changes in bone tissues among dinosaurs (Nopcsa and Heidsieck 1933) and general issues on tetrapod evolution (Nopcsa 1930). During the same period Moodie (1923) described several tissue structures among early tetrapods, notably dinosaurs, in the context of pathological interpretations.

Simultaneously, efforts in the comparative histology of compact bone tissue of long bone shafts, especially the femur, in extant vertebrates brought a great deal of new data to the histodiversity of this bone among mammals, birds, reptiles, and amphibians (Foote (1913, 1916), introducing some terminological novelties for tissue classification. Those extensive studies were illustrated by numerous comparative, semi-diagrammatic drawings of deceptive simplicity, a method followed by Matyas (1929). A little-known summary of Foote's observations, also covering his findings on dermal bone and teeth, was published posthumously (Foote 1928).

The fundamental contributions to bone histogenesis and biology offered by Weidenreich (1930) and Petersen (1930) influenced later works, notably the extensive comparative, structural and functional research of Rodolfo Amprino (1912–2007: Figure 1.10) and his coworkers. His approach to bone histology was simultaneously comparative and experimental. He pioneered the analysis of the complex causality that can explain the puzzling variability, local and taxonomic, of compact bone tissue noted by Murray (1936). Starting with ontogenetic and comparative studies in humans (Amprino 1943; Amprino and Bairati 1936, 1938), he extended his inquiry to tetrapods (Amprino and Godina 1944–1945, 1947; Godina 1946, 1947), and ultimately other vertebrates (Amprino and Godina 1956) using plentiful microphotographic illustrations. This allowed him to offer evidence that the histovariability of primary compact bone first and foremost expresses differences in growth rates (Amprino 1947), a milestone later known as "Amprino's rule" (Castanet et al. 1996; Margerie et al. 2002), which revolutionized interpretations of bone as a tissue. Simultaneously Amprino and his research fellows elaborated a histophysiology of bone as a tissue, thanks to various experimental approaches, with special emphasis on the significance of Haversian substitution in compact bone (Amprino 1948, 1967; Frost 1964; Glimcher 1976; Hancox 1972; Ponlot 1960).

The famous series of papers by Enlow and Brown (1956–1958; Figure 1.11), C*omparative histological study of fossil and recent bone tissue,* represent the first (and only) attempt at a comparative description of bone histology encompassing the whole systematic spectrum of vertebrates, with some emphasis on tetrapods. They offer a tentative nomenclature and classification of bone tissue patterns and diversity. Augmented by later works by Donald Enlow (Enlow 1963, 1966, 1968, 1969), this seminal work was influential in many ways (Ricqlès 1975–1978, 1979, 2007). From the same period also came important papers by Smith (1960) and, Currey (1960, 1962) on the fibrillary organization and vascularization of primary compact bone in mammals and dinosaurs.

As already noted, from the beginning of paleohistology there was an implicit assumption that histological character states have a systematic (phylogenetic) importance, similar to the significance of gross morphological-anatomical character states, i.e., Quekett's (1849a,b) "program." In other words, it was assumed that the straightforward transposition from the anatomical to the histological levels of integration did not raise special problems, and that, accordingly, histological

VetBooks.ir



FIGURE 1.9 Franz Nopcsa. (Austro-Hungary, 1877–1933.) A Hungarian nobleman from Transylvania, Nopcsa remains one of the most extraordinary and romantic personalities of the history of vertebrate paleontology. With his sister, he discovered dinosaurs at age 18 (1895) on his family properties and started a meteoric career as a paleontologist, defending his PhD at age 22 in Vienna. Nothing can be said here of his adventurous life as a spy and an ethnologist in the Balkan turmoil during World War I. Nopcsa was active in several domains of paleontology and geology, often with an almost prophetic power, and he may be regarded as a founding father of paleobiology and paleoecology. He fully realized the paleobiological value of paleohistology and built an important collection of thin sections of fossil reptiles, working especially on the secondary adaptation of tetrapods to aquatic life. He also pioneered dinosaur histology, discussing the taxonomic versus ontogenetic interpretations of the data. A good part of Nopcsa's fossil collections, including thin sections, are preserved in the Natural History Museum, London.

characters should have a systematic value, just like anatomical ones. This was the basis of the first historical phase of comparative compact bone histology and paleohistology of tetrapods, where the prevailing interpretation was systematic. For example, it was long believed that primary osteons were "primitive" and that dense Haversian bone expressed the evolutionary "summit" of compact bone evolution. Similarly, it was assumed that coarse woven bone was primitive (both ontogenetically and phylogenetically) compared to finely lamellar bone (Crawford 1940; Foote 1913, 1916, 1928; Matyas 1929; see Ricqlès 1975–1978).

Nevertheless, the accumulation of descriptive and comparative data gradually raised doubts about the systematic value of bone histology among tetrapods and about a "straightforward," linear evolution of tissue types (Enlow 1963, 1966). Functional (rather than historical) interpretations of bone histovariability (within an organism) and at broader comparative levels (histodiversity) integrate several "explanatory" causes or "factors" (ontogenetic, physiological, biomechanical, environmental) that may all interact to account for the character states of bone tissue at a given spot in a bone section (Murray 1936). In other words, the *vera causa* of histological diversity is to be found in the "functional" (*sensu lato*) activities of the living organism, its systematic/evolutionary pedigree then appearing as a more medial, or remote, "cause" for explaining comparative data. The massive amount of histological convergence among similarly adapted taxa that are only remotely related fits very well with this interpretation (Ricqlès 1993).

The contributions of Amprino and Enlow were instrumental in shifting emphasis in the study of tetrapod bone histodiversity from systematic-evolutionary causes to ontogenetic-functional causes, opening new avenues to explain how and why various kinds of tissues are laid down under a variety of local and general circumstances (Ricqlès 1993, 2007). This trend started in the 1960s with several descriptive works of great value, such as Currey (1960, 1962), Smith (1960) and Pritchard (1972). By the 1960s the number of available comparative descriptions of compact bone tissue diversity among tetrapods permitted the development of tentative syntheses from structural, functional, and evolutionary points of view (Ricqlès 1975–1978, 1976). This work also tackled the terminological conundrum induced by the long use of rather profuse and contradictory terminologies, as an effort toward a more standardized classification and nomenclature of tissue types.

The tentative conclusion stemming from the abovementioned studies, notably about the general evolution of thermometabolic physiology among synapsids and archosaurs (Bonis et al. 1972; Ricqlès 1976, 1980), stirred a renewal of interest in dinosaur paleohistology, with a rapidly increasing number of descriptive works and discussions on the functional significance of the data. This took place during the last two decades of the twentieth century. The expansion of comparative histological inquiries was especially active regarding dinosaurs (Chinsamy 1995, 2005; Erickson 2005; Horner et al. 1999, 2000, 2001; Reid 1981, 1983, 1984, 1985, 1996; Sander 2000), pterosaurs (Ricqlès et al. 2000; Steel 2003), and birds (Amprino and Godina 1944–1945; Chinsamy et al. 1995; Margerie 2002; Ricqlès et al. 2000, 2001b, 2003; Zavattari and Cellini 1956 (see chapter 27 in this book on Avemetatarsalia). During the same period, other tetrapod groups were also analyzed histologically, notably early reptiles (Ricqlès and Bolt 1983) and especially various synapsids (e.g., Botha 2003). Various histological specializations (e.g., pachyostosis) linked to the secondary adaptations of tetrapods to aquatic environments were also described, both among mammals (Fawcett 1942; Felts and Spurrel 1966; Buffrénil et al. 1990; Perrin and Mirrick 1980), and among various reptilian clades (Buffrénil 1982; Buffrénil et al. 1987, 1990; Caldwell et al. 2003; Houssaye et al. 2008; Hugi et al. 2011; Ricqlès and Buffrénil (2001); Wiffen et al. 1995; Zangerl 1935).

Simultaneously, experimental and comparative work on extant model animals attempted to get quantitative data on the relationships between growth trajectories and histological patterns (Castanet et al. 1996, 2000; Margerie et al. 2002).

Roughly, up to the 1990s, comparative-descriptive paleohistological studies had been taxonomically extensive but, perforce, also opportunistic. There was often little control on the material available for study. It was very difficult, for

VetBooks.ir



FIGURE 1.10 Rodolfo Amprino. (Italy, 1912–2007.) A medical doctor and anatomist, Amprino enjoyed an active international career in developmental biology. He led, with several collaborators, breakthrough research on bone biology, especially on the histophysiological significance of compact bone remodeling. Because he used various approaches, both experimental and comparative, he brought a significant amount of new data on the histodiversity of primary bone tissues among extant vertebrates, and its physiological significance in terms of growth rates. This was later popularized under the term Amprino's rule and applied to paleohistological research.

example, to standardize histological descriptions at functionally analogous sections (Enlow 1963) within homologous bones (Padian 2011). Considering the all-important histovariability demonstrated in the skeleton of every extant tetrapod taxon, it gradually became possible to master those variables somewhat better among extinct taxa as soon as better samples became available for histological analyses (Horner et al. 1999, 2000). This has greatly improved the reliability and importance of paleohistological descriptions, now supplemented by intensive quantitative analyses and statistical treatments (Cubo et al. 2012).

In parallel with the development of general comparative paleohistology among dinosaurs and other fossil tetrapods, a complementary approach to bone histology was developed in the late twentieth century: the use of natural "growth marks" in compact hard tissues to assess growth dynamics, individual age, and longevity. The "recording" of time and of various life events, (e.g., hatching, seasonal cycles, general cessation of linear growth) in the structure of growing hard tissues demonstrates the causal importance of external (environmental) factors to shaping tissue structures and patterns. The latter may then be deciphered, retrieving life history traits (e.g., individual age) of the organisms, extant and ancient (see Chapter 31).

The method has a very ancient origin. It was used by the Swedish ichthyologist Hans Hederström in the eighteenth century (Meunier 2003), but it started to develop much later, with pioneer works on bone tissue by Bryuzgin (1939), Klevezal and Kleinenberg (1967), and Kleinenberg and Smirina (1969) in the USSR, and Peabody (1961) and Warren (1963) in the United States. It was later considerably expanded, under the name of skeletochronology, by the Paris group (Caetano et al. 1985; Castanet 1974, 1985, 1986–1987; Castanet et al. 1993, 2000; Meunier 1988) and their colleagues and followers (Baglinière et al. 1992). The value of those approaches is now acknowledged in a great number of ecological studies dealing with extant terrestrial and aquatic vertebrates, as well as in paleontological (Steyer et al. 2004) and archaeological applications (Burke and Castanet 1995; Casteel 1976).

Following Peabody's (1961) early suggestion, it was first assumed that the occurrence of "lines of arrested growth," "annuli," and other evidence of cyclical bone deposition were mostly restricted to ectothermic ("cold-blooded") vertebrates; hence, it could be used as an index of thermo-metabolism among fossils, notably dinosaurs (Ricqlès 1980). It took some time to recognize that "growth marks" were also widespread in compact bone tissues among endothermic mammals as well (Castanet 2006; Klevezal and Kleinenberg 1967; Perrin and Mirrick 1980). Accordingly, the consensual meaning of growth marks shifted from thermophysiological issues toward the more general study and deciphering of "life history traits" among extant and extinct vertebrates (Horner et al. 1999; Reid 1981; Ricqlès et al. 2004).

Because the size, shape, and density of bone cellular spaces (periosteocytic lacunae and canaliculi) are so often well preserved in fossil bone, various attempts have been made to extract information from these kinds of data. Osteocytic density is now measured to describe and assess the functional significances of various bone tissues (Cubo et al. 2012; Rensberger and Watabe 2000). The size of the bone lacunae may be used as a proxy for the cell (and nucleus) size, and hence of the genome size and its evolution. Early works along such lines (Brambilla 1972; Sacchi-Vialli 1967; Thomson 1972; Vialli and Vialli 1969) were followed by more quantitative analyses (Pawlicki 1984; Rensberger and Watabe 2000) and this approach is currently experiencing an explosive development in paleohistology; see Organ et al. (2016) for a recent synthesis.

Beyond the historical phase when tetrapod paleohistology mostly developed in the framework of functional (rather than phylogenetical) interpretations (1960–2000), as mentioned above, a new trend developed: a renewal of interest in the systematic-phylogenetic importance of bone histodiversity. Actually, the ancient quest for diagnostic characters in osseous tissues that would allow us to sort out fossil fragments and classify them reliably never really ended (Cuijpers 2006), in spite of its rather poor practical results in many cases (Enlow 1963; Ricqlès et al. 2004). The new trend derives from the generalization of cladistic approaches, and also from the development of new statistical analyses and further reasoning on the comparative method in biology (Blomberg and Garland 2002; Harvey and Pagel 1991).

Trying to find characters of systematic values at the histological level is theoretically sensible because, like any

VetBooks.ir



FIGURE 1.11 Donald Enlow. (USA, 1927–2014.) D. H. Enlow is especially well known and remembered in the biomedical area for his masterful syntheses on the human face and its growth, analyzed by bone histology, and he demonstrated the paramount importance of such knowledge in the practical fields of orthodontics and pedodontics. This occupied most of his later academic career. However, before that Enlow played an equally important role in the field of comparative bone histology and paleohistology of long bone growth and helped to decipher several complex issues in this domain. His famous research on bone paleohistology and reptilian comparative histology proved to be very influential. His enormous thin section collection is currently preserved at New York University's College of Dentistry.

intrinsic character of the semaphoront, bone tissue should convey a "phylogenetic signal," along with other structural and functional signals (Ricqlès et al. 2004, 2008). A phylogenetic signal can be defined for our purpose by the postulate that closely related species should have a statistically higher correlation of bone tissue features than would be expected from a random sample of taxa (Cubo et al. 2012). Considerable research has recently discovered that a phylogenetic signal indeed exists at the levels of bone histology and microanatomy (Cubo et al. 2005, 2008, 2012; Laurin et al. 2004), thus allowing us to separate the phylogenetic-systematic (historical) component of bone histodiversity.

All of the foregoing points to the complex, multifactorial causality of bone and other hard tissue structures and distributions at every level of perception. Rather than opposing historicism to structuralism or functionalism, and thus putting forward univocal causation where phylogeny, topology, the environment, and biomechanics are viewed as the unique efficient cause (or explanation, or constraint) of observed data, one may prefer an approach of causality that is multifactorial and tries to take into account simultaneously the relevant factors, their interactions, and their integration (Murray 1936; Padian 2004, 2011; Ricqlès and Cubo 2010). New statistical tools can even help to quantify the relative weight and influence of phylogenetic, functional, and structural factors determining the segregation of bone tissues in a phylogenetic context (Cubo et al. 2008). This gives an operational power to theoretical approaches to multifactorial causality, as expressed in the famous "triangle" developed by Seilacher (1970) and Gould (2002).

Epiphyses and Endochondral Ossification

It is historically interesting to notice how the problem of the lengthening of long bones during growth (and of growth of the endoskeleton generally) through the processes of cartilage growth and endochondral ossification has been studied rather independently of the radial growth of compact bone shafts (Enlow 1963, 1968; Ricqlès 1993). Both are distinct but intimately related expressions of the general growth modeling and remodeling processes that ultimately shape every adult bone as an organ (Enlow 1963; Ricqlès 1979). Nevertheless, for a very long time those studies remained rather distinct from each other. This dissociation can be easily accounted for, retrospectively, by technical constraints (Ricqlès 1993). Although the radial growth of compact cortices in shafts could best be studied with undecalcified ground sections, even in large bones, the study of endochondral ossification required decalcified, paraffin-embedded and colored longitudinal sections. Those techniques of classical histology, requiring the use of a microtome, could be best practiced on embryonic material or on adults of very small species, the developing mouse or chicken embryos being the most common examples (Fell 1925).

One of the major and long-lasting controversies in the history of skeletal histology has been linked to the processes of endochondral ossification. Early authors believed that cartilage was actually changed into bone by "metaplasia," a process of direct transformation of one tissue (cartilage) into another one (bone). Others observed the actual destruction of cartilage and its local substitution by the deposition of a new tissue, such as bone. This debate was settled by Müller's (1858) contribution in favor of "neoplasia," which is the local destruction of cartilage and its replacement by bone. This new tissue is laid down by osteoblasts, at the periphery of the erosion bays carved by chondroclasts into the remains of cartilage. Although it is uncontroversial that most endochondral bone is formed by this process, especially among mammals and birds, some apparently contradictory situations were persistently described, especially among urodeles (Quilhac et al. 2014). General surveys of the matter (Beresford 1981; Bohatirchuk 1969; Haines and Mohuiddin 1968), as well as a great deal of research in developmental biology (Hall 1975, 1978, 2005; Huysseune and Verraes 1986, Huysseune and Sire 1990), have emphasized that a full spectrum of connective tissues could be produced, sometimes making formal definitions of tissues ambiguous.

In this context, current cell biology acknowledges the possibility of several back-modulations of already differentiated cell lineages into a more generalized condition, in which other differentiation pathways can take place (e.g., Bianco et al. 1998; Ereinpreisa and Roach 1996; Hall 2005). This may well be the

VetBooks.ir

case in endochondral ossification, when a tiny fraction of the hypertrophied cartilage cells does not experience apoptosis or destruction by chondroclasts. They may back-differentiate into osteoblasts, forming around them the so-called "globuli ossei" that become integrated into the new bone laid down by normal osteoblastic deposition around the resorption bays of the endochondral front of ossification, e.g., in metaphyses of the long bones of urodeles. For a recent review see Quilhac et al. (2014).

From a comparative-evolutionary point of view, important surveys on epiphyseal structures and processes of endochondral ossification among tetrapods include those of Moodie (1908) on reptiles and von Eggeling (1911) on urodele amphibians, with a later general review (von Eggeling 1938); Kastschenko (1881) and Froböse (1927) on anuran amphibians; Heidsieck (1928, 1929) on squamates and *Sphenodon*; and Lubosch (1927) on the issue of permanent cartilage. A little-known massive synthesis of those questions was published in Russian (Roumiantsiev 1958). However, the most significant comparative syntheses on the matter were provided by R.W. Haines (1938, 1942, 1969). For practical reasons, most studies on cartilaginous epiphyses dealt with extant animals, but a few hints at the possible conditions among extinct tetrapods were clearly offered by Haines (1938, 1942). Haines' publications heavily influenced later works, such as those of Ricqlès (1979) on tetrapods, Francillon (1981) on anurans, and Rhodin (1985) on marine turtles.

A point of special interest is the development of "secondary centers" of ossification within the cartilaginous epiphyses in some clades. Lack of secondary centers appears to be the plesiomorphic condition for tetrapods, widespread among various clades of limbed vertebrates from the Devonian to the Triassic periods. It may be linked to an indeterminate growth curve, where organisms grow all their lives, at a slower and slower pace. In some clades where secondary centers of ossifications have independently evolved (by convergence, e.g., anurans, squamates, mammals), it may be that they are linked to the evolution of a more determinate growth curve, in which the body size of adults is more or less constant and highly species specific. It also may be linked to the selection and control of small body sizes, in which the welding of secondary centers with the shaft prevents further longitudinal growth.

Although cartilage was generally considered a nonvascular tissue, comparative research has emphasized the occurrence of a system of cartilage canals (Haines 1933; Kuettner and Pauli 1983; Thorpe 1988) that has important functions in living cartilage, not only in its physiology but also in its spatial structuring (Wilsman and Van Sickle 1972; Fyfe 1964). This question of cartilage canals is intimately linked to the comparative issues dealing with the general evolution of endochondral ossification among osteichthyans (in a phylogenetic sense, including tetrapods).

Among fossils, the occurrence of calcified cartilage in the long bone epiphyses and elsewhere, with histological preservation of their structures, was described by Hasse (1878) in fossil vertebrae and by Seitz (1907) in the Triassic temnospondyl *Mastodonsaurus* and extensively discussed by Ørvig (1951) among early finned vertebrates. This was gradually



FIGURE 1.12 Historical dinosaur thin sections. Examples of two ancient thin sections of dinosaurs, from Professor Paul Gervais' collection preserved at the Muséum National d'Histoire Naturelle, Paris (circa 1876). The first one, processed in Paris by P. Bourgogne, reads "Reptile de la Nerthe (Matheron) niveau (?) inférieur." From La Nerthe tunnel (near Marseille) Matheron described the sauropod *Hypselosaurus* and the ornithopod *Rhabdodon*. The second thin section, processed by C. M. Topping and likely of English origin, is wrapped in red and gold paper and labeled *Iguanodon*.

recognized by the community, and the possibility of studying growth directly among fossils, thanks to paleohistological approaches to cartilage and endochondral ossification developed along several lines.

First, there has been a strong interest in the evolution of endochondral ossification through heterochronic processes, especially among tetrapod clades that are secondarily adapted to aquatic environments (Buffrénil et al. 1987, 1990; Nopcsa 1923a,b, 1930; Nopcsa and Heidsieck 1934; Ricqlès 1979, 1989; Ricqlès and Buffrénil 2001). Heterochronic regression of endochondral ossification is sometimes (but not necessarily) linked to other skeletal specializations, especially pachyostosis *sensu lato*, a subject that has stimulated a great deal of research and speculation (Gervais 1875; Houssaye et al. 2008; Kaiser 1960, 1970; Lubosch 1927; Nopcsa 1923a,b; Nopcsa and Heidsieck 1934; Zangerl 1935).

Second, it became obvious that in early terrestrial vertebrates, the structure of calcified cartilages preserved in epiphyseal regions could provide several clues to relative and absolute longitudinal growth dynamics. The relative amount of growth provided by the two epiphyses of a given long bone can vary extensively. This is faithfully recorded in the patterns and thickness of the fossilized calcified cartilage. The offsetting of the "neutral section" in the shaft – the part that can most completely record radial growth of the shaft – toward the slower growing epiphysis is important to consider for skeletochronology, because the geometrical midshaft may actually be remote from this neutral section and hence poorly record radial growth.

Observations of dinosaur epiphyses have stimulated experimental tests on living birds (Montes et al. 2005), asking whether the thickness and organization of preserved calcified cartilage could reflect the relative activity of the uncalcified (not preserved) epiphyseal contributions to growth.

VetBooks.ir

Observations of extant models have vindicated the hypotheses derived from the paleohistological observations (Barreto 1997; Horner et al. 2001).

A massive coating of calcified cartilage forms the corrugated surface of epiphyses, as preserved among sauropod dinosaurs (Ricqlès 1972; Rimblot-Baly et al. 1995). This coating by no means approximates the functional, articular surfaces of epiphyses, which are formed of noncalcified cartilage, not preserved by fossilization. Actually, the corrugated surface corresponds to the "blue line" of histologists, at the boundary between calcified and uncalcified cartilage. Corrugation increased the surface contact between both, perhaps improving cohesion between neighboring tissues with different biomechanical properties and functions.

Considerable attention to epiphyseal structures in extant and extinct tetrapods, notably in "embryonic" (actually late fetal) and juvenile dinosaurs and various archosaurs, is obvious in some paleohistological studies (Barreto 1997; Barreto and Wilsman 1994; Barreto et al. 1993; Horner et al. 2001, Reid 1984, Ricqlès et al. 2001a) and many new results on growth dynamics, growth stages, maturity, and so forth should be expected.

Concluding Remarks

Starting with what is known from extant vertebrates, where the relationships of hard tissues to every aspect of animal biology and natural history traits can be observed and experimented on, paleohistology tries to expand this knowledge into the deep time of vertebrate evolution. This allows (and will allow) a new view of early vertebrates as "living machines," with a better appreciation of species- and clade-specific characteristics dealing with various life history traits and physiology. Moreover, it allows (and will allow) further understanding of the large-scale evolution of important structural innovations and of physiological functions in Deep Time.

Current research in bone and other hard tissue biology is now dominated by work at the molecular level, in connection with cell physiology, biomolecules involved in mineralization of extracellular matrices, transduction of mechanical strains into cell behaviors, and so forth. Such studies can bring to light the deep origins (biochemical, genetical, epigenetic, biomechanical, etc.) of skeletal organization at the cell and tissue levels in extant and extinct vertebrates. However, they do not make irrelevant the many studies at the tissue, organ, organismal, and higher levels that allow us to build an integrative evolutionary biology.

Necessarily, paleohistological studies remain dominated by structural-comparative approaches at the tissue level of integration. They share much with comparative histology of extant organisms, where experimental approaches are possible. Both can now be extended and refined by new technological breakthroughs (3D virtual reconstruction, synchrotron light, etc.). Comparative hard tissue histology and paleohistology are invaluable because they combine the three points of view of structural knowledge, functional interpretations, and evolutionary prospects. The study of histology remains a most important level of biological integration because it is intimately linked to the great problem shared by developmental and evolutionary biology*: the creation and changes of Form*.

Acknowledgments

I thank Lars Werdelin and Philippe Janvier for sharing photographs; Vivian de Buffrénil, Philippe Janvier and Michel Laurin for information, numerous suggestions and practical help; and Kevin Padian for his linguistic revision.

REFERENCES

Agassiz, L. 1833–1843. *Recherches sur les poissons fossiles*. Neuchatel: Petitpierre.

Agassiz, L. 1844–1845. *Monographie des poissons fossiles du vieux grès rouge ou Système Dévonien (Old Red Sandstone) des Iles Britanniques et de Russie*. Neuchatel: A. Sorrel, Atlas, A. Nicollet.

Aldinger, H. 1937. Permische ganoidfische aus Ostgrönland. *Medd. Grön*. 102: 1–392.

Amprino, R. 1943. La struttura della ossa nell'uomo in relazione a turbe dell' accressimento. Richerche negli scheletri di un gigante e di un nano. *Arch. Ital. Anat. Embryol*. 49: 161–193.

Amprino, R. 1947. La structure du tissu osseux envisagée comme expression de différences dans la vitesse de l'accroissement. *Arch. Biol*. 58: 315–330.

Amprino, R. 1948. A contribution to the functional meaning of the substitution of the primary by secondary bone tissue. *Acta Anat*. 5: 291–300.

Amprino, R. 1967. Bone histophysiology. *Guy's Hosp. Rep*. 116: 51–69.

Amprino, R., A. Bairati. 1936. Processi di ricostruzione e di riassorbimente nella sostanza compatta della ossa dell'uomo. *Zeitsch. Zellforsch*. 24: 439–511.

Amprino, R., A. Bairati. 1938. La variazoni nella struttura dell'osso in relazione al eta e la loro importanze medico forenze. *Arch. Anthrop. Criminol*. 16: 61–74.

Amprino, R., G. Godina. 1944–1945. Osservationi sui processi di rimaneggiamento strutturale della sostanza compatta delle ossa lunghe degli ucelli coridori. *Anat. Anz*. 95: 191–214.

Amprino, R., G. Godina. 1947. La struttura della ossa nei vertebrate. Richerche comparative negli amfibi e negli amnioti. *Comment. Pont. Acad. Sci*. 11: 329–467.

Amprino, R., G. Godina. 1956. Osservazioni sul rinnovamento strutturale dell'osso in pesci teleostei. *Publ. Staz. Zool. Napoli* 28: 62–71.

Anderson, J. R. 2004. Les outils: dans quelles espèces, et ce qu'ils signifient? In *L'éthologie cognitive* [on line]. Paris: Éditions de la Maison des sciences de l'homme. http://books.openedition.org/editionsmsh/7107.

Asfaw B., et al. 1999. *Australopithecus garhi*: a new species of early hominid from Ethiopia. *Science* 284: 629–35.

Baglinière, J. L., eds. 1992. *Tissus durs et âge individual des vertébrés*. Bondy: Colloques et Séminaires OSTROM-INRA.

Barreto, C. 1997. Dinosaur growth plates and dinosaur bone growth. In *Dino fest international*, Wolberg, D. L., E Stump and G. D. Rosenberg eds., 95–100. Philadelphia: Academy of Natural Sciences.

VetBooks.ir

Barreto, C., et al. 1993. Evidence of the growth plate and the growth of long bones in juvenile dinosaurs. *Science* 262: 2020–2023.

Barreto, C., N. J. Wilsman. 1994. Hypertrophic chondrocyte volume and growth rates in avian growth plates. *Resch. Veter. Sci.* 56: 53–61.

Baud, C. A., P. W. Morgenthaler. 1953. Sur l'ultrastructure du tissu osseux d'un poisson téléostéen fossile: *Diplomystus brevissimus* (Fam. Clupeidae). *Bull. Mus. Hist. Nat. Paris* 25: 641–645.

Baudelot, M. E. 1873. Recherches sur la structure et le développement des écailles des poissons osseux. *Arch. Zool. exp. gén.* 2: 87-244, 429–480.

Belchier, J. 1736. An account of the bones of animals being changed to a red colour by aliment only. *Phil. Trans. R. Soc. Lond.* 34: 287–299.

Belon du Mans, P. 1555. *Histoire naturelle des oiseaux*. Paris: Gilles Corrozet et Cavellat.

Beresford, W. A. 1981. *Chondroid bone, secondary cartilage and metaplasia*. Munich: Urban and Schwarzemberg.

Bertin, L. 1958. Ecailles et sclérifications dermiques. In *Traité de Zoologie*, Vol. 13, Grassé, P. P. ed., 482–504. Paris: Masson et Cie.

Bianco P., et al. 1998. Bone formation via cartilage models: the "borderline" chondrocyte. *Matrix Biol.* 17: 185–192.

Biederman, W. 1913. Physiologie der Stütz- und Skelettsubstanzen. In *Handbuch der vergleichenden Physiologie III (7–8)*, Winterstein, H. ed., X – Das Knorpelgewebe, 1024–1085, XI – Das Knochengewebe,1085–118. Iena: Fischer.

Blanc, M. 1953. Contribution à l'étude de l'ostéogenèse chez les poissons téléostéens. *Mém. Mus. Nat. Hist. Nat.* 7: 1–145.

Blieck, A., et al. 2010. Fossils, histology and phylogeny: why conodonts are not vertebrates. *Episodes* 33: 234–241.

Blomberg, S., T. J. Garland. 2002. Tempo and mode in evolution: phylogenetic inertia, adaptation and comparative method. *J. Evol. Biol.* 15: 899–910.

Bloom, W., D. Fawcett eds. 1968. *A textbook of histology.* 9th edition. Philadelphia: W. B. Saunders Co.

Bohatirchuk, F. P. 1969. Metaplasia of cartilage into bone – a study by stain historadiography. *Am. J. Anat.* 126: 243–254.

Bonis L. de, et al. 1972. Etude de la répartition des types de tissus osseux chez les vertébrés tétrapodes au moyen de l'analyse factorielle des correspondances. *C.R. Acad. Sci. Paris. Ser. D.* 274: 3084–3087.

Bordat, C. 1987. Etude ultrastructurale de l'os des vertèbres du sélacien *Scyliorhinus canicula* L. *Can. J. Zool.* 65: 1435–1444.

Botha, J. 2003. Biological aspects of the Permian dicynodont *Oudenodon* (Therapsida: Dicynodontia) deduced from bone histology and cross-sectional geometry. *Paleont. Afr.* 39: 37–44.

Bourne, G. H. ed. 1972. *The biochemistry and physiology of bone.* 2nd edition, New York: Academic Press.

Brambilla, G. 1972. Primi dati morfometrici sulle lacune ossee di Vertebrati fossili: *Kritosaurus notabilis* (Lambe). *Atti Soc. Ital. Sci. Nat. Mus. Civ. Storia Nat. Milano.* 113: 313–327.

Bryant, W. L. 1936. A study of the oldest known vertebrates, *Astraspis and Eryptichius. Proc. Amer. Philos. Soc.* 76: 409–427.

Bryuzgin, V. L. 1939. A procedure for investigating age and growth in Reptilia. *C. R. (Doklady) Acad. Sci. USSR (N.S.)* 2: 403–405.

Buffrénil, V. de 1982. Morphogenesis of bone ornamentation in extant and extinct crocodilians. *Zoomorphology* 99: 155–166.

Buffrénil, V. de, et al. 2011. An enamel-like tissue, osteodermine, on the osteoderms of a fossil Anguid (Glyptosaurinae) lizard. *C.R. Palevol.* 10: 427–437.

Buffrénil, V. de, et al. 1990. Bone histology of the ribs of Archaeocetes (Mammalia, Cetacea). *J. Vertebr. Paleont.* 10: 455–466.

Buffrénil, V. de, J. M. Mazin.1990. Bone histology of the Ichthyosaurs: comparative data and functional interpretation. *Paleobiology* 16: 435–447.

Buffrénil, V. de, et al. 1987. Caractères structuraux et mode de croissance du fémur d'*Omphalosaurus nisseri*, ichthyosaurien du Trias moyen du Spitzberg. *Ann. Paléont.* 73: 195–216.

Burke, A., J. Castanet. 1995. Histological observations of cementum growth in horse teeth and their application to archaeology. *J. Archaeol. Sci.* 22: 479–493.

Butler, P. M., K. A Joyesy eds. 1978. *Development, function and evolution of teeth*. London: Academic Press.

Bystrow, A. P. 1935. Morphologische Untersuchungen der Deckknochen des Schädels der Wirbeltiere, 1 Mitt: Schädels der Stegocephalen. *Acta Zool.* 16: 64–141.

Bystrow, A. P. 1938a. *Dvinosaurus* als neotenische Form der Stegocephalen. *Acta Zool.* 19: 137–164.

Bystrow, A. P. 1938b. Zahnstruktur der Labyrinthodonten. *Acta Zool.* 19: 387–425.

Bystrow, A. P. 1939. Zahnstruktur des Crossopterygier. *Acta Zool.* 20: 283–338.

Bystrow, A.P. 1942. Deckknochen und Zähne des *Osteolepis* und *Dipterus*. *Acta Zool.* 23: 263–289.

Bystrow, A. P. 1944. *Kottlassia* prima Amalitzky. *Bull. Geol. Soc. Amer.* 55: 379–416.

Bystrow, A.P. 1947. Hydrophilous and xerophilous labyrinthodonts. *Acta Zool.* 28: 137–164.

Bystrow A. P. 1957a. *Man. past, present, future* (in Russian). Leningrad: Medical Literature.

Bystrow, A.P. 1957b. The microstructure of dermal bones in Arthrodires. *Acta Zool.* 38: 239–275.

Bystrow, A. P. 1959. The microstructure of skeleton elements in some vertebrates from the Lower Devonian deposits of the USSR. *Acta Zool.* 40: 59–83.

Caetano, M. H., et al. 1985. Détermination de l'âge de *Triturus marmoratus marmoratus* (Latreille 1800) du Parc national de Peneda-Gêres (Portugal) par squelettochronologie. *Amphibia-Reptilia* 6: 117–132.

Caldwell, M. W., et al. 2003. Histology of tooth attachment tissues in the Late Cretaceous mosasauroid *Platecarpus*. *J. Vertebr. Paleontol.* 23: 622–630.

Carlson, S. 1990. Vertebrate dental structures. In *Skeletal biomineralisation: patterns, processes and evolutionary trends*, Vol. 1, Carter, J. G. ed., 531–556. New York: Van Nostrand and Reinhold.

Castanet, J. 1974. Etude histologique des marques squelettiques de croissance chez *Vipera aspis* L. *Zool. Scripta*. 3: 137–151.

Castanet, J. 1985. La squelettochronologie chez les reptiles 1. Résultats expérimentaux. *Ann. Sci. Nat. Zool.* 7: 223–240.

Castanet, J. 1986–1987. La squelettochronologie chez les reptiles 3. Applications. *Ann. Sci. Nat. Zool.* 8: 157–172.

Castanet, J. 2006. Time recording in bone microstructures of endothermic animals; functional relationships. *C. R. Palevol.* 5: 629–636.

Castanet J., A. de Ricqlès. 1986–1987. Sur la relativité des notions d'ostéones primaires et secondaires et de tissus osseux primaires et secondaires en général. *Ann. Sci. Nat. Zool.* 8: 103–109.

Castanet, J., et al. 2003. The skeletal histology of the Amphibia. In *Amphibian biology*, Vol. 5, Heatwole, H. ed, 1598–1683. Chipping Norton, NSW: Surrey Beatty and Sons.

Castanet, J., et al. 1993. Bone and individual aging. In *Bone*, Vol. 7, Hall, B. K. ed., 254–283. Boca Raton: CRC Press.

Castanet, J., et al. 1996. Expression de la dynamique de croissance de l'os périostique chez *Anas platyrhynchos*. *C. R. Acad. Sci. Paris* 319: 301–308.

Castanet, J., et al. 2000. Periosteal bone growth rates in extant Ratites (ostrich and emu). Implications for assessing growth in dinosaurs. *C. R. Acad. Sci. Paris* 323: 543–550.

Casteel, R. W. 1976. *Fish remains in archaeology and paleo-environmental studies*. London: Academic Press.

Chibon, P., A.de Ricqlès. 1995. Dents et tissus dentaires. In *Traité de zoologie. amphibiens*, Vol. XIV (1 A), Grassé, P. P and M. Delsol eds., 167–187. Paris: Masson et Cie.

Chinsamy, A. 1995. Ontogenic changes in the bone histology of the Late Jurassic Ornithopod *Dryosaurus lettowvorbecki*. *J. Vertebr. Paleontol.* 15: 96–104.

Chinsamy, A. 2005. *The microstructure of dinosaur bone: deciphering biology with fine scale techniques*. Baltimore: John Hopkins University Press.

Chinsamy, A., et al. 1995. Mesozoic avian bone microstructure: physiological implications. *Paleobiology* 21: 561–574.

Colbert, E. H. 1955. Scales in the Permian amphibian *Trimerorachis*. *Am. Mus. Novit.* 1740: 1–17.

Courvoisier, B., eds. 1978. *Fluoride and bone*. Genève: Médecine et Hygiène.

Crawford, G. N. C. 1940. The evolution of the haversian pattern in bone. *J. Anat.* 74: 284–299.

Credner, H. 1893. Die Stegocephalen und Saurier aus dem Rothliegenden des Plauenschen Grundes bei Dresden. *Deutsch Geol. Ges. Z.* 45: 639–704.

Cubo, J., et al. 2008. Phylogenetic, functional and structural components of variation in bone growth rate in Amniotes. *Evol. Dev.* 10: 217–227.

Cubo, J., et al. 2012. Paleohistological estimation of bone growth rate in extinct archosaurs. *Paleobiology* 38: 335–349.

Cubo, J., et al. 2005. Phylogenetic signal in bone microstructure of Sauropsids. *Syst. Biol.* 54: 562–574.

Cuijpers, A. G. 2006. Histological identification of bone fragments in Archaeology: telling humans apart from horses and cattle. *Int. J. Osteoarcheol.* 16: 465–480.

Currey, J. D. 1960. Difference in the blood supply of bone of different histological types. *Q. J. Microsc. Sci.* 101: 351–370.

Currey, J. D. 1962. The histology of the bone of a prosauropod dinosaur. *Paleontology* 5: 238–246.

Currey, J. D. 1984. *The mechanical adaptations of bones*. Englewood Cliffs, NJ: Princeton University Press,

Dawson, J. B. 1992. First thin section of experimentally melted igneous rocks: Sorby's observations on magma crystallization. *J. Geol.* 100: 251–257.

Dean, M. N., A. P. Summers. 2006. Mineralized cartilage in the skeleton of chondrichthyan fishes. *Zoology* 109:164–168.

Delgado, S., et al. 2001. Molecular evidence for Precambrian origin of amelogenin, the major protein of vertebrate enamel. *Mol. Biol. Evol.* 18: 2146–2153.

Denison, R. H. 1963. The early history of the vertebrate calcified skeleton. *Clin. Orthop. Relat. Res.* 31:141–152.

Denison, R. H. 1967. Ordovician vertebrates from Western United States. *Fieldiana Geol.* 16: 131–192.

Denison, R. H. 1974. The structure and evolution of teeth in lungfishes. *Fieldiana Geol.* 33: 31–58.

Desse, G. 1984. *Histoire d'Os*. Paris: L'Harmattan.

Di Masi, E., L. B. Gower eds. 2016. *Biomineralization source book: characterization of biominerals and biomimetic materials*. Boca Raton, FL: CRC Press.

Donoghue, P. C., R. J. Aldridge. 2001. Origin of mineralized skeleton. In *Events in early vertebrate evolution: paleontology, phylogeny, genetics and development*. Ahlberg P.E. ed., 85–105. London: Taylor and Francis.

Donoghue, P. C., et al. 2005. *Swiss light shed on the nature of fossilized embryos from the dawn of animal evolution*. PSI Scientific report. 10–11.

Donoghue, P. C., I. J. Sansom. 2002. Origin and early evolution of vertebrate skeletonization. *Microsc. Res. Tech.* 59: 352–372.

Donoghue, P. C., et al. 2006. Early evolution of vertebrate skeletal tissues and cellular interactions, and the canalization of skeletal development. *J. Exp. Zool. B (Mol. Dev. Evol.)* 306: 1–17.

Donoghue, Ph. C. 2001. Conodonts meet cladistics: recovering relationships and assessing the completeness of the Conodont fossil record. *Paleontology* 44: 65–93.

Duhamel du Monceau, H. L. 1739. Sur une racine qui a la faculté de teindre en rouge les os des animaux vivants. 1. *Mém. Acad. R. Sci.* 52: 1–13.

Duhamel du Monceau, H. L. 1743. Quatrième mémoire sur les os. *Mém. Acad. R. Sci.* 56: 87–146.

Ebner, V. von 1875. Über den feineren Bau der Knochensubstanz. *Sitzungsber Kön Acad. Wiss. Math. Naturwiss. Wien III Abt.* 72: 49–138.

Eggeling, H. von 1911. *Den Aufbau der skeletteile in den freien Gliedmassen der Wirbeltiere. Untersuchungen an urodelen Amphibien*. Iena: Fischer.

Eggeling, H. von 1938. *Allegemeines über den Aufbau knöcherner Skeletteile*. In *Handbuch vergleichende anatomie der wirbeltiere*, Vol. 5, Bolk, L., E. Goppert, E. Kallius, W. Lubosch eds., 275–304. Berlin: Urban and Schwarzenberg.

Enlow, D. H. 1963. *Principles of bone remodeling.* Springfield, IL: Charles C Thomas.

Enlow, D. H. 1966. An evaluation of the use of bone histology in forensic medicine and anthropology. In *Studies on the anatomy and function of bone and joints*, Evans, G. ed., 92–111. Berlin: Springer.

Enlow, D. H. 1968. Wolff's law and the factors of architectonic circumstances. *Am. J. Orthod.* 54: 803–822.

Enlow, D. H. 1969. The bone of reptiles. In *Biology of the reptilia,* Vol. A 1, Gans, C. ed., 45–80. London: Academic Press.

VetBooks.ir

Enlow, D. H. and S.O. Brown. 1956–1958. A comparative histological study of fossil and recent bone tissues. Parts 1–3. *Texas J. Sci*. 8: 403–443, 9: 185–214, 10: 187–230.

Ereinpreisa J., Roach H. I. 1996. Epigenetic selection as a possible component of transdifferenciation. Further study of the commitment of hypertrophic chondrocytes to become osteocytes. *Mech. Aging Dev.* 87: 165–182.

Erickson, G. 2005. Assessing dinosaur growth patterns: a microscopic revolution. *Trends Ecol. Evol.* 20: 677–684.

Evans, F. G. 1957. *Stress and strain in bones*. Springfield, IL: Charles C Thomas.

Fawcett, D. W. 1942. The amedullary bones of the Florida manatee (*Trichechus latirostris*). *Am. J. Anat.* 71: 271–309.

Fell, H. B. 1925. The histogenesis of cartilage and bone in the long bones of the embryonic fowl. *J. Morphol. Physiol.* 40: 417–459.

Felts, W. J. L., Spurrell F.A. 1966. Some structural and developmental characteristics of cetacean (odontocetes) radii. a study of adaptive osteogenesis. *Amer. J. Anat.* 118: 103–134.

Findlay, G. H. 1968. On the structure of the skin in *Uranocentrodon* (*Rhinesuchus*) *senegalensis* Van Hoepen. *Paleontol. Afr.* 11: 15–21.

Findlay, G. H. 1970. Skin structure of small Pareiasaurs. *Paleontol. Afr.* 13: 15–23.

Foote, J. S. 1913. *The comparative histology of the femur,* 61 (publ. 2232). Washington, DC: Smithsonian Institute.

Foote J. S. 1916. *A contribution to the comparative histology of the femur*, (publ.328): 1-242. Washington, DC: Smithsonian Institute.

Foote J. S. 1928. *Bone as a measure of development and when and why we acquired our teeth. Parts 1--3 (Opus posthumus)*, Omaha, NE: Douglas.

Francillon, H. 1974. Développement de la partie postérieure de la mandibule de *Salmo trutta fario. Zool. Scripta*. 3: 41–51.

Francillon, H. 1977. Développement de la partie antérieure de la mandibule de *Salmo trutta fario. Zool. Scripta*. 6: 245–251.

Francillon, H. 1981. Contribution à l'étude des structures et du fonctionnement des épiphyses fémorales chez les amphibiens anoures. *Arch. Zool. exp. gén*. 122: 289–310.

Francillon-Vieillot, H., et al. 1990. Microstructure and mineralization of vertebrate skeletal tissues. In *Skeletal biomineralization: patterns, processes and evolutionary trends,* Vol. 1, Carter, J. G. ed., 471–530. New York: Van Nostrand Reinhold.

Froböse, H. 1927. Der Aufbau des skeletteile in den freien Gliedmassen der anuren amphibien. *Jahrb. Morphol. Mikrosk. Anat*. 58: 473–566.

Frost, H. M. ed. 1964. *Bone biodynamics (Henry Ford Hosp. Intern. Sympos.*). Boston: Little, Brown and Co.

Frost, H. M. 1988. Vital biomechanics: proposed general concept for skeletal adaptation to mechanical usage. *Calcif. Tissue Int*. 42: 145–156.

Fyfe, F.W. 1964. Predominance of epiphyseal over metaphyseal blood supply in nourishment of epiphyseal cartilage demonstrated by 35 S radioautography and vascular ablation. J. Anat. 98: 471–472.

Galileo, G. 1638. *Discorsi e demonstrazioni matematische in torno a due scienze attenanti alla mecanica ed i movimenti locali*. Leiden: Elsevier.

Gayet, M., F. J. Meunier. 1992. Polypteriformes (Pisces Cladistia) du Maastrichtien et du Paléocène de Bolivie. *Geobios. Mem. Spec.* 14: 159–168.

Gayet, M., Fr. J. Meunier. 1986. Apport de l'étude de l'ornementation microscopique de la ganoïne dans la détermination de l'appartenance générique et/ou spécifique des écailles isolées. *C. R. Acad. Sci. Paris 303*: 1259–1262.

Gebhardt, W. 1901–1906. Ueber functionell wichtige Anordnungs weisen der gröseren und feineren Bauelemente des Wirbeltiere knochens. I-1901. *Archs. Entw. Mechan*. 11 (1901): 383–498; 12 (1901): 1–52, 123–167; 16 (1903): 377–410; 20 (1906): 187–322.

Gebhardt, W. 1910. Die spezielle functionelle Anpassung der Röhrenknochen Diaphyse. *Archs. Entw. Mechan*. 30: 516–534.

Geraudie, J. 1988. Fine structural peculiarities of the pectoral fin dermoskeleton of two Brachiopterygii, *Polypterus senegalus* and *Calamoichthys calabaricus*. *Anat. Rec*. 221: 455–468.

Geraudie J., F. J. Meunier. 1980. Elastoidin actinotrichia in coelacanth fins: a comparison with teleosts. *Tissue Cell* 12: 367.

Geraudie, J., F. J. Meunier. 1982. Comparative fine structure of the Osteichthyan dermotrichia. *Anat. Rec*. 202: 325–328.

Gervais, P. 1875. De l'hyperostose chez l'homme et chez les animaux (I: Mammifères, Oiseaux, Reptiles). *J. Zool*. 4: 272–284; (II: Poissons) id. 4: 445–462.

Giraud, M. M., et al. 1978. The fibrous structure of Coelacanth scales: a twisted "plywood". *Tiss. Cell* 10: 671–686.

Glimcher, M. J. 1976. Composition, structure, and organization of bone and other mineralized tissues and the mechanism of calcification. In *Handbook of physiology/endocrinology*, 25–116. Baltimore: William and Wilkins Co.

Glimcher, M. J. 1981. On the form and function of bone: from molecules to organs. Wolff's law revisited. In *The Chemistry and Biology of mineralized connective tissues*. Veis, A. ed., 617–675. Amsterdam, NY., Oxford: Elsevier.

Glimcher, M. J., J. B. Lian eds. 1989. *The chemistry and biology of mineralized tissues.* New York: Gordon and Breach Science Publishers.

Godina, G. 1946. Transformazioni strutturali della compatta delle ossa lunghe degli Equidi durante l' accrescimento e nella senescenza. *Arch. Ital. Anat. Embriol*. 51: 219–241.

Godina, G. 1947. Transformazioni strutturali durante l'accrescimento nelle ossa lunghe in cani di diffenrente mole somatica. *Arch. Ital. Anat. Embriol*. 52: 161–178.

Goodrich, E. S. 1904. On the dermal fin-rays of fishes – living and extinct. *Q. J. Microsc. Sci.* 47: 465–521.

Goodrich, E. S. 1907. On the scales of fishes – living and extinct and their importance in classification. *Proc. Zool. Soc. London*. 751–574.

Goodrich, E. S. 1913. On the structure of bone in fishes: a contribution to Palaeohistology. *Proc. Zool. Soc. London*. 80–85.

Gould, S. J. 2002. *The structure of evolutionary theory.* Cambridge, MA: Belknap Press Harvard University.

Gould, B. S., G. N. Ramachandran eds. 1968. *Treatise on collagen*. New York: Academy Press.

Gross, W. 1930. Die Fische des mittleren Old Red Süd-Livlands. *Geol. Paläontol*. 18: 121–156.

Gross, W. 1934. Die Typen des mikroskopischen Knochenbaues bei fossilen Stegocephalen und Reptilien. *Z. Anat.* 103: 731–764.

Gross, W. 1935. Histologische studien am Ausenskelett fossiler Agnathen und Fische. *Paleontographica 83 A* 1–60.

Gross, W. 1956. Uber Crossopterygier und Dipnoer aus dem Oberdevon im Zussamenhang einer verglecheinden Untersuchung des Porenkanalsystems paläozoischer Agnathen und Fische. *Kung. Svensk. Vetensk. Acad. Band 5*: 1–140.

Gross, W. 1961. Aufbau der Panzers obersilurischer Heterostraci und Osteostraci Norddeutschlands (Geshiebe) und Oesels. *Acta Zool*. 42: 73–150.

Gross, W. 1967. Uber Thelodontier-Schuppen. *Paleontographica* 127: 1–67.

Gross, W. 1971. Downtonische und Dittonische Acanthodier-Reste des *Ostseegebietes. Paleontographica A* 136: 1–82.

Haines, R.W. 1933. Cartilage canals. *J.of Anat*. 68: 45–64.

Haines, R. W. 1934. Epiphysial growth in the branchial skeleton of fishes. *Q. J. Microsc. Sci*. 77: 79–97.

Haines, R. W. 1937. Posterior end of Meckel's cartilage and related ossification in bony fishes. *Q. J. Microsc. Sci*. 80: 1–38.

Haines, R. W. 1938. The primitive form of epiphysis in the long bones of tetrapods. *J. Anat*. 72: 323–343.

Haines, R. W. 1942. The evolution of epiphyses and of endochondral bone. *Biol. Rev.* 174: 267–292.

Haines, R. W. 1969. Epiphyses and sesamoids. In *Biology of the Reptilia,* Vol. A 1, Gans, C. ed., 81–115. New York: Academic Press.

Haines, R. W., A. Mohuiddin. 1968. Metaplastic bone. *J. Anat*. 103: 527–538.

Hall, B. K. 1975. Evolutionary consequences of skeletal differentiation. *Am. Zool*. 15: 329–350.

Hall, B. K. 1978. *Developmental and cellular skeletal biology.* London and New York: Academic Press.

Hall, B K. 2005. *Bones and cartilage – developmental and evolutionary skeletal biology.* Amsterdam: Elsevier.

Halstead-Tarlo, L. B. 1963. Aspidin: the precursor of bone. *Nature* 199: 46–48.

Halstead-Tarlo, L. B. 1964–1965. Psammosteiforms (Agnatha). A review with description of new material from the Lower Devonian of Poland. Parts 1-2: *Paleont. Polonica* 13: 1–133; 15: 1–167.

Halstead-Tarlo, L. B. 1969. Calcified tissues in the earliest vertebrates. *Calc. Tissue Res.* 3: 107–124.

Halstead-Tarlo, L. B. 1973. The Heterostracan fishes. *Biol. Rev.* 48: 279–332.

Halstead L. B., J. Middleton. 1972. *Bare bones, an exploration in arts and sciences*. Edinburgh: Oliver and Boyd.

Hancox, N. M. 1972. *Biology of Bone*. Cambridge, UK: Cambridge University Press.

Harvey, P. H., M. D. Pagel. 1991. *The comparative method in evolutionary biology.* Oxford, UK: Oxford University Press.

Hasse, C. 1878. Die fossilen Wirbel. Die Histologie fossiler Reptilien-wirbel. *Morphol. Jahrb.* 4: 480–502.

Havers, C. 1691. *Osteologia nova*. London: Samuel Smith.

Heidsieck, E. 1928. Der bau der Sketteile der freien Extremitäten bei den Reptilien. 1Mitt. Gekkonidae und Agamidae. *Morphol. Jahrb.* 59: 343–492.

Heidsieck, E. 1929. Der bau der Sketteile der freien Extremitäten bei den Reptilien. 2Mitt. *Hatteria* (*Sphenodon*) *punctata*. *Morphol. Jahrb.* 62: 319–354.

Hérissant, F.-D. 1758. Eclaircissements sur l'ossification. *Mém. Acad. R. Sci*. 322–336.

Hertwig, O. 1874a. Über Bau und Entwicklung der Placoidshuppen und Zähne der Selachier. *Jnaer Z. Naturwiss.* 8: 331–402.

Hertwig, O. 1874b. Uber den Zahnsystem der Amphibien und seine Bedeutung für die Genese des Skeletts der Mundhöle. *Arch. Mikrosc. Anat*. 11 (A33–A84).

Hertwig, O. 1876–1882. Uber des Hautskelett der Fische. 1–3: *Morphol. Jahrb. Z. Anat. Entwickl*., 2: 328–396, 5: 1–21, 7: 1–4.

Higham, N. 1963. *A very scientific gentleman: the major achievements of Henry Clifton Sorby.* Oxford, UK: Pergamon Press.

Horner, J. R., et al. 1999. Variation in skeletochronological indicators of the Hadrosaurid dinosaur *Hypacrosaurus*: implications for age assessment of dinosaurs. *Paleobiology* 25: 295–304.

Horner, J. R., et al. 2000. The bone histology of the hadrosaurid dinosaur *Maiasaura peeblesorum:* growth dynamics and physiology based on an ontogenetic series of skeletal elements. *J. Vertebr. Paleontol*. 20: 115–129.

Horner, J. R., et al. 2001. Comparative osteohistology of some embryonic and neonatal archosaurs: implications for variable life histories among dinosaurs. *Paleobiology* 27: 39–58.

Houssaye, A., et al. 2008. An analysis of vertebral pachyostosis in *Carentonosaurus mineaui* (Mosasauroidea, Squamata) from the Cenomanian (early Late Cretaceous) of France, with comments on its phylogenetic and functional significance. *J. Vertebr. Paleontol*. 28: 685–691.

Hugi, J., et al. 2011. Long bone microstructure gives new insights into the life of pachypleurosaurids from the Middle Triassic of Monte San Giorgio, Switzerland/Italy. *C. R. Palevol.* 10: 413–426.

Huysseune, A., J.-Y. Sire. 1990. Ulrastructural observations on chondroid bone in the teleost fish *Hemichromis bimaculatus. Tissue and Cell* 23 (3): 371–383.

Huysseune, A., W. Verraes. 1986. Chondroid bone in the upper pharyngeal jaws and neurocranial bones in the adult fish *Astatotilapia elegans. Am. J. Anat.* 177: 527–535.

Janvier, P. 1996. *Early vertebrates.* Oxford, UK: Clarendon Press.

Janvier, P. 2003a. Vertebrate characters and the Cambrian vertebrates. *C. R. Palevol.* 2: 523–531.

Janvier, P. 2003b. Skeleton keys. *Nature* 424: 493.

Janvier, P. 2003c. Armoured fish from deep time: from Hugh Miller's insights to current questions of early vertebrate evolution. In *Celebrating the life and times of Hugh Miller – Scotland in the early 19th Century.* Borely, L. ed., 177–196. Cromarty, Scotland: The Cromarty Arts Trusts.

Janvier, P. 2013. *Inside-out turned upside-down. Nature* 502: 457–458.

Janvier, P., M. Arsenault. 2002. Calcification of early vertebrate cartilage. *Nature* 417: 609.

Jing, Lu, et al. 2016. The oldest Actinopterygian highlights the cryptic early history of the hyperdiverse ray-finned fishes. *Current Biol*. 26: 1–7.

Johnson, D. R. 1986. *The genetics of the skeleton*. Oxford, UK: Clarendon Press.

Kaiser, H. E. 1960. Untersuchugen zur vergleichenden Osteologie der fossilen und rezenten Pachyostosen. *Paleontographica* 114: 113–196.

Kaiser, H. E. 1970. *Das abnorme in der evolution*. Leyden, the Netherlands: Brill.

VetBooks.ir

Kastschenko, M. 1881. Ueber die Genese und Architektur der Batrachier Knochen. *Arch. Microsc. Anat.* 19: 1–52.

Kemp, A. 2002. Hyaline tissue of thermally unaltered conodont elements and the enamel of vertebrates. *Alcheringa* 26: 23–36.

Kemp, N. E., S. K. Westrin. 1979. Ultrastructure of calcified cartilage in the endoskeletal tesserae of sharks. *J. Morphol.* 160: 75–102.

Kerr, T. 1952. The scales of the primitive living actinopterygians. *Proc. Zool. Soc. London* 122: 55–78.

Kiprijanoff, V. 1881–8183. Studien über die fossilen Reptilien Russlands. *Mem. Acad. Imp. Sci. St. Petersbourg* Ser. 7, Vol. 28–31.

Klaatsch, H. 1890. Zur Morphologie der Fischuppen und zur Geschichte der Hartsubstanzgewebe. *Morphol. Jb.* 16: 97-203; 209–258.

Kleinenberg, S. E., E. M. Smirina.1969. Contribution to the method of age determination in Amphibians (in Russian). *Zool. Zh.* 48: 1090–1094.

Klevezal, G. A., S.E. Kleinenberg. 1967. Age determination of mammals from lamellar structures of teeth and bone (in Russian). *Nauka*. English translation by Slatkin, J. 1969. Israel Program for Scientific Transl.

Kölliker, A. von 1859. On the different types in the microstructure of the skeletons of osseous fish. *Proc. R. Soc. London* 9: 656–668.

Kuettner, K. E., B. U. Pauli. 1983. Vascularity of cartilage. In *Cartilage, structure, function and biochemistry*, Hall, B. K. ed., 281–312. London and New York: Academic Press.

Kummer, B. K. F. 1972. Biomechanics of bone: mechanical properties, functional structure, functional adaptation. In *Biomechanics – its foundations and objectives*, Fung, Y. C., N. Perrone and M. Anliker eds., 237–271. Englewood Cliffs, NJ: Prentice-Hall.

Lacroix, P. 1971. The internal remodeling of bone. In *The biochemistry and physiology of bone*, Bourne, G. H. ed., 119–142. London, New York: Academic Press.

Lamm, E.-T. 2013. Preparation and sectioning of specimens. In *Bone histology of fossil tetrapods*, Padian, K. and E.-T. Lamm eds., 55–160. Berkley, CA: University of California Press.

Laurin, M., et al. 2004. The Evolution of Long Bone Microanatomy and Lifestyle in Lissamphibians. *Paleobiology* 30 (4): 589–613.

Lester K., W. von Koenigswald. 1989. Crystallite orientation discontinuities and the evolution of mammalian enamel – or where is a prism?. *Scan. Microsc.* 3: 645–663.

Leeuwenhoek, A. van 1674. Microscopical observations concerning blood, milk, bones, the brain, spittle, and cuticula. Letter to the publisher. *Phil. Trans. R. Soc. London*. 106: 125.

Leeuwenhoek, A. van 1693. Several observations on the texture of the bones of animals compared with that of wood. *Philos. Trans. R. Soc. London* 17: 838–843.

Levrat-Calviac, V., L. Zylberberg. 1986. The structure of the Osteoderms in the Gekko: *Tarentola mauritanica*. *Am. J. Anat.* 176: 437–446.

Lison L. 1941. Recherches sur la structure et l'histogenèse des dents des poissons dipneustes. *Arch. Biol.* 52: 279–320.

Lubosch, W. 1927. Das perennierende Kalkskelett der Wirbeltiere und der fibrillar Bau der Knorpelingen Skeletteile. *Z. Mikro Anat. Forsch.* 9: 69–121.

Maisey, J. G. 1988. Phylogeny of early vertebrate skeletal induction and ossification patterns. *Evol. Biol.* 22: 1–36.

Mandl, L. 1839. Recherches sur la structure intime des écailles des poissons. *Ann. Sci. Nat.* 2: 337–371.

Margerie, E. de 2002. Laminar bone as an adaptation to torsional loads in flapping flight. *J. Anat.* 201: 521–526.

Margerie, E. de, et al. 2002. Bone typology and growth rate: testing and quantifying "Amprino's rule" in the mallard (*Anas platyrhynchos*). *C. R. Acad. Sci. Paris (Sci. Vie)* 325: 221–230.

Märss, T. 2006. Exoskeletal ultrastructure of early vertebrates. *J. Vertebr. Paleontol.* 26: 235–252.

Matyas, J. 1929. Die microanatomischen Knochenstrukturen und die Abstammungsgeschichte einzelner Wirbeltieregruppen. In *10th Congr. Int. Zool. Budapest*, 66–74.

McGonnel, I., A. Graham. 2002. Trunk neural crest has skeletogenic potential. *Curr. Biol.* 12: 767–771.

Meinke, D. K. 1984. A review of cosmine: its structure, development, and relationship to other forms of the dermal skeleton in Osteichthyans. *J. Vertebr. Paleontol.* 4: 457–470.

Meinke, D. K., K. S. Thomson. 1983. The distribution and significance of enamel and enameloid in the dermal skeleton of osteolepiform rhipidistian fishes. *Paleobiology* 9: 138–149.

Meunier, F. J. 1981. Données générales sur la structure de l'écaille et l'organisation spatiale des fibres de collagène de la plaque basale chez les Osteichthyens. *Icthyophysiol. Acta* 5: 41–49.

Meunier, F. J. 1984. Spatial organization and mineralization of the basal plate of elasmoid scales in osteichthyans. *Am. Zool.* 24: 953–964.

Meunier, F. J. 1987. Os cellulaire, os acellulaire et tissus derivés chez les Ostéichthyens: les phénomènes de l'acellularisation et de la perte de minéralisation. *Ann. Biol.* 26: 201–233.

Meunier, F. J. 1988. Détermination de l'âge individual chez les Osteichthyens à l'aide de la squelettochronologie: historique et méthodologie. *Acta Oecol. General.* 9: 299–329.

Meunier, F. J. 2003. Hans Hederström (1710-1792), un précurseur avisé de la squelettochronologie pour la determination de l'âge individual des poissons et la gestion des stocks. In *La mer dévorée. Le poisson bon à manger, le poisson bon à penser*, Geistdoerfer, A., J. Ivanoff and J. Matras-Guin eds., 23–28. Lorient: Anthropologie maritime/CCSTI.

Meunier, F. J. 2011. The Osteichthyes, from the Paleozoic to the extant time, through histology and paleohistology of bony tissues. *C. R. Palevol.* 10: 347–356.

Meunier, F. J., Y. François. 1980. L'organisation spatiale des fibres collagènes et la minéralisation des écailles des Dipneustes actuels. *Bull. Soc. Zool. Fr.* 105: 215–226.

Meunier, F. J., M. Herbin. 2014. La collection histologique du squelette des "poissons" de Paul Gervais. *Cybium* 8: 23–42.

Miles, A. E. W. ed. 1967. *Structural and chemical organization of teeth*. London, New York: Academic Press.

Mongera, A., C. Nüsslein-Volhard. 2013. Scales of fish arise from mesoderm. *Curr. Biol.* 23: 338–339.

Montes, L., et al. 2005. Relationship between bone growth rate and the thickness of calcified cartilage in the long bones of Galloanserae (Aves). *J. Anat.* 206: 445–452.

Moodie, R. W. 1908. Reptilian epiphyses. *Am. J. Anat.* 7: 443–467.

Moodie, R. W. 1923. *Paleopathology.* Urbana, IL: University of Illinois Press.

Morrison-Low, A., R. H. Nuttall. 2003. Hugh Miller in an Age of Microscopy. In *Celebrating the life and times of Hugh Miller – Scotland in the early 19th Century*, Borely, L. ed., 214–226. Cromarty, Scotland: The Cromarty Arts Trusts.

Moss, M. L. ed. 1963. Comparative biology of calcified tissues. *Ann. NY Acad. Sci.* 109: 1–410.

Moss, M. L. 1964. The phylogeny of mineralized tissues. *Int. Rev. Gen. Exp. Zool.* 1: 297–331.

Moss, M. L. 1968. The origin of vertebrate skeletal tissues. In *Current problems of lower Vertebrates phylogeny. Nobel symposium 4*, Ørvig, T. ed., 359–371. New York: J. Wiley and Sons.

Moss, M. L. 1972. The vertebrate dermis and the integumental skeleton. *Am. Zool.* 12: 27–34.

Moss, M. L. 1977. Skeletal tissues in sharks. *Am. Zool.* 17: 335–342.

Müller, H. 1858. Über die Entwicklung der Knochensubstanz nebst Bemerkungen über den Bau rachitischer Knochen. *Z. Zool.* 9: 147–233.

Murdoch, D. J. E., et al. 2013. The origin of conodonts and of vertebrate mineralized skeletons. *Nature* 502: 546–549.

Murray, P. D. F. 1936. *Bones. A study of the development and structure of the vertebrate skeleton*. Cambridge, UK: Cambridge University Press. (New edition 1985 with an introduction by B.K. Hall.)

Nicol, W. 1828. Observations on the fluids contained in crystallized minerals. *Edinburgh New Philos. J.* 5: 94.

Nicol, W. 1831. Observations of the fossil trees of Van Diemen's land. *Edinburgh New Philos. J.* 12: 361.

Nicol, W. 1834. Observations on the structure of recent and fossil Coniferae. *Edinburgh New Philos. J.* 16: 137–158.

Nicol, W. 1835. On the structure of some fossil woods found in the islands of Mull, Northern Africa and in the Karoo ground to the North-East of the Cape of Good Hope. *Edinburgh New Philos. J.* 18: 335.

Noda, M. 1993. *Cellular and molecular biology of Bone*. New York: Academic Press.

Nopcsa, F. von 1923a. *Eidolosaurus* und *Pachyophis*: Zwei neue Neocom-reptilien. *Paleontographica* 55: 97–154.

Nopcsa, F. von 1923b. Vorläufige Notiz über die Pachyostose und Osteosklerose einiger mariner Wirbeltiere. *Anat. Anz.* 56: 353–359.

Nopcsa, F. von 1930. Notes on Stegocephalia and Amphibia. *Proc. Zool. Soc. London* 64: 979–995.

Nopcsa, F. von, E. Heidsieck. 1933. On the histology of the ribs in immature and half-grown trachodont dinosaurs. *Proc. Zool. Soc. London* 1: 221–226.

Nopcsa, F. von, E. Heidsieck. 1934. Über eine pachyostotische Rippe auf der Kreide Rügens. *Acta Zool.* 15: 431–455.

Organ, C., et al. 2016. Macroevolution of genome size in sarcopterygians during the water-land transition. *C. R. Palevol* 15: 65–73.

Ørvig, T. 1951. Histologic studies of placoderms and fossil elasmobranchs 1: the endoskeleton with remarks on the hard tissues of lower vertebrates. *Ark. Zool.* 2: 321–456.

Ørvig, T. 1965. Paleohistological notes 2. Certain comments on the phyletic significance of acellular bone tissue in early lower vertebrates. *Ark. Zool.* 16: 551–556.

Ørvig, T. 1966. Histologic studies of Ostracoderms, Placoderms and fossil Elasmobranchs. 2. On the dermal skeleton of two late Paleozoic Elasmobranchs. *Ark. Zool.*19: 1–39.

Ørvig, T. 1967. Phylogeny of tooth tissues: evolution of some calcified tissues in early Vertebrates. In *Structure and chemical organization of teeth*, Miles, A. E. W. ed., 45–110. London and New York: Academic Press.

Ørvig, T. 1968. The dermal skeleton: general considerations. In *Current problems of lower tetrapod phylogeny*, Ørvig, T. ed., 373–397. New York: John Wiley and Sons.

Ørvig, T. 1977. A survey of odontodes ("dermal teeth") from developmental, structural, functional and phyletic points of view. In *Problems in vertebrate evolution, Zoological Society. London Symp. Ser 4*, Andrews, S. M., R. S. Miles and A. D. Walker, eds., 53–75. London, New York: Academic Press.

Ørvig, T. 1978a,b,c. Microstructure and growth of the dermal skeleton in fossil Actinopterygian fishes. a: *Birgeria and Scanilepis. Zool. Scr.* 7: 33–56; b: *Boreosomus, Plegmolepis and Gyrolepis,* id. 7: 125–144, c: *Nephrotus* and *Colobodus*, with remarks on the dentition of other forms. Id. 7: 297–326.

Owen, R. 1840–1845. *Odontography or a treatise on the comparative anatomy of the teeth*. London: Baillière.

Owen, R. 1842a. On the teeth of species of the genus *Labyrinthodon* (*Mastodonsaurus* of Jaeger) common to the German Keuper-formation and the Lower sandstone of Warwick and Leaningston. *Trans. Geol. Soc. London* 6: 503–513.

Owen, R. 1842b. Report on British fossil Reptiles. Part II. Report. British Assoc. *Adv. Sci.* 60–204.

Owen, R. 1861. The fossil Reptilia of the Liassic Formations. Part first: *Scelidosaurus harrisonii*. *Paleontogr. Soc. London* 13: 1–14.

Padian, K. 2004. *De Darwin au dinosaures: essais sur l'idée d'Evolution*. Paris: Odile Jacob.

Padian, K. 2011. Vertebrate paleohistology then and now: a retrospective in the light of the contributions of Armand de Ricqlès. *C. R. Palevol.* 10: 303–309.

Paine, G. 1937. Fossilization of bone. *Am. J. Sci.* 234: 148–157.

Pander, C. H. von 1856–1860. *Fossilen Fische der Russisch-Baltischen Gouvernements*, Vol. 4, Academy of Sciences, Saint Petersbourg.

Patterson, C. 1977. Cartilage bones, dermal bones and membrane bones, or the exoskeleton versus the endoskeleton. In *Problems in vertebrate evolution. Zoological Society London Symp. Ser 4*, Andrews, S. M., R. S. Miles and A. D. Walker, eds., 77–121. London, New York: Academic Press.

Pawlicki, R. 1984. Metabolic pathways of fossil dinosaur bone. IV. Modes of linkage between osteocytes and a variety of nexuses of osteocyte processes. *Folia Histochem. Cytobiol.* 22: 99–104.

Payen, A., J. Rossignon. 1843. *Manuel du cours de chimie organique appliquée aux arts industriels et agricoles.* Lyon, Franche: Béchet.

Peabody, F. E. 1961. Annual growth zones in vertebrates (living and extinct). *J. Morphol.* 108: 11–62.

Peck, W. A. ed. 1987. *Bone and mineral research/5*. Amsterdam, New York: Elsevier.

Perrin, W. F., A. C. Mirrick. 1980. *Age determination of toothed whales and sirenians*, Report IWC spec. issue 3. Cambridge, UK: International Whaling Commission.

Petersen, H. 1930. Die Organe des Skelettsystems. In *Handbuch der mikroskopischen Anatomie des Mensche*, von Mollendorff, W. ed., 529–676. Berlin: Springer.

VetBooks.ir

Peyer, B. 1931. Hartgebilde der Integuments. In *Handbuch vergleichende anatomie der wirbeltiere,* Vol. 1, Bolk, L., E. Goppert, E. Kallius and W. Lubosch eds., 703–752. Berlin: Urban and Schwartzenberg.

Peyer, B. 1968. *Comparative odontology*, R. Zangerl, ed. Chicago, London: Chicago University Press.

Piveteau, J. 1934. L'histoire du tissu osseux. *Terre et Vie* 4: 515–522.

Ponlot, R. 1960. *Le radiocalcium dans l'étude de l'os*. Paris: Masson et Cie.

Poole, D. F. G. 1967. Phylogeny of tooth tissue: enameloid and enamel in recent vertebrates, with a note on the history of cementum. In *Structural and chemical organization of teeth*, Miles, A. E. W. ed., 11–149. London and New York: Academic Press.

Poplin, C., et al. 1976. Quelques particularités anatomiques et histologiques du rostre de l'espadon (*Xiphias gladius L.*). *C. R. Acad. Sci. Paris 282*: 1105–1108.

Pritchard, J. J. 1972. General histology of bone. In *The biochemistry and physiology of bone.* 2nd edition, G. H. Bourne ed. London and New York: Academic Press.

Quekett, J. 1849a. On the intimate structure of bone as composing the skeleton of the four great classes of vertebrates viz. mammals, birds, reptiles and fish with some remarks on the great value of such structures to assess the affinities of minute fragments of organic remains. *Trans. R. Microsc. Soc. London 2*: 46–58

Quekett, J. 1849b. Additional observations on the intimate structure of bones. *Trans. R. Microsc. Soc. London 2*: 40–42.

Quekett, J. 1855. *Descriptive and illustrated catalogue of the histological series contained in the Museum of the Royal College of surgeons of England*. Vol. 2. London.

Quilhac, A., et al. 2014. *Globuli ossei* in the long limb bones of *Pleurodeles waltl* (Amphibia, Urodela, Salmandridae). *J. Morphol*. 275: 1226–1237.

Reid, R. E. H. 1981. Lamellar-zonal bone with zones and annuli in the pelvis of a sauropod dinosaur. *Nature* 292: 49–51.

Reid, R. E. H. 1983. High vascularity in bones of dinosaurs, mammals and birds. *Geol. Mag.* 120: 191–194.

Reid, R. E. H. 1984. The histology of dinosaurian bone, and its possible bearing on dinosaurian physiology. In *The structure, development and evolution of reptiles*, Fergusson, M. W. J. ed., 629–663. London: *Symp. Zool. Soc. London,* 52.

Reid, R. E. H. 1985. On supposed Haversian bone from the Hadrosaur *Anatosaurus* and the nature of compact bone in dinosaurs. *J. Paleontol*. 59: 140–148.

Reid, R. E. H. 1996. Bone histology of the Cleveland-Lloyd dinosaurs and of dinosaurs in general, part 1: Introduction: introduction to bone tissues. *Brigham Young Univ. Geol. Studies* 41: 25–71.

Reif, W. E. 1982. Evolution of dermal skeleton and dentition in vertebrates – the odontode regulatory theory. *Evol. Biol*. 15: 287–368.

Rensberger, J. M., M. Watabe M. 2000. Fine structure of bone in dinosaurs, birds and mammals. *Nature* 406: 619–622.

Rhodin, A. G. J. 1985. Comparative chondro-osseous development and growth of marine turtles. *Copeia* 3: 752–771.

Ricqlès, A. de 1972. Nature et signification des surfaces épiphysaires chez les tétrapodes fossiles. *C. R. Acad. Sci. Paris* 274: 3527–3530.

Ricqlès, A. de 1975–1978. Recherches paléohistologiques sur les os longs des tétrapodes (part. 7). Sur la classification, la signification fonctionnelle et l'histoire des tissus osseux des tétrapodes). 1 – Structures. *Ann. Paléont*. 61 (1975): 51–129. 2 – Fonctions, id. 62 (1976): 71–126; 63 (1977): 33–56, 133–160. 3 – Evolution, id. 64 (1978): 85–111, 153–184.

Ricqlès, A. de 1976. On bone histology of fossil and living reptiles, with comments on its functional and evolutionary significance. In *Morphology and biology of reptile*, Bellairs, A. d'A. and C.B. Cox eds., 123–150. London: Linn. Soc. Sympos. Ser. 3.

Ricqlès, A. de 1979. Quelques remarques sur l'histoire évolutive des tissus squelettiques chez les vertébrés et plus particulièrement chez les tétrapodes. *Ann. Biol*. 18: 1–35.

Ricqlès, A. de 1980. Tissue structure of dinosaur bone: functional significance and possible relations to dinosaur physiology. In *A cold look at the warm-blooded dinosaurs (AAAS Symposium 28)*, Olson, E. C. and R. D. K. Thomas eds., 103–139. Boulder, CA: Westview.

Ricqlès, A. de 1989. *Les mécanismes hétérochroniques dans le retour des tétrapodes au milieu aquatique*. Lyon, France: *Geobios. Spec. Mem*. no. 12, 337–348.

Ricqlès, A. de 1993. Some remarks on Paleohistology from a comparative-evolutionary point of view. In *Histology of ancient human bone: methods and diagnosis*, Grupe, G. and A. N. Garland eds., 37–77. Berlin: Springer.

Ricqlès, A. de1995a. Les vertébrés des grès de Harding: ce que Vaillant a pu observer. In *Premiers vertébrés et vertébrés inférieurs, VIIIth Int. Congress*, H. Lelièvre, S. Wenz., A. Blieck. and R. Cloutier eds., 51–56. Lyon, France: Geobios Spec. Mem. no. 19.

Ricqlès, A. de 1995b. Tissus squelettiques. In *Traité de zoologie. Amphibiens,* Vol. XIV A, Grassé, P. P. and M. Delsol eds., 49–96. Paris: Masson et Cie.

Ricqlès, A. de 2007. Fifty years after Enlow and Brown's Comparative histological study of fossil and recent bone tissue (1956-58): a review of Professor Donald H. Enlow's contribution to palaeohistology and comparative histology of bone. *C. R. Palevol*. 6: 591–601.

Ricqlès, A. de, J. Bolt. 1983. Jaw growth and tooth replacement in *Captorhinus aguti* (Reptilia, Captorhinomorpha): a morphological and histological analysis. *J. Vertebr. Paleontol.* 3: 7–24.

Ricqlès A. de, V. de Buffrénil. 2001. Bone histology, heterochronies and the return of Tetrapods to life in water: where are we? In *Secondary adaptations of tetrapods to life in water*, Mazin, J. M. and V. de Buffrénil, eds., 289–310. Munchen: Fr. Pfeil Verlag.

Ricqlès, A. de, et al. 2004. The "message" of bone tissue in Paleoherpetology. *Ital. J. Zool*. (Suppl.1): 3–12.

Ricqlès, A. de, J. Cubo. 2010. Le problème de la causalité complexe aux sources de la relation structuro-fonctionnelle: 1/ généralités, 2/ l'exemple du tissu osseux. In *Les fonctions: des organismes aux artefacts*, Gayon, J. and A. de Ricqlès eds., 179–188. Paris: PUF.

Ricqlès, A. de, et al. 2001a. Histomorphogenesis of embryos of Upper Jurassic Theropods from Lourhina (Portugal). *C. R. Acad. Sci. Paris. Ser. III*, 332: 647–656.

Ricqlès A. de, et al. 1991. Comparative microstructure of bone. In *Bone matrix and bone specific products*, Vol. 3, Hall, B. K. ed., 1–78. Boca Raton, FL: CRC Press.

Ricqlès, A. de, et al. 2001b. The bone histology of basal birds in phylogenetic and ontogenetic perspectives. In *New perspectives on the origin and early evolution of birds*, Gauthier, J. A. and L. F. Gall, eds., 411–425. New Haven, CT: Yale University Press.

Ricqlès, A. de, et al. 2000. Paleohistology of the bones of Pterosaurs (Reptilia, Archosauria): anatomy, ontogeny and biomechanical implications. *Zool. J. Linn. Soc*. 129: 349–385.

Ricqlès, A. de, et al. 2003. Osteohistology of *Confuciusornis sanctus* (Theropoda, Aves), *J. Vertebr. Paleontol*. 23: 373–386.

Ricqlès, A. de, et al. 2001c. Histology of dermal ossifications in an Ankylosaurian dinosaur from the Late Cretaceous of Antarctica. In *VIIth. Internatl. Sympos. on Mesozoic Terrestrial Ecosystems*, 171–174. Assoc. Paleont. Argentina.

Ricqlès, A. de, et al. 2009. Rediscovery of Paul Gervais' paleohistological collection. *Geodiversitas* 31: 943–971.

Rimblot-Baly, F., et al. 1995. Analyse paléohistologique d'une série de croissance chez *Lapparentosaurus madagacariensis* (Jurassique moyen): essai sur la dynamique de croissance d'un dinosaure sauropode. *Ann. Paléontol*. 81: 49–86.

Rodahl, K., et al. 1960. *Bone as a tissue*. New York: Mc Graw-Hill Company.

Romer, A. S. 1963. The ancient history of bone. *Ann. N.Y. Acad. Sci*. 109: 168–176.

Romer, A. S. 1964. Bone in early vertebrates. In *Bone biodynamics*, Frost, H. M. ed., 13–40. Boston: Little, Brown and Co.

Roumiantsiev, A. V. 1958. *Essay on the evolution of cartilaginous and bony tissues* (in Russian). Moscow: *Akad. Nauk. USSR*.

Ruibal, R., J. Shoemaker. 1984. Osteoderms in Anurans. *J. Herpetol*. 18: 313–328.

Sacchi-Vialli, G. 1967. Contributo alla conoscenza paleoistologica di ossa fossili. *Atti Instit. Geol. Univ. Pavia* 18: 65–81.

Sander, P. M. 1997a. Glossary of terms used for enamel microstructure. In *Tooth enamel microstructure*, Koenigswald, W. von and P. M. Sander, eds., 267–280. Rotterdam: Balkema.

Sander, P. M. 1997b. Non-mammalian Synapsid enamel and the origin of mammalian enamel prisms: the bottom-up perspective. In *Tooth enamel microstructure, Koenigswald* W. von and P. M. Sander eds., 41–62. Rotterdam: Balkema.

Sander, P. M. 2000. Long bone histology of the Tendaguru sauropods: implications for growth and biology. *Paleobiology* 26: 466–488.

Sansom, I. J., et al. 1992. Presence of the earliest vertebrate hard tissues in conodonts. *Science* 256: 1308–1311.

Sansom, M. W. 1996. *Pseudooneotodus*: a histological study of an Ordovician to Devonian vertebrate lineage. *Zool. J. Linn. Soc*. 118: 47–57.

Sansom, M. W., D. K. Elliott. 2002. A Thelodont from the Ordovician of Canada. *J. Vertebr. Paleontol*. 22: 867–870.

Sansom, M. W., et al. 1994. Dentine in conodonts. *Nature* 368: 591.

Schaeffer, B. 1977. The dermal skeleton in fishes. In *Problems in vertebrate evolution*, Andrews, S. M., R. S. Miles and A. D. Walker, eds., *Linn. Soc. Symp.* Ser 4, 25–52. London and New York: Academic Press.

Schaffer, J. 1889. Über den feineren Bau fossiler Knochen. *Sitzungsber Kaiserl. Akad. Wiss. Math. Naturwiss.* 98: 319–382.

Schmidt, W. J., A. Kiel. 1971. *Polarizing microscopy of dental tissues*. Oxford, UK: Pergamon Press.

Schmitt, S. 2005. From eggs to fossils: epigenesis and transformations of species in Pander's biology. *Int. J. Dev. Biol*. 49: 1–8.

Schönbörner, A., et al. 1981. The fine structure of calcified Mandl's corpuscles in teleost fish scales. *Tissue Cell* 13: 589–597.

Schultze, H. P. 1966. Morphologische und histologische Untersuchungen an Schuppen mesozoischer actinopterygier. Übergang von Ganoid-zu Rund-Schuppen. *N. Jahrb. Geol. Palaontol*. 126: 232–314.

Schultze, H. P. 1969. Die Faltenzähne der Rhipidistiiden Crossopterygier, der Tetrapoden und der Actinopterygier-Gattung *Lepisosteus*. *Paleontol. Ital.* 65: 63–136.

Schultze, H. P. 1977. Ausgangsformen und Entwicklung der rombischen Schuppen des Osteichthyes (Pisces). *Paleont. Z*. 51: 152–168.

Schultze, H. P. 1996. Conodont histology: an indicator of vertebrate relationship? *Mod. Geol*. 20: 275–285.

Schultze, H. P. 2009. The international influence of the Stockholm School. *Acta Zool. (Stockholm)* 90 (suppl. 1): 22–37.

Schultze, H. P. 2016. Scales, enamel, cosmine, ganoine, and early Osteichthyans. *C. R. Palevol*. 15: 83–102.

Seilacher, A. 1970. Arbeitskonzept zur Konstructionsmorphologie. *Lethaia* 3: 393–396.

Seitz, A. L. 1907. Veirgleichende Studien über den mikroscopischen Knochenbau fossiler und rezenter Reptilien. *Nova Acta Acad. Leop. Carol. Naturforsch*. 87: 230–370.

Serafini-Fracassini, A., J. W. Smith. 1974. *The structure and biochemistry of cartilage*. Edinburgh and London: Churchill Livingstone.

Shahar, R., S. Wiener. 2017. Open questions on the 3D structures of collagen containing vertebrate mineralized tissues: a perspective. *J. Struct. Biol*. 201: 187–198.

Shu, D. G., et al. 2003. Head and backbone of the Early Cambrian vertebrate *Haikouichthys*. *Nature* 421:526–529.

Simkiss, K. 1975. *Bone and biomineralization* (Studies in Biology 53). London: Edward Arnold.

Sire, J.-Y., et al. 2009. Origin and evolution of the integumentary skeleton in non-tetrapod vertebrates. *J. Anat*. 214: 409–440.

Sire, J. Y., et al. 1987. On the origin of Ganoin: histological and ultrastructural data on the experimental regeneration of the scales of *Calamoichthys calabaricus* (Osteichthyes, Brachyopterygii, Polypteridae). *Am. J. Anat*. 180: 391–402.

Sire, J.-Y., A. Huysseune. 2003. Formation of dermal skeletal and dental tissues in fish: a comparative and evolutionary approach. *Biol. Rev.* 78: 219–249.

Sloan, P. R. ed. 1992. *Richard Owen's Hunterian Lectures in comparative anatomy (May and June 1837)*. Chicago: University of Chicago Press.

Smith, J. W. 1960. Collagen fiber patterns in mammalian bone. *J. Anat*. 94: 329–344.

Smith, M. M. 1984. Petrodentin in extant and fossil Dipnoan dentitions: microstructure, histogenesis and growth. *Proc. Linn. Soc. NSW.* 107: 367–407.

Smith, M. M. 1988. The dentition of Paleozoic lungfishes: a consideration of the significance of teeth, denticles and tooth plates for dipnoan phylogeny. *Mém. Mus. Nat. Hist. Nat*. 53: 179–194.

VetBooks.ir

Smith, M. M., K. S. W. Campbell. 1987. Comparative morphology, histology and growth of the dental plates of the Devonian Dipnoan *Chirodipterus*. *Philos. Trans. R. Soc. London B* 317: 329–363.

Smith, M. M., M. I. Coates. 1998. Evolutionary origins of the vertebrate dentition: phylogenetic patterns and developmental evolution. *Eur. J. Oral Sci*. 106 (suppl. 1): 482–500.

Smith, M. M., et al. 1987. The relationships of *Uronemus*: a carboniferous Dipnoan with highly modified tooth plates. *Philos. Trans. R. Soc. London B 317*: 299–327.

Sognnaes, R. F., ed. 1960. *Calcification in biological systems*. Washington, DC: American Association for the Advancement of Science. 64.

Soressi, M., et al. 2013. Neandertals made the first specialized bone tools in Europe. *PNAS* 110 (35): 14186–14190 https://doi.org/10.1073:pnas.1302730110

Steel, L. 2003. John Quekett's sections and the earliest pterosaur histological studies. In *Evolution and paleobiology of Pterosaurs*, Buffetaut, E. and J.M. Mazin, eds., 325–334. Geol. Soc. Special Publ. 217.

Stephan, P. 1900. Recherches histologiques sur la structure du tissus osseux des poissons. *Bull. Soc. Fr. Belg.* 33: 281–429.

Steyer, J. S., et al. 2004. First histological and skeletochronological data on temnospondyl growth: paleoecological and paleoclimatological implications. *Paleogeography, Paleoclimatol. Paleoecol*. 206: 193–201.

Stockwell, R. A. 1979. *Biology of cartilage cells*. Cambridge, UK: Cambridge University Press.

Tchudinov, P. K. 1970. *About skin structure among therapsids (Estemmenosuchus uralensis)*. Moscow: *Nauka*, 45–50.

Thomasset, J. J. 1930 Recherches sur les tissus dentaires des poissons fossiles. *Arch. Anat, Histol. Embryol*. 11: 5–153.

Thomson, K. S. 1972. An attempt to reconstruct evolutionary changes in the cellular DNA content of Lungfish. *J. Exp. Zool*. 180: 363–372.

Thomson, K. S. 1975. On the biology of cosmine. *Bull. Peabody Mus. Nat. Hist*. 40: 1–59.

Thorpe, B.H. 1988. Pattern of vascular canals in the bone extremities of the pelvic appendicular skeleton in broiler type fowls. *Rec. Veter. Sci*; 44: 112–124.

Tomes, C. S. 1875. On the development of the teeth of the newt, frog, slowworm, and green lizard. *Philos. Trans. R. Soc. London* 165: 285–296.

Tomes, C. S. 1878. On the structure and development of vascular dentine. *Philos. Trans. R. Soc. London* 169: 1–3.

Tomes, C. S. 1897. On the development of marsupial and other tubular enamels, with notes upon the development of enamel in general. *Philos. Trans. R. Soc. B* 189: 107–122.

Tomes C. S. 1898. Upon the structure and development of the enamel in the elasmobranch fishes. *Philos. Trans. R. Soc. London* 190: 7

Tomes, J., C. De Morgan. 1853. Observations on the structure and development of bone. *Philos. Trans. R. Soc. London* 143 (1): 109–139.

Tretjakoff, D., F. Chinkus. 1927. Das knochengewebe des Fische. *Z. Anat. Entwickl*. 83: 363–396.

Tretjakoff, D., F. Chinkus. 1930. Die Hautschuppen des Anamnia. *Z. Wiss. Zool*. 136: 3–4.

Turner, S., et al. 2010. False teeth: conodont-vertebrate phylogenetic relationships revisited. *Geodiversitas* 32: 545–594.

Vaillant, L. 1902. Sur la présence du tissue osseux chez certains poissons des terrains paléozoïques de Canyon City (Colorado). *C. R. Acad. Sci. Paris* 134: 1321–1322.

Valentin, G. G. 1861. *Dien Untersuchungen der Pflanzen-und Tiergewebe in polarisierten licht*. Leipzig.

Veis, A. ed. 1981. *The chemistry and biology of mineralized connective tissues*. Amsterdam, New York: Elsevier.

Vesalius, A. 1543. *De humanis corpori fabrica*. Basel, Switzerland: J. Oporinus.

Vialli, M., G. S. Vialli. 1969. Morfometria delle lacune ossee di Vertebrati attuali e fossili alla luce delle conoscenze di biologia cellular. *Rend. Inst. Lombardo Acad. Sci. Lett*. 103: 234–254.

Vickaryous, M. K., J.-Y.Sire. 2009. The integumentary skeleton of tetrapods: origin, evolution and development. *J. Anat*. 214: 441–464.

Wang, N-Z., et al. 2005. Histology of the Galeaspid dermoskeleton and endoskeleton, and the origin and early evolution of the vertebrate cranial endoskeleton. *J. Vertebr. Paleontol*. 25: 745–756.

Warren, J. W. 1963. Growth zones in the skeleton of recent and fossil vertebrates. PhD (unpublished). *Univ. of California, Los Angeles. Dissert. Abstracts (USA)*: 24(2): 908–909.

Weidenreich, F. 1930. Das Knochengewebe. In *Handbuch der mikroscopischen Anatomie des Menschen*, von *Mollendorff*, W., ed., Vol. II (2), 391–520. Berlin: Springer.

Weishampel, D. B., W.-E. Reif. 1984. The work of Franz Baron Nopcsa (1877-1933): dinosaurs, evolution and theoretical tectonics. *J. Geol. Bundesanstalt Wien*. 127: 187–203.

Wiffen, J., et al. 1995. Ontogenic evolution of bone structure in Late Cretaceous Plesiosauria from New Zealand. *Geobios* 28: 625–640.

Williamson, W. C. 1849. On the microscopic structure of the scales and dermal teeth of some ganoid and placoid fishes. *Philos. Trans. R. Soc. London B* 139: 435–475.

Williamson, W. C. 1851. Investigations into the structure and development of the scales and bones of fishes. *Philos. Trans. R. Soc. London B* 141: 643–702.

Wilsman, N. J., D. C. Van Sickle. 1972. Cartilage canals: their morphology and distribution. *Anat. Rec*. 173: 79–94.

Witham, H. 1831. *Observations of fossil vegetables* (reference by Geikie A. in *The founders of Geology*. 1897). Baltimore: John Hopkins University.

Wolff, J. 1892. *Das Gesetz des Transformation der Knochen*. Berlin: Hirschwald.

Wurmbach, H. 1932. Das Wachstum des Selachierwirbels und seiner Gewebe. *Zool. Jahrb*. 55: 1–136.

Young, G. C., et al. 1996. A possible late Cambrian vertebrate from Australia. *Nature* 383: 810–812.

Zangerl, R. 1935. *Pachypleurosorus edwardii*, Cornalia. Osteologie, Variationsbreite, Biologie. In *Triasfauna der Tessiner Kalkalpen IX Pachypleurosaurus*, Peyer, B. ed., 1–80 Mem. Soc. Pal. Suisse 66.

Zavattari E., L. Cellini. 1956. La minutta architettura delle ossa degli ucelli e il suo valore nelle sistematica dei grandi gruppi. *Monit. Zool. Ital*. 64: 189–200.

Zhu, M., et al. 2006. A primitive fish provides key characters bearing on deep Osteichthyan phylogeny. *Nature* 440: 77–80.

VetBooks.ir

Zilhão, J., 2012. Personal ornaments and symbolism among the Neanderthals. In *Origins of human innovation and creativity*, J. J. M. van der Meer ed., Developments in Quaternary Science, vol. 16, pp. 35–49. Amsterdam: Elsevier.

Zipkin, I. ed. 1973. *Biological mineralization*. New York: John Wiley and Sons.

Zylberberg, L. 1988. Ultrastructural data on the scales of the Dipnoan *Protopterus annectens* (Sarcopterygii, Osteichthyes). *J. Zool. London* 216: 55–71.

Zylberberg, L., J. Castanet. 1985. New data on the structure and the growth of the osteoderms in the reptile *Anguis fragilis* L. (Anguidae, Squamata). *J. Morphol.* 186: 327–342.

Zylberberg, L., et al. 1980. Structure of the dermal scales in Gymnophiona (Amphibia). *J. Morphol.* 165: 41–54.

Zylberberg, L., et al. 1992. Biomineralization in the integumental skeleton of the living lower Vertebrates. In *Bone metabolism and mineralization*, Vol. 4, Hall, B. K. ed., 171–224. Boca Raton, FL: CRC Press.

Zylberberg, L., et al. 2010. A microanatomical and histological study of the postcranial dermal skeleton in the Devonian sarcopterygian *Eusthenopteron foordi*. *Acta. Paleont. Pol.* 55: 459–470.

Zylberberg, L., M. H. Wake. 1990. Structure of the scales of *Dermophis* and *Microcaecilia* (Amphibia, Gymnophiona), and a comparison to dermal ossifications in other vertebrates. *J. Morphol.* 206: 25–43.

VetBooks.ir

Section II

Morphology and Histology of the Skeleton

VetBooks.ir



Taylor & Francis
Taylor & Francis Group
http://taylorandfrancis.com

VetBooks.ir

2

An Overview of the Embryonic Development of the Bony Skeleton

Vivian de Buffrénil and Alexandra Quilhac

CONTENTS

Introduction 29
Late Gastrulation and the Tridermic Organization 29
The Inductive Role of the Chord 31
Skeletogenic Involvement of Neural Crests, Somites and Lateral Plates 31
Neural Crests and the Cephalic Domain 31
Somites and the Axial and Paraxial Skeleton 33
Lateral Plates and the Zono-Appendicular Skeleton 34
References 36

Introduction

Skeletal development is one of the most important pillars of evo-devo studies, because it allows direct experimental approaches to mechanisms that may have been at work in the evolutionary modifications of anatomical structures in extinct organisms. Today, the main stages of embryonic development have been richly documented for numerous taxa encompassing most of vertebrate diversity (reviews in Hall 2005; Long and Ornitz 2013; Berendsen and Olsen 2015; Hirasawa and Kuratani 2015; see also De Vos and Van Gansen 1980).

Because descriptive (anatomical and histological) data have been relatively well established, fundamental questions now shift to genetic processes, local messengers and other tissue interactions that control both, the differentiation of chondrogenic and osteogenic cells and the integrated morphological patterning of skeletal elements. Considering this molecular dimension in detail is beyond the goals of this book. Here we aim mainly to summarize the main stages of bone organogenesis in Tetrapoda, so that basic concepts frequently used in this book, such as *dermal* and *endochondral* bone, can have specific meanings. Substantial differences in early skeletal development among vertebrate classes (see Hall 2005; Hirasawa and Kuratani 2015) will be glossed over to describe only larger qualitative trends.

Late Gastrulation and the Tridermic Organization

By the end of the complex cell drifts and morphogenetic processes that characterize gastrulation (reviews in Solnica-Krezel 2005; Wang and Steinbeisser 2009), the tridermic organization of the embryo is complete (Figure. 2.1A).

The deep endodermal archenteron located in the core of the embryo, in ventral and lateral positions, is then covered dorsally and laterally by the chordomesoderm; these two cell layers are enclosed by the superficial ectodermic envelope (Figure 2.1B). When gastrulation ends, a sagittal flexible rod called the notochord, which is wedged between the top of the archenteron and the axial part of the ectoderm, differentiates within the dorsalmost region of the chordomesoderm (Figure 2.1C). This rod is composed of the closely stacked cells that form the chordoderm. Initially simple, this structure later complexifies with the differentiation of three histological compartments: (1) a relatively stiff core occupying most of the chord volume and composed of fluid-filled vacuolated cells; (2) a thin layer of outer epithelial-like cells surrounding the core and (3) a thick acellular sheath, called the perinotochordal basement membrane, which is composed of several extracellular matrix proteins, enveloping the whole structure (reviews in Stemple 2005, Corallo et al. 2015; Trapani et al. 2017). The occurrence of a chordoderm in early embryos is a diagnostic feature of the phylum Chordata; the vertebrates are chordates that develop an internal skeleton, as opposed to the prochordates. In most craniates, the chord is a transient structure, whereas it is permanent in some vertebrates such as agnathans and chondrosteans (Stemple 2005). Parallel with chordal development, the part of the ectoderm situated just above the chord forms the *neural plate* (Figure 2.1C), a sagittal band of ectodermal cells basically (but not exclusively) destined to differentiate into neural tissues.

VetBooks.ir

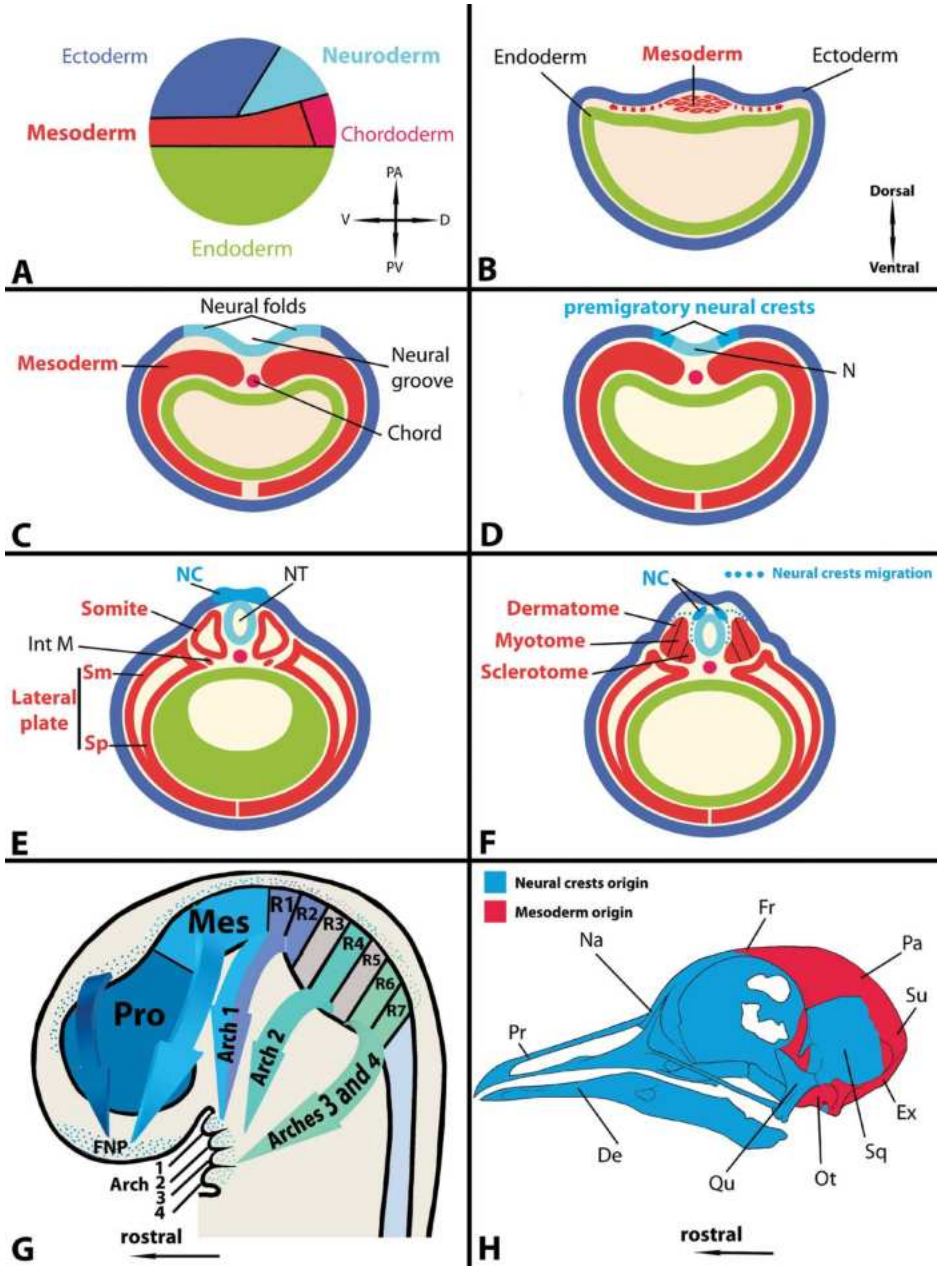


FIGURE 2.1 Embryonic development of osteogenic territories. Cell layers involved in osteogenesis are bold. A, Schematic map of vertebrate early gastrula. During gastrulation, cell movements result in a three-layer organization. The future endodermal cells lie at the vegetal pole (PV). The area of the animal pole (PA) forms the ectoderm where the future neuroderm is already determined. The third area, between the ectoderm and endoderm, called the mesoderm, contains the future chordoderm. B–F, Schematic representations of cross sections during gastrulation, neurulation and somitogenesis. B, During vertebrate gastrulation, endoderm and ectoderm interact to produce a three-germ layer called mesoderm. Some of the invaginated epiblast cells invade the space between endoderm and ectoderm and migrate laterally. C, The axial mesoderm forms the notochord, while other mesodermal cells follow their migration. The notochord induces the formation of the neural plate within the ectoderm located above it. D, The neural plate (N) bends ventrally and the neural folds begin to join to form the neural tube (NT). Above the NT, neural crest cells (NCs) differentiate. E, The NT is complete, and premigratory NCs are lying above it. The mesoderm subdivides into paraxial mesoderm, which gives rise to somites, intermediate mesoderm (Int M) and lateral plates, which split into two layers: somatic (Sm) and splanchnic mesoderm (Sp). F, NCs start migrating under the ectoderm and between the mesoderm and endoderm. Each somite splits into three parts: the ventromedial part is induced to become a sclerotome by factors secreted by the ventral part of the neural tube and the notochord. The medial part of the somite becomes a myotome later involved in muscle development, and the dorsal part of the somite becomes a dermatome that will contribute to the development of the dermis. G, Segmental migration of cranial NCs in a vertebrate embryo. Arrows represent the patterns of migration of prosencephalic (Pro), mesencephalic (Mes) and rhombencephalic NCs into the frontonasal process (FNP) and pharyngeal arches 1–4. NCs from the prosencephalon and the anterior mesencephalon migrate toward the FNP, whereas the NCs of the posterior mesencephalon and the first and second rhombomere (R1 and R2) fill the first pharyngeal arch (Arch 1). NCs from R4 fill the second arch and those of R6 and R7 both fill arches 3 and 4. H, Embryonic origin of the skull in bird model. Neural crest derived territories are in blue and paraxial mesoderm derived territories are in red. D, dorsal; De, dentary; Ex, exoccipital; Fr, frontal; Na, nasal; Ot, otic capsule; Pa, parietal; Pr, premaxilla; Qu, quadrate; Sq, squamosal; V, ventral.

VetBooks.ir

The Inductive Role of the Chord

The chordoblasts exert an inductive action on the mesodermal formations bordering them laterally, the ectodermic cells located above them and the underlying endodermal cells. Several molecular signals, among which are the Hedgehog protein family (Hh), playing a general and prominent role (Jia and Jiang 2006), are involved in this process and transmit information on both the spatial situation of the embryo parts (ventral vs. dorsal, left vs. right) and the fate of targeted cells (reviews in Stemple 2005, Corallo et al. 2015; see also Nicollet 1971, Pownall et al. 1996). In the ectoderm, these signals influence the neurulation process (Figure 2.1D, E), resulting in the formation of the *neural tube*. Simultaneously, the differentiation of ectodermal excrescences, the *neural crests*, on the dorsolateral walls of the neural groove, at the junction with epidermal cells, is initiated (Figure 2.1E, F). Neural crests are distributed in the anterior half of the embryo (future cephalic and trunk territories), where they appear as two symmetric ridges along the sides of the neural tube. Several neural crest-inducing molecular signals, emitted by neighboring tissues including the notochord, and belonging to the broad families of *bone morphogenetic proteins* (BMPs), *Wingless-Int* (Wnt) and *fibroblast growth factors* (FGF), control this transformation process (reviews in Rogers et al. 2012; Pegoraro and Monsoro-Burq 2013). Although derived from polarized, fixed epithelial cells, neural crest cells acquire new characteristics through the so-called *epithelial to mesenchymal transition* (EMT) process (review in Lim and Thiery 2012): they lose polarity and gain migration capabilities, finally to become multipotent mesenchymal cells (e.g., Thiery et al. 2009, Theveneau and Mayor 2014). Moreover, topographic specialization (i.e., *regionalization*), relative to the skeletal elements they later produce (Figure 2.1G, H), has been observed among them (reviews in Le Douarin et al. 2004, Hall 2005, Schilling and Le Pabic 2014).

In parallel with this process, the inductive action of the chord and the ectoderm (Fan and Tessier-Lavigne 1994; Fleming et al. 2003, 2015) provokes a segmentation of the parachordal mesoderm into metameric units, the somites (Figure 2.1E) (reviews in Tajbakhsh and Spörle 1998; Geetha-Loganathan et al. 2008; Bénazéraf and Pourquié 2013). The number of somites varies among taxa and is characteristic of the species (Flint et al. 1978; Pourquié 2001). Segmentation of the parachordal mesoderm into somites is a sequential process, developing in the craniocaudal direction with a species-specific periodicity that reflects the action of a genetic clock in presomitic mesoderm cells (Tam 1981; Oates et al. 2012; Saga 2012).

By the time somites are differentiating, the broad mesodermal sheets situated more laterally turn into two symmetric *lateral plates* that cover most of the surface of the archenteron (Figure 2.1E, F). Like the somites, these plates are composed of mesodermal cells. Each lateral plate subsequently laminates into two cell blades separated by a gap that will increase to become the coelomic cavity. The lateral, subepidermal layer constitutes the somatopleura, and the inner, perivisceral layer is the splanchnopleura.

Skeletogenic Involvement of Neural Crests, Somites and Lateral Plates

Neural Crests and the Cephalic Domain

In subsequent stages of the embryonic development the ectomesenchymal cells of the neural crests start migrating to various locations, as seen *in vivo* and *in vitro* by the use of antibody labeling (e.g., Sadaghiani and Vielkind 1990) and cell labeling with ^{3}H thymidine (Johnston 1966; Chibon 1967). Detailed reviews of this complex migratory process, in which there are many activating and inhibiting regulators involved, attractive and repulsive factors, along with local epigenetic tissue interactions, are given by Hall (2008), Theveneau and Mayor (2014), and Pegoraro and Monsoro-Burq (2013). Neural crest cells are likely to follow two main pathways in their migrations: a dorsal pathway for the cells originating from the cephalic region (Figure 2.1G), and a ventral one for the trunk cells (Loring and Erickson 1987; Olsson and Hanken 1996; Kuratani et al. 2018). Many embryonic territories are targeted, including the future cephalic (Figure 2.1H), mandibular, pharyngeal, cardiac and thoracic domains (reviews in Le Douarin et al. 2004; Theveneau and Mayor 2012). A list of the numerous derivatives of the sole cephalic neural crest cells is given by Le Douarin and Dupin (2014). Once settled in putative skeletal regions, skeletogenic ectomesenchymal cells aggregate to form discoid (flat bones) or various-shaped condensations (Figure 2.2A).

As pointed out by Hall and Miyake (1992, 1995), mesenchymal condensations (whether at the origin of the membrane or endochondral bones) are key elements for the development of the skeleton. They are the sites of three major processes i.e., cell aggregation, proliferation and differentiation, controlled by a complex cascade of genetic expressions and local regulation factors (for review see Hall and Miyake 1995, 2000; Hall 2005; Long and Ornitz 2013). During the differentiation process, mesenchymal cells undergo a gradual restriction of their initial totipotent capability (Le Douarin 2004). Substantial progress toward a detailed understanding of osteoblast differentiation in membrane ossification was accomplished with Abzhanov et al.'s (2007) study of the development of cranial bones in the chicken and the mouse (see also Zelzer and Olsen 2003; Yamashiro et al. 2004 and Dobreva et al. 2006 for genetic aspects). This study showed that only a part of the cells derived from neural crests differentiate directly into osteoblasts (as was currently considered; see the review by Kobayashi and Kronenberg 2005). Rather, there is a gradual maturation, in response to initial mesenchymal-epithelial interactions, of proliferating mesenchymal cells into early preosteoblasts, then preosteoblasts and finally mature osteoblasts (Figure 2.2B, C). At each stage of this maturation process, the cells successively express several combinations of skeletal markers and morphogenetic factors that are characteristic of membrane ossification and distinct from those involved in endochondral bone development. Moreover, retroaction loops modulate the expression of each factor (see also reviews in Dunlop and Hall 1995; Sieber-Blum 2000; Le Douarin and Dupin 2003; Aubin 2008).

VetBooks.ir

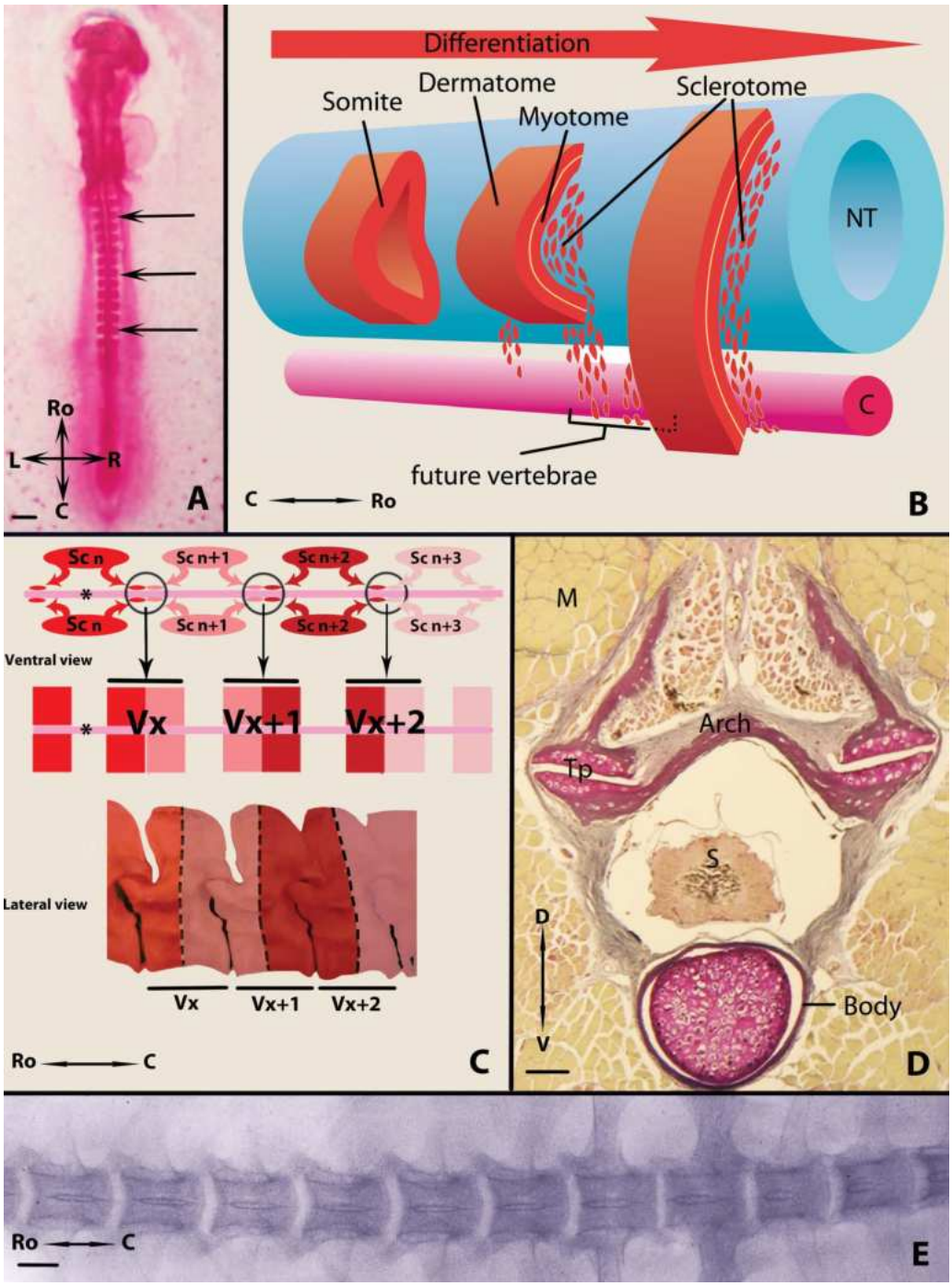


FIGURE 2.2 Somite contribution to the spine. A, Dorsal view of a chick embryo. Presomitic mesoderm on both sides of the neural tube becomes subdivided into somites (black arrows) in the craniocaudal direction. Scale bar: 250 µm. B, Schematic representation of somite maturation and subdivision along the craniocaudal axis. Each somite ultimately subdivides into a dermatome, myotome and sclerotome. Sclerotome cells migrate medially, ventrally and laterally. Cells from the ventral part condense around the notochord and give rise to the vertebral body and intervertebral disc. The transverse process is derived from the central part of the sclerotome and the spinous process from the dorsal part. The neural arch has a double origin: central and dorsal (see D and Figure 2.5). NT, neural tube; C, chord. C, Illustration of resegmentation of the sclerotome. Each sclerotome (Sc) splits into two halves. Thus, one vertebra is formed by the recombination of two neighboring sclerotome halves. Vertebral bodies (V) form by the fusion of the caudal end of one sclerotome with the cranial end of the sclerotome caudal to it. D, Developing vertebra in an amphibian larva. Specific component of a vertebra such as the vertebral body (Body), vertebral arch (Arch) and transversal processes (Tp) are more or less ossified at this stage. Spinous process (dorsally) is not complete at this stage. S, spinal cord; M, muscles. Scale bar: 150 µm. E, Dorsal view of lumbar and sacral vertebrae in a post-hatching *Crocodylus niloticus*. C, caudal; D, dorsal, L, left; R, right; Ro, rostral; V, ventral. Scale bar: 0.5 cm.

VetBooks.ir

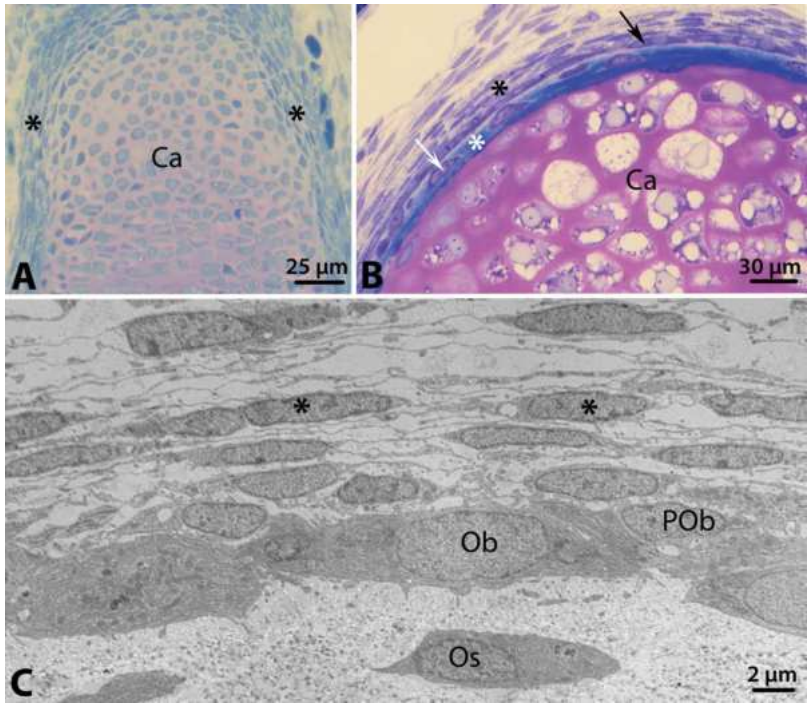


FIGURE 2.3 Condensation of mesenchymal cells in presumptive territories of skeletal elements and ossification. A–B, Thin sections of skeletal elements of stage 12–13 *Pogona* embryo. A, Longitudinal section of phalange. Concentric layers of elongated mesenchymal cells (asterisks) surround a cartilage template (Ca) issued from the differentiation of chondrogenic progenitor cells. B, Cross section of femur. Black asterisk indicates the mesenchymal cells differentiating into osteoblasts (black arrow). Osteoblasts form the osteoid (white asterisk) where osteocytes are "buried". C, Ultrathin cross section of femur of stage 12–13 *Pogona* embryo. Elongated, flattened mesenchymal cells (asterisks) condensate and differentiate into preosteoblasts (POb), and then into secreting osteoblasts (Ob) rich in mitochondria and rough endoplasmic reticulum. An osteocyte (OS) showing a cytoplasmic process is surrounded by the unmineralized extracellular fibrillar matrix.

In superficial territories of the cephalic and pectoral regions, newly differentiated osteoblasts in the condensations begin to produce the extracellular matrix of the osseous tissue in the form of nonmineralized osteoid. Osteoid-producing cells are progressively entrapped in their own secretion and definitively remain there, in the form of osteocytes, when local mineralization of the osteoid is complete (a detailed review of this process is presented in Franz-Odendaal et al. 2006). The osteoid then starts mineralizing to become the early template of a bone. Such a direct mode of bone formation characterizes the *membrane ossification* process, also called *dermal* ossification, and the bony elements produced by it are the *membrane bones*. Most skeletal elements resulting from this process have an ectomesenchymal origin, except the clavicle, which has a mesodermal origin. Some bones that arise from the alternative ossification way, i.e., endochondral ossification (see below), can also originate from neural crest ectomesenchymal cells, as is the case for middle-ear bones (Long and Ornitz 2013).

Somites and the Axial and Paraxial Skeleton

Somites are repetitive structures along the rostrocaudal axis (Figure 2.2A). Each somite initially consists of a homogeneous epithelial sphere with a small central lumen. The ventral part of the early somite, close to the notochord, turns into a thick formation of mesodermal mesenchyme through the EMT process. In the mature somite (Figures 2.1F, 2.2B), this part constitutes the sclerotome, which is later involved in the development of vertebrae and ribs. In the meantime, the dorsolateral region of the early somite becomes a two-compartment formation, the myodermatome, comprising, both peripheral cells (dermatome) that will be at the origin of the dermis of the back and the musculature of the axial skeleton, and the subjacent myotome (wedged between the sclerotome and the dermatome), the cells of which will be involved in the organogenesis of skeletal muscles and tendons (reviews in Pourquié 2001 and Christ et al. 2007; see also Christ and Wilting 1992).

The skeletogenic role of the somites results from the migration and subsequent condensations of sclerotomal cells around the chord, facing the present pairs of somites locally. An additional migration, located more laterally, also occurs toward the thoracic region, again in spatial correspondence with the somites on each side. Several molecular interactions between these cells and the notochord, neural tube and other target tissues (review in Lawson and Harfe 2017; see also Krück et al. 2013) are involved in both migration pathways and resulting local condensations. In addition, a topographical subdivision exists among mesenchymal cells, within a single sclerotome and between neighboring sclerotomes, concerning the skeletal elements that they will contribute to produce (Verbout 1985, Bagnall et al. 1989, Christ and Wilting 1992). Cells located laterally and centrally in the sclerotome are involved in the organogenesis of ribs (Evans 2003). Cells located centrally and dorsally create the neural arches and their processes, and

VetBooks.ir

cells located in the ventral part of the sclerotome constitute vertebral centra and intervertebral discs (see reviews in Chal and Pourquié 2009; Scaal 2016). The formation of one vertebral centrum requires mesenchymal contributions from the caudal half of one somite pair plus the cranial half the adjacent pair following it (Figure 2.2B, C). Conversely, a neural arch (Figure 2.2D) derives from the caudal part of the sclerotome of a single pair of somites. In the thoracic region, migrating cells originating from the ventrolateral part of the sclerotome of each somite create a condensation at the origin of the proximal part of one rib. Spine organogenesis is thus a perfect illustration of metamerization in vertebrates, a process that remains perceptible through the succession of vertebrae far beyond embryonic development proper (Figure 2.2E).

The genetic controls, cellular mechanisms, local molecular regulators and tissue interactions involved in the initiation and growth of the condensations of mesodermal mesenchymal cells are reviewed in Hall and Miyake (1995; 2000) (see also reviews by Karsenty and Wagner [2002] and Karaplis [2008]).

Once settled in the sites of future skeletal elements, aggregated sclerotomal cells undergo a differentiation process that successively transforms them into prechondroblasts and chondroblasts (see Chapter 7 for details on these cells). Various transcriptional factors that influence the expression of specific genes (Han and Lefevre 2008), along with local regulators and their specific receptors, are involved in this transformation (recent reviews in Danks et al. 2011; Long and Ornitz 2013; Kaucka and Adameyko 2017; see also Day et al. 2005; Lehti et al. 2018). Chondroblasts initially create cartilaginous anlagen of the future bones through interstitial multiplication and secretion of extracellular matrix. When the anlage size increases, an outer membrane, the perichondrium, which contains active chondroblasts in its basal layer, forms around the bone and contributes to cartilage growth through superficial accretion. Complex morphogenetic processes, combined with a cascade of regulating factors, are involved in the shaping and growth of individual bone templates and the patterning of composite skeletal regions. Reviews of these factors and processes are available in Olsen et al. (2000); Hall (2005) and Eames and Schneider (2008). The ossification and growth processes occurring in later ontogenetic stages in the bones derived from the cartilaginous templates created by mesodermal mesenchyme are typical of the so-called endochondral mode of ossification (Figure 2.3A-C shows its initial steps), and the bones derived from it are thus designated as endochondral bones. These processes are further considered in Chapter 9.

The development of the pectoral girdle is a puzzling issue, further complexified by new, contrasting data. The initial ortho- and heterotopic graft experiments conducted by Chevallier (1975, 1977) in bird embryos led to the conclusion that, in addition to being involved in the formation of vertebrae and ribs, somite mesoderm also contributes to the organogenesis of the scapula. No details were given in this study on whether the mesoderm was from sclerotomes or dermomyotomes. Chevallier (1975, 1977) pointed out that somite contribution follows a strict "principle of vicinity", i.e., each somite supplies the mesenchymal material to build the part of the scapula immediately adjacent to it. Therefore, the development of the scapula does not correspond to a craniocaudal extension of that bone; instead, it corresponds to a step-by-step construction progressing rearward. The studies by Huang et al. (2000, 2005) confirmed the contribution of the somites (with the topographical pattern presented by Chevallier) but restricted it to the scapular blade; the "head and neck" of the scapula is then derived from lateral plate mesoderm. Moreover, within the somites, the dermomyotome was designated as the source of mesodermal cells (see also Christ et al. 2007). The use of three-dimensional reconstructions of quail chick chimeras by Shearman et al. (2011) led to questioning the actual importance of somite contribution and considering the "majority of the avian scapula" as derived from lateral plate mesoderm. The issue remains incompletely settled. In nonamniote vertebrates, the pectoral girdle as a whole is derived from lateral plate mesenchyme (Hall 2005).

Lateral Plates and the Zono-Appendicular Skeleton

In parallel with somite maturation, the development of future limbs (fins for nontetrapod vertebrates) is initiated in each somatopleural (outer) lateral plate. This process starts with the induction of *limb fields* in determinate spots, through the local expression of Hox genes combined with the action of several specific regulators of these genes (reviews in Krumkauf 1994; Capdevila and Izpisua Belmonte 2001). Failure of this process disorganizes at various degrees the position or spatial structure of future limbs (Mallo 2018).

In all land vertebrates, there are four limb buds per embryo (Figure 2.4A). Their position is constant with respect to the level of Hox-gene expression along the anteroposterior axis. Retinoic acid is critical for the initiation of limb bud outgrowth by regulation of FGF-10 expression (Stratford et al. 1996). Once relevant fields are established, the development of one limb bud (i.e., a limb *primordium)* involves preferential mitotic activity in the relevant field, which results in the outgrowth of the primordium. At this stage, bud structure consists of a homogeneous mass of mesenchymal cells covered by a layer of epithelial ectoderm. A precise functional framework, integrating positional and spatial information relative to anteroposterior, dorsoventral and proximodistal axes, is then established in the bud. Distinct contributions to growth are assigned to mesenchymal cells according to their position in the bud volume. However, most of the cells on which the growth of the bud depends are located along its distal margin, in the so-called progress zone (PZ; Ten Berge et al. 2008). The overlying ectoderm forms an equatorial crest called the apical ectodermal ridge (AER), which contributes to maintain a dominant outward lateral direction to the bud (Verheyden and Sun 2017). A cascade of genetic expressions, as well as paracrine and autocrine regulators originating from the somatopleura, the AER, the rest of the overlying ectoderm and possibly also the intermediate mesoderm (small bilateral cell masses, at the origin of kidneys, flanking the somites laterally), is involved in the control of growth and the patterning of limb buds (reviewed by Capdevila and Izpisua Belmonte 2001, Towers and Tickle 2009, Zuniga 2015). FGF-10, expressed in the lateral plate mesoderm, is capable of initiating the limb-forming interactions between the ectoderm and the mesoderm (Sekine et al. 1996). FGF-10 induces the AER, which expresses FGF factors,

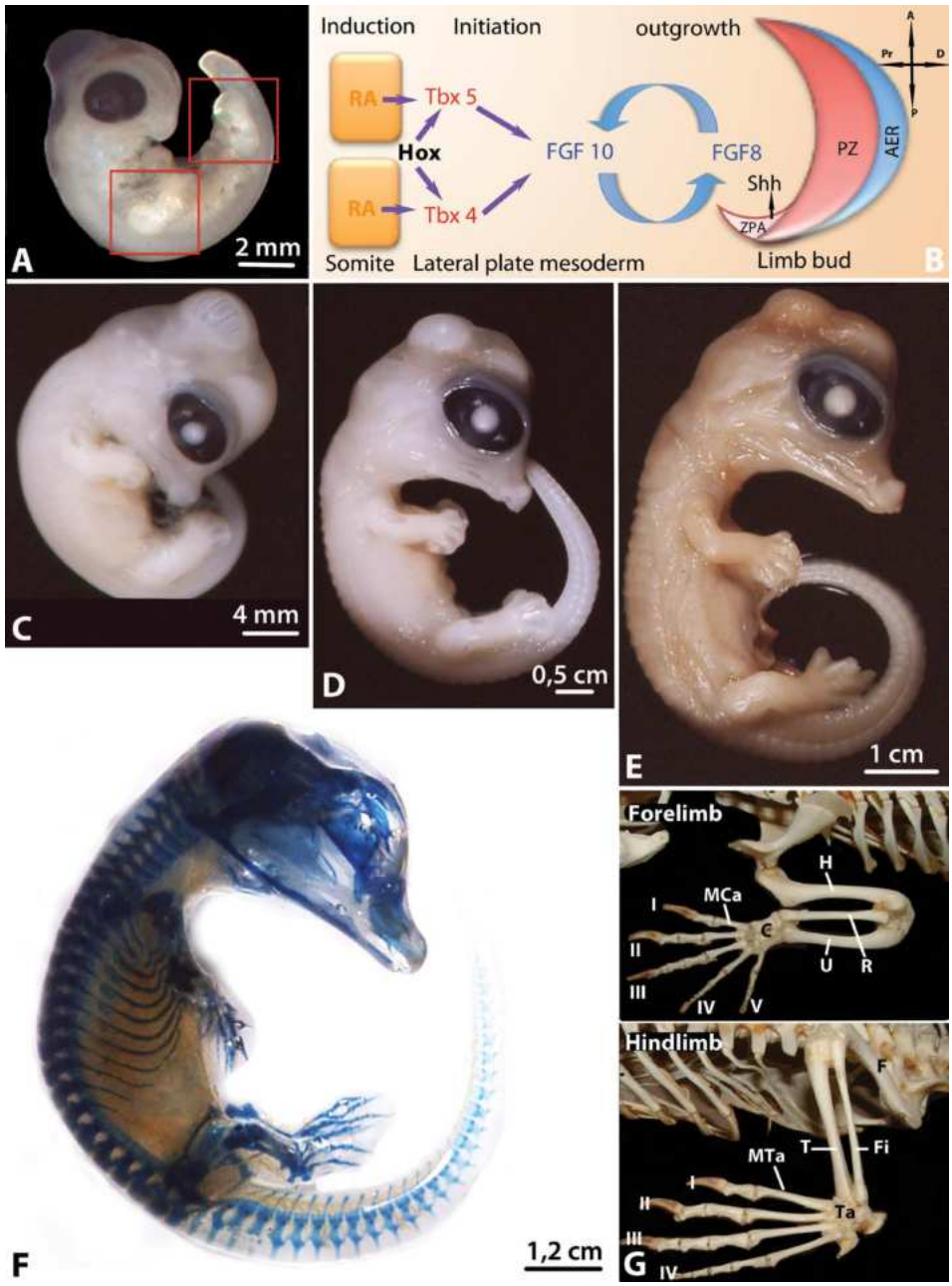


FIGURE 2.4 Limb development. A, C–F, Embryonic stages of *Crocodylus niloticus* in lateral view. A, C–E, *In toto* embryos. F, Diaphonized specimen stained with Alcian blue. During limb development, cells differentiate and the cartilage forms. The digital plate and digital serration in limbs develop progressively. Condensation of cartilage cells occurs in a proximodistal sequence (for the forelimb: humerus, radius, ulna, carpals and digits; for the hindlimb: femur, tibia, fibula, tarsals and digits). This will be followed by replacement of cartilage with bone, vascularization and innervation. A, This is a 17-day-old embryo. Red squares indicate right forelimb and hindlimb buds. The digital plate is well developed. B, Scheme showing the key regulatory network during limb formation. Retinoic acid (RA) regulates limb bud induction and initiation. It acts with Hox genes to regulate Tbx gene expression. The early limb bud has a core of mesenchymal mesoderm and an epithelial ectodermal layer. The progress zone (PZ) is at the tip of the bud and is composed of rapidly dividing and proliferating cells. The apical ectodermal ridge (AER) lays above PZ and is essential for outgrowth and proximodistal patterning of the limb. The dorsoventral ectoderm determines the dorsoventral polarity of the distal part of the limb. A zone called zone of polarizing activity (ZPA) where Sonic hedgehog (Shh) is expressed, is responsible for the anteroposterior polarization of the limb. The position of the limb field along the axis is controlled by antagonism between RA and fibroblast growth factor-8 (FGF-8). Tbx genes previously controlled the limb bud emergence (initiation) by upregulating FGF-10 expression in the mesenchyme. An epithelial-mesenchymal feedback loop, established between FGF-10 in the mesenchyme and FGF-8 in the AER, is involved in limb bud outgrowth. C, This is a 23-day-old embryo. The digital grooves are pronounced, and a weak demarcation of the digits is visible. D, This is a 24-day old embryo. Demarcation of the digits is clear. Elbow and knee are visible. E, This is a 26-day old embryo. Elbow and knee are slightly flexed at the joint. F, This is a 31-day-old embryo. The digits of the forelimb and hindlimb are complete. Interdigital grooves are distinct at this stage. G, Adult forelimb (upper panel) and hindlimb (lower panel) of *C. niloticus*. Note the loss of the fifth digit of the hindlimb (extant archosaurs show several instances of digit loss). C, carpal bones; F, femur; Fi, fibula; H, humerus; MCa, metacarpal bones; MTa, metatarsal bones; R, radius; T, tibia; Ta, tarsal bones; U, ulna; I, II, III, IV, and V, respectively, digits I, II, III, IV, and V.

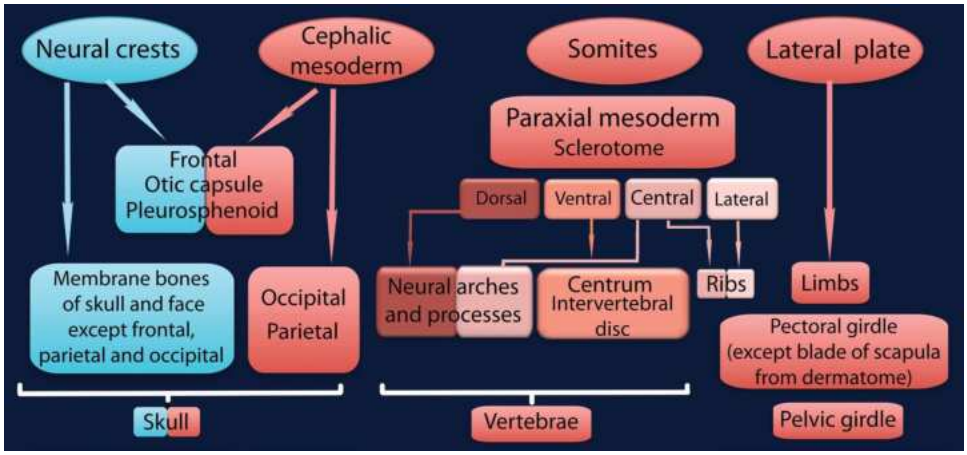


FIGURE 2.5 Origin of the skeletal elements in vertebrates. Summary diagram showing the contribution of cells from cranial neural crests, mesoderm, somites and lateral plates in the craniofacial, axial and limb skeleton.

and a retroaction loop occurs between these molecular signals. as illustrated in Figure 2.4B, the specification of forelimb and hindlimb is under the control of Tbx genes (Figure 2.4B).

The cells located inside the bud subsequently differentiate into prechondroblasts and chondroblasts that start producing the cartilaginous anlagen of the bones (Figure 2.4 C–G). As pointed out by Danks et al. (2011), the creation of the anlage of the femur in the human fetus is a particularly complex process involving 161 cartilage-specific genes. Among the individual osseous elements composing a limb, the template of the proximal bone (stylopod in tetrapods) is formed first, and followed by those of more distal elements (review in Towers and Tickle 2009). Reviews by Shubin et al. (1997), Abbasi (2011), Hopyan et al. (2011) and Zuniga (2015) (see also Sheth et al. 2012) consider the many factors controlling the fate of the cells produced during bud development (these cells can contribute to a bone's design template or be eliminated by apoptosis) and the morphogenetic processes involved in the shaping of limb bones. The typical growth pattern of endochondral long bones relies on complex apposition and resorption processes and is further considered in Chapter 9.

Within the thoracic region, the anterior articular part of the scapula, the coracoid (this bone is distinct from the scapula in nonmammalian vertebrates but fused to it, as the coracoid process, in mammals; see Kardong 1998), the clavicle and the sternum arise exclusively from the somatopleural mesenchyme, as is the case for the pelvic girdle in totality (Chevallier 1977; Hall 2001). Distinct morphogenetic fields are involved in each of these skeletal elements, which suggests an early regionalization (previous to somatic segmentation) within the somatopleura. As mentioned above, the blade of the scapula derives from the mesoderm of the somites. The genetic controls and molecular interactions contributing to a correct development of the bones of the zonal skeleton, both pectoral and pelvic, are presented in Kuijper et al. (2005) and Capellini et al. (2010, 2011).

All the elements of the pectoral and pelvic girdles undoubtedly originate from mesodermal mesenchyme, whether initially located in the somites or the somatopleura. The clavicle is no exception to this general situation, but its development involves a complex, unexpected pattern, with the lateral part of this bone developing by direct ossification of the mesenchymal condensation, as do typical membrane bones, and the medial part developing as an endochondral bone, with ossification of cartilage (Huang et al. 1997; Hall 2005; see also Hall 2001). Membrane ossification of bones originating from mesodermal condensations occurs also in some skull elements, as exemplified by the mammalian parietals, which (unlike most bones of the cranial vault and the face) are mesodermal in origin but develop as membrane bones under interaction with the (neural crest derived) meninges (Jiang et al. 2002). As mentioned above, the reverse situation also exists, i.e., bones form from condensations of neural crest cells but have an endochondral mode of growth (e.g., mammalian temporal bones). Therefore, the mode of development and growth of a bone (membrane vs. endochondral) is clearly not synonymous with the origin of the embryonic cell populations (ectodermal vs. mesodermal mesenchyme) from which it derives. Skeletogenic derivatives of both cranial neural crests and mesoderm are summarized in Figure 2.5.

REFERENCES

Abbasi, A. A. 2011. Evolution of vertebrate appendicular structures: insight from genetic and palaeontological data. *Dev. Dyn.* 240: 1005–1016.

Abzhanov, A., et al. 2007. Regulation of skeletogenic differentiation in cranial dermal bone. *Development* 134: 3133–3134.

Aubin, J. E. 2008. Mesenchymal stem cells and osteoblast differentiation. In Bilezikian J. P., L. G. Raisz and T. J. Martin (eds.) *Principles of bone biology*, 3rd edition, vol. 1, 85–108. Amsterdam: Elsevier-Academic Press.

Bagnall, K. M., et al. 1989. The contribution made by cells from a single somite to tissues within a body segment and assessment of their integration with similar cells from adjacent segments. *Development* 107: 931–943.

Bénazéraf, B. and O. Pourquié. 2013. Formation and segmentation of the vertebrate body axis. *Annu. Rev. Cell Dev. Biol.* 29: 1–26.

Berendsen, A. D. and B. R. Olsen. 2015. Bone development. *Bone* 80: 14–18.

Capdevila J. and J. C. Izpisua Belmonte. 2001. Patterning mechanisms controlling vertebrate limb development. *Annu. Rev. Cell Dev. Biol.* 17: 87–132.

Capellini, T. D., et al. 2010. Scapula development is governed by genetic interactions of Pbx1 with its family members and with Emx2 via their cooperative control of Alx1. *Development* 137: 2559–2569.

Capellini, T. D., et al. 2011. Control of pelvic girdle development by genes of the Pbx family and *Emx*2. *Dev. Dyn.* 240: 1173–1189.

Chal, J. and O. Pourquié. 2009. Patterning and differentiation of the vertebrate spine. In *The skeletal system: Cold Spring Harbour Monographs*, vol. 53, 41–116. Pourquié, O. (ed.). New York: Cold Spring Harbor Laboratory Press.

Chevallier, A. 1975. Rôle du mésoderme somitique dans le développement de la cage thoracique de l'embryon d'oiseau. I. origine du segment sternal et mécanismes de la différenciation des côtes. *J. Embryol. Exp. Morph.* 33: 291–311.

Chevallier, A. 1977. Origine des ceintures scapulaires et pelviennes chez l'embryon d'oiseau. *J. Embryol. Exp. Morph.* 42: 275–292.

Chibon, P. 1967. Marquage nucléaire par la thymidine tritiée des derivés de la crête neurale chez l'Amphibien Urodèle *Pleurodeles waltlii* Michah. *J. Embryol. Exp. Morph.* 18: 343–358.

Christ, B. et al. 2007. Amniote somite derivatives. *Dev. Dyn.* 236: 2382–2396.

Christ, B. and J. Wilting. 1992. From somites to vertebral column. *Ann. Anat.* 174: 23–32.

Corallo, D., et al. 2015. *Cell Mol. Life Sci.* 72: 2989–3008.

Danks, J., et al. 2011. Evolution of the parathyroid hormone family and skeletal formation pathways. *Gen. Comp. Endocr.* 170: 79–91.

Day, T. F., et al. 2005. Wnt/β-Catenin signaling in mesenchymal progenitors controls osteoblast and chondrocyte differentiation during vertebrate skeletogenesis. *Dev. Cell.* 8: 739–750.

De Vos, L. and P. Van Gansen. 1980. *Atlas d'embryologie des vertébrés.* Paris: Masson S. A.

Dobreva, G., et al. 2006. SATB2 is a multifunctional determinant of craniofacial patterning and osteoblast differentiation. *Cell* 125: 971–986.

Dunlop, L. L. T. and B. K. Hall. 1995. Relationships between cellular condensation, preosteoblast formation and epithelial-mesenchymal interactions in initiation of osteogenesis. *Int. J. Dev.* 39: 357–371.

Eames, B. F. and R. A. Schneider. 2008. The genesis of cartilage size and shape during development and evolution. *Development.* 135: 3947–3958.

Evans, D. J. 2003. Contribution of somatic cells to the avian ribs. *Dev. Biol.* 256: 114–126.

Fan, C. M. and M. Tessier-Lavigne. 1994. Patterning of mammalian somites by surface ectoderm and notochord: evidence for sclerotome induction by a hedgehog homolog. *Cell.* 79: 1175–1186.

Fleming, A., et al. 2003. A central role for the notochord in vertebral patterning. *Development.* 131: 873–880.

Fleming, A., et al. 2015. Building the backbone: the development and evolution of vertebral patterning. *Development.* 142: 1733–1744.

Flint, O. P., et al. 1978. Control of somite number in normal and amputated mutant mouse embryos: an experimental and a theoretical analysis. *J. Embryol. Exp. Morph.* 45: 189–202.

Franz-Odendaal, T. A., et al. 2006. Buried alive: how osteoblasts become osteocytes. *Dev. Dyn.* 235: 176–190.

Geetha-Loganathan, P., et al. 2008. Wnt signalling in somite development. *Ann. Anat.* 190: 208–222.

Hall, B. K. 2001. Development of the clavicles in birds and mammals. *J. Exp. Zool.* 289: 153–161.

Hall, B. K. 2005. *Bones and cartilage: developmental and evolutionary skeletal biology.* Amsterdam: Elsevier-Academic Press.

Hall, B. K. 2008. The neural crest and neural crest cells: discovery and significance for theories of embryonic organization. *J. Biosci.* 33: 781–793.

Hall, B. K. and T. Miyake. 1992. The membranous skeleton: the role of cell condensations in vertebrate skeletogenesis. *Anat. Embryol.* 186: 107–124.

Hall, B. K. and T. Miyake. 1995. Divide, accumulate, differentiate: cell condensation in skeletal development revisited. *Int. J. Dev. Biol.* 39: 881–893.

Hall, B. K. and T. Miyake. 2000. All for one and one for all: condensations and the initiation of skeletal development. *BioEssays* 22: 138–147.

Han, Y. and V. Lefevre. 2008. L-Sox5 and Sox6 drive expression of the aggrecan gene in cartilage securing binding of Sox9 to a far-upstream enhancer. *Mol. Cell. Biol.* 28: 4999–5013.

Hirasawa, T. and S. Kuratani. 2015. Evolution of the vertebrate skeleton: morphology, embryology, and development. *Zool. Lett.* 1: 1–17.

Hopyan, S., et al. 2011. Budding behaviors: growth of the limb as a model of morphogenesis. *Dev. Dyn.* 240: 1054–1062.

Huang, B. K., et al. 2000. Insulin-like growth factor 1 production is essential for anabolic effects of thyroid hormone in osteoblasts. *J. Bone Miner. Res.* 15: 188–197.

Huang, F. M., et al. 2005. Induction of interleukin-6 and interleukin-8 gene expression by root canal sealers in human osteoblastic cells. *J. Endod.* 31: 679–683.

Huang, L.-F., et al. 1997. Mouse clavicular development: analysis of wild-type and cleidocranial dysplasia mutant mice. *Dev. Dyn.* 210: 33–40.

Jia, J. and J. Jiang. 2006. Decoding the hedgehog signal in animal development. *Cell. Mol. Life Sci.* 63: 1249–1265.

Jiang, X., et al. 2002. Tissue origins and interactions in the mammalian skull vault. *Dev. Biol.* 241: 106–116.

Johnston, M. C. 1966. A radioautographic study of the migration and fate of cranial neural crest cells in the chick embryo. *Anat. Rec.* 156: 143–156.

Karaplis A. C.2008. Embryonic development of bone and regulation of intramembranous and endochondral bone formation. In Belizekian, P., L. G. Raisz and T. J. Martin (eds.) *Principles of bone biology*, 3rd edition, vol. 1, 53–84. Amsterdam: Elsevier-Academic Press.

Kardong, K. V. 1998. *Vertebrates. Comparative anatomy, function, evolution.* Boston: WCB-McGraw-Hill.

Karsenty, G. and E. F. Wagner. 2002. Reaching a genetic and molecular understanding of skeletal development. *Dev. Cell.* 2: 389–406.

Kaucka, M. and I. Adameyko. 2017. Evolution and development of the cartilaginous skull: from a lancelet towards a human face. *Semin. Cell dev. Biol.* 91: 2–12.

Kobayashi, T. and H. Kronenberg. 2005. Minireview: transcriptional regulation in development of bone. *Endocrinology* 146: 1012–1017.

Krück, S., et al. 2013. Development of somites, muscle, and skeleton is independent of signals from the Wolffian duct. *Dev. Dyn*. 242: 941–948.

Krumkauf, R. 1994. Hox genes in vertebrate development. *Cell*. 78: 191–201.

Kuijper, S., et al. 2005. Function and regulation of Alx4 in limb development: complex genetic interactions with Gli3 and Shh. *Dev. Biol*. 285: 533–544.

Kuratani, S., et al. 2018. The neural crest and evolution of the head/trunk interface in vertebrates. *Dev. Biol*. https://doi.org/10.1016/j.ydbio.2018.01.017.

Lawson, L. Y. and B. D. Harfe. 2017. Developmental mechanisms of intervertebral disc and vertebral column formation. *Wiley Interdiscip. Rev. Dev. Biol*. 6: e283.doi :10.1002/wdev.283.

Le Douarin, N., et al. 2004. Neural crest plasticity and its limits. *Development* 131: 4637–4650.

Le Douarin, N. and E. Dupin. 2003. Multipotentiality of the neural crest. *Curr. Opin. Genet. Dev*. 13: 529–536.

Le Douarin, N. M. and E. Dupin. 2014. The neural crest, a fourth germ layer of the vertebrate embryo: significance in chordate evolution. In Trainor, P. (ed.) *Neural crest cells. Evolution, development and disease*, 3–26. Amsterdam: Elsevier-Academic Press.

Lehti, M. S., et al. 2018. Cilia-related protein SPEF2 regulates osteoblast differentiation. *Sci. Rep*. 8: 1–11.

Lim, J. and J.-P. Thiery. 2012. Epithelial-mesenchymal transitions: insights from development. *Development* 139: 3471–3486.

Long, F. and D. M. Ornitz. 2013. Development of the endochondral skeleton. *Cold Spring Harb. Perspect. Biol*. 5: a008334.

Loring, J. F and C. A. Erickson. 1987. Neural crest cell migratory pathways in the trunk of the chick embryo. *Dev. Biol*. 121: 220–236.

Mallo, M. 2018. Reassessing the role of *Hox* genes during vertebrate development and evolution. *Trends Genet*. 34: 209–217.

Nicollet, G. 1971. Avian gastrulation. *Adv. Morphog*. 9: 231–262.

Oates, A. C., et al. 2012. Patterning embryos with oscillations: structure, function and dynamics of the vertebrate segmentation clock. *Development*. 139: 625–639.

Olsen, B. R., et al. 2000. Bone development. *Annu. Rev. cell. Dev. Biol*. 16: 191–220.

Olsson, L. and J. Hanken. 1996. Cranial neural-crest migration and chondrogenic fate in the oriental fire-bellied toad Bombina orientalis: defining the ancestral pattern of head development in anuran amphibians. *J. Morphol*. 229: 105–120.

Pegoraro, C. and A. H. Monsoro-Burq. 2013. Signaling and transcriptional regulation in neural crest specification and migration: lessons from Xenopus embryo. *Dev. Biol*. 2: 247–259.

Pourquié, O. 2001. Vertebrate somitogenesis. *Annu. Rev. cell. Dev. Biol*. 17: 311–350.

Pownall, M. E., et al. 1996. Notochord signals control the transcriptional cascade of myogenic bHLH genes in somites of quail embryos. *Development* 122: 1475–1488.

Rogers, C.D., et al. 2012. Neural crest specification: tissues, signals, and transcription factors. *Dev. Biol*. 1: 52–68.

Sadaghiani, B. and J. R. Vielkind. 1990. Distribution and migration pathways of HNK-1-immunoreactive neural crest cells in teleost fish embryos. *Development* 110: 197–209.

Saga, Y. 2012. The mechanism of somite formation in mice. *Curr. Op. Genet. Dev*. 22: 331–338.

Scaal, M. 2016. Early development of the vertebral column. *Sem. Cell Dev. Biol*. 49: 83–91.

Schilling, T. F. and P. Le Pabic. 2014. Neural crest cells in craniofacial skeletal development. In Trainor, P. (ed.) *Neural crest cells. Evolution, development and disease*, 127–151. Amsterdam: Elsevier-Academic Press.

Sekine, K., et al. 1999. FgF10 is essential for limb and lung formation. *Nat. Genet*. 21: 138–141.

Shearman, R. M., et al. 2011. 3D reconstructions of quail-chick chimeras provide a new fate map of the avian scapula. *Dev. Biol*. 355: 1–11.

Sheth, R., et al. 2012. Hox genes regulate digit patterning by controlling the wavelength of a Turing-type mechanism. *Science* 338: 1476–1480.

Shubin, N., et al. 1997. Fossils, genes and the evolution of animal limbs. *Nature* 388: 639–648.

Sieber-Blum, M. 2000. Factors controlling lineage specification in the neural crest. *Int. Rev. Cytol*. 197: 1–33.

Solnica-Krezel, L. 2005. Conserved patterns of cell movements during vertebrate gastrulation. *Curr. Biol*. 15: 213–226.

Stemple, D. L. 2005. Structure and function of the notochord: an essential organ for chordate development. *Development* 132: 2503–2512.

Stratford, T., et al. 1996. Retinoic acid is required for the initiation of outgrowth in the chick limb bud. *Curr. Biol*. 6: 1124–1133.

Tajbakhsh, S. and R. Spörle. 1998. Somite development: constructing the vertebrate body. *Cell*. 92: 9–16.

Tam, P. P. L. 1981. The control of somitogenesis in mouse embryos. *J. Embryol. Exp. Morph*. 65: 103–128.

Ten Berge, D., et al. 2008. Wnt and FGF signals interact to coordinate growth with cell fate specification during limb development. *Development* 135: 3247–3257.

Theveneau, E. and R. Mayor. 2012. Neural crest cell migration: interplay between chemorepellents, chemoattractants, contact inhibition, epithelial-mesenchymal transition, and collective cell migration. *WIREs Dev. Biol*. 1: 435–445.

Theveneau, E. and R. Mayor. 2014. Neural crest cell migration: guidance, pathways, and cell-cell interactions. In Trainor, P. (ed). *Neural crest cells. Evolution, development and disease* 73–88. Amsterdam: Elsevier-Academic Press.

Thiery, J. P., et al. 2009. Epithelial-mesenchymal transitions in development and disease. *Cell*. 139: 871–890.

Towers, M. and C. Tickle. 2009. Generation of pattern and form in the developing limb. *Int. J. Dev. Biol*. 53: 805–812.

Trapani, V., et al. 2017. Role of the ECM in notochord formation, function and disease. *J. Cell Sci*. 130: 3203-3211.

Verbout, A. J. 1985. The development of the vertebral column. *Adv. Anat. Embryol. Cell Biol*. 90: 1–122.

Verheyden, J. M. and X. Sun. 2017. Embryology meets molecular biology: deciphering the apical ectodermal ridge. *Dev. Biol*. 429: 387–390.

Wang, Y. and H. Steinbeisser. 2009. Molecular basis of morphogenesis during vertebrate gastrulation. *Cell. Mol. Life Sci*. 66: 2263–2273.

Yamashiro, T., et al. 2004. Possible roles of Runx1 and Sox9 in incipient intramembranous ossification. *J. Bone Min. Res*. 19: 1671–1676.

Zelzer, E. and B. R. Olsen. 2003. The genetic basis for skeletal diseases. *Nature* 423: 343–348.

Zuniga, A. 2015. Next generation limb development and evolution: old questions, new perspectives. *Development* 142: 3810–3820.

VetBooks.ir

3

The Vertebrate Skeleton: A Brief Introduction

Michel Laurin, Alexandra Quilhac and Vivian de Buffrénil

CONTENTS

Classifying Bones and Bone Groups 39
Homology and Analogy: Two Central Concepts in Anatomy 41
The Dermal Skeleton 41
The Endoskeleton 44
Accessory Skeletal Elements: Sesamoids and Calcified Tendons 49
  Sesamoids 49
  Calcified tendons 51
The Shape of Bones 51
  A Significant but General Criterion 51
  Long Bones 51
  Short Bones 52
  Flat Bones 52
Remarks on the Mineralization of Skeletal Elements 52
Acknowledgments 52
References 52

Classifying Bones and Bone Groups

In this chapter we review the regions, forms and relative positions of the elements of the vertebrate skeleton, as a preface to examining their histology and paleohistology.

The vertebrate skeleton is a complex biological apparatus organized at various levels of integration to fulfill four main roles: (1) it contributes to structuring the body into distinct regions (head, neck, thorax, spine and limbs), defined anatomically and functionally; (2) it constitutes a tough, rigid envelope protecting fragile vital organs such as the brain, the heart and the lungs; (3) it constitutes a mechanical assemblage able to support body weight against gravity and transform muscle contraction into movement and displacement in space and (4) it is a reservoir of calcium, phosphorus and other minerals for ionic homeostasis. The first three functions are generally relevant to the domain of skeletal anatomy, and the fourth deals with physiology and is considered in subsequent chapters.

In general, the many elements constituting a skeleton (the human skeleton, for example, has around 206 bones) may differ in these four main characteristics. A basic classification refers to the three origins of the embryonic cell populations from which the bones arise: the ectodermal cells of the neural crest, the mesodermal mesenchyme of the somites and the population of mesodermal cells from the lateral plate mesenchyme. This classification, rarely used in anatomical literature, was presented in Chapter 2 and will not be further considered here.

A second criterion discriminating the bones of a skeleton refers to their two main modes of development (Figure 3.1): direct ossification of membrane-like mesenchymal condensations and replacement of a previous cartilaginous anlage. In the latter case, osteogenesis is double; it occurs both within the anlage, through endochondral ossification, and on its surface, through periosteal accretion, in a process basically comparable to membrane ossification. The term *endochondral bones*, applied to the second category, is universally accepted (Francillon-Vieillot et al. 1990, Kardong 1998, Hall 2005). Conversely, two terms, *dermal bone* and *membrane bone*, are often used for the first category. These terms are not strictly equivalent, because membrane bone refers to the ossification process only, whereas dermal bone also considers the position of the bones within the dermis (Hall 2005). This nuance must be mentioned, although it is of little practical importance, because nearly all membrane bones have an intradermal development, with very few exceptions such as the clavicle.

A third feature that distinguishes the bones refers to their positions in the body and their relationships to other bones. This feature can be expressed in reference either to the anteroposterior (craniocaudal) axis of the body, or to the transverse plane. In the first case three large, integrative sets of bones defining skeletal regions can be distinguished: cephalic (head),

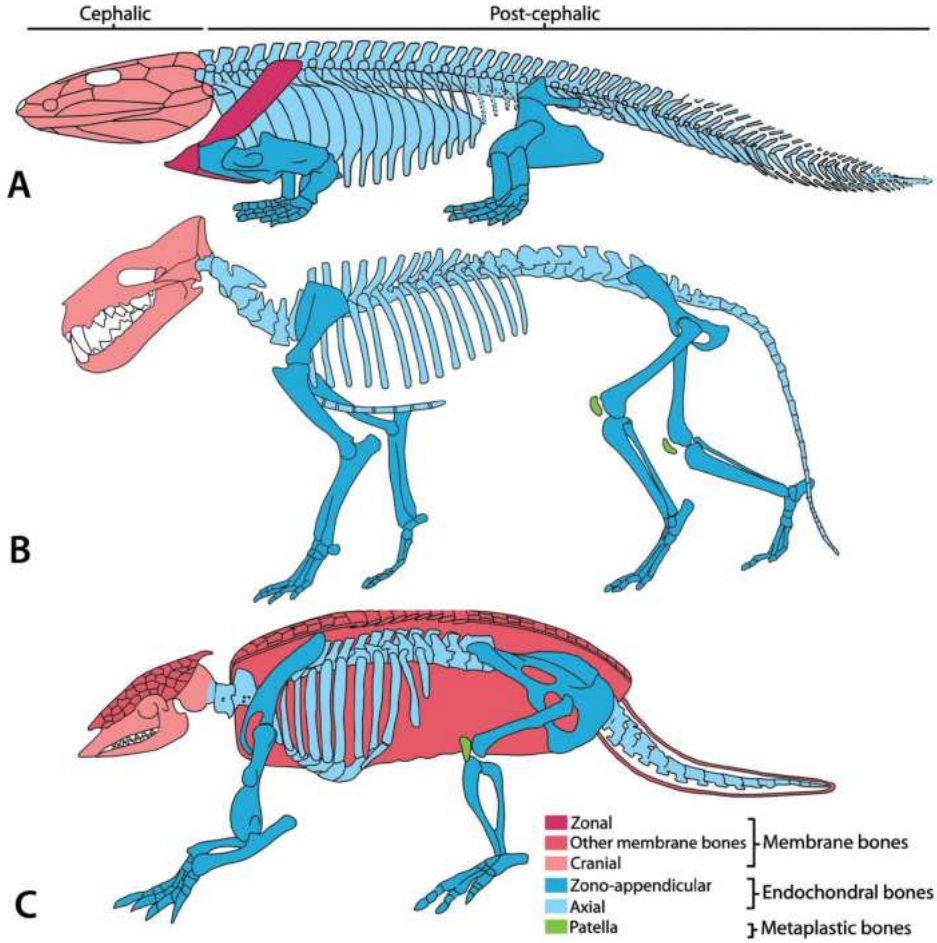


FIGURE 3.1 Distinction of bones by their mode of formation, and broad skeletal regions. Three taxa are considered here. A, A basal stem-tetrapod, *Ichthyostega* sp., from the Upper Devonian of Greenland. (Modified from Jarvik 1959.) B, A relatively unspecialized mammalian predator, the creodont *Hyaenodon* sp. from the Eocene-Miocene of the palearctic region. (From Romer 1956.) C, The nine-banded armadillo, *Dasypus novemcinctus*, an extant xenarthran mammal.

axial (spine, ribs and sternum) and zonoappendicular (limbs and girdles) (Figure 3.1). In reference to the transverse plane, two types of skeletal elements are currently recognized, endoskeletal bones and dermal bones. Deep bones, located in the core of the body and separated from the skin by muscles, constitute the *endoskeleton* (literally *the skeleton within*). This concept is basically topographic, and not synonymous with the term endochondral, although most (but not all) endoskeletal bones are also endochondral. The term *dermal skeleton* (or *dermoskeleton*, as used by Francillon-Vieillot et al. 1990) designates a diverse set of calcified skeletal structures that partly or entirely develop within the skin, or dermis; they include true membrane bones, osteoderms, scales, teeth and tooth-like structures. These elements may result from diverse histogenetic processes (odontogenesis, metaplasia, etc.), in addition to membrane ossification. The term *exoskeleton* (literally: *external skeleton*) has at least two distinct definitions. According to Francillon-Vieillot et al. (1990), the term designates non-osseous, hard keratinized structures of epidermal origin that differentiate from the external surface of the skin (nails, horns, horny scutes, etc.). These authors do not consider such elements parts of the skeleton *sensu stricto*. For Hall (2005, p. 4), in contrast, the exoskeleton is a "skeletal system that forms in contact with the ectoderm or endoderm" by "intramembranous ossification" and comprises "dermal bones, scales, fin rays, gill rakers, teeth". We will adopt here the terminology proposed by Francillon-Vieillot et al. (1990), and exclude the exoskeleton, as defined by these authors, from the scope of this chapter.

Finally, osseous skeletal elements can be classified according to their shapes. Among dermal and endoskeletal bones, three main morphologies are documented, long bones, flat bones and short bones; moreover, the morphology of intradermal osteoderms may be spherical, discoid, pyramidal, vermiform and so forth.

The short anatomical account given below aims to define, in a comparative evolutionary context, the various types of bones, or groups of bones, observed in vertebrate skeletons. Some authors (e.g. Kardong 1998) also consider the functional role of bones (e.g. protection, locomotion, etc.) as a classification criterion, but we will restrict ourselves to anatomy, namely, the position of skeletal elements within the body (third criterion mentioned above), and the shape of the bones (fourth criterion). The second classification criterion, mode of formation, is addressed in Chapters 2 and 9.

VetBooks.ir

Homology and Analogy: Two Central Concepts in Anatomy

In its most basic form, homology is the relationship between two structures that share a common evolutionary origin; in other words, it is similarity due to common origin. This is now often called historical or secondary homology, especially when this relationship has been validated by an evolutionary analysis that shows continuity between a hypothetical common ancestor and two descendants that share the homologous character. In contrast, primary homology refers to similarity in structure, composition and embryological origin that suggests the same origin. Serial homology is the relationship between structures that share structural and developmental similarities, but that may never have been identical in the past. For instance, the mandibular arch of gnathostomes is usually considered serially homologous with gill arches, although there is no proof that it derives from a gill arch that would have been present in a stem-gnathostome. However, much has been written on homology; for more information, see Minelli and Fusco (2013) and references cited therein.

Analogy, in contrast, is similarity that reflects a common function and that typically does not reflect shared ancestry. For instance, the limbs of vertebrates and arthropods are analogous; they both serve in walking, but they have different evolutionary origins, as shown by their extensive differences in structure, embryological origin and by the taxonomic distribution of limbs in metazoans.

The Dermal Skeleton

Membrane elements of the dermal skeleton include much of the skull, a variable part of the shoulder girdle, and in some taxa, scales, bony plates or osteoderms that cover part of the body. Most of these bones are fairly flat and located superficially, beneath the skin, or within the dermis.

In the skull (Figure 3.2A), the dermal skeleton of stegocephalians (tetrapods and other limbed vertebrates; see Laurin 2020a, b) includes, when complete, a set of 19 elements (excluding the mandible). Many of them, however, have been lost or fused in most extant tetrapods, especially in mammals. In superficial (or peripheral) locations, the nasal,

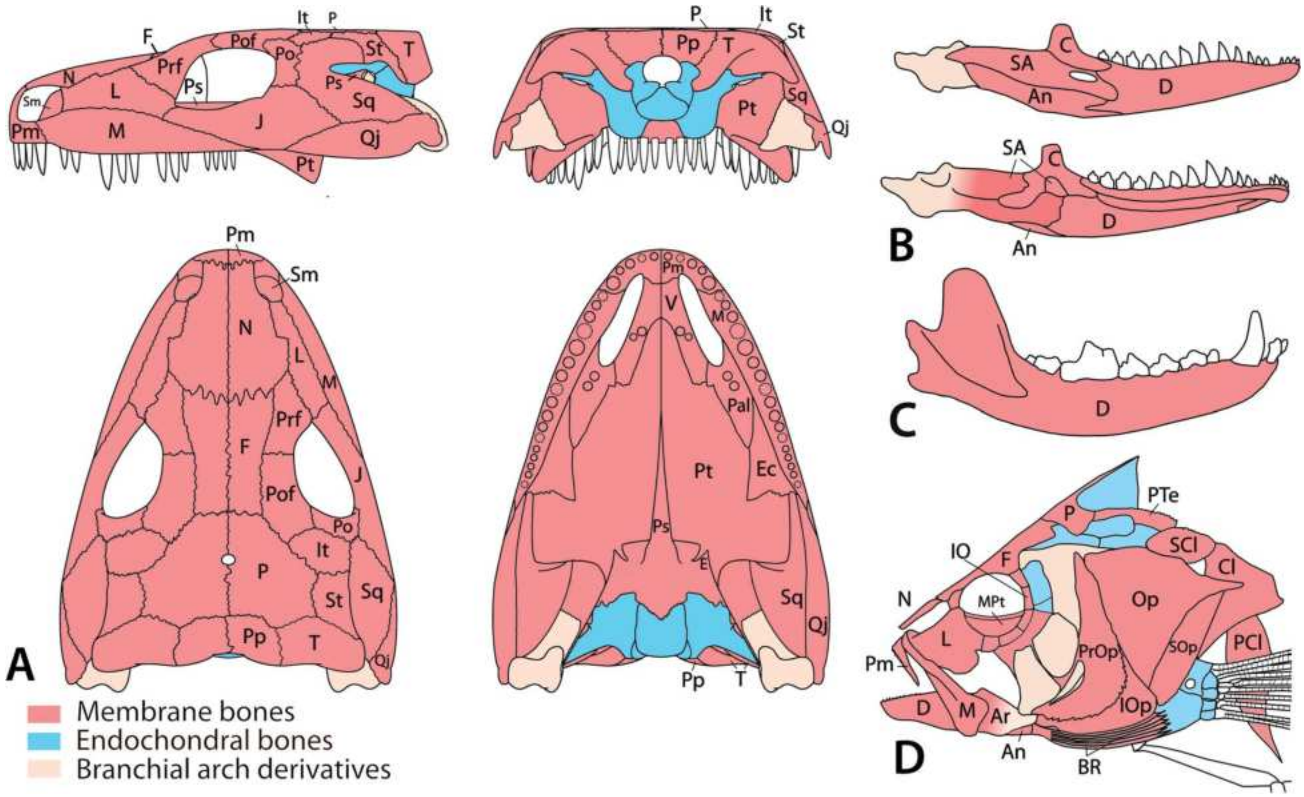


FIGURE 3.2 Dermal bones of the skull. A, Calvarium of *Seymouria baylorensis*, a seymouriamorph (probably a stem-tetrapod, although it has long been considered a stem-amniote) from the Early Permian of North America, in left lateral, occipital, dorsal and ventral views. (From Laurin 2000.) B, Lower jaw of an undetermined squamate, in labial (upper) and lingual (lower) views. C, A dog mandible in right lateral view. (B and C redrawn from Kardong 1998). D, An extant actinopterygian, the perch *Perca flavescens*, in left lateral view. (Modified from De Luliis and Pulerà 2007) List of abbreviations: A: E, epipterygoid; Ec, ectopterygoid; F, frontal; It, intertemporal; J, jugal; L, lacrimal; M, maxilla; N, nasal; P, parietal; Pal, palatine; Pm, premaxilla; Po, postorbital; Pof, postfrontal; Pp, postparietal; Prf: prefrontal; Ps, parasphenoid; Pt, pterygoid; Qj, quadratojugal; Sm, septomaxilla; Sq, squamosal; St, supratemporal; T, tabular; V, vomer. In B and C: An, angular; C, coronoid; D, dentary; SA, surangular. In D: An, angular; Ar, articular; BR, branchial rays; Cl, cleithrum D, dentary; F, frontal; IO, infraorbital; IOp, interopercular; L, lacrimal; M, maxillary; MPt, metapterygoid; N, nasal; Op, opercular; P, parietal; PCl, postcleithrum; Pm, premaxilla; PrOp, preopercular; PTe, posttemporal; SCl, supracleithrum; SOp, subopercular.

VetBooks.ir

frontal, parietal and postparietal form the central portion of the skull roof; the prefrontal, postfrontal, postorbital and jugal surround the orbit; the supratemporal and tabular complete the skull table; the squamosal and quadratojugal form the cheek (along with the jugal); and the premaxilla and maxilla form the upper jaw. On the palatal surface of the skull, the vomer, palatine, ectopterygoid, pterygoid and parasphenoid form the palate. The lower jaw, or mandible (Figure 3.2B) mainly comprises the dentary, angular, surangular, prearticular and up to three coronoids (Kardong 1998). The skull of mammals lacks many of these elements, which have been reduced gradually in synapsid evolution by a process known as "Williston's law" (Sidor 2001), which is a misnomer because it is no law; notable exceptions occur (Ascarrunz et al. 2019). The elements lost in mammals include the prefrontal, postfrontal and postorbital around the orbit. All dermal bones except the dentary have been eliminated from the lower jaw (Figure 3.2C), although some of the other dermal elements appear to be retained as minute structures in the middle ear. The supratemporal, tabular and postparietal have been eliminated from the skull table (synthesis in Kardong 1998). Conversely, actinopterygians have more elements (Figure 3.2D), such as a supramaxilla, suborbitals, an opercular series with a variable number of elements covering the gill chamber and so forth (Grande and Bemis 1998). Some of these elements have no homologues in tetrapods; for instance, the opercular series disappeared, along with the internal gills (Laurin 2010). Others may be homologous with certain tetrapod bones, although the exact homology is not always clear, and some bones that bear the same names in actinopterygians, early sarcopterygians and tetrapods (such as the frontal) may not be homologous (Borgen 1983; Arratia and Cloutier 1996). Homologies of the cranial dermal bones outside Osteichthyes are even more challenging to establish, given that various taxa (placoderms, acanthodians, osteostracans, heterostracans, etc.) have strongly divergent morphologies, with different numbers of elements (Janvier 1996a). In most gnathostomes (except placoderms, which originally lack them), the mouth includes teeth, which typically consist of a single large odontode. Teeth are composed of enamel, dentine and attachment bone, but recent research raises the possibility that enamel appeared first on dermal scales and spread to teeth a bit later (Qu et al. 2015). Teeth were originally simple conical structures, but they evolved toward a much more complex and variable morphology in mammals (Carroll 1988).

The shoulder girdle of gnathostomes originally included several dermal elements. It articulated tightly to the skull anteriorly and extended from the ventral to the dorsal surface (Figure 3.2D). In stegocephalians, the shoulder girdle became progressively reduced in a dorsal-to-ventral direction. Thus, most Permo-Carboniferous stegocephalians retain only the median interclavicle ventrally, as well as paired clavicles and cleithrum more dorsally (Figure 3.3A–C). The cleithrum has disappeared in most extant tetrapods, and the interclavicle has also been lost in several taxa. Birds retain a well-developed clavicle in the form of the furcula (Figure 3.3D), inherited from their dinosaurian ancestors, and some therian mammals still have it as a pair of variably sized bony rods (Figure 3.3E) (review in Romer and Parsons 1977).

Posterior to the skull and shoulder girdle, most of the body is covered by dermal skeletal elements in most euvertebrates. These elements first appeared in the earliest euvertebrates

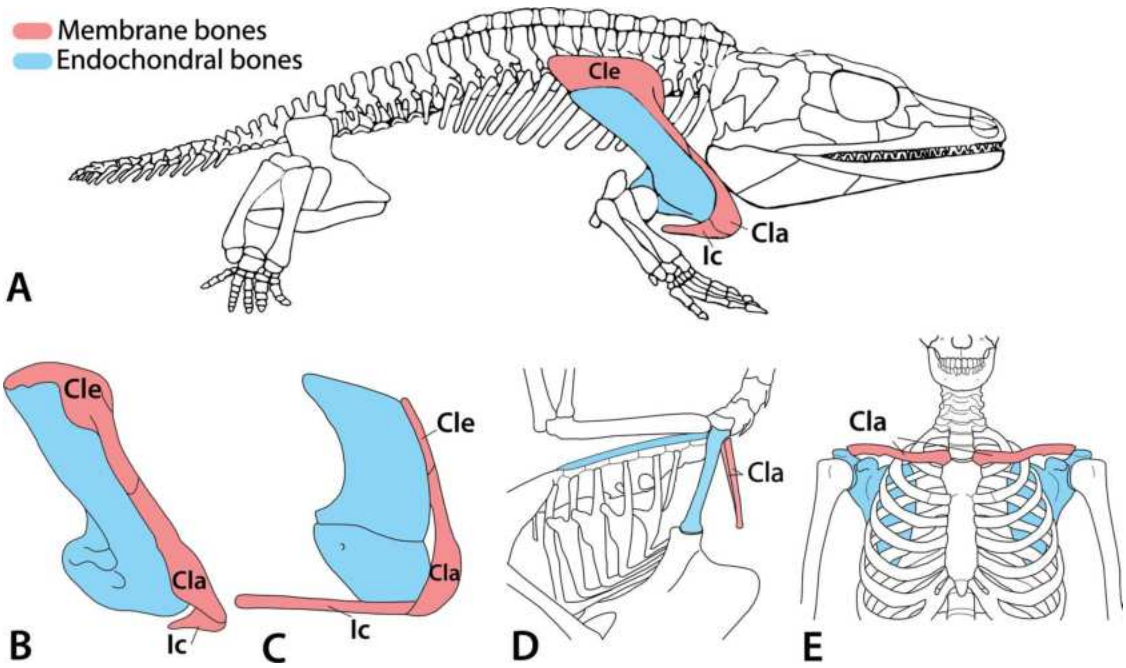


FIGURE 3.3 Dermal (membrane) and endochondral bones in the shoulder girdle of diverse tetrapods. A, *Cacops aspidephorus*, a temnospondyl (probably a stem-tetrapod) from the Early Permian of North America (From Williston 1910.) B, Shoulder girdle of the Early Permian temnospondyl *Eryops megacephalus* (From Gregory 1911.) C, Shoulder girdle of *Seymouria* sp. (From Kardong, 1998.) D, The furcula (clavicle), scapula and coracoid of an extant bird. E, The shoulder girdle of a mammal, the extant primate *Homo sapiens*. List of bone abbreviations: Cla, clavicle; Cle, cleithrum; Ic, interclavicle.

VetBooks.ir

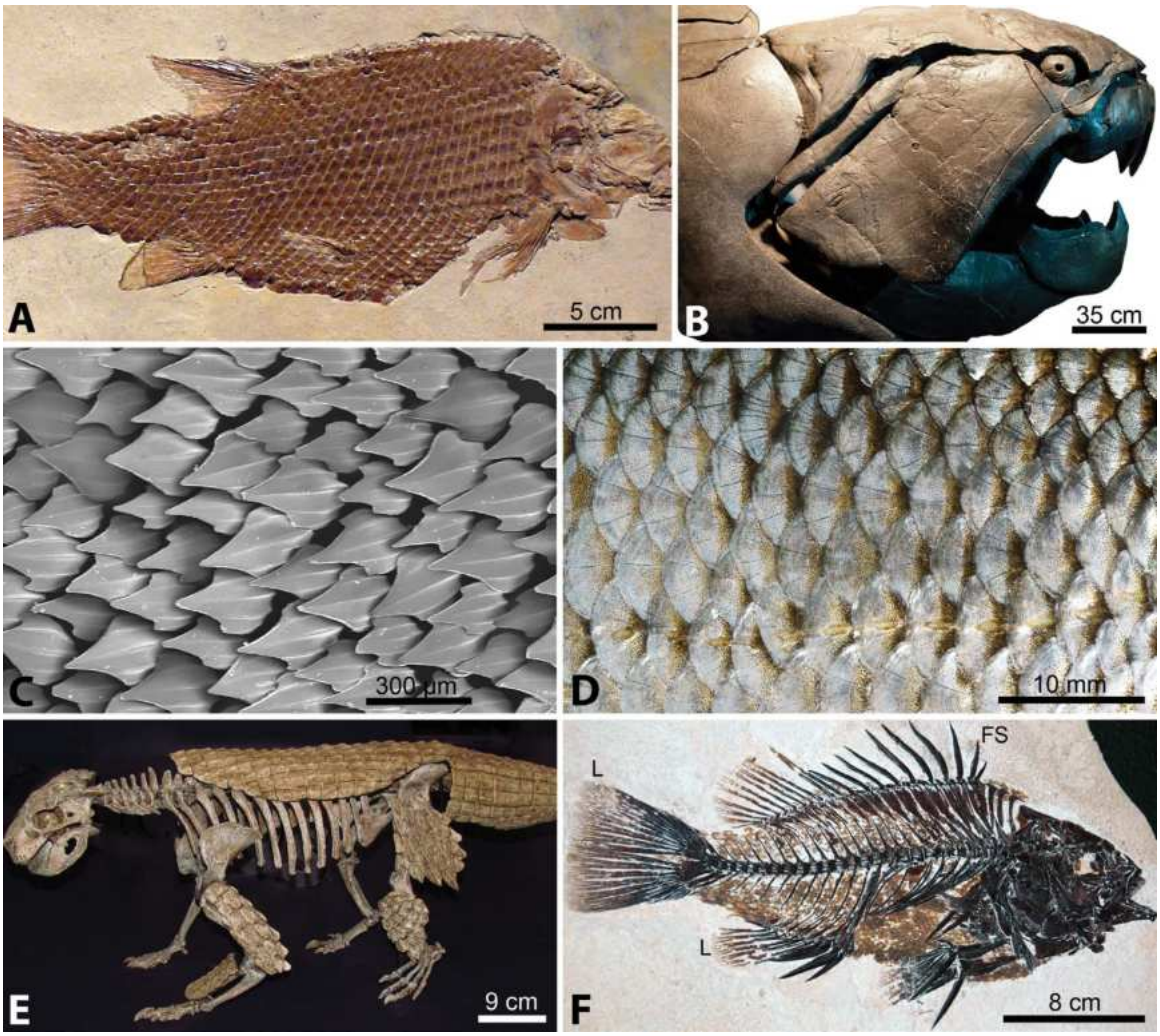


FIGURE 3.4 Scales, dermal plates and osteoderms. A, *Lepidotes notopterus,* modified (by erasing metallic supports visible in the original picture) from a picture by Wikipedia Commons user Haplochromis, licensed under the GNU Free Documentation License, Version 1.2. B, *Dunkleosteus*. Picture by Neil Conway, licensed under the Creative Commons Attribution 2.0 Generic license. C, Denticules of *Scyliorhinus canicula*. Picture by Wikipedia Commons user Isurus, licensed under the Creative Commons license. D, *Rutilus rutilus* scales. Picture by Wikipedia Commons user kallerna, licensed under the Creative Commons Attribution-Share Alike 3.0 Unported license. E, *Simosuchus clarki* skeleton. Picture by D. Gordon E. Robertson, licensed under the Creative Commons Attribution-Share Alike 3.0 Unported license. F, *Priscacara serrata* skeleton. Picture by James St. John, licensed under the Creative Commons Attribution 2.0 Generic license.

(Janvier 1996a, Sire et al. 2009), and they still cover most of the body in extant, primitively aquatic vertebrates (Khemiri et al. 2001; Figure 3.4A–D), in gymnophionans, crocodilians, turtles, some sauropsids and a few mammals (Vickaryous and Sire 2009). Among extant gnathostomes, chondrichthyans have only placoid (tooth-like) scales in the dermis (Figure 3.4C), and some early stem-gnathostomes, the possibly paraphyletic thelodonts, likewise had only small scales. The scales that covered the body in most Paleozoic vertebrates were either micromeric (consisting of small dermal elements including a single odontode, which is a structure resembling a tooth and probably preceded teeth in evolution) or macromeric (consisting of larger dermal elements covered by an odontocomplex or several odontodes, if such tissues are present). Which condition originally prevailed for vertebrates and osteichthyans is an unresolved, ancient debate (Pearson 1982, Zylberberg et al. 2016). Among extant faunas, shields of intradermal elements occur in gymnophionans, crocodilians (Figure 3.4E), turtles, some sauropsids and a few mammals (Vickaryous and Sire 2009).

The fins of most euvertebrates are supported by lepidotrichia (Figure 3.4F), which may be modified scales (Zylberberg et al. 2016). These are composed of bone and may be covered by dentine and enamel (the latter is modified into ganoine in actinopterygians). However, extant chondrichthyans have ceratotrichia, which lack mineralization and appear to be homologous to actinotrichia, which are present at the tip of actinopterygian fins (Géraudie and Meunier 1984). Extant dipnoans possess camptotrichia, which are less mineralized than lepidotrichia. However, contrary to early reports (e.g. Jarvik 1959, p. 48), these are not "horny" structures; they are composed of bone that is only superficially mineralized. Paleozoic dipnoans possessed regular lepidotrichia.

VetBooks.ir

The Endoskeleton

In the cephalic region, the bones of the base of the skull (floor of the braincase) and of the occipital complex are parts of the endoskeleton and typically result from endochondral ossification (Figure 3.5). They constitute the chondrocranium. The number of ossified elements that it contains varies according to the taxon. For instance, in early amniotes, it included prootic and opisthotic, which form the otic capsule, the supraoccipital dorsally and the basioccipital and basisphenoid ventrally. The interorbital septum also ossified (sphenethmoid), at least in some taxa (see Kardong 1998 for review). A braincase is found in all vertebrates, although in hagfishes it does not protect the brain, which is surrounded by fibrous tissue (Janvier 1996a).

The visceral skeleton (Figure 3.6A–E) is also endoskeletal. The first two branchial arches (mandibular and hyoid; see Figure 3.6A) are integrated into the skull. The first (mandibular) arch forms a variable part of the jaws. Chondrichthyans are the only extant vertebrates in which the skeleton of the jaws is composed exclusively of the mandibular arch (Figure 3.6B). In other extant vertebrates, the jaw skeleton is completed by membrane bones of the dermal skeleton that cover the mandibular arch. Consequently, the contribution of the arch to the jaw may be restricted to cartilage and two ossified elements forming the jaw articulation, the quadrate that derives from the rear region of the palatoquadrate (i.e. the dorsal half of the arch) and the articular that originates from Meckel's cartilage. In amniotes, the anterior part of the palatoquadrate, called the epipterygoid, often has a dorsal process that braces the upper jaw against the skull roof, thus strengthening the skull. In mammals, the articular and quadrate migrate to become the malleus and incus of the middle ear (Figure 3.6D, E), and the anterior part of the palatoquadrate is ossified into an alisphenoid (homologous with the epipterygoid of other tetrapods) and integrated into the braincase.

The second (hyoid) visceral arch originally helped link the mandibular arch to the skull (Figure 3.6A, B). This supportive function, assumed almost exclusively by the hyomandibular (a dorsal element in the second arch), is best shown in the hyostylic suspension that characterizes elasmobranchs and gives the upper jaw a mobility unknown in other vertebrates (Figure 3.6B). However, the original condition is almost certainly an amphistylic suspension, in which the palatoquadrate also articulates with the neurocranium. This mechanical function of the hyomandibular persisted in the first tetrapods, even though we call this element a "stapes", but in many extant tetrapods, the stapes has become more slender as its distal contact shifted from the palatoquadrate to the tympanum. Its new role as a middle ear ossicle requires minimal inertia; hence, it has a more slender, lighter shaft (Laurin 2010). This transformation occurred at least a few times. Among extant tetrapods alone, this event occurred near the origin of anurans, in therapsids before the origin of mammals and once or twice in sauropsids, depending on the phylogenetic position of turtles. Among extinct stegocephalians, a parallel change may have occurred in seymouriamorphs (Laurin 2010) and in parareptiles (Müller and Tsuji 2007), which may include most of the stem-group of turtles (Laurin and Piñeiro 2017).

The ventral part of the second arch constitutes, along with more posterior arches, part of the cartilages in the throat that are involved in swallowing and vocalization in tetrapods. But in gnathostomes, these arches (the second and more caudally) were originally involved in breathing and in a buccal pump also involved in feeding. Lampreys have cartilaginous branchial arches, but hagfishes lack them (Janvier 1996a). It is unclear if the absence of cartilaginous support for gill arches

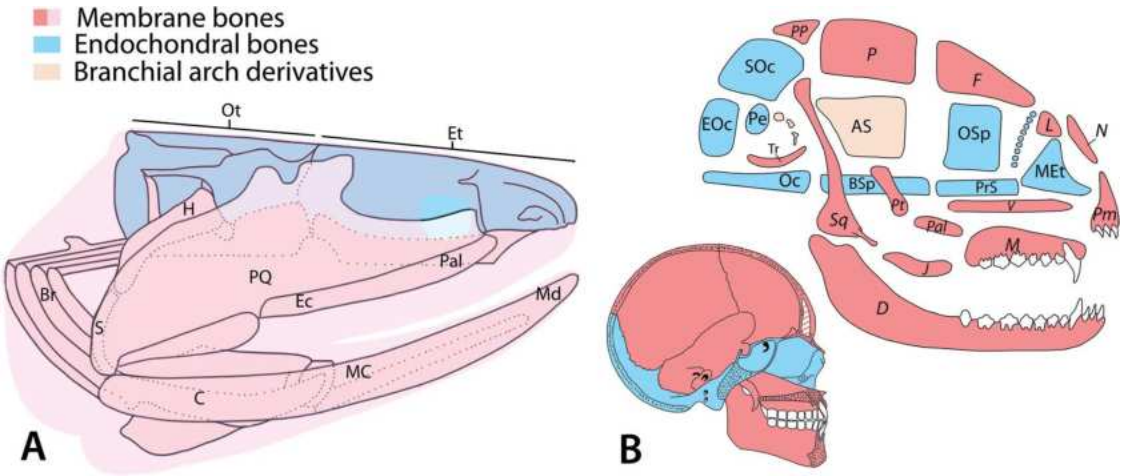


FIGURE 3.5 Endochondral bones of the skull (chondrocranium). A, General view of the position of the chondrocranium in the Devonian tetrapodomorph *Eusthenopteron*. (Redrawn after Kardong1988) B, Schematic view of the osseous composition of a mammalian skull. (Redrawn after Kardong 1988) Insert, Human skull in sagittal section showing the basal position of endochondral bones. AS, alisphenoid; Br, epibranchial and ceratobranchial; BSp, basisphenoid; C, ceratohyal; D, dentary; Ec, ectopterygoid; EOc, exoccipital; Et, ethmosphenoid region; F, frontal; H, hyomandibula; J, Jugal; L, lacrimal; M, maxilla; MC, Meckel's cartilage; Md, mandible; MEt, mesethmoid; N, nasal; Oc, basioccipital; OSp, orbitosphenoid; Ot, otoccipital region; P, parietal; Pal: palatine; Pe, petromastoid; Pm, premaxilla; PP, interparietal; PQ, palatoquadrate; PrS, presphenoid; Pt, pterygoid; S, symplectic; SOc, supraoccipital; Tr, tympanic ring; V, vomer.

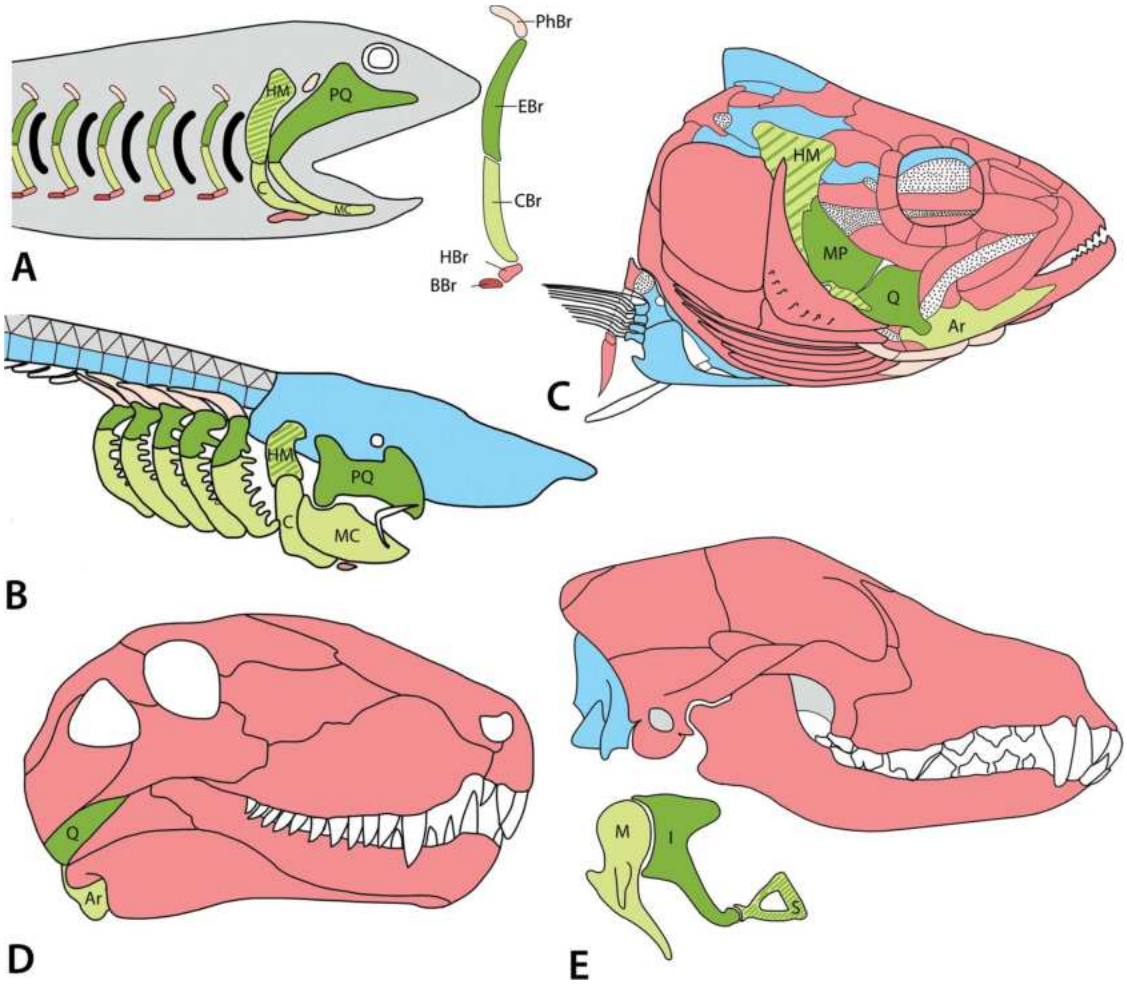


FIGURE 3.6 The branchial arches and their fate. A, Initial situation of a basal gnathostome, with two morphologically specialized arches, i.e. the mandibular arch (arch 1, comprised of the palatoquadrate and Meckel's cartilage) and the hyoid arch (arch 2), followed by five nonspecialized branchial arches. Each of these five arches has five segments. B, Branchial arches of a chondrichthyan. C, Osseous structures derived from the mandibular and hyoid arches of a typical osteichthyan. D, Osseous structures, i.e. the quadrate and the articular, derived from the mandibular arch in a basal synapsid (the eupelycosaur *Dimetrodon*). E, In a eutherian mammal (here, a dog), the only cranial remnants of the mandibular and hyoid arches are the ear ossicles, which are here much enlarged. Ar, articular; BBr. basibranchial; C, ceratohyal; CBr, ceratobranchial; EBr, epibranchial; HBr, hypobranchial; HM, hyomandibular; I, incus; M, malleus; MC, Meckel's cartilage; MP, metapterygoid; PhBr, pharyngobranchial; PQ, palatoquadrate; Q, quadrate; S, stapes.

in hagfishes is primitive or derived; if Cyclostomata is a clade, both hypotheses are equally parsimonious. Thus, the main function of the bulk of the visceral arches is to support the gills (Figure 3.6B, C), the primary respiratory organ of most primitively aquatic vertebrates. This function even persists in larval lissamphibians, where most arches support external gills, which are probably not homologous with internal gills; nevertheless, they are involved in breathing.

The bulkiest part of the endoskeleton in most vertebrates forms the axial skeleton: vertebrae, ribs and sternum (Figure 3.7A–H). Vertebrae are absent in hagfishes; only *arcualia* (in the position of neural arches and probably homologous with the interdorsals and basidorsals of gnathostomes) are present in lampreys (Janvier 1996a). Complete vertebrae, including centrum, neural and hemal arches are present only in gnathostomes. The neural arch surrounds the spinal cord, and the centrum surrounds and stiffens the notochord (when it persists in adults; see Figure 3.7C), whereas the hemal arch surrounds a large caudal artery. The hemal arch is apparently serially homologous with ventral ribs (Romer and Parsons 1977).

Figure 3.7 gives some characteristic vertebral patterns encountered in gnathostomes. The centrum is composed of a variable number of elements. In chondrichthyans, the cylindrical amphicoelous centrum includes arch bases for the neural and hemal arches. These arch bases are composed of a different type of cartilage and are often continuous with the arches. In osteichthyans, some taxa such as *Latimeria*, dipnoans, sturgeons and paddlefishes (Polyodontidae) have a poorly developed centrum comprising only bases of arches, but most extant actinopterygians have a single cylindrical centrum (Romer 1956; see also Figure 3.7C, D). Among stegocephalians, centrum evolution has been complex. Figure 3.8 summarizes the main stages of this evolution. The earliest, Devonian stegocephalians (see chapter 16), had a large, ventral crescentic intercentrum and a smaller dorsal pleurocentrum, both of which were paired (Coates 1996), a

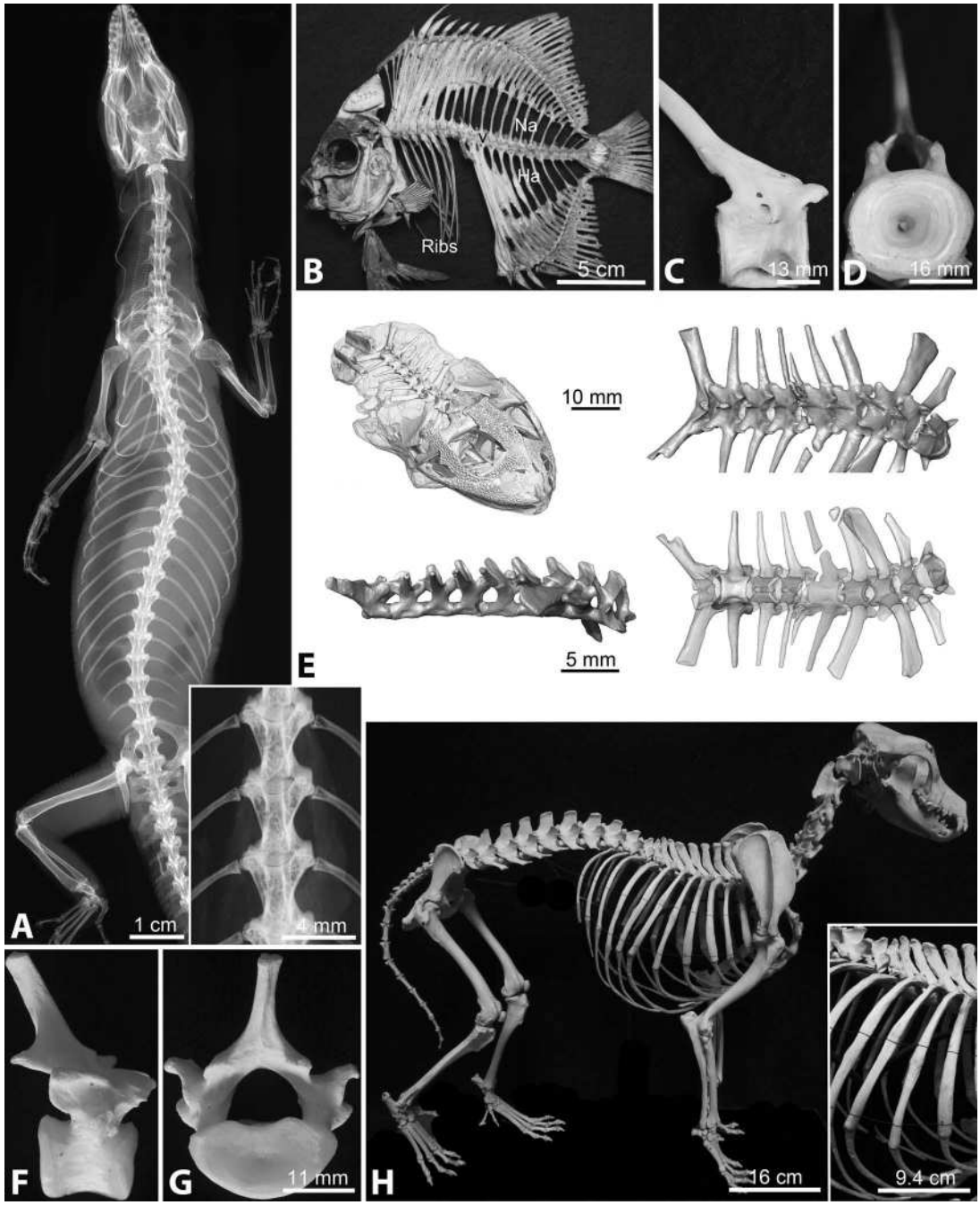


FIGURE 3.7 The axial skeleton including vertebrae and ribs. A, The axial skeleton in a tetrapod, the squamate *Varanus pilbarensis*. Inset shows a closer view of the vertebrae and ribs (X-ray proof). B, Axial skeleton of the teleost *Chaetodon* sp. [specimen MNHN-ZM-AC-A 7290, in the comparative anatomy collection of the Muséum National d'Histoire Naturelle (MNHN) in Paris, France]. C and D, Typical aspect of a teleost, here *Lutjanus* sp., vertebra (unnumbered specimen in MNHN-ZM-AC [Anatomie Comparée] collections). The small pit in the center of the vertebra in D is a remnant of the notochord canal. E, Typical aspect of lissamphibian vertebrae; here, the anuran *Thaumastosaurus*, from the Eocene of France. Upper left: head and anterior axial skeleton of this taxon; lower left: lateral view of the spine; upper right: dorsal view; lower right: ventral view. (Modified from Laloy et al. 2013.) F and G: Typical aspect of a eutherian mammal (*Castor fiber*) dorsal vertebra in left lateral (F) and posterior (G) views. As in most amniotes, the centrum consists exclusively of the pleurocentrum. H, The skeleton and thoracic region of a dog, *Canis lupus familiaris* (MNHN-ZM-AC-2020-1587).

configuration vaguely reminiscent of the Devonian sarcopterygian *Eusthenopteron* (Andrews and Westoll 1970). This basic pattern was soon modified: by the Carboniferous, the temnospondyls (then the most speciose stegocephalians) had evolved a rhachitomous vertebra, with a single median intercentrum, whereas embolomeres had two cylindrical elements (still the pleurocentrum and intercentrum). In seymouriamorphs and crown tetrapods, the intercentrum became much smaller, and the pleurocentrum dominated the centrum; the pleurocentrum is often the only remaining central element in extant tetrapods (Laurin 1998b; see also Figure 3.7F, G).

VetBooks.ir

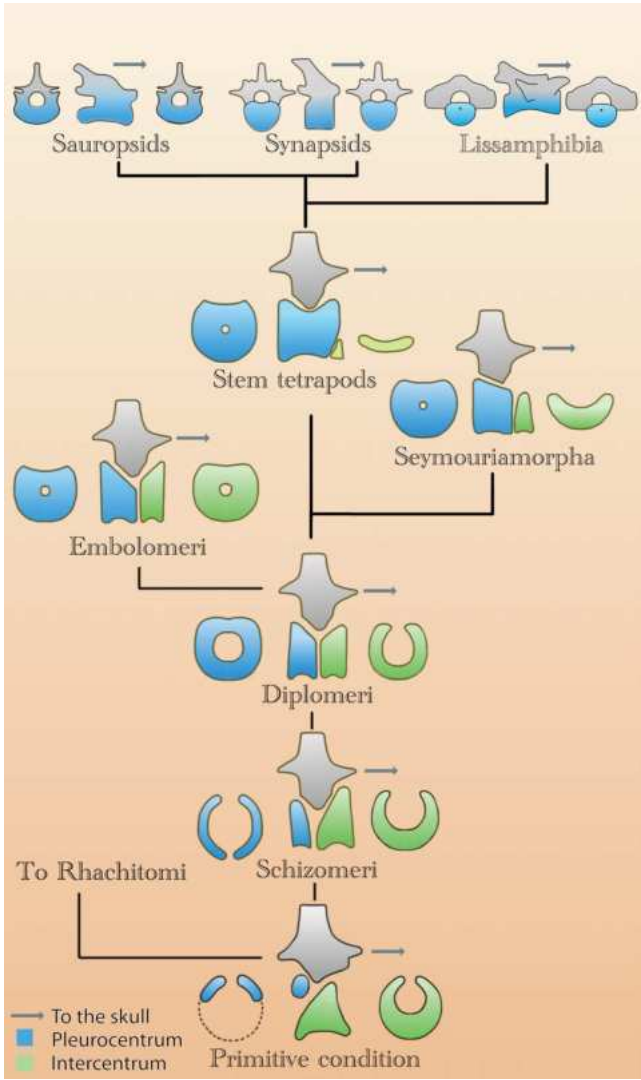


FIGURE 3.8 Evolution of the vertebral centrum. See comments in the text. (Redrawn from Romer 1956.)

Tetrapods possess only one type of ribs (Figures 3.1 and 3.7A, H), which surround the abdominal cavity. These are homologous with the ventral ribs that occur in other vertebrates, along with dorsal ribs, which may occur at the intersection of myocommata (tendinous sheets that separate myomeres) and a longitudinal septum that separates the axial musculature into dorsal and ventral portions (Romer and Parsons 1977). The development of ribs is highly variable. They are absent in cyclostomes, little developed (ventral ribs only) in extant chondrichthyans, more developed in actinopterygians (which may have dorsal and ventral ribs) and generally well developed in tetrapods (anurans are exceptions: Figure 3.7E), where they may display much regionalization, especially in mammals and birds, in which ribs are absent in the neck and tail (in mammals, they are also absent in the lumbar region). In most tetrapods, ribs play an important role in costal ventilation of the lungs.

The endoskeleton also contributes to the appendages (Figures 3.1 and 3.9). In hagfishes, the only fin is the caudal fin, which is supported (in part) by cartilaginous radials. Lampreys also have a dorsal fin, similarly supported by cartilaginous radials. The pectoral fin appeared among stem-gnathostomes and is present in the jawless osteostracans, in addition to placoderms and crown-gnathostomes (Janvier 1996a, b). The pelvic fin appeared a bit later, though still in stem-gnathostomes. They appear to be a synapomorphy of placoderms and crown-gnathostomes (Janvier 1996a, b). These paired fins (Figure 3.9A) are supported both by endoskeletal radials and dermal elements (lepidotrichia). Proximally, they articulate with girdles; the pelvic girdle is entirely endochondral, whereas the pectoral girdle includes both membrane bones and endochondral elements.

Several taxa have a metapterygial axis (i.e. a succession of robust bones along the fin axis, which feature prominently in appendage development; Figure 3.9B) in the appendicular skeleton. It is unclear if it was originally present in crown-gnathostomes, but it is very common in several early gnathostomes, such as chondrichthyans (Pradel et al. 2010). This axis gave rise to the tetrapod limb (Cohn et al. 2002), but it was lost in other taxa, such as teleosts (Laurin 2011). The articulation between the radials and the girdle may be monobasal (i.e. it involves a single element and occurs only when a metapterygial axis is present; Figure 3.9B), or polybasal (several elements articulate with the girdle). There is a debate about which of these conditions is original for gnathostomes. With the transformation of fins into limbs associated with the origin of stegocephalians, the dermal fin supports (lepidotrichia) disappeared, and some radials that were part of the metapterygial axis or located postaxially to it became incorporated into the limbs (Figure 3.9C). The homologies among proximal elements (stylopod, zeugopod and some carpal and tarsal elements) is clear, but whether or not the more distal elements of a sarcopterygian fin gave rise to the more distal parts of the limbs (metapodials and phalanges) is controversial; the majority view is that most such structures are neomorphs, but supporting evidence for this is tenuous (Laurin 2006, 2011).

The extensive development of appendages in stegocephalians justifies a brief description. In these taxa, the girdles include up to three endochondral ossifications. In the shoulder girdle, these are represented by the scapula and the anterior and posterior coracoids (Figures 3.3, 3.9D). In the pelvic girdle they consist of the ilium, ischium and pubis of the pelvic girdle. All are originally relatively flat, broad elements. Some of them may be missing in some taxa, or remain cartilaginous. The proximal part of the limbs, the stylopod (Figure 3.9D, E), comprises the humerus in the forelimb and the femur in the hindlimb. More distally, the zeugopod includes the radius and ulna in the forelimb, and the tibia and fibula in the hindlimb. These stylopod and zeugopod elements typically have a constricted waist with expanded epiphyses, although this is much more obvious in the stylopod than in the zeugopod, and in early stegocephalians than in birds and mammals (Romer 1956), in which all these elements become fairly tubular, except in the epiphyses. In some taxa, such as anurans, both elements of the zeugopod may be fused.

More distally, the carpus (wrist) and tarsus (ankle) include a variable number of polygonal elements that form a mosaic. These may have evolved progressively as neomorphs, or by transformation of distal radials. In Devonian stegocephalians, three proximal elements (ulnare, intermedium and radiale in

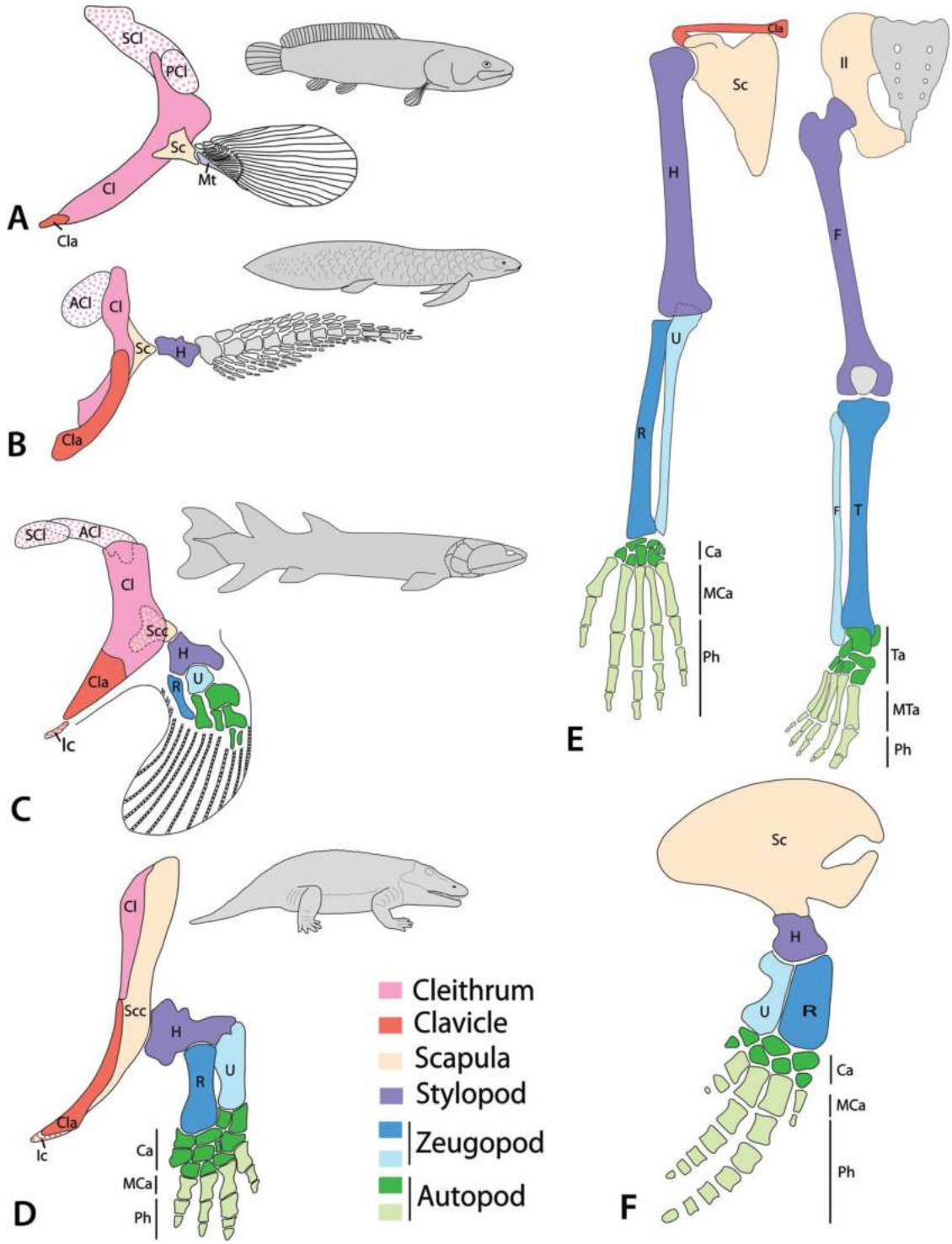


FIGURE 3.9 Origin of the limb and homology of its main bones. A, Pectoral fin structure in a fairly basal actinopterygian, *Amia calva*. B, Pectoral fin of the extant dipnoan *Neoceratodus forsteri* and its sagittal bony axis. The basal-most element is considered homologous to the tetrapod humerus by some authors (e.g. Laurin 2008). C, Condition of the tetrapodomorph *Eusthenopteron*. D, Condition of the stem-tetrapod *Eryops*. (Sketches A–D are redrawn from Kardong, 1998) E, Conservative structure of the zonoappendicular skeleton (thoracic and pelvic) of a eutherian mammal, *Homo sapiens*. Most bones displayed by the early tetrapods remain present (except in the carpus and tarsus; the number of phalanges is somewhat reduced). F, Forelimb of a cetacean (Mammalia, Eutheria). Long-bone morphology is dedifferentiated (loss of a differentiated shaft), and the number of phalanges is increased (hyperphalangy), which are two typical traits encountered in pelagic tetrapods. ACl, anocleithrum; Ca, carpals; Cl, cleithrum; Cla, clavicle; F, femur; H, humerus; Ic, interclavicle; Il, ilium; MCa, metacarpals; Mt, metapterygium; MTa, metatarsal; PCl, postcleithrum; Ph, phalanges; R, radius; Sc, scapula; Scc, scapulocoracoid; SCl, supracleithrum; T, tarsal; U, ulna.

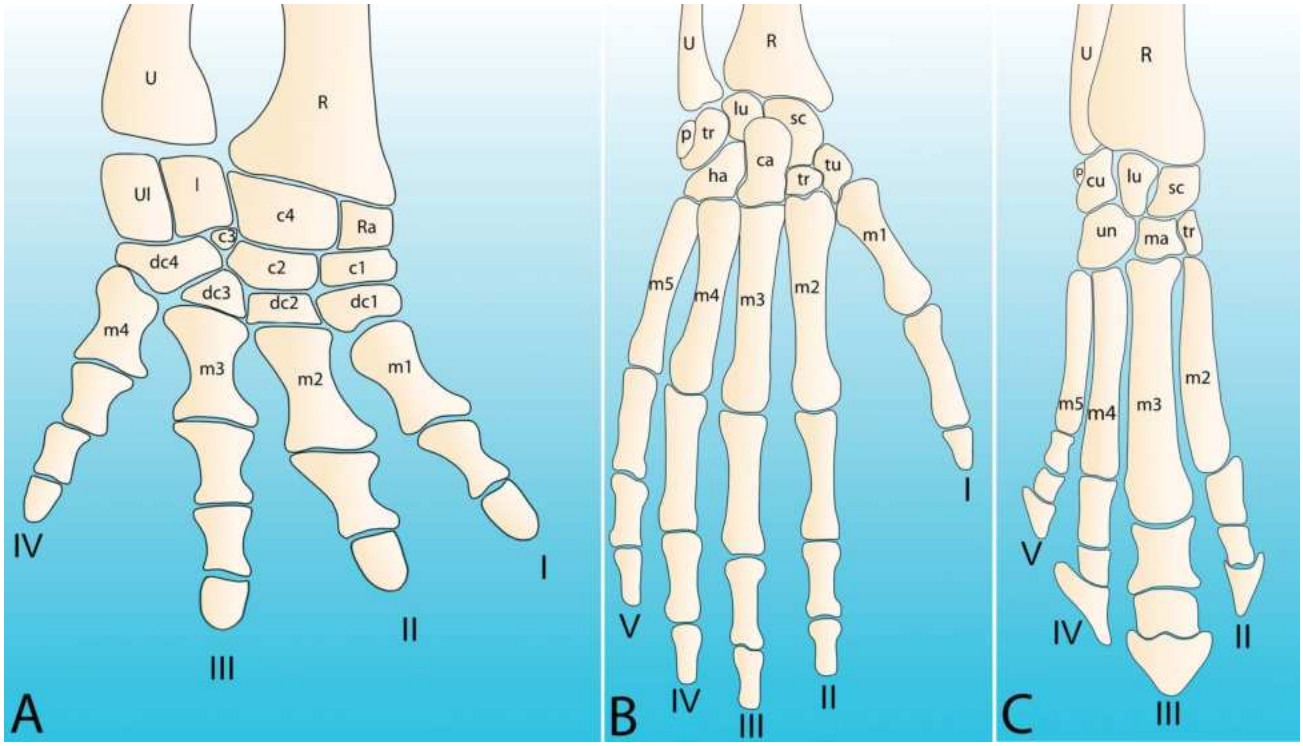


FIGURE 3.10 The autopodia of tetrapods. A, The forelimb autopodium of the basal tetrapod *Eryops* B, The conservative anterior autopodium of *Homo sapiens*. C, Anterior autopodium of a tapir (*Tapirus terrestris*). Only four digits remain. c, centralia; ca, capitate; cu, cuneiform; dc, distal carpal; ha, hamate; I, intermedium; lu, lunar; m, metacarpal; ma, magnum; p, pisiform; R, radius; Ra, radiale; sc, scaphoid; tr, trapezoid; tu, trapezium; U, ulna; Ul, ulnare; un, uncinate. The metapodials are designated by m1 to m5, and the digits by Latin numbers.

the carpus; fibulare, intermedium and tibiale in the tarsus) and a variable number of distal elements are ossified in the carpus and tarsus (Dilkes 2015); additional elements may have remained cartilaginous. The variations in number of elements are too great to give a detailed account, but the temnospondyl condition can illustrate the configuration found in many Permo-Carboniferous stegocephalians. The carpus of *Eryops megacephalus* and the tarsus of *Acheloma cumminsi* (Figure 3.10A), which were recently thoroughly described by Dilkes (2015), will form the basis of this description. Proximally, from medial to lateral, the radiale, centrale 4, intermedium and ulnare articulate with the radius and ulna. More distally, the three other centralia articulate with the distal carpals (in *Eryops* and *Dissorophus*, centrale 1 also articulates with metacarpal 1, but this is not the general stegocephalian condition). Temnospondyls have four digits in the hand, hence, four metacarpals that articulate with phalanges distally, but the original condition for Permo-Carboniferous stegocephalians is the presence of five digits in the hand. The reduction to four digits in the hand of temnospondyls is often interpreted as a synapomorphy with lissamphibians, but it may be convergent with a clade that includes most or all lepospondyls and lissamphibians, according to other hypotheses (Laurin 1998a). The phalangeal formula is documented in few temnospondyls, but in *Archegosaurus decheni* and *Eryops*, the formula is 2, 2, 3, 2 (Witzmann and Schoch 2006), which is lower than the original condition for Permo-Carboniferous stegocephalians, which is 2, 3, 4, 5, 3, as seen in some seymouriamorphs (Laurin 2000) and amniotes (Reisz 1986). Metacarpals and phalanges have a tubular diaphysis and expanded extremities, except for the terminal phalanges, called "unguals", which are pointed distally and presumably bore horny claws at least in some taxa. The foot follows a similar pattern, although the tarsus has different proximal elements (tibiale, intermedium and fibulare) and five digits in nearly all early stegocephalians. From that pattern, there was a trend toward reduction of the number of elements throughout the evolution of amniotes (Figure 3.10B, C), with the exception of the hyperphalangy of some marine amniotes such as the ichthyosaurs and the cetaceans (Romer and Parsons 1977).

Accessory Skeletal Elements: Sesamoids and Calcified Tendons

In addition to the main bones, which develop under the close control of genetic programs and are constant in shape and relative size, other skeletal elements occur, but their development is less regular and more affected by local circumstances. Such is the case with sesamoids and calcified tendons.

Sesamoids

A sesamoid is a small lenticular or spheroid ossified piece (Figure 3.11A, B) localized in the core, or along the trajectory, of a strong tendon, between the muscle and the insertional site of the tendon on the bone (general reviews in Haines 1969,

VetBooks.ir

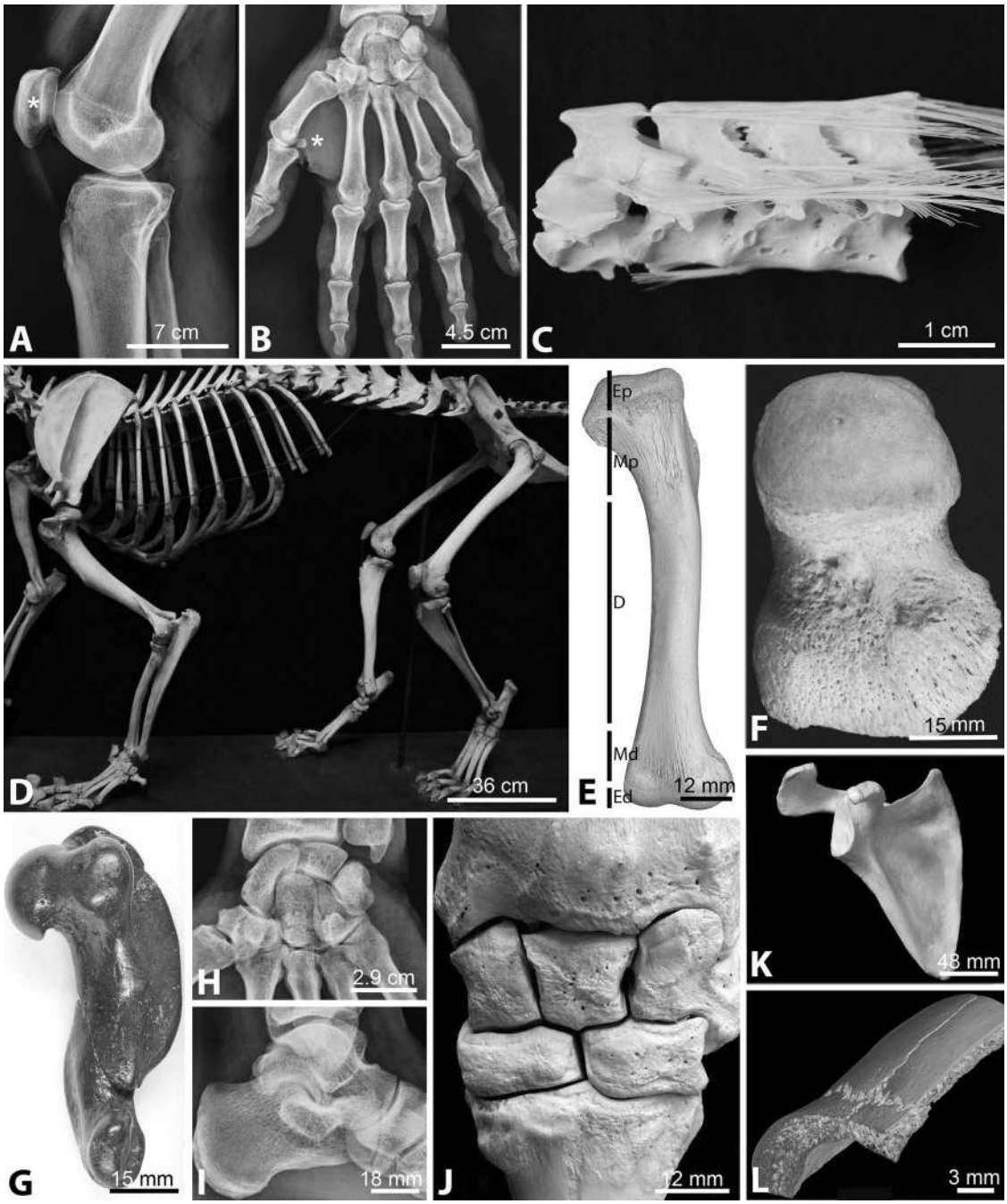


FIGURE 3.11 Accessory elements and the morphology of the bones. A, A large sesamoid (asterisk): the patella (in *Homo sapiens*). B, Small accidental sesamoid (asterisk) at the base of the first phalanx of digit 1 in the hand of a *H. sapiens* individual. C, Calcified tendons around the thoracic vertebrae of a bird [*Grus antigone,* unnumbered specimen in Muséum National d'Histoire Naturelle (MNHN-ZM-AC collections). D, Aspect of long bones in the three regions of the limbs of a tetrapod (here, a lion, *Panthera leo*, MNHN-ZM-AC-2020-1586). E, Typical aspect of a long bone (humerus of a young crocodilian, *Alligator mississippiensis).* Such bones typically display three main regions: epiphyseal (proximal, or Ep and distal, or Ed), metaphyseal (Mp and Md) and diaphyseal (D). F, Poorly differentiated humerus of a cetacean, the common dolphin (*Delphinus delphis*). G, An example of the complex, derived shape that a mammal "long" bone may display. This is the humerus of a seal, *Monachopsis khromi* (Upper Miocene of Eastern Europe). H and I, Short bones in the carpus (H) and tarsus (I) of a primate, *H. sapiens*. J, Short bones in the carpus of an artiodactyl, *Bos taurus*. K, A typical flat bone, the scapula from *H. sapiens*. L, Curved and sutured flat bones in the skull vault of a small xenarthran (Mammalia), *Dasypus* sp.

VetBooks.ir

Mottershead 1988, Vikaryous and Olson 2007). Sesamoids are considered to have appeared in tetrapods some 200 Ma ago (Carter et al. 1998). They typically occur, with substantial variability (see, for example, the statistical data on the human hand presented by Bizarro 1921), in the appendicular skeleton, close to articulations or bone protuberances where tendons undergo strong, repetitive elongation. Sesamoid size is generally small compared with that of neighboring main bones. In the hands of large anthropoids, for example, they are a few millimeters in diameter (Bizarro 1921, Sarin et al. 1999; see also Figure 3.11B); however, the patella (Figure 3.11A), located in the knee of most quadrupedal amniotes, is much larger (several centimeters in great apes). The *patellar index*, used comparatively (Haxton 1944), quantifies the relative development of this sesamoid. In extant tetrapod faunas, sesamoids occur, at least in the form of a knee patella, in most clades: lissamphibians (Ponssa et al. 2010), squamates (Jerez et al. 2010, Regnault et al. 2016), birds (Shufeldt 1884, Barnett and Lewis 1958) and mammals (Samuels et al. 2017).

Sesamoids receive strong tendinous insertions on both the muscle and bone sides (Blend and Ashhurst 1997, Toumi et al. 2006). Their functional role remains uncertain. Comparative data by Haxton (1944) suggest that the size of sesamoids depends on the strength of the muscles inserting on them. According to Schindler and Scott (2011) (see also Eyal et al. 2015), sesamoids increase the distance between bone and muscle and thus enhance the moment arm of the muscle.

Calcified Tendons

The calcification or complete ossification of tendons in various parts of the skeleton is common in tetrapods. In humans and other domestic animals, it is considered either pathological (calcific tendinopathy) if it occurs following a lesion of the tendinous tissue (e.g. Oliva et al. 2012, Zhang et al. 2016), or provoked by gradual degradation of tendon quality due to aging, with possible genetic predisposition (Agabalyan et al. 2013, Skelly and Dyson 2014, Arora and Arora 2015). Tendinous calcifications are best seen on X-ray proofs, where they appear as diffuse (when apatite crystals are loosely distributed within the tendon tissue) or clearly differentiated (when an ossification process occurs) radio-opaque nodules of moderate size, affecting parts of only the largest tendons in the appendicular skeleton. However, in one tetrapod clade, the dinosaurs, especially the ornithischians and the extant avian representatives of the theropods, tendinal ossification is both a normal condition, integrated into the regular development of the skeleton, and an extensive process involving limb (Vanden Berge and Storer 1995, Landis and Silver 2002), paravertebral (Organ 2006) and vertebral (Klein et al. 2012) domains (Figure 3.11C). The detailed morphology, orientation and anatomical relations of tendons are preserved in this process; however, through metaplasia (cf. Haines and Mohuiddin 1968), tendons are entirely transformed into osseous tissue that may undergo the same internal or external transformations (remodeling and modeling, see Chapter 11) as genuine bone (Adams and Organ 2005, Organ and Adams 2005) and fossilize as well.

The functional role of calcified or ossified tendons is generally considered biomechanical: they apparently stiffen skeletal regions submitted to severe bending or stretching stresses (Bledsoe et al. 1993, Organ 2006).

The Shape of Bones

A Significant but General Criterion

Description of the gross external morphology of bones currently encompasses three categories: long, short and flat (Figure 3.11D–I). These categories are not defined by strict anatomical or morphometric criteria; rather, they represent a global and relatively subjective appreciation of bone shape. Many ambiguous, peripheral situations are likely to occur with relatively short long bones such as the phalanges of most tetrapods, or flat long bones as represented by the rib shafts of many artiodactyls. Bone shape categories are loosely related to the early embryonic origin or the mode of formation (endochondral vs. membranous) of skeletal elements. Although all long bones derive from mesodermal mesenchyme (from the somites for ribs; the lateral plates for girdles and limb bones), flat and short bones can be either ectodermal or mesodermal. Similarly, whereas the endochondral ossification of a cartilaginous anlage is the basic mode of formation of long and short bones, a few exceptions such as the clavicle mainly result from membrane ossification. Flat bones derive from membrane ossification in the cephalic region, but from endochondral ossification in the postcranial skeleton. Of course, as Currey (2002) pointed out, the shape of bones is "intimately related to their functions" and its description (completed by microanatomical analyses) is a prerequisite to functional interpretations. General textbooks on comparative anatomy (e.g. Kardong 1998; see also Francillon-Vieillot et al. 1990) consider in detail the morphologic differences among bones.

Long Bones

This category (Figure 3.11D–G) occurs in two regions of the tetrapod skeleton: (1) the limbs, represented by stylopod (humerus and femur), zeugopod (radius and ulna in the forelimb, tibia and fibula in the hindlimb) and, *pro parte*, the autopod (metacarpals, metatarsals and phalanges) and (2) the thoracic region, with the ribs. Most long bones occur as individual elements; however, in some taxa, they can be fused, thus creating apomorphic anatomical entities such as the avian tibiotarsus and the anuran radio-ulna. Irrespective of size, a long bone shaft is basically characterized by the existence of a slender, cylindrical central region, the diaphysis, merging at both extremities with a broader, cone-shaped metaphysis, ending in a terminal dome-shaped or flat surface covered with cartilage, the epiphysis (Figure 3.11D). Broad variations in this general pattern exist between taxa; the most important variations are the relative length and diameter of the diaphysis. As exemplified by the humerus, a bone present in all extant tetrapods, except the limbless squamates and gymnophionans, the diaphyseal region can be extremely extended in some taxa (e.g. pterosaurs), or entirely undifferentiated in others (e.g. most cetaceans). The bone is then formed only by metaphyses and epiphyses (Figure 3.11F). Long bones also show various

VetBooks.ir

external structures designated as crests, tuberosities, trochanters and so forth, on which tendons insert (Figure 3.11G).

Short Bones

Wherever their location in the skeleton, these bones result from endochondral ossification. They are typically represented by the vertebral centra, the carpal and tarsal elements (Figure 3.11H–J) and, in some taxa, the phalanges. The bones of the floor of the braincase, although very complex in shape, may also belong to this category. Short bones have very diverse morphologies, from cylindrical (vertebral centra; see Figure 3.7D, F, G), to irregular polyhedric shapes (tarsals and carpals; see Figure 3.11H–J). All are, nevertheless, characterized by the absence of differentiated diaphysis and metaphyses. Vertebral centra have two regular epiphyses comparable in position and function to those of long bones. Conversely, carpals and tarsals may have several articular surfaces, and neighboring bones can be partly or entirely fused.

Flat Bones

Flat bones typically have a very low thickness-to-surface ratio (Figures 3.5B and 3.11K, L). Those of ectodermal origin and membranous formation occur in the cephalic region, where they constitute the compound osseous assemblages of the face and skull roof. Their borders are indented and mutually imbricated to form sutures. Flat bones of mesodermal origin, e.g. the scapulae, sternum and the ilium, ischium and pubis comprising the pelvic girdle, may or may not (scapulae) be jointed and display sutures, at least along their articular borders. Each mammalian scapula has two large processes (coracoid and acromion: Figure 3.11K) in addition to its main blade, which testifies that this bone is formed by the fusion of three distinct elements. The articular surfaces of girdles consist of hemispherical cavities (glenoid and acetabulum) to which the proximal epiphyses of stylopod bones articulate. Vertebral apophyses (neurapophyses and transverse apophyses) represent an ambiguous case between long bones, of which they have the slender morphology and one (distal) epiphysis, and flat bones, of which they have the blade-like aspect. In various clades of amphibians and sauropsids, membrane flat bones often display structured, repetitive patterns of pits, grooves or dome-like excrescences, designated as *bone ornamentation* or *bone sculpture*.

Remarks on the Mineralization of Skeletal Elements

The elements of the vertebrate skeleton are generally composed of mineralized and unmineralized tissues. These mineralized tissues include bone, which itself is composed of mineralized and unmineralized tissues and forms the bulk of the skeleton of extant osteichthyans, in addition to enamel and dentine (Romer and Parsons 1977). Cartilage represents a peculiar case because it coexists, in most taxa, in both unmineralized and mineralized forms, although in most vertebrates, most cartilage remains unmineralized. Mineralized cartilage may be permanent or transitory. Mineralized cartilages are permanent in chondrichthyans, in which a layer of mineralized cartilage (prismatic superficially and spheritic more deeply) typically covers a core of unmineralized cartilage, except in vertebral centra, which undergo areolar mineralization, a process creating concentric rings that record growth (Dean and Summers 2006). Permanent mineralized cartilage also occurs in some long bones, which may retain a core of calcified cartilage that reveals the occurrence of a neotenic process in skeletal growth (Quilhac et al. 2014, Buffrénil et al. 2015). Calcified cartilage may also be transitory and undergo chondroclastic resorption, as typically happens at the level of the growth plates of endochondral bones. Mobile articulations between skeletal elements usually involve unmineralized cartilage (Romer and Parsons 1977).

Acknowledgments

We are extremely grateful to Professor Christine Lefèvre (Muséum National d'Histoire Naturelle [MNHN], Paris) and Mr. Eric Pellé (MNHN, Paris) for their efficient and courteous help in finding the right specimens in the MNHN comparative anatomy collections to illustrate this article.

REFERENCES

Adams, J. S. and C. L. Organ. 2005. Histologic determination of ontogenetic patterns and processes in hadrosaurian ossified tendons. *J. Vert. Paleont.* 25: 614–622.

Agabalyan, N. A., et al. 2013. Investigating tendon mineralization in the avian hindlimb: a model for tendon aging, injury and disease. *J. Anat.* 223: 262–277.

Andrews, S. M., and T. S. Westoll. 1970. The postcranial skeleton of *Eusthenopteron foordi* Whiteaves. *Trans. R. Soc. Edinburgh.* 68(9): 207–329.

Arora, A. J. and R. Arora. 2015. Ossification of the bilateral Achilles tendon: a rare entity. *Acta Radiol.* 4: 1–3.

Arratia, G. and R. Cloutier. 1996. Reassessment of the morphology of *Cheirolepis canadensis* (Actinopterygii); pp. 165–197 in H.-P. Schultze and R. Cloutier (ed.), *Devonian Fishes and Plants of Miguasha*, Quebec, Canada vol. Dr. Friedrich Pfeil, München.

Ascarrunz, E., M. R. Sánchez-Villagra, R. Betancur-R, and M. Laurin. 2019. On trends and patterns in macroevolution: Williston's law and the branchiostegal series of extant and extinct osteichthyans. *BMC Evolutionary Biology* 19:117.

Barnett, C. H. and O. J. Lewis. 1958. The evolution of some traction epiphyses in birds and mammals. *J. Anat.* 92: 593–601.

Bizarro, A. H. 1921. On sesamoids and supernumerary bones of the limbs. *J. Anat.* 55: 256–268.

Bledsoe, A. H., et al. 1993. Evolution and functional significance of tendon ossification in woodcreepers (Aves: Passeriformes: Dendrocolaptinae). *J. Morphol.* 215: 289–300.

Blend, Y. S. and D. E. Ashhurst. 1997. Fetal and postnatal development of the patella, patellar tendon and suprapatella in the rabbit; changes in the distribution of the fibrillar collagens. *J. Anat.* 190: 327–342.

VetBooks.ir

Borgen, U. J. 1983. Homologizations of skull roofing bones between tetrapods and osteolepiform fishes. *Palaeontology.* 26(4): 735–53.

Buffrénil, V. de, et al. 2015. Histological study of karaurids, the oldest known (stem) urodeles. *Historical Biology* 27: 109–114.

Carroll, R. L. 1988. *Vertebrate paleontology and evolution*. New York: W. H. Freeman.

Carter, D. R., et al. 1998. Epigenetic mechanical factors in the evolution of long bone epiphyses. *Zool. J. Linn. Soc.* 123: 163–178.

Coates, M. I. 1996. The Devonian tetrapod *Acanthostega gunnari* Jarvik: postcranial anatomy, basal tetrapod interrelationships and patterns of skeletal evolution. *Trans. R. Soc. Edinburgh*. 87(6288): 363–421.

Cohn, M. J., et al. 2002. Branching, segmentation and the metapterygial axis: pattern versus process in the vertebrate limb. *BioEssays.* 24: 460–465.

Currey, J. D. 2002. Bones. *Structure and mechanics.* Princeton and Oxford: Princeton University Press.

Dean, M. N., and A. P. Summers. 2006. Mineralized cartilage in the skeleton of chondrichthyan fishes. *Zoology.* 109: 164–168.

De Luliis and Pulerà. 2007. *The dissection of vertebrates.* Amsterdam: Academic Press.

Dilkes, D. 2015. Carpus and tarsus of Temnospondyli. *Vertebr. Anat. Morph. Palaeontol.* 1(1): 51–87.

Eyal, S., et al. 2015. On the development of the patella. *Development*. 142: 1831–1839.

Francillon-Vieillot, et al. 1990. Microstructure and mineralization of vertebrate skeletal tissues. In *Skeletal biomineralization: patterns, processes and evolutionary trends*, vol. 1, ed. J. G. Carter, 471–530. New York: Van Nostrand Reinhold.

Géraudie, J. and F. J. Meunier. 1984. Structure and comparative morphology of camptotrichia of lungfish fins. *Tissue & Cell* 16: 217–236.

Grande, L., and W. E. Bemis. 1998. A comprehensive phylogenetic study of amiid fishes (Amiidae) based on comparative skeletal anatomy. An empirical search for interconnected patterns of natural history. *J. Vertebr. Paleontol.* 18(Supp 1): 1–688.

Gregory, W. K. 1911. The limbs of *Eryops* and the origin of paired limbs from fins. *Science* 33: 848–849.

Haines, R. W. 1969. Epiphyses and sesamoids. In *Biology of the Reptilia. Morphology A*, vol. 1, ed. C. Gans, 81–115. London: Academic Press.

Haines, W. R. and A. Mohuiddin. 1968. Metaplastic bone. *J. Anat.* 103: 527–538.

Hall, B. K. 2005. *Bones and cartilage: developmental and evolutionary skeletal biology.* Amsterdam: Elsevier-Academic Press.

Haxton, H. 1944. The patellar index in mammals. *J. Anat.* 78: 106–107.

Janvier, P. 1996a. *Early vertebrates.* Oxford, UK: Oxford University Press.

Janvier, P. 1996b. The dawn of the vertebrates: characters versus common ascent in the rise of current vertebrate phylogenies. *Palaeontology.* 39(2): 259–287.

Jarvik, E. 1959. Dermal fin-rays and holmgren's principle of delamination. *Kungl. Svenska Vetens. Handl.* 6(1): 1–61.

Jerez, A., et al. 2010. Occurrence and distribution of sesamoid bones in squamates: a comparative approach. *Acta Zool. (Stockh.).* 91: 295–305.

Kardong, K. V. 1998. *Vertebrates – comparative anatomy, function, evolution*. Boston: McGraw-Hill.

Khemiri, S., et al. 2001. Morphology and structure of the scales in the Gadiformes (Actinopterygii: Teleostei: Paracantopterygii) and a comparison to the elasmoid scales of other Teleostei. *Cash. Biol. Mar.* 42(4): 345–362.

Klein, N., et al. 2012. Histology shows that elongated neck ribs in sauropod dinosaurs are ossified tendons. *Biol. Lett.* 8: 1032–1035.

Laloy, F., et al. 2013. A re-interpretation of the Eocene anuran *Thaumastosaurus* based on microCT examination of a 'mummified' specimen. *PLoS One.* 8: 1–11.

Landis, W. J. and F. H. Silver. 2002. The structure and function of normally mineralizing avian tendons. *Comp. Biochem. Physiol. A.* 133: 1135–1157.

Laurin, M. 1998a. A reevaluation of the origin of pentadactyly. *Evolution.* 52(5): 1476–1482.

Laurin, M. 1998b. The importance of global parsimony and historical bias in understanding tetrapod evolution. Part II. Vertebral centrum, costal ventilation, and paedomorphosis. *Ann. Sci. Nat., Zool., 13 Ser.* 19(2): 99–114.

Laurin, M. 2000. Seymouriamorphs. In *Amphibian biology*, eds. H. Heatwole and R. L. Carroll, 1064–1080. Chipping Norton: Surrey Beatty & Sons.

Laurin, M. 2006. Scanty evidence and changing opinions about evolving appendages. *Zool. Scr.* 35: 667–68.

Laurin, M. 2008. Systématique, paléontologie et biologie évolutive moderne. *L'exemple de la sortie des eaux chez les vertébrés*. Paris: Ellipses.

Laurin, M. 2010. *How vertebrates left the water. Translated by Michel Laurin*. Berkeley: University of California Press.

Laurin, M. 2011. Limb origin and development. In *Mémoires Du Muséum National D'histoire Naturelle*, eds. V. Bels, A. Casinos, J. Davenport, J.-P. Gasc, M. Jamon, M. Laurin and S. Renous, 75–89. Paris: Muséum National d'Histoire Naturelle.

Laurin, M. 2020a. *Stegocephali;* pp. 741–745 in K. de Queiroz, P. D. Cantino, and J. A. Gauthier (ed.), *Phylonyms: An Implementation of PhyloCode* CRC Press, Boca Raton, Florida.

Laurin, M. 2020b. *Tetrapoda;* pp. 759–764 in K. de Queiroz, P. D. Cantino, and J. A. Gauthier (ed.), *Phylonyms: An Implementation of PhyloCode* CRC Press, Boca Raton, Florida.

Laurin, M., and G. Piñeiro. 2017. A reassessment of the taxonomic position of mesosaurs, and a surprising phylogeny of early amniotes. *Front. Earth Sci.* 5(88): 1–13.

Minelli, A., and G. Fusco. 2013. Homology. In *The philosophy of biology: a companion for educators*, ed. K. Kampourakis, *History, philosophy and theory of the life sciences* book series, 289–322. Dordrecht: Springer.

Mottershead, S. 1988. Sesamoid bones and cartilages: an enquiry into their function. *Clin. Anat.* 1: 59–62.

Müller, J., and L. A. Tsuji. 2007. Impedance-matching hearing in Paleozoic reptiles: evidence of advanced sensory perception at an early stage of amniote evolution. *PLoS One.* 2007(9): 1–7.

Oliva, F., et al. 2012. Physiopathology of intratendinous calcific deposition. *BMC Med.* 10: 95.

Organ, C. L. 2006. Biomechanics of ossified tendons in ornithopod dinosaurs. *Paleobiology.* 32: 652–665.

VetBooks.ir

Organ, C. L. and J. Adams. 2005. The histology of ossified tendons in dinosaurs. *J. Vert. Paleont*. 25: 602–613.

Pearson, D. 1982. Primitive bony fishes, with especial reference to *Cheirolepis* and palaeonisciform actinopterygians. *Zool. J. Linn. Soc.* 74(1): 35–67.

Ponssa, M. L., et al. 2010. Sesamoids in anurans: new data, old issues. *Anat. Rec.* 293: 1646–1668.

Pradel, A., et al. 2010. Study of the pectoral girdle and fins of the Late Carboniferous sibyrhynchid iniopterygians (Vertebrata, Chondrichthyes, Iniopterygia) from Kansas and Oklahoma (USA) by means of microtomography, with comments on iniopterygian relationships. *C. R. Palevol*. 9(6–7): 377–387.

Qu, Q., et al. 2015. New genomic and fossil data illuminate the origin of enamel. *Nature*. 526: 108–111.

Quilhac, A., et al. 2014. *Globuli ossei* in the long bones of *Pleurodeles waltl* (Amphibia, Urodela, Salamandridae). *J. Morphol*. 275: 1226–1237.

Regnault, S., et al. 2016. Anatomy, morphology and evolution of the patella in squamate lizards and tuatara (*Sphenodon punctatus*). *J. Anat*. 228: 864–876.

Reisz, R. R. 1986 Pelycosauria. In *Encyclopedia of paleoherpetology*, ed. P. Wellnhofer, 1–102. Stuttgart: Gustav Fischer.

Romer, A. S. 1956. *Osteology of the reptiles*. Chicago: University of Chicago Press.

Romer, A. S., and T. S. Parsons. 1977. *The vertebrate body*. 5 ed. Philadelphia: W. B. Saunders.

Samuels, M. E., et al. 2017. Evolution of the patellar sesamoid in mammals. *PeerJ*. 5: e3103.

Sarin, V. K., et al. 1999. Coincident development of sesamoid bones and clues to their evolution. *Anat. Rec.* 257: 174–180.

Schindler, O. S. and N. W. Scott. 2011. Basic kinematics and biomechanics of the patello-femoral joint. Part1: The native patella. *Acta. Orthop. Belg.* 77: 421–431.

Shufeldt, R. W. 1884. Concerning some of the forms assumed by the patella in birds. *Proc. U. S. Natl. Mus.* 7: 324–331.

Sidor, C. A. 2001. Simplification as a trend in synapsid cranial evolution. *Evolution* 55(7): 1419–1442.

Sire, J.-Y., et al. 2009. Origin and evolution of the integumentary skeleton in non-tetrapod vertebrates. *J. Anat.* 114: 409–440.

Skelly, E. and S. Dyson. 2014. Mineralization or ossification of the interosseous ligament of the centrodistal joint of the horse: is there an association with osteoarthritis? *Equine Vet. J.* 46(Suppl. 47): 2–25.

Toumi, H., et al. 2006. Regional variations in human patellar trabecular architecture and the structure of the proximal patellar tendon enthesis. *J. Anat*. 208: 47–57.

Vanden Berge, J. C. and R. W. Storer. 1995. Intratendinous ossification in birds: a review. *J. Morphol.* 226: 47–77.

Vickaryous, M. K. and W. M. Olson. 2007. Sesamoids and ossicles in the appendicular skeleton. In *Fins into limbs: evolution, development and transformation*, ed. B. K. Hall, 323–341. Chicago: University of Chicago.

Vickaryous, M. K. and J.-Y. Sire. 2009. The integumentary skeleton of tetrapods: origin, evolution, and development. *J. Anat.* 214: 441–464.

Williston, S. W. 1910. *Cacops, Desmospondylus*: new genera of Permian vertebrates. *Bull. Geol.l Soc. Am*. 21:249–284.

Witzmann, F., and R. M. Schoch. 2006. The postrcanium of *Archegosaurus decheni*, and a phylogenetic analysis of temnospondyl postcrania. *Palaeontology*. 49(6): 1211–1235.

Zhang, K., et al. 2016. Tendon mineralization is progressive and associated with deterioration of tendon biomechanical properties, and requires BMP-Smad signaling in the mouse Achilles tendon injury model. *Matrix Biol.* 52–54: 315–324.

Zylberberg, L., et al. 2016. A microanatomical and histological study of the postcranial dermal skeleton of the Devonian actinopterygian *Cheirolepis canadensis*. *Acta Palaeont. Pol*. 61(2): 363–76.

VetBooks.ir

Methodological Focus A

The New Scalpel: Basic Aspects of CT-Scan Imaging

Damien Germain and Sandrine Ladevèze

CONTENTS

Introduction 55
Basic Principles of the Method 55
Two Examples of CT Scan Use in Anatomy 57
Mammalian Inner Ears and Species Ecology 57
Virtual Dissections in Paleontology: The Example of "Cuvier's Opossum" 58
References 58

Introduction

Tomography literally means "slice drawing," and this activity has long been one of the main tasks of paleohistologists, Traditionally, these were pen-and-ink renderings, usually labeled, of the tissues and microstructures exposed on histological slides. The term now mainly refers to X-ray computed tomography scanning, or CT scanning, which is a technical approach that currently plays a crucial and prominent role in morphology.

Soon after their discovery by Röntgen in 1895, X-rays were used in paleontological studies. Blot (1910) proposed that radiographs could be an additional source to access the internal organization of fossils, complementary to thin sections. However, radiographs are projections in a single plane of the entire depth of the sample, and the images thus obtained are not equivalent to thin sections. During the same epoch, the mathematician Radon (1917) demonstrated that it was theoretically conceivable to reconstruct virtual sections from many projections (radiographs, for instance), but at that time, this was technically impossible to calculate. The development of computers and efficient calculators in the 1970s made the modern CT-scanning method feasible, and it quickly flourished (Beckmann 2006). At the beginning of X-ray CT, image resolution was not high enough to explore bone microanatomy or histology, but today these techniques have acquired sufficient power and are much more affordable, allowing a great multiplication of paleohistological studies at various scales.

Basic Principles of the Method

CT scanning consists of taking radiographs of a sample around a single rotational axis. Each radiograph corresponds to one angle of rotation, and this is called a projection. All projections are analyzed by an algorithm to reconstruct the virtual sections. These reconstructed virtual sections are oriented in a plane perpendicular to that of the projections. During this reconstruction process, artifacts can be removed. In three-dimensional (3D) digital pictures, the smallest unit of information is the voxel. This is the 3D equivalent of the pixel for two-dimensional (2D) pictures. The smaller the voxel is, the better the resolution and the bigger the data sets. All reconstructed slices are in gray levels (indicating the brightness of the voxel) and are assembled in a stack (Figure A.1).

Various technical applications can be used. Medical CT scans have been designed for health care to minimize the dose of X-rays received by the patient. The scanning process must be as fast as possible and the coupled X-ray tube/detector rotates around the immobile, lying patient. The voxel sizes in such CT scans are often too large for studying histology, but in certain cases they allow the study of bone microanatomy, through such parameters as cortical compactness or trabecular architecture (if the trabeculae are thick enough).

In industrial CT scans, as used in paleohistology, the X-ray tube and the detector are fixed, and the (nonliving) specimen is mounted on a rotating table. Industrial CT scans work under a tension as high as 240 kV, whereas the voltage of a classical (medical) X-ray generator is 100 kV at the most. Of course, absolute stability and accurate centering of the specimen are prerequisites for good results. The X-ray beam is then conical. This technique is particularly adapted for the study of trabecular architecture, but it is of limited use for histology proper, because the voxel size is often too large (>5 µm) to accurately visualize, e.g., osteocyte lacunae. Synchrotron light then takes the relay.

Because voxels are cubes of a known dimension, basic spatial coordinates can be automatically generated by the CT scan, which allows accurate measurements of the specimen (lengths, angles, areas, volumes, densities etc.). The size of the pixels of the detector is determined by the size of its captors; however, it is possible to change the reconstructed voxel size by modifying acquisition parameters. Voxel size is mainly influenced by the relative distance of the sample between the source and the detector. Because the beam is conical, when the sample is close to the source and far from the detector the

VetBooks.ir

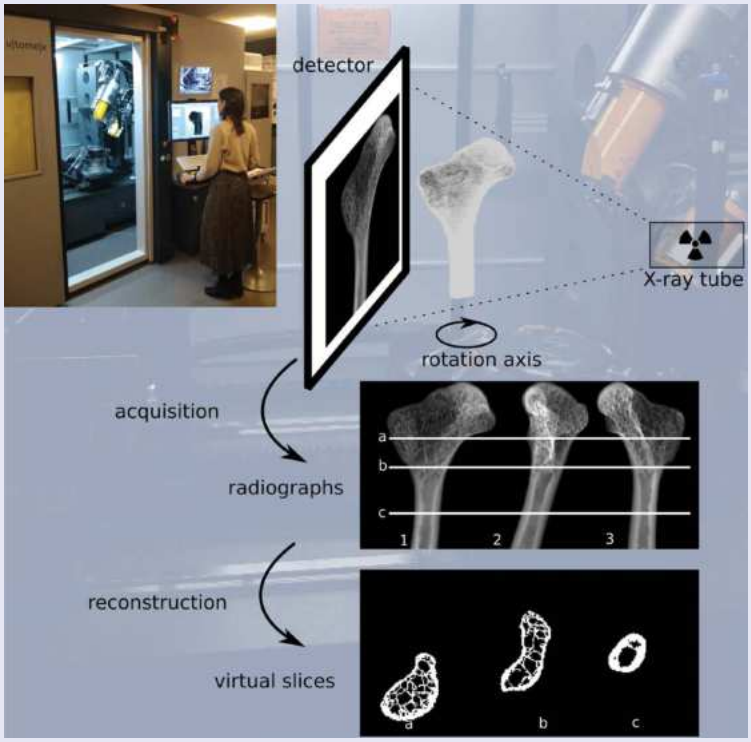


FIGURE A.1 Various steps in the CT image acquisition process. The specimen (here a schematic turtle humerus) rotates while it is exposed to a conic X-ray beam. The X-ray images are acquired by a detector, and processed by an algorithm for reconstructing a stack of virtual slices. 1, 2, 3 correspond to X-ray images at three different angles. a, b, c show three different virtual sectional planes.

magnification is higher, and the relative size of the voxel, compared to that of the receptor captors, is smaller.

Although it is often better to have small voxels, the most important thing is to have a high contrast, and it may be necessary to choose bigger voxels to improve contrast. Initial CT scan pictures are in gray levels, often coded in 8 bits ($2^8 = 256$ gray levels) or 16 bits ($2^{16} = 65{,}536$ gray levels). Properly setting the histogram of gray levels is therefore of prime importance for optimizing the visibility of details (Figure A.2). In CT scans, gray levels are proportional to the absolute radio-opacity of the specimens, a characteristic that reflects X-ray absorption by the tissues. X-ray opacity is proportional to both the local mineralization rate of the specimen (in bone: parameter *BMC*, for *bone mineral content*, according to the official microanatomical nomenclature), and to the volume of the mineralized tissue through which the X-ray beam propagates (parameter *BV*, for

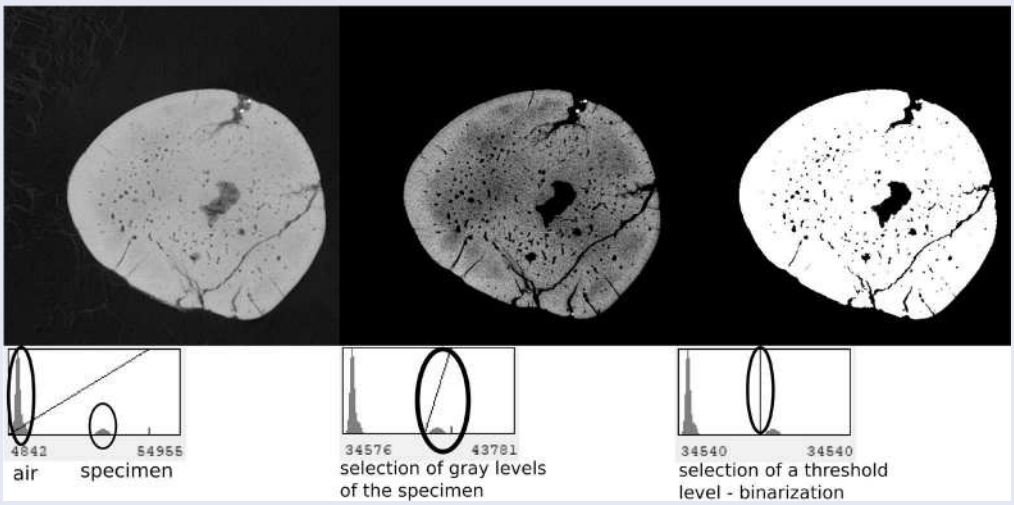


FIGURE A.2 Thresholding virtual slices of a fossil specimen (humerus of *Claudiosaurus germaini*, collection number MNHN.F.MAP9) on Fiji (Schindelin et al. 2012). Left: all gray levels are represented proportionally. Center: gray levels corresponding to the air are removed and only gray levels corresponding to the specimen are represented proportionally. Right: all gray levels corresponding to the specimen are equalized; the image is binarized (air in black, bone in white).

VetBooks.ir

bone volume); the darkest gray values correspond to lowest X-ray opacity, (e.g. the air around the specimen), and brightest values to the highest opacity (e.g. bone, enamel). In medical CT scans, gray values in a CT-scan image can be measured in Hounsfield units, which basically correspond to the relative X-ray opacity observed in a voxel compared to the reference opacity values of air and water.

Virtual sections can be analyzed as mere 2D images, but other methods are available for studying 3D bone structure. In most cases, a step of segmentation is required. Segmentation consists of selecting the region of interest (ROI) inside each virtual section. This can be done by thresholding the relevant gray values when contrasts are good enough, for instance, in extant bones. In fossil specimens, the internal spaces of bone are often filled by minerals or the bone is still enclosed in a rock matrix. Thresholding is then more difficult or insufficient (because parts of the matrix may be more opaque than bone, whereas others may be less opaque, depending on composition), which implies the selection of ROIs on each slide, which is a long and tedious task. Fortunately, segmentation software, such as Avizo (Visualization Sciences Group), Mimics (Materialise), VG StudioMax (Volume Graphics) or SPIERS (Sutton et al. 2012), is now quite efficient. These programs allow us to treat not only CT-scan data, but also data obtained by serial grinding or serial thin sectioning. In addition to the basic image of the object in gray values, the basic structure of a 3D CT-scan file also includes acquisition parameters (voltage, intensity, voxel size, filters etc.). Generally, the size of a data set is about 5 Gb, much smaller than in synchrotron data sets, which can reach several hundred Gb.

Two Examples of CT Scan Use in Anatomy

Mammalian Inner Ears and Species Ecology

Since the 1960s, the morphology and structure of the inner ear, viewed as an integrative center for hearing and equilibration, have been considered in reference to the animal's behavior (Jones and Spells 1963; Mayne 1965). However, technical constraints long prevented a full quantification of the shape of the inner ear organs; therefore, the veracity of such causal relations remained untested. The bony labyrinth of the inner ear is particularly difficult to investigate, because its complex 3D shape is hidden inside the dense (and highly opaque to ordinary X-ray beams) otic capsule of the petrosal bone. The recent use of high-resolution CT scan, with a voxel size less than 20 µm (e.g. David et al. 2016; Costeur et al. 2018), has allowed much better documentation.

In hominids, the pioneer studies based on CT-scan files resulted in the first morphometric analyses of the osseous inner ear in both large extant samples and rare anthropological specimens. The specimens were scanned with overlapping slices (slice increment 0.75 mm), which took approximately 20 transverse and 20 sagittal scans to cover the entire human labyrinth (Spoor et al. 1994; Spoor and Zonneveld 1995). Spoor and colleagues defined procedures for repeatable linear measurements of the bony labyrinth, and these procedures proved to be repeatable and accurate. The final result of their studies was to point out that the inner ear of *Homo erectus* was already very similar to that of *H. sapiens*, in pace with modern running and jumping. More recent studies benefited from higher resolution micro-CT scans, and are preferentially based on geometry rather than on linear measurements, because geometry better approximates 3D shape. Figure A.3 shows the bony labyrinth of the inner ear virtually extracted from the skull, with fixed landmarks and semilandmarks reproducing the shape of its semicircular canal system. Micro-CT imagery coupled with 3D geometric morphometry is a powerful method for determining phylogenetic and functional patterns of mammalian inner ears, and it allows systematic biologists to better understand the relationships among the shape of the bony labyrinth, phylogeny and ecology. Mammals have adapted to a large array of adaptive zones and, consequently, display a broad range of locomotion patterns, apparently consistent with variations of the bony semicircular system of the inner ear. However, predicting the ecology from the shape of the semicircular canals would require visualization of not only the bone but the inner soft tissues in order to fully investigate the sensory biology of the organ of balance (David et al. 2016).

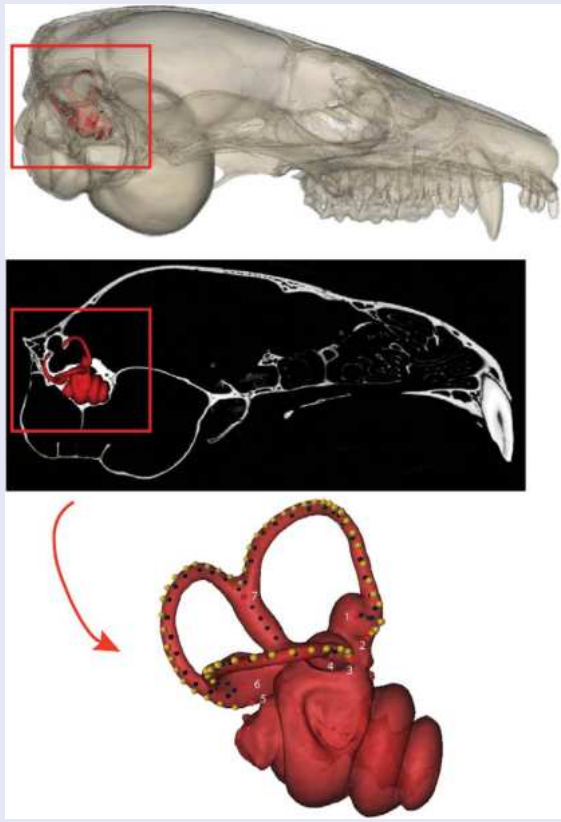


FIGURE A.3 A 3D reconstruction of the cranium and right bony labyrinth of *Phascogale tapoatafa* (collection number MNHN.ZM.MO.2007-18). The bony labyrinth, in red, is virtually extracted from the rest of the skull. Upper field: 3D reconstruction. Middle field: parasagittal virtual section at the level of the left canine. Lower field: the bony labyrinth reconstructed in 3D. The shape of the semicircular duct system is approximated by fixed (red) and sliding (yellow and black) landmarks, which run all over the external surface and midline of the semicircular canals. Seven independent curves are defined on the semicircular canals, each of which starts with a fixed homologous landmark (type I). This procedure allows assessment of the angles, lengths, thicknesses and twists of the semicircular canals, as well as the length of the crus commune.

VetBooks.ir

Virtual Dissections in Paleontology: The Example of "Cuvier's Opossum"

Micro-CT technique and 3D imagery have become the reference method with which to access fossil material embedded in rock matrices, and it allows large-scale, nondestructive comparative studies. A recent study dealing with an historical fossil, "Cuvier's opossum," exemplifies this situation. In 1804, Georges Cuvier described the almost complete skeleton of a small quadrupedal mammal found in the late Eocene layer of the Montmartre gypsum (now in Paris, France). This small fossil was at the origin of the demonstration of the *principle of correlations* and became one of the most emblematic historical specimens of the Muséum National d'Histoire Naturelle (Paris). It nevertheless partly remained in a stony matrix. Cuvier, using the principles of correlative anatomical inference (related to taxonomy but not to phylogeny), predicted that beneath the matrix were the epipubic bones, a typical marsupial feature of extra pelvic bones associated taxonomically with the opossum-like molars. In the presence of other *savants*, the overlying matrix was removed and the epipubic bones were revealed, validating Cuvier's principle. More than two centuries later, the fossil had not yet revealed all its secrets until the use of micro-CT techniques, which allowed a virtual removal of the rest of the matrix (Figure A.4) and a 3D reconstruction of hidden bones (Selva and Ladevèze 2017). Anatomical comparisons with extant and extinct taxa reveal that Cuvier's "opossum" is not a crown-group opossum (recalling that opossums, or didelphimorphss, are the most basal diverging group of marsupials) and is not closely related to recent opossums; instead, it belongs to an ancient and bygone European radiation of small omnivorous marsupials (Herpetotheriidae) close to didelphimorphs (Ladevèze et al. 2020). Still, his demonstration of the principles of comparative anatomy stands.

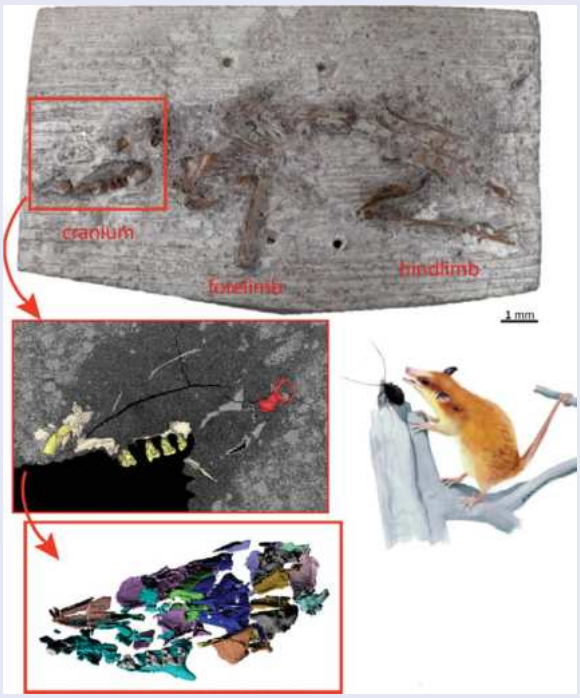


FIGURE A.4 Skeleton of Cuvier's "opossum" (*Peratherium cuvieri*) trapped inside a gypsum slab (MNHN.F.GY.697b). Its cranium was scanned through micro-CT imaging, and the maxillary with emerging teeth (middle box, in yellow), as well as the bony labyrinth (in red), have been virtually extracted in 3D. Most of the cranial bones have been found in the gypsum matrix, and the 3D reconstructed skull is shown in ventral view (bottom box). This work (Selva and Ladevèze 2017) inspired an artistic interpretation of the fossil. (Courtesy of B. Duhem, Muséum National d'Histoire Naturelle, Paris.)

REFERENCES

Beckmann, E. C. 2006. CT scanning: the early days. *Brit. J. Radiol*. 79: 5–8.

Blot, M. 1910. La radiographie d'un fossile. *La Nature*. 38: 400.

Costeur, L., et al. 2018. The bony labyrinth of toothed whales reflects both phylogeny and habitat preferences. *Sci. Rep.* 8: 1–6.

David, R., et al. 2016. Assessing morphology and function of the semicircular duct system: introducing new in-situ visualization and software toolbox. *Sci. Rep.* 6: 32772.

Jones, G. M. and Spells, K. E. 1963. A theoretical and comparative study of the functional dependence of the semicircular canal upon its physical dimensions. *Proc. Roy. Soc. Lond. B: Biol. Sci.* 157: 403–419.

Keklikoglou, K., et al. 2019. Micro-computed tomography for natural history specimens: a handbook of best practice protocols. *Eur. J. Taxon*. 522: 1–55.

Ladevèze, S., et al. 2020. What are "opossum-like" fossils? The phylogeny of herpetotheriid and peradectid metatherians, based on new features from the petrosal anatomy. *J. Syst. Palaeontol*. 18: 1463–1479.

Mayne, R. 1965. The "match" of the semicircular canals to the dynamic requirements of various species. *The Role of the Vestibular Organs in the Exploration of Space*. NASA SP-77: 57–67.

Radon, J. 1917. Uber die Bestimmung von Funktionen durch ihre Integralwerte Langs Gewisser Mannigfaltigkeiten [On the determination of functions from their integrals along certain manifolds]. *Ber. Saechsische Akad. Wiss*. 29: 262.

Schindelin, J., et al. 2012. Fiji: an open-source platform for biological-image analysis. *Nat. Methods*. 9: 676–682. https://doi.org/10.1038/nmeth.2019

Selva, C. and S. Ladevèze. 2017. Computed microtomography investigation of the skull of Cuvier's famous 'opossum' (Marsupialiformes, Herpetotheriidae) from the Eocene of Montmartre. *Zool. J. Linn. Soc*. 180: 672–693.

Spoor, F., et al. 1994. Implications of early hominid labyrinthine morphology for evolution of human bipedal locomotion. *Nature* 369: 645–648.

Spoor, F. and F. Zonneveld. 1995. Morphometry of the primate bony labyrinth: a new method based on high-resolution computed tomography. *J. Anat*. 186: 271–286.

Sutton, M. D., et al. 2012. SPIERS and VAXML; a software toolkit for tomographic visualisation and a format for virtual specimen interchange. *Palaeontol. Electr.* 15: 1–14.

VetBooks.ir

4

Microanatomical Features of Bones and Their Basic Measurement

Vivian de Buffrénil, Eli Amson, Alexandra Quilhac, Dennis Voeten and Michel Laurin

CONTENTS

An Intermediate Level of Integration: Microanatomy 59
Gross Microanatomical Structure of Long Bones 61
The Outer Envelopes of Bone 61
Diaphyseal Region 61
Metaphyses 64
Epiphyses 66
Microanatomy of Short Bones 68
Gross Microanatomy of Flat Bones 70
Remarks on Some Basic Concepts Used in Microanatomical Descriptions 71
Cortex versus Medulla 71
Compact versus Cancellous Bone 71
Tubular versus Diploe 71
Qualitative Classification of Cancellous Bone 72
An Overview of Vascular Canals in Bone 72
General Characteristics of Cortical Vascularization 72
Cartilage Canals 75
Remark on Dermal Bone Vascularization 75
Acknowledgments 76
References 76

An Intermediate Level of Integration: Microanatomy

Between the anatomical level described above and the histological level in which observation bears on details invisible to the naked eye, the intermediate level of microanatomy deals with inner structural features some tens of microns to a few millimeters in size. This level of morphological integration can be considered relevant both to anatomy (e.g., Burr and Akkus 2014), and to histology (Francillon-Vieillot et al. 1990; Ricqlès et al. 1991). Histological features, i.e., the characteristics of cells and extracellular matrices as observed in optical and electronic microscopy, are independent of typical microanatomical details such as the thickness of bone cortices and the geometrical architecture of medullary spongiosa (Ricqlès 1975, 1976). Such characteristics depend on causes more relative to growth and functional constraints than to the organization of the tissues themselves. This is why histological aspects proper are excluded from the field of microanatomy. This level of integration applies to all skeletal elements, osseous or not. In the case of the bony skeleton, the term microanatomy will be restricted to the gross inner architecture of the bones that results from the distribution of extracellular matrices and cavities, including vascular canals. Basic concepts in this field are the antagonistic notions of compact and cancellous. An osseous formation is generally considered cancellous when cavities occupy a broader volume (or area in 2D) than the bone tissue proper (Francillon-Vieillot et al. 1990). However, in current practice, the theoretical threshold of 50% (e.g., Currey 2002) that should distinguish a compact (i.e., a compacta) from a cancellous (i.e., a spongiosa) tissue is very seldom considered. The decision to use one or the other of these terms remains largely subjective, although precise quantification of local bone compactness may be given.

Microanatomy is the typical domain of histomorphometrical studies, in which principal aspects of skeletal biology are approached, such as the local development of bone volume during ontogeny or phylogeny, its architectural organization in

VetBooks.ir

relation to mechanical constraints, and the density and geometry of intracortical vascular networks. From a functional perspective, the microanatomical level is one of the most important. In relation to the monitoring of various pathologies of the human skeleton, medical histomorphometry has considerably developed in theoretical and practical terms (see Chapter 32). Numerous parameters, indices, reference values, and other standardized measurement protocols have been created for this purpose and are the subject of abundant publications (reviews in Kalender et al. 1989; Glorieux et al. 2000; Dempster et al. 2013). However, only some of them prove to be usable in comparative biology, and still less in paleohistology; therefore, the descriptions presented below are focused on the aspects of bone histomorphometry that can be equally applied, and with similar results, to extant and extinct taxa. This, of course, excludes parameters related to nonmineralized tissues such as osteoid or hyaline cartilage: the basic measurements of bone tissue considered here refer to mineralized bone and represent a set of parameters currently designated by the suffix *Md* in standard nomenclature (Parfitt et al. 1987; Dempster et al. 2013). Table 4.1 summarizes some of the basic,

TABLE 4.1

Name and Content of Some Basic Microanatomic Parameters

Name and Content	Abbreviation (2D)
A. Qualitative Parameter Relative to Tissue	
Bone: mineralized or nonmineralized osseous matrix	B
Cancellous: tissue in which cavities are predominant (≈ spongiosa)	Cn
Cartilage: mineralized or nonmineralized cartilaginous matrix	Cg
Canal: vascular canal or perilacunar canalicula(r)	Ca
****Compact***: tissue with few (less than 50% in area) inner cavities	Co
Lacuna: hollow compartment (mainly cell), excluding Howship lacunae	Lc
Mineralized: for bone or cartilage	Md
Matrix: intercellular substance	Mx
Osteon: either primary or secondary	On
Osteocyte: bone cell	Ot
Spongiosa: cancellous tissue made of trabeculae	Sn
Tissue: entire bone formation including matrix + cavities	T
Trabecula(r): relative to rod- or plate-like bone struts	Tb
B. Topography, Position, and Orientation	
Cort(ex) (ical): Bone cortex or relative to the cortex	Ct
Diaphys(is) (eal): shaft between metaphyses; see text	Dp
Epiphys(is) (seal): bone extremity between articular surface and metaphysis	Ep
Endost(eal): produced by endosteal cells; not exclusively perimedullar	Es
External: outside the volume or surface of a bone or bone sample	Ex
Horizontal: relative to the horizontal plane	Hz
Internal: inside the volume or surface of a bone or bone sample	In
Inter-: between designated structures	Ir
Intersection: crossing of structures	I
Longitudinal: along the major axis of a skeletal element	Lo
Medullary: central cavity, with or without trabeculae, in long bones	Me
Metaphys(is) (eal): part of a bone between epiphysis and diaphysis	Mp
Node: branching point of structures	Nd
Periost(eum) (eal): external osteogenic membrane or bone produced by it	Ps
Radi(us) (al): parallel to radius (transverse plane)	Rd
Region of interest (ROI): selected field in tissue area	ROI
Sample: entire or fragmentary skeletal element	Sa
Section: thin or virtual slicing of sample	Se
Transverse: sectional plane orthogonal to long axis or bone surface	Tv
Vertical: orthogonal to horizontal	Vt
C. Length, Area, Number, and Density	
Area: usual meaning	Ar
Diameter: usual meaning	Dm
Length: longer dimension of a structure	Le
Number: usual meaning	N
Separation: spacing between structures	Sp
***Total*:** whole tissue and cavities in a section or a- ROI (≈ tissue)	Tt
Width: dimension of a structure orthogonal to length	Wt

Source: This table is mainly based on the nomenclature reviews by Parfitt et al. (1987) and Dempster et al. (2013)

VetBooks.ir

descriptive histomorphological parameters most commonly used in comparative studies and applicable to both recent and fossil bone samples.

Our scope will be limited to the tetrapod skeleton, describing bones according to their gross morphology, i.e., long, short, or flat bones. The dermal or endochondral origin of flat bones will be ignored because it has little specific influence on their gross inner structure; otherwise, long or short bones are generally endochondral, with few exceptions (jugal, clavicle, etc.; synthesis in Kardong 1998).

All techniques that allow a 2D or 3D imaging of calcified matrices without distortion are suited to microanatomical studies: thin sections in recent and fossil samples, stained sections of decalcified bone, scanning electron microscopy, X-ray proofs, virtual sections from computerized tomographs, and so forth (for 2D techniques, review in Recker 1983; see also Hordon et al. 2000; for 3D, see, e.g., Fejardo and Müller 2001, Ito et al. 2003, Gross et al. 2014). For best results, a researcher should know as precisely as possible the location and orientation of the anatomical samples to be analyzed and, for sections, their thickness. Considering the relatively modest definition generally required for microanatomical studies (most often a 10–20 µm of nominal resolution is sufficient), the use of computed tomography (CT scans) looks attractive, because it is nondestructive and allows considerable flexibility in the handling of sectional planes and sampled volumes (Fajardo et al. 2002; see also Baiker et al. 2012 for automatic procedures). In general, there is a good correlation between 2D and 3D analyses, i.e., between area and volumetric measurements (Hildebrand et al. 1999; Jia et al. 2010). However, for some parameters such as trabecular thickness and spacing in cancellous formations, the use of 3D micro-tomography (µCT) may give overestimated values (Chappard et al. 2005, see also Hildebrand et al. 1999). The concept of "relative resolution" (Sode et al. 2008) was developed to account for this potential bias. Instead of relying on an absolute pixel size, one should compute the ratio between the trabecular thickness (*Tb.Th*) and the pixel size, which assesses how many pixels define a trabecula at a certain location. A review of technical solutions for nondestructive skeletal imaging is given by Allen and Krohn (2014).

Gross Microanatomical Structure of Long Bones

The Outer Envelopes of Bone

At a microanatomical level, the periosteum appears as a membrane some 50 to 200 µm in total thickness, depending on the size of the bones (e.g., Fan et al. 2008; Burr and Akkus 2014). It covers continuously the diaphyseal and metaphyseal regions (Figure 4.1A, B), and is tightly attached by tough bundles of Sharpey's fibers onto the superficial cortex. Its gross structure (reviews in Allen et al. 2004; Seeman 2007) consists of two very distinct layers. The outer (most superficial) layer is mainly fibrous, with collagen and elastin fibers associated with fibroblastic cells and a rich vascular supply (Simpson 1985). It protects the inner, cellular stratum and allows the attachment of muscle tendons and ligaments. The inner, or cambial, layer is mainly composed of osteoblasts responsible for the accretion of nonmineralized bone tissue matrix, the osteoid. Cambial osteoblasts are progressively trapped in the osteoid which they secrete to become osteocytes after matrix calcification. The gross structure of the perichondrium is basically similar to that of the periosteum, with chondroblasts replacing osteoblasts. The narrow junction between the periosteum and the perichondrium comprises a zone where the metaphyseal cortex ends and where the cartilaginous cap of the epiphysis begins. In a growing long bone, this narrow zone displays a short notch, wedged between the cartilaginous and the osseous parts of the bone, the so-called Ranvier's ossification notch.

Diaphyseal Region

In most cases the diaphysis has a roughly tubular organization, with a compact peripheral cortex surrounding a medullary cavity that can either be entirely hollow, or show some sparse trabeculae. This structure is best differentiated in the middle of the diaphysis, as revealed by transverse sections sampled approximately near the pit marking the entrance of the nutrient artery into the bone (Figure 4.1C–E). On either side of this plan, toward the metaphyses, the tubular structure progressively disappears with the multiplication of bone trabeculae within the medullary cavity (Figure 4.1F–H). Although very frequent in long bones, the tubular structure is not a plesiomorphic feature in limbed vertebrates because, in the most basal stegocephalians (e.g., *Acanthostega*), the medullary cavity is always occupied by an extensive spongiosaa (Sanchez et al. 2016). It instead constitutes an architectural pattern resulting from the evolution of terrestrial locomotion by early amniotes (Sanchez et al. 2010). In fully aquatic amniotes, when the skeleton no longer maintains its basic weight-bearing, antigravitational role (as in marine reptiles and mammals), the tubular morphology changes toward either entirely cancellous, or entirely compact amedullary structures. Of course, the bones in which the diaphyseal region disappeared by dedifferentiation in relation to peculiar adaptations (e.g., limb bones of numerous secondarily aquatic tetrapods) do not display a tubular organization (Felts and Spurrell 1965; Fawcett 1942; Ricqlès and Buffrénil 2001).

The degree to which a bone is tubular, i.e., the contrast between its hollow core and its compact periphery at midshaft or in any other transverse plane, is a complex but functionally very important characteristic. It can be accurately assessed by the simple 2D analysis of a cross section with Bone Profiler (Girondot and Laurin 2003), a computer program specifically designed for this purpose (Figure 4.2A–E). This software extracts several useful compactness parameters to compute a "compactness profile". The term *compactness* (and its opposite, *porosity*) is generally used in comparative studies instead of the standard term *bone area fraction* (*B.Ar.f*) or *bone volume fraction (B.V.f)*, which is common in biomedical histomorphometric literature (Parfitt et al. 1987; Dempster et al. 2013). In a sectional plane, bone compactness, or *BC*, corresponds to the actual area occupied by mineralized bone tissue (i.e., parameter *Md.Ar* in the standardized nomenclature list by Dempster et al. 2013), expressed as a proportion of total area (parameter *T.Ar*, i.e., bone tissue + cavities) in either an entire section, or a

VetBooks.ir

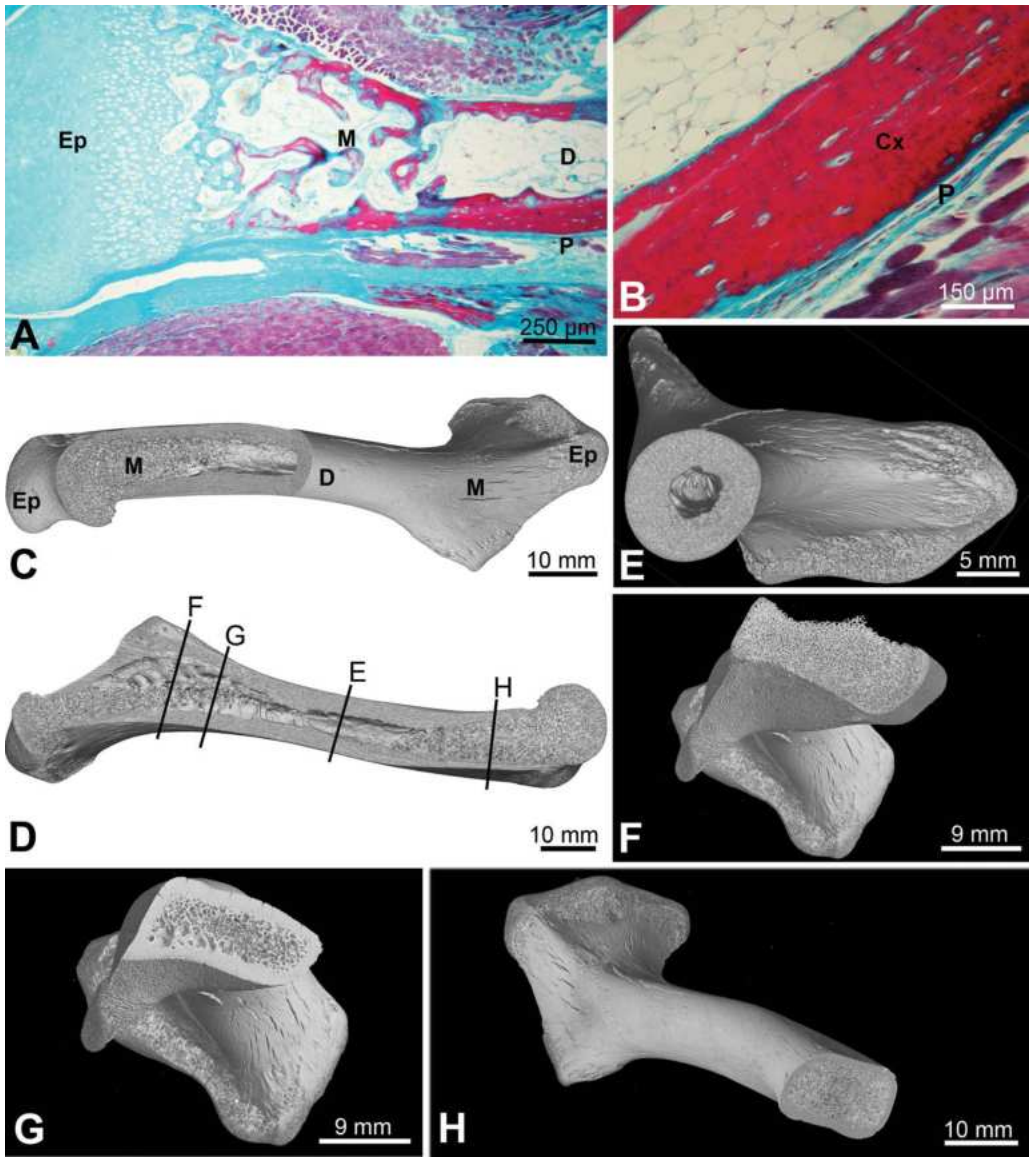


FIGURE 4.1 The periosteum and the main regions of a long bone. A, Location and general aspect of the periosteum in a lissamphibian femur (the newt *Pleurodeles waltl*). Ep, epiphysis; M, metaphysis; D, diaphysis; P, periosteum. B, Closer view of the periosteum in *P. waltl* femur. Cx, diaphyseal cortex. C, Outer and inner aspects of the three main regions of the humerus of the crocodilian *Alligator mississippiensis*, a typical long bone (CT scan 3D reconstruction). D, Inner architecture of the epiphyseal, metaphyseal, and diaphyseal regions of the alligator femur viewed in longitudinal section. The positions of the cross sections shown in E through H are indicated. E, Cross section of the tubular diaphysis. F and G, Two cross sections in the proximal metaphysis. H, Cross section in the distal metaphysis.

particular region of interest (*ROI*). In a tubular bone analyzed with Bone Profiler, compactness is calculated in 3060 cells created by the intersection of 60 sectors (6° each) and 51 concentric rings parallel to the section outline. This computer program can cope with a progressive transition, through cancellous tissue, between a compact cortex and a hollow medulla (other methods do not specifically address this problem), because it fits a sigmoid model to bone compactness along the radius of the bone section. Local measurements are then used to represent the topographical distribution of bone compactness, called the *compactness profile*, as a sigmoid (Figure 4.2B–E) with four parameters *S*, *P*, *Min*, and *Max*. *S* is the reciprocal of the slope at the curve inflection point; it is proportional to the relative width of the transition zone between the medulla and the compact cortical regions. *P* is the position of the curve inflection point on the *x*-axis; it materializes the position of the transition area between the medulla and the cortex. *Min* and *Max* are the lower and upper asymptotes, respectively; they typically (but not always) represent the minimum and maximum values of bone compactness in a section. In addition to these four variables, estimated from 51 compactness values extracted from as many concentric, roughly circular rings (in vaguely circular sections), there are radial versions of the same variables (*RS*, *RP*, *Rmin*, and *Rmax*), which are the average of 60 values of these variables, each computed from the 51 compactness values of a single 6° sector. Other parameters

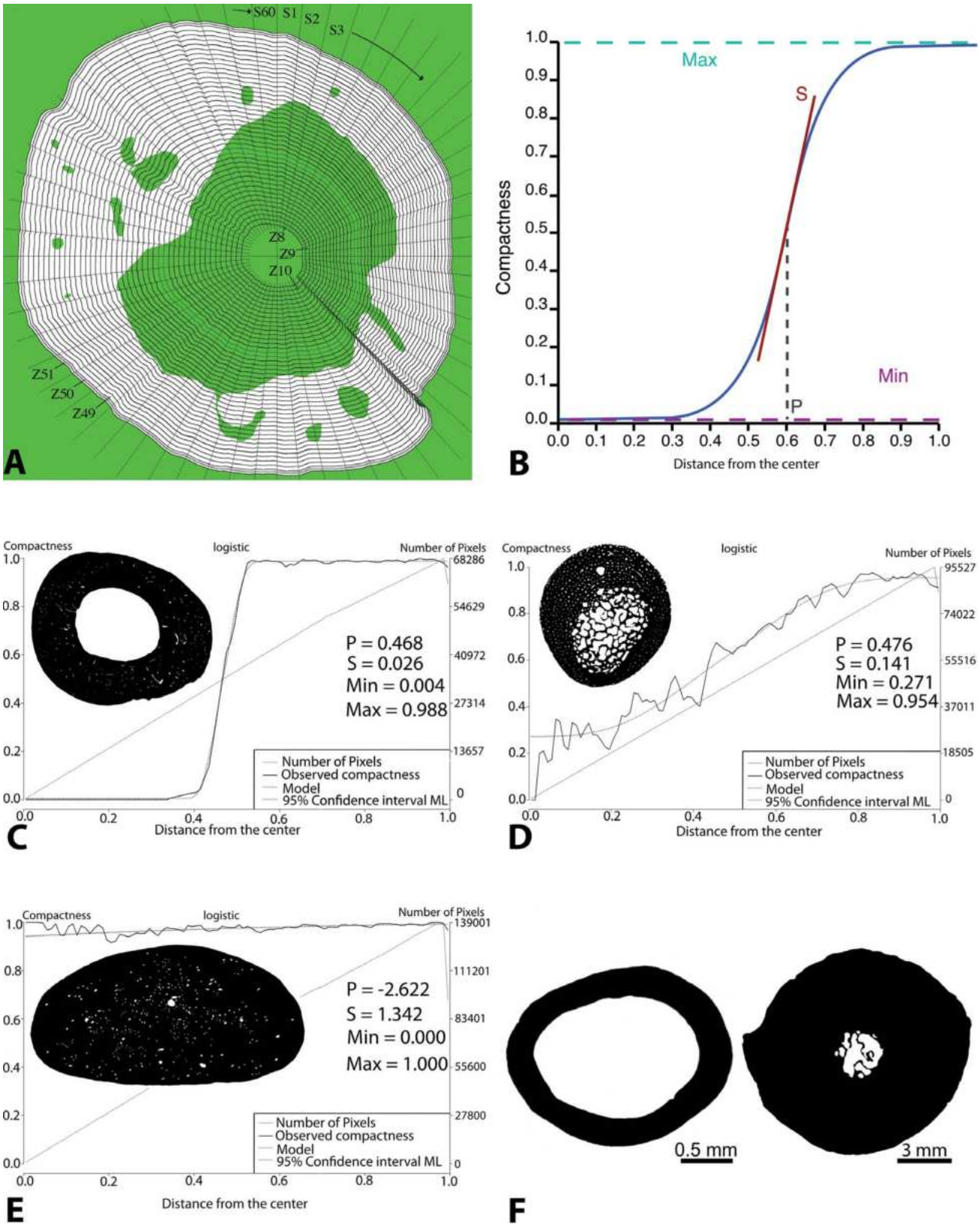


FIGURE 4.2 Basic histomorphometry of tubular diaphyses. A and B, Principles of local compactness measurements with Bone Profiler, and main structural parameters analyzed by this program. Further comments in the text. C to E, Examples of distinct compactness profiles shown by the femur of the European mink (*Mustela lutreola*), the same bone of the turtle (*Chelydra serpentina*), and the rib of the extinct dugongid *Prototherium* sp. F, Two examples of different corticodiaphyseal indices (CDI), i.e., a low CDI value (ca. 29%) in the small arboreal lemurine *Microcebus murinus*, and a high CDI value (ca. 77%) in the aquatic penguin *Aptenodytes patagonicus.*

VetBooks.ir

can also be given by Bone Profiler: *CC* (compactness at sectional center), *SC* (compactness at the periphery of the cortical region), *MC* (global compactness predicted by the model), and *Cg*, the observed global compactness (a parameter not to be confounded with *cg*, the centroid of a surface) in articles based on the use of Bone Profiler.

Another index is commonly used for the comparative study of tubular bones, the *corticodiaphyseal index* (*CDI*), also called *cortical index* (Kaur and Jit 1990; Castanet et al. 1993). This linear index does not quantify the tubular or nontubular structure of a bone; instead, it quantifies the relative thickness of its cortex. It consists of the ratio (sometimes expressed in percent) of the mean cortical thickness (*Ct.Th* in standard nomenclature), expressed as a fraction of the mean diaphyseal radius (Figure 4.2F). The *K* index proposed by Currey and Alexander (1985) (*K* = mean diameter of the medullary cavity/mean external diameter) and Bone Profiler's parameter P have a similar basic meaning to that of *CDI* (see also Sanchez et al. 2008) and equal 1 – *CDI*. At a practical level, the assessment of CDI and K was often imprecise (before Bone Profiler was introduced) when the transition zone between cortex and medulla comprises extensive cancellous tissue, or is otherwise irregular. Bone Profiler was precisely designed to cope with this situation, and automatically measures CDI through the integration of 60 sectors. Other software such as ImageJ and its plug-in BoneJ (Schneider et al. 2012) also give *CDI*, *K,* and *Cg* measurements. In intraspecific comparisons, the respective value of CDI can be a qualitative indicator of age (Kaur and Jit 1990); otherwise, it has a strong mechanical meaning for the stiffness (resistance to buckling) of a bone diaphysis (Currey 2002).

Bone mineral density (*BMD*), is frequently used in human and veterinary medicine for quantifying the local amount of osseous tissue at diverse skeletal sites. This index is given by an opacity measurement on X-ray proofs (including scanner documents) made under standard conditions (Kleerekoper and Nelson 1997). As Meunier and Boivin (1997) pointed out, *BMD* values result from both the mineralization rate of the osseous tissue, i.e., its content in hydroxyapatite per volume unit, and its compactness; therefore, the meaning of this index is ambiguous. For this reason, it is of limited interest in comparative biology and especially in paleohistology.

Metaphyses

The gross inner structure of the metaphyseal regions of long bones is strongly constrained by the process of endochondral osteogenesis (see Chapters 9 and 11); consequently, it is basically similar among taxa, except in lissamphibians and in some temnospondyls. The main causes that create some diversity in metaphyseal structure among amniotes are related both to the intensity and direction of the local mechanical involvement of the bones and to individual age. Most of the metaphyseal volume is occupied by a spongiosaa, surrounded by a compact cortex, the thickness of which gradually decreases toward the epiphyses (Figure 4.3A, B). When a crest, a strong muscular insertion, or a superficial resorption field locally exists, the spongiosa can extend up to the bone periphery, locally interrupting the continuity of the cortex (Ricqlès 1976; see also Figure 4.1F). Detailed description of metaphyseal structure, especially of its cancellous part, is commonly performed with a rich set of histomorphometric parameters briefly considered below. The morphology of individual bone trabeculae, in long bone metaphyses as in any other spongiosa, is variable and generally altered by insufficient physical activity and aging (Bergot et al. 1990; see also Castanet et al. 1993 and Chapter 32). Individual trabeculae can consist of either roughly cylindrical rods or flattened, blade-like platelets (Stauber and Müller 2006). Important differences in the mechanical behavior of these two morphological types have been shown (Arlot et al. 2008; Fields et al. 2009; Liu et al. 2009). The current use of 3D microanatomy shows that the rod-like trabeculae visible in 2D sections may not represent struts, but strong plates forming interconnected networks in the actual bone volume (Odgaard 1997; Schnapper et al. 2002). Two-dimensional descriptions are thus to be considered with some caution, and viewed as an approximation of the true architectural design that locally occurs in a skeletal element.

The inner structure of metaphyses in numerous anuran lissamphibians, as described by Haines (1942), Ricqlès (1979), Francillon (1981), and Castanet et al. (2003), diverges from the common situation of tetrapods because it has very few, or no, endosteal trabeculae and a mere tubular structure (Figure 4.3C). Moreover, in the adults of some species, the metaphyses can be separated from the epiphyses by a thin, continuous plate of bone that extends transversely across the metaphysis (in, e.g., *Uperoleia rugosa*: Francillon 1981).

The cancellous core of metaphyses is of major importance for the mechanical capacities of the bones, and its general architecture must fit the dominant trajectory of mechanical loads. This "trajectorial theory" is the basis of Wolff's Law (1892; see also Currey 2002; Pontzer et al. 2006), later enriched by Murray (1936) to integrate developmental constraints as an accessory factor influencing trabecular architecture. This structural accommodation is operated by repeated processes of trabecular erosion and reconstruction, called *adaptive remodeling*. As a result, the general trabecular orientation in long bone metaphyses is nonrandom and highly polarized (structural *anisotropy*), at least in the planes parallel to load direction, thus creating the so-called *trabecular bone* (Figure 4.3D, E). In the planes orthogonal to this direction (these planes represent sections perpendicular to the bone major axis), metaphyseal spongiosae often display a rough honeycomb (isotropic) architecture (Figure 4.3F).

The histomorphometric description of cancellous bone is of prime importance in the metaphyseal region because of the functional involvement of this region in long bones. Parameters and indices used in this purpose can be derived from either 2D measurements (from ground sections or virtual tomographic slices), or from 3D CT-scan reconstructions. The respective advantages and limitations of these approaches have been exposed and discussed in several publications (e.g., Hildebrand et al. 1999; Ito et al. 2003). Most of the current histomorphometric parameters exist in 2D or 3D versions; the former refers to area (suffix *Ar* in current histomorphometric nomenclature, e.g., *Tb.Ar* for trabecular area), and the latter to volume (suffix *Vol*, or simply *V*: Dempster et al. 2013; Allen and Krohn 2014). Two-dimensional studies, however, are strongly dependent on

VetBooks.ir

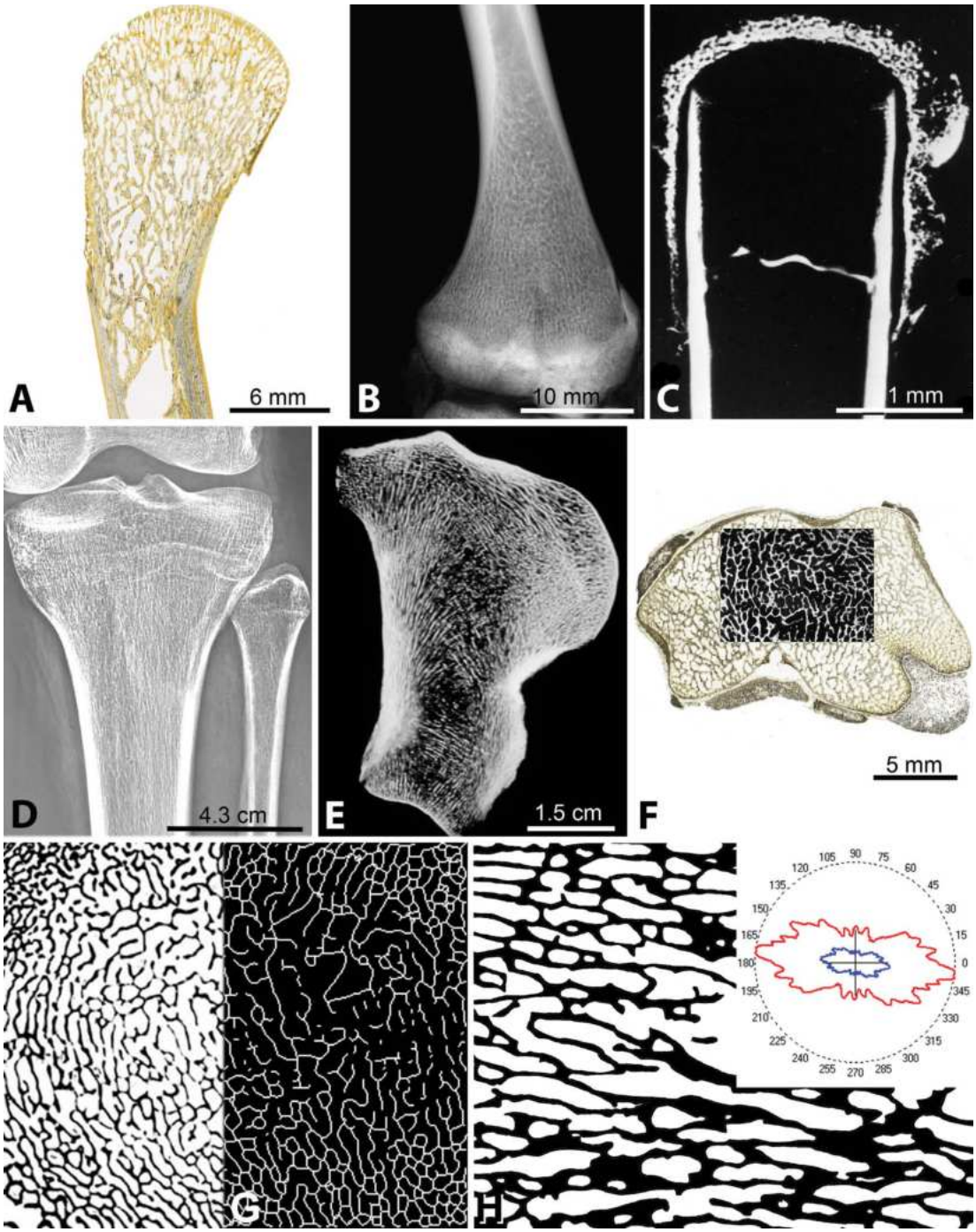


FIGURE 4.3 Microanatomical features of metaphyseal regions. A, Longitudinal section in the metaphysis and epiphysis of a juvenile spectacled caiman (*Caiman crocodilus*), a form having "primitive" epiphyses. B, X-ray proof of the distal metaphysis and epiphysis of the tibia in the Nile monitor lizard (*Varanus niloticus*), a taxon that has secondary ossification centers. C, Microradiograph of a longitudinal section in the proximal metaphysis and epiphysis of the femur of the anuran *Chiromantis xerampelina* (Courtesy of H. Francillon-Vieillot.) D and E, X-ray proofs showing the polarized, adaptive architecture of the "trabecular bone" in the proximal metaphysis of a human tibia and the humerus of a dolphin *Delphinus delphis*. F, Cross section in the distal metaphysis of a Nile monitor femur. In this sectional plane, the spongiosa has an isotropic, honey-comb-like architecture. The black area shows a region of interest (ROI) in which compactness and trabecular parameters can be measured. G, Skeletonization under ImageJ (right half of the field) of the trabecular network in a ROI from a cross section in the *Delphinus delphis* humerus. ROI size: ca. 20 × 15 mm. H, Analysis of trabecular polarization in the humeral metaphysis of a grey seal (*Halichoerus grypus*) with the computer program MPSAK v.2.9 (National Museum "L. Pigorini", Rome, Italy.) With a value of 0.406, parameter *Pol* (i.e., structural polarization) is relatively high. ROI dimensions: ca. 16 × 12 mm.

VetBooks.ir

the orientation of bone trabeculae compared with the sectional plane (whatever the orientation of this plane), a geometrical constraint that can heavily bias area measurements. Three-dimensional studies are free of this constraint, and likely to reflect with limited bias actual trabecular volume and architecture. In paleohistology, 2D measurements are generally used because the recourse to 3D tomographic reconstructions in fossils is much more problematic and time-consuming than in recent bones, due to the filling of intraosseous cavities by highly mineralized matrix (but see recent developments that are able to cope with this problem in Dunmore et al. 2018). The measurement of *trabecular area fraction*, or *Tb.Ar.f* (*Tb.Vol.f* in 3D studies), describing the relative amount of cancellous tissue in an ROI, is the most commonly used index. Its calculation requires two descriptive parameters: total trabecular area, *Tb.Ar* (*Tb.Vol* in 3D) and total tissue area, *T.Ar* (*T.Vol* in 3D): $Tb.Ar.f = 100 Tb.Ar/T.Ar$ (Figure 4.3F). Several other basic parameters and indices, specific to cancellous bone tissue and well suited to comparative studies, are of special interest and can be obtained by simple, direct measurements on 2D documents (the same can be obtained in 3D).

1. Total length of trabecular network (Dumont et al. 2013), equivalent to Mellish et al.'s (2009) *total strut length*. This parameter can be measured under ImageJ after previous skeletonization of a binary image (Figure 4.3G), a process that reduces bone trabeculae to their central axis on a thickness of one pixel. The length of the trabecular network is that of this "skeleton" (moreover, dividing *T.Ar* by this parameter gives a mean estimation of trabecular width).
2. Trabecular connectivity, or *N.Nd*, that corresponds to the number of nodes in the trabecular network. This parameter reflects the number of junctions between bone trabeculae in the virtual "skeletonized" trabecular network. A trabecular junction is then defined as a pixel having more than two contacts with neighboring ones (Mellish et al. 2009).
3. Mean trabecular orientation. and structural polarization of the trabecular network, i.e., parameters α and *Pol*, respectively (Dumont et al. 2013). These two complementary parameters are of great interest for the morphofunctional interpretation of spongy bone tissue. Parameter α expresses the angular deviation (in degrees) of trabecular orientation compared to a horizontal reference axis (after proper orientation of the bone section). Parameter *Pol* (a number ranging from 0 to 0.5) gives the standard deviation of trabecular orientation when measured according to a grid rotating over 180° (Figure 4.3H). Low *Pol* values indicate a random variation of trabecular orientation (e.g., dominant orthogonal intersections), whereas high values indicate steep orientation differences and a high structural polarity. *Pol* values thus reflect the isotropic or anisotropic structure of cancellous bone. Fundamentals of this approach, commonly called line fraction deviation (LFD), are exposed in Geraets (1998) and Geraets et al. (2008).

Epiphyses

Unlike diaphyseal and metaphyseal regions, which are normally composed of bone tissue only (some exceptions exist in neotenic tetrapods and aquatic amniotes), epiphyseal regions may contain three distinct tissues: bone, in the form of trabecular networks enclosed in a thin cortex and forming intraepiphyseal (secondary) ossification centers; calcified cartilage; and nonmineralized cartilage. In adult amniotes, when somatic growth is finished or has dropped to a residual level, epiphyses consist of a layer (0.2 to 6 mm in humans) of non-calcified hyaline cartilage, the articular cartilage, covering a stratum of calcified cartilage of variable thickness that rests on the first metaphyseal trabeculae (Figure 4.4A). The histological features of these tissues are described specifically in chapter 7. Both are often separated by a thin but strongly mineralized layer of a tissue that might be akin to bone and result from a metaplastic process, i.e., a direct transformation of cartilage matrix into bone matrix (Haines 1975; Haines and Mohuiddin 1968; Ricqlès 1975; see also Krstić 1985 and Chapter 12). Epiphyseal surfaces of fossil bones often consist of this peculiar tissue (Ricqlès 1972). In young, actively growing specimens, epiphyseal surfaces of dry or fossil bones merely consist of a layer of calcified cartilage (Figure 4.4B).

During early growth stages in all amniote taxa, long bone epiphyses are composed of a thick cap of hyaline cartilage, limited toward the metaphysis by the so-called "growth plate", responsible for the growth in length of the bones, and further described below (see Chapter 9). The growth plate constitutes the primary center of ossification. In later growth stages, two main types of epiphyses (with some variations in both cases) distinguish mammals and most squamates from all other tetrapods (reviews in Haines 1938, 1942, 1969; see also Ricqlès 1979).

In the former group, epiphyses are characterized by the development, in the core of the hyaline cartilage cap, of a secondary ossification center through osteogenic processes similar to those of the primary center (Figure 4.4C). A network of bone trabeculae comparable to that of the metaphysis, but with distinct (and variable) architecture and compactness (see, e.g., Haines 1975), is thus created. By the end of somatic growth, the secondary center nearly occupies the whole volume of the epiphysis (Figure 4.4D) and fuses with the metaphyseal spongiosa, thus provoking the disappearance of the growth plate (Figure 4.4E). Growth then becomes impossible (Haines 1941, 1969, 1975). At this stage, the epiphyseal region acquires the adult structure described above. A faint hypercalcified line may occasionally remain (this feature is highly variable) at the level where the former growth plate was (Figures 4.3D, 4.4A). The chronology of epiphyseal fusion can be variable among the bones of a single skeleton (Maisano 2002) and, in the adults of some taxa (e.g., the large varanids studied by Buffrénil et al. 2004 and Frydlova et al. 2017), it does not occur within the limits of individual longevity. Some bones have only one intraepiphyseal center of ossification, located in either the proximal or the distal epiphysis. Such is the case, for example, of the phalanges in the juveniles of numerous mammalian species, including *Homo sapiens* (Wong and Carter 1990).

VetBooks.ir

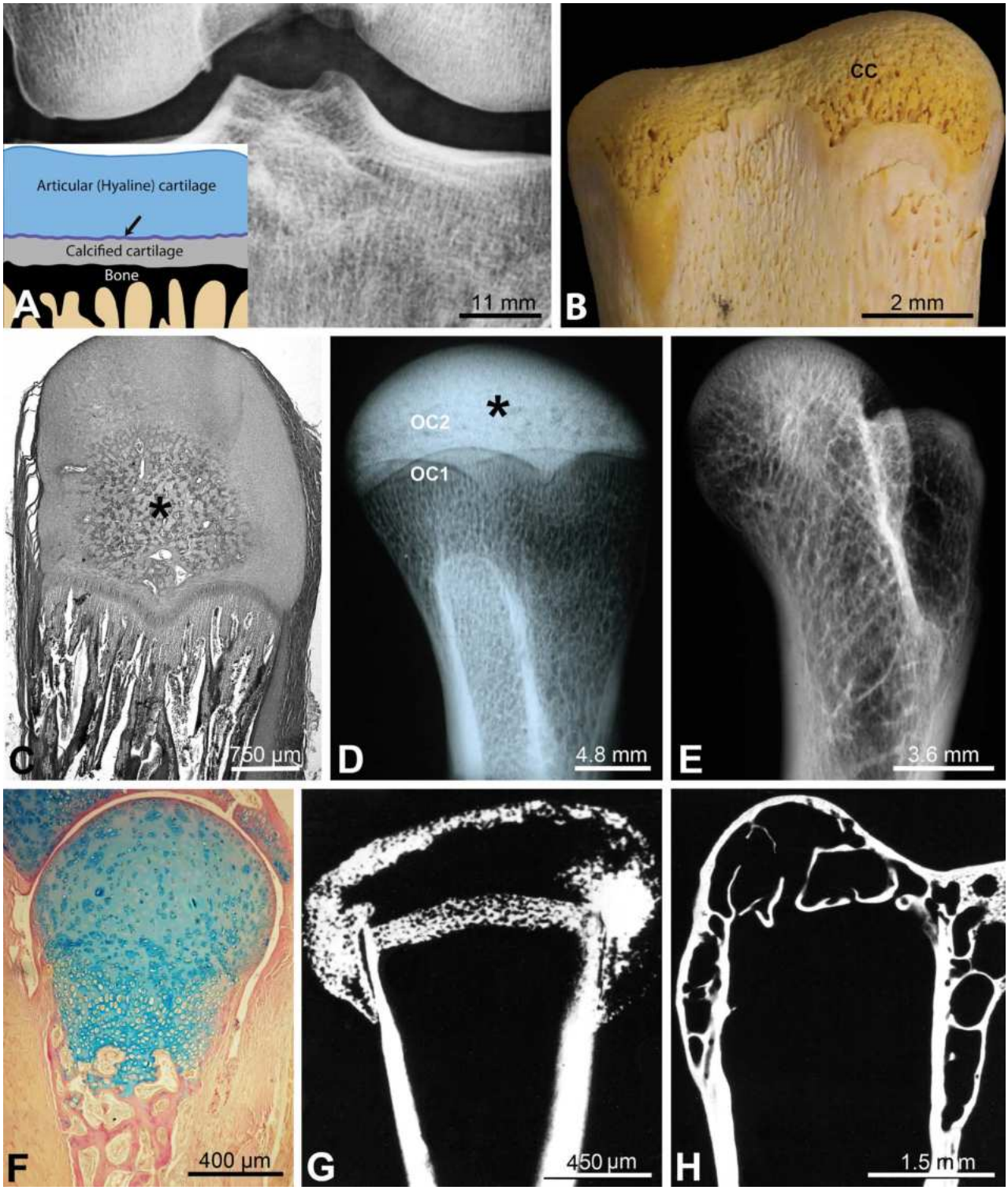


FIGURE 4.4 Structural features of the epiphyses. A, Tissues forming the epiphyseal surface in the long bone of an adult tetrapod (X-ray proof of the knee articulation of a human). The inset shows the four main tissues present at the epiphyseal surface. The arrow points to the so-called "blue line", a metaplastic tissue between hyaline and calcified cartilages. B, Aspect of the epiphyseal surface of a dry bone in a juvenile (fast-growing) spectacled caiman. When articular cartilage is removed, the epiphyseal surface is composed of calcified cartilage (CC). C, General epiphyseal structure in a tetrapod having secondary ossification centers. In this femur from a juvenile Nile monitor lizard, the secondary ossification center (asterisk) is developing within the mass of hyaline cartilage. D, Fully developed (but still unfused) secondary ossification center (OC2; asterisk) in the femur of an adult Nile monitor (X-ray proof). E, Aspect of an epiphysis when primary and secondary ossification centers have fused, and growth plate has disappeared. Femur of a small monitor lizard, *Varanus glebopalma*. F, Primitive epiphysis in an actively growing newt, *Pleurodeles waltl*. G, Calcification of epiphyseal cartilage in the anuran *Uperoleia rugosa* (X-ray proof). H, Development of osseous trabeculae in the femoral epiphysis of the anuran *Mixophyes fasciolatus* (G and H: Courtesy of H. Francillon-Vieillot)

VetBooks.ir

The situation is simpler in the latter group, comprising numerous extant and extinct taxa: all amphibians, archosaurs, chelonians, sauropterygians, early synapsids, and so forth (Haines 1942; Ricqlès 1979). Epiphyses of juvenile, actively growing (supposed so in fossils) specimens are indeed similar to those of adults, but with proportionally much thicker layers of calcified and noncalcified cartilages. According to Haines (1938, 1969; see also Ricqlès 1972; Rimblot-Baly et al. 1995), this relatively simple type of epiphyses should be considered "primitive" (i.e., plesiomorphic) among tetrapods, and is otherwise close to the epiphyseal type generally encountered in finned osteichthyans. All other epiphyseal structures, including the highly derived forms in some nonamniote taxa, are supposed to arise from it (Haines 1942).

Among extant nonamniotic tetrapods, the Caudata (urodeles) have epiphyses (Figure 4.4F) corresponding basically to the primitive type (Castanet et al. 2003). Available data for basal tetrapods suggest that temnospondyls, seymouriamorphs, and so forth shared the same type of epiphyses (Sanchez et al. 2008; Castanet et al. 2003). Conversely, the anurans have a distinct epiphyseal organization, commonly designated as "match-head" (Figure 4.4G). Some variation exists in this peculiar morphology, but its general characteristics can be summarized as follows (see Haines 1942; Ricqlès 1972; Francillon 1981; Castanet et al. 2003 for reviews). In juvenile specimens, both extremities of long bones are capped by a subspherical, solid formation of noncalcified cartilage in which the metaphyses penetrate deeply. A part of the cartilage enters the metaphysis cavity, initially devoid of bone trabeculae, and forms a cork-like plug. The basal part of this cartilaginous plug is structured as a normal growth plate, with a deep layer of calcified cartilage that undergoes erosion, to be replaced by sparse osseous trabeculae. By the end of growth and in the adults of some taxa, such trabeculae may extend to most of the volume of the epiphyseal cap and fuse with the outer, peripheral surface of the metaphysis (Figure 4.4H). The nonmineralized parts of the epiphysis are then limited to a thin peripheral hyaline layer. Conversely, in other taxa, the cartilaginous cap does not mineralize (a rich set of comparative data can be found in Francillon 1981). In anurans, the osseous trabeculae (when present) colonizing the epiphyseal cap do not show any definite or polarized geometrical orientation, regardless of the extent of trabecular formations.

Microanatomy of Short Bones

The inner structure of short bones is prone to great variation, consistent with their morphological diversity. Some of them are roughly similar to long bones but, of course, without a well-differentiated diaphyseal region. A typical example of this structure is given by vertebral centra, as well as metapodials and phalanges in some taxa. Others such as carpals and tarsals have a more complex structure, with a variable number of articular surfaces and an irregular, convoluted morphology (e.g., Galateanu et al. 2013; Candela et al. 2017).

The inner organization of short bones that have a proximal and a distal epiphysis requires few specific comments: it is comparable to that of long bones less, of course, the presence of a tubular diaphysis with an open medullary cavity. Such bones thus consist of two symmetrical units, each comprising a functional epiphysis (that may have a secondary ossification center or not) and a metaphyseal part (Figure 4.5A). These two units face each other in a transverse plane often located approximately in the middle of the bone (but this location is variable; see Chapter 9), where the process of ossification began. Endosteoendochondral spongiosae as well as periosteal cortices regularly occur in this kind of bone. In vertebral centra, this basic structure is clearly visible in juveniles, but it is generally blurred in adults by remodeling. It may nevertheless remain, even in late ontogenetic stages, in various aquatic tetrapods (Figure 4.5B) in which bone turnover is reduced or inhibited, a situation commonly encountered in nothosaurs and placodonts (see Chapters 21 and 22), champsosaurs (Buffrénil et al. 1990), Cenomanian marine squamates (Buffrénil et al. 2008a; Houssaye et al. 2008), and so forth.

Short bones with complex morphologies (they can be cuboid, lenticular, trapezoidal, etc.) display a juvenile structure reminiscent of the epiphyses in which a secondary ossification center develops: cartilage replacement by bone trabeculae starts in the core of the cartilaginous anlagen of the bone and spreads centrifugally in all directions up to occupy most of the bone volume (examples in Gardner 1971; McLaughlin and Doige 1982; Stafford and Thorington 1998; and Shapiro 2002), while new cartilage is added by both interstitial growth and subperichondral accretion (Krstić 1985; Fawcett and Jensh 1997; see also Francillon-Vieillot et al. 1990). A limited contribution of subperiosteal accretion occurs in some bones such as the calcaneum (Fritsch et al. 1996). The ossification process in carpals and tarsals is delayed compared to neighboring long bones, and it does not occur at all in some neotenic newts (Cabrera-Téllez et al. 2010). In adult individuals, all short bones, whether autopodial or vertebral, display a similar microanatomical structure (Figure 4.5A–G), and most of the bone volume is occupied by a spongiosa surrounded by a relatively thin compact cortex (e.g., Sinha 1985). Cortices gradually merge with the spongiosa occupying the core region (a case of compact bone made cancellous); the latter thus includes trabeculae from either a periosteal or an endosteoendochondral origin.

Most research on short bone structure deals with the human spine and, to a lesser extent, carpal and tarsal bones. Unfortunately, precise comparative data are relatively few. The studies by Dumont et al. (2013) and Houssaye et al. (2014) of vertebral centra in broad samples of mammal species revealed considerable differences between taxa, involving not only bone compactness at global and local scales, but the proportion of the periosteal and endochondral components of the centra, the length and width of the trabeculae, the relative spatial density of trabecular intercepts, and so forth. Moreover, a significant influence of specific body size was shown: vertebral centra in small species have low compactness values (Figure 4.5E), thin periosteal cortices, and few trabeculae. Conversely, large species display considerable extents of trabecular networks (Figure 4.5D, F, G). The orientation of bone trabeculae and the degree of isotropy in spongiosae are also highly variable in mammals (even among taxa sharing close phylogenetic relationships and similar adaptations), squamates (Buffrénil and Rage 1993; Houssaye et al. 2010), and

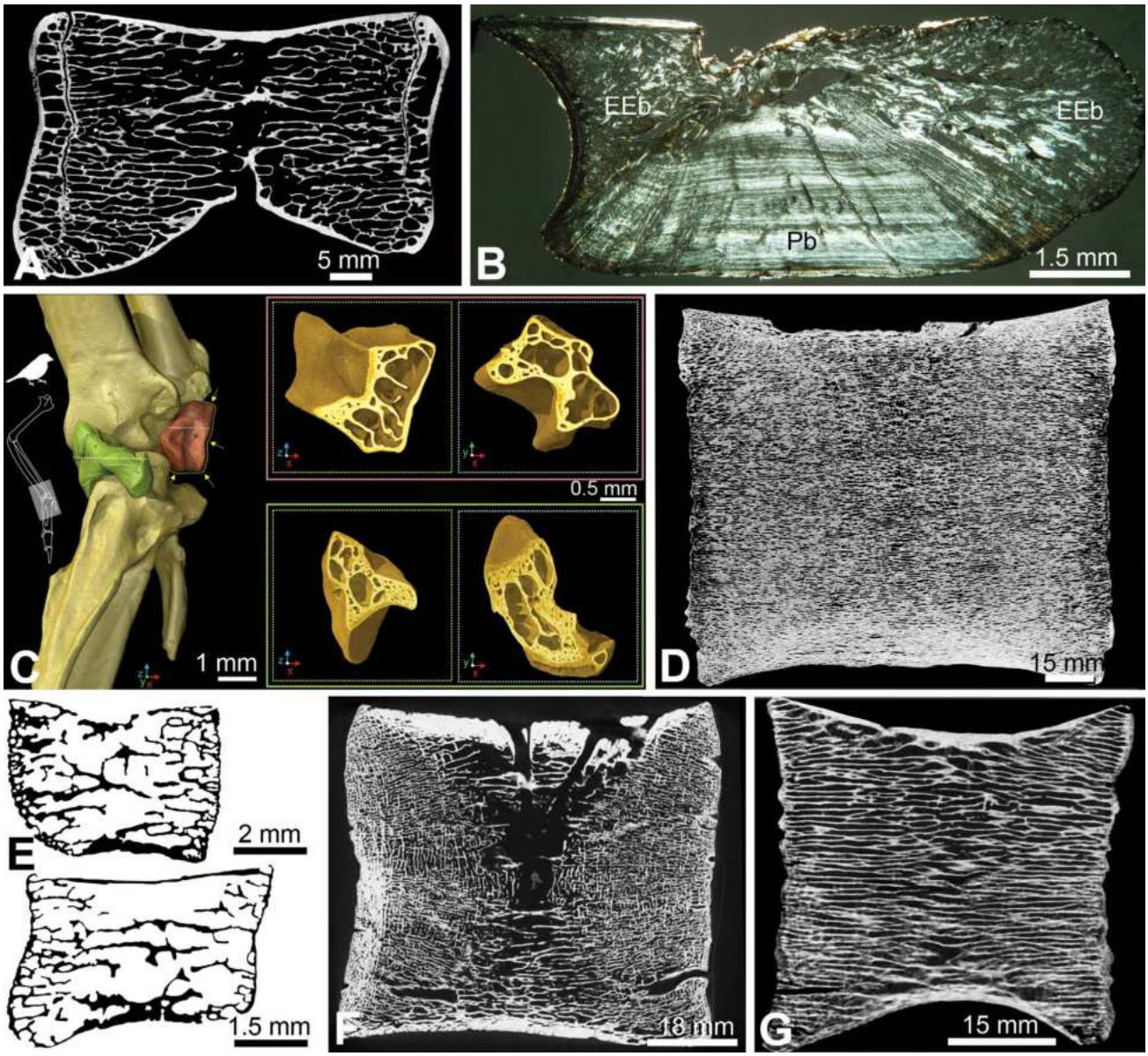


FIGURE 4.5 Microanatomy of short bones. A, Longitudinal sagittal virtual section (CT scan) in a lumbar vertebra of a juvenile seal *Pagophilus groenlandicus*. The two secondary ossification centers are not yet fused. B, Osteosclerotic vertebral centrum of the Cenomanian marine squamate *Simoliophis rechebrunei* in sagittal section. The endosteoendochondral (EEb) and the periosteal (Pb) regions remain clearly visible due to remodeling inhibition. C Structure of short autopodial bones in a passerine bird. D, Extreme density of the trabecular network in a vertebra of a juvenile from a very large mammal, the whale *Balaenoptera* sp. (virtual section from CT scan). E, Sparse trabeculae in the vertebral centra of the small mammals *Erynaceus europeus* (the hedgehog; above), and *Didelphis virginiana* (the opossum; below). F, Orthogonal intersection of bone trabeculae in the centrum of a sirenian, *Dugong dugon* (virtual section from CT scan). H, Subparallel and sagittally oriented trabeculae in the centrum of a dorsal vertebra from the Irrawaddy dolphin, *Orcella brevirostris* (virtual section from CT scan).

among a large sample of diverse basal tetrapods and amniotes from Paleozoic and Mesozoic faunas (Danto et al. 2016). Although some peculiar patterns occur only in certain taxa, as exemplified by the orthogonal intersection of trabeculae frequently observed in primates (including humans) and sirenians (Figure 4.5F), and the dominant sagittal trabecular orientation (Figure 4.5G) displayed by some cetaceans (Buck et al. 2002; Dumont et al. 2013), available data remain insufficient to ascertain clear tendencies. In human vertebral centra, several studies have pointed out contrasting mechanical involvement of the trabeculae according to their individual orientation (Fields et al. 2011) and morphology (plates vs. rods: Liu et al. 2009). In autopodial bones, trabecular structure has been shown to display substantial diversity, and a poor functional signal in the wrist of primates (Schilling et al. 2014) and some human tarsals (Sinha 1985). Conversely, the compliance of trabecular architecture with Wolff's law was shown in the calcaneum of several species, including e.g., *Potorous tridactylus*, a small marsupial (Biewener et al. 1996) and the mule deer, *Odocoileus hemionus* (Skedros et al. 2004), in addition

to humans (Jhamaria et al. 1983). In limb bones without a differentiated diaphysis such as the cetacean humerus (Felts and Spurrell 1965) and radius (Felts and Spurrell 1966), trabecular orientation may be elaborate and similar to that observed in the metaphyseal regions of typical long bones (see, e.g., Fig. 4.3E). As elsewhere in the skeleton, aging strongly affects the volume and continuity of trabecular networks in short bones (e.g., Bergot et al. 1988; Krause et al. 2013).

Gross Microanatomy of Flat Bones

Flat bones share a similar inner structure whatever the origin of the mesenchymal cells from which they derive (ectodermal mesenchyme vs. mesodermal mesenchyme). Intradermal osseous plates, the osteoderms, produced by a metaplastic process (i.e., a direct, local transformation of dermal tissue into bone), at least in the initial stage of their formation (review in Vickaryous and Sire 2009; see also Zylberberg and Castanet 1985), also share the same basic structure. All these bones are organized as diploes, which basically consist of a cancellous core of variable compactness, framed in lateral and in medial positions by compact cortical layers of periosteal origin (Francillon-Vieillot et al. 1990; Scheyer and Sanchez-Villagra 2007; see also Figure 4.6A–C). In medical and anthropological articles, the term "diploe" has a more restrictive meaning: it is used to designate exclusively the cancellous core of flat bones, especially in the cranial vault (e.g., Balzeau 2013; Copes et al. 2018). This terminological discrepancy between biomedical and comparative literature is to be kept in mind. Moreover, the convenient terms "outer" and "inner" are frequently used (e.g., Boruah et al. 2015) for naming the lateral and medial cortices of a diploe (*sensu* Francillon-Vieillot et al. 1990).

Conspicuous differences in the relative thickness of the cortices, or the extent and compactness of the central spongiosa, exist between taxa for homologous bones, and between juveniles and adults of the same taxon: in some bones, the core spongiosa is extensive and loose, while in others it is nearly compact (see, e.g., Amson et al. 2018 for quantitative data). Moreover, flat bones most often display a morphological asymmetry, with a convex lateral (i.e., "outer") surface and a concave medial (i.e., "inner") surface (Figure 4.6B). The lateral cortex (in superficial position) can be thicker than the medial (deep position) one (Boruah et al. 2015).

Two kinds of flat bone exist: bones firmly articulated to their neighbors by sutures to form integrated anatomical structures (e.g., the bones of the face and skull roof, or the plates of a turtle carapace), and individual nonrigidly articulated flat bones with free edges such as the scapula. In the first category, the two periosteal cortices are subparallel and not in continuity (Figure 4.6A, B). At the periphery of the bone, they are separated by the osseous tissue produced by the sutures. Sutural bone displays microanatomical patterns (and histological characteristics as well) distinct from the periosteal layers (Figure 4.6D and E); in particular, it is deeply indented in vertical and horizontal planes (e.g., Khonsari et al. 2012). Converging data show that the main factors controlling the geometric pattern of cranial and facial sutures are related to local mechanical strains (Renzuli-Jaslow 1990; Herring and Mucci 1991; Rafferty and Herring 1999; Sun et al. 2004). In the second category of flat bones, the periosteal cortex is continuous around the bone. Frequently, a single bone can

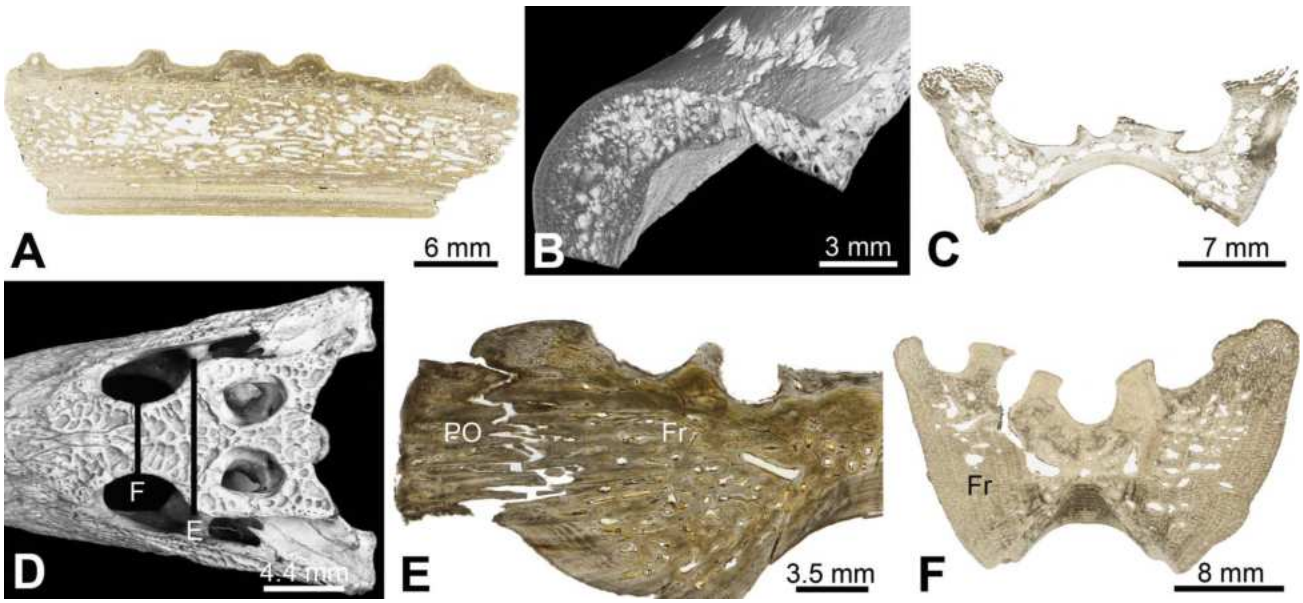


FIGURE 4.6 Flat bone microanatomy. A, Typical flat bone in the carapace of the turtle *Trionyx triunguis*. The "diploe" structure of this bone comprises two compact cortices framing a broad cancellous core. B, Similar structure in the cranial vault of the xenarthran *Dasypus* sp. C, Frontal of a juvenile alligator. The initial architecture of the bone is that of a typical flat bone. D, Outer view of the rear part of the skull of an adult Nile crocodile (*C. niloticus*). The two transverse segments localize the sections shown, respectively, in parts E and F. E, Complex, indented microanatomical aspect of the bone deposited by sutures Rear part of the frontal of an adult *Diplocynodon ratelii* (extinct alligatorid). At this growth stage, the bone displays a high compactness. F, Structure of the frontal in a zone (interorbital part) devoid of sutures.

VetBooks.ir

correspond to both situations, depending on the orientation of sectional planes, as exemplified by the crocodile frontal bone shown in Figure 4.6D and F: it is limited by sutures anteriorly and posteriorly, but has free lateral (interorbital) edges.

Flat bones of ectomesenchymal origin (*membrane* or *dermal* bones) grow by simple periosteal (growth in thickness) and sutural (growth in width) accretion, combined with relevant remodeling. The organization of sutures was described in detail and illustrated by Pritchard et al. (1956). In brief, at a microanatomical level, neighboring bones are covered and maintained in place by the outermost fibrous layer of the periosteum. The sutures are mere symmetrical *diverticula* of the periosteum and consist, on each of their sides, of a cambial (cellular and osteogenic) layer covered by a fibrous layer. A loose conjunctive formation is wedged between the two symmetrical fibrous layers. Dermal flat bones display roughly comparable microanatomical characteristics in juvenile, actively growing individuals and in adults; however, the typical indented aspect of sutural bone tissue tends to be erased in adults by the intense remodeling of the central spongiosa that accompanies the peripheral expansion of the bones (review in Opperman 2000).

In relation to the current practice of iliac crest biopsies, the histomorphometric techniques applied to flat bones became extremely sophisticated. In comparative bone histology and paleohistology, the parameters and indices presented above about the cancellous tissue of long bone metaphyses are generally sufficient for the analysis of diploe-like flat bones.

Remarks on Some Basic Concepts Used in Microanatomical Descriptions

Some of the most common terms used in microanatomical descriptions of bones (including the descriptions made just above) are often associated in couples of opposite concepts, which suggest that the structures to which they refer are sharply distinct and mutually exclusive. Such is particularly the case for the notions of cortex versus medulla, cancellous versus compact bone, and tubular versus diploe architectures. As Francillon-Vieillot et al. (1990) mentioned, the reality of microanatomical observations suggests that the actual differences between the structures designated by these terms is less clear-cut and more gradual.

Cortex versus Medulla

In long bones of the limbs, periosteal cortices, whatever the morphology of the skeletal element to which they belong, are generally considered to be made of compact bone tissue. Conversely, the medulla is viewed as a central hollow region that can be either free of osseous trabeculae or occupied by a loose spongiosa initially formed, in endochondral bones, by endosteoendochondral ossification. This structure is indeed frequent, but by no means a mandatory or "normal" state for all tetrapods; rather, it reflects an adaptation to terrestrial locomotion (including flying and digging). Long bones in several extant or extinct tetrapod lineages readapted to life in water can have, in physiological conditions, a cancellous cortex, as exemplified by cetaceans, ichthyosaurs, marine turtles, and so forth, or a strongly compact medulla, as observed in sirenians, some marine birds and reptiles, and so forth (Ricqlès and Buffrénil 2001; see, e.g., Figure 4.2E and Chapter 35). Likewise, the bone trabeculae located in the cancellous core of the bones (a region commonly considered medullary) can often be of periosteal origin and result from local resorption (followed or not by superficial reconstruction) of deep cortical layers (Ricqlès 1975). This situation is very common, although the initial origin of the trabeculae can be partly or entirely masked by the active remodeling process that develops during growth and aging. Therefore, the terms *cortex* and *medulla* do not necessarily refer to definite structural characteristics, or to sharply distinct formation processes; in numerous instances, they represent mere topographic concepts that may retain some subjectivity when used in the description of a bone section, especially when the transition from cortex to medulla is progressive.

Compact versus Cancellous Bone

The concepts of compact bone and cancellous bone also call for some comments. Bone compactness has no close relationship with the histological structure of an osseous formation and by no means contributes to define it (Ricqlès 1975). A single bone deposit may present, during its maturation process, a cancellous stage, followed by a compact stage. Such is the case, for example, of the so-called *woven-parallel complexes,* which are initially deposited as a trabecular scaffolding (the so-called fine cancellous bone) that is later compacted by intertrabecular deposits (examples in Castanet et al. 2000; Margerie et al. 2004; Cubo et al. 2012). Conversely, as mentioned above, compact bone can be made cancellous through local, patchy resorption processes; and it is even possible that, due to the filling of intertrabecular spaces by subsequent secondary deposits, this tissue turns again to compact bone (compacted spongiosa). Such complex morphogenetic processes (described in more detail in Chapter 9) occur in, for example, the metaphyseal regions of most long bones (Enlow 1963). In the developmental course of a bone, the cancellous or compact structure that it may present at a local scale is often a transitory characteristic, related to the immediate context of its growth, not a permanent feature that would define it.

Tubular versus Diploe

The distinction between tubular and diploe structures (the term diploe is used here in the sense of Francillon-Vieillot et al. 1990) is clear-cut and unambiguous only when extreme cases are compared, for example a flat bone from the skull roof versus the diaphysis of a long bone from a terrestrial amniote. Numerous intermediate situations exist in which a more or less clearly characterized diploe structure can result locally from the lateral expansion or morphological flattening of an otherwise tubular bone. Such is typically the case of the distal part of ribs in many mammalian taxa (e.g., artiodactyls, proboscideans, etc.) and long bone regions where strong crests develop. Osteoderms also offer a rich demonstration of the diploe pattern (Scheyer and Sander 2004; Buffrénil et al. 2015, 2016).

VetBooks.ir

Qualitative Classification of Cancellous Bone

Cancellous bone formations have been classified into *fine cancellous* or *coarse cancellous* (Ricqlès 1975; Enlow 1975, review in Francillon-Vieillot et al. 1990). Though apparently referring to the textural compactness of the spongiosa, a feature roughly equivalent to several comparable parameters such as *trabecular bone volume* or *bone area fraction*, these expressions have a distinct meaning, loosely related to mere compactness features. According to the definitions recalled by Ricqlès 1975, the expression *fine cancellous* tissue designates the scaffolding of woven-fibered bone typical of the woven-parallel (i.e., fibrolamellar) complexes before the centripetal accretion of primary osteons (for further details, see Chapter 8). Conversely, *coarse cancellous* tissue designates the ordinary spongiosa found in metaphyseal regions and around the medullary cavity of diaphyses. Therefore, the main difference between fine and coarse cancellous tissues refers to their respective origins, periosteal for the former, and generally endosteal for the latter, more than to their textural aspects. In addition, within the coarse cancellous type of spongiosa, the expression *trabecular bone* refers to a distinct architectural pattern: the occurrence of a clearly polarized orientation of the trabeculae, in compliance with the (measured or theoretical) trajectory of dominant mechanical stress within the bone.

An Overview of Vascular Canals in Bone

General Characteristics of Cortical Vascularization

During life, bone tissue is vascularized by blood capillaries (arterial and venous) of variable diameter, and houses nerve fibers (reviews in Brookes 1971; Rhinelander 1972; Singh et al. 1991; Brandi and Collin-Osdoby 2006). In comparative skeletal histology (a research field often using dry collection skeletons) and, *a fortiori*, in paleohistology, blood vessels themselves are seldom preserved; therefore, the notion of bone vascularization, as well as the studies conducted on this character, generally refer to the occurrence of intracortical networks of tunnels (Figure 4.7A), the vascular canals, in which the capillaries and neural fibers were once housed (Francillon-Vieillot et al. 1990). Of course, blood vessels also exist in the medulla and the intertrabecular spaces of cancellous formations (Iwaku 1989; Singh et al. 1991; Saint-Georges and Miller 1992), but they leave no trace in the calcified osseous matrix. A review of bone vasculature (blood vessels proper) was recently presented by Chen et al. (2020). Preservation of blood vessels, and even blood cells, in Cretaceous fossils has been mentioned in some publications (Martill and Unwin 1997; Pawlicki and Nowogrodska-Zagorska 1998; Schweitzer and Horner 1999), but this situation is very exceptional. The relationship between capillary diameter and canal diameter is extremely loose and variable (see, e.g., Clarac et al. 2017) and no reliable estimation of the first parameter can be made from the second (see Figure 4.7B).

Bone vascularization in long bones is an important character in comparative skeletal biology, not only for its contribution to cortical porosity; but also for its use in the classification of bone tissue types (review in Ricqlès 1975), and the assessment of cortical growth speed and specific metabolic rates in fossils (Castanet et al. 2000; Legendre et al. 2016). However, the occurrence of vascularized cortices is extremely irregular among taxa and within the bones of a single skeleton. In a given taxon (of generic rank for example), some species may have avascular cortices (Figure 4.7C), whereas others (although closely related) have strongly vascularized cortices. In a sample of extant lissamphibians (71 species, distributed among 34 urodeles and 37 anurans), cortical vascularization in stylopod bones occurs in only 3.7% of the urodele species and 40.7% of the anurans (Canoville et al. 2017). In sauropsids, this frequency is 77% in 30 bird species, and 37% in the 54 lepidosaur species studied by Cubo et al. (2014) (see also Buffrénil et al. 2008b). Up to now the reasons considered for explaining these discrepancies, such as the body size of the taxa, their growth rates, and their resting metabolic rates, do not fully resolve the question (Canoville et al. 2017).

In an endochondral long bone, vascularization has several origins (Brookes 1971; Rhinelander 1972; Singh et al. 1991). The blood vessels that colonize medullary tissues and deep (often cancellous) cortical regions in the diaphyseal territory result from the ramification of relatively large arteries and veins, the nutrient vessels, that penetrate the element (then represented by a cartilaginous anlage) through the initial diaphyseal cortex at early stages of skeletal development. In metaphyseal regions, smaller vessels that originate from periarticular plexuses enter and leave the bone through numerous minute pits. They mainly ramify within the metaphyseal spongiosa. Finally, in medium and peripheral cortical regions, blood capillaries originate from the periosteum vascularization and are incorporated into the newly formed (osteoid) cortical layers.

This incorporation can occur in two distinct ways. The simpler is a direct and relatively close entrapment of the blood vessel within the osteoid. When the matrix becomes calcified, the vessels are then housed in small tunnels some 20 to 50 µm in diameter, perforating the bone cortex, the *simple vascular canals* (Figure 4.7D). Conversely, when *primary osteons* are formed, the vessels are contained in broad cavities (150 µm or more), which are progressively narrowed by centripetal bone deposits to some tens of microns in width (15 – 40 µm are common diameters; cf. Figure 4.7E). A third, variable and facultative modality of vascular development within bone cortices is related to *Haversian remodeling*. This process is indeed initiated by local angiogenesis, or burgeoning of vascular *diverticula* (Cooper et al. 2003), and it results in the creation of *secondary osteons* (further considered in Chapter 11), i.e., thick-walled tubes created by a dual mechanism of resorption and reconstruction (Figure 4.7F).

The geometric organization of vascular canals, as well as their spatial density (i.e., the number of canals per surface or volume units) in bone cortices, vary greatly among taxa in homologous bones, among the various bones of an individual skeleton, and among different regions within a single section. Up to now, six main patterns for the geometrical structuring of vascular networks in primary cortices (Figure 4.8A, B) have been described (review in Ricqlès 1975), in addition, of course, to the frequent situation in which no intracortical canal exists, except the canal housing the initial nutrient artery or arteries.

VetBooks.ir

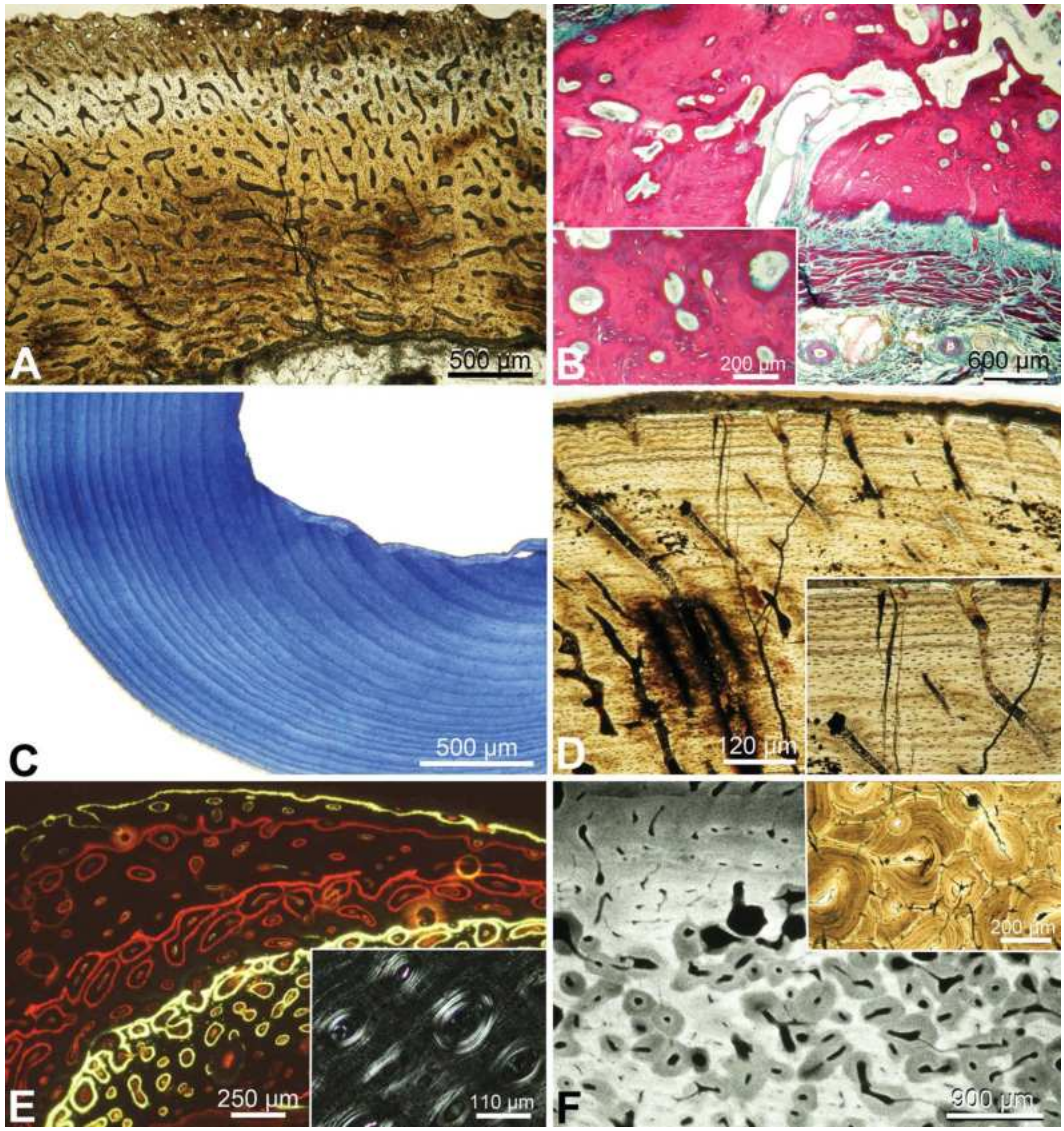


FIGURE 4.7 General aspects of bone vascularization. A, Dense vascular supply in the femoral cortex of the early archosauromorph *Erythrosuchus*. B, Relationship of blood vessel diameter to vascular canal diameter. Eosin-stained decalcified section in an osteoderm of a juvenile Nile crocodile, *Crocodylus niloticus*. C, Avascular bone cortex in the femur of a tuatara (*Sphenodon punctatus*). Hematoxylin-stained decalcified section. D, Integration of simple vascular canals into the peripheral cortex. Femur of the eupelycosaur *Ophiacodon insignis*. E, Formation of longitudinal primary osteons in the femoral cortex of the mallard, *Anas platyrhynchos*. Skeletal growth in this specimen was labeled with injections of two fluorescent markers, DCAF (calcein: yellow labels) and Alizarin (red labels) (Courtesy of Jacques castanet.) The inset shows fully formed primary osteons in the femur of the toad *Rhinella marina* (cross section in polarized light). F, Main frame: formation and mineral content of secondary osteons in the scapula of a sirenian, the dugong (*Dugong dugon*). The inset shows densely packed secondary osteons in the femur of a fossil seal, *Nanophoca vitulinoides*.

As observed in transverse sections, vascular networks in bone, whether represented by simple canals or primary osteons, can be composed of longitudinal canals (i.e., canals oriented parallel to the long axis of the bone; Figure 4.8A1, A2) that can be united or not by transverse anastomoses. Three distinct modes of distribution have been described for longitudinal canals: they can have a random distribution within the cortex or be disposed in radial or circular rows. Nonlongitudinal canals, especially when represented by primary osteons, can display five distinct patterns. They can be *oblique*, with a variable angle compared to the bone's sagittal axis (Figure 4.8A3, A4; see also Figure 4.9A). They form a network with no dominant orientation in the *reticular* pattern (Figure 4.8A5, A6). Canals extend roughly in parallel with the radii of a long bone cross section in the *radiating* pattern (Figure 4.8B1, B2). Canals are circular (i.e., parallel to the outer contour of the cortex) and constitute parallel strata united by numerous radial anastomoses in the *plexiform pattern* (Figure 4.8B3). They have a similar orientation but with few anastomoses in the *laminar pattern* (Figure 4.8B4). It often occurs that two or more of these patterns are associated in a single section; the transition from one pattern to another then depends on either the depth of the canals within the bone cortex, or on local growth circumstances, such as the development of a crest, the insertion of a muscle (Goldman et al. 2009), or a process of asymmetrical development of the bone.

VetBooks.ir

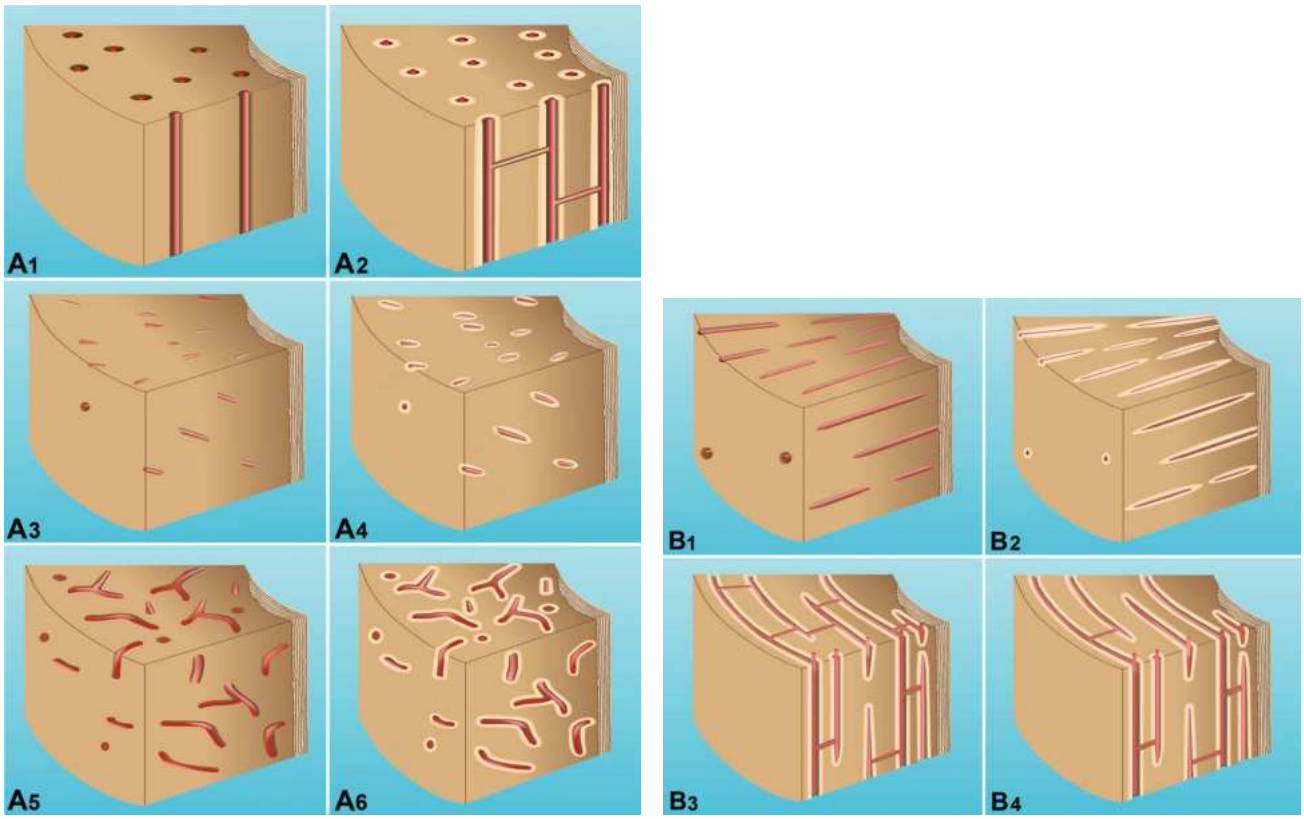


FIGURE 4.8 Vascular network patterns in cortical bone. A1 and A2, Longitudinal canals (simple canals: A1; primary osteons: A2). A3 and A4, Oblique canals. A5 and A6, Reticular canal network. B1 and B2, Radial canals. B3, Plexiform canal network. B4, Laminar canal network. The two latter patterns mainly involve primary osteons.

The nature (simple canals or osteons) and orientation of vascular canals contribute to the distinction of bone tissue categories and represent a major clue to the interpretation of local growth rates and morphogenetic processes (see Chapters 8 and 10). The aspect of vascular networks, and their "legibility" (i.e., the possibility to precisely distinguish their geometric pattern) broadly differ between 2D and 3D images. Even though these networks possess a definite geometric architecture, clearly visible in 2D pictures, this pattern is distinguishable in 3D reconstructions only if anastomoses among canals are few or absent, a relatively rare situation (Figure 4.9A). If anastomoses occur (by far the most frequent situation; Figure 4.9B, C) then 3D images fail to reveal a definite geometric organization of the canals because of the superimposition of planes. Conversely, these kinds of images impressively show the complexity and richness of the vascular supply of cortices, and allow detailed, accurate and realistic measurements of vascular density.

To our knowledge, little mention has been made of vascular characteristics or indices that quantify the development of cortical vascularization in the lists of acknowledged histomorphometric descriptors of bone structure. Dempster et al. (2013) mentioned four measurements for intracortical canals: canal area (*Ca.Ar*), canal volume (*Ca.V*), canal radius (*Ca.Rd*), and canal number (*N.Ca*). In comparative skeletal biology, the quantitative parameters and indices used for vascular assessment in bone cortices frequently consist of "customized" measurements proposed by each author for documenting a particular question. Some of them consider the spatial density of vascular canals, i.e., the total number of canals per unit of cortical area (n/mm²; Cubo et al. 2014), whereas others measure the relative area of the canals in the percentage of the whole cortical area in a section or a ROI (e.g., Cubo et al. 2014; Buffrénil et al. 2008b). The spatial density of vascular canals has a clear, unquestionable biological meaning only in the case of longitudinal canals. When other orientations occur, there is an obvious risk of counting the same canal several times, because a possible sinuous trajectory may make the canal outcrop more than once in the sectional plane. According to the procedure used by Cubo et al. (2014), the *relative vascular area* is assessed through direct measurements of canal and cortex areas (computerized image analysis). Another approach to obtain the total area of the vascular canals in a whole section or a selected ROI is to first establish the total length of the visible vascular network after skeletonization, and then multiply this length by the mean width (i.e., diameter) of the canals measured in a significant sample of canals (Buffrénil et al. 2008b). An index equivalent to the *relative vascular area*, but obtained through different technical procedures, is called the *area fraction of vascular canals* (A_A) by Tonar et al. (2011).

Histomorphometric data relative to the area of bone vascularization are to be handled with caution, especially when vascular canals are represented by primary or secondary osteons,

VetBooks.ir

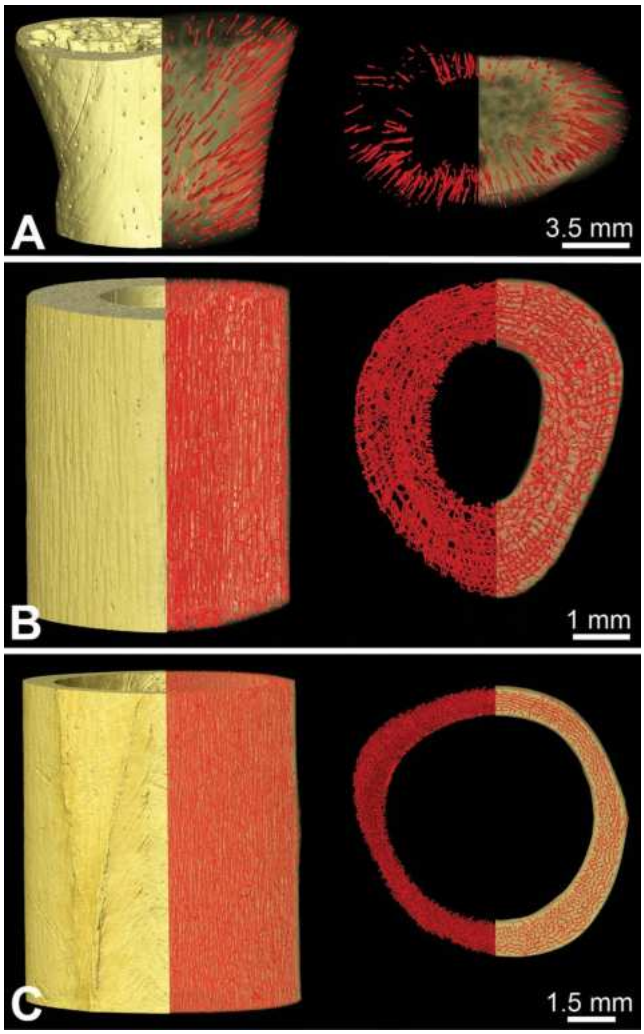


FIGURE 4.9 Three-dimensional reconstructions of vascular networks by synchrotron imaging. A, Simple oblique canals devoid of anastomoses in the femur of the amphibian *Andrias* sp. This simple vascular geometry is easily legible in 3D reconstructions. B and C, Complex 3D structure and high spatial density of vascular canals in the nandu, *Rhea americana* (B) and the albatross *Diomedea* sp. (C). Canal anastomoses and the superimposition of planes in the bone volume tend to blur the basic geometry of vascular networks.

because the reduction of osteonal lumen by centripetal deposits is a gradual process that basically depends on the age of the osteon and the developmental stage of the bone. More generally, measurements of bone vascularity based on the relative area or volume of vascular canals give only a caricature of the real development of vascular networks because the relationship between canal width and the actual blood vessel diameter is most often unknown.

Up to now, 3D quantification of vascular development in bone, such as the study conducted by Jia et al. (2010) in the rat femur (see also Roche et al. 2012), remains relatively scarce. Although they are much more complex to handle, 3D reconstructions have an obvious superiority over 2D ones: they provide an exhaustive and realistic picture of canal development and distribution within cortices.

Cartilage Canals

The occurrence, in early stages of skeletal growth, of blood vessels housed in canals that ramify in cartilaginous epiphyses, i.e., the cartilage canals (Figure 4.10A, B), is a common feature, encountered in large lizards, some giant turtles (Dermochelyidae), eutherian mammals, birds, and so forth (reviews in Haines 1933, 1942; Wilsman and Van Sickle 1972; Blumer et al. 2008; see also Rhodin et al. 1981, 1996). It occurs not only in the epiphyses of long bones, but also in vertebral centra (Chandraraj and Briggs 1988) and other short bones (Agrawal et al. 1984, 1986), as well as in rib heads (Craatz et al. 1999). Cartilage canals are initially derived from the perichondrium. They penetrate the epiphyses and locally ramify (see Blumer et al. 2008 for review of the complex local mechanisms involved in this process) to supply growth cartilage with blood during the most active stages of growth (fetal development and early postnatal growth). The occurrence of these vessels is not closely related to that of secondary ossification centers because, as Haines (1933) mentioned, they can occur in the absence of such centers (birds, Dermochelyidae) or be absent while secondary centers exist (e.g., marsupials and some small eutherian mammals). Recent experimental studies nevertheless have shown the key role played by the canals in the development and ossification of secondary centers, although other mechanisms may intervene when normal, local angiogenetic processes fail (Blumer et al. 2008). Some of the canals pierce the calcified cartilage of growth plates to enter the metaphyses; conversely, blood vessels derived from the diaphyseal medullary vascularization can reach the epiphyses and fuse with cartilage canals (in Haines 1942: "perforating" and "communicating" canals; see also Krstić 1985). These canals can be surrounded by a bony sheath. The occurrence of dense bundles of cartilage canals and communicating canals is generally associated with the sustained growth rates that characterize relatively large amniotes (e.g., Rhodin et al. 1981). In some fossil taxa (e.g., ichthyosaurs, large marine turtles, etc.), the locations where communicating canals perforated growth plates can be extremely conspicuous on the epiphyseal surfaces of long bones (Figure 4.10C), and the bony sheaths of these canals can be preserved deep into the metaphyses (e.g., Buffrénil et al. 1987; see also Figure 4.10D, E). Such microanatomical details give a first, general clue for interpreting the growth activity of extinct taxa. Cartilage canals are transitory structures. With the progression of bone growth, they are incorporated into the vascular networks of bony epiphyses, when present, and finally into metaphyseal vascularization.

Remark on Dermal Bone Vascularization

The vascular supply of dermal bones has received less attention than that of long bones. Developing mesenchymal concentrations are initially avascular, to be later invaded by blood vessels originating from the neighboring tissues (e.g., meningeal, or dermal vessels). According to the model proposed by Percival and Richtsmeier (2013), this vascular invasion occurs just before the beginning of osteoid mineralization in the mesenchymal condensation and is triggered by both "a reduction

VetBooks.ir

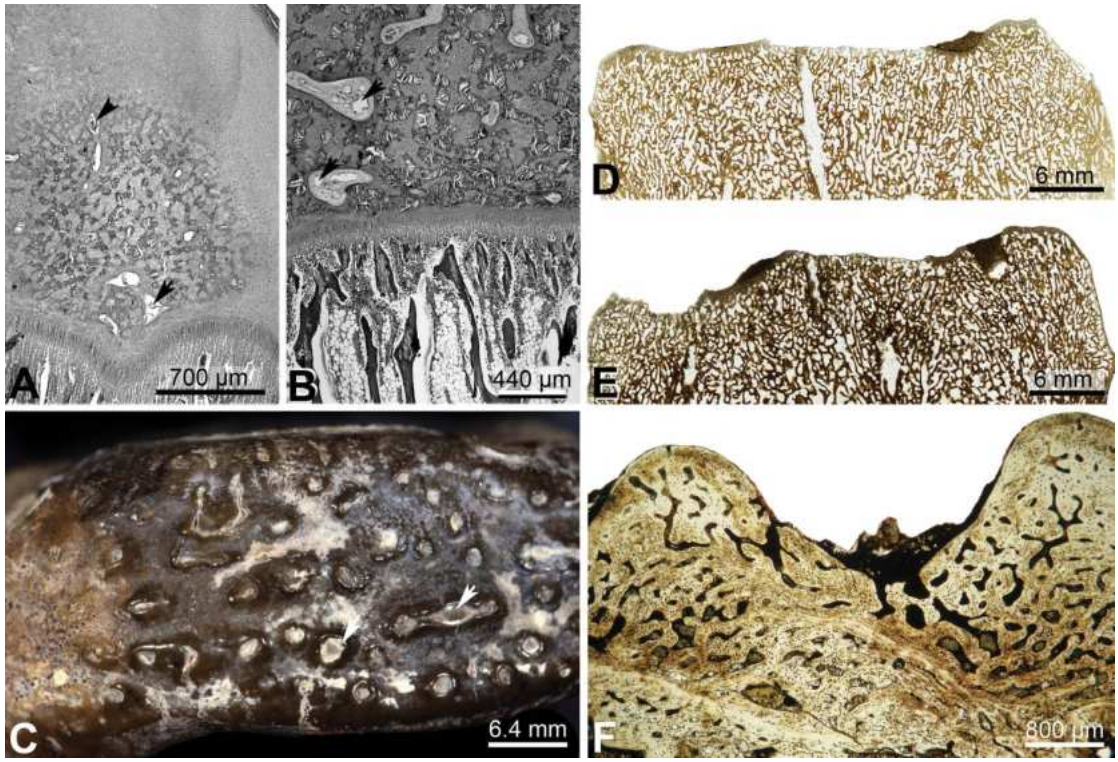


FIGURE 4.10 Cartilage canals. A, B, Cartilage canals (arrows) in the incipiently forming secondary ossification center in the proximal epiphysis of the femur of a juvenile Nile monitor lizard. B, Detail of the canals and the blood vessels that they contain (arrows) in the fully developed secondary ossification center of an adult Nile monitor. C, Superficial outcrop of the bony sheaths surrounding perforating metaphyseal canals (arrows). Proximal epiphyseal surface of the humerus of the early ichthyosaur *Omphalosaurus nisseri*. D and E, Two longitudinal sections in the femur of *O. nisseri*, showing the course of perforating canals. F, Dense, reticular vascular network outcropping at the cortex surface in a membrane bone of the skull roof of the Late Triassic temnospondyl *Benthosuchus sushkini*.

in the expression of currently identified antiangiogenic factors and an increase in the expression of proangiogenic factors" (see Chapters 2 and 9). The outer surfaces of dermal bones are densely riddled by vascular pits of various diameters related to the penetration or the outcrop (Figure 4.10F) of, respectively, superficial and intracortical capillary networks (Ricqlès 1976; Iwaku 1989). In relatively thick dermal flat bones, the inner organization of vascular networks is comparable to that of long bones, with distinct cortical and medullary vessels. In thin bones (less than 0.4 mm), medullary vessels become scarce (Pannarale et al. 1997).

Acknowledgments

Dr. Sophie Sanchez (Upsala University, Sweden) generously gave us access to the rich Synchrotron image resources that she constructed; we warmly thank her for that. For 3D documents, we are also grateful to supporting organizations, i.e., the European Synchrotron Radiation Facility (Proposal EC 203), and the Wenner-Gren Foundation (Fellowship UPD-2018_250). We also thank Drs. Damien Germain (Muséum National d'Histoire Naturelle, Paris), John. R. Nudds (University of Manchester, UK), and Didier Berthet (Musée des Confluences, Lyon, France) for granting access to comparative material.

REFERENCES

Agrawal, P., et al. 1984. The role of cartilage canals in the calcification of the talus. *Acta Anat.* 199: 238–240.

Agrawal, P., et al. 1986. The participation of cartilage canals in the calcification of the human fetal calcaneum. *J. Anat.* 147: 135–142.

Allen, M. R., et al. 2004. Periosteum: biology, regulation, and response to osteoporosis therapies. *Bone.* 35: 1003–1012.

Allen, M. R. and K. Krohn. 2014. Skeletal imaging. In *Basic and applied bone biology*, ed. D. B. Burr and M. R. Allen, 93–113. London: Academic Press.

Amson, E., et al. 2018. Evolutionary adaptation to aquatic lifestyle in extinct sloths can lead to systemic alteration of bone structure. *Proc. Biol Sci.* 285: 20180270.

Arlot, M. E., et al. 2008. Microarchitecture influences microdamage accumulation in human vertebral trabecular bone. *J. Bone Min. Res.* 23: 1613–1618.

Baiker, M., et al. 2012. Automated bone volume and thickness measurements in small animal whole-body micro-CT data. *Mol. Imaging Biol.* 14: 420–430.

Balzeau, A. 2013. Thickened cranial vault and parasagittal keeling: correlated traits and autapomorphies of Homo erectus? *J. Human Evol.* 64: 631–644.

Bergot, C., et al. 1988. Measurement of anisotropic vertebral trabecular bone loss during aging by quantitative image analysis. *Calcif. Tissue Int.* 43: 143–149.

Bergot, C., et al. 1990. Variation du volume osseux et de la densité minérale au cours du vieillissement chez l'homme. *Rev. Rhum. Mal. Osteoartic*. 57: 791–798.

Biewener, A. A., et al. 1996. Adaptive changes in trabecular architecture in relation to functional strain patterns and disuse. *Bone*. 19: 1–8.

Blumer, M. J. F., et al. 2008. Structure, formation and role of cartilage canals in the developing bone. *Ann. Anat*. 190: 305–315.

Boruah, S., et al. 2015. Variation of bone layer thickness and trabecular volume fraction in the adult male human calvarium. *Bone*. 77: 120–134.

Brandi, M. L. and P. Collin-Osdoby. 2006. Perspective: vascular biology of the skeleton. *J. Bone Min. Res*. 21: 183–192.

Brookes, M. 1971. *The blood supply of bone*. London: Butterworth & Co.

Buck, A. M., et al. 2002. An investigation of thoracic and lumbar cancellous vertebral architecture using power-spectral analysis of plain radiographs. *J. Anat*. 200: 445–456.

Buffrénil, V. de et al. 1987. Caractères structuraux et mode de croissance du fémur d'*Omphalosaurus nisseri*, ichthyosaurien du Trias moyen du Spitsberg. *Ann. Paléontol. (Vert.)*. 73: 195–216.

Buffrénil, V. de, et al. 1990. L'histologie osseuse des Champsosauridés: données descriptives et interprétation fonctionnelle. *Ann. Paléontol. (Vert.)*. 76: 255–275.

Buffrénil, V. de, et al. 2004. Comparative data on epiphyseal development in the family Varanidae. *J. Herpetol*. 37: 328–335.

Buffrénil, V. de, et al. 2008a. Specialization of bone structure in *Pachyvaranus crassispondylus* Arambourg, 1952, an aquatic squamate from the late Cretaceous of the southern Tethyan margin. *Lethaia*. 41: 59–69.

Buffrénil, V. de, et al. 2008b. Bone Vascular supply if monitor lizards (Squamata: Varanidae): influence of size, growth and phylogeny. *J. Morphol*. 269: 533–543.

Buffrénil V de, et al. 2015. Differentiation and growth of bone ornamentation in vertebrates: a comparative histological study among the Crocodylomorpha. *J. Morphol*. 276: 425–445.

Buffrénil V. de, et al. 2016. Comparative data on the differentiation and growth of bone ornamentation in gnathostomes (Chordata: Vertebrata). *J. Morphol*. 277: 634–670.

Buffrénil, V. de and J.-C. Rage. 1993. La pachyostose vertébrale de *Simoliophis* (Reptilia, Squamata): données comparatives et considérations fonctionnelles. *Ann. Plaéontol. (Vert.)*. 79: 315–335.

Burr, D. B. and O. Akkus. 2014. Bone morphology and organization. In *Basic and applied bone biology*, eds. D. B. Burr and M. A. Allen, 3–25. Amsterdam: Academic Press.

Cabrera-Téllez, L., et al. 2010. Morphology and posthaching ontogeny of the autopodial skeleton of *Bolitoglossa nicefori* (Caudata: Plethodontidae). *J. Morphol*. 271: 1374–1385.

Candela, A. M., et al. 2017. The tarsal-metatarsal complex of caviomorph rodents: anatomy and functional-adaptive analysis. *J. Morphol*. 278: 828–847.

Canoville A., et al. 2017. Quantitative data on bone vascular supply in the Lissamphibia: comparative and phylogenetic aspects. *Zool. J. Linn. Soc*. 20: 1–22.

Castanet, J., et al. 1993. Bone and individual aging. In *Bone. Vol. 7: Bone growth – B*, ed. B. K. Hall, 245–283. Boca Raton, FL: CRC Press.

Castanet, J., et al. 2000. Periosteal bone growth rates in extant ratites (ostriche and emu). Implications for assessing growth in dinosaurs. *C. R. Acad. Sci. Paris, Sciences de la Vie*. 323: 543–550.

Castanet, J., et al. 2003. The skeletal histology of the Amphibia. In *Amphibian biology*, ed. H. Heatwole and M. Davies, vol. 5, 1598–1683. Chipping Norton: Surrey Beatty & Sons.

Chandraraj, S. and C. A. Briggs. 1988. Role of cartilage canals in osteogenesis and growth of the vertebral centra. *J. Anat*. 158: 121–136.

Chappard, D., et al. 2005. Comparison insight Bone measurements by histomorphometry and µCT. *J. Bone Min. Res*. 20: 1177–1184.

Chen, J. et al. 2020. Bone vasculature and bone marrow vascular niches in health and disease. *J. Bone Min. Res*. 35: 2103–2120.

Clarac F., et al. 2017. Vascularization in ornamented osteoderms: physiological implications in ecthothermy and amphibious lifestyle in the Crocodylomorphs? *Anat. Rec*. 301: 175–183.

Copes, L. E., et al. 2018. Locomotor activity, growth hormone, and systemic robusticity: an investigation of cranial vault thickness in mouse lines bred for high endurance running. *Am. J. Phys. Anthropol*. 166: 442–458.

Cooper, D. M. L., et al. 2003. Quantitative 3D analysis of the canal network in cortical bone y micro-computed tomography. *Anat. Rec*. 274B: 169–179.

Craatz, S., et al. 1999. Histologisch-histochemische und immunohistochemische Untersuchungen an Knorpelkanälen menschlicher Rippenknorpel. *Ann. Anat*. 181: 359–363.

Cubo, J., et al. 2012. Paleohistological estimation of bone growth rate in extinct archosaurs. *Paleobiology*.38: 335–349.

Cubo, J., et al. 2014. Geometric and metabolic constraints on bone vascular supply in diapsids. *Biol. J. Linn. Soc*. 112: 668–677.

Currey, J. D. 2002. *Bones. Structure and mechanics*. Princeton and Oxford: Princeton University Press.

Currey, J. D. and R. Mc N. Alexander. 1985. The thickness of the walls of tubular bones. *J. Zool. Lond*. 206: 453–468.

Danto, M., et al. 2016. Vertebral development in Paleozoic and Mesozoic tetrapods revealed by paleohistological data. *PLoS One*. 11: e0152586. https://doi.org/10.1371/journal.pone.0152586

Dempster, D. W., et al. 2013. Standardized nomenclature, symbols, and units for bone histomorphometry: A 2012 update of the report of the ASBMR Histomorphometry Nomenclature Committee. *J. Bone Min. Res*. 28: 1–16.

Dumont M., et al. 2013. Inner architecture of vertebral centra in terrestrial and aquatic mammals: a two-dimensional comparative study. *J. Morphol*. 274: 570–584.

Dunmore, C. J., et al. 2018. MIA-Clustering: a novel method for segmentation of paleontological material. *PeerJ*. 6: e4374.

Enlow, D. H. 1963. *Principles of bone remodeling*. Springfield, IL: Charles C Thomas.

Enlow, D. H. 1975. *Handbook of facial growth*. Philadelphia, W.B. Saunders Company.

Fajardo, R. J., et al. 2002. Assessing the accuracy of high-resolution X-Ray computed tomography of primate trabecular bone by comparisons with histological sections. *Am. J. Phys. Anthropol*. 118: 1–10.

Fajardo, R. J. and R. Müller, R. 2001. Three-dimensional analysis of nonhuman primate trabecular architecture using micro-computed tomography. *Am. J. Phys. Anthropol.* 115: 327–336.

Fan, W., et al. 2008. Structural and cellular differences between metaphyseal and diaphyseal periosteum in different aged rats. *Bone.* 42: 81–89.

Fawcett, D. W. 1942. The medullary bones of the Florida manatee (*Trichechus latirostris*). *Am. J. Anat.* 71: 271–309.

Fawcett, D. W. and R. P. Jensh. 1997. *Bloom and Fawcett: concise histology.* London: Chapman & Hall.

Felts, W. and F. A. Spurrell. 1965. Structural orientation and density of cetacean humeri. *Am. J. Anat.* 116: 171–203.

Felts, W. and F. A. Spurrell. 1966. Some structural and developmental characteristics of cetacean (Odontocete) radii. A study of adaptive osteogenesis. *Am. J. Anat.* 118: 103–134.

Fields A. J., et al. 2009. Role of trabecular microarchitecture in whole-vertebral body mechanical behavior. *J. Bone Min. Res.* 24: 1523–1530.

Fields, A. J., et al. 2011. Influence of vertebral trabeculae on the compressive strength of the human vertebra. *J. Bone Min. Res.* 26: 263–269.

Francillon, H. 1981. Contribution à l'étude des structures et du fonctionnement des épiphyses fémorales chez les amphibiens anoures. *Arch. Zool. Exp. Gen.* 122: 289–310.

Francillon-Vieillot, H., et al. 1990. Microstructure and mineralization of vertebrate skeletal tissues. In *Skeletal biomineralization: patterns, processes and evolutionary trends*, vol. 1, ed. J. G. Carter, 471–530. New York: Van Nostrand Reinhold.

Fritsch, H., et al. 1996. The ossification centre of the talus. *Ann. Anat.* 178: 455–459.

Frydlova, P., et al. 2017. Patterns of growth in monitor lizards (Varanidae) as revealed by computed tomography of femoral growth plates. *Zoomorphology.* 136: 95–106.

Galateanu, G., et al. 2013. Canine tarsal architecture as revealed by high-resolution computed tomography. *Vet. J.* 196: 374–380.

Gardner, E. 1971. Osteogenesis in the human embryo and fetus. In *The biochemistry and physiology of bone, Vol. 3: Development and growth*, ed. G. H. Bourne, 77–118. New York: Academic Press.

Geraets, W. G. M. 1998. Comparison of two methods for measuring orientation. *Bone.* 23: 383–388.

Geraets, W. G. M., et al. 2008. Spatial orientation in bone samples and Young's modulus. *J. Biomech.* 41: 2206–2210.

Girondot, M. and M. Laurin. 2003. Bone profiler: a tool to quantify, model, and statistically compare bone section compactness profiles. *J. Vert. Paleontol.* 23: 458–461.

Glorieux, F. H., et al. 2000. Normative data for iliac bone histomorphometry in growing children. *Bone.* 26: 103–109.

Goldman, H. M., et al. 2009. Ontogenetic patterning of cortical bone microstructure and geometry at the human mid-shaft femur. *Anat. Rec.* 292: 48–64.

Gross, T., et al. 2014. A CT-image-based framework for the holistic analysis of cortical and trabecular bone morphology. *Palaeontol. Elect.* 17: 1–13.

Haines, R. W. 1933. Cartilage canals. *J. Anat.* 68: 45–64.

Haines, R. W. 1938. The primitive form of epiphyses in the long bones of tetrapods. *J. Anat.* 72: 323–343.

Haines, R. W. 1941. Epiphyseal structure in lizards and marsupials. *J. Anat.* 75: 282–294.

Haines, R. W. 1942. The evolution of epiphyses and of endochondral bone. *Biol. Rev.* 17: 267–292.

Haines, R. W. 1969. Epiphyses and sesamoids. In *Biology of the reptile: morphology A*, vol. 1, ed. C. Gans, 81–115. London: Academic Press.

Haines, R. W. 1975. The histology of epiphyseal union in mammals. *J. Anat.* 120: 1–25.

Haines, R. W. and A. Mohuiddin. 1968. Metaplastic bone. *J. Anat.* 103: 527–538.

Herring, S. W. and R. J. Mucci. 1991. In vivo strain in cranial sutures: the zygomatic arch. *J. Morphol.* 207: 225–239.

Hildebrand, T., et al. 1999. Direct three-dimensional morphometric analysis of human cancellous bone: microstructural data from spine, femur, iliac crest, and calcaneus. *J. Bone Miner. Res.* 14: 1167–1174.

Hordon, L. D., et al. 2000. Trabecular architecture in women and men of similar bone mass with and without vertebral fracture: I. Two-dimensional histology. *Bone.* 27: 271–276.

Houssaye, A., et al. 2008. An analysis of vertebral "pachyostosis" in *Carentonosaurus mineaui* (Mosasoroidea, squamata) from the Cenomanian (Early Late Cretaceous) of France, with comments on its phylogenetic and functional significance. *J. Vert. Paleontol.* 28: 685–691.

Houssaye, A., et al. 2010. Vertebral microanatomy in squamates: structure, growth and ecological correlates. *J. Anat.* 217: 715–727.

Houssaye, A., et al. 2014. Amniote vertebral microanatomy. What are the major trends. *Biol. J. Linn. Soc.* 112: 735–746.

Ito, M., et al. 2003. Bone structure and mineralization demonstrated using synchrotron radiation computed tomography (SR-CT) in animal models: preliminary findings. *J. Bone Miner. Metab.* 21: 287–293.

Iwaku, F. 1989. Microvasculature of bone. III Microvasculature of the bone marrow of the rat's femur by means of vascular corrosion-cast SEM method. *J. Bone Min. Metab.* 7: 13–17.

Jhamaria, N.L., et al. 1983. The trabecular pattern of the calcaneum as an index of osteoporosis. *J. Bone Joint Surg. B.* 65: 195–198.

Jia, F., et al. 2010. Imaging and quantitative assessment of long bone vascularization in the adult rat using microcomputed tomography. *Anat. Rec.* 293: 215–224.

Kalender, W. A., et al. 1989. Reference values for trabecular and cortical vertebral bone density in single and dual-energy quantitative computed tomography. *Eur. J. Radiol.* 9: 75–80.

Kardong, K. V. 1998. *Vertebrates. Comparative anatomy, function, evolution*. Boston: WCB-McGraw-Hill.

Kaur, H. and I. Jit. 1990. Age estimation from cortical index of the human clavicle in northwest Indians. *Am. J. Phys. Anthropol.* 83: 297–305.

Khonsari, R. H., et al. 2012. High-resolution imaging of craniofacial sutures: new tools for understanding the origins of craniosynostoses. *Childs Nerv. Syst.* 28: 1465–1469.

Kleerekoper M. and D. A. Nelson. 1997. Which bone density measurements? *J. Bone Miner. Res.* 12: 712–714.

Krstić, R. V. 1985. *General histology of the mammal*. Berlin: Springer Verlag.

VetBooks.ir

Krause, M., et al. 2013. Bone microarchitecture of the talus changes with aging. *Clin. Orthop. Relat. Res.* 471: 3663–3671.

Legendre, L. J., et al. 2016. Palaeohistological evidence for ancestral high metabolic rate in archosaurs. *Syst. Biol.* 65: 989–996.

Liu, X. S., et al. 2009. Micromechanical analyses of vertebral trabecular bone based on individual trabeculae segmentation of plates and rods. *J. Biomech*. 42: 249–256.

Maisano, J. A. 2002. Terminal fusions of skeletal elements as indicators of maturity in squamates. *J. Vert. Paleontol*. 22: 268–275.

Margerie, E. de, et al. 2004. Assessing a relationship between bone microstructure and growth rate: a fluorescent labeling study in the king penguin chick (*Aptenodytes patagonicus*). *J. Exp. Biol*. 207: 869–879.

Martill, D. M. and D. M. Unwin. 1997. Small spheres in fossil bones: blood corpuscles or diagenetic product? *Palaeontology.* 40: 619–624.

McLaughlin, B. G. and C. E. Doige. 1982. A study of ossification of carpal and tarsal bones in normal and hypothyroid foals. *Can. Vet. J.* 23: 164–168.

Mellish, R. W. E, et al. 2009. A new manual method for assessing two-dimensional cancellous bone structure: Comparison between iliac crest and lumbar vertebra. *J. Bone Miner. Res.* 6: 689–696.

Meunier, P. J. and G. Boivin. 1997. Bone mineral density reflects bone mess but also the degree of mineralization of bone: therapeutic implications. *Bone.* 21: 373–377.

Odgaard, A. 1997. Three-dimensional methods for quantification of cancellous bone architecture. *Bone.* 20: 315–28.

Opperman, L. A. 2000. Cranial sutures as intramembranous bone growth sites. *Dev. Dyn*. 219: 472–485.

Pannarale, L., et al. 1997. SEM corrosion-casts study of the microcirculation of the flat bones in the rat. *Anat. Rec*. 247: 462–471.

Parfitt, A. M., et al. 1987. Bone histomorphometry: standardization of nomenclature, symbols, and units. *J. Bone Miner. Res*. 2: 595–610.

Pawlicki, R. and M. Nowogrodska-Zagorska. 1998. Blood vessels and red blood cells preserved in dinosaur bones. *Ann. Anat*. 180: 73–77.

Percival, C. J. and J. T. Richtsmeier. 2013. Angiogenesis and intramembranous osteogenesis. *Dev. Dyn.* 242: 909–922.

Pontzer, H., et al. 2006. Trabecular bone in the bird knee responds with high sensitivity to changes in load orientation. *J. Exp. Biol*. 209: 57–65.

Pritchard, J. J., et al. 1956. The structure and development of cranial and facial sutures. *J. Anat*. 90: 73–86.

Rafferty, K. L. and S. W. Herring. 1999. Craniofacial sutures: morphology, growth, and in vivo masticatory strains. *J. Morphol*. 242: 167–179.

Recker, R. R. (ed.). 1983. *Bone histomorphometry: techniques and interpretation*. Boca Raton, FL: CRC Press.

Renzuli-Jaslow, C. 1990. Mechanical properties of cranial sutures. *J. Biomech*. 23: 313–321.

Rhinelander, F. W. 1972. Circulation in bone. In *The biochemistry and physiology of Bone*, vol. 2, ed. G. H. Bourne, 1–77. New York: Academic Press.

Rhodin, A. G. J., et al. 1981. Chondro-osseous morphology of *Dermochelys coriacea*, a marine reptile with mammalian skeletal features. *Nature.* 290 (5803): 244–246.

Rhodin, A. G. J., et al. 1996. Electron microscopic analysis of vascular cartilage canals in the humeral epiphysis of hatchling leatherback turtles, *Dermochelys coriacea*. *Chelonian Conserv. Biol*. 2: 250–260.

Ricqlès, A. de. 1972. Nature et signification des « surfaces épiphysaires chez les tétrapodes fossiles. *C. R. Acad. Sci. Paris.* 274: 3527–3530.

Ricqlès, A. de. 1975. Recherches paléohistologiques sur les os longs des tétrapodes. VII – Sur la classification, la signification fonctionnelle et l'histoire du tissu osseux des tétrapodes (Première partie). *Ann. Paléont*. 61: 51–81.

Ricqlès, A. de. 1976. Recherches paléohistologiques sur les os longs des tétrapodes. VII – Sur la classification, la signification fonctionnelle et l'histoire du tissu osseux des tétrapodes (Deuxième partie). *Ann. Paléont*. 62: 71–126.

Ricqlès, A. de. 1979. Quelques remarques sur l'histoire évolutive des tissus squelettiques chez les vertébrés et plus particulièrement chez les tétrapodes. *Ann. Biol*. 18: 1–35.

Ricqlès, A. de, et al. 1991. Comparative microstructures of bone. In: *Bone, Vol. 3: Bone matrix and bone specific products*, ed. B. K. Hall, 1–78. Boca Raton, FL: CRC Press.

Ricqlès A. de and V. de Buffrénil. 2001. Bone histology, heterochronies and the return of tetrapodsti life in water: where are we? In *Secondary adaptation of tetrapods to life in water*, eds. J-M. Mazin and V. de Buffrénil, 287–310. München: Verlag Dr. Friedrich Pfeill.

Rimblot-Baly, F., et al. 1995. Analyse paléohistologique d'une série de croissance partielle chez *Lapparentosaurus madagascarensis* (Jurassique moyen): essai sur la dynamique de croissance d'un dinosaure sauropode. *Ann. Paleont*. 81: 49–86.

Roche, B., et al. 2012. Structure and quantification of microvascularisation within mouse long bones: what and how should we measure? *Bone.* 50: 390–399.

Saint-Georges, L. de and S. C. Miller. 1992. The microcirculation of bone and marrow in the diaphysis of the rat hemopoietic long bones. *Anat. Rec.* 233: 169–177.

Sanchez, S., et al. 2008. Salamander-like development in a seymouriamorph revealed by paleohistology. *Biol. Let. (Paleont).* 4: 411–414.

Sanchez, S., et al. 2010. Limb-bone histology of temnospondyls: implications for understanding the diversification of palaeoecologies and patterns of locomotion of Permo-Triassic tetrapods. *J. Evol. Biol*. 3: 2076–2090.

Sanchez, S., et al. 2016. Life history of the stem tetrapod *Acanthostega* revealed by synchrotron microradiography. *Nature.* 537: 408–411.

Scheyer, T. M. and M. R. Sanchez-Villagra. 2007. Carapace bone histology in the giant pleurodiran turtle *Stupendemys geographicus*: ohylogeny and function. *Acta Paleontol. Pol*. 52: 137–154.

Scheyer, T. M. and M. Sander. 2004. Histology of ankylosaur osteoderms: implications for systematics and function. *J. Vert. Paleontol*. 24: 874–893.

Schilling, A. M., et al. 2014. Trabecular bone structure in the primate wrist. *J. Morphol*. 275: 572–585.

Schnapper, A., et al. 2002. The architecture of growing compact bone in the dog: visualization by 3D-reconstruction of histological sections. *Ann. Anat*. 184: 229–233.

Schneider, C. A., et al. 2012. NIH Image to ImageJ: 25 years of image analysis. *Nat. Methods*. 9: 671–675.

VetBooks.ir

Schweitzer, M. H. and J. R. Horner. 1999. Intravascular microstructures in trabecular bone tissues of Tyrannosaurus rex. *Ann. Paléontol.* 85: 179–192.

Seeman, E. 2007. The periosteum – a surface for all seasons. *Osteoporos. Int.* 18: 123–128.

Shapiro, M. D. 2002. Developmental morphology of limb reduction in *Hemiergis* (Squamata: Scincidae): chondrogenesis, osteogenesis, and heterochrony. *J. Morphol.* 254: 211–231.

Simpson, A. H. R. W. 1985. The blood supply of the periosteum. *J. Anat.* 140: 697–704.

Singh, I. J., et al. 1991. Bone vascularity. In: *Bone. Vol. 3: Bone matrix and bone specific products*, ed. B. K. Hall, 141–164. Boca Raton, FL: CRC Press.

Sinha, D. N. 1985. Cancellous structure of tarsal bones. *J. Anat.* 140: 111–117.

Skedros, J. G., et al. 2004. Relationships of loading history and structural and material characteristics of bone: development of the mule deer calcaneus. *J. Morphol.* 259: 281–307.

Sode, M., et al. 2008. Resolution dependence of the mon-metric trabecular structure indices. *Bone.* 42: 728–736.

Stafford, B. I. and R. W. Thorington. 1998. Carpal development and morphology in archontan mammals. *J. Morphol.* 235: 135–155.

Stauber, M. and R. Müller. 2006. Volumetric spatial decomposition of trabecular bone into rods ad plates – A new method for local bone morphometry. *Bone.* 38: 475–484.

Sun, Z., et al. 2004. Cranial sutures and bones: growth and fusion in relation to masticatory strain. *Anat. Rec.* 276A: 150–161.

Tonar, Z., et al. 2011. Quantification of compact bone microporosities in the basal and alveolar portions of the human mandible using osteocyte lacunar density and area fraction of vascular canals. *Ann. Anat.* 193: 211–219.

Vickaryous, M. K. and J.-Y. Sire. 2009. The integumentary skeleton of tetrapods: origin, evolution, and development. *J. Anat.* 214: 441–464.

Wilsman, N. J. and D. C. Van Sickle. 1972. Cartilage canals, their morphology and distribution. *Anat. Rec.* 173: 79–94.

Wong, M. and D. R. Carter. 1990. A theoretical model of endochondral ossification and long bone architectural construction in long bone ontogeny. *Anat. Embryol.* 181: 523–532.

Zylberberg, L. and J. Castanet. 1985. Newdata on the structure and the growthof the osteoderms inthe reptile *Anguisfragilis* L. (Anguidae. Squamata). *J. Morphol.* 186: 327–342.

VetBooks.ir

Methodological Focus B

Basic Aspects of 3D Histomorphometry

Eli Amson and Damien Germain

CONTENTS

From 2D to 3D Histomorphometry 81
Indications of 3D Analyses and VOI Sampling 81
Characteristics of Usable 3D Files and VOIs 81
Basic 3D Parameters and Indices 82
Acknowledgements 83
References 83

From 2D to 3D Histomorphometry

Indications of 3D Analyses and VOI Sampling

Although many aspects of bone structure can be described with two-dimensional (2D) sections (either physical thin sections or virtual ones), investigations are increasingly oriented toward three-dimensional (3D) data acquisition and analysis to characterize skeletal microanatomical organization in a more realistic manner. This methodology is especially relevant to describe the complex architecture of cancellous bone and the microstructural details of diaphyseal cortices. Whereas serial grinding or thin sectioning methods remove extensive parts of the specimen, and especially trabeculae that become difficult to follow from one section to another, computed tomography (CT) scans – on which 3D analyses most often rely – keep the specimen intact and preserve the connectivity between trabeculae when voxel size is small enough.

Basic 3D reconstructions, whatever the device producing them (classical CT scan or synchrotron), are all based on a virtual X-ray slicing of bone volume, as revealed in the "focus" relative to the CT scan. Two main approaches ("sampling strategy") can be developed for the subsequent analysis and quantification of bone structure.

The approach based on *volumes of interest* (VOIs) relies on the sampling, within a broad osseous 3D reconstruction, of a geometric figure, usually a sphere or cube, to which the analysis will be restricted. An interesting development of this approach is mechanically testing 3D printed VOIs (Wood et al. 2019). Although single VOIs are usually compared to one another, several VOIs can also be used to describe broader structures, including entire skeletal elements (Gross et al. 2014). Within a VOI, most methods allow automatic separation of trabecular and cortical bone, along with a mapping of cortical thickness, where the highest wavelengths (red) represent the highest thickness values (Puymerail 2013).

The other approach, "compartment-scale" sampling, usually relies on a series of parallel cross sections, i.e., an oriented stack of 2D images, subsequently analyzed independently to describe the evolution of the parameters of interest along an anatomical profile (Doube et al. 2010; Houssaye et al. 2018; Amson 2019). This sampling mode has been mostly used so far to study the inner diaphyseal geometry of long bones. Further developments of this approach have also implemented a reorientation of the sections depending on the bone curvature (e.g., Behrooz et al. 2017).

The precise methodological option adopted to quantify 3D microanatomy often depends on the type of bone analyzed. The most common skeletal elements analyzed in 3D are long bones and vertebral centra (e.g., Fajardo et al. 2013; Tsegai et al. 2018; but see Amson 2019 for a whole vertebral structure approach). Flat bones, such as those of the skull roof and of the zonal skeleton, often require specific acquisition procedures, such as the modeling of cortical thickness on complex shapes (Baab et al. 2018).

Characteristics of Usable 3D Files and VOIs

The choice of conventional CT scan or synchrotron light to obtain usable acquisitions depends on the precision needed. Image stacks are usually coded in gray levels (the relative brightness of a voxel), and a step of binarization is often required: the stack levels are then ascribed to either foreground (bone) or background (surrounding space or any other tissue). This binarization can be done through automatic thresholding or manual selection. In both cases, great care is required in rendering the trabecular architecture as accurately as possible. After binarization and VOI extraction, the files are much smaller (100 Mo) than the original stacks (5 – 10 Gb or more).

Voxel size must be small enough to properly reflect the shape and size of the trabeculae. For a given object, a better resolution (i.e., a smaller voxel size) will bring more precision to the analysis (if no other CT acquisition parameters are forfeited for that purpose). But resolution is limited by technical constraints of the data acquisition, such as the capabilities of the CT scanner, the morphology of the specimens, the size of

VetBooks.ir

the data files thus produced, and so forth. Furthermore, resolution, a principal parameter expressing the sharpness of an image, should always be considered in regard to the size of the object of interest. To guide the selection of a scan resolution adjustment before the acquisition stage has started, Sode et al. (2008) recommended setting a lower threshold for the *relative resolution*. This index is defined as the mean trabecular thickness (see definition of this parameter below) divided by the resolution. For instance, if a minimum relative resolution is set at 5 pixels (a value supposed *a priori* to be sufficient to characterize the trabeculae in a sample), the femoral trabeculae of a small mammal such as the Etruscan shrew, which have an actual mean trabecular thickness (*Tb.Th*) of 40 µm (Doube et al. 2011), will require an 8 µm or lower scanning resolution. On the other hand, a large animal such as an Asian elephant (*Tb.Th* = 500 µm; Doube et al. 2011) will require a scanning resolution of 100 µm or lower. Some authors, concerned with the potential bias represented by disparate resolutions within a data set, use a correction for resolution discrepancy (Ryan and Shaw 2012).

For approaches aimed to analyze the content of a VOI, the criteria used to define the shape, size, and position of that VOI will naturally be of prime importance (Kivell et al. 2011). VOIs are usually cubic or spherical (irregular volumes can be used as well to capture an entire compartment, for instance) and their position defined in reference to anatomical landmarks (e.g., center of the femoral head; Figure 1A, B). Their size is either restricted by the tissues intended to be sampled (e.g., a VOI as large as possible including only cancellous bone) or chosen to reflect the specimen size (VOI size is then indexed on a reference linear measurement for instance). In cancellous tissue, a caveat intrinsic to the VOI-based approaches may occur when the trabeculae comprised in the total VOI are too few.

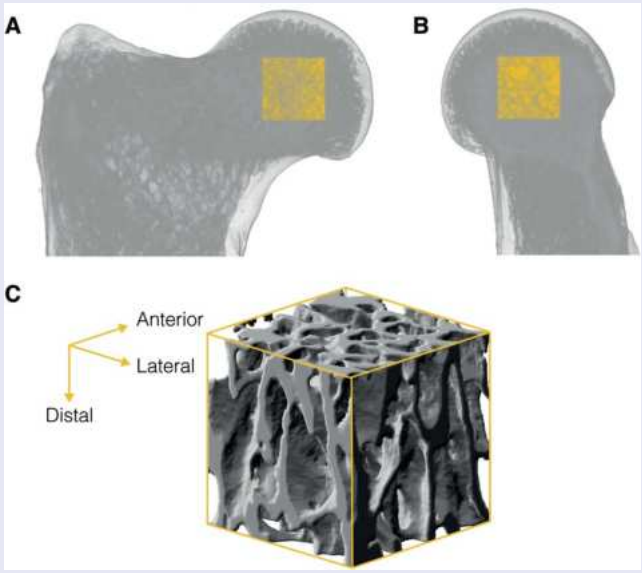


FIGURE B.1 Example of a cubic volume of interest (VOI) within the center of the right femoral head of an Asian small-clawed otter (*Amblonyx cinereus*; collection number ZMB_MAM 43245). Whole epiphysis in A, anterior, and B, medial views. C, Extracted cube comprising only trabecular bone and the space surrounding it. Cube side: 5.13 mm.

This situation can possibly make the acquisition of some parameters dubious, in particular those related to structural anisotropy or those assuming that the sampled trabecular network is assimilated to a continuum (Harrigan et al. 1988).

Basic 3D Parameters and Indices

The main parameters that specifically deserve 3D imaging and analyses, as opposed to parameters accessible with a much simpler 2D approach, mainly deal with cancellous bone formations, and they allow precise and reproducible measurement of the basic architectural characteristics of bone spongiosae. Several efficient computer programs for data analysis are available. A free program, BoneJ v. 1.4.3 (Doube et al. 2010), a collection of plug-ins for Fiji (Schindelin et al. 2012), will be referred to here. The initial files to be analyzed then consist of a binary file (Fiji reads many file formats, e.g., tiff, jpg, etc.), previously submitted to optimal thresholding under the command *Optimize Threshold* in BoneJ.

1. ***Bone volume fraction*** *(B.V.f)* – Quantification of the volume of the trabeculae comprised in a VOI (*Tb.V*) relative to the total volume of the VOI (*Tt.V*; see Figure 1C): *B.V.f* = *Tb.V/Tt.V*, expressed as a rough ratio (ranging from 0 to 1), or in percentage. The acronyms used here refer to the list of standard histomorphometric nomenclature by Dempster et al. (2013); however, other designations, such as *BV/TV* or *compactness* (in comparative literature), are also frequently used for this index. The most straightforward way to compute it is, for a given thresholded stack, to count the number of voxels defining bone tissue and divide that by the total number of voxels of the stack. Command: *BoneJ* > *Volume Fraction* (option *Voxel* method).
2. ***Trabecular thickness and separation*** *(Tb.Th* and *Tb.Sp)* – Usually expressed as, respectively, the mean thickness of the trabeculae enclosed in a VOI, and their mean separation i.e., the space separating them (Figure 2A). BoneJ relies on a local thickness assessment approach, which consists of fitting spheres as large as possible at all points within the solid trabecular network (for *Tb.Th*) or within the empty space surrounding the trabeculae (for *Tb.Sp*). The diameters of these spheres are then used to compute mean *Tb.Th* and mean *Tb.Sp*, respectively. Command: *BoneJ* > *Thickness*
3. ***Trabecular network parameters*** – Prior to acquisition of these parameters, the trabecular network has to be skeletonized, i.e., reduced to a one-voxel-thick shape that is equidistant to the initial network's boundaries. It is then possible to retrieve parameters describing the network, such as the number of branches as well as the length of these branches and the number of nodes (also referred to as junctions or trabecular intersections). Command: *BoneJ* > *Skeletonise* ≥ *Analyse skeleton*.

VetBooks.ir

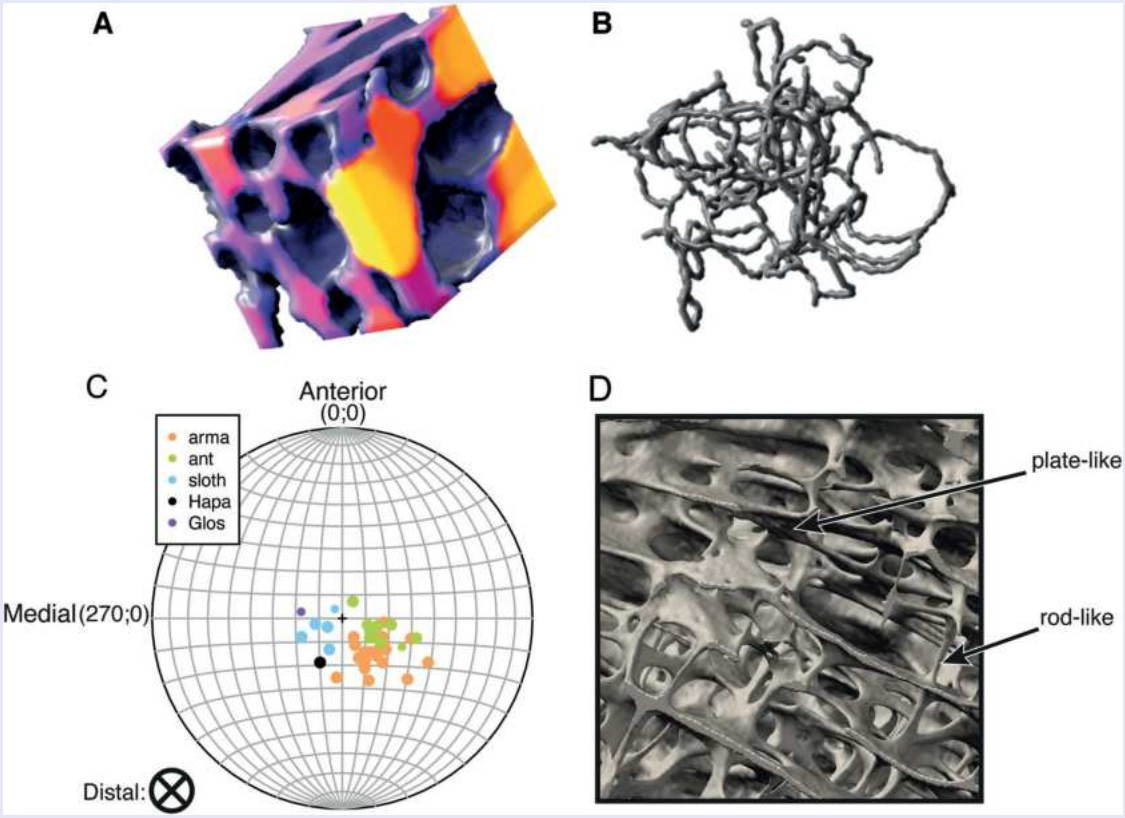


FIGURE B.2 Illustration of selected 3D bone microanatomy parameters. A, Trabecular thickness (Tb.Th; higher values represented by warmer colors). B, Same trabecular network, but skeletonized. C, Stereographic projection of the mean direction of trabeculae in the distal radius of various xenarthrans (a dot found near the center of the circle will, for instance, represent a purely proximodistal direction, whereas a dot at the periphery at three o'clock will denote a purely mediolateral direction). D, Example of rod-like and plate-like trabeculae. Abbreviations: arma, armadillos; ant, anteaters; sloth, extant sloths; Hapa, *Hapalops*; Glos, *Glossotherium*.

4. ***Polarization degree and orientation of trabecular networks*** – The 3D anisotropy of a trabecular network within a VOI is most commonly assessed with the mean intercept length method (MIL; Harrigan and Mann 1984). In brief, a series of a great number of lines are traced with random orientations across the sample. The algorithm detects when these lines cross the trabeculae and computes vectors accordingly. The preferential alignment of the trabeculae of interest is first defined by the degree of anisotropy (DA), analogous to the parameter Pol described in the section "From 2D to 3D Histomorphometry". Depending on the acquisition definition, DA can range from either 0 (perfect isotropy) to 1 (perfect anisotropy; e.g., Saers et al. 2019), or from 1 to infinity (e.g., Fajardo and Müller 2001). The 3D anisotropy of a trabecular network is also defined by its major, intermediate, and minor directions, which are derived from the ellipsoid used for its computation (Odgaard 1997). The major direction of anisotropy is often the most significant parameter, in a comparative context, for instance (Figure B.2C). Command: *BoneJ > Anisotropy.*
5. ***Trabecular morphology*** – The morphology of individual trabeculae can range from a rod-like (i.e., a slender cylinder) to a plate-like shape. Its computation is based on the *ellipsoid factor* (EF), which relies on the average shape of a series of ellipsoids fitted to the contour of trabeculae (Doube 2015). Aiming to make a similar assessment, the widely used *structure model index* has been shown to be seriously flawed (Doube 2015). *BoneJ > Ellipsoid factor.*

Acknowledgements

EA was supported by the German Research Council (Deutsche Forschungsgemeinschaft; grant number AM 517/1-1).

REFERENCES

Amson, E. 2019. Overall bone structure as assessed by slice-by-slice profile. *Evol. Biol.* 46: 343–348.

Baab, K. L., et al. 2018. Using modern human cortical bone distribution to test the systemic robusticity hypothesis. *J. Hum. Evol.* 119: 64–82.

Behrooz, A., et al. 2017. Automated quantitative bone analysis in in vivo x-ray micro-computed tomography. *IEEE Trans. Med. Imaging* 36: 1955–1965.

VetBooks.ir

Dempster, D. W., et al. 2013. Standardized nomenclature, symbols, and units for bone histomorphometry: A 2012 update of the report of the ASBMR Histomorphometry Nomenclature Committee. *J. Bone Min. Res.* 28: 2–17.

Doube, M. 2015. The ellipsoid factor for quantification of rods, plates, and intermediate forms in 3D geometries. *Front. Endocrinol.* 6: 1–5.

Doube, M., et al. 2010. BoneJ: Free and extensible bone image analysis in ImageJ. *Bone* 47: 1076–1079.

Doube, M., et al. 2011. Trabecular bone scales allometrically in mammals and birds. *Proc. R. Soc. B: Biol. Sci.* 278: 3067–3073.

Fajardo, R. J., et al. 2013. Lumbar vertebral body bone microstructural scaling in small to medium-sized strepsirhines. *Anat. Rec.* 296: 210–226.

Fajardo, R. J., and R. Müller. 2001. Three-dimensional analysis of nonhuman primate trabecular architecture using micro-computed tomography. *Am. J. Phys. Anthrop.* 115: 327–336.

Gross, T., et al. 2014. A CT-image-based framework for the holistic analysis of cortical and trabecular bone morphology. *Palaeontol. Electron.* 17: 1–13.

Harrigan, T. P., et al. 1988. Limitations of the continuum assumption in cancellous bone. *J. Biomech.* 21: 269–275.

Harrigan, T. P., and R. W. Mann. 1984. Characterization of microstructural anisotropy in orthotropic materials using a second rank tensor. *J. Mater. Sci.* 19: 761–767.

Houssaye, A., et al. 2018. 3D quantitative comparative analysis of long bone diaphysis variations in microanatomy and cross-sectional geometry. *J. Anat.* 232: 836–849.

Kivell, T. L., et al. 2011. Methodological considerations for analyzing trabecular architecture: an example from the primate hand. *J. Anat.* 218: 209–225.

Odgaard, A. 1997. Three-dimensional methods for quantification of cancellous bone architecture. *Bone* 20: 315–328.

Puymerail, L. 2013. The functionally-related signatures characterizing the endostructural organisation of the femoral shaft in modern humans and chimpanzee. *C. R. Palevol.* 12: 223–231.

Ryan, T. M., and C. N. Shaw. 2012. Unique suites of trabecular bone features characterize locomotor behavior in human and non-human anthropoid primates. *PLoS ONE.* 7: e41037.

Saers, J. P. P., et al. 2019. Trabecular bone functional adaptation and sexual dimorphism in the human foot. *Am. J. Phys. Anthrop.* 168: 154–169.

Schindelin, J., et al. 2012. Fiji: an open-source platform for biological-image analysis. *Nature Meth.* 9: 676–682.

Sode, M., et al. 2008. Resolution dependence of the mon-metric trabecular structure indices. *Bone* 42: 728–736.

Tsegai, Z. J., et al. 2018. Systemic patterns of trabecular bone across the human and chimpanzee skeleton. *J. Anat.* 232: 641–656.

Wood, Z., et al. 2019. Are we crying Wolff? 3D printed replicas of trabecular bone structure demonstrate higher stiffness and strength during off-axis loading. *Bone* 127: 635–645.

5

Bone Cells and Organic Matrix

Louise Zylberberg

CONTENTS

Bone as a Tissue 85
The Cells of Bone 86
The Lineage of Osteoblasts 86
From Preosteoblasts to Osteoblasts 86
The Osteoblast 86
Pathways of Osteoblast Differentiation 89
The Bone-Lining Cells 90
The Osteocytes 90
The Osteoclasts 92
Pathway of Osteoclast Formation 92
The Osteoclast 93
Bone Mineral Dissolution 96
Organic Dissolution 96
Osteoclast Regulation. 96
Bone Matrix 97
The Organic Matrix 97
The Collagen Family 98
Collagens in the Bone Matrix 98
Noncollagenous Proteins 101
Proteoglycans 101
Glycoproteins 101
Osteonectin 102
Gla-Containing Proteins 102
RGD-Containing Proteins 102
Lipids 102
Other Components 102
The Mineral Phase 102
Mineral Matrix Relationships 103
Acknowledgments 103
References 103

Bone as a Tissue

Like other connective tissues, bone consists of cells and an abundant extracellular matrix (ECM) comprising fibers embedded in a ground substance. However, bone matrix is mineralized, unlike that of other connective tissues, a property that makes the mechanical function of skeletal elements possible. The osseous tissue is a composite material: some 60–66% of its weight is inorganic material, 8–10% is water and the remainder is organic (Gong et al. 1964; Currey 2002). By volume the inorganic material is approximately 40%, water 25% and organic substance 35% (Einhorn 1994). The inorganic phase is an impure form of hydroxyapatite, whereas the organic component predominantly consists of type I collagen and a variety of noncollagenous proteins, along with cells.

Despite its hardness and inert, stony appearance, bone is an active tissue. Once formed, it undergoes continual growth, at least at a local scale, along with modeling and remodeling to maintain the size, shape and structural integrity of each

skeletal element. In addition, it contributes to regulating mineral homeostasis because it is a huge calcium and phosphorous reservoir that can be drawn upon as needed for the balance of the blood levels of these ions.

Whatever the mode of formation of the bones (intramembranous vs. endochondral ossification; see Chapter 3), the osseous tissue houses two specific cell categories: the bone-forming cells, i.e. osteoblasts (a term coined by Gegenbauer 1864, 1867), osteocytes and bone-lining cells, which all originate from mesenchymal stem cells (MSCs), and voluminous, polynuclear resorbing cells: the osteoclasts. The latter result from the fusion of mononuclear precursors of the hematopoietic lineage.

Numerous reviews of bone cells and their interactions have been published over the last decades (e.g., Dudley and Spiro 1961; Hall 1978, 1988, 2005; Olsen et al. 2000; Bilezikian et al. 2002; Yuehuei and Martin 2003; Crowder and Stout 2011; Burr and Allen 2014; Florencio-Silva et al. 2015). All emphasize the importance of cell regulation, because bone generation and maintenance are the result of a subtle interplay between osteogenic and osteoclastic activities, under the influence of intrinsic, local and systemic factors. Recent studies have also revealed the complexity of bone cell involvements: osteoblasts may not be only osteoid-producing cells, and osteocytes might not only be the final avatar of osteoblasts (Capulli et al. 2014). Research on bone ECM has also exploded in recent decades; for example, over 200,000 articles have been published on collagen only. This review briefly summarizes the most important data about bone cells and organic matrix. It is not intended to be exhaustive, and only key issues will be addressed.

The Cells of Bone

Continuous layers of cells cover the outer (periosteal) and inner (endosteal, trabecular) surfaces of the bones (Figure 5.1A). The periosteum is a tough membrane that comprises two layers, an outer fibrous layer or mantle housing fibroblasts and an inner layer or cambium of preosteoblasts and osteoblasts. Only the latter are able to form bone (Hall 2005). In addition, a rich network of blood vessels, along with sensory nerves, occurs in the periosteum. The endosteum is a thin layer of connective tissue gathering preosteoblasts, osteoblasts and bone-lining cells interspersed with osteoclasts.

Within the osseous matrix, scattered osteocytes are inserted in lacunae (Figure 5.1A, B) and connected both to neighbors and to the cells lining the bone surface by cytoplasmic processes passing through fine channels or canaliculi.

The Lineage of Osteoblasts

Osteogenic cells synthesize almost all the constituents of the bone matrix and its subsequent mineralization. Like other connective tissue cells, they differentiate from pluripotent MSCs. Their development into osteoblasts follows a sequence of cellular transition described using morphological characteristics and molecular criteria (Aubin and Liu 1996).

MSC cells, with the proper stimulation, can differentiate into preosteoblasts or osteoprogenitors and then osteoblasts (e.g., Caplan, 1991). Osteoblast proliferation and differentiation is controlled by cell-cell and cell-matrix interactions, both of which may involve cytoskeletal proteins (Lomri and Marie 1996). Osteogenic differentiation is prevalent in MSCs with a stiff, spread actin cytoskeleton and numerous focal adhesions (specialized structures involved in actin cytoskeleton organization and signal transduction (Mathieu and Loboa 2012)). The regulation of cell-cell adhesion and cell-matrix interaction in bone is complex due to the multitude of factors possibly involved (see below).

From Preosteoblasts to Osteoblasts

MSCs are spindle shaped or flattened and resemble the fibroblasts of the connective tissues, but they accumulate glycogen. Preosteoblasts are located between the fibroblasts of the connective tissues and the fully differentiated osteoblasts lining the bone surface. They form a preosteoblastic layer in the midshaft periosteum of long bones. They are also found in the loose connective tissue in bone marrow, especially near the small blood vessels.

At the beginning of the differentiation of the MSCs into preosteoblasts an important morphological change is observed. The preosteoblasts become nearly spherical or cuboidal and, at this stage, they can be distinguished from osteoblasts only by their location and by their function, not by their morphology or fine structure. Preosteoblasts are stacked close to the developing bone but not in contact with the bone surface. They can still divide, an ability lost by the osteoblasts, and thus provide the population of cells in which the recruitment of future osteoblasts will occur. They can produce some components of the ECM such as alkaline phosphatase (ALP), but they cannot induce its mineralization.

The Osteoblast

Osteoblasts do not function individually. They are cuboidal cells found in clusters of 100–400 per mm^3 located along the advancing bone surface.

In light microscopy, osteoblasts appear as polarized cells containing a round nucleus located in their apical zone, opposite to the face bordering the bone surface. Basic stains such as methyl blue or toluidine blue reveal one of their most obvious characteristics: the strongly basophilic cytoplasm of their apical part with the exception of the vicinity of the nucleus, where an area less intensively stained represents the Golgi complex (Holtrop 1990). Osteoblasts are always found lining a layer of unmineralized bone matrix or osteoid that they are producing. The presence of osteoid reflects the time lag between matrix deposition and its subsequent mineralization (Figure 5.1C, D).

At the ultrastructural level, osteoblasts display the characteristics of a high synthetic activity (Figure 5.1C). Their large globular nucleus, often eccentrically located, contains one to three well-developed nucleoli. The rough endoplasmic reticulum (RER) occupies most of the cells. It is composed of extensive paired membrane sheets with dilated cisternae filled with an amorphous material (Figure 5.1D, E). There are frequent anastomoses between the paired membrane systems. A large Golgi complex is located close to the nucleus. It comprises

VetBooks.ir

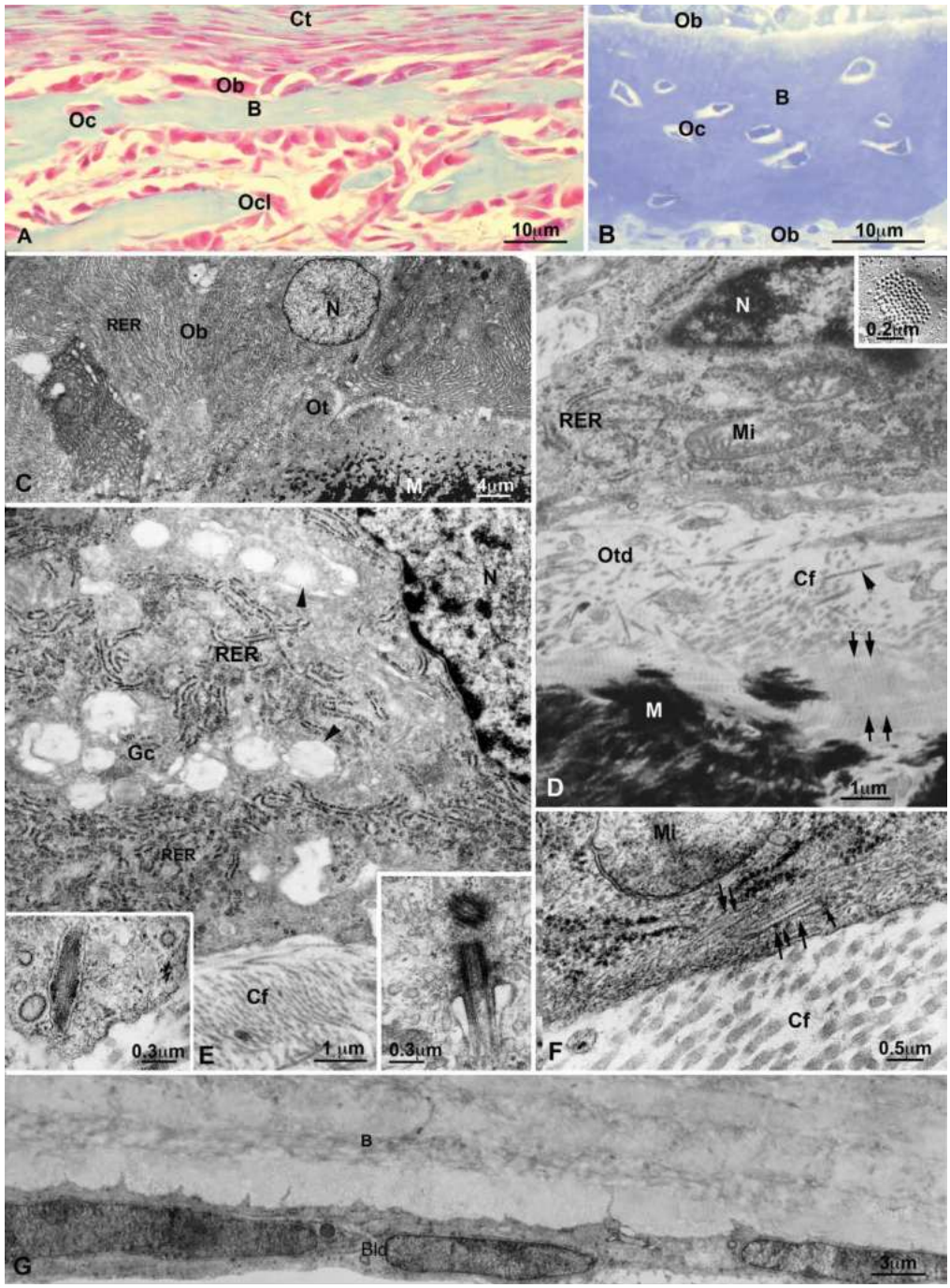


FIGURE 5.1 Osteoblasts. A, B, Light micrographs. A, Rat. Cross section of the femur. One step trichrome. Trabecular bone. The surface of the trabeculae is covered by the bone cells. B, bone; Ob, osteoblast; Oc, osteocyte; Ocl, osteoclast. B, Human. Femur of a 12-week-old fetus. Semithin section. Toluidine blue. Note osteoblasts (Ob) lining the marrow side (to the top) or the connective tissue (to the below) shows a different shape. B, bone; Oc, osteocyte. C–G: Transmission electron micrographs. C, *Cyprinus carpio*. Vertebra. Partially demineralized section. Osteoblasts (Ob) show a well-developed rough endoplasmic reticulum (RER). The osteoid (Ot) forms a layer of unmineralized collagen fibrils in the vicinity of the osteoblasts. Mineral invades the matrix (M) of the osteoid. N, nucleus. D, Human. Femur of a 12-week old fetus. Osteoblast shows a well-developed RER and mitochondria (Mi). Isolated unmineralized collagen fibrils (arrowhead) of the osteoid (Otd) close to the osteoblast form a loose network (Cf), those that are farther fuse to form bundles (double arrows). The crystals are distributed along the collagen fibrils in the mineralized matrix (M). N, nucleus. Inset shows a gap junction observed in a cryofracture. E, Human. Femur of a 12-week-old fetus. Osteoblast with a well-developed Golgi complex (Gc) with large saccules filled with an amorphous material (arrowheads) and abundant RER. Unmineralized collagen fibrils (Cf) show an approximately parallel orientation. Inset at the bottom left shows a Golgi secretory globule containing parallel-oriented filaments. Inset at the bottom right show a cross-sectioned centriole and a longitudinally sectioned cilium. F, Human. Femur of a 12-week-old fetus. Cytoskeletal filaments (arrows) are coaligned with the collagen fibrils (Cf) of the osteoid. Mi, mitochondria. G, Rat. Femur. Demineralized section. Bone-lining cells (Blc) are flat cells forming a thin cellular layer on inactive bone surface (B). Few organelles are seen in these cells.

multiple vacuoles and interconnected stacks of flattened saccules showing dilations. The saccules are filled with a network of thin filaments (0.5–2 nm in diameter) (Figure 5.1E, inset). Coated vacuoles occur at the periphery of the Golgi complex and the secretory region and tend to fuse with the plasmatic membrane.

The sequence of different structural aspects of the RER and Golgi areas is related to the sequence of the synthesis of collagen. This sequence has been elucidated at an ultrastructural level using radioautography and immunostaining for labeling type I procollagen (the precursor of collagen fibrils). The increasing gradient of labeled procollagen that occurs from the RER cisternae through the Golgi saccules and ultimately to the secretory granules illustrates the pathway of the collagen synthesis (Wright and Leblond 1981). Accumulation of particulate glycogen is observed at one or both poles of the cells.

Mitochondria are scattered in the cytoplasm between the sheets of the RER, outside the Golgi area (Figure 5.1D, E). Electron-dense particles (*ca.* 60 nm in diameter) bonded to the inner membrane are reported in osteoblasts involved in a very active synthetic activity that occurs in the early stages of skeletal development (Martin and Matthews 1970) or during fracture repair (Gothlin 1973). These particles have a high content of calcium and phosphorus as revealed by electron microscopic observations (Landis et al. 1977a, b) and microprobe analysis (Sutfin et al. 1971; Manston and Katchburian 1984). Lysosomes are rarely observed in osteoblasts. When present, they consist of spherical bodies limited by a single membrane surrounding a characteristic uniform dense central matrix. Lysosomes contain acid hydrolases (Vaes 1965; Doty and Schofield 1984), but their function in osteoblasts remains to be elucidated (Tsukuba et al. 2017).

Centrioles and solitary cilia have been described in osteoblasts but are extremely rare (Figure 5.1E, inset). A possible role of cilia in anabolic signaling between osteoblasts and osteocytes is considered by Xiao et al. (2006). An alternate hypothesis suggests that the cilia could be involved in shear amplification (Myers et al. 2007). Ultrastructural studies show that the cytoskeleton of osteoblasts is composed of microtubules and two types of microfilaments. The microtubules (*ca.* 25 nm in diameter) are particularly abundant in the vicinity of cell-cell contacts and close to the cell membrane facing the bone surface (Aubin et al. 1983; Arena et al. 1991) (Figure 5.1F). Filaments of intermediate size (*ca.* 10 nm in diameter) run singly or in thin bundles. Actin microfilaments are thinner (5–7 nm), but represent the major part of osteoblast microfilaments (Chen et al. 2015). They play a prominent role in the mechanical loading-dependent proliferation of the cells during bone formation (Sakai et al. 2011).

The cytoskeleton is of fundamental importance in MSCs and preosteoblasts because it regulates their shape and their osteogenic potential (Rodriguez et al. 2004; Mathieu and Loboa 2012). It remains of fundamental importance in osteoblasts because it is involved in cell proliferation, adherence and differentiation; cell-matrix interactions and gene expression (Lomri and Marie 1996). The plasma membrane of the osteoblasts is rich in alkaline and neutral phosphatases and has been shown to house receptors for diverse systemic or local hormones (see below).

Adjacent osteoblasts are frequently joined by adherens junctions and desmosomes, which perform a mechanical function by linking their cytoskeleton (Palumbo et al. 1990). Adherens junctions are associated with cadherins, i.e., transmembrane proteins that function to join cells through their cytoskeleton. The apposed cell surfaces of contiguous osteoblasts are also occasionally very close and dense, a situation indicative of gap junctions (Figure 5.1D, inset), as already observed between other bone cells (Doty 1981). Such intercellular communications allow small molecules (molecular mass < 1 kD) to pass from cell to cell. Gap junctions are composed of connexin 43 (Cx43), which is a specific gap junction protein known to influence the function of osteoblasts and osteocytes (Buo and Stains 2014) because both of these cells are also joined to each other through gap and adherens junctions (Palumbo et al. 1990). Gap junctions may be involved in bone development or remodeling by coordinating the responses of bone cells to physical or hormonal signals (Donahue et al. 1995). Altered gap junctional communication between osteoblasts may have an indirect stimulating effect on osteoclasts that results in decreased bone strength (Watkins et al. 2011).

Secretion of osteoblasts is generally polarized toward bone surfaces and only the cell surface facing the bone surface displays short microvilli. The latter increase in length as the osteoblasts become surrounded by the matrix. They thus contact similar processes originating from the osteocytes and housed within the bone tissue in thin tunnels called *canaliculi*. Osteoblasts orchestrate the bone formation process. They produce bone ECM in two steps. First they synthesize an unmineralized ECM, the osteoid, which later becomes mineralized under their influence. The fibrillar type I collagen represents approximately 90% of the total organic component of osteoid (see below).

In addition to collagen, osteoblasts also synthesize noncollagenous proteins including proteoglycans, glycoproteins, Gla-containing proteins and RDG-containing proteins (Groot et al. 1986; Fisher et al. 2001; Gehron Robey 2002; Gehron Robey and Boskey 2006). These calcium-phosphate binding proteins may be involved in an ordered deposition of the mineral by regulating the amount and the size of hydroxyapatite crystals (see Chapter 6). The matrix extracellular phosphoglycoprotein (MEPE) is a highly phosphorylated protein also synthesized by osteocytes. It acts as an inhibitor of osteoblastic activity (Rowe 2004).

Osteoblasts are also a target for bone morphogenetic proteins (BMPs), i.e., pleiotropic cytokines belonging to the transforming growth factor (TGF)-β superfamily (Katagiri and Tsukamoto 2013). BMPs were originally identified by their ability to induce ectopic bone formation when demineralized bone was implanted in ectopic sites in mammals (Urist 1965). This unique bone inductive activity indicates that BMPs provide a primordial signal for osteoblastogenesis because BMPs induce the expression of Runx2 and osterix, the most important transcription factors involved in osteoblast differentiation (see below and Ducy et al. 1997; Lee et al. 2000). In the TGF-β superfamily, BMPs are nearly the sole proteins having osteogenic properties (Wozney 1992). BMP signaling is known to be mediated by the Smad family of proteins (Heldin et al. 1997).

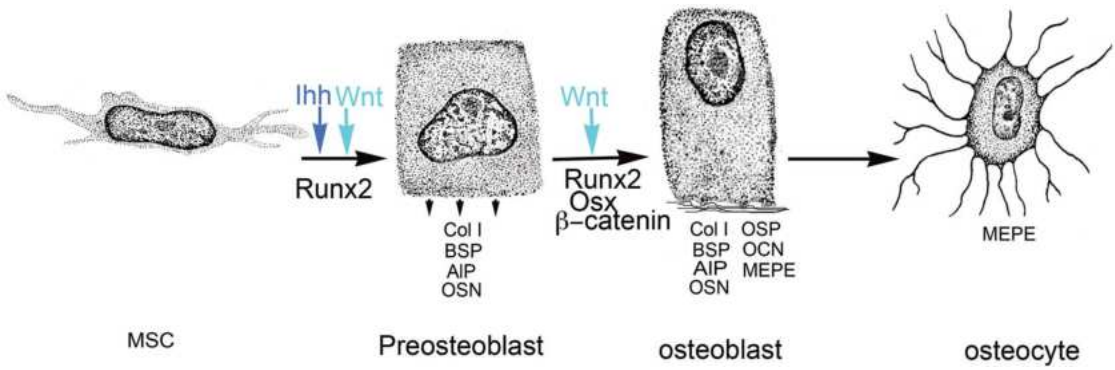


FIGURE 5.2 Schematic representation of the osteoblast differentiation pathway. Observations from these studies (Harada and Rodan 2003; Hu et al. 2005; Rodda and McMahon 2006; Florencio-Silva et al. 2015) have been used to synthesize this model. Blue and green arrows indicate the requirement for Ihh and Wnt signaling, respectively. AIP, alkaline phosphatase; BSP, bone sialoprotein; Col I, type I collagen; MEPE, matrix extracellular phosphoglycoprotein; OCN, osteocalcin; OSN, osteonectin; OSP, osteopontin.

Pathways of Osteoblast Differentiation

A central role in osteoblast differentiation is played by the Wnt protein family, which is involved in the early development of organs and tissues (Hartmann, 2007) (Figure 5.2). The Wnt genes encode a large family of protein growth factors identified in animals from hydra to humans. In mammals, Wnts are a family of 19 lipid-modified glycoproteins sharing a 27–83% amino-acid sequence identity and a conserved pattern of 23 or 24 residues of cysteine (Miller 2001). Wnt proteins interact with the Frizzled receptor, which transduces the signal through either the canonical β-catenin pathway or the non-canonical β-catenin pathway (Gordon and Nusse 2006).

Canonical Wnt signaling regulates renewal of stem cells and the stimulation of preosteoblast duplication. It promotes differentiation of osteoblast precursors into mature osteoblasts, and it prevents osteoblast apoptosis (Karsenty and Wagner 2002; Westerndorf et al. 2004; Hill et al. 2005; Krishnan et al. 2006; Kobayashi et al. 2008). However, Notch, a transmembrane receptor, may inhibit the differentiation of MSCs into osteoblasts through a temporal interaction with Wnt signaling (Ji et al. 2017; Shao et al. 2018).

Together with canonical Wnt signaling, the Indian Hedgehog (IHh; a member of the Hedgehog gene family encoding proteins implicated in cell-cell contact) pathway is implicated in the osteogenic program in endochondral ossification but not in intramembranous bone formation (Hill et al. 2005; Hu et al. 2005; Rodda and McMahon 2006). The canonical Wnt pathway promotes bone formation through the activation of master osteogenic transcription factor Runx2 (previously Cbfa1), a member of the runt family, which drives mesenchymal cells to osteogenic lineage (Ducy et al. 1997; Gaur et al. 2005).

Osteoblast differentiation nevertheless requires the sequential activity of two transcription factors, Runx2/Cbfa1 and osterix (osx), also known as Sp7, which is a finger zinc-containing transcription factor (Nakashima et al. 2002).

Runx2 is the earliest marker of osteoblast differentiation (Ducy et al. 1997; Komori et al. 1997; Otto et al. 1997; Ducy 2000; Karsenty and Wagner 2002). It upregulates genes coding for proteins specifically produced by the osteoblasts (i.e., markers of these cells) such as osteocalcin, bone sialoproteins (BSPs), ALP and type I collagen. Runx2 activity is required for bone matrix deposition (Ducy et al. 1999; Ducy 2000); however, the transcription factor osx is also required for the differentiation of preosteoblasts into functional osteoblasts (Nakashima et al. 2002). Its inactivation in mice results in arrested osteoblast differentiation and absence of bone formation (Nakashima et al. 2002). Osx was shown to be able to induce a decrease of osteoblast proliferation that, in contrast, is stimulated by the Wnt pathway activity. This experiment suggests that osx inhibits Wnt/β-catenin signaling (Zhang et al. 2006). Osx acts downstream of Runx2 in the transcriptional cascade of osteoblast differentiation (Nakashima et al. 2002). It is an essential transcription factor for osteoblast differentiation and bone formation, not only during embryonic development, but also in postnatal skeletal growth (Zhou et al. 2010). Runx2 and osterix are the master genes for osteoblast differentiation and function.

The canonical Wnt signaling induces a downregulation of RANKL (receptor activator of nuclear factor kappa B ligand belonging to the tumor necrosis factor [TNF] superfamily). In osteoblasts, its binding with the RANK receptor results in the inhibition of bone resorption (Kobayashi et al. 2008) and in the upregulation of osteoprotegerin (OPG) expression (Figure 5.2). OPG is a cytokine receptor of the TNF belonging to the receptor superfamily expressed in the osteoblast lineage cells (Simonet et al. 1997). Because of the importance of Wnt proteins during bone formation, the Wnt signaling pathway is considered an interesting target for therapeutics for bone diseases (e.g., Boudin et al. 2013).

Recent insights into the transcriptional regulation of osteoblasts identified LRP5 as a molecule involved in bone homeostasis (Harada and Rodan 2003), and LRP4 is thought to promote osteoclast genesis by inhibiting Wnt/catenin signaling. Leptin, a small polypeptide hormone, regulates bone mass through the control of the osteoblast function (Ducy et al. 2000; Reseland and Gordeladze 2002).

The normal fate of osteoblasts is ultimately to differentiate into bone-lining cells or osteocytes. Approximately 30–50% of the osteoblast population becomes one or the other of these two cell types, whereas some 50–70% undergo apoptosis.

VetBooks.ir

The Bone-Lining Cells

Bone-lining cells are quiescent cells, defined by their location and morphology (Figure 5.1G). They have an elongated shape parallel to the bone surfaces where neither accretion nor resorption occurs (Florencio-Silva et al. 2015). They contain slightly ovoid nuclei and their cytoplasmic organelles, such as profiles of RER, free ribosomes, Golgi complex and mitochondria, are sparse. Bone-lining cells are often connected to each other and to nearby osteocytes by gap junctions (Miller et al. 1980).

Little is known of the function of these cells, which are nevertheless much more abundant than osteoblasts. They may remove an organic protective material and induce a direct exposure of the mineralized matrix to contact the osteoclast (Chambers 1980; Andersen et al. 2009). During the remodeling process of cancellous bone, bone-lining cells locally lift off the trabeculae to form a velum-like structure currently named canopy, under which bone resorption and reconstruction will occur (Hauge et al. 2001). Together with other cells, bone-lining cells are an important component of the so-called bone multicellular units (BMUs), transitory structures that form during the remodeling cycle (Everts et al. 2002; see the chapter 11).

Everts et al. (2002) showed that bone-lining cells contribute to cleaning Howship's lacunae, digesting the collagen remnants left by the osteoclasts. Once the lacuna is cleaned the bone-lining cells deposit a thin layer of collagen fibrils over its surface. Removal of collagen left by the osteoclasts is considered a necessary step between resorption and subsequent secondary accretion (Everts et al. 2002). In addition, bone-lining cells participate in osteoclast differentiation through the production of OPG and RANKL (Andersen et al. 2009). They may also regulate influx and efflux of mineral ions such as calcium and phosphate into and out of bone extracellular fluid, serving as a blood-bone barrier. Moreover, they retain the ability to redifferentiate into osteoblasts under exposure to parathyroid hormone (PTH) or mechanical forces (Dobnig and Turner 1995; Matic et al. 2016).

The Osteocytes

Osteoblasts become osteocytes when they are trapped within the matrix during bone deposition (Fig. 5.3A–C). Two processes of encasement are hypothesized: self-entrapment or embedding by adjacent cells. In the first case, some osteoblasts remain behind their collagen synthesis and become trapped within the matrix. In the other case, the nascent osteocytes degrade their surrounding matrix to create the lacuna-canalicular system (Holmbeck et al. 2005).

During their transition to entrapped osteocytes, osteoblasts undergo a dramatic morphological transformation and extend their microvilli toward the mineralizing front. Three cell types were distinguished from osteoblasts to mature osteocytes: type I preosteocytes (or osteoblastic osteocytes) that start to be embedded in the mineralizing matrix resemble mature osteoblasts. Type II preosteocytes (osteoid osteocytes) have decreased in size and lost some 30% of their initial volume (Marotti et al. 1976). Type III preosteocytes are partially surrounded by mineral (Palumbo et al. 1990; Bonewald 2011).

Osteocytes are the most abundant cellular components of mammalian bone, representing up to 95% of all bone cells. Their survival within the mineralized matrix is estimated to reach 25 years in humans, whereas osteoblasts live approximately 3 months on the average.

The nuclei of "young" osteocytes have nucleoli (Figure 5.3D). The cytoplasm of these cells contains large amounts of RER that form irregular dilations filled with an amorphous material, extensive Golgi complex, mitochondria, microtubules, microfilaments and some lysosomes (Figure 5.3C, D). These cells thus retain the machinery for synthesizing the matrix (Baylink and Wergedal 1971). Only young osteocytes show neutral and acidic phosphatase activity on their cell membranes. They continue to secrete the matrix and appear to play a role in the initiation and control of matrix mineralization (Barragan-Adjemian et al. 2006). They also express osteocalcin, osteonectin, and osteopontin. More mature osteocytes show a decrease of ALP activity (Aarden et al. 1996). Osteocytes express MEPE much more than osteoblasts do (Bonewald 2007), and they are enriched in proteins (less abundant in osteoblasts) associated with resistance to hypoxia.

The differentiation of osteoblasts into osteocytes is supposed to be regulated by oxygen tension that may also play a role in disuse-mediated bone resorption (Dallas and Bonewald 2010). It is also promoted by Notch, a transmembrane receptor that inhibits the differentiation of MSCs into osteoblasts. Notch action involves a temporal interaction with Wnt signaling in the terminal stages of osteocyte differentiation (Ji et al. 2017; Shao et al. 2018). Notch affects both osteoblast and osteoclast lineages (Ashley et al. 2015). Moreover, the inhibition of Wnt signaling by sclerostin, a glycoprotein produced by osteocytes, results in an inhibition of osteoblast differentiation into preosteocytes (Delgado-Calle et al. 2017; Sebastian and Loots 2017). It has been shown that sclerostin, which promotes osteoclastic bone resorption by modulating the RANKL/OPG ratio in osteocytes, may play a catabolic role in bone (Wijenayaka et al. 2011).

Fully mature osteocytes are recognized by their stellate morphology and by their location within the lacunocanalicular network of bone. However, their size and shape differ depending on the bone type (Figure 5.3E). Osteocytes from woven bone are more rounded than osteocytes from parallel-fibered or lamellar bone, which are more slender (Currey 2003; Kerschnitzki et al. 2011). New methods developed for two-dimensional (2D) and three-dimensional (3D) imaging facilitate the study of the complex lacunocanalicular system and its environment (Webster et al. 2013; Bach-Gansmo et al. 2015; Kamel-Elsayed et al. 2015). The size of the lacunae as well as the space between the osteocyte and the mineralized matrix within the lacunae are variable. Some osteocytes are closely surrounded by mineralized matrix, whereas others are surrounded by a network of collagen fibrils that can be compared to the osteoid (Holtrop 1990). Each osteocyte extends slender processes within canaliculi through the matrix to contact processes of neighboring osteocytes and with those of cells lining the bone surface (Franz-Odendaal et al. 2006). The 3D network of lacunae and canaliculi contain a non-mineralized organic matrix rich in osteopontin. Osteocytes acquire a typical cytoskeletal organization related to their

VetBooks.ir

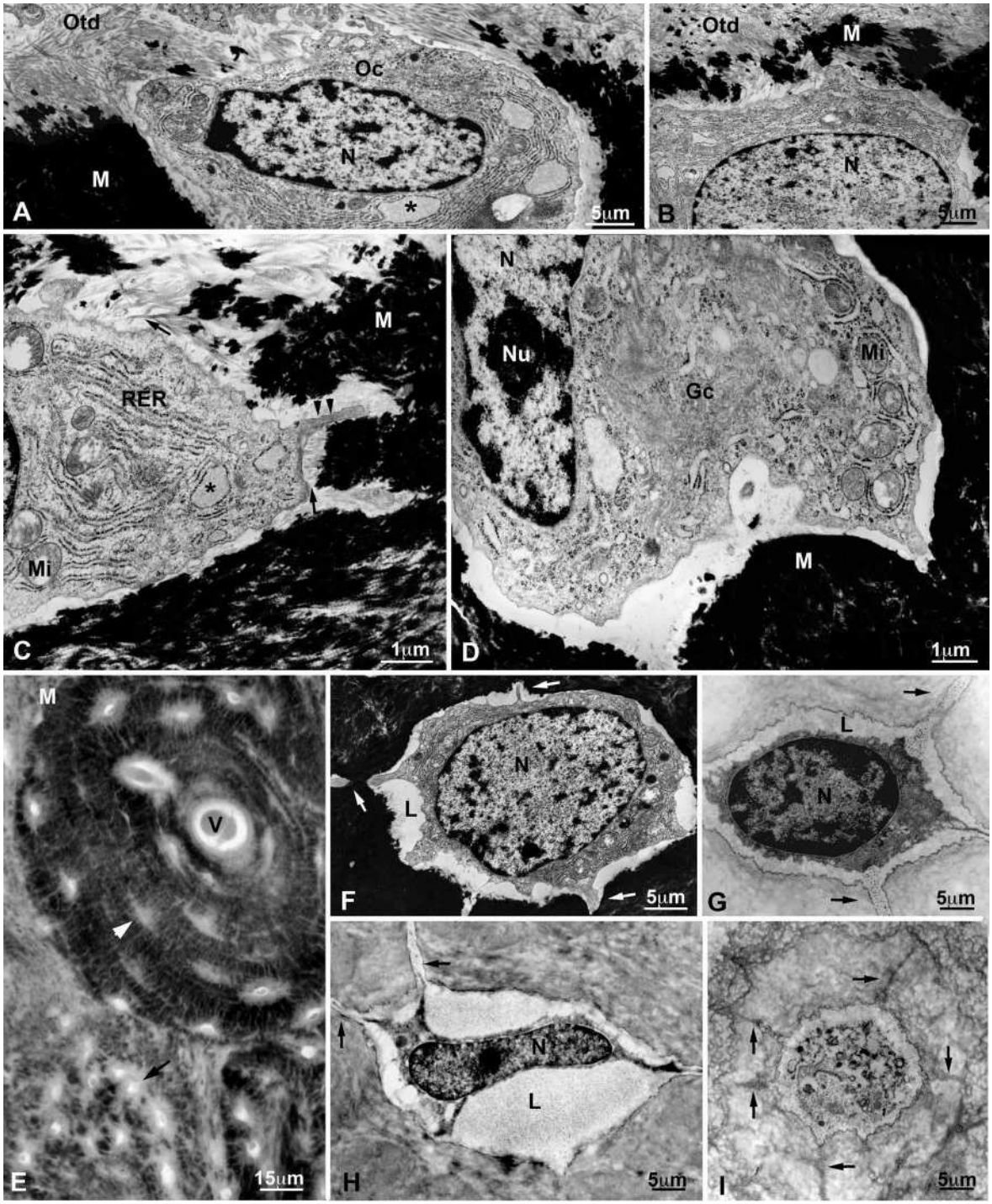


FIGURE 5.3 Osteocytes at different stages of maturation. A–D, F–I, Transmission electron micrographs. E, Light micrograph. A–D, Human. Femur of a 12-week-old fetus. A–C, "Young osteocytes". A, The osteocyte (Oc) is not entirely engulfed in the mineralized matrix (M). It shows a well-developed rough endoplasmic reticulum with dilated cisternae containing an amorphous material (asterisk). N, nucleus; Otd, osteoid. B, The osteocyte is almost entirely surrounded by the mineralized matrix (M). C, Human embryo. Femur. A young osteocyte extends slender processes (arrowheads). It shows dilated cisternae of RER containing an amorphous material (asterisk) and numerous mitochondria (Mi). D, Femur of a 12-week-old fetus. An osteocyte entirely encased in the mineralized matrix (M) has a developed RER surrounding a large Golgi area (Gc). It contains a voluminous nucleolus (Nu) and numerous mitochondria (Mi). N, nucleus. E, Cat. Cross section of the femur. Hematoxylin staining. Flat osteocytes inserted between the concentrically arranged lamellae of the osteon (arrow head) and connected by slender canaliculi differ from the round osteocytes located in the spaces between the osteons (arrow). F, Human. Femur of a 12-week-old fetus. Osteocyte surrounded by mineralized matrix extends many cell processes (arrows). L, lacuna; N, nucleus. G, Duck. Femur. Demineralized tissue. Osteocyte with a reduced cytoplasm layer around the nucleus. Osteoid fills the lacuna (L). Part of cell processes (arrows). N, nucleus. H, Duck. Femur. Demineralized tissue. Osteocyte at a degenerative stage is surrounded by osteoid, which fills the lacuna (L). Cell processes (arrows). N, nucleus. I, Rat. Femur. Demineralized tissue. Cellular debris. Parts of canaliculi (arrows).

VetBooks.ir

stellate morphology. Actin bundles run in their processes (Figure 5.3C). A dramatic change of the distribution of actin binding proteins such as fimbrin, filamin and α-actinin occurs in osteocytes compared to osteoblasts (Kamioka et al. 2004). A single nucleus occupies most of the cellular space, and the relatively sparse cytoplasm contains small Golgi saccules, a few mitochondria and occasional lysosomes (Figure 5.3F). The extent of RER areas varies greatly depending on the age and state of activity of the osteocytes (Figure 5.3F, G).

As osteocytes become located deeper within the bone, their morphology gradually changes and becomes a resorptive stage followed by a degenerative one (Holtrop 1990). In the resorptive stage, RER and the Golgi complex are greatly diminished although still observable, and lysosomes have proliferated. Old osteocytes no longer exhibit cell membrane ALP. They decrease in size and their lacunae are filled with more osteoid (Figure 5.3H). Most of them die (Figure 5.3I) by apoptosis (see apoptosis in chapter 7). Some are phagocytosed by osteoclasts during bone resorption (Bronkers et al. 1987; Elmardi et al. 1990).

To some extent, osteocytes can initiate and control osteoid production and mineralization (Mikuni-Tagaki et al. 1995; Barragan-Adjemian et al. 2006; Repp et al. 2017). They prevent the mineralization of the matrix around the lacunocanalicular network (Schneider et al. 2010) and dissolve the mineral on their walls. Recent data suggest that this action is made possible by the capacity of osteocytes to acidify their environment, dissolve the mineral, and transfer it to the bloodstream, in addition to allowing the transport of oxygen, nutrients and waste products through the lacunocanalicular network (Nango et al. 2016). In brief, osteocytes remodel their perilacunar environment by removing or replacing its components. They can also extend or retract their dendritic processes (Dallas and Bonewald 2010). TGF-β is thought to be one of the regulators of perilacunar/lacunar remodeling (Dole et al. 2017).

The pericellular space is filled by a fluid that separates the osteocyte from the surrounding mineralized matrix (Schaffler et al. 2014); the space between them is approximately 0.5–1.0 μm at the level of the cell body, and 50–100 nm around the dendritic processes (You et al. 2004). Osteocyte processes are not free-floating structures; instead, they are connected by transverse tethers to the wall of the canaliculi. They play a central role in the mechanosensitive function of the osteocytes by amplifying the fluid flux provoked by mechanical load forces aligned with the pericellular space (You et al. 2004). In this process, integrins are mediating factors for cell-matrix interactions at the somatic as well as the dendritic levels (McNamara et al. 2009). Such interactions generating and amplifying the signals created by tissue deformation are essential for the mechanosensitive function of osteocytes (Wang et al. 2007). Signals are also transmitted from osteocytes to bone surface cells through the Wnt/β-catenin pathway that also appears to be associated with a decrease of osteocyte apoptosis (Bonewald and Johnson 2008; Tu et al. 2015). Osteocytes located on the endosteal surface communicate with bone marrow cells by extending dendrites and by secreting diverse molecules: sclerostin, PTH-related peptide (PTHrP), prostaglandin E2 (PGE2), fibrocyte growth factor (FGF), RANKL and OPG (Zhang et al. 2006).

Osteocytes not only control their perilacunar environment but also regulate bone remodeling by controlling osteoblasts and osteoclasts. Their network within bone may act as a functional syncytium. Indeed, despite their location deep within the bone matrix, osteocytes communicate with osteoblasts and osteoclasts on the surface by sending signals (Atkins and Findlay 2012). Their plasmic membrane possesses receptors for PTH and estrogens, through which they control bone remodeling (Prideaux et al. 2016). Xiong et al. (2015) suggested that osteocytes, in contrast to osteoblasts or lining cells, are the main source of RANKL required for osteoclast formation. As in osteoblasts, RANKL is mainly localized in lysosomes in osteocytes (Honma et al. 2013). Considering that osteocytes orchestrate both osteoblast and osteoclast activities, they are viewed as the masters of remodeling (Bonewald 2011).

The Osteoclasts

Pathway of Osteoclast Formation

Osteoclasts, discovered and named by Kölliker (1873), are located on the endosteal bone surface and on the periosteal surface beneath the bone periosteal surface. They are usually isolated cells or aggregated in low numbers with only two or three per μm^3 (Roodman 1996).

These multinucleated cells are larger than the other bone cells (150–200 μm in diameter in human) and are derived from the fusion of mononuclear precursor cells of the monocyte-macrophage lineage (Fishman and Hay 1962) under the influence of several factors. Proliferation of precursor cells and their differentiation are driven by two factors: the macrophage colony-stimulating factor (M-CSF), secreted by the osteoprogenitor mesenchymal cells and the osteoblasts, and RANKL, secreted by osteoblasts, osteocytes and stromal cells. M-CSF and RANKL are critical for osteoclast formation (Figure 5.4). Binding of M-CSF to its receptor (cFMS) in the osteoclast precursor stimulates its proliferation and inhibits its apoptosis (Yavropoulou and Yovos 2008).

The binding of RANKL to its receptor RANK in osteoclast precursors induces osteoclast formation. Osteoblasts also produce OPG, a soluble decoy receptor that binds to RANKL and prevents from its binding to RANK, thus inhibiting osteoclast formation and stopping osteoclastogenesis. The relative concentration of RANKL and OPG determines the extent of proliferation and differentiation of osteoclast precursors in bone (Boyce and Xing 2008). The RANKL/RANK/OPG system is a key mediator of osteoclastogenesis and is possibly stimulated through the noncanonical Wnt pathway. Osteoblasts also control the movement of osteoclast precursors to the bone surface through the release of chemoattractants such as osteocalcin and type I collagen, deposited in the matrix by osteoblasts during bone formation. Such chemoattractants are also released during bone resorption and continue bone resorption by attracting osteoclast precursors (Malone et al. 1982). Interestingly, unmineralized bone osteoid is protected against osteoclastic resorption. Additionally, osteoclastogenesis is promoted by sclerostin through a modulation of the RANKL/OPG ratio in osteocytes (Wijenayaka et al. 2011). Together

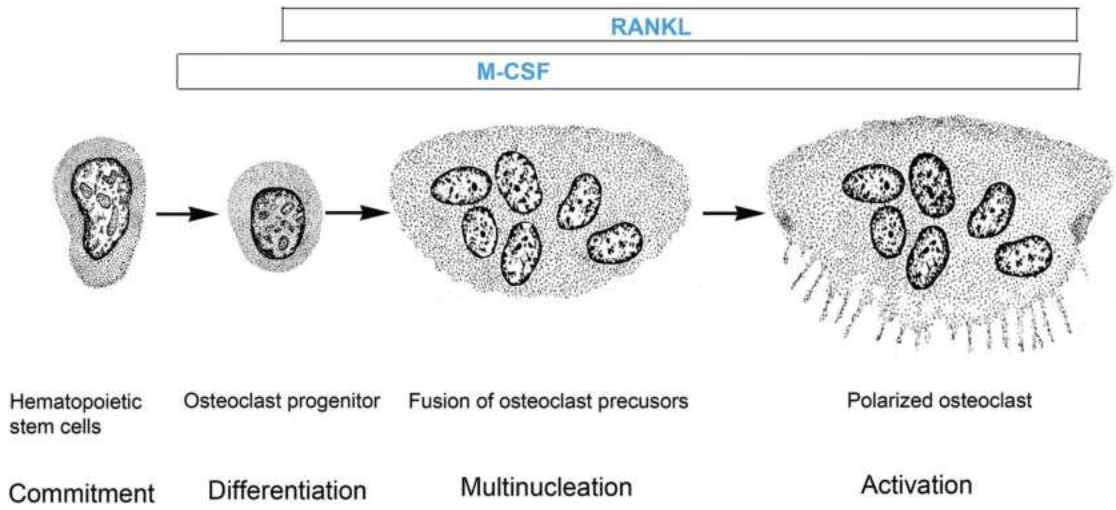


FIGURE 5.4 Osteoclast differentiation pathway. Proposed pathway of osteoclast differentiation based on the observations from Karsenty and Wagner (2002), Kobayashi and Kronenberg (2005) and Florencio-Silva et al. (2015). MCSF, macrophage colony-stimulating factor; RANKL, receptor activator of nuclear factor kappa B ligand.

M-CSF and RANKL are factors promoting the activation of the corresponding receptors at the cell surface of osteoclast precursors. This activation induces the regulated expression of genes including those encoding cathepsin K_1, and $\alpha_V\beta_3$ integrin, such as tartrate-resistant acid phosphatase (TRAcP) specific to osteoclasts (Yavropoulou and Yovos 2008). The production of acid-phosphatase isoenzyme resistant to inhibition by tartrate (TRAcP) is generally accepted as a marker for osteoclasts and their immediate precursors (Scheven et al. 1986; van de Wijngaert and Burger 1986), whereas the acid-phosphatase isoenzyme of monocytes and macrophages is tartrate sensitive (Wergedal 1970; Seifert 1984).

Bone marrow monocyte-macrophage precursor cells give rise to most osteoclasts. The fusion of cells takes place in the vicinity of the bone surface. The diversity of osteoclast shape suggests that these cells may wander on the bone surface to be guided to the sites that are determined to be resorbed. The presence of snail track lacunae on the surface of bone ECM reveals their movement (Jones et al. 1985); however, the typical clue to osteoclastic erosion is the occurrence of shallow cup-like pits, the Howship's lacunae. Differences in size and depth of the lacunae reflect variations in the resorbing activity of osteoclasts (Jones and Boyde 1977). Sometimes, cells can be identified in the lacuna, but the latter are often empty and ready to be secondarily filled. Although the factors determining the resorption site remain elusive, the retraction of the bone-lining cells can be considered the early stage of a resorption process (Jones and Boyde 1977). This retraction leaves a free surface of bone on which the osteoclasts can be fixed. Moreover, osteoclast precursors expressing RANK are found in the vicinity of osteoblasts, which could suggest that osteoblasts also contribute to provide a site for osteoclast activity (Maeda et al. 2012).

Osteoclasts alternate between migration with a flat morphology and resorption with polarization. Between nonresorbing and resorbing cycles, they undergo dramatic modifications. For each cell, a resorbing cycle involves complicated multistep processes including the attachment of the osteoclast to the bone surface, its polarization, the formation of a sealing zone and a ruffled border, the resorption proper and the cell detachment. Polarization of osteoclasts begins as soon as they are in contact with the mineralized ECM of bone. Active osteoclasts differentiate into four types of membrane domains: (1) the apical domain (the ruffled border), (2) the sealing zone (these two domains are in contact with the bone ECM), (3) the basolateral domain and (4) the basal functional secretory domain (FSD) (these last two domains are not in contact with the bone ECM). FDS is morphologically different from the rest of the membrane and has been shown to be a target for transcytotic vacuoles carrying bone degradation products (Salo et al. 1997b) (Figure 5.5). These domains are not observed in nonresorbing osteoclasts.

The Osteoclast

Resulting from the fusion of mononuclear cells, osteoclasts contain many nuclei heterogeneous in size, shape and in basophilia, which reflects an asynchronous fusion of mononuclear precursors. The largest osteoclasts may have several hundred nuclei, the smallest two or three, although most have from 5 to 20 (Figure 5.5A, B). Nuclei contain conspicuous nucleoli. Compared to osteoblasts, the osteoclasts have a highly heterogenous, poorly basophilic cytoplasm, which suggests a less developed RER (Figure 5.5B). The latter is usually located in the basal portion of the cytoplasm in active polarized osteoclasts (Figure 5.5B, C). Cisternae are sparse but the numerous nonmembrane ribosomes, often associated into clusters, are probably responsible for the basophilia of these cells. Their cytoplasm is characterized by abundant mitochondria (Figure 5.5C) containing dense granules comparable to those of osteoblasts and similarly rich in calcium (Landis et al. 1977b). Mitochondria provide energy for bone resorption through cell respiration, which is an energy-dependent process. The CO_2 that they produce plays a role in the acidification processes

VetBooks.ir

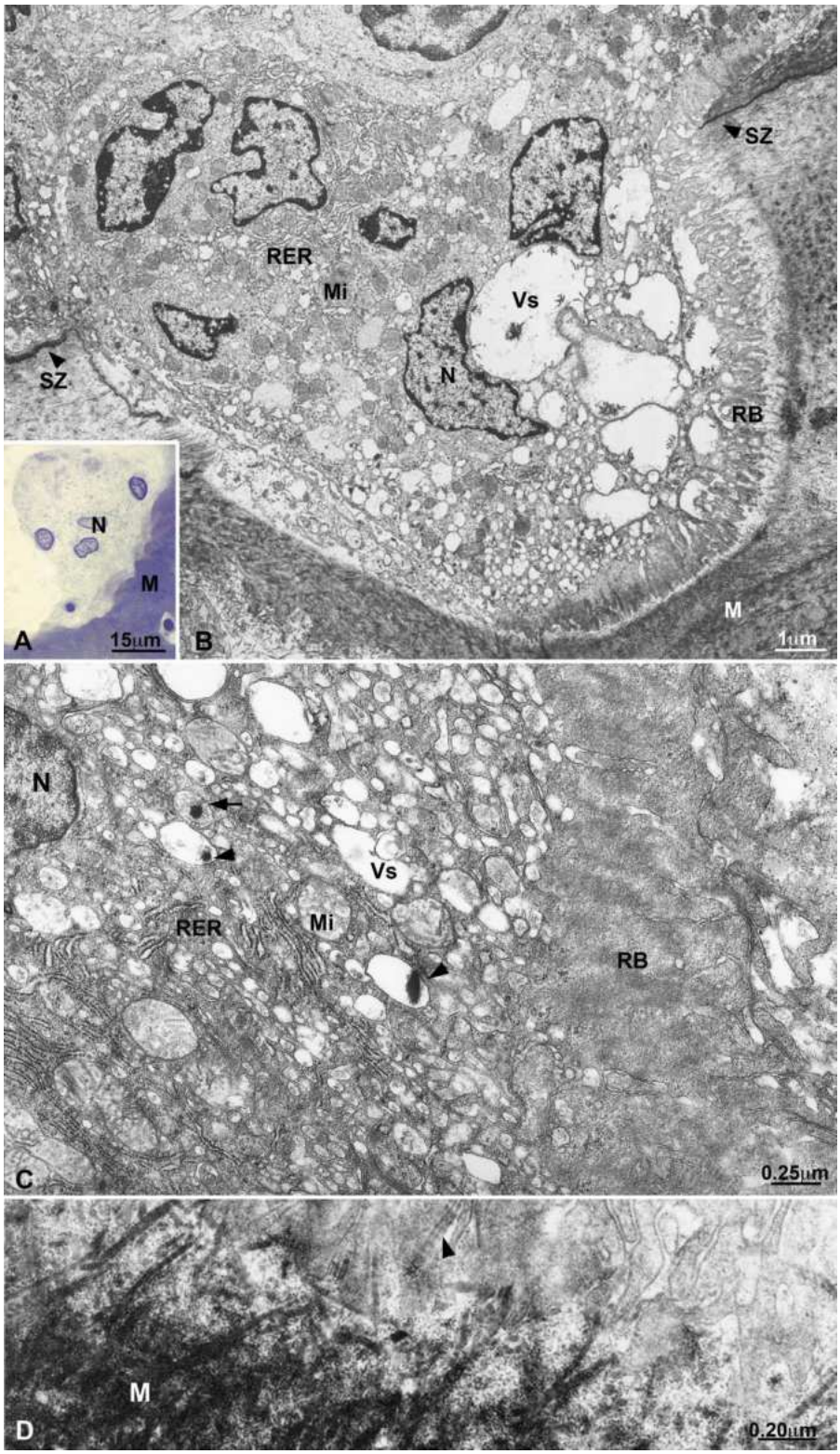


FIGURE 5.5 Osteoclasts. A, Human. Femur of a 12-week-old fetus. Light microscopy. Semithin section. Toluidine blue. This large cell shows osteoclast characteristics: a dome-shape and many nuclei (N) and a foamy aspect of the cytoplasm. M, mineral. B–D, Transmission electron micrographs (TEMs). B, Osteoclast. TEM. This typical osteoclast is characterized by large and numerous vacuoles (Vs) near of the ruffled border (RB) with some containing debris, numerous mitochondria (Mi), flat cisternae of rough endoplasmic reticulum (RER) present mostly in the vicinity of the nuclei (N) and the sealing zone (SZ). (Holtrop 1990). C, Human. Femur of a 12-week-old fetus. Cisternae of the RER. Mitochondria are distributed between the nucleus (N) and the ruffled border (RB). One mitochondrion (Mi) contains a dense granule (arrow). Vacuoles (Vs) are numerous in the vicinity of the ruffled border, and some contain dense material (arrowhead). D: Detail of the bone-ruffled border interface. Some partially demineralized collagen fibrils show a characteristic periodic striation (arrowhead) (Holtrop 1990). M, mineral.

VetBooks.ir

occurring at the ruffled border. The Golgi complex, usually close to the nuclei, is less developed than in osteoblasts.

Cytochemical studies reveal that lysosomal enzymes, including acid phosphatases and acid hydrolases, are concentrated in the cisternae of the RER, in the saccules of the Golgi complex and in numerous small and coated vacuoles, and are abundant between the nuclei and the deep portions of the ruffled border membrane folds (Figure 5.5B, C). This differentiation of the cell membrane is the most characteristic morphological feature of active osteoclasts. The ruffled border (also called striated border or brush border; Kölliker (1873) is considered a resorbing organ (see below and Figure 5.4). Its ultrastructure was described by Scott and Pease (1956).

Lysosomes are frequent especially near the ruffled border in active osteoclasts, whereas a few larger uncoated vacuoles are concentrated mostly in the basal part of the cell facing the bone compartment. Microtubules are randomly distributed within the cytoplasm but can be more abundant in the vicinity of the centrioles, which form clusters close to the Golgi complex. Microtubules are involved in the delivery of matrix-degrading enzymes and influence the stability of podosomes (Blosse Duplan et al. 2014). The latter are small punctate cytoskeletal structures that form early in osteoclast differentiation. Each podosome consists of an F-actin-rich central core surrounded by a loose web of actin filaments called the cloud. In addition to actin microfilaments, the podosomes contain other proteins known to occur at sites of cell-substratum interaction: fimbrin, α-actinin and gelsolin all closely associated with the actin microfilaments in the core of the podosome. Two additional proteins, vinculin and talin, appear to form rosette structures surrounding the podosome core (Teti et al. 1991). Both the core and the cloud are sites of constant actin polymerization. The diameter of the core is about 300 nm, that of the cloud is 3 µm and the average distance between the cores of the two podosomes is 750 nm (Luxenburg et al. 2007). Podosomes first form clusters, and several clusters can exist within an osteoclast. They are mostly arranged as a band at the periphery of the flat nonresorbing cells. In actively resorbing osteoclasts, podosomes accumulate in the areas facing the bone surface. Gradually podosomes increase in density and are collected in a circular belt under the control of microtubules (Jurdic et al. 2006). This rapid podosome turnover is required for the mobility of the osteoclasts and for efficient sealing of a bone-resorbing compartment. In the zone of contact with the bone matrix, the fibrillar actin cytoskeleton of the osteoclast organizes into a ring, initiating the formation of the sealing zone (Figure 5.5B). The reversible passage among clusters, the circular belt, and the sealing zone is unique characteristics of osteoclasts (Jurdic et al. 2006; Luxenburg et al. 2007).

The sealing zone is characterized by a narrow space (0.2–0.5 nm) between the cell membrane of the osteoclast and the surface of the bone ECM. At these sites, the actin ring and other proteins including talin, vinculin, paxilin and tensin are anchored by integrins (Figure 5.4) As in osteoblasts, the integrin αvβ3 present in osteoclasts recognizes the RGD sequence of bone matrix proteins, such as osteopontin, vitronectin and BSP, in facilitating bone resorption. Integrin mediates cytoskeleton organization through the cytoplasmic domain of the β3 subunit. The β family of integrin receptors in osteoclasts binds to components of the bone matrix such as collagen, fibronectin and laminin. Intracellular signaling mediates the cytoskeletal reorganization required for adhesion to bone. Much of the signaling is mediated by the intracellular tyrosine kinase Src, which is also activated in osteoclasts in response to RANKL/RANK interaction.

The sealing zone defines and isolates an acidified apical resorbing compartment from the surrounding bone surface. Toward the center of this apical resorbing compartment, the osteoclast first develops microvilli, which appear progressively as deeper infoldings ("ruffles") that form the characteristic sea anemone-like ruffled border facing the bone (Figure 5.5B, C). The infoldings fan out from the cell surface to end up on the bone surface. In sections, the infoldings appear as finger-like projections that show a great variability in shape, length and width. These infoldings increase the surface area from which lysosomal enzymes are actively secreted within the resorbing compartment.

The ruffled border is composed of two different domains, lateral and central, where exocytosis and endocytosis occur, respectively (Zhao et al. 2000). This allows the simultaneous proton and enzyme secretion and the endocytosis of degradation products (Figure 5.6). The ruffled border represents a means whereby the membrane-associated activities required for bone resorption are concentrated. Disruption of either the ruffled border or actin ring blocks bone resorption.

The abundant prominent cytoplasmic vacuoles close to the ruffled border contain an adenosine triphosphatase: H^+-adenosine triphosphatase (H^+-ATPase) that transports protons to acidify the resorption compartment (pH is about 4.5). The high concentration of acid on a basic mineral liberates calcium. The source of the cytoplasmic protons is carbonic acid, which is generated by cytoplasmic carbonic anhydrase from carbon dioxide and water: ($CO_2 + H_2O \leftrightarrow H_2CO_3 \leftrightarrow H^+ + HCO_3^-$). To maintain electron neutrality Cl^- is also transported into the extracellular resorbing compartment through Cl^- channels, which are charge-coupled to H^+-ATPase and present in the ruffled border membrane (Schlesinger et al. 1997). Hydrochloric acid is formed in the resorbing compartment to demineralize bone and expose the organic matrix (Figure 5.5D). The secretion of protons across the ruffled border membrane into the extracellular resorbing compartment leaves the conjugate base (HCO_3^-) inside the cytoplasm of the osteoclast and it must be removed from the cell. Furthermore, the osteoclast also must continuously supply Cl^- ions for secretion into the extracellular resorbing compartment. These two works are accomplished by a passive chloride-bicarbonate exchanger in the basal lateral membrane (Teti et al. 1989).

Osteoclasts produce a number of enzymes, among which the most important is an acid phosphatase that dissolves both the inorganic phase and the collagen (Table 5.1).

Dissolution of the mineral precedes the degradation of the organic matrix (Pierce et al. 1991). Mineralized bone is first broken into fragments; the osteoclast then engulfs the fragments and digests them within cytoplasmic vacuoles. At the ultrastructural level, the vacuoles appear to contain bone salt crystals and bits of collagen (Figure 5.5D).

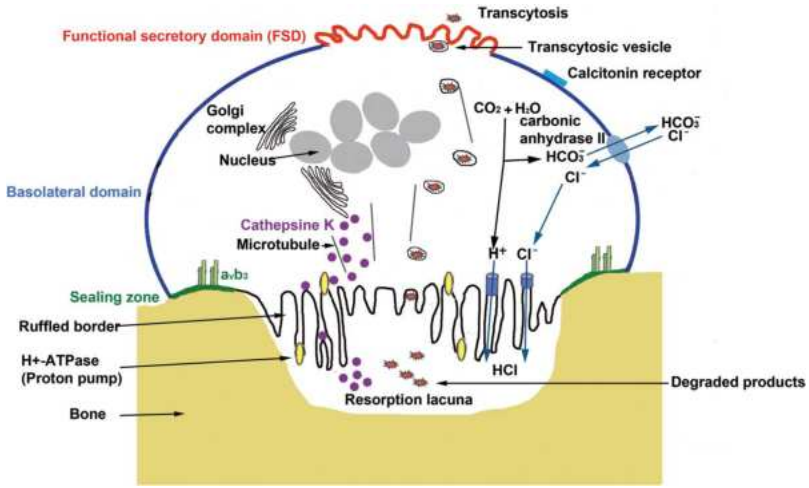


FIGURE 5.6 Diagrammatic representation of an osteoclast showing the different cellular membrane domains, and the molecular machinery involved in the dissolution of the bone matrix. (Modified from Väänänen and Zhao 2002.)

TABLE 5.1

Some Secretory Products of the Osteoclasts

Lysosomal Enzymes
Tartrate resistant acid phosphatase
β-Glycerophosphate
Arylsulfatase
β-Glucuronidase
Cathepsins
Non-Lysosomal Enzymes
Collagenase
Metalloproteinases
Lysozyme
Other (matrix) proteins
Bone sialoprotein
Osteopontin
TGF-β

Bone Mineral Dissolution

Hydroxyapatite can be solubilized in biological environments at low pH. The acidification of the resorbing compartment is mediated by a vacuolar H^+-ATPase under the ruffled membrane (Li et al. 1999). The low pH in the resorbing compartment results from the action of the proton pump at the ruffled border and in the intracellular vacuoles. Initial acidification of the compartment is achieved by the exocytosis of acid during the fusion of intracellular vacuoles to the ruffled border. This ensures rapid mineral dissolution. Pumping protons from the cytoplasm is balanced by the secretion of anions. The outflow of chloride anions through the ruffled border is most likely compensated by the action of a HCO_3^-/Cl^- exchanger in the basal membrane. Calcium and phosphorus liberated by the breakdown of the mineralized bone are released into the bloodstream.

Organic Dissolution

The organic matrix is degraded after dissolution of the mineral phase. Two major classes of proteolytic enzymes, lysosomal cysteine proteinases and metalloproteinases (MMPs), are identified. The lysosomal proteolytic enzyme cathepsin K is the main collagenase in osteoclasts; it is highly expressed in osteoclasts that degrade type I collagen. MMPs also function as collagenases at neutral pH and are involved in the migration of osteoclasts and in the initiation of bone resorption at new sites (Delaisse et al. 2003).

A set of different hydrolases additionally contributes to the degradation of noncollagenous proteins. The removal of the degraded products is accomplished by transcytosis through a vesicular process. Transcytosis includes several steps: degraded products are first endocytosed, then transported along a transcytotic vesicular pathway toward the nonresorptive side of the cell, and finally released out (Nesbitt and Horton 1997; Salo et al. 1997b).

Osteoclast Regulation

Several positive and negative regulators of osteoclast life span have been identified, including hormones, cytokines and growth factors.

Osteoclastic regulation seems to be mediated by cells of the osteoblastic lineage. These cells are capable of inducing, stimulating and inhibiting bone resorption by mature osteoclasts (Bingham et al. 1969).

Two systemic factors, PTH and $1.25(OH)_2$ vitamin D_3, prevent osteoclast apoptosis. PTH is a peptide hormone that regulates calcium homeostasis in the serum. However, osteoclasts do not have a receptor for PTH. This hormone binds to osteoblasts the only bone cells that have receptors for it: the stimulation of osteoclast activity is thus indirect. Binding stimulates osteoblasts to increase their expression of RANKL and inhibits their secretion of OPG. Free OPG competitively binds to RANKL as a decoy receptor, preventing RANKL from interacting with RANK, a receptor for RANKL (Figure 5.7). The relative concentration of RANKL and OPG are likely to be important determinants of osteoclast survival and formation (Xing and Boyce 2005). As a result, calcium concentration in blood rises, while collagen synthesis decreases.

VetBooks.ir

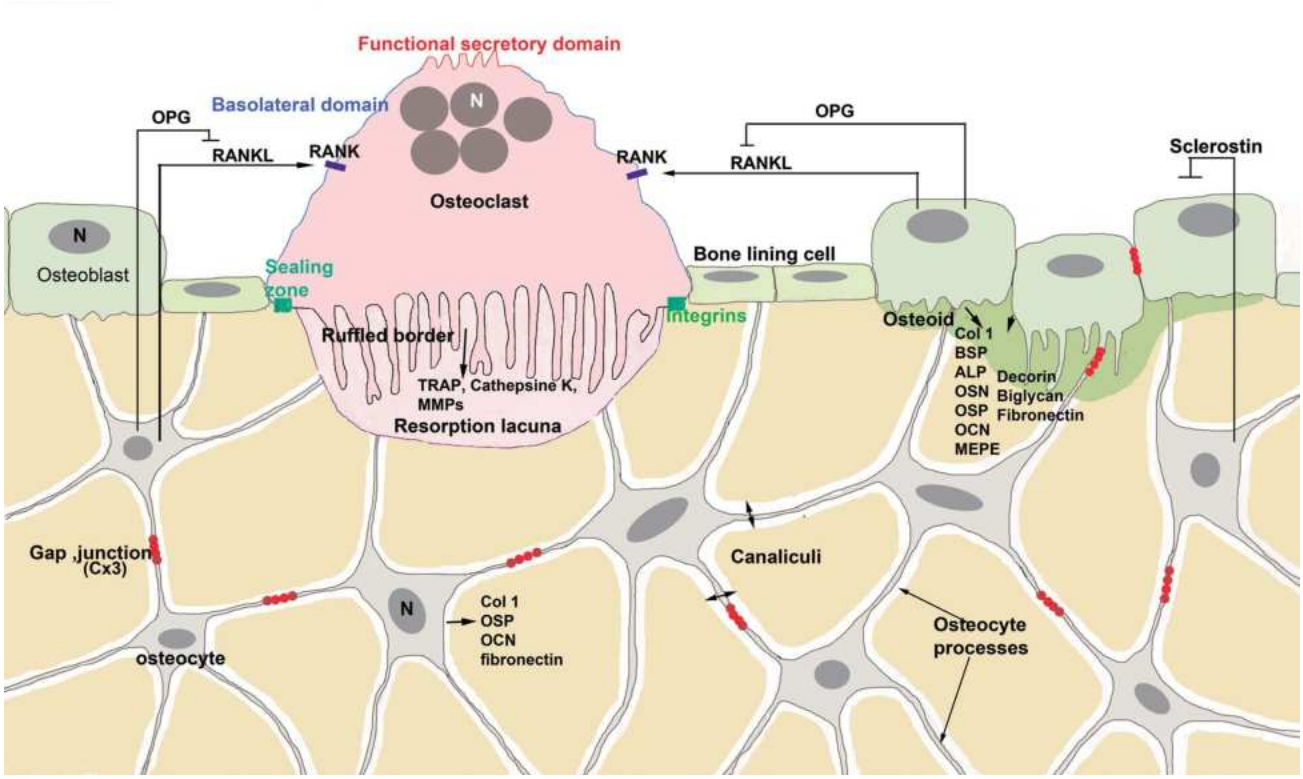


FIGURE 5.7 Simplified view of cellular interactions between the bone cells within the RANK/RANKL/OPG system. ALP, alkaline phosphatase; BSP, bone sialoprotein; Col 1, collagen type I; MEPE, matrix extracellular phosphoglycoprotein; MMP, metalloproteinases; N, nucleus; OCN, osteocalcin; OSN, osteonectin; OSP, osteopontin; TRAP, tartrate-resistant acid phosphatase. (Modified from Florencio-Silva et al. 2015.)

A direct control is exerted on osteoclasts by calcitonin. This hormone is synthesized by clear cells of the thyroid, and it inhibits osteoclastic activity through the suppression of cell motility, retraction of cell spreading and inhibition of the secretion of the lysosomal enzymes. These enzymes are rerouted to intracellular vacuoles, and eventually their synthesis is arrested (Baron et al. 1990). Estrogen acts synergistically with calcitonin by downregulating the proliferation of hematopoietic stem cells through the interleukin (IL)-7–dependent mechanism. They thus exert antiresorbing effects through stimulation of OPG expression in osteoblasts. Osteoclasts may go through apoptosis under the influence of numerous factors, but they can experience more than one cycle during their life span.

The quality and quantity of bone is determined by the balance between osteoblast and osteoclast numbers and activity (Delaisse 2014). Cells of these lineages may communicate through three modes. They can make direct contact, allowing membrane-bound ligands and receptors to interact and initiate intracellular signaling. Osteoblasts and osteoclasts may also be connected by gap junctions, which allow the passage of small molecules. Communication may also depend on diffusible paracrine factors, such as growth factors, cytokines and other small molecules secreted by either cell type and acting on the other by diffusion. Resorption of the bone matrix by osteoclasts may liberate molecules such as growth factors originating from the osteoblasts. Communication of bone cells with other cells such as neurons and endothelial cells is critical for bone integrity (Matsuo and Irie 2008).

Bone Matrix

The bone organic matrix is composed of a wide range of macromolecules that fulfill a variety of biochemical and biomechanical functions; it is composed of fibrillar collagenous proteins (90% of total proteins) and noncollagenous proteins including glycoproteins and proteoglycans. Noncollagenous proteins form the ground substance that fills the space between the cells and the collagen fibrils (there are relatively few cells per volume or mass in mature bone). The mineral phase is in the form of crystals of hydroxyapatite. The third major component of the bone ECM is water, located between the triple-helical molecules, in the gaps, within the fibrils, between the fibrils and between the fibers. It also binds to the surface of hydroxyapatite crystals (Dorvee and Veis 2013). Water is important for the mechanical functioning of bone, as evidenced by the differences in the responses of dry and wet osseous samples to stress, strain and shear (Currey 2002) (Figure 5.8).

The Organic Matrix

Because of its high collagen content, the bone matrix is stained green or blue by specific topographic stains (one step trichrome, Goldner's trichrome, Azan, etc.) in demineralized bone sections. Sirius red is used to stain collagen fibers; the sections are then observed under a polarized microscope. Bone matrix is also stained by the periodic acid Schiff (PAS)

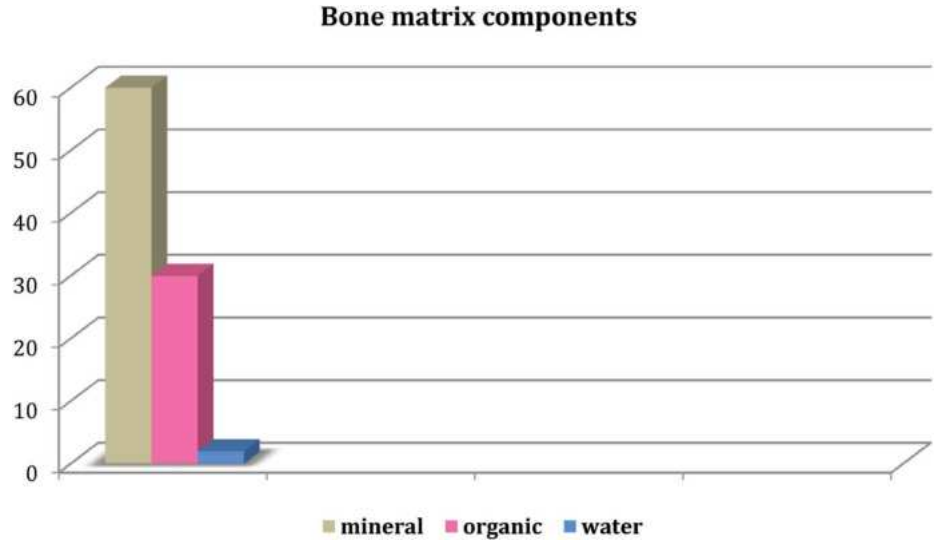


FIGURE 5.8 Bone matrix components. (Data from Zhang et al. 2018.)

technique, with a variation in color intensity depending on the quantity of glycoproteins. Collagen and noncollagenous proteins of the ECM are identifiable using immunocytochemical techniques.

The Collagen Family

In bone as in all connective tissues the most abundant components of ECMs belong to the collagen family, which is an ancient protein group. The first collagen-related gene was identified in the choanoflagellate (a sister group of Metazoa that diverged more than 600 million years ago) *Monosiga brevicollis* (Haq et al. 2019). Therefore, the formation of the α chain that characterizes collagen molecules occurred before the metazoan radiation (Exposito et al. 2010). Collagen genes are thought to be derived by gene duplication processes Boot-Handford and Tuckwell 2003; Aouacheria et al. 2004; Exposito et al. 2010). To date the vertebrate collagen gene family comprises 44 genes encoding 28 collagen types, each type being composed of three α chains.

The main characteristic of collagens is to be a triple helical molecule made of three α chains of peptides, each forming a left-handed helix, which intertwines with each other to form a right-handed helix. Collagen α chains are characterized by a Gly-X-Y repeating triplet, where glycine (Gly) occurs in every third position and where X is usually proline and Y is often hydroxylysine. Glycine, the smallest amino acid, occupies a restricted space where the three helical α chains come together in the center of the triple helix. Its position is crucial for appropriate folding of the molecule. Proline and hydroxylysine are rigid amino acids that limit the rotation of the polypeptide backbone and thus contribute to the stability of the triple helix (e.g., Prockop et al. 1979; Eyre 1980; Olsen 1991; van der Rest 1991; Brodsky and Persikov 2005; Hulmes 2008; Ricard-Blum 2011). The three α chains can vary in size from 662 up to 3152 amino acids for the human α1(X) and α3(VI) chains, respectively (Ricard-Blum 2011). The three α chains can be identical to form homotrimers or different to form heterotrimers.

On the basis of differences in their structural features, collagens are divided into different groups. Fibril-forming collagens, one of the most ancient collagen groups (Haq et al. 2019), already have a major triple helix. Fibrillar collagens (types I, III, V and XI), the most abundant ones, are present in connective tissues. Type I collagen is predominant in all connective tissues except cartilage, which predominantly contains type II collagen. Types III and V collagens are found in tissues where type I collagen is predominant, whereas type XI collagen is associated with type II collagen.

Nonfibrillar collagens are characterized by triple-helical domains that are either shorter or longer than those of the fibrillar collagens, and they may contain parts of nontriple-helical domains. The nonfibrillar collagens are subdivided into subfamilies according to their similarities in their supramolecular assemblies.

The fibril-associated collagens with interrupted triple helix (FACITs collagens) (types IX, XII, XIV and XIX–XXI) contain several triple-helical domains. FACITs do not form fibrils by themselves or may form very thin fibrils. They are located at the surface of collagen fibrils and serve as molecular bridges involved in the organization and stability of the ECMs.

Different groups of collagens are distinguished according to the network they form: collagens organized in hexagonal networks, collagens of the basement membranes, collagens forming the anchoring fibrils of the basement membrane, collagens forming beaded filaments and collagens that have transmembrane domains (Ricard-Blum 2011).

Collagens in the Bone Matrix

Bone matrix proper contains a rather limited array of collagen types. The main type is the fibrillar type I collagen, a heterotrimer made of two identical α1(I) chains and one α2(I) chain. Like other fibril-forming collagens, it is

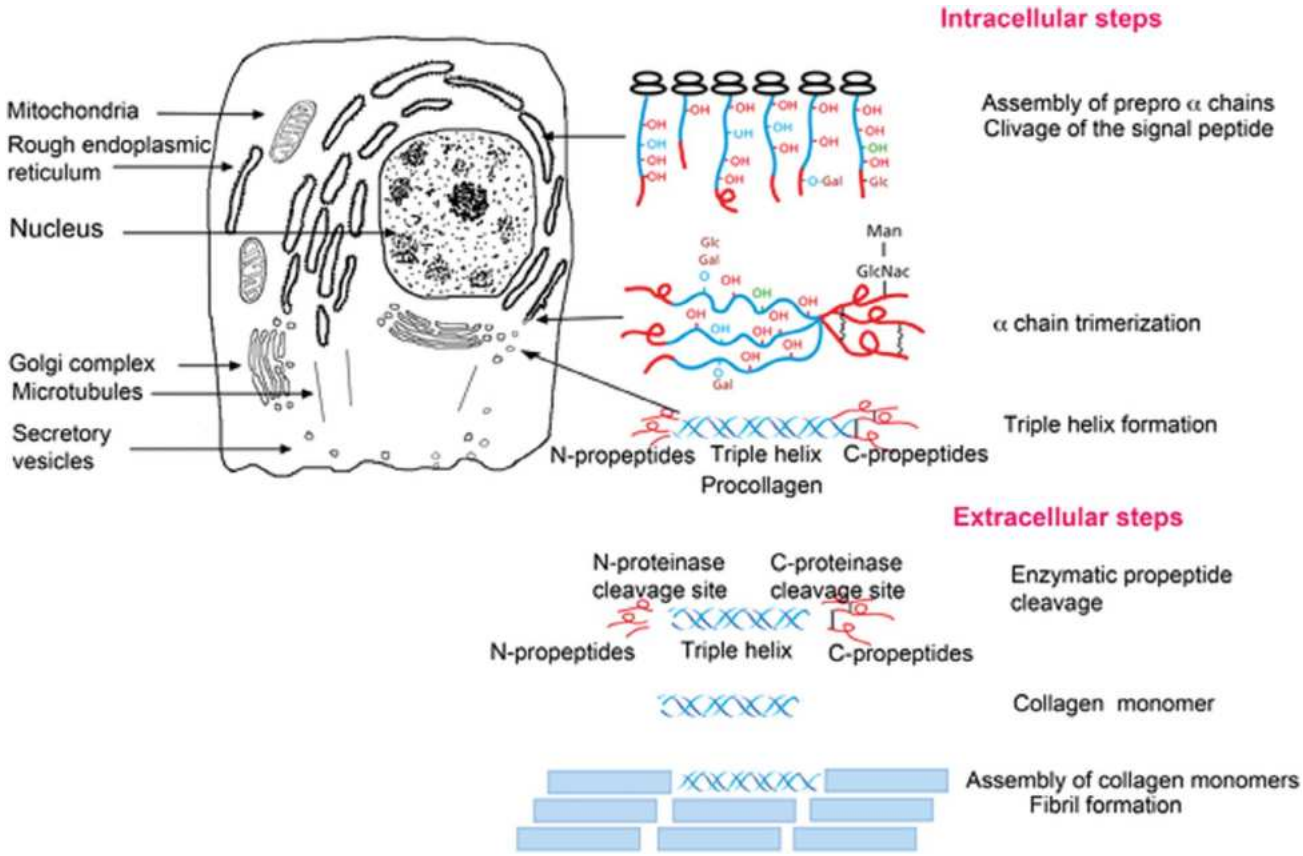


FIGURE 5.9 Steps of fibrillar collagen synthesis. Gal, galactose; Glc: glucose; GlcNac: N-acetyl-D glucosamine; Man, mannose.

synthesized as a procollagen molecule composed of a central triple helical domain for each of the three chains, which gives the molecule the shape of a long rod about 300 nm in length and about 1.5 nm in diameter. The central domain is bordered at each side by short nonhelical domains, the amino terminal propeptides: the nonhelical N-telopeptide and C-telopeptide. The telopeptides play an important role in the formation of the cross-links that stabilize the fibrillar assembly.

Collagen undergoes extensive posttranslational processing. Polypeptide procollagens are imported into the RER, where after a series of posttranslational steps, the three α chains combine to make a procollagen molecule (Figure 5.9). Stabilization is due to the hydroxylation of proline and hydroxyproline and the glycosylation of hydroxylysine that occurs after its hydroxylation. Different collagen types have variable amounts of carbohydrates (galactose or glycol galactose) linked to hydroxylysine. There are differences between soft and mineralized tissue type I collagen resulting from different posttranslational modifications (Glimcher 1976; Glimcher and Krane 1968; van der Rest 1991; Ricard-Blum 2011; Sherman et al. 2015). Interestingly, it has been shown that the type I collagen of rat cortical and trabecular bone differs in the extent of posttranslational modifications: the former contains a higher amount of hydroxylysine residues, whereas in the latter, the degree of hydroxylysine glycosylation is higher and the number of cross-links reduced. The result is a different mechanical resistance of the fibrils, higher in cortical than in trabecular bone, due to the differing number of structures stabilizing cross-links (Suarez et al. 1996). Procollagen molecules transit via the Golgi complex, where they are packaged into secretory vacuoles (Sherman et al. 2015).

After secretion from the cell, procollagen molecules are enzymatically cleaved into collagen. Two proteases are required, an N-proteinase that removes the N-telopeptides and a C-proteinase that removes the C-propeptide. The fibrils are stabilized by formation of covalent cross-links based on the reactions of aldehydes that are generated enzymatically from lysine or hydroxylysine side chains and by disulfide bridges (van der Rest 1991). Once cleavage of the procollagen ends occurs, each type I collagen molecule relates to the adjacent molecule in a quarter-stagger array, so that the composite fibrils show the characteristic light and dark bands and interbands observed in electron micrographs (Figure 5.10A). The contrast between dark and light bands may be increased by using electron-dense staining such as phosphotungstic acid, lead salts, and uranyl salts (van der Rest 1991). The type I collagen fibrils show an axial repeating period between 64 and 70 nm (Hodge and Petruska 1963; Hulmes et al. 1995; see Landis et al., chapter 6). The longitudinal staggering of the molecules involves slightly less than one quarter of the length

VetBooks.ir

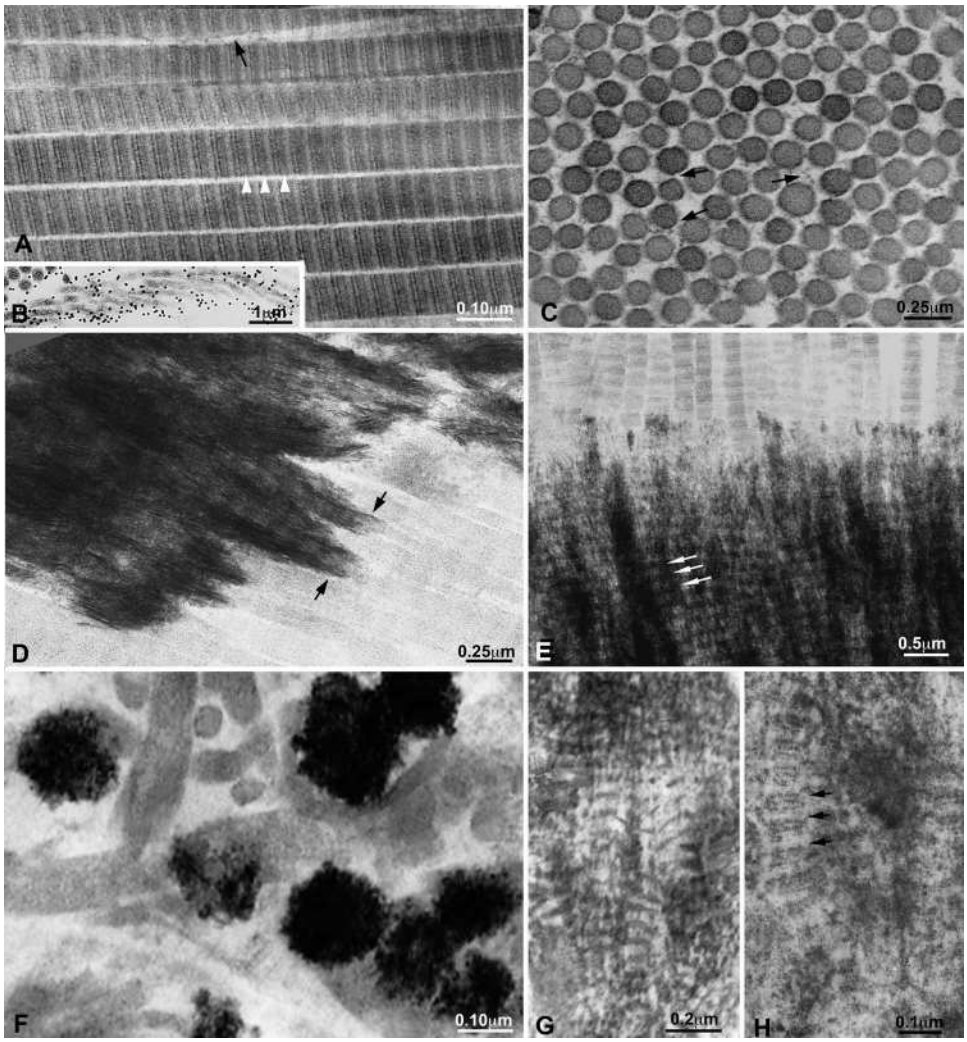


FIGURE 5.10 Bone matrix in transmission electron micrographs. A, *Protopterus annectens*. Scale basal plate. Collagen fibrils longitudinally sectioned show the characteristic striation of type I collagen fibrils (arrowheads). A microfibrillar network occupies the space between the collagen fibrils (arrow). B, *Carassius auratus*. Immunogold staining of a scale with an anti-type I collagen antibody adsorbed to 10-nm gold particles. Gold particles are distributed along the collagen fibrils. C, *Protopterus annectens*. Scale basal plate. Note the regular arrangement of the collagen fibrils connected by thin microfibrils (arrows). D, Human. Femur of a 12-week-old fetus. Crystals are oriented along the collagen fibrils (arrows). Inotropic mineralization. E, *Protopterus annectens*. Scale basal plate. Longitudinally sectioned mineralized collagen fibrils. Mineralization front. The ordered deposition of the crystals (arrows) along the axial direction of the collagen fibrils enhances their periodic structure. F, *Chalcides viridanus*. Osteoderm. Spheritic mineralization. Crystals do not show relationships with the collagen fibrils. G, *Lapparentosaurus madagascariensis*. Femur. Fibrils parallel to each other show a periodic striation similar to the one of modern collagen. H, *Lapparentosaurus madagascariensis*. Femur. The periodic striation of the fibrils is composed of electrolucent and electrodense bands (arrows) as in the fibrils of modern collagen.

of the molecule and leaves a "hole" between the end of one triple helix and the beginning of the next. The hole provides a site for the deposition of hydroxyapatite crystals in bone formation (Glimcher and Krane 1968; Glimcher 1984, 1989 and see Table 5.2).

Trace amounts of fibrillar type III and V collagens are also identified in bone matrix (van der Rest 1991). Type III collagen is occasionally found, especially in the early stages of bone development. Type V collagen appears as very thin striated fibrils associated with type I collagen. Type V regulates the thickness of the fibrils but has no effect on the tissues once they become mineralized (Linsenmayer et al. 1985; Veis and Sabsay 1987; Birk et al. 1988).

Other collagen types are also present in bone matrix but at lower levels. FACITs (types XII and XIV) have been identified associated with type I collagen fibrils. They are supposed to contribute to the regulation of the matrix structure (Wu et al. 2010).

Type XXIV collagen, restricted to bone tissue, is considered a marker of bone formation. Col 24α1 gene transcription is activated simultaneously with osteocalcin gene and increases in pace with osteoblast activity. Type XXIV collagen may be implicated in bone matrix competence for mineralization (Matsuo et al. 2008).

Collagen fibrils aggregate into large units in a highly specific arrangements to form collagen fibers. Collagen fibers may be packed to form fiber bundles. Fibers and fiber bundles are

VetBooks.ir

TABLE 5.2

Collagens in Bone

Collagen Types	α Chains	Functions
Fibrillar Collagens		
Type I collagen	$(\alpha I(I)_2\alpha 2(I))$	90% of the organic matrix Most abundant protein of the bone matrix Serves as scaffolding Binds with other proteins which nucleate hydroxyapatite deposition and orients the crystals
Type III collagen	$\alpha I(III)_3$	Present in trace in embryos May regulate fibril diameter
Type V collagen	$(\alpha I(V)_2\alpha 2(V))$ $(\alpha I(V)\alpha 2(V)\alpha 3(V))$	Associated with type I collagen Regulates the diameter of the fibrils
Type XXIV collagen	αI(XXIV)	May be considered as a marker of bone formation
FACIT Collagens		
Type XII collagen Type XIV collagen	αI(XII) αI(XIV)	FACIT collagens are associated with the fibrillar type I collagen and may be involved in regulation of the matrix

Abbreviations: FACIT, fibril-associated collagens with interrupted triple helix.

distinguishable at the level of light and electron microscopy (*inter alia* Reznikov et al. 2014). Higher orders of organization reflect the spatial organization of the fiber bundles and give rise to the basic types of bone tissues (see chapter 8).

Noncollagenous Proteins

They form the ground substance filling the space between the cells and the collagen fibrils. A wide variety of proteins is produced by the bone cells. However, components can be also absorbed from circulation or synthesized by neighboring cells, such as endothelial cells, marrow stromal cells, hemopoietic cells and hypertrophic chondrocytes. Moreover, the mineral phase is a powerful attractant for molecules including immunoglobulins, glycoproteins, albumin, and lysozyme derived from other tissues via vascular pathways and for molecules related to bone cells such as lysosomal enzymes, ALP, collagenase and calmodulin (Table 5.3).

Proteoglycans

Decorin and biglycan are the most abundant proteoglycans found in the bone matrix. Decorin is produced by preosteoblasts and osteoblasts, but its synthesis is not maintained in osteocytes, which indicates its role in the regulation of initial mineral deposition. The proposed functions of decorin are the regulation of collagen fibril diameter and fibril orientation, and possibly the prevention of premature osteoid calcification. Decorin has a low affinity to hydroxyapatite but a high affinity to type I collagen (Hoshi et al. 1999; Zhu et al. 2010). Biglycan is produced by osteoblasts and osteocytes and is expressed at later stages than decorin. Biglycan is thought to stimulate osteoblastic differentiation, but the underlying mechanism has not been elucidated (Ye et al. 2012).

Glycoproteins

Numerous glycoproteins mainly produced by osteoblasts have been identified in mineralized bone matrix. ALP is a hallmark of the osteoblast lineage. Although this protein is associated with the cell surface, a glycoprotein with ALP activity has nevertheless been found in the mineralized matrix of bone, suggesting that ALP can be shed from the cell surface of the osteoblast or occurs in a membrane-bound form. A function of ALP in the mineralization process could be to hydrolyze phosphate esters to provide a source of inorganic phosphate (Zhu et al. 2010).

TABLE 5.3

Some Noncollagenous Proteins of Bone Matrix

Noncollagenous proteins	Functions
Proteoglycans	
Decorin	Regulator of collagen fibril diameter
Biglycan	Cell surface associated, binds TGF-β Regulates fibrillogenesis Induces osteogenesis
Hyaluron, glycosaminoglycan without core protein	Capture space destined to become bone
Glycoproteins	
Alkaline phosphatase	Inhibitor of mineral deposition
Osteonectin	Regulator of collagen fibrillogenesis Positive regulator of bone formation May influence cell cycle, strong affinity for Ca^{2+}
RDG-Containing Proteins	
Osteopontin	Supports osteoclast attachment to bone Inhibits mineralization in bone
Bone sialoprotein	Binds to cells, strong affinity for Ca^{2+}
MEPE	Possible regulator of phosphate metabolism
Fibronectin	Binds to cells and collagen
Vitronectin	Binds to cells and collagen
Gla-Containing Proteins	
Osteocalcin	Restricted to the osteoblast lineage Vitamin K dependent Regulator of osteoclast recruitment and activity
Matrix Gla-protein	Negative regulator of mineralization

Abbreviations: MEPE, matrix extracellular phosphoglycoprotein; TGF, transforming growth factor.

VetBooks.ir

Osteonectin

A 32-kDa acidic phosphoprotein rich in glutamic residues (Termine et al. 1981) is one of the most abundant glycoproteins in bone mineralized matrix, in which it can constitute up to 15% of the noncollagenous proteins depending on the animal species and the developmental stage considered (Hoshi and Ozawa 2004). Newly differentiated osteoblasts secrete osteonectin, which is mainly incorporated into mineralized bone matrix (Ishigaki et al. 2002). Osteonectin is found in other connective tissues, but it is accumulated only in the bone mineralized matrix where it binds with calcium and hydroxyapatite, as well as with type I collagen (Tracy and Mann 1991). Whether it has a specific function or simply accumulates within the tissue because of its affinity for hydroxyapatite remains to be determined.

Gla-Containing Proteins

These proteins are posttranslationally modified by vitamin K-dependent enzymes to form γ-carboxyglutamic residues. Osteocalcin (bone Gla protein) is the most abundant noncollagenous protein in human bone matrix, and it makes up 10–20% of the noncollagenous proteins of the bone matrix. This small vitamin-dependent peptide (5800 MW), characterized by its Gla residues, is almost exclusively synthesized by the osteoblasts and is thus restricted to bone tissues (Hauschka et al. 1975; Price 1985; Lian et al. 1989). It is a late marker characteristic of mature osteoblasts (Mark et al. 1987; Lian and Gundberg 1988). Its biosynthesis is stimulated by 1.25-dihydroxy vitamin D. Osteocalcin binds strongly to hydroxyapatite crystals and more weakly to free calcium ions (Cole and Hanley 1991). Osteocalcin isolated from different vertebrate species shows a homology of the primary sequences with conservation of key structural features. Matrix Gla protein (MGP) is a protein unrelated to osteocalcin. It is a 15-kDa protein containing five γ-carboxyglutamic acid (Gla) residues. It may play a role in bone development (Price et al. 1983).

RGD-Containing Proteins

Bone ECM is composed of proteins containing the sequence arginine-glycine-aspartate (RGD). These proteins include collagen, thrombospondin, fibronectin, vitronectin and the two members of the small integrin-binding ligand, N-linked glycoprotein (SIBLING), BSP and osteopontin. These last two can associate with other proteins as well as with the mineral phase (Fisher et al. 2001).

BSP, an early marker of osteoblast differentiation, is a phosphorylated glycoprotein implicated in the nucleation of hydroxyapatite during bone formation. It is expressed at a high level by osteoblasts at the onset of bone formation (Hunter and Goldberg 1993). BSP may also be produced by osteoclasts and be involved in the attachment of the osteoclasts to bone.

Osteopontin is secreted by osteoblasts in the early stages of osteogenesis. It inhibits mineral formation and crystal growth. Osteopontin binds to osteoclasts and promotes the adherence of osteoclasts to the mineralized bone matrix during resorption processes.

The RDG sequence of both BSP and osteopontin is recognized by members of the class of cell surface receptor: the integrins. Integrins are transmembrane α, β heterodimers that mediate cell-cell and cell-matrix recognition (Ruoslahti 1991). They belong to a large family of N-glycosylated glycoproteins of heteromeric cell surface receptors composed of α and β subunits that interact with the ECM proteins of the extracellular face of the cell membrane and with the cytoskeletal proteins and actin filaments through their cytoplasmic domain (Clark and Brugge 1995). The bone-forming cells show different patterns of integrin expression at successive stages of the osteoblast lineage (review in Bennett et al. 2001). Osteoblasts and osteoclasts use different integrin subunits to attach to specific ligands of the bone matrix. Thus, integrins mediate interactions between cells of the osteoblast and osteoclast lineages and these cells and the bone matrix (Clover et al. 1992; Hughes et al. 1993).

In addition to the major proteins, other proteinic molecules absorbed from circulation, such as albumin and α2HS glycoprotein, a partially phosphorylated glycoprotein, occur in bone matrix, as well as large amounts of TGF. Bone matrix is the largest reservoir of this growth factor that regulates osteogenic or osteoclastic cellular differentiation.

Lipids

Lipids, especially phospholipids, occur in bone. Acidic phospholipids and proteolipids are thought be involved in the initial deposition of hydroxyapatite because they are abundant in the mineralization front.

Other Components

In addition to the major proteins secreted by the bone cells, other protein molecules absorbed from circulation, such as albumin and α2HS glycoprotein, occur in the bone matrix as well as large amounts of TGF-β. Bone matrix is the largest reservoir of this growth factor, which regulates osteogenic and osteoclastogenic cellular differentiation.

The Mineral Phase

The von Kossa silver method is most often used to stain the mineral component of bone matrix. It becomes black whereas the unmineralized osteoid remains unstained. Bone mineral is not pure hydroxyapatite. The crystals contain impurities, most often carbonate-replacing phosphate groups. This carbonated bone mineral associated with the collagen fibrils shows similarities to the carbonate apatite considered dahlite ($Ca_5(PO_4, CO_3)_3(OH)$) (Weiner and Wagner 1998). Carbonate is one of a large number of possible substitutions. It occurs in two distinct phases, calcium carbonate and a carbonate apatite, where CO_3^{-2} may replace phosphate. Hydroxyl HPO_4^{-2} may replace phosphate ions; chlorine and fluorine may replace OH^- and sodium, potassium, magnesium and strontium may replace calcium (Fratzl et al. 2004). Trace elements including zinc, boron, copper, manganese and potassium are also present. All these impurities reduce the crystallinity of the apatite and may alter properties critical for mineral homeostasis, such as solubility.

In transmission electron micrographs (TEMs), the crystals of hydroxyapatite appear in the form of very thin platelets (Robinson 1952). Robinson (1952) reported an average size of

VetBooks.ir

$50 \times 25 \times 10$ nm for normal human bone. Significant variations in platelet size have been reported, based on observations using TEM, X-ray diffraction or scattering and atomic force microscopy. Crystals range in length from 15 to 150 nm, in width from 10 to 50 nm, and in thickness from 2 to 5 nm.

Mineral Matrix Relationships

Mineralization of bone is a well-regulated biological process whose mechanism is related to the spatial arrangement of the collagen scaffold where type I collagen (Figure 5.10A, B) is the major constituent implicated, although a number of minor collagen types are present (Table 5.2). In cortical and trabecular bone, fibrils maintain a regular parallel arrangement, and show a regular outline as well as a uniform diameter distribution (Figure 5.10A, C). The collagen fibrils are bound with a network of thin microfibrils of noncollagenous proteins dispersed around them (Figure 5.10A, B).

The relationship between the crystals and collagen fibrils is evident: the flat platelets of crystals are oriented with their long axis (crystallographic *c*-axis) parallel to the long axis of the collagen fibrils with which they are associated (Figure 5.10D, E). The plate-shaped crystals are not randomly deposited along the collagen fibrils but are distributed in a highly ordered manner accentuating the axial periodic striation of the collagen fibrils (Glimcher 1989; Landis 1999 and chapter 6 this book).

Woven bone contains a higher amount of noncollagenous material and a looser collagen network where the interfibrillary spaces are larger than in fibrolamellar bone (Currey 2002). When accessible organic material is removed from a woven bone, it retains a pattern of spherical mineral clusters with little evidence of the collagen network (Boyde 1972). Mineralized globules (Figure 5.10F) are also found in areas of the postcranial dermal skeleton, including teleostean scales and reptile osteoderms, where collagen fibrils are organized in a loose network (Zylberberg et al. 1992). Such mineral deposition of hydroxyapatite crystals without any relationships to the collagen fibrils was named spheritic mineralization. It does not reflect the spatial organization of the bone's organic matrix (Boyde and Sela 1978; Hur and Ornoy 1984). This process of mineralization differs from the inotropic mineralization of typical bony tissues, where the crystals oriented by collagen fibrils are found within and/or around the fibrils (see chapter 6). According to Ørvig (1951, 1968), spheritic mineralization should be considered the phylogenetic precursor of the inotropic mineralization that may represent "ultimate stages" in a phyletic process of increasing complexity.

Numerous histological studies carried out on fossil bone refer to their remarkable preservation, including the persistence of the birefringence observed in fresh bone where it reflects the original alignment of apatite crystals parallel to the collagen fibrils (Bromage et al. 2003; Sahar and Weiner, 2018). Collagen fibrils of mineralized fossil bone can be preserved down to the ultrastructural level when observed in replica (Pawlicki et al. 1966; Doberenz and Wyckoff 1967; Armitage 2001). Ultrastructural analyses performed after demineralization of fossil bones show that reasonably well-preserved fibrils can be identified (Rimblot-Baly et al. 1995; Schweitzer et al. 2008; Zylberberg et al. 2010; Zylberberg and Laurin 2011; Bertazzo et al. 2015). Examination of the femur of *Lapparentosaurus madagascariensis* composed of secondary Haversian bone reveals that the matrix contains patches of striated fibrils oriented in parallel. (Figure 5.10G) The periodic striation is due to the sequences of electrodense and electron lucent zones that are themselves made of thin striations, as in fibrils of extant collagen (Figure 5.10H).

The intimate association of bone mineral with the organic matrix appears to protect the collagen molecules in fossil bone. Conversely, collagen provides protection for hydroxyapatite crystals so that bone hydroxyapatite crystals and collagen fibrils ensure a mutual protection affording a greater stability to both components in fossil remains.

Acknowledgments

I thank my colleague Alexandra Quilhac for providing micrographs of duck osteocytes. All studies reviewed in this chapter were performed following regulatory requirements for human and animal rights, and informed consent statements have been obtained from each patient.

REFERENCES

Aarden, E.M., et al. 1996. Immunocytochemical demonstration of extracellular matrix proteins in isolated osteocytes. *Histochem Cell Biol*. 106: 495–501.

Andersen, T.L., et al. 2009. A physical mechanism for coupling bone resorption and formation in adult human bone. *Am J Pathol*. 174: 239–247.

Arena, N., et al. 1991. Characterization of the cytoskeleton in human normal and otosclerotic osteoblast-like cells. *Acta Anat (Basel)*. 141: 311–315.

Armitage, M. 2001. Scanning electron microscope study of mummified collagen fibers in fossil *Tyrannosaurus rex bone*. CRS Q 38: 61–66.

Ashley, J.W., et al. 2015. Notch signalling promotes osteoclast maturation and resorbing activity. *J Cell Biochem*. 116: 2596–2609.

Atkins, G.J., D.M. Findlay. 2012. Osteocyte regulation: a little give and take. *Osteoporos Int*. 23: 2067–2079.

Aubin, J.E., et al. 1983. A primary role for microfilaments, but not microtubules, in hormone-induced cytoplasmic retraction. *Exp Cell Res*. 143: 439–450.

Aubin, J.E., F. Liu. 1996. The osteoblast lineage. In *Principles of bone biology*, ed. J.P. Bilezikian, L.G. Raisz, G.A. Rodan, 51–67. San Diego, CA: Academic Press.

Aouacheria, A., et al. 2004. Invertebrate data predict an early emergence of vertebrate fibrillar collagen clades and anti-incest model. *J Biol Chem*. 279: 4711–4719.

Bach-Gansmo, F.L., et al. 2015. Osteocyte lacunar properties in rat cortical bone: differences between lamellar and central bone. *J Struct Biol*. 191: 59–67.

Baron, R., et al. 1990. Selective internalization of the apical plasma membrane and rapid redistribution of lysosomal enzymes and mannose 6-phosphate receptors during osteoclast inactivation by calcitonin. *J Cell Sci*. 97: 439–447.

Barragan-Adjemian, C., et al. 2006. Mechanism by which MLO-A5 late osteoblasts/early osteocytes mineralize in culture: Similarities with mineralization of lamellar bone. *Calcif Tissue Res*. 79: 340–353.

Baylink, J.D., J.E. Wergedal. 1971. Bone formation by the osteocytes. *Am J Physiol*. 221: 669–678.

Bennett, J.H., et al. 2001. Patterns of integrin expression in a human mandibular explant model in osteoblast differentiation. *Arch Oral Biol*. 46: 229–238.

Berner, H.S., et al. 2004. Adiponectin and its receptors are expressed in bone forming cells. *Bone*. 35: 842–849.

Bertazzo, S., et al. 2015. Fibres and cellular structures preserved in a 75-millions year-old dinosaur specimen. *Nat Commun*. 6: 7352.

Bilezikian, J.P., et al. 2002. *Principles of bone biology*. 2nd edition. San Diego, CA: Academic Press, Vol. 1.

Bingham, P.J., et al. 1969. The effect of parathyroid extraction on cellular activity and plasma calcium level in vivo. *J Endocrinol*. 45: 387–400.

Birk, D.E., et al. 1988. Collagen type I and type V are present in the same fibril in the avian cornel stroma. *J Cell Biol*. 106: 999–1008.

Blosse Duplan, M., et al. 2014. Microtubule dynamic instability controls podosome patterning in osteoclasts through EB1, cortancil, and Src. *Mol Cell Biol*. 34: 16–29.

Bonewald, L.F. 2007. Osteocytes as dynamic multifunctional cells. *Ann N Y Acad Sci*. 1116: 281–290.

Bonewald, L.F. 2011. The amazing osteocyte. *J Bone Miner Res*. 26: 229–238.

Bonewald, L.F., M.L. Johnson. 2008. Osteocytes and mechanosensing and Wnt signalling. *Bone*. 42: 606–615.

Boot-Handford, R.P., D.S. Tuckwell. 2003. Fibrillar collagen the key to vertebrate evolution? A tale of molecule incest. *BioEssays News Rev Mol Cell Dev Biol*. 25: 142–151

Boudin, E., et al. 2013. The role of extracellular modulators of canonical Wnt signalling in bone metabolism and diseases. *Semin Arthritis Rheum*. 43: 220–240.

Boyce, B.F., L. Xing. 2008. Functions of RANKL/RANK/OPG in bone modelling. *Arch Biochem Biophys*. 473: 139–146.

Boyde, A. 1972. Scanning electron microscope studies of bone. In *The biochemistry and physiology of bone*, ed. G.H. Bourne, 259–310. New York: Academic Press.

Boyde, A., J. Sela 1978. Scanning electron microscope study of separated calcospherites from the matrices of different mineralizing systems. *Calcif Tissue Res*. 26: 47–49.

Brodsky, B., A.V. Persikov. 2005. Molecular structure of the collagen triple helix. *Adv Protein Chem*. 70: 301–339.

Bromage, T. G., et al. 2003. Circulary polarized light standards for investigations of collagen fiber orientation in bone. *Anat Rec*. 274B: 157–168.

Bronkers, A.L.J.J., et al. 1987. Developmental appearance of gla proteins (osteocalcin) and alkaline phosphatase in tooth germs and bone of the rat. *Bone Miner*. 2: 361–373.

Buo, A. M., J.P. Stains. 2014. Gap junctional regulation of signal transduction in bone cells. *FEBS Lett*. 588: 1315–1321. http://dx.doi.org/10.1016/j.febslet.2014.01.025

Burr, D. B., M.R. Allen. 2014. *Basic and applied bone biology*, ed. D.B. Burr and M.R. Allen. London: Academic Press.

Caplan, A.I. 1991. Mesenchymal stem cells. *J Orthop Res*. 9: 641–650.

Capulli, M., et al. 2014. Osteoblast and osteocyte: Games without frontiers. *Arch Biochem Biophys*. 61: 3–12.

Chambers, T.J. 1980. The cellular basis of resorption. *Clin Orthop Rel Res*. 151: 283–293.

Chen, L., et al. 2015. Inhibiting actin depolymerisation enhances osteoblast differentiation and bone formation in human stromal stem cells. *Stem Cell Res*. 15: 281–289.

Clark, E.A., J.S. Brugge. 1995. Integrins and signal transduction pathways: Road taken. *Science*. 268: 233–239.

Clover, J., R.A. Dodds, M. Gowen. 1992. Integrin subunit expression by human osteoblast and osteoclasts *in situ* and in culture. *J Cell Sci*. 103: 267–271.

Cole, D.E.C., D.A. Hanley. 1991. Osteoclacin. In *Bone vol 3, Bone matrix and bone specific products*, ed. B.K. Hall, 239–294. Boca Raton, FL: CRC Press.

Crowder, C., S. Stout. 2011. *Bone histology: an anthropological perspective*. Boca Raton, FL: CRC Press.

Currey, J.D. 2002. Bones. *Structure and mechanics*. Princeton, NJ: Princeton University Press.

Currey, J.D. 2003. The many adaptations of bone. *J Biomech*. 36: 1487–1495.

Dallas, S.L., L.F. Bonewald. 2010. Dynamics of the transition from osteoblast to osteocyte. *Ann NY Acad Sci*. 1192: 437–443.

Delaisse, J. M. 2014. The reversal phase of the bone remodelling cycle: cellular prerequisites for coupling resorption and formation. *Bonekey Rep*. 3: 561.

Delaisse, J.M., et al. 2003. Matrix metalloproteinases (MMPs) and cathepsin K contribute differently to osteoclastic activities. *Microsc Res Tech*. 61: 504–513.

Delgado-Calle, J., et al. 2017. Role and mechanism of action of sclerostin in bone. *Bone*. 96: 29–37.

Doberenz, A.R., W.G. Wyckoff. 1967. Fine structure in fossil collagen. *Proc Natl Acad Sci USA*. 57: 539–541.

Dobnig, H., R.T. Turner. 1995. Evidence that intermittent treatment with parathyroid hormone increases bone formation in adult rats by activation of bone lining cells. *Endocrinology*. 136: 3632–3638.

Dole, N.S., et al. 2017. Osteocyte-intrinsic TGF-β signalling regulates bone quality through perilacunar/canalicular remodeling. *Cell Rep*. 21: 2585–2596.

Donahue, H.J., et al. 1995. Cell-to-cell communication in osteoblastic networks: Cell line-dependent hormonal regulation of gap junction function. *J Bone Miner Res*. 10: 881–889.

Dorvee, J.R., A. Veis. 2013. Water in the formation of biogenic minerals: peeling away the hydration layers. *J Struct Biol*. 183: 278–303.

Doty, S.B. 1981. Morphological evidence of gap junctions between bone cells. *Calcif Tissue Int*. 33: 509–512.

Doty, S.B., B.H. Schofield. 1984. Ultrahistochemistry of calcified tissues. In *Methods of calcified tissues preparation*, ed. G.R. Dickson, 149–198. Amsterdam: Elsevier Science Publisher.

Ducy, P. 2000. CBFA1: A molecular switch in osteoblast biology. *Dev Dyn*. 219: 461–471.

Ducy, P., et al. 1997. Osf2/Cbfa1: a transcriptional activator of osteoblast differentiation. *Cell*. 89: 747–754.

Ducy, P., et al. 1999. A Cbfa1-dependent genetic pathway controls bone formation beyond embryonic development. *Genes Dev*. 13: 1025–1036.

Ducy, P., et al. 2000. Leptin inhibits bone formation through a hypothalamus relay: a central control of bone mass. *Cell*. 100: 197–207.

Dudley, H. R., D. Spiro. The fine structure of bone cells. 1961. *J Biophys Biochem Cytol*. 11: 627–649.

Einhorn, T.A. 1994. Bone metabolism and metabolic bone disease. In *Orthopaedic knowledge update 4 home study Syllabus*, ed. J.W. Frymoyer, 69–88. Rosemont, IL: American Academy of Orthopedic Surgeons.

VetBooks.ir

Elmardi, A.S., et al. 1990. Electron microscopy of developing calvaria reveals images that suggest that osteoclasts engulf and destroy osteocytes during bone resorption. *Calcif Tissue Int*. 46: 239–245.

Everts, V., et al. 2002. The bone lining cells: Its role in cleaning Howship's lacunae and initiating bone formation. *J Bone Miner Res*. 17: 77–90.

Exposito, J.-Y., et al. 2010. The fibrillar collagen family. *Int J Mol Sci*. 11: 407–426.

Eyre, D.R. 1980. Collagen: molecular diversity in the body's protein scaffold. *Science* 207: 1315–1322.

Fisher, L.W., et al. 2001. Flexible structures of SIBLING proteins, bone sialoprotein, and osteopontin. *Biochem Biophys Res Commun*. 280: 460–465.

Fishman, D.A., E.D. Hay. 1962. Origin of osteoclasts from mononuclear leucocytes in regenerating newt limbs. *Anat Rec*. 143: 329–337.

Florencio-Silva R., et al. 2015. Biology of bone tissue: structure, function, and factors that influence bone cells. *Biomed Res Int*, 2015: 421746.

Franz-Odendaal, T., et al. 2006. Buried alive: How osteoblast become osteocytes. *Dev Dyn*. 235: 176–190.

Fratzl, P., et al. 2004. Structure and mechanical quality of the collagen-mineral nano-composite in bone. *J Mater Chem*. 14: 2115–2123.

Gaur, T., et al. 2005. Canonical WNT signalling promotes osteogenesis by directly stimulating *Runx*2 gene expression. *J Biol Chem*. 280: 33132–33140.

Gegenbauer, C. 1864. Ueber die Bildung des Knochengewebes. *Jena Zeitschr Med Naturwissen*. 1: 343–369.

Gegenbauer, C. 1867. Ueber die Bildung des Knochengewebes. 2Mitt. *Jena Zeitschr Med Naturwissen*: 206–246.

Gehron Robey, P. 2002. Bone matrix proteoglycans and glycoproteins. In *Principles of bone biology*, eds. J.P. Bilezikian, L.G. Raisz, G.A. Rodan, 225–238. San Diego, CA: Academic Press.

Gehron Robey, P., A.L. Boskey. 2006. The composition of bone. In *Primer on the metabolic bone diseases and disorders of mineral metabolism*, ed. C. J. Rosen, 32–38. Washington, DC: American Society for Bone and Mineral Research.

Glimcher, M.J. 1976. Composition, structure and organization of bone and other mineralized tissues and the mechanism of calcification. In *Handbook of physiology*, eds. R.O. Greep, E.B. Astwood, Endocrinology Vol. BII, 26–116. Washington, DC: American Physiological Society.

Glimcher, M.J. 1984. Recent studies of mineral phase in bone and its possible linkage to the organic matrix by protein-bound phosphate bonds. *Philos Trans R Soc Lond B Biol Sci*. 304: 479–508.

Glimcher, M.J. 1989. Mechanism of calcification: Role of collagen fibrils and collagen-phosphoprotein complexes in vitro and in vivo. *Anat Rec*. 224: 139–153.

Glimcher, M.J., S.M. Krane. 1968. The organization and the structure of bone and the mechanism of calcification. In *Treatise on collagen*, eds. G.N. Ramachandran, B. Bould, 67–251. London: Academic Press.

Gong, J.K., et al. 1964. Composition of trabecular and cortical bone. *Anat Rec*. 149: 325–332.

Gordon, M.D., R. Nusse. 2006. Wnt signalling: multiple pathways, multiple receptors and multiple transcription factors. *J Biol Chem*. 281: 22429–22433.

Gothlin, G. 1973. Electron microscopic observations on fracture repair in the rat. *Acta Pathol Microbiol Scand (A)*. 81: 507–522.

Groot, C.G., et al. 1986. Light and electron microscopic demonstration of osteocalcin antigenicity in embryonic and adult rat bone. *Bone*. 7: 379–385.

Hall, B.K. 1978. *Developmental and cellular skeletal biology*. New York: Academic Press.

Hall, B.K. 1988. The embryonic development of bone. *Sci Amer*. 76: 174–181.

Hall, B.K. 2005. *Bone and cartilage*. In *Developmental and evolutionary skeletal biology*. San Diego, CA: Elsevier.

Haq, F., et al. 2019. Comparative genomic analysis of collagen gene diversity. *3 Biotech* 9: 83. https://doi.org/10.1007/s13205-019-1616-9

Harada, S., G.A. Rodan. 2003. Control of osteoblast function and regulation of bone mass. *Nature*. 423: 349–355.

Hartmann, C. 2007. Skeletal development - Wnts are in control. *Mol Cells*. 24: 177–184.

Hauge, E.M., et al. 2001. Cancellous bone remodelling occurs in specialized compartments lined by cells expressing osteoblastic markers. *J Bone Miner Res*. 16: 1575–1582.

Hauschka, P.V., et al. 1975. Direct identification of the calcium-binding amino acid gamma-carboxyglutamate in mineralized tissue. *PNAS*. 72: 3925–3929.

Heldin, C.H., et al. 1997. TGF-beta signalling from cell membrane to nucleus through SMAD proteins. *Nature*. 390: 465–471.

Hill, T.P., et al. 2005. Canonical Wnt/β-catenin signaling prevents osteoblasts from differentiating into chondrocytes. *Dev Cell*. 8:727–738.

Hodge A.J., J.A. Petruska. 1963. Recent studies with the electron microscope on ordered aggregates of the tropocollagen macromolecule. In *Aspects of protein structure*, ed. G.N. Ramachandran, 289–300. New York: Academic Press.

Holmbeck, K., et al. 2005. The metalloproteinase MT1-MMP is required for normal development and maintenance of osteocyte processes in bone. *J Cell Sci*. 118: 147–156.

Holtrop, M.E. 1990. Light and electron microscopic structure of bone-forming cells. The osteoblast and osteocyte. In *Bone*, ed. B.K. Hall, Vol. 1, 1–40. Caldwell, NJ: The Telford Press.

Honma, M., et al. 2013. RANKL subcellular trafficking and regulatory mechanisms in osteocytes. *J Bone Miner Res*. 28: 1936–1949.

Hoshi, K., et al. 1999. The primary calcification in bones follows removal of decorin and fusion of collagen fibrils. *J Bone Miner Res*. 14: 273–280.

Hoshi, K., H. Ozawa. 2004. Control of calcification by extracellular matrix. *Clin Calcium*. 14: 16–22.

Hu, H., et. al. 2005. Sequential roles of Hedgehog and Went signalling in osteoblast development. *Development*. 132: 49–60.

Hughes, D.H., et al. 1993. Integrin expression in human bone. *J Bone Miner Res*. 8: 527–533.

Hulmes, D.J.S. 2008. Collagen, diversity, synthesis, and assembly. In *Collagen structure and mechanics*, ed. P. Fratzel, 15–48. New York: Springer.

Hulmes, D.J.S., et al. 1995. Radial packing, order, and disorder in collagen fibrils. *Biophys J*. 68: 1661–1670.

Hunter, G.K., H.A. Goldberg. 1993. Nucleation of hydroxyapatite by bone sialoprotein. *PNAS USA*. 90: 8562–8565.

Hur, H. B., A. Ornoy. 1984. Ultrastructural studies of initial stages of mineralization of long bones and vertebrae in human fetuses. *Acta Anat (Basel).* 118: 33–39.

Ishigaki, R., et al. 2002. Gene expression and immunohistochemical localization of osteonectin in association with early bone formation in the developing mandible. *Histochem J.* 34: 57–66.

Ji, Y., et al. 2017. Intermittent activation of notch signalling promotes bone formation. *Am J Transl Res*. 9: 2933–2944.

Jones, S.J., A. Boyde. 1977. Some morphological observations on osteoclasts. *Cell Tissue Res*. 185: 387–397.

Jones, S.J., et al. 1985. A review of bone cells and substratum interactions. *Scanning.* 7: 5–24.

Jurdic, P., et al. 2006. Podosome and sealing zone: specificity of the osteoclast model. *Eur Cell Biol*. 85: 195–202.

Kamel-Elsayed, S.A., et al. 2015. Novel approach for two and three dimensional multiplexed imaging of osteocytes. *Bone*. 76: 129–140.

Kamioka, H., et al. 2004. Terminal differentiation of osteoblasts to osteocytes is accompanied by dramatic changes in the distribution of actin-binding proteins. *J Bone Miner Res*. 19: 471–478.

Karsenty, G., E.F. Wagner. 2002. Reaching a genetic and molecular understanding of skeletal development. *Dev Cell*. 2: 399–406.

Katagiri, T., S. Tsukamoto. 2013. The unique activity of bone morphogenetic proteins in bone: a critical role of the Smad signaling pathway. *Biol Chem*. 394: 703–714. doi: 10.1515/hsz-2012-0310

Kerschnitzki, M., et al. 2011. The organisation of the osteocyte network mirrors the extracellular matrix orientation in bone. *J Struct Biol*. 173: 303–311.

Kobayashi, T., H. Kronenberg. 2005. Mini review: transcriptional regulation in development of bone. *Endocrinology.* 146: 1012–1017.

Kobayashi, Y., et al. 2008. Roles of Wnt signaling in bone formation and resorption. *Jap Dental Sci Rev*. 44: 76–82.

Kölliker, A. 1873. *Die normale Resorption des Knochengewebes und ihre Bedeutung für die Entstehung der typische Knochenformen*. Leipzig: F.C.W. Vogel.

Komori, T., et al. 1997. Targeted disruption of Cbfa1 results in a complete lack of bone formation owing to maturational arrest of osteoblasts. *Cell*. 89: 756–764.

Krishnan, V., et al. 2006. Regulation of bone mass by Wnt signaling. *J Clin Invest*. 116: 1202–1209.

Landis, W.J. 1999. An overview of vertebrate mineralization with emphasis on collagen interaction. *Gravit Space Biol Bull*. 12: 15–26.

Landis, W.J., et al. 1977a. Electron microscopic observations of bone tissue prepared by ultracryotomy. *J. Ultrastruct Res*. 59: 185–206.

Landis, W.J., et al.. 1977b. Electron microscopic observations of bone tissue prepared anhydrously in organic solvents. *J Ultrastruct Res*. 59: 1–30.

Lee, K.S., et al. 2000. Runx2 is a common target of transforming growth factor β1 and bone morphogenetic protein 2, and cooperation between Runx2 and Smad 5 induces osteoblast-specific gene expression in the pluripotent mesenchymal precursor cell line C2C12. *Mol Cell Biol*. 20: 8783–8792.

Li, Y.-P., et al. 1999. *Atp*6i-deficient mice exhibit severe osteopetrosis due to loss of osteoclast-mediated extracellular acidification. *Nat Genet*. 23: 447–451.

Lian, J.B., C.M. Gundberg. 1988. Osteocalcin. Biochemical considerations and clinical applications. *Clin Orthop.* 226: 267–291.

Lian, J.B., et al. 1989. Gene expression and functional studies of the vitamin K-dependent protein of bone, osteocalcin. In *Clinical impact of bone and connective tissue markers*, eds. E. Lindh, J.J. Torell, 121–132. San Diego, CA: Academic Press.

Lomri, A., P.J. Marie. 1996. The cytoskeleton in the biology of bone cells. In *Cytoskeleton in specialized tissues and in pathological states*, eds. J.E. Hesketh, I.F. Pryme, Vol. 3, 229–264. Greenwich, CT: JAI Press Inc.

Linsenmayer, T.F., et al. 1985. Are collagen fibrils in the developing avian cornea composed of two different collagen types? Evidence from monoclonal antibody studies. *Ann NY Acad Sci*. 460: 232–245.

Luxenburg, C., et al. 2007. The architecture of the adhesive apparatus of cultured osteoclasts: from podosome formation to sealing zone assembly. *PLoS One*. 2:e179.

Maeda, K., et al. 2012. Wnt5a-Ror2 signaling between osteoblast-lineage cells and osteoblast precursors enhances osteoclastogenesis. *Nat Med*. 18: 405–412.

Malone, J.D., et al. 1982. Recruitment of osteoclasts precursors by purified bone matrix constituents. *J Cell Biol*. 92: 227–230.

Manston, J., E. Katchburian. 1984. Demonstration of mitochondrial mineral deposits in osteoblasts after anhydrous fixation and processing. *J Microsc.* 134: 177–182.

Mark, M.P., et al. 1987. Bone gamma-carboxyglutamic acid-containing protein (osteocalcin) expression by osteoblasts during mandibular bone development in fetal rats: absence of correlation with the mineralization process. *Med Sci Res*. 15: 1299–1300.

Marotti, G., et al. 1976. Number size and arrangement of osteoblasts in osteons at different stages of formation. *Calcif Tissue Res*. 21Suppl: 96–101.

Martin, J.H., J.L. Matthews. 1970. Mitochondrial granules in chondrocytes, osteoblasts and osteocytes. An ultrastructural and microincineration study. *Clin Orthop.* 68: 273–278.

Mathieu, P.S., E.G. Loboa. 2012. Cytoskeletal and focal adhesion influences on mesenchymal stem cells shape, mechanical properties and differentiation down osteogenic, adipogenic, chondrogenic pathways. *Tissue Eng Part B Rev.* 18: 436–444.

Matic, I., et al. 2016.Queiscent bone lining cells are major source of osteoblasts during adulthood. *Stem Cells* 34: 2930–2942.

Matsuo K., N. Irie. 2008. Osteoclast-osteoblast communication. *Arch Biochem Biophys.* 473: 201–209.

Matsuo, N., et al. 2008. Collagen XXIV (Col24α1) gene expression is a specific marker of osteoblast differentiation and bone formation. *Connect Tissue Res.* 49: 68–75.

McNamara, L.M., et al. 2009. Attachment of osteocyte cell processes to the bone matrix. *Anat Rec.* 292: 355–363.

Mikuni-Tagaki, Y., et al. 1995. Matrix mineralization and the differentiation of osteocyte-like cells in culture. *J Bone Miner Res.* 10: 231–242.

Miller, J.R. 2001. The Wnts. *Genome Biol.* 3: 3001.1–3001.15.

VetBooks.ir

Miller, S.C., et al. 1980. Characterization of endosteal bone-lining cells from fatty marrow bone sites in adult beagles. *Anat Rec*. 198: 163–173.

Myers, K.A., et al. 2007. Osteoblast-like cells and fluid flow: Cytoskeleton-dependent shear sensivity. *Biochem Biophys Res Commun*. 364: 214–219.

Nakashima, K., et al. 2002. The novel zinc finger-containing transcription factor osterix is required for osteoblast differentiation and bone formation. *Cell*. 108: 17–29.

Nango, N., et al. 2016. Osteocyte-directed bone demineralization along canaliculi. *Bone*. 84: 279–288.

Nesbitt, S.A., M.A. Horton. 1997. Trafficking of matrix collagen through bone-resorbing osteoclasts. *Science*. 276: 266–269.

Olsen, B.R. 1991. Collagen biosynthesis. In *Cell biology of extracellular matrix*. 2nd edition, ed. E.D. Hay, 177–220. New York: Plenum Press.

Olsen, B.R., et al. 2000. Bone development. *Annu Rev Cell Dev Biol*. 16: 191–220.

Ørvig, T. 1951. Histologic studies of Placoderms and fossil Elasmobranchs. I. The endoskeleton, with remarks on the hard tissue of lower vertebrates in general. *Ark Zool*. 2: 321–454.

Ørvig, T. 1968.The dermal skeleton; general considerations. In *Current problems of lower vertebrate phylogeny*, eds. T. Ørvig, J. Weyley, 373–397. New York: Interscience Publishers.

Otto, F., et al. 1997. Cbfa1, a candidate gene for cleidocranial dysplasia syndrome, is essential for osteoblast formation and bone development. *Cell*. 89: 765–771.

Palumbo, C., et al. 1990. Morphological study of intercellular junctions during osteocytes differentiation. *Bone*. 11: 401–406.

Pawlicki, R., et al. 1966. Cells, collagen fibrils and vessels in dinosaur bone. *Nature*. 211: 655–657.

Pierce, A.M., et al. 1991. Osteoclasts: structure and function. *Electron Microsc Rev*. 4: 1–45.

Price, P.A. 1985. Vitamin K-dependent formation of bone Gla protein (osteocalcin) and its function. *Vitam Horm*. 42: 65–108.

Price, P.A., et al. 1983. Matrix Gla protein, a new γ-carboxyglutamic acid-containing protein which is associated with the organicmatrix of bone. *Biochem Biophys Res Commun*. 117: 765–771.

Prideaux, M., et al. 2016. Osteocytes: the master cell in bone remodelling. *Curr Opin Pharmacol*. 28: 24–30.

Prockop, D.J., et al. 1979. The biosynthesis of collagen and its disorders. *N Engl J Med*. 301: 13-23 and 77–85.

Repp, F, et al. 2017. Coalignment of osteocyte canaliculi and collagen fibers in human osteonal bone. *J Struct Biol*. 199: 177–186.

Reseland, J.E., J.O. Gordeladze. 2002. Role of leptin in bone growth: central player or peripheral supporter? *FEBS Lett*. 528: 40–52.

Reznikov, N., et al. 2014. Three dimensional structure of human lamellar bone: the presence of two different materials and new insights into the hierarchical organization. *Bone*. 59: 93–104.

Ricard-Blum, S. 2011. The collagen family. *Cold Spring Harb Perspect Biol*. 3: a004978.

Rimblot-Baly, F., et al. 1995. Analyse paléohisologique d'une série de croissance partielle chez *Lappentosaurus madascariensis* (Jurassique moyen): essai sur la dynamique de croissance d'un dinosaur sauropode. *Ann. Paléontol*. 81: 49–86.

Robinson, R. 1952. An electron microscopic study of the crystalline inorganic component of bone and its relationship to the organic matrix. *J Bone Joint Surg Am*. 34-A: 389–435.

Rodda, S., A.P. McMahon. 2006. Distinct roles for Hedgehog and canonical Went signalling in specification, differentiation and maintenance of osteoblast progenitors. *Development*. 133: 3231–3244.

Rodriguez, J.P., et al. 2004. Cytoskeletal organization of human mesenchymal stem cells (MSC) changes during their osteogenic differentiation. *J Cell Biochem*. 93: 721–731. doi: 10.1002/jcb.20234.

Roodman, G.D. 1996. Advances in bone biology: the osteoclast. *Endocrinol Rev*. 17: 308–332.

Rowe, P.S. 2004. The wrikkened pathways of FGF23, MEPE, and PHEX. *Crit Rev Oral Biol Med*. 15: 264–281.

Ruoslahti, E. 1991. Integrins. *J Clin Invest*. 87: 1–5.

Sahar, R., S. Weiner. 2018. Open question on the 3D structures of collagen containing vertebrate mineralized tissues: a perspective. *J Struct Biol*. 201: 187–198. https://doi.org/10.1016/j.sb.2017.11.008

Sakai, D., I. Kii, K. Nakagawa, et al. 2011. Remodelling of actin cytoskeleton in mouse periosteal cells under mechanical loading induces periosteal cell proliferation during bone formation. *PLoS One*. 6(9): e24847.

Salo, T., et al. 1997a. Identification of the membrane-type matrix metalloproteinase MTI-MMP in osteoclasts. *J Cell Sci*. 110: 589–596.

Salo, T., et al. 1997b. Removal of osteoclast bone resorption products by transcytosis. *Science*. 276: 270–273.

Schaffler, M.B., et al. 2014. Osteocytes: master orchestrators of bone. *Calcif Tissue Int*. 94: 5–24.

Scheven, B.A.A., et al. 1986. *In vitro* osteoclast generation from different marrow fractions, including a highly enriched hematopoietic stem cell population. *Nature*. 321: 79–81.

Schlesinger, P.H., et al.1997 Characterization of osteoclast ruffled border chloride channel and its role in bone resorption. *J Biol Biochem*. 272: 18636–18643.

Schneider, P., et al. 2010. Towards quantitative 3D imaging of the osteocyte lacuno-canalicular network. *Bone*. 47: 848–858.

Schweitzer, M.H., et al. 2008. Microscopic, chemical, and molecular methods for examining fossil preservation. *C R Palevol*. 7: 159–184.

Scott, B.L., D.C. Pease. 1956. Electron microscopy of the epiphyseal apparatus. *Anat Rec*. 126: 465–495.

Sebastian, A., G.G. Loots. 2017. The transcriptional control of *Sost* in bone. *Bone*. 96: 76–84.

Seifert, M.F. 1984. The biology of macrophages in osteopetrosis. Structure and function. *Clin Orthop RelatRes*. 182: 270–277.

Shao, J., et al. 2018. The regulatory roles of Notch in osteocyte differentiation via the crosstalk with canonical Wnt pathways during transition of osteoblast to osteocytes. *Bone*. 108: 165–178.

Sherman, V.R., et al. 2015. The material science of collagen. *J Mech Behav Biomed Mater*. 52: 22–50.

Simonet, W.S., et al. 1997. Osteoprotegerin: a novel secreted protein involved in bone density. *Cell*. 89: 309–319.

Suarez, K.N., et al. 1996. Collagen type I cortical and trabecular bone differs in the extent of posttranslational modifications. *Calcif Tissue Res*. 58: 65–69.

Sutfin, L.V., et al. 1971. Microanalysis of individual granules with diameters less than 1000 Angstroms. *Science*. 174: 947–949.

Termine, J.D., et al. 1981. Osteonectin, a bone-specific protein linking mineral to collagen. *Cell*. 26: 99–105.

Teti, A., et al. 1989. Extracellular protons acidify osteoclasts, reduce cytosolic calcium and promote expression of cell-matrix attachment structures. *J Clin Invest*. 84: 773–780.

Teti, A., et al. 1991. Clear zone in osteoclast function: role of podosomes in regulation of bone-resorbing activity. *Am J Physiol*. 261: C1–C7.

Tracy, R.P., K.G. Mann. 1991. Osteonectin. In *Bone vol 3 Bone matrix and bone specific products*, ed. B.K. Hall, 295–320. Boca Raton, FL: CRC Press.

Tsukuba, T., et al. 2017. New functions of lysosomes in bone cells. *J Oral Biosci*. 59: 92–95.

Tu, X., et al. 2015. Osteocytes mediate the anabolic actions of canonical Wnt/beta-catenin signaling in bone. *PNAS*. 112: E478–E486.

Urist, M.R. 1965. Bone: formation by induction. *Science*. 150: 893–899.

Väänänen, K., H. Zhao. 2002. Osteoclast functions: Biology and mechanisms. In *Principles of bone biology*, eds. J.P. Bilezikian, L.G. Raisz, G.A. Rodan, 127–139. San Diego, CA: Academic Press.

Vaes, G. 1965. Excretion of acid and lysosomal hydrolytic enzymes during bone resorption induced in tissue culture by parathyroid extract. *Exp Cell Res*. 39: 470–474.

Van de Wijngaert, F.P., E.H. Burger. 1986. Demonstration of tartrate-resistant acid phosphatase in un-decalcified, glycomethacrylate-embedded mouse bone: a possible marker for (pre)osteoclast identification. *J Histochem Cytochem*. 34: 1317–1323.

Van der Rest, M. 1991. Collagens of bone. In *Bone vol 3. Bone matrix and bone specific products*, ed. B.K. Hall, 187–237. Boca Raton, FL: CRC Press.

Veis, A., B. Sabsay. 1987. The collagen of mineralized matrices. *Bone Mineral Res*. 5: 1–63.

Wang, Y., et al. 2007. A model for the role of integrins in flow induced mechnanotransduction in osteocytes. *PNAS*. 104: 15941–15946.

Watkins, M., et al. 2011. Osteoblast connexin 43 modulates skeletal architecture by regulating both arms of bone remodeling. *Mol Biol Cell*. 22: 1240–1251.

Webster, D. J., et al. 2013. Studying osteocytes and their environment. *Bone*. 54: 285–295.

Weiner, S., H.D. Wagner. 1998. The material bone: Structure-mechanical function relations. *Ann Rev Mater Sci*. 28: 271–298.

Wergedal, J. E. 1970. Characterization of bone acid phosphatase activity. *Proc Soc Exp Biol Med*. 134: 244–247.

Westerndorf, J.J., et al. 2004. Wnt signaling in osteoblasts and bone diseases. *Gene*. 341: 19–39

Wijenayaka, A.R., et al. 2011. Sclerostin stimulates osteocyte support of osteoclast activity by a RANKL-dependent pathway. *PLoS One*. 6: e25900.

Wozney, J.M. 1992. The bone morphogenetic protein family and osteogenesis. *Mol Repro Dev*. 32: 160–167.

Wright, G.M., C.P. Leblond. 1981. Immunohistochemical localization of procollagens. III. Type I procollagen antigenicity in osteoblasts and prebone (osteoid). *J Histochem Cytochem*. 29: 791–804.

Wu, J.J., et al. 2010. Type III collagen, a fibril network modifier in articular cartilage. *J Biol Chem*. 285: 18537–18544.

Xiao, Z., et al. 2006. Cilia-like structures and polycystin-1 in osteoblasts/osteocytes and associated abnormalities in skeletogenesis and RUNX2 expression. *JBC*. 281: 3088–30895. http://www.jbc.org/cgi/doi/10.1074/jbc.M604772200

Xing, L., B.F. Boyce. 2005. Regulation of apoptosis in osteoclast and osteoblast cells. *Biochem Biophys Res Commun*. 328: 709–720.

Xiong, J., et al. 2015. Osteocytes not osteoblasts or lining cells, are the main source of the RANKL required for osteoclastes formation in remodeling bone. *PLoS One*. 10: e0138 189.

Xiong, L., et al. 2015. Lrp4 in osteoblasts suppresses bone formation and promotes osteoclastogenesis and bone resorption. *PNAS*. 112: 34887–3492.

Yavropoulou, M.P., J.G. Yovos. 2008. Osteocladogenesis – Current knowledge and future perspectives. *J Musculoskelet Neuronal Interact*. 8: 204–216.

Ye, Y., et al. 2012. Glycosaminoglycan chains of biglycan promote morphogenetic protein-4-induced osteoblast differentiation. *Inter J Mol Med*. 30: 1075–1080.

You, L.-D., et al. 2004. Ultrastructure of the osteocyte process and its pericellular matrix. *Anat Rec*. 278A: 505–513.

Yuehuei, H.A., K.L. Martin. 2003. *Handbook of histology methods for bone and cartilage*. New York: Springer.

Zhang, D., et al. 2018. The development of collagen based composite scaffolds for bone regeneration. *Bioact Mater*. 3: 129–138.

Zhang, K., et al. 2006. El 1/gp38 selective expression in osteocytes: regulation by mechanical strain and role in dendrite elongation. *Mol Cell Biol*. 26: 4539–4552.

Zhao, H., et al. 2000. Osteoclast ruffled border membrane contains different subdomains for exocytosis and endocytosis. *Calcif Tissue Int*. 52: S63.

Zhou, X., et al. 2010. Multiple functions of Osterix are required for bone growth and homeostasis in postnatal mice. *PNAS*. 107: 12919–12924.

Zhu, W., et al.. 2010. The regulatory role of matrix proteins in mineralization of bone. In *Fundamental of osteoporosis*, 3rd edition, eds. R. Marcus, D. Feldman, D. Nelson, C.J. Rosen, 153–202. Amsterdam: Elsevier.

Zylberberg, L., et al. 1992. Biomineralization in the integumental skeleton in living lower vertebrates. *Bone vol 4*, ed. B.K. Hall, 171–224. Boca Raton, FL: CRC Press.

Zylberberg, L., et al. 2010. A microanatomical and histological study of the postcranial dermal skeleton in the Devonian sarcopterygian *Eusthenopteron foordi*. *Acta Palaeontol Pol*. 55: 559–570.

Zylberberg, L., M. Laurin. 2011. Analysis of fossil bone organic matrix by transmission electron microscopy. *C R Palevol*. 10: 357–366.

VetBooks.ir

6

Current Concepts of the Mineralization of Type I Collagen in Vertebrate Tissues

William J. Landis, Ph.D., Tengteng Tang, Ph.D., and Robin DiFeo Childs, M.S.

CONTENTS

Introduction 109
Collagen Basic Structure 109
Collagen Synthesis and Secretion 110
The Mineralization Process 110
The Normally Mineralizing Avian Leg Tendon Model 110
Type I Collagen Self-Assembly 111
Ultrastructural Appearance of Mineralized Type I Collagen 112
Intrafibrillar Mineralization of Type I Collagen 112
Interfibrillar Mineralization of Type I Collagen 117
Noncollagenous Proteins: Bone Sialoprotein 117
Noncollagenous Proteins: Osteopontin 118
Noncollagenous Proteins: Osteocalcin 118
Possible Temporal and Spatial Relationships Between Interfibrillar and Intrafibrillar Collagen Mineralization 119
Conclusions 119
Acknowledgments 120
References 120

Introduction

Collagen Basic Structure

With the exception of enamel, the mineralization of bone, dentin, cementum and calcifying cartilage and tendon in vertebrate species by and large is founded on the presence of the protein collagen, of which there are 28 types now identified. In bone, dentin, cementum and calcifying tendon, type I collagen is the most abundant, whereas type II collagen is most prominent in calcifying cartilage. Collagen structure, biochemistry, biomechanical properties and other characteristics have been studied for some time, and fundamental reviews and journal articles addressing these topics are extensive (for example, Fratzl 2008; Shoulders and Raines 2009; Stock 2015). The basis for collagen structure lies in a three amino-acid repeating motif, glycine-X-Y, where X and Y may be any amino acid, but they are commonly proline and hydroxyproline, to form three helical polypeptide chains (Figure 6.1).

For type I collagen, critical for vertebrate mineralization of bone, dentin, cementum and tendon, two such chains are identical and designated as α1(I). The third chain, α2(I), is different from α1(I) in its amino acid content and number of carbohydrate residues bound to the chain (Kuhn and Glanville 1980). Type I collagen is then comprised as 2α1(I)α2(I) chains. Type II collagen, important in cartilage mineralization (calcification) of vertebrates, has three identical α1(II) chains and is represented structurally as 3α1(II). Whether type I or type II, each of the three collagen chains is characterized by a slight twist and a left-handed helical conformation imparted by the presence of the repetitious proline in the primary peptide structure. The three chains associate to generate a right-handed triple helical molecule, stabilized in part by numerous hydrogen bonds bridging both within and between the three individual chains principally through amino- and carboxy-peptide groups. The glycine residues comprising every third amino acid of collagen are located inside and proline residues are outside each molecule. Since collagen molecular movement, particularly rotation, is limited by the twist induced by proline residues and the pyrrolidine side chains of proline are bulky, there is rigidity to the collagen helix. Moreover, the side chains of proline and hydroxyproline along with the side chains of any other

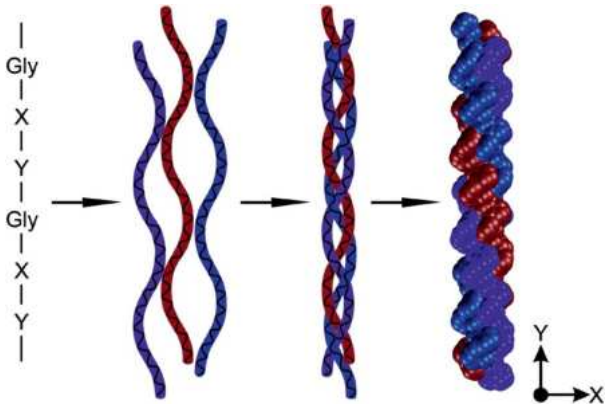


FIGURE 6.1 Left-to-right, the transition from the basic Gly-X-Y amino acid structure of collagen to its three α-chains (two identical α1(I) chains [blue], one α2(I) chain [red] for type I collagen). The three single chains form a right-handed triple helical molecule on their association and become cross-linked and more stable in the depiction by molecular modeling using VMD software (Humphrey et al. 1996.)

amino acids occupying the X- and Y-positions of the glycine-X-Y motif are directed outward from the collagen helix and, consequently, from the surfaces of aggregates of the molecules formed by lateral bonding between other helices and molecules. Additional cross-links provide further collagen chain stability (Eyre 1987; Yamauchi et al. 1989; Otsubo et al. 1992).

Collagen Synthesis and Secretion

Type I and II collagen and their other family members are synthesized and posttranslationally modified by phosphorylation, glycosylation and sulfation in a manner generally similar to that of other proteins in a variety of cells. The details of such synthesis and processing through endoplasmic reticulum and Golgi vacuoles and then transport of molecules by means of exosomes and intracellular vesicles will not be elaborated here (for relevant literature, see, for instance, Bornstein 1980; Shapiro et al. 2015). However, the larger synthesized and processed procollagen precursor molecules are cleaved of their amino- and carboxy-terminal extension peptides by enzymatic action at the cell envelope (Bornstein 1980). The resulting smaller collagen (or tropocollagen) molecules are then secreted to the extracellular environment where they may undergo subsequent structural changes that yield self-assembled aggregates of individual secreted molecules. Although a list of cells synthesizing collagen family members includes fibroblasts, vascular endothelial cells and others, for the normally mineralizing tissues of vertebrates and type I collagen, the relevant cells are osteoblasts (bone), odontoblasts (dentin), cementoblasts (cementum) and tenocytes (tendon) as well as chondrocytes (cartilage) for type II collagen.

The Mineralization Process

The Normally Mineralizing Avian Leg Tendon Model

As it is related to protein synthesis and secretion, a recent study of type I collagen gene expression correlated with the expression of several other genes and the appearance of mineralization in the normally mineralizing avian leg tendon has provided insight into the temporal and spatial sequence of collagen gene regulation and mineral formation in this mineralizing model (Chen et al. 2019). Certain birds, including the domestic turkey, *Meleagris gallopavo*, naturally mineralize their wing and leg tendons (Johnson 1960; Likens et al. 1960; Nylen et al. 1960). Investigations of the tendon mineralization events (Landis 1986; Arsenault 1988, 1991, 1992; Landis et al. 1993; Landis and Silver 2002) have demonstrated that this model closely resembles and may serve to represent many of the related events in bone, dentin and other vertebrate mineralizing tissues (Landis 1986; Bigi et al. 1988; Christoffersen and Landis 1991; Arsenault 1992). The model, therefore, has been utilized in this chapter to describe mineral deposition in vertebrate tissues in general.

By way of understanding the mineralization of turkey leg tendons, and the gastrocnemius (Achilles) tendon in particular (Figure 6.2), there is a well-defined temporal and spatial progression to mineral deposition that occurs in these tissues (Landis 1986; Arsenault et al. 1991). The gastrocnemius tendon of the domestic turkey is its largest leg tendon in size and extends from the claw of the bird to insertion sites in two shank (hip) muscles of the animal (Landis 1986) (Figure 6.2A). As the gastrocnemius tendon passes through a sheath behind the single upper leg joint, the tendon undergoes an anatomical division or bifurcation proximal to the joint in which its distal aspect, approximately 1 cm in diameter (for birds ~14–16-weeks of age), becomes two separate segments, each ~0.5 cm in diameter (Landis 1986) (Figure 6.2B). With aging and maturation of the tendon and the animal and for other factors that remain to be determined fully, each tendon segment begins to mineralize proximal to the gastrocnemius bifurcation point (Figure 6.2B). The segments continue mineralizing with time from these sites further proximal and toward their insertion into the shank muscles, yielding as a result tissues that present successive events of mineral deposition precisely correlated temporally and spatially along the proximal-to-distal direction of the tendons (Landis 1986). This progressive transition can therefore provide data of gene expression, synthesis and secretion of proteins and other molecules, and additional parameters uniquely and directly correlated between the youngest (proximal) and oldest (distal) mineral deposits in the bifurcated tendon aspects (Chen et al. 2015, 2019).

With this backdrop, gene expression and corresponding stages of mineralization have been correlated by sampling along the lengths of several gastrocnemius tendons in 12- and 15-week-old turkeys (Chen et al. 2019). As shown in Figure 6.3, type I collagen is expressed by tenocytes at a steady and relatively consistent level along tendons regardless of their degree of mineralization from younger (proximal) to older (distal) regions and animal and tissue age. The expression levels of several other genes that were examined with type I collagen vary, most notably that of bone sialoprotein, osteopontin and osteocalcin at the same sites and tissue and animal ages (Figure 6.3; Chen et al. 2019). The latter three proteins will be considered and discussed in regard to their possible roles in association with collagen and mineralization events in a subsequent part of this chapter.

VetBooks.ir

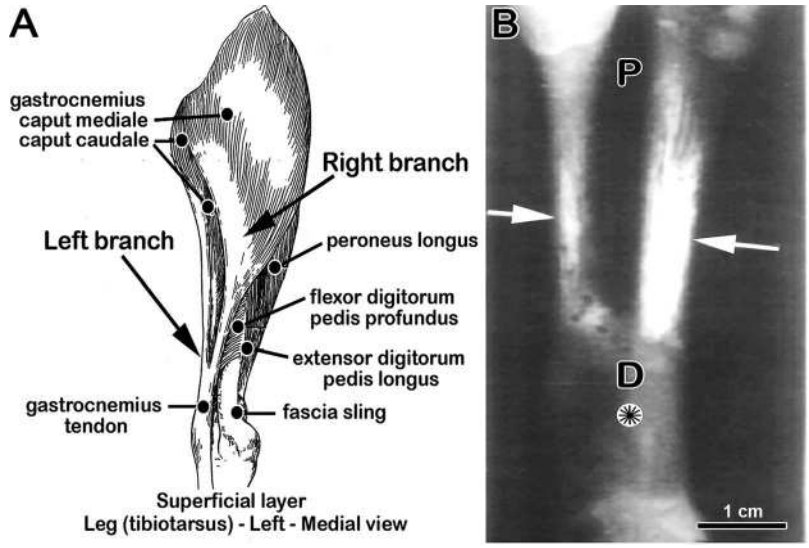


FIGURE 6.2 A, Illustration of the gastrocnemius (Achilles) tendon from the tibiotarsus of the domestic turkey, *Meleagris gallopavo*, demonstrating the bifurcation of this tissue into two branches that insert into separate muscles (caput mediale and caput caudale) of the hip of the animal. The bifurcation occurs proximal to a joint in the turkey leg at the level of the labeled gastrocnemius tendon and fascia sling. B, A radiograph of a gastrocnemius tendon dissected from a 16-week-old domestic turkey, showing the bifurcation of the tissue (asterisk) and the formation of mineral as opaque streaks (arrows) in both bifurcated segments. Mineral deposition begins distally (D) and progresses proximally (P) from the point of gastrocnemius tendon bifurcation. The tendon region distal to the point of bifurcation (asterisk) never mineralizes as here the tendon slides through a sheath and must be flexible at the joint of the leg. (Images adapted and reprinted with permission from Harvey et al. (1968) [Figure 2A] and Landis (1986) [Figure 2B].)

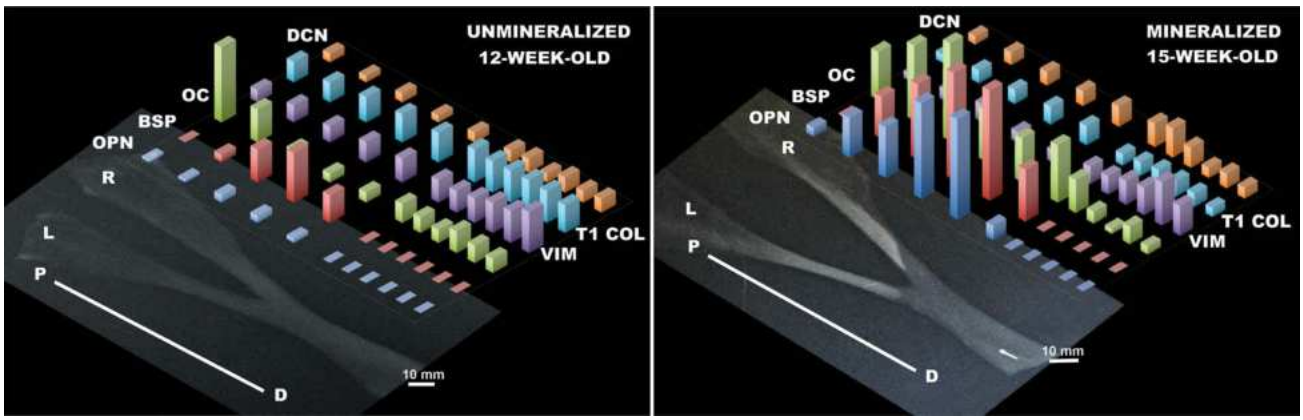


FIGURE 6.3 Graphic plots showing the relative expression levels of several different genes corresponding to their locations along the right (R) branch of the gastrocnemius tendons dissected from 12- and 15-week-old domestic turkeys. The genes are osteopontin (OPN), bone sialoprotein (BSP), osteocalcin (OC), vimentin (VIM), type I collagen (T1 COL), and decorin (DCN). The 12-week-old turkey maintains a tendon that is unmineralized as determined by radiography, whereas the 15-week-old turkey has a tendon that is partially mineralized. Type I collagen expression is relatively constant over the full tendon length examined at both 12 and 15 weeks of age. The same can be concluded for DCN. For the 12-week-old tendon, BSP expression markedly rises and falls along the proximal tendon region that will mineralize by 15 weeks. OC expression is greater in proximal tendon regions near the tendon-muscle insertion site at the turkey shank. Levels of expression of OPN and BSP are minimal in regions distal to the bifurcation point of the tendon, whereas VIM expression increases along the same distal portions of the tissue. For the 15-week-old tendon, OPN, BSP and OC expression levels each rise and fall in a somewhat corresponding manner through the mineralized proximal tissue region, and the levels of the same genes are minimal over much of the tendon region distal to the point of bifurcation. VIM expression is lower in the tissue proximal to its bifurcation point and increasingly greater distal to the point, presenting an expression pattern opposite to that of OC. L, left tendon branch; P, proximal; D, distal. (Images reprinted with permission from Chen et al. 2019.)

Type I Collagen Self-Assembly

Following its cellular synthesis, type I procollagen is secreted to the extracellular matrix at the cell envelope where its amino- and carboxy-terminal peptides are cleaved, as noted above. Individual triple helical collagen molecules, ~300 nm in length and comprised of 1038 amino acids, are now replete in the matrix and spontaneously self-assemble by bonding laterally between overlapping ends of molecules. The overlap domain of such bonding is 234 amino acids and ~27 nm in length. Molecules form dimers, trimers and other groupings and intermolecular cross-linking stabilizes such associations to create so-called gaps or holes in two-dimensional collagen assemblages (Figure 6.4). The holes

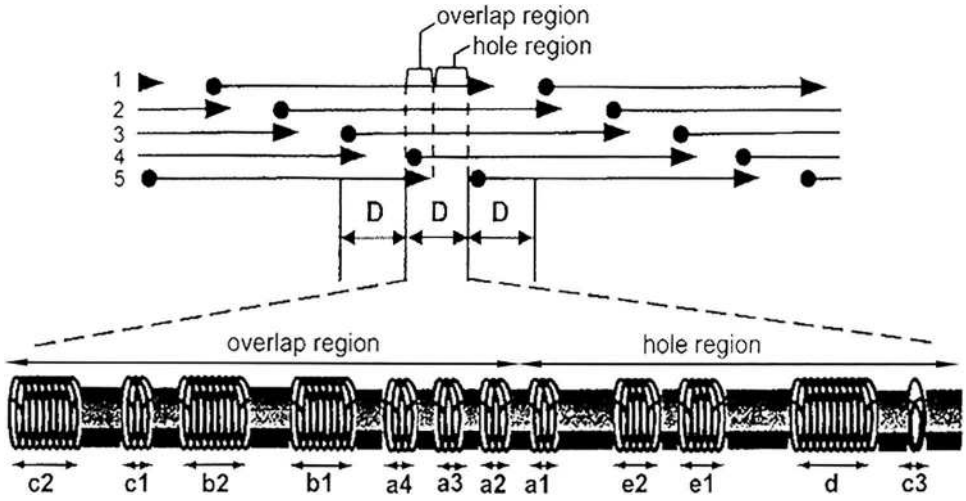


FIGURE 6.4 The two-dimensional arrangement of collagen following the Hodge-Petruska quarter-staggered model (Hodge and Petruska 1963) and containing five molecules in a subfibrillar unit. Individual collagen molecules, 4.46 *D* in length and shown as segments (arrows) 1–5 above, cross-link to form head and tail overlap regions between molecules. Packing of five molecules along their long-axis direction shifts them with respect to each other by a length *D* = 67 nm, comprised of an overlap region ~0.4 *D* and a hole region ~0.6 *D*. When packed microfibrils are stained with metal ions and observed by electron microscopy, a series of 12 dark (stained) bands is detected along them and designated c1, c2, b2 … c3 for their identification and differentiation. The width of the bands is proportional to the number of their composite amino acids. Bands are shown as springs to denote their flexible nature resulting from their relative absence of proline and hydroxyproline. They alternate with more rigid interband regions with relatively greater numbers of these amino acids and depicted as cylinders (Silver et al. 2001). (Image modified and reprinted with permission from Silver et al. 2001.)

are ~40 nm in length and, together with the overlap domains, generate a length of ~67 nm that repeats along the long axis of collagen. This periodicity is particular to collagen, although it may vary slightly from ~64 to 70 nm depending on the degree of hydration and vertebrate species involved. The self-assembly of collagen in this manner results in a structure with a period of about one-fourth of the collagen molecule length of 300 nm. Thus, it leads to the "quarter-staggered" model of collagen association in two dimensions developed by Hodge (1989), Hodge and Petruska (1963) and Petruska and Hodge (1964) (Figure 6.4). Studies utilizing high-voltage transmission electron microscopy and tomography demonstrated that collagen arrays associate in three dimensions in a manner such that their overlap and hole domains align and cross-link strictly in register (McEwen et al. 1991, Landis et al. 1993). This three-dimensional organization yields 64–70 nm periodic channels that extend into the arrays from proposed openings at the surfaces of the collagen assemblages (Landis et al. 1993; Figure 6.5).

Ultrastructural Appearance of Mineralized Type I Collagen

The 64–70 nm periodicity resulting from the assembly and packing of the molecular or higher ordered arrays of collagen produces the characteristic banded appearance of the protein on electron microscopy (Figure 6.6). The presence of mineral principally in collagen hole zones and channels enhances such ultrastructural periodicity (Figure 6.6A). Images such as these demonstrate that mineral deposition associated with type I collagen occurs both within (intrafibrillar) and along the surfaces and outside (interfibrillar) of the protein (Figures 6.6A, B). Electron diffraction studies have shown that the orientation and alignment of apatite mineral crystals are different in intra- and interfibrillar regions of collagen: the crystals are highly aligned within collagen such that their crystallographic *c*-axes are oriented principally along collagen long axes, whereas they are randomly oriented at the collagen surfaces and between collagen assemblages in the extracellular matrices (Landis et al. 1996). These results suggest that the mechanism of apatite nucleation, growth and development is distinct in intra- and interfibrillar collagen regions.

Intrafibrillar Mineralization of Type I Collagen

The location of early mineral crystals principally within the hole zones or channels of type I collagen arrays (Figures 6.5, 6.6A) is intriguing to consider. These zones provide ample available space for crystal nucleation and growth to occur, but space is not the only factor in crystal formation and subsequent crystal orientation and alignment. In this context, the hole zone and channels are surrounded in large part by a three-dimensional neighborhood of collagen molecules. The channels contain and maintain a fluid environment supersaturated in calcium and phosphate ions, and nucleation events are not thought to be spontaneous but highly regulated and controlled. From the critical studies by Orgel et al. (2006, 2014), a single collagen molecule was found to associate with five other molecules to form a quasi-hexagonal or microfibrillar packing unit (Figure 6.7). The order of adjacent collagen molecules in a microfibril was determined to be 1-4-1-3-2-3, in which 2, 3 and 4 describe molecules that are staggered, respectively, 234 amino acids, 2 × 234 amino acids, and 3 × 234 amino acids in relation to molecule 1 (Figure 6.7). This molecular configuration envelopes a collagen hole zone channel (Figure 6.7), and the association is repetitive as collagen molecules form larger groupings of fibrils, fibers and fiber bundle aggregates.

VetBooks.ir

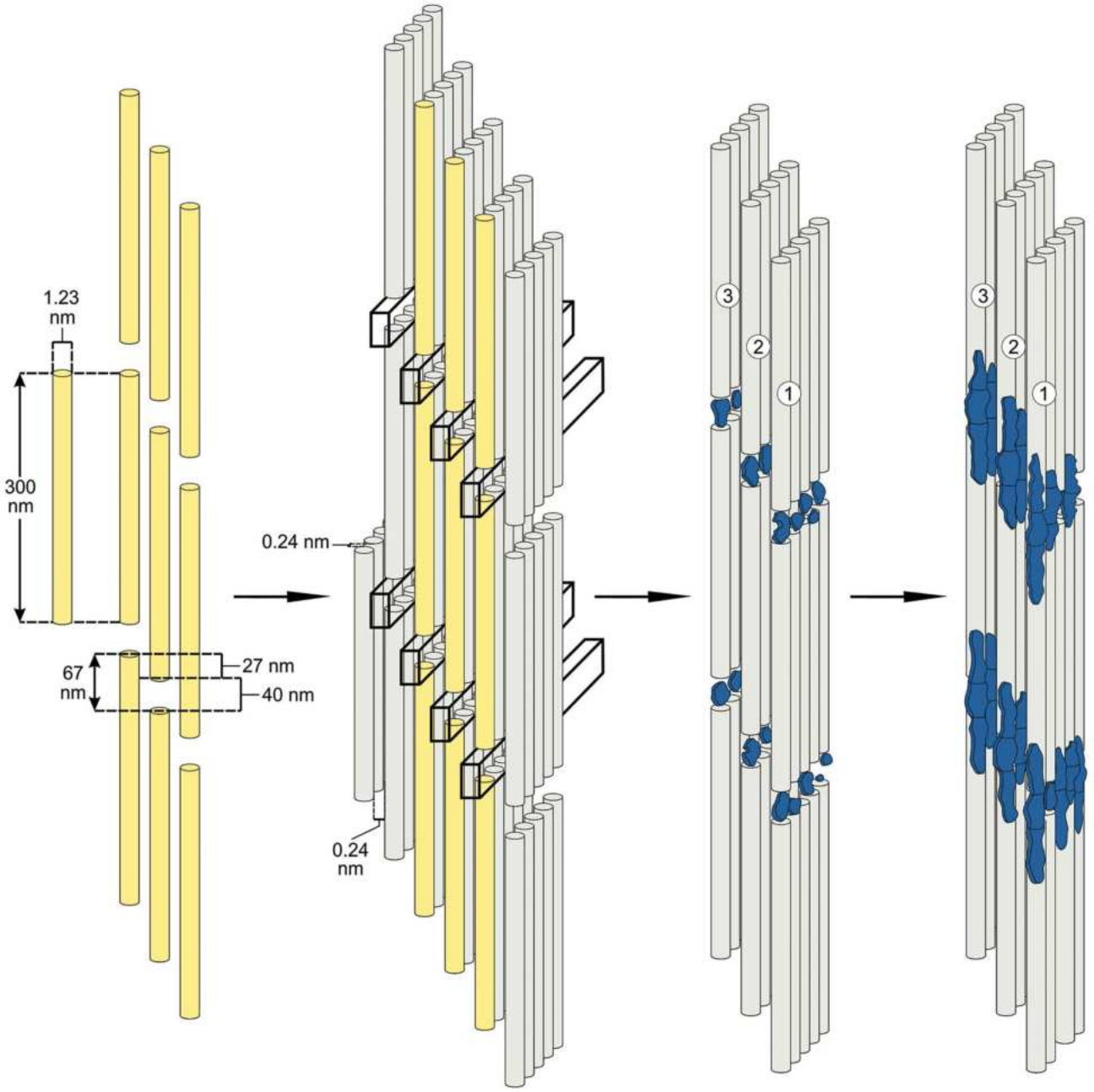


FIGURE 6.5 Assembly of collagen molecules to form the so-called quarter-staggered model of Hodge and Petruska (1963) (yellow) and the subsequent creation of hole zone channels or gaps that traverse the collagen assemblages in three dimensions (rectangles). Intrafibrillar nucleation of apatite mineral crystals (blue) begins principally in the channels, and crystal growth follows nucleation events to form a series of platelet-shaped crystals developing preferentially lengthwise with their crystallographic *c*-axes parallel to the long axes of collagen molecules. The largest developing faces of the crystals, their (100) planes, become generally parallel to each other and to the long axes of the collagen molecules with which they associate. The crystals increase in width within the channels by putatively fusing with one another. (Image modified and reprinted with permission from Landis et al. 1993, which describes additional features of collagen assembly and mineralization.)

The characteristic 64–70 nm period of collagen, the basic D-stagger of collagen molecules first described by Hodge and Petruska (1963), is conserved through the various hierarchical assemblages of microfibrils to fiber bundles.

The amino acid sequence of human type I collagen has been published (see www.ncbi.nlm.nih.gov/protein) and, as a result, the residues of neighboring molecules, each staggered by a specific multiple of 234 amino acids, may be identified in the vicinity of collagen hole zone regions. An example of the sequence for five molecules, each successively staggered by 234 residues, demonstrates several characteristics of importance for mineralization (Figure 6.8). While the majority of sequence is comprised of an uncharged repeating tripeptide, Gly-X-Y, noted earlier (Figure 6.1), there are numerous charged residues present in the X- and Y-positions of type I collagen molecular structure. Such charged residues are particularly abundant in the 12 bands

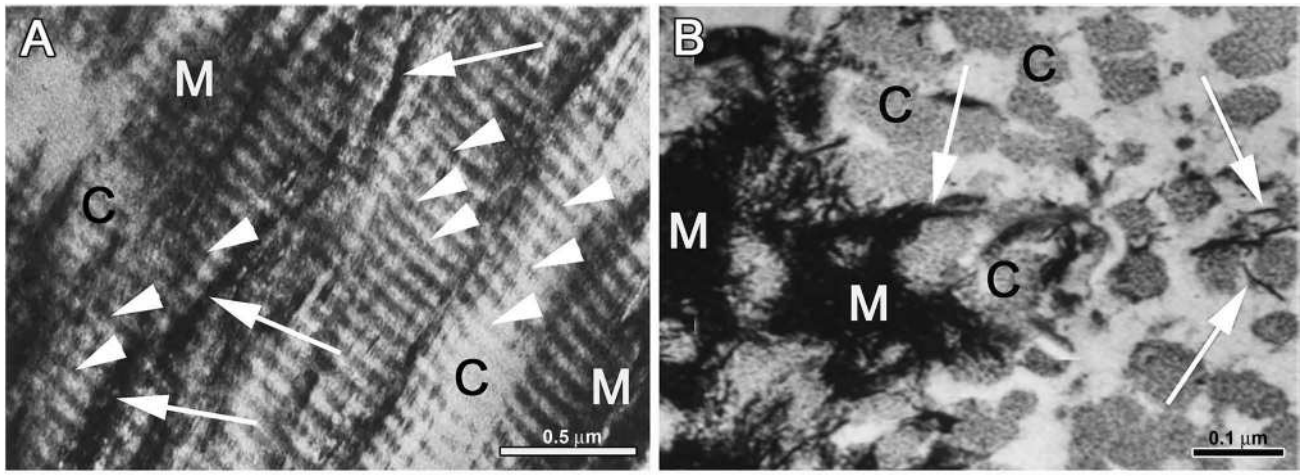


FIGURE 6.6 A, Transmission electron micrograph of a leg tendon from an 18-week-old turkey. The specimen was prepared by conventional fixation in glutaraldehyde-osmium tetroxide and stained with uranyl acetate and lead citrate. Sectioned along the longitudinal profiles of collagen fibrils (C), the tissue shows the distinct 64–70 nm periodicity of collagen and highly ordered deposition of crystals having the same intrafibrillar periodicity (arrowheads). Mineral deposition (M) also may be found in interfibrillar spaces between fibrils of different diameters (arrows). B, Transmission electron micrograph of a 16-day-old embryonic chick bone, prepared with glutaraldehyde and stained with uranyl acetate and lead citrate. Sectioned transversely to the long axes of collagen fibrils (C), the tissue shows mineral (M) along and encompassing several generally circular-shaped profiles of fibrils (arrows), representing interfibrillar deposition, as well as completely encasing fibrils, which are examples of intrafibrillar deposition. Scale bars = 0.5 µm (A), 0.1 µm (B). (Images adapted and reprinted with permission from (A) Christoffersen and Landis 1991 and (B) Landis et al. 1977.)

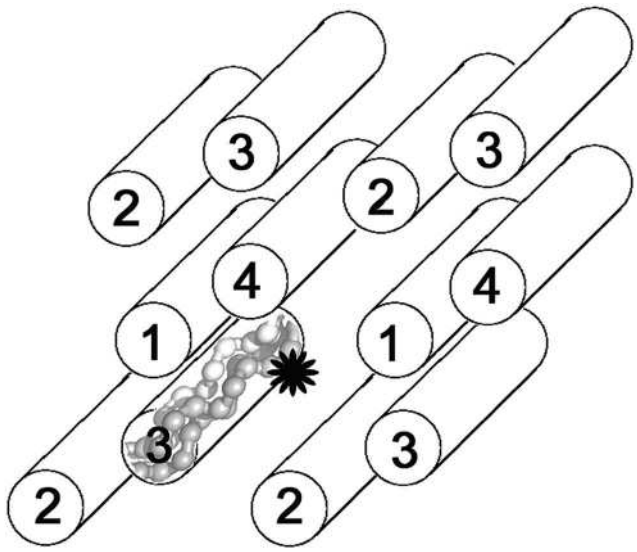


FIGURE 6.7 The neighborhood of collagen molecules surrounding a hole zone region (asterisk) in the three-dimensional molecular packing model following Orgel et al. (2006, 2014). A repeating quasi-hexagonal unit of segments of collagen molecules is shown in an order of the molecules as 1-4-1-3-2-3, respectively D-staggered as noted above. Molecular segment 3 is depicted with its three composite amino acid chains. The void space (asterisk) results from the absence of molecular segment 5 in the hole zone region. The stagger of the other five molecules with respect to segment 1 is known and so is the amino acid sequence of a single collagen molecule. Thus, the amino acids can be precisely defined about a hole zone. (Schematic reprinted with permission from Silver and Landis 2011.)

defining the hole and overlap regions of collagen (Figures 6.4 and 6.8) and are responsible for the higher density of heavy metal staining and resulting periodicity of collagen (Chapman 1974; Chapman and Hardcastle 1974). Indeed, the binding of calcium and phosphate ions to these charged residues is predicted to yield the same periodic banding that is characteristic of collagen (Glimcher 2006). Inspection of the amino acid sequence of each type I collagen molecule within a microfibril (Silver and Landis 2011; Figures 6.4 and 6.8) reveals the following features: (1) numerous sites in which the same charged amino acid (glutamic acid, aspartic acid, arginine, lysine and hydroxylysine) lies adjacent in all three helical peptide chains [2α1(I) and α2(I)], (2) sites in which the adjacent amino acids of the 2α1(I) and the α2(I) chains are different but are of the same charge, (3) sites in which two or three amino acids of the same charge are close to the same two or three amino acids in the three peptide chains, (4) sites in which two or three glutamic or aspartic acid residues are close to their respective counterpart two or three aspartic or glutamic acid residues in the three peptide chains, (5) sites in which the same two or three amino acids of one charge are close to the same two or three amino acids of the opposite charge in the three peptide chains and (6) sites in which lysine or arginine residues are replaced by a hydroxylysine residue to contribute identically charged groups in the three peptide chains.

Additional examination of the compositional character of type I collagen molecules is interesting regarding the presence of serine and threonine residues and their structural relation to the charged amino acids described above. Serine particularly is notable in the collagen bands of high charge density (Figure 6.8). Serine and threonine are frequently phosphorylated in a wide spectrum of proteins in which such residues perform a variety of functions, and phosphoproteins have been implicated in mineralization events through multiple lines of research (Glimcher 2006; George and Veis 2008; Huang et al. 2008; Robey 2008; Boskey and Robey 2013). Further analysis of these two residues in type I collagen is ongoing and may yield new data related to binding of calcium ions and putative nucleation of apatite crystals.

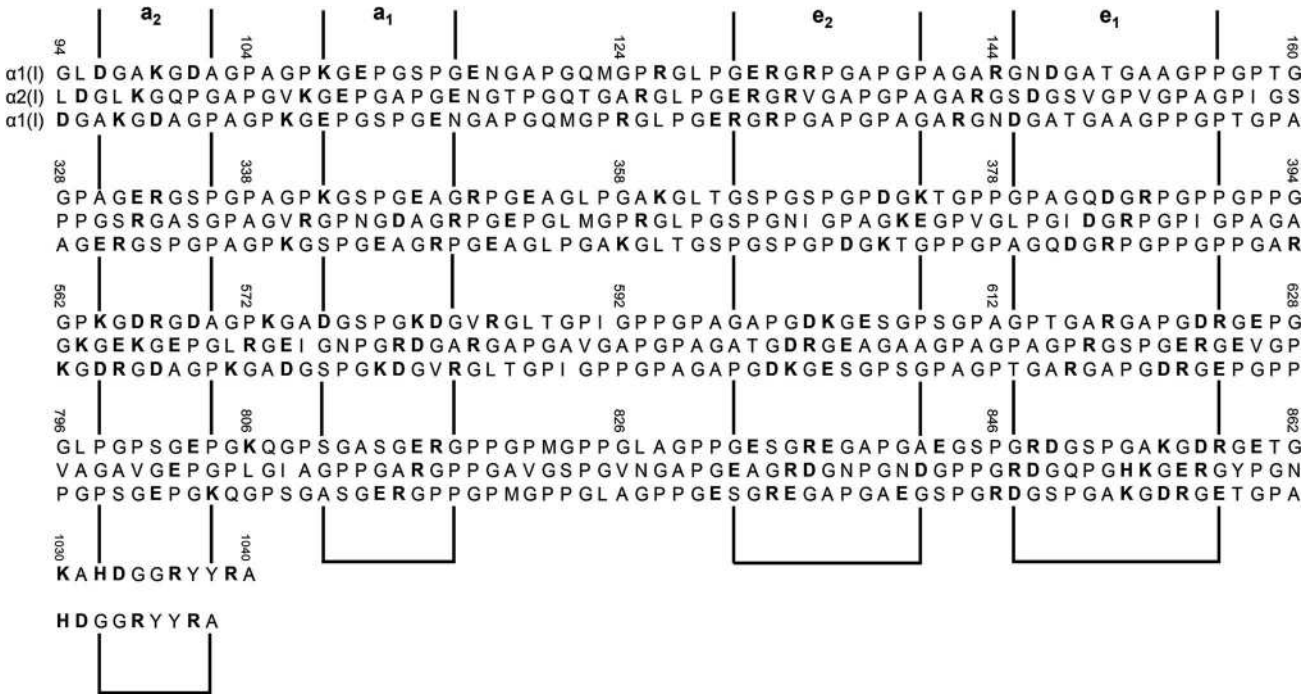


FIGURE 6.8 Numbered amino acid residues in a selected portion of the human type I collagen microfibril (see www.ncbi.nlm.nih.gov/protein) that includes 4 (a2, a1, e2 and e1) of the total of 12 bands defined by Hodge and Petruska (1963). Five molecular segments of collagen are shown with their N- to C-termini left to right. The four segments illustrate several features of the amino acid sequence potentially important to calcium and phosphate ion binding and subsequent apatite crystal nucleation and growth. Each molecular segment of the microfibril is presented with its α2(I) chain between its two α1(I) chains. Residues are staggered by 234 amino acids between respective segments, representing 1D, 2D, 3D and 4D units from the second to fifth (top to bottom) segments of the figure, respectively. The fifth segment (bottom-most) shown is part of the extrahelical terminal peptide of the microfibril whose α2(I) chain ended at residue 1028. Charged residues in the segments are highlighted in bold. The remaining eight bands comprising the collagen hole and overlap zones have amino acid residues with several features common to those depicted for a2–e1. (Schematic reprinted with permission from Silver and Landis 2011.)

There is a great fundamental and functional significance of these previous observations relevant to the amino acid composition of type I collagen peptide chains and vertebrate mineralization: Calcium and phosphate ions supersaturated in the circulating fluid around and within collagen molecules may be bound by the charged amino acid residues comprising hole and overlap regions of the protein (Silver and Landis 2011). Grouping and close spatial location of the charged residues to each other imply that calcium and phosphate ions bound to the amino acids may be brought into stereochemical positions that accommodate apatite (calcium phosphate) crystal nucleation (Silver and Landis 2011; Xu et al. 2015).

Silver and Landis (2011) utilized the three-dimensional packing model of type I collagen described by Orgel et al. (2006) (Figure 6.7) together with the known type I collagen amino acid sequence (Figure 6.8) to depict the charged residues in the e2 band and putative calcium and phosphate ion binding to this aspect of the collagen hole zone region. Figure 6.9 presents a composite image of the quasi-hexagonal assemblage of the molecules shown with their charged residues identified and putative ion association in the e2 band vicinity of the hole zone. This example of proposed ion binding may be extrapolated to the entirety of the hole and overlap regions of type I collagen molecules to define the nucleation of apatite crystals within the protein, that is, its intrafibrillar mineralization as noted previously in this chapter and illustrated in Figure 6.6 at an ultrastructural level.

The suggested presence of calcium and phosphate ion binding in hole zone regions of collagen rests on the assumption that the side chains of the charged residues enveloping those regions point inward and toward the hole zone spaces. Validation of such an assumption was recently established utilizing molecular dynamics simulation (Xu et al. 2015). In this study, the ensemble of atoms and molecules comprising the charged residues in the e1 and e2 bands of type I collagen molecules in their 1-4-1-3-2-3 configuration (Figure 6.7) surrounding a hole zone region was allowed to interact dynamically for a known time interval and the final state of atom and molecule interplay was recorded (Figure 6.10). The neighborhood of molecules envisioned in this manner showed that the side chains of each charged amino acid were principally directed toward and into the collagen hole zone regions and that the length and direction of side chains for the different charged amino acids varied and extended to different degrees into the hole zones (Xu et al. 2015).

Variable lengths and directions of the charged residue side chains extending toward and into collagen hole zones suggest that these regions are not uniform but differ in their diameter across the hole space. The holes or channels in collagen assemblages are then wider or narrower, winding and convoluted, as they traverse the arrays (Xu et al. 2018). Furthermore, the positions and configurations of certain collagen molecules comprising the assemblages may effectively block some channels from extending completely through the arrays (Xu et al. 2018).

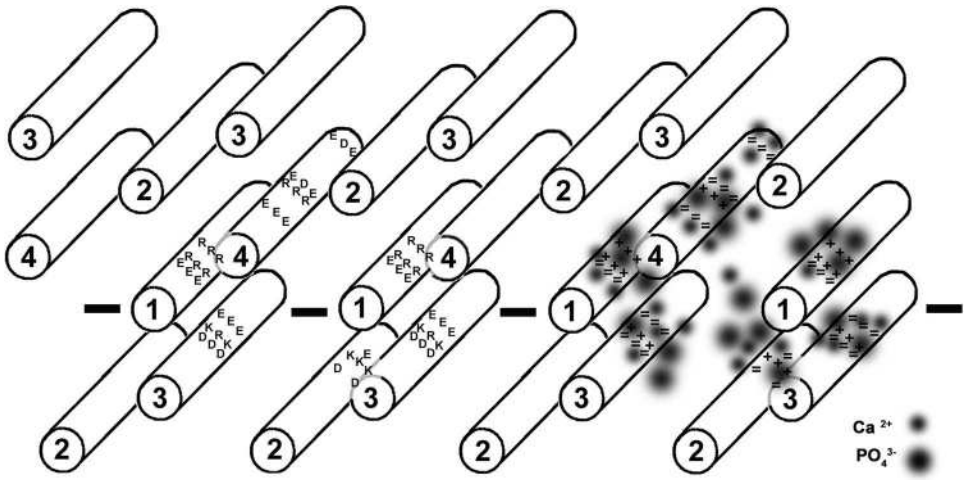


FIGURE 6.9 Axial location and distribution of charged amino acid residues in the e2 band surrounding a portion of the hole zone region of type I collagen and in the three-dimensional packing model according to Orgel et al. (2006). Charges corresponding to the residues are shown with conceptual association of calcium and phosphate ions and the several possible binding sites presented by the charges. Amino acid residues (glutamic acid [E], aspartic acid [D], lysine [K] and arginine [R]) that comprise each molecular segment correspond to their identification and order given in Figure 6.8 and are in precise spatial registration with the residues in respective segments. In three dimensions, ion-binding sites would be found within the hole zone volume defined by the surrounding six molecular segments. The position of void spaces constituting the hole zone of the e2 band is denoted by black bars in the schematic. Together these regions comprise a portion of the channel or gap in type I collagen assembly. (Figure reprinted with permission from Silver and Landis 2011.)

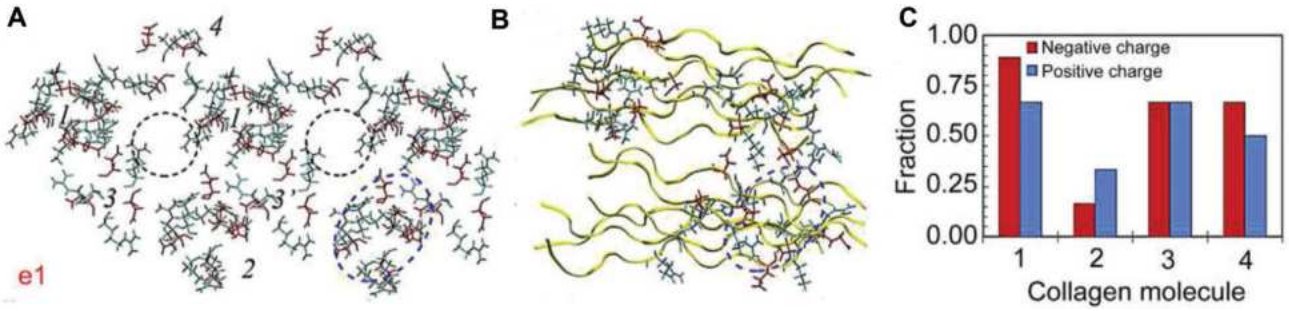


FIGURE 6.10 A, Molecular dynamics simulation of the distribution of side chains of charged residues of collagen molecules comprising the e1 band about the hole zones in a fully hydrated system and in the presence of sodium and chloride ions. Collagen segments are numbered 1-4-1-3-2-3 according to Orgel et al. (2006). Side chains are shown as positively (blue) and negatively (red) charged groups as viewed down the crystallographic *c*-axis of collagen. B, View parallel to the collagen *c*-axis and where the backbone of the various molecular segments is shown by yellow ribbons. Positions of the hole zones are depicted by dashed black circles and the blue ellipse indicates an area of closely interacting charged side chains. C, Plot of the fraction of charged side chains comprising the e1 band directed toward the hole zone for each of the collagen molecules surrounding the hole region. (Figure adapted and reprinted with permission from Xu et al. 2015.)

These factors may influence molecular diffusion, dehydration of ion species, nucleation events in intrafibrillar collagen mineralization, interaction and growth of apatite by fusion of crystals within the same hole zone channels, and crystal shape, alignment and orientation.

Data from molecular dynamics analysis demonstrate that certain fractions of the side chains of the charged amino acids of collagen are not directed toward the void spaces of hole zones and channels (Xu et al. 2015). These particular chains could also attract and bind calcium and phosphate ions from the supersaturated solution, leading to nucleation events in regions of collagen other than those describing holes and channels. Nucleation away from the channels would result in additional mineral formation between and about intrafibrillar collagen chains.

Intrafibrillar collagen mineralization appears to be directed by charged amino acids that line and surround the hole zones and channels of quasi-hexagonal molecular assemblages. Side chains of such residues are thought to bind calcium and phosphate ions from solution and bring these ions into sufficiently close proximity so that they may interact to form initial calcium phosphate nuclei. Conceptually, such ion clusters are suggested to be amorphous in nature, ~1.3 to 1.6 nm in size, ripening and transforming on recruitment of additional solution ions to a poorly crystalline calcium phosphate phase (Xu et al. 2015). Growth and development of crystals within and ultimately beyond the holes and channels could possibly break collagen bonding or occlude or encase the collagen chains to provide further intrafibrillar collagen-mineral interaction.

VetBooks.ir

Interfibrillar Mineralization of Type I Collagen

Mineralization of type I collagen occurs within fibrils and their higher ordered aggregates, as just described, as well as on their surfaces and between them as they comprise the bulk of the extracellular matrices of vertebrate tissues (Figure 6.6). Such interfibrillar mineral deposition is understood to some degree at the present time, but many questions concerning its underlying mechanisms remain unanswered. As noted previously, there is certain agreement that openings of the hole zone channels exist at various surface sites of collagen assemblages, allowing fluid flow of the solution environment and diffusion of supersaturated calcium and phosphate ions between the outside and inside of the arrays. Further, as also mentioned earlier, the X- and Y-positions of the commonly repeating tripeptide motif of collagen are directed outward from collagen helical molecules and therefore collagen surfaces so that side chains of amino acids, including charged residues, project from the surfaces of fibrils, fibers and fiber bundles. Such side chains of charged amino acids may attract calcium and phosphate ions from solution and bind them, conceptually presenting sources for the nucleation of apatite crystals over the collagen surfaces. Growth and development of crystals would follow to provide collagen surface propagation of mineral (Landis et al. 1996; Landis and Jacquet 2013; Landis 2018).

A host of noncollagenous proteins may be found in the extracellular matrices of mineralizing vertebrate tissues and many have collagen binding motifs comprising their peptide sequences. Among such proteins is the SIBLING family of *s*mall *i*ntegrin-*b*inding *lig*and, *N*-linked *g*lycoproteins that are also phosphorylated (Fisher et al. 2001). Bone sialoprotein (Ganss et al. 1999), dentin matrix protein 1 (George et al. 1993), osteopontin (Sodek et al. 2000), matrix extracellular phosphoglycoprotein (Nampei et al. 2004) and dentin sialophosphoprotein (D'Souza et al. 1997) are the known SIBLING members, having a common human chromosome source and related intron-exon structure, amino acid sequence, and exon location (MacDougall et al. 1997; Ganss et al. 1999). Sibling members function variously in osteogenesis, chondrogenesis and dentinogenesis, cellular development, cell and extracellular matrix interaction and communication and other roles (Huang et al. 2008; Sun et al. 2010). Additionally, non-SIBLING, noncollagenous proteins involved in mineralization of extracellular matrices of vertebrates are osteocalcin (Hauschka 1986), fetuin (Jahnen-Dechent et al. 2011), matrix Gla-protein (Kiefer et al. 1988), and numerous other molecules.

Several of these noncollagenous proteins commonly share an abundant number of aspartic and glutamic acid residues in their peptide chains, a structural feature resulting in their high acidity (Boskey 2003). They are also phosphorylated, as noted for SIBLING members, most prominently at their serine and threonine residues, and they are glycosylated to yield molecules that are net negatively charged. In the case of osteocalcin and matrix Gla-protein, the presence of γ-carboxyglutamic acid residues imparts a negative charge to these proteins. Given their negative character, these noncollagenous proteins have the capacity to interact with and bind calcium ions in the extracellular fluid or mineral crystals or particle aggregates that might be present in extracellular matrices. Interestingly, some of the same noncollagenous proteins have a collagen-binding motif so that they may serve to transport bound calcium, crystals or mineral particles to collagen surfaces where they might contribute to mineralization events at specific surface sites. In this regard, such noncollagenous proteins, on binding solution calcium, may be involved themselves in events of apatite nucleation in the tissue extracellular matrices or, carrying calcium and tethered to collagen surfaces, they may modulate nucleation, growth and development of crystals in their size, shape and degree of crystallinity. In consideration of such conceptual roles, the functional changes to mineral deposition may be either facilitative or inhibitory, all occurring with respect to interfibrillar mineralization of type I collagen (Landis and Jacquet 2013). Type I collagen, then, may undergo both interfibrillar and intrafibrillar mineralization events as summarized and depicted in Figure 6.11.

Noncollagenous Proteins: Bone Sialoprotein

Of the noncollagenous proteins noted above and others, bone sialoprotein, osteopontin and osteocalcin have been studied more extensively, particularly with respect to their matrix localization, association with type I collagen, and their possible functional roles in mineralization. Their properties provide novel and important considerations in type I collagen-mineral interaction in vertebrate tissues. Bone sialoprotein is an extracellular protein secreted by mineralizing tissue cells, first thought to be bone-specific but also found in dentin, cementum and calcifying cartilage and tendon (Bianco et al. 1991; Chen et al. 1991; Ganss et al. 1999; Moses et al. 2006; Chen et al. 2019). Bone sialoprotein has a molecular weight of about 34 kDa with an unstructured and flexible conformation, and it is highly glycosylated and additionally phosphorylated (Qin et al. 2004). Its sequence of residues is principally basic at its amino terminus and acidic at its carboxy terminus whereas its central domain is comprised of numerous repeating polyglutamic acid residues and multiple phosphorylated serine residues (Ohnishi et al. 1993; Shapiro et al. 1993). Bone sialoprotein contains an Arg-Gly-Asp (RGD) motif for integrin binding (Shapiro et al. 1993) and a collagen-binding region, highly conserved over several different vertebrate species (Tye et al. 2005).

There are numerous functional roles reported for the molecule (Ganss et al. 1999), and it has been widely accepted that bone sialoprotein is a critical determinant in binding calcium and phosphate ions and mediating apatite nucleation and subsequent events of vertebrate tissue mineralization (Ganss et al. 1999; Qin et al. 2004; Kärner et al. 2009). In this regard, expression of bone sialoprotein was recently found to coincide temporally and spatially with sites of early and ongoing mineral formation in normal avian tendon (Figure 6.3; Chen et al. 2019), and immunocytochemical localization demonstrated bone sialoprotein along the surfaces of type I collagen or outside the fibrils, conceptually promoting interfibrillar collagen mineralization (Chen et al. 2019). As a consequence of its relatively large size among noncollagenous proteins, bone sialoprotein has been suggested as being excluded from penetrating collagen arrays in vivo (Toroian et al. 2007), but it may attach to collagen surfaces by interaction of its collagen-binding

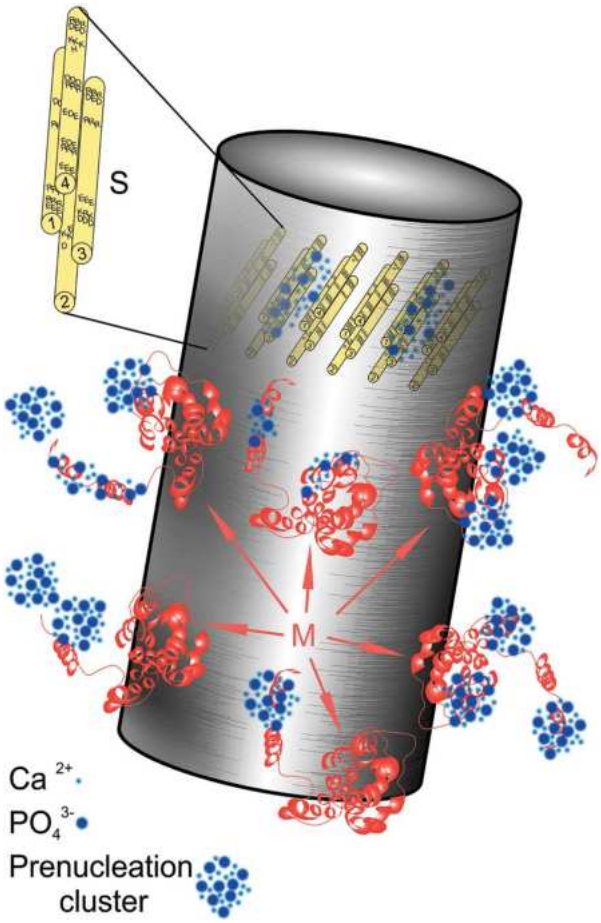


FIGURE 6.11 Both intrafibrillar and interfibrillar mineralization of a type I collagen fibril (gray cylinder). Numbers of collagen molecules structurally organized in parallel arrangement with ordered hole and overlap zones comprise the collagen fibril. Intrafibrillar mineral formation is represented by four segments (S, yellow) of the e1 and e2 bands of collagen molecules, slightly shaded and hidden to indicate their location within the larger cylindrical collagen fibril. As detailed previously, these two segments and their 10 additional segments of high charge density comprising the hole and overlap zones of collagen are proposed to be mineralized through calcium and phosphate ion binding to the template of their composite charged residues. Events of apatite crystal nucleation, growth and development occur to form a series of platelets whose (100) faces are approximately parallel to each other and to the long axes of collagen molecules with which they associate. Propagation of the platelets and their increases in size with time ultimately lead to a poorly crystalline apatite network throughout the internal collagen structure. Interfibrillar mineralization is suggested to occur through two possibilities: (1) binding of calcium and phosphate ions or their putative prenucleation clusters (Dey et al. 2010) to side chains of charged amino acid residues of collagen exposed at the collagen surfaces and/or (2) binding of calcium and phosphate ions or prenucleation clusters to certain noncollagenous molecules (M, red) themselves bound and attached to various collagen surface sites. Six such molecules, for example, bone sialoprotein, are shown conceptually in the diagram. These molecules may initially bind calcium phosphate ions and prenucleation clusters from solution and carry them to collagen surfaces or the molecules themselves may become bound to collagen surfaces and subsequently attract and bind calcium and phosphate ions and clusters. As with intrafibrillar mineralization, propagation of apatite crystals and their increasing size with time provide a means of developing interfibrillar mineralization of a poorly crystalline network over the extracellular spaces between collagen fibrils and their higher ordered structures. (Figure adapted and reprinted with permission from Landis and Jacquet 2013.)

domain. Such binding and localization of bone sialoprotein at collagen surfaces may be supported by attachment of decorin, another noncollagenous protein, to both bone sialoprotein and collagen (Hunter et al. 2001). Experimental animal studies in which the bone sialoprotein gene has been functionally reduced or ablated altogether (knocked-out) demonstrate phenotypic results that are consistent with the proposed roles for the protein in apatite nucleation and mineral deposition (Malaval et al. 2009; Bouleftour et al. 2014).

Noncollagenous Proteins: Osteopontin

Osteopontin is an acidic, phosphorylated glycoprotein of about 34 kDa in molecular weight, present in extracellular matrices of bone, certain cartilages, dentin, cementum and normally mineralizing tendons of some avian species as well as in several nonmineralizing tissues (Nomura et al. 1988; Butler 1989; Sodek et al. 2000; Qin et al. 2004; Moses et al. 2006; Sun et al. 2010; Chen et al. 2019). Sequence data are published of the unstructured, flexible nature of the molecule, having numerous phosphorylated serine and threonine residues and binding motifs for collagen, apatite, integrin, and transglutaminase (McKee and Nanci 1995; Sodek et al. 2000).

Osteopontin gene expression in the avian leg tendon, like that of bone sialoprotein, may be correlated with the onset and progression of mineralization in this tissue (Figure 6.3; Chen et al. 2019), and its localization in the same tissue by immunocytochemistry shows that it attaches to type I collagen fibrils and other higher ordered collagen structures at their surfaces and throughout extracellular matrix sites (Chen at al. 2015, 2019). The localization pattern for osteopontin is similar to that reported for bone sialoprotein (Chen et al. 2015, 2019). These two proteins are also alike in that they are too large to enter collagen arrays, so they are excluded from such domains (Toroian et al. 2007) and confined to participate in interfibrillar collagen mineralization events. From numerous lines of evidence in both mineralizing and nonmineralizing tissues and in experimental systems in vitro, osteopontin has been documented to bind calcium as a means of inhibiting mineral formation (Boskey et al. 1993, 2002; Hunter et al. 1994; Sodek et al. 2000; Zaka and Williams 2006), and recently it has been proposed that osteopontin interacts with osteocalcin to mediate collagen mineralization in this principal role (Poundarik et al. 2018). Experimentally modifying the osteopontin gene in animals has yielded certain evidence consistent with osteopontin inhibition of mineral formation and crystal growth and development. For example, bones from osteopontin knockout mice showed increased crystal size, crystal perfection and mineral mass, proteoglycan loss and reduced articular content in the skeletal tissues of the animals (Boskey et al. 2002; Matsui et al. 2009).

Noncollagenous Proteins: Osteocalcin

Osteocalcin is a small protein of molecular weight of about 5.8 kDa in humans and the most abundant (~10%) of the noncollagenous proteins of bone (Hauschka and Carr 1982). It may be referred to as bone Gla (γ-carboxyglutamic acid)-protein because in most species it contains three Gla residues (Hauschka and Carr 1982; Hauschka 1986). Carboxylation of

VetBooks.ir

glutamate residues is vitamin K-dependent and provides osteocalcin the capacity to bind calcium ions or interact with apatite crystals (Hauschka and Carr 1982; Hauschka et al. 1989; Gundberg et al. 2012; Simon et al. 2018). Osteocalcin expression is reported in all bones of vertebrate tissues (Bronckers et al. 1987; Camarda et al. 1987; McKee et al. 1992; Chen et al. 2019), and it coincides with osteoblast and tenocyte differentiation occurring before or during mineralization of bone and tendon (in avian species) (Aronow et al. 1990; Chen et al. 2019). There appears to be no obvious phenotype to the skeleton of osteocalcin gene knockout animals (Ducy et al. 1996; Boskey et al. 1998) and studies in vitro suggest that the protein inhibits mineralization, perhaps by limiting apatite nucleation (Hunter et al. 1996). Immunocytochemical localization of osteocalcin in normally mineralizing avian tendons (Figure 6.3; Chen et al. 2015) showed the protein in its carboxylated form along the surfaces of type I collagen fibrils and both within and outside the fibrils. Within the fibrils, osteocalcin was found to reside specifically in collagen hole zone regions, where it was suggested to function in nucleation, stabilization of mineral ions or phases, and growth, alignment, orientation and/or development of apatite crystals during intrafibrillar collagen mineralization (Chen et al. 2015, 2019). Outside and on the surfaces of collagen fibrils, osteocalcin was proposed to mediate interfibrillar collagen mineralization (Chen et al. 2015). More recent work has hypothesized that osteocalcin interacts with osteopontin (Poundarik et al. 2018) and with octacalcium phosphate, a possible precursor to apatite, in the mineralization of collagen (Simon et al. 2018). A further consideration regarding the presence of osteocalcin in collagen hole zones and along the surfaces of collagen is that mineralized tissues and particularly apatite are known to serve as storage reservoirs for small molecules, anions and cations (Glimcher 2006; Burger et al. 2008). In this instance, osteocalcin may be sequestered at sites associated with collagen and mineral, to be released at a time of mineral remodeling, for example, to the circulating serum as a functional hormone in the vertebrate body (Karsenty and Ferron 2012; Karsenty and Oury 2014).

Possible Temporal and Spatial Relationships Between Interfibrillar and Intrafibrillar Collagen Mineralization

Given that collagen mineralization occurs at the surfaces and outside of the fibrils (interfibrillar collagen mineralization) and within the fibrils (intrafibrillar collagen mineralization) and that collagen may not serve as a singular template for apatite deposition in the presence of bone sialoprotein and osteocalcin acting as potential mediators of nucleation, it is interesting to address the question of whether a temporal or spatial relation exists between interfibrillar and intrafibrillar mineralization of collagen. In this context, recent work is being conducted utilizing high-pressure freezing and automated freeze substitution, techniques intended to impart strict preservation of hydrated mineralizing specimens, coupled with sample examination by focused ion beam/scanning electron microscopy (FIB/SEM) and high-resolution image reconstruction in three dimensions. Well aligned collagen fibrils undergoing defined mineralization in avian leg tendons as described above have been investigated in 26-week-old adult turkeys (Zou et al. 2020).

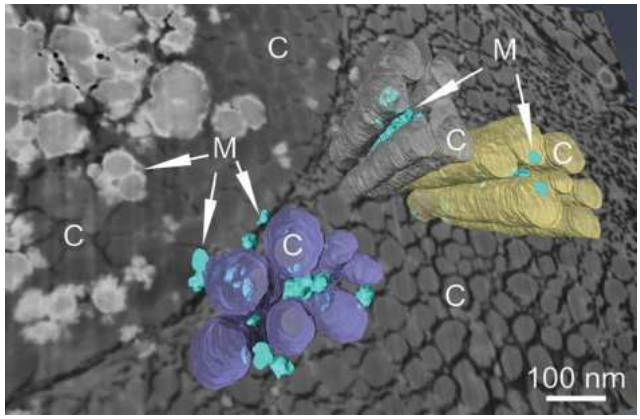


FIGURE 6.12 A color-rendered image of collagen fibrils (C) and mineral (M) in a leg tendon from a 26-week-old turkey. The sample was treated by high-pressure freezing and automated freeze substitution to minimize artifacts of sample preparation, stained with uranyl acetate and osmium tetroxide, and viewed following focused ion beam/scanning electron microscopy (FIB/SEM) serial surface imaging. FIB/SEM images of selected small groups of collagen fibrils (color-rendered in yellow, gray and purple) and mineral particles (turquoise) were reconstructed in three dimensions and show a close association between collagen and mineral. Collagen is disposed as smaller, discrete individual fibrils or fibers to the right of the image or as a more homogeneous and mineralized fiber bundle mass to the left of the image. A distinct, continuous semicircular dark interface separates the fiber bundle from its neighboring collagen fibrils and fibers. (Image courtesy of Drs. Zhaoyong Zou and Peter Fratzl, Department of Biomaterials, Max Planck Institute of Colloids and Interfaces, Golm Research Campus, Potsdam, Germany.)

Initial results, an example of which is shown in Figure 6.12, present intriguing images of mineral deposits that are observed in putative cell processes extending from tenocytes and located outside and adjacent to collagen fibrils at several sites in the tissue (Zou et al. 2020). At some of these sites, the deposits appear to be related spatially to mineral deposits appearing within the fibrils, across the collagen surfaces separating collagen exterior and interior spaces (Figure 6.12). Similar spatial relations have been reported with avian tendon samples preserved by anhydrous techniques, examined by conventional transmission electron microscopy and imaged in two dimensions (Landis 1986). Novel reconstructed FIB/SEM images demonstrate in a compelling manner that inter- and intrafibrillar collagen mineral deposition is spatially related. The further observations that interfibrillar mineralization apparently occurs at numerous sites in the absence of intrafibrillar deposition suggest that a temporal relation exists as well, that is, interfibrillar mineralization precedes intrafibrillar mineralization of collagen in the avian tendon model (Zou et al. 2020). Additional studies will provide more data from which definitive conclusions may be drawn regarding the timing and location of collagen mineralization in this vertebrate system.

Conclusions

From the perspective of this chapter, the current view associated with the onset of type I collagen mineralization in vertebrates is one in which collagen may serve as a principal template to

VetBooks.ir

nucleate apatite crystals within its intrafibrillar spaces and on its surfaces through its unique stereochemical character. It may function in this capacity in conjunction with osteocalcin, a small noncollagenous protein located in the hole zone channels of collagen. Additionally, collagen may act as a principal template, binding bone sialoprotein, osteopontin and osteocalcin, which attract and bridge calcium and phosphate ions or their possible prenucleation ion clusters to mediate nucleation (bone sialoprotein and osteocalcin) and inhibition (osteopontin) of crystal formation at collagen surfaces and in interfibrillar spaces outside the fibrils. Thus, the role of type I collagen acting alone to mediate vertebrate mineral deposition may be modified to include contributions from certain noncollagenous proteins and possibly other molecules as well.

Clearly, many concepts concerning collagen mineralization of vertebrate tissues require more detailed elaboration. For example, the presence and influence of water (Dorvee and Veis 2013; Stock 2015; Xu et al. 2015), the transport and diffusion of calcium and phosphate ions, and the presence, transport and diffusion of putative prenucleation clusters are not well understood as factors in collagen mineralization. They await further investigations to clarify their possible roles in these events. Interactions of noncollagenous proteins, such as the three noted above, with calcium and phosphate ions and conceptual prenucleation ion clusters in the interfibrillar spaces of mineralizing tissues are likewise poorly characterized, and so, too, is the potential involvement of osteocalcin in mineralization as it resides directly within the hole zone channels of type I collagen. Finally, the subtle points of cellular and extracellular ultrastructure of mineralizing matrices and possible temporal, spatial and functional interrelations between interfibrillar and intrafibrillar collagen mineralization need greater clarification.

The current work with high-pressure freezing and FIB/SEM analysis of the ultrastructure and apatite crystal formation detected in the avian leg tendon model (Zou et al. 2020) suggests novel results and may be relevant to understanding more completely those and additional uncertainties just noted. Such studies also may yield new insight into the mineralization processes of normal bone, dentin and cementum and into events of pathological and abnormal mineral formation in vertebrate tissues.

Acknowledgments

The authors are extremely grateful for valuable discussions with Drs. Peter Fratzl, Luca Bertinetti, Zhaoyong Zou and Elena Macias, as well as the use of FIB/SEM instrumentation and facilities in the Department of Biomaterials, Max Planck Institute of Colloids and Interfaces, Golm Research Campus, Potsdam, Germany.

REFERENCES

Aronow, M. A., et al. 1990. Factors that promote progressive development of the osteoblast phenotype in cultured fetal rat calvaria cells. *J. Cell. Physiol.* 143: 213–221.

Arsenault, A. L. 1988. Crystal-collagen relationships in calcified turkey leg tendons visualized by selected-area dark field electron microscopy. *Calcif. Tiss. Int.* 43: 202–212.

Arsenault, A. L. 1991. Image analysis of collagen-associated mineral distribution in cryogenically prepared turkey leg tendons. *Calcif. Tiss. Int.* 48: 56–62.

Arsenault, A. L. 1992. Structural and chemical analyses of mineralization using the turkey leg tendon as a model tissue. *Bone and Mineral* 17: 253–256.

Arsenault, A. L., et al. 1991. Vectorial sequence of mineralization in the turkey leg tendon determined by electron microscopic imaging. *Calcif. Tiss. Int.* 48: 46–55.

Bianco, P., et al. 1991. Expression of bone sialoprotein (BSP) in developing human tissues. *Calcif. Tiss. Int.* 49: 421–426.

Bigi, A., et al. 1988. Calcified turkey leg tendon as structural model for bone mineralization. *Int. J. Biol. Macromol.* 10: 282–286.

Bornstein, P. 1980. The biosynthesis, secretion and processing of procollagen. In *Biology of Collagen*, Viidik, A. and J. Vuust, eds., 61–75. London: Academic Press.

Boskey, A. L. 2003. Biomineralization: an overview. *Connect. Tiss. Res.* 44: 5–9.

Boskey, A. L., et al. 1993. Osteopontin-hydroxyapatite interactions in vitro: inhibition of hydroxyapatite formation and growth in a gelatin gel. *Bone and Mineral* 22: 147–159.

Boskey, A. L., et al. 1998. Fourier transform infrared microspectroscopic analysis of bones of osteocalcin-deficient mice provides insight into the function of osteocalcin. *Bone* 23: 187–196.

Boskey, A. L., et al. 2002. Osteopontin deficiency increases mineral content and mineral crystallinity in mouse bone. *Calcif. Tiss. Int.* 71: 145–154.

Boskey, A. L., and P. G. Robey. 2013. The regulatory role of matrix proteins in mineralization of bone. In *Osteoporosis*, 4th Edition, Marcus, R., et al., eds. 235–255. London: Elsevier.

Bouleftour, W., et al. 2014. Skeletal development of mice lacking bone sialoprotein (BSP) – Impairment of long bone growth and progressive establishment of high trabecular bone mass. *PLoS One* 9: e95144.

Bronckers, A. L., et al. 1987. Immunolocalization of Gla proteins (osteocalcin) in rat tooth germs: comparison between indirect immunofluorescence, peroxidase-antiperoxidase, avidin-biotin-peroxidase complex, and avidin-biotin-gold complex with silver enhancement. *J. Histochem. Cytochem.* 35: 825–830.

Burger, C., et al. 2008. Lateral packing of mineral crystals in bone collagen fibrils. *Biophys. J.* 95: 1985–1992.

Butler, W. T. 1989. The nature and significance of osteopontin. *Connect. Tiss. Res.* 23: 123–136.

Camarda, A. J., et al. 1987. Immunocytochemical localization of gamma-carboxyglutamic acid-containing proteins (osteocalcin) in rat bone and dentin. *Calcif. Tiss. Int.* 40: 349–355.

Chapman, J. A. 1974. The staining pattern of collagen fibrils: I. An analysis of electron micrographs. *Connect. Tiss. Res.* 2: 137–150.

Chapman, J. A., and R. A. Hardcastle. 1974. The staining pattern of collagen fibrils: II. A comparison with patterns computer-generated from the amino acid sequence. *Connect. Tiss. Res.* 2: 151–159.

Chen, J. K., et al. 1991. Localization of bone sialoprotein (BSP) expression to sites of mineralized tissue formation in fetal rat tissues by in situ hybridization. *Matrix* 11: 133–143.

Chen, L., et al. 2015. Refinement of collagen-mineral interaction: A possible role for osteocalcin in apatite crystal nucleation, growth and development. *Bone* 71: 7–16.

VetBooks.ir

Chen L., et al. 2019. Correlations between gene expression and mineralization in the avian leg tendon. *Bone* 121: 42–59.

Christoffersen, J., and W. J. Landis. 1991. A contribution with review to the description of mineralization of bone and other calcified tissues in vivo. *Anat. Rec.* 230: 435–450.

Dey, A., et al. 2010. The role of prenucleation clusters in surface-induced calcium phosphate crystallization. *Nature Materials* 9: 1010–1014.

Dorvee, J. R., and A. Veis. 2013. Water in the formation of biogenic minerals: peeling away the hydration layers. *J. Struct. Biol.* 183: 278–303.

D'Souza, R. N., et al. 1997. Gene expression patterns of murine dentin matrix protein 1 (Dmp1) and dentin sialophosphoprotein (DSPP) suggest distinct developmental functions in vivo. *J. Bone Min. Res.* 12: 2040–2049.

Ducy, P., et al. 1996. Increased bone formation in osteocalcin-deficient mice. *Nature* 382: 448–452.

Eyre, D. 1987. Collagen cross-linking amino acids. *Meth. Enzymol.* 144: 115–139.

Fisher, L. W., et al. 2001. Flexible structures of SIBLING proteins, bone sialoprotein, and osteopontin. *Biochem. Biophys. Res. Comm.* 280: 460–465.

Fratzl, P., ed. 2008. *Collagen-Structure and Mechanics.* New York: Springer.

Ganss, B., et al. 1999. Bone sialoprotein. *Crit. Rev. Oral Biol. Med.* 10: 79–98.

George, A., et al. 1993. Characterization of a novel dentin matrix acidic phosphoprotein. Implications for induction of biomineralization. *J. Biol. Chem.* 268: 12624–12630.

George, A., and A. Veis. 2008. Phosphorylated proteins and control over apatite nucleation, crystal growth, and inhibition. *Chemical Rev.* 108: 4670–4693.

Glimcher, M. J. 2006. Bone: nature of the calcium phosphate crystals and cellular, structural, and physical chemical mechanisms in their formation. *Rev. Miner. Geochem.* 64: 223–282.

Gundberg, C. M., et al. 2012. Vitamin K-dependent carboxylation of osteocalcin: Friend or foe? *Advances in Nutrition* 3: 149–157.

Harvey, E. B., et al. 1968. *An Atlas of the Domestic Turkey (Meleagris Gallopavo): Myology and Osteology.* U.S. Atomic Energy Commission, Division of Biology and Medicine: Washington D.C., p. 105.

Hauschka, P. V. 1986. Osteocalcin: the vitamin K-dependent Ca^{2+}-binding protein of bone matrix. *Haemostasis* 16: 258–272.

Hauschka, P. V., and S. A. Carr. 1982. Calcium-dependent α-helical structure in osteocalcin. *Biochemistry* 21: 2538–2547.

Hauschka, P. V., et al. 1989. Osteocalcin and matrix Gla protein: vitamin K-dependent proteins in bone. *Physiol. Rev.* 69: 990–1047.

Hodge, A. J. 1989. Molecular models illustrating the possible distribution of "holes" in simple systematically staggered arrays of type I collagen molecules in native-type fibrils. *Connect. Tiss. Res.* 21: 137–147.

Hodge, A. J., and J. A. Petruska. 1963. Recent studies with the electron microscope on ordered aggregates of the tropocollagen macromolecule. In *Aspects of Protein Structure*, Ramachandran, G. N. ed., 289–300. New York: Academic Press.

Huang, B., et al. 2008. Distribution of SIBLING proteins in the organic and inorganic phases of rat dentin and bone. *Europ. J. Oral Sci.* 116: 104–112.

Humphrey, W., et al. 1996. VMD – visual molecular dynamics. *J. Mol. Graph.* 14: 33–38.

Hunter, G. K., et al. 1994. Modulation of crystal formation by bone phosphoproteins: structural specificity of the osteopontin-mediated inhibition of hydroxyapatite formation. *Biochem. J.* 300: 723–728.

Hunter, G. K., et al. 1996. Nucleation and inhibition of hydroxyapatite formation by mineralized tissue proteins. *Biochem. J.* 317: 59–64.

Hunter, G. K., et al. 2001. Induction of collagen mineralization by a bone sialoprotein-decorin chimeric protein. *J. Biomed. Mat. Res.* 55: 496–502.

Jahnen-Dechent, W., et al. 2011. Fetuin-A regulation of calcified matrix metabolism. *Circulation Res.* 108: 1494–1509.

Johnson, L. C. 1960. Mineralization of turkey leg tendon. I. Histology and histochemistry of mineralization. In *Calcification in Biological Systems.* Sognnaes, R. F. ed., 117–128. Washington, D.C.: American Association for the Advancement of Science.

Kärner, E., et al. 2009. Dynamics of gene expression during bone matrix formation in osteogenic cultures derived from human embryonic stem cells in vitro. *Biochim. Biophys. Acta* 1790: 110–118.

Karsenty, G., and M. Ferron. 2012. The contribution of bone to whole-organism physiology. *Nature* 481: 314–320.

Karsenty, G., and F. Oury. 2014. Regulation of male fertility by the bone-derived hormone osteocalcin. *Molec. Cell. Endocrinol.* 382: 521–526.

Kiefer, M. C., et al. 1988. The cDNA and derived amino acid sequences for human and bovine matrix Gia protein. *Nucleic Acids Res.* 16: 5213.

Kuhn, K., and R. W. Glanville. 1980. Molecular structure and higher organization of different collagen types. In *Biology of collagen*, Viidik, A., and J. Vuust eds., 1–14. London: Academic Press.

Landis, W. J. 1986. A study of calcification in the leg tendons from the domestic turkey. *J. Ultrastruct. Molec. Struct. Res.* 94: 217–238.

Landis, W. J. 2018. Current aspects of type I collagen mineralization in vertebrates. In *Ten Cate's Oral Histology. Ninth Edition*, Nanci, A., ed., 10–11. St. Louis, MO: Elsevier.

Landis, W. J., and R. Jacquet. 2013. Association of calcium and phosphate ions with collagen in the mineralization of vertebrate tissues. *Calcif. Tiss. Int.* 93: 329–337.

Landis, W. J., and F. H. Silver. 2002. The structure and function of normally mineralizing avian tendons. *Comp. Biochem. Physiol. A* 133: 1135–1157.

Landis, W. J., et al. 1977. Electron microscopic observations of bone tissue prepared anhydrously in organic solvents. *J. Ultrastruct. Res.* 59: 1–30.

Landis, W. J., et al. 1993. Mineral and organic matrix interaction in normally calcifying tendon visualized in three dimensions by high voltage electron microscopic tomography and graphic image reconstruction. *J. Struct. Biol.* 110: 39–54.

Landis, W. J., et al. 1996. Mineralization of collagen occurs on fibril surfaces: Evidence from conventional and high voltage electron microscopy and three-dimensional imaging. *J. Struct. Biol.* 117: 24–35.

Likens, R. C., et al. 1960. Mineralization of turkey leg tendon. III. Chemical nature of the protein and mineral phases. In *Calcification in Biological Systems*, Sognnaes, R. F. ed., 143–149. Washington, D.C.: American Association for the Advancement of Science.

VetBooks.ir

MacDougall, M., et al. 1997. Dentin phosphoprotein and dentin sialoprotein are cleavage products expressed from a single transcript coded by a gene on human chromosome 4. Dentin phosphoprotein DNA sequence determination. *J. Biol. Chem.* 272: 835–842.

Malaval, L., et al. 2009. Absence of bone sialoprotein (BSP) impairs cortical defect repair in mouse long bone. *Bone* 45: 853–861.

Matsui, Y., et al. 2009. Accelerated development of aging-associated and instability-induced osteoarthritis in osteopontin deficient mice. *Arthritis Rheumatol.* 60: 2362–2367.

McEwen, B. F., et al. 1991. Quantitative determination of the mineral distribution in different collagen zones of calcifying tendon using high voltage electron microscopic tomography. *J. Computer-Assisted Microsc.* 3: 201–210.

McKee, M. D., and A. Nanci. 1995. Osteopontin and the bone remodeling sequence – colloidal-gold immunocytochemistry of an interfacial extracellular matrix protein. *Ann. NY Acad. Sci.* 760: 177–189.

McKee, M. D., et al. 1992. High-resolution immunolocalization of osteopontin and osteocalcin in bone and cartilage during endochondral ossification in the chicken tibia. *Anat. Rec.* 234: 479–492.

Moses, K., et al. 2006. Immunohistochemical study of small integrin-binding ligand, N-linked glycoproteins in reactionary dentin of rat molars at different ages. *Europ. J. Oral Sci.* 114: 216–222.

Nampei, A., et al. 2004. Matrix extracellular phosphoglycoprotein (MEPE) is highly expressed in osteocytes in human bone. *J. Bone Min. Metabol.* 22: 176–184.

Nomura, S., et al. 1988. Developmental expression of 2ar (osteopontin) and SPARC (osteonectin) RNA as revealed by in situ hybridization. *J. Cell Biol.* 106: 441–450.

Nylen, M. J., et al. 1960. Mineralization of turkey leg tendon. II. Collagen-mineral relations as revealed by electron and x-ray microscopy. In *Calcification in Biological Systems*, Sognnaes, R. F. ed., 129–142. Washington, D.C.: American Association for the Advancement of Science.

Ohnishi, T., et al. 1993. Molecular cloning and sequence analysis of cDNA for a 59 kD bone sialoprotein of the rat: Demonstration that it is a counterpart of human α2-HS glycoprotein and bovine fetuin. *J. Bone Min. Res.* 8: 367–377.

Orgel, J. P. R. O., et al. 2006. Microfibrillar structure of type I collagen in situ. *Proc. Natl. Acad. Sci., U.S.A.* 103: 9001–9005.

Orgel, J. P. R. O., et al. 2014. Variation in the helical structure of native collagen. *PLoS One* 9: e89519.

Otsubo, K., et al. 1992. Cross-linking connectivity in bone collagen fibrils: The COOH-terminal locus of free aldehyde. *Biochemistry* 31: 396–402.

Petruska, J. A., and A. J. Hodge. 1964. A subunit model for the tropocollagen macromolecule. *Proc. Natl. Acad. Sci., U.S.A.* 51: 871–876.

Poundarik, A. A., et al. 2018. Biomolecular regulation, composition and nanoarchitecture of bone mineral. *Scientif. Rep.* 8: 1191.

Qin, C., et al. 2004. Post-translational modifications of sibling proteins and their roles in osteogenesis and dentinogenesis. *Crit. Rev. Oral Biol. Med.* 15: 126–136.

Robey, P. G. 2008. Noncollagenous bone matrix proteins. In *Principles of bone biology*, 3rd Edition, Bilezikian, J. P., et als. eds., 335–349. London: Elsevier.

Shapiro, H. S., et al. 1993. Characterization of porcine bone sialoprotein: Primary structure and cellular expression. *Matrix* 13: 431–440.

Shapiro, I. M., et al. 2015. Matrix vesicles: Are they anchored exosomes? *Bone* 79: 29–36.

Shoulders, M. D., and R. T. Raines. 2009. Collagen structure and stability. *Ann. Rev. Biochem.* 78: 929–958.

Silver, F. H., and W. J. Landis. 2011. Deposition of apatite in mineralizing vertebrate extracellular matrices: A model of possible nucleation sites on type I collagen. *Connect. Tiss. Res.* 52: 242–254.

Silver, F. H., et al. 2001. Molecular basis for elastic energy storage in mineralized tendon. *Biomacromolecules* 2: 750–756.

Simon, P., et al. 2018. First evidence of octacalcium phosphate@ osteocalcin nanocomplex as skeletal bone component directing collagen triple-helix nanofibril mineralization. *Scientif. Rep.* 8: 13696.

Sodek, J., et al. 2000. Osteopontin. *Crit. Rev. Oral Biol. Med.* 11: 279–303.

Stock, S. R. 2015. The mineral-collagen interface in bone. *Calcif. Tiss. Int.* 97: 262–280.

Sun, Y., et al. 2010. Distribution of small integrin-binding ligand, N-linked glycoproteins (SIBLING) in the articular cartilage of the rat femoral head. *J. Histochem. Cytochem.* 58: 1033–1043.

Toroian, D., et al. 2007. The size exclusion characteristics of type I collagen: Implications for the role of noncollagenous bone constituents in mineralization. *J. Biol. Chem.* 282: 22437–22447.

Tye, C. E., et al. 2005. Identification of the type I collagen-binding domain of bone sialoprotein and characterization of the mechanism of interaction. *J. Biol. Chem.* 280: 13487–13492.

Xu, Z., et al. 2015. Molecular mechanisms for intrafibrillar collagen mineralization in skeletal tissues. *Biomaterials* 39: 59–66.

Xu, Z., et al. 2018. Structure analysis of collagen fibril at atomic-level resolution and its implications for intra-fibrillar transport in bone biomineralization. *Phys. Chem. Chem. Phys.* 20: 1513–1523.

Yamauchi, M., et al. 1989. Cross-linking and stereospecific structure of collagen in mineralized and nonmineralized skeletal tissues. *Connect. Tiss. Res.* 21: 159–169.

Zaka, R., and C. J. Williams. 2006. Role of the progressive ankylosis gene in cartilage mineralization. *Current Opinion Rheumatol.* 18: 181–186.

Zou, Z., et al. 2020. Three-dimensional structural interrelations between cells, extracellular matrix and mineral in normally mineralizing avian leg tendon. *Proc. Natl. Acad. Sci., U.S.A.* 117: 14102–14109.

VetBooks.ir

7

An Overview of Cartilage Histology

Alexandra Quilhac

CONTENTS

Introduction 123
An Ancient and Essential Tissue 123
Cartilage Location 124
The Main Types of Cartilage 124
Hyaline Cartilage 124
Cartilages of the Growth Plate, or Growth Cartilages 126
Articular Cartilage of an Adult Bone 126
Fibrocartilage 126
Elastic Cartilage 126
Calcified Cartilage 127
Chondrogenesis and Chondrocyte Structure 128
Basic Aspects of Chondrogenesis 128
Chondrocyte Ultrastructure 129
Ultrastructure of the Extracellular Matrix 131
Collagen 131
Glycosaminoglycans 131
Proteoglycans 131
Noncollagenous Proteins 132
Water and Ions 132
Cartilage Vascularization and Innervation 132
The Functions of Cartilage and Their Regulation 132
Modalities of Cartilage Growth 132
Function of Growth Plates 132
Mechanical Behavior 133
Repair 133
Cells Death, Degradation and Resorption of Cartilage 133
Cells 133
Matrix 134
References 135

Introduction

An Ancient and Essential Tissue

Cartilage is found in a broad range of taxa and is a predominant tissue at all ontogenetic stages in the vertebrate skeleton from early ontogeny. Many groups, especially water-dwelling forms, retain parts of their endoskeleton as cartilage throughout life. When calcified, cartilage often resists fossilization processes. A long and complex evolutionary history of this tissue is revealed in fossil bones (e.g., Hall 2005; Zhang et al. 2009; see also Ricqlès 1975). Like other connective tissues, cartilage is composed of cells, here known as chondrocytes, that are located within lacunae embedded in a hydrated extracellular matrix mainly comprising diverse collagen types (Type II is typical, but other types also occur) and proteoglycans. Cartilage in the basal, jawless vertebrates can be noncollagenous but, in any case, fibrous proteins constitute the extracellular matrix (Cole and Hall 2004) and collagen-based cartilage is also present (Ohtani et al. 2008). The absence of nerves, blood vessels and lymphatics, which can be related to a low metabolic rate and a limited capacity for repair, is a peculiar feature of this tissue. Depending on cartilage type, the extracellular matrix may or may not mineralize. The main functions of cartilage are to assist in skeletal growth, facilitate bone movements, absorb mechanical stress in articulations and support soft tissues and organs.

VetBooks.ir

Cartilage Location

In the skeletons of juvenile and adult osteichthyans (whether finned or limbed), cartilage is a typical feature of endochondral bones and has two main locations. Most conspicuously, it covers articular surfaces of long and short bones (the latter may have more than two articular surfaces) as well as some sectors of the periphery of flat bones. Cartilage also occurs in the so-called *growth plates*, at the junction between epiphyses and metaphyses, during the growth in length of endochondral bones. Most studies deal with articular and growth cartilages. In adult elasmobranchs and some actinopterygians, the chondrocranium is made of cartilage in early development and remains cartilaginous in adults. The notochord of elasmobranchs is partly replaced by calcified cartilaginous vertebrae; moreover, the pelvic and pectoral girdles of adult *Pleurodeles* and parts of mammal ribs remain cartilaginous in adults.

In the first part of this chapter, the main types of cartilage are introduced with a description at the histological level. The ultrastructural aspect is then approached, highlighting the diversity of cellular and matrix components. The "birth, life and death" cycle of cartilage is detailed in the last part: the molecular aspect of chondrogenesis is discussed, the numerous functions of cartilage and their regulation are described and the different processes of cell death and matrix degradation and repair are detailed.

The Main Types of Cartilage

Four forms of this tissue are distinguished, based mainly on their functions, but they also differ in matrix composition and chondrocyte distribution (Figure 7.1).

Hyaline cartilage (Figure 7.1A), the matrix of which is composed predominantly of glycosaminoglycans (GAGs) and type II collagen, is the most common, and the best studied. *Fibrous cartilage* (also called *fibrocartilage*; Figure 7.1B) has a matrix rich in collagen type I, whereas elastic fibers are abundant in *elastic cartilage* (Figure 7.1C). *Calcified cartilage* (Figure 7.1D) includes collagen types I and II, but its main characteristic is to become mineralized. This tissue is most often eroded just before local bone accretion.

Hyaline Cartilage

Histological reviews of this type of cartilage have been published by Boyde and Jones (1983), Hall (1983, 2005) and Mescher (2013). In vertebrates, bones develop either directly from mesenchymal cells or through a preexisting cartilage model that is secondarily replaced by bone (i.e., endochondral ossification). This model, frequently called *anlage,* is initially made of hyaline cartilage and prefigures the morphology of the future endochondral bone (Figure 7.2A, B).

Hyaline cartilage persists later inside the bones, where it occurs in both the growth plates and over the bone epiphyses, as a highly specialized joint tissue (Figure 7.2C). The free (or "external") joint surface of hyaline cartilage is covered by the synovial membrane. In other parts of the bones, free cartilage surfaces are covered by the perichondrium, a strong connective tissue membrane that contains blood vessels supplying the cartilage in oxygen and nutrients through diffusion. The lower, cellular (cambial) layer of the perichondrium is also responsible for the accretional growth of cartilage, and the fibrous (lateral) perichondral layer in metaphyseal regions is involved in the early differentiation of tendinous and ligamentous insertions. When growth and ossification are completed, permanent

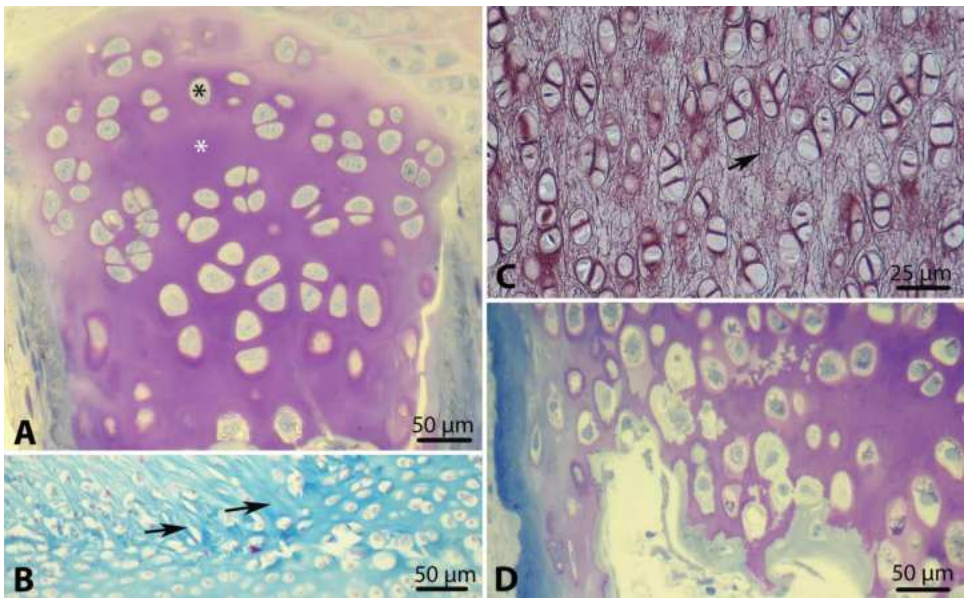


FIGURE 7.1 Cartilage types. Semithin sections in cartilage of long limb bone (A, B, D) and in epiglottis (C). A, Hyaline cartilage. Toluidine blue. Sagittal section of the distal part of the femur of *Pleurodeles waltl*. Chondrocytes (black asterisk) are embedded in an abundant matrix (white asterisk). B, Fibrocartilage. Azan. Articular fibrocartilage in *Mus musculus*. Black arrows point to the fibrous matrix. C, Elastic cartilage. Human epiglottis stained with orcein. The extracellular matrix contains elastic fibers (black arrows). D, Calcified cartilage. Toluidine blue. Sagittal section of the distal part of the femur of *P. waltl* in the metaphysis. The oldest chondrocytes are surrounded by a calcified matrix.

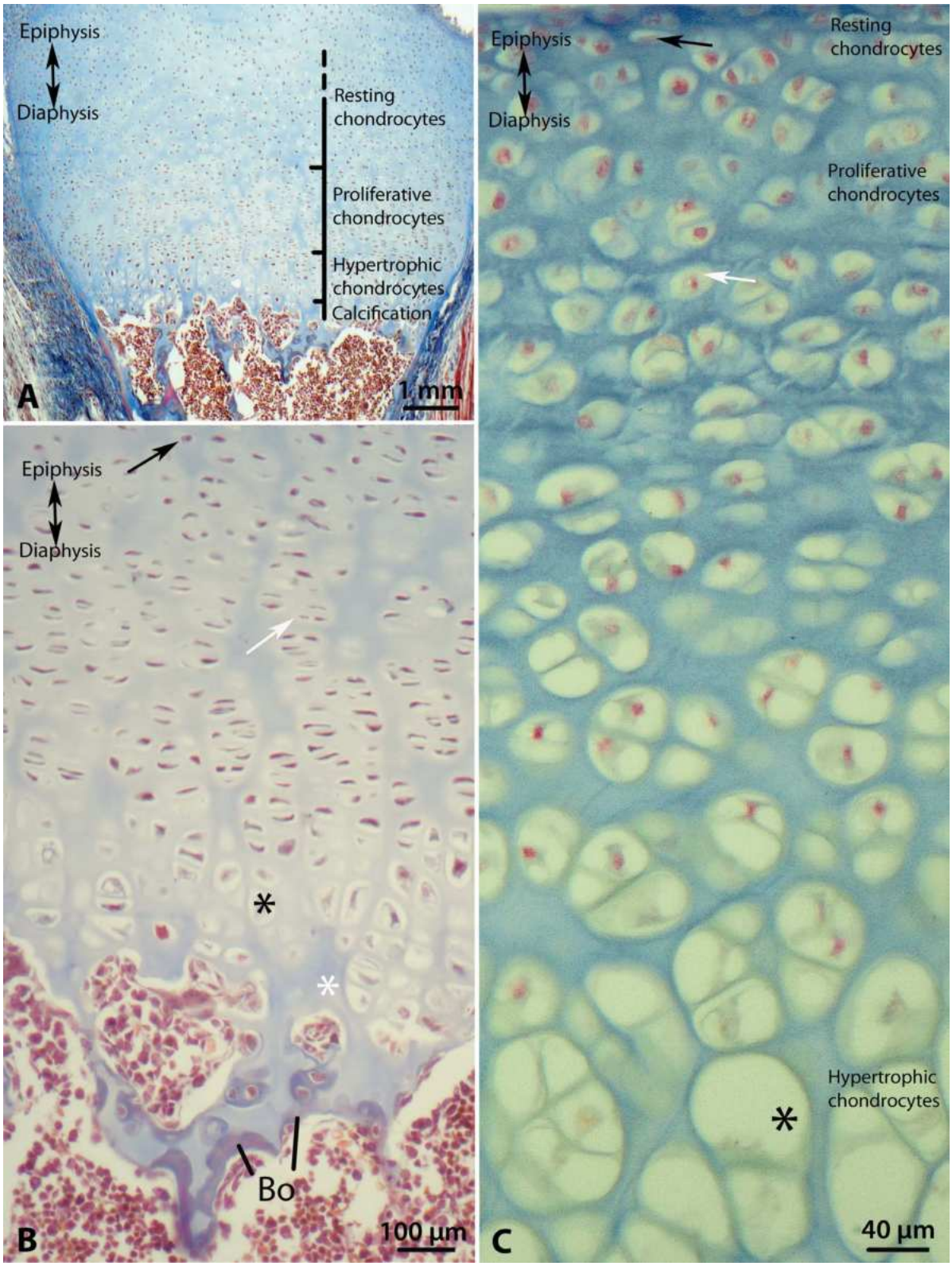


FIGURE 7.2 Hyaline cartilage. Semithin section of mammal femur. A, B, One-step trichrome. C, toluidine blue. A, This image represents the classic picture of endochondral ossification from the proximal part of the metaphysis to the distal part. B, In the growth plate, chondrocytes are first rather globular (black arrow) then divide and are arranged in columns (white arrow) and follow a maturation leading to hypertrophic cells (black asterisk). The cartilage mineralizes (white asterisk). Cartilage anlage is finally destroyed and replaced by bone (Bo). C, Structure of articular cartilage. In the proximal zone, the chondrocytes are flattened (black arrow); in the second zone, the cells are globular (white arrow); in the third zone, the chondrocytes are hypertrophic (black asterisk); in the fourth zone, the calcified cartilage is anchored to the subchondral bone (not shown in the picture).

VetBooks.ir

hyaline cartilages are normally restricted to thin articular caps. Histologically, hyaline cartilage is easily recognizable by its abundant homogeneous matrix. Toluidine blue or Alcian blue, often used to stain it, reflect the abundance of sulfated GAGs.

Cartilages of the Growth Plate, or Growth Cartilages

Growth cartilages are initially in hyaline form, and they undergo a series of histological transformations resulting in their multiplication, hypertrophy and final calcification (e.g., Francillon-Vieillot et al. 1990; Leonore et al. 1995). This process is gradual and continuous, but distinct stages can be recognized through the occurrence of clearly distinct strata (or zones) from the joint to the diaphysis (Figure 7.2A, B); the whole structure forms the growth plate. The first, proximalmost stratum, the *reserve zone*, has the typical aspect of hyaline cartilage, with relatively small, spherical chondrocytes scattered in an abundant and homogeneous matrix. In the second zone, the *proliferation zone*, the chondrocytes proliferate through an active mitotic activity. This is a typical process of interstitial growth, the local thickening of the cartilage resulting from an increase in chondrocyte number and an accumulation of extracellular matrix (Bush et al. 2008). In amniotes, daughter cells tend to align to form sagittal columns, the so-called isogenic groups of the seriated cartilage. In other taxa, chondrocyte alignment is far less regular (Karaplis 2002; Hall 2005; Wuelling and Vortkamp 2010; for review, see also Bausenhardt 1951 and Cubo et al. 2002). Chondrocytes gradually become larger toward the bone metaphyses, so the third zone, or hypertrophic zone, is composed of large cells some ~40 µm in diameter (vs. ~10 µm for the cells of the hyaline cartilage). The fourth zone consists of calcified cartilage embedding the dying hypertrophic chondrocytes.

In several vertebrate taxa (teleosteans, chelonians and some archosaurs), growth cartilage forms an uninterrupted mass from the articular surface down to the marrow cavity in the diaphysis. In most lepidosaurs and mammals, a second center of ossification (called secondary ossification center) develops, to a variable extent, within the epiphyseal cartilage. In anurans calcification is limited and a second center of ossification rarely occurs.

Articular Cartilage of an Adult Bone

In an articulation, the convex cartilage of a bone works under pressure against the concave cartilage of the adjacent bone in an articular pocket lubricated with synovial fluid. In articular cartilage, collagen fiber orientation, along with chondrocyte arrangement and amount, contribute to differentiate four zones (Figure 7.2C). The collagen fibers of the superficial zone are parallel to the articular surface and form a dense network. Chondrocytes are numerous and flattened. This zone is the first to face the compression forces imposed by the articulation. Its cells play a key role in maintaining frictionless joint motion through the production of hyaluronate, phospholipids and lubricin (Jay et al. 2001). Under the superficial layer, collagen fibers are obliquely organized or run perpendicular to the surface toward deeper regions of the epiphysis. Chondrocytes there are spherical and less numerous than in the superficial layer. The third zone is characterized by collagen fibers orthogonal to the articular surface, and chondrocytes forming more or less regular columns parallel to the collagen fibers (Dodds 1930). These deeper zones are chiefly involved in resistance to compressive forces. The deepest layer is the calcified cartilage where collagen fibrils anchor the subjacent bone. The population of chondrocytes is scarce and cells are hypertrophic.

Fibrocartilage

Fibrocartilage (Figure 7.1B) occurs in the intraarticular discs of joints, in knee joint menisci and at the pubic and other symphyses and sites of attachment of tendons to bones. This type of cartilage may also cover hyaline cartilage. Fibrocartilage appears as a transitional tissue between dense fibrous connective tissue and hyaline cartilage. The cells of fibrocartilage are irregularly arranged or lie in longitudinal rows. They are variably flattened, some of them being more like fibroblasts than chondrocytes (Ghadially 1983), but their ultrastructure is typical of chondrocytes and similar to that of the hyaline cartilage cells. Generally, the cells in the center of fibrocartilage are morphologically closer to chondrocytes, while more peripheral cells are closer to fibroblasts. Fibrocartilage matrix contains large collagen fibers arranged irregularly or running aligned with the long axis of the ligament or tendon (Woo et al. 1988). However, fibers may occasionally run at right angles to the long axis of the tendon (Merrilees and Flint 1980). Type I collagen remains the most abundant. The relative paucity of type II collagen is a key biochemical feature that distinguishes fibro- from hyaline cartilage (Arnoczky et al. 1988). Minor collagen components such as types V, VI, IX, XI and M may be important in anchoring chondrocytes to the matrix and allowing collagen fibers to interact with one another and with proteoglycans (Eyre 1988; Melrose and Ghosh 1988). Elastic fibers occur in intervertebral discs, menisci and tendon or ligament attachment zones. There are fewer proteoglycans in fibrocartilage than in the hyaline form. In addition, proteoglycans in fibrocartilage differ biochemically from those of hyaline cartilage (Eyre et al. 1988). Fibrocartilage is poorly vascularized or avascular, a feature probably due to anti-angiogenetic factors. Mechanoreceptors are present in areas related to extreme movement (Zimny 1988). The mechanical properties of fibrocartilage are intermediate between hyaline cartilage and tendon (Yamada 1970). Benjamin and Evans (1990) reviewed the structure, development, growth, degeneration and repair of fibrocartilage.

Elastic Cartilage

The structure of elastic cartilage (Figure 7.1C) is roughly similar to that of hyaline cartilage but, due to the presence of elastic fibers, it is more susceptible to deformation (regions submitted to compression versus traction and shearing). This type of cartilage is therefore highly flexible and is found in intervertebral discs and in ear auricle, epiglottis, larynx and auditory tubes. Elastic cartilage has been extensively studied in extraskeletal sites, especially the external ear in mammals (Kostovic-Knezevic et al. 1981; Calderon-Komaromy et al. 2015).

VetBooks.ir

At the histological level, cells are roundish and variable in size. They occur singly or in pairs rather than in clusters. TEM data distinguish cells of the perichondrium, which are ovoid and contain classical organelles, glycogen granules and cytoplasmic filaments, from the fully differentiated chondrocytes in the central zone. The cytoplasm of the latter cells contains common organelles like those of hyaline cartilage, a large amount of lipids and few big Golgi vesicles (Cox and Peacock 1977). Their nucleus is flattened, cytoplasmic organelles are scarce and cytoplasmic filaments are abundant and closely packed. The chondrocytes of elastic cartilage synthesize the elastic components of the matrix as well as various proteins constituting the extracellular matrix. The matrix consists of a dense network of fibrils (6–25 nm in diameter) depending on the distance from the chondrocyte. Interestingly, chondrocytes contain matrix-vesicles-like inclusions linked to the secretion of elastic fibers rather than to mineralization (Hall 2005). Mineralization of elastic cartilage has nevertheless been reported (Svajger 1970).

Calcified Cartilage

Calcified cartilage results from the impregnation of the organic extracellular matrix by hydroxyapatite, forming a mineral phase. In simple ground sections, this tissue can be distinguished from subchondral bone by its histological appearance, i.e., large rounded cell lacunae in an amorphous, monorefringent matrix (Figure 7.3A).

This tissue is also clearly revealed by Safranin-O/Fast green staining (Gabe 1968; Mescher 2013; Wang et al. 2009). In all endochondral bones of actively growing individuals, the mineralization of cartilage occurs in the lower (metaphyseal) part of growth plates, as well as under the cap of articular cartilage (if a secondary ossification center exists). In adults, calcified cartilage is limited to the latter location, except in neotenic amphibians and some rare marine tetrapods (mostly extinct; review in Ricqlès and Buffrénil 2001) in which it may persist at a distance from the epiphyses. In typical endochondral ossification, the calcified cartilage of growth plates is a transitory tissue, sequentially replaced *in situ* by endosteal bone through a resorption and reconstruction process. Cartilage usually does not fossilize because the proteinaceous scaffold and the cells normally degrade postmortem. However, fossilized calcified cartilage (Figure 7.3B) has been broadly described in the literature, especially in long limb bones (de Ricqlès 1972; Horner et al. 2000; Schwarz et al. 2007; Bonnan et al. 2010; Padian and Lamm 2013). It may thus provide information about the ontogenetic stages of fossils (Bailleul et al. 2012), and about the biomechanical, physiological or ecological characteristics of extinct organisms (Ossa-Fuentes et al. 2017).

The hyaline cartilage is anchored to the bone by collagen fibers through the tidemark, a thin wavy stratum between the deep cartilage and subchondral bone. The tidemark is better defined by biochemical methods than by morphology. A high concentration of calcium phospholipid phosphate complexes has been characterized by Dmitrovsky et al. (1978). This line is a symbol of skeletal maturation (Lyons et al. 2005, 2006).

Hydroxyapatite crystals are deposited around the lacunae of hypertrophic chondrocytes, which suggest that the latter could play a role in cartilage calcification (Amizuka et al. 2012).

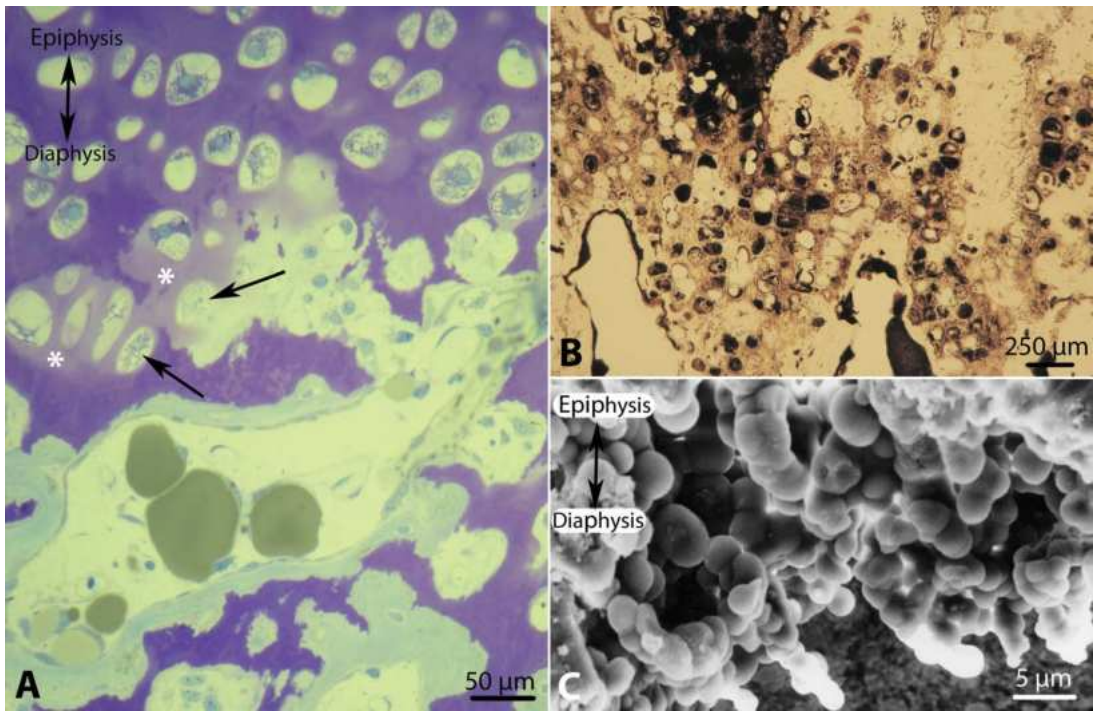


FIGURE 7.3 Calcified cartilage. A, In growth plate, in the distal part of the metaphysis, the matrix calcifies (asterisk) around dying hypertrophic chondrocytes (arrows). *Pleurodeles waltl*. Toluidine blue. B, Dorsal vertebrae of *Simoedosaurus*. C, Scanning electron microscopy General view of the distal part of the hypertrophic cartilage of the hemal part of a vertebrae. Numerous mineralized globules appear like pillars. *Cyprinus carpio.*

VetBooks.ir

Glycogen, in association with phosphorylase, produces phosphorylated sugars within the matrix of calcifying cartilage. During the subchondral bone formation, the deposition and absorption of calcium salts are balanced in the cartilage matrix. After skeletal maturation, calcium salts are no longer absorbed and the calcified cartilage forms (Frisbie et al. 2006). The calcified cartilage interrupts the transfer of the interstitial fluid between hyaline cartilage and bone and affects the ability of nutrients to diffuse between tissues (Oegema et al. 1997). The limited permeability stabilizes the microenvironment of hyaline cartilage and modulates the forces between the two tissues, which differ in their biomechanical properties. Calcified cartilage plays an important role in transferring load from the hyaline cartilage to the subchondral bone (Mente and Lewis 1994).

The mineral component of calcified cartilage is a form of hydroxyapatite close to that of bone, but with a different carbonate concentration (Rey et al. 1991). The molecular structure of hydroxyapatite in calcified cartilage, and its interface with the organic matrix, are described in detail in Duer et al. (2009). The organic matrix of mineralized cartilage mainly includes collagen types II and X, along with GAGs such as chondroitin sulfate. The collagen bundles provide a scaffold for the deposition of calcium phosphate particles. Fine hydroxyapatite crystals are arranged radially around a calcification center and expanding globules, the calcospherites, are formed; these globules then fuse in larger masses. This pattern of mineral deposit, designated *spheritic mineralization* (Ørvig 1951, 1968) is usually observed in cartilage (Hall 2005; Zylberberg and Meunier 2008) (Figure 7.3C).

In sharks, calcified cartilage generally occurs in the endoskeleton. The surface of the cartilage has a unique prismatic pattern, making it unmistakable when found in fossils. Because of their calcification, the vertebral centra, part of the jaw, and the rostral node are the most common fossil remains in sharks. Here, mineralization is not spheritic but rather inotropic as in bone tissue (Kemp and Westrin 1979). In the mandibular condyle of mammals, a slowly growing cartilage close to fibrocartilage mineralizes by way of calcospherites (Boyde and Jones 1983). This secondary cartilage develops in the dermal skeleton of embryonic birds and mammals in regions functioning as hinges (Francillon-Vieillot et al. 1990).

Chondrogenesis and Chondrocyte structure

Basic Aspects of Chondrogenesis

The formation of cartilage, or chondrogenesis, takes place during the embryonic development and persists until adulthood. It is also involved in fracture repair. Through a cytogenetic process typical of connective tissue, mesenchymal cells are recruited and migrate, leading to a condensation of progenitor cells (skeletal stem cells [SSCs]) that locally differentiate into chondroblasts (Hall 1983, 2005; Day et al. 2005; Hill et al. 2005). Progenitor cells become growth plate chondrocytes by proceeding through an intermediate, bipotent osteochondroprogenitor stage (with osteoblastic or chondrocytic potentials), while they become articular chondrocytes through a distinct pathway marked by a multipotent joint progenitor stage. Chondrogenesis is controlled by cell interactions with the surrounding matrix and different factors such as growth and differentiation factors, and the temporal-spatial expression of specific genes is involved in this process (Cole 2011; see Gomez-Picos and Eames 2015 for review). In addition, lineage specification and fine functional differentiation of chondrocytes and their progenitors are controlled by numerous transcription factors that contribute to the great diversity in size, shape and properties of cartilage tissues (see Liu et al. 2017 for review).

Within the cartilage anlagen of developing limbs, flattened and condensed mesenchymal cells appear in the putative joint site. This zone is defined as the *interzone* (Holder 1977; Mitrovic 1977). Three different embryonic cell populations contribute to the formation of cartilage. The cranial neural crest cells, the lateral plate mesoderm and the paraxial mesoderm (Kuratani et al. 2008) are, respectively, involved in cartilage formation in the cephalic, zonoappendicular and axial parts of the skeleton (see also Chapter 2). Neural crest derived cartilage constitutes much of the endoskeleton of the head and is also found in the clavicle (Dupin et al. 2018). Neural crest derived mesenchyme has the capacity to orchestrate the spatiotemporal programs of chondrogenesis and to control cartilage size and shape across embryonic stages and between species (Eames and Schneider 2008). These authors showed that neural-crest mesenchyme regulates fibroblast growth factor (FGF) signaling and the expression of downstream effectors such as sox9 and col2a1. Cartilage derived from the mesoderm occurs not only in the endoskeleton, but also in tendons, ligaments and soft connective tissues.

The complexity of chondrogenesis is enhanced by numerous developmental phases. The gene regulatory network (GNR) for vertebrate chondrogenesis is separated into four categories: GNR involved in recruitment, condensation, differentiation and hypertrophy (Goldring et al. 2006). The induction of the chondrogenic differentiation process resembles osteogenesis in sharing with it a Sox 9 progenitor (Lefevre et al. 2007; Han and Lefevre 2008; Long 2011). By binding to DNA, Sox9 is responsible for the expression of several cartilage-specific components including type II collagen (Bell et al. 1997) and type XI collagen (Bridgewater et al. 1998). The lack of Sox 9 leads to the complete loss of cartilage within an organism. Mesenchymal stem cells (MSCs) entering a chondrogenesis process have unique characteristics, expressing many biomolecules that are typically associated with cartilage, such as type II collagen and proteoglycan aggrecan (Solchaga et al. 2011; Grässel et al. 2012). Assis-Ribas et al. (2018) reviewed the main mechanisms involved in chondrogenesis. To summarize, transforming growth factor (TGF)-β (particularly bone morphogenetic proteins [BMPs]; Chubinskaya and Kuettner 2003), Wnt, Runx, Hh, FGFs and parathyroid hormone (PTH)-related peptide (Jüppner 2000; Katagiri and Takahashi 2002; Komori 2015; Hojo et al. 2016) are involved in the regulation of signaling pathways of MSC lineage commitment (Figure 7.4).

The run-related transcription factors Runx are required for chondrocyte hypertrophy (Yoshida 2004). Indian hedgehog (Ihh) and PTH-related peptide control chondrocyte

VetBooks.ir

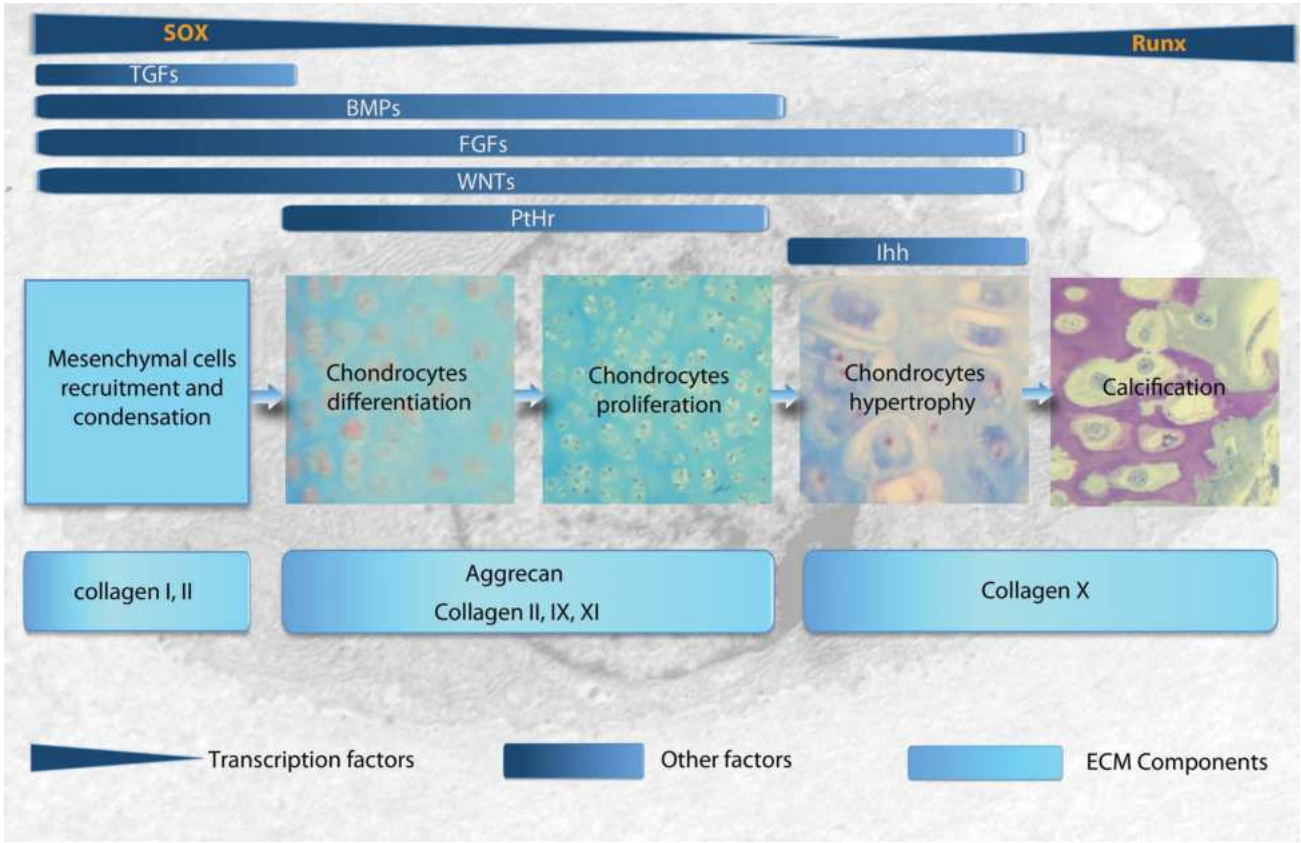


FIGURE 7.4 Chondrogenesis. Various stage of chondrogenesis. Main key factors and extracellular matrix components (ECM) involved in each stage are mentioned. The process of chondrogenesis is initiated with the stimulation of mesenchymal stem cells to differentiate into prechondrocytic cells, which migrate and condense to form cartilage. The cells differentiate into chondrocytes and start to proliferate. In hyaline cartilage, cells become hypertrophic and die. Cartilage differentiates under the control of SOX and Runx transcription factors. Above each stage, the relevant factors involved appear. Underneath each stage, ECM-specific components are mentioned. BMP, bone morphogenetic protein; FGF, fibroblast growth factor; Ihh, Indian hedgehog; PtHr, parathyroid hormone related peptide; TGF, transforming growth factor.

differentiation at multiple steps through the mutual regulation of their activities (Kobayashi et al. 2002). Recently, Bai et al. (2019) showed that the redox status controls chondrocyte differentiation and chondrogenesis as an endogenous regulator of signaling kinases and transcription factors. Chondroblasts give rise to chondrocytes by mitoses. The chondrocyte is the fully mature cartilage cell. Its shape is rounded, and it is located in a chondroplast (i.e., a chondrocyte lacuna) within the extracellular matrix that it produces.

Therefore, the immature cartilage (growth plate and articular cartilage) and the mature cartilage (hypertrophied or dying cells, mineralized cartilage and degraded matrix) have distinct gene and protein expression profiles. Both express collagen XI, biglycan and decorin. Immature cartilage expresses high levels of collagen II and IX, aggrecan and fibromodulin. Mature cartilage expresses high levels of collagen X (see Gomez-Picos and Eames 2015 for review).

Epigenetics, including DNA methylation and histone modification, has recently emerged as an essential regulatory system for gene expression. Transcriptional coregulators are predominantly involved in this epigenetic process and regulate gene expression during chondrogenesis (Hata 2015).

Chondrocyte Ultrastructure

Chondrocytes are highly specialized cells varying in shape, size and number, depending on the cartilage type and the zone observed. They occupy a small part of the tissue volume (0.01–2% of the total tissue volume in articular cartilage). Unlike bone cells, chondrocytes are not connected with each other.

As described above, chondrocytes undergo an orderly series of spatiotemporal morphological changes and have specific features during their life (Figure 7.5).

At the ultrastructural level, all chondrocytes share common structures (Figure 7.5A). They are bordered by a limiting plasma membrane with cytoplasmic processes extending into the surrounding matrix. A rough endoplasmic reticulum (RER) involved in enzyme and protein synthesis is present in variable amounts, as are mitochondria. A Golgi complex operates the transport of the molecules synthesized by the chondrocyte, as well as one or more areas with dilations and vesicles of variable size and number. Micropinocytotic vesicles transport material into the cell from the exterior. Lipid drops and glycogen are often observed. Microtubules are generally present, and many chondrocytes contain intracytoplasmic filaments.

VetBooks.ir

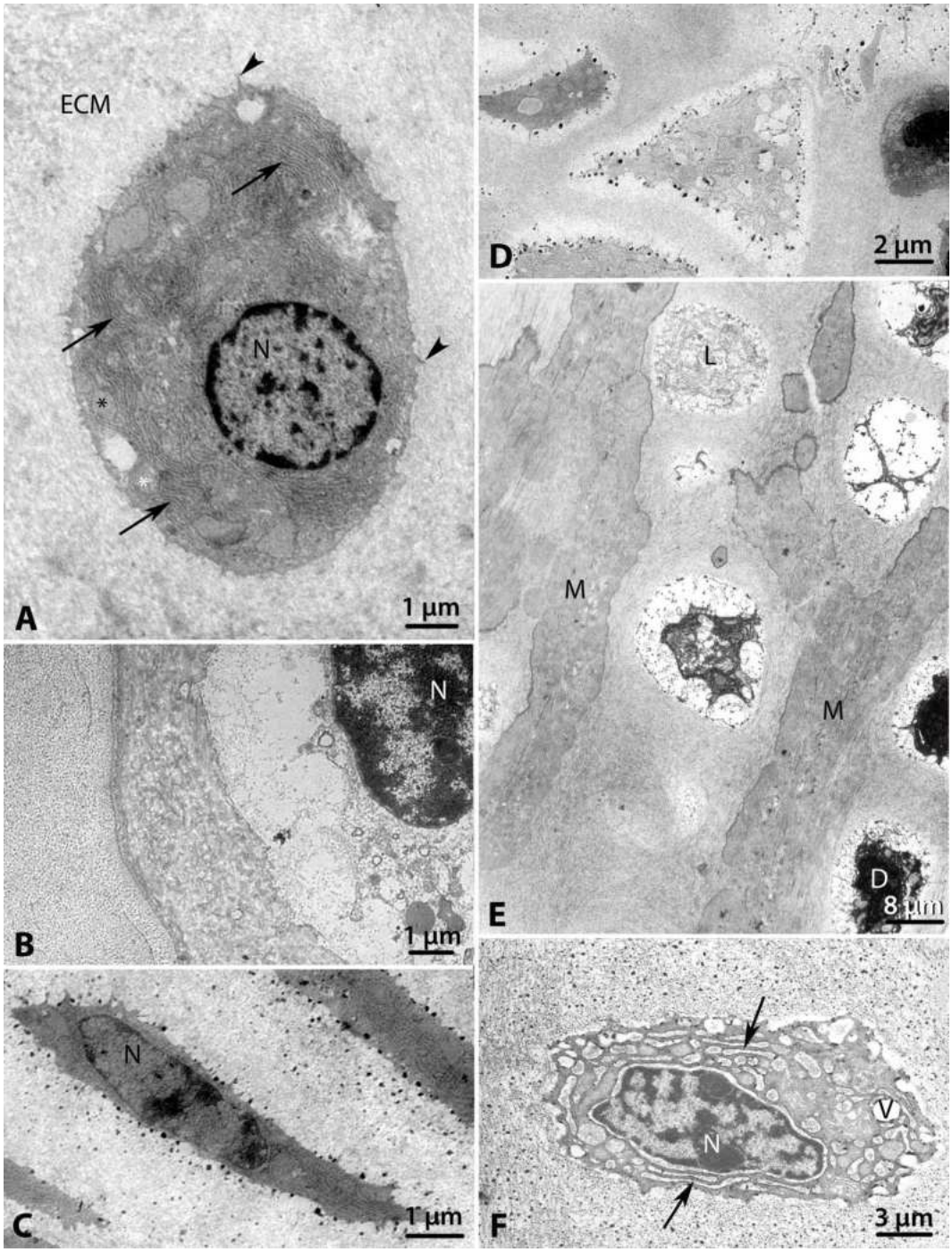


FIGURE 7.5 Chondrocyte ultrastructure. Transmission electron microscopy images of chondrocytes. A, Globular healthy chondrocyte with numerous organelles. *Mus musculus* femur. B: Extracellular matrix (ECM) next to the chondrocyte. *Pleurodeles waltl* femur. C, Elongated cells in the superficial zone of articular cartilage of *M. musculus* femur. D, Chondrocyte in a proliferative zone of the growth plate of the femur of *M. musculus* femur. E, Hypertrophic chondrocyte at different stages of maturation. Chondrocyte columns are separated by mineralized septa. *Cyprinus carpio,* hemal part of a vertebra. F, Hypertrophic chondrocyte with abundant rough endoplasmic reticulum (RER) and vacuoles (V), becoming dark. *Cyprinus carpio.* Hemal part of a vertebra. D, dark chondrocyte; L, light chondrocyte, M, mineral; N, nucleus. Black arrows, RER; arrowheads, cytoplasmic processes.

The nucleus is like that of many other tissues, but there is much variation in its shape in chondrocytes. The walls of the lacunae individually housing each of these cells differ in aspect from the rest of the matrix (they display a higher chromophilia; Figure 7.5B).

In hyaline cartilage, flattened chondrocytes lie near the perichondrium, in the proximal part of the metaphyses (Figure 7.5C). Chondrocytes of various shapes (triangular or globular) are characterized by a voluminous, globular nucleus surrounded by abundant flat reticulum saccules and mitochondria

typical of growth plates (Figure 7.5D). Some of them divide, and several cells may occur in the same lacuna, thus forming cell clusters. In the metaphyses, larger cells, the hypertrophic chondrocytes, display a high glycogen content and a voluminous, globular nucleus surrounded by reticulum saccules. Their cytoplasmic membrane is intact and close to the matrix. These types of cells are called "light chondrocytes" (Figure 7.5E). Some chondrocytes have a globular nucleus with a condensed nucleus and swollen saccules of RER. These cells correspond to "dark chondrocytes" (Figure 7.5E), as described by Wilsman et al. (1981), Ereinpresa and Roach (1998), Zylberberg and Meunier (2008) and Quilhac et al. (2014) in various vertebrate taxa. Hypertrophic cells follow various degeneration programs near the distal part of the metaphyses (see the section "Cell Death, Degradation and Resorption of Cartilage"). Some of them have a ruptured membrane, lose their organelles and look necrotic. Others may have an abundant reticulum at first (Figure 7.5F), and then a shrunken nucleus surrounded by vacuoles of autodigestion. Hypertrophic chondrocytes may also show a convoluted cell membrane, along with apoptotic bodies. Empty lacunae are encountered near the erosion front.

Ultrastructure of the Extracellular Matrix

Cartilage matrix is an amorphous, gel-like substance. Because it is a dynamic system, its biochemical composition (Figure 7.6A, B) varies considerably depending on several factors.

However, the matrix is basically composed of collagen, proteoglycans, noncollagenous proteins, glycoproteins, lipids and phospholipids; it is highly hydrated. In endochondral ossification, it undergoes mineralization close to the erosion front (see above: calcified cartilage).

Collagen

Collagen is produced by chondroblast activity. It is the most abundant component of the matrix. Fibers are thin and composed of fibrils arranged in a meshwork that encloses large amounts of proteoglycans. Type II collagen is dominant (90% of the collagens and about 60% of cartilage dry weight), whereas Type II fibers, found in articular cartilage, are thicker and resemble, ultrastructurally, type I collagen fibers. The cross-banding of Type II collagen is less obvious than that of Type I, due to the masking effect of an abundant interfibrillar material. Collagen Types I, III–VI and IX–XI are also present (1–10% of collagens) and help to form and stabilize the Type II networks (Seyer et al. 1974; Von der Mark and Von der Mark 1977; Galotto et al. 1994; Eyre et al. 2006; Zelenski et al. 2015). In hyaline cartilage, collagen represents about 75% of the cartilage dry weight. Its relative weight is highest in the superficial zone and gradually decreases in deeper strata (Brocklehurst et al. 1984).

Glycosaminoglycans

GAGs are carbohydrates made of repeated disaccharide units, which results in six major subunits in articular cartilage: chondroitin sulfate 4 and 6, keratin sulfate, dermatan sulfate, heparin sulfate and hyaluronan. They are negatively charged, repelling each other while attracting ions and water. Therefore, they ensure their main functional role: absorbing water and thus maintaining the hydration and the mechanical properties of the matrix (Culav et al. 1999; Brody 2015). The hyaluronan is important for matrix structure because it forms a linear aggregate interwoven with collagen fibril networks.

Proteoglycans

Proteoglycans are hydrophilic proteins that present GAG chains covalently attached to a protein core. They represent 20–40% of the dry weight in hyaline cartilage (Handley et al. 1985). In contrast to collagen, proteoglycan content is higher in the superficial than in the deeper zone of the articular cartilage (Brocklehurst et al. 1984). The latter contains a variety of proteoglycans such as aggrecan, decorin, biglycan and fibromodulin. Aggrecan is the most abundant by weight. It possesses at least 100 chondroitin sulfate and keratin sulfate chains in the core protein. Aggrecan interacts with hyaluronan and occupies the interfibrillar space in the matrix. It contributes to the physical properties of cartilage, preventing the proteolytic cleavage of collagen (Pratta et al. 2003). Decorin and fibromodulin, small leucine-rich proteoglycans, interact with type II collagen and play a role in fibrillogenesis and interfibril interactions. Biglycan interacts with

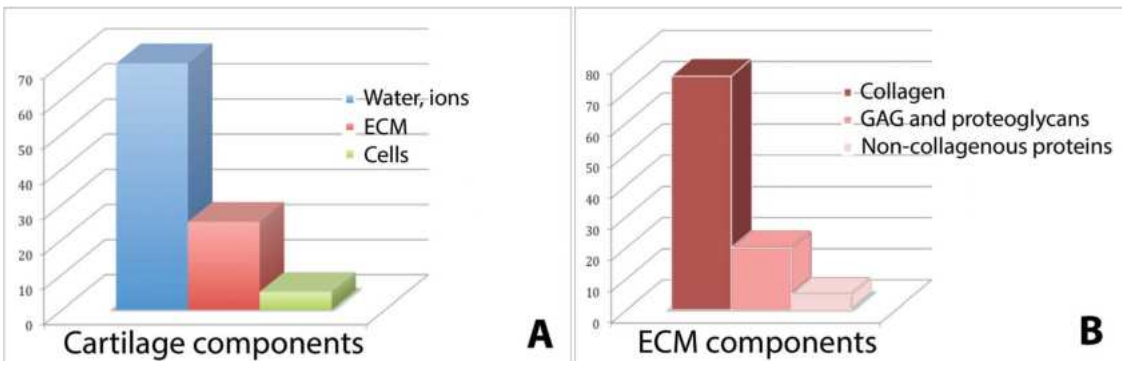


FIGURE 7.6 Bar graph illustrating the respective parts of cartilage components. A, Cartilage is an highly hydrated tissue. Cells represent only 1–5% of the all components. B, The main part of the extracellular matrix (ECM) is collagen and glycosaminoglycan (GAG).

VetBooks.ir

collagen VI. Perlecan and lubricin are present in mature cartilage (Nagakawa et al. 2016; Sadatsuki et al. 2016). Lubricin binds collagen II and fibronectin and is involved in maintaining the essential boundary lubrication of articular cartilage (Flowers et al. 2017). The proteoglycans, in conjunction with collagen networks, contribute to cartilage resilience, elasticity, shear strength and self-lubrication. The role of proteoglycans in cartilage development and maintenance is reviewed in Iozzo (1998) and Knudson and Knudson (2001).

Noncollagenous Proteins

Numerous noncollagenous proteins are present in the cartilage matrix. Structural proteins (mainly of the integrin family) interact with cellular receptors, and control adhesion, migration, proliferation and differentiation of chondrocytes, whereas regulation proteins influence cell metabolism (Roughley 2001). Fibronectin is a large, adhesive glycoprotein that aggregates near the chondrocyte membrane and in the matrix; it serves as a substrate for cell attachment. Laminins are polyvalent molecules secreted by chondrocytes and involved in the regulation of chondrocyte activities such as adhesion, migration and survival (Sun et al. 2017).

Water and Ions

Water plays a major role in supplying nutrients to chondrocytes. Hyaline cartilage has a high (60–80%) water content. However, water concentration is locally variable in the cartilage. The largest water content occurs close to articular surfaces, possibly to provide lubrication. Sodium, calcium, potassium and chloride are dissolved in water within the interfibrillar space.

Cartilage Vascularization and Innervation

The nature of the extracellular matrix allows diffusion of molecules, ions, dioxygen and CO_2 to and from the chondrocytes, but diffusion can take place over a limited distance only. The lack of blood vessels (avascularity) in cartilage is due to inhibitors of both endothelial cell growth and protease. Blood vessels may penetrate the cartilage when its thickness is more than 3 mm (Schaffer 1930; Knese 1980). Channels of vascularized mesenchyme can penetrate the hyaline cartilage of long bone epiphyses before ossification (Kuettner and Pauli 1983).

Cartilage is a basically aneural tissue. Perception and proprioception in synovial joints depend on nerves that end in the synovium capsule, muscles and subchondral bones. Cartilage canals contain nerves in addition to vessels, and they play a role in chondrocyte metabolism and functions.

The Functions of Cartilage and Their Regulation

Chondrocytes are multifunctional cells involved in matrix synthesis, maintenance and repair by producing enzymes, growth factors and inflammatory mediators.

Modalities of Cartilage Growth

Cartilage growth is due to chondroblast proliferation, hypertrophy and matrix secretion. The characteristic of cartilage is its ability to grow both from within (interstitial growth) and by the subperichondral deposit of new layers (appositional growth).

The matrix surrounding chondrocytes in hyaline cartilage is supposed to initiate signal transduction within the cartilage (Eggli et al. 1985). Matrix synthesis by chondrocytes is controlled by a number of physical factors, growth factors and cytokines. Growth factors and cytokines are soluble polypeptides capable of regulating growth, differentiation and metabolic activity of cells. They have an antagonistic effect. The results of their activity depend on the relative concentration of each mediator present in cartilage. Factors as insulin-like growth factor (IGF)-1 (a systemic hormone) and TGF-β (a cytokine) have an anabolic effect. Thus, IGF-1 directly stimulates matrix synthesis. TGF-β stimulates proteoglycans synthesis, especially when the matrix has been damaged. TGF-β interacts with decorin, a small proteoglycan that binds to collagen fibers. Recently, it has been demonstrated that TGF-β1 plays a role in both cartilage health and disease (Zhen et al. 2013; Handorf et al. 2014). Chondrocytes have specific membrane receptors that bind matrix components such as collagen and fibronectin. Integrins mediate many cellular processes including tissue morphogenesis, homeostasis and repair. The extracellular matrix adjacent to the cellular elements has a relatively high turnover compared with proteoglycans (weeks to months) and collagens (several years) located more distantly. PTH and thyroxine stimulate matrix synthesis.

Function of Growth Plates

In endochondral ossification, the differentiating chondrocytes within the growth plate are organized along a continuum: The resting and the actively proliferating chondrocytes are closer to the epiphysis and the hypertrophic and apoptosing chondrocytes are in the metaphysis. During their differentiation, chondrocytes express and secrete various molecules such as collagens, proteoglycans and other matrix components (Karsenti and Wagner 2002; Samsa et al. 2017 for review). Indian hedgehog (Ihh), which is predominantly expressed in prehypertrophic chondrocytes, stimulates the expression of parathyroid hormone (PTH)-related peptide, which negatively regulates terminal chondrocyte differentiation (Kobayashi et al. 2002). The role played by hypertrophic chondrocytes in the attraction of blood vessels and the facilitation of biomineralization (through the expression of specific proteins) is clear (Leboy et al. 1989).

Hypertrophic chondrocytes secrete matrix vesicles, containing diverse enzymes that degrade and mineralize the matrix (Wuthier et al. 1985; Kirsh et al. 2000). Behonick and Werb (2003) gave an overview of the relationship between the matrix and the chondrocytes at each step of their differentiation. Matrix vesicles bind to collagen and have a well-defined function as initiators of mineralization; however, the mechanisms leading to the biogenesis of matrix vesicles and the process through which the mineral phase forms remain unclear (Bottini et al. 2018).

VetBooks.ir

Hypertrophic chondrocytes normally die and leave empty lacunae that are invaded by blood vessels (Farnum and Wilsman 1989a, b; Roach et al. 1998). In the salamander (Caudata) *Pleurodeles waltl*, Quilhac et al. (2014) showed that a subpopulation of chondrocytes called *dark chondrocytes* undergoes degeneration through chondroptosis (see section "Cell Death, Degradation and Resorption of Cartilage" below), whereas others die through apoptosis and necrosis (Roach and Clarke 2000; Roach et al. 2004; Elmore 2007). In hypertrophic chondrocyte populations, some cells survive and play a direct role in osteogenesis (Aubin et al. 1995; Shapiro et al. 2005; Kouri and Lavalle 2006): they secrete matrix molecules such as osteopontin, osteonectin and bone sialoprotein, which were once thought to be uniquely produced by osteoblasts. These molecules create a scaffold for the attachment and differentiation of osteoblast and osteoclast precursor cells (White and Wallis 2001).

Mechanical Behavior

In the vicinity of the pericellular zone, the cartilage matrix becomes richer in collagen and forms a fine network protecting the cell against mechanical stress (Gannon et al. 2014). The chondrocyte microenvironment is regularly renewed, which prevents cell-to-cell communication. A chondrocyte can respond to growth factors and mechanical forces. The mechanical behavior of cartilage depends on the interaction between its fluid and solid components. The ability of articular cartilage to withstand mechanical constraints arises from its frictional resistance to water pressure and flow. The relationship between proteoglycans and interstitial fluid provides compressive resilience to cartilage through negative electrostatic repulsion forces (Kheir and Shaw 2009). Articular cartilage is viscoelastic. The fluid pressure absorbs a significant part of total load, thereby reducing the stress acting on the solid matrix. The low permeability of articular cartilage prevents fluid from being quickly squeezed out of the matrix (Frank and Grodzinski 1987). Fluid flow induced by mechanical loading helps to expel waste products from cartilage and transport nutrients, such as salts or glucose, and growth factors into the tissue (Fox et al. 2009; Albro 2011). As reviewed by Di Domenico et al. (2018), the transport of solutes through cartilage is multifaceted due to the intrinsic heterogeneities of the tissue (collagen orientation and matrix composition). Interestingly, molecules larger than the pore size of the tissue can diffuse through the matrix.

Repair

Cartilage repair capacity is impeded by the poor replication power of chondrocytes and their limited ability to produce enough matrix when mature. However, recovery from mild damage is possible (review in Carballo et al. 2017). There are indications that immature cartilage has at least a partial regeneration capacity, but this is subsequently lost (Calandruccio et al. 1962; Ikegawa et al. 2016). The main reason mature cartilage is unable to self-repair seems to be its avascular structure; thus, blood clots cannot form (Mow and Rosewasser 1988). Various growth factors are potentially involved in repair (Freyria and Mallein-Gerin 2012), such as the platelet-derived growth factor (Zhao et al. 2016). When injury or other damage occurs to articular cartilage, several different cell types are mobilized and can produce new matrix with, however, different properties compared with the original matrix (Redman et al. 2005; Morito et al. 2008; Sekiya et al. 2012). Chondrocytes near the lesion can proliferate and secrete new matrix, but repair is not complete. Cells such as MSCs can also migrate from the synovial fluid and, in the presence of growth factors, fill the lesion with regenerative tissue, but they produce a fibrocartilage tissue the material properties of which are inferior to those of true hyaline cartilage.

Cell Death, Degradation and Resorption of Cartilage

Cell death results from a series of morphological and molecular events. The aim of this section is not to review the different forms of cell death but to give an overview of the diversity and regulation of chondrocyte death. Research on this process revealed an association between cell death proper and matrix degradation (Thomas et al. 2007).

Cells

In physiological conditions, chondrocyte death is associated with apoptosis, necrosis or chondroptosis (Figure 7.7).

As explained above, chondrocytes occur in several forms: "light" and "dark" cells. Among light hypertrophic chondrocytes with fragmented nuclei and membranes, some die by necrosis as defined by Golstein and Kroemer (2006), Ahmed et al. (2007) and Nikoletopoulou et al. (2013). These cells have a ruptured nuclear membrane and condensed chromatin. Their cytoplasm becomes vacuolated, their organelles are disintegrated and their plasmic membrane soon breaks. Other chondrocytes follow a cell death program such as apoptosis (Kuhn et al. 2003; Hwang and Kim 2015). These cells have condensed chromatin and a discontinuous nuclear membrane. Their well-preserved organelles are compacted together, and their cell membrane is intact but convoluted. Finally, their nucleus and cytoplasm fragment. The light and dark cells die by a mechanism morphologically distinct from apoptosis (Ereinpresa and Roach 1998). In teleosts, amphibians, birds and mammals, dark chondrocytes probably undergo degeneration through chondroptosis, a specific cell death process (Wilsman et al. 1981; Ereinpresa and Roach 1998; Elmore 2007; Zylberberg and Meunier 2008; Quilhac et al. 2014). Dying dark chondrocytes undergo a progressive extrusion of cytoplasm, and their nucleus fragments into condensed patches of chromatin. Light chondrocytes appear to disintegrate within their well-preserved plasmic membrane. The appearance of their nucleus is variable, and their organelles progressively disintegrate. A difference exists in the timing of nuclear and cytoplasmic changes between apoptosis and other ways of cell death. In apoptosis, nuclear changes precede cytoplasmic alterations, whereas in other processes the reverse situation prevails (Ahmed et al. 2007).

VetBooks.ir

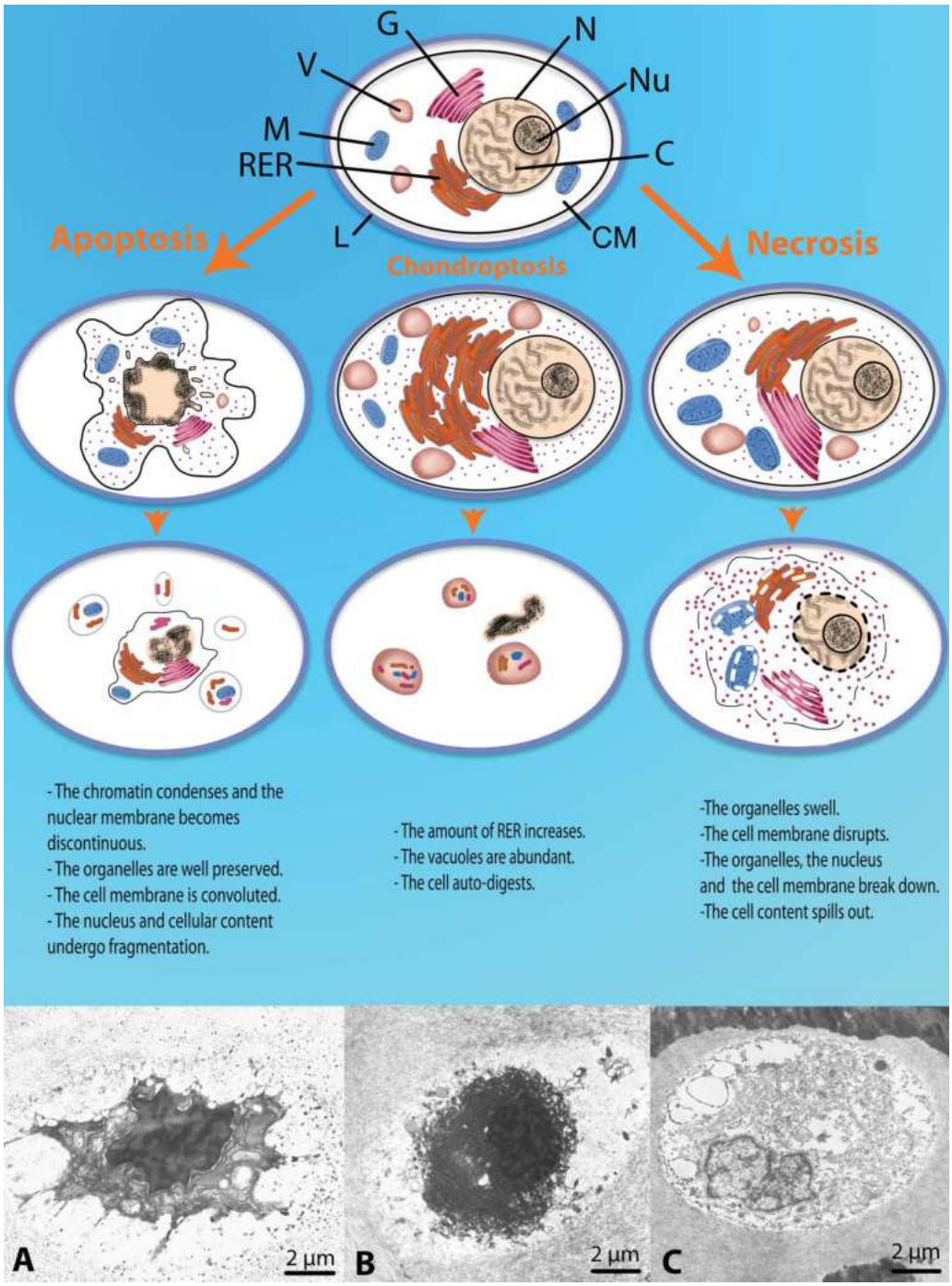


FIGURE 7.7 Chondrocyte death. The major differences among apoptosis, chondroptosis and necrosis of chondrocytes. Normal hypertrophic chondrocyte can follow one of the three ways of cell death. The cell fills its lacuna (L) within the matrix. Rough endoplasmic reticulum (RER), Golgi (G), mitochondria (M) and vacuoles (V) are present. Nucleus (N) contains chromatin (C) and nucleolus (Nu). There is a narrow space between the cytoplasmic membrane (CM) and the lacunae limits. In apoptosis nuclear changes precede the modifications of the cytoplasm. In chondroptosis and necrosis, the cytoplasm aspect changes before nuclear modifications. Transmission electron micrographs of dying chondrocytes. A, Apoptosis. B, Chondroptosis. C, Necrosis.

Matrix

Cell death may lead to altered extracellular matrix structure and abnormal mechanical function. The ability of chondrocytes, synovial cells and inflammatory cells to degrade matrix components relies on the synthesis and secretion of proteases. The latter enzymes are thus involved in cartilage turnover. Four classes of proteases, active at different pH, have been identified in cartilage: aspartic and cysteine proteases, as well as serine and metalloproteases (MMPs). MMPs are responsible for breaking the bond between collagen and proteoglycans. Proteases are found either within the cells, in lysosomes, or outside them.

VetBooks.ir

They are currently important therapeutic targets because of their involvement in mammalian osteoarthritis; their role has thus been extensively studied (Zhen et al. 2013; Handorf et al. 2014). For example, MMP 13 degrades both collagen II and aggrecan (Leong et al. 2011). Collagenases degrade collagen fibrils, and gelatinase denatures type II and type IV collagen. Normal cartilage contains large amounts of protease inhibitors. Cytokines induce synthesis of proteases and reduce the synthesis rate of proteoglycans and other matrix components.

Cartilage resorption occurs during endochondral ossification, growth of cartilaginous structures and local vascular proliferation. Chondroclasts are the specialized cells destroying, by phagocytosis, most of the hypertrophic calcified cartilage (cells and matrix) at the level of the so-called erosion front. They only leave *in situ* a network of trabeculae made of the matrix of the calcified cartilage. The accretion of endochondral bone tissue then occurs over these trabeculae. A thin coat of nondestroyed embryonic cartilage matrix may persist around the medullary cavity in the diaphyseal region of growing long bones. In cross sections, this layer appears as a line, known as Kastchenko's line (Francillon-Vieillot et al. 1990). Chondroclasts are large, multinuclear cells similar in origin to the osteoclasts (Jee and Nolan 1963). Anderson and Parker (1966) proposed that chondroclasts first resorb calcified cartilage and that mononuclear clastic cells then resorb uncalcified cartilage. Both types of cells seem to be involved in cartilage resorption, depending on the stages of development and the vascular density of this tissue (Silvestrini et al. 1979; Sorell and Weiss 1980).

REFERENCES

Ahmed, Y. A., et al. 2007. Physiological death of hypertrophic chondrocytes. *Osteoarthritis Cartilage.* 15: 575–586.

Allen, M. R., D. B. Burr. 2014. Basic and Applied Bone Biology. *Bone modeling and remodeling.* SanDiego. Academic Press.

Albro, M.B. 2011. Dynamic loading of immature epiphyseal cartilage pumps nutrients out of vascular canals. *J. Biochem.* 44: 1654–1659.

Amizuka, N. T. et al. 2012. Histology of epiphyseal cartilage calcification and endochondral ossification. *Front. Biosci.* 1(4): 2085–2100.

Anderson, H.C., J. Parker. 1966. Invasion and resorption in endochondral ossification. An electron microscopic study. *J. Bone jt. Surg.* 48A: 899–914.

Arnoczky, S., et al. 1988. Meniscus. In *Injury and repair of the musculoskeletal soft tissues*, eds. S.L.Y. Woo and J. A. Buckwalter. 487–537. Rosemont, IL: American Academy of Orthopaedic Surgeons.

Assis-Ribas, T., et al. 2018. Extracellular matrix dynamics during mesenchymal stem cells differentiation. *Dev. Biol.* 437: 63–74.

Aubin, J. E., et al. 1995. Osteoblast and chondroblast differentiation. *Bone.* 17: 77–83.

Bai, Y., et al. 2019. Redox control of chondrocyte differentiation and chondrogenesis. *Free Radic. Biol. Med.* 132: 83–89.

Bailleul, A. M., et al. 2012. First evidence of dinosaurian secondary cartilage in post-hatching skull of *Hypacrosaurus stebingeri* (Dinosauria, Ornithischia). *PLoS One* 7(4): e36112. doi:10.1371/journal.pone.0036112.

Bausenhardt, D. 1951. Vergleichend-anatomische untersuchungen über die encoche d'ossification. *Anat. Anz.* 97(suppl): 223–230.

Behonick, D. J., Z. Werb. 2003. A bit of give and take: the relationship between the extracellular matrix and the developing chondrocyte. *Mech. Dev.* 120: 1327–1336.

Bell, D. M., et al. 1997. SOX9 directly regulates the type-II collagen gene, *Nat. Genet.* 16: 174–178.

Benjamin, M., E. J. Evans. 1990. Fibrocartilage. *J. Anat.* 171: 1–15.

Bonnan, M. F., et al. 2010. Calcified cartilage shape in archosaur long bones reflects overlying joint shape in stress-bearing elements: implications for non-avian dinosaur locomotion. *Anat. Rec.* 293: 2044–2055.

Bottini, M., et al. 2018. Matrix vesicles from chondrocytes and osteoblasts: their biogenesis, properties, functions and biomimetic models. *Biochim. Biophys. Acta Gen. Subj.* 1862: 532–546.

Boyde, A., S. J. Jones. 1983. Scanning electron microscopy of cartilage. In *Cartilage I: Structure, function and biochemistry*, ed. B. K. Hall, 105–148. New York: Academic Press.

Bridgewater, L. C., et al. 1998. Chondrocyte-specific enhancer elements in the Col11a2 gene resemble the Col2a1 tissue-specific enhancer, *J. Biol. Chem.* 273: 14998–15006.

Brocklehurst, R., et al. 1984. The composition of normal and osteoarthritic articular cartilage from tissue engineering zonal cartilage human knee joints. With special reference to unicompartmental replacement and osteotomy of the knee. *J. Bone Joint Surg. Am.* 66: 95–106.

Brody, L. T. 2015. Knee osteoarthritis: clinical connections to articular cartilage structure and function. *Phys. Ther. Sport.* 16(4): 301–316.

Bush, P. G., et al. 2008. The osmotic sensitivity of rat growth plate chondrocytes in situ: clarifying the mechanisms of hypertrophy. *J. Cell. Physiol.* 214: 621–629.

Calandruccio, R. A., et al. 1962. Proliferation, regeneration, and repair of articular cartilage of immature animals. *J. Bone Joint. Surg. Am.* 44: 431–455.

Calderon-Komaromy, A., et al. 2015. Osificacion bilateral del cartilage auricular. *Actas Dermosifiliogr.* 433–435.

Carballo, C. B., et al. 2017. Basic science of articular cartilage. *Clin. Sports Med.* 36: 413–425.

Chubinskaya, S., K. E. Kuettner. 2003. Regulation of osteogenic proteins by chondrocytes. *Int. J. Biochem. Cell Biol.* 35: 1323–1340.

Cole, A. G. 2011. A review of diversity in the evolution and development of cartilage: the search for the origin of chondrocyte. *Eur. Cells Mater.* 21: 122–129.

Cole, A. G., B. K. Hall. 2004. Cartilage is a metazoan tissue; integrating data from nonvertebrate sources. *Acta Zool.* 85: 69–80.

Cox, R. W., M. A. Peacock. 1977. The fine structure of developing elastic cartilage. *J. Anat.* 123(2): 283–296.

Cubo, J., et al. 2002. Heterochronic patterns in primate evolution: evidence from endochondral ossification. *Eur. J. Morphol.* 40(2): 81–88.

Culav, E. M., et al. 1999. Connective tissues: matrix composition and its relevance to physical therapy. *Phys. Ther.* 79(3): 308–319.

Day, T. F., et al. 2005. Wnt/betacatenin signaling in mesenchymal progenitors controls osteoblast and chondrocyte differentiation during vertebrate skeletogenesis. *Dev. Cell.* 8: 739–750.

Di Domenico, C. D., et al. 2018. Molecular transport in articular cartilage. What have we learned from the past 50 years. *Rheumatology*. 14: 393–403.

Dmitrovsky, E., et al. 1978. The characterization of the tidemark in human articular cartilage. *Metab. Bone Dis. Rel. Res.* 1: 115–118.

Dodds, G. S. 1930. Row formation and other types of arrangement of cartilage cells in endochondral ossification. *Anat. Rec.* 46: 385–399.

Duer, M. J, et al. 2009. The mineral phase of calcified cartilage: its molecular structure and interface with the organic matrix. *Biophys. J.* 96: 3372–3378.

Dupin, E., et al. 2018. The issue of the multipotency of the neural crest cells. *Dev. Biol*. 444: 847–859.

Eames B. F., R. A. Schneider. 2008. The genesis of cartilage size and shape during development and evolution. *Development*. 135: 3947–3958.

Eggli, P. S., et al. 1985. Matrix compartments in the growth plate of the proximal tibia of rats. *Anat. Rec.* 211: 246–257.

Elmore, S. 2007. Apoptosis. A review of programmed cell death. *Toxicol. Pathol*. 35: 495–516.

Ereinpresa, J., H. I. Roach. 1998. Aberrant death in dark chondrocytes of the avian growth plate. *Cell Death Differ.* 5: 60–66.

Eyre, D. R. 1988. Collagens of the disc. In *The biology of the intervertebral disc*, ed. P. Gosh, Vol. 1, 171–188. Boca Raton, FL. CRC press.

Eyre D., et al. 1988. Intervertebral disc. Part B. Basic science perspectives. In *New perspectives on low back pain*, eds. J. W. Frymoyer and S. L. Gordon, 147–207. Rosemont, IL: American Academy of Orthopaedic Surgeons.

Eyre, D. R., et al. 2006. Articular cartilage collagen: an irreplaceable framework? *Eur. Cell Mater.* 12: 57–63.

Farnum, C. E., N. J. Wilsman. 1989a. Cellular turnover at the chondro-osseous junction of the growth plate cartilage: analysis by serial sections at the light microscopical level. *J. Orthop. Res.* 7: 654–666.

Farnum, C. E., N. J. Wilsman. 1989b. Condensation of hypertrophic chondrocytes as the chondro-osseous junction of the growth plate cartilage swine: relationship to long bone growth. *Am. J. Anat.* 186: 346–358.

Flowers, S. A., et al. 2017. Lubricin binds cartilage proteins, cartilage oligomeric matrix protein, fibronectin and collagen II at the cartilage surface. *Sci. Rep.* 7(1): 13140. doi:10.1038/s41598-017-13558-y.

Fox, S., et al. 2009. The basic science of articular cartilage: structure, composition and function. *Orthopaedics*. 1: 461–468.

Francillon-Vieillot, H., et al. 1990. Microstructure and mineralization of vertebrate skeletal tissues. In *Skeletal biomineralization: patterns, processes and evolutionary trends*, ed. J. G. Carter, Vol. 20, 471–530. New York: Van Nostrand Reinhold.

Frank, E. H., A. J. Grodzinski. 1987. Cartilage electromechanics: I: Electrokinetic transduction and effect of electrolyte pH and ionic strength. *J. Biomech*. 20: 615–627.

Freyria, A. M., F. Mallein-Gerin. 2012. Chondrocytes or adult stem cells for cartilage repair: the indisputable role of growth factors. *Injury Int. J. Care Injured*. 43: 259–265.

Frisbie, D. D., et al. 2006. A comparative study of articular cartilage thickness in the stifle of animal species used in human preclinical studies compared to articular cartilage thickness in the human knee. *Vet. Comp. Orthop. Traumatol*. 3: 142–146.

Gabe, M. 1968. *Techniques histologiques*. Paris: Masson.

Galotto, M., et al. 1994. Hypertrophic chondrocytes undergo further differentiation to osteoblast-like cells and participate in the initial bone formation in developing chick embryo. *J. Bone Miner. Res*. 9: 1239–1249.

Gannon, A., et al. 2014. Postnatal changes to the mechanical properties of articular cartilage are driven by the evolution of its collagen network. *Eur. Cell Mater.* 29: 105–121.

Ghadially, F. N. 1983. *Fine structure of synovial joints*. London: Butterworth.

Goldring, M.B., et al. 2006. The control of chondrogenesis. *J. Cell. Biochem*. 97(1): 33–44.

Golstein, P., G. Kroemer. 2006. Cell death by necrosis: towards a molecular definition. *Trends Biochem. Sci.* 32: 37–43.

Gomez-Picos P., B. F. Eames. 2015. On the evolutionary relationship between chondrocytes and osteoblasts. *Front. Genet.* 6: 297–325.

Grässel, S., et al. 2012. Isolation, culture, and osteogenic/chondrogenic differentiation of bone marrow-derived mesenchymal stem cells. *Methods Mol. Biol*. 879, 203–267.

Hata, K. 2015. Epigenetic regulation of chondrocyte differentiation. *Jap. Dental Rev.* 51: 105–113.

Hall, B. K. 1983. *Cartilage. Development, differentiation, and growth*. New York: Academic Press.

Hall, B. K. 2005. Bones and cartilage. *Development and evolutionary skeletal biology*. New York: Elsevier.

Han, Y., V. Lefevre. 2008. L-Sox5 and Sox6 drive expression of the aggrecan gene in cartilage securing binding of Sox9 to a far-upstream enhancer. *Mol. Cell. Biol*. 28: 4999–5013.

Handley, C. J., et al. 1985. The structure and synthesis of proteoglycans of articular cartilage. *Cell Biol. Int. Rep.* 9: 753–782.

Handorf, A. M., et al.. 2014. Endogenously produced Indian hedgehog regulates TGF β-driven chondrogenesis of human bone marrow stroma/stem cells. *Stem Cells Dev.* 24: 995–1007.

Hill, T. P., et al. 2005. Canonical Wnt/betacatenin signaling prevents osteoblasts from differentiating into chondrocytes. *Dev. Cell*. 8: 727–738.

Hojo, H., et al. 2016. An emerging regulatory landscape for skeletal development. *Trends Genet*. 32(12): 774–787.

Holder, N. 1977. An experimental investigation into the early development of the chick elbow joint. *J. Embryol. Exp. Morphol*. 39: 115–127.

Horner, J. R., et al. 2000. Long bone histology of the hadrosaurid dinosaur *Maiasaura peeblesorum*: growth dynamics and physiology based on ontogenetic series of skeletal elements. *J. Vert. Paleontol*. 20: 115–129.

Hwang, H. S, H. A. Kim. 2015. Chondrocyte apoptosis in the pathogenesis of osteoarthritis. *Int. J. Mol. Sci.* 16 (11): 26035–26054.

Ikegawa, N., et al. 2016. Identification of genes required for the spontaneous repair of partial-thickness cartilage defects in immature rats. *Connect. Tissue Res*. 57(3): 190–199.

Iozzo, R.V. 1998. Matrix proteoglycans: from molecular design to cellular function. *Annu. Rev. Biochem*. 67: 609–652.

VetBooks.ir

Jay, G.D., et al. 2001. Homology of lubricin and zuperficial zone protein (SZP): products of megakaryocyte stimulating factor (MSF) gene expression by human synovial fibroblasts and articular chondrocytes localized to chromosome 1q25. *J. Orthop. Res.* 19: 677–687.

Jüppner, H. 2000. Role of parathyroid hormone-related peptide and Indian hedgehog in skeletal development. *Pediatr. Nephrol.* 14: 606–611.

Karaplis, A.C. 2002. Embryonic development of bone and the molecular regulation of intramembranous and endochondral bone formation. In *Principles of bone biology*, eds. Bilekizian, J.P., L. G. Raiz, G. A. Rodan. San Diego: Academic Press.

Karsenti, G., E.F. Wagner. 2002. Reaching a genetic and molecular understanding of skeletal development. *Cell*. 2: 389–406.

Katagiri, T., N. Takahashi. 2002. Regulatory mechanisms of osteoblast and osteoclast differentiation. *Oral Dis.* 8: 147–159.

Kemp, N.E., S.K. Westrin. 1979. Ultrastructure of calcified cartilage in the endoskeletal tesserae of sharks. *J. Morphol.* 160. 75–102.

Kheir, E., D. Shaw. 2009. Hyaline articular cartilage. *Orthop. Trauma*. 23(6): 450–455.

Kirsh, T., et al. 2000. Regulatory roles of zinc in matrix vesicle-mediated mineralization of growth plate cartilage. *J. Bone Miner. Res.* 15: 261–270.

Knese, K.H. 1980. Die Knorpelgefâsse und der Knochenkern. Der metamorphosierende Knorpel: II *Mitteilung. Gegenbaurs. Morphol. Jahrb.* 126: 86–101.

Knudson, C.B., W. Knudson. 2001. Cartilage proteoglycans. *Semin. Cell Dev. Biol.* 12: 69–78.

Kobayashi, T., et al. 2002. PTHrP and Indian hedgehog control differentiation of growth plate chondrocyte at multiple steps. *Development.* 129: 2977–2986.

Komori, T. 2015. The functions of Runx family transcription factors and Cbfb in skeletal development. *Oral Sci. Int.* 12: 1–4.

Kostovic-Knezevic, L., et al. 1981. Ultrastructure of elastic cartilage in the rat external ear. *Cell Tissue Res.* 218(1): 149–160.

Kouri, J.B., C. Lavalle. 2006. Do chondrocytes undergo "activation" and "transdifferentiation" during pathogenesis of osteoarthritis, A review of the ultrastructural and immunohistochemical evidence. *Histol. Histopathol.* 21: 793–802.

Kuettner, K.E., B.U. Pauli. 1983.In *Cartilage structure, function and biochemistry.* ed. B. K. Hall, 281–312. Academic Press: New York.

Kuhn, K., et al. 2003. Cell death in cartilage. *Osteoarthritis Cartilage*. 12: 1–16.

Kuratani et al. 2008. Embryonic development of bone and regulation of intramembranous and endochondral bone formation. In *Principles of bone biology*, 3rd edition, eds. Belizekian, P., L.G. Raisz and T.J. Martin. Amsterdam: Elsevier-Academic Press.

Leboy, P.S., et al. 1989. Ascorbic acid induces alkaline phosphatase, type X collagen, and calcium deposition in cultured chick chondrocytes. *J. Biol. Chem.* 264(29): 17281–17286.

Lefevre, V., et al. 2007. Control of cell fate and differentiation by Sry related high mobility-group box (Sox) transcription factors. *Int. J. Biochem. Cell Biol.* 39: 2195–2214.

Leong, D.J., et al. 2011. Physiological loading of joints prevents cartilage degradation through CITED2. *FASEB J.* 25(1): 182–191.

Leonore, C., et al. 1995. Normal cartilage structure, biochemistry, and metabolism: a review of the literature. *J. Oral Maxillofac. Surg.* 53: 924–929.

Liu, C.F., et al. 2017. Transcriptional control of chondrocyte specification and differentiation. *Semin. Cell Dev. Biol.* 62: 34–49.

Long, F. 2011. Building strong bones: molecular regulation of the osteoblast lineage. *Nat. Rev. Mol. Cell Biol.* 13 (1): 27–38.

Lyons, T.J., et al. 2005. The tidemark of the chondro-osseous junction of the normal human knee joint. *J. Mol. Histol.* 36:207–215.

Lyons, T.J., et al. 2006. The normal human chondro-osseous junctional region: evidence for contact of uncalcified cartilage with subchondral bone and marrow spaces. *BMC Musculoskelet. Discord.* 7–52.

Melrose, J., P. Ghosh 1988. The non-collagenous proteins of the intervertebral disc. In *The biology of the intervertebral disc*, Vol. 1, 189–237. Ed. Ghosh, P. Boca Raton, FL: CRC.

Mente, P.L., J.L. Lewis. 1994. Elastic modulus of calcified cartilage in an order of magnitude less than that of the subchondral bone. *J. Orthop. Res.* 12: 637–647.

Merrilees, M.J., M.H. Flint. 1980. Ultrastructural study of tension and pressure zones in a rabbit flexor tendon. *Am. J. Anat.* 157: 87–106.

Mescher, A. L. 2013. Cartilage. In *Junqueira's Basic histology: text and atlas*, 130–139. New York: McGraw-Hill Lange.

Mitrovic, D.R. 1977. Development of the metatarsophalangeal joint of the chick embryo: morphological, ultrastructural and histochemical studies. *Am. J. Anat.* 150: 333–347.

Morito, T.T. et al. 2008. Synovial-fluid derived mesenchymal stem cells increase after intra-articular injury in humans. *Rheumatology (Oxford).* 47: 1137–1143.

Mow, V.C., M. Rosewasser. 1988. Articular cartilage: biomechanics. In *Injury and repair to the musculoskeletal soft tissues*, eds. Woo, S.L.Y. and J.A. Buckwalter, 427–446. Rosemont, IL: American Academy of Orthopedic Surgeons.

Nagakawa, Y., et al. 2016. Cartilage derived from bone marrow mesenchymal cells expresses lubricin in vitro and in vivo. *PLoS One*. 11(2): e0148777. doi:10.1371/journal.pone.0148777.

Nikoletopoulo, V., et al. 2013. Crosstalk between apoptosis, necrosis and autophagy. *Biochem. Biophys. Acta*. 1833: 3448–3459.

Oegema Jr. T.R., et al. 1997. The interaction of the zone of calcified cartilage and subchondral bone in osteoarthritis. *Miscrosc. Res. Tech.* 37: 324–332.

Ohtani, K., et al. 2008. Expression of Sox and fibrillar collagen genes in lamprey larval chondrogenesis with implications for the evolution of vertebrate cartilage. *J. Exp. Zool.* 310: 596–607.

Ørvig T. 1951. Histologic studies of Placoderms and fossil Elasmobranchs. I. The endoskeleton, with remarks on the hard tissues of lower vertebrates in general. *Ark. Zool.* 2: 321–454.

Ørvig T. 1968. The dermal skeleton: General considerations. In *Current problems of lower vertebrate phylogeny*, ed. T. Ørvig, 373–397. Stockholm: Almqvist and Wiksell.

Ossa-Fuentes, L., et al. 2017. Microanatomy and osteohystology of a juvenile elasmosaurid plesiosaur from the upper Maastrichtian of Marambo (=Seymour) Island, Antarctica. *Bol. Mus. Nac. Hist. Nat.* 66 (2): 149–160.

Padian, K., E.T. Lamm (eds). 2013. *Bone histology of fossil tetrapods: advancing methods, analysis, and interpretation.* Berkeley, CA: University of California Press.

Pratta, M.A., et al. 2003. Aggrecan protects cartilage collagen from proteolytic cleavage. *J. Biol. Chem.* 278: 45539–455545.

Quilhac, A., et al. 2014. Globuli ossei in the long limb bones of *Pleurodeles waltl* (Amphibia, urodela, Salamandridae). *J. Morphol.* 0: 1–12.

Redman, S.N., et al. 2005. Current strategies for articular cartilage repair. *Eur. Cell Mater.* 9: 23–32.

Rey, C., et al. 1991. Structural studies of the mineral phase of calcifying cartilage. *J. Bone. Miner. Res.* 6: 515–521.

Ricqlès, A. de. 1972. Nature et signification des "surfaces épiphysaires" chez les tétrapodes fossiles. *C. R. Acad. Sci.* 274: 3527–3530.

Ricqlès, A. de. 1975. Recherches paléohistologiques sur les os longs de tétrapodes. Sur la classification, la signification fonctionnelle et l'histoire de tissus osseux des tétrapodes (première partie). *Ann. Paleontol.* 61: 51–129.

Ricqlès, A. de. and V. de Buffrénil. 2001. Bone histology, heterochronies and the return of tetrapods to life in water: where are we? In *Secondary Adaptation of Tetrapods to Life in Water*, Mazin J.-M. and V. de Buffrénil (eds.), 289–310. München: Verlag Dr. Friedrich Pfeil.

Roach, H.I., et al. 1998. Initiation of the bony epiphysis in long bone: chronology of interactions between the vascular system of the chondrocytes. *J. Bone Miner. Res.* 13: 950–961.

Roach H.I., et al. 2004. Chondroptosis: a variant of apoptotic cell death in chondrocytes? *Apoptosis.* 9: 265–277.

Roach, H.I., N.M.P. Clarke. 2000. Physiological cell death of chondrocytes in vivo is not confined to apoptosis. *J. Bone Joint Surg.* 82B: 601–613.

Roughley, P.J. 2001. Articular cartilage and changes in arthritis: non collagenous proteins and proteoglycans in the extracellular matrix of cartilage. *Arthritis Res.* 3(6): 342–347.

Sadatsuki, R., et al. 2016. Perlecan is required for the chondrogenic differentiation of synovial mesenchymal cells through regulation of sox9 gene expression. *J. Orthop. Res.* 35: 837–846.

Samsa, W.E., et al. 2017. Signaling pathways regulating cartilage growth plate formation and activity. *Semin. Cell Dev. Biol.* 62: 3–15.

Schaffer, J. 1930. Das Stutzgewebe. 1-314. In *Handbuch der mikroskopischen*, ed. Mollendorff W.v., Anatomie des Menschen. Bd.II/2. Berlin: Springer Verlag.

Schwarz, D., et al. 2007. Super sizing the giants: first cartilage preservation of a sauropod limb joint. *J. Geol. Soc.* 164: 61–65.

Sekiya, I., et al. 2012. Human mesenchymal stem cells in synovial fluid increase in the knee with degenerated cartilage and osteoarthritis. *J. Orthop. Res.* 30: 943–949.

Seyer, J.M., et al. 1974. Identification of two types of collagen in articular cartilage of postnatal chickens. *Calcif. Tissue Res.* 17: 43–55.

Shapiro, I.M., et al. 2005. Fate of the hypertrophic chondrocyte: microenvironmental perspectives on apoptosis and survival in the epiphyseal growth plate. *Birth Defects Res. C Embryo Today.* 75: 330–339.

Silvestrini, G., et al. 1979. Resorption of uncalcified cartilage in the diaphysis of the chick embryo tibia. *Cell Tissue Res.* 196: 221–235.

Solchaga, L.A., et al. 2011. Chondrogenic differentiation of bone marrow derived mesenchymal stem cells: tips and tricks. *Methods Mol. Biol.* 698: 253–278.

Sorell, J.M., L. Weiss. 1980. A light and electron microscopic study of the region of cartilage resorption in the embryonic chick femur. *Anat. Rec.* 198: 513–530.

Sun, Y., et al. 2017. The role of laminins in cartilaginous tissues: from development to regeneration. *Eur. Cells Mater.* 34: 40–54.

Svajger, A. 1970. Chondrogenesis in the external ear of the rat. *Z. Anat. Entwicklungsgesch.* 131: 236-242.

Thomas, C.M., et al. 2007. Chondrocyte death by apoptosis is associated with cartilage matrix degradation. *Osteoarthritis Cartilage.* 15: 27–34.

Von der Mark, K., H. Von der Mark. 1977. The role of three genetically distinct collagen types in endochondral ossification and calcification cartilage. *J. Bone Joint Surg.* 59: 458–464.

Wang, F., et al. 2009. Histomorphometric analysis of adult articular calcified cartilage zone. *J. Struct. Biol.* 168 (3): 359–365.

White, A., G. Wallis. 2001. Endochondral ossification: a delicate balance between growth and mineralisation. *Curr. Biol.* 11(15): 589–591.

Wilsman, N.J, et al. 1981. Ultrastructure evidence of a functional heterogeneity among physeal chondrocytes in growing swine. *Am. J. Vet. Res.* 42: 1547–1553.

Woo, S., et al. 1988. Ligament, tendon and joint capsule insertions to bone. In *Injury and repair of the musculoskeletal soft tissues*, eds. Woo S.L.Y. and J. A. Buckwalter, 133–166. Rosemont, IL: American Academy of Orthopaedic Surgeons.

Wuelling, M., A. Vortkamp. 2010. Transcriptional networks controlling chondrocyte proliferation and differentiation during endochondral ossification. *Pediatr. Nephrol.* 25: 625–631.

Wuthier, R.E., et al. 1985. Isolation and characterization of calcium-accumulating matrix vesicles from chondrocytes of the chicken epiphyseal growth plate cartilage in primary culture. *J. Biol Chem.* 260: 15972–15979.

Yamada, H. 1970. *Strength of biological materials.* Baltimore: Williams & Wilkins.

Yoshida C.A. 2004. Runx2 and Runx3 are essential for chondrocyte maturation, and Runx2 regulates limb growth through induction of *Indian hedgehog. Genes Dev.* 18: 952–963.

Zelenski, N.A., et al. 2015. Type VI collagen regulates pericellular matrix properties, chondrocyte swelling, and mechanotransduction in mouse articular cartilage. *Arthritis Rheumatol.* 67(5): 1286–1294.

Zhang, G.J., et al. 2009. Evolution of vertebrate cartilage development. *Curr. Top. Dev. Biol.* 86: 15–42.

Zhao, G.Z., et al. 2016. Effect of platelet-derived growth factor on chondrocyte proliferation, migration and apoptosis via regulation of GIT1 expression. *Mol. Med. Rep.* 14: 897–903.

Zhen, G., et al. 2013. Inhibition of TGF β signalling in mesenchymal stem cells of subchondral bone attenuates osteoarthritis. *Nat. Med.* 19(6): 704–712.

Zimny, M.L. 1988. Mechanoreceptors in articular tissues. *Am. J. Anat.* 182: 16–32.

Zylberberg, L., F.J. Meunier. 2008. New data on the structure and chondrocyte populations of haemal cartilage of the abdominal vertebrae in the adult carp *Cyprinus carpio* (Ostariophysii, Cyprinidae). *Cybium.* 32: 225–239.

VetBooks.ir

Methodological Focus C

Virtual (Paleo-)Histology Through Synchrotron Imaging

Sophie Sanchez, Dennis F. A. E. Voeten, Damien Germain and Vincent Fernandez

CONTENTS

Introduction 139
Principles of Synchrotron Radiation 139
Phase-Contrast Imaging 140
Principle 140
Applications to Virtual Histology 140
Facilities Available for Virtual Histology Using Phase-Contrast Imaging 141
(Micro-)Anatomy 141
Histology and Microstructure 144
Molecular Biology and Ultrastructure 144
Tomography Combined with Various Techniques 144
Principle 144
Applications to Virtual Histology 144
Facilities Available for Virtual Histology Through SAXS or XRD-CT 145
Prospects for The Field 145
Acknowledgments 145
References 145

Introduction

Toward the end of the 20th century, progressive development of high-resolution imaging methods using powerful X-ray sources enabled virtual histological study of mineralized tissues. Numerous incentives drove the establishment and improvement of virtual histology. Biomedical researchers first started collaborating with physicists and mathematicians to develop three-dimensional (3D) imaging for reliably investigating 3D bone microstructures of their patients in great detail (Peyrin 2009). Paleontologists then recognized the potential of these methods for revealing dental and osseous microstructures in crucial vertebrate fossils that could not be physically sectioned (Tafforeau et al. 2006; Sanchez et al. 2012). Although modern and fossilized bones have markedly different material properties, X-ray computed tomography (CT) protocols should follow the same principles for comparative purposes. Because high-resolution imaging of large and/or dense samples is particularly challenging with conventional X-ray sources (e.g., laboratory or hospital CT scanners; Tafforeau et al. 2006; see "Methodological Focus A: The New Scalpel: Basic Aspects of CT-Scan Imaging"), synchrotron-based imaging techniques were developed. In this chapter, we detail the most common methods used so far.

Principles of Synchrotron Radiation

Synchrotron radiation is an electromagnetic radiation that is produced when a charged particle is accelerated in a curved path. Synchrotron facilities are particle accelerators aiming at generating synchrotron radiation usually by using electrons as charged particles (for more information see Kim et al. 2017). An electron gun delivers electrons to a booster where they reach an energy of several billion electronvolts. Accelerated electrons are then directed into the storage ring as discrete series of bunches. One of the aims of the storage ring is to preserve the overall conditions of the electrons by maintaining a constant energy and keeping the bunches focused, avoiding dispersal of the electrons. Various types of magnets guide the electrons along curved trajectories to excite synchrotron radiation. The simplest magnets used are long dipole bending electromagnets that curve the path of electrons. More complex magnets, called insertion devices, consist of a series of

VetBooks.ir

dipole electromagnets that create an undulating path for the electrons. Because the intensity of the synchrotron radiation depends on the degree of curvature, an undulating path generates a radiation several orders of magnitude more intense than a simple curve.

Synchrotron radiation (also called synchrotron light) comprises a wide spectrum ranging from microwaves to X-rays. Synchrotron facilities mostly produce X-rays, although some facilities also channel other types of radiation such as infrared. Once generated, the X-ray beam is channeled into laboratories (colloquially known as *beamlines*), tangentially plugged to the storage ring. Beamlines are equipped with detector and optical setups that register the various types of interactions of X-rays with matter. Among many convenient properties, the generated X-ray beams exhibit high brilliance and a wide energy range. The brilliance describes the flux (number of photons going through an area per second) and the divergence of the beam. In a synchrotron beamline, the beam has a high flux and a low divergence that helps to concentrate all the X-rays into a narrow beam. The wide range of energy allows the investigation of diverse samples, with either low or high density.

Synchrotrons are among the most powerful sources of high-energy X-ray radiation suitable for penetration of dense samples and high-resolution visualization. The brilliance of the light emitted in a synchrotron is about 10^{10} times higher than in a conventional micro-CT scanner (Peyrin 2009). Generations of synchrotrons have succeeded each other, and each new iteration has marked a significant leap in brilliance. Currently most facilities are third-generation synchrotrons. High-resolution virtual dental and bone histology (e.g., Tafforeau et al. 2006; Sanchez et al. 2012; Peyrin 2009; Giles et al. 2013; Davesne et al. 2020) was developed using a third-generation synchrotron such as the European Synchrotron Radiation Facility (ESRF; France), the Swiss Light Source (SLS; Switzerland) and the Diamond Light Source (Diamond; UK). The various imaging beamlines installed in these synchrotrons provide different ranges of energy, beam properties and optical resolutions. This experimental diversity not only allows multiscale investigations (Tafforeau et al. 2007; Müller 2009), but also inspires and enables the development of new investigative tools (Dierolf et al. 2010; Langer et al. 2012; Peyrin et al. 2014; Mürer et al. 2018).

Phase-Contrast Imaging

Principle

Traditional X-ray radiography and CT rely on the attenuation of the X-ray beam by the sample. The created pattern reflects on the composition of the sample but does not distinguish among materials with similar densities. Phase contrast is an effect resulting from a property of light called coherence, which indicates how light waves remain constant in space and time. Temporal coherence reflects the way in which waves conserve their frequency and amplitude, while spatial coherence describes the shape of the wavefront: the more planar the wavefront, the higher the spatial coherence. Waves of synchrotron radiation have a high spatial coherence compared to more classic X-ray sources (e.g., laboratory or hospital X-ray CT) (Snigirev et al. 1995; Wilkins et al. 1996). Once the beam penetrates a sample, the interactions with the medium(s) perturb the wavefront. This disruption of the wavefront creates a phase shift, and this results in interference patterns that highlight local changes in density (Snigirev et al. 1995). Classic X-ray CT and radiography rely on the attenuation of the X-ray beam by the sample. The attenuation depends on the composition of the sample and cannot distinguish among materials with very similar densities. Depending on the energy, phase contrast can be a thousand times more sensitive in discerning material densities (Snigirev et al. 1995; Baruchel et al. 2006). Although phase-contrast imaging can be performed with any type of X-ray source, the high degree of coherence of the synchrotron beam improves the observation of interference fringes when the distance between the sample and the detector is increased (Baruchel et al. 2006; Tafforeau et al. 2006). Different techniques exploit this phenomenon, including phase-contrast microradiography (Wilkins et al. 1996), propagation phase-contrast synchrotron radiation microtomography (PPC-SRμCT) (Cloetens et al. 1996; Lak et al. 2008), holotomography where both attenuation and phase contrast are informative (Cloetens et al. 1999), grating-based X-ray phase tomography (Zanette et al. 2011; Gradl et al. 2016), speckle-based X-ray phase tomography (Zdora et al. 2020) and ptychography where phase contrast is combined with scattering (Dierolf et al. 2010).

Applications to Virtual Histology

Individual mineralized elements can be studied using a multiscale approach (Tafforeau et al. 2007; Müller 2009; Sanchez et al. 2012) that resolves features at the organ level, the microanatomical level and the histological level in two and three dimensions (2D and 3D) (Figure C.1).

Multiple virtual thin sections (VTS) can be produced from a single tomographic data set. These can be extracted at each desired thickness and in any required orientation (Figure C.2).

With a voxel (i.e., 3D pixel) size of 0.7 μm (or smaller), such VTS reveal the same structures as traditional thin sections using a microscope under natural light (Figure C.3). High-resolution virtual dental and bone histology greatly benefit from the phase-contrast effect when identifying and characterizing vascular canals, cell lacunae, lines of arrested growth and cementing lines (Tafforeau and Smith 2008; Sanchez et al. 2012). Provided that the resolution is sufficiently high (i.e., at voxel sizes below 0.7 μm), the fibril texture of the bone matrix (Langer et al. 2012) and muscle-fiber lacunae – often referred to as Sharpey's fibers – (Sanchez et al. 2013a) may be resolvable as well. Cell canaliculi may be imaged using ptychography at high resolutions (Dierolf et al. 2010). However, contrary to polarized-light microscopy, bone-matrix apatite crystals cannot be visualized in a VTS using phase-contrast imaging (Figure C.3).

In summary, all types of mineralized microstructures (apart from apatite crystals) can be visualized using synchrotron light with phase-contrast imaging. They can be segmented to be rendered in 3D (Figure C.4).

Virtual models allow the quantification of volumes (e.g., cell-lacunar volumes, Figure C.4; Sanchez et al. 2014, and

VetBooks.ir

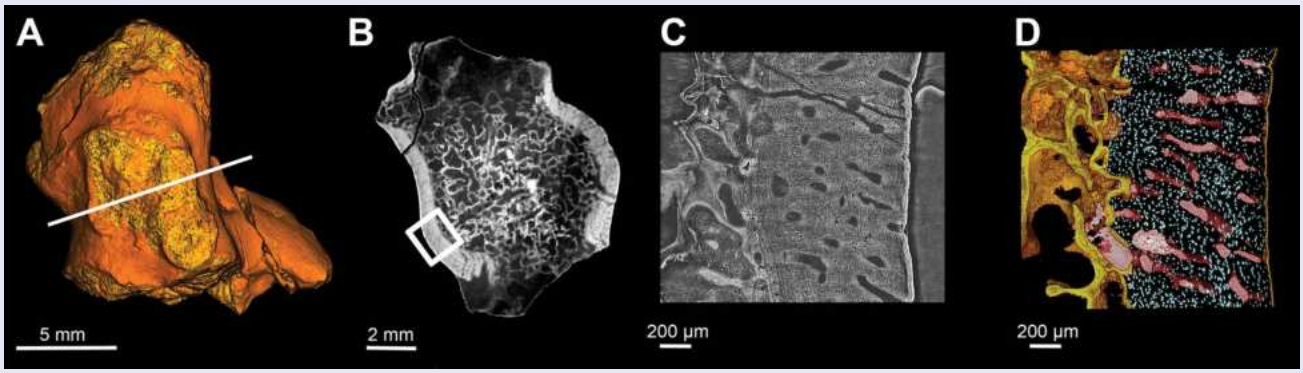


FIGURE C.1 Multiscale approach showing the 3D morphology and internal microstructure of the humerus of a 380 million-year-old finned stem tetrapod (*Eusthenopteron foordi*) as the result of propagation phase-contrast synchrotron radiation microtomography. A, 3D model showing the external morphology of the humerus (voxel size: 20 µm). B, Transverse virtual thin section at midshaft of the bone exhibiting microanatomy (voxel size: 5 µm). C, Virtual thin section of the midshaft cortex of the bone revealing the microstructure of the bone (voxel size: 0.7 µm). D, 3D model of the bone microstructure (voxel size: 0.7 µm): vascular canals in pink, cell lacunae in blue and surfaces of the bone including the trabecular surface in gold.

vascular volumes; Figure C.5) or orientations (Figure C.6) (Sanchez et al. 2013a). These quantified parameters greatly complement, refine and incidentally even rectify insights gleaned from 2D information (Prondvai et al. 2014; Stein and Prondvai 2014).

For example, even though two transverse bone cross-sections from different species can exhibit rather similar vascular orientations, the true 3D organization may strongly differ in degrees of anastomosis and longitudinal patterning (Figure C.7). Bone porosity or lacunar density can also be quantified with precision (Peyrin et al. 2014).

Finally, in data obtained using a monochromatic beam (i.e., a very narrow range of energy, typically within $\pm 10^{-2}$ keV), the degree of tissue mineralization can be accurately determined using phase-contrast parameters (Nuzzo et al. 2002), grating-based phase contrast (Gradl et al. 2016) or ptychography (Dierolf et al. 2010).

Facilities Available for Virtual Histology Using Phase-Contrast Imaging

(Micro-)Anatomy

All synchrotron facilities with tomographic beamlines are suitable for imaging bones and teeth at the (micro-) anatomical scale. Some microtomographic beamlines, such as ID19 at the ESRF, are more suitable for imaging relatively small samples (Tafforeau et al. 2006; Sanchez et al. 2012) than others (e.g., ID17, Houssaye et al. 2015; BM05, Voeten et al. 2018b and BM18 of the ESRF-EBS – Extremely Brilliant Source). Different protocols were developed for various unconventional nonhomogeneous samples (e.g., dense samples, Sanchez et al. 2013b; flat samples, Houssaye et al. 2011 and Voeten et al. 2018b and inherently low-contrast samples, Voeten et al. 2018a). The voxel sizes used in these applications typically range between circa 5 and 50 µm.

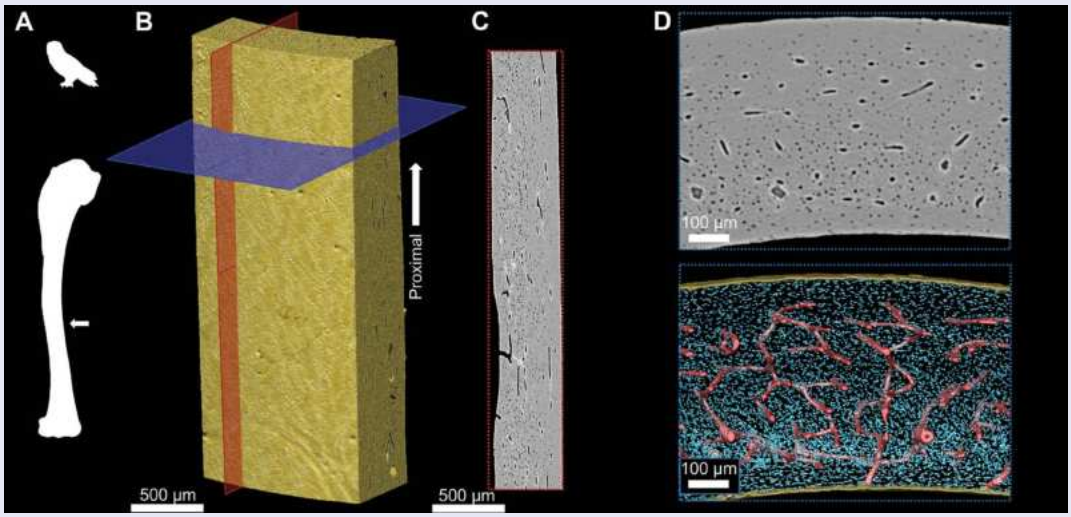


FIGURE C.2 Virtual thin sectioning allows multiple orientation visualization. A, Silhouettes of *Strix* and its humerus with the location where the tomography was performed, not to scale. B, 3D bloc of the humeral cortex at midshaft indicating the possibility of performing virtual thin sections in different orientations at different locations. C, Example of a longitudinal virtual thin section revealing the microstructure of the cortex of *S. aluco* humerus at mid-diaphysis. D, Example of a transverse section with the corresponding 250-µm-thick 3D rendering (vascular canals are in pink, cell lacunae are in blue and cortical surfaces are in gold).

VetBooks.ir

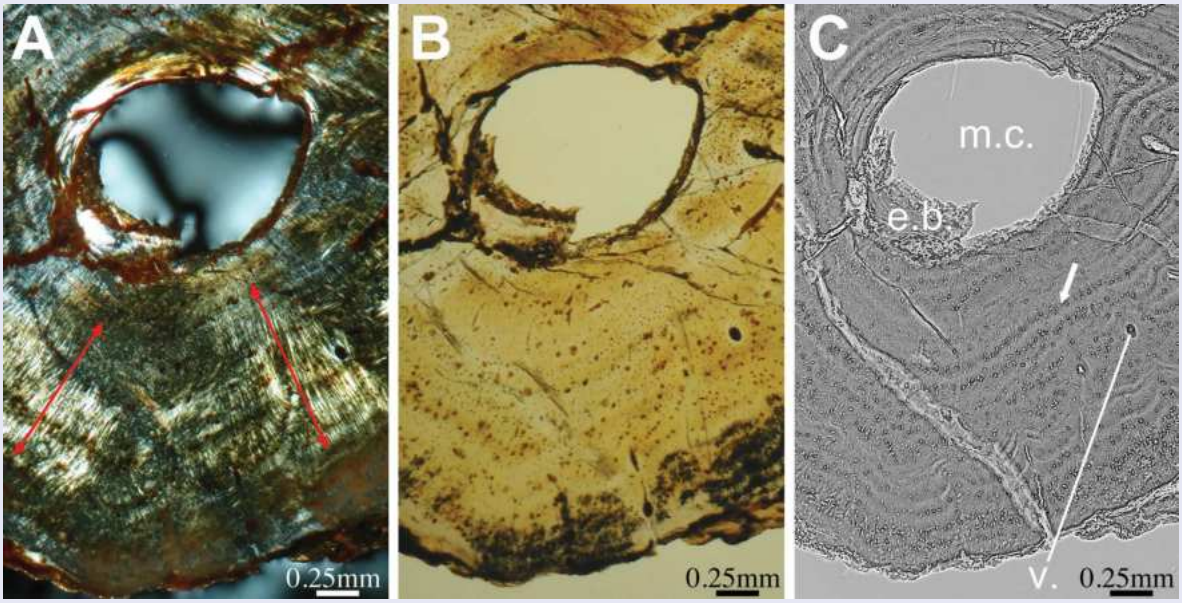


FIGURE C.3 Comparison between traditional and virtual thin sections based on a transverse section made in the tibia of *Discosauriscus austriacus*. A, Thin section observed with polarized light revealing the crystallite organization of the bone matrix and bundles of extrinsic fibers (red arrows). B, Thin section observed with natural light revealing the microstructure of the cortical bone (cell lacunae, vascularization and lines of arrested growth). C, Phase-contrast based microradiography showing the vascularization (v.), lines of arrested growth (white arrow) and the medullary cavity (m.c.) surrounded by the endosteal bone (e.b.).

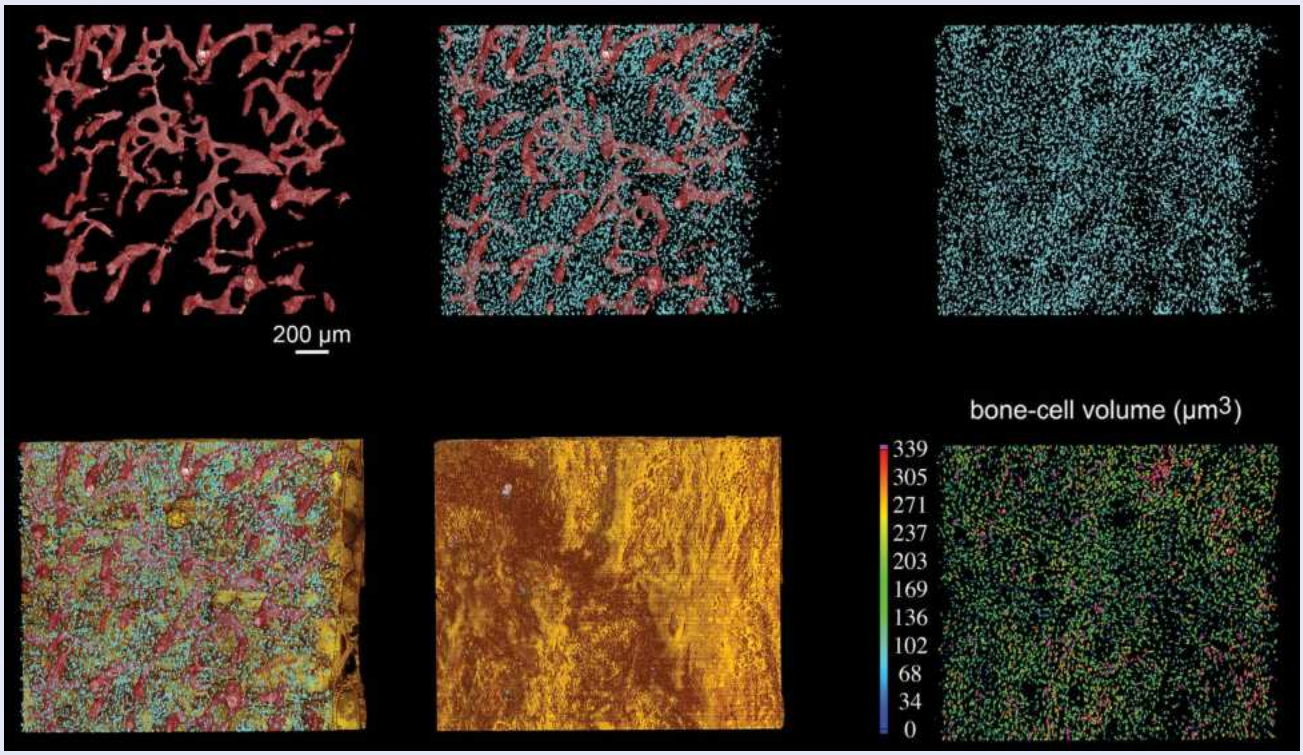


FIGURE C.4 Multiple 3D high-resolution models of the humeral midshaft of *Eusthenopteron foordi* created from data obtained with propagation phase-contrast synchrotron radiation microtomography, showing the flexibility of the technique to visualize the bone microstructures in different contexts: vascularization in pink, cell lacunae in blue and bone surfaces in gold. This technique also allows the quantification of volumes (e.g., cell lacunae).

VetBooks.ir

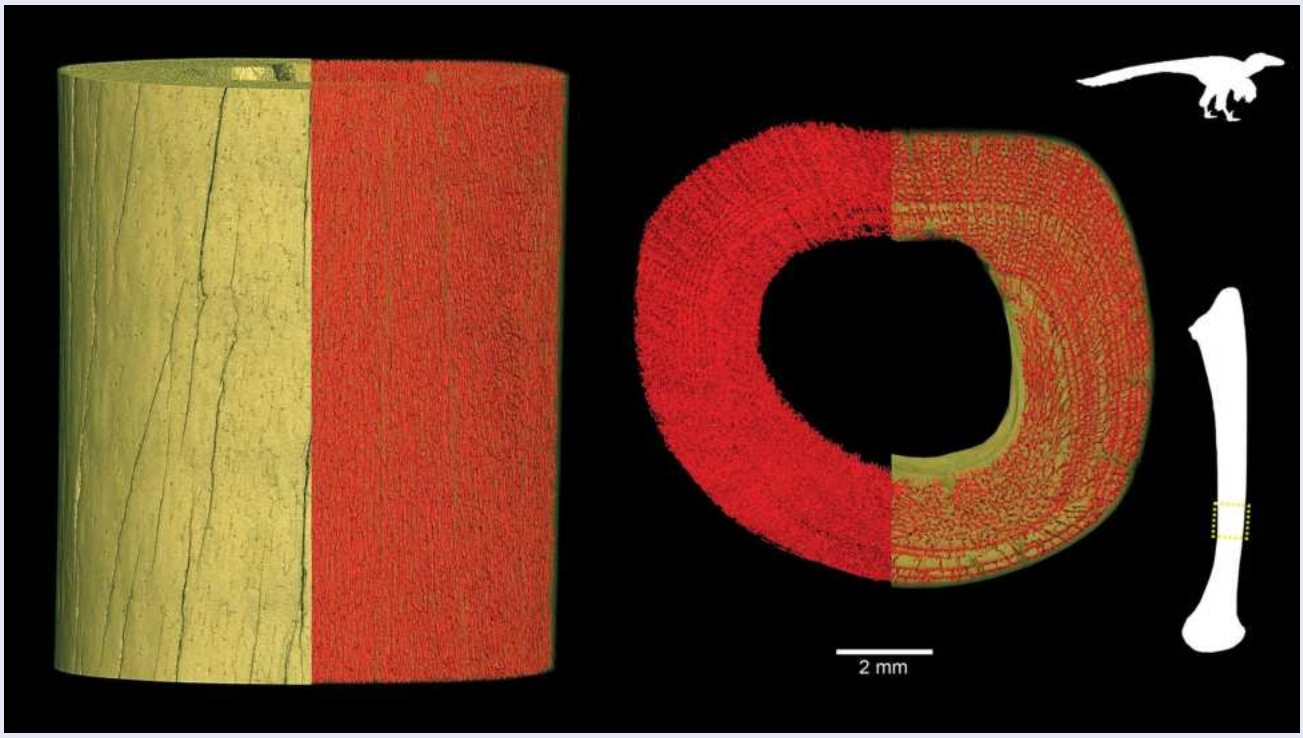


FIGURE C.5 A 3D model of the vascularization in the ulna of *Deinonychus* (silhouette of the extinct animal to the top right of the figure) from propagation phase-contrast synchrotron microtomography in longitudinal and transverse views. The yellow dotted square on the silhouette of the ulna (on the right of the figure) indicates the location where the scan was made (not to scale).

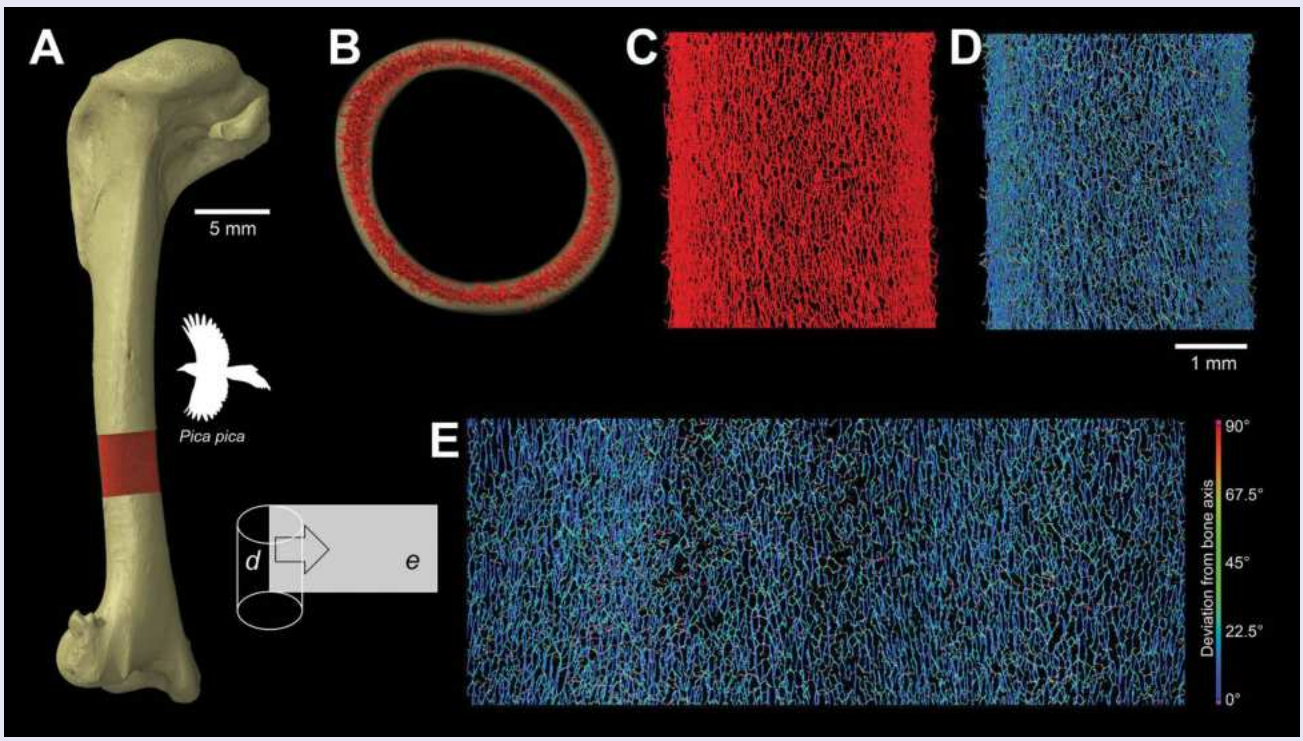


FIGURE C.6 A 3D quantification of the vascular orientation in the humerus of *Pica pica* based on propagation phase-contrast synchrotron microtomography. A, Humerus and silhouette of *P. pica*. B, Virtual cross section in the diaphysis of the humerus. C, Longitudinal view of the diaphyseal vascularization in the same location as B. D, Color-coded quantification of the longitudinality of the vascular mesh modeled in C. E, Unrolled cortex allowing the color-code quantification of both the longitudinality and circularity of the vascular mesh.

VetBooks.ir

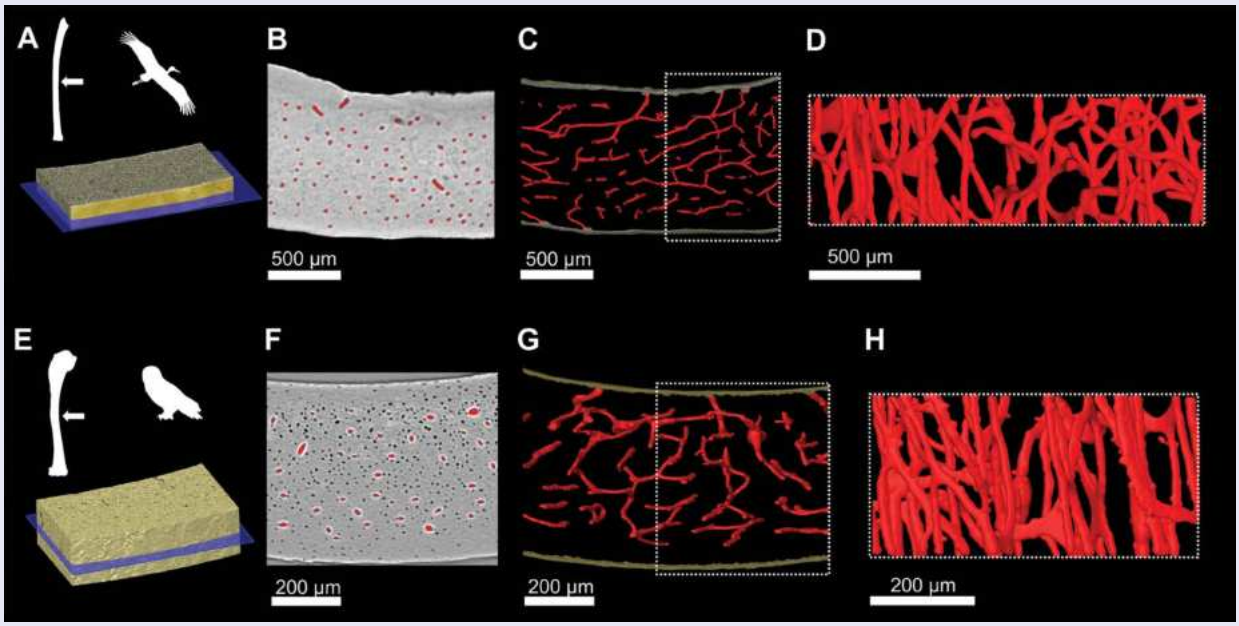


FIGURE C.7 A 2D versus 3D histology using propagation phase-contrast synchrotron radiation microtomography. A, Silhouettes of *Ciconia* and its ulna with virtual sample location indicated, not to scale. B, Virtual thin section in the cortex of *C. ciconia* ulna at mid-diaphysis in proximal view showing predominantly subcircular canal cross sections (indicated in red) suggesting a largely longitudinal plexus. C, A 250-µm-thick 3D rendering of the canal plexus showing a more complex mesh than expected. D, A 3D rendering of the canal plexus in longitudinal view revealing the numerous transverse anastomoses. E, Silhouettes of *Strix* and its humerus with virtual sample location indicated, not to scale. F, Virtual thin section in the cortex of *S. aluco* humerus at mid-diaphysis in proximal view showing predominantly subcircular canal cross sections (indicated in red) among osteocyte lacunae, suggesting a largely longitudinal plexus as in B. G, A 250-µm-thick 3D rendering of the canal plexus showing a different plexus organization than in C. H, A 3D rendering of the canal plexus in longitudinal view revealing an unexpected higher density of longitudinal canals than in D.

Histology and Microstructure

ID19 and ID16 (ESRF) (Tafforeau and Smith 2008; Dierolf et al. 2010; Sanchez et al. 2012, 2013a), Tomcat (SLS) (Giles et al. 2013) and I13-2 (Diamond) (Davesne et al. 2020) are beamlines optimized for microtomography through configurations that facilitate virtual (paleo-) histological investigations. These beamlines vary according to the levels of resolution and energy available. ID19 and Tomcat can achieve voxel sizes from 0.6 to 0.7 µm for samples measuring a couple of centimeters; I13-2 and ID19 can achieve 0.33 and 0.14 µm for samples smaller than 1 cm and ID16A and B, both being true nanotomographic beamlines, can reach 25 and 50 nm, respectively, for samples smaller than 1 mm.

Molecular Biology and Ultrastructure

Tomographic visualization of molecular ultrastructures is currently only possible at the nanotomographic beamline ID16A (ESRF), where a voxel size down to 25 nm can be reached (Langer et al. 2012).

Tomography Combined with Various Techniques

Principle

As mentioned above, even though phase-contrast imaging can reveal the microstructure of mineralized tissues, it fails to reveal their crystallite 3D organization. Toward accomplishing this, new developments combine attenuation-based tomography with diffraction and scattering techniques (Schaff et al. 2015; Mürer et al. 2018; Mürer et al. 2021). Diffraction techniques, such as X-ray diffraction CT (XRD-CT), can detect crystals measuring only a few micrometers/nanometers and reliably reveal their geometry, orientation and nature (Mürer et al. 2018; Mürer et al. 2021). Scattering techniques, such as small-angle X-ray scattering (SAXS), can provide the orientation of collagen fibers (Schaff et al. 2015).

Applications to Virtual Histology

SAXS tomography recently revealed, for the first time, the 3D orientation of collagen fibers in the dentine of a tooth (Schaff et al. 2015) and may also be applied to other mineralized tissues such as bone (Rinnerthaler et al. 1999) and cartilage (Moger et al. 2007). This is of great interest for (1) understanding the pattern of bone matrix deposition through the 3D organization of collagen fibers and (2) identifying extrinsic fibers (e.g., Sharpey's fibers) to locate muscle insertions on bones (Hieronymus 2006; Sanchez et al. 2013a; Mürer et al. 2018).

XRD-CT recently revealed the 3D orientation of apatite crystals across an entire fossil bone (Mürer et al. 2018) and the mineralisation front of a piglet's femur (Mürer et al. 2021) which permitted investigations into the process of bone mineralization. In addition, because the arrangement of apatite crystals is intimately related to that of collagen fibers (Bromage et al. 2003; Georgiadis et al. 2016), the 3D

VetBooks.ir

organization of the collagen matrix can be indirectly inferred as well. During fossilization, the mineral composition of bones often alters; this technique also permits the identification and localization of crystallite elements incorporated into the fossil bone (Mürer et al. 2018).

Facilities Available for Virtual Histology Through SAXS or XRD-CT

Among other techniques, SAXS tomography can be performed at the beamline cSAXS (SLS), and experiments involving XRD-CT can be carried out at the beamline ID15 (ESRF).

Prospects for The Field

These recently developed state-of-the-art techniques pave the way for realizing new opportunities in the field of (paleo-) histology. Because bones are 3D organs with an intricate spatial architecture, traditional 2D thin sections only reveal limited insight into their microstructural arrangement (e.g., Sanchez et al., 2012; Stein and Prondvai 2014). Our understanding of the 3D complexity of, e.g., the vascular mesh and trabecular organizations, would greatly benefit from comparative analyses in (quantitative) 3D virtual bone histology.

Synchrotron facilities also present certain limitations. For example, it is not conceivable to image an entire bone as large as a sauropod femur at submicron resolution due to (1) the large amount of data that would be generated and (2) the time it would take to perform such experiments. Nevertheless, the rapid development of synchrotron-beam power, optical instruments, processing and storage solutions will continue to alleviate particular hurdles. Notably, the fourth generation of synchrotrons has recently emerged, and includes MAX IV (Sweden) and the ESRF-EBS (upgraded version of the ESRF, France). This new generation of facilities should offer a significant leap in image quality, notably for virtual histology of dense tissues, but are yet to be tested in this domain. In addition, the combination of different techniques that emerge from a fruitful environment in which physicists, biologists and paleontologists intensively collaborate promises great technological advancements that will benefit the ever-evolving field of (paleo-)histology.

Acknowledgments

This project was supported by two stipends from the Wenner-Gren Foundations (grants UPD2018-0250 and UPD2019-0076, D.F.A.E.V. and S.S.), as well as two grants from the Vetenskapsrådet (2015-04335 and 2019-04595, S. S.). Scan data were produced using beamtime allocated by the European Synchrotron Radiation Facility (ESRF) through accepted proposals (EC203, EC519 and EC1017) and in-house beamtime (D.F.A.E.V., P. Tafforeau). We thank P. Tafforeau and M. di Michiel (ESRF) for their help performing experiments. We are grateful to the editorial board of this book, who helped to edit this chapter.

REFERENCES

Baruchel, J., et al. 2006. Advances in synchrotron radiation microtomography. *Scripta Mater.* 55: 41–46.

Bromage, T. G., et al. 2003. Circularly polarized light standards for investigations of collagen fiber orientation in bone. *Anat. Rec. Part B* 274: 157–168.

Cloetens, P., et al. 1996. Phase objects in synchrotron radiation hard x-ray imaging. *J. Phys. D Appl. Phys.* 29: 133.

Cloetens, P., et al. 1999. Holotomography: quantitative phase tomography with micrometer resolution using hard synchrotron radiation x rays. *Appl. Phys. Lett.* 75: 2912–2914.

Davesne, D., et al. 2020. Three-dimensional characterization of osteocyte volumes at multiple scales, and its relationship with bone biology and genome evolution in ray-finned fishes. *J. Evolution. Biol.* 33: 808–830.

Dierolf, M., et al. 2010. Ptychographic X-ray computed tomography at the nanoscale. *Nature* 467: 436–440.

Georgiadis, M., et al. 2016. Techniques to assess bone ultrastructure organization: orientation and arrangement of mineralized collagen fibrils. *J. Roy. Soc. Interface* 13: 20160088.

Giles, S., et al. 2013. Histology of "placoderm" dermal skeletons: Implications for the nature of the ancestral gnathostome. *J. Morphol.* 274: 627–644.

Gradl, R., et al. 2016. Mass density measurement of mineralized tissue with grating-based x-ray phase tomography. *PLoS One* 11: e0167797.

Hieronymus, T. L. 2006. Quantitative microanatomy of jaw muscle attachment in extant diapsids. *J. Morphol.* 267: 954–967.

Houssaye, A., et al. 2015. Transition of Eocene whales from land to sea: evidence from bone microstructure. *PLoS One* 10: e0118409.

Houssaye, A., et al. 2011. Three-dimensional pelvis and limb anatomy of the Cenomanian hind-limbed snake *Eupodophis descouensi* (Squamata, Ophidia) revealed by synchrotron-radiation computed laminography. *J. Vertebr. Paleontol.* 31: 2–7.

Kim, K.-J., et al. 2017. *Synchrotron radiation and free-electron lasers*. Cambridge, UK: Cambridge University Press.

Lak, M., et al. 2008. Phase contrast X-ray synchrotron imaging: opening access to fossil inclusions in opaque amber. *Microsc. Microanal.* 14: 251–259.

Langer, M., et al. 2012. X-ray phase nanotomography resolves the 3D human bone ultrastructure. *PLoS One* 7:e35691.

Moger, C. J., et al. 2007. Regional variations of collagen orientation in normal and diseased articular cartilage and subchondral bone determined using small angle X-ray scattering (SAXS). *Osteoarthritis Cartilage* 15: 682–687.

Müller, R. 2009. Hierarchical microimaging of bone structure and function. *Nat. Rev. Rheumatol.* 5: 373–381.

Mürer, F. K., et al. 2018. 3D maps of mineral composition and hydroxyapatite orientation in fossil bone samples obtained by x-ray diffraction computed tomography. *Sci. Rep.* 8: 10052.

Mürer, F.K., et al. 2021. Quantifying the hydroxyapatite orientation near the ossification front in a piglet femoral condyle using X-ray diffraction tensor tomography. Sci Rep 11, 2144. https://doi.org/10.1038/s41598-020-80615-4

VetBooks.ir

Nuzzo, S., et al. 2002. Synchrotron radiation microtomography allows the analysis of three-dimensional microarchitecture and degree of mineralization of human iliac crest biopsy specimens: effects of etidronate treatment. *J. Bone Miner. Res.* 17: 1372–1382.

Peyrin, F. 2009. Investigation of bone synchrotron radiation imaging: from micro to nano. *Osteoporosis Int.* 20: 1057–1063.

Peyrin, F., et al. 2014. Micro-and nano-CT for the study of bone ultrastructure. *Curr. Osteoporos. Rep.* 12: 465–474.

Prondvai, E., et al. 2014. Development-based revision of bone tissue classification: the importance of semantics for science. *Biol. J. Linn. Soc.* 112: 799–816.

Rinnerthaler, S., et al. 1999. Scanning small angle X-ray scattering analysis of human bone sections. *Calcified Tissue Int.* 64: 422–429.

Sanchez, S., et al. 2012. Three dimensional synchrotron virtual paleohistology: a new insight into the world of fossil bone microstructures. *Microsc. Microanal.* 18: 1095–1105.

Sanchez, S., et al. 2013a. 3D microstructural architecture of muscle attachments in extant and fossil vertebrates revealed by synchrotron microtomography. *PLoS One* 8:e56992.

Sanchez, S., et al. 2013b. Homogenization of sample absorption for the imaging of large and dense fossils with synchrotron microtomography. *Nat. Protoc.* 8: 1708–1717.

Sanchez, S., et al. 2014. The humerus of *Eusthenopteron*: a puzzling organization presaging the establishment of tetrapod limb bone marrow. *Proc. Roy. Soc. B* 281: 20140299.

Schaff, F., et al. 2015. Six-dimensional real and reciprocal space small-angle X-ray scattering tomography. *Nature* 527: 353–356.

Snigirev, A., et al. 1995. On the possibilities of X-ray phase contrast microimaging by coherent high-energy synchrotron radiation. *Rev. Sci. Instrum.* 66: 5486–5492.

Stein, K. and Prondvai, E. 2014. Rethinking the nature of fibrolamellar bone: an integrative biological revision of sauropod plexiform bone formation. *Biol. Rev.* 89: 24–47.

Tafforeau, P., et al. 2006. Applications of X-ray synchrotron microtomography for non-destructive 3D studies of paleontological specimens. *Appl. Phys. A-Mater.* 83: 195–202.

Tafforeau, P., et al. 2007. Nature of laminations and mineralization in rhinoceros enamel using histology and X-ray synchrotron microtomography: potential implications for palaeoenvironmental isotopic studies. *Palaeogeogr. Palaeocl.* 246: 206–227.

Tafforeau, P. and Smith, T. M. 2008. Nondestructive imaging of hominoid dental microstructure using phase contrast X-ray synchrotron microtomography. *J. Hum. Evol.* 54: 272–278.

Voeten, D. F. A. E., et al. 2018a. Synchrotron microtomography of a *Nothosaurus marchicus* skull informs on nothosaurian physiology and neurosensory adaptations in early Sauropterygia. *PLoS One* 13: e0188509.

Voeten, D. F. A. E., et al. 2018b. Wing bone geometry reveals active flight in *Archaeopteryx*. *Nat. Commun.* 9: 923.

Wilkins, S. W., et al. 1996. Phase-contrast imaging using polychromatic hard X-rays. *Nature* 384: 335–338.

Zanette, I., et al. 2011. Quantitative phase and absorption tomography with an X-ray grating interferometer and synchrotron radiation. *Phys Status Solidi A*208: 2526–2532.

Zdora, M.-C., et al. 2020. X-ray phase tomography with near-field speckles for three-dimensional virtual histology. *Optica* 7: 1221–1227.

VetBooks.ir

8

Bone Tissue Types: A Brief Account of Currently Used Categories

Vivian de Buffrénil and Alexandra Quilhac

CONTENTS

Introduction 148
Relevant Descriptors of Bone Microstructure 148
Global Topography and Origin of Bone Deposits 148
Cortical and Medullary Formations 148
Periosteal and Endosteal Tissues 150
Primary and Secondary Bone Tissues 150
Classifying Tissues in Static and Dynamic Osteogenesis 150
Microanatomical Description as a Prerequisite to Histological Analysis 151
Distinction of Osseous Tissues Based on Compactness 151
Vascular Canals in Cortices 152
Types of Intercellular Matrix 155
Woven-Fibered Collagen Networks 155
The Parallel-Fibered Matrix 157
The Lamellar Matrix 157
Degraded Matrix of Hypermineralized Bone Tissue 158
Osteocytes and Their Diversity 158
Other Significant Features of Bone Matrices 159
Osteons 159
Cyclical Growth Marks, Rest Lines and Reversion Lines 161
Sharpey's Fibers 163
Current, Integrative Classification of Primary Compact Tissues 163
Woven-Fibered Tissue 163
Parallel-Fibered Bone Tissue 165
The Lamellar Tissue 165
Specialized Terminology Related to Lamellar or Parallel-Fibered Tissues 166
External and Internal Fundamental Systems 166
On Intermediate Tissue Types 166
Remarks on the "Lamellar-Zonal" Tissue 166
Some Peculiar Cases of Lamellar Bone in Basal Gnathostomes 168
Acellular Bone and Aspidin 168
Isopedin 168
Composite Tissues: The Woven-Parallel [Fibrolamellar] Complexes 169
Woven-Parallel Complexes With Longitudinal Osteons 171
Reticular Woven-Parallel Complex 171
Radial Woven-Parallel Complex 171
Laminar and Plexiform Woven-Parallel Complexes 171
Dense Haversian Bone: A Secondary Compact Tissue 172
Osseous Tissues in Cancellous Formations 172
Tissues Forming the Primary Trabeculae 172
The Tissues of Secondary, Endosteal Trabeculae 174
Trabeculae Resulting from Patchy Cortical Resorption 174
Remarks on Fine Cancellous Bone 174
Histological Features of Compacted Coarse Cancellous Bone (CCCB) 174

Between Bone and Cartilage: Chondroid Bone 175
Acknowledgments 176
References 176

VetBooks.ir

Introduction

The power and reliability of paleohistology for reconstructing biological traits in extinct taxa rest on the accuracy and precision of the descriptions of histological sections. These in turn depend on the concepts used for analyzing, interpreting and naming bone tissue structures. They also reflect the validity of a description independently of the sample considered (universality criterion) and of the person observing it (reproducibility criterion). Since the beginning of histology, considerable discrepancies have existed among authors in both the descriptive options adopted for coping with the diversity of osseous tissues and the meaning and importance given to obvious structural features such as compactness, matrix characteristics, cell shape and density, occurrence and arrangement of vascular canals and so forth. A frequent tendency in early authors was to focus the diagnosis of bone tissues preferentially or exclusively on one of these characteristics at the exclusion of the others. For example, Foote's (1911, 1913, 1916) classifications, like those of Enlow and Brown (1956, 1957, 1958), were mainly based on cortical vascularization (see also Locke 2004), whereas, e.g., Weidenreich (1930) and Gross (1934) privileged matrix structure. As a consequence, little consensus existed about the bone tissue categories built on these observational choices and the words used for defining them. For this reason, many ancient descriptions are now hardly usable in current comparative practice.

Our purpose here is neither to reconstruct the historical course of the concepts and terminology applied to skeletal tissues, nor to list the contents, synonymy, convergence or divergence of the terms invented by the pioneers of bone histology. This has already been done in reviews by Enlow and Brown (1956, 1957, 1958), Enlow (1963) and Ricqlès (1975, 1976, 1977, 1978) (see also the historical introduction to this book). Ricqlès' (1975-1978) quasi-exhaustive synthesis, based on the hierarchical subdivision of bone features into "integration levels" as initially proposed by Petersen (1930) (see also Reznikov et al. 2014a), resulted in a graded description and classification system in which the internal structure of a bone, as defined by the knowledge available at the beginning of the 1970s, was considered at both microanatomical and histological levels (structural features), and in reference to the local conditions of bone accretion and resorption (growth events). This system, updated and adapted to the English vocabulary in 1990 (Francillon-Vieillot et al. 1990), has accompanied the progress of paleohistology for 50 years, and it remains a universal tool for deciphering the microstructure and growth processes of bones in a comparative perspective (e.g., Horner and Padian 2004; Chinsamy-Turan and Ray 2012; Martinez-Maza 2014; Orlandi-Oliveras et al. 2018). With the exception of the classification proposals of Stein and Prondvai (2014) and Prondvai et al. (2012), further considered below, the categories of bone tissue defined by Ricqlès have not been fundamentally questioned hitherto, although other authors proposed slightly different hierarchical subdivisions (e.g., Weiner and Wagner 1998; Reznikov et al. 2014a). Therefore, they will be presented with the pragmatic approach of following the gradual stages of the description of a section, from the broadest to the finest structural characteristics accessible to optical techniques, X-ray scanning and, to a lesser extent, electron microscopy. When necessary, brief accounts of recent advances, as typically yielded by modern three-dimensional, computerized approaches (e.g., Reznikov et al. 2014a), will be cited.

The accumulation of comparative data in extant and extinct vertebrates tends to confirm what several authors noticed decades ago (e.g., Ricqlès 1975; Margerie et al. 2002, 2004): the histological structure of bone cortices often appears intermediate between currently acknowledged tissue types, and is seldom in total compliance with typical categories. Bone structure varies along a continuum, rather than being a strictly discrete character. This is an essential concept for both histological descriptions and the inferences (functional, developmental, phylogenetic, etc.) that can be drawn from them.

Relevant Descriptors of Bone Microstructure

Global Topography and Origin of Bone Deposits

One of the main reasons for identifying bone tissue types is to reconstruct the local course of the growth of a bone in chronological and topographical perspectives. Therefore, provided that the position and orientation of a section are precisely controlled (a very basic and essential condition for conducting histological analyses, e.g., Prondvai et al. 2014; Faure-Brac et al. 2019), the most elementary descriptors of bone structure refer to the (1) location of osseous formations that can be cortical or medullary; (2) cell populations, either periosteal or endosteal, involved in their accretion and (3) relative order, either primary or secondary, of their deposition.

Cortical and Medullary Formations

These concepts (already considered in Chapter 4) are essentially topographical and rank among the most currently used in comparative bone histology. They nevertheless rest on a somewhat unclear and ambiguous conceptual basis. In the case of tubular bones (Figure 8.1A) that have a well-differentiated medullary cavity occupying a central position, the cortical territory corresponds to the bony ring (parallel layers in the case of a diploe; Figure 8.1B) surrounding or framing (diploe) this cavity. However, the central position of the medullary region is far from being general: when off-centered growth occurs (the normal situation of, e.g., ribs), the medulla can be relocated to one side of the bone.

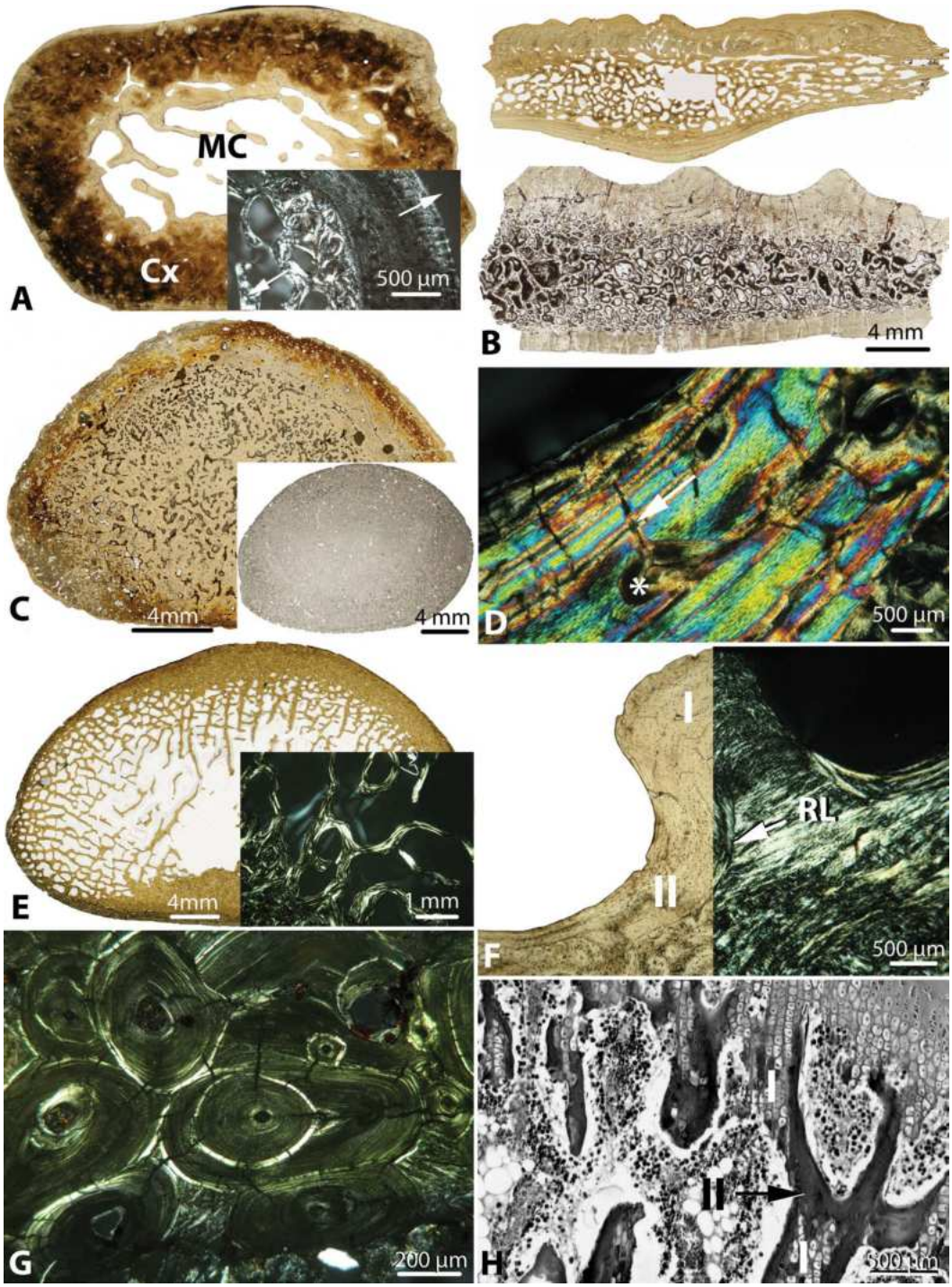


FIGURE 8.1 Basic dichotomies: cortex versus medulla, periosteal versus endosteal and primary versus secondary. A, Main frame: cross section in the tibia of the mammalian carnivore *Potamotherium valletoni* (Miocene of Europe); inset: cross section in the femur of an extant reptile, *Varanus niloticus* (Varanidae), viewed in polarized light. Cx, periosteal cortex; MC, medullary cavity. Endosteal bone (here in the form of trabeculae) is indicated by the inward directed arrow; periosteal bone is indicated by the outward directed arrow. B, Diploe structure of the osteoderms of an extant turtle, *Trionyx triunguis* and a phytosaur (Upper Triassic archosauromorph). C, Feeble difference in compactness between the medulla and the cortex in two sirenian mammals, *Pezosiren portelli* (Lower Eocene of Jamaica) and *Dugong dugon* (extant Dugongidae). D, Vascularized and remodeled endosteal bone in the tibia of the extant elephant *Loxodonta africana*. Polarized light. The arrow points to a vascular canal and the asterisk indicates a secondary osteon. E, Secondary endosteal trabeculae in a rib from the Early Pliocene seal *Callophoca obscura*. The inset is an enlarged view of the trabeculae in polarized light. F, Remodeled outer surface of the frontal of *Diplocynodon ratelii*, an Early Miocene alligatorid from Europe. A single bone layer is both primary (indicated by I) on top of the ridge and secondary (II) over the bottom of a pit. Right half: polarized light. G, Secondary osteon inside the wall of another secondary osteon. H, Primary trabeculae composed of a core of calcified cartilage (primary tissue indicated by I), covered by endosteal bone sheets (secondary tissue, or II). Section of decalcified bone stained with hematoxylin in the proximal epiphysis of the femur of *Varanus niloticus*.

VetBooks.ir

In this meaning, the cortex is often heterogeneous because it includes strata deposited by distinct cell populations (periosteal and endosteal), following different accretion modalities (centrifugal vs. centripetal). As Ricqlès (1975) and Francillon-Vieillot et al. (1990) pointed out, the term *cortex* has no explicit connotation with local compactness, although the frequent (if not general) difference in compactness between cortical and medullary regions sometimes leads to a mistaken synonymy between the concepts of cortex and compacta. In the case of, e.g., the stylopod bones of terrestrial mammals, it is simple to discriminate the cortex, which is compact, from the medullary region, which is hollow or contains only a few trabeculae (e.g., Buie et al. 2007; see also Girondot and Laurin 2003). However, when a gradual transition occurs between the most cancellous part of the medulla and the most compact part of the cortex (Figure 8.1C) – a situation that can even lead to a total absence of either compact or cancellous tissue layers in a bone section (often observed in marine tetrapods: Figure 8.1C, inset) – assessing cortical limits becomes difficult because they cease to be defined by criteria of location or compactness. The cortex is then implicitly assimilated into the primary periosteal formations deposited centrifugally, as opposed to a medullary region where centripetal endosteal deposits prevail. Of course, this distinction needs the origin of local tissues to be identified unambiguously. It appears that the terms *cortex* and *medulla*, both indispensable in practical mapping of histological observations, can hardly be defined only by topographic clues, although the final meaning of these terms is essentially topographic.

Periosteal and Endosteal Tissues

In contrast to the terms presented above, the terms periosteal and endosteal (Figure 8.1A, inset) have a common use and a precise, nonambiguous meaning. Periosteal tissues are cortical and created as centrifugal deposits by the osteoblasts of the cambial layer of the periosteum. They can be vascularized or not and can comprise any histological bone tissue type. Moreover, periosteal tissues may contain extrinsic fibers such as Sharpey's or elastic fibers, incorporated into the unmineralized osteoid during cortical accretion. Conversely, endosteal deposits are represented by only two categories of osseous tissue, lamellar and parallel-fibered bone (see below). They are often avascular, but may occasionally contain simple canals, oriented radially (e.g., Figure 8.1D; see also Margerie et al. 2002), or secondary osteons resulting from local remodeling (Enlow and Brown 1957). The accretion of these deposits progresses in a basically centripetal direction (it tends to fill the lumen of inner bone cavities), although it occurs on the complex and variable surface of medullary trabeculae (Figure 8.1A, inset, 8.1E). The term *endosteal* refers to an osteoblast population that does not constitute a consistent and tough membrane like the periosteum. The endosteum is instead a loose and variable cell layer (Marotti et al. 1992; Burr and Akkus 2014) that covers the walls of bone inner cavities, including the medullary cavity, the eventual trabecular network that it may contain, and resorption bays within bone cortices. The origin of endosteal osteoblasts is still debated and could well be multiple (early periosteal cells, mesenchymal stem cells, etc.; review in Aubin 2008). Endosteal deposits can often be distinguished easily from periosteal ones by the *reversion lines* bordering them and marking a structural discontinuity between these two kinds of tissues. The so-called *medullary bone*, exclusive to ornithodiran archosaurs, is a special tissue considered specifically in the chapter dealing with this clade.

Primary and Secondary Bone Tissues

Understanding the chronology, i.e., the order of formation, of the osseous deposits visible in a section is an obvious prerequisite for reconstructing the local morphogenesis of a bone. The two basic descriptors in this field are the concepts of primary and secondary deposits. Their definition is simple and used straightforwardly in all descriptions of bone histology. A primary osseous deposit occurs *de novo* in a spot and does not replace *in situ* a previous skeletal formation; conversely, a secondary deposit locally replaces preexisting tissue after its resorption by osteoclasts. As such, the notions of primary and secondary deposits simultaneously integrate topography and chronology and are therefore constrained in time and space (Castanet and Ricqlès 1987). For example, a single bone layer covering a relatively broad area can be both primary and secondary, depending on its precise location and the previous events that occurred in the spots where it is observed (space constraint: Figure 8.1F). Similarly, depending on the relative chronology of its deposit, it can be secondary if compared to the preexisting substrate, or primary if it has been submitted to a remodeling process subsequent to its formation (time constraint; Figure 8.1G). Moreover, the notion of secondary bone does not imply that the preexisting (primary) and replacing (secondary) tissues be of the same type. Bone deposited in a site after the resorption of, e.g., cartilage (a general situation in endochondral ossification; Figure 8.1H), is considered secondary (see Ricqlès 1975). This nuance is important if skeletal microstructures are to be interpreted in terms of local morphogenetic patterns. When they occur in a mere osseous context, secondary layers are always bordered by a reversion line that clearly shows the limit of the initial resorption stage and the starting point of the subsequent secondary reconstruction.

Classifying Tissues in Static and Dynamic Osteogenesis

The studies by Marotti et al. (1999) and Ferretti et al. (2002) showed that, in the process of membrane ossification (including subperiosteal accretion), the secretion of the bone matrix and the entrapment of osteoblasts in it may follow two patterns, respectively, designated as *static* and *dynamic* osteogenesis. In static osteogenesis (SO), osteoblasts are randomly arranged and oriented in the osteogenic cell layer (periosteal cambium; Figure 8.2A). Each of them is functionally polarized and excretes matrix components through only a part of its plasmic membrane; however, because the orientation of these cells is random, they are surrounded by the osteoid that they collectively produce, and finally become embedded in it in the place where they are (Figure 8.2B). Conversely, in *dynamic*

VetBooks.ir

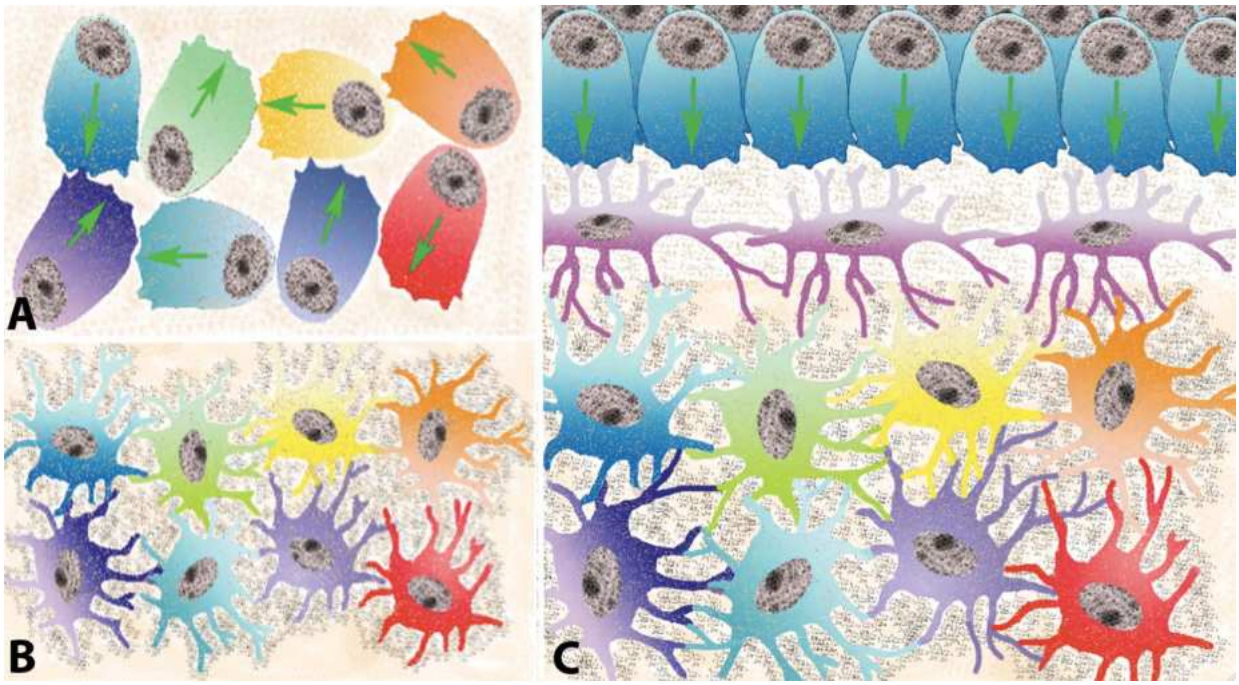


FIGURE 8.2 Static and dynamic osteogenesis. A and B, Static osteogenesis. The osteoblasts of the periosteal cambial layer are oriented randomly and the osteoid excreted through their basal surface surrounds them entirely (A). Consequently, when trapped within the mineralizing osteoid, the osteocytes display no organized position or orientation (B). C, In dynamic osteogenesis, osteoblasts are oriented in a single direction, as a polarized set of cells, and they move back with the accumulation of their secretion. Some of them are trapped within the osteoid in the position that they had in the cambial layer.

osteogenesis (DO), active osteoblasts are organized in one layer (Figure 8.2C), and osteoid excretion occurs in the same direction for all the cells. An osteoblast layer is thus highly polarized morphologically and functionally. Secreting cells therefore tend to move backward in pace with the accumulation of their own production, although a small number of them are trapped within the osseous matrix. In Marotti et al.'s (1999) model, SO locally precedes DO during the growth of a bone, a generalization criticized by Cubo et al. (2017).

As further explained below (Chapter 10), accretion rate is the main factor influencing the local pattern of osteoblast organization and activity (the now universally acknowledged Amprino's [1947] rule). A given osteoblast population often works *in situ* (for example, at mid-diaphyseal level) in SO during embryonic and early postnatal growth, when growth rate is greatest, and in DO in later ontogenetic stages, when accretion rate decreases. Moreover, local accretion modalities cyclically fluctuate from one type to another with the formation of yearly growth marks, the zones (fast SO) and the annuli (slower DO: see, e.g., Castanet 1974). Although obviously valid in a general perspective, comparative data suggest that Marotti et al.'s (1999) model deals with the extreme terms of a gradual continuum, characterized by great plasticity and the capacity of a single osteoblast population to radically change its activity pattern.

In reference to Marotti et al.'s (1999) model, Stein and Prondvai (2014) and Prondvai et al. (2014) proposed some terminological adjustments in bone tissue nomenclature, dealing mainly with the so-called *fibrolamellar complexes*. This question is further considered below, with the description of these tissue types.

Microanatomical Description as a Prerequisite to Histological Analysis

Bone microanatomical features have been presented in a previous chapter (Chapter 4); they will nevertheless be briefly reviewed here because they are, in the current practice of histological descriptions, closely imbricated with histological traits in the perspective of an integrative approach to bone microstructures. Indeed, many histological categories, along with the terms associated with them, directly refer to either the local compactness of the bones or their vascular pattern, two basic microanatomical concepts.

Distinction of Osseous Tissues Based on Compactness

A basic dichotomy distinguishes cancellous bone, or *spongiosa*, and compact bone, or *compacta*. These concepts are intrinsically quantitative and refer to the local quantity of solid bone tissue, expressed as a percentage of the total area (or volume) in a selected spot or in a section as a whole. However, in current practice, they do not refer to a precise threshold, although the value of 50% compactness should logically represent the upper limit of cancellous tissue and the lower limit of compact bone. Consequently, the terms spongiosa and compacta may designate fairly different structural realities according to the authors who use them. Precise quantitative measurements, now easily accessible with free software like Bone Profiler or BoneJ, are recommended to avoid possible inconsistencies. In addition to the

VetBooks.ir

basic distinction between compact and cancellous osseous formations (Figure 8.3A), three kinds of spongiosae and one peculiar kind of compact bone are currently distinguished in the literature, in reference to both their actual compactness level and the conditions of their formation.

Coarse Cancellous Bone

This kind of spongiosa is defined by a relatively loose network of slender trabeculae (Figure 8.3B), separated by broad intertrabecular cavities (i.e., parameter *trabecular separation*, or *Tb.Sp.*, in histomorphometric nomenclature). The latter measures some 1.2 to 1.5 mm in mean width in the proximal head of the femur of a medium-sized mammal such as *Homo sapiens* (Hildebrand et al. 1999). Consequently, the compactness of this type of spongiosa (*ca.* 25% in the anatomical site quoted above) is relatively low. In long bones, coarse cancellous formations result from the intensive and repeated remodeling of the so-called *primary* trabeculae initially formed in the metaphyseal region after the resorption of calcified cartilage during the growth in length of the bones. For this reason, this type of spongiosa is mainly (although not exclusively) confined to metaphyseal and epiphyseal regions. In dermal bones, the same type of spongiosa is created by an imbalanced resorption/reconstruction process in the core of diploes. Considering their mode of formation, the trabeculae of the coarse cancellous tissue are secondary structures, resulting from a long cascade of local remodeling and thus, at least in adults, of predominant endosteal origin. Their histological traits are further considered below. When the architecture of coarse cancellous bone displays a particular, nonisotropic pattern seemingly adapted to withstand mechanical constraints, the term *trabecular bone* is applied to it by some authors.

Fine Cancellous Bone

This type of cancellous formation (Figure 8.3C), first identified by Weidenreich (1930) and later named in English by Pritchard (1956), greatly differs from the previous one by most of its characteristics: it has a cortical location and a periosteal origin, and the intertrabecular spaces that it contains are small (100–200 µm in diameter or width in most cases); therefore, sometimes it is hardly distinguishable from compact tissue. Intertrabecular spaces in this type of spongiosum house abundant blood vessels, once present in the periosteum and incorporated into the developing cortex. The vascular networks that are thus created form several characteristic patterns (further described below) that condition the whole geometrical structuration of the fine cancellous bone. The latter is transitory during cortical growth. Its compactness quickly increases due to intertrabecular centripetal deposits progressing in pace with the centrifugal accretion of new periosteal layers. The general fate of fine cancellous bone is thus to become compact. In some rare exceptions this osseous formation maintains its cancellous state throughout life. This has been described in some tetrapods that secondarily returned to an aquatic life, such as ichthyosaurs (e.g., Buffrénil et al. 1987; Buffrénil and Mazin 1990; Houssaye et al. 2014; see also Figure 8.3C) and placodonts (Buffrénil and Mazin 1992; Klein et al. 2015a).

Compact Bone Made Cancellous

In all vertebrate groups the base of periosteal cortices is frequently submitted to a patchy but extensive resorption process that transforms originally compact bone into a cancellous formation (Figure 8.3D). In best characterized cases, e.g., short metapodial bones and vertebrae, this process leaves only a thin compact layer that constitutes the most peripheral stratum of periosteal cortices. Stylopodials and, to a lesser extent, rib cortices in numerous extant and extinct marine tetrapods are almost entirely composed of this type of spongiosa, derived from compact tissue. The basic histogenetic process involved is imbalanced remodeling, a process that favors resorption to the detriment of reconstruction and results in a local loss of bone volume (e.g., Buffrénil and Schoevaert 1988). Although nonpathological in marine tetrapods, this process is roughly comparable to that causing disuse or senile osteoporosis. From a histological perspective, compact cortices made cancellous are easily recognizable by the presence of broad remnants of primary cortical bone (whatever its histological structure) in the core of the trabeculae (Figure 8.3D).

Compacted Coarse Cancellous Bone (CCCB)

This tissue (described and interpreted in detail by Enlow 1963) results from the filling of intertrabecular spaces of coarse cancellous bone by centripetal endosteal deposits. Loose cancellous formations are thus made compact (Figure 8.3E, F). According to the classic models of Lacroix (1945, 1949) and Enlow (1963), this process is a normal and general aspect of the growth in length of long bones. It mainly occurs in the metaphyseal regions, which are thus prepared to be sequentially incorporated into the compact wall of the diaphysis. An abundant vascularization that has a medullary origin and is poorly structured geometrically occurs in CCCB and gives it a "disorganized" aspect. During growth, this tissue is normally erased by the enlargement of the medullary cavity and is no longer visible in the diaphyseal region. Its occurrence in the mid-shaft territory is relatively infrequent, and it depends on local morphogenetic events (especially an off-centered pattern of growth in diameter). The recent multiplication of detailed comparative studies, chiefly conducted in mammals, shows that, depending on the morphology and growth patterns of long bones, the CCCB formed in the metaphyseal territory can remain in variable quantity up to the middle of the shaft, as observed in the aardvark, *Orycteropus afer* (Legendre and Botha-Brink 2018), the rodent *Bathyergus suillus* (Montoya-Sanhueza and Chinsamy 2017) and the xenarthran *Dasypus novemcinctus* (Heck et al. 2019).

Vascular Canals in Cortices

The importance given to intracortical vascular canals in early attempts to discriminate bone tissue categories has been mentioned above. Although the use of this character is more nuanced today, it remains a central element in the description and categorization of bone tissues, in part because of the considerable functional meaning currently attributed to it. The multiplication of quantitative data, considered in a comparative

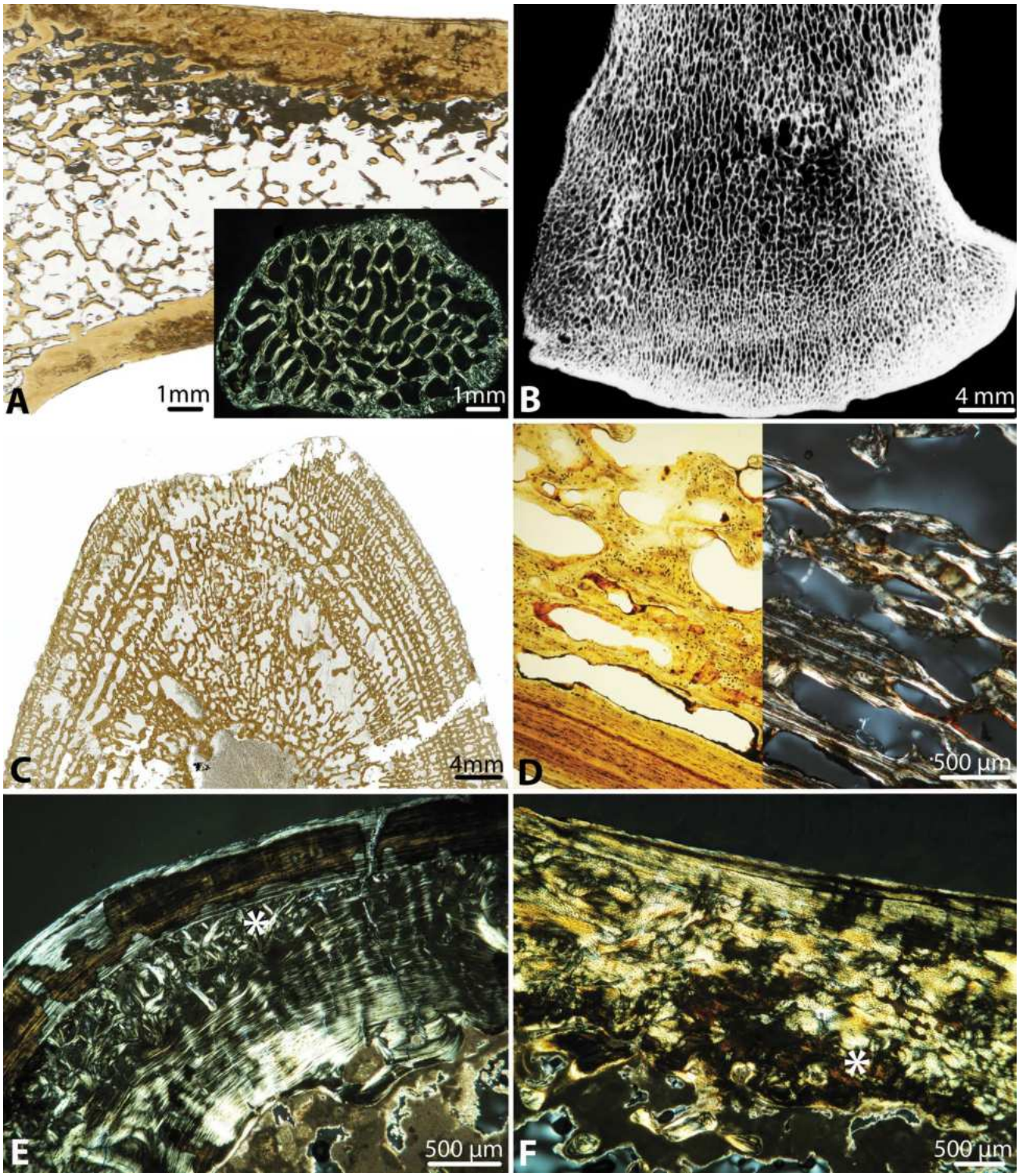


FIGURE 8.3 Cancellous tissues and bone compactness. A, Compact and cancellous bone in the metaphysis of *Potamotherium valletoni* tibia. Sagittal section. Inset: Cross section in the metaphysis of the same bone (polarized light). B, Coarse cancellous bone forming most of the humerus volume in the extant cetacean *Delphinus delphis*. X-ray proof of longitudinal section. C, Fine cancellous bone in the humerus of the Middle Triassic ichthyosaur from Spitzbergen, *Omphalosaurus nisseri* (cross section). D, Compact, cortical bone (lower left field) submitted to patchy resorption and transformed into a spongiosa in the vertebra of the Paleocene-Eocene Choristodera *Simoedosaurus* sp. E, Compacted coarse cancellous bone (CCCB; asterisk) in the femur of *P. valletoni*. Cross section in polarized light. F, Same tissue in a sagittal section of *P.* tibia metaphysis.

perspective (e.g., Cubo et al. 2005; 2014; Buffrénil et al. 2008; Canoville et al. 2017), suggests that the occurrence, density and geometric structuring of vascular canals are likely to respond to their own (still incompletely understood) deterministic factors, and that the latter could, to some extent, be independent from the processes that influence the character states of other descriptive features of bone structure.

Avascular Bone

Avascular cortices (Figure 8.4A) are frequent and even general in the skeleton of small vertebrates, regardless of their taxonomic position, and in the smallest bones of larger forms. Avascular bone is also more often associated with certain tissue types than with others. The lack of intracortical vascularity is compensated by superficial capillaries originating from

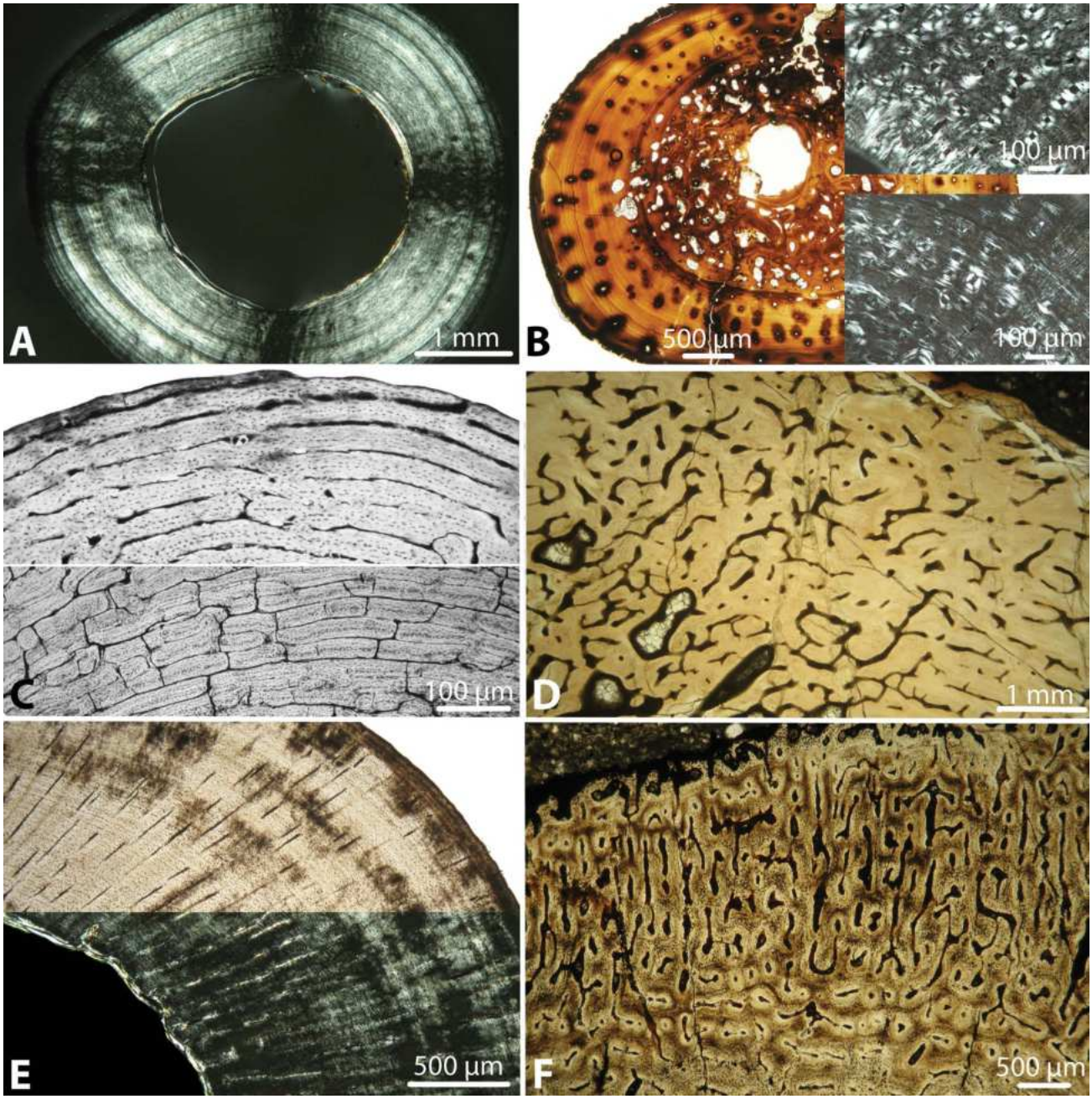


FIGURE 8.4 Vascular networks in the bone cortex. A, Totally avascular cortex in the femur of the extant marine iguana *Amblyrhynchus cristatus*. Polarized light. B, Longitudinal canals. Main frame: simple canals in the femoral cortex of the Upper Permian basal diapsid *Claudiosaurus germaini*. Upper inset: canals (primary osteons) in radial files in the femur of the extant anuran *Amietophrynus regularis*. Lower inset: primary osteons in circular files in the femur of the anuran *Rhinella marina*. C, Laminar (upper half) and plexiform (lower half) vascular patterns in the femur cortex of the extant duck *Anas platyrhynchos*. D, Reticular vascular pattern in the Upper Permian therapsid *Lystrosaurus* sp. E, Radial orientation of the canals (here, simple canals) in the femur of *Varanus niloticus*. Lower half: polarized light. F, Association of variably oriented (longitudinal, radial, oblique) canals in the peripheral cortex of the femur of the Middle Triassic therapsid *Kannemeyeria* sp.

VetBooks.ir

medullary and periosteal tissues (e.g., Roche et al. 2012; see also Simpson 1985). Cubo et al. (2014) elaborated on the possible influence of functional and geometrical constraints on the blood supply of bone cortices. However, whether the size of skeletal elements is considered, or the composition and structure of their tissues, the presence or absence of intracortical vascular canals presents paradoxical exceptions that remain to be explained (examples of such situations in sauropsids are given by Cubo et al. 2014, and in lissamphibians by Canoville et al. 2017).

Vascular Patterns in Bone Cortices

This subject has already been considered in detail in Chapter 4. Here we will briefly recall that two main features of cortical vascularization must be considered in the description of bone sections: the type of the canals and their geometrical arrangement. Primary periosteal cortices may thus house two types of primary vascular canals (the case of secondary osteons is considered below): simple canals (Figure 8.4B), which are mere tunnels circulating through the cortex, and primary osteons (Figure 8.4C, F), whose lumen is surrounded by a layer of centripetally deposited bone tissue without any previous perivascular resorption. Whatever their form or the osseous substrate in which they are inserted, vascular canals may display five distinct orientations.

The simplest orientation is longitudinal. This orientation mainly occurs in long bones, and the canals are then parallel, or slightly oblique, to the bone sagittal axis. In cross section, they appear as small discs (Figure 8.4B) and in longitudinal section as long, straight segments. Longitudinal canals can also form diverse patterns within the cortices and be distributed either randomly or in radial, circular or concentric rows (Figure 8.4B, insets).

In the *circular* (or *laminar*) pattern, vascular canals, as observed in standard cross sections of adult bones, have a circular course and are distributed in successive parallel layers, centered around the axis of the bone if the latter is tubular (Figure 8.4C, upper field). Some sparse anastomoses oriented radially connect the canals of adjacent layers. A pattern equivalent to the circular one may occasionally occur in flat or irregularly shaped skeletal elements: vascular canals are then oriented parallel to the outer bone surface. An increase in the frequency of radial anastomoses defines the *plexiform* vascular pattern (Figure 8.4C, lower field), whereas in the *reticular* pattern, vascular canals do not display any preferential orientation. They thus form a dense network of random and irregular structure (Figure 8.4D). The *radial* orientation (Figure 8.4E) is less frequent than the others. Canals are then oriented parallel to the radii of tubular bones (as viewed in cross section), or perpendicular to the outer surface of periosteal cortices in flat bones.

The occurrence of a single, homogeneous canal orientation within a bone section is relatively infrequent. Although a dominant vascular orientation generally stands out, which allows the use of a single term to describe it, differently oriented canals also occur as minor elements (Figure 8.4F). Each vascular orientation pattern thus coexists with one or several other patterns (see synthetic sketches in Ricqlès 1975): for example, longitudinal canals are commonly developed in circular, plexiform or radial networks; similarly, radial canals are also normal constituents of the circular and plexiform types. The quantitative analysis proposed by Boef and Larsson (2007; see also Pratt and Cooper 2017, 2018) is designed to cope with the multiplicity of vascular orientations in a single section, and gives, in the form of an index (*laminarity index*), the proportion of each orientation.

Types of Intercellular Matrix

The spatial structure of collagen networks in bone matrices is of major importance for the definition of bone tissue types. In the early classification of Weidenreich (1922, 1930), fiber orientation is the only feature considered. Three tissue categories are thus defined: woven-fibered, parallel-fibered and lamellar. Considering only the osseous matrix proper, this classification and the terms expressing it remain valid and unchanged today. Their meaning has nevertheless been extended to designate more integrative histological categories including cells, in addition to matrices. For the present, only the characteristics of collagen matrices relevant to tissue classification will be considered.

In current histological practice, collagen fiber orientation can be observed through several technical approaches (review in Georgiadis et al. 2016). One of the simplest, most useful approaches in recent and fossil material is polarized light microscopy, especially in its modern version as circularly polarized light (CPL), coupled with computerized image analysis (e.g., Bromage et al. 2003). Applied to standard ground sections sampled in strictly controlled planes (transverse and/or longitudinal), this technique allows calibrated color representations of fiber orientation in large fields. Practical examples of CPL are given in, e.g., Boyde and Riggs (1990). A new and highly efficient method for small field analysis in recent bone samples is the so-called *serial surface view* (SSV). In brief, this specialized technique of scanning electron microscopy consists of a serial "slicing" and imaging of the sample surface, followed by computerized three-dimensional (3D) reconstruction (see the *Methodological Focus* on this technique below). A nanometric resolution can thus be reached, and local fibrillar networks are revealed in detail, each fibril visible individually (Reznikov et al. 2013, 2014a, b; Mitchell and van Heteren 2016). Substantial progress in matrix description was made with this approach.

Woven-Fibered Collagen Networks

An outstanding review of this type of matrix was recently presented by Shapiro and Wu (2019). The reader is encouraged to consult this article. Woven-fibered matrices are typical products of SO. Because the orientation of the osteoblasts that secrete collagen monomers is random, the fibrils and subsequently the fibers and fiber bundles that form from them also have no preferential orientation (isotropic, or "disorganized" structure, following Reznikov's (2014a, b) vocabulary; see also Chapter 5). In polarized light (Figure 8.5A), this situation results in monorefringence. This type of matrix structure is supposed to occur when large amounts of osseous tissue are quickly deposited by periosteal osteoblasts to

VetBooks.ir

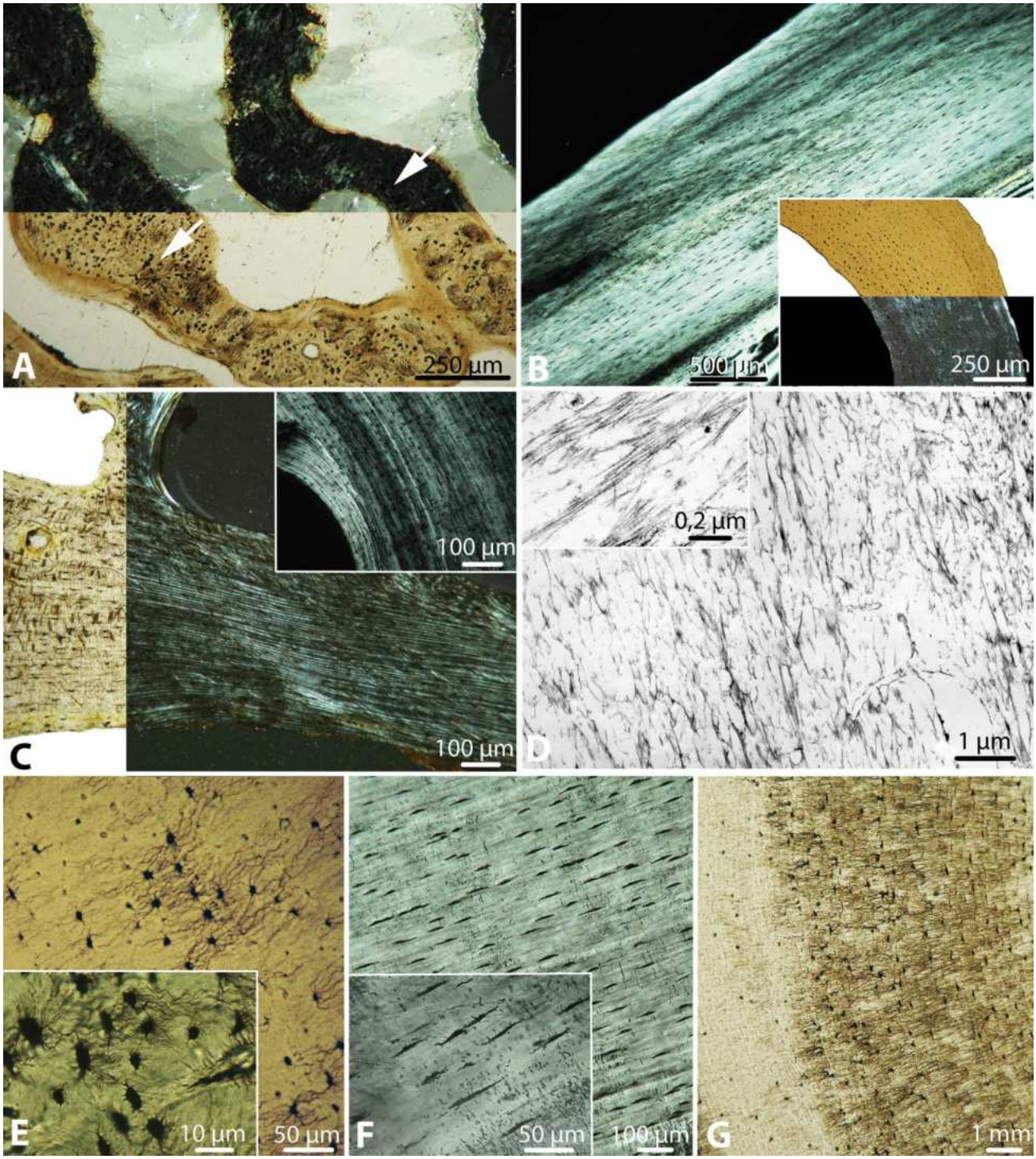


FIGURE 8.5 Diversity of bone matrices and cell morphology. A, Woven-fibered matrix (arrows) in the core of the trabeculae forming the fine cancellous bone of the *Omphalosaurus* humeral cortex. Upper part: view in polarized light showing the monorefringence of this kind of matrix. B, Typical parallel-fibered bone. The main frame shows a longitudinal section, viewed in polarized light, of the femoral cortex of the extant giant frog *Conraua robusta*. The bone matrix displays a bright mass birefringence indicative of a longitudinal orientation of collagen fibers (parallel to the sectional plane). Inset: in natural (upper field) and polarized light (lower field), the aspect of this kind of matrix in cross section; the matrix is then monorefringent. C, Lamellar bone matrix in the basal cortex of a *Placosaurus rugosus* osteoderm. Right half: polarized light. The inset shows a perimedullar layer of typical lamellar osseous tissue in the femur of *Amblyrhynchus cristatus*. D, View in transmitted electron microscopy of the degraded collagenous meshwork in the matrix of *Mesoplodon densirostris* (an extant ziphiid cetacean) premaxillae. Inset: closer view at the collagen fibrils. E, Multipolar osteocyte lacunae with well-developed canaliculi. Lacunae of this kind are typically oriented at random in woven-fibered matrices. Inset: closer view at the lacunae. Details of cross sections in *Omphalosaurus* humerus. F, Detail of longitudinal sections in the femur of *C. robusta* showing the spindle-shaped or flat osteocytes associated with parallel-fibered and lamellar matrices. G, Local differences in the development of *canaliculi* within a single matrix type (here, parallel-fibered bone in the femur of *Varanus niloticus*, viewed in cross section).

VetBooks.ir

build bone cortices, most often in the initial form of loose scaffolds (see the section "Fine Cancellous Bone" above) in embryos or fast-growing juveniles. In subadults and adults (residual growth), this kind of matrix is no longer produced and seldom visible in cortices because it was eroded long ago by remodeling during growth.

Beyond this general description, which was clearly settled by Frost (1960; the woven-fibered tissue was then called "fibrous bone"), recent SSV studies by, e.g., Reznikov et al. (2013, 2014a, b) have shown that randomly oriented fibrils may also occur as a minor element in other matrix types than the woven-fibered (i.e., parallel-fibered and lamellar) matrices. The "disorganized fibrils" are then wedged between strong, evenly spaced fiber bundles and fill up (as mortar would do) free spaces between the bundles (Reznikov 2014a, b). A typical woven-fibered matrix has a relatively low collagen content but abundant noncollagenic proteins (e.g., Currey 2003; Reznikov et al. 2014a, b). Its mineral content, some 70% ash weight, is higher than that of other matrix types. Specific measurements of the mechanical properties of "pure" (i.e., nonremodeled) woven-fibered matrices are scarce in theliterature. Considering the strong correlation between the mineral content of bones and their mechanical properties (Currey 1984; Currey and Brear 1990; see also the study of woven-fibered tissue by Garcia et al. 2012)), the hardness and Young's modulus of woven-fibered matrices should be high, but their work of fracture should be low: such matrices are thus likely to be hard and stiff, but also brittle (see also Currey 2003).

The Parallel-Fibered Matrix

This highly polarized type of matrix is typically produced by DO. In this case, osteoblasts are aligned and similarly polarized; consequently, their collagen products are also polarized (Marotti et al. 1999; Ferretti et al. 2002; Prondvai et al. 2014; see also Ozasa et al. 2017). The fiber network of parallel-fibered matrices is thus highly ordered, with fibers and fiber bundles basically oriented in a single consistent direction. In transmitted polarized light, such matrices are easily recognizable by a strong mass birefringence if the sectional plane is parallel to the direction of the fibers or, conversely, a total monorefringence if the plane is orthogonal to the direction of the fibers (Figure 8.5B). In long bone cortices, fiber networks may be either aligned with the bone's sagittal axis (longitudinal fibers) or perpendicular to it (circular fibers). The alignment of longitudinal fibers is seldom strictly parallel to the bone major axis; a slight angulation often exists, creating a spiral orientation of the collagen network in the shaft. In diploes, the fiber bundles of parallel-fibered matrices are aligned with the outer surface of the bone, although their course can be deflected by vascular canals. As mentioned above, recent SSV analyses (Reznikov et al. 2013, 2014a, b) revealed the presence of small amounts of woven-fibered matrix filling the interstices between fiber bundles. The collagen compartment of parallel-fibered matrices is proportionally more important than that of the woven-fibered tissue (e.g., Reznikov et al. 2014a); consequently, their mineral phase is somewhat less (66–67%; e.g., Currey 1984), and their mechanical properties shifted accordingly toward flexibility and compliance.

The Lamellar Matrix

The lamellar matrix derives from the same dynamic osteogenic process as parallel-fibered bone; both therefore share a similar basic structure with one major difference: collagen fibers in a lamellar matrix are not all oriented in a unique, exclusive direction. They are rather arranged in a series of stacked, well-differentiated strata, the lamellae. Broadly diverging estimates of the thickness of individual lamellae (2–7 µm) have been proposed. Most frequently, a thickness of 5–7 µm is attributed to the lamellae forming the walls of the osteons (review in Mitchell and van Heteren 2016). According to a current view, prevailing in many publications since the study by Gebhardt (1906) (see also Frasca et al. 1978; Giraud-Guille 1988; Weiner et al. 1997), each lamella comprises only fibers parallel to each other, and fiber orientation changes between adjacent lamellae, either in a clockwise or counterclockwise direction. A plywood-like structure is thus created with either a simple roughly orthogonal crossing of adjacent lamellae (orthogonal plywood), or a more complex, twisted structure considered in more detail below (see the section "Isopedin").

A quite different interpretation, based on observations with light and electron microscopy in human secondary osteons, was proposed by Marotti (1993) and Marotti et al. (2013): lamellar matrices consist of the alternation of two types of "lamellae" (i.e., collagen-poor and cellular, collagen-rich and acellular lamellae). Both are made of interwoven (i.e., woven-fibered or disorganized) collagen networks; the main difference between them is their respective textural densities (high for collagen-rich, low for collagen-poor lamellae) and their content in cell lacunae. To some extent, the SSV data by Reznikov et al. (2013, 2014a, b) lead to an interpretation of lamellar structure intermediary between the models of Gebhardt (1906) and Marotti (1993). Lamellar bone is described by Reznikov et al. (2013, 2014a, b) as a composite structure: the interstitial, woven-fibered matrix described for parallel-fibered tissue occurs also in lamellar matrices. This "disordered material" is inserted between the fiber bundles ("ordered material") within each lamella, and between adjacent lamellae. In current comparative histology and paleohistology, the lamellar pattern, when clearly differentiated, is unambiguously recognizable in ground sections observed in transmitted polarized light by the alternate reaction of monorefringence and birefringence exhibited by successive lamellae or groups of lamellae (Figure 8.5C). The accretion of lamellar bone is slow (less than 2 µm day^{-1}: Margerie et al. 2002), especially when occurring in periosteal cortices (the endosteal accretion of this tissue seems to be somewhat faster: Margerie et al. 2002). The formation of the lamellae obviously reflects a basic and very stable endogenous biological rhythm akin to that regulating the inscription of Retzius striae in tooth enamel (Bromage et al. 2009).

Lamellar and parallel-fibered matrices constitute the major part of bone cortices in vertebrates, either as primary periosteal deposits, as observed in small species (e.g., all extant lissamphibians and squamates, numerous mammals, etc.), or as secondary, mainly endosteal layers. Most of the attention paid to the mechanical properties of osseous tissues deals with these kinds of matrices, especially the lamellar bone in the walls of osteons. The mineral contents of lamellar and parallel-fibered

VetBooks.ir

tissues are similar, with a maximum value *ca*. 65–67% (Ziv et al. 1996), and their mechanical properties are characterized by a sharp anisotropy that basically reflects the polarization of their fiber networks. In a single specimen, quantitative values for hardness, Young's modulus or work of fracture can thus greatly differ with the location or direction of measurements (Bonfield and Grynpas 1977; Ziv et al. 1996; Faingold et al. 2013).

Degraded Matrix of Hypermineralized Bone Tissue

The facial bones (premaxillae, vomer, maxillae *pro parte*) of a few cetacean taxa among the Ziphiidae (or "beaked whales" i.e., odontocetes highly specialized for deep diving) have an unusual feature studied in detail in the rostrum of *Mesoplodon densirostris*. The mineral content of these bones is extremely high (85–90%; Buffrénil and Casinos 1995; Zioupos et al 1997), and their collagen meshwork is degraded and lacunar (Figure 8.5D). Ultrastructural data by Zylberberg et al. (1998) show that this sparse meshwork is made of thin fibrils (17 nm in average diameter), creating an irregular and loose system of longitudinal "tubes". A large volume is consequently available for the mineral phase, which explains the exceptional mineralization of the rostrum. Consistent with the organization of the collagen meshwork, the mineral phase of the rostrum is distributed in the form of rod-like structures. The physical properties of the rostrum of *M. densirostris* are steeply polarized and, when measured in the sagittal direction, they consistently reflect the unusual ultrastructural characteristics of the bones it comprises: density (2.7 g/cm^3), hardness (200–220 Vickers Hardness Number [VHN]) and Young's modulus (46.9 GPa) are the highest encountered hitherto in bone, making the rostrum an exceptionally stiff structure. Conversely, its binding strength (56 MPa) is that of a very brittle tissue (Zioupos et al. 1997). Such a hypermineralized matrix, although rare among vertebrates, occurs in ziphiids under normal physiological conditions. It is not a pathological feature, and it must be considered a highly specialized form of osseous matrix.

Osteocytes and Their Diversity

The embedding of osteoblasts in the osteoid that they have secreted, and their subsequent transformation into osteocytes, is accompanied by considerable morphological reconfiguration (reviews in Franz-Odendaal et al. 2006; Klein-Nulend and Bonewald 2008; Dallas and Bonewald 2010; see also Webster et al. 2013 for a review of the techniques employed in osteocyte studies). Active osteoblasts have a grossly cubic morphology; however, depending on whether the local osteogenic process is static or dynamic, the osteocytes derived from them have two distinct morphologies: they are multipolar or stellate and oriented at random within the bone matrix in SO (Figure 8.5E), or they have a spindle-like or flat shape, and the long axis of the soma is aligned (with some degree of obliquity: cf. Marotti 1979) with the general direction of collagen fibers, in the lamellar or parallel-fibered matrices produced by DO (Figure 8.5F). As Kerschnitski et al. (2011) showed, the dominant orientation of osteocyte somas generally "mirrors" the spatial geometry of the matrix. When osteoblast embedding is complete, each osteocyte thus created is encased in a lacuna whose morphology closely reflects that of the cell, and is thus highly characteristic of bone tissue types. Fossilization seldom drastically alters the morphology of cell lacunae, which thus constitute a precious clue to tissue identification in paleohistology. A pericellular space, most often some 170 to 300 nm wide (Baud 1962), separates the cell from the wall of its lacuna. Quantitative data by Marotti et al. (1985a) indicate that the osteocytes (as well as the former osteoblasts) in woven-fibered matrices (i.e., SO) are larger than those of lamellar bone. However, osteocyte size is highly variable, even for morphologically similar cells within a single bone layer (see the study of osteons by Hannah et al. 2010).

The most spectacular aspect of osteoblast transformation into osteocytes is the development of cytoplasmic, dendrite-like processes of variable abundance and direction (recent morphological review in Weinkamer et al. 2019). These processes are slender (50–410 nm in diameter; average 104 nm) and housed within the bone matrix in a complex network of interconnected tunnels 80–710 nm in diameter (with a 260 nm mean value) called the *canaliculi*. A 70- to 80 nm gap separates each cell process from its canaliculus (detailed quantitative data in You et al. 2004). The supply of oxygen and nutrients to intracortical cell populations depends on intercellular communications through the canalicular networks (reviews in Bonewald 2011 and Bellido et al. 2014). These networks are chiefly involved in the transduction and transmission of mechanical information through bone cortices (e.g., You et al. 2001, 2004). Within woven-fibered matrices, perisomatic canaliculi develop in all directions as bushy, highly branching formations; conversely, in parallel-fibered and lamellar matrices, the canaliculi of a single osteocyte develop perpendicular to the major axis of the cell and tend to be subparallel to each other, creating a peg-like pattern mainly oriented toward blood vessels (Marotti 1979). According to Reznikov et al. (2013, 2014a, b), canaliculi in parallel-fibered and lamellar tissues mainly extend into the "disordered" (i.e., woven-fibered) interstitial formations.

Although quantitative data for the stellate osteocytes of the woven-fibered tissue are scarce, these cells seem to have more dendrite processes (and their lacunae more canaliculi) than the flat or spindle-like osteocytes of lamellar and parallel-fibered tissues do (Marotti et al. 1985b). In a normal secondary osteon, the global, accumulated length of the canalicular network per volume unit, as computed by Repp et al. (2017), reaches 0.074 µm/µm^3 (i.e., 74 km/cm^3). However, these authors emphasized the spatial heterogeneity of canalicular distribution within a single section. It is common to observe broad fields in a section where canaliculi are absent around cell lacunae, whereas neighboring sectors may display dense canalicular networks (Figure 8.5G). In secondary osteons, canalicular density is not influenced by the size of the osteons or by the relative volume (or area) occupied by osteocyte somas. The spatial density of cell lacunae is also highly variable. To our knowledge, the only study (Hernandez et al. 2004) comparing this parameter in woven-fibered and lamellar tissues with the same methodology (cell density per mm^2, observed in cross sections from cortical bone) shows that woven-fibered matrices generally contain more cell lacunae (10% to 36% more) than lamellar matrices. However, this difference is statistically significant only in fracture calluses, in which osteocyte density is 125% greater than in

VetBooks.ir

lamellar bone (1875 cells per mm^2 vs. 834 cells per mm^2). Along with cell morphology and orientation, cell lacuna density is an important clue for bone tissue classification.

Osteocyte populations, as well as the morphology of individual cells, are often exquisitely preserved in fossils and may allow sophisticated 3D reconstructions and morphometric analyses (e.g., Neves and Tarlo 1965; Cadena and Schweitzer 2012). Cell characteristics prove to be fairly conservative among vertebrates, although clear differences, mainly related to canalicular development, have been observed between teleosts and tetrapods (Cao et al. 2011).

Other Significant Features of Bone Matrices

Osteons

In its current meaning, the term osteon designates thick-walled intracortical tubes, resulting from a centripetal osseous deposit centered around a blood vessel. Typical tubular osteons are mainly observed in compact cortices; their occurrence is rarer in cancellous formations. A basic dichotomy distinguishes primary osteons (Figure 8.6A), which form at the surface of growing periosteal cortices in pace with the accretion of new cortical layers, from secondary osteons, or Havers' systems (Figure 8.6B), which result from a remodeling process (Haversian substitution) comprising initial local resorption of bone cortices, followed by secondary (reconstructive) deposition. Enlow and Brown (1957) described another type of primary osteons that they named *protohaversian systems*. The latter develop (without a previous resorption phase) within medullary cancellous tissues, at the intersections of endosteal trabeculae. The expression *hemi-osteon* (Parfitt 1994) refers to similar structures as secondary osteons, but they are located on the surface of trabeculae in cancellous formations (see Chapter 11). Hemi-osteons (Figure 8.6C) also result from a resorption-reconstruction process, and they reflect the basic form of trabecular remodeling in cancellous bone.

Whatever the location and the mode of formation of osteons, they consist of constant and easily recognizable structures, contributing to define several types of osseous tissues. Primary and secondary osteons are known in early gnathostomes such as the Devonian placoderms *Bothriolepis* (Downs and Donoghue 2009) and *Incisoscutum* (Giles et al. 2013); however, their frequency among vertebrate taxa, as well as their location in the bones of a single skeleton and their spatial density in the sectors of a single section, are greatly variable in connection with several factors interacting with each other in conditions still incompletely understood. The walls of all osteons have a lamellar or parallel-fibered matrix. Previous paragraphs of this review reported the controversy about the basic structure of lamellar matrices. Studies of this issue were nearly all based on osteonal material; it is thus unnecessary to consider this topic again.

Primary Osteons in Compact Cortices

While the centrifugal osteogenic activity of periosteal osteoblasts proceeds, periosteal blood vessels are trapped within the yet unmineralized osseous tissue (osteoid) to finally constitute most of the vascular network of the cortex (review in Francillon-Vieillot et al. 1990). Although some cortical blood vessels may originate from the medullary region, the capillaries that form primary osteons are always derived from the periosteum (Gabe 1967). Unfortunately, the numerical and geometrical relationships between them and the periosteal vascularization remain poorly documented. A wide groove lined by periosteal osteoblasts and filled with a loose connective tissue initially surrounds the blood capillary within the osteoid. The open part of the groove is then progressively closed by converging deposits from the osteoblasts of the cambial periosteal layer, and the groove becomes an intracortical tunnel. The osteoblasts lining the lumen of this tunnel proceed, through typical DO, to the centripetal accretion of a thick layer of lamellar or parallel-fibered matrix around the blood capillary; a primary osteon is thus created. Figure 8.6D shows some stages of osteonal formation, as seen in the femur of a fossil crocodile, *Goniopholis*. The spindle-like or flat osteonal cells display numerous cytoplasmic processes (and thus canaliculi) converging toward the central capillary (Figure 8.6B, inset). Primary osteons are structurally continuous with the matrix of the cortex, which can be either woven-fibered or parallel-fibered tissue (primary osteons are only exceptionally present in lamellar bone). No gap ever occurs between them; however, when the cortical matrix is of the parallel-fibered type, it is deflected around the osteons. The average diameter of primary osteons is variable (50–100 µm are commonly observed: Burr and Akkus 2014), as are their possible orientations within the cortex, as described above. When inserted within woven-fibered matrices, primary osteons constitute the so-called fibrolamellar complexes. Tissues of this kind are presented in more detail below. The mode of formation of primary osteons in endosteal tissues remains poorly documented.

Secondary Osteons

Considerable research has been dedicated for decades to the structure, mode of formation and role of secondary osteons, which are chiefly involved in the mechanical and physiological functions of the skeleton. In extant and extinct vertebrates, secondary osteons are mainly distributed in medium- to large-sized tachymetabolic species, but they may nevertheless occur, in lesser density, in smaller or bradymetabolic taxa (see Enlow and Brown 1956, 1957). As a result of inner cortical remodeling, secondary osteons do not properly define a type of osseous tissue, unless their spatial density is so high that they totally occupy the area of a section (at least at a local scale), excluding any trace of the previous, primary periosteal bone.

Morphologically, secondary osteons (Figure 8.6B) are roughly similar in structure to primary ones, but several important differences distinguish them. (1) They have a broader diameter (100–250 µm) and their wall contains up to 25 lamellae versus less than 10 (Burr and Akkus 2014). (2) Because they result from secondary accretion, following previous local resorption, their outer contour is always bordered by a reversion line (also called "cementing line"; Figures 8.6B inset, 8.6E and 8.6F), further described below. This line, and the outermost osteonal lamellae in contact with it, appear birefringent in polarized light and translucent in fossil material. (3) The blood vessel housed in the central canal, the Havers' canal, of each secondary osteon anastomoses with those of neighboring osteons through short orthogonal branches

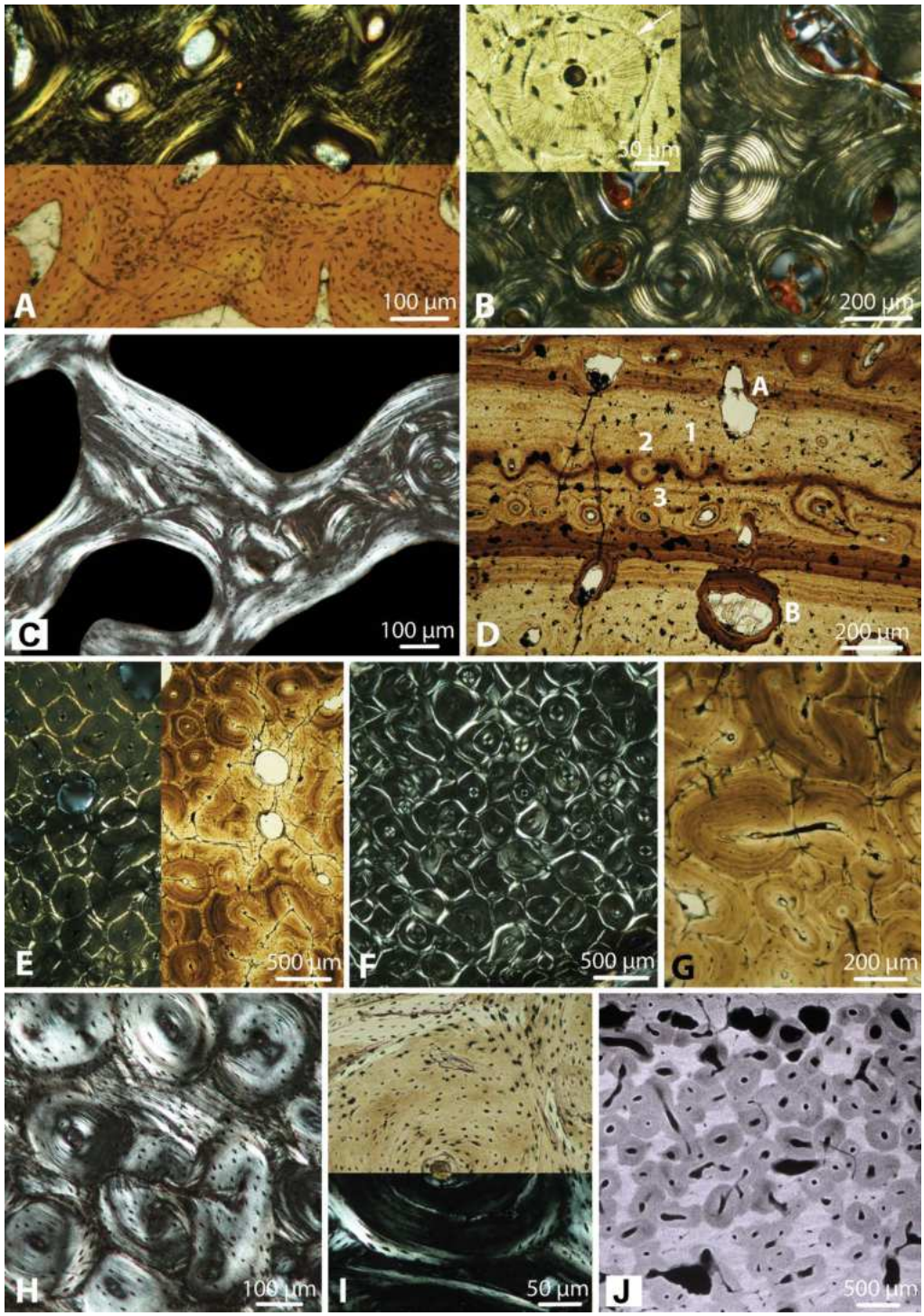


FIGURE 8.6 The osteons. A, Primary osteons in the limb bone cortex of an undetermined hadrosaurian dinosaur (possibly *Telmatosaurus*) from the Upper Cretaceous (Maastrichtian) of Western Europe. Upper field: polarized light. B, Secondary osteons in a rib of the Miocene desmostylian (afrotherian mammal) *Paleoparadoxia tabatai*. Inset: typical aspect of a secondary osteon, bordered by a reversion line (arrow) in a rib of the extant fur seal *Otaria flavescens*. C, Hemi-osteons in the medullar trabeculae of a rib from a beluga *(Delphinapterus leucas)*. Polarized light. D, Basic stages of the formation of primary and secondary osteons in the femur of an extinct crocodilian, *Goniopholis* sp. (Upper Jurassic–Lower Cretaceous). The numbers 1, 2 and 3 indicate three stages of primary osteon formation. The letters A and B indicate two stages of the formation of secondary osteons. E and F, Aspect of reversion lines in ground sections from fossil (E) and extant (F) bone samples from, respectively, the Upper Miocene (Tortonian) xenarthran *Thalassocnus littoralis* and the artiodactyl *Hexaprotodon*. G, Volkmann's canal in the rib cortex of *T. littoralis*. H, Atypical secondary osteons made of nonlamellar, brightly birefringent parallel-fibered tissue in the humerus of the dwarf seal *Nanophoca vitulinoides* (Miocene of Northern Europe). I, Atypical secondary osteon made of a nonlamellar, poorly birefringent parallel-fibered tissue in the premaxillae of the Miocene ziphiid cetacean *Choneziphius leidyi*. Polarized light. J, X-ray proof showing secondary osteons in the exoccipital bone of the extant sirenian (afrotherian mammal) *Dugong dugon*. Compared to the surrounding bone, the osteons are undermineralized.

VetBooks.ir

(Figure 8.6G) running in Volkmann's canals (e.g., Cooper et al. 2003; Pazzaglia et al. 2012; Maggiano et al. 2016). As observed in cross sections in polarized light, the lamellar matrix in the walls of secondary (as well as primary) osteons may have three distinct appearances (e.g., Marotti 1979; Marotti and Muglia 1992; Ascenzi et al. 2003; Bromage et al. 2003; Ascenzi and Lomovtsev 2006): (1) alternate birefringence and monorefringence (the most common appearance; Figure 8.6B) due to a quasi-orthogonal crossing of the fibers between adjacent lamellae; (2) homogeneous birefringence (Figure 8.6H), indicative of a dominant orientation of collagen fibers parallel to the sectional plane in adjacent lamellae and (3) homogeneous monorefringence (Figure 8.6I), indicative of a gross longitudinal orientation (i.e., orthogonal to sectional plane) of the fibers in all lamellae. Havers' systems are often less mineralized than the surrounding bone because mineralization proceeds much more slowly in their walls than in primary tissues (Figure 8.6J; see also Marotti et al. 1972). In long bone cortices, secondary osteons tend to be quasi-aligned, with some obliquity, with the bone's sagittal axis (Heřt et al. 1994). Their direction can, however, be different or locally deflected under entheses (see Ricqlès 1975) or when sharp relief exists. Haversian remodeling is a cumulative process that ceases only with death. Consequently, the bone cortices of many taxa display densely packed osteonal populations representing several successive generations of osteons (see below).

Cyclical Growth Marks, Rest Lines and Reversion Lines

Annuli and lines of arrested growth (LAGs), i.e., the cyclical growth marks, result from an annual (sometimes biannual) drop in skeletal growth rate that leaves a trace in primary periosteal cortices (reviews in Warren 1963; Castanet 1981; Klevezal 1996). Initially considered typical of taxa with ecto- and poikilothermic metabolic regimes, annuli and LAGs are now known to occur in all vertebrates, including humans, and reflect, at least in part, a highly plesiomorphic and ancient endogenous rhythmicity of constant (usually annual) periodicity. Growth marks, in one form or another, occur in all types of bone tissue, and their sharpness often depends on the influence of external, stochastic factors related to climate and local ecology. As such, they cannot be considered true histological characteristics that define any type of osseous tissue. Their presence, and occasional absence, in primary periosteal deposits are nevertheless significant structural features that must be mentioned in the description of bone sections. The utility of growth marks is considerable in two respects: age determination and reconstruction of local morphogenetic events. Cyclical growth marks are often very well preserved in fossil material and even enhanced by the impregnation of bone matrix by natural dyes (see below and Chapter 31). Some basic traits of annuli and LAGs, considered only in the frame of osseous matrices, are briefly reviewed here.

Annuli

Any cyclical modification in the matrix structure of primary cortices should be considered an annulus, provided it is represented by a layer more than *ca.* 10 µm. There is no unique histological definition of annuli: their structure, as well as their sharpness, width and spacing are a matter of context (Figure 8.7A, B). They basically reflect a temporary decrease in growth rate, and many structural details in osseous matrices (as well as cells and vascular canals) can express this phenomenon. For example, when the type of matrix deposited during active growth phases is woven fibered, the annuli are then of either the parallel-fibered or the lamellar types. Similarly, if the "background matrix" is parallel fibered, the annuli will then consist of lamellar bone.

Lines of Arrested Growth

Some terminological imprecision has persisted about LAGs and, more generally, the category of so-called "cementing lines". Several authors (e.g., Klevezal 1996), used the term cementing lines to designate the LAGs, whereas others (e.g., Francillon-Vieillot et al. 1990) considered the *rest line* identical to the LAG, both being placed within cementing lines, along with reversion (or resorption) lines. It is preferable to distinguish among these three types of lines which, beyond an obvious morphological similarity, do not have exactly the same histogenetic meaning. Designating them by the same expression could therefore result in a loss of information.

In decalcified sections of recent bone, LAGs are easily revealed by topographic dyes (especially Ehrlich's hematoxylin), because they are strongly chromophilic (Figure 8.7C). Their structural definition is much more precise than that of the annuli. In simple ground sections of recent bone viewed in transmitted polarized light (Figure 8.7C), they appear as thin (i.e., 5–10 µm; Castanet 1981), brightly birefringent layers (e.g., Buffrénil and Castanet 2000). In fossils, their aspect varies with taphonomic conditions, but they often appear as black lines (Figure 8.7D). On X-ray proofs, LAGs generally appear slightly more mineralized than the surrounding bone. Measurements by Castanet (1979, 1982) showed a 2–3% difference between them, with broad variability. Due to their relatively high mineral content, LAGs are quite visible on tomographic documents, even in very ancient material such as the Early Silurian anaspids studied by Keating and Donoghue (2016). Their collagen network seems sparser than that of the surrounding matrix, but their content in "ground substance" (i.e., noncollagenous proteins) is higher (Castanet 1981). These characteristics may explain their relative hypermineralization.

Rest Lines

Rest lines are very similar to LAGs in both structural and functional aspects. They are set in place when periosteal (and less frequently endosteal) accretion resumes after a period of arrest. Their structure, like that of the LAGs, is also characterized by sparse collagen fibers, abundant noncollagenous proteins and a relatively high mineral content (Frasca 1981). The only difference they have from LAGs is that their formation is not cyclical; it depends instead on local morphogenetic events and therefore reflects fairly distinct subjacent deterministic factors.

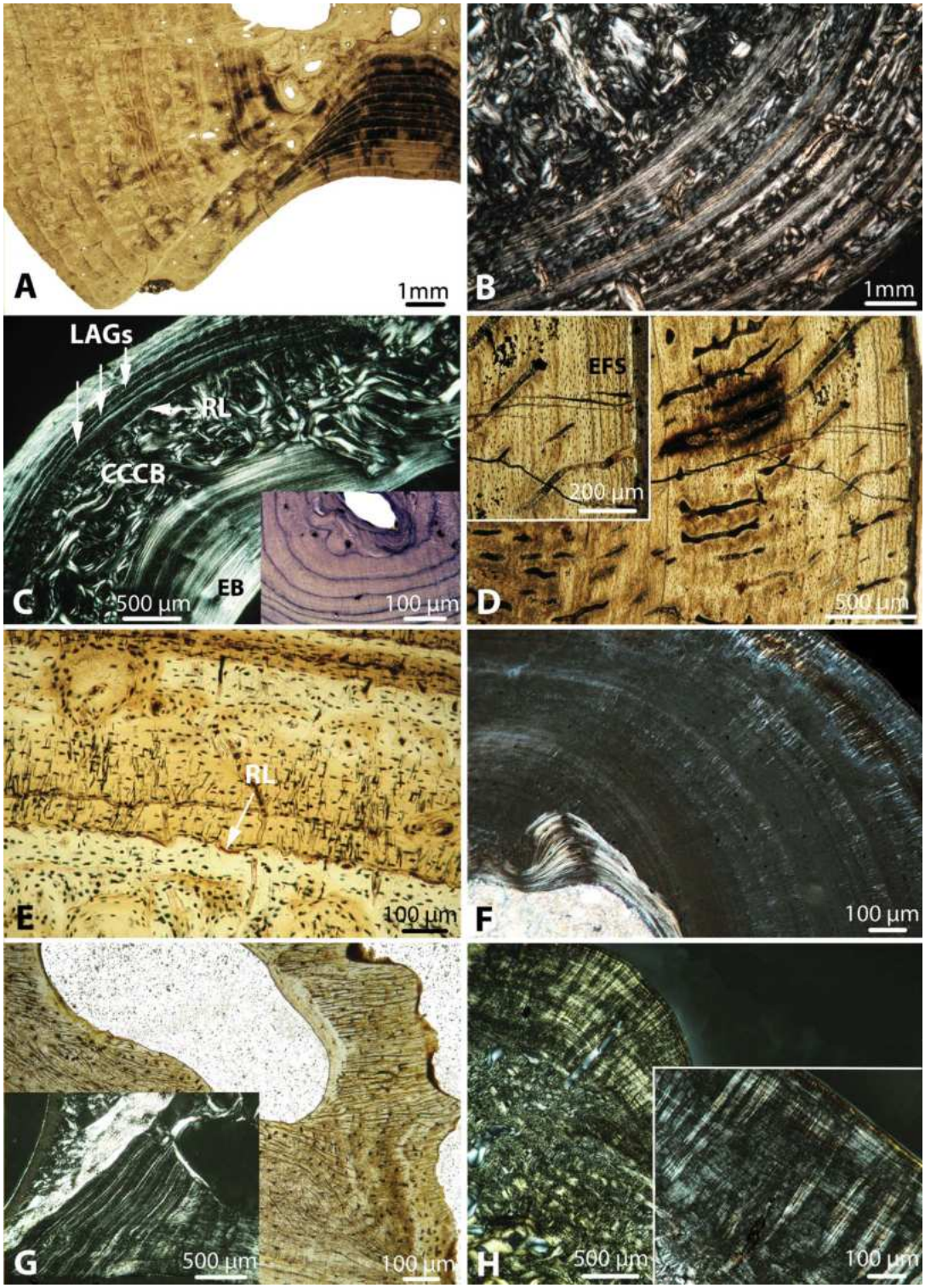


FIGURE 8.7 Other, accessory components of the bone matrix: annuli, lines of arrested growth (LAGs), resorption lines and Sharpey's fibers. A, Annuli and zones in the frontal bone of the early Miocene (Aquitanian) alligatorid *Diplocynodon ratelii*. B, Diffuse, birefringent annuli made of parallel-fibered tissue in the humerus of *Nanophoca vitulinoides*. Polarized light. C, LAGs. Main frame: birefringent aspect of the LAGs in polarized light. Femur of the extant river otter, *Lutra lutra*. Inset: chromophilic LAGs in a section of decalcified bone stained with Ehrlich's hematoxylin in the femur of the urodele *Triturus marmoratus*. CCCB, compacted coarse cancellous bone; EB, endosteal bone; RL, resorption line. D, Closely spaced LAGs forming an external fundamental system (EFS) in the femur of the Late Carboniferous/Early Permian synapsid *Ophiacodon insignis*. E, Typical crenellated aspect of a line of reversion (RL) in the humerus of *N. vitulinoides*. F, Short birefingent (likely mineralized) Sharpey's fibers in the femur of the Middle Miocene anuran *Latonia gigantea*. Polarized light. G, Long anchorage equatorial fibers in an osteoderm from *Placosaurus rugosus*. Inset: same kind of fibers in the centrum of a vertebra from *Varanus niloticus*. H, Main frame and inset: long anchorage fibers orthogonal to the bone surface in an osteoderm of the turtle *Trionyx triunguis*. Polarized light.

VetBooks.ir

Reversal (Cementing or Resorption) Lines

These lines (Figure 8.7E) share with LAGs and rest lines a similar (though slightly lesser) thickness of some 5 µm at most (Milovanovic et al. 2018), a strong chromophilia, and some degree of hypermineralization (6–8%, compared to osteonal lamellae: Philipson 1965; Castanet 1982; see also Skedros et al. 2005; Milovanovic et al. 2018 and Burr et al. 1988 for contrasting data). They can, however, be easily distinguished by at least two conspicuous characteristics: they are typically scalloped, an aspect revealing that they are constituted by the linear addition of Howship's lacunae resulting from osteoclast activity, and the geometrical orientation and, most often, the histological structure of bone layers on both sides of a reversion line are discordant. These lines are thus characteristic of a remodeling process, showing the limit reached by the initial resorption and the level from which the subsequent reconstruction process started. Their functional meaning is therefore clearly different from that of LAGs and resting lines. The ultrastructure of reversion lines remains incompletely documented. They basically constitute a gap in matrix structure, characterized by scarceness of collagen fibrils and a relative abundance of noncollagenous proteins (especially glycosaminoglycans and osteopontin; Burr and Akkus 2014). In fossils, the visibility of these lines is often enhanced by the local infiltration of the bone matrix by natural dyes. Like cyclic growth marks and rest lines, reversal lines are essential elements for understanding the growth and remodeling events once at work in a bone. For this reason, they must be considered in the description of sections. However, these lines (along with LAGs and rest lines), likely to occur in all types of osseous matrix, are by no means a diagnostic character for any of them.

Sharpey's Fibers

A current trend is to designate as "extrinsic" or, more commonly, "Sharpey's" fibers, all fibers that anchor to a bone, a tissue or an organ external to the bone (review in Aaron 2012). Other terms such as the early but misleading expression "perforating fibers" (e.g., Quigley 1970) are occasionally used. The most frequent situation is the anchorage of teeth into alveolar bone, or that of the fibrous layer of the periosteum, skin or muscle tendons into primary cortices. However, according to Aaron (2012), Sharpey's fibers might have broader and diversified functions. These fibers occur only in periosteal deposits; endosteal layers are necessarily devoid of such fibers (moreover, the endosteum has no fibrillar layer; e.g., Marotti et al. 1992). Aaron (2012) described periosteal Sharpey's fibers extending up to the wall of the medullary cavity, presented as the "endosteal" surface of a bone. Of course, this situation can occur only if no secondary endosteal bone layer has been previously deposited around the medullary cavity. Sharpey's fibers are liable to be resorbed with the substrate in which they are inserted, and when marked cyclical growth occurs, they may either be continuous through the cortex or show a cyclically interrupted pattern (Figure 8.7F). Up to now, the great majority of studies of Sharpey's fibers deal with the periodontium. Few detailed data are available about, e.g., the anchorage of the periosteum in the superficial layers of cortices, or the processes through which Sharpey's fibers are incorporated into bone.

Sharpey's fibers are principally made of collagen Type I, with variable contributions of Types III and VI, in periodontal bundles (Aaron 2012) as well as muscle entheses (Saino et al. 2003; Luther et al. 2003). Within the bone matrix, they consist of relatively thick bundles 6–7 µm in average diameter (up to 25 µm in the periodontium) for a broadly variable length (Jones and Boyde 1974; Hieronymus 2006). The fibers anchoring the diaphyseal periosteum of limb bones are relatively short (some 30–80 µm in the *Latonia* femur shown in Figure 8.7F), but in sutures or in the cortex of vertebral centra, their length may be much more important (Figure 8.7G). Similarly, the spatial density of Sharpey's fibers can be low or very high (Jones and Boyde 1974), as typically exemplified by extensive muscle insertions, suture regions or the extensive bundles running at right angles in the outer cortex of turtle shells (e.g., Hieronymus 2006; Buffrénil et al. 2016; see also Figure 8.7H). Sharpey's fibers can be in such high density locally that the bone matrix housing them is specifically called *Sharpey's fiber bone* (e.g., Boyde and Jones 1968). Extrinsic fibers may occur in any type of matrix, provided it is a primary periosteal formation. Within bone cortices, the bundles of Sharpey's fibers mineralize by the superficial adjunction of hydroxyapatite crystals in variable thickness (Jones and Boyde 1974). Most often, the core of the bundles remains unmineralized, especially when the accretion rate of cortices is high (Boyde 1972). Except for the so-called Sharpey's fiber bone, which can be considered a special kind of matrix because of the volume occupied by extrinsic fibers, Sharpey's fibers are additional structural details, which deserve to be mentioned in the histological description of a section for the many details they can reveal about, e.g., muscle attachment in cortices, but they are irrelevant to define any osseous matrix category.

Current, Integrative Classification of Primary Compact Tissues

Tissue types are independent of the identity of individual elements, i.e., homologous bones of diverse taxa may have very different tissue types in the same anatomical region (e.g., at mid-diaphysis). Tissue types are only loosely related to the morphology (long, flat and short) of the bones, their intraskeletal location (endoskeleton vs. dermal skeleton) and the gross organogenetic process from which they derive (endochondral vs. membrane ossification). Comparative data currently available tend to confirm the synthesis of Ricqlès (1975, 1977): the factors involved in the intraskeletal and interspecific distribution of bone tissue types are to be sought in the absolute size of skeletal elements (not their relative size, compared to other elements) and their accretion rate.

Woven-Fibered Tissue

This tissue basically consists of a woven-fibered matrix housing large, multipolar osteocytes randomly oriented within the matrix (Figure 8.8A). These cells have a rich arborescence of ramified cytoplasmic processes spreading in all directions around the soma. According to histomorphometric

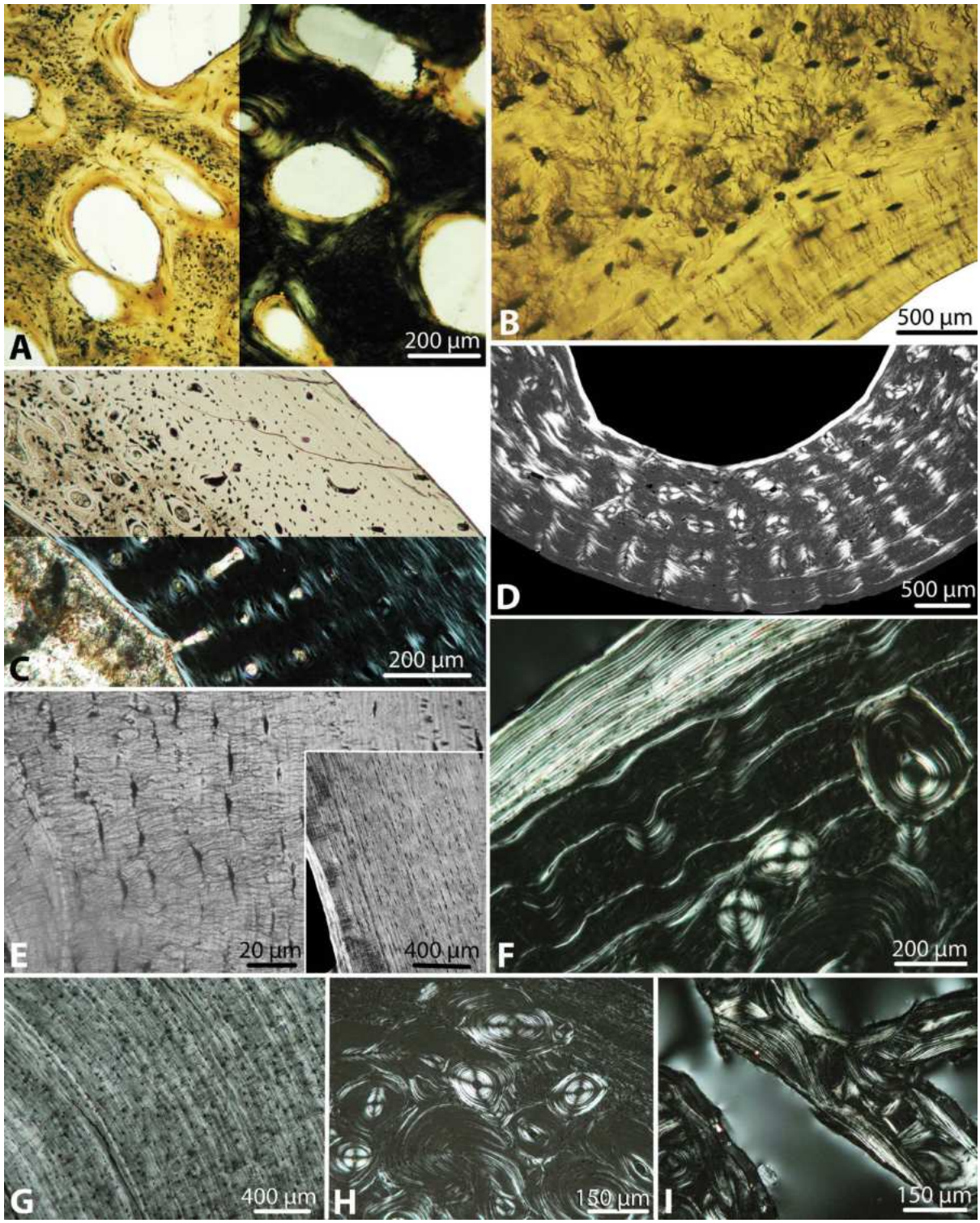


FIGURE 8.8 Simple tissue types. A, Woven-fibered bone tissue in the humerus of *Omphalosaurus nisseri*. Right half: polarized light. B, Different aspect of cell lacunae in woven-fibered (upper left) and lamellar (lower right) tissues. *Varanus niloticus* femoral shaft. C, Woven-fibered bone tissue (lower third of the cortex) with both simple canals and primary osteons in the femur of the Early Carboniferous synapsid *Clepsydrops limbatus*. Lower half: polarized light. D, Parallel-fibered tissue with a longitudinally oriented collagen meshwork and longitudinal primary osteons in the femur of *Varanus niloticus*. E, Two aspects of the parallel-fibered tissue viewed in longitudinal section. In the main frame (femur of the lizard *Amblyrhynchus cristatus*), the osteocyte lacunae have abundant *canaliculi*, whereas in the inset (femur of the anuran *Conraua robusta*), the *canaliculi* are much less developed. Polarized light. F, Haversian remodeling in the parallel-fibered tissue of the river otter (*Lutra lutra*) femur. Polarized light. The parallel-fibered tissue appears monorefringent here (longitudinal fibers cut transversally). It is covered by a layer of birefringent lamellar tissue. G, Lamellar tissue in the femoral cortex of *Iguana iguana*. Polarized light. H, Secondary osteons made of lamellar bone in the femur of *L. lutra*. Polarized light. I, Lamellar tissue in the hemi-osteons of the remodeled trabeculae of a *Desmostylus* sp. rib.

VetBooks.ir

measurements in the rat femur by Hernandez et al. (2004), cell lacuna density is not significantly different in primary lamellar (834 ± 83 lacunae/mm^2) and woven-fibered (921 ± 204 lacunae/mm^2) tissues. However, considering the larger size of the osteocytes in woven-fibered tissue (Figure 8.8B), the *total fractional lacunar volume* (i.e., the volume, or area, occupied by all cell lacunae compared to the total volume, or area, of local mineralized bone) is much greater in the woven-fibered tissue than in other types of bone (Parfitt 1983). Moreover, the woven-fibered tissue in fracture calluses has 100% more osteocyte lacunae (1875 ± 270 cells/mm^2) than lamellar tissue does (Hernandez et al. 2004).

When it is well characterized, woven-fibered tissue is easily recognizable under both ordinary transmitted light (the morphology and orientation of cell lacunae are then diagnostic) and polarized light that reveals the monorefringence of its matrix, whatever the orientation of the sectional plane (Figure 8.8A). Woven-fibered tissue typically forms from subperiosteal accretion through SO during stages of fast growth (Castanet et al. 2000; Margerie et al. 2002). It is thus a primary tissue normally unknown in secondary and/or endosteal deposits. An exception could possibly be the endosteal tissue (of uncertain interpretation) observed by Chinsamy et al. (2016) in the bones of *Saltasaurus loricatus*, a titanosaurian sauropod. When it constitutes the main component of compact cortices, woven-fibered bone is principally observed in fetuses and juveniles of medium-sized or large species (Parfitt 1983; Ricqlès 1975), principally (but not exclusively) endotherms. This tissue is most often transitory, and it is soon erased and replaced by secondary deposits of parallel-fibered and lamellar tissues, through the combined effect of intra-cortical remodeling and the enlargement of the medullary cavity. It is seldom observed in adults, except in small parts of the deep cortex spared by resorption. Woven-fibered tissue commonly occurs in the core of the trabeculae forming fine cancellous bone (e.g., Buffrénil and Mazin 1990), especially in the initial scaffold of woven-parallel complexes, as further described below. Compact formations of woven-fibered tissue are generally vascularized, and may contain simple vascular canals, primary or secondary osteons. All possible orientations and spacing patterns of canals (including the combination of diverse orientations) are likely to occur; however, considering the short duration of woven-fibered tissue during ontogeny and its restricted occurrence in adults, only some vascular patterns (mainly longitudinal canals; Figure 8.8C) are commonly observed. Like all bone tissue types, woven-fibered tissue can display reversion lines if locally remodeled, and cyclical growth marks in the form of annuli and LAGs. When inserted between annuli, it forms the so-called "zones" that represent the fast growth stages of yearly growth cycles (e.g., Castanet 1974).

Parallel-Fibered Bone Tissue

This tissue is extremely common in extant and extinct vertebrates. In ectotherms (Figure 8.8D), it constitutes the major part of primary periosteal cortices in most taxa and all kinds of bones (see, e.g., comparative reviews in Enlow and Brown 1957, 1958; Ricqlès 1976; Ricqlès et al. 1991 and Castanet et al. 2003). In endotherms, this tissue often occurs in annuli and in a broad part of the peripheral cortex (when spared by remodeling), especially in the *external fundamental system* (further considered below), which marks the end of local skeletal growth. Parallel-fibered bone, however, is not exclusively periosteal in origin; it may also be observed, although less frequently, in endosteal deposits (see Figure 8.1D). It consists of a parallel-fibered matrix including spindle-like or flat osteocytes (cell lacunae in dry and fossil bone) oriented parallel to the general direction of the collagen fibers; the latter are parallel to the outer contours of the bones (Figure 8.8E). Specific data on osteocyte lacuna density in parallel-fibered bone remain scarce because most studies are relative to densely remodeled human long bones, where remnants of parallel-fibered tissue between the osteons are scarce. A density of 312 lacunae · mm^{-2} in the interstitial tissue, and 274 lacunae · mm^{-2} in monorefringent osteons (i.e., parallel-fibered bone in both cases) were observed by Bromage et al. (2016). Similarly, morphometric data on individual cell lacunae in parallel-fibered bone are, to our knowledge, still needed. Considering the similarity of lacunar morphology in the tissues resulting from DO (i.e., slender spindle-like morphology), the data dealing with lamellar bone can also be considered to represent parallel-fibered bone. According to Dong et al. (2014), the mean dimensions of individual lacunae in such tissues in humans is 409.5 ± 149.7 µm^3, 336.2 ± 94.5 µm^2 and 18.9 ± 4.9 × 9.2 ± 2.1 × 4.8 ± 1.1 µm. The development of *canaliculi* around the cell lacunae is variable: *canaliculi* may be very sparse or occur at higher densities (Figure 8.8E). In ground sections from recent and fossil bone, parallel-fibered tissue is easily recognizable by its mass birefringence in polarized light (Figure 8.8E, inset). However, as mentioned above, this aspect occurs only if collagen fibers are oriented parallel to the sectional plane, which prompts the use of two perpendicular sections to avoid interpreting a parallel-fibered tissue with fibers and cells cut orthogonally as woven-fibered bone (monorefringence) (Figure 8.8D; see on this topic Stein and Prondvai 2014 and Canoville et al. 2017). Cyclical growth marks, in the form of lamellar annuli or LAGs, are seldom absent within parallel-fibered primary (and sometimes secondary) formations, including in tachymetabolic animals such as eutherian mammals (Klevezal 1996, Castanet 2006). Similarly, Sharpey's fibers often occur in this tissue type, and are made conspicuous by the high translucence of the bone matrix. Parallel-fibered bone can be either totally avascular, as exemplified by most extant lissamphibians (Canoville et al. 2017) and squamates (Buffrénil et al. 2008), or house a dense vascular network of simple canals or/and primary osteons (Figure 8.8D). For both types of canals, several orientations may occur; however, to our knowledge, well-characterized laminar and plexiform orientations have not yet been documented in parallel-fibered cortices. Remodeling can be active in this tissue (Figure 8.8F), but it seldom results in densely packed secondary osteons, as is commonly observed in woven-fibered tissue.

The Lamellar Tissue

Most fundamental knowledge about bone biology refers to the lamellar tissue that, in one form or another, constitutes most of the volume of "mature" bone in adult eutherian mammals, and especially humans and other primates (e.g., Cummaudo

VetBooks.ir

et al. 2018). Because parallel-fibered and lamellar tissues both result from DO, they share a matrix basically made of parallel fiber bundles, along with spindle-like or flat cells (and cell lacunae) oriented parallel to the fiber meshwork in which they are embedded. Their main difference is, of course, the occurrence of lamellae, as described above, within the matrix of the lamellar tissue (Figure 8.8F). In its most common form, lamellar tissue is an orthogonal plywood, as described above. The more complex structure of twisted plywood is less frequent (the peculiar case of isopedin, a specialized form of twisted plywood, is further considered below). Lacunar density in lamellar bone is *ca*. 340 * mm^{-2} (Bromage et al. 2016; see also Metz et al. 2003). A density of some 20,000 cell lacunae per cubic millimeter has been recorded by Dong et al. (2014).

When representing primary periosteal bone, lamellar tissue may occur in the whole cortex of small taxa or small bones (Figure 8.8G). In larger taxa, or larger skeletal elements, it forms a part of the walls of primary osteons and the outermost (terminal, during growth) external fundamental system (Figure 8.8F). Additionally, it is the main, and by far the most common, component of secondary osseous deposits, whether located around the medullary cavity to form the so-called *inner fundamental system* (Figure 8.8E, inset), on the walls of secondary osteons, or on the surface of remodeled trabeculae (Figure 8.8H, I). As mentioned above, lamellar deposits are then bordered by a reversion line and appear in discordance with neighboring bone strata. Vascular canals, mainly represented by simple longitudinal canals, are sparse in lamellar bone; however, radial canals housing vessels derived from the medullary vascularization are commonly observed in birds and mammals (examples in Enlow and Brown 1958; Margerie et al. 2002). Sharpey's fibers in lamellar bone are restricted to primary subperiosteal deposits.

Specialized Terminology Related to Lamellar or Parallel-Fibered Tissues

Such terms relate either to contingent characteristics (e.g., cyclical growth marks) or the position of parallel-fibered and lamellar tissues in a section. They are convenient, synthetic designations, but they do not necessarily imply a definite, original structure at a histological level.

External and Internal Fundamental Systems

The terms *external* and *internal* fundamental systems (also called *outer* and *inner circumferential lamellae*; see Enlow 1963) both designate layers of parallel-fibered or lamellar tissues, variable in thickness, located either along the outer (or peripheral) margins of periosteal cortices in fully developed adult individuals (external fundamental system), or on the wall of the medullary cavity (internal fundamental system; Figure 8.8E, F). The external fundamental system reflects the steep decrease in subperiosteal accretion rate that occurs at the end of somatic growth. It is most often a primary deposit continuous with underlying osseous strata, but it can occasionally be secondary in relation to local morphogenetic processes, especially in mammals (see Chapter 29). Conversely, the formation of the internal fundamental system is not closely dependent on individual growth stage and is unrelated to the rate of local skeletal growth. It is always a secondary (and centripetal) endosteal deposit, bordered by a reversion line. It partly reconstructs the wall of the medullary cavity after an episode of resorption. The internal fundamental system is often asymmetrical, reflecting a drift in the growth in diameter of the medullary cavity.

On Intermediate Tissue Types

As mentioned above, the histological characteristics of osseous tissue are not discrete variables with clear-cut and perfectly differentiated categories. Many authors (e.g., Ricqlès 1975; Margerie et al. 2004, etc.) have described intermediate or ambiguous forms of tissue organization. This is especially the case with parallel-fibered bone, which may locally display some features of lamellar tissue (faint differentiation of lamellae; Figure 8.9A) or turn to the woven-fibered type (feeble mass birefringence and randomly distributed cell lacunae; Figure 8.9B, C). This situation has prompted some authors to create new, self-defined descriptive terms. For example, atypical parallel-fibered bone with features reminiscent of woven-fibered tissue was named *coarse parallel-fibered bone* by Klein et al. (2016) or *uncommon parallel-fibered* bone by Houssaye et al. (2013). The many variations encountered in intermediate forms of tissue challenge any attempt to regulate the terminology used for these tissue types. Therefore, some degree of "verbal creativity" should be tolerated, provided it is supported by precise histological descriptions and illustrations.

Remarks on the "Lamellar-Zonal" Tissue

The expression *lamellar-zonal* is frequently used as a collective designation for primary lamellar or parallel-fibered formations of periosteal origin regardless of whether or not they are vascularized (by simple canals or primary osteons). Although the occurrence of cyclical growth marks is not formally mentioned in the authoritative definition that Ricqlès (1975, p. 102) gave of this tissue, Currey (2002) pointed out that, in addition to the above-quoted characteristics, lamellar-zonal bone is "particularly characterized by zones where growth comes to a halt then starts again". Therefore, this tissue should be viewed, in brief, as lamellar or parallel-fibered primary bone with evidence of cyclic growth (annuli or LAGs). As such, the actual meaning of the term *lamellar-zonal* would seem clear; however, its current use in comparative histology has become eclectic. It encompasses, on the one hand, the pure avascular, nonremodeled and homogeneous formations of lamellar or parallel-fibered bone with LAGs encountered in small ectopoikilothermic tetrapods (i.e., most lissamphibians and squamates; Castanet 1978; Castanet et al. 2003; Hugi and Sánchez-Villagra 2012) as well as small, highly tachymetabolic endotherms (insectivores, bats, rodents and small primates among mammals; see Chapter 29) and, on the other hand, the well-vascularized and occasionally remodeled tissue formed by the alternation of zones and annuli differing by their histological structure (Figure 8.9D). The zones are made of either woven-fibered or parallel-fibered bone (typical or atypical), while the annuli consist of a thin layer of lamellar or typical parallel-fibered bone. The latter type of lamellar-zonal tissue

VetBooks.ir

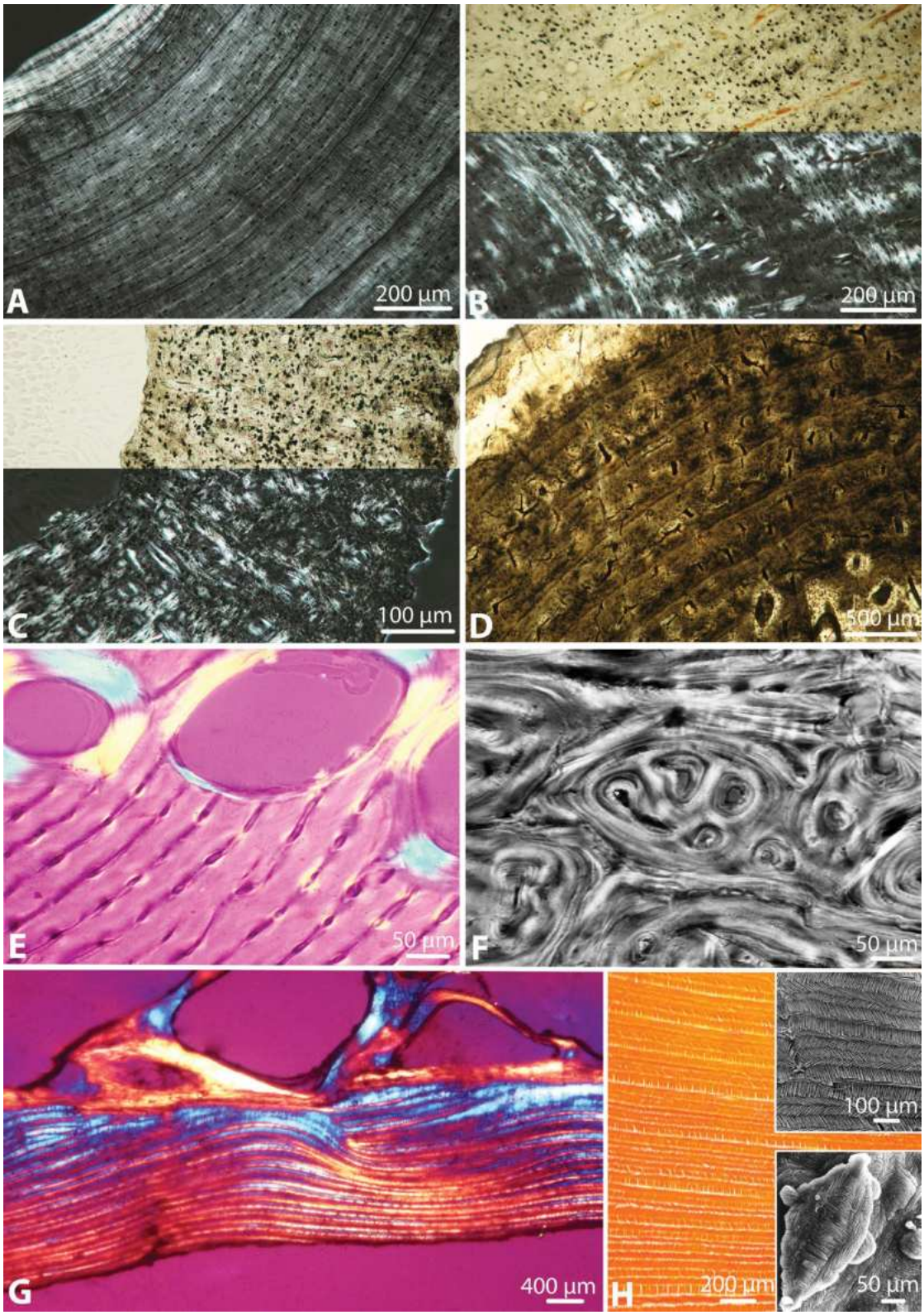


FIGURE 8.9 Other simple bone tissue types. A. Tissue intermediate between the lamellar and the parallel-fibered types in the femur of *Amblyrhynchus cristatus*. B and C, Tissue types intermediate between parallel-fibered and woven-fibered tissue types. Femur of *Varanus niloticus*. D, The so-called lamellar-zonal tissue in the femur of *Diplocynodon ratelii*. E, Acellular bone tissue in the perciform (Actinopterygii) *Drepane africana*. F, Remodeled acellular bone tissue in the rostrum of the extant teleost *Xiphias gladius*. G, General view of isopedin in a scale of the coelacanthiform (Sarcopterygii) *Latimeria chalumnae*. Polarized light. H, Main frame: closer view of the structure of isopedin *in L. chalumnae*. The upper inset shows a detail of isopedin structure (in a scale of the dipneust *Neoceratodus forsteri*), viewed with scanning electron microscopy. The lower inset shows a Mandl corpuscle in the amiiform (Actinopterygii) *Amia calva*.

VetBooks.ir

is observed in many large extant and extinct ectotherms (and occasionally some rare endotherms; Köhler and Moya-Solà 2009) such as crocodiles, varanids and tortoises, along with large temnospondyls and early "anapsid", diapsid and synapsid reptiles (review in Castanet et al. 1993; see also Ricqlès 1979; Ricqlès et al. 2003; Botha-Brink and Smith 2011; Hugi et al. 2011; Klein et al. 2015a, b). In this context, the term lamellar-zonal refers to such a broad tissue spectrum that it loses any precise descriptive power. For this reason, it might seem preferable to restrain the use of this term to the osseous tissue that reflects its etymological construction (i.e., primary cortical bone made of a succession of accretion cycles, each consisting of different tissue types in the zones and annuli). Conversely, homogenous formations of typical primary parallel-fibered or lamellar bone, with or without vascular canals but with cyclical growth marks, should then be called what they merely are; for example, a description could be "parallel-fibered tissue with simple longitudinal canals and LAGs".

Some Peculiar Cases of Lamellar Bone in Basal Gnathostomes

The tissue type descriptions presented above reflect the relatively simple histodiversity of the tetrapod skeleton. The situation is more complex in basal gnathostomes, which display several additional types of primary osseous, or osseous-like, tissues variably distributed among extinct and extant taxa. Concise reviews of these tissue types are available in, e.g., Francillon-Vieillot et al. (1990), Meunier and Huysseune (1992), Meunier (2011), Sire et al. (2009) and Davesne et al. (2018a). Three of these tissue types, which actually represent specialized forms of lamellar or parallel-fibered bone, are briefly described below.

Acellular Bone and Aspidin

The occurrence of acellular or, more properly named, anosteocytic bone tissue is a dominant condition in teleosts (recent review in Davesne et al. 2018a). It occurs in all endoskeletal and dermal bones, as well as scales, of the phylogenetically most derived taxa (euteleosts). More basal forms have bones with normal osteocyte populations trapped within the bone matrix, although a variable degree of acellularity may occur in the scales of some taxa (Davesne et al. 2018a).

From a histological perspective, the basic structure of acellular bone matrix is comparable to that of lamellar or parallel-fibered tissues (Figure 8.9E); however, its mineral content is significantly higher than that of the cellular bone of osteichthyans. For example, the mineral rate of the opercular of a tilapia (*Oreochromis aureus*), an acellular bone, is 64.49%, whereas that of a cell-containing carp opercular (*Cyprinus carpio*) is 57.58% (Cohen et al. 2012; see also Meunier 1984a). The appositional process resulting in anosteocytic tissue is reminiscent of DO: osteoblasts move back in place with the secretion of osteoid, but they do not get trapped in the matrix (Ekanayake and Hall 1987, Davesne et al. 2018a). Moss (1961) and Ricqlès et al. (1991) nevertheless mention the entrapment of young osteocytes that soon die; their lacunae are then filled with mineralized matrix. This situation was recently confirmed with Synchrotron 3D reconstructions by Ofer et al. (2019), who showed the possible occurrence of such occluded cell lacunae in large bone volumes in the medaka, *Oryzias latipes* (see also Hughes et al. 1994). Strong bundles of noncalcified collagen fibers oriented perpendicular to the direction of lamellae frequently occur in acellular bone tissue (Moss 1963; Atkins et al. 2015). Anosteocytic bone can be vascularized (Moss 1961) and remodeled through Haversian substitution in conditions very similar to those prevailing in ordinary (cellular) bone (Witten and Huysseune 2009), although the walls of the secondary osteons are also acellular (Atkins et al. 2014; Currey et al. 2016). A very peculiar pattern of osteons (Figure 8.9F), colonizing the walls of other larger osteons, was observed in the acellular rostral bone of the swordfish (*Xiphias gladius*) by Poplin et al. (1976).

The origin and evolutionary course of anosteocytic bone in osteichthyans, as currently reconstructed (reviews on this topic in Schultze 2018; Davesne et al. 2018a,b; see also Meunier and Huysseune 1992), proves to be complex and still incompletely settled. Among the earliest forms of bone tissue known in vertebrates, aspidin, a tissue present in the Silurian to Devonian jawless pteraspidomorphs (heterostracans), was acellular and made of a parallel-fibered matrix containing strong additional fiber bundles (e.g., Halstead-Tarlo 1963; Sire et al. 2009; Keating et al. 2015, 2018). It occupied the middle, trabecular layer of diploe-like dermal bones and was deposited centripetally. Aspidin trabeculae were associated, in the carapace plates of heterostracans, with a superficial layer formed by dentine odontodes, and a basal acellular layer of a plywood-like tissue interpreted as isopedin (e.g., Keating et al. 2015). However, another nearly contemporaneous Silurian group, the osteostracans, had cellular bone (Donoghue and Sansom 2002). Extinct and extant basal actinopterygians, including basal teleosts, display cellular bone, as illustrated by, e.g., the Devonian taxon *Cheirolepis canadensis* and nearly all noneuteleostean actinopterygians (Davesne et al. 2018a). Acellularity is a derived condition in teleosts, and it could well be an ancestral trait of euteleosts, which represent by far the most diversified vertebrate taxon in extant faunas. It underwent a reversion, with the reacquisition of cellular bone, in some of the physiologically most advanced euteleosts, including Salmonidae, Lampriididae and, among the Scombridae, the Thunnini, or true tunas (Sire et al. 2009; Schultze 2018; Davesne et al. 2018b). The latter situation, often concomitant with dense Haversian remodeling in bone cortices, could possibly be related to a specialization toward a tachymetabolic physiology, at least during some periods of the year (review of this question in Davesne et al. 2018a, b).

Isopedin

A peculiar plywood structure, isopedin, is commonly encountered in the scales of several osteichthyan clades (Giraud et al. 1978; Francillon-Vieillot et al. 1990; Ricqlès et al. 1991; Meunier 2011; Schultze 2018). Initially, isopedin was confused with elasmodin, another plywood-like tissue found in elasmoid scales and now considered nonosseous but derived from dentine (Sire and Huysseune 2003; Sire et al. 2009). The terminology applied to scale tissues, as well as their phylogenetic

occurrence, remain controversial issues, and important discrepancies still exist among authors (see, e.g., Schultze 2018). The term isopedin will be used here to designate the poorly mineralized or nonmineralized, acellular and complex plywood (Figure 8.9G, H) that forms the basal plate of scales in most teleosts (Giraud et al. 1978). This tissue is currently acknowledged as a form of lamellar bone and merely presented as such by some authors, who thus question the relevance of a specific name for it (e.g., Sire et al. 2009). Several isopedin forms exist (review in Meunier and Castanet 1982), which form a relatively thick lamellar deposit, lying under a superficial scale stratum made of variable tissues (e.g., Meunier 1980). Although representing a derived form of lamellar osseous tissue, isopedin is characterized by three main features that clearly distinguish it from other types of bone.

Its most obvious histological trait is to be composed of a stack of lamellae (several tens of lamellae may occur in large individuals). Lamellar orientation follows a complex pattern prone to vary among taxa. Figure 8.10 summarizes isopedin structure in the well-documented case of the coelacanth (*Latimeria chalumnae*) studied by Giraud et al. (1978) (see also Meunier and Castanet 1982). In addition to its peculiar fibrillar geometry, isopedin is characterized by a complete or quasi-complete absence of cells (a general feature in the teleost skeleton; see above) and a low mineral content, if any (quantitative data in Meunier and Huysseune 1992; see also Meunier 1981). When a mineral phase occurs in this tissue, it involves, in addition to the common inotropic mineralization, an original process, i.e., the proliferation of irregularly shaped calcified concretions some 5-40 µm in diameter (Figure 8.9H, inset), Mandl' corpuscles (Schönbörner et al. 1981, Meunier 1984b). Isopedin is viewed as a specialized and derived tissue. According to the phylogenetic study by Schultze (2018), it is a homoplastic character, independently evolved in many lineages of osteichthyans. Its low or missing mineral phase could have been selected for one functional advantage: reducing skeletal mass and, consequently, improving the locomotory capabilities of the taxa (Meunier and Huysseune 1992).

Composite Tissues: The Woven-Parallel [Fibrolamellar] Complexes

The term *fibrolamellar* has long been and is still currently used to designate the types of primary periosteal tissues that comprise a woven-fibered component (formerly called "fibrous") and a lamellar component in the form of primary osteons. The initial stage of their formation is the fast subperiosteal accretion (through SO) of a loose scaffold of thin trabeculae (fine cancellous bone) made of woven-fibered tissue (Figure 8.11A). The geometrical structure of the scaffolding, as well as that of the capillary network of periosteal origin that it houses, are variable according to the five patterns presented in more detail below.

Following Amprino's (1947) study, the geometrical structure of fibrolamellar complexes has been shown to be influenced by accretion rate (e.g., Castanet et al. 1996, 2000; Margerie et al. 2002); however, contrasting data exist on this topic (Margerie et al. 2004). Many questions remain about the mechanism that controls at once the structuring of vascular networks and the work of the osteoblasts involved in the production of the distinct geometrical patterns of these tissues. Fibrolamellar complexes are typical of early (juvenile) and most active stages of skeletal growth in medium-sized and

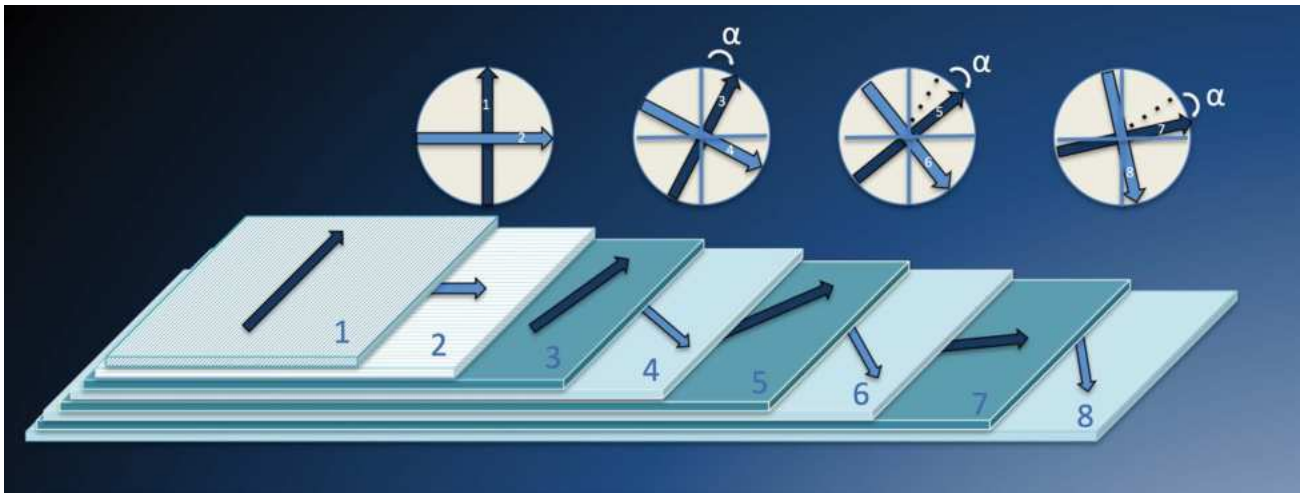


FIGURE 8.10 A schematic representation of an isopedin structure. Eight layers (in four pairs) of parallel fibered bone lamellae with different fibrillar orientations are represented here. Much more pairs of layers may occur in isopedin formations. The angle between two successive lamellae is 90° plus a small additional angle designated as α/2 (Figure 8.10). When considered from one pair of lamellae to the following pair, the total rotation angle is thus 180 + α, or simply α. The value of angle α may range from 10 to 50° (average 26°), depending on the location of the scales on the body, or other factors. In the whole lamella stack, there is thus a right-handed accumulation of α increments, which finally results in a 360° twist of the fibrillar structure for a number of lamellae varying with the value of α. This model is characteristic of a twisted plywood. Other, generally simpler patterns exist among teleost elasmoid scales: rotation can be double or simple, right- or left-handed and with variable angles, thus creating different twisted structures. In some taxa, there is a mere orthogonal pattern, corresponding to that of ordinary lamellar bone (synthetic data in Meunier and Castanet 1982.)

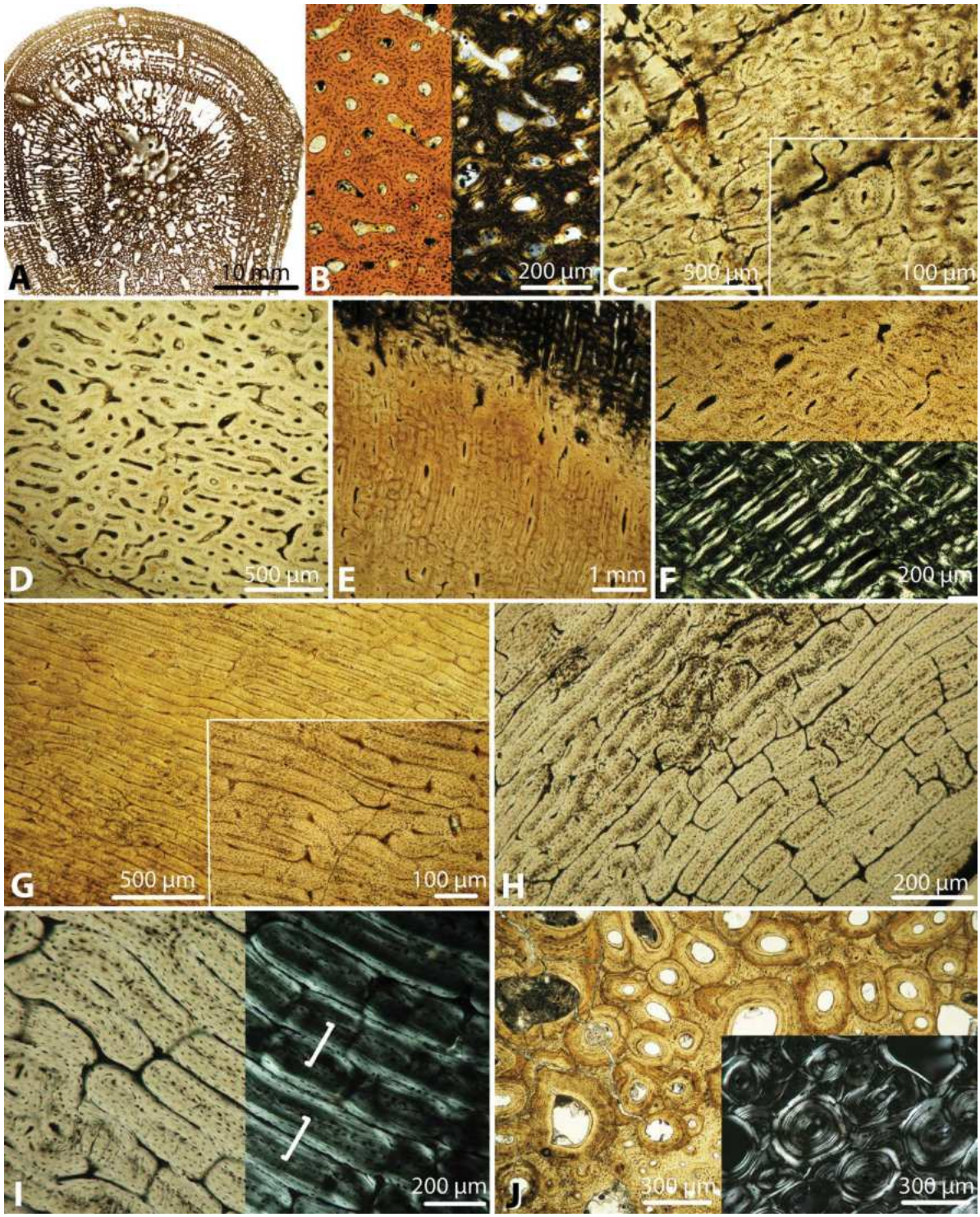


FIGURE 8.11 Woven-parallel (i.e., fibrolamellar) complexes. A, The initial woven-fibered "scaffolding" of woven-parallel complexes. In the ichthyosaur (*Omphalosaurus nisseri*) presented here, this scaffolding remains as fine cancellous bone and intertrabecular spaces are not filled by primary osteons. B, Woven-parallel tissue with longitudinal primary osteons in the tibia of *Maiasaura peeblesorum*, an Upper Cretaceous ornithopod dinosaur. Right half: polarized light. C, Reticular woven-fibered complex in the Triassic archosauriform *Erythrosuchus africanus*. Inset: closer view at the vascular network. D, Mixed type of woven-parallel complex, with reticular, longitudinal and circular primary osteons, in the humerus of a Middle Permain anomodont (Therapsida). E, Radial woven-parallel complex in a premaxilla of the Miocene ziphiid cetacean *Aporotus recurvirostris*. F, Closer view at the reticular woven-parallel complex of *A. recurvirostris*. Lower half: polarized light. G, Laminar tissue in a premaxilla of *A. recurvirostris*. Inset: closer view at the bone structure. H, Plexiform woven-parallel complex in the femur of a roe deer (*Capreolus capreolus*). I, Closeup view of the structure of the laminae (roe deer femur). The white brackets show the limits of laminae, according to the definition by Ricqlès (1975). Right half: polarized light. J, Dense Haversian bone in the core of a rib from the Upper Jurassic marine crocodile *Metriorhynchus geoffroyi*. The inset shows a detail of tightly packed secondary osteons in dense Haversian tissue (femur of the extant African buffalo *Syncerus caffer*).

VetBooks.ir

large endothermic tetrapods. They occur neither in basal gnathostomes nor in small taxa generally, whether they are tachy- or bradymetabolic (Enlow and Brown 1956, 1958; Ricqlès 1976; Cubo et al. 2012), and their mere presence is considered a strong argument in favor of a high, sustained metabolic activity (Ricqlès 1979; Sander et al. 2004; Ricqlès et al. 2008; Legendre et al. 2016). Moreover, in a bone section, there is a close correspondence between the cortical distribution of fibrolamellar complexes and that of Haversian remodeling. These osseous complexes are extensively erased and replaced by dense Haversian bone (see below) in the lower strata of periosteal cortices in subadults and adults.

The studies by Marotti et al. (1999) and Ferretti et al. (2002) on static and dynamic osteogenesis resulted in relatively few consequences for the terminology currently used in histological descriptions, although the terms static and dynamic osteogenesis (SO and DO, respectively) are now commonly used. The most important (although loosely related to the findings of Marotti et al. 1999) innovation that they inspired is the proposal by Stein and Prondvai (2014) and Prondvai et al. (2014) to replace the expression *fibrolamellar complexes* with *woven-parallel complexes*. Although still uncommon, the use of this novel expression is to be recommended for simple, straightforward reasons. The term *fibrous bone* is now abandoned and universally replaced by *woven-fibered bone,* which is far better if one considers the structural characteristics of bone tissue as a whole (all osseous tissues are principally made of fibers) and those of woven-fibered bone in particular; namely, fiber networks tend to be looser in this tissue than in parallel-fibered or lamellar tissues (Francillon-Vieillot et al. 1990; Reznikov et al. 2014a, b). The term woven-parallel has a much higher descriptive power than fibrolamellar because it clearly evokes the geometric characteristics of fiber networks in the bone matrix.

Woven-Parallel Complexes With Longitudinal Osteons

This tissue type (Figure 8.11B; see also Figure 8.6A) may occur in two distinct forms. In its most common aspect, primary osteons are relatively thin (35–100 µm in diameter) and widely spaced, and do not show branching or anastomoses (Margerie et al. 2002; see also diagnosis in Ricqlès 1975). Moreover, the initial woven-fibered deposit is compact. This kind of tissue is seen in many skeletal sites (long bones, jaws, vertebral apophyses, etc.) in many tetrapod clades, from basal amniotes (e.g., Ricqlès and Bolt 1983 for *Captorhinus* jaws) to extant mammals. It can be observed in the deep cortex (described by Ray et al. 2012 and Botha-Brink et al. 2012 in therapsids), and often occurs in peripheral layers of bone cortices, deposited when an originally fast accretion rate begins to decline (e.g., Jordana et al. 2016). In another form of this tissue, encountered for example in ungulates (e.g., equids and cervids), primary osteons have a larger sectional area and a roughly square shape in cross section, and are closely packed in circular files (see Chapter 29 for further details). Stover et al. (1992) used the expression "saltatory primary osteonal formation" to designate this peculiar structure, which is actually intermediate between woven-parallel bone with longitudinal primary osteons and the plexiform tissue type described below.

Reticular Woven-Parallel Complex

In this tissue type (Figure 8.11C, D), the primary osteons have no definite orientation. They display a variable, convoluted course with frequent branching and they generally coexist with longitudinal osteons. When spared by remodeling, the lowest part of the cortex of numerous large or fast-growing taxa such as dinosaurs (Horner et al. 2001; Klein and Sander 2008), pterosaurs (Enlow and Brown 1957; Ricqlès et al. 2000), derived synapsids (Ray et al. 2009; Chinsamy-Turan and Ray 2012) and mammals (Enlow and Brown 1958) frequently show this kind of tissue.

Radial Woven-Parallel Complex

The name of this tissue type (Figure 8.11E, F) refers to the orientation of primary osteons, which are roughly parallel to the radii of tubular diaphyses (as seen in cross section) or perpendicular to the outer surface of diploes. In some taxa, the radial woven-parallel complex represents the highest subperiosteal accretion rate ever measured with experimental methods (Margerie et al. 2002). As in the reticular tissue type, the primary osteons of the radial woven-parallel complex show branching, and are often mixed with longitudinal or variably oblique osteons, as well as simple canals.

Laminar and Plexiform Woven-Parallel Complexes

Both these complexes (Figure 8.11G–I) have a dominant circular orientation of primary osteons that form concentric sheets throughout the cortex. They are structurally close to each other; their main difference is the frequency of radial anastomoses between successive canal layers: anastomoses are sparse in the laminar type and more numerous in the plexiform. Laminae are the basic structural element of laminar tissue. In cross sections of dry or fossil bone observed in transmitted light, each lamina comprises a primary osteon, framed on both sides with a thin stratum of hypermineralized woven-fibered tissue. In their study, Stein and Prondvai (2014) had tentatively created the term *highly organized primary bone* (HOPB) to designate the part of a lamina resulting from DO (the primary osteon); however, this term was soon abandoned (Prondvai et al. 2014). Among all woven-parallel complexes, laminar bone is by far the most studied and best known.

The study of this tissue by Magal et al. (2014), based on the SSV approach, showed that initial woven-fibered trabeculae of the cortex scaffold are thin (some 10–12 µm in the specimens that they studied), and their core forms a *primary hypermineralized layer* (PHL, also called *bright line* by Currey 1960 or *hypercalcified line* by Mori et al. 2003). Intertrabecular spaces are subsequently filled (centripetal deposits) by parallel-fibered bone and ultimately by lamellar tissue in the close vicinity of blood vessels. The originally fine cancellous tissue is thus made compact. These observations enriched the common interpretation of the laminar and plexiform tissue types by showing that the lamellar bone forming a part of the walls

VetBooks.ir

of the primary osteons is a minor component, opposite to the situation prevailing in secondary osteons. The results of Magal et al. (2014) closely agree with the detailed observations made by Stein and Prondvai (2014) in light microscopy on ground sections from dinosaur bones. The latter study pointed out the importance of sectional planes for a precise assessment of laminar structure, and for the accuracy of the histomorphometric measurements that can be made on laminae (see also Faure-Brac et al. 2019). In a long bone, the collagen meshwork in parallel-fibered bone that forms most of the osteon wall is generally oriented longitudinally (parallel to the long axis of the bones) and therefore appears as monorefringent in cross section. It might then be confused with woven-fibered bone in this kind of section, and thus induce considerable overestimation of the thickness of the woven-fibered part of laminar and plexiform tissues. False deductions about growth rate and metabolic activity could then be derived from this basic error.

Ricqlès (1975) settled an old debate about the true limits of laminae by showing that one lamina is actually defined by the vascular canal and the bone tissues located between two successive PHLs. Therefore, centripetally from the PHLs toward the central vascular canal of one lamina, the osseous tissues encountered are woven-fibered, parallel-fibered and lamellar bone, ; Figure 8.11I). This interpretation was confirmed by the studies of Stein and Prondvai (2014) and Magal et al. (2014). Laminar and plexiform tissues are very common in medium-sized and large ornithodirans and mammals (see Ricqlès et al. 2000 for pterosaurs, Klein and Sander 2008 for dinosaurs, Enlow and Brown 1958 for mammals). Histomorphometric data by Sander and Tuckmantel (2003) and Hofmann et al. (2014) showed that the mean spatial density of laminae in sauropod dinosaurs (4.8 lamina per millimeter, range: 4–6) is significantly different from that of mammals ($4.1*mm^{-1}$).

Although they reflect a high growth rate consistent with tachymetabolism, woven-parallel complexes (except the tissue type containing longitudinal primary osteons, which may occur, at least in local spots, in ectotherms), often display sharp cyclical growth marks, as mentioned above about matrices.

Dense Haversian Bone: A Secondary Compact Tissue

This tissue occurs in compact cortices and results from the local accumulation of secondary osteons (sustained Haversian remodeling), which are eventually present in such density that all traces of the once-present primary cortex are erased. Several generations of osteons, partly destroying each other, are thus set in place (review in Lacroix 1970; Parfitt 1994; Allen and Burr 2014; see also Chapter 11). This tissue is easily observable in transmitted light in ground sections from recent and fossil samples (Figure 8.11J; see also Figure 8.6B, E, F). The development of dense Haversian bone is progressive and reaches full completion in subadults and adults; this is why histology textbooks often present it as "mature bone". This expression is misleading because dense Haversian bone, as a secondary formation, replaces primary tissues and by no means represents their "mature" stage. These tissues can be of any type, but the spreading of dense Haversian bone does not usually touch the inner fundamental system (although isolated secondary osteons may occur locally; see Figure 8.1D) and such tissues often colonize only a part of the total cortical area. Dense Haversian bone occurs exclusively in medium-sized to large tachymetabolic vertebrates. In extant faunas, for which accurate and precise data on resting metabolic rate exist, this tissue is restricted to mammals, birds and some teleosteans such as true tunas or billfishes (Meunier 2011; Atkins et al. 2014; Davesne et al. 2018a). Several estimates of osteonal density in the Haversian tissue of extant and extinct taxa have been published. Maximal density values are, for example, 8.261 entire osteons$*mm^{-2}$ in the humerus of the sauropod dinosaur *Phuwiangosaurus sirindhornae* (Mitchell et al. 2017), and 10.1 osteons$*mm^{-2}$ in the sixth rib of *H. sapiens* (Wu et al. 1970). The meaning of these results may appear questionable in the case of well-differentiated dense Haversian bone, because the proportion of "missing osteons", i.e., osteons that once existed but have been erased by subsequent osteonal generations, cannot be estimated. Considering the delay for a full mineralization of secondary osteons, and the continued renewal of the osteons in dense Haversian bone, microradiographic and CT-scan images of this tissue resemble a patchwork or unevenly radiopaque osteons (see Figure 8.6J).

Osseous Tissues in Cancellous Formations

There is no osseous tissue specific to cancellous formations. Depending on its location and mode of formation, a trabecula may be made of one, two or several of the basic tissue types presented above. Moreover, trabeculae can (at least partly) integrate endosteal or periosteal, primary or secondary osseous tissues in their structure. Calcified cartilage is also an important component of some types of trabeculae. The cancellous formations located in the medullary region of the bones are normally submitted to intense and extensive remodeling and thus, early or late, become mainly formed of secondary endosteal tissue. An exception to this basic trend is encountered in some extant and extinct aquatic tetrapods whose skeletons show evidence of a neotenic process, variably pronounced among taxa and resulting in remodeling inhibition.

Tissues Forming the Primary Trabeculae

Primary trabeculae comprise a core of hypertrophic calcified cartilage, covered by thin layers of lamellar endosteal bone (Figure 8.12A). Bone deposits often infill empty chondrocyte lacunae after the death (through an apoptotic process) of the chondrocytes. This process results in subspherical bony globules some 30–80 µm in diameter, continuous with endosteal deposits (Figure 8.12B, C), the *globuli ossei* (e.g., Quilhac et al. 2014). Primary trabeculae, and the endosteoendochondral spongiosa that they build, occur in the metaphyseal part adjacent to the epiphysis, a zone where the conjunctivovascular erosion front attacks the thick layer of calcified cartilage formed at the base of the growth plate (see above, Figure 8.1H). Therefore, the true primary part of such trabeculae is their cartilage core; the superficial osseous platings, although deposited early in growth, are already secondary deposits (Ricqlès 1975). Primary trabeculae represent an initial scaffold from which

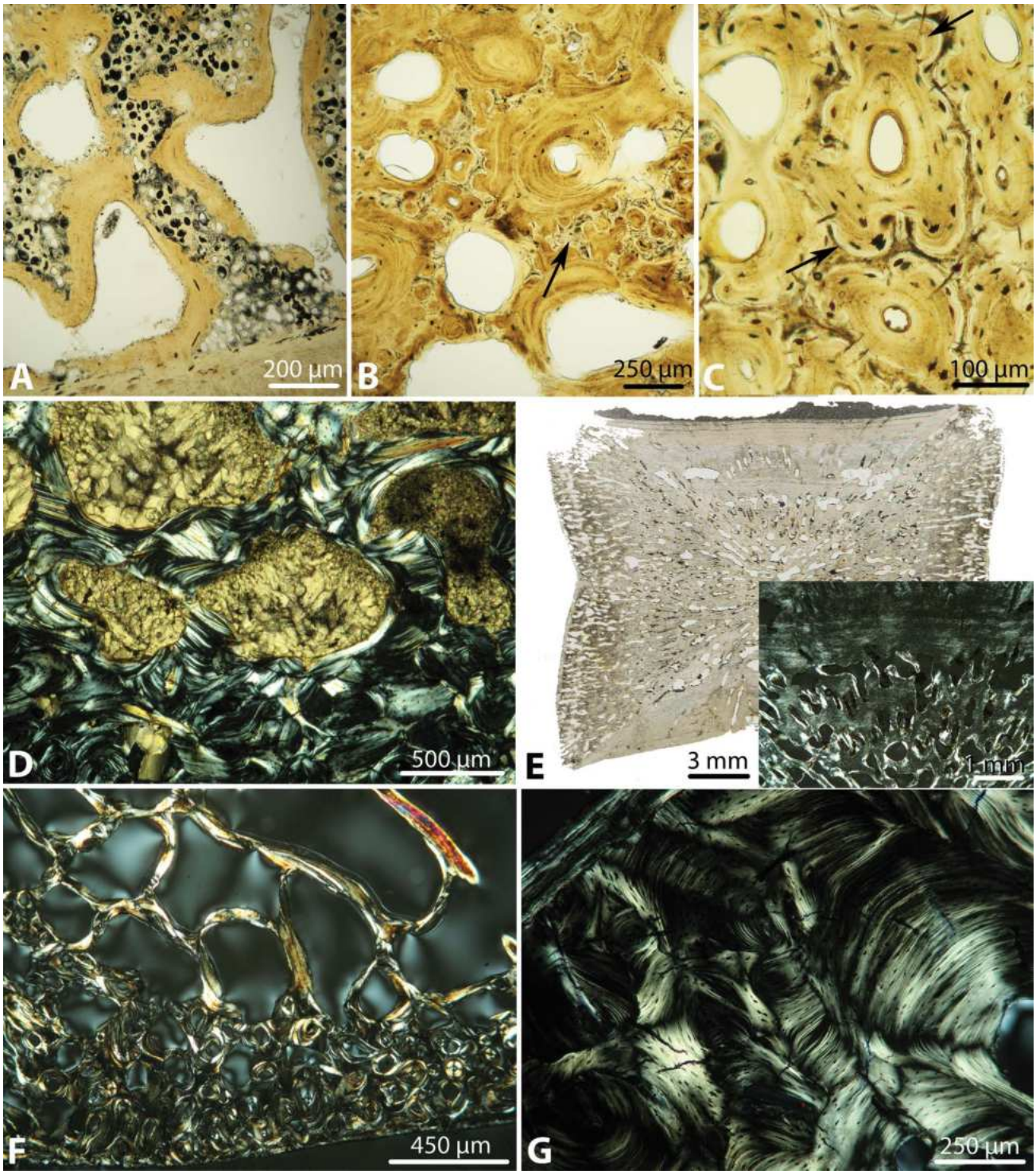


FIGURE 8.12 Histology of bone trabeculae. A, A typical primary trabecula in the femur of *Simoedosaurus* sp. Cross section in the femoral metaphysis. The trabecula consists of a core of calcified cartilage matrix, covered with a sheet of endosteal lamellar bone. B, Cross section of primary trabeculae in a rib of *Zygorhiza kochii*. The core of the trabeculae shows remnants of calcified cartilage matrix (arrow), with *globuli ossei* protruding in it. C, Closer view of the *globuli ossei* (arrows). D, Densely remodeled secondary trabeculae in a rib of *Desmostylus* sp. E, Resorption of the deep periosteal cortex, which turns from compact to cancellous, in a *Simoedosaurus* vertebra. The inset (polarized light) shows that the trabeculae thus created are mildly remodeled, and the primary periosteal tissue remains visible in them. F, Resorption of the deep cortex, that turns from compact to cancellous, in a rib of the extant primate *Macaca radiata*. Opposite to the situation observed in *Simoedosaurus*, the cortex as well as the trabeculae created by its resorption are densely remodeled. Polarized light. G, Detail of the histological structure of compacted coarse cancellous bone in the tibia of *Potamotherium valletoni*. Polarized light.

VetBooks.ir

the future endosteal coarse cancellous bone occupying most of the metaphyseal volume will develop. In a normal situation, as in basal aquatic taxa and all terrestrial tetrapods, primary endosteoendochondral trabeculae are transitional structures. Their fate is to be densely remodeled (resorption and reconstruction) and to be replaced by *secondary endosteal trabeculae* in metaphyses. Calcified cartilage is then eliminated from the core of the trabeculae. However, in skeletal neoteny, a frequent condition in secondarily aquatic tetrapods, this remodeling stage does not occur. Typical primary trabeculae persist, and can be sequentially relocated toward the middle of the diaphysis, while protracted endosteal deposits tend to obturate intertrabecular spaces (review in Ricqlès and Buffrénil 2001).

The Tissues of Secondary, Endosteal Trabeculae

This kind of trabeculae results from the intense and repeated remodeling of diverse types of cancellous tissue, regardless of whether they are primary (as mentioned above) or created by the patchy resorption of deep cortices. Consequently, the trabeculae consist entirely of an imbrication of variably shaped (but most often crescent-like), brightly birefringent layers of endosteal lamellar tissue, medially bordered by reversion lines (hemi-osteons; Figure 8.12D). In long bones, this remodeling process mainly occurs in metaphyses, but it also involves diaphyseal spongiosae, if any. True secondary osteons may also occur in broad intertrabecular intersections (Figure 8.6C). Secondary trabeculae are the basic component of the so-called coarse cancellous bone that occupies most of the osseous volume in metapodials, vertebrae and long bone metaphyses. Their intense and permanent remodeling is the basis of the structural fitting of the bones to the specific mechanical loads they have to face (Wolff's Law; Wolff's 1892). Most of the research effort dealing with cancellous bone refers to secondary, endosteal trabeculae, considered from a biomedical perspective.

Trabeculae Resulting from Patchy Cortical Resorption

Spongiosa created by the resorption of deep cortical layers are extremely common, especially in short bones, where they sequentially replace compact periosteal formations during the course of local skeletal growth. Histologically, the trabeculae, when newly differentiated by resorption, are composed of the same tissue as the deep cortex (Figure 8.12E, F; see also Figure 8.3D). In juveniles, which still retain early deposited bone layers, this tissue may potentially comprise any kind of primary periosteal bone; conversely, in adults, it often consists of parallel-fibered bone, with or without cyclical growth marks. Soon after their formation, the trabeculae are submitted to further remodeling by surficial resorption and reconstruction. During this process, the remnants of cortical bone become gradually scarcer toward the bone core, until they disappear entirely. The trabeculae then turn into the secondary endosteal type described above (Figure 8.12D, F).

Remarks on Fine Cancellous Bone

The woven-fibered tissue comprising the trabeculae of fine cancellous bone (i.e., the initial scaffold of woven-parallel tissues) has already been described above. In brief, it does not differ histologically from the general woven-fibered type, except for the occurrence of a hypermineralized line running in the middle of the trabeculae, especially in the laminar and plexiform patterns. This line is similar to a rest line marking the limit between the successive accretion cycles from which the repetitive structure of cortical woven-parallel complexes arises. The normal fate of the fine cancellous bone is to become compacted through the centripetal, intertrabecular deposit of parallel-fibered or lamellar tissues.

Histological Features of Compacted Coarse Cancellous Bone (CCCB)

The classification of this tissue among, on the one hand, compact or cancellous formations and, on the other hand, primary or secondary bone, is a debatable question. Although it is compact, CCCB is originally a spongiosa, and it often occurs in association with true cancellous bone; moreover, it combines secondary trabeculae with primary intertrabecular deposits.

During the growth in length and diameter of long bones, this tissue forms at two distinct sites: the metaphyseal and, less frequently, the diaphyseal region. It occurs also in concave flat bones (a morphology requiring a strongly asymmetrical growth pattern, cf. Enlow 1963; see also Chapters 4 and 9), but most studies about this tissue deal with tubular limb bones. Basically, CCCB comprises an initial cancellous tissue made of either secondary metaphyseal trabeculae, as defined above, or a trabecular network resulting from the patchy resorption of the deep part of primary cortices (diaphyseal region). In relation to local morphogenetic processes developing during growth, these cancellous formations must be made compact to be relocated into solid cortices. This result is obtained by the centripetal accretion of endosteal parallel-fibered or lamellar tissues filling intertrabecular spaces (Figure 8.12G; see also Figure 8.3E, F). In addition, CCCB is remodeled and integrates variably oriented secondary osteons. Residues of calcified cartilage matrix may also occur in this tissue (Heck et al. 2019). The combination of these components eventually results in a complex histological structure that appears "disorganized" (a term frequently used in literature since Enlow and Brown 1958) and highly convoluted, especially when observed in transmitted polarized light (Figure 8.12G). When formed in the metaphyseal region, CCCB is a transitional tissue, supposed (according to the classical growth model by Lacroix 1945 and Enlow 1963) to be normally eliminated by the enlargement of the medullary cavity in the diaphyseal region. However, recent data by Montoya-Sanhueza and Chinsamy (2017), Legendre and Botha-Brink (2018) and Heck et al. (2019) suggest that it can be spared by resorption and integrated into the diaphyseal cortex in some mammalian taxa (see also Chapter 29).

VetBooks.ir

Between Bone and Cartilage: Chondroid Bone

In addition to clearly identifiable bone and cartilage, chondroid bone integrates the characteristics of both these tissues, and is thus a spectacular form of intermediate histological structure. It was first mentioned in the histological literature by the middle of the 19th century (historical survey in Beresford 1981), and has since been observed in endochondral and dermal formations (limb bones and skull bones) in extant and extinct finned vertebrates (e.g. Huysseune and Sire 1990; Witten et al. 2010) and most tetrapod clades (e.g. Goret-Nicaise 1984; Bailleul et al. 2016, 2019; Prondvai et al. 2020). It seems particularly common in sutural regions (including mandibular symphyses) of the fetal face, cranial vault and mandible of all vertebrate clades. It is also suspected to contribute in mammals to the formation of some peculiar skeletal elements such as the baculum and the antlers. This tissue, associated with fast local osteogenesis, also occurs during the initial stages of bone fracture repair (Beresford 1981; Li and Stocum 2014). Histogenetic processes resulting in chondroid bone formation seem to be complex and variable, and remain to be further deciphered.

The histological characteristics of chondroid bone are variable, depending on where the tissue is formed and the stage of its development (Figure 8.13A, B). As a consequence, different terminologies and categorizations have been used to characterize chondroid bone (reviewed in Beresford 1981; see also Witten et al. 2010). Most of the detailed histological and cytological data available about chondroid bone originate from Huysseune et al. (1986), Huysseune and Verraes (1986), Huysseune and Sire (1990), for finned vertebrates, from Goret-Nicaise (1984) and Goret-Nicaise and Dhem (1987) for mammals, and from Bailleul et al. (2016) and Prondvai et al. (2020) for dinosaurs and birds, respectively.

Chondroid bone matrix is fully mineralized by hydroxyapatite. Its mineral proportion is high, and comparable to that of woven-fibered bone (Goret-Nicaise and Dhem 1985, 1987), except for pericellular spaces and for a thin superficial layer equivalent to osteoid when the matrix is initially produced by the periosteum. According to Huysseune and Sire (1990), mineralization in chondroid bone involves spheritic mineralization (see Chapter 12), instead of the inotropic process common in bone. The gross spatial organization of the matrix is of the woven-fibered type, with a fibrillar meshwork including as major components Collagen I (an osseous character) and, in pericellular areas, Collagen II (a feature of cartilage: Goret-Nicaise 1984). This matrix has no preferential fiber orientation (Huysseune and Sire 1990) and appears monorefringent in polarized light. In addition to collagen, chondroid bone matrix contains a ground substance displaying dense interfibrillar granular material and matrix vesicles that coalesce at the mineralization front (Goret-Nicaise 1984; Huysseune and Sire 1990).

The morphology and cytological characteristics of chondroid bone cells are highly variable: these cells can be similar to chondrocytes and devoid of cytoplasmic processes (see e.g. Huysseune and Sire 1990; Bailleul et al. 2016; Prondvai et al. 2020), or present short cytoplasmic processes with intercellular gap junctions (Goret-Nicaise and Dhem 1987) Their overall morphology is then reminiscent of the stout, multipolar osteocytes encountered in the woven-fibered tissue. They may occur as single elements, broadly spaced within an abundant extracellular matrix, or form clusters that gather a few units, sometimes aligned in isogenic groups (Prondvai et al. 2020). Beyond great morphological diversity, most descriptions of these cells mention abundant endoplasmic reticulum, well-developed golgi apparatus and the presence of vacuoles.

The mode of formation of chondroid bone remains incompletely understood, and diverse conjectural interpretations have been proposed. This tissue is generally considered to result from an accretional (appositional) process, and its matrix is supposed to be produced by preosteoblasts and osteoblasts deriving from fibroblasts located in the periosteum (Huysseune and Sire 1990). As in bone, matrix-secreting cells

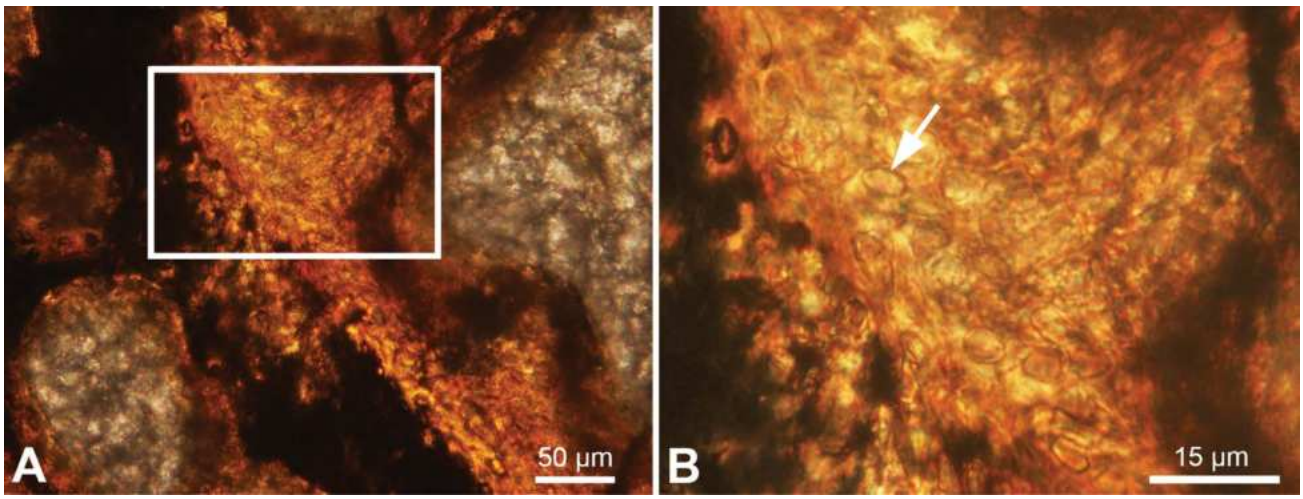


FIGURE 8.13 – Chondroid bone in a dinosaur. A, Broad view of a trabecula from the surangular bone of a hadrosaur embryo (Hadrosauridae indet; Campanian of Montana, USA). Chondroid bone occurs in the core of the trabecula. The box indicates the field shown in B. B, Closeup view of chondroid bone. The cell lacunae (arrow) display a chondrocyte-like morphology and lack canaliculi. For A and B: polarized light. Image of MOR 1038 by A. Bailleul; courtesy of the Museum of the Rockies, Montana State University.

VetBooks.ir

are then trapped in their own secretions (unmineralized osteoid-like substance) and enter a maturation process to finally become chondrocyte-like cells (secreting Type II collagen) mentioned above. Some authors (e.g., Witten et al. 2010) used the terms "metaplasia" or "transdifferentiation" to designate this transformation. The latter, however, is a gradual process involving several intermediary steps, which may not fully correspond to these concepts. Moreover, the cells resulting from it are not identical to chondrocytes *stricto sensu*. A distinct interpretation, developed by Prondvai et al. 2020, is suggested by the occurrence of cell clusters and isogenic groups within the chondroid bone (see also Gillis et al. 2006). The periosteum possess a chondrogenic potential (which quickly decreases with age), a characteristic possibly due to the local contribution of undifferentiated mesenchymal cells located in the cambial layer (O'Driscoll et al. 2001). Unmineralized chondroid bone might then be initially deposited by subperiosteal apposition and increase, through interstitial growth, before being mineralized. Its cells would then be transformed to variable degrees into osteocyte-like cells; the whole process is close to the transformation of cartilage into bone, as observed by Hall (1972) in immobilized chick embryos. In this interpretation, the transformation of chondrocytes into osteocyte-like cells might be considered, in a broad and integrative meaning, as a case of metaplasia, although the resulting cells are not typical, fully differentiated osteocytes.

As pointed out by several authors, chondroid bone is typical of fetal and early postnatal stages. It disappears, through resorption, in later ontogeny to be locally replaced by lamellar bone (e.g., Goret-Nicaise 1984). This tissue can fossilize under the same conditions as bone. It is just beginning to be specifically considered in the paleohistological literature (Bailleul et al. 2016, 2019).

Acknowledgments

We are extremely grateful to our colleague, Dr. Alida Bailleul (Institute of Vertebrate Paleontology and Paleoanthropology, Chinese Academy of Sciences, Beijing, China) for her generous loan of the photo of dinosaurian chondroid bone. For this article, as for others in this book, our colleague, Prof. Kevin Padian (University of California, Berkeley, USA), greatly contributed to improve the quality of the text. We warmly thank him for his irreplaceable help.

REFERENCE

Aaron, J. E. 2012. Periosteal Sharpey's fibers: a novel bone matrix regulator system? *Front. Endocrinol.* 3: article 98.

Allen, M. R. and D. B. Burr. 2014. Bone modeling and remodeling. In *Basic and applied bone biology*, eds. D. B. Burr, and M. R. Allen, 75–89. London: Academic Press.

Ascenzi, M.-G., et al. 2003. Structural differences between "dark" and "bright" isolated human osteonic lamellae. *J. Struct. Biol.* 141: 22–33.

Ascenzi, M.-G. and A. Lomovtsev. 2006. Collagen orientation patterns in human secondary osteons, quantified in the radial direction by confocal microscopy. *J. Struct. Biol.* 153: 14–30.

Amprino, R. 1947. La structure du tissu osseux envisagée comme l'expression de différences dans la vitesse de l'accroissement. *Arch. Biol.* 58: 315–330.

Atkins, A., et al. 2014. Remodeling in bone without osteocytes: billfish challenge bone structure-function paradigms. *PNAS* 111(45): 16047–16052.

Atkins, A., et al. 2015. The three-dimensional structure of anosteocytic lamellated bone of fish. *Acta Biomater.* 13: 311–323.

Aubin, J. E. 2008. Mesenchymal stem cells and osteoblast differentiation. In *Principles of bone biology*, eds. Bilezikian, J. P., L. G. Raisz and T. J. Martin, eds., 85–107. New York:, Academic Press.

Bailleul, A., et al. 2016. Chondroid bone in dinosaur embryos and nestlings (Ornithischia : Hadrosauridae): insights into the growth of the skull and the evolution of skeletal tissues. *C. R. Palevol* 15: 49–64.

Bailleul, A., et al. 2019. Dinosaur paleohistology: review, trends and new avenues of investigation. *PeerJ* 7: e7764 DOI 10.7717/peerj.7764.

Baud, C. A. 1962. Morphologie et structure inframicroscopique des ostéocytes. *Acta Anat.* 51: 209–225.

Bellido, T., et al. 2014. Bone cells. In: *Basic and applied bone biology*, eds. D. B. Burr and M. R. Allen, 27–45. New York: Academic Press.

Beresford, W. A. 1981. *Chondroid bone, secondary cartilage and metaplasia*. Baltimore: Urban and Schwartzenberg.

Boef, M. de and H. C. E. Larsson. 2007. Bone microstructure: quantifying bone vascular orientation. *Can. J. Zool.* 85: 63–70.

Bonfield, W. and M. D. Grynpas. 1977. Anisotropy of the Young's modulus of bone. *Nature* 270: 453–454.

Bonewald, L. F. 2011. The amazing osteocyte. *J. Bone Miner. Res.* 26: 229–238.

Botha-Brink, J., et al. 2012. The radiation and osteohistology of nonmammaliaform cynodonts. In *Forerunners of mammals*, ed. Chinsamy-Turan, A., 223–246. Bloomington: Indiana University Press.

Botha-Brink, J. and R. M. H. Smith. 2011. Osteohistology of the Triassic archosauromorphs *Prolacerta*, *Proterosuchus*, *Euparkeria*, and *Erythrosuchus* from the Karoo basin of South Africa. *J. Vert. Paleontol.* 31: 1238–1254.

Boyde, A. 1972. Scanning electron microscope studies of bone. In *The biochemistry and physiology of bone*, 2nd edition, ed. Bourne, G. H. ed., Vol. 1, 259–310. New York:, Academic Press.

Boyde, A and S. J. Jones. 1968. Scanning electron microscopy of cementum and Sharpey fibre bone. *Z. Zellforsch. Mikrosk. Anat.* 92: 536–548.

Boyde, A. and C. M. Riggs. 1990. The quantitative study of the orientation of collagen in compact bone slices. *Bone* 11: 35–39.

Bromage, T. G., et al. 2003. Circularly polarized light standards for investigations of collagen fiber orientation in bone. *Anat. Rec.* 274B: 157–168.

Bromage, T. G., et al. 2009. Lamellar bone is an incremental tissue reconciling enamel rhythms, body size, and organismal life history. *Calcif. Tissue Int.* 84: 388–404.

Bromage, T. G., et al. 2016. The scaling of human osteocyte lacuna density with body size and metabolism. *C. R. Palevol.* 15: 32–39.

Buffrénil, V. de, et al. 1987. Caractères structuraux et mode de croissance du fémur d'*Omphalosaurus nisseri*, ichthyosaurien du Trias moyen du Spitsberg. *Ann. Paléontol. (Vert.).* 73: 195–216.

Buffrénil, V. de, et al. 2008. Bone Vascular supply if monitor lizards (Squamata: Varanidae): influence of size, growth and phylogeny. *J. Morphol.* 269: 533–543.

Buffrénil V. de, et al. 2016. Comparative data on the differentiation and growth of bone ornamentation in gnathostomes (Chordata: Vertebrata). *J. Morphol.* 277: 634–670.

Buffrénil, V. de and A. Casinos. 1995. Observations histologiques sur le rostre de *Mesoplodon densirostris* (Mammalia, Cetacea, Ziphiidae): le tissu osseux le plus dense connu. *Ann. Sci. Nat., Zoologie*, 13ème sér., 16: 21–32.

Buffrénil, V. de and J. Castanet. 2000. Age estimation by skeletochronology in the Nile monitor (*Varanus niloticus*), a highly exploited species. *J. Herpetol.* 34: 414–424.

Buffrénil, V. de and J.-M. Mazin. 1990. Bone histology of the ichthyosaurs: comparative data and functional interpretation. *Paleobiology.* 16: 435–476.

Buffrénil, V. de and J.-M. Mazin. 1992. Contribution de l'histologie osseuse à l'interprétation paléobiologique du genre *Placodus* Agassiz, 1833 (Reptilia, Placodontia). *Rev. Paléobiol.* 11: 397–407.

Buffrénil, V. de and D. Schoevaert. 1988. On how the periosteal bone of the delphinid humerus becomes cancellous: ontogeny of a histological specialization. *J. Morphol.* 198: 149–164.

Buie, H. R., et al. 2007. Automatic segmentation of cortical and trabecular compartments based on a dual threshold technique for in vivo micro-CT bone analysis. *Bone.* 41: 505–515.

Burr, D. B., et al. 1988. Composition of the cement line and its possible mechanical role as a local interface in the human compact bone. *J. Biomech.* 21: 939–945.

Burr, D. B. and O. Akkus. 2014. Bone morphology and organization. In *Basic and applied bone biology*, eds. Burr, D. B. and M. R. Allen, 3–25. Amsterdam:, Academic Press.

Cadena, E. A. and M. H. Schweitzer. 2012. Variation in osteocyte morphology vs bone type in turtle shell and their exceptional preservation from the Jurassic to the present. *Bone.* 51: 614–620.

Canoville A., and et al. 2017. Quantitative data on bone vascular supply in the Lissamphibia: comparative and phylogenetic aspects. *Zool. J. Linn. Soc.* 20: 1–22.

Cao, L., et al. 2011. Comparative morphology of the osteocyte lacunocanalicular system in various vertebrates. *J. Bone Miner. Metab.* 29: 662–670.

Castanet, J. 1974. Etude histologique des marques squelettiques de croissance chez *Vipera aspis* (L.) (Ophidia: Viperidae). *Zool. Scripta.* 3: 137–151.

Castanet, J. 1978. Les marques de croissance osseuse comme indicateurs de l'âge chez les lézards. *Acta Zool. (Stockh.).* 59: 35–48.

Castanet, J. 1979. Données comparatives sur la minéralisation des marques de croissance squelettiques chez les Vertébrés. Etude par microradiographie quantitative. *C. R. Acad. Sci.* Paris D 289: 405–408.

Castanet, J. 1981. Nouvelles données sur les lignes cimentantes de l'os. *Arch. Biol.* 92: 1–24.

Castanet, J. 1982. *Recherche sur la croissance du tissu osseux des reptiles. Application: la méthode squelettochronologique.* Thèse d'Etat, Université Paris VII, Paris, June 1982.

Castanet, J. 2006. Time recording in bone microstructures of endothermic animals; functional relationships. *C. R. Palevol.* 5: 629–636.

Castanet, J. and A. de Ricqlès. 1987. Sur la relativité de la notion d'ostéones primaires et secondaires et de tissu osseux primaire et secondaire en général. *Ann. Sci. Nat. (Zool.).* 8: 103–109.

Castanet, J., et al. 1993. Bone and individual aging. In *Bone. Vol. 7: Bone Growth B*, ed. Hall, B. K., 245–283. Boca Raton, FL:, CRC Press.

Castanet, J., et al. 1996. Expression de la dynamique de croissance dans la structure de l'os périostique chez *Anas platyrhynchos*. *C. R. Acad. Sci.* 319: 301–308.

Castanet, J., et al. 2000. Periosteal bone growth rates in extant ratites (ostriche and emu). Implications for assessing growth in dinosaurs. *C. R. Acad. Sci.* 323: 543–550.

Castanet, J., et al. 2003. The skeletal histology of the Amphibia. In *Amphibian biology*, eds. Heatwole H. and M. Davies, Vol. 5, 1598–1683., Chipping Norton, NSW: Surrey Beatty.

Chinsamy, A., et al. 2016. Vascularized endosteal bone tissue in armoured sauropod dinosaurs. *Scientif. Rep.* 6: 24858. DOI: 10.1038/sirep24858.

Chinsamy-Turan, A., and S. Ray. 2012. Bone histology of some therocephalians and gorgonopsians, and evidence of bone degradation by fungi. In *The forerunners of mammals: radiation, histology and biology*, ed. A. Chinsamy-Turan, 199–222. Bloomington, IN: Indiana University Press.

Cohen, L., et al. 2012. Comparison of structural, architectural and mechanical aspects of cellular and acellular bone in two teleost fishes. *J. Exp. Biol.* 215: 1983–1993.

Cooper, D. M. L., et al. 2003. Quantitative 3D analysis of the canal network in cortical bone by micro-computed tomography. *Anat Rec.* 274B: 169–179.

Cubo, J., et al. 2005. Phylogenetic signal in bone microstructure of sauropsids. *Syst. Biol.* 54: 562–574.

Cubo, J., et al. 2012. Paleohistological estimation of bone growth rate in extinct archosaurs. *Paleobiology* 38: 335–349.

Cubo J, et al. 2014. Geometric and metabolic constraints on bone vascular supply. *Biol. J. Linn. Soc.* 112: 668–677.

Cubo, J., et al. 2017. Static osteogenesis does not precede dynamic osteogenesis in periosteal ossification of *Pleurodeles* (Caudata, Amphibia) and Pogona (Squamata, Lepidosauria). *J. Morphol.* 278: 621–628.

Cummaudo, M., et al. 2018. Histomorphological analysis of the variability of the human skeleton: forensic implications. *Int. J. Legal Med.* 132: 1493–1503.

Currey, J. D. 1960. Differences in the blood-supply of bone of different histological types. *Q. J. Microsc.* 101: 351–370.

Currey, J. D. 1984. Effects of differences in mineralization on the mechanical properties of bone. *Philos. Trans. R. Soc. Lond.* B 304: 509–518.

Currey, J. D. 2002. Bones. *Structure and mechanics.* Princeton, NJ:, Princeton University Press.

Currey, J. D. 2003. The many adaptations of bone. *J. Biomech.* 36: 1487–1495.

Currey, J. D. and K. Brear. 1990. Hardness, Young's modulus and yield stress in mammalian mineralized tissues. *J. Mater. Sci.* 1: 14–20.

Currey, J. D., et al. 2016. Revisiting the links between bone remodeling and osteocytes: insights from across phyla. *Biol. Rev.* 92: 1702–1719.

Dallas, S. L. and L. F. Bonewald. 2010. Dynamics of the transition from osteoblast to osteocyte. *Ann. N Y Acad. Sci.* 1192: 437–443.

Davesne, D., et al. 2018a. The phylogenetic origin and evolution of acellular bone in teleost fishes: insights into osteocyte function in bone metabolism. *Biol. Rev. Camb. Philos. Soc.* doi.org/ 94: 1338–1363.

Davesne, D., et al. 2018b. Histology of the endothermic opah (*Lampris* sp.) suggests a new structure-function relationship in teleost fish bone. 2018. *Biol. Lett.* 14: 20180270.

Dong, P., et al. 2014. 3D osteocyte lacunar morphometric properties and distributions in human femoral cortical bone using synchrotron radiation micro-CT images. *Bone* 60: 172–185.

Downs, J. P. and P. C. J. Donoghue. 2009. Skeletal histology of *Bothriolepis canadensis* (Placodermi, Antiarchi) and evolution of the skeleton at the origin of jawed vertebrates. *J. Morphol.* 270: 1364–1380.

Donoghue P. C. J. and I. J. Sansom. 2002. Origin and early evolution of vertebrate skeletonization. *Microsc. Res. Tech.* 59: 352–372.

Ekanayake, S. and B. K. Hall. 1987. The development of acellularity of the vertebral bone of the Japanese Medaka, *Oryzias latipes* (Teleostei; Cyprinidontidae [sic]). *J. Morphol.* 193: 253–261.

Enlow, D. H. and S. O. Brown. 1956. Comparative histological study of fossil and recent bone tissues. Part I. *Texas J. Sci.* 8: 405–443.

Enlow, D. H. and S. O. Brown. 1957. Comparative histological study of fossil and recent bone tissues. Part II. *Texas J. Sci.* 9: 186–214.

Enlow, D. H. and S. O. Brown. 1958. Comparative histological study of fossil and recent bone tissues. Part III. *Texas J. Sci.* 10: 187–230.

Enlow, D. H. 1963. *Principles of bone remodeling.* Springfield (Illimois, USA): Charles C. Thomas.

Faingold, A., et al. 2013. Osteonal lamellae elementary units: lamellar microstructure, curvature and mechanical properties. *Acta Biomater.* 9: 5956–5962.

Faure-Brac, M., et al. 2019. The influence of plane of section on the identification of bone tissue types in amniotes with implications for paleophysiological inferences. *J. Morphol.* 280: 1282–1291.

Ferretti, M., et al. 2002. Static and dynamic osteogenesis: two different types of bone formation. *Acta Embryol.* 206: 21–29.

Foote, J. S. 1911. The comparative histology of femoral bones. *Trans. Am. Microsc. Soc.* 30: 87–140.

Foote, J. S. 1913. The comparative histology of the femur. *Smith. Miscell. Coll.* 61: publ. 2232.

Foote, J. S. 1916. A contribution to the comparative histology of the femur. *Smith. Contrib. Knowl.* 35: publ. 2382

Francillon-Vieillot, H., et al. 1990. Microstructure and mineralization of vertebrate skeletal tissues. In *Skeletal biomineralization: patterns, processes and evolutionary trends*, ed. J. G. Carter, Vol. 1, 471–530. New York:, Van Nostrand Reinhold.

Franz-Odendaal, T. A., and et al. 2006. Buried alive: how osteoblasts become osteocytes. *Dev. Dyn.* 235: 176–190.

Frasca, P. 1981. Scanning-electron microscopy studies of "ground substance" in the cement lines, resting lines, hypercalcified rings and reversal lines of human cortical bone. *Acta Anat.* 109: 115–121.

Frasca, P., et al. 1978. Mineral and collagen fiber orientation in human secondary osteons. *J. Dent. Res.* 57: 526–533.

Frost, H. M. 1960. Observations on fibrous and lamellar bone. *Med. Bull.* 8: 199–207.

Gabe, M. 1967. Cartilage, tissue osseux et ostéogenèse. In *Traité de zoologie*, XVI, fasc., ed. Grassé, P. P., XVI, fasc. 1, 259–333. Paris:, Masson.

Garcia, J., and J. Martinez -Reina. and 2017. Elastic properties of woven bone: effect of mineral content and collagen fibrils orientation. *Biomech. Model Mechanobiol.*16: 159–172.

Gebhardt, W. 1906. Ueber funktionell wichtige Anordnungs weisen der gröberen und feineren Bauelemente des Wirbeltiere Knochens. II. Spezieller Teil: 1. Des Bau der Haversshen Lamellensysteme und seine funktionelle Bedeutung. *Arch. Entw. mechan.* 20: 187–322.

Georgiadis, M., et al. 2016. Techniques to assess bone ultrastructre organization: orientation and arrangement of mineralized collagen fibrils. *J. R. Soc. Interface* 13: 20160088.

Giles, S., et al. 2013. Histology of "Placoderm" dermal skeletons: implications for the nature of the ancestral gnathostome. *J. Morphol.* 274: 627–644.

Gillis, J. A., et al. 2006. Chondroid bone and secondary cartilage contribute to apical dentary growth in juvenile Atlantic salmon. *J. Fish Biol.* 68: 1133–1143.

Giraud, M.-M., et al. 1978. The fibrous structure of coelacanth scales: a twisted "plywood". *Tissue Cell* 10: 671–686.

Giraud-Guille, M. M. 1988. Twisted plywood architecture of collagen fibrils in human compact bone osteons. *Calcif. Tissue Int.* 42: 167–180.

Girondot, M. and M. Laurin. 2003. Bone Profiler, a tool to quantify, model, and statistically compare bone section compactness profiles. *J Vert Paleontol.* 23: 458–461.

Goret-Nicaise, M. 1984. Identification of collagen type I and type II in chondroid tissue. *Calcif. Tissue Int.* 36: 682–689.

Goret-Nicaise, M. and M. Dhem. 1985. Comparison of the calcium content of different tissues present in the human mandible. *Acta Anat.* 124: 167–172.

Goret-Nicaise, M. and M. Dhem. 1987. Electron microscopic study of chondroid tissue in the cat mandible. *Calcif. Tissue Int.* 40: 219–223.

Gross, W. 1934. Die typen des mikroscopischen Knochenbaues bei fossilen Stegocephalen und Reptilien. *Zeit. Anat.* 103: 731–764.

Hall, B. K. 1972. Immobilization and cartilage transformation into bone in the embryonic chick. *Anat. Rec.* 173: 391–404.

Halstead-Tarlo, L. B. 1963. Aspidin: the precursor of bone. *Nature* 199: 46–48.

Hannah, K. M., et al. 2010. Bimodal distribution of osteocyte lacunar size in the human femoral cortex as revealed by micro-CT. *Bone.* 47: 866–871.

Heck, C. T., et al. 2019. Ontogenetic changes in the long bone microstructure in the nine-banded armadillo (*Dasypus novemcinctus*). *PLoS One* 14(4): e0215655.

Hernandez, C. J., et al. 2004. Osteocyte density in woven bone. *Bone.* 35: 1095–1099.

Heřt, J., et al. 1994. Osteon orientation of the diaphysis of the long bones in man. *Bone* 15: 269–277.

Hieronymus, T. L. 2006. Quantitative microanatomy of jaw muscle attachment in extant diapsids. *J. Morphol.* 267: 954–967.

Hildebrand, T., et al. 1999. Direct three-dimensional morphometric analysis of human cancellous bone: microstructural data from spine, femur, iliac crest, and calcaneus. *J. Bone Miner. Res.* 14: 1167–1174.

VetBooks.ir

Hofmann, R., et al. 2014. Constraints on the lamina density of laminar bone architecture of large-bodied dinosaurs and mammals. *Acta Palaeontol. Pol.* 59: 287–294.

Horner, J. R., et al. 2001. Comparative osteohistology of some embryonic and perinatal archosaurs: developmental and behavioral implications for dinosaurs. *Paleobiology.* 27: 39–58.

Horner, J. R. and K. Padian. 2004. Age and growth dynamics of *Tyrannosaurus rex*. *R. Soc. Lond. Proc.*B 271 (1551): 1875–1880.

Houssaye A., et al. 2013. Jack-of-all-trades master of all? Snake vertebrae have a generalist inner organization. *Naturwissenschaften* 100: 997–1006.

Houssaye, A., et al. 2014. New look at ichthyosaur long bone microanatomy and histology. Implications for their adaptation to an aquatic life. *PLoS One* 9: e95637.doi:.

Hughes, D. R., et al. 1994. Histological identification of osteocytes in the allegedly acellular bone of the sea breams *Acanthopagrus australis*, *Pagrus auratus* and *Rhabdosargus sarba* (Sparidae, Perciformes, Teleostei). *Anat. Embryol.* 190: 163–179.

Hugi, J., et al. 2011. Long bone microstructure gives new insights into the life of pachypleurosaurids from the Middle Triassic of Monte San Giorgio, Switzerland/Italy. *C. R. Palevol.* 10: 413–426.

Hugi, J. and M. R. Sánchez-Villagra. 2012. Life history and skeletal adaptations in the Galapagos marine iguana (*Amblyrhynchus cristatus*) as reconstructed with bone histological data – A comparative study of Iguanines. *J. Herpetol.* 46: 312–324.

Huysseune, A., et al. 1986. The contribution of chondroid bone in the growth of the parasphenoid bone of a cichlid fish as studied by oblique computer-aided reconstructions. *Biol. Jaarb. Dodonaea* 54: 131–141.

Huysseune, A. and W. Verraes. 1986. Chondroid bone on the upper pharyngeal jaws and neurocranial base in the adult fish *Astatotilapia elegans*. *Am. J. Anat.* 177: 527–535.

Huysseune, A. and J.-Y. Sire. 1990. Ultrastructural observations on chondroid bone in the teleost fish *Hemichromis bimaculatus*. *Tissue Cell* 22: 371–383.

Jasinoski, S. C. and A. Chinsamy. 2012. Mandibular histology and growth of the nonmammaliaform cynodont *Tritylodon*. *J. Anat.* 220: 564–579.

Jones, S. J. and A. Boyde. 1974. The organization and gross mineralization patterns of the collagen fibers in Sharpey fibre bone. *Cell Tissue Res.* 148: 83–96.

Jordana, X., et al. 2016. Ontogenetic changes in the histological features of zonal bone tissues of ruminants: a quantitative approach. *C. R. Paleovol.* 15: 255–266.

Keating, J. N. and P. C. J. Donoghue. 2016. Histology and affinity of anaspids, and the early evolution of the vertebrate dermal skeleton. *Proc. R. Soc. B.* 283: 20152917.

Keating, J. N., et al. 2015. Histology of the heterostracan dermal skeleton: insight into the origin of the vertebrate mineralised skeleton. *J. Morphol.* 276: 657–680.

Keating, J. N., et al. 2018. The nature of aspidin and the evolutionary origin of bone. *Nat. Ecol. Evol.* 21: 1501–1506.

Kerschnitski, M., et al. 2011. The organization of the osteocyte network mirrors the extracellular matrix orientation in bone. *J. Struct. Biol.* 173: 303–311.

Klein, N. and M. Sander. 2008. Ontogenetic stages in the long bone histology of sauropod dinosaurs. *Paleobiology.* 34: 247–263.

Klein, N., et al. 2015a. Long bone histology and microanatomy of Placodontia (Diapsida: Sauropterygia). *Contrib. Zool.* 84: 59–84.

Klein, N., et al. 2015b. Growth pattern and life history strategies in Placodontia (Diapsida: Sauropterygia). *R. Soc. Open sci.* 2: 140440.

Klein, N., et al. 2016. Diverse aquatic adaptations in *Nothosaurus* spp. (Sauropterygia) – Inferences from humeral histology and microanatomy. *PLoS One* 11: e0158448. doi:.

Klein-Nulend, J. and L. F. Bonewald. 2008. The osteocyte. In *Principles of bone biology.*(3rd edition, eds. Bilezikian, J. P., L. G. Raisz and T. J. Martin, 153–174. Amsterdam,: Academic Press.

Klevezal, G. A. 1996. *Recording structures of mammals: determination of age and reconstruction of life history.* Brookfield: A. A. Balkema.

Köhler, M. and S. Moya-Solà. 2009. Physiological and life history strategies of a fossil large mammal in a resource-limited environment. *PNAS.* 106: 20354–20358.

Lacroix, P. 1945. Remarques sur le mécanisme de l'allongement des os. *Arch. Biol.* 56: 185–197.

Lacroix, P. 1949. *L'organisation des os*. Paris: Masson et Cie.

Lacroix, P. 1970. Recherches sur le remaniement interne des os. *Arch. Biol. (Liège).* 81: 275–304.

Legendre, L. J., et al. 2016. Palaeohistological evidence for ancestral high metabolic rate in archosaurs. *Syst. Biol.* 65: 989–996.

Legendre, L. J. and J. Botha-Brink. 2018. Digging the compromise: investigating the link between bone histology and fossoriality in the aardvark (*Orycteropus afer*). *PeerJ* 6: e5216;.

Li, J. and D. L. Stocum. 2014. Fracture healing. In *Basic and Applied bone biology*, eds. Burr, D. B. and M. R. Allen, 205–223. Amsterdam: Academic Press.

Locke, M. 2004. Structure of long bones in mammals. *J. Morphol.* 262: 546–565.

Luther, F., et al. 2003. Evidence for an extensive collagen type III/VI proximal domain in the rat femur. I: Diminution with ovariectomy. *Bone* 32: 652–659.

Magal, R. A., et al. 2014. Three-dimensional structure of minipig fibrolamellar bone: adaptation to axial loading. *J. Struct. Biol.* 186: 253–264.

Maggiano, I. S., et al. 2016. Three-dimensional reconstruction of Haversian systems in human cortical bone using synchrotron radiation-based micro-CT: morphology and quantification of branching and transverse connections across age. *J. Anat.* 228: 719–732.

Margerie, E. de, et al. 2002. Bone typology and growth rate: testing and quantifying "Amprino's rule" in the mallard (*Anas platyrhynchos*). *C. R. Biol.* 325: 221–230.

Margerie, E. de, et al. 2004. Assessing a relationship between bone microstructure and growth rate: a fluorescent labeling study in the king penguin chick (*Aptenodytes patagonicus*). *J. Exp. Biol.* 207: 869–879.

Marotti, G. 1979. Osteocyte orientation in human lamellar bone and its relevance to the morphometry of periosteocytic lacunae. *Metab. Bone Dis. Rel. Res.* 1: 325–333.

Marotti, G. 1993. A new theory of bone lamellation. *Calcif. Tissue Int.* 53(suppl. 1): S47–S56.

VetBooks.ir

Marotti, G., et al. 1972. Quantitative analysis of the rate of secondary bone mineralization. *Calcif. Tissue Res.* 10: 67–81.

Marotti, G., et al. 1985a. A SEM study of osteocyte orientation in alternately structured osteons. *Bone*. 6: 331–334.

Marotti, G., et al. 1985b. Quantitative investigation on osteocyte canaliculi in human compact and spongy bone. *Bone*:. 6: 335–337.

Marotti, G., et al. 1992. A quantitative evaluation of osteoblast-osteocyte relationships on growing endosteal surface of rabbit tibiae. *Bone*. 13: 363–368.

Marotti, G., et al. 1999. Static and dynamic bone formation and the mechanism of collagen fiber orientation. *Bone*. 25: 156.

Marotti, G., et al. 2013. The problem of bone lamellation: an attempt to explain different proposed models. *J. Morphol.* 274: 543–550.

Marotti, G. M. and M. A. Muglia. 1992. The structure of primary and secondary osteons studied with the scanning electron microscope (abstract from *Bone Morphology*, 1992). *Bone*. 13: A22.

Martinez-Maza, C., et al. 2014. Life-History traits of the Miocene *Hipparion concudense* (Spain) Inferred from *bone histological structure*. *PLoS One*. 9(8): e103708.

Metz, L. N., et al. 2003. Histomorphometric analysis of the effects of osteocyte density on osteonal morphology and remodeling. *Bone*. 33: 753–759.

Meunier, F. J. 1980. Les relations isopédine-tissu osseux dans le post-temporal et les écailles de la ligne latérale de *Latimeria chalumnae* (Smith). *Zool. Scripta*. 9: 307–317.

Meunier, F. J. 1981. "Twisted plywood" structure and mineralization in the scales of a primitive living fish Amia calva. *Tissue Cell*. 13: 165–171.

Meunier, F. J. 1984a. Etude de la minéralisation de l'os chez les téléostéens à l'aide de la microradiographie quantitative. Résultats préliminaires. *Cybium*. 8: 43–49.

Meunier, F. J. 1984b. Spatial organization and mineralization of the basal plate of elasmoid scales in osteichthyans. *Am. Zool*. 24: 953–964.

Meunier, F. J. 2011. The osteichtyes [*sic*], from the Paleozoic to the extant time, through histology and paleohistology of bony tissues. *C. R. Palevol*. 10: 347–355.

Meunier, F. J. and J. Castanet. 1982. Organisation spatiale des fibres de collagène de la plaque basale des écailles des Téléostéens. *Zool. Scripta*. 11: 141–153.

Meunier, F. J. and A. Huysseune. 1992. The concept of bone tissue in Osteichthyes. *Nether. J. Zool*. 42: 445–458.

Milovanovic, P., et al. 2018. Bone tissue aging affects mineralization of cement lines. *Bone*. 110: 187–193.

Mitchell, J. and A. H. van Heteren. 2016. A literature review of the spatial organization of lamellar bone. *C. R. Palevol*. 15: 23–31.

Mitchell, J., et al. 2017. Can secondary osteons be used as ontogenetic indicators in sauropods? Extending the histological ontogenetic stages into senescence. *Paleobiology*. 43: 321–342.

Montoya-Sanhueza, G. and A. Chinsamy. 2017. Long bone histology of the subterranean rodent *Bathyergus suillus* (Bathyergidae: ontogenetic pattern of cortical bone thickening. *J. Anat*. 230: 203–233.

Mori, R., et al. 2003. Comparative histology of the laminar bone between young calves and foals. *Cell. Tissue Org.* 175: 43–50.

Moss, M. L. 1961. Osteogenesis of acellular teleost fish bone. *Am. J. Anat*. 108: 99–110.

Moss, M. L. 1963. The biology of acellular teleost bone. *Ann. N. Y. Acad. Sci*. 109: 337–350.

Neves, R. and L. B. Halstead-Tarlo. 1965. Isolation of fossil osteocytes. *J. R. Microsc. Soc*. 84: 217–219.

O'Driscoll, W. M., et al. 2001. The chondrogenic potential of periosteum decreases with age. *J. Orthop. Res*. 19: 95–103.

Ofer, L., et al. 2019. New insights into the process of osteogenesis in anosteocytic bone. *Bone*. 125: 61–73.

Orlandi-Oliveras, G., et al. 2018. Bone histology provides insights into the life history mechanisms underlying dwarfism in hipparionids. *Sci. Rep*. 8: 1–15.

Ozasa, R., et al. 2017. Preferential arrangement of mature osteoblast from juvenile mouse calvariae on the oriented collagen substrate. *J. Japan Inst. Met. Mater.* 81: 480–484.

Parfitt, A. M. 1983. The physiologic and clinical significance of bone histomorphometric data. In *Bone histomorphometry: techniques and interpretations*, ed. Recker, R. R., 143–223. Boca Raton, FL:, CRC Press.

Parfitt, A. M. 1994. Osteonal and hemi-osteonal remodeling: the spatial and temporal framework for signal traffic n adult human bone. *J. Cell Biochem*. 55: 273–286.

Pazzaglia, U. E., et al. 2012. A model of osteoblast-osteocyte kinetics in the development of secondary osteons in rabbits. *J. Anat*. 220: 372–-383.

Petersen, H. 1930. Die Organe des Skeletsystems. In *Handbuch der Mikroskopischen Anatomie des Menschen II*, ed. Möllendorff, W. v. ed., 521–678. Berlin:, Springer Verlag.

Philipson, B. 1965. Composition of cement lines in bone. *J. Histochem. Cytochem*. 13: 270–281.

Poplin, C., et al. 1976. Quelques particularités anatomiques et histologiques du rostre de l'espadon (*Xiphias gladius L.*). *C. R. Acad. Sci*. 282: 1105–1108.

Pratt, I. V. and D. M. L. Cooper. 2017. A method for measuring the three-dimensional orientation of cortical canals with implications for comparative analysis of bone microstructure in vertebrates. *Micron* 92: 32–38.

Pratt, I. V. and D. M. L. Cooper. 2018. The effect of growth rate on the three-dimensional orientation of vascular canals in the cortical bone of broiler chickens. *J. Anat*. 233: 531–541.

Pritchard, J. J. 1956. General anatomy and histology of bone. In *The biochemistry and physiology of bone*, 1st edition, ed. Bourne, G. H. ed., 1–25. London and New York:, Academic Press.

Prondvai, E., et al. 2014. Development-based revision of bone tissue classification: the importance of semantics for science. *Biol. J. Linn. Soc*. 112: 799–816.

Prondvai, E., et al. 2020. Extensive chondroid bone in juvenile duck limbs hints at accelerated growth mechanism in avian skeletogenesis. *J. Anat*. 236: 463–473.

Quigley, M. B. 1970. Perforating (Sharpey's) fibers of the periodontal ligament and bone. *Alabama J. Med. Sci*. 7: 336–342.

Quilhac, A., et al. 2014. Globuli ossei in the long limb bones of *Pleurodeles waltl* (Amphibia, Urodela, Salamandridae). *J. Morphol*. 275: 1226–1237.

Ray, S., et al. 2009. Growth patterns of fossil vertebrates as deduced from bone microstructure: case studies from India. *J. Biosci*. 34: 661–672.

Ray, S., et al. 2012. Dicynodont growth dynamics and lifestyle adaptations. In *Forerunners of mammals*, ed. Chinsamy, A., 121–148. Bloomington: Indiana University Press.

Repp, F., et al. 2017. Spatial heterogeneity in the canalicular density of the osteocyte network in human osteons. *Bone Rep.* 6: 101–108.

Reznikov, N., et al. 2013. Three-dimensional imaging of collagen fibril organization in rat circumferential lamellar bone using a dual beam electron microscope reveals ordered and disordered sub-lamellar structures. *Bone*,. 52: 676–683.

Reznikov, N., et al. 2014a. Bone hierarchical structure in three dimensions. *Acta Biomater.* 10: 3815–3826.

Reznikov, N., et al. 2014b. Three-dimensional structure of human lamellar bone: the presence of two different materials and new insights into the hierarchical organization. *Bone*:. 59: 93–104.

Ricqlès, A. de. 1975. Recherches paléohistologiques sur les os longs des tétrapodes VII. – Sur la classification, la signification fonctionnelle et l'histoire des tissus osseux des tétrapodes. Première partie, structures. *Ann. Paléontol.* 61: 51–129.

Ricqlès, A. de. 1976. Recherches paléohistologiques sur les os longs des tétrapodes VII. – Sur la classification, la signification fonctionnelle et l'histoire des tissus osseux des tétrapodes (deuxième partie : fonctions). *Ann. Paléontol.* 62: 71–126.

Ricqlès, A. de. 1977. Recherches paléohistologiques sur les os longs des tétrapodes VII. – Sur la classification, la signification fonctionnelle et l'histoire des tissus osseux des tétrapodes (deuxième partie, fin). *Ann. Paléontol.* 63: 33–56, 63: 133–160.

Ricqlès, A. de. 1978. Recherches paléohistologiques sur les os longs des tétrapodes VII. – Sur la classification, la signification fonctionnelle et l'histoire des tissus osseux des tétrapodes. (troisième partie: évolution). *Ann. Paléontol.* 64: 33–56, 64: 153–184.

Ricqlès, A. de. 1979. Quelques remarques sur l'histoire évolutive des tissus squelettiques chez les vertébrés et plus particulièrement chez les tétrapodes. *Ann. Biol.* 18: 1–35.

Ricqlès, A. de, et al. 1991. Comparative microstructure of bone. In *Bone, Vol. 3 Bone matrix and bone specific products*,. Eed. Hall, B. K., 1–78. Boca Raton, FL:, CRC Press.

Ricqlès, A. de, et al. 2000. Paleohistology of the bones of pterosaurs (Reptilia: Archosauria): anatomy, ontogeny, and biomechanical implications. *Zool. J. Linn. Soc.* 129: 349–385.

Ricqlès, A. de, et al. 2003. On the bone histology of some Triassic pseudosuchian archosaurs and related taxa. *Ann. Paléontol.* 89: 67–101.

Ricqlès, A. de, et al. 2008. On the origin of high growth rates in archosaurs and their ancient relatives: Complementary histological studies on Triassic archosauriforms and the problem of a "phylogenetic signal" in bone histology. *Ann. Paléontol.* 94: 57–76.

Ricqlès, A. de and J. R. Bolt. 1983. Jaw growth and tooth replacement in *Captorhinus aguti* (Reptilia: Captorhinomorpha): a morphological and histological analysis. *J. Vert. Paleontol.* 3: 7–24.

Ricqlès, A. de. and V. de Buffrénil. 2001. Bone histology, heterochronies and the return of tetrapods to life in water: where are we? In *Secondary Adaptation of Tetrapods to Life in Water*, eds. Mazin J.-M. and V. de Buffrénil, 289–310. München: Verlag Dr. Friedrich Pfeil.

Roche, B., et al. 2012. Structure and quantification of microvascularization within mouse long bones: what and how should we measure. *Bone* 50: 390–399.

Saino, H., F., et al. 2003. Evidence for an extensive collagen type III proximal domain in the rat femur. II: Expansion with exercise. *Bone* 32: 660–668.

Sander, M. P., et al. 2004. Adaptive radiation in sauropod dinosaurs : bone histology indicates rapid evolution of giant body size through acceleration. *Organ. Divers. Evol.* 4: 165–173.

Sander, M. P. and C. Tückmantel. 2003. Bone lamina thickness, bone apposition rates, and age estimates in sauropod humeri and femora. *Paläontol. Zeitschr.* 77: 161–172.

Schultze, H.-P. 2018. Hard tissues in fish evolution: history and current issues. *Cybium.* 42: 29–39.

Shapiro, F. and J. Y. Wu. 2019. Woven bone overview: structural classification based on its integral role in developmental, repair and pathological bone formation throughout vertebrate groups. *Eur. Cells Mater.* 38: 137–167.

Schönbörner, A. A., et al. 1981. The fine structure of calcified Mandl's corpuscles in teleost fish scales. *Tissue & Cell* 13: 589–597.

Simpson, A. H. R. W. 1985. The blood supply of the periosteum. *J. Anat.* 140: 697–704.

Sire, J.-Y. and A. Huysseune. 2003. Formation of dermal skeletal and dental tissues in fish: a comparative and evolutionary approach. *Biol. Rev.* 78: 219–249.

Sire, J.-Y., et al. 2009. Origin and evolution of the integumentary skeleton in non-tetrapod vertebrates. *J. Anat.* 214: 409–440.

Skedros, J. G., et al. 2005. Cement lines of secondary osteons in human bone are not mineral-deficient: new data in a historical perspective. *Anat. Rec.* 286A: 781–803.

Stein, K. and E. Prondvai. 2014. Rethinking the nature of fibrolamellar bone: an integrative biological revision of sauropod plexiform bone formation. *Biol. Rev.* 89: 24–47.

Stover, S. M., et al. 1992. Histological features of the dorsal cortex of the third metacarpal bone mid-diaphysis during postnatal growth in thoroughbred horses. *J. Anat.* 181: 455–469.

Warren, J. W. 1963. *Growth zones in the skeleton of recent and fossil vertebrates.* University Microfilms Inc., n° 63-4544. University of California, Los Angeles.

Webster, D. J., et al. 2013. Studying osteocytes within their environment. *Bone*:. 54: 285–295.

Weidenreich, F. 1922. Uber die Bezichungen Zwischen Muskelapparat und Knocken und der Charakter des Knockengewebes. *Anat. Anz.* 55: 28–53.

Weidenreich, F. 1930. Das Knochengewebe. In *Handbuch der miroscopischen Anatomie des Menschen (II-2)*, ed. Möllendorff, W. v., 391–520. Berlin:, Springer Verlag.

Weiner, S. and H. D. Wagner. 1998. The material bone: structure-mechanical function relations. *Ann. Rev. Mat. Sci.* 28: 271–298.

Weiner, S., et al. 1997. Rotated plywood structure of primary lamellar bone in the rat: orientations of the collagen fibril arrays. *Bone.* 20: 509–514.

Weinkamer, R., et al. 2019. Towards a connectomic description of the osteocyte lacunocanalicular network in bone. *Curr. Osteoporosis Rep.* https://doi.org/10.1007/s11914-019-00515-z.

VetBooks.ir

Witten, P. E., et al. 2010. A practical approach for the identification of the many cartilaginous tissues in teleost fish. *J. Appl. Ichthyol*. 26: 257–262.

Witten, P. E. and A. Huysseune. 2009. A comparative view on mechanisms and functions of skeletal remodeling in teleost fish, with special emphasis on osteoclasts and their function. *Biol. Rev.* 84: 315–346.

Wolff, J. 1892 (transl. 1986). *The law of bone remodeling*. Berlin,: Springer.

Wu, K., et al. 1970. Haversian bone formation rate determined by a new method in a mastodon, and in human *diabetes mellitus* and osteoporosis. *Calcific. Tissue Res*. 6: 204–219.

You, L.D., et al. 2001. A model for strain amplification in the actin cytoskeleton of osteocytes due to fluid drag on pericellular matrix. *J. Biomech*. 34: 1375–1386.

You, L.-D., et al. 2004. Ultrastructure of the osteocyte process and its pericellular matrix. *Anat. Rec.* 278A: 505–513.

Ziv, V., et al. 1996. Microstructure-microhardness relations in parallel-fibered and lamellar bone. *Bone*. 18: 417–428.

Zioupos, P., et al. 1997. Mechanical properties of the rostrum of the whale *Mesoplodon densirostris*, a remarkably dense bony tissue. *J. Zool. Lond*. 241: 725–737.

Zylberberg, L., et al. 1998. Rostrum of a toothed whale: ultrastructural study of a very dense bone. *Bone*. 23: 241–247.

VetBooks.ir

Methodological Focus D

FIB-SEM Dual-Beam Microscopy for Three-Dimensional Ultrastructural Imaging of Skeletal Tissues

Natalie Reznikov and Katya Rechav

CONTENTS

Use of Dual-Beam FIB-SEM 3D Imaging in Skeletal Biology 183
Fundamental Principles and Practical Use 184
General Geometry and Some Customized Geometries 184
Specimen Preparation 187
Imaging Parameters 187
3D Image Processing 188
Conclusion 189
Acknowledgments 189
References 189

Use of Dual-Beam FIB-SEM 3D Imaging in Skeletal Biology

The focused ion beam scanning electron microscope (FIB-SEM) is a versatile instrument that can be used for both three-dimensional (3D) imaging of a bulky specimen at nanometer-scale resolution (Kizilyaprak et al. 2019), or as a powerful sample preparation platform for subnanometer imaging (Langelier et al. 2017, Grandfield et al. 2018). Both of these capacities can be used in a complementary fashion for studying the same object. FIB-SEM used as a 3D imaging tool (the serial surface view (SSV), or serial slice and view) was originally developed for materials science and semiconductor research for site-specific imaging and failure analysis. From there it eventually made its way into the life sciences (Narayan and Subramaniam 2015). As a 3D imaging tool, FIB-SEM occupies an intermediate niche between other common 3D imaging approaches such as µCT tomography and electron tomography (see the continuity of their respective imaging power in Table D.1).

Considering the 3D nature of our world and the prevailing hierarchical complexity of biological materials, the position of the FIB-SEM among other tomographic analytical tools is of particular value because it allows contextualization of high-resolution features relative to larger-scale features, which in turn form even larger-scale structures, and so on. Having a rich structural context in life sciences is generally important for any data from biological tissues, and particularly so for biomineralization research because of the remarkable hierarchical complexity of mineralized tissues such as bone (Reznikov et al. 2014a) and tooth dentin (Earl et al. 2010) and enamel (Goldberg et al. 2014). Along with having remarkably extended spatial complexity, skeletal tissues in particular have additional chronological complexity, as they form, grow and remodel, following intricate development (Akiva et al. 2015; Kerschnitzki et al. 2016; Hasegawa et al. 2017; Buss et al. 2020) and turnover pathways and eventually enter pathophysiological scenarios of decline and involution leading to degeneration and disease (Milovanovic et al. 2016). From a functional perspective, skeletal tissues form multifaceted interfaces or, more precisely, 3D interphases with soft tissues and cells. Any such interphase studied in 3D inevitably yields fascinating novel results that hardly could be detectable from two-dimensional (2D) section-based imaging methods, perhaps only extrapolated. Inspiring examples of FIB-SEM imaging include 3D analyses of the bone-tendon attachment structure (Kanazawa et al. 2016), the bone-marrow niche with its unique adrenergic adipocytes and associated capillaries (Robles et al. 2019), the close interphase apposition between the mineralized extracellular matrix and osteocytes (Hasegawa et al. 2018), the precisely and heterogeneously architected periodontal ligament situated between the tooth root and the alveolar bone socket (Hirashima et al. 2020) or even the structure of the hinge ligament of a bivalve mollusk that has been perfected over millions years of evolution to incorporate a fine gradient of elastic moduli by combining fibrous organic material with embedded aragonite crystals (Suzuki et al. 2019).

As an illustration of a FIB-SEM application in the life sciences that has boosted the pace of scientific discovery in biomineralized tissues, we will consider the 3D hierarchical architecture of bone. More than three centuries ago, Clopton Havers described five nested structural levels in the skeleton (Havers 1691). However, coincident with the advent of FIB-SEM technology in the life sciences, our understanding of 3D bone structural organization has rapidly expanded, extending down to the nanoscale. In particular, it was only possible with submicrometer 3D imaging to unveil the combination of built-in, synergistic

VetBooks.ir

TABLE D.1

Comparison of Several 3D Imaging Methods in Terms of Pixel Size and Volume of Acquisition

Tomographic Method	Interaction With Sample	Pixel Size	Volume of Interest
µCT	Nondestructive	0.1–50 µm	10^{10} voxels
FIB-SEM SSV	Destructive	3–100 nm	10^{10} voxels
E-tomography	Semidestructive	0.3–5 nm	10^{8}–10^{9} voxels

coexistence of order and disorder in the most common type of mammalian bone, lamellar bone (Reznikov et al. 2013, 2014b, 2015) (Figure D.1). After having been discovered in mammalian lamellar bone, a disordered motif was then also identified in 3D in mammalian fibrolamellar bone (Almany-Magal et al. 2014) and in teleost fish bone (Atkins et al. 2015). Soon thereafter, in porcine alveolar bone, the relative proportions of order and disorder were found to invert, apparently in response to its specific biomechanical environment (Maria et al. 2019).

Why would nature insert chaotic, disordered motifs into an otherwise overall neat and periodically ordered structure (Shahar and Weiner 2018)? It turns out there are many implications, from regulating and controlling the extent of local bone deformation on loading, to containment of noncollagenous organic molecules in bone matrix for long-term regulation of skeletal metabolism, to accommodating the network of bone-resident cells (osteocytes) with their extensively branching and interconnected cellular processes. In this latter case, these cellular networks of osteocytes entombed within the mineralized extracellular matrix have a distinct density, connectivity and morphology identifiable in primary bone, plexiform bone and lamellar bone (Schneider et al. 2011; Cadena and Schweitzer 2012), and because the osteocyte networks are sometimes exceptionally well preserved despite diagenetic changes in the surrounding matrix (see Figure D.2, an archaeological specimen), three-dimensional imaging can assist in studies of bone histology, functional adaptation and metabolic status, even in extinct animals. Also within the last decade, the same SSV method confirmed and quantified a previously reported (Boyde and Hobdell 1969) composition of lamellar bone as layers of twisted bundles (Reznikov et al. 2014a). In its sample-preparation tool capacity, being able to handle hard, dense and heterogeneous materials (all natural descriptors of the bone extracellular matrix), FIB-SEM methodology contributed to the discovery of the self-similarity of bone structural organization across many hierarchical levels (Reznikov et al. 2018), thus putting "good old" bones on par with such natural phenomena as mountain ridges, thunderbolts, trees and snowflakes. There is no doubt that the application of FIB-SEM in skeletal biology is still dawning, and other exciting discoveries are on the way.

Fundamental Principles and Practical Use

General Geometry and Some Customized Geometries

In a dual-beam microscope, the electron beam (and associated detectors) comprises the core component of an essentially self-standing SEM that is capable of collecting images of the substrate with the contrast originating from the substrate composition and/or its topographic features. The focused ion beam component of a FIB-SEM traditionally uses gallium as the agent of the ion beam enabling high-precision substrate ablation – the mass of a Ga atom is higher than the mass of an electron by about 1.3×10^5 and this renders the focused beam significantly more effective, where it acts as a fine, nanoscale "knife" removing surface material of the sample. The third component of the system that is not reflected in the instrument name but is nevertheless an important component of a FIB-SEM is a gas injection system (GIS) that contains one or more crucibles with metalloorganic compounds. A tiny cloud of such compounds - injected locally near the substrate surface and subjected to the Ga beam of appropriate tension - decomposes such that the metallic component precipitates on the surface while the volatile organic component evaporates. This intentionally deposited surface layer, as a preparation step prior to FIB milling, is protective for the substrate and allows even more selective and precise rendering using the I-beam. In combination with the GIS-injected compound, the I-beam becomes even more versatile; it precisely ablates and cuts substrate surfaces and deposits compounds accurately at selective sites on the surface of the substrate. Thus, highly controlled ablation and subsequent imaging of a freshly "dissected" surface makes FIB-SEM systems unique among other 3D imaging instruments. A serial, iterative operation of the I- and E-beams is the basis for true tomographic imaging (*tomos,* slice; *graphy,* imaging), also known as slice and view, serial slice and view or serial surface view.

The two beams (E and I) operate at an angle with respect to each other, which is usually about 52–54°. This brings about some peculiarities because, as the name implies, the ion beam is focused, and not collimated. Therefore, the most predictable, uniform and precise dissection is at the specimen surface close to the I-beam incidence point. The deeper the milling, the less accurate and smooth will be the exposed surface. This means that from the E-beam point of view, the area near the top of the exposed surface will be of better quality than that at the bottom. The exact extent of the quality difference depends on the I-beam milling parameters, the uniformity of the internal structure of the specimen and the quality of the protective layer deposited onto the surface of the specimen. Careful calibration of these factors may result in the difference being negligible, and, conversely, ill fitting milling parameters will inevitably result in the formation of artifacts.

In most common FIB-SEM configurations, the E-beam rasters the exposed surface at an acute angle and automatically applies dynamic focus correction. This, however, does not fully compensate for partial shading, or the brightness gradient of

VetBooks.ir

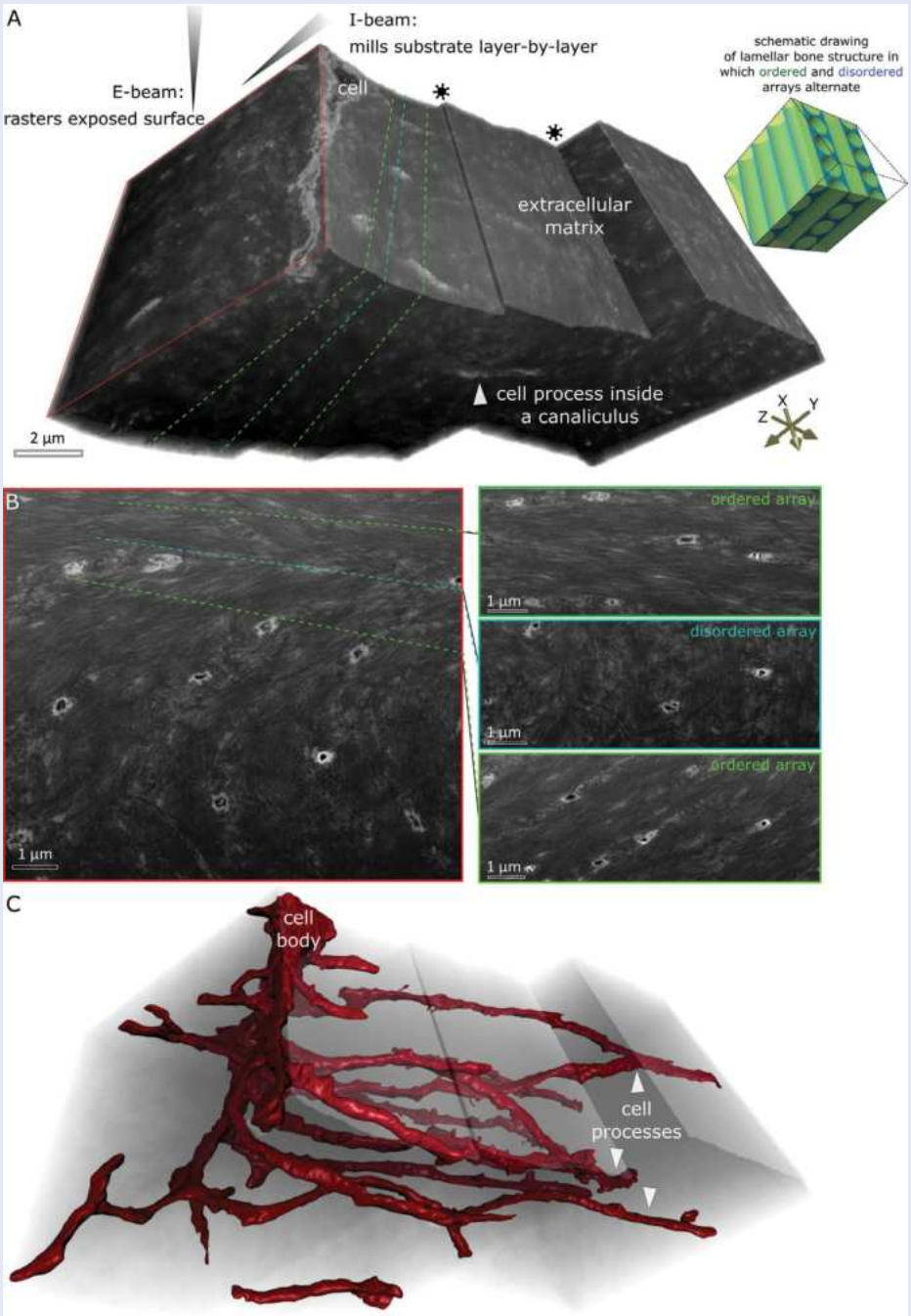


FIGURE D.1 Geometry of a focused ion beam scanning electron microscope (FIB-SEM, Helios 600) serial surface view (SSV) experiment and examples of the features in a modern specimen of human bone. A, Reconstructed and aligned SSV stack of about 1500 2D slices from a demineralized and OTOTO-stained human lamellar bone sample from a healthy 20-year-old female donor. Conventional angulated orientation of the ion beam (I-beam) and electron beam (E-beam) with respect to each other results in a nonorthogonal overall geometry of the stack. During acquisition, the E-beam focus is automatically corrected and adjusted with respect to the shifting exposed surface. The angled geometry results in a brightness gradient and requires readjustment to the field of view (two times, as indicated by asterisks). FIB-SEM instrument models that either tilt the stage to the right angle with respect to the E-beam for each acquisition step, or have a built-in right angle between the beams, do not produce such artifacts. The dashed lines indicate the planes shown in panel B. B, Stained collagen arrays, with some brighter cross sections of osteocyte processes in canaliculi (as also seen in the original plane of image acquisition; in the red-frame area in A) are readily identifiable. Note the vertical brightness gradient in this generally good quality image. Although the D-spacing of collagen fibrils is well visualized and differential staining of noncollagenous organic components is evident, this plane of view is oriented in a slightly oblique orientation with respect to the lamellar boundaries, and this results in a nested arching pattern also known as a Bouligand pattern. Virtual reslicing of the reconstructed volume in the exact orientation of the lamellar boundaries allows identification of sublamellar structural motifs such as alternating ordered (high-angle and low-angle) and disordered collagen assemblies. Examples of the sublamellar motifs are shown in colored frames (top green, low-angle ordered; blue, disordered; bottom green, high-angle ordered), and their location within the stack and original slice is indicated by dashed lines of corresponding colors. C, From within the stack of images, surface rendering of part of an osteocyte cell body and its extended dendritic cell processes reconstructed using Dragonfly™ software (Object Research Systems Inc., Montréal).

VetBooks.ir

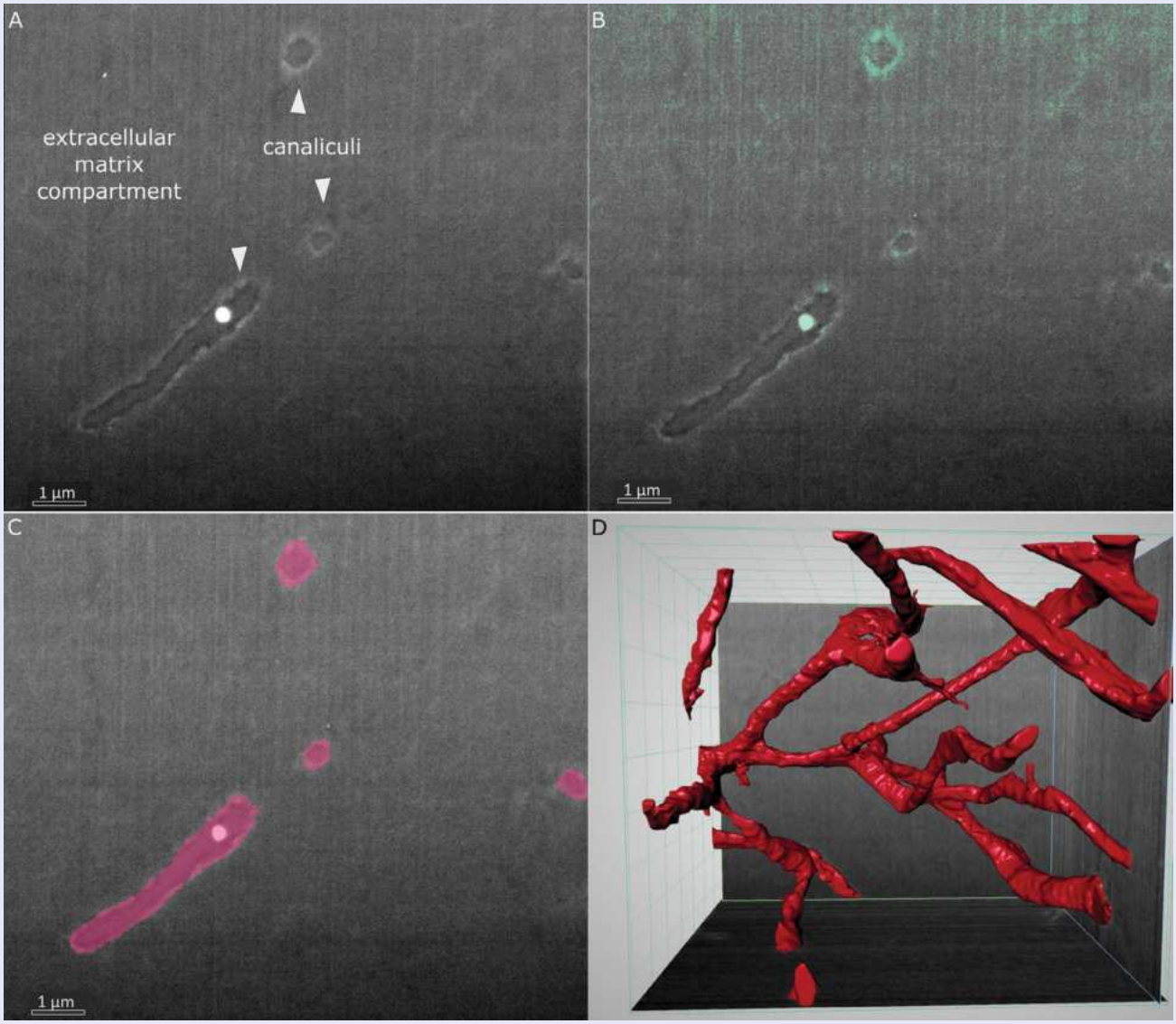


FIGURE D.2 Focused ion beam scanning electron microscope (FIB-SEM) serial surface view (SSV) images and 3D reconstruction of an archaeological bone specimen (Levant, Late Chalcolithic, about 5000 BP). This specimen had unusually high protein content (12 wt%), and for this reason was processed using the same demineralization and staining protocol as the modern sample shown in Figure D.1, as an attempt to visualize collagen arrays of lamellar bone. A, B, Despite the high content of organic matter, the tertiary and quaternary structure of collagen is lost, and no D-spacing or differential osmium stain uptake can be visualized. However, the inner surfaces of the canaliculi show high stain uptake. Note the bright spot thought to be a sediment grain in the lumen of a longitudinally sectioned canaliculus. Because of the poor contrast, the brightness gradient is more pronounced than in Figure D.1, to the extent that global grayscale thresholding is not applicable for segmentation of the canalicular network, see teal label in (B). Note that due to partial degradation of the preserved organic material, another staining method could have been used instead of the OTOTO method, for example, iodine vapor staining. C, D, Application of a deep learning-based segmentation algorithm (UNet Convoluted Neural Network, Dragonfly™) nevertheless allows for a tracing of the cross sections of the canaliculi (C) and results in a fair-quality surface rendering of the preserved interfaces in this archeological sample (D).

the deeper parts of the exposed sample face. Moreover, signal collection from deeper, shaded areas is more prone to decay of the signal-to-noise ratio. Some instruments overcome this problem of angled E-beam incidence and dynamic focusing by iteratively tilting the stage by 38° between every step of milling and imaging so that despite having 52° between the two beams, the sample would face the E-beam at a right angle during the scanning steps, and face the I-beam at a right angle during the milling steps. Other ways to modify the incidence angles include holder modifications (Ohta et al. 2012), angulation of the stage for I-beam incidence at 38° (instead of the right angle) and E-beam imaging at a right angle (De Winter et al. 2009) or complete customization of the system so that the two beams are orthogonal (Xu et al. 2017). Note that the change of incidence angle of each beam does not cancel the limitation of high-quality milling depth.

VetBooks.ir

Specimen Preparation

3D imaging using FIB-SEM in the SSV mode is mainly obtained from compositional contrast within the specimen that can be either native or enhanced by staining. The imaging is done within the bulk, below the original specimen surface as the I-beam rastering exposes the interior. The positive side, and the ultimate goal of the FIB-SEM SSV method, is that it is always exciting to visualize the structure of interest in its full 3D volume at high resolution. However, subsurface features of interest can be accidentally missed and/or destroyed during I-beam ablation, or certain artifacts or undesired features can be mistakenly included in the field of view. Although small-scale unwanted features cannot be avoided by coarse resolution "survey" methods for initial examination of a specimen, it is nearly always useful to precede SSV tomography with a larger-scale imaging method such as light microscopy or X-ray imaging in a correlative setup (Leser et al. 2009) for better, directed localization of the exact volume of interest, or at least for familiarization with some possible subsurface artifacts or defects.

Another issue related to the exposure of the sample interior is that the inherent contrast within the bulk might be insufficient for the study objective. For that reason, more often than not, contrast enhancement is achieved by heavy metal staining. While most soft, cell membrane-rich samples usually stain sufficiently well by most conventional methods developed for contrasting/staining 2D sections (as for transmission electron micrography [TEM]), either mineralized or demineralized/unmineralized extracellular matrices such as bone, ligaments, cartilage and dental tissues are too dense for conventional staining protocols. Because of their high density, stain penetration is poor, and connective tissues typically bind staining agents only within a couple of micrometers of the surface of the specimen instead of permitting deep infiltration of the stain into the bulk. For uniform bulk staining of dense tissues, one can use microwave-assisted processing (Weston et al. 2010; Kremer et al. 2015) where the stain (or demineralizing agent, or fixative – for the same reason) are agitated at the molecular scale by microwaves, and percolate into a more substantial depth of the sample. Of note, microwave-assisted processing requires thorough monitoring of the temperature in the vicinity of the sample to avoid the loss of structural water and denaturation of proteins.

To avoid the formation of artifacts (and their subsequent imaging and interpretation) within a bulky biological sample, a strategic decision that must be made prior to running an SSV experiment is what to do with the water content of the sample. Trivial room-temperature desiccation usually results in gross deformities of unmineralized/demineralized samples and the formation of voids within the interior of the sample. Critical-point drying might be adequate in some cases (Drobne et al. 2007; Schatten 2011) as it more or less preserves the overall geometry of a sample, but high-resolution structural observations can be disappointing because of the formation of micropores and structural irregularities. Plunge freezing for stabilization of structural water is limited in depth to not more than 10 µm, and that depth is adequate for imaging entire cells. However, such depth might be insufficient for the size of larger samples that are within the feasible range of the volume of interest in FIB-SEM SSV tomography. Hence, the accepted standard specimen preparation strategy is high-pressure freezing where water vitrification can be achieved within a volume up to 200 µm in depth (Dubochet et al. 1988). High-pressure frozen samples can be further processed for low-temperature FIB-SEM imaging if the inherent contrast is deemed attainable (Vidavsky et al. 2015, 2016), or can be streamed to the room-temperature preparation routine via freeze substitution. During freeze substitution, the temperature is slowly elevated in a controlled, stepwise manner over several days, where solid vitrified water is gradually replaced by liquid organic solvent, and during that time the specimen can be chemically fixed, contrasted and infiltrated by an embedding medium (Hayat 2000).

Imaging Parameters

Imaging by electron microscopy is based on the principles of the interaction of an electron beam with the substrate. This interaction is not limited to the substrate surface, but also involves the subsurface volume. Because (1) the signal in each pixel is a result of integration of secondary and back-scattered electrons coming both from the surface and the subsurface volume, and (2) the collection of 2D images is iterated with ablation of thin slices of material from the sample face, it would be unreasonable to have the volume of E-beam interaction exceeding the thickness of the ablated slice. Because FIB-SEM users are often interested in minimizing the voxel size, and therefore reducing the slice thickness, the E-beam of a FIB-SEM typically operates at low voltage (sometimes below 1 keV). The current used in electron imaging is a compromise between the pixel size (lower current gives a smaller spot) and the acceptable signal-to-noise ratio (higher current improves the signal-to-noise ratio). In the frequent cases in which the highest practically possible current still results in an unacceptably high noise level, the quality of the image can be improved by increasing dwell time or applying pixel-, line-, or frame-averaging. However, increasing the dwell time per pixel proportionally increases the duration of the experiment, sometimes beyond the limits of an instrument availability in shared facilities (FIB-SEM SSV tomography is one of the slowest image acquisition methods, often requiring days of acquisition). Moreover, both increased dwell time and averaging can result in charging of the exposed nonconductive surface. The presence of charging artifacts leads to image distortion, drift, and obstruction of features. Therefore, it is often useful to test a mock specimen of representative composition in terms of image acquisition parameters and sometimes to resort to conductive staining where the sample is saturated with heavy metal compounds and remains charge free (Chissoe et al. 1995; Reznikov et al. 2013).

An important question that a FIB-SEM operator faces before each experiment is the exact size of the pixel in the *XY*-dimension, and the step size in the *Z*-direction (the slice thickness). Whereas the *XY* pixel size can be reduced as much as the contrast and signal-to-noise ratio allow, the *Z*-step is not so much the function of the I-beam diameter, but of the

VetBooks.ir

electron optics of the system, i.e., the ability to accurately shift the I-beam, the quality of its focus and stability. As a general rule, it is disadvantageous to set the *Z*-step size to larger values than the *XY* pixel size. The reason for this lies in the objective of 3D imaging: the beauty of producing volumetric data relates to the ability to digitally reslice the acquired volume in any arbitrary way and to visualize the features from any angle, and not necessarily aligned with the original plane of imaging, the *XY* plane. When the *Z*-dimension of a voxel exceeds that of the *XY*-dimension, any image derived from the 3D data set that is not in the original plane of imaging will be composed of anisotropic pixels and will appear "astigmatic." If the objective of a FIB-SEM SSV experiment is to conduct a coarse survey of the specimen along the *Z*-axis, it is more than reasonable to increase the *XY* pixel size accordingly. This will result in a larger total volume available for analysis. On a practical note, the nominal slice thickness may not truthfully reflect the resolution along the *Z*-axis because the accuracy of milling decays with its depth, and the control of the I-beam shift can be less precise and stable than needed (Jones et al. 2014, Narayan et al. 2014). Therefore, it is sometimes reasonable to set the *Z*-slice thickness even to a smaller value than the lateral *XY* pixel size. Then, the acquired volume can be downsampled along the *Z*-axis, overcoming the inherent imperfections of I-beam milling.

Because of the technical restraints, such as low voltage and current, higher dwell time due to weak sample contrast and aspirations to minimize the voxel size, FIB-SEM SSV experiments are often long and expensive. Considering the destructive nature of the method as well, it is obviously important for the operators to explicitly familiarize themselves with the sample using quicker and/or nondestructive methods such as (polarized) light microscopy, X-ray tomography, traditional SEM imaging of the specimen's fractured or polished surface, and/or, if possible, using conventional TEM sections. Although these auxiliary techniques likely will not address the original research question that requires 3D FIB-SEM imaging, they will provide guidance regarding the size and nature of structural features, the adequacy of the natural or enhanced contrast, and avoiding possible artifacts and the ways to control or minimize them. False starts or aborted experiments are nearly as lengthy and expensive as good ones, but they are also demoralizing and discouraging for a microscopist. Because there is no single recipe for 3D acquisition, a good practice before starting SSV imaging is to dedicate a small area of the sample for optimization of the parameters (voltage, current, dwell time, different staining and embedding methods, etc.). Observing the outcome of different combinations of these settings side by side allows the making of a more informed choice regarding the "real-time" experimental conditions.

Another way to limit the typically long durations of 3D acquisition is to use FIB-SEM systems that allow better coordinated milling and scanning, so that instead of discrete steps of having one beam on while the other beam is blanked out, the rastering of the beams can be interlaced within each cycle. Although the two beams do not operate simultaneously, the use of time becomes more advantageously parsimonious.

Advanced dedicated software (Atlas 3D, Fibics) permits taking key frames at desired intervals, while continuing high-resolution acquisition over a smaller area with the minimal *Z*-step (Narayan et al. 2014). Such simultaneous acquisition at two different scales is a way to incorporate a correlative imaging approach within one experiment. It also allows amending an area of interest for high-resolution imaging, customizing its shape or even acquiring more than one high-resolution frame at each step (Narayan et al. 2014). These large-scale key frames provide larger-scale context for the ease of interpretation of the high-resolution data.

Finally, after advance planning for the dimensions of the volume of interest, pixel size, milling and acquisition parameters, the operator might face a scenario when a follow-up expanded analysis is needed. Or, for example, the preplanned SSV run has to be terminated to preserve a certain area for electron tomography using a different imaging tool (TEM or STEM). In such cases, efforts made to protect the sample material around the immediate volume of interest by generous GIS deposition of protective coating will undoubtedly pay off.

Successful 3D SSV acquisition is very rewarding, but the operation is neither trivial nor flexible. Few contingencies can be corrected "on the go," and the generic answer to most methodological inquiries would be to carefully "plan ahead." While attempting not to be discouraging, other realistic answers might be "try out mock samples/areas" and "prepare thoroughly" because all specimens are unique in terms of their general geometry, 3D structure, composition, behavior during preparation stages and, of course, in terms of finding the optimal combination of experimental settings. Successful strategic planning and careful implementation of an SSV experiment brings the operator to the next important step – the processing of a stack of images.

3D Image Processing

The raw output of an SSV experiment is a series of several hundreds or thousands of sequential 2D images spatially related to each other by bodily translation, the 3D stack. Although each of the serial 2D images may contain interesting information, there is a minimal set of procedures to be accomplished prior to 3D visualization of the object. The first and essential step is the alignment, or registration, of each and every 2D image with respect to its adjacent neighbors. Although theoretically image *n* comes from the same physical position along the *X*- and *Y*-axes as the image $n + 1$, minor fluctuations of magnetic fields near the specimen surface cause small and random lateral offsets of the adjacent images, with the offset value being comparable to the pixel size. Prior to stack registration, no viewing in a derived plane (i.e., any plane that is not the original imaging plane) is possible because of this random shuffling of the voxels originating from the same continuous feature. Most available imaging software packages are equipped with effective stack registration plug-ins, so that manual adjustment is rarely needed (although not always and totally excluded).

The next step that might be required prior to 3D viewing is histogram balancing, which means normalization of brightness and contrast in adjacent images, so that the same structure in images *n* and $n + 1$ would have the same grayscale value (otherwise it will not appear as the same continuous structure in the

VetBooks.ir

derived views). In the case that the data set will be processed by traditional manual or (semi)automated methods, a vast toolkit of filters is available in most contemporary software packages dedicated for 3D image handling. For example, commonly occurring vertical stripes (or so-called "curtains") induced by the decaying quality of milling in depth or irregular substrate surface can be eliminated by Fourier transform-based wavelet subtraction. Shading, or brightness gradient, can be corrected by a background subtraction or polynomial filters. Edges of the features of interest can be sharpened by a variety of "Derivative of Gaussians" filters. Of note, all these useful operations can be applied to the entire data set, although that is both time and labor intensive. Alternatively, segmentation can be accomplished with higher precision and in shorter time by a deep learning-assisted approach, which is subdomain of machine learning (Reznikov et al. 2020). Deep learning for image segmentation typically employs a UNet – a variety of a convolutional neural network, and it requires a training dataset - a small representative fragment segregated from the working (registered and balanced) data set, and segmented to the best capacity of an expert operator. Of note, the training dataset can be duplicated for smoothing, denoising, filtering, edge detection and manual segmentation. Then, the segmentation labels generated using the manipulated duplicate fragment are overlaid on the pristine representative fragment and that will serve as the "ground truth" for the UNet segmentation: a deep learning model needs a small fraction of high-fidelity segmentation labels ("output") to be associated with pristine data ("input") for self-training and validation. After the deep-learning model has been trained to the operator's satisfaction, the whole 3D data set can be processed automatically, sometimes resulting in surprisingly precise segmentation results that would otherwise take a disproportionate amount of time to be produced manually.

The recent introduction of artificial intelligence for image processing, feature recognition, classification and analysis is of tremendous significance in bioimaging because it abolishes the bottleneck of large data handling. Needless to say, the application of dedicated graphic software with an option for deep learning based segmentation imparts certain technical hardware requirements. Here, however, the same common denominators can be used as in the recommended SSV experimental conduct: plan ahead and prepare thoroughly.

Conclusion

This methodological insert chapter highlights the power and peculiarities of the FIB-SEM SSV workflow, with the latter meant not in any way to discourage its use in the life sciences in general, and in skeletal biology in particular, but rather with an intent quite the opposite – to illustrate the *big effort/big reward* combination characteristic of the method. Such a method is "luxurious" in the sense of it having not only a significant amount of invested time and labor, but perhaps more so in the sense of providing astonishingly beautiful, informative 3D imaging output that was heretofore unattainable. As such, FIB-SEM SSV 3D imaging is rarely quick or easy, but when properly planned and implemented, it nearly guarantees exciting discoveries that enrich our understanding of biological structures in all their sublime complexity.

Acknowledgments

The authors thank professor Marc D. McKee (McGill University, Montréal) for critical reading of this manuscript.

REFERENCES

Akiva, A., et al. 2015. On the pathway of mineral deposition in larval zebrafish caudal fin bone. *Bone* 75: 192–200.

Almany-Magal, R., et al. 2014. Three-dimensional structure of minipig fibrolamellar bone: adaptation to axial loading. *J. Struct. Biol.* 186: 253–264.

Atkins, A., et al. 2015. The three-dimensional structure of anosteocytic lamellated bone of fish. *Acta Biomater.* 13: 311–323.

Boyde, A. and M. H. Hobdell. 1969. Scanning electron microscopy of lamellar bone. *Z. Zellforsch.* 93: 213–231.

Buss, D. J., et al. 2020. Crossfibrillar mineral tessellation in normal and Hyp mouse bone as revealed by 3D FIB-SEM microscopy. *J. Struct. Biol.* 212: doi.org/10.1016/j.jsb.2020.107603.

Cadena, E. A. and M. H. Schweitzer. 2012. Variation in osteocytes morphology vs bone type in turtle shell and their exceptional preservation from the Jurassic to the present. *Bone* 51: 614–620.

Chissoe, W. F., et al. 1995. The use of osmium-thiocarbohydrazide for structural stabilization and enhancement of secondary electron images in scanning electron microscopy of pollen. *Grana* 34: 317–324.

De Winter, D. A. M., et al. 2009. Tomography of insulating biological and geological materials using focused ion beam (FIB) sectioning and low-kV BSE imaging. *J. Microsc.* 233: 372–383.

Drobne, D., et al. 2007. Surface damage induced by FIB milling and imaging of biological samples is controllable. *Microsc. Res. Tech.* 70: 895–903.

Dubochet, J., et al. 1988. Cryo-electron microscopy of vitrified specimens. *Q. Rev. Biophys.* 21: 129–228.

Earl, J. S., et al. 2010. Characterization of dentine structure in three dimensions using FIB-SEM. *J. Microsc.* 240: 1–5.

Goldberg, M., et al. 2014. Comparative studies between mice molars and incisors are required to draw an overview of enamel structural complexity. *Front. Physiol.*: doi.org/10.3389/fphys2014.00359.

Grandfield, K., et al. 2018. Ultrastructure of bone: hierarchical features from nanometer to micrometer scale revealed in focused ion beam sections in the TEM. *Calcif. Tissue. Int.* 103: 606–616.

Hasegawa, T., et al. 2017. Biological application of focus ion beam-scanning electron microscopy (FIB-SEM) to the imaging of cartilaginous fibrils and osteoblastic cytoplasmic processes. *J. Oral Biosci.* 59: 55–62.

Hasegawa, T., et al. 2018. Three-dimensional ultrastructure of osteocytes assessed by focused ion beam-scanning electron microscopy (FIB-SEM). *Histochem. Cell Biol.* 149: 423–432.

Havers, C. 1691. *Osteologia Nova*. London: Samuel Smith.

Hayat, A. M. 2000. *Principles and techniques of electron microscopy: biological applications*, 4th ed. Cambridge, UK: Cambridge University Press.

Hirashima, S., et al. 2020. Three-dimensional ultrastructural imaging and quantitative analysis of the periodontal ligament. *Anat. Sci. Int.* 95: 1–11.

Jones, H. G., et al. 2014. Investigation of slice thickness and shape milled by a focused ion beam for three-dimensional reconstruction of microstructures. *Ultramicroscopy* 139: 20–28.

Kanazawa, T., et al. 2016. Histomorphometric and ultrastructural analysis of the tendon-bone interface after rotator cuff repair in a rat model. *Sci. Rep.* 6: 33800.

Kerschnitzki, M., et al. 2016. Bone mineralization pathways during the rapid growth of embryonic chicken long bones. *J. Struct. Biol.* 195: 82–92.

Kizilyaprak, C., et al. 2019. Volume microscopy in biology: FIB-SEM tomography. *Tissue Cell* 57: 123–128.

Kremer, A., et al. 2015. Developing 3D SEM in a broad biological context. *J. Microsc.* 259: 80–96.

Langelier, B., et al. 2017. Atomic scale chemical tomography of human bone. *Sci. Rep.* 7: 39958.

Leser, V., et al. 2009. Comparison of different preparation methods of biological samples for FIB milling and SEM investigation. *J. Microsc.* 233: 309–319.

Maria, R., et al. 2019. An unusual disordered alveolar bone material in the upper furcation region of minipig mandibles: A 3D hierarchical structural study. *J. Struct. Biol.* 206: 128–137.

Milovanovic, P., et al. 2016. The formation of calcified nanospherites during micropetrosis represents a unique mineralization mechanism in aged human bone. *Small* 13(3).

Narayan, K. and S. Subramaniam. 2015. Focused ion beams in biology. *Nat. Methods* 12: 1021–1031.

Narayan, K., et al. 2014. Subramaniam, S. Multi-resolution correlative focused ion beam scanning electron microscopy: applications to cell biology. *J. Struct. Biol.* 185: 278–284.

Ohta, K., et al. 2012. Beam deceleration for block-face scanning electron microscopy of embedded biological tissue. *Micron* 43: 612–620.

Reznikov, N., et al. 2013. Three-dimensional imaging of collagen fibril organization in rat circumferential lamellar bone using a dual beam electron microscope reveals ordered and disordered sub-lamellar structures. *Bone* 52: 676–683.

Reznikov, N., et al. 2014a. Bone hierarchical structure in three dimensions. *Acta Biomater.* 10: 3815–2826.

Reznikov, N., et al. 2014b. Three-dimensional structure of human lamellar bone: the presence of two different materials and new insights into the hierarchical organization. *Bone* 59: 93–104.

Reznikov, N., et al. 2015. The 3D Structure of the collagen fibril network in human trabecular bone: relation to trabecular organization. *Bone* 71: 189–195.

Reznikov, N., et al. 2018. Fractal-like hierarchical organization of bone begins at the nanoscale. *Science* 360: eaao2189.

Reznikov N., et al. 2020. Deep learning for 3D imaging and image analysis in biomineralization research. *J. Struct. Biol.* 212: doi.org/10.1016/j.jsb.2020.107598.

Robles, H., et al. 2019. Characterization of the bone marrow adipocyte niche with three-dimensional electron microscopy. *Bone* 118: 89–98.

Schatten, H. 2011. Low voltage high-resolution SEM (LVHRSEM) for biological structural and molecular analysis. *Micron* 42: 175–185.

Schneider, P., et al. 2011. Serial FIB/SEM imaging for quantitative 3D assessment of the osteocyte lacuno-canalicular network. *Bone* 49: 304–311.

Shahar, R. and S. Weiner. 2018. Open questions on the 3D structures of collagen containing vertebrate mineralized tissues: A perspective. *J. Struct. Biol.* 201: 187–198.

Suzuki, M., et al. 2019. A unique methionine-rich protein–aragonite crystal complex: Structure and mechanical functions of the Pinctada fucata bivalve hinge ligament. *Acta Biomater.* 100: 1–9.

Vidavsky, N., et al. 2015. Mineral-bearing vesicle transport in sea urchin embryos. *J. Struct. Biol.* 192: 358–365.

Vidavsky, N., et al. 2016. Cryo-FIB-SEM serial milling and block face imaging: Large volume structural analysis of biological tissues preserved close to their native state. *J. Struct. Biol.* 196: 487–495.

Weston, A. E., et al. 2010. Towards native-state imaging in biological context in the electron microscope. *J. Chem. Biol.* 3: 101–112.

Xu, C. S., et al. 2017. Enhanced FIB-SEM systems for large-volume 3D imaging. *eLife* 6: 325916.

VetBooks.ir

Section III

Dynamic Processes in Osseous Formations

VetBooks.ir



Taylor & Francis
Taylor & Francis Group
http://taylorandfrancis.com

VetBooks.ir

9

Basic Processes in Bone Growth

Vivian de Buffrénil and Alexandra Quilhac

CONTENTS

Interpreting Skeletal Growth 194
Initial Growth of Membrane Bones 194
From Mesenchymal Condensations to Bones 194
Remarks on Local Growth Controls 195
Basic Growth Pattern of Endochondral Bones 195
Ossification of the Cartilaginous Anlage 195
Basic Mechanisms of the Growth in Length of the Bones 197
Epiphyseal Structure and the Course of Growth 197
Subperiosteal Growth of Bone Cortices 199
Systemic Regulators of Skeletal Growth 199
Multiple Systemic Regulators 199
Action of GH, IGF-1 and the GH/IGF-1 Axis on Skeletal Growth 200
Molecular Structure and Secretion Context 200
Actions of GH and IGF-1 on Cartilage and Bone Cells 201
Thyroid Hormones 201
Nature and Secretion of Thyroid Hormones 201
Actions on the Growing Skeleton 202
Sex Steroids, Androgens and Estrogens 203
Secretion and Regulation of Sex Steroids 203
Action of Sex Steroids in Bone 205
Glucocorticoids (GCs) 205
Growth and Morphology of Bones 207
The Constraint of Rigidity 207
Basic Shaping Processes in the Growth of Bones 207
The Peculiar Growth Geometry of Some Flat Bones 207
Differentiation of Superficial Relief Through Accretion Rate, or Resorption 207
Morphogenetic Role of Heterochrony in Local Bone Deposits 207
Sequential Growth Remodeling in Appendicular Long Bones 209
Growth Off-Centering and Diaphyseal Curvature 210
Differential Contribution of Proximal and Distal Epiphyses 210
Brief Overview at the Problem 210
Chronology of Epiphyseal Fusion 210
The Quantitative Study of Epiphyseal Contribution to Growth 212
Integral Preservation of Endochondral Bone Formations 212
Interpreting Growth Patterns in the Cephalic Region 212
An Essential but Complex Issue 212
Cephalometry 213
Modeling of Facial Bone: The Histologic Mechanisms 214
References 215

VetBooks.ir

Interpreting Skeletal Growth

Interpreting the growth pattern of a bone and its microstructural history in detail is the most fruitful result of comparative skeletal histology and paleohistology. This operation can be complex because it relies on deciphering a series of processes that develop in time and space, and are influenced by internal and external factors, as well as developmental and functional constraints. As the previous chapter showed, identifying the tissue types that occur locally in a section or an entire bone is the first step of this reconstruction. Other, more general processes integrate the global morphology of the bones and contribute to understanding them at each developmental stage. This chapter (as well as Chapters 10, 11 and 12, dealing with dynamic processes in osseous formations) describes some of the most fundamental and common processes involved in the growth of individual bones and composite skeletal regions.

Initial Growth of Membrane Bones

From Mesenchymal Condensations to Bones

The growth of membrane bones (Figure 9.1A–C) is a relatively simple process, compared to endochondral ossification (see, e.g., Krstić 1985). Mature osteoblasts, in the core of mesenchymal condensations, are involved in intense protein synthesis and secrete bone matrix in the form of nonmineralized osteoid. Calcification of the osteoid occurs relatively early (see Bernard and Pease 1969 for description of this process); in the cranial vault of the chick embryo, it starts at stage E10 (i.e., 10 days post conception [dpc]) and is advanced and clearly visible at stage E15 (in the mouse, at stages 5 and E17.5, respectively; review in Abzhanov et al. 2007). Histologically, the initial calcified tissue in the core of flat membrane bones is of the woven-fibered type and displays the microanatomical organization of a fine trabecular scaffolding (Percival and Richtsmeier 2013).

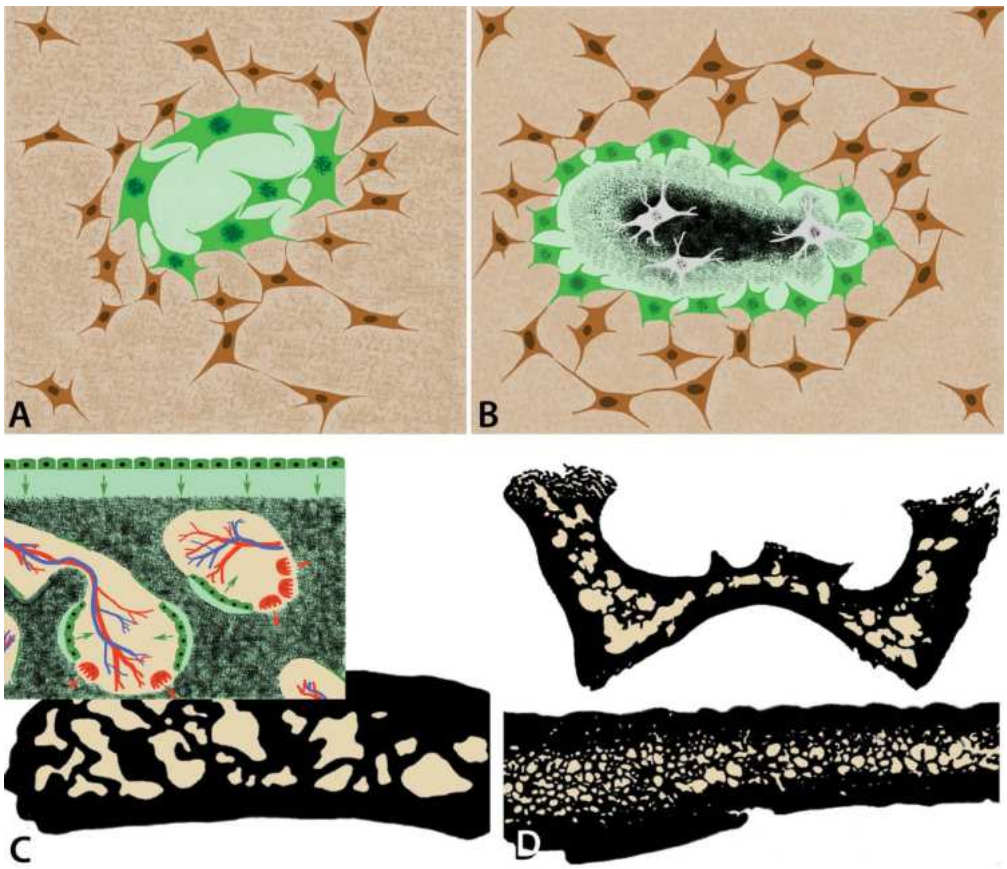


FIGURE 9.1 Early formation of membrane bones. A, Mesenchymal cells aggregate to create mesenchymal condensations in the presumptive territory of membrane bones. These cells start functioning as osteoblasts and secrete nonmineralized bone matrix, i.e., osteoid. B, Calcification starts in the central-most core of the osteoid to spread outwardly. In the meantime, the differentiation of mesenchymal cells into osteoblasts, organized as a membrane around the future bone, proceeds and some of these cells become entrapped in the recently secreted osteoid to become osteocytes. C, A local angiogenetic process results in the proliferation of blood vessels. The latter perforate the developing bone through osteoclastic resorptive activity and numerous cavities, resulting from strongly imbalanced remodeling, start colonizing the bone core. Lower view: general inner architecture of the bone at this stage. Inset: detail of the resorption-reconstruction activities inside the bone. D, A diploe architecture differentiates through the imbalanced remodeling process. In further developed bones, and throughout individual life, the trabeculae in the core of the diploe are remodeled through resorption and secondary reconstruction. Upper field: cross section in the frontal of a juvenile *Alligator mississippiensis*. Lower field: section in a carapace plate of the turtle *Cyclanorbis*.

VetBooks.ir

Vascularization plays an important role in the onset and development of the ossification process of both membrane and endochondral bones (reviews in Percival and Richtsmeier 2013; Sivaraj and Adams 2016). Just before the differentiation of their cells into osteoblasts, the mesenchymal condensations of future membrane bones are surrounded by an avascular zone, a situation that also occurs around prechondrogenic condensations of limb bones, and possibly reflects the transitory action of a factor inhibiting local invasion of the condensation by blood vessels (Brandi and Collin-Osdoby 2006). By the time calcification starts, this repelling factor is inhibited, and neighboring blood vessels penetrate the osseous primordium and quickly ramify (angiogenesis) inside it. They thus allow the local supply of the developing skeletal element in gases, nutrients and the precursors of osteoclasts (brought *in situ* by the bloodstream) and osteoblasts that will be involved in inner bone remodeling in later ontogenetic stages (Figure 9.1C, D). Maes et al. (2010) showed that the osteoblasts penetrating the bones along the external surface of the invading blood vessels are precursor cells, not mature fully differentiated osteoblasts. They will constitute the initial population of endosteal osteoblasts.

Although the precise mechanism of this vascular invasion remains incompletely elucidated, a central role is attributed to proangiogenetic factors in both the attraction of external blood vessels toward the bone primordium and the angiogenic sprouting of the vessels inside it. The most important of these factors, the vascular endothelium growth factors (or VEGFs), secreted by osteoblasts in hypoxic conditions (review in Beamer et al. 2010; see also Maes et al. 2012), act not only on the endothelial cells of the blood vessels, thus stimulating angiogenesis, but also on the osteoblasts themselves through an autocrine process (Hu and Olsen 2016). Additionally, bone morphogenetic proteins (BMPs), further described below, could contribute to the control of this angiogenetic process (David et al. 2009).

When skeletal elements increase in volume, the osteoblasts differentiated around them construct a dense cellular layer that acquires the structure of a periosteum (Hall 2005). Growth of membrane bones has two fundamental characteristics: (1) it is appositional, which means that new bone layers are formed on the bone surface above the layers already deposited, and (2) it occurs on a free surface and proceeds centrifugally. In other words, when mesenchymal condensations have acquired their definitive size, then subsequent growth relies only on apposition (also called accretion), not on interstitial (intussusception) processes as do most other nonmineralized tissues. Most membrane bones are flat and have a diploe structure (the clavicle is a rare exception). When they form a compound assemblage (skull roof), they tend to come closer to each other while their peripheral expansion proceeds. In the narrow space between contiguous elements, the periosteal membrane locally becomes a suture; its gross structural organization is described in Chapter 4. In later stages of growth, the periosteum covering the upper (or lateral) and inner (medial) surfaces of a bone is responsible for its growth in thickness, while the sutures control its growth in diameter (radial growth). Bone accretion under sutures can be very fast in juveniles: up to 100 µm/day in the human skull (Henderson et al. 2004). The contribution of chondroid bone, a tissue intermediary between bone and cartilage described in Chapter 8, also contributes to variable degrees to the growth of the flat bones of the face and skull vault (e.g., Goret-Nicaise and Dhem 1982; Lengelé et al. 1996; Bailleul et al. 2016).

Remarks on Local Growth Controls

The growth activity of membrane bones (like that of all other skeletal elements) is under the control of systemic endocrine factors (described below), acting in synergy with several local molecular regulators and their specific receptors (reviews in Mundy et al. 2001; Karaplis 2008; Ho 2015; Graf et al. 2016). Some of these are common to intramembranous and endochondral ossification processes (Day et al. 2005; Abzhanov et al. 2007). The totality of these factors (new ones are regularly discovered) are beyond the scope of this book. The most important of these regulators, the transforming growth factor (TGF)-β, belongs to a broad superfamily of cytokines. They are produced in most tissue types and are active from the early embryo until the latest ontogenetic stages (review in Weiss and Attisano 2013). Along with their receptors, these molecules are involved in a multitude of paracrine and autocrine regulations, especially cell proliferation and differentiation in developing skeletal elements (reviews in Caestecker 2004; Massagué 2012). Among TGF-β factors, the many forms of BMPs, and their receptors (BMPRs), are ubiquitous growth regulators of prominent importance for skeletal development (detailed reviews in Hiepen et al. 2016; Yadin et al. 2016). In synergy with their antagonists, *noggin* and *chordin* (review in Canalis et al. 2003), they induce the differentiation of mesenchymal cells into preosteoblasts, their condensation, and contribute to controlling the activity of differentiated osteoblasts. Tissue interactions, especially epithelial-ectomesenchymal interactions, also contribute to membrane bone morphogenesis (Hall 1980; Jiang et al. 2002).

Basic Growth Pattern of Endochondral Bones

Ossification of the Cartilaginous Anlage

Figure 9.2 summarizes the main steps of the development of a long bone. Once the cartilaginous template, entirely made of hyaline cartilage, is fully constituted, its cells start a differentiation process that creates several zones of chondrocyte modification: the cartilage remains hyaline at the extremities of the anlage (future epiphyseal regions), while zones of cell proliferation, hypertrophy and matrix calcification successively occur toward the middle of the anlage, in the future metaphyseal and diaphyseal regions of the bone (detailed review in Long and Ornitz 2013).

In the meantime, the perichondrium, initially homogeneous all around the anlage, undergoes a different development in the middle (future diaphyseal) region, where its cells differentiate into preosteoblasts and mature osteoblasts to form a functional periosteal membrane, and at the extremities of the anlage, in the territory of future epiphyses, where it retains its initial perichondral structure.

The osteogenic activity of the newly formed periosteum first creates the so-called *bone collar* that surrounds the middle (diaphyseal) region of the cartilaginous template. This regular,

VetBooks.ir

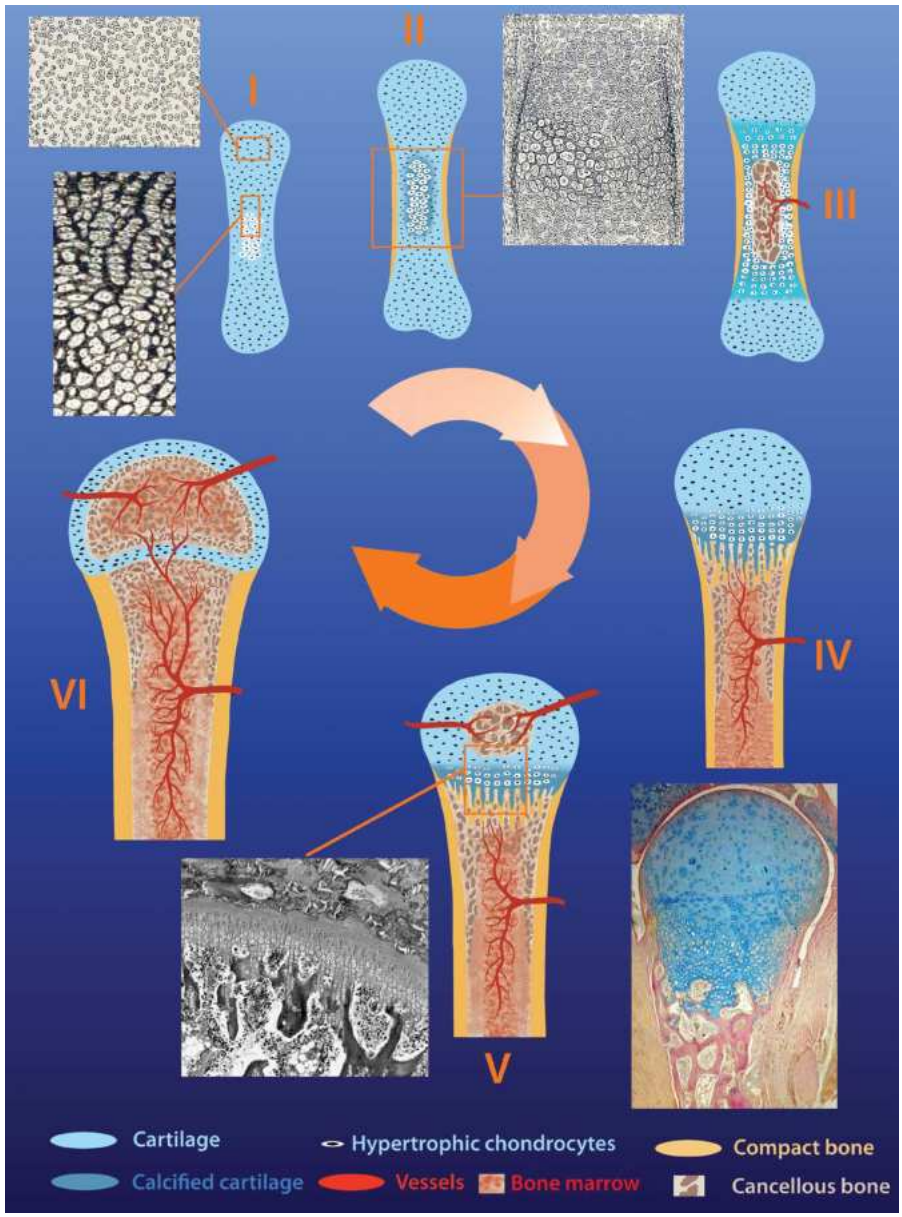


FIGURE 9.2 Main steps of endochondral ossification. Six stages of the development of endochondral long bones are considered. Stage I: the cartilaginous anlage of the bone is constituted and chondrocytes enter a hypertrophic process in its core. Stage II: in the diaphyseal territory, cartilage matrix calcifies and a peripheral bone collar is formed through the secretion of osteoblasts differentiated from perichondrium cells. Stage III: vascular invasion occurs through the perforation of the osseous collar by the nutrient artery. Populations of osteoclasts and osteoblasts thus enter the core of the bone, forming the conjunctivovascular invasion front. The latter resorbs the calcified cartilage, which results in the local differentiation of the marrow cavity and cancellous bone formations. Vascularization of the bone is initiated. Stage IV: the spreading of the conjunctivovascular invasion front toward both extremities of the bone results in the formation of growth plates. The latter are then responsible for the growth in length of the bone. Stage V: blood vessels invade the cartilaginous masses of the epiphyses and, in some amniote clades (mainly lepidosaurs and mammals), cartilage matrix starts calcifying and ossifying, thus forming a secondary ossification center in the core of each epiphysis. Stage VI: the spreading of this center finally reduces the hyaline cartilage to a layer under the articular surface. In the final stage of growth, the growth plates disappear through resorption and, when present, the secondary ossification center of each epiphysis fuses with the neighboring metaphyseal spongiosa. Lowest right picture: primitive epiphysis (no secondary center) in *Pleurodeles waltl.*

subperiosteal accretion process is like that occurring over membrane bone surfaces. Just under the collar, the chondrocytes of the anlage are fully hypertrophied and the intercellular matrix between them mineralizes to form an initial mass of calcified cartilage. The collar is then perforated through the action of osteoclasts and a tunnel, the *nutrient canal*, is excavated through the bone cortex. Its opening on the bone surface constitutes the initial *nutrient foramen* that remains visible throughout life. This process allows the penetration, up to the core of the calcified cartilage, of some blood vessels that quickly proliferate through angiogenesis (see Carlevaro et al. 2000; Beamer et al. 2010). Osteoclast progenitors (monocytes) are then brought *in situ* by the bloodstream, while osteoblast precursors originating from the basal (cambial) cellular layer

VetBooks.ir

of the periosteum migrate into the core of the anlage along the walls of the nutrient canal.

Basic Mechanisms of the Growth in Length of the Bones

The whole set of capillaries, osteogenic and osteoclastic cells gathered in the core of the calcified cartilage form the conjunctivovascular invasion front, which has a key role in the growth in length of endochondral bones. Its action is twofold. The osteoclasts that it contains, acting locally as chondroclasts, resorb the calcified cartilage and excavate in it deep resorption bays separated by thin trabeculae. The osteoblasts of the front partly reconstruct the surface of the trabeculae by thin secondary deposits of lamellar tissue. By this process, endosteoendochondral primary trabeculae with a core of calcified cartilage and superficial osseous plating are created (Figure 9.3A–D). They will subsequently be submitted to intense and repeated remodeling (see Chapter 8) that erases all remnants of calcified cartilage matrix. Secondary trabeculae entirely composed of lamellar bone platings separated by resorption lines are thus created (Figure 9.3E). In the diaphyseal region of the bones, this process is strongly imbalanced toward resorption, which most often results in the differentiation of the medullary cavity through a total resorption of local trabeculae. In pace with the expansion of the conjunctivovascular erosion front in proximal and distal directions, an intense chondrogenic activity occurs at the epiphyseal extremities of the bones, through both the accretion of new cartilage by the perichondrium, and the inner, interstitial growth of the hyaline cartilage.

Epiphyseal cartilages in a growing bone display a characteristic transformation gradient of the chondrocytes (Figure 9.3F, G). The peripheral zone, called the *reserve zone*, is made of hyaline cartilage with few small and rounded chondrocytes in an abundant intercellular matrix. In the intermediary zone, called the *proliferation zone*, the chondrocytes multiply by intense mitotic activity, forming columns of flat daughter cells stacked on one another, the *isogenic groups*. Finally, in the deeper zone, these cells are submitted to gradual hypertrophy while the extracellular matrix containing them becomes calcified. The deep side of the hypertrophic calcified cartilage is then attacked by the conjunctivovascular invasion front, according to the process described above, to form primary and secondary trabeculae in the metaphyseal region of the bones. The growth in length of endochondral bones, whatever their morphology, basically results from the double, combined movement of epiphyseal addition of new cartilage layers and replacement of the deep, hypertrophied and calcified cartilage layers by bone trabeculae.

As for intramembranous ossification, BMPs, along with their receptors and antagonists, are key regulators at all stages of endochondral osteogenesis (review in Pogue and Lyons 2006). In addition to BMPs, six extracellular (paracrine) factors and two nuclear factors contribute to control growth plate development and activity at various levels, i.e., proliferation, maturation and hypertrophy (reviews in Kronenberg 2006; Long and Ornitz 2013; Tickle and Barker 2013; Ornitz and Itoh 2015).

Flat bones of mesodermal origin have an endochondral mode of growth roughly comparable to that of long bones, but their growth cartilages can be located in several primary growth centers distributed along the peripheral edges of the bones. For example, in most mammals, humans included, the scapula has three main growth centers (subdivided into seven functional units in humans by Gray 1918) normally located on top of the acromion and coracoid processes, and along the medial border of the bone (some variation exists; see Nesslinger 1956 for the opossum). Similarly, the pubis and ischium (two bones of the pelvic girdle) have a triradiate morphology with three primary ossification centers (Verbruggen and Nowlan 2017). Comparable situations occur in amphibians (Shearman 2008) and sauropsids (Sheil 2005). Juvenile specimens thus display typical growth plates at the periphery of these bones, along with endosteoendochondral trabeculae in their core. Depending on the location and orientation of sectional planes, calcified cartilage can be observed or not in young individuals. In adults, inactive "epiphyseal" surfaces are like those described above for long bones.

Epiphyseal Structure and the Course of Growth

As described in Chapter 4, epiphyses in finned vertebrates and most clades of limbed vertebrates have the simple, "primitive" structure (according to the terminology of Haines 1938), whereas the appendicular skeleton of lepidosaurs and most endochondral bones of mammals have secondary centers of ossification (with associated vascularization) developing within the noncalcified cartilaginous mass of the epiphyses. In the latter situation, growth cartilages are wedged between the base of the secondary center and the first trabeculae of the metaphyseal region of the bone (e.g., Fawcett and Jensh 1997). They then form a disc of variable thickness, called the *growth plate*, which includes what remains of the reserve zone, the proliferation zone and the subjacent hypertrophic calcified cartilage (Figure 9.3A, B). The development of secondary ossification centers results in a progressive decrease in the mass of cartilage directly involved in the growth in length of the bones. In sagittal sections, the growth plate thus appears as a band of decreasing width (Figure 9.3A, B). When it disappears completely, with the fusion of the secondary center with the metaphysis, growth in length stops. Some of the main factors influencing epiphyseal development and functioning during growth are considered below (see the section "Systemic Regulators of Skeletal Growth").

The thickness of the growth plate gives an indication of the growth stage reached by an animal and shows the chronology of growth of the diverse bones or regions in a single skeleton (e.g., Stevenson 1924; Washburn 1946; Maisano 2002). In humans, the thickness of growth plates in the hand or knee can be compared to standard values for assessing the "skeletal age" of an individual (review in De Sanctis et al. 2014). This parameter allows prediction of final height in reference to the statistical development table created by Bayley and Pinneau (1952) (critical review in Waal et al. 1996).

The lack of intraepiphyseal ossification centers is generally associated with the concept of *indefinite or indeterminate growth*. In this case, the growth of the skeleton and, by extension, that of the whole animal, is supposed to proceed throughout life (although at lower rates in late ontogenetic stages).

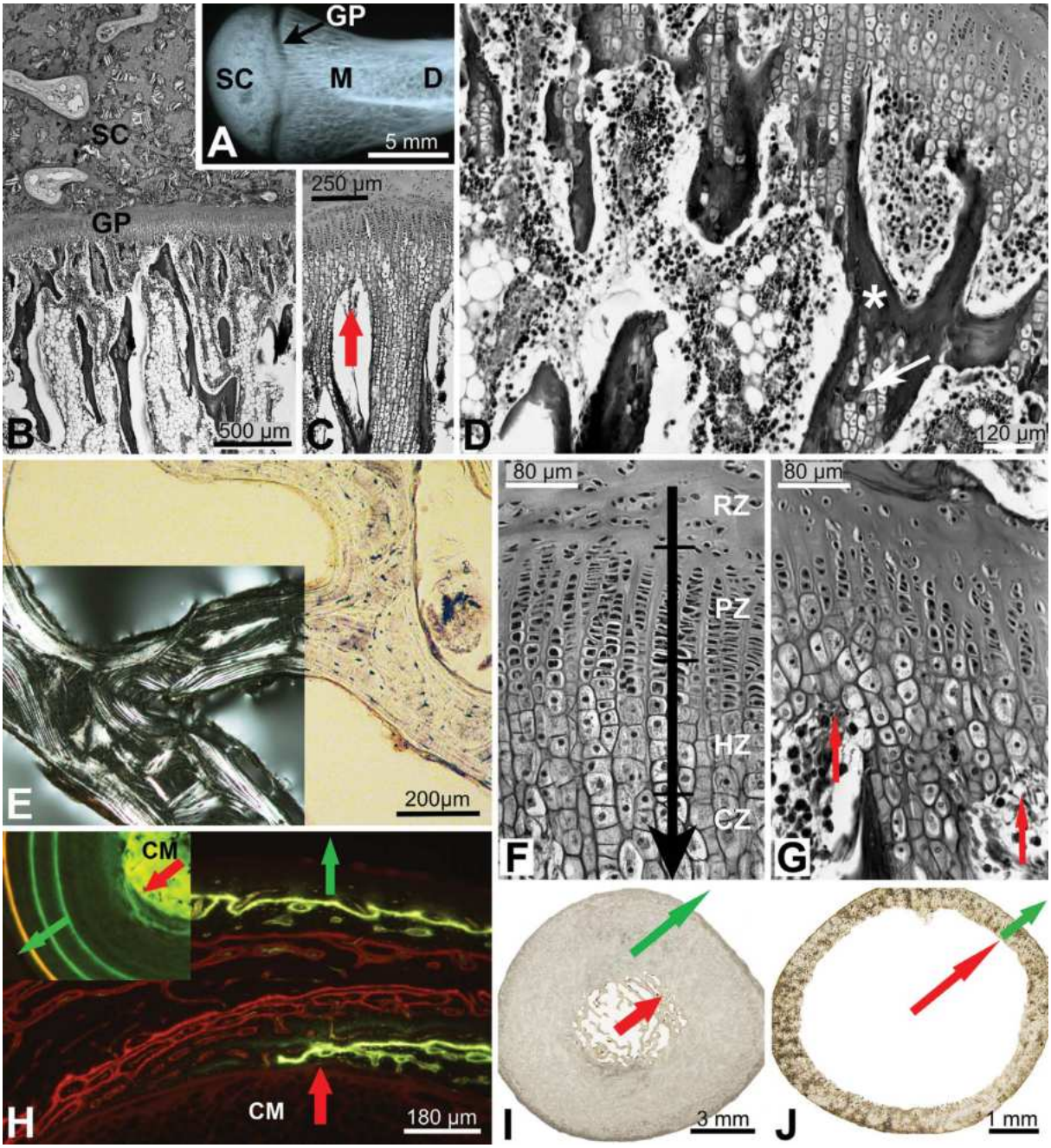


FIGURE 9.3 Microanatomical and histological aspects of long bone growth. A, External view of the metaphyseal and epiphyseal regions of an actively growing bone. Noncalcified cartilage in the growth plate (GP) (arrow) is still thick. Femur of a monitor lizard, *Varanus niloticus*. SC, secondary, intraepiphyseal ossification center; M, metaphyseal region; D, beginning of the diaphyseal region. B, Longitudinal section in the femur of *V. niloticus*, showing the base of the secondary ossification center, the growth plate and the first metaphyseal trabeculae. C, Structure of the primary trabeculae in a fast-growing *V. niloticus*. These trabeculae result from the resorption of the calcified cartilage into rods, subsequently covered with endosteal layers of lamellar bone. The red arrow indicates the movement of the conjunctivovascular invasion front. D, Closer view of a primary trabecula. The core still contains calcified cartilage (arrow), and the surface is covered with endosteal lamellar bone (asterisk). E, Structure of an intensely remodeled secondary trabecula. The lower left field is seen in polarized light. Femur of an adult *V. niloticus*. F, Maturation gradient of the chondrocytes and subdivision of the growth cartilages into four zones: the reserve zone (RZ), the proliferation zone (PZ), the zone of hypertrophy (HZ) and the zone of matrix calcification (CZ). The specimen represented here (femur of a juvenile *V. niloticus*) was actively growing, and the proliferation zone is thick. G, Maturation gradient of the chondrocytes in the growth plate of an adult *V. niloticus*. Growth is slower, and the PZ is relatively thin. Red arrows: movement of the conjunctivovascular invasion front. H, Increase in the diameter of the femoral diaphysis through subperiosteal accretion. Main frame: fast growth in *Anas platyrhynchos*. Inset: slower growth in *Lacerta lepida*. Skeletal growth in these specimens was evidenced by *in vivo* labeling by calcein (yellow labels) and alizarine (red labels). CM: medullary cavity. Green arrow: subperiosteal cortical growth. Red arrow: perimedullary resorption. I and J, Species-specific differences in the relative dynamics of cortical thickening and medullary cavity widening. In I (tibiotarsus of the penguin *Aptenodytes patagonicus*), the medullary cavity develops more slowly than the cortex and the wall of the bone is thick. In J (tibiotarsus of *Anas platyrhynchos*) the expansion of the medullary cavity is much more active, and the cortex is thin.

VetBooks.ir

Conversely, if secondary ossification centers develop, resulting in the elimination of growth plates when adult size is reached, growth is considered finite and limited to juvenile and subadult stages. In extant faunas, these broad principles reflect the situation in certain taxa, but by no means all. Primitive epiphyses associated with long-lasting growth (at least within the limits of individual longevity) have been recorded in, e.g., some crocodilians (Bellairs 1969; see also Erickson and Brochu 1999 for the extinct *Deinosuchus*) and testudines (Patterson and Brattstrom 1972). Reciprocally, most mammals and squamates associate the presence of secondary ossification centers with a growth activity strictly limited in time. However, reverse examples, showing a relative independence of growth duration from epiphyseal structure, are numerous. The presence of "primitive" epiphyses coexists with limited growth in all birds and possibly also in other dinosaurs (Horner and Padian 2004; Erickson 2014), and most lissamphibians, even of large size (e.g., Gramapurohit et al. 2004). Woodward et al. (2011) showed that *Alligator mississippiensis,* a species that has typical primitive epiphyses and is commonly considered for this reason (like all crocodilians) to grow throughout life (e.g., Chabreck and Joanen 1979), has limited somatic growth (see also Congdon et al. 2013 and Omeyer et al. 2018 for testudines). An opposite situation was described in the Nile monitor (*Varanus niloticus*) and other large varanid species by Buffrénil et al. (2008) and Frydlova et al. (2017): the fusion of secondary ossification centers with primary centers is so delayed in these animals that it does not occur within the limits of their longevity. Functional growth plates are thus maintained and, according to environmental conditions, growth may potentially continue even in large and old adults.

These comparative data tend to support Parfitt's (2002) statement that epiphyseal fusion is a consequence, not the real cause, of growth cessation. The complete disappearance of growth plates is nevertheless an irreversible process that makes further growth impossible. As such, it is an important target for selective pressures that, in the short or long term, closely constrain the somatic size of taxa to their ecological specialization.

Subperiosteal Growth of Bone Cortices

In pace with the epiphyseal growth in length, the growth in diameter of the bone shaft is realized by the combined action of the osteoblasts of the cambial layer of the periosteum (increase in cortical thickness), and the osteoclasts located over both the walls of the medullary cavity and the surface of the medullary trabeculae (Figure 9.3H). Depending on the relative dynamics of both cortical thickening and the expansion of the medullary cavity, the corticodiaphyseal index of a bone shaft will be of variable value (Figure 9.3I, J).

During active growth, the morphological differentiation of an endochondral bone (whatever its shape) results from an interplay between the chondrogenic activity of the epiphyseal regions, responsible for the growth in length of the bone, and the osteogenic activity of the periosteum, responsible for its growth in diameter. Allometric trends in this relationship result in a modification of the bone shape (e.g., Kilbourne and Makovicky 2012). Moreover, according to the so-called Amprino's (1947) rule, the basic histological features of bone deposits basically depend on their accretion rate, as measured in $\mu m \cdot day^{-1}$. This primary and universally acknowledged relationship is a central clue for interpreting the dynamic aspects of bone accretion in paleohistology. It is presented in more detail in Chapter 10.

The model of static and dynamic osteogenesis by Marotti et al. (1999) and Ferretti et al. (2002) (see also Marotti 2010; Stein and Prondvai 2014 and Prondvai et al. 2014) is a major contribution to the description of periosteal osteogenesis modalities. This model has been presented and commented on above (see Chapter 8). In brief, in static osteogenesis, the osteoblasts are randomly distributed and oriented in the cambial layer of the periosteum. Although each of them is functionally polarized (osteoid excretion occurs through only a part of the plasmic membrane), because of their random orientation, they become surrounded by the osteoid that they collectively produce and are finally embedded where they are. The result is the production of fast-growing woven-fibered bone tissue. Conversely, in dynamic osteogenesis, active osteoblasts are organized in one layer and the osteoid excretion occurs in the same direction for all the cells. Secreting cells tend to move backward in pace with the accumulation of their own production, but a small number of them get entrapped in the matrix. This kind of osteogenesis characterizes slow accretion processes that correspond to parallel-fibered or lamellar bone tissues.

Systemic Regulators of Skeletal Growth

Multiple Systemic Regulators

In addition to the many local regulators briefly evoked above, the growth of the skeleton, and more generally that of the organism as a whole, is under the control of several endocrine (systemic) factors that may or may not interact with paracrine and autocrine factors. They have a principal role in skeletal biology either through the direct action that they exert on bone cells, or by the activation of paracrine or autocrine signals (indirect action). Interactions, known to be variable among taxa and influenced by the ontogenetic stage of development, occur among the systemic regulators of bone growth. Five of these factors will be considered here. The two most important are the growth hormone (GH) and the insulin-like growth factor 1 (IGF-1). For a part of their physiological activity, these hormones depend on each other and, along with their own receptors and regulators, they form an integrated functional unit, the so-called GH/IGF-1 axis. Thyroid, sex steroids and glucocorticoid (GC) hormones are also importantly involved in skeletal growth control. Numerous reviews and syntheses, most often oriented toward human pathology, have been produced on this topic, e.g., Eerden (2003), Bellido and Hill Gallant (2014) and Pozo et al. (2014) for general surveys; Yakar et al. (2002) and Yakar and Isaksson (2016) for the GH/IGF-1 axis and Bassett and Williams (2008, 2016) for thyroid hormones (TH; see also Ducornet et al. 2005). Other endocrine and systemic agents are involved in the control of bone cell proliferation or activity; with direct or indirect, activating or inhibiting effects on bone growth. Such is the case, for example, of leptin (Roubos et al. 2012; Londraville et al. 2014), prolactin (Yamaguchi and Yasumasu 1977; Coss et al. 2000) and vitamin D metabolites (Miller et al. 1983; Ciresi and Giordano 2017). However, their

actions are more closely related to long-term regulation of bone metabolism and remodeling than to the modulation of growth plates or periosteal osteoblast activities in the developing juvenile skeleton. Therefore, these factors will not be considered specifically in the present chapter.

Action of GH, IGF-1 and the GH/IGF-1 Axis on Skeletal Growth

Molecular Structure and Secretion Context

GH is a polypeptide that occurs in all vertebrates. It comprises some 190 amino acids (191 amino acids in humans; Kopchick et al. 2002), with a very similar structure among taxa. Comparative data in vertebrates (Miller and Eberhardt 1983; Ávila-Mendoza et al. 2014) reveal only minor differences, generally distributed in compliance with acknowledged phylogenetic relationships. Some unexplained phylogenetic inconsistencies may nevertheless exist in the molecular structure of the GH, as exemplified by, e.g., the closer proximity of the anurans (frogs and toads) to the amniotes than to the urodeles (newts and salamanders), as displayed by the cladogram from Ávila-Mendoza et al. (2014).

The secretion process and action on skeletal cells of GH and IGF-1 are summarized in Figure 9.4. GH is secreted intermittently by the somatotrophic cells of the anterior, glandular part

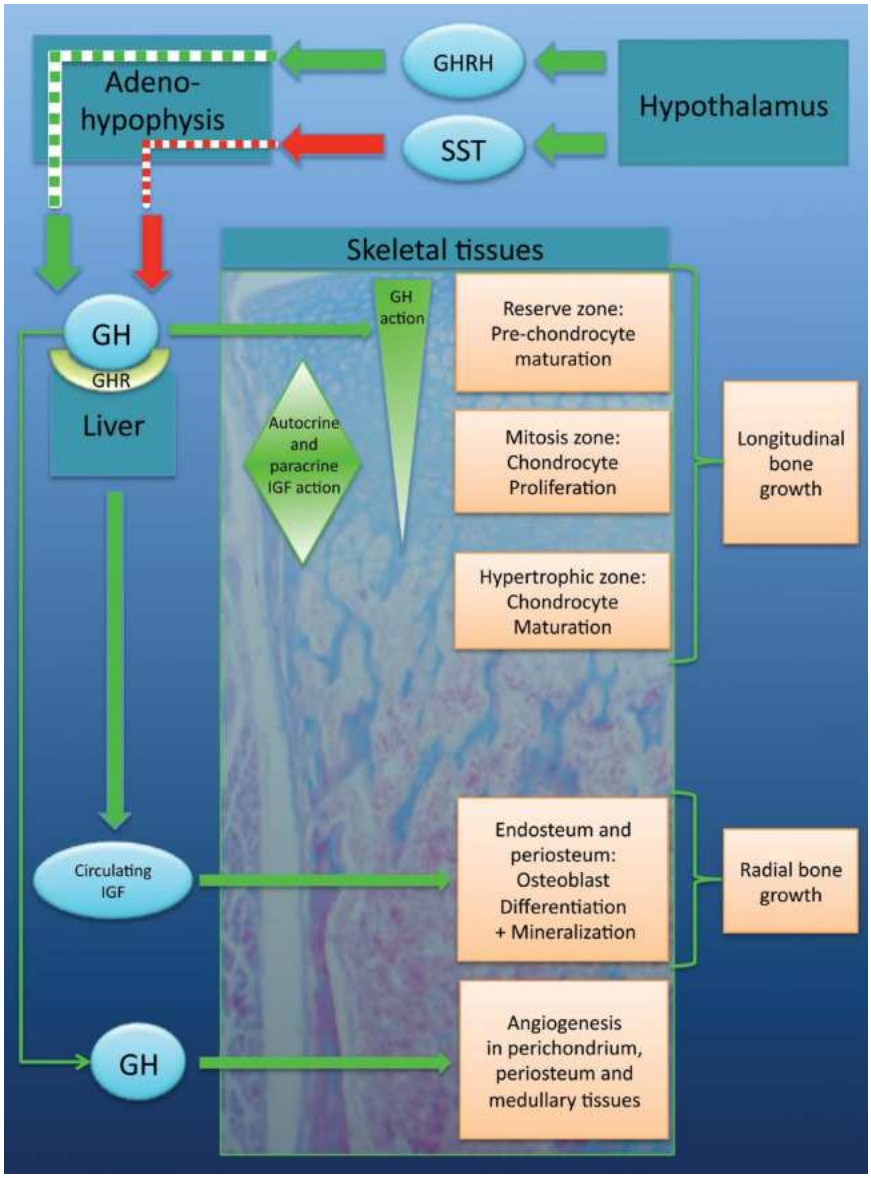


FIGURE 9.4 Growth hormone (GH) and skeletal development. GH is a growth promoting hormone produced by the pituitary gland. The hypothalamus secretes the GH-releasing hormone (GHRH) and somatostatin (SST), which increases and decreases GH secretion, respectively. GH action is maximal in the reserve zone, where it enhances prechondrocytes maturation, and null in the hypertrophic zone. This hormone also stimulates the production of insulin-like factor 1 (IGF-1) in multiple target organs, especially the liver. IGF-1 has several target cells in bone and acts at all levels to enhance longitudinal and radial growth. IGF-1 action is maximal in the proliferation zone. Additionally, GH stimulates angiogenesis in perichondrium, periosteum and medullary tissues. Negative feedback on the production of GH is induced by IGF-1 (not shown). GHR, growth hormone receptor.

VetBooks.ir

of the hypophysis (adenohypophysis) and enters the systemic blood flow by the jugular veins. The secretion of GH is under the direct positive control of the hypothalamic arcuate nucleus whose neurons secrete a releasing factor, the GH releasing hormone (GHRH). On somatotrophic cells, this neuropeptide acts through the stimulation of specific receptors (review in Gaylinn 1999). The activity of the arcuate nucleus is regulated by the diencephalon and, as such, is submitted to strong influences, both daily and seasonal, from environmental conditions (see Tannenbaum and Martin 1976; Root and Diamond 2000). In embryos and early fetuses, in the absence of differentiated adenohypophysis (and thus of pituitary GH secretion), the GH gene along with the GH receptors (GHRs; see below) are expressed in numerous tissues (reviews in Harvey 2013; Harvey and Baudet 2014); local GH then acts as an autocrine or paracrine factor (Harvey and Hull 1997; Harvey et al. 1998). Embryonic growth, prior to organogenesis, seems to depend on the action of such extrapituitary GH, in addition to placental growth hormone in mammals (Lacroix et al. 2002). Limited GH amounts are still produced by numerous peripheral, nonpituitary tissues during postnatal life (review in Harvey 2010). The blood level of GH steeply varies with age. In humans, its peak value occurs in late adolescence; it then drops progressively to fall to residual levels after the sixth decade (Root and Diamond 2000).

The presence of circulating IGF-1 is entirely dependent on, and controlled by, the level of serum GH. IGF-1 is a 7 kDa polypeptide comprising 70 amino acids (in mammals). It is secreted by the hepatocytes (liver cells), under the stimulating action of the growth hormone that targets specific receptors (GHRs) present in the plasmic membrane of these cells (review in Rosen and Niu 2008). Other tissues such as cartilage, bone, fat and muscles are also known to produce this hormone under the control of GH (Sjögren et al. 2002). However, their importance is minor: according to Yakar and Isaksson (2016), 75% of the circulating IGF-1 originates from the liver. Discrepancies between authors exist on this topic (reviewed by Ohlsson et al. 2009). In the bloodstream, IGF-1 molecules are bound to specific binding proteins (IGFBPs), which increase their half-life.

From the hypothalamic neurons down to the membrane receptors of skeletal cells, the GH/IGF-1 axis thus comprises at least four main links depending on each other in cascade: the neurons of the arcuate nucleus, the somatotroph cells of the adenohypophysis, the cells of the liver and the skeletal tissue cells. This integrated cascade justifies the term GH/IGF-1 axis.

Actions of GH and IGF-1 on Cartilage and Bone Cells

GH and IGF-1 have distinct though partly overlapping effects on skeletal tissues. Their respective actions on cells are mediated by specific receptors, the GHRs and IGFRs, which occur in the plasmic membrane of all bone cells, including chondroblasts, chondrocytes, osteoblasts, osteocytes and osteoclasts. The structure and function of these receptors are reviewed by Kopchick et al. (2002) for GHRs, and by D'Ercole (1996), Clemens and Chernausek (2004) and Rosen and Niu (2008) for IGFRs.

Many reviews have been published on the action of GH and IGF-1 on skeletal tissues. Among the most recent ones are Giustina et al. (2008), Bellido and Hill Gallant (2014) and Forbes (2016). In epiphyses, GH basically stimulates the differentiation of prechondrocytes into mature cells in the reserve zone. The action of this hormone on cartilage cells is thus maximal at this level, and gradually decreases to become quasi-null in hypertrophic calcified cartilage. The actual morphological result of GH activity is bone elongation. GH also stimulates angiogenesis in the perichondrium, periosteum and medullary tissues. Additionally, it increases the production of local IGF-1 not only by the cells of the reserve zone, but also by the osteoblasts of the periosteum in the metaphyseal and diaphyseal regions.

In growth plate cartilages, the action of local IGF-1 is mainly to stimulate, through paracrine and autocrine processes, the mitotic activity of chondrocytes (intussusception) in the proliferation zone. Topographically, the activity of this hormone is quasi-null in the reserve zone, maximal in the proliferation zone and progressively less toward the hypertrophy zone (Yakar and Isaksson 2016). Conversely, circulating IGF-1 mainly targets periosteal and endosteal osteoblasts in metaphyseal and diaphyseal regions. Its action is then to stimulate osteoid secretion by osteoblasts, with two main morphological results: a stimulation of the growth in diameter of the diaphyseal region through the control of periosteal cortex thickness; and a similar stimulating action of endosteal accretion over medullary trabeculae, thus preserving the mechanical competence of the bones.

The secretion of GH is inhibited by a small polypeptide that is also synthesized in the hypothalamus (SST). This neurohormone acts as an antagonist of GHRH on somatotrophic cells and inhibits GH production (review in Barnett 2003). In addition to SST action, serum GH and IGF-1 exert a feedback resulting in both a stimulation of SST synthesis and a direct inhibition of GH secretion (Cuttler 1996; Minami et al. 1998; Rosen and Niu 2008). Other hormones such as sexual steroids or thyroid hormones (THs) decrease GH production.

Thyroid Hormones

Nature and Secretion of Thyroid Hormones

THs are secreted by the follicular cells (thyrocytes) of the acini that occupy most of the volume of the thyroid gland. The initial form of this secretion is a colloid composed principally of a large (660 kDa) glycoprotein, the thyroglobulin that consists of repeated domains containing tyrosine (an amino acid) residues. The colloid also contains iodine atoms that bind to the tyrosine molecules to form either simply or doubly iodinated tyrosine, i.e., monoiodo- or diiodotyrosine, respectively. The coupling of two doubly iodinated molecules constitutes tetraiodothyronine (T_4), which represents 80% of the native form of THs. At this stage, triiodothyronine (T_3; coupling of one simply plus one doubly iodinated tyrosine) is much less than T_4. Tri- and tetraiodothyronine are then split from thyroglobulin by a protease within the thyrocytes, and they enter the bloodstream (recent review in Di Jeso and Arvan 2016). In various tissues, e.g., the liver and, to a lesser extent, skeletal

muscles, brown fat, and so forth, T_4 is converted into T_3 by the action of a deiodinase enzyme (review in Gereben et al. 2008). In target tissues, T_3 is by far the most active form of TH.

The activity of follicular cells is under the stimulation of the thyroid-stimulating hormone (TSH), which is produced by the thyrotroph cells of the anterior pituitary lobe. The follicular cells of the thyroid gland have specific receptors to TSH (TSHRs). Upstream, thyrotroph pituitary cells are controlled by a hypothalamic neurohormone, the thyrotropin-releasing hormone (TRH), which acts on receptors of the thyrotrophs. From the hypothalamus down to the thyroid gland, a cascade of regulating factors justifies the term hypothalamic-pituitary-thyroid axis (HPT; Bassett and Williams 2008; Fekete and Lechan 2014). The secretion of TRH, as well as that of TSH (and consequently the resulting secretion of TH), are directly regulated by a negative retroaction depending on the level of circulating T_3 and T_4 (reviews in Gogakos et al. 2010; Waung et al. 2012). The general structure of the HPT, and its action on skeletal targets is summarized in Figure 9.5.

Actions on the Growing Skeleton

THs target a considerable variety of tissues (liver, heart, fat, brain, etc.) through the expression of receptors (TRs, of which three types exist: TRα, TRβ1, TRβ2), and they are involved in the control of vital functions such as metabolism, heart rate and bone growth and remodeling (review in Yen 2001). The most active form, T_3, enters target cells via specific membrane binding proteins. Its action within the cells is then mediated by nuclear receptors, TRα and TRβ, which trigger the expression

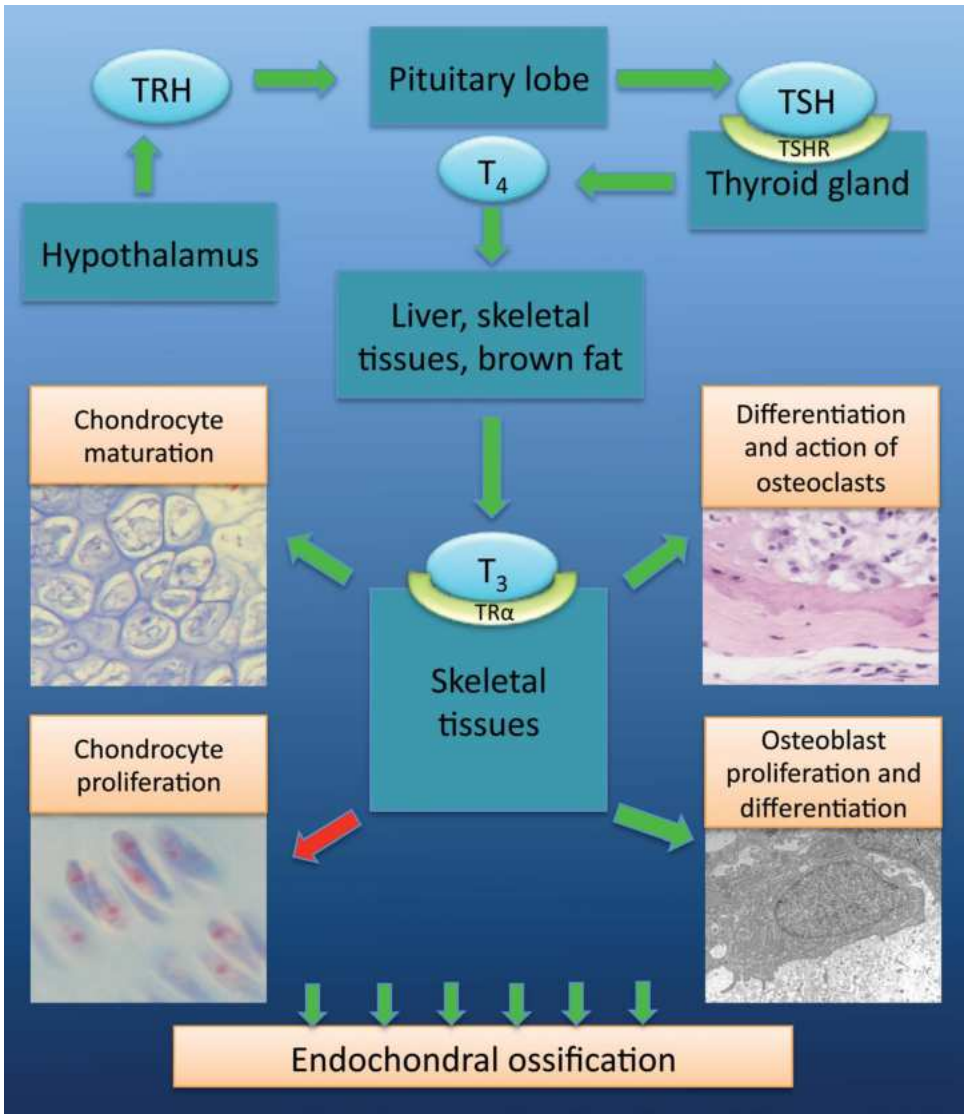


FIGURE 9.5 Thyroid hormones and skeletal development. Thyrotropin-releasing hormone (TRH) is secreted in the hypothalamus. The target of this neurohormone is the adenohypophysis, which releases thyroid-stimulating hormone (TSH) in response. The bloodstream brings TSH to the thyroid gland, where it binds to the TSH receptor (TSHR) and stimulates the production and release of thyroxin (T_4). T_4 is converted into T_3 in several organs as liver, brown fat and skeletal tissues. T_3 mainly binds to TRα receptors in bone cells. In the growth plate, T_3 promotes chondrocyte maturation and matrix mineralization, osteoclast differentiation and action, osteoblast proliferation and differentiation. In contrast, T_3 inhibits chondrocyte proliferation. The result is an enhancement of endochondral ossification.

VetBooks.ir

of specific genes (review in Cheng et al. 2010; see also Forrest et al. 1990). This process occurs in all target cells, whether in peripheral tissues, including bone, or in the central nervous system (hypothalamus, pituitary gland), where they are involved in the feedback regulation loop of T_4 and T_3 secretion.

In bone, THs (mainly T_3) actions are principally mediated by the TRα receptor and may be either direct on bone cells (Robson et al. 2000) or exerted via the modulation of the activity of other regulators of bone growth such as GH and IGF-1 (Huang et al. 2000), fibroblast growth factors (Barnard et al. 2005) or other histogenetic agents (Stevens et al. 2000; Eerden et al. 2003; Wang et al. 2007). A review of thyroxin interactions with other hormones on skeletal cells is presented in Williams et al. (1998; see also Gouveia et al. 2018).

Contrasted actions on chondrocytes and osteoblasts are attributed to T_3. In the growth plates of the developing skeleton, T_3 stimulates the maturation of chondrocytes toward hypertrophy and the mineralization of the cartilage matrix, while it inhibits cell proliferation (Robson et al. 2000; Bassett and Williams 2016). Conversely, in osteoblasts, this hormone stimulates cell proliferation, differentiation and matrix synthesis by both direct and indirect actions; however, it also increases apoptosis (Waung et al. 2012) and accelerates the differentiation and action of osteoclasts (Bassett and Williams 2016). These combined effects result in stimulating endochondral ossification in fetuses and juveniles, since both osteoblasts and osteoclasts are simultaneously involved in this process (Muira et al. 2002). Moreover, recent data suggest that TSH and its specific receptor, TSHR, also influence the activity of chondrocytes, osteoblasts and osteoclasts in synergy with T_3 (Bassett and Williams 2016).

In juvenile, actively growing mammals (most data deal with humans), the skeletal syndromes typically associated with hypothyroidism consist of slow endochondral ossification, decreased mineralization of the osteoid and delayed growth in length of the bones (Bellido and Gallant 2014; Bassett and Williams 2016). The resulting condition is short stature and mechanically fragile bones due to remodeling impairment. Hyperthyroidism in juveniles accelerates endochondral ossification and calcification of bone matrix and provokes precocious arrest of growth plate activity (Waung et al. 2012; Bellido and Gallant 2014). These disorders also result in short stature and mechanically weakened bones due to excessive and imbalanced remodeling (Allain and McGregor 1993; see also Chapter 11). TH dysfunctions are often due to mutations affecting the HPT axis at any level, including receptors TRα and TRβ, in target tissues (Bassett and Williams 2016).

Sex Steroids, Androgens and Estrogens

Secretion and Regulation of Sex Steroids

In male and female vertebrates, steroidal hormones, mainly produced by the gonads (testes and ovaries), play an important role in the development and functioning of essential organs or systems, and have a crucial role in bone growth and maintenance (recent review in Almeida et al. 2017). Chemically, they are all derived from the cholesterol molecule. Androgens and estrogens both occur in all individuals, whatever their gender because, in addition to the main organs that produce them preferentially, they are also secreted in lesser quantities by other, nongenital cells or organs such as the reticulate zone of the adrenals, the adipose tissue, the liver and so forth. Males thus have a significant amount of circulating estrogens and females have a similar impregnation of androgens. Of course, testosterone is in much greater concentration (sixfold more elevated) in males than in females, and vice versa for the estrogens in females.

Androgens, mainly represented by testosterone and its metabolites, are the masculinizing hormones. In males, they are principally produced by the interstitial (Leydig) testicular cells, in addition to the other tissues also able to secrete them. In females, androgens can be accessorily secreted by the thecal and ovarian cells of the ovarian follicle. Estrogens are feminizing steroid hormones. They basically result from a chemical modification (aromatization) of the androgens. In females, their main origin is the follicular ovarian cells and, in gravid mammals, the placenta (steroid hormones occur in the yolk of sauropsid eggs; review in Elf 2003). However, they are also released by the diverse tissues mentioned above. In general, a part of circulating androgens is transformed into estrogens within the peripheral tissues that they target (e.g., nervous tissue, fat or bone). Figure 9.6 summarizes the production and the action on bone cells of male and female sex steroids.

The secretion of sex steroids starts early during embryonic life. In humans, functional precursors of Leydig cells differentiate at embryonic age 6–7 weeks (7 days in the rat) and testosterone is detectable after this developmental stage (Svechnikov et al. 2010). As for THs, sex steroid secretion corresponds to an "axis", the gonadotroph axis or HPG, starting at the hypothalamic level and ending, via the adenohypophysis, in the gonads. The hypothalamic-releasing hormone for sex steroid is the gonadotrophin-releasing hormone (GnRH), a neurohormone secreted in a relatively broad hypothalamic region in the floor of the third ventricle (review in Ducornet et al. 2005). GnRH targets the gonadotroph cells of the anterior pituitary and, through the action of a specific receptor (GnRHR), it controls the production of two stimulating (gonadotrophin) hormones: the so-called interstitial cell-stimulating hormone (ICSH; also called LH) that principally targets Leydig cells and acts through LH specific receptors (LHRs; review in Svechnikov et al. 2010; see also Saez et al. 1995; Faugeron-Ruel and Christin-Maitre 2005), and the FSH, targeting the ovarian follicle through FSH-specific receptors (FSHRs; Fan and Hendrickson 2005). A negative retroactive loop, based on the level of circulating androgens and estrogens, regulates both the release of GnRH in the hypothalamus and the secretion of ICSH and FSH in the pituitary gland. Two additional, recently discovered neurohormones, GnIH (an inhibiting factor; review in Tsutsui et al. 2012) and kisspeptin (Kanasaki et al. 2017), are possibly also involved in the regulation of GnRH and gonadotropin secretions. Comparative data by Kah et al. (2007) and Kawauchi and Sower (2006) underline the extremely ancient phylogenetic rooting, and the possible evolutionary specialization pathways, of GnRH and GnRHRs in metazoans in general and vertebrates in particular.

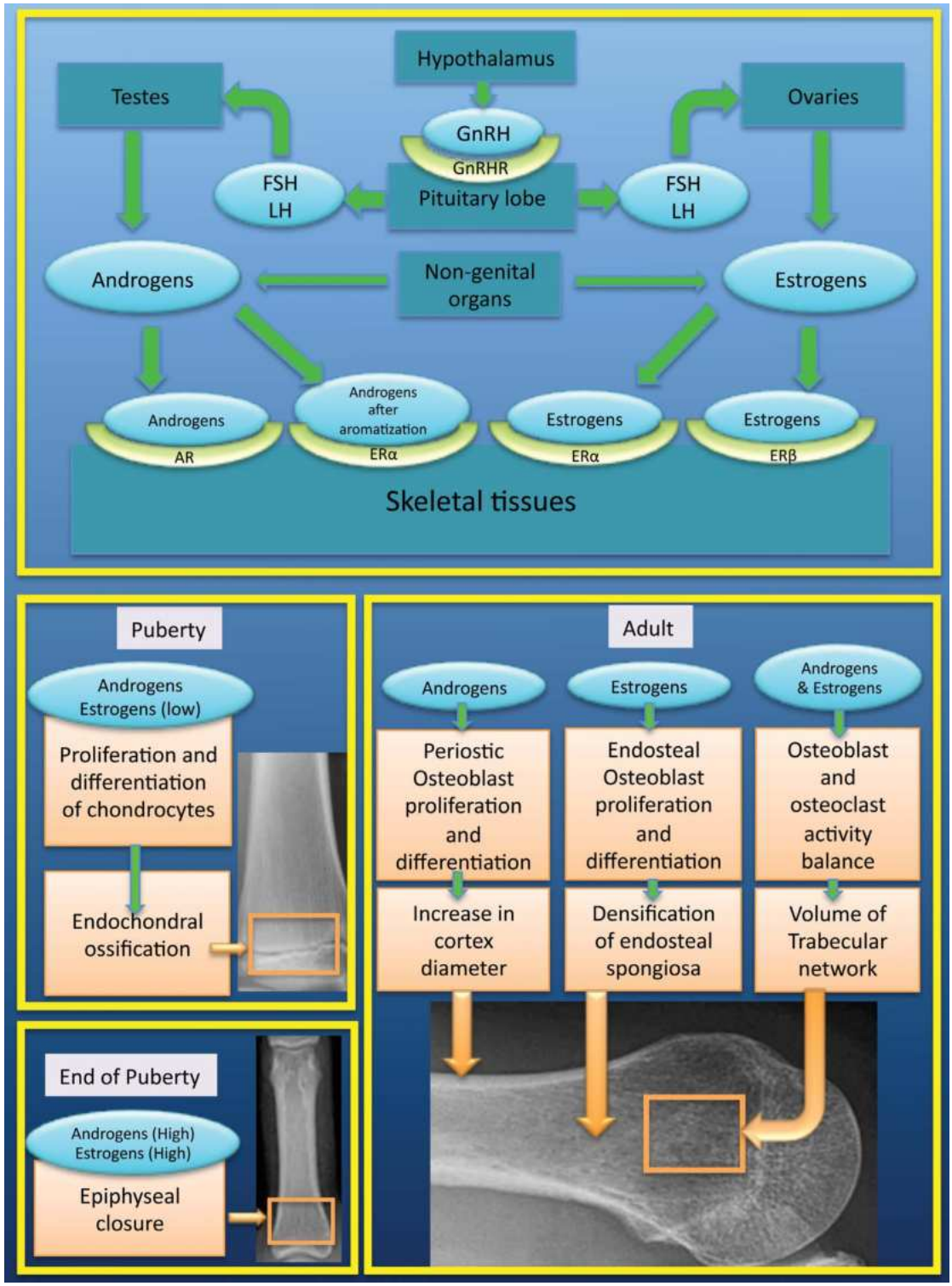


FIGURE 9.6 Sex steroids and skeletal growth and maturation. The gonads regulate bone physiology through the complex and variable action of the sex steroid hormones they produce. The hypothalamus secretes gonadotropin-releasing hormone (GnRH), which stimulates the cells of the pituitary anterior (glandular) lobe to release luteinizing hormone (LH) and follicle-stimulating hormone (FSH). The targets of LH and FSH are the gonads. Testosterone and estrogen are then secreted by testes and ovaries (to a lesser extent, they can also be secreted by nongenital organs). The main receptors of sex steroid in bone are the androgen receptor (AR) for androgens, the estrogen receptor ERα for estrogens and for androgens after aromatization, and the specific estrogen receptor ERβ for estrogens. During puberty, androgens and a low concentration of estrogens stimulate endochondral ossification. At the end of puberty, a high concentration of both hormones promotes a decline in growth and epiphyseal closure. This results in a complete arrest of the growth in length of bones. In adults, androgens are responsible for cortex diameter increase, estrogens for the densification of endosteal spongiosae, and both hormones for the balance between osteoblast and osteoclast activity during bone remodeling. GnRHR: gonadotrophin-releasing hormone receptor.

VetBooks.ir

Action of Sex Steroids in Bone

Although the detailed processes involved in the action of androgens and estrogens on their target tissues are not yet fully elucidated (Steffens et al. 2015), available data show that this action is mediated by two types of nuclear receptors, the AR receptor for testosterone and the two forms of ER receptors, i.e., ERα and ERβ, for estrogens (general reviews in Imai et al. 2013; Almeida et al. 2017; see also Vanderschueren et al. 2004; Wiren. 2008 for androgens and Turner et al. 2008 for estrogens). These receptors are distributed in many tissues of the male and female vertebrate bodies (Compston 2001). In well-documented taxa (basically mammals), their expression (as well as the release of their regulators) is chronologically variable during ontogeny: it is relatively high in fetal life, then it decreases in juveniles to steeply rise again during puberty (Svechnikov et al. 2010). In postpubertal stages, AR and ERs expressions gradually drop and finally reach low levels in late ontogenetic stages.

In the skeleton, the respective actions of androgens and estrogens are partly synergic and overlap, at least in the control of growth plate activity. Conversely, they have distinct effects on bone cortices. Moreover, estrogens only provoke the expression of estrogen receptors, whereas androgens aim at both receptors: AR and, after a local transformation (aromatization) into estrogen in target tissues, receptor ERα (Bord et al. 2001; Wiren 2008; Iravani et al. 2017). During growth, and especially the pubertal growth spurt, sex steroids are synergic of, and mediated by, the growth hormones GH/IGF-1 (Almeida et al. 2017).

In growth plates of the fast-growing pubertal individual androgens and, when present in low concentration, estrogens, both stimulate the proliferation and differentiation of chondrocytes (Kusec et al. 1998; Vanderschueren 2004; Bellido and Hill Gallant 2014). This strongly accelerates endochondral bone formation and growth in length. By the end of puberty, when the concentration of sex steroids is maximal, estrogens then have an inhibitory effect on the proliferation and synthetic activities of chondrocytes. The growth in length of endochondral bones is consequently slowed, a process that finally results in epiphyseal closure (i.e., disappearance of growth plates) and growth arrest. Circulating estrogen concentration is higher in females, which consistently results in earlier epiphyseal fusion. In pathological or experimental contexts, when estrogen action in bone is made impossible, growth plates remain present and active far beyond the end of puberty (e.g., Eerden et al. 2003; Bellido and Hill Gallant 2014).

In the diaphyseal region, the actions of androgens and estrogens are opposite. Androgens stimulate the proliferation and synthetic activity of periosteal osteoblasts. The result of this action is a marked increase in thickness of the diaphyseal cortex, combined with an increase in diameter of the medullary cavity. This outward-directed growth pattern is characteristic of males with high testosterone concentration. Conversely, through receptor ERβ, estrogens tend to decrease the proliferation and activity of periosteal osteoblasts, while those of endosteal osteoblasts are increased. The bone shafts then have a limited expansion in diameter but thick endosteal formations. This growth pattern prevails in females, characterized by high estrogen concentration (Bellido and Hill-Gallant 2014). Such sex-contrasted processes are the basis of sexual dimorphism in the skeleton and are responsible for greater robusticity (otherwise consistent with higher muscular development) in males.

In the metaphyseal regions and in other cancellous formations of adult bones, both hormones contribute to maintaining the volume of trabecular networks (generally measured through bone mineral density [BMD] values) by activating both the osteoblasts and osteoclasts involved in bone remodeling and creating the conditions of a balanced action of these cells (see Chapter 11 for further details). The action of sex steroids on skeletal target cells gradually decreases with aging; a senescence process that finally results in net bone loss (osteoporosis) due to imbalanced remodeling (e.g., Raisz et al. 2008; Imai et al. 2013; see also Chapter 32).

Glucocorticoids (GCs)

Corticosteroid hormones, mainly (but not exclusively) cortisol and, to a lesser extent, corticosterone, are steroid hormones secreted by the cells located, in mammals, in one of the three histological zones forming the cortex of the adrenal gland, the *zona fasciculata* (Xing et al. 2015). The molecular structure of GCs, as well as their roles and physiological involvements, are highly conservative. They share similar features in all vertebrates, from finned osteichthyans to mammals (Nesan and Vijayan 2013). These hormones are principally involved in the physiological answers to distress, or "stress", situations (Habib et al. 2001), having a powerful action on glucose metabolism, an immunosuppressive role and an enhancing effect on apoptosis in diverse cell populations. The secretion and skeletal action of GCs are shown in Figure 9.7.

As for THs, glucocorticoid secretion is controlled by a stimulating hormone, adrenocorticotrophin hormone (ACTH), produced and released in the bloodstream by the anterior lobe of the pituitary gland. ACTH secretion is regulated by the releasing action of a hypothalamic neurohormone, the corticotrophin-releasing factor (CRF). Through a retroaction loop, the concentration of circulating GCs regulates the secretion of CFR and ACTH (review in Ducornet et al. 2005). At each level, from hypothalamus to peripheral target tissues, specific membrane GC receptors (GRs) are involved. The expression of receptors to GCs has been reported in numerous tissues and, within bones, in growth plate chondrocytes (in the proliferation and hypertrophic zones), osteoblasts and osteocytes.

At blood concentrations comparable to severe stress situations, GCs have a generally negative effect on the growth in length of endochondral bones (review in Hartmann et al. 2016). Pathological observations in, e.g., Cushing syndrome (review in Arnaldi et al. 2003), along with experimental results, show that these hormones reduce chondrogenesis in the proliferation zone of growth plates and inhibit the maturation of chondrocytes toward hypertrophy (Eerden et al. 2003). In all bones and all bone regions (metaphyses and diaphyses, compact cortices and medullary spongiosae), they also impede the proliferation of osteoblasts, reduce their matrix secretion and enhance their apoptosis rate (Weinstein and Manolagas 2000; reviews in Jilka et al. 2008; Bellido and Hill Gallant 2014). The expression of receptors to GCs (GRα) has been seen in the chondrocytes, osteoblasts and osteocytes of rats and humans (Silvestrini et al. 1999; Abu et al. 2000), which confirms that

VetBooks.ir

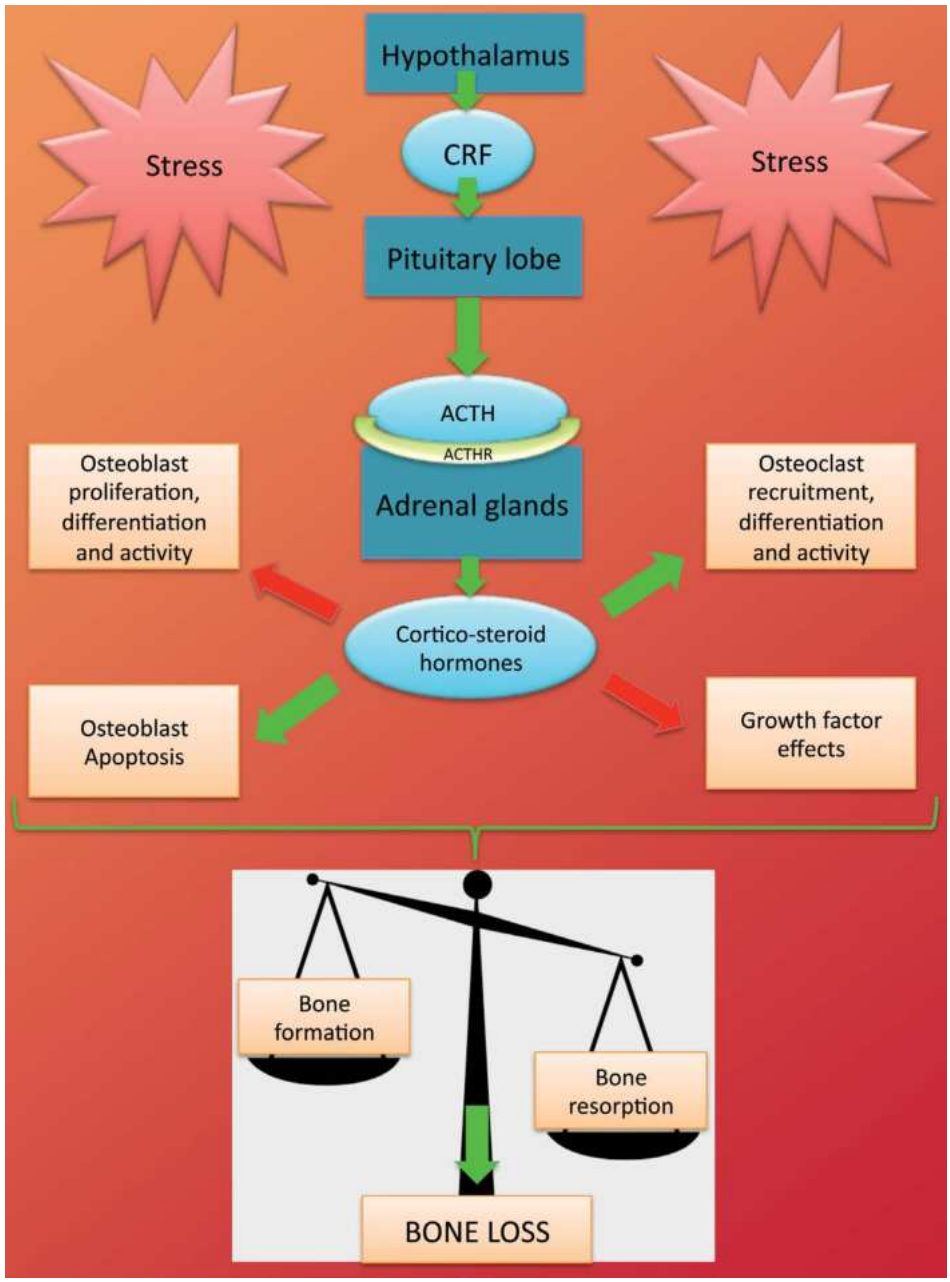


FIGURE 9.7 Corticosteroid and bone loss. In a stress situation, the hypothalamus secretes cortico-releasing factor (CRF) that stimulates the production of adrenocorticotrophin hormone (ACTH) by the anterior pituitary lobe. ACTH targets the adrenal glands, stimulating the production of corticosteroid hormones. Corticosteroid hormones enhance osteoclast activity and osteoblast apoptosis and decrease growth factor effects and osteoblast activity. The negative result of the action of corticosteroid hormones is a loss of bone mass. ACTHR, ACTH receptor.

bone tissue cells are indeed targets for GC hormones. In addition to these direct and proper effects, GCs disturb the activity of important growth regulators: they inhibit the pituitary release of GH, even at low concentrations (Malerba et al. 2005), and interfere with GH and IGF-1 receptors or binding proteins in target cells (Allen 1996; Robson et al. 2002; Kream et al. 2008). Conversely, osteoclasts (which do not express GRs) are not affected. GCs are supposed to be involved in the modulation of T_3 activity in growth plates (Eerden et al. 2003). The final consequences of GC excess in the bones of juvenile, actively growing individuals is growth retardation (review in Allen 1996; Rosenfeld 1996). In adults, high GC concentrations induce imbalance in the remodeling process of compact cortices (Haversian remodeling) and spongy formations, resulting in osteoporotic processes (review in Lane and Lukert 1998). It is worth noting, however, that, at small doses, *in vitro* studies show that the negative effects of GCs on bone growth are mild or absent (Kream et al. 2008). Although the effects of GCs on skeletal growth were mainly studied in mammals (humans and rodents), the studies conducted in osteichthyans (Nesan and Vijayan 2013) and birds (Bellamy and Leonard 1965) yielded comparable results.

VetBooks.ir

Growth and Morphology of Bones

The Constraint of Rigidity

Once mineralized, bone and other calcified tissues can increase their size and control the differentiation of their morphology during growth by two basic mechanisms. Accretion at various rates by osteoblasts adds new tissue volume, and resorption by osteoclasts removes tissue volume. This is a basic developmental constraint, occurring at all ontogenetic stages, because it is fundamentally related to the rigidity of the extracellular matrix of bone. When accretion and resorption operate independently from each other to modify the morphology of a bone, either from inside or on the outer bone surface, they contribute to *modeling*; when they occur in close functional coordination, with accretion following resorption in time and space, they contribute to bone *remodeling*, a process that mainly (but not exclusively) renews and repairs osseous tissue (review in Allen and Burr 2014). Details on the remodeling process are given in Chapter 11.

Deciphering the course of local bone modeling is a principal goal of developmental studies and is of special interest to evolutionary biology because it can reveal the sequence of local growth events, expressed during ontogeny, through which the shape of a bone can be progressively modified during the evolution of a given clade. In extant taxa, modeling processes can be conveniently studied by the experimental labeling of bone growth with fluorescent markers (see below, Chapter 10). This possibility is, of course, out of reach in fossils; however, mineralized tissues can keep inscribed in their structure, in the form of natural growth marks (see Chapter 31 on *Skeletochronology*), the traces of local growth events, including accretion rate and direction, resorption, local growth arrest and bone contours at various ages.

Reading and interpreting these clues in terms of local morphogenetic processes is one of the most exciting fields in paleohistology. Both modeling and remodeling can be of great geometrical complexity, especially when they are combined. Here we consider only the most basic aspects of this question through some relatively simple cases.

Basic Shaping Processes in the Growth of Bones

The Peculiar Growth Geometry of Some Flat Bones

The diploe structure that characterizes flat bones is related to a strong remodeling activity, through resorption and reconstruction, that occurs both in the core and the surface of the bones. This process is strongly imbalanced toward resorption, which provokes an expansion of the cancellous core to the detriment of compact cortices as long as the bone increases its overall size (Figure 9.8A). Moreover, when flat dermal bones are part of a complex skeletal assemblage and present a convex and a concave surface, as is typically the case for the bones forming the skull roof, their growth pattern is characterized by a strong asymmetry. In actively growing individuals, subperiosteal accretion is fast on the convex surface, but much slower on the concave surface, which can even be subjected to extensive resorption (Enlow 1963; Francillon-Vieillot et al. 1990; Garcia Gil et al. 2016). Consequently, the central spongiosa of the diploe can be gradually shifted toward the concave (generally medial) side of the bone and may outcrop superficially (Figure 9.8B). When growth stops, a new medial cortex develops again.

Differentiation of Superficial Relief Through Accretion Rate, or Resorption

Variations in accretion rate and local resorption are the most common and simplest mechanisms for modifying the local shape of a skeletal piece. In bones submitted to no (or mild) inner remodeling, the trace of growth acceleration is clearly visible in the spacing of cyclical growth marks, or in other histological details such as a local proliferation of vascular canals, or a change in the refringence properties of the bone matrix (Figure 9.8C, D). Similarly, the occurrence of a resorption front is revealed by Howship's lacunae or reversion lines. In recent, as in fossil bones, it is thus possible to follow (sometimes year by year) the process operating during individual ontogeny for the elevation of a crest, the excavation of a depression, their migration on the bone surface and their local replacement by reverse relief (Figure 9.8E, F). Although apparently simple, interpretations of this kind nevertheless require that histological details in a given sectional plane be interpreted in reference to the global growth dynamics of a bone in diameter and in length, and to recall that deep (early) cortical layers may not represent, in absolute and relative terms, the same anatomical regions as more superficial (later) layers. Examples of these kinds of morphogenetic reconstructions are given by the studies on bone ornamentation in the dermal skeleton of extant and extinct vertebrates by Jasinoski and Chinsamy (2012) and Buffrénil et al. (2015).

Morphogenetic Role of Heterochrony in Local Bone Deposits

At a local scale, chronological differences in the timing of bone deposits, even in the absence of discrepancies in absolute growth rate, may create positive or negative relief or otherwise contribute to modeling the shape of a bone. In this situation, the type of bone tissue occurring locally may not change, compared to the rest of the bone, but the relative duration of its accretion is either longer or shorter. In extant and extinct taxa, if cyclical growth marks occur, their spacing does not change; however, their number may differ in neighboring territories, thus reflecting a protraction (positive relief), or a shortening (negative relief), in the duration of local bone accretion. An example (among many other possible examples) of these kinds of heterochronic processes is given by the differentiation of pseudoteeth (Figure 9.8G) in the Late Pliocene/Early Pleistocene (*ca*. 2.5 Ma) marine bird *Pelagornis mauretanicus*, as interpreted by Louchart et al. (2013). The pseudoteeth are made of an osseous tissue (dense Haversian bone) whose structure is identical to, and in perfect continuity with, that of the jaw bones (Figure 9.8H). The most parsimonious interpretation that can be proposed to explain the topographical arrangement of the microanatomical details displayed by the pseudoteeth and the jaw bones (these details reveal the local operations of

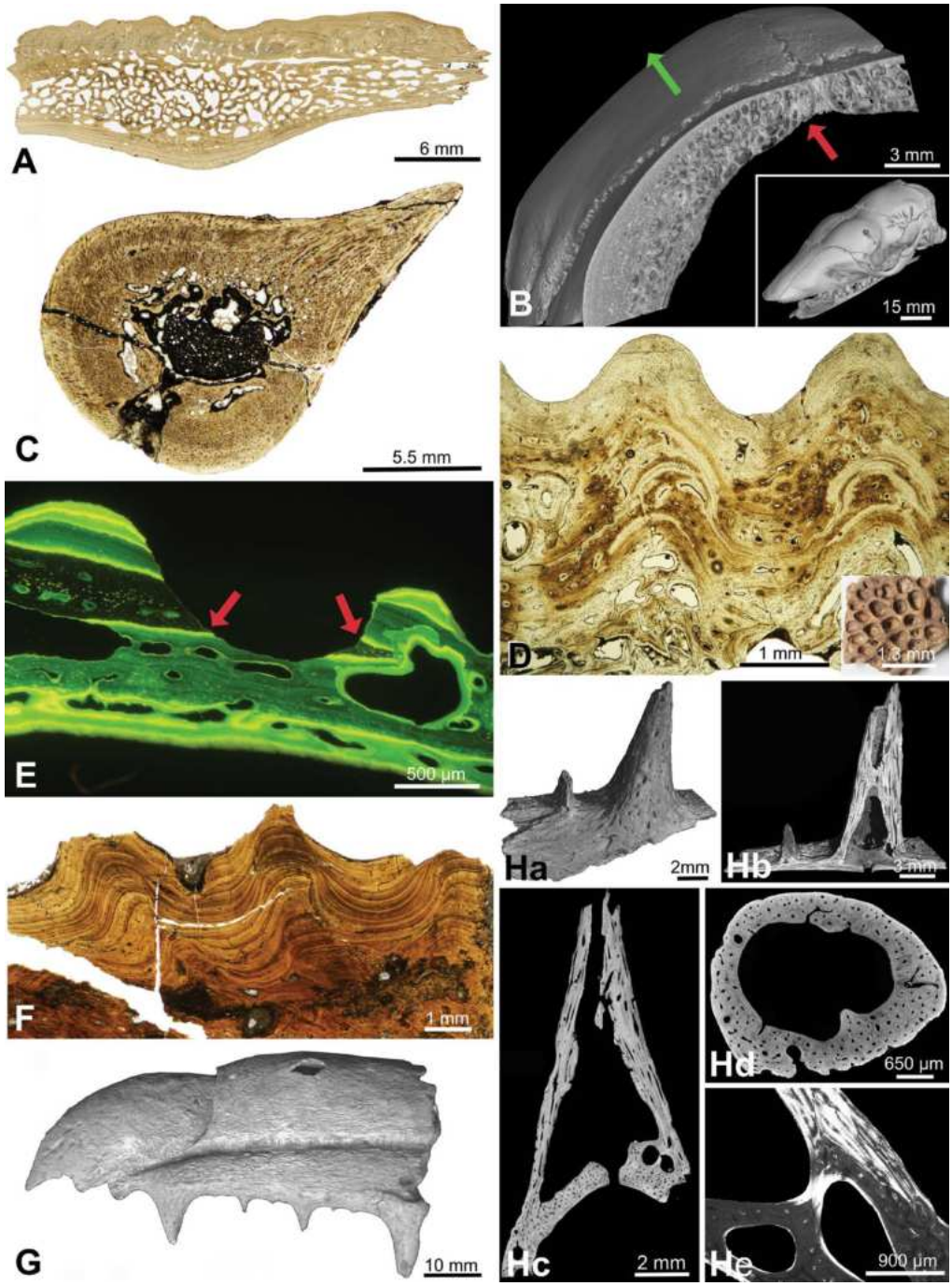


FIGURE 9.8 Growth of diploes and superficial relief formation. A, Roughly symmetric growth of a diploe (carapace plate of the turtle *Trionyx triunguis*). Accretion occurs on both the deep (inner) and superficial (outer) cortices of the osteoderm. B, Asymmetrical growth of a diploe in the skull of a nine-banded armadillo, *Dasypus novemcinctus*. CT-scan 3D reconstruction. Accretion (green arrow) occurs on the outer surface of the bone, while its inner surface is partly eroded (red arrow). The inset shows the entire skull of *D. novemcinctus*. C, Differentiation of a crest through local acceleration of bone growth in the femur of the early synapsid *Ophiacodon insignis*. D, Differentiation of bone ornamentation through local growth acceleration in a fragment of the parietal of an unidentified temnospondyl (cf. *Stanocephalosaurus*) from the Early Triassic beds of Zarzaitine, Algeria. The inset shows the typical aspect of the pit-and-ridge ornamentation pattern. E, Differentiation of bone ornamentation through a complex resorption and reconstruction process. Osteoderm of a juvenile *Caiman crocodilus* labeled *in vivo* with fluorescent markers. The red arrows indicate a resorptive process. F, Superficial layer in the frontal bone of the extinct *Crocodylus affinis* (Crocodylidae), from the Middle Eocene of Wyoming. Growth marks and resorption lines reveal the mode of formation of bone ornamentation in this taxon. G: Pseudoteeth on the maxillary of the bird *Pelagornis mauretanicus*. Ha, General view of pseudoteeth on the mandible of *Pelagornis*. CT-scan 3D reconstruction. Hb, General view of a sagittal section in a *Pelagornis* pseudotooth. Hc, The bone plate closing the base of the tooth is part of the jawbone wall and is made of dense Haversian tissue with longitudinal osteons, cut transversally here. Hd, Cross section in a pseudotooth showing dense Haversian bone with longitudinal secondary osteons (the osteons are then quasi-orthogonal to those of the jawbone). He, Pseudotooth histology in polarized light. Depending on the direction of the osteons in this sectional plane, the bone is monorefringent or birefringent.

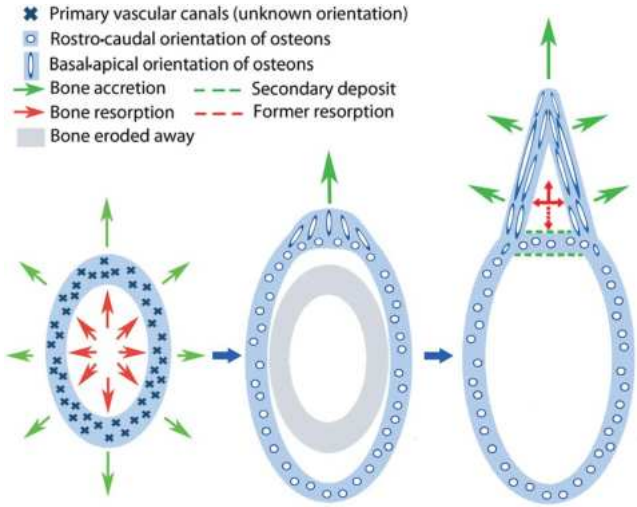


FIGURE 9.9 A possible model for explaining pseudotooth growth in *Pelagornis mauretanicus*. This model is derived from Louchart et al. (2013, 2018). The differentiation of the pseudoteeth is due to a local protraction of periosteal osteogenic activity, likely controlled by ancient and highly plesiomorphic, tooth-specific epithelial signals.

accretion or resorption which occurred locally) leads to the conclusion that each tooth must have differentiated through a local protraction of bone accretion on the surface of the jaw, while accretion had ceased in the neighboring territories of the jaw surface (Figure 9.9). Moreover, the developmental model proposed by Louchart et al. (2018) hypothesized that the differentiation, size and spatial distribution of the pseudoteeth depend on local interactions between the osteoblasts of the jaw periosteum and signaling factors from the neighboring epithelium. These interactions are supposed to have involved a series of morphogenetic fields, remotely derived from the molecular mechanism controlling the patterning of true tooth sequences along the jaws.

Sequential Growth Remodeling in Appendicular Long Bones

The typical shape of tetrapod long bones, with a narrow, subcylindrical diaphyseal region and broader metaphyses and epiphyses, creates a constraint on the growth in length of these bones. Such a morphology cannot be realized in a simple manner through the combined processes of epiphyseal endochondral osteogenesis and subperiosteal accretion over diaphyseal and metaphyseal cortices. The fate of newly formed metaphyseal regions is to be incorporated during growth into the diaphysis, which has a much smaller diameter. The pioneer analyses of this problem by, e.g., Lacroix (1945, 1949) and Enlow (1963), are seminal studies that contributed to define the conceptual principles of studies dealing with the local shaping of bones during growth. In its basic version, the models of long bone growth by Lacroix (1945, 1949) and Enlow (1963) can be summarized as in Figure 9.10A, B.

To become parts of the diaphysis, proximal and distal metaphyses must be reduced in diameter through a strong peripheral, outer resorption process. The latter erodes the metaphyseal cortex up to provoking a superficial outcrop of the underlying spongiosa. To be then incorporated into the diaphysis, the latter must be compacted by intertrabecular deposits, to form the so-called *compacted coarse cancellous bone*. In further growth, new periosteal layers of cortical tissue shall cover the compacted metaphyseal spongiosa, in harmony with diaphyseal widening. In the meantime, the expansion of the medullary cavity broadly erases the compacted cancellous formations of metaphyseal origin and lets persist *in situ* only the periosteal cortex. At every stage of its course, this complex process is closely adjusted, in its spatial and temporal dimensions, to the osteogenic activity of the epiphyses. Exceptions to this general growth pattern are relatively rare. Notable ones are the shortened flipper bones of some pelagic and highly hydrodynamic tetrapods, such as cetaceans and ichthyosaurs (e.g., Felts and Spurrell 1965, 1966). The stylopod and, to a lesser extent, zeugopod elements of these animals (the humerus and radius only in cetaceans) have lost a differentiated diaphysis and are amedullary (see Chapters 35 and 36). Their growth pattern is accordingly simplified and relies only on endochondral osteogenesis and periosteal accretion, with no need for complex inner and outer modeling and remodeling operations (Figure 9.10C, D).

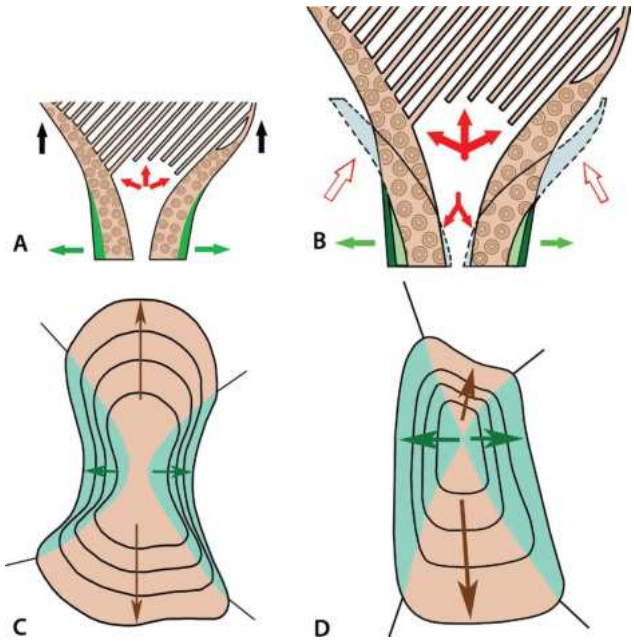


FIGURE 9.10 Modeling the growth pattern of long bone growth. A and B, The classical model developed by Lacroix (1945, 1949) and Enlow (1963) for typical long bones with well-differentiated diaphysis and metaphysis. In the bone metaphysis, this model involves the combination of outer resorption and inner compaction of the peripheral cancellous tissue. Solid red arrows: inner resorption. Hollow red arrows: outer superficial resorption. Green arrows and areas: bone resulting from periosteal accretion. Beige areas: endosteal bone formations. Among these formations, the solid surface with concentric circles indicates compacted coarse cancellous bone, and the hatched areas indicate noncompacted cancellous bone. (Freely derived from Enlow 1963). C and D, Simple, homothetic growth pattern of long bones lacking a differentiated diaphyseal region (C, femur of the ichthyosaur *Stenopterygius quadriscissus*; D, radius of the cetacean *Delphinus delphis*). The green areas and arrows indicate the periosteal territories; the beige areas and brown arrows indicate the endosteoendochondral territories.

VetBooks.ir

Growth Off-Centering and Diaphyseal Curvature

In ribs and some limb long bones (tibia, femur) of the amniote skeleton, the shaft shows a curvature that can be strongly pronounced. Considering the basic constraints on growth in mineralized, rigid parts of the skeleton, one of the basic mechanisms to create, maintain or increase this curvature during growth is an asymmetric appositional activity on the lateral and medial shaft surfaces, with or without additional resorption on one of the bone sides. As in concave flat bones, this process results in a strong off-centering of growth, with a drift of the diaphyseal axis that, in absolute terms, moves progressively in the lateral direction compared with the position of the epiphyses. This process involves both the cortex as a whole and the medullary cavity (Figure 9.11A–D).

Intense remodeling within the bone cortex and around the medullary cavity often results in the disappearance of the histological traces formed by the growth history of the bone. However, when remodeling is mild (e.g., in finned vertebrates or ectothermic tetrapods) or inhibited in relation to some particular ecomorphological adaptations (e.g., secondary adaptation to life in water), histological evidence of growth off-centering can be clear, in recent bones as in fossil bones. In this situation, consistent with Amprino's (1947) rule, the fast-growing side of the cortex displays either a type of bone matrix different from that prevailing in the slow-growing side, or a distinct vascular pattern, or both. The expansion of the medullary cavity by resorption is also off-centered, in the same direction and sense as the drift of the cortex. Resorption thus occurs on the cavity edge under the fast-growing part of the cortex, and reconstructive endosteal deposits on the opposite edge (e.g., Figure 9.11C). In a bone with a strong curvature (e.g., ribs), the concave face of the shaft is frequently under extensive superficial resorption that comes in addition to the drift processes described above. In such cases, the perimedullary region may outcrop at the bone surface, a situation frequently observed in marine tetrapods showing osteosclerosis or pachyostosis (Figure 9.11D).

Differential Contribution of Proximal and Distal Epiphyses

Brief Overview at the Problem

Endochondral long bones increase their length at both their extremities, but observations suggest that the contribution to growth of the proximal "epiphysis" (i.e., its growth plate) may not be strictly equal to that of the distal epiphysis, a situation designated as differential growth (Wilsman et al. 1996). Of course, such a process is of great morphogenetic consequence insofar as, in combination with the growth in diameter occurring at both the periphery of growth plates (subperichondral cartilage accretion) and the cortical surface of diaphyseal and metaphyseal regions (subperiosteal accretion), it will be responsible for the actual shape of a bone at any stage of the growth process. Considered from an evolutionary perspective, a heritable modification touching one of these three parameters will result in a transformation of bone shape. The proper dynamics of each epiphysis is a key element conditioning not only the shape of a bone but also its overall size, as spectacularly shown, for example, by the bones of flippers in cetaceans (e.g., Felts and Spurrell 1965, 1966), compared to the forelimb skeleton of their terrestrial artiodactyl relatives and their closer ancestors such as *Pakicetus* (Muizon 2001; Uhen 2007) or *Indohyus* (Muizon 2009).

In most taxa, the sagittal and radial enlargement of the medullary cavity erases the traces of early bone deposits. Therefore, the total quantity of bone produced at each extremity of a bone during the life of an individual is not immediately accessible. Taxa in which such deposits are preserved throughout life are rare and most of them are extinct. Several approaches to cope with the problem of differential epiphyseal contributions have been proposed.

Chronology of Epiphyseal Fusion

The chronology of epiphyseal fusion is only partly related to the question of differential growth because it documents only the time interval during which growth plates retain the potential capability to contribute to bone growth, although at low rates, because of their anatomical and histological integrity. Of course, unfused epiphyses are not evidence, but nevertheless constitute a presumption of active osteogenic activity (Parfitt 2002). In this respect, considering the timing of local epiphyseal fusion is relevant to the problem of differential growth. In early studies, the chronology of epiphyseal fusion was merely based on naked-eye observation of bones prepared by maceration (Washburn 1946). The current technique now rests on 2D or 3D radiographic documents (e.g., Maisano 2002; Stern et al. 2015; see also Figure 9.11E). Most studies have dealt with mammals including, in addition to humans, various primates, artiodactyls and rodents (see Geiger et al. 2014 for comparative data). Studies on lizards are scarce and recent (Maisano 2002; Buffrénil et al. 2004; Frydlova et al. 2017).

Information yielded by these studies can be summarized in three main results: (1) In mammals as well as in lizards, epiphyseal fusion is not straightforwardly related to the notion of "skeletal maturity" and still less to that of sexual maturity. Although it generally occurs during the first half of life in most mammals, it can be delayed until advanced ontogenetic stages in some marsupials (Washburn 1946) or rodents (Dawson 1925). A similar condition also occurs in large varanids (Buffrénil et al. 2004; Frydlova et al. 2017). (2) In a single skeleton, differences in the chronology of proximal and distal epiphyseal fusion is not necessarily parallel and comparable among the bones, even if they represent similar skeletal elements. For example, the distal epiphysis of the humerus is the first to fuse in the skeleton of most mammals, whereas the same epiphysis in the femur, a functionally similar stylopod element, is among the last to fuse (Koch 1935). (3) The detailed chronological pattern of epiphyseal fusion in a single skeleton is not a matter of individual bones; rather, it is related to anatomical regions defined both by the topographical proximity and common functional involvement of the epiphyses of the bones that compose them. For example, in many mammalian taxa, the fusion of the distal humeral

VetBooks.ir

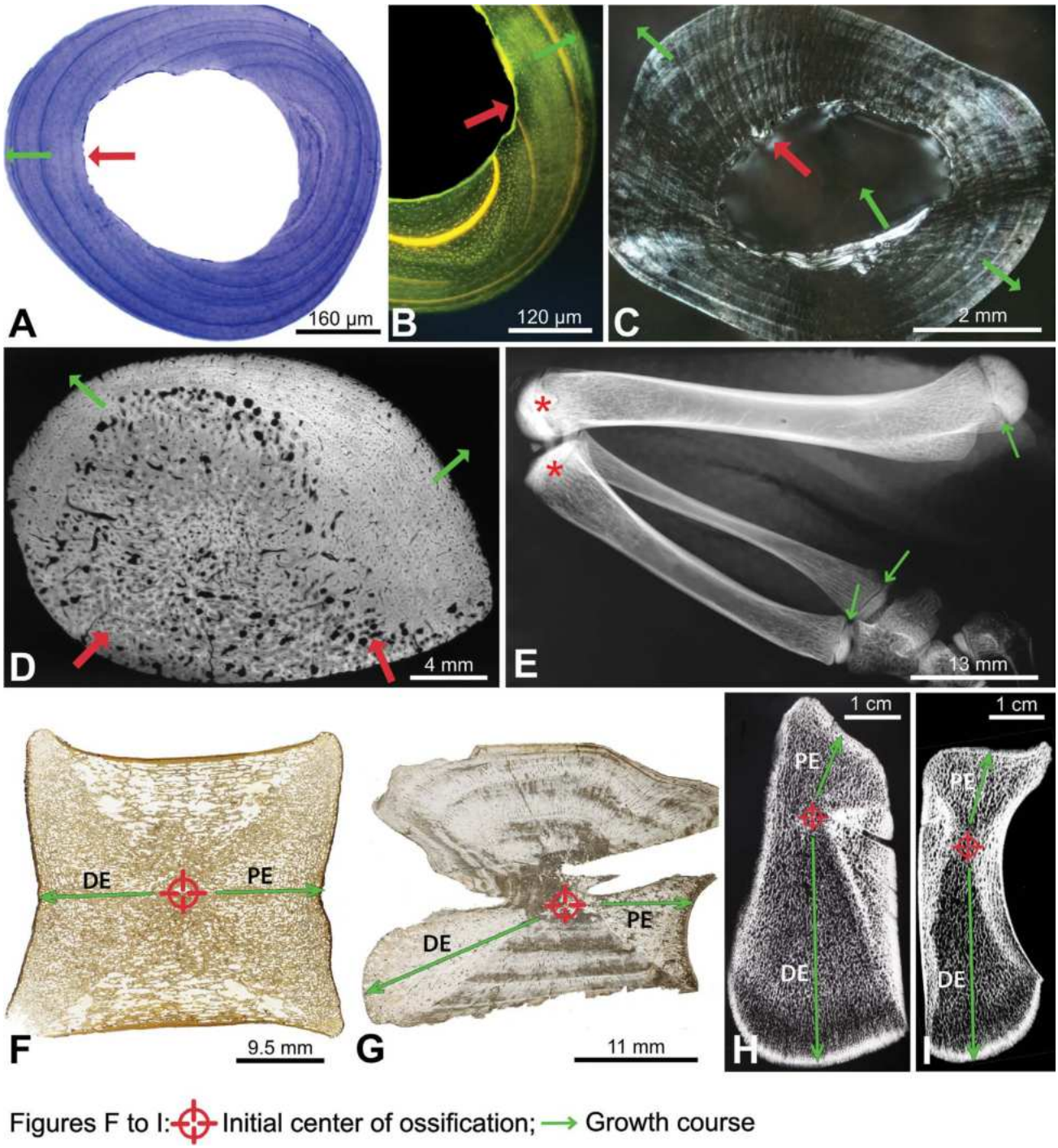


FIGURE 9.11 Off-centercentered growth and imbalanced epiphyseal contributions. A, Strong drift of diaphyseal growth in the femur of *Lacerta muralis*. Decalcified bone section stained with hematoxylin. The red arrow indicates resorption and the green arrow shows bone growth (here, by subperiosteal accretion). B, Partial view of the same phenomenon in the femur of *L. viridis*. Same symbols as in all other figures. *In vivo* fluorescent labeling makes the asymmetric resorption process clearer. C, Tibia of a Nile monitor, *V. niloticus*. Polarized light. D, Strong growth off-centering in the rib of a dugong. Resorption of the concave side of the bone brings the medullary core (compacted in this taxon) of the bone to the surface. X-ray proof of a ground section. E, Different timing of proximal and distal epiphyseal fusion in the rear leg of *Varanus pilbarensis*. X-ray proof. The green arrows indicate "open", still active growth plates and unfused epiphyses, while the red asterisks show "closed" (inactive) growth plates and fused epiphyses. F, Balanced contributions of proximal (PE) and distal (DE) epiphyses in the vertebral centrum of *Champsosaurus* sp., an Upper Paleocene choristodere (Archosauromorpha). The contribution ratio EP/DP is then *ca*. 0.96. G, Strongly imbalanced epiphyseal contributions in the vertebral centrum of the Late Cretaceous squamate *Pachyvaranus crassispondylus*. The ratio is *ca*. 0.48. H, Strongly imbalanced epiphyseal contributions in the radius (left) and ulna (right) of *Delphinus delphis*. The ratio for both these bones is ca. 0.41.

VetBooks.ir

epiphysis is approximately synchronous with the fusion of the proximal epiphyses of the ulna and radius (together they form the elbow region); similarly, the distal epiphysis of the femur fuses by the same time as the proximal epiphyses of the tibia and fibula in the knee region (Stevenson 1924; Koch 1935; see also Figure 9.11E).

The Quantitative Study of Epiphyseal Contribution to Growth

Since the early 20th century, differential growth has been assessed by measuring the distance (say, distance D_x) separating each growth plate from a precise benchmark, at a single growth stage or at several consecutive stages (radiographic follow-up). According to the method used in the early study by Digby (1916) and more recently (e.g., Lee 1968), the benchmark is an estimate of the position of the initial point from which the ossification of the former cartilaginous template began; this position is given by a projection of the axis of the nutrient canal(s) onto the sagittal axis of the bone (see also Payton 1934). In later experimental studies, the benchmark is a metallic implant inserted in the bone cortex and precisely located on X-ray proofs (e.g., Sarnat 1968; Juster and Plachot 1975). In both cases the proper effective contribution of each epiphysis to the total growth of the bone (*TL*) at a given stage of ontogeny is given by the ratio 100 D_x/TL (Figure 9.11F–H). Another method aims to quantify specifically the thickness of calcified cartilage formed per time unit, using fluorescent markers administered at known dates. As for the Mineral Accretion Rate (MAR) index (see Chapter 10) of bone cortices, this approach gives a proxy of the rate of cartilage growth and differentiation in the hypertrophic zone of the growth plate.

The results yielded by these approaches in humans (e.g., Digby 1916), rats (Juster and Plachot 1975; Wilsman et al. 2008), pigs (Payton 1932), cattle (Graham and Price 1981) and rabbits (Sissons 1953) show that the contribution indices of the epiphyses of a single bone can differ greatly. In the human humerus, for example, the proximal epiphysis can be four times more active than the distal one. In general, epiphyseal contributions are convergent among taxa and consistent with the chronology of epiphyseal fusion. In the forelimb of *Homo sapiens*, taken here as the example of a general trend, available data indicate that a high contribution to growth (up to 81%) characterizes the proximal epiphysis of the humerus (shoulder field) and the distal epiphyses of the radius (75%) and ulna (81%), both participating in the wrist field. Figure 9.11H shows a similar situation in the radius of the common dolphin, *Delphinus delphis*. Conversely, the elbow field in humans is characterized by low indices (19% for the distal epiphysis of the humerus, 25 and 19%, respectively, for the proximal epiphysis of the radius and ulna). As for epiphyseal fusion, a reverse pattern is observed in the hindlimb, with low indices for the proximal femur (hip field) and distal tibia and fibula (ankle field), but high indices for the knee field, with 79% for the distal femur and values of 57 and 60% for the proximal tibia and fibula, respectively.

Payton (1932) and later Wilsman et al. (2008) produced data based on measurements of instantaneous growth rates at both extremities of the bone, whereas the data from Digby (1916) represent the total (cumulative) contribution of each growth plate to growth, from embryo to adult. The convergence of the results from all these authors and with the studies on the chronology of epiphyseal fusion shows that the final contribution of proximal and distal epiphyses to the total growth of a long bone depends on both the rate of cartilage differentiation and the duration of epiphyseal functioning, among other possible factors (Wilsman et al. 2008).

Integral Preservation of Endochondral Bone Formations

Among tetrapods, all documented cases of an integral preservation of endosteoendochondral formations, which thus reveal the "production" of each epiphysis, are encountered only in tetrapods secondarily adapted to aquatic life. This condition reflects an inhibition of perimedullary resorption and the lack of a differentiated medullary cavity. It principally concerns limb long bones, ribs and, to a lesser extent, vertebrae. In recent forms (Figure 9.11H), it is observed in the long bones of some marine turtles (Rhodin 1985), the flippers of cetaceans (Felts and Spurrell 1965, 1966) and the humerus of sirenians (Kaiser 1974). In extinct taxa, it is reported in numerous marine clades, including choristoderes (Buffrénil et al. 1990), Cenomanian marine lizards and snakes (Buffrénil et al. 2008; Houssaye et al. 2008), ichthyosaurs (Buffrénil and Mazin 1990), and some mosasaurs (Houssaye 2008). Sagittal sections of bones reveal the precise position of the growth center and the quantity of bone produced by each growth plate. Obvious differences in the growth "strategy" of similar bones in different lineages then become obvious. For example, in the short cylindrical centrum of the choristodere *Champsosaurus* sp. (Figure 9.11F), the contribution of the distal growth plate is just 105.3% of that of the proximal growth plate (from Buffrénil et al. 1990); conversely, this ratio is much higher in the elongated centra of the marine lepidosaurs *Paleophis maghrebianus* (140%; from Houssaye et al. 2013), *Pachyvaranus crassispondylus* (167%; from Buffrénil et al. 1990; see also Figure 9.11G) and H*aasiasaurus gittelmani* (240%; from Houssaye 2008).

Interpreting Growth Patterns in the Cephalic Region

An Essential but Complex Issue

Most of the apomorphic traits that diagnose vertebrate taxa are located in the cephalic region; it therefore exhibits the greatest morphological diversity, and its growth pattern can provide important phylogenetic information (see, for example, the studies on cranial growth in fur seals by Tarnawski et al. 2015 and in crocodilians by Piras et al. 2010). In comparative and evolutionary perspectives, reconstructing the growth pattern of skull bones and skull regions (i.e., the braincase, the face or the mandible) is an essential prerequisite for documenting the immediate (or terminal) mechanisms that contribute to morphological diversification within vertebrate lineages (genetic

VetBooks.ir

divergence is the initial cause). However, this operation proves to be delicate because it involves bones with irregular shapes, or composite skeletal regions including closely imbricated elements that may themselves have complex individual morphology and growth pattern (e.g., Zelditch et al. 1992, 1993). Moreover, local growth processes vary during ontogeny and are influenced by the functional activity of the skeletal territory considered (e.g., Moore 1965; Herring 1993; Helm and German 1996), two circumstances that make their deciphering still more complicated (Herring and Ochareon 2005), especially in extinct taxa.

The short overview given here briefly considers the two main methodological approaches, i.e., cephalometry and histology, applied to the study of mandibular and face growth in mammals, along with some of the results that they yielded. Attention will be paid principally to postnatal growth. At this ontogenetic stage, the basic shape of skeletal elements is settled; the problem for an organism is then to increase the size of bones, or integrated skeletal regions, while maintaining their specific morphological traits. Up to now, this question has been principally considered in humans and some other monkeys, along with a few laboratory animals. Studies of nonmammalian vertebrates remain scanty, at least for the histological aspect of the question. Several specific reviews have been published, among which a fundamental, necessary reference is the handbook by D. H. Enlow (Enlow 1975).

Cephalometry

This approach aims to quantify the ontogenetic transformation of either the size of skull bones or, more frequently, the distance between characteristic landmarks. Three main methodological options are used to this purpose.

External descriptive cephalometry (also called craniometry) relies on the measurement of distances between external landmarks on the surface of bones in growth series of whole skulls from anatomical collections (review in Sirianni and Swindler 1979 for primates). A derived version of this classical approach is based on geometric morphometry analyses applied to surface-scanning documents (e.g., Martinez-Maza et al. 2016). This technique allows a clear separation of size from shape and the handling of a dense series of landmarks. External cephalometry is currently used, alone or with other approaches (X-ray imaging or histology), in comparative anatomy, and has been applied to a great variety of vertebrates (see Porto et al. 2013 for mammals). It is also used in paleontology, provided that a growth series of well-preserved fossils is available for a given species. Of course, in extant and extinct forms, the recourse to growth series must face the basic problem of interindividual variability in facial and mandibular shapes.

Radiographic cephalometry (often called *roentgenographic cephalometry*) is the most commonly used method for the morphometric analysis of braincase, face and mandible growth during postnatal and prenatal ontogeny. In its descriptive version, this method is based on X-ray proofs taken *in vivo* at regular time intervals in growing specimens. It may also be applied to specimens in collections. Originally based on 2D X-ray proofs, roentgenographic cephalometry is now performed on 3D tomographic documents (e.g., Hildebolt et al. 1990; Barbeito-Andrés et al. 2012). The geometric center of the *sella turcica,* a conspicuous depression of the sphenoid dorsal surface that houses the pituitary gland and marks the geometric center of the skull, is used as a reference point, from which are projected most measurements to the facial and mandibular landmarks (e.g., Sirianni and Newell-Morris 1980; Ghafari et al. 1987; Begnoni et al. 2018). The most currently used landmarks (they vary to some extent with the questions considered by each author) are distributed in several spots on each facial bone and mandible (e.g., McNamara et al. 1976; Helm and German 1996; Zumpano 2002). Moreover, a qualitative assessment of sutural contribution to growth is accessible (Scott 1956). Recent trends in the treatment of radiographic cephalometric data involve, in addition to classical statistical analyses, finite-element scaling analyses (FESA) for building 2D or 3D models of skull and facial growth (e.g., Takeshita et al. 2001; Zumpano 2002).

Experimental radiographic craniometry is based on the implantation *in vivo* of metallic (tantalum) pins in both a reference spot (in primates, the deep surface of the sphenoid at the level of the *sella turcica*) and various other peripheral landmarks (e.g., Björk 1968; Sarnat 1968; McNamara et al. 1976), including the symmetric edges of sutures (Sarnat 1981, 1986b). The other aspects of this method are like those of descriptive radiographic cephalometry. Precise quantitative measurements can thus be obtained, through individual radiographic follow-up of cranial growth. This technique allows a quantitative measurement of the osteogenic activity of sutures, a key element for assessing the global drift of compound facial regions.

The general results of descriptive cephalometry are consistent with those of experimental methods (comparative data in Sarnat 1986a). They indicate the gross trends and growth directions of cranial regions during postnatal development. The neurocranial region, including the various bones of the braincase situated above an axis uniting the anterior margin of the foramen magnum with the dorsal-most point of the orbits, via the center of the *sella turcica*, grows in a backward and upward direction, whereas the facial territory, including the maxillae, premaxillae and nasals, below this axis, grows in a forward and downward direction. This situation was described in primates (McNamara et al. 1976; Martinez-Maza 2016) and rodents (Asling and Frank 1963; Engström et al. 1982; Rizos et al. 2001). On each side of the skull, the general common movement of facial bones is due to the osteogenic activity of the sutures between the maxillae and the frontal, zygomatic, ethmoid and palatine bones and to the accretion of bone on the maxillary tuberosity (Enlow and Bang 1965; Enlow 1975). Similarly, the mandible follows a forward movement, in pace with that of the face, under the impetus of strong accretion activity, directed backward and upward, along the caudal edge of the ramus, coronoid process and articular condyle (Enlow and Harris 1964; Sirianni et al. 1982; see also Bang and Enlow 1967; Sarnat 1968, 1986a for nonprimate mammals). Most of the active mandibular growth is thus posterior to the tooth row; the apparent forward movement of the mandibular corpus and the tooth row that it bears is then a passive consequence of the caudad growth of the ramus and condyle (Figure 9.12).

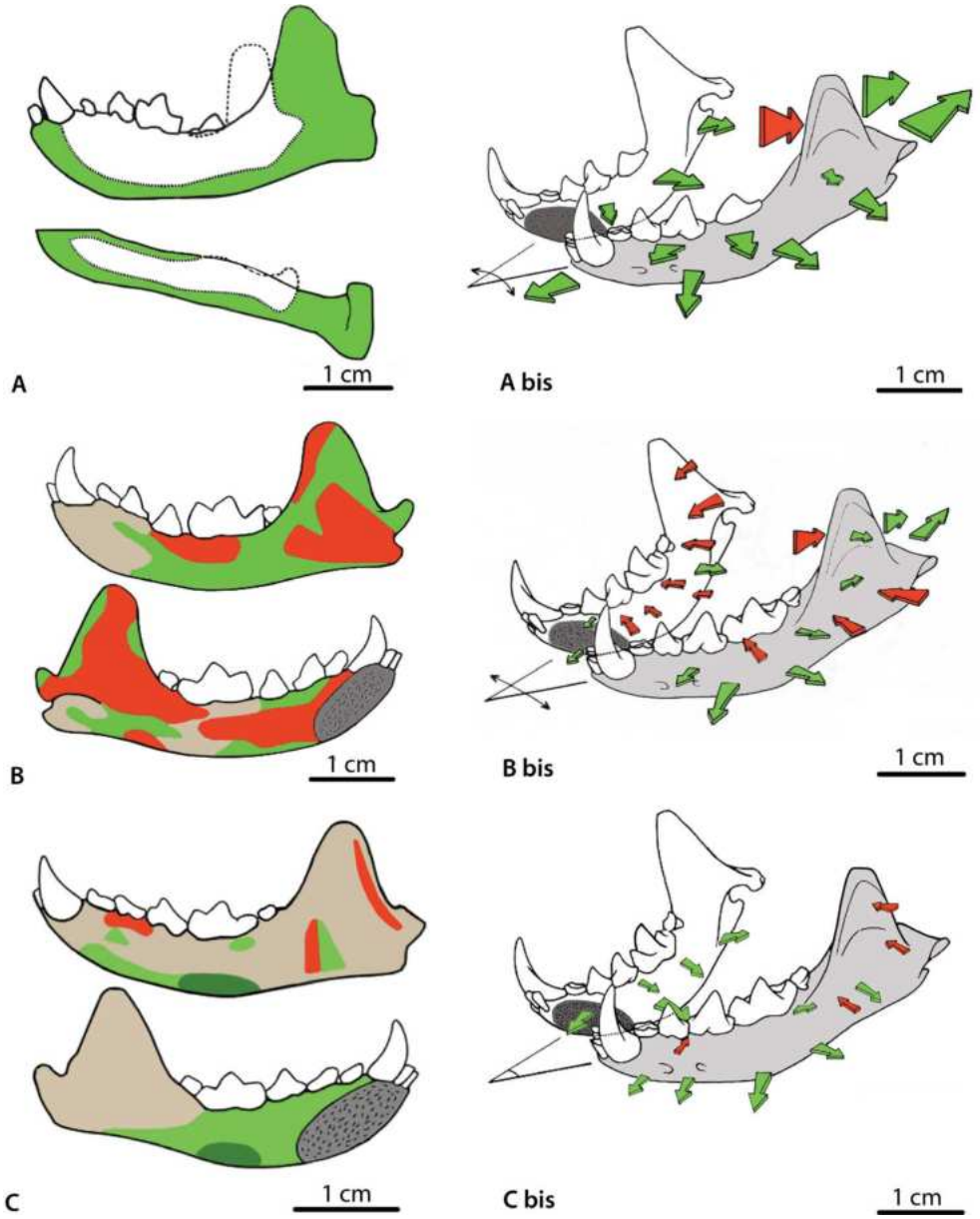


FIGURE 9.12 Osteogenic events in the growth of the mink (*Neovison vison*) mandible. Reconstructions (from Buffrénil and Pascal 1984) were based on *in vivo* labeling of skeletal growth with calcein and alizarin. A and Abis, Actively growing early juvenile. The sketch in (A) shows lateral (above) and occlusal views of the dentary. The sketch in (Abis) shows an anterolateral view of the mandible in which the left ramus (in gray) is in labial view and the right ramus (white) is in lingual view. Green areas and green arrows: accretion in progress. Red areas and red arrows: resorption in progress (these symbols have the same meaning in all parts of this figure). B and Bbis, Late juvenile. C and Cbis, Young, fully developed adult. The dark green area indicates a zone where accretion on mandibular surface is long-lasting during adulthood. In B and C, the upper sketch shows the bone in labial view and the lower sketch, in lingual view.

Modeling of Facial Bone: The Histologic Mechanisms

Radiographic follow-up of growth with implants can reveal the gross shape modifications resulting from osteogenic processes, but it gives no definite information about the nature of these processes, except sutural contributions. A relevant complement to this approach is the study of the *bone modeling pattern*, or *BModPat*, an expression used by Martinez-Maza et al. (2016) to designate the apposition, stagnation or resorption activities that occur on the surface of growing mandibular and cranial bones (see also Martinez-Maza 2013). The non-destructive method proposed by these authors to identify the functional status of bone surfaces relies on microscopic observations in reflected light. Accretion surfaces are characterized by "mineralized collagen fiber bundles", whereas resorption surfaces are riddled by small randomly distributed depressions, the Howship's lacunae. Of course, this method is limited to outer bone surfaces accessible to observation.

VetBooks.ir

The classical histological procedures for identifying the functional status of bone surfaces involve serial cross sections performed as either decalcified and colored sections, or ground sections of dry (nondecalcified) bone. Classical microscopic techniques in transmitted natural or polarized light are then applied to these preparations. In his classic studies, Enlow (1963, 1975; Enlow and Harris 1964; Enlow and Bang 1965) considered the basic occurrence, in superficial bone layers, of either periosteal bone deposits (defined by several histological features detailed and illustrated in Enlow 1975) indicative of active outward or forward-directed (centrifugal) growth, or endosteal bone formations reflecting the superficial outcrop of inner bone layers due to resorption. Bone accretion then occurs on the deep, endosteal surface or bone cortices and proceeds in a direction (inward, centripetal direction) opposite to that of periosteal layers.

In extant taxa, the most efficient procedure to investigate local accretion or resorption activities is the *in vivo* multiple labeling of bone growth (two injections at least) by fluorescent markers, as explained in Chapter 10. This technique gives unambiguous results, not only on the nature of local osteogenic processes (including growth arrest) but also on their absolute rate. Studies based on this approach have been conducted in many taxa, including humans (Baer 1954), macaques (Craven 1956), rats (Massler and Schour 1951; Cleall et al. 1969), rabbits (Isotupa et al. 1965) and carnivorans (Buffrénil and Pascal 1984). An example of the use of this approach for the study of the mink mandibular growth is developed in Figure 9.12. In primates (see Enlow and Bang 1965; Martinez-Maza et al. 2016), the mapping of apposition and resorption fields shows complex forward (periosteal) and backward (endosteal) local movements on the surface of the face that come in complement, or in addition, to the general forward-downward growth of this region. For example, on each side of the face, the anterior region of the zygomatic arch and the neighboring lateral sector of the maxillary progress backward under extensive superficial resorption, while the lateral region of the zygomatic arch and the medial maxillary surface proceed outward under active subperiosteal accretion. Mandibular growth in mammals also involves a similar patchy distribution of appositional (e.g., on the rear edge of the ramus or the ventral surface of the mandibular body) and resorptive (e.g., lateral and anterior surfaces of the ramus) fields. These minute adjustments of local growth trends are responses to the need to reconcile the maintenance of the shape of individual bones with the overall expansion of a complex skeletal region. They are observed in all vertebrate taxa and show great consistency with the gross morphology of the bones.

Because methods for the study of local modeling patterns of the skeleton rely on relatively simple histological clues, they are applicable without restriction to fossils, provided that well-preserved material conducive to sectioning is available. Relatively few studies have been conducted so far on extinct forms; among them, one of the most characteristic deals with the mandible of the cynodont *Tritylodon* (Jasinoski and Chinsamy 2012). A considerable and nearly inexhaustible reservoir of original studies are open to paleontologists and comparative anatomists.

REFERENCES

Abu, E. O., et al. 2000. The localization of the functional glucocorticoid receptor α in human bone. *J. Clin. Endocr. Metab.* 85: 883–889.

Abzhanov, A., et al. 2007. Regulation of skeletogenic differentiation in cranial dermal bone. *Development* 134: 3133–3144.

Allain, T. J. and A. M. McGregor. 1993. Thyroid hormones and bone. *J. Endocr.* 139: 9–18.

Allen, D. B. 1996. Growth suppression by glucocorticoid therapy. *Endocrinol. Metab. Clin. N. Am.* 25: 699–716.

Allen, M. R. and D. B. Burr. 2014. Bone modeling and remodeling. In *Basic and applied bone biology*, eds. Burr, D. B. and M. R. Allen, 75–89. Amsterdam: Elsevier-Academic Press.

Almeida, M., et al. 2017. Estrogens and androgens in skeletal physiology and pathophysiology. *Physiol. Rev.* 97: 135–187.

Amprino, R. 1947. La structure du tissue osseux envisagé comme l'expressions de differences dans la vitesse de l'accroissement. *Arch. Biol.* 58: 317–330.

Arnaldi, G., et al. 2003. Diagnosis and complications of Cushing's syndrome: a consensus statement. *J. Clin. Endocr. Metab.* 88: 5593–5602.

Asling, C. W. and H. R. Frank. 1963. Roentgen cephalometric studies on skull development in the rat. I. Normal and hypophysectomized females. *Am. J. Physiol.* 21: 527–537.

Ávila-Mendoza, et al. 2014. Characterization of pituitary growth hormone and its receptor in the green iguana (*Iguana iguana*). *Gen. Comp. Endocr.* 203: 281–295.

Bailleul, A., et al. 2016. Chondroid bone in dinosaur embryos and nestlings (Ornithischia : Hadrosauridae): insights into the growth of the skull and the evolution of skeletal tissues. *C. R. Palevol* 15: 49–64.

Bang, S. and D. H. Enlow. 1967. The postnatal growth of the rabbit mandible. *Arch. Oral Biol.* 12: 993–998.

Barbeito-Andrés, J., et al. 2012. Measurement error of 3D cranial landmarks of an ontogenetic sample using computed tomography. *J. Oral Biol. Craniofac. Res.* 2: 77–82.

Barnard, J. C., et al. 2005. Thyroid hormones regulate fibroblast growth factor receptor signaling during chondrogenesis. *Endocrinol.* 146: 5568–5580.

Barnett, P. 2003. Somatostatin and somatostatin receptor physiology. *Endocrine* 20: 255–264.

Bassett, J. H. D. and G. R. Williams. 2008. Critical role of the hypothalamic-pituitary-thyroid axis in bone. *Bone* 43: 418–426.

Basset, J. H. D and G. R. Williams. 2016. Role of thyroid hormones in skeletal development and bone maintenance. *Endocr. Rev.* 37: 135–187.

Bayley, N. and S. R. Pinneau. 1952. Tables for predicting adult height from skeletal age: revised for use with the Greulich-Pyle hand standards. *J. Pediatr.* 40: 423–441.

Beamer, B., et al. 2010. Vascular endothelial growth factor: an essential component of angiogenesis and fracture healing. *HSSJ* 6: 85–94.

Baer, M. J. 1954. Patterns of growth of the skull as revealed by vital staining. *Hum. Biol.* 26: 80–126.

Begnoni, G., et al. 2018. Craniofacial structures' development in prenatal period: an MRI study. *Orthod. Craniofac. Res.* 21: 96–103.

Bellairs, A. 1969. *The life of reptiles*. London: Weidenfeld and Nicolson.

Bellamy, D. and R. A. Leonard. 1965. Effect of cortisol on the growth of chicks. *Gen. Comp. Endocrinol.* 5: 402–410.

Bellido, T. and K. M. H. Hill Gallant. 2014. Hormonal effects on bone cells. In *Basic and applied bone biology*, ed. D. B. Burr, and M. R. Allen, 299–314. London: Academic Press.

Bernard, G. W. and D. C. Pease. 1969. An electron microscopic study of initial intramembranous osteogenesis. *Am. J. Anat.* 125: 271–290.

Björk, A. 1968. The use of metallic implants in the study of facial growth in children: method and applications. *Am. J. Phys. Anthrop.* 29: 243–254.

Bord, S., et al. 2001. Estrogen receptors α and β are differentially expressed in developing human bone. *J. Clin. Endocrinol. Metab.* 86: 2309–2314.

Brandi, M.-L. and P. Collin-Osdoby. 2006. Vascular Biology and the skeleton. *J. Bone Miner. Res.* 21: 183–191.

Buffrénil, V. de, et al. 1987. Caractères structuraux et mode de croissance du fémur d'*Omphalosaurus nisseri*, ichthyosaurien du Trias moyen du Spitsberg. *Ann. Paléont. (Vert.)* 73: 195–216.

Buffrénil, V. de, et al. 1990. L'histologie osseuse des Champsosauridés: données descriptives et interprétation fonctionnelle. *Ann. Paléont. (Vert.)* 76: 255–275.

Buffrénil, V. de, et al. 2004. Comparative data on epiphyseal development in the family Varanidae. *J. Herpetol.* 39: 328–335.

Buffrénil, V. de, et al. 2008. Specialization of bone structure in *Pachyvaranus crassispondylus* Arambourg, 1952, an aquatic squamate from the late Cretaceous of the southern Tethyan margin. *Lethaia*, 41: 59–69.

Buffrénil V de, et al. 2015. Differentiation and growth of bone ornamentation in vertebrates: a comparative histological study among the Crocodylomorpha. *J. Morphol.* 276: 425–445.

Buffrénil, V. de and J.-M. Mazin. 1990. Bone histology of the ichthyosaurs: comparative data and functional interpretation. *Paleobiology* 16: 435–476.

Buffrénil, V. de and M. Pascal. 1984. Croissance et morphogenèse postnatales de la mandibule du vison (*Mustela vison*): données sur la dynamique et l'interprétation fonctionnelle des dépôts osseux mandibulaires. *Can. J. Zool.* 62: 2026–2037.

Caestecker, M. 2004. The transforming growth factor-β. *Cytokine Growth Factor Rev.* 15: 1–11.

Canalis, E., et al. 2003. Bone morphogenetic proteins, their antagonists and the skeleton. *Endocr. Rev.* 24: 218–235.

Carlevaro, M. F., et al. 2000. Vascular endothelial growth factor (VEGF) in cartilage neovascularization and chondrocyte differentiation: auto-paracrine role during endochondral bone formation. *J. Cell. Sci.* 113: 59–69.

Chabreck, R. H. and T. Joanen. 1979. Growth rates of American alligators in Louisiana. *Herpetologica* 35: 51–57.

Cheng, S.-Y., et al. 2010. Molecular aspects of thyroid hormone action. *Endocr. Rev.* 31: 139–170.

Ciresi, A. and C. Giordano. 2017. Vitamin D across growth hormone (GH) disorders: from GH deficiency o GH excess. *Growth Horm. IGF Res.* 33: 35–42.

Cleall, J. F., et al. 1969. Normal craniofacial skeletal growth in the rat. *Am. J. Phys. Anthrop.* 29: 225–242.

Clemens, T. L. and S. D. Chernausek. 2004. Genetic strategies for elucidating insulin-like growth factor action in bone. *Growth Horm. IGF Res.* 14: 195–199.

Compston, J. E. 2001. Sex steroids and bone. *Physiol. Rev.* 81: 419–447.

Congdon, J. D., et al. 2013. Indeterminate growth in long-lived freshwater turtles as a component of individual fitness. *Evol. Ecol.* 27: 445–459.

Coss, D., et al. 2000. Effects of prolactin on osteoblast alkaline phosphatase and bone formation in the developing rat. *Am. J. Physiol. Endocrinol. Metab.* 279: E1216–E1225.

Craven, A. H. and M. Holland. 1956. Growth in width of the head of the macaca rhesus monkey as revealed by vital staining. *Am. J. Orthodont.* 42: 341–362.

Cuttler, L. 1996. The regulation of growth hormone secretion. *Endocr. Metab. Clin. North Am.* 25: 541–571.

David, L., et al. 2009. Emerging role of bone morphogenetic proteins in angiogenesis. *Cytokine Growth Fact. Rev.* 20: 203–212.

Day, T. F., et al. 2005. Wnt/β-Catenin signaling in mesenchymal progenitors controls osteoblast and chondrocyte differentiation during vertebrate skeletogenesis. *Dev. Cell* 8: 739–750.

D'Ercole, A. J. 1996. Insulin-like growth factors and their receptors in growth. *Endocr. Metab. Clin. North Am.* 25: 573–590

De Sanctis, V., et al. 2014. Hand X-Ray in pediatric endocrinology: skeletal age assessment and beyond. *Indian J. Endocr. Metab.* 18(suppl. S1): 63–71.

Digby, K. H. 1916. The measurement of diaphyseal growth in proximal and distal directions. *J. Anat. Physiol.* 50: 187–188.

Di Jeso, B. and P. Arvan. 2016. Thyroglobulin from molecular and cellular biology top clinical endocrinology. *Endocr. Rev.* 37: 2–36.

Ducornet, B., et al. 2005. Contrôle hypothalamique des sécrétions hormonales antéhypophysaires. *EMC-Endocrinol.* 2: 209–230.

Eerden, B. C. J. van der, et al. 2003. Systemic and local regulation of the growth plate. *Endocr. Rev.* 24: 782–801.

Elf, P. K. 2003. Yolk steroid hormones and sex determination in reptiles with TSD. *Gen. Comp. Endocrinol.* 132: 349–355.

Engström, C., et al. 1982. Craniofacial morphology and growth in the rat. Cephalometric analysis of the effects of a low calcium and vitamin D-deficient diet. *J. Anat.* 134: 299–314.

Enlow, D. H. 1963. *Principles of bone remodeling.* Springfield (Illimois, USA): Charles C. Thomas.

Enlow, D. H. 1975. *Handbook of facial growth.* Philadelphia: W.B. Saunders Company.

Enlow, D. H. and S. Bang. 1965. Growth and remodeling of the human maxilla. *Am. J. Orthodont.* 51: 446–464.

Enlow, D. H. and D. B. Harris. 1964. A study of the postnatal growth of the human mandible. *Am. J. Orthodont.* 50: 25–49.

Erickson, G. M. 2014. On dinosaur growth. *Annu. Rev. Earth Planet. Sci.* 42: 675–697.

Erickson, G. M. and C. A. Brochu. 1999. How the "terror crocodile" grew so big? *Nature* 398: 205–206.

Fan, Q. R. and W. A. Hendrickson. 2005. Structure of human follicle-stimulating hormone in complex with its receptor. *Nature* 433: 269–277.

Faugeron-Ruel, I. and S. Christin-Maitre. 2005. Mutations des récepteurs des gonadotrophines. *Med. Reprod.* 7: 91–99.

Fawcett, D. W. and R. P. Jensh. 1997. *Bloom and Fawcett: concise histology.* London: Chapman and Hall.

Fekete, C. and R. M. Lechan. 2014. Central regulation of hypothalamic-pituitary-thyroid axis under physiological and pathophysiological conditions. *Endocr. Rev.* 35: 159–194.

VetBooks.ir

Felts, W. and F. A. Spurrell. 1965. Structural orientation and density of cetacean humeri. *Am J Anat* 116: 171–203.

Felts, W. and F. A. Spurrell. 1966. Some structural and developmental characteristics of cetacean (Odontocete) radii. A study of adaptive osteogenesis. *Am. J. Anat.* 118: 103–134.

Ferretti, M., et al. 2002. Static and dynamic osteogenesis: two different types of bone formation. *Anat. Embryol.* 206: 21–29.

Forbes, B. E. 2016. Two years in IGF research. *Growth Horm. IGF Res.* 216: 70–74.

Forrest, D., et al. 1990. Contrasting developmental and tissue-specific expression of α and β thyroid hormone receptor genes. *EMBO J.* 9: 1519–1528.

Francillon-Vieillot, et al. 1990. Microstructure and mineralization of vertebrate skeletal tissues. In *Skeletal biomineralization: patterns, processes and evolutionary trends*, vol. 1, ed. Carter, J. G., 471–530. New York: Van Nostrand Reinhold.

Frydlova, P., et al. 2017. Patterns of growth in monitor lizards (Varanidae) as revealed by computed tomography of femoral growth plates. *Zoomorphology* 136: 95–106.

Garcia Gil, O., et al. 2016. Investigating histomorphological variations in human cranial bones through ontogeny. *C. R. Palevol.* 15: 527–535.

Gaylinn, B. D. 1999. Molecular and cell biology of the growth hormone-releasing hormone receptor. *Growth Horm. IGF Res.* 9: 37–44.

Geiger, M., et al. 2014. Heterochrony and post-natal growth in mammals – an examination of growth plates in limbs. *J. Evol. Biol.* 27: 98–115.

Gereben, G., et al. 2008. Cellular and molecular basis of deiodinase-regulated thyroid hormone signaling. *Endocr. Rev.* 29: 898–938.

Ghafari, J., et al. 1987. Cephalometric superimposition of the cranial base: a review and comparison of four methods. *Am. J. Orthod. Dentofac. Orthop.* 91: 403–413.

Giustina, A., et al. 2008. Growth hormone, insulin-like growth factors, and the skeleton. *Endocr. Rev.* 29: 535–559.

Gogakos A. I., et al. 2010. Thyroid and bone. *Arch. Biochem. Biophys.* 503: 1229–136.

Goret-Nicaise, M. and A. Dhem. 1982. Presence of chondroid tissue in the symphyseal region of the growing human mandible. *Cells Tiss. Org.* 113: 189–195.

Gouveia, C. H. A., et al. 2018. Thyroid hormone and skeletal development. *Vitam. Horm.* 106: 383–472.

Graf, D., et al. 2016. Common mechanisms in development and disease: BMP signaling in craniofacial development. *Cytokine Growth Fact. Rev.* 27: 129–139.

Graham, N. C. and M. A. Price. 1981. A technique for measuring linear bone growth during short time intervals in cattle. *Can. J. Zool.* 61: 1049–1053.

Gramapurohit, N. P., et al. 2004. Growth, sexual maturation and body size dimorphism in the Indian bullfrog, *Hoplobatrachus tigerinus* (Daud.). *Herpetologica* 60: 414–419.

Gray, H. 1918. *Anatomy of the human body*, 20th edition. Philadelphia: Lea & Febiger.

Habib, K. E., et al. 2001. Neuroendocrinology of stress. *Endocr. Metab. Clin. North Am.* 30: 695–727.

Haines, R. W. 1938. The primitive form of epiphyses in the long bones of tetrapods. *J Anat.*72: 323–343.

Hall, B. K. 1980. Tissue interactions and the initiation of osteogenesis and chondrogenesis in the neural crest-derived mandibular skeleton of the embryonic mouse as seen in isolated murine tissues and in recombinations of murine and avian tissues. *J. Embryol. Exp. Morphol.* 58: 251–264.

Hall, B. K. 2005. *Bones and cartilages. Developmental and evolutionary skeletal biology.* Amsterdam: Elsevier-Academic Press.

Hartmann, K., et al. 2016. Molecular actions of glucocorticoids in cartilage and bone during health, disease, and steroid therapy. *Physiol. Rev.* 96: 409–447.

Harvey, S. 2010. Extrapituitary growth hormone. *Endocrine* 38: 335–359.

Harvey, S. 2013. Growth hormone and growth? *Gen. Comp. Endocr.* 190: 3–9.

Harvey, S. and K. L. Hull. 1997. Growth hormone: a paracrine or autocrine? *Endocrine* 7: 267–279.

Harvey, S. C. and M.-L. Baudet. 2014 Extrapituitary growth hormone and growth? *Gen. Comp. Endocr.* 205: 55–61.

Harvey, S. C. et al. 1998. Growth hormone: a paracrine growth factor in embryonic development? *Comp. Biochem. Physiol. C Phramacol. Toxicol. Endocrinol.* 119: 305–315.

Helm, J. W. and R. Z. German. 1996. The epigenetic impact of weaning on craniofacial morphology during growth. *J. Exp. Zool.* 276: 243–253.

Henderson, J. H., et al. 2004. Sutural bone deposition rate and strain magnitude during cranial development. *Bone* 34: 271–280.

Herring, S. W. 1993. Formation of the vertebrate face: epigenetic and functional influences. *Amer. Zool.* 33: 472–483.

Herring, S. W. and P. Ochareon. 2005. Bone – special problems of the craniofacial region. *Orthod. Craniofac. Res.* 8: 174–182.

Hiepen, C., et al. 2016. Actions from head to toe: an update on bone/body morphogenetic proteins in health and disease. *Cytokine Growth Fact. Rev.* 27: 1–11.

Hildebolt, C. F. et al. 1990. Validation study of skull three-dimensional computerized tomography measurements. *Am. J. Phys. Anthrop.* 82: 283–294.

Ho, T.-V., et al. 2015. Integration of comprehensive 3D microCT and signaling analysis reveals differential regulatory mechanisms of craniofacial bone development. *Dev. Biol.* 400: 180–190.

Houssaye, A. 2008. A preliminary report on the evolution of the vertebral microanatomy within mosasauroids (Reptilia squamata). *Proc. Sec. Mosasaur Meeting, Fort Hays Studies* Spec. issue 3, 81–90. Fort Hays State University, Hays, Kansas.

Houssaye, A., et al. 2008. An analysis of vertebral "pachyostosis" in *Carentonosaurus mineaui* (Mosasauroidea, Squamata) from the Cenomanian (early Late Cretaceous) of France, with comments on its phylogenetic and functional significance. *J. Vert. Paleontol.* 28: 685–691.

Houssaye, A., et al. 2013. New highlights about the enigmatic marine snake *Palaeophis maghrebianus* (Palaeophiidae; Palaeophiinae) from the Ypresian (Lower Eocene) phosphates of Morocco. *Palaeontology* 56: 647–661.

Horner, J. R. and K. Padian.2004. Age and growth dynamics of *Tyrannosaurus rex*. *Proc. Biol. Sci.*271(1551): 1875–1880.

Hu, K. and B. R. Olsen. 2016. Osteoblast-derived VEGF regulates osteoblast differentiation and bone formation during bone repair. *J. Clin. Invest.* 126: 509–526.

Huang, B. K., et al. 2000. Insulin-like growth factor 1 production is essential for anabolic effects of thyroid hormone in osteoblasts. *J. Bone Miner. Res.* 15: 188–197.

Imai, Y., et al. 2013. Nuclear receptors in bone physiology and diseases. *Physiol. Rev.* 93: 481–523.

Iravani, M., et al. 2017. Regulation of bone growth via ligand-specific activation of estrogen receptor alpha. *J. Endocr.* 232: 403–410.

Isotupa, K., et al. 1965. Changing architecture of growing cranial bones at sutures as revealed by vital staining with alizarin red S in the rabbit. *Am. J. Phys. Anthropol.* 23: 19–22.

Jasinoski, S. C. and A. Chinsamy. 2012. Mandibular histology and growth of the non-mammaliaform cynodont *Tritylodon*. *J. Anat.* 220: 564–579.

Jiang, X., et al. 2002. Tissue origins and interactions in the mammalian skull vault. *Dev. Biol.* 241: 106–116.

Jilka, R. L., et al. 2008. Apoptosis of bone cells. In *Principles of bone biology*, third edition, eds. Bilezikian J. P., L. G. Raisz and T. J. Martin, Vol. 1, 237–261. Amsterdam: Elsevier-Academic Press.

Juster, M. and J.-J. Plachot. 1975. Sur la formation du squelette. IX. – Croissance d'un os long. Sur la dynamique de la croissance diaphysaire. *Bull. Assoc. Anat.* 59 (165): 443–455.

Kah, O., et al. 2007. GnRH and GNRH receptors in metazoa: a historical, comparative, and evolutive perspective. *Gen. Comp. Endocr.* 153: 346–364.

Kaiser, H. E. 1974. Morphology of the sirenian. A macroscopic X-ray atlas of the morphology of recent species. Basel: S. Kargel.

Kanasaki, H., et al. 2017. How is GnRH regulated in GnRH-producing neurons? Studies using GT1-7 cells as a GnRH-producing cell model. *Gen. Comp. Endocr.* 247: 138–142.

Karaplis, A. C. 2008. Embryonic development of bone and regulation of intramembranous and endochondral bone formation. In *Principles of bone biology*, third edition, eds. Bilezikian J. P., L. G. Raisz and T. J. Martin, Vol. 1, 53–84. Amsterdam: Elsevier-Academic Press.

Kawauchi, H. and S. A. Sower. 2006. The dawn and evolution of hormones in the adenohypophysis. *Endocrinology* 148: 3–14.

Kilbourne, B. M. and P. J. Makovicky. 2012. Postnatal long bone growth in terrestrial placental mammals: allometry, life history, and organismal traits. *J. Morphol.* 273: 1111–1126.

Koch, W. 1935. The age order of epiphyseal union in the skeleton of the European bison (*Bos bonasus* L.). *Anat. Rec.* 61: 371–376.

Kopchick, J. J., et al. 2002. Growth hormone receptor antagonists: discovery, development, and use in patients with acromegaly. *Endocr. Rev.* 23: 623–646.

Kream, B. E., et al. 2008. Clinical and basic aspects of glucocorticoid action in bone. In *Principles of bone biology*, third edition, eds. Bilezikian J. P., L. G. Raisz and T. J. Martin, Vol. 2, 955–981. Amsterdam: Academic Press.

Kronenberg, H. M. 2006. PTHrP and skeletal development. *Ann. N.Y. Acad. Sci.* 1068: 1–13.

Krstić, R. V. 1985. *General histology of the mammal*. Berlin: Springer Verlag.

Kusec, V., et al. 1998. Localization of estrogen receptor-α in human and rabbit skeletal tissues. *J. Clin. Endocr. Metab.* 83: 2421–2428.

Lacroix, P. 1945. Remarques sur le mécanisme de l'allongement des os. *Arch. Biol.* 56: 185–197.

Lacroix, P. 1949. *L'organisation des os*. Paris: Masson et Cie.

Lacroix, M.-C., et al. 2002. Placental growth hormones. *Endocrine* 19: 73–79.

Lane, N. E. and B. Lukert. 1998. The science and therapy of glucocorticoid-induced bone loss. *Endocrinol. Metab. Clin. N. Am.* 27: 465–483.

Lee, M. M. C. 1968. Natural markers in bone growth. *Am. J. Phys. Anthropol.* 29: 295–310.

Lengelé, B. et al. 1996. Chondroid tissue in the early facial morphogenesis of the chick embryo. *Anat. Embryol.* 193: 505–513.

Londraville, R. L., et al. 2014. Comparative endocrinology of leptin: assessing function in a phylogenetic context. *Gen. Comp. Endocr.* 203: 146–157.

Long, F. and D. M. Ornitz. 2013. Development of the endochondral skeleton. *Cold Spring Harb. Perspect. Biol.* 5: a008334.

Louchart, A., et al. 2013. Structure and growth pattern of pseudoteeth in *Pelagornis mauretanicus* (Odontopterygiformes: Pelagornithidae). *PLoS One* 8(11): 1–12.

Louchart, A., et al. 2018. Bone pseudoteeth of extinct pelagic birds (Aves, Odontopterygiformes) formed through a response of bone cells to tooth-specific epithelial signals under unique conditions. *Sci. Rep.* 8: 1–9.

McNamara, J. A. Jr., et al. 1976. Growth of the maxillary complex in the rhesus monkey (*Macaca mulatta*). *Am. J. Phys. Anthropol.* 44: 15–26.

Maes, C., et al. 2010. Osteoblast precursors, but not mature osteoblasts, move into developing and fractured bones along with invading blood vessels. *Dev. Cell* 19: 329–344.

Maes, C., et al. 2012. Hypoxia-driven pathways in bone development, regeneration and disease. *Nat. Rev. Rheumatol.* 8: 358–566.

Maisano, J. A. 2002. Terminal fusions of skeletal elements as indicators of maturity in squamates. *J. Vert. Paleontol.* 22: 268–275.

Malerba, M., et al. 2005. Growth hormone response to growth hormone releasing hormone is reduced in adult asthmatic patients receiving long-term inhaled corticosteroid treatment. *Chest J.* 127: 515–521.

Marotti, G. 2010. Static and dynamic osteogenesis. *Ital. J. Anat. Embryol.* 115: 123–126.

Marotti, G., et al. 1999. Static and dynamic bone formation and the mechanism of collagen fiber orientation. *Bone* 25: 156.

Martinez-Maza, C., et al. 2013. Postnatal changes in the growth dynamics of the human face revealed from bone modeling patterns. *J. Anat.* 223: 228–241.

Martinez-Maza, C., et al. 2016. Bone growth dynamics of the facial skeleton and mandible in *Gorilla gorilla* and *Pan troglodytes*. *Evol. Biol.* 43: 60–80.

Massagué, J. 2012. TGF-β signaling in context. *Nat. Rev. Mol. Cell Biol.* 13: 616–630.

Massler, M. and I. Schour. 1951. The growth pattern of the cranial vault in the albino rat as measured by vital staining with alizarine red "S". *Anat. Rec.* 83–101.

Miller, S. C., et al. 1983. Studies on the role of vitamin D in early skeletal development, mineralization, and growth in rats. *Calcif. Tissue Int.* 35: 455–460.

Miller, W. L. and N. L. Eberhardt. 1983. Structure and evolution of the growth hormone gene family. *Endocr. Rev.* 4: 97–130.

Minami, S., et al. 1998. Growth hormone inhibits its own secretion by acting on the hypothalamus through its receptors on neuropeptide Y neurons in the arcuate nucleus and somatostatin neurons in the periventricular nucleus. *Endocr. J.* 45(Suppl.): S19–S26.

Moore, W. J. 1965. Masticatory function and skull growth. *J. Zool.* 146 123–131.

Mundy, G. R., et al. 2001. Growth regulatory factors and bone. *Rev. Endocr. Metab. Dis.* 2: 105–115.

Muira, M., et al. 2002. Thyroid hormones promote chondrocyte differentiation in mouse ATDC5 cells and stimulate endochondral ossification in fetal mouse tibias through iodothyronine deiodinase in the growth plate. *J. Bone Miner. Res.* 17: 443–454.

Muizon, C. de. 2001. Walking with whales. *Nature* 413: 259–260.

Muizon, C. de. 2009. L'origine et l'histoire évolutive des cétacés. *C. R. Palevol.* 8: 295–309.

Nesan, D. and M. M. Vijayan. 2013. Role of glucocorticoid in developmental programming: evidence from zebrafish. *Gen. Comp. Endocrinol.* 181: 35–44.

Nesslinger, C. L. 1956. Ossification centers and skeletal development in the postnatal Virginia opossum. *J. Mammal.* 37: 282–394.

Ohlsson, C., et al. 2009. The role of liver-derived insulin-like growth factor-1. *Endocr. Rev.* 30: 494–535.

Omeyer, L. C. M., et al. 2018. Determinate or indeterminate growth? Revisiting the growth strategy of sea turtles. *Mar. Ecol. Prog. Ser.* 596: 199–211.

Ornitz, D. M. and N. Itoh. 2015. The fibroblast growth factor signaling pathway. *Dev. Biol.* 4: 215–266.

Parfitt, A. M. 2002. Misconceptions (1): Epiphyseal fusion causes cessation of growth. *Bone* 30: 337–339.

Patterson, R. and B. Brattstrom. 1972. Growth in captive *Gopherus agassizi*. *Herpetologica* 28: 169–171.

Payton, C. G. 1932. The growth in length of the long bones in the madder-fed pig. *J. Anat.* 66: 414–425.

Payton, C. G. 1934. The position of the nutrient foramen and the direction of the nutrient canal in the long bones of the madder-fed pig. *J. Anat.* 68: 500–510.

Percival, C. J. and J. Richtsmeier. 2013. Angiogenesis and intramembranous osteogenesis. *Dev. Dyn.* 242: 909–922.

Piras, P., et al. 2010. The *Gavialis-Tomistoma* debate: the contribution of skull ontogenetic allometry and growth trajectories to the study of crocodilian relationships. *Evol. Dev.* 12: 568–579.

Pogue, R. and K. Lyons. 2006. BMP signaling in the cartilage growth plate. *Curr. Top. Dev. Biol.* 76: 1–48. Doi: 10.1016/30070-2153(06)76001-X.

Porto, A., et al. 2013. Size variation, growth strategies, and the evolution of modularity in the mammalian skull. *Evolution* 67: 3305–3322.

Pozo, E. del, et al. 2014. Radiometrical, hormonal and biological correlates of skeletal growth in the female rat from birth to senescence. *Growth Horm. IGF Res.* 24: 83–88.

Prondvai, E., et al. 2014. Development-based revision of bone tissue classification: the importance of semantics for science. *Biol. J. Linn. Soc.* 112: 799–816.

Raisz, L. G., et al. 2008. Pathophysiology of osteoporosis. In *Principles of bone biology*, third edition, eds. Bilezikian J. P., L. G. Raisz and T. J. Martin, Vol. 2, 1635–1647. Amsterdam: Academic Press.

Rhodin, A. G. J. 1985. Comparative chondro-osseous development and growth of marine turtles. *Copeia* 1985(3): 752–771.

Rizos, M., et al. 2001. The quantitative and qualitative analysis of the craniofacial skeleton of mice lacking the iGF-1 gene. *Clin. Orthop. Res.* 4: 206–219.

Robson, H., et al. 2000. Thyroid hormone acts directly on growth plate chondrocytes to promote hypertrophic differentiation and inhibit clonal expansion and cell proliferation. *Endocrinology* 141: 3887–3897.

Robson, H., et al. 2002. Interactions between GH, IGF-1, Glucocorticoids, and thyroid hormones during skeletal growth. *Pediatr. Res.* 52: 137–147.

Root, A. W. and F. B. Diamond. 2000. Regulation and clinical assessment of growth hormone secretion. *Endocrine* 12: 137–145.

Rosen, C. J. and T. Niu. 2008. Insulin-like growth factors and the IGF-binding proteins: implications for bone biology. In *Principles of bone biology*, third edition, eds. Bilezikian J. P., L. G. Raisz and T. J. Martin, Vol. 2, 1069–1094. Amsterdam, Academic Press.

Rosenfeld, R. L. 1996. Essentials of growth diagnosis. *Endocrinol. Metab. Clin. N. Am.* 25: 743–758.

Roubos, E. W., et al. 2012. Leptin and the hypothalamo-pituitary-adrenal stress axis. *Gen. Comp. Endocrinol.* 177: 28–36.

Saez, J. M., et al. 1995. Le contrôle des fonctions différenciées des cellules de Leydig. *Médecine/Science* 11: 547–553.

Sarnat, B. G. 1968. Growth of bones as revealed by implant markers n animals. *Am. J. Phys. Anthropol.* 29: 255–286.

Sarnat, B. G. 1981. Sutural bone growth of the turtle *Chrysemys scripta* plastron: a serial radiographic study by means of radiopaque implants. *Growth* 45: 123–134

Sarnat, B. G. 1986a. Growth pattern of the mandible: some reflections. *Am. J. Orthod. Dentofac. Orthop.* 90: 221–233.

Sarnat, B. G. 1986b. Something of the nature of gross sutural growth. *Ann. Plastic Surg.* 17: 339–349.

Scott, J. H. 1956. Growth at the facial sutures. *Am. J. Orthod.* 42: 381–387.

Shearman, R. M. 2008. Chondrogenesis and ossification of the lissamphibian pectoral girdle. *J. Morphol.* 269: 479–495.

Sheil, C. A. and H. Alamillo. 2005. Osteology and skeletal development of Phyllomedusa vaillanti (Anura: Hillidae: Phyllomedusinae) and a comparison of this arboreal species with a terrestrial member of the genus. *J. Morphol.* 265: 343–368.

Silvestrini, G., et al. 1999. Cytochemical demonstration of the glucocorticoid receptor in skeletal cells of the rat. *Endocr. Res.* 25: 117–128.

Sirianni J. E. and L. Newell-Morris. 1980. Craniofacial growth of fetal *Macaca nemestrina*: a cephalometric roentgenographic study. *Am. J. Phys. Anthropol.* 53: 407–421.

Sirianni, J. E. and D. R. Swindler. 1979. A review of postnatal craniofacial growth in old world monkeys and apes. *Yearb. Phys. Anthropol.* 22: 80–104.

Sirianni, J. E., et al.1982. Growth of the mandible in adolescent pigtail macaques (*Macaca nemestrina*). *Hum. Biol.* 54: 31–44.

Sissons, H. A. 1953. Experimental determination of rate of longitudinal bone growth. *J. Anat.* 87: 228–236.

Sivaraj, K. K. and R. H. Adams. 2016. Blood vessels formation and function in bone. *Development* 143: 2706–2715.

VetBooks.ir

Sjögren, K., et al. 2002. A model for tissue-specific inducible insulin-like growth factor-1 (IGF-1) inactivation to determine the physiological role of liver-derived IGF-1. *Endocrine* 19: 249–256.

Steffens, J. P., et al. 2015. Androgen receptors and experimental bone loss – an *in vivo* and in *vitro study. Bone* 81: 683–690.

Stein, K. and E. Prondvai. 2014. Rethinking the nature of fibrolamellar bone: an integrative biological revision of sauropod plexiform bone formation. *Biol. Rev.* 89: 24–47.

Stern, T., et al. 2015. Isometric scaling in developing long bones is achieved by an optimal epiphyseal growth balance. *PLoS Biol. 13: e1002212*.

Stevens, D. A., et al. 2000. Thyroid hormones regulate hypertrophic differentiation and expression of parathyroid-hormone related peptide and its receptor during endochondral bone formation. *J. Bone Miner. Res.* 15: 2431–2442.

Stevenson, P. H. 1924. Age order of epiphyseal union in man. *Am. J. Phys. Anthropol*. 7: 53–95

Svechnikov, K., et al. 2010. Origin, development and regulation of human Leydig cells. *Horm. Res. Paediatr.* 73: 93–101.

Takeshita, S., et al. 2001. The nature of human craniofacial growth studied with finite element analytical approach. *Clin. Orthod. Res.* 4: 148–160.

Tannenbaum, G. S. and J. B. Martin. 1976. Evidence for an endogenous ultradian rhythm governing growth hormone secretion in the rat. *Endocrinology* 98: 562–570.

Tarnawski, B. A., et al. 2015. A comparative analysis of cranial ontogeny of south American fur seals (Otariidae: *Artocephalus*). *Zool. J. Linn. Soc.* 173: 249–269.

Tickle, C. and H. Barker. 2013. The Sonic hedgehog gradient in the developing limb. *Dev. Biol.* 2: 275-290.

Tsutsui, K., et al. 2012. Gonadotropin-inhibitory hormone (GnIH): Discovery, progress and prospect. *Gen. Comp. Endocr.* 177: 305–314.

Turner, R. T. et al. 2008. Estrogens and progestin. In *Principles of bone biology*, third edition, eds. Bilezikian J. P., L. G. Raisz and T. J. Martin, Vol. 1, 855–886. Amsterdam: Academic Press.

Uhen, M. D. 2007. Evolution of marine mammals: back to the sea after 300 million years. *Anat. Rec.* 290: 514–522.

Vanderschueren, D., et al. 2004. Androgens and bone. *Endocr. Rev.* 25: 389-425.

Verbruggen, S. W. and N. C. Nowlan. 2017. Ontogeny of the human pelvis. *Anat. Rec.* 300: 643–652.

Waal, W. J., et al. 1996. Accuracy of final height prediction and effect of growth-reductive therapy in 362 constitutionally tall children. *J. Clin. Endocrinol. Metab. 81*: 1206–1216.

Wang, L., et al. 2007. Thyroid hormone interacts with the Wnt/β-Catenin signaling pathway in the terminal differentiation of growth plate chondrocytes. *J. Bone Miner. Res.* 22: 1988–1995.

Waung, J. A., et al. 2012. Thyroid hormone metabolism in skeletal development and adult bone maintenance. *Trends Endocr. Metab.* 23: 155–162.

Washburn, S. L. 1946. The sequence of epiphyseal union in the opossum. *Anat. Rec.* 95: 353–363.

Weinstein, R. S. and S. C. Manolagas. 2000. Apoptosis and osteoporosis. *Am. J. Med.* 108: 153–164.

Weiss, A. and L. Attisano. 2013. The TGF beta superfamily signaling pathway. *Dev. Biol.* 2: 47–63.

Williams, G. R., et al. 1998. Thyroid hormone actions on cartilage and bone: interactions with other hormones at the epiphyseal plate and effects on linear growth. *J. Endocrinol.* 157: 391–403.

Wilsman, N. J., et al. 1996. Differential growth by growth plates as a function of multiple parameters of chondrocytic kinetics. *J. Orthop. Res.* 14: 927–936.

Wilsman, N. J., et al. 2008. Age and pattern of the onset of differential growth among growth plates in rats. *J. Orthop. Res.* 26: 1457–1465.

Wiren, K. M. 2008. Androgen receptor expression and steroid action in bone. In *Principles of bone biology*, third edition, eds. Bilezikian J. P., L. G. Raisz and T. J. Martin, Vol. 1, 1001–1023. Amsterdam: Academic Press.

Woodward, H. N., et al. 2011. Osteohistological evidence for determinate growth in the American alligator. *J. Herpetol.* 45: 339–342.

Xing, Y., et al. 2015. Development of adrenal cortex zonation. *Endocrinol. Metab. Clin. N. Am.* 44: 243–274.

Yadin, D., et al. 2016. Structural insights into BMP receptors: specificity, activation and inhibition. *Cytokine & Growth Fact. Rev.* 27: 13–34.

Yakar, S. and O. Isaksson. 2016. Regulation of skeletal growth and mineral acquisition by the GH/IGF-1 axis: lessons from mouse models. *Growth Horm. IGF Res.* 28: 26–42.

Yakar, S., et al. 2002. The role of circulating IGF-1. *Endocrine* 19: 239–248.

Yamaguchi, K., and I. Yasumasu. 1977. Effects of thyroxine and prolactin on the rates of protein synthesis in the thigh bones of the tadpole of *Rana catesbeiana*. *Dev. Growth. Differ.* 19: 161–169.

Yen, P. M. 2001. Physiological and molecular basis of thyroid hormone action. *Physiol. Rev.* 81: 1097–1142.

Zelditch, M. L., et al. 1992. Ontogeny of integrated skull growth in the cotton rat *Sigmodon fulviventer. Evolution* 46: 1164–1180.

Zelditch, M. L., et al. 1993. The ontogenetic complexity of developmental constraints. *J. Evol. Biol.* 6: 621–641.

Zumpano, M. P. 2002. Size and shape changes during late fetal growth (137–157 gestational days) in the pigtailed macaque (*Macaca nemestrina*) craniofacial complex: an application using three-dimensional coordinate data and finite element scaling analysis. *Anat. Rec.* 267: 307–320.

VetBooks.ir

10

Accretion Rate and Histological Features of Bone

Vivian de Buffrénil Alexandra Quilhac and Jorge Cubo

CONTENTS

A Keystone for Paleobiological Inferences 221
Quantifying Appositional Rate of Primary Periosteal Cortices 222
Histological Features and Apposition Rate: Comparative Results 223
Semiquantitative Approach 223
Recent Efforts Toward a Full Quantitative Approach 225
References 227

A Keystone for Paleobiological Inferences

As explained in Chapter 8, primary periosteal bone tissue is remarkable for its great histological diversity. The morphology, density and spatial pattern of osteocytes, the orientation of collagen fibers in extracellular matrices, and the density and orientation of vascular canals may differ greatly among taxa, bones of a single skeleton, and even the areas of a thin section. Early comparative studies tended to consider phylogeny as a prominent explanation of bone histodiversity (see historical account in Ricqlès 1976); however, more modern syntheses discarded such a close, unequivocal relationship (Ricqlès 1977, 1978; Padian and Lamm 2013).

Although certain types of osseous tissue invariably occur in some taxa, for example, parallel-fibered bone in the appendicular skeleton of all lissamphibians (e.g., Enlow and Brown 1956), phylogeny was shown to explain only a part of bone histodiversity (Ricqlès 1978; Ricqlès et al. 2004; Cubo et al. 2005; see also Chapter 30). Similarly, local biomechanical forces on the skeleton generally have limited influence (if any) on the features of primary periosteal cortices, considered at the level of cells and intercellular matrix, although they have much greater influence on bone microanatomical organization and remodeling (Ricqlès 1976; Currey 2000; Robling et al. 2014).

Until now, the most consistent and integrative interpretation of the cause of histological diversity in primary periosteal cortices remains "Amprino's rule" (Amprino 1947). This generalization was formulated in 1947 in conclusion to a comparative histological study of tetrapod long bones: "Variations in the rate of bone tissue formation determine the variations in its structure" (Amprino 1947, p. 329; see also Amprino and Godina 1947). This general statement remains the keystone for most functional interpretations in paleohistology and paleophysiology, because it allows the double transformation of histological observations into (1) gross, qualitative estimates of bone growth rate and (2) assessments of the kind of metabolic activity most likely related to such a growth rate (e.g., Castanet et al. 2001).

Amprino's rule was based on relatively few observations of amphibian and mammalian bones and referred to no experimental demonstration. This is possibly why it remained unnoticed and of limited practical application until it was revived by Ricqlès (1976, 1977, 1978) and his followers, and has to the present been applied to the interpretation of the dynamic aspects of bone tissue formation in extant and extinct taxa. The question was first considered on the basis of qualitative observations, an approach still currently practiced today, especially by paleontologists (e.g., Ricqlès et al. 2008; Mitchell and Sander 2014; Buffrénil et al. 2016). In brief, osseous tissue types, viewed as discrete qualitative categories as defined in Chapter 8, are ranked in a hierarchical order referring to their estimated growth rate, as suggested by empirical, comparative observations. The hierarchy that they form can be summarized as follows. (1) Fibrolamellar complexes indicate faster growth than woven-fibered tissue with simple vascular canals. (2) The latter results from faster apposition than parallel-fibered bone, whether or not it is vascularized. (3) vascularized parallel-fibered tissue is formed at a higher rate than the same tissue devoid of vascular canals. (4) True lamellar bone has the slowest depositional rates (Ricqlès 1976; Mitchell and Sander 2014). This qualitative use of Amprino's rule has yielded and continues to yield important insights into paleobiology. It has led to fruitful inferences about the growth rates and metabolism of extinct taxa that were subsequently supported by independent lines of evidence. Today, the use of *in vivo* labeling of bone growth creates an opportunity to increase greatly the basic dataset to test Amprino's rule. It is now possible to document, quantitatively and experimentally, the relationship between the main

VetBooks.ir

categories of bone tissue structure and the apposition rates of periosteal and endosteal deposits. Astonishingly, few publications specifically deal with this question. Most relevant data are from Ricqlès et al. (1991), Castanet et al. (1996, 2000), Margerie et al. (2002, 2004) and Cubo et al. (2012) (see also Gomez et al. 2013), and they relate to various taxa of amphibians, lizards, turtles, and crocodilians, as well as birds and mammals.

Quantifying Appositional Rate of Primary Periosteal Cortices

Since the pioneering studies of the 1930s (e.g., Schour 1936), many authors have conducted experimental measurements of cortical accretion rates through *in vivo* labeling of bone growth. Such studies have had various aims, mainly related to biomedical research or to the validation of the skeletochronological method of age determination (see Chapter 31). As a result, a substantial database on bone apposition rates is available for several taxa, often domestic or laboratory animals. The basic methodological approach for quantifying the rate of periosteal (as for endosteal) bone accretion (Figure 10.1A–D) is relatively simple, and it proceeds in two stages. In a growing animal, the mineralizing osteoid is labeled *in vivo*, at a known date, with one of the many substances (oxytetracycline, alizarine, DCAF-fluoresceine also called "calcein", or xylenol-orange; see Castanet 1982 for practical synthesis) that bind permanently with calcium. Such dyes create a fluorescent signal, visible as a colored line, when a thin section of the bone (most often a cross section) is observed in transmitted ultraviolet light. One or several injections combining various markers can be done, creating one or several fluorescent lines that show the position of the mineralization front in the growing bone cortex at the time of the injection (Figure 10.1D).

Several indices are then used to assess bone apposition rate. Syntheses of the nomenclature acknowledged worldwide to designate these indices, and the procedures to compute them are given in Revell (1983), Parfitt et al. (1987), Recker et al. (2011) and Dempster et al. (2013). The simplest and most commonly used method is to measure, on a cross section sampled at mid-diaphysis, the spacing between two fluorescent lines or, more rarely, between the last line and the outer margin of the bone. This measurement is then divided by the time, expressed in days or hours, elapsed between either two consecutive labeling operations or between the last labeling and the date of bone sampling (Figure 10.1D). A formal morphometric index is thus created called the *mineral accretion rate* (MAR; of which *apposition rate* is a frequent synonym), expressed in µm*day^{-1} or in µm*hour^{-1} (example in Wronski et al. 1981). Another procedure is to consider the area (instead of the width) of the entire bone layer located between two fluorescent lines and divide it by time, giving a result in mm^2*day^{-1} or in µm^2*day^{-1}. This method was used, but not named, by Cubo et al. (2008). A third currently used index is *bone formation rate* (BFR), which has a more complex structure than the two previous ones. For example, in a layer of bone bordered by two fluorescent lines, BFR integrates the mean perimeter of these lines (as a substitute for the accretion surface) multiplied by MAR (Revell 1983;

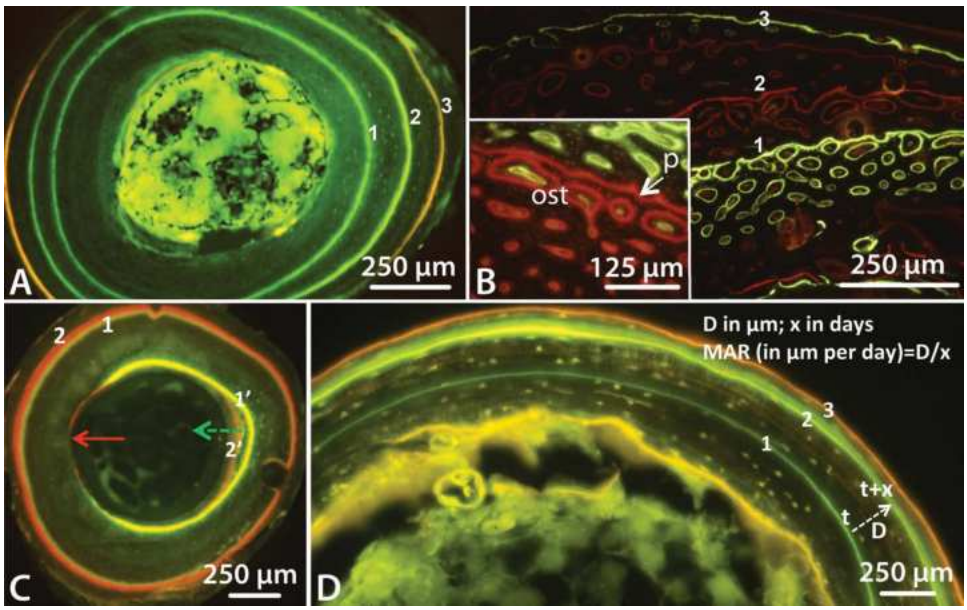


FIGURE 10.1 Bone labeling and mineral accretion rate (MAR) calculation. A, Cortical growth labeling in a tubular bone (femur of *Lacerta viridis*). The first two marks (1, 2) correspond to DCAF (calcein) injection, and the third mark (3) to xylenol-orange. B, Labeling of woven-parallel tissue in the femur of the mallard *Anas platyrhynchos*. Three successive injections were made in the following order: (1) first calcein injection, (2) alizarine injection and (3) second calcein injection. The inset shows the simultaneous labeling of bone tissue at periosteal (p) and osteonal (ost) levels. C, Double labeling with DCAF (yellow-green) and alizarin (red) in periosteal (1, 2) and endosteal (labels 1′ and 2′) bone deposits in a femur of *L. viridis*. The medullary cavity expends through resorption in one direction only (red arrow), whereas endosteal secondary reconstruction (green arrow) occurs on the other side of the cavity. D, Computation of the MAR index. Two successive DCAF labels (1, 2) were made at times t and $t + x$ (in days). The thickness of the bone deposit (D) is measured in microns between the two DCAF labels and divided by x to obtain the MAR value, in µm*d^{-1}.

VetBooks.ir

Parfitt et al. 1987). BFR is then expressed in $mm^2*mm^{-1}*day^{-1}$. Of course, it must be assured that the interval of deposition in question did not experience any growth hiatus, and this can be investigated histologically.

The meaning of MAR differs from those of the other two indices. BFR and Cubo et al.'s (2008) indices both reflect the total amount of mineralized bone tissue produced in the sectional plane by time unit. They express a quantity, whereas MAR denotes a vector expressing the local speed of cortical expansion in the precise place where the thickness of the interlabel layer is measured. For relating the histological structure of primary periosteal deposits to appositional quickness, MAR is the only relevant index because bone histological characteristics are basically defined at a very local scale and seldom appear constant across the entire area of a section.

Observed growth rates in periosteal deposits range from 0.043 $\mu m*day^{-1}$ in some regions of the adult mink (*Neovison vison*) mandible (Buffrénil and Pascal 1984), up to 171 $\mu m*day^{-1}$ in the femur of the king penguin, *Aptenodytes patagonicus* (Margerie et al. 2004). Important differences exist, not only between homologous bones of distinct taxa, but also among the bones of a single skeleton (Tam et al. 1978). The functional meaning of such differences, as well as the upstream biological factors that may explain them, are beyond the scope of this chapter, but they are more closely considered in Chapter 31.

Histological Features and Apposition Rate: Comparative Results

Semiquantitative Approach

Studies specifically aimed at confirming Amprino's rule with experimental evidence were initially conducted by Castanet (1996, 2000) and Margerie et al. (2002, 2004) in actively growing specimens of four bird species: the mallard (*Anas platyrhynchos*), the ostrich (*Struthio camelus*), the emu (*Dromaius novaehollandiae*) and the king penguin (*Aptenodytes patagonicus*). These studies were based on a semiquantitative approach because, although the apposition rate (MAR) was quantitatively measured with experimental methods as an accurate, continuous variable (in $\mu m*d^{-1}$), the bone tissue categories remained defined qualitatively by peculiar histological *tableaux* combining at once the visible characteristics of bone matrix (refringence properties in polarized light), cell lacunae (multipolar vs. spindle-like morphology) and vascular networks (occurrence, nature and spatial structuring of the canals). Four basic types of bone tissue were thus distinguished and defined by Margerie et al. (2002, 2004). Three types of lamellar or parallel-fibered tissues were all considered equivalent and designated collectively as L (Figure 10.2A–D), and the various fibrolamellar complexes (now called woven-parallel complexes after Prondvai et al. 2014) were collectively designated as WP (Figure 10.2F–J). In the L group of tissues, the various patterns of vascular supply distinguish three types: nonvascular tissue, or L_{nv}; tissue with simple vascular canals, or L_{sv} and tissue with primary osteons, or L_{po}. Among the WP group, the geometric organization of vascular networks defines the classical tissue types: radial (WP_{rad}), laminar (WP_{lam}), reticular (WP_{ret}) and longitudinal (WP_{long}). The categories considered by Margerie et al. (2002, 2004) were mainly suited to the situation of the limb bones of medium to large bird species; they excluded several important types of bone tissue commonly encountered in vertebrates, such as woven-fibered tissue with simple vascular canals (Figure 10.2E). Of course, miscellaneous data mentioning (or illustrating) definite bone tissue types, together with the apposition rates associated with them in various taxa, are occasionally given in the literature (synthesis in Ricqlès et al. 1991).

To consider only the specific studies mentioned above, data can broadly diverge among taxa, as between the various bones of a single taxon. Considerable overlap exists among the marginal values of MAR that correspond to distinct tissue types, a situation that results in some confusion. Figure 10.3, derived from the results of Margerie et al. (2002), and supplemented by data from the literature, shows that there is an actual ranking of bone tissue types according to their mean (or median) MAR values: $WP_x > L_{po} > L_{sv} > L_{nv}$ (see also Figure 10.2A–D vs. F–J). This situation was confirmed by the statistical tests applied by Margerie et al. (2002) to the 288 observations collected for the mallard. Therefore, Amprino's rule reflects biological reality, at least for the four broad categories mentioned above, and with a collective representation of all woven-parallel tissue types (WP_x). Another condition must be added to the validity of Amprino's rule: it must be applied only to primary periosteal bone deposits. Several studies (e.g., Buffrénil and Pascal 1984; Margerie et al. 2002; Gomez et al. 2013; Van Hof et al. 2017) showed that endosteal deposits of lamellar or parallel-fibered tissues can form as rapidly (close to, or more than, 2.5 $\mu m*day^{-1}$) as woven-fibered bone in primary cortices. As already pointed out by Ricqlès et al. (1991), available data suggest that endosteal and periosteal apposition processes do not share the same dynamics.

The validity of Amprino's rule becomes less clear when comparisons are made within the WP_x group. Table 10.1 summarizes the experimental data obtained by Castanet et al. (2000) from the emu and the ostrich, and by Margerie et al. (2002, 2004) from the mallard and the king penguin, respectively. In the last species, the ranking within the WP group is consistently: $WP_{rad} > WP_{ret} > WP_{long} > WP_{lam}$. Conversely, in the other three species, different and fairly variable rankings are observed. Consequently, the general relationship between apposition rate and vascular organization in woven-parallel bone tissues is equivocal. It remains possible that radial woven-parallel bone (WP_{rad}; Figure 10.2J) is the most rapidly growing tissue of all because the apposition rate that it reaches (up to 171 $\mu m*d^{-1}$, with a mean value above 100 $\mu m*day^{-1}$) is unknown up to now in any other kind of osseous tissue, whatever the bone or the taxon considered. Moreover, according to the results of Margerie et al. (2002), the apposition rate of woven-parallel tissues could also be related to the volume of primary osteons (i.e., their relative area in cross sections), in addition to their orientation: the bigger the osteons are, the more rapid the apposition of the tissue. This interesting issue requires further study.

The occurrence of discrepancies in the relationships of MAR values to histological categories is obvious, and it may have complex causes. Moreover, although tissue types have

VetBooks.ir

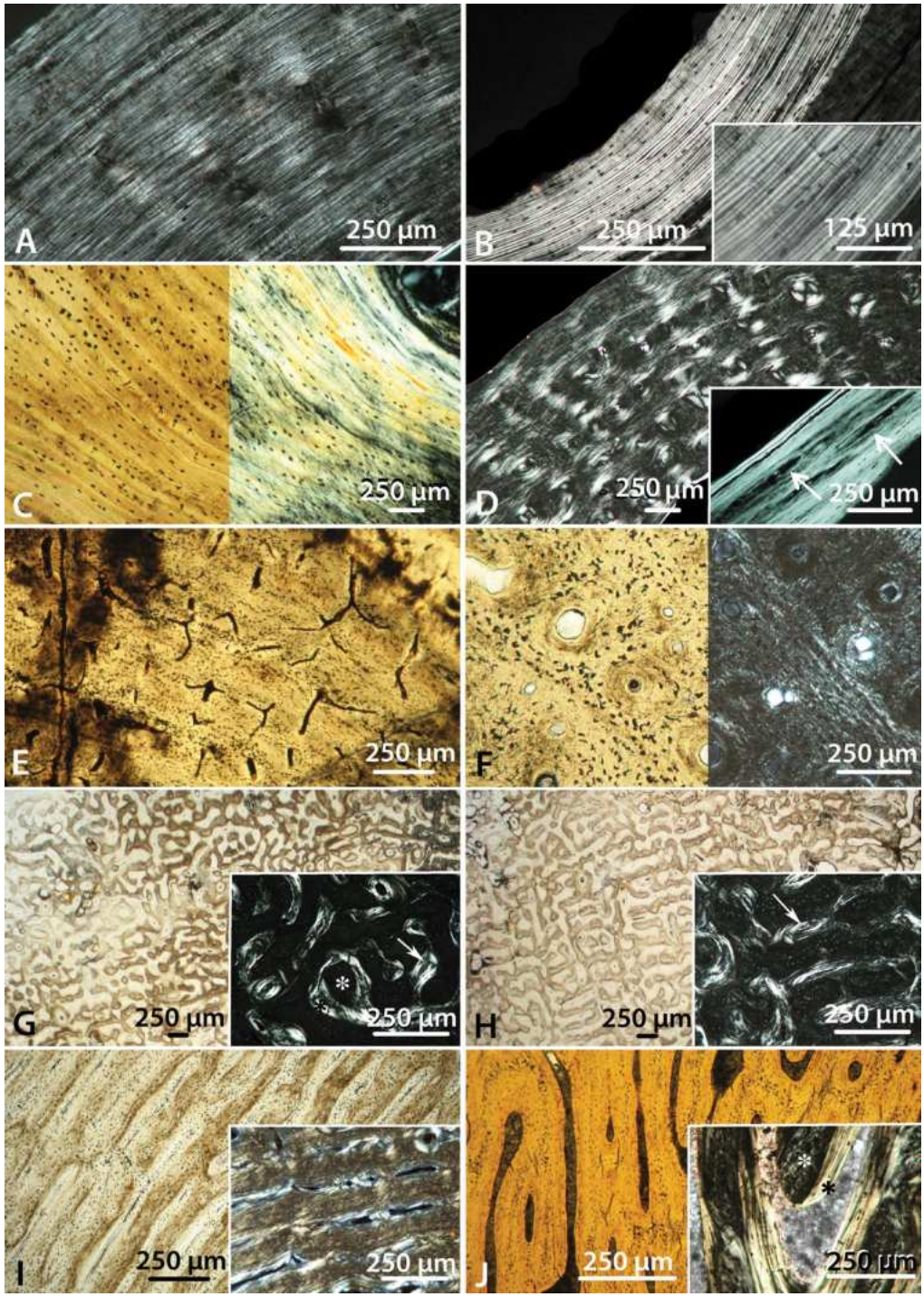


FIGURE 10.2 Main bone tissue types for which quantitative data on apposition rates are available. A, Periosteal tissue akin to the lamellar type in the femur of a small monitor lizard (*Varanus eremius*). Polarized transmitted light. B, Endosteal lamellar tissue in the femur of the squamate *Iguana iguana*. The inset is an enlargement showing the bone lamellae. Polarized transmitted light. C, Avascular parallel-fibered bone in the femur of *Andrias japonicus* (Amphibia, Caudata). Left half: ordinary transmitted light. Right half: polarized light showing the strong mass birefringence of this type of tissue. D, Parallel-fibered tissue with numerous longitudinal primary osteons in the femoral cortex of the toad (Amphibia, Anura) *Rhinella marina*. Polarized light. The inset shows the strong mass birefringence of the parallel-fibered tissue between the primary osteons (arrows) in a longitudinal section of the femur of the frog *Amietophrynus regularis*. E, Woven-fibered bone tissue with simple vascular canals in the femur of the Aquitanian crocodilian *Diplocynodon ratelii*. F, Woven-parallel bone tissue in a rib of the Callovian marine crocodile *Metriorhynchus superciliosus*. Right half: polarized light. G, Reticular woven-parallel tissue in the premaxilla of the Miocene beaked whale (Ziphiidae) *Globicetus hiberus*. Inset: closer view in polarized light. The arrow points to the lamellar bone of aprimary osteon, and the white asterisk is on woven-fibered tissue. H, Plexiform-like bone tissue in the premaxilla of *G. hiberus*. Inset: closer view in polarized light. Same symbols as in G. I, Laminar tissue in the premaxilla of *G. hiberus*. Inset: closer view in polarized light. J, Radial woven-parallel complex in the rib of an early Bartonian cetacean, *Eocetus wardii*. Inset: view in polarized light. The white asterisk is on woven-fibered tissue and the black asterisk on lamellar tissue.

VetBooks.ir

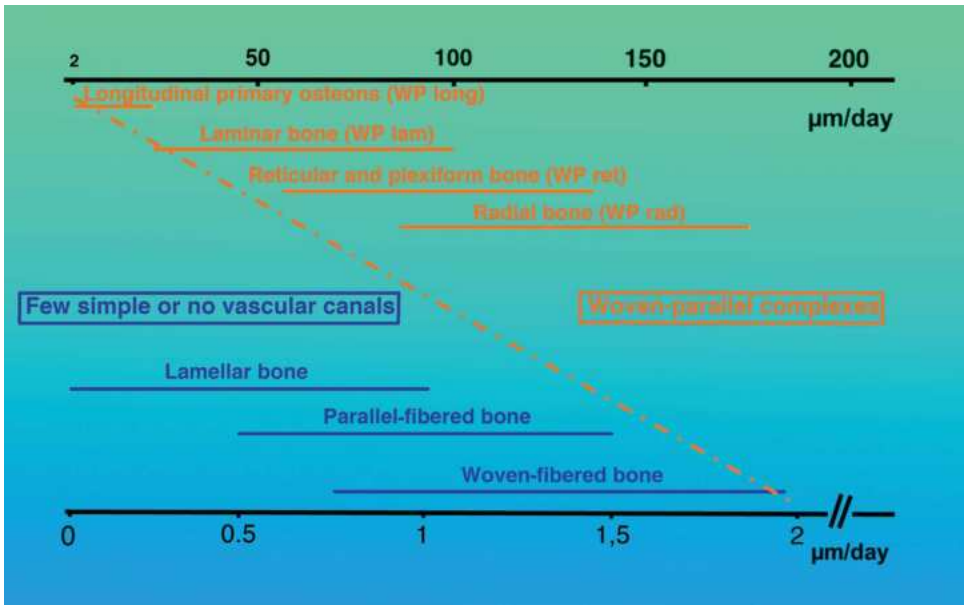


FIGURE 10.3 Apposition rates of bone tissue types. Tissues belonging to the broad category of non-WP tissue types are indicated in dark blue below the dotted line. Tissues belonging to the WP category (woven-parallel tissue types) are in orange, above the line. Within non-WP and WP categories, the growth rates of the diverse tissues broadly overlap.

sometimes been described as if they were pure, archetypal categories, this is not the most common situation: intermediate conditions between typical categories exist, and the actual variation between bone tissue types looks like a continuum (Margerie et al. 2002; see also Chapter 8). The problem is made more complex by the fact that each of the three main parameters (matrix, cell lacunae and vascular canals) that contribute to current descriptions of bone tissue categories may vary with apposition rate according to its own characteristics (Margerie et al. 2002). In addition, these characteristics can differ among taxa or among the various elements of a single skeleton in relation to, e.g., bone morphology or local functional contexts. The influences of such factors can result in imprecise and sometimes contradictory inferences, a situation justifying that a different approach needs to be developed.

Recent Efforts Toward a Full Quantitative Approach

In the quantitative studies developed by Cubo et al. (2012), bone histological structure and apposition rates (MAR) were analyzed using continuous numerical variables in a relatively large and diverse sample of amniotes (three long bones in 52 specimens representing 16 species: three mammals, three testudines, four squamates, one crocodile and five birds). In this study, the histological structure of bone tissue was no longer summarized as a series of integrative categories, but subdivided into the main basic features that comprise it, at least for the density, morphology and size of osteocyte lacunae (three distinct variables), as well as the development and geometrical structuration of vascular networks (four variables). Some of these variables had already been quantified (for other purposes than comparative histology) in relation to growth rate in previous studies, e.g., the spatial density of cell lacunae (Qiu et al. 2002; see also Hernandez et al. 2004) and vascular canals (McKenzie and Silva 2011). In Cubo et al.'s (2012) model, the structural features of the bone matrix were not considered specifically (to some extent, cell density and shape are related to this feature; see, e.g., Jones and Boyde 1976; Kerschnitzki et al. 2011).

The relationship of each of these variables with the appositional rate was then quantified using a multiple regression method taking into account the redundancy of information (collinearity) among independent (explanatory) variables. A synthetic equation was proposed that allows the retrocalculation of MAR (then considered the dependent, or response, variable) from the quantitative character states of the basic histological descriptors of bone structure. For the femur of amniotes, this equation is

Femoral growth rate = –13.5753 – 0.2574 * Vascular density + 20474.2882 * Cellular density – 101.5837 * Cellular shape + 1.9660 * Cellular size + 60.0438 * Proportion of circular canals – 34.7885 * Proportion of oblique canals – 30.2255 * Proportion of radial canals.

Although this method proved to be correct only for the femur (with $P = 0.02551$ in cross-validation tests) among the 16 sampled taxa (significant results could not be obtained for the other bones), it is likely to open considerable perspectives in paleobiology provided the method can be further substantiated by additional data (larger and more diversified samples, precise quantification of matrix properties, etc.). Back-calculations applied to any section from recent or fossil (well preserved) bone tissue should then provide definite numerical values of MAR. Subsequently, these values could be used to assess quantitatively the resting metabolic rate of a taxon with the calculation method presented by Montes et al. (2007) and Cubo et al. (2008) (see also Chapter 37).

Such inferences represent the core of the paleohistological approach and are one of its perennial goals (Ricqlès 1969, 1972,

VetBooks.ir

TABLE 10.1

Relationship Between Growth Rate (in µm*day $^{-1}$) and the Orientation of Primary Canals in Woven-Parallel Complexes Observed in the Limb Bones of Four Bird Species

	Mallard [1]	Emu [2]	Ostrich [2]	Penguin [3]
Humerus				
Radial	-	-	-	**100** (45–165)
Laminar	**19.2** (7.1–62)	-	**20**	**24.4** (10–46)
Reticular	**12.8** (4.5–66.2)	**9.5** (8.1–11)	**12.4** (10.1–15.5)	**84.7** (48–110)
Longitudinal	**21.5** (4.7–54.5)	**7.4** (5.5–9.2)	**7.8** (9.2–6.4)	**47.4** (32–60)
Radius				
Radial	-	-	-	**67.8** (28–101)
Laminar	**19.2** (7.1–62)	-	-	**19.8** (9–39)
Reticular	**12.8** (4.5–66.2)	-	**6.1**	**43.8** (19–82)
Longitudinal	**21.5** (4.7–54.5)	**11.3** (6.6–16)	**4.6** (3.5–6.4)	**20.4** (8–45)
Ulna				
Radial	-	-	-	-
Laminar	**19.2** (7.1–62)	-	-	-
Reticular	**12.8** (4.5–66.2)	-	**7.1** (4.8–9.4)	-
Longitudinal	**21.5** (4.7–54.5)	**3.6**	**3.9** (2.7–5.5)	-
Digit				
Radial	-	-	-	-
Laminar	-	-	**10.7**	-
Reticular	-	-	**13.3**	-
Longitudinal	-	-	**4.1** (3.2–5.6)	-
Femur				
Radial	-	-	-	**113** (76–171)
Laminar	**19.2** (7.1–62)	**30.3** (18.1–58.1)	**24.2** (13.4–35.9)	**36.8** (12–72)
Reticular	**12.8** (4.5–66.2)	**53.5** (29.8–89.4)	**33.8** (13.3–39.6)	**52.8** (21–101)
Longitudinal	**21.5** (4.7–54.5)	-	**4.2**	**61.5** (30–91)
Tibiotarsus				
Radial	-	-	-	**86.8** (34–135)
Laminar	**19.2** (7.1–62)	**33.5**(31.5–35.5)	**31.9** (22.5–34.9)	**30.6** (17–60)
Reticular	**12.8** (4.5–66.2)	**30.1** (11.7–55)	**38.9** (35.8–42)	**39** (30–48)
Longitudinal	**21.5** (4.7–54.5)	-	**7.8**	**54.2** (15–105)
Tarsometatarsus				
Radial	-	-	-	-
Laminar	**19.2** (7.1–62)	-	**47.3**	-
Reticular	**12.8** (4.5–66.2)	**19.4** (10–29.2)	**39.9**	-
Longitudinal	**21.5** (4.7–54.5)	-	-	-
Digit III				
Radial	-	-	-	-
Laminar	-	**12.9** (10.7–15.1)	**10.7**	-
Reticular	-	**10** (11–19.1)	**29.2** (18–40.4)	-
Longitudinal	-	**4.4** (2.5–7)	-	-

Notes: Numbers in bold: mean values; numbers in parentheses: variation range.

Source: Data from [1] Margerie et al. (2002), [2] Castanet et al. (2000) and [3] Margerie et al. (2004). Data for the mallard are mean values for each tissue type, irrespective of the bone categories in which it occurs.

2000; Ray et al. 2009; Legendre et al. 2016; Olivier et al. 2017). However, the present state of knowledge about the quantitative correlations between apposition rate and bone histological characteristics and about the local histogenetic factors likely to explain such correlations is still insufficient to allow strong conclusions. This is especially true for woven-parallel tissue types. Progress in these fields will depend on the development and improvement of the quantitative methods proposed by Margerie et al. (2002, 2004) and by Cubo et al. (2012), which are currently the only procedures to address the basic uncertainty inherent to a qualitative (and necessarily subjective; cf. Prondvai et al. 2014) identification of bone structure.

VetBooks.ir

Despite the possible biases mentioned above, the conclusions derived from the application of Amprino's rule to fossils have generally proved to be correct and have been supported by other lines of evidence. This has been the case for the pioneering interpretations of dinosaurian growth rate and physiology proposed by Currey (1962) and Ricqlès (1968) (see also Ricqlès 1975, 1976, 1977), and for the inference derived from histological evidence by Buffrénil and Mazin (1990, 1992) and by Wiffen et al. (1995) that some Mesozoic marine reptiles i.e., the ichthyosaurs, placodonts and plesiosaurs, might have had high growth rates and a thermometabolic regime close to endothermy and homeothermy. These conclusions were confirmed 20 years later by isotopic analyses in tooth tissues (Amiot et al. 2006; Bernard et al. 2010; see also Chapter 26 for contrasting elements).

REFERENCES

Amiot, R., et al. 2006. Oxygen isotopes from biogenic apatites suggest widespread endothermy in Cretaceous dinosaurs. *Earth Planet. Sci. Let.* 246: 41–54.

Amprino, R. 1947. La structure du tissue osseux envisagé comme l'expressions de differences dans la vitesse de l'accroissement. *Arch. Biol.* 58: 317–330.

Amprino, R. and G. Godina. 1947. La struttura della ossa nei; vertebrate. Ricerche comparative neigli amfibi e neigli amnioti. *Comment. Pont. Acad. Sci.* 11: 329–467.

Bernard, A., et al. 2010. Regulation of body temperature by some Mesozoic marine reptiles. *Science* 328: 1379–1381.

Buffrénil, V. de and J.-M. Mazin. 1990. Bone histology of the ichthyosaurs: comparative data and functional interpretation. *Paleobiology* 16: 435–476.

Buffrénil, V. de and J.-M. Mazin. 1992. Contribution de l'histologie osseuse à l'interprétation paléobiologique du genre *Placodus* Agassiz, 1833 (Reptilia, Placodontia). *Rev. Paléobiol.* 11: 397–407.

Buffrénil, V. de and M. Pascal. 1984. Croissance et morphogenèse postnatales de la mandibule du vison (*Mustela vison* Schreiber): données sur la dynamique et l'interprétation fonctionnelle des dépôts osseux mandibulaires. *Can. J. Zool.* 62: 2026–2037.

Buffrénil, V. de, et al. 2016. Comparative data on the differentiation and growth of bone ornamentation in gnathostomes (Chrodata: Vertebrata). *J. Morphol.* 277: 634–670.

Castanet, J. 1982. *Recherches sur la croissance du tissu osseux des reptiles. Application: la méthode squelettochronologique*, PhD thesis. Paris: University Paris VII-Denis Diderot.

Castanet, J., et al. 1996. Expression de la dynamique de croissance dans la structure de l'os périostique chez *Anas platyrhynchos*. *C. R. Acad. Sci. Paris, Sciences de la Vie* 319: 301–308.

Castanet, J., et al. 2000. Periosteal bone growth rates in extant ratites (ostriche and emu). Implications for assessing growth in dinosaurs. *C. R. Acad. Sci. Paris, Sciences de la Vie* 323: 543–550.

Castanet, J., et al. 2001. Signification de l'histodiversité osseuse: le message de l'os. *Biosystema* 19: 133–147.

Cubo, J., et al. 2005. Phylogenetic signal in bone microstructure of Sauropsids. *Syst. Biol.* 54: 562–574.

Cubo, J., et al. 2008. Phylogenetic, functional, and structural components of variation in bone growth rate of amniotes. *Evol. Dev.* 10: 217–227.

Cubo, J., et al. 2012. Paleohistological estimation of bone growth rate in extinct archosaurs. *Paleobiology* 38: 335–349.

Currey, J. D. 1962. The histology of the bone of a prosauropod dinosaur. *Palaeontology* 5: 238–246.

Currey, J. D. 2000. *Bones. Structure and mechanics.* Princeton and Oxford, Princeton University Press.

Dempster, D. W., et al. 2013. Standardized nomenclature, symbols and units for bone histomorphometry: A 2012 update of the report of the ASBMR histomorphometry nomenclature committee. *J. Bone Miner. Res.* 28: 1–6.

Enlow, D. H. and S. O. Brown. 1956. A comparative histological study of fossil and recent bone tissues. Part 1. *Texas J. Sci.* 8: 405–443.

Gomez, S., et al. 2013. Labelling studies on cortical bone formation in the antlers of red deer (*Cervus elaphus*). *Bone* 52: 506–515.

Hernandez, C. J., et al. 2004. Osteocyte density in woven bone. *Bone* 35: 1095–1099.

Jones, S. J. and A. Boyde. 1976. Is there a relationship between osteoblasts and collagen orientation in bone? *Israel J. Med. Sci.* 12: 98–107.

Kerschnitzki, M., et al. 2011. The organization of the osteocyte network mirrors the extracellular matrix orientation in bone. *J. Structural Biol.* 173: 303–311.

Legendre, L., et al. 2016. Palaeohistological evidence for ancestral high metabolic rate in Archosaurs. *Syst. Biol.* 65: 989–996.

Margerie, E. de, et al. 2002. Bone typology and growth rate: testing and quantifying "Amprino's rule" in the mallard (*Anas platyrhynchos*). *C. R. Biol.*325: 221–230.

Margerie, E. de, et al. 2004. Assessing a relationship between bone microstructure and growth rate: a fluorescent labeling study in the king penguin chick (*Aptenodytes patagonicus*). *J. Exp. Biol.* 207: 869–879.

McKenzie, J. A. and M. J. Silva. 2011. Comparing histological, vascular and molecular responses associated with woven and lamellar bone formation induced by mechanical loading in the rat ulna. *Bone* 48: 250–258.

Mitchell, J. and M. Sander. 2014. The three-front model: a developmental explanation of long bone diaphyseal histology of Sauropoda. *Biol. J. Linn. Soc.* 112: 765–781.

Montes, L., et al. 2007. Relationships between bone growth rate, body mass and resting metabolic rate in growing amniotes: a phylogenetic approach. *Biol. J. Linn. Soc.* 92: 63–76.

Olivier, C., et al. 2017. First paleohistological inference of resting metabolic rate in an extinct synapsid, *Moghreberia nmachouensis* (Therapisa: Anomodontia). *Biol. J. Linn. Soc.* 121: 409–419.

Padian, K. and E.-T. Lamm (eds.). 2013. *Bone histology of fossil tetrapods: advancing methods, analysis and interpretation*. Berkeley, CA, University of California Press.

Parfitt, M., et al. 1987. Bone histomorphometry: standardization of nomenclature, symbols and units. *J. Bone Miner. Res.* 2: 595–610.

Prondvai, E. K., et al. 2014. Development-based revision of bone tissue classification: the importance of semantic for science. *Biol. J. Linn. Soc.* 112: 799–816.

Qiu, S., et al. 2002. Relationship between osteocyte density and bone formation rate in human cancellous bone. *Bone* 31: 709–711.

Ray, S., et al. 2009. Growth patterns of fossil vertebrates as deduced from bone microstructure: case studies from India. *J. Biosci.* 34: 661–672.

VetBooks.ir

Recker, R. R., et al. 2011. Issues in modern bone histomorphometry. *Bone* 49: 955–964.

Revell, P. A. 1983. Histomorphometry of bone. *J. Clin. Pathol.* 36: 1323–1331.

Ricqlès, A. de 1968. Quelques observations paléohistologiques sur le dinosaurien sauropode *Bothriospondylus*. *Ann. Univ. Madagascar* 6: 157–209.

Ricqlès, A. de 1969. L'histologie osseuse envisagée comme indicateur de la physiologie thermique chez les tétrapodes fossiles. *C. R. Acad. Sci. Paris D* 268: 782–785.

Ricqlès, A. de 1972. Vers une histoire de la physiologie thermique I: Les données histologiques et leur interprétation fonctionnelle. *C. R. Acad. Sci. Paris D* 275: 1745–1749.

Ricqlès, A. de 1975. Quelques remarques paléo-histologiques sur le problème de la néoténie chez les stégocéphales. *Colloque International du CNRS* 218: 351–363.

Ricqlès, A. de 1976. Recherches paléohistologiques sur les os longs des tétrapodes. VII. Sur la classification, la signification fonctionnelle et l'histoire des tissus osseux des tétrapodes (Deuxième partie). *Ann. Paléontol.* 62: 71–126.

Ricqlès, A. de 1977. Recherches paléohistologiques sur les os longs des tétrapodes. VII. Sur la classification, la signification fonctionnelle et l'histoire des tissus osseux des tétrapodes (Deuxième partie, suite). *Ann. Paléontol.* 63: 33–56.

Ricqlès, A. de 1978. Recherches paléohistologiques sur les os longs des tétrapodes. VII. Sur la classification, la signification fonctionnelle et l'histoire des tissus osseux des tétrapodes (Troisième partie, fin). *Ann. Paléontol.* 64: 153–184.

Ricqlès, A. de 2000. L'origine dinosaurienne des oiseaux et de l'endothermie avienne: les arguments histologiques. *Année Biol.* 39: 69–100.

Ricqlès A. de, et al. 1991. Comparative microstructure of bone. In *Bone matrix and bone specific products*, vol. 3, ed. Hall, B. K., 1–78. Boca Raton, FL, CRC Press.

Ricqlès A. de, et al. 2004. The « message » of bone tissue in paleoherpetology. *Ital. J. Zool.*, Suppl. 1: 3–12.

Ricqlès, A. de, et al. 2008. On the origin of high growth rates in archosaurs and their ancient relatives: complementary histological studies on Triassic archosauriformes and the problem of a "phylogenetic signal" in bone histology. *Ann. Paléontol.* 94: 57–76.

Robling, A. G., et al. 2014. Mechanical adaptation. In *Basic and applied bone biology*, eds. Burr, D. B. and M. R. Allen, 175–204. Amsterdam: Elsevier -Academic Press.

Schour, I. 1936. Measurements of bone growth by alizarine injections. *Proc. Soc. Exp. Biol. Med.* 34: 140–141.

Tam, C. S., et al. 1978. Bone apposition rate as an index of bone metabolism. *Metabolism* 27: 143–150.

Van Hof, R. J., et al. 2017. Open source software for semi-autyomated histomorphometry of bone resorption and formation parameters. *Bone* 99: 69–79.

Wiffen, J., et al. 1995. Ontogenetic evolution of bone structure in Late Cretaceous Plesiosauria from New Zealand. *Geobios* 28: 625–640.

Wronski, T. J., et al.1981. Variation in mineral apposition rate of trabecular bone within the beagle skeleton. *Calcif. Tissue Int.* 33: 583–586.

VetBooks.ir

11

Bone Remodeling

Vivian de Buffrénil and Alexandra Quilhac

CONTENTS

The Multiple Functional Involvements of Bone Remodeling 229
Basic Multicellular Unit and Bone Structure Unit, the Basic Units of Bone Remodeling 231
General Characteristics 231
Basic Structure and Functioning of the Haversian BMU 231
The Haversian BSU, i.e. the Secondary Osteon 233
Histological Structure of BMU and BSU in Trabecular Remodeling 236
The Multiple Regulation Processes of Bone Remodeling 237
Remodeling and Bone Damage Repair 237
Remarks on the Regulation of Adaptive Remodeling 237
Phosphocalcic Homeostasis and the Endocrine Regulation of Bone Remodeling 238
Contribution of Vitamin D to Phosphocalcic Homeostasis 238
Influence of the Central and Sympathetic Nervous Systems on Remodeling 239
The Message of Remodeling in Fossil Bones 239
A Basic Clue in Paleophysiology 240
Remark on the Histomorphometry of Bone Remodeling in Extant and Extinct Taxa 241
Remodeling Pattern as a Clue for the Estimation of Ontogenetic Age in Fossils 241
References 242

The Multiple Functional Involvements of Bone Remodeling

The stiffness of the intercellular matrix of bone, as well as the close inclusion of the osteocytes in lacunae, do not only result in constraining bone growth in length and diameter, as described above. They also prevent internal renewal of the osseous tissue by the common processes of cell multiplication and apoptosis that prevail in nonmineralized tissues. Consequently, bone renewal necessarily requires removing, through resorption, the parts to be replaced, and the apposition *in situ* of new bone layers. These substitutive layers are thus defined as *secondary*, and the double process combining resorption and reconstruction from which they result is called bone *remodeling*. Bone *modeling* is a concept close to remodeling, but they differ in one principal aspect: modeling refers to a local modification of the outer or inner morphology of a bone through a single process of apposition or resorption (Ricqlès et al. 1991, Martin et al. 2015). Conversely, the coupling of these two processes, resulting in local replacement of osseous tissue with limited (or no) modification in bone shape, is an exclusive characteristic of remodeling.

Remodeling is one of the most essential aspects of bone biology. Its study is an important part of the research effort on skeletal tissues, and reviews are periodically published on the fundamental histogenetic aspects of this process (e.g., Parfitt 1984, Huffer 1988, Jaworski 1992, Allen and Burr 2014, Martin et al. 2015). The brief synthesis presented below does not pretend to be exhaustive, or to report all advances in this complex question; rather, it will focus on the basic knowledge required to interpret paleohistological observations. At a broad, comparative level, the taxonomic distribution of bone remodeling, at least in its Haversian form, is a puzzling issue on which contradictory statements have been (and can still be) written. The critical synthesis proposed by Ricqlès (1977a, b) remains largely relevant today.

Two main forms of remodeling (Figure 11.1A, B) are generally distinguished, depending on whether it occurs on the trabeculae of internal spongiosae, or within compact cortices, in the particular form of Haversian remodeling (also called Haversian substitution), which is a term created in reference to the early descriptions by Havers (1691). To a lesser extent, remodeling may occur on the external surfaces of the bones (superficial remodeling), where it contributes to local growth and morphogenetic processes. This peculiar case was considered in Chapter 9. The fundamental process of bone remodeling is the same in all cases and involves local populations of osteoclasts and osteoblasts (along with their respective

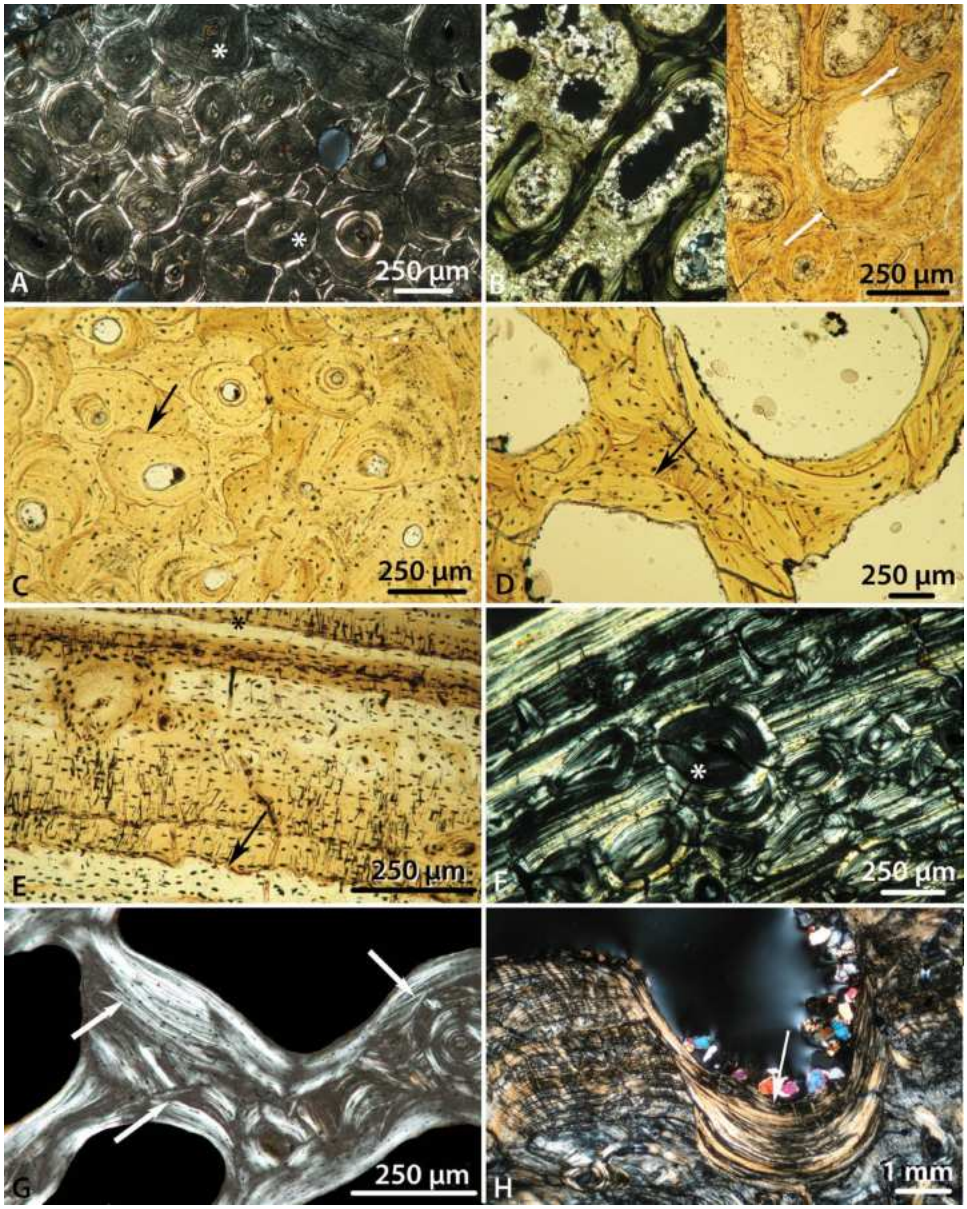


FIGURE 11.1 General diagnostic features of bone remodeling. A, Typical aspect of Haversian remodeling in transmitted polarized light, with closely packed secondary osteons (asterisks), in the femur of the fossil (Early Pliocene) sloth *Thalassocnus natans*. B, Remodeled trabeculae in the humerus of the ichthyosaur *Stenopterygius quadriscissus* (Lower Jurassic). Arrows point to reversion lines. Left half, transmitted polarized light; right half: ordinary light. C, Haversian bone in the radius of the fossil (Miocene) seal *Nanophoca vitulinoides*. The secondary osteons are bordered by conspicuous resorption lines (arrow). D, Remodeled trabeculae in a rib of the Pliocene sloth *Thalassocnus littoralis*, with conspicuous resorption lines (arrow). E, Difference between a smooth line of arrested growth (asterisk) and a scalloped resorption line (arrow) in the humerus of *N. vitulinoides*. F, Typical geometrical discordance between the bone tissue forming the wall of a secondary osteon (asterisk) and the primary (or even secondary) bone tissue surrounding this osteon. Polarized transmitted light. Rib of the fossil sloth *T. littoralis*. G, Geometrical discordance (arrows) of bone layers in a remodeled trabecula from the medulla of a beluga rib (*Delphinapterus leucas*). H, Geometrical discordance and histological difference between primary and secondary (arrow) bone in the remodeled, superficial layer of an osteoderm from the fossil (Early Eocene) crocodile *Asiatosuchus depressifrons*. Polarized light.

precursors) that form an integrated functional unit called by Frost (1969) the *basic multicellular unit* (BMU). The expression *bone metabolic unit*, used by Seeman (2008), is a rarely used synonym.

Whatever the spatial (location in bones) or chronological (ontogenetic developmental stages) context in which it occurs, bone remodeling is directly involved in the most fundamental mechanical and physiological functions of the skeleton. In addition to its contribution to the growth processes of endochondral and dermal bones described above, remodeling has a major role in three functional domains: (1) it is responsible, during development, for the fitting of inner bone architecture to local mechanical loading; (2) it repairs the osseous tissue in which fatigue damages (due to long-lasting, cyclical loading

VetBooks.ir

of the bones) accumulate, and thus contributes to delay bone aging and (3) by the release and recycling of the mineral salts contained in bone matrix, it is a key factor in phosphocalcic homeostasis.

The histological traces of bone remodeling are extremely clear and legible in all kinds of sections from fresh or fossil bone samples. Haversian substitution (Figure 11.1A) is the most easily recognizable, and thus the most studied and best known form of remodeling. All vertebrates can display it, with variable intensity, from Silurian agnathans (Downs and Donoghue 2009, Giles et al. 2013) to mammals, with the notable exceptions of the long bones of lissamphibians and squamates, in which it is unusual (Enlow and Brown 1956, 1957, 1958, Ahmed et al. 2017, Canoville et al. 2017; see also Chapters 17 and 20). Histological signs of remodeling in extant and extinct vertebrates can be precious clues for interpreting the functional context (biomechanical, physiological or morphogenetic) that prevailed when these structural details were recorded in the bones, and they provide crucial information.

Basic Multicellular Unit and Bone Structure Unit, the Basic Units of Bone Remodeling

General Characteristics

The BMU is a temporary morphofunctional structure, directly involved in local bone replacement and comprising, in addition to the cell populations mentioned above, an arterial and a venous capillary, along with nervous fibers. Inside each BMU, the number of osteoclasts is fewer than that of the osteoblasts, in a proportion of about 1 to 400 (Jaworski 1992). This basic cellular composition has three main characteristics. (1) It is restricted in space to a definite spot, or *locus*. Although each BMU is necessarily subject to spreading, it remains distinct from other, neighboring BMUs, if any.. (2) BMUs are also limited in time. In Haversian remodeling, a BMU remains active for 6–7 months, a period in which the reconstruction stage is three to four times longer than the previous resorption stage (Manolagas 2000). However, bone remodeling is basically an iterative process (unlike modeling), and several successive BMUs can occur at the same locus or in closely spaced, partly overlapping loci. (3) The activity of each BMU is divided into three stages, commonly designated by the letters A, R and F. The initial stage is the *in situ* activation (A) of the BMU, with the recruitment of the osteoclast population and the creation of a vascular diverticulum. A resorption stage then follows (R), accompanied, with a certain time lag by a stage of secondary bone formation (F) by osteoblasts. Parfitt (1984) and Martin et al. (2015) considered two additional stages: a quiescence stage preceding and following the activity period of the BMU, and a reversion stage, inserted between the resorption and the formation stages.

The origin, differentiation and *in situ* transportation of BMU cells is a complex and still incompletely elucidated problem (reviews in Manolagas 2000, Eriksen 2010, Bellido and Hill Gallant 2014, Domenech 2017). Osteoclast precursors, the monocytes, are of the blood cell lineage and originate from hematopoietic stem cells (HSCs) in bone marrow (see Chapter 5). They are brought to remodeling loci by the blood flow. The constitution of a BMU thus requires the proximity of arterial and venous capillaries which can be part of (1) intracortical vascular networks (in Haversian remodeling); (2) be housed in the tissues filling the medullary cavities (trabecular and perimedullary remodeling) or (3) derive from the periosteum vascularization or constitute the superficial outcrop of intracortical blood vessels, in the case of superficial remodeling. Syntheses of the contribution of blood vessels to local bone remodeling can be found in Barou et al. (2002), Cooper et al. (2003) and Lafage-Proust et al. (2015).

The origin of BMU osteoblasts has long been debated. There is currently some agreement that, in the case of inner remodeling (in bone cortices or on medullary trabeculae), they originate from populations of mesenchymal stem cells (MSCs) located in the medullary stroma (e.g., Krampera et al. 2006). However, contrasting statements have also been published on this topic (e.g., Otsuru et al. 2017). The complex pathways involved in the differentiation of these MSCs into preosteoblasts are discussed in Aubin (2008), Domenech (2017) and Tamma and Riballi (2017) (see also Suda et al. 1995 and Kristensen et al. 2014). The preosteoblasts integrated into Haversian BMUs are supposed to be brought *in situ* by blood vessels, as are the monocytes (Zaidi et al. 2012). In the case of superficial remodeling, active osteoblasts obviously belong to the cambial layer of the periosteum. The structures of Haversian and trabecular BMUs have some different characteristics, as explained below.

At the end of the five main stages of BMU activity, a typical histological structure called the *bone structural unit* (BSU) is created. The detailed organization of BSUs varies with the substrate on which the BMUs operate (see below); however, all BSUs display two unequivocal diagnostic characteristics. (1) Each BSU is bordered by a *reversion line* (also called *resorption line* or *cementing line*) that marks the boundary of the previous resorption (Figure 11.1B–D). Reversion lines are not usually mistaken for other histological features, except maybe *lines of arrested growth* (see Chapter 31), from which they differ by having a crenellated contour typically due to the action of osteoclasts (Figure 11.1E). (2) On both sides of a reversion line, bone deposits are most often of different histological types, and they always show conspicuous geometrical discordance (Figure 11.1F–H).

Basic Structure and Functioning of the Haversian BMU

The histological structure, as well as the developmental dynamics, of bone multicellular units in Haversian remodeling have been abundantly documented and illustrated, since the pioneering work by Frost (1969; see also Huffer 1988, Jaworski 1992, Parfitt 1994, Martin et al. 2015). However, the initial events immediately subsequent to their activation in a given locus remain poorly understood and have not, up to now, been precisely described. According to Tappen (1977), Haversian BMUs begin with the transverse branching of an intracortical capillary at a “breakout zone”. A similar interpretation, based on three-dimensional (3D)-reconstructions of vascular networks in cortices, was proposed by Cooper et al. (2003),

VetBooks.ir

who described the initial development of a BMU in the form of the lateral, angled diverticulum of a vascular canal. Although a close link seems to exist between the onset of Haversian BMUs and the spatial density of local blood vessels, the precise relationship between preexisting vascularization (whether it is housed in simple vascular canals, primary osteons or already constituted Haversian systems) and the local activation of a Haversian BMU remains obscure. Moreover, it is not clearly settled whether Haversian BMUs progress, in parallel with longitudinal blood vessels, in both proximal and distal directions and are thus double ended, or whether they develop in one direction only (see, for example, Cooper et al. 2003, Figure 10). Additional information on this question, for which contrasting data exist, is given below.

Once fully formed within bone cortices, Haversian BMUs show a characteristic structure summarized in Figure 11.2. Other reconstructions based on similar principles are given in Lacroix (1970), Parfitt (1994), and Martin et al. (2015). The quantitative data given below are mainly from Jaworski (1992) and Parfitt (1994). Morphologically and functionally, a Haversian BMU is a polarized structure displaying a roughly conical apical pole, the *cutting cone,* that houses 8–10 typical polynucleated osteoclasts. In human bones, the cutting cone is generally about 200 µm in basal diameter, with a length of about 300 µm. It is followed by a shorter (150- to 200-µm-long) cylindrical part of the same diameter, called the *reversion zone*, the walls of which are covered with osteoblasts in the course of their differentiation (preosteoblasts). This zone merges distally with the so-called *closing cone*, where several thousand (up to 4000) functional osteoblasts, distributed over a length of about 1.5 mm, centripetally deposit a thick layer of osteoid tissue around the central capillaries. The osteoid gradually mineralizes and turns into lamellar or parallel-fibered bone. At the terminal (distal) end of the closing cone, the reconstruction of the walls of the tunnel is completed, less the width of the central neurovascular canal, the Haversian canal. Haversian BMUs thus feature intracortical tunnels, which are blind at both ends.

The cutting cone excavates the bone cortex (stage R), through classical osteoclastic resorption, at a rate of about 40–50 µm per day in a longitudinal direction, and about 5 µm*day^{-1} in a radial direction. In parallel with resorption, but with a delay corresponding to the time required for the differentiation of preosteoblasts into functional osteoblasts, the reconstruction of the walls of the tunnel begins (stage F). Local bone formation in a given transverse plane lasts about 40–60 days, at a rate of 1–2 µm*day^{-1} (this rate decreases progressively). Cell kinetics strongly differs between osteoclast and osteoblast populations (Jaworski and Hooper 1980). Osteoclasts are mobile cells that migrate within the cortex in pace with the resorption they exert on it. They are partly regenerated by the adjunction of new monocytes, but the same cells remain active as long as the resorptive stage occurs. Conversely, once recruited, osteoblasts stay in place. Their population follows the stretching of the BMU by recruiting new cells in the reversion zone. When bone deposition on the walls of the Haversian system is completed, the osteoblasts become quiescent, lose the organelles related to active protein secretion, and display a flat shape. They thus constitute *lining cells* that cover the surface of the Haversian canal, which remains indefinitely open to house the blood vessels and nervous fibers mentioned above.

The mineralization of the thick osteoid layer formed by the osteoblasts is delayed for about 10 days and then progresses gradually over a period of about 6–7 months (up to 12 months, according to Parfitt 1994), which is the normal life span of an osteonal BMU. Two-thirds of the mineral content is deposited within the first three weeks.

At all stages of the life of a BMU (be it Haversian or not), osteoclasts, preosteoblasts, osteoblasts and osteocytes communicate with and react with each other through gap junctions and multiple intercellular (paracrine) messengers. This complex subject is beyond the scope of this book. Recent reviews are available in Xiong and O'Brian (2012), Schaffler et al. (2014),

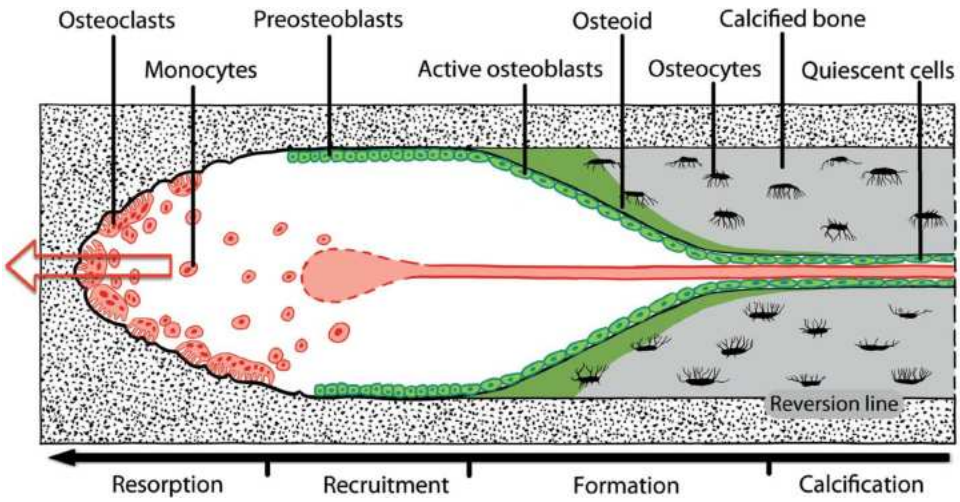


FIGURE 11.2 Structure of Haversian BMU. Basic developmental processes and cell population of a BMU. The processes (i.e., resorption, recruitment of preosteoblasts and osteoblasts, formation of new osteoid and calcification) are indicated below the sketch, and the various cell populations of the BMU are indicated above.

VetBooks.ir

Sims and Martin (2014) and Lassen et al. (2017). Through this *coupling* process (a concept proposed by Baylink and Liu 1979; see also Parfitt 1982), the amount of bone eroded by the osteoclasts is entirely balanced (less the volume of the Haversian canal) by the tissue deposited by the osteoblasts. Coupling failure results in imbalance, most often toward bone resorption, thus creating a net loss of bone mass . This situation is the cause of a general, age-dependent skeletal pathology, osteoporosis (see Chapter 32). Excess apposition of reconstructive bone during stage F also occurs. It results in sealed osteons (review in Skedros et al. 2018). According to Congiu and Pazzaglia (2011), osteon sealing might be a result (instead of a cause) of a collapse and degeneration of the central blood vessels of the BMUs. In terrestrial tetrapods, the diverse situations of imbalanced remodeling are clearly pathological. However, a propensity to develop them in early growth stages may be advantageous for some types of locomotory adaptations (e.g., flying, swimming) and undergo positive selection. This question is further considered in Chapters 35 and 36.

The Haversian BSU, i.e., the Secondary Osteon

In general textbooks of histology, the osseous tissue is essentially described in reference to Haversian bone, a tissue made of closely packed secondary osteons (Figure 11.3A). Detailed descriptions of Haversian systems are available in Krstić (1985) and Fawcett and Jensh (1997).

When a Haversian BMU stops functioning, the resulting secondary osteon acquires its definitive structure (Figures 11.1A, C, F; 11.3A), although its mineralization is not yet fully completed (Figure 11.3B). In humans, longitudinal sections show that a secondary osteon consists of a tube several millimeters long for a width (i.e., diameter) of about 200 µm. In other taxa, the dimensions of the osteons can be different; for example, they reach 300–500 µm in diameter in the ziphiid whale *Mesoplodon densirostris* (Buffrénil and Casinos 1995). When fully developed, at the onset of the final quiescent stage, the walls of this tube are about 70–80 µm thick, and the lumen of the central Haversian canal is usually 20–50 µm wide in young, healthy adults (Jaworski 1992, Qiu et al. 2003). However, osteons with a much smaller Haversian canal (less than 10 µm; Figure 11.3C) or even entirely occluded (sealed osteons) have been observed in diverse taxa (review in Skedros et al. 2018; see also Lambert et al. 2011, Dewaele et al. 2019). Sagittal sections (e.g., Krstić 1985) and tomographic 3D reconstructions (Cooper et al. 2003) suggest that a secondary osteon first appears as two blind tubes of similar or different lengths (3–5 mm), developing symmetrically on both sides of the vascular diverticulum formed in the early stage of BMU activation. This diverticulum, Volkmann's canal, actually consists of a transverse anastomosis between the Haversian canals of two neighboring osteons. It is a simple tube (Figure 11.3D) excavated within the bone cortex. The whole set of Haversian systems in the cortex of a bone thus appears as a network of roughly parallel elements, united by short transverse bridges (Figure 11.3E). Recent synchrotron observations by Maggiano et al. (2016) revealed a more complex pattern, with strongly oblique Volksmann's canals, branching osteons or osteons developing in one direction only from the Volksmann 's canals. In the long bones of humans and some domestic artiodactyls, Haversian systems are oriented longitudinally, with a slight helical rotation in opposite directions on the medial and lateral walls of the bones (Dhem 1967, Petrtyl et al. 1996).

The spatial density of Haversian BSUs among taxa varies broadly with phylogeny (Enlow and Brown 1956, 1957, 1958, Ricqlès 1977a, b), individual life history traits (age, sex, reproductive status: Kerley 1965, Martin 1991, Mitchell et al. 2017), the bones considered in an individual skeleton, the regions of a single bone (Klein et al. 1990, McFarlin et al. 2008) and the immediate physiological requirements of an animal. In most vertebrate taxa, Haversian remodeling tends to spread gradually from deeper (older) to more superficial (recent) cortical layers (Figure 11.3F, G). When secondary osteons occur in high density, a situation encountered in large tachymetabolic tetrapods (see Chapter 37), they form so-called *dense Haversian tissue*. In this kind of tissue, several generations of secondary osteons occur subsequently, overlapping each other (Figures 11.1A–C and 11.3A–D). Cross sections of dense Haversian bone often show BMUs at various periods of their activity (Figures 11.3B and 11.4A), i.e., osteons at various stages of achievement. In a single sectional plan, fully completed osteons may coexist with a cutting cone (cavity of smaller diameter than the osteons), a reversion zone (cavity of same diameter as the osteons) and a closing cone that was active when the animal died (broader Haversian canal than in an osteon). Concentric osteons, representing two distinct generations centered on the same Haversian canal, were described by Lacroix (1970), and recently observed by Dewaele et al. (2019) in the osteosclerotic bones of a fossil seal (Figure 11.4B). Similarly, a secondary osteon may develop within the wall of another, already present osteon (Figure 11.4C). Histologically, the walls of secondary osteons most often consist of pure lamellar bone tissue displaying an orthogonal plywood structure (Figure 11.4D, F; see also Chapter 8). In cross section, secondary osteons can occasionally be monorefringent in polarized light (Figure 11.4A, E, F); this aspect reveals the occurrence of parallel-fibered tissue with a dominant longitudinal fiber orientation.

In the same kind of sections, secondary osteons are typically lined with a reversion line that shows the boundary between the osteoclastic resorption front and the contour of the reversion zone once present when the BMU was active (e.g., Figure 11.1C). Osteoblastic reconstruction of the tunnel walls started at this level. The reversion line is an absolute and diagnostic signature of bone remodeling, whatever the substrate on which this process takes place. It is the sole morphological clue that distinguishes a secondary from a primary osteon (the latter lacks the reversion line). As mentioned above, another diagnostic feature of bone remodeling is the geometric discordance of osseous layers (which can additionally be of different kinds) on both sides of the reversion line.

Osteocyte populations embedded in the walls of secondary osteons are morphologically typical of the lamellar and parallel-fibered tissues (i.e., the products of so-called dynamic osteogenesis). They generally display abundant canaliculi converging toward the lumen of the Haversian canal and the capillaries housed in it (Figure 11.4G). The canaliculi develop either symmetrically on the sides of the osteocyte soma, or asymmetrically from the medial side of the cell body. They are

VetBooks.ir

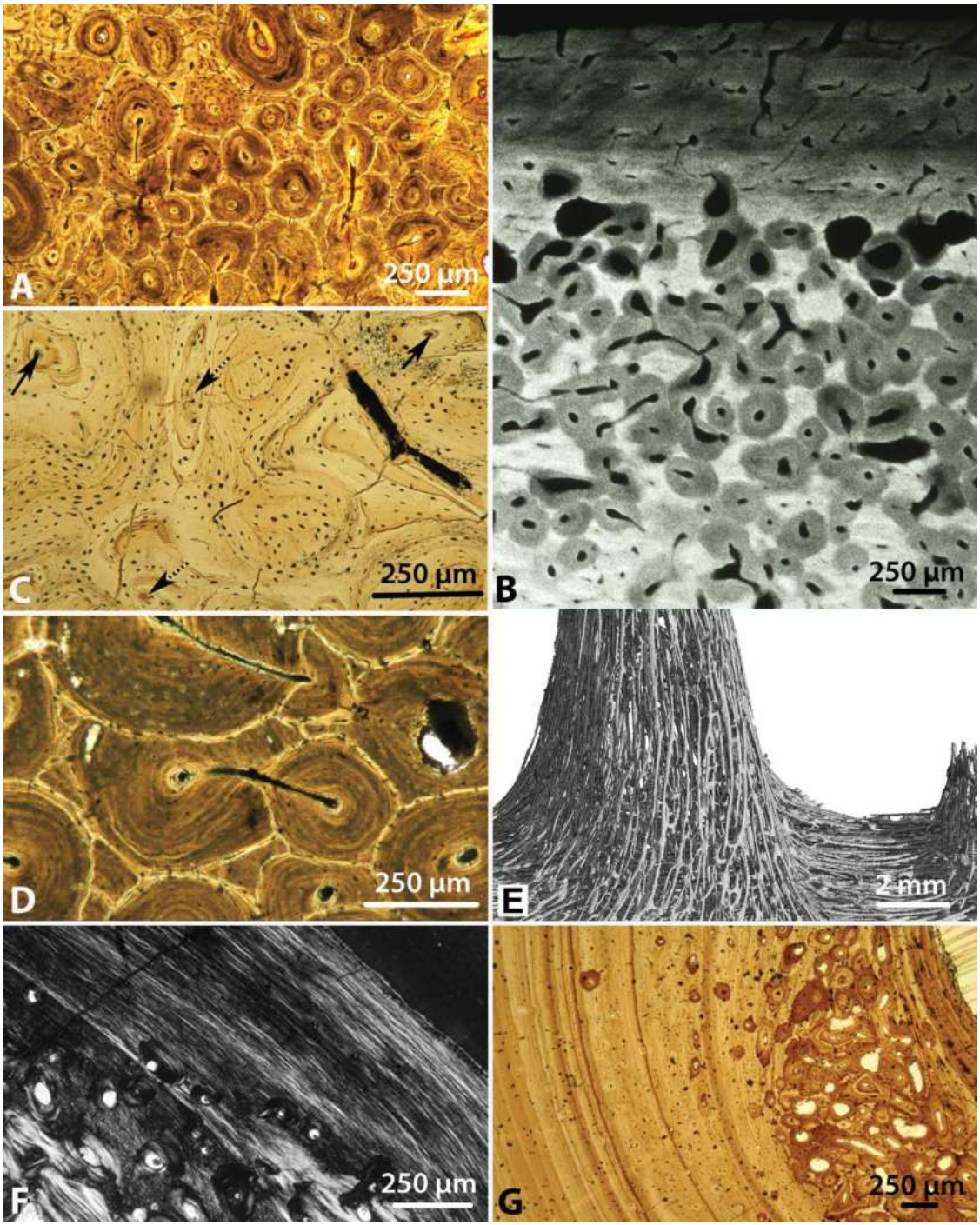


FIGURE 11.3 Characteristics of Haversian BSU. A, Closely packed secondary osteons forming dense Haversian tissue. Polarized light. B, Differences in mineralization rates of the osteons according to the timing of their formation. Microradiograph of a section in the exoccipital of a sirenian mammal (*Dugong dugon*). Older osteons, located in the deep cortical region, are more mineralized (i.e., more radiopaque) than more recent ones in superficial layers. Several Haversian BMUs were still active, at the R or F stages, when the bone was sampled. C, Minute (solid arrows) or occluded (dotted arrows) Haversian canals in the osteons of the compact premaxillae of the fossil (Neogene) ziphiid whale *Choneziphius* sp. D, Close view of a Volkmann's canal uniting the Haversian canals of two neighboring secondary osteons. Humerus of *Thalassocnus littoralis*. E, Haversian and Volkmann's canals in the remodeled mandible and pseudotooth of the Miocene toothed bird *Pelagornis mauretanicus*. Computed tomography (CT)-scan 3D reconstruction. F, Mild Haversian remodeling in the basal cortex of the femur of *Iberosuchus macrodon*, an Eocene crocodile. Polarized light. G. Spreading of Haversian remodeling from the deep, perimedullary region of a bone to its superficial cortical layers. Femur of the Upper Jurassic crocodile *Goniopholis* sp.

VetBooks.ir

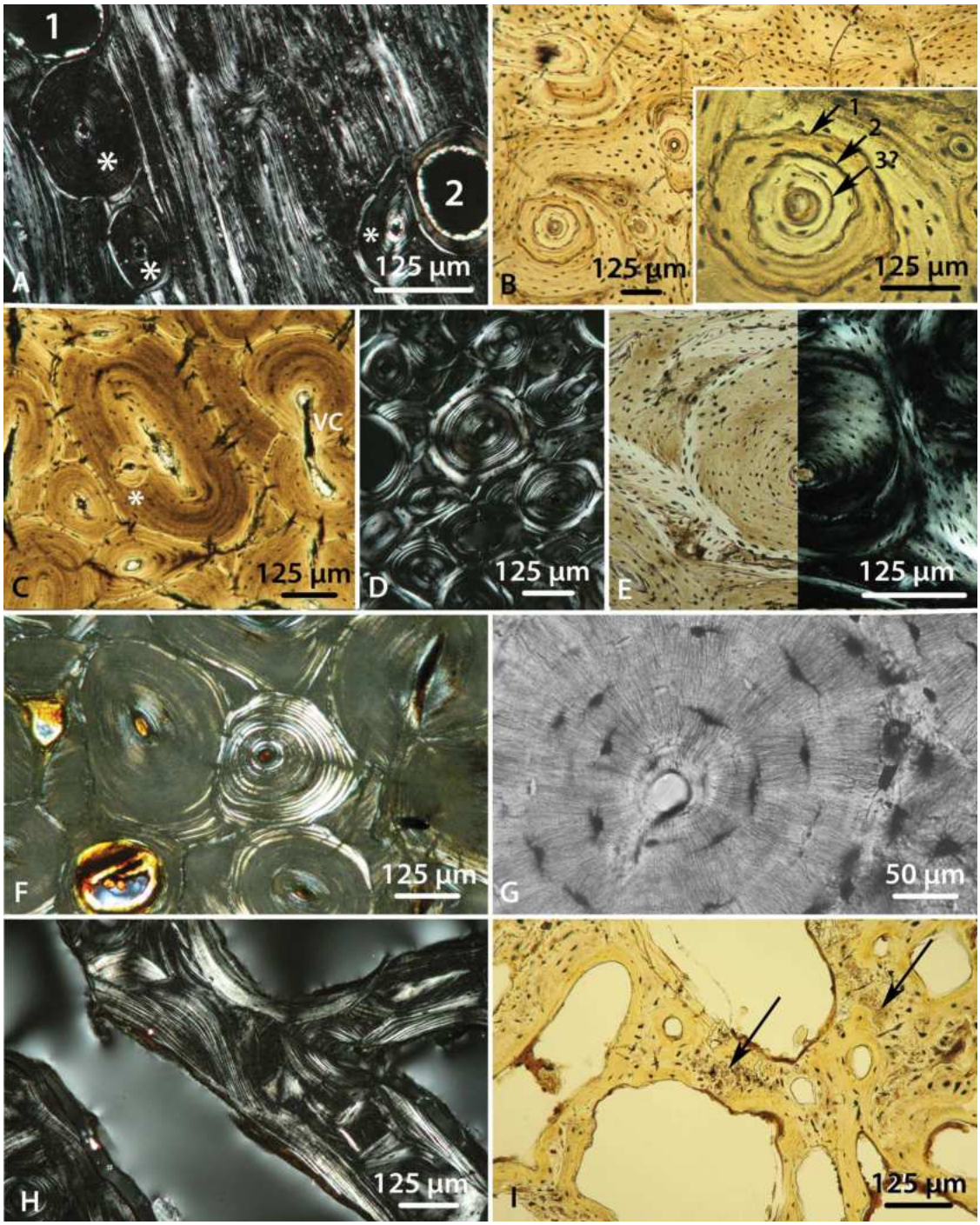


FIGURE 11.4 Peculiarities of remodeling BSUs. A, Haversian BMU and BSU at various stages. The cavity at the left upper corner (1) represents the reversion zone of a BMU, whereas that located at the lower right corner (2) shows the beginning of the formation zone. Three complete osteons (i.e., quiescent stage) are indicated by asterisks. Rib of a harbor porpoise *Phocoena phocoena*. B, Concentric secondary osteons (general and closer views) in the radius of *Nanophoca vitulinoides*. The resorption lines corresponding to two osteon generations (1 and 2) are well visible, and a third line is possible (3). C, Secondary osteon within the wall of another osteon (asterisk). A Volkmann's canal (VC) is visible along the right border of the picture. Rib of *Thalassocnus littoralis*. D, Secondary osteons made of lamellar bone in a rib of a common dolphin, *Delphinus delphis*. Polarized light. E, Osteon made of parallel-fibered bone tissue in the rostrum of the beaked whale *Mesoplodon densirostris*. Right half: polarized light. F, Coexistence of osteons made of lamellar and parallel-fibered tissues within a single bone section. Rib of the Upper Oligocene whale *Squalodon calvernensis*. Polarized light. G, Close view of a secondary osteon (rib of *P. phocoena*) showing the osteocytes and their canaliculi converging toward the Haversian canal. H, Complex assemblage of trabecular BSUs in the rib of *Desmostylus* sp. (Mammalia, Desmostylia). Polarized light. I, Persistence at mid-diaphysis of non-resorbed remnants of calcified cartilage matrix (arrows) in the medulla trabeculae of a rib from the Late Eocene whale (basilosaurid) *Zygorhiza kochii*.

in contact through gap junctions, and thus form a consistent network around the Haversian canal (e.g., Curtis et al. 1985 and Chapters 5 and 8).

Histological Structure of BMU and BSU in Trabecular Remodeling

Trabecular remodeling in the metaphyseal and diaphyseal regions starts earlier than Haversian remodeling in compact cortices (although the latter can already be active in the fetus; Burton et al. 1989). It appears when endochondral ossification begins and progresses in pace with the conjunctivovascular erosion front toward the proximal and distal epiphyses of the bones. The result of this process is the creation of primary endochondral trabeculae, composed of a core of calcified cartilage, covered by lamellar deposits. As soon as they are formed, these trabeculae show evidence of remodeling in their superficial osseous layer. Remodeling will then persist, with variable intensity, up to the latest stages of life. Each year, about 25% of the total volume of cancellous bone is replaced through trabecular remodeling in humans (Huiskes et al. 2000, Parfitt 2002).

The basic structural organization of trabecular BMUs (Figure 11.5), i.e., an osteoclastic resorption front followed by a reversion zone with preosteoblasts and a formation zone with active osteoblasts (e.g., Parfitt 1994, Delaisse 2014), is roughly comparable to that of Haversian BMUs, as is their general functioning. This is why the trabecular BMU is often designated as a *hemiosteon*. Several structural details nevertheless distinguish these two BMU types. Osteoclastic resorption in trabecular BMUs is superficial. Although it can initially have the shape of a groove, it does not result in a tunnel, but in a shallow, irregular pit housing ramified blood vessels (Delaisse 2014). However, the main difference between a Haversian and a trabecular BMU is the presence of a veil-like formation of cells, called the *canopy* (Hauge et al. 2001), covering the marrow side of the trabecular BMU (Figure 11.5). The cells of the canopy are interpreted as quiescent osteoblasts derived from endosteal lining cells (Eriksen 2010, Delaisse 2014). They are supposed to play an important role in both osteoblast recruitment, by supplying the reversion zone in preosteoblasts, and in cellular coupling (Hauge et al. 2001, Eriksen 2010, Jensen et al. 2015). The whole structure of a trabecular BMU thus features a distinct compartment closed by the canopy; for this reason, it is often called the bone remodeling compartment (BRC).

The origin of the cell populations in trabecular BMUs is still debated. Recent studies have pointed out the primary role of marrow vascularization on local remodeling (Barou et al. 2002, Lafage-Proust et al. 2010, Maes and Clemens 2014), and the *in situ* supply of monocytes by capillaries seems unquestionable (Blair and Zaidi 2006, Andersen et al. 2009). However, the origin of the osteoblasts is less clear. Two main recruitment pathways (both hypothetical) have been considered: (1) osteoprogenitors derived from marrow MSCs and (2) the canopy lining cells mentioned above (Kristensen et al. 2014, Sims and Martin 2014, Jensen et al. 2015).

According to data from Eriksen et al. (1984a, b) that deal with the human iliac crest, the average resorption rate in a trabecular BMU is 1.4 µm*day^{-1} for 48 days, up to a depth of about 65 µm. The mean apposition rate during the F stage is 1.1 µm*day^{-1} for 150 days. Therefore, a trabecular BMU is active during about 200 days; then its osteoblasts become quiescent lining cells in continuity with the endosteum. Recent data by Lassen et al. (2017) show that bone apposition in the formation zone begins only when a threshold of cell density is reached in the reversion zone. The coupling of osteoblastic and osteoclastic activities results in properly balanced remodeling. In long-lived animals, this process can be affected by age, which results in a general loss of bone mass and a collapse of the mechanical competence of the cancellous parts of the bones. As in Haversian BMUs, the mineralization process of the osteoid secondarily deposited in the formation zone starts

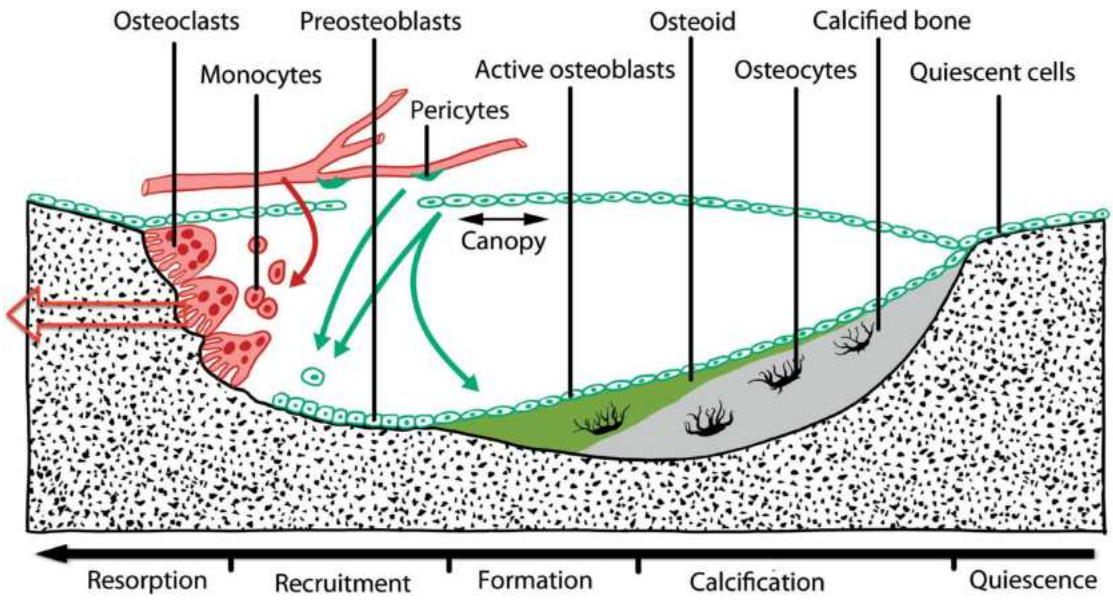


FIGURE 11.5 Structure of trabecular BMU. The basic processes and cell population are the same as described in Figure 11.2.

VetBooks.ir

with a delay of some 15 days and proceeds as long as the BMU is active.

In cross section, a trabecular BSU appears as a crescent, or a meniscus, of lamellar bone tissue bordered on its deep side by a reversion line (Figures 11.1D, G and 11.4H) and, on its superficial side, by lining cells. There is no differentiated vascular canal. In the bones of adult individuals of most vertebrate taxa, osseous trabeculae (whether located in the diaphysis, the metaphyses or the epiphyses) are always entirely formed of a dense accumulation of overlapping BSUs (Figures 11.1D, G and 11.4H). This obviously reflects sustained remodeling. The only exceptions are encountered in neotenic forms (e.g., amphibians) or in some tetrapods secondarily adapted to an aquatic life (Ricqlès and Buffrénil 2001), in which an alteration of the normal sequence of endochondral ossification results in a life-long maintenance of calcified cartilage in the core of the trabeculae (Figure 11.4I; see also Chapter 37).

The Multiple Regulation Processes of Bone Remodeling

Remodeling and Bone Damage Repair

It is currently accepted that one of the basic functions (if not the main one, according to Martin 2002) of bone remodeling, whether Haversian or trabecular, is to locally renew the bone tissue in which fatigue microfractures have accumulated and compromise its mechanical capabilities (e.g., Burr et al. 1985). Repeated mechanical stresses indeed provoke, at the relatively low threshold of 1500 loading cycles (in, e.g., a dog skeleton; Burr et al. 1985), small lesions in bone extracellular matrix in the form of cracks 150–250 µm long and a number of microns wide (Lee et al. 2003, Landrigan et al. 2011). The coalescence of these fractures may result in a collapse of bone resistance (Danova et al. 2003), a process particularly frequent in long-lived species such as *Homo sapiens* (Schaffler et al. 1995). Remodeling involvement in the biomechanical preservation of bone tissue occurs at two levels: (1) it blocks the propagation of the cracks and (2) it operates the replacement of the degraded tissue. Histomorphometric data by Norman and Wang (1997) showed that an important proportion (62.4%) of secondary osteons is topographically related to the local presence of microcracks. Moreover, the rich set of experimental data summarized by Mohsin et al. (2006) and O'Brian et al. (2007) reveal that reversion lines act as barriers able to stop the propagation of microcracks less than 300 µm long. The hypothesis considering that all (100%) of Haversian BMUs are associated with microcracks, and that their prominent function is thus to repair mechanical damage, was tested and supported by 3D mathematical models (Martin 2002) integrating the dynamic aspects of Haversian remodeling (i.e., travel through bone of the cutting cone). Such a conclusion otherwise agrees with previous experimental data (Verborgt et al. 2000) designating microcracks as the main activator of bone remodeling. The diverse and complex biological implications of the model of Norman and Wang (1997) are further discussed below.

The role of microcracks in BMU activation was considered questionable in the 1990s (cf. Burr 1993); it is now viewed as the best hypothesis to resolve the topographical and chronological problems related to the involvement of bone remodeling in microdamage repair. An accumulation of data (reviewed by Florencio-Silva et al. 2015) shows that osteocyte apoptosis can be directly caused by microcrack propagation. Live osteocytes secrete a factor close to a *transforming growth factor* (TGF)-β that inhibits osteoclast differentiation and activity (Heino et al. 2002). When the osteocytes die, this factor is no longer secreted, and this situation results in osteoclast stimulation and BMU activation. Moreover, osteocytes act as mechanoreceptors and can be affected by the disturbance of their immediate neighboring environment due to microcrack propagation. In such conditions, they secrete "soluble factors" (Verborgt et al. 2000, Kurata et al. 2007), identified as macrophage colony-stimulating factors (M-CSF), which stimulate osteoclast differentiation (Zao et al. 2002, Henriksen et al. 2009, Schaffler et al. 2014).

Although the influence of microcracks on local bone remodeling is no longer questioned, elementary comparative data suggest that the mere presence of these lesions is unlikely to be, by itself, the sole and exclusive explanation for BMU activation (as proposed by Martin 2002). Instead, they should represent a frequent, but circumstantial, correlate of this process. Indeed, bones undergoing strong mechanical constraints can be devoid of any intracortical remodeling, as in the whole skeleton of lissamphibians and squamates, including large active predators such as Varanidae or Teiidae (see Chapters 17 and 20). Conversely, bones with limited mechanical involvement (e.g., skull or face bones) can be made of dense Haversian tissue (e.g., Marotti 1968). These observations imply that, if osteocyte lesions or apoptosis rank among the fundamental causes of BMU activation, as suggested by experimental studies, in the reality of histological facts, this situation should be directly due to microfractures in only 62.4% of cases, according to Norman and Wang (1997). The remaining 37.6% should then be due to other causes. Several authors considering nonmammalian models questioned the prevalence of mechanical strain in the causality of secondary osteon proliferation (e.g., Meers 2002 in crocodiles). Padian et al. (2016), pointing out that large stylopod elements are poorly remodeled in dinosaurs, whereas smaller zeugopodial bones are proportionally more densely remodeled, hypothesized that, in reference to nutrient allocation, the largest bones "grow too rapidly to deposit secondary tissues". Nutrients would then "largely be used in primary bone deposition". This interesting hypothesis calls for further substantiation.

Remarks on the Regulation of Adaptive Remodeling

The activation and control of the remodeling process responsible for the accommodation of trabecular architecture to the mechanical loading patterns of the bones, i.e., the adaptive remodeling as defined by Lanyon et al. (1982), is not due to apoptosis of the osteocytes, but to their mechanoreceptive capabilities. A direct involvement of nondestructive mechanical constraints in remodeling control was initially proposed by Justus and Luft (1970), but in reference to a causal process, i.e.,

VetBooks.ir

a chemical modification of apatite crystals, no longer accepted today. Experimental data by Tan et al. (2007), as well as finite-element models (Huiskes et al. 2000, Smit and Burger 2000; see also Tsubota et al. 2002), show that the activity of cell populations in trabecular BMUs (and probably also of Haversian BMUs; see Smit and Burger 2000) respond to the mechanical stresses traveling through cortices and spongiosae. Osteocytes are likely to detect such stresses through the tiny movements thus provoked in the fluid filling the gap between their soma, with dendritic extensions, and the walls of the lacunae and canaliculi that house them (Mak et al. 1997, Tan et al. 2007, see also You et al. 2001).

Although osteocyte mechanosensitivity is now firmly settled (review in Florencio-Silva et al. 2015), the process by which live osteocytes trigger and regulate BMU activity remains hypothetical (see, for example, the model proposed by Burger et al. 2003). *In vitro*, mechanically stimulated osteocytes have an inhibiting action on osteoclast recruitment and activity (Tan et al. 2007, You et al. 2008). Moreover, the progression of BMUs within bone volumes or on bone surfaces tends to be aligned with the direction of main local stresses (Burger et al. 2003, Oers et al. 2008). Data currently available suggest that osteocytes have a double and contrasting effect on BMU osteoclasts: under mechanical stimulation, live osteocytes have an inhibiting influence on the osteoclasts; conversely, injured or dead osteocytes stop exerting this negative influence, and indirectly favor osteoclast recruitment and activity. These limited and, to some extent, paradoxical results (remodeling necessarily begins by active osteoclastic resorption) are far from exhausting the particularly complex subject of adaptive remodeling, especially for the "geometrical competence" underlying this process.

Phosphocalcic Homeostasis and the Endocrine Regulation of Bone Remodeling

The main systemic regulator of bone remodeling is the antagonistic couple formed by parathormone (PTH) and calcitonin (CT). The role of PTH as a factor increasing blood calcium has been suspected since the beginning of the 20th century, and experimentally revealed in the first quarter of this century (review in Potts 2005). The antagonistic role of CT, a hormone provoking a decrease in calcemia, was first shown in the 1960s (review in MacIntyre 1967). These two hormones mainly operate through their influence on bone remodeling. This is a universal process in vertebrates, including forms (e.g., osteichthyans) that lack differentiated parathyroid glands. In this case, the secretions of PTH and CT are made by the ultimobranchial bodies. The genetic equipment involved in the hormonal control of calcemia in vertebrates is supposed to have already been acquired by the Placoderms about 400 MA ago (Sasayama 1999).

PTH is a protein of variable structure and molecular weight among taxa (e.g., it includes 84 amino acids and weighs 9400-Da in mammals: reviews in Potts 2005, Danks et al. 2011). Beyond these discrepancies, the physiologically active part of this molecule, i.e., its terminal region, is fairly conservative and has a broad interspecific activity (Potts 2005). Similarly, CT, a protein about 3600 Da in weight, also proves to be very conservative, with considerable overlap in amino acid sequences among vertebrate taxa (MacIntyre 1967, Sasayama et al. 1992). Its interspecific efficiency has also been shown (synthetic data in Dix et al. 1970, see also Filipović et al. 2017).

The numerous experimental data accumulated since Collip's (1925) study show that PTH secretion responds to a state of hypocalcemia detected by the calcium-sensitive receptors of the parathyroid cell membrane (reviews in Brown 2008). In its osseous target, PTH directly or indirectly influences several cell populations through a specific (though roughly similar in all types of target cells) receptor, PTH1R (Jüppner 1995, Potts 2005, Gardella et al. 2008). Available data suggest that, paradoxically, the first targets of PTH are the membrane receptors of osteocytes (Xiong and O'Brian 2012). At this level, PTH stimulates the expression of *receptor activator of nuclear factor kappa-B ligands* (RANKLs), a particular family of cytokines involved in the differentiation of bone cells, and subsequently the emission of other cytokines that favor the recruitment and activation of both osteoclasts and osteoblasts (review in Bellido et al. 2014, see also Xiong and O'Brian 2012). The overall result of this process is, nevertheless, a relative increase in bone resorption. Although the general action of PTH on its osseous target cells, the intensity of bone remodeling and, finally, the level of blood calcium, are relatively well settled, the detailed role of this hormone in the initial activation of BMUs remains insufficiently documented.

CT secretion is a response to calcemia increase, as detected by the receptors of C-cell membranes. In bone, this hormone binds to specific receptors in osteoclast membranes, stops the activity of these cells and provokes a regression of the plasmic organelles involved in bone resorption (Hu and Gagel 2008). However, CT is poorly active in adult individuals, at least in mammals (in other taxa, it has a much stronger action: Sasayama et al. 1992), and its actual role in BMU regulation seems to be limited (Hadjidakis and Androulakis 2006).

Other hormones can influence bone remodeling in diverse directions. Sexual steroids (estrogens and androgens) tend to reduce osteoclast activity and maintain remodeling balance (Matsumoto 2006, Wiren 2008). Conversely, an excess of thyroxine increases remodeling intensity and creates imbalance toward resorption, resulting in a net loss in bone mass (Stern 2008). Bone turnover and mineralization are also influenced by direct and indirect actions of vitamin D_3 on bone cells (Huffer 1988, Driel and van Leeuwen 2017, Williamson et al. 2017).

Contribution of Vitamin D to Phosphocalcic Homeostasis

Vitamin D is an important factor for the endocrine machinery that regulates levels of calcium and phosphorus in the blood. Most of the vitamin D required daily (most studies deal with humans) is synthesized, in the form of vitamin D_3 (cholecalciferol), from the cholesterol molecule by the skin exposed to ultraviolet light (review in Holik 2008). Despite its name, vitamin D_3 is a steroid hormone rather than a vitamin. Complementary incomes of vitamin D, absorbed by the intestine, are provided by plants (in the form of vitamin D_2, or ergocalciferol) or animals (D_3; general reviews in Norman 2008).

VetBooks.ir

Vitamin D circulates in the bloodstream associated with a binding protein, DBP, which carries it to its various target cells (Bouillon and van Baelen 1981, Bishop et al. 1994). In the liver, cholecalciferol and ergocalciferol are transformed into hydroxylated forms ($25(OH)D_{2,3}$) that are further hydroxylated in the kidneys into $1\alpha,25(OH)_2D$, a process partly controlled by the parathyroid hormone, in relation to the level of calcemia (review in DiMeglio and Ilem 2014). Other tissues (e.g., placenta) are considered to have the capacity for producing $1\alpha,25(OH)_2D$ (Norman 2008). The metabolite resulting from vitamin D_3 transformation ($1\alpha,25(OH)_2D_3$) is physiologically the most active form (Heaney et al. 2011).

Vitamin D metabolites act as typical hormones on target tissues, through the action of specific receptors, VDRs, which can be located in the plasmic membrane (VDR_{mem}) or the nucleus (VDR_{nuc}) of target cells (Jurutka et al. 2001, Norman 2008). VDRs occur in many tissues (33, according to Norman 2008), including renal proximal tubules, the intestine, and the cells of the osteoblastic and osteoclastic lineages (review in DiMeglio and Ilem 2014). In the kidneys, they stimulate calcium reabsorption (e.g., Friedman and Gesek 1993), whereas in the intestine they enhance calcium and phosphorus absorption (Wasserman and Fullmer 1995; see also review in Christakos 2008). The action of vitamin D on its skeletal target is complementary to that on the gut and kidneys. It is a complex process, with contradictory effects on bone remodeling, depending on the immediate status of phosphocalcic homeostasis (review in Lieben and Carmeliet 2013). Moreover, vitamin D has both a direct action on bone cells (reviews in St-Arnaud 2008, Eisman and Bouillon 2014) and an indirect action, synergistic with that of the parathyroid hormone and other systemic factors (Raisz 1990, Christakos 2008). When calcemia and phosphoremia decrease, the renal production of $1\alpha,25(OH)_2D$ increases and this hormone activates the differentiation of osteoclasts through either a direct action on VDRs in the monocytes (Kogawa et al. 2010), or an indirect action through paracrine factors released by osteoblasts (Suda et al. 1992, Takeda et al. 1999). It also stimulates osteoclastic activity, finally resulting in an increase in BMU formation rate and a decrease of bone mass (Sowers et al. 1990). Elevation in blood phosphocalcic levels has a negative feedback effect on the kidney's enzymatic activities involved in $1\alpha,25(OH)_2D3$ production. In skeletal tissues, it then increases osteoblast differentiation (Zhou et al. 2010), stimulates the production of proteins (osteocalcin, osteopontin) involved in the mineralization of the osteoid tissue, and inhibits osteoclast activity (Bellido and Hill Gallant 2014, van Driel and van Leeuwen 2017; see also Lanske et al. 2014); the result is an increase in bone mass (Williamson et al. 2017). Severe deficiencies in vitamin D result in rickets and osteomalacia (i.e., a deficit in bone mineralization).

Influence of the Central and Sympathetic Nervous Systems on Remodeling

One of the most innovative research fields in remodeling regulation relates to the contribution of the central and sympathetic nervous systems (reviews in Takeda and Ducy 2008; Elefteriou et al. 2014). Three receptor categories, called $\beta_{1,2,3}$ *adrenergic receptors* (AR), occur in the plasmatic membrane of the osteoblast, osteocyte and osteoclast. The stimulation of these receptors by the sympathetic system activates the osteoclasts and probably also induces RANKL secretion by the osteocytes (Elefteriou et al. 2014); conversely, osteoblastic activity seems to be negatively influenced by the βARs (Ducy et al. 2000). The combination of these effects creates an imbalance toward resorption in bone remodeling (coupling disturbance), resulting in a net loss of bone volume. The whole nervous chain involved in this process is initially triggered, within the central nervous system, by the action of leptin on the hypothalamus (Ducy et al. 2000). Leptin, the so-called *satiety hormone,* a 16 kDa protein, is secreted by the adipocytes of white fat. It is a powerful regulator of food intake and energetic metabolism (Buettner et al. 2006). Its strong antiosteogenic action has been shown experimentally (Elefteriou et al. 2004), but this action is indirect, and mediated by the sympathetic nervous system (Hansen et al. 2003, Elmquist and Strewler 2005). A relatively tight relationship thus exists, through the effect of leptin, between fat metabolism and remodeling intensity.

The discovery of leptin action suggests that a general link exists between bone remodeling and energy metabolism (Karsenty and Oury 2010). Studies developed on this topic during the last 10 years revealed that this link is twofold: hormones chiefly involved in the regulation of energy metabolism (i.e., leptin, thyroxine) are active on bone cells and, conversely, bone behaves like an endocrine organ and influences energetic metabolism, mainly through the release of osteocalcin, a molecule that stimulates insulin secretion (Karsenty 2006, Lee et al. 2007, Confavreux et al. 2009). This situation sheds some light on the distribution of intense bone remodeling (resulting in dense Haversian tissue) in extant and extinct vertebrates, as briefly presented below.

Figure 11.6 summarizes the main regulation factors influencing bone remodeling.

The Message of Remodeling in Fossil Bones

The main functional meaning of Haversian substitution, and consequently the reason for the uneven distribution of this process among vertebrates, have long been and still partly remain puzzling issues. Diverse and sometimes contradictory hypotheses have been published (a brief historic account of this question is given by Ricqlès 1977b; see also Enlow 1962), but they generally fail to give a comprehensive explanation of available comparative data. Bone remodeling is under the influence of multiple and, to some extent, competing factors; for this reason, the issue is particularly complex, and caution is required in interpretations and inferences. Since the critical review of data, arguments and historical contributions given by Ricqlès (1977b), the so-called "state of the art" has not evolved spectacularly; however, the extent, as well as the limits, of the information provided by the characteristics of Haversian tissues is now more precisely defined. The study of cortical remodeling in fossils is acknowledged to give meaningful clues to two main biological questions: the gross metabolic features of the taxa, and their relative ontogenetic ages.

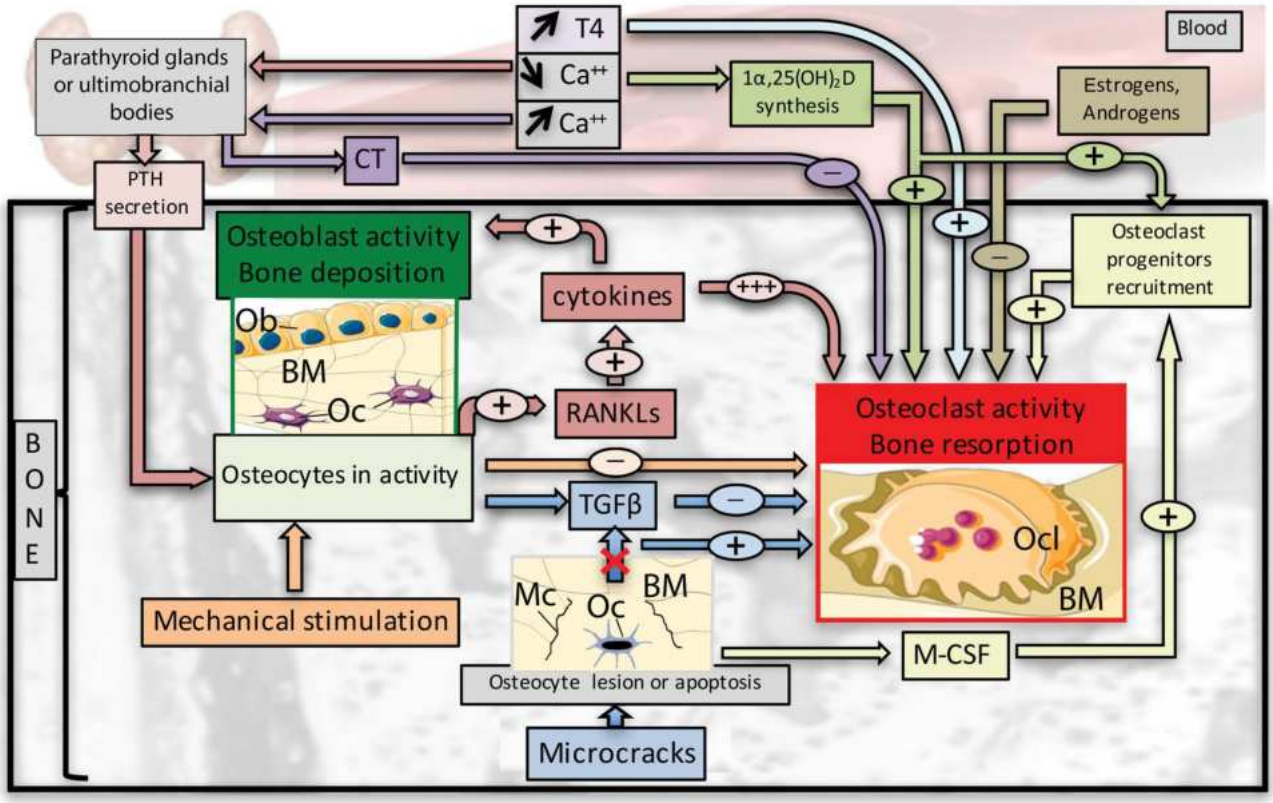


FIGURE 11.6 Main regulation factors influencing bone remodeling. The balance between osteoblasts (Obs) producing bone matrix (BM) and osteoclasts (Ocl), which degrade mineralized bone, is under multifactorial control. In blue: osteocyte (Oc) activity produces a factor close to transforming growth factor (TGF)-β that inhibits osteoclast activity. Microcracks (Mc) cause osteocyte apoptosis and this factor is no longer secreted, which permits osteoclast activity. In yellow: osteocytes affected by microcrack propagation secrete macrophage colony-stimulating factor (M-CSF), which stimulates osteoclast differentiation. In orange: under mechanical stimulation, live osteocytes have an inhibiting effect on the osteoclasts. In pink: hypocalcemia is detected by parathyroid cells, which secrete parathormone (PTH). When PTH binds PTH receptors on osteocytes, they express RANKLs and consequently permit the emission of cytokines, which activate the recruitment and activity of osteoclasts. In purple: calcitonin (CT) is produced when hypercalcemia is detected by parathyroid cells. CT binds to osteoclast receptors and inhibits their activity. In green: hypocalcemia leads to the production of $1,25(OH)_2D$, which activates osteoclast differentiation and activity. In light brown: sexual steroids reduce osteoclast activity. In light blue: thyroxine (T_4) increases remodeling intensity.

A Basic Clue in Paleophysiology

A consensus exists among paleohistologists to consider, after the pioneer work by Amprino (1948, 1967) and Ricqlès (1969, 1977a, b, 1978), that the involvement of bone remodeling in the general homeostatic processes of vertebrates is the most robust line of explanation for the taxonomic distribution and the ontogenetic development of Haversian tissue. In brief, this interpretation refers to the critical role played by the release and recycling, through bone remodeling, of fixed calcium and phosphate ionic reserves. Therefore, remodeling intensity should reflect the need of an organism for calcium and phosphate ions. This need is supposed to be primarily influenced by growth (as measured in bone cortices) and metabolic rates, two physiological features otherwise known to be closely related to each other (Montes et al. 2007, Cubo et al. 2012; see also Tam et al. 1978). In extant faunas, taxa that have a high metabolic level but a small size (e.g., small mammalian "insectivores" and rodents, small birds) generally lack dense Haversian tissue (see Chapters 27 and 29). Conversely, most organisms that are medium to large sized and have a tachymetabolic regime display this kind of tissue, at least when they reach late ontogenetic stages (comparative reviews in Enlow and Brown 1957, 1958, Ricqlès 1977a, b). In the context of this comparative argument and an actualistic point of view, a relatively high metabolic activity has been attributed to extinct taxa in which bone cortices are made of dense Haversian tissue. This is characteristically the case for, e.g., large dinosaurs and non-mammalian synapsids (Ricqlès 1972a, b; see also Chapter 27). Frequently, these taxa also present another qualitative feature interpreted in similar terms: their primary periosteal cortices, when known, are made of one of the many forms of woven-parallel bone tissue. The latter is indicative of fast growth (see Chapter 10); its occurrence is thus poorly compatible with the hypothesis of a low metabolic rate. Up to now, the conclusions derived from the nature of primary cortical tissues and the intensity of Haversian substitution were supported by geochemical methods used to assess the metabolism of extinct taxa through oxygen isotope ratios (Amiot et al. 2006, Bernard et al. 2010). Moreover, the recently discovered role of leptin in both the physiology of the skeleton (especially bone

VetBooks.ir

remodeling) and the general energetic metabolism of tetrapods can provide a meaningful reference in support of the physiological interpretation of dense Haversian bone in fossils.

All paleophysiological inferences referring to remodeling intensity were based on qualitative observations. Such observations constituted an essential intellectual advance, on which a large part of comparative bone histology is built. However, future progress in the functional deciphering of bone remodeling calls for a quantitative approach and recourse to histomorphometric methodologies.

Remark on the Histomorphometry of Bone Remodeling in Extant and Extinct Taxa

Numerous publications relate to the quantitative assessment of bone remodeling because this approach is best suited to the diagnosis and control of skeletal metabolic diseases. The aim is then to quantify the dynamics of bone remodeling in terms of frequency of BMU appearance, duration of BSU formation and total bone turnover in standardized locations (e.g., the iliac crest in humans), which are considered representative of the whole skeleton. It is thus in humans and laboratory rodents that most studies are conducted. Classical (two-dimensional [2D]) remodeling histomorphometry is based on multiple *in vivo* labeling of bone growth with fluorescent markers such as tetracyclines for humans, or other calcium-binding substances like alizarine, calcein, orange xylenol and so forth for non-human animals. A rich set of descriptive variables, the *primary* (or *static*) *variables,* is now available, allowing the computation of *derived* variables such as BMU *formation period* (FP), BMU *activation frequency* (*Ac. f*) or BMU *mineralization lag time* (*MLt*), which are the true goals of remodeling histomorphometry because they actually express the essential dynamic trends of this process. Detailed reviews of these diverse variables, along with their measurement and computation protocols, are given in Parfitt et al. (1987), Recker et al. (2011), Dempster et al. (2013) and Allen and Burr (2014). Today, non-invasive techniques based on computerized tomography (CT scan) are becoming a routine tool for *in vivo* long-term control of bone turnover (e.g., Schulte et al. 2011, Altman et al. 2015, van't Hof et al. 2017).

A common feature of these approaches is that they are inapplicable to fossil material because they are ultimately based on *in vivo* operations. Only some static variables, listed and precisely described in Dempster et al. (2013), can be collected and interpreted in fossils. They are related, for example, to the total cortical area (or *bone area* [*B.Ar*]), the spatial density of intact or fragmentary osteons in bone cortices (P_i and P_f, respectively, in Wu et al. 1970), the unitary osteon area (*On.Ar*) or perimeter (*On.Pm*), the Haversian canal area (*HC.Ar*) or perimeter (*HC.Pm*) and the number of osteocyte lacunae per osteon (*Lc.N*). With these descriptive variables, diverse indices can be computed, such as the spatial density of osteons ($P_i + P_f$ /*B.Ar*) or that of the lacunae per osteon (*Lc.N*/*On.Ar*). Examples of an efficient use of simple variables and indices of this sort are given by Fiala (1980), Qiu et al. (2003) and Skedros et al. (2011). To our knowledge, only one study (Wu et al. 1970) has tried to compute dynamic remodeling variables in a fossil—the rib of a "mastodon" [*sic*] from the Pleistocene of Michigan. However, this study, conducted jointly with that of human ribs analyzed with classical histomorphometric procedures (including bone labeling), has methodological shortcuts that make the understanding of its results difficult. Thus far it has not been followed up.

In the case of the dense Haversian tissue occurring in some fossil mammals and dinosaurs, including birds, an accurate assessment of the dynamic trends of bone remodeling is precluded because two necessary variables, the number of missing osteons (i.e., osteons that have been entirely eroded and disappeared) and individual age determination (dynamic trends must be referred to time), remain out of reach. Of course, in the case of mild remodeling activity with nonoverlapping osteons (as encountered in numerous extant and extinct vertebrates, including ectotherms and endotherms; see Chapter 31), this double restriction does not exist. No osteons are missing and age can often be determined by skeletochronology, unless resorption around the medullary cavity has extensively erased early growth marks. Haversian tissue can, nevertheless, be used in fossils for estimating, at least in general terms, the relative ontogenetic age of individuals when skeletochronology is not usable.

Remodeling Pattern as a Clue for the Estimation of Ontogenetic Age in Fossils

Since the initial study by Kerley (1965; see also Kerley and Ubelaker 1978), four histological parameters related to Haversian remodeling in standard sites of human long bone cortices have been used to assess individual age: the number of the entire osteons and the number of fragmentary osteons, the number of "primary" vascular canals (primary osteons and simple canals) and the relative area of the remnants of primary periosteal tissue. Although originally based on a relatively small sample (126 subjects from 0 to 95 years with a 75% ratio for males), Kerley's method proved to be reasonably accurate: in a control sample, more than 83% of age estimates were within ±5 years of real age, and all estimates were within ±10 years. This method is still currently used in forensic medicine, anthropology and archaeology (e.g., Thomas et al. 2000). Of course, Kerley's method rests on the fact that cortical remodeling is progressive during ontogeny, and that, consequently, the formation of dense Haversian tissue is a cumulative process. Another characteristic of this method is to merely ignore the problem of missing osteons.

In the numerous vertebrate taxa devoid of dense Haversian bone, age determination by skeletochronology is a much more efficient and precise approach than quantifying remodeling (if any). However, in taxa developing very dense Haversian tissue and lacking cyclical growth marks, simplified versions of Kerley's method have been used for gross estimates of individual developmental stages (distinction of juveniles from adults) in studies on dwarfism and gigantism (Sander 2000, Klein and Sander 2008, Stein et al. 2010).

The *remodeling stage* (RS) index recently developed for this purpose by Mitchell et al. (2017) is the continuation, restricted to Haversian remodeling, of a broader-based index previously proposed by Klein and Sander (2008), called the *histological ontogenetic stage* (HOS). The latter was based on an integration of three kinds of histological clues, the

VetBooks.ir

basal histological features of primary periosteal cortices, the number of cyclical growth marks and the degree of proliferation of secondary osteons, for assessing gross developmental categories in the long bones of 12 sauropod taxa. Mitchell et al.'s (2017) *RS* index also relates to sauropods (8 taxa). On cross sections from the mid-diaphysis, the RS index considers the number of successive generations of secondary osteons (be they entire or fragmentary) occurring in standardized 50-mm^2 fields located in the deep, middle and superficial thirds of bone cortices already defined for HOS estimates (see also Stein et al. 2010). The three mean values of osteonal generations thus obtained are then added to compute a global score reflecting the RS value for the bone studied. This index proved to be positively correlated with femoral length (a substitute of size) in five taxa, which justified the conclusion that RS is a valid age clue for these species. Mitchell et al.'s (2017) method is potentially applicable to all vertebrates that have entirely remodeled cortices, provided that a precise calibration in a growth series is previously made for each taxon. However, because this method does not take into account the problem of missing osteons (an unavoidable question), the age indication that it gives can be suspected to be of increasing inaccuracy with increasing age.

In paleohistology, the heuristic potential of remodeling analyses for a great variety of studies (biomechanics, physiology, growth studies, taxonomic discrimination, etc.) is considerable and has been little exploited up to now. This field constitutes one of the major avenues for future investigations.

REFERENCES

Ahmed, Y., et al. 2017. Absence of typical Haversian system from the compact bone of some reptile and bird species. *Asian J. Biol. Sci.* 10: 98–103.

Allen, M. R. and D. B. Burr. 2014. Bone modeling and remodeling. In *Basic and applied bone biology*, eds. D. B. Burr, and M. R. Allen, 75–89. London: Academic Press.

Altman, A. R., et al. 2015. Quantification of skeletal growth, modeling, and remodeling by *in vivo* micro computed tomography. *Bone* 81: 370–379.

Amiot, R., et al. 2006. Oxygen isotopes from biogenic apatites suggest widespread endothermy in Cretaceous dinosaurs. *Earth Planet Sci. Lett.* 246: 41–54.

Amprino, R. 1948. A contribution to the functional meaning of the substitution of primary by secondary bone tissue. *Acta Anat.* 5: 291–300.

Amprino, R. 1967. Signification fonctionnelle du remaniement osseux. *J. Médic Montpellier* 2: 105–109.

Andersen, T. L., et al. 2009. A physical mechanism for coupling bone resorption and formation in adult human bone. *Am. J. Pathol.* 174: 239–247.

Aubin, J. E. 2008. Mesenchymal stem cells and osteoblast differentiation. In *Principles of bone biology,* 3rd edition, vol. 1, eds. J. P. Belizikian, L. G. Raisz and T. J. Martin, 85–107. San Diego, CA: Academic Press.

Barou, O., et al. 2002. Relationships between trabecular bone remodeling and bone vascularization; a quantitative study. *Bone* 30: 604–612.

Baylink, D. J. and C. C. Liu. 1979. The regulation of endosteal bone volume. *J. Periodont.* 50: 43–49.

Bellido, T. and K. M. H. Hill Gallant. 2014. Hormonal effects on bone cells. In *Basic and applied bone biology*, eds. D. B. Burr, and M. R. Allen, 299–314. London: Academic Press.

Bellido, T., et al. 2014. Bone cells. In: *Basic and applied bone biology*, eds. D. B. Burr and M. R. Allen, 27–45. New York: Academic Press.

Bernard, A., et al. 2010. Regulation of body temperature by some Mesozoic marine reptiles. *Science* 328: 1379–1381.

Bishop, J. E., et al. 1994. Profile of ligant specificity of the vitamin D binding protein for 1α,25-Dihydroxyvitamin D_3 and its analogs. *J. Bone Miner. Res.* 9: 1277–1288.

Blair, H. C. and M. Zaidi. 2006. Osteoclastic differentiation and function regulated by old and new pathways. *Rev. Endocrinol. Metab. Dis.* 7: 23–32.

Bouillon, R. and H. van Baelen. 1981. Transport of vitamin D: significance of free and total concentrations of the vitamin D metabolites. *Calcif. Tissue Int.* 33: 451–453.

Brown, E. M. 2008. Biology of the extracellular Ca^{2+} sensing receptor. In *Principles of bone biology,* 3rd edition, vol. 1, eds. J. P. Belizikian, L. G. Raisz and T. J. Martin, 533–553. San Diego, CA: Academic Press.

Buettner, C., et al. 2006. Critical role of STAT3 in leptin's metabolic actions. *Cell. Metab.* 4: 49–60.

Buffrénil, V. de and A. Casinos. 1995. Observations histologiques sur le rostre de *Mesoplodon densirostris* (Mammalia, Cetacea, Ziphiidae): le tissu osseux le plus dense connu. *Ann. Sci. Nat., Zool.*, 16: 21–32.

Burger, E. H., et al. 2003. Strain-derived canalicular fluid flow regulates osteoclast activity in a remodeling osteon – a proposal. *J. Biomech.* 36: 1453–1459.

Burr, D. B. 1993. Remodeling and the repair of fatigue damage. *Calcif. Tissue Int/* 53: S75–S81.

Burr, D. B., et al. 1985. Bone remodeling in response to *in vivo* fatigue microdamage. *J. Biomech.* 18: 189–200.

Burton, P., et al. 1989. Haversian bone remodeling in human fetus. *Acta Anat.* 135: 171–175.

Canoville A., et al. 2017. Quantitative data on bone vascular supply in the Lissamphibia: comparative and phylogenetic aspects. *Zool. J. Linn. Soc.* 182: 107–128.

Christakos, S. 2008. Vitamin D gene regulation. In *Principles of bone biology,* 3rd edition, vol. 1, eds. J. P. Belizikian, L. G. Raisz and T. J. Martin, 779–794. San Diego, CA: Academic Press.

Collip, J. B. 1925. The extraction of a parathyroid hormone which will prevent or control parathyroid tetany and which regulates the level of blood calcium. *J. Biol. Chem.* 63: 395–438.

Confavreux, C. B., et al. 2009. A paradigm of integrative physiology, the crosstalk between bone and energy metabolisms. *Mol. Cell. Endocrinol.* 310: 21–29.

Congiu, T. and U. E. Pazzaglia. 2011. The sealed osteons of cortical diaphyseal bone. Early observations revisited with scanning electron microscopy. *Anat. Rec.* 294: 193–198.

Cooper, D. M. L., et al. 2003. Quantitative 3D analysis of the canal network in cortical bone by micro-computed tomography. *Anat. Rec.* 274B: 169–179.

Cubo, J., et al. 2012. Paleohistological estimation of bone growth rate in extinct archosaurs. *Paleobiology* 38: 335–349.

Curtis, T. A., et al. 1985. Canalicular communication in the cortices of human long bones. *Anat. Rec.* 212: 336–344.

Danks, J. A., et al. 2011. Evolution of the parathyroid hormone family and skeletal formation pathways. *Gen. Comp. Endocrinol.* 170: 79–91.

Danova, N. N., et al. 2003. Degradation of bone structural properties by accumulation and coalescence of microcracks. *Bone* 33: 197–205.

Delaisse, J.-M. 2014. The reversal phase of the bone remodeling cycle: cellular prerequisites for coupling resorption and formation. *Bonekey Rep.* 3: 561.

Dempster, D. W., et al. 2013. Standardized nomenclature, symbols, and units for bone histomorphometry: a 2012 update of the report of the ASBMR Histomorphometry Nomenclature Committee. *J. Bone Miner. Res.* 28: 1–16.

Dewaele, L., et al. 2019. Generalized osteosclerotic-like condition in the skeleton of *Nanophoca vitulinoides*, a dwarf seal from the Neogene of Belgium. *J. Mammal. Evol.* 26: 517–543.

Dhem, A. 1967. *Le remaniement de l'os adulte*. Bruxelles and Paris: Arscia/Maloine.

DiMeglio, L. A. and E. A. Ilem. 2014. Calcium and phosphate: hormonal regulation and metabolism. In *Basic and applied bone biology*, eds. D. B. Burr, and M. R. Allen, 261–282. London: Academic Press.

Dix, M. W., et al. 1970. Lizard calcium metabolism: lack of effect of mammalian calcitonin on serum calcium and phosphate levels in normal and parathyroidectomized lizards, *Anolis carolinensis*. *Gen. Comp. Endocrinol.* 14: 243–247.

Domenech, J. 2017. What are mesenchymal stromal cells? Origin and discovery of mesenchymal stromal cells. In *Mesenchymal stromal cells as tumor stromal modulators*, eds. M. Garcia and M. Bolontrade, 1–37. Amsterdam: Elsevier Inc.

Downs, J. P. and P. C. J. Donoghue. 2009. Skeletal histology of *Bothriolepis canadensis* (Placodermi, Antiarchi) and the evolution of the skeleton at the origin of jawed vertebrates. *J. Morphol.* 270: 1364–1380.

Driel, M. van and J. van Leeuwen. 2017. Vitamin D endocrinology of bone mineralization. *Mol. Cell. Endocrinol.* 453: 46–51.

Ducy, P., et al. 2000. Leptin inhibits bone formation through a hypothalamic relay: a central control of bone mass. *Cell* 100: 197–207.

Eisman, J. A. and R. Bouillon. 2014. Vitamin D: direct effects of vitamin D metabolites on bone: lessons from genetically modified mice. *Bonekey Rep.* 3: 499.

Elefteriou, F., et al. 2004. Serum Leptin level is a regulator of bone mass. *PNAS* 101: 3258–3263.

Elefteriou, F., et al. 2014. Control of bone remodeling by the peripheral sympathetic nervous system. *Calcif. Tissue Int.* 94: 140–151.

Elmquist, J. K. and G. J. Strewler. 2005. Do neural signals remodel bone? *Nature* 434: 447–448.

Enlow, D. H. 1962. Functions of the Haversian system. *Am. J. Anat.* 110: 269–306.

Enlow, D. H. and S. O. Brown, 1956. A comparative histological study of fossil and recent bone tissues. Part I. *Texas J. Sci.* 8: 403–443.

Enlow, D. H. and S. O. Brown, 1957. A comparative histological study of fossil and recent bone tissues. Part II. *Texas J. Sci.* 9: 185–214.

Enlow, D. H. and S. O. Brown, 1958. A comparative histological study of fossil and recent bone tissues. Part III. *Texas J. Sci.* 10: 187–230.

Eriksen, E. F. 2010. Cellular mechanisms of bone remodeling. *Rev. Endocrinol. Metab. Dis.* 11: 219–227.

Eriksen, E. F., et al. 1984a. Reconstruction of the formative site in iliac trabecular bone in 20 normal individuals employing a kinetic model for matrix and mineral apposition. *Metab. Bone Dis. Rel. Res.* 5: 243–252.

Eriksen, E. F., et al. 1984b. Reconstruction of the resorptive site in iliac trabecular bone: a kinetic model for bone resorption in 20 normal individuals. *Metab. Bone Dis. Rel. Res.* 5: 235–242.

Fawcett, D. W and R. P. Jensh. 1997. *Bloom and Fawcett: concise histology.* London: Chapman & Hall.

Fiala, P. 1980. Structure of the long limb bones and its significance in determining age in man. *Folia Morphol.* 28: 259–263.

Filipović, B., et al. 2017. Response of trabecular bone, thyroid C and follicular cells to synthetic salmon calcitonin in middle-aged orchidectomized male rats. *J. Anat.* 230: 787–795.

Florencio-Silva, R., et al. 2015. Biology of bone tissue: structure, function, and factors that influence bone cells. *BioMed. Res. Int.* 2015: 421746.

Friedman, P. A. and F. A. Gesek. 1993. Vitamin D accelerates PTH-dependent calcium transport in distal convoluted tubule cells. *Am. J. Physiol.* 265: F300–F308.

Frost, H. M. 1969. Tetracycline-based histological analysis of bone remodeling. *Calcif. Tissue Res.* 33: 211–237.

Gardella, T. J., et al. 2008. Receptors for parathyroid hormone (PTH) and PTH-related protein. In *Principles of bone biology,* 3rd edition, vol. 1, eds. J. P. Belizikian, L. G. Raisz and T. J. Martin, 555–576. San Diego, CA: Academic Press.

Giles, S., et al. 2013. Histology of the "Placoderm" dermal skeletons: implication for the nature of the ancestral gnathostome. *J. Morphol.* 274: 627–644.

Hadjidakis, D. J. and I. I. Androulakis. 2006. Bone remodeling. *Ann. NY Acad. Sci.* 1092: 385–396.

Hansen, K. R., et al. 2003. Activation of the sympathetic nervous system by galanin-like peptide – a possible link between leptin and metabolism. *Endocrinology*, 144: 4709–4717.

Hauge, E.-M., et al. 2001. Cancellous bone remodeling occurs in specialized compartments lined by cells expressing osteoblastic markers. *J. Bone Miner. Res.* 16: 1575–1582.

Havers, C. 1691. Osteologia nova. 304. London.

Heaney, R. P., et al. 2011. Vitamin D_3 is more potent than vitamin D_2 in humans. *J. Clin. Endocrinol. Metab.* 96: E447–E452.

Heino, T. J., et al. 2002. Osteocytes inhibit osteoclastic bone resorption through transforming growth factor-beta: enhancement by estrogens. *J. Cell. Biochem.* 85: 185–197.

Henriksen, K., et al. 2009. Local communication on and within bone controls bone remodeling. *Bone* 44: 1026–1033.

Holik, M. F. 2008. Photobiology and noncalcemic actions of vitamin D. In *Principles of bone biology,* 3rd edition, vol. 1, eds. J. P. Belizikian, L. G. Raisz and T. J. Martin, 795–811. San Diego, CA: Academic Press.

Hu, M. I. and R. F. Gagel. 2008. Calcitonin gene family of peptides. In *Principles of bone biology,* 3rd edition, vol. 1, eds. J. P. Belizikian, L. G. Raisz and T. J. Martin, 813–836. San Diego, CA: Academic Press.

Huffer, W. E. 1988. Morphology and biochemistry of bone remodeling: possible control by vitamin D, parathyroid hormone, and other substances. *Lab. Invest.* 59: 418–442.

Huiskes, R., et al. 2000. Effect of mechanical forces on maintenance and adaptation of form in trabecular bone. *Nature* 405: 704–706.

Jaworski, Z. F. and C. Hooper. 1980. Study of cell kinetics within evolving secondary Haversian systems. *J. Anat*. 131: 91–102.

Jaworski, Z. F. G. 1992. Haversian systems and Haversian bone. In *Bone Metabolism and Mineralization*, vol. 4, ed. B. K. Hall, 21–44. Boca Raton, FL: CRC Press.

Jensen, R., et al. 2015. A joined role of canopy and reversal cells in bone remodeling – Lessons from glucocorticoid-induced osteoporosis. *Bone* 73: 16–23.

Jüppner, H. 1995. Functional properties of the PTH/PTHrP receptor. *Bone* 17: 39S–42S.

Jurutka, P. W., et al; 2001. Molecular nature of the vitamin D receptor and its role in regulation of gene expression. *Rev. Endocr. Metab. Disord*. 2: 203–216

Justus, R. and J. H. Luft. 1970. A mechanochemical hypothesis for bone remodeling induced by mechanical stress. *Calcif. Tissue Res.* 5: 222–235.

Karsenty, G. 2006. Convergence between bone and energy homeostases: review of leptin regulation of bone mass. *Cell. Metab.* 4: 341–348.

Karsenty, G. and F. Oury. 2010. The central regulation of bone mass, the first link between bone remodeling and energy metabolism. *J. Clin. Endocrinol. Metab.* 95: 4795–4801.

Kerley, E. R. 1965. The microscopic determination of age in human bone. *Am. J. Phys. Anthropol*. 23: 149–164.

Kerley, E. R. and D. H. Ubelaker. 1978. Revision of the microscopic method of estimating age at death in human cortical bone. *Am. J. Phys. Anthropol*. 49: 545–546.

Klein, L., et al. 1990. Variation of resorption rates *in vivo* of various bones in immature rats. *Bone Miner.* 3: 169–175.

Klein, N. and P. M. Sander. 2008. Ontogenetic stages in the long bone histology of sauropod dinosaurs. *Paleobiology* 34: 247–263.

Kogawa, M., et al. 2010. Osteoclastic metabolism of 25(OH)-Vitamin D_3: a potential mechanism for optimization of bone resorption. *Endocrinology* 151: 4613–4625.

Krampera, M., et al. 2006. Mesenchymal stem cells for bone, cartilage, tendon and skeletal muscle repair. *Bone* 39: 678–683.

Kristensen, H. B., et al. 2014. Osteoblast recruitment routes in human cancellous bone remodeling. *Am. J. Pathol*. 184: 778–789.

Krstić, R. V. 1985. *General histology of the mammal*. Berlin: Springer Verlag.

Kurata, K., et al. 2007. Role of mechanically damaged osteocytes in the initial phase of bone remodeling. *Int. J. Fatigue* 29: 1010–1018.

Lacroix, P. 1970. Recherches sur le remaniement interne des os. *Arch. Biol. (Liège)* 81: 275–304.

Lafage-Proust, M.-H., et al. 2010. Bone vascularization and remodeling. *Joint Bone Spine*, 77: 521–524.

Lafage-Proust, M.-H., et al. 2015. Assessment of bone vascularization and its role in bone remodeling. *Bonekey Rep.* 4: 662.

Lambert O., et al. 2011. Hyperdense rostral bones of ziphiid whales: diverse processes for a similar pattern. *C. R. Palevol.* 10: 453–468.

Landrigan M. D., et al. 2011. Contrast-enhanced micro-computed tomography of fatigue microdamage accumulation in human cortical bone. *Bone* 48: 443–450.

Lanske, B., et al. 2014. Vitamin D endocrine system and osteocytes. *Bonekey Rep.* 3: 494.

Lanyon, L. E., et al. 1982. Mechanically adaptive bone remodeling. *J. Biomech*. 15: 141–154.

Lassen, N. E., et al. 2017. Coupling of bone resorption and formation in real time: new knowledge gained from human Haversian BMUs. *J. Bone Miner. Res.* 32: 1395–1405.

Lee, N. K., et al. 2007. Endocrine regulation of energy metabolism by the skeleton. *Cell* 130: 456–469.

Lee, T. C., et al. 2003. Detecting microdamage in bone. *J. Anat*. 203: 161–172.

Lieben, L. and G. Carmeliet. 2013. Vitamin D signaling in osteocytes: effects on bone and mineral homeostasis. *Bone* 54: 237–243.

MacIntyre, I. 1967. Calcitonin: a general review. *Calcif. Tissue Res.* 1: 173–182.

Maes, C. and T. L. Clemens. 2014. Angiogenic-osteogenic coupling: the endothelial perspective. *Bonekey Rep.* 3: 578.

Maggiano, I. S., et al. 2016. Three-dimensional reconstruction of Haversian systems in human cortical bone using synchrotron radiation-based micro-CT: morphology and quantification of branching and transverse connections across age. *J. Anat*. 228: 719–732.

Mak, A. F. T., et al. 1997. Deformation-induced hierarchical flows and drag forces in bone canaliculi and matrix microporosity. *J. Biomech*. 30: 11–18.

Manolagas, S. C. 2000. Birth and death of bone cells: basic regulatory mechanisms and implications for the pathogenesis and treatment of osteoporosis. *Endocr. Rev*. 21: 115–137.

Marotti, G. 1968. The dynamics of osteon formation in inert bones. *Calcif. Tissue Res*. 2, Suppl.: 86.

Martin, R. B. 1991. On the significance of remodeling space and activation rate changes in bone remodeling. *Bone* 12: 391–400.

Martin, R. B. 2002. Is all cortical bone remodeling initiated by microdamage? *Bone* 30: 8–13.

Martin, R. B., et al. 2015. Growth, modeling and remodeling of bone. In *Skeletal tissue mechanics*, 2nd edition, eds. R. B. Martin, D. B. Burr, N. A. Sharkey and D. P. Fyhrie, 95–173. New York: Springer Science + Business Media.

Matsumoto, C., et al. 2006. Estrogens and androgens play distinct roles in bone turnover in male mice before and after reaching sexual maturity. *Bone* 38: 220–226.

McFarlin, S. C., et al. 2008. Regional variability in secondary remodeling within long bone cortices of catarrhine primates: the influence of bone growth history. *J. Anat*. 213: 308–324

Meers, M. B. 2002. Cross-sectional geometric properties of the crocodilian humerus: an exception to Wolff's law? *J. Zool. Lond*. 258: 405–418.

Mitchell, J., et al. 2017. Can secondary osteons be used as ontogenetic indicators in sauropods? Extending the histological ontogenetic stages into senescence. *Paleobiology* 43: 321–342.

Mohsin, S., et al. 2006. Osteonal crack barriers in ovine compact bone. *J. Anat*. 208: 81–89.

Montes, L. et al. 2007. Relationships between bone growth rate, body mass and resting metabolic rate in growing amniotes: a phylogenetic approach. *Biol. J. Linn. Soc*. 92: 63–76.

Norman, A. W. 2008. 1α,25$(OH)_2$ vitamin D_3. Vitamin D nuclear receptor (VDR) and plasma vitamin-binding protein (BDP) structures and ligand shape preferences for genomic and

rapid biological responses. In *Principles of bone biology,* 3rd edition, vol. 1, eds. J. P. Belizikian, L. G. Raisz and T. J. Martin, 749–778. San Diego, CA: Academic Press.

Norman, T. L. and Z. Wang. 1997. Microdamage of human cortical bone: incidence and morphology in long bones. *Bone* 20: 375–379.

O'Brian, F. J., et al. 2007. Bone as a composite material: the role of osteons as barriers to crack growth in compact bone. *Int. J. Fatigue* 29: 1051–1056.

Oers, R. F. M., et al. 2008. Relating osteon diameter to strain. *Bone* 43: 476–482.

Otsuru, S., et al. 2017. Hematopoietic derived cells do not contribute to osteogenesis as osteoblasts. *Bone* 94: 1–9.

Padian, K., et al. 2016. A hypothesis of differential secondary bone formation in dinosaurs. *C. R. Palevol.* 15: 41–49.

Parfitt, A. M. 1982. The coupling of bone formation to bone resorption: a critical analysis of the concept and of its relevance to the pathogenesis of osteoporosis. *Metab. Bone Dis. Rel. Res.* 4: 1–6.

Parfitt, A. M. 1984. The cellular basis of bone remodeling: the quantum concept examined in light of recent advances in the cell biology of bone. *Calcif. Tissue Int.* 36: S37–S45.

Parfitt, A. M. 1994. Osteonal and hemi-osteonal remodeling: the spatial and temporal framework for signal traffic n adult human bone. *J. Cell. Biochem.* 55: 273–286.

Parfitt, A. M. 2002. Misconceptions (2): turnover is always higher in cancellous than in cortical bone. *Bone* 30: 807–809.

Parfitt, A. M., et al. 1987. Bone histomorphometry: standardization of nomenclature, symbols, and units. *J. Bone Miner. Res.* 2: 595–610.

Petrtyl, M., et al. 1996. Spatial organization of the Haversian bone in man. *J. Biomech.* 29: 161–169.

Potts, J. T. 2005. Sterling review – Parathyroid hormone: past and present. *J. Endocrinol.* 187: 311–325.

Qiu, S., et al. 2003. Histomorphometric assessment of Haversian canal and osteocyte lacunae in different-sized osteons in human ribs. *Anat. Rec.* 272A: 520–525.

Raisz, L. G. 1990. Recent advances in bone cell biology: interactions of vitamin D with other local and systemic factors. *Bone Miner.* 9: 191–197.

Recker, R. R., et al. 2011. Issues in modern bone histomorphometry. *Bone* 49: 955–964.

Ricqlès, A. de 1969. L'histologie osseuse envisagée comme indicateur de la physiologie thermique chez les tétrapodes fossiles. *C. R. Acad. Sci. (Paris), Série D* 268: 782–785.

Ricqlès, A. de 1972a. Vers une histoire de la physiologie thermique. L'apparition de l'endothermie et le concept de reptile. *C. R. Acad. Sci (Paris), Série D* 275: 1875–1878.

Ricqlès, A. de 1972b. Vers une histoire de la physiologie thermique. Les données histologiques et leur interprétation fonctionnelle. *C. R. Acad. Sci. (Paris), Série D* 275: 1745–1749.

Ricqlès, A. de 1977a. Recherches paléohistologiques sur les os longs des tétrapodes. VII – Sur la classification, la signification fonctionnelle et l'histoire des tissus osseux des tétrapodes (deuxième partie). *Ann. Paléontol.* 62: 71–126.

Ricqlès, A. de 1977b. Recherches paléohistologiques sur les os longs des tétrapodes. VII – Sur la classification, la signification fonctionnelle et l'histoire des tissus osseux des tétrapodes (deuxième partie, suite). *Ann. Paléontol.* 63: 33–56.

Ricqlès, A. de 1978. Recherches paléohistologiques sur les os longs des tétrapodes. VII – Sur la classification, la signification fonctionnelle et l'histoire des tissus osseux des tétrapodes (troisième partie). *Ann. Paléontol.* 64: 85–111.

Ricqlès, A. de and V. de Buffrénil. 2001. Bone histology, heterochronies and the return of tetrapods to life in water: Where are we? In *Secondary adaptation of tetrapods to life in water*, eds. J.-M. Mazin and V. de Buffrénil, 289–310. Verlag Dr. Müchen: Friedrich Pfeil.

Ricqlès, A. de, et al. 1991. Comparative microstructure of bone. In *Bone matrix and bone specific products*, vol. 3, ed. B. K. Hall, 1–78. Boca Raton, FL: CRC Press.

Sander, M. 2000. Longbone histology of the Tendaguru sauropods: implications for growth and biology. *Paleobiology* 26: 466–488.

Sasayama, Y. 1999. Hormonal control of Ca homeostasis in lower vertebrates: considering the evolution. *Zool. Sci.* 16: 857–869.

Sasayama, Y., et al. 1992. Calcitonin of the stingray: comparison of the hypocalcemic activity with other calcitonins. *Gen. Comp. Endocrinol.* 86: 269–274.

Schaffler, M. B., et al. 1995. Aging and microdamage accumulation in human compact bone. *Bone* 17: 521–525.

Schaffler, M. B., et al. 2014. Osteocytes: master orchestrators of bone. *Calcif. Tissue Int.* 94: 5–24.

Schulte, F. A., et al. 2011. *In vivo* micro-computed tomography allows direct three-dimensional quantification of both bone formation and bone resorption parameters using time-lapsed imaging. *Bone* 48: 433–442.

Seeman, E. 2008. Modeling and remodeling. The cellular machinery responsible for the gain and loss of bone's material and structural strength. In *Principles of bone biology*, 3rd edition, vol. 1, eds. J. P. Belizikian, L. G. Raisz and T. J. Martin, 3–28. San Diego, CA: Academic Press.

Sims, N. A. and T. J. Martin. 2014. Coupling the activities of bone formation and resorption: a multitude of signals within the basic multicellular unit. *Bonekey Rep.* 3: 481.

Skedros, J. G., et al. 2011. Analysis of the effect of osteon diameter on the potential relationship of osteocyte lacuna density and osteon wall thickness. *Anat. Rec.* 294 1472–1485.

Skedros, J. G., T. R. Henrie, M. S. Doutré and R. D. Bloebaum. 2018. Sealed osteons in animals and humans: low prevalence and lack of relationship with age. *J. Anat.* 232: 824–835.

Smit, T. H. and E. H. Burger. 2000. Is BMU-coupling a strain-regulated phenomenon? A finite element analysis. *J. Bone Miner. Res.* 15: 301–307.

Sowers, M. R., et al. 1990. The relationship of 1,25-Dihydroxyvitamin D and radial bone mass. *Bone Miner.* 10: 139–148.

St-Arnaud, R. 2008. The direct role of vitamin D on bone homeostasis. *Arch. Biochem. Biophys.* 473: 273–230.

Stein, K., et al. 2010. Small body size and extreme cortical bone remodeling indicate phyletic dwarfism in *Magyarosaurus dacus* (Sauropoda: Titanosauria). *PNAS* 107: 9258–9263.

Stern, P. 2008. Thyroid hormone and bone. In *Principles of bone biology*, 3rd edition, vol. 1, eds. J. P. Belizikian, L. G. Raisz and T. J. Martin, 935–954. San Diego, CA: Academic Press.

Suda, T., et al. 1992. Role of vitamin D in bone resorption. *J. Cell. Biochem.* 49: 53–58.

VetBooks.ir

Suda, T., et al. 1995. Modulation of osteoclast differentiation by local factors. *Bone* 17: 87S–91S.

Takeda, S. and P. Ducy. 2008. Regulation of bone remodeling by central and peripheral nervous signals. In *Principles of bone biology*, 3rd edition, vol. 1, eds. J. P. Belizikian, L. G. Raisz and T. J. Martin, 1059–1068. San Diego, CA: Academic Press.

Takeda, S., et al. 1999. Stimulation of osteoclast formation y 1,25-Dihydroxyvitamin D requires its binding to vitamin D receptor (VDR) in osteoblastic cells: studies using VDR knockout mice. *Endocrinology* 140: 1005–1008.

Tam, C. S., et al. 1978. Bone apposition rate as an index of bone metabolism. *Metabolism* 27: 143–149.

Tamma, R. and D. Riballi. 2017. Bone niches, hematopoietic stem cells, and vessel formation. *Int. J. Mol. Sci*. 18: 1–13.

Tan, D., et al. 2007. Osteocytes subjected to fluid flow inhibit osteoclast formation and bone resorption. *Bone* 41: 745–751.

Tappen, N. C. 1977. Three-dimensional studies of resorption spaces and developing osteons. *Am. J. Anat*. 149: 301–332.

Thomas, C. D. L., et al. 2000. Determination of age at death using combined morphology and histology of the femur. *J. Anat*. 196: 463–471.

Tsubota, K.-I., et al. 2002. Functional adaptation of cancellous bone in human proximal femur predicted by trabecular surface remodeling simulation toward uniform stress state. *J. Biomech*. 35: 1541–1551.

van't Hof, R. J., et al. 2017. Open source software for semi-automated histomorphometry of bone resorption and formation parameters. *Bone* 99: 69–79.

Verborgt, O., et al. 2000. Loss of osteocyte integrity in association with microdamage and bone remodeling after fatigue *in vivo*. *J. Bone. Miner. Res*. 15: 60–67.

Wasserman, R. H. and C. S. Fullmer. 1995. Vitamin D and intestinal calcium transport: facts, speculations and hypotheses. *J. Nutr*. 125: 1971S–1979S.

Williamson, L., et al. 2017. High dose dietary vitamin D_3 increases bone mass and strength in mice. *Bone Rep*. 6: 44–56.

Wiren, K. M. 2008. Androgens receptor expression and steroid action in bone. In *Principles of bone biology*, 3rd edition, vol. 1, eds. J. P. Belizikian, L. G. Raisz and T. J. Martin, 1001–1023. San Diego, CA: Academic Press.

Wu, K., et al. 1970. Haversian bone formation rate determined by a new method in a mastodon, and in human *diabetes mellitus* and osteoporosis. *Calcif. Tissue Res*. 6: 204–219.

Xiong, J. and C. A. O'Brian. 2012. Osteocyte RANKL: new insights into the control of bone remodeling. *J. Bone Miner. Res*. 27: 499–505.

You, L., et al. 2001. A model for strain amplification in the actin cytoskeleton of osteocytes due to fluid drag on pericellular matrix. *J. Biomech*. 34: 1375–1386.

You, L., et al. 2008. Osteocytes as mechanosensors in the inhibition of bone resorption due to mechanical loading. *Bone* 42: 172–179.

Zaidi, M., et al. 2012. Special stem cells for bone. *Cell Stem Cell* 10: 233–234.

Zao, S., et al. 2002. MLO-Y4 osteocyte-like cells support osteoclast formation and activation. *J. Bone Miner. Res*. 17: 2068–2079.

Zhou, S., et al. 2010. Vitamin D metabolism and action in human bone marrow stromal cells. *Endocrinology* 151: 14–22.

VetBooks.ir

12

Remarks on Metaplastic Processes in the Skeleton

Vivian de Buffrénil and Louise Zylberberg

CONTENTS

Definition and Development of Metaplastic "Osseous" Tissues 247
Osteoderms and Dermo-osseous Metaplasia 248
Calcified Tendons of Ornithodirans 251
References 254

Definition and Development of Metaplastic "Osseous" Tissues

"Normal" bone is produced through the secretion of organic matrix components by fully differentiated osteoblasts, followed by calcification of the matrix. But another pathway exists in several manifestations that all produce, without recognizable osteoblasts, calcified matrices that are structurally and functionally reminiscent of bone to various degrees. In these processes, a non-osseous (cartilaginous, tendinous or dermal) tissue mineralizes, while its cells become trapped in the matrix and may or may not alter their shapes to produce a morphology similar to that of osteocytes. The bone-like formation may proliferate through the secretions of non-osteoblastic cells that act like osteoblasts. The final result is that, *in situ*, one tissue, including matrix and cells, has seemingly been transformed into another roughly bone-like one. Such an anosteoblastic osteogenesis is commonly called *metaplasia*.

In addition to bone, similar processes can also take place in most skeletal sites and tissues (except teeth), and various composite or intermediate formations, such as fibrocartilage or chondroid bone, occur in nearly all finned and limbed vertebrates (reviews in Haines and Mohuiddin 1968; Beresford 1981; Hall 2005). Beyond the skeleton, metaplastic processes may also occur in nearly all tissues (Slack 2009). The term metaplasia, however, has been interpreted in several distinct, contrasting and contradictory ways, which we will try to explain and sort out.

The concept of metaplasia was initially based on anatomical and histological observations of the unexpected appearance of foreign tissues at ectopic sites. It was used in particular by pathologists, but in recent years it has tended to be replaced by *transdifferentiation*. These two terms actually refer to distinct phenomena (Figure 12.1; see also Slack and Tosh 2001; Shen et al. 2004). Transdifferentiation designates the conversion, through an irreversible switch, of one fully differentiated cell type into another (Eguchi and Kodama 1993; Tosh and Slack 2002; Slack 2009). It only involves cells, whereas metaplasia may also involve the extracellular compartment (matrices), especially in skeletal tissues. Metaplasia thus semantically includes transdifferentiation as a subordinate (more restricted) concept. According to the hypothesis by Cervantes-Diaz et al. (2017), endochondral ossification might have evolved from a chondroosseous process of transdifferentiation (see also Aghajanian et al. 2017; Giovannone et al. 2019).

Whether a cell undergoes transdifferentiation directly or through a dedifferentiated state varies with the type of cell studied. Some cases of transdifferentiation involve cellular division and loss of apparent differentiation; however, this situation is only occasional (Figure 12.1; see also Beresford 1990 and Tosh and Horb 2004). Aghajanian and Mohan (2018) use the terms "direct" and "indirect" transdifferentiation to distinguish both cases (a stricter definition, promoted by e.g., Okada 1991, restricts the concept of transdifferentiation to direct mature-cell to mature-cell transformation; see also Slack and Tosh 2001 and Slack 2009). Some cells, such as fibroblasts, are capable of both processes, and may either dedifferentiate into pluripotent cells (e.g., He et al. 2014), or be directly transformed into a new, fully differentiated cell type (e.g., fibroblasts into neurons: Xu et al. 2016).

Transdifferentiation and metaplasia generally modify cellular morphology. These modifications are associated with a change in the expression of master regulatory genes, which in turn, induce changes in the Hedgehog and Wnt signaling pathways. They can also be associated with growth factors (fibroblast growth factors [FGF]), transforming growth factors (TGF) (e.g., TGF-β) and bone morphogenetic proteins (Li et al. 2005; Slack 2009; Cho et al. 2014). This molecular cascade acts in close cooperation with molecules of the extracellular matrix (Eguchi and Kodama 1993). The whole set of these factors regulates cellular identity under the influence of epigenetic reprogramming; therefore, metaplasia responds to environmental stimuli. Studies carried out at a cellular level have shown that a switch of cell components such as rough

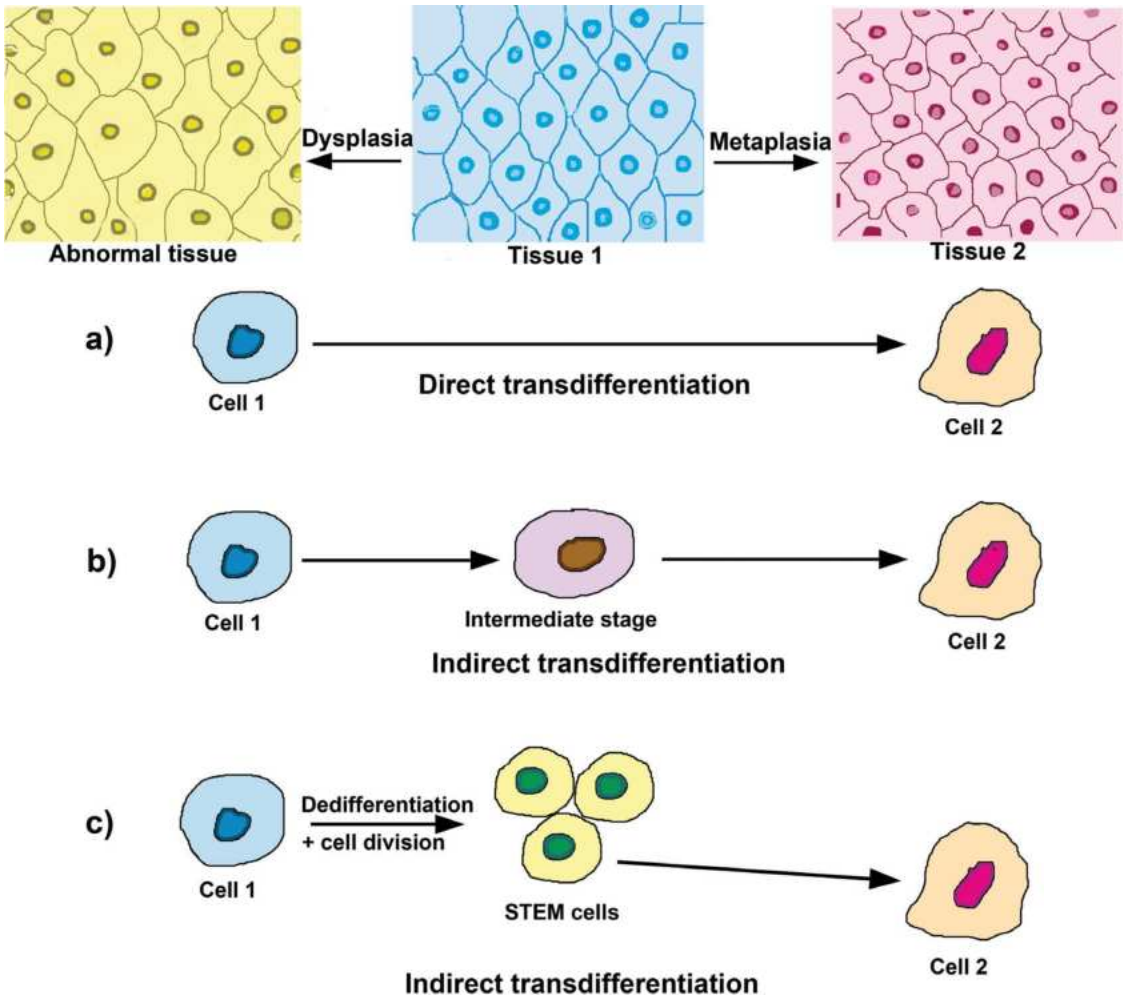


FIGURE 12.1 Metaplasia, transdifferentiation. Upper sketches: In metaplasia, a differentiated tissue is changed from one type to a different one; in dysplasia, a normal, differentiated tissue is changed into an abnormal, pathological one. The lower sketches show different mechanisms of transdifferentiation: (a) through the direct conversion of one cell type into another; (b) through an intermediate cell type and (c) through cell division, dedifferentiation and redifferentiation into a different cell type.

endoplasmic reticulum (RER), Golgi areas and cytoskeleton organization may facilitate the change of cell phenotype without dedifferentiation (Beresford 1990).

Pathological, extraskeletal formations of bone through metaplasia may occur in locations such as lungs (e.g., Shuangshoti 1995; Usami et al. 2005), thyroid (Chun et al. 2013; Aurora et al. 2017) and kidneys (Bataille et al. 2010; Ozkanli et al. 2012). Metaplastic processes were long suspected to occur as normal (physiological) events in skeletal organogenesis; however, beyond their obvious interest, they received little attention in a comparative perspective, except some outstanding syntheses like those of Haines and Mohuiddin (1968), Ricqlès (1975) and Beresford (1981). Interest in the subject, particularly in zoology and paleontology, was renewed during the last 10 years, in pace with worldwide advances in paleohistological studies. The brief review presented below focuses on two main tissues that are formed by metaplastic processes in extant and extinct tetrapods: the osseous or osseous-like tissues in the osteoderms of some taxa and the calcified tendons of ornithodirans, principally dinosaurs, including birds. Chondroid bone is a relatively common tissue showing (with substantial variability) structural characteristics and matrix-staining properties intermediate between cartilage and bone (e.g. Beresford 1981; Huysseune and Sire 1990; Bailleul 2016; Prondvai et al. 2020). It has been suspected to form, at least partly, through a metaplastic process (see Chapter 8). However, this tissue is neither true cartilage nor true bone. It is a third, distinct tissue type, and the actual involvement of metaplasia or transdifferentiation in its formation is a complex and insufficiently documented question. For this reason chondroid bone will be omitted from further consideration here.

Osteoderms and Dermo-osseous Metaplasia

In several tetrapod taxa, osteoderms consist of osseous tissue for which no specific argument suggests that it could have been the result of any process other than osteoblastic

VetBooks.ir

osteogenesis. This situation is found in the carapace of the xenarthran *Dasypus novemcinctus*, in which Vickaryous and Hall (2006) (see also Hill 2006; Krmpotic et al. 2009) found initial osteoblast condensations, secreting osteoid and marking the initial point of osteoderm organogenesis. Similarly, histological studies of other tetrapod taxa, including temnospondyls (*Gerrothorax*, *Aspidosaurus*, *Cacops* and *Platyhystrix*; Witzmann and Soler-Gijón 2010), pareiasaurs (*Bradysaurus*, *Pareiasaurus*, *Anthodon*; Scheyer and Sander 2009) and aetosaurs (*Aetosauroides*; Cerda and Desojo 2011), concluded that typical osteoblastic osteogenesis is at the origin of the osteoderms that form the heavy dermal shields of these taxa.

In other studies, osteoderm development is explained by another osteogenic process, commonly, but sometimes inaccurately, called metaplasia. A key role of metaplasia was initially considered in various scincid, anguid and gerrhosaurid lizards by Moss (1969), and subsequently developed with much more detailed observations in the gekkonid *Tarentola* sp. and the anguid *Anguis fragilis* by Zylberberg and Castanet (1985), Levrat-Calviac and Zylberberg (1986), Levrat-Calviac et al. (1986), Levrat-Calviac (1986–1987), Vickaryous and Sire (2009) and Vickaryous et al. (2015). Osteoderms in these taxa have a roughly comparable structure. They are inserted in the dermis (Figure 12.2A, B), and comprise two distinct structural regions: a superficial layer, composed of a translucent, poorly chromophilic matrix located within the loose dermis (*stratum superficiale*), and a deep, thick layer composed of a strongly chromophilic matrix located within the *stratum compactum* of the dermis. Light and electron microscopy studies have shown that the superficial layer has a loose and poorly organized (woven) fiber meshwork, whereas the matrix of the deep layer has a dense collagen meshwork coarsely organized as a lamellar-like plywood (Figure 12.2C). Apart from lizards, a similar structure was briefly described by Ricqlès et al. (2001) in a dinosaur osteoderm. To some extent, the structure of *Tarentola* and *Anguis* osteoderms closely reflects what prevails in the local dermis (loose or dense) in which they are embedded. Matrix mineralization in gekkos is of the spheritic type in the superficial layer, and of the inotropic type in the deep layer (Levrat-Calviac and Zylberberg 1986). In the basal layer, strong bundles corresponding to the "structural fiber bundles" described by Scheyer and Sander (2004) in ankylosaur osteoderms are continuous with the bundles of the surrounding dense dermis (Figure 12.2B–F). In the superficial layer, extrinsic (Sharpey's) fibers penetrate orthogonally into the osteoderm and anchor it in the surrounding dermis and dermal-epidermal membrane (Figure 12.2B). Squamate osteoderms that share this type of organization are most often totally compact and not, or very marginally, subjected to internal or external remodeling. A comparable structure, with strong, variably oriented bundles of fibers in compact osteoderms, can be observed in an extinct Pleistocene xenarthran (Mylodontidae), *Glossotherium* (Figure 12.2D).

In *Tarentola* as well as in *Anguis*, well-differentiated osteoblasts (Figure 12.2B, G) occur around the osteoderms and, in the form of osteocytes, within them (Zylberberg and Castanet 1985; Levrat-Calviac and Zylberberg 1986; Vickaryous et al. 2015). Osteoderm organogenesis was considered a form of metaplasia by the authors quoted above, mainly because its initial stage starts with the "deposit of mineral crystals in a preexisting dermal tissue" (Figure 12.2H). Of course, the occurrence of normal, functional osteoblasts and osteocytes is hardly compatible with the first meaning of the term metaplasia, i.e., an irreversible shift in the cell type of a tissue. It also conflicts with the possibility of a change in the secretion of these cells, because the osteoderms are made of bone, i.e., the normal product of osteoblasts. Finally, a metaplastic interpretation could mainly rely on the hypothesis that the initial calcification of the dermis is controlled by fibroblasts (functional shift) and/or that these cells later turn into trapped osteocyte-like cells (structural shift). This hypothesis was proposed by Vickaryous et al. (2015). Matrix calcification, considered per se and unrelated to cellular processes, cannot properly define a metaplastic process, according to the various formal meanings of this term.

The general model of the metaplastic osteogenesis of osteoderms summarized above has been applied by several authors to a number of extant and extinct taxa in which osteoderm structure reflects the integration and calcification of massive fiber bundles (up to 250 µm in diameter or more; see e.g. figure 3 in Scheyer and Sander 2004). These are distinguished from Sharpey's fibers by both their diameter and their orientation parallel to the osteoderm surfaces. Moreover, they are not linked to the insertion of connective tissue such as tendons, ligaments or muscle attachments to bone. Such fibers, currently designated *structural fiber bundles* (Scheyer and Sander 2004), are likely to originate from the surrounding dermis. Examples of the metaplastic interpretations of osteoderm formation are given by Witzmann and Soler-Gijón (2010) in the temnospondyl *Plagiosuchus*, Bhullar and Bell (2008) in the anguid lizard *Anniella*, Burns and Currie (2014) in ankylosaurian dinosaurs and Cerda and Powell (2010) and Cerda et al. (2015) in sauropod dinosaurs. The increase in the number of comparative studies suggests that complex situations, in which an initial metaplastic process may subsequently be replaced by normal osteoblastic osteogenesis, are relatively common. A typical (and perhaps the best documented) case is the differentiation and growth of crocodilian osteoderms and palpebrals. Vickaryous and Hall (2008) and Vickaryous and Sire (2009) showed in *Alligator mississippiensis* that, at an initial stage, osteoderms develop as mere knots of non-calcified, standard dermic tissue, "in the absence of differentiated osteoblasts, osteoid and periosteum and via the direct transformation of the preexisting connective tissue". Osteoderm and palpebral primordia nevertheless contain fibroblast-like cells, but the latter are seemingly inactive. Mineralization occurs with some delay, proceeding centrifugally through the dermal collagen meshwork, and creating a calcified nodule that reacts like bone to histochemical dyes. Cells are trapped in it and display the appearance of osteocytes (presence of canaliculi). This early mode of formation is interpreted by the authors as metaplasia, and it is implicitly considered the sole active process that produce osteoderms. Recently Dubansky and Dubansky (2018) showed in a growth series of *A. mississippiensis* that endothelial cells migrate in the dermis and turn into osteoblasts to form osteoderms. Of course, this observation would falsify the model presented by Vickaryous and Hall (2008) and

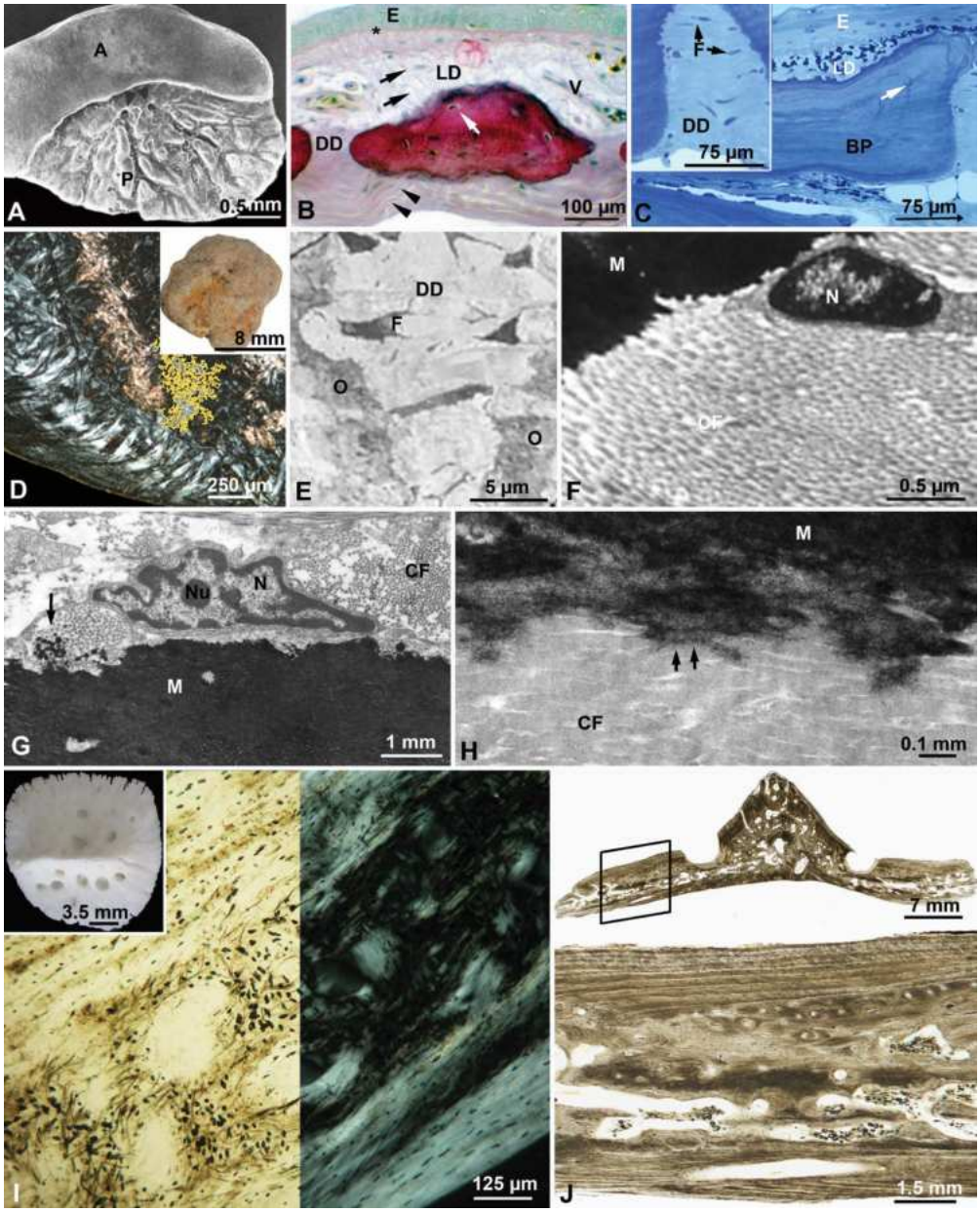


FIGURE 12.2 Metaplasia in osteoderms. A, *Anguis fragilis*. Scanning electron micrograph of the outer surface of an osteoderm. The anterior field (A) appears as a flat surface, while the posterior field (P) is ornamented with grooves and ridges. B, *Anguis fragilis* (young specimen). Section of an osteoderm stained with one-step trichrome. The osteoderm is inserted between the superficial loose dermis (LD) and the compact dense dermis (DD). Cells are present within the osteoderm (white arrow). Thin bundles (upper black arrows) connect the outer surface of the osteoderm to the epidermal layer (E). In the dense dermis, thick bundles pass from one osteoderm to another (arrowheads). V, blood vessel; C, *Chalcides sexlineatus*. Demineralized semithin section stained with toluidine blue. Inset: dense dermis (DD) between two osteoderms. F and arrows, fibroblasts; BP, basal plate, E, epidermis; LD, loose dermis. The white arrow points to a line of arrested growth. D, Histological structure of *Glossotherium* sp. (Mammalia, Xenarthra, Pilosa) osteoderms. The inset shows the outer morphology of an osteoderm. Main frame: strong fiber bundles (birefringent on the section) originating from the dermis occupy a large part of the osteoderm volume. Transmitted polarized light. E, *Chalcides sexlineatus*. Transmission electron micrography (TEM). Low magnification of a demineralized thin section. Fibroblasts (F) are scattered in the dense dermis (DD) between two osteoderms (O; shows the limits of the osteoderms). F, *Anguis fragilis*. TEM. A fibroblast surrounded by the collagen fibrils (CF) of the dense dermis contacts the mineralized osteoderm (M). N, nucleus of the fibroblast. G, *Anguis fragilis*. TEM. Osteoblast at the surface of an osteoderm. Mineral deposit (arrow) is found in the collagen fibrils (CF) in the vicinity of the osteoderm. M, mineralized basal layer; N, nucleus; Nu, nucleolus. H, *Anguis fragilis*. TEM. Mineralization front in the basal plate of an osteoderm. M, mineralized basal layer. At the mineralization front, the mineral crystals are oriented by the collagen fibrils (arrows). CF: collagen fibrils of the dense dermis. I, Histological structure of an osteoderm from a juvenile *Alligator mississippiensis*. Inset shows the size and general aspect of the osteoderm. Main frame: histological structure in ordinary (left half) and polarized (right half) light. The core of the osteoderm is occupied by a monorefringent tissue with randomly oriented cells and numerous fiber bundles. This formation possibly results from dermo-osseous metaplasia. J, Structure of an osteoderm from an adult *Crocodylus niloticus* (ordinary transmitted light). Extensive remodeling occurs in the core of the osteoderm, erasing the early formed fiber-rich tissue. Upper field: general view of the osteoderm (the box indicates the field shown in the lower field); lower field: closer view of the osteoderm structure.

VetBooks.ir

Vickaryous and Sire (2009). Complementary observations in several extant and extinct crocodilian taxa (Buffrénil 1982; Buffrénil et al. 2015) show that the diploe-shaped osteoderms of subadult and adult crocodiles have a complex histological structure (Figure 12.2I, J; see also Scheyer and Sander 2004). They are made of woven-fibered bone, mainly located in their core region, along with very typical (matrix and cells) parallel-fibered and lamellar tissues, in their compact cortices. The distribution of these tissues is totally unrelated to dermis strata (the thickness of the osteoderms at this stage is incommensurate with that of the dermis). In addition, crocodilian osteoderms are intensely and repeatedly remodeled from both inside, in their core region, and outside, over their outer ("lateral") cortical surface; therefore, an important part of their volume is occupied by secondary lamellar bone. This remodeling process, along with the occurrence of parallel-fibered and lamellar tissues in the whole cortical region of the osteoderms, implies that active osteoclasts and osteoblasts are present around and inside the osteoderms, and that the further growth of these elements is due to regular "dynamic osteogenesis" (according to the terminology of Marotti et al. 1999), depending on a population of osteoblasts spatially ordered to form a kind of periosteum. Crocodilian osteoderms thus exemplify a non-exclusive osteogenic process, combining early metaplasia (the tissues then formed are most often erased by remodeling) and subsequent normal osteoblastic osteogenesis. A very similar growth pattern was described in the osteoderms of *Placosaurus rugosus*, a large anguid lizard from the European Miocene (Buffrénil et al. 2011). It is likely to be common in a number of taxa, depending on the size and shape of the osteoderms.

Calcified Tendons of Ornithodirans

The calcification of tendons in various parts of the musculoskeletal system (Figure 12.3A, B) is considered by some authors (reviews in Van den Berge and Storer 1995; Bailleul et al. 2019) as a typical case of metaplasia, through which tendinous tissue is "transformed" into bone (e.g., Haines and Mohuiddin 1968; Abdalla 1979; Organ and Adams 2005). The propension to develop this process under tensile stress seems to be exclusive to birds and their dinosaurian relatives (e.g. Summers and Koob 2002). In non-dinosaurian tetrapods, tendon calcification is rare under normal physiological conditions; however, it is a relatively common pathology, including in humans (e.g., Oliva et al. 2012). Much more attention has been paid to this process than to the development of osteoderms; therefore, the general information available on this topic, briefly summarized here, is relatively more precise.

The basic structure of tendons, as reviewed by Organ and Adams (2005), consists of fibers, with fibrils made of collagen Type I and, to a small degree (5–10%), Types V and III (Canty and Kadler 2002; Landis and Silver 2002). The fibrils are principally associated in parallel to form fibers, and the fibers are parallel to each other, oriented longitudinally, and gathered into increasingly integrative structural units. Kannus (2000) considered six distinct integration levels, from individual fibrils to the entire tendon. Each large fiber bundle (fascia) within the tendon is enveloped in a membrane, the endotenon, and the whole tendon, formed of several fascia, is surrounded by an external envelope, the peritenon. In addition to collagen fibrillar material, the tendon matrix also contains elastic fibers (Grant et al. 2013), and a rich set of noncollagenous proteins similar to those encountered in bone: osteocalcin, osteopontin, fibronectin, bone sialoproteins and various kinds of proteoglycans (Glimcher 1989; Canty and Kadler 2002; Agabalyan et al. 2013). Glimcher et al. (1979) observed in the matrix of calcified tendons of the turkey some biochemical peculiarities in peptide composition that do not occur in non-calcified tendons. Tendon cells, the tenoblasts and tenocytes, are of the fibroblast lineage. During fibrillogenesis, their plasmic membrane develops deep and narrow recesses, separated by processes and open to the extracellular compartment, where collagen fibrillogenesis occurs (Birk and Trelstad 1986). When fully differentiated, the cells within a tendon can be very similar morphologically to osteocytes, with a spindle-like soma and dendrite-like processes housed in *canaliculi* (Adams and Organ 2005). The processes, connected to each other by gap junctions (Tanji et al. 1995), form extensive networks (McNeilly et al. 1996). Tenocytes are interspersed among collagen fiber bundles and fascia; their long axis is parallel to the general direction of the fibers. In cross section, their aspect is strikingly reminiscent of multipolar osteocytes (Krstić 1985). Like a periosteum, the peritenon comprises an external fibrillar stratum and a deep layer of tenoblasts devoid of processes and oriented parallel to the outer contour of the tendon. Sparse vascular canals, mainly oriented longitudinally, occur between the fibrillar fascia.

Histologically, the calcified tendons of adult birds, as exemplified by the Indian crane (*Grus antigone*) studied for this review, appear in cross section like a totally compact formation, the core of which consists of dense Haversian bone, and the periphery of a layer of primary tissue variable in thickness (Figure 12.3C). Between the osteons, remnants of primary tissue are sparse. Strong remodeling in the tendons of other bird species was observed by Abdalla (1979); Adams and Organ (2005) and Organ and Adams (2005). In *G. Antigone*, vascularization of calcified tendons mainly consists of Haversian and Volkmann's canals. Although the secondary osteons are morphologically well-characterized, their histological structure is atypical compared to other species (e.g., Abdalla 1979): they are not made of lamellar bone, but of a homogeneous tissue showing "rods" about 10–15 µm in diameter, framed by darker material (Figure 12.3C, insets). This structure suggests the occurrence of longitudinal calcified fiber bundles. Interstitial and cortical bone formations are comparable in structure to the osteons. In polarized light, primary (cortical and interstitial) and secondary (Haversian) tissues are totally monorefringent (Figure 12.3D). Wherever located, cell lacunae are multipolar and surrounded by short canaliculi.

In the most studied case, the gastrocnemius tendon of the domestic turkey, *Meleagris gallopavo* (Landis 1986; Landis et al. 2002; Chen et al. 2019), calcification develops progressively, from the central region of the tendon toward its forked proximal extremity. The mineral phase of the calcified tendon

VetBooks.ir

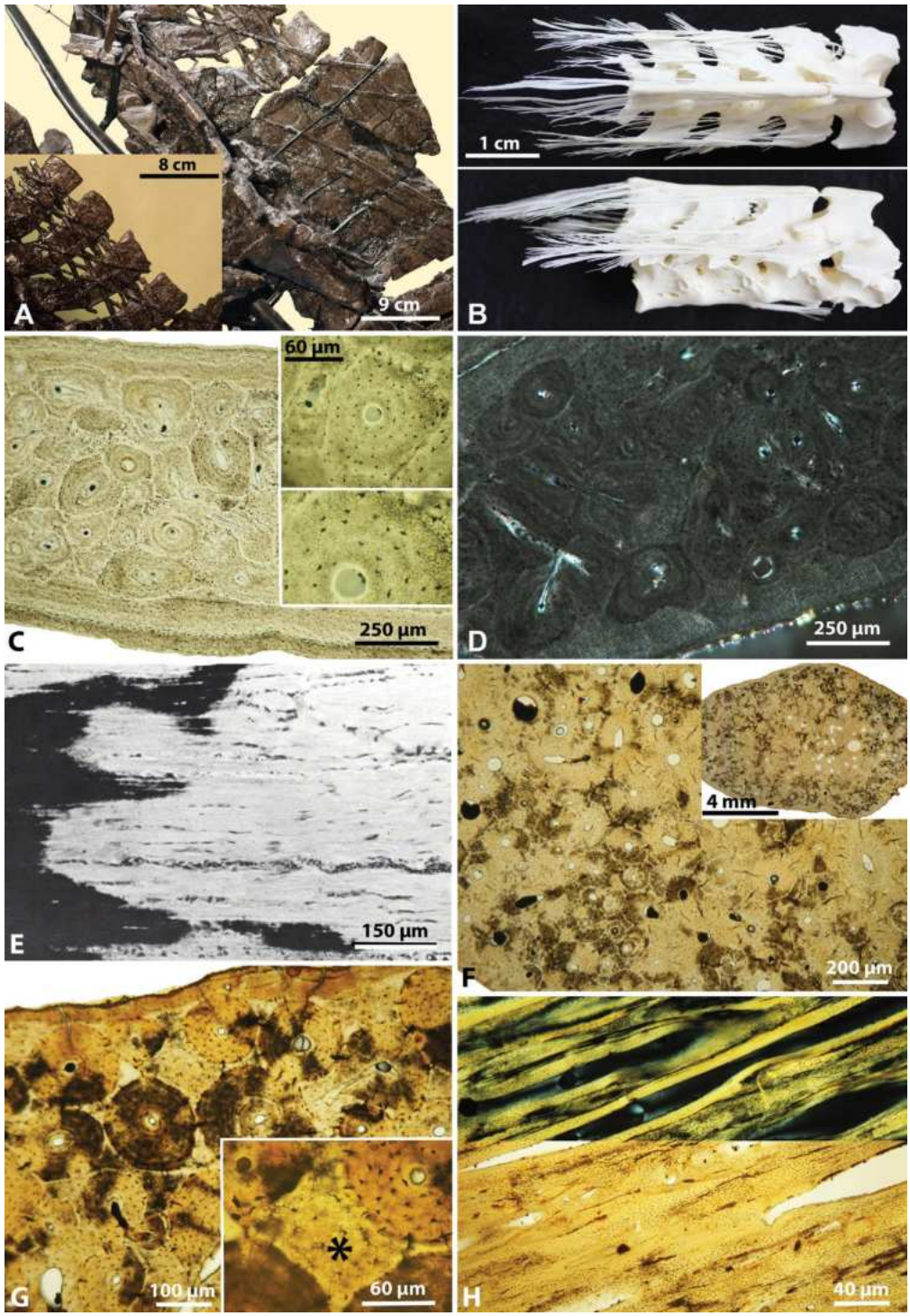


FIGURE 12.3 General histological traits of calcified tendons. A, Aspect of the calcified tendons around the spine of the ornithischian dinosaur *Iguanodon bernissartensis*, from the Cretaceous of western Europe (courtesy of the Institut Royal des Sciences Naturelles de Belgique, Brussels, Belgium). B, Aspect of calcified tendons around the vertebrae of the extant bird *Grus antigone* (Guiformes). C, Cross section in a calcified tendon of *G. antigone*. The tendon is mainly composed of Haversian bone, but the walls of the osteons are made of an atypical, non-lamellar tissue (insets). D, The tissue composing the bird calcified tendon is monorefringent on cross sections in both the secondary osteons and the interstitial tissue. Polarized light. E, Mineralization front in the tendon of a turkey, *Meleagris gallopavo*. (Transmission electron microscopy image, courtesy of Dr. William Landis). F, Cross section of the calcified tendon of the ornithischian dinosaur *Edmontosaurus*, from the Upper Cretaceous of North America. At low (inset) and medium (main frame) enlargement, the histological structure of this sample is identical to that observed in the bird tendon. G, Closer view of the Haversian and interstitial tissues of *Edmontosaurus* calcified tendon. Notice the total similitude with the bird tendon, and the occurrence of osteocyte-like cells, derived from tenoblasts, in the interstitial tissue (asterisk in the inset). H, Longitudinal section in *Edmontosaurus* tendon, showing that the tendon tissue, whether primary or secondary, is birefringent in polarized light. This reveals the longitudinal orientation of the fibrillar meshwork in osteons and interstitial tissue.

VetBooks.ir

relies on a small form of hydroxyapatite crystals (Moradian-Oldak et al. 1991). Recent analyses of the mechanisms involved in normal tendon mineralization in the turkey gastrocnemius tendon pointed out a close parallel between the progression of the calcification front (Figure 12.3E), the local expression of several genes and the resulting synthesis and secretion of non-collagenous matrix proteins by the tenocytes (Chen et al. 2019). Two kinds of mineral nucleation sites (i.e., initial spots of mineral deposition) have been described by Landis (1986; see also Arsenault 1992; Landis et al. 1992; Landis and Silver 2002). The earliest to appear during the local mineralization process of a tendon are extracellular "matrix vesicles", i.e., small (ca. 0.01–0.2 µm in diameter) interfibrillar mineral spherules developing in chaplets, at variable distance from the tenocytes in the vicinity of the progressing mineralization front (see Arsenault 1992 and Shapiro et al. 2015 for structural details on the matrix vesicles). The following stage is ordinary inotropic mineralization, which can occur either in contact with the matrix vesicles or away from them and from the tenocytes. Both mineralization processes are considered independent from each other (Landis and Silver 2002). Very different results were obtained by Agabalyan et al. (2013) in the domestic chicken (*Gallus gallus*). These authors observed the coexistence of several cell types in the matrix of calcified tendons, including well-differentiated tenocytes and cells phenotypically comparable to either chondrocytes or osteocytes. Based on additional histochemical and immunochemical data, Agabalyan et al. (2013) inferred the possibility "that a process akin to endochondral ossification is responsible for the non-pathological mineralization of the tendon". To our knowledge, this interpretation has not been supported by other studies.

The calcified tendons of dinosaurs are often presented as comparable in structure to those of birds (e.g., Horner et al. 2015), a statement supported by our own observations in the ornithischian *Edmontosaurus* (Upper Cretaceous of North America). They indeed contain a primary tissue that represents the original calcified tendons itself and extensive formations of densely packed secondary osteons (Figure 12.3F, G). Primary interstitial tissue may remain, interspersed between the osteons, in the core of the tendons (Figure 12.3G; see also Organ and Adams 2005). The *Edmontosaurus* calcified tendon is monorefringent in cross section, like the tendons of *G. antigone*, but it is strongly birefringent in longitudinal section (Figure 12.3H), showing the longitudinal orientation of its fiber bundles.

A conspicuous difference between dinosaurs and birds is the possible occurrence of cyclical growth marks (CGMs), *annuli* and lines of arrested growth, as well as longitudinal primary osteons in the peripheral layers of the tendons from large dinosaurs. These features confer to the peripheral tendon layer a striking resemblance to the external fundamental systems so frequently observed in tetrapod bones. When present, the CGMs show that the growth in diameter of the tendons proceeded by apposition under the peritenon, which clearly functioned like a periosteum. This situation is spectacularly exemplified by a cross section from the hadrosaurian *Hypacrosaurus stebingeri* described by Organ and Adams (2005). These authors considered the peripheral layer true bone tissue and named it accordingly. However, the formal presence of osteocytes was not mentioned and the detailed histological structure of the local matrix was not described. As a result, it remains dubious whether this tissue is real bone, secreted by osteoblasts and housing osteocytes, or a tendon tissue, cyclically produced by the tenoblasts of the peritenon and subsequently calcified. Several figures in Organ and Adams (2005) tend to support the second hypothesis.

Following Haines and Mohuiddin (1968), several authors designate the primary tissue of dinosaurian calcified tendons as "bone" and refer to its mode of formation as metaplasia. A problematic issue is that both the matrix and cells of this tissue differ from bone (however, secondary tissues are unambiguously osseous, as pointed out by Horner et al. 2015). Until now, cells undoubtedly identifiable as osteocytes, as well as a different matrix type than strong bundles of longitudinal fibers (i.e., tendon-like matrix), have not been convincingly shown in dinosaurian calcified tendons. The question of cell morphology, density and location in the so-called metaplastic bone is at best considered allusively (see Bailleul et al. 2019 and Horner et al. 2015). Conversely, in extant birds, the cells in the primary tissue of calcified tendons are generally identified as tenocytes or fibroblasts (e.g., Adams and Organ 2005). Their actual transdifferentiation into osteoblasts and osteocytes is seldom proposed, although the study of tendon mineralization in chicks (*G. gallus domesticus*) by Abdalla (1979; see also Agabalyan et al. 2013) concluded to the occurrence of "fibroblasts transformed into osteoblasts which secreted around the cells and later between the fibers".

Although sophisticated methods have been used for extant species, contrasting and contradictory results have been obtained. This situation suggests that some variation may occur among taxa in the processes involved in tendon calcification and remodeling. Moreover, available information may create some ambiguity about the relevance of the concept of metaplasia, viewed as "a direct transformation of tendon into bone" (Francillon-Vieillot et al. 1990), as applied to dinosaur (including bird) calcified tendons. Most reference studies on the histology of extant birds do not formally use the term metaplasia. In this context, this term could have two distinct meanings. In one case, tenoblasts become osteoblasts (transdifferentiation *sensu stricto*) and experience the normal fate of these cells i.e., they secrete osteoid before being embedded in it as osteocytes. But this situation has never been unambiguously shown through appropriate techniques in any study. Considering the close morphological resemblance between tenocytes and osteocytes, a diagnostic clue based on cell morphology is barely usable in fossils. In the other case, the tendon cells remain tenoblasts and tenocytes, but they function as osteoblasts or osteocytes, including in their secretions (a functional shift of the cells). This situation differs little from the previous one, and identifying it in fossils is hampered by the same difficulties. A third solution might be that tenoblasts and tenocytes remain tendon cells morphologically and functionally, and secrete a tendon matrix that becomes mineralized through the mechanisms partly understood in extant birds. Subsequent remodeling extensively ossifies the tendons through the replacement of their primary tissue by secondary bone. In this situation, which closely fits histological and paleohistological observations, the recourse to a metaplastic

VetBooks.ir

model would be unnecessary because at no time is there a real transformation of one type of cells, matrix or both into other types. Replacement of tendon tissue by bone during remodeling is a very different question, unrelated to the problem of metaplasia proper. This conclusion is close to Bailleul et al.'s (2019) based on similar arguments.

REFERENCES

Abdalla, O. 1979. Ossification and mineralization in the tendons of the chicken (*Gallus domesticus*). *J. Anat.* 129: 351–359.

Adams, J. S. and C. L. Organ. 2005. Histologic determination of ontogenetic patterns and processes in hadrosaurian ossified tendons. *J. Vert. Paleontol.* 25: 614–622.

Agabalyan, N. A., et al. 2013. Investigating tendon mineralization in the avian hindlimb: a model for tendon aging, injury and disease. *J. Anat.* 223: 262–277.

Aghajanian, P., et al. 2017. Epiphyseal bone formation occurs via thyroid hormone regulation of chondrocyte to osteoblast transdifferentiation. *Scient. Rep.* 7: 10432 DOI:10.1038/s41598-017-11050-1.

Aghajanian, P. and S. Mohan. 2018. The art of building bone: emerging role of chondrocyte-to-osteoblast transdifferentiation in endochondral ossification. *Bone Res.* 6: 19. Doi.org/10.1038/s41413-018-0021-z.

Arsenault, A. L. 1992. Structural and chemical analyses of mineralization using the turkey leg tendon as a model tissue. *Bone Miner.* 17: 253–256.

Aurora, N., et al. 2017. A rare presentation: a case report of osseous metaplasia and mature bone formation in a follicular adenoma of the thyroid. *Int. J. Surg Case Rep.* 37: 83–86.

Bailleul, A. M., et al. 2016. Chondroid bone in dinosaur embryos and nestings (Ornithischia: Hadrosauridae): insights into the growth of the skull and the evolution of skeletal tissues. *C. R. Palevol* 15: 49–64.

Bailleul, A. M., et al. 2019. Dinosaur paleohistology: review, trends and new avenues of investigation. *Peer J.* 7: e7764 DOI 10.7717/peerj.7764

Bataille, S., et al. 2010. Osseous metaplasia in a kidney allograft. *Nephrol. Dial. Transplant.* 25: 3796–3798.

Beresford, W. A. 1981. *Chondroid bone, secondary cartilage and metaplasia*. Baltimore and Munich: Urban & Schwarzenberg.

Beresford, W. A. 1990. Direct transdifferentiation: can cells change their phenotype without dividing? *Cell Diff. Dev.* 29: 81–93.

Bhullar, B.-A. S. and C. J. Bell. 2008. Osteoderms of the California legless lizard *Anniella* (Squamata: Anguidae) and their relevance for considerations on miniaturization. *Copeia* 2008: 785–793.

Birk, D. E. and R. L. Trelstad. 1986. Extracellular compartments in tendon morphogenesis: collagen fibril, bundles, and macroaggregate formation. *J. Cell Biol.* 103: 231–240.

Buffrénil, V. de. 1982. Morphogenesis of bone ornamentation in extant and extinct crocodilians. *Zoomorphology* 99: 155–166.

Buffrénil V. de, et al. 2011. An enamel-like tissue, osteodermine, on the osteoderms of a fossil anguid (Glyptosaurinae) lizard. *C.R. Palevol*. 10: 427–437.

Buffrénil V de, et al. 2015. Differentiation and growth of bone ornamentation in vertebrates: a comparative histological study among the Crocodylomorpha. *J. Morphol.* 276: 425–445.

Burns, M. E. and P. J. Currie. 2014. External and internal structure of ankylosaur (Dinosauria, Ornithischia) osteoderms and their systematic relevance. *J. Vert. Paleontol*. 34: 835–851.

Canty, E. G. and K. R. Kadler. 2002. Collagen fibril biosynthesis in tendon: a review of recent insights. *Comp. Biochem. Physiol. A* 133: 979–985.

Cerda, I. A. and J. E. Powell. 2010. Dermal armor histology of *Saltasaurus loricatus*, an Upper Cretaceous sauropod dinosaur from Northwest Argentina. *Acta Palaeontol. Pol.* 55: 389–398.

Cerda, I. A. and J. B. Desojo. 2011. Dermal armour histology of aetosaurs (Archosauria: Pseudosuchia), from the Upper Triassic of Argentina and Brazil. *Lethaia* 44: 417–428.

Cerda, I. A., et al. 2015. Morphology, microanatomy, and histology of Titanosaur (Dinosauria, Sauropoda) osteoderms from the Upper Cretaceous of Patagonia. *J. Vert. Paleontol*. 35: e905791. DOI 10.1080/02724634.2014.905791.

Cervantes-Diaz, F., et al. 2017. Evolutionary origin of endochondral ossification: the transdifferentiation hypothesis. *Dev. Genes Evol*. 227: 121–127.

Chen, L., et al. 2019. Correlations between gene expression and mineralization in the avian leg tendon. *Bone* 121: 42–59.

Cho, Y.-D., et al. 2014. Epigenetic modifications and canonical wingless/int-1class (WNT) signaling enable transdifferentiation of non-osteogenic cells into osteoblasts. *J. Biol. Chem*. 289: 20120–20128.

Chun, J. S., et al. 2013. Osseous metaplasia with mature bone formation of the thyroid gland: three case reports. *Oncol. Lett.*6: 977–979.

Dubansky, B. H. and B. D. Dubansky. 2018. Natural development of dermal ectopic bone in the American alligator (*Alligator mississippiensis*) resembles heterotopic ossification disorders in humans. *Anat. Rec.* 301: 56–76.

Eguchi, G. and R. Kodama. 1993. Transdifferentiation. *Curr. Opin. Cell Biol*. 5: 1023–1026.

Francillon-Vieillot, H., et al. 1990. Microstructure and mineralization of vertebrate skeletal tissues. In *Skeletal biomineralization: patterns, processes and evolutionary trends*, vol. 1, ed. J. G. Carter, 471–530. New York: Van Nostrand Reinhold.

Giovannone, D., S. et al. 2019. Programmed conversion of hypertrophic chondrocytes into osteoblasts and marrow adipocytes within zebrafish bones. *eLife* 8: e 42736. Doi: https://doi.org/10.7554/eLife.42739.

Glimcher, M. J. 1989. Mechanism of calcification: Role of collagen fibrils and collagen-phosphoprotein complexes in vitro and in vivo. *Anat. Rec.* 224: 139–153.

Glimcher, M. J., et al. 1979. Phosphopeptides and γ-carboxyglutamic acid-containing peptides in calcified turkey-tendon: Their absence in uncalcified tendon. *Calcif. Tiss. Int.* 27: 281–284.

Grant, T. M., et al. 2013. Elastic fibers are broadly distributed in tendon and highly localized around tenocytes. *J. Anat.* 222: 573–579.

Haines, R. W. and A. Mohuiddin. 1968. Metaplastic bone. *J. Anat.* 103: 527–538.

Hall, B. K. 2005. Bone and cartilage. *Development and evolutionary skeletal biology.* Amsterdam: Elsevier-Academic Press.

He, X., et al. 2014. Human fibroblast reprogramming to pluripotent stem cells regulated by the miR19a/b-PTEN Axis. *PLoS One* 9(4): e95213. DOI 10.1371/journal.pone.0095213.

Hill, R. V. 2006. Comparative anatomy and histology of xenarthran osteoderms. *J. Morphol.* 267: 1441–1460.

Horner, J., et al. 2015. Mineralized tissues in dinosaurs interpreted as having forms through metaplasia: a preliminary evaluation. *C. R. Palevol.* 15: 176–196.

Huysseune, A. and J.-Y. Sire 1990. Ultrastructural observations on chondroid bone in the zebrafish *Hemichromis bimaculatus*. *Tissue Cell* 22: 371–383.

Kannus, P. 2000. Structure of the tendon connective tissue. *Scand. J. Med. Sci. Sports* 10: 312–320.

Krmpotic, C. M., et al. 2009. Osteoderm morphology in recent and fossil euphractine xenarthrans. *Acta Zool. (Stockholm)* 90: 339–351.

Krstić, R. V. 1985. *General histology of the mammal*. Berlin: Springer Verlag.

Landis, W. J. 1986. A study of calcification in the leg tendons from domestic turkey. *J. Ultrastruc. Mol. Struct. Res.* 94: 217–238.

Landis, W. J. and F. H. Silver. 2002. The structure and function of normally mineralizing avian tendons. *Comp. Biochem. Physiol. A*133: 1135–1157.

Landis W. J., et al. 1992. Extracellular vesicles of calcifying turkey leg tendon characterized by immunocytochemistry and high voltage electron microscopic tomography and 3-D graphic image reconstruction. *Bone Miner.* 17: 237–241.

Landis W. J., et al. 2002. Vascular-mineral spatial correlation in the calcifying turkey leg tendon. *Connect. Tissue Res.* 43: 59–605.

Levrat-Calviac, V. 1986–1987. Etude comparée des ostéodermes de *Tarentola mauritanica* et de *T. neglecta* (Gekkonidae, Squamata). *Arch. Anat. Micr. Morphol. Exp.* 75: 29–43.

Levrat-Calviac, V. and L. Zylberberg. 1986. The structure of osteoderms in the gecko: *Tarentola mauritanica*. *Am. J. Anat.* 176: 437–446.

Levrat-Calviac, V., et al. 1986.The structure of the osteoderms of two lizards: *Tarentola mauritanica* and *Anguis fragilis*. In *Studies in herpetology*, ed. Rocek, Z., 341–344. Prague.

Li, W.-C., et al. 2005. The molecular basis of transdifferentiation. *J. Cell. Mol. Med.* 9: 569–582.

Marotti, G., et al. 1999. Static and dynamic bone formation and the mechanism of collagen fiber orientation. *Bone* 25: 156.

McNeilly, C. M., et al. 1996. Tendon cells in vivo form a three-dimensional network of cell processes linked by gap junctions. *J. Anat.* 189: 593–600.

Moradian-Oldak, J., et al. 1991. Electron diffraction study of individual crystals of bone, mineralized tendon and synthetic apatite. *Connect. Tissue Res.* 25: 219–228.

Moss, M. L. 1969. Comparative histology of dermal sclerifications in reptiles. *Acta Anat.* 73: 510–533.

Okada, T. S. 1991. *Transdifferentiation. Flexibility in cell differentiation*. Oxford: Clarendon Press.

Oliva, F., et al. 2012. Physiopathology of intratendinous calcific deposition. *BMC Med.* 10: 95.

Organ, C. L. and J. Adams. 2005. The histology of ossified tendons in dinosaurs. *J. Vert. Paleontol.* 25: 602–613.

Ozkanli, S., et al. 2012. Osseous metaplasia and bone marrow elements in a case of renal carcinoma. *Case Rep. Urol.* 2012: 649257.

Prondvai, E., et al. 2020. Extensive chondroid bone in juvenile duck limbs hints at accelerated growth mechanism in avian skeletogenesis. *J. Anat.* 236: 463–473.

Ricqlès, A. de 1975. Recherches paléohistologiques sur les os longs des tétrapodes VII. – Sur la classification, la signification fonctionnelle et l'histoire des tissus osseux des tétrapodes. Première partie, structures. *Ann. Paléontol.* 61: 51–129.

Ricqlès, A. de, et al. 2001. Histology of dermal ossifications in an ankylosaurian dinosaur from the Late Cretaceous of Antarctica. *Assoc. Paleontol. Argent., Publ. Esp.* 7: 171–174.

Scheyer, T. M. and P. M. Sander. 2004. Histology of ankylosaur osteoderms: implications for systematics and function. *J. Vert. Paleontol.* 24: 874–893.

Scheyer, T. M. and P. M. Sander. 2009. Bone microstructure and mode of skeletogenesis in osteoderms of three pareiasaur taxa from the Permian of South Africa. *J. Evol. Biol.* 22: 1153–1162.

Shapiro, I. M., et al. 2015. Matrix vesicles: are they anchored exosomes? *Bone* 79: 29–36.

Shen, C.-N., et al. 2004. Transdifferentiation, metaplasia and tissue regeneration. *Organogenesis* 1: 36–44.

Shuangshoti, S. 1995. Metaplasia of bone in lungs and bronchi: report of 2 cases. *J. Med. Assoc. Thai.* 78: 103–107.

Slack, J. M. W. 2009. Metaplasia and somatic cell reprogramming. *J. Pathol.* 217: 161–168.

Slack, J. M. W. and D. Tosh. 2001. Transdifferentiation and metaplasia – switching cell types. *Curr. Opin. Genet. Dev.* 11: 581–586.

Summers, A. P. and T. J. Koob. 2002. The evolution of tendon – morphology and material properties. *Comp. Biochem. Physiol.* A 133: 1159–1170.

Tanji, K., et al. 1995. Gap junctions between fibroblasts in rat myotendon. *Arch. Histol. Cytol.* 58: 97–102.

Tosh, D. and M. E. Horb. 2004. How cells change their phenotype. *Handb. Stem Cells*2: 138–145.

Tosh, D. and J. M. W. Slack. 2002. How cells change their phenotype. *Nat. Rev. Mol. Cell Biol.* 3: 127–194.

Usami, M. D., et al. 2005. Primary lung adenocarcinoma with heterotopic bone formation. *Jpn. J. Thorac. Cardiovasc. Surg.* 53: 102–105.

Van den Berge, J. C. and R. W. Storer. 1995. Intratendinous ossification in birds: a review. *J. Morphol.* 226: 47–77.

Vickaryous, M. K. and B. K. Hall. 2006. Osteoderm morphology and development in the nine-banded armadillo, *Dasypus novemcinctus* (Mammalia, Xenarthra, Cingulata). *J. Morphol.* 267: 1273–1283.

Vickaryous, M. K. and B. K. Hall. 2008. Development of the dermal skeleton in *Alligator mississippiensis* (Archosauria, Crocodylia) with comments on the homology of osteoderms. *J. Morphol.* 269: 398–422.

Vickaryous, M. K. and J.-Y. Sire. 2009. The integumentary skeleton of tetrapods: origin, evolution, and development. *J. Anat.* 214: 441–464.

VetBooks.ir

Vickaryous, M. K., et al. 2015. Armored gekkos: a histological investigation of osteoderm development in *Tarentola* (Phyllodactylidae) and *Gekko* (Gekkonidae) with comments on their regeneration and inferred function. *J. Morphol.* 276: 1345–1357.

Witzmann, F. and R. Soler-Gijón. 2010. The bone histology of osteoderms in temnospondyl amphibians and in the chroniosuchian *Bystrowiella*. *Acta Zool. (Stockholm)* 91: 96–114.

Xu, Z., et al. 2016. Direct conversion of human fibroblasts to induced serotoninergic neurons. *Molec. Psychiatry* 21: 62–70.

Zylberberg, L. and J. Castanet. 1985. New data on the structure and the growth of the osteoderms in the reptile *Anguis fragilis* L. (Anguidae, Squamata). *J. Morphol.* 186: 327–342.

VetBooks.ir

Section IV

Teeth

VetBooks.ir



Taylor & Francis
Taylor & Francis Group
http://taylorandfrancis.com

VetBooks.ir

13

Histology of Dental Hard Tissues

Alan Boyde and Timothy G. Bromage

CONTENTS

Tooth Germs and The Embryonic Origins of Dentine, Enamel and Cementum 260
Basics of Tooth Form 261
Dentine Histology 262
General Features 262
Mineralisation and Mineralizing Front Morphology 262
Matrix Vesicles, Calcospherites, Interglobular Dentine and Secondary Nucleation 262
Periodic growth layer lines in dentine 264
Annual Growth Layers and Growth Layer Groups 264
Matrix Daily 264
Mineral Daily 264
Longer Interval Incremental Lines: A Few Too Many Days 264
Much Longer Aperiodic Growth Disturbance Lines: Neonatal Line 264
Calcospherites and Polarized Light Microscopy 264
Von Korff Fibers in Early Dentine Mineralization 265
Tubule-Centered Mineralization 266
Collagen Orientation in the Tubule Wall 266
Peritubular Dentine 266
Side Branches of Dentine Tubules. 267
Postmortem Changes: Microbial and Fungal Bore Holes in Dentine 267
Dentine Resorption 268
Curvature of Dentine Tubules: Sinusoidal Oscillations and Decussations 268
Vasodentine and Osteodentine in Beaked Whales. 268
Secondary, Tertiary and Responsive Reparative Dentine Phases 268
Calcified Dental Pulp 270
Pulp Stones. 270
Enamel 270
Prisms and Packing Patterns. 270
Prism Decussation 272
Relative Cell Movement Within the Ameloblast Layer 272
Rodent Incisor Inner-Enamel Decussation 272
Hunter-Schreger Bands 272
Periodic Growth Layer Lines in Enamel 272
Cross Striations or Varicosities: Circadian Rhythms 272
Regular-Period Striae of Retzius: Multidien Rhythms 277
Perikymata or Imbrication Lines at Tooth Surface: Prism-Free Layer 277
Growth Disturbance Lines: Hypoplasia 277
Daily, Ultradian Lines 277
Maturation and Surface Enamel Composition 277
Iron in Surface Enamel. 277
Enamel Tubules and Spindles, Tufts and Lamellae 278
Enamel Tubules 278
Spindles 278
Tufts and Lamellae 278

Roots and Cementum: Crowns and Coronal Cementum. 278
Primary Cementum 278
Secondary Cementum (See Also Dentine Resorption). 278
Coronal Cementum 278
The Cement-Dentine Junction Region in Murine Molars. Incorporation of Hertwig's Root Sheath. 279
Cartilage Cementum 279
Annual Period of Cementum Deposition 279
Preparation Methods We Either Like or Disdain 279
Etching 279
Air Polishing and Airbrasion. 279
Replica Films for LM 281
TEM of Carbon Replicas 282
Replicas and 3D Resin Casts for Scanning Electron Microscopy 282
'Thin' Sections and Laser Ablation Microtomy (LAM). 282
Plastic Slides 282
Cyanoacrylate Glue 282
Imaging Methods We Either Like or Disdain 282
Reflected Light Confocal Microscopy 282
Reflected Light Metallurgical Microscope 284
Rotating Condenser Aperture 284
Polarized Light Microscopy (PLM) 284
Flatbed Scanner: 3D Images 284
BSE-SEM "at Bad Vacuum", High Chamber Pressure, No Coating and Instant Gratification SEM. 285
Faxitron™ Point Projection Digital Microradiography 285
Scanning X-Ray Microscopy 285
X-Ray Microtomography (XMT or μCT) 285
Simultaneous-Inductively Coupled Plasma-Mass Spectrometry (si-LA-ICP-MS) 285
Summary 285
Acknowledgments 286
References 286

Tooth Germs and the Embryonic Origins of Dentine, Enamel and Cementum

Tooth germs originate from epithelial swellings (dental buds) on an epithelial dental lamina corresponding to the position and shape of the future dental arch. Mesenchymal (embryonic connective tissue) cells multiply and congregate around and within the epithelial buds when these invaginate on the pole (aboral) facing away from the oral cavity to form cap stage tooth germs. The most peripheral layer of cells now surrounded by epithelium will go on to differentiate as tall columnar cells called odontoblasts, which secrete the substantially collagenous dentine matrix against the epithelial-derived noncellular basement membrane, which later mineralizes.

Not all mammalian teeth have enamel, but all have enamel organs (sometimes called epithelial dental organs). If enamel will develop, and it does in the future biting ends of most mammalian teeth, it is always the case that the epithelium of the dental cap further proliferates to form a multilayered "bell" stage tooth germ (Figure 13.1). The inner layer of cells (the inner enamel epithelium [IEE]) opposite the "mesenchymal papilla" (the future dental pulp that is surfaced with the presumptive odontoblasts) become elongated, their nuclei migrate to the ends of the cells against the basement membrane away from the mesenchyme and they eventually secrete enamel matrix toward the dentine, when they are called ameloblasts.

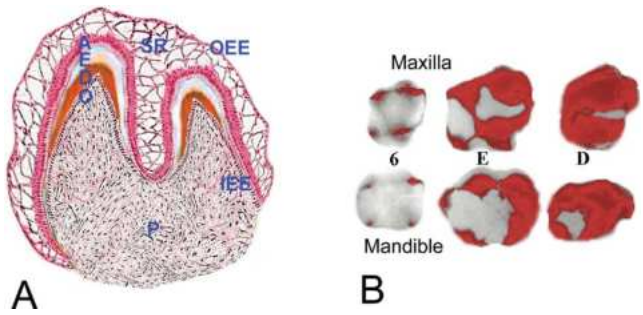


FIGURE 13.1 Tooth germs and embryonic origins of dental tissues. A, Diagram of a late bell stage tooth germ showing odontoblasts (O), dentine (D), ameloblasts (A) and enamel (E), surrounding the dental pulp (P; mesenchymal papilla) facing the inner enamel epithelium (IEE) and the stellate reticulum (SR) bounded by the outer enamel epithelium (OEE) (abbreviations lay over the layer or structure). Note that dentine formation toward the pulp and enamel formation starting from dentine is progressing along the slopes of two cusps that eventually will be bridged by these mineralizing matrices to form the crown. B, Diagram of alizarin red S–stained developing human molar tooth germs, first permanent molar left (6), second deciduous molar center (E) and first deciduous molar (D) right. Mineralized tissue phases (enamel and dentine) are stained red. Al cusps are fused in D, most in E and none in 6 in this individual. The tooth germ of 6 will continue to grow to become bigger than E before its separate cusp elements fuse together to outline the occlusal surface.

VetBooks.ir

All other epithelial cells secrete away from the basement membrane with an adjacent connective tissue; this is called "the reversal of polarity".

Epithelial-mesenchymal interactions at the basement membrane interface called "reciprocal induction" orchestrates these processes. The invaginating dental lamina induces the proliferation and condensation of mesenchyme. Following the cap stage and bell stage, the elaboration of dentine matrix by odontoblasts then induces the differentiation of ameloblasts and enamel matrix formation. Three basic rules can be considered in dental histogenesis. Rule 1: no dentine = no enamel and no cementum. Rule 2: if the epithelial component of the tooth germ becomes multilayered, it will make enamel. Rule 3: ameloblasts do not act alone in making enamel. They are backed up by a layer of cells (stratum intermedium [SI]) between them and the bulk epithelial layer in the late "bell" stage of organogenesis, the "stellate reticulum" (SR) or enamel pulp. SI is always present next to functioning ameloblasts, even if the SR disappears in later stages of amelogenesis, when SI then constitutes the papillary layer of the enamel organ.

SR is an extremely unusual multilayered epithelium that contains a very large proportion of intercellular substance and forms a soft protective cushioning layer for the hard parts growing inside it. It is soft and squishy and bounded by a single layer of cells at the external surface of the developing dental organ, the external, or outer enamel epithelium (OEE). Remarkably, blood vessels do not penetrate the enamel organ in early stages of development, whereas capillary blood vessels dominate the scene in the dental papilla and may actually lie between odontoblasts.

Mammalian teeth are separate organs that develop inside spaces called crypts in the jawbone; in most gnathostomes the dental lamina invaginates into mesenchyme, although the first cycle of crocodilian teeth evaginate from the lamina. The jawbone is the first line of protection for the initially incredibly delicate tissues within the developing dental organ. However, the enamel organ is a main protective buffer layer, especially the SR. The mesenchymal papilla, the future dental pulp, cushions the developing hard tissue layers internally. The tooth grows as the jaw grows and as the crypt space within it increases. All this has to be integrated with bone growth and drift processes. Bone resorbing osteoclasts make the space within the bone necessary for tooth growth. Compensatory addition of bone has to follow to keep the whole jaw stable and functional. However, it is a remarkable fact that the shell of bone separating the crypt and the tooth germ from the buccal and lingual surfaces of the mandible and the buccal surface of the maxilla can be astonishingly thin, and even absent in fetal stages in large mammals.

Varieties of occlusal form are shaped by the lead given to it by the IEE, the inner, folded continuation of the OEE. IEE turns on odontoblast formation, thus dentinogenesis; then the IEE cells differentiate into ameloblasts and secrete enamel matrix on the dentine. Enamel-forming fronts appear first over tips of dentine horns located at positions of future cusps, incisal edges or plates of enamel.

Single-cusped teeth in mammals begin to form dentine in one place only. A spatulate-shaped incisor tooth with a ridge connecting mesial and distal ends may begin to form dentine at each end, but these regions are soon connected to form incisal edges. Teeth with more than a single simple conical or ridge element begin to form dentine in as many places as there will be cusps in the finished tooth; these are the premolars and molars of mammals with "typical" heterodont dentitions. This is achieved by an increase in extent of the layers of future odontogenic tissues at the epithelial-mesenchymal interface in the tooth germ, with differential growth leading the elevations in this plane corresponding to the future "cusps". Future cusps grow apart from one another during the expansion of the epithelial-mesenchymal interface, but eventually dentine formation in each element joins with that of the next, when the extent of the future occlusal surface of the tooth is determined (Figure 13.1B).

The layer of mesenchymal cells that concentrates around the outside of the tooth bud, and the cap and bell stages thereof, will give rise to other major components of the "gomphosis" system of tooth attachment, i.e., a periodontal ligament (PDL), "alveolar" (socket) bone, and dental cementum. No tooth exists without its basis substance, dentine. No tooth can possibly function without being attached to bone. PDL fiber bundles insert on one side of the socket into bone and the other, but not the same bundles, into cementum, which is in this sense the second most important tissue in the tooth organ. However, it is not the second tissue to form, but the third, unless there is no enamel formed (e.g., aardvarks, sloths and some toothed whales).

Basics of Tooth Form

A good guide to extant mammalian tooth forms may be found in Hillson (2005). Teeth that have shearing crests between cusps are common among insectivores (Figure 13.2A) and some carnivores. Incisal edges of all mammals with heterodont dentition are also a form of shearing crest. Bunodont molars adapted to crushing and grinding have low rounded cusps separated by basins or grooves that accommodate the cusps of occlusal opponents (Figure 13.2B). Such teeth are typical of omnivorous mammals.

Teeth with occlusocervical infoldings deep to the occlusal surface and from the sides of the crowns generate complex wear morphologies and may be found in arvicoline rodents, lagomorphs, rhinos, horses and ruminants (Figure 13.2C–E). What would be erstwhile empty occlusal surface fissures/spaces between separate cusp elements are frequently filled with coronal cementum, which packs out the space and binds the cusps together. Infundibula are the deep depressions in crowns, common among ruminants, which are not so filled. An infundibulum between crescent-shaped curved ridges of enamel and dentine is normal in the selenodont crown form common in artiodactyls, which are among side-to-side chewing ungulates (Figure 13.2D). Ridges on molars of herbivores run in the direction perpendicular to the main axis of jaw motion; this movement has to be permitted by the morphology of the jaw and temporomandibular joint and the jaw musculature. In lophodont elephant molars, tall flat cusps form transverse plates, united by coronal cementum, used in a mainly back and forth chewing/grinding (Figure 13.2E).

VetBooks.ir

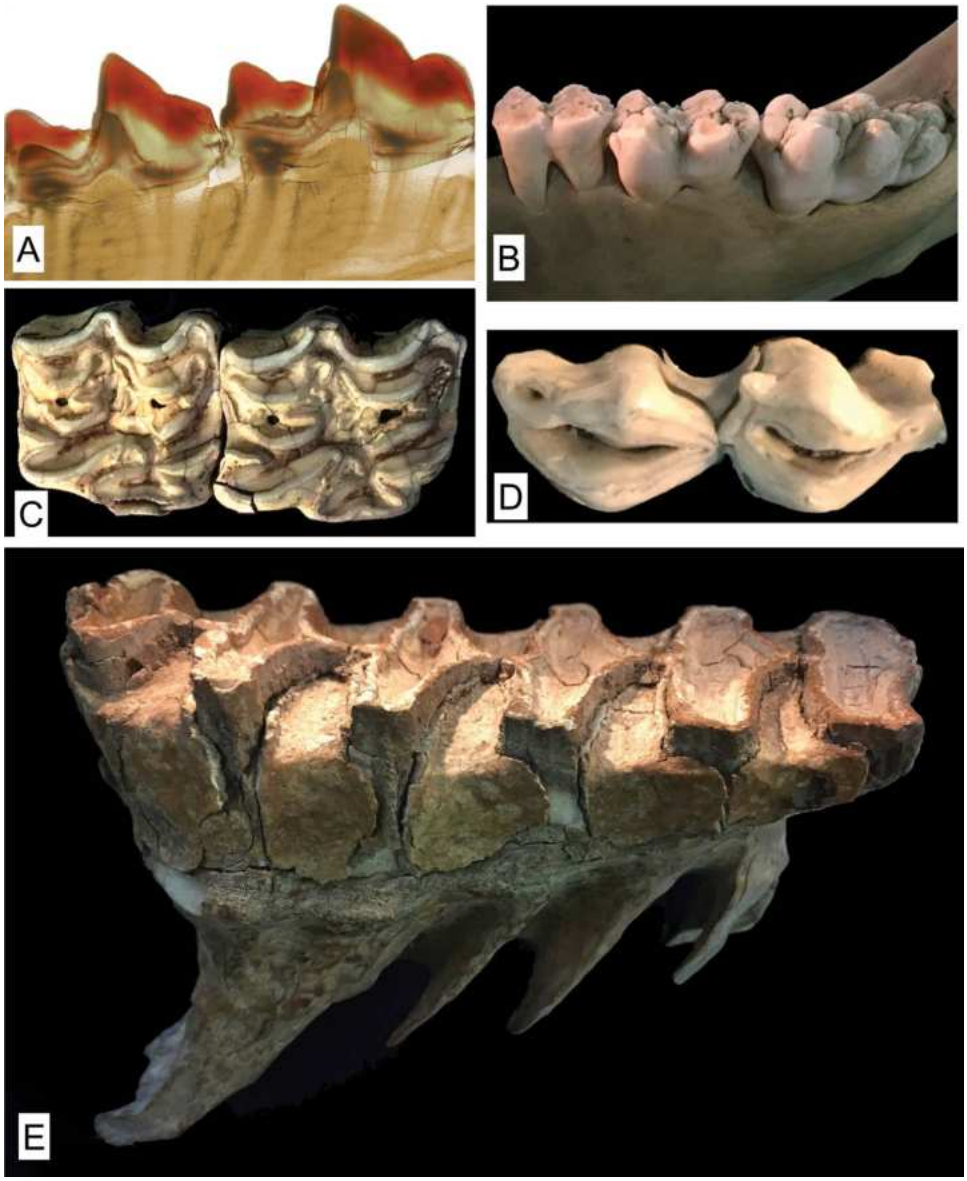


FIGURE 13.2 Some tooth forms. A, Northern short-tailed shrew (*Blarina brevicauda*) lower M1-M2. Red color is due to iron incorporation in enamel. Field width 4 mm. B, Boar (*Sus scrofa*) lower M1-M3 illustrating bunodont cheek teeth. Mesial-distal length of combined teeth 7.0 cm. C, Zebra (*Equus quagga*) upper M1-M2 illustrating complex anatomy. Mesiodistal length of combined teeth 4.8 cm. D, White-tailed deer (*Odocoileus virginianus*) lower M2 illustrating selenodont crown form. Mesiodistal breadth 3.5 cm. E, Subfossil forest elephant (*Loxodonta cyclotis*) lower deciduous premolar illustrating lophodont tooth form. Mesiodistal length 14.5 cm.

Dentine Histology

General Features

Dentine-secreting odontoblasts generate a major cell process with a variable number of side branches that they leave inside the forming dentine, forming the cylindrical spaces which are called dentine tubules. These are analogous to osteocyte canaliculi in bone, but, unlike in bone, the cell bodies of the odontoblasts remain outside the dentine in the dental pulp.

The dentine matrix collagen is generally constituted as fibrils with diameters from 0.05 to 0.2 µm which are too small to be resolved with conventional optical microscopy. These are layered in a feltwork arrangement with the fibrils parallel with the formative surface (Figure 13.3A). However, in some cases the collagen is constrained to from much larger "bundles" generally parallel with the tooth long axis (Figure 13.3B). The dentine matrix mineralizes via several mechanisms special to dentine.

Mineralization and Mineralizing Front Morphology

Matrix Vesicles, Calcospherites, Interglobular Dentine and Secondary Nucleation

Mineralization in the most peripheral, i.e., the first formed, mantle dentine is initiated by matrix vesicles (MVs), which are spherical blebs of odontoblastic cell membrane deposited

VetBooks.ir

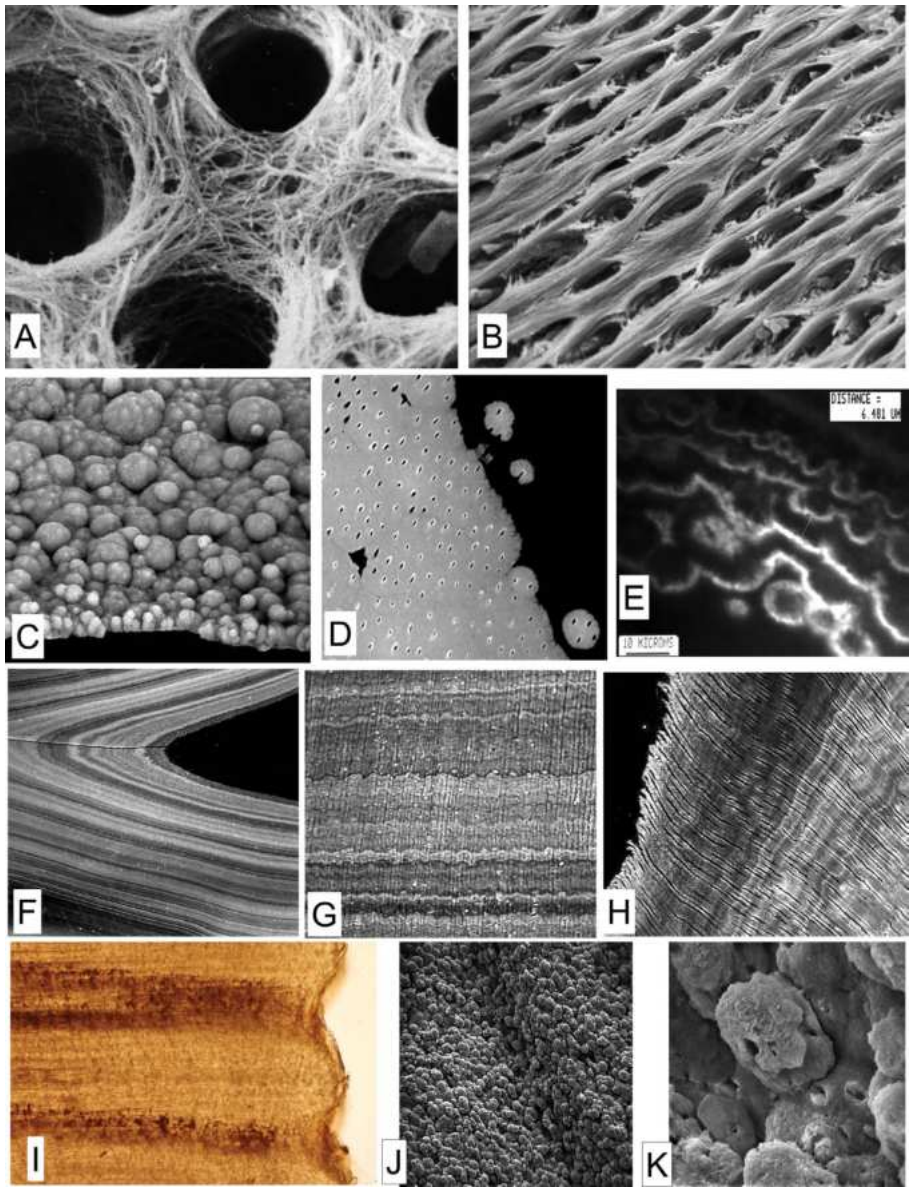


FIGURE 13.3 Predentine: dentine mineralization: calcospherites: interglobular dentine. A, Secondary electron image in the scanning electron microscope (SE-SEM). Predentine surface in a human premolar after removal of the odontoblasts, showing the typical feltwork arrangement of collagen fibrils that form parallel with this surface. Most forming mammalian dentine looks like this. Field width 17 µm. B, SE-SEM. Predentine surface in a sperm whale (*Physeter catodon*) tooth. The sample was treated with 5% sodium hypochlorite for 30 minutes to remove unmineralized collagen, but here we see the collagen fibers indicating that they were mineralized so there had been an arrest in the process of dentine matrix formation and mineralization. Note that the collagen fibers are organized more as bundles running in the longitudinal axis of the tooth. Field width 74 µm. C, Mineralizing front in dentine in an anorganic (deproteinized) developing human third mandibular molar crown. The growing edge with the first-formed dentine at the lower margin of the image shows large numbers of small calcospherites. At the top of the image, where the dentine has considerably thickened, we see a reduced number of larger calcospherites, each of which covers the secretory territory of many odontoblasts. Field width 174 µm. D, Back-scattered electron (BSE)-SEM. Polymethyl methacrylate (PMMA)-embedded human permanent molar showing a formative surface region: only mineralized tissue shows in this mode, and denser regions are whiter. The section plane is at a tangent to the mineralizing front such that the dentine tubules are cut more transversely: most tubules have a lining of peritubular dentine (PTD). Calcospherites appear isolated from the bulk of the dentine on the right-hand side of the image. A small interglobular dentine patch is seen on the left. Field width 200 µm. E, Confocal fluorescence image of the surface of polished PMMA-embedded block surface showing the mineralizing front position at 24-hour intervals. Very-low-dose calcein (0.1 mg/kg) injections were given via an ear vein in a 2-kg adult New Zealand white rabbit. Earliest dentine left; latest dentine, bottom right corner. Field width 68 µm. F, BSE-SEM. Surface of longitudinal section of pilot whale (*Globicephala melaena*) tooth showing multiple growth layer group lines. Sample was etched with dilute acetic acid for 23 hours then hypochlorite bleach for 2 minutes. Field width 4.5 mm. G, BSE-SEM. Pilot whale tooth showing multiple growth layer lines. Field width 450 µm. H, BSE-SEM. Surface (left) of carious human tooth root. Daily mineralization layer lines become much more prominent when dentine is demineralized in caries. Field width 450 µm. I, narwhal (*Monodon monoceros*) tusk. Transversal ground section (TS) in ordinary transmitted light microscopy, growing pulpal surface to the right. The poorly mineralized interglobular dentine (IGD)-rich radial longitudinal zone(s) appear dark because they scatter the transmitted light. Field width 405 µm. J, SE-SEM. Anorganic, mineralizing front preparation of Narwhal tusk showing one of the spiral longitudinal groves seen at the forming dentine surface: defective, IGD-rich dentine forms deep in this. Field width 225 µm. K, Higher magnification showing the calcospherite morphology. Field width 22 µm.

VetBooks.ir

in the dentine matrix. The mineral component, which forms in all mammalian tissues that calcify (bone, enamel, dentine, cement and some cartilage, ligament and tendon), is an imperfect, carbonated hydroxyapatite (HA). All extracellular fluid is supersaturated with calcium and phosphate ions with respect to HA, so the question arises as to why all tissues do not calcify. The answer lies in inorganic pyrophosphate (PPi), which is a ubiquitous inhibitor of mineralization. Phosphatase enzymes on the MV cleave PPi to kill the inhibition, liberate free phosphate and allow spontaneous precipitation to occur. The initial crystals formed have unstable surfaces so that ionic clusters can leave – as well as join the growing crystal surface. Such clusters can congregate to form new crystals by a process called secondary nucleation; to understand this aspect of dentine mineralization, we might regard it as "seeding".

Large numbers of MVs form to initiate dentine mineralization, but once the process has started, it seems that not so many (or even no more) are needed and the process is self-sustaining. The tiny volumes of dentine that are calcified grow as spheres and are known as calcospherites (CSs; Figure 13.3C–K). Generally, there are large numbers of small CSs in early dentine formation and small numbers of large CSs in later dentine formation. However, many mammals make more CSs of moderate magnitude throughout dentinogenesis. All these features can be easily seen by scanning electron microscopy (SEM) of mineralizing front preparations of developing teeth made by dissolving away superficial uncalcified matrix with, for example, sodium hypochlorite bleach (Figure 13.3C, J, K).

CSs grow forward in 3D into newly secreted *pre*dentine matrices as well as sideways and backward to join with surrounding mineralized regions. When they fail to join, intervening regions of uncalcified matrix persist as interglobular dentine (IGD) patches (Figure 13.3D, left). Poorly mineralized dentine generally consists of a mixture of properly mineralized tissue with IGD (Figure 13.3F–I). Normal mineralization requires normal vitamin D and phosphate metabolism. Conditions that cause rickets in bone also cause an increase in IGD. However, many large mammalian teeth, e.g., those of toothed whales (Figure 13.3F, G) and elephant tusks, have a high proportion of IGD, and its concentration varies in succeeding growth layer increments (Perrin and Myrick 1980).

Periodic Growth Layer Lines in Dentine

Annual Growth Layers and Growth Layer Groups

Dentine in large teeth of large wild mammals shows wide variations in the degree of mineralization of successive layers. There may be layers of layers, which show a periodicity and such "growth layer groups" (GLGs) frequently demonstrating annual growth layering. This is of particular interest for marine mammals in determining the age of animals killed in commercial fishing operations and strandings (Perrin and Myrick 1980; Waugh et al. 2018).

Matrix Daily

Von Ebner's lines are high frequency incremental or growth layers in dentine that are clearly circadian. These can be seen in decalcified sections as regular flattened planes, a few microns apart, parallel with the layers of collagen of the matrix feltwork. These reflect the daily layers of new matrix deposited upon the preexisting predentine.

Mineral Daily

Comparable frequency near-daily growth lines are seen by back-scattered electron imaging in the scanning electron microscope (BSE-SEM) of undermineralized or slightly demineralized polished surfaces as regular layers with varying mineral concentration, but their contours reflect the morphology of the mineralizing front (MF), thus showing details of calcospheritic progression of mineralization. Such lines become much more prominent after dentine demineralization *in vivo* as the consequence of bacterial acid attack in caries (Figure 13.3H). Why should a similar process not occur postmortem, prior to fossilization?

Since there is a time delay between matrix deposition and calcospheritic mineralization, these mineral-concentration daily lines cannot exactly overlap or correspond with the matrix-deposition-daily lines. In human teeth, the matrix and mineral layers would be expected to be roughly 20–30 μm apart (the thickness of predentine) reflecting a time delay difference of about 4 or 5 days. The existence of this second different class of mineralization-progress layers shows that there is a second circadian rhythm in CS-MF calcification, which is separate from that of the matrix deposition. (*Note* that this is the first time that this has been described in the literature.)

Longer Interval Incremental Lines: A Few Too Many Days

The "Andresen's lines" in dentine reflect systemic disturbances a number of days apart within the whole organism, and they correspond to similar periodicities in enamel, seen as the subsurface, regular interval Retzius lines. The biological significance of many-days rhythms is briefly described in the enamel section below (see part on Regular-Period Striae of Retzius: Multidien Rhythms).

Much Longer Aperiodic Growth Disturbance Lines: Neonatal Line

The "Owen's lines" in dentine reflect systemic disturbances to the whole organism, such as disease, malnutrition and starvation, which relate to much longer and less regular time intervals. Like the irregular, aperiodic growth lines in enamel, the pattern of these lines is the same in all portions of dentine being formed in all teeth at the same time. A neonatal line may be found in dentine forming at birth in the deciduous teeth of mammals with diphyodont tooth succession.

Calcospherites and Polarized Light Microscopy

At the nanostructural level, mineral is deposited in what was water-filled space in collagen fibrils and bundles, but not in the centers of microfibrils, which are enshrouded in a continuous mineral phase that hangs together when we remove the organic matrix. Mineral in collagen is parallel with the

VetBooks.ir

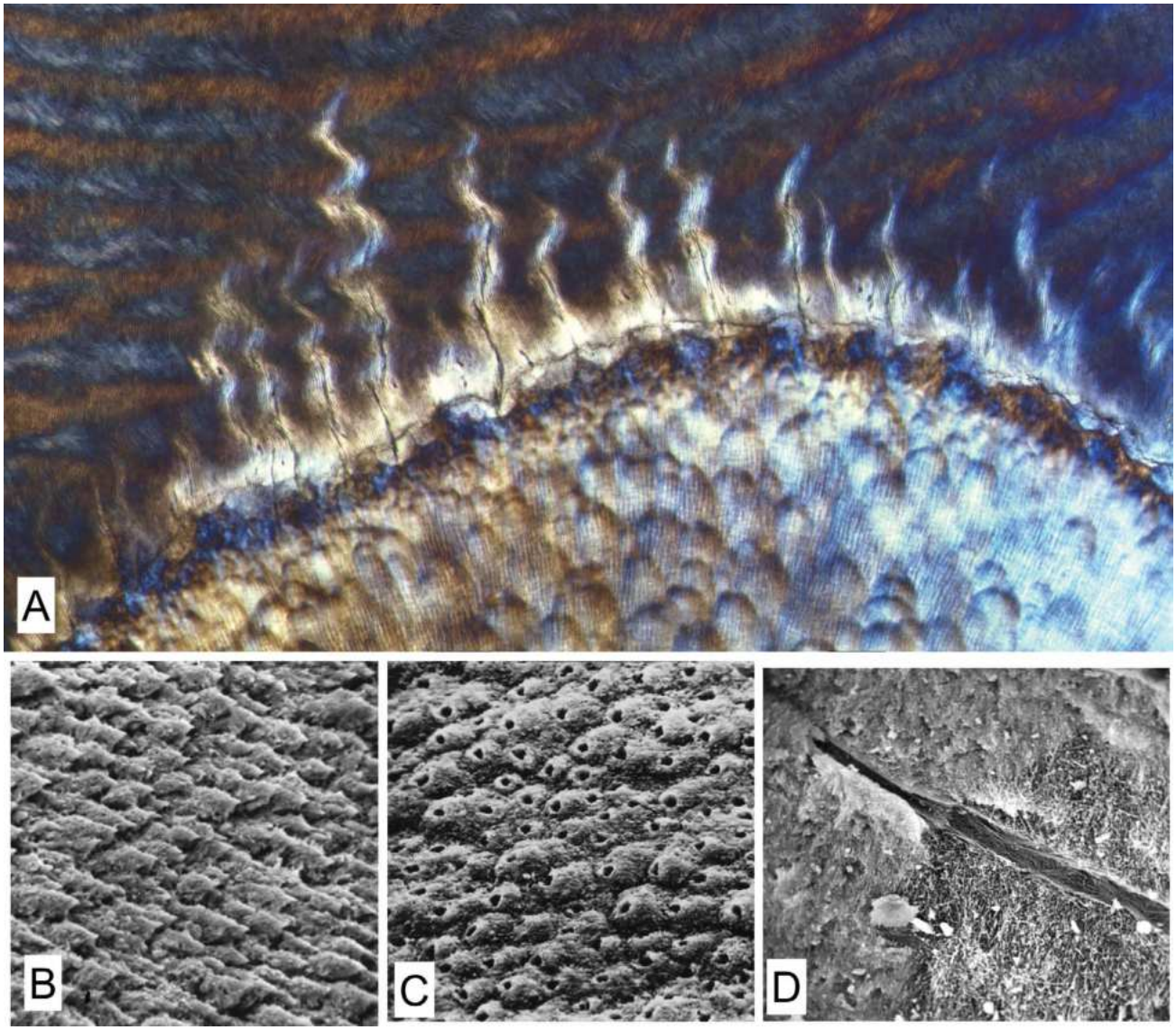


FIGURE 13.4 Dentine mineralization continued. A, Ground section of human permanent tooth, oblique *en face* to the enamel dentine-junction (EDJ), enamel top and dentine below, in polarized light microscopy (PLM), showing that the calcospheritic domains seen in PLM have a spherical surface facing toward the EDJ (or cementum-dentine junction). Note bands of enamel with different prism orientations and vertical, wavy, "tuft" planes. Field width 1.65 mm. B, Secondary electron-scanning electron microscopy (SE-SEM). Anorganic preparation of rat incisor dentine showing the von Korff fiber-centered mineralization front. Field width 50 µm. C, SE-SEM. Anorganic preparation of a rhesus monkey (*Macaca mulatta*) molar showing the most advanced level of the mineralizing front to lie where the dentine tubules pass through. Field height and width 67 µm. D, Human developing mandibular third molar coronal dentine, freeze-fractured, freeze-dried, showing mineralized dentine to the right and above and predentine (left). Detail in the tubule wall is obscured by the deposition of peritubular dentine at the level of the mineralizing front. This field is also of interest because it shows an unusual orientation of collagen fibrils of the intertubular dentine matrix parallel with the long axis of the tubule in the wall of the tubule. Field width 18 µm.

collagen. However, there is some space, which is not within collagen and in which extra mineral can pack. All the HA mineral, wherever located, is elongated in the vertical, or *c*-axis. It is possible that this extracollagenous fraction of the mineral is predominantly oriented as a function of the local MF surface of the local CS, since their territories are clearly seen by polarized light microscopy (PLM) but not in ordinary transmitted light microscopy (TLM) of undecalcified "ground" sections (Shellis 1983). Their profiles are reversed from that of the MF proper as seen in BSE-SEM, light microscopy (LM) of decalcified sections and 3D MF preparations (Figure 13.4A).

Von Korff Fibers in Early Dentine Mineralization

In many mammals, the earliest dentine mineralization is led by another phenomenon. The von Korff fibers (VKFs) are collagen fiber bundles that lie between odontoblasts, even before they themselves start secreting dentine matrix. They are continuous with a collagen fiber network in the dental pulp, and in most respects are similar to the collagen continuum that pervades environments in which immature "woven" bone forms. Like the latter, VKFs become incorporated in the new collagen-rich matrix secreted by the odontoblasts. For whatever

reason, perhaps because they are the oldest, they start to mineralize first. The process of secondary (seeding) nucleation (mineralization) within the centers of the VKFs dominates any other tendency, and the MF consists of spikes centered in the VKFs (Figure 13.4B).

Tubule-Centered Mineralization

In some cases, the most advanced points in the mineralizing front in dentine are centered where the tubules pass through this front (Figure 13.4C).

Collagen Orientation in the Tubule Wall

In some instances, the dentine matrix collagen next to the tubule has an orientation parallel with the tubule axis (Figure 13.4D). This is rare; it is much more common for the collagen to lie at a large angle to the tubule axis, parallel with the predentine surface (Figure 13.3A, B). The major solid component of dentine containing the collagen feltwork is the shared secretory product of the adjacent odontoblasts at one spot called intertubular dentine (ITD).

Peritubular Dentine (Figure 13.5)

Most mammals make another dentine product with a noncollagenous, watery (i.e., low solids concentration) proteoglycan matrix within the dentine tubule. This is called peritubular dentine (PTD; Figure 13.5A–E).

Not all dentine and not all tubules have PTD. It may form "at a later date", but, in species where it is a conspicuous feature, its mineralization (i.e., its formation) may occur at the same level (i.e., time) as that of the ITD (see Figure 13.5A, B), and at least in elephant molars it may precede ITD (Figure 13.5C).

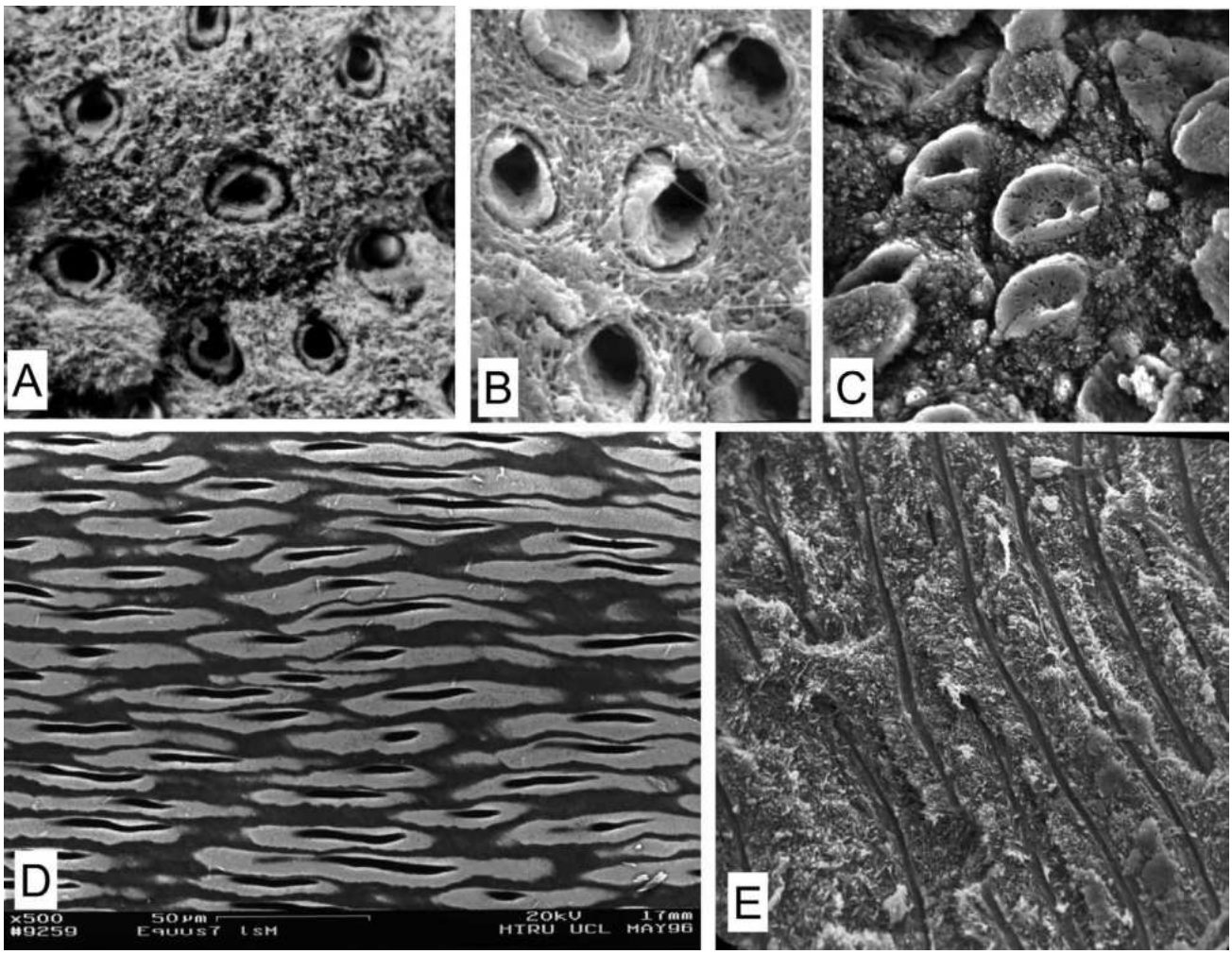


FIGURE 13.5 Peritubular dentine. A, Secondary electron-scanning electron microscopy (SE-SEM). Anorganic preparation of developing human third molar, showing peritubular dentine (PTD) deposition in the tubules at the level of the mineralizing front. Field width 20 µm. B, SE-SEM. Developing bovine molar dentine, predentine removed by papain digestion, showing eccentric distribution of PTD forming at the mineralizing front. Field height 15 µm. C, SE-SEM. African elephant (*Loxodonta*) molar dentine mineralizing front with PTD forming ahead of the mineralizing front of the intertubular dentine and almost completely occluding the tubules at the outset. Field width 26 µm. D, Back-scattered electron (BSE)-SEM. Polished surface of polymethyl methacrylate (PMMA)-embedded horse molar, showing a very high volume fraction of PTD. 50 µm scale bar in image. E, SE-SEM. Walrus (*Odobenus*) dentine fractured parallel with the tubule axis, showing PTD lining the tubules. This is a broken fragment from one of the Lewis chessmen in the British Museum. Field width 54 µm.

VetBooks.ir

Mammals with vast amounts of PTD (Figure 13.5C, D) are herbivorous and all have large teeth subject to severe lifetime wear. PTD is more densely mineralized than ITD and more wear resistant. At a microscopic scale, PTD forms low protuberances on wear surfaces, which help to bruise plant cell walls. Thus, apart from merely plugging the tubules, PTD enhances tooth function. It would be anticipated that high-PTD-fraction dentine would be better preserved during fossilization.

Another interesting aspect of PTD is that it may form eccentrically and in some cases mainly or only on one side of a tubule, particularly when the tubules enter the formative surface at a very oblique angle (Figure 13.5B; Jones and Boyde 1984).

Side Branches of Dentine Tubules

Lateral branches of the tubules reflect lateral extensions of the odontoblast processes at the time of formation (Figures 13.6A, B). They extend into ITD and may be very numerous within PTD (Figure 13.5C; Jones and Boyde 1984).

Postmortem Changes: Microbial and Fungal Bore Holes in Dentine (Figure 13.5C)

Dentine, like bone, can be subject to a variety of internal structural taphonomic (postmortem) changes that are somewhat equivalent to those induced by carious decomposition in living human teeth. New dentine "tubules" may be generated by postmortem fungal boring (Figure 13.6C). There is no reason not to suppose that analogous invasion by bacterial and fungal species may occur prior to fossilization. A distinct subtype of change in dental caries *in vivo* is caused by motile organisms that move along dentinal tubules and then tunnel out sideways, channeling along the matrix collagen fibers which are, of course, more or less perpendicular to the tubule axis (as seen in Figure 13.3H, left).

At their most intense, growth disturbances may cause a complete interruption of mineralization, followed by a restart. In this case, if we make fresh tooth specimens "anorganic" or "deproteinized" with sodium hypochlorite or hydroxide treatment, they will fall apart at such fault lines (Figure 13.6D).

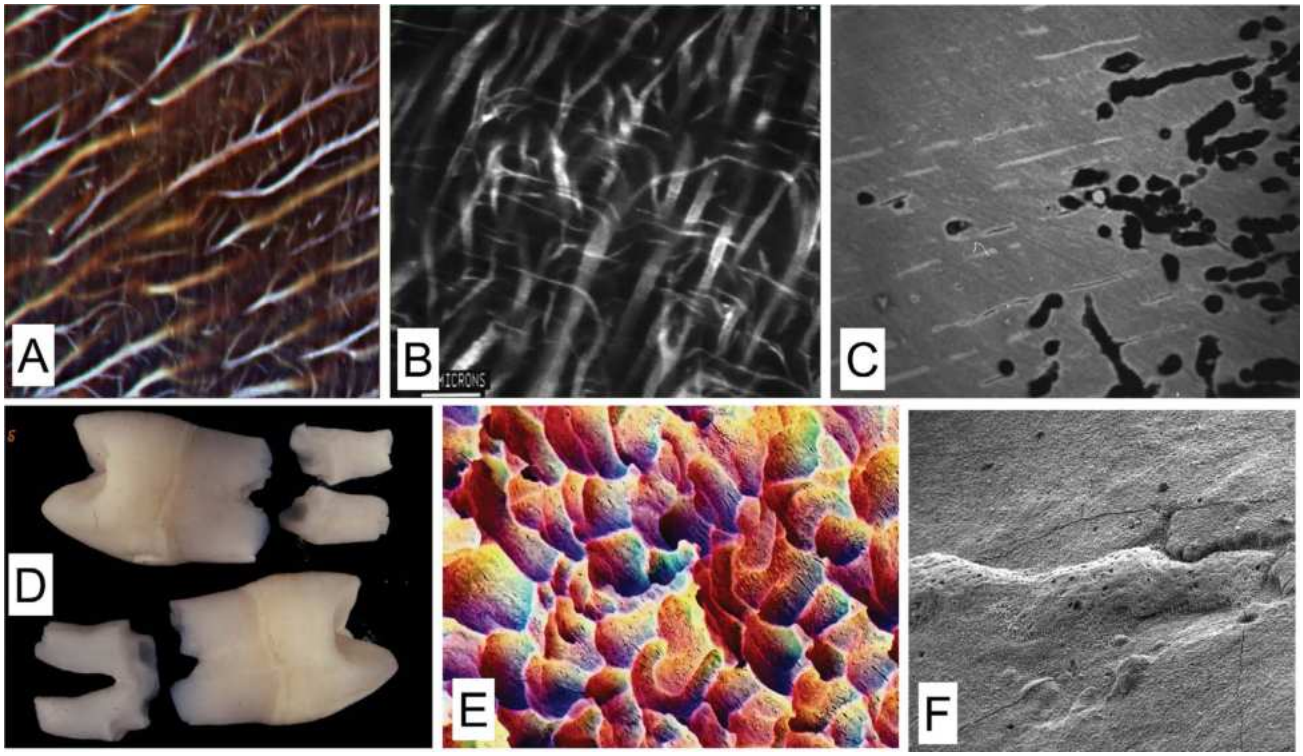


FIGURE 13.6 Dentine tubules side branches, postmortem (PM) changes, resorption. A, Rat incisor dentine, polymethyl methacrylate (PMMA)-embedded, polished, showing multiple side branches of tubules. Back-scattered electron-scanning electron microscopy (BSE-SEM) images were recorded at 10, 15 and 25 kV and superimposed using red, green and blue channels to make a composite image. Increasing the accelerating voltage increases the transparency of the tissue. Field width 40 µm. B, Confocal fluorescence image of rabbit incisor dentine showing numerous side branches of the dentine tubules and their considerable lateral extent. Field width 68 µm. C, BSE-SEM. PMMA-embedded polished tooth sample showing, at right, postmortem submarine fungal invasion canals in human mandibular premolar dentine from a sailor who drowned in the Mary Rose in 1545 (https://maryrose.org/the-history-of-the-mary-rose/). Field height 200 µm. D, Photograph of a pair of human upper first premolar teeth extracted for "orthodontic reasons" that were treated with hypochlorite bleach for several weeks and fell apart, demonstrating complete failure of mineralization at one time due to unknown causes, but followed by recovery. E, Three-dimensional BSE-SEM. Resorbed undersurface of a human deciduous tooth that shed because the root dentine was removed by osteoclasts (odontoclasts). The colored image was synthesized from images recorded using separate BSE detector segments for directional coding. Field width 260 µm. F, Secondary electron (SE)-SEM. Anorganic root surface of human lower third molar. An area of prior resorption of acellular, extrinsic fiber cementum has been repaired by the deposition of new cellular, mixed intrinsic and extrinsic fiber cementum. Field width 833 µm.

VetBooks.ir

Analogous faulting due to postmortem, taphonomic decomposition of less-well or unmineralized layers is found is semi-fossil teeth, for example, mammoth tusks from Siberia, which simply peel apart along the major incremental layer lines. Modern elephant ivory can be similarly spoilt and split by cooking/boiling.

Dentine Resorption

The dentine of the roots of mammalian deciduous teeth is resorbed so that they may be shed and replaced by the successional permanent teeth (Figure 13.6E). This process is undertaken by massive teams of osteoclasts supported by a rich blood vessel capillary system. The deep undermining osteoclastic resorption lacunae lead to large chunks of dentine being separated from the bulk when this process is rapid. If shedding is a little delayed, then dental enamel may also be resorbed, as in human teeth. In the hypsodont, selenodont or lophodont teeth of herbivores, resorption also involves both enamel and coronal cementum. Within dentine, the densely mineralized PTD is resistant to resorption and stands proud of resorbed surfaces (Boyde and Lester 1967a).

Teeth move within jawbones because the socket bone moves, translating the position over time of the PDL (socket) space. The integrated control of this process is essential to the normal growth of the entire craniofacial dental system in all mammals. In a subgroup of humans subject to intervention by "orthodontists", untoward forces applied to teeth may result in the resorption of the cement surface of a toothbut hopefully, its eventual repair by secondary cementum deposition. However, in human teeth, it would seem that normally occurring but unusual impact forces are directly responsible for initiating secondary cementum deposition on root surfaces consequent on prior resorption (Figure 13.6E). This is probably related to sudden impaction of the tooth into its socket due to accidental masticatory overload. Information for all other mammals is, to the authors' knowledge, still completely lacking.

Curvature of Dentine Tubules: Sinusoidal Oscillations and Decussations

Dentine tubules preserve or fossilize the courses of the odontoblasts throughout the period of formation of dentine. Details depend on the morphology and rate of formation of the individual tooth in the particular species, but some generalizations are valid. The first part of the main tubule axis stands more perpendicular to the forming tooth surface and the enamel-dentine junction (EDJ) or the cementum-dentine junction (CDJ). Later formed dentine has tubules that deviate toward the then-forming (cervical/apical) end of the tooth because the whole odontoblastic sheet is moved by the mass of tissue being or has been accreted. In even later dentine, toward the center of the tooth or tooth element, the course becomes akin to that at the start. These considerations explain the primary curvatures of the tubules. Deviations from the idealized primary courses are seen as "wiggles" that can be resolved when the tubules can be resolved and are known as secondary curvatures.

Another set of curvatures can be seen in some large mammals and are best exemplified in elephant tusks. Here, extensive vertical columns or armies of odontoblasts move ahead relatively more toward the formative end, balanced by equal territories in which columns of cells move in the opposing sense. This ensures that a balance is obtained: the numbers of cells (and tubules) is always the same. Within any one such vertical column of odontoblasts, the direction of motion alternates over a period so that it adopts the direction seen in the opposing group in antiphase. In longitudinal sections, an oscillation is seen at the millimetric scale. In transverse sections, a kind of deformed, curved checkerboard pattern develops. Since light is reflected differently from different orientations of dentine tubules at a polished surface and also depends on the direction of the incident light, a most beautiful pattern is seen on elephant tusk dentine. It is highly probable that this is the central reason for the commercial value of ivory and the endangerment of elephants due to "poaching" for an Eastern Asian market (Figure 13.7A–C).

Vasodentine and Osteodentine in Beaked Whales (Figure 13.7D–F)

The family of the beaked whales is unusual in that nearly all of them have a dentition reduced to two teeth, one on each side of the anterior mandible, showing great sexual dimorphism, with much larger and more prominent teeth in males. These project above the contour of the protruding beak (rostrum, premaxilla) and are used to inflict damage by scoring and scarring the body surface of other males. The teeth are, nevertheless, small in proportion to the total bulk of the animal. The "starter-pack" portions of these teeth are basically simple cones or small pegs of regular orthodentine with a thin layer of overlying enamel (lost by wear in older animals), but this element is embedded in a large mass in which the central portion is *vaso*dentine (dentine containing capillary blood vessel canals) mixed with *osteo*dentine (resembling bone by the inclusion of the formative cells into the calcified matrix). The vasodentine is in turn embedded in the largest mass of the tooth, which is composed of *vaso*cementum-containing regions in which capillary blood vessel canal inclusion is obvious (Figure 13.7D–F: Boyde 1968, 1980). Altogether, these are the least known of all the large mammals and contain the deepest and longest-duration divers. Some species are actively pursued in Japanese commercial fisheries.

Secondary, Tertiary and Responsive Reparative Dentine Phases

Teeth subject to heavy attrition could possibly run the dangerous risk of exposing a completely unprotected soft connective tissue, the dental pulp, to the outside world. Nowhere is this allowed in nature. Much has been made of naming the types of tissue formed and the responses to this potential danger. The plain issue is that microbial invasion of the living pulp would lead to an inflammatory response, the "tumor" aspect of which might lead to occlusion of the blood vessel supply at the tooth "apex", because swelling cannot occur inside the rigid capsule which is the tooth organ and the ensuing death of the

VetBooks.ir

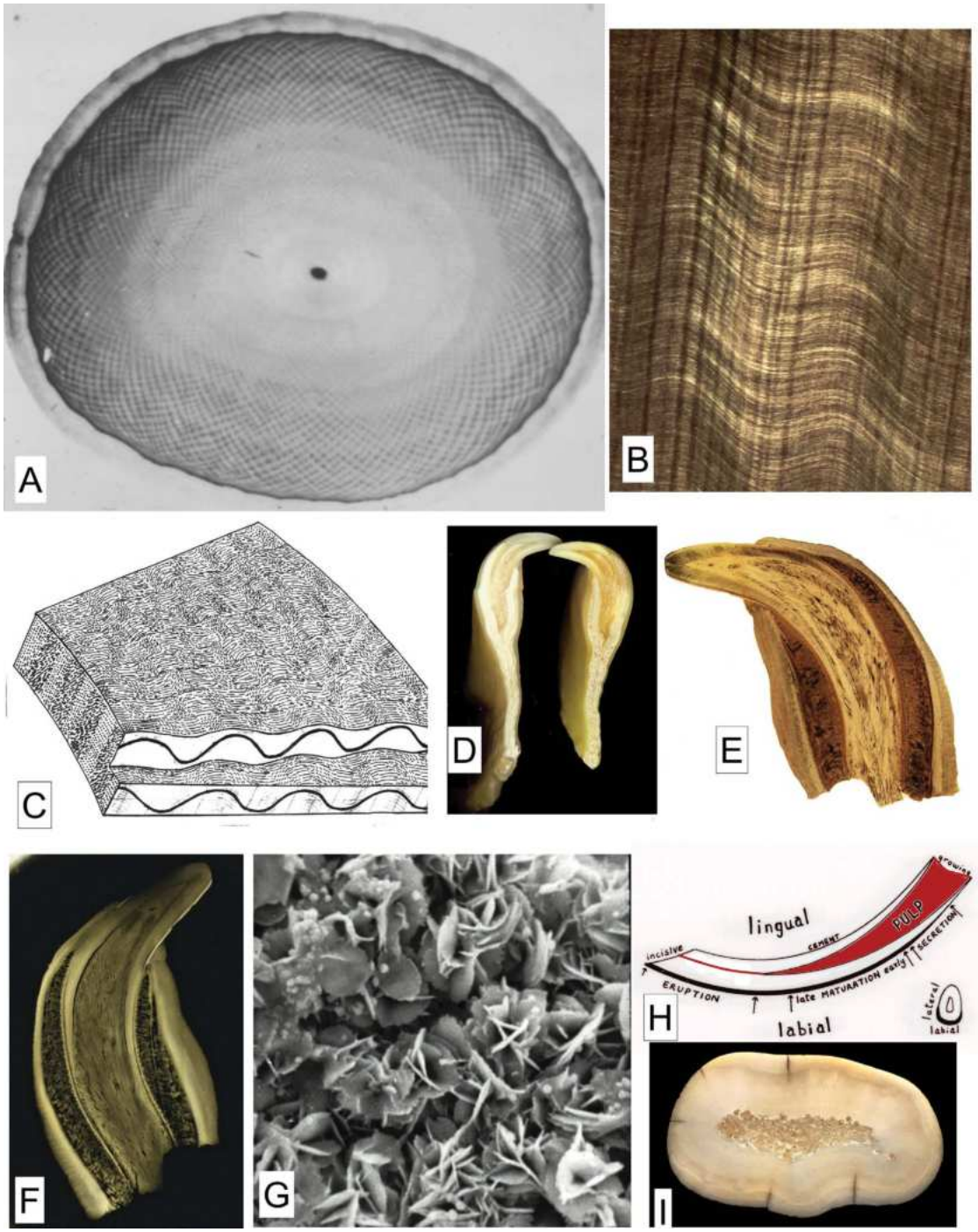


FIGURE 13.7 Elephant tusk ivory; *Mesoplodon layardii* pulp calcification and pulp stones. A, Photograph of a complete 8-cm diameter transverse section of a *Loxodonta* tusk showing six annual layers. Notice the deformed checkerboard pattern of light reflection from the outer layers of dentine. B, Transmitted light micrograph of a radial longitudinal section in more peripheral elephant tusk (*Loxodonta*) dentine showing the vertical sinusoidal oscillation of the paths of the dentine tubules. Note also the high frequency incremental lines, which appear dark because of the reflection/scattering of light from poorly calcified interglobular dentine rich layers. Field width 1.5 mm. C, Diagram of elephant tusk dentine structure showing how alternate radial wedges have the sinusoidal oscillations in antiphase. The left (central) surface of the diagram corresponds to an incremental surface during growth where vertical stripe(s) have odontoblasts moving in opposite directions. (Analogous movements of vast sheets of cells in opposite vertical directions on a formative hard tissue surface occur in the formation of the inner layers of enamel in rhinoceroses). D, Photograph of bisected *M. layardii* (Layard's beaked whale) tooth. As is typical for this group of whales, the bulk phase is vasocementum and cementum. Much of the dentine is vasodentine. Photo height 10 cm. E, *M. layardii* tooth section mounted dry. Field width 5 cm. F, The same section seen in a microradiograph recorded directly on a 2-inch photoplate. Field height 5 cm. G, Secondary electron (SE)-scanning electron microscopy (SEM). Anorganic preparation of longitudinally sectioned rat incisor, showing the form of the mineral deposited within the dead, central pulp cells. Field width 25 µm. H, Diagram of a longitudinal section through a rodent incisor showing the pulp as red. I. Photo of polished transverse section of a walrus tusk showing the fused calcified pulp stone mass that occludes the erstwhile pulp chamber. Specimen width 4.7 cm.

VetBooks.ir

tooth, abscess formation and death of the animal. This must be avoided at all costs.

In human teeth, breaches in the external covering of the tooth frequently occur through the microbially induced demineralization and destruction of enamel, dentine and cementum in "caries". The physiological response is to activate odontoblasts and create a new dentine barrier to ward and wall off the approaching "insult". Toothbrushing to reduce the risk of cervical caries reliably removes cervical cementum, exposing dentine tubules, and the physiological response is the same. Trauma resulting in fracture of dentine, but not exposing the pulp, may be likewise patched up, saving the tooth and the living pulp, especially after timely clinical intervention. These considerations are, however, of little relevance in wild nature.

Pulp also risks being exposed where enamel and thence dentine are removed by attrition. This occurred and occurs regularly in archaeological and/or third-world human populations with a more abrasive diet. The physiological response is the same as above, responsive secondary dentine formation.

Although it may be impossible to have a controlled experiment to clinch this argument, it would seem that mammals with heavy dental tissue loss due to wear do not "wait" for a physiological response. The tooth-forming system obliterates any possibility of pulp exposure by making additional "dentine" tissues to eradicate the pulp space long before the risk might be incurred. The management strategy is to keep the world at bay. Pulp space is plugged with an anticipatory calcified tissue long before "invasion" or "exposure" could occur. Such dentine is only secondary in that it formed later, but *not* in response to experiences in the living life history of the individual.

Calcified Dental Pulp (Figure 13.7G, H)

Calcified dental pulp is another phase that should be considered with dentine. It plugs holes in a tooth that might arise from the removal of dentine by attrition, risking the exposure of dental pulp to the oral cavity with its microbiota. This is particularly important in the case of the continuously and rapidly growing incisor teeth of rodents and lagomorphs. The narrow central part of the pulp dies and the cells are calcified to make a tissue that plugs the erstwhile opening from the worn surface through to the living pulp (Figure 13.7G, H; Bishop and Boyde 1986). The preservation of the general cell morphology by mineralization is good enough that the pulp appears to extend all the way through to the exposed, worn dentine surface in decalcified sections.

Pulp Stones

"Pulp stones" are tissue masses created as an extracellular secretory product. They usually have a substantially collagenous matrix closely resembling dentine. Pulp stone tissue may contain tubules as in regular orthodentine, but it may also be free of cell inclusions. Pulp stones become incorporated within dentine as its formative surface advances into prior pulp space.

In walrus tusks (maxillary canines), the entire former dental pulp space is filled with a fused mass of calcified pulp stones (Figure 13.7I). This creates a distinctive feature in walrus ivory that enables its recognition from any other large mammal dentine.

In sperm whales, there is evidence that the frequency of inclusions of pulp stones has the same cycle period as pregnancy and lactation (see Scheffer and Myrick 1980, Figure 1, p. 52).

Enamel

Dental enamel is practically a "fossil" when it is complete in the living organism, and it has, embedded within it, strong records of life history events. If a tissue is defined as being composed of cells and intercellular substance, then enamel is *not* a tissue. It contains no cells. It is a calcified extracellular secretory product.

Ameloblasts secrete proteins that regulate nucleation and growth of crystallites. During very early enamel formation, enamel contains a high percentage of protein that is enzymatically removed whilst crystallites grow in diameter. Enamel reaches 95–98% by weight carbonated hydroxyapatite $Ca_{10}(PO_4)_6(OH)_2$ (usually just called hydroxyapatite [HA]), and the balance is protein and water (Chadwick and Cardew 1997; Lacruz et al. 2012).

Prisms and Packing Patterns (Figure 13.8)

The cellular activities involved in making this amazing material are fossilized within its structure. Each enamel-forming cell (ameloblast) leaves a track in the material, which it is secreting, and has secreted, so that we can see where it was at any time during its life history. These paths or tracks divide the structure into units marked by a boundary at which there is a change in the orientation of the (ca. 0.05- to 0.1 µm cross section) crystallites (Figure 13.8A–J). This relates to the shape of the interface between the ameloblast and its secretory product (Boyde 1964, 1989). The resulting boundary discontinuity may be closed to make a circular "prism" as in pattern 1 (Figure 13.8E, H) or it may be absent on one side as in pattern 2 (Figure 13.8F, I) and pattern 3 (Figure 13.8B, G, J).

Ameloblasts are tall cells that are closely packed as hexagonal columns. Considering the basically hexagonal cross-sectional shape of these cells, the deficient bit of the prism boundary discontinuity may face the side of a hexagon (Pattern 2) or a corner (Pattern 3). Different mammalian orders show a marked predisposition to the frequency at which these different prism packing patterns occur. The patterns also relate to the cross-sectional area of the cells: very roughly 20 μm^2 for Pattern 2, 30 μm^2 for Pattern 1 and 40 μm^2 for Pattern 3 (Figure 13.8A). We should interpose here that the cross-sectional size of the cells does not relate to the amount of "matrix" secreted per unit of time. This is determined by the thickness of the layer of protein manufacturing cells – the length of the ameloblasts.

An extra declivity is present in the lower side of each "Tomes' process" pit in bats, which causes the formation of an

VetBooks.ir

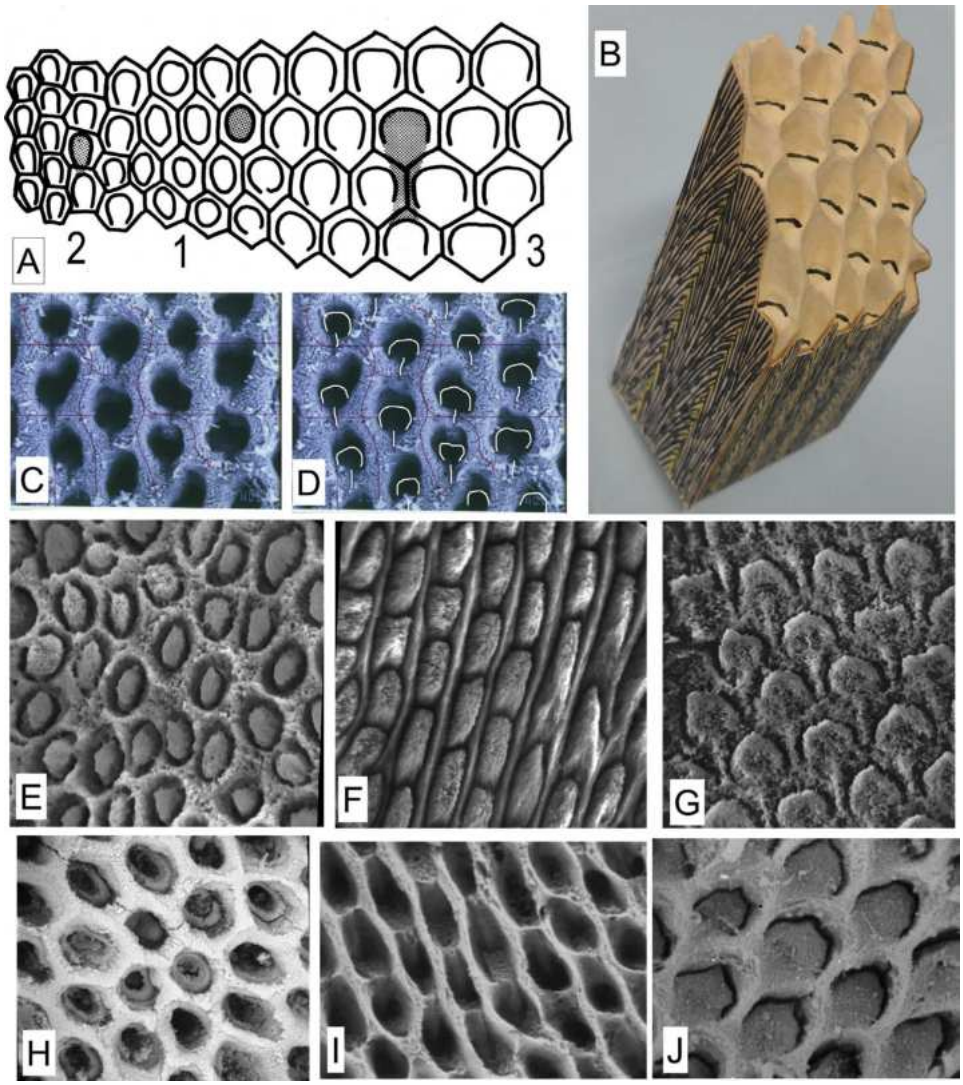


FIGURE 13.8 Enamel prism patterns and development. A, Diagram showing the relationship between the size of the secretory territories of the ameloblasts and the "Pattern" of the prism. The results are based on data from Boyde (1968) derived from examining the development of enamel across a range of mammalian orders. The hexagonal outlines show the amount of enamel made at the forming front by each ameloblast. The horseshoe shaped line within each hexagon shows the site of the prism boundary (crystallite orientation) discontinuity. The largest cross-sectional ameloblasts (at ~40 μm^2) have the open side of the prism boundary discontinuity facing the corner of the hexagon and make Pattern 3 prisms in which components are derived altogether from four ameloblasts, but mainly from three, with the greatest part derived from one cell. This is shown by the dotted shading indicating the extent of one prism. All the enamel is attributed to prisms, including that released in the interpit position: there is no interprismatic substance. Smaller than Pattern 3 prisms are Pattern 1 prisms (repeating at ~30 μm^2). They have a more or less complete cylindrical prism boundary discontinuity such that circular to hexagonal cross section prisms are separated by a continuous interprismatic phase formed from the matrix released between ameloblasts (the interpit material). Smaller still are Pattern 2 (repeating at ~20 μm^2) prisms that form when the pits form longitudinal rows: the prism boundary discontinuity faces the side of a hexagon and is continuous with that of the next prism in the same row (note shading extending between prisms). This leaves a discontinuous interprismatic phase comprising the material which was released in the interpit position and forms an interrow sheet interprismatic phase. B, Photograph of a model illustrating the development of Pattern 3 prisms in a human deciduous incisor. The shape of the model was derived by direct 3D reproduction of the stereoscopic 3D optical model formed from a stereoscopic pair of images recorded by 10-kV secondary electron (SE)-scanning electron microscopy (SEM). The sides of the model show the interpolated crystallite orientation as determined both by transmission electron microscopy (TEM) of thin sections and direct observation of suitable SEM samples. The black lines drawn in the floors of the Tomes' process pits show where crystallite orientation changes (the site of the prism boundary discontinuity). C, SE image in the SEM of plasma-ashed embedded developing enamel surface of the microchiropteran bat (*Chalinolobus gouldii*). This field is the same as Lester and Boyde (1987, Figure 13.10, left) where the surface profiles corresponding to the several marked lines as analyzed with a stereo comparator will be found in Figures 13.11–17 of that publication. Field width 16 µm. D, Same with positions of the prism boundary discontinuities and the seam features as marked. E, SE-SEM. Ethylene-diamine-tetra-acetic acid (EDTA)-etched enamel of African hedgehog *Atelerix algirus*, showing Pattern 1 prisms. Field width 21 µm. F, SE-SEM. Acid-etched pig (*Sus scrofa*) enamel showing Pattern 2 prisms separated by longitudinal interrow sheets of interprismatic (interpit origin) enamel. Field width 20 µm. G, SE-SEM. Acid-etched human permanent enamel showing Pattern 3 prisms. Field width 28 µm. H, SE-SEM. Developing black rhinoceros deciduous molar enamel surface at completion showing Pattern 1 arrangement but with "prisms within prisms" due to a two-level filling-in process of the Tomes' process pits. Field width 21 µm. I, SE-SEM. Developing pig enamel surface showing Pattern 2 arrangement with longitudinal rows of pits separated by interrow ridges in which the interrow sheets of interprismatic enamel form. Field width 17 µm. J, SE-SEM. Developing human permanent third molar enamel showing Pattern 3 prisms. Field width 20 µm.

VetBooks.ir

extra crystallite orientation discontinuity called the "seam of Lester" (Figure 13.8C, D; Lester and Boyde 1987).

Examples of etched enamels corresponding to Patterns 1–3 are shown in Figure 13.8E–G and developing enamel surfaces in Figure 13.8H, I. Fractured Pattern 2 enamel is seen in Figure 13.9A and Pattern 3 in Figure 13.9B.

Prism Decussation

Relative Cell Movement Within the Ameloblast Layer

Cells within the ameloblastic sheet move not only in the direction in which they propel themselves by secreting enamel, but they may move relative to their neighbors within the plane of the sheet. This gives rise to an element of crisscrossing of prism boundary discontinuities, called decussation (after the Roman numeral *decus*, X). The tendency is extremely developed in carnivores and rodents.

Rodent Incisor Inner-Enamel Decussation

In the formation of the inner layer of the enamel of myomorph (Figure 13.10A) and sciuromorph (Figure 13.10B) rodent incisors, single transverse rows of cells may move past each other making layers of prisms crossing at 90°. This specialization might favor the cleavage of the resultant sheets of enamel prisms to contribute to a mechanism for generating self-sharpening cutting edges to the continuously growing, gnawing teeth (Boyde 1964, 1978, 1989). However, the width of the decussating "zones" in hystricomorphs is a few prisms (transverse bands of four or five ameloblasts move against each other during development [Figure 13.10C]) and the final cutting edges are still sharp. In all rodent incisors, prisms in the outermost zone are parallel to each other (decussation ceases) and they slope strongly toward the incisal edge. Exact details of the arrangements across a large number of rodent species were determined by Korvenkontio (1934). See also the many papers by Koenigswald (1982, 2004) for more structural aspects and Boyde (1969, 1978) for developmental studies.

Sciuromorph fractured incisor enamel is shown in Figure 13.10D and myomorph enamel in Figure 13.10E. Etched hystricomorph enamel is shown in Figure 13.10F and myomorph enamel in Figure 13.10G. The crystallites proper constituting the bundles, which form prisms and the interrow sheets, can be resolved using ultrathin sections of developing enamel studied by transmission electron microscopy (TEM), as shown in *Myocastor coypu* (hystricomorph) enamel in Figure 13.16H. They can also be resolved by high-resolution SEM of fractured enamel.

Hunter-Schreger Bands

The name Hunter-Schreger bands (HSBs) has been given to the arrangement of enamel prisms deriving from the relative cell movement within the ameloblastic sheet as revealed in human teeth and which might also be regarded as illustrative for the great majority of mammalian teeth in which decussation is obvious. If we examine the inner enamel layer, we find several adjacent prisms (which represent the paths of the ameloblasts during their secretory life history) in the longitudinal direction of the tooth deviating to one side and then the course changes to the other side and so on, down the length of the tooth (Figure 13.11A, B; see also Figure 13.4A). Details of the arrangement are different to a degree in all species that have been studied in sufficient detail; not all species have evident decussation, and not all layers of the enamel are the same, with deeper layers, nearer to the EDJ, more affected (Boyde 1969).

Gnarled enamel is a name given to deep enamel near cusp tips in which the courses of the prisms appear to be very complex reflecting substantial relative movements of ameloblast during secretion. The thick enamel of elephant molars shows great complexity in decussation (Figure 13.11C, D).

Rhinoceroses have HSBs turned through 90° in the inner part of the enamel (Figure 13.11E, G). To achieve this, the bands of ameloblasts with common directional properties move up and down the formative tooth surface instead of across it as in all other extant mammals. In function, enamel exposed at sloping occlusal surfaces wears more rapidly where the prism boundary discontinuities are more parallel with the surface and is resistant to wear when they are perpendicular (Figure 13.11G). Thus occlusal surfaces naturally generate a microserrated relief suited to a browsing diet (Fortelius 1985; Boyde and Fortelius 1986).

Periodic Growth Layer Lines in Enamel

Cross Striations or Varicosities: Circadian Rhythms

Ameloblasts secrete enamel incrementally. Two main types of growth incremental lines can be observed by LM: the cross striations and the striae of Retzius. These features, concealed beneath the intact tooth surface, have a long history of observation and inquiry (Havers 1691; Retzius 1837; Andresen 1898; Schour and Poncher 1937; Boyde 1964; Dean 1987).

The amount of enamel formed each day is shown by the cross striation repeat interval and measuring this distance gives the daily secretion rate, which varies greatly owing to biological necessity and life history, ranging roughly from 2–20 μm/day.

At least in Pattern 3 enamels such as human and dog, 3D SEM of fractured samples in which the fracture plane follows the boundary discontinuities show alternating varicosities and constrictions of the prisms corresponding to the cross striations (Figure 13.9B). Strictly, the prism "body" (pit floor-filling material developmentally) expands at the expense of the prism "tail" (the interpit phase developmentally: interprismatic in Pattern 1). This is due to a variation in the ratio of the material released by the ameloblasts in the pit floor versus the interpit (intercellular) locations, with less interpit during faster secretion and more during slower secretion (Boyde 1964, 1989).

Compositional BSE-SEM imaging of polished enamel samples (where the information is derived from a thin layer in the surface) show the cross striations as variations in intensity reflecting variations in the concentration or composition of the mineral phase (Figure 13.12A, B; Boyde 1989).

VetBooks.ir

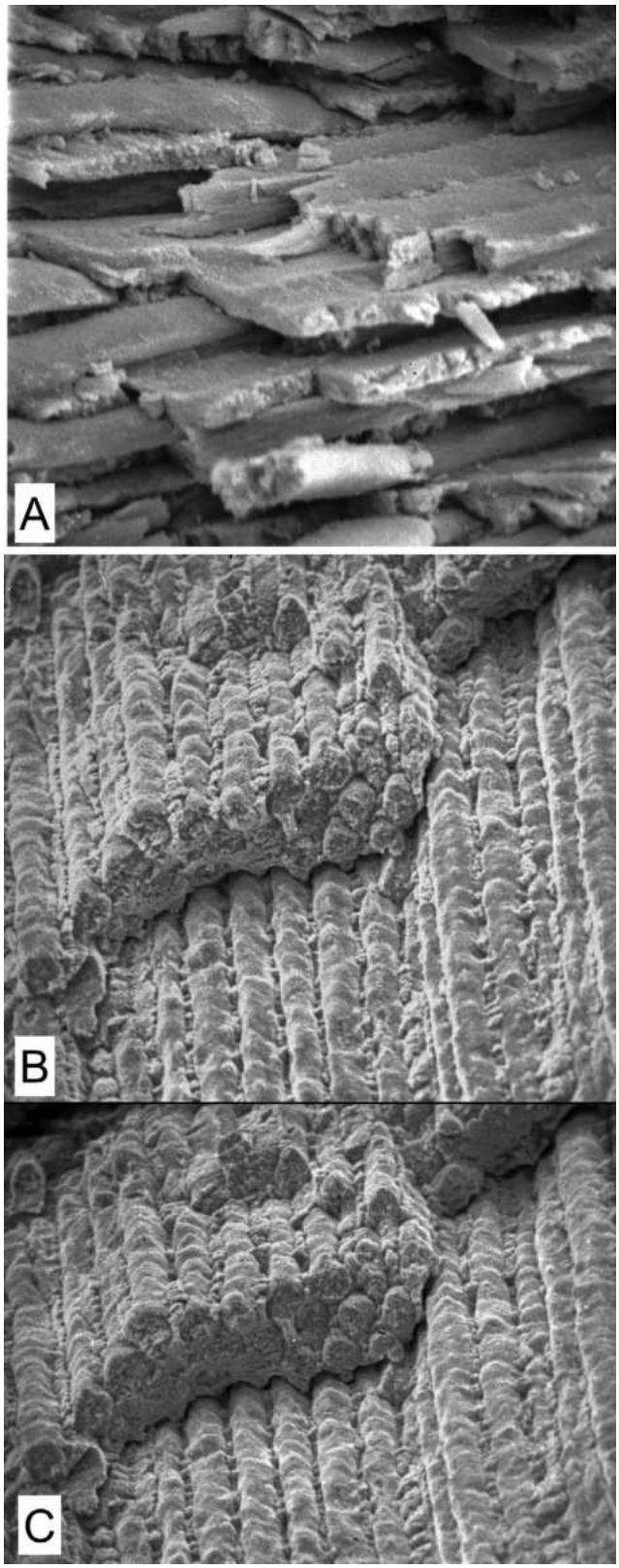


FIGURE 13.9 Fractured Pattern 2 and 3 enamel. A, Secondary electron (SE)-scanning electron microscopy (SEM). Fractured sheep (*Ovis aries*) enamel showing rows of prisms separated by continuous interrow sheets (IRS) of interprismatic (interpit origin) enamel. Since crystallites in the prisms are nearly parallel with the prism long axes, it can be seen the those in the IRS are more or less perpendicular. Field width 22 µm. B, SE-SEM. Fractured human permanent enamel (Pattern 3) showing the cross striations of the prisms as varicosities, i.e., variations in the width of the prism bodies at the expense of the interpit origin phase "prism tails". Field width 82 µm. C, Same field of view at a 10° higher tilt angle: rotate the page 90° and gaze to view B and C in stereo.

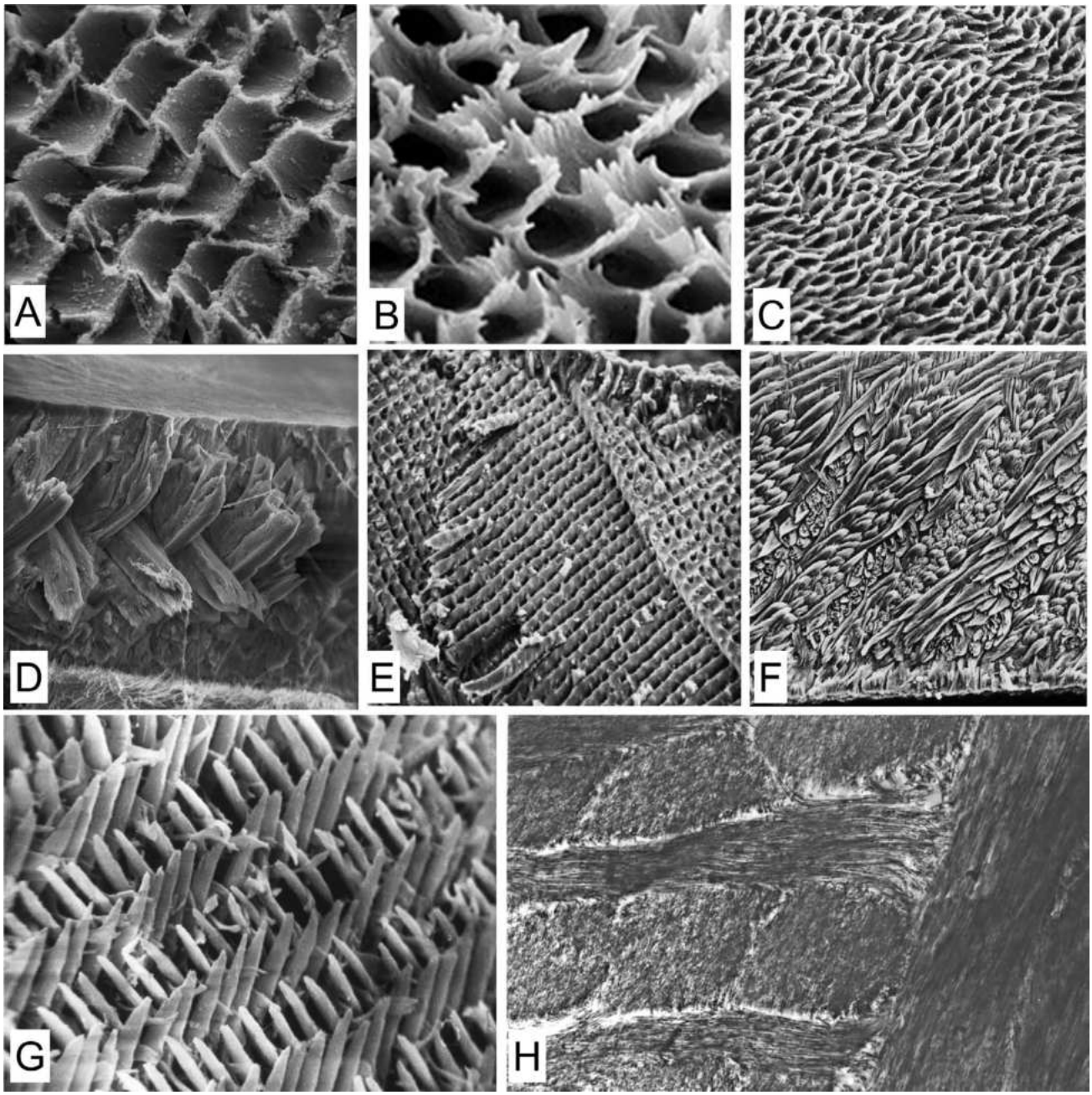


FIGURE 13.10 Enamel prism decussation characteristics in rodents. A, Secondary electron (SE)-scanning electron microscopy (SEM). Squirrel, a sciuromorph rodent (*Sciurus carolinensis*), developing surface of inner enamel of lower incisor, showing alternate transverse rows of Tomes' process pits with alternate slopes (entry/exit directions) corresponding to the formation of transverse 90° decussating rows of prisms (uniserial lamellae after Korvenkontio 1934). Field width 19 µm. B, SE-SEM. Myomorph rodent, rat (*Rattus norvegicus domestica*), developing surface of inner enamel of lower incisor, showing alternate transverse rows of Tomes' process pits with alternate slopes (entry/exit directions) corresponding to the formation of transverse decussating rows of prisms (again, uniserial lamellae after Korvenkontio 1934). Here, however, the pits also enter at 45° in the third sense, from incisal toward apical, making the interpit phase much more obvious. Field width 20 µm. C, SE-SEM. Hystricomorph rodent, guinea pig (*Cavia*), developing surface of inner enamel of lower incisor, showing Tomes' process pits in zones with alternate slopes (entry/exit directions) at intervals of four to five pits corresponding to the formation of transverse decussating zones of prisms (pauciserial lamellae after Korvenkontio 1934). Field width 100 µm. D, SE-SEM. Longitudinally fractured squirrel incisor showing the 90° differently oriented transverse rows of prisms in the inner enamel. Tooth surface at top, dentine below. Field width 20 µm E, SE-SEM. A 45° oblique transversely fractured rat lower incisor enamel, parallel with the decussating sheets of prisms in the inner enamel. Field width 100 µm. F, SE-SEM. Ethylene-diamine-tetra-acetic acid (EDTA)-etched longitudinal section (LS) cut surface through guinea pig (hystricomorph) lower incisor showing the decussating zones of prisms. Field width 100 µm. G, SE-SEM. EDTA-etched transversal section (TS) rat lower incisor developing enamel. Field width 100 µm. H, Transmission electron microscopy (TEM) of coypu (*Myocastor coypu*) hystricomorph developing enamel showing the enamel crystallites organized as parallel bundles in prisms and interprismatic (interpit phase in development) regions. Field width 9 µm.

VetBooks.ir

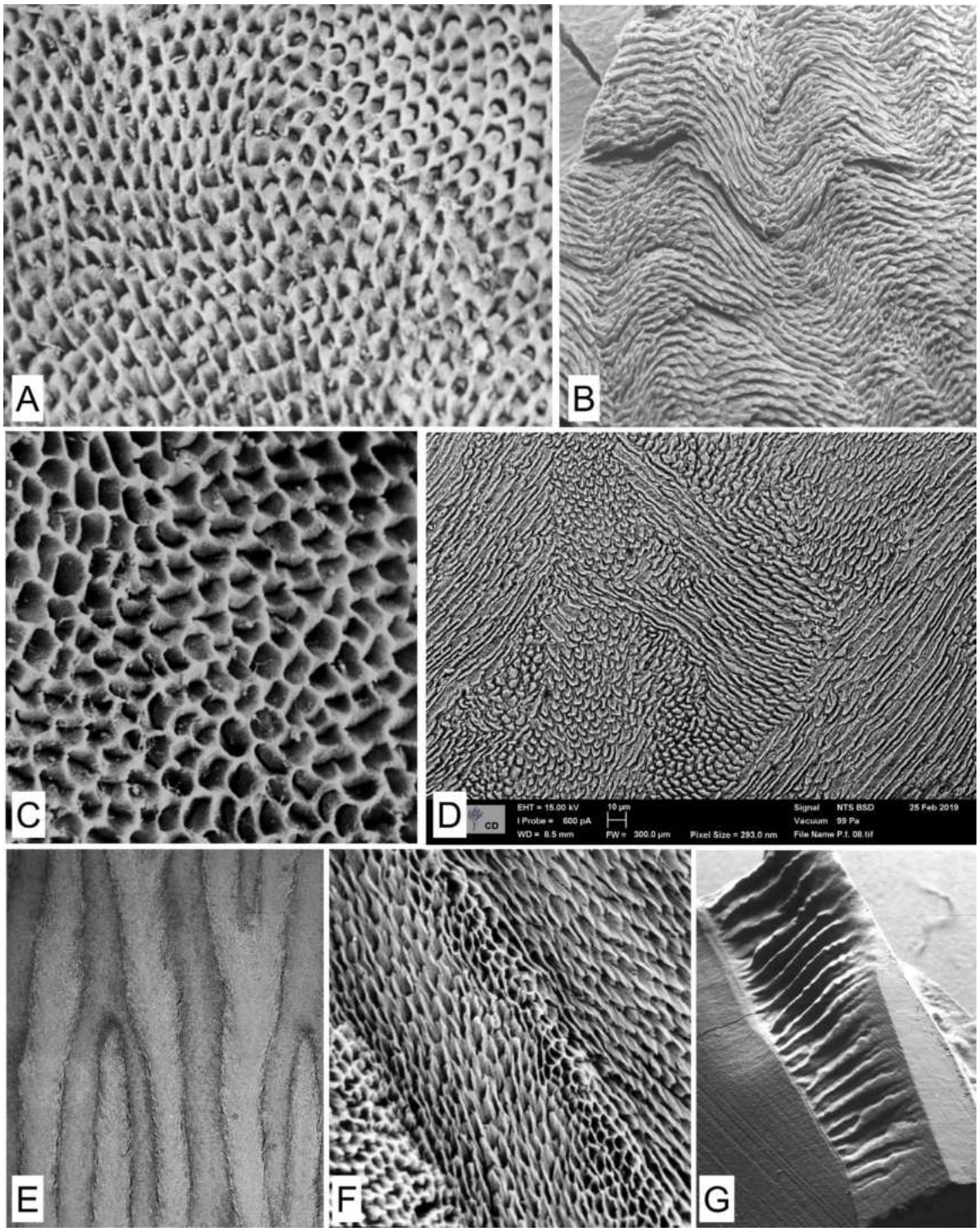


FIGURE 13.11 Hunter-Schreger bands in man, elephants and rhinos. A, Secondary electron (SE)-scanning electron microscopy (SEM). Human third permanent molar developing enamel surface showing the gradual change in the entry direction of the pits in keeping with the translatory motion of the ameloblasts across the surface. Field width 160 µm. B, SE-SEM. Deep etched (first NaOCl, then potassium citrate) human premolar enamel TS, enamel-dentine junction (EDJ) top left corner. Note the deeply etched tuft-lamellar planes. Field width 220 µm. C, SE-SEM. African elephant (*Loxodonta africana*) developing molar enamel surface showing apparently random exit direction of Tomes' process pits. Such a surface may have dimensions of square inches, whereas the area of each pit is around 40 μm^2. Many tooth plates, each several inches high (roughly 10 cm), are worn away in the life span of the animal. Field width 78 µm. D, Back-scattered electron (BSE)-SEM. Maltese pygmy elephant (*Palaeoloxodon falconeri*) molar enamel showing a complex array of decussating prisms. Phosphoric acid etched for 5 seconds. Field width 300 µm. E, SE-SEM. White rhinoceros developing enamel surface showing the vertical zones in which ameloblasts move "up and down" the surface resulting in vertical decussation of the enamel prisms. Field height 1 mm. F, SE-SEM. White rhinoceros developing enamel surface. Field height 100 µm. G, Simulated wear surface of a black rhinoceros molar. Occlusal surface was beveled at 45° toward cervical before air polishing. Converted BSE image achieved by applying negative potential to sample holder to capture SE. Field width 2.94 mm.

VetBooks.ir

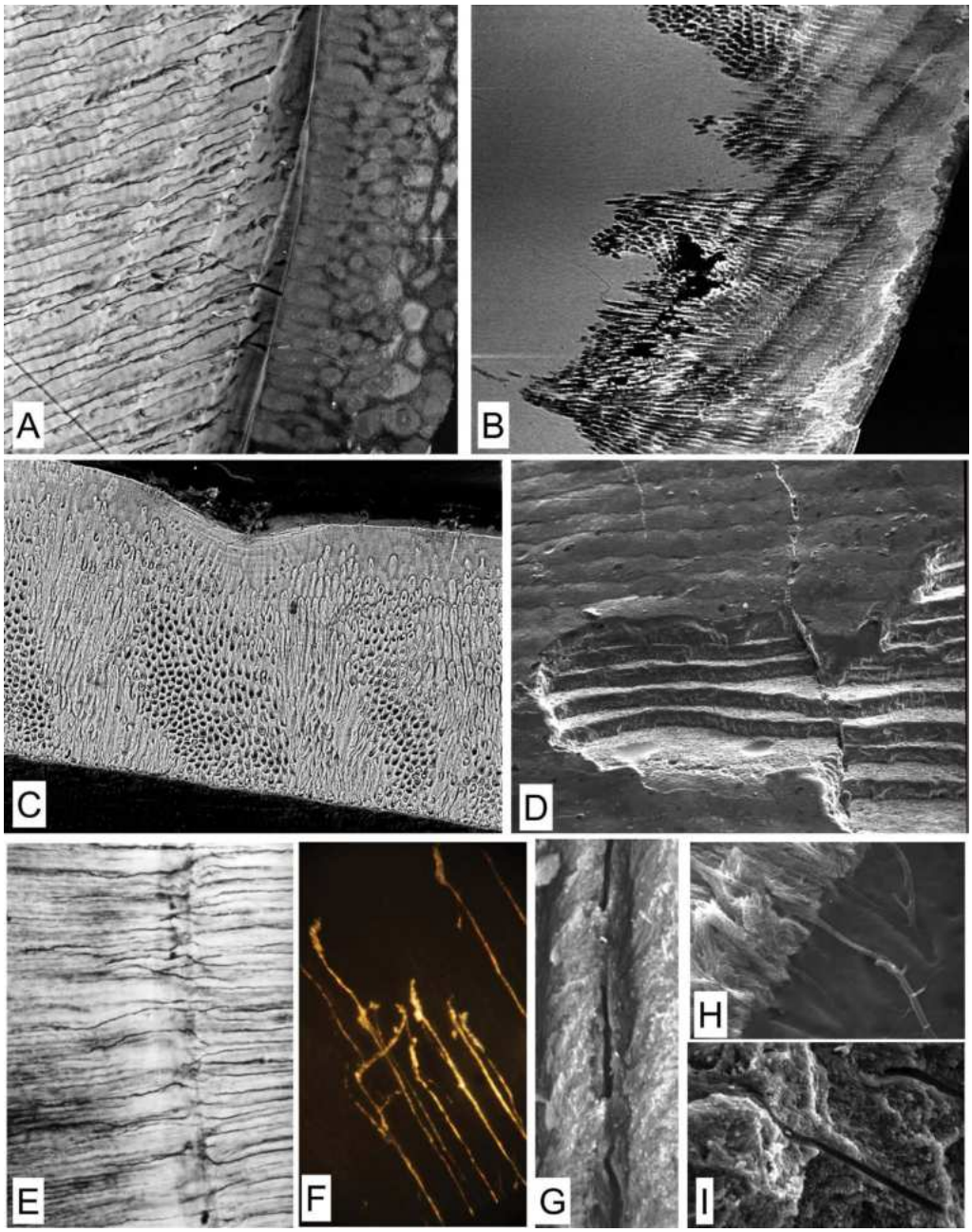


FIGURE 13.12 Growth layer lines (cross striations and striae) in enamel. Enamel tubules. A, Back-scattered electron (BSE)-scanning electron microscopy (SEM). Micromilled polymethyl methacrylate (PMMA)-embedded, immature, human 12-year-old unerupted third permanent molar, fixed in OsO4, enabling us also to image the maturation ameloblasts *in situ* on the surface. Note the cross striations of the enamel prisms and supradian, regular Retzius lines. Field height and width 150 µm. B, BSE-SEM. Natural carious lesion in a human premolar showing the prominence of the cross striations and the striae in the affected tissue. Field width 438 µm. C, BSE-SEM. Antarctic fur seal (*Arctocephalus australis*) decussating enamel prism zones, etched. Note aprismatic enamel at top presenting daily incremental lines. Field width 326 µm. D, Secondary electron (SE)-SEM. Epoxy cast of silicone rubber impression replica of human premolar with damage of unknown origin but probably caused during extraction, showing perikymata at top, and fractures parallel with the regular striae below and to right. Field width 1 mm. E, Photomicrograph of longitudinal ground section (LS) of Galago (Primate) tooth made by J. Thornton-Carter showing dentine tubules (right) crossing the enamel-dentine junction (EDJ; center vertical boundary) from right and continuing as enamel tubules (left). Scanned from an original 3¼-inch square lantern slide made by Thornton-Carter (Zoology Department University College London ca.1920). Field height ~200 µm. F, Reflected light confocal image made with Tracor-Northern TSM. Enamel in LS of *Diprotodon* – a giant fossil marsupial mammal – tooth showing swollen ends of enamel tubules in mid-enamel, interpreted here as encapsulated dead ameloblast cell bodies. These features are very similar to enamel spindles in human teeth. Extended depth-of-field image made by summing several focal planes over a range of a few microns directly onto color transparency film. One member of a stereoscopic pair. Field height 84 µm. G, SE-SEM. Fractured kangaroo (*Macropus* sp., marsupial) enamel showing one tubule running parallel with the prism direction. Field width 4 µm. H, EDJ in LS, etched PMMA-embedded preparation of *Trichosurus vulpecula* (marsupial) mammal showing continuity of replica cast of dentine (right) with enamel (left) tubules. Field width 10 µm. I, SE-SEM. EDJ in LS fractured kangaroo tooth showing continuity of a dentine tubule between enamel (dark gray region at right) and dentine (bright region at left). Field width 10 µm.

VetBooks.ir

Regular-Period Striae of Retzius: Multidien Rhythms

Beyond the daily enamel formation rhythm is a longer period incremental line, the regular-period striae of Retzius. These represent temporary perturbations of enamel development and show the successive positions of the once forming fronts of the developing tooth crown. For reasons having to do with interspecific organismal life history and body size, regular striae of Retzius in different mammalian species are variously formed every 2–14 days (Bromage et al. 2009, 2011; Bromage and Janal 2014). The number of daily striations between adjacent regular striae of Retzius is termed the repeat interval, or period, and when varying within a species, is the same value in all teeth of the same individual. Whereas cross striations are formed on a circadian (24 hour) rhythm, striae of Retzius correspond to a multidien rhythm, meaning a many-days biological period, most frequently 8 or 9 days in humans.

It is well known from the literature on human dental caries that Retzius lines, cross striations and prism boundary markings are brought into great prominence during the parallel demineralization and remineralization phenomena occurring in dental caries (Figure 13.12B). It might be anticipated that analogous subsurface redistribution of mineral phase material might occur during taphonomy and fossilization.

Perikymata or Imbrication Lines at Tooth Surface: Prism-Free Layer

Perikymata or imbrication lines are outer surface manifestations of outcropping and overlapping striae of Retzius that appear as undulations or shallow steps, which most of us can see on the front-facing surfaces of our upper incisors. The famous Dutch pioneer of microscopy, Antonie van Leeuwenhoek (1632–1723) was the first to describe them, as "kringsgewijze rimpels", i.e., circular wrinkles. Their microscopic anatomy in human teeth is considered in detail by Boyde (1989). In essence, where enamel formation stopped earlier and the thickness is thus slightly less in the troughs or the grooves of the perikymata, the surface shows shallow Tomes' process pits and the prism boundary discontinuities continue to the surface. At the ridges and in the overlapping layer lines, the pits may be scarcely detectable and the surface layer is "prism free". Thus, the enamel of all mammalian taxa is predominantly prismatic, although toward the end of outer enamel formation, aprismatic enamel is common (Figure 13.12C).

The regular striae have an important functional significance, because enamel has a strong predisposition to fracture parallel with these planes. Many human dental clinical procedures induce this type of fracture (Figure 13.12D).

Growth Disturbance Lines: Hypoplasia

Accentuated, irregular striae (also of Retzius), also parallel with lesser growth increments, represent periods of stress to the individual when the crown was forming. The neonatal line is one, and the best understood, of these but is of course only found in the enamel of teeth forming at birth. In humans, these are the deciduous teeth and the principal cusp of the first permanent molars.

Gross growth disturbances may further result in the inability of the affected secretory stage ameloblast to recover and proceed to make full-thickness enamel afterward, leading to the development of hypoplastic grooves, which are essentially very well marked perikymata.

Daily, Ultradian Lines

There are additional finer bandings crossing the enamel prism axes that can be seen with higher resolution BSE-SEM. They would be explained by "ultradian" rhythms i.e., those occurring within the 24-hour diurnal cycle at every several to 12 hours. They may also be seen as finely spaced cross striations by LM, but here there are problems regarding the physical and optical section thicknesses and overlap and interference effects. They are more reliably seen as mineralization density variations in density-dependent imaging in BSE-SEM. There has been no systematic investigation of these lines across species.

Maturation and Surface Enamel Composition

Ameloblasts continue with a very important function after they have completed secretion of all the tissue for which they are responsible by regulating the entry of more calcium and phosphate mineral and the exit of more protein matrix. This maturation phase of the ameloblast life history may last for several years in a human permanent molar or be as short as a few days in a small rodent incisor.

Iron in Surface Enamel

Iron is incorporated in the most superficial, late stages of pre-eruptive enamel maturation-mineralization in the incisor teeth of most, but not all, rodent incisors and the cheek teeth in some shrews (insectivores; Figure 13.2A) and has been shown in extinct fossil mammal groups in both incisors and cheek teeth (Moya-Costa et al. 2019). In all extant mammals, those with yellow, orange or red incisors are rodents, and the color is in proportion to the iron content. However, many rodents have white teeth, with no iron.

The first estimation of maximal iron content in the surface enamel of rat incisors was made by scanning electron probe wavelength dispersive x-ray emission microanalysis at ~10% (Boyde et al. 1961), since confirmed in many other studies.

Upper incisor teeth in rodents are roughly half the length of lower incisor teeth, grow at roughly half the speed of lower incisors, contain roughly twice as much iron in the surface enamel and are more intensely colored. The color is not uniform, and it shows a striking variation as transverse or oblique transverse bands corresponding to the daily growth rate of the tooth. There is thus a circadian rhythm of enamel iron pigmentation, which might be used as a surrogate for estimating tooth formation and eruption rates.

It has recently been proposed that the iron content hardens the enamel, causing the sharp cutting edges (Gordon et al. 2015). The hardening due to iron deposition as nanocrystalline

VetBooks.ir

ferrihydrite (Wen and Paine 2013; Gordon et al. 2015) may be highly significant in shrew cheek tooth cusp tips because of the small size of the teeth, the short life span of the individual, the thinness of the enamel, the hardness of insect exoskeletal chitin and the abrasiveness of rock particles in soil. However, the fact that all rodent incisors have very sharp edges is due to the internal arrangement of the prisms and the resulting inbuilt tendency to cleave parallel with the decussating sheets of prisms, many of which are removed per hour in normal function. Although the iron content might contribute, it can hardly matter, given that white rodent and lagomorph incisors function in the same way. Rodent incisor self-sharpening is only possible because of the form of the jaw and the jaw joint and musculature, which permits a large range of anteroposterior movement. The upper incisor is used to cut back the lower incisor and vice versa. This is performed as a tooth grooming routine, and the activity emits a high-pitched squeaking or screeching noise (Boyde, personal observations on captive coypu, *Myocastor coypus*).

Enamel Tubules and Spindles, Tufts and Lamellae

Enamel Tubules

Enamel may also have tubules (Figure 13.12F–I: Boyde and Lester 1967b). Ameloblasts have attachments to odontoblasts and leave a cell process within the enamel matrix, which, in some species, continues for a considerable distance into the enamel, defining a tubular space. Classically, it is stated that tubules are the hallmark of marsupial enamel (Figure 13.12G–I) with the sole exception of the wombats. They are also ubiquitous in insectivores, and lemurs among the primates (Figure 13.12E; Thornton-Carter 1922). They also exist in many other mammalian teeth, including human, but are of such small dimensions that they routinely escape detection.

Spindles

The standard dental histology texts have been unable to explain the origin and the significance of features called "enamel spindles". By examination of marsupial enamel, and especially in the fossil macropod *Diprotodon,* it is clear that the terminal expansions of the enamel tubules have the same dimensions of secretory ameloblasts, and are the tombs of defunct ameloblasts (Figure 13.12F). Spindles, which are only found close to the EDJ, are the same, but with a very short tubule.

Tufts and Lamellae

Features called tufts and lamellae form in what would be in geological terms described as faulting planes in the enamel structure. During maturation, the period in which enamel protein matrix is removed from the enamel, we assume that shifts occur and natural routes for matrix exits are impaired, leading to regions that remained enriched with undegraded enamel matrix proteins. These features typically run in the longitudinal direction of a tooth and are most exaggerated in the first-formed layers of enamel near the EDJ where decussation is most marked (Tuft planes may be identified in Figures 13.4A and 13.11B).

Roots and Cementum: Crowns and Coronal Cementum

For descriptive purposes teeth are said to have crowns and roots. The term crown may refer to those portions of the tooth normally exposed in the oral cavity (tusks are teeth projecting outside the oral cavity) but, if the tooth has enamel, that part covered with enamel may also be called the (anatomical) crown. Cementum is the tissue which, together with the PDL, serves to attach teeth to the jawbone, and it always covers those parts of teeth that are to be so attached, whether they are crown or root. The majority of the inorganic mass of cementum is 65% by weight HA, whose crystals measure approximately 55 nm in width and 8 nm in thickness (Berkovitz et al. 2017).

Primary Cementum

Primary cementum is a simple tissue by means of which external, penetrating, extrinsic Sharpey's fibers are attached to the surface of root dentine. This layer may be as thin as 50 μm in human teeth. It is composed of roughly 95% extrinsic fibers. It contains no cell remnants or spaces such as the lacunae and canaliculi found in bone.

Secondary Cementum (See Also Dentine Resorption)

Secondary cementum forms layers on a primary cementum basis and may contain cementocytes and their lacunae and canaliculi.

It is extremely important to distinguish Sharpey's fiber centers in cementum from dentine tubules. It is a characteristic of this layer that the central axis of each extrinsic collagen bundle fails to mineralize: thus, it has a much lower refractive index than the periphery and it may appear in conventional transmitted light microscopy like a dentine tubule. In BSE-SEM of polished preparations, the centers of the Sharpey's fibers appear dark because they are unmineralized. In anorganic, deproteinized preparations, these bundles appear to be hollow where the nonmineralized matrix has been removed.

Coronal Cementum

Plant diets can cause huge amounts of tooth wear. To compensate, many herbivorous mammals have evolved extremely tall, enamel-covered crowns that take a correspondingly long time to wear away. These teeth have cementum deposited on (and in) the surface of the "crown", which has to act as a root before there is an anatomical root. The enamel must first reach full maturation to become hard and wear resistant. The ameloblasts survive long enough to fulfill this, their last function, and then move away to permit connective tissue cells to deposit a bonelike tissue on the enamel surface, which is called cement because it is in a tooth. Such "hypsodont" crowns are formed by extreme elongation of individual tooth cusp elements to make plates or "lophs". The potential weakness of having very deep erstwhile "fissures" in the crown surface is overcome by filling the space with packing and binding

VetBooks.ir

cementum, which contains blood vessel canal spaces as well as (osteocyte) cementocyte lacunae and canaliculi.

To get a grip between coronal cementum and enamel, the most common stratagem adopted in evolution has been to stop enamel secretion while the ameloblasts still have their secretory-pole Tomes' processes, so that the enamel surface is micro-rough at this scale. Cementum is deposited after the enamel maturation phase (Figure 13.13A–D).

However, some groups of mammals have adopted the general strategy used in bone in bone organs to stick one layer to the next: namely, osteoclasts are employed to resorb the enamel surface, on which the bony tissue (cementum) is deposited. In extant mammals this is only found in the Equidae (Figure 13E–J; Jones and Boyde 1974).

There are many examples of teeth in which an important fraction of the total bulk is cement, including elephant tusks and the homodont (usually simple conical shapes, all the same and not obeying the typical mammalian dental formula) teeth of many odontocetes. A vascularized tissue "vasocementum" bulks out the whole tooth form in the beaked whales and is usually the predominant tissue (Figure 13.7D–F; Boyde 1968, 1980).

The Cement-Dentine Junction Region in Murine Molars: Incorporation of Hertwig's Root Sheath

During tooth development, the growing edge of the epithelial component of the tooth germ composed of only the inner and outer dental epithelia, by mutual inductive processes, allows the differentiation of the odontoblasts, which form the dentine of the root portion of the tooth. The residue of this epithelial sheet remains incorporated, in a perforated form, within the periodontal membrane or ligament (PDL). However, in murine rodents (rats and mice and congeners) the epithelial root sheath of Hertwig becomes incorporated in part within the plane of the cement-dentine junction (Figure 13.14A, B; Lester and Boyde 1970). It has not been established what the ubiquity or frequency of this phenomenon may be in other mammals. This epithelium within the whole tooth structure remains uncalcified, but we have no evidence as to how long the cells remain "alive".

Cartilage Cementum

In the Caviidae (Hystricomorpha) family, including *Cavia porcellus* the domesticated guinea pig, connective tissue fiber bundles of the PDL attach to the surface of even rather immature molar enamel, as judged by the degree of retention of the unmineralized matrix in decalcified sections (Figure 13.14C, D. In addition, connective tissue differentiates into plain hyaline cartilage, which calcifies and becomes one of the dental tissues as a coronal cementum (Listgarten and Shapiro 1974).

Annual Period of Cementum Deposition

Acellular cementum is secreted and mineralized in incremental layers over the root surface with an annual periodicity that persists throughout life without undergoing remodeling. The annual periodicity appears in PLM as alternating light and dark bands, which are used for estimation of age (Klevezal and Kleinenberg 1969; Grue and Jensen 1979; Kagerer and Grupe, 2001) and season (Spiess 1976; Klevezal and Shishlina 2001; Wedel 2007) at death in a variety of mammals, including humans.

Cementum also dynamically responds to a variety of external (environmental) and internal (hormonal, metabolic) factors that are physiologically impactful. A recent study on human cementum samples has confirmed that events related to female reproductive physiology (pregnancy and menopause), systemic illnesses (malaria and human immunodeficiency virus [HIV]) and lifestyle traumas (major move and imprisonment) all leave a permanent mark in cementum, which can be accurately timed (Cerrito et al. 2020).

Preparation Methods We Either Like or Disdain

Etching

Wet acid etching of recent or fossil skeletal and dental tissue samples is commonly employed to generate morphologic surface relief. We make a strong warning that new structures may develop in an etching process that were never present in the original sample. This is notorious in etching procedures for recent dental enamel, where sample surfaces are frequently completely artifactual. This does not mean that such a roughened surface would not be suitable for a specific clinical dental procedure, but one should be careful when making interpretations about the original ultrastructure.

Many valuable museum samples would be damaged beyond redemption by immersion etching procedures. However, in this context, we may recommend the use of two products. One product, Icon-Etch by DMG™ (https://www.dmg-dental.com/en/products; Boyde 2019), is hydrochloric acid supported in a viscous gel of silicic acid. The other is a 37.5% phosphoric acid gel (https://www.kerrdental.com/kerr-restoratives/gel-etchant-bonding-agents-0). Both may be precisely applied as tiny drops, down even to 1 mm in diameter, to chosen spots on a sample surface We recommend limiting exposure to a maximum of 30 seconds followed by vigorous washing with water. This focused approach will lead to more information being obtained from potentially valuable fossils.

Precise, focused "etching" can also be achieved by culturing osteoclasts on any flat sample surface. A good example showing discrete etching of elephant molar plate enamel and dentine is seen in Jones et al. (1995).

Air Polishing and Air Abrasion

Air polishing is a technique using jet propulsion of soft materials, such as sodium bicarbonate powder shrouded in a water jet, to erode sample surfaces. It can be applied to limited areas by using suitable physical masks. It is excellent for revealing differences in structure related to either orientation or degree of mineralization (Boyde 1984a, b). It is related to soft polishing, such as when a hard surface is polished on a soft lap

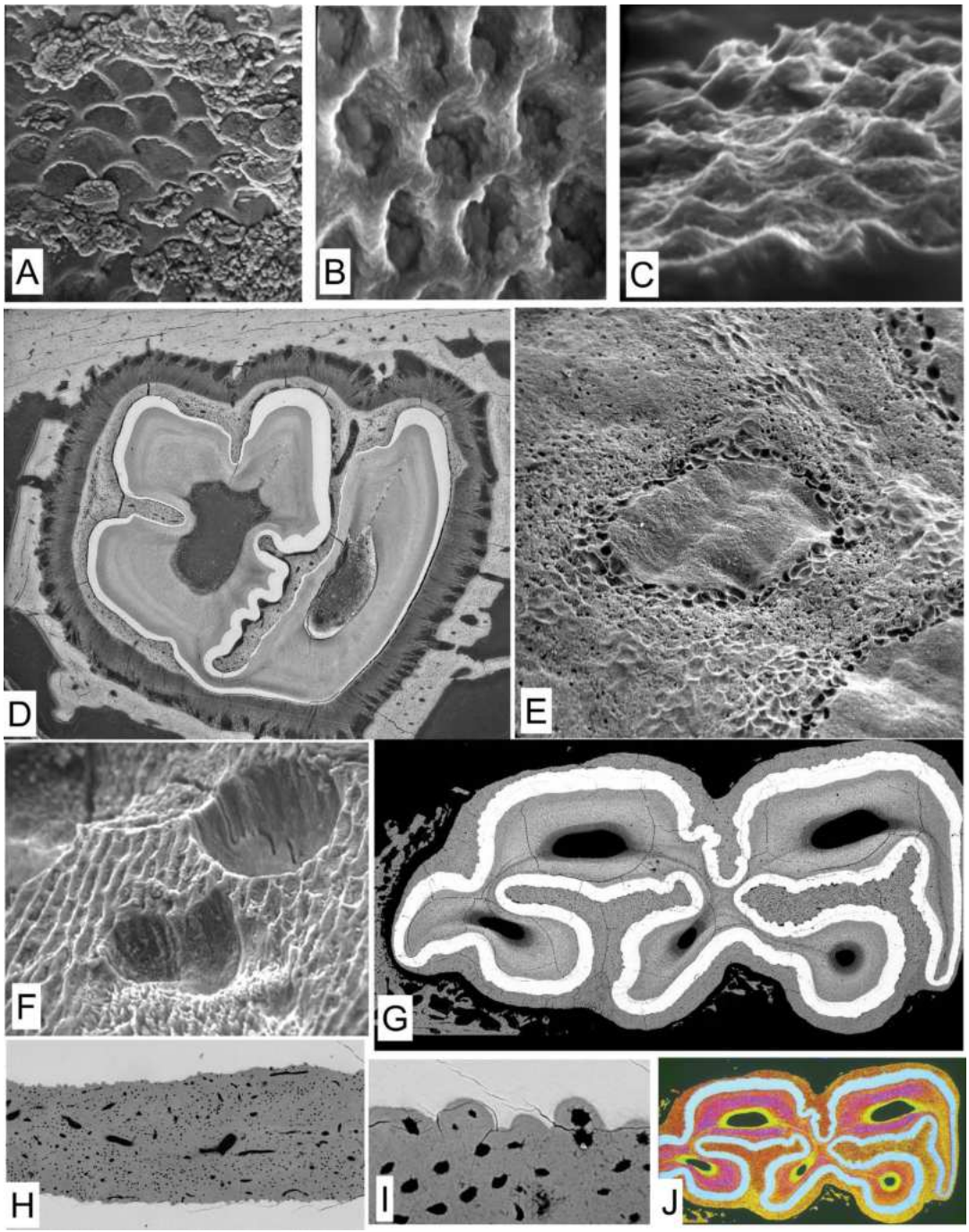


FIGURE 13.13 Coronal cementum. A, Secondary electron (SE)-scanning emission microscopy (SEM). Surface of developing *Loxodonta* molar plate. The completed enamel surface in the background shows typical Tomes' process pits. These are partly filled with calcified coronal cementum matrix. The two tissues are joined via this interdigitation. Field width 47 µm. B, SE-SEM. Surface of developing rabbit molar showing the morphology of the completed enamel surface from which the coronal cementum had detached during shrinkage on drying. Field width 10 µm. C, SE-SEM. Developing rabbit molar showing coronal cementum that had detached from the completed enamel surface during drying shrinkage. Field width 11 µm. D, Back-scattered electron (BSE)-SEM. (TS) rabbit molar *in situ*, embedded in polymethyl methacrylate (PMMA), polished surface, stained with iodine in ammonium iodide solution to show soft tissue elements, including the Sharpey's fibers in the periodontal ligament. Field height 5.3 mm. E, Three-dimensional (3D) SE-SEM. Enamel surface in full-term Arabian horse fetal foal deciduous molar showing areas that have been etched by osteoclastic resorption of enamel and partly filled with coronal cementum. Some unresorbed enamel areas remain. Field width 1 mm. F, Same as E, showing detail of osteoclastic resorption pits penetrating the completed enamel surface, which shows a pattern 2 arrangement of Tomes' process pits. Field width 72 µm. G, BSE-SEM. Very low magnification montage of a 2-year-old Thoroughbred racehorse developing molar TS. The white tissue is enamel. Dentine density varies according to the proportion of highly mineralized peritubular dentine, which it contains. The darkest is "secondary" dentine, which is infilling the pulp chamber space (black). Coronal cementum outside of the tooth is attachment cementum. This is continuous with the internal packing and binding cementum. Mesiodistal width of the tooth is 34 mm. H and I, Higher magnification views showing attachment of cementum to resorbed enamel. Field heights 1.5 mm and 150 µm. J, Same as G but pseudocolored to show relative densities.

VetBooks.ir

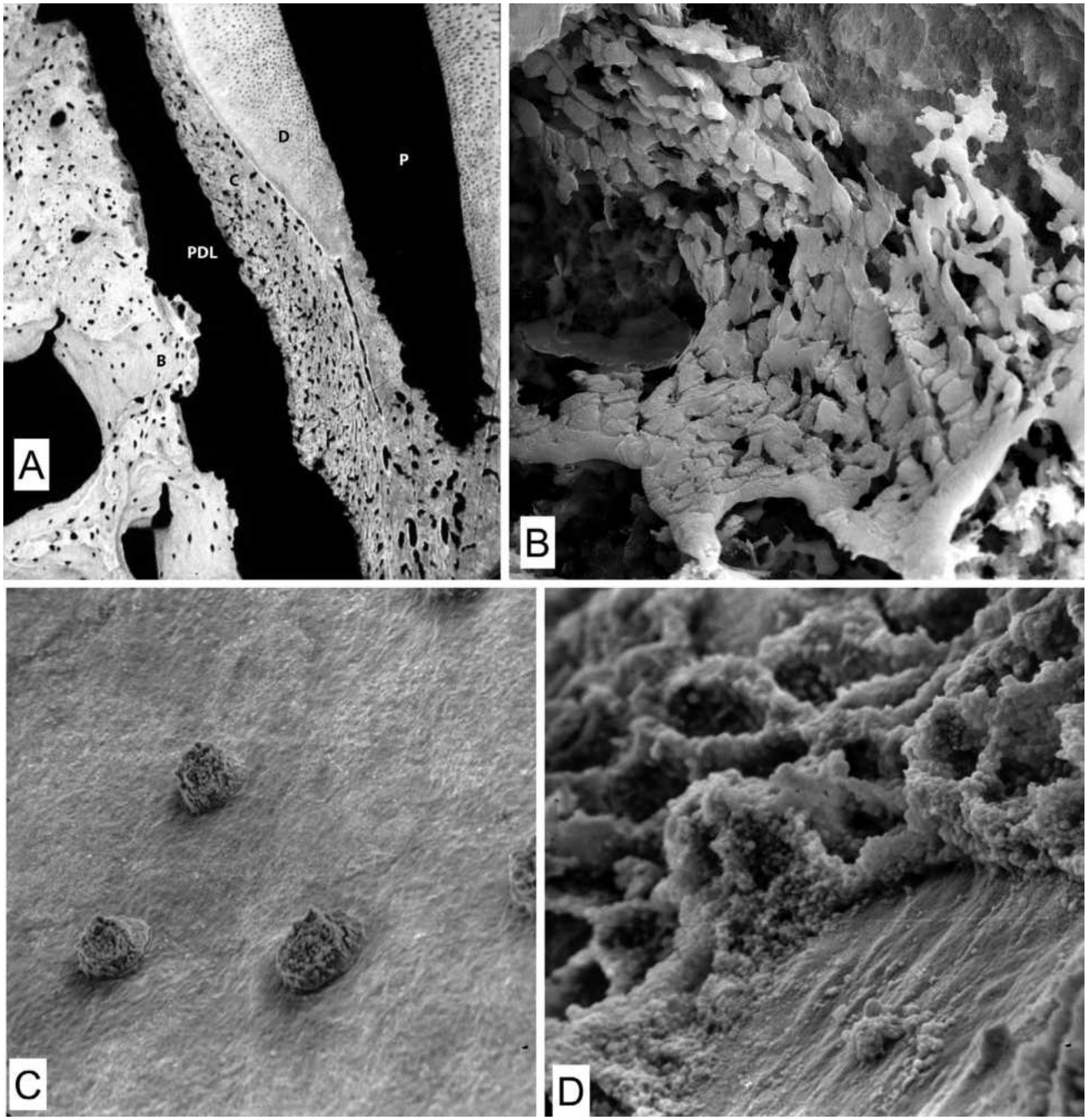


FIGURE 13.14 Inclusion of root sheath at cementum-dentine junction (CDJ) in murine molars. Cartilage cementum. A, Back-scattered electron (BSE)-scanning electron microscopy (SEM). Mouse mandibular molar *in situ* embedded in polymethyl methacrylate (PMMA), polished surface (P, pulp; D, dentine; C, cementum; PDL, location of the periodontal ligament and B, alveolar bone). Note the thin dark space separating dentine and cementum, which represents the zone in which Hertwig's epithelial root sheath is incorporated into the tooth structure. Field width 450 µm. B, A similar preparation, which was treated sequentially with HCl and NaOCl to destroy all calcified tissue matrices, thus leaving a PMMA cast of the space occupied by Hertwig's epithelial root sheath. Field width 100 µm. C, Secondary electron (SE)-SEM. Guinea pig molar anorganic preparation showing a site of direct attachment of PDL to enamel surface. Field width 500 µm. D, SE-SEM. Guinea pig molar anorganic preparation showing calcifying cartilage on enamel surface. Field width 47 µm.

and similar topographic relief develops. This has often been used in hard tissue research without the mechanism being comprehended.

Air abrasion is a closely related and older technique in which abrasive particles are propelled in a dry gas stream. Various grades of alumina and dolomite are commonly employed.

Replica Films for LM

Before the advent of the SEM, it was common to study surface morphology of mineralized tissue samples by applying a thin replica film of a resin, which could be either dissolved or softened with a solvent. This was applied to the sample surface and

VetBooks.ir

stripped off, becoming the LM slide. This method is extremely cheap and could be applied in the field while excavating a fossil. The "extraction replica" is a variant of this technique in which the aim is to remove small particles or features in the replica film.

TEM of Carbon Replicas

TEM of thin replica films is very much out of vogue, but it has extreme advantages of simplicity and low cost if one may be permitted to destroy small scraps of a sample, particularly from samples too large for the microscope chamber. Simply evaporate carbon onto the sample surface, for example, fractured enamel, and then dissolve the sample in any acid. The carbon film floats in the liquid. It is fished out using an uncoated copper TEM grid, washed in distilled water, dried and ready for microscopy. The TEM image will apparently have very low contrast, but, as soon as stereopair images are recorded by tilting the sample through a few degrees, the surface morphology is revealed at the highest resolution (Lester and Boyde 1968).

Replicas and 3D Resin Casts for Scanning Electron Microscopy

High-resolution resin replicas may be made of surfaces for the study of developmental details or taphonomic effects (Pfefferkorn and Boyde 1974; Bromage 1985, 1987). This technique typically employs a silicone-based dental impression material for constructing the negative replica, and a reasonably low-viscosity resin for reestablishing the positive replica. Simple techniques for generating surface histology typically reflect detail on the order of 0.1–0.3 µm (Bromage 1985).

If a sample is embedded or included in a resin that has low viscosity before polymerization, we can, if permitted, dissolve the sample to produce a 3D cast of spaces in the tissue (Boyde 2019). This can be of great value, at least in recent material, in studying the 3D distribution and connectedness of dentine tubules and their side branches, enamel tubules, cementocyte canaliculi and blood vessel canal spaces. Again, in recent material we can recover polymethyl methacrylate (PMMA) resin casts from relatively poorly or nonmineralized regions, such as IGD.

"Thin" Sections and Laser Ablation Microtomy (LAM)

Transmitted light microscopy with conventional optics requires thin sections. Contrasts are commonly generated by scattering or reflection of light at interfaces where the refractive index changes. Such features therefore appear darker. If viewed in reflection mode, the identical features appear bright.

Regarding the preparation of very thin sections, we highly commend the use of laser ablation microtomy (LAM; Boyde 2018, 2019). With this technique, a flat polished surface of a sample is glued to a glass LM slide with cyanoacrylate glue. A pulsed laser beam is focused through the slide and at a desired distance into the sample. This is scanned over the entire area of the block, ablating material in the focused plane, leaving a section attached to the slide. This has the extreme advantage that the same section may be the surface of a volume reconstructed by x-ray microtomography (XMT) and it may be examined by any LM or SEM method.

Plastic Slides

PMMA LM slides are commonly used because they are readily produced in custom sizes and they may resist breakage. However, they are polarizing filters and interfere with serious PLM.

Cyanoacrylate Glue

Superglues are often used to cement the polished surface of a sample to a glass or plastic LM slide prior to cutting close to the slide surface to leave a section, which is then polished. If your aims include the use of PLM, then try to use as thin a film as possible because the cyanoacrylate will interfere.

Imaging Methods We Either Like or Disdain

Reflected Light Confocal Microscopy

Confocal scanning LM is made for fossils, but not all fossils are made for confocal microscopy. To overcome this problem, in 1983 we designed the first confocal microscope ever to be used with fossils to approach large samples from almost any angle (Boyde et al. 1983, Figure 86).

In the original "two-sided" spinning disk tandem scanning reflected light microscope (TSRLM) configuration invented by Petran and Hadravsky (Petran et al. 1985, 1990), the sample is illuminated by multiple focused beams defined by holes in a spinning Nipkow disk (Figure 13.15A–E). Reflected (or fluorescent) light from brightly illuminated spots in the sample is collected by matching pinholes on the opposite side of the same disk, providing excellent discrimination of an optical section plane but also a formidable challenge in optical alignment.

This instrument (Figure 13.15A) was used in a large number of studies of fossil dental tissues in the 1980s (Boyde and Martin 1984, 1987). Images were permanently recorded on film (Figure 13.15B–E). This was a white light-illuminated system. No computer was involved. No sample preparation was required. To minimize the strongest reflection, which arises at the outer surface of a sample, it was desirable to use oil immersion objectives with light microscope immersion oil, which had to be removed from the surface with a solvent. Glycerin is nearly as good and has the advantage that it can be washed off with water.

When illuminated with a mercury arc source, we could exploit the nonuniformity of the spectrum, which was dominated with blue and green spectral lines. Even the most

VetBooks.ir

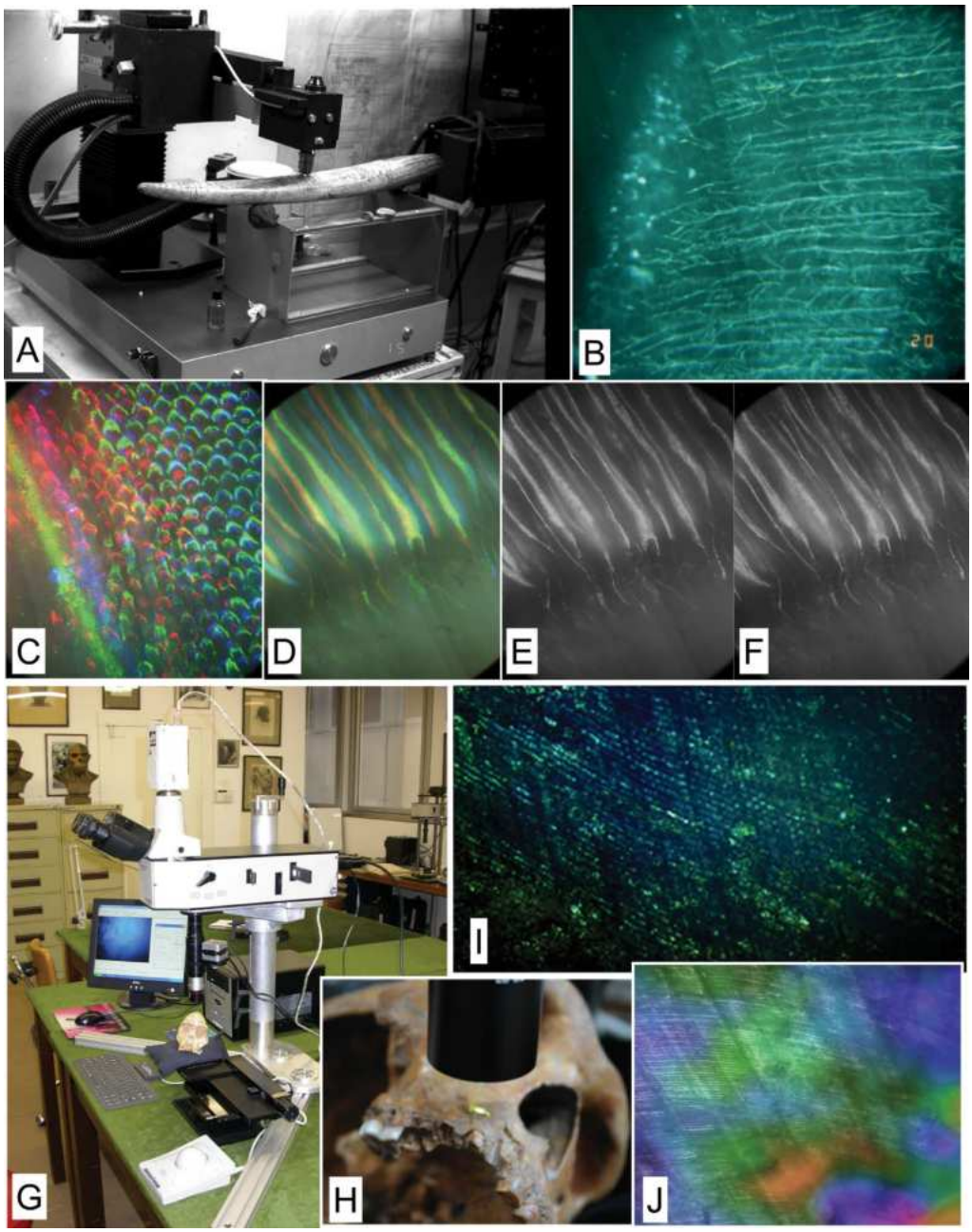


FIGURE 13.15 Confocal microscopy. A, The tandem scanning reflected light microscope (TSRLM) system constructed in Plzen in 1983 for the hard Tissue Unit at University College London (UCL) was designed to permit the examination of very large samples. The system is being used with a walrus tusk. B, Reflected light confocal image made with the Petran-Hadravsky TSRLM at UCL. Longitudinal ground section of human tooth root showing dentine tubules and their side branches. Toward the left is the granular layer of Tomes. Field height 71 µm. C, Reflected light confocal image made with the Petran-Hadravsky TSRLM at UCL in January 1984. *Paranthropus boisei* subsurface enamel in intact fossil tooth. Three images where focused at 10-µm red, 12-µm green and 14-µm blue below the enamel surface: color synthesized from three separate monochrome negatives. The lateral shift of the image of the prism boundary discontinuity illustrates the 3D paths of the prisms. Field height 74 µm. D–F: Show the same field. Reflected light confocal images made with the Petran-Hadravsky TSRLM at UCL in 1984. Longitudinal section (LS) surface of *Anchitherium aurelianense*, a fossil equid, tooth showing giant dentine tubules at the enamel-dentine junction (EDJ) with no terminal or side branches and enamel tubules. Field height 74 µm. D, Six images at 2-µm focus intervals are combined in a depth map in the color sequence red, yellow, green, cyan, blue and magenta. E and F, A stereo pair made by reprojecting the stack of images using ImageJ. G, The Bromage portable TSRLM set up at the University of the Witwatersrand, Republic of South Africa, Department of Anatomy, early hominin repository, imaging the Taung skull (*Australopithecus africanus*). H, The same portable TSRLM set up at the Natural History Museum, London, fossil hominin collections, imaging the Broken Hill 1 cranium (*Homo heidelbergensis/H. rhodesiensis*). I, Portable TSRLM below-surface reflection image of fractured *H. rudolfensis* (UR 501) enamel from northern Malawi, showing prisms, cross striations (daily secretory events) and striae of Retzius. Natural color resulting from the use of mercury arc lamp illumination. Field width 240 µm. J, Portable TSRLM through-focus image set over a field containing high topographic relief of *Paranthropus robustus* enamel showing prisms, regular Retzius lines and cross striations. All in-focus content was united in a single pseudocolor depth map image using Syncroscopy (Cambridge, UK) Auto-Montage software: deeper levels in blue, intermediate levels in green and nearest levels in orange. Field width 450 µm.

VetBooks.ir

expensive achromatic objectives have a significant longitudinal chromatic dispersion, and this TSRLM proved to be a most useful tool for inspecting lens properties. Because different colors are focused at different distances, we could simultaneously image two focal planes separated by ~1 µm in one recorded image. Using monochromatic light, through-focus series were profitably recorded at as little as 1-µm separation.

In a further development, we designed and constructed special objective lenses with extremely small front elements, for example, 2–3 mm in diameter in a high numerical aperture (NA) lens. This permitted approach to difficult regions in difficult samples. A typical commercially available objective might be 2 cm wide with a focal distance of 200 µm. We can omit any form of coverslip because immersion oil has the same refractive index as glass but, nevertheless, small physical size of the front objective is a major advantage in working with fossils.

In addition, we made some of these lenses have a high and linear longitudinal chromatic dispersion. This permitted the recording of an entire deep-focus range, rainbow-colored images in single frames on color film. With a binocular viewing head with prisms in opposite orientations for the two eyes, we could convert the live image into a real-time dynamic 3D image, the only instantaneous gratification 3D confocal imaging method (Maly and Boyde 1994).

A "one-sided" TSM, including a polarizer and one-quarter lambda plate to eliminate unwanted reflections and, thus, to image in reflected circularly polarized light, is probably the world's best configuration. It typically gives subsurface information from up to 50 µm in fossil samples. In a single-sided TSRLM, the pinholes are only used on one side of the disk; i.e., the same pinhole is used to define the illuminated spot and the collection from that identical volume. This presents the difficulty that intense reflection from the surface of the disk can overwhelm the real imaging information. To overcome this, a polarizing filter is used in illumination with a one-quarter lambda plate in or on the objective. Since we are dealing with reflected light, the same one-quarter lambda plate is oriented effectively at 90° and the same applies to the polarizing filter, which is now, as it were, the analyzer. This is the exact specification to achieve circularly polarized light illumination, which is simply the best mode of illumination of general application for the study of mineralized tissues.

Bromage constructed a portable TSRLM with this configuration (Figure 13.15F–I), designed to be carried around the world to fossils sitting in remote museums and locations (Bromage et al. 2004, 2005). This unique instrument, specifically designed for the job, is, in our modest opinions, the very best microscope ever invented for work with fossil hard tissue histology (Figure 13.15G–I).

Reflected Light Metallurgical Microscope

Reflected light microscopy (RLM) of polished or nearly flat sample surfaces is an excellent and almost universally applicable method for fossil studies. Only the sample surface morphology is examined, but because we only look at the surface, we have in effect the infinitely thin optical section, which satisfies the fundamental requirement for a stereological approach to sample analysis. Indeed, stereology was invented in the context of examining rock surfaces. The disadvantages only stem from the limited depth of field with suitable high NA objectives, but this may be overcome by taking through-focus image sets, which are then processed by computer to produce a perfect in-focus image. Excellent software was available for this purpose from Syncroscopy called Auto-Montage.

Rotating Condenser Aperture

Oblique illumination in the LM can be used to produce direct view 3D images. Several methods have been published (Greenberg and Boyde 1997) and all depend on using one part of the total cone of illumination. The simplest is simply to obscure half the illumination aperture for one member of a stereoscopic pair, followed by the other. By using, for example, one-quarter of the illuminating cone, and rotating this around the optic axis, a 3D impression will be obtained either by direct viewing down the microscope, or with a video image on a monitor. Binocular microscopes with two long working distance objectives will be used by everyone for low magnification 3D inspection. The advantage of oblique illumination through a single objective is that 3D imaging is available at much higher NA, magnifications and resolutions.

Polarized Light Microscopy (PLM)

PLM is in great favor with current and paleo bone and tooth histologists. Certainly, beautiful images are produced, but it has to borne in mind that a thick physical section (more than 50 µm) is a retardation plate of undefined thickness and optical properties, which will seriously interfere with interpretation of the resultant image. One will find instances in the literature where the use of a single polarizing filter is described as "PLM". In fact, here the sample is the second polarizing filter, which would otherwise be called the analyzer. This interference is an insoluble problem.

PLM should involve the use of two crossed linearly polarizing filters and a thin sample. Colors can be introduced by using the standard one-half lambda plate, commonly called the "sensitive tint". If the sample shows color without any additional retardation plate, it is simply too thick. We conclude that this method is overused and unjustified in a large number of cases. The solution is to use a reflection confocal microscopic method, which automatically gives optical section properties so that the total thickness of the sample does not matter.

Flatbed Scanner: 3D Images

Flatbed scanners are extremely cheap and typically generate a pixel size ≤20 µm. Thus, any reasonably flat sample can be documented as a colored image. However, these devices also

VetBooks.ir

produce excellent 3D imaging, either of rough surfaces or subsurface layers of translucent samples. Simply record one image and then move the sample 1 inch (ca. 2.5 cm) in the direction along the line axis of the scanner. These two images are a stereoscopic pair. With smaller movement increments, you can generate a through-tilt sequence for obtaining a 3D image. To enable the movement without "moving" the sample, it is placed on a thin acetate sheet.

BSE-SEM "at Bad Vacuum", High Chamber Pressure, No Coating and Instant Gratification SEM

Modern SEMs offer the option of imaging uncoated insulating samples by using what can most simply be described as a "bad" vacuum; i.e., a relatively high pressure in the vacuum chamber. This is a huge advantage when examining fossils. No preparation is needed whatsoever. This should lead museum curators to be generous with their permissions. This approach works best with back-scattered electrons (BSE-SEM) and has the following advantages: (1) with polished flat-surface samples, atomic number (compositional) contrast will be obtained, demonstrating differences in mineral concentration or composition and (2) with samples having topographic relief, different detector segments can be used to emulate illumination with light from contrasting directions to generate genuine colored SEM images with valuable information in the pseudocolor (Boyde 2003, 2019).

Faxitron™ Point Projection Digital Microradiography

Soft x-ray images are very simply produced with a Faxitron™ apparatus. At the maximal projective magnification, the pixels equate to 10 µm at the sample scale. It is brilliant for imaging either sections or none-too-thick whole samples.

Scanning X-Ray Microscopy

Scanning x-ray microscopy is a technique in which a thin sample is scanned mechanically relative to a narrow, monochromatic soft x-ray beam (Elliott et al. 1992). Resolution is limited by the beam diameter. Quantitative results are obtained very simply because the method is self-calibrating. It can be used for, among other things, preparations prepared for LM on either glass or plastic slides.

X-Ray Microtomography (XMT or µCT)

X-ray microtomography (XMT) is now so common in the study of fossil mineralized tissues that it may be regarded as routine. An issue is how to correlate XMT with other microscopic methods. Here we make the strong recommendation that any sample preparation for any other method of microscopy, for example, confocal LM or BSE-SEM, be done before the XMT. Then, in the 3D rendering, the block surface is automatically the same surface as seen with the other methods (Zikmund et al. 2012).

Simultaneous-Inductively Coupled Plasma-Mass Spectrometry (si-LA-ICP-MS)

In simultaneous-inductively coupled plasma-mass spectrometry (si-LA-ICP-MS) the complete relevant inorganic spectrum of elements from lithium ($Z = 3$) to uranium ($Z = 92$) is simultaneously detected and measured in parts per million, billion and trillion. The focused beam can be on spots or track widths as little as 2 µm and up to a maximum of 160 µm. This method enables isotope identification in the context of imaging information obtained with any of the methods considered above.

Summary

Biological hard tissue structures can only be fully comprehended through a thorough understanding of developmental mechanisms. This is possible to achieve through the study of living animals. We limit our coverage here to dental tissues in extant mammals. Opportunities for the study of fossils will necessarily be limited. Nevertheless, understanding some of the ranges of possibilities found today in the extraordinarily wide variety of dental tissue structure, arrangements, attachment mechanisms and tooth morphology within mammals will further our curiosity into what may have happened, and evolutionary sequences, in the distant past.

Most knowledge of dental histology is in fact limited to human teeth and to those of common laboratory rodents. These are so profoundly different within themselves that it is a wonder that so much attention is paid to the latter. But this concentration has blinkered vision, and we hope to open a view to a wider horizon.

We describe the nature of mammalian tooth germs; the embryonic origins of dentine, enamel and cementum; and the basics of tooth form. We explore the histology of dental tissues in respect to variability in cell behaviors, matrix and mineralization strategies, their periodic and sometimes aperiodic growth expression and the adaptive structural patterns that emerge. We also relay the advantages and pitfalls of preparation and imaging methods particularly useful to the paleohistologist.

We are particularly focused on the sophisticated heterodont dentitions of mammals among the gnathostomes. Yet, the diversity explored here is expected to be a vast underestimate of the real variability among living and extinct mammals. Ample room exists for advancement. In particular, comparative studies of cementum are practically nonexistent, but such investigations would contribute the necessary integration with form and function of dentine and enamel histology in relation to tooth form. Although paleohistologists have concentrated their attentions principally on bone, more research on dental hard tissues will be required to firm up the connections bridging the locomotor and feeding niches of toothed animals.

VetBooks.ir

Acknowledgments

We thank the many colleagues who have helped us over the years in many different ways including Sheila Jones, Maureen Arora, Roy Radcliffe, Keith Lester, Mikael Fortelius, Lawrence Martin, Rodrigo Lacruz, Meike Kohler, Friedemann Schrenk, Ottmar Kullmer, Oliver Sandrock, Igor Smolyar, Haviva Goldman, Shannon McFarlin, Johanna Warshaw, Alejandro Perez-Ochoa, Russell Hogg, Jeremy Tausch, Bin Hu, Paola Cerrito and Lou Terracio

REFERENCES

Andresen, V. 1898. Die Querstreifung des Dentins. *Deutsche Monatsschrift fuer Zahnheilkunde* 16: 386–389.

Berkovitz, B. K., et al. 2017. *Oral Anatomy, Histology and Embryology E-Book*. London: Elsevier Health Sciences.

Bishop, M. A. and A. Boyde. 1986. Distribution of capillaries in relation to the life cycle of odontoblasts in the rat incisor - the fate of the pulp at the incisal end. *Anat. Embryol.* 175: 189–198.

Boyde, A. 1964. *The Structure and Development of Mammalian Enamel*, PhD thesis, Department of Anatomy, The London Hospital Medical College, University of London, London. https://qmro.qmul.ac.uk/xmlui/handle/123456789/1410

Boyde, A. 1968. Dental histology of the ziphioid whales: a new calcified tissue (vasocementum). In *Les Tissus Calcifiés*, Milhaud, G. et al. eds. Paris: Société d'édition d'enseignement supérieur.

Boyde, A. 1969. Electron microscopic observations relating to the nature and development of prism decussation in mammalian dental enamel. *Bull. Groupe Int. Rech. Sci. Stomatol.* 12: 151–207.

Boyde, A. 1978. Development of the structure of the enamel of the incisor teeth in the three classical subordinal groups of the rodentia. In *Development, Function and Evolution of Teeth*, chap 4, Butler, P. M. and K. A. Joysey eds., 43–58. London: Academic Press.

Boyde, A. 1980. Histological studies of dental tissues of Odontocetes. *In Growth of Odontocetes and Sirenians: Problems in Age Determination: Proceedings of the International Conference on Determining Age of Odontocete Cetaceans [and Sirenians]*, Perrin W. F. and A. C. J. Myrick eds., 65–87. La Jolla, California, September 5–19, 1978. International Whaling Commission.

Boyde, A. 1984a. Airpolishing effects on enamel, dentine, cement and bone. *Brit. Dent. J.* 156: 287–291.

Boyde, A. 1984b. Dependence of rate of physical erosion on orientation and density in mineralised tissues. *Anat. Embryol.* 170: 57–62.

Boyde, A. 1989. Enamel. In *Handbook of Microscopic Anatomy*, A. Oksche and L. Vollrath eds. Berlin: Springer Verlag.

Boyde, A. 2003. Improved digital SEM of cancellous bone: scanning direction of detection, through focus for in-focus and sample orientation. *J. Anat.* 202: 183–194.

Boyde, A. 2018. Evaluation of laser ablation microtomy for correlative microscopy of hard tissues. *J. Microsc.* 271: 17–30.

Boyde, A. 2019. Scanning electron microscopy of bone. In *Bone Research Protocols. Methods in Molecular Biology*, A. Idris ed. New York: Humana Press.

Boyde, A. and M. Fortelius. 1986. Development, structure and function of rhinoceros enamel. *Zool. J. Linn. Soc.* 87: 181–214.

Boyde, A. and K. S. Lester. 1967a. Electron microscopy of resorbing surfaces of dental hard tissues. *Z. Zellforsch.* 83: 538–548.

Boyde, A. and K. S. Lester. 1967b. The structure and development of marsupial enamel tubules. *Z. Zellforsch.* 82: 558–576.

Boyde, A. and L. B. Martin. 1984. A non-destructive survey of prism packing patterns in primate enamels. In *Tooth Enamel,* Vol. IV, R. W. Fearnhead and S. Suga eds. Amsterdam: Elsevier.

Boyde, A. and L. B. Martin. 1987. Tandem scanning reflected light microscopy of primate enamel. *Scan. Microsc.* 1: 1935–1948.

Boyde, A., et al. 1961. Application of the scanning electron-probe x-ray microanalyser to dental tissues. *J. Ultrastruct. Res.* 5: 201–207.

Boyde, A., et al. 1983. Tandem scanning reflected light microscopy of internal features in whole bone and tooth samples. *J. Microsc.* 132: 1–7.

Bromage, T. G. 1985. Systematic inquiry in tests of negative/positive replica combinations for SEM. *J. Microsc.* 137: 209–216.

Bromage, T. G. 1987. The scanning electron microscopy/replica technique and recent applications to the study of fossil bone. *Scan. Microsc.* 1: 607–613.

Bromage, T. G. and M. N. Janal. 2014. The Havers-Halberg oscillation regulates primate tissue and organ masses across the life history continuum. *Biol. J. Linn. Soc.* 112: 649–656.

Bromage, T. G., et al. 2004. Nuevas posibilidades en la investigación Palaeantropologica utilizando un microscopio confocal patátil. In *Miscelánea en Homenaje a Emiliano Aguirre, Volumen III, Paleoantropología*, Baquedano E. and S. R. Jara eds. Madrid: Museo Arqueologico Regional.

Bromage, T. G., et al. 2005. Portable confocal microscope reveals fossil hominid microstructure. *Microsc. Anal.* 19: 5–7.

Bromage, T. G., et al. 2009. Lamellar bone is an incremental tissue reconciling enamel rhythms, body size, and organismal life history. *Calcif. Tissue Int.* 84: 388–404.

Bromage, T. G., et al. 2011. Enamel-calibrated lamellar bone reveals long period growth rate variability in humans. *Cells Tissues Organs* 194: 124–130.

Carter, J. T. 1922. On the Structure of the Enamel in the Primates and some other Mammals. *J. Proc. Zool. Soc. Lond.* 92: 599–608.

Cerrito, P., et al. 2020. Parturitions, menopause and other physiological stressors are recorded in dental cementum microstructure. *Sci. Rep.* 10: 5381.

Chadwick, D. J. and G. Cardew. 1997. *Dental Enamel, Ciba Symposium Foundation* West Sussex: John Wiley & Sons Ltd.

Dean, M. C. 1987. Growth layers and incremental markings in hard tissues; a review of the literature and some preliminary observations about enamel structure in *Paranthropus boisei*. *J. Human Evol.* 16: 157–172.

Elliott, J. C., et al. 1992. X-ray microtomographic studies of bones and teeth. In *X-Ray Microscopy III*, Michette, A. G., G. R. Morrison, and C. J. Buckley eds. Berlin Heidelberg: Springer-Verlag.

Fortelius, M. 1985. Ungulate cheek teeth: developmental, functional, and evolutionary interrelations. *Acta Zool. Fenn.* 180: 1–76.

Gordon, L. M., et al. 2015. Dental materials. Amorphous intergranular phases control the properties of rodent tooth enamel. *Science* 347: 746–750.

Greenberg, G. L., and A. Boyde. 1997. Convenient and controllable direct-view 3D imaging in conventional optical microscopes: approaches via illumination and inspection. *Proc. R. Microsc. Soc.* 32: 87–100.

Grue, H. and B. Jensen. 1979. Review of the formation of incremental lines in tooth cementum of terrestrial mammals [age determination, game animal, variation, sex, reproductive cycle, climate, region, condition of the animal]. *Danish Rev. Game Biol. (Denmark)* 11: 1–48.

Havers, C. 1691. *Osteologia Nova: Or, Some New Observations of the Bones, and the Parts Belonging to them: With the Manner of their Accretion and Nutrition*. London: Samuel Smith.

Hillson, S. 2005. Teeth. In *Cambridge Manuals in Archaeology*, 2nd ed., Barker G., ed. Cambridge, UK: Cambridge University Press.

Jones S. J. and A. Boyde 1974. Coronal cementogenesis in the horse. *Archs. Oral Biol.* 19: 605–614.

Jones, S. J. and A. Boyde. 1984. Ultrastructure of dentin and dentinogenesis. In *Dentin and Dentinogenesis*, Linde A. ed. Boca Raton, FL: CRC Press.

Jones S. J., et al. 1995. The rate of osteoclastic destruction of calcified tissues is inversely proportional to mineral density. *Calcif. Tissue Int.* 56: 554–558.

Kagerer, P. and G. Grupe. 2001. Age-at-death diagnosis and determination of life-history parameters by incremental lines in human dental cementum as identification aid. *Forensic Sci. Int.* 118: 75–82.

Klevezal, G. A. and S. E. Kleinenberg. 1969. *Age determination in mammals from annual layers in teeth and bone*. Jerusalem Israel Program for Scientific Translations.

Klevezal, G. A. and N. I. Shishlina. 2001. Assessment of the season of death of ancient human from cementum annual layers. *J. Archaeol. Sci.* 28: 481–486.

Koenigswald, W. von. 1982. Enamel structure in the molars of Arvicolidae (Rodentia, Mammalia), a key to functional morphology and phylogen. In *Teeth: Form, Function and Evolution*, Kurtén B. ed. New York: Columbia University Press.

Koenigswald, W. von. 2004. Enamel microstructure of rodent molars, classification, and parallelisms, with a note on the systematic affiliation of the enigmatic Eocene rodent *Protoptychus*. *J. Mammal. Evol.* 11: 127–142.

Korvenkontio, V. A. 1934. Mikroskopische Untersuchungen an Nagerincisiven unter Hinweis auf die Schmelzstruktur der Backenzähne. Histologisch-phyletisch Studie. *Ann. Bot. Soc. Zool.-Bot. Fenn. "Vanamo"* 2: 1–274.

Lacruz, R. S., et al. 2012. Requirements for ion and solute transport, and pH regulation during enamel maturation. *J. Cell. Physiol.* 227: 1776–1785.

Lester K. S. and A. Boyde. 1968. The surface morphology of some crystalline components of dentine. In *Dentine and Pulp*, Symons N. B. B. ed., 197–219. Edinburgh, Dundee: Livingstone.

Lester K. S. and A. Boyde. 1970. Scanning electron microscopy of developing roots of molar teeth of the laboratory rat. *J. Ultrastruct. Res.* 33: 80–94.

Lester, K. S. and A. Boyde. 1987. Relating developing surface to adult ultrastructure in chiropteran enamel by scanning electron microscopy. *Adv. Dental Res.* 1: 181–190.

Listgarten, M. A. and I. M. Shapiro. 1974. Fine structure and composition of coronal cementum in guinea-pig molars. *Arch. Oral Biol.* 19: 679–696.

Maly, M and A. Boyde. 1994. Real time stereoscopic confocal reflection microscopy using objective lenses with linear longitudinal chromatic dispersion. *Scanning* 16: 187–192.

Moya-Costa, R., et al. 2019. Structure and composition of the incisor enamel of extant and fossil mammals with tooth pigmentation. *Lethaia* 52: 370–388.

Perrin, W. F. and A. C. Myrick, Jr. eds. 1980. Growth of odontocetes and sirenians: problems in age determination: Proceedings of the International Conference on Determining Age of Odontocete Cetaceans [and Sirenians]. *Reports of the International Whaling Commission*, Special Issue 3. Cambridge: International Whaling Commission.

Petran, M., et al. 1985. The tandem-scanning reflected light microscope. Part 1—the principle and its design. *Proc. R. Microsc. Soc.* 20: 125–139.

Petran, M., et al. 1990. Direct view confocal microscopy. In *Confocal Microscopy*, T. Wilson ed. London: Academic Press.

Pfefferkorn, G. and A. Boyde. 1974. Review of replica techniques for scanning electron microscopy. *Scan. Electron Microsc.* 1974: 75–82.

Retzius, A. 1837. Bemerkungen über den innern Bau der Zähne, mit besonderer Rücksicht auf dem im Zahnknochen vorkommenden Röhrenbau. *Arch. Anat., Physiol. Wissenschaft. Med.* 1837: 486–566.

Scheffer, V. B. and A. C. Myrick. 1980. A review of studies to 1970 of growth layers in the teeth of marine mammals. In *Growth of Odontocetes and Sirenians: Problems in Age Determination: Proceedings of the International Conference on Determining Age of Odontocete Cetaceans [and Sirenians]*, Perrin W. F. and J. A.C. Myrick eds., 51–64. *Reports of the International Whaling Commission*, Special Issue 3. Cambridge: International Whaling Commission.

Schour, I. and H. G. Poncher. 1937. Rate of apposition of enamel and dentin, measured by the effect of acute fluorosis. *Am. J. Dis. Child.* 54: 757–776.

Shellis, R. P. 1983. Structural organization of calcospherites in normal and rachitic human dentine. *Arch. Oral Biol.* 28: 85–95.

Spiess, A. 1976. Determining season of death of archaeological fauna by analysis of teeth. *Arctic* 29: 53–55.

Thornton-Carter, J. 1922. On the structure of the enamel in the primates and some other mammals. *Proc. Zool. Soc. London* 92: 599–608. https://doi.org/10.1111/j.1096-3642.1922.tb02159.x

VetBooks.ir

Waugh, D. A., et al. 2018. Validation of Growth Layer Group (GLG) depositional rate using daily incremental growth lines in the dentin of beluga (*Delphinapterus leucas* (Pallas, 1776)) teeth. *PLoS One.* 13:e0190498

Wedel, V. L. 2007. Determination of season of death using dental cementum increment analysis. *J. Forensic Sci*. 52: 1334–1337.

Wen, X. and M. L. Paine. 2013. Iron deposition and ferritin heavy chain (Fth) localization in rodent teeth. *BMC Res. Notes*. 6: 1.

Zikmund, T., et al. 2012. Correlation between 3D imaging methods in studying bone architecture: SEM, microCT and confocal LM. *J. Anat*. 221: 86–86.

VetBooks.ir

Section V

Phylogenetic Diversity of Skeletal Tissues

VetBooks.ir



Taylor & Francis
Taylor & Francis Group
http://taylorandfrancis.com

14

Introduction

Michel Laurin

Considering the number of studies that present mutually incompatible results about vertebrate phylogenetic relationships, a concise presentation of the reference phylogeny used in this book is indispensable.

The phylogeny of basal chordates (Figure 14.1) follows Janvier (1996) except that, according to most recent molecular phylogenies and a recent morphology-based paleontological study by Miyashita et al. (2019), hagfishes and lampreys are considered to form a clade, the Cyclostomata. The position of chondrichthyans, nested within taxa formerly considered acanthodians, follows Maisey et al. (2017). Placoderm phylogeny follows Zhu et al. (2016) in suggesting that they are paraphyletic, whereas other studies suggest monophyly (e.g., King et al. 2017). The phylogeny of early stegocephalians (Figure 14.2) follows Marjanović and Laurin (2019), for whom lissamphibians are nested within lepospondyls. This is a controversial issue, and many other studies support an origin among temnospondyls (e.g., Ruta and Coates 2007); however, the topology presented here is supported by various lines of evidence (Laurin et al. 2019). Early amniote phylogeny follows the long-accepted divisions between Synapsida and Sauropsida and Eureptilia and Parareptilia (e.g., Laurin and Reisz 1995), even though recent studies raise doubts about the validity or boundaries of these subdivisions (Laurin and Piñeiro 2017, 2018; MacDougall et al. 2018; Ford and Benson 2020). Therapsid phylogeny follows Sidor (2001), except for cynodonts, which follow Liu and Olsen (2010) (Figure 14.2). Basal diapsid phylogeny follows Neenan et al. (2013) and Simões et al. (2018). Thus, ichthyosaurs and sauropterygians are placed on the diapsid stem, even though the latter have often been considered lepidosauromorphs (e.g., Rieppel and Reisz 1999; Bickelmann et al. 2009). Ichthyosaurs have typically been placed on the

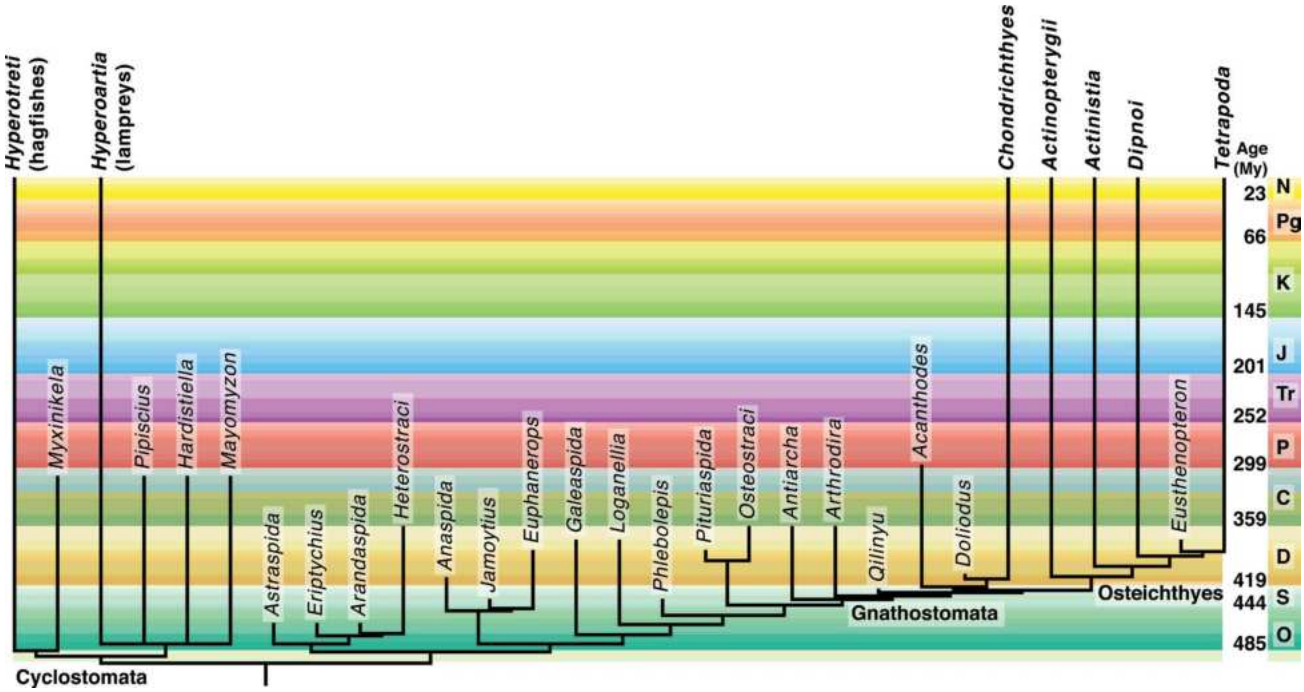


FIGURE 14.1 Vertebrate phylogeny. This whole tree is covered in chapter 15 on finned vertebrates. In conformity with Recommendation 6.1A of the PhyloCode (Cantino and de Queiroz 2020), which was implemented in April 2020 after decades of preparation (Laurin 2019), all taxon names are italicized (in this figure, in the next one, and in the captions), not only genus and species names. This convention has not been adopted in the main text to match the typographic convention used by the authors of other chapters of this book, most of whom were presumably unaware of this recommendation of the PhyloCode. Abbreviations of geological periods: C, Carboniferous; D, Devonian; J, Jurassic; K, Cretaceous; N, Neogene; P, Permian; Pg, Paleogene and Tr, Triassic.

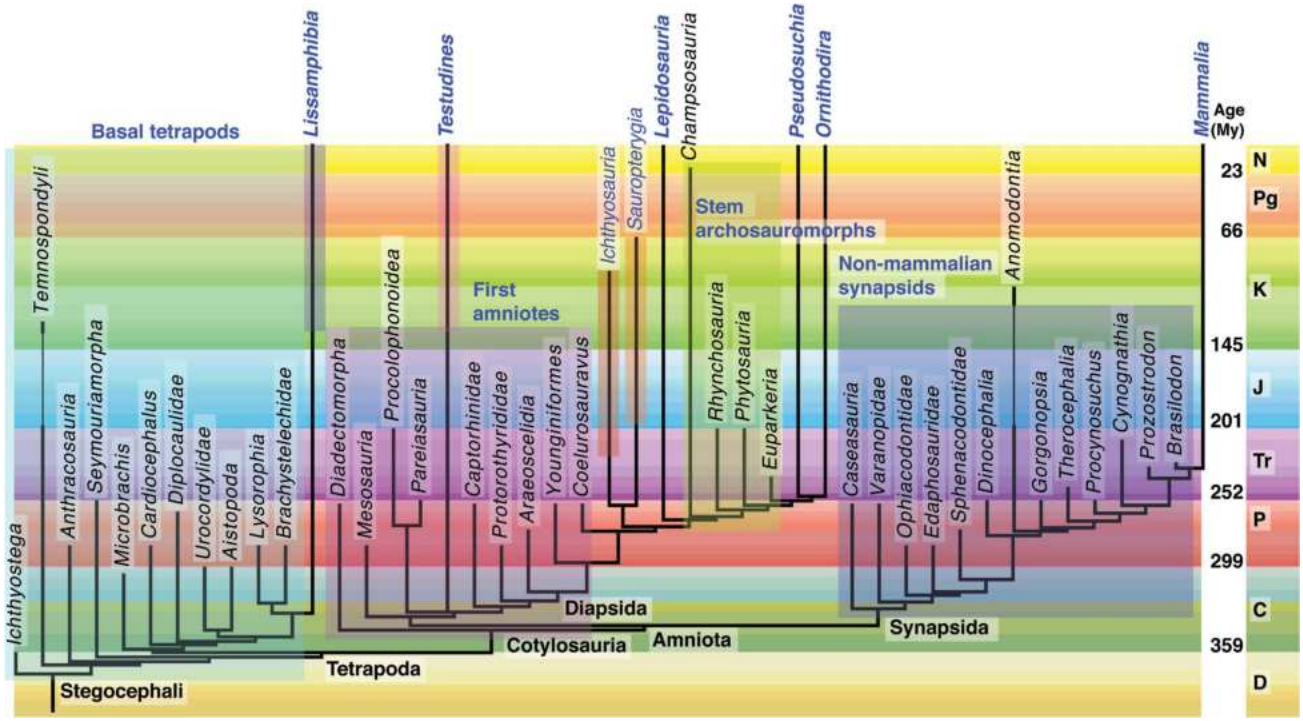


FIGURE 14.2 Stegocephalian phylogeny. The taxonomic coverage of the chapters is shown using polygons on the tree. When a chapter deals with a single terminal taxon, this taxon name is highlighted in blue (gray), rather than being repeated. Chapter 26 (*Crocodylomorpha*) is not shown, but this taxon fits within *Pseudosuchia*. The phylogenetic definitions of taxa that have been established under the PhyloCode have been used. Thus, *Tetrapoda* is restricted to the crown group and *Stegocephali* is used for a larger clade that includes all currently known limbed vertebrates. Abbreviations as in Figure 14.1.

diapsid stem (e.g., Bickelmann et al. 2009) and may form a clade with euryapsids (Simões et al. 2018).

Some chapters in this section (15, 16, 18, 22, 25, and 28) cover paraphyletic groups for practical reasons; they would have been far too long if they had dealt with clades. For instance, Archosauromorpha had to be split into three major chapters, two of which deal with clades (26, Crocodylomorpha; 27, Avemetatarsalia), whereas the other (25) deals with a paraphyletic taxon composed of stem archosauromorphs and early pseudosuchians (crurotarsans). This was required to summarize the abundant information on ornithodirans and crocodylomorphs, two clades with intensively studied, well-resolved phylogenies (Nesbitt 2011; Lee and Yates 2018).

The stratigraphic ranges were taken from the literature, and these account for some rare survivors that sometimes persisted in isolated areas, such as Australia. This is the case for the last, Cretaceous dicynodont (Thulborn and Turner 2003) and temnospondyl (Warren et al. 1991), which are geologically much younger than all their known close relatives. These ranges were transformed into absolute time using a recent geological timescale (Ogg et al. 2016).

REFERENCES

Bickelmann, C., et al. 2009. The Enigmatic Diapsid *Acerosodontosaurus piveteaui* (Reptilia: Neodiapsida) from the Upper Permian of Madagascar and the Paraphyly of ''Younginiform'' Reptiles. *Can. J. Earth Sci.* 46: 651–661.

de Queiroz, K. & Cantino, P. D. 2020. *International Code of Phylogenetic Nomenclature (PhyloCode): A Phylogenetic Code of Biological Nomenclature*. CRC Press, Boca Raton, Florida.

Ford, D. P. and R. B. Benson. 2020. The Phylogeny of Early Amniotes and the Affinities of Parareptilia and Varanopidae. *Nat. Ecol. Evol.* 4: 57–65.

Janvier, P. 1996. The Dawn of the Vertebrates: Characters Versus Common Ascent in the Rise of Current Vertebrate Phylogenies. *Palaeontology* 39: 259–287.

King, B., et al. 2017. Bayesian Morphological Clock Methods Resurrect Placoderm Monophyly and Reveal Rapid Early Evolution in Jawed Vertebrates. *Syst. Biol.* 66: 499–516.

Laurin, M. 2019. Développements Importants Pour Les *Comptes Rendus Palevol*: Nouveaux Rédacteurs Associés, Meilleur Facteur D'impact Et Entrée En Vigueur Du Phylocode/ Important Developments for the Comptes Rendus Palevol: New Associate Editors, Increased Impact Factor, and the Forthcoming Implementation of the Phylocode. *C.R. Palevol.* 18: 909–912.

Laurin, M. and G. Piñeiro. 2017. A Reassessment of the Taxonomic Position of Mesosaurs, and a Surprising Phylogeny of Early Amniotes. *Front. Earth Sci.* 5(88): 1–13.

Laurin, M. and G. Piñeiro. 2018. Response: Commentary: A Reassessment of the Taxonomic Position of Mesosaurs, and a Surprising Phylogeny of Early Amniotes. *Front. Earth Sci.* 6(220): 1–9.

Laurin, M. and R. R. Reisz. 1995. A Reevaluation of Early Amniote Phylogeny. *Zool. J. Linn. Soc.* 113: 165–223.

VetBooks.ir

Laurin, M., et al. 2019. What Do Ossification Sequences Tell Us About the Origin of Extant Amphibians? *PCI Paleontology*. DOI 10.1101/352609v3.

Lee, M. S. and A. M. Yates. 2018. Tip-Dating and Homoplasy: Reconciling the Shallow Molecular Divergences of Modern Gharials with Their Long Fossil Record. *Proc. R. Soc. Edin. B*285(1881): 20181071.

Liu, J. and P. Olsen. 2010. The Phylogenetic Relationships of Eucynodontia (Amniota: Synapsida). *J. Mammal. Evol.* 17: 151–176.

MacDougall, M. J., et al. 2018. Response: A Reassessment of the Taxonomic Position of Mesosaurs, and a Surprising Phylogeny of Early Amniotes. *Front. Earth Sci.* 6: 99.

Maisey, J. G., et al. 2017. Pectoral Morphology in *Doliodus*: Bridging the "Acanthodian"-Chondrichthyan Divide. *Am. Mus. Novit.* 3875: 1–15.

Marjanović, D. and M. Laurin. 2019. Phylogeny of Paleozoic Limbed Vertebrates Reassessed through Revision and Expansion of the Largest Published Relevant Data Matrix. *PeerJ* 6: e5565.

Miyashita, T., et al. 2019. Hagfish from the Cretaceous Tethys Sea and a Reconciliation of the Morphological–Molecular Conflict in Early Vertebrate Phylogeny. *Proc. Natl Acad. Sci. USA* 116: 2146–2151.

Neenan, J. M., et al. 2013. European Origin of Placodont Marine Reptiles and the Evolution of Crushing Dentition in Placodontia. *Nat. Commun.* 4(1621): 1–7.

Nesbitt, S. J. 2011. The Early Evolution of Archosaurs: Relationships and the Origin of Major Clades. *Bull. Am. Mus. Nat. Hist.* 352: 1–292.

Ogg, J. G., et al. 2016. *A Concise Geologic Time Scale: 2016*. Amsterdam: Elsevier.

Rieppel, O. and R. R. Reisz. 1999. The Origin and Early Evolution of Turtles. *Annu. Rev. Ecol. Syst.* 30: 1–22.

Ruta, M. and M. I. Coates. 2007. Dates, Nodes and Character Conflict: Addressing the Lissamphibian Origin Problem. *J. Syst. Palaeontol.* 5: 69–122.

Sidor, C. A. 2001. Simplification as a Trend in Synapsid Cranial Evolution. *Evolution* 55: 1419–1442.

Simões, T. R., et al. 2018. The Origin of Squamates Revealed by a Middle Triassic Lizard from the Italian Alps. 557(7707): 706.

Thulborn, T. and S. Turner. 2003. The Last Dicynodont: An Australian Cretaceous Relict. *Proc. R. Soc. Lond. B* 270: 985–93.

Warren, A. A., et al. 1991. An Early Cretaceous Labyrinthodont. *Alcheringa* 15: 327–32.

Zhu, M., et al. 2016. A Silurian Maxillate Placoderm Illuminates Jaw Evolution. *Science* 354(6310): 334–336.

VetBooks.ir

15

Finned Vertebrates

Jorge Mondéjar-Fernández and Philippe Janvier

CONTENTS

Introduction 294
The Clades (Or Presumed Clades) 302
Myllokunmingiida 302
Euconodonta 302
Cyclostomi 302
Euphaneropida 302
Jamoytiida 303
Anaspida 304
Pteraspidomorphi 304
Thelodonti 307
Galeaspida 308
Osteostraci 309
Pituriaspida 311
Gnathostomata 311
Chondrichthyes 311
Acanthodii 311
Placodermi 313
Osteichthyes 315
Conclusion 318
References 319

Introduction

The earliest descriptions of vertebrate hard tissues were based on those of extant animals, which were used to define such hard tissues as bone, cartilage, dentine and enamel, and were later compared to hard tissues of supposedly related fossil vertebrates. This entailed the rise of microscopical techniques (e.g., polished sections, glass-mounted thin sections) developed by geologists and paleobotanists in the first half of the 19th century. Paleohistology first became widely used to try to identify and classify the earliest vertebrates known at that time; that is, the Paleozoic "fishes" (in the broad sense of vertebrates that are not tetrapods) (Figures 15.1–15.5). Most of them had odd morphologies and an extensively mineralized dermal skeleton; therefore, they were primarily compared to extant "armored" fishes, such as catfishes and sturgeons. In the early 20th century, paleontologists began to explore the detailed anatomy of these fishes, notably using the destructive technique of serially ground sections (e.g., Stensiö 1927, 1964). Thanks to this method, Stensiö (1927) demonstrated that one group of these armored vertebrates, the osteostracans, possessed a median dorsal nasohypophysial opening and only two vertical semicircular canals of the labyrinth, like lampreys, thereby confirming Cope's (1889) intuition that osteostracans were indeed jawless and allied to lampreys. Cope (1889) coined the name Ostracodermi for these fossil taxa that had no evidence of jaws or teeth, although they possessed bone and dentinous tissues in the dermal skeleton.

The phylogenetic position of "ostracoderms" has been a matter of heated debate during most of the 20th century, notably because of the question of their relationships to the major living vertebrate clades (reviewed in Janvier 1996a, b, 2008, 2015). Kiaer (1924) regarded some of them (anaspids, osteostracans) as stem cyclostomes and others (heterostracans) as jawless stem gnathostomes, respectively. In contrast, Stensiö (1927) considered anaspids and osteostracans stem lampreys because of their small, median dorsal nasohypophysial opening, and heterostracans as stem hagfishes, essentially by default, because of the absence of this character, associated with the absence of jaws (Stensiö's [1927] so-called

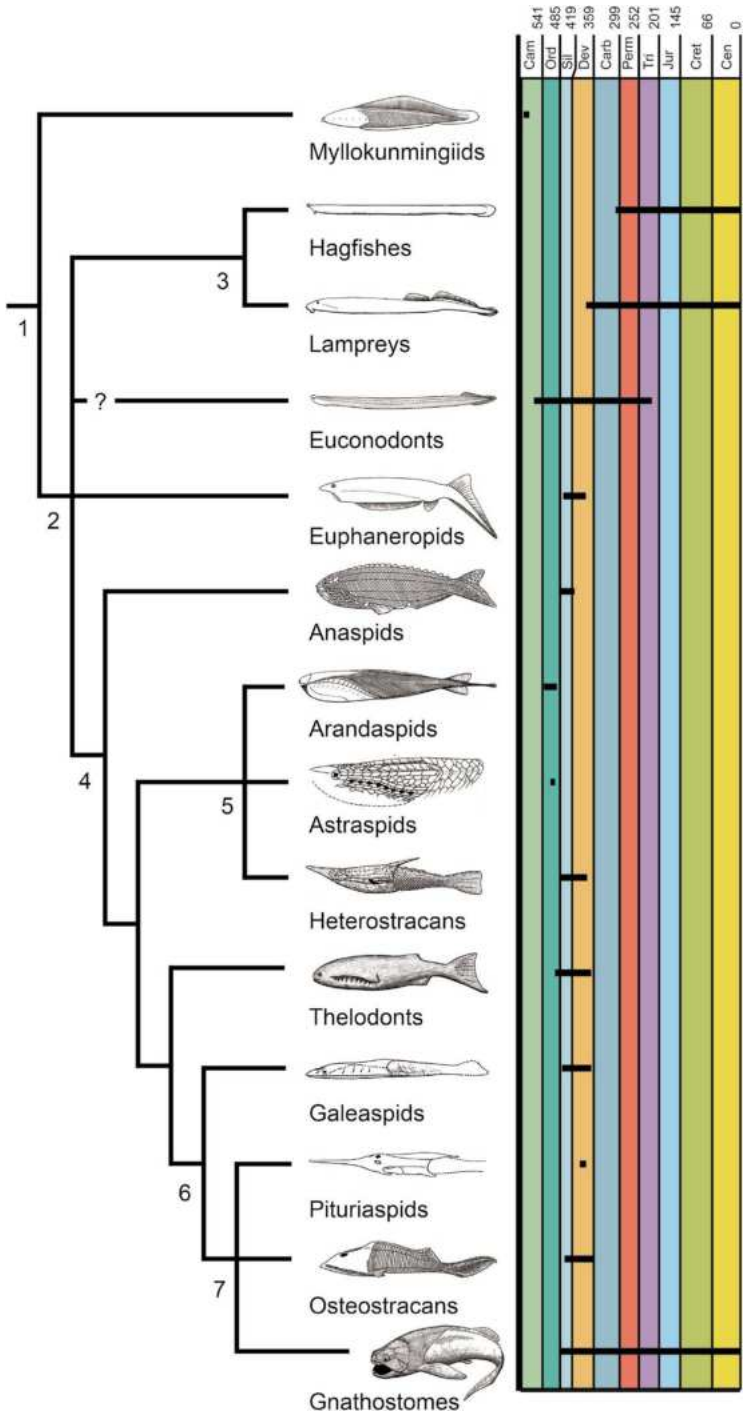


FIGURE 15.1 The currently accepted tree of the major extant and fossil vertebrate taxa (left side) and their distribution in geologic time (right side). Major histological characters are indicated at nodes: 1, total group vertebrates (migrating and delaminating neural crest cells); 2, crown group vertebrates (apatite mineralization in some tissues); 3, cyclostomes (production of keratinized epidermal tissues, localized calcified cartilage); 4, total group osteognathostomes (production of either acellular or cellular bone made of bioapatite in the dermal skeleton); 5, pteraspidomorphs (acellular bone, or aspidine, in an extensive dermal skeleton); 6, unnamed taxon (mineralized perichondral lamella); 7, unnamed taxon (perichondral bone, cellular bone in dermal skeleton).

"diphyletic origin of the cyclostomes") (Figure 15.6). The bases for these early hypotheses were essentially some anatomical characters of the oral, nasal and hypophysial regions, which were nevertheless poorly documented at that time. The debate went on until the 1980s. Kiaer's (1924) hypothesis of a closer heterostracan-gnathostome relationships was generally favored because of the assumption of the presence of paired olfactory organs in the two groups (the "diplorhinal" condition) (Heintz 1962). Nevertheless, with the rise of phylogenetic systematics and the consideration of more

VetBooks.ir

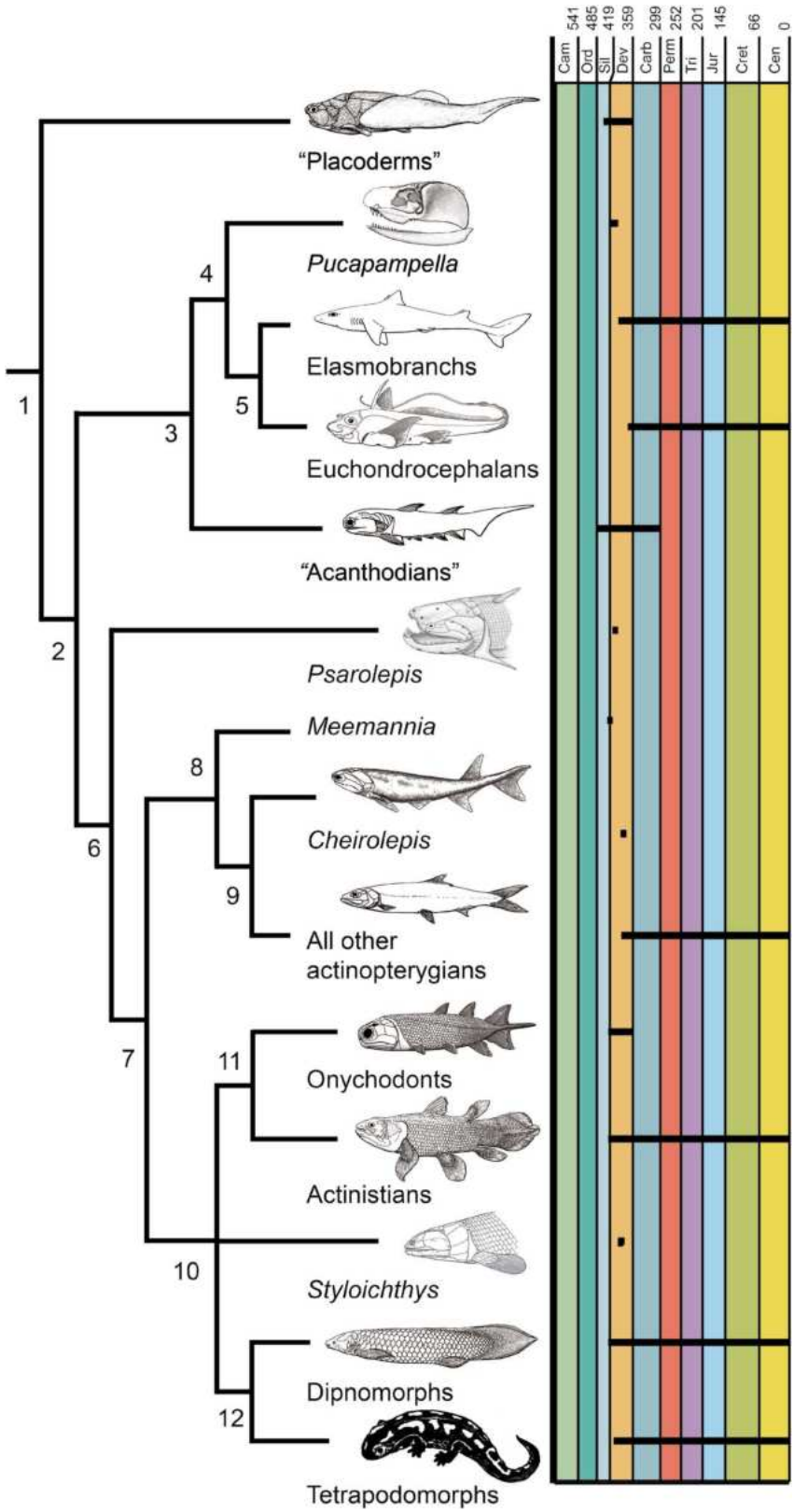


FIGURE 15.2 Simplified tree of the total group gnathostomes (jawed vertebrates) (left side) and their distribution in geologic time (right side). Major histological characters are indicated at nodes: 1, total group gnathostomes (jaws and teeth); 2, crown-group gnathostomes; 3, total group chondrichthyans (micromeric or mesomeric dermal skeleton); 4, euchondrichthyans (placoid scales, extensive tessellated calcified cartilage); 5, crown group chondrichthyans (lyodont teeth); 6, total group osteichthyans (endochondral bone); 7, crown group osteichthyans (multilayered cosmine, plicidentine, presence of enamel in the teeth); 8, total group actinopterygians; 9, unnamed taxon (multilayered enamel = ganoine, acrodine tooth cap); 10, total group sarcopterygians; 11, total group coelacanthiforms; 12, rhipidistians (single-layered cosmine).

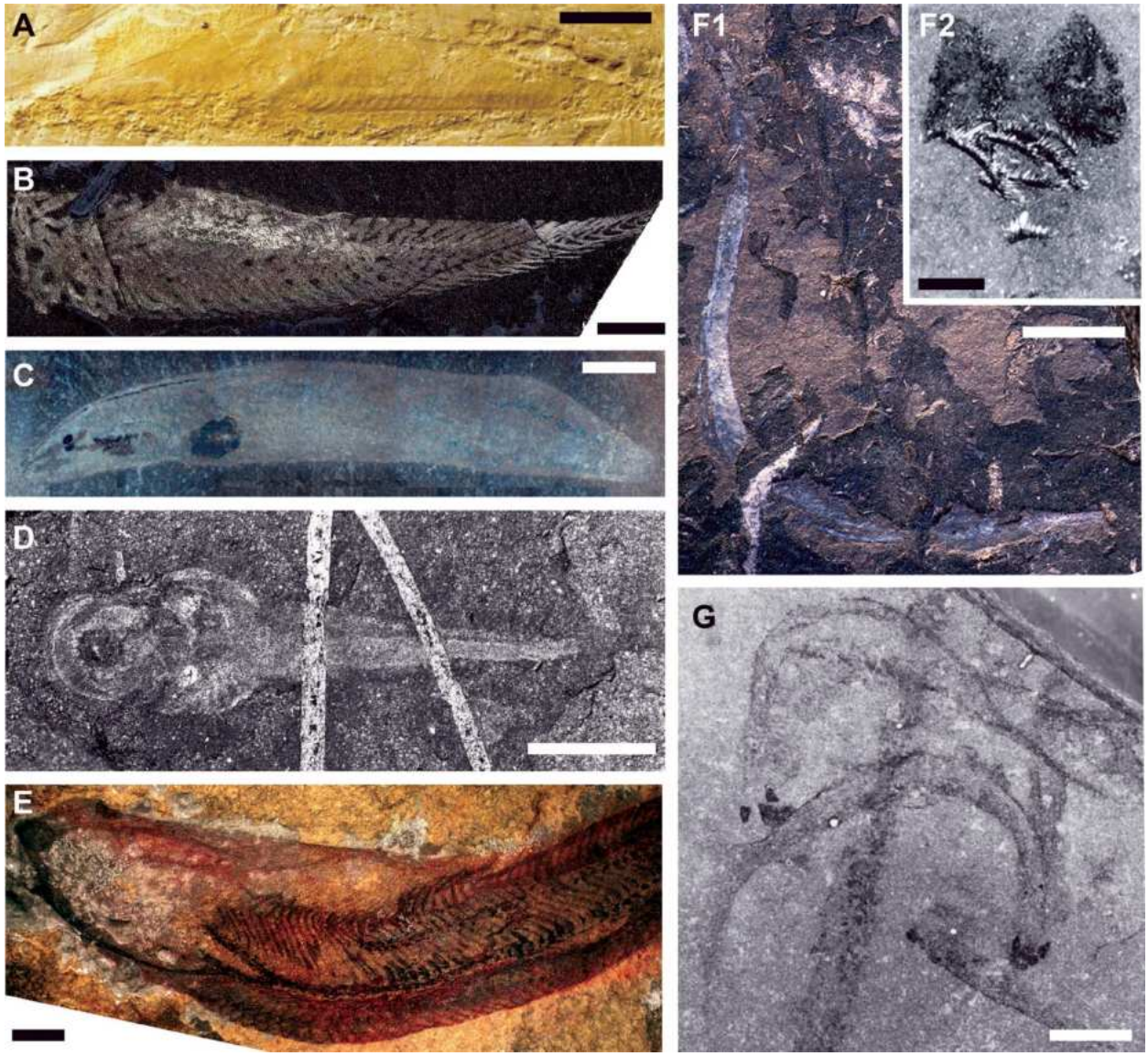


FIGURE 15.3 Early vertebrates. A, The myllokunmingiid *Haikouichthys ercaicunensis* (ELI-0001001 172), Lower Cambrian, China (after Shu et al. 2003, figure 1J). Scale bar = 5 mm. B, *Metaspriggina walcotti* (USNM198612), Lower Cambrian of the United States (after Conway-Morris and Caron 2014, ED figure 1G). Scale bar = 5 mm. C, The putative hagfish *Myxinikela siroka* (NEIU MCP 126), Pennsylvanian (Upper Carboniferous) of the United States (after Donoghue and Keating 2014, figure 2F). Scale bar = 10 mm. D, The lamprey *Priscomyzon riniensis* (AM5750), Upper Devonian of South Africa (after Gess et al. 2006, figure 1B). Scale bar = 10 mm. E, The jamoytiid *Jamoytius kerwoodi* (NHM PI1284a), Lower Silurian of Scotland (after Sansom et al. 2010, plate 1). Scale bar = 10 mm. F1 and F2, The conodont *Clydagnathus windsorensis* (IGSE 13821), Mississippian (Lower Carboniferous) of Scotland. Inset (F2) illustrates the feeding apparatus (after Donoghue and Keating 2016, figure 2L, M). Scale bar = 5 mm (F1) and 500 um (F2). G, The euphaneropid *Achanarella trewini* (NEWHM1999.H1801), Middle Devonian of Scotland (after Newman 2002, figure 2). Scale bar = 10 mm.

characters, paleontologists generated a series of trees (Janvier 1981, 1984) (Figure 15.6) where "ostracoderms" appeared as a paraphyletic array of clades in which hagfishes, lampreys and gnathostomes were independently rooted, and where gnathostomes were the sister group of the clade that included osteostracans, anaspids and lampreys (Stensiö's "cephalaspidomorphs"), all sharing notably muscularized paired fins. Shortly thereafter, using the first computer phylogenetic programs, Gagnier (1993a, b) proposed a radically new tree, in which cyclostomes, whether mono- or paraphyletic, were all basal to "ostracoderms" and gnathostomes (Figure 15.1), with osteostracans as the sister group to gnathostomes (Forey 1995), and all "ostracoderms" and gnathostomes essentially characterized by the presence of at least a mineralized dermal skeleton (Hennig's "Osteognathostomata") (Mickoleit 2004). This position of "ostracoderms" as jawless stem gnathostomes was further supported by more extensive character analyses (Janvier 1996b; Donoghue et al. 2000), as cyclostome monophyly became more and more strongly supported by molecular sequence data (Kuraku et al. 1999; Heimberg et al. 2010).

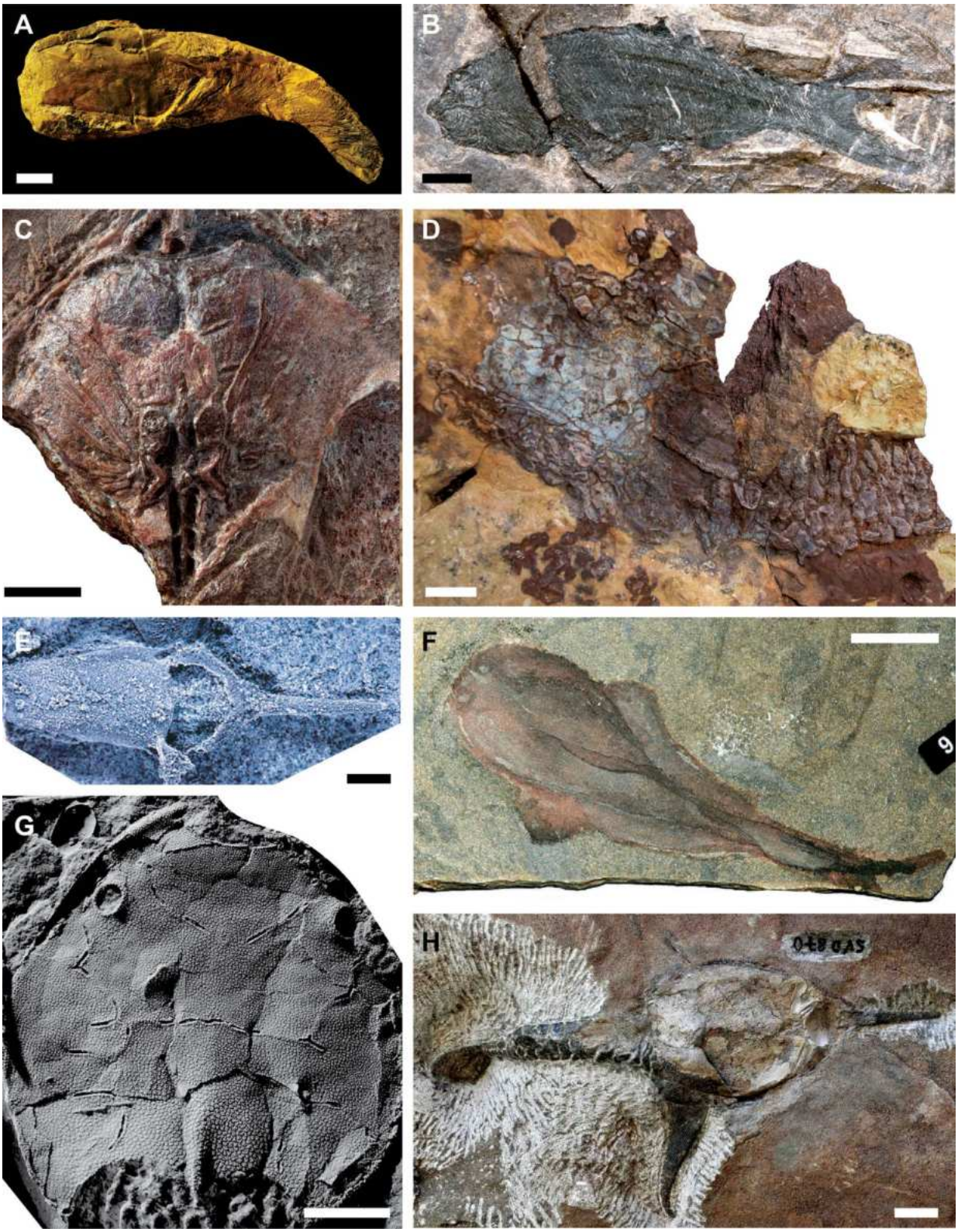


FIGURE 15.4 "Ostracoderms". A. The arandaspid *Sacabambaspis janvieri* (MNHAO 02), Middle Ordovician of Bolivia. Scale bar = 10 mm. B, The anapsid *Birkenia elegans* (NHMUK P10141), Lower Silurian of Scotland (after Donoghue and Keating 2014 figure 2B). Scale bar = 10 mm. C, The osteostracan MNHN (SVD1001), Lower Devonian of Spitzbergen. Scale = 5 mm. D, The astraspid *Astraspis desiderata* (BU 2472), Upper Ordovician of the United States (courtesy of I. Sansom). Scale bar = 10 mm. E, The pituriaspid *Pituriaspis*, Lower Devonian of Australia (after Young and Lu 2020, figure 2B). Scale bar = 10 mm. F, The thelodont *Loganellia scotica* (GLAHMV8304), Lower Silurian of Scotland (after Donoghue and Keating 2014, figure 2C) Scale bar = 10 mm. G, The galeaspid *Polybranchiaspis liaojaoshanensis* (BT 246), Lower Devonian of Vietnam. Scale bar = 10 mm. H. The heterostracan *Doryaspis nathorsti* (MNHN SVD870), Lower Devonian of Spitsbergen. Scale bar = 10 mm.

VetBooks.ir

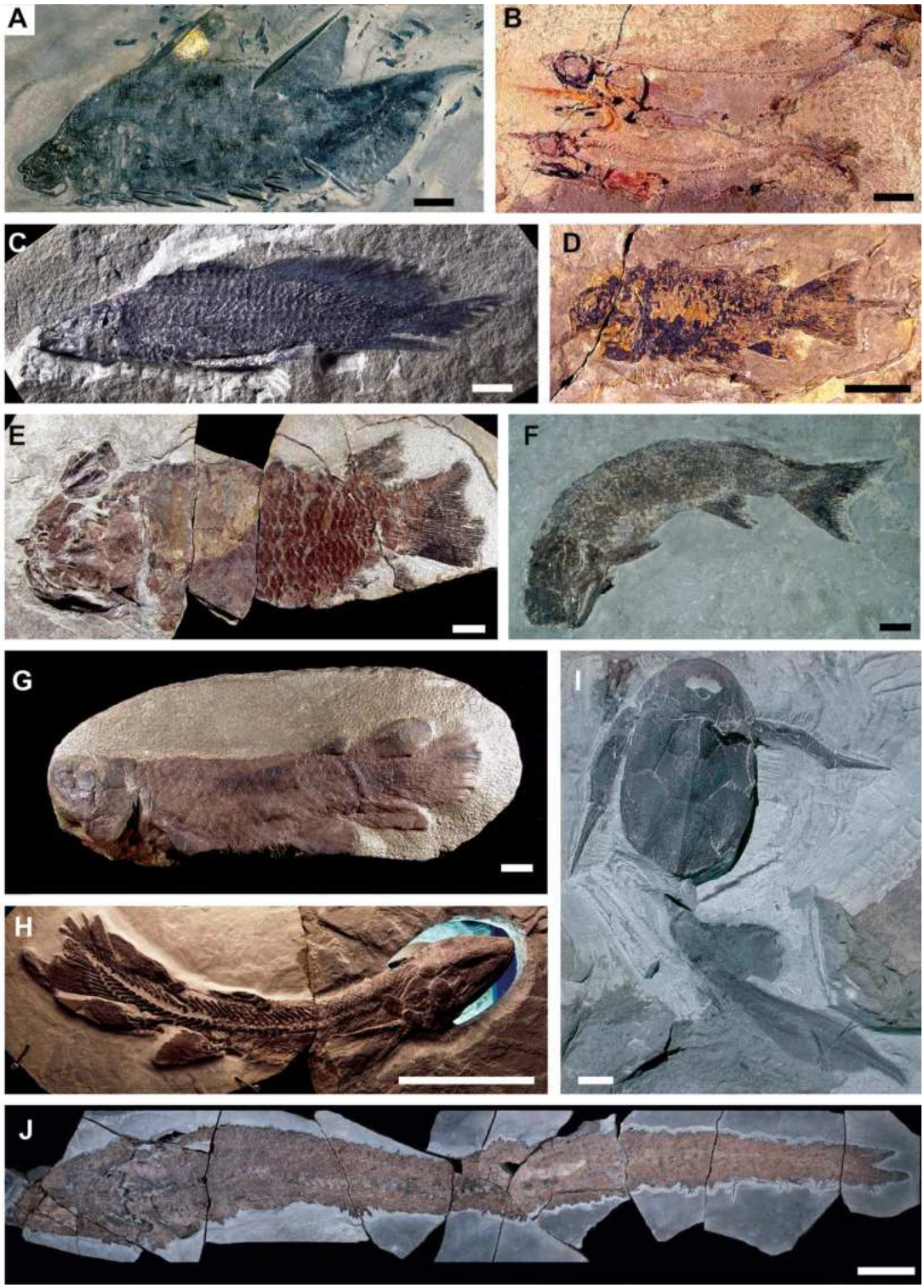


FIGURE 15.5 Gnathostomes. A, The acanthodian *Brochoadmones milesi* (UALVP 41495), Lower Devonian of Canada (after Hanke and Wilson 2006, figure 3C). Scale bar = 1 cm. B, The chondrichthyan *Falcatus falcatus* (MV 5385 and MV 5386), Mississippian (Lower Carboniferous) of the United States (courtesy of R. Lund). Scale bar = 1 cm. C. The dipnoan *Scaumenacia curta* (MNHN.F.1968.8.2), Upper Devonian of Canada. Scale bar = 1 cm. D, The onychodont *Strunius walteri* (MB.f.5224), Upper Devonian of Germany. Scale bar = 1 cm. E, The actinistian *Miguashaia bureaui* (MHNM 06-494), Upper Devonian of Canada (courtesy of R. Cloutier). Scale bar = 1 cm. F. The actinopterygian *Cheirolepis canadensis* (MHNM 05-71), Upper Devonian of Canada (courtesy of R. Cloutier). Scale bar = 1 cm. G, The porolepiform *Holoptychius jarviki* (AMNH 11593), Upper Devonian of Canada (courtesy of R. Cloutier). Scale bar = 1 cm. H, The osteolepiform *Eusthenopteron foordi* (CMNH 8158), Upper Devonian of Québec (Canada) (courtesy of R. Cloutier). Scale bar = 10 cm. I, The placoderm *Bothriolepis canadensis* (MHNM 02-2676) from the Upper Devonian of Canada (courtesy of R. Cloutier). Scale bar = 1 cm. J, The elpistostegalian *Elpistostege watsoni* (MHNM 06-2067), Upper Devonian of Canada (courtesy of R. Cloutier). Scale bar = 10 cm.

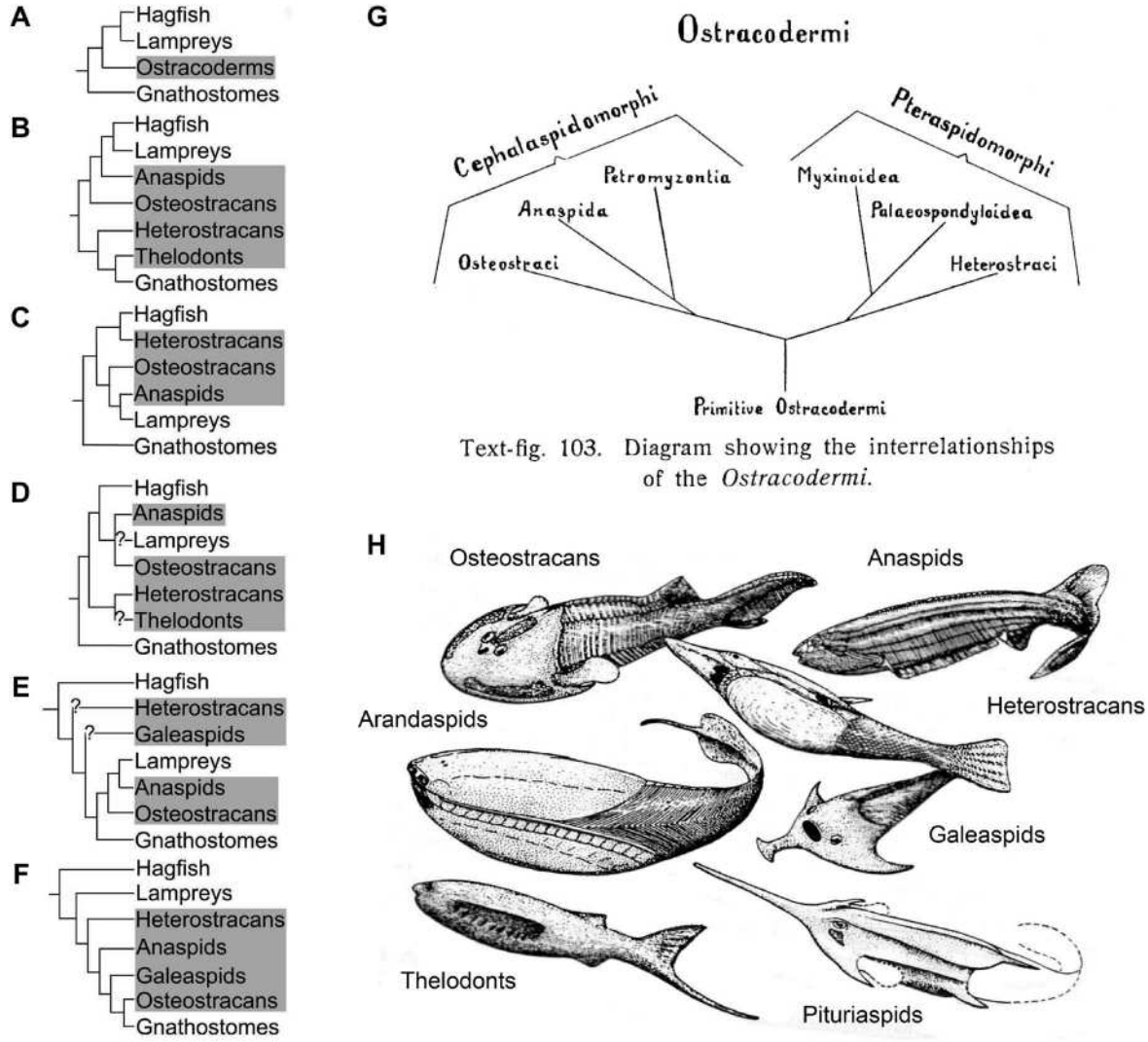


FIGURE 15.6 Interrelationships of the major living and fossil vertebrate clades and the position of "ostracoderms". A-F, series of trees showing the interrelationships of the vertebrates including "ostracoderms" published during the 19th and 20th century. A, After Cope 1889. B, After Kiaer (1924) and most other authors of the 20th century. C, After Stensiö (1927, and see also facsimile of his original figure in G). D, After Moy-Thomas and Miles (1971). E, after Janvier (1978). F, After Janvier (1996a, Gagnier 1993a, b, and Gess et al. (2006). After Janvier 2008. G, Facsimile of the original diagram by Stensiö 1927, illustrating the so-called diphyletic origin of the cyclostomes. H, Reconstructions of representatives of the major Ordovician to Devonian "ostracoderm" taxa. See Figure 15.1 for their distribution through time.

Since the beginning of the 20th century, a large number of essentially soft-bodied organisms have been described from the Lower Cambrian Lagerstätte of either the Burgess Shale (Canada) or Chengjiang (China), some of which were considered possible vertebrate relatives because of their vaguely segmented body or because of possible serially arranged gill openings. An iconic example is *Pikaia*, long regarded as a possible cephalochordate (see historical background of this interpretation in Conway-Morris and Caron 2012). Nevertheless, the presence of a segmented trunk mesoderm remains one of the most commonly invoked arguments to refer these often enigmatic fossils to the vertebrates. Many of these peculiar Cambrian organisms, such as the vetulicolians and yunnanozoans, are now regarded as stem deuterostomes (Gee 2001, 2018), although *Cathaymyrus* may be a stem cephalochordate (Shu et al. 1996). However, only the Myllokunmingiids (*Myllokunmingia*, *Haikouichthys*) and *Metaspriggina* (Shu et al. 1999; Conway-Morris and Caron 2014) are unanimously accepted as Cambrian stem vertebrates, although their nonmineralized endoskeleton is still poorly known (Janvier 2015). It was once suggested that these taxa could be stem cyclostomes on the basis of very tenuous character analyses, but a position as stem vertebrates remains most likely.

The current vertebrate tree (Figure 15.1) including the major jawless taxa seems to be relatively stable given the currently available characters. However, some of them clearly deserve further scrutiny, such as the histological data from the mineralized tissues and the rare data from exceptionally preserved soft tissues, which new technologies now allow us to investigate much better (e.g., Keating and Donoghue 2016; Qu et al. 2017; see also Table 15.1).

VetBooks.ir

TABLE 15.1

Diversity and Phylogenetic Distribution of the Calcified Tissues in Vertebrates

		Dermoskeleton						
				Bone		Endoskeleton		
Taxon		**Enamel/oid**	**Dentine**	**Structure**	**Cellularity**	**Cartilage**	**Bone**	**Scales**
Myllokunmingiida		–	–	–	–	?	–	–
Euconodonta		Enamel?	Dentine?	?	?	–	–	–
Cyclostomi	Myxinoidea	–	–	–	–	"Soft"/"hard" cartilage	–	–
	Petromyzontida	–	–	–	–	"Soft"/"hard" Calcified cartilage		–
Euphaneropida		–	–	–	–	Calcified cartilage	–	–
Jamoytiida		?	?	?	?	–	–	–
Anaspida		Enameloid	Spheritic dentine	Vascular (reduced) and parallel-fibered (aspidine/ isopedine?)	Acellular	–	–	Micromeric Monodontode
Pteraspidomorphi	Astraspida	Enameloid	Orthodentine	Cancellar (aspidine) and lamellar (isopedine)	Acellular	Calcified cartilage	–	Micromeric Polyodontode
	Arandaspida	Enameloid	Orthodentine	Cancellar (aspidine) and lamellar (isopedine)	Acellular?	–	–	Micromeric Polyodontode
	Heterostraci	Enameloid	Orthodentine	Cancellar (aspidine) and lamellar (isopedine)	Acellular	–	–	Micromeric Polyodontode
Thelodonti		Enameloid	Orthodentine	Bone of attachment	Acellular	–	–	Micromeric Monodontode
Galeaspida		–	–	Lamellar (galeaspidine)	Acellular	Calcified cartilage	–	Micromeric
Osteostraci		Enameloid	Mesodentine	Vascular and lamellar (isopedine)	Cellular/ acellular	Calcified cartilage	Perichondral bone	Micromeric Polyodontode
Pituriaspida		?	?	?	?	?	?	?
Placodermi		Enameloid/ none	Semidentine/ orthodentine/ none	Vascular and pseudo-lamellar?	Cellular	Calcified cartilage	Perichondral/ endochondral bone?	Micromeric Polyodontode
Acanthodii		Enameloid	Meso/ orthodentine	Pseudolamellar	Cellular	Calcified cartilage	–	Micromeric Polyodontode
Chondrichthyes		Enameloid	Mesodentine	Bone of attachment	Cellular	Calcified prismatic cartilage	Perichondral bone (reduced)	Micromeric Poly/ monodontode
Osteichthyes	Actinopterygii	Enamel (multilayered = ganoine)/ none	Orthodentine/ none	Vascular (reduced) and pseudolamellar	Cellular	Calcified cartilage	Perichondral and endochondral bone	Macromeric Polyodontode
	Sarcopterygii	Enamel/none	Orthodentine/ none	Vascular and lamellar (isopedine)	Cellular	Calcified cartilage	Perichondral and endochondral bone	Macromeric Polyodontode

VetBooks.ir

The Clades (Or Presumed Clades)

Here we will follow the order in which the taxa appear in the tree in Figure 15.1 and 15.2, which roughly reflects the order of their divergence, from the oldest to the most recent.

Myllokunmingiida

Myllokunmingiids are known from the famous Lower Cambrian (335- and 310-My-old, respectively) "Konservat-Lagerstätten" of Chengjiang (China) and the Burgess Shale (Canada); that is, fossil sites that preserve nonmineralized soft tissues, usually in the form of "compressions". In fact, these are collapsed soft-bodied organisms sealed on the bottom by bacterial films. The vertebrate affinity of myllokunmingiids is suggested by the series of postcephalic V- or W-shaped myomeres, a series of cephalic gills with filaments, imprints of paired eyes and olfactory organs, and traces of median fins supported by radials. Only *Metaspriggin*a and *Haikouichthys* (Figure 15.3A, B) display series of apparently sclerotinized endoskeletal elements in the gill apparatus and median fin radials, but their histology remains unknown, and they may well be cartilaginous or collagenous. Currently, Myllokunmingiids are regarded as the sister group of all other vertebrates because they apparently lack any of the derived features that characterize either the cyclostomes or gnathostomes, such as a complex "lingual apparatus", jaws, and dermal skeleton (Figure 15.1).

Euconodonta

Euconodonts are part of the Conodonta, a very large group known from the Upper Cambrian to the Upper Triassic (ca. 500–240 My) and long known exclusively by minute tooth or comb-shaped denticles made of calcium phosphate, similar to the dentine and enamel of vertebrate odontodes. The affinities of euconodonts were an enigma until the discovery of articulated body fossils preserved as imprints and associated with assemblages of conodont denticles of euconodont type in the Carboniferous (Briggs et al. 1983; Aldridge et al. 1993; Donoghue et al. 2000). This revealed that the "conodont animal" possessed chevron-shaped myomeres, median fin radials and large anterior eyes; that is, characters that strongly suggested their vertebrate affinity (Figure 15.3F1). The interpretation of euconodonts as vertebrates has raised heated debate during the last 20 years (e.g., Turner et al. 2010; Blieck et al. 2011; Schultze 1996) and this ended with the demonstration that conodont growth is at odds with that of vertebrate odontodes, because they grew in an opposite way (Murdock et al. 2013). It is provisionally concluded that euconodonts are actually vertebrates, but that their denticles are convergent with the odontodes of the total-group gnathostomes. They may be an early offshoot of the cyclostomes, possibly allied to hagfishes (Goudemand et al. 2011), whose feeding apparatus would be functionally compatible with that of the known euconodont assemblages (Figure 15.3F2).

Cyclostomi

The cyclostomes include two extant taxa, hagfishes (Myxinoidea or Hyperotreti) and lampreys (Petromyzontida or Hyperoartia), and a small number of fossil taxa that are only preserved in Konservat-Lagerstätte, essentially of Devonian (Gess et al. 2006), Carboniferous (Bardack and Zangerl 1968; Bardack and Richardson 1977; Bardack 1991; Janvier 1996a), and Cretaceous (Chang et al. 2006, 2014) ages (369-, 300- and 110-My-old, respectively). The early fossil lampreys are clearly identified by their oral disk (or "sucker") strengthened by an annular cartilage, but generally lack clear evidence of keratinous teeth, which may, however, be preserved sometimes in the form of impressions (Gabbott et al. 2016; Janvier and Sansom 2015) (Figure 15.3C, D). Cyclostomes display two different types of cartilage: the "soft cartilage" and "hard cartilage", which depend on their respective composition in collagen. Hard cartilage contains small chondrocytes surrounded by a large amount of extracellular matrix, whereas soft cartilage contains large, hypertrophic chondrocytes. Collagen 2 and 1 are component of the soft cartilages, but not of hard ones. Soft cartilages are more prone to decay, but this must be taken with reservations, depending on the processes of preservation involved in the sediment (Sansom et al. 2010, 2013). Some cases of calcification of the cartilage in lampreys have been mentioned (although not studied in detail) in living specimens (Bardack and Zangerl 1971) and can occur *in vitro* (Langille and Hall 1993) in a phosphate-saturated environment. A Cretaceous lamprey displays traces of calcified cartilage with large chondrocytic spaces in the annular and subocular cartilages (P. Janvier, pers.obs.)

Euphaneropida

Euphaneropids are known from the Silurian and Devonian (ca. 380–420 Mya) and were once referred to as "naked anaspids" because of their overall anapsid-like morphology, notably their strongly hypocercal tail and elongate "branchial basket". They are entirely devoid of a mineralized dermal skeleton, but many large (and presumably aged) specimens have a mineralized endoskeleton, in the form of calcified cartilage with large chondrocytic spaces enclosed by a thin "shell" of calcium phosphate (Janvier and Arsenault 2007) (Figure 15.7). Again, the most complete euphaneropid specimens come from the Devonian Konservat-Lagerstätten of Miguasha (Canada), in which soft tissues are preserved in pyrite, thanks to biofilms, in a quiet and reducing benthic environment (Chevrinais et al. 2018). Euphaneropids have a somewhat lamprey-like vertebral column made of arcualia, large calcified fin supports, and large calcified radials in both median (anal, caudal) and paired fins. The skull is composed of several large plates that are suggestive of the tectal cartilages of lampreys, and the branchial apparatus is made up of sinuous branchial arches that meet ventrally in a series of copular elements that may have supported a tongue-like structure (Figure 15.7B, C). Euphaneropids also possess a rounded annular cartilage that may support their close relationships to lampreys (Figure 15.7D, E). Currently, euphaneropids are considered either the

VetBooks.ir

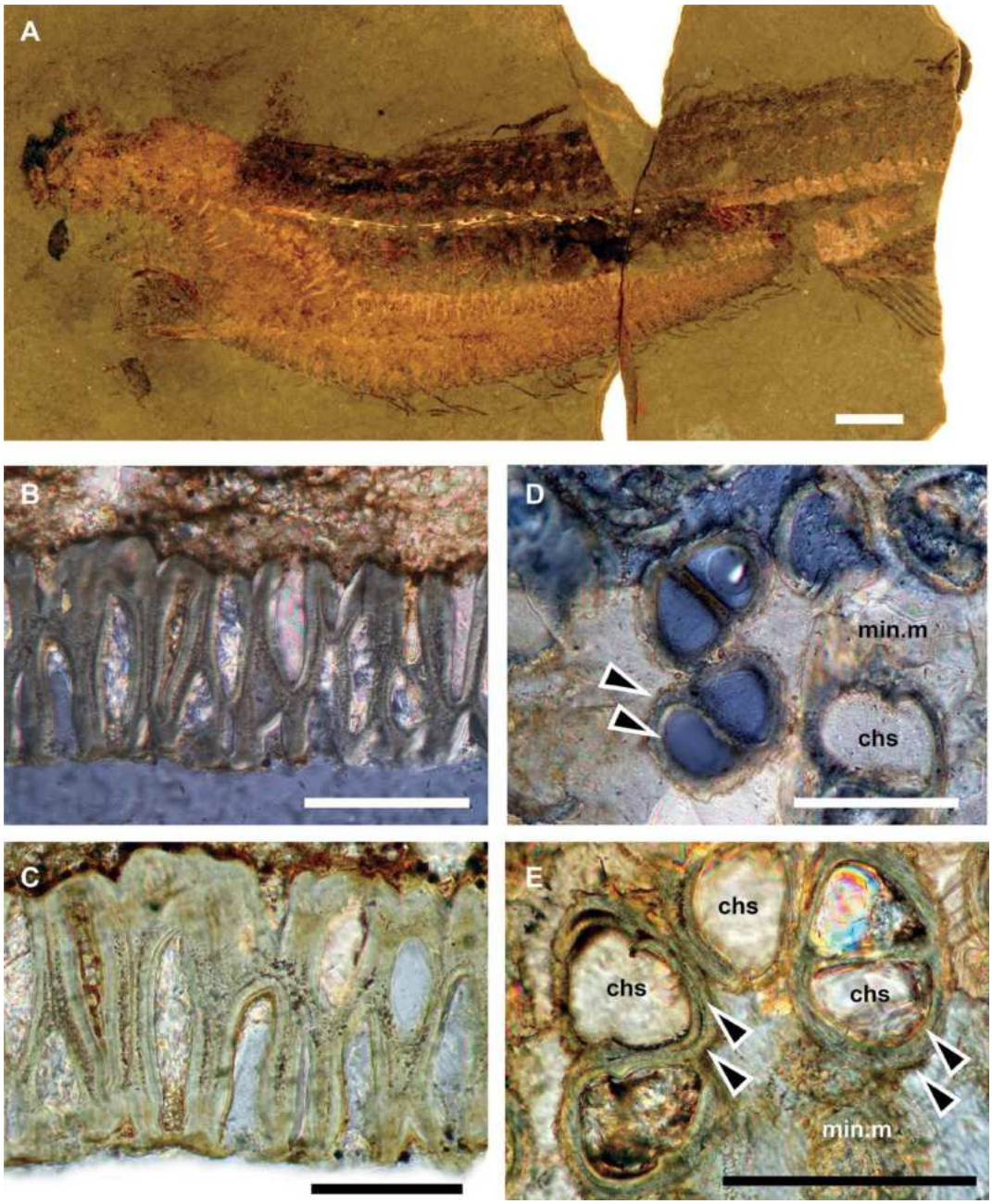


FIGURE 15.7 Histology of *Euphanerops*. A, The euphaneropid *Euphanerops longaevus* (MHNM 01-123), Upper Devonian of Canada. Scale bar = 10 mm. B and C, Sections through "gill rods". Scale bars = 100 µm. D and E, Sections through a "copular element". Scale bars = 100 µm. Arrowheads indicate growth lines. Abbreviations: chs, chondrocytic spaces; min.m, mineralized matrix.

sister group to cyclostomes (Janvier 2015) or a highly derived form of anaspids with a secondarily regressed dermoskeleton (Sansom et al. 2010; Keating and Donoghue 2016). The long enigmatic Middle Devonian fish-like fossil *Achanarella* is now proven to be a juvenile euphaneropid (Figure 15.3G).

Jamoytiida

The Jamoytiida are essentially known from the Silurian (ca. 438 Mya). *Jamoytius kerwoodi*, long considered as a potential "vertebrate ancestor" (White 1946), then as a "naked anaspid" (Ritchie 1968, 1984), is now proven to possess thin mineralized scales of unknown histology (Sansom et al. 2010). A peculiar result of this recent revision of *Jamoytius* is the total absence of scales on the head and tail. These authors consider *Jamoytius* the sister group of euphaneropids, both nested among anaspids. *Jamoytius* strongly differs from *Euphanerops* by its much shorter branchial apparatus, which comprises only 10 pairs of gill openings, and the absence of well-developed median fins (Figure 15.3E).

Anaspida

The Anaspida are known from the mid-Silurian to the Lower Devonian (ca. 430-410 Mya). They possess an extensive dermal skeleton covering the head and body and a long slanting series of gill openings (Figure 15.4B) (Blom 2012). However, anaspids possess no mineralized endoskeleton, and their internal anatomy is only inferred from the morphology of the dermal plates covering the head and shoulder girdle, such as the presence of a median dorsal nasohypophysial opening (Figure 15.6H). The flank scales of anaspids are characteristically elongated and were long said to contain no dentine. However, recent investigations have shown that the superficial layer of the scales is made up of spheritic dentine covered with a thin enameloid layer and rests on a basal layer of parallel-fibered acellular bone that contains a canal network (Keating and Donoghue 2016), an arrangement that is regarded by these authors as derived from a generalized three-layered condition through the early loss of an osteonal middle layer of vascular bone (Figures 15.8 and 15.12).

Pteraspidomorphi

Pteraspidomorphs are a very large group of armored jawless vertebrates, including arandaspids, astraspids and heterostracans (Figures 15.4A, D, H and 15.9–15.11), but the monophyly of the group is still unclear. The taxon is named after the Devonian heterostracan *Pteraspis*, which illustrates the basic anatomy of the group; that is, a "headshield" composed of several paired and unpaired plates that cover the brain, sensory capsules and branchial apparatus, posteriorly followed by generally polygonal scales covering the body and tail (Janvier 1996a). The tail consists of several lobes arising from a hypocercal axial lobe (Figures 15.4H and 15.6H). The internal surface of the headshield plates often displays impressions of the underlying organs, notably the brain, olfactory and optic capsules, vertical semicircular canals of the labyrinth and gill pouches that, in heterostracans, opened to the exterior by a single laterally or dorsally placed common exhalent branchial opening (Figure 15.6H). The lower lip of the mouth was covered ventrally by a series of oral plates for grazing but that did not "bite" against any dorsal structure (*contra* Halstead 1973). Therefore, pteraspidomorphs were essentially grazers or suspension feeders (Purnell 2002), but nothing suggests that their feeding apparatus prefigures gnathostome jaws.

Janvier (1996a) gathered most heterostracans in a large ensemble referred to as "higher heterostracans", which includes the Cyathaspidiformes and the Pteraspidiformes (Denison 1964, 1970, Blieck 1984), two once supposedly monophyletic taxa (Figure 15.12). Cyathaspidiforms are characterized by a superficial dermal bone ornamentation that is composed of longitudinal, more or less parallel ridges of orthodentine capped by an enameloid layer and separated by grooves devoid of dentine (Figure 15.9). The margins of the dentine ridges are gently crenulated. The dorsal headshield of cyathaspidiforms consists of a single plate composed of the fusion of several units, or epitega, that remain separate in pteraspidiforms. In some cyathaspidiforms, notably the amphiaspidids, all the plates of the dermal armor are fused into a single "box" and the entire head is flattened, suggesting benthic or burrowing habits. In some amphiaspidid genera, the anterior part of the armor is elongated into a tube-shaped structure and the orbits are lacking, suggesting the loss of the eyes. In other amphiaspidids, there is a peculiar opening, the adorbital opening, close to the orbits, which has been interpreted as either a spiracular (or prespiracular) opening (Halstead 1973; Novitskaya 1971),

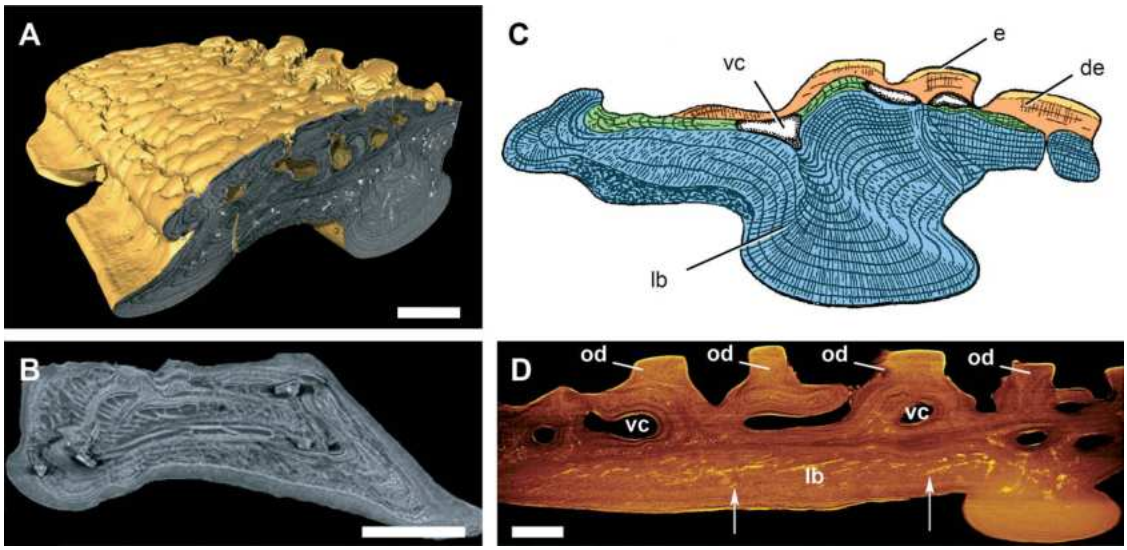


FIGURE 15.8 Histology of anaspids. A, Transverse section through a body scale of *Vesikulepis funiforma* (NHM PV P73708), Lower Silurian of Estonia (after Keating and Donoghue 2016, figure 3A). Scale bar = 100 µm. B, Transverse section through a body scale of *Birkenia robusta*, Lower Silurian of Estonia (after Sire et al. 2009, figure 5B). Scale bar = 200 µm. C, Schematic illustration of a section through a generalized anapsid scale (after Janvier 1996a). D, Transverse section of the dermal skeleton of *Rhyncholepis butriangula* (NHM PV P73705), Lower Silurian of Estonia. Arrows point to the coarse extrinsic fabric of fiber spaces infilled with pyrite (after Keating and Donoghue 2016, figure 4E). Scale bar = 100 µm. Abbreviations: de, dentine; e, enameloid; lb, lamellar bone; od, odontode; vc, vascular canal.

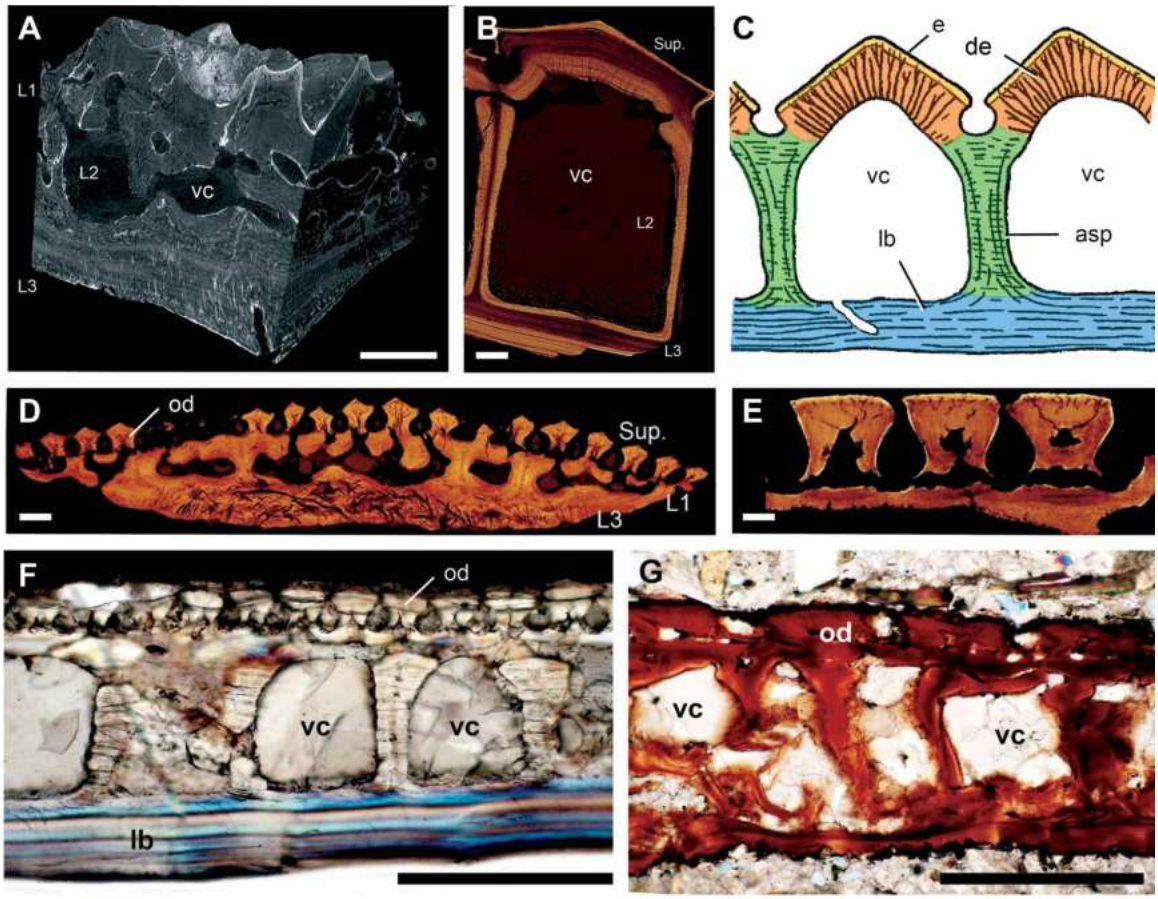


FIGURE 15.9 Histology of heterostracans. A, Virtual section through a scale of *Tesseraspis tesselata* (NHM P.73617), Lower Devonian of England (after Keating et al. 2015, figure 3A). Scale bar = 200 µm. B, D, E, Synchrotron radiation x-ray tomographic microscopy sections of the cephalothoracic shield of *Anglaspis macculloughi* (NHM P.73620), Lower Devonian of England (after Keating et al. 2015, figures 7A and 8D, E) showing the histological structure of the shield: Sup., superficial layer comprising broad round tubercles made of enameloid and dentine (odontodes); L1, compact layer comprising an anastomosing network of vascular canals, defined by centripetal lamellar walls; L2, cancellous middle layer, comprising a network of polygonal cancellae subdivided by robust intersecting radial walls of acellular bone (aspidine) and L3, lamellar basal layer consisting of an avascular orthogonal arrangement of bone lamellae (isopedine). Scale bars = 100 µm (B), 50 µm (D), and 150 µm (E). C, Schematic illustration of the dermal skeleton of a generalized heterostracan (after Janvier 1996a). F and G, Cross sections through the dermal bone of an indeterminate heterostracan (MNHN), Lower Devonian of Spitzbergen. Scale bars = 500 µm. Abbreviations: asp, aspidine; de, dentine; e, enameloid; lb, lamellar bone; od, odontode; vc, vascular canal.

or a laterally displaced, inhalant nasal or nasohypophysial opening (Janvier 1974). In pteraspidiforms, the dorsal headshield is composed of several plates that roughly correspond to the epitega of cyathaspidiforms.

The extensive phylogenetic analysis combining cyathaspidiforms and pteraspidiforms shows that cyathaspidiforms are paraphyletic if they include anchipteraspidids, which appear as the sister group of pteraspidiforms (Randle and Sansom 2016; Glinskiy 2017). The largest heterostracan group is the psammosteididae, which includes very large forms in which the headshield is composed of the same canonical plates as in the pteraspididae (viz. rostral, orbital, pineal, median dorsal, median ventral, branchial and cornual plates), but these are separated by numerous smaller, growing platelets, sometimes erroneously referred to as "tesserae". Because of their histological diversity and the abundance of their remains in the Devonian, psammolepids have been an abundant source of histological studies (Ørvig 1965, 1968). Glinskiy (2017) considered psammosteids the sister group of the pteraspidoidei within Janvier's (1996a) "higher heterostracans". Heterostracan growth is also documented by exceptional growth series (Greeniaus and Wilson 2003).

In addition to the "higher heterostracans", a number of taxa are sometimes gathered in the heterostracans because they possess large median dorsal and ventral plates, although they lack the other canonical heterostracan plate elements, such as the branchial, cornual, orbital and rostral plates. In addition, some of them show a "tessellate" pattern of the dermoskeleton which is made up of small, polygonal, growing units centered around a primordial odontode (Blieck et al. 2018; Dineley & Loeffler 1976). Contrary to higher heterostracans, these taxa show no evidence of a common external branchial opening, but display lateral series of gill openings. An iconic example of these forms is the Middle Ordovician *Astraspis* (Elliott 1987; Sansom et al. 1997; Lemierre and Germain 2019), long regarded as the earliest known vertebrate (Figure 15.4D) and

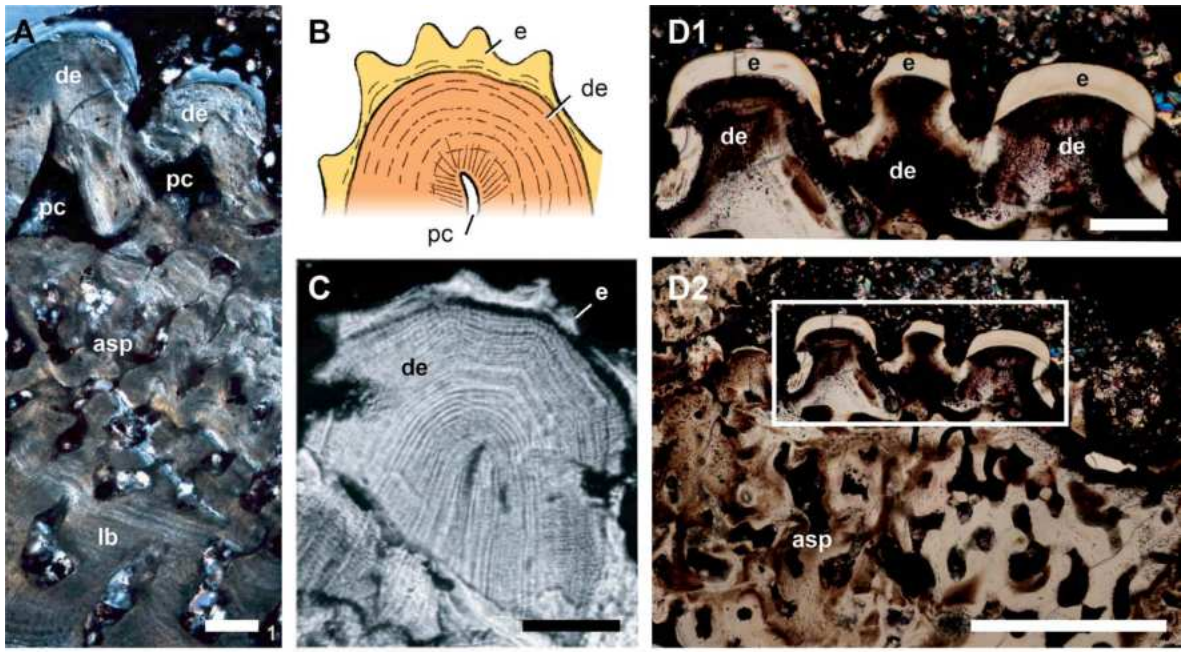


FIGURE 15.10 Histology of astraspids. A, Section through the dermal armor of *Astraspis desiderata* (BU 4471), Middle Ordovician of the United States, illustrating two tubercles capped by monocrystalline enameloid overlying a middle layer made of acellular bone (aspidine) and the lamellar basal layer (isopedine) (after Donoghue et al. 2006, figure 2.1). Scale bar = 100 µm. B, Schematic illustration of an odontode of *Astraspis* (after Janvier 1996a). C, Detailed section of an odontode of *Astraspis* (after Donoghue and Sansom 2002, figure 2.2). Scale bar = 100 µm. D1 and D2, Detailed section of the odontodes from a dermal plate of *Astraspis* (MNHN-F-1891-20). Scale bars = 100 µm (D1) and 500 µm (D2). Abbreviations: asp, aspidine; de, dentine; e, enameloid; lb, lamellar bone; pc, dentinal pulp cavity.

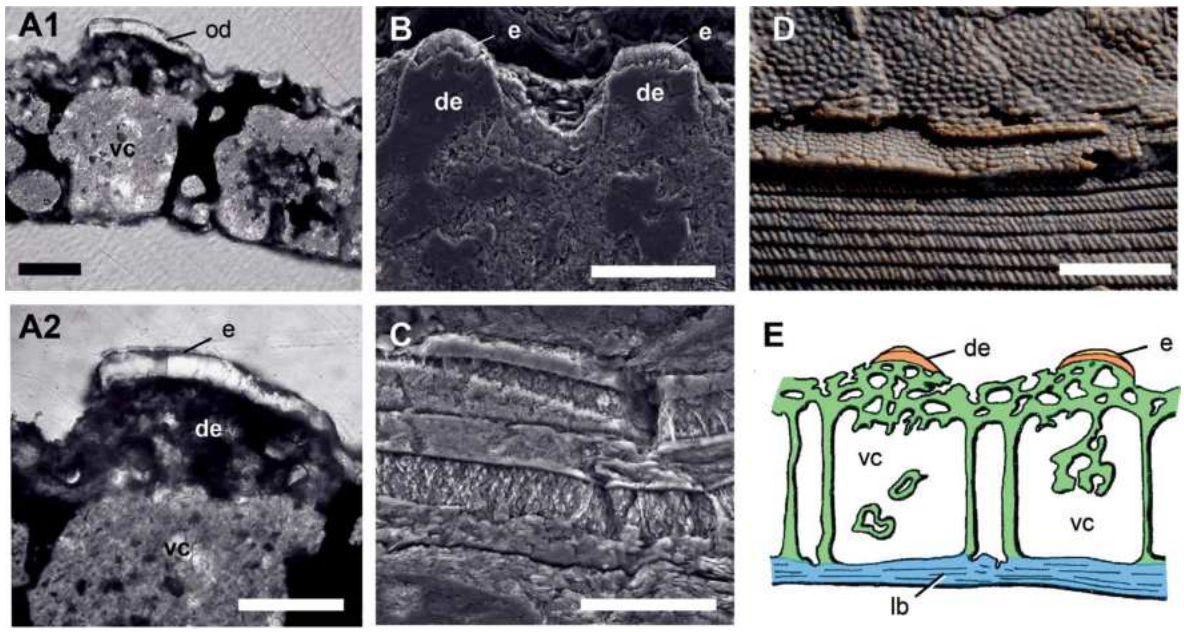


FIGURE 15.11 Histology of arandaspids. A1 and A2, Cross sections through tesserae of *Sacabambaspis janvieri* (CORDMP 9101), Middle Ordovician of Bolivia, illustrating, from the base upward, the fragmented basal layer, cancellous middle layer and cap of enameloid on the upper surface. Scale bar = 100 µm. B and C, Detailed insets of tesserae (MHNC 13261) illustrating the organization of the odontodes (B) and the laminated basal layer (isopedine) (C). Scale bar = 50 µm (after Sansom et al. 2005, figure 1A–D). D, Odontode ornamentation of the squamation of *S. janvieri*. Scale bar = 10 mm. E, Schematic illustration of a section through the dorsal shield of *S. janvieri* (after Janvier 1996a). Abbreviations: de, dentine; e, enameloid; lb, lamellar bone; od, odontode; vc, vascular cavity.

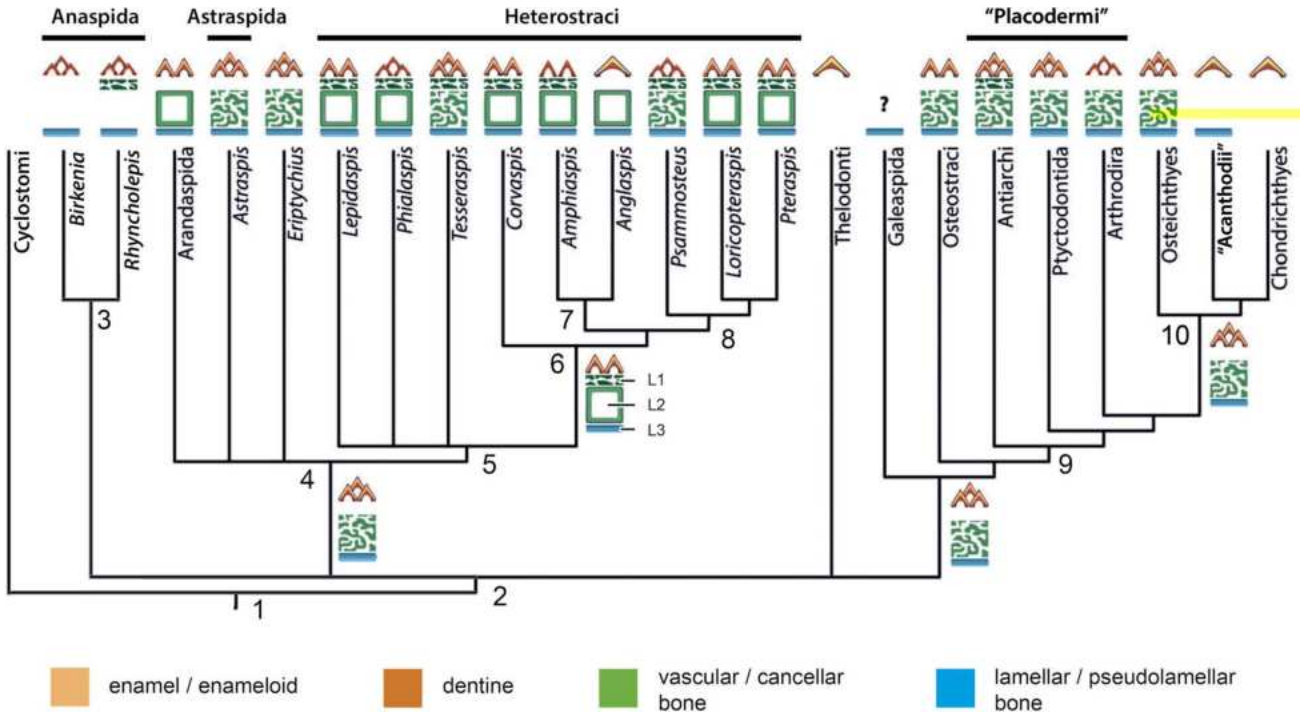


FIGURE 15.12 Evolutionary distribution of mineralized tissue types among vertebrates (modified after Donoghue and Keating 2014 and Keating and Donoghue 2016). Phylogenetic hypothesis after Janvier (1996a), Zhu et al. (2013), Donoghue and Keating (2014) and Keating and Donoghue (2016). Symbols and colors represent the layered structure of the dermal skeleton: adjacent orange triangles correspond to dentine tubercles; yellow caps correspond to a capping layer of enamel/enameloid; stacked orange triangles correspond to stacked tubercle generations; dark green reticular band corresponds to superficial vascular bone (L1); green square box corresponds to cancellar bone (L2); light green reticular box corresponds to trabecular bone (L2); blue bottommost band corresponds to lamellar or pseudolamellar bone (L3). Symbols adjacent to internal branches represent the reconstructed ancestral state. Nodes: 1, vertebrates; 2, total group gnathostomes; 3, anaspids; 4, pteraspidomorphs; 5, heterostracans; 6, "higher heterostracans"; 7, pteraspidiforms; 8, cyathaspidiforms; 9, jawed vertebrates; 10, crown gnathostomes.

dethroned by the discovery of the coeval arandaspids (e.g., *Sacabambaspis*) (Figure 15.4A). All these taxa are nevertheless gathered with heterostracans in the Pteraspidomorphi, essentially on the basis of the histology of their dermoskeleton, whose middle and basal layer is made of a type of acellular bone called aspidin (Keating et al. 2018), while its upper layer is ornamented by small stacking odontodes made of dentine, capped by enameloid (Figures 15.10 and 15.11). Investigations on *Astraspis* have revealed the presence of globular calcified cartilage (Denison 1967, Ørvig 1989) and probable chondroid metaplastic bone indicating the presence of a partially mineralized endoskeleton (Lemierre and Germain 2019).

Thelodonti

Thelodonts are supposedly jawless vertebrates (Figure 15.6H) whose dermoskeletons are entirely micromeric and composed of small scales that generally bear a single odontode. The orbits are surrounded by slightly larger and curved scales. The mouth opens anteroventrally and the ventral lip is covered by rows of scales that are basically similar to those covering the rest of the body. Dorsal to the mouth is the large opening of the nasohypophysial duct, which is covered by minute monodontode scales made of dentine and generally capped by a thin layer of enameloid with a sharp, forwardly oriented apex and associated bone of attachment (Figure 15.13) (Märss et al. 2007; Sire et al. 2009; Keating et al. 2015). The scales that cover the fins are long. Very few thelodonts are known from articulated specimens (Märss & Ritchie 1999). The best examples are *Turinia* (Donoghue and Smith 2001), *Loganellia* (Figure 15.4F), *Phlebolepis* (Wilson and Märss 2012) and the so-called "fork-tailed thelodonts" (e.g., *Canonia*, *Furcacauda*) (Wilson and Caldwell 1993, 1998). Because of this paucity of macroanatomical information on the group, thelodont systematics has been essentially based on scale morphology and histology, in particular whether the dentine contains tubules that arise either directly from the base (the now disused "acanolepid" type), from a large pulp cavity (loganiid type) or from large common canals (katoporid type) (Figure 15.13). The most recent summary of thelodont scale histology has been provided by Märss et al. (2007) and Žigaitė et al. (2013), who established 11 histological scale types: Sandivia, Loganellia, Shielia, Helenolepis, Trimerolepis, Thelodus, Turinia, Barlowodus, Apalolepis, Canonia and Talimaalepis types. These histological characters have been used to reconstruct a phylogeny of the thelodonts (Wilson and Märss 2009), which surprisingly concludes that the group is monophyletic. This result contrasts with Janvier's (1981, 1996a, b) vertebrate trees, where thelodonts appeared as a paraphyletic ensemble of taxa that populates the stem of all other major skeletonized

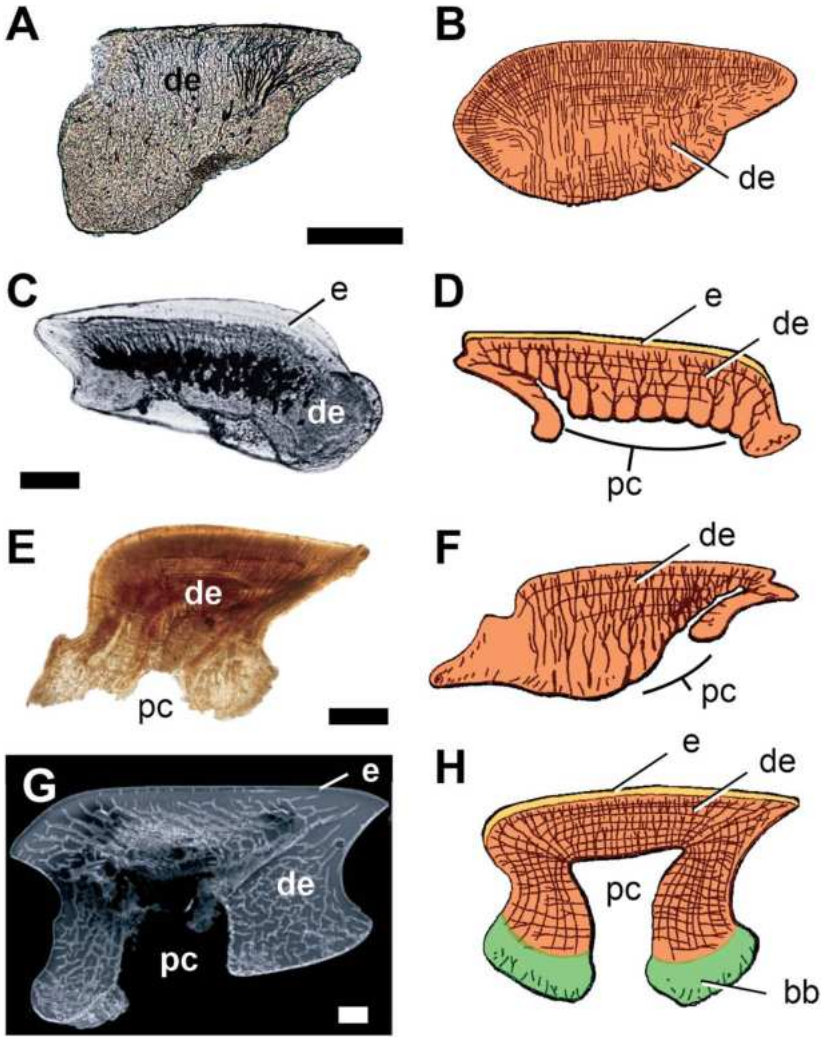


FIGURE 15.13 Histology of thelodonts. A, Cross sections of the scales of *Loganellia cuneata* (GIT 456-119), Upper Silurian of Estonia (after Märss 2006, fig.2A). Scale bar = 100 µm. B, Schematic illustration of an "achanolepid" type thelodont scale (after Janvier 1996a). C, *Loganellia matura* (PI 7624), Lower Silurian of Russia (after Märss and Karatajute-Talimaa 2002, fig. 6A). Scale bar = 100 µm. D, Schematic illustration of a loganiid type thelodont scale (after Janvier 1996a). E, *Neoturinia hutkensis* (AEU 548), Upper Devonian of Iran (after Hairapetian et al. 2016, fig.6C). Scale bar = 100 µm. F. Schematic illustration of a katoporid type thelodont scale (after Janvier 1996a). G, *Thelodus* sp. (BRISUG 27770) (after Sire et al. 2009, fig.6D). Scale bar equals 100 µm. E. Schematic illustration of a katoporid type thelodont scale (after Janvier 1996a). H, Schematic illustration of a thelodontid type thelodont scale (after Janvier 1996a). Abbreviations: bb, bony base; de, dentine; e, enameloid; pc, pulp cavity.

vertebrate clades. Janvier's suggestion was based on the frequent presence, even in macromeric vertebrates, of micromeric scales, the shape of which recalls thelodont scales, in many such stem taxa, including gnathostomes.

Galeaspida

The Galeaspida are a clade of jawless vertebrates that are known exclusively from the Silurian and Devonian of China and Vietnam (Sansom 2009) (Figure 15.6H). They possess, like osteostracans, a large headshield that comprises an endoskeletal braincase covering the gills and an abdominal division, but they entirely lack paired fins and girdles (Figure 15.4G). The endoskeleton of most galeaspids displays a very large number of branchial fossae that housed the gills (up to about 50 pairs), but this amazing specialization only appears in Devonian forms; the earliest (and presumably plesiomorphic) condition is a much smaller number of gill fossae, comparable to that of osteostracans. The main characteristic of galeaspids is a large, oval or slit-shaped anterodorsal opening that opens toward a space that contains the nasal capsules and the hypophysial duct, and communicates ventrally with the oral cavity (Gai et al. 2011).

The histology of galeaspids has been extensively discussed (Janvier 1990; Zhu and Janvier 1998; Wang et al. 2005) because of the apparent absence of cell lacunae and odontoblastic lacunae in the tubercles of the dermoskeleton, which suggested an acellular structure. It differs in many respects from the aspidine of heterostracans by the orthogonal plywood-like arrangement of thin collagen fibrils (recalling the isopedine of osteichthyans) and has therefore been termed "galeaspidin" (Wang et al. 2005; Donoghue et al. 2006; Qu et al. 2013) (Figure 15.14).

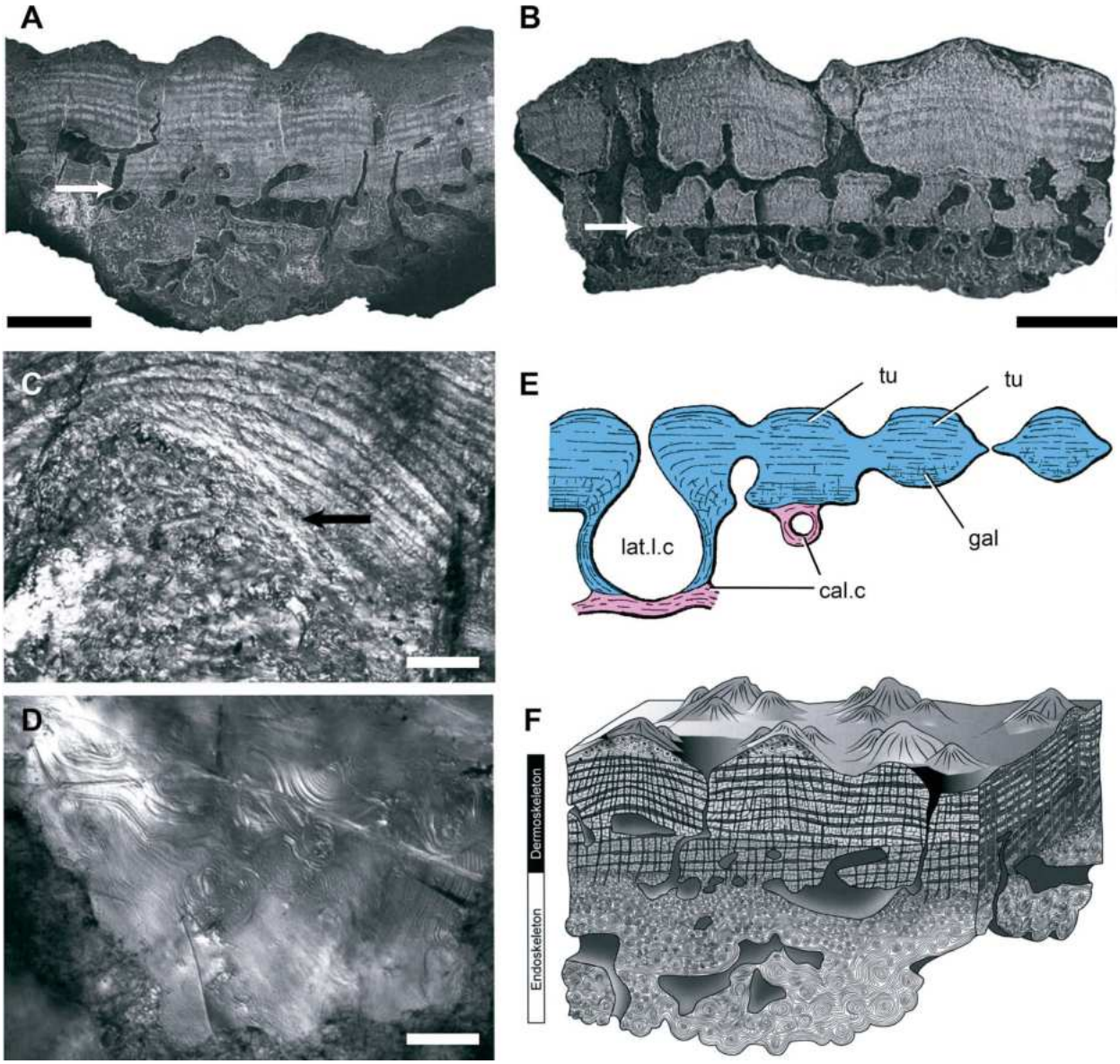


FIGURE 15.14 Histology of galeaspids. A and B, Cross sections through the cephalothoracic skeleton of a pectoral cornual process of a polybranchiaspid indet (IVPP V12599.2), Lower Devonian of China. The arrow indicates the junction between the dermoskeleton (upper) and endoskeleton (lower). Scale bars = 500 µm. C, Detailed inset showing the junction between the dermoskeleton (upper) and endoskeleton (lower). Scale bar = 50 µm. D, Detailed inset (IVPPV 12607.1) illustrating the structure of the endoskeleton comprising the progressive infilling of undulations on the inner surface of the endoskeleton with laminations of cartilage. Scale bar = 50 µm. E, Schematic illustration of the headshield of a generalized galeaspid (after Janvier 1996a). F, Diagrammatic reconstruction of the skeletal histology of the galeaspid dermoskeleton (after Wang et al. 2005, figures 2, 4 and 5). Abbreviations: cal.c, calcified cartilage; gal, galeaspidine; lat.l.c, lateral line canal; tu, tubercles.

The tubercles of the dermoskeleton are made of a spheritic calcified tissue that seems comparable to the superficial layer of the elasmoid scales of teleosts, and contains no dentine or enameloid. The endoskeleton of galeaspids is entirely made of calcified cartilage, and the sheath that surrounds the internal structures contains no perichondral bone, only spheritic calcified cartilage (Wang et al. 2005) (Figure 15.14D). The otic capsule of galeaspids possesses only two vertical semicircular canals, and the saccular division of the labyrinth is small and devoid of the large canals leading to the lateral and dorsal fields in osteostracans.

Osteostraci

The Osteostraci are a clade of jawless vertebrates that are only known from the Silurian and Devonian of the Euramerican continent. Like galeaspids, their headshield comprises a braincase that covers the oral and pharyngeal region, which is separated from the abdominal region by a postbranchial wall that also includes the shoulder girdle (Stensiö 1964). The pectoral fins are covered by small, elongated scales (Figure 15.15A, B) and their endoskeletal supports are made of calcified cartilage (Figure 15.15E, F), and articulate with the endoskeletal

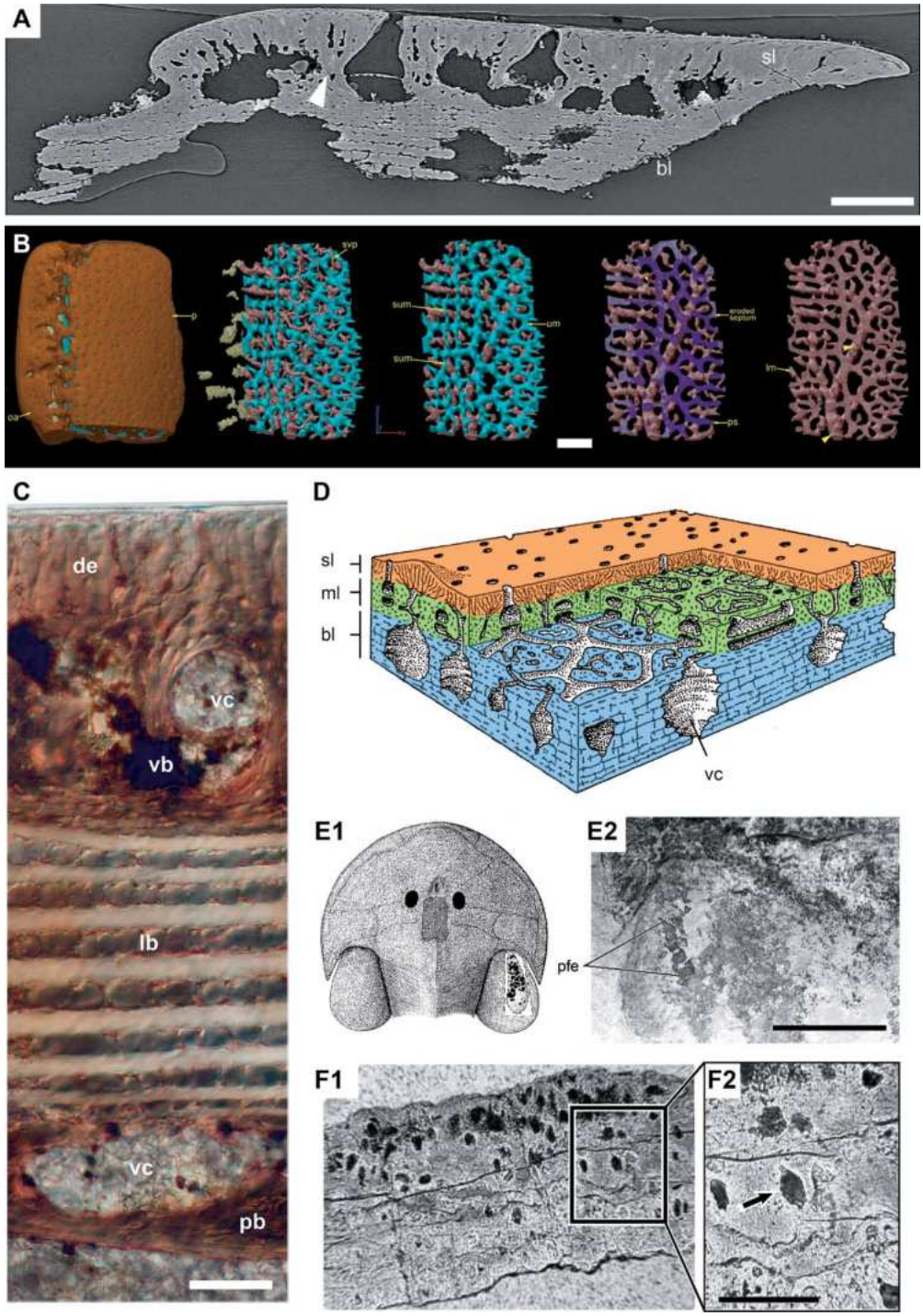


FIGURE 15.15 Histology of osteostracans. A, Vertical section of a caudal trunk scale of *Trematapsis mammillata* (NHMUK P25008), Silurian of Estonia, showing superficial and basal layer tissue. Arrowhead shows a patch of middle layer tissue (after O'Shea et al. 2019, figure 10A). B, Scanned scale of *T. schmidtii* (GIT 712-1) and virtual reconstruction of the internal system of canals: turquoise indicates upper mesh canals, yellow indicates basal canals, pink indicates the lower mesh canals plus subepidermal vascular plexus, and dark and light purple indicate perforated septa. Yellow arrowheads indicate the main trunk canals of the lower mesh canal system (after Qu et al. 2015, figure 2). C, Cross section through the dermoskeleton and underlying endoskeleton of *Trematapsis* sp. (FM4109) revealing a superficial layer of dentine, a middle layer of vascular bone, and a basal layer of lamellar bone. D, Schematic illustration of a dermal plate of *Trematapsis* (after Janvier 1996a). E and F, The endoskeleton of *Escuminaspis laticeps* (MHNM 01–09), Upper Devonian of Canada (after Janvier et al. 2004). E, Detailed view of the paired fins and endoskeleton of the right fin in black. Scale bar = 100 µm. F, Histology of the patches of calcified cartilage in the paired fins showing the successive zones of calcification and detail of some chondrocyte spaces. Scale bar = 5 cm. Arrow indicates the chondrocyte space. Abbreviations: bl, basal layer; de, dentine; lm, lower mesh canals; ml, middle layer; oa, overlapped area as part of basal layer; p, pore openings; pb, perichondral bone; pfe, patches of calcified cartilage from the fin endoskeleton; ps, perforated septum; sl, superficial layer; svp, subepidermal vascular plexus; um, upper mesh; vb, vascular bone; vc, vascular canal.

VetBooks.ir

shoulder girdle laterally to the postbranchial wall. The dermoskeleton of osteostracans is made of cellular bone and covered with tubercles of mesodentine (Figure 15.15) capped by a thin layer of enameloid in certain forms. Underneath it lies a middle layer of vascular bone pervaded by a complicated network of canals (Figure 15.15B), which recalls the cosmine of osteichthyans. The basal portion of the dermoskeleton is composed of a homogenous acellular basal layer with an orthogonal arrangement of thick collagen bundles (isopedine) (Gross 1935, 1961; Denison 1947, 1951; O'Shea et al. 2019; Mondéjar-Fernández and Meunier 2020).

The structure of the dermoskeleton of osteostracans is far more complex than that of all other "ostracoderms" and was the first to be elucidated using electron scanning microscope (Gross 1968). Now its organization and mode of growth are well understood, thanks to Synchrotron x-ray microtomography (Qu et al. 2015; O'Shea et al. 2019) (Figure 15.15). The dermoskeleton of the headshield is composed of growing polygonal tesserae bearing either sensory-line grooves or including sensory-line canals. The endoskeleton is essentially made of perichondral bone that lines the internal structures (Figure 15.15C), but it also contains spheritic calcified cartilage. The dorsal surface of the head is pierced by two closely set, round orbits that are separated by a pineal plate bearing the pineal foramen.

A unique character of osteostracans is the lateral and median dorsal fields, which are shallow depressions of unknown function, covered by free tesserae, and connected internally to large branching canals that lead to the otic capsule (Figure 15.6H). These "fields" have been tentatively interpreted as housing either electromotor organs or dynamosensory organs. Anterior to the pineal foramen, the dorsal surface of the head is pierced by a slit-shaped nasohypophysial foramen, by which opens the ethmoid cavity that prolongs the brain cavity anteriorly, and which housed the olfactory capsule and the hypophysial tube. As in galeaspids, the otic capsule possesses only two vertical semicircular canals, but the vestibular division is enlarged by the proximal swellings of the enigmatic canals connecting with the cephalic fields. Because of the presence of a dorsally upturned nasohypophysial duct, the soft tissue anatomy of osteostracans (e.g., gill organization, central and peripheric nerve system, blood vessels) has been classically interpreted in the light of lamprey anatomy (Stensiö 1927, 1964; Wängsjö 1952; Janvier 1985a, b, 1996a-c) (Figure 15.6G), despite an increasingly strong support for their sister group relationship to gnathostomes (Janvier 1984, 1996b, 2008; Forey 1995; Donoghue et al. 2000) (Figure 15.6F).

Pituriaspida

The Pituriaspida (Young 1991) is a small group of presumably jawless vertebrates that is known exclusively from the Lower Devonian of Australia. It comprises only two genera, *Pituriaspis* and *Neeyambaspis*. The few specimens known to date are only preserved as impressions in a sandstone sediment and provide only little anatomical information and no histological information (Figure 15.4E). Their headshield is reminiscent of that of osteostracans by its large ventral oralobranchial chamber. The orbits face laterally and lie close to a small adorbital depression of unknown function. Pituriaspids show no evidence of dorsal "fields" of the osteostracan type, but *Pituriaspis* displays a pectoral fenestra for the attachment of the pectoral fin, situated, as in osteostracans, just posterior to the cornual process. At the posterior end of the long abdominal division of the headshield, a laterally expanded horizontal process suggests the presence of possible pelvic fins. Current phylogenies suggest that pituriaspids form a trichotomy with osteostracans and gnathostomes (Figures 15.1 and 15.6H).

Gnathostomata

The Gnathostomata (gnathostomes) include all the vertebrates in which the mandibular arch is developed into articulated jaws composed of a dorsal palatoquadrate and a ventral Meckelian cartilage, both bearing teeth and toothed dermal bones. They also possess a large number of unique anatomical characters, such as the horizontal, lateral and semicircular canals of the labyrinth, and many unique physiological characters. All gnathostomes produce dentinous tissues (diverse types of dentine, viz. orthodentine, mesodentine, semidentine) and most of them produce bone and calcified cartilage (Table 15.1). The living gnathostomes fall into two major extant clades, the Chondrichthyes (chondrichthyans) and the Osteichthyes (osteichthyans), and two major extinct grades, the Placodermi (placoderms) and the Acanthodii (acanthodians), which are stem gnathostomes and stem chondrichthyans, respectively (Figure 15.2).

Chondrichthyes

Living chondrichthyans (sharks, rays, torpedoes) produce dentine and enameloid, but no endoskeletal bone, apart from extremely thin layers of perichondral bone that lines the underlying tessellate made of calcified cartilage. The loss of bone in chondrichthyans allowed an increased flexibility of their skeleton, whose dermal covering is only composed of small monodontode scales, the so-called "placoid" scales that are initially formed by a single odontode tightly anchored to the dermis by fibers (Goodrich 1907; Andreev et al. 2016a). However, in some fossil forms (e.g., *Mongolepis*), several odontodes can fuse basally or fuse at the papillary stage, resulting in a polyodontode structure of the scales (Karatajūtė-Talimaa 1995, 1998; Donoghue 2002; Andreev et al. 2016b) (Figure 15.16).

Acanthodii

"Acanthodians", or stem chondrichthyans, are generally small, "sharklike" fishes known from the Upper Ordovician (470 Mya) to the Lower Permian (300 Mya). They are covered with minute polyodontode scales that display a characteristic onion-shaped structure where the odontodes made of mesodentine and a thin layer of enameloid in certain taxa grow successively over a central primordium (Figure 15.17A–D) (Valiukevičius and Burrow 2005). Valiukevičius (1995) defined four main types of scales: the *Nostolepis* type (thick basal plate of cellular bone, crown

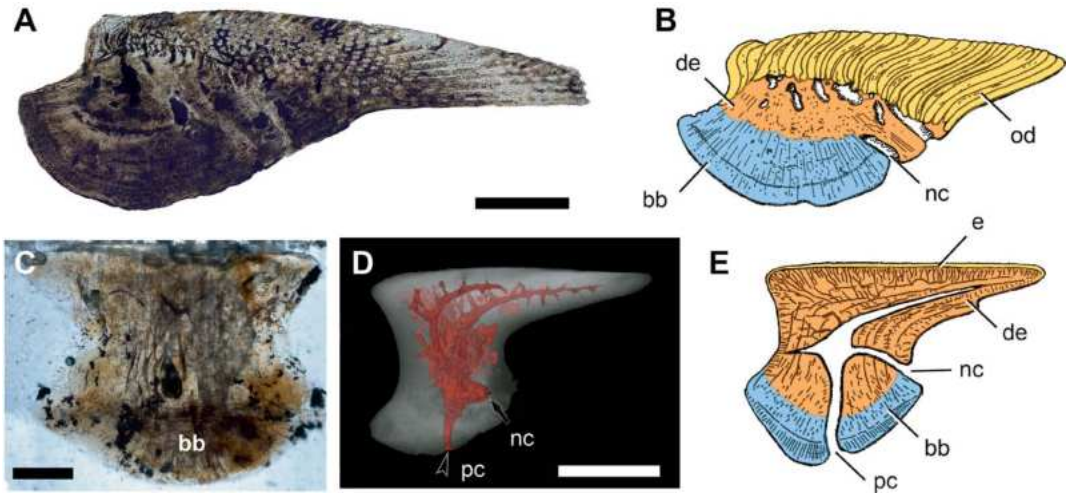


FIGURE 15.16 Histology of chondrichthyans. A, Cross section of a scale of *Mongolepis rozmanae* (BU5297), Silurian of Russia (after Andreev et al. 2016b, figure 6A). Scale bar = 500 µm. B, Schematic illustration of a scale of *Mongolepis* (after Janvier 1996a). C, Cross section of a scale of *Elegestolepis grossi* (BU5292), Silurian of Mongolia (after Andreev et al. 2016a, figure 5F). Scale bar = 100 µm. D, Volume rendering of the scale of *E. grossi* (BU5284) (after Andreev et al. 2016a, figure 9B) illustrating the canal system (in red). Scale bar = 100 µm. E, Schematic illustration of a scale of *Elegestolepis* (after Janvier 1996a). Abbreviations: bb, bony base; de, dentine; e, enameloid; nc, neck canal; od, odontode; pc, pulp canal.

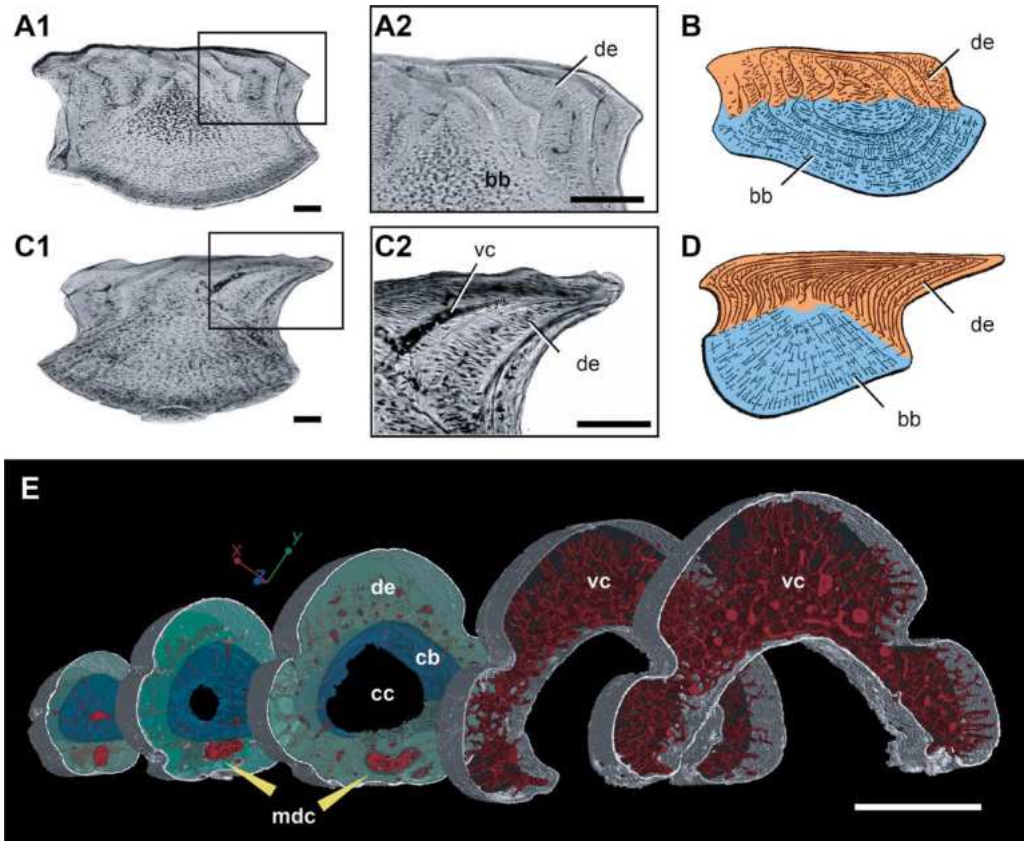


FIGURE 15.17 Histology of acanthodians. A1 and A2, Cross section and detailed inset of the scales of *Vesperalia perplexa* (LIGG 3679), Lower Devonian of Russia (Valiukevičius and Burrow 2005, figures 2–4). Scale bar = 100 µm. B, Schematic illustration of a *Nostolepis* scale (after Janvier 1996a). C1 and C2, Cross sections and detailed inset of the scales of *V. perplexa* (LIGG 3678) (after Valiukevičius and Burrow 2005, figures 2–4). Scale bar = 100 µm. D, Schematic illustration of a *Gomphonchus* scale (after Janvier 1996a). E, Synchrotron data 3D reconstruction of the vascular organization of the fin spine of an indeterminate acanthodian from the Upper Silurian of Sweden (after Jerve et al. 2017, figure 5.7). Scale bar = 500 µm. Abbreviations: bb, bony base; cb, compact bone; cc, central canal; de, dentine or osteodentine; mdc, median canal; vc, vascular canal.

VetBooks.ir

of mesodentine, no enameloid), the *Diplacanthus* type (vascularized basal plate of acellular bone, crown of mesodentine, no enameloid), the *Poracanthodes* type (basal plate of either acellular or cellular bone, crown of either orthodentine, mesodentine or both, with a pore canal system, no enameloid) and the *Acanthodes* type (basal plate of acellular bone with narrow vascular canals, crown of mesodentine, presence of enameloid). Each scale type supposedly characterizes an acanthodian order, but their phylogenetic status is questionable. In addition, acanthodians possess large, bony dermal plates that cover the shoulder girdles and part of the head, and bear dentine tubercles. A characteristic of acanthodians is the presence of large spines anterior to the paired and median fins that display a tripartite structure consisting of a basal layer of lamellar bone or osteodentine, a middle layer of trabecular dentine and an external layer of mesodentine (Figure 15.17E) (Jerve et al. 2017).

For a long time, the relationships of acanthodians have been a matter of debate (Woodward 1891; Denison 1979; Janvier 1996a; Brazeau 2009; Maisey et al. 2017). They have long been considered possibly related to chondrichthyans despite the paucity of information about their endoskeletal anatomy, until they became regarded as a paraphyletic group, part of which was related to chondrichthyans, and part of which was more closely related to osteichthyans (Janvier 1996a). Finally, new information about their endoskeletal anatomy strongly supported chondrichthyan affinities (Davis et al. 2012), as had been proposed earlier by Jarvik (1977, 1980). The definitive answer to this question was recently provided by the discovery of a shoulder girdle of acanthodian type with multiple prepectoral and prepelvic spines in the undisputed early Devonian chondrichthyan *Doliodus* (Maisey et al. 2017). Moreover, *Doliodus* possesses typical chondrichthyan teeth arranged into "families", as are the teeth of some acanthodians. Nevertheless, there remains the question of the histological structure of the endoskeleton of *Doliodus,* which shows no clear evidence for either tessellate prismatic calcified cartilage or continuous perichondral bone. Histological characters are widely used to reconstruct the phylogenetic relationships of neoselachians (living extant elasmobranch taxa), which are characterized by extensively calcified vertebral centra and three-layered enameloid on the odontodes and teeth (Maisey 2012; Cuny et al. 2017). The histology of the dermal skeleton of acanthodians is diverse and includes both ortho- and mesodentine and enameloid in either the scale odontodes or the teeth (Karatajūtė-Talimaa 1998). In contrast, the dermal skeleton of euchondrichthyans (i.e., conventionally defined chondrichthyans, characterized by tessellate prismatic calcified cartilage) is essentially made of orthodentine and osteodentine, that is, tissues that remain relatively stable throughout the phylogeny of the group, although combined in various ways, notably in the fin spines (Jerve et al. 2017) (Figure 15.17).

Placodermi

The Placodermi ("placoderms") is an ensemble of jawed vertebrates whose dermal skeleton is arranged into large plates or platelets that cover the head and trunk, respectively, and articulate at the level of the craniothoracic junction (Goujet 1984; Young 2010). The dermal skeleton of placoderms is generally organized into three layers: a superficial layer of compact bone ornamented with tubercles, a middle layer of vascular, cancellous bone, and a basal layer of lamellar bone (Figure 15.18). In most placoderms, in particular the most plesiomorphic ones, the dermal plates bear odontodes that are made of a thin layer of enameloid and semidentine (Burrow and Turner 1999; Giles et al. 2013) (Figure 15.18A–C), the latter long regarded as an autapomorphy of the group. Semidentine is a type of dentine in which the pulp cavities (odontoblast lacunae) are unipolar and isolated in the extracellular matrix (Goujet 1984). However, many placoderms are secondarily devoid of odontodes and the ornamentation is solely made of cellular bone. It is thus difficult to test the degree of generality of semidentine. The jaws of placoderms are covered with dermal plates bearing large tubercles that gather into cutting blades and are made up by semidentine (Johanson and Smith 2005; Giles et al. 2013; Smith et al. 2017). Placoderms also display a number of macroanatomical features that have long been supporting their monophyly (Young 2010), notably the medial position for the adductor muscle fossa on the palatoquadrate. However, the recent discovery of placoderms in the Upper Silurian of China has raised important debates about the relationships of the group and the diversity of the anatomy of its earliest members (Zhu et al. 2013). Thanks to these new data, placoderms now appear as a paraphyletic array of stem jawed vertebrates that illustrate the stepwise assembly of the gnathostome body plan (Figure 15.12). Yet it is unclear whether or not some members of this ensemble are related to any particular clade of either the total group Chondrichthyes or the total group Osteichthyes. Nevertheless, the character analyses published by both Zhu et al. (2013, 2016) and Dupret et al. (2014) yield all placoderms as being stemward to the total group Chondrichthyes (acanthodians + euchondrichthyans) and thus stem gnathostomes.

The phylogenetic relationships of placoderms is currently extensively debated, but the most recent and best supported trees (Zhu et al. 2013; Dupret et al. 2014) consistently show antiarchs in the basalmost position, then acanthothoracids, rhenanids, petalichthyids, ptyctodontids and arthrodires, and finally *Qilinyu* and *Entelognathus* (the so-called maxillate placoderms) as successive sister groups to crown gnathostomes (Figure 15.12). This phylogeny is probably bound to change considerably in the future, as new well-preserved Silurian forms turn up. However, current data suggest that placoderms straddle the morphological gap between crown gnathostomes and the most crownward "ostracoderms", such as osteostracans. Currently, the most heated debates about placoderms are centered around the question of whether the gnathal plates arming the jaws bear real teeth, or mere tubercles (odontodes) (Smith and Johanson 2003; Young 2003; Rücklin and Donoghue 2015; Burrow et al. 2016) (Figure 15.18J).

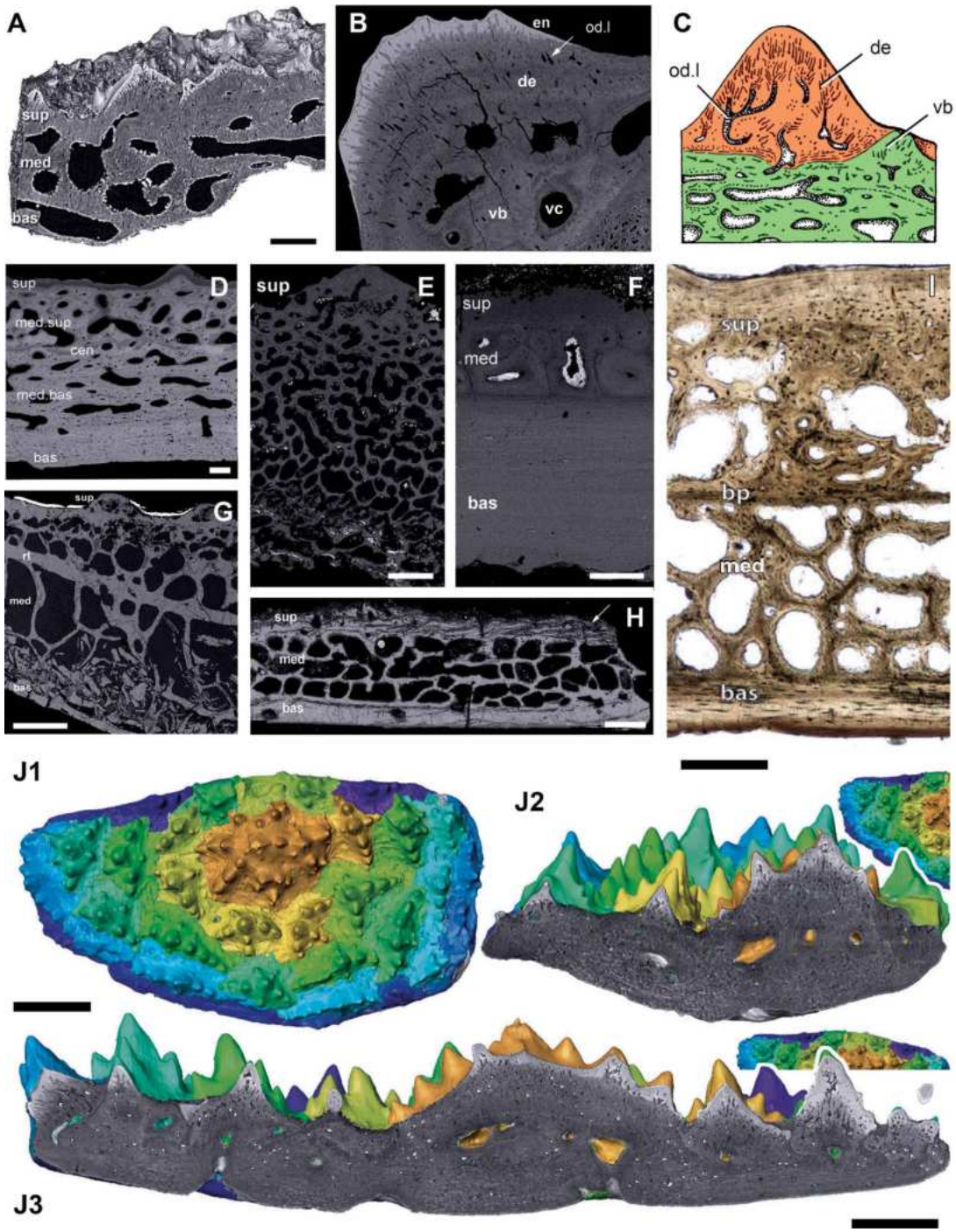


FIGURE 15.18 Histology of placoderms. A, Virtual reconstruction of a skull plate of the acanthothoracid *Romundina stellina* (NRM-PZ.15951), Lower Devonian of Arctic Canada, Scale bar = 50 µm. B, Detail of the superficial layer with enameloid cap and semidentine forming a tubercle. C, Schematic illustration of the dermoskeleton of a generalized arthrodire (after Janvier 1996a). D–I, Vertical cross sections of the dermoskeleton of selected placoderms illustrating the three-layered organization, composed of a superficial layer ornamented with tubercles, a cancellous middle layer, and a lamellar basal layer (A-B, D-I after Giles et al. 2013, figures 2–8). D, The arthrodire *Incisoscutum* sp. (NHMUK PV P 57639), Upper Devonian of Australia. Scale bar = 100 µm. E, The arthrodire *Antineosteus* sp. (BRSUG 29371.1), Middle Devonian of Morocco. Scale bar = 500 µm. F, The arthrodire *Phyllolepis* sp. (NHMUK PV P.50928), Upper Devonian of the United States. Scale bar = 100 µm. G, The antiarch *Yunnanolepis* sp. (MNHN HISTPAL 2801), Lower Devonian of Vietnam. Scale bar = 500 µm. H, The petalichthyid *Lunaspis* sp. (ANSP 21405), Middle Devonian of Germany. Scale bar = 100 µm. I, The antiarch *Bothriolepis canadensis* (MHNM 02-616), Upper Devonian of Canada. Scale bar = 500 µm. J1–J3. Virtual segmentation and reconstruction of the upper dental plate (supragnathal bone) of *R. stellina* (NRM-PZ P.15956) in (1) ventral view (scale bar = 200 µm) and transverse (2) and longitudinal (3) sections (scale bar = 100 µm). Color scheme (from gold to purple) represents the radial and centrifugal sequence of tooth addition (after Rücklin and Donoghue 2015, figure 2). Abbreviations: bas, basal layer; bp, boundary plane between superficial and middle layers; cen, central cancellous tissue; de, dentine; en, enameloid; med, medial layer; med.bas, basal-most zone of the medial layer; med.sup, superficial-most zone of the medial layer; od.l, odontoblastic lacunae; rl, resting line ; vb, vascular bone; vc, vascular canal; sup, superficial layer.

Osteichthyes

Along with these spectacular discoveries of Silurian placoderms, the same outcrops from China also yielded the earliest known (ca. 410–430 Mya) osteichthyans, which are readily recognizable by their typical dermal bone pattern, with tooth-bearing jaw bones (premaxillary, maxillary, dentary), shoulder and pelvic girdles, and generally large rhombic scales. These taxa display some traces of endochondral bone, which may be foreshadowed in some placoderms whose braincases show some trabeculae that are internal to the perichondral bone layer (Brazeau et al. 2020). These early osteichthyans have often been referred to either of the two extant osteichthyan clades Actinopterygii and Sarcopterygii, essentially on the basis of histological characters of the dermal skeleton, but a number of them are possible stem osteichthyans (Zhu et al. 2012).

In general, the presence of ganoine (multilayered enamel) on isolated scales and dermal bones was regarded as a "signature" of actinopterygians, as in the case of the Silurian *Andreolepis*, although this character has sometimes been somewhat misused for merely overlying enamel layers that do not necessarily bear intervening dentine layers (Schultze 2016, 2018) (Figures 15.19–15.21). In the same way, cosmine

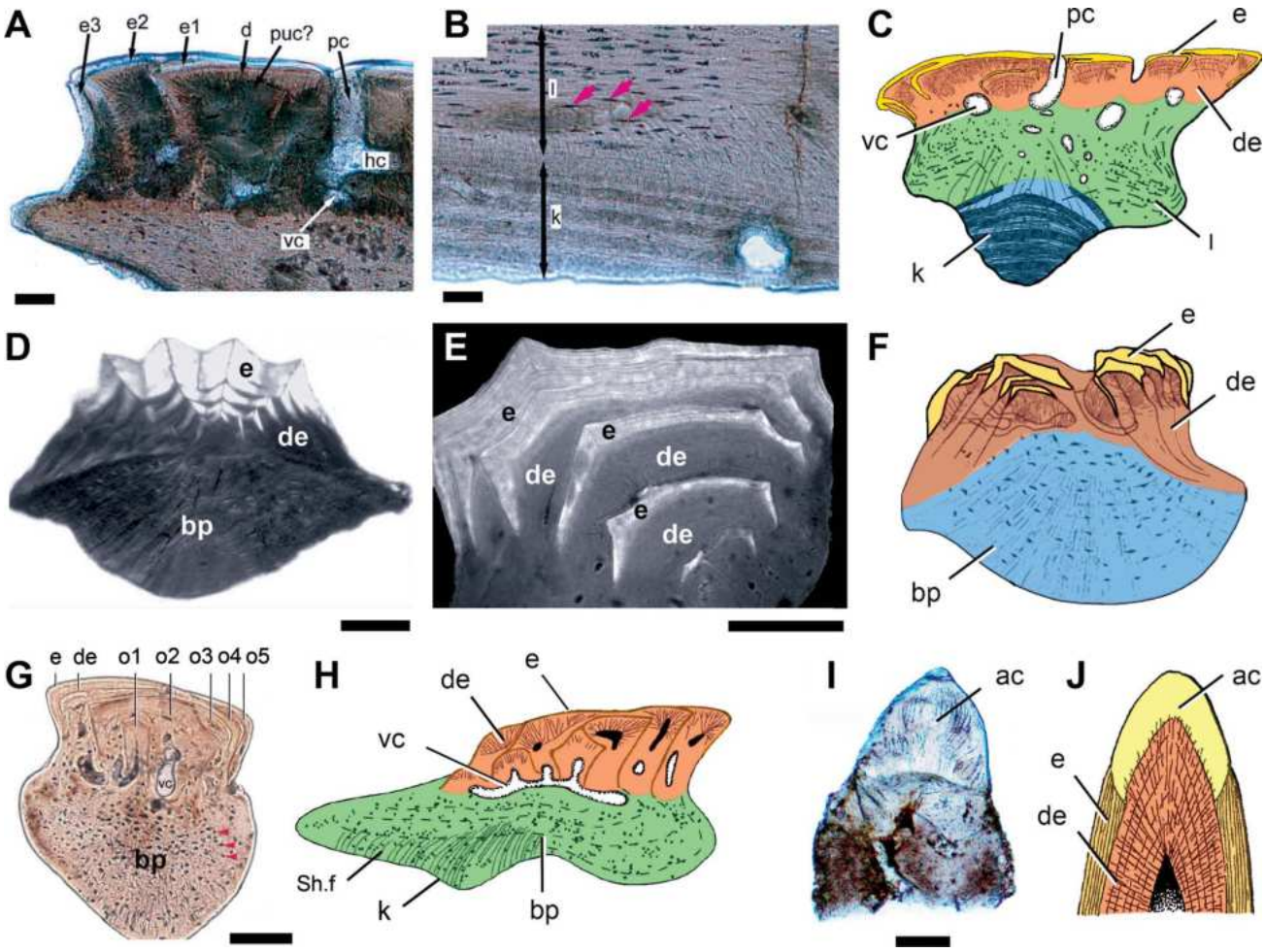


FIGURE 15.19 Histology of osteichthyans. A and B, Cross section of the scales of the stem osteichthyan *Psarolepis romeri* (IVPP V17757.19), Lower Devonian of China (after Qu et al. 2013a, figure 5B, C). A, Detailed inset of the crown showing the odontode overlap pattern. Scale bar = 100 µm. B, Detailed inset of the base showing the lamellar bone (isopedine) forming the keel. Pink arrowheads indicate osteocyte lacunae. Scale bar = 100 µm. C. Schematic illustration of the scales of *Psarolepis* (modified after Qu et al. 2013a). D and E, Cross section of the scales of the actinopterygian *Cheirolepis canadensis* (MHNM 05-132), Upper Devonian of Canada (after Zylberberg et al. 2016, figures 2B3, 3H). D, General view of the scale. Scale bar = 100 µm. E, Detail of the odontode overlap. Scale bars = 100 µm. F, Schematic illustration of the scales of *Cheirolepis* (after Janvier 1996a). G, Cross section of a scale of the stem osteichthyan *Andreolepis hedei* (PMU 24784), Upper Silurian of Sweden (after Qu et al. 2013b, figure 2D). Pink arrowheads indicate osteocyte lacunae. H, Schematic illustration of the scales of *Andreolepis*. I, Isolated tooth tentatively attributed to *Ligulalepis toombsi* (MMC 4755), Lower Devonian of Australia, showing the acrodine cap (after Schultze 2016, figure 13). Scale bar = 100 µm. J, Schematic illustration of the tooth of a generalized actinopterygian (after Janvier 1996a). Abbreviations: ac, acrodine; bp, basal plate; de, dentine; e1-3, enamel layers of several generations of odontodes; hc, horizontal canal; k, keel; l, ledge; o1-5, odontodes; pc, pore cavity; puc?, probable recrystallized pulp cavity; Sh.f, Sharpey's fibers; vc, vascular canal.

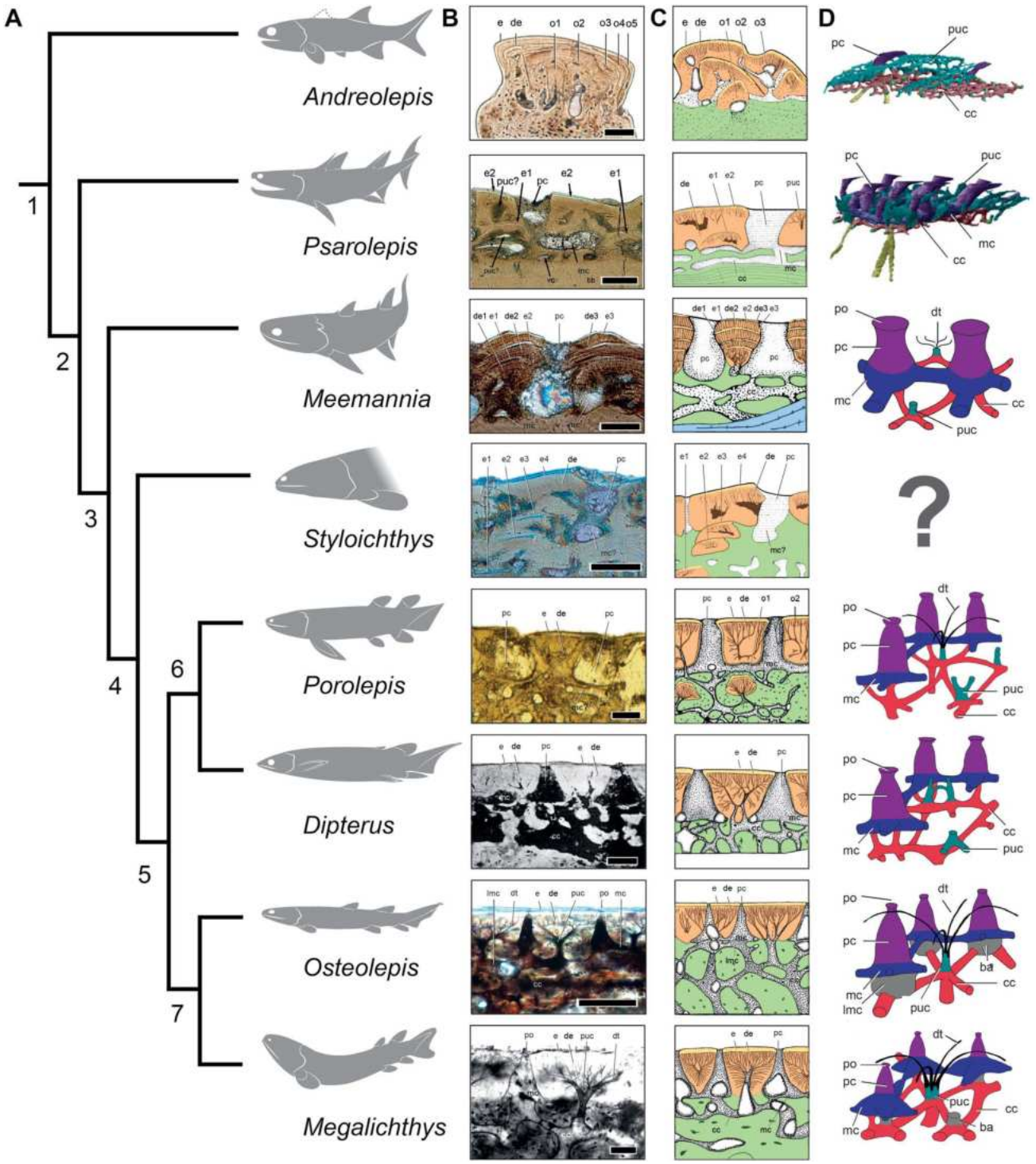


FIGURE 15.20 The evolution of cosmine in osteichthyans. A, phylogenetic interrelationships of selected osteichthyans (after Lu et al. 2017) and interpretive reconstructions of the taxa; B, Histological cross sections. C, Illustrations of the histological structures from the cross sections; D, Virtual and idealized reconstructions of the pore-canal system of the cosmine. Nodes: 1, total group osteichthyans (scales ornamented with superimposed ridgelike odontodes); 2, total group osteichthyans (ridgelike ornamentation of the scales is replaced by a uniform enamel layer overlying a system of pores and canals in the dentine = cosmine); 3, crown osteichthyans (larger superimposed odontodes associated with a pore-canal system); 4, total group sarcopterygians (well-developed basal layer of lamellar bone = isopedine); 5, rhipidistians (the cosmine is composed of a single layer of odontodes and a uniform layer of enamel); 6, dipnomorphs (the enamel usually penetrates the pore cavities of the dentine) and 7, tetrapodomorphs (the enamel does not penetrate the pore cavities). Sources of cross sections and drawings: *Andreolepis*: Zhu et al. 2010, Qu et al. 2013b, 2017; *Psarolepis*: Qu et al. 2013a, 2017 *Meemannia:* Zhu et al. 2010; *Styloichthys:* Zhu et al. 2006; *Porolepis:* Gross 1956, Mondéjar-Fernández and Clément 2012; *Dipterus*: Gross 1956; *Osteolepis*: Gross 1956, Schultze 2016; *Megalichthys:* Gross 1956; Thomson 1975. Scale bar = 100 µm. Abbreviations: ba, basal extension; cc, cross canal; de1-3, dentine from several generations of odontodes; dt, dentinal tubules; e1-4, enamel from several generations of odontodes; lmc, lower mesh canal; mc, mesh canal; o1-5, odontodes; pc, pore cavity; po, pore opening; puc, pulp cavity.

VetBooks.ir

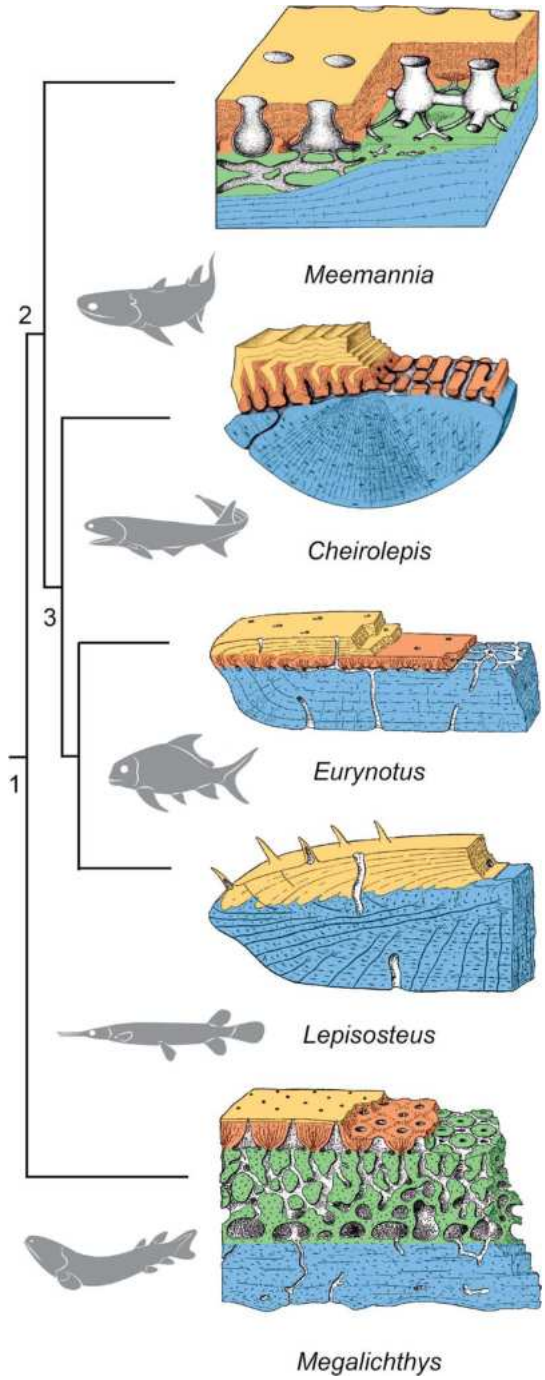


FIGURE 15.21 Comparison and evolution of the dermoskeleton organization in osteichthyans. Nodes: 1, Osteichthyans (scales composed of three layers: a superficial layer of superimposed odontodes made of enamel (yellow) and dentine (orange), a middle layer of vascular bone (green), and a basal layer of lamellar or pseudolamellar bone (blue) with the cosmoid scale as the primitive condition displayed in *Meemannia* and retained in sarcopterygians such as *Megalichthys*); 2, total group actinopterygians (the evolution of multilayered enamel (=ganoine) is a consequence of the primitive odontode superposition condition) and 3, unnamed taxon (loss of the middle vascular layer, establishment of multilayered enamel, retention of underlying dentine in the primitive ganoid scale of "paleonisciforms" [*Cheirolepis*, *Eurynotus*], loss of the dentine in the derived lepisosteoid scale [*Lepisosteus*]. Drawings modified after Zhu et al. 2010 (*Meemannia*), Moy-Thomas and Miles 1971 (*Cheirolepis*), and Goodrich 1907 (*Eurynotus*, *Lepisosteus* and *Megalichthys*).

(the combined occurrence of enamel, dentine and bone pervaded by a complex pore-canal system) has been regarded as the "signature" of sarcopterygians, because it is widely present in Paleozoic piscine tetrapodomorphs (e.g., "osteolepiforms") and dipnomorphs (Mondéjar-Fernández 2018) (Figure 15.20). However, cosmine-like tissues with large pores are also seen in the Silurian *Meemannia*, whose braincase anatomy clearly displays actinopterygian characters (Zhu et al. 2010; Lu et al. 2016) (Figure 15.2). The early Devonian and late Silurian *Psarolepis* (Yu 1998; Zhu et al. 1999) and *Guiyu* (Zhu et al. 2009, 2012; Qiao and Zhu 2010) all possess a typically sarcopterygian-like cranial anatomy with a bipartite braincase and an intracranial articulation (or juncture apparatus), and in the case of *Psarolepis*, its dermal bones and scales are also covered by a cosmine-like tissue (Figure 15.19A–C). Yet their paired fins remain polybasal, as in actinopterygians (Zhu and Yu 2009; Zhu et al. 2012), suggesting that cosmine constitutes a primitive feature of osteichthyans (Figure 15.20).

The cosmine of sarcopterygians is basically made of orthodentine that surrounds small flask-shaped cavities that are interconnected by a network of canals. It displays two clearly distinct structures. In dipnomorphs (porolepiforms and dipnoans), the internal walls of the flask-shaped cavities are lined with enamel, whereas in cosmine-covered piscine tetrapodomorphs (e.g., "osteolepiforms"), the enamel layer does not penetrate the cavities and remains on the external surface of the dentine (Figure 15.20). The structure of the cosmine-like tissue of *Psarolepis* and *Meemannia* is different from that of sarcopterygians, because it is composed of several generations of odontodes with intervening enamel layers, and the canal network that connects its cavities are more irregular (Qu et al. 2013a; Mondéjar-Fernández 2018). Another often cited histological character of sarcopterygians is the presence of prismatic enamel covering the dentine. But this character may also be present in actinopterygians in the form of the "collar enamel", which differs from the acrodine cap, which is a mere hypermineralized dentine (Figure 15.19I, J). True enamel may not be initially present in the teeth of the earliest sarcopterygians, because it is lacking in the teeth of *Psarolepis* (Qu et al. 2013a) but present in its scales (Figure 15.19A–C).

Sarcopterygian teeth are also well known for the folded structure of the dentine (i.e., plicidentine), which is well exemplified by the "labyrinthodont" teeth of early piscine tetrapodomorphs and dipnomorphs, where both dentine and enamel are strongly folded (Figure 15.22). A somewhat comparable folding of the dentine is also seen in the plicidentine at the base of the attachment tooth tissue in other sarcopterygians (e.g., coelacanths and onychodonts) (Meunier et al. 2015; Mondéjar-Fernández 2020), and even actinopterygians (e.g., gars) (Schultze 1969), and crown group tetrapods (e.g., varanoids and ichthyosaurs) (Meunier et al. 2018). The selective advantage of this complex structure of the dentine may rest on its mechanical resistance to stress during bite. The teeth of osteichthyans, although originally conical in shape, may evolve into a large variety of shapes, becoming either very long and slender in some actinopterygians, or forming crushing plates through early fusion of odontodes,

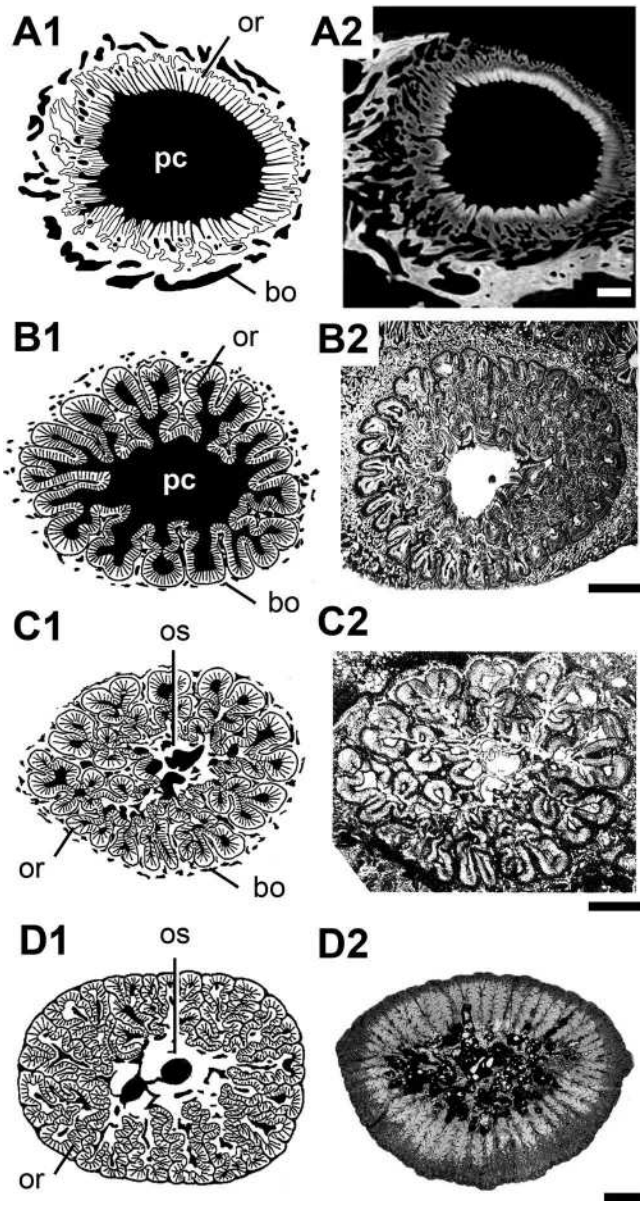


FIGURE 15.22 Types of plicidentine in sarcopterygians. A1 and A2, Simplexodont (*Latimeria*): pulp cavity free from osteodentine, orthodentine folded with primary branches only, bone of attachment not extending between the folds (after Meunier et al. 2015, figure 12). Scale bar = 1 mm. B1 and B2, Polyplocodont (*Panderichthys*): pulp cavity free from osteodentine, orthodentine folded simply and irregularly with branches of first or second degree, bone of attachment extending between the folds (after Schultze 1969, plate 14). Scale bar = 1 cm. C1 and C2, Eusthenodont (*Eusthenodon*): pulp cavity filled with osteodentine, orthodentine folding usually more complicated, bone of attachment extending between the folds (after Schultze 1969, plate 24). Scale bar = 1 cm. D1 and D2, Dendrodont (*Laccognathus*): pulp cavity filled with osteodentine, orthodentine displaying complicated and regular folding ("firelike" branching), bone of attachment restricted to the base of the tooth, not extending between the folds. Scale bar = 1 cm (drawings B–D after Schultze 1970, figure 1). Abbreviations: bo, attachment bone; or, orthodentine; os, osteodentine, pc, pulp cavity.

as in lungfishes (Chang and Yu 1984). The "tooth plates" of lungfishes have long been a riddle in sarcopterygian phylogeny (Mondéjar-Fernández et al. 2020); therefore, they were used as an argument to consider the possibility of a close relationship of lungfishes to chimaeroids (holocephalans), which display a similarly "pitted" surface of their tooth plates. This similarity is due to the abrasion of the tubular dentine (osteodentine) that forms the plates. This question was settled by the discovery of the early Devonian lungfish *Diabolepis* (Chang and Yu 1984), which demonstrates the progressive formation of the pterygoid and prearticular tooth plates by fusion of the odontodes they bear. Many other characters demonstrate that lungfishes are nested within the dipnomorphs as the sister group to porolepiforms (Figure 15.20). Similarly, the origin of the chimaeroid tooth plates is shown by the progressive fusion of the typically lyodont teeth of stem holocephalans ("bradyodonts") into statodont tooth plates.

Some early digited tetrapods still retain dermal scales, notably in *Ichthyostega*, *Acanthostega*, and *Tulerpeton* (Mondéjar-Fernández et al. 2014). Dermal scales persist in some crown tetrapods, such as temnospondyls (Witzmann 2011) and apodans (Zylberberg et al. 1980). However, the transition of tetrapods to land during the Devonian and Carboniferous affected the squamation modifying the size, shape, overlapping pattern, and the bone tissue of the scales. The scales of tetrapods differ from those of aquatic sarcopterygians by their simplification relative to the primitive cosmoid scale (Figure 15.20). In tetrapods, the scales are solely made of compact bone and lack the enamel, dentine and basal layer of lamellar bone (isopedine) (Figure 15.23).

Conclusion

The suite of paleontological data that document the rise and evolution of vertebrate mineralized hard tissues is now relatively complete. However, some questions remain, notably about the earliest stages of this evolution in the dermal skeleton (Donoghue and Sansom 2002), for which euconodonts and *Anatolepis* were once suggested as possible proxies, yet now largely dismissed (Bockelie and Fortey 1976; Smith and Sansom 1995). Did the rise of the dermal skeleton have an effect on the rise of the endoskeleton through some induction process? (Smith and Hall 1990). And what is the developmental and physiological link between the two vertebrate skeletons (exo- and endoskeleton), if any? How did the regression of perichondral (and endochondral) bone occur, notably during the acanthodian euchondrichthyan evolutionary transition? And what triggered it? The same kind of question arises about the breakdown of the neurocranium or the endoskeletal shoulder girdle into separate units, and the subsequent rise of sutures between long-separated skeletal units.

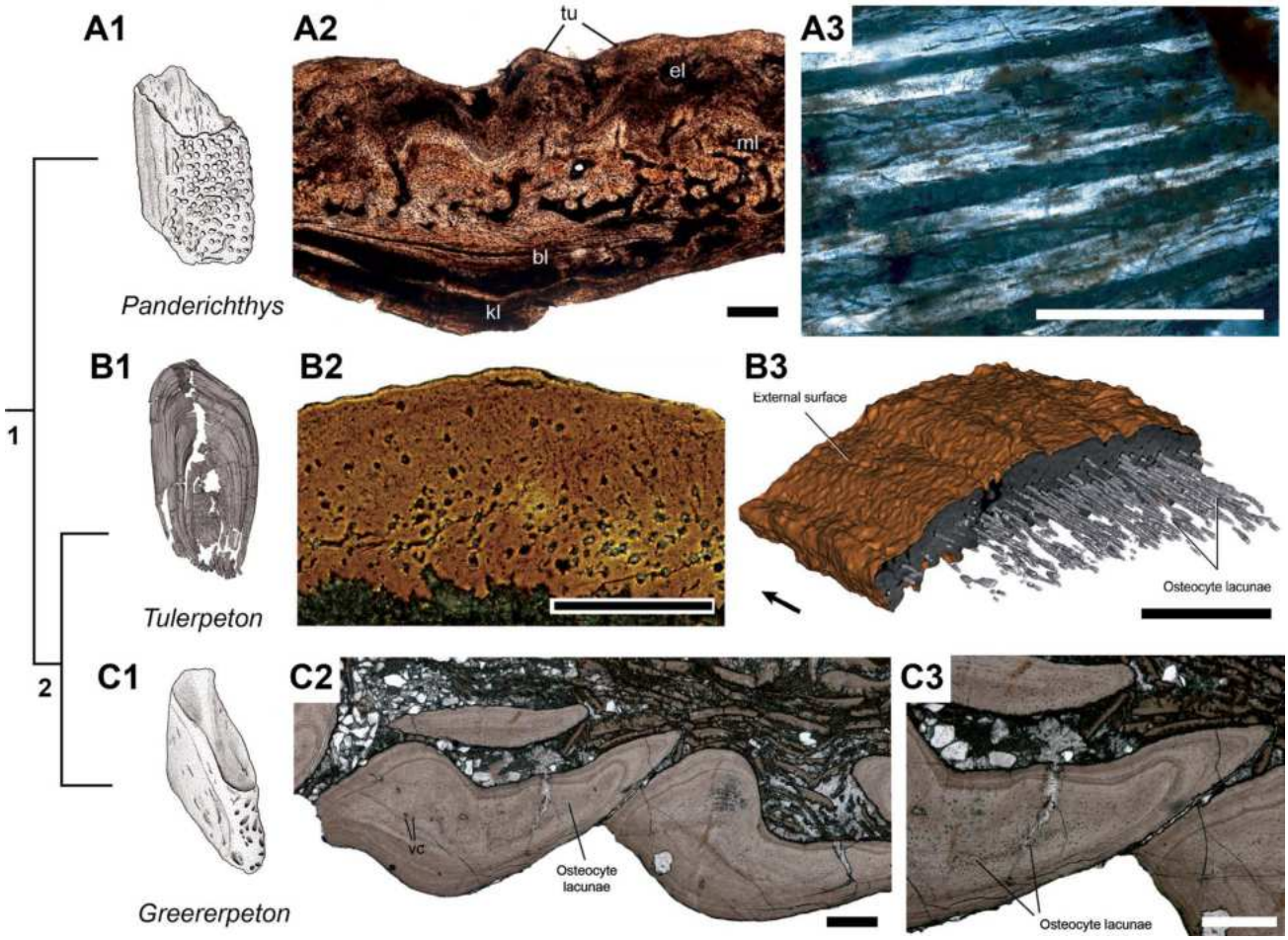


FIGURE 15.23 Histology of the tetrapod dermoskeleton. A1–A3, The elpistostegalian *Panderichthys rhombolepis* (MB.Hi.415), Upper Devonian of Latvia (after Witzmann 2011, figures 2A and 7A, B). B1–B3, The Devonian tetrapod *Tulerpeton curtum* (PIN 2921/3238), Upper Devonian of Russia (after Mondéjar-Fernández et al. 2014). The arrow points anteriorly. C1–C3, The Carboniferous tetrapod *Greererpeton burkemorani* (CMNH 11113), Mississippian (Lower Carboniferous) of Scotland (after Witzmann 2011, figures 4A and 7A, B). Nodes: 1, Elpistostegalia (rhombic scales composed of three layers: an external layer of compact bone ornamented with bony tubercles, a middle layer of vascular bone, and a basal layer of lamellar bone (isopedine) and 2, Tetrapoda (scales reduced and variable in shape with only a single layer of cellular bone, generally avascular, absence of the isopedine layer). Scale bar = 100 µm. Abbreviations: bl, basal layer; el, external layer; kl, keel; ml, middle layer; tu, tubercles; vc, vascular canals.

REFERENCES

Aldridge, R. J., et al. 1993 The anatomy of conodonts. *Philos. Trans. R. Soc. B* 340: 405–421

Andreev, P., et al. 2016a. The systematics of the Mongolepidida (Chondrichthyes) and the Ordovician origins of the clade. *PeerJ* 4: e1850.

Andreev, P. S., et al. 2016b. *Elegestolepis* and its kin, the earliest monodontode chondrichthyans. *J. Vert. Paleontol.* 37: e1245664.

Bardack, D. 1991. First fossil hagfish (Myxinoidea): a record from the Pennsylvanian of Illinois. *Science* 254: 701–703.

Bardack, D. and E. S. Richardson, Jr. 1977. New agnathous fishes from the Pennsylvanian of Illinois. *Fieldiana Geol.* 33: 489–510.

Bardack, D. and R. Zangerl. 1968. First fossil lamprey: A record from the Pennsylvanian of Illinois. *Science* 162: 1265–1267.

Bardack, D. and R. Zangerl. 1971. Lampreys in the fossil record. In *The Biology of Lampreys*, M. W. Hardisty and I. C. Potter eds., Vol. 1, 67–84. London: Academic Press.

Blieck, A. 1984. *Les Hétérostracés Ptéraspidiformes. Systématique, phylogénie, biostratigraphie, biogéographie. Cahiers de Paléontologie*. Paris: Editions du Centre National de la Recherche Scientifique.

Blieck, A., et al. 2011. Fossils, histology, and phylogeny: Why conodonts are not vertebrates. *Episodes*33: 237–241.

Blieck, A., et al. 2018. A redescription of *Tesseraspis mosaica* Karatajūtė-Talimaa (Vertebrata: †Pteraspidomorphi: Heterostraci) from the Lochkovian (Lower Devonian) of Severnaya Zemlya, Russia, with a review of tessellated heterostracan taxa. *Acta Geol. Pol.* 68: 275–306.

Blom, H. 2012. New birkeniid anaspid from the Lower Devonian of Scotland and its phylogenetic implications. *Palaeontology* 55: 641–682.

Bockelie, T.G. and R. Fortey. 1976. An Early Ordovician vertebrate. *Nature* 260: 36–38.

Brazeau, V. 2009. The braincase and jaws of a Devonian 'acanthodian' and modern gnathostome origins. *Nature* 457: 305–308.

Brazeau, M., et al. 2020. Endochondral bone in an early placoderm from Mongolia. *Nat. Ecol. Evol.* 4: 1477–1484.

Briggs, D. E. G., et al. 1983. The conodont animal. *Lethaia* 20: 1–14.

Burrow, C. J. and S. Turner. 1999. A review of placoderm scales, and their significance in placoderm phylogeny. *J. Vert. Paleontol.* 19: 204–219.

Burrow, C. J., et al. 2016. Placoderms and the evolutionary origin of teeth: a comment on Rücklin and Donoghue (2015). *Biol. Lett.* 12: 20160159.

Chang, M. M. et al. 2006. A lamprey from the Cretaceous Jehol Biota of China. *Nature* 441:972–974.

Chang, M. M. and X. Yu. 1984. Structure and phylogenetic significance of *Diabolichthys speratus* gen. et sp. nov., a new dipnoan-like form from the Lower Devonian of eastern Yunnan, China. *Proc. Linn. Soc. New South Wales* 107: 171–184.

Chang, M. M., et al. 2014. Discovery of fossil lamprey larva from the Lower Cretaceous reveals its three-phased life cycle. *Proc. Natl Acad. Sci. USA* 111: 15486–15490.

Chevrinais, M., et al. 2018. Evolution of vertebrate postcranial complexity: axial skeleton regionalization and paired appendages in a Devonian jawless fish. *Palaeontology* 61: 949–961.

Conway-Morris, S. and J.-B. Caron. 2012. *Pikaia gracilens* Walcott, a stem-group chordate from the Middle Cambrian of British Columbia. *Biol. Rev. Camb. Philos. Soc.* 87: 480–512.

Conway-Morris, S. and J.-B. Caron. 2014. A primitive fish from the Cambrian of North America. *Nature* 512: 419–422.

Cope, E. D. 1889. Synopsis of the families of vertebrata. *Am. Nat.* 23: 1–29.

Cuny, G., et al. 2017. *Evolution of Dental Tissues and Paleobiology in Selachians*, 97–103. st. Louis, MO: Elsevier.

Davis, S. P., et al. 2012. *Acanthodes* and shark-like conditions in the last common ancestor of modern gnathostomes. *Nature* 486(7402): 247–250.

Denison, R. H. 1947. The exoskeleton of *Trematapsis*. *Am. J. Sci.* 245: 337–367

Denison RH. 1951. The exoskeleton of early Osteostraci. *Fieldiana Geol.* 11:199–218.

Denison, R. H. 1964. The Cyathaspididae: a family of Silurian and Devonian jawless vertebrates. *Fieldiana Geol.* 13: 309–473.

Denison, R. H. 1967. Ordovician vertebrates from Western United States. *Fieldiana Geol.* 16: 269–288.

Denison, R. H. 1970. Revised classification of Pteraspididae with description of new forms from Wyoming. *Fieldiana Geol.* 20: 1–41.

Denison, R. H. 1979. Acanthodii. In *Handbook of Paleoichthyology*, H.-P. Schultze ed., 1–62. Stuttgart: Gustav Fischer.

Dineley, D. L. and J. Loeffler. 1976. Ostracoderm faunas of the Delorme and associated Siluro-Devonian formations, North West Territories, Canada. *Palaeontology*, Special Paper 18: 1–214.

Donoghue, P. C. J. 2002. Evolution of development of the vertebrate dermal and oral skeletons: unraveling concepts, regulatory theories, and homologies. *Palaeobiology* 28: 474–507.

Donoghue, P. C. J. and R. J. Aldridge. 2001. Origin of a mineralized skeleton, *In Major Events in Early Vertebrate Evolution*, P. E. Ahlberg ed., 85–105. London: Taylor and Francis.

Donoghue, P. C., J. and J. N. Keating. 2014. Early vertebrate evolution. *Palaeontology* 57: 879–893.

Donoghue, P. C. J. and I. J. Sansom. 2002. Origin and early evolution of vertebrate skeletonization. *Microsc. Res. Tech.* 59:352–372.

Donoghue, P. C. J. and M. P. Smith, M. P. 2001. The anatomy of *Turina pagei* (Powrie), and the phylogenetic status of the Thelodonti. *Trans. R. Soc. Edinburgh: Earth Sci.* 92: 17–37.

Donoghue, P. C. J., et al. 2000. Conodont affinity and chordate phylogeny. *Biol. Rev.* 75: 191–251.

Donoghue, P. C. J., et al. 2006. Early evolution of vertebrate skeletal tissues and cellular interactions, and canalization of skeletal development. *J. Exp. Zool. Mol. Dev. Evol.* 306: 278–294.

Dupret, V., et al. 2014. A primitive placoderm sheds light on the origin of the jawed vertebrate face. *Nature* 507: 500–503.

Elliott, D. K. 1987. A reassessment of *Astraspis desiderata*, the oldest North American vertebrate. *Science* 237: 190–192.

Forey, P. L. 1995. Agnathans recent and fossil, and the origin of jawed vertebrates. *Rev. Fish Biol. Fisheries* 5: 267–303.

Gabbott, S. E., et al. 2016. Pigmented anatomy in Carboniferous cyclostomes and the evolution of the vertebrate eye. *Proc. R. Soc. B* 283: 20161151.

Gagnier, P. Y. 1993a. *Sacabambaspis janvieri*, Vertébré ordovicien de Bolivie. 1. Analyse morphologique. *Ann. Paléontol.* 79: 19–69.

Gagnier, P. Y. 1993b. *Sacabambaspis janvieri*, Vertébré ordovicien de Bolivie. 2. Analyse phylogénétique. *Ann. Paléontol.* 79: 119–166.

Gai, Z., et al. 2011. Fossil jawless fish from China foreshadows early jawed vertebrate anatomy. *Nature* 476: 324–327

Gee, H. 2001. "On being Vetulicolian." *Nature* 414: 407–409.

Gee, H. 2018. *Across the Bridge. Understanding the Origin of the Vertebrates*. Chicago: The University of Chicago Press.

Gess, R. W., et al. 2006. A lamprey from the Devonian period of South Africa. *Nature* 443(7114): 981–984.

Giles, S., et al. 2013. Histology of ''Placoderm'' dermal skeletons: implications for the Nature of the Ancestral gnathostome. *J. Morphol.* 274: 627–644.

Glinskiy, V. 2017. Phylogenetic relationships of psammosteid heterostracans (Pteraspidiformes), Devonian jawless vertebrates. *Biol. Commun.* 62: 219–243.

Goodrich, E.S. 1907. On the scales of fish living and extinct, and their importance in classification. *Proc. Zool. Soc. Lond.* 47: 751–774.

Goudemand, N., et al. 2011. Synchrotron-aided reconstruction of the conodont feeding apparatus and implications for the mouth of the first vertebrates. *Proc. Natl. Acad. Sci. USA*, 108(21): 8720–8724.

Goujet, D. 1984. *Les poissons Placodermes du Spitsberg. Cahiers de Paléontologie*. Paris: Editions du Centre National de la recherche Scientifique.

VetBooks.ir

Greeniaus, J. W. and M. V. H. Wilson. 2003. Fossil juvenile Cyathaspididae (Heterostraci) reveal rapid cylomorial development of the dermal skeleton. *J. Vert. Paleont.* 23: 483–487.

Gross, W. 1935. Histologische Studien am Aussenskelett fossiler Agnathen und Fische. *Palaeontographica Abt A*. 83: 1–60.

Gross, W. 1956. Über Crossopterygier und Dipnoer aus dem baltischen Oberdevon im Zusammenhang einer vergleichenden Untersuchung des Porenkanalsystems paläozoischer. *Agnathen und Fische. K. Sven. Vetenskapsakad. Handl., 4e Ser.* 5: 1–140.

Gross, W. 1961. Aufbau des Panzers obersilurischer Heterostraci un Osteostraci Norddeutschlands (Geschiebe) und Oesels. *Acta Zool. Stockholm* 42: 73–150.

Gross, W. 1968. Beobachtung mit dem Elektronenraster-Auflichtmikoskop an den Siebplatten und dem Isopedin von *Dartmuthia* (Osteostraci). *Paläont. Z.* 42: 74–82.

Halstead, L. B. 1973. The heterostracan fishes. *Biol. Rev.* 48: 279–332.

Hanke, G. F. and Wilson, M. V. 2006. Anatomy of the Early Devonian acanthodian Brochoadmones milesi based on nearly complete body fossils, with comments on the evolution and development of paired fins. *J. Vert. Paleontol.* 26: 526–537.

Heimberg, A. M., et al. 2010. microRNAs reveal the interrelationships of hagfish, lampreys, and gnathostomes and the nature of the ancestral vertebrate. *Proc. Natl Acad. Sci. USA*. 107(45): 19379–19383.

Heintz, A. 1962. Les organes olfactifs des Hétérostracés; In *Evolution des Vertébrés*, J.-P. Lehman, ed. Paris: Colloques internationaux du Centre National de la Recherche Scientifique.

Janvier, P. 1974. The structure of the naso-hypophysial complex and the mouth in fossil and extant cyclostomes, with remarks on amphiaspiforms. *Zool. Scripta* 3: 193–200.

Janvier, P. (1978). On the oldest known teleostome fish Andreolepis hedei Gross (Ludlow of Gotland), and the systematic position of the lophosteids. Eesti NSV Teaduste Akadeemia Toimetised, Geoloogia, 27, 86–95.

Janvier, P. 1981. The phylogeny of the Craniata, with particular reference to the significance of fossil 'agnathans.' *J. Vert. Paleont.* 1: 121–159.

Janvier, P. 1984. The relationships of the Osteostraci and Galeaspida. *J. Vert. Paleont.* 4: 344–358.

Janvier, P. 1985a. *Les Céphalaspides du Spitsberg. Cahiers de Paléontologie*. Paris: Centre National de la Recherche Scientifique.

Janvier, P. 1985b. Les Thyestidiens (Osteostraci) du Silurien de Saaremaa (Estonie). Deuxième partie: Analyse phylogénétique, répartition stratigraphique, remarques sur les genres *Auchenaspis*, *Timanaspis*, *Tyriaspis*, *Didymaspis*, *Sclerodus* et *Tannuaspis*. *Ann. Paléontol.* 71: 187–216.

Janvier, P. 1985c. Les Thyestidiens (Osteostraci) du Silurien de Saaremaa (Estonie). Première partie: Morphologie et anatomie. *Ann. Paléontol.* 71: 83–147.

Janvier, P. 1990. La structure de l'exosquelette des Galeaspida (Vertebrata). Comptes Rendus de l'Académie des Sciences, Paris. 310:655–659.

Janvier, P. 1996a. *Early vertebrates. Oxford Monographs in Geology and Geophysics n 33*. Oxford, UK: Oxford University Press.

Janvier, P. 1996b. The dawn of the vertebrates: Characters versus common ascent in the rise of current vertebrate phylogenies. *Palaeontology* 39: 259–287.

Janvier, P. 2008. Early jawless vertebrates and cyclostome origins. *Zool. Sci.* 25: 1045–1056.

Janvier, P. 2015. Facts and fancies about early fossil chordates and vertebrates. *Nature* 520, 483–489.

Janvier, P. and M. Arsenault. 2007. The anatomy of *Euphanerops longaevus* Woodward, 1900, an anaspid-like jawless vertebrate from the Upper Devonian of Miguasha, Quebec, Canada. *Geodiversitas* 29: 143–216.

Janvier, P. and R. S. Sansom. 2015. Fossil hagfishes, fossil cyclostomes, and the lost world of 'ostracoderms.' In *Hagfish Biology,* S. Edwards and G. Goss eds., 73–93. Boca Raton, FL: Taylor and Francis.

Janvier, P., et al. 2004. Calcified cartilage in the paired fins of the osteostracan Escuminaspis laticeps (Traquair 1880), from the Late Devonian of Miguasha (Québec, Canada), with a consideration of the early evolution of the pectoral fin endoskeleton in vertebrates. *Journal of Vertebrate Paleontology.* 24: 773–779.

Jarvik, E. 1977. The phylogenetic position of the acanthodian fishes. In *Problems in Vertebrate Evolution*, S. M. Andrews, R. S. Miles and A. D. Walker, eds. London: Academic Press.

Jarvik, E. 1980. *Basic Structure and Evolution of Vertebrates,* Vol. 1, London: Academic Press.

Jerve, A., et al. 2017. Morphology and histology of acanthodian fin spines from the late Silurian Ramsåsa E locality, Skåne, Sweden. *Palaeontol. Electron.* 20.3.56A.

Johanson, Z. and M. M. Smith. 2005. Origin and evolution of gnathostome dentitions: a question of teeth and pharyngeal denticles in placoderms. *Biol. Rev.* 80: 303–345.

Karatajūtė-Talimaa, V. 1995. The Mongolepidida: scale structure and systematic position. *Geobios* 28: 35–37.

Karatajūtė-Talimaa, V. N. 1998. Determination methods for the exoskeletal remains of early vertebrates. *Fossil Rec.*1: 21–51.

Keating, J. N. and P. C. J. Donoghue. 2016. Histology and affinity of anaspids, and the early evolution of the vertebrate dermal skeleton. *Proc. R. Soc. B* 283: 20152917.

Keating, J. N., et al. 2015. Histology of heterostracan dermal skeleton: insights into the origin of the origin of the vertebrate mineralized skeleton. *J. Morphol.* 276: 657–680.

Keating, J. N., et al. 2018. The nature of aspidin and the evolutionary origin of bone. *Nat. Ecol. Evol.* 2: 1501–1506.

Kiaer, J. 1924. The Downtonian fauna of Norway. 1. Anaspida. Skrifter utgitt af det Norske Videnskapsakademien, 1, matematisk-naturvidenskapslige Klasse. 6: 1–139

Kuraku, S., et al. 1999. Monophyly of lampreys and hagfishes supported by nuclear DNA-coded genes. *J. Mol. Evol.* 49:729–35.

Langille, R. M. and B. K. Hall. 1993. Calcification of cartilage from the lamprey *Petromyzon marinus* (L.) *in vitro. Acta Zool. Stockholm* 74: 31–41.

Lemierre, A. and D. Germain. 2019. A new mineralized tissue in the early vertebrate *Astraspis*. *J. Anat.* 235: 1105–1113.

Lu, J., et al. 2016. The oldest actinopterygian highlights the cryptic early history of the hyperdiverse ray-Finned Fishes. *Current Biol.* 26: 1602–1608.

Lu, J., et al. 2017. A new stem sarcopterygian illuminates patterns of character evolution in early bony fishes. *Nature Commun*. 8: 1–8.

Maisey, J. G. 2012. What is an 'elasmobranch'? The impact of palaeontology in understanding elasmobranch phylogeny and evolution. *J. Fish Biol*. 80: 918–951.

Maisey, J. G., et al. 2017. Pectoral morphology in *Doliodus* bridges the 'acanthodian'-euchondrichthyan divide. *Am. Mus. Novitates* 3875: 1–15.

Märss, T. and A. Ritchie. 1999. Articulated thelodonts (Agnatha) of Scotland. *Trans. R. Soc. Edinburgh, Earth Sciences* 88: 143–195.

Märss, T., et al. 2007. Agnatha II – Thelodonti. In: *Handbook of Palaeoichthyology*, Vol. 1B. Munchen: Verlag Dr. Friedrich Pfeil.

Meunier, F. J., et al. 2015. Presence of plicidentine in the oral teeth of the coelacanth *Latimeria chalumnae* Smith 1939 (Sarcopterygii; Actinistia). *J. Struct. Biol*., 190: 31–37.

Meunier, F. J., et al. 2018. Histological study of the jaw teeth in the Devonian actinopterygian† *Cheirolepis canadensis* (Whiteaves). *Cybium* 42: 67–74.

Mickoleit, G. 2004. *Phylogenetische Systematik der Wirbeltiere*. Munich: Pfeil.

Mondéjar-Fernández, J. 2018. On cosmine: Its origins, biology and implications for sarcopterygian interrelationships. *Cybium* 42: 41–65.

Mondéjar-Fernández, J. 2020. A new onychodont (Osteichthyes; Sarcopterygii) from the Middle Devonian of Morocco and its bearing on early osteichthyan evolution. *J. Syst. Palaeontol*. 18: 573–606.

Mondéjar-Fernández, J. and G. Clément. 2012. Squamation and scale microstructure evolution in the Porolepiformes (Sarcopterygii, Dipnomorpha) based on *Heimenia ensis* from the Devonian of Spitsbergen. *J. Vert. Paleontol*. 32: 267–284.

Mondéjar Fernández, J. and F. J. Meunier. 2020. New histological information on *Holoptychius* Agassiz, 1839 (Sarcopterygii, Porolepiformes) provides insights into the palaeoecological implications and evolution of the basal plate of the scales of osteichthyans. *Hist. Biol*. 1–13.

Mondéjar-Fernández, J., et al. 2014. New insights into the scales of the Devonian tetrapod *Tulerpeton curtum* Lebedev, 1984. *J. Vert. Paleont*. 34: 1454–1459.

Mondéjar-Fernández, J., et al. 2020. A lungfish (Sarcopterygii, Dipnomorpha) tooth–plate from the Lower Devonian of Vietnam and the onset of modern dipnoan dental organization. *J. Vert. Paleontol*., 40: e1772274. DOI 10.1080/02724634.2020.1772274.

Moy-Thomas, J. A. and Miles, R. S. 1971. *Palaeozoic fishes*. Chapman and Hall, London.

Murdock, D. J. E., et al. 2013. The origin of conodonts and of vertebrate mineralized skeletons. *Nature* 502: 546–549.

Newman, M. J. 2002. A new naked jawless vertebrate from the Middle Devonian of Scotland. *Palaeontology*. 45: 933–941.

Novitskaya, L. I. 1971. Les Amphiaspides (Heterostraci) du Dévonien de la Sibérie. *Cahiers de Paléontologie*. Paris: Centre National de la Recherche Scientifique.

Ørvig, T. 1965. Palaeohistological notes. 2. Certain comments on the phyletic significance of acellular bone tissue in early lower vertebrates. *Arkiv Zool*. 16: 551–556.

Ørvig, T. 1968. The dermal skeleton: general consideration. In *Current Problems of Lower Vertebrate Phylogeny*, T. Ørvig ed., 373–397. Stockholm: Almqvist and Wiksell.

Ørvig, T. 1969. Cosmine and cosmine growth. *Lethaia* 2: 241–260.

Ørvig, T. 1989. Histologic studies of ostracoderms, placoderms and fossil elasmobranchs. 6. Hard tissues of Ordovician vertebrates. *Zool. Scripta* 18: 427–446.

O'shea, J., et al. 2019. The dermal skeleton of the jawless vertebrate *Tremataspis mammillata* (Osteostraci, stem-Gnathostomata). *J. Morphol*. 280: 999–1025.

Purnell, M. A. 2002. Feeding in extinct jawless heterostracan fishes and testing scenarios of early vertebrate evolution. *Proc. R. Soc*. B269(1486): 83–88.

Qiao, T. and M. Zhu. 2010. Cranial morphology of the Silurian sarcopterygian. *Sci. China Earth Sci*. 53: 1836–1848.

Qu, Q., et al. 2013a. Scales and dermal skeletal histology of an early bony fish, *Psarolepis romeri* and their bearing on the evolution of rhombic Scales and hard tissues. *PLoS One* 8: e61485.

Qu, Q., et al. 2013b. Scales and tooth whorls of ancient fishes challenge distinction between external and oral 'teeth'. *PLoS One* 8: e71890.

Qu, Q., et al. 2015. Three-dimensional virtual histology of silurian osteostracan scales revealed by synchrotron radiation microtomography. *Journal of morphology 276*(8): 873–888.

Qu, Q. S., et al. 2017. The origin of novel features by changes in developmental mechanisms: ontogeny and three-dimensional microanatomy of polyodontode scales of two early osteichthyans. *Biol. Rev. Camb. Philos. Soc*.92: 1189–1212.

Randle, E. and R. S. Sansom. 2016. Exploring phylogenetic relationships of Pteraspidiformes Heterostracans (stemgnathostomes) using continuous and discrete characters. *J. Syst. Palaeont*. 15: 583–599.

Ritchie, A. 1968. New evidence on *Jamoytius kerwoodi* White, an important ostracoderm from the Silurian of Lanarkshire, Scotland. *Paleontology* 11: 21–39.

Ritchie, A. 1984. Conflicting interpretations of the Silurian agnathan. *Jamoytius. Scot. J. Geol*. 20: 249–256.

Rücklin, M. and P. C. J. Donoghue. 2013. Development of teeth and jaws in the earliest jawed Vertebrates. *Nature* 491: 758–781.

Rücklin, M. and P. C. J. Donoghue. 2015. *Romundina* and the evolutionary origin of teeth. *Biol. Lett*. 11: 20150326.

Sansom, I. J., et al. 1997. *Astraspis* - The anatomy and histology of an Ordovician fish. *Palaeontology*, 30: 625–643.

Sansom, I. J., et al. 2005. Histology and affinity of the earliest armoured vertebrate. *Biol. Lett*. 1: 446–449.

Sansom, R. S. 2009. Phylogeny, classification and character polarity of the Osteostraci. *J. Syst. Palaeont*. 7: 95–115.

Sansom, R. S., et al. 2010. Taphonomy and affinity of an enigmatic Silurian vertebrate, Jamoytius kerwoodi White. *Palaeontology*, 53: 1393–1409.

Sansom, R. S., et al. 2013. Atlas of vertebrate decay: a visual and taphonomic guide to fossil interpretation. *Palaeontology*, 56: 457–474.

VetBooks.ir

Schultze, H. P. 1969. Die Faltenzähne der Rhipidistiden Crossopterygier, der Tetrapoden und der Actinopterygier-gattung *Lepisosteus*. *Palaeontogr. Ital*. 65: 63–136.

Schultze, H. P. 1970. Folded teeth and the monophyletic origin of tetrapods. *Am. Mus. Novit.* no. 2408.

Schultze, H. P. 1996. Conodont histology: an indicator of vertebrate relationship? *Modern Geol.* 20: 275–285.

Schultze, H. P. 2016. Scales, enamel, cosmine, ganoine, and early osteichthyans. *C. R. Palevol.* 1–2: 83–102.

Schultze, H. P. 2018. Hard tissues in fish evolution. *Cybium* 218: 29–42.

Shu, D. G., et al. 1996. A *Pikaia*-like chordate from the Lower Cambrian of China. *Nature* 384: 157–158.

Shu, D. G., et al. 1999. Lower Cambrian vertebrates from South China. *Nature* 402: 42–46.

Shu, D. G., et al. 2003. Head and backbone of the early Cambrian vertebrate *Haikouichthys*. *Nature* 421: 526–529.

Sire, J. Y., et al. 2009. Origin and evolution of the integumentary skeleton in non-tetrapod vertebrates. *J. Anat.* 214: 409–440.

Smith, M. M. and B. K. Hall. 1993. A developmental model for evolution of the vertebrate exoskeleton and teeth. The role of cranial and trunk neural crest. *Evol. Biol.* 27: 387–448.

Smith, M. M. and Z. Johanson. 2003. Separate evolutionary origins of teeth from evidence in fossil jawed vertebrates. *Science* 299: 1235–1236.

Smith, M. M., et al. 2017. Evolutionary origins of teeth in jawed vertebrates: conflicting data from acanthothoracid dental plates ('Placodermi'). *Palaeontology*, 60: 829–836.

Smith, M. P. and I. J. Sansom. 1995. The affinity of *Anatolepis* Bockelie and Fortey [L'affinité d' Anatolepis Bockelie & Fortey]. *Geobios* 19: 61–63.

Stensiö, E. A. 1927. The Devonian and Downtonian vertebrates of Spitsbergen. 1. Family Cephalaspidae. *Skr. Svalbard Ishavet* 12: 1–391.

Stensiö, E. A. 1964. Les Cyclostomes fossiles ou Ostracodermes; In *Traité de Paléontologie,* Vol. 4(1), J. Piveteau ed., 96–383. Paris: Masson.

Thomson, K. S. 1975. On the biology of cosmine. *Bull. Peabody Mus. Nat. Hist.* 40: 1–57.

Turner, S., et al. 2010. False teeth: conodont-vertebrate phylogenetic relationships revisited. *Geodiversitas* 32: 545–594.

Valiukevicius, J. 1995. Acanthodian histology: some significant aspects in taxonomical and phylogenetical research. *Geobios*, 28(suppl.): 157–159.

Valiukevicius, J. and C. J. Burrow. 2005. Diversity of tissues in acanthodians with Nostolepis-type histological structure. *Acta Palaeontol. Pol.* 50: 635–649.

Wang, N.-Z., et al. 2005. Histology of the galeaspid dermoskeleton and endoskeleton, and the origin and early evolution of the vertebrate cranial skeleton. *J. Vert. Paleont.* 25: 745–756.

Wängsjö, G. 1952. The Downtonian and Devonian vertebrates of Spitsbergen. 9. Morphologic and systematic studies of the Spitsbergen cephalaspids. *Norsk Polarinst.Skr.* 97: 1–611.

White, E. I. 1946. *Jamoytius kerwoodi*, a new chordate from the Silurian of Lanarkshire. *Geol. Mag.* 83: 89–97.

Wilson, M. V. and M. W. Caldwell. 1993. New Silurian and Devonian fork-tailed'thelodonts' are jawless vertebrates with stomachs and deep bodies. *Nature* 361(6411): 442–444.

Wilson, M. V. H. and M. W. Caldwell. 1998. The Furcacaudiformes: a new order of jawless vertebrates with thelodont scales, based on articulated Silurian and Devonian fossils from Northern Canada. *J. Vert. Paleont.* 18: 10–29.

Wilson, M. V. H. and T. Märss. 2009. The thelodont phylogeny revisited, with inclusion of key scale-based taxa. *Estonian J. Earth Sci.* 58: 297–310.

Wilson, M.V.H. and T. Märss. 2012. Anatomy of the Silurian thelodont *Phlebolepis elegans* Pander. *Estonian J. Earth Sci.* 61: 261–276.

Witzmann, F. 2011. Morphological and histological changes of dermal scales during the fish-to-tetrapod transition *Acta Zool. Stockholm* 92: 281–302.

Woodward, A. S. 1891. *Catalogue of Fossil Fishes in the British Museum (Natural History). Part 2. Containing the Elasmobranchii (Acanthodii), Holocephali, Ichthyodorulites, Ostracodermi, Dipnoi, and Teleostomi (Crossopterygii and chondrostean Actinopterygii).* London: Taylor & Francis.

Young, G. C. 1991. The first armoured agnathan vertebrates from the Devonian of Australia. In *Early Vertebrates and Related Problems of Evolutionary Biology*, M. M. Chang, Y. H. Liu and G. R. Zhang eds., 67–85. Beijing: Science Press.

Young, G. C. 2003. Did placoderm fish have teeth? *J. Vert. Paleontol*. 23: 987–990.

Young, G. C. 2010. Placoderms (Armored Fish): Dominant Vertebrates of the Devonian Period. *Ann. Rev. Earth Planet. Sci.* 38: 523–550.

Young, G. C. and Lu, J. 2020. Asia–Gondwana connections indicated by Devonian fishes from Australia: palaeogeographic considerations. *Journal of Palaeogeography*. 9: 1–22.

Yu, X. 1998. A new porolepiform-like fish, *Psarolepis romeri*, gen. et sp. nov. (Sarcopterygii, Osteichthyes) from the Lower Devonian of Yunnan, China. *J. Vertebr. Paleontol.* 18: 261–274.

Zhu, M. and P. Janvier. 1998. The histological structure of the endoskeleton in galeaspids (Galeaspida, Vertebrata). *J. Vert. Paleontol.* 18: 650–654.

Zhu, M. and X. Yu. 2009. Stem sarcopterygians have primitive polybasal fin articulation. *Biol. Lett.* 5(3): 372–375.

Zhu, M., et al. 1999. A primitive fossil fish sheds light on the origin of bony fishes. *Nature* 397(6720): 607–610.

Zhu, M. et al. 2006. A primitive fish provides key characters bearing on deep osteichthyan phylogeny. *Nature* 441: 77–80.

Zhu, M., et al. 2009. The oldest articulated osteichthyan reveals mosaic gnathostome characters. *Nature* 458: 469–474.

Zhu, M., et al. 2010. *Meemannia eos*, a basal sarcopterygian fish from the Lower Devonian of China – expanded description and significance. In *Morphology, Phylogeny and Paleobiogeography of Fossil Fishes*, D. K. Elliot, J. G. Maisey, X. Yu and D. Miao eds., 199–214. München, Germany: Friedrich Pfeil.

VetBooks.ir

Zhu, M., et al. 2012. Fossil fishes from China provide first evidence of dermal pelvic girdles in Osteichthyans. *PLoS One* 7: e35103.

Zhu, M., et al. 2013. A Silurian placoderm with osteichthyan-like marginal jaw bones. *Nature* 502: 188–193.

Zhu, M., et al. 2016. A Silurian maxillate placoderm illuminates jaw evolution. *Science*, 354(6310): 334–336.

Žigaitė, Ž., et al. 2013. Tissue diversity and evolutionary trends of the dermal skeleton of Silurian thelodonts. *Hist. Biol*. 25: 143–154.

Zylberberg, L., et al. 1980. Structure of the dermal scales in Gymnophiona (Amphibia). *J. Morphol*. 165: 41–54.

Zylberberg, L., Meunier, F. J. and Laurin, M. 2016. A microanatomical and histological study of the postcranial dermal skeleton of the Devonian actinopterygian *Cheirolepis canadensis*. *Acta Palaeontologica Polonica*. 61: 363–376.

VetBooks.ir

16

Early Tetrapodomorphs

Sophie Sanchez, François Clarac, Michel Laurin and Armand de Ricqlès

CONTENTS

Phylogenetic, Evolutionary and Biological Considerations 326
General Characteristics 326
Finned Stem-tetrapods 327
Limbed Stem-tetrapods 327
Temnospondyls 327
Embolomeres 328
Seymouriamorphs 328
Lepospondyls 328
Bone Microanatomy and Histology 328
Finned Stem-tetrapods 328
Tooth Microstructure 329
Postcranial Dermal Bone Microstructure (Scales and Rays) 329
Cosmine Evolution 329
Skull and Girdle Bone Microstructure 329
Fin Bone Microanatomy and Histology 329
General Conclusion 331
Limbed Stem-tetrapods 331
Tooth Microstructure 331
Postcranial Dermal Bone Microstructure (Scutes and Rays) 331
Skull and Girdle Bone Microstructure 332
Limb Bone Microanatomy and Histology 332
General Conclusion 332
Temnospondyls 333
Limb Bone Microanatomy and Histology 333
Skull Bone Microstructure 333
Scute and Osteoderm Microstructure 335
Vertebral Microstructure 335
Tooth Microstructure 335
General Conclusion 335
Embolomeres 336
Long Bone Microanatomy and Microstructure 336
Scute Microstructure 336
General Conclusion 336
Seymouriamorphs 336
Limb Bone Microanatomy and Histology 336
Skull Bone Microstructure 337
Vertebral Microstructure 338
Scute Microstructure 338
General Conclusion 338

Lepospondyls 338
Jawbone Histology 338
Skull Bone Microstructure 338
Vertebral Microstructure 339
Scute Microstructure 339
General Conclusion 339
Acknowledgments 339
References 339

Phylogenetic, Evolutionary and Biological Considerations

General Characteristics

Tetrapodomorphs (Ahlberg 1991) comprise extant limbed vertebrates including amphibians and pan-amniotes (crown-tetrapods) as well as the extinct taxa that are more closely related to them than to lungfish (Dipnoi) (Figure 16.1). These extinct groups are called stem-tetrapods and form a paraphyletic grade (Figure 16.1).

Major morphological changes related to the water-to-land transition occurred within stem-tetrapods (Laurin 2010; Clack 2012). Notably, the internal nostril ("choana") evolved during the Early Devonian, about 403 million years (My) ago. The migration of this nostril between the maxilla and premaxilla has been observed in one of the earliest known stem-tetrapods, *Kenichthys* (Figure 16.1) (Zhu and Ahlberg 2004). It probably enhanced olfaction for hunting more than air-breathing abilities (Janvier 2004). The intracranial joint that allowed mobility between ethmoid and otico-occipital portions of the skull is an adaptation to breathing and feeding underwater (Downs et al. 2008). It was involved in bite force generation and probably increased the range of prey the animal could feed on (Dutel et al. 2015). It is present and mobile in *Eusthenopteron*, still present, even though immobile in *Panderichthys* (Ahlberg et al. 1996) and *Tiktaalik* (Downs et al. 2008), and fused in limbed stem-tetrapods (*Acanthostega*, *Ichthyostega*) (Ahlberg et al. 1996). The body shape rapidly became crocodile-like in stem-tetrapods: the skull roof flattened, the midline fins disappeared, the gill apparatus was reduced with the disappearance of the bony gill cover and the shoulder girdle became independent of the skull (Janvier 1996; Clack 2012; Ahlberg 2019). The hyomandibular bone was modified into a stapes presumably more than 390 My ago (Brazeau and Ahlberg 2006; Niedzwiedzki et al. 2010; Ahlberg 2019) and evolved later into the tetrapod middle ear (Clack, 2002). Recent studies describing the earliest limbed vertebrate complete enough to be reconstructed (*Parmastega*, dated from 372 My, Beznosov et al. 2019) and limb tracks dated from 395 My (Niedzwiedzki et al. 2010) show that all these features probably appeared even earlier than expected in the evolutionary history of stem-tetrapods. Until recently, limbs were thought to have evolved from bony fins in the late Devonian (Clack 2012). The recent discovery of tetrapod trackways attests to the evolution of paired finned appendages into limbs more than 395 My ago, in the late Early Devonian (Niedzwiedzki et al. 2010). In parallel, the pelvis became connected to the vertebral column (Ahlberg et al. 2005; Clack 2009; Shubin et al. 2014). The combination of these morphological innovations played a major role in the adaptation of four-legged vertebrates to land and their radiation worldwide (Clack 2012).

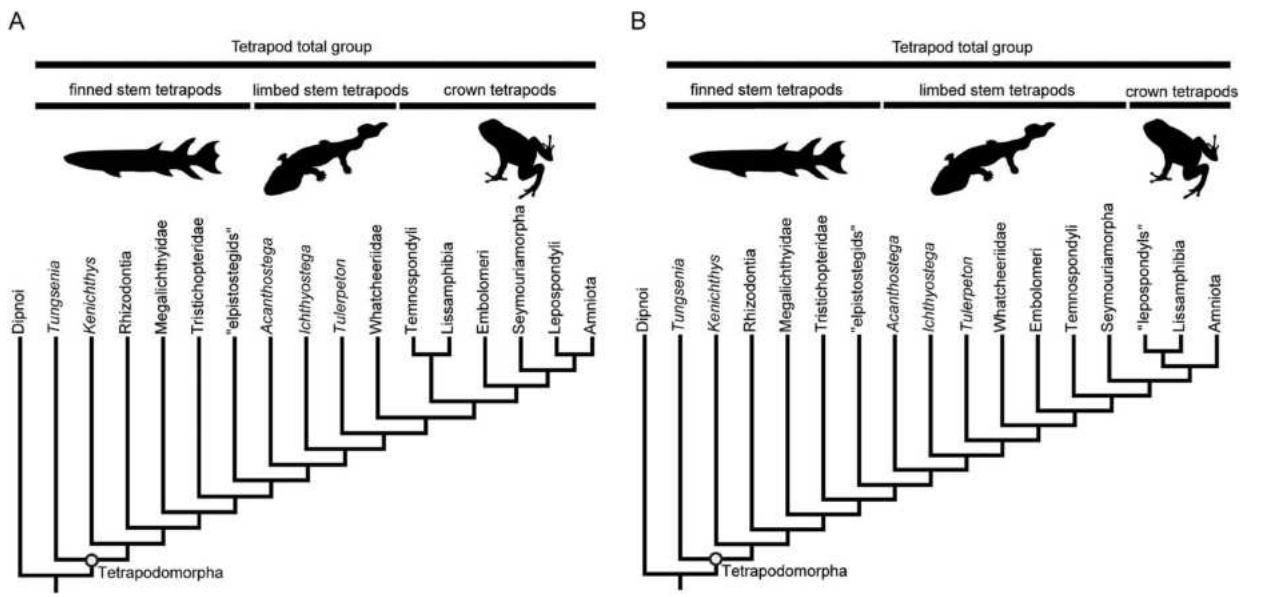


FIGURE 16.1 Phylogenetic relationships of tetrapodomorphs. A, Hypothesis modified from the phylogenies proposed by Ruta and Coates (2007), Ruta et al. (2003, 2007) and Pardo et al. (2017a,b). B, Hypothesis modified from the phylogenies proposed by Vallin and Laurin (2004) and Marjanović and Laurin (2019).

VetBooks.ir

Limbed tetrapods, called stegocephalians by Laurin (2020), comprise a large diversity of non-amniotic taxa including stem limbed tetrapods, temnospondyls, seymouriamorphs and lepospondyls. These groups encompass a total of about 30 clades (Marjanović and Laurin 2019) spanning from the Middle or late Early Devonian, i.e., 395 My (*Ichthyostega*-like tetrapod, Niedzwiedzki et al. 2010) to the Early Cretaceous, i.e.,120 My (*Koolasuchus*, Warren et al. 1997). They evolved a large range of locomotor abilities and occupied a great diversity of ecological and adaptive zones (e.g., Laurin 2010; Sanchez et al. 2010b; Schoch 2014). For many reasons (discussed in Chapter 17), their phylogenetic distribution relative to crown-tetrapods has long been debated (Ruta et al. 2003, 2007; Vallin and Laurin 2004; Anderson 2007; Marjanović and Laurin 2009, 2019; Pardo et al. 2017a, b; Laurin et al. 2019) (Figure 16.1) and will certainly continue to be until new fossils are discovered (Parsons and Williams 1963; Ahlberg 2019). Evolutionary implications of bone histological studies in stegocephalians will be discussed in the context of various reference phylogenies.

Finned Stem-tetrapods

Finned stem-tetrapods were most diverse during the Middle and Late Devonian (Clack 2012; Swartz 2012). They formed a very large and speciose paraphyletic group (Ahlberg and Johanson 1997, 1998) (Figure 16.1). Finned stem-tetrapods include the most basal member of the grade, *Tungsenia,* from the Early Devonian of China (Lu et al. 2012); *Kenichthys*, dated from about 403 My (Zhu and Ahlberg 2004), and more apical forms such as the rhizodonts, one of the clades of finned stem-tetrapods that survived the Devonian-Carboniferous crisis and persisted until the Pennsylvanian, i.e., late Carboniferous (Swartz 2012). Many small clades formerly recognized as "osteolepidids," including some megalichthyids, survived until the Permian (Witzmann and Schoch 2012), as did the large monophyletic group of Devonian tristichopterids (Ahlberg and Johanson 1998) and members of the Devonian "elpistostegid" grade (Daeschler et al. 2006; Swartz 2012). They were distributed worldwide because faunal interchanges already existed during the Middle-Late Devonian between the southern and northern paleocontinents (Johanson 2004; Young et al. 2013). In turn, this suggests marine dispersal capabilities for many of these taxa (Janvier 2003; Goedert et al. 2018). They display a great variety of body shapes: some taxa such as *Kenichthys, Gogonasus* and *Osteolepis* are rather small with a generalized fusiform body shape (Ahlberg and Johanson 1998), whereas tristichopterids have a larger, longer trunk similar to that of recent ambush predators (Ahlberg and Johanson 1997; Young et al. 2013), and only elpistostegids show tetrapod features such as a crocodile-like skull with dorsal raised orbits, derived humeral morphology and an elongated tail fin (e.g., *Tiktaalik*, Shubin et al. 2006; *Elpistostege*, Ahlberg 2019; Cloutier et al. 2020). Extremely large forms emerged within the tristichopterids (e.g., *Hyneria* with a body length up to 3 m, Daeschler and Downs 2018; Kamska et al. 2019; *Edenopteron* with a body length up to 2.5 m, Young et al. 2013) and rhizodonts (Andrews 1985; Ahlberg and Johanson 1998).

Limbed Stem-tetrapods

Limbed stem-tetrapods include the earliest four-legged vertebrates, which spanned from the Middle Devonian (Stössel 1995; Niedzwiedzki et al. 2010; Stössel et al. 2016) to at least the Carboniferous (Ruta and Coates 2007; Anderson et al. 2015), and possibly well into the Cretaceous (Warren et al. 1991; Marjanović and Laurin 2019), depending on the reference phylogeny used. They form a paraphyletic group.

Most Devonian limbed stem-tetrapods were located in Laurasian (sub)tropical regions (including Europe, Greenland, North America and Russia) (Clément et al. 2004; Clack 2012; Beznosov et al. 2019), but a few Devonian tetrapods from Gondwana were discovered in Australian localities (trackways, Warren and Wakefield 1972; *Metaxygnathus*, Campbell and Bell 1977), Chinese localities (Zhu et al. 2002) and southern polar regions from South Africa (Gess and Ahlberg 2018). They were mainly aquatic, even though some of them could venture out of the water (Ahlberg et al. 2005; Shubin et al. 2006; Laurin 2010; Niedzwiedzki et al. 2010; Clack 2012; Pierce et al. 2012). They could be relatively small (the smallest is estimated at 25 cm, Ahlberg and Clack 2020) or 2–3 m long (Niedzwiedzki et al. 2010). More taxa than previously thought survived the end-Devonian extinction event (Anderson et al. 2015; Ahlberg and Clack 2020). The Carboniferous taxa suffered from a taphonomic bias called Romer's gap (Romer 1956; Coates and Clack 1995; Clack and Carroll 2000; Smithson and Clack 2018). However, recent studies have demonstrated that, when a window into this time period was discovered, a rich fauna of tetrapods was flourishing (Anderson et al. 2015). A few main localities provided a great diversity of limbed stem-tetrapods (the Tournaisian Ballagan Formation of the Scottish Borders, Clack et al. 2016 and Otoo et al. 2019; the Tournaisian locality of Blue Beach in Canada, Anderson et al. 2015; the mid-Viséan Ducabrook Formation in central Queensland, Australia, Parker and Webb 2008). In these localities were discovered extinct forms with reduced limbs and elongated bodies (e.g., *Colosteus*, *Crassigyrinus*, *Greererpeton*) and others with strong and well-ossified legs (*Ossinodus, Pederpes*). This diversity probably correlates with a large range of paleoecologies, among which amphibious and terrestrial lifestyles have been described (Mansky and Spencer 2013). Not only do the Carboniferous tetrapods show a great variety of forms but they also obviously diverge in their size range, with small forms such as *Diploradus* (lower jaw length: 30 mm) and *Aytonerpeton* (reconstructed skull length: 50 mm), and others about twice as large such as *Koilops* (skull length: 80 mm) and *Perittodus* (lower jaw length: 68 mm) (Clack et al. 2016; Ahlberg and Clack 2020). Although debated (Marjanović and Laurin 2019), the tetrapod *Lethiscus*, from the Middle Viséan of Scotland, has recently been suggested to be a stem-tetrapod (Pardo et al. 2017a). As such, it would represent the oldest known limbless stem-tetrapod and thus participate in increasing the flourishing morphological diversity of the Devonian/Carboniferous tetrapod stem.

Temnospondyls

They form the most diversified and largest group of extinct non-amniotic tetrapods (Schoch 2013a). Depending on the hypothesis favored regarding the origin of lissamphibians, temnospondyls

VetBooks.ir

are considered a grade (Ruta et al. 2007; Anderson 2008; Pardo et al. 2017b) or a clade (Vallin and Laurin 2004; Marjanović and Laurin 2019) (Figure 16.1). They comprise 200 genera and more than 290 species that lived for about 250 My over the Paleozoic and Mesozoic (Warren and Davey 1992; Warren 2000; Schoch 2013a; Fortuny and Steyer 2019). They originated in the Early Carboniferous (Milner 1990; Milner and Sequeira 1993), reached a peak of diversity in the Permian and Triassic (Milner 1990; Ruta and Benton 2008) and fully disappeared in the Cretaceous (the latest occurrence of a temnospondyl, identified as a brachyopoid, is dated from the Early Cretaceous, Warren 2000; Warren and Davey 1992; Warren et al. 1991, 1997). They have been excavated worldwide (Milner 1990; Warren et al. 2001; Steyer and Damiani 2005; Steyer et al. 2006; Maisch and Matzke 2005; Sidor et al. 2005; Jenkins et al. 2008; Steyer and Jalil. 2009) and displayed a large developmental and physiological plasticity (Schoch 2004, 2013a; Witzmann 2006; Fröbisch et al. 2010; Sanchez et al. 2010a; Sanchez and Schoch 2013) to adapt to all kinds of ecological zones. Some temnospondyls lived in aquatic environments that differed in the nature and size of the water body, as well as the degree of salinity (Boy 1993; Laurin and Soler-Gijón 2010; Schoch and Witzmann 2014); some were more amphibious to terrestrial, and inhabited coal swamps to tropical forests, or even lived in harsh dry conditions (e.g., Schoch 2014; Canoville and Chinsamy 2015). They ranged in size from the 5-cm-long *Apateon* (Schoch 2004) to the 6-m-long *Mastodonsaurus* (Schoch 1999). Some isolated remains of the skull of a brachyopoid even suggested a temnospondyl of about 7 m (Steyer and Damiani 2005). Although greatly dependent on the aquatic environment for reproduction and development, they evolved a diversity of locomotor abilities (Sanchez et al. 2010b; Marsicano et al. 2014; Mujal and Schoch 2020).

Embolomeres

They are represented by crocodile-like anthracosaurs (Smithson 2000; Ruta and Clack 2006). Depending on the phylogenetic reconstructions and nomenclature used (Laurin and Smithson 2020), anthracosaurs can be considered a grade or a clade, and may be stem amniotes (Smithson 2000; Ruta and Clack 2006) or stem-tetrapods (Marjanović and Laurin 2019) (Figure 16.1). Embolomeres are characterized by terrestrial forms and aquatic taxa that could reach about 2 m for the largest species (Holmes 1984; Smithson 2000). They are found from the Carboniferous (e.g., *Proterogyrinus*, Romer 1970) to the Permian (e.g., *Archeria*, Romer 1957). They are known from Europe and North America (Smithson 2000).

Seymouriamorphs

Depending on hypotheses, the seymouriamorphs are either a clade of stem-tetrapods (Laurin and Reisz 1997; Marjanović and Laurin 2019) or stem amniotes (Ruta et al. 2003; Ruta and Coates 2007) (Figure 16.1). They represent a relatively small group of tetrapods, with fewer than 10 genera discovered so far (Klembara and Ruta 2005b; Ruta et al. 2007). They are known from the Late Carboniferous to the Late Permian in Europe, Asia (Kazakhstan former microcontinent) and America (White 1939; Bystrow 1944; Zhang et al. 1984; Berman et al. 1987; Klembara and Meszároš 1992; Berman and Martens 1993; Laurin 1996a, b). Seymouriamorphs are relatively small compared to temnospondyls. The largest adult seymouriamorph has a maximal skull length of about 15 cm (*Seymouria*, Laurin 2000). The developmental biology of seymouriamorphs is relatively well documented: many specimens of different sizes have been thoroughly investigated for each species (Klembara and Ruta 2004a, 2005a; Klembara et al. 2006). However, some disparities in their developmental distributions can be observed: hundreds of discosauriscid fossils have been excavated, but most of them were identified as larvae and juveniles (Sanchez et al. 2008), and many fewer specimens of *Seymouria* were discovered, but both juvenile and adult forms could be studied (Berman et al. 2000). Although they all exhibit an early development in the aquatic environment, they lose their lateral line canal, ampullary organs and external gills at the adult stage (Klembara 1994), suggesting that adults were terrestrial (Kriloff et al. 2008). They had a sprawling gait with a relatively slow pace (Marchetti et al. 2017), and they used a marked lateral movement of the body trunk to move (Marchetti et al. 2017).

Lepospondyls

They have long been considered both a clade (Ruta et al. 2003; Ruta and Coates 2007) and a grade (Vallin and Laurin 2004; Marjanović and Laurin 2019) of tetrapods (Figure 16.1). Some recent studies have suggested that they were a polyphyletic group (e.g., Pardo et al. 2017a). They lived from the Viséan (Middle Carboniferous) to the late Permian (Anderson 2001; Anderson et al. 2003; Germain 2010). They were essentially discovered in North America and Europe, meaning that most of them were probably living in the tropical region of the northern supercontinent of Pangea, Laurasia. Nevertheless, some occurrences of diplocaulids in Morocco suggest that some lepospondyls were living in Gondwana (North Africa), at least during the late Permian (Germain 2010). They are often classified into five orders. They are on average smaller than temnospondyls (Anderson 2001). Most lepospondyls were aquatic, with a rather long body and reduced limbs, even though the most diverse group of lepospondyls, represented by Microsauria, also includes short terrestrial morphotypes (e.g., *Archerpeton anthracos*, Reisz and Modesto 1996). Some nectrideans had some anatomical peculiarities such as “horns” (actually hyperelongated posterolateral skull roof bones) at the rear of the cranium, giving a boomerang-like shape to their skull (e.g., *Diplocaulus*, Cruickshank and Skews 1980).

Bone Microanatomy and Histology

Finned Stem-tetrapods

Very few paleohistological studies have been carried out on finned stem-tetrapods. Most of them have focused on tooth histology (Schultze 1970) as a tool to identify isolated remains (Clément 2002; Clément and Janvier 2004; Davesne et al. 2015). Nevertheless, the evolution of scale histology has gained more attention (Zylberberg et al. 2010; Witzmann 2011; Mondéjar-Fernández et al. 2014), and more specifically the

VetBooks.ir

evolution of cosmine within sarcopterygians has been a topic of debate (Qu et al. 2017; Mondéjar-Fernández 2018; see also Chapter 15). Endoskeletal elements have barely been investigated. Jarvik (1952) described the bone histology of vertebrae in a finned stem-tetrapod, *Eusthenopteron*, but no follow-up on this topic was provided. Recent studies have somehow shifted the focus of paleohistological investigations to long-bone histology to understand a key evolutionary event: the fin-to-limb transition (Laurin et al. 2007; Meunier and Laurin 2012; Sanchez et al. 2014; Kamska et al. 2019).

Tooth Microstructure

Schultze (1970) was the first contemporary researcher to describe in detail the tooth microstructure of finned stem-tetrapods. His work laid the foundation for many other researchers to recognize taxa on the basis of their dental histology (Clément 2002; Clément and Janvier 2004; Davesne et al. 2015). Schultze (1970) identified three different tooth microstructural configurations in finned stem-tetrapods: (1) *simple conical teeth* with little or no folding of the orthodentine (e.g., *Gyroptychius, Latvius, Osteolepis, Thursius*); (2) *polyplocodont teeth* with a simply folded orthodentine associated with irregular branches, free pulp cavities and a bone of attachment extended between folds (e.g., *Eusthenopteron, Megalichthys, Panderichthys, Rhizodopsis, Rhizodus, Sauripteris, Strepsodus, Tristichopterus*) and (3) *eusthenodont teeth* with a more complicated folding of the orthodentine, pulp cavities filled with osteodentine and a bone of attachment extended between folds (e.g., *Eusthenodon*, *Litoptychus*, *Platycephalichthys*).

Postcranial Dermal Bone Microstructure (Scales and Rays)

Major morphological changes of the scales first evolved in elpistostegids, accompanying terrestrialization (Witzmann 2011; Mondéjar-Fernández et al. 2014). The rhombic scales of finned stem-tetrapods differentiated into ventral gastral and dorsal round scales. This morphological change persisted in limbed stem-tetrapods (Witzmann 2011) and permitted a greater anteroposterior overlap between the scale rows, allowing a greater flexibility of the body (Witzmann 2011). In parallel, the scale microstructure became simplified: the superficial cosmine layer disappeared, the bone matrix became parallel-fibered and bore a succession of growth marks and the thick basal layer of isopedin was drastically reduced (Castanet et al. 1975; Witzmann 2011; Mondéjar-Fernández et al. 2014). This simplification began in some taxa of tristichopterids such as *Eusthenopteron* (Zylberberg et al. 2010). It possibly lowered the body weight, limited the visceral compression and likely improved trunk flexibility (Zylberberg et al. 2010; Mondéjar-Fernández et al. 2014).

Regarding the fin-rays (lepidotrichia) of finned stem-tetrapods, little histological investigation has been carried out so far (Zylberberg et al. 2010). As in actinopterygians (Hall 2008; Zylberberg et al. 2016), the rays of the tristichopterid *Eusthenopteron* form a series of long slender elements in the proximal region of the fin and separate into hemisegments where the lepidotrichia branch more distally. They display a (hemicylindrical) compact organization with concentric annuli and lines of arrested growth (Zylberberg et al. 2010; Sanchez et al. 2014). Longitudinal sections of rays show that the cell lacunae are flattened and align along longitudinally oriented fibers (Zylberberg et al. 2010). A skeletochronological analysis of the proximal section of lepidotrichia allowed the assessment of the overall development of *Eusthenopteron* and suggested a life span of at least 11 years with a long prereproductive period (Sanchez et al. 2014).

Cosmine Evolution

Cosmine (eucosmine) is "a combination of dermal tissues composed of a single layer of enamel and dentine incorporating a well-developed pore canal system overlying a vascular bone layer" (cited from Sire et al. 2009; Mondéjar-Fernández 2018; see also Chapter 15). A thick layer of cosmine covers the remnants of dermal skull and lower jaw of the most basal stem-tetrapod, *Tungsenia* (Mondéjar-Fernández 2018). *Kenichthys* also displays a layer of cosmine on dermal bones and rhombic scales (Zhu and Ahlberg 2004; Mondéjar-Fernández 2018). However, it is unknown so far in all rhizodontids and it is absent in some osteolepiforms (e.g., *Canowindra*, tristichopterids) (Mondéjar-Fernández 2018). In the osteolepiforms, where odontogenetic tissues are found, cosmine is present under different forms (Qu et al. 2017; Mondéjar-Fernández 2018): (1) complete cosmine sheets in *Gogonasus*, (2) cosmine separated by areas of naked bone like Westoll line (e.g., *Osteolepis* and *Gyroptychius*), (3) blisters of cosmine in *Ectosteorhachis*, (4) unfinished cosmine, considered an early ontogenetic stage in *Ectosteorhachis,* and (5) tubercles of cosmine (e.g., *Ectosteorhachis* and *Lamprotolepis*). Cosmine is lost in the dermoskeleton of elpistostegids and limbed stem-tetrapods (Thomson 1975; Mondéjar-Fernández 2018; see also Chapter 38).

Skull and Girdle Bone Microstructure

In his large review on dermal bone microstructure, Witzmann (2009) studied the dermal bone of one finned stem-tetrapod, *Panderichthys*. The bone has a compact external and internal layer framing a spongy middle layer. The external layer is relatively vascularized with primary vascular canals and a few osteons, whereas the inner layer is thinner but more compact. Both layers exhibit a pseudolamellar bone matrix. The middle layer is very cancellous. This overall microstructural organization greatly resembles the dermal bone histology of the porolepiform *Laccognathus* (Witzmann 2009). This means that both the histology and morphology of dermal bone largely remain conservative despite the evolution of numerous crownward anatomical features in the rest of the body in elpistostegids.

Fin Bone Microanatomy and Histology

Although mentioned occasionally in the literature (e.g., Ricqlès 1981; Castanet et al. 2003), the long-bone micro-anatomy and histology of finned stem-tetrapods has only recently been more thoroughly studied. These analyses have been restricted to the tristichopterids (Figure 16.2A). Laurin et al. (2007) and Meunier and Laurin (2012) carried out complete investigations on the

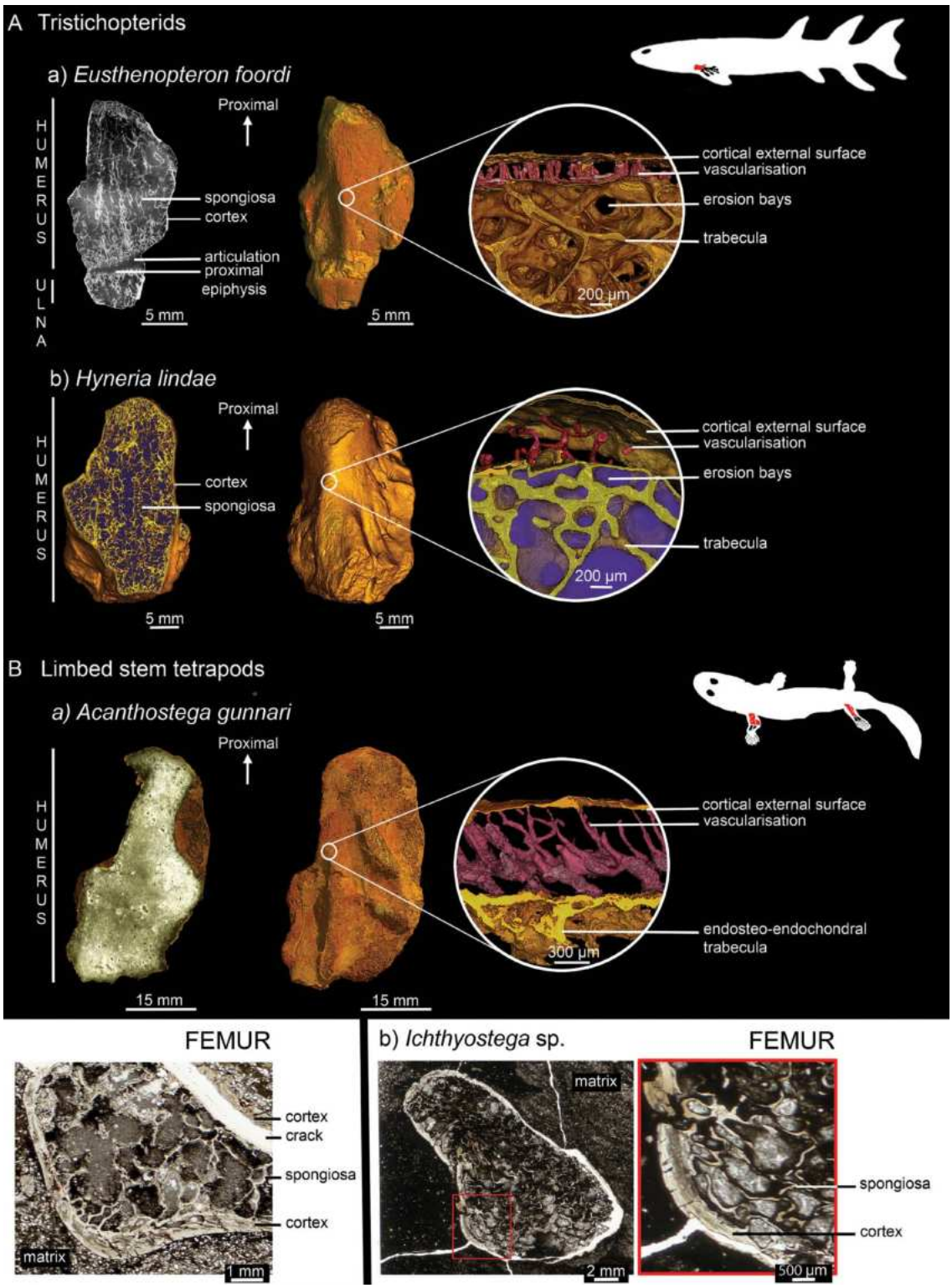


FIGURE 16.2 Long-bone microanatomy and histology of finned stem-tetrapods and limbed stem-tetrapods. A, Silhouette of a tristichopterid showing the location of the humerus illustrated in the following specimens. (a) *Eusthenopteron foordi*, NRM P248d, Naturhistoriska riksmuseet, Stockholm, Sweden. From left to right: longitudinal virtual thin section, 3D model in mesial view and high-resolution 3D model at midshaft (investigated by Sanchez et al. 2014). (b) *Hyneria lindae*, ANSP 21483, Academy of Natural Sciences of Philadelphia, USA. From left to right: longitudinal virtual thin section, 3D model in posteromesial view and high-resolution 3D model at midshaft (investigated by Kamska et al. 2019). B, Silhouette of a limbed stem-tetrapod showing the location of the humerus and femur illustrated in the following specimens. (a) *Acanthostega gunnari*, humerus MGUH 29020, Natural History Museum of Denmark. From left to right, up to down: longitudinal virtual thin section, 3D model in dorsal view and high-resolution 3D model at midshaft (investigated by Sanchez et al. 2016). *Acanthostega* sp., femur T1a, Muséum national d'Histoire naturelle, in transverse section. (b) *Ichthyostega* sp., femur T2a, Muséum national d'Histoire naturelle, in transverse section.

VetBooks.ir

species *Eusthenopteron foordi*. A microanatomical investigation of the fin-bone compactness confirmed the aquatic lifestyle of *Eusthenopteron* (Laurin et al. 2007). This inference was mainly based on the microstructure of the humerus. Meunier and Laurin (2012) thereafter focused on the development of tristichopterid fin-bones and revealed a tetrapod-like long bone development, including a cortical appositional growth through perichondral and periosteal ossification as well as a long-bone elongation through endochondral ossification (Meunier and Laurin 2012). Articulations between cartilaginous epiphyses of the fin elements are diarthroses (Meunier and Laurin 2012). Studies based on classic thin sections were rapidly followed by three-dimensional (3D) virtual histological investigations (Sanchez et al. 2014; Kamska et al. 2019) (Figure 16.2) including an additional tristichopterid called *Hyneria* (Kamska et al. 2019) (Figure 16.2Ab). The combination of both two-dimensional (2D) and 3D studies of these taxa revealed a large medullary cavity (Figure 16.2A) surrounded by remnants of Kastschenko's line (Laurin et al. 2007; Sanchez et al. 2014), suggesting a late onset of ossification during the juvenile stage (Sanchez et al. 2014; Kamska et al. 2019). Periosteal bone was deposited cyclically (Meunier and Laurin 2012; Sanchez et al. 2014). Although lines of arrested growth are only visible in older individuals (Sanchez et al. 2014; Kamska et al. 2019), repetitive cycles based on an alteration of smaller and larger cell-lacunae can be observed in the cortex of younger individuals (Sanchez et al. 2014). The density and primary nature of the vascularization, as well as the thickness of the growth marks, suggest a relatively slow growth rate (Sanchez et al. 2014; Kamska et al. 2019). In addition, the new 3D approach revealed tubular structures of bone marrow processes shaping the trabecular architecture of the humerus of both tristichopterids *Eusthenopteron* and *Hyneria* (Sanchez et al. 2014; Kamska et al. 2019).

General Conclusion

Finned stem-tetrapods form a grade whose morphological skeletal features have been largely investigated to illustrate the emergence of limbed-tetrapod characters (e.g., Janvier 1996; Clack 2012). Microanatomical and histological patterns, however, have been studied independently. Their combined review here shows a mosaic of patterns at these levels. The tooth infolding in *Panderichthys* is similar to that of *Ichthyostega* (Schultze 1970). The scales of tristichopterids and elpistostegids have differentiated into morphologically different gastral and dorsal scales, as in Paleozoic limbed tetrapods (Witzmann 2011). Their histology also simplifies with the reduction of isopedin (Witzmann 2011) and loss of cosmine (Mondéjar-Fernández 2018). Tristichopterid fin bones, such as the humerus (Figure 16.2A), form as periosteal and endochondral ossifications. Because endochondral ossification has been observed in some actinopterygian long bones (Haines 1934), it is considered a plesiomorphic character. However the development of an extended spongiosa in the stylopod of finned stem-tetrapods (Figure 16.2A) (Sanchez et al. 2014, 2016) looks more like that of limbed vertebrates (Meunier and Laurin 2012). Dermal skull and girdle bone tissues, retain plesiomorphic states as observed in the porolepiform *Laccognathus* (Witzmann 2009). All these features (apart from the tooth folding) seem to converge toward a lightening of the skeleton favoring trunk mobility (Zylberberg et al. 2010; Mondéjar-Fernández et al. 2014).

Limbed Stem-tetrapods

Although crucial for understanding the fin-to-limb transition and tetrapod terrestrialization, Devonian limbed stem-tetrapods have a poor fossil record (Clack 2012; Anderson et al. 2015). Consequently, the histological study of their hard tissues has essentially been performed on fragmentary elements (e.g., Jarvik 1952; Ricqlès 1973, 1981; Witzmann 2009, 2011), limiting the interpretation of life histories of Devonian and even Carboniferous stem-tetrapods. Recently, the use of novel non-destructive virtual techniques revealed the histology of scarce and exceptionally well-preserved fossil material of these taxa (Bishop 2014; Mondéjar-Fernández et al. 2014; Bishop et al. 2015; Sanchez et al. 2016).

Tooth Microstructure

All early limbed vertebrates share a folded tooth microstructure of the dentine forming a stellate (or petaloid, according to Warren and Turner 2005) pattern. However, this pattern slightly differs among taxa (e.g., *Ossinodus* and *Megalocephalus*, Warren and Turner 2005; *Crassigyrinus*, Panchen 1985; *Whatcheeria*, Lombard and Bolt 1995). For example, the tooth histology of the Carboniferous stem-tetrapod *Ossinodus*, thoroughly described by Warren and Turner (2005), exhibits a simple pattern forming up to 41 folds, the number of folds correlating with the diameter of the tooth. In the baphetid *Megalocephalus*, however, the folding is distinct from that of *Ossinodus* in that each primary bend is extended by a branch so that individual folds display a zigzag appearance (Warren and Turner 2005).

Postcranial Dermal Bone Microstructure (Scutes and Rays)

The scale microstructure became simplified with the loss of cosmine already observed in finned stem-tetrapods associated with a loss of ornamentation and vascularization in limbed stem-tetrapods (Mondéjar-Fernández et al. 2014). The scale microstructure only consists of parallel-fibered bone and lamellar bone which may form a thick, plywood-like structure housing substantial osteocyte populations. Witzmann (2011) designated this tissue as isopedin, a term that remains controversial because isopedin has often been presented as acellular (e.g., Francillon-Vieillot et al. 1990; Sire et al. 2009; but see also Meunier 2011). Morphological traits of the scales evolved in limbed stem-tetrapods: they differentiated into gastral, dorsal and ventral scales with a larger overlapping surface between each scale (Witzmann 2011). This overall (i.e., morphological and microstructural) derived condition in Devonian and later stem-tetrapods has been suggested to be linked to a lightening of the skeleton and increased flexibility of the trunk (Witzmann 2011).

The dermal fin-rays of *Ichthyostega* seem to display a relatively compact microstructure with flattened cells aligning with the surrounding longitudinal collagen fibers (Jarvik 1952, Figure 4) similar to the histological organization of *Eusthenopteron* (Zylberberg et al. 2010).

VetBooks.ir

Skull and Girdle Bone Microstructure

Two limbed stem-tetrapods were investigated by Witzmann (2009): *Acanthostega*, an early tetrapod from the Devonian of Greenland, and *Greererpeton*, a colosteid from the Carboniferous of North America. They both exhibit a dermal bone diploë microanatomy with a pseudolamellar-to-sublamellar vascularized external layer, a cancellous middle layer and pseudo-to-lamellar compact inner layer. This microstructural organization is comparable to the dermal bone structure of the porolepiform *Laccognathus* and the finned stem-tetrapod *Panderichthys* (Witzmann 2009). These observations reveal no change of the skull and girdle dermal microorganization around the origin of limbed stem-tetrapods (Witzmann 2009). However, Janis et al. (2012) observed an increase of dermal sculpture of the skull bones from finned to limbed stem-tetrapods (*Eusthenopteron*, Jarvik 1944; e.g., *Pederpes*, Clack and Finney 2005), suggesting physiological adaptation to the terrestrial environment through acidosis buffering to maintain homeostasis while on land. Because several partially contradictory hypotheses have been proposed to explain changes in dermal skull sculpturing (e.g., cutaneous respiration, Bystrow 1947; reinforcement of bone-dermis contact, Romer 1947; strengthening adaptation, Coldiron 1974; coossification, Seibert et al. 1974; see reviews by Witzmann et al. 2010 and Chapter 38), further investigations are needed.

Limb Bone Microanatomy and Histology

As part of his doctoral dissertation (1973), Ricqlès conducted an extensive skeletal analysis of early (Devonian to Triassic) non-amniotic limbed vertebrates. This includes 24 genera of limbed stem-tetrapods (e.g., *Ichthyostega*), embolomeres, seymouriamorphs, temnospondyls, and lepospondyls. Only some of his main results have been published so far (Ricqlès 1975b, 1981) using photographs of a restricted number of his thin sections (Ricqlès 1975b). The current chapter extends on this hitherto unseen dataset in the figures 16.2, 16.3 and 16.4. Notably, Ricqlès (1981) made a cross section of the long bone of a rib of *Ichthyostega* during his doctoral work. He presented evidence of a very spongy element surrounded by a thin compact layer of cortical bone that recalls the microanatomy of the fin elements of finned stem-tetrapods (Figure 16.2A) (e.g., *Eusthenopteron*, Meunier and Laurin 2012; Sanchez et al. 2014; *Hyneria*, Kamska et al. 2019). The study of the humeral and femoral structure of *Ichthyostega* and *Acanthostega* (Sanchez et al. 2016; Figure 16.2B) confirmed the extremely cancellous architecture of proximal limb elements in early limbed stem-tetrapods. Ricqlès (1981) associated this very loose spongy microanatomy of early tetrapod long-bones with their aquatic lifestyle. The humeral cortices of *Ichthyostega* (Ricqlès 1981) and *Acanthostega* (Sanchez et al. 2016) display a primary tissue pierced by vascular canals and sparse primary osteons (Figure 16.2B). They are formed of lamellar bone (Ricqlès 1981) (Figure 16.2B). The humeral cortex of *Acanthostega* exhibits a very regular pattern of six lines of arrested growth (Sanchez et al. 2016) at a distance of 65 µm from each other (Estefa et al. 2020). This combination of microstructural features suggests a relatively slow deposition rate in both *Ichthyostega* and *Acanthostega*. Based on a 3D paleohistological investigation of the humerus of *Acanthostega*, Sanchez et al. (2016) were able to identify some remnants of cartilage from Kastschenko's line on the inner surface of the cortex, suggesting that the formation of the large initial rod of cartilage was only covered by a cylinder of cortical compact bone. This strongly implies that the humerus only began to ossify after several years of development. The limb development of *Acanthostega*, at least, seems relatively slow as in *Eusthenopteron* (Sanchez et al. 2016). Because Carboniferous tetrapods have been less investigated than Devonian forms, no life history traits can be provided so far. The orientation and degree of remodeling of the trabecular mesh in the radius of *Ossinodus*, revealed by the microanatomy, suggests a biomechanically demonstrable adaptation to terrestrial locomotion (Bishop et al. 2015).

General Conclusion

Although Devonian stem-tetrapods are the first vertebrates to evolve limbs with digits and potentially leave the water (Niedzwiedzki et al. 2010; Clack 2012; Ahlberg 2019), their hard tissue histology barely differs from that of finned stem-tetrapods. Dental microstructure remains folded as in *Panderichthys* (Schultze 1970). The scale histology follows the same pattern of simplification as in finned stem-tetrapods (Witzmann 2011). Dermal bone of Devonian and Carboniferous forms is mostly cancellous, as in *Panderichthys* and *Laccognathus* (Witzmann 2009), suggesting no changes in skull and girdle dermal microorganization over the origin of limbed vertebrates. The appendicular skeleton persists as very spongy elements in *Acanthostega* (Sanchez et al. 2016). The genome size of these groups was investigated through the study of their bone cell lacunae. No major shift could be associated with the emergence of limbed stem-tetrapods (Organ et al. 2016). Skeletochronological analyses revealed a slow bone growth rate and late onset of limb ossification in *Acanthostega* (Sanchez et al. 2016). This confirms the weakness of the limb skeleton for this Devonian tetrapod, restricting it to the aquatic environment (Sanchez et al. 2016). The limb bones of some Carboniferous forms, such as *Ossinodus*, however, can show obvious evidence of trabecular resistance to terrestrial activity (Bishop et al. 2015). Increased robustness of the cortical bone seems to co-occur with the more prominent terrestrial activity of the Carboniferous stem-tetrapod *Ossinodus* (Bishop et al. 2015). This suggests that microstructural changes of the appendicular skeleton would be related to strong biomechanical changes associated with increased terrestriality of tetrapods rather than morphological changes reflecting the fin-to-limb transition. The sculpturing of the dermal skull bones may be related to physiological adaptations to the terrestrial environment (Janis et al. 2012). All these hypotheses rely on a limited number of histological studies due to the rarity of fossils from the Devonian and Carboniferous periods. These speculations need to be tested at a larger scale using non-destructive techniques such as virtual bone paleohistology (see Methodological Focus C: Virtual (Paleo-)Histology Through Synchrotron Imaging) and comparative statistical analyses.

VetBooks.ir

Temnospondyls

Temnospondyls comprise the most diversified and largest known group of non-amniotic extinct tetrapods (Schoch 2013b). They have survived for more than 280 million years (Fortuny and Steyer 2019). They have been discovered with abundant growth series that suggest a great developmental plasticity (Schoch 2009; Fröbisch et al. 2010). This obviously raised the interest of paleohistologists who largely focused on investigating their successful survival strategies (e.g., Sanchez and Schoch 2013; Canoville and Chinsamy 2015). Most paleohistological studies carried out on temnospondyls have been conducted on limb bones, but a few tooth, dermal (cranial and postcranial) and vertebral bone histological analyses have been conducted too (e.g., Warren and Davey 1992; Konietzko-Meier et al. 2014; Witzmann 2009; Buffrénil et al. 2016).

Limb Bone Microanatomy and Histology

Numerous investigations have been carried out on the limb bones of temnospondyls. Their long bones generally comprise a well-developed central spongiosa of endosteo-endochondral origin, surrounded by a periosteal compacta (Enlow and Brown 1956; Ricqlès 1981). The cortical histodiversity and thickness seem mostly related to the hypothesized lifestyles, bone growth rates, body sizes and/or developmental strategies of these taxa. All temnospondyls have fully cartilaginous limb-bone epiphyses.

Temnospondyls are characterized by a large range of body sizes (Schoch 2013a). Bone microanatomy and histology show obvious differences (Figure 16.3) that reveal depositional growth rates resulting in this size diversity (Ricqlès 1975b, 1981; Castanet et al. 2003). Small taxa (e.g., *Apateon, Doleserpeton*) have tubular limb bones characterized by a relatively empty medullary cavity and an (almost) avascular periosteal cortex made of lamellar to parallel-fibered bone (Figure 16.3h, i) (Castanet et al. 2003; Sanchez et al. 2010a). Large temnospondyls (e.g., *Mastodonsaurus*, *Dutuitosaurus*, *Eryops*) have a highly vascularized cortex mainly made of lamellar-zonal bone tissue (see Chapter 8) which may, at least locally, turn to woven-fibered or fibrolamellar bone, and be subject to active remodeling (Figure 16.3b, d, k) (Ricqlès 1981; Castanet et al. 2003; Steyer et al. 2004; Mukherjee et al. 2010; Sanchez et al. 2010b; Konietzko-Meier and Sander 2013).

Despite this size-related histodiversity, the long-bone microanatomy of temnospondyls obviously reflects lifestyles (e.g., Damiani 2000; Girondot and Laurin 2003; Steyer et al. 2004; Mukherjee et al. 2010; Sanchez et al. 2010b; Quémeneur et al. 2013; McHugh 2014; Canoville and Chinsamy 2015; McHugh 2015). Consistent with anatomical analyses, temnospondyl limb bone compactness suggests a variety of lifestyles from fully aquatic to terrestrial. Most aquatic taxa are characterized by spongy limb bones (e.g., *Benthosuchus*, *Gerrothorax*, *Mastodonsaurus*, *Rhinesuchus*, *Wetlugasaurus*, Figure 16.3a–c, e; Ricqlès 1981; Castanet et al. 2003; Sanchez et al. 2010b; Quémeneur et al. 2013; McHugh 2014), whereas terrestrial species have tubular structures with an empty marrow cavity (e.g., *Acheloma*, *Doleserpeton*, *Lydekkerina*, Figure 16.3i, j; Castanet et al. 2003; Laurin et al. 2006; Sanchez et al. 2010b; Canoville and Chinsamy 2015; McHugh 2015). Even though this distinction can be made, Triassic stereospondyls display a great trabecular plasticity, resulting from differential degrees of erosion (Figure 16.3a–e). This reflects different locomotory behaviors. For example, as aquatic bottom-dwellers in a shallow-water environment, some populations of *Gerrothorax* exhibit a pachy-osteosclerotic appendicular skeleton (Ricqlès 1992), while other members of the same genus display lighter spongy limb bones resulting from a higher degree of resorption, probably associated with more active swimming abilities in dynamic freshwater currents (Sanchez and Schoch 2013). Microanatomical analyses could also reveal unexpected changes in the lifestyle of certain taxa during their development: the evolution from an extended spongiosa in the juveniles of *Dutuitosaurus* toward an unusual development of the compacta – distinct from the spongiosa – in adult forms may reflect a shift from a more amphibious lifestyle in the juveniles toward a fully aquatic lifestyle in adults (Steyer et al. 2004).

The long-bone cortical microstructure of temnospondyls is marked by lines of arrested growth highlighting successive biological cycles that define an overall developmental strategy. Several skeletochronological analyses have been performed on growth series of selected temnospondyls and have shown a prereproductive period lasting between 1 and 7 years, depending on the taxa: 5–7 years for *Apateon* (Sanchez et al. 2010a, c), 3–6 years for *Gerrothorax* (Sanchez and Schoch 2013), 6–7 years for *Dutuitosaurus* (Steyer et al. 2004) and 1 year for *Lydekkerina* (Canoville and Chinsamy 2015). Apart from *Lydekkerina* and a population of *Gerrothorax*, most temnospondyls studied thus far demonstrate a relatively late onset of sexual maturity.

Skull Bone Microstructure

Dermal bones in temnospondyls exhibit a diploë structure (Gross 1934; Bystrow 1935, 1947; Castanet et al. 2003; Buffrénil et al. 2016). The bone matrix of the superficial compact layer displays a variety of bone types from parallel-fibered to woven-fibered bone (Castanet et al. 2003; Witzmann 2009) that can be punctuated by growth marks. This compact layer is barely to moderately vascularized in Permian forms except in *Archegosaurus*, which is characterized by moderate to high vascularization. In stereospondyls, vascularization increases (Witzmann 2009). The innermost compact layer of the dermal bone is largely made of parallel-fibered tissue. If not avascular, it is only slightly vascularized in Permian temnospondyls. Stereospondyls, however, have a more variable degree of vascularization. The middle layer of the diploë has a fine-to-coarse cancellous structure made of parallel-fibered-to-woven-fibered trabeculae that can be more or less remodeled (Witzmann 2009). The differences in vascular density may correspond to differences in growth rate and local bone repair (Witzmann 2009). The compactness of the dermal bone, however, relates to the lifestyle and paleoecology of the animals. Indeed, *Edops*, *Chenoprosopus*, *Eryops*, *Metoposaurus*, *Gerrothorax*, *Kupferzellia* and *Mastodonsaurus* are represented by a heavily ossified dermal bone with thick remodeled trabeculae, as shown by Witzmann (2009). This coincides with osteosclerotic and pachyostotic conditions observed in the rest of the skeleton of some of them (Ricqlès and Buffrénil 2001).

VetBooks.ir

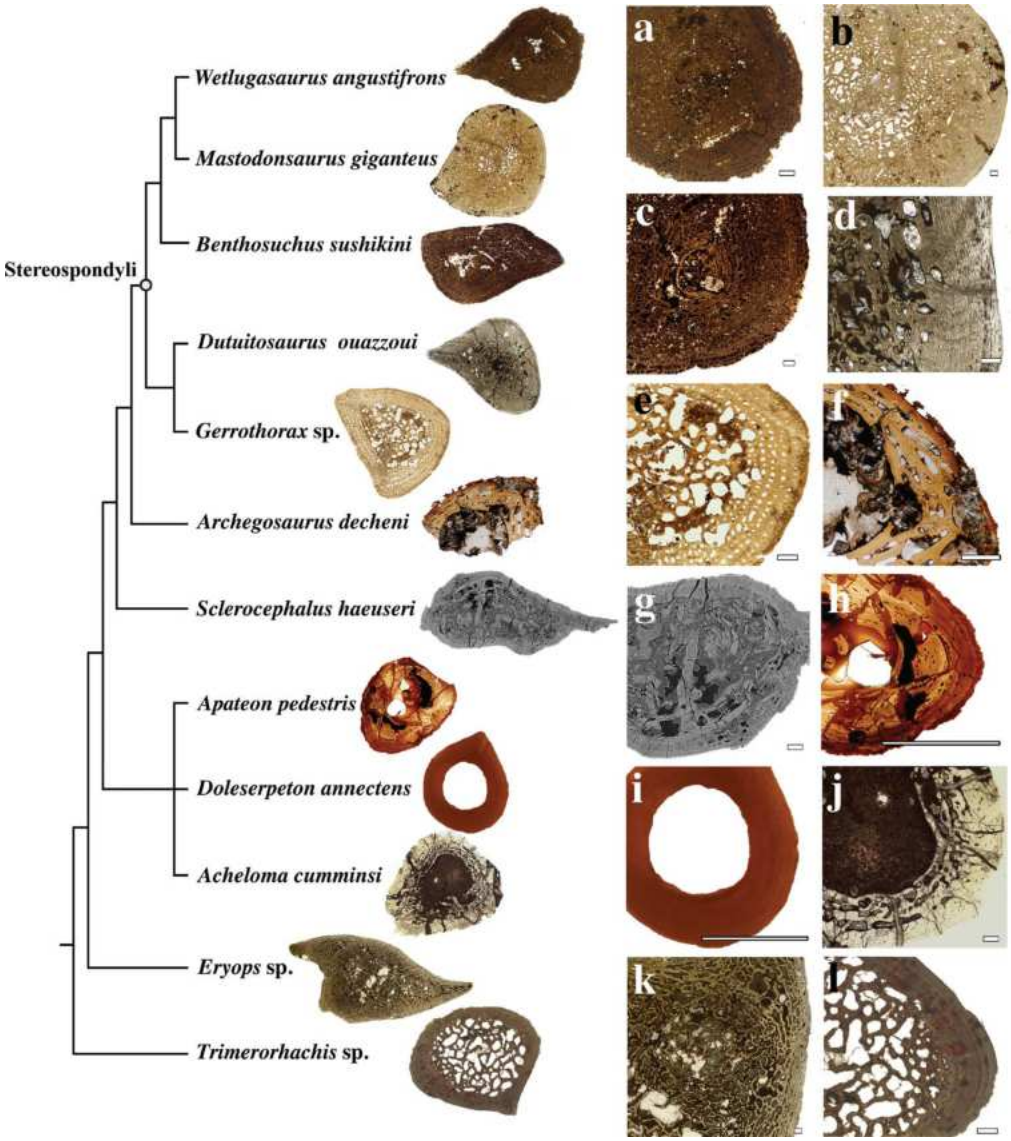


FIGURE 16.3 Long-bone microanatomy and histology of temnospondyls. Phylogenetic relationships of the studied temnospondyls illustrated with diaphyseal thin sections (modified from Schoch 2013b, 2018.) Some details of the cortex of these thin sections are presented as follows: (a) femur of *Wetlugasaurus angustifrons* (603.1.2.T, Muséum national d'Histoire naturelle, Paris, France); (b) femur of *Mastodonsaurus giganteus* (SMNS 84254, c, Stuttgart, Germany); (c) humerus of *Benthosuchus sushkini* (44.1.3.T, Muséum national d'Histoire naturelle, Paris, France); (d) femur of *Dutuitosaurus ouazzoui* (AZA 74, Muséum national d'Histoire naturelle, Paris, France); (e) femur of *Gerrothorax* sp. (SMNS 41466, Staatliches Museum für Naturkunde, Stuttgart, Germany); (f) femur of *Archegosaurus decheni* (MB.Am.236.b2, Museum für Naturkunde, Berlin, Germany); (g) humerus of *Sclerocephalus haeuseri* (SMNS 90055; Staatliches Museum für Naturkunde, Stuttgart, Germany); (h) femur of *Apateon pedestris* (SMNS 54981, Staatliches Museum für Naturkunde, Stuttgart, Germany); (i) femur of *Doleserpeton annectens* (919.5.3T, Muséum national d'Histoire naturelle, Paris, France); (j) femur of *Acheloma cumminsi* (38.11.T, Muséum national d'Histoire naturelle, Paris, France); (k) femur of *Eryops* sp. (12.6.2.T, Muséum national d'Histoire naturelle, Paris, France) and (l) femur of *Trimerorhachis* sp. (40.11.1.T, Muséum national d'Histoire naturelle, Paris, France.) Scale bars = 0.5 mm.

This feature is characteristic of aquatic bottom-dwellers and/or ambush predators (Schoch 2009). *Eryops* is an exception to this rule because it has recently been considered amphibious by some authors (e.g., Pawley and Warren 2006; Quémeneur et al. 2013). Nevertheless, *Eryops* is supposed to have fed under water (Schoch 2009) and this could be the reason for a heavily ossified dermal skeleton.

The dermal skull bones of temnospondyls are heavily sculptured. Large bundles of Sharpey's fibers suggest strong regions of soft tissue anchoring and a better resistance of the integument against dehydration and mechanical load (Witzmann 2009).

A recent study was conducted on *Metoposaurus* to investigate the dermal bone's resistance to feeding load (Konietzko-Meier et al. 2018). It revealed a great variability in compactness among different bones of the skull that probably reflect different biomechanical properties of these bones. This could have played a major role in distributing the stresses along the skull. Based on this assumption, the researchers concluded that *Metoposaurus* may have used two foraging techniques in hunting: bilateral

VetBooks.ir

biting as a bottom-dweller, and lateral strikes of the head as an ambush predator (Konietzko-Meier et al. 2018).

Scute and Osteoderm Microstructure

Most temnospondyls have ossified dermal scales. As in early limbed stem-tetrapods, temnospondyl scales have neither enamel nor dentine (Witzmann 2007). They consist only of bone tissue and have concentric growth rings (Witzmann 2011). Visible bundles of Sharpey's fibers penetrate the bone matrix, suggesting that the scales were strongly anchored to the integumentary dermis (Witzmann 2011). In Paleozoic forms, thin circular or elliptical scales cover the body of larvae (Witzmann 2007). During ontogeny, the scales in the ventral region differentiate into elongated or rhombic gastral scales whose arrangement provided some flexibility to the body (Witzmann 2007). In parallel, the compact scales of juveniles became cancellous in adults (e.g., *Australerpeton*, Dias and Richter 2003) through erosion and bone redeposition. In the plagiosaurids *Gerrothorax* and *Plagiosuchus*, however, the gastral scales are compact (Witzmann 2011). The bone cells are elongated and numerous, the density of vascular canals is poor to moderate, and they mainly consist of simple canals (Witzmann 2011). Many Mesozoic forms of aquatic temnospondyls clearly show a reduction in the thickness of their scalation that may be related to a demand for cutaneous respiration, body flexibility, or the absence of body protection against predation by large stereospondyls (Witzmann 2007).

In addition to scales, several temnospondyls evolved plate-like postcranial osteoderms. A histological study of these osteoderms was conducted on *Peltobatrachus*, dissorophids such as *Aspidosaurus*, *Cacops* and *Platyhystrix*, as well as plagiosaurids such as *Gerrothorax* and *Plagiosuchus* (Witzmann and Soler-Gijón 2010; Buffrénil et al. 2016). It revealed different microstructural organizations and developmental origins. The osteoderms of *Peltobatrachus* and *Gerrothorax* show a parallel-fibred bone matrix of periosteal origin, whereas the osteoderms of dissorophids have a cancellous middle layer surrounded by thin plywood-type cortices. The osteoderms of *Plagiosuchus* have a fibrous bone matrix of metaplastic origin. These differences among taxa suggest convergent evolutionary paths. The osteoderms of *Gerrothorax* recorded periodic events of osteoclastic resorption that might relate to cyclical changes in environmental salinity. *Gerrothorax* lived in a brackish environment where freshwater incursions could cause physiological stress (Schoch and Wild 1999), probably compensated by the use of calcium in osteoderms to readjust their osmotic balance (Witzmann and Soler-Gijón 2010). These interpretations remain conjectural because all extant crocodylians have a full dermal shield of cyclically resorbed osteoderms whether they live in fresh, brackish or saline waters (Clarac et al. 2015, 2017). Osmoregulation is regulated by salt glands that are located in the oral cavity (Taplin et al. 1982), therefore not involving any mineralized tissue. The cancellous microanatomy of dissorophoid osteoderms, however, would instead be involved in strengthening the vertebral column for terrestrial locomotion (Dilkes and Brown 2007). Finally, in *Peltobatrachus*, osteoderms may have served as protection due to their massive compact organization (Witzmann and Soler-Gijón 2010).

Vertebral Microstructure

This was recently described in temnospondyls (Konietzko-Meier et al. 2013, 2014; Danto et al. 2016). The main focus of these studies relates to the development of the vertebral centrum of temnospondyls. They have multipartite vertebral centra that ossify late in development from cartilaginous precursors (Danto et al. 2016). Their histological structure can play an important role in ecological adaptations. For example, aquatic stereospondyls retain large amounts of calcified cartilage that increase the density of the vertebral column (Konietzko-Meier et al. 2014; Danto et al. 2016), acting as a ballast (Ricqlès and Buffrénil, 2001). In addition, in some bottom-dwelling plagiosaurids, the vertebrae are pachyostotic (Danto et al. 2016). Miniaturization also seems to influence vertebral histology: *Doleserpeton* exhibits a microstructure similar to the vertebral inner organization of the small lepospondyl *Microbrachis* (Danto et al. 2016). All these observations suggest that the histological organization of temnospondyl vertebrae might exhibit more functional than phylogenetic signals. Further analyses using comparative phylogenetic methods will be required to test this hypothesis.

Tooth Microstructure

Within Triassic temnospondyls, the complexity of infolding at the base of the tooth seems to be related to the size of the tooth (smallest denticles vs largest tusks) (Warren and Davey 1992). In addition, the number of folds also seems to express a phylogenetic signal because the teeth of capitosaurids, mastodonsaurids and metoposaurids have more bends than teeth of similar size from brachyopids, chigutisaurids and trematosaurids (Warren and Davey 1992). Trematosaurs and chigutisaurs occasionally can have unbent teeth, whereas rhytidosteids only barely have infolds in their larger tusks, and no bends were found in plagiosaurid teeth (Warren and Davey 1992). The unbent state in these taxa is considered a derived state.

General Conclusion

Contrary to Devonian and Carboniferous non-amniotic tetrapods, Permo-Triassic temnospondyls exhibit a large diversity of hard-tissue microstructures (Figure 16.3). Depending on the type of mineral tissue, this histodiversity reflects either growth factors and adaptations to environmental stress or phylogenetic relatedness. The development of dermal and endoskeletal elements probably relates to body size, development, lifestyle, biomechanics and environmental stress (e.g., Ricqlès 1981; Castanet et al. 2003: Witzmann 2009: Witzmann and Soler-Gijón 2010; Witzmann 2011; Danto et al. 2016; Konietzko-Meier et al. 2018), whereas tooth histology seems to be phylogenetically driven (Warren and Davey 1992). Temnospondyls constitute one of the few groups that survived the greatest biological crisis of the Phanerozoic: the Permo-Triassic biodiversity loss. This histodiversity reflects a physiological plasticity that may have contributed to this survival (Sanchez and Schoch 2013). Indeed, the temnospondyls from the Triassic exhibit a larger range of microstructural patterns (e.g., Witzmann 2009; Sanchez and Schoch 2013 ; Canoville and Chinsamy 2015) than the Permian forms (e.g., Ricqlès 1981;

VetBooks.ir

Castanet et al. 2003; Sanchez et al. 2010b). Convergently, skeletochronological analyses also revealed a greater variability in the life history traits of Triassic taxa compared to the Permian groups. It seems that both *Gerrothorax* and *Lydekkerina* were probably able to adjust their development (and timing of sexual maturity) to survive drastic environmental conditions (Sanchez and Schoch 2013; Canoville and Chinsamy 2015).

This large diversity of histological patterns, as well as their potential relationships with environmental and biological factors, blur the phylogenetic signal that could potentially relate temnospondyls to lissamphibians. The vertebral histology of *Doleserpeton* greatly resembles that of extant amphibians (Castanet et al. 2003) as much as that of the small lepospondyl *Microbrachis* (Danto et al. 2016). The diaphyseal and metaphyseal limb bone microstructures of *Doleserpeton* (Figure 16.3i) and other dissorophoids such as *Apateon* (Figure 16.3h) (Sanchez et al. 2010a, c; Estefa et al. 2021) also recall those of lissamphibians. Because no limb bone histology of lepospondyls has been investigated thus far, it is hard to tell whether these histological similarities are phylogenetically related or characterizations of miniaturization. This line of research should be pursued before we can draw strong conclusions on that topic.

Embolomeres

Only a few mineralized elements of these taxa have been studied at the histological level (Enlow and Brown 1956; Ricqlès 1975b, 1981; Witzmann 2011). They give a preliminary view of the organization of hard tissues in embolomeres.

Long Bone Microanatomy and Microstructure

The femoral diaphysis of *Archeria* is very spongy (Ricqlès 1975b). The cortex is relatively thick, only leaving space for a small medullary cavity (Figure 16.4Aa). The cortex is lamellar with numerous flattened bone-cell lacunae. The bone forming the walls of vascular canals is highly remodeled, showing large erosion bays partly reconstructed, as well as secondary osteons (Figure 16.4Aa). The endosteal margin constitutes a broad transitional zone between a compact cortex and a central medullary spongiosa. The spongiosa, made of endosteal bone, is of secondary origin, and has a relatively tight texture. Rib cortices also show secondary osteons (e.g., *Pteroplax*, Figure 16.4Ab; see also Enlow and Brown 1956; Ricqlès 1981). Lines of arrested growth are well recognizable in the rib cortex (Figure 16.4Ab). The remodeling intensity in these long bones, as well as numerous lines of arrested growth, suggest that embolomeres had a long life span and a moderate growth rate (Ricqlès 1981). The extended spongiosa observed in most long bones might reflect an aquatic lifestyle (Ricqlès 1981).

Scute Microstructure

As in temnospondyls, embolomeres have rhombic gastral scales (Witzmann 2011). Dorsal scales have rarely been described for embolomeres but one illustration of caudal scales was provided by Panchen (1970). It revealed round scales with concentric growth rings that greatly resemble the dorsal scales of temnospondyls (Witzmann 2011).

General Conclusion

Based on the histological data collected so far, embolomeres would seem to have a long life span and a moderate growth rate (Ricqlès 1981), like many Devonian stem-tetrapods (Sanchez et al. 2014, 2016; Kamska et al. 2019). The phylogenetic position of embolomeres is debated. If embolomeres are considered stem amniotes (Figure 16.1A; Smithson 2000; Ruta and Clack 2006), the developmental plasticity observed in temnospondyls can be viewed as a derived character state unique to this group. If embolomeres are considered stem-tetrapods (Figure 16.1B; Marjanović and Laurin 2019), the developmental plasticity of temnospondyls can be seen as a first step toward a change of developmental strategy in the crown group of tetrapods. Before drawing strong conclusions on these phylogenetic considerations, it will be necessary to investigate more widely the hard tissues of embolomeres in addition to those of other non-amniotic extinct tetrapods.

Seymouriamorphs

Although seymouriamorphs can be crucial for the study of stem-amniote evolution (depending on the phylogenetic hypotheses proposed so far), the histological structure of their bones has only rarely been investigated. Only a few genera have been analyzed at the microstructural level; these include *Seymouria* (e.g., Danto et al. 2016; Bazzana et al. 2020; Estefa et al. 2020), *Discosauriscus* (e.g., Klembara and Ruta 2004a; Sanchez et al. 2008; Danto et al. 2016) and *Utegenia* (Klembara and Ruta 2004a).

Limb Bone Microanatomy and Histology

A first study was carried out on *Discosauriscus* in 2008 using classical thin sectioning. It revealed that limb bone development followed the classical pattern of endochondral and periosteal ossification, and epiphyses remained cartilaginous in adults (Sanchez et al. 2008). At first sight, the diaphyseal bone histology seemed to result from a slow deposition rate: the cortex exhibits very little vascularization, and is made of parallel-fibered to lamellar tissue (Figure 16.4Ba). However, a recent three-dimensional study restricted the distribution of this tissue to the metaphyses (Estefa et al. 2020). The exact mid-shaft microstructure in the humerus of *Discosauriscus* rather suggests a higher growth rate on the basis of a greater vascular density and a large number of rounded cell lacunae (Estefa et al. 2020). A 3D analysis of the humerus of *Seymouria* (as well as the femur; Figure 16.4Bb) additionally revealed a very high degree of remodeling in this taxon, supporting a faster growth rate at least in this taxon (Estefa et al. 2020). Although the growth rate seems to have been relatively rapid in seymouriamorphs compared to temnospondyls, a skeletochronological analysis suggested that *Discosauriscus* would retain a long prereproductive period (lasting about 10 years; Sanchez et al. 2008), whereas *Seymouria* would have had a short premetamorphic stage (Bazzana et al. 2020). If seymouriamorphs are considered stem amniotes, this combination of

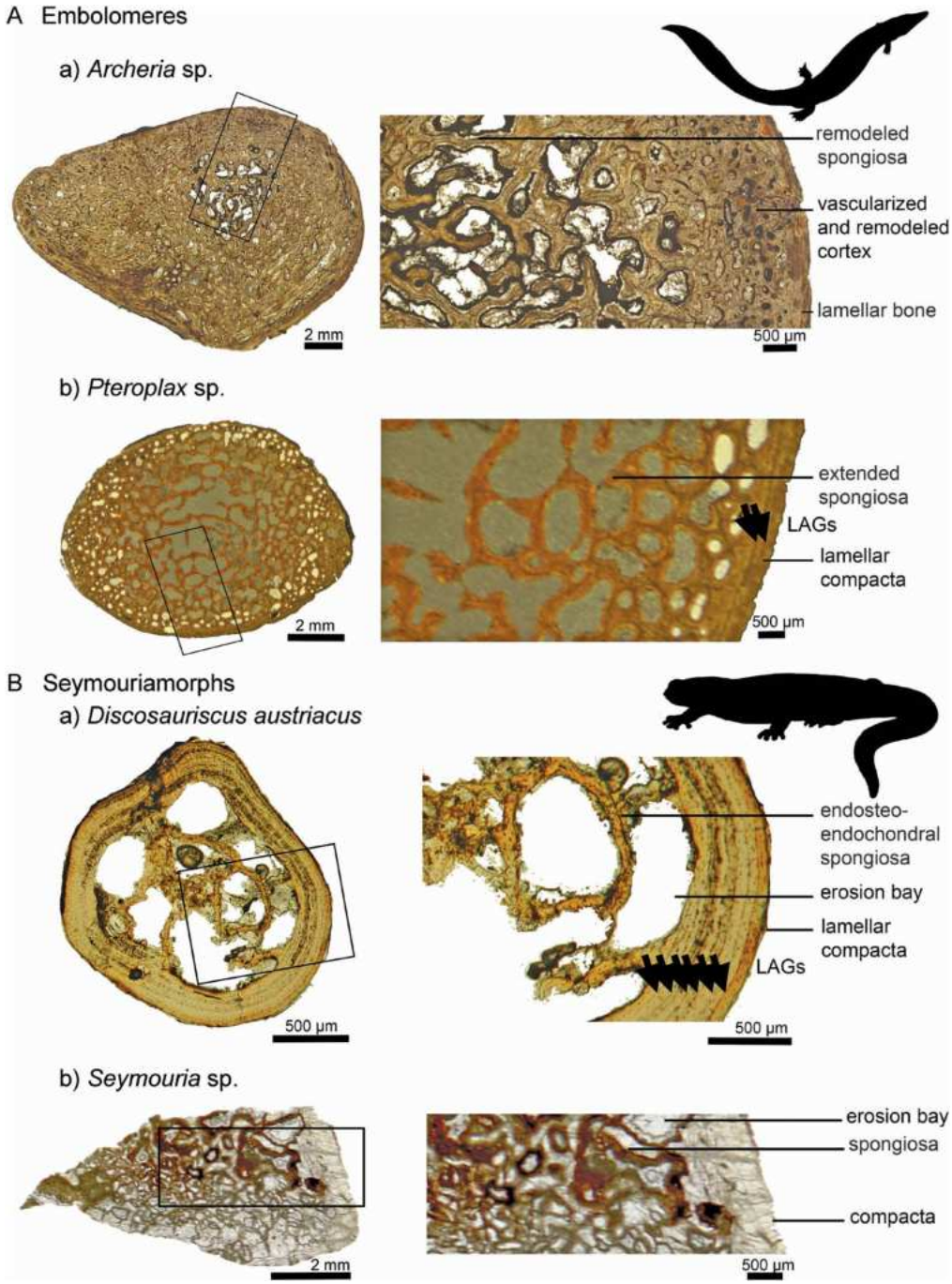


FIGURE 16.4 Long-bone microanatomy and histology of embolomeres and seymouriamorphs. A, Silhouette of an embolomere. (a) Transverse section through the femur of *Archeria* sp. (1.1.3.T, Muséum national d'Histoire naturelle, Paris, France.) (b) Transverse section through the rib of *Pteroplax* sp. (322.1.2.T, Muséum national d'Histoire naturelle, Paris, France). B, Silhouette of a seymouriamorph. (a) Transverse section through the femur of *Discosauriscus austriacus* (Z15697, Slovak National Museum, Bratislava, Slovakia) (investigated by Sanchez et al. 2008). (b) *Seymouria* sp. (femur 30.4.1.1.T, Muséum national d'Histoire naturelle) in transverse section. LAG, lines of arrested growth.

fast deposition rate but mixed developmental rates (Bazzana et al. 2020; Estefa et al. 2020) favors a progressive shift toward an amniotic growth strategy (Estefa et al. 2020). However, if seymouriamorphs are considered stem-tetrapods (Marjanovíc and Laurin 2019), the histology of seymouriamorphs suggests a unique increase of metabolic activity in the stem group of tetrapods (Estefa et al. 2020).

Skull Bone Microstructure

Witzmann (2009) described the microstructure of dermal bones in *Seymouria* as a diploë bone with an external layer made of a coarse parallel-fibered bone matrix displaying irregular birefringence and a moderate to high degree of vascular density. The inner cortex is greatly vascularized. Both

VetBooks.ir

cortices frame a fine cancellous middle layer. Sanchez et al. (2012) revealed the dermal bone histology of *Discosauriscus* but neither described nor discussed it. It also exhibits a diploë structure with poorly vascularized superficial and deep cortices. The middle layer is very thin and comprises a coarse cancellous tissue. The absence or reduction of vascular density in *Discosauriscus*, as well as in *Enosuchus* (Bystrow 1935, 1947), was hypothesized to be related to the absence of cutaneous respiration in these terrestrial taxa (Bystrow 1947). However, Coldiron (1974) challenged the argument solely relating vascular density to cutaneous respiration on the basis of observations made on temnospondyl dermal bones. Indeed, the vascular network, even though dense in the outermost cortex of the dermal skeleton of aquatic temnospondyls, displays an irregular pattern that would have been inefficient for cutaneous respiration. The absence of vascularization in the dermal bone of *Discosauriscus* and *Enosuchus* would then rather play a role in increasing the bone compactness, thereby improving mechanical properties of the skeleton in terrestrial conditions (Witzmann 2009).

Vertebral Microstructure

Very few studies have investigated the vertebral microstructure of seymouriamorphs. Danto et al. (2016) described the pleurocentral histology of *Discosauriscus* and *Seymouria*. The development of vertebrae in seymouriamorphs is of endochondral origin. Sparse remnants of calcified cartilage can be observed on the internal surface of the notochordal canal in both juveniles and adults, but no remnants of calcified cartilage were found in the trabecular mesh of the pleurocentrum (Danto et al. 2016). The strongly remodeled endochondral spongiosa (Danto et al. 2016), as well as the early ossification of the pleurocentrum into a full ring (Klembara and Bartík 2000), greatly reflect the intensity of the ossification dynamics. This differs from the low endochondral bone deposition rate observed in temnospondyl stereospondyls (with retention of calcified cartilage, Danto et al. 2016).

Scute Microstructure

The body of discosauriscids was largely covered with round to oval scales (Spinar 1952; Bulanov 2003). Microstructural observations revealed concentric growth rings crossing radial striae (Klembara and Bartík 2000; Klembara and Ruta 2004b), as in temnospondyls (Witzmann 2011).

General Conclusion

Seymouriamorphs seem to show an obvious heterogeneity in life history traits: *Discosauriscus* had a long prereproductive period (Sanchez et al. 2008) while *Seymouria* seemed to have a faster development with a short premetamorphic period (Bazzana et al. 2020). Although our data set is limited to two taxa, these observations tend to show a developmental heterogeneity among seymouriamorphs that could recall the plasticity of stereospondyls.

The bone deposition rate tends to differ between seymouriamorphs and temnospondyls in both long bones (Estefa et al. 2020) and vertebrae (Danto et al. 2016). The bone microstructure of seymouriamorphs suggests that it is more intense in this clade. More data should be collected to construct a broad picture of the evolution of life history traits in these early tetrapods.

Lepospondyls

Some authors have proposed lepospondyls as potential candidates for the origin of lissamphibians (Figure 16.1B) (Vallin and Laurin 2004; Marjanović and Laurin 2019). For this reason, this group should be thoroughly investigated. However, only a few studies have been carried out on the bone histology of lepospondyls. Despite their scarcity, these studies cover a large range of tissue types from diverse skeletal elements including endochondral jawbone, dermal bone (both cranial and postcranial) and vertebral bone. This gives a fairly complete overview of the paleohistology of this group.

Jawbone Histology

Most lepospondyls have reduced limbs that are rarely found. The easiest way to investigate periosteal ossification in lepospondyls relies on jawbone histological studies. Peabody (1961) sectioned the dentary of *Euryodus* and *Cardiocephalus*. He revealed the presence of growth marks characterized by zones rich in osteocyte lacunae alternating with annuli poor in cell spaces (Peabody 1961). The vascularization is very simple and radially oriented (Castanet et al. 2003). Ricqlès (1981) investigated the dentary of *Diplocaulus*. He showed that this bone was more cancellous and vascularized although still punctuated by cyclic growth marks.

Skull Bone Microstructure

The dermal bone histology of the skull of *Diplocaulus* was described by Ricqlès (1981) and Witzmann (2009). Both studies revealed a reduced external compact layer with respect to the extensive middle cancellous layer. Although the outermost region of the superficial compact layer exhibits a relatively simple, almost avascular microstructure, the innermost region of this cortex is densely vascularized with primary osteons (Witzmann 2009). The bone matrix is predominantly constituted of woven-fibered tissue. The middle layer has been extensively remodeled and results in a very porous microstructure. The trabeculae have a thin layer of secondary lamellar bone. Although the vascularization is slightly less dense in the external cortex, the dermal bone microstructure of *Pantylus* greatly resembles that of *Diplocaulus*, with an extensively remodeled middle layer (Witzmann 2009). The core of the middle layer and internal compact cortex are eroded in *Pantylus*. In both lepospondyls, contrary to temnospondyls, the dermal skeleton is extremely porous (Witzmann 2009) and somewhat reminiscent of the "osteoporotic-like" condition observed in the long bone cortices of some marine amniotes (e.g., Ricqlès and Buffrénil 2001). The reduced mass of the skull probably played a role in improving hydrodynamic abilities. The boomerang-like skull of *Diplocaulus* was suggested to have hydrofoil properties that could help the body lift into the water column using currents

(Cruickshank and Skews 1980). A light porous skeleton could increase the agility of the animal (Witzmann 2009).

Vertebral Microstructure

Lepospondyls have monospondylous vertebrae, once supposed to be formed through direct, intramembranous ossification from the outside in (Carroll 1989). However, several studies demonstrated the endochondral origin of the vertebrae with remnants of calcified cartilage (e.g., *Diplocaulus*; Ricqlès 1975b) despite the precocious and rapid ossification over their development (Danto et al. 2016). As for temnospondyls, lepospondyl vertebral microstructure likely relates to ecological adaptations; for example, the vertebral column of nectrideans is characterized by a very light (osteoporotic-like) architecture that might have contributed to lighten their skeleton for floating and swimming (Bossy and Milner 1998; Danto et al. 2016). Once again, a very limited phylogenetic signal might emerge from the vertebral microstructure, but phylogenetic comparative methods will be required to test this idea.

Scute Microstructure

Within lepospondyls, microsaurs are largely covered with scales (trunk, tail and limbs, Fritsch 1883; Carroll 1998). The gastral scales are longer and thicker than the dorsal scales. On the flanks, the scales are rounded to oval and sometimes ornamented with ridges and striae that resemble temnospondyl scale sculpture (Witzmann 2011). Most nectrideans exhibit variably sculptured spindle-shaped gastral scales (Bossy and Milner 1998). Aïstopods have needle-like gastral scales (Anderson 2003) and dorsal rounded scales (Witzmann 2011).

General Conclusion

The skeleton of lepospondyls shows a reduction of bone mass in dermal bones (Witzmann 2009), jaws (Ricqlès 1981) and vertebrae (Danto et al. 2016). This lightening of the skeleton may have contributed to increase hydrodynamic abilities and the agility to move in the water column (Cruickshank and Skews 1980). This conspicuous skeletal sponginess along with limb reduction in this taxon hampers skeletochronological analysis on a large scale. It markedly limits our understanding of life history and growth-rate evolution in lepospondyls. The use of new technologies such as virtual paleohistology based on synchrotron imaging (see Metodological Focus C) will probably help to fill in this gap through the investigation of rare lepospondyl limb bones.

Acknowledgments

This project was supported by two grants from the Vetenskapsrådet (2015-04335 and 2019-04595, S. S.). Scan data were produced using beamtime allocated by the European Synchrotron Radiation Facility via proposals accepted (EC203, SS) and in-house beamtime (P. Tafforeau). S. S. was also funded by the European program Synthesys for collecting samples in museums. We thank all the collection managers who gave access to their collections: D. Germain from the Muséum national d'Histoire naturelle (Paris, France), F. Witzmann from the Museum für Naturkunde (Berlin, Germany), R. Schoch from the Staatliches Museum für Naturkunde (Stuttgart, Germany), A. Durišová from the Slovak National Museum (Bratislava, Slovakia), T. Mörs from the Naturhistoriska Riksmuseet (Stockholm, Sweden), E. B. Daeschler from the Academy of Natural Sciences of Philadelphia (ANSP, USA), B. E. Kramer Lindow from the Natural History Museum of Denmark (Copenhagen, Denmark), and M. Lowe from the University Museum of Zoology (Cambridge, UK). We are grateful to B. Le Dimet and M. Lemoine (MNHN, Paris) for casting the bones and preparing the thin sections of *Apateon*. We thank V. Kamska who modeled the humerus of *Hyneria*. We show our gratitude to P. Ahlberg, J. Castanet, J. A. Clack, E. B. Daeschler, J. P. Downs, J. Klembara, R. Schoch, J.-S. Steyer, P. Tafforeau and F. Witzmann for fruitful discussions. We are grateful to the editorial board of the book who helped edit this article.

REFERENCES

Ahlberg, P. E. 1991. A re-examination of sarcopterygian interrelationships, with special reference to the Porolepiformes. *Zool. J Linn. Soc.* 103: 241–287.

Ahlberg, P. E. 2019. Follow the footprints and mind the gaps: a new look at the origin of tetrapods. *Trans. R. Soc. Edinburgh Earth. Sci.* 109: 115–137.

Ahlberg, P. E. and Clack, J. A. 2020. The smallest known Devonian tetrapod shows unexpectedly derived features. *R. Soc. Open Sci.* 7: 192117.

Ahlberg, P. E. and Johanson, Z. 1997. Second tristichopterid (Sarcopterygii, Osteolepiformes) from the Upper Devonian of Canowindra, New South Wales, Australia, and phylogeny of the Tristichopteridae. *J. Vertebr. Paleontol.* 17: 653–673.

Ahlberg, P. E. and Johanson, Z. 1998. Osteolepiforms and the ancestry of tetrapods. *Nature* 395: 792–794.

Ahlberg, P. E., et al. 1996. Rapid braincase evolution between *Panderichthys* and the earliest tetrapods. *Nature* 381: 61–64.

Ahlberg, P. E., et al. 2005. The axial skeleton of the Devonian tetrapod *Ichthyostega*. *Nature* 437: 137–140.

Anderson, J. S. 2001. The phylogenetic trunk: maximal inclusion of taxa with missing data in an analysis of the lepospondyli (Vertebrata, Tetrapoda). *Syst. Biol.* 50: 170–193.

Anderson, J. S. 2003. A new Aïstopod (Tetrapoda: Lepospondyli) from Mazon Creek, Illinois. *J. Vertebr. Paleontol.* 23: 79–88.

Anderson, J. S. 2007. Incorporating ontogeny into the matrix: a phylogenetic evaluation of developmental evidence for the origin of modern amphibians. In *Major Transitions in Vertebrate Evolution*, eds. Anderson, J. S. and Sues, H. D., 182–227. Indiana University Press, Bloomington.

Anderson, J. S. 2008. Focal review: the origin (s) of modern amphibians. *Evol. Biol.* 35: 231–247.

Anderson, J. S., et al. 2003. New information on *Lethiscus stocki* (Tetrapoda: Lepospondyli: Aistopoda) from high-resolution computed tomography and a phylogenetic analysis of Aistopoda. *Can. J. Earth Sci.* 40: 1071–1083.

Anderson, J. S., et al. 2015. A diverse tetrapod fauna at the base of 'Romer's Gap'. *PLoS One* 10: e0125446.

Andrews, S. M. 1985. Rhizodont crossopterygian fish from the Dinantian of Foulden, Berwickshire, Scotland, with a re-evaluation of this group. *Trans. R. Soc. Edinburgh Earth. Sci.* 76: 67–95.

Bazzana, K. D., et al. 2020. Postcranial anatomy and histology of *Seymouria*, and the terrestriality of seymouriamorphs. *PeerJ* 8: e8698

Berman, D. S. and Martens, T. 1993. First occurrence of *Seymouria* (Amphibia: Batrachosauria) in the Lower Permian Rotliegend of Central Germany. *Ann. Carnegie Mus.* 62: 63–79.

Berman, D. S., et al. 1987. *Seymouria sanjuanensis* (Amphibia, Batrachosauria) from the Lower Permian Cutler Formation of north-central New Mexico and the occurrence of sexual dimorphism in that genus questioned. *Can. J. Earth Sci.* 24: 1769–1784.

Berman, D. S., et al. 2000. Redescription of *Seymouria sanjuanensis* (Seymouriamorpha) from the Lower Permian of Germany based on complete, mature specimens with a discussion of paleoecology of the Bromacker locality assemblage. *J. Vertebr. Paleontol.* 20: 253–268.

Beznosov, P. A., et al. 2019. Morphology of the earliest reconstructable tetrapod *Parmastega aelidae*. *Nature* 574: 527–531.

Bishop, P. J. 2014. The humerus of *Ossinodus pueri*, a stem-tetrapod from the Carboniferous of Gondwana, and the early evolution of the tetrapod forelimb. *Alcheringa*. 38: 209–238.

Bishop, P. J., et al. 2015. Oldest pathology in a tetrapod bone illuminates the origin of terrestrial vertebrates. *PLoS One* 10:e0125723.

Bossy, K. A. and Milner, A. C. 1998. Order Nectridea. In *Encyclopedia of Paleoherpetology*, eds. Carroll, R. L, Bossy, K. A., Milner, A. C, Andrew, S. M, and Wellstead, C. F., Lepospondyli, Part 1: 73–131. Gustav Fischer, Stuttgart.

Boy, J.A. 1993. Synopsis of the tetrapods from the Rotliegend (Lower Permian) in the Saar-Nahe Basin (SW-Germany). In *New Research on Permo-Carboniferous Faunas*, ed. Heidtke U, Vol. 29: 155–169. Pollichia-Buch, Bad Dürkheim.

Brazeau, M. D. and Ahlberg, P. E. 2006. Tetrapod-like middle ear architecture in a Devonian fish. *Nature* 439: 318–321.

Buffrénil, V. de et al. 2016. Comparative data on the differentiation and growth of bone ornamentation in gnathostomes (Chordata: Vertebrata). *J. Morphol.* 227: 634–670.

Bulanov, V. 2003. Evolution and systematics of seymouriamorph parareptiles. *Paleontol. J.* 37(1): 1–105.

Bystrow, A. P. 1935. Morphologische Untersuchungen der Deckknochen des Schädels der Stegocephalen. 1. Mitteilung. Schädel der Stegocephalen. *Acta Zool.-Stockholm* 16: 65–141.

Bystrow, A. P. 1944. *Kotlassia prima* Amalitzky. *Geol. Soc. Am. Bull.* 55: 379–416.

Bystrow, A. P. 1947. Hydrophilous and xerophilous labyrinthodonts. *Acta Zoolog.- Stockholm* 28: 137–164.

Campbell, K. S. W. and Bell, M. W. 1977. A primitive amphibian from the Late Devonian of New South Wales. *Alcheringa* 1: 369–381.

Canoville, A. and Chinsamy, A. 2015. Bone Microstructure of the Stereospondyl *Lydekkerina huxleyi* reveals adaptive strategies to the harsh post Permian-Extinction environment. *Anat. Rec.* 298: 1237–1254.

Carroll, R. L. 1989. Developmental aspects of lepospondyl vertebrae in Paleozoic tetrapods. *Hist. Biol.* 3: 1–25.

Carroll, R. L. 1998. Order Microsauria. In *Encyclopedia of Paleoherpetology*, Lepospondyli, ed. Wellnhofer, P., vol. 1, 1–72. Verlag Dr. Friedrich Pfeil, München.

Castanet, J., et al. 1975. Données préliminaires sur les structures histologiques du squelette de *Latimeria chalumnae*. Problèmes Actuels de Paléontologie—Evolution des Vertébrés, Colloque International. *CNRS* 218:159-175.

Castanet, J., et al. 2003. The Skeletal Histology of the Amphibia. In *Amphibian Biology*, eds. Heatwole, H., Davies, M., Osteology 5, 1598–1683. Surrey Beatty & Sons, Chipping Norton.

Clack, J. A. 2002. Patterns and processes in the early evolution of the tetrapod ear. *J. Neurobiol.* 53: 251–264.

Clack, J. A. 2009. The fin to limb transition: New Data, interpretations, and hypotheses from paleontology and developmental biology. *Annu. Rev. Earth Planet. Sci.* 37: 163–179.

Clack, J. A. 2012. *Gaining Ground*. Indiana University Press, Bloomington.

Clack, J. A. and Carroll, R. L. 2000. Early Carboniferous tetrapods. In *Amphibian Biology*, eds. Heatwole, H. and Carroll, R. L., The evolutionary history of amphibians. Palaeontology 4, 1030–1043. Surrey Beatty & Sons, Chipping Norton.

Clack, J. A. and Finney, S. M. 2005. *Pederpes finneyae*, an articulated tetrapod from the Tournaisian of Western Scotland. *J. Syst. Palaeontol.* 2: 311–346.

Clack, J. A., et al. 2016. Phylogenetic and environmental context of a Tournaisian tetrapod fauna. *Nat. Ecol. Evol.* 1: 1–11.

Clarac, F., et al. 2015. A quantitative assessment of bone area increase due to ornamentation in the Crocodylia. *J. Morphol.* 276: 1183–1192.

Clarac, F., et al. 2017. The evolution of bone ornamentation in Pseudosuchia: morphological constraints versus ecological adaptation. *Biol. J. Linn. Soc.* 121: 395–408.

Clément, G. 2002. Large Tristichopteridae (Sarcopterygii, Tetrapodomorpha) from the Late Famennian Evieux Formation of Belgium. *Palaeontology* 45: 577–593

Clément, G. and Janvier, P. 2004. *Powichthys spitsbergensis* sp. nov., a new member of the Dipnomorpha (Sarcopterygii, lobe-finned fishes) from the Lower Devonian of Spitsbergen, with remarks on basal dipnomorph anatomy. *Foss. Strat.* 50: 92–112.

Clément, G., et al. 2004. Devonian tetrapod from western Europe. *Nature* 427: 412–413.

Cloutier, R., et al. 2020. *Elpistostege* and the origin of the vertebrate hand. *Nature* 579: 549–554.

Coates, M. I. and Clack, J. A. 1995. Romer's gap: Tetrapod origins and terrestriality. *Bull. Mus. Natl. Hist. Nat.* 17: 373–388.

Coldiron, R. W. 1974. Possible functions of ornament in labyrinthodont amphibians. *Occ. Pap. Mus. Nat. Hist. Kansas* 33: 1–19.

Cruickshank, A. R. I. and Skews, B. W. 1980. The functional significance of nectridean tabular horns (Amphibia: Lepospondyli). *Proc. Roy. Soc. B-Biol. Sci.* 209: 513–537.

Daeschler, E. B. and Downs, J. P. 2018. New description and diagnosis of *Hyneria lindae* (Sarcopterygii, Tristichopteridae) from the Upper Devonian Catskill Formation of Pennsylvania, USA. *J. Vertebr. Paleontol.* 38: e1448834.

Daeschler, E. B., et al. 2006. A Devonian tetrapod-like fish and the evolution of the tetrapod body plan. *Nature* 440: 757–763.

Damiani, R. J. 2000. Bone histology of some Australian Triassic temnospondyl amphibians: preliminary data. *Mod. Geol.* 24: 109–124.

VetBooks.ir

Danto, M., et al. 2016. Vertebral development in Paleozoic and Mesozoic tetrapods revealed by paleohistological data. *PLoS One* 11: e0152586.

Davesne, D., et al. 2015. A new large tetrapodomorph sarcopterygian from the Late Devonian of Iran. *Palaeontol. Z.* 89: 661–667.

Dias, E. V. and Richter, M. 2003. On the squamation of *Australerpeton cosgriffi* Barberena, a temnospondyl amphibian from the Upper Permian of Brazil. *An. Acad. Bras. Cienc.* 74(3): 477–490.

Dilkes, D. and Brown, L. E. 2007. Biomechanics of the vertebrae and associated osteoderms of the Early Permian amphibian *Cacops aspidephorus*. *J. Zool*. 271: 396–407.

Downs, J. P., et al. 2008. The cranial endoskeleton of *Tiktaalik roseae*. *Nature* 455: 925–929.

Dutel, H., et al. 2015. Bite force in the extant coelacanth *Latimeria*: the role of the intracranial joint and the basicranial muscle. *Curr. Biol.* 25: 1228–1233.

Enlow, D. H. and Brown, S. O. 1956. A Comparative histological study of fossil and recent bone tissues. Part I. *Tex. J. Sci*. 8: 405–443.

Estefa, J., et al. 2021. New light shed on the early evolution of limb-bone growth plate and bone marrow. *Elife.*

Estefa, J., et al. 2020. Limb-bone development of seymouriamorphs: implications for the evolution of growth strategy in stem amniotes. *Front. Earth Sci.* 8: 97.

Fortuny, J. and Steyer, J. S. 2019. New insights into the evolution of temnospondyls. *J. Iber.Geol*. 45: 247–250.

Fritsch, A. 1883. *Fauna der Gaskohle und der Kalksteine der Permformation Bohmens*. Bd.1, Prague.

Fröbisch, N. B., et al. 2010. Amphibian development in the fossil record. *Semin. Cell Dev. Biol.* 21: 424–431.

Germain, D. 2010. The Moroccan diplocaulid: the last lepospondyl, the single one on Gondwana. *Hist. Biol.* 22: 4–39.

Gess, R. and Ahlberg, P. E. 2018. A tetrapod fauna from within the Devonian Antarctic Circle. *Science* 360: 1120–1124.

Girondot, M. and Laurin, M. 2003. Bone profiler: a tool to quantify, model, and statistically compare bone-section compactness profiles. *J Vertebr. Paleontol*. 23: 458–461.

Goedert, J., et al. 2018. Euryhaline ecology of early tetrapods revealed by stable isotopes. *Nature* 558: 68–72.

Gross, W. 1934. Die Typen des mikroskopischen Knochenbaues bei fossilen Stegocephalen und Reptilien. *Z. Anat. Entwicklungsgesch*. 103: 731–764.

Haines, R. W. 1934. Epiphysial growth in the branchial skeleton of fishes. *Quat. J. Micros. Sci*. 77: 77–97.

Hall, B. K, ed. 2008. *Fins into limbs: evolution, development and transformation*. University of Chicago Press, Chicago.

Holmes, R. 1984. The Carboniferous amphibian *Proterogyrinus scheelei* Romer, and the early evolution of tetrapods. *Proc. R. Soc. B-Biol. Sci.* 306: 431–524.

Janis, C. M., et al. 2012. Dermal bone in early tetrapods: a palaeophysiological hypothesis of adaptation for terrestrial acidosis. *Proc. R. Soc. B-Biol. Sci.* 279: 3035–3040.

Janvier, P. 1996. *Early Vertebrates*. Clarendon Press, Oxford.

Janvier, P. 2004. Wandering nostrils. *Nature* 432: 23–24.

Jarvik, E. 1944. *On the Dermal Bones, Sensory Canals and Pitlines of the Skull in Eusthenopteron Foordi Whiteaves, With Some Remarks on E. Säve-Söderberghi Jarvik*. Almqvist & Wiksell, Stockholm.

Jarvik, E. 1952. On the fish-like tail in the Ichthyostegid Stegocephalians: with descriptions of a new Stegocephalian and a new Crossopterygian from the Upper Devonian of East Greenland. *Meddelelser om Grønland* 114: 1–90.

Jenkins, J. F. A., et al. 2008. *Gerrothorax pulcherrimus* from the Upper Triassic Fleming fjord formation of East Greenland and a reassessment of head lifting in Temnospondyl feeding. *J. Vertebr. Paleontol*. 28: 935–950.

Johanson, Z. 2004. Late Devonian sarcopterygian fishes from eastern Gondwana (Australia and Antarctica) and their importance in phylogeny and biogeography. In *Recent Advances in the Origin and Early Radiation of Vertebrates*, eds. Arratia, G, Wilson, MVH, Cloutier, R., 287–308. Verlag Dr. Friedriech Pfeil, Munich.

Kamska, V., et al. 2019. Long-bone development and life-history traits of the Devonian tristichopterid *Hyneria lindae*. *Earth Environ. Sci. Trans. R Soc. Edinb.* 109: 75–86.

Klembara, J. 1994. Electroreceptors in the Lower Permian tetrapod *Discosauriscus austriacus*. *Palaeontology* 37: 609–626.

Klembara, J. and Bartík, I. 2000. The postcranial skeleton of *Discosauriscus* Kuhn, a seymouriamorph tetrapod from the Lower Permian of the Boskovice Furrow (Czech Republic). *Trans. R. Soc. Edinburgh Earth. Sci*. 90: 287–316.

Klembara, J. and Meszároš, S. 1992. New finds of *Discosauriscus austriacus* (Makowsky 1876) from the Lower Permian of Boskovice Furrow (Czecho-Slovakia). *Geol. Carpath*. 43: 305–312.

Klembara, J. and Ruta, M. 2004a. The seymouriamorph tetrapod *Utegenia shpinari* from the? Upper Carboniferous-Lower Permian of Kazakhstan. Part I: Cranial anatomy and ontogeny. *Trans. R. Soc. Edinburgh Earth. Sci*. 94: 45–74.

Klembara, J. and Ruta, M. 2004b.The seymouriamorph tetrapod *Utegenia shpinari* from the? Upper Carboniferous–Lower Permian of Kazakhstan. Part II: Postcranial anatomy and relationships. *Trans. R. Soc. Edinburgh Earth. Sci*. 94: 75–93.

Klembara, J. and Ruta, M. 2005a. The seymouriamorph tetrapod *Ariekanerpeton sigalovi* from the Lower Permian of Tadzhikistan. Part I: Cranial anatomy and ontogeny. *Trans. R. Soc. Edinburgh Earth. Sci* 96: 43–70.

Klembara, J. and Ruta, M. 2005b. The seymouriamorph tetrapod *Ariekanerpeton sigalovi* from the Lower Permian of Tadzhikistan. Part II: Postcranial anatomy and relationships. *Trans. R. Soc. Edinburgh Earth. Sci* 96: 71–93.

Klembara, J., et al. 2006. Comparison of cranial anatomy and proportions of similarly sized *Seymouria sanjuanensis* and *Discosauriscus austriacus*. *Ann. Carnegie Mus.* 75: 37–49.

Konietzko-Meier, D. and Sander, P. M. 2013. Long bone histology of *Metoposaurus diagnosticus* (Temnospondyli) from the Late Triassic of Krasiejów (Poland) and its paleobiological implications. *J Vertebr. Paleontol.* 33: 1003–1018.

Konietzko-Meier, D., et al. 2014. The microstructural variability of the intercentra among temnospondyl amphibians. *Biol. J Linn. Soc.* 112: 747–764.

Konietzko-Meier, D., et al. 2018. Merging cranial histology and 3D-computational biomechanics: a review of the feeding ecology of a Late Triassic temnospondyl amphibian. *PeerJ*6:e4426.

Kriloff, A., et al. 2008. Evolution of bone microanatomy of the tetrapod tibia and its use in palaeobiological inference. *J Evol. Biol.* 21:807–826.

Laurin, M. 1996a. A reappraisal of *Utegenia*, a Permo-Carboniferous seymouriamorph (Tetrapoda: Batrachausairia) from Kazakhstan. *J. Vertebr. Paleontol.* 16: 374–383.

Laurin, M. 1996b. A reevaluation of *Ariekanerpeton*, a Lower Permian seymouriamorph (Vertebrata: seymouriamorpha) from Tadzhikistan. *J. Vertebr. Paleontol*. 16: 653–665.

Laurin, M. 2000. Seymouriamorphs. In *Amphibian Biology*, eds. Heatwole, H. and Carroll, R. L., Palaeontology, The evolutionary history of amphibians, vol. IV, 1064–1080. Surrey Beatty & Sons, Chipping Norton.

Laurin, M. 2010. *How Vertebrates Left the Water*, 199. University of California Press, Berkeley.

Laurin, M. 2020. Stegocephali. In *Phylonyms: An Implementation of PhyloCode*, eds. de Queiroz, K., Cantino, P. D., and Gauthier, J. A., 741–745. CRC Press, Boca Raton.

Laurin, M. and Reisz, R. R. 1997. A new perspective on tetrapod phylogeny. In *Amniote Origins*, eds. Sumida, S. S., and Martin, K. L. M., 9–59. Academic Press, San Diego.

Laurin, M. and R. Soler-Gijón. 2010. Osmotic tolerance and habitat of early stegocephalians: indirect evidence from parsimony, taphonomy, paleobiogeography, physiology and morphology, eds. M. Vecoli and G. Clément, pp. 151–179. The Geological Society of London, London.

Laurin, M. and T. R. Smithson. 2020. Anthracosauria. In *Phylonyms: An Implementation of PhyloCode*, eds. K. de Queiroz, P. D. Cantino, and J. A. Gauthier (ed.), pp. 751–754. CRC Press, Boca Raton.

Laurin, M., et al. 2006. Données microanatomiques sur la conquête de l'environnement terrestre par les vertébrés. *C R Palevol*. 5: 603–618.

Laurin, M, et al. 2007. A microanatomical and histological study of the paired fin skeleton of the Devonian sarcopterygian *Eusthenopteron foordi*. *J. Paleontol*. 81: 143–153.

Laurin, M., et al. 2019. What do ossification sequences tell us about the origin of extant amphibians? *PCI Paleontol.* 1–36.

Lombard, E. and Bolt, J. R. 1995. A new primitive tetrapod, *Whatcheeria deltae*, from the Lower Carboniferous of Iowa. *Palaeontology* 38: 471–94.

Lu J., et al. 2012. The earliest known stem-tetrapod from the Lower Devonian of China. *Nat. Commun.* 3: 1160.

Maisch, M. W. and Matzke, A. T. 2005. Temnospondyl amphibians from the Jurassic of the southern Junggar Basin (NW China). *Paläontol. Z.* 79: 285–301.

Mansky, C. F. and Spencer, L. G. 2013. Romer's Gap revisited: continental assemblages and ichno-assemblages from the basal Carboniferous of Blue Beach, Nova Scotia, Canada. *Bull. N. M. Mus. Nat. Hist. Sci.* 60: 244–273.

Marchetti, L., et al. 2017. An unusual *Amphisauropus* trackway and its implication for understanding seymouriamorph locomotion. *Lethaia* 50: 162–174.

Marjanović, D. and Laurin, M. 2009. The origin(s) of modern amphibians: a commentary. *Evol. Biol.* 36: 336–338.

Marjanović, D. and Laurin, M. 2019. Phylogeny of Paleozoic limbed vertebrates reassessed through revision and expansion of the largest published relevant data matrix. *PeerJ* 6: e5565.

Marsicano, C. A., et al. 2014. A temnospondyl trackway from the Early Mesozoic of Western Gondwana and its implications for basal tetrapod locomotion. *PLoS one* 9: e103255.

McHugh, J. B. 2014. Paleohistology and histovariability of the Permian stereospondyl *Rhinesuchus*. *J. Vertebr. Paleontol.* 34: 59–68.

McHugh, J. B. 2015. Paleohistology of *Micropholis stowi* (Dissorophoidea) and *Lydekkerina huxleyi* (Lydekkerinidae) humeri from the Karoo Basin of South Africa, and implications for bone microstructure evolution in temnospondyl amphibians. *J. Vertebr. Paleontol.* 35: e902845.

Meunier, F. J. 2011. The Osteichthyes, from the Paleozoic to the extant time, through histology and paleohistology of bony tissues. *C. R. Palevol*. 10: 347–355.

Meunier, F. J. and Laurin, M. 2012. A microanatomical and histological study of the fin long bones of the Devonian sarcopterygian *Eusthenopteron foordi*. *Acta Zool*. 81: 143–153.

Milner, A. R. 1990. The radiations of temnospondyl amphibians. In *Major Evolutionary Radiations*, eds. Taylor, P. D. and Larwood, G. P., 321–349. The Systematics Association, Oxford.

Milner, A. R. and Sequeira, S. E. K. 1993. The temnospondyl amphibians from the Viséan of east Kirkton, West Lothian, Scotland. *Trans. R. Soc. Edinburgh Earth. Sci.* 84: 331–361.

Mondéjar-Fernández, J. 2018. On cosmine: its origins, biology and implications for sarcopterygian interrelationships. *Cybium* 42: 41–65.

Mondéjar-Fernández, J., et al. 2014. New insights into the scales of the Devonian tetrapod *Tulerpeton curtum* Lebedev, 1984. *J Vertebr. Paleontol*. 34: 1454–1459.

Mujal, E. and Schoch, R. R. 2020. Middle Triassic (Ladinian) amphibian tracks from the Lower Keuper succession of southern Germany: Implications for temnospondyl locomotion and track preservation. *Palaeogeogr. Palaeoclimatol. Palaeoecol*. 543: 109625.

Mukherjee, D., et al. 2010. Preliminary observations on the bone microstructure, growth patterns, and life habits of some Triassic temnospondyls from India. *J Vertebr. Paleontol*. 30: 78–93

Niedzwiedzki, G., et al. 2010. Tetrapod trackways from the early Middle Devonian period of Poland. *Nature* 463: 43–48.

Organ, C., et al. 2016. Macroevolution of genome size in sarcopterygians during the water-land transition. *C. R. Palevol.* 15: 67–75.

Otoo, B. K. A., et al. 2019. A fish and tetrapod fauna from Romer's Gap preserved in Scottish Tournaisian floodplain deposits. *Palaeontology* 62: 225–253.

Panchen, A. L. 1970. Anthracosauria. In *Encyclopedia of Paleoherpetology*, ed. Kuhn, O., vol. 5A: Batrachosauria, pp. 1–82. Gustav Fischer Verlag, Stuttgart.

Panchen, A. L. 1985. On the amphibian *Crassigyrinus scoticus* Watson from the Carboniferous of Scotland. *Philos. T. R. Soc. B*. 309: 505–68.

Pardo, J. D., et al. 2017a. Hidden morphological diversity among early tetrapods. *Nature* 546: 642–645.

Pardo, J. D., et al. 2017b. Stem caecilian from the Triassic of Colorado sheds light on the origins of Lissamphibia. *PNAS* 114: E5389–E5395.

Parker, K. E. and Webb, J. A. 2008. Estuarine deposition of a mid-Visean tetrapod unit, Ducabrook Formation, central Queensland: implications for tetrapod dispersal. *Aust. J. Earth Sci.* 55: 509–530.

Parsons, T. S. and Williams, E. E. 1963. The relationships of the modern Amphibia: a re-examination. *Q. Rev. Biol*. 38: 26–53.

VetBooks.ir

Pawley, K. and Warren, A. 2006. The appendicular skeleton of *Eryops megacephalus* Cope, 1877 (Temnospondyli: Eryopoidea) from the Lower Permian of North America. *J Paleontol*. 80:561–580.

Peabody, F. E. 1961. Annual growth zones in living and fossil vertebrates. *J. Morphol*. 108: 11–62.

Pierce, S. E., et al. 2012. Three-dimensional limb joint mobility in the early tetrapod *Ichthyostega*. *Nature* 486: 523–526.

Qu, Q., et al. 2017. The origin of novel features by changes in developmental mechanisms: ontogeny and three-dimensional microanatomy of polyodontode scales of two early osteichthyans. *Biol. Rev.* 92: 1189–1212.

Quémeneur, S., et al. 2013. Microanatomy of the amniote femur and inference of lifestyle in limbed vertebrates. *Biol. J Linn. Soc.* 109: 644–655.

Reisz, R. R. and Modesto, S. P. 1996. *Archerpeton anthracos* from the Joggins Formation of Nova Scotia: a microsaur, not a reptile. *Can. J. Earth Sci.* 33: 703–709.

Ricqlès, A. de. 1973. Recherches paléo-histologiques sur les os longs des tétrapodes. PhD thesis, Université Paris VII, Paris.

Ricqlès, A. de. 1975a. Quelques remarques paléo-histologiques sur le problème de la néoténie chez les Stégocéphales. C.N.R.S., ed., 351–363.Colloque international C. N. R. S., Paris.

Ricqlès, A. de. 1975b. Recherches paléohistologiques sur les os longs des tétrapodes. VII- Sur la classification, la signification fonctionnelle et l'histoire des tissus osseux de tétrapodes (Première partie: Structures). *Ann. Paléontol.* 61: 49–129.

Ricqlès, A. de. 1981. Recherches paléohistologiques sur les os longs des tétrapodes - VI.- Les Stégocéphales. *Ann. Paléontol.* 67: 141–157.

Ricqlès, A. de. 1992. Paleoherpetology now: a point of view. In *Herpetology: current research on the biology of amphibians and reptiles. Proceedings of the first World Congress of Herpetology*, ed. Adler K., 97–120. Soc. Study of Amphib. and Rept., Oxford.

Ricqlès, A. de. and Buffrénil, V. de. 2001. Bone histology, heterochronies and the return of tetrapods to life in water: where are we? In *Secondary Adaptation of Tetrapods to Life in Water*, eds. Mazin J.-M. and Buffrénil M., de, 289–310. Verlag Dr. Friedrich Pfeil, München.

Romer, A. S. 1947. Review of the Labyrinthodontia. *Bull. Mus. Comp. Zool.* 99: 1–368.

Romer, A. S. 1956. The early evolution of land vertebrates. *Proc. Am. Philos. Soc.* 100: 157–167.

Romer, A. S. 1957. The appendicular skeleton of the Permian embolomerous amphibian *Archeria*. *Contributions from the Museum of Paleontology University of Michigan* 13: 103–159.

Romer, A. S. 1970. A new anthracosaurian labyrinthodont, *Proterogyrinus scheelei*, from the Lower Carboniferous. *Kirtlandia* 10: 1–16

Ruta, M. and M. J. Benton. 2008. Calibrated diversity, tree topology and the mother of mass extinctions the lesson of temnospondyls. *Palaeontology* 51:1261–1288.

Ruta, M. and Clack, J. A. 2006. A review of *Silvanerpeton miripedes*, a stem amniote from the Lower Carboniferous of East Kirkton, West Lothian, Scotland. *Earth Environ. Sci. Trans. R. Soc. Edinb.* 97(1): 31–63.

Ruta, M. and Coates, M. I. 2007. Dates, nodes and character conflict: addressing the Lissamphibian origin problem. *J. Syst. Paleontol.* 5: 69–122.

Ruta, M., et al. 2003. Early tetrapod relationships revisited. *Biol. Rev.* 78: 251–345.

Ruta, M., et al. 2007. A supertree of Temnospondyli: cladogenetic patterns in the most species-rich group of early tetrapods. *Proc. R. Soc. B Biol. Sci.* 274, 3087–3095.

Sanchez, S., and Schoch, R. R. 2013. Bone histology reveals a high environmental and metabolic plasticity as a successful evolutionary strategy in a long-lived homeostatic Triassic temnospondyl. *Evol. Biol.* 40: 627–647.

Sanchez, S., et al. 2008. Salamander-like development in a seymouriamorph revealed by palaeohistology. *Biol. Lett.* 4: 411–414.

Sanchez, S., et al. 2010a. Developmental plasticity of limb bone microstructural organization in *Apateon*: histological evidence of paedomorphic conditions in branchiosaurs. *Evol. Dev.* 12: 315–328.

Sanchez, S., et al. 2010b. Limb-bone histology of temnospondyls: implications for understanding the diversification of palaeoecologies and patterns of locomotion of Permo-Triassic tetrapods. *J. Evol. Biol.* 23: 2076–2090.

Sanchez, S., et al. 2010c. Palaeoecological and palaeoenvironmental influences revealed by long-bone palaeohistology: the example of the Permian branchiosaurid *Apateon*. *Geol. Soc. Spec. Pub.* 339: 139–149.

Sanchez, S., et al. 2012. Three dimensional synchrotron virtual paleohistology: a new insight into the world of fossil bone microstructures. *Microsc. Microanal.* 18:1095–1105.

Sanchez, S., et al. 2014. The humerus of *Eusthenopteron*: a puzzling organization presaging the establishment of tetrapod limb bone marrow. *Proc. R. Soc. B-Biol. Sci.* 281: 20140299.

Sanchez, S., et al. 2016. Life history of the stem-tetrapod *Acanthostega* revealed by synchrotron microtomography. *Nature* 537: 408–411.

Schoch, R. R. 1999. Comparative osteology of *Mastodonsaurus giganteus* (Jaeger, 1828) from the Middle Triassic (Lettenkeuper: Longobardian) of Germany (Baden-Württemberg, Bayern, Thüringen). *Stuttg. Beitr. Naturkd.* 278: 1–175.

Schoch, R. R. 2004. Skeleton Formation in the Branchiosauridae: a case study in comparing ontogenetic trajectories. *J. Vertebr. Paleontol.* 24: 309–319.

Schoch, R. R. 2009. The evolution of life cycles in early amphibians. *Annu. Rev. Earth Planet. Sci.* 37: 135–162.

Schoch, R. R. 2013a. How body size and development biased the direction of evolution in early amphibians. *Hist. Biol.* 25: 155–165.

Schoch, R. R. 2013b. The evolution of major temnospondyl clades: an inclusive phylogenetic analysis. *J. Syst. Palaeontol.* 11: 673–705.

Schoch, R. R. 2014. Life cycles, plasticity and palaeoecology in temnospondyl amphibians. *Palaeontology* 57: 517–529.

Schoch, R. R. 2018. The putative lissamphibian stem-group: phylogeny and evolution of the dissorophoid temnospondyls. *J. Paleontol.* 93: 137–156.

Schoch, R. R. and Wild, R. 1999. Die Wirbeltier-Fauna im Keuper von Süddeutschland. In *Die Trias – Eine Ganz Andere Welt Hauschke*, eds. Hauske, N., and Wilde, V., 395–408. Dr. Friedrich Pfeil, München.

Schoch, R. R. and Witzmann, F. 2014. Cranial morphology of the plagiosaurid *Gerrothorax pulcherrimus* as an extreme example of evolutionary stasis. *Lethaia* 45: 371–385.

Schultze, H.P. 1970. *Folded teeth and the monophyletic origin of tetrapods. American Museum Novitates; no. 2408*. American Museum of Natural History, New York.

Seibert, E. A., et al. 1974. Cranial co-ossification in frogs: relationship to rate of evaporite water loss. *Physiol. Zool.* 47: 261–265

Shubin, N. H., et al. 2006. The pectoral fin of *Tiktaalik roseae* and the origin of the tetrapod limb. *Nature* 440: 764–771.

Shubin, N. H., et al. 2014. Pelvic girdle and fin of *Tiktaalik roseae*. *PNAS* 111: 893–899.

Sidor, C. A., et al. 2005. Permian tetrapods from the Sahara show climate-controlled endemism in Pangaea. *Nature* 434: 886–889.

Sire, J. Y., et al. 2009. Origin and evolution of the integumentary skeleton in non-tetrapod vertebrates. *J. Anat.* 214: 409–440.

Smithson, T. R. 2000. Anthracosaurs. In *Amphibian Biology*, eds. Heatwole, H., and Carroll, R. L., Palaeontology, vol. 4, 1053–1063. Surrey Beatty, Chipping Norton.

Smithson, T. R. and J. A. Clack. 2018. A new tetrapod from Romer's Gap reveals an early adaptation for walking. *Earth Environ. Sci. Tr. R. Soc.* 108: 89–97.

Spinar, Z. V. 1952. Revision of some Moravian Discosauriscidae (Labyrinthodontia). *Rozpravy UUG* 15: 1–115.

Steyer, J. S. and Damiani, R. J. 2005. A giant brachyopoid temnospondyl from the Upper Triassic or Lower Jurassic of Lesotho. *B. Soc. Géol. Fr.* 176: 243–248.

Steyer, J. S. and Jalil, N. E. 2009. First evidence of a temnospondyl in the Late Permian of the Argana Basin, Morocco. *Palaeontology* 81: 155–160.

Steyer, J. S., et al. 2004. First histological and skeletochronological data on temnospondyl growth: palaeoecological and palaeoclimatological implications. *Palaeogeogr. Palaeoclimatol., Palaeoecol.* 206: 193–201.

Steyer, J. S., et al. 2006. The vertebrate fauna of the Upper Permian of Niger. IV. *Nigerpeton ricqlesi* (Temnospondyli: Cochleosauridae), and the Edopoid colonization of Gondwana. *J. Vertebr. Paleontol.* 26: 18–28.

Stössel, I. 1995. The discovery of a new Devonian tetrapod trackway in SW Ireland. *Geol. Soc. Spec. Publ.* 152: 407–413.

Stössel, I., et al. 2016. Ichnology and depositional environment of the Middle Devonian Valentia Island tetrapod trackways, south-west Ireland. *Palaeogeogr. Palaeoclimatol. Palaeoecol.* 462: 16–40.

Swartz, B. 2012. A marine stem-tetrapod from the Devonian of Western North America. *PLoS One* **7**: e33683.

Taplin, L. E., et al. 1982. Lingual salt glands in *Crocodylus acutus* and *C. johnstoni* and their absence from *Alligator mississippiensis* and *Caiman crocodilus*. *J. Comp. Physiol.* 149: 43–47.

Thomson, K. S. 1975. *On the biology of cosmine: Peabody Museum of Natural History*, Yale University, New Haven, CT.

Vallin, G. and Laurin, M. 2004. Cranial morphology and affinities of *Microbrachis*, and a reappraisal of the phylogeny and lifestyle of the first amphibians. *J. Vertebr. Paleontol.* 24: 56–72.

Warren, A. 2000. Secondarily aquatic temnospondyls of the Upper Permian and Mesozoic. In *Amphibian Biology*, eds. Heatwole, H. and Carroll, R. L., Palaeontology, vol. IV, 1121–1149. Surrey Beatty & Sons, Chipping Norton.

Warren, A. and Davey L. 1992. Folded teeth in temnospondyls — a preliminary study, *Alcheringa* 16(2): 107–132.

Warren, A. and Turner, S. 2005. Tooth histology patterns in early tetrapods and the presence of "dark dentine". *Trans. R. Soc. Edinburgh Earth Sci.* 96: 118–130.

Warren, A., et al. 1997. The last labyrinthodonts. *Paleontogr. ABT. B.* 247: 1–24.

Warren, A., et al. 2001. Palaeobiogeography of Australian fossil amphibians. *Hist. Biol.* 15: 171–179.

Warren, A., et al. 1991. An Early Cretaceous labyrinthodont. *Alcheringa* 15: 327–332.

Warren, J. W. and Wakefield, N. A. 1972. Trackways of tetrapod vertebrates from the Upper Devonian of Victoria, Australia. *Nature* 238: 469–470.

White, T. E. 1939. Osteology of *Seymouria baylorensis Broili*. *Bull. Mus. Comp. Zool.* 85: 325–409.

Witzmann, F. 2006. Developmental patterns and ossification sequence in the Permo-Carboniferous temnospondyl *Archegosaurus decheni* (Saar-Nahe Basin, Germany). *J. Vertebr. Paleontol.* 26: 7–17.

Witzmann, F. 2007. The evolution of the scalation pattern in temnospondyl amphibians. *Zool. J Linn. Soc.* 150: 815–834.

Witzmann, F. 2009. Comparative histology of sculptured dermal bones in basal tetrapods, and the implications for the soft tissue dermis. *Palaeodiversity* 2: 233–270.

Witzmann, F. 2011. Morphological and histological changes of dermal scales during the fish-to-tetrapod transition. *Acta Zool.* 92: 281–302.

Witzmann, F. and Schoch, R. R. 2012. A megalichthyid sarcopterygian fish from the Lower Permian (Autunian) of the Saar-Nahe Basin, Germany. *Geobios* 45: 241–248.

Witzmann, F. and Soler-Gijón, R. 2010. The bone histology of osteoderms in temnospondyl amphibians and in the chroniosuchian *Bystrowiella*. *Acta Zool.* 91: 96–114.

Witzmann, F., et al. 2010. Sculpture and vascularization of dermal bones, and the implications for the physiology of basal tetrapods. *Zool. J. Linn. Soc.* 160: 302–340.

Young, B., et al. 2013. A gigantic sarcopterygian (tetrapodomorph lobe-finned fish) from the Upper Devonian of Gondwana (Eden, New South Wales, Australia). *PLoS One* 8: e53871.

Zhang, F. K., et al. 1984. A new occurrence of Permian-Seymouriamorphs in Xinjiang, China. *Vertebrata PalAsiatica* 22: 294–304.

Zhu, M. and Ahlberg, P. E. 2004. The origin of the internal nostril of tetrapods. *Nature* 432: 94–97.

Zhu, M., et al. 2002. First Devonian tetrapod from Asia. *Nature* 420: 760–761.

Zylberberg, L., et al. 2010. A microanatomical and histological study of the postcranial dermal skeleton in the Devonian sarcopterygian *Eusthenopteron foordi*. *Acta Palaeontol. Pol.* 55: 459–470

Zylberberg, L., et al. 2016. A microanatomical and histological study of the postcranial dermal skeleton of the Devonian actinopterygian †*Cheirolepis canadensis* (Whiteaves). *Acta Palaeontol. Pol.* 61: 363–376.

VetBooks.ir

17

Lissamphibia

Vivian de Buffrénil and Michel Laurin

CONTENTS

Introduction 345
General Characteristics 345
Definition of Lissamphibians and General Phylogenetic Affinities 345
A Basic Trichotomy 346
Gymnophiona 346
Caudata 346
Anura 346
Microanatomical and Histological Features of Long Bones 347
Microanatomical Features in the Caudata 347
Bone Histology in Caudata 348
Microanatomical Features of Long Bones in the Anura 351
Histology of Anuran Long Bone Cortices 352
Remarks on Other Skeletal Elements 353
Cranial Bones 353
Gross Vertebral Organization in Lissamphibians 355
Anuran Osteoderms and Gymnophiona "Scales" 356
An Overview of Skeletal Neoteny 357
Some Concluding Remarks 359
References 359

Introduction

General Characteristics

Lissamphibians currently include 7944 recognized extant and recently extinct species (see Amphibiaweb at https://amphibiaweb.org/lists/index.shtml, accessed on November 9, 2018) and at least 319 long-extinct nominal species known from the fossil record (Marjanović and Laurin 2014). The taxon Lissamphibia, erected by Haeckel (1866), originally included only Anura (frogs and toads) and taxa now included in Caudata or Urodela (salamanders and newts), even though the latter was split by Haeckel into Perennibranchiata (neotenic urodeles that retain external gills into adulthood) and Caudata proper, a distinction that is no longer accepted today. As the name Lissamphibia indicates, a characteristic of this group is the smooth, scaleless skin. Subsequently, the limbless gymnophionans (Gymnophiona, Caecilia or Apoda) were added to this taxon, even though their skin includes dermal (bony) scales.

Lissamphibians live on every continent except Antarctica (Hopkins and Brodie 2015), but biogeographic data have long suggested that lissamphibians were once present there too (Goin and Goin 1972), and this suggestion has been upheld by more recent biogeographic analyses (Pyron 2014) and the fossil record (Mörs et al. 2020). Oviparity is common in lissamphibians, but viviparous species are encountered in urodeles as well as anurans and gymnophionans; fertilization is most frequently external, but it is internal in several taxa (Duellman and Trueb 1986).

Definition of Lissamphibians and General Phylogenetic Affinities

Lissamphibians, in the current usage, as well as in phylogenetic nomenclature (Laurin et al. 2020), is the crown-group of Amphibia. The monophyly of this taxon is supported by several characters, including the loss (which may have been achieved, in some cases, by fusion to other neighboring elements) of several cranial bones that were present in Paleozoic stegocephalians, such as the postorbital, angular and surangular (Marjanović and Laurin 2013: appendix 1). But perhaps the most often discussed synapomorphies of lissamphibians are two dental characters: the presence of pedicely and of two cuspids on the crown. Parsons and Williams (1962) first drew attention to the fact that pedicely (the presence of a poorly mineralized zone between the crown and the base of the tooth) was

VetBooks.ir

shared by most lissamphibians and was probably a synapomorphy of the group. Bolt (1969) pointed out that most lissamphibians have bicuspid (rather than simple conical) teeth, when he discovered that the Early Permian temnospondyl *Doleserpeton* shared this character (and pedicely) with lissamphibians. Since then, these two dental characters have played a prominent role in discussions about the origin of lissamphibians.

Now, the most widespread (though not necessarily best supported) hypothesis about the origin of lissamphibians is that they are nested among temnospondyls. This hypothesis has been argued to be supported, among others, by dental characters (Bolt 1969), cranial ossification sequences (Schoch and Carroll 2003) and phylogenetic analyses of large data matrices (e.g., Ruta and Coates 2007). Bolt and Lombard (1985) also hypothesized the presence of an anuran-style tympanic middle ear in temnospondyls. However, there are problems with most of these arguments. The tympanic middle ear is absent in gymnophionans and urodeles, and this absence may well be primitive (Laurin 1998). The similarities in cranial ossification sequences displayed by the temnospondyl *Apateon* and lissamphibians are apparently largely primitive (Schoch 2006, Schoch and Fröbisch 2006), are in any case not as convincing as originally claimed (Germain and Laurin 2009), and actually support an origin of lissamphibians among lepospondyls (Laurin et al. 2019). The largest data matrix that has been used to support temnospondyl affinities of lissamphibians (Ruta and Coates 2007) has been thoroughly restudied, with many characters and taxa rescored, and the resulting matrix supports lepospondyl affinities of lissamphibians (Marjanović and Laurin 2019). This leaves the dental characters that still support an origin of lissamphibians among temnospondyls, but many other characters suggest affinities between lissamphibians and some lepospondyls, such as the loss of various cranial bones (postparietal, ectopterygoid, postsplenial, third coronoid, etc.), loss of the parasternal process of the interclavicle, and so forth (Marjanović and Laurin 2013, 2019).

A Basic Trichotomy

Extant lissamphibians belong to three large clades, Gymnophiona, Caudata and Anura, whose interrelationships remain unclear. Two main hypotheses coexist in the literature. The most popular one is that Caudata and Anura form a taxon called Batrachia, but a less frequently supported hypothesis places Gymnophiona and Caudata in Procera, to the exclusion of Anura (Marjanović and Laurin 2013). The extinct Albanerpetontidae (formerly called Prosirenidae) may also be lissamphibians, or close relatives. This chapter will mainly focus on the three main extant clades because no histological work has been done on albanerpetontids, except the study of *Albanerpeton* frontal bones (Skutschas et al. 2021), which was published too late to be integrated into this review.

Gymnophiona

The limbless gymnophionans inhabit the tropics and are either aquatic or fossorial; the latter live in superficial, loose soil layers. This, along with their low biodiversity (209 extant species currently recognized according to the Amphibiaweb site, accessed on November 9, 2018), may explain why they are the most poorly known major lissamphibian clade. Gymnophionans include both oviparous (about 70% of species) and viviparous taxa, but fertilization is always internal (Duellman and Trueb 1986). Eggs may be laid in water or on land; in the first case, there is usually an aquatic larva. The eyes of extant taxa have regressed and are covered by skin, and in some cases bone. All have a chemosensory tentacle between the eyes and the nostrils. The skull is characterized by the fusion of several elements, such as the nasopremaxilla, maxillopalatine, and *os basale* that includes the parasphenoid and most of the braincase. Their body is greatly elongated: the number of vertebrae ranges from fewer than 70 to nearly 300, with a total body length from about 15 cm to more than 1.3 m (Renous and Gasc 1989).

Gymnophionans have a relatively scant fossil record (Santos et al. 2020). The oldest known stem-gymnophionan is *Eocaecilia*, from the Early Jurassic. It retained paired limbs and more cranial bones (such as separate palatine and premaxillae) than crown-gymnophionans (Jenkins et al. 2007). Two more gymnophionans are known from the Late Cretaceous and two from the Paleogene; their affinities with extant taxa are unclear (Marjanović and Laurin 2014).

Caudata

Caudata include the salamanders and newts. They retain the most generalized body plan of extant amphibians because most have four well-developed limbs, even though these have regressed in size in a few taxa (such as *Amphiuma*), and the hind limbs have disappeared in sirenids (Duellman and Trueb 1986). Caudata are moderately diverse, with 716 currently recognized extant species, according to the Amphibiaweb site. Reproductive modes are diverse, ranging from external fertilization of aquatic eggs that give rise to aquatic larvae (probably the primitive condition for Caudata) to viviparity. Many intermediates are known, such as internal fertilization of aquatic or terrestrial eggs. Larvae (feeding or not) or terrestrial juveniles may hatch from terrestrial eggs (Duellman and Trueb 1986, p. 22). Caudata have a reasonably good fossil record, at least for the aquatic taxa, which develop with various degrees of neoteny. The oldest known Caudata date from the Middle Jurassic and most (perhaps all) of them are karaurids, which are probably stem-Caudata (Marjanović and Laurin 2014).

Anura

Anurans include the frogs and toads. Anurans are by far the most speciose of the three main lissamphibian clades, with 7019 currently recognized extant species (Amphibiaweb site accessed on November 9, 2018). Nearly all anurans have external fertilization, but they use many oviposition sites; in addition to standing or flowing fresh water, some taxa also lay eggs on leaves located above ponds, in water-filled cavities of trees or in epiphytic bromeliads (a few bufonids and hylids), in foam nests (some myobatrachids and leptodactylids), or near water, in or on the ground, sometimes in a nest or burrow, and so forth. Similarly, larvae (tadpoles) may or may not feed, and some (such as all leiopelmatids) even have direct development. At least five species are known to be viviparous or

VetBooks.ir

ovoviviparous (Duellman and Trueb 1986). Most are specialized for a saltatory locomotion, with a few exceptions such as the highly aquatic pipids. Many have a moist skin like most other lissamphibians, but toads have somewhat drier skin and a few, like the spadefoot toad, inhabit arid areas, even though this involves spending most of their life in burrows and coming out in the rainy season to breed. A few tree frogs can secrete a lipid-based cocoon and spend the dry season on a branch. Anurans include a few invasive taxa, such as the cane toad *Rhinella marina* (formerly known as *Bufo marinus*), which has caused a great deal of ecological damage since it was introduced in Australia (Phillips et al. 2006). Anurans are the most salt-tolerant lissamphibians (even though a few caudates and gymnophionans have limited brackish water tolerance), and at least one species (*Fejervarya cancrivora*) can swim in seawater, a fact that was already known to Darwin; at least one other species (*Bufotes viridis*) has nearly as good an osmotic tolerance (Hopkins and Brodie 2015). Many other species of anurans tolerate brackish water.

Anurans have a reasonably good fossil record, at least for the aquatic taxa. The emergence of anurans is documented in the fossil record through several stem-anurans dating from the Early Triassic to the Early Cretaceous. The oldest crown-anurans date from the Middle Jurassic (Marjanović and Laurin 2014).

Microanatomical and Histological Features of Long Bones

Since the classic comparative syntheses by Foote (1911, 1916), Amprino and Godina (1947), Enlow and Brown (1956) and Ricqlès (1979) (see also the historical account in Part I) on the histology of tetrapod skeletons, based on the shaft cortices of long bones, only two more recent reviews have considered the skeletal tissues of lissamphibians specifically and synthetically, Ricqlès (1995) and Castanet et al. (2003). In many respects, these two articles remain central references. Our purpose here is merely to summarize and update them on some questions for which new data or interpretations have been proposed.

Microanatomical Features in the Caudata

At a microanatomical level, long bones in most terrestrial and amphibious urodeles (that experience full metamorphosis have a common "generalized" structure (Figure 17.1A), with a tubular diaphysis presenting an open medullary cavity and well-differentiated metaphyses and epiphyses (Castanet et al. 2003). In juveniles and subadults, the latter house hyaline, hypertrophic and calcified cartilages, as well as some endosteoendochondral trabeculae, as in most other tetrapods (Figure 17.1B). In the adults, long bones have a roughly tubular diaphysis, their metaphyses contain networks of endosteal trabeculae of variable spatial density, and their epiphyseal surfaces are covered with a cap of hyaline articular cartilage (Haines 1942, 1969; Ricqlès 1964, 1965, 1979, 1995; Castanet et al. 2003; see also Skutschas and Stein 2015). In nonneotenic taxa, the basic endochondral growth process of long bones complies with the general pattern prevailing in tetrapods (Figure 17.1C; see also Chapter 9). The situation of neotenic forms is different, especially for the fate of the cartilages produced by the epiphyses during growth: resorption of calcified cartilage is more or less severely inhibited in such forms and the entire medullary region can be obstructed by this tissue. This question is specifically considered in the section about heterochronic processes. Urodele epiphyses are of a typical primitive type (Haines 1938; Ricqlès 1979, 1995; Castanet et al. 2003).

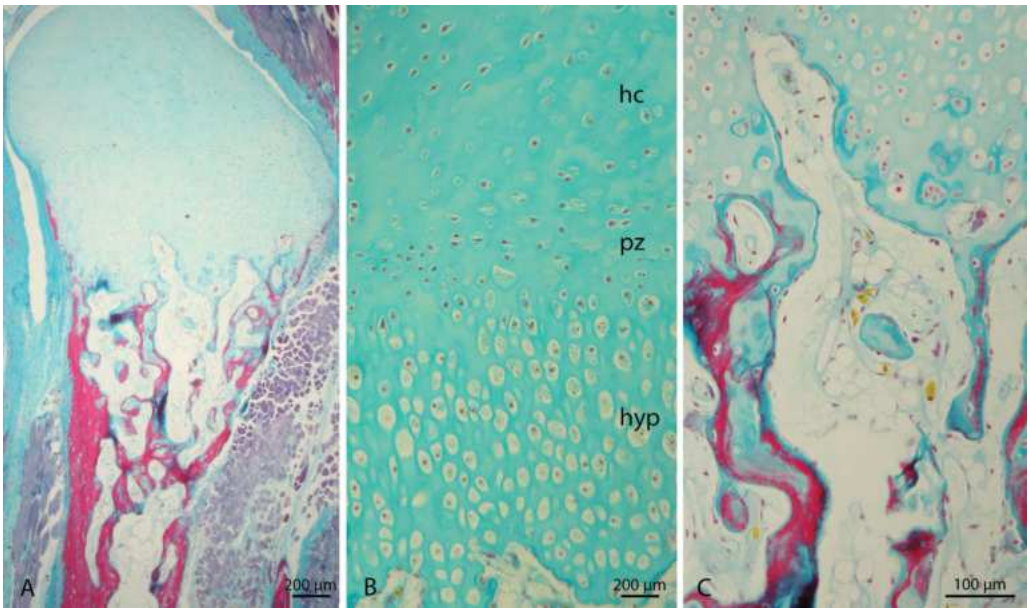


FIGURE 17.1 Epiphyseal and metaphyseal regions of an urodele long bone (here, the femur of *Pleurodeles waltl*). A, Longitudinal section including the diaphysis, metaphysis and epiphysis. The noncalcified cartilage is blue; the bone is red. B, Detail of (A) showing the distribution of the hyaline cartilage (hc), the proliferation zone (pz) and the hypertrophic cartilage (hyp). C, Detail of (A) showing the chondroclastic resorption of the hypertrophied cartilage and its replacement by endosteal osseous tissue (red areas).

VetBooks.ir

In mid-diaphyseal reference sections, general compactness profiles differ considerably among urodele taxa, even when neotenic forms are ignored. Detailed quantitative studies of the relationship between specific habitat (terrestrial, amphibious, fully aquatic) and compactness profile parameters in stylopodial bones conducted by Laurin et al. (2004) on the femur and by Canoville and Laurin (2009) on the humerus revealed that the bones of aquatic taxa (Figure 17.2A, B) have narrower medullary cavities, thicker cortices and higher global compactness than do amphibious or terrestrial forms (see also Chapter 35). When pronounced neoteny exists, diaphyseal compactness can be close to 100% due to the local retention of calcified cartilage; however, as exemplified by the humerus of *Salamandra salamandra* figured by Alcobendas and Castanet (2000), a total occlusion of the medullary cavity may also result from excessive endosteal deposits during the remodeling process that normally affects the periphery of this cavity.

A frequent and striking feature of urodele long bones is the occurrence within the shaft cortex of numerous large (up to 1.3 mm in mean diameter in *Andrias*) resorption bays bordered by Howship's lacunae (Figure 17.2A, C, D, H). This feature has been observed in the juveniles as well as the adults of many species of different body sizes, including, for example, *Pleurodeles waltl* (Ricqlès 1964), *Triturus cristatus* (Castanet et al. 2003), *Andrias japonicus* (Canoville et al. 2018) and so forth. The lacunae are distributed at random within the cortices and never show any sign of secondary reconstruction. Their functional significance remains obscure.

Cortical vascularization is extremely rare in extant Caudata. The extensive study (34 species) by Canoville et al. (2018) revealed the occurrence of sparse simple vascular canals only in the femur of *Andrias japonicus* and *A. davidianus*, the two largest extant urodele species (the humerus is avascular in these species). A clearly higher (though not quantified) vascular density was observed in computed tomography (CT-scan) sections of the humerus of a large adult *A. japonicus* by Sanchez et al. (2014; cf. additional illustrations), an observation contrasting with the descriptions by Canoville et al. (2018). This discrepancy suggests that substantial interindividual variability in vascular density may occur in *Andrias*. With the exception of this taxon, the bones of extant urodeles can be considered quasi-avascular (Figure 17.2A, B). Among extinct forms, the outer surface of the femoral cortices of *Aviturus exsecratus*, from the Paleocene-Eocene of Mongolia (Vasilyan and Böhme 2012), and *Ukrainurus hypsognathus*, from the Miocene of Ukraine (Vasilyan et al. 2013), two taxa of larger body size than *Andrias* (femur diameter at mid-diaphysis is 6.3 mm, at most, in extant *Andrias* vs 8.08 mm in *Ukrainurus* and 10 mm in *Aviturus*), display a dense pitting that most likely reflects the former existence of blood vessels perforating the cortex. These various observations suggest that there is a size threshold (at least for the femur) above which urodele long bones are vascularized and below which they are avascular. According to Canoville et al.'s (2018) data, this threshold should correspond approximately to the size (i.e., the bone area in cross section at mid-diaphysis) of extant adult *Andrias*. It is noteworthy, however, that Castanet et al. (2003) mentioned the occurrence of vascularization, appearing as "one row of longitudinally oriented primary simple vascular canals", in long bone cortices of *Ambystoma tigrinum*, a large American salamander up to 25 cm in total length (TL). If so, the threshold could be lower, although the diameter of the *A. tigrinum* femoral shaft is unknown. In two smaller *Ambystoma* species (*A. andersoni*: 15 cm TL; *A. opacum*: 10 cm), no vascular canals were observed by Canoville et al. (2018). This could indicate that the occurrence of vascularization in caudate long bones does not closely depend on phylogeny.

The gross morphology and microanatomical features of the femur in the early (Bathonian) forms, *Kokartus honorarius* (Skutschas and Stein 2015), *Marmorerpeton* sp. and Salamander A (Buffrénil et al. 2015), share similarities, but they also have marked differences that distinguish these taxa from each other and from extant urodele species. Beyond the fact that the femur of *Kokartus* has a relatively large medullary cavity (albeit peripherally bordered by a layer of calcified cartilage), a feature seldom encountered in urodeles, the main peculiarity of this bone is to have vascularized cortices in spite of its small size (2.2 mm in diameter for the largest individuals), according to the measurements of Skutschas and Stein (2015), and to display traces of Haversian remodeling, two characteristics contrasting with the condition of other Caudata.

As in many extant urodeles, the long bone cortices of *Marmorerpeton* and Salamander A display numerous, large and randomly distributed resorption lacunae showing no trace of peripheral reconstruction (Figure 17.2D). Conversely, intracortical resorption in *Kokartus* is much less pronounced, or is absent in some of the sections shown by Skutschas and Stein (2015); in addition, it is distributed differently (the lacunae are concentrated around the medullary cavity). These three Jurassic salamanders have several other microanatomical peculiarities (especially the very high compactness of long bones in *Marmorerpeton* and Salamander A), due to neoteny; these features will be considered below, in the chapter relative to this developmental pattern.

Bone Histology in Caudata

The histological structure of epiphyses and metaphyses in urodele long bones has been described in detail in several studies including Haines (1942), Ricqlès (1964, 1965), and Quilhac et al. (2014). In nonneotenic growing individuals, epiphyseal structure is roughly comparable to that of "primitive epiphyses" encountered in many amniote taxa (see Chapter 4); however, in the proliferation and hypertrophy zones, the chondrocytes do not tend to be aligned in axial isogenic groups (Fig. 1B) as is so commonly observed in amniotes. According to Haines (1942; see also Ricqlès 1979), this condition is supposed to be a derived feature; the ancestral character state in tetrapods is the occurrence of axially aligned isogenic groups. The calcification of hypertrophic cartilage is of the spheritic type, a process (common in cartilage) in which apatite crystals aggregate independent of collagen fibers to form spherical units, the calcospherites, typical of globular cartilage (e.g., Ricqlès 1965 and Chapter 7).

VetBooks.ir

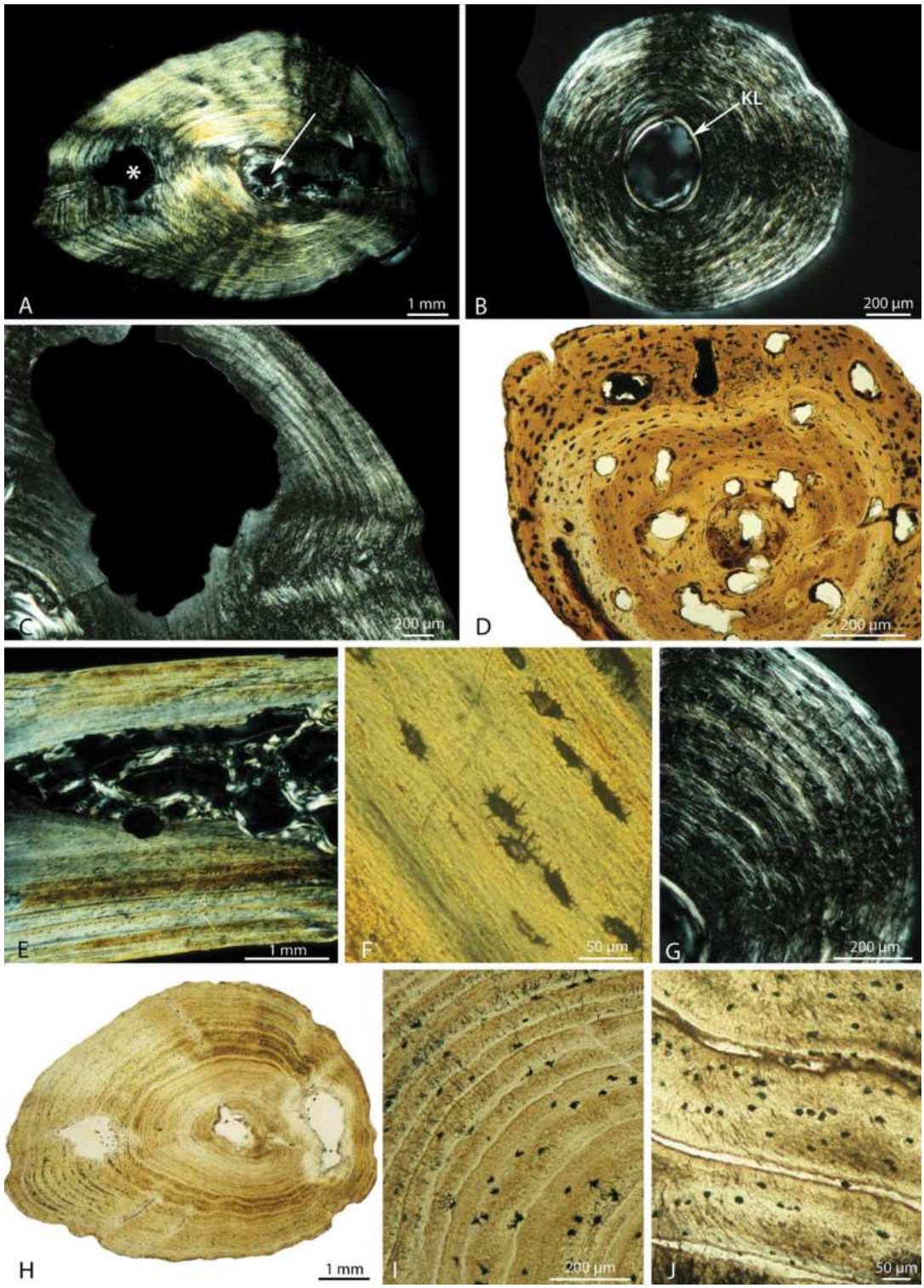


FIGURE 17.2 General histology of long bones in the urodeles. A, General view of a cross section of the femur of *Andrias japonicus*. The arrow points to the medullary cavity and the asterisk indicates a large erosion lacuna within the cortex. B, Cross section of the femur of *Necturus maculosus*. The avascular cortex is made of parallel-fibered tissue. The thin birefringent layer around the medullary cavity is Kastschenko's line (KL and arrow). Transmitted polarized light. C, Detail of an erosion lacuna in the femur of *Andrias japonicus*. D, Multiple resorption lacunae in the humerus of *Marmorerpeton* sp. E, Longitudinal section of the humeral shaft of *Andrias davidianus*. The cortex, made of pure parallel-fibered tissue, shows mass birefringence in polarized light. F, Detail of cortical histology in the femur of *A. davidianus* in longitudinal section. The bone matrix is strongly birefringent, and the osteocyte lacunae are flat, parallel to the surface of the bone and have few *canaliculi*. G, Diffuse annuli in the femoral cortex of *N. maculosus*. Transmitted polarized light. H, Cross section of the femur of *A. japonicus* showing the succession of numerous annuli. I, Detail of the femoral cortex of *A. davidianus* showing lines of arrested growth (LAGs) associated with annuli. J, Detail of the stratification of the cortex into cyclical growth marks in the femur of *A. davidianus*. Very conspicuous LAGs are visible.

VetBooks.ir

Comparative studies of extant taxa show that the periosteal cortices of long bone diaphyses in urodeles are made of well characterized parallel-fibered tissue. In cross-sections observed in polarized light, this tissue may either appear as monorefringent or display irregular and variable birefringence (in, e.g., *Necturus maculosus* and *Andrias*; Figure 17.2A, B). Conversely, in all specimens, birefringence is much more pronounced in longitudinal sections (Figure 17.2E, F). These observations suggest that the orientation of collagen fibers in the osseous matrix of urodele long bones is basically longitudinal, but that it may also include a spiral component. The periphery of the medullary cavity is generally covered with secondary, reconstructive deposits of true lamellar tissue, set in place by the endosteum after local resorption (enlargement of the medullary cavity) has ceased (Figure 17.2C).

The tens of skeletochronological studies conducted hitherto on urodele populations show that most taxa have well differentiated growth marks, although the marks can be missing in populations living in stable conditions or growing to adult size in less than one year (Castanet 1975). Histologically, urodele cyclic growth marks, as seen in cross sections, consist of annuli or, more frequently, lines of arrested growth (LAGs) regularly spaced within the cortex. The annuli are layers of lamellar tissue 20–50 µm thick appearing clear in ordinary transmitted light, an aspect due to the rarefaction of canaliculi, and birefringent in polarized light (Figure 17.2G, H). LAGs are thinner (5–10 µm), acellular and strongly birefringent (Figure 17.2I, J). In decalcified sections stained with hematoxylin, they appear as strongly chromophilic lines. Skeletal cyclic growth marks and the age determination based on them, i.e., the skeletochronological method, are fully described in Chapter 31. Such marks are very sharp in most urodele taxa and are sometimes split (each LAG being double), especially in mountain-dwelling populations (e.g., in *Euproctus asper*; Montori 1990); otherwise, they do not differ in their structure and ecophysiological significance (an annulus reflects a decrease in growth rate and LAGs reflect a growth cessation) from the marks in other vertebrates. Sharpey's fibers are frequent in long bones, including phalanges, where they appear as strong oblique bundles in the cortex (Kolenda et al. 2018). Occasionally, between the cortical and medullary regions, a thin layer of a tissue displaying different optical properties than the rest of the cortex encircles the medullary cavity. This line, known as Kastschenko's line (first description in Kastschenko 1881) is considered to represent a remnant of calcified cartilage matrix spared by perimedullary resorption (see Figure 17.2B). When present, it would then mark the initial boundary, in a given transverse plane, of the periosteal cortex when it started to develop (see also Skutschas and Stein 2015).

Consistent with the spatial orientation of the collagen matrix, osteocyte lacunae are predominantly circular in transverse sections, with some variability in their morphology and orientation, whereas they are flattened and oriented parallel to the surface of the cortices in longitudinal sections (Figure 17.2F). Canaliculi are often poorly developed.

Comparative data on bone histology in extinct urodeles are relatively scarce, but detailed information exists for *K. honorarius* (Skutschas and Stein 2015), *Marmorerpeton* sp. and Salamander A (Buffrénil et al. 2015), all of which date from the Middle Jurassic. *Kokartus* retained perimedullar calcified cartilage and a clear Kastschenko line at mid-diaphysis. Cartilage retention was much more pronounced in *Marmorerpeton* and Salamander A, and their medullary cavity was entirely filled with this tissue. Failure of cartilage resorption at a distance from the epiphyses reveals a process of skeletal neoteny. The histological characteristics of femoral cortices in *Marmorerpeton* and Salamander A are comparable to those of extant urodeles, although these two taxa (as is also the case for *Kokartus*) do not display LAGs, but feebly differentiated annuli (Figure 17.2D). Otherwise, *Kokartus* seems different from all other urodeles. Although bone tissue in this taxon is of the common parallel-fibered type, it displays some secondary osteons in subadults and adults in addition to having a significant vascularization consisting of longitudinal primary osteons, two features nearly unknown in other urodeles of its size. According to Skutschas and Stein (2015), these characteristics are plesiomorphic in urodeles (see also Ricqlès 1979) and were lost when this taxon evolved toward miniaturization.

To our knowledge, measurements of the spatial density of cell lacunae in lissamphibian bones have not yet been conducted; however, the individual volume of the lacunae was studied in *Marmorerpeton* sp. for documenting its possible relation to genome size (Laurin et al. 2016). The volume of osteocyte lacunae indeed appears to be proportional to the size of a specific genome (Organ et al. 2007), a relationship that allows inference from extant to extinct taxa (Organ et al. 2011). Extant Caudata are known to have the largest genome size among tetrapods, with a 10-fold difference among taxa. This had long been attributed to differences in life cycle between taxa experiencing full metamorphosis (small genome) and the neotenic forms; however, the latest study did not find a significant link between genome size and life cycle (Liedtke et al. 2018). Similarly, an inverse relationship between genome size and metabolic rate was long hypothesized, but the latest study did not find unambiguous support for this idea (Gardner et al. 2020). The study by Laurin et al. (2016) showed that the volume of *Marmorerpeton* osteocyte lacunae was already large and corresponded to an estimated genome size comparable to that of extant Caudata. This result suggests that stem-urodeles had evolved this characteristic at least by the Middle Jurassic, some 167 Ma ago. To some extent, *K. honorarius* also displays large cell lacunae, but Skutschas and Stein (2015) proposed to explain this feature by another possible cause, periosteocytic osteolysis. This is a resorption process seen in numerous vertebrates (e.g., Alcobendas et al. 1991) that is operated by the osteocytes themselves and results in an increase in lacunar size.

Finally, available comparative data therefore suggest that, at both microanatomic and histologic levels, the basal, plesiomorphic condition of long bones in the Caudata might have had four characteristics: (1) variably pronounced neoteny, (2) vascularized cortices, (3) mild intracortical Haversian remodeling and (4) large osteocytic lacunae likely related to large genome size. Two of these features (vascularization and Haversian remodeling) were subsequently lost (possibly only once) with size reduction and are absent in most taxa.

VetBooks.ir

Microanatomical Features of Long Bones in the Anura

At a microanatomical level, the long bones of all anuran taxa have a typical tubular architecture, with a slender cylindrical diaphysis and cortices lacking the wide erosion bays observed in the urodeles (Canoville et al. 2018, Rozenblut and Ogielska 2005). Conversely, metaphyseal and epiphyseal regions have a highly apomorphic structure, unparalleled among other tetrapods. The comparative studies by Haines (1942), Ricqlès (1979, 1995), Francillon (1981), Francillon-Vieillot (1987) and Castanet et al. (2003) give a synthetic idea of the basic epiphyseal characteristics of anurans, along with their variations among species and during ontogeny (Figure 17.3). In brief, long bone metaphyses are variably differentiated and may differ little in diameter from the diaphysis; they also contain few endosteal trabeculae, if any (Figure 17.4). Anuran epiphyses are covered by a thick subspherical cap of cartilage that extends both inside the neighboring metaphyseal part to form a metaphyseal cartilaginous plug and outside the metaphysis to form a cartilaginous "muff" (Figure 17.3). The space between this muff and the surface of the metaphyseal wall, the so-called *encoche d'ossification* (ossification notch), contains a loose connective tissue housing active osteoblasts (located along the outer surface of the metaphyseal cortex) and chondroblasts (along the opposite, cartilaginous side). The whole morphology of anuran epiphyses thus evokes the head of a match and is designated as "matchlike" for this reason. In early growth stages, the epiphyses are made of a homogeneous mass of hyaline cartilage. During growth, the peripheral part of the cap remains hyaline but its basal part, just above the metaphyseal cartilaginous plug, differentiates into a lenticular cell aggregation where chondrocytes appear flat and oriented parallel to the outer contour of the epiphysis (Figure 17.3). This zone is equivalent to the proliferation zone of other, less specialized tetrapod epiphyses. At the same time, the cartilage in the basal part of the metaphyseal cartilaginous plug turns into hypertrophied calcified cartilage before being resorbed and ultimately replaced by sparse endosteal bone trabeculae (if any), whereas active periosteal osteogenesis occurs at the level of the ossification notch and contributes to the growth in length of the bone (Francillon-Vieillot 1987, Rozenblut and Ogielska 2005, Miura et al. 2008). In large adults, calcification spreads to variable extents into the epiphyseal cartilage, which can be ultimately replaced by more or less extensive networks of endosteal trabeculae (Figure 17.4; see also Francillon 1981). As in most other tetrapods, sesamoids are present in the vicinity of articulations in the skeleton of anurans. Documentation of this topic is nevertheless meager; the most precise studies are by Hoyos (2003) and Ponssa et al. (2010).

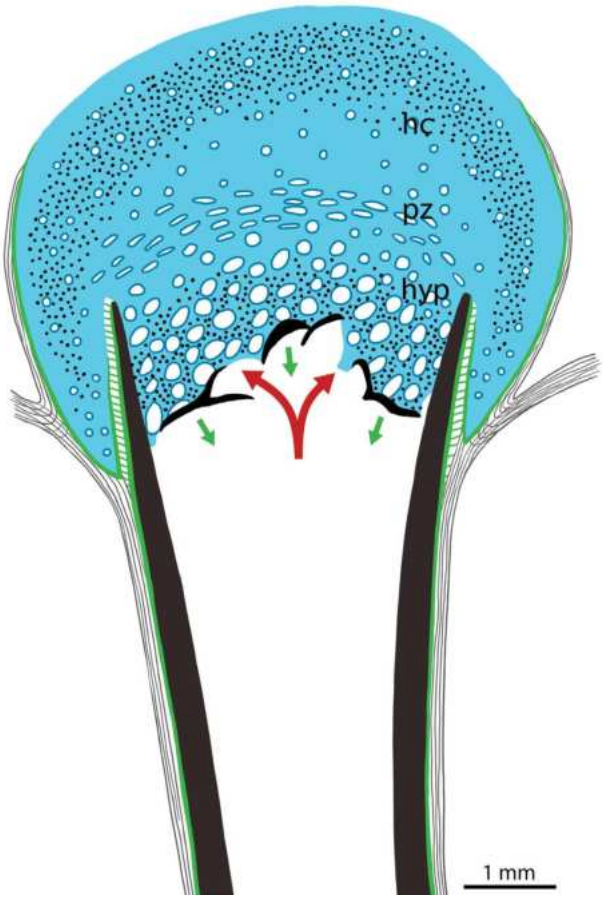


FIGURE 17.3 Basic organization of the epiphyseal and metaphyseal regions of an anuran long bone. Same abbreviations as for Figure 17.1B. In addition, osteogenic (periosteum) and chondrogenic (perichondrium) membranes are indicated in green. The match-head structure, typical of anuran long bones (see text), creates the ossification notch, in which the activity of osteoblasts stimulates the growth in length of the bone shaft. The red arrows indicate the resorption of the hypertrophic cartilage by the conjunctivovascular erosion front. The green arrows indicate the apposition of endosteal bone layers over the eroded cartilage.

In the diaphysis, cortical thickness is broadly variable both among taxa and among the various bones of a single limb. Environment has the same influence on the compactness profile parameters of long bones as observed in Caudata: aquatic forms tend to have more compact bones (up to 89% in *Pipa pipa*) than amphibious or terrestrial taxa (typically 50–80%: Laurin et al. 2004; Canoville and Laurin 2009). Contradictory data on this topic (i.e., skeletal weight is less in aquatic forms) were presented by Leclair et al. (1993) and Castanet and Caetano (1995). This contradiction may result from methodological discrepancies (use of long bones vs whole skeleton, measurement of weight vs compactness profile). Irrespective of specific habitat, phalanges and the tibiofibula tend to have an extremely narrow medullary cavity, and consequently very thick cortices, due to limited perimedullary resorption (e.g., Leclair 1990, Esteban et al. 1998).

The occurrence of vascular canals in anuran long bones is relatively common; they are present in 32.3% of the 62 bones (humerus and/or femur) from 37 species studied for this purpose by Canoville et al. (2018) (see also Castanet et al. 2003). The canals are mostly represented by primary osteons, whose lumen varies from 10 to 40 µm in diameter, depending on the position of the canal in the section, and the individual or species considered (Figure 17.5A, C). Besides the primary osteons, sparse secondary osteons may occasionally be present in the deep cortex, as exemplified by *Nanorana vicina* (Canoville et al. 2018). Simple vascular canals (Figure 17.5B), often associated with primary osteons, can also be observed. In *Amietophrynus regularis*, both may coexist in a single

VetBooks.ir

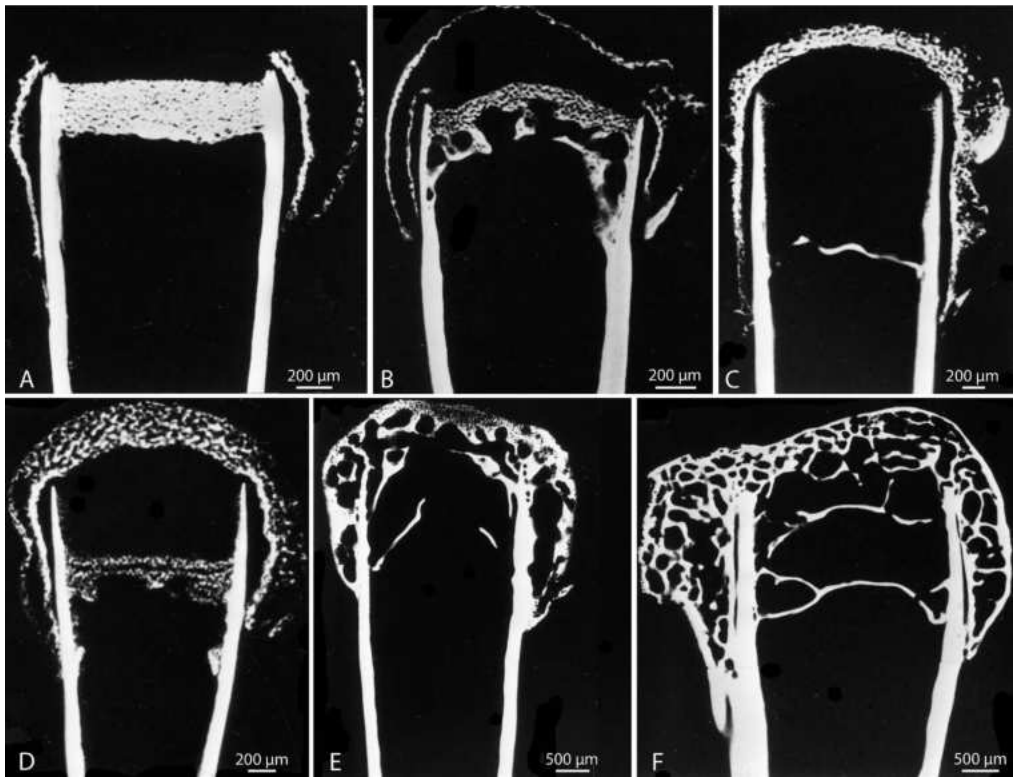


FIGURE 17.4 Various aspects of the calcification of cartilage and the differentiation of bone trabeculae in the epiphyseal territory of adult anurans. A, *Adelotus brevis* (Myobatrachidae). B, (*Phrynomerus bifasciatus* (Microhylidae). C, *Chiromantis xerampelina* (Rhacophoridae). D, *Breviceps gibbosus* (Brevicipitidae). E, *Mixophyes fasciolatus* (Myobatrachidae). F, *Dryopsophus caeruleus* (Pelodryadinae).

section, depending on the sectional sector considered. In the humerus, canals do not occur in bones smaller than 0.9 mm^2 in sections sampled at mid-diaphysis; in the femur, this threshold is 1.2 mm^2. The occurrence of vascular canals seems unrelated to phylogeny and is imperfectly associated with size (the largest species in Canoville et al.'s (2018) sample, *Conraua goliath,* has avascular bones). So far, the main factors that influence vascular density in anuran bones remain to be clearly identified. Vascular canals have a preferential longitudinal orientation; however, oblique or radial canals can occasionally be associated with longitudinal ones. Vascular canals, regardless of their orientation, can be distributed randomly (Figure 17.5A), but this condition is rare; they rather tend to be organized either in radial rows (Figure 17.5B), in circumferential layers or in a combination of both. In *Rhinella marina*, the primary osteons are arranged in concentric layers and tend to have an incipient circumferential orientation (Figure 17.5C); this locally gives the bone an apparent sublaminar organization (but the latter does not represent, of course, a fibrolamellar complex).

Histology of Anuran Long Bone Cortices

Diaphyseal cortices in anurans are made of parallel-fibered tissue, like those of the urodeles; however, in cross-section, they are more markedly monorefringent (Figure 17.5D). Likewise, in longitudinal sections, the birefringence of the bone matrix is particularly strong, with alternation of total extinction or total illumination when the microscope stage is rotated (Figure 17.5E, F). These observations indicate that the fibers of the collagenous matrix have a marked longitudinal orientation in anurans. Some faint differences may nevertheless exist among taxa in the regularity of the spatial orientation of the bone collagenous meshwork. Sharp cyclical growth marks, in the form of LAGs or birefringent annuli, occur in most anuran bones (Figure 17.5D), as do bundles of radial and oblique Sharpey's fibers (Figure 17.5G, H) originating from either the periosteum or muscular entheses. Castanet et al. (2003) and Francillon-Vieillot et al. (1990) mention the occasional occurrence of a Kastschenko's line in the long bone diaphyses of anurans.

In longitudinal sections, osteocyte lacunae appear flat and parallel to the sagittal axis of the bones (Figure 17.5G), an aspect confirming that long bone cortices are made of well characterized parallel-fibered bone tissue. Osteocyte lacunae are generally circular in cross section (Figure 17.5H), but minor differences may exist among taxa in the apparent shape (i.e., the orientation in reference to the sectional plane) of the lacunae. Although the canaliculi appear short in longitudinal section, the cross sections of most limb bones reveal the presence of complex canalicular networks in the vicinity of the osteocyte bodies (Figure 17.5I). The canaliculi have a primarily radial orientation but tend to converge toward the lumen of vascular canals, when present. They constitute a complex network, with ramifications mainly developing at some distance from osteocyte bodies. Opposite to the situation prevailing in the Caudata, the volume of anuran osteocytes is only moderately increased compared to the primitive tetrapod condition (Laurin et al. 2016).

VetBooks.ir

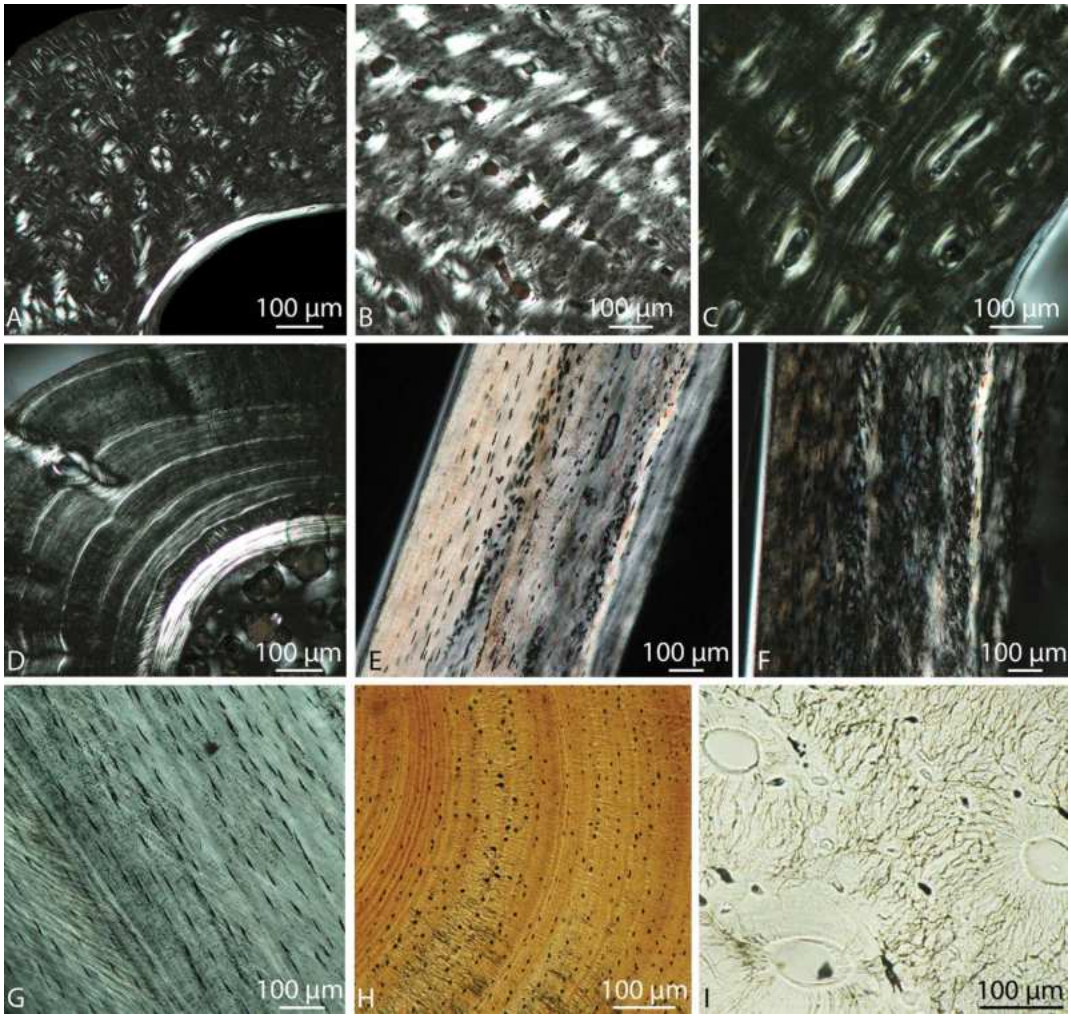


FIGURE 17.5 General histological features of the shaft of anuran long bones. A, Vascularization in the femoral cortex of *Amietophrynus regularis* (Bufonidae) consists of longitudinal primary osteons distributed randomly in the cortex. The latter is made of parallel-fibered tissue with a longitudinal orientation of the collagen meshwork (monorefringent aspect of cross-sections in polarized light). B, Another view of bone vascularization in the femoral cortex of *Amietophrynus regularis*; in this case, the canals are simple, and oriented longitudinally in radial rows. C, Femoral cortex of *Rhinella marina* (Bufonidae). The primary osteons are distributed in concentric rows and have an oblique or subcircular orientation. The cortex itself is made of parallel-fibered tissue with collagen fibers oriented longitudinally. D, Cortex of parallel-fibered tissue with a clear longitudinal orientation of the collagenous meshwork (*Nanorana vicina*: Dicroglossidae). Six sharp lines of arrested growth (LAGs) are visible. E and F, Longitudinal section of the femoral cortex of *Hoplobatrachus occipitalis* (Dicroglossidae), viewed in transmitted polarized light. With the rotation of the microscope stage, the cortex turns from totally illuminated (E) to totally dark (F), which reveals the clear, dominant longitudinal orientation of its collagenous meshwork. G, Aspect and orientation of cell lacunae in a longitudinal section of the femur of *Conraua goliath* (Conrauidae). Birefringence is strong, and the cells are all oriented parallel to the bone surface. Sharpey's fibers occur (lower left part). H, Femoral cortex of *Latonia gigantea* (an extinct alytid from the Middle Miocene of Europe) in cross section. The cortical tissue is of the parallel-fibered type. Osteocyte lacunae, cut transversely here, have a discoid aspect whereas their real morphology is spindle-like. I, Close view of the cell lacunae and their canaliculi in the femoral cortex of *Trichobatrachus robustus* (Arthroleptidae).

Remarks on Other Skeletal Elements

Cranial Bones

As in most other vertebrates, the membrane bones of the skull of lissamphibians are, at a microanatomical level, basically structured as diploes (Figure 17.6A–D). Precise descriptions are scanty and most often anecdotical, compared to the many studies conducted on the anatomy, morphometry and "ossification sequences" of extant and extinct taxa (see, e.g., Hanken and Hall 1984, Djorović and Kalezić 2000, Germain and Laurin 2009). The sparse documents hitherto available show that sharp compactness differences exist between the diverse skull bones and among taxa. For example, in anurans, the dermal part of the ethmoid of *Hyla septentrionalis* (Hylidae) has a very loose architecture and a low apparent compactness, with two (dorsal and ventral) thin cortices united by sparse, slender trabeculae (Trueb 1966). A similar architecture is observed in the frontoparietal of the "ceratophryid" *Ceratophrys cornuta* (Buffrénil et al. 2016); conversely, the same bone in *Latonia gigantea* displays a more compact structure (Buffrénil et al. 2016) and the skull roof elements

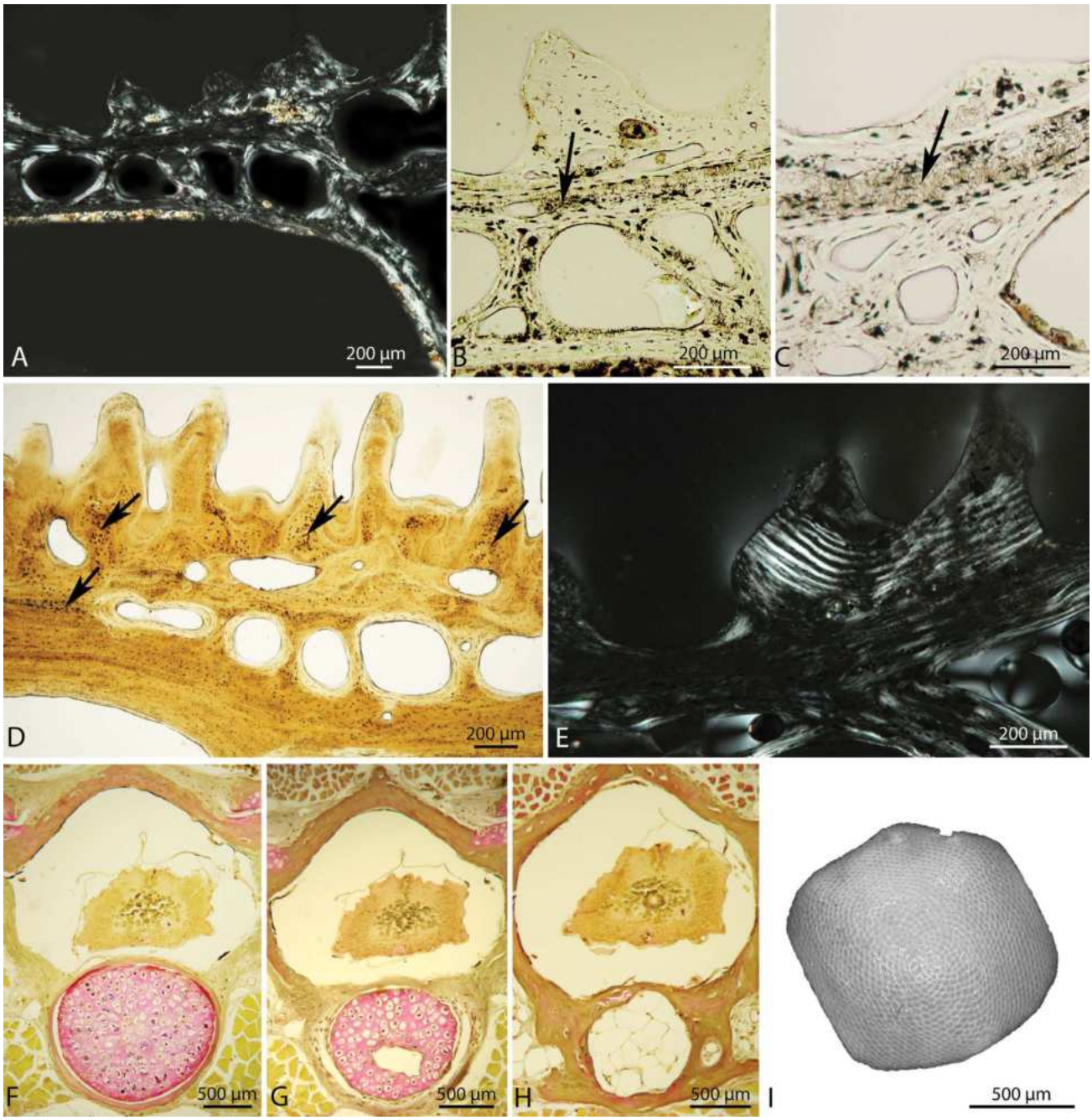


FIGURE 17.6 Microstructures in the lissamphibian skull, vertebrae and "scales". A, Cross section. The diploe structure of the frontoparietal of ceratophryid *Ceratophrys aurita* (cross section in polarized light). B, Closer view of the same bone in ordinary transmitted light. The arrow points to the tissue located in the core of the outer layer. C, Detail of the tissue designated by the arrow in B. D, Cross section of the frontoparietal of *Latonia gigantea*. The arrow points to the core layer mentioned in A and B. E, Plywood bone formation on top of the frontoparietal of *C. aurita*. Transmitted polarized light. F–H, Cross sections through the growth cartilage of a *Pleurodeles waltl* vertebra. The sectional planes are shown in the sketch in Figure 17.7. Sections F and G are through the cartilage, whereas section H is through the part occupied by the remnants of the notochord. I, General aspect of the scales of the gymnophione *Hypogeophis* sp.

of *Brachycephalus ephippium* (Brachycephalidae) are entirely compact (Clemente-Carvalho et al. 2009). The squamosal of the basal urodele *K. honorarius* is a typical diploe, with a broad central spongiosa of low compactness, whereas the frontal of *Eoscapherpeton asiaticum* (Late Cretaceous urodele) is more compact and somewhat less characteristic of the diploe architecture (Skutschas and Boitsova 2017).

From a histological perspective, information on urodele and anuran skull bones is also scarce. To our knowledge, three studies (not including the study on albanerpetontids by Skutschas et al. 2021), specifically consider these bones: Clemente-Carvalho et al. (2009), Buffrénil et al. (2016) and Skutschas and Boitsova (2017). The three regions comprising the diploe, i.e., the central, cancellous region, the deep (basal)

VetBooks.ir

cortex and the superficial (dorsal) cortex, display contrasting histological features. The basal layer is always made of a well characterized lamellar or parallel-fibered tissue devoid of vascular canals. Skutschas and Boitsova (2017) showed that the trabeculae of the spongy core region of the squamosal in *K. honorarius* were extensively remodeled. The local remnants of primary bone consist of parallel-fibered tissue with rounded osteocyte lacunae. The trabeculae of the core spongiosa in the frontoparietals of *Ceratophrys* and *Latonia* are also made of remodeled parallel-fibered tissue, coated by secondary deposits of lamellar bone (Buffrénil et al. 2016); however, just above the spongiosa, a thin, poorly birefringent layer with multipolar cells presenting abundant *canaliculi* (two features reminiscent of woven-fibered bone) may occur in spots spared by remodeling (Figure 17.6B, C, D). The superficial ornamented layer displays different histological characteristics in the three taxa considered (cf. Skutschas and Boitsova 2017, for *Kokartus* and Buffrénil et al. 2016 for *Ceratophrys* and *Latonia*). The squamosal of *Kokartus* consists of a simple, homogeneous formation of parallel-fibered tissue, and the differentiation of the reliefs forming the bone ornamentation merely results from local differences in accretion rate (high on top of ridges and lower or nil over the bottom of pits and grooves). Beyond some similarity, the situation in *Latonia* differs from that prevailing in *Kokartus* by two characteristics: (1) the core of the ridges includes an excrescence of the subjacent woven-like tissue and (2) the growth of the ridges not only involves faster accretion on their top, but also remodeling by resorption and partial reconstruction on the bottom of the pits and grooves (Figure 17.6D). In *Ceratophrys*, the histological structure of the superficial layer is more complex than in the other two taxa. This layer includes, in its basal part, parallel-fibered tissue, but this tissue is covered by a thick layer displaying a plywood-like structure (Figure 17.6E), with the succession of brightly birefringent strata (about 6–7 µm thick) and monorefringent strata (8–12 µm). This aspect shows the orthogonal orientations of successive strata (Francillon-Vieillot et al. 1990). In a peripheral-most position, the plywood turns into a layer of parallel-fibered bone containing few cell lacunae. Skull roof ornamentation in *Ceratophrys* is integrated with this last layer and mainly results from a remodeling process, with the excavation of pits (resorption) and a partially asymmetrical reconstruction of their walls; the whole process is reminiscent of that observed in crocodiles (Buffrénil et al. 2016).

The skull sections of *Brachycephalus pitanga* (extant anuran) presented by Clemente-Carvalho et al. (2009) shed some light on the nature and origin of the plywood-like layer observed in the *Ceratophrys* frontoparietal. The development of "ornamental" reliefs in *Brachycephalus* involves the incorporation of collagen fibers into the growing bony ridges located within the dermis. These fibers display the same laminated disposition, and apparently the same size, as the strata observed in the plywood formation of *Ceratophrys*. The direct incorporation of dermal matrix into the growing surface of membrane bones has already been described by Trueb (1966) in *H. septentrionalis* (see also Ruibal and Shoemaker 1984). Such a process might be considered metaplastic because originally soft dermis locally becomes a calcified osseous-like tissue that fuses to bone. Another interpretation refers to the fusion of cephalic osteoderms with skull bones (see below), a process currently designated as coossification (Seibert et al. 1974, Lynch 1992, Evans et al. 2014; see also Toledo and Jared 1993). This situation would not discard the contribution of a metaplastic process, but the latter would be chiefly involved in the differentiation of the osteoderms before their fusion to skull bones.

Gross Vertebral Organization in Lissamphibians

At a microanatomical level, the organization of lissamphibian vertebrae differs from that of amniotes by the persistence of the notochord within the vertebral centrum. The embryonic chord regresses in pace with the differentiation of the vertebral centra in most nonamphibian tetrapods (see Chapters 2 and 9), to persist only as the *nucleus pulposus* in the core of intervertebral disks. The structure of the notochord (mirrored by that of the *nucleus pulposus*) comprises large vacuolar chordal cells, along with chondrocytes, collagen fibers and proteoglycans (review in Colombier et al. 2014; see also Mookerjee et al. 1953 for the development and structure of the amphibian notochord). In lissamphibians, however, the chord is part of the centrum, where it occupies a significant, but variable volume during life (e.g., Goodrich 1986, Carroll et al. 1999, Castanet et al. 2003). As recently shown by Danto et al.'s (2016) synthetic study, this feature is also common in all Paleozoic and Mesozoic amphibians, whatever their phylogenetic position, provided at least that a complete, cylindrical centrum (of intercentral or pleurocentral origin) exists.

Classic comparative studies of the structure and development of lissamphibian vertebrae include those of Mookerjee (1931), Mookerjee and Das (1939) for the anurans and Wake (1970) and Wake and Lawson (1973) for the urodeles, among the numerous articles published on this topic since the 19th century (see, e.g., Gadow 1896). In an adult urodele, the basic structure of a vertebral centrum comprises three different components, as shown on Figures 17.7 and 17.6F-H. (1) The central region is occupied by a part of the notochord that displays a roughly cylindrical aspect with at least one pronounced constriction in the anterior (cranial) half of the centrum. (2) The outer cortex consists of a compact layer of parallel-fibered or lamellar bone tissue. This bony sheath confers to the centrum its characteristic subcylindrical morphology (centrum diameter shows a neat median constriction). (3) Thick cartilaginous formations occupy the rest of the centrum volume, around the notochord and in contact with it. This cartilage may be hypertrophic and mineralized or remain unmineralized

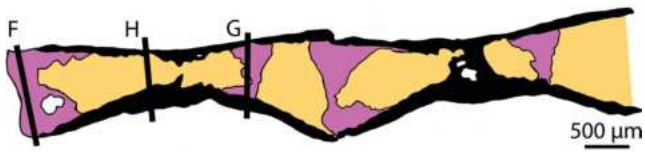


FIGURE 17.7 Sketch of a sagittal section through two contiguous vertebrae in *Pleurodeles waltl*. Black area: bone; purple areas: cartilage; yellow areas: territory occupied by the notochord. The transverse segments localize the sections shown in Figure 17.6 F, H

VetBooks.ir

(neotenic taxa), but it undergoes no ossification process and lacks osseous trabeculae in the urodeles. In addition to these principal tissues, the cranial (condylar) extremity of the centrum is covered by a layer of fibrocartilage to form an articular surface with the cotyle of the preceding vertebra; moreover, a disk of cartilage ("vertebral notochordal cartilage," according to Wake and Lawson's 1973 terminology; "intravertebral cartilage" according to Goodrich 1986) may develop in the narrowest part of the centrum, interrupting the continuity of the notochord. Detailed descriptions of the ontogenetic developmental processes resulting in the vertebral structure of urodeles are given in, e.g., Lawson (1966), Wake and Lawson (1973) and Skutschas and Baleeva (2012). Beyond this general organization, significant differences may exist among taxa, especially in the occurrence or absence of notochordal cartilage, or the continuity of the notochord from one vertebra to the neighboring ones. In terrestrial forms such as the Salamandridae, the chord in often obliterated (e.g., Gadow 1896, Goodrich 1986); therefore, the cranial and caudal articular surfaces of the centra have no open notochordal canal; rather, they display continuous cartilaginous caps.

The inner structure of vertebrae, as well as the timing and pattern of vertebral development, are closely comparable in the Caudata and the Gymnophiona (Lawson 1966), which suggested that both taxa could be more closely related to each other than to the Anura (Carroll et al. 1999). Beyond the rough similarity of adult vertebral structure in all lissamphibians, both taxa differ from the Anura by the fact that, during embryonic development, the chondrification and subsequent ossification of the vertebral centra occur before those of the neural arches; conversely, neural arches chondrify and ossify before the centra in the Anura, as in at least some finned tetrapodomorphs and the amniotes (Carroll et al. 1999). The second condition is considered primitive in tetrapods, while the first is derived (Boisvert 2009). This difference led to diverse (and conflicting) speculations on the pattern of lissamphibian evolution. Otherwise, another significant difference between anurans and other lissamphibians is related to the occurrence of endosteoendochondral bony trabeculae, and the replacement of the notochord by marrow tissues, in the centra of some terrestrial toads, as exemplified by the *Bufo melanostictus* studied by Mookerjee (1931).

Anuran Osteoderms and Gymnophionan "Scales"

Osteoderms occur in several anuran taxa (e.g., Hylidae, Ceratophryidae, Brachycephalidae). Apparently, their presence or absence is not clearly related to phylogeny, because some species of a genus may have or lack these structures, whereas distantly related taxa may display very similar osteoderms (Ruibal and Shoemaker 1984). Anuran osteoderms are generally small (at most several square millimeters in area for a thickness of 0.1–0.2 mm), but can also consist of large plates covering the skull and/or the vertebrae, as exemplified by *Brachycephalus* (Campos et al. 2010) and ceratophryids (Quinzio and Fabrezi 2012). Anuran osteoderms bear surficial sculpture in the form of spines or pits and ridges. They are distributed, as individual elements or compound shields, over the back, head, flanks and sometimes the limbs of the animals (see, e.g., the radiography of *Brachycephalus crispus* in Condez et al. 2014). Over the head and the vertebrae, they often fuse with the underlying bone (coossification). The inner structure of anuran osteoderms is still scantily documented. The major comparative reference on this topic remains the study by Ruibal and Shoemaker (1984; see also Campos et al. 2010), from which most of the information presented below is derived.

At a microanatomical level, the osteoderms covering the postcranial region do not display a diploe structure as commonly observed in tetrapods; they are solid and compact. However, in some taxa (e.g., *Phyllomedusa bicolor*), they house a relatively abundant vascular network that outcrops on the outer (ornamented) surface as small, regularly spaced pits. In other taxa, the osteoderms are avascular. In *Ceratophrys*, the plates, fused to skull bones, house numerous large cavities, which tend to create a spongiosa framed by two (dorsal and ventral) compact cortices (Quinzio and Fabrezi 2012). Histologically, three osteoderm types are described by Ruibal and Shoemaker (1984). The first type, observed in *Phyllomedusa bicolor* and *Phyllomedusa vaillantii*, consists of vascularized osteoderms principally made of well characterized parallel-fibered bone tissue. Inner remodeling on the walls of the vascular canals occurs, thus creating secondary osteons, but it is poorly pronounced. A periosteal-like cell formation surrounds this type of osteoderm. The second type (in *Megophrys* and *Hylactophryne*) is avascular. Its matrix includes collagen fibers organized in several horizontal layers crossing orthogonally, along with bundles of vertical fibers; the whole fiber meshwork is in continuity with the fibers of the dermis. Cell lacunae are spherical and disposed randomly. Osteoderms of the third type (in *Lepidobatrachus, Ceratophrys* and *Brachycephalus*) are made of vascularized woven-fibered bone. Signs of extensive inner remodeling (with secondary deposit of lamellar bone tissue) are conspicuous around the vascular canals.

Ruibal and Shoemaker's (1984) descriptions suggest that the second type of osteoderm entirely results from metaplasia, a process of nonosteoblastic osteogenesis frequently involved in the differentiation of dermal ossicles (e.g., Zylberberg and Wake 1990, Scheyer et al. 2014). Type 1 and Type 3 could also derive from this mechanism, but for a minor part of their growth. The tissues forming the osteoderms, especially the parallel-fiber tissue (in *Phyllomedusa*) and the lamellar tissue covering the walls of vascular canals in the Ceratophryidae and Brachycephalidae (third type) indicate that osteoblasts are involved, at least in the advanced stages of osteoderm growth. This conclusion is substantiated by the observation of a periosteum around *Phyllomedusa* osteoderms. Again, such a double origin of the osteoderms is supposed to occur in several other tetrapod taxa, as exemplified by pseudosuchians (Buffrénil et al. 2014) and some squamates (Buffrénil et al. 2011). Considering the uneven phylogenetic distribution of frog osteoderms, as well as the diversity of their microstructure, Ruibal and Shoemaker (1984) do not consider them strictly homologous among anuran taxa; they might have evolved independently and thus reflect convergence rather than homology. In

VetBooks.ir

a broader comparative perspective, lissamphibian osteoderms, whatever their detailed structure, are roughly comparable to those observed in other tetrapods and seem to result from similar, albeit diverse, osteogenic processes. Similarly, the sculpture pattern over the plates coossified with skull bones in *Ceratophrys* were shown to result from mechanisms (i.e., surficial remodeling) similar to those that produce the ornamentation on the bones and osteoderms of pseudosuchians for example (Buffrénil et al. 2014, 2016).

Several gymnophione genera and families (e.g., *Dermophis*, *Microcaecilia*, *Epicrionops*, Typhlonectidae, etc.) have small, roughly ovoid "scales" (their shape can vary in a single individual; Donnelly and Wake 2013) measuring 0.4–4.5 mm, depending on the taxa considered (Taylor 1972). They are invisible from the outside, because they are located deep in the skin, below the epidermis, and between large intradermal exocrine poison glands. Each scale is inserted in a pocket-like slit within the loose layer of the dermis, and oriented obliquely to the skin surface (e.g., Wake 1975). In general, four to five scale pockets are packed side by side in the same spot. At both morphological (Figure 17.6I) and histological levels, these structures differ totally from the osteoderms mentioned above and have no equivalent (at least at a phenotypic level) in other extant tetrapods. The histological characteristics of such "scales" were described in detail in *Dermophis*, *Ichthyophis, Hypogeophis, Microcaecilia,* in three main studies: Casey (1979), Zylberberg et al. (1980) and Zylberberg and Wake (1990) (see also Cockrell 1912 and Castanet et al. 2003). Caecilian scales typically comprise a relatively thick, nonmineralized basal plate and superficial rectangular or rhomboid mineralized elements, the *squamulae*. The latter are small (about 0.03–0.05 mm in mean diameter) and distributed in several concentric rings (up to 20 in *Brasilotyphlus*, Taylor 1971; tens of rings in *Herpele squalostoma*, Perret 1982). They result from the activity of local osteoblasts. Ultrastructural data from Zylberberg et al. (1980) and Zylberberg and Wake (1990) show that each *squamula* includes a peripheral layer, in which mineralization is of the spheritic type and develops in a noncollagenic meshwork, and a deep core that houses a typical collagen matrix mineralized through a common inotropic process. The basal plate exhibits the rough structure of a biological plywood, with three to five layers of parallel collagen fibers, each layer orthogonal to those framing it above and below. This structure is reminiscent of the isopedin encountered in the elasmoid scales of teleosteans (see Chapters 8 and 15). The developmental and evolutionary meaning of gymnophionan scales remains a matter of conjecture, as is also their function. Several interpretations were proposed, the most consistent of which are reviewed and discussed in Castanet et al. (2003).

An Overview of Skeletal Neoteny

Although many taxa among extant lissamphibians have a direct development pattern in which the juvenile is morphologically and physiologically similar to the adult, as exemplified by *Eleutherodactylus*, a neotropical taxon that includes more than 400 recognized species, the most common situation, in Caudata and Anura, is to go through a larval stage, with aquatic tadpoles swimming by undulating their tail and breathing through external gills, followed by preadult and adult forms breathing air with lungs and having an amphibious or terrestrial lifestyle (reviews in Hanken 1989, Pough et al. 2004). The passage from one stage to another, i.e., the metamorphosis, is normally marked by a complex cascade of physiological transformations, including the involution of the gills, the onset of a pulmonary respiration and, in anurans, the regression of the tail (reviews in, e.g., Lynn 1961). When proceeding normally, this process characterizes the so-called metamorphic species. Amphibian metamorphosis is mainly triggered and controlled by the interplay of several endocrine factors, among which thyroidian and adrenal hormones play a major role (reviews in Duellman and Trueb 1986, Dent 1988, and Pough et al. 2004; see also Wolffe and Shi 1999). This determinism was shown more than a century ago by experimental studies (e.g., Allen 1918, Swingle 1918). In numerous taxa, however, genetic (mandatory) controls, as well as the epigenetic influence of environmental conditions (life in cold water, confinement to dark areas, etc.; see Denver 1997, Boorse and Denver 2004), may prevent or interfere with metamorphic processes. This situation either results in an irreversible suppression of somatic adulthood integrated into the species genome, as exemplified by neotenic (or "perennibranchiates") taxa such as Proteidae or Sirenidae, or provokes retardation in somatic development, including a partial, but permanent, inhibition or a mere (and possibly reversible) delay in somatic maturation that may be variably pronounced among taxa or among local populations of a single species. This situation is well documented in e.g., several species of *Ambystoma* and *Triturus* (comparative data in, e.g., Wakahara 1996). In all cases, the development of gonads and gametes remains untouched and somatically juvenile specimens are able to mate, a condition designated as neoteny (the precise meaning of this term as applied to amphibians is discussed in Pierce and Smith 1979) and documented not only in extant lissamphibians, but also in temnospondyls (e.g., Ricqlès 1975, Fröbisch and Schoch 2009) and in the stem-urodeles (Evans et al. 1988, Buffrénil et al. 2015, Skutschas and Stein 2015, see also Carroll and Zheng 2012). Neotenic states are much more frequent and more sharply characterized in urodeles than in anurans (Lynn 1961). Like all heterochronic processes, neoteny and its interspecific and intraspecific variations can be interpreted in adaptive terms, referring mainly to the general need to optimize, in ecological contexts, the energy allocation between somatic development and reproduction (Hayes 1997, Iwasaki and Wakahara 1999, Denoël and Joly 2000; see also Schoch 2010).

The typical set of neotenic features involves definite skeletal manifestations (Figure 17.8), collectively designated as "skeletal neoteny" (Ricqlès 1964, 1965, 1975; Castanet et al. 2003). In endoskeletal elements, especially the appendicular skeleton and the spine, skeletal neoteny is characteristically related to a delay in endosteoendochondral ossification, and the life-long preservation of calcified cartilages as described in detail by Terry (1918). Periosteal accretion is normal during the growth

VetBooks.ir

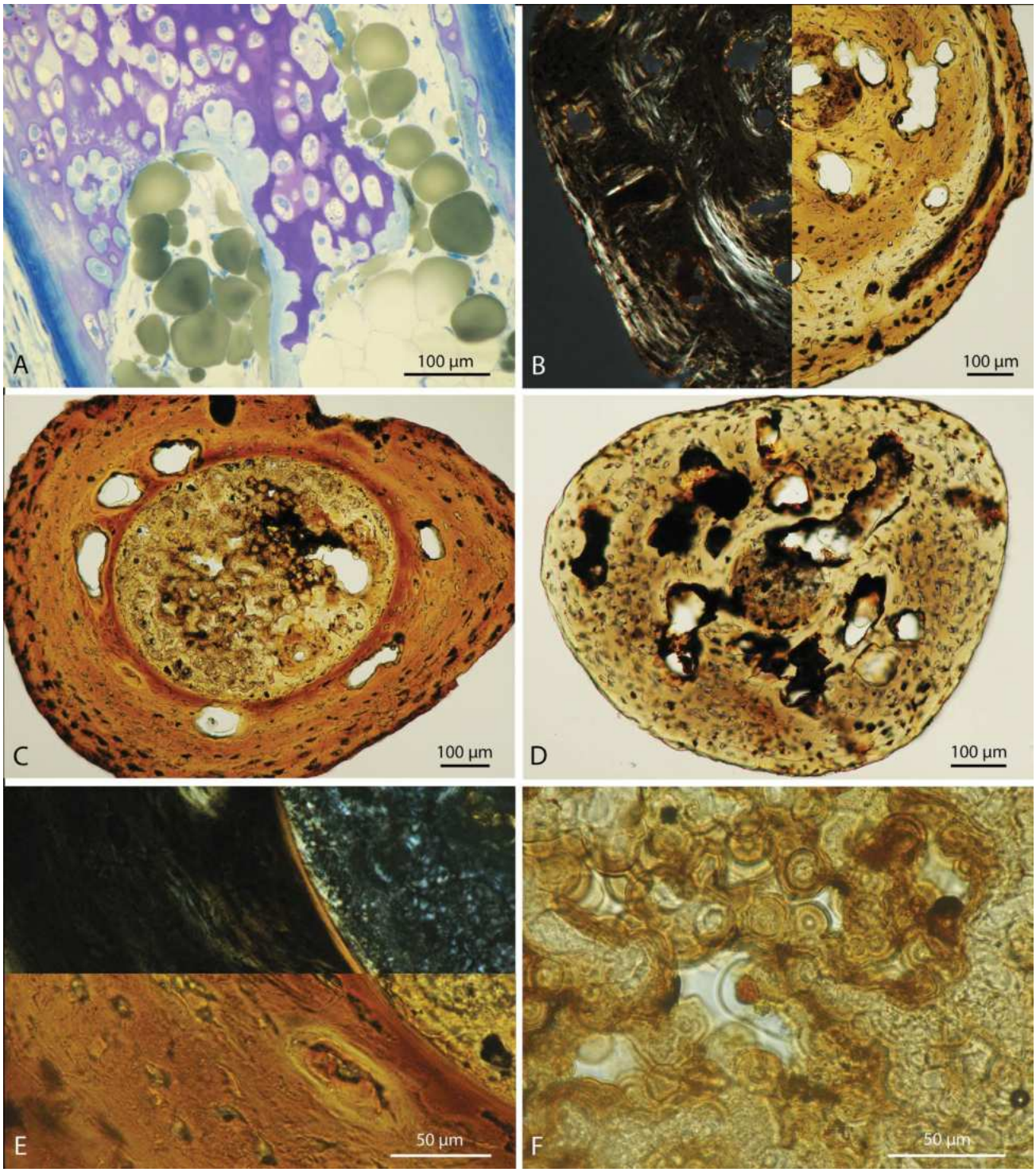


FIGURE 17.8 Aspects of skeletal neoteny. A, *Globuli ossei* in the femur of a mildly neotenic *Pleurodeles waltl* raised in experimental conditions (semi-thin section stained with Alcian blue, periodic acid–Schiff stain (PAS) and Groat's hematoxylin). B, Cross section of the humerus of a *Marmorerpeton* specimen. Left half: transmitted polarized light. C, Cross section of the humerus of another *Marmorerpeton* specimen. D, Cross section of the humerus of Salamander A (cf. Evans et al. 1988). These two karaurid taxa display skeletal neoteny, with an occlusion of the medullary cavity by remnants of calcified cartilage. E, Occurrence of a Kastschenko's line in *Marmorerpeton*. Upper half: transmitted polarized light. F, Close view of the spheritic mineralization in globular calcified cartilage remnants in *Marmorerpeton*.

VetBooks.ir

of the bones and diaphyseal cortices are well developed: skeletal neoteny mainly affects endochondral ossification, not periosteal ossification. In this process, the production, maturation and calcification of the cartilage produced by growth plates most often occurs normally, but the subsequent resorption of the hypertrophic calcified cartilage by chondroclasts and its replacement by endosteal trabeculae (see Chapter 9) is more or less severely inhibited (see reviews by Ricqlès 1995, Castanet et al. 2003). As a consequence, calcified cartilages, with the characteristic structural details that they present, including *globuli ossei* (Figure 17.8A), Kastschenko's line (Figure 17.8C, E) and globular calcified cartilage (Figure 17.8F) (see Quilhac et al. 2014 for the description of *globuli ossei* and Ricqlès 1975a for the globular cartilage) may persist far from the epiphyses (Figure 17.8B-D) in neotenic or partly neotenic forms. In well-characterized neoteny, as exemplified by the proteid *N. maculosus*, a species in which this feature is genetically determined (comparative data in Wakahara 1996), the medullary region of long bone shafts can be entirely occupied by calcified cartilage in some individuals (Castanet et al. 2003).

Skeletal neoteny is likely to be a very ancient feature in urodeles (the situation of anurans is less documented). Limb long bones (humerus and femur) in the oldest forms attributed to this taxon, *K. honorarius*, *Marmorerpeton* sp. and Salamander A, from the Middle Jurassic of Europe, retain persistent calcified cartilage in the middle of their diaphysis (Figure 17.8B-F). Considering the size of the open medullary cavity, this process looks relatively mild in *Kokartus* (Skutschas and Stein 2015), but more pronounced in the other two taxa, in which there is no open medullary cavity at mid-diaphysis (Buffrénil et al. 2015). Otherwise, neotenic forms are recorded in all geological epochs and at all stages of lissamphibian evolutionary history (e.g., Wang and Rose 2005, Carroll and Zheng 2012). Temnospondyls, which most authors consider the stem-group of the lissamphibians, include taxa displaying variable degrees of neoteny, such as the Branchiosauridae (Schoch and Fröbisch 2006, Fröbisch and Schoch 2009; see also Witzmann and Pfretzschner 2003 for Dissorophoidea). However, the ontogeny of most Paleozoic stegocephalians is poorly known. Among lepospondyls, the lysorophians, which may also be closely related to lissamphibians (Marjanović and Laurin 2018), are occasionally neotenic (Wellstead 1991).

The histological consequences of neotenic processes in the vertebrae and, to a lesser extent, the skull, seem to be basically similar to those described in long bones, though few comparative data have been published on this topic after the pioneer study by Terry (1918) (see also Duellman and Trueb 1986, Castanet et al. 2003). In thyroidless specimens of *Rana pipiens*, a neotenic-like condition is experimentally created, and this condition is expressed (among several characteristics) in endochondral skull elements by variably pronounced delay of ossification. In vertebrae, it provokes maintenance of hypertrophic calcified cartilage in the neural arch and the vertebral body: typically, the replacement of cartilage by endosteal bone is delayed or blocked (Terry 1918). Although the whole pattern of skeletal neoteny in the skull and vertebrae approximately mirrors that prevailing in long bones, some discrepancies have been noticed. For example, the partial neoteny occasionally displayed in the postcranial skeleton of the eastern newt, *Notophthalmus viridescens* does not occur in its skull (Reilly 1986).

Some Concluding Remarks

The developmental, physiological and ecological characteristics of Lissamphibians remain intriguing questions, despite the growing but still relatively limited set of data. The frequent occurrence of neoteny in this group is an original feature, seldom encountered in other tetrapod taxa, and obviously relevant to the evolution of the ecophysiological characteristics of tetrapods. Fortunately, it can be traced and studied in fossils through the typical consequences that it has on skeletal structure, as described above. Skeletal neoteny also evolved in at least a few major Paleozoic stegocephalians, and is relatively well documented in temnospondyls (reviews in Ricqlès 1975b, Schoch 2009). Other peculiarities of the lissamphibian skeleton, such as the uneven occurrence of vascularization in long bone cortices and the microanatomical and histological features of vertebrae, remain insufficiently documented issues for which further knowledge is wanted. Future studies should address these specific topics.

REFERENCES

Alcobendas, M. and J. Castanet. 2000. Bone growth plasticity among populations of *Salamandra Salamandra*: interactions between internal and external factors. *Herpetologica* 56: 14–26.

Alcobendas, M., et al. 1991. Structural changes of the periosteocytic area in *Vipera aspis* (L.) (Ophidia, Viperidae) bone tissue in various physiological conditions. *Calcif. Tissue Int.* 49: 53–57.

Allen, B. M. 1918. The results of thyroid removal in the larvae of *Rana pipiens*. *J. Exp. Zool.* 24: 499–519.

Amprino, R. and G. Godina. 1947. La struttura delle ossa nelle vertebrati. Ricerche comparative neigli amphibi et neigli amnioti. *Comment. Pontif. Acad. Sci.* 11: 328–463.

Boisvert, C. A. 2009. Vertebral development of modern salamanders provides insights into a unique event of their evolutionary history. *J. Exp. Zool. B (Mol. Dev. Evol.)* 312B: 1–29.

Bolt, J. R. 1969. Lissamphibian origins: possible protolissamphibian from the lower Permian of Oklahoma. *Science* 166: 888–891.

Bolt, J. R. and R. E. Lombard. 1985. Evolution of the amphibian tympanic ear and the origin of frogs. *Zool. J. Linn. Soc.* 24: 83–99.

Boorse, G. C. and R. J. Denver. 2004. Endocrine mechanisms underlying plasticity in metamorphic timing in spadefoot toads. *Integr. Comp. Biol.* 43: 646–657.

Buffrénil V. de, et al. 2011. An enamel-like tissue, osteodermine, on the osteoderms of a fossil anguid (Glyptosaurine) lizard. *C.R. Palevol.* 10: 427–438.

Buffrénil V de, et al. 2014. Differentiation and growth of bone ornamentation in vertebrates: a comparative histological study among the Crocodylomorpha. *J. Morphol.* 276: 425–445.

Buffrénil, V. de, et al. 2015. Histological study of karaurids, the oldest known (stem) urodeles. *Hist. Biol.* 27: 109–114.

Buffrénil V. de, et al. 2016. Comparative data on the differentiation and growth of bone ornamentation in gnathostomes (Chrodata: Vertebrata). *J. Morphol.* 277: 634–670.

Bulfinch, T. 2012. *The age of fable: stories of gods and heroes.* Auckland, New Zealand: The Floating Press.

Campos, L. A., et al. 2010. Morphology and development of additional bony elements in the genus *Brachycephalus* (Anura: Brachycephalisae). *Biol. J. Linn. Soc.* 99: 752–767.

Canoville, A. and M. Laurin. 2009. Microanatomical diversity of the humerus and lifestyle in lissamphibians. *Acta Zool. (Stockholm)* 90: 110–122.

Canoville, A., et al. 2018. Quantitative data on bone vascular supply in lissamphibians: comparative and phylogenetic aspects. *Zool. J. Linn. Soc.* 182: 107–128.

Carroll, R. L. and A. Zheng. 2012. A neotenic salamander, *Jeholotriton paradoxus*, from the Doaohugou beds in inner Mongolia. *Zool. J. Linn. Soc.* 164: 659–668.

Carroll, R. L., et al. 1999. Vertebral development and amphibian evolution. *Evol. Dev.* 1: 36–48.

Castanet, J. 1975. Quelques observations sur la présence et la structure des marques squelettiques de croissance chez les amphibiens. *Bull. Soc. Zool. Fr.* 100: 603–620.

Castanet, J. and M.-H. Caetano. 1995. Influence du mode de vie sur les caractéristiques pondérales et structurales du squelette chez les amphibiens anoures. *Can. J. Zool.* 73: 234–242.

Castanet, J., et al. 2003. The skeletal histology of the Amphibia. In Heatwole H. and M. Davies (eds.) *Amphibian biology*, vol. 5, 1598–1683. Chipping Norton, UK: Surrey Beatty.

Clemente-Carvalho, R. B. G., et al. 2009. Hyperossification in miniaturized toadlets of the genus *Brachycephalus* (Amphibia: Anura: Brachycephalidae): microscopic structure and macroscopic patterns of variation. *J. Morphol.* 270: 1285–1295.

Cockrell, T. D. A. 1912. The scales of *Dermophis*. *Science* 36: 681.

Colombier, P., et al. 2014. The lumbar intervertebral disk: from embryonic development to degeneration. *Joint Bone Spine* 81: 125–129.

Condez, T. H., et al. 2014. A new species of *Brachycephalus* (Anura: Brachycephalidae) from the highlands of the Atlantic forest, southwestern Brazil. *Herpetologica* 70: 89–99.

Danto, M., et al. 2016. Vertebral development in Paleozoic and Mesozoic tetrapods revealed by paleohistological data. *PLoS One*. 11: e0152586.

Denoël, M. and P. Joly. 2000. Neoteny and progenesis as two heterochronic processes involved in paedomorphosis in *Triturus alpestris* (Amphibia: Caudata). *Proc. R. Soc. Lond.* 267: 1481–1485.

Dent, J. N. 1988. Hormonal interaction in Amphibian metamorphosis. *Am. Zool.* 28: 297–308.

Denver, R. J. 1997. Proximate mechanisms of phenotypic plasticity in amphibian metamorphosis. *Am. Zool.* 37: 172–184.

Djorović A. and M. Kalezić. 2000. Paedogenesis in European newts (*Triturus*: Salamandridae): cranial morphology during ontogeny. *J. Morphol.* 243: 127–139.

Donnelly, M. A. and M. H. Wake. 2013. A new *Microcaecilia* (Amphibia: Gymnophiona) from Guyana with comments on *Epicrionops niger*. *Copeia* 2013(2): 223–231.

Duellman, W. E. and L. Trueb. 1986. *Biology of amphibians*. New York: McGraw-Hill Book Company.

Enlow, D. H. and S. O. Brown. 1956. A comparative histological study of fossil and recent bone tissues. Part 1. *Texas J. Sci.* 8: 405–443.

Esteban, M., et al. 1998. Inferring age and growth from remains of fossil and predated recent anurans: a test case using skeletochronology. *Can. J. Zool.* 76: 1689–1695.

Evans, S. E., et al. 1988. The earliest known salamanders (Amphibia, Caudata): a record from the Middle Jurassic of England. *Geobios* 21: 539–552.

Evans, S. E., et al. 2014. New material of *Beelzebufo*, a hyperossified frog (Amphibia: Anura) from the Late Cretaceous of Madagascar. *PLoS One* 9: e87236.

Foote, J. S. 1911. The comparative histology of femoral bones. *Trans. Am. Micros. Soc.* 30: 87–140.

Foote, J. S. 1916. A contribution to the comparative histology of the femur. *Smiths. Contr. Knowl.* 35: 1–242.

Francillon, H. 1981. Contribution à l'étude des structures et du fonctionnement des épiphyses fémorales chez les amphibiens anoures. *Arch. Zool. Exp. Gen.* 122: 289–310.

Francillon-Vieillot, H. 1987. *La croissance des os longs chez les amphibiens. Son utilisation comme critère d'âge*. PhD thesis, Paris: University Paris.

Francillon-Vieillot, H., et al. 1990. Microstructure and mineralization of vertebrate skeletal tissues. In J. G. Carter (ed.) *Skeletal biomineralization: patterns, processes and evolutionary trends*, vol. 1, 471–530. New York: Van Nostrand Reinhold.

Fröbisch, N. B. and R. R. Schoch. 2009. The largest specimen of *Apateon* and the life history pathway of neoteny in the Paleozoic temnospondyl family Branchiosauridae. *Fossil Rec.* 12: 83–90.

Gadow, H. 1896. On the evolution of the vertebral column in Amphibia and Amniota. *Philos. Trans. Roy. Soc. London B* 187: 1–58.

Gardner, J. D., M. Laurin, and C. L. Organ. 2020. The relationship between genome size and metabolic rate in extant vertebrates. *Philos. Trans. Roy. Soc. London B* 375:20190146.

Germain, D. and M. Laurin. 2009. Evolution of ossification sequence s in the salamanders and urodele origins assessed through event-pairing and new methods. *Evol. Dev.* 11: 170–190.

Goin, C. J. and O. B. Goin. 1972. Antarctica, Isostacy, and the Origin of Frogs. *Q. J. Fl. Acad. Sci.* 35: 113–29.

Goodrich, E. S. 1986. *Studies on the structure and development of vertebrates*. Chicago: University of Chicago Press.

Haeckel, E. 1866. *Generelle Morphologie der Organismen*, 2 vols. Berlin: Reimer.

Haines, R. W. 1938. The primitive form of epiphysis in the long bones of tetrapods. *J. Anat. Lond.* 72: 323–343.

Haines, R. W. 1942. The evolution of epiphyses and of endochondral bone. *Biol. Rev.* 17: 267–292.

Haines, R. W. 1969. Epiphyses and sesamoids. In Gans, C. and A. d'A. Bellairs (eds.) *Biology of the reptilia 1A*, 81–115. London: Academic Press.

Hanken, J. 1989. Development and evolution in Amphibians. *Am. Sci.* 77: 336–343.

Hanken, J. and B. K. Hall. 1984. Variation and timing of the cranial ossification sequence of the oriental fire-bellied toad, *Bombina orientalis* (Amphibia, Discoglossidae). *J. Morphol.* 182: 245–255.

Hayes, T. B. 1997. Amphibian metamorphosis: an integrative approach. *Am. Zool.* 37: 121–123.

Hopkins, G. R. and E. D. Brodie Jr. 2015. Occurrence of amphibians in saline habitats: a review and evolutionary perspective. *Herpetol. Monogr.* 29: 1–27.

Hoyos, J. M. 2003. Additions to our knowledge of anuran sesamoids. *Herp. Rev.* 34: 112–116.

Iwasaki, F. and M. Wakahara. 1999. Adaptable larval life histories in different populations of the salamander, *Hynobius retardatus*, living in various habitats. *Zool. Sci.* 16: 667–674.

Jenkins, F. A., Jr., et al. 2007. Anatomy of *Eocaecilia micropodia*, a limbed caecilian of the Early Jurassic. *Bull. Mus. comp. Zool. Harv.* 158: 285–365.

Kastschenko, M. 1881. Über die genes end Architecture der Batrachier Knochen. *Archiv. Mikrosk. Anat.* 19: 1–52.

Kolenda, K., et al. 2018. Common occurrence of Sharpey's fibres in amphibian phalanges. *Zoomorphology* 137: 329–336.

Laurin, M. 1998. The importance of global parsimony and historical bias in understanding tetrapod evolution. Part I. Systematics, middle ear evolution, and jaw suspension. *Ann. Sci. Nat., Zool. 13 Ser.* 19: 1–42.

Laurin, M., et al. 2004. The evolution of long bone microstructure and lifestyle in lissamphibians. *Paleobiology* 30: 589–613.

Laurin, M., et al. 2016. Early genome size increase in urodeles. *C.R. Palevol.* 15: 77–85.

Laurin, M., et al. 2019. What do ossification sequences tell us about the origin of extant amphibians? *Peer Community in Paleontology.* https://www.biorxiv.org/content/10.1101/352609v4

Laurin, M., et al. 2020. Lissamphibia in *Phylonyms: An implementation of PhyloCode*, eds. K.de Queiroz, P. D. Cantino, and J. A.Gauthier, 773–778. Boca Raton, FL: CRC Press.

Lawson, R. 1966. The development of the centrum of *Hypogeophis rostratus* (Amphibia, Apoda) with special reference to the notochordal (intravertebral) cartilage. *J. Morphol.* 118: 137–148.

Leclair, R. 1990. Relationships between relative mass of the skeleton, endosteal resorption, habitat and precision of age determination in ranid amphibians. *Ann. Sci. Nat.*11: 205–209.

Leclair R., et al. 1993. Allométrie de la masse du squelette chez les amphibiens anoures. *Can. J. Zool.* 71: 352–357.

Liedtke, H. C., et al. 2018. Macroevolutionary shift in the size of amphibian genomes and the role of life history and climate. *Nat. Ecol. Evol.*2: 1792–99.

Lynch, J. D. 1992. A new species of *Eleutherodactylus* (Amphibia: Leptodactilidae) from western Colombia with cranial coossification. *Copeia* 1992(3): 826–831.

Lynn, G. W. 1961. Types of amphibian metamorphosis. *Am. Zool.* 1: 151–161.

Marjanović, D. and M. Laurin. 2013. The origin(s) of extant amphibians: a review with emphasis on the "Lepospondyl Hypothesis." *Geodiversitas*35: 207–272.

Marjanović, D. and M. Laurin. 2014. An updated paleontological timetree of lissamphibians, with comments on the anatomy of Jurassic crown-group salamanders (Urodela). *Hist. Biol.* 26: 535–50.

Marjanović, D. and M. Laurin. 2019. Phylogeny of Paleozoic limbed vertebrates reassessed through revision and expansion of the largest published relevant data matrix. *PeerJ* 6: e5565.

Miura, S., et al. 2008. Skeletogenesis in *Xenopus tropicalis*: characteristic bone development in an anuran amphibian. *Bone* 43: 901–909.

Montori, A. 1990. Skeletochronological results in the Pyrenean newt *Euproctus asper* (Dugès, 1852) from the prepyrenean population. *Ann. Sci. Nat., Zool. 13ème série* 11: 209–211.

Mookerjee, H. K. 1931. On the development of the vertebral column in Anura. *Philos. Trans. R. Soc. London B* 219: 165–196.

Mookerjee, H. K. and S. K. Das. 1939. Further investigation on the development of the vertebral column in Salientia (Anura). *J. Morphol.* 64: 167–209.

Mookerjee, H. K., et al. 1953. The morphogenesis of the notochord in Amphibia. *J. Embryol. Exp. Morphol.* 1: 399–409.

Mörs, T., et al. 2020. First fossil frog from Antarctica: implications for Eocene high latitude climate conditions and Gondwanan cosmopolitanism of Australobatrachia. *Sci. Rep.* 10:1–11.

Organ, C. L., et al. 2007. Origin of avian genome size and structure in non-avian dinosaurs. *Nature* 446: 180–184.

Organ, C. L., et al. 2011. Paleogenomic data suggest mammal-like genome size in the ancestral amniote and derived large genome size in amphibians. *J. Evol. Biol.* 24: 372–380.

Parsons, T. S. and E. E. Williams. 1962. The teeth of Amphibia and their relation to amphibian phylogeny. *J. Morphol.* 110: 375–89.

Perret, J.-L. 1982. Les écailles de deux gymnophiones africains (Batraciens apodes), observées au microscope à balayage. *Bonn. zool. Beitr.* 33: 343–347.

Phillips, B. L., et al. 2006. Invasion and the evolution of speed in toads. *Nature*439(7078): 803.

Pierce, B. A. and H. M. Smith. 1979. Neoteny or paedogenesis? *J. Herpetol.* 13: 119–121.

Ponssa, M. L., et al. 2010. Sesamoids in anurans: new data, old issues. *Anat. Rec.* 293: 1646–1668.

Pough, F. H., et al. 2004. *Herpetology.* 3rd ed., vol. 1. Upper Saddle River, NJ: Prentice Hall.

Pyron, R. A. 2014. Biogeographic analysis reveals ancient continental vicariance and recent oceanic dispersal in amphibians. *Syst. Biol.* 63: 779–97.

Quilhac, A., et al. 2014. Globuli ossei in the long limb bones of *Pleurodeles waltl* (Amphibia, Urodela, Salamandridae). *J. Morphol.* 275: 1226–1237.

Quinzio, S. and M. Fabrezi. 2012. Ontogenetic and structural variation of mineralizations and ossifications in the integument within Ceratophryid frogs (Anura, Ceratophryidae). *Anat. Rec.* 295 2089–2103.

Reilly, S. M. 1986. Ontogeny of cranial ossification in the eastern newt, *Notophthalmus viridescens* (Caudata: Salamandridae), and its relationship to metamorphosis and neoteny. *J. Morphol.* 188: 315–36.

Renous, S. and J.-P. Gasc. 1989. Body and vertebral proportions in Gymnophiona (Amphibia): diversity of morphological types. *Copeia* 1989(4): 837–847.

Ricqlès A de. 1964. Formation des os longs des membres de *Pleurodeles waltii* (Michahelles). *Bull. Soc. Zool. France* 34: 797–808.

Ricqlès A de. 1965. Formation des os longs des membres de *Pleurodeles waltii* (Michahelles). Deuxième partie. *Bull. Soc. Zool. France* 40: 267–286.

Ricqlès, A. de. 1975a. Recherches paléohistologiques sur les os longs des tétrapodes VII. – Sur la classification, la signification fonctionnelle et l'histoire des tissus osseux des tétrapodes. Première partie, structures. *Ann. Paléontol.* 61: 51–129.

Ricqlès, A. de. 1975b. Quelques remarques paléo-histologiques sur le problème de la néoténie chez les stégocéphales. *Colloq. Int. CNRS* 18 (Paris: 4–9 June 1973): 351–363.

Ricqlès, A. de. 1979. Quelques remarques sur l'histoire évolutive des tissus squelettiques chez les vertébrés et plus particulièrement chez les tétrapodes. *Ann. Biol.* 18: 1–35.

Ricqlès, A. de. 1995. Les tissus squelettiques. In P. P. Grassé (ed.) *Traité de Zoologie, Amphibiens*, vol. XIV, 1A, 49–96. Paris: Masson.

Rozenblut, B. and M. Ogielska. 2005. Development and growth of long bones in European water frogs (Amphibia: Anura: Ranidae), with remarks on age determination. *J. Morphol.* 265: 304–317.

Ruibal, R. and V. Shoemaker. 1984. Osteoderms in anurans. *J. Herpetol.* 18: 313–328.

Ruta, M. and M. I. Coates. 2007. Dates, nodes and character conflict: addressing the lissamphibian origin problem. *J. Syst. Palaeontol.* 5: 69–122.

Sanchez, S., et al. 2014. The humerus of *Eusthenopteron*: a puzzling organization presaging the establishment of tetrapod limb bone marrow. *Proc. R. Soc. B* 281: 2014.0299.

Santos, R. O., M. Laurin, and H. Zaher. 2020. A review of the fossil record of caecilians (Lissamphibia; Gymnophionomorpha) with comments on its use to calibrate molecular timetrees. *Biol. J. Linn. Soc.* 131:737–755.

Scheyer, T. M., et al. 2014. Bone histology of phytosaur, aetosaur, and other archosauriform osteoderms (Eureptilia, Archosauromorpha). *Anat. Rec.* 297: 240–60.

Schoch, R. R. 2006. Skull ontogeny: developmental patterns of fishes conserved across major tetrapod clades. *Evol. Dev.* 8: 524–36.

Schoch R. R. 2009. The evolution of life cycles in early amphibians. *Ann. Rev. Earth Planet Sci.* 37: 135–162.

Schoch, R. R. 2010. Heterochrony: the interplay between development and ecology exemplified by a Paleozoic amphibian clade. *Paleobiology* 36: 318–334.

Schoch, R. R. and R. L. Carroll. 2003. Ontogenetic evidence for the Paleozoic ancestry of salamanders. *Evol. Dev.* 5: 314–24.

Schoch, R. R. and N. B. Fröbisch. 2006. Metamorphosis and neoteny: alternative pathways in an extinct amphibian clade. *Evolution* 60: 1467–1475.

Seibert, E. A., et al. 1974. Cranial co-ossification in frogs: relationship to rate of evaporative water loss. *Physiol. Zool.* 47: 261–265.

Skutschas, P. P. and N. V. Baleeva. 2012. The spinal cord supports of vertebrae in the crown-group salamanders (Caudata, Urodela). *J. Morphol.* 273: 1031–1041.

Skutschas, P. and K. Stein. 2015. Long bone histology of the stem salamander *Kokartus honorarius* (Amphibia: Caudata) from the Middle Jurassic of Kyrgyzstan. *J. Anat.* 226: 334–347.

Skutschas, P. and E. A. Boitsova. 2017. Histology of sculptured cranial dermal bones of the stem salamander *Kokartus honorarius* (Amphibia: Caudata) from the Middle Jurassic of Kyrgyzstan. *Hist. Biol.* 29: 423–429.

Skutschas, P. P., et al. 2021. Microanatomy and histology of frontal bones in two species of *Albanerpeton* senso lato (Lissamphibia: Albanerpetontidae) from the Upper Cretaceous in southeastern Alberta, Canada. *Hist. Biol.* DOI:10.1080/08912963.2021.1881084.

Swingle, W. W. 1918. The acceleration of metamorphosis in frog larvae by thyroid feeding, and the effects upon the alimentary tract and sex glands. *J. Exp. Zool.* 24: 521–543.

Taylor, E. H. 1971. Scale and cranial characteristics of the caecilian *Brasilotyphlus braziliensis* (Dunn). *J. Herpetol.* 5: 181–183.

Taylor, E. H. 1972. Squamation in caecilians, with an atlas of scales. *Univ. Kansas Sci. Bull.* 59: 989–1164.

Terry, G. S. 1918. Effects of the extirpation of the thyroid gland upon ossification in *Rana pipiens*. *J. Exp. Zool.* 24: 567–587.

Toledo, R. C. and C. Jared. 1993. The calcified dermal layer in Anuran. *Comp. Biochem. Physiol.* 104A: 443–448.

Trueb, L. 1966. Morphology and development of the skull in the frog *Hyla septentrionalis*. *Copeia* 1966(3): 562–573.

Vasilyan, D. and M. Böhme. 2012. Pronounced peramorphosis in lissamphibians – *Aviturus exsecratus* (Urodela, Cryptobranchidae) from the Paleocene-Eocene thermal maximum of Mongolia. *PLoS One*: e40665.

Vasilyan, D., et al. 2013. A new giant salamander (Urodela, Pancryptobrancha) from the Miocene of Eastern Europe (Grytsiv, Ukraine). *J. Vert. Paleont.* 33: 301–318.

Wakahara, M. 1996. Heterochrony and neotenic salamanders: possible clues for understanding the animal development and evolution. *Zool. Sci.* 13: 765–776.

Wake, M. 1970. Aspects of vertebral evolution in the modern Amphibia. *Forma Funtio* 3: 33–60.

Wake, M. and R. Lawson 1973. Developmental and adult morphology of the vertebral column in the plethodontid salamander *Eurycea bislineata*, with comments on vertebral evolution in the Amphibia. *J. Morphol.* 139: 251–300.

Wake, M. H. 1975. Another scaled caecilian (Gymnophiona: Typhlonectidae). *Herpetologica* 31: 134-136.Wake, D. B. and R. Lawson. 1973. Developmental and adult morphology of the vertebral column of the plethodontid salamander *Eurycea bislineata*, with comments on vertebral evolution in the Amphibia. *J. Morphol.* 139: 251–300.

Wang, Y. and C. S. Rose. 2005. *Jeholotriton paradoxus* (Amphibia: Caudata) from the Lower Cretaceous of southeastern Inner Mongolia, China. *J. Vert. Paleont.* 25: 523–532.

Wellstead, C. F. 1991. Taxonomic revision of the lysorophia, Permo-Carboniferous lepospondyl amphibians. *Bull. Am. Mus. Nat. Hist.* 209: 1–90.

Witzmann, F. and H.-U. Pfretzschner. 2003. Larval ontogeny of *Micromelerpeton credneri* (Temnospondyli, Dissorophoidea). *J. Vert. Paleont.* 23: 750–768.

Wolffe, A. P. and Y-B. Shi. 1999. A hypothesis for the transcriptional control of amphibian metamorphosis by the thyroid hormone receptor. *Am. Zool.* 39: 807–817.

Zylberberg, L. and M. H. Wake. 1990. Structure of the scales of *Dermophis* and *Microcaecilia* (Amphibia: Gymnophiona), and comparison to dermal ossifications of other vertebrates. *J. Morphol.* 206: 25–43.

Zylberberg, L., et al. 1980. Structure of the dermal scales in Gymnophiona (Amphibia). *J. Morphol.* 165: 41–54.

VetBooks.ir

18

Early Amniotes and Their Close Relatives

Aurore Canoville, Michel Laurin and Armand de Ricqlès

CONTENTS

Introduction 363
Histological Survey and Paleobiological Inferences 364
Diadectomorphs 364
Skeletal Microstructure in *Diadectes* 364
Bone Microstructure in *Limnoscelis* 365
Mesosauria 365
Bone Microstructure in Mesosaurs 366
Dental Microstructure in Mesosaurs 368
Parareptiles 368
Bone Microstructure in Procolophonoids 368
Dental Microstructure in Procolophonoids 370
Dental Microstructure of Other Basal Parareptiles 370
Bone Microstructure in Pareiasaurs 370
Undetermined Small "Romeriid" Amniote (Protorothyrididae or Diapsida) 372
Captorhinids 372
Bone Microstructure in *Captorhinus* 372
Bone Microstructure in *Labidosaurus* 374
Bone Microstructure in *Moradisaurus* 374
Concluding Remarks 374
Dental Microstructure in *Captorhinus* 374
Dental Microstructure in *Moradisaurus* 376
Araeoscelidia 376
Bone Microstructure in *Dictybolos* 377
Bone Microstructure in *Araeoscelis* 377
Avicephala 377
Bone Microstructure in *Coelurosauravus* 377
Synthetic Remarks 379
Bone Histodiversity of Early Amniotes and Their Relatives 379
Dental Microstructure and Insertion in Early Amniotes 379
Early Amniote Paleobiology and the Permo-Triassic Crisis 379
References 381

Introduction

The origin of amniotes remains contentious. Most studies conclude that the amniote stem includes the seymouriamorphs, which retained aquatic, gilled larvae, as well as the geologically older embolomeres (e.g., Ruta and Coates 2007). However, rescoring of some matrices that initially supported this hypothesis suggests that the amniote stem includes only diadectomorphs, with the addition, perhaps, of the enigmatic *Solenodonsaurus*, whose affinities remain debated (Marjanović and Laurin 2019). This chapter will deal only with early amniotes and diadectomorphs.

VetBooks.ir

Within amniotes, there is a broad consensus that the basalmost division is between synapsids (the mammal total group) and sauropsids (the reptile total group). The nonmammalian synapsids are presented elsewhere by Botha-Brink (Chapter 28), so among amniotes, only early sauropsids will be described here. Within sauropsids, many authors recognize a fairly basal division between parareptiles, which include on the one hand pareiasaurs, procolophonids, millerettids and related taxa, and on the other eureptiles, which include captorhinids, protorothyridids (a possibly paraphyletic group) and diapsids (Gauthier et al. 1988, Laurin and Reisz 1995). Both taxa were originally erected by Olson (1947), though with a different composition; in addition to the taxa mentioned above, Parareptilia included diadectomorphs and seymouriamorphs, whereas Eureptilia included Synapsida.

The position of mesosaurs is still debated. Some consider them basal parareptiles (Gauthier et al. 1988, MacDougall et al. 2018), whereas others consider them the sister-group of reptiles (Laurin and Reisz 1995, Laurin and Piñeiro 2018).

The position of turtles is even more problematic. Until the mid-1990s, they were thought to be closely related to captorhinids and, hence, to be eureptiles. Parareptiles were considered extinct (Gauthier et al. 1988). Later, some paleontologists placed turtles within parareptiles, as close relatives of procolophonids (Laurin and Reisz 1995), pareiasaurs (Lee 1997a), or *Eunotosaurus* (Lyson et al. 2013, Bever et al. 2015). To complicate matters, *Eunotosaurus* may be a caseid synapsid (Lee 1995), in which case it is unlikely to be relevant to the origin of turtles. Other paleontologists considered turtles lepidosauromorph diapsids that lost the temporal fenestrae (deBraga and Rieppel 1997, Rieppel and Reisz, 1999). This last suggestion is the most compatible with the bulk of molecular phylogenies that place turtles within crown diapsids, most often as archosauromorphs (Hugall et al. 2007, Chiari et al. 2012), but sometimes as lepidosauromorphs (Lyson et al. 2012). However, significant conflict in the signal of various genes casts doubts about the reliability of molecular phylogenies to assess the affinities of turtles (Lu et al. 2013).

Recent analyses raise doubts on several points of the previous opinions on Permo-Carboniferous amniote phylogeny (no consensus has existed for a while about the origin of the geologically more recent turtles). The monophyly of eureptiles and of synapsids (as currently delimited) have both been questioned because the tree of MacDougall et al. (2018) places the presumed ophiacodontid *Archaeothyris* and varanopids closer to eureptiles than to other synapsids, whereas the analysis of Laurin and Piñeiro (2017) places turtles as parareptiles, and that clade within diapsids. Ford and Benson (2020) confirmed these results to a large extent by placing varanopids among reptiles, and parareptiles among stem-diapsids (turtles were not included in their analysis). These studies should be viewed as preliminary, but they suggest that traditional views may not be as strongly supported as often assumed. Nevertheless, recognition of the most generally accepted large taxa (Synapsida/Sauropsida; Parareptilia/Eureptilia) will form the phylogenetic basis of our histological review.

In addition to early amniotes with anapsid skulls, more or less covering the old precladistic concept of "Cotylosauria", we also discuss a few basal (stem) diapsid groups for which some histological data are available. There is almost no histological information so far on these taxa in the literature, hence, the interest of our new data.

Histological Survey and Paleobiological Inferences

Diadectomorphs

Diadectomorpha includes the only known undisputed stem-amniotes. This name is based on the Early Permian genus *Diadectes* from the Texas Red Beds, a massively built tetrapod about 2 m in length or more, probably mostly terrestrial, with an anapsid skull and specialized teeth adapted to feeding on plants. However, diadectomorphs are also represented by predatory taxa that may have been more aquatic (limnoscelids).

Skeletal Microstructure in Diadectes

Early histological studies of *Diadectes* include descriptions by Warren (1963) and Ricqlès (1974). Warren (1963) was mainly concerned with the study of growth marks in bone, following Peabody's (1961) pioneering work. In *Diadectes*, Warren (1963: 68–73, plates XXI–XXIII) showed that the flat articular surfaces of vertebral zygapophyses display a number of "wavelike" structures, constant in a given individual, likely expressing yearly growth cycles. Accordingly, he suggested an age between 17 and 23 years for individuals whose shoulder height reaches between 66 cm and 1 m. This estimate implies growth rates similar to those of extant crocodilians (Warren 1963, p. 72), which seems reasonable. He also noted that much evidence of annuli and zones is lost in the long bones because of extensive perimedullary erosion and remodeling.

Ricqlès (1974: 174–179, figure 12; plate I) histologically described the femoral shaft of two bones of different sizes, the largest one being apparently less ossified than the smaller one. The periosteal cortex of the smaller femur is thin (2–3 mm) and formed of thin periosteal lamellae organized in 4–5 thicker layers, although no clear annuli and lines of arrested growth (LAGs) could be observed. Vascularization is rather dense, with simple longitudinal vascular canals and primary osteons aligned in radial rows (Figure 18.1A). Some short anastomoses allow communications between the canals. In the smaller bone, the endosteal margin is abrupt, with a large number of circular erosion bays destroying the deep cortex; no typical secondary osteons are formed in the process (Figure 18.1B). The inner part of the bone is entirely built by an extensively developed spongiosa made of irregular trabeculae of secondary endosteal bone. This spongiosa extrudes outwardly, forming the fourth trochanter. There is no free marrow cavity devoid of bony trabeculae (Figure 18.1A). Detailed histological differences (Ricqlès 1974: 178) suggest that the larger femur grew faster but was ontogenetically younger than the smaller femur.

Le Blanc and Reisz (2013) described the tooth insertion in *Diadectes* as an ankylosis on the dentigerous bone through mineralized tissues that may include acellular and cellular cementum, and perhaps also a component from the mineralized periodontal ligament.

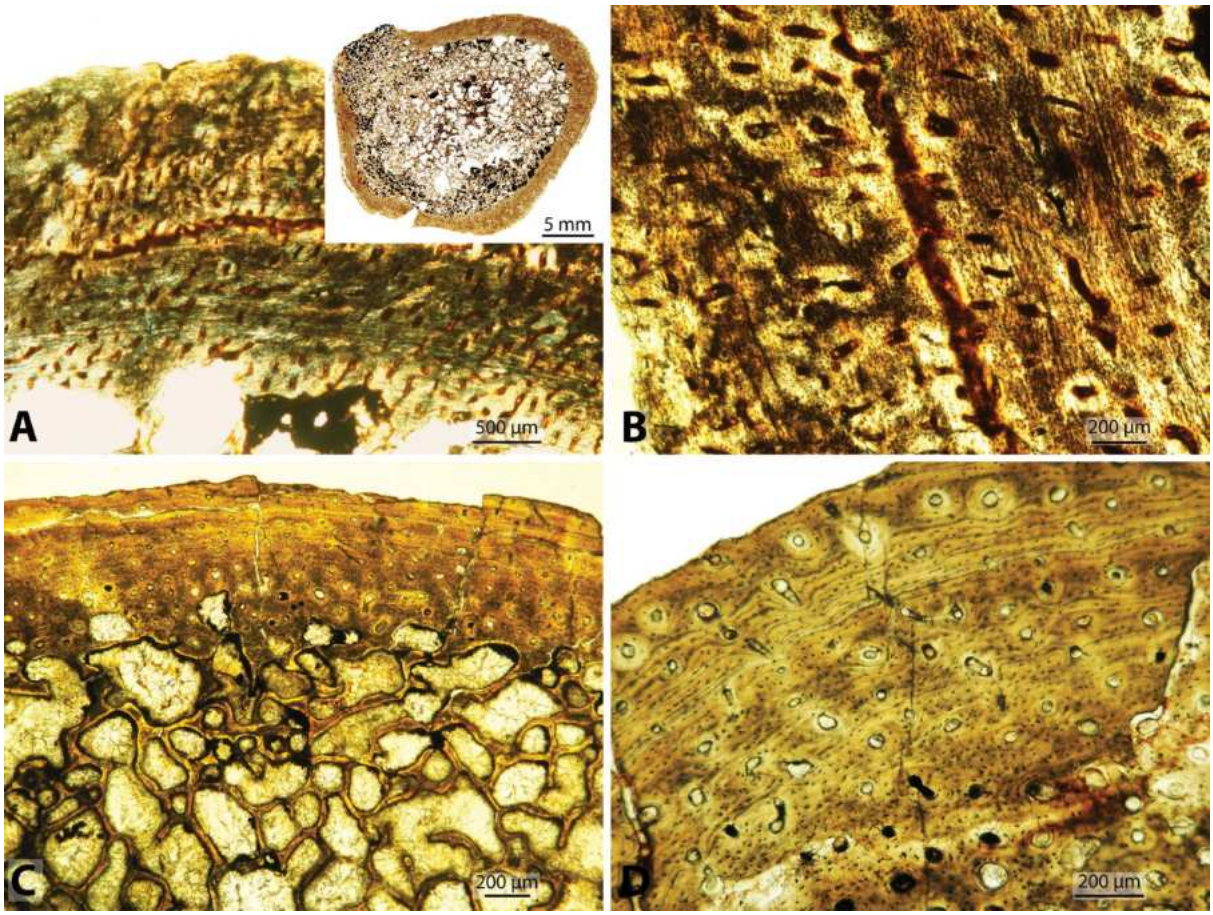


FIGURE 18.1 Diadectomorphs. A, *Diadectes*, femoral cross section, general view (inset). The cortex is densely vascularized by primary osteons set in radial rows. B, Same material, detail of the lamellar-zonal cortex with some evidence of cyclical deposition. C, *Limnoscelis*, undetermined long bone. General view of cross section. As in *Diadectes,* the deep primary cortex experiences generalized erosion resulting in an extensively developed spongiosa. D, Same material, detail of the primary cortex. Lamellar-zonal bone permeated by primary osteons.

Bone Microstructure in Limnoscelis

This early diadectomorph from the Lowermost Permian of New Mexico had an anapsid skull, with sharp teeth that indicate a carnivorous or piscivorous diet (it may have been amphibious); it reached a total body length of about 1.50 m. Thus, the habitus and diet of *Limnoscelis* are very different from those of *Diadectes*. Its rib histology was described by Enlow and Brown (1957: 186, plate XV, figure 5) and Enlow (1969: 71, figure 31). The rib has an almost avascular, lamellar cortex circling a well-developed endosteal spongiosa. The transitional region (endosteal margin) contains some secondary osteons.

Our specimen (Figure 18.1C, D) is a small part of a long bone shaft displaying a circular section 10 mm in diameter. It has a rather thin periosteal cortex (1 mm) relative to the bone diameter. The central part of the bone is entirely occupied by an extensive spongiosa formed of regularly organized endosteal trabeculae of constant thickness, leaving between them slightly polygonal medullary spaces (Figure 18.1C). The erosion front is rather abrupt, leaving almost no cortical bone in the external spongiosa, and is devoid of secondary osteons. The cortex entirely consists of periosteal bone with a grossly lamellar organization (Figure 18.1D). Vascularization comprises longitudinal primary osteons with very few anastomoses and sparse simple vascular canals also oriented longitudinally. The whole lamellar cortex is organized into six to seven poorly defined growth cycles, some of them marked by a LAG.

Mesosauria

The mesosaurs form a small group of early amniotes of the Early Permian of South Africa and South America, ostensibly adapted to an aquatic life. Their geographical distribution has been a classic argument for the progressive discovery and understanding of "continental drift", ultimately integrated into the global plate tectonics synthesis (du Toit 1927, Oelofsen and Araujo 1987).

The anatomy of the mesosaurs has stirred considerable attention, both to decipher their phylogenetic affinities and to better understand their adaptation to an aquatic lifestyle. They are the earliest group of amniotes known to have followed the pathway of an adaptation to aquatic life (Canoville and Laurin 2010, Villamil et al. 2016, Nuñez Demarco et al. 2018), which has subsequently been followed, in various ways, by numerous, geologically more recent clades of amniotes (Houssaye et al. 2016).

VetBooks.ir

Bone Microstructure in Mesosaurs

Mesosaurs were first described histologically by Nopcsa and Heidsieck (1934: 442–443, figures 4 and 5) in the more general context of the study of pachyostosis (Abel 1912: 93–94; Abel 1924), a somewhat complex condition of skeletal morphological and histological characters often associated with the adaptations of amniotes to aquatic life (Ricqlès and Buffrenil 2001). The most familiar morphological examples of pachyostosis are the "banana-like" swollen ribs of mesosaurs, pachypleurosaurs, some squamates and sirenians (e.g., Houssaye et al. 2016).

Many museum specimens of mesosaurs, especially of large individuals, consist of natural molds of the external surfaces of bones left in connection. Such fossils are effective for producing excellent anatomical casts (Modesto 1999, 2006, 2010; Bickelmann and Tsuji 2018, etc.), but lack actual bone remains that could be used for histology. Fortunately, the actual skeletal material is preserved in some localities. This is the case at the "Passo di São Boriga", Lower Permian Irati formation (Rio Grande do Sul, Brazil), from where some of the histologically described material originates, and in the Mangrullo Formation in the Lower Permian of Uruguay (Piñeiro et al. 2012).

Nopcsa and Heidsieck (1934) gave excellent histological descriptions of the ribs of both *Mesosaurus* (pp. 442–443, figure 4) and the closely related *Stereosternum* (pp. 444–445, figure 5). This was supplemented by Ricqlès (1974: 203–207, figure 11; plate VII, figures 4 and 5). A brief account of *M. brasiliensis* is given below.

The ribs are 2 to 4 mm in diameter, and have a roughly circular cross section. The cortex is very thick (at least 60% of the bone radius), which suggests osteosclerosis, and is entirely composed of periosteal bone made of ill-defined circumferential lamellae likely made of parallel-fibered (rather than truly lamellar) tissue with a longitudinal fiber orientation (Figure 18.2A). Several LAGs, which become closer and closer toward the external margin of the bone, occur in this tissue (Figure 18.2B). Some local peculiarities of the tissue at the level of a few LAGs suggest that the latter might actually be subperiosteal lines of resorption, reflecting local morphogenetic processes. The cortex is vascularized by longitudinal simple vascular canals and primary osteons distributed throughout the cortex. The canals are more numerous in the perimedullary region, where some of them experience resorption from bays extruding from the medulla. Subsequent endosteal deposition changes them into secondary osteons closely associated with the endosteal tissue.

The central part of the ribs has a specialized structure, often described as osteosclerotic (see Ricqlès and Buffrenil 2001), although rather variable. In some ribs, about half the surface of the medullary region is made of globular calcified cartilage, set as irregular islands surrounded by highly irregular deposits of endosteoendochondral bone associated with tortuous vascular canals and marrow spaces (Figure 18.2C). Those canals send some anastomoses outwardly beyond the endosteoendochondral region, into the deepest periosteal cortex, where they are responsible, as noted above, for some local Haversian remodeling. Other sections are remarkable for their extreme compactness (Ricqlès 1974: 206). Cartilage is reduced to small, scattered islets (Figure 18.2D) or disappears entirely. Marrow spaces are rare, and the central region consists of a massive endosteal compacta mostly formed by very irregular endosteal secondary osteons, similar to the structure described in the ribs of *Claudiosaurus germaini* (Buffrenil and Mazin 1989).

Observation of a long bone in longitudinal section (Ricqlès 1974: plate VII, figure 3) demonstrates a very simple "egg cup" growth pattern (Figure 18.2E) where no sequential resorptive remodeling of the metaphyses is needed to maintain the morphology of the bone when its size increases (the growth of the bone has an homothetic pattern; see Chapter 9). Therefore, one diaphyseal cross section may record the full course of bone growth in diameter. In mesosaurs, as in many aquatic amniotes, the endosteoendochondral spongiosae were not extensively resorbed to create a medullary cavity in bone diaphyses. Rather, they persisted throughout life (sometimes housing remnants of calcified cartilage) in the form of a tight and irregular trabecular formation with a convoluted plexus of small marrow spaces.

An exceptionally well preserved 2/3-grown individual (Ricqlès 1974: 201–203, figure 10; plate VII) offers the opportunity to observe details of the cyclical growth of the skeleton (Figure 18.2F). The epiphyseal regions of the long bones and of the short bones of the carpus and tarsus are formed by calcified cartilage pervaded by the irregular endosteoendochondral component just described. Annuli and zones in the periosteal cortex of the diaphysis (growth in diameter) precisely match successive bursts of longitudinal (and radial) growth in the cartilages. More precisely, the wide zones in the cortex match thick cartilaginous deposits in epiphyses of short bones. Conversely, the thin annuli in the cortex match thin partitions in the cartilage, probably made of endosteal bone. In the short bones, the partitions are circular, superimposed and parallel to the bone surface. At most, five growth cycles can be observed in the specimen (their number differs among epiphyses as among short bones), suggesting a minimal age of 6 years for this specimen. A rather similar system may be observed in the cartilaginous conical component of the axonost-baseost complex of the unpaired fins of gadid teleosts (A. de Ricqlès, personal observation).

A recent study (Klein et al. 2019) compared histologically the main taxa of mesosaurs, with an emphasis on *Stereosternum*. This was the first study to describe systematically the histology of several skeletal elements (vertebrae, ribs, hemal arch, humeri and femora) in 10 individuals. Comparisons were made to *Brazilosaurus* (one individual); all individuals had reached about 65% of maximal known body length. Although it generally agrees with earlier histological descriptions, the new study shows that *Brazilosaurus* had a highly organized avascular lamellar tissue and a high number of regularly deposited LAGs in the ribs, suggesting a growth pattern distinct from those of *Mesosaurus* and *Stereosternum*. Especially in the latter, the number of LAGs is variable and poorly correlated to body size. The ribs of the three genera are clearly distinguishable by the proportions in area of periosteal and endosteal regions, with the last one distinctly larger in *Brazilosaurus* than in *Stereosternum*. This is in line with the shape of *Brazilosaurus* ribs that are rather gracile, exhibiting no obvious morphological pachyostosis, contrary to those of

VetBooks.ir

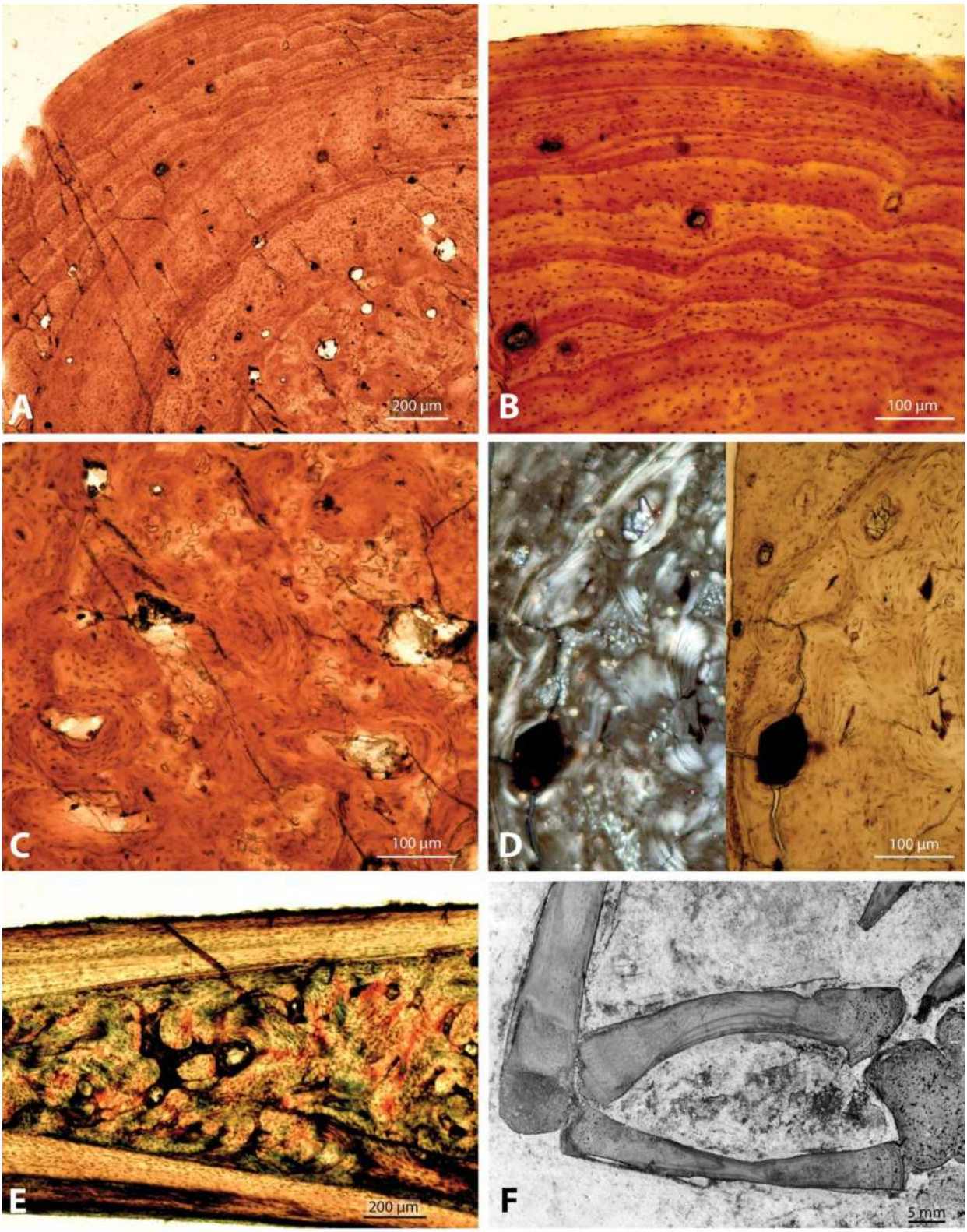


FIGURE 18.2 Mesosaurs. A, *Mesosaurus brasiliensis*. Pachyostotic rib, cross section, general view. The thick cortex surrounds a dense medullary region. B, Same material, detail of the poorly vascularized external cortex. C, Same material, detail of the medullary region and deep cortex. In this specimen, extensive amounts of globular calcified cartilage remain between the endosteal bone deposits. D, Rib of another specimen. In this specimen the long bones have experienced more complete osteosclerosis with dense compaction of the endosteal bone. Only small islands of calcified cartilage remain. E, Same material, longitudinal section of the metaphysis of a long bone. The medullary region is almost entirely filled up by convoluted endosteal bone deposits. F, Same material, preservation allows matching the cycles of deposition in the periosteal cortex with those in the calcified cartilage of epiphyseal regions and short bones.

VetBooks.ir

Mesosaurus and *Stereosternum*, which have an intermediate morphological condition. Nevertheless, osteosclerosis is well developed in the three genera.

This work raises the issue of the relative amount of periosteal bone compared to the endosteal region in several bones, notably ribs. It seems that this question is mainly a matter of anatomical location of the sections, relative to the shape and growth pattern of each skeletal element. Everything else being equal, the proportion of calcified cartilage in a cross section increases as the section is further from the neutral plane, set (theoretically) at mid-diaphysis in long bones (limbs), but not in ribs. Moreover, in each cross section, the amount of calcified cartilage locally replaced by endosteal bone is a time-dependent process. Obviously, more time has been available to replace the cartilage with endosteal bone (and to secondarily remodel it) in the ontogenetically oldest parts of a bone (close to the neutral plane in the diaphysis) than in epiphyseal regions laid down much later as growth took place.

The complexity of all such bone-specific growth circumstances may often preclude the ability to attribute *a priori* the observed histological differences to a systematic (taxonomic) causation among closely related genera. As long as the factors of time/shape/growth variability have not been comparatively mastered in the context of strict homology, down to the level of homologous sections localized within homologous bones, the observed differences among sections are best explained by taking into account the influence of morpho-ontogenetic factors (Nopcsa and Heidsieck 1934).

Klein et al. (2019; see p. 106) pointed out a contradiction between Nopcsa and Heidsieck (1934) and Ricqlès and Buffrénil (2001) regarding the immediate cause of osteosclerosis, the latter suggesting that "osteosclerosis is caused by incomplete endochondral ossification" (and correlated retention of calcified cartilage). Actually, we do not see a contradiction but ask for a more complete definition of physiological (nonpathological) osteosclerosis, as observed in several aquatic vertebrates (Ricqlès and Buffrénil 2001: 293–296, 301, figure 5). It seems unquestionable to us that osteosclerosis is somehow linked ontogenetically to a relative delay of the endochondral ossification process in the endoskeleton (a heterochronic phenomenon: Alberch et al. 1979), hence, the extensive amount and wide distribution of calcified cartilage even at large, subadult body sizes. We do not overlook the fact that later, the calcified cartilage may be entirely eroded and ultimately replaced by secondary endosteal bone in adults, forming the compact bony medulla that appears as the final ontogenetic stage of osteosclerosis, as observed in several cases, such as in mesosaurs and in *Claudiosaurus* (de Buffrenil and Mazin 1989).

Dental Microstructure in Mesosaurs

A recent histological study provides detailed data for mesosaur teeth and tooth insertion (Pretto et al. 2014). The study deals mainly with *Stereosternum*, a taxon with medium-sized teeth, compared to *Brazilosaurus* (shorter teeth) and *Mesosaurus* (longer teeth). The tooth structure and insertion show a great number of characters that may be adaptations to deal with breakage risks. The teeth are very long, thin, and covered by a thin coating of enamel. Limits of the enamel and dentine are not obvious because the externalmost dentine, in contact with the enamel, may have been partially modified by enamel proteins (durodentinous metaplasia). The external dentine appears to be an orthodentine with few but long dentinal tubules. Inside it there is a region made of globular dentine, itself divided in two by a central region where the dentine was incompletely mineralized. The innermost sheet of mineralized globular dentine borders the pulp cavity. This mixed arrangement may have increased tooth resistance to lateral tensions. Vascular dentine and denteons were also described as forming regions associated with globular dentin. The tooth base is covered by a thin layer of cementum. The mature teeth became ankylosed to the dentigerous bone through a very complex system. Teeth are located inside shallow tooth sockets and are held in place by a tripartite periodontium (composed of alveolar bone, cementum and possibly soft periodontal tissue) and accessory structures, the anchorage trabeculae (mainly composed of cementum). Fully grown teeth are ankylosed to the bottom of the tooth socket.

Parareptiles

Scheyer et al. (2010) reviewed the paleohistological analyses carried out on Reptilia. They noted that only a few studies had investigated the paleohistology of Permo-Triassic parareptiles, a group comprising ecologically and morphologically diverse forms and whose phylogenetic relationships are still debated (e.g., Laurin and Piñeiro 2018, MacDougall et al. 2018). Since then, new data have been produced, but mostly on the bone and tooth microstructure of a few clades, i.e., procolophonoids, pareiasaurs, and some more basal parareptiles. These studies, as well as their paleobiological implications, are presented below.

Bone Microstructure in Procolophonoids

Procolophonoids are small animals that constitute the most diverse and successful group of Parareptilia, as well as the only one that survived the End-Permian mass extinction event (unless turtles are parareptiles).

To date, only two studies have looked at the bone histology of procolophonoids with the aim to decipher their growth strategies and/or test the hypothesis of a fossorial lifestyle. Ricqlès (1974: 187–189, figure 5, plate IV) was the first to investigate the histology of isolated skeletal elements of *Procolophon trigoniceps* from the Early Triassic of South Africa and *Phaanthosaurus ignatjevi* from the Triassic of Russia. This pioneer study showed that the limb microstructure of both taxa was very similar, with thick compact cortices made of a poorly to moderately vascularized lamellar bone tissue. More recently, Botha-Brink and Smith (2012) undertook a comprehensive study of Triassic South African procolophonoids. Their sample comprised limb elements of different-sized individuals from the Early Triassic *Sauropareion anoplus* and *P. trigoniceps*, and from the Middle Triassic *Teratophon spinigenis*. Based on an ontogenetic series, their study revealed that the early ontogeny of *P. trigoniceps* was characterized by a relatively slow growth, with deposition of a poorly vascularized parallel-fibered bone, followed by an acceleration of growth rates at the subadult stage, associated with an increase in vascularization (Figure 18.3A, B). Interestingly, this taxon

VetBooks.ir

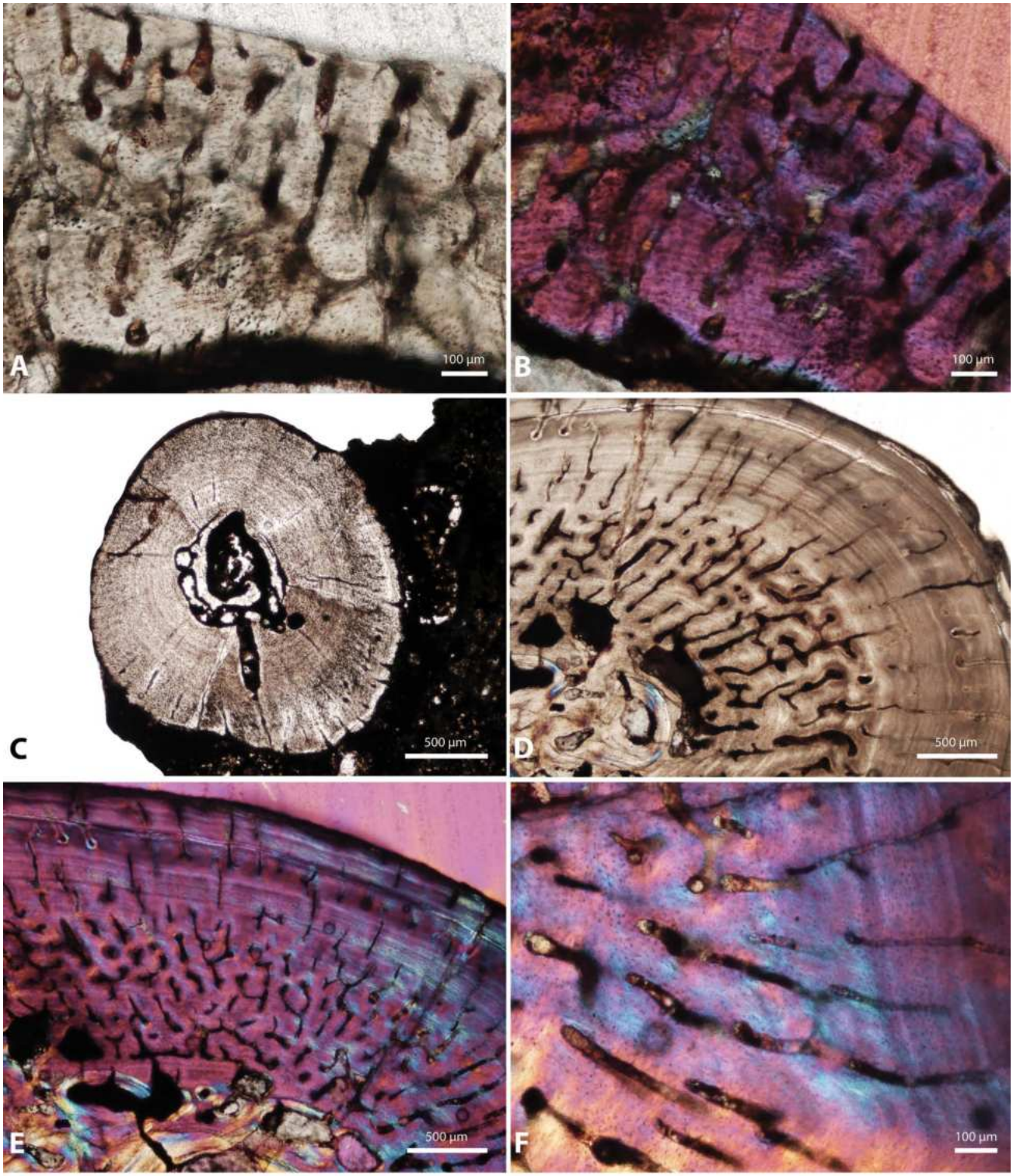


FIGURE 18.3 Procolophonids. Limb bone histology of the Triassic procolophonids *Procolophon trigoniceps* (NMQR3944b, A, B), *Teratophon spinigenis* (SAM-PK-K10183, C), and an undetermined procolophonid, possibly *T. spinigenis* (SAM-PK-7711, D–F). A, Diaphyseal cross section of femur in normal light. B, Femur in polarized light with lambda compensator showing parallel-fibered bone. C, Diaphyseal cross section of the radius showing a thick compact cortex composed of parallel-fibered bone with simple radial canals. D, Cross section of the humerus shaft showing a thick bone wall composed of a well-vascularized deep cortex with a subreticular vascularization and a less vascularized outer cortex with simple radial canals. Numerous annuli are visible throughout the cortex. E, Humerus in polarized light with lambda compensator showing a parallel-fibered bone matrix. F, High magnification of humerus in polarized light with lambda compensator showing numerous simple radial canals. Images reproduced with the permission of Jennifer Botha.

VetBooks.ir

does not exhibit any growth marks in its bone cortices, suggesting that its bone deposition was not affected by seasonal variation or that it reached somatic maturity in less than a year. The individuals sampled from the geologically younger *T. spinigenis* show relatively well vascularized (radial and reticular) parallel-fibered bone tissues (Figure 18.3C–F) and differ from the Early Triassic taxa *S. anoplus* and *P. trigoniceps* in forming annuli throughout the cortex.

Dental Microstructure in Procolophonoids

The evolution of procolophonid dentition and its specializations for herbivory have been recognized as crucial for the success of the group throughout the Triassic (e.g., Cisneros 2008). However, until recently, our knowledge of procolophonid tooth histology was limited to some scanning electron microscopy (SEM) observations of *P. trigoniceps* (Sander 1999). Over the last decade, several independent studies investigated this feature in different species.

Cabreira and Cisneros (2009) studied the dental histology of one procolophonid specimen of *Soturnia caliodon* from the Upper Triassic of Brazil. The teeth of this taxon had a low replacement rate and present a thick aprismatic enamel layer on the cusps, as well as a thick secondary dentine, features indicating an extended functional life span of the teeth, which would have been advantageous for the hypothesized fiber-rich herbivorous diet of *Soturnia*. Although the teeth are set in a shallow bony groove and ankylosed by bone of attachment, these authors described the implantation of *Soturnia*'s teeth as acrodont (a term normally used when the tooth is set at the top of the jawbone without a socket; see Bertin et al. 2018), contradicting previous hypotheses about the implantation of procolophonid dentition (based on gross visual observations only). Their interpretation was challenged by MacDougall and Modesto (2011), who investigated the tooth histology of *S. anoplus* from the Lower Triassic of South Africa. They found that although tooth replacement seems to have also been rare in *Sauropareion*, it was still present. They noted that the presence of tooth replacement and bone of attachment in their specimen and *Soturnia* (Cabreira and Cisneros 2009) rather suggest a protothecodont dentition (teeth implanted in shallow alveoli; see Bertin et al. 2018) in procolophonids, an implantation common to most early amniotes (see Bertin et al. 2018: figure 7).

Dental Microstructure of Other Basal Parareptiles

MacDougall et al. (2014) investigated the presence of plicidentine, a pattern of dentine infolding around the pulp cavity, in various clades of parareptiles from the Lower Permian of Texas and Oklahoma. This tooth structural specialization was previously thought not to occur in amniotes, but is now known from various amniote clades (Maxwell et al. 2011). Using thin-sectioning and microcomputed tomography, the authors found that plicidentine was fairly common among basal parareptiles, but could assume very diverse forms. Whereas plicidentine structure can be very complex and convoluted in the largest teeth of taxa with shallowly implanted dentition, such as *Colobomycter pholeter*, *Feeserpeton oklahomensis*, and to a lesser extent *Delorhynchus* sp., it is fairly simple or absent in taxa with deeply rooted teeth, such as *Bolosaurus striatus*. Their observations support the hypothesis that plicidentine occupies an increased surface of attachment between the dentine and the tooth-bearing element in parareptiles.

Haridy et al. (2017) also studied the dental histology of *Delorhynchus*. However, their investigations mostly focused on the coronoid dentition because the marginal dentition had already been described by MacDougall et al. (2014). They found that the histology of the coronoid teeth is similar to that of the marginal teeth. Although no plicidentine was observed in the small coronoid teeth, the teeth are anchored to the underlying coronoid ossification by alveolar bone. Finally, the crowns of these teeth are covered by a thick layer of enamel that makes up one-third of the total tooth height.

Bone Microstructure in Pareiasaurs

Pareiasaurs represented an abundant and taxonomically diverse tetrapod group in Middle to Late Permian continental ecosystems (Smith et al. 2012, Pearson et al. 2013). They included some of the largest and most heavily built herbivores of the time (with an anapsid skull, stout skeletal elements and osteoderms partially or completely covering the body). They achieved a significant radiation and extensive geographic distribution in only a few million years before becoming extinct around the end of the Permian.

Ricqlès (1974: 190–197, figures 6–9, plates V, VI) was the first to investigate the limb bone and rib histology of a few South African taxa (*Pareiasaurus serridens*, *Pareiasaurus* sp., *Bradysaurus* sp.) to describe their structure and possibly decipher their growth strategies. After a gap of nearly 25 years, researchers regained interest in these poorly known animals and provided new data on the osteoderm and limb bone microstructure of various species, i.e., mostly South African taxa (Kriloff et al. 2008, Scheyer and Sander 2009, Lyson et al. 2013, 2014, Canoville and Chinsamy 2017), and other forms such as *Bunostegos akokanensis* from Niger (Looy et al. 2016), *Pareiasuchus nasicornis* from Zambia (Tsuji et al. 2015), *Deltavjatia rossica* and *Scutosaurus karpinskii* from Russia (Boitsova et al. 2019) and *Provelosaurus americanus* from Brazil (Macedo Farias et al. 2019).

All these studies revealed that the bone microstructure and related life history traits of pareiasaurs are relatively uniform among species. Early in development, the primary periosteal bone deposited in limbs consists of a well-vascularized woven to parallel-fibered tissue interrupted by annuli and/or LAGs and attests to a relatively rapid (although discontinuous) growth (Figure 18.4D). Periosteal deposition later slowed (after the attainment of sexual maturity) but was prolonged for several years during adulthood, resulting in the formation of a thick layer of avascular lamellar bone interrupted by closely spaced LAGs (Figure 18.4B, F, H). Therefore, appositional growth continued for several years in mature individuals, suggesting a protracted and slow increase in bone diameter, a phenomenon that could contribute to the bulky appearance of pareiasaur skeletons (Canoville and Chinsamy 2017). Finally, Haversian substitution appears relatively early in ontogeny and is uniformly strong, such that most of the cortices can be formed of a dense Haversian tissue at adulthood (Figure 18.4G). Canoville

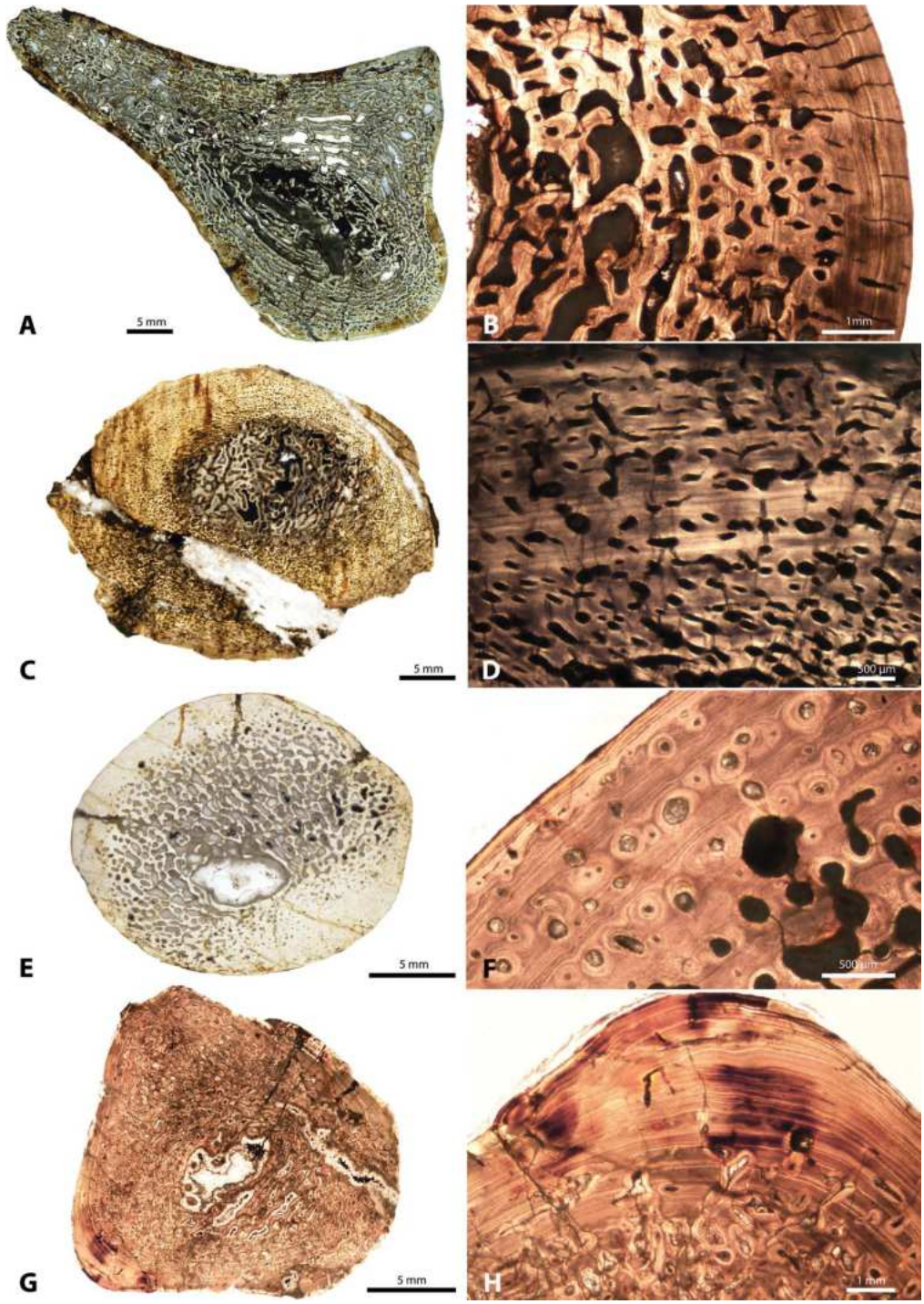


FIGURE 18.4 Pareiasauria. Bone histology of Permian pareiasaurs *Pareiasaurus* sp. (BP/I/5282, A and B), *Bradysaurus seeleyi* (SAM-PK-9137, C and D), *Pareiasuchus nasicornis* (SAM-PK-K6607, E and F) and *Anthodon serrarius* (SAM-PK-10074, G and H). A, Mid-diaphyseal cross section of a femur. Note that the section has an overall spongy organization, with a very thin compact cortex, B, Detail of the cortex in A. The deep and middle cortex is highly remodeled, although a few islands of primary lamellar-zonal bone tissue interrupted by growth marks are still visible. The oldest primary osteons are changed by erosion and reconstruction processes into secondary osteons that retain a wide Haversian canal. By this process, the deepest part of the primary cortex is progressively changed into a spongiosa. The outermost cortex is formed by a slowly deposited lamellar bone interrupted by lines of arrested growth (LAGs). Even though this outer layer is poorly vascularized, it contains a few simple radial canals attesting to a slow but prolonged periosteal deposition of bone. C, Diaphyseal cross section of a fibula. D, Detail of the inner cortex of the fibula in C. The cortex is highly vascularized and formed of a lamellar-zonal bone tissue. The vascularization mostly consists of enlarged primary osteons and incipient secondary osteons. E, Cross section of a rib, with asymmetrical bone remodeling. F, Detail of the outer cortex of the rib in E. The primary bone is lamellar-zonal and the vascularization is organized in concentric layers. The vascular canals are longitudinal. Some faint rest lines as well as cementing lines are visible in this area of the cortex. G, Diaphyseal cross section of a fibula. H, Closeup of the cortex in G. The midcortical region is highly remodeled with several generations of secondary osteons. The outer layer is formed of a poorly vascularized lamellar bone interrupted by several closely spaced LAGs.

VetBooks.ir

and Chinsamy (2017) hypothesized that this could be related to an important phosphocalcic metabolism linked to the formation and maintenance of osteoderms, as proposed for other organisms with dermal bones (Stein et al. 2013)

Undetermined Small "Romeriid" Amniote (Protorothyrididae or Diapsida)

A very small indeterminate reptile from the Fort Sill fauna (Lower Permian, Oklahoma) was mentioned by Richards (2016) and described histologically in a comparison of all the taxa known from Fort Sill.

Our material (femora) from this locality (OMNH [Sam Noble Oklahoma Museum of Natural History, Norman, Oklahoma] 56891, lent by Richard Cifelli) suggests that this small reptile may be a protorothyridid or a diapsid (="Romeriid"). The possibly paraphyletic Protorothyrididae includes several Late Carboniferous (*Hylonomus, Paleothyris*) and Early Permian (*Protorothyris*) genera. They are generally considered very early basal eureptile amniotes of small body size with an anapsid skull and a single row of teeth on the maxillary and dentary. Anatomically, they are close to Captorhinids and were once regarded as ancestral to them, but recent phylogenetic analyses suggest that they are more closely related to diapsids (i.e., Ford and Benson 2020).

Our material includes sections from two femoral shafts. The sections are fairly circular with a diameter of 2 mm (Figure 18.5A). There is a free marrow cavity, devoid of bone trabeculae, coated with a thin deposit of endosteal bone, with local evidence of erosion/reconstruction processes. This perimedullary endosteal bone coating is well separated from the deep primary (periosteal) cortex by a line of reversion; hence, the deepest cortex has been entirely resorbed (Figure 18.5C). The periosteal cortex is homogeneously formed by lamellar-like bone. The bone cell spaces are flattened parallel to the bone surface and the canaliculi are radially oriented. The cortex is almost devoid of vascularization (Figure 18.5B), apart from a few simple vascular canals oriented longitudinally and one very large nutrient canal. There is an annulus-like structure located deep in the cortex without a clear LAG. Several twin LAGs (about 6) are set closer and closer in the external cortex, separating the external-most bone deposits that become thinner toward the external bone surface.

Our material is histologically similar to that of the specimen described by Richards (2016: chapter 3, figure 3c) and likely belongs to the same taxon. The histological structure differs sharply from that of *Captorhinus aguti* from Fort Sill and other localities and of closely related taxa (*C. magnus, Protocaptorhinus*) histologically described by Richards (2016). Differences include the very sparse vascularization of the cortex, the slight development of secondary endosteal bone around the marrow cavity with hardly any endosteal trabeculae, and the external cortex, apparently always associated with LAGs completed by a thin external-most layer of bone. Among the Fort Sill tetrapod community, this taxon is closer histologically to the microsaur *Cardiocephalus* (Richards 2016: chapter 3, figure 2c) than to any other amniote, and it differs sharply from temnospondyls. Similarities in developmental dynamics offer the simplest explanations of the resemblances.

Captorhinids

It is generally accepted that captorhinids are closely related to the protorothyridids and diapsids. Protorothyridids are all small, probably insectivorous predators, with only a single row of teeth on the jaw margin plus palatal teeth on several bones (see above). They are known from the Late Carboniferous and the Permian. The earliest captorhinids (and the earliest amniotes in general), such as the Late Carboniferous *Concordia*, retained small body size and one row of marginal teeth. In Early Permian taxa such as *Captorhinus*, we see the appearance of several rows of teeth, which may have evolved up to three times in captorhinids (Brocklehurst 2016). Patterns in body size evolution in this clade are complex (Modesto et al. 2014, Brocklehurst 2016): maximal body size increased until the Late Permian (*Moradisaurus)*, but small taxa also persisted until the Late Permian, when the group became extinct.

Bone Microstructure in Captorhinus

Enlow and Brown (1957: 188, plate XV; 1969: 71, figure 28) described the histology of several bones (skull and jawbones, long limb bones, ribs). Peabody (1961: 48, figures 34, 35, 56–69) also studied the growth marks in the precoracoid, dentary and humerus and Warren (1963: plate XVII, figures 1, 2) studied the zygapophyses in *Captorhinus*. Later, a humerus and an ulna were histologically described by Ricqlès (1974: 180–182, plate II, figures 1–7). All the material studied came from the famous Lower Permian Richards Spur fissure fills of Oklahoma, which date from the Artinskian (deBraga et al. 2019).

The main histological features of long bone shafts include a thick primary cortex formed of fine lamellae of periosteal origin, permeated by a variably developed vascular system, formed by mostly longitudinal vascular canals around which there is a little centripetal deposition. Hence, these canals become poorly developed primary osteons (Figure 18.5D, E). In the deeper cortex, some regions are crossed by irregularly oriented vascular anastomoses and the bone tissue matrix becomes more irregular, forming an incipiently woven tissue. There is some cyclicity in the structure of the cortex but the annuli are difficult to decipher on thin sections (Figure 18.5D), and there are apparently no LAGs. Cyclicity may be easier to observe in rather thick sections (Peabody 1961). There is a free but narrow medullary cavity surrounded by some well-developed endosteal deposition associated with a few secondary osteons in the deepest cortex (Figure 18.5E).

More recently, a growth series of femora (from 15 to 34 mm in length) of *Captorhinus* has been histologically studied in the context of a comparative histological survey of the vertebrate community preserved in the Richards Spur fissure fill at the Dolese quarry, Oklahoma (Richards 2016). The new histological findings add many data to *Captorhinus* histovariability and generally concur with the (sometimes unquoted) previous descriptions with, however, a major difference: Richards (2016) describes the histology of *Captorhinus* as entirely devoid of growth marks, whereas all other members of the fauna (small synapsids, temnospondyls, lepospondyls)

VetBooks.ir

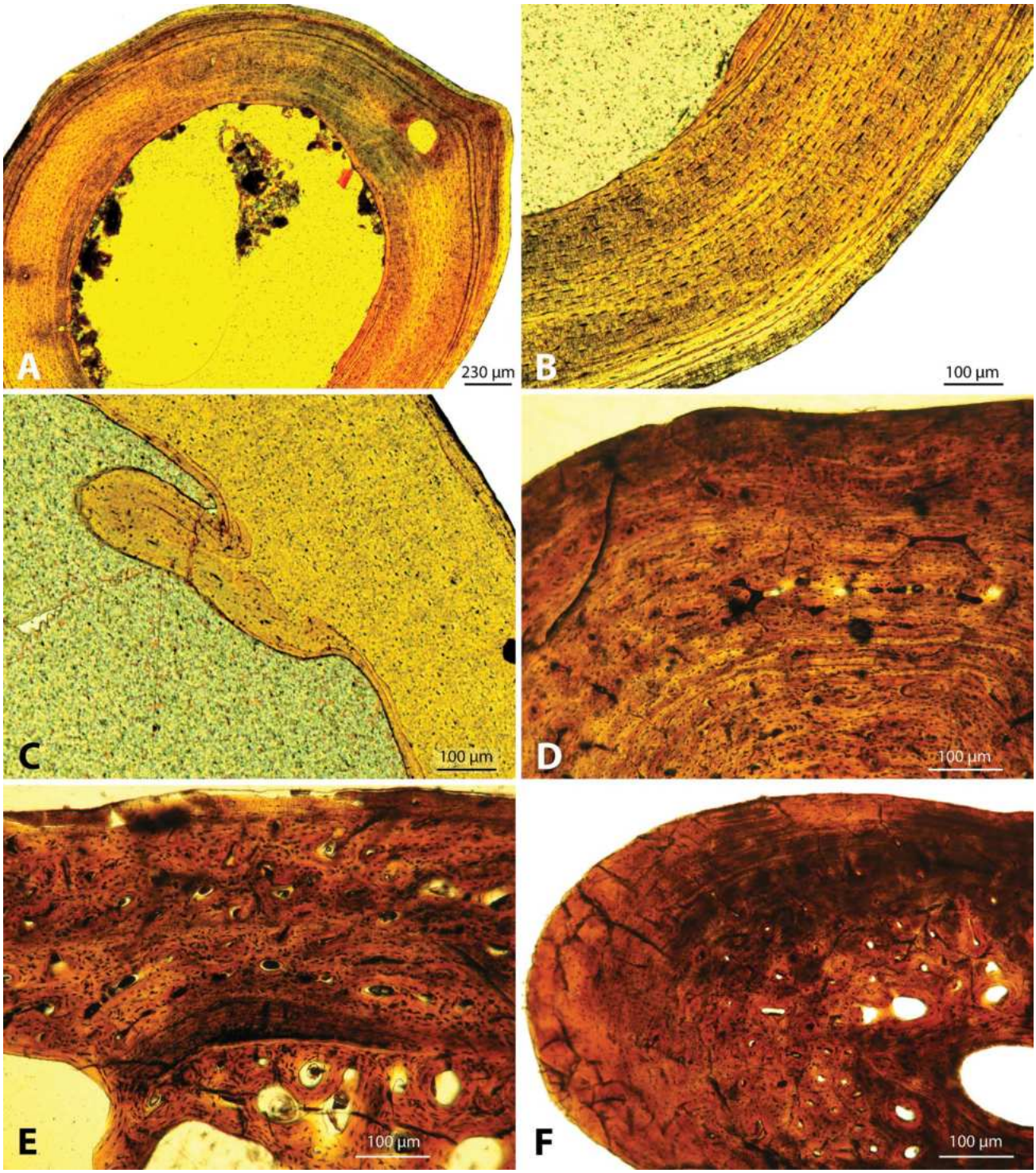


FIGURE 18.5 Protorothyridids (Romeriids) and Captorhinomorphs. A, "Romeriid" femoral shaft, cross section. The diaphysis is tubular and almost nonvascular, apart from a few simple vascular canals and one large nutrient canal. B, Same material. The lamellar cortex shows evidence of lines of arrested growth (LAGs) close to its periphery. C, Same material, endosteal trabeculae are minimally developed but a thin coating of endosteal bone is laid down uncomformably on the deep cortex around most of the marrow cavity. D, *Captorhinus*. Humeral cortex at mid-shaft. The thick diaphyseal cortex covers a small central marrow cavity. The cortex is permeated by numerous irregularly oriented vascular canals. Cycles of bone deposition are not apparent. E, Same material closer to the metaphysis. The marrow cavity is largely expanded and contains well-developed endosteal trabeculae. One LAG may be present in the middle of the cortex. F, *Captorhinus*. cross section of the ulna diaphysis. The small marrow cavity is associated with well-developed endosteal deposition and erosion/reconstruction took place in the deep cortex.

VetBooks.ir

show obvious growth marks, most often LAGs. We agree that growth cycles are not obvious in *Captorhinus* shaft cross sections since LAGs are lacking. We concur with Richards (2016) that *Captorhinus* was probably able to maintain some year-round growth and could reach maturity probably more quickly than most other vertebrates in the community (Ricqlès 1974: 186–187; see the discussion below).

Richards (2016: 24, figure 5) also reports the histology of specimens of *Captorhinus* from other deposits than the Dolese Quarry, and also from *Protocaptorhinus*, and compares long bones from *C. aguti* with *C. magnus*. Beyond several details linked to bone preservation, section localization, and so forth, the general histological pattern of bone cortex is similar.

Bone Microstructure in Labidosaurus

This captorhinid from the Permian Texas Red Beds is distinctly larger than *Captorhinus* but retains a single tooth row (Modesto et al. 2007). The histology of the ribs was described by Enlow and Brown (1957:186–188, plate XV, figure 1) and Enlow (1969: 71) as characterized by a great density of longitudinal vascular canals, a poorly developed spongiosa and no Haversian reconstruction. Ricqlès (1974: 183, figure 4; plate II, figures 8 and 9) described the shaft of a humerus and a femur. The cortex is lamellar and permeated by simple primary vascular canals that are radial or longitudinal with a radial organization. A general cyclicity of bone deposition is not obvious (Figure 18.6A–C). The periphery of the marrow cavity forms an abrupt region of generalized bone resorption, with some endosteal deposition locally (Figure 18.6A). There are interesting local modifications of structure, linked to muscular insertions. For example, the adductor crest of the femur is formed by a tissue much more densely and irregularly vascularized than the "regular" cortex and pervaded by numerous erosion bays spreading from the endosteal margin.

Bone Microstructure in Moradisaurus

The histology of the largest and geologically most recent (uppermost Permian from Niger) captorhinid, *Moradisaurus*, has been described from several bone fragments including an adult-sized ulna shaft and neural spine, and smaller radius, femur and tibia (Ricqlès 1974: 184; plate III, figures 1–5). Dentigerous bones and teeth have also been histologically described (Ricqlès and Taquet 1982: 63–73, figure 20; plates IX–XI). Several later additions to the anatomical knowledge of the genus have been published (O'Keefe et al. 2005, Richards et al. 2007, Modesto et al. 2018).

The bone cortex is typically lamellar-zonal in the shaft of the adult-sized ulna and in the radius. The thin lamellae together form higher-order zones that are set apart by annuli. The zones are variably vascularized by simple small vascular canals or by primary osteons, oriented longitudinally (Figure 18.6F). Vascularization may be entirely lacking, especially in the more superficial zones. Sharpey's fibers may be very numerous locally. The annuli are formed by a few lamellae, more translucent than the material of the zones in transmitted light, and devoid of vascular canals (Figure 18.6E, F). Occurrence of LAGs associated with the annuli is not obvious. The deep cortex is progressively eroded by subcircular erosion bays, some of them ultimately forming isolated secondary osteons. The inner part of the bones is formed by an extensive spongiosa made of secondary endosteal bone trabeculae. The structure of the smaller bones (radius, femur, tibia, possibly from subadult individuals) is very similar to that of the adult-sized ulna. On the contrary, an adult-sized neural spine has a very light structure, formed by an endosteal spongiosa, in clear contrast with the thick cortex of the limb bones.

Concluding Remarks

Captorhinus histology suggests that it was fairly insensitive to environmental yearly cycles (Richards 2016) and could probably grow rather quickly to adult size (Enlow 1969: 71; Ricqlès 1974: 186). During the Permian, some captorhinid taxa appear to have retained the modest body size of *Captorhinus* (Ricqlès 1984). On the contrary, most captorhinids more recent than *Captorhinus* show a distinct body size increment and changes in skull shape, associated with an increase in the number of tooth rows. This is illustrated by several genera such as *Rothianiscus*, *Kahneria* and *Gecatogomphius* (review in Ricqlès 1984 and more recently in Modesto et al. 2007, 2014, 2018, Richards et al. 2007). Ricqlès (1979, 1980, 1983) argued that the evolution of captorhinids expresses the recurrent exploration of "K" demographic strategies, starting from an ancestral "r" strategy (Pianka 1970), expressed in early taxa, such as *Captorhinus*. More recently, Brocklehurst (2017) used a timetree of 20 captorhinid taxa and various quantitative analyses to study evolutionary patterns. He showed that the shift to a herbivorous diet in the smallest clade that includes *Captorhinikos* and *Moradisaurus* (and comprises mostly Middle and Late Permian captorhinids) is associated with an increased evolutionary rate and increased disparity, compared to the predatory and omnivorous captorhinids. Note that this shift toward a less nutritious herbivorous diet should result in lower maximal growth rate, which is coherent with the shift toward a K-strategy postulated by Ricqlès (1979, 1980, 1983). This scenario can be tested through histological data. Comparisons between the bone structures of *Captorhinus* and *Moradisaurus* suggest that the former had a rather continuous (rather than strongly cyclical) and perhaps initially rapid growth, with no evidence of extended longevity. On the contrary, *Moradisaurus* histology strongly suggests a protracted longevity that allowed the animal to reach a large body size through slow, cyclical growth. Moreover, many morphological specializations of *Moradisaurus* and other large captorhinids, such as the multiple tooth rows, may be the automatic consequences of unchanged growth trajectories extended through a longer ontogenetic interval (peramorphosis through hypermorphosis of Alberch et al. 1979).

Dental Microstructure in Captorhinus

The histology of teeth and their insertion system was observed by Ricqlès and Bolt (1983) and more recently by Modesto (1998), Le Blanc and Reisz (2015) and Richards (2016). Ricqlès

VetBooks.ir

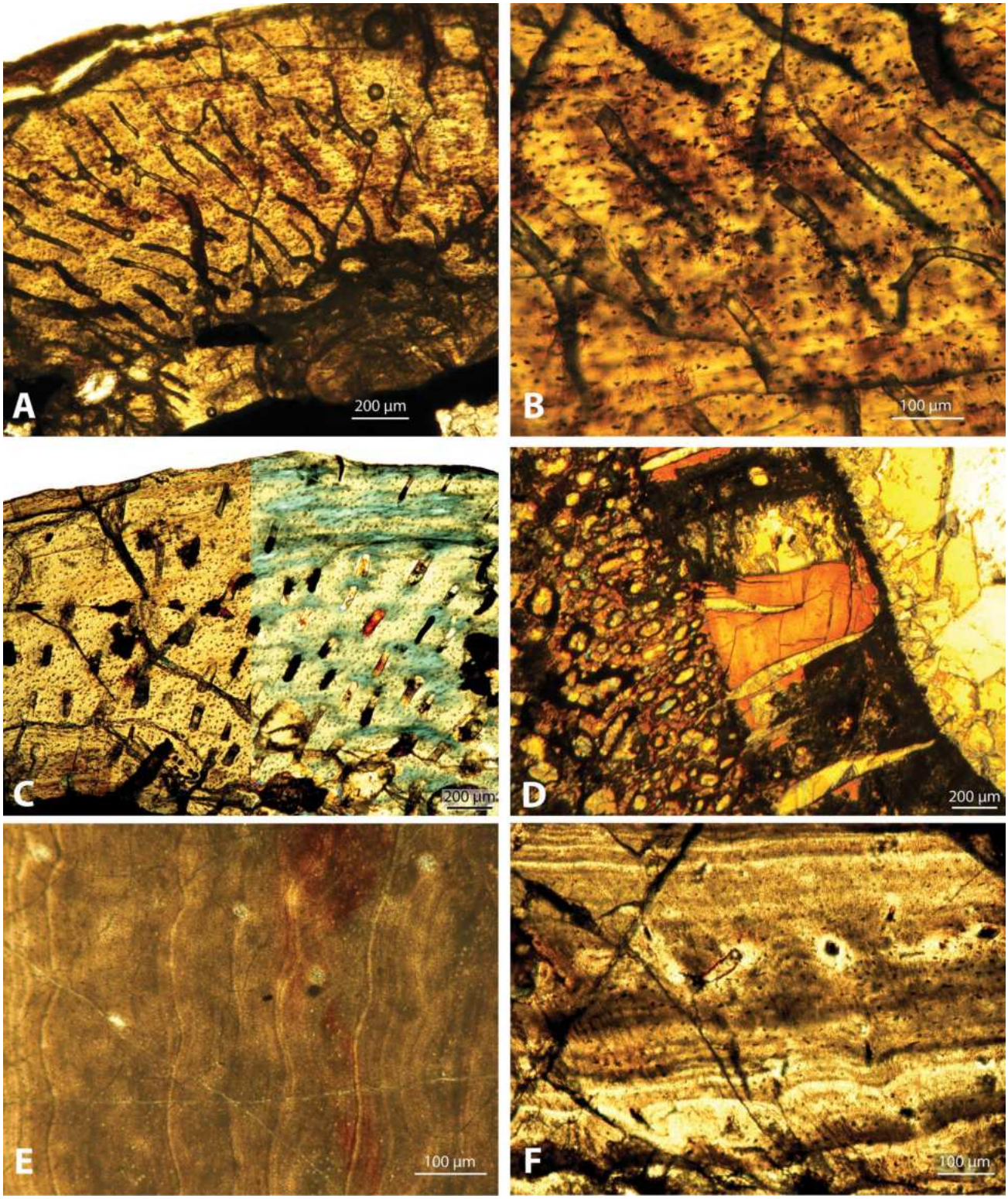


FIGURE 18.6 Captorhinids. A, *Labidosaurus* femur. General view of the cortex suggesting an incipient cyclicity; the free marrow cavity is locally surrounded by thick endosteal bone. B, Same material, detail of the cortical bone. The lamellar-like tissue is permeated by radially oriented primary vascular canals. C, Same material; in this region the vascular canals are more obliquely oriented. Polarized light suggests that most of the bone is parallel-fibered. D, *Moradisaurus*. Horizontal section of the base of an ankylosed tooth. The pulp cavity is at the right; in the middle, the thin coating of dentine is poorly preserved; at the left is the alveolar or "attachment bone". E, *Moradisaurus*. Radius. Detail of the superficial cortex. Cycles of almost non-vascular bone lamellae are set apart by thin lines. F, Same material, lamellar-zonal bone with a large "zone" containing a few vascular canals lined by nonvascularized annuli. Sharpey's fibers are well developed locally.

VetBooks.ir

and Bolt (1983) were especially interested in understanding the growth of the jaw apparatus as a whole and replacement of the tooth rows in the context of the "Zahnreihen" theory. Their approach was to devise a growth model exclusively derived from gross morphological data, then to test the model by independent histological data. This could explain the paradoxical "motion" of teeth and tooth rows ankylosed to the dentigerous bones. The histology of the tooth was described as relatively simple: a thin cap of enamel covers the orthodentine, which is very rich in tubules opening into the pulp cavity. The massive bulk of orthodentine, slightly folded at the tooth base, increases the surface for tooth insertion, which was described as subthecodont, or rather protothecodont, according to MacDougall and Modesto (2011). Maxwell et al. (2012) suggested that *Captorhinus* possessed cementum covering the tooth base. Following the recent review of Bertin et al. (2018), the exact type of tissue(s) by which the tooth became ankylosed to the dentigerous bone (cementum, alveolar bone, attachment bone or interdental bone) remains problematic. The microcancellous tissue that developed between and below the tooth bases and formed the bulk of the tooth attachment material is cellular, vascularized and primary but capable of erosion/redeposition phases and hence structurally and functionally closer to bone than to cementum. In addition, a very thin sheet of what is probably an avascular cementum developed at the interface of the dentine and the surrounding microcancellous issue.

LeBlanc and Reisz (2015) considerably built on former studies by histologically comparing patterns of tooth replacement in early captorhinids with a single tooth row (*Concordia cunninghami*, *Captorhinus magnus*) and multiple tooth rows (*C. aguti*). Hence they documented the morphogenetic changes that ultimately led to the evolution of the multiple-rowed captorhinids.

Locally, the older teeth (and neighboring cementum or attachment bone) are always those eroded close to the younger teeth and tooth-bearing tissues.

Captorhinus teeth were also described and figured by Richards (2016: 25–26, figure 6), who used the number of daily accretion lines in the dentin (von Ebner's lines) of the teeth pertaining to successive rows to get an idea of the rate of tooth row replacement. The oldest row of teeth (labial) has 603 (daily) lines, the middle row has 384 lines and the youngest row (lingual) has 299 lines. This suggests an age of at least 2 years for the specimen examined. This approach had been suggested but not implemented for the multiple-rowed *Moradisaurus* by Ricqlès and Taquet (1982: 64, plates IX and X).

The occurrence of dentine folding, or plicidentine, among captorhinid taxa is variable, as discussed by Maxwell et al. (2011), with the absence of dentine folding reported in *Labidosaurus* (Broili 1904) and *Moradisaurus* (Ricqlès and Taquet 1982). Actually, the modest folds observed in *Captorhinus* can hardly be called plicidentine.

Dental Microstructure in Moradisaurus

The anterior part of the jaws bears large teeth organized into one row; the teeth are slightly incurved and flattened parallel to the labial curvature of the bones. They have not been observed histologically. Posteriorly, the teeth are organized into several parallel rows (up to 11 on the maxillary, and to 10 on the dentary). Starting from the lingual region, the longest rows are numbers 5–8, bearing as many as 23 teeth. The total number of ankylosed teeth exceeds 600 on the holotype specimen. New material (Modesto et al. 2018) includes a slightly smaller lower jaw.

The teeth from the multirowed area have a rather simple and constant morphology; the crown is 6–7 mm high with a diameter of 4–6 mm at the base (Figure 18.6D). The section is circular. It is roughly conical with a rather pointed tip and some convexity on the flanks, giving a slightly globular shape. There is no evidence of abrasion on the tip, but some wear occurs on the lateral sides (labial and lingual) of some teeth. The crown is entirely covered by enamel of the pseudoprismatic type (Schmidt and Kiel 1971), thickest at the tooth tip and becoming very thin and disappearing at the crown base. The pulp cavity is very narrow at the tip and greatly expands only in the basal region of the tooth crown. The bulk of the tooth is made of orthodentine containing a great density of thin dentinal tubules, running from the enamel junction toward the pulp cavity, and also along a direction from the tip toward the tooth base. The dentine does not have a globular structure. It contains a very high number of fine concentric von Ebner's lines (probably deposited daily) and two or three more obvious concentric lines, likely recording a higher order time cycle.

There are no indications of plicidentine at the base of the tooth. The radial structures observed in the dentine are fossilization artefacts. The tooth insertion is probably complex and involved firm ankylosis of the teeth on the jawbones. There is an alveola under each tooth, the basis of the crown being attached at its periphery. The basis of the crown is surrounded by a peculiar tissue, very rich in canals of small diameter that also forms the bottom of the alveolar cavity (Figure 18.6D). This tissue is different from the cancellous bone that forms the bulk of the bony plates bearing the tooth rows. It is microcancellous with a multitude of parallel canals set vertically, especially at the bottom of the alveola, but also forming the material that surrounds the basis of the crown. This tissue differentiates only within, below and immediately around each alveola. It experiences phenomena of erosion and reconstruction just like bone. With reference to the structurofunctional definitions of attachment tissues (Bertin et al. 2018), the tissue is more akin to bone than to ligament or cementum.

Araeoscelidia

This group of early amniotes from the Late Carboniferous and Early Permian of Laurasia includes the earliest diapsids, generally small terrestrial (less than 1 m long) tetrapods that retained the primitive amniote habitus and long limbs. The most salient apomorphy of most taxa is the occurrence of the two typical temporal fossae, as in *Petrolacosaurus*. The genus *Araeoscelis* has received various interpretations (Vaughn 1955) because it lacks the lower temporal fossa, but on the balance of other evidence it is now generally recognized as

VetBooks.ir

a somewhat aberrant early araeoscelidian. Other taxa include *Aphelosaurus* (reviewed by Falconnet and Steyer 2007), *Spinoaequalis* and *Kadaliosaurus* (reviewed by deBraga and Rieppel 1997). The taxon *Dictybolos* from the Early Permian of Oklahoma was put into this group by Olson (1970), although this has been disputed (Evans 1988).

Bone Microstructure in Dictybolos

Our specimen is a small long bone. The cortex has a thickness of about 3–4 mm for a bone shaft of oval section with a diameter of 11*8 mm. The bone has a free central marrow cavity surrounded by a well-developed spongiosa that spreads outwardly and forms a rather progressive transition with the deep cortex. The spongiosa comprises irregularly shaped trabeculae of endosteal origin, lining irregular medullary bays, with the most external ones eroding the deep cortex. No typical secondary osteons develop in this endosteal margin. The cortex is entirely primary bone of periosteal origin and is clearly divided into a few growth cycles (Figure 18.7A). The bone tissue has a thin lamellar-like organization, underlined by the orientation of the bone cell lacunae. There is evidence of radially oriented Sharpey's fibers locally. Vascularization of the cortex is composed of primary vascular canals with a longitudinal but also a strongly oblique to radial component in their orientation. There are no anastomoses between the canals. The deep cortex forms a thick homogenous region, forming about one-third of the total cortical thickness. It is limited outwardly by a LAG. The more external cortex, slightly less vascularized, is divided into at least two well-marked superimposed growth cycles. The free bone surface may correspond to a final LAG at the end of the animal's life.

Bone Microstructure in Araeoscelis

Our specimen consists of small rib fragments of different shapes, some with a circular section (diameter 2 mm) (Figure 18.7C), others with an oval section (1.5*2.5 mm) (Figure 18.7B). The thin cortex circles a wide marrow cavity devoid of bone trabeculae. A thin endosteal deposit forms the innermost cortex locally, and is sometimes associated with one or two erosion bays in the deep cortex. In other regions, endosteal bone is entirely lacking and the deep cortex is formed by a periosteal bone experiencing a perimedullary resorption (Figure 18.7D). Where an endosteal deposit is present (Figure 18.7F), it is always set apart from the deep periosteal cortex by a scalloped resorption line. Hence there is no Kastschenko's line and the entire sequence of periosteal bone deposition is never present. The deep periosteal cortex is very rich in large, stellate bone cell spaces and its matrix is formed of obliquely oriented sheets (Figure 18.7E). Locally there are some short Sharpey's fibers packed together. Tiny primary osteons and simple vascular canals oriented longitudinally pervade the whole cortex. One LAG is generally located at the middle of the cortex, but it may be localized more outward. Outside the LAG, the cortex has a more lamellar structure, with a lesser density of cells (Figure 18.7D–F). Structural differences between opposite quadrants in a section offer good evidence of lateral drift associated with the overall bone growth. Those small ribs show, on a minute scale, all the regular tissue components observed in much larger bones.

Avicephala

Avicephala is a group of small early diapsids of the Late Permian and Triassic with a pointed head. Among them, the drepanosaurids show various peculiarities of the limbs and tail that strongly suggest an arboreal life and analogical comparisons have been attempted with chameleons and sloths. Other taxa, such as *Longisquama* and the coelurosauravids, evolved peculiar specializations possibly linked to parachuting or gliding flight. Whereas the highly specialized Upper Triassic drepanosaurs (*Drepanosaurus, Megalancosaurus*, etc.) appear to form a monophyletic group (Renesto et al. 2010) perhaps close to the prolacertiforms, the validity of the group Avicephala as a clade is still open to question.

Bone Microstructure in Coelurosauravus

Among Coelurosauravids, the Late Permian genus *Coelurosauravus* (also known as *Weigeltisaurus*) is famous as the oldest known amniote apparently adapted to gliding or parachuting flight. It was reviewed by Schaumberg et al. (2007: 167, 169, figures 7–9) who gave the first histological description of the bone tissue of the femur and of the rods supporting the flying membrane.

The femur has a cortex formed of avascular bone with a parallel-fibered or lamellar aspect, likely organized in successive cycles (a double annulus may be observed). The bone cell spaces are lenticular and organized conformably to the bone lamellae. Around the marrow cavity there seems to be a line of resorption and a centripetal deposition of endosteal bone.

A spar supporting the wing membrane has been observed in cross and longitudinal sections. Figure 7C in Schaumberg et al. (2007) is a schematic reconstruction of three cross sections of spars showing that growth in diameter took place in two opposite preferential directions, giving a distinct flattened shape to the spar's sections. The histological structure of the spar is identical to that of the femur: an avascular lamellar-like bone with flattened osteocytic lacunae and radiating canaliculi. Around the central cavity, the cross section observed at higher magnification again suggests a resorption line covered by a centripetal endosteal bone deposition. The histological structure of the spar is almost identical to that of the femur: a typical cellular, avascular bone, as also observed in most extant small squamates (see Chapter 20). Perimedullary erosion and endosteal deposition suggest that the spar bone tissue grew just like the normal femoral bone tissue.

The origin of the spars has been discussed (review in Schaumberg et al. 2007: 161): hypotheses include a costal (endoskeletal) or a dermal origin of those neomorphic organs, perhaps implying metaplasia of a preexisting tissue into bone. The actual tissue observed in the spar, as well as the occurrence of an internal (marrow) cavity, is compatible with an endoskeletal (rib) origin, although no typical endoskeletal component (i.e., endochondral ossification) is observed. Morphological

VetBooks.ir

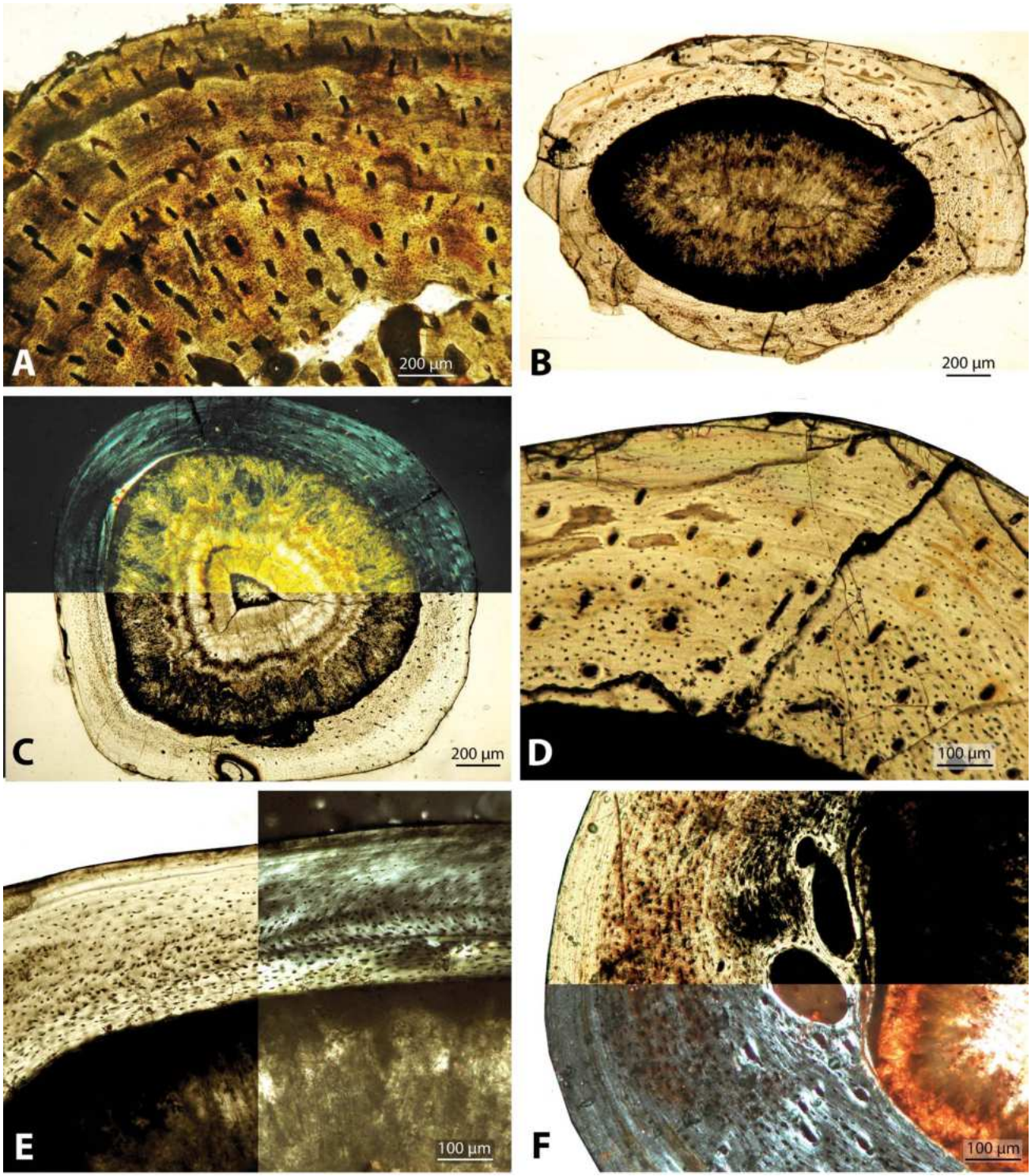


FIGURE 18.7 Areoscelids. A, *Dictybolos*. Long bone shaft cross section. The lamellar-zonal external cortex shows good evidence of cyclical growth. B–F, *Areoscelis*. B, Flattened rib. In spite of the small size of the bone, the vascular canals system is well developed. C, Cylindrical rib. Some regions of the deep cortex experience perimedullary resorption and endosteal deposition at the opposite side. Upper half, polarized light. D, Detail of a region in B. Fine structural differences between the deep and superficial cortex are well marked. E, In this cylindrical rib, the complex fibrillar and cellular organization of the deep cortex is noteworthy. One line of arrested growth (LAG) is located in the external cortex. Right half, polarized light. F, In this rib, the thick internal cortex is associated with endosteal erosion/reconstruction forming an incipient spongiosa. Lower half, polarized light.

VetBooks.ir

observations suggest a dermal rather than a costal origin for the spars (Schaumberg et al. 2007). This could have taken place through a direct neomorphic ossification within the skin dermis. There is no histological evidence of a metaplastic transformation of a preexisting dense connective tissue (tendinous or ligamentous like tissues) into the spar's bone tissue.

Synthetic Remarks

Bone Histodiversity of Early Amniotes and Their Relatives

In spite of the obvious diversity and the debatable interrelationships of the various groups of early cotylosaurs reviewed in this chapter, some generalizations may be attempted about their bone histology. The compact bone tissue forming the cortex of long bone shafts appears mostly built by primary periosteal bone tissue of a lamellar or parallel-fibered organization. Vascularization is low to moderately dense, formed by simple primary vascular canals or, to a lesser extent, by primary osteons oriented longitudinally, sometimes with an important radial component. Sharpey's fibers are locally developed, in connection with regions of tendinous or ligamentous insertions (either at the time of death, or earlier in ontogeny). Some regions of especially extensive insertions, such as the fourth trochanter of the femur, have a specialized structure. Evidence of cyclical growth is widespread in the form of LAGs and avascular thin *annuli* alternating with thicker vascularized zones (Peabody 1961). The endosteal margin may be very progressive and associated with erosion bays and secondary osteons. The medullary cavity in several groups (especially large vertebrates: diadectids, pareiasaurs) appears more or less invaded by a well-developed system of endosteal bone trabeculae.

On this general pattern, which is typical of several taxa, some variants occur, depending on several variables, the importance of which has been recognized for a long time: specific body size, bone/specific shape, size and localization, ecological adaptation and systematics (Padian et al. 2004). For example, small early captorhinids and small procolophonids have a thick cortex around a rather free marrow cavity, and few growth marks. Some pareiasaurs may have some fast-growing woven bone tissue during early ontogeny and most species show well developed dense Haversian bone (secondary osteons) later. Mesosaurs evolved beyond the generalized pattern described above a spectrum of histological specializations (pachyostosis and osteosclerosis) that had already independently evolved among some lineages of secondarily aquatic anamniotic stegocephalians (Ricqlès and Buffrenil 2001) and that evolved time and time again among later clades of secondarily aquatic amniotes (Houssaye et al. 2016). Small, light animals, such as weigeltisaurids, reduced the cortical bone vascular system just as among small squamates (see Chapter 20), although this is not the case for *Araeoscelis*.

In sum, it seems that the general bone histology of early amniotes is not fundamentally different from that of other stegocephalians, with the restriction that some traits may show a more frequent and generalized adaptation to locomotion on the ground and even sometimes to some fossorial adaptations (procolophonids). From a paleobiological point of view, and by comparison with extant vertebrates, bone histology suggests that most early amniotes (except maybe pareiasaurs; see discussion in Canoville and Chinsamy 2017) retained the grade of a general ectothermic metabolic physiology, hence a generalized, plesiomorphic condition of vertebrate thermometabolism.

Dental Microstructure and Insertion in Early Amniotes

The recent review of Bertin et al. (2018) offers a modern framework for an evolutionary synthesis on tooth implantation, attachment and replacement in amniotes. From a general evolutionary point of view, the traditional morphological division of tooth insertions as acrodont, pleurodont and thecodont, derived from the analysis of extant vertebrates, can hardly describe the situation observed among early vertebrates, especially in a phylogenetic framework (Gaengler 2000, Caldwell et al. 2003). The situations observed in early amniotes, such as mesosaurs and captorhinids, namely the occurrence of alveolae, specialized alveolar bone and cementum (and the possible presence of a soft periodontal ligament in mesosaurs), suggest that these tissues may have been widespread among early amniotes, rather than being exclusive to mammals and archosaurs (Bertin et al. 2018). Occurrence of the periodontal ligament is especially contentious. Among mammals and archosaurs with a thecodont insertion, the ligament is nonmineralized, and accordingly replaced by exogenous minerals in fossils. Evidence for the ligament thus paradoxically relies on its absence but also on its mineralized ends, anchored in the alveolar bone and cementum, respectively (Bertin et al. 2018). In the captorhinids that we observed, a "subthecodont" insertion is associated with a firm tooth ankylosis with a very thin cementum, but we have not observed evidence of a periodontal ligament that, in our case, should have been entirely mineralized. No space is left between the tooth material and the peridental bone-like tissue, and no evidence of ligamentous fibers could be observed.

This raises the issue of which kind of tooth insertion was the primitive condition for amniotes. Although several specialized tissues including cementum, attachment bone, alveolar bone and especially periodontal ligaments were already differentiated among, e.g., mesosaurs, this suggests a very early evolution of those tissues, perhaps even among nonamniotic tetrapods. It also suggests that the most significant apomorphy in the evolution of the tooth insertion system, as observed among archosaurs and mammals, is the differentiation of the dental root itself, at once associated with the possibly preexisting systems of cementum, periodontal ligaments and specialized alveolar wall.

Early Amniote Paleobiology and the Permo-Triassic Crisis

Although pareiasaurs have been the focus of numerous morphological descriptions and phylogenetic analyses (see for example Lee 1997a,b, Tsuji 2011, Van den Brandt 2020, and literature therein), reconstructing their lifestyle and paleobiology has proven challenging.

VetBooks.ir

It remains difficult to draw paleoecological interpretations from the long bone microanatomy of pareiasaurs. Based on morphological, taphonomic and recent isotopic studies (see discussions in Canoville et al. 2014, Canoville and Chinsamy 2017, Rey et al. 2019 and references therein), these animals have been alternatively inferred as fully aquatic, amphibious or strictly terrestrial; the latter hypothesis is the current favored one (Benton et al. 2012, Canoville et al. 2014, Smith et al. 2015, Rey et al. 2019). However, the ecological signal contained in their limb bone microanatomy remains difficult to interpret. Indeed, in the limb bones studied to date (mostly stylopodial and zeugopodial elements), the medullary region is almost always infilled by a loose to dense spongiosa (Figure 18.4) and the weight-bearing bones (such as femur, humerus, tibia) tend to display an extensive spongiosa, with relatively thin compact cortices (e.g., Canoville and Chinsamy 2017, Boitsova et al. 2019, see also Figure 18.4A, B). This overall bone inner architecture is due to an imbalance between resorption and reconstruction (in favor of resorption) during ontogeny, which results in the progressive transformation of the deep periosteal cortices into a spongiosa. As Canoville and Chinsamy (2017) discussed, this bone organization is reminiscent of the long bone microanatomy observed in pelagic marine tetrapods, such as extant whales and seals and even some extinct marine reptiles (e.g., Ricqlès and Buffrénil, 2001, Canoville and Laurin 2010). However, such a bone architecture is completely unusual for amphibious and terrestrial tetrapods (see Canoville et al. 2014 and Chapter 35).

The ontogeny of pareiasaurs is also challenging to infer because their bones often display intensive Haversian remodeling, at least in a part of the cortex, which obliterates some of the growth marks, as does the conversion of the deepest cortex into an extended secondary spongiosa. Accordingly, only a part of the lifespan may be histologically recorded in the long limb bone shafts of the adults. This situation is not unlike what has been observed in the long bones of large terrestrial turtles (Amprino and Godina 1947). So it may be that long-lived giant land tortoises offer some possible extant analogy to pareiasaur life history traits regarding growth and longevity. Histological, morphological (e.g., early fusion and ossification of girdle elements) and taphonomic observations suggest that these animals had a relatively short juvenile period compared to adulthood (Spencer and Lee 2000, Turner et al. 2015).

Pareiasaurs and captorhinids both became extinct in the Late Permian, but whereas captorhinid diversity decreased gradually in the Permian after a peak around the Kungurian (Brocklehurst 2017), pareiasaurs appear to have been among the major casualties of the end-Permian mass extinction event (Ward et al. 2005). Thus, it may be useful to compare their situations. In both cases one is dealing with medium- to large-sized terrestrial plant eaters, perhaps more or less associated with continental freshwaters but without any obvious adaptations to a clearly aquatic ecology. In both cases, bone histology suggests a long period of subadult and adult growth at low rates and probably an extended individual longevity. Those traits have been regarded, for the late captorhinid *Moradisaurus*, as expressing a "K" demographic strategy (Ricqlès 1979, 1980, 1983). We suggest that a generally similar situation may have existed among pareiasaurs. It is generally assumed that "K" strategists are successful in environments that are fairly stable on the very long run but are very sensitive to rapidly changing environmental situations, especially when the new situations become erratic and unpredictable at the short scales of ecological time. In such situations, the survivors appear to be the "r" strategists, with small body sizes, rapid growth, short longevity and fast population turnover (MacArthur and Wilson 1967, Pianka 1970). Thus, it may be that the optimal adaptation of late captorhinids and pareiasaurs to the Late Permian terrestrial ecosystems precisely spelled their demise at the time of the end-Permian crisis.

Procolophonids are the only parareptile clade and one of the (very) few vertebrate groups that survived the end-Permian extinction event. They then flourished and diversified during the Triassic and dispersed all across Pangaea (Cisneros 2008, Ruta et al. 2011). Studying their lifestyle and growth strategies through bone paleohistology may provide crucial data for understanding why this group survived such a cataclysmic event at the end of the Permian and prospered in the dry, unpredictable environmental conditions of the Early Triassic (Smith and Botha-Brink 2014), whereas most other aquatic and terrestrial vertebrates became extinct. Several studies hypothesized that specific lifestyle adaptations (i.e., [opportunistic] fossoriality) and/or growth strategies (i.e., fast growth, shortened development) enhanced survival of a few, yet taxonomically and morphologically diverse, tetrapod groups (sometimes called "disaster taxa") at the end of the Permian and beginning of the Triassic. These hypotheses have been supported by taphonomical, morphological and histological studies of several therapsid (Botha and Chinsamy 2005, Fernandez et al. 2013, Huttenlocker and Botha-Brink 2014, Botha-Brink et al. 2016, Botha-Brink 2017) and temnospondyl taxa (Fernandez et al. 2013, Canoville and Chinsamy 2015, McHugh 2015), but a rigorous statistical, comparative test of these hypotheses remains to be performed.

Published bone histological observations suggest that the Early Triassic members of South African procolophonoids (such as *Sauropareion anoplus* and *Procolophon trigoniceps*) had an unusual growth strategy (sustained growth without interruption) compared to geologically younger relatives (such as *Teratophon spinigenis*), which may have been advantageous for survival and diversification (Botha-Brink and Smith 2012). Moreover, morphological and taphonomical observations suggest that at least some procolophonoids were fossorial. These animals show anatomical characteristics of the skull and postcrania that suggest digging activities (deBraga 2003, MacDougall et al. 2013). Several specimens of procolophonid taxa such as *Procolophon* and *Teratophon* have often been collected in close association with burrow casts (Groenewald 1991, Botha-Brink and Smith 2012). Studies have shown that burrowing and digging tetrapods often exhibit thicker limb bone walls than their nonfossorial terrestrial relatives (Magwene 1993, Nasterlack et al. 2012, Montoya-Sanhueza and Chinsamy 2017, Legendre and Botha-Brink 2018). The limb bone microanatomy of procolophonoids, i.e., relatively thick bone wall (see Figure 18.3C, D), and numerous Sharpey's fibers in the cortices implying strong muscle insertions, is congruent with taphonomical and morphological data and supports previous hypotheses that these animals were burrowers (Botha-Brink and Smith 2012).

VetBooks.ir

REFERENCES

Abel, O. 1912. *Grundzüge der Paleobiologie des Wirbeltiere*. Stuttgart: E. Schweizerbart'sche Verlagsbuchhandlung.

Abel, O. 1924. *Die Eroberungszüge der Wirbeltiere in die Meere der Vorzeit*. Iena: G. Fischer.

Alberch, P., et al. 1979. Size and shape in ontogeny and phylogeny. *Paleobiology* 5:296–317.

Amprino, R. and G. Godina. 1947. La struttura delle ossa nei vertebrti. Ricerche comparative negli amfibi e negli amnioti. *Comment. Pont. Acad. Sci.* 11: 329–467.

Benton, M. J., et al. 2012. Preservation of exceptional vertebrate assemblages in Middle Permian fluviolacustrine mudstones of Kotel'nich, Russia: stratigraphy, sedimentology, and taphonomy. *Palaeogeogr. Palaeoclimatol. Palaeoecol.* 319: 58–83.

Bertin, T. J., et al. 2018. Current perspectives on tooth implantation, attachment, and replacement in Amniota. *Front. Physiol.* 9:1630.

Bever, G., et al. 2015. Evolutionary origin of the turtle skull. *Nature* 525:239–242.

Bickelmann, C. and L. A. Tsuji. 2018. A case study of developmental palaeontology in *Stereosternum tumidum* (Mesosauridae, Parareptilia). *Foss. Rec.* 21:109–118.

Boitsova, E. A., et al. 2019. Bone histology of two pareiasaurs from Russia (*Deltavjatia rossica* and *Scutosaurus karpinskii*) with implications for pareiasaurian palaeobiology. *Biol. J. Linn. Soc.* 128:289–310.

Botha, J. and A. Chinsamy. 2005. Growth patterns of *Thrinaxodon liorhinus*, a non-mammalian cynodont from the Lower Triassic of South Africa. *Palaeontology* 48:385–394.

Botha-Brink, J. 2017. Burrowing in *Lystrosaurus*: preadaptation to a postextinction environment? *J. Vertebr. Paleontol.* 37: e1365080.

Botha-Brink, J. and R. M. H. Smith. 2012. Palaeobiology of Triassic procolophonids, inferred from bone microstructure. *C. R. Palevol.* 11:419–433.

Botha-Brink, J., et al. 2016. Breeding young as a survival strategy during Earth's greatest mass extinction. *Sci. Rep.* 6:24053.

Brocklehurst, N. 2016. Rates and modes of body size evolution in early carnivores and herbivores: a case study from Captorhinidae. *PeerJ* 4:e1555.

Brocklehurst, N. 2017. Rates of morphological evolution in Captorhinidae: an adaptive radiation of Permian herbivores. *PeerJ* 5:e3200.

Broili, F. 1904. Permische Stegocephalen und Reptilien aus Texas. *Palaeontographica* 51:1–120.

Buffrenil, V. de and J.-M. Mazin. 1989. Bone histology of *Claudiosaurus germaini* (Reptilia, Claudiosauridae) and the problem of pachyostosis in aquatic vertebrates. *Hist. Biol.* 2:311–322.

Cabreira, S. F. and J.C. Cisneros. 2009. Tooth histology of the parareptile *Soturnia caliodon* from the Upper Triassic of Rio Grande do Sul, Brazil. *Acta Palaeontol. Pol.* 54:743–748.

Caldwell, M. W., et al. 2003. Histology of tooth attachment tissues in the late Cretaceous mosasaurid *Platecarpus*. *J. Vertebr. Paleontol.* 23:622–630.

Canoville, A. and M. Laurin. 2010. Evolution of humeral microanatomy and lifestyle in amniotes, and some comments on paleobiological inferences. *Biol. J. Linn. Soc.* 100:384–406.

Canoville, A. and A. Chinsamy. 2015. Bone microstructure of the stereospondyl *Lydekkerina huxleyi* reveals adaptive strategies to the harsh post Permian-extinction environment. *Anat. Rec.* 298:1237–1254.

Canoville A. and A. Chinsamy. 2017. Bone microstructure of pareiasaurs (Parareptilia) from the Karoo Basin, South Africa: implications for growth strategies and lifestyle habits. *Anat. Rec.* 300:1039–1066.

Canoville, A., et al. 2014. Insights into the habitat of Middle Permian pareiasaurs (Parareptilia) from preliminary isotopic analyses. *Lethaia* 47:266–274.

Chiari, Y., et al. 2012. Phylogenomic analyses support the position of turtles as the sister group of birds and crocodiles (Archosauria). *BMC Biol.* 10:65.

Cisneros, J. C. 2008. Phylogenetic relationships of procolophonid parareptiles with remarks on their geological record. *J. Syst. Palaeontol.* 6:345–366.

DeBraga, M. 2003. The postcranial skeleton, phylogenetic position, and probable lifestyle of the Early Triassic reptile *Procolophon trigoniceps*. *Can. J. Earth Sci.* 40:527–556.

DeBraga, M. and O. Rieppel. 1997. Reptile phylogeny and the interrelationships of turtles. *Zool. J. Linn. Soc.* 120:281–354.

DeBraga, M., et al. 2019. A new captorhinid from the Permian cave system near Richards Spur, Oklahoma and the taxic diversity of *Captorhinus* at this locality. *Front. Earth Sci.* 7:112.

du Toit, A. L. 1927. *A geological comparison of South America with South Africa*. Washington, D.C: Carnegie Institute Publications.

Enlow, D. H. 1969. The bone of reptiles. In *Biology of the Reptilia*. Vol Ia, ed. C. Gans, and A. d'A Bellairs, 45–80. London: Academic Press.

Enlow, D. H. and S. O. Brown. 1957. A comparative histological study of fossil and recent bones tissues (part II). *Texas J. Sci.* 9:189–214.

Evans, S. E. 1988. The early history and relationships of the Diapsida. In *The Phylogeny and Classification of the Tetrapods, Volume 1: Amphibians, Reptiles, Birds*, ed. M. J. Benton, 221–260. Oxford, UK: Clarendon Press.

Falconnet, J. and J.-S. Steyer. 2007. Revision, osteology and locomotion of *Aphelosaurus*, an enigmatic reptile from the Lower Permian of France. *J. Morphol.* 268: 1071–1072.

Fernandez, V., et al. 2013. Synchrotron reveals Early Triassic odd couple: injured amphibian and aestivating therapsid share burrow. *PLoS One* 8:e64978.

Ford, D. P. and R. B. Benson. 2020. The phylogeny of early amniotes and the affinities of Parareptilia and Varanopidae. *Nat. Ecol. Evol.* 4:57–65.

Gaengler, P. 2000. Evolution of tooth attachment in lower vertebrates to tetrapods. In *Development, Function and Evolution of Teeth*, ed. M. F. Teaford, M. M. Smith, and M. W. J. Ferguson, 173–185. Cambridge, UK: Cambridge University Press.

Gauthier, J., et al. 1988 The early evolution of the Amniota. In *The Phylogeny and Classification of the Tetrapods, Volume 1: Amphibians, Reptiles, Birds*, ed. M. J. Benton, 103–55. Oxford, UK: Clarendon Press.

Groenewald, G. H. 1991. Burrow casts from the *Lystrosaurus-Procolophon* Assemblage-zone, Karoo Sequence, South Africa. *Koedoe* 34:13–22.

Haridy, Y., et al. 2017. The lower jaw of the Early Permian parareptile *Delorhynchus*, first evidence of multiple denticulate coronoids in a reptile. *Zool. J. Linn. Soc.* 184:791–803.

Houssaye, A., et al. 2016. Adaptive patterns in aquatic amniote bone microanatomy—more complex than previously thought. *Integr. Comp. Biol.* 56:1349–1369.

Hugall, A. F., et al. 2007. Calibration choice, rate smoothing, and the pattern of tetrapod diversification according to the long nuclear gene Rag-1. *Syst. Biol.* 56:543–63.

Huttenlocker, A. K. and J. Botha-Brink. 2014. Bone microstructure and the evolution of growth patterns in Permo-Triassic therocephalians (Amniota, Therapsida) of South Africa. *PeerJ* 2:e325.

Klein, N., et al. 2019. Microanatomy and growth of the mesosaurs *Stereosternum tumidum* and *Brazilosaurus sanpauloensis* (Reptilia , Parareptilia). *Foss. Rec.* 22: 91–110.

Kriloff, A., et al. 2008. Evolution of bone microanatomy of the tetrapod tibia and its use in palaeobiological inference. *J. Evol. Biol.* 21:807–826.

Laurin, M. and G. H. Piñeiro. 2017. A reassessment of the taxonomic position of mesosaurs, and a surprising phylogeny of early amniotes. *Front. Earth Sci.* 5:1–13.

Laurin, M. and G. Piñeiro. 2018. Response: commentary: a reassessment of the taxonomic position of mesosaurs, and a surprising phylogeny of early amniotes. *Front. Earth Sci.* 6:1–9.

Laurin, M. and R. R. Reisz. 1995. A reevaluation of early amniote phylogeny. *Zool. J. Linn. Soc.* 113:165–223.

LeBlanc, A. R. H. and R. R. Reisz. 2013. Periodontal ligament, cementum, and alveolar bone in the oldest herbivorous tetrapods, and their evolutionary significance. *PLoS One* 8:e74697.

LeBlanc, A. R. H. and R. R. Reisz. 2015. Patterns of tooth development and replacement in captorhinid reptiles: a comparative approach for understanding the origin of multiple tooth rows. *J. Vertebr. Paleontol.* 35:e919928.

Lee, M. S. Y. 1995. Historical burden in systematics and the interrelationships of 'parareptiles'. *Biol. Rev.* 70:459–547.

Lee, M. S. Y. 1997a. A taxonomic revision of pareiasaurian reptiles: implications for Permian terrestrial palaeoecology. *Mod. Geol.* 21:231–298.

Lee, M. S. Y. 1997b. Pareiasaur phylogeny and the origin of turtles. *Zool. J. Linn. Soc.* 120:197–280.

Legendre, L. J. and J. Botha-Brink. 2018. Digging the compromise: investigating the link between limb bone histology and fossoriality in the aardvark (*Orycteropus afer*). *PeerJ* 6: e5216.

Looy, C. V., et al. 2016. Biological and physical evidence for extreme seasonality in central Permian Pangea. *Palaeogeogr. Palaeoclimatol. Palaeoecol.* 451:210–226.

Lu, B., et al. 2013. Using genes as characters and a parsimony analysis to explore the phylogenetic position of turtles. *PLoS One* 8:e79348.

Lyson, T. R., et al. 2012. MicroRNAs support a turtle + lizard clade. *Biol. Lett.* 8:104–107.

Lyson, T. R., et al. 2013. Evolutionary origin of the turtle shell. *Curr. Biol.* 23:1113–1119.

Lyson, T. R., et al. 2014. Origin of the unique ventilatory apparatus of turtles. *Nat. Commun.* 5:5211.

MacArthur, R. H. and E. O. Wilson. 1967. *The Theory of Island Biogeography.* Princeton, NJ: Princeton University Press.

MacDougall, M. J. and S. P. Modesto. 2011. New information on the skull of the Early Triassic parareptile *Sauropareion anoplus*, with a discussion of tooth attachment and replacement in procolophonids. *J. Vertebr. Paleontol.* 31:270–278.

MacDougall, M. J., et al. 2013. The postcranial skeleton of the Early Triassic parareptile *Sauropareion anoplus*, with a discussion of possible life history. *Acta Palaeontol. Pol.* 58:737–750.

MacDougall, M. J., et al. 2014. Plicidentine in the Early Permian parareptile *Colobomycter pholeter*, and its phylogenetic and functional significance among coeval members of the clade. *PLoS One* 9:e96559.

MacDougall, M. J., et al. 2018. Commentary: a reassessment of the taxonomic position of mesosaurs, and a surprising phylogeny of early amniotes. *Front. Earth Sci.* 6:99.

Macedo Farias, B. D. et al. 2019. Bone microstructure of the pareiasaur *Provelosaurus americanus* from the Middle Permian of southern Brazil. *Hist. Biol.* 1–12.

Magwene, P. M. 1993.What's bred in the bone: histology and cross-sectional geometry of mammal-like reptile long bones. *Evidence of Changing Physiological and Biomechanical Demands*. M.Sc. diss., Harvard University.

Marjanović, D. and M. Laurin. 2019. Phylogeny of paleozoic limbed vertebrates reassessed through revision and expansion of the largest published relevant data matrix. *PeerJ* 6:e5565.

Maxwell, E. E., et al. 2011. The structure and phylogenetic distribution of amniote plicidentine. *J. Vertebr. Paleontol.* 31:553–561.

Maxwell, E. E., et al. 2012. Tooth histology, attachment, and replacement in the Ichthyopterygia reviewed in an evolutionary context. *PalZ* 86:1–14.

McHugh, J. B. 2015. Paleohistology of *Micropholis stowi* (Dissorophoidea) and *Lydekkerina huxleyi* (Lydekkerinidae) humeri from the Karoo Basin of South Africa, and implications for bone microstructure evolution in temnospondyl amphibians. *J. Vertebr. Paleontol.* 35:e902845.

Modesto, S. P. 1998. New information on the skull of the Early Permian reptile *Captorhinus aguti*. *PaleoBios* 18:21–35.

Modesto, S. P. 1999. Observations on the structure of the Early Permian reptile *Stereosternum tumidum* Cope. *Palaeont. Afr.* 35:7–19.

Modesto, S. P. 2006. The cranial skeleton of the Early Permian aquatic reptile *Mesosaurus tenuidens*: implications for relationships and palaeobiology. *Zool. J. Linn. Soc.* 146:345–368.

Modesto, S. P. 2010. The postcranial skeleton of the aquatic parareptile *Mesosaurus tenuidens* from the Gondwanan Permian. *J. Vertebr. Paleontol.* 30:1378–1395.

Modesto, S. P., et al. 2007. The skull and the palaeoecological significance of *Labidosaurus hamatus* a captorhinid reptile from the Lower Permian of Texas. *Zool. J. Linn. Soc.* 149:237–262.

Modesto, S. P., et al. 2014. The captorhinid reptile *Captorhinikos valensis* from the lower Permian Vale Formation of Texas and the evolution of herbivory in eureptiles. *J. Vertebr. Paleontol.* 34:291–302.

Modesto S.P., et al. 2018. The vertebrate fauna of the Upper Permian of Niger—X. The mandible of the captorhinid reptile *Moradisaurus grandis*. *J. Vertebr. Paleontol.* 38: e1531877.

VetBooks.ir

Montoya-Sanhueza, G. and A. Chinsamy. 2017. Long bone histology of the subterranean rodent *Bathyergus suillus* (Bathyergidae): ontogenetic pattern of cortical bone thickening. *J. Anat.* 230:203–233.

Nasterlack, T., et al. 2012. New insights into the biology of the Permian genus *Cistecephalus* (Therapsida, Dicynodontia). *J. Vertebr. Paleontol.* 32:1396–1410.

Nopcsa, F. von and E. Heidsieck. 1934. Uber eine pachyostotische Rippe aus der Kreide Rügens. *Acta Zool.* 14: 431–455.

Nuñez Demarco, P., et al. 2018. Was *Mesosaurus* a fully aquatic reptile? *Front. Ecol. Evol.* 6:109.

Oelofsen, B. W. and D. C. Araujo. 1987. *Mesosaurus tenuidens* and *Stereosternum tumidum* from the Permian Gondwana of both southern Africa and South America. *S. Afr. J. Sci.* 83:370–372.

O'Keefe, F. R., et al. 2005. The vertebrate fauna of the Upper Permian of Niger—III. Ontogeny and morphology of the hindlimb of *Moradisaurus grandis* (Reptilia: Captorhinidae). *J. Vertebr. Paleontol.* 25:309–319.

Olson, E. C. 1947. The family Diadectidae and its bearing on the classification of reptiles. *Fieldiana Geol.* 11:1–53.

Olson, E. C. 1970. New and little known genera and species of vertebrates from the Lower Permian of Oklahoma. *Fieldiana Geol.* 18:359–434.

Padian, K., et al. 2004. Growth in small dinosaurs and pterosaurs: the evolution of archosaurian growth strategies. *J. Vertebr. Paleontol.* 24:555–571.

Peabody, Fr. E. 1961. Annual growth zones in living and fossil vertebrates. *J. Morphol.* 108:11–62.

Pearson, M. R., et al. 2013. Reconstructing the diversity of early terrestrial herbivorous tetrapods. *Palaeogeogr. Palaeoclimatol. Palaeoecol.* 372:42–49.

Pianka, E. R. 1970. On r and K selection. *Am. Nat.* 104:592–597.

Piñeiro, G., et al. 2012. Unusual environmental conditions preserve a Permian mesosaur-bearing konservat-lagerstätte from Uruguay. *Acta Palaeont. Pol.* 57:299–318.

Pretto, F. A., et al. 2014. Tooth microstructure of the Early Permian aquatic predator *Stereosternum tumidum*. *Acta Palaeontol. Pol.* 59:125–133.

Renesto, S., et al. 2010. The taxonomy and paleobiology of the Late Triassic (Carnian-Norian: Adamanian-Apachean) drepanosaurs (Diapsida: Archosauromorpha: Drepanosauromorpha). *Bull. N. M. Mus. Nat. Hist. Sci.* 46:1–81.

Rey, K., et al. 2019. Oxygen isotopes and ecological inferences of Permian (Guadalupian) tetrapods from the main Karoo Basin of South Africa. *Palaeogeogr. Palaeoclimatol. Palaeoecol.* 538:109485.

Richards, E. J. 2016. *The ontogenetic osteohistology of the eureptile Captorhinus aguti (Reptilia, Captorhinidae) and the community histology of the Early Permian fissure-fill fauna Dolese Quarry, Richards Spur, Oklahoma*. Master of Sci. Univ. of Toronto, p. 60.

Richards, C., et al. 2007. The mandible of *Moradisaurus grandis* (Reptilia: Captorhinidae) and its implications for herbivory in moradisaurines. *J. Vertebr. Paleontol.* 27:134A.

Ricqlès, A. de. 1974. Recherches paléohistologiques sur les os longs des tétrapodes V.-Cotylosaures et Mésosaures. *Ann. Paléontol.* 60:171–216.

Ricqlès, A. de. 1976. On bone histology of fossil and living reptiles, with comments on its functional and evolutionary significance. *Linn. Soc. Symp. Ser.* 3:123–151.

Ricqlès, A. de. 1979. Relations entre structures histologiques, ontogenèse, stratégies démographiques et modalités évolutives: le cas des reptiles captorhinomorphes et des stégocéphales temnospondyles. *C.R. Acad. Sci. Paris. Ser. II* 288:1147–1150.

Ricqlès, A. de. 1980. Croissance périodique, ontogenèse, phylogenèse et stratégies démographiques: le cas des reptiles captorhinomorphes. *Bull. Soc. Zool. France* 105:363–369.

Ricqlès, A. de. 1983. Documentation paléontologique, interprétation des données et mécanique évolutive: étude d'un castype "moyen", les Captorhinidés. In *Modalités, rythmes et mécanismes de l'évolution biologique*, ed. J. Chaline, 200–209. Dijon, France: Colloque International, CNRS.

Ricqlès, A. de. 1984. Remarques systématiques et méthodologiques pour servir à l'étude de la famille des Captorhinidés. *Ann. Paléontol.* 70:1–39.

Ricqlès, A. de and J. R. Bolt. 1983. Jaw growth and tooth replacement in *Captorhinus aguti* (Reptilia, Captorhinomorpha): a morphological and histological analysis. *J. Vertebr. Paleontol.* 3:7–24.

Ricqlès, A. de and V. Buffrenil de. 2001. Bone histology, heterochronies and the return of tetrapods to life in water: Where are we? In *Secondary Adaptation of Tetrapods to Life in Water*, ed. J. M. Mazin, and V. de Buffrénil, 289–310. Munchen: Pfeil Verlager.

Ricqlès, A. de and P. Taquet. 1982. La faune de vertébrés du Permien supérieur du Niger 1 - Le captorhinomorphe *Moradisaurus grandis* (Reptilia, Cotylosauria) - le crâne. *Ann. Paléontol.* 68:33–106.

Rieppel, O. and R. R. Reisz. 1999. The origin and early evolution of turtles. *Annu. Rev. Ecol. Syst.* 30:1–22.

Ruta, M. and M. I. Coates. 2007. Dates, nodes and character conflict: addressing the lissamphibian origin problem. *J. Syst. Palaeontol.* 5:69–122.

Ruta, M., et al. 2011. Amniotes through major biological crises: faunal turnover among parareptiles and the end-Permian mass extinction. *Palaeontology* 54:1117–1137.

Sander, P. M. 1999. The microstructure of reptilian tooth enamel: terminology, function and phylogeny. *Münch. Geowiss. Abh. A Geol. Paläontol.* 38:1–102.

Schaumberg, G., et al. 2007. New information on the anatomy of the Late Permian gliding reptile *Coelurosauravus*. *PalZ* 81:160–173.

Scheyer, T. M. and P. M. Sander. 2009. Bone microstructures and mode of skeletogenesis in osteoderms of three pareiasaur taxa from the Permian of South Africa. *J. Evol. Biol.* 22:1153–1162.

Scheyer, T. M., et al. 2010. Developmental palaeontology of Reptilia as revealed by histological studies. *Sem. Cell Dev. Biol.* 21:462–470.

Schmidt, D. T. and A. Kiel. 1971. *Polarizing microscopy of dental tissues*. Oxford, UK: Pergamon Press.

Smith, R., et al. 2012. Therapsid biodiversity patterns and paleoenvironments of the Karoo Basin, South Africa. In: *Forerunners of Mammals: Radiation, Histology, Biology*, ed. A. Chinsamy-Turan, 31–62. Bloomington, IN: Indiana University Press.

VetBooks.ir

Smith, R. M. and J. Botha-Brink. 2014. Anatomy of a mass extinction: sedimentological and taphonomic evidence for drought-induced die-offs at the Permo-Triassic boundary in the main Karoo Basin, South Africa. *Palaeogeogr. Palaeoclimatol. Palaeoecol*. 396:99–118.

Smith, R. M., et al. 2015. Sedimentology and vertebrate taphonomy of the Moradi Formation of northern Niger: a Permian wet desert in the tropics of Pangaea. *Palaeogeogr. Palaeoclimatol. Palaeoecol*. 440:128–141.

Spencer, P. S. and M. S. Y. Lee. 2000. A juvenile *Elginia* and early growth in pareiasaurs. *J. Paleontol*. 74:1191–1195.

Stein, M., et al. 2013. Long bone histology and growth patterns in ankylosaurs: implications for life history and evolution. *PLoS One* 8:e68590.

Tsuji, L. A. 2011. Evolution, morphology and paleobiology of the Pareiasauria and their relatives (Amniota: Parareptilia). PhD Dissertation.

Tsuji, L. A., et al. 2015. The Permian and Triassic parareptiles of Tanzania and Zambia: Review of diversity and new life history insights provided by osteohistology. *J. Vertebr. Paleontol*. 35(supplement):227.

Turner, M. L., et al. 2015. The vertebrate fauna of the upper Permian of Niger—IX. The appendicular skeleton of *Bunostegos akokanensis* (Parareptilia: Pareiasauria). *J. Vertebr. Paleontol*. 35:e994746.

Van den Brandt, M. J., et al. 2020. Cranial morphology and phylogenetic relationships of the Middle Permian pareiasaur *Embrithosaurus Schwarzi* from the Karoo Basin of South Africa. *Zool. J. Linn. Soc*. 188:202–241.

Vaughn, P. P. 1955. The Permian reptile *Araeoscelis* restudied. *Bull. Mus. Comp. Zool*. 113:305–467.

Villamil, J., et al. 2016. Optimal swimming speed estimates in the Early Permian mesosaurid *Mesosaurus tenuidens* (Gervais 1867) from Uruguay. *Hist. Biol*. 28:963–971.

Ward, P. D., et al. 2005. Abrupt and gradual extinction among Late Permian land vertebrates in the Karoo Basin, South Africa. *Science* 307:709–714.

Warren, J. W. 1963. *Growth-Zones in the Skeleton of Recent and Fossil Vertebrates*. Dissert, LA: University of California.

VetBooks.ir

19

Testudines

Torsten M. Scheyer and Ignacio A. Cerda

CONTENTS

Introduction 385
Phylogenetic Position and Anatomical Peculiarities 385
Early Histological Studies 386
An Overview of Recent Histological Studies 386
Skeletal Microstructures in Turtles 387
Endoskeletal Elements 387
Scleral Ossicles 389
Shell Bones and Osteoderms 389
Preliminary Remarks 389
The General Construction of Turtle Shell Bones 389
The Plywood-Like Pattern of Soft-Shelled Turtles 389
External Ornamentation of Shell Bones 393
Sutural Growth of Shell Bones 393
Ossicles of the Secondary Epithecal Shell of Dermochelyidae 393
Osteocytes and Osteocyte Lacunae 393
Accessory Osteoderms and Ossicles 394
Summary and Outlook 394
Institutional Abbreviations 394
Acknowledgments 394
References 394

Introduction

Phylogenetic Position and Anatomical Peculiarities

Testudines, comprising both the aquatic and semiaquatic turtles and the terrestrial tortoises (i.e., Testudinidae) are, due to their unique body armor in the form of a shell, among the most recognizable tetrapods living today. Whereas Testudines refers to the crown group, Testudinata includes also stem taxa such as the Late Triassic terrestrial forms *Proganochelys quenstedti* and *Proterochersis robusta* from Europe, *Palaeochersis talampayensis* and the enigmatic *Waluchelys cavitesta* from South America (Fraas 1913; Gaffney 1990; Joyce et al. 2013; Rougier et al. 1995; Sterli et al. 2007, 2020), as well as the more aquatic forms *Odontochelys semitestacea* from South China and *Pappochelys rosinae* from Germany (Li et al. 2008; Schoch and Sues 2015, 2018). In the following, the general term "turtle" is used to refer to the whole group of Testudinata/Testudines rather than reflecting habitat preferences.

Based on their skull and neck retraction system, crown turtles are divided into two groups (e.g., Pereira et al. 2017), the Cryptodira or "hidden-necked" turtles, which can usually withdraw their necks and heads into the shell, and the Pleurodira or "side-necked" turtles, which put their head and neck under the rim of the shell. The origins and evolutionary history of this peculiar neck and head protection system involving different shell parts is still an active field of research (e.g., Anquetin et al. 2017; Joyce and Sterli 2012; Werneburg et al. 2015).

In contrast to other armored tetrapods such as armadillos or crocodylians, the turtle's shell cannot simply be removed or shed to reveal the underlying endoskeleton of the animal. This is due to the unique incorporation of parts of the axial and appendicular skeleton into the turtle shell (Zangerl 1969). The shell consists of a dorsal domed part, the carapace and a ventral part, the flattened plastron; both parts are usually connected by a bony bridge. In the typical modern turtle body plan, the bony shell is covered by an alternate set of keratinous scutes, although a few groups independently lost the scutes and carry a leathery skin instead, such as the soft-shelled turtles, Trionychidae, and the giant marine leatherback turtle, *Dermochelys coriacea* (e.g., Frazier et al. 2005; Meylan 1987; Sánchez-Villagra et al. 2009; Scheyer et al. 2007; Zangerl 1969). *D. coriacea*

VetBooks.ir

is the last surviving representative of the Dermochelyidae, a group of marine turtles in which the primary "thecal" shell was largely reduced to a few bony remnants, while a secondary, somewhat flexible mosaic "epithecal" shell, composed of hundreds of polygonal ossicles, evolved (e.g., Bever and Joyce 2005; Chen et al. 2015; Delfino et al. 2013; Frazier et al. 2005; Völker 1913; Wood et al. 1996).

There is a general consensus that the dorsal carapace incorporates the ribs in the costal plates and the vertebral neural arches in the neural series, whereas the ventral plastron includes part of the shoulder girdle (i.e., clavicles = epiplastra; interclavicle = entoplastron) along with three to five paired bony elements, likely derived from the gastral apparatus of ancestral reptiles, the belly ribs, being incorporated into the paired hyo-, hypo-, and xiphiplastra (e.g., Burke 1989; Cebra-Thomas et al. 2005, 2007; Cherepanov 1984; Gilbert et al. 2007, 2008; Młynarski 1956; Nagashima et al. 2013; Rice et al. 2015, 2016; Zangerl 1939, 1969, and references therein). The remaining elements, the nuchal (neck plate), the peripheral series, the suprapygals and the pygal bone are dermal ossifications that do not incorporate endoskeletal elements. Thus, the shell of modern turtles consists of about 50 carapacial and nine plastral bones in total (not counting additional mesoplastral elements; e.g., Zangerl 1969). Stem-turtles, on the other hand, show higher disparity, especially in the number of shell elements (Szczygielski and Sulej 2019) and, potentially, in histology and microstructure of peripherals (Sterli et al. 2020).

There is an ongoing debate about the evolutionary origins of the turtle shell and where the turtles fit into the amniote tree of life (e.g., Hirasawa et al. 2013, 2015; Joyce 2015; Laurin and Piñeiro 2017; Lyson et al. 2010; MacDougall et al. 2018; Rieppel 2013; Scheyer et al. 2013; Werneburg and Sánchez-Villagra 2009, among others). Most recent molecular analyses favor a close relationship of turtles with archosaurs (e.g., Crawford et al. 2012; Field et al. 2014; Shaffer et al. 2013; Wang et al. 2013, but see Joyce 2015 for further discussion) and some new morphological studies also recover turtles within Eureptilia (despite their apparent anapsid skull configuration), although not necessarily close to archosaurs (e.g., Bever et al. 2015; Schoch and Sues 2015, 2018).

Early Histological Studies

Following Richard Owen's lead on the value of microscopic observations of fossil plants and teeth, reptile bones, including those of turtles, were sectioned in the first comparative histological and anatomical studies during the 19th century (Aeby 1878; Quekett 1849a, b, 1855). The main aim was then to clarify relationships of extinct animal remains. One of the first turtle bones that was histologically sectioned was a toe bone (Quekett 1849b) of *Megalochelys atlas* (formerly *Colossochelys atlas*) from the Himalayas, India, the largest extinct tortoise discovered so far (Badam 1981). Shortly thereafter, sections (longitudinal and cross sections) of a humerus and carapace of the extant marine cheloniid eucryptodire *Chelonia mydas*, an ilium of the extant Galapagos giant tortoise *C. nigra* (then *Testudo elephantopus*) and a sectioned costal plate of a large indeterminate turtle were studied (Quekett 1849a, 1855).

Although focusing on details of vascular canal and bone cell lacunae distribution and diameter, Quekett (1849b) already recognized the similarity of the general organization of the turtle shell bone with that of tetrapod skull bones, namely a diploe framed by external and internal compact bone layers. This author also pointed out differences in the presence and number of Haversian canals (as parts of secondary osteons) compared, for example, to bones from mammals or birds. The numerous Haversian canals found in a carapace section of *Chelonia mydas* are also known from other marine turtles and were recently used in a large-scale comparative histological study including extant semiaquatic, marine and terrestrial turtles to elucidate the paleoecology of important stem-turtles such as the Late Triassic *Proganochelys quenstedti* and *Proterochersis robusta* from southern Germany (Scheyer and Sander 2007).

Quekett (1849b) noted that turtle short bones are usually solid, whereas long bones are either purportedly hollow or cancellous in the center. However, modern analyses indicate that turtle long bones are generally cancellous inside, most lacking a large central medullary cavity. Marine forms such as *Dermochelys coriacea* retain life-long hourglass-shaped endochondral bone cones extending proximally and distally from the bone growth center (Nakajima et al. 2014; Rhodin 1985; Rhodin et al. 1981). Aeby (1878) studied carapace bones from the plesiochelyid eucryptodire *Plesiochelys solodurensis* (Late Jurassic, Solothurn, Switzerland) and the emydid cryptodire *Emys* from the Molasse basin of Aarwangen ("Untere Süsswassermolasse"), Canton Bern, Switzerland. These histological descriptions were very brief and focused mainly on the infilling of the vascular system and bone cell lacunae (Aeby 1878).

An Overview of Recent Histological Studies

In recent decades, various histological approaches to estimate and determine age and growth rates have been carried out on turtle bones (e.g., Castanet 1986–1987, 1988; Castanet and Cheylan 1979; Chinsamy and Valenzuela 2008; Çiçek et al. 2016; Coles et al. 2001; Klinger and Musick 1992, 1995; Peters 1983; Snover and Hohn 2004; Turner Tomaszewicz et al. 2015; Zug and Glor 1998; Zug and Parham 1996; Zug et al. 1986; 2001). These studies, focusing mainly on long bone material or, in a few cases, on the scleral (i.e., sclerotic) ossicles of marine turtles such as *D. coriacea* and *Lepidochelys kempii* (Avens and Goshe 2007; Avens et al. 2009; Zug and Parham 1996), are invaluable for investigating population structure and conservation biology in these long-lived animals. With the exception of a few studies (e.g., Kälin, 1945; Meylan 1987; Suzuki 1963; Wallis 1928; Zangerl 1953, 1969), comparative data on the histology of turtle shell bone remained scarce in the literature until recently, with only occasional descriptions and illustrations of thin sections.

Paleohistological studies of turtle bones have proven useful for addressing several evolutionary and paleobiological issues including (1) shell origin and development (Delfino et al. 2013; Lyson et al. 2014, 2016; Scheyer and Sánchez-Villagra, 2007; Scheyer et al. 2007), (2) the origin of shell ornamentation

VetBooks.ir

(Buffrénil et al. 2016; Jannello et al. 2016; Scheyer et al. 2015), (3) paleoecology (Cerda et al. 2016; Scheyer and Sander 2007; Scheyer et al. 2014) and (4) systematics (Lyson et al. 2013; Nakajima et al. 2017; Scheyer 2009; Scheyer and Anquetin 2008; Scheyer et al. 2017). Given the importance of bone microstructure to these questions, histological descriptions have also been included in recent anatomical and systematic studies of extinct turtles (e.g., Cadena et al. 2013; de la Fuente et al. 2015; Gaffney et al. 2008; Jannello et al. 2018; Marmi et al. 2009; Pereyra et al. 2020; Pérez-García et al. 2013; Scheyer et al. 2015; Sena et al. 2020; Skutchas et al. 2017; Slater et al. 2011; Sterli et al. 2013), as well as in studies of ecological adaptations and lifestyle in extant and extinct turtles (e.g., Canoville and Laurin 2010; Germain and Laurin 2005; Kriloff et al. 2008; Nakajima et al. 2014; Rhodin 1985; Snover and Rhodin 2008).

Skeletal Microstructures in Turtles

Endoskeletal Elements

Most histological studies of the turtle endoskeleton have focused on long bones, mainly the humerus and the femur. Histological data from long bones have been commonly used to determine age (skeletochronology) and reconstruct growth curves in extant taxa, including marine (e.g., the giant leatherback *D. coriacea*, as well as *Caretta caretta*, *Lepidochelys olivacea*, and *Chelonia mydas*), terrestrial (e.g., the tortoises *Testudo hermanni*, *Gopherus agassizii, G. polyphemus*) and freshwater forms (e.g., the Arrau side-necked turtle *Podocnemis expansa*: Castanet and Cheylan 1979; Chinsamy and Valenzuela 2008; Coles et al. 2001; Curtin et al. 2008; Ehret 2007; Zug et al. 1986, 2001, 2006; Zug and Parham 1996). These contributions have mainly focused on counting growth marks in cortical bone, but otherwise have provided little information about additional aspects of the bone histology of these taxa (e.g., vascularization pattern, intrinsic fiber arrangement, distribution of Sharpey's fibers, etc.). With the exception of the study of *P. expansa* (Chinsamy and Valenzuela 2008), histological studies of turtle long bones have been conducted on decalcified samples; skeletochronological studies based on long bone histology of extinct taxa, such as *G. laticuneus* and *Stylemys nebrascensis* from the late Eocene/Oligocene White River Group, NW Nebraska, USA (Ehret 2007), are still scarce.

The relationship between turtle long bone microanatomy (i.e., compactness profile) and lifestyle adaptations was investigated by several authors, including Canoville and Laurin (2010), Germain and Laurin (2005), Kriloff et al. (2008) and Nakajima et al. (2014). These studies independently found that extant turtles show an atypical pattern in long bone microanatomy compared to other amniotes: they do not show a clear relationship between shaft compactness and habitat. This peculiarity may be linked to the unique body plan of turtles or to a phylogenetic effect. Based on whole element x-rays and CT-scan data, it was recently shown that the ossification center (see Chapter 9) is not located at midshaft, but slightly shifted toward the proximal epiphysis (Nakajima et al. 2014). This has implications for estimating the ideal plane of histological cross-sectional cuts, as well as for interpreting the vascularization and compactness at the growth center in histological and microanatomical studies, because midshaft sections might underestimate the growth record or might not provide the best bone compactness data for the bones.

In general, turtle long bones are compact with a central spongiosa and either no free medullary cavity or only a small one (Castanet 1985; Ricqlès et al. 2004), surrounded by a compact periosteal cortex mainly composed of annually deposited parallel-fibered bone tissue (e.g., Castanet 1985; Foote 1911, 1916; Ricqlès 1976). However, microanatomical and histological variation (linked to the outer shape of the bone) can be quite extensive, even for the same element in closely related species, as exemplified by the comparison of two limb bones in three land-living tortoises (Figure 19.1), two of which are closely related and share the same burrowing lifestyle. This question requires broader systematic and anatomic samples.

Vascularization is common in turtle long bones and usually consists of longitudinally or radially oriented simple primary vascular canals, the former often arranged in circular rows (e.g., Ricqlès et al. 2004; see also summary in Houssaye 2013). The density of vascular networks closely depends on the ecology of the taxa, with lower vascular density in terrestrial and semiaquatic turtles, and higher densities in fully aquatic forms. In open sea forms such as the giant leatherback *D. coriacea*, the cortical tissue of long bones might be completely spongy, with a very progressive transition from the innermost spongiosa to the peripheral cortical layers (e.g., Ricqlès et al. 2004). In addition, histological studies using longitudinal sections of long bone epiphyses have provided important data on growth dynamics in this highly specialized pelagic form. With the exception of *D. coriacea*, all living turtles have thin avascular layers of noncalcified cartilage in their epiphyses during growth (Haines 1942, 1969; Rhodin 1985). Conversely, in leatherbacks, the noncalcified epiphyseal cartilage remains thick throughout ontogeny with what was described as "transphyseal as well as perichondral vascularization through cartilage canals" (Rhodin 1985; Rhodin et al. 1981). These canals are considered to provide additional cartilage nutrition in relation to the extremely high growth rate of *Dermochelys*, which is unique not only for turtles but also for reptiles in general (Snover and Rhodin 2008). Vascularized cartilage on the epiphyseal surface is supposed to have occurred as well in the appendicular bones of the extinct giant sea turtle *Archelon ischyros*, from the Cretaceous Western Interior Seaway in North America (Rhodin et al. 1981).

Secondary remodeling can be observed in the form of large erosion cavities and/or secondary osteons in the deeper cortex (Ricqlès 1976; Ricqlès et al. 2004) and can be extensive. This can cause remodeling of most or all of the primary cortical bone (thus erasing the growth record), as shown by an old individual of the extinct *Gopherus* cf. *laticuneus*, from Nebraska, USA (Ehret 2007).

Although not focusing on Testudinata, data from long bone histology in some extant turtles have been included in several comparative studies of variation of bone growth rates in amniotes (e.g., Cubo et al. 2012; Legendre et al. 2012; Montes et al. 2010, 2007). Using *in vivo* fluorescent labeling, apposition rates

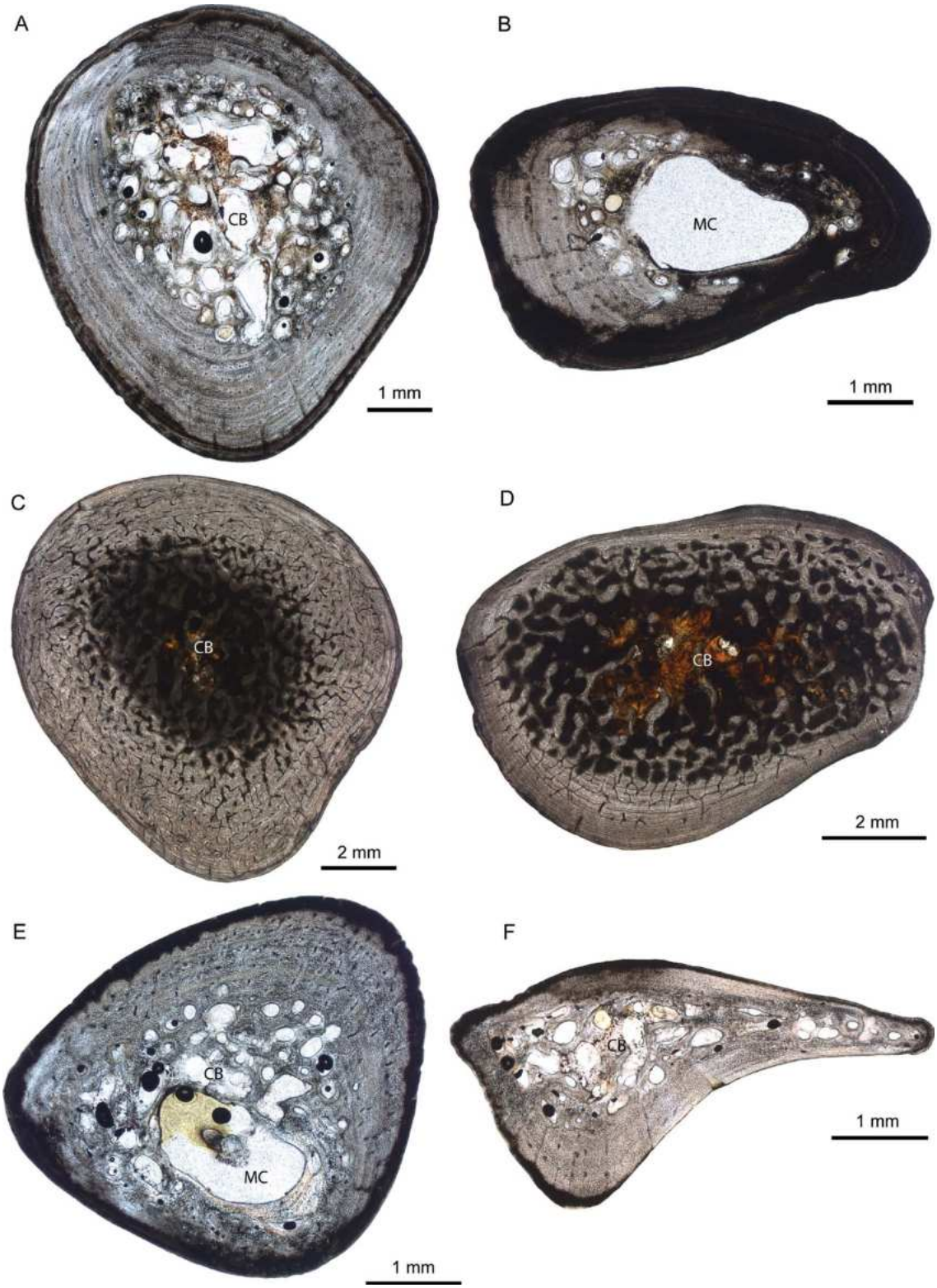


FIGURE 19.1 Microanatomy and histology of the humeri and ulnae of three extant tortoises (Cryptodira, Testudinidae), the North American desert tortoise *Gopherus agassizi* (A and B, USNM 560934), the Bolson tortoise/Mexican giant tortoise *G. flavomarginatus* (C and D, USNM 51357) and the Indian star tortoise *Geochelone elegans* (E and F, USNM 293724). Sections were taken at homologous points in the limb bones and all pictures are in normal transmitted light. A, C, and E, Left humeri. B, D, and F, Left ulnae. Note the shape variation, and the differences in microstructural organization and level of vascularization among these terrestrial taxa, with open medullary cavities being present in B and E. The periosteal cortices of all bones consist of lamellar-zonal bone. Vascularization consists of longitudinal and radially arranged primary canals in *G. agassizi* and *Geochelone elegans*, whereas the cortex of the *G. flavomarginatus* bones is extensively vascularized by a reticular network of primary canals. Abbreviations: CB, cancellous bone; MC, medullary cavity.

VetBooks.ir

(parameter *MAR*, as described in Chapter 10) on the femur shaft cortex, were measured by Cubo et al. (2012) for some taxa, including the North American pond slider *Trachemys scripta* (*MAR* = 3.55 µm*day^{-1} ± 1.59), the Chinese soft-shelled turtle *Pelodiscus sinensis* (1.53 µm*day^{-1} ± 0.41) and the Australo-Indonesian northern snake-necked turtle *Chelodina siebenrocki* (0.24 µm*day^{-1} ± 0.1). The rates of periosteal apposition in these turtles were found to be not only much lower than those of the fast-growing birds and mammals studied by Cubo et al. (2012; see also Kolb et al. 2015 for lower accretion rates assessments based on classical growth zone measurements in some cervid femora), but also lower than that observed in the larger reptiles sampled, such as *Crocodylus niloticus* (9.54 µm*day^{-1} ± 3.85), *Varanus exanthematicus* and *V. niloticus* (7.6/4.5 µm*day^{-1} ± 1.39). However, apposition rates in turtles proved to be similar to those of the small lacertid squamates *Lacerta vivipara* and *Podarcis muralis* (1.03/1.19 µm*day^{-1} ± 0.18/0.68). Based on this amniote data set, Cubo et al. (2012) found that appositional rates are significantly correlated with femur size, thus providing support for the generalization proposed by Case (1978) that larger taxa in a tetrapod clade show higher growth rates than their smaller relatives.

Scleral Ossicles

Skeletochronological studies using scleral ossicles of marine turtles (Avens and Goshe 2007; Avens et al. 2009; Zug and Parham 1996) indicate that these dermal bones have an appositional growth and are made of avascular lamellar-zonal bone tissue with well-defined annual zones and lines of arrested growth (LAGs). Haversian remodeling occurs in the primary tissue, along with large erosion cavities in the center. Compaction of growth marks at the lateral edges can be quite extensive, so the growth record is best visible and more complete in the narrow and wider ossicle tips (Avens et al. 2009).

Shell Bones and Osteoderms

Preliminary Remarks

The turtle shell is composed mainly of flat bones, i.e., the costals, keeled and nonkeeled neurals, and plastral elements, whereas the peripheral elements (including the nuchal and pygal bone) can be somewhat thickened, producing an enlarged interior cancellous bone area (Figure 19.2). After the initial descriptions of turtle shell bones in a few selected taxa (e.g., Kälin 1945; Meylan 1987; Suzuki 1963; Wallis 1928; Zangerl 1969), a comparative study of turtle shell bones over a broad taxonomic and systematic basis was performed by Scheyer (2007). This initial publication signaled a series of articles on several turtle clades (Scheyer and Anquetin 2008; Scheyer and Sánchez-Villagra 2007; Scheyer and Sander 2007; Scheyer et al. 2007, 2014, 2017).

More recently, other working groups have also contributed strongly to add to the database on shell bone histology in extant and extinct turtles (e.g., Buffrénil et al. 2016; Cadena et al. 2013; de la Fuente et al. 2015; Gaffney et al. 2008; Jannello et al. 2016; 2018; Marmi et al. 2009; Nakajima et al. 2017; Pérez-García et al. 2012, 2013; Skutchas et al. 2017; Slater et al. 2011; Sterli et al. 2013). While all these studies agree that the typical buildup of the turtle primary shell consists of a diploe, i.e., a central cancellous area framed by compact internal and external compact bone layers (Figure 19.2), details of the bone tissue types, vascularization and thickness of individual cancellous and compact layers vary among taxa. Furthermore, shell bones, like the endoskeletal elements (see Cubo et al. 2008), are influenced to various degrees by the phylogenetic position of the taxa and by structural and functional constraints. It thus appears that semiaquatic or aquatic lifestyles have profound effects on shell bone microanatomy and histology (e.g., Scheyer and Sander 2007; Pérez-García et al. 2012). In general, and compared to turtles that live in water, terrestrial turtle shells (and osteoderms: Figure 19.2A–C), including those of the stem turtles *Proganochelys quenstedti* and *Proterochersis robusta* (Scheyer and Sander 2007, Figure 2), show more compact diploes framed by well-developed cortices (often of similar thickness), low levels of cortical vascularization (up to avascular internal cortices), and a clear-cut difference in the compactness of cortical and cancellous bone tissues. Semiaquatic and fully aquatic turtles, in contrast, have less compact diploes, moderate to strong vascularization of the cortices and a frequent reduction in the thickness of the internal (deep) cortex (Figure 19.2D–F). In addition, open sea forms show high levels of cortical and cancellous bone tissue homogenization (Figure 19.2G, H; see also Scheyer and Sander 2007).

The General Construction of Turtle Shell Bones

The internal cortex (Figure 19.3A, B) of the primary turtle shell bones usually consists of parallel-fibered tissue (Scheyer and Sander 2007), although lamellar bone or a mixture of both tissues can also be present (Scheyer and Sánchez-Villagra 2007). The cancellous bone in the core area of shell bones can be primary or secondary, varying in the spongiosa of extant and extinct taxa (Figure 19.3A, B). Furthermore, the transition from the cancellous core to the external and internal compact cortices can be sharp or very gradual. The external cortices (Figure 19.3C–J), on the contrary, can differ from each other by the presence or absence of a cortical zonation, ornamentation patterns and bone fiber arrangement. In some cases, the observable structures are diagnostic for a turtle clade. The occurrence of interwoven structural fiber bundles (e.g., Figure 19.3D, F, J), a metaplastically ossified part of the dermis, in the external cortex in both cryptodirans and pleurodirans as well as in shelled stem-turtles (see e.g., Scheyer and Sander 2007), can be viewed as the plesiomorphic condition for the turtle crown.

The Plywood-Like Pattern of Soft-Shelled Turtles

Soft-shelled turtles (Trionychidae, Figure 19.4) have a unique, complex plywood-like system in their external shell cortices (e.g., Nakajima et al. 2017; Scheyer et al. 2007, 2012; Vlachos et al. 2015). Beneath the external ornamentation pattern of the trionychid shell bones, the plywood-like system has the

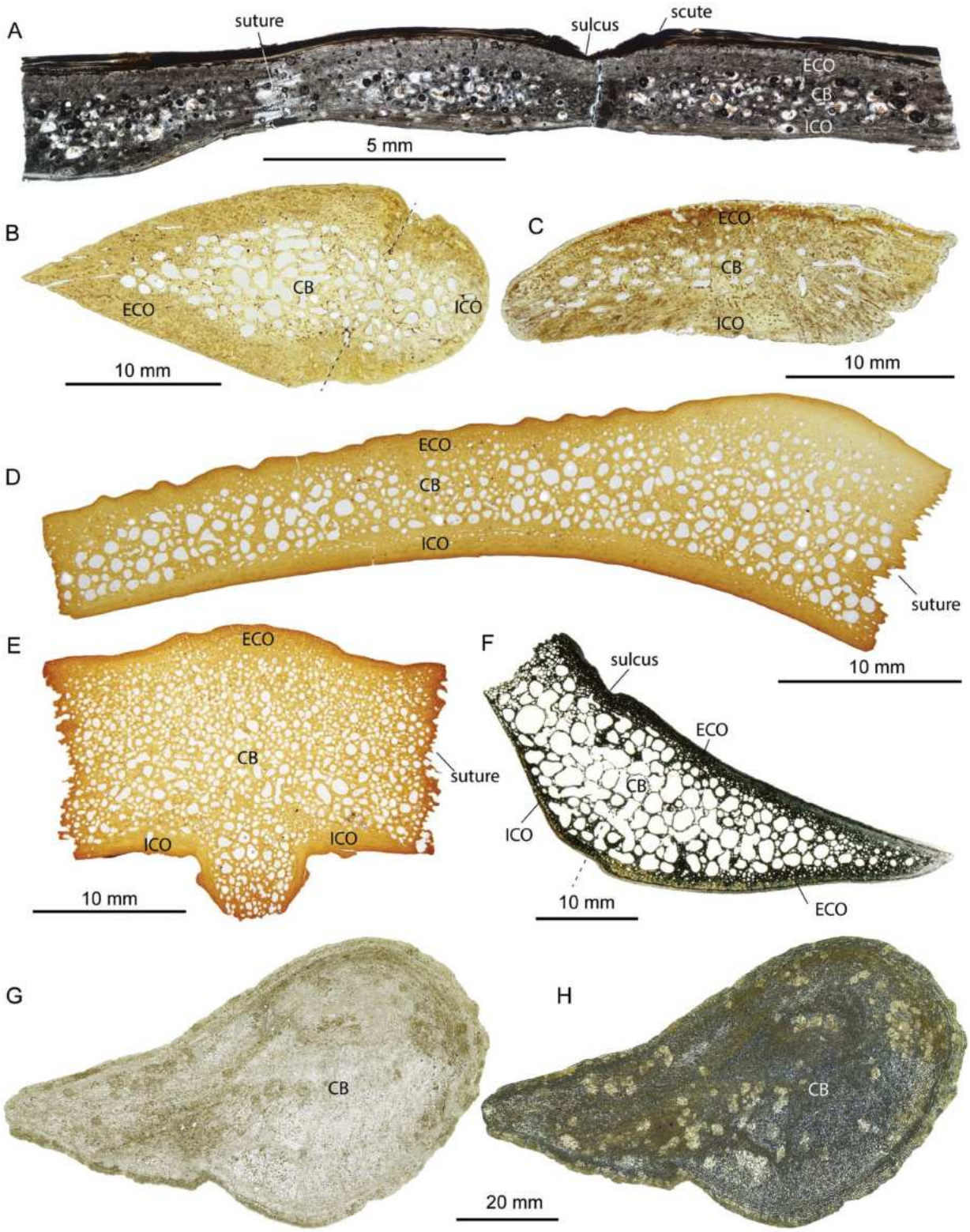


FIGURE 19.2 Microanatomy of selected shell bones and limb osteoderms of extant and extinct turtles. All pictures are viewed in normal transmitted light except H, which is in cross-polarized light. A, Cross section (drilled core) of partial neural and right costal bone of the extant Indian star tortoise *Geochelone elegans* (StIPB R561a). B and C, Osteoderms of the extinct giant tortoise cf. *Hesperotestudo* (flat: TMM 30967-1010.1, spiked: TMM 30967-1010.2) from the Pleistocene of North America. Dotted black lines indicate transition from external to internal cortices. D–F, Cross sections of shell elements of the pond slider *Trachemys scripta* (D, costal fragment ROM 34289; E, neural ROM 34287; F, peripheral ROM 33693; dotted black line indicates transition from external to internal cortex) from the Pleistocene of Florida, USA. G and H, Cross section of a peripheral bone (YPM 1783) of a giant marine turtle from the Late Cretaceous of North America (possibly from the Niobrara Fm., South Dakota, USA). Note overall tissue homogenization in the specimen. Abbreviations: CB, cancellous bone; ECO, external cortex; ICO, internal cortex.

VetBooks.ir

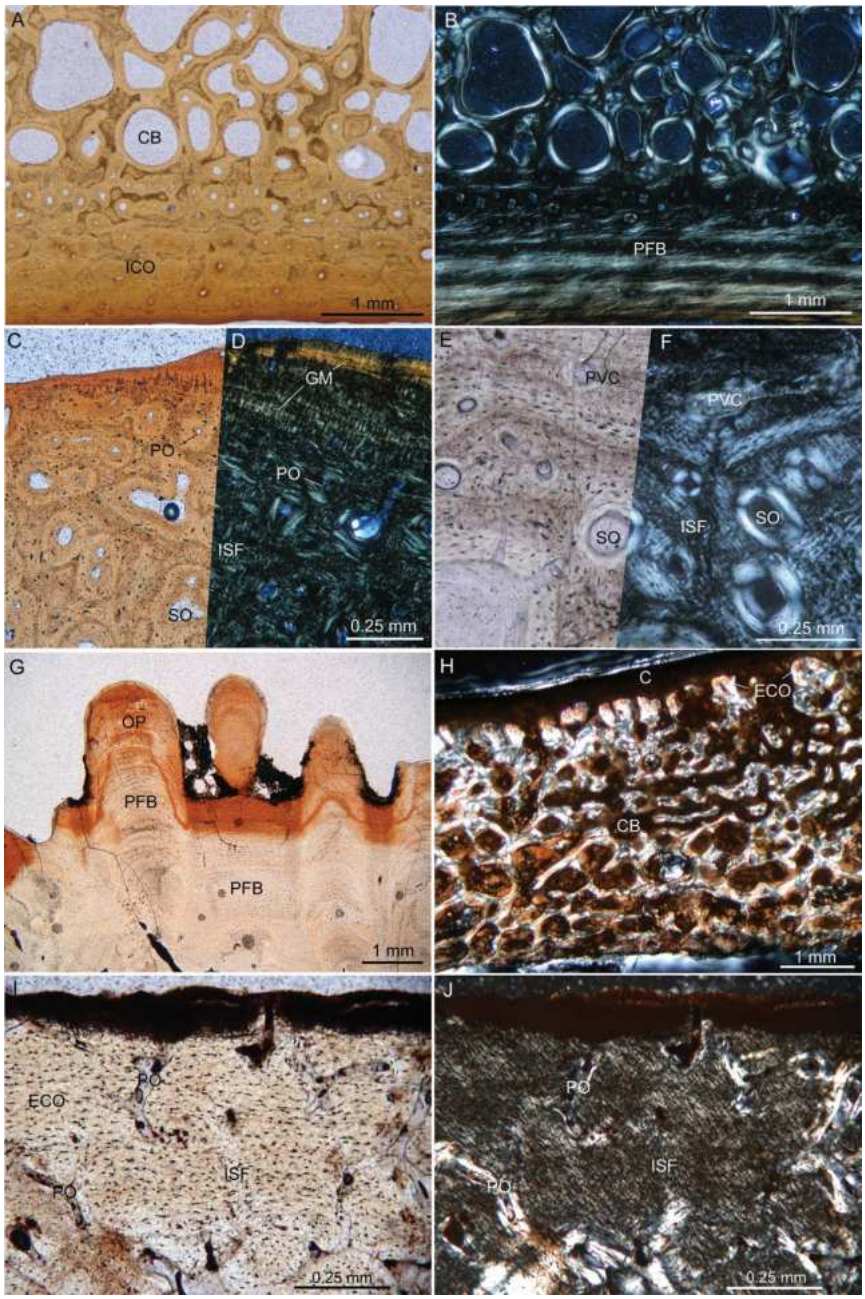


FIGURE 19.3 Histology of selected thecal and epithecal shell bones of extant and extinct turtles. Pictures in A, C, E, G and I are viewed in normal transmitted light, and B, D, F, H and J in cross-polarized light. A and B, Close-up of the internal cortex and cancellous bone of a costal fragment of the cryptodiran emydid *Trachemys scripta* (ROM 34289, see Figure 19.2D) from the Pleistocene of Florida, USA. The internal cortex consists of parallel-fibered bone, vascularized by small primary osteons. The trabeculae of the cancellous bone retain a primary bone core, and the intertrabecular spaces are mostly lined with lamellar bone. C and D, Close-up of the external cortex of the same specimen (ROM 34289). The external cortex is composed of a matrix of interwoven structural fiber bundles, vascularized by primary osteons and scattered secondary osteons. Growth marks (i.e., lines of arrested growth) are found only in the outer periphery of the cortex. E and F, Close-up of the external cortex of a costal fragment of the pleurodiran chelid *Emydura* sp. (UCMP V5762/57055) from the Miocene Etadunna Formation, South Australia. Although the cortical matrix is superficially similar to woven bone, it consists of metaplastically ossified fiber bundles of the dermis extending in different directions, which provide the tissue its structure. G, Outer, strongly ornamented part of the external cortex of a peripheral (RTMP 90.60.07) of the Helochelydridae (=Solemydidae) aff. *Naomichelys* sp. (perichelydian stem-turtles) from the Late Cretaceous Foremost Formation (Campanian) of Pinhorn Ranch, southeastern Alberta, Canada. The pillars and the surrounding cortical tissue are composed of almost avascular parallel-fibered bone. H, Cross section of a ridge ossicle (QM J73979) from the epithecal shell of an adult specimen of the extant cryptodiran leatherback turtle, *Dermochelys coriacea*. Note the overall spongy nature of the ridge ossicle. I and J, Cross section of the external cortex of a flat epithecal ossicle of the extinct cryptodiran leatherback turtle *Psephophorus* sp. (MB.R. 25.321) from the Miocene of Boom near Antwerp, Belgium. The cortex is composed of interwoven structural fiber bundles and vascularized by scattered and branching primary osteons. Abbreviations: C, epidermal cuticle; CB, cancellous bone; ECO, external cortex; GM, growth mark; ICO, internal cortex; ISF, interwoven structural fiber bundles; OP, ornamentation pattern; PFB, parallel-fibered bone; PO, primary osteon; PVC, primary vascular canal; SO, secondary osteon.

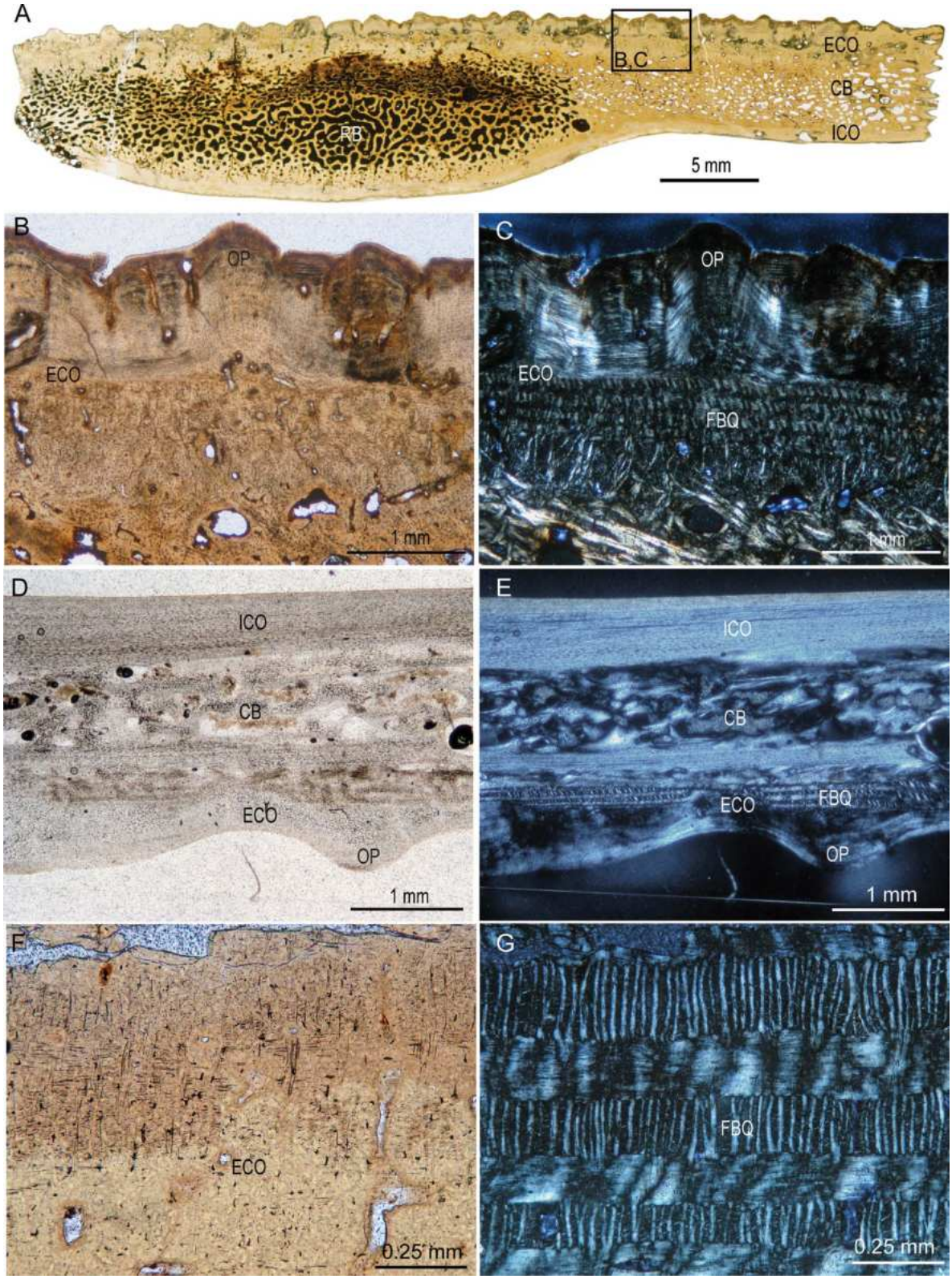


FIGURE 19.4 Histology of extant and extinct cryptodiran soft-shelled turtles (Trionychidae). Picture in A, B, D and F in normal transmitted light and C, E and G in cross-polarized light. A–C, Cross section of a costal fragment of plastomenine stem-trionychid *Helopanoplia* sp. (UCMP V87051/150193) from the Late Cretaceous Hell Creek Formation, Montana, USA. D and E, Longitudinal section of a right xiphiplastron of extant trionychine *Apalone ferox* (YPM13874), southeastern USA. F and G, Close-up of plywood-like structure in the external cortex of a costal fragment (longitudinal section) of trionychine *Trionyx* sp. (HLMD-Me 8084) from the Middle Eocene, Messel pit near Darmstadt, Germany. Note the peculiar pattern of fiber-bundle quadrangles forming the plies of the plywood-like system. Abbreviations: CB, cancellous bone; ECO, external cortex; FBQ, fiber-bundle quadrangles; ICO, internal cortex; OP, ornamentation pattern, RB, rib bulge.

VetBooks.ir

following hierarchical organization: (1) a stack of plies variable in thickness, in which each alternating ply is rotated; (2) the individual plies combine sets of alternating, horizontally and vertically arranged fiber bundle quadrangles and (3) each fiber bundle quadrangle consists of a set of parallel, tubular fiber bundles, in which the horizontal quadrangles contain more fiber bundles than the thinner vertically arranged quadrangles (e.g., Scheyer et al. 2007).

The posterior peripheral ossicles of the extant Asian flapshell turtle *Lissemys punctata* (together with its sister species *L. scutata*) have posterior peripheral ossicles, a peculiarity among trionychid turtles that otherwise have completely reduced the peripheral bones of their shell (Delfino et al. 2010). The posterior peripheral ossicles share the same histological features as other trionychid shell bones, including a diploe, the plywood-like structure in the external cortex reflecting metaplastically ossified soft tissue and parallel-fibered bone tissue in the internal cortex. These structural criteria, together with positional and transitional criteria (the latter involving ontogeny and phylogeny), suggested that the posterior peripheral ossicles of *Lissemys* are homologous to the "standard" peripherals of other turtles with a fully developed primary thecal shell (Delfino et al. 2010).

External Ornamentation of Shell Bones

Turtle shell bones can be smooth, show imprints of superficial integumentary vascular networks or have distinct ornamentation patterns (e.g., Figures 19.3G and 19.4A–C) with ridges and valleys, pockmarks or columns and tubercles of different heights. These patterns are often reflected in the bone cross sections (e.g., Jannello et al. 2016; Joyce et al. 2014; Scheyer and Anquetin 2008; Scheyer et al. 2007, 2015, 2017). Cross sections thus potentially reveal the shell formation through ontogeny, including the osteogenic processes involved in the differentiation and eventual changes of ornamental relief during growth (e.g., Buffrénil et al. 2016). One of the most peculiar forms of ornamentation is found in Helochelydridae (=Solemydidae), a group of perichelydian stem turtles that were distributed over Europe and North America between the Late Jurassic and the Late Cretaceous (Joyce 2017). Members of this group can build reticular patterns of raised ridges to low tubercles and, most peculiarly, tightly spaced high tubercles or columns, as in the North American *Naomichelys speciosa* (Scheyer et al. 2015). In cross sections, these tubercles are traceable throughout ontogeny (Figure 19.3G), having a growth center at the transition between an inner zone (consisting of coarse and irregularly interwoven fiber bundles) and an outer zone (more finely fibered) within the external cortex (e.g., Scheyer and Anquetin 2008; Scheyer et al. 2015).

Sutural Growth of Shell Bones

During shell growth, individual bones converge until their margins meet; an interdigitating tight suture is thus formed, consisting of a three-dimensional relief of bony pegs or laminae and respective sockets and grooves in the adjacent bones (Krauss et al. 2009; Meylan 1987). As long as these sutures stay open and the bones do not fuse, additional appositional growth of the shell bones remains possible (Zangerl 1969). In cross section (e.g., Figure 19.2A, D, E), suture zones display the same tissue as in the external cortex and the vascularization and growth marks can be traced from the external to the lateral plate margins as well. Sharpey's fibers extend at variable angles into the sutural bone, anchoring the two adjacent elements to each other (e.g., Chen et al. 2015; Pérez-García et al. 2013).

Ossicles of the Secondary Epithecal Shell of Dermochelyidae

The ossicles of the secondary shell of dermochelyids, e.g., *Psephophorus polygonus* from the Middle Miocene and the extant *D. coriacea* (see Figure 19.3F–H), were also studied (Delfino et al. 2013). The ossicles of the former are thick bones with a relatively compact diploe structure and retain an internal compact coarsely fibrous layer; conversely, those of *Dermochelys* are thinner bones with a more vascularized external compacta, a less compact cancellous core and a tendency to reduce the thickness of the internal compact cortex. Compared to other animals that produce an armor of polygonal ossicles (e.g., placodont reptiles and armadillos), the ossification centers of dermochelyid ossicles generally lie more superficially below the external bone surface, instead of being centrally situated within the element (Delfino et al. 2013).

Osteocytes and Osteocyte Lacunae

Cadena and Schweitzer (2012) studied the shape variation and distribution patterns of osteocyte lacunae in extant and extinct turtle shell samples, in addition to the extraction of osteocytes from artificially digested tissue of the extant taxa and morphologically similar structures (=osteocyte-like microstructures) from demineralized tissue of the fossils. The authors divided the lacunae, and thus the original osteocytes once residing in them, into two types: flattened cells and stellate cells. The former type was supposed to occur mostly in the internal cortex and in the secondary deposits of the cancellous bone (lamellar tissue in both cases), whereas the latter type was considered more typical of interstitial lamellae between secondary osteons and in the external cortex. In a later study revising the definition and description of fibrolamellar bone, Stein and Prondvai (2014), however, prompted a careful interpretation of flattened and stellate lacunar morphologies in ground sections, because the orientation of the cutting plane can strongly influence the two-dimensional appearance of the lacunae. For these authors, the succession of flattened and stellate osteocyte lacunae in the internal cortex of the extant Arrau side-necked turtle *Podocnemis expansa* (Cadena and Schweitzer 2012, Figure 3k,i) could simply reflect alternating lamellae in the plywood organization, instead of documenting true changes in lacunar morphology.

Structures resembling osteocytes, blood vessels, and collagen fibrils were also extracted from demineralized turtle shell bone from the Eocene of the Eocene Messel pit in Germany. These structures were tentatively interpreted as preserved soft tissues and studied for internal and external microstructure and elemental composition (Cadena 2016). They were composed of a ca. 50-nm thin layer, whose external and internal texture was mottled

VetBooks.ir

and showed weak striations, whereas external circular to linear marks of the osteocyte-like details were interpreted as microbial troughs (Cadena 2016). Whether the osteocyte-like or blood vessel–like entities truly represent preserved soft tissue structures in the extinct turtles, or are instead mere organic or inorganic molds of lacunae and canals, currently remains under study.

Accessory Osteoderms and Ossicles

Many extinct and extant terrestrial turtles including extant tortoises (members of Testudinidae) bear osteoderms in the skin of the neck region, the limbs and the tail (see Figure 19.2B, C). Barrett et al. (2002) used histological and geological evidence to identify hitherto enigmatic "granicones" (small sculptured conical bones from the Early Cretaceous Purbeck Limestone Formation of Dorset, UK), as limb osteoderms of helochelydrid (=solemydid) turtles (see also Scheyer et al. 2015). Other sampled turtle osteoderms include an ornamented limb osteoderm of aff. *Naomichelys* sp., from the Early Cretaceous of Montague County in Texas (Scheyer et al. 2015), and spiked and ridged ornamented osteoderms of unknown position belonging to the extinct nanhsiungchelyid *Basilemys* sp. from the Late Cretaceous Belly River Group in Alberta, Canada (Scheyer et al. 2017). In each taxon, osteoderm ornamentation mirrors that seen in the external cortex of the shell bones. The thicker internal regions of the osteoderms can be cancellous, and the osteoderm base usually shows some regular meshwork of longitudinally and transversely arranged thick structural fiber bundles, by which the osteoderm was anchored in the surrounding integumentary tissue (Scheyer et al. 2017).

Summary and Outlook

With greater study, our understanding of the microanatomy and histological features of the shell and long bones of turtles has increased distinctively over the last decade. Extinct taxa have been especially intensively studied, whereas comparative data on extant forms are less readily available. There is great potential for future comparative anatomical and histological studies combining both extant and extinct taxa. In addition, intraspecific variation, both within and among shell and long bones, has received little attention so far, although this aspect is paramount in understanding and interpreting histological and microanatomical results. Recent advances in imaging and analysis such as high-resolution microcomputed tomography should be further used to elucidate microstructural details hidden within specimens without destructive sampling. This approach can put the two-dimensional classical histological slice data into a more biologically informative, three-dimensional framework.

Institutional Abbreviations

HLMD, Hessisches Landesmuseum Darmstadt, Darmstadt, Germany; StIPB, Steinmann Institute for Geology, Mineralogy and Palaeontology, Division of Paleontology, University of Bonn, Germany; MB.R., Museum für Naturkunde, Paläontologische Sammlung, Berlin, Germany; QM, The Queensland Museum, Brisbane, Queensland, Australia; ROM, Royal Ontario Museum, Toronto, Ontario, Canada; TMM, Texas Memorial Museum, University of Texas at Austin, Austin, Texas, USA; UCMP, University of California at Berkeley, Museum of Paleontology, California, USA; USNM, National Museum of Natural History (formerly United States National Museum) Smithsonian Institution, Washington, DC, USA and YPM, Peabody Museum of Natural History at Yale University, New Haven, Connecticut, USA.

Acknowledgments

We thank N. Micklich (former curator HLMD), J. Gauthier (YPM) and W. Joyce (former collections manager YPM), P. Holroyd and H. Hutchison (UCMP), K. de Queiroz (USNM), D. Brinkman and J. Gardner (RTMP), K. Seymour (ROM), M. Sander (StIPB), J. Sterli and E. Ruigómez (Museo Paleontológico Egidio Feruglio), D. Unwin (former curator MB), A. Amey and P. Couper (QM) and T. Rowe (TMM) for access to specimens under their care. T. Lyson (Denver Museum of Nature and Science), M. Delfino (University of Torino), N. Klein (StIPB), and S. Salisbury (QM) and many unnamed colleagues are thanked for collaboration and discussions, and O. Dülfer (StIPB) and C. Kolb (former University of Zurich) are acknowledged for help with preparing thin sections.

REFERENCES

Aeby, C. 1878. Das histologische Verhalten fossilen Knochen- und Zahngewebes. *Arch. f. Mikros. Anat.* 15:371–382.

Anquetin, J., et al. 2017. A Jurassic stem pleurodire sheds light on the functional origin of neck retraction in turtles. *Sci. Rep.* 7:42376 [doi: 10.1038/srep42376].

Avens, L., et al. 2009. Use of skeletochronological analysis to estimate the age of leatherback sea turtles *Dermochelys coriacea* in the western North Atlantic. *Endanger. Species Res.* 8:165–177 [doi: 10.3354/esr00202].

Avens, L. and L. R. Goshe. 2007. Comparative skeletochronological analysis of Kemp's ridley (*Lepidochelys kempii*) and loggerhead (*Caretta caretta*) humeri and scleral ossicles. *Mar. Biol.* 152:1309–1317 [doi: 10.1007/s00227-007-0779-9].

Badam, G. L. 1981. *Colossochelys atlas*, a giant tortoise from the Upper Siwaliks of North India. *Bull. Deccan College Research Inst.* 40:149–153.

Barrett, P. M., et al. 2002. Morphology, histology and identification of the 'granicones' from the Purbeck Limestone Formation (Lower Cretaceous: Berriasian) of Dorset, southern England. *Cretaceous Res.* 23:279–295 [doi:10.1006/cres.2002.1002].

Bever, G. S. and W. G. Joyce. 2005. Dermochelyidae - Lederschildkröten; pp. 235–248 in U. Fritz (ed.), *Handbuch der Reptilien und Amphibien Europas. Band 3/IIIB: Schildkröten (Testudines) II (Cheloniidae, Dermochelyidae, Fossile Schildkröten Europas).* Aula-Verlag, Wiebelsheim.

Bever, G. S., et al. 2015. Evolutionary origin of the turtle skull. *Nature* 525:239–242 [doi: 10.1038/nature14900].

Buffrénil, V. de, et al. 2016. Comparative data on the differentiation and growth of bone ornamentation in gnathostomes (Chordata: Vertebrata). *J. Morphol.* 277:634–670 [doi: 10.1002/jmor.20525].

Burke, A. C. 1989. Development of the turtle carapace: implications for the evolution of a novel bauplan. *J. Morphol.* 199:363–378.

Cadena, E. A. 2016. Microscopical and elemental FESEM and Phenom ProX-SEM-EDS analysis of osteocyte and blood vessel-like microstructures obtained from fossil vertebrates of the Eocene Messel Pit, Germany. *PeerJ* 4:e1618 [doi: 10.7717/peerj.1618].

Cadena, E. A. and M. H. Schweitzer. 2012. Variation in osteocytes morphology vs bone type in turtle shell and their exceptional preservation from the Jurassic to the present. *Bone* 51:614–620 [doi: 10.1016/j.bone.2012.05.002].

Cadena, E. A., et al. 2013. New material of *Mongolemys elegans* Khosatzky and Młynarski, 1971 (Testudines: Lindholmemydidae), from the Late Cretaceous of Mongolia with comments on bone histology and phylogeny. *Am. Mus. Novit.* 3766:1–27.

Canoville, A. and M. Laurin. 2010. Evolution of humeral microanatomy and lifestyle in amniotes, and some comments on palaeobiological inferences. *Biol. J. Linn. Soc.* 100:384–406 [doi: 10.1111/j.1095-8312.2010.01431.x].

Case, T. J. 1978. Speculations on the growth rate and reproduction of some dinosaurs. *Paleobiology* 4:320–328.

Castanet, J. 1985. La squelettochronologie chez les reptiles I. Resultats experimentaux sur la signification des marques de croissance squelettiques chez les lezards et les tortues. *Ann. Sci. Nat., Zool., Paris. 13e Sér.* 7:23–40.

Castanet, J. 1986–1987. La squelettochronologie chez les reptiles III - application. *Ann. Sci. Nat., Zool., Paris.13e Sér.* 8:157–172.

Castanet, J. 1988. Les méthodes d'estimation de l'âge chez les chéloniens. *Mésogée* 48:21–28.

Castanet, J. and M. Cheylan. 1979. Les marques de croissance de l'âge chez *Testudo hermanni* et *Testudo graeca* (Reptilia, Chelonia, Testudinidae). *Can. J. Zool.* 57:1649–1665.

Cebra-Thomas, J., et al. 2005. How the turtle forms its shell: a paracrine hypothesis of carapace formation. *J. Exp. Zool. (Mol. Dev. Evol.)* 304B:558–569.

Cebra-Thomas, J. A., et al. 2007. Evidence that a late-emerging population of trunk neural crest cells forms the plastron bones in the turtle *Trachemys scripta*. *Evol. Dev.* 9:267–277.

Cerda, I. A., et al. 2016. Bone shell microstructure of *Condorchelys antiqua* Sterli 2008, a stem turtle from the Jurassic of Patagonia [Special issue: Current advances in paleohistology: A tribute to a generation of French Paleohistologists; Laurin, M., Cubo, J. (eds.)]. *C. R. Palevol.* 15:128–141 [doi: 10.1016/j.crpv.2015.01.004].

Chen, I. H., et al. 2015. Leatherback sea turtle shell: a tough and flexible biological design. *Acta Biomater.* 28:2–12 [doi: 10.1016/j.actbio.2015.09.023].

Cherepanov, G. O. 1984. On the nature of the plastron anterior elements in turtles [in Russian]. *Zool. Zh.* 63:1529–1534.

Chinsamy, A. and N. Valenzuela. 2008. Skeletochronology of the endangered side-neck turtle, *Podocnemis expansa*. *S. Afr. J. Sci.* 104:311–314.

Çiçek, K., et al. 2016. A skeletochronological study of age, growth and longevity in two freshwater turtles, *Emys orbicularis* and *Mauremys rivulata*, from Mediterranean Turkey (Reptilia: Testudines). *Zool. Mid. East* 62:29–38 [doi: 10.1080/09397140.2016.1144277].

Coles, W. C., et al. 2001. Skeletochronology validation from an adult loggerhead (*Caretta caretta*). *Copeia* 2001(1):240–242.

Crawford, N. G., et al. 2012. More than 1000 ultraconserved elements provide evidence that turtles are the sister group of archosaurs. *Biol. Lett.* 8:783–786 [doi: 10.1098/rsbl.2012.0331].

Cubo, J., et al. 2012. Paleohistological estimation of bone growth rate in extinct archosaurs. *Paleobiology* 38:335–349 [doi: 10.1666/08093.1].

Cubo, J., et al. 2008. Phylogenetic, functional, and structural components of variation in bone growth rate of amniotes. *Evol. Dev.* 10:217–227.

Curtin, A. J., et al. 2008. Assessing age in the desert tortoise *Gopherus agassizii*: testing skeletochronology with individuals of known age. *Endanger. Species Res.* 5:21–27 [doi: 10.3354/esr00108].

De la Fuente, M. S., et al. 2015. Long-necked chelid turtles from the Campanian of northwestern Patagonia with comments on K/P survivorship of the genus *Yaminuechelys*. *C. R. Palevol.* 14:563–576 [doi: 10.1016/j.crpv.2015.04.008].

Delfino, M., et al. 2010. An integrative approach to examining a homology question: shell structures in soft-shelled turtles. *Biol. J. Linn. Soc.* 99:462–476 [doi: 10.1111/j.1095-8312.2009.01356.x].

Delfino, M., et al. 2013. Gross morphology and microstructure of type locality ossicles of *Psephophorus polygonus* Meyer, 1847 (Testudines, Dermochelyidae). *Geol. Mag.* 150:767–782 [doi: 10.1017/S001675681200091X].

Ehret, D. 2007. Skeletochronology: a method for determining the individual age and growth of modern and fossil tortoises (Reptilia: Testudines). *Bull. Florida Mus. Nat. Hist.* 47:49–72.

Field, D. J., et al. 2014. Toward consilience in reptile phylogeny: miRNAs support an archosaur, not lepidosaur, affinity for turtles. *Evol. Dev.* 16:189–196 [doi: 10.1111/ede.12081].

Foote, J. S. 1911. The comparative histology of femoral bones. *Trans. Am. Micros. Soc.* 30:87–140.

Foote, J. S. 1916. A contribution to the comparative histology of the femur. *Smithson. Contrib. to Knowledge* 35:1–242.

Fraas, E. 1913. *Proterochersis*, eine pleurodire Schildkröte aus dem Keuper. *Jahresh. Ver. Vaterl. Naturkd. Wuerttemb.* 80:1–30.

Frazier, J., et al. 2005. *Dermochelys* Blainville, 1816 - Lederschildkröten; pp. 249–328 in U. Fritz (ed.), *Handbuch der Reptilien und Amphibien Europas. Band 3/IIIB: Schildkröten (Testudines) II.* Aula-Verlag, Wiebelsheim.

Gaffney, E. S. 1990. The comparative osteology of the Triassic turtle *Proganochelys*. *Bull. Am. Mus. Nat. Hist.* 194:1–263.

Gaffney, E. S., et al. 2008. Two new species of the side necked turtle genus, *Bairdemys* (Pleurodira, Podocnemididae), from the Miocene of Venezuela [in M. R. Sánchez-Villagra (ed.), Contributions on Vertebrate Paleontology in Venezuela]. *PalZ* 82:209–229 [doi: 10.1007/BF02988411].

Germain, D. and M. Laurin. 2005. Microanatomy of the radius and lifestyle in amniotes (Vertebrata, Tetrapoda). *Zool. Scripta*. 34:335–350.

Gilbert, S. F., et al. 2007. The contribution of neural crest cells to the nuchal bone and plastron of the turtle shell. *Integr. Comp. Biol*. 47:401–408 [doi:10.1093/icb/icm020].

Gilbert, S. F., et al. 2008. How the turtle got its shell; pp. 1–16 in J. Wyneken, M. H. Godfrey, and V. Bels (eds.), *Biology of Turtles*. CRC Press, Boca Raton.

Haines, R. W. 1942. The evolution of epiphyses and of endochondral bone. *Biol. Rev.* 17:267–292 [doi: 10.1111/j.1469-185X.1942.tb00440.x].

Haines, R. W. 1969. Epiphyses and sesamoids; pp. 81–115 in C. Gans, A. d. A. Bellairs, and T. S. Parsons (eds.), *Biology of the Reptilia*, Vol. 1. Morphology A. Academic Press, London.

Hirasawa, T., et al. 2013. The endoskeletal origin of the turtle carapace. *Nat. Commun*. 4:2107 [doi:10.1038/ncomms3107].

Hirasawa, T., et al. 2015. The evolutionary origin of the turtle shell and its dependence on the axial arrest of the embryonic rib cage. *J. Exp. Zool. (Mol. Dev. Evol.)* 324:194–207 [doi: 10.1002/jez.b.22579].

Houssaye, A. 2013. Bone histology of aquatic reptiles: what does it tell us about secondary adaptation to an aquatic life? *Biol. J. Linn. Soc*. 108:3–21 [doi: 10.1111/j.1095-8312.2012.02002.x].

Jannello, J. M., et al. 2016. Shell bone histology of the long-necked chelid *Yaminuechelys* (Testudines: Pleurodira) from the late Cretaceous—early Palaeocene of Patagonia with comments on the histogenesis of bone ornamentation. *Naturwissenschaften* 103:26 [doi: 10.1007/s00114-016-1346-3].

Jannello, J. M., et al. 2018. *Linderochelys rinconensis* (Testudines: Pan-Chelidae) from the Upper Cretaceous of northern Patagonia: new insights from shell bone histology, morphology and diagenetic implications. *Cretaceous Res.* 83:47–61 [doi: 10.1016/j.cretres.2017.05.011].

Joyce, W. G. 2015. The origin of turtles: a paleontological perspective. *J. Exp. Zool. (Mol. Dev. Evol.)* 324B:181–193 [doi: 10.1002/jez.b.22609].

Joyce, W. G. 2017. A review of the fossil record of basal Mesozoic turtles. *Peabody Mus. Nat. Hist. Yale Univ. Bull.* 58:65–113.

Joyce, W. G. and J. Sterli. 2012. Congruence, non-homology, and the phylogeny of basal turtles. *Acta Zool. (Stockh.)* 93:149–159 [doi: 10.1111/j.1463-6395.2010.00491.x].

Joyce, W. G., et al. 2013. The girdles of the oldest fossil turtle, *Proterochersis robusta*, and the age of the turtle crown. *BMC Evol. Biol*. 13:266:[doi: 10.1186/1471-2148-13-266].

Joyce, W. G., et al. 2014. The skeletal morphology of the solemydid turtle *Naomichelys speciosa* from the Early Cretaceous of Texas. *J. Paleontol*. 88:1257–1287 [doi: 10.1666/14-002].

Kälin, J. 1945. Zur Morphogenese des Panzers bei den Schildkröten. *Acta Anat.* 1:144–176.

Klinger, R. C. and J. A. Musick. 1992. Annular growth layers in juvenile loggerhead turtles (*Caretta caretta*). *Bull. Mar. Sci.* 51:224–230.

Klinger, R. C. and J. A. Musick. 1995. Age and growth of loggerhead turtles (*Caretta caretta*) from Chesapeake Bay. *Copeia* 1995:204–209.

Kolb, C., et al. 2015. Growth in fossil and extant deer and implications for body size and life history evolution. *BMC Evol. Biol*. 15:19 [doi: 10.1186/s12862-015-0295-3].

Krauss, S., et al. 2009. Mechanical function of a complex three-dimensional suture joining the bony elements in the shell of the red-eared slider turtle. *Adv. Mater.* 21:407–412 [DOI: 10.1002/adma.200801256].

Kriloff, A., et al. 2008. Evolution of bone microanatomy of the tetrapod tibia and its use in palaeobiological inference. *J. Evol. Biol*. 21:807–826.

Laurin, M. and G. Piñeiro. 2017. A reassessment of the taxonomic position of mesosaurs, and a surprising phylogeny of early amniotes. *Front. Earth Sci*. 5:88 [doi: 10.3389/feart.2017.00088].

Legendre, L., et al. 2012. Phylogenetic signal in bone histology of amniotes revisited. *Zool. Scripta* 42:44–53 [doi:10.1111/j.1463-6409.2012.00564.x].

Li, C., et al. 2008. An ancestral turtle from the Late Triassic of southwestern China. *Nature* 456:497–501 [doi: 10.1038/nature07533].

Lyson, T., et al. 2014. Origin of the unique ventilatory apparatus of turtles. *Nat. Commun*. 5:5211 [doi: 10.1038/ncomms6211].

Lyson, T. R., et al. 2010. Transitional fossils and the origin of turtles. *Biol. Lett*. 6:830–833 [doi: 10.1098/rsbl.2010.0371].

Lyson, T. R., et al. 2013. Evolutionary origin of the turtle shell. *Curr. Biol*. 23:1113–1119 [doi: 10.1016/j.cub.2013.05.003].

Lyson, T. R., et al. 2016. Fossorial origin of the turtle shell. *Curr. Biol*. 26:1887–1894 [doi: 10.1016/j.cub.2016.05.020].

MacDougall, M. J., et al. 2018. Commentary: A reassessment of the taxonomic position of mesosaurs, and a surprising phylogeny of early amniotes. *Front. Earth Sci*. 6:99 [doi: 10.3389/feart.2018.00099].

Marmi, J., et al. 2009. *Solemys* (Chelonii, Solemydidae) remains from the Maastrichtian of Pyrenees: evidence for a semi-aquatic lifestyle. *Cretaceous Res.* 30:1307–1312 [doi: 10.1016/j.cretres.2009.07.008].

Meylan, P. A. 1987. Phylogenetic relationships of soft-shelled turtles (Family Trionychidae). *Bull. Am. Mus. Nat. Hist.* 186:1–101.

Młynarski, M. 1956. Studies on the morphology of the shell of recent and fossil tortoises. *Acta Zool. Cracov.* 1:1–13.

Montes, L., et al. 2010. Relationship between bone growth rate and bone tissue organization in amniotes: first test of Amprino's rule in a phylogenetic context. *Anim. Biol*. 60:25–41.

Montes, L., et al. 2007. Relationships between bone growth rate, body mass and resting metabolic rate in growing amniotes: a phylogenetic approach. *Biol. J. Linn. Soc*. 92:63–76.

Nagashima, H., et al. 2013. Origin of the turtle body plan: the folding theory to illustrate turtle-specific developmental repatterning; pp. 37–50 in D. B. Brinkman, P. A. Holroyd, and J. D. Gardner (eds.), *Morphology and Evolution of Turtles. Proceedings of the Gaffney Turtle Symposium (2009) in Honor of Eugene S Gaffney. Vertebrate Paleobiology and Paleoanthropology Series*. Springer, Dordrecht.

Nakajima, Y., et al. 2014. Turtle humeral microanatomy and its relationship to lifestyle. *Biol. J. Linn. Soc.* 112:719–734 [doi: 10.1111/bij.12336].

Nakajima, Y., et al. 2017. Morphological and histological evidence for the oldest known softshell turtles from Japan. *J. Vertebr. Paleontol.* 37:2, e1278606 [doi: 10.1080/02724634.2017.1278606].

Pereira, A. G., et al. 2017. Multilocus phylogeny and statistical biogeography clarify the evolutionary history of major lineages of turtles. *Mol. Phylog. Evol*. 113:59–66 [doi: 10.1016/j.ympev.2017.05.008].

Pereyra, M. E., et al. 2020. Growth dynamics and body size evolution of South American long-necked chelid turtles: A bone histology approach. *Acta Palaeontol. Pol.* 65:535–545 [doi: 10.4202/app.00702.2019].

Pérez-García, A., et al. 2012. New interpretations on *Dortoka vasconica* Lapparent de Broin and Murelaga, a freshwater turtle with an unusual carapace. *Cretaceous Res.* 36:151–161 [doi: 10.1016/j.cretres.2012.03.006].

Pérez-García, A., et al. 2013. The turtles from the uppermost Jurassic and Early Cretaceous of Galve (Iberian Range, Spain): anatomical, systematic, biostratigraphic and palaeobiogeographical implications. *Cretaceous Res.* 44:64–82 [doi: 10.1016/j.cretres.2013.03.011].

Peters, R. H. 1983. *The Ecological Implications of Body Size*; p. 329. Cambridge University Press, Cambridge, UK.

Quekett, J. T. 1849a. Additional observations on the intimate structure of bone. *Trans. Micros. Soc. Lond.* 2:59–64.

Quekett, J. T. 1849b. On the intimate structure of bone as composing the skeleton in the four great classes of animals, [viz., mammals, birds, reptiles, and fishes, with some remarks on the great value of the knowledge of such structure in determining the affinities of minute fragments of organic remains]. *Trans. Micros. Soc. Lond.* 2:46–58.

Quekett, J. T. 1855. Descriptive and Illustrated Catalogue of the Histological Series contained in the Museum of the Royal College of Surgeons of England. *Volume II. Structure of the Skeleton of Vertebrate Animals*; p. 305. Taylor and Francis, London.

Rhodin, A. G. J. 1985. Comparative chondro-osseous development and growth of marine turtles. *Copeia* 1985(3):752–771.

Rhodin, A. G. J., et al. 1981. Chondro-osseous morphology of *Dermochelys coriacea*, a marine reptile with mammalian skeletal features. *Nature* 290:244–246.

Rice, R., et al. 2015. Emerging from the rib: resolving the turtle controversies. *J. Exp. Zool. (Mol. Dev. Evol.)* 324:208–220 [doi: 10.1002/jez.b.22600].

Rice, R., et al. 2016. Development of the turtle plastron, the order-defining skeletal structure. *PNAS* 113:5317–5322 [doi: 10.1073/pnas.1600958113].

Ricqlès, A. de 1976. On bone histology of fossil and living reptiles, with comments on its functional and evolutionary significance; pp. 123–150 in A. d. A. Bellairs, and C. B. Cox (eds.), *Linnean Society Symposium Series No. 3. Morphology and Biology of Reptiles*. Academic Press, London.

Ricqlès, A. de, et al. 2004. The 'message' of bone tissue in paleoherpetology. *Ital. J. Zool.* 71:3–12 [doi: 10.1080/11250000409356599].

Rieppel, O. 2013. The evolution of the turtle shell; pp. 51–62 in D. B. Brinkman, P. A. Holroyd, and J. D. Gardner (eds.), *Morphology and Evolution of Turtles. Proceedings of the Gaffney Turtle Symposium (2009) in Honor of Eugene S Gaffney. Vertebrate Paleobiology and Paleoanthropology Series*. Springer, Dordrecht.

Rougier, G. W., et al. 1995. Late Triassic turtles from South America. *Science* 268:855–858 [DOI: 10.1126/science.268.5212.855].

Sánchez-Villagra, M. R., et al. 2009. Skeletal development in the Chinese soft-shelled turtle *Pelodiscus sinensis* (Testudines: Trionychidae). *J. Morphol.* 270:1381–1399 [doi: 10.1002/jmor.10766].

Scheyer, T. M. 2007. Comparative bone histology of the turtle shell (carapace and plastron): implications for turtle systematics, functional morphology, and turtle origins. *Doctoral Thesis, Mathematisch-Naturwissenschaftliche Fakultät*, University of Bonn, Germany [http://hss.ulb.uni-bonn.de/2007/1229/1229.htm].

Scheyer, T. M. 2009. Conserved bone microstructure in the shells of long-necked and short-necked chelid turtles (Testudinata, Pleurodira). *Fossil Rec.* 12:47–57 [doi: 10.1002/mmng.200800009].

Scheyer, T. M. and J. Anquetin. 2008. Bone histology of the Middle Jurassic turtle shell remains from Kirtlington, Oxfordshire, England. *Lethaia* 41:85–96 [doi: 10.1111/j.1502-3931.2007.00044.x].

Scheyer, T. M. and M. R. Sánchez-Villagra. 2007. Carapace bone histology in the giant pleurodiran turtle *Stupendemys geographicus*: phylogeny and function. *Acta Palaeontol. Pol.* 52:137–154.

Scheyer, T. M. and P. M. Sander. 2007. Shell bone histology indicates terrestrial palaeoecology of basal turtles. *Proc. R. Soc. Lond. B* 274:1885–1893 [doi:10.1098/rspb.2007.0499].

Scheyer, T. M., et al. 2007. A plywood structure in the shell of fossil and living soft-shelled turtles (Trionychidae) and its evolutionary implications. *Org. Divers. Evol.* 7:136–144 [doi: 10.1016/j.ode.2006.03.002].

Scheyer, T. M., et al. 2012. First record of soft-shelled turtles (Cryptodira, Trionychidae) from the Late Cretaceous of Europe. *J. Vertebr. Paleontol.* 32:1027–1032 [doi: 10.1080/02724634.2012.685036].

Scheyer, T. M., et al. 2013. Three ways to tackle the turtle: integrating fossils, comparative embryology, and microanatomy [published 16. August 2012]; pp. 63–70 in D. B. Brinkman, P. A. Holroyd, and J. D. Gardner (eds.), *Morphology and Evolution of Turtles. Proceedings of the Gaffney Turtle Symposium (2009) in Honor of Eugene S Gaffney. Vertebrate Paleobiology and Paleoanthropology Series*. Springer, Dordrecht.

Scheyer, T. M., et al. 2014. The shell bone histology of fossil and extant marine turtles revisited. *Biol. J. Linn. Soc.* 112:701–718 [doi: 10.1111/bij.12265].

Scheyer, T. M., et al. 2015. Shell bone histology of solemydid turtles (stem Testudines): palaeoecological implications. *Org. Divers. Evol.* 15:199–212 [doi: 10.1007/s13127-014-0188-0].

Scheyer, T. M., et al. 2017. Turtle shell bone and osteoderm histology of Mesozoic and Cenozoic stem-trionychian Adocidae and Nanhsiungchelyidae (Cryptodira: Adocusia) from Central Asia, Mongolia, and North America. *Fossil Rec.* 20:69–85 [doi: 10.5194/fr-20-69-2017].

Schoch, R. R. and H.-D. Sues. 2015. A Middle Triassic stem-turtle and the evolution of the turtle body plan. *Nature* 523:584–587 [doi: 10.1038/nature14472].

Schoch, R. R. and H.-D. Sues. 2018. Osteology of the Middle Triassic stem-turtle *Pappochelys rosinae* and the early evolution of the turtle skeleton. *J. Syst. Palaeontol.* 16:927–965 [doi: 10.1080/14772019.2017.1354936].

Sena, M. V. A., et al. 2020. Osteohistology and microanatomy of a new specimen of *Cearachelys placidoi* (Testudines: Pleurodira) a side-necked turtle from the Lower Cretaceous of Brazil. *Anat. Rec.* 2020:1–11 [doi: 10.1002/ar.24556].

Shaffer, B. S., et al. 2013. The western painted turtle genome, a model for the evolution of extreme physiological adaptations in a slowly evolving lineage. *Genome Biol.* 14:R28 [doi: 10.1186/gb-2013-14-3-r28].

Skutchas, P., et al. 2017. Shell bone histology of the pan-carettochelyid turtle *Kizylkumemys schultzi* from the Upper Cretaceous of Uzbekistan and shell bone morphology transformations in the evolution of pan-trionychian turtles. *Cretaceous Res.* 79:171–181 [doi: 10.1016/j.cretres.2017.07.010].

Slater, B. J., et al. 2011. A new Late Jurassic turtle from Spain: phylogenetic implications, taphonomy and palaeoecology. *Palaeontology* 54:1393–1414 [doi: 10.1111/j.1475-4983.2011.01100.x].

Snover, M. L. and A. A. Hohn. 2004. Validation and interpretation of annual skeletal marks in loggerhead (*Caretta caretta*) and Kemp's Ridley (*Lepidochelys kempii*) sea turtles. *Fish. Bull.* 102:682–692.

Snover, M. L. and A. G. J. Rhodin. 2008. Comparative ontogenetic and phylogenetic aspects of chelonian chondro-osseous growth and skeletochronology; pp. 17–43 in J. Wyneken, M. H. Godfrey, and V. Bels (eds.), *Biology of Turtles*. CRC Press, Boca Raton.

Stein, K. and E. Prondvai. 2014. Rethinking the nature of fibrolamellar bone: an integrative biological revision of sauropod plexiform bone formation. *Biol. Rev.* 89:24–47 [doi: 10.1111/brv.12041].

Sterli, J., et al. 2007. Anatomy and relationships of *Palaeochersis talampayensis*, a Late Triassic turtle from Argentina. *Palaeontographica Abt. A*281:1–61.

Sterli, J., et al. 2013. A new species of meiolaniform turtle and a revision of the Late Cretaceous Meiolaniformes of South America. *Ameghiniana* 50:240–256.

Sterli, J., et al. 2020. Appearances can be deceptive: bizarre shell microanatomy and histology in a new Triassic turtle (Testudinata) from Argentina at the dawn of turtles. *Pap. Palaeontol.* 2020: 1–36 [doi: 10.1002/spp2.1334].

Suzuki, H. K. 1963. Studies on the osseous system of the slider turtle. *Ann. N Y Acad. Sci.* 109:351–410 [doi: 10.1111/j.1749-6632.1963.tb13476.x].

Szczygielski, T. and T. Sulej. 2019. The early composition and evolution of the turtle shell (Reptilia, Testudinata). *Palaeontology* 62:375–415 [doi: 10.1111/pala.12403].

Turner Tomaszewicz, C. N., et al. 2015. Age and residency duration of loggerhead turtles at a North Pacific bycatch hotspot using skeletochronology. *Biol. Conserv.* 186:134–142 [doi: 10.1016/j.biocon.2015.03.015].

Vlachos, E., et al. 2015. The first record of a soft-shelled turtle (Testudines: Pan-Trionychidae) from southern Balkans (Pliocene, Gefira, N. Greece) and new information from bone histology. *Sci. Nat.* 102:45 [doi: 10.1007/s00114-015-1295-2].

Völker, H. 1913. Über das Stamm-, Gliedmaßen- und Hautskelet von *Dermochelys coriacea* L. *Zool. Jahrb., Abt. Anat. Ontog. Tiere* 33:431–552.

Wallis, K. 1928. Zur Knochenhistologie und Kallusbildung beim Reptil (*Clemmys leprosa* Schweigg.). *Z. Zellforsch. Mikrosk. Anat.* 6:1–26.

Wang, Z., et al. 2013. The draft genomes of soft-shell turtle and green sea turtle yield insights into the development and evolution of the turtle-specific body plan. *Nat. Gen.* 45:701–706 [doi: doi:10.1038/ng.2615].

Werneburg, I. and M. R. Sánchez-Villagra. 2009. Timing of organogenesis support basal position of turtles in the amniote tree of life. *BMC Evol. Biol.* 9:82 [doi:10.1186/1471-2148-9-82].

Werneburg, I., et al. 2015. Evolution of neck vertebral shape and neck retraction at the transition to modern turtles: an integrated geometric morphometric approach. *Syst. Biol.* 64:187–204 [doi: 10.1093/sysbio/syu072].

Wood, R. C., et al. 1996. Evolution and phylogeny of leatherback turtles (Dermochelyidae), with descriptions of new fossil taxa. *Chelonian Conserv. Biol.* 2:266–286.

Zangerl, R. 1939. The homology of the shell elements in turtles. *J. Morphol.* 65:383–409.

Zangerl, R. 1953. The vertebrate fauna of the Selma Formation of Alabama. Part III: The turtles of the family Protostegidae. *Fieldiana, Geol. Mem.* 3:57–133.

Zangerl, R. 1969. The turtle shell; pp. 311–339 in C. Gans, A. d. A. Bellairs, and T. S. Parsons (eds.), *Biology of the Reptilia*, Vol. 1. Morphology A. Academic Press, London.

Zug, G. R. and R. E. Glor. 1998. Estimates of age and growth in a population of green sea turtles (*Chelonia mydas*) from the Indian River lagoon system, Florida: a skeletochronological analysis. *Can. J. Zool.* 76:1497–1506.

Zug, G. R. and J. F. Parham. 1996. Age and growth in leatherback turtles, *Dermochelys coriacea* (Testudines: Dermochelyidae): a skeletochronological analysis. *Chelonian Conserv. Biol.* 2:244–249.

Zug, G. R., et al. 1986. Age determination of loggerhead sea turtles, *Caretta*, by incremental growth marks in the skeleton. *Smithon. Contrib. Zool.* 427:1–34.

Zug, G. R., et al. 2001. Age and growth of Hawaiian green seaturtles (*Chelonia mydas*): an analysis based on skeletochronology. *Fish. Bull.* 100:117–127.

Zug, G. R., et al. 2006. Age and growth in olive ridley seaturtles (*Lepidochelys olivacea*) from the North-central Pacific: a skeletochronological analysis. *Mar. Ecol.* 27:263–270 [doi:10.1111/j.1439-0485.2006.00109.x].

VetBooks.ir

20

Lepidosauria

Vivian de Buffrénil and Alexandra Houssaye

CONTENTS

Introduction 399
Preliminary Remarks 399
An Overview of Studies of Skeletal Histology in Lepidosaurs 400
Squamates 400
"Lizards" and Snakes 400
Microanatomical and Histological Structure of Limb Long Bones in Lizards 400
Occurrence of Sesamoids 404
Vertebrae and Ribs in Lizards and Snakes 404
Remarks on Skull Bones and Teeth in Lizards and Snakes 406
Osteoderms 409
"Aigialosaurs" and Mosasaurs 410
General Features of Mosasauroidea 410
Microanatomy and Histology of Ribs 411
Microanatomy and Histology of Vertebrae 411
Microanatomy and Histology of Limb Long Bones 413
Cranial Bones and Teeth 415
Paleobiological and Paleoecological Inferences 415
The Strange Case of Marine Cenomanian Snakelike Forms 416
"Dolichosaurs" and Hind-Limbed Snakes 416
Structure of the Ribs and Vertebrae 417
A Note on the Inner Structure of Reduced Limbs 419
Paleobiological and Paleoecological Inferences 419
Rhynchocephalia 419
A Once Diverse Taxon 419
Overview of Rhynchocephalian Skeletal Structures 419
Acknowledgments 420
References 420

Introduction

Preliminary Remarks

Lepidosauria (Romer 1956) is a group of diapsids that includes the last common ancestor of rhynchocephalians and squamates and all its descendants (Evans and Jones 2010). The divergence between Rhynchocephalia and Squamata is dated from the Early to Middle Triassic (Evans and Jones 2010), or even Late Permian (Cleary et al. 2018).

In this review of skeletal microstructure, lepidosaurs will be grouped into four sets that do not strictly reflect current opinions on their phylogenetic relationships. The first three sets are gathered under the heading Squamates. Squamata is a natural taxon that encompasses extant "lizards", snakes and amphisbaenians and their fossil relatives, including highly specialized forms such as the mosasauroids and the enigmatic pachyostotic "limbed snakes" from the Cenomanian. Although the oldest squamate fossils are known from the Early or Middle Jurassic (Evans 1994, Evans et al. 2002) or even the Middle Triassic (Simoes et al. 2018), it is in the Cretaceous that this taxon reached the highest diversity. Opinions still diverge on the precise phylogenetic relationships of mosasaurs and Cenomanian "limbed snakes" to other squamates (lizards and snakes). We will avoid prejudging these open questions and, for our purposes, we subdivide the Squamata into three sets that do not strictly overlap the phylogenetic frames acknowledged at present. The first set comprises the paraphyletic

VetBooks.ir

lizards and snakes (considered individually or collectively). It gathers the extant and extinct representatives of the Squamata, with the exception of the mosasauroids and the Cenomanian limbed snakes. This set constitutes a paraphyletic construction because, in one manner or another, mosasaurs and limbed snakes are rooted among lizards and snakes. The second set includes the Mosasauroidea (i.e., Mosasauridae and "Aigialosauridae"). The third set comprises the limbed snake–like taxa from the Cenomanian-Turonian ("Dolichosauridae" and Pachyophiidae). Finally, we consider a fourth, nonsquamate taxon, the Rhynchocephalians. This is a true, unquestionable natural clade. Our approach has one basic advantage in addition to avoiding prejudging some phylogenetic issues that are still debated: it makes the presentation simpler and shorter because it describes broad, consistent patterns in the microstructural organization of the skeleton that are related to gross ecophysiological characteristics and specific life history traits.

An Overview of Studies of Skeletal Histology in Lepidosaurs

Lepidosaur bones have been described and analyzed in pioneering works on the diversity of bone tissue types in tetrapods (e.g., Foote 1911, 1916, Amprino and Godina 1947, Enlow and Brown 1957, Enlow 1969, Ricqlès 1976). Because these taxa are ectotherms and poikilotherms, their long bones have notably been studied in the context of species-specific skeletochronological studies (Castanet 1978, Buffrénil and Castanet 2000, Pal et al. 2009, Petermann and Gauthier 2020), but more inclusive questions relative to somatic growth and ecology have also been considered (e.g., Haines 1939, Buffrénil and Francillon-Vieillot 2001, Buffrénil et al. 2005, 2008). Many squamate forms are limbless; therefore, their vertebrae have proved useful in similar analyses (e.g., Houssaye et al. 2010). These bones were analyzed in large data sets to reveal functional adaptive patterns and make paleoecological inferences (e.g., Houssaye 2013, Houssaye et al. 2013a). The structure and growth of osteoderms in various taxa have also been considered in detailed studies (Zylberberg and Castanet 1985, Buffrénil et al. 2011, Vickaryous et al. 2015).

Squamates

"Lizards" and Snakes

Lizards and snakes include about 10, 000 extant species (Uetz et al. 2018) and are distributed nearly worldwide. They show a large range of body sizes, from tiny chameleonids (e.g., *Brookesia minima*, about 3 cm in total length) to giant forms such as the lizard *Varanus* [*Megalania*] *priscus* and the snake *Eunectes murinus* (7 m total length: Bellairs 1969; Pianka 2004). They are also ecologically diverse, with semiaquatic (marine iguana), aquatic (*Pelamis*), fossorial (amphisbaenids) and arboreal (green iguana) taxa. Their reproductive modes include degrees of viviparity, oviparity, and even parthenogenesis (Kearney et al. 2009). Lizards and snakes have evolved key adaptations such as cranial kinesis, a venom-delivery apparatus, elongated bodies, and limblessness, along with some unusual locomotory abilities such as scansoriality (Gekkonidae), bipedal running on water (*Basiliscus*), gliding (*Draco*), walking on strongly inclined and narrow supports (*Chamaeleo*), and blowing resistance (*Anolis*). The phylogenetic relationships within extant squamates remain debated, notably the position of snakes (e.g., Townsend et al. 2004, Pyron et al. 2013, Streicher and Wiens 2017). Snakes are a monophyletic group. No one seriously considers snakes a separate evolutionary lineage from lizards; rather, snakes evolved from a group of lizards whose identity is still disputed, so lizards form a monophyletic group if they include snakes.

Microanatomical and Histological Structure of Limb Long Bones in Lizards

Though the limbs of most quadrupedal lizards look proportionally short compared to, for example, those of mammals (e.g., Blob 2000), they have well differentiated and slender long bones (Figure 20.1A), including phalanges, with clearly distinguishable epiphyseal, metaphyseal and diaphyseal regions (Romer 1956). Adaptations to running, digging, swimming and climbing have limited influence on the basic morphological characteristics of long bones in lizards (e.g., Johnson et al. 2005), but their overall size can be drastically affected: even the fossorial serpentiform gymnophthalmid *Bachia bicolor* or the scincid *Hemiergis*, for example, retain well-conformed, albeit residual, limb bones (Shapiro 2002, Jerez and Tarazona 2009; see also Lee and Caldwell 1998).

The inner architecture of lizard long bones is typically tubular (Figure 20.1B-E), with broad discrepancies among skeletal elements and taxa. For the same bone, some species have high compactness values (e.g., *ca*. 80% on average for the femur of large male *Varanus niloticus*; 79% in *Gerrhonotus imbricatus*), reflecting robust, thick-walled bones, whereas others, such as *Iguana iguana* and *Sceloporus horridus,* have more gracile bones (compactness: 53% and 34%, respectively; see Figure 20.1D–F). Several comparative studies of the humerus (Canoville and Laurin 2010), the radius (Germain and Laurin 2005), the femur (Quémeneur et al. 2013) and the tibia (Kriloff et al. 2008) of amniotes, including good samples of lizards, have shown that interspecific differences are only loosely related to habitat and locomotory mode. The main ecological adaptation influencing the microanatomical features of limb bones is an exclusively aquatic lifestyle (e.g., Laurin et al. 2011). This adaptation is absent in lizards: the most aquatic taxa, e.g., *Amblyrhynchus cristatus*, *V. salvator*, *V. niloticus* and *V. varius* are more amphibious than fully aquatic.

Sexual dimorphism of long bone robusticity has been documented at least in one species, *V. niloticus*. Buffrénil and Francillon-Vieillot (2001) showed a gradual decrease in the cortical thickness of the femur in mature females. This bone is submitted to repeated perimedullary resorption for calcium recycling during egg growth. From year to year, the volume of eroded tissue is not entirely compensated by subsequent secondary deposits. As a consequence, a deficit in the reconstruction of cortices and a progressive decrease in their thickness take place with age.

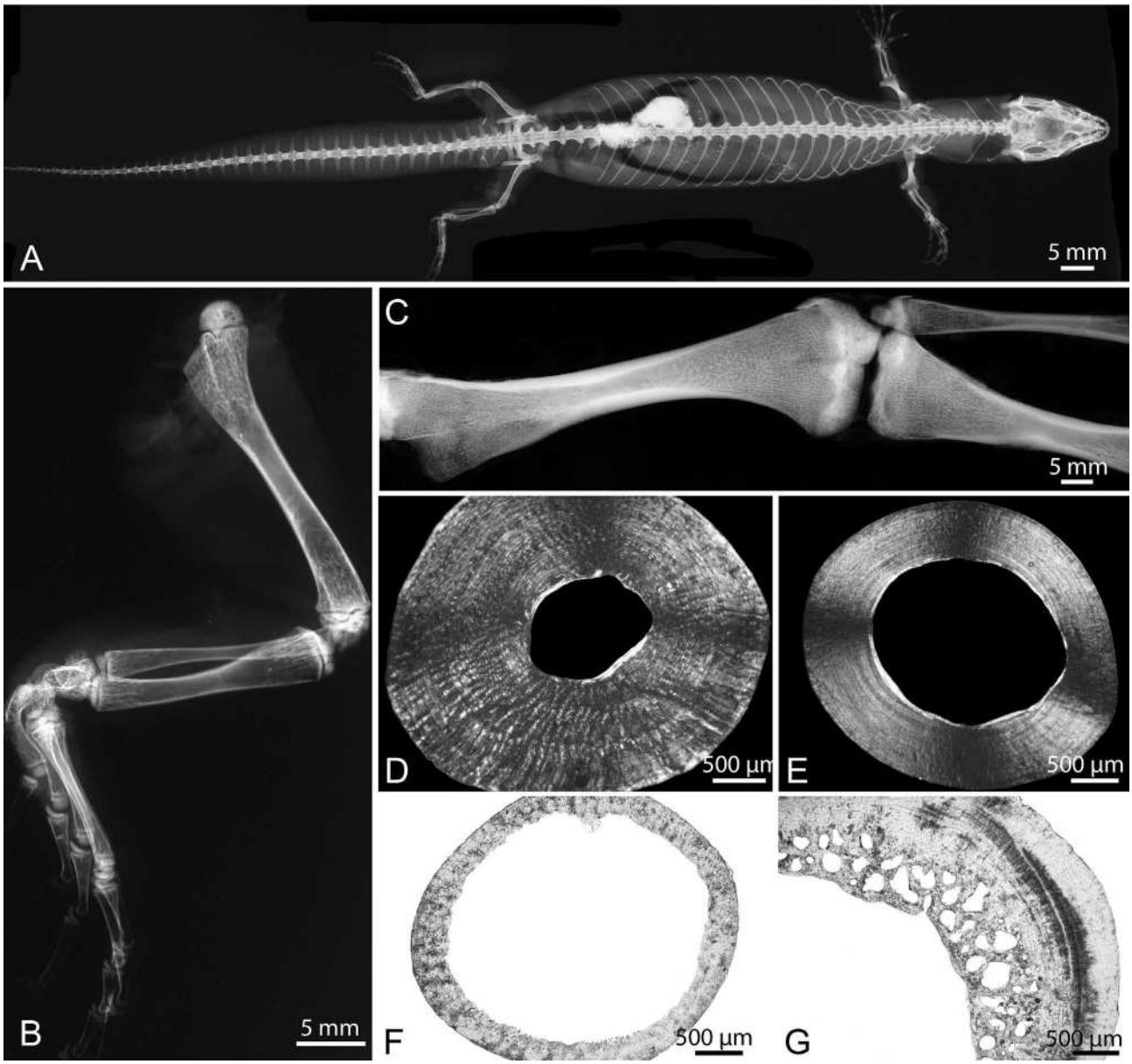


FIGURE 20.1 Gross anatomy and microanatomical features of a lizard skeleton. A, X-ray proof showing the general aspect of the skeleton of a small varanid, *Varanus brevicauda* (maximum snout-vent length: 120 mm). B, Limb bones of an arboreal varanid, *V. prasinus*. The cortices of stylopodial and zeugopodial elements are relatively thin. C, Femur, tibia and fibula in *V. exanthematicus*. Bone cortices are much thicker than in *V. prasinus*. D, Mid-diaphyseal cross section of the femur of *V. exanthematicus* (transmitted polarized light). The cortex is thick and the corticodiaphyseal index (CDI) of this bone (79%) is high. The transition between the cortex and the medullary cavity is very sharp. E, Mid-diaphyseal cross section of the femur of *V. prasinus* (transmitted polarized light). The cortex is thinner, with a CDI value of 40%. F, Mid-diaphyseal cross section of the femur of *V. rudicollis*. The cortex is very thin (CDI = 16%). G, Patchy resorption around the medullary cavity in *Tupinambis teguixin* (Teiidae).

In most lizard species, the transition between the cortex and the medullary cavity is clear-cut (Figure 20.1D–F; see also Enlow and Brown 1957, Ricqlès 1976), with values close to 0 for Bone Profiler parameter *S* that reflects the steepness of this transition (see Chapter 4). Such a feature is typically associated with terrestrial locomotion (see Chapter 35). The main exceptions are the femurs of large taxa such as some monitor lizards, teiids and iguanas, which may display in some individuals a belt of cancellous tissue due to patchy resorption around the medullary cavity (Figure 20.1G). Cancellous formations are normally differentiated in the metaphyseal and epiphyseal regions of lizard long bones (Enlow and Brown 1957); however, their detailed trabecular architecture and its eventual variations have remained nearly undocumented up to now.

As exposed in Chapter 4, extant limbed lepidosaurs differ from other extant and extinct sauropsids by the presence of secondary ossification centers in the core of the cartilaginous epiphyses of long bones. This feature culminates in conspicuously developed secondary centers housing abundant vascularity in large monitor lizards (Haines 1941). This peculiar

condition, closely convergent with that of mammals, reflects the relatively high (though markedly cyclic and variable) growth rates that characterize many varanid species compared to other extant lizards (e.g., Buffrénil et al. 1994, Buffrénil and Hémery 2002).

The pattern and timing of epiphyseal fusion in 21 lizard taxa were extensively investigated by Maisano (2002), while Buffrénil et al. (2005) and Frydlova et al. (2017; see also review in Griffin et al. 2020) focused on the Varanidae, a taxon absent from Maisano's (2002) sample. Epiphyseal fusion in the stylopodial and zeugopodial bones of the taxa studied by Maisano (2002) may start either before or during sexual maturation, and end when maturation is complete or afterward. Therefore, entirely fused epiphyses in these bones undoubtedly designate sexually mature individuals. Similarly, when epiphyseal fusion occurs, 80% of maximum specific size is reached (only 65% in some species). Therefore, epiphyseal fusion may not be synonymous with total cessation of growth in squamates. In monitor lizards, a characteristic difference exists in the timing of epiphyseal fusion between small and large species. In small forms such as *V. brevicauda*, *V. kingorum* (maximum snout-vent length ca. 120 mm in both), *V. timorensis* (274 mm) and *V. tristis* (305 mm), epiphyseal fusion occurs early and is complete, thus causing the disappearance of growth plates (Figure 20.2A). Conversely, in larger species (Figure 20.2B), such as *V. gouldii* (SVL max = 670 mm), *V. niloticus* (980 mm) and *V. salvator* (1170 mm), fusion is so delayed that it does not occur within the normal limits of individual longevity (data from Buffrénil et al. 2005). In such taxa, epiphyseal fusion is observed only in very old individuals (Frydlova et al. 2017); therefore, potentially functional growth plates may remain nearly throughout life. The timing of epiphyseal fusion is likely to constrain the growth potential of varanid species (and the whole set of their morpho-functional features) to the requirements of specific ecological niches. Data from Petermann et al. (2017) showed a complex interplay between the chronology of suture fusion in cranial and postcranial bones and the detailed niche characteristics of populations of *Aspidoscelis tigris*, a small insectivorous teiid from Central America. Epiphyseal fusion, with complete loss of growth cartilages and with determinate growth, seems to be the ancestral condition of lizards, as settled by Frydlova et al. (2020) in the conclusion to a broad comparative study. The long-lasting maintenance of functional growth plates during ontogeny (with potentially indeterminate growth) is thus a derived condition that appeared several times independently.

Cortical vascularization (Figure 20.2C, D) is an important microanatomical feature of bones, but it is very unevenly distributed in the limb skeleton of squamates. Only two taxa regularly possess vascular canals: the Varanidae (genus *Varanus*) and the Teidae (*Tupinambis* and, to a lesser extent, *Dracaena* and *Callopistes*), which are all large, active opportunistic predators. Other extant and extinct lizards investigated hitherto, including relatively large species such as the green and marine iguanas (*I. iguana* and *Amblyrhynchus cristatus*, respectively) have avascular (Figure 20.2E) or quasi-avascular cortices (Buffrénil et al. 2008, Cubo et al. 2014). When vascular canals occur, they are generally restricted to the larger species and to the larger bones. In monitors (Figure 20.2C, D), where the subject has been more precisely studied, there is a threshold of 398-mm SVL at least, below which species have avascular bones and above which the femur, the humerus, and occasionally the tibia have vascular canals in variable density (Buffrénil et al. 2008). Vascularization in thin bones such as the fibula may occur but is rare and sparse. Cortical vascular supply in limb long bones has been quantified in 54 extant squamate taxa (Cubo et al. 2014), using methods described in Chapter 4. Large tegus (*Tupinambis*) and varanids are close in bone vascular density; however, the abundance of vascular canals in their femora is at best one-half and often one-tenth that of birds, the only diapsids for which precise data are available (Cubo et al. 2014). Morphologically, the canals are either simple (Fig. 2C) or consist of primary osteons (Figure 20.2, D). Until now, only three distinct canal orientations have been observed in squamate long bones: longitudinal, oblique and radial. When present, radial canals (Figure 20.2C) are more frequent in the femur and the rapidly growing part of the tibial cortex (the tibia often presents pronounced off-centered growth; Figure 20.2D).

At histological level, the great homogeneity of the basic traits of all bones in lizards and snakes has been pointed out by Enlow and Brown (1957), Enlow (1969) and Ricqlès (1976). This is particularly true for limb bones in lizards, whatever the size or the geological age of the taxa. In these animals, the expression of Amprino's (1947) rule (cf. Chapter 10) seems to be mainly substantiated by the presence and density of vascular canals, with paradoxical exceptions such as the avascular bones of large iguanids.

In small species, long bone cortices are made of variably differentiated lamellar bone (Figure 20.2E), displaying the typical traits of this tissue type (see Chapter 8). However, the most common type of osseous tissue in lizard limbs is parallel-fibered bone (Figure 20.2F), with a birefringent matrix and spindle-like cell lacunae, oriented parallel to each other and to the general direction of bone layers (Figure 20.2F). According to the dominant geometrical orientation of the collagen meshwork, cross sections may (Figure 20.2F) or may not (Figure 20.2H) express this basic birefringence. Parallel-fibered tissue in lizard long bones can nevertheless turn locally into two different types. Toward the outer cortical layers, it can be progressively replaced by lamellar bone, which is an effect of the decrease in accretion rate in fully developed adults. Conversely, the tissue occurring in basal cortical layers of juveniles in large species (mainly varanids) can display ambiguous characteristics, with a matrix poorly and irregularly birefringent and with large round cell lacunae, randomly distributed within the matrix (Figure 20.2G). This histological structure is intermediate between the true parallel-fibered and the true woven-fibered types. It was named "uncommon parallel-fibered bone" by Houssaye et al. (2013a) but will be called "atypical parallel-fibered tissue" in this chapter. In adults, perimedullary resorption generally erases this tissue.

The growth rate of periosteal cortices (the parameter MAR considered in Chapters 4 and 10) has been experimentally measured in several lizard taxa by *in vivo* skeletal labeling. The parallel-fibered type predominantly encountered in stylopodials reflects accretion speeds *ca.* 0.15–0.60 $\mu m*day^{-1}$. These values are roughly similar to those observed in the

VetBooks.ir

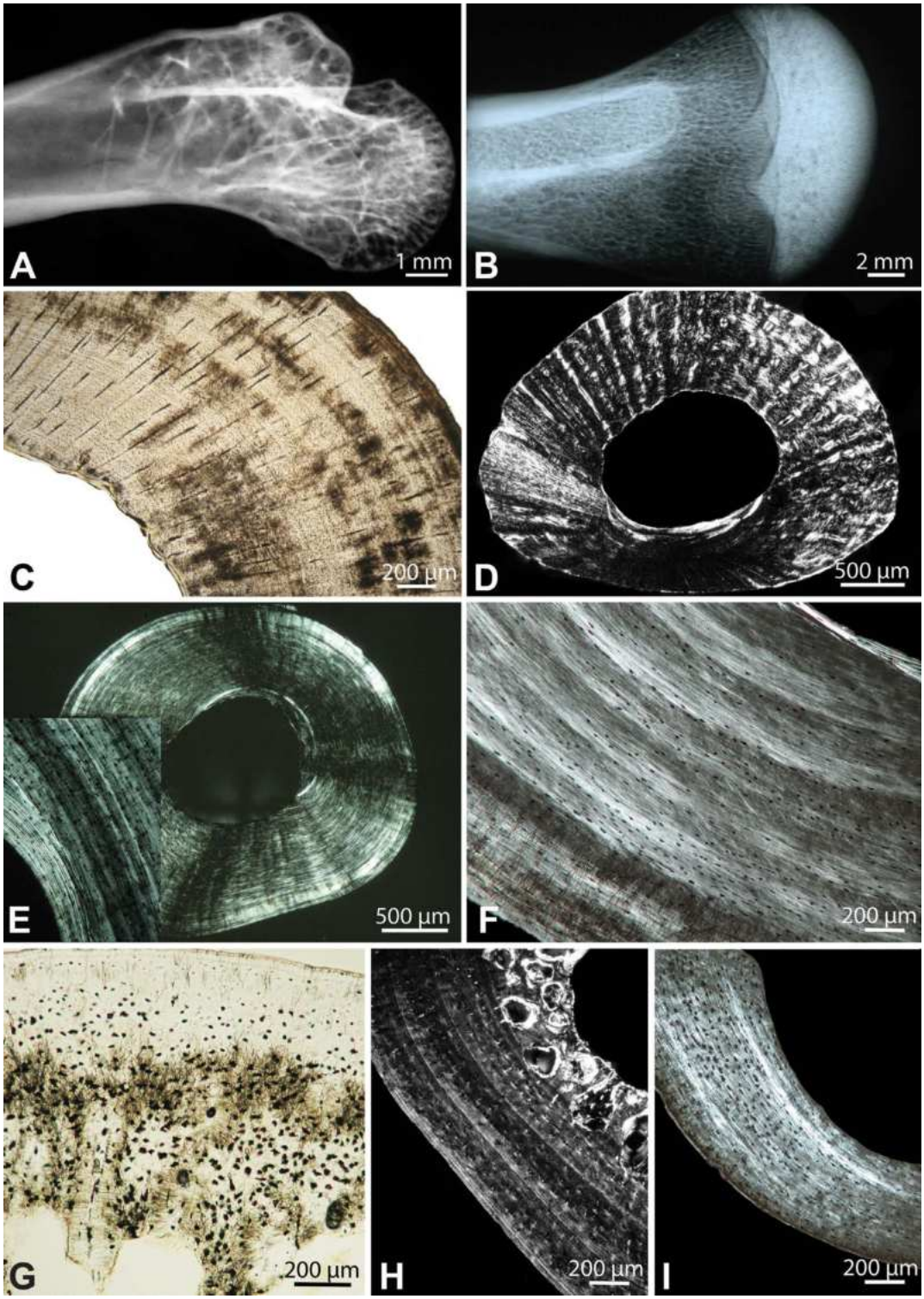


FIGURE 20.2 Microanatomical and histological features of limb bones in lizards. A, X-ray proof showing complete fusion between epiphysis and metaphysis in an adult of a small varanid, *Varanus glebopalma* (maximal snout-to-vent length, or SVL max = 350 mm). B, Aspect of the epiphysis in the adult of a large species, the Nile monitor *V. niloticus* (SVL max = 980 mm). Epiphysis and metaphysis do not fuse within the natural limits of individual longevity. C, Radial vascular canals in the femur of a Nile monitor. D, Asymmetric vascularization in the tibia of the Nile monitor. The lateral, rapidly growing part of the cortex is richly vascularized, whereas the slowly growing medial part of the cortex is avascular (transmitted polarized light). E, A tissue structure intermediate between the parallel-fibered and the lamellar types in the femoral cortex of *Crocodilurus amazonicus* (Teidae). The inset shows the aspect of the true lamellar bone secondarily deposited by the endosteum around the medullary cavity (transmitted polarized light). F, Typical parallel-fibered tissue in the femur of the iguanid *Amblyrhynchus cristatus* (transmitted polarized light). G, Atypical parallel-fibered tissue in the deep cortex of the femur of *V. niloticus*. The expansion of the medullary cavity generally erases this type of tissue. H, Sharp lines of arrested growth in the tibia of *V. niloticus* (transmitted polarized light). I, Two brightly birefringent annuli in the femoral cortex of *Sauromalus obesus* (Iguanidae).

VetBooks.ir

same kind of tissue in other tetrapods (e.g., Castanet 1982, Buffrénil and Castanet 2000). Moreover, comparative data on osteocyte lacunar density (parameter OLD, expressed in cell lacunae*mm^{-3}) presented by Stein and Werner (2013) show that this parameter is of comparable value, between 40*10^3 and 60*10^3 cl*mm^{-3} in three relatively large lizard species (*Tupinambis teguixin*, *V. niloticus* and *V. timorensis*) and a sample of two bird species, *Buteo buteo* and *Struthio camelus*. However, another large lizard, *I. iguana*, has a smaller OLD value, 20*10^3 cl*mm^{-3}. Paradoxically, OLD in teiids and varanids is higher than in mammals (20*10^3 to 40*10^3 cl*mm^{-3}), which suggests that this parameter is not closely related to resting metabolism.

Yearly cyclical growth marks are prone to occur in all bones of all squamate taxa and age can be determined by counting growth cycles (e.g., Peabody 1961, Castanet 1985), a method called skeletochronology after Castanet (1978). Details of this method are given in Chapter 31. The great number of squamate species studied hitherto shows that annual growth cycles in lizard long bones consist of either lines of arrested growth (i.e., 5–10 µm-thick layers strongly birefringent and chromophilic; Figure 20.2H) separated by strata of lamellar or parallel-fibered bone, or annuli (Figure 20.2E, I), which are layers of lamellar bone several tens of microns thick, regularly distributed within parallel-fibered formations. The sharpness, spacing and even the existence of the marks may show conspicuous variations among species or conspecific populations (Buffrénil and Castanet 2000). Cyclical growth marks basically reflect the local and instantaneous dynamics of periosteal bone accretion. Their structure depends on both internal parameters and numerous external influences likely to vary greatly with individual ecological context (see e.g., Pertermann and Gauthier 2018). This explains why typical ectopoikilothermic animals such as lizards and snakes may vary greatly in the sharpness and pattern of their growth marks (Peabody 1958, Buffrénil and Castanet 2000).

In the current histological literature, the tissue organization observed in squamates (as in numerous other vertebrates), i.e., a combination of parallel-fibered or lamellar tissues with cyclic growth marks and sparse vascularization, if any, is often designated by the term "lamellar-zonal" (cf. terminological review in Francillon-Vieillot et al. 1990; see also Ricqlès 1975, 1976, 1979). It is noteworthy, however, that two of these characteristics, vascular canals and growth marks, are prone to extreme variability and may even be absent. Moreover, the basic structure of the bone matrix can vary substantially.

Perimedullary remodeling occurs in all long bones. It can be either symmetrical and centered around the bone long axis, a situation characteristic of straight, cylindrical bones such as the fibula, or strongly asymmetrical in bones having a bent diaphysis, as frequently exemplified by the tibia (Figure 20.2D). In the latter situation, asymmetry involves both periosteal accretion on the outer surface of the cortex, with fast accretion on one side and slow or no accretion on the opposite side, and the expansion of the medullary cavity that proceeds by resorption in the direction of faster growth and secondary reconstruction on its opposite side (see Chapter 9). In lizard long bones, remodeling around the medullary cavity involves regular, continuous resorption and reconstruction fronts, thus giving a smooth contour to the medullary cavity. As mentioned above, patchy remodeling in the form of small units dispersed in the deep cortex is observed only in the femur or humerus of some large taxa (e.g., Figure 20.1G, 2H).

Haversian remodeling is rare in the long bones of lizards. Sparse secondary osteons have been observed by one of us (VB) in the cortex of the fibula of *V.* [*Megalania*] *priscus* (the largest known lizard, from the Pleistocene of Australia) and the femur of a young *V. komodoensis*; otherwise, lizard long bones are basically devoid of intracortical remodeling. Some limited remodeling activity can nevertheless occasionally occur near or within the secondary deposits bordering the medullary cavity and result in closed cavities partly infilled later by centripetal endosteal deposits (Figure 20.3A). Such structures, comparable to secondary osteons, were designated "endosteal Haversian systems" by Enlow and Brown (1957). As in all other vertebrates, the trabeculae of endosteoendochondral spongiosae in epiphyses and metaphyses are densely remodeled in lizards.

Occurrence of Sesamoids

Well-differentiated sesamoids can be observed near the joints of long bones in many lizards. The reviews by Haines (1969) and Jerez et al. (2010) show that these accessory ossicles are prone to occur, with variable frequency, at all articular levels: between phalanges, metapodials, tarsal and carpal bones as well as zeugopodial and stylopodial elements. They appear as cartilaginous masses during embryonic development and are fully ossified in large adults. Their inner structure does not differ from that of the sesamoids observed in mammals, for example. Squamate sesamoids were classified into four groups by Jerez et al. (2010), depending on whether they (1) occur inside tendons ("embedded sesamoids"), (2) are placed between bones but outside tendons ("intraosseous sesamoids"), (3) provide a gliding surface to tendons ("glide sesamoids") or (4) serve for muscle attachment ("supporter sesamoids"). According to Regnault et al. (2016), the patella (i.e., knee joint sesamoid) is an ancestral character in lepidosaurs.

Vertebrae and Ribs in Lizards and Snakes

The number of investigations dealing specifically with the inner structure of the vertebrae in lizards and snakes is astonishingly low compared to studies of their anatomy or biomechanical characteristics. To our knowledge, only five contributions give detailed data on this topic: Buffrénil and Rage (1993), and Houssaye et al. (2010, 2013a, b, 2014). Miscellaneous observations are found in Tschopp (2015) and Petermann and Gautier (2018).

The inner architecture of vertebral centra in lizards and snakes is basically similar in all taxa; exceptions are few and mainly restricted to some fossil forms. As in most vertebrae, the centrum includes two conelike formations (they appear as triangles in sagittal sections) of endosteoendochondral spongy tissue opposed at their apices; the remaining osseous parts of the centrum are composed of periosteal tissue in the form of a compact cortex turning into a remodeled spongiosa in the deeper region. As shown in Chapter 9, when remodeling

VetBooks.ir

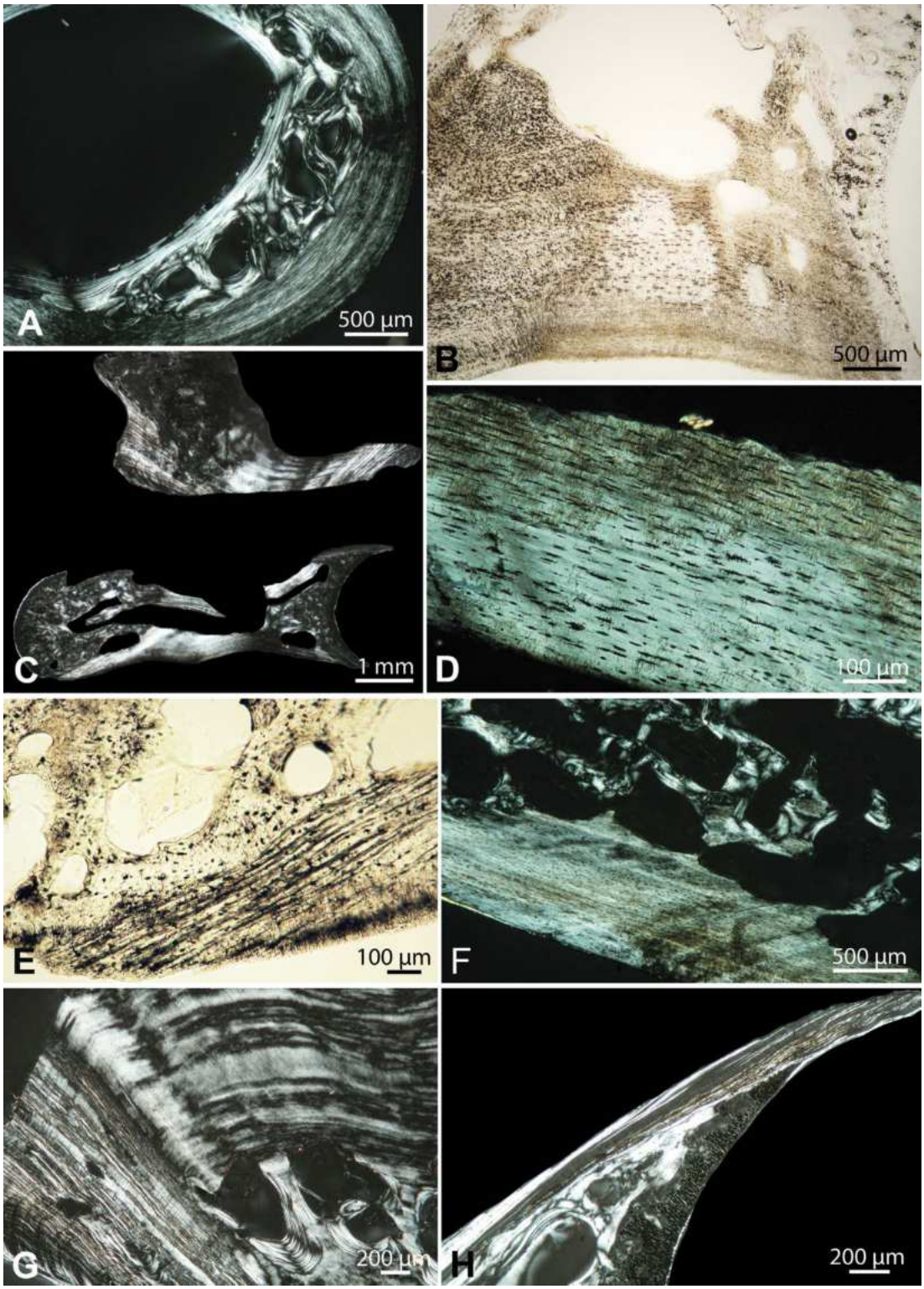


FIGURE 20.3 Long bone remodeling and vertebral structure in squamates. A, Perimedullary secondary osteons in the femur of *Heloderma horridum* (transmitted polarized light). B, Atypical parallel-fibered tissue in the deep vertebral cortex (temporarily spared by resorption) of a young *Python reticulatus*. C, Lightly built vertebral centrum in the colubrid *Natrix natrix* (transmitted polarized light). D, Sagittal section in the cortex of the vertebral centrum of *Amblyrhynchus cristatus*. The cortex is made of pure parallel-fibered tissue (transmitted polarized light). E, Sharpey's fibers in the posteroventral region of the vertebral centrum of *N. natrix*. F, Resorption of the deep cortex of a *Varanus bengalensis* vertebral centrum. The trabeculae occupying the core of the centrum are intensely remodeled (transmitted polarized light). G, Sharpey's fibers and inner remodeling in the neural apophysis of a *Bothrops lanceolatus* (Viperidae) vertebra (transmitted polarized light). H, The secondary osseous formation containing Sharpey's and elastic fibers that frequently forms the dorsal, protruding edge of the squamate vertebral cotyle (sagittal section of a *B. lanceolatus* vertebra in transmitted polarized light).

VetBooks.ir

activity in the endosteoendochondral spongiosa is mild, the growth center of the centrum can be localized with reasonable precision. In lizards and snakes (and in squamates as a whole), the position of this point is generally not at mid-length between the cotyle and the condyle: the contribution of the caudal (condylar) growth cartilages to the overall growth in length of the centrum is greater than that of the cranial (cotylar) cartilages. This is a characteristic trait of squamates, documented with quantitative data by Houssaye et al. (2010).

The compactness of the centrum is variable (Figure 20.3B, C). Compactness values measured in longitudinal sections by Houssaye et al. (2010, 2013a) range in extant lizards (28 species) between 38 and 80%, and in snakes (54 species) between 43 and 90%. Transverse sections give roughly similar results. Precise data for extinct taxa are restricted to *Palaeophis maghrebianus*, a very large coastal snake from the Ypresian of Morocco (Houssaye et al. 2013b). The vertebral centrum of this taxon shows exceptionally high compactness indices (up to 92% in longitudinal and transverse sections) and signs of osteosclerosis. Such features also occur in *P. colossaeus*. The variation among taxa cannot be clearly related to phylogeny, habitat or locomotory mode, except some peculiar adaptations such as bottom feeders (e.g., Palaeophiidae) or heavy-bodied strikers (e.g., *Bitis* vipers); however, specific size is suspected to influence vertebral microstructure (Houssaye et al. 2013a). When several specimens are available for one species, individual compactness values can be fairly different. As in long bones, compactness measurements in vertebrae are likely to be sensitive to gender, age, growth activity and reproductive status (not considering environmental stochastic factors): they must therefore be considered and interpreted with some caution, especially in fossils. Until now, there are no specific descriptions of the inner architecture of vertebral apophyses in lizards and snakes. Miscellaneous observations and illustrations in Buffrénil and Rage (1993), Houssaye et al. (2010, 2013a), and Petermann and Gautier (2018) suggest that their inner architecture is a mere continuation of that prevailing in the centrum.

The histological structure of periosteal cortices in vertebrae is like that in long bones. The tissue is generally parallel-fibered bone (Figure 20.3D), which may turn to either the atypical parallel-fibered type (when the deep cortex is spared by resorption, as shown in Figure 20.3B) or to the lamellar type, if the taxon considered is, respectively, of large or small size. Skeletal growth marks are common in the cortices of the centrum and neural arch (e.g., Buffrénil and Rage 1993). Vertebral centra in lizards and snakes have strong bundles of Sharpey's fibers mainly located at the cranial and caudal ends of periosteal cortices (Figure 20.3E). Radiating or oblique simple vascular canals, sometimes densely ramified (see, e.g., Houssaye et al. 2013b), occur in the cortex of the centrum of large (mainly snake) species. As in long bones, intracortical (Haversian) remodeling is absent in vertebral bodies.

The trabeculae of the spongy formations occupying the core of the centrum are densely remodeled. Some of them are of endosteoendochondral origin and are composed exclusively of endosteal lamellar tissue in the form of crescent-like hemiosteons (see Chapter 11). In no extant taxon, whatever its ecological specialization, has calcified cartilage been observed in the core of these trabeculae at a distance from epiphyseal (cotylar and condylar) surfaces. Another part of trabecular networks is of periosteal origin. Although the periosteal cortex of squamate vertebral centra is deposited as compact bone, its basal part undergoes an extensive resorption that transforms it into a loose spongiosa (Figure 20.3F). Toward the core of the centrum, the trabeculae are actively remodeled to become entirely composed of secondary lamellar tissue. The basic histological characteristics of apophyses (Figure 20.3G) are similar to those of the centrum: their cortex is made of parallel-fibered tissue with conspicuous cyclical growth marks and Sharpey's fibers, whereas their inner spongiosae (if any) are intensely remodeled. Superficial (outer) remodeling also occurs on the floor of the neural canal, where it is extremely pronounced and extensive. Most of the bone present at this level consists of secondary deposits that tend to form a thick caplike layer, rich in anchoring fibers and resting on a reversion line, in the anterior part of the neural canal floor (Figure 20.3H).

Few publications specifically consider the inner structure of ribs in lizards and snakes, a subject that may have some potential interest, especially in snakes in which the ribs are both weight-bearing and involved in locomotion. Brief references to these bones can be found in Enlow and Brown (1957), Peabody (1961) and Ricqlès (1976), who all pointed out the structural similarity between ribs and long bones. The extensive comparative study of rib microanatomy in amniotes by Canoville et al. (2016) (27 extant lizard species, 32 snakes) showed that the general pattern observed in long bones, i.e., a clear-cut boundary between a medullary cavity devoid of trabeculae and the compact cortex also occurs in ribs; however, as in long bones, the medullary cavity of the ribs in large lizards (several varanids and iguanids) can be partly occupied by trabeculae. Rib compactness among lizard taxa ranges from 50.9% (in *Hydrosaurus pustulatus*, an amphibious agamid) to 99.6% (in *Salvator merianae*, a terrestrial teiid). In snakes, it ranges from 66.5% (in the amphibious colubrid *Natrix natrix*) to 99% (in *Liasis fuscus*, a terrestrial pythonid). High compactness values in both groups are not obviously related to habitat, but are frequently associated with large body size. Cortices in lizard and snake ribs are avascular.

Histologically, there is no noticeable difference between ribs and long bones. Cortices are of the same basic parallel-fibered tissue type. Cyclic growth marks (annuli and lines of arrested growth) regularly occur, as well as abundant bundles of Sharpey's fibers. Off-centered growth, resulting in a characteristic drift in the position of the medullary cavity, is a general trait of ribs. When present, medullary trabeculae are intensely remodeled, but there is no trace of intracortical Haversian remodeling.

Remarks on Skull Bones and Teeth in Lizards and Snakes

Studies dealing specifically with the microanatomical or histological structure of skull elements in lizards and snakes long remained scarce and mainly related to tooth-bearing bones, especially the dentary. The current use of tomography changed this situation, but data on the architecture of calvarial bones are still anecdotal. In *Uromastyx*, the tomographic evidence

VetBooks.ir

from Moazen et al. (2009) revealed a lightly built but otherwise classical diploe structure in the jugal, postorbital and parietal. Similar data were obtained through the same technique for the skull bones of *Shinisaurus* (Bever et al. 2005). The broad tomographic survey of the cranial microanatomy of squamates recently conducted by Ebel et al. (2020) revealed an ecological signal in the bones of the skull roof. These bones are proportionally thicker and much more compact (they often display osteosclerotic-like characteristics) in fossorial lepidosaurs compared to non- or semifossorial forms. This trait evolved convergently in several taxa and may have regressed (a reversion process) in the clades that returned to a nonfossorial lifestyle. For the mandible, several anecdotal descriptions or illustrations can be found in the literature, in studies dealing with either tooth implantation and replacement or skeletochronological age assessments. The squamate upper jaw is composed of two bones, and the mandible includes up to six bones (see, e.g., Romer 1956, Kardong 1998), each having its own microanatomical features and its own pattern of transformation during growth. The precise location of sectional planes is thus important, but rarely considered. In *V. niloticus*, Maxwell et al.'s (2011) illustrations show the dentary as a fairly compact bone, as is also the case in, e.g., *Cylindrophis ruffus* (Rieppel 1978); however, comparative data suggest that this bone has a much lighter fabric in juveniles (e.g., Smirina and Anajeva 2007, Haridy 2018). In the absence of broad comparative series, no general conclusion can be drawn from the miscellaneous data available hitherto on calvarial and mandibular architecture in lizards and snakes. It nevertheless seems obvious that this feature is highly variable and prone to important ontogenetic modifications, and that it may have adaptive meaning. Future studies based on large sampling and computed tomography (CT)-scan reconstructions should address these interesting issues.

A common opinion, following the classic syntheses by Enlow and Brown (1957), Enlow (1969) and Ricqlès (1976), is to consider the histological structure of all bones in lizards and snakes as identical to that of the long bone cortices, i.e., basically avascular parallel-fibered or lamellar tissues. Observations by Castanet (1974a, b) of cross sections in the mandibular plate of *Vipera aspis* (a flat and thin region composed of the fused angular and surangular bones, and forming a dorsally protruding blade) have shown that the growth of this bone is strongly asymmetric, with a rapid (1.3–2.1 µm*day^{-1}) accretion directed upward on top of the mandibular plate, and a much slower bone deposition on lateral and ventral surfaces. Consistent with this growth pattern, lateral cortices are made of lamellar tissue, whereas the part of the cortex situated in the major growth axis is formed by a succession of growth cycles; each cycle comprises a zone of woven-fibered tissue resulting from fast accretion, associated with an *annulus* made of parallel-fibered or lamellar tissues and a line of arrested growth. Vascular canals are sparse or absent in this bone, especially in the annuli. The reference definition of the structure of cyclical growth marks in reptile bones (e.g., Castanet et al. 1993) was mainly inspired by this description (see also Chapter 31). The histological structure of the mandible can be somewhat different in large species such as the Nile monitor: unpublished observations by one of us (VB) reveal that the deep part of primary cortices in the thickest regions of the adult dentary may include a relatively broad formation of woven-fibered bone (Figure 20.4A). Cyclic growth marks are locally absent in this tissue, but vascularization is abundant in the form of primary osteons, oriented parallel to the long axis of the mandible. Therefore, the deep cortex of the dentary in adult Nile monitors is, at least in some places, made of a fibrolamellar complex with longitudinal osteons. This tissue can be remodeled and exhibit secondary osteons (Figure 20.4B). All these features are in strong contrast with classical descriptions and show that the histological structure of squamate bones is more plastic than previously thought. Again, future comparative studies should further document this interesting question.

The occurrence of sesamoids in various cranial locations has recently been shown by Montero et al. (2017) in several lizard taxa. This feature was previously considered restricted, among reptiles, to the crocodiles and turtles.

Tooth characteristics in squamates were reviewed by Edmund (1969) and Carlson (1990; see also Chapter 13); interest will be focused here on the relationship between bone and teeth. The two main modes of tooth implantation in lizards and snakes, acrodonty and pleurodonty, are very unevenly distributed. Acrodonty is observed in only two lizard families, the Agamidae and the Chamaeleonidae (united for this reason in the clade Acrodonta), and in some Amphisbaenia (Zaher and Rieppel 1999). By definition (cf. Edmund 1969, Zaher and Rieppel 1999), acrodont teeth are implanted on the occlusal ridge of the maxillae, premaxillae and dentary bones, to which they are ankylosed at their base and lower lateral faces in a shallow groove bordered on both sides by bony crests, the dental groove (also called "alveolar groove" by Zaher and Rieppel 1999). As pointed out by Zaher and Rieppel (1999), beyond this morphological definition, the most constant and characteristic trait of acrodont teeth is that they are not replaced in adult individuals. Therefore, they undergo continuous wear during aging, and may disappear entirely in old animals. The latter then use their jawbones for food processing. Pleurodont teeth (Figure 20.4C) are mainly ankylosed at the lateral (labial) wall and, to a lesser extent, their base on the oblique inner (lingual) side of the labial crest of tooth-bearing bones. The base of the lingual wall of a pleurodont tooth typically has a large opening created by resorption to accommodate the growing replacement tooth. Minor morphological variations in acrodont and pleurodont implantations were described by Edmund (1969) and Zaher and Rieppel (1999). A combination of pleurodont teeth in the anterior part of the jaws and acrodont teeth in the rear part occurs in some taxa, such as the agamid *Pogona vitticeps* (Haridy 2018).

Nearly all squamate teeth, whether acrodont or pleurodont, have a synostotic mode of ankylosis to the jawbones; the tooth-to-bone union is accomplished by a specific tissue, the attachment bone (Figure 20.4D, E). The histological characteristics of this tissue closely resemble those of woven-fibered bone (Edmund 1969) with a coarse monorefringent matrix housing numerous large roundish osteocyte lacunae making it different from cementum. Attachment bone can extend between the teeth and constitute interdental ridges. The surface of attachment bone in pleurodont teeth is covered with Howship's lacunae set in place by extensive osteoclastic

VetBooks.ir

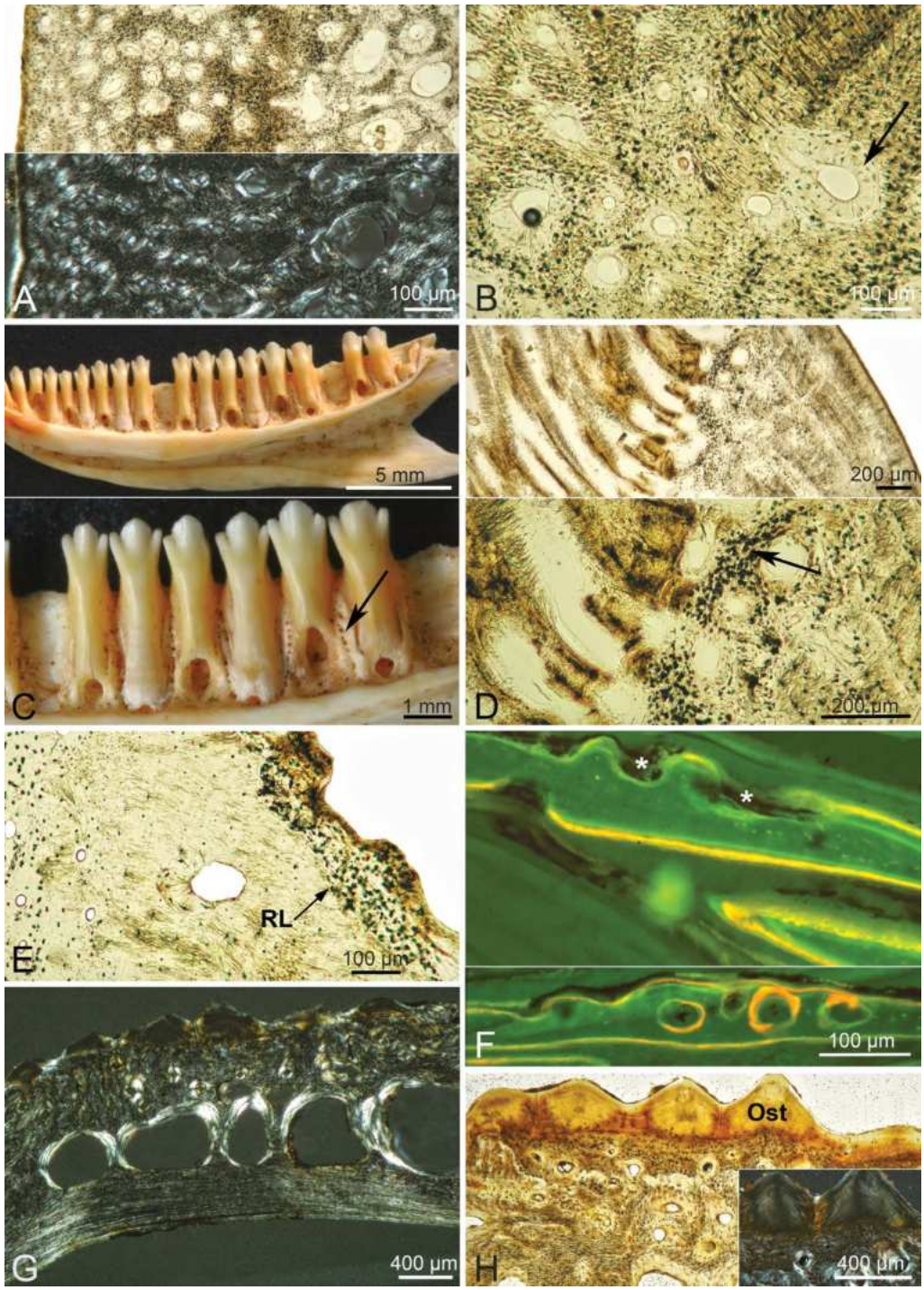


FIGURE 20.4 Squamate mandible and osteoderms. A, Local formation of a woven-parallel complex in the mandible of *Varanus niloticus*. Lower part: transmitted polarized light. B, Closer view of the tissue mentioned in A. Secondary osteons (arrow) also occur in this tissue. C, Lingual view of *Gallotia* sp. mandible at two distinct enlargements. The tooth implantation is typically pleurodont. Attachment bone (arrow) partly fills interdental gaps. The holes in the tooth roots accommodated developing replacement teeth. D, Attachment bone (arrow) in the mandible of *V. salvator*. The lower view is a detail of the upper one. The tooth root in this taxon consists of plicidentine. E, Reversion line (RL and arrow) separating the attachment bone from the dentary in *V. salvator* mandible. F, *In vivo* labeled (by DCAF and xylenol-orange) osteoderms of the anguid *Anguis fragilis*. The upper field shows (a) the tilelike overlap of contiguous osteoderms, (b) their initial compactness and (c) the patchy resorption (asterisks) that creates ornamentation on the osteoderm surface. The lower field shows the inner resorption and incomplete reconstruction resulting in the creation of a spongiosa in the core of an osteoderm. G, Section of an osteoderm from a Middle to Late Eocene indeterminate glyptosaurine lizard (possibly *Placosaurus* sp.). The osteoderm is made of three distinct tissues: (1) lamellar tissue in its basal cortex, (2) strongly fibrillar metaplastic tissue, with extensive traces of remodeling in its outer cortex and (3) osteodermine, a tissue akin to hypermineralized tissues, forming a superficial coating with domelike protuberances (transmitted polarized light). H, Closer view of the outer cortex showing its coarse fibrillar structure (due to the dermo-osseous metaplasia that initiates the osteoderm growth) and the acellular, monorefringent osteodermine (ost.). Inset: osteodermine in transmitted polarized light.

VetBooks.ir

resorption (e.g., Delgado et al. 2005). During tooth replacement, the base of a functional tooth and the attachment bone covering it are eroded (Figure 20.4C) until the shedding of the tooth; a new tooth of larger size then comes to position against the labial crest of the jawbone and is ankylosed to it by attachment bone. In cross sections, the latter is often bordered by a cementing line (Figure 20.4E) that separates it from the tooth-bearing bone (Edmund 1969). Though the teeth of snakes are undoubtedly pleurodont, their attachment to bone includes an important ligament, shaping a crescent along the rear (caudolingual) side of the tooth base. This ligament is normally embedded in attachment bone to form the mineralized periodontal ligament (PDL; LeBlanc et al. 2017). In some species, however, attachment bone is absent, and the ligament is unmineralized (Savitzky 1981). This situation confers to the teeth a capacity to incline backward under frontal pressure, defining the so-called "hinged teeth". This characteristic is interpreted as an adaptation to swallowing hard, shelled prey (Savitzky 1981, Patchell and Shine 1986, LeBlanc et al. 2017). According to Budley et al. (2006), this feature might have been already present in a Cretaceous snake, *Dinilysia*.

Osteoderms

In extant and extinct Lepidosauria, osteoderms are encountered only in lizards. The clades displaying the most conspicuous osteoderm shields are predominantly the Anguimorpha and the Scincomorpha. Among the Anguimorpha, osteoderms occur in the Anguidae (review in Hoffstetter 1962; see also Bhullar and Bell 2008, Bochaton et al. 2015), the Shinisauridae (Bever et al. 2005, Conrad 2006), the Helodermatidae and other Monstersauria (Mead et al. 2012), and several varanoid forms such as the Paleovaranidae (Necrosaurinae), the Lanthanotidae (Maisano et al. 2002) and the largest Varanidae: *V. komodoensis* (Auffenberg 1981) and *V.* (*Megalania*) *priscus* (Erickson et al. 2003). Among the Scincomorpha, well-developed osteoderms mainly occur in the Scincidae, exemplified by *Chalcides* (Hoffstetter 1962) and *Corucia* (Moss 1969).

The morphology of squamate osteoderms is highly variable, as well as their size, compared to that of the body. Most osteoderms are single elements (juxtaposed or partly overlapping: Figure 20.4F), but in the scincids, they are compound (Hoffstetter 1962). They can appear as irregular parallelepipeds (e.g., *Tarentola*), hemispheric volumes (Helodermatids), discoid or ovoid elements often showing a convex outer side, a sagittal keel and a concave inner side, or convoluted "vermiform bones" (large varanids). Ornamentation (Figure 20.4F) on the outer surface of osteoderms is a general trait in lizards (as in most other vertebrates; e.g., Buffrénil et al. 2016). Conversely, the inner (lower) surface is smooth. Ornamentation may consist of a network of vermicular interconnected grooves (e.g., *Anguis*; Zylberberg and Castanet 1985), apparently reflecting the trajectories of superficial blood vessels, or appear as roundish pits separated by ridges (e.g., Monstersauria and *Lanthanotus*). A rarer form of ornamentation is created by positive reliefs that may have a hemispheric shape (skull osteoderms of helodermatids; Mead et al. 2012) or develop as ogival domes, as in the Eocene glyptosaurine *Placosaurus* (Buffrénil et al. 2011).

Few studies clearly figure and describe the inner architecture of squamate osteoderms. Data currently available suggest that two main patterns may occur, with a possible transition from one to another during ontogeny. In the small spheroid osteoderms observed in *Tarentola* by Levrat-Calviac (1986), as in the hemispheric ones sampled by Moss (1969) from *Heloderma*, the osteoderm's inner structure is solid, with only sparse and minute cavities housing blood vessels. Though not measured specifically, the overall compactness should apparently be close to 100% in such cases. Conversely, lenticular or discoid osteoderms display the gross structure of a diploe, the compactness of which is highly variable. In specimens of *Celestus occiduus* and *Diploglossus monotropis* (Diploglossidae) observed by Bochaton et al. (2015), and in the *Placosaurus* osteoderms described by Buffrénil et al. (2011), compactness is high in some specimens, while others may show relatively large coalescent cavities creating a central spongiosa (Figure 20.4G). A similar (though much less pronounced) situation occurs in the osteoderms of *Anguis fragilis* studied by Zylberberg and Castanet (1985). It seems likely that the core of osteoderms organized as a diploe is gradually made cancellous by imbalanced remodeling.

At the histological level, osteoderms are merely composed of osseous tissue in most of the tetrapod taxa in which they occur (e.g., temnospondyls, pseudosuchians, dinosaurs and mammals; e.g., Vickaryous and Sire 2009, Buffrénil et al. 2016); however, they may differ from this general situation in some lizard taxa. In the gekkonid *Tarentola mauritanica*, the detailed studies in optic and electronic microscopy by Levrat-Calviac (1986), Levrat-Calviac and Zylberberg (1986) and Levrat-Calviac et al. (1986) revealed that osteoderms show two histologically distinct strata. The outer stratum includes both sparse collagen fiber bundles anchoring the osteoderm into the surrounding dermis, and a "fuzzy network" of microfilaments displaying a radiating arrangement. The whole organic phase in this stratum is loose and displays feeble chromophily. Mineralization is of the inotropic type (i.e., apatite crystals distributed along the fibrils) within the collagen bundles, and of the spheritic type (apatite globules) between the microfibrils. The basal stratum, more chromophilic, contains densely packed bundles of collagen fibers oriented variably. Local mineralization is inotropic. Comparative data by Moss (1969) and Vickaryous and Sire (2009) have shown that this general histological structure is also encountered in the osteoderms of helodermatids; moreover, the pictures of a *V.* (*Megalania*) *priscus* osteoderm section given by Erickson et al. (2003) suggest that it occurs as well in varanid osteoderms. Following the interpretation of these authors, this structure results from a metaplastic transformation of the local dermis into osseous tissue, in the absence of differentiated osteoblasts (see also Chapter 12). The superficial, poorly chromophilic layer is then supposed to derive from the *stratum laxum* (loose layer) of the dermis, and the more chromophilic basal layer from the *stratum compactum*.

Although the flat, diploe-like osteoderms of anguids and several other lizard taxa have been interpreted by some authors (e.g., Levrat-Calviac et al. 1986) as also resulting from metaplasia, they differ importantly from those of

VetBooks.ir

geckos and deserve specific descriptions and comments. The histological structure of this kind of osteoderms has been studied, with variable precision and clarity, in extant anguids (Moss 1969, Zylberberg and Castanet 1985, Vickaryous and Sire 2009, Bochaton et al. 2015), scincids and gerrhosaurids (Moss 1969), fossil glyptosaurids (Buffrénil et al. 2011) and a paleovaranid (Buffrénil et al. 2016). A simple structure is encountered in *Anguis fragilis*: the outer (superficial) layer is composed of woven-fibered tissue with a relatively loose collagenous meshwork and a high mineral content. Conversely, the basal layer is made of somewhat less mineralized typical lamellar bone (Zylberberg and Castanet 1985). The illustrations by Zylberberg and Castanet (1985) suggest that in *Anguis* osteoderms, ornamentation is due to patchy superficial resorption of the outer layer (Figure 20.4F), a process also described in the Necrosauridae by Buffrénil et al. (2016). Descriptions by Bochaton et al. (2015) reveal some minor differences between *Anguis* and two other anguimorphs *Diploglossus* and *Celestus*. In these taxa (1) the outer cortex is made of a tissue "intermediate between parallel-fibered and lamellar bone", not of woven-fibered tissue; (2) the woven-fibered component is restricted, as a thin layer, to the core of the osteoderms and (3) this central region is submitted to intense remodeling that creates a local spongiosa (inner remodeling is milder in *Anguis*). Moreover, in all anguids, the lamellar tissue forming the basal layer of the osteoderms displays conspicuous cyclic growth marks. Most of these characteristics were also observed in the osteoderms of the fossil glyptosaurine *Placosaurus* (Figure 20.4G, H) by Buffrénil et al. (2011).

Detailed observations by Vickaryous et al. (2015) pointed out some inconsistency between actual osteoderm characteristics and a growth model based on metaplasia alone. Briefly, in anguids, as in other lizards and nonlepidosaurian reptiles (e.g., crocodiles), metaplasia is likely to occur during the earliest stages of osteoderm morphogenesis but typical osteoblast-like cells secreting osteoid soon appear around the osteoderm primordium and are directly responsible for its further growth. In addition, as noted by Buffrénil et al. (2011), superficial and inner remodeling of the osteoderms necessarily implies the presence of both osteoclasts (resorption) and osteoblasts (reconstruction).

The superficial layer of *Placosaurus* osteoderms shows a very peculiar tissue, osteodermine, in the form of ogival protuberances. This tissue displays none of the typical features of bone: it is vitreous, monorefringent and acellular (Figure 20.4H); moreover, its mineral content, as revealed by x-ray images and electronic probe analyses, is clearly higher than that of the surrounding bone (Buffrénil et al. 2011). Osteodermine is apparently akin to enamel and other hypermineralized tissues resulting in vertebrates from dermo-epidermal interactions. The molecular machinery involved in its production was thought to have completely disappeared outside the oral cavity in tetrapods, an opinion that should now be revised. Osteodermine was recently identified and described with further precision in the osteoderms of geckos by Vickaryous et al. (2015) and Kirby et al. (2020). It had been suspected long ago by Moss (1969) and Vickaryous and Sire (2009) to occur in *Heloderma*. This tissue might be relatively frequent in lizards.

Aigialosaurs and Mosasaurs

General Features of Mosasauroidea

Mosasauroids are large aquatic squamate predators forming the clade Mosasauroidea. They comprise the most recent ancestor of *Aigialosaurus* and *Mosasaurus* and all its descendants; it includes the taxa previously assigned to the families Aigialosauridae and Mosasauridae (Bell 1997, Bardet et al. 2008), comprising about 30 genera and 70 species (Garcia et al. 2015). Mosasauroids quickly diversified from the early Late Cretaceous (Cenomanian) to somewhere near the end of the Cretaceous (K/Pg boundary), when they became extinct. Their phylogenetic position within squamates remains strongly debated, ever since Cope (1869). They are generally considered either the sister group of snakes, or members (or at least close relatives) of the Anguimorpha (e.g., Reeder et al. 2015, Pyron 2017).

Mosasauroids are varanoid-like squamates with elongated skull, body and tail; the tail is laterally compressed. They were essentially marine, though some forms have been discovered in freshwater deposits (Makádi et al. 2012, Garcia et al. 2015). They display three general morphotypes (Bell and Polcyn 2005; Caldwell and Palci 2007). The first consists of plesiopedal (with terrestrial-like limbs; Figure 20.5A) and plesiopelvic (ilium anchored to the vertebral column) forms, previously referred to as "aigialosaurs" and now considered a polyphyletic group (Polcyn and Bell 2005; e.g., *Komensaurus*: Figure 20.5B). They were up to 2 m long and are supposed to have lived in the shallow waters of the northern and southern margins of the Mediterranean Tethys and the Caribbean zone, from the Early Cenomanian to the Early Turonian. The

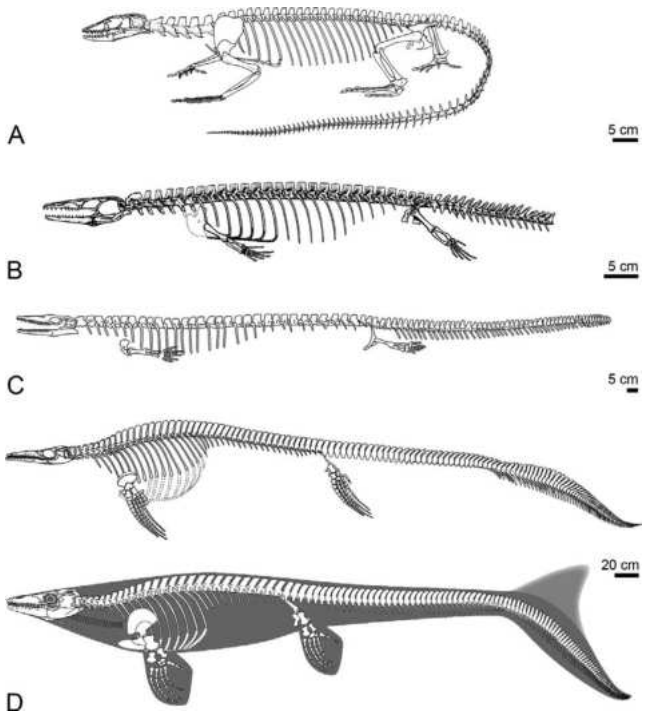


FIGURE 20.5 Skeletal reconstructions of characteristic varanoid and mosasauroid taxa. A, *Varanus salvator*. B, *Komensaurus carrollii*. C, *Dallasaurus turneri*. D, *Platecarpus tympaniticus*. A and B are from Caldwell et al. (1995) and D is from Lindgren et al. 2010.

second morphotype comprises plesiopedal and hydropelvic (no sacrum) forms up to 3 m long (e.g., *Dallasaurus*; Figure 20.5C), known from the Turonian of Texas and Morocco. The third morphotype is represented by hydropedal (with paddles displaying hyperphalangy) and hydropelvic forms ("true mosasaurs") that could reach up to 15 m (e.g., *Prognathodon*, *Mosasaurus*; Figure 20.5D) and lived from the Late Turonian to the Late Maastrichtian. They were distributed worldwide across a broad latitudinal range (Lindgren and Siverson 2002, Fernández and Gasparini 2012). The discovery of a gravid "aigialosaur" (Caldwell and Lee 2001) showed that, from their early origin, some if not all mosasauroids had evolved some degree of viviparity (Field et al. 2015), and were thus independent from the terrestrial environment. Most mosasauroids propelled themselves by body and tail undulations, but some derived forms had hypocercal tail indicating a shift from an anguilliform/subcarangiform to a carangiform swimming mode (Lindgren et al. 2011; Figure 20.5D).

The group shows significant cranial and dental diversity, reflecting different diets and consistent with three main types of food intake and processing: piercing, cutting and crushing (Figure 20.6). While some mosasauroids appear to have been generalists, feeding on invertebrates, fish and reptiles, like opportunist top predators, others were small and gracile with teeth more specialized for eating small fishes, or were robust durophagous forms (Bardet et al. 2005, 2015; Figure 20.6).

Microanatomy and Histology of Ribs

Mosasauroid ribs were notably studied by Sheldon (1997). She focused her work on the three most common mosasauroids from the Western Interior Seaway of North America, *Clidastes*, *Platecarpus* and *Tylosaurus*, which are hydropedal and hydropelvic forms, and she also analyzed the plesiopedal and hydropelvic *Dallasaurus*.

Diaphyseal rib sections in adult hydropedal mosasauroids show no large open medullary cavity, but a spongiose medullary area (Figure 20.7A). The thickness of the compact cortex surrounding the medullary area and the tightness of the spongiosa differ significantly among taxa and result in compactness indices ranging from 54 to 79% (Houssaye and Bardet 2012). Homogeneity in the microstructure (size of the intertrabecular spaces and trabecular thickness) appears to increase during ontogeny, while compactness decreases (Houssaye and Bardet 2012). Conversely, a diaphyseal section of *Dallasaurus* illustrates a tubular organization, with a compactness index of 78% (Sheldon and Bell 1998, Houssaye and Bardet 2012; Houssaye et al. 2013c; Figure 20.8A). The compactness values obtained for these taxa do not significantly differ from the ranges observed in extant forms; therefore, neither osteosclerosis nor decrease of bone tissue mass are observed in hydropelvic mosasauroid ribs (Houssaye and Bardet 2012). Conversely, pachyostosis is observed in the ribs of plesiopelvic mosasauroids and the broken parts of articulated specimens suggest osteosclerosis (Houssaye et al. 2013c). However, no rib sections of plesiopelvic taxa are so far available for study.

In *Dallasaurus*, periosteal bone in ribs consists essentially of parallel-fibered tissue. In the innermost, perimedullary region, localized endosteal deposits of secondary parallel-fibered and lamellar tissues occur. Vascularization consists only of a few local primary osteons oriented longitudinally (Houssaye et al. 2013c). Histological features in the ribs of hydropelvic mosasauroids have not been described in detail, but primary osteons also occur in the outer compact cortex, and the trabeculae of the spongiosa consist of secondary lamellar bone (Sheldon 1997).

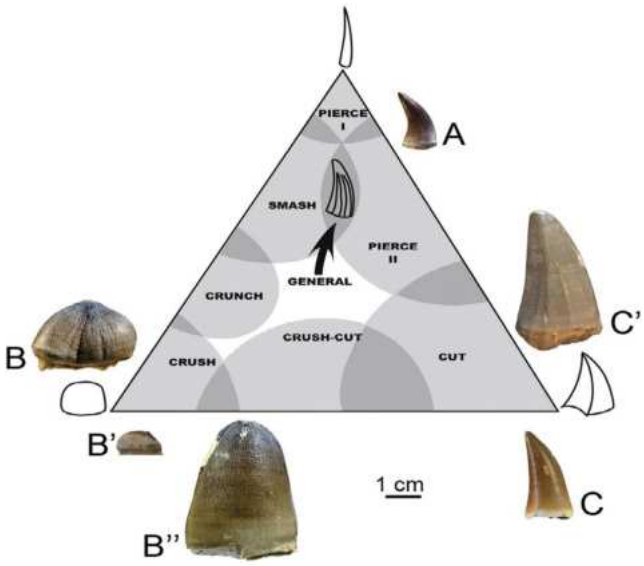


FIGURE 20.6 Diagram illustrating the feeding guilds of mosasauroid species, including piercing, cutting and crushing extremes, with some teeth illustrating shape variation. A, *Halisaurus arambourgi*. B, *Globidens phosphaticus*; B′, *Carinodens minalmamar*. B″, *Prognathodon* nov. sp. (from Bardet et al. 2015.) C, *Eremiasaurus heterodontus*. C′, *Mosasaurus beaugei*.

Microanatomy and Histology of Vertebrae

The inner structure of vertebral centra has been studied in various hydropedal (e.g., *Clidastes*, *Prognathodon*, *Platecarpus*, *Plotosaurus*), plesiopedal and hydropelvic (*Dallasaurus*, *Tethysaurus*) as well as plesiopedal and plesiopelvic (*Haasiasaurus*) mosasauroids.

The compactness of vertebral centra in hydropelvic mosasauroids is variable, in part with size (Figure 20.7B, C). Compact cortical tissue is restricted to a thin layer at the bone periphery and at the dorsal margin of the centrum. It consists of parallel-fibered bone with either primary osteons oriented longitudinally and organized in circumferential rows (Figure 20.9A, B), or simple vascular canals predominantly oriented longitudinally and radially, with some anastomoses. Juvenile specimens show radially oriented vascular canals illustrating the logical occurrence of higher growth rates at early ontogenetic stages (Houssaye and Tafforeau 2012, Houssaye and Bardet 2013). Osteons at the periphery often show a limited centripetal infilling, as opposed to deeper osteons, and can thus appear more like cavities than true osteons (Figure 20.9A, B; Houssaye and Bardet 2012). They thus represent immature/incipient primary osteons following Klein (2010). During growth they become filled until resorption occurs so that the vascular spaces evolve from large to

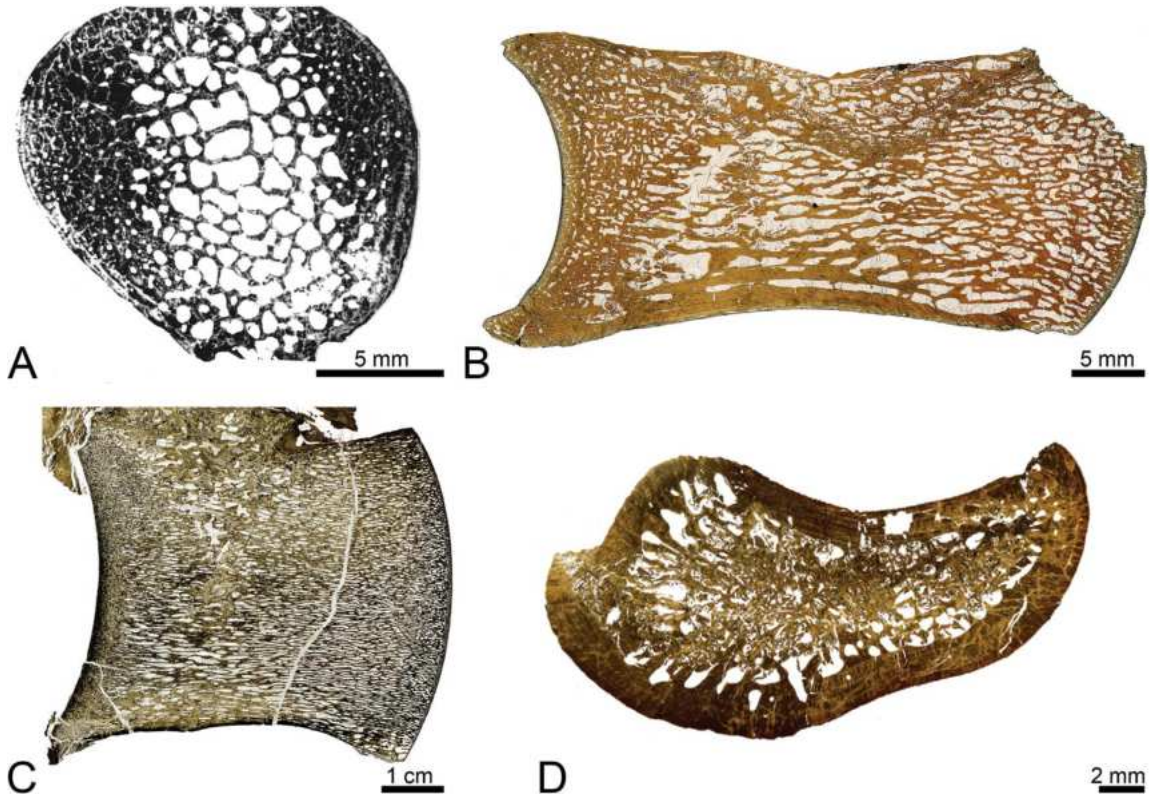


FIGURE 20.7 Ground sections of bones from hydropedal mosasauroids showing their microanatomical organization. A, Rib section of *Platecarpus* sp. (from Houssaye and Bardet 2012). B, Mid-sagittal section of the vertebral centrum of *Clidastes propython*. C, Mid-sagittal section of the vertebral centrum of *Plotosaurus bennisoni*. D, Cross-section of the humeral diaphysis of *Clidastes* sp.

reduced and to large again, from the outer to the inner cortex (Figure 20.9A). Cyclical growth marks in the form of zones and annuli (Chapter 31) occur in compact cortices (Figure 20.9A). Osteocyte density, along with the development of vascular canals, appears clearly higher in zones (the annuli are generally avascular). The trabeculae in the core of the centrum are thin and mostly made of secondary lamellar bone. There seems to be an increase with individual size and species size in the number of trabeculae, coupled with a reduction of their width and of the width of intertrabecular spaces (Houssaye and Bardet 2012, Houssaye and Tafforeau 2012). Despite these differences, a similar vertebral microanatomical organization is observed in juvenile and adult specimens, which suggests that their ecology remained rather constant throughout growth and that the functional requirements of juvenile hydropedal mosasauroids were rather similar to those of adults (Houssaye and Tafforeau 2012).

The global vertebral compactness in hydropedal mosasauroids is similar to that observed in various terrestrial squamates: the compactness of the centrum varies between 50.6 and 52.8% in the specimens studied by Houssaye and Bardet (2012), versus 36.5 to 79.7% in extant squamates (Houssaye et al. 2010). However, these taxa are peculiar because they distribute the osseous tissue inside the centrum to form a relatively tight spongiosa throughout most of the bone volume and a very thin, compact cortex. The resulting architecture clearly differs from the pattern described above for terrestrial squamates (see also Figure 20.14E)

In the plesiopedal and hydropelvic *Dallasaurus* and *Tethysaurus*, the trabecular network in the core of the vertebral centrum is looser, with few but relatively thick trabeculae and irregularly shaped intertrabecular spaces. Moreover, the compact layer of the cortex is proportionally thicker (Houssaye and Bardet 2012; Figure 20.8B). Primary bone also consists of parallel-fibered tissue, but vascularization is scarcer (Figure 20.9C, D). Remodeling is intense, as in hydropedal forms (Figure 20.9E–F), and the trabeculae are entirely made of secondary lamellar bone (Figure 20.9F).

Inner vertebral organization in *Haasiasaurus* completely differs from the patterns considered above. Its vertebrae are osteosclerotic with high compactness (compactness index of 86% in the centrum longitudinal section, 98% in the transverse section; Houssaye 2008; Figure 20.9G, H). A thick formation of compact periosteal bone extends from the growth center to the ventral surface (Figure 20.8E). The dorsal extension of periosteal tissue is limited by the expansion of the neural canal during growth. In general, periosteal formations are extremely compact and show a dense network of simple vascular canals oriented radially but no osteons (Figure 20.9H). The two cones of endosteoendochondral bone formed at epiphyseal levels consist of very tight spongiosae (Figures 20.8E and 20.9G; see also Houssaye 2008). Important remains of calcified cartilage occur in the core of trabeculae, from articular surfaces to the centrum core (Figure 20.9G). They are covered by thin plates of feebly remodeled lamellar bone (Houssaye 2008).

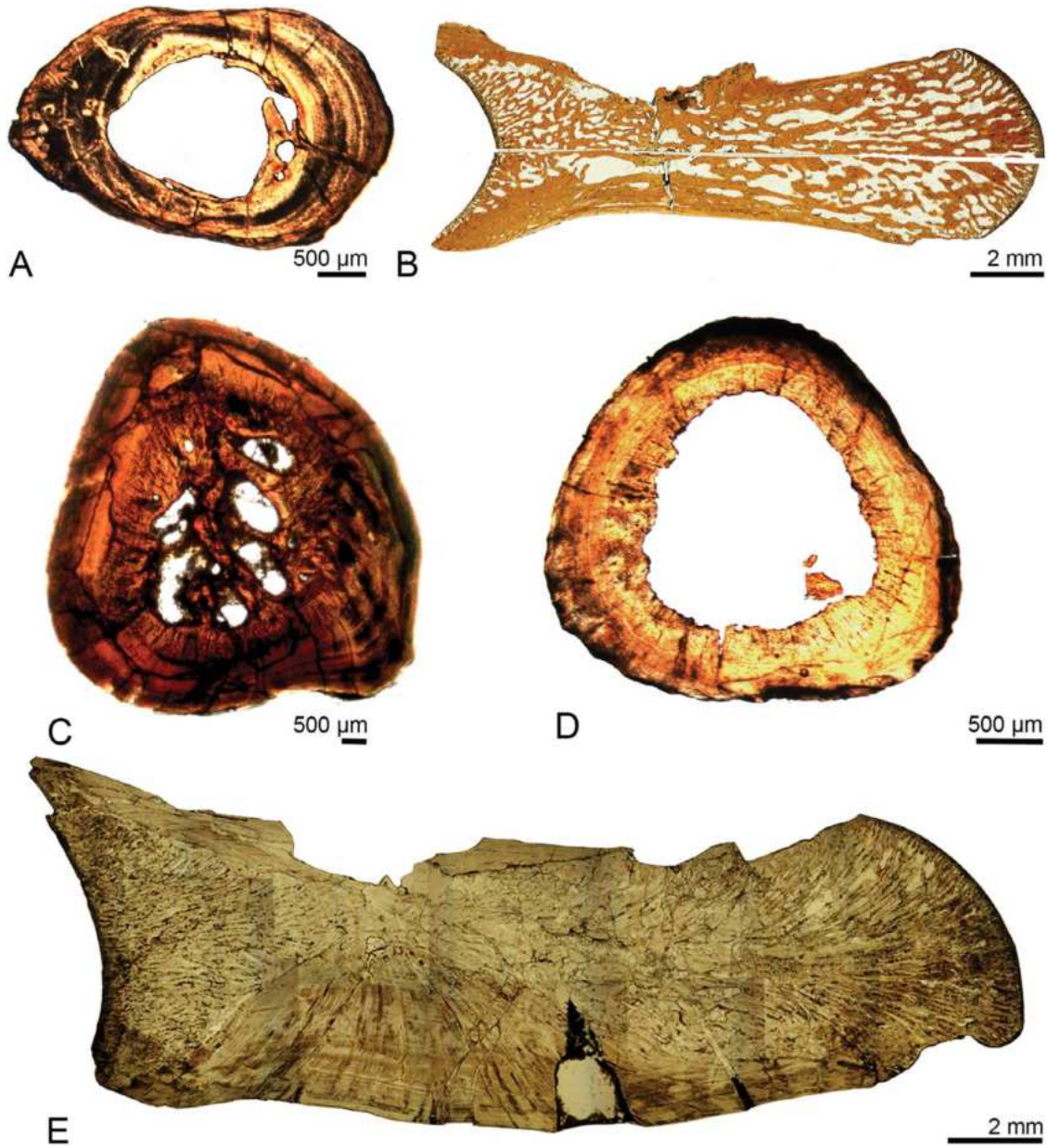


FIGURE 20.8 Bone sections in plesiopedal mosasauroids. A–D, The hydropelvic *Dallasaurus turneri*. E, The plesiopelvic *Haasiasaurus gittelmani*. A, Transverse rib section showing a tubular organization. B and E, Mid-sagittal sections of the centra of dorsal vertebrae showing cancellous (B) and osteosclerotic (E) organizations. C, Osteosclerotic humerus transverse section. D, Transverse section in a tubular femur.

Microanatomy and Histology of Limb Long Bones

Mid-diaphyseal sections in the humerus of several hydropedal mosasaurine mosasauroids (*Clidastes*, *Globidens*, *Mosasaurus*, and *Prognathodon*) show a wide spongiosa surrounded by a relatively thin compact cortex that can be slightly wider in some taxa or much wider at muscle attachment sites (e.g., *Clidastes*; Houssaye et al. 2013c; Figure 20.7D). Primary bone is of various tissue types. Within zones, it represents the atypical parallel-fibered bone described above (see the section "Lizards" and Snakes). Woven-fibered bone also occurs locally (Figure 20.10A); it surrounds longitudinal primary osteons organized in circumferential rows separated by annuli. The latter consist of true parallel-fibered bone often devoid of vascularization (Figure 20.10A). Radial simple vascular canals are more locally distributed (Figure 20.10B). Bone trabeculae in the core of the spongiosa consist of secondary lamellar tissue but remnants of primary bone occur in the trabeculae of the outer spongiosa (Houssaye et al. 2013c).

In contrast, the humerus of *Dallasaurus* strongly differs from that of hydropedal mosasauroids. It shows a thick layer of compact cortex and there is no open medullary cavity (Figure 20.8C). The medullary area is occupied by a spongiosa with a few thick trabeculae and large randomly shaped

VetBooks.ir

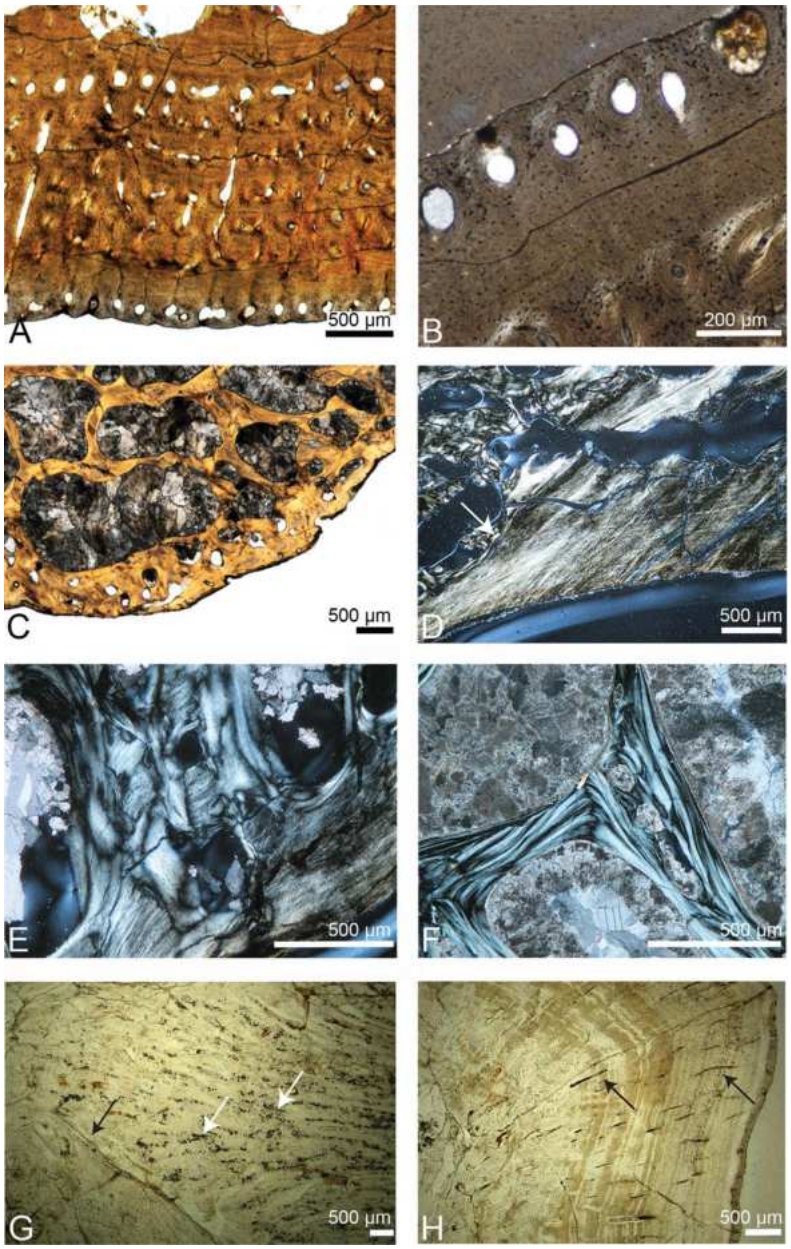


FIGURE 20.9 Histological features of mosasauroid vertebrae. A, Primary cortical bone in a transverse section of *Clidastes propython* showing circumferential layers of longitudinal primary osteons and cyclical growth marks. B, Detail of longitudinal canals showing the filling of the osteons from the outer (top) to the inner (bottom) cortex and the variation in osteocyte size and density between the vascularized zones and the annuli. C, Incipient primary osteons in the vertebral cortex of *Tethysaurus nopcsai*. Cross-section. D, The arrow points to the limit between primary periosteal bone (parallel-fibered bone; right) and remodeled endosteo-endochondral cancellous formations (left). Longitudinal section. E, Highly remodeled lamellar bone in a transverse section (primary bone at the bottom right). F, Secondary lamellar bone in trabeculae from the spongiosa of a *Tethysaurus nopcsai* vertebra. Cross-section. G, Remains of calcified cartilage (white arrows) in the trabeculae of the compacted spongiosa in a vertebral centrum of *Haasiasaurus gittelmani*. Mid-sagittal section. The limit between periosteal and endosteo-endochondral territories is indicated by the black arrow. H, Radial canals (black arrows) in the centrum cortex of *Haasiasaurus gittelmani*. Transverse section. D–F: Polarized light.

intertrabecular spaces. Periosteal bone is made of parallel-fibered tissue that only shows vascularization as radially oriented simple vascular canals in the inner cortex (Figure 20.10C). The inner cortex also shows the atypical parallel-fibered bone that, associated with vascularization, suggests a higher growth rate in early ontogenetic stages (Figure 20.10C).

The femur of *Dallasaurus* shows a tubular organization, with a compact cortex surrounding a large medullary cavity free of trabeculae (Figure 20.8D). Histological features are similar to those observed in the humerus (Figure 20.10D).

A skeletochronological analysis of long bones (humerus, tibia, fibula) in several hydropedal mosasauroids (*Clidastes*, *Platecarpus*, *Tylosaurus*) was conducted by Pellegrini (2007). This study illustrated a decrease in growth rate after sexual maturity, likely between five and seven years (as in *Varanus komodoensis*), and a long-lasting growth.

VetBooks.ir

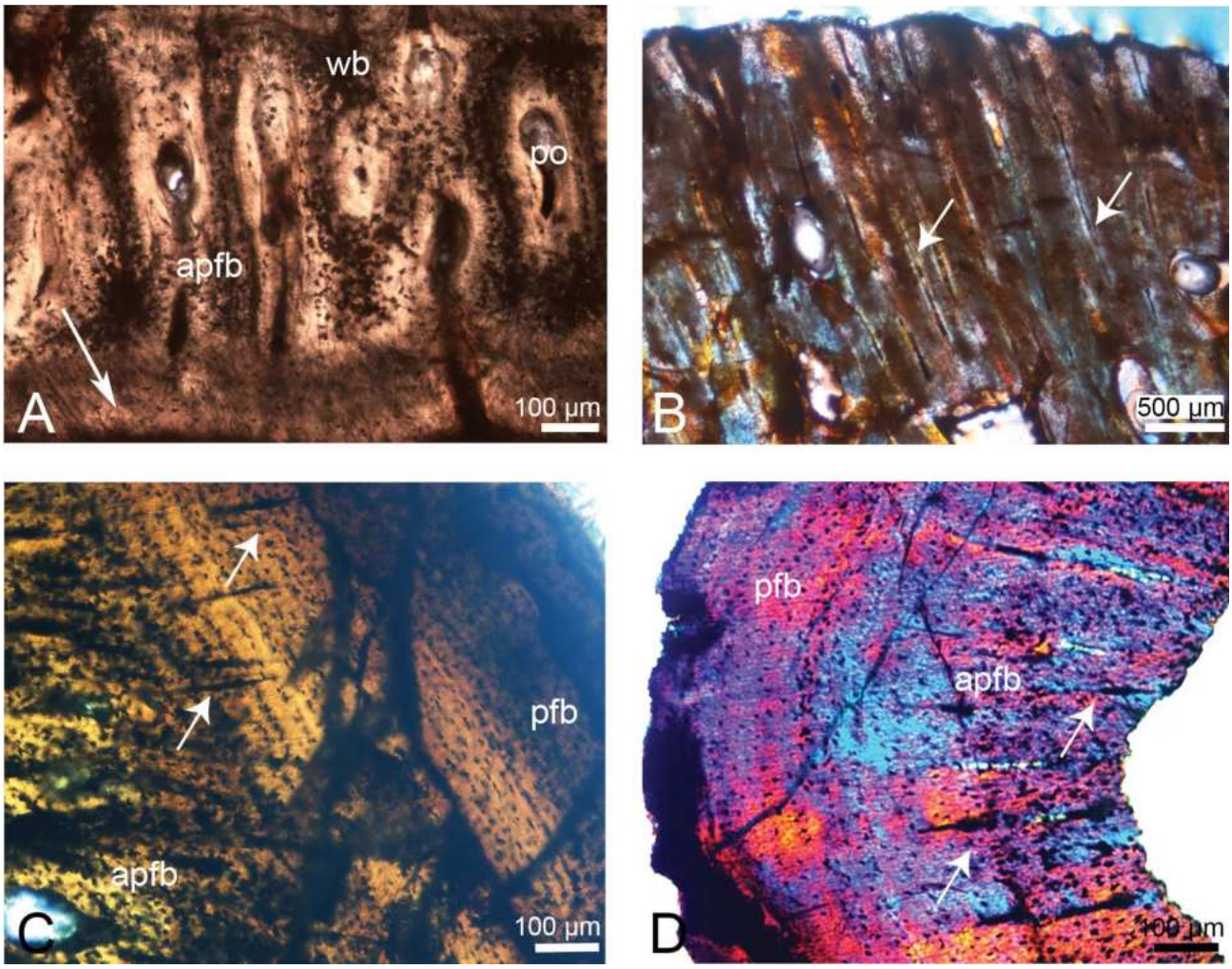


FIGURE 20.10 Histological features of mosasauroid long bones. A, Woven-fibered bone (wb) and atypical parallel-fibered bone (apfb) surrounding primary osteons (po) in a zone within the humeral cortex of a hydropedal mosasaurine (transversal section). The arrow points to an annulus. B, Radial vascular canals (arrows) in the humeral cortex of a hydropedal mosasaurine. Cross-section. C, Cross-section in the humeral cortex of *Dallasaurus turneri* showing apfb and radial vascular canals in its deep part, and avascular parallel-fibered bone (pfb) in its outer part. D, Same as C, but in the femur.

Cranial Bones and Teeth

Caldwell (2007) analyzed the modes of tooth attachment and replacement in hydropedal mosasauroids. The dentition is thecodont and teeth follow a unique "movement-path" during development: a developing tooth forms posterolingual to a functional tooth, and then migrates anterolabially, causing root resorption. The developing tooth then sinks into the alveolus and continues to grow, eventually erupting into the oral cavity and causing the older tooth to be shed. Caldwell's (2007) study also highlighted the extensive amount of root cementum and the deep and well-developed alveolus hosting the root and root cementum, which are unique features among squamates. Luan et al. (2009) described the architecture of tooth attachment in mosasaurs as a quadruple-layer structure with acellular and cellular cementum, mineralized PDL and alveolar bone. LeBlanc et al. (2017) revised this hypothesis, proposing that the previously described cellular cementum represents mineralized and partly mineralized ligament fiber bundles of the PDL itself (Figure 20.11A, B). The PDL, which also occurs in most snakes, persists temporarily as a soft tissue as the tooth erupts into its functional position, and then completely calcifies in most mosasauroids (Figure 20.11). In its unmineralized state the PDL presumably offers a flexible connection between the teeth and the jaw, allowing teeth to cope with the compressive impact of high bite forces (LeBlanc et al. 2017).

Paleobiological and Paleoecological Inferences

Isotopic studies of dental tissues estimated high body temperatures (between 35 ± 2°C and 39 ± 2°C) in hydropelvic mosasauroids, suggesting at least partial homeothermy in mosasaurs (Bernard et al. 2010). Considering these results, Motani (2010) inferred gigantothermy (a form of inertial

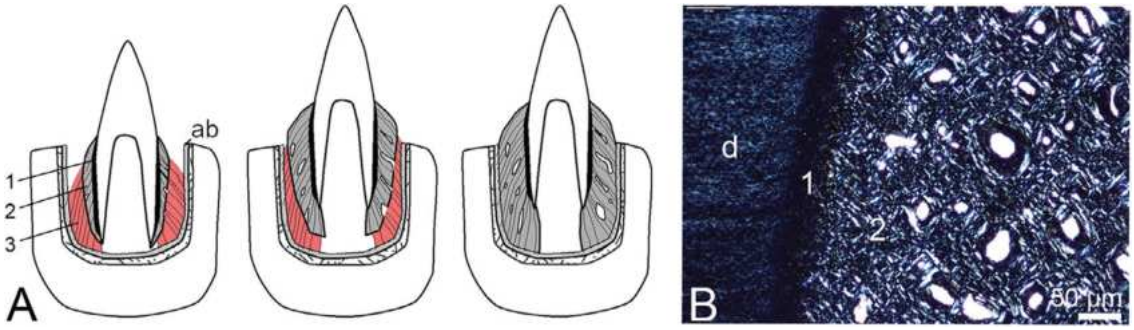


FIGURE 20.11 Mosasaur tooth histology. A, Schematic drawing illustrating mosasaurid dental attachment during ontogeny (from early eruption to ankylosis). 1, acellular cementum; 2, cellular cementum and partly mineralized periodontal ligament (pdl); 3, unmineralized pdl. ab, alveolar bone. B, Transverse section of a *Platecarpus* tooth showing part of the attachment tissue. (Courtesy A. LeBlanc.) Abbreviations: d: dentin.

homeothermy), i.e., the ability to maintain a high body temperature through large body size and possible insulation, as exemplified by the extant leatherback turtle, *Dermochelys coriacea* (Paladino et al. 1990). This hypothesis would agree with the occurrence of similar histological features in the skeletons of hydropelvic mosasauroids and the leatherback turtle, with a likely higher basal metabolic rate in the former than in the latter because mosasauroids show, from their origin, a much higher degree of bone vascularization than *Dermochelys* (Houssaye 2008, Houssaye et al. 2013c). Plesiopelvic mosasauroids display parallel-fibered bone housing numerous simple radially oriented vascular canals with some anastomoses. These features might indicate a higher growth rate than in extant squamates, except large monitor lizards and large tegus (see above). Hydropedal mosasauroids display atypical parallel-fibered bone with longitudinally oriented primary osteons organized in circumferential rows (though simple radial vascular canals also occur locally), which suggests much higher growth rates possibly reflecting gigantothermy for mosasaurs (Motani 2010, Houssaye et al. 2013c).

Interestingly, the hypothesis that mosasaurs shifted during their evolution from a coastal habitat toward the open-ocean realm, and therefore increased their ability for more efficient swimming, is reflected in the microanatomical and histological features of these animals. Plesiopedal and plesiopelvic forms show osteosclerosis often associated with pachyostosis in their vertebrae and probably also ribs. These traits can be expected in coastal divers performing long dives at shallow depths (Houssaye 2013). Conversely, hydropedal and hydropelvic mosasauroids display cancellous bones well suited for fast and agile swimmers. Interestingly, the plesiopedal and hydropelvic mosasauroid *Dallasaurus* displays an intermediary pattern with terrestrial-like (tubular) ribs and femora, lightly built vertebrae and osteosclerotic humeri. These contrasting skeletal features probably reflect an intermediary ecology with a trade-off among distinct functional requirements (Houssaye et al. 2013c). The maintenance of one type of microanatomical specialization through ontogeny in mosasauroids highlights that a hydrodynamic control of buoyancy associated with active swimming already occurred at a very young age in hydropedal mosasauroids, and that the type of osseous specialization is not correlated with body size in mosasauroids.

The Strange Case of Marine Cenomanian Snakelike Forms

"Dolichosaurs" and Hind-Limbed Snakes

In the Late Cretaceous, aquatic snakelike forms with legs radiated in the marine realm. They are part of the Ophidiomorpha, which is a taxon erected by Palci and Caldwell (2007) to include the most recent common ancestor of Dolichosauridae, *Aphanizocnemus*, adriosaurs and Ophidia and all its descendants.

Dolichosauridae, *Aphanizocnemus*, and adriosaurs were previously referred to as "dolichosaurs" following Nopcsa (1908). These nonophidian ophidiomorphs, or stem-ophidians, constitute a paraphyletic group (Palci and Caldwell 2010). They are slender-bodied lizards, no more than a meter long, displaying a long neck, a very long laterally compressed tail, and reduced limbs (Bardet et al. 2008, and Figure 20.12). They occurred in coastal environments of the Mediterranean Tethys from the Lower Cenomanian to the Lower Turonian, with the exceptions of *Dolichosaurus* and *Coniasaurus* (which could be synonymous), which are considered open-marine forms. Remains of *Coniasaurus* occur in the Western Interior Seaway of North America up to the Middle Santonian (Bardet et al. 2008).

Marine Ophidia, notably Pachyophiidae, often referred to as "hind-limbed snakes," also lived during the Late Cretaceous. Pachyophiidae include *Pachyophis*, *Pachyrhachis*, and all taxa more closely related to these genera than to extant snakes (Lee and Caldwell 1998). The status and phylogenetic position of this group remain debated (Palci et al. 2013a, b, Martill et al. 2015, Reeder et al. 2015). Pachyophiidae are known from the Early to Late Cenomanian of the Mediterranean Tethys (Europe, North Africa, Middle-East; Bardet et al. 2008). They have a long laterally compressed body (1–1.5 m long) that ends in a short tail (Figure 20.12B) with a strong lateral compression that forms a small paddle, at least in *Eupodophis*

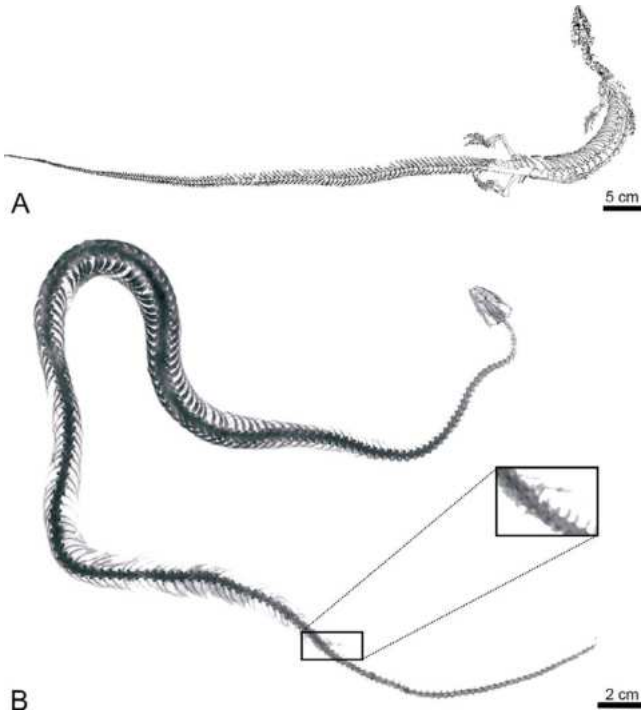


FIGURE 20.12 Skeletal reconstructions. A, The stem-ophidiomorph *Pontosaurus kornhuberi*. B, The pachyophiid snake *Haasiophis terrasanctus*, with a zoom-in on a hind limb.

(Rage and Escuillié 2000). These forms are characterized by the possession of reduced though normally formed hind limbs and a reduced pelvic girdle. Whereas three genera (*Pachyrhachis*, *Eupodophis* and *Haasiophis* shown in Figure 20.12B) are unquestionable hind-limbed snakes, three others (*Simoliophis*, *Mesophis*, *Pachyophis*) are attributed to this group despite the absence of preserved limbs; their identification is based on cranial or vertebral morphological features (Rage and Escuillié 2003).

Structure of the Ribs and Vertebrae

Most stem-ophidians and all pachyophiids display pachyostosis (see also Chapter 36) in their ribs and dorsal vertebrae, as shown by the bloated aspect of these bones (Figure 20.13A,B). Pachyostosis appears much milder in cervical vertebrae and absent in sacral and caudal ones (Houssaye 2013). The degree of pachyostosis varies among taxa, from rather light (e.g., in *Pontosaurus*; Figure 20.13A) to strong with almost no intercostal spaces (e.g., *Adriosaurus*, Figure 20.13B, P*achyophis*). Conversely, the stem-ophidians *Dolichosaurus, Coniasaurus* and *Aphanizocnemus* do not show pachyostosis (Figure 20.13C).

Pachyostotic taxa also display strong osteosclerosis with an extremely high inner compactness in their postcranial axial skeleton (Figures 20.14A, B, D and 20.15). Vertebrae show only a few rather small cavities in the endochondral territories or near the growth center (Figures 20.14A and 20.15B). Ribs have no medullary cavity (Figures 20.14D and 20.15E)

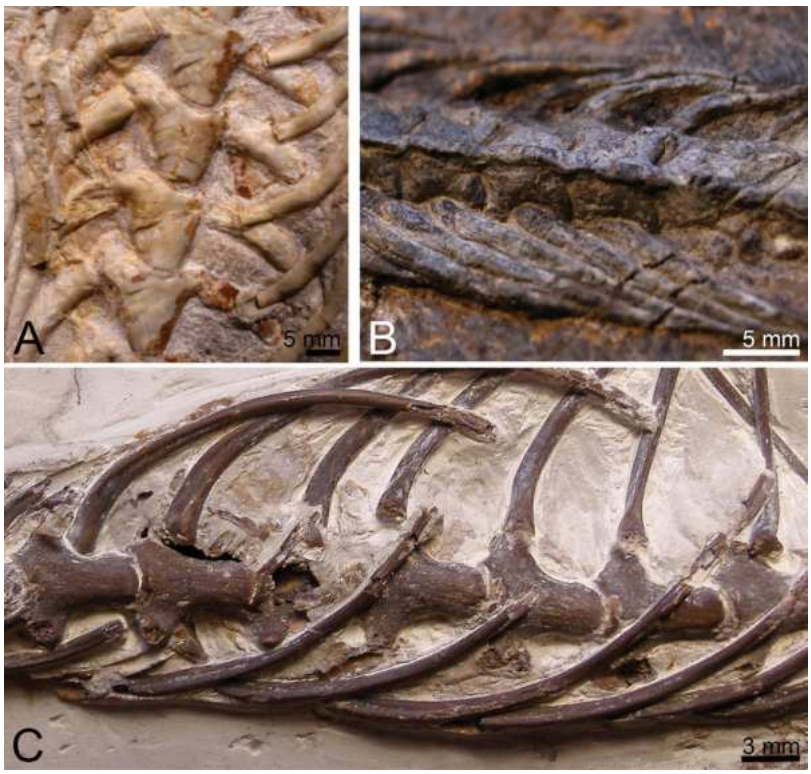


FIGURE 20.13 Anterior dorsal region of stem-ophidians. A, Feeble pachyostosis in *Pontosaurus lesinensis*; ventral view. B, Pronounced pachyostosis in *Adriosaurus* sp., dorsal view. C, Absence of pachyostosis in *Dolichosaurus longicollis*. Ventral view.

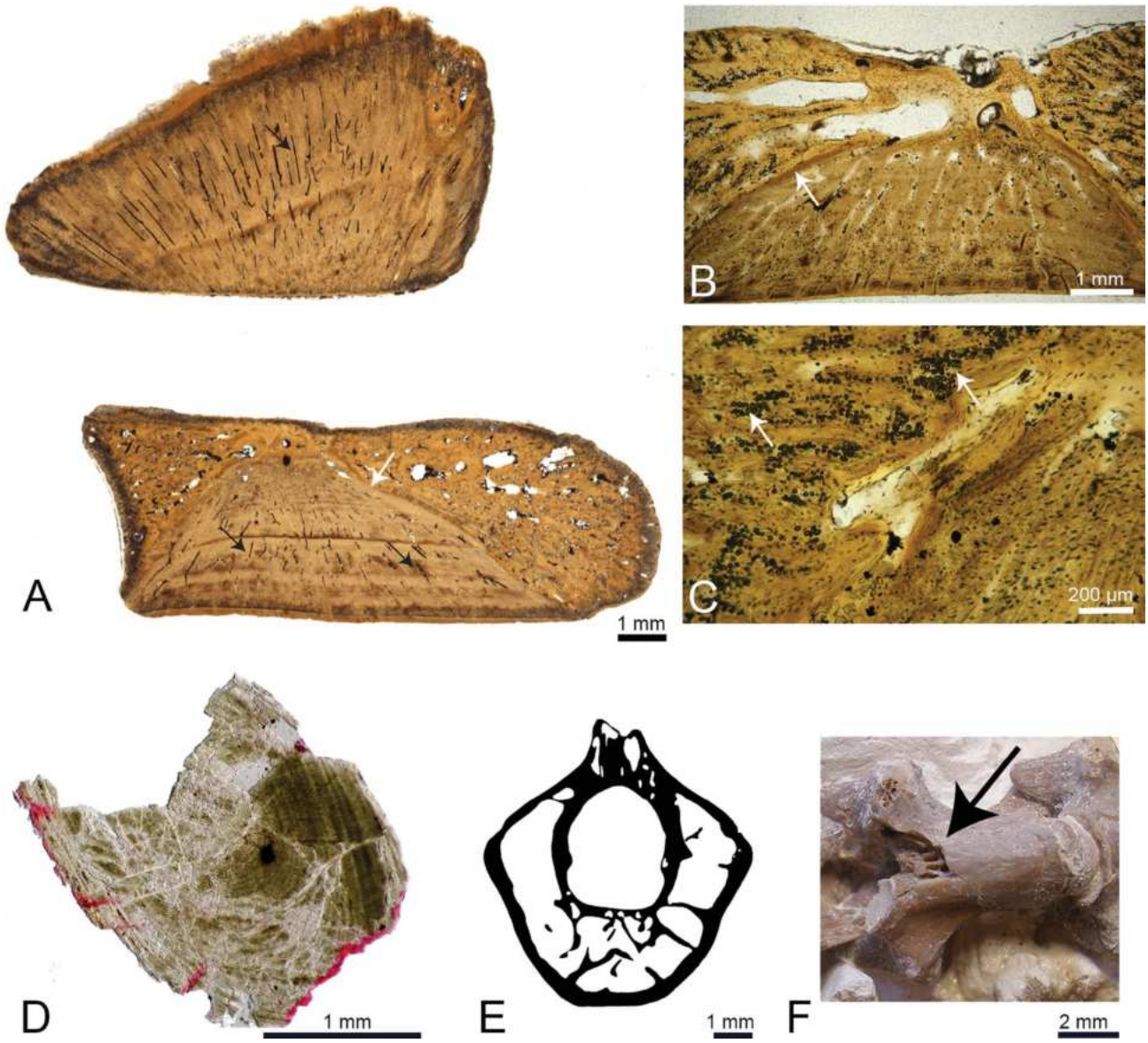


FIGURE 20.14 Bone histological features in stem-ophidians. A–C: Mid-sagittal sections of vertebrae of the stem-ophidian *Carentonosaurus mineaui*. A, Whole vertebra. The black arrow points to vascular canals and the white one to the limit between the periosteal and endosteo-endochondral territories. B, Partial section of a centrum. The white arrow points to the limit between the periosteal and endosteo-endochondral territories. C, Remnants of calcified cartilage (arrows) in the endosteo-endochondral region (left). D, Rib section of the stem-ophidian *Pontosaurus lesinensis*. E, Schematic drawing of a transverse section of a vertebra of the stem-ophidian *Coniasaurus* sp. (black, osseous tissue). F, Ventral view of a broken vertebra of the stem-ophidian *Dolichosaurus longicollis* illustrating the cancellous inner structure of the centrum (black arrow).

and only scarce cavities, essentially near the articular region. There is a clear inhibition of remodeling with entirely compact, periosteal cortices extending from the growth center to the ventral border of the centrum in longitudinal vertebral sections (Figures 20.14A and 20.15B). The boundary between the periosteal and endochondral territories is clear-cut (Figure 20.14A and 20.15B), and important remains of calcified cartilage occupy the core of the trabeculae in the rather compact spongiosae (Figures 20.14C). In transverse section, vertebrae are almost entirely compact (Figure 20.15A). As for pachyostosis, osteosclerosis does not occur in *Dolichosaurus* and *Coniasaurus* (Figure 20.14E, F). In cross section, *Coniasaurus* vertebrae clearly show a double-ringed structure: one osseous ring surrounds the neural canal, while the other surrounds the bone as a whole (Figure 20.14E). Both rings are connected by a few thin trabeculae. Such a structure is common in extant squamates (Buffrénil and Rage 1993, Houssaye et al. 2010; Houssaye 2013). In all taxa, primary bone consists of parallel-fibered tissue with conspicuous annuli and, in vertebrae but not in ribs, numerous simple vascular canals oriented radially (Figures 20.14A, B, D and 20.15C–E).

VetBooks.ir

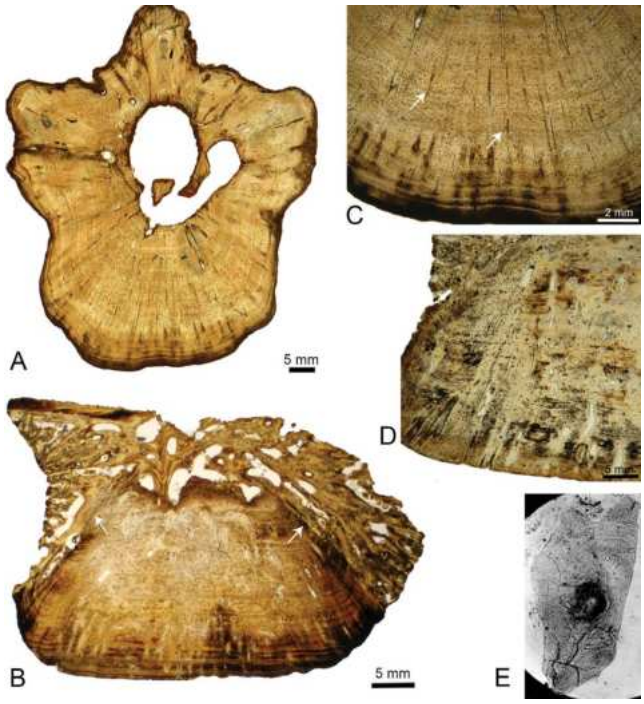


FIGURE 20.15 Bone histological features in pachyophiids. A–D, Vertebral sections of *Simoliophis rochebrunei*. A, Transverse section of a vertebra. B, Mid-sagittal section of a vertebral centrum. Arrows: boundary between periosteal and endosteo-endochondral osseous formations. C, Close-up view of a cross section in a vertebral centrum. The arrows point to vascular canals. D, Detail of a sagittal section in a centrum. E, Cross section in a rib of the pachyophiid *Mesophis nopcsai*. (Courtesy A. de Ricqlès; no scale available.)

A Note on the Inner Structure of Reduced Limbs

The inner structure of limb bones in the pachyophiid *Eupodophis* is characterized by an absence of increase in bone mass, whereas the postcranial axial skeleton in this taxon is pachy-osteosclerotic. This paradoxical situation shows that bone mass increase is not a generalized feature in these taxa, though it occurs in almost all elements of the axial postcranial skeleton (Houssaye et al. 2011).

Paleobiological and Paleoecological Inferences

The stem-ophidians and pachyophiids that show strong pachyosteosclerosis in their postcranial axial skeleton are considered shallow divers and poorly active ambush predators (Houssaye 2013). Conversely, *Dolichosaurus* and *Coniasaurus* are supposed to have been surface (or subsurface) swimmers (like the pelagic snake *Pelamis*; Houssaye 2013). Despite their relatively small size, stem-ophidians and pachyophiids show, as plesiopedal mosasauroids, numerous simple, radially oriented and anastomosed vascular canals. This feature, contrasting with the condition commonly encountered in extant snakes, suggests higher growth rates than in extant squamates and could mean that the swollen pachyostotic cortices of stem-ophidians and hind-limbed snakes resulted from accelerated periosteal accretion rather than from protracted local periosteal accretion.

Rhynchocephalia

A Once Diverse Taxon

Rhynchocephalia are known from the Middle Triassic to the present. Although they are represented today by a single genus, *Sphenodon*, this group is much more diverse in the fossil record, especially from the Late Triassic to the Late Jurassic, and it reached a worldwide distribution (Jones et al. 2013). Rhynchocephalians disappeared from Asia after the Early Jurassic, and from Euramerica by the mid-Cretaceous, but they survived in South America until the Late Cretaceous, becoming restricted to southern continents afterward (Evans and Jones 2010). Their decline since the Late Cretaceous is interpreted by some authors as a consequence of squamate diversification (Carroll 1985), but there is no clear evidence for this. Fossils are diverse notably in their body proportions, with elongated, gracile, large-bodied, and large-headed forms, and varied tooth structures and arrangements. The variety of these features suggests diverse ecologies and feeding strategies (insectivorous, omnivorous and herbivorous: Jones 2008). Their fossil record shows distinct episodes of adaptation to an aquatic lifestyle, as exemplified by pleurosaurs (Carroll and Wild 1994) and *Ankylosphenodon* (Reynoso 2000), and to herbivory (Rasmussen and Callison 1981).

Overview of Rhynchocephalian Skeletal Structures

Microanatomical and histological data from the skeletons of rhynchocephalians are sparse and mainly deal with long bone epiphyses (Haines 1939), the shaft of the femur and phalanges of *Sphenodon punctatus* (Castanet et al. 1988), and the mandible and teeth of this species and some fossil forms (Jenkins et al. 2017). However, the recent study by Klein and Scheyer (2017) describes bone microstructures in *Paleopleurosaurus posidoniae*, an incipiently aquatic form from the Early Jurassic of Germany. In general, the information so far available suggests that there is no important difference in bone and tooth structures between rhynchocephalians and squamates of similar size (*Sphenodon* snout-vent length is 210–270 cm in adults; Castanet et al. 1988). *P. posidoniae* slightly differs by some characteristics from the extant *Sphenodon*.

Long bone epiphyses in the tuatara contain secondary ossification centers, but these are incipient and less extensive and differentiated than in squamates; moreover, they are devoid of vascularization (Haines 1942, Ricqlès 1979). Sesamoids occur in *Sphenodon punctatus*, notably a well-differentiated (though relatively small in volume) patella (Regnault et al. 2016). Otherwise, the microstructure of the femur in this species is comparable to that of terrestrial lizards, though its global compactness at mid-diaphysis, some 85% in old specimens (Quémeneur et al. 2013; see also Castanet et al. 1988), ranks among the highest values encountered in extant lepidosaurs. Phalanges may show still higher compactness and their medullary cavity can even be entirely absent, as observed in an 11-year-old individual by Castanet et al. (1988). Femoral and phalangeal cortices in *Sphenodon* are avascular. In old individuals, deep cortical layers in the femur may show the

VetBooks.ir

irregular patchy resorption observed in some large lizards (see above). The same dynamic processes (centered or off-centered growth, etc.) occur in tuatara and squamate bones. At a microanatomical level, two main differences distinguish *Paleopleurosaurus* from *Sphenodon*: (1) the gastralia and, to a lesser extent, the ribs of *P. posidoniae* show some signs of osteosclerosis, an increase in internal bone tissue volume typical of aquatic amniotes and totally absent in *Sphenodon*, and (2) the femur of *P. posidoniae* is vascularized by thin longitudinal and oblique simple vascular canals.

At a histological level, there is no difference in cortical structure between the long bones of *Sphenodon* and those of lizards of similar size: both basically display the same parallel-fibered tissue with cyclic growth marks. However, longevity in *Sphenodon* (up to 35 years in the wild population studied by Castanet et al. 1988) looks much greater than in lizards. As a consequence, their thick cortices display impressive series of successive growth marks, which confers on them quite a distinctive cachet. Though long bone cortices of adult *P. posidoniae* are also made of parallel-fibered tissue, the growth marks that they display are both much less numerous and more irregular in their spatial patterning than those of the adult *Sphenodon* individuals studied by Castanet et al. (1988). These elements suggest fairly different life history parameters between these two taxa (Klein and Scheyer 2017).

Acknowledgments

We are extremely grateful to Professor Jacques Castanet for his detailed revision of the initial version of this manuscript and his useful suggestions. We sincerely thank Sophie Fernandez (CR2P, National Museum of natural History, Paris) for the line drawing of the *Dallasaurus* mosasaur skeleton, and Aaron LeBlanc (University of Alberta, Canada) for his explanations and comments about mosasaur tooth histology.

REFERENCES

Amprino, R. 1947. La structure du tissue osseux envisagé comme l'expressions de differences dans la vitesse de l'accroissement. *Arch. Biol.* 58: 317–330.

Amprino, R. and G. Godina. 1947. La struttura delle ossa nei vertebrati. Ricerche comparative negli anfibi e negli amnioti. *Comment. Pontif. Acad. Sci.* 11: 328–463.

Auffenberg, W. 1981. *The behavioral ecology of the Komodo monitor.* Gainesville, FL: University of Florida Press.

Bardet, N., et al. 2005. A new species of *Halisaurus* from the Late Cretaceous phosphates of Morocco, and the phylogenetical relationships of the Halisaurinae (Squamata: Mosasauridae). *Zool. J. Linn. Soc.* 143: 447–472.

Bardet, N., et al. 2008. The Cenomanian-Turonian (Late Cretaceous) radiation of marine squamates (Reptilia): the role of the Mediterranean Tethys. *Bull. Soc. Géol. Fr.* 179: 605–622.

Bardet, N., et al. 2015. Mosasaurids (Squamata) from the Maastrichtian phosphates of Morocco: Biodiversity, palaeobiogeography and palaeoecology based on tooth morphoguilds. *Gondwana Res.* 27: 1068–1078.

Bell, G. L. Jr. 1997. A phylogenetic revision of North American and adriatic Mosasauroidea. In *Ancient Marine Reptiles*, eds. Callaway, J. M. and E. L. Nicholls, 293–332. San Diego: Academic Press.

Bell, G. L. Jr. and M. J. Polcyn. 2005. *Dallasaurus turneri*, a new primitive mosasauroid from the Middle Turonian of Texas and comments on the phylogeny of Mosasauridae (Squamata). *Neth. J. Geosci.* 84: 177–194.

Bellairs, A. 1969. *The life of Reptiles*. London: Weidenfeld & Nicolson.

Bernard, A., et al. 2010. Regulation of body temperature by some Mesozoic marine reptiles. *Science*. 328: 1379–1382.

Bever, G. S., et al. 2005. The ossified braincase and cephalic osteoderms of *Shinisaurus crocodilurus* (Squamata, Shinisauridae). *Palaeont. Electron.* 8: 1–35.

Bhullar, B.-A. and C. J. Bell. 2008. Osteoderms of the California legless lizard *Anniella* (Squamata: Anguidae) and their relevance for consideration of miniaturization. *Copeia* 2008(4): 785–793.

Blob, R. W. 2000. Interspecific scaling of the hindlimb skeleton in lizards, crocodilians, felids and canids: does bone shape correlate with limb posture? *J. Zool. Lond.* 250: 507–531.

Bochaton, C., et al. 2015. Body location and tail regeneration effects on osteoderm morphology – Are they useful tools for systematic, paleontology, and skeletochronology in Diploglossine lizards (Squamata, Anguidae)? *J. Morphol.* 276: 1333–1344.

Budley, L. A., et al. 2006. Tooth socket histology in the Cretaceous snake *Dinilysia*, with a review of amniote dental attachment tissues. *J. Vert. Paleont.* 28: 138–145.

Buffrénil, V. de and J. Castanet. 2000. Age estimation by skeletochronology in the Nile monitor (*Varanus niloticus*), a highly exploited species. *J. Herpetol.* 34: 414–424.

Buffrénil, V. de and H. Francillon-Vieillot. 2001. Ontogenetic changes in bone compactness in male and female Nile monitors. *J. Zool.(Lond.)* 254: 539–546.

Buffrénil, V. de and G. Hémery. 2002. Variation in longevity, growth and morphology in exploited Nile monitors (*Varanus niloticus*) from Sahelian Africa. *J. Herpetol.* 36: 419–426.

Buffrénil, V. de and J.-C. Rage. 1993. La "pachyostose" vertébrale de *Simoliophis* (Reptilia, Squamata): données comparatives et considérations fonctionnelles. *Ann. Plaéont. (Vert.)* 79: 315–335.

Buffrénil, V. de, et al. 1994. Données préliminaires sur la taille, la croissance et la longévité du varan du Nil (*Varanus niloticus*) dans la région du lac Tchad. *Can. J. Zool.* 72: 262–273.

Buffrénil, V. de, et al. 2005. Comparative data on epiphyseal development in the family Varanidae. *J. Herpetol.* 39: 328–335.

Buffrénil, V. de, et al. 2008. Bone Vascular supply if monitor lizards (Squamata: Varanidae): influence of size, growth and phylogeny. *J. Morphol.* 269: 533–543.

Buffrénil V. de, et al. 2011. An enamel-like tissue, osteodermine, on the osteoderms of a fossil anguid (Glyptosaurine) lizard. *C. R. Palevol* 10: 427–438.

Buffrénil V. de, et al. 2016. Comparative data on the differentiation and growth of bone ornamentation in gnathostomes (Chrodata: Vertebrata). *J. Morphol.* 277: 634–670.

Caldwell, M. W. 2007. Ontogeny, anatomy and attachment of the dentition in mosasaurs (Mosasauridae: Squamata). *Zool. J. Linn. Soc.* 149: 687–700.

VetBooks.ir

Caldwell, M. W. and M. S. Y. Lee. 2001. Live birth in Cretaceous marine lizards (mosasauroids). *Proc. R. Soc. B: Biol. Sci.* 268: 2397–2401.

Caldwell, M. W. and A. Palci. 2007. A new basal mosasauroid from the Cenomanian (U. Cretaceous) of Slovenia with a review of mosasauroid phylogeny and evolution. *J. Vert. Paleontol.* 27: 863–880.

Caldwell, M. W., et al. 1995. The pectoral girdle and forelimb of *Carsosaurus marchesetti* (Aigialosauridae), with a preliminary phylogenetic analysis of mosasauroids and varanoids. *J. Vert. Paleontol.* 15: 516–531.

Canoville, A. and M. Laurin. 2010. Evolution of humeral microanatomy and lifestyle in amniotes, and some comments on paleobiological inferences. *Biol. J. Linn Soc.* 100: 384–406.

Canoville, A., et al. 2016. Microanatomical diversity of amniotes ribs: an exploratory quantitative study. *Biol. J. Linn. Soc.* 118: 706–733.

Carlson, S. J. 1990. Vertebrate dental structures. In *Skeletal biomineralization: patterns, processes and evolutionary trends*, vol. 1, ed. J. G. Carter, 531–556. New York: Van Nostrand Reinhold.

Carroll, R. L. 1985. Evolutionary constraints in aquatic diapsid reptiles. *Sp. Pap. Palaeontol.* 33: 145155.

Carroll, R. L. and R. Wild. 1994. Marine members of the Sphenodontia. In *In the Shadow of the Dinosaurs*, eds. Fraser, N. C. and H.-D. Sues, 70–83. Cambridge: Cambridge University Press.

Castanet, J. 1974a. Données expérimentales sur la valeur des marques squelettiques comme indicateur de l'âge chez *Vipera aspis*. *Zool. Scr.* 3: 201–208.

Castanet, J. 1974b. Etude histologique des marques squelettiques de croissance chez *Vipera aspis* (L.) (Ophidia, Viperidae). *Zool. Sc.* 3: 137–151.

Castanet, J. 1978. Les marques de croissance osseuse comme indicateurs de l'âge chez les lézards. *Acta Zool. (Stockh.)* 59: 35–48.

Castanet, J. 1982. *Recherches sur la croissance du tissu osseux des reptiles. Application: la méthode squelettochronologique*. PhD thesis, Paris: University Paris.

Castanet, J. 1985. La squelettochronologie chez les reptiles. I. Résultats expérimentaux sur la signification des marques de croissance squelettique chez les lézards et les tortues. *Ann. Sci. Nat. Paris* 7: 23–40.

Castanet, J., et al. 1988. Skeletochronological data on the growth, age, and population structure of the Tuatara, *Sphenodon punctatus*, on Stephens and Lady Alice islands, New Zealand. *Herpetologica* 44: 25–37.

Castanet, J., et al. 1993. Bone and individual aging. In *Bone, Vol. 7: bone growth – B*, ed. Hall, B. K., 245–283. Boca Raton, FL: CRC Press.

Cleary, T. J., et al. 2018. Lepidosaurian diversity in the Mesozoic–Palaeogene: the potential roles of sampling biases and environmental drivers. *Roy. Soc. Op. Sci.* 5: 171830.

Conrad, J. L. 2006. An Eocene shinisaurid (Reptilia: Squamata) from Wyoming, USA. *J. Vert. Paleontol.* 26: 113–126.

Cope, E. D. 1869. On the Reptilian orders, Pythonomorpha and Streptosauria. *Proc. Boston Soc. Nat. Hist.* 12: 250–269.

Cubo J., et al. 2014. Geometric and metabolic constraints on bone vascular supply. *Biol. J. Linn. Soc.* 112: 668–677.

Delgado, S., et al. 2005. Tooth development in a scincid lizard, *Chalcides viridanus* (Squamata), with particular attention to enamel formation. *Cell Tissue Res.* 319: 71–89.

Edmund, A. G. 1969. Dentition. In *Biology of the Reptilia 1A*, eds. Gans, C., A. d'A. Bellairs and T. S. Parsons, 117–200. London: Academic Press.

Enlow, D. H. 1969. The bone of reptiles. In *Biology of the Reptilia 1A*, eds. Gans, C. and A. d'A. Bellairs, 45–80. London: Academic Press.

Enlow, D. H. and S. O. Brown. 1957. A comparative histological study of fossil and recent bone tissues. Part II. *Texas J. Sci.* 9: 186–214.

Erickson, G., et al. 2003. Vermiform bones and the evolution of gigantism in *Megalania* – How a reptilian fox became a lion. *J. Vert. Paleontol.* 23: 966–970.

Evans, S. E. 1994. A new anguimorph lizard from the Jurassic and Lower Cretaceous of England. *Palaeontology* 37: 33–50.

Evans, S. E. and M. E. Jones. 2010. The origin, early history and diversification of lepidosauromorph reptiles. In *New aspects of mesozoic biodiversity*, ed. Bandyopadhyay, S., 27–44. New York: Springer.

Evans, S. E., et al. 2002. Fossil lizards from the Jurassic Kota Formation of India. *J. Vert. Paleontol.* 22: 299–312.

Fernández, M. S. and Z. Gasparini. 2012. Campanian and Maastrichtian mosasaurs from Antarctic Peninsula and Patagonia, Argentina. *Bull. Soc. Geol. France.* 183: 93–102.

Field, D. J., et al. 2015. Pelagic neonatal fossils support viviparity and precocial life history of Cretaceous mosasaurs. *Palaeontology* 58: 401–407.

Foote, J. S. 1911. The comparative histology of femoral bones. *Trans. Am. Micros. Soc.* 30: 87–140.

Foote, J. S. 1916. A contribution to the comparative histology of the femur. *Smiths. Contr. Knowl.* 35: 1–242, publ. 2382.

Francillon-Vieillot, H., et al. 1990. Microstructure and mineralization of vertebrate skeletal tissues. In *Skeletal biomineralization: patterns, processes and evolutionary trends*, vol. 1, ed. J. G. Carter, 471–530. New York: Van Nostrand Reinhold.

Frydlova, P., et al. 2017. Patterns of growth in monitor lizards (Varanidae) as revealed by computed tomography of femoral growth plates. *Zoomorphology* 136: 95–106.

Frydlova, P., et al. 2020. Determinate growth is predominant and likely ancestral in squamate reptiles. *Proc. R. Soc. B* 287. http://doi.org/10.1098/rspb.2020.2737.

Garcia, G., et al. 2015. Mosasauroid (Squamata) discovery in the Late Cretaceous (Early Campanian) continental deposits of Villeveyrac–L'Olivet, southern France. *C. R. Palevol* 14: 495–505.

Germain, D. and M. Laurin. 2005. Microanatomy of the radius and lifestyle in amniotes (Vertebrata, Tetrapoda). *Zool. Scripta.* 34: 335–350.

Griffin, C. T., et al. 2020. Assessing ontogenetic maturity in extinct saurian reptiles. *Biol. Rev.* Doi: 10.1111/brv.12666.

Haines, R. W. 1939. The structure of epiphyses in *Sphenodon* and the primitive form of secondary centre. *J. Anat. Physiol.* 74: 80–90.

Haines, R. W. 1941. Epiphyseal structure in lizards and marsupials. *J. Anat. Lond.* 75: 282–294.

Haines, R. W. 1942. The evolution of epiphyses and of endochondral bone. *Biol. Rev.* 17: 267–292.

Haines, R. W. 1969. Epiphyses and sesamoids. In *Biology of the Reptilia 1A*, eds. Gans, C. and A. d'A. Bellairs, 81–115. London: Academic Press.

Haridy, Y. 2018. Assessing acrodont dentition in Reptilia, with special attention to replacement and wear adaptations. *Master of Science thesis*, University of Toronto.

Hoffstetter, R. 1962. Observations sur les ostéodermes et la classification des anguidés actuels et fossiles (Reptiles, Sauriens). *Bull. Mus. Nat. Hist. Nat.2ème ser.* 34: 149–157.

Houssaye, A. 2008. A preliminary report on the evolution of the vertebral microanatomy within mosasauroids (Reptilia, Squamata). In *Proceedings of the Second Mosasaur Meeting*, ed. M. J, Everhart, 81–89. Fort Hays State University.

Houssaye, A. 2013. Palaeoecological and morphofunctional interpretation of bone mass increase: an example in Late Cretaceous shallow marine squamates. *Biol. Rev.* 88: 117–139.

Houssaye, A. and N. Bardet. 2012. Rib and vertebral microanatomical characteristics of hydropelvic mosasauroids. *Lethaia* 45: 200–209.

Houssaye, A. and N. Bardet. 2013. A baby mosasauroid (Reptilia, Squamata) from the Turonian of Morocco – *Tethysaurus* 'junior' discovered? *Cretaceous Res.* 46: 208–215.

Houssaye, A. and P. Tafforeau. 2012. What vertebral microanatomy reveals about the ecology of juvenile mosasaurs (Reptilia, Squamata). *J. Vert. Paleontol.* 32: 1042–1048.

Houssaye, A., et al. 2010. Vertebral microanatomy in squamates: structure, growth and ecological correlates. *J. Anat.* 217: 715–727.

Houssaye, A., et al. 2011. Three-dimensional pelvis and limb anatomy of the Cenomanian hind-limbed snake *Eupodophis descouensi* (Squamata, Ophidia) revealed by synchrotron-radiation computed laminography. *J. Vert. Paleontol.* 31: 2–7.

Houssaye A., et al. 2013a. Jack-of-all-trades master of all? Snake vertebrae have a generalist inner organization. *Naturwissenschaften* 100: 997–1006.

Houssaye, A., et al. 2013b. New highlights about the enigmatic marine snake *Paleophis maghrebianus* (Palaeophiidae; Paleophiinae) from the Ypresian (Lower Eocene) phosphates of Morocco. *Palaeontology* 56: 647–661.

Houssaye, A., et al. 2013c. Microanatomical and histological features in the long bones of mosasaurine mosasaurs (Reptilia, Squamata) - implications for aquatic adaptation and growth rates. *PLoS One*. 8: e76741.

Houssaye, A., et al. 2014. Amniote vertebral microanatomy – what are the major trends? *Biol. J. Linn. Soc.* 112: 735–746.

Jenkins, K. M., et al. 2017. A review of tooth implantation among rhynchocephalians (Lepidosauria). *J. Herpetol.* 51: 300–306.

Jerez, A. and O. A. Tarazona. 2009. Appendicular skeleton in *Bachia bicolor* (Squamata: Gymnophthalmidae): osteology, limb reduction and postnatal skeletal ontology. *Acta Zool. (Stockh.)* 90: 42–50.

Jerez, A., et al. 2010. Occurrence and distribution of sesamoid bones in squamates: a comparative approach. *Acta Zool. (Stockholm)* 91: 295–305.

Johnson, M. K., et al. 2005.Locomotor morphometry of the *Pachydactylus* radiation of lizards (Gekkota: Gekkonidae): a phylogenetically and ecologically informed analysis. *Can. J. Zool.* 83: 1511–1524.

Jones, M. E. H. 2008. Skull shape and feeding strategy in Sphenodon and other Rhynchocephalia (Diapsida: Lepidosauria). *J. Morphol.* 269: 945–966.

Jones, M. E., et al. 2013. Integration of molecules and new fossils supports a Triassic origin for Lepidosauria (lizards, snakes, and tuatara). *BMC Evol. Biol.* 13: 208.

Kardong, K. V. 1998. *Vertebrates – Comparative anatomy, function, Evolution*. Boston, MA: McGraw-Hill.

Kearney, M., et al. 2009. Lost sex in the reptiles: Constraints and correlations. In *Lost sex: The evolutionary biology of parthenogenesis*, eds. Schön, I., et al., 447–474. Dordrecht: Springer Netherlands.

Kirby, A., et al. 2020. A comparative histological study of the osteoderms in the lizards *Heloderma suspectum* (Squamata: Helodermatidae) and *Varanus komodoensis* (Squamata: Varanidae). *J. Anat.* 236: 1035–1043

Klein, N. 2010. Long bone histology of Sauropterygia from the Lower Muschelkalk of the Germanic Basin provides unexpected implications for phylogeny. *PLoS One*. 5: e11613.

Klein, N. and T. M. Scheyer. 2017. Microanatomy and life history in *Palaeopleurosaurus* (Rhynchocephalia: Pleurosauridae) from the Early Jurassic of Germany. *Sci. Nat.* 104: 4.

Kriloff, A., et al. 2008. Evolution of bone microanatomy of the tetrapod tibia and its use in palaeobiological inference. *J. Evol. Biol.* 21: 807–826.

Laurin, M., et al. 2011. Bone microanatomy and lifestyle: a descriptive approach. *C. R. Palevol* 10: 381–402.

LeBlanc, A. R. H., et al. 2017. Mosasaurs and snakes have a periodontal ligament: timing and extent of calcification, not tissue complexity, determines tooth attachment mode in reptiles. *J. Anat.* 231: 869–885.

Lee, M. Y. S and M. W. Caldwell. 1998. Anatomy and relationships of *Pachyrhachis problematicus*, a primitive snake with hindlimbs. *Philos. Trans. R. Soc. Lond. B* 353: 1521–1552.

Levrat-Calviac, V. 1986. Etude comparée des ostéodermes de *Tarentola mauritanica* et de *T. neglecta* (Gekkonidae, Squamata). *Arch. Anat. Microsc. Morphol. Exp.* 75: 29–43.

Levrat-Calviac, V. and L. Zylberberg. 1986. The structure of osteoderms in the gecko: *Tarentola mauritanica*. *Am. J. Anat.* 176: 437–446.

Levrat-Calviac, V., et al. 1986. The structure of the osteoderms of two lizards: Tarentola mauritanica and Anguis fragilis. In *Studies in herpetology*, ed. Rocek, Z., 341–344. Prague: Charles University.

Lindgren, J. and M. Siverson. 2002. *Tylosaurus ivoensis*: a giant mosasaur from the early Campanian of Sweden. *Trans. R. Soc. Edin: Earth Sci.* 93: 73–93.

Lindgren, J., et al. 2010. Convergent evolution in aquatic tetrapods: insights from an exceptional fossil mosasaur. *PLoS One* 58: e11998.

Lindgren, J., et al. 2011. Landlubbers to leviathans: evolution of swimming in mosasaurine mosasaurs. *Paleobiology* 37: 445–469.

Luan, X., et al. 2009. The mosasaur tooth attachment apparatus as paradigm for the evolution of the gnathostome periodontium. *Evol. Dev.* 11: 247–259.

Maisano, J. A. 2002. Terminal fusion of skeletal elements as indicators of maturity in squamates. *J. Vert. Paleont.* 22: 268–275.

Maisano, J. A., et al. 2002. The osteoderms and palpebral in *Lanthanotus borneensis* (Squamata: Anguimorpha). *J. Herpetol.* 36: 678–682.

Makádi, L., et al. 2012. The first freshwater mosasauroid (Upper Cretaceous, Hungary) and a new clade of basal mosasauroids. *PLoS One*. 7: e51781.

Martill, D. M., et al. 2015. A four-legged snake from the Early Cretaceous of Gondwana. *Science*. 349: 416–419.

Maxwell, E. E., et al. 2011. Histology of tooth attachment tissues and plicidentine in *Varanus* (Reptilia: Squamata), and a discussion of the evolution of amniote tooth attachment. *J. Morphol*. 272: 1170–1181.

Mead, J. I. et al. 2012. Helodermatid lizard from the Mio-Pliocene oak-hickory forest of Tennessee, eastern USA, and a review of monstersaurian osteoderms. *Acta Paleontol. Pol*. 57: 111–121.

Moazen, M., et al. 2009. Assessment of the role of sutures in a lizard skull: a computer modelling study. *Proc. R. Soc. B* 276: 39–46.

Montero, R., et al. 2017. How common are cranial sesamoids among squamates? *J. Morphol*. 1400–1411.

Moss, M. L. 1969. Comparative histology of dermal sclerifications in reptiles. *Acta Anat*. 73: 510–533.

Motani, R. 2010. Warm-blooded "sea dragons"? *Science*. 328: 1361–1362.

Nopcsa, F. 1908. Zur Kenntnis der fossilen Eidechsen. *Beit. Paläontol. Geol. Österreich-Ungarns und des Orients*. 21: 33–62.

Pal, A., et al. 2009. Long bone histology and skeletochronology in a tropical Indian lizard, Sitana ponticeriana (Sauria: Agamidae). *Curr. Herpetol*. 28: 13–18.

Paladino, F. V., et al. 1990. Metabolism of leatherback turtles, gigantothermy, and thermoregulation of dinosaurs. *Nature*. 344: 858–860.

Palci, A. and M. W. Caldwell. 2007. Vestigial forelimbs and axial elongation in a 95 million-year-old non-snake squamate. *J. Vert. Paleontol*. 27: 1–7.

Palci, A. and M. W. Caldwell. 2010. Redescription of *Acteosaurus tommasinii* von Meyer, 1860, and a discussion of evolutionary trends within the clade Ophidiomorpha. *J. Vert. Paleontol*. 30: 94–108.

Palci, A., et al. 2013a. Emended diagnosis and phylogenetic relationships of the Upper Cretaceous fossil snake *Najash rionegrina* Apesteguía and Zaher, 2006. *J. Vert. Paleontol*. 33: 131–140.

Palci, A., et al. 2013b. Reevaluation of the anatomy of the Cenomanian (Upper Cretaceous) hind-limbed marine fossil snakes *Pachyrhachis*, *Haasiophis*, and *Eupodophis*. *J. Vert. Paleontol*. 33: 1328–1342.

Patchell, F. C. and R. Shine. 1986. Hinged teeth for hard-bodied prey: a case of convergent evolution between snakes and legless lizards. *J. Zool. Lond. A* 208: 269–275.

Peabody, F. E. 1958. A Kansas drouth recorded in growth zones of a bullsnake. *Copeia* 1958(2): 91–94.

Peabody, F. E. 1961. Annual growth zones in living and fossil vertebrates. *J. Morphol*. 108: 11–62.

Pellegrini, R. 2007. Skeletochronology of the limb elements of mosasaurs (Squamata; Mosasauridae). *Trans. Kansas Acad. Sci*. 110: 83–99.

Petermann, H. and J. A. Gautier. 2018. Fingerprinting snakes: paleontological and paleoecological implications of zygantral growth rings in Serpentes. *PeerJ.* 6: e4819.

Petermann, H. and J. A. Gautier. 2020. Skeletochronology reconcilies differences in growth strategies and longevity in the common chuckwalla (*Sauromalus ater*) with implications for squamate life-history studies. *Copeia* 108: 72–82.

Peterman, H., et al. 2017. Osteology and sequence of suture fusion reveal complex environmentally influenced growth in the teiid lizard Aspidoscelis tigris - Implications for fossil squamates. Palaeogeogr. Palaeoclim. Palaeoecol. 475: 12–22.

Pianka, E. R. 2004. Evolution of body size and reproductive tactics. In *Varanoid lizards of the world*, eds. Pianka, E. R. and D. R. King, 549–570. Bloomington, IN and Indianapolis, IN: Indiana University Press.

Polcyn, M. J. and G. L. Jr. Bell. 2005. *Russellosaurus coheni* n. gen., n. sp., a 92 million-year-old mosasaur from Texas (USA), and the definition of the parafamily Russellosaurina. *Neth. J. Geosci*. 84: 321–333.

Pyron, R. A., et al. 2013. A phylogeny and revised classification of Squamata, including 4161 species of lizards and snakes. *BMC Evol. Biol*. 13: 93.

Pyron, R. A. 2017. Novel approaches for phylogenetic inference from morphological data and total-evidence dating in squamate reptiles (lizards, snakes, and amphisbaenians). *Syst Biol*. 66: 38–56.

Quémeneur, S., et al. 2013. Microanatomy of the amniote femur and inference of lifestyle in limbed vertebrates. *Biol. J. Linn. Soc*. 109: 644–655.

Rage, J.-C. and F. Escuillié. 2000. Un nouveau serpent bipède du Cénomanien (Crétacé). Implications phylétiques. *CR Acad. Sci. IIA*. 330: 513–520.

Rage, J.-C. and F. Escuillié. 2003. Le Cénomanien: étage des serpents bipèdes. *Carnets de Géologie/Notebooks on Geology*, Maintenon, Article 1.

Rasmussen, T. E. and G. Callison. 1981. A new herbivorous sphenodontid (Rhynchocephalia: Reptilia) from the Jurassic of Colorado. *J. Paleontol*.: 1109–1116.

Reeder, T. W., et al. 2015. Integrated analyses resolve conflicts over squamate reptile phylogeny and reveal unexpected placements for fossil taxa. *PLoS One*. 10: e0118199.

Regnault, S., et al. 2016. Anatomy, morphology and evolution of the patella in squamate lizards and Tuatara (*Sphenodon puntatus*). *J. Anat*. 228: 864–876.

Reynoso, V. H. 2000. An unusual aquatic sphenodontian (Reptilia: Diapsida) from the Tlayua Formation (Albian), central Mexico. *J. Paleontol*. 74: 133–148.

Ricqlès, A. de 1975. Recherches paléohistologiques sur les os longs des tétrapodes. VII. Sur la classification, la signification fonctionnelle et l'histoire des tissus osseux des tétrapodes (Première partie). *Ann. Paléontol*. 61: 51–129.

Ricqlès A. de. 1976. On bone histology of fossil and living reptiles, with comments on its functional and evolutionary significance. In *Morphology and biology of reptiles*, eds. Bellairs, A. d'A. and C. Barry Cox, 123–151.

Ricqlès, A. de. 1979. Quelques remarques sur l'histoire évolutive des tissus squalettiques chez les vertébrés et plus particulièrement chez les tétrapodes. *Ann. Biol*. 18: 1–35.

Rieppel, O. 1978. Tooth replacement in anguinomorph lizards. *Zoomorphologie* 91: 77–90.

Romer, A. S. 1956. *Osteology of the reptiles*. Chicago: University of Chicago Press.

Savitzky, A. H. 1981. Hinged teeth in snakes: an adaptation for swallowing hard-bodied prey. *Science* 212: 346–349.

Shapiro, M. D. 2002. Developmental morphology of limb reduction in *Hemiergis* (Squamata: Scincidae): chondrogenesis, osteogenesis, and heterochrony. *J. Morphol*. 254: 211–231.

Sheldon, A. 1997. Ecological implications of mosasaur bone microstructure. In *Ancient marine reptiles*, eds. Callaway, J. M. and E. L. Nicholls, 293–332. San Diego, CA: Academic Press.

Sheldon, A. and G. L. Bell. 1998. Paedomorphosis in Mosasauroidea (Squamata): evidence from fossil bone microstructure. *Paludicola* 2: 190–205.

Simoes, T. R., et al. 2018. The origin of squamates revealed by a Middle Triassic lizard from the Italian Alps. *Nature* 557: 706–709.

Smirina, E. M. and N. B. Anajeva. 2007. Growth layers in bone and acrodont teeth of the agamid lizard *Laudakia stoliczkana* (Blanford, 1875) (Agamidae, Sauria). *Amphibia-Reptilia* 28: 193–204.

Stein, K. W. H. and J. Werner. 2013. Preliminary analysis of osteocyte lacunar density in long bones of tetrapods: all measures are bigger in sauropod dinosaurs. *PLoS One* 8: e77109.

Streicher, J. W. and J. J. Wiens. 2017. Phylogenomic analyses of more than 4000 nuclear loci resolve the origin of snakes among lizard families. *Biol. Lett.* 13: 20170393.

Townsend, T., et al. 2004. Molecular phylogenetics of squamata: the position of snakes, amphisbaenians, and dibamids, and the root of the squamate tree. *Syst. Biol.* 53: 735–757.

Tschopp, E. 2015. Nomenclature of vertebral laminae in lizards, with comments on ontogenetic and serial variation in lacertine (Squamata; Lacertidae). *PLoS One* 11(2): e0149445.

Uetz, P., et al. (eds). 2018. *The Reptile Database*. http://www.reptile-database.org.

Vickaryous, M. K. and J.-Y. Sire. 2009. The integumentary skeleton of tetrapods: origin, evolution, and development. *J. Anat.* 214: 441–464.

Vickaryous, M. K., et al. 2015. Armored geckos: a histological investigation of osteoderm development in *Tarentola* (Phyllodactilidae) and *Gekko* (Gekkonidae) with comments on their regeneration and inferred function. *J. Morphol.* 276: 1345–1367.

Zaher, H. and O. Rieppel. 1999. Tooth implantation and replacement in squamates, with special reference to mosasaur lizards and snakes. *Am. Mus. Novit.* 3271.

Zylberberg, L. and J. Castanet. 1985. New data on the structure and the growth of the osteoderms in the reptile *Anguis fragilis* L. (Anguidae, Squamata). *J. Morphol.* 186: 327–342.

VetBooks.ir

21

Sauropterygia: Placodontia

Torsten M. Scheyer and Nicole Klein

CONTENTS

Introduction 425
Overview of Endoskeletal Element Studies 425
Overview of Studies of Dermal Armor Elements 426
New Data from *Cyamodus hildegardis* from the Besano Formation of Monte San Giorgio, Switzerland 430
Conclusions 430
Institutional Abbreviations 430
Acknowledgments 430
References 432

Introduction

Placodontia, hereafter referred to as placodonts, are an enigmatic group of Mesozoic marine reptiles that were restricted to the Triassic. Placodonts are sister to the remaining eosauropterygians (Rieppel 2000) within Sauropterygia, one of the three major clades of marine reptiles (the others are the ichthyosaurs and the thalattosaurs) that lived in the Mesozoic seas (Bardet et al. 2014; Neenan et al. 2013; Rieppel 2000). Most placodonts are generally considered semiaquatic to near-shore bottom dwellers, because their morphology suggests that they were not highly agile swimmers, feeding mostly on sessile or slow-moving prey (e.g., Klein et al. 2015a, b; Mazin and Pinna 1993; Scheyer et al. 2012). Placodonts have an array of globular to flattened teeth in their upper jaws, especially on the palatine bones, and in the lower jaws, suitable for crushing hard-shelled prey items (Crofts et al. 2017; Scheyer et al. 2012). Recently, a small juvenile skull, *Palatodonta bleekeri*, was described from Middle Triassic Muschelkalk deposits of Winterswijk, The Netherlands, which constitutes the first and so far only nonplacodont placodontiform (Neenan et al. 2013). *Palatodonta* was found to represent a transitional morphology between animals with jaws carrying palatal denticles, i.e., the plesiomorphic diapsid condition, and the specialized placodont durophagous dentition.

Along with their dentition, most placodonts also show a diversity of specialized postcranial features in the form of dermal armor. Traditionally, the group was split into the non-armored placodontoid genera, i.e., *Paraplacodus* (completely lacking any armor), *Placodus* (carrying a single row of armor elements over the vertebral column) and *Pararcus* (an animal likely carrying a loose array of dermal armor, but the context to the endoskeleton is not known) and the heavily armored cyamodontoid genera, which bore almost turtle-like shells (Klein and Scheyer 2014; Pinna and Nosotti 1989; Renesto and Tintori 1995; Rieppel 2000, 2002). Although the latter group is generally considered monophyletic, the former is often recovered as a successive grade of taxa (e.g., Klein and Scheyer 2014; Neenan et al. 2015).

Prior to the new millennium, placodont remains were exclusively known and described from sediments of the western Tethyan Province, from central and southern Europe to the Middle East (e.g., Buffetaut and Novak 2008; Drevermann 1933; Huene 1936; Rieppel 2000; Rieppel and Hagdorn 1998; Rieppel et al. 1999). Since 2000, however, several new placodont species have also been described from the eastern Tethyan Province, i.e., from outcrops in southern China (Jiang et al. 2008; Li 2000; Li and Rieppel 2002; Zhao et al. 2008) and new and exciting finds in that area –and from Europe– are still coming to light, which will further increase the knowledge on these animals in the near future (De Miguel Chaves et al. 2018, 2020; Gere et al. 2020; Wang et al. 2019a,b; 2020). Until recently, bones of placodonts were seldom thin sectioned and thus played only a minor role in comparative histological studies (Ricqlès and Buffrénil 2001).

Overview of Endoskeletal Element Studies

The first study to describe the histology of a placodont was that of a long bone from the Ladinian (Upper Muschelkalk) of the Germanic Basin (Crailsheim, southern Germany; Buffrénil and Mazin 1992). The histology of that specimen showed a poorly developed medullary cavity and periosteal "woven-fibered" bone tissue with a very abundant vascular supply. These data were later incorporated into comparative reviews of

VetBooks.ir

the histological and microstructural changes in bone accompanying a return of tetrapods to a secondary aquatic lifestyle (Houssaye 2013; Ricqlès and Buffrénil 2001). Klein et al. (2015b) pointed out that the original identification of the placodont humerus by Buffrénil and Mazin (1992) as pertaining to the genus *Placodus*, also used by Canoville and Laurin (2010) for lifestyle inference, is equivocal and should be treated with caution (however, the specimen is undoubtedly a placodont). Based on its microanatomy and resulting compactness parameters (using the program Bone Profiler) and according to various models, the bone was supposed to have derived from an animal with an amphibious lifestyle (Canoville and Laurin 2010). The authors, however, noted that this interpretation is to be used with caution only, because the bone fell out of the three lifestyle clusters of extant amniotes.

Klein (2010) studied two long bones (one humerus and one femur) of Placodontia indet. from the Anisian (Middle Muschelkalk) of the Germanic Basin (Freyburg, River Unstrut, Germany) in a study of Sauropterygia and reported a high vascular density of placodont long bones. These bones confirmed the absence of a large medullary cavity (compared to some other studied sauropterygian bones) and the presence of thick cortices made of a fibrolamellar (i.e., woven-parallel) complex. Bone compactness is relatively high, although vascularization is dense. Vascular networks include both simple canals and primary osteons, and they display a relatively atypical plexiform-like structure.

In a follow-up study, the histology and microstructure focused on a larger sample of long bones (humeri and femora) of armored and nonarmored placodonts (Klein et al. 2015b). Only long bones that were found in association with other postcranial or cranial material could be identified to the genus or even species level, whereas the remaining isolated long bones could be identified only as Placodontia with affinities to certain taxa. The study revealed a hitherto unknown and not phylogenetically or stratigraphically related disparity in histological structures and microanatomical details, as well as growth strategies (Klein et al. 2015a). Some armored and nonarmored placodonts have unexpectedly low vascularized lamellar-zonal bone tissue (Figure 21.1).

Other taxa, again including both armored and nonarmored forms, have a spongy architecture throughout most of the cortex and deposited fibrolamellar bone tissue in their main growth phase (Figure 21.2), as previously described for placodonts by Buffrénil and Mazin (1992) and Klein (2010). Fibrolamellar complexes result from fast subperiosteal apposition (Castanet et al. 1996; Margerie et al. 2004) and are considered to reflect relatively high metabolic rates (e.g., Cubo et al. 2008; Montes et al. 2007). Among marine reptiles, the latter also occur, for example, in thunniform ichthyosaurs, a group of pelagic forms supposed to have been fast-swimming, tachymetabolic predators (Buffrénil and Mazin 1992; Houssaye et al. 2014; Klein et al. 2015b). All placodont humeri that show this high vascular density additionally have secondarily widened primary osteons, resulting in a secondarily spongy tissue (Figure 21.2). However, the microanatomy of all placodonts shows a tendency toward osteosclerosis (i.e., bone mass increase), supporting an aquatic lifestyle in shallow marine habitats (Houssaye et al. 2016).

Differences in microanatomy, bone histology, and growth patterns suggest different ecological adaptations, including differences in lifestyle, as well as swimming modes and capabilities in Placodontia. These differences may have reduced competition in the shallow marine environments of the Tethys and might be a key to the success and diversity of Placodontia. A certain developmental plasticity among studied placodonts, as revealed by inter- and intraspecific histological variation, is interpreted as a response to different environmental conditions.

In addition to the bones mentioned above, Weidemeyer (2001) studied histological sections of a clavicle (SMNS 81889; Ladinian, upper Muschelkalk of Bindlach near Bayreuth, Germany) and a jaw fragment (SMNS 81890; Ladinian, upper Muschelkalk of Mistlau near Crailsheim, Germany) of *Placodus*. Both specimens were described as overall compact bones made of lamellar-zonal tissue, with larger vascular cavities restricted to the bone center. It is difficult, however, to compare these data with the aforementioned long bones studied (Klein et al. 2015b) because differences are to be expected between dermal bones and appendicular long bones and size-related differences in histology cannot be ruled out among cranial, forelimb and girdle elements.

Overview of Studies of Dermal Armor Elements

There have been very few studies focusing on the histology and/or microanatomy of placodont armor. Westphal (1976) discussed growth patterns of hexagonal to polygonal placodont armor plates, showing a sketch of a cross section of plates of *Psephosaurus suevicus*, from the Late Ladinian of southern Germany (Rieppel 2002) exclusively known from its dermal armor. The sketch indicates that the plates did not change much in shape during ontogeny. They were depicted as having an internal growth center surrounded by compact bone with vascular canals radiating toward the plate borders and peripheral growth marks (see also Chapter 31 on skeletochronology). Weidemeyer (2001) later included a bowl-shaped armor plate of *P. suevicus* in his comparative histological work, corroborating the findings of Westphal (1976) and specifically mentioning the radial vascular canals in the center of the plate, whereas marginal regions displayed avascular parallel-fibered bone tissue with cyclic growth marks. Concentrations of osteocyte lacunae were presented as highly irregular throughout the plate, whereas Sharpey's fibers converging toward the center of the plate were abundant. Scheyer (2007b) then sectioned a sample of placodont armor plates from *Placodus gigas* and the cyamodontoids *P. suevicus*, cf. *Placochelys*, and *Psephoderma*. That study showed for the first time a distinction between (1) completely ossified placodontoid and cyamodontoid plates, which are very similar to each other in exhibiting a meshwork of interwoven fiber bundles and parallel-fibered bone tissue (usually in the peripheral parts of the plates), and (2) nonhexagonal/polygonal cyamodontoid plates that consist of various bone tissue types and a tissue resembling calcified fibrocartilage (Figure 21.3). Scheyer (2007b) coined the term "postcranial fibrocartilaginous bone" (PFCB) for the latter condition, raising the issue of the possible nonhomology of these armor plates with true osteoderms that form within the dermis without a cartilaginous precursor. What Weidemeyer (2001) interpreted as parallel-fibered tissue in the plate of

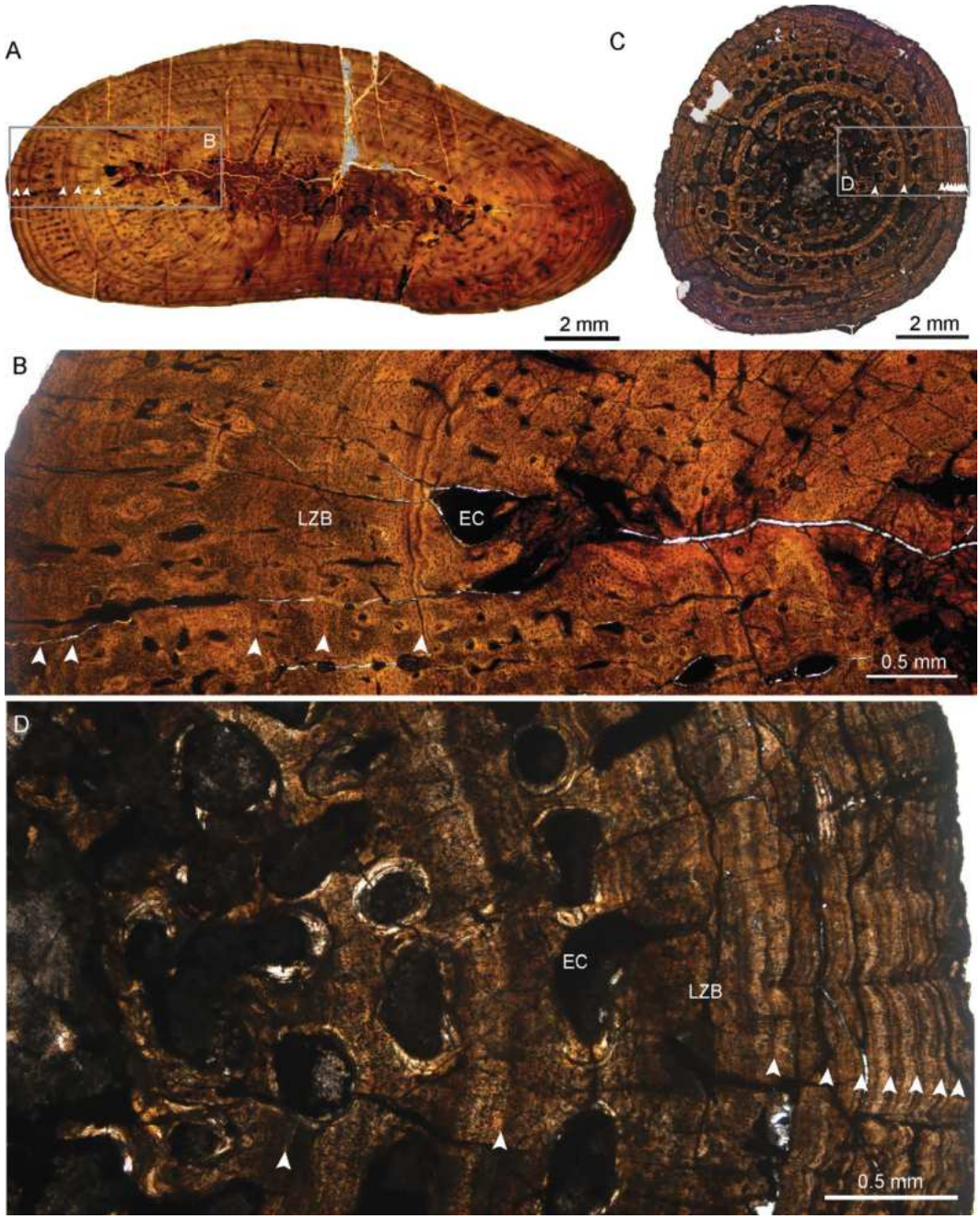


FIGURE 21.1 Long bone histology of placodonts showing slower bone deposition (see also (Klein et al. 2015a, b). A and B, Humerus of *Paraplacodus broilii* (PIMUZ T5845) from the Middle Triassic (Late Anisian, Middle Besano Fm.) of Meride, Switzerland. C and D. Femur of *Psephoderma alpinum* (PIMUZ A/III 0735) from the Late Triassic (Rhaetian) of Switzerland. In both taxa, the thick cortex is composed of lamellar-zonal bone (LZB) and the perimedullary region shows bone resorption in the form of erosion cavities (EC). Lines of arrested growth are indicated by white arrowheads.

P. suevicus is reinterpreted here as mostly longitudinally and transversely sectioned structural fiber bundles, as encountered in other placodont plates.

Scheyer (2008) used neutron tomography imaging in addition to external morphology to identify the then allegedly oldest turtle shell fragment, *Priscochelys hegnabrunnensis* (Muschelkalk of southern Germany), as belonging to a cyamodontoid placodont instead. These tomographic data could not be used, however, for further histological work on the specimen, due to insufficient resolution.

De Miguel Chaves et al. (2020) recently presented histological descriptions of diverse armor plates discovered among Middle Triassic placodont remains from Canales de Molina, Central Spain. Because of similar general histological features (including the absence of PFCB), the presence of few growth marks in the larger and thicker specimens only, and the external morphology of the plates, the authors concluded that the sample reflects different ontogenetic stages of the same species, possibly *Psephosauriscus*. Furthermore, it was proposed that PFCB is generally absent in the common type

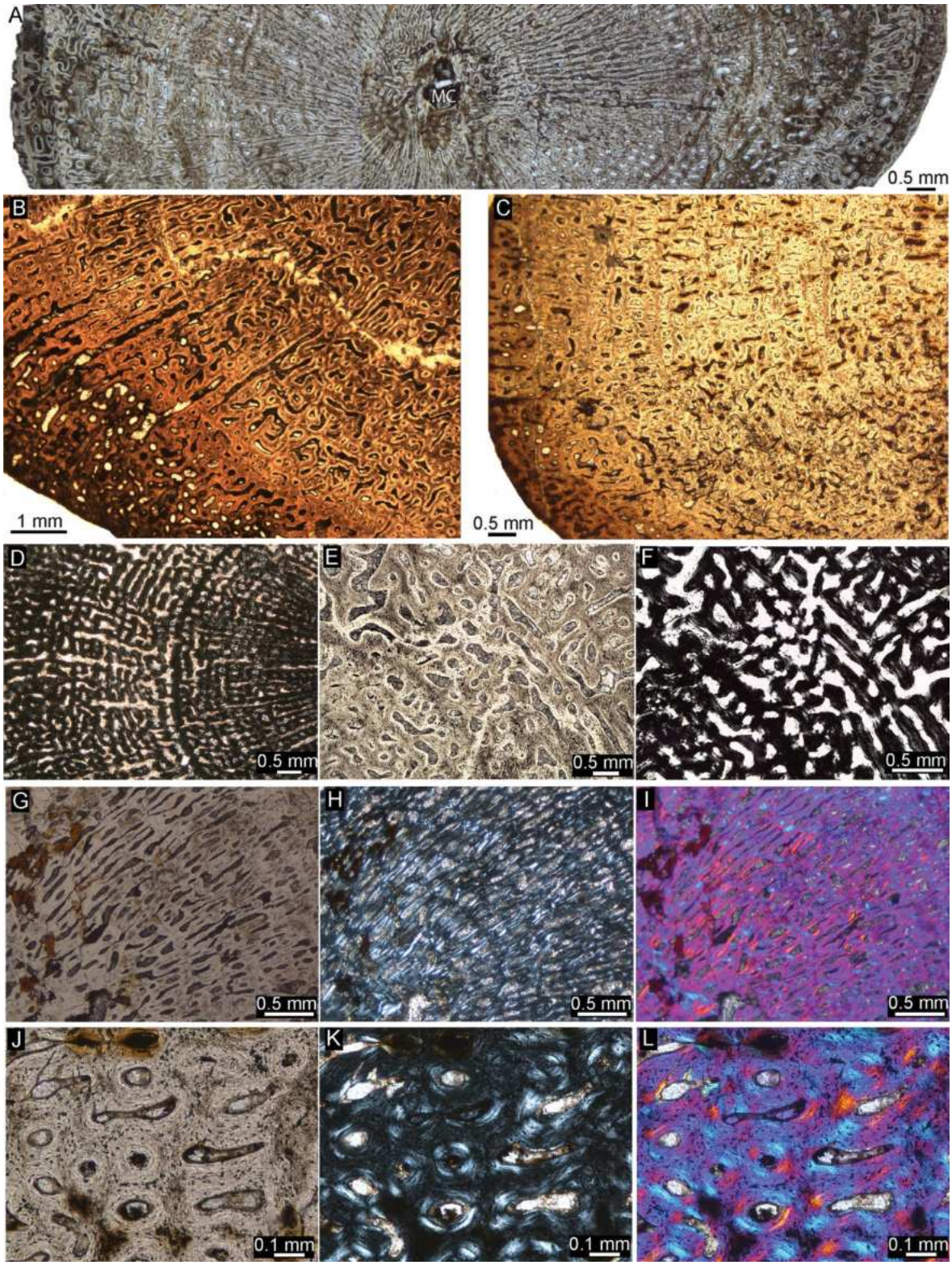


FIGURE 21.2 Long bone histology of placodonts showing faster bone deposition in various humeri of Placodontia indet. aff. *Cyamodus* from the Middle Triassic (Ladinian; Upper Muschelkalk) of southern Germany (see also Klein et al. 2015a, b). In all specimens, the thick cortex is composed of highly vascularized fibrolamellar bone tissue. Note the highly diverse vascular systems ranging from radial to plexiform and radiating. A, Humeral cross section of the entire cortex from the medial to the lateral bone side (MHI 1096) in normal light. Note the very small medullary cavity (MC). B, Middle and outer cortex (MHI 2112/6) in normal light. C, Middle and outer cortex (MHI 697) in normal light. D–F. Details of the cortex (SMNS 15981) in cross-polarized (D and F) and normal light (E). G–I. Details of radial primary osteons in the middle cortex (MNS 54582) in normal light (G), cross-polarized light (H), and cross-polarized light with gypsum filter (I). J–L. Details of longitudinal primary osteons and elongated simple vascular canals (MHI 697) in normal light (J), cross-polarized light (K), and cross-polarized light with gypsum filter (L).

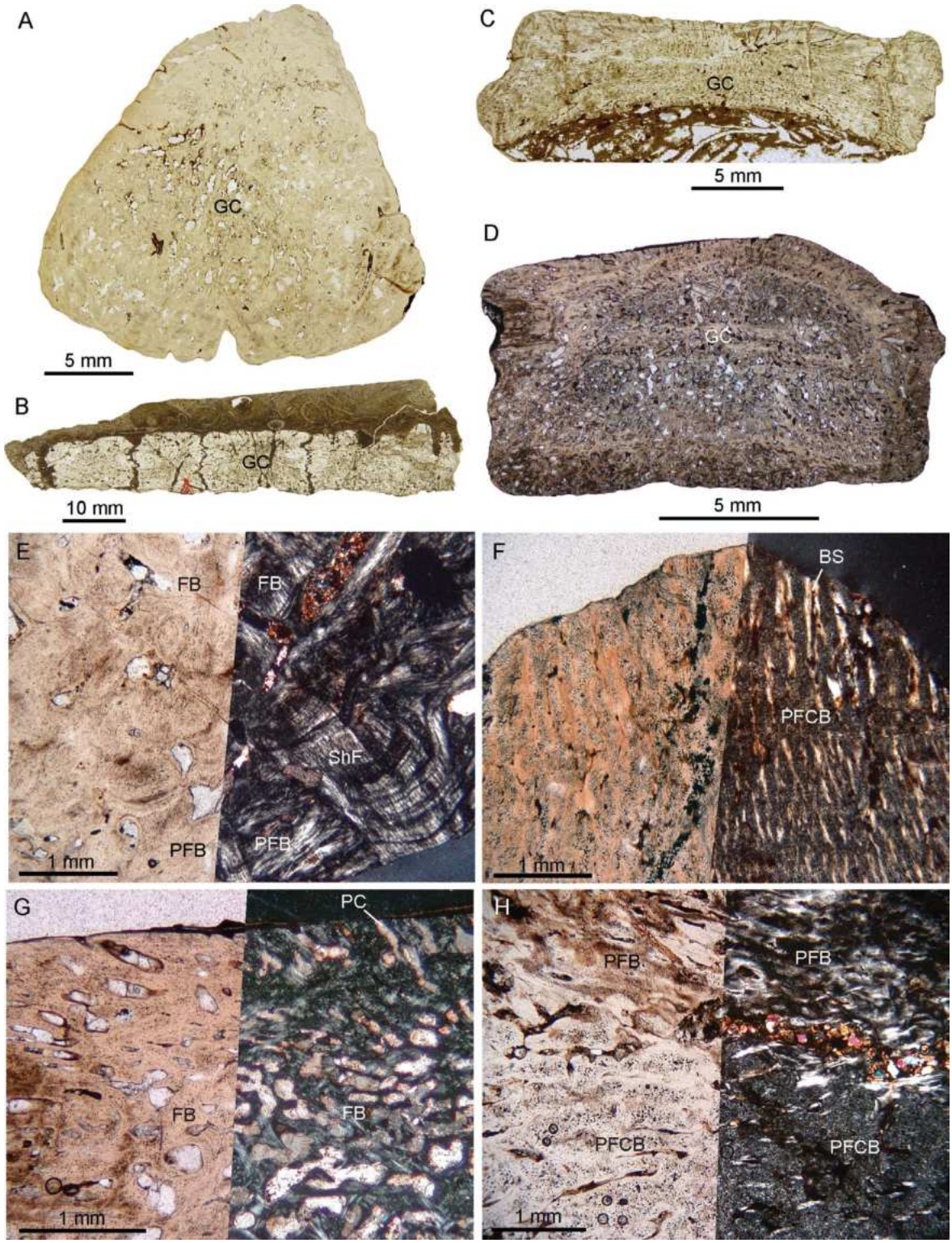


FIGURE 21.3 Placodont armor plate histology (see also Scheyer 2007a, b). A–D, Overview images of complete sections. E–F. Close-ups of bone tissues in normal transmitted (left sides) and cross-polarized light (right sides of images). A and E, Plate of *Placodus gigas* (SMNS 91006) from the Middle Triassic (Ladinian) of Bühlingen near Rottweil, Germany. B, Polygonal plates of *Psephoderma* sp. (NRM-PZ R.1759a) from the Middle Triassic (Muschelkalk) of Wadi Raman (Makhtesh Ramon), Negev, Israel. C, Isolated hexagonal flat plate of *Psephosaurus* sp. (SMNS 91008) from the Middle Triassic (Ladinian) of Hoheneck near Ludwigsburg, Germany. D and G, Isolated small hexagonal plate of *Psephosaurus suevicus* (MHI 1426/3) from the Middle Triassic (Ladinian) of Kirchberg/Jagst, Germany. F, Small recumbent spike of *P. suevicus* (SMNS 91007). H, Rhomboidal plate of possible plastral region of *Psephosaurus* sp. (SMNS 91009); both are from the Middle Triassic (Ladinian) of Hoheneck near Ludwigsburg, Germany. BS, bone spicule; FB, fiber bundle; GC, growth center; PC, primary canal; PFB, parallel-fibered bone; PFCB, postcranial fibrocartilaginous bone (*sensu* Scheyer 2007b); ShF, Sharpey's fibers.

VetBooks.ir

of hexagonal/polygonal plates, and that its presence in some bones should not be linked to ontogeny, but to other morphogenetic differences among placodont taxa (De Miguel Chaves et al. 2020).

New Data from *Cyamodus hildegardis* from the Besano Formation of Monte San Giorgio, Switzerland

The cyamodontoid *Cyamodus hildegardis* (Peyer 1931) is one of the best documented placodonts from the Middle Triassic of Europe (Pinna 1980, 1992, Scheyer 2010). Although several specimens are present in Swiss (Paläontologisches Institut und Museum der Universität Zürich) and Italian collections (e.g., Museo Civico di Storia Naturale di Milano), it has never been subjected to histological study. Recently, several small fragments of the postcranium of the holotype specimen of *C. hildegardis* (PIMUZ T 4763, upper Late Anisian Besano Fm. of Val Porina, Meride, Canton Ticino, Switzerland), stored separately for several decades in the collections apart from the exhibited specimen, were available for sectioning. These fragments included two keeled armor plates and three other bone fragments (from either the appendicular or the axial skeleton) from the trunk region (Figures 21.4 and 21.5). It is likely that the latter comes from either long bones, ribs, or the prominent transverse processes of vertebrae; however, due to the lack of further morphological external details, they are treated as indeterminate endoskeletal bones herein.

The two keeled armor plates are compact structures (>90% bone tissue) with few larger cavities and scattered vascular canals. Their core consists of an irregular meshwork of longitudinally and transversely oriented structural fibers, while their peripheral cortex is made of parallel-fibered tissue showing growth marks in the form of zones separated by lines of arrested growth (LAGs) or annuli. Sharpey's fibers regularly cross the parallel-fibered tissue at steep angles. The vascularization is overall low, consisting of small, scattered primary vascular canals and a few larger vascular spaces in the deep cortex. Histologically, these armor plates are similar in build to the hexagonal/polygonal plates of other cyamodontoids sectioned previously, such as those of *Psephoderma* and *Psephosaurus* (Scheyer 2007b).

The other three samples represent either cross sections (two samples) or longitudinal sections (one sample) from indeterminate bones. The longitudinal and transverse sections (Figure 21.4) reveal that the bones had a central marrow cavity with some bone trabeculae (usually collapsed), surrounded by thick cortical bone that is increasingly compact toward the periphery. Adjacent to the medullary cavity, the bone tissue consists of a parallel-fibered type devoid of cyclical growth marks. It turns to lamellar tissue bearing growth marks toward the outer bone surface. Vascularization is low, consisting of scattered secondary osteons in the deep cortex and longitudinal canals arranged in circular rows toward the periphery. Growth marks (10 in the cross section in Figure 21.4A–F), in the form of LAGs and thin zones, are conspicuous in this outer cortex, hinting at the presence of an outer circumferential layer (*sensu* Ponton et al. 2004). If so, the large holotype specimen of *C. hildegardis* had reached skeletal maturity.

The endoskeletal bone sample of *C. hildegardis* shares the presence of lamellar-zonal bone tissue and overall low level of vascularization with the previously sampled *Paraplacodus* and *Psephoderma,* also from the Alpine Triassic. These taxa are likely to have shared similar ecological traits (Klein et al. 2015b). *C. hildegardis* thus differed considerably from the other species of *Cyamodus* (i.e., bones attributed to aff. *Cyamodus*) that inhabited the Germanic Basin of the Muschelkalk Sea and bear more rapidly deposited fibrolamellar tissue in their long bones (Klein et al. 2015a, b).

Conclusions

Dermal armor plates of placodonts typically show a centrally situated growth center, an interwoven meshwork of structural fibers in the core and parallel-fibered bone with growth marks in the outer cortical periphery, and radial vascularization patterns. The dense structure of the armor plates could indicate that they also contributed to bone ballast and buoyancy control of the animals under water. In the case of long bones, differences in microanatomy, bone histology and growth patterns, as shown above, likely indicate different ecological adaptations, including differences in lifestyle, as well as swimming modes and capabilities in Placodontia. The plexiform to radiating fibrolamellar bone tissue and the implied high growth rates observed in some placodonts are without any analogue among modern reptiles. Tissue type and growth rate are only comparable to those of Ichthyosauria (see Chapter 24 on Ichthyosauria). These animals, however, were sustained swimmers in the open sea hunting actively for mobile prey, whereas placodonts have been interpreted as slow bottom walkers that feed on immobile or sessile prey items. The question remains why some placodonts evolved such high growth rates and whether documented differences among taxa from the Alpine Triassic and the Germanic Basin are really related to these environments.

Institutional Abbreviations

MHI, Muschelkalkmuseum Hagdorn, Ingelfingen, Germany; NRM, Naturhistoriska riksmuseet, Stockholm, Sweden; PIMUZ, Paläontologisches Institut und Museum, Universität Zürich, Switzerland; SMNS, Staatliches Museum für Naturkunde Stuttgart, Germany (R. Schoch).

Acknowledgments

We acknowledge O. Dülfer (Institute of Geosciences, University of Bonn), Ch. Wimmer-Pfeil (SMNS), V. Jaquier and C. Kolb (formerly PIMUZ) for the production of the thin sections. We thank H. Hagdorn (MHI), T. Mörs (NRM), H. Furrer (former curator) and C. Klug (PIMUZ), and R. Schoch (SMNS) for access to specimens under their care.

VetBooks.ir

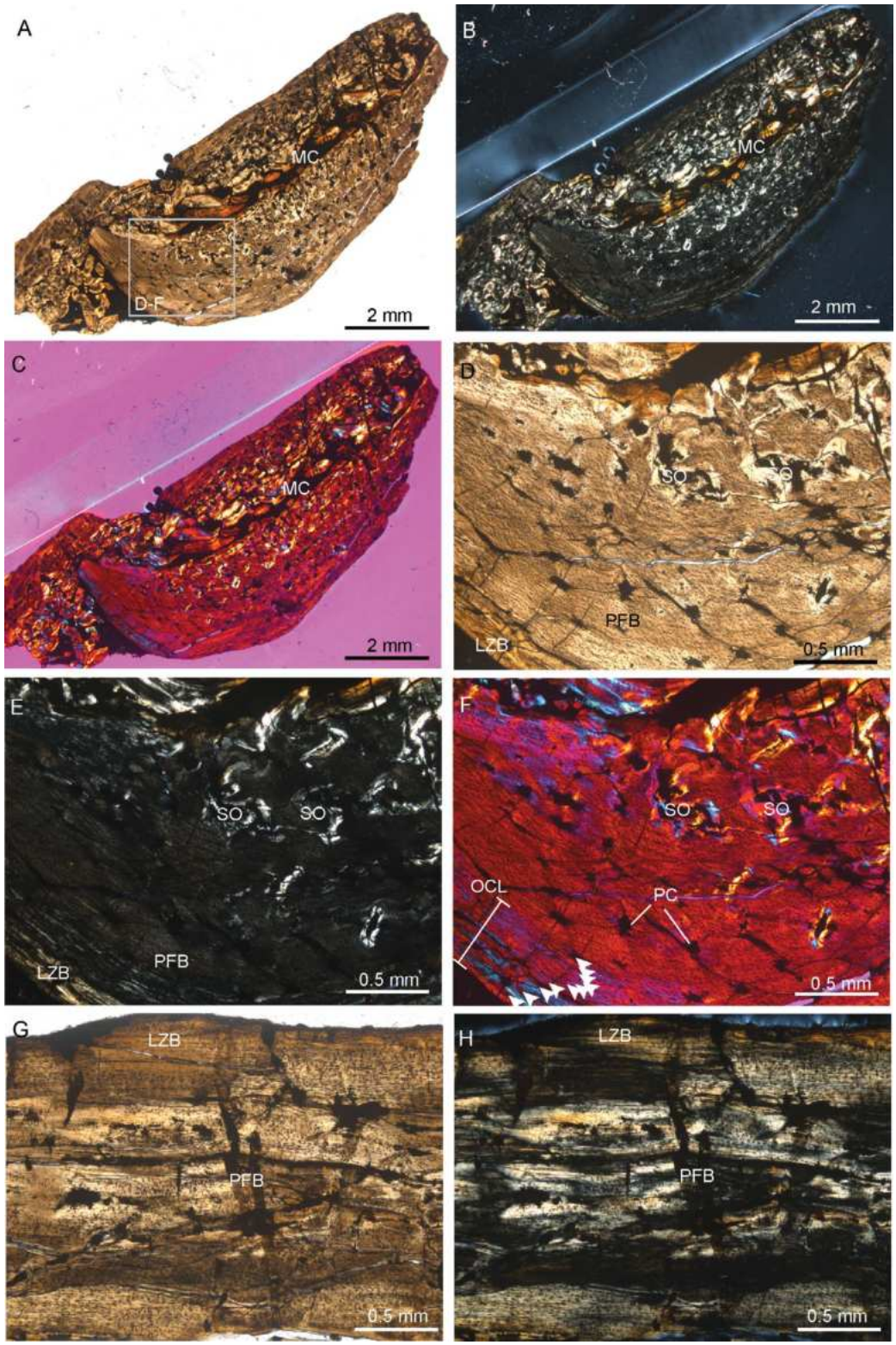


FIGURE 21.4 Histology of two indeterminate endoskeletal bones of *Cyamodus hildegardis* (holotype specimen PIMUZ T 4763) from the Middle Triassic (Late Anisian, Middle Besano Fm.) of Meride, Switzerland. A–F, Cross-sectioned bone fragment. G–H. Longitudinally sectioned bone fragment. Images in A, D, and G are in normal transmitted light, B, E, and H in cross-polarized light, and C and F in cross-polarized light using a lambda compensator. Note the thick cortex, which is increasingly compact toward the bone periphery. The cortex is composed of parallel-fibered tissue adjacent to the medullary cavity and turns into lamellar-zonal tissue toward the outer bone surface. Vascularization is low with scattered secondary osteons in the perimedullary region and circumferentially arranged longitudinal primary vascular canals toward the outer bone surface. The presence of an outer circumferential layer in F (OCL; lines of arrested growth marked by white arrowheads) is assumed to indicate skeletal maturity of the specimen. LZB, lamellar-zonal bone; MC, medullary cavity; PC, primary canal; PFB, parallel-fibered bone; SO, secondary osteon.

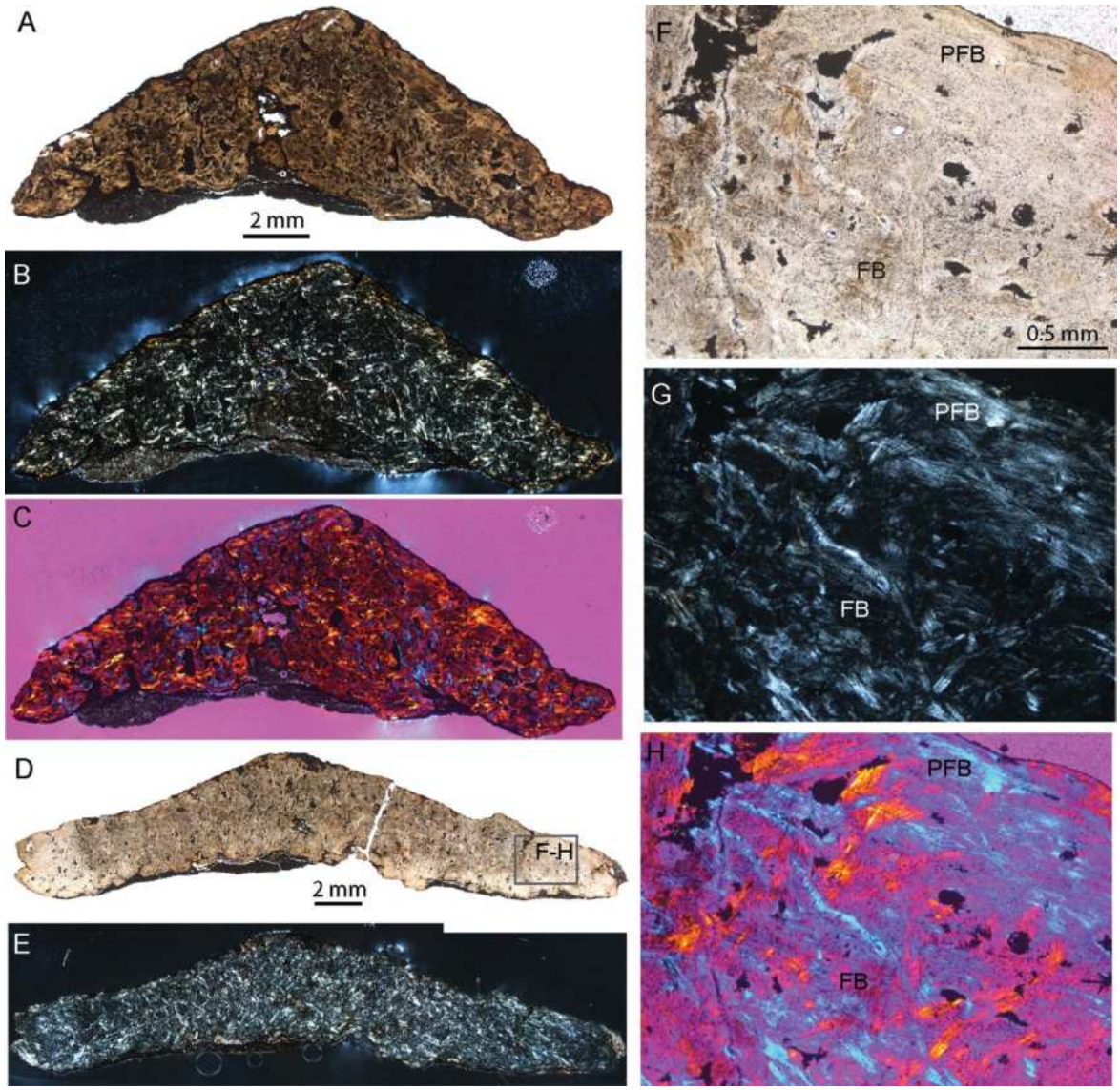


FIGURE 21.5 Histology of keeled armor plates of *Cyamodus hildegardis* (holotype specimen PIMUZ T 4763) from the Middle Triassic (Late Anisian, Middle Besano Fm.) of Meride, Switzerland. Images in A, D, and F are in normal transmitted light, B, E, and G in cross-polarized light, and C and H in cross-polarized light using a lambda compensator. Note the compactness of the armor plates. The center of the plates consists of structural fiber bundles extending longitudinally and transversely, whereas the outer surficial layer is composed of a parallel-fibered bone matrix. Clear growth centers are not discernible in the two specimens. FB, fiber bundle; PFB, parallel-fibered bone.

REFERENCES

Bardet, N., et al. 2014. Mesozoic marine reptile palaeobiogeography in response to drifting plates. *Gondwana Res.*26:869–887 [doi: 10.1016/j.gr.2014.05.005].

Buffetaut, E., and M. Novak. 2008. A cyamodontid placodont (Reptilia: Sauropterygia) from the Triassic of Slovenia. *Palaeontology* 51:1301–1306.

Buffrénil, V. de, and J.-M. Mazin. 1992. Contribution de l'histologie osseuse à l'interprétation paléobiologique du genre *Placodus* Agassiz, 1833 (Reptilia, Placodontia). *Rev. Paléobiol.* 11:397–407.

Canoville, A., and M. Laurin. 2010. Evolution of humeral microanatomy and lifestyle in amniotes, and some comments on palaeobiological inferences. *Biol. J. Linn. Soc.* 100:384–406 [doi: 10.1111/j.1095-8312.2010.01431.x].

Castanet, J., et al. 1996. Expression de la dynamique de croissance dans la structure de l'os périostique chez *Anas platyrhynchos*. *C. R. Acad. Sci. Paris* 319:301–308.

Crofts, S. B., et al. 2017. Tooth occlusal morphology in the durophagous marine reptiles, Placodontia (Reptilia: Sauropterygia). *Paleobiology* 43:114–128 [doi: 10.1017/pab.2016.27].

Cubo, J., et al. 2008. Phylogenetic, functional, and structural components of variation in bone growth rate of amniotes. *Evol. Dev.* 10:217–227.

De Miguel Chaves, C., et al. 2018. A new placodont from the Upper Triassic of Spain provides new insights on the acquisition of the specialized skull of Henodontidae. *Pap. Palaeontol.* 4:567–576 [doi: 10.1002/spp2.1218].

De Miguel Chaves, C., et al. 2020. The placodonts (Sauropterygia) from the Middle Triassic of Canales de Molina (Central Spain), and an update on the knowledge about this clade in the Iberian record. *Hist. Biol.* 32:34–48 [doi: 10.1080/08912963.2018.1462805].

Drevermann, F. 1933. Die Placodontier. 3. Das Skelett von *Placodus gigas* Agassiz im Senckenberg-Museum. *Abh. Senckenb. Naturforsch. Ges.* 38:321–364.

Gere, K., et al. 2020. Placodont remains (Sauropsida, Sauropterygia) from the Triassic of Hungary (Transdanubian Range and Villány Mountains). *Palaeobiodivers. Palaeoenviron.* 100: 1047–1063 [doi: 10.1007/s12549-020-00432-5].

Houssaye, A. 2013. Bone histology of aquatic reptiles: what does it tell us about secondary adaptation to an aquatic life? *Biol. J. Linn. Soc.* 108:3–21 [doi: 10.1111/j.1095-8312.2012.02002.x].

Houssaye, A., et al. 2014. A new look at ichthyosaur long bone microanatomy and histology: Implications for their adaptation to an aquatic life. *PLoS One* 9(4):e95637 [doi:10.1371/journal.pone.0095637].

Houssaye, A., et al. 2016. Adaptive patterns in aquatic amniote bone microanatomy—More complex than previously thought. *Integr. Comp. Biol.* 56:1349–1369 [doi: 10.1093/icb/icw120].

Huene, F. von 1936. *Henodus chelyops*, ein neuer Placodontier. *Palaeontogr. Abt. A* 84:99–148.

Jiang, D.-Y., et al. 2008. First record of Placodontoidea (Reptilia, Sauropterygia, Placodontia) from the Eastern Tethys. *J. Vertebr. Paleontol.* 28:904–908.

Klein, N. 2010. Long bone histology of Sauropterygia from the Lower Muschelkalk of the Germanic Basin provides unexpected implications for phylogeny. *PLoS One* 5(7):e11613 [doi: 10.1371/journal.pone.0011613].

Klein, N., and T. M. Scheyer. 2014. A new placodont sauropterygian from the Middle Triassic of the Netherlands. *Acta Palaeontol. Pol.* 59:887–902 [doi: 10.4202/app.2012.0147].

Klein, N., et al. 2015a. Growth patterns and life history strategies in Placodontia (Diapsida: Sauropterygia). *R. Soc. Open Sci.* 2 [doi: 10.1098/rsos.140440].

Klein, N., et al. 2015b. Long bone histology and microanatomy of Placodontia (Diapsida: Sauropterygia). *Contrib. Zool.* 84:59–84 [doi: 10.1163/18759866-08401005].

Li, C. 2000. Placodont (Reptilia: Placodontia) from Upper Triassic of Guizhou, Southwest China [in Chinese with English summary]. *Vertebr. PalAsiat.* 38:314–317.

Li, C., and O. Rieppel. 2002. A new cyamodontoid placodont from Triassic of Guizhou, China [in Chinese]. *Chinese Sci. Bull.* 47:156–159.

Margerie, E. de, et al. 2004. Assessing a relationship between bone microstructure and growth rate: a fluorescent labelling study in the king penguin chick (*Aptenodytes patagonicus*). *J. Exp. Biol.* 207:869–879.

Mazin, J.-M., and G. Pinna. 1993. Palaeoecology of the armoured placodonts. *Paleontologia Lombarda N. S.* 2:83–91.

Montes, L., et al. 2007. Relationships between bone growth rate, body mass and resting metabolic rate in growing amniotes: a phylogenetic approach. *Biol. J. Linn. Soc.* 92:63–76.

Neenan, J. M., et al. 2013. European origin of placodont marine reptiles and the evolution of crushing dentition in Placodontia. *Nat. Commun.* 4:1621 [doi: 10.1038/ncomms2633].

Neenan, J. M., et al. 2015. The cranial anatomy of Chinese placodonts and the phylogeny of Placodontia (Diapsida: Sauropterygia). *Zool. J. Linn. Soc.* 175:415–428 [doi: 10.1111/zoj.12277].

Peyer, B. 1931. Die Triasfauna der Tessiner Kalkalpen III. Placodontia. *Schweiz. palaeontol. Abh.* 51:1–25.

Pinna, G. 1980. Lo scheletro postcraniale di *Cyamodus hildegardis* Peyer, 1931 descritto su un esemplare del Triassico Medio Lombardo (Reptilia Placodontia). *Atti Soc. ital. sci. nat., Mus. civ. stor. nat. Milano* 121:275–306.

Pinna, G. 1992. *Cyamodus hildegardis* Peyer, 1931 (Reptilia, Placodontia). *Mem. Soc. ital. sci. nat. Mus. civ. stor. nat. Milano* 26:1–21.

Pinna, G., and S. Nosotti. 1989. Anatomia, morfologia funzionale e paleoecologia del rettile placodonte *Psephoderma alpinum* Meyer, 1858. *Mem. Soc. ital. sci. nat. Mus. civ. stor. nat. Milano* 25:17–50.

Ponton, F., et al. 2004. Variation of the outer circumferential layer in the limb bones of birds. *Acta Ornithol. (Warsaw)* 39:21–24.

Renesto, S., and A. Tintori. 1995. Functional morphology and mode of life of the Late Triassic placodont *Psephoderma alpinum* Meyer from the Calcare di Zorzino (Lombardy, N Italy). *Riv. Ital. Pal. Strat.* 101:37–48.

Ricqlès, A. de, and V. de Buffrénil. 2001. Bone histology, heterochronies and the return of tetrapods to life in water: w[h]ere are we? In: *Secondary Adaptations of Tetrapods to Life in Water*, ed. J.-M. Mazin, and V. de Buffrénil, 289–310. München: Verlag Dr. Friedrich Pfeil.

Rieppel, O. 2000. Sauropterygia I - Placodontia, Pachypleurosauria, Nothosauroidea, Pistosauroidea. *Handbuch der Paläoherpetologie* 12A:1–134.

Rieppel, O. 2002. The dermal armor of the cyamodontoid placodonts (Reptilia, Sauropterygia): morphology and systematic value. *Fieldiana (Geology), new. ser.* 46:1–41.

Rieppel, O., and H. Hagdorn. 1998. Fossil reptiles from the Spanish Muschelkalk (Mont-Ral and Alcover, Province Tarragona). *Hist. Biol.* 13:77–97 [doi: 10.1080/08912969809386575].

Rieppel, O., et al. 1999. Sauropterygia from the Middle Triassic of Makhtesh Ramon, Negev, Israel. *Fieldiana (Geology), new. ser.* 40:1-85.

Scheyer, T. M. 2007a. Comparative bone histology of the turtle shell (carapace and plastron): implications for turtle systematics, functional morphology, and turtle origins. PhD Thesis, University of Bonn, Germany [http://nbn-resolving.de/urn:nbn:de:hbz:5N-12299].

Scheyer, T. M. 2007b. Skeletal histology of the dermal armor of Placodontia: the occurrence of 'postcranial fibro-cartilaginous bone' and its developmental implications. *J. Anat.* 211: 737–753 [doi: 10.1111/j.1469-7580.2007.00815.x].

Scheyer, T. M. 2008. Aging the oldest turtles: the placodont affinities of *Priscochelys hegnabrunnensis*. *Naturwissenschaften* 95:803–810 [doi: 10.1007/s00114-008-0386-8].

Scheyer, T. M. 2010. New interpretation of the postcranial skeleton and overall body shape of the placodont *Cyamodus hildegardis* Peyer, 1931 (Reptilia, Sauropterygia). *Palaeontologia Electronica* 13(2) [http://palaeo-electronica.org/2010_2/232/index.html].

Scheyer, T. M., et al. 2012. Revised paleoecology of placodonts – with a comment on 'The shallow marine placodont *Cyamodus* of the central European Germanic Basin: its evolution, paleobiogeography and paleoecology' by C. G. Diedrich (Historical Biology, iFirst article, 2011, 1–19, doi: 10.1080/08912963.2011.575938). *Hist. Biol.* 24:257–267 [doi: 10.1080/08912963.2011.621083].

Wang, W., et al. 2019a. A new species of Cyamodus (Placodontia, Sauropterygia) from the early Late Triassic of south-west China. J. Syst. Palaeontol. 17:1457–1476 [doi: 10.1080/14772019.2018.1535455].

Wang, W., et al. 2019b. An adult specimen of Sinocyamodus xinpuensis (Sauropterygia: Placodontia) from Guanling, Guizhou, China. *Zool. Linn. Soc.* 185:910–924 [doi: 10.1093/zoolinnean/zly080].

Wang, W., et al. 2020. First subadult specimen of Psephochelys polyosteoderma (Sauropterygia, Placodontia) implies turtle-like fusion pattern of the carapace. *Pap. Palaeontol.* 6:251–264 [doi: 10.1002/spp2.1293].

Weidemeyer, S. 2001. Untersuchung der Knochenhistologie aquatischer Reptilien und Amphibien des Mesozoikums. *Diploma Thesis*, Eberhard-Karls-Universität Tübingen, Germany.

Westphal, F. 1976. The dermal armour of some Triassic placodont reptiles. In: *Linnean Society Symposium Series No. 3. Morphology and Biology of Reptiles*, ed. A. d'A. Bellairs, and C. B. Cox, 31–41. London: Academic Press.

Zhao, L.-J., et al. 2008. A new armored placodont from the Middle Triassic of Yunnan Province, southwestern China. *Vertebr. PalAsiat.* 46:171–177.

VetBooks.ir

22

Sauropterygia: Nothosauria and Pachypleurosauria

Torsten M. Scheyer, Alexandra Houssaye and Nicole Klein

CONTENTS

Introduction 435
Overview of Histological Studies 436
Conclusions and Outlook 441
Institutional Abbreviations 441
Acknowledgments 441
References 441

Introduction

Sauropterygia, one of the most successful clades of Mesozoic marine reptiles, commonly includes the following subgroups: the placodonts (and possibly saurosphargids), pachypleurosaurs, nothosaurs and pistosauroids, which also include the only sauropterygians not restricted to the Triassic, namely the plesiosaurs (Rieppel 2000; Scheyer et al. 2017; see also chapters on Placodontia (Chapter 21) and Plesiosauria (Chapter 23). Pachypleurosaurs, nothosaurs, and pistosauroids are grouped together as Eosauropterygia, in which the pachypleurosaurs and nothosaurs traditionally form the clades Pachypleurosauria and Nothosauroidea, respectively (Rieppel 2000; see also Neenan et al. 2013). Other studies, however, indicate that Nothosauroidea, consisting of the genera *Simosaurus*, *Germanosaurus*, *Nothosaurus*, *Lariosaurus* and *Ceresiosaurus* (see taxonomic discussion on the two latter taxa in Hänni 2004 and Rieppel 2007), could represent a clade within a larger paraphyletic grade of pachypleurosaur-like reptiles (e.g., Cheng et al. 2016; Sato et al. 2014). The position of European pachypleurosaurs (*Neusticosaurus*, *Serpianosaurus*, *Dactylosaurus* and *Anarosaurus*) appears quite stable, but other taxa such as the Chinese eosauropterygians *Wumengosaurus*, *Dawazisaurus* and the pachypleurosaur *Keichousaurus*, often fall out as "wild card" taxa in different phylogenetic analyses (Cheng et al. 2016; Wu et al. 2011). In addition, the monophyly of the *Nothosaurus* and *Lariosaurus* group has recently been questioned (Liu et al. 2014).

The fossil record of nothosaurs and pachypleurosaurs is restricted to the Triassic; the first representatives are known from the late Early Triassic and extend into the early Late Triassic (e.g., Bardet et al. 2014; Kelley et al. 2014; Neenan et al. 2013; Scheyer et al. 2014). They inhabited near-shore habitats of the Tethys Ocean, as well as connected epicontinental seas. Isolated bones of pachypleurosaurs and nothosaurs occur in high individual numbers in the bone beds of the Germanic Basin (i.e., Muschelkalk deposits), whereas articulated material is extremely rare in these localities. However, complete skeletons are well known from the Alpine Triassic (e.g., localities in the Southern Alps, such as from Monte San Giorgio, Switzerland and Italy (e.g., Rieppel 2000) and the eastern Tethyan province of South China (summarized in Liu et al. 2014 and Lu et al. 2017). Nothosaurs and pachypleurosaurs have a relatively uniform postcranial morphology of elongated necks and tails, as well as a dorsoventrally flattened skull. Pachypleurosaurs tend to be small animals with maximum body lengths usually well below 1 m (e.g., Carroll and Gaskill 1985; Peyer 1932; Rieppel 1989; Sander 1989), whereas nothosaurs have a larger size spectrum from very small forms such as *Lariosaurus buzzi* with a body length of less than 1 m (Tschanz 1989) to *Nothosaurus giganteus* with lengths reaching 4 m and more (Peyer 1939; Liu et al. 2014). In addition, the postorbital portion of the nothosaur skull became greatly elongated, producing extremely long upper temporal fenestrae that are much larger than the round orbits (Rieppel 1994, 2000).

Morphological convergences among these taxa are essentially associated with adaptation to an aquatic lifestyle. With the exception of *Anarosaurus heterodontus*, pachypleurosaurs have a homodont dentition consisting of small pointed teeth (Klein 2009; Rieppel 1995). Among Nothosauroidea, *Simosaurus* was durophagous (Rieppel 2002) and nothosaurs have a heterodont dentition with large fangs (Rieppel 2000). Pachypleurosaurs and nothosaurs most likely fed on various metazoans, such as actinopterygians and other reptiles (e.g., Liu et al. 2014; Rieppel 2002; Sander 1989). Some of the largest nothosaurs were also among the highest, if not top, predators

VetBooks.ir

in oceanic food webs (Liu et al. 2014; Rieppel 2002). Based on their morphology, pachypleurosaurs are regarded as anguilliform swimmers (review in Houssaye 2013), which kept their slender forelimbs appressed to the body. Nothosaurs might have made use of their usually more massive forelimbs during swimming, for example, for fast steering, while the main propulsion was still likely provided by their long tails (Carroll 1985; Klein et al. 2015a, 2016; Storrs 1993). An alternative modified rowing or punting (in which the forelimb paddle tips dug into the seafloor sediment) swimming style using both forelimbs simultaneously was recently proposed based on swimming tracks possibly formed by a large nothosaur (Zhang et al. 2014).

High individual numbers of the Chinese pachypleurosaur *Keichousaurus* and of the pachypleurosaurs from the Alpine Triassic (*Neusticosaurus* spp. and *Serpianosaurus mirigiolensis*) enabled detailed studies of intraspecific, including ontogenetic, variation, which clearly documented sexual dimorphism in size and morphology (Cheng et al. 2009; Lin and Rieppel 1998; Rieppel 1989; Rieppel and Lin 1995; Sander 1989, 1988; Xue et al. 2015). Live-bearing was documented by pregnant females of *Keichousaurus* (Cheng et al. 2004) and was most likely present in *Neusticosaurus* (Sander 1988) and *Nothosaurus* (Renesto et al. 2003).

Overview of Histological Studies

Hasse (1878) was one of the first to report on some histological details of a vertebra of *Nothosaurus mirabilis* from the Upper Muschelkalk of Poland (Tarnowskie Góry area). He described lamellar bone in the neural arch and the centrum, showing compact periosteal bone and internal cancellous bone. Seitz (1907) included more samples of *Nothosaurus mirabilis* (ribs, femur and girdle elements from Crailsheim, Germany, and one femur from the Upper Muschelkalk of the Tarnowskie Góry area, Poland) and noted a clear distinction between a compacta composed of lamellar-zonal bone, and a cancellous core area whose trabeculae are lined with thin layers of lamellar bone. The vascularization was shown to consist mainly of simple primary canals and primary osteons, with only a few scattered resorption cavities, close to the deep cancellous area and partly lined by secondary lamellar bone. In addition, Seitz (1907) mentioned a subdivision of the cortical bone into 18 zones in the Crailsheim femur. Gross (1934) also described cyclically deposited periosteal bone ("zonarer Periostknochen," but tissue type was not further identified) in the compacta, with lamellar and radial vascularization, in a humerus (and other elements such as a femur and ribs) of *Nothosaurus* from eastern Germany (Saxony) and western Poland, the latter likely again from the Tarnowskie Góry area. Because these studies did not provide additional information on the external morphology of the samples, the taxonomic assignment to species and even genus should be treated with caution. Zangerl (1935) later added information on pachypleurosaur and nothosaur ribs (based on a sample of 80 sections, mainly of thoracic ribs) from the Middle Triassic of Monte San Giorgio, southern Switzerland/northern Italy. Zangerl admitted the limited taxonomic value of his nothosaurid histological rib data but stressed the importance of homologous sampling localities of the ribs.

Ricqlès (1976) was the first to review histological features of both nothosaurs and pachypleurosaurs, including long bones. He reported pachyostosis in the ribs, the persistence of calcified cartilage in the middle part of the long bone shaft and the presence of lamellar periosteal bone with numerous longitudinally oriented primary osteons arranged in concentric circumferential rows. Later, Sander (1990) studied the cyclic growth marks of the pachypleurosaurs *Neusticosaurus pusillus* and *N. peyeri* by counting the minimum number of lines of arrested growth (LAGs) and describing the spacing pattern of growth cycles. He found a minimum age between 7 and 10 years and inferred that sexual maturity was reached at an age between 3 and 4 years (Sander 1990). Subsequently, Hugi et al. (2011) did a comprehensive histological and skeletochronological study of the three species of *Neusticosaurus* and *Serpianosaurus mirigiolensis* from the fossiliferous beds of the Besano and Meride formations at Monte San Giorgio, Switzerland/Italy. The study indicated that *S. mirigiolensis* became sexually mature between the second and fourth years of life and that the oldest individual died in its 14th year, whereas the sexual maturity in *N. edwardsii* began between the fourth and seventh years, while it reached ages above 15 years (Hugi et al. 2011). Variation in the spacing pattern of the growth cycles might indicate possible climate-dependent reproductive seasons comparable to what is observed in modern iguanids (Hugi and Sánchez-Villagra 2012). Germain and Laurin (2005) inferred the probable lifestyle of *N. edwardsii* based on compactness parameters of a zeugopodial element, the radius. Using linear discriminant analysis (LDA), they found the fossil specimen to cluster with extant amphibious taxa but also close to terrestrial ones. A subsequent study by Canoville and Laurin (2010), using a humerus of *N. edwardsii* in LDA inferred that these animals were predominantly aquatic instead (i.e., the extinct taxon was close to but not within the field of extant aquatic amniotes in the LDA).

According to Hugi et al. (2011), *Neusticosaurus* spp. and *S. mirigiolensis* long bones show an embryonic bone layer consisting of woven bone, followed by a succession of growth cycles consisting of a zone, an annulus a LAG toward the bone periphery. The growth zones formed of parallel-fibered bone are usually wider in the deeper cortex and become reduced in thickness toward the outer bone surface, whereas, *vice versa*, the annuli that consist of more organized lamellar tissue become relatively thicker toward the periphery. This histological change likely reflects a general decrease in growth rate during ontogeny (see also Chapter 31 on Skeletochronology). An outer circumferential layer (*sensu* Ponton et al. 2004; =external fundamental system) of closely spaced LAGs at the bone periphery indicates skeletal maturity in adult pachypleurosaurs.

Cortical vascularization varies slightly between the pachypleurosaur taxa, with vascular canals being mainly simple radial and longitudinal, but some primary osteons can also be present. Hugi et al. (2011) measured high compactness values (e.g., between 89 and 96% in *N. edwardsii* and between 95 and 99% in *S. mirigiolensis*) in the long bones of these taxa. This is due to the occurrence of pachyosteosclerosis, a (nonpathological) condition in which hyperplasic compact cortices (pachyostosis) are associated with the persistence of calcified cartilage infilling the medullary region of the bones (osteosclerotic and amedullary bones).

This feature stands in contrast to other pachypleurosaurs such as *A. heterodontus* and *Dactylosaurus* in which a medullary cavity exists (Figure 22.1A, B).

Klein and Griebeler (2018) studied bone tissue, microanatomy, and growth of the oldest pachypleurosaur known so far, *Dactylosaurus*, from the early Anisian of Poland (Kowal-Linka and Bodzioch 2017; Rieppel 2000). *Dactylosaurus* (Figures 22.1C, D and 22.2C, D) shares a similar bone tissue type and microanatomy (Figures 22.1 and 22.2) with the *Neusticosaurus–Serpianosaurus* clade. Although *Dactylosaurus* can retain a very narrow medullary cavity and does not show calcified cartilage at midshaft, bone compactness values are nevertheless high in this taxon.

The pachypleurosaur *A. heterodontus* distinctly differs in microanatomy and bone tissue type from other European taxa (Klein 2010, 2012; Klein and Griebeler 2018) in growing with incipient fibrolamellar bone (*sensu* Klein 2010; Klein et al. 2016; meaning that the parallel-fibered bone tissue is intermixed with woven bone, while primary osteon formation of canals has only partially started). They have a higher proportion of woven-fibered bone and a higher vascular density throughout the cortex, along with numerous developing or fully developed primary osteons (Figure 22.2A, B). *Anarosaurus* is the only pachypleurosaur studied so far that displays a relatively large free medullary cavity (Figures 22.1A, B and 22.2A, B). This feature, combined with high vascular density, results in generally lower compactness values (bone compactness [BC]: 67–90%) compared to other pachypleurosaurs (BC > 90%, in most samples >95%).

Histological comparison thus reveals distinct taxon-specific differences in microanatomy and bone tissue type between *Anarosaurus* and *Dactylosaurus* and the *Neusticosaurus–Serpianosaurus* clade. The persistence of a relatively large free medullary cavity in *Anarosaurus* likely reflects a somewhat lesser degree of aquatic adaptation (Klein and Griebeler 2018), and although more developed than in other pachypleurosaurs, this medullary cavity is nevertheless narrower than that, for example, in a terrestrial tetrapod. Differences in bone tissue type indicate different growth patterns (i.e., higher growth rate in *Anarosaurus*) and thus different life history strategies.

One of the most striking features in nothosaur long bones is the wide spectrum of diaphyseal microanatomical patterns (Figure 22.3), most likely reflecting differences in habitat and swimming style (Klein and Griebeler 2016; Klein et al. 2016; Krahl et al. 2013). In their microanatomy, nothosaur long bones exhibit a range from thick (= bone mass increase/osteosclerosis) to very thin-walled cortices (= extreme bone mass decrease). Early Anisian small and large nothosaurs generally display a relatively narrow free medullary cavity (i.e., bone mass increase/osteosclerosis) compared to potential terrestrial

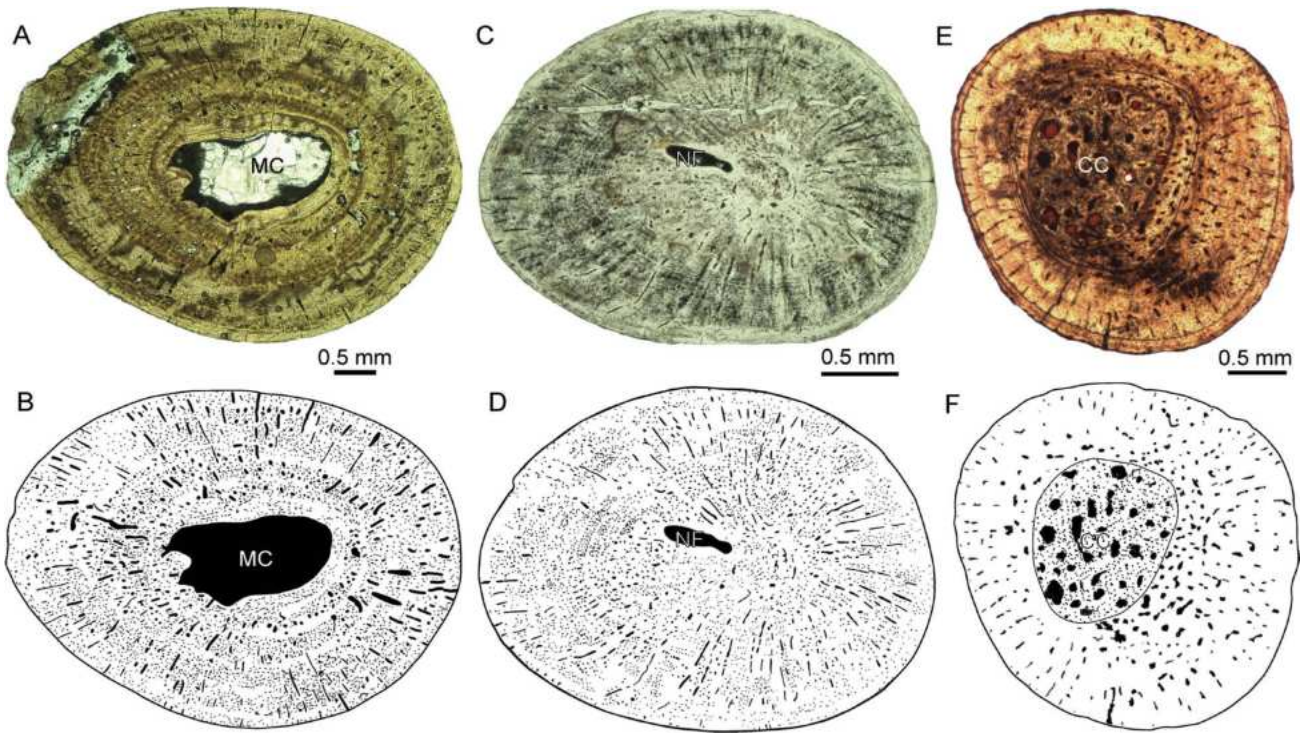


FIGURE 22.1 Humerus microanatomy and interpretative drawings of Pachypleurosauria at midshaft from the Middle Triassic of the Germanic Basin (Germany, Poland, The Netherlands) and from the Alpine region, Monte San Giorgio, Switzerland/Italy (see also Klein 2010; Klein and Griebeler 2018). A, C, and E in normal transmitted light. A and B. *Anarosaurus heterodontus* (Wijk07-50; 4.15 cm proximodistal length) from the middle Anisian of Winterswijk, The Netherlands, depicting a free medullary cavity and a dense vascular system of longitudinally and radially arranged canals. C and D. *Dactylosaurus* cf. *D. gracilis* (MB. R 776.2; 3.82 cm proximodistal length) from the early Anisian of Poland depicting a medullary region completely filled in by endosteal bone and the trace of the nutrient foramen. E and F. *Neusticosaurus peyeri* (PIMUZ T 4270) from the middle Ladinian of the Alpine Triassic with a central core of calcified cartilage surrounded by a weakly vascularized cortex. Note remodeling processes in the calcified cartilage. Abbreviations: CC, calcified cartilage; MC, medullary cavity; NF, nutrient foramen.

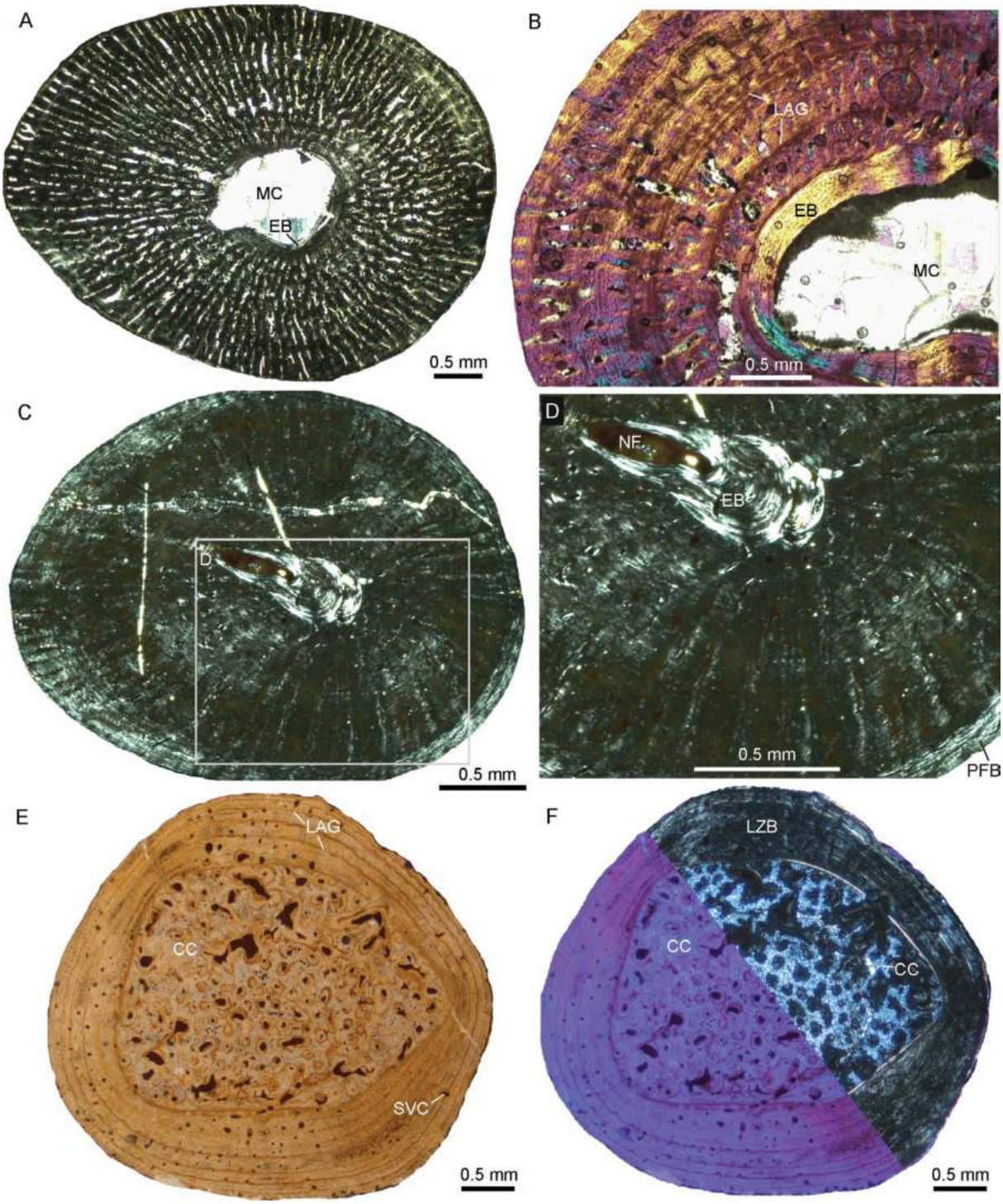


FIGURE 22.2 Long bone (humeri) histology of Pachypleurosauria from the Middle Triassic of the Germanic Basin (Germany, Poland, The Netherlands) and from the Alpine region, Monte San Giorgio, Switzerland/Italy (see also Hugi et al. 2011; Klein 2010; Klein and Griebeler 2018). All sections were taken at humerus midshaft. A and B, *Anarosaurus heterodontus* from the middle Anisian of Winterswijk (The Netherlands). C and D, *Dactylosaurus* cf. *D. gracilis* from the early Anisian of Poland. E and F, *Neusticosaurus pusillus* from the early Ladinian Cava Inferiore beds, Meride Formation, Monte San Giorgio, Switzerland. A, C, and D and the upper part of F are taken in cross-polarized light; B and the lower part of F in cross-polarized light using a lambda compensator and E in normal transmitted light. A, Complete section of Wijk09-543 (3.6 cm) in polarized light showing a radial vascular system. B, Close-up view of Wijk07-50 (4.15 cm proximodistal length) showing a free medullary cavity lined with secondary, endosteal lamellar bone. C and D, MB.R. 776.2 (3.82 cm proximodistal length) depicting a medullary region completely filled in by secondary, endosteal lamellar bone. The nutrient foramen is also partially lined by lamellar bone. E and F. Complete overview of section of PIMUZ T4178 (1.6 cm proximodistal length). Note sharp transition between interior core area retaining calcified cartilage and secondary bone infillings surrounding vascular spaces and the cortex composed of lamellar-zonal bone. Abbreviations: CC, calcified cartilage; EB, endosteal bone consisting of lamellar bone tissue; LAG, line of arrested growth; LZB, lamellar-zonal bone; MC, medullary cavity; NF, nutrient foramen; PFB, parallel-fibered bone; SVC, simple vascular canal.

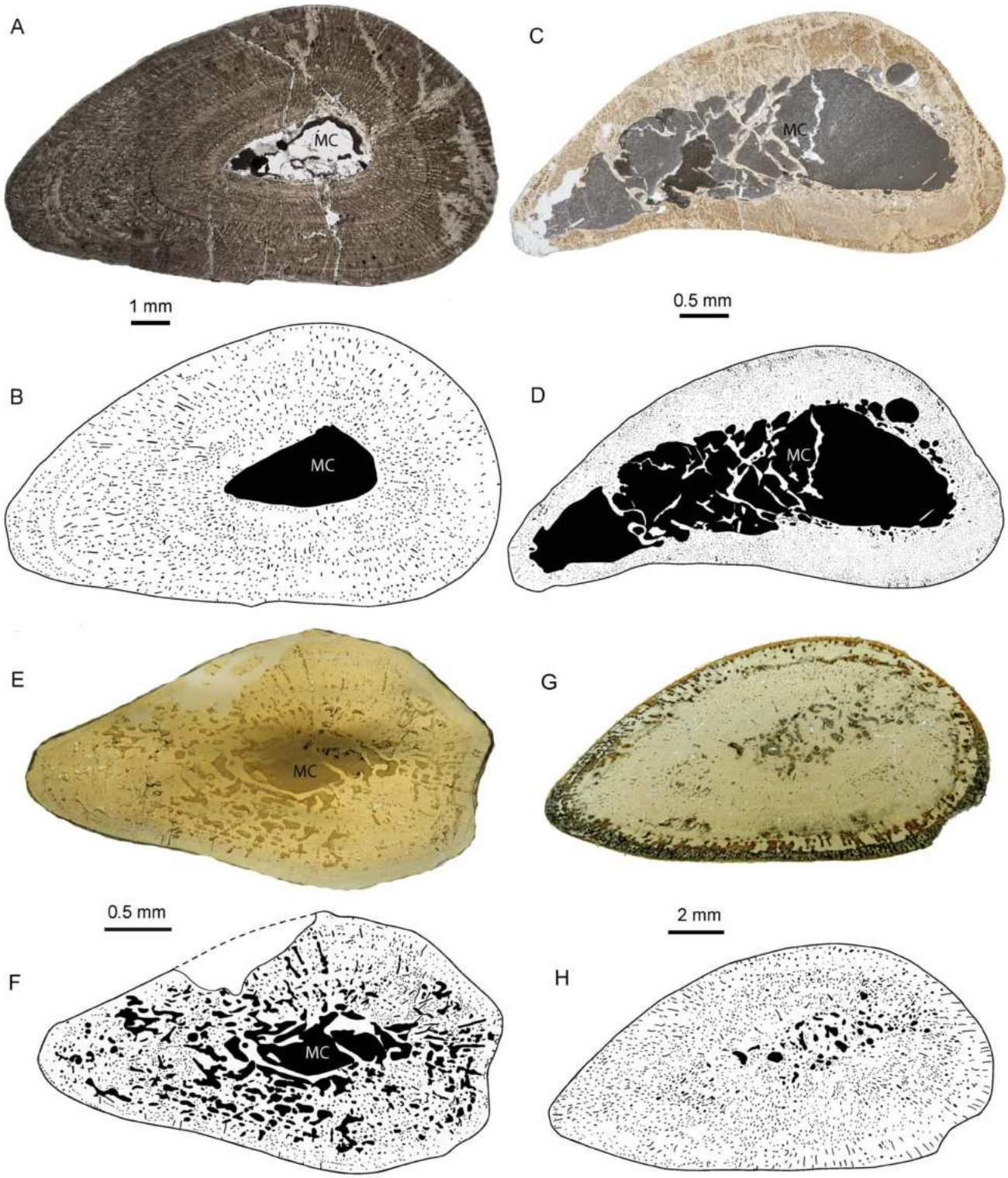


FIGURE 22.3 Humerus microanatomy at midshaft and interpretative drawings of *Nothosaurus* spp. from the Middle Triassic of the Germanic Basin (Muschelkalk deposits in Germany and The Netherlands); see Klein et al. (2016). A, C, E, and G are in normal transmitted light. A and B. Cross section of humerus Wijk11-265 (7.3 cm proximodistal length) with single free medullary cavity (MC) whose outline is similar to the external shape of the bone. C and D, Cross section of humerus SMNS 81988 (~31 cm proximodistal length) with enlarged and irregular MC traversed by some trabeculae. E and F, Cross section of humerus SMNS 84772 (16.5 cm proximodistal length) with open MC and an irregular (rather random) resorption pattern affecting the cortex. G and H, Cross section of humerus GPIT 1339f (8.4 cm proximodistal length) in which an open MC is absent; only a few small cavities occur in the medullary area.

relatives. In the middle to late Anisian, small nothosaurs retain this microanatomy, whereas larger forms tend to increase the size of their medullary cavity, resulting in a decrease in bone mass. During the latest Anisian to early Ladinian, when nothosaurs have the highest taxonomical diversity, small and some large nothosaurs have small free medullary cavities, whereas the majority of large forms show a relative increase in the size of their medullary cavities, so that some individuals have extremely thin-walled humeri (and in general a decrease in bone mass). The medullary cavity of *Simosaurus* is also enlarged (Klein and Griebeler 2016) but to a lesser extent than in some similar-sized *Nothosaurus* spp. (Klein et al. 2016). Conversely, *Ceresiosaurus* always retained a reduced medullary cavity (Hugi 2011) and thus a high bone mass.

Bone histology of nothosaurs has been the focus of some recent comparative studies (Hugi 2011; Klein 2010; Klein and Griebeler 2016; Klein et al. 2016; Krahl et al. 2013). Studied taxa include *Simosaurus*, *Ceresiosaurus* and a variety of *Nothosaurus* species covering most of the evolutionary history of this clade, from the early middle Anisian until the Ladinian. All these taxa generally share lamellar-zonal cortices with moderate vascular density (Figure 22.4). Vascularization consists of simple longitudinal and radial canals, with occasional primary osteons. The inner cortex is usually more loosely organized and consists of coarse parallel-fibered bone (*sensu* Klein et al. 2015b, 2016; meaning that the fibers building up the tissue are especially thick and coarse) and, more rarely and locally, woven bone tissue, whereas highly organized parallel-fibered and lamellar tissues increase in proportion toward the outer cortex. Funnel-shaped organization of crystallites (meaning that crystallites adjacent to a canal extend steeply angled toward the outer bone surface) can occur adjacent to radially arranged simple vascular canals (Figure 22.4B; see Hugi 2011). In some nothosaur samples, incipient or true fibrolamellar bone (*sensu* Klein 2010; Klein et al. 2016) can occur, but it is always locally restricted.

It cannot be clarified at present whether microanatomical differences in *Nothosaurus* spp. are related to taxonomy, developmental plasticity, sexual dimorphism and/or differences in swimming style (see discussion in Klein et al. 2016). Based on microanatomical observations, small-bodied *Nothosaurus* spp. and *Ceresiosaurus* are interpreted as bound to near-shore, shallow marine environments throughout their evolution. Some large-bodied *Nothosaurus* spp. followed the same trend, while some others might have become more active swimmers or subsurface swimmers that possibly inhabited open marine environments.

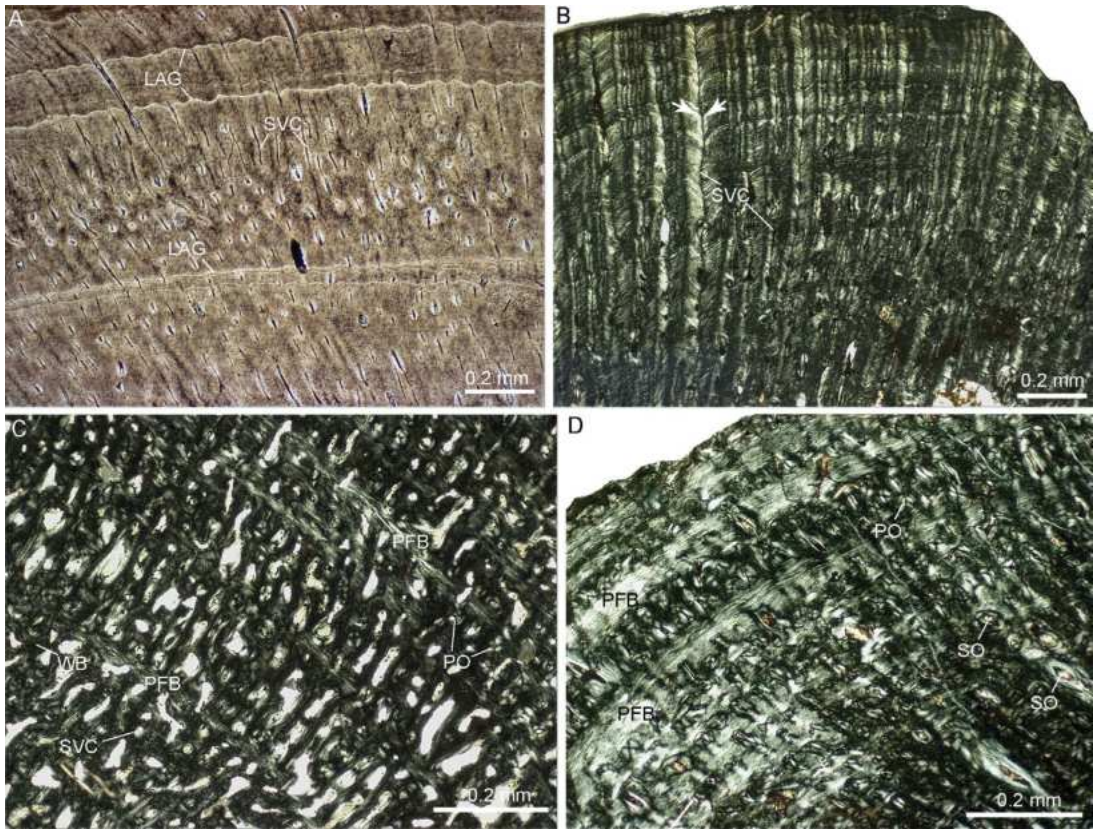


FIGURE 22.4 Humerus histology at midshaft of *Nothosaurus* spp. from the Middle Triassic of the Germanic Basin (Muschelkalk deposits in Germany and The Netherlands; see also Klein et al. 2016). A, Normal transmitted light. B, C and D in cross-polarized light. A, Part of the cortex of MB.R. 269 (~40 cm proximodistal length) showing lamellar-zonal bone organization. B, Part of the cortex of humerus SMNS 17214 with funnel-shaped crystallite orientation (marked by white arrows) adjacent to radiating simple vascular canals. C, More internal part of the cortex of humerus SMNS 84851 (~18 cm proximodistal length). D, More external part of the cortex of humerus MB.R. 941 (21 cm proximodistal length). Abbreviations: LAG, line of arrested growth; PFB, parallel-fibered bone; PO, primary osteon; SO, secondary osteon; SVC, simple vascular canal; WB, woven bone.

VetBooks.ir

Two microanatomical categories documented among *Nothosaurus* spp. are so far unique among marine amniotes: (1) a highly heterogeneous spongy organization because of rather randomly located resorption of periosteal bone without redeposition and (2) an extremely thin-walled cortex only traversed/connected by a few thin trabeculae, resulting from an extreme enlargement of the medullary cavity (Klein et al. 2016). Finally, mathematical growth modeling of the growth mark record preserved in humeri of nothosaurs also supported possible viviparity for this group (Griebeler and Klein 2019).

In addition, Klein et al. (2019) studied the microstructure of vertebrae, ribs, and gastral ribs using a large dataset of nothosaurs and pachypleurosaurs from Muschelkalk and Lettenkeuper outcrops in the Germanic Basin and from the Alpine Triassic of Monte San Giorgio. The authors noted the peculiar well-delineated cavity in their vertebral sample, as well as proximodistal changes of the periosteal vs. endosteal tissue thicknesses along the rib samples. Furthermore, according to Klein et al. (2019), the processes leading to (pachy-) osteosclerosis (see Chapter 36) in the ribs and vertebrae are the same as those of the sauropterygian long bones.

Conclusions and Outlook

Although in general the bone tissues of pachypleurosaurs and nothosaurs are dominated by parallel-fibered bone and longitudinal and radial vascular canals, they show intraspecific variability as well as developmental plasticity. Growth rates deduced from bone tissue organization and vascular density are higher compared to extant reptiles including some marine and aquatic forms, which might be related to an overall warmer climate during the Middle Triassic. Future work should focus on taxa from the Eastern Tethys (e.g., pachypleurosaur *Keichousaurus*, *Nothosaurus* spp.) and the Western Pacific realm (e.g., *Corosaurus*) to investigate taxonomic and environmentally related differences. Samples of large *Nothosaurus* with a reliable taxonomic assignment would clarify causes of observed humeral microanatomical diversity.

Institutional Abbreviations

MB.R., Museum of Natural History, Leibniz Institute for Research on Evolution and Biodiversity at the Humboldt University Berlin, Germany; MHI, Muschelkalkmuseum Ingelfingen, Germany; PIMUZ, Paläontologisches Institut und Museum der Universität Zürich, Switzerland; SMNS; Stuttgart State Museum of Natural History, Germany; StIPB, Steinmann-Institute of Geology, Mineralogy and Paleontology; Division of Paleontology. University of Bonn. Germany. Wijk, material labeled with this abbreviation is stored in the National Museum of Natural History (NCB Naturalis), Leiden, The Netherlands.

Acknowledgments

We acknowledge O. Dülfer (StIPB), Ch. Wimmer-Pfeil (SMNS), and J. Hugi (formerly PIMUZ) for the production of the thin sections. C. Klug (PIMUZ), H. Furrer (formerly PIMUZ), H. Hagdorn (MHI), N. Hauschke (Martin-Luther-University Halle-Wittenberg), P. Havlik (former Universität Tübingen), R. Schoch (SMNS), and D. Schwarz-Wings (Museum für Naturkunde Berlin) kindly gave permission for the histological sampling of bones.

REFERENCES

Bardet, N., et al. 2014 Mesozoic marine reptile palaeobiogeography in response to drifting plates. *Gondwana Res.* 26:869–887 [doi: 10.1016/j.gr.2014.05.005].

Canoville, A., and M. Laurin. 2010. Evolution of humeral microanatomy and lifestyle in amniotes, and some comments on palaeobiological inferences. *Biol. J. Linn. Soc.* 100:384–406 [doi: 10.1111/j.1095-8312.2010.01431.x].

Carroll, R. L. 1985. Evolutionary constraints in aquatic diapsid reptiles. *Spec. Pap. Palaeontol.* 33:145–155.

Carroll, R. L., and P. Gaskill. 1985. The nothosaur *Pachypleurosaurus* and the origin of plesiosaurs. *Philos. Trans. R. Soc. Lond. B* 309:343–393.

Cheng, Y.-N., et al. 2004. Triassic marine reptiles gave birth to live young. *Nature* 432:383–386.

Cheng, Y.-N., et al. 2009. Sexual dimorphism and life history of *Keichousaurus hui* (Reptilia: Sauropterygia). *J. Vertebr. Paleontol.* 29:401–408 [doi: 410.1671/1039.1029.0230].

Cheng, Y.-N., et al. 2016. *Dawazisaurus brevis*, a new eosauropterygian from the Middle Triassic of Yunnan, China. *Acta Geol. Sin. (Engl. Ed.)* 90:401–424.

Germain, D., and M. Laurin. 2005. Microanatomy of the radius and lifestyle in amniotes (Vertebrata, Tetrapoda). *Zool. Scr.* 34:335–350.

Griebeler, E.-M., and N. Klein. 2019. Viviparity in *Nothosaurus* spp. (Sauropterygia) is indicated by similarities in their life-history strategies to modern squamates and live-bearing extinct pachypleurosaurs (Sauropterygia). *Palaeontology* 62:697–713.

Gross, W. 1934. Die Typen des mikroskopischen Knochenbaues bei fossilen Stegocephalen und Reptilien. *Z. Anat. Entwicklungsgesch.* 203:731–764 [doi: 10.1007/BF02118752].

Hänni, K. 2004. *Die Gattung Ceresiosaurus. Ceresiosaurus calgagnii Peyer und Ceresiosaurus lanzi n.sp. (Lariosauridae, Sauropterygia).* Zürich: vdf Hochschulverlag AG.

Hasse, C. 1878. Die fossilen Wirbel. Morphologische Studien aus dem anatomischen Institut zu Breslau. Die Histologie fossiler Reptilwirbel. *Morphol. Jahrb.* 4:480–502.

Houssaye, A. 2013. Bone histology of aquatic reptiles: what does it tell us about secondary adaptation to an aquatic life? *Biol. J. Linn. Soc.* 108:3–21 [doi: 10.1111/j.1095-8312.2012.02002.x].

Hugi, J. 2011. The long bone histology of *Ceresiosaurus* (Sauropterygia, Reptilia) in comparison to other eosauropterygians from the Middle Triassic of Monte San Giorgio (Switzerland/Italy). *Swiss J. Palaeontol.* 130:297–306 [doi: 210.1007/s13358-13011-10023-13356].

Hugi, J., and M. R. Sánchez-Villagra. 2012. Life history and skeletal adaptations in the Galapagos marine iguana (*Amblyrhynchus cristatus*) as reconstructed with bone histological data—a comparative study of iguanines. *J. Morphol.* 46:312–324 [doi: 310.1670/1611-1071].

Hugi, J., et al. 2011. Long bone microstructure gives new insights into the life of pachypleurosaurids from the Middle Triassic of Monte San Giorgio, Switzerland/Italy. *C. R. Palevol* 10:413–426 [doi: 410.1016/j.crpv.2011.1003.1009].

Kelley, N. P., et al. 2014. Selective extinction of Triassic marine reptiles during long-term sea-level changes illuminated by seawater strontium isotopes. *Palaeogeogr., Palaeoclimatol., Palaeoecol.* 400:9–16 [doi: 10.1016/j.palaeo.2012.1007.1026].

Klein, N. 2009. Skull morphology of *Anarosaurus heterodontus* (Reptilia: Sauropterygia: Pachypleurosauria) from the lower Muschelkalk of the Germanic Basin (Winterswijk, the Netherlands) *J. Vertebr. Paleontol.* 29:665–676 [doi: 610.1671/1039.1029.0327].

Klein, N. 2010. Long bone histology of Sauropterygia from the Lower Muschelkalk of the Germanic Basin provides unexpected implications for phylogeny. *PLoS One* 5:e11613 [doi: 10.1371/journal.pone.0011613].

Klein, N., and E. M. Griebeler. 2016. Bone histology, microanatomy, and growth of the nothosauroid *Simosaurus gaillardoti* (Sauropterygia) from the Upper Muschelkalk of southern Germany/Baden-Württemberg. *C. R. Palevol.* 15:142–162 [doi: 110.1016/j.crpv.2015.1002.1009].

Klein, N., and E. M. Griebeler. 2018. Growth patterns, sexual dimorphism, and maturation modeled in Pachypleurosauria from Middle Triassic of central Europe (Diapsida: Sauropterygia). *Foss. Rec.* 21:137–157 [doi: 10.5194/fr-21-137-2018].

Klein, N., et al. 2015a. Postcranial material of *Nothosaurus marchicus* from the Lower Muschelkalk (Anisian) of Winterswijk, The Netherlands, with remarks on swimming styles and taphonomy. *Paläont. Z.* 89:961–981 [doi: 910.1007/s12542-12015-10273-12545].

Klein, N., et al. 2015b. Long bone histology and microanatomy of Placodontia (Diapsida: Sauropterygia). *Contrib. Zool.* 84:59–84 [doi: 10.1163/18759866-08401005].

Klein, N., et al. 2016. Diverse aquatic adaptations in *Nothosaurus* spp. (Sauropterygia)—inferences from humeral histology and microanatomy. *PLoS One* 11:e0158448 [doi: 10.1371/journal.pone.0158448].

Klein, N., et al. 2019. Microstructure of vertebrae, ribs, and gastralia of Triassic sauropterygians—New insights into the microanatomical processes involved in aquatic adaptations of marine reptiles. *Anat. Rec.* 302:1770–1791 [doi: 10.1002/ar.24140].

Kowal-Linka, M., and A. Bodzioch. 2017. Genesis of the Lower Triassic bonebeds from Gogolin (S Poland): The impact of microbial mats on trapping of vertebrate remains. *Palaeogeogr., Palaeoclimatol., Palaeoecol.* 466:38–58 [doi: 10.1016/j.palaeo.2016.1011.1010].

Krahl, A., et al. 2013. Evolutionary implications of the divergent long bone histologies of *Nothosaurus* and *Pistosaurus* (Sauropterygia, Triassic). *BMC Evol. Biol.* 13:1–23 [doi: 10.1186/1471-2148-13-123].

Lin, K., and O. Rieppel. 1998. Functional morphology and ontogeny of *Keichousaurus hui* (Reptilia, Sauropterygia). *Fieldiana (Geology) new. ser.* 39:1–35.

Liu, J., et al. 2014. A gigantic nothosaur (Reptilia: Sauropterygia) from the Middle Triassic of SW China and its implication for the Triassic biotic recovery. *Sci. Rep.* 4:7142 [doi: 10.1038/srep07142].

Lu, H., et al. 2017. Middle Triassic Xingyi Fauna: showing turnover of marine reptiles from coastal to oceanic environments. *Palaeoworld* 27:107–116 [doi: 10.1016/j.palwor.2017.05.005].

Neenan, J. M., et al. 2013. European origin of placodont marine reptiles and the evolution of crushing dentition in Placodontia. *Nat. Commun.* 4:1621 [doi: 10.1038/ncomms2633].

Peyer, B. 1932. Die Triasfauna der Tessiner Kalkalpen. V. *Pachypleurosaurus edwardsii* Corn. spec. *Abhandlungen der schweizerischen Paläontologischen Gesellschaft* 52:1–18.

Peyer, B. 1939. Die Triasfauna der Tessiner Kalkalpen XIV. *Paranothosaurus amsleri* nov. gen. nov. spec. *Abhandlungen der schweizerischen Paläontologischen Gesellschaft* 62:1–87.

Ponton, F., et al. 2004. Variation of the outer circumferential layer in the limb bones of birds. *Acta Ornithol.* 39:21–24.

Renesto, S., et al. 2003. Nothosaurid embryos from the Middle Triassic of northern Italy: an insight into the viviparity of nothosaurs? *J. Vertebr. Paleontol.* 23:957–960 [doi: 910.1671/1840-1621].

Ricqlès, A. de. 1976. On bone histology of fossil and living reptiles, with comments on its functional and evolutionary significance. In: *Linnean Society Symposium Series No. 3. Morphology and Biology of Reptiles*, ed. A. d'A. Bellairs, and C. B. Cox, 123–150. London: Academic Press.

Rieppel, O. 1989. A new pachypleurosaur (Reptilia: Sauropterygia) from the Middle Triassic of Monte San Giorgio, Switzerland. *Philos. Trans. R. Soc. Lond. B* 323:1–73.

Rieppel, O. 1994. Osteology of *Simosaurus gaillardoti* and the relationships of stem-group Sauropterygia. *Fieldiana (Geology) new ser.* 28:1–85.

Rieppel, O. 1995. The status of *Anarosaurus multidentatus* von Huene (Reptilia, Sauropterygia), from the Lower Anisian of the Lechtaler Alps (Arlberg, Austria). *Paläont. Z.* 69: 289–299.

Rieppel, O. 2000. Sauropterygia I - Placodontia, Pachypleurosauria, Nothosauroidea, Pistosauroidea. *Handbuch der Paläoherpetologie* 12A:1–134.

Rieppel, O. 2002. Feeding mechanics in Triassic stem-group sauropterygians: the anatomy of a successful invasion of Mesozoic seas. *Zool. J. Linn. Soc.* 135:33–63.

Rieppel, O. 2007. On the nothosaurian genera *Ceresiosaurus* and *Lariosaurus*. *Geologia Insubrica* 10:1–4.

Rieppel, O., and K. Lin. 1995. Pachypleurosaurs (Reptilia: Sauropterygia) from the Lower Muschelkalk, and a review of the Pachypleurosauroidea. *Fieldiana (Geology) new ser.* 32:1–44.

Sander, P. M. 1988. A fossil reptile embryo from the Middle Triassic of the Alps. *Science* 239:780–783.

Sander, P. M. 1989. The pachypleurosaurids (Reptilia: Nothosauria) from the Middle Triassic of Monte San Giorgio (Switzerland) with the description of a new species. *Philos. Trans. R. Soc. Lond. B* 325:561–666 [doi: 510.1098/rstb.1989.0103].

Sander, P. M. 1990. Skeletochronology in the small Triassic reptile *Neusticosaurus*. *Ann. Sci. Nat. (B Zool.)* 11:213–217.

Sato, T., et al. 2014. *Diandongosaurus acutidentatus* Shang, Wu & Li, 2011 (Diapsida: Sauropterygia) and the relationships of Chinese eosauropterygians. *Geol. Mag.* 151:121–133 [doi: 110.1017/S0016756813000356].

Scheyer, T. M., et al. 2014. Early Triassic marine biotic recovery: the predators' perspective. *PLoS One* 9:e88987 [doi: 10.1371/journal.pone.0088987].

Scheyer, T. M., et al. 2017. A new, exceptionally preserved juvenile specimen of *Eusaurosphargis dalsassoi* (Diapsida) and implications for Mesozoic marine diapsid phylogeny. *Sci. Rep.* 7:4406 [doi: 10.1038/s41598-017-04514-x].

Seitz, A. L. L. 1907. Vergleichende Studien über den mikroskopischen Knochenbau fossiler und rezenter Reptilien, und dessen Bedeutung für das Wachstum und Umbildung des Knochengewebes im allgemeinen. *Nova Acta, Abh. der Kaiserl. Leop-Carol. Deutschen Akademie der Naturforscher* 87:230–370.

Storrs, G. W. 1993. Function and phylogeny in sauropterygian (Diapsida) evolution. *Am. J. Sci.* 293-A:63–90.

Tschanz, K. 1989. *Lariosaurus buzzii* n. sp. from the Middle Triassic of Monte San Giorgio (Switzerland) with comments on the classification of nothosaurs. *Palaeontogr. Abt. A* 208:153–179.

Wu, X.-C., et al. 2011. New information on *Wumengosaurus delicatomandibularis* Jiang et al. 2008 (Diapsida: Sauropterygia), with a revision of the osteology and phylogeny of the taxon. *J. Vertebr. Paleontol.* 31:70–83 [doi: 10.1080/02724634.02722011.02546724].

Xue, Y., et al. 2015. New information on sexual dimorphism and allometric growth in *Keichousaurus hui*, a pachypleurosaur from the Middle Triassic of Guizhou, South China. *Acta Palaeontol. Pol.* 60:681–687 [doi: 610.4202/app.00006.02013].

Zangerl, R. 1935. B. Peyer, Die Triasfauna der Tessiner Kalkalpen. IX. *Pachypleurosaurus edwardsi*, Cornalia sp. *Schweiz. palaeontol. Abh.* 56:1–80.

Zhang, Q., et al. 2014. Nothosaur foraging tracks from the Middle Triassic of southwestern China. *Nat. Commun.* 5:3973 [doi: 10.1038/ncomms4973].

VetBooks.ir

23

Sauropterygia: Histology of Plesiosauria

P. Martin Sander and Tanja Wintrich

CONTENTS

Introduction 444
History of Research on Plesiosaur Histology 445
Descriptions by Skeletal Region 446
Skull: Dental Histology Only 446
Propodials 446
Vertebrae 449
Ribs and Gastralia 451
Girdle Bones 451
Limb Bones Other Than Propodials 452
Growth, Skeletochronology and Life History 452
Qualitative Indicators of Fast Growth 452
Ontogenetic Changes and Histologic Ontogenetic Stages 452
Histomorphometry 453
Growth Rates and Resting Metabolic Rates 453
Bone Density: Vertebrae and Propodials 454
Red Blood Cell Size 454
Paleobiological and Evolutionary Implications 454
Fast Growth and Endothermy 454
Aquatic Adaptation 455
Evolutionary Success 455
Conclusions 455
Acknowledgments 455
References 455

Introduction

Plesiosaurs are iconic marine reptiles that inhabited Mesozoic seas from the latest Triassic to the very end of the Cretaceous (Benson et al. 2012; Benson and Druckenmiller 2014; Wintrich et al. 2017a). They were denizens of the open sea (pelagic habitat), because their remains are found in open marine sediments of the Jurassic and Cretaceous (Figure 23.1) from around the world (Bardet et al. 2014).

However, unlike ichthyosaurs, the other major clade of Mesozoic marine reptiles, plesiosaurs also inhabited large rivers, as documented, e.g., from the Campanian Dinosaur Park Formation of Alberta, Canada (Sato et al. 2005), like extant dolphins but not larger cetaceans.

Plesiosaurs are instantly recognizable by their four flippers of even size used in a unique mode of locomotion called four-winged underwater flight (Figure 23.2). Form following function, the forelimbs and hind limbs are very similar to each other in their osteology, more so than in any other tetrapod.

Plesiosaurs have many other unique features in their anatomy and biology, which must have been key to the great diversity and longevity of the clade. Plesiosaurs inherited from their ancestors a very long neck with the highest number of vertebrae among tetrapods (Müller et al. 2010). Early plesiosaurs have around 30 cervical vertebrae (Soul and Benson 2017), a great increase over the basal seven or eight of most tetrapods, and the Late Cretaceous Elasmosauridae had up to 76 (Zammit et al. 2008). Several times independently in their phylogeny, however, plesiosaurs evolved large-headed, short-necked forms, the pliosauromorph type (e.g., Pliosauridae, Polycotylidae) (Figure 23.1). Only recently was it recognized that plesiosaurs also have a unique bone histology (Wintrich et al. 2017a; O'Keefe et al. 2019) that is difficult to compare to that of any other amniote clade. Here we review the histology of plesiosaur bones, provide some new information and discuss studies that use plesiosaur bone histology for inferences about lifestyle, metabolism, ecology and evolution.

VetBooks.ir

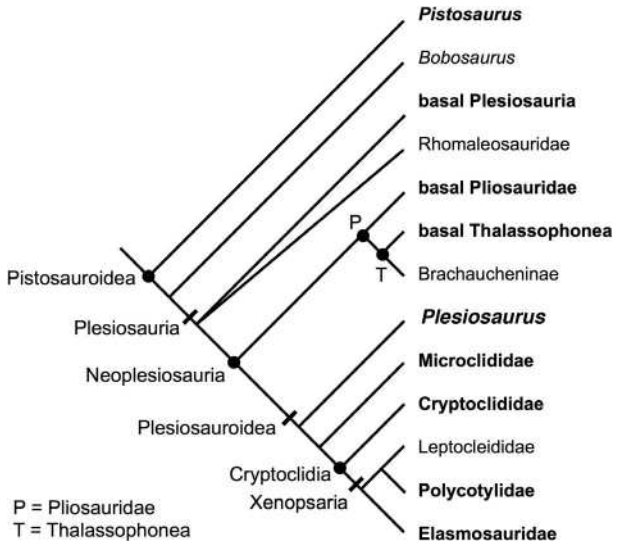


FIGURE 23.1 Simplified plesiosaur phylogeny based on Benson and Druckenmiller (2014), Wintrich et al. (2017a) and Fischer et al. (2017). Taxa in bold have been sampled histologically.

Because bone histology is mainly an expression of growth (Amprino and Godina 1947; Montes et al. 2007; Cubo et al. 2012), determining the ontogenetic stage of the sampled individual is of particular importance. Little histological work has been done in this regard, but Brown (1981) proposed a suite of morphological features that distinguish juveniles from adults. The most common indicators of an immature ontogenetic stage are unfused neurocentral sutures (e.g., Brown 1981), as in many amniote clades. Plesiosaur centra are commonly found in isolation, and such centra are generally attributed to juveniles (e.g., Wiffen et al. 1995; Wintrich et al. 2017b). A remarkable amount of isolated fetal bones have been described for plesiosaurs as well (Kiprijanoff 1881–1883; Moodie 1911; O'Gorman et al. 2017; Wintrich et al. 2017b; O'Keefe et al. 2019), although only one pregnant female is known (O'Keefe and Chiappe 2011). Apart from this specimen, fetal status is inferred from incomplete ossification and small size.

The purpose of this chapter is to compile what is known about plesiosaur bone histology and to analyze how this information can be used for paleobiological inferences, in particular with regard to ontogeny, physiology and ecology.

Plesiosauria is a subclade of Pistosauroidea, which is first recorded in the form of the early Middle Triassic *Augustasaurus* (Anisian, 244 Ma) (Sander et al. 1997). Pistosauroidea is represented by other Triassic stem taxa (*Pistosaurus*, *Yunguisaurus*, *Bobosaurus*). The first Plesiosauria are recorded from the latest Triassic (Rhaetian, 205 Ma); *Rhaeticosaurus* is the only named and diagnostic taxon (Wintrich et al. 2017a). The closest sister taxon to Plesiosauria is *Bobosaurus* (Dalla Vecchia 2006, 2017; Fabbri et al. 2014) from the Carnian (235 Ma). Thus, Plesiosauria and their stem relatives are separated from each other by an enormous 30-Ma gap, during which the typical plesiosaur features must have arisen. The length of the gap is consistent with the great difference in morphology between stem taxa and Plesiosauria (Ketchum and Benson 2010; Fabbri et al. 2014; Wintrich et al. 2017a). Recently, it became apparent that already in the Late Triassic, plesiosaurians must have diversified into the clades dominating the Jurassic and Cretaceous (Benson et al. 2012; Wintrich et al. 2017a). Currently, over 120 valid genera of plesiosaurs are recognized (Fischer et al. 2017). A consensus on the phylogenetic relationships of plesiosaurs is emerging (Figure 23.1), as represented by the analyses of Fischer et al. (2017) based on the matrix of Benson and Druckenmiller (2014). Apart from the Rhomaleosauridae, which became extinct in the Middle Jurassic, the two main clades are the Pliosauridae and the Plesiosauroidea (Figure 23.1). The Pliosauridae evolved the most pronounced pliosauromorph body plan in the Middle Jurassic to Early Cretaceous. The Plesiosauroidea contain basal Early Jurassic taxa such as the eponymous *Plesiosaurus* and the large clades Cryptoclididae, Leptoclidia, and Elasmosauridae. The Leptoclidia include the Polycotylidae, another clade of pliosauromorphs.

Histological coverage of this diversity of clades is far from comprehensive (Figure 23.1) and is patchy and uneven, and there are clades that have not been sampled (Rhomaleosauridae, Brachaucheninae, Leptoclididae). Sample clade coverage specifics will be noted below in the histological descriptions.

History of Research on Plesiosaur Histology

Given that plesiosaurs were among the first reptiles from deep time for which the skeleton became completely known (Conybeare 1824), decades before the dinosaurs, it is perhaps

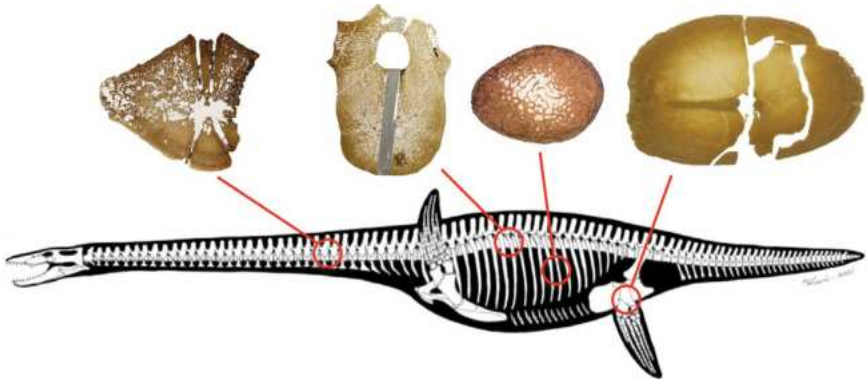


FIGURE 23.2 Plesiosaur skeleton (*Rhaeticosaurus*) with small images of microanatomy (photos) of skeletal regions. Plesiosaur reconstruction by Takahashi Oda in Wintrich et al. (2017a). See Figures 23.3 and 23.4 for explanation and scales of histology images.

VetBooks.ir

surprising that only recently has their histology been studied intensively. Although Owen (1840–1845) figured and discussed plesiosaur tooth histology and Kiprijanoff (1881–1883) published lavish lithographs providing astonishing detail, also of plesiosaur tooth histology, the study of plesiosaur bone histology lagged behind that of archosaurs, in particular dinosaurs. As for all major amniote taxa, plesiosaur bone histology was illustrated and discussed in the comparative compendia of Seitz (1907), Enlow and Brown (1957) and Ricqlès (1976). Naturally, at least since Armand de Ricqlès' early work, the question of how aquatic adaptation has influenced plesiosaur histology has attracted serious attention (Ricqlès and Buffrénil 2001; Houssaye 2013; Houssaye et al. 2016). Perhaps this adaptive focus explains the relatively poor understanding of other aspects of histology, such as the growth record found in plesiosaur long bones. In fact, not a single plesiosaur taxon has been studied from a proper growth series, and no micrographs of a histological section covering entire midshaft cross sections of plesiosaur humeri and femora were figured before 2017 (Wintrich et al. 2017a), a type of illustration that has been standard in paleohistology for decades. Partially, this lack of midshaft cross section illustrations may have been influenced by the very short and morphologically simplified plesiosaur propodials and zeugopodials. Location of the plane of section is crucial (see below), and any section slightly off the neutral zone will have a great deal of endochondral bone. Earlier and even contemporary studies (Wiffen et al. 1995; Fostowicz-Frelik and Gazdzicki 2001; Salgado et al. 2007; Araújo et al. 2015; O'Gorman et al. 2017; Ossa-Fuentes et al. 2017) missed their full potential because of imprecise section sampling.

Work on plesiosaur histology in the modern era, i.e., since de Ricqlès redefined the field of paleohistology, shows a peculiar and presumably unintentional focus on elasmosaurs from the Late Cretaceous of the Southern Hemisphere (Wiffen et al. 1995; Fostowicz-Frelik and Gazdzicki 2001; Salgado et al. 2007; Araújo et al. 2015; O'Gorman et al. 2017; Ossa-Fuentes et al. 2017). The first extensive study of plesiosaur bone histology that also took an ontogenetic perspective was that by Wiffen et al. (1995) on plesiosaurs from the Late Cretaceous of New Zealand. The authors concluded that juveniles of a single taxon showed pachyostosis, whereas the adults showed secondary cancellous bone, suggesting an ontogenetic shift from near-shore to open marine habitats. Fostowicz-Frelik and Gazdzicki (2001) studied plesiosaur long bones and ribs from the Late Cretaceous of Seymour Island, Antarctica, and noted the presence of extensive Haversian remodeling. Further histological studies of plesiosaurs from this region are those by Salgado et al. (2007), O'Gorman et al. (2017) and Ossa-Fuentes et al. (2017). O'Gorman et al. (2017) studied the histology of a perinatal humerus and noted the abundance of calcified cartilage. This is due to the early ontogenetic stage and distal location of the plane of section in this study. Similarly, Ossa-Fuentes et al. (2017) found abundant calcified cartilage and an "osteosclerotic-like" skeleton as well as a thin cortex in a juvenile. The latter is clearly due to the plane of section being far from the neutral zone. Araújo et al. (2015) also focused on an apparent early juvenile from the Late Cretaceous of Angola, but argued that its histology indicates it was a pedomorphic adult because the bone tissue was mainly cancellous. However, the apparent presence of abundant calcified cartilage suggests that this interpretation is problematic. Clearly, the thin sections from all the other Southern Hemisphere plesiosaurs discussed above also need restudy in light of the current understanding of plesiosaur bone histology and its change through ontogeny.

It is perhaps surprising that the iconic plesiosaurs from the Lower Jurassic beds of the United Kingdom and Germany have received so little sampling. A single mature propodial was studied by Krahl et al. (2013), but the first extensive skeletal histological study was only done more recently (Wintrich et al. 2017a). Middle and Upper Jurassic plesiosaur histology remains largely unstudied (but see below) except for a few specimens figured by Liebe and Hurum (2012) and Wintrich et al. (2017a). The former mainly focused on microanatomy, comparing juvenile and adult propodials from the Upper Jurassic of Svalbard (Liebe and Hurum 2012). The latter described a midshaft cross section of the femur of the common Oxford Clay plesiosaur *Cryptoclidus*. The specimen is on display at the Goldfuß Museum of the University of Bonn (Germany) and was sampled systematically from all skeletal regions except the skull. Although a detailed description of the resulting sections is beyond the scope of this chapter, below we will provide basic information on histovariability across the skeleton.

Cretaceous plesiosaurs of the Northern Hemisphere have received little histological study. Street and O'Keefe (2010) noted pachyostosis in the gastralia of the Middle Jurassic plesiosaur *Tatenectes*. The best, albeit still rather incomplete, histological growth series of any plesiosaur is known from the primarily Late Cretaceous Polycotylidae, comprising two fetal individuals, one early juvenile and two adults, one of which is the mother of one of the fetuses (O'Keefe et al. 2019). The other is represented by an isolated bone.

Descriptions by Skeletal Region

Skull: Dental Histology Only

Knowledge of the histology of the skull bones of plesiosaurs is poor. This is partly because such material is rare, so it is less amenable to consumptive sampling than other body regions. Only tooth histology has been studied (Kiprijanoff 1881–1883; Sander 1999; Kear et al. 2017), but details are beyond the scope of this chapter. Suffice it to say that plesiosaur dental histology conforms to the general amniote pattern and is not nearly as unusual as the histology of their bones.

Propodials

Here we deviate from the proper anatomical order of description by focusing on propodials first, because propodials of plesiosaurs are by far the best sampled and understood bones. The histological and microanatomical patterns described here for the propodials are generally found with modifications in the other postcranial endoskeletal elements and hence are described first and in more detail (Figure 23.2).

As noted above, a distinction between isolated humeri and femora can be difficult in plesiosaurs because the morphology

VetBooks.ir

of the bones is so simplified. Accordingly, several studies only identify the bones in question as propodials (e.g., Araújo et al. 2015; Ossa-Fuentes et al. 2017). As noted above, during pistosauroid evolution, propodial morphology became ever more simplified, accompanied by a simplification of the relationship of the periosteal and endochondral domains (Wintrich et al. 2017a). These domains have a very similar relationship in vertebral centra (see below). As well described by Liebe and Hurum (2012), plesiosaur propodials comprise long, flattened cones of endochondral bone surrounded by a cortex of periosteal bone. The arrangement resembles an hourglass surrounded by a double-funnel-shaped mantle. The two cones meet at the embryonic center of ossification, which is commonly resorbed by a small medullary cavity. Growth thus proceeded proximally and distally as well as circumferentially from this region, also known as the "neutral zone" (Francillon-Vieillot et al. 1990). Importantly, the location of the center of ossification may vary from the middle of the proximodistal midlength of the bone to considerably more distally (e.g., Liebe and Hurum 2012; Wintrich et al. 2017a). Neutral zone location must be identified before sectioning to obtain exact midshaft sections.

The only unequivocal method for detecting the location of the center of ossification is computed tomography (CT) scanning to reveal the internal end of the nutrient canal where it inserts into the primordium (Wintrich et al. 2017a). However, in most plesiosaurs, the canal runs proximally from the ossification center to the posterior margin of the bone, exiting there as the nutrient foramen, and thus the plane of section should be placed well distal to the nutrient foramen in the absence of CT scans.

Longitudinal sections should also intersect the center of ossification, if at all possible. Hitting the correct plane of section is more crucial in plesiosaurs than in terrestrial amniotes (but similar to the situation in nonamniote tetrapods) because the shaft of the bones is short and thick, and the thickness of the periosteal domain rapidly decreases toward both ends. Plesiosaur propodials thus resemble the vertebral centra of amniotes, including plesiosaurs (see below), in their morphogenesis and microanatomy. Reports of a thin cortex (Wiffen et al. 1995; Araújo et al. 2015; O'Gorman et al. 2017; Ossa-Fuentes et al. 2017) and abundant calcified cartilage in the cortex of plesiosaur bones almost certainly result from suboptimal placement of the sections either proximally or distally. The published location of the sections confirms this suspicion in the cases of Wiffen et al. (1995), Araújo et al. (2015) and O'Gorman et al. (2017), whereas Fostowicz-Frelik and Gazdzicki (2001) and Ossa-Fuentes et al. (2017) did not provide a plane of section.

The primary bone tissue of the periosteal domain is a highly unusual bone tissue (Figures 23.3–23.5) only recognized in plesiosaurs so far (Wintrich et al. 2017a) and termed plesiosaur radial fibrolamellar bone (pFLB). This tissue was found in the somewhat taxonomically representative sample of plesiosaur propodials in this study as well as by O'Keefe et al. (2019) in an additional clade, North American polycotylids. Descriptions and images in the literature (Fostowicz-Frelik and Gazdzicki 2001, Figure 4a; Araújo et al. 2015, Figure 8c, h; Ossa-Fuentes et al. 2017, Figure 3b, d, f, h; O'Gorman et al. 2017, Figure 5d, e) suggest the presence of this tissue in the propodials of Cretaceous Antarctic elasmosaurids as well. The unusual bone tissue also occurs in all other plesiosaur endoskeletal elements that have been sampled so far (see below). The pFLB belongs to the fibrolamellar complex, consisting of radially oriented (at least at midshaft) primary osteons set in a matrix of woven bone (Figures 23.3 and 23.4). The tissue superficially looks like the laminar fibrolamellar bone of many dinosaurs and large mammals, but rotated by 90° (Figures 23.3F–I and 23.5B). The woven bone matrix shows densely packed lacunae of large (diameter averaging 20 µm) static osteocytes (Stein and Prondvai 2014). The density of these lacunae exceeds that in fibrolamellar bone of other tetrapods, and in places, the lacunae take up most of the volume of the tissue (Figures 23.3I and 23.4D, E). The primary osteons in the pFLB are made of a centripetal infill of parallel-fibered bone with flattened lacunae of dynamic osteocytes (Figure 23.3I). Vascularity is relatively low, although it has not been quantified yet across the board, so in longitudinal sections few vascular canals are intersected (Figure 23.4B, C). The radial orientation of the primary osteons in pFLB at midshaft gradually changes to a longitudinal orientation toward the epiphysis. In this region, the primary osteons are parallel to the boundary between the periosteal and endochondral domains. In longitudinal sections of entire bones, the primary osteons are seen to fan out from the center of ossification, as already depicted by Lydekker (1889, Figure 6) in the earliest illustration of plesiosaur propodial microanatomy.

The formation of the pFLB is interrupted by growth marks, most prominently by the first-year line (Wintrich et al. 2017a; O'Keefe et al. 2019) (Figure 23.3B, F, G). The presence of a birth line is suggestive but cannot be affirmed because the pFLB is already formed from the onset of ossification, well before birth. Cyclical growth marks (Figures 23.3B, C, D, J and 23.5A) in pFLB mainly consist of an abrupt change in orientation of the vascular canals (Figure 23.3F, G, J), from radial to nearly circumferential and then, beyond the growth mark, from nearly circumferential to fully radial again (Wintrich et al. 2017a). It is peculiar that this distinctive pattern was not mentioned or illustrated by earlier workers. For example, Liebe and Hurum (2012) particularly noted the "absence of zonation", which is quite distinctive in most of our midshaft cross sections (Figures 23.3B, C, D, J and 23.5A). This lack of earlier mention may partially be because no full cross sections of bones or transects across the cortex were figured before and partially because sections placed too proximally or distally only revealed the final part of the growth record.

The final stage of periosteal bone deposition appears to be an external fundamental system (EFS) (O'Keefe et al. 2019) after a limited number of cycles (<5) had been laid down (Wintrich et al. 2017a). The pFLB is peculiar in that it looks rather different in longitudinal section with seemingly much lower vascularization (Figure 23.4). This may be an artifact of section location because the vascular canals that are radial at midshaft become increasingly longitudinal, fanning away from the center of ossification. However, the vascular architecture of pFLB remains incompletely understood.

Tissues from the endochondral domain are not seen in midshaft cross sections, of course, but are seen in more proximally and distally placed cross sections and in longitudinal sections

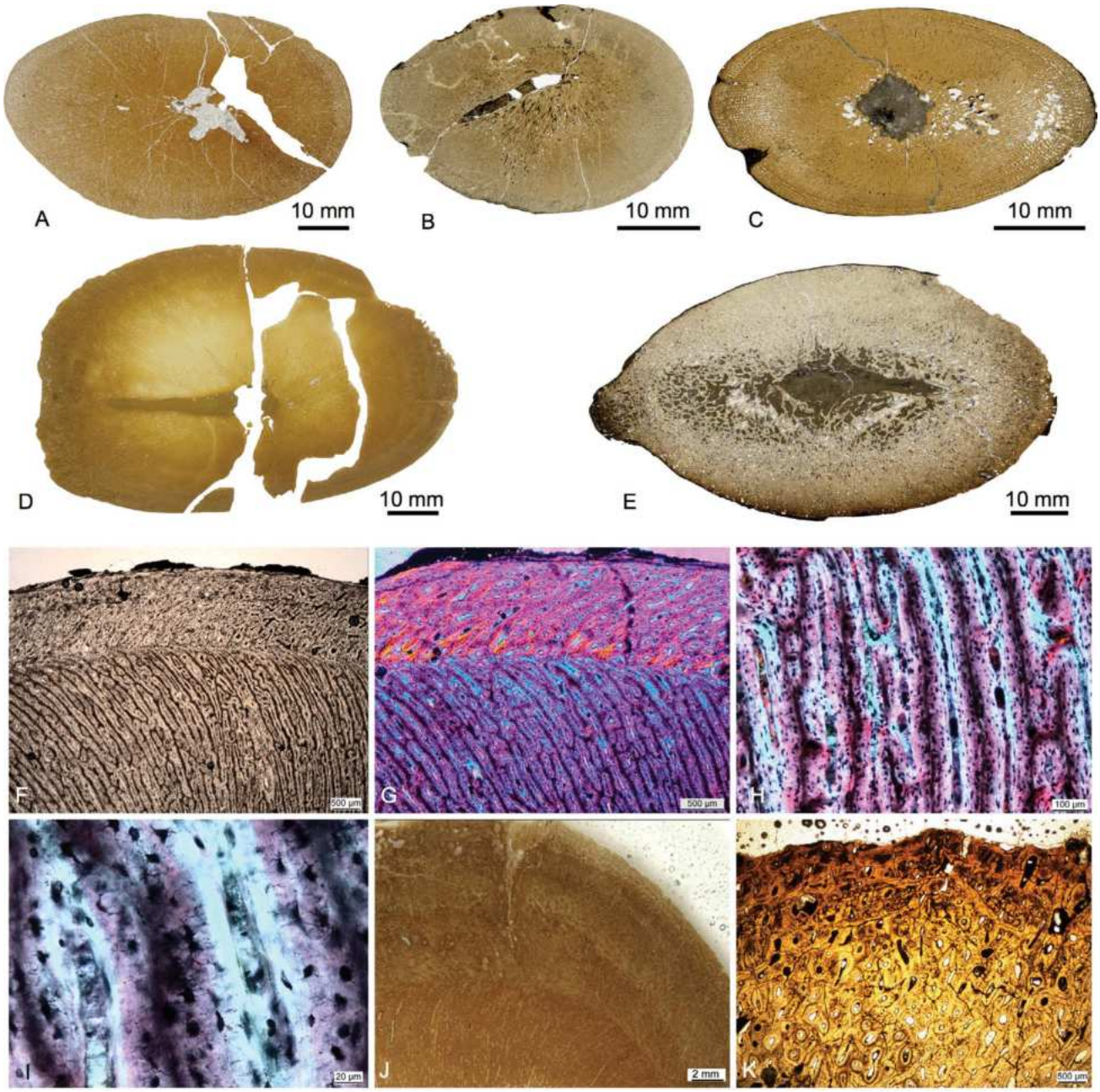


FIGURE 23.3 Microanatomy and histology of plesiosaur propodials. A–E, Midshaft cross sections arranged in ontogenetic order. Midshaft location of all sections is indicated by at least part of the nutrient canal being intersected. Images in normal transmitted light. A, Humerus of the indeterminate juvenile elasmosaur OMNH MV 85. Note the lack of growth marks, the high vascularity and the wavy course of the radial vascular canals. This is a juvenile in its first year. B, Femur of the holotype of the basal pliosaurid *Rhaeticosaurus mertensi* WMNM P 64049. Note the abrupt directional change of the vascular canals at the growth cycle boundary. This animal laid down one growth mark and died in its second year of life. C, Femur of *Plesiosaurus dolichodeirus* IPB R 89. This animal laid down two growth marks. D, Femur of cryptoclidid plesiosaurian *Crytpoclidus eurymerus* IPB R 324. This animal laid down three growth marks. E, Humerus or femur of indet. Pliosauridae SMNS 54025. Note that the cortex is completely remodeled by Haversian substitution and that there is an inner region of cancellous bone. This is an old individual, although its age at death cannot be determined. F, Closeup of the outer part of the first growth cycle and of the second growth cycle of the *Rhaeticosaurus* figure in B. Note the abrupt directional change of the vascular canals at the growth mark and the plesiosaur radial fibrolamellar bone (pFLB) seen in all postcranial elements of plesiosaurs. Image in normal light. G, same as F, but in polarized light with lambda filter. H, pFLB of the first growth cycle in polarized light with lambda filter. I, Closeup of G. Note the woven bone scaffold (magenta) surrounded by primary osteons (light blue). In addition, note the plump and densely spaced osteocyte lacunae in the woven bone and the lenticular ones in the primary osteons. J, Closeup of D (*Cryptoclidus*) showing the growth cycles in the mid- and outer cortex. K, Closeup of the outer cortex of (Pliosauridae indet.) showing the nearly complete replacement of the primary cortex by secondary osteons. These echo the radial arrangement of the primary osteons. IPB, Institute of Geosciences, University of Bonn, Germany; OMNH, Osaka Museum of Natural History, Osaka, Japan; SMNS, Staatliches Museum für Naturkunde, Stuttgart, Germany; WMNM, Westfälisches Museum für Naturkunde, Münster, Germany.

VetBooks.ir

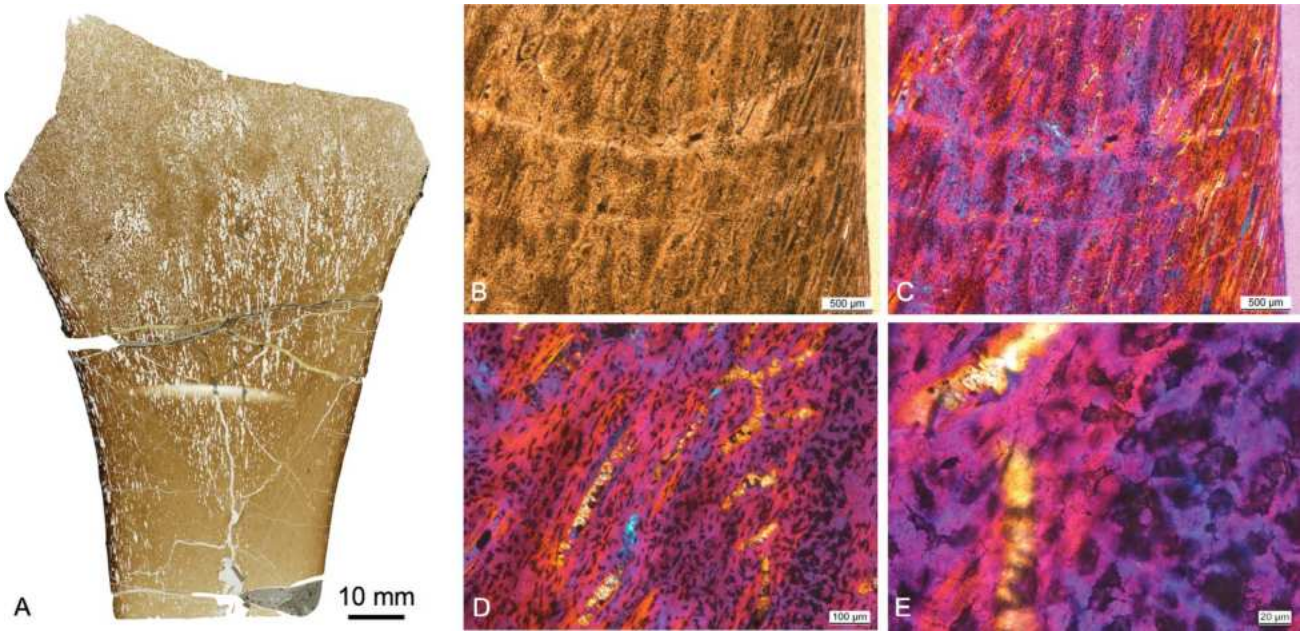


FIGURE 23.4 Microanatomy and histology of plesiosaur propodials in longitudinal sections. A, Longitudinal section cut in the dorsoventral plane of the distal half of humerus or femur of *Plesiosaurus dolichodeirus* IPB R 90 in normal light. The articular surface of the specimen is damaged. Note the dense cortex of periosteal origin and the large cancellous cone of endochondral bone. B, Longitudinal section of the midshaft region of the femur of the holotype of *Rhaeticosaurus mertensi* WMNM P 64049. Outer bone surface is to the left. Note the low number of vascular canals that gradually extend from the center of ossification to the bone surface. C, Same as B, but in polarized light with a lambda filter. The first growth mark is at the color change from magenta to orange. Note the dominance of woven bone (magenta) with a few primary osteons (light blue) in the cortex to the left of the first growth mark. D, Closeup of C. Note the extreme density of plump, irregular osteocyte lacunae in the woven bone indicating dominance of static osteogenesis consistent with rapid tissue formation. Primary osteons are less distinct than in the cross section. E, Closeup of D. IPB, Institute of Geosciences, University of Bonn, Germany; WMNM, Westfälisches Museum für Naturkunde, Münster, Germany.

(Liebe and Hurum 2012). Primary endochondral bone replaces cartilage along the walls of abundant longitudinally oriented vascular canals, including distinctive large pipes a few millimeters across that penetrate the bone from the articular surface proximally as well as distally (Liebe and Hurum 2012; Figure 4a; Araújo et al. 2015, Figure 8g; O'Gorman et al. 2017, Figure 5b; Ossa-Fuentes et al. 2017, Figure 3a). There is ample cartilage preserved interstitially between the bone tissues, increasing toward the articular surface and thus the younger bone tissue (Fostowicz-Frelik and Gazdzicki 2001). However, the details of the pattern of replacement of cartilage by bone and of the vascular network have not been studied yet. Like the periosteal domain, the endochondral domain is characterized by high vascular density but low vascular area, producing low porosity values (Ossa-Fuentes et al. 2017).

Secondary remodeling is an important process in the life history of plesiosaur propodials and in the skeleton in general. As described by the three-front model (Mitchell and Sander 2014), remodeling starts from the center of ossification; secondary osteon formation initially follows the radial canals (e.g., in *Rhaeticosaurus* and *Plesiosaurus*). Eventually, several generations of secondary osteons completely replace the primary periosteal bone (Figure 23.3E, K) and show a predominantly longitudinal orientation even at midshaft (Wiffen et al. 1995; Krahl et al. 2013; Wintrich et al. 2017a; O'Keefe et al. 2019). The details of this process and how secondary osteons ontogenetically change direction from radial to longitudinal have not yet been studied and would require a good ontogenetic series. As already noted by Krahl et al. (2013), plesiosaur secondary osteons are irregular in outline (Figure 23.3K) and not circular or oval as in other amniotes.

In plesiosaur propodials, the resorption front lags very much behind the apposition front in the model of Mitchell and Sander (2014) and appears to lag well behind the remodeling front, resulting in a small or nonexistent medullary cavity up to the time when skeletal maturity is reached (Figure 23.3A–D). Later in ontogeny, there appears to be resorption of the secondary bone, which produces an interior region of more cancellous bone (Figure 23.3E). The patterns of remodeling and resorption in the more proximal and distal parts of the bone, mainly belonging to the endochondral domain, are insufficiently understood. However, there are repeated reports of a great increase in cancellous bone toward the bone ends (Wiffen et al. 1995; Fostowicz-Frelik and Gazdzicki 2001).

Vertebrae

No systematic comparative study of plesiosaur vertebral histology has been conducted, but the microanatomy of several taxa in particular has been studied with respect to potential aquatic adaptations and ontogenetic change (Wiffen et al. 1995; Houssaye et al. 2016). However, most of these studies do not seem to have closely controlled the planes of section. Although there is only one true sagittal section in any vertebral centrum (i.e., that following the sagittal plane of the body), transverse and horizontal sections should be placed with equal

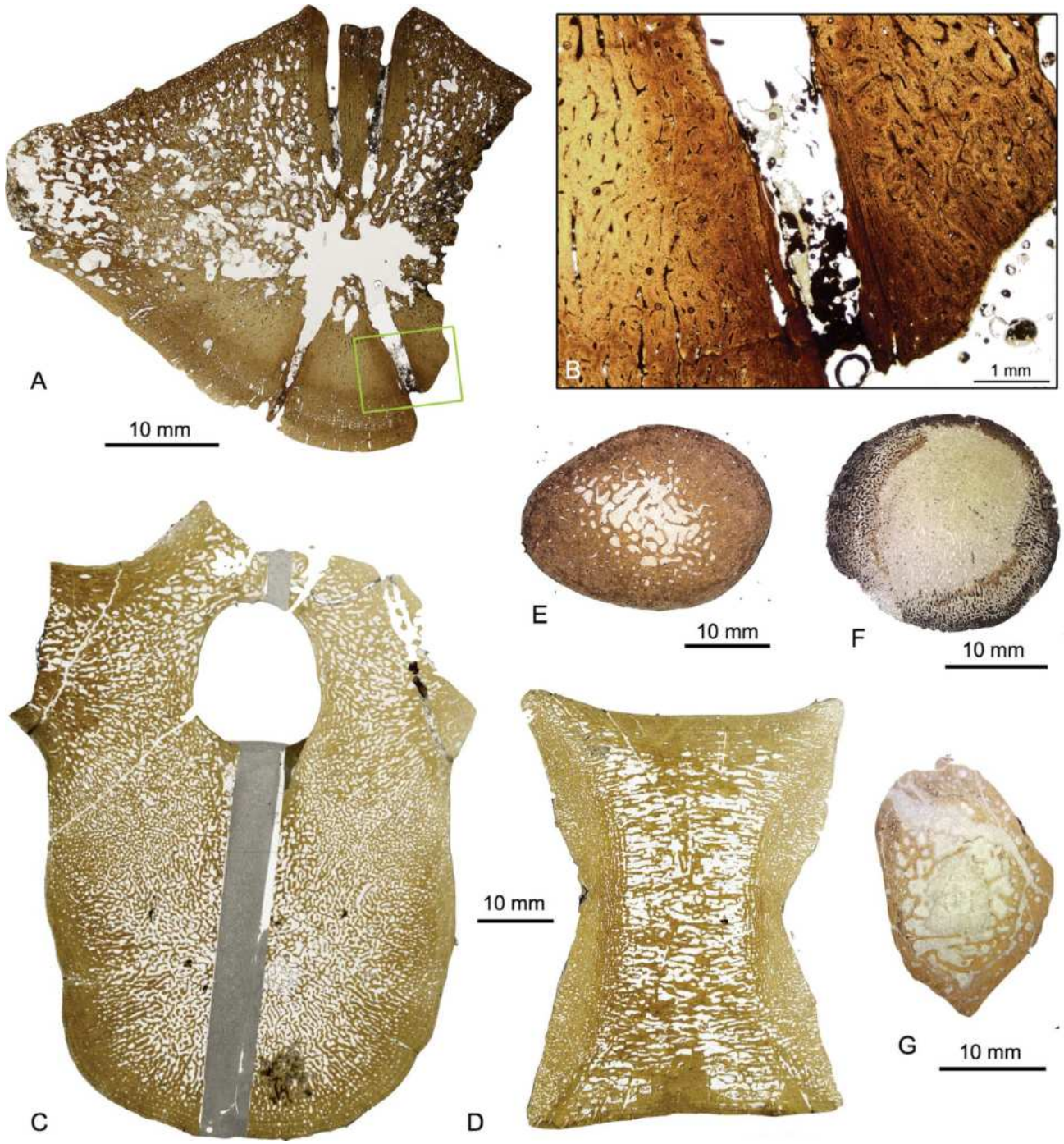


FIGURE 23.5 Microanatomy and histology of plesiosaur vertebrae and ribs. A, Transverse section through posterior cervical centrum of an indet. Toarcian plesiosaur SMNS 50845. The specimen is juvenile because of the unfused neurocentral suture, the extensive preservation of primary cortex in the ventral region and the low number of growth marks. Resorption activity in the dorsal half of the centrum leads to the formation of cancellous bone. Note the paired intersegmental artery canals dorsoventrally traversing the centrum. Green box marks field of view in (B). B, Close-up of ventral cortex, note the plesiosaur radial fibrolamellar bone (pFLB) on either side of the intersegmental artery canals. This pFLB is also seen in all other postcranial plesiosaur elements. C, transverse section through vertebral centrum no. 40 of *Cryptoclidus eurymerus* IPB R 324. Note the fused neurocentral suture. The transverse processes and the neural spine are damaged. The vertical gray area in the middle of the section is the location of the sagittal section of the same vertebra figured in (D). There is only a thin layer of primary cortex of the centrum preserved. D, sagittal section, note the clearly set-off endochondral bone of the articular surface. The two sections reveal that the secondary trabeculae in the interior of the vertebra are primarily longitudinally arranged. E, rib cross section of *C. eurymerus* IPB R 324. Note the cortex of secondary osteons and the cancellous medullary region. F, rib cross section of Plesiosauria indet. IPB R uncatalogued. Note the radial fibrolamellar bone also seen in all other postcranial plesiosaur elements. G, rib cross section of indet. Japanese elasmosaur NMNH 40-16. Note the cancellous internal structure resulting from secondary remodeling. All images in transmitted light. IPB, Institute of Geosciences, University of Bonn, Germany; NMNH, Nakagawa Museum of Natural History, Nakagawa, Japan; SMNS, Staatliches Museum für Naturkunde, Stuttgart, Germany.

VetBooks.ir

precision, intersecting the growth center of the bone. In plesiosaur cervical centra, the proper plane of a transverse section cuts through the paired intervertebral artery canals that connect the ventral and dorsal surface of the centra (Wintrich et al. 2017b) (Figure 23.5A). These are present in all plesiosaur cervical vertebral centra. The horizontal section should intersect the growth center, but the location of the embryonic primordial region of the bone is usually resorbed by expansion of the small medullary cavity, making exact placement of such sections more difficult.

Wiffen et al. (1995) first noted the great difference in histology and microanatomy between juvenile and adult cervical vertebral centra. Wiffen et al. (1995, Figure 3) described highly compact primary tissue in transverse sections of a juvenile elasmosaurid and a juvenile "pliosaurid" from the Late Cretaceous of New Zealand. Although these sections were cut from the anteroposterior middle of the centra, it is not clear if they intersect the growth center of the centrum because there is no indication that the intervertebral artery canals were intersected. The figured section (Wiffen et al. 1995, Figure 3a) shows a small central cavity but not the canals entering and leaving it, as described by Wintrich et al. (2017b) in a juvenile posterior cervical vertebra of an indeterminate Toarcian plesiosaur (Figure 23.5A, B). This specimen shows compact primary fibrolamellar bone of the periosteal domain with the typical radial canal arrangement (Figure 23.5A, B) also observed by Wiffen et al. (1995). This pFLB seen in the Toarcian juvenile is typical of plesiosaurs and was described in detail in the propodial bones (above), where it is best studied. Wiffen et al. (1995) also noted and figured the primary bone of the vertebral centra and noted the presence of abundant interstitial calcified cartilage. This indicates that their sections were not placed strictly transversely because a strictly transverse section in a vertebral centrum does not intersect the endochondral domain. No sagittal sections of juvenile plesiosaurs have been published or are available to provide details of the histology of the endochondral domain, but the description by Wiffen et al. (1995) indicates the retention of cartilage in the trabecular interstices of the endochondral domain.

According to Houssaye et al. (2016), sagittal sections of vertebral centra (cervical and dorsal) reveal an even fill of loose cancellous bone, where trabeculae are preferentially oriented in the axial direction. Wiffen et al. (1995, Figure 3) described a similar loose trabecular architecture in transverse sections of an adult elasmosaurid and an adult "pliosaurid" from the Late Cretaceous of New Zealand. The results of the two studies are compatible, indicating the presence of longitudinally oriented trabeculae that apparently extend across the center of growth without interruption. We observed this pattern in all vertebral centra of *Cryptoclidus* (Figure 23.5F, G) and an indeterminate elasmosaurid from Japan. Although it was not noted in the descriptions of Wiffen et al. (1995) and Houssaye et al. (2016), these trabeculae must be of secondary origin. Their longitudinal orientation indicates a radical reorganization of the histology of the vertebral centra during growth from the primary compact pFLB to the longitudinally oriented secondary trabeculae. A dorsal vertebra of *Cryptoclidus* (vertebra 40, Figure 23.5F) preserves laminar FLB with growth marks in a limited area of the primary dorsal and ventral cortex, different from what is observed in juveniles. Presumably, the predominantly radial vascularization of the juveniles changes to laminar vascularization with more closely spaced growth marks as skeletal maturity is approached.

The question of whether there are histological differences among the different regions of the vertebral column has not been explicitly addressed in the published literature; mostly cervicals have been studied. This bias toward cervicals is not surprising because there are many more cervicals in most plesiosaur taxa than dorsals. A series of cervical and dorsal centra of a single adult skeleton of *Cryptoclidus*, however, reveals little variation along the column. A similar result was obtained for the Japanese elasmosaurid. This may be surprising given the seemingly different biomechanical conditions experienced by the different sections of the column. However, recent work (Wintrich et al. 2019) suggests that the cervical vertebral column was similarly immobilized as the dorsal column by muscles, connective tissue and osteological stops. This limited mobility of the neck thus is consistent with the microanatomical similarity of cervicals and dorsals. The longitudinal orientation of the trabeculae is consistent with axial loading of the centra, as would be expected in a neck of limited mobility.

Descriptions of caudal centrum histology are lacking, as are specific descriptions of the histology of the neural arch.

Ribs and Gastralia

Although easily sampled, ribs of plesiosaurs have only been studied to a limited extent, and the locations of samples on the rib shafts have been poorly constrained. Thus histovariability along the shaft of the ribs has not been studied systematically. Nopcsa and Heidsieck (1934) described plesiosaur ribs in a comparative fashion as pachyostotic. Wiffen et al. (1995) described juvenile and adult anterior dorsal ribs: the juvenile ones (ontogenetic stage determined by size only) showed compact primary bone and little central resorption, whereas the adult rib showed secondary cancellous bone and a large central resorption cavity. Our own rib samples of *Cryptoclidus* (Figure 23.3C) and the Japanese elasmosaurid (Figure 23.3E) conform to the adult pattern described by Wiffen et al. (1995). An indeterminate plesiosaur rib fragment (Figure 23.3D), on the other hand, shows the distinctive pFLB seen in propodials and vertebrae, suggesting that the sample came from a juvenile.

Girdle Bones

Girdle bone histology has not been studied in a systematic fashion in plesiosaurs, but a range of isolated bones and ontogenetic stages has been published. Ossa-Fuentes et al. (2017) described the histology of a fragmentary juvenile elasmosaurid scapula, whereas O'Keefe et al. (2019) described the same in the polycotylid fetus *in utero* mentioned above (O'Keefe and Chiappe 2011). Both scapulae share a cortex of highly vascularized radial FLB. Surprisingly, the fetal scapula lacks any indication of cartilage preservation and already shows signs of remodeling in the innermost region. The juvenile scapula, on the other hand, shows abundant interstitial cartilage in the primary endochondral bone. This difference may be due to

VetBooks.ir

the sampling location, which was at midshaft in the fetus (core sample traversing the entire bone thickness, O'Keefe et al. 2019) but uncertain in the juvenile.

The histology of mature girdle bones was also briefly described by Fostowicz-Frelik and Gazdzicki (2001) as compact throughout, with abundant secondary osteons and no preservation of cartilage. Our own observations of *Cryptoclidus* cover the flat parts of the coracoids, which were sampled at different locations by coring. The core samples reveal a diploe structure of the coracoid with a cancellous interior and compact outer layers of secondary bone.

Limb Bones Other Than Propodials

Limb bones other than propodials also have not been studied in a systematic fashion in plesiosaurs, but a range of isolated bones and ontogenetic stages has been described. Wiffen et al. (1995) compared juvenile and adult phalanges of a Late Cretaceous New Zealand elasmosaur. They found abundant calcified cartilage interstitially to the typical plesiosaur endochondral primary bone and primary periosteal bone. In the adult phalanx, only secondary trabeculae similar to those in the vertebrae were found.

The most extensive study of limb bones distal to the propodials is that by Liebe and Hurum (2012) on the Jurassic Svalbard plesiosaurs, comparing two juvenile, one subadult and one adult individual. The study did not, however, include zeugopodial bones. Concomitant with bone shape, the distribution and shape of the periosteal domain varied between the flat bones of the carpus and the long bones of the metapodium and phalanges. This was already described morphologically by Caldwell (1997), who used the term "perichondral" bone for the bone tissue of the periosteal domain. The study by Liebe and Hurum (2012) basically confirmed what Wiffen et al. (1995) observed based on only two phalanges, i.e., juveniles show a clear difference between the domains, and this difference is obliterated by the formation of secondary trabeculae through remodeling. Liebe and Hurum (2012) also described circumferentially oriented trabeculae in some phalangeal cross sections, but it is not clear whether the trabeculae are primary.

Our own observations of *Cryptoclidus* are the first of the histology of the radius and ulna. In accordance with morphology, the leading edge of the radius and the trailing edge of the ulna consist of periosteal bone, whereas the medial margins have endochondral bone at the surface (see also Caldwell 1997).

Growth, Skeletochronology and Life History

Qualitative Indicators of Fast Growth

A cursory consideration of the primary cortical histology of plesiosaurs reveals three features typically associated with very fast growth (Cubo et al. 2008): fibrolamellar bone with radial vascular canals, high density of osteocyte lacunae and preponderance of isometric osteocyte lacunae. In addition, a low number of growth marks relative to the size of the animal also suggests fast growth.

Quantification of the growth mark record in terms of number and spacing of the growth marks supports these qualitative observations, as does histomorphometry (see below). Because there was almost no medullary resorption and Haversian remodeling until after final size was reached, plesiosaur midshaft cortices preserve an unusually complete growth record (Wintrich et al. 2017a; O'Keefe et al. 2019). Thus, the first bone tissue deposited soon after the onset of ossification may be preserved even in fully grown individuals. A neonatal line, however, is not distinctive and could not be recognized in the sample of Wintrich et al. (2017a) but appears to be present at least in polycotylids (O'Keefe et al. 2019). The first-year mark, on the other hand, is always distinctive (Figure 23.3B–D, F, G, J and 23.4) and marks the largest change in bone appositional style before EFS deposition. Remarkably, over 65% of final cortical thickness had been laid down at the end of the first year of life in all plesiosaurs studied by Wintrich et al. (2017a). The remaining thickness of the cortex was then laid down in two to four more cycles of generally diminishing thickness before final size was reached (Wintrich et al. 2017a). Cortical apposition rates calculated from cycle thickness are in the range of extant mammals and an order of magnitude higher than for extant reptiles (Wintrich et al. 2017a).

Although the Wintrich et al. (2017a) sample was admittedly small (n = 3), it is distributed widely over the plesiosaur tree, suggesting the generality of the observed pattern. All other available evidence (Liebe and Hurum 2012; Araújo et al. 2015; O'Gorman et al. 2017; Ossa-Fuentes et al. 2017; O'Keefe et al. 2019) is consistent with this pattern, and no single plesiosaur propodial has been described that would show a thinner first cycle and a higher number of more closely spaced growth marks than those described by Wintrich et al. (2017a). We conclude that plesiosaurs grew very rapidly during their first year, retaining high fetal growth rates, and only took a few more years to reach skeletal maturity. Currently, it is difficult to determine when sexual maturity occurred, and it is likely that it coincided with skeletal maturity (see below), as is the case in some large mammals.

Plesiosaurs thus may have evolved this pattern convergently to mammals from the ancestral amniote condition, in which sexual maturity is reached well before final size (Sander 2000; Klein and Griebeler 2018).

Ontogenetic Changes and Histologic Ontogenetic Stages

Wiffen et al. (1995) were the first to systematically address ontogenetic changes in plesiosaur bone histology, although earlier workers, beginning with Kiprijanoff (1881–1883), repeatedly noted differences between juveniles and adults. Wiffen et al. (1995) in particular focused on the effect that ontogenetic changes would have had on bone mass. They described the dense bone of the juveniles as osteosclerotic and the cancellous bone of the adults as osteoporotic-like, inferring a change in habitat shift from near-shore to open marine. They also noted the presence of cartilage remains in the trabecular tissue of the endochondral domain in juveniles and the lack of cartilage in adults. However, the differences between juveniles and adults were not quantified, and other explanations for the ontogenetic

VetBooks.ir

change in tissue structure than habitat shift appear possible, such as the extremely fast growth of juveniles (see below).

Although no complete growth series have been sampled for any plesiosaur taxon, seemingly precluding the definition of histologic ontogenetic stages (HOS; Klein and Sander 2008), the general uniformity of histology across taxa and bones in plesiosaurs, together with a good representation of very early ontogenetic stages (fetal, perinatal), we nevertheless define HOS for plesiosaurs in this chapter (Table 23.1). Plesiosaurs also appear suitable for the HOS approach because of the slow resorption front and the moderately slow remodeling front (see Mitchell and Sander 2014). This means that almost the entire growth record is preserved in many plesiosaur bones, in particular the propodials. In addition, propodials are particularly suitable for the HOS approach because of their large absolute amount of periosteal cortex laid down at midshaft. HOS stages are defined based on the sequence and relative thickness of different bone tissue types and other features such as growth marks and the EFS exactly at midshaft (Klein and Sander 2008).

At present, only four tissue types can be recognized in plesiosaurs: woven bone with radial and plexiform vascularization (type A), pFLB (type B), secondary compact bone (Haversian bone) and secondary cancellous bone. Cortical growth marks are distinctive, and an EFS may be well developed. We thus recognize eight HOS and their corresponding biological ontogenetic stages in propodials: HOS 1, fetus; HOS 2, neonate; HOS 3, juvenile; HOS 4, late juvenile; HOS 5, subadult; HOS 6, early adult; HOS 7, adult; HOS 8, late adult. These HOS can be applied to several individuals described in the literature from the published histological descriptions (Table 23.1).

Other specimens described in the literature are difficult to assign to a specific HOS because of insufficient descriptions and illustrations. This applies to the material described by Araújo et al. (2015), for which the histological descriptions are internally inconsistent and the conclusion, based on histology, that the material represents pedomorphic adults, is problematic.

Histomorphometry

Growth Rates and Resting Metabolic Rates

Qualitative evidence for extremely fast growth invites further quantification of growth rates, bone apposition rates and the application of phylogenetically informed inference models. Following the histomorphometric approach of Cubo et al. (2012) and Legendre et al. (2016) for fossil archosaurs, Fleischle et al. (2018) estimated bone growth rate (as cortical apposition rate) and resting metabolic rate for plesiosaurs (Figure 23.6). Using phylogenetic eigenvector modeling (Legendre et al. 2016) with the predictor variable of vascular density, Fleischle et al. (2018) inferred bone growth rates (cortical apposition rates) and resting metabolic rates for plesiosaurs in the bird range, exceeding that of mammals. Evidence for high bone apposition rates thus comes from two independent sources, growth mark spacing and histomorphometry. Unlike for terrestrial tetrapods (e.g., Griebeler et al. 2013), it has not been possible to infer absolute growth rates (in kilogram per year) for plesiosaurs because no scaling relationships between long bone dimensions (or any other skeletal size proxy) and body mass are available. Such an approach would be fraught with uncertainties because of the impossibility of validation using data from extant amniotes (there are no animals alive today that have the same body plan as plesiosaurs) and the lack of reliable mass estimates for most plesiosaurs. Mass estimates can only be obtained from physical scale models or other methods for determining body volume, such as three-dimensional (3D) mathematical slicing (Henderson 1999).

TABLE 23.1

Histologic ontogenetic stage (HOS) for Plesiosaurs and HOS Assignment of Specific Individuals Based on Descriptions in the Literature

HOS		BOS Tissue Types	Specimens	Reference
1	Fetus	Woven bone with radial and plexiform vascularization (type A)	*Polycotylus* LACM 129639b, indet. polycotylid FMNH PR 1619	O'Keefe et al. 2019
2	Neonate	Type A followed by thin radial FLB (type B), sometimes neonatal line	*Dolychorynchops* USNM 55810	O'Keefe et al. 2019
3	Juvenile	Type A followed by thick type B, sometimes neonatal line	indet. elasmosaur OMNH MV 85	Wintrich et al. 2017a
4	Late juvenile	Type A followed by thick type B with one to two growth marks	*Rhaeticosaurus* WMNM P 64049	Wintrich et al. 2017a
5	Subadult	Type A followed by thick type B with growth marks of decreasing spacing	*Plesiosaurus* IPB R 89	Wintrich et al. 2017a
6	Early adult	Type A followed by thick type B with growth marks of decreasing spacing and beginning EFS, beginning Haversian substitution	*Cryptoclidus* IPB R 324	Wintrich et al. 2017a
7	Adult	Type A followed by thick Type B followed by an EFS with substantial Haversian substitution and beginning cancellous medullary region	*Plesiosaurus* IPB R 90	Krahl et al. 2013
8	Late adult	Complete Haversian replacement with cancellous medullary region	Pliosauridae SMNS 54025, *Polycotylus* LACM 129639a, *Dolychorynchops* USNM 50133	Wintrich et al. 2017a; O'Keefe et al. 2019

Abbreviations: BOS, biological ontogenetic stage; EFS, external fundamental system; FLB, fibrolamellar bone.

VetBooks.ir

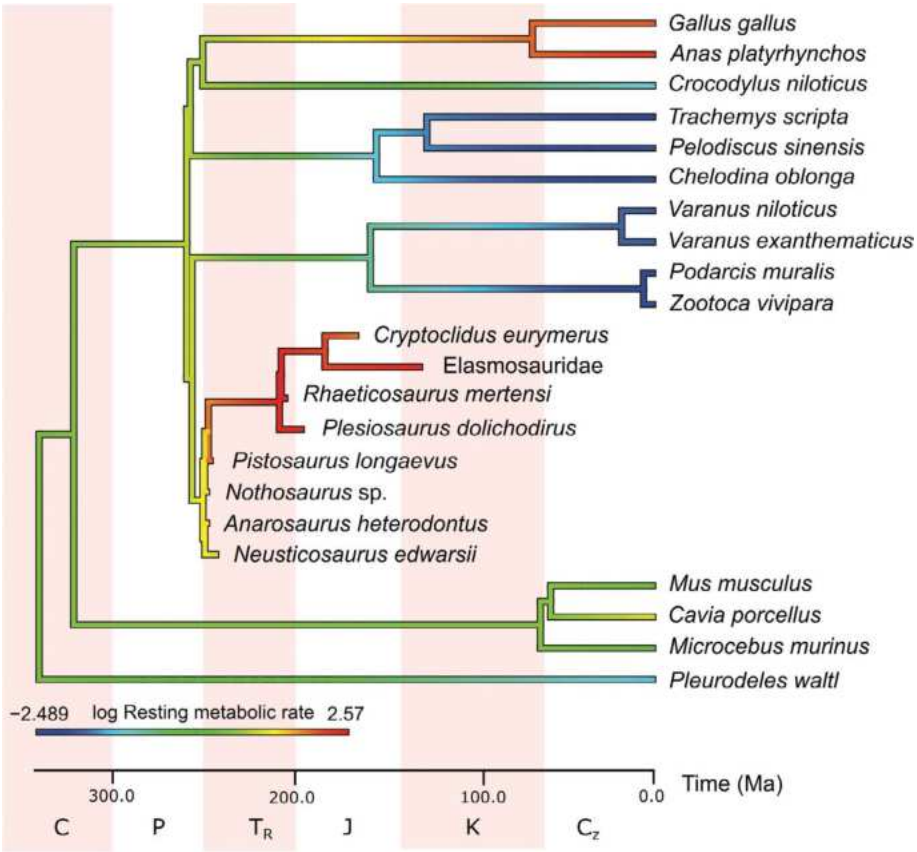


FIGURE 23.6 Inference model of metabolic rate in plesiosaurs. Measured and estimated mass-specific resting metabolic rate (RMR) in log mL O_2 h^{-1} $g^{-0.67}$ mapped color-coded on a phylogenetic tree of amniotes. In this comparison, blue represents low values, green and yellow intermediate values, and red high values. Plesiosaurs have an RMR in the range of birds. Within sauropterygians, the RMR increases evolutionarily, but even basal forms show values in the range of mammals or higher and far above the ectothermic species included in the model. (From Fleischle et al. 2018, reprinted under a CRC license.)

Bone Density: Vertebrae and Propodials

Evolutionary changes in bone density connected to secondary aquatic adaptation have long been in the focus of paleohistologists (see Houssaye et al. 2016 for a recent review). The first study to deal extensively with this issue is that by Wiffen et al. (1995), who found that juvenile plesiosaurs had dense, pachyosteosclerotic bone in all parts of the skeleton, whereas adults had secondary cancellous bone. These results are consistent with several other more recent studies as reviewed above, although proper quantification of porosity (e.g., Canoville et al. 2016) is lacking. The pachyosteosclerotic juvenile condition may represent bone mass increase, whereas the adult condition may represent a decrease in bone mass, lightening the skeleton. Alternatively, the pattern may simply reflect an ontogenetic reorganization of microanatomy while relative bone mass remains the same, as in ichthyosaurs (Houssaye et al. 2014, 2018).

In a few cases, there is clear evidence for pachyostosis in plesiosaurs, e.g., in the Jurassic *Pachycostosaurus* (Cruickshank et al. 1996) and *Tatenectes* (Street and O'Keefe 2010), but only the latter instance of pachyostosis has been confirmed histologically. However, pachyostosis is restricted to the ribs and gastralia and does not affect the entire skeleton, unlike in pachypleurosaurs, mesosaurs, hupehsuchians and aquatic stem snakes (Houssaye 2013).

Red Blood Cell Size

Finally, histomorphometry can be used to infer red blood cell (RBC) size in plesiosaurs, following the approach of Huttenlocker and Farmer (2017), using minimal vascular canal dimensions. Fleischle et al. (2019) found that RBC size increases by a factor of 3 from basal sauropterygians to plesiosaurs, a pattern that is also seen in the evolution of deep-diving marine mammals and birds from terrestrial ancestors and, less distinctively, in extant turtles and snakes. RBC size varies among higher clades, so a direct comparison between plesiosaurs and any extant clade is not meaningful, but the difference between less aquatic and deep-diving taxa within a clade is meaningful (Fleischle et al. 2019).

Paleobiological and Evolutionary Implications

Fast Growth and Endothermy

Fast growth generally requires an endothermic metabolism (Werner and Griebeler 2014), and the fast growth observed and inferred in plesiosaurs (Figure 23.6) is consistent with the histomorphometric inference of elevated resting metabolic rates (at the level of birds) in plesiosaurs (Fleischle et al. 2018). The

VetBooks.ir

evolution of endothermy in the line leading to plesiosaurs may be explained by two of the prevalent hypotheses for the origin of endothermy in general: the aerobic scope hypothesis and the parental care hypothesis (Wintrich et al. 2017a; see Clarke and Pörtner 2010). An increased aerobic scope allowed both the colonization of the pelagic habitat and parental care (Koteja 2000).

The notable skeletal fossil record of large fetal material (Moodie 1911; O'Gorman et al. 2017; Ossa-Fuentes et al. 2017; O'Keefe et al. 2019) and of a pregnant female (O'Keefe and Chiappe 2011) suggests from a morphological perspective that plesiosaurs gave birth to very large young and very few offspring. These traits are typical for K-selected reproduction, part of which in amniotes is extensive parental care. This evidence is wholly consistent with the histological evidence of very fast fetal and juvenile growth, facilitated by a high metabolic rate of the mother and by parental care.

Aquatic Adaptation

The cancellous bone of adult plesiosaurs is seen in other clades of highly marine amniotes such as ichthyosaurs, marine turtles and cetaceans (Houssaye et al. 2016). Its presence suggests that plesiosaurs had a similarly pelagic lifestyle as these other clades. The evolutionary size increase in RBCs is also consistent with this hypothesis because it is best explained as an adaptation to deep diving, where larger RBCs of the deep divers can hold more oxygen than the smaller ones of the shallow-water and terrestrial relatives.

The ontogenetic shift in bone density from an osteosclerotic to an osteoporotic condition described by Wiffen et al. (1995) is confirmed by this interpretation. Wiffen et al. (1995) had hypothesized that this shift reflects a habitat shift: the juveniles inhabited coastal waters and migrated to the open sea after reaching adulthood. This hypothesis has not been tested based on the sedimentary environment of juvenile versus adult plesiosaur finds. It also is somewhat inconsistent with extensive parental care, which would require that juveniles and at least reproductive adults lived in the same habitat.

Evolutionary Success

Our understanding of plesiosaurian bone histology and implications adds to the emerging explanation for the evolutionary success of the clade and their survival of the end-Triassic extinctions (Krahl et al. 2013; Wintrich et al. 2017a; Fleischle et al. 2018). Through extended cruising abilities, endothermy allowed the colonization of the pelagic habitat in the Late Triassic. Live birth was a prerequisite for this colonization. Although live birth was already present in basal Sauropterygia (Sander 1988; Cheng et al. 2004), a pronounced K-strategy may have been advantageous in the pelagic habitat as well. A single large offspring is also seen in extant cetaceans (O'Keefe and Chiappe 2011) but not in ichthyosaurs (Böttcher 1990), which appear to have been equally well adapted to life in the open ocean as do plesiosaurs. However, ichthyosaurs of the Jurassic and the Cretaceous show obviously lower morphological disparity and range of feeding adaptations than plesiosaurs and were less diverse and long-lived than plesiosaurs, becoming extinct at the beginning of the Late Cretaceous.

Conclusions

This review of plesiosaur bone histology finds a remarkable discrepancy between the long history of paleontological research on this iconic group of marine reptiles and the limited understanding of their bone histology. Plesiosaur bone histology is as unique as several features of plesiosaurian osteology and functional morphology. Plesiosaur cortical bone histology is characterized by a peculiar kind of radial FLB in juveniles to early adults. Later in ontogeny this tissue is remodeled into dense Haversian bone and secondary trabecular bone, resulting in an apparent ontogenetic mass decrease of bone. A low number of growth cycles indicates that plesiosaur growth was extremely fast: juveniles reached over 60% of final cortical thickness by the end of the first year and skeletal maturity in less than five years. Histomorphometry indicates cortical apposition rates and inferred resting metabolic rates in the range of extant birds. Plesiosaurs must have been endotherms that gave birth to few but very large offspring for which they provided parental care. Together with the cruising capabilities in the pelagic environment provided by endothermy, this may explain plesiosaurian survival of the end-Triassic extinction event.

Fruitful avenues of research from the taxic perspective call for a more complete coverage of the plesiosaur tree, in particular the Rhomaleosauridae, the most basal taxon to evolve large size (Benson et al. 2012). Open questions about plesiosaur bone tissues concern the 3D arrangement of the vasculature in the radial FLB, the nature and distribution of interstitial cartilage in the endochondral domain, and reorientation of the Haversian canals from radial to longitudinal.

Acknowledgments

As in most histological studies, we are deeply indebted to the curators who facilitated consumptive sampling of material under their care. Lab work for this study was performed in the usual expert fashion by Olaf Dülfer and Pia Schucht (Bonn). This review was inspired by discussions with Shoji Hayashi (Okajam), Yasuhisa Nakajima (Tokyo) and Alexandra Houssaye (Paris), who, together with Tamaki Sato (Tokyo), initiated the sampling of some material used in this chapter. We also thank the editor Vivian de Buffrénil for inviting us to write this review and the reviewer Kevin Padian for constructive criticism and editing that nicely improved the manuscript. Funding was provided by Deutsche Forschungsgemeinschaft research grant SA 469/47 to PMS.

REFERENCES

Amprino, R. and G. Godina. 1947. La struttura delle ossa nei vertebrati: ricerche comparative negli anfibi e negli amnioti. *Comment. Pontif. Acad. Scient.* 11: 329–463.

Araújo, R., et al. 2015. New aristonectine elasmosaurid plesiosaur specimens from the early Maastrichtian of Angola and comments on paedomorphism in plesiosaurs. *Netherl. J. Geosci.* 94: 93–108.

Bardet, N., et al. 2014. Mesozoic marine reptile palaeobiogeography in response to drifting plates. *Gondwana Res.* 26: 869–887.

Benson, R. B. J. and P. S. Druckenmiller. 2014. Faunal turnover of marine tetrapods during the Jurassic–Cretaceous transition. *Biol. Rev.* 89: 1–23.

Benson, R. B. J., et al. 2012. High diversity, low disparity and small body size in plesiosaurs (Reptilia, Sauropterygia) from the Triassic – Jurassic boundary. *PLoS One* 7: e31838.

Böttcher, R. 1990. Neue Erkenntnisse zur Fortpflanzungsbiologie der Ichthyosaurier (Reptilia). *Stuttgarter Beit. Naturk. B* 164: 1–51.

Brown, D. S. 1981. The English upper Jurassic Plesiosauroidea (Reptilia) and a review of the phylogeny and classification of the Plesiosauria. *Bull. Brit. Mus. (Nat. Hist.), Geol. Ser.* 35: 253–347.

Caldwell, M. W. 1997. Modified perichondral ossification and the evolution of the paddle-like limbs in ichthyosaurs and plesiosaurs. *J. Vert. Paleontol.* 17: 534–547.

Canoville, A., et al. 2016. Microanatomical diversity of amniote ribs: an exploratory quantitative study. *Biol. J. Linn. Soc.* 118: 706–733.

Cheng, Y., et al. 2004. Triassic marine reptiles gave birth to live young. *Nature* 432 (18 November 2004): 383–386.

Clarke, A. and H. O. Pörtner. 2010. Temperature, metabolic power and the evolution of endothermy. *Biol. Rev.* 85: 703–727.

Conybeare, W. D. 1824. On the discovery of an almost perfect skeleton of the *Plesiosaurus*. *Trans. Geol. Soc. Lond.* S2-S1: 381–389.

Cruickshank, A. R. I., et al. 1996. A pliosaur (Reptilia, Sauropterygia) exhibiting pachyostosis from the Middle Jurassic of England. *J. Geol. Soc.* 153: 873–879.

Cubo, J., et al. 2008. Phylogenetic, functional, and structural components of variation in bone growth rate of amniotes. *Evol. Dev.* 10: 217–277.

Cubo, J., et al. 2012. Paleohistological estimation of bone growth rate in extinct archosaurs. *Paleobiology* 38: 335–349.

Dalla Vecchia, F. M. 2006. A new sauropterygian reptile with plesiosaurian affinity from the late Triassic of Italy. *Rev. Ital. Paleont. Strat.* 112: 207–225.

Dalla Vecchia, F. M. 2017. Comments on the skeletal anatomy of the Triassic reptile *Bobosaurus forojuliensis* (Sauropterygia, Pistosauroidea). *Gortania* 38: 39–75.

Enlow, D. H. and S. O. Brown. 1957. A comparative histological study of fossil and recent bone tissues. Part II. *Texas J. Sci.* 9: 186–214.

Fabbri, M., et al. 2014. New information on *Bobosaurus forojuliensis* (Reptilia: Sauropterygia): implications for plesiosaurian evolution. *Hist. Biol.* 26: 661–669.

Fischer, V., et al. 2017. Plasticity and convergence in the evolution of short-necked plesiosaurs. *Curr. Biol.* 27: 1–10.

Fleischle, C. V., et al. 2018. Quantitative histological models suggest endothermy in plesiosaurs. *PeerJ* 6: e4955.

Fleischle, C. V., et al. 2019. Hematological convergence between Mesozoic marine reptiles (Sauropterygia) and extant aquatic amniotes elucidates diving adaptations in plesiosaurs. *PeerJ* 7: e8022.

Fostowicz-Frelik, L. and A. Gazdzicki. 2001. Anatomy and histology of plesiosaur bones from the Late Cretaceous of Seymour Island, Antarctic Peninsula. *Palaeontol. Pol.* 60: 7–32.

Francillon-Vieillot, H., et al. 1990. Microstructure and mineralization of vertebrate skeletal tissues. In *Skeletal Biomineralization: Patterns, Processes and Evolutionary Trends. Vol. 1.* J.G. Carter ed. New York, Van Nostrand Reinhold.

Griebeler, E. M., et al. 2013. Aging, maturation and growth of sauropodomorph dinosaurs as deduced from growth curves using long bone histological data. *PLoS One* 8: e67012.

Henderson, D. M. 1999. Estimating the masses and centers of mass of extinct animals by 3-D mathematical slicing. *Paleobiology* 25: 88–106.

Houssaye, A. 2013. Bone histology of aquatic reptiles: what does it tell us about secondary adaptation to an aquatic life? *Biol. J. Linn. Soc.* 108: 3–21.

Houssaye, A., et al. 2014. A new look at ichthyosaurian long bone microanatomy and histology: implications for their adaptation to an aquatic life. *PLoS One* 9: e95637.

Houssaye, A., et al. 2016. Adaptive patterns in aquatic amniote bone microanatomy – More complex than previously thought. *Integr. Comp. Biol.* 56: 1349–1369.

Houssaye, A., et al. 2018. Structural, functional, and physiological signals in ichthyosaur vertebral centrum microanatomy and histology. *Geodiversitas* 40: 161–170.

Huttenlocker, A. K. and C. G. Farmer. 2017. Bone microvasculature tracks red blood cell size diminution in Triassic mammal and dinosaur forerunners. *Curr. Biol.* 27: 48–54.

Kear, B. P., et al. 2017. Exceptionally prolonged tooth formation in elasmosaurid plesiosaurians. *PLoS One* 12: e0172759.

Ketchum, H. F. and R. B. J. Benson. 2010. Global interrelationships of Plesiosauria (Reptilia, Sauropterygia) and the pivotal role of taxon sampling in determining the outcome of phylogenetic analyses. *Biol. Rev.* 85(2): 361–392.

Kiprijanoff, A. V. 1881–1883. Studien über die fossilen Reptilien Russlands. *Mém. Acad. Impér. Sci. Saint Petersbourg* 7: 1–144.

Klein, N. and E. M. Griebeler. 2018. Growth patterns, sexual dimorphism, and maturation modeled in Pachypleurosauria from Middle Triassic of central Europe (Diapsida: Sauropterygia). *Foss. Rec.* 21: 137–157.

Klein, N., and P. M. Sander. 2008. Ontogenetic stages in the long bone histology of sauropod dinosaurs. *Paleobiology* 34: 247–263.

Koteja, P. 2000. Energy assimilation, parental care and the evolution of endothermy. *Proc. R. Soc. B* 267: 479–484.

Krahl, A., et al. 2013. Evolutionary implications of the divergent long bone histologies of *Nothosaurus* and *Pistosaurus* (Sauropterygia, Triassic). *BMC Evol. Biol.* 13: 1–23.

Legendre, L. J., et al. 2016. Palaeohistological evidence for ancestral high metabolic rate in archosaurs. *Syst. Biol.* 65: 989–996.

Liebe, L. and J. H. Hurum. 2012. Gross internal structure and microstructure of plesiosaur limb bones from the Late Jurassic, central Spitsbergen. *Norw. J. Geol.* 92: 285–309.

Lydekker, R. 1889. *Catalogue of the Fossil Reptilia and Amphibia in the British Museum, Part 2*. London, Trustees of the British Museum.

Mitchell, J. and P. M. Sander. 2014. The three-front model: a developmental explanation of long bone diaphyseal histology of Sauropoda. *Biol. J. Linn. Soc. Lond.* 112: 765–781.

Montes, L., et al. 2007. Relationships between bone growth rate, body mass and resting metabolic rate in growing amniotes: a phylogenetic approach. *Biol. J. Linn. Soc.* 92: 63–76.

VetBooks.ir

Moodie, R. L. 1911. An embryonic plesiosaurian propodial. *Trans. Kansas Acad. Sci.* 23/24: 95–101.

Müller, J., et al. 2010. Homeotic effects, somitogenesis and the evolution of vertebral numbers in recent and fossil amniotes. *Proc. Natl. Acad. Sci. USA* 107: 2118–2123.

Nopcsa, F. and E. Heidsieck. 1934. Über eine pachyostotische Rippe aus der Kreide Rügens. *Acta Zoologica* 15: 431–455.

O'Keefe, F. R. O. and L. M. Chiappe. 2011. Viviparity and K-selected life history in a Mesozoic marine plesiosaur (Reptilia, Sauropterygia). *Science* 333 (12 August 2011): 870–873.

O'Keefe, F. R. O., et al. 2019. Ontogeny of polycotylid long bone microanatomy and histology. *Integr. Organismal Biol.* 1 (1): oby007.

O'Gorman, J. P., et al. 2017. Osteology of a perinatal aristonectine (Plesiosauria; Elasmosauridae). *Antarctic Sci.* 29: 61–72.

Ossa-Fuentes, L., et al. 2017. Microanatomy and osteohistology of a juvenile elasmosaurid plesiosaur from the Upper Maastrichtian of Marambio (Seymour) Island, Antarctica. *Bol. Mus. N. Hist. Natl. Chile* 66: 149–160.

Owen, R. 1840–1845. *Odontography. 2 vols.* London, H. Baillière.

Ricqlès, A. de. 1976. On bone histology of fossil and living reptiles, with comments on its functional and evolutionary significance. In *Morphology and Biology of Reptiles*, A. d'A. Bellairs and C. B. Cox eds., 123–150. London, Academic Press.

Ricqlès, A. de and V. de Buffrénil. 2001. Bone histology, heterochronies and the return of tetrapods to life in water: where are we? In *Secondary Adaptation of Tetrapods to Life in Water*, J.-M. Mazin and V. de Buffrénil eds., 289–310. Munich, Verlag Dr. Friedrich Pfeil.

Salgado, L., et al. 2007. Observaciones histologicas en reptiles marinos (Elasmosauridae y Mosasauridae) del Cretacico Tardio de Patagonia y Antartida. *Ameghiana* 44: 513–523.

Sander, P. M. 1988. A fossil reptile embryo from the Middle Triassic of the Alps. *Science* 239: 780–783.

Sander, P. M. 1999. *The Microstructure of Reptilian Tooth Enamel: Terminology, Function, and Phylogeny. Münchner geowissenschaftliche Abhandlungen*, Vol. 38, 1–102. Munich, Verlag Dr. Friedrich, Pfeil.

Sander, P. M. 2000. Long bone histology of the Tendaguru sauropods: Implications for growth and biology. *Paleobiology* 26: 466–488.

Sander, P. M., et al. 1997. A new pistosaurid (Reptilia: Sauropterygia) from the Middle Triassic of Nevada and its implications for the origin of plesiosaurs. *J. Vert. Paleontol.* 17: 526–533.

Sato, T., et al. 2005. Plesiosaurian remains from non-marine to paralic sediments. In *Dinosaur Provincial Park: A Spectacular Ancient Ecosystem Revealed*, P. J. Currie and E. B. Koppelhus eds., 249–276. Bloomington and Indianapolis, Indiana University Press.

Seitz, A. L. 1907. Vergleichende Studien über den mikroskopischen Knochenbau fossiler und rezenter Reptilien. *Nov. Acta Leopol.* 87: 230–370.

Soul, L. C. and R. B. J. Benson. 2017. Developmental mechanisms of macroevolutionary change in the tetrapod axis: a case study of Sauropterygia. *Evolution* 71: 1164–1177.

Stein, K. and E. Prondvai. 2014. Rethinking the nature of fibrolamellar bone: an integrative biological revision of sauropod plexiform bone formation. *Biol. Rev. Cambridge Philos. Soc.* 89: 24–47.

Street, H. P. and F. R. O. O'Keefe. 2010. Evidence of pachyostosis in the cryptocleidoid plesiosaur *Tatenectes laramiensis* from the Sundance Formation of Wyoming. *J. Vert. Paleontol.* 30: 1279–1282.

Werner, J. and E. M. Griebeler. 2014. Allometries of maximum growth rate versus body mass at maximum growth indicate that non-avian dinosaurs had growth rates typical of fast growing ectothermic sauropsids. *PLoS One* 9: e88834.

Wiffen, J., et al. 1995. Ontogenetic evolution of bone structure in Late Cretaceous Plesiosauria from New Zealand. *Geobios* 28: 625–640.

Wintrich, T., et al. 2017a. A Triassic plesiosaurian skeleton and bone histology inform on evolution of a unique body plan. *Sci. Adv.* 3: e1701144, 1–11.

Wintrich, T., et al. 2017b. Foramina in plesiosaur cervical centra indicate a specialized vascular system. *Foss. Rec.* 20: 279–290.

Wintrich, T., et al. 2019. Neck mobility in the Jurassic plesiosaur *Cryptoclidus eurymerus*: finite element analysis as a new approach to understanding the cervical skeleton in fossil vertebrates. *PeerJ* 7: e7658.

Zammit, M., et al. 2008. Elasmosaur (Reptilia: Sauropterygia) neck flexibility: implications for feeding strategies. *Comp. Biochem. Physiol. A* 150: 124–130.

VetBooks.ir

24

Ichthyosauria

P. Martin Sander

CONTENTS

Introduction 458
On Ichthyosaurs 458
Ichthyosaur Evolution 458
History of Research on Ichthyosaur Histology 459
Descriptions by Skeletal Region 459
Skull 459
Axial Skeleton 461
Vertebrae 461
Ribs and Gastralia 461
Appendicular Skeleton 461
Girdle Bones 461
Propodials 462
Lower Limb Bones 463
Ontogenetic Changes 463
Growth, Skeletochronology and Life History 463
Histomorphometry 464
Paleobiological and Evolutionary Implications 464
Conclusions 464
Acknowledgments 465
References 465

Introduction

On Ichthyosaurs

Ichthyosaurs are iconic marine reptiles that inhabited the Mesozoic seas from the Early Triassic to the early Late Cretaceous Cenomanian (Sander 2000, Motani 2005, 2009). Records from open marine sediments around the world from the Early Triassic to the mid-Cretaceous (Bardet et al. 2014) indicate that ichthyosaurs were clearly denizens of the open sea (pelagic). Among all Mesozoic marine reptiles, ichthyosaurs appear to have been the most pelagic: their remains have never been recorded from brackish or freshwater deposits, unlike those of the other major clade of Mesozoic marine reptiles, the sauropterygians, including the plesiosaurs.

Ichthyosaurs, especially the post-Triassic forms, the Neoichthyosauria, are instantly recognizable by their streamlined, fish-shaped body propelled through the water by a vertical fluke-like tail fin (Sander 2000, Motani 2005, 2009). The morphological convergence with dolphins is underscored by the small dorsal fin, not supported by any part of the skeleton, and the reduction or near loss of the hind fins. The fore fins served only in steering, as in dolphins and whales. Among the Triassic forms, more elongate body forms predominate that suggest swimming more like an eel than a dolphin. Jurassic ichthyosaurs were among the earliest large reptiles from the Mesozoic to become known to science: discoveries from Germany and England date to the middle of the 18th century. Ichthyosaur bone histology, and especially the histology of their teeth, also has a long history of study, and it had been recognized for some time that their bone histology was convergent in many respects with cetaceans (Buffrénil and Mazin 1990, Houssaye et al. 2016). Here I review the histology of ichthyosaur bones and discuss studies that have used ichthyosaur bone histology for inferences on lifestyle, metabolism, ecology, and evolution.

Ichthyosaur Evolution

Even the earliest records of ichthyosaurs come from open marine sediments, from localities scattered around the Northern Hemisphere, including Japan, South China, Thailand, Europe, Svalbard and western North America (Jiang et al. 2016). The age of these localities is roughly the same and postdates the devastating end-Permian extinction by only about 3 million

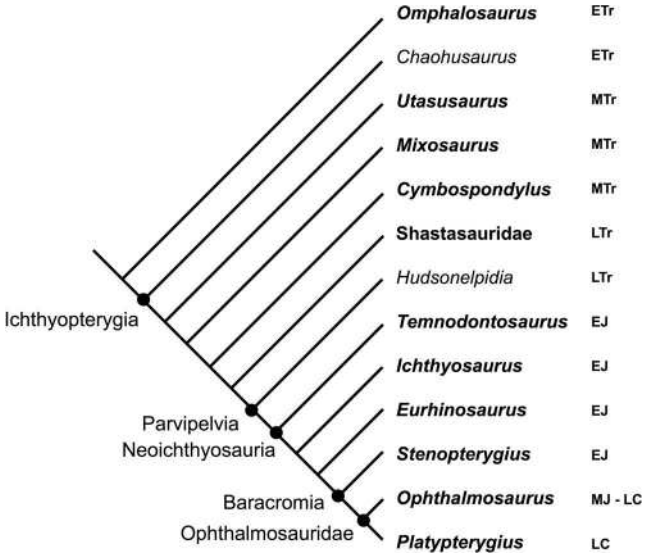


FIGURE 24.1 Simplified ichthyosaur phylogeny including temporal occurrence. Phylogeny based on Moon (2019). Taxa in bold have been sampled histologically. Abbreviations of geologic ages: EJ, Early Jurassic; ETr, Early Triassic; LC, Late Cretaceous; LTr, Late Triassic; MJ, Middle Jurassic; MTr; Middle Triassic.

years (middle Olenekian). As suggested by the stratigraphic record (Motani et al. 2017), ichthyosaurs evolved during this time period from terrestrial ancestors into obligatorily marine reptiles. An Olenekian Chinese ichthyosaur locality has even yielded a pregnant female (Motani et al. 2014). This indicates that even the oldest ichthyosaurs were live-bearing, a crucial adaptation of amniotes to the marine environment (Sander 2012). The basal grade of ichthyosaurs is small- and medium-sized forms such as *Utatsusaurus* and *Chaohusaurus* from the Early Triassic (Jiang et al. 2016, Moon 2019) as well as the probable ichthyosaur *Omphalosaurus*, which survived into the Middle Triassic (Figure 24.1). Next up the phylogenetic tree are the generally small-bodied and large-eyed mixosaurs and the medium- to large-bodied (>10 m) cymbospondylids. The former inhabited coastal waters and the latter the open ocean (Sander 2000). Together, these forms dominate the Middle Triassic faunas of China, Europe and Nevada, USA.

Late Triassic ichthyosaurs are generally poorly known but reached gigantic size (>20 m), only being surpassed by extant whales (Sander 2000, Motani 2005, 2009, Fischer et al. 2014) among marine amniotes. In the middle of the Late Triassic, the first parvipelvian ichthyosaurs, of the body plan so familiar from the Jurassic, evolved. Thus, diversity and disparity of ichthyosaurs was greatest during the Triassic, but the group did not fare well during the end-Triassic mass extinction; only the Neoichthyosauria survived (Figure 24.1). These became ever more adapted to a cruising pelagic lifestyle and deep diving, as indicated by their enormous eyes. This is reflected in the genus name *Ophthalmosaurus*, the namesake of a highly successful clade of Middle Jurassic to Early Cretaceous ichthyosaurs (Figure 24.1). The evolution of ichthyosaurs ends with a whimper, not a bang, because they disappeared in the early Late Cretaceous (Fischer et al. 2016), unlike the other major clades of marine reptiles, the plesiosaurs and mosasaurs, which became extinct near or at the very end of the Cretaceous in the latest Maastrichtian (Bardet et al. 2014).

History of Research on Ichthyosaur Histology

Given that ichthyosaurs were among the first fossil reptiles for which the skeleton became completely known (De la Beche and Conybeare 1821), many decades before the dinosaurs, it is perhaps surprising that only recently has ichthyosaur histology been studied intensively (Figure 24.1). Although Quekett (1855) figured and discussed ichthyosaur bone histology and Kiprijanoff (1881) published lavish lithographs of microscopic images providing astonishing detail, also of ichthyosaur tooth histology, the study of ichthyosaur bone histology lagged behind that of archosaurs, in particular dinosaurs. As for all major amniote taxa, ichthyosaur bone histology was illustrated and discussed in the comparative studies of Seitz (1907), Gross (1934), Enlow and Brown (1957) and Ricqlès (1976). Naturally, as least since Ricqlès' early work, the question of how aquatic adaptation influenced ichthyosaur histology has attracted serious attention (Buffrenil and Mazin 1990, Ricqlès and Buffrenil 2001, Houssaye 2013, Houssaye et al. 2016, 2018). In particular, the work by Buffrenil (Buffrenil and Schoevaert 1988, Buffrenil and Mazin 1990) has been important in understanding this relationship. Since then, several papers have dealt with ichthyosaur histology, as compiled by Anderson et al. (2019) and reviewed below. Three studies stand out among these for having sampled comprehensively across the skeleton: Kolb et al. (2011) on *Mixosaurus*, Nakajima et al. (2014) on *Utatsusaurus*, and Anderson et al. (2019) on *Stenopterygius*. The broadest comparative approach across taxa was taken by Houssaye et al. (2014) for the limbs and Houssaye et al. (2018) for the vertebrae.

Descriptions by Skeletal Region

Skull

Knowledge of the histology of the skull bones of ichthyosaurs is relatively scanty, as for many tetrapod clades. Ichthyosaurian tooth histology, on the other hand, has been studied extensively and for a long time (Owen 1840–1845, Kiprijanoff 1881, Sander 1999, Scheyer and Moser 2011, Anderson et al. 2019) but details are beyond the scope of this review. Suffice it to say that ichthyosaur dental histology is more unusual than their bone histology because of the plicidentine of ichthyosaurs. Plicidentine refers to the deep infolding of the dentine toward the pulp cavity. This tissue type is a synapomorphy of Ichthyosauria (Maxwell et al. 2012) but is also found in varanid lizards and temnospondyl amphibians among tetrapods. Further data on and illustrations of ichthyosaur tooth histology, including plicidentine, may be found in Besmer (1947), Sander and Faber (2003), Massare et al. (2011) and, especially, Maxwell et al. (2012).

Among the most informative studies of ichthyosaurian skull histology is that by Anderson et al. (2019) who sampled the rostral portions of the premaxilla and dentary. They noted the presence of radial to reticular fibrolamellar bone tissue. As seen in their figures (figure 2A, C), the fibrolamellar bone has

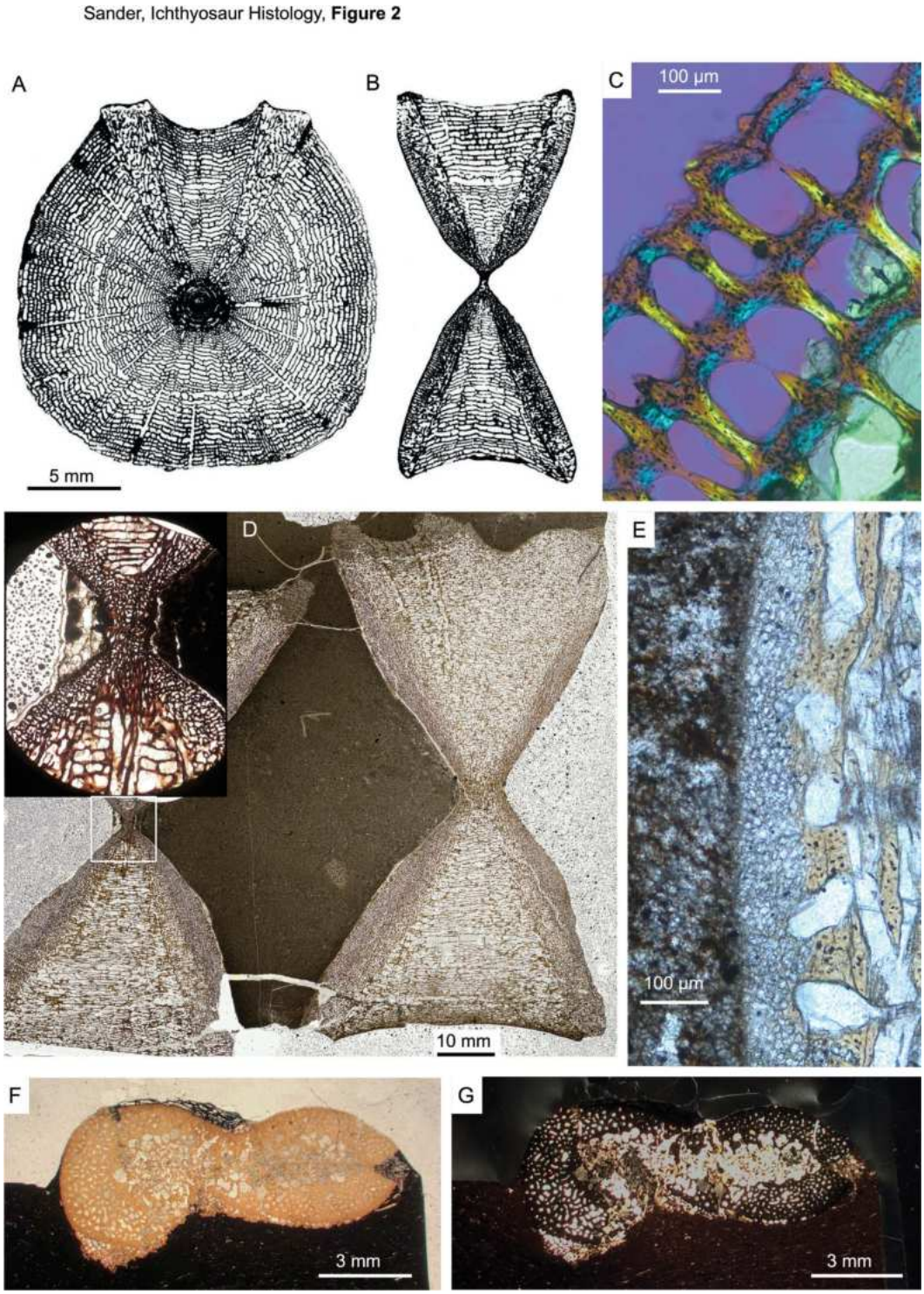


FIGURE 24.2 Microanatomy and histology of ichthyosaur vertebrae and ribs. A–C, cf. *Stenopterygius* sp. SMNS uncat., centrum of juvenile cervical vertebra, Posidonienschiefer Formation, Holzmaden area, Germany. A, Transverse section. B, Sagittal section rendered as black and white to show porosity. Note the regular arrangement of the trabeculae and the single, distinctive growth mark. C, Transverse section, primary cancellous bone of periosteal origin in cross-polarized light with lambda filter. D, cf. *Cymbospondylus* IGPB R 660, Vikinghøgda Formation, Early Triassic, Svalbard, Norway. Two articulated posterior dorsal vertebral centra, sagittal section. Note the proportions of the centrum; they are much taller than long, and have limited contribution from the perichondral domain, as in all later ichthyosaurs. E, *Stenopterygius* sp. IGPB R 661, Posidonienschiefer Formation, Holzmaden, Germany. Sagittal section, peripheral region of anterior articular surface of an anterior dorsal vertebral centrum. Note the anteroventrally directed files of cartilage cells. F and G, *Stenopterygius* sp. IGPB uncat, Posidonienschiefer Formation, Holzmaden area, Germany. Section from middle dorsal rib at midshaft. F, Normal light. Note the strong vascularization with longitudinal canals and the cancellous medullary region. G, Same in cross-polarized light, emphasizing the patterns of vascularization. IGPB, Section Paleontology, Institute of Geosciences, University of Bonn, Germany; SMNS, State Museum of Natural History, Stuttgart, Germany.

VetBooks.ir

completely filled in primary osteons, approaching the osteosclerotic condition. Similarly dense rostra are also known from ziphiid whales, in particular (Lambert et al. 2011). The rostral bones show a low number of growth marks, described as annuli by Anderson et al. (2019). There is little remodeling of this primary bone, but resorption bays produce a medullary region. Although Kiprijanoff (1881) provided extensive section images of *Platypterygius* sp. skull bones, these images are not informative, unlike those of the dental histology.

Axial Skeleton

Vertebrae

The histology of the vertebrae of ichthyosaurs has attracted much attention because of the distinctive disk-like, amphicoelous centra. In thin section, the amphicoelous shape can be seen to result from relatively fast peripheral apposition of the periosteal cortex combined with little endochondral growth in an axial direction (Figure 24.2). There is no cone of endochondral bone, only a thin layer covering the articular surfaces between the centra (e.g., Houssaye et al. 2018). This thin layer of endochondral bone is often covered by an even thinner layer of fossilized cartilage (e.g., Houssaye et al. 2018, Anderson et al. 2019, Wintrich et al. 2020) (Figure 24.2). This pattern of limited endochondral tissue formation is seen in the earliest-branching ichthyosaurs, although their centra are plesiomorphically longer than high, and the trabeculae are coarser and less organized. Disk-shaped centra first originated in mixosaurs and are correlated with finer trabeculae. This general internal structure of the centra remains the same throughout ichthyosaurian evolution (still seen in *Platypterygius*: Kiprijanoff's 1881 plate 11, Lopuchowycz and Massare 2002). The boundaries between the periosteal and endochondral domains persist throughout life despite extensive remodeling (Houssaye et al. 2018). Distinctive Sharpey's fibers run roughly parallel to this boundary in the periosteal bone. These fibers probably indicate the insertion of intervertebral ligaments.

Importantly, all known ichthyosaur centra so far lack a thick cortex but show cancellous bone (>50% porosity) throughout, and the trabeculae parallel the periosteal surface to varying degrees (Figure 24.2). Fetal and juvenile specimens, even of Middle Triassic ichthyosaurs, indicate that the cancellous bone in the periosteal domain is of primary origin (Figure 24.2C). Later in ontogeny, the primary cancellous bone is replaced by secondary trabeculae without an appreciable change in trabecular architecture (Houssaye et al. 2018). The secondary trabeculae consist of lamellar bone, whereas the primary ones have a woven bone matrix and plump osteocytes, indicating rapid apposition (Houssaye et al. 2018). The longitudinal orientation of the trabeculae is also seen in other pelagic amniotes and results from the pattern of loading of the bones (Dumont et al. 2013). A special case appears to be represented by *Omphalosaurus,* which shows very loose trabeculae (Sander and Faber 2003), often leading to poor preservation of the entire bone (Ekeheien et al. 2018) because of trabecular collapse. Note that some limb material from the Lower Triassic of Svalbard was previously assigned to *Omphalosaurus* and investigated histologically under this assignment (Buffrénil et al. 1987), but this material is now assigned to the genus *Pessopteryx* (Houssaye et al. 2014, Ekeheien et al. 2018).

Ribs and Gastralia

Ribs are the elements most available for histological study and are most easily processed into thin sections. However, a common problem with published histological work on ribs is that sampling location along the rib shaft was not known or not recorded, even in recent studies (e.g., Talevi et al. 2012). However, when ribs are systematically sampled along their length, considerable microanatomical and histological variation becomes apparent, and ichthyosaurs are no exception. Anderson et al. (2019) (on *Stenopterygius*) showed that rib microanatomy is most homogeneous in the proximal section, and that coarse trabeculae of secondary origin dominates the sections. This is seen in a *Cymbospondylus* section located close to the rib head (Sander and Faber 2003). In the middle of the shaft of the *Stenopterygius* rib (Figure 24.2F, G), there is a central medullary region set off from a fairly thick cortex, which in the distal rib becomes thin and surrounds a large medullary region (Anderson et al. 2019). The same pattern was observed in the basal ichthyosaur *Utatsusaurus* and described in detail by Nakajima et al. (2014). On the other hand, *Omphalosaurus* ribs lack a cortex along their entire length and show the same very loose trabeculae as the vertebrae of this taxon (Sander and Faber 2003).

Talevi and Fernández (2012) described a sample from a proximal rib of the ophthalmosaurid *Mollesaurus* and compared it to a rib of the related *Caypullisaurus*. The *Mollesaurus* sample shows a dense microanatomy with a distinct cortex, whereas the *Caypullisaurus* sample is cancellous. The results of Talevi and Fernández (2012) and their inference that *Mollesaurus* ribs reflect bone mass increase are difficult to evaluate because the *Caypullisaurus* sample could simply have come from the distal part of the rib. Similarly, the dorsal rib samples from two adult and one juvenile of *Caypullisaurus* described by Talevi et al. (2012) are not localized along the rib, making the observation that they are entirely cancellous with a large open medullary cavity difficult to evaluate in a comparative context.

Gastralia have been little studied in ichthyosaurs. Kolb et al. (2011) figured nearly avascular gastralia in *Mixosaurus* with distinct growth lines. Anderson et al. (2019) reported dense parallel-fibered bone with some secondary trabeculae in the center but no growth marks in *Stenopterygius*.

Appendicular Skeleton

Girdle Bones

Girdle bone histology has not been studied extensively in ichthyosaurs. The few reports available (Kolb et al. 2011, Pardo-Perez et al. 2018, Anderson et al. 2019) are from mixosaurs, *Stenopterygius*, and *Eurhinosaurus*. In *Mixosaurus*, the scapula and the ischium were sampled by Kolb et al. (2011). Both bones show the same pattern as the ribs, which is an originally dense cortex of first fibrolamellar and then lamellar-zonal bone transformed into secondary cancellous bone.

In the ischiopubis of *Stenopterygius*, there is only a thin cortical layer of woven bone, and most of the section consists of secondary cancellous bone (Anderson et al. 2019). However, the thin cortex may be an artifact of sectioning because the ischiopubis was not sampled at midshaft but at the ends. In *Eurhinosaurus* there also remains a distinction between a thick cortex set off distinctly from the center of the cancellous bone (Pardo-Perez et al. 2018), similar to what is seen in terrestrial amniote scapulae.

Propodials

Among propodials, the humerus has been studied extensively in ichthyosaurs (Buffrénil et al. 1987, Buffrenil and Mazin 1990, Kolb et al. 2011, Houssaye et al. 2014, Nakajima et al. 2014, Anderson et al. 2019), with a focus on the basal *Utatsusaurus* and *Mixosaurus* and classical Jurassic neoichthyosaur taxa (Figure 24.3). Basal merriamosaur histology is poorly described for the limb bones. The broadest sample is that of Houssaye et al. (2014). The femur has received much

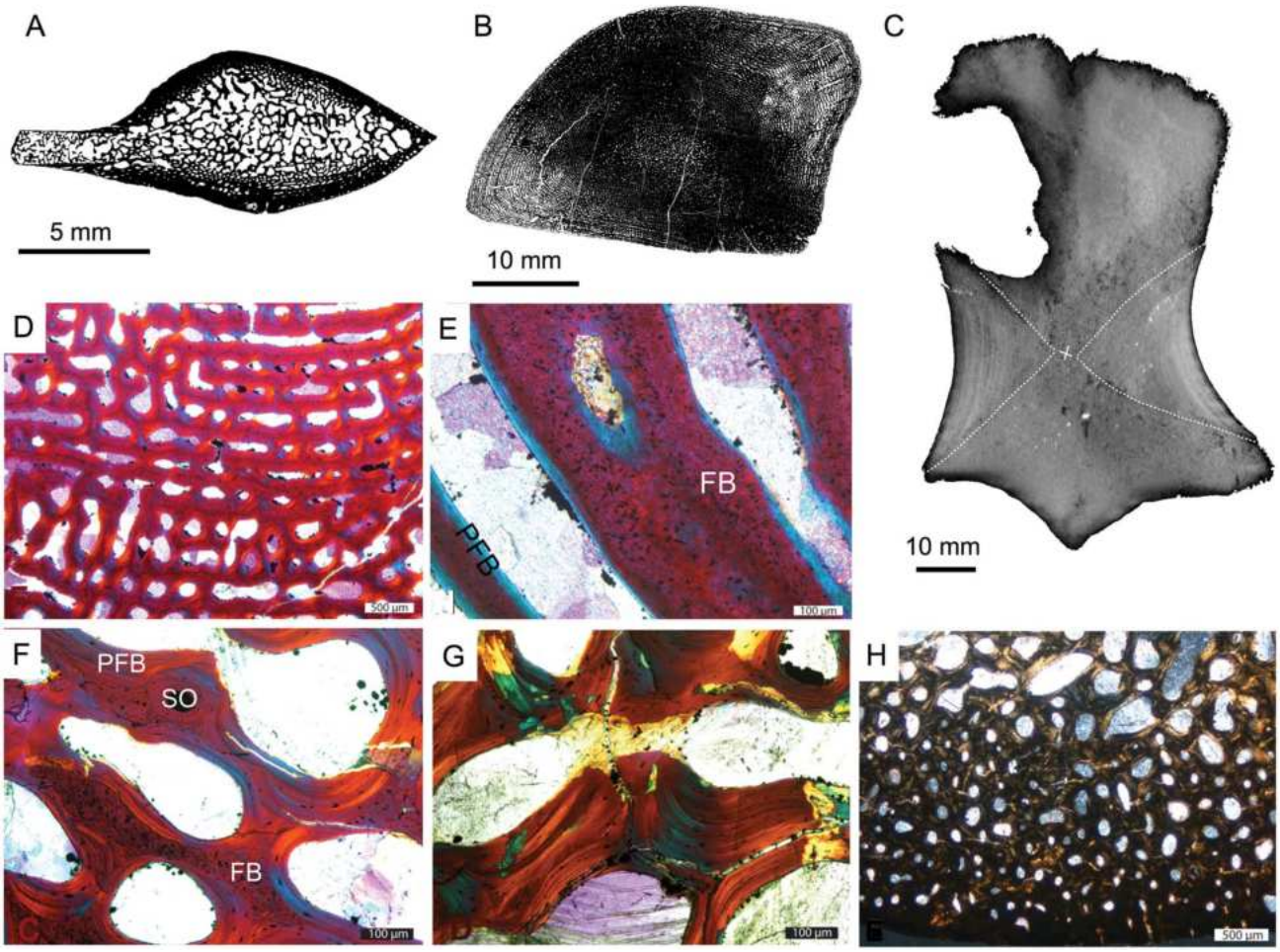


FIGURE 24.3 Microanatomy and histology of ichthyosaur humeri, modified from Houssaye et al. (2014). A, *Mixosaurus* sp. (PIMUZ T 2046, Besano Formation, Middle Triassic, Monte San Giorgio, Switzerland). Humerus midshaft section. Black and white rendering of the microanatomy. Note that the initially compact cortex is turned into cancellous bone by remodeling. B, *Ichthyosaurus* sp. (SMNS uncat., Lower Jurassic, Lyme Regis, Dorset, England). Humerus midshaft section. Black and white rendering of the microanatomy. The section consists of primary cancellous bone, lacking a distinction between cortex and cancellous central regions. C, *Ophthalmosaurus* sp. (ULg 2013-11-19, Kimmeridgian, Dorset, England). Virtual longitudinal sections in the dorsoventral plane produced by CT scanning of the humerus. The dotted lines indicate the boundary between the osseous tissues of periosteal (left to right) and endochondral (top to bottom) origin. Note the growth marks in the primary periosteal bone. The cross indicates the point of origin of growth. D and E, *Ichthyosaurus* sp. (IGPB R222, Lower Jurassic, Lyme Regis, Dorset, England). Thin sections of outer cortex in cross-polarized light with lambda filter. D, Primary fibrolamellar bone, note the laminar organization. E, Dominant primary fibrous bone in the osseous trabeculae. F and G, *Stenopterygius* (SMNS uncat., Posidonienschiefer Formation, Holzmaden area, Germany). F, Trabeculae located slightly away from the bone periphery; note the remains of primary fibrous bone and the secondary lamellar and parallel-fibered bone; G, Central region of section; the trabeculae are entirely secondary in origin. H, *Ichthyosaurus* sp. (SMNS uncat., Lower Jurassic, Lyme Regis, Dorset, England). Dense secondary osteons with large vascular canals in the core of the section. FB, fibrous bone; IGPB, Section Paleontology, Institute of Geosciences, University of Bonn, Germany. PFB, parallel-fibered bone; PIMUZ, Paleontological Institute and Museum, University of Zurich, Switzerland; SMNS, State Museum of Natural History, Stuttgart, Germany; SO, secondary osteon; ULg: Palaeontological Collections, Université de Liège, Belgium.

VetBooks.ir

less attention (Buffrénil et al. 1987, Buffrénil and Mazin 1990, Kolb et al. 2011, Houssaye et al. 2014), probably because it is much smaller than the humerus in many (particularly the parvipelvian) ichthyosaurs. Virtually all sections of propodials described in this literature are cross sections at midshaft. The exception is the serial sections of the early ichthyosaur *Pessopteryx* studied by Buffrénil et al. (1987). The humeri of the basal ichthyosaurs *Utatsusaurus* and *Mixosaurus* have a similar histology in that there is a cortex of first fibrolamellar and then parallel-fibered bone, which is quickly resorbed and remodeled into secondary trabeculae, as described for the ribs and girdle bones of these taxa. However, the largest specimen in the study by Kolb et al. (2011) does not fit this pattern in that it shows distinctive radial vascular canals and lacks growth marks (Kolb et al. 2011; Figure 24.3D). These features suggest much faster growth than in the other specimens. The femur of *Pessopteryx* studied by Buffrénil et al. (1987) has primary cancellous periosteal bone but not much remodeling into secondary trabeculae. This is also seen in a zeugopodial element of the same taxon (Houssaye et al. 2014) and thus is probably not an ontogenetic feature.

There is no real medullary cavity in any ichthyosaur long bone (Figure 24.3). Using the three-front model of Mitchell and Sander (2014) for periosteal bone shafts, the remodeling front in ichthyosaur propodials closely follows the apposition front, whereas the resorption front was extremely slow. The ontogenetic end result is an entirely cancellous cross section. This concept is already implicit in the study of Buffrenil and Mazin (1990) where the same pattern was described for the neoichthyosaurs *Stenopterygius* and *Ichthyosaurus.* In younger individuals of these taxa, the primary bone consists of cancellous woven bone, which later in ontogeny changes to more compact woven bone, which then is turned into secondary trabeculae as described above. In general, this pattern was also found in other neoichthyosaurs such as *Temnodontosaurus* and *Ophthalmosaurus* as well as in further specimens of *Stenopterygius* and *Ichthyosaurus* by Houssaye et al. (2014) (Figure 24.3). However, the larger sample base revealed that in these taxa the primary cortex is already formed as cancellous bone consisting of woven bone tissue and is not the result of remodeling. In addition, this primary cancellous tissue shows cyclical growth, as already had been noted for *Pessopteryx* (Buffrénil and Mazin 1990). Femoral histology is essentially the same as humerus histology in neoichthyosaurs (Houssaye et al. 2014) but not in *Mixosaurus*. The midshaft cross section of this taxon is round, and there is a distinct cortex of lamellar-zonal bone sharply set off from the medullary region filled in by loose secondary trabeculae (Kolb et al. 2011).

Lower Limb Bones

Limb bones other than propodials have not been studied in a systematic fashion in ichthyosaurs, but a number of isolated data points covering a range of bones and ontogenetic stages exist. In general, lower limb bones, including phalanges, follow the same pattern as the propodials. Basal ichthyosaurs have secondary cancellous bone replacing primary woven and parallel-fibered compact bone (e.g., in *Mixosaurus,* Kolb et al. 2011) but neoichthyosaurs have uniformly cancellous bone, some of which is primary. Importantly, however, all bones distal to the propodials have an incomplete shaft of periosteal bone, described as a loss of perichondral bone by Caldwell (1997a, b). This loss is seen in cymbospondylids and more derived ichthyosaurs, in which the zeugopodials, metapodials and phalanges are dorsoventrally flattened and form a tight mosaic in the flippers together with the mesopodials (carpals, respectively, tarsals). These bones thus consist of a dorsal and ventral plate of periosteal bone with endochondral bone sandwiched in between and forming the periphery of the elements. Only in basal forms such as *Chaohusaurus* do the flipper bones retain their morphological identity, which becomes increasingly lost in evolution (Caldwell 1997a, b, Sander 2000, Motani 2009).

Ontogenetic Changes

Only a single growth series has been sampled for any ichthyosaur, that of *Mixosaurus* (Kolb et al. 2011); however, the largest specimen in the series may belong to a different taxon (see above). Mention of ontogenetic change is frequent in the literature, beginning with Kiprijanoff (1881) who noted differences between juveniles and adults. In vertebral centrum microanatomy, fetus and early juveniles show primary cancellous bone, whereas subadults and adults show secondary cancellous bone but retain essentially the same trabecular arrangement as laid out in the primary bone (Houssaye et al. 2018). The rib of the juvenile *Caypullisaurus* studied by Talevi et al. (2012) shows primary cancellous bone with a clearly offset medullary cavity, whereas the two adult individuals show secondary cancellous bone. As noted, these observations are difficult to evaluate. Primary cancellous bone theoretically could still be found at the growing tip of a nearly fully grown ichthyosaur, whereas closer to the head, the ribs might consist entirely of secondary cancellous bone (see Waskow and Sander (2014) on sauropod ribs).

In long bones of basal ichthyosaurs and some neoichthyosaurs, the juveniles are reported to have laid down fibrolamellar bone followed by parallel-fibered bone in the adults (Kolb et al. 2011, Houssaye et al. 2018). The ontogenetic coverage of ichthyosaur histology is currently insufficient to define histologic ontogenetic stages as opposed to sauropods (Klein and Sander 2008) and plesiosaurs (Chapter 23). Patterns of secondary remodeling have not been studied systematically in ichthyosaurs either, and dense Haversian bone has not been reported. This probably is because any primary cortical bone ontogenetically turned into secondary cancellous bone, precluding the development of dense secondary osteons.

Growth, Skeletochronology and Life History

A cursory consideration of the primary cortical histology of ichthyosaurs reveals three features typically associated with fast growth (Cubo et al. 2008): fibrolamellar bone, sometimes with radial vascular canals; a high density of osteocyte lacunae and preponderance of isometric (“plump”) osteocyte lacunae (Houssaye et al. 2014, 2018, Nakajima et al. 2014).

VetBooks.ir

In addition, a low number of growth marks relative to the size of the animal also hints at fast growth, particularly in neoichthyosaurs, as seen in the rostrum of *Stenopterygius* (Anderson et al. 2019).

In general, skeletochronology in ichthyosaurs has not been possible so far because of the lack of any bone preserving a good growth record. This is probably due to the scarcity of primary compact bone in the ichthyosaur skeleton. In basal ichthyosaurs, this bone type is quickly replaced by secondary cancellous bone and in more derived ichthyosaurs, all primary bone is cancellous, except the bones of the rostrum. Although there is cyclical growth in the humeral and femoral primary periosteal cancellous bone (Buffrénil et al. 1987, Houssaye et al. 2014), the cycles are usually too indistinct in the Jurassic taxa to give reliable skeletochronological ages (Houssaye et al. 2014). Basal ichthyosaurs apparently grew more slowly, and growth marks in the gastralia of a medium-sized *Mixosaurus* suggest an age of 14 years at the time of death (Kolb et al. 2011). A neonatal line has not been described for any ichthyosaur.

Because of the abundant pregnant specimens of *Stenopterygius*, it is possible to determine when sexual maturity occurred, which is well before skeletal maturity (Anderson et al. 2019). In fact, *Stenopterygius* is by far the most abundant ichthyosaur (with over 3000 specimens excavated; Anderson et al. 2019) and seemingly would offer an exceptional sample for histologic study of life history parameters.

Histomorphometry

Evolutionary changes in bone density connected to secondary aquatic adaptation have long been a focus of paleohistologists (see Houssaye et al. 2016 for a recent review). The first study to deal extensively with this issue was by Buffrénil and Mazin (1990) who hypothesized that the cancellous bone of ichthyosaur centra and long bones represents a case of bone mass decrease as an adaptation to the aquatic environment. However, quantification of bone compactness (Houssaye et al. 2014, 2018) indicates that there is no decrease in bone mass but a reorganization of the bone from the compact cortex and medullary cavity of terrestrial taxa to an even network of trabeculae, both in the long bones (Houssaye et al. 2014) and in the centra (Houssaye et al. 2018). Similarly, the limb bone microanatomy and histology of merriamosaurian ichthyosaurs shows this evolutionary redistribution, even leading to a very dense bone in some taxa. The original hypothesis of Buffrénil and Mazin (1990) appears to posit that the cancellous composition of the long bones resulted from the immediate remodeling of the primary cortical bone to trabeculae only in the basal *Utatsusaurus* and *Mixosaurus* but not in more derived ichthyosaurs, which have primary cancellous bone. In *Mixosaurus*, this process of remodeling was well documented by Kolb et al. (2011) for most bones of the skeleton, including a girdle bone (ischium) and limb bones. The humerus, however, as the largest bone in the *Mixosaurus* skeleton, shows a primary cortex that is nearly cancellous with very large vascular spaces (Kolb et al. 2011) that are then turned into a loose trabecular network by remodeling.

To date there is no convincing evidence for bone mass increase in the ichthyosaur postcranial skeleton; the description of a relatively dense rib cortex in the Middle Jurassic ophthalmosaurid *Mollesaurus* (Talevi and Fernández 2012) is not tenable in light of the results by Anderson et al. (2019). However, some ichthyosaur humeri appear rather dense (Houssaye et al. 2014) and are approaching the osteosclerotic condition, as does the rostrum of the common Lower Jurassic ichthyosaur *Stenopterygius* (Anderson et al. 2019)

Paleobiological and Evolutionary Implications

The presence of fibrolamellar bone even in the earliest and most basal ichthyosaurs sampled, i.e., *Utatsusaurus*, indicates fast growth and has generally been interpreted to reflect the endothermic physiology of ichthyosaurs (Buffrénil and Mazin 1990, Kolb et al. 2011, Nakajima et al. 2014, Anderson et al. 2019). A high basal metabolic rate has also been inferred for neoichthyosaurs based on how their body shape adapted to cruising in the open ocean (Buffrénil and Mazin 1990, Motani 2010) and is also supported by evidence from stable isotope geochemistry (Bernard et al. 2010).

The cancellous bone of ichthyosaurs is seen in other clades of highly marine amniotes such as plesiosaurs, marine turtles and cetaceans (Buffrénil and Mazin 1990, Houssaye 2013, Houssaye et al. 2016). Its presence suggests that ichthyosaurs had a pelagic lifestyle similar to these other clades. The small red blood cells recently reported by Plet et al. (2017) are inconsistent with such a pelagic lifestyle (see discussion in Chapter 23).

The evolutionary success of ichthyosaurs during the Triassic can be partially ascribed to the strong aquatic adaptation and endothermy, which allowed rapid dispersal around the globe by the Early Triassic (Bardet et al. 2014). Ichthyosaurian diversity and disparity remained high throughout the Triassic, but the clade appears to have been hard-hit by the end-Triassic extinctions (Thorne et al. 2011, Fischer et al. 2014), and only the streamlined fish-shaped Neoichthyosauria survived. Evidence from bone histology is unable to explain the pattern of early extinction of the clade in the early Late Cretaceous, however.

Conclusions

This review of ichthyosaur bone histology finds consistent patterns in histology and its evolutionary change:

1. Ichthyosaur bones, except skull bones, are generally cancellous and lack a thick cortex.
2. Cancellous bone is both primary fibrolamellar bone and secondary, resulting from remodeling.
3. Lack of compact bone explains the lack of Haversian bone.
4. Ichthyosaur bone compactness and microanatomy is similar to that of other aquatic amniotes.

5. Patterns of variation among skeletal elements result from differences in local bone apposition rate.
6. Skeletochronology is difficult to apply in ichthyosaurs because they lack compact bone.
7. Evolutionary trends are evident from basal taxa to Neoichthyosauria, but incomplete sampling of intermediate Triassic forms currently precludes a comprehensive evolutionary narrative.
8. Abundance of fibrolamellar bone indicates rapid growth and suggests endothermy.
9. Future work should aim at a more continuous coverage of ontogenetic series and phylogeny.

Acknowledgments

As in most histological studies, we are deeply indebted to the curators who facilitated consumptive sampling of material under their care. This review benefited greatly from discussions with Alexandra Houssaye (Paris), Yasuhisa Nakajima (Tokyo), Nicole Klein (Bonn), and Tanja Wintrich (Bonn). I also thank the editors for inviting me to write this review and for helpful suggestions and editing. Funding was provided by DFG research grant 388659338 to PMS.

REFERENCES

Anderson, K. L., et al. 2019. Skeletal microstructure of *Stenopterygius quadriscissus (Reptilia, Ichthyosauria) from* the Posidonienschiefer (Posidonia Shale, Lower Jurassic) of Germany. *Palaeontology* 62: 433–449.

Bardet, N., et al. 2014. Mesozoic marine reptile palaeobiogeography in response to drifting plates. *Gondwana Res.* 26: 869–887.

Bernard, A., et al. 2010. Regulation of body temperature by some Mesozoic marine reptiles. *Science* 328: 1379–1382

Besmer, F. 1947. Die Triasfauna der Tessiner Kalkapen VI. Beiträge zur Kenntnis des Ichthyosauriergebisses. *Schweizerische Palaeontol. Abh.* 65:1–21.

Buffrénil, V. de and J.-M. Mazin. 1990. Bone histology of the ichthyosaurs: comparative data and functional interpretation. *Paleobiology* 16 (4): 435–447.

Buffrénil, V. de and D. Schoevaert. 1988. On how the periosteal bone of the delphinid humerus becomes cancellous: ontogeny of a histological specialization. *J. Morphol.* 198: 149–164.

Buffrénil, V. de, et al. 1987. Caractères structuraux et mode de croissance du fémur d´*Omphalosaurus nisseri*, Ichthyosaurien du trias moyen de Spitsberg. *Ann. Paléont.* 73: 195–216.

Caldwell, M. W. 1997a. Modified perichondral ossification and the evolution of the paddle-like limbs in ichthyosaurs and plesiosaurs. *J. Vert. Paleontol.* 17: 534–547.

Caldwell, M. W. 1997b. Limb ossification patterns of the ichthyosaur Stenopterygius and a discussion of the proximal tarsal row of ichthyosaurs and other neodiapsid reptiles. *Zool. J. Linn. Soc.* 120: 1–25.

Cubo, J., et al. 2008. Phylogenetic, functional, and structural components of variation in bone growth rate of amniotes. *Evol. Dev.* 10: 217–277.

De la Beche, H. and W. Conybeare. 1821. Notice of the discovery of a new fossil animal, forming a link between the ichthyosaurs and crocodile, together with general remarks on the osteology of the *Ichthyosaurus*. *Geol. Soc. Lond.* 5: 559–594.

Dumont, M., et al. 2013. Inner architecture of vertebral centra in terrestrial and aquatic mammals: a two-dimensional comparative study. *J. Morphol.* 274: 570–584.

Ekeheien, C. P., et al. 2018. Preliminary report on ichthyopterygian elements from the Early Triassic (Spathian) of Spitsbergen. *Norw. J. Geol.* 98: 219–237.

Enlow, D. H. and S. O. Brown. 1957. A comparative histological study of fossil and recent bone tissues. Part II. *Texas J. Sci.* 9: 186–214.

Fischer, V., et al. 2014. Ichthyosaurs from the French Rhaetian indicate a severe turnover across the Triassic–Jurassic boundary. *Naturwissenschaften* 101: 1027–1040.

Fischer, V., et al. 2016. Taxonomy of *Platypterygius campylodon* and the diversity of the last ichthyosaurs. *PeerJ* 4: e2604.

Gross, W. 1934. Die Typen des mikroskopischen Knochenbaues bei fossilen Stegocepahlen und Reptilien. *Z. Anat. Entwicklungsgesch.* 203: 731–764.

Houssaye, A. 2013. Bone histology of aquatic reptiles: what does it tell us about secondary adaptation to an aquatic life? *Biol. J. Linn. Soc.* 108: 3–21.

Houssaye, A., et al. 2014. A new look at ichthyosaurian long bone microanatomy and histology: Implications for their adaptation to an aquatic life. *PLoS One* 9 (4): e95637.

Houssaye, A., et al. 2016. Adaptive patterns in aquatic amniote bone microanatomy - More complex than previously thought. *Integr. Comp. Biol.* 56: 1349–1369.

Houssaye, A., et al. 2018. Structural, functional, and physiological signals in ichthyosaur vertebral centrum microanatomy and histology. *Geodiversitas* 40: 161–170.

Jiang, Da-Y., et al. 2016. A large aberrant stem ichthyosauriform indicating early rise and demise of ichthyosauromorphs in the wake of the end-Permian extinction. *Sci. Rep.* 6: 26232.

Kiprijanoff, W. 1881. Studien über die fossilen Reptilien Russlands I. Theil Gattung *Ichthyosaurus* König aus dem severischen Sandstein oder Osteolith der Kreide-Gruppe. *Mém. Acad. Imper. Sci. St. Petersbourg, VIIe Sér.* 28: 1–103.

Klein, N. and P.M. Sander. 2008. Ontogenetic stages in the long bone histology of sauropod dinosaurs. *Paleobiology* 34: 247–263.

Kolb, C., et al. 2011. The palaeohistology of the basal ichthyosaur *Mixosaurus* (Ichthyopterygia, Mixosauridae) from the Middle Triassic: Palaeobiological implications. *C. R. Palevol.* 10: 403–411.

Lambert, O., et al. 2011. Hyperdense rostral bones of ziphiid whales: diverse processes for a similar pattern. *C. R. Palevol* 10: 453–468.

Lopuchowycz, V. B. and J. A. Massare. 2002. Bone microstructure of a Cretaceous ichthyosaur. *Paludicola* 3: 139–147.

Massare, J. A., et al. 2011. Tooth histology in the Cretaceous ichthyosaur *Platypterygius australis* and its significance for the conservation and divergence of mineralized tooth tissues in amniotes. *J. Morphol.* 272: 129–135.

Maxwell, E. E, et al. 2012. Tooth histology attachment, and replacement in the Ichthyopterygia reviewed in an evolutionary context. *Paläontol. Zeitschr.* 86: 1–14.

VetBooks.ir

Mitchell, J. and P. M. Sander. 2014. The three-front model: a developmental explanation of long bone diaphyseal histology of Sauropoda. *Biol. J. Linn. Soc. Lond.* 112: 765–781.

Moon, B. 2019. A new phylogeny of ichthyosaurs (Reptilia: Diapsida). *J. Syst. Palaeontol.* 17: 1–27.

Motani, R. 2005. Ichthyosauria: evolution and physical constraints of fish-shaped reptiles. *Ann. Rev. Earth Planet. Sci* 33: 395–420.

Motani, R. 2009. The evolution of marine reptiles. *Evol. Educ. Outreach* 2: 224–235.

Motani, R. 2010. Warm-blooded "sea dragons"? *Science* 328 (5984): 1361–1362.

Motani, R., et al. 2014. Terrestrial origin of viviparity in Mesozoic marine reptiles indicated by Early Triassic embryonic fossils. *PLoS One* 9: e88640.

Motani, R., et al. 2017. Pre- versus post-mass extinction divergence of Mesozoic marine reptiles dictated by time-scale dependence of evolutionary rates. *Proc. R. Soc. B* 284: 20170241.

Nakajima, Y., et al. 2014. Osteohistology of *Utatsusaurus hataii* (Reptilia: Ichthyopterygia): Implications for early ichthyosaur biology. *Acta Palaeontol. Pol.* 59: 343–352.

Owen, R. 1840–1845. *Odontography. 2 vols*. London, H. Baillière.

Pardo-Perez, J. M., et al. 2018. Ichthyosaurian palaeopathology: evidence of injury and disease in fossil 'fish-lizards'. *J. Zool.* 304: 21–33.

Plet, C., et al. 2017. Palaeobiology of red and white blood cell-like structures, collagen and cholesterol in an ichthyosaur bone. *Sci. Rep.* 7: 13776.

Quekett, J. 1855. *Descriptive and illustrated catalogue of the histological series contained in the museum of the Royal College of Surgeons of England: Structure of the skeleton of vertebrate animals. Vol. 2*. London, R. & J. E. Taylor.

Ricqlès, A. de. 1976. On bone histology of fossil and living reptiles, with comments on its functional and evolutionary significance. In *Morphology and Biology of Reptiles*, A.d'A. Bellairs and C.B. Cox eds., 123–150. London, Academic Press.

Ricqlès, A. de and V. de Buffrénil. 2001. Bone histology, heterochronies and the return of tetrapods to life in water: Where are we? In *Secondary Adaptation of Tetrapods to Life in Water*, J.-M. Mazin and V. de Buffrénil eds., 289–310. Munich, Verlag Dr. Friedrich Pfeil.

Sander, P. M. 1999. The microstructure of reptilian tooth enamel: terminology, function, and phylogeny. *Münchner geowissenschaft. Abh.* 38: 1–102.

Sander, P. M. 2000. Ichthyosauria: their diversity, distribution, and phylogeny. *Paläontol. Zeitschr.* 74: 1–35.

Sander, P. M. 2012. Reproduction in early amniotes. *Science* 337: 806–808.

Sander, P. M. and C. Faber. 2003. The Triassic marine reptile *Omphalosaurus*: osteology, jaw anatomy, and evidence for ichthyosaurian affinities. *J. Vert. Paleontol.* 23: 799–816.

Scheyer, T. M. and M. Moser 2011. Survival of the thinnest: rediscovery of Bauer's (1898) ichthyosaur tooth sections from Upper Jurassic lithographic limestone quarries, south Germany. *Swiss J. Geosci.* 104 (Suppl. 1): S147–S157.

Seitz, A. L. 1907. Vergleichende Studien über den mikroskopischen Knochenbau fossiler und rezenter Reptilien. *Nova Acta Leopoldina* 87: 230–370.

Talevi, M., et al. 2012. Variación ontogenética en la histología ósea de *Caypullisaurus bonapartei* Fernández, 1997 (Ichthyosauria: Ophthalmosauridae). *Ameghiniana* 49: 38–46.

Talevi, M. and M. S. Fernández. 2012. Unexpected skeletal histology of an ichthyosaur from the Middle Jurassic of Patagonia: implications for evolution of bone microstructure among secondary aquatic tetrapods. *Naturwissenschaften* 99: 241–244.

Thorne, P. M., et al. 2011. Resetting the evolution of marine reptiles at the Triassic-Jurassic boundary. *Proc. Natl. Acad. Sci.* 108: 8339–8344.

Waskow, K. and P. M. Sander. 2014. Growth record and histological variation in the dorsal ribs of *Camarasaurus* sp. (Sauropoda). *J. Vert. Paleontol.* 34: 852–869.

Wintrich, T., et al. 2020. Palaeontological evidence reveals convergent evolution of intervertebral joint types in amniotes. *Sci. Rep.* 10: 14106.

VetBooks.ir

25

Archosauromorpha: From Early Diapsids to Archosaurs

Armand de Ricqlès, Vivian de Buffrénil and Michel Laurin

CONTENTS

Introduction 467
Historical Background 468
Choristodera 468
Champsosaurus and *Simoedosaurus* 469
Non-Archosauriform Archosauromorphs 469
The "Protorosauria" 469
Aenigmastropheus parringtoni 470
Tanystropheus and *Macrocnemus* (Tanystropheidae) 471
The Rhynchosauria 472
Stenaulorhynchus stockleyi 472
Hyperodapedon and *Teyumbaita sulcognathus* 472
The Allokotosauria 473
Trilophosaurus buettneri 473
Azendohsaurus laaroussii 473
Prolacerta broomi 474
The Archosauriformes 475
Proterosuchidae 475
Erythrosuchidae 476
The Proterochampsia 476
Doswelliidae 476
Proterochampsidae 476
The Euparkeriidae 476
Euparkeria (Figure 25.5F, G) 477
The Phytosaurs (Parasuchia) 477
Rutiodon 477
The Archosauria: Noncrocodylomorph Pseudosuchia 477
Ornithosuchidae 477
Erpetosuchidae 477
Aetosauria (Stagonolepididae) 477
Paracrocodylomorpha 480
Rauisuchidae 481
Discussion 481
Acknowledgments 483
References 483

Introduction

The bone paleohistology of the amniotes, ranging from the earliest diapsids (Reisz 1977) to the archosaurs and lepidosaurs, is fascinating because it records important clues about the early evolution of thermometabolic regimes in amniotes (Cubo and Huttenlocker 2019). It also may bear on the general evolutionary consequences of the biodiversity crisis that marked the transition from the Paleozoic to the Mesozoic eras (Smith and Botha-Brink 2014). This subject was relatively static for quite a long time, but new research has modified and clarified the general picture. Starting with early research (1900–1970), we will briefly review the main methodological breakthroughs that have more recently advanced the question. Then we will

VetBooks.ir

summarize new histological data, set in the currently accepted phylogenetic context. Finally, we will discuss some paleobiological issues that emerge from these new analyses.

Historical Background

In an early paleohistogical study, Seitz (1907) described some "thecodont" (basal archosaur, in this case phytosaur) bone tissues (*Phytosaurus*, *Termatosaurus*) that suggested extensive histological similarities with crocodylians (Games 1990). In contrast, the discovery by Gross (1934) of dinosaur-like fibrolamellar tissues in the large thecodont (in this case, basal archosauriform) *Erythrosuchus*, from the Early Triassic, subsequently raised the issue of which tissue types were basal for archosaurians. The situation, taking into account the histological data and the systematic philosophy then dominant (the "new systematics" of the Modern Synthesis), was summarized by Ricqlès (1976) and extensively discussed (Ricqlès 1978: 94–96). One of the main suggestions was that the crocodylian pattern of bone histology does not represent the basal situation among archosaurs, but it is perhaps linked to a return to an ectothermic physiology associated with an amphibious lifestyle.

Starting in the 1970s, three general methodological breakthroughs changed our views about the relationships, diversity and importance of early diapsids. First, the introduction of phylogenetic systematics (cladistics) in diapsid paleontology (Benton 1984, 1985, Evans 1984, 1988, Gauthier 1984, Sereno and Arcucci 1990, Carroll and Currie 1991, Laurin 1991, Sereno 1991, etc.) profoundly modified the classical view (Hoffstetter 1955, Romer 1966, 1968, Charig and Reig 1970, Reig 1970, Cruickshank 1972) of the interrelationships and systematics of the Permo-Triassic forerunners and allies of squamates, crocodylians, pterosaurs and dinosaurs, including birds.

Second, worldwide efforts in field research, discoveries of new taxa and redescriptions of previously known material have enormously enriched our knowledge of the diversity of early diapsids and extended the data set of anatomical character states used to build stronger phylogenetic hypotheses about early diapsid interrelationships (see Nesbitt 2011, Ezcurra 2016 and extensive references therein).

Third, the renewal of paleohistology from a broad qualitative-descriptive approach (Enlow and Brown 1957, Enlow 1969, Ricqlès 1976, Francillon-Vieillot et al. 1990) to the progressive availability of much more complete comparative fossil material, including several bones in a given skeleton, growth series in a species and so forth (Horner et al. 1999, 2000) allowed paleobiologists to analyze and decipher the anatomical, ontogenetic, and other factors that play important roles in histovariability (Padian et al. 2004).

Finally, the use of new quantified and statistically controlled methods in paleohistology (Montes et al. 2007, Cubo et al. 2012, Legendre et al. 2013, 2016, Cubo and Jalil 2019) has allowed us to hypothesize more objective and testable results in descriptions and functional inferences.

Once a basic knowledge was acquired of the osteohistological characteristics of dinosaurs and crocodylians (e.g., Enlow 1969, Ricqlès 1980, Chinsamy 1990, Chinsamy-Turan 2005, Reid 1996, Horner et al. 2000), it became important to infer the evolutionary relationships among all archosaurs (Ricqlès et al. 2003), archosauriforms and archosauromorphs (Ricqlès et al. 2008, Nesbitt et al. 2009, Botha-Brink and Smith 2011, Werning and Irmis 2011, Legendre et al. 2013, 2016, Werning 2013, Ezcurra et al. 2014, Mukherjee 2015, Veiga et al. 2015, Ezcurra 2016, Werning and Nesbitt 2016, Jaquier and Scheyer 2017, Klein et al. 2017, Cubo and Jalil 2019) to get a broader and more precise picture of how, where and when particular histological features (and likely correlated traits in growth dynamics and thermometabolism) evolved.

Simultaneously, another part of archosauriform skeletal histology, the flat bones and osteoderms, so often well developed in this clade, received greater attention. Apart from systematics, external armor bears on several issues of general paleobiological interest: growth, ecology, locomotion, biomechanics and thermoregulation. More specifically, these investigations have bearing on the problem of the role of bone tissue in calcium homeostasis, and on the regulation of acid–base balance related to excess blood carbon dioxide and/or lactate acidosis when shifting from aquatic to terrestrial environments (Cubo and Huttenlocker 2019). Some recent work on these questions among Triassic archosauriforms, especially aetosaurs, includes Cerda and Desojo (2010, 2011), Cerda et al. (2013), Scheyer and Desojo (2011), Desojo et al. (2013), Taborda et al. (2013, 2015), Scheyer et al. (2014), Cerda et al. (2015, 2018), Hoffman (2017, 2019) and Parker (2018).

A consequence of the abovementioned phylogenetic work has been to progressively decipher the interrelationships among long-recognized classic taxa within diapsids, such as araeoscelids, choristoderes, prolacertiforms, rhynchosaurs, sphenodontids, thalattosaurs, trilophosaurs, younginiforms and now even chelonians, which may be diapsids that lost their temporal fenestrae (Li et al. 2018). Recent phylogenetic analyses of these groups have produced cladograms (see reviews in Nesbitt 2011, Ezcurra et al. 2014 and Ezcurra 2016) that have disagreed about the specific relative positions of various taxa. Recognizing that the number of taxa analyzed histologically to date is still a poor sample, and that samples have not always been made consistently with respect to element and position, the following summary attempts to put available observations in systematic, ontogenetic, and other contexts. Differences from other studies and additional observations are noted. The remainder of the chapter will proceed from the most distant to the most proximal relatives of Archosauria, and then within Pseudosuchia.

Choristodera

The champsosaurs (Choristodera) are a group of small- to medium-sized quadrupedal diapsids with gavial-like habits, best known from classic Cretaceous and Paleocene forms (*Champsosaurus* and *Simoedosaurus*) adapted to freshwater environments. They were originally thought to have evolved from a basal diapsid ancestry because their morphological features are so unusual, and for a long time they remained an isolated group with unclear phylogenetic relationships. The discovery of early (Middle Jurassic) taxa such as *Cteniogenys* (Evans 1990) and of late (Oligocene) champsosaurs such as *Lazarussuchus* (Hecht 1992) less specialized to aquatic life

VetBooks.ir

than *Champsosaurus* promoted this clade as an example of the incompleteness of the fossil record (Evans and Hecht 1993, but see Matsumoto and Evans 2010 and Skutschas and Vitenko 2017). Recent phylogenetic analyses (Ezcurra 2016) put Choristodera in a basal trichotomy with lepidosauromorphs and archosauromorphs.

Champsosaurus and *Simoedosaurus*

The histology of champsosaurs was studied with the issue of adaptation to aquatic life very much in mind (Nopcsa and Heidsieck 1934, Erickson 1972, Ricqlès 1992, Ricqlès and Buffrénil 2001). The most detailed account of bone histology in connection with ontogeny in both genera is that of Buffrénil et al. (1990). Champsosaurs have a rather generalized bone histology dominated by (1) parallel-fibered or lamellar periosteal tissues forming the dense cortex of shafts (Figure 25.1A, B), with evidence of numerous growth cycles (Figure 25.1C), and (2) secondary endosteal spongiosa forming the epiphyseal regions with variably developed cancellous trabeculae in and around the marrow cavity (Buffrenil et al. 1990).

Following this general pattern, some tissue specializations are generally expressed under the syndrome of "pachyosteosclerosis", combining external thickening of the bone (pachyostosis) and internal compactness of the medullary region (osteosclerosis) (Houssaye et al. 2016). In champsosaurs, the cancellous perimedullary tissue of endosteoendochondral origin contains remains of calcified cartilage that form isolated "islands" inside the bone trabeculae (Figure 25.1C–E), even in the central shafts of long bones of adult size and in the cores of vertebral centra (Figure 25.1E), far from the epiphyses (Ricqlès 1992). This process can result in an extensive conservation of primary trabeculae, with persistence of a distinct Kastschenko's line at a distance from the epiphyses in adult individuals (Figure 25.1F). This peculiarity can be interpreted as a kind of heterochronic development inasmuch as the ontogenetic trajectory of endochondral ossification is not fully completed, or at least retarded. Such a phenomenon is often found among aquatic tetrapods (Ricqlès and Buffrénil 2001), where it pertains to the osteosclerosis syndrome (no pathological connotation being implied), and can sometimes reach spectacular development such as in mesosaurs and pachypleurosaurs (see Chapters 18 and 21 on these taxa). Another aspect of osteosclerosis in endoskeletal bones is the progressive thickening, through endosteal deposits, of the medullary trabeculae during ontogeny. In champsosaurs, the erosion/reconstruction processes within the bones produce more deposition than resorption, such that the internal (marrow) bone cavities become progressively filled by endosteal bone, with an overall decrease of porosity and increase of bone density and weight. Traditional (external) pachyostosis is caused by a hyperplasic development of the bone cortices of periosteal origin. This occurs to some degree in champsosaurs, too, but moderately at the level of the main long bones, which do not acquire the typical "swollen" aspect. The dermal skeleton of champsosaurs appears to be less affected by pachyostosis than the endoskeleton, although the clavicles can become completely compact (Ricqlès 1992). The ontogenetic evolution of pachyosteosclerosis in the western European *Simoedosaurus* and *Champsosaurus* suggests that juveniles were probably more terrestrial, or at least less strictly restricted to aquatic habitats than adults. Comparisons of the histological situations among the two genera have also suggested that *Simoedosaurus* was perhaps slightly more aquatic (Buffrenil et al. 1990).

North American champsosaurs from the Upper Cretaceous and Paleocene were studied histologically by Katsura (2010), especially in paleobiological and paleoecological perspectives. Although his conclusions differ from those of Buffrénil et al. (1990) regarding some histological changes during ontogeny, and consequently on the degree of adaptation to aquatic life of adults versus juveniles, his findings regarding the basic histological structure of the primary cortical bone are similar.

Champsosaurs from Siberia were recently reviewed by Skutschas and Vitenko (2017) with some emphasis on bone microanatomy and histology. The best known taxon is *Khurendukhosaurus,* from the Mogito locality from the Lower Cretaceous of Transbaikalia. Sections of adult-sized humeri, ribs and gastralia show that the primary periosteal bone forming the thick cortices is grossly lamellar, or parallel-fibered and poorly vascularized, or avascular. The medullary region of the humerus has no free marrow cavity but is formed by large secondary endosteal osteons associated with stout, short endosteal trabeculae, forming a dense spongiosa. The same kind of tissue forms the deep cortex of the rib, which contains a small free marrow cavity. The gastralia are entirely formed of solid, compact bone. Skutschas and Vitenko (2017) concluded that there is good evidence for a pachyosteosclerotic condition, suggesting a mostly aquatic lifestyle in *Khurendukhosaurus.* This is interesting because this genus seems to be remote phylogenetically from the "classic" Upper Cretaceous and Paleocene "neochampsosauria" and, accordingly, the histological specializations linked to aquatic life would be widespread in the choristoderan clade as a whole.

Non-Archosauriform Archosauromorphs

The "Protorosauria"

Currently understood as a questionably monophyletic group (clade) located among basal archosauromorphs, the concept of Protorosauria broadly conceived has a long and complex history (Piveteau 1955). Based on the earliest recognized taxon, *Protorosaurus* from the Upper Permian of Thuringia, a medium-sized terrestrial quadrupedal reptile with a generalized early diapsid habitus, the protorosaurs were long associated with the rhynchocephalians and squamates, on the lepidosauromorph side of the diapsids. Gauthier (1984) found evidence that *Protorosaurus, Prolacerta*, tanystropheids and several other long-necked Permo-Triassic taxa could form a natural group under the general term Protorosauria. The Triassic tanystropheids were later associated with protorosaurids and drepanosaurids within the clade Protorosauria (Modesto and Sues 2004). However, Ezcurra et al. (2014) and other more recent studies have failed to recover a monophyletic Protorosauria, and there is general consensus that the group needs further phylogenetic study. The name is used informally here.

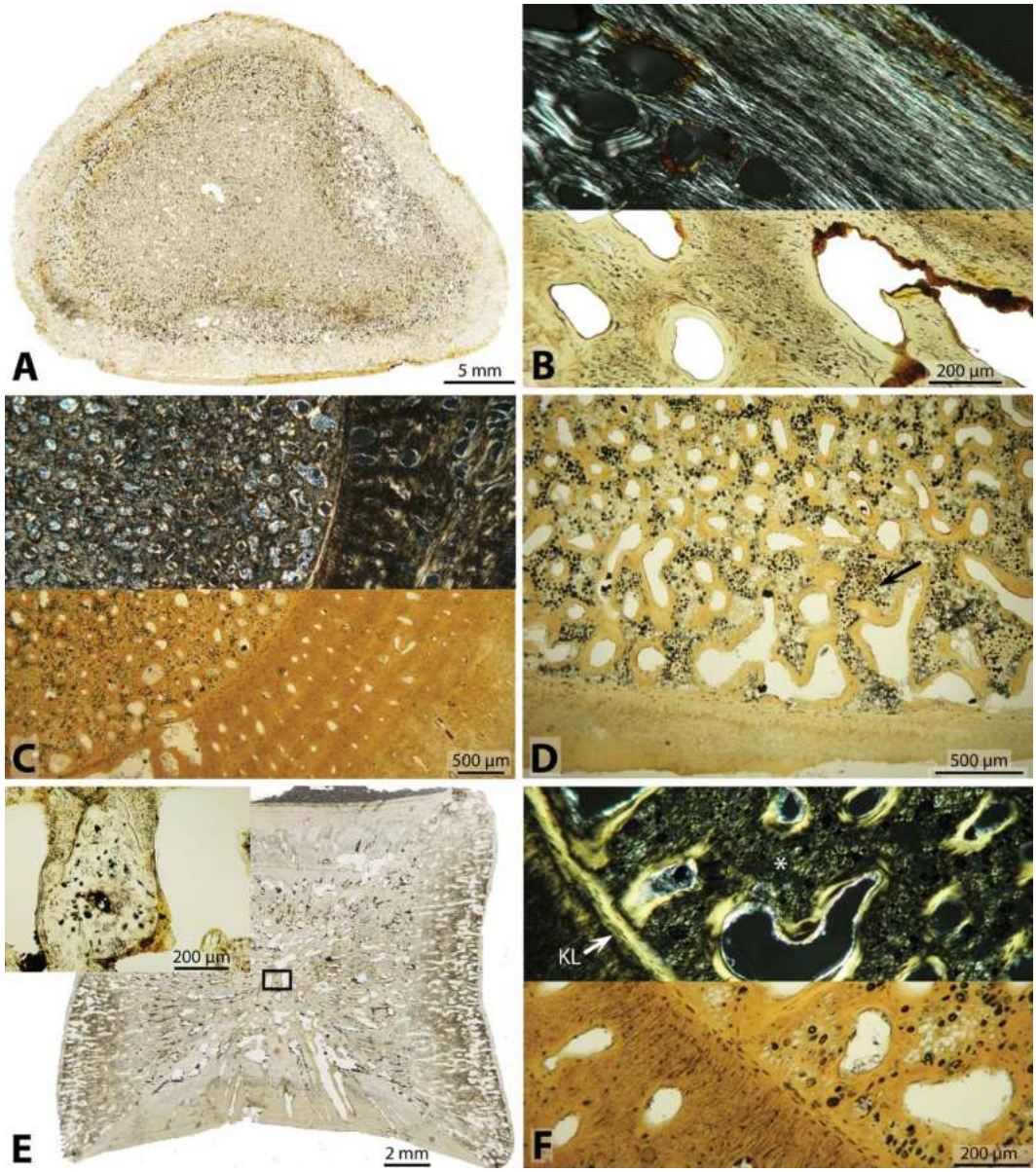


FIGURE 25.1 Choristodera (Champsosaur) bone histology. A, *Simoedosaurus*, adult size. Femoral shaft cross section. General view showing the dense spongiosa filling up most of the bone, with hardly any free marrow cavity left. B, *Simoedosaurus*, adult size. Femoral shaft cross section. Detail of the periosteal cortex mostly formed of finely parallel fibered bone. Some erosion bays are partially filled up by secondary bone deposition. C, *Simoedosaurus*, adult size. Rib cross section. The thick vascular bone cortex suggests some cyclicity in its deposition. The medullar region is densely filled up by bony trabeculae. D, Same material, detail. The core of the medullary bone trabeculae is formed by extensive remains of calcified cartilage (arrow). The marrow was located within the cavities lined by the bone tissue. E, *Champsosaurus*, adult size, vertebral centrum. Periosteal component at top and bottom, and endochondral component at right and left. Inset: an island of calcified cartilage close to the center of the centrum. F, Same material as C. The growth process has not required resorption at the limit between endochondral and periosteal bone components, hence, Kastschenko's line (KL; arrow) remains unchanged.

Aenigmastropheus parringtoni

The histology of this basal archosauromorph from the Late Permian, Songea Group, Ruhuhu Basin of southwestern Tanzania was described by Ezcurra et al. (2014). Their phylogenetic analysis recovered it as the sister-group of *Protorosaurus* among Protorosauria and other archosauromorphs. The shaft of a long bone (possibly the left humerus) has a rather thin cortex with a few bone trabeculae in the endosteal margin around a circular free marrow cavity. The deep cortex is made of fibrolamellar tissue containing longitudinal primary osteons circumferentially arranged. The middle cortex is to a large degree made of parallel-fibered tissue interspaced with thin layers of woven bone, and some more reticular organization of the vascular canals develops. The outer cortex is formed of lamellar-zonal bone poorly vascularized by some radially oriented simple vascular canals. The cortex contains up to eight growth cycles marked by three annuli in the deeper cortex and five lines of arrested growth (LAGs) centrifugally.

VetBooks.ir

Tanystropheus and *Macrocnemus* (Tanystropheidae)

These two Middle Triassic Protorosauria were studied by Jaquier and Scheyer (2017). In both genera the cervical vertebrae are unusually long, a general characteristic for protorosaurs but particularly pronounced in Tanystropheidae, especially in the eponymous taxon *Tanystropheus*. The morphology of *Macrocnemus* suggests a terrestrial habit (Rieppel 1989). In contrast, the lifestyle of the extraordinary *Tanystropheus* remains problematic in spite of numerous hypotheses based on osteological analyses. For *Tanystropheus* (several species), nine bones, including cervical vertebrae, ribs, postcloacal bone, femora and humerus were considered. A femur (SMNS 54622) was selected as the only long bone preserved well enough three-dimensionally to conduct an analysis. The midvertebral section of MHI 1104 was also histologically analyzed. For *Macrocnemus bassanii*, a femur, a cervical vertebra and a humerus were studied. The bone histology of the analyzed elements of *Tanystropheus* (Figure 25.2A, B) and M*acrocnemus* is virtually identical except that Sharpey's fibers are present only in the cervical region of *Macrocnemus*. Both genera have a common basic bone tissue, lamellar-zonal compact bone consisting of a primary compact lamellar to

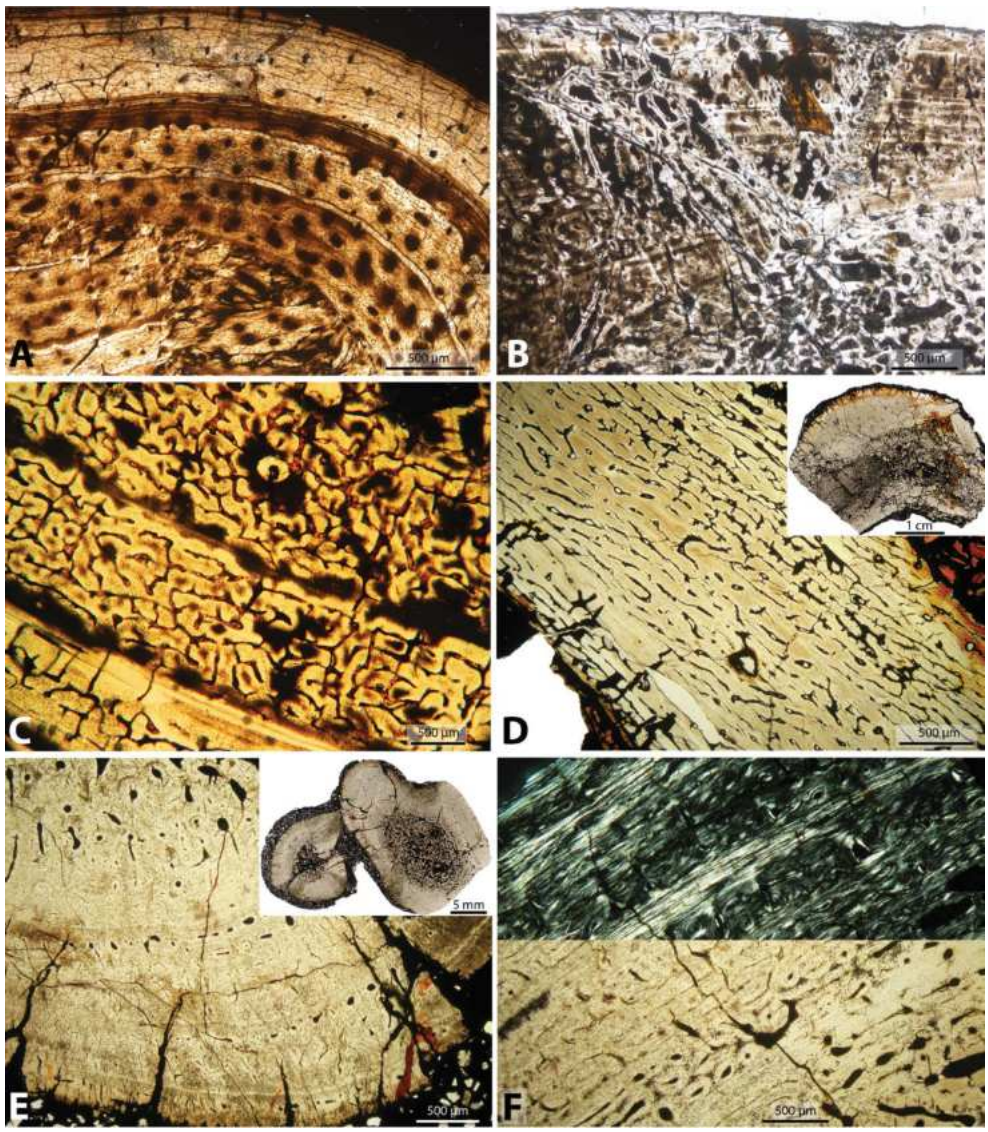


FIGURE 25.2 Protorosauria and Rhynchosauria bone histology. A, *Tanystropheus* femur, cross section. The cortex is formed by a lamellar-zonal tissue with clear evidence of growth cycles and moderate vascularization. The deep cortex has been apparently displaced by *postmortem* crushing. B, Same material; low magnification. The cortex with several growth cycles (top) surrounds a rather cancellous perimedullar region (bottom). Both are permeated by multiple fractures bringing extraneous minerals. (Photos courtesy of Drs. V. Jaquier and T. Scheyer.) C, *Teyumbaita sulcognathus* tibia, shaft cross section. Most of the deep cortex is formed by thick zones of fibrolamellar tissue of the plexiform pattern alternating with lamellar annuli. (Photo courtesy of Drs. F. Veiga, M. B. Soares and J. M. Sayao.) D, *Hyperodapedon* ("*Scaphonyx*") sp. undetermined long bone. The thick perimedullar cortex is entirely formed by an irregular laminar to poorly sub-plexiform pattern of fibrolamellar tissue (insert: general view of the section). E, Same material, rib cross section (smaller bone in the inset). Most of the cortex is formed by poorly vascularized periosteal tissue with growth cycles and a rich component of radially oriented Sharpey's fibers. F, Same material, tibia? (cf. Werning and Nesbitt 2016, p. 172; larger bone in the inset in E). Alternation of lamellar annuli and ill-defined zones with some fibrolamellar components.

VetBooks.ir

a parallel-fibered matrix of periosteal origin, with extensive evidence for cyclical growth. This bone type contains longitudinal simple primary vascular canals. Small variations in vascularization occur locally in a section or among different bones. The growth pattern here is a typical slow-growing one found in many extant reptiles, notably squamates, in contrast to *Aenigmastropheus,* another basal archosauromorph close to *Protorosaurus* (Ezcurra et al. 2014), which shows some histological characters perhaps closer to those observed among more crownward archosauromorph clades.

The Rhynchosauria

The Rhynchosauria form a large and well-delineated group of fairly large and massive diapsids mostly known from the Upper Triassic with a worldwide range. They were terrestrial, and some limb anatomical features suggest burrowing behaviors (Huene 1935–1942). Early forms, such as *Mesosuchus* and *Howesia* from the *Cynognathus* zone of South Africa, are small, but later, more typical rhynchosaurs of the Late Triassic reached 3–5 m or more with skulls 80 cm wide. Rhynchosaurs had a wide skull, actually wider than long, to accommodate extensive rows of crushing/grinding teeth. They have been interpreted as herbivores, perhaps burrowers feeding on rhizomes or tubercles. The peculiar plier-shaped anterior skull that bears large incisor teeth and a downturned beak somewhat resembles those of rhynchocephalians (sphenodontids), and rhynchosaurs were for a long time put close to them on the lepidosaurian side of the diapsids (Hoffstetter 1955). More recent phylogenetic analyses have put them among archosauromorphs but at various levels in the phylogeny, and generally not very close to archosauriforms.

Early paleohistological descriptions by Enlow and Brown (1957), Enlow (1969) and Ricqlès et al. (2008) on *Scaphonyx sanjuanensis* (now *Hyperodapedon sanjuanensis*) (Figure 25.2D–F) were based on samples (MCZ FN 354-58) that were too small to allow significant assessments of rhynchosaur bone histology, although the group was used as a potential histological outgroup of archosauriforms in those early analyses. Further research (Mukherjee 2015, Veiga et al. 2015, Werning and Nesbitt 2016) has offered a more precise assessment of the bone histology of this important group, with extensive analyses of its developmental, anatomical, biomechanical and phylogenetic factors. Werning and Nesbitt (2016) compared femoral and tibial histology in an individual of *Stenaulorhynchus*, Veiga et al. (2015) sectioned long bones and ribs of *Hyperodapedon* and *Teyumbaita sulcognathus* from Brazil (Figure 25.2C) and Mukherjee (2015) sectioned several long bones from *H. huxleyi* and *H. tikiensis* from India, including a femoral growth series. Although Late Triassic hyperodapedontine rhynchosaurs are now well sampled, little is known about growth in earlier diverging rhynchosaurs, or whether these later forms are representative of the entire clade.

Stenaulorhynchus stockleyi

Werning and Nesbitt (2016) described the femoral and tibial histology of a single individual of *Stenaulorhynchus stockleyi*, a Middle Triassic rhynchosaur from the Manda beds of the Ruhuhu basin of Tanzania, a species about 1 m long at adult size. The femur has a fairly circular section at the shaft and a marrow cavity entirely filled by a dense spongiosa of endosteal bone, with a well-developed endosteal margin forming a progressive transition to the deep cortex. The femoral cortex is largely composed of moderately vascularized parallel-fibered bone tissue, which becomes almost avascular and more lamellar approaching the periosteum. Twelve cycles of growth are recorded, the three innermost ones by groups of LAGs in the deep cortex, the latter ones by LAGs in the external cortex, which become closer and closer to each other toward the periosteal surface. The deep cortex seems to be partly formed by a fibrolamellar tissue permeated by longitudinal primary osteons; however, the whole region is obscured by a diffuse endosteal erosion/reconstruction that does not produce many typical secondary osteons.

The shaft section of the tibia is also mainly circular, with a concavity close to the anterior crest and an overall dense structure, with a tiny free marrow cavity surrounded by an extensive inner region of cancellous bone trabeculae and erosion bays progressively invading the deep cortex. The histology of the cortex has a pattern generally similar to that of the femur, but the structure of its inner cortex, i.e., a fibrolamellar tissue with longitudinal primary osteons, is better preserved. The more external cortex is lamellar-zonal and sparsely vascularized. It shows at least five well-separated LAGs. The outermost cortex contains six to seven closely packed LAGs and may be described as an external fundamental system (EFS). In Werning and Nesbitt's (2016) figure 4C, it is suggested that the line labeled as a LAG is actually an artifactual fracture filled by calcite that underscores the local tissue's fine structure.

Another specimen of *Stenaulorhynchus* (NMT RB154), a limb bone mid-diaphysis, was illustrated by Sanchez et al. (2012) in the context of new technological developments in paleohistology. According to Werning and Nesbitt (2016), its histology and kidney-shaped cross section suggest that it is also a tibia. This individual is smaller than NHMUK PV R 36618 and differs histologically by its thicker cortical compacta relative to the cancellous region. Its primary cortex is similarly vascularized to the inner cortex of NHMUK PV R 36618, but it has more radial and radially oblique anastomoses. Growth marks are also present, but less distinct than those of the larger NHMUK PV R 36618.

Hyperodapedon and *Teyumbaita sulcognathus*

Veiga et al. (2015) examined several bones (humerus, radius, femur, tibia and ribs) of these two taxa from the Santa Maria 2 Sequence (Upper Triassic) of southern Brazil. The humeri of both taxa have a deep cortex formed of fibrolamellar bone showing a dense vascular network of longitudinal primary osteons, or plexiform or less regular patterns interrupted by annuli and LAGs. (Figure 25.2C–F). The spongiosa is well developed and resorbs the deep cortex irregularly. The more external cortex becomes lamellar-zonal. The radius has a deep cortex formed of typical plexiform tissue while the external cortex is lamellar-zonal.

Only one femur of *Hyperodapedon* was available to Veiga et al. (2015), and it was sectioned from fragments near the

VetBooks.ir

proximal end (UFRGS PV-0271-T). It shows a thin cortex vascularized by longitudinal primary osteons that decrease in number periosteally, similar to *Stenaulorhynchus*. The primary tissues of that specimen are described as fibrolamellar based on osteocyte shape and arrangement, and no growth marks are visible. Differences in femoral cortical thickness and growth mark presence between the femur of *Stenaulorhynchus* and that of *Hyperodapedon* partly reflect differences in sampling location. The tibial histology of *T. sulcognathus* and *Hyperodapedon* from the Santa Maria 2 Sequence was studied from several bones. The cortices of smaller individuals are composed of fibrolamellar bone with a significant woven-fibered component. The tissues are well vascularized by primary osteons arranged in a typical plexiform pattern. Larger individuals sometimes preserved similar tissues in the perimedullary region, interrupted by annuli, but their cortices were mainly composed of parallel-fibered bone, poorly vascularized by longitudinal primary osteons, and with several LAGs or annuli. Some ribs have a dense lamellar-zonal external cortex (Veiga et al. 2015, figure 1 A2), but some are extensively involved in Haversian reconstruction. Moreover, the taxa from Brazil differ from *Stenaulorhynchus* from Tanzania in the presence of more densely vascularized fibrolamellar bone with a high complexity of vascular canal patterns.

Mukherjee (2015) published a thorough histological survey of rhynchosaurs from India, reporting on two coeval species of *Hyperodapedon: H. tikiensis* from the Tiki Formation and *H. huxleyi* from the Maleri Formation. A large sample was examined, including the mid-diaphyseal sections of humeri, radius, ulna, femora, tibiae and fibula, and a transverse section of a phalanx of the pes, a pubis, several ribs and centra. The sample includes growth series of several bones, notably femora. Statistical techniques were used to produce growth curves for humeri, radius, ulna, femora and tibiae, and put individual bones in four growth classes (juveniles, early and late subadults, adults), characterized by their histology. The many photos provided in their study obviates the need for detailed analytical comments here. There are disagreements among authors about the observed presence of an EFS in rhynchosaurs. By and large, the observations concur with those on the Brazilian rhynchosaurs (Veiga et al. 2015), but with some differences. The Indian material suggests a more important development of fast-growing fibrolamellar tissues, and during a longer part of the ontogeny than previously expected. Accordingly, Mukherjee (2015) states that "predominance of fibrolamellar bone tissue and peripheral lamellar bone with growth rings in most of the adult skeletal elements suggest that *Hyperodapedon* had an initial fast growth which slowed and became punctuated later in ontogeny". Hence, "rapid growth strategy is inferred for the Late Triassic rhynchosaurs, that is the hyperodapedontines" and "rapidly growing fibrolamellar bone tissue gained predominance not only in the archosauriforms but also within the basal archosauromorphs, and rapid growth strategy was already present within members of the basal archosauromorphs" (Mukherjee 2015, p. 336).

Some additional material from the Ischigualasto Formation of Argentina (Ricqlès et al. 2008) was studied (Figure 25.2D–F) for this chapter and generally agrees with the histological patterns and variation described above.

The Allokotosauria

According to Nesbitt et al. (2015) (see also Ezcurra 2016), the Allokotosauria form the sister-group of the clade *Prolacerta* + archosauriforms. However, some analyses put this clade in a more remote position than rhynchosaurs, relative to archosauriforms.

Trilophosaurus buettneri

The Upper Triassic trilophosaurs have long been an enigmatic group because their durophagous dentition and peculiar anatomical organization of the temporal region did not readily allow their recognition as diapsids, a conclusion that was reached by recent phylogenetic analyses. They have been placed among archosauromorphs at highly variable nodes (Ezcurra 2016). The recent identification of the clade Allokotosauria (Nesbitt et al. 2015) includes trilophosaurs, *Azendohsaurus,* and their kin. Werning and Irmis (2010, 2011) published abstracts of a thorough histological study of *T. buettneri*, well known from hundreds of individual elements from a monodominant Late Triassic (~220 Ma) bone bed near Otis Chalk, Texas. Statistical analyses of 300 bones were based on a growth series of femora and tibiae to obtain skeletochronological age estimates. Adult humeri and ulnae were also analyzed. The authors described the bone microstructure of this taxon as low to moderately vascularized lamellar-zonal bone. This type of bone tissue, in association with multiple LAGs, was evident throughout ontogeny and indicates an overall slow and cyclical growth (Werning and Irmis 2010). Additional first-hand observations made for this review (Figure 25.3A, B) generally confirm this description.

Azendohsaurus laaroussii

The bone histology of this taxon from the Carnian of Morocco was thoroughly analyzed by Cubo and Jalil (2019) as a basis for inferring its thermometabolic regime by comparison with archosauriforms. Stylopodial and zeugopodial bones (Figure 25.3C–E) show three tissue types: (1) avascular lamellar-zonal bone formed at low growth rates, (2) a scaffold of parallel-fibered bone containing either small primary osteons or simple vascular canals and (3) fibrolamellar bone formed at high growth rates. The tibial cortex differs in structure according to its anatomical orientation. The medially oriented part of the cortex is nearly nonvascular, whereas the posterior part is densely vascularized by longitudinally oriented primary osteons (Figure 25.3E). The fibrillar organization of the periosteal tissue is longitudinally parallel-fibered. The femoral and humeral shaft cross sections are rather different because they are formed by fibrolamellar tissue of a laminar pattern (Figure 25.3D), with minor local differences in vascular canal density and orientation. Overall, the histological differences between stylopodial and zeugopodial elements are well marked, and may be linked to differences in anatomical orientation, biomechanical function and size of the elements. The quantitative inferences of resting metabolic rate (RMR) conducted by Cubo and Jalil (2019) on *Azendohsaurus* put this taxon in close agreement with several archosauriforms regarding its RMR as distinctly higher than that of extant ectotherms, although not as high as among extinct theropods and extant birds.

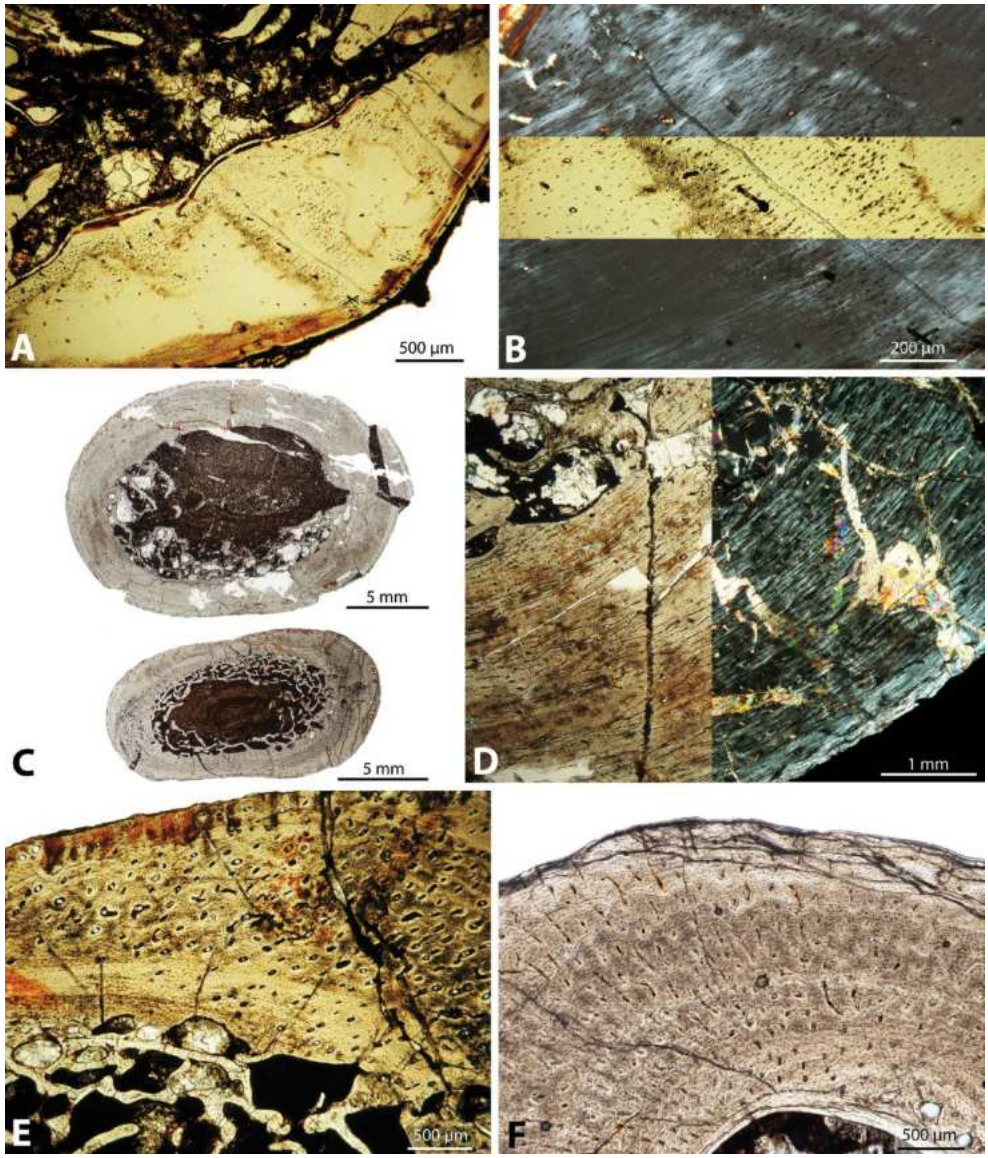


FIGURE 25.3 Allokotosauria and *Prolacerta* bone histology. A, *Trilophosaurus buettneri*. Humeral shaft. General view of the cortex surrounding a free marrow cavity. The cortex is entirely lamellar-zonal with a weak vascular component and little evidence of growth cycles. B, Same material. Detail of the cortex. The compact bone tissue appears to be finely parallel-fibered. C, *Azendohsaurus laaroussii*. Cross sections of femoral (above) and tibial shafts. D, Same material, general view of the femoral cortex, mostly formed of densely vascularized fibrolamellar tissue. E, Same material, general view of the tibia. The longitudinally parallel-fibered bone tissue is permeated by a moderately dense network of primary osteons. (Photos courtesy of Pr. J. Cubo-Garcia.) F, *Prolacerta broomi*. Humerus. The inner cortex is formed by an ill-defined fibrolamellar tissue with a suggestion of three to four growth cycles and the outermost cortex becomes more lamellar. (Photo courtesy of Dr. J. Botha.)

Prolacerta broomi

Prolacerta is recognized (Ezcurra 2016) as the closest well-known sister-group of Archosauriformes. A tibia from a presumably fully adult individual was histologically described and illustrated by Botha-Brink and Smith (2011). A cross section of the humerus (Figure 25.3F) generally agrees with the description of the tibia.

The cortex is entirely primary and made of compact periosteal bone permeated by a regular network of vascular canals organized longitudinally (Figure 25.3F). The canals reflect poorly defined primary osteons that, according to Botha-Brink and Smith (2011), are embedded in a rather woven tissue, thus forming together a poorly defined "fibrolamellar" complex. However, other parts of the cortex appear to be built of circumferential lamellae. There is little evidence of secondary osteons in the cortex, although the perimedullary region shows obvious endosteal resorption/redeposition activity. The poorly developed endosteal trabeculae circling the free marrow cavity appear to be abruptly set apart from the deep periosteal cortex. This unconformity may suggest an earlier phase of complete resorption of the latter. If so, a large part of early ontogeny is not recorded in the section. No obvious evidence of growth cyclicity ("LAGs") is observed through the cortex. The "fibrolamellar" organization seems more prevalent in the deeper cortex, while

the external cortex becomes lamellar, thus revealing a progressive slowdown of radial growth. There is no evidence of an EFS at the cortical periphery although the bone size is close to the largest known body size for the species. Botha-Brink and Smith (2011) put *Prolacerta*, a relatively basal archosauromorph, as a sister-taxon to the archosauriforms, perhaps exemplifying the basal pattern of growth dynamics of archosauriforms.

The Archosauriformes

This great clade contains the crown archosaurs and a number of closely related groups sharing some important archosaurian character states such as thecodont tooth implantation and a preorbital fenestra. Otherwise, basal archosauriforms retain some plesiomorphic diapsid character states and lack some crown archosaur apomorphies. The traditional "proterosuchians" are now an informal (paraphyletic) group of Early to Middle Triassic nonarchosaurian archosauriforms (Charig and Reig 1970, Reig 1970, Cruickshank 1972, Ezcurra 2016).

Proterosuchidae

Proterosuchidae constitutes an Early Triassic group (*Lystrosaurus* zone) of basal quadrupedal archosauriforms with moderate body sizes and crocodylian-like habitus. The front of the upper jaw forms a characteristic "hook" common to many basal archosauromorphs. *Proterosuchus* is very similar to the perhaps congeneric *Chasmatosaurus* (*Proterosuchus*) *fergusi*; Figure 25.4A). The bone histology of *Proterosuchus* was described for the first time by Botha-Brink and Smith (2011)

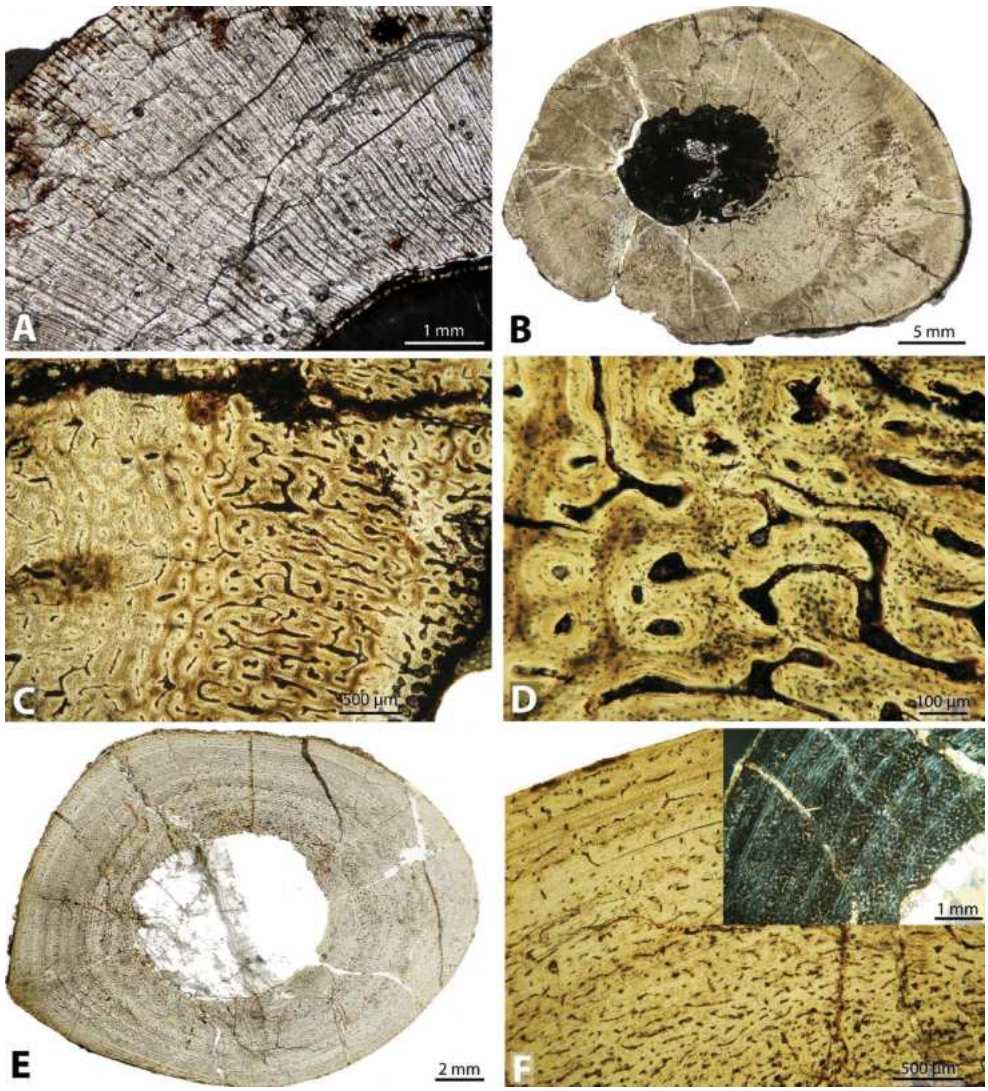


FIGURE 25.4 Archosauriforms: Proterosuchidae, Erythrosuchidae, Proterochampsidae. A, Proterosuchidae: *Proterosuchus fergusi.* Tibia of a two-thirds grown individual. The cortex is formed by the radiating variety of fibrolamellar bone, where radially oriented primary osteons dominate the structure. This suggests a very high rate of radial growth of the bone. (Photo courtesy of Dr. J. Botha-Brink.) B, Erythrosuhidae: *Erythrosuchus* sp. Fibular shaft cross section. The thick cortex has an abrupt transition with the free marrow cavity. C, Same material. The deep cortex is entirely formed by fibrolamellar bone of the general plexiform type. D, Same material. Detail of the fibrolamellar tissue. E, Proterochampsidae: *Chanaresuchus.* Long bone shaft cross section. The cyclicity of the cortical bone deposition is apparent. F, Same material. The inner cortex is fibrolamellar, turning to lamellar-zonal near the bone surface. The general cyclicity of bone deposition is enhanced under polarized light (inset).

VetBooks.ir

and is very interesting. They studied material from three individuals inferred to be about two-thirds grown to fully grown, as well as some isolated bones, and they identified some histological changes through ontogeny as well as specific histological peculiarities of some elements. The femur and tibia of a presumably immature individual (about two-thirds maximal known body size) have a cortex entirely formed of a peculiar tissue dominated by radially oriented primary osteons embedded in a matrix identified as woven-fibered bone (radiating fibrolamellar bone). The dense vascular system also contains longitudinally oriented primary osteons set in radial rows. The cortex is eroded endosteally by a free marrow cavity, only uncomformably coated locally by a very thin layer of endosteal bone. In adult-sized bones (femur and fibula) the aforementioned cortical bone tissue becomes relocated in the deep cortex, where it experiences some erosion/reconstruction cycles. Externally, further periosteal growth has progressively laid down a less vascularized lamellar-zonal tissue, with more longitudinally oriented canals. This tissue shows a great number of LAGs. In the fibula vascular canals are longitudinal but set in radial rows. The external cortex is distinctly lamellar-zonal with evidence of growth cycles and lower vascular density. There is a well-developed endosteal margin, along with erosion bays (not developed into completed secondary osteons) in the deep cortex, and perimedullary endosteal trabeculae. The prevalence of radial fibrolamellar tissue in nonadult *Proterosuchus* is striking and suggests a very high rate of radial growth of the shaft. A similar example from the Beaufort Series was described from a radius of the whaitsid therocephalian *Notosollasia* from the *Cistecephalus* Zone (Ricqlès 1969).

Erythrosuchidae

Erythrosuchidae comprises a group of Lower to Middle Triassic (*Cynognathus* Zone, South Africa), mostly terrestrial quadrupedal predators with a large, high skull and massive body. *Erythrosuchus* (Figure 25.4B–D) is a famous taxon in paleohistology because the early description by Gross (1934) of its dinosaur-like (rather than crocodile-like) histology subsequently raised the issue of the origin and evolution of bone tissue types among dinosaurs and related taxa – and in particular what rapidly growing tissue might imply about the physiological regimes of basal archosauromorphs. Later descriptions (Ricqlès et al. 2008) were amplified by Botha-Brink and Smith (2011), and more material has now been described histologically. This includes stylopodial and zeugopodial elements, metatarsals and rib fragments of triangular and circular sections, with some of these bones coming from the same individual. Although the ontogenetic situation of most fragments could not be controlled by direct comparison with the largest (presumably adult or nearly so) bones known for this taxon, it appears that most may reflect a still very active growth phase from about two-thirds to three-quarters or more of maximal body size.

Histological descriptions of *Erythrosuchus* note a cortical bone of the general fibrolamellar type, becoming modified in the largest limb bones into the plexiform pattern, and into a pattern dominated by longitudinally oriented primary osteons in the ribs. Some regions in various bones contain vascular canals in oblique and radial orientations that give the local tissue a subplexiform or reticular pattern. The perimedullary region often presents an image of a general erosion front without many scattered erosion bays in the deep cortex and little secondary reconstruction. Dense Haversian bone has not been observed. LAGs, when present, are restricted to the most superficial cortex in some ribs. To sum up, the general picture suggests a continuously fast-growing skeleton even at large subadult body size.

The Proterochampsia

According to recent analyses (Ezcurra 2016), the North American Late Triassic armored Doswelliidae (*Doswellia* and *Vancleavea*) form a clade of semiaquatic archosauriforms located within the Proterochampsia, as a sister-group to the Proterochampsidae.

Doswelliidae

Nesbitt et al. (2009) described the femoral bone histology of the Late Triassic archosauriform *Vancleavea campi* as formed by a poorly vascularized lamellar-zonal tissue with distinct LAGs throughout the cortex. This suggests a generally slow and cyclical pattern of growth. They also described a particularly thick cortex and a medullary cavity infilled by bone, and this, in association with morphological features, suggests that *Vancleavea* was semiaquatic (Nesbitt et al. 2009).

Proterochampsidae

This clade of generally long-snouted, semiaquatic archosauriforms is only known from South America, mainly from the Middle Triassic. Recent research (Arcucci et al. 2019, Marsà et al. 2020) suggests that their ecological adaptations may have been more varied than previously thought. Long bone histology is represented by *Chanaresuchus* (Figure 25.4E, F), a crocodile-like proterochampsid from the Chañares Formation, Middle Triassic (Anisian) of Argentina. A long bone shaft (MCZ 4036) was briefly described by Ricqlès et al. (2008) as having an inner cortex formed by a thick region of densely vascularized fibrolamellar tissue. Toward the bone periphery, cortical structure progressively turns to lamellar-zonal with a far less dense vascular component. Several growth cycles are conspicuous. Hence, the histology of this bone appears rather similar to that observed among phytosaurs. Recent descriptions of another femur of *Chanaresuchus* (PULR-V 125) and of the femur of the Proterochampsid *Tropidosuchus* (PVL-4604) by Marsà et al. (2020, figures 5 and 6) generally agree with previous observations.

The Euparkeriidae

Euparkeriids were lightly built, small archosauriforms from the Lower Triassic of South Africa, traditionally considered the sister-group of crown Archosauria. Nesbitt (2011) found that Phytosauria (Parasuchia) was the first sister-group outside Archosauria and *Euparkeria* was just outside that clade, whereas Ezcurra (2016) recovered Proterosuchia as the first sister-group outside Archosauria and *Euparkeria* just outside that clade, with Parasuchia as the most basal group of Pseudosuchia.

VetBooks.ir

Euparkeria (Figure 25.5F, G)

Preliminary histological descriptions by Ricqlès et al. (2008) were considerably supplemented by Botha-Brink and Smith (2011) and Legendre et al. (2013). Long bone shafts (humeri, femur, tibia and fibula) were studied among presumably adult individuals (although no EFS was observed; see below). They generally show a tubular structure with a free marrow cavity. A distinct fibrolamellar organization of the innermost and middle cortex is observed in the humerus, tibia and fibula, but a large part of the cortex is formed by parallel-fibered bone (especially in the femur) with a lower vascular density, and one to three LAGs are present. Secondary endosteal bone with a very moderate complement of secondary osteons surrounds the marrow cavity. The amount and organization of the calcified cartilage in the femoral epiphysis (Botha-Brink and Smith 2011, figure 6c) suggest the possibility of further longitudinal growth.

The Phytosaurs (Parasuchia)

Phytosaurs were traditionally considered a clade of basal pseudosuchian archosaurs but some analyses now put them outside crown archosaurs (e.g., Nesbitt 2011). Alternatively, phytosaurs are within Archosauria (Ezcurra 2016) as the sister-group of all other pseudosuchians (i.e., Crurotarsi *sensu* Sereno and Arcucci 1990). Phytosaurs are well known for their crocodylian-like or gavial-like habitus and ecologies, and are mostly restricted to the Upper Triassic. Several taxa reached considerable body size (8–10 m). One of the earliest histological descriptions was by Seitz (1907). Osteoderm structure is complex and rather similar to that of crocodylians (Figure 25.5A). The superficial region is ornamented, the result of extensive localized erosion/reconstruction processes, including lateral drift. The basal region is formed by dense lamellar bone. The deep (inner) region locally still contains well-vascularized primary periosteal bone but is mostly formed of a secondary endosteal spongiosa. The long bone histology was described by Ricqlès et al. (2003). Quantitative histological assessment of the same material allowed estimates of RMRs in phytosaurs and other basal archosauriforms (Legendre et al. 2013, 2016), which yielded RMR values higher than in extant ectotherms.

Rutiodon

Ricqlès et al. (2003) described the histology of the femoral shafts of a specimen labeled as *Rutiodon* (UCMP 25921; Figure 25.5B, C), but possibly referable only to Phytosauria (Werning 2013, p. 59) and an indeterminate large phytosaur reported as "UCMP 2186" (Figure 25.5D, E) but more likely UCMP 32186 (Werning 2013, p. 59). The internal cortex is formed by several thick zones of fibrolamellar tissues, with a dense vascularization of laminar to subplexiform patterns. There is evidence of active erosion/redeposition of bone at the endosteal margin, resulting in convoluted endosteal lamellar systems and secondary osteons (Figure 25.5B, C). About half of the external cortex is formed by lamellar-zonal tissue, progressively less vascularized toward the periosteal margin (Figure 25.5D, E). Some external zones can nevertheless be formed of a well-vascularized fibrolamellar tissue, interrupting the cycles of mostly lamellar bone. Haversian reconstruction is scattered through the whole cortex, but can be very dense in the perimedullary region, obscuring previously deposited laminar tissue.

The Archosauria: Noncrocodylomorph Pseudosuchia

Within the crown group Archosauria our review is restricted to pseudosuchians (crocodile-line archosaurs) that are outside Crocodylomorpha, a taxon that includes extant crocodylians and some of their close relatives. For crocodylomorphs, see chapter 26.

Ornithosuchidae

These gracile, possibly facultatively bipedal archosaurs of the Upper Triassic were classified by Alick Walker (1964) as basal saurischian dinosaurs, in spite of their crurotarsan ankle joint which, however, has a very peculiar construction (Sereno and Arcucci 1990, Sereno 1991). Gauthier (1984) recovered ornithosuchians as the most basal group of bird-line archosaurs, but subsequent analyses placed them at the base of the pseudosuchian (crocodile-line) archosaurs (Sereno and Arcucci 1990), depending on the placement of phytosaurs (Parasuchia) within or outside Archosauria. *Ornithosuchus,* from the Elgin Sandstone of Scotland (BM R 3142), is known histologically (Ricqlès et al. 2008) only from a triangular rib fragment. A secondary endosteal spongiosa is surrounded by a thin cortex of likely fibrolamellar bone containing several rows of longitudinally oriented primary osteons and punctuated by one LAG. The deep cortex contains secondary osteons.

Erpetosuchidae

Tarjadia (Figure 25.6A, B), from the Chañares Formation, Middle Triassic (Anisian) of Argentina, is histologically known from a fragment of a large bone shaft (MCZ 4077, originally referred to as *Luperosuchus*). The external cortex is a typical lamellar-zonal bone tissue with six to seven growth cycles (Ricqlès et al. 2008). The inner cortex has a denser complement of longitudinal primary osteons connected by circular and radial anastomoses. The bone tissue in the zones of the deep cortex attains a fibrolamellar organization. Overall, the general tissue organization of the cortex is similar to that observed among phytosaurs, aetosaurs and poposaurs.

Aetosauria (Stagonolepididae)

This large group of terrestrial quadrupedal plant-eating pseudosuchians is principally known from the Upper Triassic and remarkable for the spectacular development of ornamented osteoderms organized in several large rows. Apparently, aetosaurs covered a wide range of species-specific adult body sizes (up to 8 m; Heckert et al. 1996, Heckert and Lucas 1999). A large number of histological studies on the osteoderms of this group have been recently published (review in Hoffman et al. 2019). Several long bones from three aetosaur genera from the Upper Triassic of the southwestern United States, such as *Typothorax, Stagonolepis (Calyptosuchus*) (see Parker

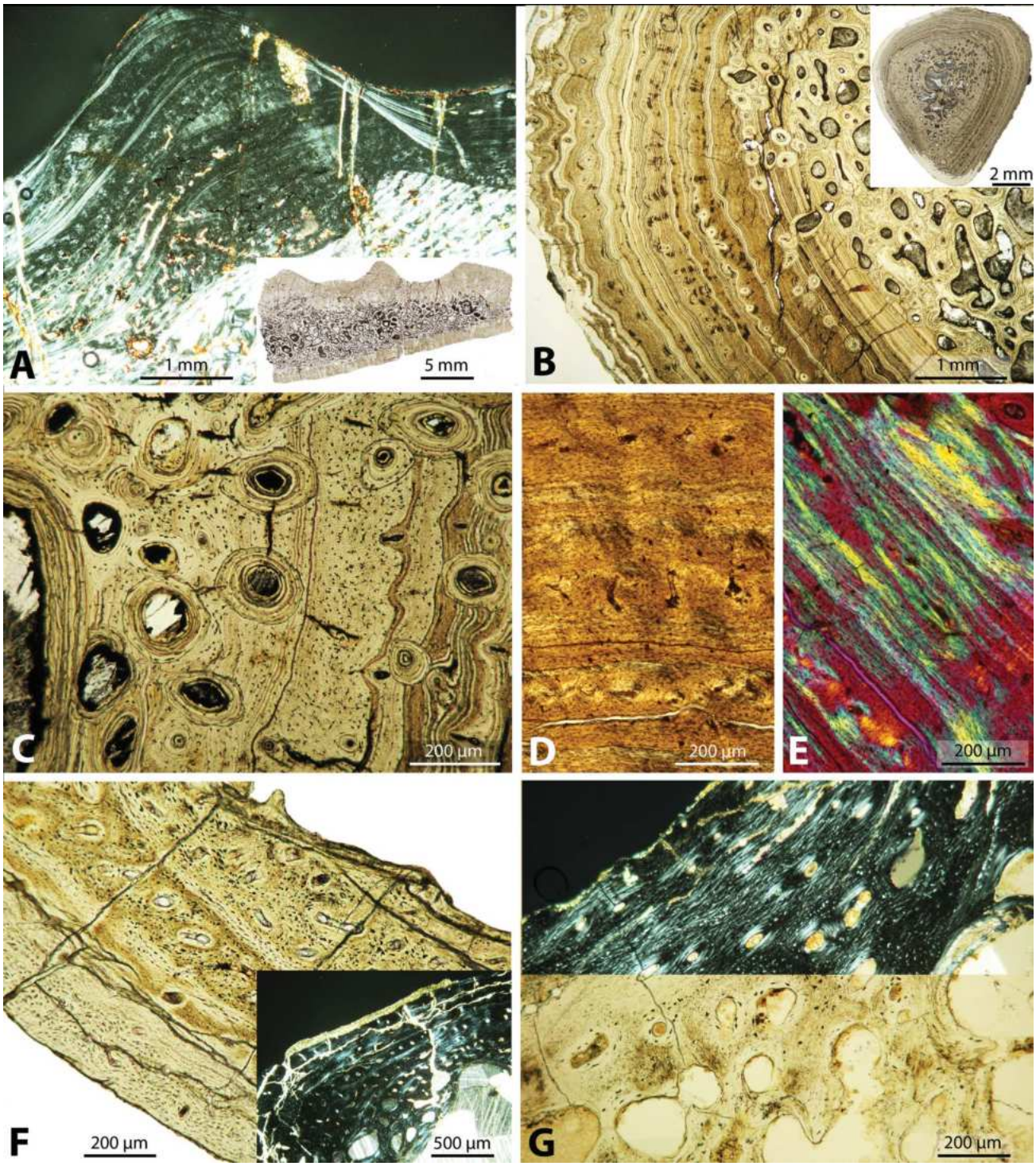


FIGURE 25.5 Archosauriforms: Phytosauria, Euparkeriidae. A, Parasuchia (Phytosauria). Phytosaur osteoderm. Superficial ornamentation results from cycles of bone deposition and erosion associated with extensive lateral drifts, as among crocodylians (insert: general view). B, "*Rutiodon*" femoral shaft. The endosteal margin is very progressive around the marrow cavity and associated with secondary osteons. Most of the cortex is lamellar-zonal (insert: general view). C, Same material, detail. The deep lamellar-zonal cortex is progressively invaded by secondary osteons. D and E, Phytosaur, undetermined large femur. Detail of the external cortex. Cyclical lamellar-zonal tissue. F and G: Archosauriforms; Euparkeriidae: *Euparkeria capensis*, femur. The inner cortex is fibrolamellar and the external cortex lamellar, with evidence of growth cycles (insert F: general view; upper half of G: polarized light).

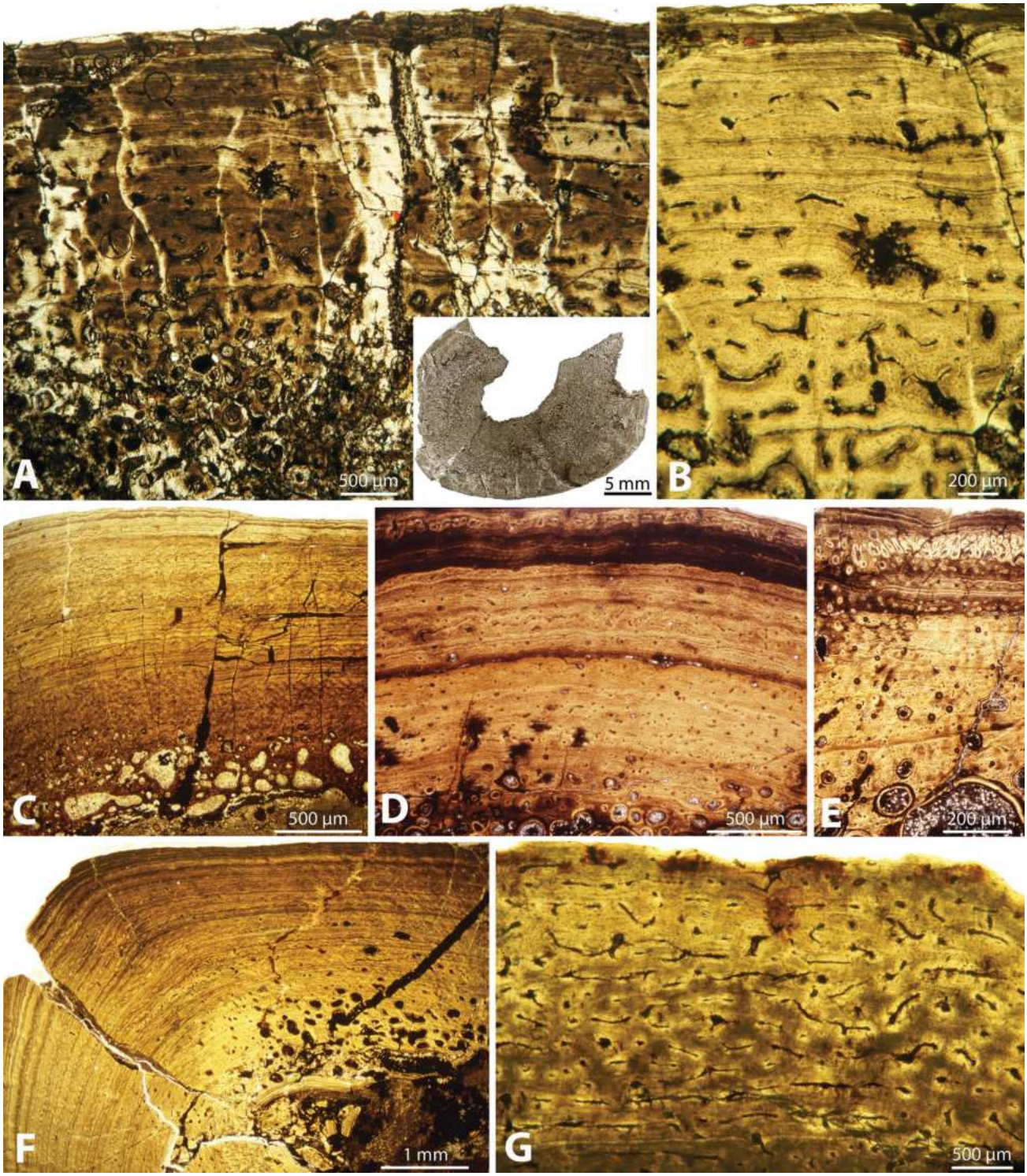


FIGURE 25.6 Archosauriforms; Archosauria, Pseudosuchia: Erpetosuchidae, Aetosauria, Paracrocodylomorpha. A, B, Archosauria, Pseudosuchia (Crurotarsi), Erpetosuchidae: *Tarjadia*. Large long bone shaft. The deep cortex is fibrolamellar with growth cycles, and turns into lamellar-zonal outwardly (insert: general view). C, Archosauria, Pseudosuchia (Crurotarsi), Aetosauria: *Stagonolepis* (*Calyptosuchus*), femoral shaft. The deep and middle cortical regions are fibrolamellar, whereas the external cortex is lamellar. The whole cortex is structured by several growth cycles. D, Aetosauria: *Typothorax*, radius shaft. Lamellar-zonal tissue forms the whole cortex. E, Same material, in this growth direction, a fast deposit of fibrolamellar bone has temporarily interrupted the deposition of lamellar tissue. F, Pseudosuchia (Crurotarsi), Rauisuchidae: *Postosuchus kirkpatricki*. humerus. The cortex has different structures on various bone sides, in connection with differences in radial growth rates. Numerous growth cycles are clear. G, Archosauria, Pseudosuchia (Crurotarsi), Paracrocodylomorpha: *Mandasuchu*s, femur. External cortex. Fibrolamellar bone tissue of a laminar to subplexiform pattern with one thin annulus.

VetBooks.ir

2018 for nomenclatural discussion) and *Desmatosuchus,* have been histologically described (Ricqlès et al. 2003). Recently the long bones and osteoderms of a single individual of *Coahomasuchus chathamensis* have been described (Hoffman et al. 2019), which allows interesting comparisons. Observations are summarized below.

In *Desmatosuchus*, a humerus (UCMP 32178) and radius (UCMP 28354) show a generally similar pattern but also extensive local differences linked to bone-specific morphogenetic constraints (Ricqlès et al. 2003). The deep cortex is formed by several thick zones separated by thin, nonvascular annuli associated with one LAG. The zones are made of a fibrolamellar tissue that locally displays a clear laminar type. The external cortex progressively becomes less vascularized, lamellar-zonal tissue with several LAGs, closer to each other toward the periosteal surface, and almost forming an EFS locally. The endosteal margin is complex, with several endosteal trabeculae in and around the marrow cavity, and erosion bays progressively spreading outward up to the external cortex locally. Haversian reconstruction is scattered but can be very dense in specific radial directions. The radius section has deep zones of a less laminar pattern, vascularized only by longitudinal canals. It offers a graphic example of sequential relocation during the growth of former, smaller metaphyseal cancellous bone into the later, larger diaphysis.

A femur of *Stagonolepis* ("*Calyptosuchus*") (specimen UCMP 25914; Figure 25.6C) has a thick cortex generally similar to that observed in *Desmatosuchus* (Ricqlès et al. 2003). There is a well-developed endosteal margin associated with larger and smaller erosion bays in the deep cortex. The latter is formed of wide fibrolamellar zones, with a reticular-like vascularization by primary osteons. Externally, the cortex progressively becomes a lamellar-zonal tissue with several cycles of deposition. Some especially thick external zones may revert to fibrolamellar tissue.

A proximal humerus of *Typothorax* (UCMP 25905) and a radius shaft (UCMP 25905; Figure 25.6D, E) give additional details (Ricqlès et al. 2003). The proximal epiphyseal surface of the (at least nearly) adult-sized humerus was observed in longitudinal section. The epiphysis is formed by cancellous trabeculae of endosteoendochondral origin that do not have a clear longitudinal orientation. A very thin (four to five cells thick) coating of hypertrophied calcified cartilage caps the bone tissue externally. The structure suggests that active longitudinal growth had ceased. In the distal shaft of the radius, which has a well-developed cancellous endosteal margin, an interesting detail in the external lamellar-zonal cortex is the local deposition of a fibrolamellar zone (Figure 25.6E), capped by later deposition of slow-growing tissue.

For *C. chathamensis*, we restrict our review here (but see Hoffman et al. 2019) to the long bones, a fibula (NCSM 16441) and a radius (NCSM 19765). In the radius, the inner cortex up to the first LAG is formed of woven-fibered bone, with few secondary osteons. Endosteal lamellar bone forms five separate layers indicative of cortical drift. Bone is deposited on one side of the section, opposite an area of resorption. In the cortex, subsequent LAGs occur between progressively thinner layers of parallel-fibered bone. LAG spacing decreases toward the periosteal surface, becoming tightly packed and suggesting the presence of an EFS. Seven LAGs are observed in the outermost cortical layer. In the fibula, vascularity decreases gradually from endosteal to periosteal regions, while growth marks (4) are recorded throughout the cortex. There is evidence of some Haversian remodeling near the endosteal margin of the woven-fibered bone.

Paracrocodylomorpha

This potential clade covers basally a nexus of crurotarsan carnivorous pseudosuchians, mostly quadrupedal, with limbs that reflect semierect to almost parasagittal gaits. Practically, the group more or less covers the older concept of "Rauisuchians" *sensu lato*, a polyphyletic assemblage, as recognized by Parrish (1993), which contained at least three distinct clades, including Prestosuchids and Rauisuchids *sensu stricto,* as well as Poposaurs.

Pending the formal description of *Mandasuchus* material from the Lower Triassic of Tanzania, Ricqlès et al. (2008) put this taxon as an *incertae sedis* archosauriform. The formal description of the material (Butler et al. 2017) now places it as a relatively basal paracrocodylomorph. We observed the histology of a small rib (BM R 692-11) and a femur (BMR 6791-63R) of *Mandasuchus* (Ricqlès et al. 2008). The rib has a lamellar-zonal structure with evidence of growth cycles and is diffusely eroded by bays, some of them turned into typical secondary osteons. The much larger femur (Figure 25.6G) is quite different, formed of an ill-defined fibrolamellar tissue containing irregular vascular anastomoses. Two annuli are well developed.

Batrachotomus, from the Middle Triassic of southern Germany, was a large (5–6 m) predator that recently received a detailed histological description (Klein et al. 2017). It is closer to the Rauisuchians *sensu stricto* (Butler et al. 2017) than to *Mandasuchus.* Samples from the femur, rib and gastralia of three individuals were studied. The femoral cortex comprises laminar fibrolamellar tissue throughout and is marked by three annual growth cycles, suggesting that the individual died in its fourth year of life, at which time it had reached 87% of maximum known femur length. The rib and gastralium both show an inner spongy organization surrounded by a ring of compact, avascular, highly organized parallel-fibered and/or lamellar bone largely covered by short fibers. According to some authors, *Batrachotomus* achieved its large body size in a very short time by fast, although interrupted, growth and not by protracted longevity, in contrast with most other Pseudosuchia and their relatives (e.g., phytosaurs, aetosaurs and most crocodylomorphs, including marine taxa). Such fast growth as well as the organization of the tissue is similar to the condition observed in ornithodirans. The pseudosuchians *Effigia* (Nesbitt 2006) and *Postosuchus* (Ricqlès et al. 2003) also show fibrolamellar tissue, but vascular density is lower when compared with *Batrachotomus*, and dominated by a longitudinal organization of primary osteons. Maximal growth cycle count suggests reduction of growth rate after the sixth cycle.

Rauisuchidae

This Middle-Upper Triassic clade, situated outside the crocodylian crown group, is now understood as the most crownward noncrocodylomorph pseudosuchians (Butler et al. 2017). It

VetBooks.ir

comprises several possibly facultatively bipedal pseudosuchians, represented in histological studies by *Postosuchus kirkpatricki*, formerly thought to be a poposaur (Ricqlès et al. 2003, p. 91). Chinsamy (1994) figured a cross section of its femur as exemplifying "zonal bone", with three LAGs. A humerus (UCMP 28353; Figure 25.6F) and a tibia (UCMP 25906, reidentified as a distal right femur by Werning 2013) were histologically described by Ricqlès et al. (2003). The humeral shaft has a well-developed layer of secondary endosteal bone, with signs of complex erosion/reconstruction phases, around its marrow cavity. The latter is free of bone trabeculae. The cortex is mainly lamellar and moderately vascularized by longitudinal primary osteons. There is clear evidence of several growth cycles. The cortex shows interesting histological differences on its two sides, linked to shape modeling that implies very different radial growth rates in different directions. The slower growing side is dominated by growth cycles with zones mostly formed by lamellar-zonal tissues in the external half of the cortex. On the fast-growing side, most zones become thicker and are fibrolamellar, with subplexiform to laminar patterns, overall very "dinosaur-like". Only the most external cortex remains in part lamellar-zonal.

Discussion

Recent studies of comparative bone tissue histology among archosauromorphs are set within a relatively consensual phylogenetic context (Figure 25.7), even though the positions of various clades remain debated (Nesbitt et al. 2009, Botha-Brink and Smith 2011, Nesbitt 2011, Werning and Irmis 2011, Legendre et al. 2013, 2016, Werning 2013, Ezcurra et al. 2014, Mukherjee 2015, Veiga et al. 2015, Ezcurra 2016, Werning and Nesbitt 2016, Jaquier and Scheyer 2017, Klein et al. 2017, Cubo and Jalil 2019). It is generally assumed that, among archosaurs, ornithodirans express a derived condition in their growth patterns: the generalized occurrence of fast growth during most of their ontogeny, as revealed by typical fibrolamellar tissues in primary bone cortices, along with high RMR to sustain this costly growth. This contrasts with a plesiomorphic condition among basal amniotes, retained among basal diapsids: a cyclical, gradual growth at low rates, reflecting a low RMR. Accordingly, the obvious question would be to discover how, when and where the transition from the basal to the derived physiological condition took place. Practically, bone histology could provide an answer because there is a clear relationship between the fine structural organization of primary periosteal bone and its rate of deposition ("Amprino's rule"; Montes et al. 2010). Nevertheless, this rule is complex to apply in practice because high growth rates are commonplace during early development, and low rates prevail at adult stages among most tetrapods, irrespective of other factors, such as RMR. Similarly, histological differences linked to growth-, shape- and size-specific peculiarities of each skeletal component introduce a histovariability that may hide other factors, such as those linked to general phylogenetic kinship. A case in point is the respect of strict conditions of homology (Cubo and Jalil 2019) to obviate as far as possible the problems linked to intra- and interspecific histodiversity comparisons. Apparent histological homoplasies are also very often encountered (Ricqlès 1992, Ricqlès et al. 2008), although they may result from a deep homology at the genetic level (see below, discussion).

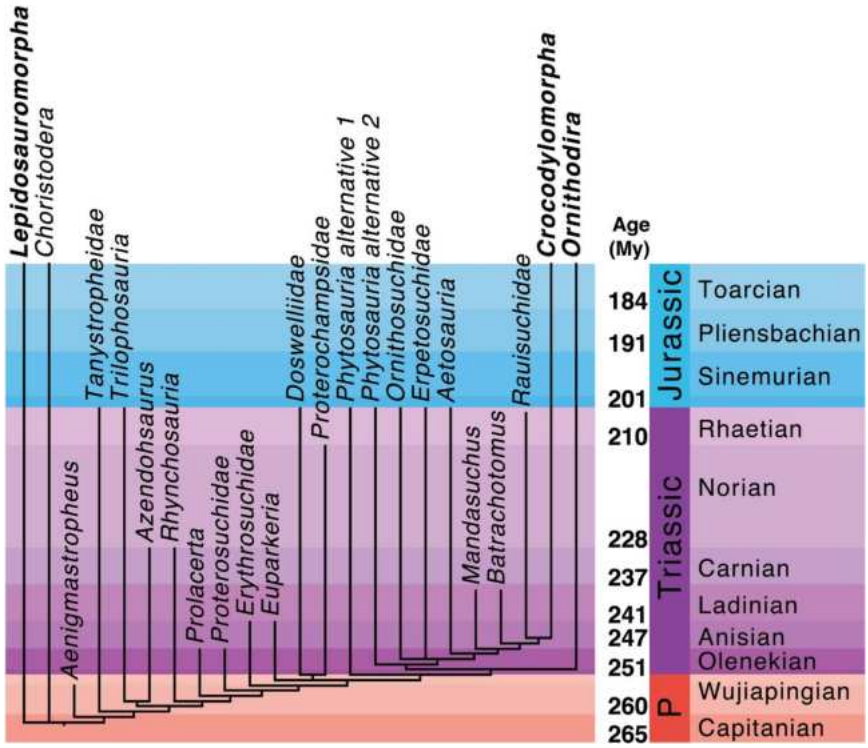


FIGURE 25.7 Time-calibrated tree of the Permo-Triassic archosauromorphs showing the phylogenetic positions and stratigraphic range of the main groups histologically surveyed. P, Permian.

VetBooks.ir

For all that, conclusions about evolution of general life history traits can hardly be extracted from comparative qualitative bone histology without careful, detailed qualifications.

Despite local phylogenetic anomalies, the consensus of the literature appears to be that, among crown archosaurs, the Ornithodira (bird-line archosaurs, including pterosaurs, dinosaurs and closely related taxa) basally had a high RMR and endothermic thermometabolism. Among Pseudosuchia, the situation is ambiguous: the RMR could have been close to those of the Ornithodira in some groups (ornithosuchians, prestosuchians, basal crocodylomorphs) and lower in phytosaurs and aetosaurs, with values possibly higher than among extant ectothermic tetrapods (Cubo and Jalil 2019). Some more crownward pseudosuchians (crown crocodylians) mostly reverted to an RMR of ectothermic scale.

Within crown archosaurs, the imperfect correspondence between the categories of bone tissue types and the dichotomy between ornithodirans and pseudosuchians is not surprising. If a more or less endothermic regime (high RMR) were the plesiomorphic condition for both, it may have been simply retained in several groups of pseudosuchians with a more or less "dinosaurian" morphology and histology (such as ornithosuchids and *Batrachotomus*).

Among nonarchosaurian archosauriforms the situation is variable: some groups have dinosaur-like RMR (erythrosuchids, euparkeriids) while others (proterosuchids, proterochampsids) are closer to the pseudosuchian lower mean RMR values (phytosaurs, aetosaurs) or definitely lower (*Vancleavea*).

Among nonarchosauriform archosauromorphs, the situation is equally variable. Basal archosauromorphs (Tanystropheidae) such as the mid-Triassic *Macrocnemus* and *Tanystropheus* seem to retain a basically slow and cyclical growth, as suggested by their histology. But the situation is more complex in the Permian *Aenigmastropheus*, a basal archosauromorph outside tanystropheids and *Protorosaurus* (Ezcurra et al. 2014), where, according to these authors, bone "exhibited high growth rates during early development, as exemplified by the short period of fibrolamellar bone formation. The steady decrease in vascularization coupled with the increase in spatial organization of the bone matrix up until the formation of lamellar-zonal bone indicates, however, that the animal was growing more slowly for most of its life" (Ezcurra et al. 2014, pp. 31–32). If so, the incipient origins of endothermy among archosauromorphs would have appeared during the Permian, whereas some taxa (e.g., tanystropheids) later either returned to a more generalized growth pattern linked to ectothermy, or retained the primitive ectothermic condition.

The problem is that histological samples for these taxa are so limited. Ideally, to obtain a full picture of the rate of growth reflected by skeletal tissues, a fairly complete ontogenetic sequence of individuals is desirable, and sections should be taken of standard elements (femur or tibia) at midshaft (Padian 2013). Without these controls, the deposition of tissues at a single random stage of ontogeny can be mistaken for the overall growth regime of a taxon.

Whether rhynchosaurs or allokotosaurians are the sister-group of the clade *Prolacerta* + Archosauriformes, in both groups, early growth, at least, could have been accomplished at very high speed. The high estimated RMR of *Azendohsaurus* is similar to that of most archosauriforms (Cubo and Jalil 2019), suggesting endothermy. Rhynchosaurs do produce typical plexiform bone tissue, but the later protracted cyclical growth toward adult size among most rhynchosaurs appears similar to the pattern observed in several groups of archosauriforms, and especially pseudosuchians. The histology of *Trilophosaurus* (an allokotosaur) may appear, in this context, indicative of a return to lower RMR and ectothermy, similar to the situation in *Vancleavea*.

Finally, and taking into account the specialized histological features linked to aquatic adaptations, the choristoderes (champsosaurs), as a close sister-group of archosauromorphs, illustrates the more generalized (plesiomorphic) pattern of cyclical growth at fairly low rates associated with low RMR and ectothermy.

From a histological point of view, the issue of an EFS among archosauromorphs, and the correlated problems of determinate (finite) versus indeterminate (indefinite) growth (with all their bearings on population structure and biology) raises the question of what, if any, is a species-specific adult body size among archosauromorphs. There may be a decoupling between slight diametral increments at the EFS (or EFS-like structures) and linear increments in skeletal growth. In a large individual, a slight EFS increment may indicate a significant change in overall body mass (with its consequences for reproductive fitness, etc.) without significant linear growth. Linear increments can be better evaluated through longitudinal sections of epiphyseal regions, which may indicate whether or not a given epiphysis is still active in longitudinal growth (Ricqlès et al. 2003 on *Typothorax*; Botha-Brink and Smith 2011 on *Euparkeria*).

To some extent, the current "race" to discover fast-growing bone tissue types in tetrapods ever more remote from extant archosaurs, to discover evidence for (or against) endothermy, suggests the fallacious trap of thinking that there are endothermic versus ectothermic bone tissues. The usual dichotomous polarity of plesiomorphic and apomorphic character states of cladistic analyses would naturally encourage us to take this approach to various tissue types (but see below). However, for nearly all workers in the field, and for quite some time (Ricqlès 1992), there is no such thing as endothermic (or ectothermic) bone *per se*. We can expect to find plexiform bone tissues outside archosauromorphs, perhaps even as far as placoderms. As soon as cellular and vascular bone emerged as an apomorphy among some early vertebrates, it brought a broad phenotypic plasticity that can be expressed under various circumstances mainly linked to the growth program, biomechanics and environment, hence integrating genetic and epigenetic factors. Depending on local growth and other circumstances, the basic genetic system controlling bone as a tissue can produce, in time and space, the entire continuum of bone tissue types, which scientists name and characterize for the practical purposes of recognition and description.

Similar functional circumstances of growth produce similar tissue types in different vertebrate groups, even those remote in time and in phylogenetic position. This is a *de facto* convergence (homoplasy) because each new appearance of the same tissue in distinct lineages does not derive from a common, unique ancestral tissue type that appeared in their most recent common ancestor. It is a novel and independent historical event that has the value of an apomorphy in each case in

VetBooks.ir

which it evolves. Nevertheless, it is likely that the resulting tissue homoplasies among various distinct clades (e.g., synapsids and archosaurs) express a deep homology at the level of the genes that control bone as a tissue or in their regulation.

The molecular basis of the functions of some genes related to endothermy in birds is now well understood (Cubo and Huttenlocker 2019). This may encourage a clear-cut dichotomy between those who have the genes conductive to endothermy and those who do not (ectotherms). But because very little is known about the control of the expression(s) of the gene(s) involved, it is not possible to rule out the evolution of more or less intermediate patterns of thermometabolic physiologies ("mesothermy" *sensu lato*). One approach is the estimates of RMR evaluated from histological data as a proxy for thermometabolic physiological regimes among extinct taxa (Cubo and Jalil 2019). The estimated RMR values in some Triassic archosauriforms are indeed "in between", close to those of some mammals but distinctly lower than among some nonavian theropods and birds. From an evolutionary point of view, it makes sense that high RMR regimes coevolved progressively, in correlation with many other anatomical and physiological advances, rather than having happened as a discrete evolutionary novelty. This is the current message of paleohistology. To conclude, we offer again (Ricqlès et al. 2008, p. 58) the idea that "the Triassic may have been a time of 'experimentation' in growth strategies for several archosauriform [we would say now archosauromorph] lineages, only one of which (the ornithodirans) eventually stayed with the higher investment strategy successfully".

Acknowledgments

The authors warmly thank Drs. J. Botha, V. Jacquier and T. Scheyer; F. Veiga, H. Soares and J. Sayao; Pr. J. Cubo-Garcia and N.-E. Jalil for providing the photos of (respectively) *Proterosuchus*, *Prolacerta*, *Tanystropheus*, *Teyumbaita* and *Azendohsaurus* published here and to Pr. K. Padian for phylogenetic and other information and linguistic revision.

REFERENCES

Arcucci, A., et al. 2019. Ecomorphology and bone microstructure of Proterochampsia from the Chañares Formation. *Acta Palaeont. Pol.* 64: 157–170.

Benton, M. J. 1984. The relationships and early evolution of the Diapsida. *Symp. Zool. Soc. Lond.* 52: 575–596.

Benton, M. J. 1985. Classification and phylogeny of the diapsid reptiles. *Zool. J. Linn. Soc.* 84: 97–164.

Botha-Brink, J. and R. M. H. Smith. 2011. Osteohistology of the Triassic archosauromorphs *Prolacerta, Proterosuchus, Euparkeria*, and *Erythrosuchus* from the Karoo Basin of South Africa. *J. Vert. Paleontol.* 31: 1238–1254.

Buffrénil, V de, et al. 1990. L'histologie osseuse des champsosauridés: données descriptives et interprétations fonctionnelles. *Ann. Paléont. (Vertébrés)* 76: 255–275.

Butler, R. J., et al. 2017. *Mandasuchus tanyauchen*, gen.et sp.nov., a pseudosuchian archosaur from the Manda beds (? middle Triassic) of Tanzania. Soc. of Vert. Pal Memoirs. 17. *J. Vert. Pal.* 37 (suppl 6): 96–121.

Carroll, R. L. and P. J. Currie. 1991. The early radiation of diapsid reptiles In *Origins of the higher groups of tetrapods*, Schultze, H. P. and L. Trueb eds., 354–424. Ithaca: Comstock, Cornell Univ. Press.

Cerda, I. A. and J. B. Desojo. 2010. Dermal armour histology of *Aetosauroides* Casamiquela, 1960 (Archosauria: Aetosauria) from the Upper Triassic of Argentina and Brazil. *Ameghiniana* 47: 70R.

Cerda, I. A. and J. B. Desojo. 2011. Dermal armour histology of aetosaurs (Archosauria: Pseudosuchia), from the Upper Triassic of Argentina and Brazil. *Lethaia* 44: 417–428.

Cerda, I. A., et al. 2013. Osteoderm microstructure of "rauisuchian" archosaurs from South America. *Geobios* 46: 273–283.

Cerda, I. A., et al. 2015. Osteoderm histology of Proterochampsia and Doswellidae (Reptilia, Archosauriformes) and their evolutionary and paleobiological implications. *J. Morphol.* 276: 385–402.

Cerda, I. A, et al. 2018. Novel data on aetosaur (Archosauria, Pseudosuchia) osteoderm microanatomy and histology: palaeobiological implications. *Palaeontology* 61: 721–45.

Charig, A. J and O. A. Reig. 1970. The classification of the Proterosuchia. *Biol. J. Linnean Soc.* 2: 125–171.

Chinsamy, A. 1990. Physiological implications of the bone histology of *Syntarsus rhodesiensis* (Saurischia: Theropoda). *Palaeontol. Afr.* 27, 77–82.

Chinsamy A. 1994. Dinosaur bone histology: implications and inferences. Paleontol.Society (special publ.) 7: 213–228.

Chinsamy-Turan, A. 2005. *The microstructure of dinosaur bone–deciphering biology with fine-scale techniques*. Baltimore-London: Johns Hopkins University Press.

Cruickshank, A. R. I. 1972. The proterosuchian thecodonts. In *Studies in vertebrate evolution*, Joysey, K. A. and T. S. Kemp, eds., 89–119. Edinburgh: Oliver and Boyd.

Cubo, J. and A. K. Huttenlocker. 2019. Vertebrate paleophysiology—introduction. *Philos. Trans R. Soc. B* 375: 20190130.

Cubo, J. and N.-E. Jalil. 2019. Bone histology of *Azendohsaurus laaroussii*: implication for the evolution of thermometabolism in archosaumorpha. *Paleobiology* 45: 317–330.

Cubo, J., et al. 2012. Paleohistological estimation of bone growth rate in extinct archosaurs. *Paleobiology* 38: 335–349.

Desojo, J. B., et al. 2013. Aetosauria: a clade of armoured pseudosuchians from the Upper Triassic continental beds. *Geol. Soc. London Spec. Pub.* 379: 203–239.

Enlow, D. H. 1969. The bone of reptiles. In *Biology of the reptilia*, Vol. 1 Morphology A, Gans, C., A. d'A. Bellairs and T. S. Parsons, eds., 45–80. London: Academic Press.

Enlow, D. H. and S. O. Brown. 1957. A comparative histological study of fossil and recent bone tissues. Part II. *Texas J. Sci.* 9: 186–214

Erickson, B. R. 1972. *The lepidosaurian reptile Champsosaurus in North America*, Monograph Vol 1. St. Paul, MN: The Science Museum of Minnesota.

Evans, S. E. 1984. The classification of the Lepidosauria. *Zool. J. Linn. Soc.* 82: 87–100.

Evans, S. E. 1988. The early history and relationships of the Diapsida. In *The phylogeny and classification of the tetrapods*, Vol. 1, Benton, M. J. ed., 221–253. Oxford, UK: Oxford University Press.

Evans S. 1990. The skull of Cteniogenys, a Choristodere (Reptilia, Archosaumorpha) from the Middle Jurassic of Oxfordshire. Zool. J. Linn. Soc. 99: 205–237.

Evans, S. E. and M. K. Hecht. 1993. A history of an extinct reptilian clade, the Choristodera: longevity, Lazarus-taxa, and the fossil record. *Evol. Biol*. 27: 323–338.

Ezcurra, M. D. 2016. The phylogenetic relationships of basal archosauromorphs, with an emphasis on the systematics of proterosuchian archosauriforms. *PeerJ* 4: e1778.

Ezcurra, M. D., et al. 2014. The origin and early evolution of Sauria: reassessing the Permian saurian fossil record and the timing of the crocodile-lizard divergence. *PLoS One* 9: e89165

Francillon-Vieillot, H., et al. 1990. Microstructure and mineralization of vertebrate skeletal tissues. In *Skeletal biomineralization: patterns, processes and evolutionary trends*, Carter, J. G. ed., 471–548. New York: Van Nostrand Reinhold.

Games, I. 1990. Growth curves for the Nile crocodile as estimated by skeletochronology. In *Crocodiles. Proc 10th Working Meeting of the Crocodile Specialist Group*, IUCN, Volume 1, 111–121. Gland, Switzerland: The World Conservation Union.

Gauthier, J. A. 1984. *A cladistic analysis of the higher categories of the Diapsida*. PhD thesis, University of California, Berkeley.

Gross, W. 1934. Die Typen des mikroskopischen Knochenbaues bei fossilen Stegocephalen und Reptilien. *Z. Anat. Entwicklungs.* 203: 731–764.

Hecht, M. K. 1992. A new choristodere (Reptilia, Diapsida) from the Oligocene of France: an example of the Lazarus effect. *Geobios* 25:115–131.

Heckert, A. B. and S. G. Lucas. 1999. A new aetosaur (Reptilia: Archosauria) from the Upper Triassic of Texas and the phylogeny of aetosaurs. *J. Vertebr. Paleontol*. 19: 50–68.

Heckert, A. B., et al. 1996. Redescription of *Redondasuchus reseri,* a Late Triassic aetosaur (Reptilia: Archosauria) from New Mexico (USA), and the biochronology and phylogeny of aetosaurs. *Geobios* 29: 619–632.

Hoffman, D. K. 2017. *X-ray computed tomographic reconstruction and bone histology of the aetosaur* Coahomasuchus chathamensis *(Archosauria:Stagonolepididae) from the upper Triassic Pekin formation, Deep River Basin, North Carolina and a re-analysis of its phylogenetic relationships*. B.S. thesis, Department of Geology, Appalachian State University, Boone, NC.

Hoffman, D. K., et al. 2019. Disparate growth strategies within Aetosauria: novel histologic data from the aetosaur *Coahomasuchus chathamensis*. *Anat. Rec*. 302: 1504–1515.

Hoffstetter, R. 1955. Thecodontia. In *Traité de paléontologie*, Vol. V: Amphibiens, Reptiles, Oiseaux, Piveteau, J. ed., 665–694. Paris: Masson et Cie.

Horner, J. R., et al. 1999. Variation in dinosaur skeletochronology indicators: implications for age assessment and physiology. *Paleobiology* 25: 295–304.

Horner, J. R., et al. 2000. Long bone histology of the hadrosaurid dinosaur *Maiasaura peeblesorum*: growth dynamics and physiology based on an ontogenetic series of skeletal elements. *J. Vertebr. Paleont*. 20: 115–129.

Houssaye, A., et al. 2016. Adaptive patterns in aquatic amniote bone microanatomy – more complex than previously thought. *Integr. Comp. Biol*. 56: 1349–1369.

Huene, F. von. 1935–1942. *Die fossilen Reptilien des südamerikanischen Gondwanalandes*. München: C.H. Becksche Verlagsbuchhandlung.

Jaquier, V. P. and T. M. Scheyer. 2017. Bone histology of the Middle Triassic long-necked reptiles *Tanystropheus* and *Macrocnemus* (archosauromorpha, Protorosauria). *J. Vertebr. Paleont*. 37: e1296456.

Katsura, Y. 2010. Ontogenetic change of bone microstructures and its ethological implication in *Champsosaurus* (Diapsida, Choristodera). *Hist. Biol* 22: 380–386.

Klein, N., et al. 2017. Preliminary observations on the bone histology of the Middle Triassic pseudosuchian archosaur *Batrachotomus kupferzellensis* reveal fast growth with laminar fibrolamellar bone tissue. *J. Vertebr. Paleont*. 37 (4): e1333121. doi: 10.1080/02724634.2017.1333121.

Laurin, M. 1991. The osteology of a Lower Permian eosuchian from Texas and a review of diapsid phylogeny. *Zool. J. Linn. Soc*. 101: 59–95.

Legendre, L. J., et al. 2013. Evidence for high bone growth rate in *Euparkeria* obtained using a new paleohistogical inference model for the humerus. *J. Vertebr. Paleont*. 33: 1343–1350.

Legendre, L. J., et al. 2016. Palaeohistological evidence for ancestral high metabolic rate in Archosaurs. *Syst. Biol*. 65: 989–996.

Li, C., et al. 2018. A Triassic stem turtle with an edentulous beak. *Nature* 560: 476.

Marsà, J. A. G., et al. 2020. Comparative bone microstructure of three archosauromorphs from the Carnian, Late Triassic Chañares Formation of Argentina. *Acta Palaeont. Pol*. 65: 387–398. doi: 10.4202/app.00644.2019.

Matsumoto, R. and S. E. Evans. 2010. Choristoderes and the freshwaters assemblages of Laurasia *J. Iberian Geol*. 36 (2): 253–274.

Modesto S.P., Sues H.D. 2004. The skull of the Early Triassic arhosauromoph Prolacerta broomi and its phylognetic significance. Zool. J. Linn. Soc. 140: 335–351.

Montes, L., et al. 2007. Relationships between bone growth rate, body mass and resting metabolic rate in growing amniotes: a phylogenetic approach. *Biol. J. Linn. Soc*. 92: 63–76.

Montes, L., et al. 2010. Relationship between bone growth rate and bone tissue organization in amniotes: first test of Amprino's rule in a phylogenetic context. *Anim. Biol*. 60: 25–41.

Mukherjee, D. 2015. New insights from bone microanatomy of the Late Triassic *Hyperodapedon* (Archosauromorpha, Rhynchosauria): implications for archosauromorph growth strategy. *Palaeontology* 58: 313–339.

Nesbitt, S. J. 2006. The anatomy of *Effigia okeeffeae* (Archosauria, Suchia), theropod-like convergence, and the distribution of related taxa. *Bull. Am. Mus. Nat. Hist*. 302: 1–84.

Nesbitt, S. J. 2011. The early evolution of archosaurs: relationships and the origin of major clades. *Bull. Am. Mus. Nat. Hist*. 352: 1–292.

Nesbitt, S. J., et al. 2009. The osteology and relationships of *Vancleavea campi* (Reptilia: archosauriformes). *Zool. J. Linn. Soc*. 157: 814–864.

Nesbitt, S. J., et al. 2015. Postcranial anatomy and relationships of *Azendohsaurus madagaskarensis*. *Bull. Am. Mus. Nat. Hist*. 398: 1–126.

Nopcsa, F. and E. Heidsieck. 1934 Uber eine pachyostotische Rippe aus der Kreide Rügens. *Acta Zool. (Stockholm)* 15: 431–455.

Padian K. 2013. Why study the bone microstructure of fossil tetrapods? In *Bone histology of fossil tetrapods*, Padian, K and E. T. Lamm eds., 1-12. Berkeley: Univ. of California Press.

Padian, K., et al. 2004. Growth in small dinosaurs and pterosaurs: the evolution of archosaurian growth strategies. *J. Vertebr. Paleont.* 24: 555–571.

Parker, W. G. 2018. Redescription of *Calyptosuchus wellesi* (Archosauria: Pseudosuchia, Aetosauria) from the Late Triassic of the Southwestern United States with a discussion of genera in vertebrate paleontology. *PeerJ* 6: e4291. doi: 10.7717/peerj.4291.

Parrish, J. M. 1993. Phylogeny of Crocodylotarsi, with reference to archosaurian and crurotarsan monophyly. *J. Vertebr. Paleont.* 13: 287–308.

Piveteau, J. 1955. Synaptosauria. In *Traité de paléontologie*, Vol. V: Amphibiens, Reptiles, Oiseaux, Piveteau, J. ed., 412–419. Paris: Masson et Cie.

Reid, R. E. H. 1996. Bone histology of the Cleveland Lloyd dinosaurs and of dinosaurs in general. Part I: Introduction to bone tissues. *Brigham Young Univ. Geol. Stud.* 41: 25–72.

Reig, O. A. 1970. The Proterosuchia and the early evolution of the archosaurs; an essay about the origin of a major taxon. *Bull. Mus. Comp. Zool.* 139: 229–292.

Reisz, R. R. 1977. *Petrolacosaurus*, the oldest known diapsid reptile. *Science* 196: 1091–1093.

Ricqlès, A. de. 1969. Recherches paléohistologiques sur les os longs des tétrapodes. II quelques observations sur la structure des os longs des Theriodontes. *Ann. Paléont.* 55: 3–52.

Ricqlès, A. de. 1976. On bone histology of fossil and living reptiles, with comments on its functional and evolutionary significance. In *Morphology and biology of reptiles*, Bellairs, A. d'A. and C. B. Cox eds., 123–150. London: Academic Press.

Ricqlès A.de. 1978. Recherches paléohistologiques sur les os longs des tétrapodes. Part VII (Third part: Evolution): *Ann. Paléont.* 64 (1): 85–111.

Ricqlès A. de. 1980. Tissue structures in dinosaur bone-functional significance and possible relation to dinosaur physiology. Pp 103–139 in Thomas R.D.K., Olson E.C. (Ed.) A cold look at the warm blooded dinosaurs. AAAS Symposium 28. Westview, Boulder, Col.

Ricqlès, A. de. 1992. Paleoherpetology now: a point of view. In *Herpetology: current research on the biology of amphibians and Reptiles*, Adler, K. ed., 97–120. Oxford (Ohio): First World Congress of Herpetology; Society for the Study of Amphibians and Reptiles.

Ricqlès, A. de and V. de Buffrénil. 2001. Bone histology, heterochronies and the return of tetrapods to life in water: w[h]ere are we? pp. 289–310 in J. M. Mazin and V. de Buffrénil. Verlag Dr. Friedrich Pfeil, München.

Ricqlès, A. de, et al. 2003. On the bone histology of some Triassic pseudosuchian archosaurs and related taxa. *Ann. Paléont.* 89: 67–101.

Ricqlès, A. de, et al. 2008. On the origin of high growth rates in archosaurs and their ancient relatives: complementary histological studies on Triassic archosauriforms and the problem of a "phylogenetic signal" in bone histology. *Ann. Paléont.* 94: 57–76.

Rieppel, O. 1989. The hind limb of *Macrocnemus Bassanii* (Nopcsa) (Reptilia, Diapsida): development and functional anatomy. *J. Vertebr. Paleontol.* 9: 373–87.

Romer, A. S. 1966. *Vertebrate paleontology.* 3rd edition. Chicago: University of Chicago Press.

Romer, A. S. 1968. *Notes and comments on vertebrate paleontology*. Chicago: University of Chicago Press.

Sanchez, S., et al. 2012. Three-dimensional synchrotron virtual paleohistology: a new insight into the world of fossil bone microstructures. *Microsc. Microanal.* 18: 1095–1105.

Scheyer, T. M. and J. B. Desojo. 2011. Palaeohistology and microanatomy of rauisuchian osteoderms (Archosauria: Pseudosuchia). *Palaeontology* 54: 1289–1302.

Scheyer, T. M., et al. 2014. Bone histology of phytosaur, aetosaur, and other archosauriform osteoderms (Eureptilia, Archosauromorpha). *Anat. Rec.* 297: 240–260.

Seitz, A. L. 1907. Vergleichende Studien uber den mikroskopischen Knochenbau Fossiler und rezenter Reptilien. *Nova Acta Leopold. Abh Deutsch. Akad. Naturforsch.* 37: 230–370.

Sereno, P. C. 1991. Basal archosaurs: phylogenetic relationships and functional implications. *Soc. Vert. Paleontol. Mem.* 2: 1–53.

Sereno, P. C. and A. B. Arcucci. 1990. The monophyly of crurotarsal archosaurs and the origin of bird and crocodile ankle joints. *Neues Jahrb. Geol. Paläontol. Abh.* 180: 21–52.

Skutschas, P. P. and D. D. Vitenko. 2017. Early Cretaceous choristoderes (Diapsida, Choristodera) from Siberia, Russia. *Cretaceous Res.* 77: 79–92.

Smith, R. M. H. and J. Botha-Brink. 2014. Anatomy of a mass extinction: sedimentological and taphonomic evidence for drought-induced die-offs at the Permo-Triassic boundary in the main Karoo Basin, South Africa. *Palaeogeogr. Palaeoclimatol. Palaeoecol.* 396: 99–118.

Taborda, J. R. A., et al. 2013. Growth curve of *Aetosauroides scagliai* (Pseudosuchia: Aetosauria) inferred from osteoderm histology. In *Anatomy, phylogeny and palaeobiology of early archosaurs and their kin*, Nesbitt, S. J., J. B. Desojo and R. B. Irmis, eds., 413–423. London: Geological Society.

Taborda, J. R., et al. 2015. Intraspecific variation in *Aetosauroides scagliai* Casamiquela (Archosauria: Aetosauria) from the Upper Triassic of Argentina and Brazil: An example of sexual dimorphism? *Ameghiniana* 52: 173–187.

Veiga, F. H., et al. 2015. Osteohistology of hyperodapedontine rhynchosaurs from the Upper Triassic of Southern Brazil. *Acta Palaeont. Pol.* 60: 829–836.

Walker, A. D. 1964. Triassic reptiles from the Elgin Area: Ornithosuchus and the origin of carnosaurs. *Philos. Trans. R. Soc. Lond. B* 248: 53–134.

Werning, S. A. 2013. *Evolution of bone histological characters in amniotes, and the implications for the evolution of growth and metabolism*. PhD Dissertation, University of California, Berkeley.

Werning, S. and R. B. Irmis. 2010. Reconstructing the ontogeny of the Triassic basal archosauromorph using bone histology and limb bone morphometrics. *J. Vert. Paleont.*, 30 (Suppl.): 185A–186A.

Werning, S. and R. B. Irmis. 2011. Reconstructing growth of the basal archosauromorph *Trilophosaurus. Integr. Comp. Biol.* 51: SICB 2011 Annual Meeting, Salt Lake City. Abstract 39.2/E147.

Werning, S. and S. J. Nesbitt. 2016. Bone histology and growth in *Stenaulorhynchus stockleyi* (Archosauromorpha: Rhynchosauria) from the Middle Triassic of the Ruhuhu Basin of Tanzania. *C. R. Palevol* 15: 163–175.

VetBooks.ir

26

Archosauromorpha: The Crocodylomorpha

Vivian de Buffrénil, Michel Laurin and Stéphane Jouve

CONTENTS

The Crocodylian Family Tree 486
The Eusuchians 486
An Overview of Early Crocodylomorphs 487
The Crocodylomorph Skeleton in Histological Literature 489
Eusuchia and Related Forms 489
General Microanatomic Features of Long Bones and Ribs 489
Histology of Long Bones 492
Remarks on Ribs and Vertebrae 494
Skull Roof Elements and Osteoderms 496
Microanatomical Features 496
Histological Features 496
Remarks on *Susisuchus* and *Goniopholis* 496
The Tethysuchia: Dyrosaurs and *Sarcosuchus* 497
Thalattosuchians 499
Microanatomy of Thalattosuchian Skeletons 499
Histology of Thalattosuchian Bones 499
Notosuchia and Peirosaurids 501
Notosuchia 501
Peirosaurids 503
Basal Crocodylomorphs: The Sphenosuchians *Terrestrisuchus-Saltoposuchus* and *Hesperosuchus* 504
Concluding Remarks 505
References 505

The Crocodylian Family Tree

The Eusuchians

Extant crocodylians are one of two archosaurian groups still represented today, the other being birds (i.e., Dinosauria). They are the only survivors of three clades that were differentiated and widespread in the Late Cretaceous: the Gavialoidea, Crocodyloidea and Alligatoroidea (Brochu 1999, 2001a,b). Only 27 extant species are currently recognized (Grigg and Kirshner 2015), mainly distributed in the intertropical area. This situation poorly reflects the past diversity and morphological richness of the group. Crocodylomorphs are represented by numerous well-preserved remains in the fossil record, and their evolutionary relationships are well understood. Extant forms are distributed among three clades. Crocodyloidea, comprising several genera such as *Crocodylus*, *Mecistops* and *Osteolaemus*, are more closely related to Alligatoroidea (*Alligator*, *Caiman*, *Melanosuchus*, *Paleosuchus*) than to Gavialoidea (*Gavialis*).

The phylogenetic relationships of the true gharial, *Gavialis gangeticus*, to other crocodilians is one of the most long-standing conflicts between molecular and morphological analyses. From a molecular perspective, the tub-snouted *G. gangeticus* is considered the closest living relative to the Malayan false gharial *Tomistoma schlegelii* (Gatesy et al. 2003, Janke et al. 2005, Roos et al. 2007, Willis et al. 2007, Gatesy and Amato 2008, Willis 2009, Meganathan et al. 2010, Man et al. 2011, Oaks 2011). *G. gangeticus* is thus considered a crocodyloid. Conversely, all morphological analyses including dozens of extinct taxa place *Gavialis* and close relatives as the sister taxon to all other extant crocodilians. They are the basal-most crocodylian group, the gavialoids (Norell 1989, Brochu 1997, 1999, 2013, Piras et al. 2010, Puértolas-Pascual et al. 2013, Jouve et al. 2014, Jouve 2016). A recent, total evidence

VetBooks.ir

tip-dating analysis suggests that the molecular tree is basically correct (Lee and Yates 2018), but this assumes that a proper weighting was found between morphological and molecular data sets, and ignores the problems linked with applying the Markov model to morphological data, which apparently fit that model poorly (Goloboff et al. 2019).

Extant crocodiles belong to the broad and once very diverse clade Eusuchia. The latter, distributed nearly worldwide during the Mesozoic and early Cenozoic, includes extremely large forms such as *Rhamphosuchus* (more than 10 m in total length), as well as much smaller ones such as *Pietraroiasuchus*, a small basal eusuchian comparable in size to extant *Osteolaemus* and *Paleosuchus* (total length ≤1.5 m). Most eusuchians were comparable to medium-sized extant forms such as *Crocodylus* sp. and *Alligator mississippiensis*. With some exceptions, eusuchians are characteristically amphibious forms, adapted to ambush preying in rivers, lakes and, for some of them (e.g., *Crocodylus porosus*), estuarine or coastal environments. Eusuchians are basically opportunistic predators but longirostrine forms (e.g., gharials, *Thoracosaurus isorhynchus*, *T. schlegelii*) show a marked adaptation to preying on teleosts, whereas some short-snouted extinct forms with blunt teeth were probably shell-crushers (e.g., *Gnatusuchus pebasensis*, *Brachychampsa montana*), or possibly herbivorous, such as *Acynodon* (Salas-Gismondi et al. 2015, Melstrom and Irmis 2019). One of the most peculiar groups of eusuchians, the Planocraniidae, is considered the sister taxon to the clade Crocodyloidea + Alligatoroidea, or Brevirostres (Brochu 2013). The strong lateromedial compression of teeth in the Planocraniidae, with a serration similar to that of theropod dinosaurs in some species, suggests that this Paleogene group comprised terrestrial predators (Rossmann 2000a, Brochu 2013). This hypothesis is supported by the postcranial morphology of *Boverisuchus magnifrons*, a German planocraniid: its limbs and hoof-like unguals do not match those of semiaquatic animals, like all other known crocodilians, but do match fully terrestrial species (Rossmann 2000b). Anatomically, eusuchians (judging from extant forms) have some characteristics unknown in other nonarchosaurian diapsids. Their buccal cavity is entirely separated from the upper airways by a secondary palate formed by the premaxillae, maxillae, palatines and pterygoid. Their heart is four-chambered with a nearly complete separation between arterial and venous blood systems, except for a minute connection at the base of the right and left aortic arches, the foramen of Panizza (review in Seymour et al. 2004). In addition, they have complex, multichambered lungs and use pelvic girdle movements during breathing ("pelvic aspiration"), thus increasing tidal volume and the efficiency of gas exchanges (e.g., Claessens 2004). All eusuchians also bear strong osteoderm shields covering their back and often their flanks and belly, and extending in some taxa to their legs.

An Overview of Early Crocodylomorphs

Although some morphological and ecological variations exist among living crocodilians, when extinct forms are considered, these variations are much larger, in terms of morphology and ecology, especially when considered at the crocodylomorph level, a broad clade including not only crown crocodylians, but also their extinct relatives (Figure 26.1).

The "sphenosuchians" are the first and oldest crocodylomorphs. They were relatively small terrestrial animals and looked very little like extant crocodylians. They had an erect stance and long, gracile limbs (Irmis et al. 2013). The oldest known species, *Trialestes romeri*, was discovered in the late Carnian Ischigualasto Formation of Argentina (231–225 My; Clark et al. 2001, Lecuona et al. 2016). The youngest known members, from the Late Jurassic Morrison Formation of North America, are represented by *Macelognathus vagans* and *Hallopus victor* (Walker 1970, Göhlich et al. 2005). Although some initial phylogenetic analyses recovered sphenosuchians as a clade (Wu and Chatterjee 1993, Sues et al. 2003), most recent analyses suggest that sphenosuchids form a paraphyletic group at the base of the crocodylomorphs (Nesbitt 2011, Zanno et al. 2015, Leardi et al. 2017).

Basal-most crocodyliforms were also terrestrial forms: small protosuchians bore erect limbs like the sphenosuchians. They are known from the middle Late Triassic, mainly flourished in the Early Jurassic, and eventually became extinct near the end of the Cretaceous (Bonaparte 1971, Martínez et al. 2018). Although they were sometimes considered possibly monophyletic (Hecht and Tarsitano 1983, Wu et al. 1994, 1997, Wilberg 2015, Wilberg et al. 2019), most recent work has found them paraphyletic, with at least three successive taxa at the base of the crocodyliforms (Pol et al. 2004, Pol and Norell 2004a,b, Buscalioni 2017, Martínez et al. 2018). Their possible monophyly depends on the phylogenetic relationships of the problematic thalattosuchians. In the phylogenetic analyses that find or constrain thalattosuchians as basal crocodyliforms (Jouve 2009, Wilberg 2015, Dollman et al. 2018, Wilberg et al. 2019), protosuchians form a monophyletic group. Thus, the thalattosuchian relationships determine the phyletic position of protosuchians.

The last group of completely terrestrial extinct crocodyliforms is Notosuchia. In morphological and ecological perspectives, they are particularly diverse, including small herbivores and large carnivores (Melstrom and Irmis 2019). Some of them have mammal-like teeth, an armadillo-like dorsal shield or teeth mimicking those of theropods (Marinho and Carvalho 2009, Riff and Kellner 2011, Melstrom and Irmis 2019). In addition, their limbs are long and erect. the group is largely considered monophyletic (Turner and Buckley 2008, Andrade et al. 2011, Fortier et al. 2011, Leardi et al. 2015, Turner 2015, Young et al. 2016, Martinelli et al. 2018, Wilberg et al. 2019), but the species that should be included in it are disputed: the araripesuchids and peirosaurids in particular are sometimes excluded from Notosuchia (Larsson and Sues 2007, Andrade and Bertini 2008, Turner and Buckley 2008, Fortier et al. 2011). Also, the monophyly of large terrestrial predators represented by the Late Cretaceous baurusuchids and the Paleogene sebecids (i.e., *Baurusuchus pachecoi* and *Sebecus icaeorhinus*; Leardi et al. 2015, Turner 2015, Fiorelli et al. 2016, Barrios et al. 2018, Dollman et al. 2018, Martinelli et al. 2018), has been extensively discussed, and some phylogenetic analyses have found baurusuchids more closely related to other notosuchians, and sebecids more closely related to peirosaurids (Andrade et al. 2011, Montefeltro et al. 2013), and sometimes outside Notosuchia (Larson 1994, Larsson and Sues 2007, Andrade and Bertini 2008, Young et al. 2016). The latest notosuchian has been referred to *Langstoni huilensis*,

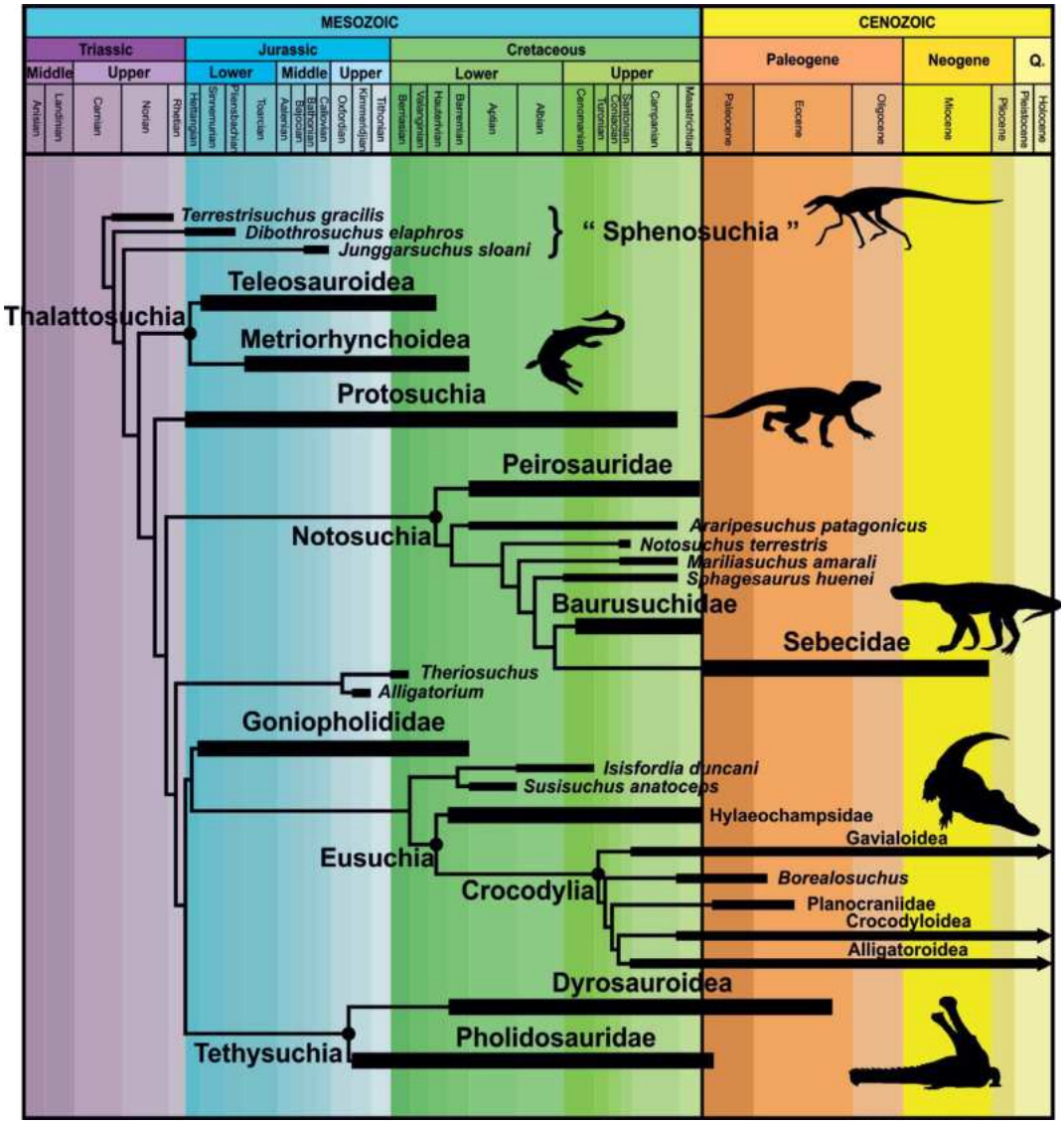


FIGURE 26.1 A consensus phylogenetic tree of the Crocodylomorpha.

a sebecid from the Late Miocene of Argentina (Busbey 1986, Paolillo and Linares 2007).

Neosuchians comprise semiaquatic crocodyliforms such as goniopholidids, tethysuchians and eusuchians, including extant crocodylians. Their general morphology is more like that of extant species, with short parasagittal limbs and a powerful tail. Goniopholidids are known from the Early Jurassic to the mid-Cretaceous, although some Late Cretaceous species have been sometimes referred to this group. Among them, the phylogenetic relationship of the Campanian *Denazinosuchus kirtlandicus* is still debated (Andrade et al. 2011, Allen 2012), and the Cenomanian *Dakotasuchus kingi* and *Woodbinesuchus byersmauricei* are probable pholidosaurids (Jouve and Jalil 2020). Goniopholidids have been alternatively described as closely related to eusuchians (Turner and Buckley 2008, Jouve 2009, Fortier et al. 2011, Montefeltro et al. 2013, Leardi et al. 2015, Turner and Pritchard 2015, Fiorelli et al. 2016, Adams et al. 2017, Wilberg et al. 2019), tethysuchians (Jouve 2009, Andrade et al. 2011, Kuzmin et al. 2018) or as the clade formed by tethysuchians and eusuchians (Young et al. 2016). The monophyly of the tethysuchians is not debated, and all recent analyses find dyrosaurids as the sister taxon to pholidosaurids, which together form the tethysuchians. Pholidosaurids appear in the Late Jurassic and were until recently considered extinct since the early Late Cretaceous; however, recent discoveries show that they survived the Late Cretaceous-Paleogene crisis, and became extinct almost 30 My later than previously thought (Jouve and Jalil 2020). They were aquatic animals and are found in marine as well as freshwater environments. Most of the dyrosaurids were found in marine environments, and their tall and powerful tail suggests that they were particularly good swimmers. The oldest known dyrosaurids are Maastrichtian. They were very diverse and survived the K-Pg crisis, further diversifying during the Paleocene, before becoming extinct by the end of the Eocene. Both pholidosaurids and dyrosaurids were mainly piscivorous longirostrine crocodyliforms, but some

VetBooks.ir

of them evolved stronger teeth and probably became more opportunistic predators.

The most aquatic crocodylomorph clade is probably the Thalattosuchia. They appeared during the Early Jurassic, and form two fairly distinct clades: the Teleosauroidea and the Metriorhynchoidea. Most of the members of both groups are found in marine environments, with some exceptions (Martin et al. 2019). The teleosauroids remained semiaquatic, although their limbs were shorter than those of extant taxa. Conversely, the more aquatic metriorhynchoids had flattened limbs and hypocercal tails, and were thus more adapted to a pelagic life than the teleosauroids. The metriorhynchoids have been extensively reviewed, and their systematic relationships are relatively well understood (Young and De Andrade 2009, Young et al. 2010, Foffa and Young 2014). In contrast, most of the teleosauroid species have been gathered, based on nondiagnostic remains, in the wastebasket genus *Steneosaurus*, which included nearly half of the known teleosauroid species, along with numerous doubtful taxa (Jouve et al. 2017). Fortunately, a recent review clarified teleosauroid taxonomy, erecting seven new genera (Johnson et al. 2020). The phylogenetic relationships of the thalattosuchians to other crocodylomorphs probably represent the most challenging problem in crocodylomorph systematics. They are often considered neosuchians, closely related to the longirostrine tethysuchians (Turner and Buckley 2008, Andrade et al. 2011, Fiorelli et al. 2016, Barrios et al. 2018, Kuzmin et al. 2018, Leardi et al. 2018), or alternatively as basal crocodyliforms (Larsson and Sues 2007, Andrade and Bertini 2008, Montefeltro et al. 2013, Turner 2015, Wilberg et al. 2019) or outside crocodyliforms (Young et al. 2016). The clade formed by thalattosuchians and tethysuchians found in some analyses is mainly formed by longirostrine species, and it has been suspected to be based on homoplasies related to this particular morphology (Benton and Clark 1988, Jouve et al. 2006, Jouve 2009, Wilberg 2015). This situation is clearly related to the lack of early thalattosuchians in the fossil record. The oldest known species, *Peipehsuchus* from the Chinese Sinemurian, already possessed the diagnostic features of teleosauroids (Vignaud 1995, Wilberg 2015).

The Crocodylomorph Skeleton in Histological Literature

The microstructure of long bones in extant crocodiles, considered mainly through the model of the American alligator (*A. mississippiensis*), was described by Quekett (1849), in the earliest comparative study of skeletal histology. Descriptions were summarized in later reviews, including Foote (1911, 1916), Amprino and Godina (1947), Enlow and Brown (1957), Peabody (1961), Warren (1963), Enlow (1969) and Ricqlès (1976). All these studies basically used the limb long bones (mainly the femur) of adult individuals. With the development of skeletochronology and its use for the management of threatened wild populations, other species such as *Crocodylus siamensis* (Buffrénil 1980a) and *C. niloticus*, and the use of other skeletal elements, especially osteoderms (e.g., Hutton 1986), were examined. Histological studies of the skeleton in extinct and noneusuchian crocodylomorphs remain scarce compared to the abundant fossil record available worldwide for this clade. Among the most detailed contributions are those for two dyrosaurs, *Dyrosaurus phosphaticus* (Buffetaut et al. 1982) and an unidentified taxon from the Early Paleocene of northwestern Brazil (Andrade and Sayão 2014); three thalattosuchians, *Steneosaurus* sp., *Teleosaurus* sp. and *Metriorhynchus superciliosus* (Hua and Buffrénil 1996); the giant alligatoroid *Deinosuchus* (Erickson and Brochu 1999); an unidentified eusuchian from the Upper Cretaceous of Spain (Company and Pereda-Suberbiola 2017); an early neosuchian, *Susisuchus anatoceps* (Sayão et al. 2016); a small cursorial notosuchian from the Eocene of Europe, *Iberosuchus macrodon* (Cubo et al. 2017); the peirosaurid *Pepesuchus deisae* (Sena et al. 2018) and the basal Triassic form *Terrestrisuchus gracilis* (Ricqlès et al. 2003). Moreover, the morphogenetic processes that differentiate bone ornamentation were studied in a variety of taxa by Buffrénil et al. (2015).

The Crocodylomorpha is of considerable interest in two macroevolutionary problems. (1) How has the thermal ecophysiology of tetrapods been adaptively modified through time? (2) How could the K/Pg environmental crisis have affected vertebrate faunas? These questions can be advanced through more intensive histological and paleohistological study of their bones. Here we review some of the most important information currently available on this topic, starting with the best documented clade, Eusuchia. In addition to published descriptions, we took bone sections (100 µm ± 20 in thickness) from a sample of limb long bones, ribs, osteoderms and the cranial roof of several extant and extinct taxa. When possible, long bone sections were made at mid-diaphysis in both transverse and longitudinal planes (i.e., orthogonal and parallel, respectively, to the long axis of the bone). The sections were then studied in transmitted ordinary or polarized light.

Eusuchia and Related Forms

General Microanatomic Features of Long Bones and Ribs

Contrary to those of squamates, the long bones of crocodylians, and more generally those of archosaurs, do not possess secondary intraepiphyseal ossification centers (a similar condition occurs also in the Testudines; see the reviews by Enlow 1969, Haines 1969 and Ricqlès 1976). In juvenile, actively growing specimens, long bone epiphyses consist of a thick cap of avascular cartilage, subdivided into the five typical histological zones: hyaline (subarticular), reserve, proliferation, hypertrophy and calcification (e.g., Haines 1938). In adults, epiphyses merely consist of a layer of hyaline articular cartilage, covering a stratum of a peculiar mineralized tissue that caps the extremities of metaphyseal trabeculae. This tissue differs from calcified cartilage by both its smaller and irregularly shaped cell lacunae and its acidophilic (instead of basophilic) matrix. It is also distinct from true bone because its cell lacunae are piled in a cartilage-like fashion and its matrix lacks a well-developed collagen meshwork. This tissue is viewed as resulting from chondro-osseous metaplasia (although it is neither true cartilage nor bone) by Haines (1938, 1969), Haines

VetBooks.ir

and Mohuiddin (1968) and Ricqlès (1972, 1975). In fresh bones, a chromophilic line (commonly designated as the "blue line") separates this tissue from the hyaline articular cartilage. The epiphyseal surfaces of well-preserved fossil specimens (especially archosaurs and turtles) are made of this "metaplastic" tissue (Ricqlès 1972). The presence of epiphyses devoid of secondary ossification centers was a general condition in basal tetrapods, and it occurs in the osteichthyans (reviews in, e.g., Haines 1942, Ricqlès 1975, 1979). Since Haines' (1938, 1942) studies, such epiphyses are therefore designated "primitive" and their occurrence is interpreted as plesiomorphic in vertebrates. All archosaurs, whatever their size and adaptation, share the same type of primitive epiphyses, except some limited skeletal sites in birds (mainly the proximal epiphysis of the tibia) in which secondary ossification centers may develop.

It is still debated whether crocodiles have a life-long (or at least long-lasting) growth activity, a trait commonly associated with the absence of secondary ossification centers, or whether they reach an asymptotic size at a given age, after which growth becomes negligible (see contrasting data presented by, e.g., Erickson and Brochu 1999 and Woodward et al. 2011). The problem is obviously made more complex by the extreme growth plasticity displayed by crocodylian taxa (e.g., Andrade et al. 2018). Most data collected in wild populations indicate a finite (or quasi-finite) growth; however, the age at which significant size increase stops, as well as the absolute rate of somatic growth during active growth periods, broadly differ among species, genders (males maintain a sustained growth activity longer than females; Chabreck and Joanen 1979) and individuals in local conspecific populations. In addition to normal yearly growth cycles (see below, chapter on *Skeletochronology*), crocodile growth can be harshly reduced or cease entirely for long periods when environmental conditions are unfavorable. It then resumes when the context improves.

A characteristic of crocodylian epiphyses that likely constitutes a consequence of the flexibility of their growth is a variation in the geometric pattern of hypertrophic and calcified cartilages. Early observations by Bausenhardt (1951) found an absence of isogenic groups and a random arrangement of chondrocytes in the proliferation, hypertrophy and calcification zones of crocodylian (as also chelonian) growth plates. Haines (1938, 1942, 1969) described and illustrated the occurrence of isogenic groups in young American alligators, but he also presented figures showing sections through the epiphyses of two other species much smaller than the American alligator, i.e., the dwarf African crocodile, *Osteolaemus tetraspis*, and the caiman, *Caiman* sp. In both of these taxa, hypertrophied chondrocytes are not aligned in recognizable isogenic groups. As Ricqlès (1976) pointed out, growth conditions, especially the absolute rate of bone lengthening, can influence both the density of proliferating chondrocytes, the degree of their hypertrophy and their geometrical patterning (Haines 1969).

Table 26.1 and Figure 26.2 summarize quantitative values expressing the inner microanatomical features (as measured with Bone Profiler) of stylopodial elements of adults or late juveniles in 16 crocodylomorphs and some noncrocodylomorph archosaurs.

TABLE 26.1

Bone Profiler Parameters in the Femur of 13 Crocodylian Species

		Bone Profiler Parameters				
	CDI	**Cg**	**Min**	**Max**	**S**	**P**
Eusuchia						
Alligator mississippiensis	0.736	0.923	0	1	0.045	0.264
Crocodylus niloticus	0.584	0.824	0	1	0.016	0.416
C. porosus	0.768	0.936	0	0.995	0.037	0.232
Diplocynodon ratelii	0.520	0.760	0	1	0.046	0.480
Gavialis gangeticus	0.568	0.810	0	0.999	0.020	0.432
Tethysuchia						
Dyrosaurus phosphaticus	0.646	0.810	0	0.932	0.033	0.354
Thalattosuchia						
Metriorhynchus superciliosus	0.306	0.518	0.038	1	0.068	0.694
Teleosaurus cadomensis	0.624	0.789	0	0.933	0.058	0.376
Notosuchia						
Trematochampsa taqueti	0.655	0.879	0	1	0.015	0.345
Iberosuchus macrodon	0.592	0.825	0	0.999	0.025	0.408
Sphenosuchia						
Hesperosuchus gracilis	0.701	0.922	0.306	1	0.081	0.299
Outgroups						
Euparkeria	0.410	0.640	0	1	0.044	0.590
Chanaresuchus	0.581	0.822	0	1	0.016	0.418

Abbreviations: CDI, corticodiaphyseal index; Cg, global compactness (CDI and Cg are direct proportions); Min, minimal local compactness; Max, maximal local compactness; S, 1/slope of the sigmoid; P, distance of the inflexion point to the bone center (see also Chapter 4).

VetBooks.ir

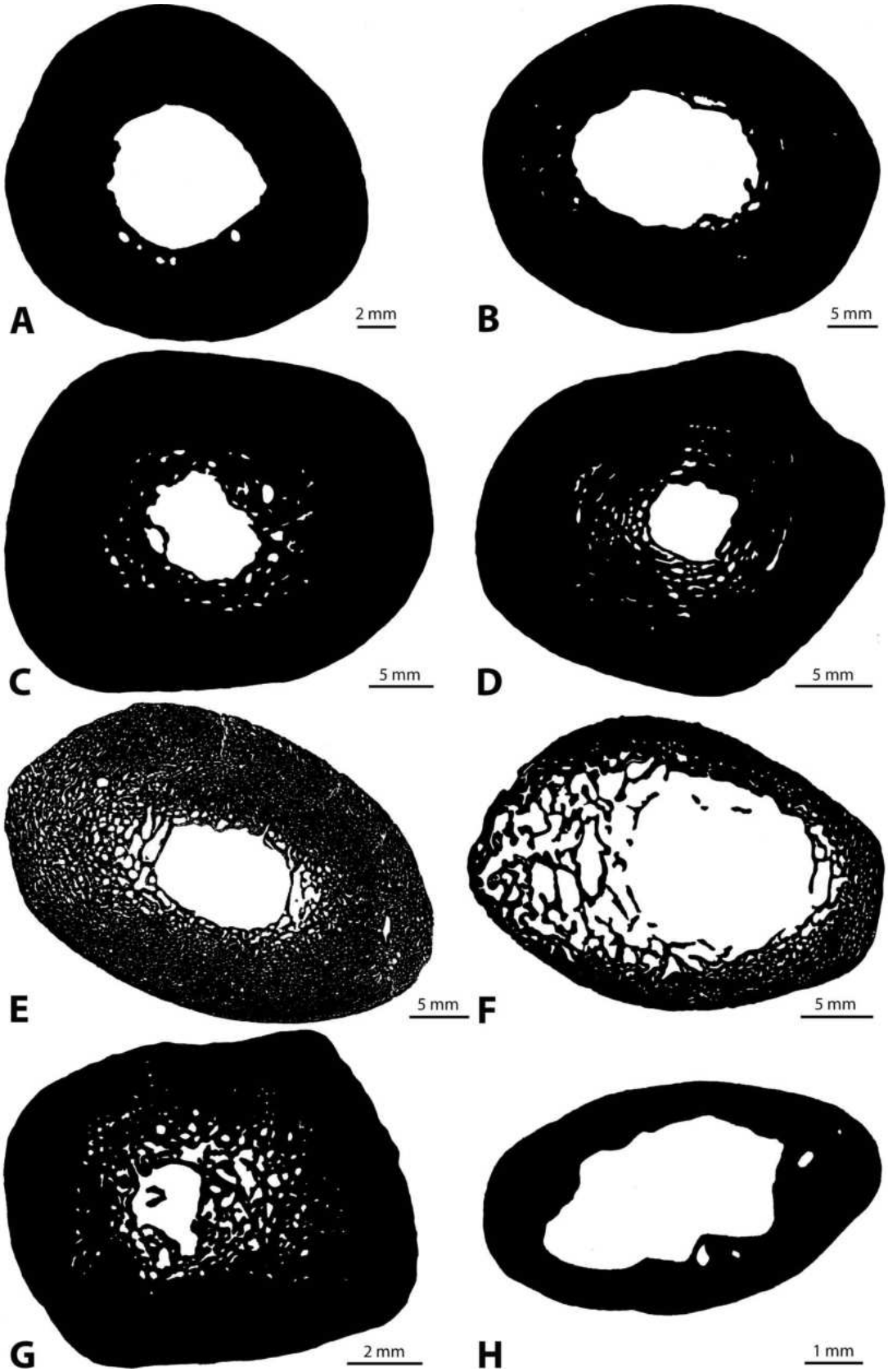


FIGURE 26.2 Some typical compactness patterns encountered in the long bones (the femur is taken here as an example) of the Crocodylomorpha, plus a basal archosauromorph, *Euparkeria*. A, *Crocodylus niloticus*. B, *Goniopholis simus*. C, *Alligator mississippiensis*. D: *C. porosus*. E, *Teleosaurus cadomensis*. F, *Metriorhynchus superciliosus*. G, *Hesperosuchus agilis*. H, *Euparkeria*. Quantitative data from *Bone Profiler* are given in Table 1.

VetBooks.ir

The values of parameter *S* indicate that all examined eusuchians have tubular bones (Figure 26.2A–D), with a thick, compact cortex sharply differentiated from a hollow medulla; however, the perimedullary part of long bone cortices often (though not in all specimens) displays numerous resorption bays, whose walls are covered by thin endosteal bone sheets (secondary reconstruction is only partial). The global compactness (Cg) and corticodiaphyseal index (CDI) of limb bones in the Eusuchians (i.e., 0.584 in a femur of *C. niloticus* to 0.767 in a femur of *C. porosus* for CDI; 0.760 to 0.936 for Cg in the femur of *Diplocynodon ratelii* and *C. porosus,* respectively) are high, which is a typical feature of semiaquatic forms in all amniotes, including birds (Meister 1962), other reptiles (Laurin et al. 2011) and mammals (Wall 1983, Stein 1989). According to Meers (2002), this characteristic creates such a disproportionately high mechanical security factor in crocodylian bones that Haversian remodeling becomes unnecessary for repairing microdamage in cortices and finely accommodating them to stresses. Remodeling, much likely related to other requirements, nevertheless occurs in all crocodylian taxa (see below).

Relatively faint sexual dimorphism occurs in the morphology of the eusuchian skeleton (*A. mississippiensis* being a reference model). This situation is seen in the external dimensions of limb bones compared to body (snout-to-vent) length: bone length, mid-diaphyseal diameter and epiphyseal width are all proportionally higher in males (Bonnan et al. 2008). Similarly, femoral robustness (an index computed from bone length and weight: robustness = bone length/$\sqrt[3]{}$ bone weight) and inner compactness (i.e., Cg index) are maximal in males, minimal in females bearing eggs or having laid their clutch recently, and intermediary in nonreproducing females (Wink and Elsey 1986). The latter data reflect the mobilization of calcium reserves through a general resorption of bones when eggshells are built. Very similar observations were made on a large squamate that commonly develops a considerable reproductive effort (especially in exploited populations), the Nile monitor, *Varanus niloticus* (Buffrénil and Francillon-Vieillot 2001; see also Buffrénil and Hémery 2007). In crocodiles, osteoderms are also resorbed from inside and outside to contribute to calcium supply, especially in females bearing advanced clutches (Dacke et al. 2015; see also Buffrénil et al. 2016). In contrast to dinosaurs (chiefly birds) and possibly pterosaurs (review in Prondvai 2017), crocodylians do not form medullary bone, a characteristic that they share with turtles and squamates (Schweitzer et al. 2007), as well as all other vertebrates. According to Canoville et al.'s (2019) definition, medullary bone consists of "highly vascularized, mostly woven, endosteally-derived tissue" that develops within large bone cavities containing marrow, to be later resorbed in pace with the progress of oogenesis (see below, Chapter 27 on the Avemetatarsalia). Crocodylian clutches can be substantial in mass (up to 16% of body weight in small forms such as *Paleosuchus* and *Caiman*; Thorbjarnarson 1996) and consist of eggs with a thick, heavily calcified shell (Ferguson 1982). Dacke et al. (2015) estimated at 200 g, at most, the total calcium amount that a female alligator uses for one clutch. This mineral is mainly supplied by food and the resorption of normal (permanent) skeletal sites, including dermal and endochondral bones from all skeletal sites. Of course, the development by crocodiles of very strong calcium reservoirs in the form of osteoderm shields and, to a lesser extent, thick (overproportioned) bone cortices, can be interpreted as a functional equivalent to the formation of medullary bone, in animals that naturally move little (crocodiles are basically ambush hunters and, when adult, have few predators; Bellairs 1969, Pough et al. 2004) and face relatively mild mechanical constraints in water and on land.

Histology of Long Bones

Eusuchian long bones share a common basic histological signature; however, due to the high ecological plasticity of these animals and their sensitivity to stochastic environmental factors, differences may exist not only among taxa, but also among the populations of a single species or the individuals of a single population. Precise histological descriptions of long bones for extinct taxa are rare; the main taxa studied have been *Deinosuchus* (a giant alligatoroid from the Late Cretaceous of North America; Erickson and Brochu 1999) and an undetermined species from the Upper Cretaceous of Spain (Company and Pereda-Suberbiola 2017).

Long bone cortices in the eusuchians are most often composed of the so-called "lamellar-zonal" tissue (Figure 26.3A–D, F, G), a broad and somewhat equivocal appellation (see above, chapter on *Bone tissue types*). Enlow (1969) used the term "laminar" for the cortical structure of long bones in crocodiles and turtles; obviously, this designation is in total discordance with the terminology used today. Lamellar-zonal tissue is basically structured by the yearly occurrence of a period of fast growth, followed by a period of slow growth that may lead to a total arrest of subperiosteal accretion on bone cortices (see also Chapter 31). During fast growth episodes, a "zone" is formed. It often consists of variably characterized parallel-fibered bone (Erickson and Brochu 1999, Klein et al. 2009, Company and Pereda-Suberbiola 2017). In cross sections observed in ordinary or polarized light, this tissue may display, at least in the deep and middle cortex, an atypical aspect strongly reminiscent of the woven-fibered type, with a monorefringent matrix and randomly distributed cell lacunae surrounded by abundant canaliculi (Figure 26.3B). The occurrence of this tissue has been observed by, e.g., Enlow (1969) and Buffrénil (1980b), in *Crocodylus* species, Tumarkin-Deratzian (2007; see also Reid 1984) in the American alligator, and Andrade et al. (2018) in *Caiman yacare*. It is noteworthy, however, that in the same species, the observation of longitudinal sections (Figure 26.3C, E, F) removes the structural ambiguity of cortical tissues by showing a clear birefringence of the matrix. The latter, straightforwardly designated woven-fibered bone (Tumarkin-Deratzian 2007); Company and Pereda-Suberbiola 2017), should actually be a rough parallel-fibered tissue that mostly includes longitudinally oriented collagen fibers. During the annual stage of slow growth, an *annulus*, made of either typical parallel-fibered or lamellar tissues, is created (Figure 26.3B). It can be, or not, followed by a line of arrested growth (LAG).

The basic histological structure just described has been observed in various Crocodylidae (Buffrénil 1980a,b) and Alligatoroidea, such as the American alligator (Lee 2004,

VetBooks.ir

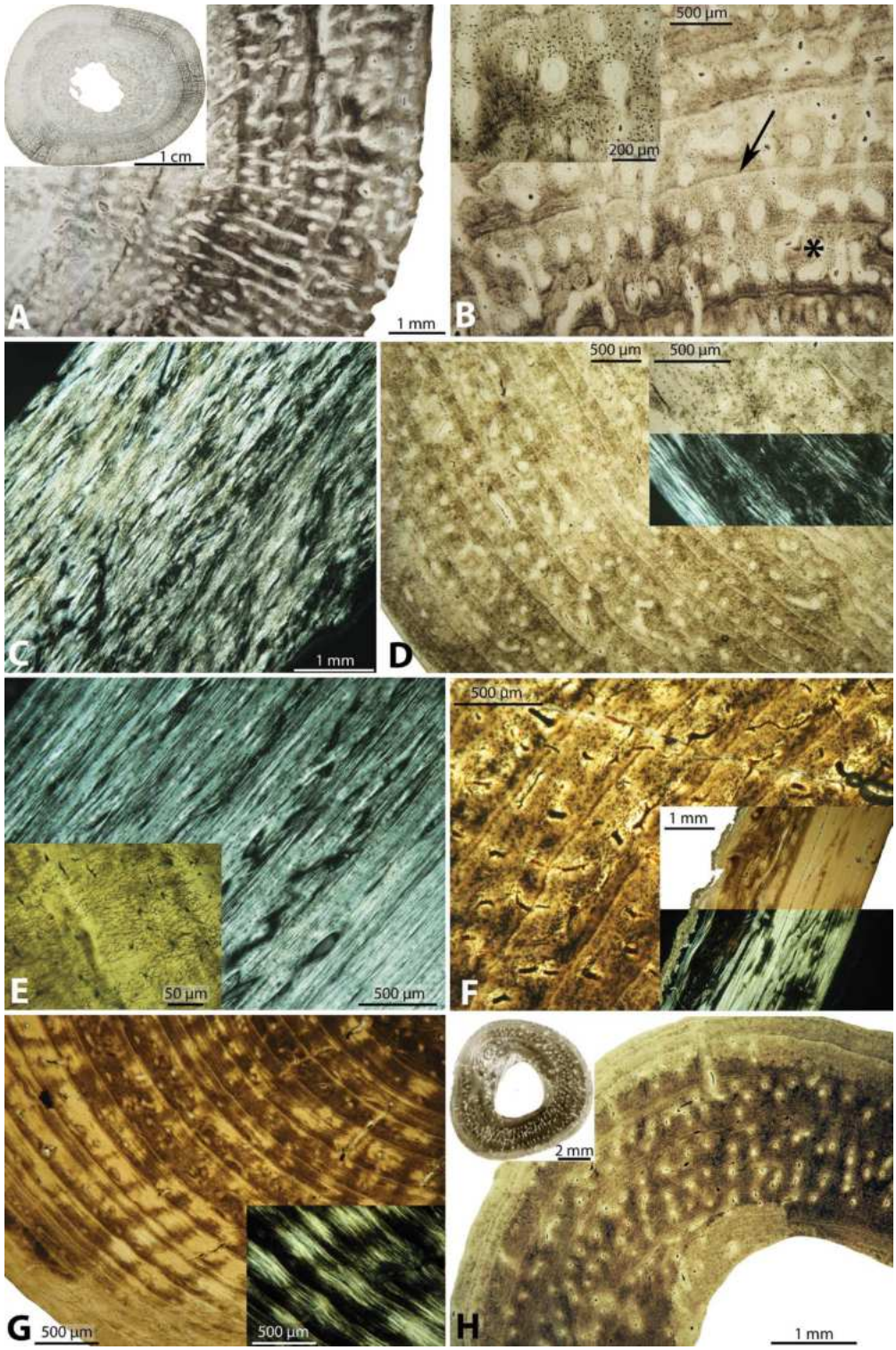


FIGURE 26.3 Microanatomy and histology of eusuchian long bones. A, Inner structure of the femur of an adult *Alligator mississippiensis* viewed in cross section. The inset shows the general aspect of the femur cross section. B, Histological features of the cortex. The inset shows in more detail the aspect and density of cell lacunae in the zones. The arrow points to an *annulus*, and the asterisk to a zone. C, Longitudinal section of the femoral cortex of an adult *Crocodylus niloticus*. Polarized light. The bone matrix displays a mass birefringence. D, Inner structure of the femur of a large adult *Gavialis gangeticus*. The inset shows a closer view of the bone structure in ordinary (upper half) and polarized (lower half) light. E, Longitudinal section of the femur of *Gavialis*. Polarized light. The inset shows the aspect of osteocyte lacunae in this bone, as viewed in a cross section. F, Histology of the femoral cortex in *Diplocynodon ratelii*. Main frame: detail of a cross section. Inset: longitudinal section viewed in natural (upper frame) and polarized light (lower frame). G, Conspicuous and numerous annuli and lines of arrested growth in the humeral cortex of *D. ratelii*. The inset shows an enlargement of the main frame in polarized light. H, Fibula of a subadult *C. niloticus* viewed in cross section. The inset shows the general aspect of the fibular cross section.

VetBooks.ir

Klein et al. 2009, Woodward et al. 2011), several Caimaninae (Andrade et al. 2018) and *Deinosuchus* (Erickson and Brochu 1999). In addition, the original observations (Figure 26.3, all images) made for this review in the extant forms *C. porosus*, *Caiman crocodilus* and *G. gangeticus*, along with the extinct eusuchian taxon *D. ratelii* (an Eocene-Miocene alligatorid from western Europe), confirm the occurrence of this type of cortical structure, but with sensible variability, in large stylopodial bones (humerus and femur) of most eusuchians. In thinner bones (radius, ulna, tibia and fibula), the cortical matrix is closer to a typical parallel-fibered tissue with, depending on shaft width, either sharp LAGs but no annuli, or both types of skeletal growth marks (SGMs). These marks remain present in animals bred in constant, artificial conditions, because SGM formation basically depends on a cyclical, endogenous rhythm in growth control (e.g., Buffrénil 1980a,b see also Chapter 31).

With the progressive decrease of growth rate in adults, the basic cortical structure of crocodylian bones turns into a typical parallel-fibered type or to lamellar bone. The occurrence of a well-characterized external fundamental system (EFS), composed of parallel-fibered or lamellar tissue with conspicuous, tightly packed LAGs, may occasionally be observed in large adults (Woodward et al. 2011). A well differentiated EFS was also observed by Company and Pereda-Suberbiola (2017) in an undetermined Upper Cretaceous eusuchian from Spain. This situation is rare; however, the most frequent pattern is a progressive tightening of cyclical growth marks toward the bone periphery, without a steep or sudden decrease in the LAG spacing. Sharpey's fibers occur as dense bundles of short fibers (periosteal insertion) or long fibers (muscle insertions) in all crocodylian long bones.

The cortex of eusuchian long bones, even when these bones have a relatively small diameter (see, e.g., the *C. siamensis* fibulae described by Buffrénil 1980b), is vascularized, at least in its deep two-thirds. Vascular canals can be either simple canals or relatively thin (diameter *ca.* 50–60 µm) primary osteons (Figure 26.3A, B, F, H). They mainly occur within the zones, and their principal orientation is longitudinal or oblique (Enlow 1969, Lee 2004), although the occurrence of a reticular-like pattern (including occasionally radial canals) in actively growing subadults is far from rare (see, e.g., Figure 26.3A, F), and can be observed in extant taxa as well as fossil forms such as *D. ratelii*. Haversian remodeling of variable intensity normally occurs in the long bones of eusuchians. It consists of longitudinal secondary osteons and remains confined lifelong to the deep half of the cortices; however, Haversian remodeling can spread outward within the cortex in crests or under the attachment areas of powerful muscles.

Some authors have concluded that the occurrence in some eusuchian specimens of primary osteons in zones composed of a tissue interpreted as woven-fibered bone locally creates a tissue type akin to a woven-parallel complex (Chinsamy and Hillenius 2004, Tumarkin-Deratzian 2007). Tumarkin-Deratzian (2007) pointed out that such a cortical structure can be encountered in wild specimens (even of poor physical condition), as well as captive-bred individuals: it does not result from an exceptional (or abnormal) growth rate, but it is a relatively frequent condition, at least in large-bodied taxa. This situation logically led some authors to question the broadly acknowledged interpretation of woven-parallel tissues, in terms of growth rate and physiological meaning (Reid 1984, Chinsamy and Hillenius 2004). The frequent occurrence of such tissues in dinosaurs was one of the most robust arguments for an endotherm-homeotherm-like thermal regime in these animals (and all those presenting this type of cortical tissue) (e.g., Ricqlès 1980). The ectopoikilothermic physiology of crocodiles, with resting metabolic rates (RMRs) slightly higher than that of squamates or turtles, but clearly lower than those of mammals and birds (Seymour et al. 2004; see also Montes et al. 2007), is well established. Therefore, if the occurrence of woven-parallel tissue in their bones proved to be real, after detailed histological analyses with both cross and longitudinal sections, it would suggest *a minima* that, provided the growth rate is indeed the main causal element explaining the structure of primary periosteal deposits (the now-classic Amprino's 1947 rule; see also, e.g., Margerie et al. 2002), the latter parameter could be more loosely related to basal metabolism than previously thought (see Reid 1984). Crocodiles are a central model for experimentally handling this kind of question. Our own observations of the 13 taxa mentioned in Table 26.1 nevertheless suggest that the occurrence of real woven-parallel complexes in eusuchians, even in the largest species, is at best dubious for the reason mentioned above.

Remarks on Ribs and Vertebrae

Eusuchian ribs are roughly oval in cross section and mainly differ from limb bones by their microanatomical characteristics. Their medullary cavity is partly obstructed by a network of trabeculae of variable spatial density (Figure 26.4A). As a consequence, Bone Profiler parameter *S* is higher, and the difference between parameters *Min* and *Max* is lesser than in limb bones. Histologically, rib cortices are made of a variably characterized parallel-fibered tissue with conspicuous cyclical growth marks (annuli and LAGs). Cortical vascularization varies with the thickness and local growth rate of the cortices (as assessed from the spacing of growth marks; see Figure 26.4A, inset). It consists of simple canals associated or not with primary osteons. As in limb bones, Haversian remodeling is of variable intensity and may occasionally be absent; however, the trabeculae in the core spongiosa are intensely remodeled.

Eusuchian vertebrae (Figure 26.4B) call for few specific comments. They display a compactness and a gross architectural pattern roughly similar to those of mammals (Dumont et al. 2013) of comparable size (data are scarce for other large tetrapods). Their histological features are also closely similar to those of other taxa: the periosteal formations are made of lamellar-zonal or parallel-fibered tissues with or without cyclical LAGs, at least in the peripheral cortical parts spared by the intense and patchy resorption that occurs in the deep cortex. As in all other endoskeletal elements of the crocodylian skeleton, the endosteoendochondral trabeculae in the core of the vertebral centra do not contain any remnant of calcified cartilage at a distance from the growth plates (such a persistence of cartilage is a feature frequently observed in aquatic or semiaquatic tetrapods).

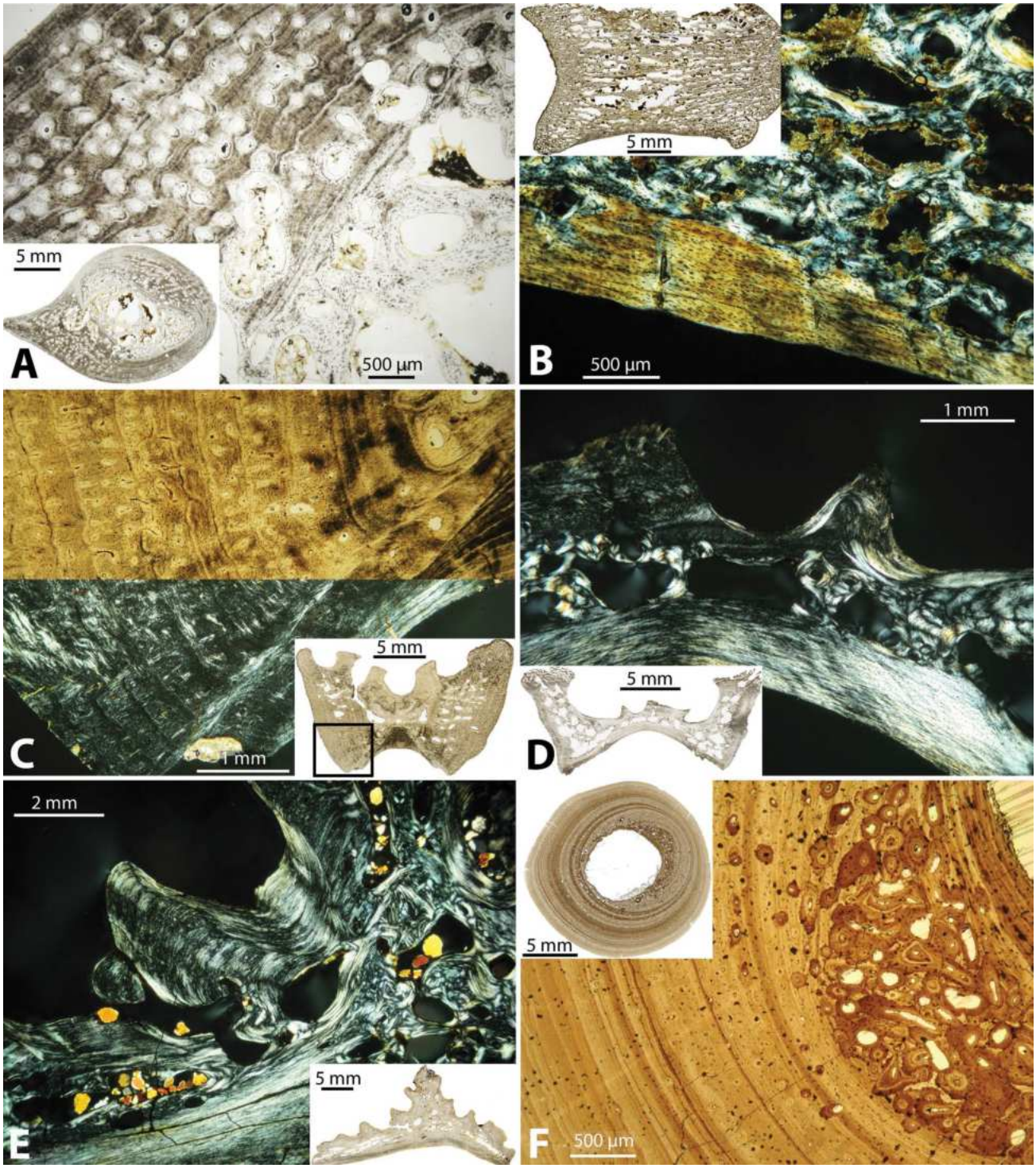


FIGURE 26.4 Structure of the ribs, vertebrae, skull bones and osteoderms in the eusuchians and *Goniopholis simus*. Throughout this figure, the insets show the general aspect of the bones in cross (all insets, except B) or longitudinal (inset in B) section. A, Macroanatomy and histological structure of the cortex in a rib from *Crocodylus niloticus*. B, Macroanatomy and histological structure of a lumbar vertebra from *Diplocynodon ratelii*. Sagittal section. Main frame: polarized light. C, Macroanatomy and histological structure in a cross section of the frontal bone of *D. ratelii*. Lower half of the main frame: polarized light. D, Macroanatomy and histological structure in a cross section of the frontal bone of a juvenile *Alligator mississippiensis*. Main frame: polarized light. E, Macroanatomy and histological structure in a section from an osteoderm of *Diplocynodon remensis*. Main frame: polarized light. F, Macroanatomy and histological structure in a cross section from a femur of *G. simus*

VetBooks.ir

Skull Roof Elements and Osteoderms

Microanatomical Features

The microanatomical organization of dermal skull bones in crocodiles has received little attention up to now, and it is mainly known by anecdotal observations. As in other vertebrates, these bones have a "diploe" structure (Figure 26.4C, D). Their compactness is very high in adults; for example, the compactness of the frontal bone, as seen in cross section at mid-length, is nearly 1 in the crocodylid *Crocodylus affinis*, and 0.889 in the alligatorid *D. ratelii* (Figure 26.4C). As for long bones, skull roof bones in juveniles are much more lightly built than those of adults (e.g., compactness is only 0.497 in the frontal bone of a young *Alligator* some 50 cm in snout-vent length: Figure 26.4D).

In all crocodyliform taxa, the whole dorsal surface of the body, from the nuchal region to the middle of the tail, is covered with osteoderms, which form a continuous shield particularly strong and extensive in the Eusuchia. Depending on individual age and the taxon considered, this shield may extend, in a more or less lightened form, toward the flanks, the belly and the legs (e.g., King and Brazaitis 1971, Grigg and Kirshner 2015; see also English 2018). The detailed microanatomical characteristics of osteoderms are better documented, in a comparative perspective, than those of dermal skull bones (e.g., Burns et al. 2013, Buffrénil et al. 2015). The inner structure of osteoderms features a robust "diploe" (Figure 26.4E), but it is highly variable in architecture and compactness with several factors, including individual age, the location of each osteoderm in the whole shield and the taxonomic position of the species. Burns et al. (2013) pointed out another variation factor, considered preponderant: a shape constraint, related to the osteoderm volume and morphology. Through the effect of this constraint, large osteoderms are less compact than small ones, so the ratio between weight and resistance is optimized. Though logical in an adaptational perspective, this interpretation nevertheless remains to be tested on a larger and more varied sample.

In both osteoderms and dermal bones, the deep cortex has a compactness close to 100%, with few vascular canals, whereas the superficial cortex is much more vascularized. Moreover, its outer surface displays an "ornamentation" made of a network of crests separating roundish pits, the bottom of which presents one or several vascular openings. Three-dimensional reconstructions of osteoderm vascularization in various extant crocodylians (e.g., Clarac et al. 2020) reveal the existence of a very dense vascular network, radiating from the center and extending radially through the cortex up to perforate the superficial and, to a lesser extent, the deep cortices. Clarac et al.'s (2017) descriptions show that blood vessels originating from the core of the osteoderms ramify within the "ornamental" pits, to form a patchy set of vascular bundles associated with the ornamentation.

Histological Features

Histologically, the structure of osteoderms is identical to that of skull bones in subadult and adult crocodiles (e.g., Buffrénil 1982). At these developmental stages, the core of these bones is occupied by an intensely remodeled secondary spongiosa, the trabeculae of which are composed of several layers of endosteal lamellar bone separated by reversion lines (Figure 26.4D, E). The basal cortex is composed of parallel-fibered or lamellar tissues, and the outer cortex is made of either typical or atypical parallel-fibered tissues (in the latter case, the tissue turns incipiently into a woven-fibered type), associated with true lamellar secondary bone (Figure 26.4C–E). Observational and experimental data (*in vivo* labeling of bone growth) show that the ornamentation of crocodylian dermal bones is due to remodeling. The pits are thus actively excavated, and partly reconstructed by secondary deposits on their bottom. This remodeling process is essentially dynamic: it accompanies bone growth, and is responsible for the creation, enlargement, relocation and eventually infilling of the pits (Buffrénil 1982, Buffrénil et al. 2015). Therefore, crocodylian ornamentation principally rests on the differentiation of its negative reliefs (pits). The development of its positive reliefs (ridges), though contributing to create the final morphological result, is of lesser importance than in other taxa that show similar sculpture patterns (e.g., temnospondyls; cf. Buffrénil et al. 2015, 2016).

Conspicuous cyclical growth marks, in the form of annuli and/or LAGs, occur in all crocodylian dermal bones, whatever their position. The pattern of these marks is often very regular, and it reveals precisely the size and shape modification of the bones during growth (Figure 26.4C). However, remodeling related to the development of ornamentation disturbs the regularity of the marks in peripheral cortices. Sharpey's fibers may occur as dense bundles located mainly in the deep (medial) cortex. When they occur in the superficial (lateral) cortex, Sharpey's fibers are confined to the top of the ridges because pit walls are permanently remodeled areas.

The origin and mode of formation of skull roof bones call for no particular comment; as in all vertebrates, they are typical membrane bones of ectomesenchymal origin. Conversely, the organogenesis of crocodylian osteoderms is less clearly settled. Vickaryous and Hall (2008) study in *A. mississippiensis* shows that the initial stage of osteoderm differentiation is a mere fibrillar condensation within the deep dermis. This primordium soon calcifies through a "metaplastic" process, in the absence of identifiable osteoblasts. It is clear, however, that the involvement of metaplasia, unquestionable in the earliest stages of osteoderm development, cannot be considered the unique mechanism through which crocodylian osteoderms grow. This interpretation fails to explain the complex histological structure of the osteoderms in subsequent ontogenetic stages, as presented above. The strong, recurrent remodeling that occurs both within and on the surface of crocodylian osteoderms, as well as their development in thickness in total independence from dermal fibrillar layers (osteoderms are much thicker than the dermis itself), altogether support the existence of osteoblast and osteoclast populations located inside and around the osteoderms, and directly involved in their growth and remodeling.

Remarks on *Susisuchus* and *Goniopholis*

S. anatoceps, known from the Early Cretaceous of Brazil, was a diminutive semiaquatic species roughly comparable in size to extant dwarf caimans (*Paleosuchus*; total length < 1.5 m).

VetBooks.ir

The phylogenetic position of this taxon is disputed, and it has been alternatively described as closely related to Eusuchia and Goniopholididae (Turner and Pritchard 2015), or outside Eusuchia (Figueiredo et al. 2011, Young et al. 2016), or as a genuine eusuchian (Andrade et al. 2011, Leite and Fortier 2018). One ulna and one rib were examined by Sayão et al. (2016). The ulna is a tubular bone, containing an extremely thin medullary cavity free of trabeculae, surrounded by a very thick cortex (CDI = 76%). Conversely, the rib fragment studied by Sayão et al. (2016) has a broad marrow cavity partly obstructed by thick trabeculae. The periosteal cortices of both bones are made of a well-characterized parallel-fibered tissue displaying conspicuous annuli and LAGs. Toward cortical depth, the morphology of cell lacunae becomes rounded and their orientation becomes irregular. Vascularization is sparse, especially in peripheral cortical regions, and mostly consists of simple longitudinal canals with rare anastomoses. The two bones display neither an EFS nor secondary osteons. Consistent with the small size of this taxon, cortical structure in both the ulna and rib suggests a growth rate lower than in other crocodylians.

The *Goniopholis* (referred to *G. simus*) femur examined for this review also displays a perfect tubular architecture with Cg and CDI values (85 and 62%, respectively) very comparable to those of eusuchians (Figure 26.4F, inset). Its cortex is made of parallel-fibered tissue, exhibiting annuli and LAGs whose sharpness is enhanced by the impregnation of the fossil by natural dyes. Its relatively sparse vascular network consists of thin simple canals and some primary osteons, mainly oriented in a longitudinal direction (Figure 26.4F). No anastomoses occur between the canals. The specimen studied differs from both true eusuchians and *Susisuchus* by a higher local density of secondary osteons (formation of dense Haversian bone) in the perimedullary region of the cortex. The bone also exhibits a strong off-centering through growth.

The Tethysuchia: Dyrosaurs and *Sarcosuchus*

In addition to the descriptions given in the two published studies of dyrosaurids (Buffetaut et al. 1982, Andrade and Sayão. 2014), two limb bones (one humerus and one femur) and one osteoderm from *D. phosphaticus* were sectioned and examined for this review.

In microanatomical and histological perspectives, dyrosaurid long bones are very similar to, though somewhat less compact than, those of the eusuchians (Figure 26.5A, B). In the specimen studied for this review (a very large and probably old individual), and in the one examined by Andrade and Sayão (2014), a wide ring of loose cancellous bone surrounds the medullary cavity (Figure 26.5A, B). The middle and outer cortices of our specimen houses numerous resorption bays, not or only partly filled by secondary centripetal deposits. As a consequence, the global compactness of the bone (81%) is relatively modest. A similar cortical pattern is commonly observed in the most aquatic crocodiles; however, in the *Dyrosaurus* specimen described here, the random distribution and the uneven size of the resorption cavities suggests that they might, at least partly, be related to mineral recycling for phosphocalcic homeostasis. This question is further considered below, about the thalattosuchians.

The periosteal cortices of our *D. phosphaticus* femur are basically made of parallel-fibered tissue, birefringent in mass in cross sections (collagen fibers parallel to the sectional plane). Cyclical growth marks in the form of *annuli* and LAGs occur, but they are unevenly spaced. In the bone periphery, the presence of six to seven tightly packed LAGs, very regularly spaced at an interval of 50 µm (Figure 26.5C), strongly suggests the occurrence of an EFS. Growth, however, was not entirely stopped. In one of the femora studied by Andrade and Sayão (2014), several LAGs were split, whereas the other femur displayed an EFS identical to that observed in our specimen, or in *A. mississippiensis* by Woodward et al. (2011). Cortical vascularization consists of simple canals and primary osteons, showing a longitudinal, oblique or incipiently circular orientation (Figure 26.5B, C), and organized in circular files in the peripheral cortex. Haversian remodeling is active in the deep half of the cortex (Figure 26.5D). In our specimen, the occurrence of numerous open resorption bays, with no trace of reconstruction, indicates that remodeling was still proceeding by the time the animal died.

The snout bones of *D. phosphaticus*, including nasals, maxillae, premaxillae and dentaries, are composed of the same kind of osseous tissue as the one observed in limb bone cortices (Buffetaut et al. 1982). Dyrosaurid osteoderms are particularly robust bony plates. Though a diploe structure, but with thick cortices and a reduced central spongiosa, is present in the osteoderms of *D. phosphaticus*, in other taxa, such as the undetermined dyrosaurid from the Paleocene of Bolivia shown in Figure 26.5E, osteoderms can be totally compact. Their basic histology is nevertheless similar to that observed in the same elements of other crocodiles. In the core of the osteoderm, the lack of remodeling and spongy tissue leaves an initial formation of woven-fibered bone containing primary osteons, oriented radially and confined to the equatorial region of the osteoderm.

Sarcosuchus is represented in our sample by only one rib fragment (originating from the central third of the bone) and some osteoderms. Most of the rib sectional area is occupied by a spongiosa, surrounded by a relatively thin compact cortex (Figure 26.5F), as compared with e.g., the *C. niloticus* rib described above. Histologically, the trabeculae forming the spongiosa are of the same remodeled endosteal lamellar tissue as in other taxa. The cortex (Figure 26.5G) consists of the lamellar-zonal tissue with annuli, LAGs and longitudinal vascular canals (simple canals and primary osteons) common to most medium and large-sized crocodiles. Haversian remodeling, with osteons at diverse completion stages, was particularly intense in the rib cortex, and still proceeded, spreading outwardly, when the animal died. *Sarcosuchus* osteoderms (Figure 26.5H) do not greatly differ in structure from those of eusuchians; however, their peripheral cortex is much more vascularized. Simple canals and primary osteons are numerous in the ridges and even abundantly colonize the thick secondary deposits in the bottom of the pits.

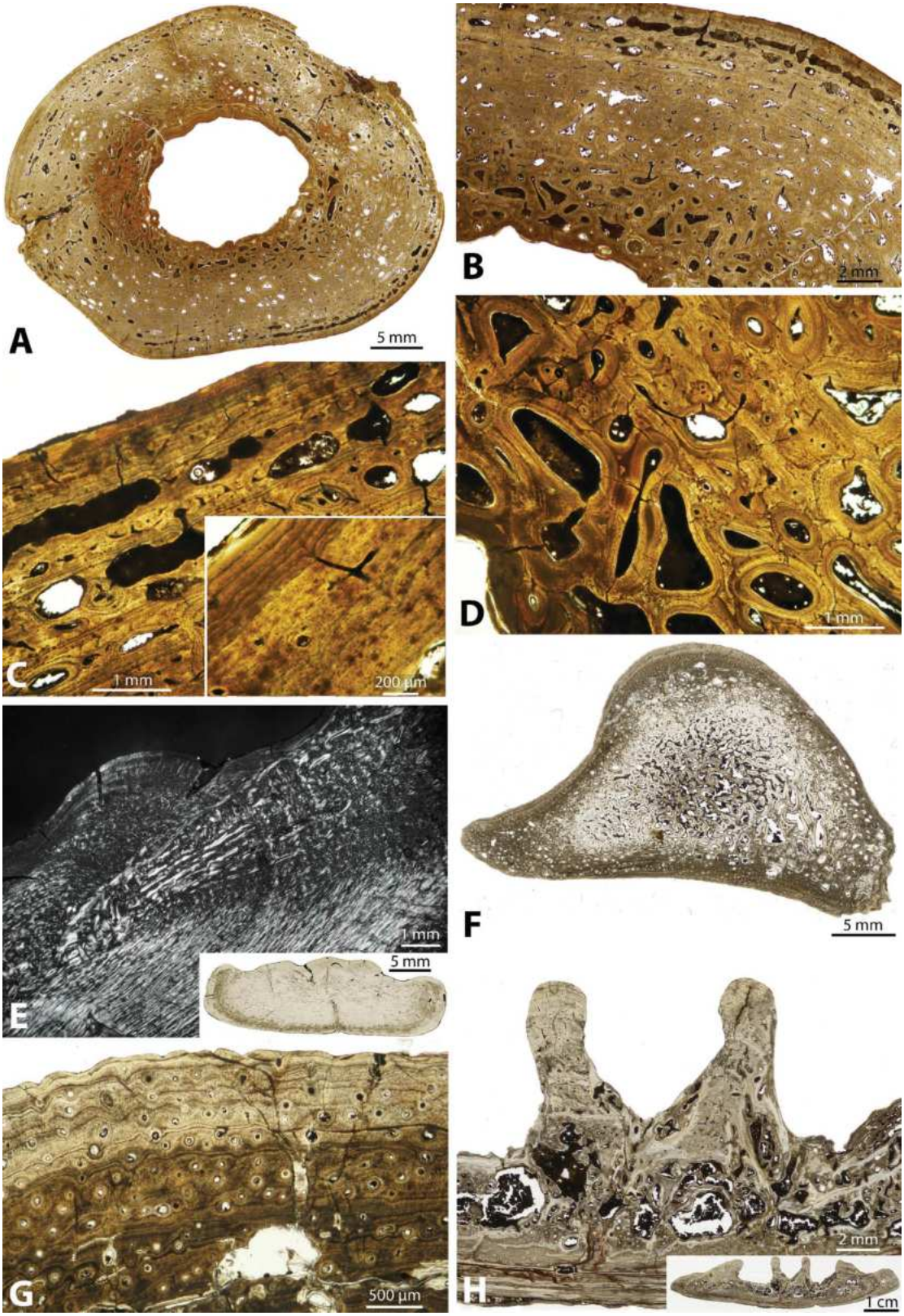


FIGURE 26.5 Basic bone microstructure in tethysuchians. A, General aspect of a cross section in the femur of a large *Dyrosaurus phosphaticus*. B, General structure of the cortex of *D. phosphaticus* femur. C, Histological characteristics of the peripheral cortex of the *D. phosphaticus* femur. The inset shows a closer view at the possible external fundamental system of this bone. D, Active Haversian remodeling in the deep cortex of *D. phosphaticus* femur. E, Microstructure of an osteoderm (entire view in the inset) from an undetermined dyrosaurid specimen from the Paleocene of Bolivia. Main frame: polarized light. F, Cross section of a rib of *Sarcosuchus imperator*. G, Cortical structure of the *Sarcosuchus* rib cortex. H, Structure of an osteoderm (general view in the inset) from *S. imperator*

VetBooks.ir

Thalattosuchians

Bone microanatomy and histology in Mesozoic marine crocodiles is mainly documented by Hua and Buffrénil's (1996) article, dealing with three taxa typical of the basic dichotomy within thalattosuchians: *Steneosaurus* sp. and *Teleosaurus* sp. for the Teleosauroidea and *Metriorhynchus* for the Metriorhynchoidea. The main results of this study are briefly summarized below, and completed with the observation of additional samples including two rib fragments of *M. superciliosus* (Callovian-Kimmeridgian of western Europe), three appendicular long bones (1 humerus, 2 femora) of *Teleosaurus* (Bathonian of western Europe) and one osteoderm (major diameter 57 mm) of the large teleosauroid *Machimosaurus hugii* (Callovian-Oxfordian of western Europe). *Teleosaurus*, *Steneosaurus* and *Metriorhynchus* were all medium-sized longirostrine forms (some 3 m in total length), but teleosauroids and metriorhynchoids greatly differed in many ecomorphological characteristics. In brief, teleosauroids were heavily built estuarine dwellers, very similar in general aspect to extant long-snouted crocodiles. Their osteoderm shield was narrow, but massive and deeply sculptured. Conversely, most derived metriorhynchoids had lost most of their osteoderms, their limbs were transformed into flippers and they were propelled by a hypocercal caudal fin (incipient lift-based propulsion). All these features reveal a pelagic, open-sea habitat (see, e.g., Hua and Buffetaut 1997, Wilberg et al. 2019).

Microanatomy of Thalattosuchian Skeletons

Appendicular long bones (humerus, femur and tibia) in teleosauroids have a robust tubular architecture, with CDI values reaching 0.758 for the humerus, and 0.624 for the femur in *Teleosaurus cadomensis* (Figures 26.2E and 26.6A, B). However, their overall compactness at mid-diaphysis (i.e., 0.903 for the humerus and 0.789 for the femur of *T. cadomensis*) seems relatively modest (see Table 26.1). This situation is due to the multiplication throughout the cortex of roundish resorption bays whose walls are not entirely reconstructed by secondary deposits (incomplete secondary osteons; Figure 26.6B). Teleosauroid osteoderms are comparable in microstructure to those of most extant eusuchians, with compactness indices of 0.720 (*Teleosaurus*) and 0.610 (*Steneosaurus*). As shown in Figure 26.6C, their deep cortices may nevertheless display an unusual porosity, reminiscent of what occurs in long bone cortices.

Quantitative measurements in *M. superciliosus* appendicular skeleton are available only for one femur (Figure 26.6D). At mid-diaphysis, this bone displays a broad spongiosa along with thin cortices (Figure 26.2F); its compactness is consequently low (0.518) compared to all other crocodylians. A similar structure, but with proportionally still broader cancellous areas, was also observed (but not measured due to bone crushing) in the humerus and coracoid. Such a tendency to skeletal lightening is also observable in the bones of the cranial table (frontal and parietals), and it is particularly pronounced in snout bones (nasal, maxillae; Figure 26.6E), which are much more lightly built, with thin cortices and extensive spongiosae, than those of extant longirostrine crocodiles (the African false gharial, *Mecistops cataphractus*, was used as a comparative element by Hua and Buffrénil 1996). Conversely, the two *Metriorhynchus* rib fragments show a thick cortex (Figure 26.6F), but the latter exhibits the same inner porosity and high remodeling activity, as observed in the long bones of other thalattosuchians (mean Cg for the entire section: 0.831).

In general terms, the set of microanatomical observations presented above is consistent with the respective ecomorphological adaptations currently attributed to teleosaurids and metriorhynchids (see, e.g., Hua and Buffetaut 1997, Wilberg et al. 2019). It agrees with what is known about the evolutionary fate of skeletal mass in both slow swimmers inhabiting shallow waters, i.e., the Teleosauroidea, which tend to maintain or increase skeletal mass as a solution to passively control their buoyancy and trim in water, and fast pelagic forms (lift-based propulsion), i.e., the Metriorhynchoidea, which tend to decrease skeletal mass as a means to reduce body inertia and improve speed and maneuverability (e.g., Webb and Buffrénil 1990, Ricqlès and Buffrénil 2001; see Chapter 36). Hua and Buffetaut 1997 assigned distinct ecological niches to the teleosauroids, which were supposed to have been near-shore bottom feeders, and the metriorhynchoids, viewed as pelagic feeders exploiting surficial levels of the water column. In both clades, however, Haversian remodeling of the cortex was imbalanced toward resorption, a situation that distinguishes the thalattosuchians and, outside this clade, the dyrosaurs (another predominantly aquatic group), from other crocodylomorphs.

Histology of Thalattosuchian Bones

The histological structure of bone cortices in Mesozoic marine crocodiles deserves few comments because it is both comparable in all skeletal elements and similar to the characteristics displayed by eusuchian skeletons. Primary periosteal deposits consist of an irregular parallel-fibered tissue, organized in conspicuous accretion cycles (Figure 26.6A, B). The annuli are made of well-characterized parallel-fibered or lamellar tissues, and sharp LAGs occur in the latest (peripheral-most) accretion cycles. Vascularization is represented by simple canals (cortical periphery) or primary osteons (cortical depth). As mentioned above, most thalattosuchian bones were submitted to sustained Haversian remodeling, with a concentration of secondary osteons around the medullary cavity and a loose extension into the mid-cortex (Figure 26.6A–F). Again, this remodeling pattern, though basically reminiscent of the situation prevailing in many crocodylomorphs, was seemingly more intense and extensive, and was characterized by some degree of imbalance to the detriment of bone reconstruction (thus creating porosity). Strong bundles of Sharpey's fibers, mainly observed here in the *Metriorhynchus* specimens, occurred in thalattosuchian bones (Hua and Buffrénil 1996). From a histological perspective, teleosauroid osteoderms (Figure 26.6C) are identical to those of similar-sized eusuchians.

The general histological pattern prevailing in the thalattosuchian bones studied up to now suggests that the skeletal growth rate of both teleosauroids and metriorhynchoids was comparable to, or somewhat lower than, those of eusuchians. Considering the broadly acknowledged relationship between

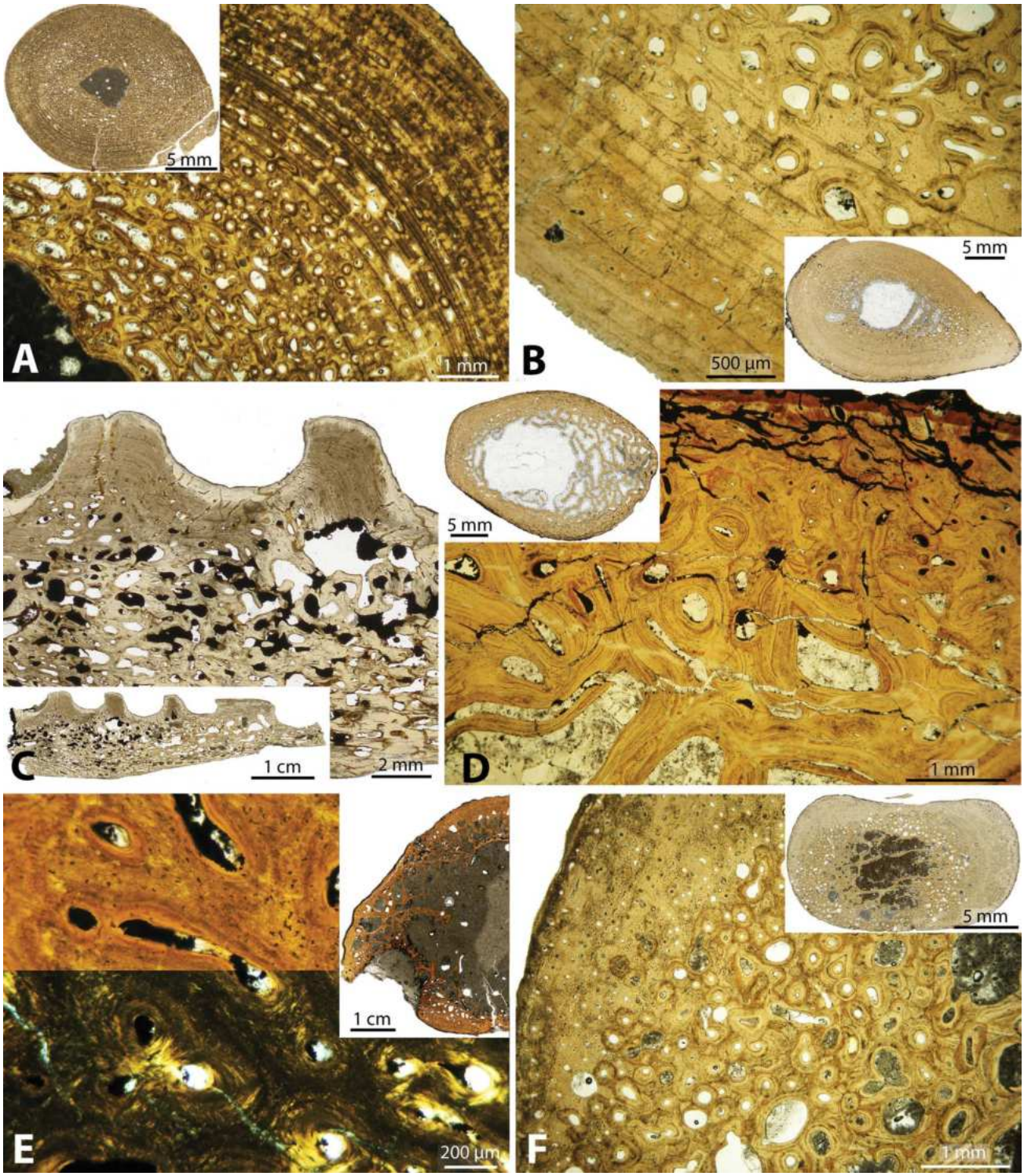


FIGURE 26.6 Basic bone microstructure in thalattosuchians. Throughout this figure, the insets show the general aspect of the bones in cross section. A, Humerus of *Teleosaurus* sp. (most probably *Teleosaurus cadomensis*) in cross section. B, Femur of *Teleosaurus* sp. in cross section. C, Osteoderm of *Teleosaurus* sp. D, Femur of *Metriorhynchus superciliosus* in cross section. E, Cross section in the snout of *M. superciliosus*. Inset, general view of the cancellous maxillary structure. F, Cross section in a rib from *M. superciliosus*.

VetBooks.ir

growth rate and basal metabolism (comparative data in, e.g., Montes et al. 2007, Cubo et al. 2012, Legendre et al. 2016, Cubo and Jalil 2019), the thermal regime of thalattosuchians should therefore be also interpreted as roughly similar to that of extant crocodiles. The only element contrasting with this qualitative inference is the seemingly higher Haversian remodeling in thalattosuchian bones, which could suggest more intense calcium recycling and consequently a higher metabolic activity in the Thalattosuchia. This question is nevertheless to be handled with caution, because Haversian remodeling is a progressive process that depends on the ontogenetic age of the specimens. It is also heavily influenced by the reproductive status of the females, the local mechanical work of the skeleton and the general health status of individuals. Finally, the meaning of secondary osteon density in a fossil bone remains equivocal. Moreover, in crocodiles, differences among taxa are a matter of nuance; they by no means reflect a massive divergence. Recent data by Gienger et al. (2018) show that the standard metabolic rate (SMR) of the extant saltwater crocodile *C. porosus*, a broadly distributed coastal species foraging in seas, is 36% higher than that of freshwater taxa such as *A. mississippiensis* or *C. johnstoni*. It is noteworthy, however, that despite this substantial difference, the histology of long bones looks strictly identical in *C. porosus* and other crocodylian species. Further documentation, based on a much broader sample and a quantitative approach, is therefore needed.

The possible cooccurrence in metriorhynchoids of a sophisticated, lift-based propulsion mode (although some contribution of the undulatory propulsion mode is likely to have persisted in these animals; see, e.g., Massare 1988), with a relatively low, crocodile-like (or barely higher) thermal regime, may seem paradoxical because aquatic tetrapods that swim in this way (e.g., cetaceans, ichthyosaurs, etc.) are endothermic and homeothermic, or supposed to have been so. Preliminary data yielded by the measurement of ^{18}O relative concentration in thalattosuchian teeth (Seon 2018) resulted in the conclusion that metriorhynchoids had a body temperature (and a corresponding metabolic activity) between that of the Teleosauroidea and that of the ichthyosaurs or plesiosaurs, the latter being interpreted as endotherms. However, the body temperature of metriorhynchoids was shown to fluctuate in pace with the variation of seawater temperature, which prompted Seon (2018) to designate these animals as endothermic poikilotherms. To some extent, this conclusion would generally agree with Gienger et al.'s (2018) data on *C. porosus*. Histological data nevertheless reveal no difference between teleosauroids and metriorhynchoids, a conclusion already reached by Enlow and Brown (1957) ("*Mystriosaurus*, *Pelagosaurus*, *Teleosaurus* and *Goniopholis*, all extinct members of the Suborder Mesosuchia, possess bone tissues that are similar in structure to the modern alligator and crocodile"); there is thus some discrepancy between the indications of histology and geochemistry in the case of thalattosuchians. Though the results of these approaches closely agree for ichthyosaurs and plesiosaurs (see, e.g., Anderson et al. 1994, Wiffen et al. 1995 and Bernard et al. 2010 for the plesiosaurs), they also diverge in the case of another group of large marine reptiles, the mosasaurs. The latter are considered endotherms and homeotherms (but not "gigantotherms") by geochemical analyses (Harrell et al. 2016), whereas their bone cortices are made of a variably vascularized and mildly remodeled parallel-fibered tissue (that may show some atypical features), roughly comparable to that commonly observed in eusuchians and thalattosuchians (Pellegrini 2007, Houssaye et al. 2013, Green 2018; see also Chapter 20). Further comparative analyses are eagerly awaited for further deciphering this complex issue that obviously has a crucial bearing on the use of both methods to infer physiological features in extinct taxa.

Notosuchia and Peirosaurids

Notosuchia

Despite the fascinating morphological diversity and related ecological specializations of the Notosuchia, only two publications (Cubo et al. 2017, 2020) deal specifically with their long bone histology. In the first of these articles the species studied was *Iberosuchus macrodon*, from the Paleogene of Spain, a sebecosuchian taxon nested in Notosuchia (Pol et al. 2012). Its general aspect suggests a land-dwelling form, roughly comparable to several sphenosuchians and protosuchians in size and morphology, though somewhat more massive. In the second article, seven notosuchian taxa, including species of various sizes, morphologies and adaptations were studied (most of them are from the Middle to Late Cretaceous of the Bauru Group, Brazil).

At mid-diaphysis, the femoral shaft of an *Iberosuchus* femur has a robust tubular architecture, with a clear-cut boundary between a hollow medulla and a compact cortex. Resorption lacunae nevertheless tend to accumulate around the medullary cavity, thus creating some porosity in the lowest cortical strata. Total bone compactness is relatively high, i.e., 0.872 in the smallest femur and 0.775 in the largest, but does not greatly diverge from the values observed in eusuchians. Histologically, the femur of *Iberosuchus* differs from what is commonly encountered in crocodylians. In cross section, periosteal cortices (Figure 26.7A, B) are mostly made of a brightly birefringent parallel-fibered tissue (collagen fibers are oriented circularly) that turns locally into the lamellar type. Conspicuous LAGs occur throughout the cortex, several of them showing a splitting that suggests the occurrence of two diapause stages during some years (see Chapter 31 on this topic). The sudden tightening of the LAGs in a narrow (*ca.* 100 µm) peripheral stratum in the largest of the two femora studied by Cubo et al. (2017) suggests that this specimen might have had a finite, asymptotic growth. Vascularization is sparse in *Iberosuchus* bones, especially in the peripheral third of the cortex, and mainly consists of simple canals oriented longitudinally.

To some extent, these histological features are more reminiscent of large squamates, such as the Teiidae and Varanidae, rather than of crocodiles. They strongly suggest that *Iberosuchus* had a similar (relatively slow and cyclic) skeletal growth, along with the low, ectopoikilothermic metabolism consistent with this growth pattern.

The study of *Iberosuchus* by Cubo et al. (2017) was based on a straightforward description and interpretation of bone histology. Conversely the more recent investigation by Cubo et al. (2020) relied on quantitative paleophysiological inferences.

VetBooks.ir

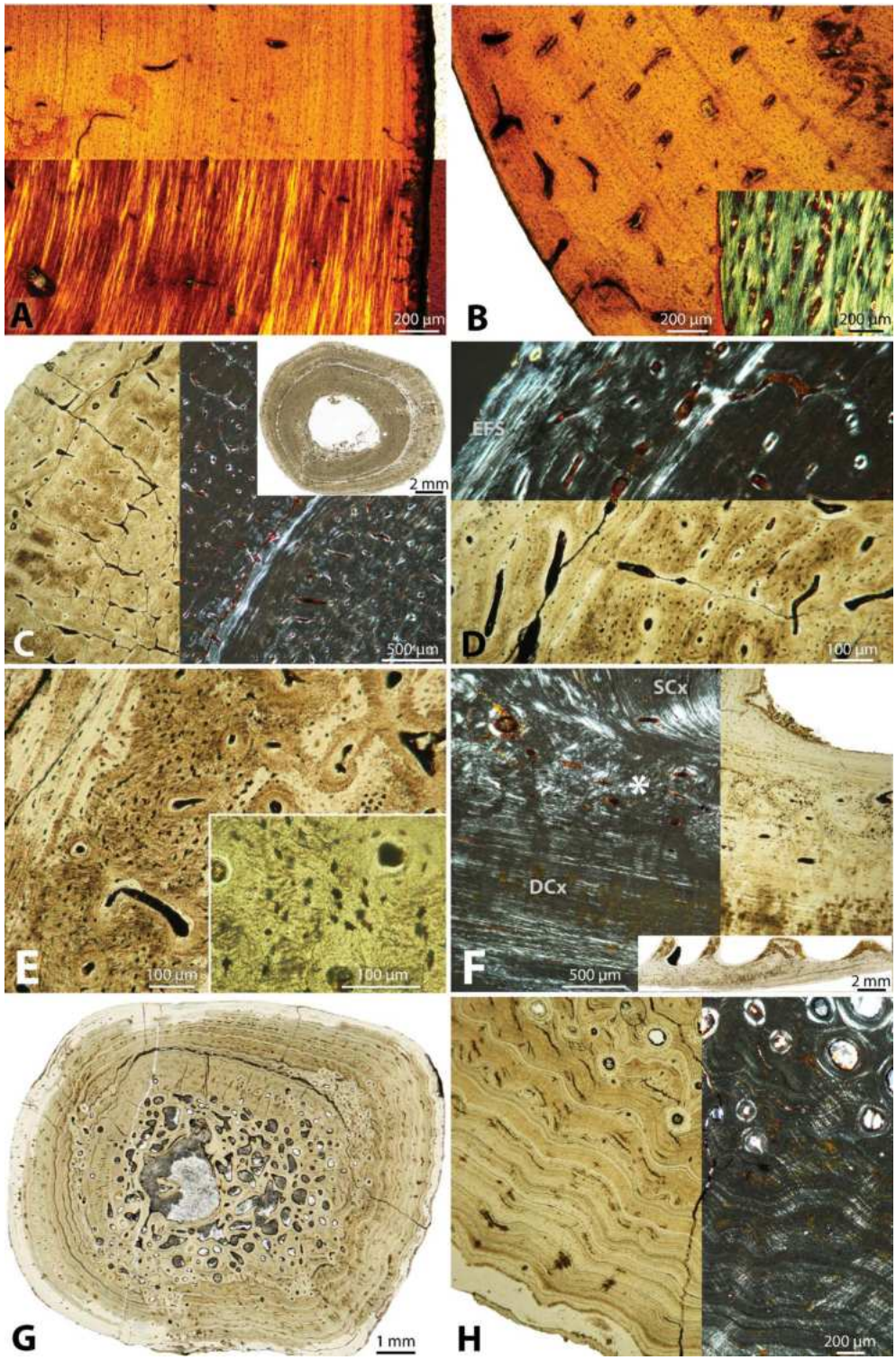


FIGURE 26.7 Basic bone microstructure in a notosuchian (*Iberosucus macrodon*), a peirosaur (*Trematochampsa taqueti*) and a sphenosuchian, *Hesperosuchus agilis*. A, Detail of the cortex in a cross section from the femur of *I. macrodon*. Lower half: polarized light. B, Detail of the cortex in a cross section from the humerus of *I. macrodon*. Inset: polarized light (detail). C, Cross section of the femur of *T. taqueti*. The right part of the main frame is viewed in polarized light. The inset shows the entire cross section of the femur. D, Closer view of the histological structure of *T. taqueti* femur. Upper half: polarized light. E, Detail of bone structure in *Trematochampsa* femur. The cell lacunae are multipolar and distributed randomly in the matrix. The inset shows the aspect of the cell lacunae at higher magnification. F, Histology of a *T. taqueti* osteoderm. Inner remodeling is mild in this osteoderm, and a broad formation of a tissue akin to the woven-fibered type (asterisk) persists in the core of the osteoderm. Left part of the main frame: polarized light. SCx, remodeled superficial (or outer, or dorsal) cortex; DCx: deep (or ventral) cortex. The inset shows the general aspect of the osteoderm section. G, General view of a cross section of the femur of *H. agilis*. H, Detail of the histological structure of the femur shown in G. Right part of the field: polarized light.

VetBooks.ir

The methodological option of this study aimed to estimate the resting metabolic rate (RMR) of the Notosuchia through two lines of evidence: (1) the relative area of primary osteons, and the shape, size and density of osteocyte lacunae (two approaches previously used by Cubo et al. 2012, Legendre et al. 2016, Fleischle et al. 2018) and (2) a reconstruction of the diameter of red blood cells from that of vascular canals. When associated with high vascular density, a small size of red blood cell is supposed to be indicative of a high (mammal-like or bird-like) aerobic efficiency (Huttenlocker and Farmer 2017), and should indirectly reveal a high metabolic activity. The technical review of these methods is beyond the scope of this chapter (see Chapter 37 for details). Their use led to a clear statement: all the notosuchian taxa considered, whatever the details of their ecological adaptations, had a low (albeit somewhat variable among taxa), lizard-like metabolic rate. This conclusion totally supported the previous histological interpretation of *Iberosuchus* femoral sections by Cubo et al. (2017).

Peirosaurids

Pepesuchus deisae, from the Upper Cretaceous of South America and Africa, is the only peirosaurid taxon for which a specific description of bone histology has been published (Sena et al. 2018). Several appendicular bones (tibia, metacarpal and ulnare) and one osteoderm from adult individuals were analyzed. To further document the basic aspects of peirosaurid osseous microstructures, several bones (femur, tibia, frontal and osteoderms) attributed to *Trematochampsa taqueti*, a taxon from the Late Cretaceous of Africa, were sampled and observed for this review. *T. taqueti* was described from isolated skull and postcranial material along with two other possible taxa (Buffetaut 1976). As Buffetaut (1976) indicated, it is particularly difficult to associate postcranial material with cranial elements when bones from several species are mixed. The association must be thus considered with caution. Moreover, the species has been considered a *nomen dubium* in recent work (e.g., Meunier and Larsson 2018), suggesting the possible presence of several taxa in the skull type material. In the present work, we consider the postcranial material to belong to the peirosaurid "*T. taqueti*", awaiting better attribution of this postcranial material. *Pepesuchus* and "*Trematochampsa*" were both medium-sized taxa with a relatively classical (i.e., eusuchian-like) gross morphology and a semiaquatic lifestyle (Buffetaut 1976, Sena et al. 2018).

The *Pepesuchus* tibia is a tubular bone with an approximate Cg value *ca*. 0.755 and a mean CDI value of 0.530 (measurements from Sena et al. 2018, Figure 8A), two values slightly below those of the *Trematochampsa* femur (Cg = 0.879, CDI = 0.655), but compatible with what is observed in most adult crocodylians (see Table 26.1). According to Sena et al.'s (2018) description, the primary cortex is made of "fibrolamellar and parallel-fibered bone intercalated over the section". A lamellar EFS exists, as well as *annuli* and LAGs, but the latter show an irregular spacing pattern. Vascularization is dense and consists of simple canals showing a longitudinal or a variable (reticular) orientation with numerous anastomoses, and of longitudinal primary osteons.

The histological characteristics of the *Trematochampsa* femur (Figure 26.7C) differ somewhat from those of the *Pepesuchus* tibia. In cross section, the matrix type prevailing in most of the cortex is an atypical parallel-fibered tissue with irregular and generally feeble birefringence. Cell lacunae are variable in aspect (often multipolar) and irregularly distributed (Figure 26.7D, E). A clear, brightly birefringent EFS occupies the bone periphery (Figure 26.7D), and variably marked but evenly spaced annuli occur throughout the cortex. Vascularization is relatively abundant. In the deep cortex, it consists of thin (diameter *ca*. 30 µm) primary osteons irregularly oriented and seldom anastomosed (Figure 26.7C, D). Osteon orientation becomes longitudinal in more peripheral regions. Haversian remodeling occurs but is mild. In general, this tissue structure differs little from the characteristics encountered in long bone cortices of most extant and extinct eusuchians (e.g., *Alligator*, *Crocodylus*, etc.).

The mid-diaphyseal region of *Pepesuchus* metacarpals is quasi-compact (see Sena et al. 2018, figure 4a). The metacarpal cortex is composed of lamellar tissue with annuli and zones. Most of the bone center is occupied by a compact formation showing evidence of intense Haversian remodeling (several generations of longitudinally oriented osteons), while the wall of the small (*ca*. 500 µm in mean diameter) medullary cavity is made of a thick deposit of lamellar tissue. Unfortunately, no other microstructural data are available for the metacarpals of other crocodylians; therefore, the degree of singularity of the features observed by Sena et al. (2018) in *Pepesuchus* cannot be estimated. Phylogenetically distant from the crocodylomorphs, a very similar structure, but extended to the whole skeleton, has been observed in an aquatic basal amniote, *Claudiosaurus germaini* (Buffrénil and Mazin 1989).

The *Pepesuchus* osteoderm studied by Sena et al. (2018) (this specimen was sampled along the sagittal keel, a nonconventional sectional plane) looks very compact, though densely vascularized, and displays a large central vascular sinus. Histologically, its basal plate is made of parallel-fibered tissue with LAGs and Sharpey's fibers oriented perpendicular to the deep surface. The core of the osteoderm is composed of woven-fibered tissue with both primary osteons and a network of simple canals, while the superficial cortex consists of parallel-fibered bone. This structure is basically consistent with what is known for other pseudosuchians; however, the *Pepesuchus* osteoderm (at least in the sectional plane used by Sena et al. 2018) is not organized as a diploe and its core does not show the extensive and imbalanced remodeling pattern observed in most crocodiles. This could explain the persistence in the core of the osteoderms of woven-fibered bone, a tissue seldom encountered in the adults of other taxa. Similar remarks could be made about *T. taqueti* osteoderms (though their sectional plane was orthogonal to that used for *Pepesuchus*). They are of modest thickness (Figure 26.7F, inset), nearly compact and comprise three histological regions: a deep cortex of parallel-fibered tissue, a median layer of woven-fibered bone housing primary osteons and a superficial layer of remodeled (differentiation of ornamentation reliefs) parallel-fibered and lamellar tissues (Figure 26.7F).

VetBooks.ir

Basal Crocodylomorphs: The Sphenosuchians *Terrestrisuchus-Saltoposuchus* and *Hesperosuchus*

Bone histology in basal crocodylomorphs is mainly known from Ricqlès et al.'s (2003) description of a humerus from *T. gracilis*, a sphenosuchian taxon that has been suspected by Allen (2003) to be the juvenile form (and junior synonym) of *Saltoposuchus connectens*. However, this synonymy was rejected by Irmis et al. (2013). The phyletic position of sphenosuchians remains uncertain (see, e.g., Clark et al. 2001) but they might represent the sister taxon of the Crocodyliformes, forming the earliest diverging lineage of Crocodylomorpha (Irmis et al. 2013). *T. gracilis-S. connectens* is thus likely to reflect the initial morphology and ecophysiological adaptation of these clades. It was a small (1.5 m in total length for *S. connectens*; Clark et al. 2001) cursorial form that lived in terrestrial Western Europe during the Norian-Rhaetian (Upper Triassic or Lower Jurassic) period. In addition to published data on "*Terrestrisuchus*", sections were made for this review at mid-diaphysis in the femur of a specimen of *H. agilis*, a typical sphenosuchian, morphologically close to *Saltoposuchus*, and originating from the early Upper Triassic (Carnian) beds of Arizona (Clark et al. 2001). *Hesperosuchus* is thus some 20 Ma older than *Terrestrisuchus-Saltoposuchus*, and almost contemporaneous with the oldest known crocodylomorph, *T. romeri* (Clark et al. 2001, Lecuona et al. 2016).

The *Terrestrisuchus* humerus was a lightly built tubular bone with a wide marrow cavity free of trabeculae. Its primary periosteal cortex, observed in cross section, mostly includes a monorefringent matrix roughly akin to the woven-fibered type (Ricqlès et al. 2003). In the bone periphery, this tissue turns into birefringent parallel-fibered tissue displaying two LAGs. The spatial density of osteocyte lacunae and the development of their canaliculi are elevated; in addition, vascular canals, represented mainly by longitudinal primary osteons, are abundant, especially in the lower layers of the cortex. Toward the bone periphery, both cell lacunae and vascular canals become sparser. No EFS was observed, which was interpreted by Ricqlès et al. (2003) as evidence that skeletal growth was still active, though clearly slower, by the time the specimen died, and that it was therefore not adult. As mentioned above, Allen's (2003) study, based on totally distinct lines of evidence, confirmed this inference by showing that *T. gracilis* could be the juvenile form of *S. connectens*.

In general, the occurrence of a well-vascularized tissue type, with a matrix somewhat intermediate between woven-fibered and parallel-fibered bone types in most of the humeral cortex, is strongly reminiscent of what is commonly encountered in extant and extinct eusuchians. The only difference is that cyclical growth marks are restricted to the bone periphery in the *Terrestrisuchus* humerus, whereas they occur in the whole cortex of eusuchian bones. As Ricqlès et al. (2003) concluded, the lack of cyclical growth marks reveals a continuous, steady cortical growth, at least in early ontogenetic stages, and might indicate a high, sustained metabolic activity. Although the early occurrence of continuous steady growth in juvenile *Terrestrisuchus* seems obvious, the interpretation of this feature in terms of absolute growth rate (in $\mu m*day^{-1}$), or in reference to metabolic activity, is more hazardous because cyclical growth marks occur in the bones (and teeth) of all vertebrates, including humans, and do not have simple, straightforward relationships with either the overall growth rate of an individual or its basal metabolic level (see, e.g., Castanet 2006, Köhler et al. 2012).

The femur shaft of *H. agilis* has a less clearly tubular architecture (Figure 26.2G) than that of *Terrestrisuchus*: in this bone, a broad spongiosa surrounds a relatively narrow medullary cavity, occupied by some robust trabeculae (Figure 26.7G). As a consequence, Cg (0.922) is high, and parameter *S* of Bone Profiler (0.081) is more elevated than in most other crocodylomorphs (Table 26.1). Such microanatomical features are very different from those of basal archosauriforms such as *Euparkeria* (Figure 26.2H), which shared with *Hesperosuchus* a similar morphology, size and possibly ecological adaptation (terrestrial, cursorial predators).

Histologically, the femoral cortex of *Hesperosuchus* is made of a parallel-fibered tissue showing some faint traces of lamellation (Figure 26.7H). In polarized light, it looks basically monorefringent (though extinction is not absolute), but the peripheral-most cortical layer, on a thickness of 200–250 µm, is more birefringent, due to the local abundance of oblique Sharpey's fibers. The gross monorefringent aspect of the cortex obviously reflects a dominant longitudinal orientation of the fiber meshwork of the bone. Consistent with this orientation, the cell lacunae appear small and rounded in cross section, as opposed to the lacunae in the walls of secondary osteons, which are much larger and oriented circularly, in compliance with the orientation of the osteonal lamellae. Cell lacunae occur at low density throughout the cortex, and so do vascular canals, which are extremely sparse and exclusively represented by simple longitudinal canals 20–30 µm in diameter. Conversely, the core of the femur, in deep cortical regions, has a dense population of secondary osteons. These appear at various stages of formation and with irregular shapes. The abundance of Sharpey's fibers is unusually high in the bone studied. Growth marks occur, especially in the form of translucent annuli showing a wavy contour (Figure 26.7H); however, they are poorly distinguishable from a general lamellar-like aspect of the bone. Considering the homogeneous monorefringence of the cortex in polarized light, this aspect is likely due to small, likely infra-annual growth cycles, enhanced by the impregnation of the bone during fossilization.

Though *Terrestrisuchus* and *Hesperosuchus* share a similar morphology, their bone structures may look divergent. However, if known specimens of *Terrestrisuchus* do represent the juveniles of a larger species (whatever the identity of this species), the histological structure of adult bones should then include a deep part made of the tissue already described under the name *Terrestrisuchus* (and now suspected to occur also in many other crocodylians, including eusuchians), plus a broad ring of parallel-fibered bone, as suggested by the peripheral-most layer incipiently present in the specimen described by Ricqlès et al. (2003). If this hypothesis is correct, then the bone structure of *Terrestrisuchus*, like that of *Hesperosuchus*, would show little divergence from what is commonly encountered in most other crownward crocodile taxa.

VetBooks.ir

Concluding Remarks

Bone histology in the Crocodylomorpha is commonly considered relatively constant, at least in post-Triassic forms. Beyond minor differences, long bone cortices are described as lamellar-zonal, with zones made of vascularized, "predominantly parallel-fibered bone", along with avascular annuli and LAGs (Ricqlès et al. 2003). The recent comparative data reviewed above tend to confirm this statement, although the structure of parallel-fibered bone in the crocodylians actually varies in a broad range from woven-fibered-like (a situation frequent in the Eusuchia) to lamellar (e.g., *H. agilis* or *I. macrodon*).

Bone histological features of early Archosauromorpha suggest that a high growth rates and the tachymetabolic physiology consistent with this feature (i.e., endothermy plus homeothermy) are likely "a basal characteristic of archosauriforms" (Ricqlès et al. 2008; see also Seymour et al. 2004, Legendre et al. 2016, Klein et al. 2017 and Cubo and Jalil 2019). In the crocodylian clade, this type of thermal physiology regressed, but the phylogenetic node(s) at which this shift occurred, as well as the type of ecological adaptation to which it was linked, remain to be defined. What bone histology positively shows is that a very basal Carnian taxon such as *Hesperosuchus* already had a type of bone histology closer to that of extant crocodiles than to early archosauromorphs. The ecophysiological divergences of the Crocodylomorpha and the Ornithodira could consequently be supposed to have occurred at least by the Carnian, and involved the Crocodylomorpha as a whole. Cubo et al. (2020) estimated that "endothermy may have been lost at the node Metasuchia (Notosuchia-Neosuchia) by the Early Jurassic". However, if the basal-most crocodylomorphs (sphenosuchians), as well as the thalattosuchians, are taken into account, this event must be considered more ancient.

A tachymetabolic physiological regime is often associated in the literature with the terrestrial, cursorial morphotype typically exemplified by basal archosauromorphs. However the histological study of *Hesperosuchus*, *Iberosuchus* and other Notosuchia suggests that the relationship between this morphology and a high metabolic activity may not be as consistent as imagined. Although histology supports such an interpretation in the Triassic, terrestrial, slender and supposedly agile archosauriforms *Teleocrater*, *Chanaresuchus* and *Euparkeria* (e.g., Ricqlès et al. 2008, Legendre et al. 2016, Cubo and Jalil 2019), it contradicts it in the case of the Notosuchia. Finally, the example of the Paleocene taxon *Iberosuchus*, studied by Cubo et al. (2017, 2020), shows that no tachymetabolic pseudosuchian persisted after the K-Pg crisis.

REFERENCES

Adams, T. L., et al. 2017. A large neosuchian crocodyliform from the Upper Cretaceous (Cenomanian) Woodbine Formation of North Texas. *J. Vert. Paleontol.* 37: e1349776. doi: 10.1080/02724634.2017.1349776.

Allen, D. 2003. When *Terrestrisuchus gracilis* reaches puberty, it becomes *Saltoposuchus connectens*. *J. Vert. Paleontol.* 23: (Suppl. n3): 29A.

Allen, E. R. 2012. *Analysis of North American goniopholidid crocodyliforms in a phylogenetic context*. Master of Science thesis, University of Iowa, Iowa City.

Amprino, R. 1947. La structure du tissue osseux envisagé comme l'expressions de differences dans la vitesse de l'accroissement. *Arch. Biol.* 58: 317–330.

Amprino, R. and G. Godina. 1947. La struttura delle ossa nei vertebrati. Ricerche comparative negli anfibi e negli amnioti. *Comment. Pontif. Acad. Scien.* 11: 328–463.

Anderson, T. F., et al. 1994. The stable isotopic records of fossils from Peterborough Member, Oxford Clay Formation (Jurassic), UK: palaeoenvironmental implications. *J. Geol. Soc. (Lond.)* 151: 125–138.

Andrade, M. de and R. J. Bertini. 2008. A new *Sphagesaurus* (Mesoeucrocodylia: Notosuchia) from the Upper Cretaceous of Monte Alto City (Bauru Group, Brazil), and a revision of the Sphagesauridae. *Hist. Biol.* 20: 101–136.

Andrade, M. de, et al. 2011. A new Berriasian species of *Goniopholis* (Mesoeucrocodylia, Neosuchia) from England, and a review of the genus. *Zool. J. Linn. Soc.* 163: S66–S108.

Andrade, R. C. L. P. de and J. M. Sayão. 2014. Paleohistology and lifestyle inferences of a dyrosaurid (Archosauria: Crocodylomorpha) from Paraiba basin (Northeastern Brazil). *PLoS One* 9: e102189.

Andrade, R. C. L. P. de, et al. 2018. Osteohistological study of both fossil and living Caimaninae (Crocodyliformes, Crocodylia) from South America and preliminary comments on growth physiology and ecology. Hist. Biol. 32: doi.org/10.10.1080/08912963.2018.1493475.

Barrios, F., et al. 2018. Re-description of the cranio-mandibular anatomy of *Notosuchus terrestris* (Crocodyliformes, Mesoeucrocodylia) from the Upper Cretaceous of Patagonia. *Cretaceous Res.* 83: 3–39.

Bausenhardt, D. 1951. Vergleichend-anatomische Untersuchungen über die Encoche d'ossification. *Anat. Anz.* 97: 223–230.

Bellairs, A. 1969. *The Life of Reptiles*. London, Widenfeld and Nicolson.

Benton, M. J. and J. M. Clark 1988. Archosaur phylogeny and the relationships of the Crocodylia. In *The Phylogeny and Classification of the Tetrapods, vol. 1: Amphibians, Reptiles, Birds*, M. J. Benton ed., 295–338. Oxford, UK, Clarendon Press.

Bernard, A., et al. 2010. Regulation of body temperature by some Mesozoic marine reptiles. *Science* 328: 1379–1382.

Bonaparte, J. F. 1971. Los tetrapodos del sector superior de la formacion Los Colorados, La Rioja, Argentina. *Opera Lilloana* 1971: 1–183.

Bonnan, M. F., et al. 2008. Using linear and geometric morphometrics to detect intraspecific variability and sexual dimorphism in femoral shape in *Alligator mississippiensis* and its implications for sexing fossil archosaurs. *J. Vert. Paleontol.* 28: 422–431.

Brochu, C. A. 1997. Morphology, fossils, divergence timing, and the phylogenetic relationships of *Gavialis*. *Syst. Biol.* 46: 479–522.

Brochu, C. A. 1999. Phylogenetics, taxonomy, and historical biogeography of Alligatoroidea. *J. Vert. Pal.* 19: 9–100.

Brochu, C. A. 2001a. Crocodylian snouts in space and time: phylogenetic approaches toward adaptative radiation. *Am. Zool.* 41: 564–585.

Brochu, C. A. 2001b. Progress and future directions in Archosaur phylogenetics. *J. Vert. Pal.* 75: 1185–1201.

Brochu, C. A. 2013. Phylogenetic relationships of Palaeogene ziphodont eusuchians and the status of *Pristichampsus* Gervais, 1853. *Earth Environ. Sci. Trans. R. Soc. Edinburgh* 103: 521–550.

Buffetaut, E. 1976. Ostéologie et affinités de *Trematochampsa taqueti* (Crocodylia, Mesosuchia) du Sénonien Inférieur d'In Beceten (République du Niger). *Géobios* 9: 143–198.

Buffetaut, E., et al. 1982. Remarques anatomiques et paléohistologiques sur *Dyrosaurus phosphaticus*, crocodilien mésosuchien des phosphates yprésiens de Tunisie. *Ann. Paléontol.* 68: 327–341.

Buffrénil, V. de. 1980a. Données préliminaires sur la structure des marques de croissance squelettiques chez les crocodiliens actuels et fossiles. *Bull. Soc. Zool. France* 105: 355–361.

Buffrénil, V. de. 1980b. Mise en évidence de l'incidence des conditions de milieu sur la croissance de *Crocodylus siamensis* (Schneider, 1801) et valeur des marques de croissance squelettiques pour l'évaluation de l'âge individuel. *Arch. Zool. Exp. Gén.* 121: 63–76.

Buffrénil, V. de. 1982. Morphogenesis of bone ornamentation in extant and extinct crocodilians. *Zoomorphology* 99: 155–166.

Buffrénil, V. de and H. Francillon-Vieillot. 2001. Ontogenetic changes in bone compactness in male and female Nile monitors. *J. Zool. Lond.* 254: 539–546.

Buffrénil, V. de and G. Hémery. 2007. Harvest of the Nile monitor, *Varanus niloticus*, in Sahelian Africa. Part II: Life history traits of harvested monitors. *Mertensiella* 16: 195–217.

Buffrénil, V. de and J.-M. Mazin. 1989. Bone histology of *Claudiosaurus germaini* (Reptilia, Claudiosauridae) and the problem of pachyostosis in aquatic tetrapods. *Hist. Biol.* 2: 311–322.

Buffrénil, V. de, et al. 2015. Differentiation and growth of bone ornamentation in vertebrates: a comparative histological study among the Crocodylomorpha. *J. Morphol.* 276: 425–445.

Buffrénil V. de, et al. 2016. Comparative data on the differentiation and growth of bone ornamentation in gnathostomes (Chordata: Vertebrata). *J. Morphol.* 277: 634–670.

Burns, M. E., et al. 2013. Histological variability in fossil and recent alligatorid osteoderms: systematic and functional interpretations. *J. Morphol.* 274: 676–686.

Busbey, A. B. 1986. New material of *Sebecus* cf. *huilensis* (Crocodilia: Sebecosuchidae) from the Miocène La Venta Formation of Colombia. *J. Vert. Pal.* 6: 20–27.

Buscalioni, Á. D. 2017. The Gobiosuchidae in the early evolution of Crocodyliformes. *J. Vert. Pal*, e1324459. doi: 10.1080/02724634.2017.1324459.

Canoville, A., et al. 2019. Systemic distribution of medullary bone in the avian skeleton: ground truthing criteria for the identification of reproductive tissues in extinct Avemetatarsalia. *BMC Evol. Biol.* 19: 71

Castanet, J. 2006. Time recording in bone microstructures of endothermic animals; functional relationships. *C. R. Palevol.* 5: 629–636.

Chabreck, R. H. and T. Joanen. 1979. Growth rates of American alligators in Louisiana. *Herpetologica* 35: 51–57.

Chinsamy, A. and W. J. Hillenius. 2004. Physiology of non-avian dinosaurs. In *The Dinosauria*, D. B. Weishampel, P. Dodson and H. Osmólska eds., 643–659. Berkeley, University of California Press.

Claessens, L. 2004. Archosaurian respiration and the pelvic girdle aspiration breathing of crocodyliforms. *Proc. Roy. Soc. B* 271: 1461–1465.

Clarac, F., et al. 2017. Vascularization in ornamented osteoderms: physiological implications in ectothermy and amphibious lifestyle in the Crocodylomorpha. *Anat. Rec.* 302: 175–183.

Clarac, F., et al. 2020. The evolution of dermal shield vascularization in Testudinata and Pseudosuchia: phylogenetic constraints versus ecophysiological adaptations. *Philos. Trans. R. Soc.* B375. doi: 10.1098/rstb.2019.0132.

Clark, J. M., et al. 2001. A new specimen of *Hesperosuchus agilis* from the Upper Triassic of New-Mexico and the interrelationships of basal crocodylomorph archosaurs. *J. Vert. Pal.* 20: 683–704.

Company, J. and X. Pereda-Suberbiola. 2017. Long bone histology of a eusuchian crocodyliform from the Upper Cretaceous of Spain: implications for growth strategy in extinct crocodiles. *Cretaceous Res.* 72: 1–7.

Cubo, J. and N.-E. Jalil. 2019. Bone histology of *Azendohsaurus laaroussii*: implications for the evolution of thermometabolism in Archosauromorpha. *Paleobiology* 45: 317–330.

Cubo, J., et al. 2012. Paleohistological estimation of bone growth rate in extinct archosaurs. *Paleobiology* 38: 335–349.

Cubo, J., et al. 2017. Bone histology of *Iberosuchus macrodon* (Sebecosuchia, Crocodylomorpha). *Lethaia* 50: 495–503.

Cubo, J. et al. 2020. Were Notosuchia (Pseudosuchia: Crocodylomorpha) warm-blooded? A palaeohistological analysis suggests ectothermy. *Biol. J. Linn. Soc.* 131: 154–162.

Dacke, C. G., et al. 2015. Alligator osteoderms as a source of labile calcium for eggshell formation. *J. Zool.* 297: 255–264.

Dollman, K. L.,et al. 2018. Convergent evolution of a eusuchian-type secondary palate within Shartegosuchidae. *Am. Mus. Nov.* 3901: 1–23.

Dumont M., et al. 2013. Inner architecture of vertebral centra in terrestrial and aquatic mammals: a two-dimensional comparative study. *J. Morphol.* 274: 570–584.

English, L. T. 2018. Variation in crocodilian dorsal scute organization and geometry with a discussion on possible functional implications. *J. Morphol.* 279: 154–162.

Enlow, D. H. 1969. The bones of reptiles. In *Biology of the Reptilia, Morphology A. 1*, C. Gans and A. Bellairs eds., 45–80. New York, Academic Press.

Enlow, D. H. and S. O. Brown. 1957. A comparative histological study of fossil and recent bone tissues. Part II. *Texas J. Sci.* 9: 186–214.

Erickson, G. M. and C. A. Brochu. 1999. How the "terror crocodile" grew so big. *Nature* 398: 205–206.

Ferguson, M. W. T. 1982. The structure and composition of the eggshell and embryonic membranes of *Alligator mississippiensis*. *Trans. Zool. Soc. Lond.* 36: 99–152.

Figueiredo, R. G., et al. 2011. Description of a new specimen of *Susisuchus anatoceps* (Crocodylomorpha: Mesoeucrocodylia) from the Crato Formation (Santana Group) with comments on Neosuchia. *Zool. J. Linn. Soc.* 163: S273–S288.

Fiorelli, L. E., et al. 2016. A new Late Cretaceous crocodyliform from the western margin of Gondwana (La Rioja Province, Argentina). *Cretaceous Res.* 60: 194–209.

Fleischle, C., et al. 2018. Quantitative histological models suggest endothermy in plesiosaurs. *PeerJ* 6: e4955.

Foffa, D. and M. T. Young. 2014. The cranial osteology of *Tyrannoneustes lythrodectikos* (Crocodylomorpha: Metriorhynchidae) from the Middle Jurassic of Europe. *PeerJ* 2: e608. doi: 10.7717/peerj.608.

Foote, J. S. 1911. The comparative histology of femoral bones. *Trans. Am. Microsc. Soc.* 30: 87–141.

Foote J. S. 1916. *A Contribution to the Comparative Histology of the Femur.* Baltimore, MD, Lord Baltimore Press, Smithsonian Institute Washington.

Fortier, D., et al. 2011. Redescription and phylogenetic relationships of *Meridiosaurus vallisparadisi*, a pholidosaurid from the Late Jurassic of Uruguay. *Zool. J. Linn. Soc.* 163: S257–S272.

Gatesy, J. and G. Amato. 2008. The rapid accumulation of consistent molecular support for intergeneric crocodylian relationships. *Mol. Phylogen. Evol.* 48: 1232–1237.

Gatesy, J., et al. 2003. Combined support for wholesale taxic atavism in gavialine crocodylians. *Syst. Biol.* 55: 403–422.

Gienger, C. M., et al. 2018. Ontogenetic comparisons of standard metabolism in three species of crocodilians. *PLoS One* 12 (2): e0171082. doi: 10.1371/journal.pone.0171082.

Göhlich, U. B., et al. 2005. The systematic position of the Late Jurassic alleged dinosaur *Macelognathus* (Crocodylomorpha: Sphenosuchia). *Can. J. Earth Sci.* 42: 307–321.

Goloboff, P. A., et al. 2019. Morphological data sets fit a common mechanism much more poorly than DNA sequences and call into question the Mkv model. *Syst. Biol.* 68 (3): 494–504.

Green, C. C. 2018. *Osteology and skeletochronology of an ontogenetic series of Clidastes (Squamata, Mosasauridae): growth and metabolism in basal mosasurids.* Master's thesis 3122, Fort Hays State University, FHSU Scholar Repository.

Grigg, G. and D. Kirshner. 2015. *Biology and Evolution of Crocodylians.* Ithaca, Comstock Publishing Associations.

Haines, R. W. 1938. The primitive form of epiphysis in the long bones of the tetrapods. *J. Anat.* 72: 323–343.

Haines, R. W. 1942. The evolution of epiphyses and of endochondral bone. *Biol. Rev.* 17: 267–292.

Haines, R. W. 1969. Epiphyses and sesamoids. In *Biology of the Reptilia, Morphology A. 1*, C. Gans, and A. Bellairs eds., 81–115. New York, Academic Press.

Haines, R. W. and A. Mohuiddin. 1968. Metaplastic bone. *J. Anat.* 103: 527–538.

Harrell, T. L. Jr, et al. 2016. Endothermic mosasaurs? Possible thermoregulation of Late Cretaceous mosasaurs (Reptilia, Squamata) indicated by stable oxygen isotopes in fossil bioapatite in comparison with coeval marine fish and pelagic seabirds. *Palaeontology* 59: 351–363.

Hecht, M. K. and S. F. Tarsitano. 1983. The tarsus and metatarsus of *Protosuchus* and its phyletic implications. In *Advances in Herpetology and Evolution*, A. G. J. Rhodin, and K. Miyata eds., 332–349. Cambridge, UK, Museum of Comparative Zoology.

Houssaye, A., et al. 2013. Microanatomical and histological features in the long bones of mosasaurine mosasaurs (Reptilia, Squamata) – Implications for aquatic adaptation and growth rates. *PLoS One* 8: e76741.

Hua, S. and E. Buffetaut; 1997. Part V: Crocodylia. Introduction. In *Ancient Marine Reptiles*, J. M. Callaway, and E. L. Nicholls eds., 357–374. London, Academic Press.

Hua, S. and V. de Buffrénil. 1996. Bone histology as a clue in the interpretation of functional adaptations in the Thalattosuchia (Reptilia, Crocodylia). *J. Vert. Paleontol.* 16: 703–717.

Huttenlocker, A. K. and C. G. Farmer. 2017. Bone microvasculature tracks red blood cell size diminution in Triassic mammal and dinosaur forerunners. *Current Biol.* 27: 48–54.

Hutton, J. M. 1986. Age determination of living Nile crocodiles from the cortical stratification of bone. *Copeia* 1986: 332–341.

Irmis, R. B., et al. 2013. Early Crocodylomorpha. *Geol. Soc. Lond. Spec. Pub.* 379: 275–302.

Janke, A., et al. 2005. Mitogenomic analyses place the Gharial (*Gavialis gangeticus*) on the crocodile tree and provide pre-K/T divergence times for most crocodilians. *J. Mol. Evol.* 61: 620–626.

Johnson, M. M., et al. 2020. The phylogenetics of Teleosauroidea (Crocodylomorpha, Thalattosuchia) and implications for their ecology and evolution. *PeerJ* 8: e9808.

Jouve, S. 2009. The skull of *Teleosaurus cadomensis* (Crocodylomorpha; Thalattosuchia), and phylogenetic analysis of Thalattosuchia. *J. Vert. Paleont.* 29: 88–102.

Jouve, S. 2016. A new basal tomistomine (Crocodylia, Crocodyloidea) from Issel (Middle Eocene; France): palaeobiogeography of basal tomistomines and palaeogeographic consequences. *Zool. J. Linn. Soc.* 177: 165–182.

Jouve, S., et al. 2014. *Maroccosuchus zennaroi* (Crocodylia: Tomistominae) from the Eocene of Morocco: phylogenetic and palaeobiogeographical implications of the basalmost tomistomine. *J. Syst. Palaeont.* 12: 1–25.

Jouve, S., et al. 2006. A new species of *Dyrosaurus* (Crocodylomorpha, Dyrosauridae) from the Early Eocene of Morocco: phylogenetic implications. *Zool. J. Linn. Soc.* 148: 603–656.

Jouve, S. and N.-E. Jalil. 2020. Paleocene resurrection of a crocodylomorph taxon: biotic crises, climatic and sea level fluctuations. *Gondwana Res.* 85: 1–18.

Jouve, S., et al. 2017. Biases in the study of relationships between biodiversity dynamics and fluctuation of environmental conditions. *Palaeont. Electron.* 20: 1–21.

King, F. W. and P. Brazaitis. 1971. Species identification of commercial crocodilian skins. *Zoologica* 56: 15–69.

Klein, N., et al. 2009. Skeletochronology and isotopic analysis of a captive individual of *Alligator mississippiensis*. Daudin, 1802. *Foss. Rec.* 12: 121–131.

Klein, N. et al. 2017. Preliminary observations on the bone histology of the Middle Triassic pseudosuchian archosaur *Batrachotomus kupferzellensis* reveal fast growth with laminar fibrolamellar bone tissue. *J. Vert. Paleontol.* 37. DOI: 10.1080/027246.2017.1333121.

Köhler, M., et al. 2012. Seasonal bone growth and physiology in endotherms shed light on dinosaur physiology. *Nature* 487: 358–361.

Kuzmin, I. T., et al. 2018. Revision of the large crocodyliform *Kansajsuchus* (Neosuchia) from the Late Cretaceous of Central Asia. *Zool. J. Linn. Soc.* 53: 335–387.

Larson, A. 1994. The comparison of morphological and molecular data in phylogenetic systematics. In *Molecular Ecology and Evolution: Approaches and Applications*, B. Schierwater, B. Streit, G. P. Wagner and R. De Salle eds., 371–390. Basel, Birkhäuser Verlag.

Larsson, H. C. E. and H. D. Sues. 2007. Cranial osteology and phylogenetic relationships of *Hamadasuchus rebouli* (Crocodyliformes: Mesoeucrocodylia) from the Cretaceous of Morocco. *Zool. J. Linn. Soc.* 149: 533–567.

Laurin, M., et al. 2011. Bone microanatomy and lifestyle: a descriptive approach. *C. R. Palevol* 10: 381–402.

Leardi, J. M., et al. 2015. The postcranial anatomy of *Yacarerani boliviensis* and the phylogenetic significance of the notosuchian postcranial skeleton. *J. Vert. Paleont.* 35: e995187. doi: 10.1080/02724634.2014.995187.

Leardi, J. M., et al. 2017. Detailed anatomy of the braincase of *Macelognathus vagans* Marsh, 1884 (Archosauria, Crocodylomorpha) using high resolution tomography and new insights on basal crocodylomorph phylogeny. *PeerJ* 5: e2801. doi: 10.7717/peerj.2801.

Leardi, J. M., et al. 2018. New Patagonian baurusuchids (Crocodylomorpha; Notosuchia) from the Bajo de la Carpa Formation (Upper Cretaceous; Neuquén, Argentina): New evidences of the early sebecosuchian diversification in Gondwana. *C. R. Palevol* 17: 504–521.

Lecuona, A., et al. 2016. Revision of the early crocodylomorph *Trialestes romeri* (Archosauria, Suchia) from the lower Upper Triassic Ischigualasto formation of Argentina: one of the oldest-known crocodylomorphs. *Papers Palaeontol.* 2: 585–622.

Lee, A. H. 2004. Histological organization and its relationship to function in the femur of *Alligator mississippiensis*. *J. Anat.* 204: 197–207.

Lee, M. S., and A. M. Yates. 2018. Tip-dating and homoplasy: reconciling the shallow molecular divergences of modern gharials with their long fossil record. *Proc. R. Soc. Edin., B* 285 (1881): 20181071.

Legendre, L. J., et al. 2016. Palaeohistological evidence for ancestral high metabolic rate in archosaurs. *Syst. Biol.* 65: 989–996.

Leite, K. J. and D. C. Fortier. 2018. The palate and choanae structure of the *Susisuchus anatoceps* (Crocodyliformes, Eusuchia): phylogenetic implications. *PeerJ* 6: e5372. doi: 10.7717/peerj.5372.

Man, Z., et al. 2011. Crocodilian phylogeny inferred from twelve mitochondrial protein-coding genes, with new complete mitochondrial genomic sequences for *Crocodylus acutus* and *Crocodylus novaeguinae*. *Mol. Phylogenet. Evol.* 60: 62–67.

Margerie, E. de, et al. 2002. Bone typology and growth rate: testing and quantifying "Amprino's rule" in the mallard (*Ana Platyrhynchos*). *C. R. Biol.* 325: 221–230.

Marinho, T. S. and I. S. Carvalho. 2009. An armadillo-like sphagesaurid crocodyliform from the Late Cretaceous of Brazil. *J. South Am. Earth Sci.* 27: 36–41.

Martin, J. E., et al. 2019. A new freshwater teleosaurid from the Jurassic of northeastern Thailand. *J. Vert. Paleontol.* 38: e31549059. doi: 10.1080/02724634.2018.1549059.

Martinelli, A. G., et al. 2018. The first *Caipirasuchus* (Mesoeucrocodylia, Notosuchia) from the Late Cretaceous of Minas Gerais, Brazil: new insights on sphagesaurid anatomy and taxonomy. *PeerJ* 6: e5594. doi: 10.7717/peerj.5594.

Martínez, R. N., et al. 2018. A new protosuchid crocodyliform (Pseudosuchia, Crocodylomorpha) from the Norian Los Colorados Formation, northwestern Argentina. *J. Vert. Paleontol.* 38: 1–12. doi: 10.1080/02724634.2018.1491047.

Massare, J. A. 1988. Swimming capabilities of Mesozoic marine reptiles: implications for method of predation. *Paleobiology* 14: 187–205.

Meers, M. B. 2002. Cross-sectional geometric properties of the crocodilian humerus: an exception to Wolff's law? *J. Zool. Lond.* 258: 405–418.

Meganathan, P. R., et al. 2010. Molecular phylogenetic analyses of genus *Crocodylus* (Eusuchia, Crocodylia, Crocodylidae) and the taxonomic position of *Crocodylus porosus*. *Mol. Phylogenet. Evol.* 57: 393–402.

Meister, W. 1962. Histological structure of long bones in penguins. *Anat. Rec.* 43: 377–386.

Melstrom, K. M. and R. B. Irmis. 2019. Repeated evolution of herbivorous crocodyliforms during the age of dinosaurs. *Curr. Biol.* 29: 2389–2395.

Meunier, L. M. V. and H. C. E. Larsson. 2018. *Trematochampsa taqueti* as a *nomen diubium* and the crocodyliform diversity of the Upper Cretaceous in Beceten Formation of Niger. *Zool. J. Linn. Soc.* 182: 659–680.

Montefeltro, F. C., et al. 2013. A new neosuchian with Asian affinities from the Jurassic of northeastern Brazil. *Naturwissenschaften* 100: 835–841.

Montes, L., et al. 2007. Relationship between bone growth rate, body mass and resting metabolic rate in growing amniotes: a phylogenetic approach. *Biol. J. Linn. Soc.* 92: 63–76.

Nesbitt, S. J. 2011. The early evolution of archosaurs: relationships and the origin of major clades. *Bull. Am. Mus. Nat. Hist.* 35: 1–292.

Norell, M. A. 1989. The higher level Relationships of the extant Crocodylia. *J. Herpetol.* 23: 325. doi: 10.2307/1564042.

Oaks, J. R. 2011. A time-calibrated species tree of Crocodylia reveals a recent radiation of the true crocodiles. *Evolution*. 65: 3285–3297.

Paolillo, A. and Linares, O. J. 2007. Nuevos cocodrilos Sebecosuchia del Cenozoico Suramericano (Mesosuchia: Crocodylia). *Contrib. Occasion. Ed. Lab. Paleobiol.* 3: 1–25.

Peabody, F. E. 1961. Annual growth zones in living and fossil vertebrates. *J. Morphol.* 108: 11–62.

Pellegrini, R. 2007. Skeletochronology of the limb elements of mosasaurs (Squamata: Mosasauridae). *Trans. Kansas Acad. Sci.* 110: 83–99.

Piras, P., et al. 2010. The *Gavialis-Tomistoma* debate: the contribution of skull ontogenetic allometry and growth trajectories to the study of crocodylian relationships: *Gavialis* and *Tomistoma* skull ontogeny. *Evol. Dev.* 12: 568–579.

Pol, D. and M. A. Norell. 2004a. A new Crocodyliform from Zos Canyon, Mongolia. *Am. Mus. Novit.* 3445: 1–36.

Pol, D. and M. A. Norell. 2004b. A new gobiosuchid crocodyliform taxon from the Cretaceous of Mongolia. *Am. Mus. Novit.* 3458: 1–31.

Pol, D., et al. 2004. Basal crocodyliforms from the Lower Cretaceous Tugulu Group (Xinjiang, China), and the phylogenetic position of Edentosuchus. *Cretaceous Res.* 25: 603–622.

Pol, D., et al. 2012. Postcranial anatomy of *Sebecus icaeorhinus* (Crocodyliformes, Sebecidae) from the Eocene of Patagonia. *J. Vert. Paleontol.* 32: 328–354.

Pough, F. H., et al. 2004. *Herpetology.* 3rd ed. Upper Saddle River, NJ, Prentice Hall.

Prondvai, E. 2017. Medullary bone in fossils: function, evolution and significance in growth curve reconstructions of extinct vertebrates. *J. Evol. Biol.* 30: 440–446.

Puértolas-Pascual, E., et al. 2013. The eusuchian crocodylomorph *Allodaposuchus subjuniperus* sp. nov., a new species from the latest Cretaceous (upper Maastrichtian) of Spain. *Hist. Biol.* 28: 91–109.

Quekett, J. T. 1849. On the intimate structure of bone as composing the skeleton in the four great classes of animals, viz., mammals, birds, reptiles, and fishes, with some remarks on the great value of the knowledge of such structure in determining the affinities of minute fragments of organic remains. *Trans. Microsc. Soc. Lond.* 2: 46–58.

Reid, R. E. H. 1984. Primary bone and dinosaurian physiology. *Geol. Mag.* 121: 589–598.

Ricqlès, A. de. 1972. Nature et signification des "surfaces épiphysaires" chez les tétrapodes fossiles. *C. R. Acad. Sci. Paris* 274: 3527–3530.

Ricqlès, A. de. 1975. Recherches paléohistologiques sur les os longs des tétrapodes. VII – Sur la classification, la signification fonctionnelle et l'histoire du tissu osseux des tétrapodes (Première partie). *Ann. Paléont.* 61: 51–81.

Ricqlès A. de. 1976. On bone histology of fossil and living reptiles, with comments on its functional and evolutionary significance. In *Morphology and Biology of Reptiles*, A. d'A. Bellairs and C. B. Cox eds., 123–151. London, Academic Press.

Ricqlès, A. de. 1979. Quelques remarques sur l'histoire évolutive des tissus squelettiques chez les vertébrés et plus particulièrement chez les tétrapodes. *Ann. Biol.* 18: 1–35.

Ricqlès, A. de. 1980. Tissue structures of dinosaur bone. Functional significance and possible relation to dinosaur physiology. In *A Cold Look at the Warm-Blooded Dinosaurs*, R. D. K. Thomas and E. C. Olson eds., 103–139. AAA Selected symposium 28, Boulder, Westview Press.

Ricqlès, A. de. and V. de Buffrénil. 2001. Bone histology, heterochronies and the return of tetrapods to life in water: where are we? In *Secondary Adaptation of Tetrapods to Life in Water*, J.-M. Mazin and V. de Buffrénil eds., 289–310. München, Verlag Dr. Friedrich Pfeil.

Ricqlès, A. de, et al. 2003. On the bone histology of some Triassic pseudosuchian archosaurs and related taxa. *Ann. Paléontol.* 89: 67–101.

Ricqlès, A. de, et al. 2008. On the origin of high growth rates in archosaurs and their ancient relatives: complementary histological studies on Triassic Archosauriforms and the problem of a "phylogenetic signal" in bone histology. *Ann. Paléontol.* 94: 57–76.

Riff, D. and A. W. A. Kellner. 2011. Baurusuchid crocodyliforms as theropod mimics: clues from the skull and appendicular morphology of *Stratiotosuchus maxhechti* (Upper Cretaceous of Brazil). *Zool. J. Linn. Soc.* 163: S37–S56.

Roos, J., et al. 2007. Extended mitogenomic phylogenetic analyses yield new insight into crocodylian evolution and their survival of the Cretaceous–Tertiary boundary. *Mol. Phylogenet. Evol.* 45: 663–673.

Rossmann, T. 2000a. Studien an känozoischen Krokodilen: 4. Biomechanische Untersuchung am Schädel und der Halswirbelsäule des paläogenen Krokodils *Pristichampsus rollinatii* (Eusuchia: Pristichampsidae). *Neues Jahrb. Geol. Paläontol. Abh.* 215: 397–432.

Rossmann, T. 2000b. Studien an känozoischen Krokodilen: 5. Biomechanische Untersuchung am postkranische Skelett des paläogenen Krokodils Pristichampsus rollinatii (Eusuchia: Pristichampsidae). *Neues Jahrb. Geol. Paläontol. Abh.* 217: 289–330.

Salas-Gismondi, R., et al. 2015. A Miocene hyperdiverse crocodylian community reveals peculiar trophic dynamics in proto-Amazonian mega-wetlands. *Proc. R. Soc. B: Biol. Sci.* 282: (1804). doi: 10.1098/rspb.2014.2490.

Sayão, J. M., et al. 2016. Paleohistology of *Susisuchus anatoceps* (Crocodylomorpha, Neosuchia): comments on growth strategies and lifestyle. *PLoS One* 11(5): e0155297. doi:10.1371/journal.pone.0155297.

Schweitzer, M. H., et al. 2007. Do egg-laying crocodilian (*Alligator mississippiensis*) archosaurs form medullary bone? *Bone* 40: 1152–1158.

Sena, M. V. A., et al. 2018. Bone microanatomy of *Pepesuchus deisae* (Mesoeucrocodylia, Peirosauridae) reveals a mature individual from the Upper Cretaceous of Brazil. *Cretaceous Res.* 90: 335–348.

Seon, N. 2018. *Thermophysiologie des Metriorhynchidae via l'analyse isotopique de l'oxygène* ($\delta^{18}O$). *Stage de recherche Master 2*. Lyon (France), Université Claude Bernard, UMR-CNRS 5276.

Seymour, R. S., et al. 2004. Evidence for endothermic ancestors of crocodiles at the stem of archosaur evolution. *Physiol. Biochem. Zool.* 77: 1051–1067.

Stein, B. R. 1989. Bone density and adaptation in semiaquatic mammals. *J. Mammal.* 70: 467–476.

Sues, H. D., et al. 2003. A new crocodylomorph archosaur from the Upper Triassic of North Carolina. *J. Vert. Paleontol.* 23: 329–343.

Thorbjarnarson, J. B. 1996. Reproductive characteristics of the order Crocodylia. *Herpetologica* 52: 8–24.

Tumarkin-Deratzian, A. R. 2007. Fibrolamellar bone in wild adult *Alligator mississippiensis*. *J. Herpetol.* 41: 341–345.

Turner, A. H. 2015. A review of *Shamosuchus* and *Paralligator* (Crocodyliformes, Neosuchia) from the Cretaceous of Asia. *PLoS One* 10: e0118116. doi: 10.1371/journal.pone.0118116.

Turner, A. H. and G. A. Buckley. 2008. *Mahajangasuchus insignis* (Crocodyliformes: Mesoeucrocodylia) cranial anatomy and new data on the origin of the eusuchian-style palate. *J. Vert. Paleontol.* 28: 382–408.

Turner, A. H. and A. C. Pritchard. 2015. The monophyly of Susisuchidae (Crocodyliformes) and its phylogenetic placement in Neosuchia. *PeerJ* 3: e759. doi: 10.7717/peerj.759.

Vickaryous, M. K. and B. K. Hall. 2008. Development of the dermal skeleton in *Alligator mississippiensis* (Archosauria, Crocodylia) with comments on the homology of osteoderms. *J. Morphol.* 269: 398–422.

Vignaud, P. 1995. *Les Thalattosuchia, Crocodiles Marins Du Mesozoique : Systématique Phylogénétique, Paléoécologie, Biochronologie et Implications Paléogéographiques*. Paléontologie, Université de Poitiers.

Walker, A. D. 1970. A revision of Jurassic reptile *Hallopus victor* (Marsh), with remarks on the classification of crocodiles. *Philos. Trans. R. Soc. London* 257: 323–372.

Wall, W. P. 1983. The correlation between high limb-bone density and aquatic habits in recent mammals. *J. Paleontol.* 57:197–207.

Warren, J. W. 1963. *Growth Zones in the Skeleton of Recent and Fossil Vertebrates*. University Microfilms Inc., n 63-4544. University of California, Los Angeles.

Webb, P. and V. de Buffrénil. 1990. Locomotion in the biology of large aquatic vertebrates. *Trans. Am. Fish. Soc.* 119: 629–641.

Wiffen, J., et al. 1995. Ontogenetic evolution of bone structure in Late Cretaceous Plesiosauria from New Zealand. *Geobios* 28: 625–640.

Wilberg, E. W. 2015. What's in an outgroup? The impact of outgroup choice on the phylogenetic position of Thalattosuchia (Crocodylomorpha) and the origin of Crocodyliformes. *Syst. Biol.* 64: 621–637.

Wilberg, E. W., et al. 2019. Evolutionary structure and timing of major habitat shifts in Crocodylomorpha. *Scient. Rep.* 9: 514. doi: 10.1038/s41598-018-36795-1.

Willis, R. E. 2009. Transthyretin gene (TTR) intron 1 elucidates crocodylian phylogenetic relationships. *Mol. Phylogenet. Evol.* 53: 1049–1054.

Willis, R. E., et al. 2007. Evidence for placing the false gharial (*Tomistoma schlegelii*) into the family Gavialidae: Inferences from nuclear gene sequences. *Mol. Phylogenet. Evol.* 43: 787–794.

Wink, C. S. and R. M. Elsey. 1986. Changes in femoral morphology during egg-laying in *Alligator mississippiensis*. *J. Morphol.* 189: 183–188.

Woodward, H. N., et al. 2011. Osteohistological evidence for determinate growth in the American Alligator. *J. Herpetol.* 45: 339–342.

Wu, X.-C. and S. Chatterjee. 1993. *Dibothrosuchus elaphros*, a crocodylomorph from the lower Jurassic of China and the phylogeny of the Sphenosuchia. *J. Vert. Paleontol.* 13: 58–89.

Wu, X.-C., et al. 1994. A new species of *Shantungosuchus* from the Lower Cretaceous of Inner Mongolia (China), with comments on *S. chuhsienensis* Young, 1961 and the phylogenetic position of the genus. *J. Vert. Paleontol.* 14: 210–229.

Wu, X.-C., et al. 1997. *Sichuanosuchus shuhanensis*, a new? Early Cretaceous protosuchian (Archosauria: Crocodyliformes) from Sichuan (China), and the monophyly of Protosuchia. *J. Vert. Paleontol.* 17: 89–103.

Young, M. T. and M. B. De Andrade. 2009. What is *Geosaurus*? Redescription of *Geosaurus giganteus* (Thalattosuchia: Metriorhynchidae) from the Upper Jurassic of Bayern, Germany. *Zool. J. Linn. Soc.* 157: 551–585.

Young, M. T., et al. 2010. The evolution of Metriorhynchoidea (mesoeucrocodylia, thalattosuchia [*sic.*]): an integrated approach using geometric morphometrics, analysis of disparity, and biomechanics. *Zool. J. Linn. Soc.* 158: 801–859.

Young, M. T., et al. 2016. Revision of the enigmatic crocodyliform *Elosuchus felixi* de Lapparent de Broin, 2002 from the Lower-Upper Cretaceous boundary of Niger: potential evidence for an early origin of the clade Dyrosauridae. *Zool. J. Linn. Soc.* 179: 377–403.

Zanno, L. E., et al. 2015. Early crocodylomorph increases top tier predator diversity during rise of dinosaurs. *Scient. Rep.* 5: 9276. doi: 10.1038/srep09276.

VetBooks.ir

27

Archosauromorpha: Avemetatarsalia – Dinosaurs and Their Relatives

Kevin Padian and Holly N. Woodward

CONTENTS

Introduction 511
Nondinosaurian Avemetatarsalia 512
  Introduction 512
  Basal (Nondinosauromorph, Nonpterosauromorph) Avemetatarsalians 514
  Ornithodira: Pterosauria 514
  Ornithodira: Nondinosaurian Dinosauromorpha 518
Dinosauria 521
  Basal Dinosauria 521
  Dinosauria: Ornithischia 522
    Heterodontosauridae 522
    Thyreophora 522
    Ceratopsia 525
    Pachycephalosauria 526
    Basal Ornithopoda 526
    Hadrosaurids 528
  Dinosauria: Saurischia 529
    Basal Sauropodomorphs 529
    Sauropoda 529
    Theropoda: Nonavian Forms 531
    Theropoda: Aves 533
  Some Functional Questions about Nonavian Dinosaurs 539
    Histological Problems in Dinosaurian Growth 539
    Interindividual Differences in Body Size Versus Age 539
    The Problem of Phyletic Dwarfism 540
    What Explains the Distribution of Secondary Bone Tissue Among Elements in a Skeleton? 541
General Conclusions to the Paleohistological Consideration of the Ornithodira 542
References 543

Introduction

Archosauromorpha (Pan-Archosauria) is a stem-group comprising all diapsid reptiles closer to *Passer* than to *Lacerta*; that is, birds, crocodiles, possibly turtles and all the extinct diapsids outside this crown-group that are closer to *Passer* than to Lepidosauromorpha (snakes and other lacertilians, rhynchocephalians and all the extinct diapsids outside this crown-group, including possibly Sauropterygia and Ichthyopterygia) that are closer to it than to Lepidosauria. Because it is a stem-group, it has no synapomorphies. Its range is from the Middle or Late Permian to the Present. Alternatively, Gauthier (2020) has defined it as a node-group comprising birds, crocodiles and several taxa outside their common ancestor.

The understanding of patterns of the evolution of growth rates, metabolic rates, and the varieties of tissues that these processes reflect has advanced considerably in the past 50 years, although the framework was laid by many workers since the 1700s, including Quekett, Hunter, Owen, Seitz, Enlow, and the "Paris School" of vertebrate bone histologists in the last half of the 20th century (see Chapter 1 and Ricqlès 2011). However, the basis for our present understanding is mainly due to Armand de Ricqlès, whose masterful series of publications in *Annales de Paléontologie* (1968–1982, and several thereafter; see Padian 2011, and Laurin 2011a, b for a bibliography through 2010) that proceeded mainly from his PhD dissertation provided the baseline descriptions of histological data for most extinct amniote (and some nonamniote) tetrapod groups.

VetBooks.ir

He has continued through the first two decades of the current millennium to add, analyze, and synthesize new information, particularly about archosauromorphs, especially dinosaurs and pterosaurs (ornithodirans).

Beginning in the 1990s, newer students of vertebrate paleohistology such as Robin Reid, John R. Horner, Anusuya Chinsamy, and their students and colleagues followed in the footsteps of de Ricqlès and the "Paris School" to expand greatly the range of extinct archosauromorphs whose osteohistological features were to some degree known. It must be stressed that until very recent times it was very difficult to study fossil bones histologically. The reason is that they must be subjected to destructive analysis, and few curators were willing to give up choice specimens to the fossil bone saw. In the last decade microcomputed tomography (CT) scans have been used to avoid destructive analysis, but the images produced to date by this technology are usually not of sufficient quality to replace traditional destructive methods – alas. Although many were well labeled, some of Armand de Ricqlès' specimens were salvaged from scraps of bone from the excavation of a skeleton, sequestered in museum drawers; sometimes it was not even clear that the sample belonged to the animal in question (this was often resolved by histological analysis); and there was no question of standardizing the section of bone from which the sample was taken, let alone the element itself (rib, femur, phalanx) or the ontogenetic stage of the specimen (which in many cases could only be estimated). The great value now perceived in our field from histological analysis of fossil bone, along with the importance of standardizing sections and the ease of molding, casting, and replacing sampled tissues, has largely alleviated this historical problem, and there are recommended protocols that can avoid confusion and facilitate sampling requests (Padian et al. 2013).

It is understood that bone tissue histology largely reflects the growth rate and, by extension in many cases, the underlying metabolic rate of its animal, although these two rates are sometimes not correlated, and it is important to consider ontogenetic stage in such assessments (Padian and de Ricqlès 2020). It has been tempting to infer these two rates from a single section of bone, but more comprehensive studies show the inherent difficulties (Padian and Stein 2013).

Current interpretations of osteohistological patterns in extinct amniotes are greatly indebted to the classic synoptic studies of colleagues such as Vivian de Buffrénil (mainly lepidosauromorphs and crocodylomorphs) and Jacques Castanet (mainly amphibians) and their students and colleagues. They provided the comparative data from living reptiles, admittedly mostly smaller and slower growing than many extinct forms, and with very different histological features, that allowed comparative inferences for dinosaurs, pterosaurs, ichthyosaurs, plesiosaurs, and many other fossil animals. Far fewer studies have been produced for mammals (e.g., Klevezal and Kleinenberg 1967), especially large ones, to which the growth of larger dinosaurs is more similar than to that of living reptiles (Köhler et al. 2012).

Anusuya Chinsamy (Chinsamy 1990) produced one of the first longitudinal histological studies of a series of homologous bones from a single species, the nonsauropod sauropodomorph dinosaur *Massospondylus carinatus* from the Early Jurassic of South Africa. Considering the size, vascularization patterns, and numbers of lines of arrested growth (LAGs) in her sample, she developed a graph that attempted to reconstruct the growth trajectory of the animal. She concluded that it reflected indeterminate growth, but it appears that no skeletally mature (or nearly mature) animals were included in her sample because they show no evidence of an external fundamental system (EFS) of virtually avascular and acellular bone that implies near-cessation of growth. (For explanation and context of these terms see chapters in Padian and Lamm 2013.) Nevertheless, her study pioneered the reconstruction of growth curves, which she applied to linear dimensions. G. M. Erickson and colleagues (Erickson et al. 2001 and later papers) translated these reconstructions of linear dinosaur growth rates to mass estimates, which accords more with procedures in ecology but exacerbates errors due to normal skeletal variation raised to the power of three (mass being a cubed function of length), a problem further complicated by small sample size and difficult data (Myrhvold 2014; Erickson et al. 2015).

Nondinosaurian Avemetatarsalia

Introduction

Although dinosaurs, particularly nonavian dinosaurs, have been most extensively studied among ornithodirans, the first studies of pterosaurs emerged at the turn of the century, and recent years have witnessed the elucidation of patterns in other dinosaurian and nondinosaurian ornithodirans, as well as an increase in the study of birds, fossil and extinct. The history of the paleohistology of dinosaurs has often been reviewed, sometimes as introductory to larger works and sometimes as extended perspectives (e.g., Ricqlès 1975, 1976a, b; Padian 2011). There was very little activity in studying dinosaur bone histology until the mid-1900s: Quekett's (1849) early rendition of a section of dinosaur bone, Owen's (1861) depiction of a *Scelidosaurus* bone cross section, sections of ornithopod bones by Seitz (1907) and Gross (1934), and a few other isolated studies (see Padian 2011). Donald H. Enlow's PhD work (published as Enlow and Brown 1956–1958) was the first synoptic study of bone histology in a variety of tetrapods, including extinct ones, and including dinosaurs. Although Enlow was only able to make a very few sections of a very few representatives of all taxa, he was able to draw generalizations about the distributions of tissues in various groups and to relate it to growth and other factors. Armand de Ricqlès took up the torch of this nascent field, publishing a series of 12 papers from his doctoral work spanning the paleohistology of most groups of terrestrial tetrapods, and emphasizing amphibians and reptiles, in *Annales de Paléontologie* from 1968 to 1981. Ricqlès was able to build on the generalizations of Enlow concerning tissues characteristic of various clades and to infer depositional rates and to compare these with living taxa, to estimate growth rates accordingly, and to infer implications for the physiological regimes of these ancient vertebrates in a variety of publications (e.g., Ricqlès 1974, 1980).

Ricqlès brought novel uses of paleohistology to a new generation of dinosaur paleontologists in the late 1970s and

VetBooks.ir

early 1980s. In 1970 John Ostrom (Ostrom 1970) published a provocative article showing that the geographic (latitudinal) distributions of admittedly "cold-blooded" extant reptiles are more equatorial and climatically limited than the distributions of dinosaurs and other ancient reptile groups. He suggested that it should not be assumed that dinosaurs had physiological and metabolic regimes with the same limits of extant reptiles. The arguments and research that this inference stimulated, as well as the history of the ideas behind them, were explored by Adrian Desmond (Desmond 1975) in a very influential book. Robert T. Bakker carried this inference further in a series of papers in which he suggested that dinosaurs were more like mammals in these respects than reptiles – notably in a provocative popular article (Bakker 1975) and in an extended original review (Bakker 1980) in which he explored a variety of lines of evidence. Most of these lines of evidence were shown to be circumstantial, although persuasive and even consilient when considered together; but Bakker's most convincing evidence came from the paleohistology of dinosaur bones, particularly secondarily remodeling. It eventuated that secondary remodeling is more a function of age (and sometimes biomechanics) than of physiology (and sometimes of the relative size of the element in the skeleton; Padian et al. 2016) in most taxa, because it occurs in a variety of extant (larger terrestrial turtles) and ancient (pareiasaurs) reptiles that did not otherwise evince rapid growth. The expression of tissue types, especially with high vascularization and osteocyte ratios, was the best guide to the growth rate and underlying physiology of an animal (Amprino 1947), although other generalized factors emerged (Padian 2013b).

The 1990s witnessed the beginning of the "modern" age of paleohistology, mostly centered on dinosaurs and other archosaurs. It was not a question of greatly improved techniques, although these began to be standardized (Lamm 2013). Rather, it was the recognition that histological analysis could provide the answers to long-standing paleobiological questions – such as how long it took for dinosaurs to reach full size. Using a slow-growing, "typical" reptilian model based on living taxa, *Tyrannosaurus* could be projected to reach maturity at well over a century, but histological analysis eventually showed that, human-like, two decades encompassed full growth (Horner and Padian 2004). These kinds of analyses were made possible by two advances: the standardization of where histological sections were sampled (usually femur or tibia, midshaft), and the willingness of curators to allow articulated specimens (in contrast to isolated, fragmentary bones) to be sampled.

The first signal advances in the field came from the work of Anusuya Chinsamy, who sampled a range of differently sized individuals of the neotheropod *Syntarsus* (now known as *Megapnosaurus*) (Chinsamy 1990), the nonsauropod sauropodomorph *Massospondylus* (Chinsamy and Rubidge 1993), and the ornithopod *Dryosaurus* (Chinsamy 1995b). These were supplemented by work on South African Permo-Triassic therapsids (Chinsamy 1993). Simultaneously Rimblot-Baly et al. (1995) published the first study of a large sauropod, the mid-Jurassic "*Bothriospondylus*" (*Lapparentosaurus*). They were the first analyses of growth series in the bones of dinosaurs. As such they provided valuable information about growth trajectories. Unfortunately, as later studies have reinforced, the series were not always complete enough to provide reasonably complete trajectories. *Syntarsus* samples (Chinsamy 1990) bore 1–6 growth rings (likely annual LAGs), and the largest samples also evinced what is likely an EFS (Horner et al. 1999), suggesting the attainment of full adult size. The situation was not clear in *Dryosaurus* because histological features were not quantified (Chinsamy 1995b). The *Massospondylus* sample (Chinsamy and Rubidge 1993) presented perhaps the first quantified ontogenetic trajectory, although regrettably the plots of size versus age were presented without data. A cross-section of an "adult" *Massospondylus* (their figure 6) showed a profile of highly regular, highly vascularized fibrolamellar complexes of cortical deposition with no signal of slowing growth or decreasing vascularization. This pattern suggests that the individual was actually not fully grown, and this is reflected in the growth curve that Chinsamy and Rubidge (1993, figure 7) devised for their specimens, which is not asymptotic; in fully grown adults we would expect to see an EFS and the flattening of the curve in its upper reaches, as has been found for other dinosaurs and for crocodiles (e.g., Woodward et al. 2011b), so it can be inferred that determinate growth is plesiomorphic for archosaurs. The authors' inference that *Massospondylus* had an "indeterminate" growth pattern cannot be sustained because they lacked fully grown specimens, but at the time this was not known.

Through the 1990s, the question of dinosaurian growth rates was often conflated with the question of dinosaurian metabolic rates. This would seem natural because high growth rates should reflect high metabolic rates, and, conversely, low growth rates should reflect low metabolic rates. Although the generalization often holds, in practice it is not that simple. For example, humans and related primates have high metabolic rates but low growth rates compared to other larger mammals, likely connected to extended parental care, altriciality, and advanced social and cognitive development. The same pattern may be found in "miniaturized" lineages of larger clades with overall high metabolic rates (Köhler and Moya-Sola 2009).

In contrast, the occasional if rare presence of fibrolamellar bone tissue in the bones of "typical reptiles" such as crocodiles and turtles was taken as an indication of high metabolic rates, because fibrolamellar bone grows at higher rates than the lamellar-zonal bone of "typical reptiles." Some authors inferred that the presence or absence of this bone tissue could not indicate anything about physiology; others inferred that because lamellar-zonal tissue was sometimes deposited in the bones of some dinosaurs, it could not be concluded that dinosaurs were endothermic (e.g., Dodson 1974; Reid 1981, 1984; Chinsamy 1990; Chinsamy et al. 1995b).

This conundrum was solved by the recognition that the characteristics of cortical bone at any given point in a section primarily indicate the rate of deposition of the bone *at that stage*, witnessed by factors such as the degree of vascularity and the orientation of canals and the density of osteocytes, as well as the type of tissue deposited (Amprino 1947; Francillon-Vieillot et al. 1990). What this means is that "cold-blooded" reptiles of today can deposit fibrolamellar tissue in parts of their skeleton at some stages of growth, but these stages are almost unexceptionally juvenile, when growth rates are high, especially in certain bones. The deposition of this tissue was not sustained

VetBooks.ir

through growth: with age, lamellar-zonal bone took over formation of the external cortex. The question became one of context: developmental, phylogenetic, and adaptive (Padian and Horner 2004). And, because larger lineages of a clade tend to grow more rapidly than smaller members (Case 1978), we expect their bone tissues to reflect higher vascularity and other similar features. Cubo and Jalil (2019), using phylogenetic eigenvector maps of quantitative histological characters, estimated that endothermy evolved at least in the last common ancestors of *Azendohsaurus* and Archosauriformes (see also Ricqlès et al. 2008). However, they were not working from complete ontogenetic sequences, although that fact alone does not invalidate their inferences.

The conclusion to be drawn from a series of studies that have compared different taxa and used a variety of ontogenetic stages, carried out in the later 1990s and beyond (e.g., Horner et al. 2000, 2001, 2009; Ricqlès et al. 2000; Erickson et al. 2001; Horner and Padian 2004; Padian et al. 2004; Goodwin et al. 2006; Knoll et al. 2010; Woodward et al. 2011b; Padian and Stein 2013, and references previously cited), is that the presence of a given type of tissue at a single stage of development is not a good direct indicator of the overall physiological regime of the animal. It does indicate instantaneous growth rate, within given ranges (Castanet et al. 1996). Full profiles throughout the skeleton and through ontogeny can put these observations into context and help to build a picture of the thermometabolic regime of the animal.

Basal (Nondinosauromorph, Nonpterosauromorph) Avemetatarsalians

Among Ornithodira, a variety of dinosaurian taxa has been studied paleohistologically, and so has a smaller group of pterosaurs, as this chapter shows (Figure 27.1). This is less true for the histology of nondinosaurian dinosauromorphs, that is, animals closer to dinosaurs than to pterosaurs. Griffin et al. (2019, p. 17–18) provided an excellent summary of studies to date on basal ornithodiran paleohistology, including basal dinosaurs. They and Werning (2013) were the first to study *Dromomeron romeri*, a lagerpetid ornithodiran somewhat closer to dinosaurs than to pterosaurs. The only other taxa in this lineage similarly studied are the silesaurids *Asilisaurus* (Griffin and Nesbitt 2016b) and *Silesaurus* (Fostowicz-Frelik and Sulej 2010), and *Nyasasaurus* (Nesbitt et al. 2013), which is either a dinosaur or a very close relative of dinosaurs (silesaurids are a beaked herbivorous clade just outside Dinosauria). Immediately outside Ornithodira is Aphanosauria, which includes *Teleocrater*, whose histology was first reported by Ricqlès et al. (2008) and elaborated by Nesbitt et al. (2017).

How do bird-line archosaurs (Avemetatarsalia: Ornithodira and outgroups) differ from crocodile-line archosaurs (Pseudosuchia) in their histological features? Overall, only a general picture is known; specimens are few and samples have been taken where available in the preserved material (i.e., not standardized to femoral or tibial midshaft as often recommended), so comparisons among elements and taxa are difficult. Also, without a relatively complete growth sequence it is difficult to assess the relative (or absolute) ontogenetic age of a specimen, as noted in this chapter for pterosaurs as well. Consequently, generalizations about growth rate are difficult to make, but as we will see, a general pattern of difference emerges between avemetatarsalians and pseudosuchians (Ricqles 1975, 1976a, b; Padian et al. 2001; Ricqles et al. 2008; Griffin et al. 2019; Marsa et al. 2020). The following section assesses some histological features in the line moving crownward toward dinosaurs. Nesbitt et al. (2017) sampled small pieces of the Triassic aphanosaur *Teleocrater rhadinus*, including a fibula with a cross section of 7–8 mm and a humerus (Figure 27.2). Both cortices are mainly composed of unremodeled primary woven-fibered bone, with some local parallel-fibered bone and no secondary osteons. The vascular canals are mostly longitudinal with some radial anastomoses, especially in the humeral segment. Sometimes longitudinal canals are aligned circumferentially. There are abundant osteocytes but they appear not to be aligned preferentially with the long axis of the bone. As Nesbitt et al. (2017) noted, these features suggest higher growth rates than in typical stem-archosaurs, but some variation among taxa, especially with size, has been observed (Padian et al. 2004). The general features of these bones suggest subadult status, but too little material is known to permit the estimation of adult size. A cross section of what is probably a metaphyseal/diaphyseal region of transition in a small metatarsal (BM R [now NHMUK] 6795) shows a cortex very densely vascularized by oblique primary osteons (Ricqlès et al. 2008). The medullary region has no free marrow cavity and is entirely made of regular trabeculae of endosteal bone.

Ornithodira: Pterosauria

Pterosaurs are the closest major sister taxon to dinosaurs (Gauthier 1984; Andres and Padian 2020). Over 100 species have been named, sometimes on fragmentary material. The group is known from the Late Triassic (Norian) to the latest Cretaceous (Maastrichtian). They were the first vertebrates to evolve active flight. Like birds, pterosaurs have very thin bone walls, and the medullary cavity is correspondingly expanded. The long bones of complete skeletons are closely appressed, which suggests very thin cartilaginous caps, as in birds, or that connective tissues may have pulled them closer after death. Occasionally thin hollow struts may traverse the medullary cavity in an oblique direction, possibly to add strength (Ricqlès et al. 2000). Cancellous bone, encased by very thin surficial laminar bone, usually comprises the skull and axial column bones. Overall the skeleton appears to be very lightly built, but it must be remembered that the bones of pterosaurs are also relatively elongated, especially in the wing, neck, and skull, so their total individual skeletal masses may not be much less than other animals of the same mass that do not fly.

Because pterosaur bones are so thin-walled, often a millimeter or less even in large forms, a single bone can capture only a brief interval of the ontogenetic trajectory. Deposition and erosion rates of bone were apparently high, judging from dense vascularization in the long bones, and this contributed to the ephemeral ontogenetic representation of individual sections. Moreover, pterosaur bone histology comprises a very broad range of tissues including fibrolamellar and lamellar cortical bone, trabecular bone struts, articular calcified cartilage,

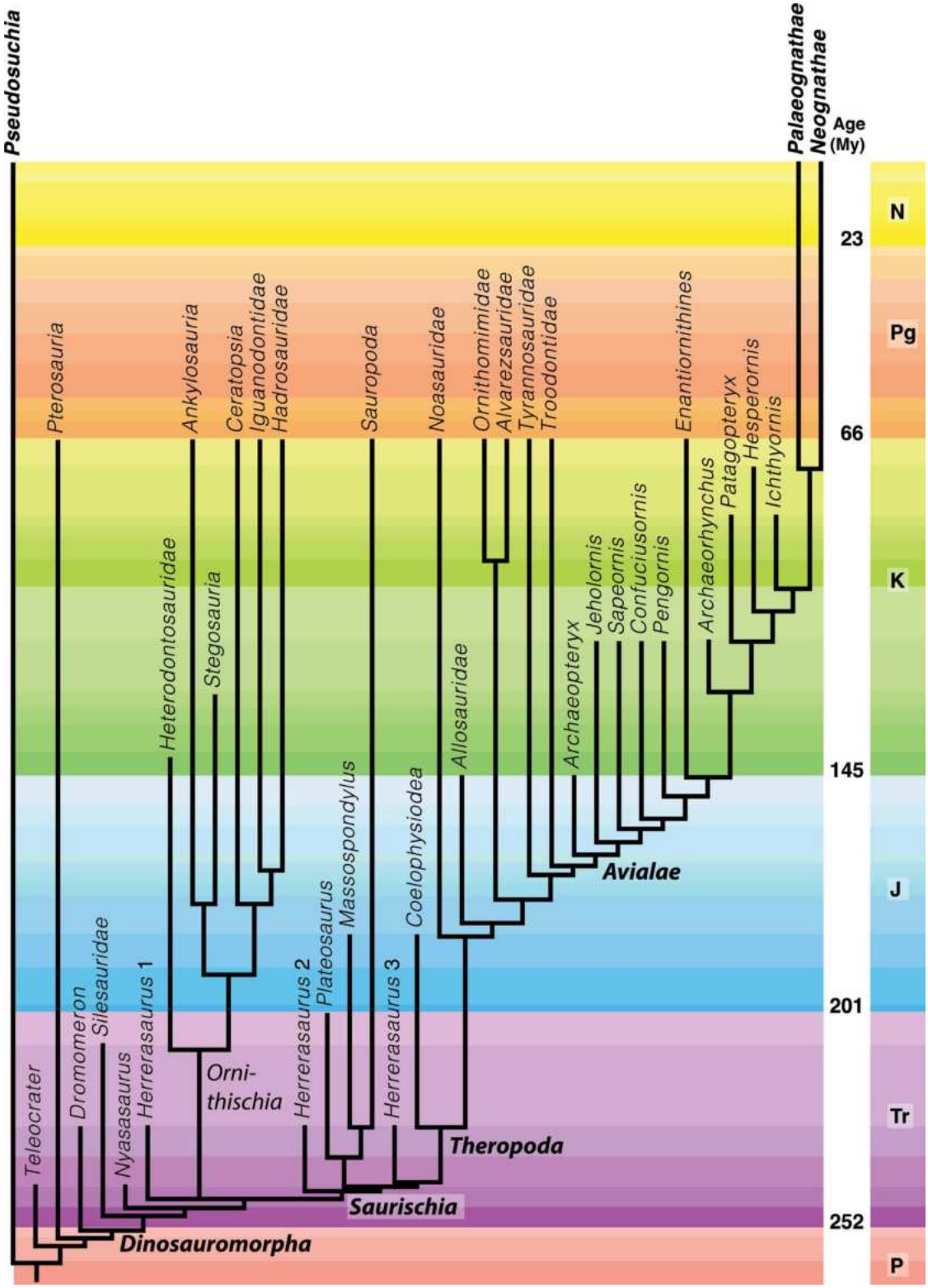


FIGURE 27.1 Phylogenetic relationships and approximate known stratigraphic ranges of the Avemetatarsalian taxa discussed in this chapter, courtesy of Michel Laurin.

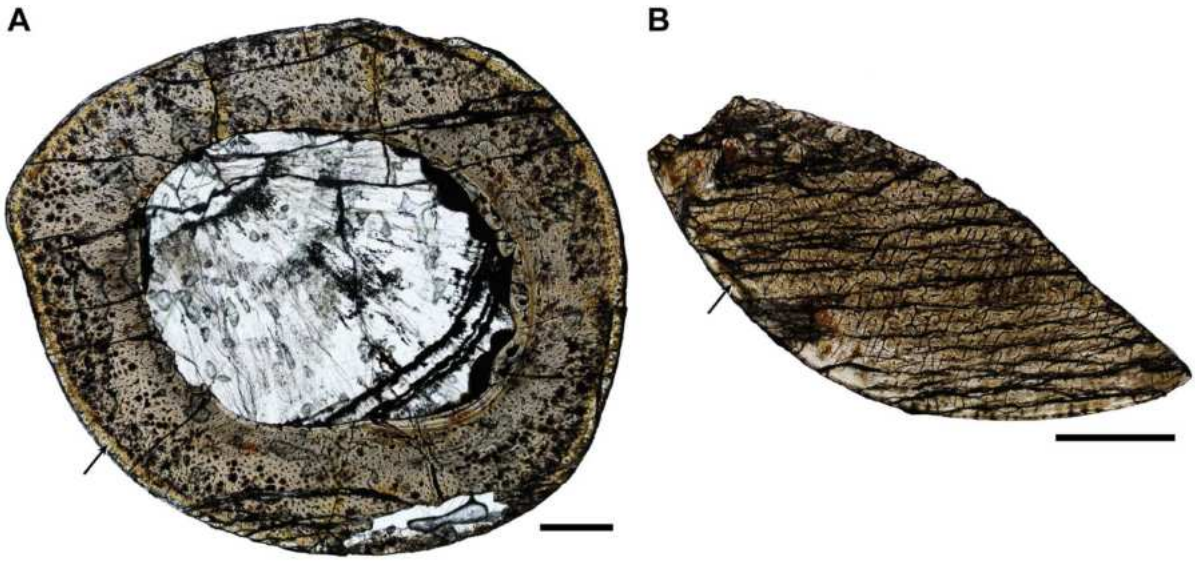


FIGURE 27.2 Histological sections of the limb bones of *Teleocrater rhadinus*. A, Histological section of the fibula (NMT RB 488) in regular transmitted light (bright field) (one-plane polarizer). B, Partial histological section of the humerus (NMT RB476) in regular transmitted light (bright field) (one-plane polarizer). Arrows indicate growth marks in the outer cortex. Scale bars = 1 mm. (From Nesbitt et al. 2017, extended data figures 2B and 2E, used with permission.)

subchondral bone plates, and Haversian bone (Ricqlès et al. 2000; Steel 2003, 2008).

Figure 27.3 shows a representative variety of pterosaur bone tissues in cross section; the description is modified from Ricqlès et al. (2000). (MOR, Museum of the Rockies, Bozeman, Montana; TMM, Texas Memorial Museum, Austin; UCMP, University of California Museum of Paleontology, Berkeley; all USA.) In these photos the external edge of the bone is up unless otherwise noted. Figure 27.3A is the cross section of a wing bone diaphysis from a small azhdarchid from the Late Cretaceous of Montana (MOR PT-C). This is obviously juvenile bone, as evidenced by its dense vascular supply (compare to Figure 27.3B) and the almost chaotic, centrifugal orientation of its reticular canals. It was clearly growing very rapidly, as it had not even reached the point where it could form scaffolded layers of typical fibrolamellar bone. The vascular canals are dark brown, visible as oblique wavering lines and also as longitudinal structures intersecting the plane of the section, with bright hollow centers. The light yellow line in the middle of each pink woven periosteal bone tissue trabecula is the "bright line" of Currey.

Figure 27.3B illustrates more "typical" rapidly growing fibrolamellar bone in the shaft of the first wing-phalanx of the azhdarchid *Quetzalcoatlus* (TMM 42422-17). Here, the tissue growth pattern has settled from the very young reticular pattern in Figure 27.3A, as seen in many dinosaurs (e.g., *Tyrannosaurus*: Horner and Padian 2004) and living birds (see below). In this more laminar pattern the bright lines are visible equidistant between the dark vascular canals. Also in the wing-phalanx of the same taxon, compacted coarse cancellous bone is heavily worked by Haversian osteons (Figure 27.3C). A triangular island of remaining primary cortical bone can be seen in the left quadrant of Figure 27.3C. Figure 27.3D shows the transition in tissue type from the endosteal margin (lower right corner) to the deep cortex (center) and finally to the outer primary (periosteal) bone cortex (ending at the upper left corner). The right side of the Figure 27.3D shows erosion bays that are frequently filled in by secondary osteons and endosteal bone. This sequence of sections of the same element demonstrates the variety of tissue types that can be found even in a single pterosaur bone.

The trabecular bone struts found in the long bone shafts of pterosaurs are very similar to those in birds (Ricqlès et al. 2000; Steel 2008). Their histology is explored in Figure 27.3E, F. The first of these two photos shows an oblique section of bone cutting through an endosteal bone strut of the pteranodontid *Pteranodon* (UCMP 124862). This strut is formed by secondary endosteal bone (tan-colored in Figure 27.3E), that has numerous obliquely sectioned osteocytic lacunae. The abrupt changes of the bone fibers and cell orientations on each side of the cementing lines (at right in photo) show that the tissue is of secondary origin. Figure 27.3F shows the transverse cross section through the base of a strut in *Montanazhdarcho* (MOR 691). This strut grows further by new deposition of endosteal bone. The direction of primary growth was from bottom to top in the photo, but erosion has removed early-deposited bone (lower corners of photo), leaving only a base of primary bone that is then invaded by secondary osteons, eroded further endosteally, and then covered with a coating of endosteal bone, suggesting that internal erosion has ceased (Steel 2008). The base of these struts is about the only place where secondary osteons have been identified in pterosaurs (Steel 2008).

An interesting and unusual tissue pattern was identified in pterosaurs by Ricqlès et al. (2000): namely, a "plywood" pattern in which successive laminae of fibrolamellar layers are oriented with the long axes of their longitudinal canals and fibers at oblique angles to each other. This was observed in the

VetBooks.ir

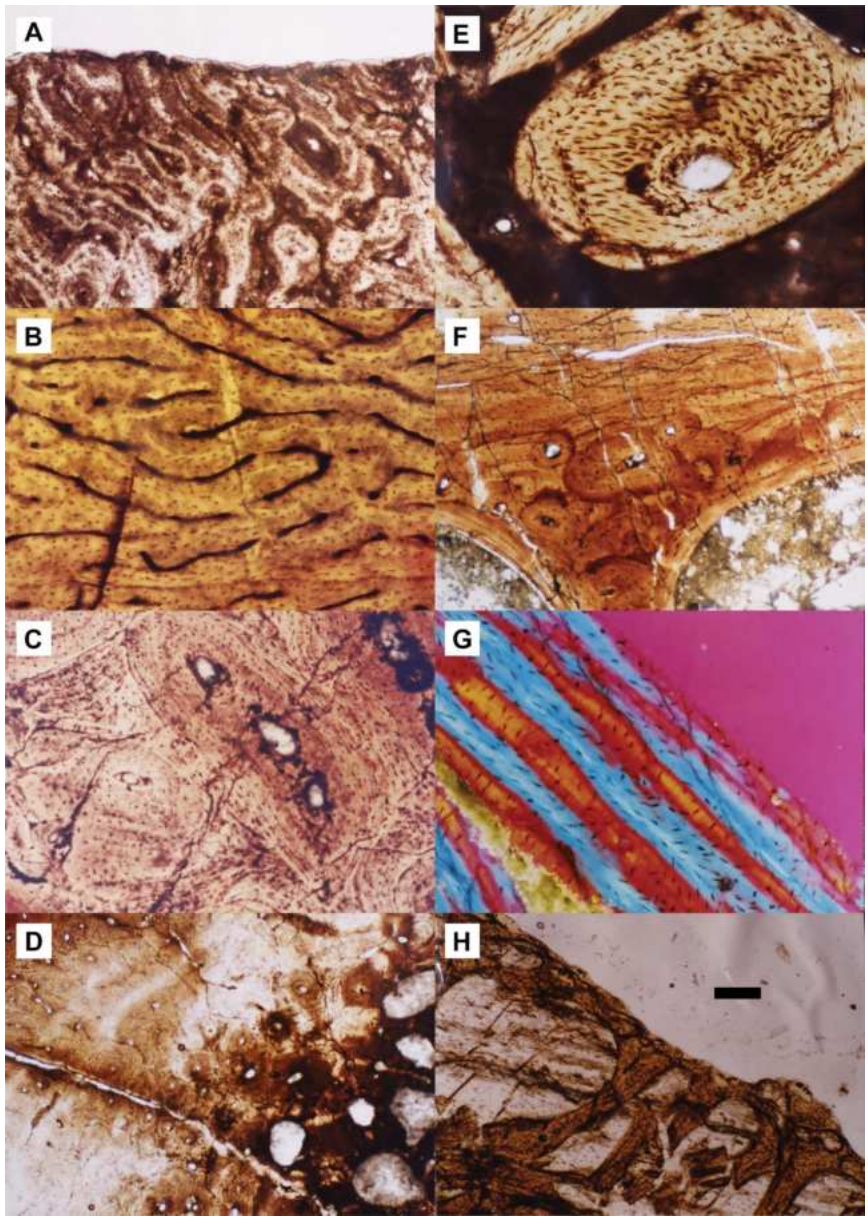


FIGURE 27.3 Cross sections of pterosaur bones. Outer edge is up unless otherwise noted. A, Azhdarchid, Late Cretaceous, Montana (MOR PT-C), cross section of wing bone diaphysis. This is rapidly growing juvenile bone, as evidenced by its dense, reticular vascular supply (compare to B). Dark brown vascular canals run both obliquely and longitudinally. The light yellow line in the middle of each pink woven periosteal bone tissue trabecula is the "bright line" of Currey. B, *Quetzalcoatlus langstoni*, TMM 42422-17, Late Cretaceous, Texas, cross section of diaphysis of first wing-phalanx. This is well vascularized, rapidly growing fibrolamellar bone, comparable to that of a living bird, with a thin cortex that is being eroded endosteally as rapidly as it is being deposited periosteally. In this laminar tissue type, the bright lines are visible equidistant between the dark vascular canals. C, Same taxon, wing bone cross section showing compacted coarse cancellous bone, heavily reworked by Haversian osteons. A triangle of primary cortical bone can be seen in the upper left quadrant. D, Same taxon, showing tissue transition from the endosteal margin (lower right corner) to the deep cortex (center) and finally to the outer primary (periosteal) bone cortex (ending at the upper left corner). Right side shows erosion bays, frequently infilled by secondary osteons and endosteal bone. E, *Pteranodon* (UCMP 124862), oblique section of bone cutting through an endosteal bone strut, which is formed by secondary endosteal bone (tan colored) with numerous obliquely sectioned osteocytic lacunae (bone cell spaces). Abrupt changes of bone fibers and cell orientations on each side of the cementing lines (at right) demonstrate the secondary origin of the tissue. F, *Montanazhdarcho* (MOR 691), showing the base of a transversely cross sectioned strut. Although the direction of primary growth has been from bottom to top, erosion has removed early-deposited bone (lower corners), leaving only a base of primary bone that is then invaded by secondary osteons, eroded further endosteally, and finally covered with a coating of endosteal bone. The strut grows further by new deposition of endosteal bone. G, *Pteranodon*, an oblique section through part of the scapula, showing alternating "plywood" layers in different colors revealed by polarized light using a quartz wedge. Note the streaklike profile of the tiny cell lacunae (black) changing their orientation, alternating in conformity with the bone fibers. H, Same taxon, longitudinal section through an epiphysis, with outer edge to the upper right. Blebs of calcified cartilage appear on the surface of the bone; the subchondral bone plate beneath it is supported by struts of endosteal bone surrounding large erosion rooms. Trabecular bone can be seen in the deep cortex at the lower left. The scale for all photos is in Fig. H; for Figures B, D, and H, it represents 250 nm; for A, C, E, F, and G, it represents 100 µm. (MOR, Museum of the Rockies, Bozeman, Montana; TMM, Texas Memorial Museum, Austin; UCMP, University of California Museum of Paleontology, Berkeley; all USA.) (Adapted from Ricqlès et al. (2000), Figure 5, used with permission.)

VetBooks.ir

scapula of *Pteranodon* (UCMP 124862), using polarized light with a quartz wedge to show alternating colors that represent alternating orientations of the plywood layers (Figure 27.3G). Steel (2008) noted a variety of vertebrate taxa and elements in which a plywood pattern appears, but as she noted nearly all of them differ from the situation in pterosaurs in various ways. Emmanuel de Margerie (Margerie 2002), building on previous studies, suggested a mechanical function for this orientation in resisting torsion.

Finally, the intersection of cartilaginous and osseous tissues is shown in Figure 27.3H, a longitudinal section through an epiphysis of a long bone of *Pteranodon* (UCMP 124862). The outer edge is seen at the upper right of the photo. Blebs of calcified cartilage appear on the surface of the bone; the subchondral bone plate beneath it is supported by struts of endosteal bone that surround large erosion rooms. Trabecular bone can be seen in the deep cortex at the lower left of the photo. These tissues show the actively growing interface at the ends of long bones, very similar to the condition in birds; these cartilaginous regions are relatively thin compared to the situation in crocodiles and other living reptiles, apart from birds.

This series of "snapshots" of pterosaur bone histology is a reflection of the spotty knowledge we have of their histodiversity. Yet some general inferences can be drawn. One of the smallest and earliest pterosaurs known, originally named *Eudimorphodon cromptonellus* by Jenkins et al. (2001), comes from the Late Triassic of Greenland (renamed *Arcticodactylus cromptonellus* by Kellner 2015). The specimen was histologically sampled and, despite extensive infilling of crystals, retained enough structure to indicate a poorly organized, very thin cortex, which is also characteristic of extant hatchling birds. Tissues sampled from an assemblage of a great many small and broken pterosaur bones from Chile revealed immature bone tissue development that suggested that the assemblage represented a kind of rookery caught in a sudden flood (Bell and Padian 1995).

At some point in ontogeny the growth pattern, which seems to have been very rapid initially, settled down from the condition represented in Figure 27.3A to that in Figure 27.3B. In some bones the plywood morphology (Figure 27.3G) evolved as a response to torsion. Secondary osteons appeared in some bones, perhaps as a result of mechanical stress, as suggested by their placement at the base of an internal cortical strut within a long bone (Figure 27.3E). It is not clear to what extent secondary osteons may have appeared with increasing age, because it is so difficult to assess age in given individual specimens. In all cases the cortices of pterosaur bones were extremely thin, and as a result any single section is likely to encapsulate only a very short period in the life of an individual. For this reason there is very little that can be generalized about histological ontogeny from a single section of pterosaur bone.

Several major issues in pterosaur osteohistology persist, and they are difficult to address. The first is that, because cortices are so thin and thus represent such a short period in the ontogeny of an animal, it will be difficult to assemble a full ontogenetic trajectory without sectioning a great many specimens, which few museum curators will agree to do. Prondvai et al. (2012) sectioned five *Rhamphorhynchus* specimens of various sizes and used their histological information in concert with that from two specimens sectioned by Padian et al. (2004) to assess patterns of change in histological expression with growth. They found evidence of a fairly typical ornithodiran pattern, but also noted that histological development did not strictly correlate with size. In other words (assuming that the specimens they used were actually conspecific and chronostratigraphically controlled), the ontogenetic stage of an individual could not be directly predicted from its size, a result also discovered by Klein (2004) for the sauropodomorph dinosaur *Plateosaurus* and by Woodward et al. (2015) for *Maiasaura*. Other examples are reviewed by Kellner (2015). As a result, Prondvai et al. (2012) rejected the inference of "year-classes" (Bennett 1995) induced by apparent gaps in size distribution. They also rejected the "super-precocial" inference of life history strategy by Unwin and colleagues (see, e.g., Lü et al. 2011) that proposed that pterosaurs could fly immediately on hatching, because the internal bone structure would not have been mature enough and because a drop in growth rate, possibly correlated with the onset of flight, did not begin until a later ontogenetic stage.

Second, histological analysis would be invaluable in assessing the taxonomic diversity of, for example, Solnhofen pterosaurs, because species names have been given to various small specimens that may belong to taxa represented by larger individuals. Alleged apomorphies, such as number of teeth and proportions, may change with age (and this may reflect ecological shifts). For example, it has long been debated whether the giant azhdarchid *Quetzalcoatlus* comprises two species or simply two "morphs" (large and small). Only a full histological analysis can approach this question: if the smaller specimens show evidence of very rapid growth, they may be juveniles of the larger morph, but if not, there could be *prima facie* evidence of separate lineages. Complete ontogenetic sequences will be very difficult to get for pterosaurs, but they hold the key to problems of taxonomy, growth rates and life history strategies and physiological regimes.

Ornithodira: Nondinosaurian Dinosauromorpha

Dinosauromorpha comprise dinosaurs (including birds) and all taxa closer to them than to pterosaurs. Lagerpetids, including *D. romeri,* are generally considered the most basal known dinosauromorphs, histologically speaking, on the line to dinosaurs. But recently Ezcurra et al. (2020) determined that lagerpetids are actually the closest sister group to pterosaurs. This phylogenetic analysis helped to fill the gap between the bizarre flight-adapted morphology of pterosaurs and more conventional ornithodiran body plans (Padian 2020b) by underscoring that pterosaurs evolved from small, agile, terrestrial bipedal animals close to dinosaurs that showed no obvious adaptations or tendencies toward arboreality or gliding. However, because the bone histology of pterosaurs is so unusual, we group the treatment of lagerpetids with basal dinosauromorphs.

Griffin et al. (2019) studied two femora of *D. romeri* histologically (Figure 27.4) and found mainly woven-fibered bone with primary osteons through most of the inner cortex, changing to more organized parallel-fibered tissue with fewer osteons in the outer cortex. The vascular canals are variably longitudinal to radial until the outer cortex, where they are

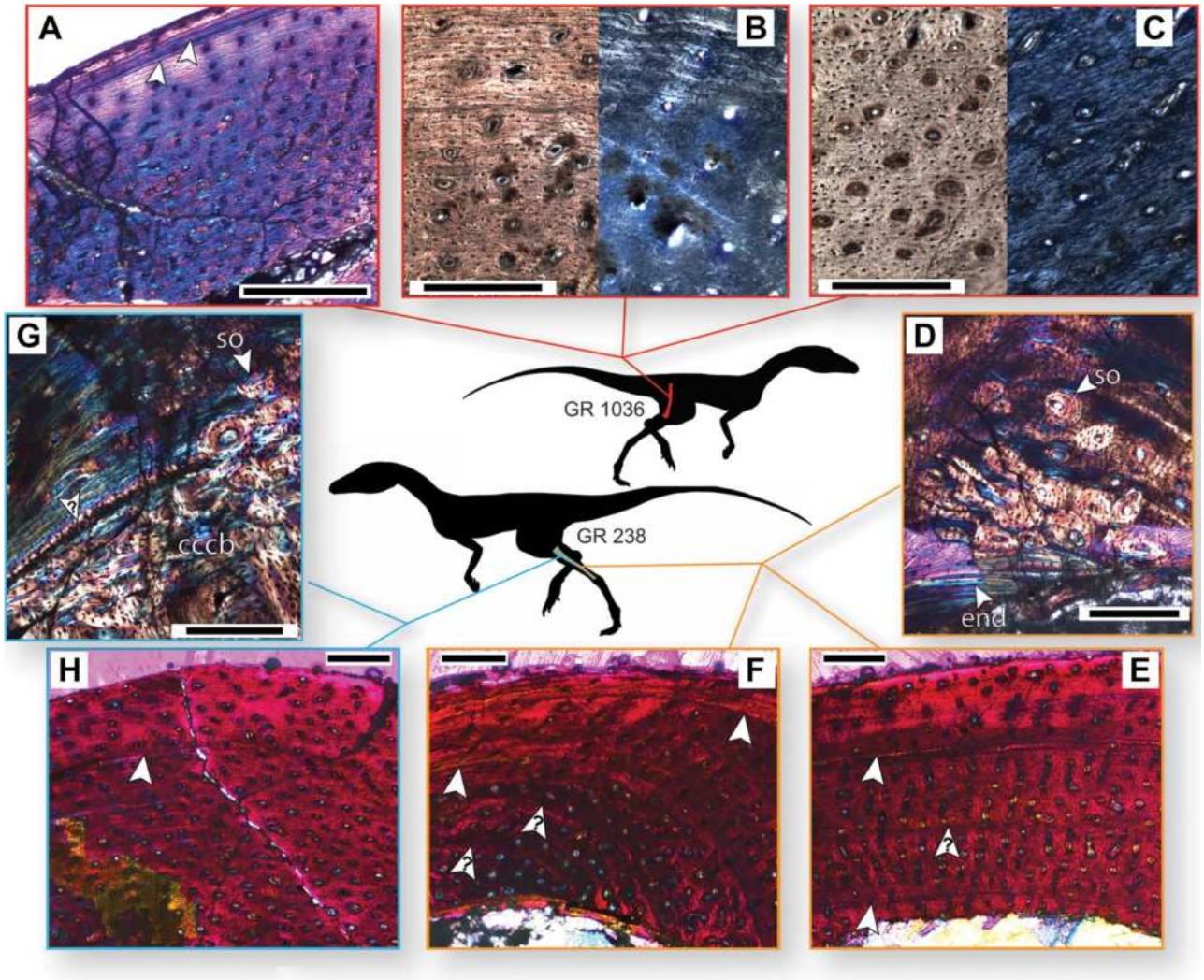


FIGURE 27.4 Bone histology of two individuals of the ornithodiran *Dromomeron romeri*. A, Femur of the smaller sampled individual (GR 1036) under cross-polarized light with a gypsum wave plate, showing two lines of arrested growth (LAGs) near the periosteal surface. B, Femur of GR 1036 under plane-polarized and cross-polarized light showing the transition from less- to more-organized tissue in the external third of the cortex. C, Femur of GR 1036 showing tissues typical of the less organized primary bone of the internal two-thirds of the cortex, under plane-polarized and cross-polarized light. D, Fibula of the midsized sampled individual (GR 238) under cross-polarized light with a gypsum wave plate, showing the boundary of the medullary bone with endosteal lamellae, secondary osteons (SO) and highly organized primary bone. E, Fibula of GR 238 under cross-polarized light with a gypsum wave plate showing two LAGs and the periosteal surface. F, Fibula of GR 238 under cross-polarized light with a gypsum wave plate showing two LAGs and the periosteal surface. G, Tibia of the midsized sampled individual (GR 238) under cross-polarized light with a gypsum wave plate showing internal compacted coarse cancellous bone (CCCB), external primary parallel-fibered bone and the boundary between these two tissues (an osteocyte-rich annulus or growth line, marked with a "?"). Note secondary osteons in the internal-most portion of the parallel-fibered bone. H, Tibia of the midsized sampled individual (GR 238) under cross-polarized light with a gypsum wave plate. Scale bars: 200 µm for A–D and G; 250 µm for E, F, and H. (From Griffin et al. 2019, Figures 3A–H, used with permission [Creative Commons Open Access license].)

sparser and mostly longitudinal. A LAG (or double LAG) appears near the subperiosteal surface in the smaller femur. The larger femur shows the same general features, but the tissues are more organized, as might be expected from a more mature individual. A tibia was also sampled, and it differs from the femoral tissue in having less organized and less vascularized bone, with denser osteocyte lacunae. The vascular canals decrease in density and increase in size centrifugally; one or two LAGs are present. A right fibula also comprised predominantly primary parallel-fibered bone, with other features much like those of the tibia (see other observations in Werning 2013). Griffin et al. (2019) suggested that the rate of growth in the aphanosaur *Teleocrater* may have persisted longer than in *Dromomeron*. This could simply reflect differences in adult body size, but available material is too limited to say.

The histology of the lagerpetid *Lagerpeton chanarensis* was studied by Marsà et al. (2020), along with that of two proterochampsids, *Chanaresuchus bonapartei* and *Tropidosuchus romeri*, all from the Chañares Formation (Late Triassic, South America). These authors noted previous work that, in contrast to placing *Lagerpeton* and the lagerpetids as dinosauromorphs, found many derived gross morphological

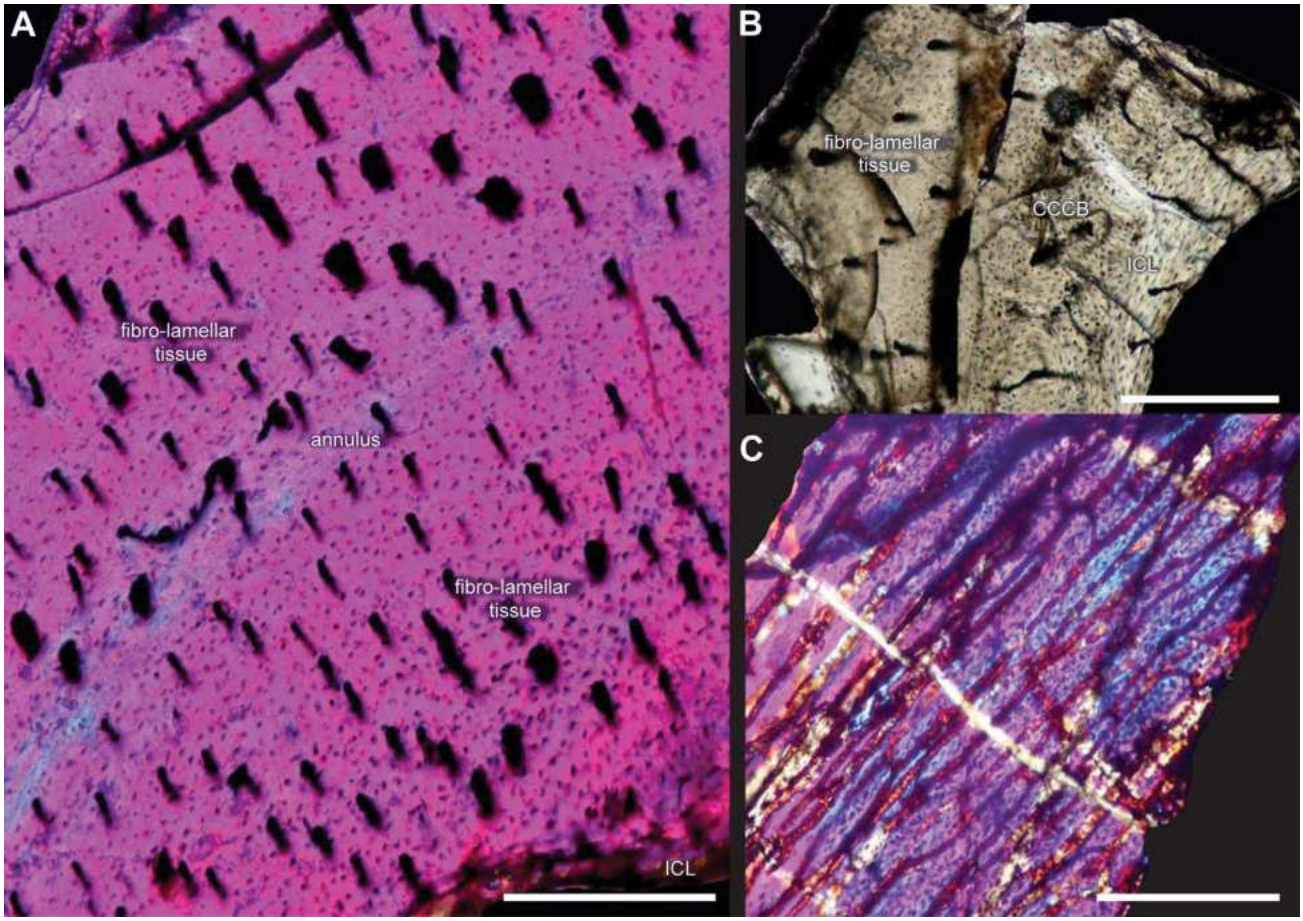


FIGURE 27.5 Femur of the ornithodiran *Lagerpeton chanarensis* (Romer 1971) (PULR-V 124, in lambda light) from La Rioja province, NW Argentina; Chañares Formation, Carnian (Late Triassic). A, Section showing the inner circumferential layer and the cortex. B, Detail of the compacted coarse cancellous bone. C, An oblique section of the same femur. Abbreviations: CCCB, compact coarse cancellous bone; ICL, inner circumferential layer. Scale bars = 300 µm. (From Marsà et al. 2020, figure 2, used with permission [Creative Commons Open Access license].)

similarities to proterochampsids, especially *Tropidosuchus*. They observed that this was also true for many histological features.

Marsà et al. (2020) studied two femora and a tibia from *Lagerpeton* (cross sections). They observed predominantly fibrolamellar tissue with generally high vascularization dominated by longitudinal canals with little to some anastomosing, and relatively dense circular osteocyte lacunae (Figure 27.5). There were limited areas of compacted coarse cancellous bone between the inner and middle cortical layers, and an annulus in both femora and a single LAG in the tibia. A thin layer of endosteal tissue surrounded the medullary cavity. No EFS was observed in any of the three bones. As they noted, vascularization does not decrease centrifugally, even after the LAG and the thin layer of CCCB. They concluded that these specimens were not of somatically mature individuals (rapid growth rate, no EFS).

Silesaurids are an unusual, beaked, herbivorous group very close to dinosaurs. The histology of *Silesaurus* was studied by Fostowicz-Frelik and Sulej (2010), and that of *Asilisaurus* by Griffin and Nesbitt (2016a). The *Asilisaurus* sample comprised several femora, a humerus, several tibiae and a fibula, from specimens of various sizes but not among the largest available specimens. Most elements were characterized by a predominance of woven-fibered tissue, with a minor proportion of circumferentially oriented fibers, increasing centrifugally. The vascular canals comprise primary osteons mostly oriented longitudinally but with extensive radial anastomoses and branches, especially in larger specimens. Osteocyte lacunae are densely distributed, with a slight decrease centrifugally (Figure 27.6). Similar features were found in *Silesaurus opolensis* by Fostowicz-Frelik and Sulej (2010), and are typical of other dinosauromorphs and basal dinosaurs.

Finally in this sequence is *Nyasasaurus parringtoni*, described as either a dinosaur or perhaps the closest taxon to dinosaurs by Nesbitt et al. (2013). A humerus sampled comprises mostly unremodeled primary woven-fibered bone, and the vascular canals are all longitudinally oriented primary osteons with substantial anastomoses oriented in all directions (Figure 27.7). Osteocyte lacunae are mostly long and oriented perpendicular to the long axis of the bone, and more globular centripetally. Canal density and size, as well as osteocyte density, decrease centrifugally, but the tissue remains woven-fibered with only primary osteons; the canals tend to become

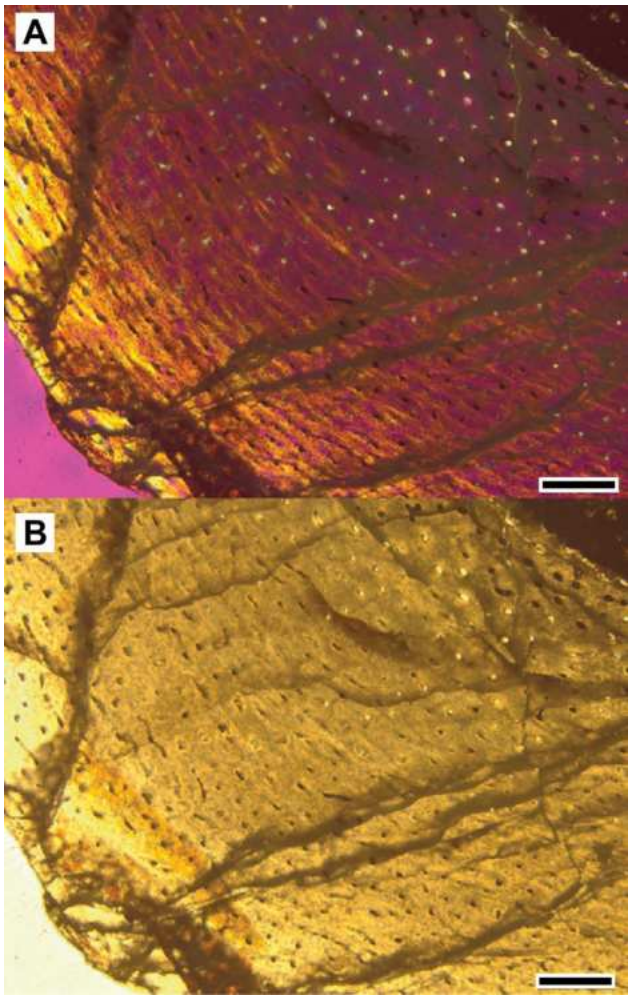


FIGURE 27.6 Cortex of a femur (NMT RB210, slide C1) of *Asilisaurus kongwe*. A, Under cross-polarized light (with quartz wedge). B, Plane-polarized light. Scale bars = 100 mm. (From Griffin and Nesbitt 2016a, Figure 4 D and E, used with permission.)

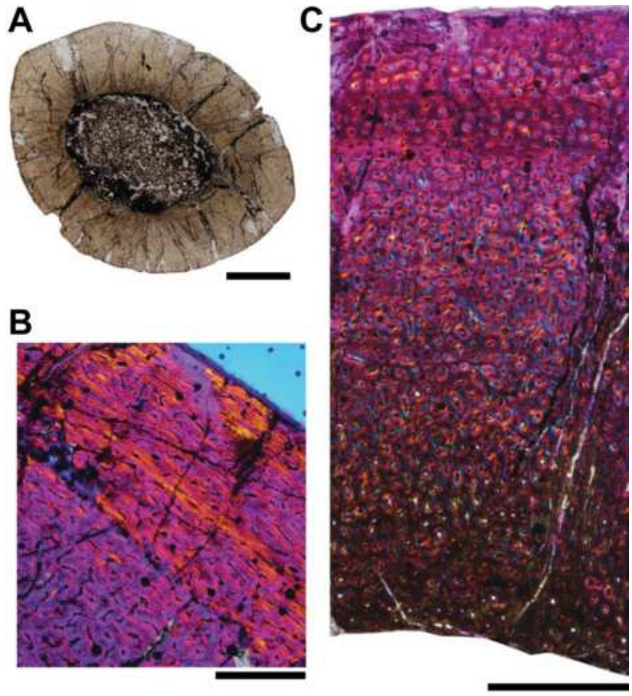


FIGURE 27.7 Humerus of *Nyasasaurus parringtoni* (NHMUK R6856). A, Complete cross section in transmitted light. B, Cross section through the outer portion of the cortex in crossed Nicols. C, Cross section through the entire cortex in crossed Nicols. Scale bars: A = 4 mm; B = 1 mm; C = 500 nm. (From Nesbitt et al. 2013, figure 1 c-e, used with permission.)

more circumferentially oriented, and anastomosis decreases. These features are consistent with the rapid growth rates seen in other ornithodirans so far; like them, in the available sample, there is no indication of cessation of growth (e.g., an EFS), so it is not possible to determine the adult body size of the animal. As Nesbitt et al. (2013) noted, some large pseudosuchians and phytosaurs (the closest major taxon outside Archosauria, or alternatively the most basal pseudosuchians) can show these features but only early in ontogeny; they do not sustain high growth rates as ornithodirans do.

Dinosauria

Basal Dinosauria

Dinosauria, by definition (Gauthier 1984), comprise the most recent common ancestor of the taxa listed by Richard Owen (Owen 1842) when he named the Dinosauria: i.e., *Megalosaurus, Iguanodon* and *Hylaeosaurus,* plus all their descendants. Seeley (1888) divided the dinosaurs into Saurischia (sauropods and theropods) and Ornithischia, which implied that Dinosauria was not a natural group but perhaps had separate ancestry. This situation persisted through most of the 20th century, although sometimes Ornithischia was affiliated with "Prosauropoda," until Gauthier (1984) showed cladistically that Dinosauria was monophyletic and comprised Saurischia (Theropoda + Sauropodomorpha) and Ornithischia (reviews in Gauthier 1984, Padian 2013a). Baron et al. (2017) produced a new phylogenetic analysis suggesting that Ornithischia and Theropoda were sister taxa, as were Sauropodomorpha and Herrerasauridae (the last taxon variously considered a basal theropod, a basal dinosaur, or outside Dinosauria but very close to it), but this proposal has not received general approval or acceptance.

Griffin et al. (2019, p. 18) listed several "early dinosaurs" that have received at least some histological analysis: "*Herrerasaurus ischigualastensis*, de Ricqlès et al. 2003a, 2008; *Tawa hallae*, Werning 2013; *Coelophysis bauri*, Colbert 1995, Nesbitt et al. 2006; *Megapnosaurus ['Syntarsus'] rhodesiensis*, Raath 1977, Chinsamy 1990, Werning 2013; *Lesothosaurus*, Knoll et al. 2010; *Scutellosaurus*, Padian et al. 2004." (Note: the specimen that Colbert [1995] illustrated, from a slide made by Armand de Ricqlès, may not be from *Coelophysis*; it is a very large specimen and its bone tissue shows that it was actively growing at death [Padian 1986]. Griffin et al. (2019) characterized a general ontogenetic shift in these taxa from depositing "predominantly disorganized woven-fibered to highly organized parallel-fibered bone tissue later in ontogeny as growth slows," which is also characteristic of dinosaurs in

VetBooks.ir

general (see below). But it must be remembered that the kind of bone tissue deposited is strongly related to size (Case 1978), both adult size in a clade and size related to the ontogenetic stage. As a result, slowly deposited parallel-fibered or lamellar tissue can occur in small vertebrates, regardless of their position on the ectothermic-endothermic metabolic spectrum (Padian et al. 2004). Early histological studies already noted the great development of dense Haversian bone among dinosaurs (Enlow and Brown 1956–1958) in contrast to other reptiles.

Herrerasaurus was a large (up to 6 m length) bipedal ornithodiran from the Upper Triassic of Argentina. It has been considered a basal theropod dinosaur, or a sister group of dinosaurs, or a form just outside Dinosauria. When preserved, the cortical structure of the long bone shaft (one humerus: MCZ FN 336-58 M and one tibia: MCZ 7064 were studied) looks similar in several specimens. It consists of typical plexiform tissue throughout the cortex (Ricqlès et al. 2003a; Padian et al. 2004). Some LAGs may develop in the most superficial cortex. This structure suggests a continuous growth at high speed with perhaps some slight growth modulations at the end of the growth phase recorded.

Dinosauria: Ornithischia

Various early dinosaurs (late Middle Triassic – Early Jurassic) have been sampled histologically, and some were discussed in previous chapters. They include *Euskelosaurus* (Ricqlès 1968), *Megapnosaurus* ("*Syntarsus*") (Chinsamy 1990), *Massospondylus* (Chinsamy 1993), *Thecodontosaurus* (Sander et al. 2004; Ricqlès et al. 2008), *Scutellosaurus* (Padian et al. 2004), *Plateosaurus* (Sander and Klein 2005) and *Lesothosaurus* (Ricqlès et al. 2008; Knoll et al. 2010). Despite specific differences among taxa, histological features reflecting more rapid growth through life are generally found in the larger taxa, notably in the sauropodomorphs among dinosaurs.

Ornithischia, as a group, has traditionally been well defined and diagnosed by a suite of characteristics, notably the predentary bone, the unusual pelvic configuration, the prevalence of crisscrossed ossified tendons on the vertebral spines and the absence of pneumatic foramina (Gauthier 1984; see also Seeley 1888). It has been viewed as the sister taxon of Sauropoda and of Theropoda, or of these two taxa together as Saurischia (Padian 2013a). What now appears astonishing, compared to the history of knowledge of dinosaurs, is that no credible ornithischian remains exist before the Early Jurassic (Nesbitt et al. 2007, 2009). Because other dinosaurian groups are known as early as the late Middle Triassic (Nesbitt et al. 2007, 2009), the 30-million-year gap could suggest that ornithischians may have evolved from a previously established dinosaurian group (Padian 2013a).

Heterodontosauridae

Among the most basal ornithischians histologically sampled is the Heterodontosauridae. Most taxa in this clade lived from the Early Jurassic to the Early Cretaceous. Adult body sizes ranged between that of a pigeon and turkey (Figure 27.8A), and their histology reflects growth to small asymptotic sizes. For instance, the Late Jurassic North American taxon *Fruitadens* is among the smallest ornithischian, at 75 cm in body length (Butler et al. 2009). Femoral bone histology reveals slow, protracted growth, reflected by a parallel-fibered cortex with longitudinal simple vascular canals. The presence of LAGs and annuli, and possibly an EFS, show that it was a young adult in its fifth year at the time of death. The histology of larger heterodontosaurids shows somewhat faster-growing tissue, but only during early ontogeny. Specifically, sampled taxa thus far show a combination of loosely organized parallel-fibered, incipient fibrolamellar, or fully fibrolamellar tissue when young (Figure 27.8B), transitioning to parallel-fibered tissue as subadults (Figure 27.8C). Some specimens had achieved adult size before death, as demonstrated by an EFS (Butler et al. 2009; Woodward et al. 2011a, 2018; Becerra et al. 2016). Woodward et al. (2011a) found that the femur and tibia microstructures of indeterminate heterodontosaurids ("hypsilophodontids") from Victoria, Australia, closely resembled those of other basal, small-bodied ornithischians from lower latitudes. Because Victoria would have been within the Antarctic Circle during the Cretaceous, these small dinosaurs would have been subjected to low mean annual temperatures and months of polar darkness. So, although considered basal dinosaurs, heterodontosaurids nevertheless were physiologically preadapted for exploiting a range of environments.

Thyreophora

Bone histology within Thyreophora is not as extensively known as it is in other ornithischian clades. The microstructure has been described for the basal members *Lesothosaurus* (traditionally considered a basal fabrosaurid, and first considered a thyreophoran by Butler et al. 2009) and *Scutellosaurus*. The femur, tibia and fibula were sampled from *Lesothosaurus* specimens ranging in body length between 1 and 2 m. Smaller specimens revealed densely vascularized longitudinal fibrolamellar bone with no LAGs and no remodeling, and a medullary cavity full of spongy bone. Larger individuals had a partially free medullary cavity and fibrolamellar bone deep within the cortex. However, the outer cortex is lamellar-zonal. Secondary remodeling is frequent, and several LAGs are visible in the cortex. There is a possible EFS, suggesting attainment of small adult body sizes (Knoll et al. 2010). *Scutellosaurus* is quite a bit smaller than *Lesothosaurus*, with a femur length of 5 cm. Long bone histology reveals fibrolamellar bone only within the innermost cortex. Vascular canals are longitudinal and sparse throughout the cortex, which becomes nearly avascular near the surface. Most of the cortex is parallel-fibered, and LAGs are common (Padian et al. 2004). As with heterodontosaurids, the bone histology of these small basal ornithischians reflects the lower growth rates expected in taxa with small adult body sizes.

Among Thyreophora, stegosaurs have thus far attracted the most attention in bone tissue studies. In 2009, two studies described the limb bone histology from ontogenetic series of *Stegosaurus stenops* (Hayashi et al. 2009) and the smaller *Hesperosaurus* (Redelstorff and Sander 2009; Maidment et al. 2018). *Stegosaurus* histology can be summarized as having fibrolamellar tissue with radial and reticular vascular canals and no LAGs in the smallest individuals, longitudinal fibrolamellar bone and some LAGs in the medium-sized individuals and fibrolamellar tissue with LAGs and an EFS in the largest

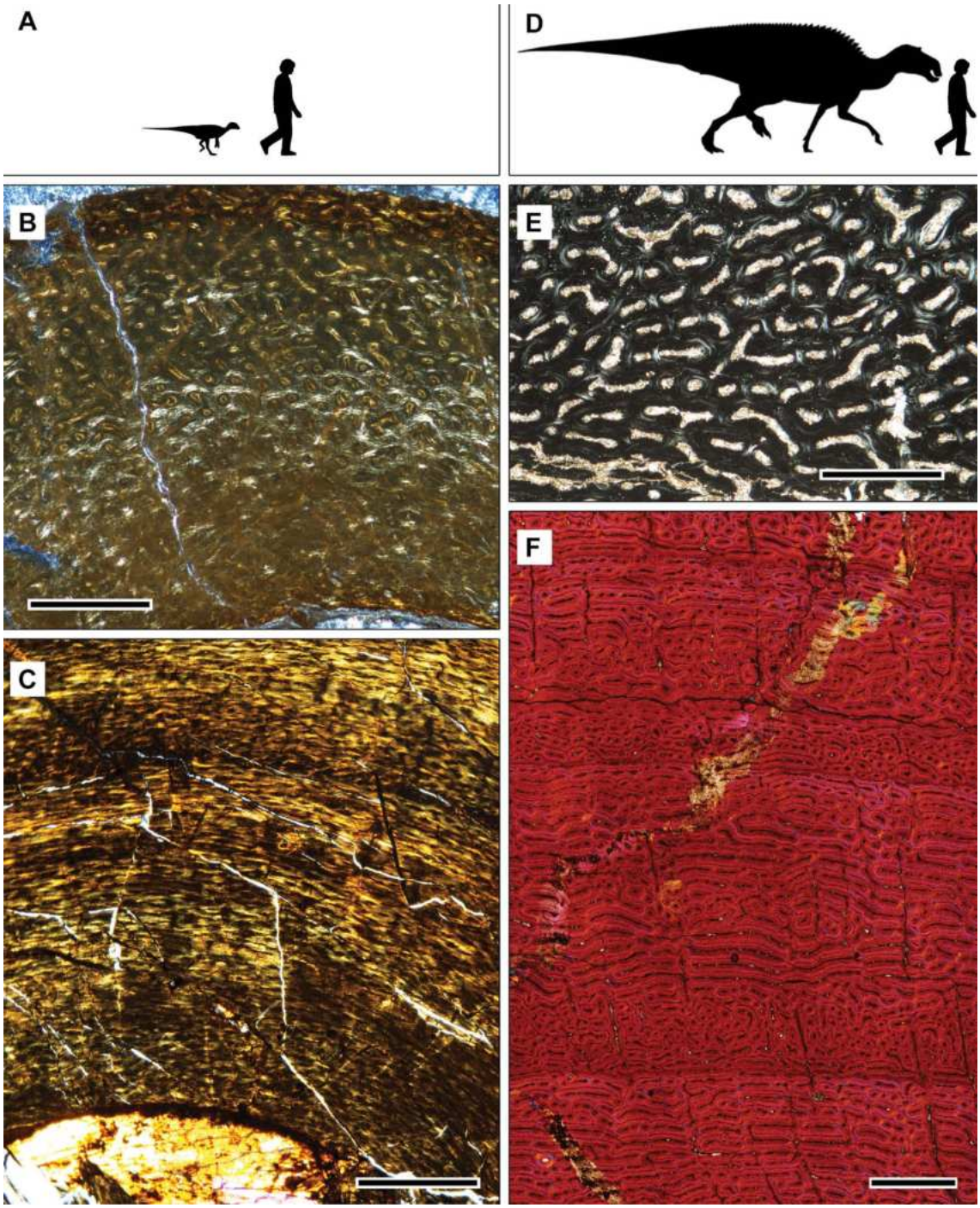


FIGURE 27.8 Ontogenetic bone histology characteristics of ornithischian dinosaurs achieving small asymptotic sizes and those reaching large asymptotic sizes. A, Schematic of a heterodontosaurid adult compared in size to a person. B, Transverse thin section of a juvenile heterodontosaurid tibia photographed in circularly polarized light. Bone fiber orientation is indicated by how bright (parallel to plane of section) or dark (perpendicular to the plane of section) the fibers appear. In this case, the entire cortex is composed of well-vascularized fibrolamellar tissue. Bone surface is at the top of the image. C, Transverse thin section of a late subadult heterodontosaurid photographed in circularly polarized light. Tissue formed when the dinosaur was younger is closest to the medullary cavity (bottom of image) and is fibrolamellar. From mid- to outer cortex, tissue takes on a more slowly formed parallel-fibered appearance. This is evident by the increased amount of bright fibers arranged in parallel with the thin section. D, Schematic of an adult *Maiasaura* hadrosaur compared in size to a person. E, Transverse thin section of a nestling-sized *Maiasaura* tibia photographed in circularly polarized light. Bone fibers are organized in a woven scaffolding and were in the process of becoming fibrolamellar bone. Large white spaces are vascular canals. F, Midcortex of an adult *Maiasaura* tibia photographed in cross-polarized light with a full wave plate. From inner to outer cortex, bone tissue is densely vascularized fibrolamellar. Bone surface is toward the top. Scale bars: B = 500 mm, C = 1 mm, E = 500 mm, F = 1 mm. (Heterodontosaurid images (A–C) by Matt Wedel, *Maiasaura* images (D–F) by Scott Hartman, and used under Creative Commons license 3.0. Image of MOR 758 NC-7-4-96.16 courtesy of Museum of the Rockies at Montana State University. Photo by H. Woodward. Image of YPM VPPU 22400 courtesy of the Division of Vertebrate Paleontology, Peabody Museum of Natural History, Yale University. Photos by H. Woodward.)

VetBooks.ir

(Hayashi et al. 2009). Maidment et al. (2018) later examined the histology of a *Hesperosaurus* specimen and found extensive secondary remodeling but that fibrolamellar bone and infrequent longitudinal canals were visible interstitially. The authors found 15 closely spaced LAGs within the outer cortex, and although no EFS was present, they suggested that the degree of remodeling and spacing of LAGs indicated a subadult individual with a smaller adult body size than the contemporaneous *Stegosaurus* (Maidment et al. 2018). Finally, the bone histology of the basal African stegosaur *Kentrosaurus* was studied to compare growth rates with *Stegosaurus* and *Scutellosaurus* (Redelstorff et al. 2013). The ontogenetic series revealed highly vascularized fibrolamellar bone with reticular and circular canals, as well as LAGs and annuli. The authors remarked that *Kentrosaurus* was growing rapidly like "typical" dinosaurs and unlike the smaller *Scutellosaurus*. It was also apparently growing more quickly than the larger and more derived *Stegosaurus*, so they suggested that *Stegosaurus* had a secondarily reduced growth rate (Redelstorff et al. 2013). However, Maidment et al. (2018) recently showed that the data set used by Redelstorff and Sander (2009) incorporated both the larger *Stegosaurus* and the smaller *Hesperosaurus*, and that it was the *Hesperosaurus* samples that were growing more slowly. Thus, it appears that Stegosauria so far conforms to the observation that animals of smaller body size in a clade tend to grow more slowly than larger ones.

A detailed examination of ankylosaur and nodosaur histology was only fairly recently published (Stein et al. 2013). Indeterminate North American ankylosaurs were sectioned, and long bone cortical histology described as a mixture of fibrolamellar and parallel-fibered tissue with poor vascularization. Ankylosaur and nodosaur limb bone histology is quite similar, and both exhibit generations of secondary osteons throughout the cortex regardless of ontogenetic status. Ankylosauridae differs from Nodosauridae in that it maintains high levels of woven tissue longer in ontogeny than does Nodosauridae, suggesting higher growth rates in the former. As in *Scutellosaurus*, vascular canal density appears to decrease toward the periosteal surface in ankylosaurs and nodosaurs. Whereas longitudinal vascular organization dominates in both groups, ankylosaurs, like stegosaurs, also occasionally shift to reticular vascularization, although of low density. Unique thus far to ankylosaurs and nodosaurs is the presence of "structural fibers" surrounding the first generation of secondary osteons (Stein et al. 2013). The Upper Cretaceous *Antarctopelta* from Antarctica is the only other ankylosaur taxon histologically examined to date. Its histology reveals that it was approaching adult size when it died, but the majority of the tissue, visible interstitially between secondary remodeling, is fibrolamellar and interrupted by LAGs (Cerda et al. 2019). Thus, the authors conclude that as with the basal heterodontosaurs from Victoria, Australia, the polar *Antarctopelta* displays no physiological differences visible in bone tissue microstructure from its lower latitude kin (Cerda et al. 2019).

Thyreophorans are distinguished by their scutes, plates and spikes, and Main et al. (2005) asked whether these had any internal histological continuity. They studied *Scutellosaurus, Scelidosaurus, Stegosaurus* and a Late Cretaceous ankylosaur. They found that "most thyreophoran scute tissues comprise secondary trabecular medullary bone that is sandwiched between layers of compact primary bone" (Figure 27.9A), and that "some scutes partly or mostly comprise anatomically metaplastic bone, that is, ossified fibrous tissue that shows incremental growth" (Figure 27.9B). Common to all taxa were erosion rooms of various size in the deep cortex, and nonvascularized channels that represented elongated spaces in larger structures (the plates and spikes of *Stegosaurus*, for example) but were smaller and more confined in smaller taxa and elements (the scutes of *Scutellosaurus, Scelidosaurus* and the ankylosaur). Variations in their relative size and shape resulted from differential growth of the element: hypertrophied structures contained hypertrophied channels. Yet a fundamental homology was seen among them, as among the layers of bone comprising the elements. The variations appeared more likely connected to forms of display, primarily species recognition, than to any function of facultative thermoregulation. The histology of

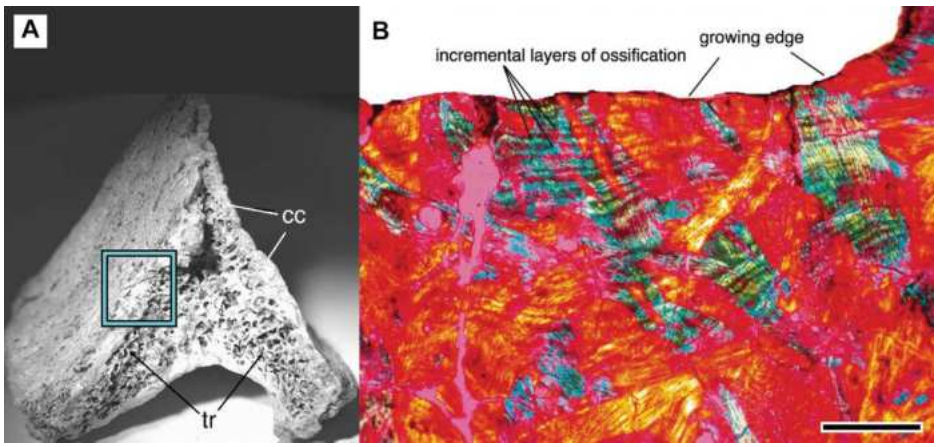


FIGURE 27.9 The osteoderm spikes and plates of ankylosaur and stegosaur thyreophorans are homologous in composition, being composed of compact (and often metaplastic) tissue sandwiching a medulla of bony trabeculae. A, Partially broken osteoderm of *Scelidosaurus* (BMNH 39516) reveals a latticework of trabeculae (tr) internally "sandwiched" by compact cortical bone (cc). The blue box indicates approximate location along an osteoderm shown in B. B, Ankylosaur osteoderm (UCMP 179282) in cross section, with bone surface toward the top of the image. The compact cortex is made of metaplastic tissue, with the fibrous bundles organized in different orientations as indicated by different interference colors. Incremental layers of fibrous metaplastic growth are evident toward the surface. Scale bar: B = 1 mm. (Images from Main et al. 2005, used with permission.)

ankylosaur osteoderms, which are generally thought to have had a protective function, was studied in major papers by Scheyer and Sander (2004), Hayashi et al. (2009) and Burns and Currie (2014), and other studies referenced in those papers. In general, the different forms of osteoderms elaborated in stegosaurs and ankylosaurs (plates, spikes, tail clubs) are variations on a basal morphology for the group as a whole, and metaplastic bone is frequently incorporated into these structures.

Ceratopsia

Within the Neoceratopsian Marginocephalia, most peer-reviewed histological studies have focused on the basal *Psittacosaurus* (Erickson and Tumanova 2000; Zhao et al. 2013; Bo et al. 2016). Bo et al. (2016) summarized the histologic differences between *P. lujiatunensis* and *P. mongoliensis*: medullary cavity expansion affects the cortex at a younger age in *P. lujiatunensis*; vascular organization of neonate *P. lujiatunensis* tibiae are typically reticular but longitudinal in *P. mongoliensis*; the adult cortex of *P. lujiatunensis* is longitudinally vascularized and reticular in *P. mongoliensis* and finally, erosion cavities appear at a younger age in *P. lujiatunensis* than in *P. mongoliensis*. The slower growth rate of *P. lujiatunensis* indicated by its histology is expected, given its smaller adult size compared with *P. mongoliensis*. Although also basal, small-bodied and abundant, there is only one extensive histological description of *Protoceratops* to date (Fostowicz-Frelik and Slowiak 2018; Figure 27.10A). The authors state that *Protoceratops* histology closely resembles that of other small ornithischians such as *Orodromeus* (see below), *Psittacosaurus*, *Kentrosaurus* and *Scutellosaurus*. In juveniles, *Protoceratops* femur tissue is fibrolamellar and well vascularized with longitudinal canals. Subadult histology resembles that of juveniles except that the cortex is now zonal (Figure 27.10B): the fibrolamellar tissue cyclically transitions to parallel-fibered and ends in a yearly annulus. In adults, the zones are closely spaced and made primarily of parallel-fibered tissue (Fostowicz-Frelik and Slowiak 2018). Although some specimens are considered adult, no EFS was reported, so an asymptotic size at skeletal maturity remains unknown.

Unfortunately, most histological studies of ceratopsids comprise currently unpublished conference papers, theses and dissertations. There are at present no peer-reviewed publications on chasmosaurine histology and only two detailed publications on centrosaurines. Erickson and Druckenmiller (2011) studied the femur of an Alaskan *Pachyrhinosaurus* (Figure 27.10C). Most of the cortex was composed of reticular fibrolamellar tissue changing to longitudinal fibrolamellar in the outer cortex. The primary tissue was separated by numerous conspicuous annuli deep within the cortex and LAGs within the outer

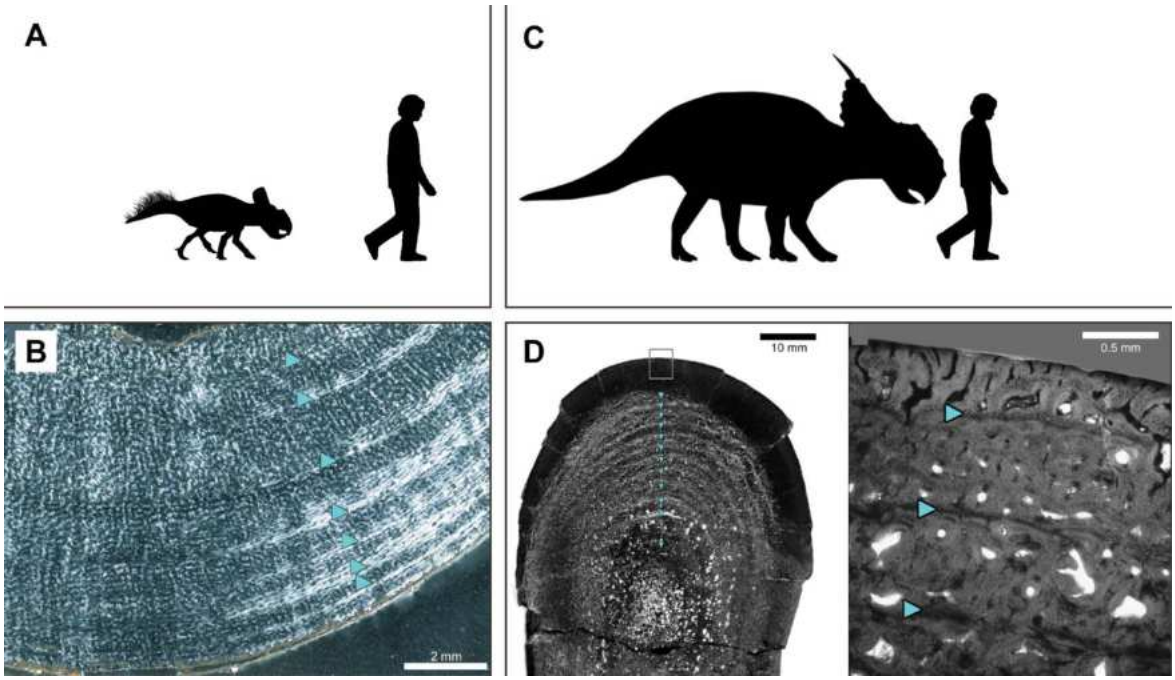


FIGURE 27.10 Ontogenetic bone histology characteristics of ceratopsid dinosaurs achieving small asymptotic sizes and those reaching larger asymptotic sizes. A, Schematic of a *Protoceratops* adult compared in size to a person. B, Transverse thin section of an adult *P. andrewsi* (ZPAL MgD-II/11a) femur in cross-polarized light. The innermost cortex nearest the medullary cavity (top of image) was formed when younger, and the bone at the periosteal surface (bottom of image) was formed most recently prior to death. The younger bone tissue is largely isotropic, indicating rapidly formed woven tissue, and closer to the surface the tissue becomes increasingly parallel-fibered, as indicated by the uniform anisotropic banded layers. Growth to adult size occurred over many years, as is indicated by the cyclical formation of parallel-fibered annuli (arrowheads). (Image taken from Zhao et al. 2013.) C, Schematic of a *Pachyrhinosaurus* compared in size to a person. D, Transverse thin section of a subadult *Pachyrhinosaurus* femur showing a richly vascularized cortex separated by annual lines of arrested growth (arrows) over many years of growth. (Image taken from Erickson and Druckenmiller 2011. *Protoceratops* image by Scott Hartman, *Pachyrhinosaurus* image by Andrew A. Farke and both used under the following license: https://creativecommons.org/licenses/by/3.0/. B is from Figure 9 in Fostowicz-Frelik and Slowiak 2018 and D is from figure 4 of Erickson and Druckenmiller 2011, both used with permission.)

VetBooks.ir

cortex (Figure 27.10D). Secondary remodeling was localized within the deep cortex (Erickson and Druckenmiller 2011).

To assess early histological trends in centrosaurines, Hedrick et al. (2020) recently sampled long bones of two basal mid-sized ceratopsids: *Avaceratops* from northwest North America and *Yehuecauhceratops* from Mexico. The *Avaceratops* humerus had fibrolamellar bone with radial and reticular vascularity grading to circumferential vascularity periosteally. These features, as well as a single LAG in the cortex and no secondary remodeling, suggest a juvenile status at death. The *Yehuecauhceratops* femur was fibrolamellar with dense laminar primary osteons, extensive secondary remodeling within the inner cortex and a scattering of secondary osteons near the periosteal surface. The femur also had several LAGs and their spacing toward the bone surface suggests a late subadult status. Because *Yehuecauhceratops* is from Mexico, this specimen demonstrates that the presence of LAGs in centrosaurines is not affected by latitude (Hedrick et al. 2020).

Horner and Lamm (2011) studied the later ontogenetic stages of the frill of *Triceratops*. They noted that in these later stages the frill became larger and thinner and developed the fenestration seen in nearly all other ceratopsians. This process occurred through an initial stage of nonpathologic hyperostosis, then external resorption and border extension of the parietal, concluded by a mineralization of the posterior end of the frill through metaplasia, a process similar to that seen in *Centrosaurus*.

Pachycephalosauria

These bizarre animals, sister taxon to Ceratopsia, are relatively poorly known among dinosaurian groups, and oddly, most preserved remains are of the thickened cranial domes that are often found isolated and worn. Postcranial remains are relatively rare and have not been assessed histologically, whereas several studies have focused on the domes (Goodwin and Horner 2004; Horner and Goodwin 2009; Evans et al. 2018). Horner and Goodwin (2009) first drew attention to the very unusual histological structures of the domes, which largely comprise metaplastic tissue that becomes altered ontogenetically along with the changing shape of the dome. They showed that the internal pattern of "radiating structures," previously identified in broken specimens as support for a "head-butting" hypothesis, diminished in size through ontogeny as the domes became enlarged, thus weakening that hypothesis. Horner and Goodwin (2009) examined the internal structure of a variety of named taxa and found that *Dracorex* and *Stygimoloch* were likely juvenile and subadult forms, respectively, of the adults known as *Pachycephalosaurus*. Through ontogeny, cranial crests and spikes were at first elaborated and then reduced, simultaneously with expansion of the cranial dome, a hypothesis supported by transitional characters among the specimens studied. Again the internal structure comprised a combination of metaplastic, fibrous and acellular tissue.

At this point it is appropriate to draw further attention to the prevalence of metaplastic tissue in the bones of dinosaurs and related reptiles. Following the pioneering work of Haines and Mohuidden (1968), Horner et al. (2016) surveyed the presence of this tissue in dinosaurs and found a great array of taxa in which the tissue is preserved. Metaplastic bone is generally defined as the permanent transformation of the identity of a cell (e.g., from chondrocytes to osteoblasts), and usually involves mineralization. Horner et al. (2016) used the accepted example of "ossified" tendons in birds to extend comparisons to the same tissues in extinct dinosaurs. They found tissues with diagnostic features of metaplasia in the tendons and a nasal bone of hadrosaurs, the scutes of the tail "club" in an ankylosaur, the neural spines of a sauropod and the stiffening tail rods of dromaeosaurs. Main et al. (2005) had identified similar tissue in the scute of an ankylosaur and it is likely that the scutes of archosaurs in general, e.g., phytosaurs, substantially comprise metaplastic tissue. The tissue is generally characterized by "fiber bundles (or fascicles) that were closely bound together and separated by arc-shaped spaces in cross section. When viewed longitudinally, they were arranged in a herringbone pattern" (Horner et al. 2016). What had previously been interpreted as osteocyte lacunae are instead the arc-shaped spaces between the fiber bundles. Mineralization of fibers is intense and proceeds centrifugally. Horner et al. (2016) hypothesized that the skeletal elements they studied formed by metaplastic transformation rather than by periosteal and intramembranous ossification, and that these processes may be more common than heretofore realized.

Basal Ornithopoda

Thus far, the small-bodied *Orodromeus* is the only parksosaurid to be described histologically in the peer-reviewed literature. In perinates, limb bone tissue is longitudinal fibrolamellar, which changes to reticular fibrolamellar in young juveniles. By the late juvenile stage, vascularity is reticular to plexiform, and several LAGs are present. Vascularity sharply decreases toward the periosteal surface and there is very little remodeling. Cortices of adults have longitudinal vascular canals; the outermost cortex is parallel-fibered, with almost no canals, but possibly with an EFS (Padian et al. 2004; Horner et al. 2009). Generally, the cortex is well vascularized throughout ontogeny, but vascular canal density is not as great as in derived ornithopods.

The femur and tibia of the basal, small-bodied (1.7 m in length) iguanodontian ornithopod *Gasparinisaura* (Figure 27.11A) were histologically examined from a partial ontogenetic series. Fibrolamellar bone predominates through most of the growth series, with a dense vascular network of longitudinal and oblique canals. The primary tissue is interrupted by diffuse annuli in younger individuals, and by more defined annuli and LAGs in older individuals. In the largest individuals, although bone tissue becomes parallel-fibered in the outermost cortex (Figure 27.11B), the tissue is not completely avascular, so an EFS is not considered to have developed (Cerda and Chinsamy 2012).

Limb bones from rhabdodontid ornithopods were among the first dinosaurs studied histologically (Taquet 2001) and were more recently sampled in a study by Ösi et al. (2012). They examined and compared *Mochlodon vorosi*, *M. suessi* and *Rhabdodon* sp., although actual bone tissue organization was never discussed. Bones sampled from *M. vorosi* were from individuals considered late juvenile, subadult and adult. Late juveniles were reported to have higher vascular density than older individuals, although secondary remodeling is already extensive. The subadult has reduced vascularity and LAGs are

VetBooks.ir

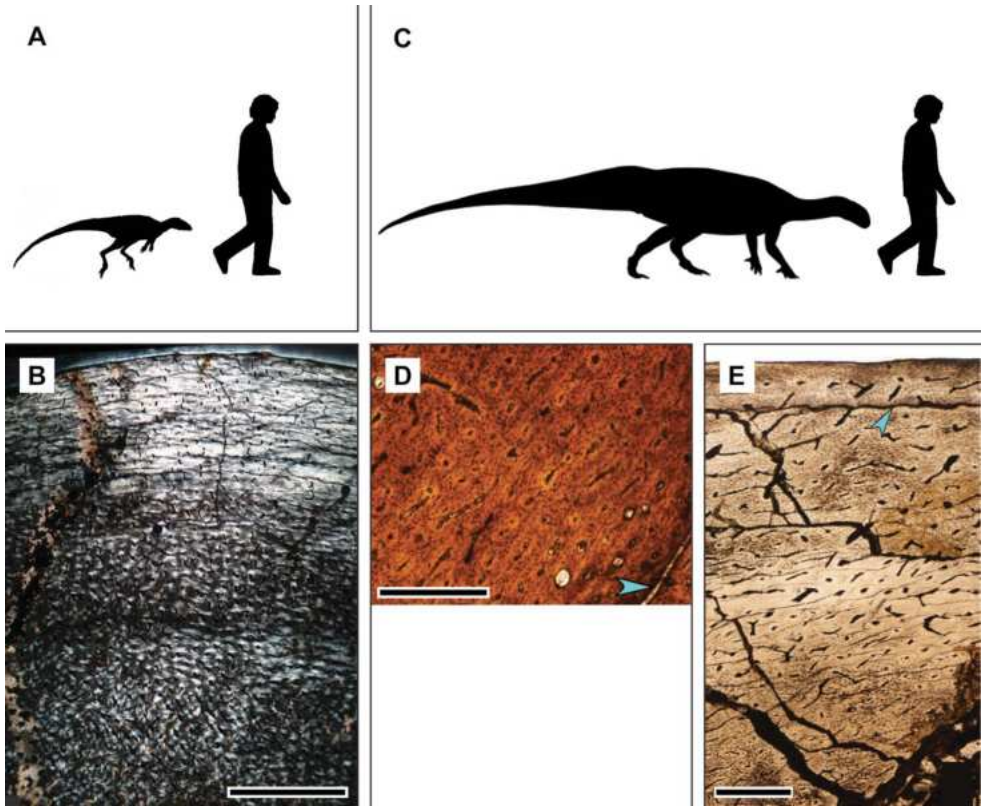


FIGURE 27.11 Osteohistology of small to medium-sized stem ornithopods. A, *Gasparinisaura*. B, Femur histology reveals an inner cortex (i.e., younger bone) of isotropic woven tissue indicating rapid growth early in life, with a mid- to outer cortex (toward the top of the image) made of more anisotropic parallel-fibered tissue, showing that growth drastically slowed as its small adult size was approached. (Image taken from Cerda and Chinsamy 2012. C, The somewhat larger *Tenontosaurus* shows a similar pattern of (D) rapid growth when young (bone surface to the right), and (E) transitioning to slower growth to medium size when older (bone surface toward the top). Lines of arrested growth indicated by arrowheads. Scale bars: B = 1 mm; D and E = 500 mm. (*Tenontosaurus* image by Matt Dempsey and used under the following license: https://creativecommons.org/licenses/by/3.0/. B is from figure 3 in Cerda and Chinsamy 2012, used with permission. D and E are from figures 7 and 8 in Werning 2012, Open Access under Creative Commons license 3.0.)

frequent and closely spaced. The adult specimen, estimated at 1.8 m in body length, has a highly remodeled cortex, sparse vascularity, tightly stacked LAGs and an avascular EFS. *M. suessi* appears to have reached a smaller adult body length (1.6 m) than *M. vorosi*, and its tibial histology displays adult features at the same body size as a subadult *M. vorosi*. The sampled specimens of *Rhabdodon* sp. displayed a wide variety of histological features at different body sizes: juveniles appeared to range between 2.7 and 5.1 m in length, while adult histology was estimated in one specimen at 1.5 m and in another at 5.9 m (Ösi et al. 2012). The histology of another small (2.5 m) rhabdodontid, *Dysalotosaurus*, was described by Hübner (2012) using several skeletal elements across an ontogenetic series. The youngest sampled femur was from an early juvenile exhibiting longitudinal fibrolamellar bone. Late juvenile histology shows more organized primary tissue, isolated secondary osteons and "growth cycles" (i.e., thick, diffuse bands of parallel-fibered tissue). Subadult individuals show an increase in secondary osteons and frequent growth cycles of fast- and slow-growing bone. Compacted coarse cancellous bone is present throughout the femoral sample (Hübner 2012), also reported by Woodward et al. (2018) in their small-bodied "hypsilophodontid" sample from Australia. The lack of an EFS in any specimen from the *Dysalotosaurus* sample indicates that the study lacks an adult individual.

Finally, a detailed ontogenetic analysis of long bones from the medium-sized (6.5–8 m in length) *Tenontosaurus* (Figure 27.11C) was presented by Werning (2012). Bone tissues from early ontogeny to subadult stage are associated with fast growth (Figure 27.11D). Femora of juveniles contain densely vascularized longitudinal fibrolamellar bone and no LAGs. Subadult tissue is also fibrolamellar, but vascularity is now laminar and there is a scattering of secondary osteons deeper within the cortex. Several LAGs are present. In the adult specimen, several generations of secondary osteons obscure the primary tissue within the inner cortex. There are scattered secondary osteons in the midcortex, and the primary cortex is plexiform fibrolamellar. The outer cortex is less densely vascularized and consists of weakly woven to parallel-fibered tissue, and the periosteal surface is completely lamellar and nearly avascular (Figure 27.11E). Ten LAGs are present, becoming more closely spaced toward the surface. Protracted slow growth appears to have begun at the subadult stage interpreted from the presence of parallel-fibered tissue. Werning (2012) hypothesized that *Tenontosaurus* retained the plesiomorphic condition of fast growth early in life, and an extended

VetBooks.ir

period of slower growth late in life. Results suggest that the iguanodontid *Tenontosaurus* grew much more slowly to adult size than larger members within Hadrosauridae.

Hadrosaurids

Within Hadrosauridae, most studies focus on Saurolophinae and are restricted to small sample sizes and/or incomplete ontogenetic series. An exception is the most extensive histological analysis of any tetrapod taxon, performed by Woodward et al. (2015) on an ontogenetic series of 50 tibiae from the Campanian saurolophine *Maiasaura peeblesorum* (Figure 27.8D). For this reason the histology of *Maiasaura* will be summarized here and used as a comparative baseline when discussing other hadrosaurid taxa. Perinatal specimens consist of completely woven tissue with reticular and radial vascularity and a fairly undifferentiated medullary cavity (Figure 27.8E). In larger perinates, the medullary cavity is better defined, and the tissue is fibrolamellar (Horner et al. 2000). In young of the first year, cortical tissue is primarily reticular to laminar fibrolamellar bone, becoming primarily subplexiform to plexiform after the second LAG (Horner et al. 2000; Woodward et al. 2015). There is considerable variation in tibia lengths (between 39 and 51 cm) for individuals at one year of age. In all tibiae with two or more LAGs, a cyclical vascular pattern manifests in each zone. Following a LAG, the primary tissue is initially reticular, then changes to laminar or plexiform for most of the zone (Figure 27.8F). This pattern then repeats to the outermost cortex, where zone spacing is only a few laminae thick with mostly longitudinal vascularity. Some specimens have an EFS in the outermost cortex. The average age at skeletal maturity is 8 years, and the oldest specimen in the sample is 15. There is also individual variation in tibia length at skeletal maturity when an EFS is observed: two tibiae with lengths of 75 and 87.5 cm have 8 LAGs before the EFS, but another tibia is 90 cm long with 10 LAGs and no EFS. The first LAG is partly present even in adult specimens, although by subadult size secondary remodeling is prevalent within the inner to middle cortex (Woodward et al. 2015).

The geologically oldest saurolophine so far histologically sampled is *Eotrachodon* from the Santonian of the southeastern United States (Prieto-Márquez et al. 2016). The sectioned tibia is estimated to correspond to an individual 4–5.1 m in body length. The cortex consists entirely of plexiform fibrolamellar bone with no remodeling. There are two possible growth rings that are only evident as polish lines. The authors suggest that because this hadrosaur is from a much lower latitude than others so far sampled, the lack of obvious LAGs may be related to more favorable environmental conditions and lesser seasonality (Prieto-Márquez et al. 2016). *Maiasaura* was estimated to be about 3 m in body length after its first year of growth, so a body length of 4–5.1 m for *Eotrachodon* within its third year of growth would be consistent with the body size of a similarly-aged *Maiasaura*.

Gates et al. (2014) described the histology of a femur 64.7 cm long of an unnamed hadrosauroid taxon close to hadrosaurids, from the Lower-Middle Campanian of Utah. The cortex consists of unordered longitudinal fibrolamellar bone within the inner cortex, and laminar to plexiform tissue in the midcortex. Vascularity is dense throughout, and there are no LAGs and no EFS, so the authors conclude that this is a juvenile individual. Compared to *Maiasaura's* limb proportions, this femur could be small enough to reflect an individual still within its first year of growth when it died; if so, it was growing more quickly during its first year and reached a larger size than did *Maiasaura* after its first year.

Probrachylophosaurus is from the Campanian of Montana and is histologically described from a single late subadult specimen (Freedman Fowler and Horner 2015). The tibia shows widely spaced LAGs within the inner cortex, becoming more closely spaced toward the periosteal surface except for a cluster of closely spaced LAGs at midcortex. The cortex is minimally remodeled and appears to be largely laminar to plexiform fibrolamellar throughout. The alternating vascular zonal cycle described in *Maiasaura* is not reported here. There are 14 LAGs within the cortex and no EFS. LAG circumferences show that *Probrachylophosaurus* was larger than *Maiasaura* at each stage of growth and achieved skeletal maturity much later than the contemporaneous *Maiasaura* (Freedman Fowler and Horner 2015).

The femur and humerus histology of the Upper Campanian *Edmontosaurus regalis* from Alberta was described from several individuals. The smallest femora sampled are 51.5 and 54.8 cm long. Femora in this size range have reticular fibrolamellar bone and no LAGs; this size range is consistent with *Maiasaura* yearlings. Femora 68.6–86 cm long show cyclical vascularity alternating between reticular and circumferential as in *Maiasaura*, but no discrete LAGs (Vanderven et al. 2014). To date, no Maastrichtian saurolophines have been histologically described from an ontogenetic series.

As with saurolophines, most lambeosaurine taxa histologically examined are from the Campanian. The type specimen of *Hypacrosaurus stebingeri*, temporally and geographically contemporaneous with *Maiasaura*, was histologically examined from most long bones and other elements (Horner et al. 1999). In the tibia and femur, primary bone in the deep cortex is reticular, becoming laminar to plexiform in midcortex. There is dense Haversian remodeling in the deeper cortex and a scattering of secondary osteons in midcortex. Growth is interrupted by 8 LAGs, and there is an EFS at the surface. The tibia displays the same cyclic reticular to plexiform vascular pattern as in *Maiasaura*. Cooper et al. (2008) modeled the growth of *Hypacrosaurus* and concluded that skeletal maturity was achieved between 10 and 12 years, and sexual maturity in 2–3 years. If so, despite achieving similar adult body lengths, skeletal maturity occurred much later in *H. stebingeri*, but sexual maturity occurred in 2–3 years as in *Maiasaura*.

The only Maastrichtian lambeosaurine histologically sampled thus far is assigned to *Pararhabdodon* from Spain (Fondevilla et al. 2018). The study examined an ontogenetic series of tibiae ranging from juveniles to adults. The youngest individuals are already 2 years old. Juvenile tibiae are reticular within the innermost cortex and primarily dominated by plexiform tissue, much as in *Maiasaura*. Resorption cavities and scattered secondary osteons in the deep cortex are present in juveniles. Subadults are defined as having tissue that has more developed secondary remodeling in the deep cortex and the outer cortex is almost exclusively longitudinal in

VetBooks.ir

vascularity. Adult individuals display more extensive remodeling within the inner cortex and secondary osteons are present to the periosteal surface. An EFS is present in adults, and skeletal maturity occurred at 14–15 years of age. Unlike *Maiasaura*, there is little variance in body size after the first year of growth. But like *Maiasaura*, final adult size varies greatly. For instance, tibiae of lengths 55–60 cm are from adults, but the largest tibia was 94 cm at skeletal maturity. Also, as in *Maiasaura*, growth rates quickly decelerated after age 3 (Fondevilla et al. 2018).

Dinosauria: Saurischia

Basal Sauropodomorphs

Basal Triassic sauropodomorphs (also called noneusauropod or nonsauropod sauropodomorphs, or "prosauropods") such as *Plateosaurus* (Figure 27.12A) achieved large body sizes (up to 10 m in length), foreshadowing the gigantism exhibited by Jurassic and Cretaceous sauropods. In general, basal sauropodomorph histology reveals well-vascularized laminar, reticular and plexiform fibrolamellar bone, interrupted by LAGs (Chinsamy 1993; Sander and Klein 2005; Klein and Sander 2007; Cerda et al. 2014; Pretto et al. 2017; Apaldetti et al. 2018) (Figure 27.12B, C). These features suggest that basal sauropodomorphs achieved large body sizes through accelerated cyclical growth (Apaldetti et al. 2018). In addition, the long bone cortices of basal sauropodomorphs, like those of theropods, are relatively thin and the marrow cavities are largely devoid of cancellous bone (Pretto et al. 2017). An extensive ontogenetic long bone histology study of *Plateosaurus* showed that with this cyclical rapid growth, a body length of 5 m could be reached in as little as 8 years (Klein and Sander 2007). However, the ontogenetic sample also revealed high individual plasticity in growth: skeletally mature individuals ranged between 6.5 and 10 m in length. In all of these respects, basal sauropodomorph bone microstructure features and related growth trends resemble more closely those of large theropods than their eusauropod descendants. But, as in all dinosaurs studied to date, there was no bimodal distribution to the size variation observed in *Plateosaurus*. So rather than inferring sexual dimorphism, the authors of the study suggest that *Plateosaurus* growth was sensitive to environmental pressures and stresses (Sander and Klein 2005). Large bones of presumably adult basal sauropodomorphs (e.g., *Euskelosaurus*) may have their cortex completely formed by dense Haversian tissue, with several superimposed generations of secondary osteons (Ricqlès 1968).

Sauropoda

Unlike the plastic growth observed in the basal sauropodomorph *Plateosaurus* and inferred for other basal taxa, the giant eusauropods ("true" sauropods, Figure 27.12D) of the Jurassic and Cretaceous show very little plasticity in growth, and generally show a high correlation between ontogenetic age and size (Griebeler et al. 2013). Also unlike basal sauropodomorphs, sauropod medullary cavities were typically filled with cancellous bone, and this feature is present even in perinatal young (Curry Rogers et al. 2016; Cerda et al. 2017; González et al. 2020). Eusauropod long bone histology has been extensively studied since the early 2000s, and the histology "typical" of the group can be generalized as well-vascularized laminar fibrolamellar bone that lacks LAGs or annuli, except at the cortical periphery when approaching adult size (Sander 2000; Sander et al. 2004, 2011; González et al. 2020). The apparent lack of cyclical growth marks within limb bones is hypothesized because sauropod bone apposition rate was so rapid, and growth paused so briefly (if at all), that no annual growth rings had time to form. At present this hypothesis is difficult to test because there is no extant vertebrate analogue for rapid continuous growth over many years and with no cyclical growth hiatuses. Growth cycles are apparent in local regions of long bones that experience lower growth rates (Ricqlès 1983).

The apparent lack of LAGs makes it difficult to determine limb bone skeletochronology and absolute age in these giants. However, brief cyclical pauses in the growth of sauropods is suggested by the presence of "polish lines," first described by Sander (2000) as rings visible within the transverse cortex of polished bone sections using reflected rather than transmitted light (Figure 27.12E). Another cyclical growth marker in sauropod long bones are "modulations" of growth rate, but are more often observed in sauropod flat bones such as the scapula (Curry 1999). Modulations, rather than being distinct lines in the bone, are rings within the bone caused by localized difference in vascular canal diameters, implying that for a brief time growth rate changed. Polish lines and modulations have since been used in place of LAGs to model growth curves for sauropods, but both structures are easily destroyed by the onset of secondary remodeling. For this reason, Klein and Sander (2008) devised a relative scale by which to age sauropods. With this method, changes in laminar fibrolamellar primary bone tissue and the density of secondary osteons define 13 "histologic ontogenetic stages" (HOS). With this system, the youngest stages are represented by partly to fully developed laminar fibrolamellar bone, and increasing secondary reconstruction is observed as the animals mature and reach later HOS stages. Recently it was reported that sauropod ribs have cyclical growth and preserve LAGs, so ribs are being used more frequently to obtain empirical ages for sauropod individuals (Waskow and Sander 2014).

The HOS model appears to work well for determining relative age in Jurassic sauropods, but it is not as effective for determining the relative ages of derived Cretaceous titanosaurs. This is because unlike Jurassic sauropods, secondary remodeling began much earlier in ontogeny in titanosaurs. In the case of the Madagascar titanosaur *Rapetosaurus*, remodeling obliterated primary growth records before individuals reached 60% maximum size (Curry Rogers and Kulik 2018). In fact, Curry Rogers et al. (2016) demonstrated that even the long bones of neonatal *Rapetosaurus* possessed a scattering of secondary osteons within the primary fibrolamellar tissue matrix. Early onset of secondary remodeling has since been observed in juvenile South American titanosaurs (González et al. 2020). There is also little evidence for the presence of an EFS in even the largest known specimens of titanosaurs (Curry Rogers and Kulik 2018), which means that their true gigantic asymptotic sizes are not yet well established. Thus,

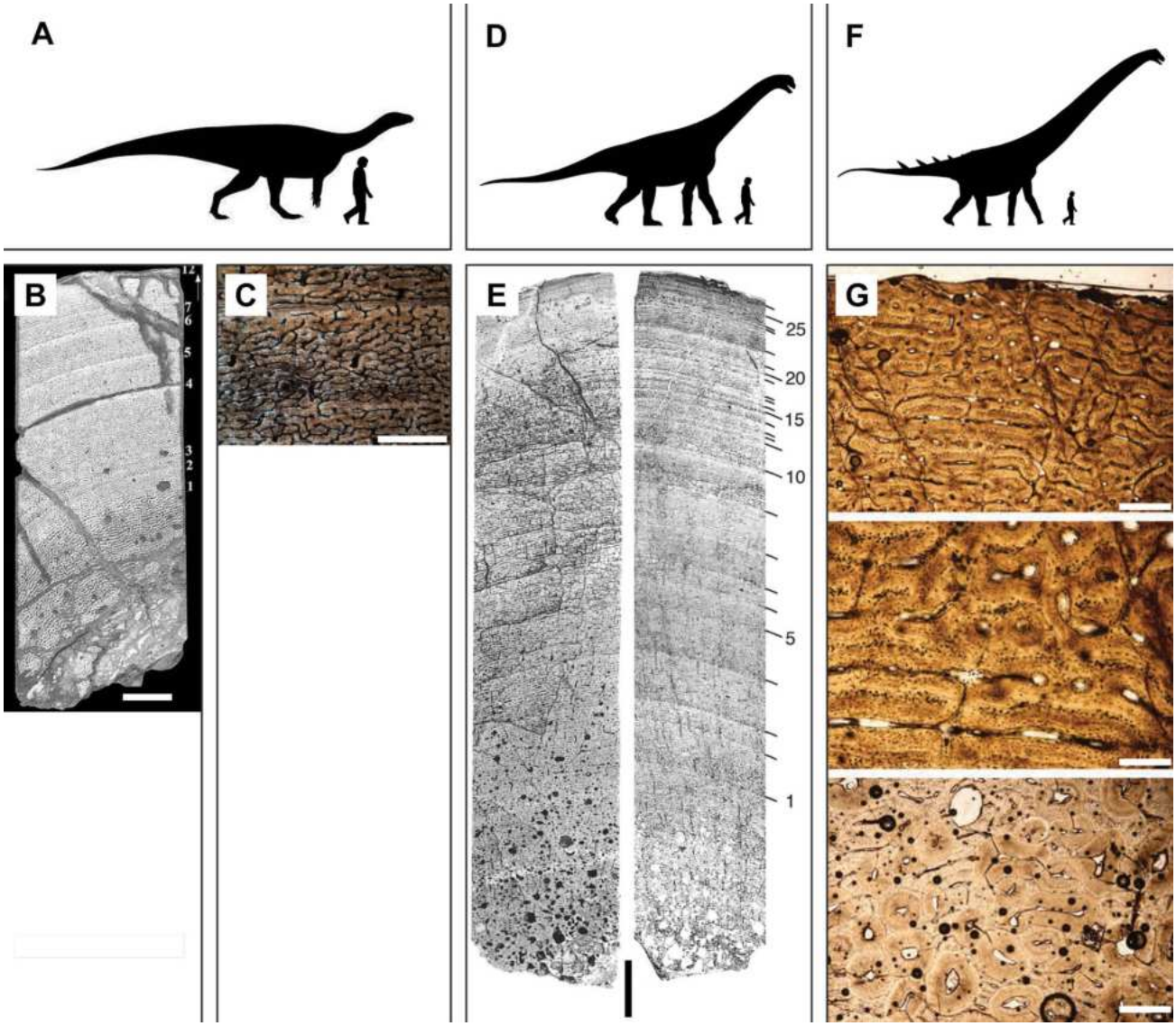


FIGURE 27.12 Examples of Sauropodomorpha histology. A, *Plateosaurus*, a basal sauropodomorph, was already a large dinosaur, which is reflected in (B) its femoral histology. Tissue is richly vascularized and fibrolamellar throughout (C), and annual lines of arrested growth (LAGs) are evident. (Images taken from Sander and Klein 2005.) D, Eusauropods such as *Janenschia* were the largest land vertebrates to date. E, Eusauropod long bone histology is very similar to that of *Plateosaurus*, except that LAGs are rarely observed (left image) from the inner cortex (bottom) to the bone surface (top). However, by polishing the bone and using reflected light, "polish lines" become evident and have been interpreted to form annually like LAGs (right image). (Image taken from Sander 2000.) F, Cretaceous titanosaurs such as *Rapetosaurus* also grew very rapidly like earlier Jurassic sauropods, but (G) underwent intense secondary remodeling earlier in life. The three panels in G show heavy remodeling deep in the cortex (bottom), with well-vascularized primary tissue still visible in the mid- to outer cortex (middle and top images). Scale bars: B = 3 mm; C = 1 mm; E = 5 mm; G = 500 µm. (Images from Curry Rogers and Kulik 2018. *Plateosaurus* image by Andrew Knight, sauropod images by Scott Hartman, all used under Creative Commons license 3.0. B and C are from figure 1 in Sander and Klein 2006. E is from Sander 2000. G is from Curry Rogers and Kulik 2018, figure 3; all used with permission.)

application of HOS to titanosaur limb bones would result in older age estimates for smaller specimens due to the degree of remodeling present, but would result in younger estimates for larger individuals due to the lack of an EFS (Curry Rogers and Kulik 2018; González et al. 2020).

Other than an ontogenetically earlier onset of secondary remodeling, the primary tissue observed in titanosaur limb bones is generally the same as that observed in Jurassic sauropods, and LAGs are seldom reported. The best histologic ontogenetic long bone series for a titanosaur thus far is that of *Rapetosaurus* (Figure 27.12F), and it has helped to fill in gaps regarding aspects of titanosaur life history. Surprisingly, in specimens smaller than 50% maximum size, a band of tightly spaced growth marks are observed within long bone cortices. The authors interpret these growth marks as a shift to slower growth rates, potentially associated with an environment stressful to small juvenile sizes. Then, at 50% maximum size, rapid primary growth resumes. Curry Rogers and Kulik (2018) observed that the growth marks are so closely spaced, together they could have been

VetBooks.ir

interpreted as an EFS if only small specimens were available for study, which would lead to the erroneous conclusion that *Rapetosaurus* was a dwarf taxon. The presence of a LAG in a juvenile titanosaur has been reported once since, in a South American taxon (González et al. 2020).

The presence of a thick stacking of LAGs in juveniles from an ontogenetic series suggests that the reports of possible dwarf sauropod taxa from Europe may be questionable, if a slowdown in growth due to stress was ubiquitous for sauropods; it may be that what has been interpreted as an EFS in dwarf taxa is instead a thick growth ring from a juvenile that did not survive past that stressful time of year. Another feature found in dwarf sauropod histology is primary tissue made of "modified lamellar bone," defined as having the rich vascular network commonly seen in rapidly growing bone, but primarily composed of parallel-fibered bone matrix (Klein et al. 2012). Curry Rogers and Kulik (2018) remarked on the highly vascularized fibrolamellar tissue observed in their *Rapetosaurus* growth series (Figure 27.12G), noting that the specimens have very large vascular canals that were subsequently infilled by lamellar primary osteons. They suggest that the "modified lamellar bone" observed in dwarf sauropod taxa could have been misidentified and is in fact fibrolamellar tissue with a rapidly deposited, fine woven matrix.

Theropoda: Nonavian Forms

Far fewer histological studies have been performed on theropods than on the herbivorous ornithischians or sauropods. Moreover, when studies on theropods are performed, they frequently consist of histological descriptions from suboptimal bones such as ribs, gastralia, fibulae, forelimbs and metatarsals. And frequently sections of long bones are not taken at midshaft, a situation that still provides interesting information but makes comparisons among taxa difficult. This review only includes papers that actually describe the theropod bone tissues observed and those that use the femur, tibia or fibula.

Despite the attention paid to life history interpretations of the iconic large carnivorous dinosaurs, most descriptions of theropod histology concern small-bodied taxa, generally much smaller than the average human is tall. These histoanalyses run the gamut from stem to crown nonavian theropods, and regardless of clade all small-bodied theropod bone tissue shares similar patterns. This observation suggests that there is a histological signal reflecting growth to small asymptotic body sizes, in much the same way as is observed for small ornithischians (e.g., Figure 27.8).

Several Triassic stem nonavian theropods have been examined histologically, including the possible theropod *Herrerasaurus* (Ricqlès et al. 2003b), an indeterminate neotheropod from New Mexico (Griffin and Nesbitt 2020), and coelophysoids including *Coelophysis bauri* (Ricqlès et al. 2003b), *C. rhodesiensis* (Chinsamy 1990) and the Early Jurassic *Segisaurus* (Carrano et al. 2005). Histology shows that even these stem theropods grew rapidly in early life, possessing highly vascularized longitudinal or plexiform fibrolamellar bone, separated cyclically by LAGs. Zero to six LAGs are present collectively, but no EFS is observed in these early theropods. However, the LAG intervals in *Segisaurus* appear to decrease toward the periosteal surface, and the authors therefore suggest it was a subadult when it died (Carrano et al. 2005).

Within Averostra, the small-bodied noasaurids are relatively well sampled (e.g., Lee and O'Connor 2013; Evans et al. 2015; Wang et al. 2017). Fibulae from nine specimens of *Limusaurus* from the Late Jurassic of China represent an ontogenetic series ranging from young of the first year to 10 years of age (Wang et al. 2017). The smallest individuals have highly vascularized longitudinal fibrolamellar bone, but already with secondary osteons within the inner two-thirds of the cortex. Late juveniles have two LAGs, the early subadult has five, and an EFS in the oldest individual shows that skeletal maturity was reached by 6 years of age (Wang et al. 2017). A growth series of tibiae and femora from *Masiakasaurus* (Figure 27.13A, B), a noasaurid from the Late Cretaceous of Madagascar, reveals dense reticular and plexiform fibrolamellar bone and a single LAG within an annulus in the smallest femur (130 mm) (Lee and O'Connor 2013). Intermediate femora (160 mm) consist of longitudinal and circumferential parallel-fibered bone, again separated by annuli and LAGs. The largest femur (202.5 mm) contains six LAGs and is primarily parallel-fibered and poorly vascularized near the periosteal surface (Lee and O'Connor 2013) (Figure 27.13B). The authors concluded that there is substantial variation in individual growth, but that an average *Masiakasaurus* would take 8–10 years to reach small adult size, and that growth rate peaked at 3–4 years of age. The slow growth to small adult size was surprising to the authors (Lee and O'Connor 2013), but it does seem consistent with emerging histologic patterns for small tetrapods.

The largest noncoelurosaurian avetheropod histologically assessed thus far is the Late Jurassic *Allosaurus*. Bybee et al. (2006) sampled an ontogenetic series of six femora and three tibiae from this iconic theropod. Throughout the sections, the tissue was circumferentially vascularized fibrolamellar bone. The age of the largest specimen, as demonstrated by LAGs, was 13–19 years. Although no EFS was found in any sample, the authors' modeling determined that *Allosaurus* would reach full somatic adult size in 22–28 years (Bybee et al. 2006).

The Coelurosauria, which includes ornithomimids, tyrannosaurids and paravians, has received the most histological attention within Theropoda. Once more, small-bodied taxa comprise the majority of studies. Tibiae of basal coelurosaurs *Albinykus* (an alvarezsauroid) (Nesbitt et al. 2011) and *Anikosaurus* (Ibiricu et al. 2013) comprise fibrolamellar bone within the innermost cortex, but primarily longitudinal to circumferential parallel-fibered tissue characterizes the majority of growth, interrupted by LAGs. No EFS was found in either specimen (Nesbitt et al. 2011; Ibiricu et al. 2013).

Small ornithomimids also demonstrate typical small-bodied histology. A basal Turonian ornithomimid growth series reveals fibrolamellar bone early in ontogeny, parallel-fibered bone by midsize and complete remodeling with an EFS in the largest individuals (maximum femur length 319 mm) (Skutschas et al. 2017). At half the size of *Struthiomimus*, the Late Campanian *Rativates* was determined to be a subadult because it has bone with a woven-parallel complex, reticular inner cortex, plexiform middle cortex and laminar outer cortex, and vascularization decreasing toward the surface. Eight LAGs were counted, but no EFS was observed (McFeeters et al. 2016).

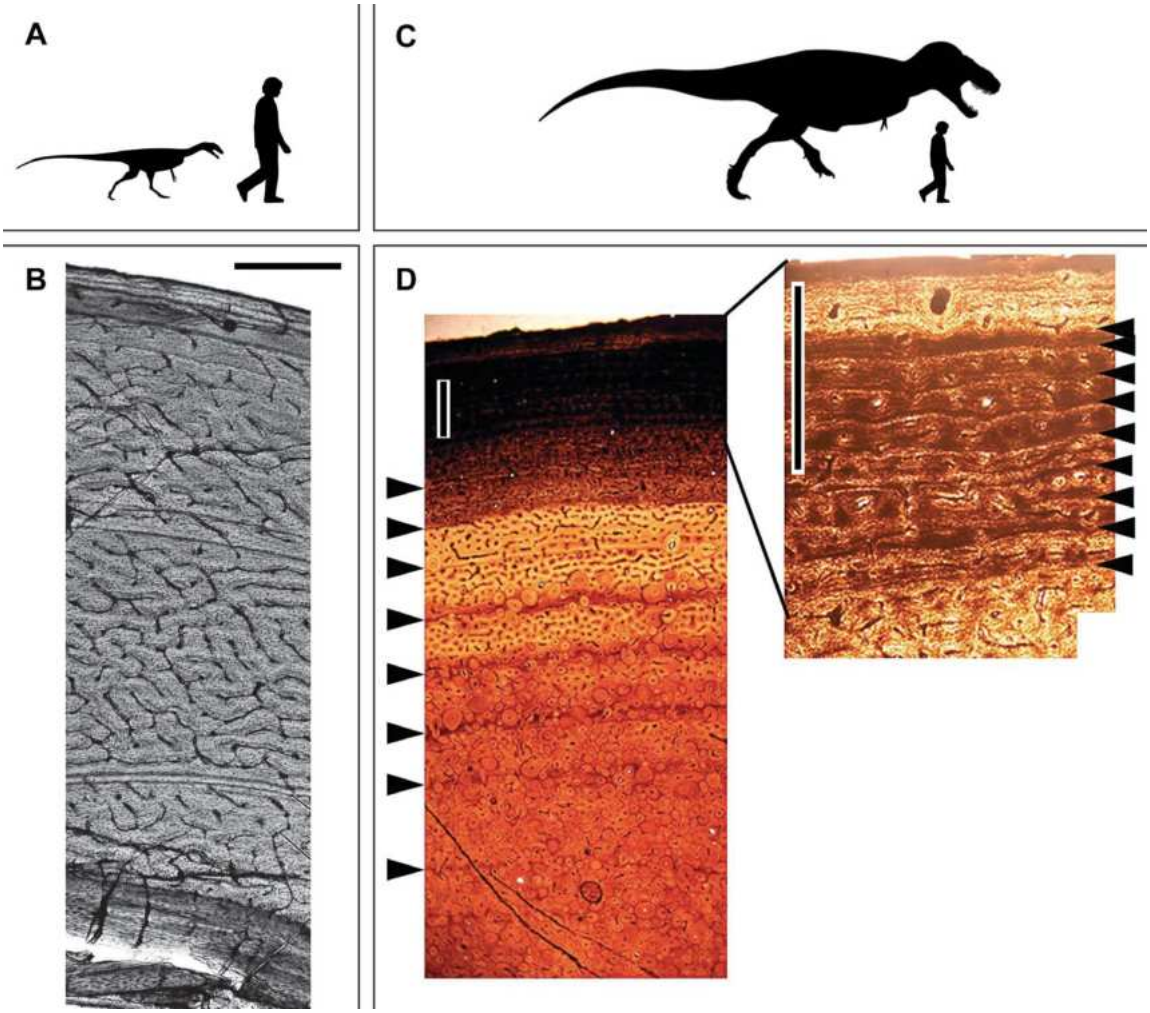


FIGURE 27.13 Examples of nonavian theropod histology. A, *Masiakasaurus* grew to a small adult size. B, A transverse transect through a tibia shows a well-vascularized cortex of fibrolamellar bone, becoming parallel-fibered tissue toward the surface. There is an EFS at the periosteal surface (top of image), indicating that this individual was an adult when it died. (Image taken from Lee and O'Connor 2013). C, *Tyrannosaurus* was one of the largest nonavian theropods, and its histology (D) shows well-vascularized woven tissue from inner to outer cortex, separated by (suposedly annual) LAGs (arrowheads). In older and larger individuals, secondary remodeling was prevalent in the inner cortex (bottom of image), and some *T. rex* started to develop an EFS (arrowheads in enlarged image to the right). Scale bars: B = 500 mm; D = 1 mm. (Image taken from Horner and Padian 2004. Dinosaur silhouettes by Scott Hartman, used under Creative Commons license 3.0. B is from figure 3 in Lee and O'Connor 2013. D is from Horner and Padian 2004; both used with permission).

Larger ornithomimids show a different histological pattern. *Sinornithomimus* from the Late Cretaceous of China has a completely reticular to laminar fibrolamellar pattern throughout the cortex of an immature individual (364-mm femur length; largest individual femur approaches 500 mm), with a minimum of four LAGs (Varricchio et al. 2008). Cullen et al. (2014) examined three ornithomimid skeletons from the Maastrichtian of Alberta, and found laminar, plexiform, and reticular vascularization within a woven-parallel complex. Three LAGs were present in the largest femur, but no EFS was visible.

Within Tyrannosauroidea, more attention has been paid to interpolating growth curves than to histological description. The geologically oldest tyrannosauroid histologically described is the small-bodied (78-kg body mass) *Moros* from the Cenomanian of Utah (Zanno et al. 2019). The femur comprised longitudinal parallel-fibered tissue, separated by LAGs. The individual was determined to be 6–7 years of age and nearing skeletal maturity. As to larger tyrannosauroids, only the histology of *T. rex* has been described (Figure 27.13C). Horner and Padian (2004) examined the tibia, femur and fibula from seven large *T. rex* specimens and found that bone tissue is completely fibrolamellar, with vascularity primarily circumferential in the femur and tibia (Figure 27.13D). By measuring the distances between LAGs, they estimated that *T. rex* achieved adult size in 16–19 years, with a longevity of approximately 22–27 years. Woodward et al. (2020) later described the femur and tibia histology of two half-grown *T. rex* specimens. The well-vascularized cortices are longitudinal to laminar, and the tissue matrix is generally loosely organized, with regions of localized fibrolamellar tissue. The specimens are estimated to be 13 and 14 years of age, respectively, when they

VetBooks.ir

died (Woodward et al. 2020). Several paravian taxa of small-bodied troodontids have been histologically examined, the first of which is *Troodon* (Varricchio 1993). Two tibiae were sampled, and the smaller is highly vascularized subplexiform to laminar fibrolamellar bone. The larger tibia is almost completely secondarily remodeled and the subperiosteal surface consists of avascular lamellar bone. Varricchio (1993) concluded that most *Troodon* growth occurred when it was very young, and that it would have reached its small adult size in about 3–5 years. *Talos*, a troodontid from the Late Cretaceous of Utah, has a similar histology: the femur consists of longitudinal fibrolamellar bone (Zanno et al. 2011). From annuli and LAGs, the authors determined that *Talos* was at least 5 years old when it died (Zanno et al. 2011).

Finally, several Late Jurassic paravian taxa were surveyed histologically by Prondvai et al. (2018): *Anchiornis*, *Aurornis*, *Eosinopteryx* and *Serikornis*. Generally, early juveniles have fibrolamellar bone and uniform vascular density, whereas late juveniles have mature primary osteons, decreasing vascularity toward the bone surface and one to three LAGs. Adults are recognized by an outer cortex of thick avascular tissue resembling either an OCL (outer circumferential layer) or an EFS, if consisting of closely spaced LAGs (Prondvai et al. 2018).

Of notable interest, within various theropod taxa there is sometimes inconsistent zonal spacing between LAGs or annuli. In other words, instead of the expected pattern of LAGs decreasing in zonal spacing as an animal matures, zonal spacing is sometimes erratic and varied. This suggests extended or truncated annual growth hiatuses, depending on relative zonal thicknesses. Inconsistent LAG spacing has been reported in the basal coelurosaur *Anikosaurus* (Ibiricu et al. 2013), the tyrannosauroid *Moros* (Zanno et al. 2019), the tyrannosaurid *Tyrannosaurus* (Woodward et al. 2020, although regular spacing was also observed by Horner and Padian 2004) and an ornithomimid (Cullen et al. 2014). Cullen et al. (2014) also discussed reports of variable LAG spacing in the ornithopods *Tenontosaurus* and *Hypacrosaurus*, and it was observed by Freedman Fowler and Horner (2015) in the hadrosaur *Probrachylophosaurus*. Cullen et al. (2014) and Woodward et al. (2020) suggested that irregular LAG spacing may reflect annual physiological responses to resource abundance, and Woodward et al. (2020) cautioned that producing growth curves for at least some dinosaurian taxa from a limited sample may be problematic as a result of this flexible growth strategy.

Theropoda: Aves

Although it had been suggested or hinted at several times in the late 19th century and early 20th century, but never really substantiated, Ostrom (1973, 1976) first proposed with substantial morphological evidence that birds evolved from theropod dinosaurs. Gauthier (1984) settled the issue with an extensive phylogenetic analysis that formed the basis for all later work. Birds are not only descended from theropod dinosaurs, they are in fact theropod dinosaurs, as humans are apes and mammals. The past 40 years have witnessed extensive work on the sequence and meaning of the series of transitions in form, function and metabolism from maniraptoran theropods through *Archaeopteryx* and basal avialians to the Cretaceous radiation of archaic birds and finally the evolution of crown birds, the Neornithae (e.g., Padian and Chiappe 1998; Padian and de Ricqlès 2009; Turner et al. 2007). Here we trace some of the major lines of inquiry in avian paleohistology.

The Transition from Basal Maniraptorans to the First Birds

Growth rate is strongly related to size (Case 1978), resulting in the formation of slowly deposited parallel-fibered or lamellar tissue in small vertebrates across the ectothermic-endothermic metabolic spectrum (Padian et al. 2004; Erickson et al. 2009). Small theropods, from which the first birds evolved, had lower growth rates than larger theropods and other dinosaurs. Basal birds resembled other small maniraptorans in many features of their bone histology and inferred growth rates. Only in the Late Cretaceous did the highly derived histological features of bird bones evolve, as we detail later (Ricqlès et al. 2001).

In general, nonavialan dinosaur bone histology reveals a highly vascularized, rapidly formed fibrolamellar cortical matrix, dense with osteocyte lacunae (Padian et al. 2001; Erickson et al. 2001, 2009). However, Erickson et al. (2009) examined histological trends in the femora of nonavialan theropod taxa from larger to smaller body sizes, and they observed a corresponding simplification of vascular canal and bone fiber organization, which would be expected according to the relationship between body size and relative growth rates in a clade. In addition, basal nonavialan deinonychosaur fossils show that miniaturization of mean theropod body sizes to less than 1 kg occurred before the evolution of powered flight, and was therefore a basal character of Paraves (Turner et al. 2007). Indeed, the femoral bone histology of the basal avialan *Archaeopteryx* reveals slowly deposited parallel-fibered cortical tissue, sparse longitudinal vascularity and the presence of annually formed LAGs, again demonstrating Case's (1978) principle (Erickson et al. 2009).

Jeholornis and *Sapeornis*, both considered basal avialans but more crownward than *Archaeopteryx*, were also histologically examined by Erickson et al. (2009) for comparison. *Jeholornis*, slightly more crownward than *Archaeopteryx*, resembles it histologically (Figure 27.14). However, *Sapeornis*, the largest and most crownward of the three basal avialans examined, had longitudinal to reticular fibrolamellar bone (Erickson et al. 2009). A reexamination of the *Jeholornis* and *Sapeornis* specimens reported by Erickson et al. (2009), carried out by O'Connor et al. (2014), incorporated additional specimens to better assess ontogenetic changes. This included an unnamed enantiornithine (STM 29-8) that showed less vascularization than *Jeholornis*, agreeing with the prediction by Erickson et al. (2009) that the smaller size of enantiornithines is correlated with slower growth and an increase in avascular bone compared to *Archaeopteryx*. On the other hand, the bone tissue of STM 29-8 is more vascularized than larger Late Cretaceous enantiornithine specimens, suggesting that the relationship between adult body size and growth rate proposed by Erickson et al. (2009) is not as clear-cut, at least within Enantiornithes. For example, Bailleul et al. (2011) and Cambra-Moo (2006) found relatively high growth rates

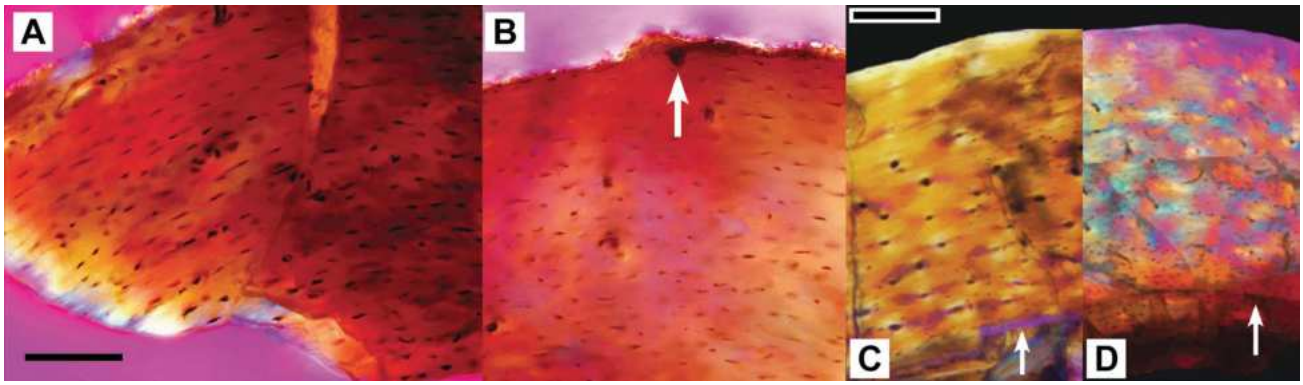


FIGURE 27.14 Bone histology of basal birds. A and B, Histological section of an *Archaeopteryx* femur (BSPG 1999 I 50) viewed with polarized microscopy. A, Parallel-fibered bone is found throughout the cortex as shown by the flattened, circumferentially oriented, lenticular osteocyte lacunae (tiny black structures) and matted bone fabric (lower left). B, Primary longitudinal vascular canals are few (large black circular structures). These are occasionally found incompletely formed at the periosteal surface (arrow) and are responsible for the fibrous surface texture of the elements and long striae seen deep within the bones of all known individuals. Scale bar: A = 0.75 mm. C and D, Femoral histology of the basal birds *Jeholornis* and *Sapeornis* viewed with polarized microscopy. C, In *Jeholornis* (IVPP 13353), parallel-fibered bone matrix similar to that of *Archaeopteryx* makes up the cortex. A growth line that locally varies between a line of arrested growth (LAG) and an annulus is shown (arrow). D, In the larger *Sapeornis* (LPM B00166), the matrix is primarily woven-fibered and shows a mix of longitudinal and reticular vascularization. Avascular parallel-fibered bone brackets a LAG (arrow) in this subadult specimen. Scale bar: C = 0.15 mm. (From Erickson et al. 2009, figures 7A and B and 8A and B used with permission from Open Access Creative Commons license 3.0.)

in juvenile stages of *Concornis*. See also Ricqlès (2000) for general remarks on the evolution of avian growth rates and physiology.

Confuciusornis sanctus, another basal bird from the Early Cretaceous of China, was studied extensively when a full skeleton was sectioned histologically without removal of surficial matrix (Ricqlès et al. 2003b). The larger long bones comprised well-vascularized fibrolamellar tissue, much as in other small dinosaurs, with sometimes a substantial coating of endosteal bone and several LAGs suggesting an age of at least 3 years (Figure 27.15). However, the cortex of these bones is thin, comprising only 37% of the bone diameter in the ulna, for example. The inner cortex of the ulna comprises rapidly growing fibrolamellar tissue with predominantly radial canals suggestive of very rapid growth. Ricqlès et al. (2003b) estimated an average growth rate of 10 µm per day, or an age to maturation of about 20 weeks, commensurate with many living birds but very different in the pace of growth. Other observations were reported by Chinsamy et al. (2013), who suggested the identification of genders in *Confuciusornis*, as previously suggested by gross morphological studies.

In addition, O'Connor et al. (2014) found that (1) *Confuciusornis*, which is much smaller than the more basal *Jeholornis* and *Sapeornis*, also has more vascularized cortical bone and (2) the increase in vascularization within *Sapeornis* compared to that of *Archaeopteryx* is greater than expected based on its only slightly larger size. Together, and *contra* Erickson et al. (2009), the study by O'Connor et al. (2014) suggests that Early Cretaceous basal enantiornithine birds exhibit nondinosaurian growth patterns. However, this inference must be tempered by the incomplete ontogenetic samples we currently have of all Jurassic and Cretaceous avialians. The paucity of sectioned specimens is compounded by the relative thinness of their bone cortices, which means that more specimens must be sectioned to "bridge the gaps" in ontogeny. Working from single specimens is an unreliable guide to inferences about growth rates and skeletochronology, because it is difficult to know which part of the ontogenetic trajectory is being represented.

In contrast, the bone microstructural patterns observed in extant birds was already present in their Late Cretaceous ornithurine ancestors (Wang and Zhou 2017, and references therein), although not in the basalmost ornithurine taxon, *Archaeorhynchus*. Rather, the bone histology of *Archaeorhynchus* reflects the basal condition noted by Erickson et al. (2009): bone slowly deposited over several years before achieving adult size. In fact, the similarities in bone microstructure between the ornithurine *Archaeorhynchus* and its enantiornithine sister taxa suggest a slow, prolonged growth period in their common ancestor, compared to living birds, and consistent with their small dinosaurian ancestors. Generally, although they evolved in the Mesozoic contemporaneously from a small, slow-growing common ancestor, ornithuromorphs evolved an extant bird-like growth pattern over time, while enantiornithines retained the plesiomorphic growth pattern (Wang and Zhou 2017). In addition, the presence of medullary bone (a gravid theropod female-specific tissue) within the femur marrow cavity of a slow-growing, immature enantiornithine supports the hypothesis that nonornithurine birds achieved reproductive maturity before skeletal maturity, like their nonavian dinosaur ancestors but unlike nearly all extant birds (Bailleul et al. 2019a, b).

History of the Question of the Evolution of Avian Growth Rates and Metabolism

Thin-sections of (mainly) the long bones of extant and extinct birds had historically been taken by several classic workers (Quekett, Foote, Enlow, etc.). The reports of these sections were understandably descriptive for the most part. With the "dinosaur renaissance" of the 1970s (see the section "Dinosauria"

VetBooks.ir

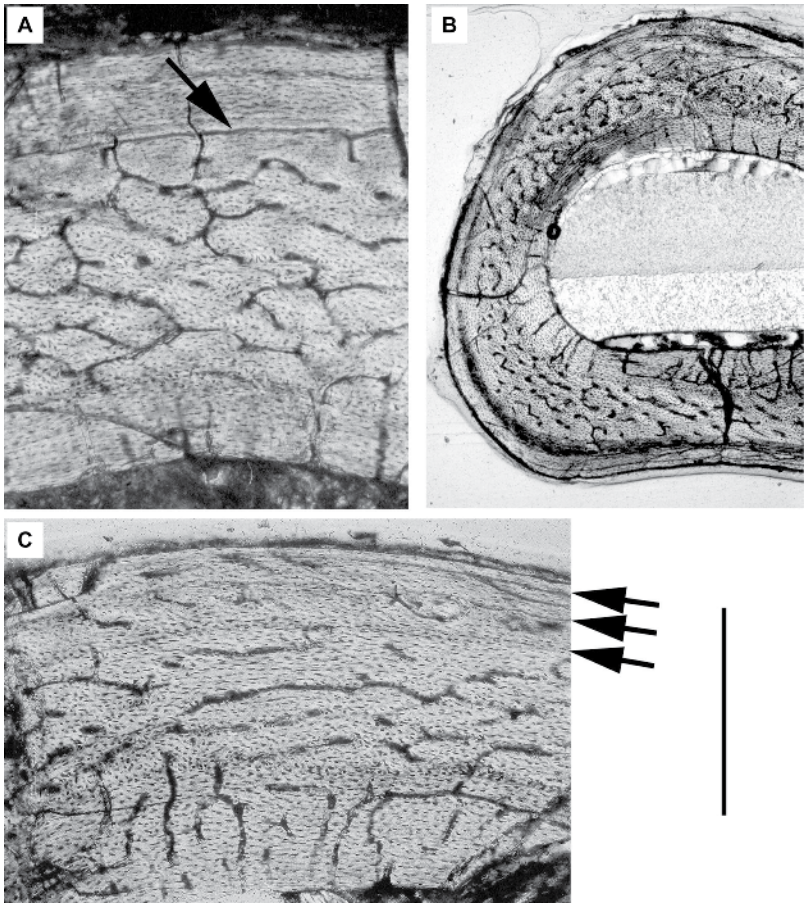


FIGURE 27.15 Thin sections of the humerus, ulna and radius of *Confuciusornis sanctus*. A, Humerus showing a line of arrested growth (LAG) and nearly avascular tissues toward the periosteal surface. Note the similar-looking endosteal bone near the marrow cavity. Scale = 0.5 mm. B, Cross section through the radius showing the open marrow space, the endosteal bone with radial canals and the vascular bone between the LAG and the periosteal surface. Scale = 1 mm. C, Detail of the ulna showing possibly two LAGs (arrows) and the external fundamental system (exterior LAG), and the radial canals in the endosteal zone. Scale = 0.5 mm. (From Ricqlès et al. 2003b, figure 3; used with permission.)

above), attention was refocused on what bone histology could reveal of the biology of ancient animals. Houde (1986, 1987, 1988) sectioned the long bones of a variety of fossil ratites and lithornithids in an attempt to discover whether their histological features revealed a phylogenetic signal that could help in taxonomic identification. He hypothesized that the Paleocene-Eocene Lithornithidae, a group that he named (Houde 1988), were paleognathous birds ancestral to crown-group ratites (but see Nesbitt and Clarke 2016). He was unable to find a consistent phylogenetic signal, although he concluded (correctly) that paleognaths (ratites, lithornithids and their relatives) and neognaths (all other birds closer to *Passer*) generally differed in their histological expressions. He also found (Houde 1987) that the ancient Cretaceous diving bird *Hesperornis* showed bone histological characteristics similar to those of neornithine birds, with dense vascular canals oriented in longitudinal, circumferential and radial directions and with extensive vascularization and considerable lamellar orientations. With the experience of several later decades of histological analysis, it now appears that Houde's hypotheses were confounded by the field's incomplete knowledge of ontogenetic and size factors, a pattern that has persisted in some studies to the present day. That is, more actively growing bone tissue tends to be deposited in earlier rather than later stages in the ontogeny of a species, and larger members of a clade grow more rapidly (and hence tend to lay down more highly vascularized tissue through growth) than their smaller relatives (Padian et al. 2004). This conundrum in no way detracts from the value of Houde's original observations. Chinsamy et al. (1998) later observed similar rapid sustained patterns of growth in *Hesperornis* and also the tern-like archaic Cretaceous bird *Ichthyornis*, as well as in an alleged "Cretaceous loon" whose identification was not substantiated (and is unlikely a loon, given the age of the Niobrara Chalk: Padian 2020). This relatively rapid rate of growth, generally relative to adult body size, was inherited from nonavian dinosaur ancestors (Padian et al. 2001).

The tendency of some workers to infer the holistic metabolic regime of an animal, either directly from a single section of bone or from a single characteristic of a bone section, created conflicting signals in late 20th century histological studies of bird (and other dinosaur) bones, sometimes within the same paper (see the section "Dinosauria" above) as extensively discussed by Ricqlès (2000). For example, Chinsamy et al. (1995a, b) studied several bones from an unidentified latest

VetBooks.ir

Cretaceous enantiornithine and from *Patagopteryx deferrariisi*, an unusual Late Cretaceous ornithuromorph of uncertain taxonomic position, both from South America. Because they found LAGs in both taxa, which were placed phylogenetically between nonavian dinosaurs and extant birds, they concluded that these birds were physiologically "intermediate" and "not fully homeothermic." (At the time LAGs in "endotherms" [e.g., birds and mammals] were not widely known, but could have been found in the plates of classic authors such as Foote). The absence of fibrolamellar bone in their enantiornithine sections was taken for an actual (global) absence during growth; they assumed that earlier deposition would not have been resorbed during medullary expansion. This is curious because bird bone is so thin, a feature inherited from other theropods, reflecting the resorption of most early stages of growth (as in pterosaurs, convergently), and because the tissue, while not rich in primary osteons, also lacks secondary osteons but is replete with osteocyte lacunae. More curiously, they reported fibrolamellar bone in *Patagopteryx*, but did not note that it is prevalent in the bone of nonavian dinosaurs, although they did say by way of introduction that dinosaur bone is "richly vascularized and endowed with dense Haversian bone," which other authors then regarded as evidence of "endothermy." They concluded that "during the transition from nonavian dinosaurs to birds, classic endothermic homeothermy evolved after, not before, the acquisition of feathers."

Why would these authors have developed such an argument when Chinsamy's own previous work (Chinsamy 1990, 1995b; Chinsamy and Rubidge 1993) showed in Triassic-Jurassic nonavian dinosaurs the presence of densely vascularized fibrolamellar bone and copious LAGs? Why would the presence of a single LAG in *Patagopteryx* outweigh for Chinsamy et al. (1995a, b) the features of fibrolamellar deposition, substantial vascularization and copious osteocytes? And more importantly, why move directly from tissue features to physiological regime without considering the primary importance of growth rate (Amprino's rule; Amprino 1947), which varies greatly (and universally diminishes) through ontogeny, even manifested in a single thin-section of bone?

A more reasonable conclusion is that the bones that Chinsamy et al. (1995a, b) sampled were those of birds that were on the latter end of their growth trajectories, reflecting lower growth rates as maturity was neared. Such patterns of growth are seen in many dinosaurs, especially small dinosaurs and basal birds (Ricqlès et al. 2001, 2003b; Padian et al. 2004), so there is nothing unusual here, either functionally or phylogenetically, with respect to the tissue patterns that Chinsamy and colleagues observed. Their notice of the deposition in LAGs in these birds was important, but innocent of their presence in living birds and mammals, which was already well known by ornithologists (Ricqlès 2000).

It now appears that nearly all living birds reach full skeletal maturity in weeks or months, but less than a year (a currently known exception is the kiwi: Bourdon et al. 2009). This pattern is likely synapomorphic of crown-group birds, but it is not clear if it preceded the evolution of crown-group birds. All living ratites apart from the kiwi (even the very large ostrich and emu) reach skeletal maturity within a year (e.g., Chinsamy 1995a), and most neognaths fully develop within a few weeks or months; they are generally smaller than most ratites (apart from the kiwi and tinamou). Turvey et al. (2005) surveyed the bones of extinct moas (Ratitae: Dinornithidae) of various sizes and found a predominance of dinosaur-like fibrolamellar bone in the cortices of the long bones, along with copious LAGs (Figure 27.16). They concluded that moas extended their somatic growth period beyond a single year. As with the kiwi, this is almost certainly secondary, given the position of both taxa within Ratites (Turvey et al. 2005). However, it suggests that the deposition of fibrolamellar tissue, even laden with frequent LAGs, is a reflection of high growth rate, and the presence of LAGs alone means little or nothing with respect to overall physiological regime. Ricqlès et al. (2016) studied the bone histology of the giant extinct Malagasy ratite *Aepyornis* (elephant bird; see also Legendre et al. 2014, and Chinsamy et al. 2020, which confirmed the observations of Ricqlès et al. 2016). They reported a variety of primary and secondary tissues, including extensive Haversian remodeling, in a matrix that showed decidedly dinosaurian characteristics such as lamellar deposition, dense osteonal and osteocytic distribution and considerable circumferential and radial canal orientation. Only one LAG was detected in a femur, but the cortex was relatively thin (1.5 cm) for a bone of up to 8 cm in diameter, so no assessment of age can be given. Although one sampled femur almost exclusively comprised secondary bone, no evidence was found of an EFS, so substantial growth and remodeling, likely reflecting substantial metabolic activity (Padian et al. 2016), presumably continued until the achievement of full somatic growth. In any case, it appears that the elephant bird, like the kiwi and moa and perhaps other large extinct ratites, took more than the single year that all other living birds take to reach somatic maturity. This is almost certainly a secondary adaptation from the condition in basal neornithines, which were small animals (Chiappe and Witmer 2002; Field et al. 2020), as are neognaths in general. It can be presumed from this that large size in ratites, which must have occurred several times given the internested position of the tinamou within ratites, was accompanied by a sustained growth period and a postponement of somatic maturity (neoteny); it is unknown when sexual maturity occurred but it was likely before somatic maturity was reached. A similar situation probably occurred in the giant Eocene neornithine *Diatryma* (Padian and Horner 2004). It is likely that maturing quickly (within weeks or months but definitely in less than a year, depending on the size of the taxon) was a basal feature of Neornithes (Paleognathae and Neognathae).

Growth in Extant (Crown-Group) Birds

All living birds mature fully within weeks to just under a year, except the kiwi, which can take 7 years or more to reach skeletal maturity (Bourdon et al. 2009). However, large extinct members of living groups, notably ratites, took several years to reach their giant size (Turvey et al. 2005). The presence of several LAGs in the bones of enantiornithines suggests that birds did not evolve the syndrome of maturing in less than a year until crown-group birds evolved, or very nearly so. This would appear to have been in the latest Cretaceous (Field et al. 2020; Padian 2020a). It is not clear whether ancient birds

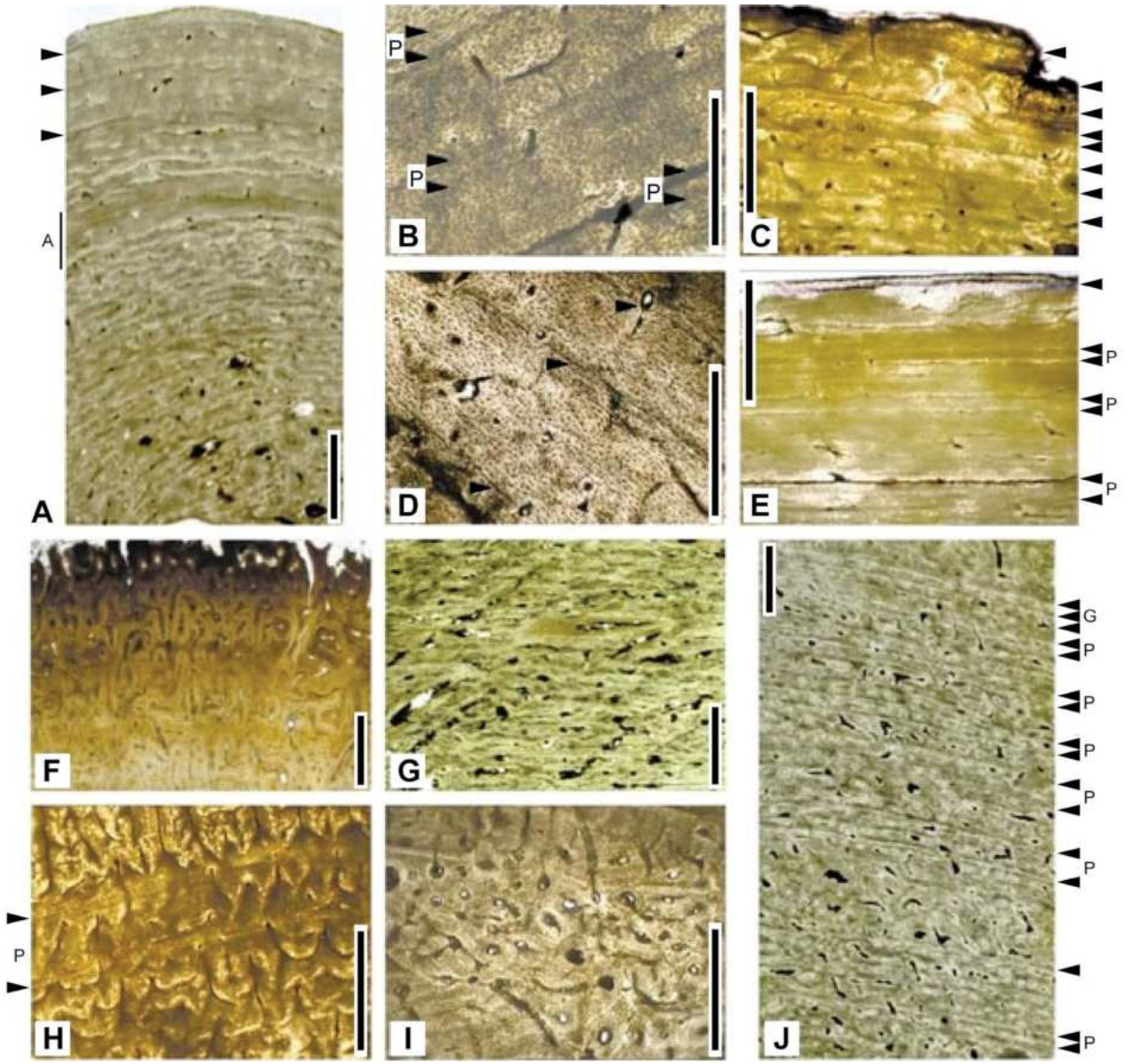


FIGURE 27.16 Transverse undemineralized diaphyseal thin sections through moa long bones. The bone periphery is at the top. All specimens are from adult individuals except where indicated. A and B, *Megalapteryx didinus* tibiotarsus (CM AV 10348). A, Cortical cross section, showing a lamellar annulus (A) in the midcortex and three lines of arrested growth (LAGs; arrows) in a second annulus in the outer cortex. B, Closeup view of three paired LAGs. C, *Anomalopteryx didiformis* tibiotarsus (MNZ S 202), showing eight single LAGs (arrows). D, *M. didinus* tibiotarsus (CM AV 9089), showing three single LAGs. E, *A. didiformis* tibiotarsus (CM AV 19187), showing four single or paired LAGs (arrows). F, Subadult *Dinornis robustus* tarsometatarsus (MNZ S 39964), showing fast-growing fibrolamellar matrix. The transverse colored bands represent tidemark stains caused by repeated penetration of swamp fluid, not growth marks. G, *Pachyornis elephantopus* tarsometatarsus (CM AV 38563), showing poorly vascularized lamellar-zonal matrix lacking annuli or LAGs. H, *D. novaezealandiae* tibiotarsus (MNZ S 24365), showing a pair of annuli each containing a LAG (arrows). I, *D. novaezealandiae* tibiotarsus (MNZ S 145), showing highly vascularized fibrolamellar matrix lacking annuli or LAGs. J, *Euryapteryx geranoides* femur (CM SB282), cortical cross section showing eight single, paired (P) or grouped (G) LAGs (arrows). Scale bars: A, C, E–J = 1 mm; B and D, 0.5 mm. (From Turvey et al. 2005, figure 2, used with permission.)

such as the Late Cretaceous *Hesperornis* and *Ichthyornis*, which were close to crown-group birds, had evolved this growth rate.

Crown-group birds generally retain the fibrolamellar complex of tissues seen in dinosaurs (Chinsamy and Elzanowski 2001), although rather than showing slower growth than larger dinosaurs, they show faster growth. In small, fast-growing birds the well-organized laminar structure of typical dinosaurs is absent, although such tissues, including laminar and subplexiform, can be recognized in birds such as the mallard (*Anas platyrhynchos*), which matures in about 22 weeks (Castanet et al. 1996). The type of tissue deposited is associated with growth rate, which is also true for the ostrich and emu (Castanet et al. 2000).

The Problem of Medullary Bone

Medullary bone is an ephemeral, finely cancellous tissue deposited along the endosteal surfaces of (and sometimes completely filling) the medullary cavity and intertrabecular spaces in ovulating female birds (Figure 27.17). It was first identified in the domestic pigeon and later in other neognath birds (review in Canoville et al. 2019), and in several ratites (Schweitzer et al. 2005; Ricqlès et al. 2016). Medullary bone provides a calcium reserve for the eggshell (and by extension the bones of the embryo). It has never been shown to occur naturally in avian males or in females too young to reproduce, but it can be stimulated by estrogen, and it is not known in crocodiles or other reptiles. In gravid females it was first noted in the long bones of the appendicular skeleton, but has since been discovered in some vertebrae and girdles (review in Canoville et al. 2019, 2020). Because the presence of medullary bone is ephemeral, it may be overlooked because it waxes and wanes in various bones as egg-producing proceeds: it may be developed or retained more in certain bones than in others (Werning 2018; Canoville et al. 2019, 2020). For example, the tibiotarsus and femur are most commonly invested with medullary bone, but the forelimb bones (especially the radius and ulna, but also the humerus) and some vertebrae (variable within regions) and skull and jawbones may be as well.

To understand medullary bone requires a *definition* and a *diagnosis*, as for phylogenetic taxa (Rowe 1987), homology (Padian 1997) and clinical diseases and manifestations. The *definition* provides the etiology of the phenomenon, and the *diagnosis* prescribes how it will be recognized. Similarly,

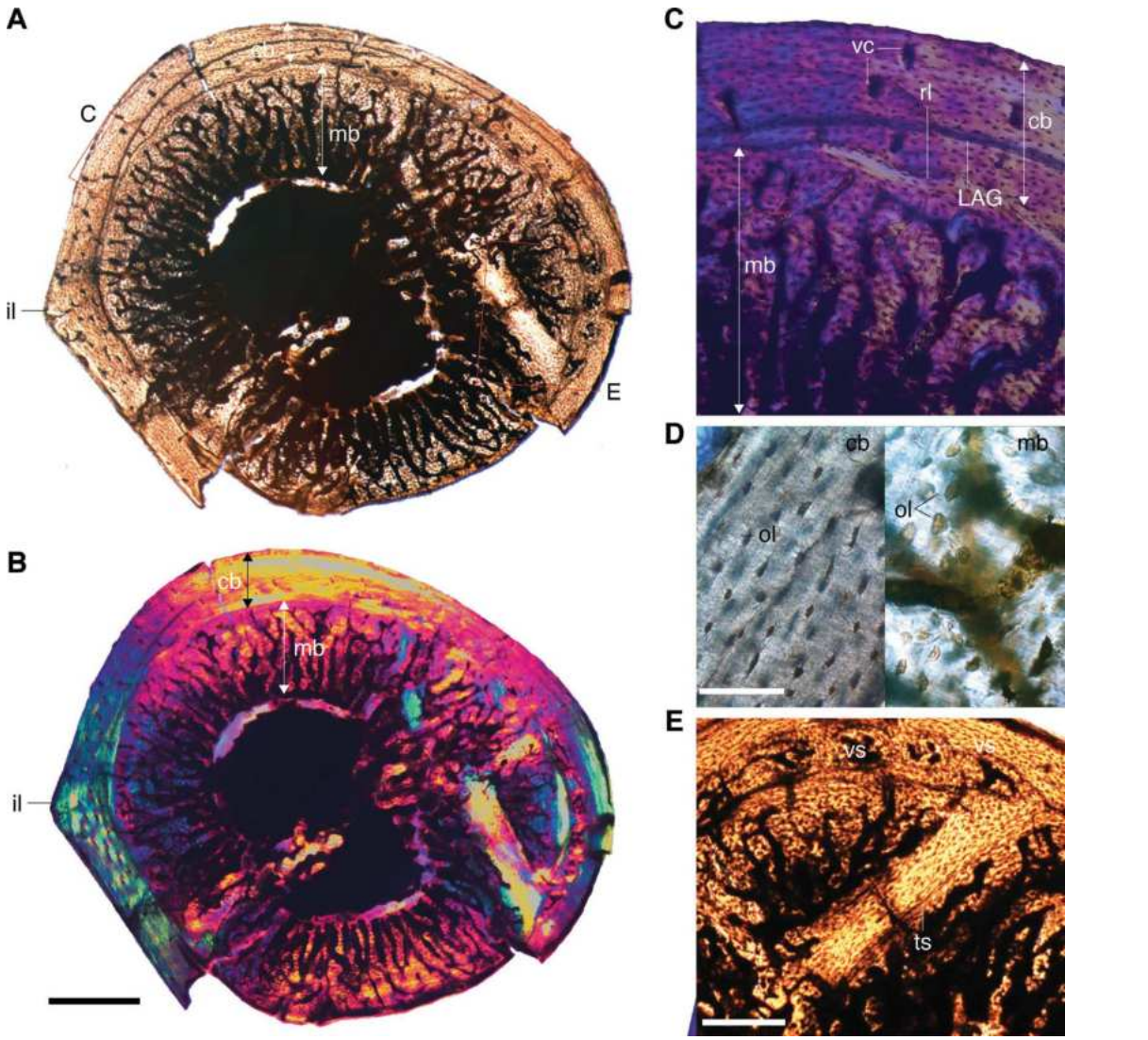


FIGURE 27.17 Femur of a pengornithid (IVPP V15576). A, Full cross section under normal light. B, Cross section under polarized light. C, LAG in the femur approached by endosteal resorption. D, Close-up of the osteocyte lacunae in the cortical bone compared with the larger and more irregular osteocyte lacunae in the medullary bone. E, Close-up of region-preserving vascular sinuses and a structure interpreted as a trabecula. Anatomical abbreviations: cb, cortical bone; il, intermuscular line; LAG, line of arrested growth; mb, medullary bone; ol, osteocyte lacunae; rl, resorption line; vc, vascular canal; vs, vascular sinus; ts, trabecular strut. Scale bars: A and B = 500 µm; C and D = 50 µm; E = 200 µm. (From O'Connor et al. 2018, figure 2, used with permission under Creative Commons Attribution 4.0 International License.)

VetBooks.ir

taxa are *defined* by ancestry and *diagnosed* by synapomorphy in the phylogenetic system. Medullary bone is defined by its production by gravid female birds, stimulated by estrogen, and resorbed for use as a calcium reservoir in the eggs and embryos. It is diagnosed by its position, its physical characteristics (which are variable among taxa), its chemical signal and other factors (O'Connor et al. 2018; Werning 2018; Canoville et al. 2019, 2020; cf. Prondvai and Stein 2014). It is usually resorbed, but sometimes incompletely, by the end of the laying cycle.

In recent years two questions about medullary bone have occupied paleohistologists: can it be produced in bones other than long appendicular elements, and do any animals besides living birds deposit it? The answer to the first question is now accepted as affirmative, because it has been discovered in other bones of living gravid female birds where it does not otherwise occur (Canoville et al. 2019). As to its taxonomic distribution, within birds O'Connor et al. (2018) identified it in a pengornithid enantiornithine, and Chinsamy et al. (2013) identified it in the basal avialian *Confuciusornis*. Within nonavian dinosaurs, Schweitzer et al. (2016 and references therein) identified it in *Tyrannosaurus rex*, and Lee and Werning (2008) identified it in *Allosaurus*, both theropods. Identification in sauropodomorphs has been difficult, but Lee and Werning (2008) identified it in the ornithopod *Tenontosaurus*. Outside dinosaurs, Prondvai and Stein (2014) identified it in the pterosaur *Bakonydraco*, but the specimens are so tiny that it is unlikely these were reproductively mature individuals, and the tissue was only found in the mandible but not the long bones (O'Connor et al. 2018). Chinsamy et al. (2009) identified it in a femur of the pterodactyloid *Pterodaustro*, but this tissue does not appear to have the diagnostic features of medullary bone and it may simply be crushed endosteal tissue. Other putative identifications have been difficult to substantiate or identified as probable pathologies. Medullary bone has never been identified or postulated in a nonornithodiran reptile, and it may be that it is confined to Dinosauria, although further work is clearly needed. Pterosaurs and other nondinosaurian avemetatarsalians grew quickly and had thin bone walls, so medullary bone may have been a good option for them to produce a calcium reservoir for ovogenesis. It should be noted that O'Connor et al. (2018) dismissed all claims of medullary bone outside crown birds except their own study of one pengornithid; some of their skepticism, however, rests mainly on inability to discern the tissue positively from published descriptions.

Some Functional Questions about Nonavian Dinosaurs

Histological Problems in Dinosaurian Growth

Why didn't all nonavian dinosaurs grow in the same way, depositing bone tissues that reflected the same growth rates? A general insight alluded to several times in the chapters on Archosauromorpha is that within a clade, taxa with larger body size grow at generally higher rates, although this does not necessarily mean that they reach adult body size sooner (Case 1978). Species-specific mean adult body size and age/size onset of reproduction are important life history traits whose independent variations allow us to describe ecophysiological diversity within clades. These life history traits are more or less recorded or reflected in bone histology, so it is not surprising to find various specific histological patterns as more and more dinosaurian taxa are analyzed.

In addition to Case's note of *interspecific* differences, and those alluded to constantly in these chapters about how growth rates and bone tissue types change *ontogenetically*, here we note briefly several other factors that contribute to differences in the growth profile of dinosaur bones. There is also the issue of tremendous *populational (interindividual)* growth rates observed in ornithischians, sauropodomorphs and theropods, which has only been noticed generally and confirmed within the past decade or so. Third, the problem of phyletic dwarfism involves the interplay of *ontogenetic and phyletic* growth change. And fourth, a hypothesis about the genesis of secondary bone tissue explores *interelemental* differences in a single skeleton. Other considerations of important biological processes in the manifestation of dinosaurian hard tissues can be found in the excellent review of Bailleul et al. (2019b) and in chapters in Padian and Lamm (2013).

Interindividual Differences in Body Size Versus Age

Klein and Sander (2007) first pointed out a great discrepancy in the adult body sizes in two collections (Trossingen and Frick localities) of the basal Triassic sauropodomorph *Plateosaurus engelhardti*. Judging from the size of the individual at the onset of the EFS, they estimated an adult body size ranging from 6.5 to 8 m (and up to 10 m) in length. No nonavian dinosaur has clearly demonstrated sexual dimorphism (Padian and Horner 2011), and Klein and Sander (2007) did not claim to have found any in their sample. They did find "gracile" and "robust" long bone elements previously noted in *Coelophysis* and other basal dinosaurs, but these differences are likely ontogenetic, reflecting a kind of thickening of the periosteal cortex (the EFS of the shaft and the ossification of tendons, ligaments and joint surfaces) at full somatic growth (the robust form), rather than sexual dimorphism (Padian and Horner 2011).

Most cortical bone of *Plateosaurus* was of the laminar fibrolamellar tissue typical for dinosaurs and other ornithodirans and indicative of rapid growth. Growth slowed peripherally, as indicated by a transition to more lamellar-zonal bone and eventually avascular lamellar bone (EFS), indicative of the overall cessation of somatic growth and the determinate growth pattern seen in all vertebrates (Padian and Stein 2013). LAGs were common in the cortices but spaced at irregular intervals, as Klein and Sander (2007) reported. They hypothesized that the growth of *Plateosaurus* may have been influenced by environmental conditions, resulting in a pattern more "reptilian" than in other dinosaurs, perhaps because of its basal phylogenetic position.

Klein and Sander (2007, p. 198) concluded: "It is striking that the longest bones do not necessarily have the highest LAG numbers […]. In fact, no correlation between bone length (= body size) and LAG number (= age) is apparent in *Plateosaurus*

VetBooks.ir

… there is no correlation between bone length and the time of growth cessation. Consequently, some individuals grew to considerably larger final sizes than others." Important here is to consider that the numbers of LAGs that they recorded only included those present and observable in the specimens represented, without extrapolation of the number of LAGs that may have been erased by expansion of the medullary cavity with growth. Therefore it is not an actual representation of age. Doing so, as they noted, would have been difficult because the distances between successive LAGs was so variable, unlike the more regular situation in *Massospondylus* that allowed Chinsamy (1993) to construct a model for retrocalculation of missing LAGs. Klein and Sander (2007) concluded that there was very high intraspecific variability in growth rates among individuals of *Plateosaurus*. They attributed this to variable ecological stress from year to year. However, because this was not found in the related South African *Massospondylus*, and because the two genera lived at comparable (if opposite) latitudes in a world with fairly homogeneous climatic conditions compared to today, some environmental factor in Europe would need to be identified to support this hypothesis.

The situation of intrapopulational variability (assuming that the thanatocoenosis, or death assemblage at hand, is in some way representative of a living population, even if time-averaged) is not clear for the larger sauropods because there is no sufficient sample of homologous bones over an adequate growth range to assess the problem.

Woodward et al. (2015) approached the question among ornithischians with histological samples of 50 tibiae of the hadrosaur *Maiasaura peeblesorum*. They found substantial variation in size for age classes. A 2-year-old individual (skeletal maturation occurred at 7–8 years) could have a tibial circumference of 19–24 cm, a variation of about 25%, which correlates well ($R^2 > 0.9$) with tibial length. In a less direct measure, the estimated mass of a 2-year-old could vary from just over 500 kg to 1200 kg, a factor of 2.4. Absent any indication of sexual dimorphism, this variation is unusual to extraordinary. They found this a greater variation than expressed in extant *Alligator*, a far smaller and slower-growing species, even with known sexual dimorphism in size trajectories.

A similar conclusion was reached by Griffin and Nesbitt (2016a), who studied a range of theropods, large and small, from the Triassic to the Cretaceous. Like Woodward et al. (2015), they found that the variability in more basal taxa such as the Triassic *Coelophysis* exceeded the range found in *Alligator*, but in more derived taxa such as *Allosaurus* and *Tyrannosaurus* the variability decreased to resemble more the condition in extant birds, which show relatively little ontogenetic variation among individuals. In the later Mesozoic Era, when members of more basal and more derived groups coexisted, the ontogenetic variability appears to have persisted, so presumably either the more basal groups were more affected by an as yet unknown environmental factor, or there are other epigenetic reasons for the variability. The deep roots of this variability may have extended outside dinosaurs to their remote ornithodiran relatives (e.g., *Dromomeron* [Griffin et al. 2019] and *Asilisaurus* [Griffin and Nesbitt 2016b]). More complete ontogenetic and "populational" series will be needed to address this question further.

The Problem of Phyletic Dwarfism

It has long been observed that certain large-bodied mammals can rapidly reduce their adult size phyletically when faced with a relatively sudden but gradual contraction of their geographic range. Changes in sea level over a short period of time can open new land connections for foraging and can as easily isolate the foragers on newly formed islands. Numerous Holocene records are known from the Mediterranean ("dwarf" mammoths and hippos) and the Channel Islands off the coast of California (Roth 1992). Some mammals, notably rodents, can become larger in contrast, and so do some birds and reptiles (Meiri et al. 2008).

Köhler et al. (2012) surveyed the bone histology of African and European ruminant mammals from the tropics to the poles and found a surprisingly uniform tissue profile among them, indicating that local climatic conditions are not a primary factor in determining bone tissue type. They also found LAGs in all the taxa, indicating that even endothermic mammals interrupt their pattern of otherwise constant growth on a yearly basis, and also that the presence of LAGs is not an indicator of ectothermic or poikilothermic metabolism. (The deposition of annual LAGs is common to all vertebrates and is likely mediated by light, according to experimental evidence: Padian 2012). The interesting thing is that, in contrast to the typical fast-growing fibrolamellar tissue found in all these ruminants, the Plio-Pleistocene dwarf island bovid *Myotragus* has lamellar-zonal bone (Köhler and Moya-Sola 2009), indicative of much lower growth rates. Curtin et al. (2012) observed histological differences in the hard tissues of neonate dwarf mammoths of the Channel Islands, compared to normally sized African elephants and the Columbian mammoth. All three taxa deposited "dinosaur-like" fibrolamellar tissue but the dwarf mammoth (*Mammuthus exilis*) showed a more advanced bone tissue stage "in terms of development of primary osteons and the beginning of secondary osteonal development in the inner cortex," as well as "a high degree of intracortical remodeling" (Curtin et al. 2012, p. 946).

Dwarfism in dinosaurs has long been suspected and recently confirmed; the association with insularity appears particularly strong. During the Jurassic and Cretaceous, Europe consisted largely of island chain archipelagos. In several European basins, fossil growth series of apparent diminutive dinosaur taxa have been collected and described since the late 1800s. Nopcsa (1914) famously proposed that the small adult sizes of some dinosaur fossils from Romania resulted from their restrictive island habitat during the latest Cretaceous (Csiki and Benton 2010). Nopcsa's observations were likely informed by Pliocene, Pleistocene and Holocene mammalian examples of island dwarfing which included fossils of small elephants, deer, hippopotamus and murine rodents (Benton et al. 2010).

The observation that after island colonization, typically small animals become large and large animals become small, was formalized by Foster (1964) and termed the "Island Rule" by Van Valen (1973). The widely accepted explanation for these insular body size changes is that dwarfing occurs as a result of limited resource abundance while an increase in size is due to lack of natural predators. Today, the generality of the Island Rule is debated: the propensity to become larger or

VetBooks.ir

smaller phyletically on newly restricted island areas appears to be taxon specific, with many exceptions (Benton et al. 2010).

To confirm fossil examples of insular dwarfism, bone histology can differentiate between small juvenile dinosaur taxa and adult dwarfed taxa (i.e., taxa that are smaller than expected compared to sister taxa), by comparing the ontogenetic growth trends in the latter to the ontogenetic histology of related members within a clade. Sander et al. (2006) were the first to use this method to address the potential for insular dwarfism in European dinosaurs. They examined an ontogenetic series of the Jurassic macronarian sauropod *Europasaurus*, for which the largest individual collected had a body length of 6.2 m. The authors noticed that LAGs appeared in the medium-sized and larger individuals; vascularization decreased with increasing body size, while secondary reconstruction increased and that skeletal maturity was indicated in the largest specimen by the presence of an EFS. These findings were unusual because at small body sizes other macronarians have richly vascularized, highly woven cortices with little secondary remodeling and no LAGs. Together these typical macronarian features imply heterochronic acceleration in growth permitting the achievement of enormous body sizes. Instead, *Europasaurus* demonstrates a reversal of the general macronarian ontogenetic growth trajectory, with a shortened and slower period of active growth compared to basal Neosauropoda and growth to a much smaller adult size.

Encouraged by the success of Sander et al. (2006), the Romanian titanosaur sauropod *Magyarosaurus* was histologically examined in 2010 to test whether it was also an insular dwarf like the Jurassic *Europasaurus* (Benton et al. 2010; Stein et al. 2010). Only the smallest specimens in the ontogenetic series had remnants of laminar fibrolamellar bone visible among the secondary remodeling. This laminar fibrolamellar bone was unusual in that it consisted of more parallel-fibered tissue than woven tissue, an arrangement not previously observed. Benton et al. (2010) named this new primary tissue modified laminar bone (MLB). The strong lamellar component of the fibrolamellar bone suggests a slower growth rate than similar-sized bones of other sauropods but still faster than reptiles. Otherwise, the histology of *Magyarosaurus* showed a degree of remodeling only seen in very large and skeletally mature titanosaur individuals. Though no EFS was found in the largest femur (550 mm in length), because secondary remodeling went right up to the bone surface, the authors suggested the EFS might have been overprinted by Haversian systems. Benton et al. (2010) concluded that the presence of MLB indicates that *Magyarosaurus* achieved its smaller body size by slowing its growth rate, rather than growing at rates similar to other titanosaurs and simply truncating growth (Benton et al. 2010; Stein et al. 2010).

Since the study on *Magyarosaurus*, MLB has been described in three additional titanosaur sauropods to date: *Ampelosaurus*, *Lirainosaurus* and *Phwiangosaurus* (Klein et al. 2012). The histology of *Lirainosaurus*, from deposits in Spain, shows intense secondary remodeling and up to 11 LAGs, though no EFS was observed. However, because the largest sampled individual would have only been 8–10 m long, and because LAGs are rare in sauropods that reach huge sizes but common in dwarf taxa, the authors concluded that *Lirainosaurus* was most likely also a dwarf (Company 2011). Despite also exhibiting MLB, the titanosaurs *Ampelosaurus* and *Phwiangosaurus* are not dwarf taxa (Klein et al. 2012). It is possible, then, that MLB is a tissue representative of a slowed growth rate evolved from fast-growing ancestors, as a possible response to resource limitations. Such a decrease in growth rate would be beneficial in repeatedly stressed environments, whether on an island or mainland (Klein et al. 2012). However, it could also be that retaining high metabolic rates while evolving smaller body sizes intensifies secondary remodeling (see below).

In addition to sauropods, the histology of a hadrosaur and an ankylosaur have since been investigated for evidence of dwarfism. An ontogenetic series from the Romanian hadrosaur *Telmatosaurus* showed primary tissue was laminar fibrolamellar, but with a strong parallel-fibered component. This tissue organization strongly resembled the MLB observed in *Magyarosaurus* and *Lirainosaurus*, suggesting that the hadrosaur was also growing more slowly than its sister taxa. The largest specimen of *Telmatosaurus*, with a femur length of 460 mm, showed a high number of LAGs (8) and dense secondary remodeling through most of the cortex; although primary tissue was still visible near the surface. Due to mechanical abrasion, the presence of an EFS could not be determined but the authors concluded that the secondary remodeling was comparable to that of an adult *Maiasaura* hadrosaur, which had a femur length approaching 1 m. Despite the lack of an EFS, Benton et al. (2010) concluded that based on other histological features it was a reasonable assumption that the largest specimen was an adult dwarf hadrosaur. An unnamed Transylvanian ankylosaur also demonstrated evidence of dwarfism. The ontogenetic series showed fibrolamellar tissue extensively replaced by secondary reconstruction in older individuals, and some specimens even preserved an EFS. Interestingly, this ankylosaur appeared to have dwarfed not by growing more slowly than its sister taxa as in the sauropods and hadrosaur, but by growing rapidly and then ceasing growth at a small size (Ösi et al. 2014). These observations indicate that versions of the processes of both neoteny and progenesis contributed to dwarfism in different lineages of dinosaurs (Alberch et al. 1979).

What Explains the Distribution of Secondary Bone Tissue Among Elements in a Skeleton?

The observation that some bones of the skeleton experience much more secondary (Haversian) reworking than others has historically been explained mostly by mechanical stresses. The repair of microcracks and the proliferation of endosteal bone, relatively reducing the medullary cavity with age, have been cited among other factors and causes (McFarlin et al. 2008; Padian et al. 2016. It has been very difficult to deduce a general explanation for the differential development of secondary osteons within and among skeletal elements, and some explanations contradict others (e.g., Amprino 1948).

Padian et al. (2016) proposed a hypothesis that, without contradicting the primacy of other explanations in particular cases, attempted to explain at least some instances of differential proliferation of secondary osteons among various elements

VetBooks.ir

of the same individual (depending, as usual, on ontogenetic stage). Begin with the premise that metabolic rates and growth rates of both entire skeletons and individual elements within a skeleton can be decoupled. Humans and some other apes are good examples. Mammals in general have high metabolic rates and high growth rates. A 20-year-old African elephant can weigh 10,000 lb, and a 20-year-old *Tyrannosaurus* may have weighed 12,000–14,000 lb or greater, whereas a 20-year-old human male mostly weighs between 150 and 200 lb. Humans do not have unusually low metabolic rates for mammals; the reason for their phyletically slowed growth likely has to do with large skull and brain sizes, extended parental care, and the processes of socialization. Humans have more extensive development of secondary osteons than most other mammalian lineages of their size (Padian et al. 2016).

Horner et al. (1999) described the histology of the skeletal elements of a single (holotype) individual of the Cretaceous hadrosaur *Hypacrosaurus stebingeri*. The recorded numbers of LAGs and the relative development of secondary osteons, which tended to obscure LAGs, varied greatly among elements. Padian et al. (2016) noted that the proliferation of secondary osteons was greatest in smaller long bone elements such as the metacarpal, metatarsal, radius and fibula. If *Hypacrosaurus* was facultatively (or mostly) quadrupedal it might be expected that narrow forelimb bones such as the radius and metacarpals would experience secondary reworking as a result of stress leading to microfractures that required repair. But how could the same be inferred for the metatarsals and radius when the femur and tibia, which bore by far most of the weight of the skeleton, showed almost no secondary reworking?

Padian et al. (2016) recognized that through ontogeny, limb elements that in hatchling stage were more nearly comparable in size (e.g., *Maiasaura*: Woodward et al. 2015) became more disparate in size and age. All histological features of their bones suggested that these large dinosaurs grew very rapidly. The femur and tibia, for example, were growing too rapidly to accommodate secondary reworking of bone until quite advanced stages. The reasoning was that high metabolic rates fueled high growth rates. But some bones, teleologically speaking, did not "want" to grow bigger proportionally. However, they had no "choice" but to accept and use the nutrients brought to them by the bloodstream as it coursed through all the skeletal elements of the body. Rather than grow, these smaller elements deployed the blood-borne nutrients to rework and remodel existing tissue without excessive increase in size. If this hypothesis is true, we would expect to see extensive secondary reworking of bone tissues in the forelimb elements of *Tyrannosaurus*, which could have borne no weight.

Amprino and Godina (1947) showed that in ostrich legs the smaller (more distal) elements experienced more Haversian substitution than the proximal ones. For the reasons given above (differential growth rates among various bones in a limb), it can be understood that the actual "biological age" of the tissues forming various bones differ, the smaller elements being "older" (most tissues laid down earlier) than rapidly growing larger bones ("allochronies"; Castanet 1986–1987; Castanet et al. 1996).

General Conclusions to the Paleohistological Consideration of the Ornithodira

The realization that birds are descended from, and formally belong to, the theropod dinosaurs (Ostrom 1973, 1976; Gauthier 1984) put a long-standing dilemma into focus. Birds are "warm-blooded" and other living reptiles are not. Therefore at some time in their history the lineage of the animals we call birds became warm-blooded. It was no longer a question of vague "thecodont" ancestry from some ancestral bubble-gram of Triassic vertebrates, but a specifically formulated, testable phylogenetic hypothesis that birds evolved from dinosaurs (Padian 2013a). At what point, then, did the growth and metabolic rates of crown-group birds evolve? The main clues that we have from this come from comprehensive analysis of their bone tissues.

In this review several principal conclusions should emerge:

1. Growth rates in Archosauromorpha did not evolve in an orthogenetic, stepwise way, but in a mosaic pattern of the evolution and reevolution of histological traits in single lineages and convergently in diverse lineages.
2. Extinct archosauromorphs follow the phylogenetic-ontogenetic patterns observed by Case (1978): in a given clade, larger taxa grow more rapidly to adult size than smaller taxa do. This is measured not in absolute years to skeletal maturity but by instantaneous growth rates measured at comparable ontogenetic stages. We should expect to see histological patterns that reflect higher overall growth rates in larger members of a clade.
3. It was traditionally thought that, whereas dinosaurs and pterosaurs (ornithodirans) display microosteological features that reflect rapid growth, crocodile-line archosaurs (pseudosuchians) and more basal members of Archosauromorpha had none of these features, and so fit the pattern of "typical reptiles." It now appears that these features evolved much more basally in the evolution of Archosauromorpha, and that living crocodiles mislead us: they are secondarily slow growers with relatively lower metabolic rates. For example, phytosaurs appear to be the closest major sister-group to the Archosauria (bird-line and crocodile-line archosaurs). Yet their histological patterns reflect rapid growth rates (Ricqlès et al. 2008), and their footprints reflect upright stance and parasagittal gait (Padian et al. 2010), again suggesting that the syndromes of living crocodiles are secondary.
4. The first animals commonly called birds (*Archaeopteryx* and *Sequinomia*) did not grow like crown-group birds; that syndrome of rapid (within a year) attainment of full somatic growth did not evolve until the origin of crown-group birds in the Late Cretaceous. More basal birds took several years to reach maturity, and slowed their growth through ontogeny, like other dinosaurs and other vertebrates.

VetBooks.ir

REFERENCES

Alberch, P., et al. 1979. Size and shape in ontogeny and phylogeny. *Paleobiology* 5: 296–317.

Amprino, R. 1947. La structure du tissu osseux envisagée comme expression de différences dans la vitesse de l'accroissement. *Arch. Biol*. 58: 315–330.

Amprino, R. 1948. A contribution to the functional meaning of the substitution of primary by secondary bone tissue. *Cells Tissue Organs* 5: 291–300.

Amprino, R. and G. Godina. 1947. La struttura delle ossa nei vertebrati. Recerche comparative negli anfibi e negli amnioti. *Pontificia Academia Scientiarum Commentationes* 11: 329–464. [In Italian].

Andres, B. and K. Padian. 2020. *Pterosauromorpha, Pterosauria, Pterodactyloidae*. In *Phylonyms: A Companion to the PhyloCode*, K. de Queiroz, P. D. Cantino and J. A. Gauthier eds., 1195–1199, 1201–1204, 1205–1207. Boca Raton, FL, CRC Press.

Apaldetti, C., et al. 2018. An early trend towards gigantism in Triassic sauropodomorph dinosaurs. *Nature Ecol. Evol.* 2: 1227.

Bailleul, A., et al. 2011. Palaeohistology and preservation of tetrapods from Las Hoyas (Lower Cretaceous, Spain). *C. R. Palevol* 10: 367–380.

Bailleul, A. M., et al. 2019a. An Early Cretaceous enantiornithine (Aves) preserving an unlaid egg and probable medullary bone. *Nat. Commun*. 10: 1275.

Bailleul, A. M., et al. 2019b. Dinosaur paleohistology: review, trends and new avenues of investigation. *PeerJ* 7: e7764.

Bakker, R. T. 1975. Dinosaur renaissance. *Sci. Am*. 232: 58–78.

Bakker, R. T. 1980. Dinosaur heresy–dinosaur renaissance. Why we need endothermic archosaurs for a comprehensive theory of bioenergetic evolution. In *A Cold Look at the Warm-Blooded Dinosaurs*, R. D. K. Thomas and E. C. Olson eds., 351–462. Boulder, CO, Westview Press.

Baron, M. G., et al. 2017. A new hypothesis of dinosaur relationships and early dinosaur evolution. *Nature* 543: 501–506.

Becerra, M. G., et al. 2016. New heterodontosaurid remains from the Cañadón Asfalto Formation: cursoriality and the functional importance of the pes in small heterodontosaurids. *J. Paleontol*. 90: 555–577.

Bell, C. M. and K. Padian. 1995. Pterosaur fossils from the Cretaceous of Chile: evidence for a pterosaur colony on an inland desert plain. *Geol. Mag.* 132: 31–38.

Bennett, S. C. 1995. A statistical study of *Rhamphorhynchus* from the southern limestone of Germany: year classes of a single large species. *J. Paleontol*. 69: 569–580.

Benton, M. J., et al. 2010. Dinosaurs and the island rule: the dwarfed dinosaurs from Haţeg Island. *Palaeogeogr. Palaeoclimatol. Palaeoecol*. 293: 438–454.

Bo, Z., et al. 2016. Histologic examination of an assemblage of *Psittacosaurus* (Dinosauria: Ceratopsia) juveniles from the Yixian Formation (Liaoning, China). *Anat. Rec*. 299: 601–612.

Bourdon, E., et al. 2009. Bone growth marks reveal protracted growth in New Zealand kiwi (Aves, Apterygidae). *Biol. Lett.* 5: 639–642.

Burns, M. E. and P. J. Currie. 2014. External and internal structure of ankylosaur (Dinosauria, Ornithischia) osteoderms and their systematic relevance. *J. Vert. Paleontol*. 34: 835–851.

Butler, R. J., et al. 2009. Lower limits of ornithischian dinosaur body size inferred from a new Upper Jurassic heterodontosaurid from North America. *Proc. Biol. Sci*.277: 375–381.

Bybee, P. J., et al. 2006. Sizing the Jurassic theropod dinosaur *Allosaurus*: assessing growth strategy and evolution of ontogenetic scaling of limbs. *J. Morphol*. 267: 347–359.

Cambra-Moo, O., et al. 2006. Histological observations of Enantiornithine bone (Saurischia, Aves) from the Lower Cretaceous of Las Hoyas (Spain). *C. R. Palevol* 5: 685–691.

Canoville, A., et al. 2019. Systemic distribution of medullary bone in the avian skeleton: ground truthing criteria for the identification of reproductive tissues in extinct Avemetatarsalia. *BMC Evol. Biol*. 19: 71.

Canoville, A., et al. 2020. Identifying medullary bone in extinct avemetatarsalians: challenges, implications and perspectives. *Philos. Trans. Roy. Soc. Lond. B* 375: 20190133.

Carrano, M. T., et al. 2005. New information on *Segisaurus halli*, a small theropod dinosaur from the Early Jurassic of Arizona. *J. Vert. Paleontol*. 25: 835–849.

Case, T. J. 1978. Speculations on the growth rate and reproduction of some dinosaurs. *Paleobiology* 4: 320–328.

Castanet, J. 1986–1987. Skeletochronology of reptiles. III. Application. *Ann. Sci. Nat.* 13(8): 157–172.

Castanet, J., et al. 1996. Expression de la dynamique de croissance de l'os périostique chez *Anas platyrhynchos*. *C. R. Acad. Sci. Paris* 319: 301–308.

Castanet, J., et al. 2000. Periosteal bone growth rates in extant ratites (ostriche and emu). Implications for assessing growth in dinosaurs. *C. R. Acad. Sci. Paris, Sciences de la Vie* 323: 543–550.

Cerda, I. A. and A. Chinsamy. 2012. Biological implications of the bone microstructure of the Late Cretaceous ornithopod dinosaur *Gasparinisaura cincosaltensis*. *J. Vert. Paleontol*. 32: 355–368.

Cerda, I. A., et al. 2014. Osteohistological insight into the early stages of growth in *Mussaurus patagonicus* (Dinosauria, Sauropodomorpha). *Hist. Biol*. 26: 110–121.

Cerda, I. A., et al. 2017. Novel insight into the origin of the growth dynamics of sauropod dinosaurs. *PLoS One* 12: e179707.

Cerda, I. A., et al. 2019. Paleobiological inferences for the Antarctic dinosaur *Antarctopelta oliveroi* (Ornithischia: Ankylosauria) based on bone histology of the holotype. *Cretac. Res.* 103: 104171.

Chiappe, L. M. and L. M. Witmer (eds.). 2002. *Mesozoic Birds: Above the Heads of Dinosaurs*. Berkeley, CA, University of California Press.

Chinsamy, A. 1990. Physiological implications of the bone histology of *Syntarsus rhodesiensis* (Saurischia: Theropoda). *Palaeontol. Afr.* 27: 77–82.

Chinsamy, A. 1993. Dicynodont (Therapsida) bone histology: phylogenetic and physiological implications. *Palaeontol. Afr.* 30: 97–102.

Chinsamy, A. 1995a. Histological perspectives on growth in the birds *Struthio camelus* and *Sagittarius serpentarius*. *Acta Palaeornithol*. 181: 317–324.

Chinsamy, A. 1995b. Ontogenetic changes in the bone histology of the Late Jurassic ornithopod *Dryosaurus lettowvorbecki*. *J. Vert. Paleontol*. 15: 96–104.

Chinsamy, A. and A. Elzanowski. 2001. Evolution of growth patterns in birds. *Nature* 412: 402–403.

Chinsamy, A. and B. S. Rubidge. 1993. Bone histology and growth trajectory of the prosauropod dinosaur *Massospondylus carinatus* (Owen). *Modern Geol.* 18: 319–32.

Chinsamy, A., et al. 1995a. Growth rings in Mesozoic birds. *Nature* 368: 196–197.

Chinsamy, A., et al. 1995b. Mesozoic avian bone microstructure: physiological implications. *Paleobiology* 21: 561–574.

Chinsamy, A., et al. 1998. Bone microstructure of the diving *Hesperornis* and the volant *Ichthyornis* from the Niobrara Chalk of western Kansas. *Cretac. Res.* 19: 225–235.

Chinsamy, A., et al. 2009. Palaeobiological implications of the bone histology of *Pterodaustro guinazui*. *Anat. Rec.* 292: 1462–1477.

Chinsamy, A., et al. 2013. Gender identification of the Mesozoic bird *Confuciusornis sanctus*. *Nature Commun.* 4: 1381.

Chinsamy, A., et al. 2020. Bone histology yields insights into the biology of the extinct elephant birds (Aepyornithidae) from Madagascar. *Biol. J. Linn. Soc.* 2020: 1–28.

Colbert, E. H. 1995. *The Little Dinosaurs of Ghost Ranch*. New York, Columbia University Press.

Company, J. 2011. Bone histology of the titanosaur *Lirainosaurus astibiae* (Dinosauria: Sauropoda) from the Latest Cretaceous of Spain. *Naturwissenschaften*. 98: 67–78.

Cooper, L. N., et al. 2008. Relative growth rates of predator and prey dinosaurs reflect effects of predation. *Proc. R. Soc. B - Biol. Sci.* 275: 2609–2615.

Csiki, Z. and M. J. Benton. 2010. An island of dwarfs – reconstructing the Late Cretaceous Haţeg palaeoecosystem. *Palaeogeogr. Palaeoclimatol. Palaeoecol.* 293: 265–270.

Cubo, J. and N.-E. Jalil. 2019. Bone histology of *Azendohsaurus laaroussii*: implications for the evolution of thermometabolism in Archosauromorpha. *Paleobiology* 45: 317–330.

Cullen, T. M., et al. 2014. Osteohistological variation in growth marks and osteocyte lacunar density in a theropod dinosaur (Coelurosauria: Ornithomimidae). *BMC Evol. Biol.* 14: 1–14.

Curry, K. A. 1999. Ontogenetic histology of *Apatosaurus* (Dinosauria: Sauropoda): new insights on growth rates and longevity. *J. Vert. Paleontol.* 19: 654–665.

Curry Rogers, K. and Z. Kulik. 2018. Osteohistology of *Rapetosaurus krausei* (Sauropoda: Titanosauria) from the Upper Cretaceous of Madagascar. *J. Vert. Paleontol.* 38: 1–24.

Curry Rogers, K., et al. 2016. Precociality in a tiny titanosaur from the Cretaceous of Madagascar. *Science* 352: 450–453.

Curtin, A. J., et al. 2012. Noninvasive histological comparison of bone growth patterns among fossil and extant neonatal elephantids using synchrotron radiation x-ray microtomography. *J. Vert. Paleontol.* 32: 939–955.

Desmond, A. J. 1975. *The Hot-Blooded Dinosaurs: A Revolution In Palaeontology*. London, Blond & Briggs.

Dodson, P. 1974. Dinosaurs as dinosaurs. *Evolution* 28: 494–497.

Enlow, D. H. and S. O. Brown. 1956–1958. A comparative histological study of fossil and recent bone tissue. *Texas J. Sci.* 8: 405–443; 9: 186–214; 10: 187–230.

Erickson, G. M. and P. S. Druckenmiller. 2011. Longevity and growth rate estimates for a polar dinosaur: a *Pachyrhinosaurus* (Dinosauria: Neoceratopsia) specimen from the North Slope of Alaska showing a complete developmental record. *Hist. Biol.* 23: 327–334.

Erickson, G. M. and T. A. Tumanova. 2000. Growth curve of *Psittacosaurus mongoliensis* Osborn (Ceratopsia: Psittacosauridae) inferred from long bone histology. *Zool. J. Linn. Soc.* 130: 551–566.

Erickson, G. M., et al. 2001. Dinosaurian growth patterns and rapid avian growth rates. *Nature* 412: 429–433.

Erickson, G. M., et al. 2009. Was dinosaurian physiology inherited by birds? Reconciling slow growth in *Archaeopteryx*. *PLoS One* 4: e7390.

Erickson, G. M., et al. 2015. Flawed analysis? A response to Myhrvold. *Anat. Rec.* 298: 1669–1672.

Evans, D. C., et al. 2015. Osteology and bone microstructure of new, small theropod dinosaur material from the early Late Cretaceous of Morocco. *Gondwana Res.* 27: 1034–1041.

Evans, D., et al. 2018. Morphology and histology of new cranial specimens of Pachycephalosauridae (Dinosauria: Ornithischia) from the Nemegt Formation, Mongolia. *Palaeogeogr. Palaeoclimatol. Palaeoecol.* 494: 121–134.

Ezcurra, M., et al. 2020. Enigmatic dinosaur precursors bridge the gap to the origin of Pterosauria. *Nature* 588: 445–449.

Field, D. J, et al. 2020. Late Cretaceous neornithine from Europe illuminates the origins of crown birds. *Nature* 579: 397–401.

Fondevilla, V., et al. 2018. Ontogeny and taxonomy of the hadrosaur (Dinosauria, Ornithopoda) remains from Basturs Poble bonebed (late early Maastrichtian, Tremp Syncline, Spain). *PLoS One* 13: e0206287.

Foster, J. B. 1964. Evolution of mammals on islands. *Nature* 202: 234–235.

Fostowicz-Frelik, L. and J. Slowiak. 2018. Bone histology of *Protoceratops andrewsi* from the Late Cretaceous of Mongolia and its biological implications. *Acta Palaeontol. Pol.* 63: 503–517.

Fostowicz-Frelik Ł. and T. Sulej. 2010. Bone histology of *Silesaurus opolensis* Dzik, 2003 from the Late Triassic of Poland. *Lethaia* 43: 137–148.

Francillon-Vieillot, H., et al. 1990. Microstructure and mineralization of vertebrate skeletal tissues. In *Skeletal Biomineralization: Patterns, Processes and Evolutionary Trends*, Vol 1, J. G. Carter ed., 471–530. New York, Van Nostrand Reinhold.

Freedman Fowler, E. A. and J. R. Horner. 2015. A new brachylophosaurian hadrosaur (Dinosauria: Ornithischia) with an intermediate nasal crest from the Campanian Judith River Formation of northcentral Montana. *PLoS One* 10: e0141304.

Gates, T. A., et al. 2014. New hadrosaurid (Dinosauria, Ornithopoda) specimens from the lower-middle Campanian Wahweap Formation of southern Utah. In *Hadrosaurs: Proceedings of the International Hadrosaur Symposium*, D. A. Eberth and D. C. Evans eds., 156–173. Bloomington, Indiana University Press.

Gauthier, J. A. 1984. *A cladistic analysis of the higher systematic categories of the Diapsida. PhD dissertation, Department of Paleontology*, Berkeley, CA, University of California.

Gauthier, J. A. 2020. Archosauromorpha. In *Phylonyms: A Companion to the PhyloCode*, K. de Queiroz, P. D. Cantino and J. A. Gauthier eds., 1179–1182. Boca Raton, FL, CRC Press.

González, R., et al. 2020. Early growth dynamics of titanosaur sauropods inferred from bone histology. *Palaeogeogr. Palaeoclimatol. Palaeoecol.* 537: 109404.

Goodwin, M. B. and J. R. Horner. 2004. Cranial histology of pachycephalosaurs (Ornithischia: Marginocephalia) reveals transitory structures inconsistent with head-butting behavior. *Paleobiology* 30: 253–267.

Goodwin, M. B., et al. 2006. The smallest known *Triceratops* skull: new observations on ceratopsid cranial anatomy and ontogeny. *J. Vert Paleontol*. 26: 103–112.

Griebeler, E. M., et al. 2013. Aging, maturation and growth of sauropodomorph dinosaurs as deduced from growth curves using long bone histological data: an assessment of methodological constraints and solutions. *PLoS One* 8(6): e67012.

Griffin, C. and S. J. Nesbitt. 2016a. Anomalously high variation in postnatal development is ancestral for dinosaurs but lost in birds. *Proc. Natl. Acad. Sci*. 113: 14757–14762.

Griffin C. T. and S. J. Nesbitt. 2016b. The histology and femoral ontogeny of the Middle Triassic (?late Anisian) dinosauriform *Asilisaurus kongwe* and implications for the growth of early dinosaurs. *J. Vert. Paleontol*. 36: e1111224.

Griffin, C. T. and S. J. Nesbitt. 2020. Does the maximum body size of theropods increase across the Triassic–Jurassic boundary? Integrating ontogeny, phylogeny, and body size. *Anat. Rec*. 303: 1158–1169.

Griffin, C. T., et al. 2019. Integrating gross morphology and bone histology to assess skeletal maturity in early dinosauromorphs: new insights from *Dromomeron*. *PeerJ7*: e6331.

Gross, W. 1934. Die Typen des mikroskopischen Knochenbaues bei fossilen Stegocephalen und Reptilien. *Zeitschr. Anat*. 103: 731–764.

Haines, R. W. and A. Mohuidden. 1968. Metaplastic bone. *J. Anat*. 103: 527–538.

Hayashi, S., et al. 2009. Different growth patterns between the skeleton and osteoderms of *Stegosaurus* (Ornithischia: Thyreophora). *J. Vert. Paleontol*. 29: 123–131.

Hedrick, B. P., et al. 2020. Filling in gaps in the ceratopsid histologic database: histology of two basal centrosaurines and an assessment of the utility of rib histology in the Ceratopsidae. *Anat. Rec*. 303: 935–948.

Horner, J. R. and M. B. Goodwin. 2009. Extreme cranial ontogeny in the Upper Cretaceous dinosaur *Pachycephalosaurus*. *PLoS One* 4(10): e7626.

Horner, J. R. and E.-T. Lamm. 2011. Ontogeny of the parietal frill of *Triceratops*: a preliminary histological analysis. *C. R. Palevol* 10: 439–452.

Horner, J. R. and K. Padian. 2004. Age and growth dynamics of *Tyrannosaurus rex*. *Proc. R. Soc. London B* 271: 1875–1880.

Horner, J. R., et al. 1999. Variation in skeletochronological indicators of the hadrosaurid dinosaur *Hypacrosaurus*: implications for age assessment of dinosaurs. *Paleobiology* 25: 295–304.

Horner, J. R., et al. 2000. The bone histology of the hadrosaurid dinosaur *Maiasaura peeblesorum*: growth dynamics and physiology based on an ontogenetic series of skeletal elements. *J Vert. Paleontol*. 20: 109–123.

Horner, J. R., et al. 2001. Comparative osteohistology of some embryonic and perinatal archosaurs: phylogenetic and behavioral implications for dinosaurs. *Paleobiology* 27: 39–58.

Horner, J. R., et al. 2009. Comparative long bone histology and growth of the "hypsilophodontid" dinosaurs *Orodromeus makelai*, *Dryosaurus altus*, and *Tenontosaurus tilletti* (Ornithischia: Euornithodpoda). *J Vert. Paleontol*. 29: 734–747.

Horner, J. R., et al. 2016. Mineralized tissues in dinosaurs interpreted as having formed through metaplasia: a preliminary evaluation. *C. R. Palevol* 15: 176–196.

Houde, P. 1986. Ostrich ancestors found in the Northern Hemisphere suggest new hypothesis of ratite origins. *Nature* 324: 563–565.

Houde, P. 1987. Histological evidence for the systematic position of *Hesperornis* (Odontornithes: Hesperornithiformes). *The Auk* 104: 125–128.

Houde, P. W. 1988. Paleognathous birds from the Early Tertiary of the Northern Hemisphere. *Pub. Nuttall Ornithol. Club* 22: 1–148.

Hübner, T. R. 2012. Bone histology in *Dysalotosaurus lettowvorbecki* (Ornithischia: Iguanodontia) – variation, growth, and implications. *PLoS One* 7: e22958.

Ibiricu, L. M., et al. 2013. The behavioral implications of a multiindividual bonebed of a small theropod dinosaur. *PLoS One* 8(5): e64253.

Jenkins, F. A. Jr., et al. 2001. A diminutive pterosaur (Pterosauria: Eudimorphodontidae) from the Greenlandic Triassic. *Bull. Mus. Comp. Zool., Harvard Univ.* 156: 151-170.

Kellner, A. W. A. 2015. Comments on Triassic pterosaurs with discussion about ontogeny and description of new taxa. *An. Acad. Brasil. Ciên*. 87: 669–689.

Klein, N. 2004. *Bone histology and growth of the prosauropod dinosaur Plateosaurus engelhardti Meyer, 1837 from the Norian bonebeds of Trossingen (Germany) and Frick (Switzerland).* PhD dissertation, University of Bonn, Germany.

Klein, N. and P. M. Sander. 2007. Bone histology and growth of the prosauropod dinosaur *Plateosaurus engelhardti* von Meyer, 1837 from the Norian bonebeds of Trossingen (Germany) and Frick (Switzerland). *Spec. Pap. Palaeontol*. 77: 169-206.

Klein, N. and P. M. Sander. 2008. Ontogenetic stages in the long bone histology of sauropod dinosaurs. *Paleobiology* 34: 248–264.

Klein, N., et al. 2012. Modified laminar bone in *Ampelosaurus* atacis and other titanosaurs (Sauropoda): implications for life history and physiology. *PLoS One* 7: 1–17

Klevezal, G. A. and S. E. Kleinenberg. 1967. *Age Determination of Mammals from Lamellar Structures of Teeth and Bone*. Moscow, Nauka (in Russian). English translation by J. Slatkin. Israel Program for Scientific Transl. 1969.

Knoll, F., et al. 2010. Ontogenetic change and adult body size of the early ornithischian dinosaur *Lesothosaurus diagnosticus*: implications for basal ornithischian taxonomy. *Gondwana Res*. 17: 171–179.

Köhler, M. and M. Moya-Sola. 2009. Physiological and life history strategies of a fossil large mammal in a resource-limited environment. *Proc. Natl Acad. Sci*. 106: 20354–20358.

Köhler, M., et al. 2012. Seasonal bone growth and physiology in endotherms shed light on dinosaur physiology. *Nature* 487: 358–361.

Lamm, E.-T. 2013. Preparation and sectioning of specimens. In *Bone Histology of Fossil Tetrapods: Advancing Methods, Analysis, and Interpretation*, Padian, K. and E.-T. Lamm eds., 55–160. Berkeley, CA, University of California Press.

Laurin, M. 2011a. A preliminary biography of Armand de Ricqlès (1938–), the great synthesizer of bone histology. *C. R. Palevol*. 10: 293–301.

Laurin, M. 2011b. A preliminary list of publications by Armand de Ricqlès. *C. R. Palevol* 10: 311–321.

Lee, A. and P. O'Connor. 2013. Bone histology confirms determinate growth and small body size in the noasaurid theropod *Masiakasaurus knopfleri*. *J. Vert. Paleontol*. 33: 865–876.

Lee, A. H. and S. Werning. 2008. Sexual maturity in growing dinosaurs does not fit reptilian growth models. *Proc. Natl. Acad. Sci.* 105: 582–587.

Legendre, L. J., et al. 2014. Bone histology, phylogeny, and palaeognathous birds (Aves, Palaeognathae). *Biol. J. Linn. Soc.* 112: 688–700.

Lü, J., et al. 2011. An egg-adult association, gender, and reproduction in pterosaurs. *Science* 331: 321–324.

Maidment, S. C., et al. 2018. A new specimen of the ornithischian dinosaur *Hesperosaurus mjosi* from the Upper Jurassic Morrison Formation of Montana, USA, and implications for growth and size in Morrison stegosaurs. *J. Vert. Paleontol*. 38: e1406366.

Main, R. P., et al. 2005. The evolution and function of thyreophoran dinosaur scutes: implications for plate function in stegosaurs. *Paleobiology* 31: 291–314.

Margerie, E. de. 2002. Laminar bone as an adaptation to torsional loads in flapping flight. *J. Anat*. 201: 521–526.

Marsà, J. A. G., et al. 2020. Comparative bone microstructure of three archosauromorphs from the Carnian, Late Triassic Chañares Formation of Argentina. *Acta Palaeontol. Pol*. 65: 387–398.

McFarlin, S. C., et al. 2008. Regional variability in secondary remodeling within long bone cortices of catarrhine primates: the influence of bone growth history. *J. Anat*. 213: 308–324.

McFeeters, B., et al. 2016. A new ornithomimid theropod from the Dinosaur Park Formation of Alberta, Canada. *J. Vert. Paleontol*. 36: e1221415.

Meiri, S., et al. 2008. The island rule: made to be broken? *Proc. R. Soc. B: Biol. Sci*. 275: 141–148.

Myrhvold, N. 2015. Problems in Erickson et al. 2009. *Anat. Rec. (Hoboken)*. 298: 489–493.

Nesbitt, S. J. and J. A. Clarke. 2016. The anatomy and taxonomy of the exquisitely preserved Green River Formation (early Eocene) lithornithids (Aves) and the relationships of Lithornithidae. *Bull. Am. Mus. Nat. Hist*. 406.

Nesbitt S. J., et al. 2006. Prey choice and cannibalistic behaviour in the theropod *Coelophysis*. *Biol. Lett*. 2: 611–614.

Nesbitt, S. J., et al. 2007. A critical re-evaluation of the Late Triassic dinosaur taxa of North America. *J. Syst. Palaeontol*. 5: 209–243.

Nesbitt, S. J., et al. 2009. Hindlimb osteology and distribution of basal dinosauromorphs from the Late Triassic of North America. *J. Vert. Paleontol*. 29: 498–516.

Nesbitt, S. J., et al. 2011. A small alvarezsaurid from the eastern Gobi Desert offers insight into evolutionary patterns in the Alvarezsauroidea. *J. Vert Paleontol*. 31: 144–153.

Nesbitt, S. J., et al. 2013. The oldest dinosaur? A Middle Triassic dinosauriform from Tanzania. *Biol. Lett*. 9: 20120949.

Nesbitt S. J., et al. 2017. The earliest bird-line archosaurs and the assembly of the dinosaur body plan. *Nature* 544(7651): 484–487.

Nopcsa, F. 1914. Über das Vorkommen der Dinosaurier in Siebenbürgen. *Verh. Zool. Bot. Ges. Wien* 54: 12–14.

O'Connor, J., et al. 2018. Medullary bone in an Early Cretaceous enantiornithine bird and discussion regarding its identification in fossils. *Nat. Commun*. 9: 5169.

O'Connor, J. K., et al. 2014. The histology of two female Early Cretaceous birds. *Vertebr. Palasiat*. 52: 112–128.

Ösi, A., et al. 2012. Phylogeny, histology and inferred body size evolution in a new rhabdodontid dinosaur from the Late Cretaceous of Hungary. *PLoS One* 7: 1–25.

Ösi, A., et al. 2014. New ankylosaurian material from the Upper Cretaceous of Transylvania. *Ann. Paléontol.* 100 (3): 257–271.

Ostrom, J. H. 1970. Terrestrial vertebrates as indicators of Mesozoic climates. North American Paleontological Convention, Chicago, 1969: Proceedings D: 347–376.

Ostrom, J. H. 1973. The ancestry of birds. *Nature* 242: 136.

Ostrom, J. H. 1976. *Archaeopteryx* and the origin of birds. *Biol. J. Linn. Soc.* 8: 91–182.

Owen, R. 1842. Report on British fossil reptiles. Part II. Report of the Eleventh Meeting of the British Association for the Advancement of Science. Plymouth, July 1841: 60–204.

Owen, R. 1861. The fossil Reptilia of the Liassic Formations. *Part first: Scelidosaurus harrisonii*. Cambridge Library Collection–*Monographs of the Palaeontographical Society*, London.

Padian, K. 1986. On the type material of Coelophysis (Saurischia: Theropoda), and a new specimen from the Petrified Forest of Arizona (Late Triassic: Chinle Formation). In *The Beginning of the Age of Dinosaurs: Faunal Change Across the Triassic-Jurassic Boundary*, K. Padian ed., 45–60. New York, Cambridge University Press.

Padian, K. 1997. The rehabilitation of Sir Richard Owen. *BioScience* 47: 446–453.

Padian, K. 2011. Vertebrate paleohistology then and now: a retrospective in the light of the contributions of Armand de Ricqlès. *C. R. Palevol* 10: 303–309.

Padian, K. 2012. A bone for all seasons. *Nature* 487: 310–311.

Padian, K. 2013a. The problem of dinosaur origins: integrating three approaches to the rise of Dinosauria. *Earth Environ. Sci. Trans. R. Soc. Edinburgh* 103: 423–442.

Padian, K. 2013b. Why study the bone microstructure of fossil tetrapods? In *Bone Histology of Fossil Tetrapods: Advancing Methods, Analysis, and Interpretation*, K. Padian and E.-T. Lamm eds., 1–11. Berkeley, CA, University of California Press.

Padian, K. 2020a. Poultry through time. *Nature* 579: 351–352.

Padian, K. 2020b. Close kin of the first flying vertebrates identified. *Nature* 588: 400–401.

Padian, K. and L. M. Chiappe. 1998. The origin and early evolution of birds. *Biol. Rev.* 73: 1–42.

Padian, K. and J. R. Horner. 2004. Physiology. In *The Dinosauria*. 2nd ed. D. Weishampel, P. Dodson and H. Osmolska eds., 660–671. Berkeley, CA, University of California Press.

Padian, K. and J. R. Horner. 2011. The evolution of 'bizarre structures' in dinosaurs: biomechanics, sexual selection, social selection or species recognition? *J. Zool*. 283: 3–17.

Padian, K. and E.-T. Lamm (eds.) 2013. *Bone Histology of Fossil Tetrapods: Advancing Methods, Analysis, and Interpretation*. Berkeley, CA, University of California Press.

Padian, K. and de Ricqlès, A. 2009. L'origine et l'évolution des oiseaux: 35 années du progres/The origin and evolution of birds: 35 years of progress. *C. R. Palevol* 8: 257–280.

Padian K. and A. de Ricqlès. 2020. Inferring the physiological regimes of extinct vertebrates: methods, limits and framework. *Philos. Trans. R. Soc. B* 375: 20190147.

Padian, K. and K. Stein. 2013. Evolution of growth rates and their implications. In *Bone Histology of Fossil Tetrapods: Advancing Methods, Analysis, and Interpretation*, K. Padian and E.-T. Lamm eds., 253–264. Berkeley, CA, University of California Press.

Padian, K., et al. 2001. Dinosaurian growth rates and bird origins. *Nature* 412: 405–408.

Padian, K., et al. 2004. Growth in small dinosaurs and pterosaurs: the evolution of archosaurian growth strategies. *J. Vert. Paleontol*. 24: 555–571.

Padian, K., et al. 2010. The trackmaker of *Apatopus*: early diversification of archosaur stance and gait. *Palaeontology* 53: 175–189.

Padian, K., et al. 2013. Selection of Specimens. In *Bone Histology of Fossil Tetrapods: Advancing Methods, Analysis, and Interpretation*, K. Padian and E.-T. Lamm eds., 35–54. Berkeley, CA, University of California Press.

Padian, K., et al. 2016. A hypothesis of differential secondary bone formation in dinosaurs. *C. R. Palevol* 15: 41–49.

Prieto-Márquez, A., et al. 2016. Anatomy and osteohistology of the basal hadrosaurid dinosaur Eotrachodon from the uppermost Santonian (Cretaceous) of southern Appalachia. *PeerJ* 4: e1872.

Pretto, F. A., et al. 2017. A juvenile sauropodomorph tibia from the 'Botucaraí hill', Late Triassic of Southern Brazil. *Rev. Brasil. Paleontol*. 19: 407–414.

Prondvai, E. and K. H. W. Stein. 2014. Medullary bone-like tissue in the mandibular symphyses of a pterosaur suggests non-reproductive significance. *Sci. Rep.* 4: 1–9.

Prondvai, E., et al. 2012. Life history of *Rhamphorhynchus* inferred from bone histology and the diversity of pterosaurian growth strategies. *PLoS One* 7: e31392.

Prondvai, E., et al. 2018. Intraskeletal histovariability, allometric growth patterns, and their functional implications in bird-like dinosaurs. *Sci. Rep.* 8: 1–16.

Quekett, J. 1849. On the intimate structure of bone as composing the skeleton of the four great classes of vertebrates viz. Mammals, birds, reptiles and fish, with some remarks on the great value of such structures to assess the affinities of minute fragments of organic remains. *Trans. R. Microsc. Soc. London* 2: 46–58.

Raath, M. A. 1977. *The anatomy of the Triassic theropod Syntarsus rhodesiensis (Saurischia: Podokesauridae) and a consideration of its biology*. PhD dissertation, Department of Zoology and Entomology. Salisbury, Rhodesia, Rhodes University.

Redelstorff, R. and P. M. Sander. 2009. Long and girdle bone histology of Stegosaurus: implications for growth and life history. *J. Vert. Paleontol*. 29: 1087–1099.

Redelstorff, R., et al. 2013. Bone histology of the stegosaur *Kentrosaurus aethiopicus* (Ornithischia: Thyreophora) from the Upper Jurassic of Tanzania. *Anat. Rec.* 296: 933–952.

Reid, R. E. H. 1981. Lamellar-zonal bone with zones and annuli in the pelvis of a sauropod dinosaur. *Nature* 292: 49–51.

Reid, R. E. H. 1984. The histology of dinosaurian bone, and its possible bearing on dinosaurian physiology. In *The Structure, Development and Evolution of Reptiles*, Vol 52, M. W. J. Fergusson ed., 629–663. London, *Symp. Zool. Soc. London*.

Ricqlès, A. de. 1968. Recherches paléohistologiques sur les os longs des tétrapodes I. – origine du tissue osseux plexiforme des dinosauriens sauropodes. *Ann. Paléontol. (Vert.)* 54: 133–145 with one plate.

Ricqlès, A. de. 1974. Evolution of endothermy: histological evidence. *Evol. Theor.* 1: 1–51.

Ricqlès, A. J. de. 1975. Recherches paléohistologiques sur les os longs des tétrapodes VII. – Sur la classification, la signification fonctionnelle et l'histoire des tissus osseux des tétrapodes. Première partie, structures. *Ann. Paléontol. (Vert.)* 61: 51–129.

Ricqlès, A. J. de. 1976a. On bone histology of fossil and living reptiles, with comments on its functional and evolutionary significance. In A. d'A. Bellairs and C. B. Cox eds., 123–150. *Linn. Soc. Symp. Ser.* 3. London, Linnean Society.

Ricqlès, A. J. de. 1976b. Recherches paléohistologiques sur les os longs des tétrapodes VII. Sur la classification, la signification fonctionnelle et l'histoire des tissus osseux des tétrapodes. Deuxième partie, fonctions. *Ann. Paléontol. (Vert.)* 62: 71–126.

Ricqlès, A. J. de. 1980. Tissue structure of dinosaur bone: functional significance and possible relation to dinosaur physiology. In *A Cold Look at the Warm-Blooded Dinosaurs*, R. D. K. Thomas and E. C. Olson eds., 103–139. Boulder, CO, Westview Press.

Ricqlès, A J. de. 1983. Cyclical growth in the long limb bones of a sauropod dinosaur. *Acta Palaeontologica Polonica* 28: 225–232.

Ricqlès, A J. de. 2000. L'origine dinosaurienne des oiseaux et de l'endothermie avienne: les arguments histologiques. *Année Biologique* 39: 69–100.

Ricqlès, A. J. de. 2011. Vertebrate paleohistology: past and future. *C. R. Palevol* 10: 509–515.

Ricqlès, A. J. de, et al. 2000. Paleohistology of the bones of pterosaurs (Reptilia: Archosauria): anatomy, ontogeny, and biomechanical implications. *Zool. J. Linn. Soc.* 129: 349–385.

Ricqlès, A. J. de, et al. 2001. The bone histology of basal birds in phylogenetic and ontogenetic perspectives. In *New Perspectives on the Origin and Early Evolution of Birds*, J. A. Gauthier and L. F. Gall eds., 411–426. New Haven, CT, Yale University Press.

Ricqlès, A. de, et al. 2003a. On the bone histology of some Triassic pseudosuchian archosaurs and related taxa. *Ann. Paléontol.* 89: 67–101.

Ricqlès, A. de, et al. 2003b. Osteohistology of *Confuciusornis sanctus* (Theropoda: Aves). *J. Vert. Paleontol*. 23: 373–386.

Ricqlès, A. J. de., et al. 2008. On the origin of rapid growth rates in archosaurs and their ancient relatives: complementary histological studies on Triassic archosauriforms and the problem of a "phylogenetic signal" in bone histology. *Ann. Paléontol*. 94: 57–76.

Ricqlès, A. J. de, et al. 2016. Preliminary assessment of bone histology in the extinct elephant bird *Aepyornis* (Aves, Palaeognathae) from Madagascar. *C. R. Palevol* 15: 197–208.

Rimblot-Baly, F., et al. 1995. Analyse paléohistologique d'une série de croissance partielle chez Lapparentosaurus madagascariensis (Jurassique Moyen): essai sur la dynamique de croissance d'un dinosaure sauropode. *Ann. Paléontol.* 81: 49–86.

Romer, A. S. 1971. The Chanares (Argentina) Triassic reptile fauna. X. Two new but incompletely known long-limbed pseudosuchians. *Breviora* 378: 1–10.

Roth, V. L. 1992. Inferences from allometry and fossils: dwarfing of elephants on islands. *Oxford Surv. Evol. Biol*. 8: 259–259.

Rowe, T. 1987. Definition and diagnosis in the phylogenetic system. *Syst. Zool.* 36: 208–211.

Sander, P. M. 2000. Longbone histology of the Tendaguru sauropods: implications for growth and biology. *Paleobiology* 26: 466–488.

Sander, P. M. and N. Klein. 2005. Developmental plasticity in the life history of a prosauropod dinosaur. *Science* 310: 1800–1802.

Sander, P. M., et al. 2004. Adaptive radiation in sauropod dinosaurs: bone histology indicates rapid evolution of giant body size through acceleration. *Organisms Diversity Evol*. 4: 165–173.

Sander, P. M., et al. 2006. Bone histology indicates insular dwarfism in a new Late Jurassic sauropod dinosaur. *Nature* 441: 739–741.

Sander, P. M., et al. 2011. Sauropod bone histology and its implications for sauropod biology. In *Biology of the Sauropod Dinosaurs: Understanding the Life of Giants*, N. Klein, K. Remes, C. T. Gee and P. M. Sander eds., 276–302. Bloomington, Indiana University Press.

Scheyer, T. M. and P. M. Sander. 2004. Histology of ankylosaur osteoderms: implications for systematics and function. *J. Vert. Paleontol*. 24: 874–893.

Schweitzer, M. H., et al. 2005. Gender-specific reproductive tissue in ratites and *Tyrannosaurus rex*. *Science* 308: 1456–1460.

Schweitzer, M. H., et al. 2016. Chemistry supports the identification of gender-specific reproductive tissue in *Tyrannosaurus rex*. *Sci. Rep.* 6: 23099.

Seeley, H. G. 1888. On the classification of the fossil animals commonly named Dinosauria. *Proc. R. Soc. London* 43: 165–171.

Seitz, A. 1907. Vergleichende Studien uber den mikroskopischen Knochenbau fossiler und rezenter Reptilien und dessen Bedeutung fur das Wachstum und Umbildung des Knochengewebes in Allgemeinen. *Nova Acta Abhand. Kaiserlichen Leopold-Carolinischen Deutsch. Akad. Naturforsch.* 87: 230–270.

Skutschas, P. P., et al. 2017. Ontogenetic changes in long-bone histology of an ornithomimid theropod dinosaur from the Upper Cretaceous Bissekty Formation of Uzbekistan. *Hist. Biol*. 29: 715–729.

Steel, L. 2003. The John Quekett sections and the earliest pterosaur histological studies. In *Evolution and Paleobiology of Pterosaurs*, Vol 217, E. Buffetaut and J. M. Mazin eds., 325–334. Oxford, Blackwell Scientific Publications.

Steel, L. 2008. The palaeohistology of pterosaur bone: an overview. *Zitteliana B*28: 109–125.

Stein, K., et al. 2010. Small body size and extreme cortical bone remodeling indicate phyletic dwarfism in *Magyarosaurus dacus* (Sauropoda: Titanosauria). *Proc. Natl. Acad. Sci.* 107: 9258–9263.

Stein, M., et al. 2013. Long bone histology and growth patterns in ankylosaurs: implications for life history and evolution. *PLoS One* 8: 368590.

Taquet, P. 2001. Philippe Matheron et Paul Gervais: deux pionniers de la découverte et de l'étude des os et des oeufs de dinosaurs de Provence (France). *Geodiversitas* 23: 611–623.

Turner, A. H., et al. 2007. A basal dromaeosaurid and size evolution preceding avian flight. *Science* 317: 1378–1381.

Turvey, S., et al. 2005. Cortical growth marks reveal extended juvenile development in New Zealand moa. *Nature* 435: 940–943.

Vanderven, E., et al. 2014. Histologic growth dynamic study of *Edmontosaurus regalis* (Dinosauria: Hadrosauridae) from a bonebed assemblage of the Upper Cretaceous Horseshoe Canyon Formation, Edmonton, Alberta, Canada. *Can. J. Earth Sci*. 51: 1023–1033.

Van Valen, L. 1973. Pattern and the balance of nature. *Evol. Theor.* 1: 31–49.

Varricchio, D. J. 1993. Bone microstructure of the Upper Cretaceous theropod dinosaur *Troodon formosus*. *J. Vert. Paleontol*. 13: 99–104.

Varricchio, D. J., et al. 2008. Mud-trapped herd captures evidence of distinctive dinosaur sociality. *Acta Palaeontol. Pol*. 54: 567–578.

Wang, M. and Z. Zhou. 2017. A new adult specimen of the basalmost ornithuromorph bird *Archaeorhynchus spathula* (Aves: Ornithuromorpha) and its implications for early avian ontogeny. *J. Syst. Palaeontol*. 15: 1–18.

Wang, S., et al. 2017. Extreme ontogenetic changes in a ceratosaurian theropod. *Curr. Biol*. 27: 144–148.

Waskow, K. and P. M. Sander. 2014. Growth record and histological variation in the dorsal ribs of *Camarasaurus* sp.(Sauropoda). *J. Vert. Paleontol.* 34: 852–869.

Werning, S. 2012. The ontogenetic osteohistology of *Tenontosaurus tilletti*. *PLoS One* 7: e33539.

Werning, S. 2013. *Evolution of bone histological characters in amniotes, and the implications for the evolution of growth and metabolism*. PhD dissertation. Berkeley, CA, University of California, Department of Integrative Biology.

Werning, S. 2018. Medullary bone is phylogenetically widespread and its skeletal distribution varies by taxon. *J. Ornithol.* 159: 527–543.

Woodward, H. N., et al. 2011a. Growth dynamics of Australia's polar dinosaurs. *PLoS One* 6: e23339.

Woodward, H. N., et al. 2011b. Osteohistological evidence for determinate growth in the American alligator. *J. Herpetol*. 45:339–342.

Woodward, H. N., et al. 2015. *Maiasaura*, a model organism for extinct vertebrate population biology: a large sample statistical assessment of growth dynamics and survivorship. *Paleobiology* 41: 503–527.

Woodward, H. N., et al. 2018. The bone microstructure of polar "hypsilophodontid" dinosaurs from Victoria, Australia. *Sci. Rep.* 8: 1162.

Woodward, H. N., et al. 2020. Growing up *Tyrannosaurus rex*: osteohistology refutes the pygmy "*Nanotyrannus*" and supports ontogenetic niche partitioning in juvenile *Tyrannosaurus. Sci. Adv.* 6: eaax6250.

Zanno, L. E., et al. 2011. A new troodontid theropod, *Talos sampsoni* gen. et sp. nov., from the Upper Cretaceous Western Interior Basin of North America. *PLoS One* 6.

Zanno, L. E., et al. 2019. Diminutive fleet-footed tyrannosauroid narrows the 70-million-year gap in the North American fossil record. *Commun. Biol.* 2: 64.

Zhao, Q., et al. 2013. Histology and postural change during the growth of the ceratopsian dinosaur *Psittacosaurus lujiatunensis*. *Nat. Commun*. 4: 2079.

VetBooks.ir

28

Nonmammalian Synapsids

Jennifer Botha and Adam Huttenlocker

CONTENTS

Introduction to Nonmammalian Synapsids 550
Nontherapsid Synapsids 551
Caseasauria 551
Eupelycosauria 551
Nonmammalian Therapsids 553
Basal Therapsids and Dinocephalians 553
Anomodonts 554
Gorgonopsians 556
Therocephalians 556
Nonmammaliaform Cynodonts 558
Summary of Nonmammalian Synapsid Histology 560
Acknowledgments 560
References 560

Introduction to Nonmammalian Synapsids

The fossil record of Permo-Triassic Synapsida has been the source of important data for studying the origin and evolution of mammalian traits (e.g., Kemp 1982, 2005, Angielczyk 2009), terrestrial community structure (e.g., Roopnarine and Angielczyk 2015, Codron et al. 2017), survival from mass extinctions (e.g., Huttenlocker 2014, Smith and Botha-Brink 2014, Day et al. 2015, Botha-Brink et al. 2016) and macroevolution (e.g., Sidor 2001, Laurin 2004, Roopnarine and Angielczyk 2012, 2016, Didier et al. 2017). Importantly, this group also produced many physiological innovations, providing some of the earliest evidence for rapidly forming fibrolamellar bone tissues, systematic skeletal remodeling, and, perhaps, endothermic thermometabolism. Synapsida includes all amniotes more closely related to mammals than to reptiles (Angielczyk 2009). The nonmammalian synapsids classically comprised two major radiations: a paraphyletic assemblage of basal synapsids commonly referred to as "pelycosaurs" and the more recent, monophyletic Therapsida. Synapsids arose during the Late Carboniferous and originally included two major clades: the extinct Caseasauria and the more diverse Eupelycosauria, which includes the therapsids (Huttenlocker and Rega 2012, Reisz 2014). These early synapsids were the dominant terrestrial vertebrates during the late Carboniferous to early Permian, but by the middle Permian they had essentially been replaced by the mammal-like therapsids. The Permo-Triassic Therapsida represent one of the most iconic evolutionary transitions in the fossil record. The first mammals evolved from therapsids by the Early Jurassic as tiny shrew-sized creatures. Despite some degree of ecological diversity, mammals remained relatively small (less than a few kilograms) until the extinction of the nonavian dinosaurs some 66 million years ago (Ma) (Kielan-Jaworowska et al. 2004).

The first researchers to document and describe the osteohistology of extinct synapsids included Moodie (1923), Gross (1934), Enlow and Brown (1957), Enlow (1969) and Ricqlès (1969, 1972, 1974a, b). However, the last two decades have seen a profusion of studies within a phylogenetic context (including, but not limited to those by Botha-Brink, Chinsamy-Turan, Huttenlocker, Jasinoski, Laurin, Ray, Shelton, among others; see below for detailed references), which have greatly improved our understanding of synapsid histology, growth, and physiology. These studies are summarized below in their phylogenetic context.

VetBooks.ir

Nontherapsid Synapsids

Caseasauria

Caseasaurs included small to very large-bodied (>200 kg) generalists and herbivores characterized by a recumbent snout with enlarged nares, some with an absurdly small skull compared to their body length (Olson 1968). During the Carboniferous-Permian transition (ca. 300 Ma), the caseids were among the first diverse group of large-bodied vertebrate herbivores, along with diadectomorphs (anamniotes) and edaphosaurids (eupelycosaurs). They also included some of the latest surviving pelycosaur-grade synapsids, with some caseids recovered from middle Permian-aged rocks. Although their lifestyle is somewhat controversial, with some researchers suggesting a possible aquatic habitus (Lambertz et al. 2016), they have mainly been interpreted as terrestrial (Olson 1968, Felice and Angielczyk 2014).

The diversity of skeletal tissues in caseids is poorly known, as they have largely been neglected in histological studies. Our first insights into caseid histology were offered by Ricqlès (1974b), who sectioned and described the midshaft histology of a femur of a subadult caseid, *Ennatosaurus tecton* from the middle Permian of Russia. The short, robust femur showed a thin cortical wall and a poorly developed free medullary cavity; most of the medullary area is occupied by a spongiosa, flanked by occasional perimedullary erosion cavities. The thin cortex was dominated by inconsistently vascularized primary lamellar bone, with sparse longitudinal canals dorsally, oblique canals ventrally (associated with the adductor ridge) and was nearly avascular posteriorly. Overall, the predominance of lamellar bone with sparse, but highly ordered vascular canals, resembles that of contemporary diadectomorphs, and it may therefore reflect the primitive state of the amniote stem. Shelton (2015) and Lambertz et al. (2016) showed similar tissue textures in limb bones of other European and North American caseids, demonstrating the paucity of nonlamellar bone and sparse vascularity, even in purported juveniles. Lambertz et al. (2016) further suggested, controversially, the possible existence of a diaphragm on the basis of Sharpey's fibers preserved in the ribs. Future histologic work on the basal eothyridids would continue to clarify the primitive condition for synapsids and for amniotes in general.

Eupelycosauria

The highest diversity of sampled tissues comes from the Permo-Carboniferous eupelycosaurs, which exhibited considerably more diversity than contemporary caseasaurs. Eupelycosauria includes all synapsids more closely related to *Dimetrodon* and mammals than to caseasaurs, and, by extension, includes therapsids as a subgroup. However, we will first discuss nontherapsid eupelycosaurs as their histology is distinctly different from therapsids and records motifs remarkably similar to modern reptile groups, notably to monitor lizards (varanids) and crocodylians. Varanopids, for example, represent an early eupelycosaur clade that shared many characteristics with extant monitor lizards, including long, slender limbs and sometimes recurved, ziphodont teeth (Evans et al. 2009). Few varanopid taxa have been examined histologically, including the varanodontine *Varanops* (Ricqlès 1974b, Huttenlocker and Rega 2012, Shelton 2015), anecdotal observations from the varanodontine *Watongia* (Ricqlès 1976, Bennett and Ruben 1986) and a mycterosaurine from the lower Permian of Oklahoma (Huttenlocker and Rega 2012, Shelton 2015). Histologically, varanopid taxa show some degree of variation in tissue texture, vascularity and growth zone formation. In *Varanops*, the cortices of the radius and femur were generally thin and dominated by lamellar primary bone with occasional growth marks. Mycterosaurine femora were slightly thicker walled with combinations of parallel-fibered bone transitioning to lamellar bone (Figure 28.1A), and numerous growth marks and growth zones incorporating mainly longitudinal vasculature arranged in radial rows. Any transition to slowed growth into adulthood was subtle as there is little evidence of distinctive, avascular outer circumferential lamellae. The bone wall was generally dense and compact, but with a distinct medullary cavity sometimes bounded by well-developed inner (endosteal) circumferential lamellae. The well-differentiated medullary cavity of varanopids contrasts with some other early tetrapods, which tended to exhibit bones with a medullary region invaded and partly occluded by a dense spongiosa. The relative lightening of the skeleton in varanopids, and the well-defined tubular architecture of their bones, may be more consistent with a more efficient terrestrial locomotion.

Ophiacodontids exhibited a curious degree of histovariability compared to contemporary groups (Enlow and Brown 1957, Enlow 1969, Ricqlès 1974b, Laurin and Buffrénil 2016). The overall structure and compactness profile of *Ophiacodon* limb bones appear similar to other early tetrapods; an irregular perimedullary margin, thick bone wall and often, an occluded medullary cavity suggested the possibility of a primitively aquatic lifestyle (though this has been questioned by numerous authors; e.g., Felice and Angielczyk 2014). However, material referred to the Carboniferous ophiacodontid *Clepsydrops collettii* shows a remarkably thinner bone wall with an abrupt transition between medulla and cortex that is more like that of *Varanops* (Laurin and Buffrénil 2016). Both *Clepsydrops* and *Ophiacodon* exhibit cortical bone tissues that are dominated by parallel-fibered and lamellar primary bone with varying degrees of vascularity. In the femoral midshaft of *Clepsydrops* (as in varanopids and many early eupelycosaurs) the vascular canals are formed by longitudinal primary osteons that are generally arranged in radial rows (Laurin and Buffrénil 2016). However, in juveniles of the larger bodied *O. retroversus* and *O. uniformis* from the Permian of Texas and Oklahoma, the vasculature may take on a variety of motifs, sometimes reticular or radial (e.g., Huttenlocker and Rega 2012, Figure 4.3C), and deep portions of the cortex in small individuals preserve woven-fibered interosteonal tissues (Figure 28.1B) (Shelton and Sander 2017). Recent sampling by Shelton (2015) and Shelton and Sander (2017) corroborated the earlier findings of Enlow and Brown (1957) who contrasted *Ophiacodon* histology with all other pelycosaur-grade synapsids in its extensive vascularization throughout the cortex. Moreover, growth marks are sparse, together suggesting relatively high growth rates for *Ophiacodon*, perhaps on par with or greater than

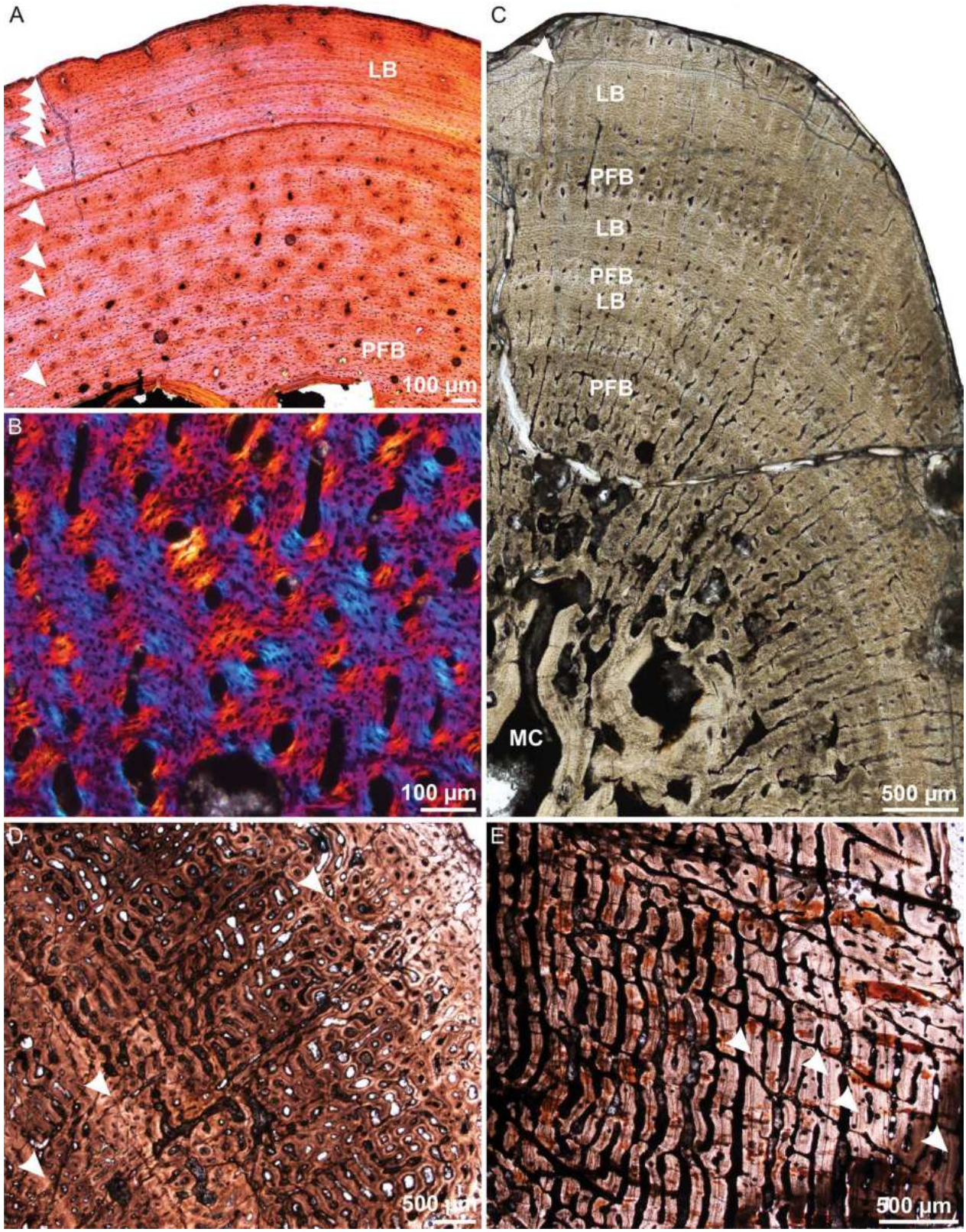


FIGURE 28.1 Basal nonmammalian synapsid and dinocephalian osteohistology. A, Mycterosaurine varanopid femur UWBM 98580 showing relatively poorly vascularized lamellar-zonal bone. B, *Ophiacodon* humerus MCZ 5926 showing woven-fibered bone in a juvenile individual. C, *Sphenacodon* humerus CM91212 showing zonal parallel-fibered and lamellar bone and vascular canals in radial rows. D, Anteosaurid dinocephalian femur BP/1/5591 showing highly vascularized zonal fibrolamellar bone. E, Titanosuchid dinocephalian femur BP/1/7242 showing a laminar vascular arrangement. Arrowheads indicate growth marks. (B, courtesy of Shelton and Sander; D and E, courtesy of Shelton and Chinsamy.) Abbreviations: LB, lamellar bone; MC, medullary cavity; PFB, parallel-fibered bone.

VetBooks.ir

extant crocodylians. These tissues are largely primary and there is no evidence of systematic cortical remodeling to the degree observed in domestic mammals, although there are perimedullary resorption cavities with concentric lamellae. Large individuals may exhibit less vascularized outer circumferential lamellae suggestive of slowed growth during adulthood (Shelton and Sander 2017).

The Permo-Carboniferous edaphosaurids were a predominantly Euramerican clade typified by a large, sometimes tuberculated, dorsal sail formed by hyperelongate neural spines. Like caseids, edaphosaurids tended toward herbivory and large body size (with the exception of the basal *Ianthasaurus,* which may have exhibited an omnivorous or insectivorous juvenile stage (Mazierski and Reisz 2010) and preserved long bone cortices constructed by sparsely vascularized lamellar-zonal bone (Enlow and Brown 1957, Enlow 1969). Primary bone deposition was incremental, mostly lamellar, and most vascular canals (either simple or primary osteons) were confined to the perimedullary areas of the limb bones and spines. The sail-supporting struts formed by the elongated neural spines tended to be constructed as a hollow cylinder with a somewhat thick bone wall composed of lamellar-zonal bone that was nearly avascular in the outer cortex (Huttenlocker et al. 2011). Prominent, short bundles of Sharpey's fibers are frequently confined to growth zones in the outer cortex. In *Edaphosaurus*, some degree of remodeling occurred in the inner third of the cortex in the spines as evidenced by large erosion cavities lined by multiple layers of concentric lamellae. Localized woven-fibered bone has been identified in *Edaphosaurus* spine tubercles, suggesting that tubercle growth was rapid in this taxon; pathologic woven bone has been identified in a fracture callus in a specimen of *Lupeosaurus* (Huttenlocker et al. 2011, Huttenlocker and Rega 2012). Among early eupelycosaurs, outer circumferential lamellae are most obvious in edaphosaurids, possibly due to the overall avascularity of their cortical bone and attainment of determinate growth.

Sphenacodontian synapsids form the sister group to edaphosaurids and include iconic predators such as the crested sphenacodontids (*Dimetrodon*) and a paraphyletic group of generally small-bodied predators traditionally called "haptodonts". Skeletal fragments from the Permian *Dimetrodon*, including pathological examples, were among the first pelycosaur-grade synapsid materials histologically studied (Moodie 1923, Enlow and Brown 1957, Enlow 1969). As in the edaphosaurids, much histological work has focused on the sail of *Dimetrodon* and its relatives—formed as an array of hyperelongated neural spines that were apparently covered by a webbing of soft tissue (Huttenlocker et al. 2010, Huttenlocker and Rega 2012, Rega et al. 2012). Histologically, however, the spines of sphenacodontids are formed by tissues strikingly different from those of edaphosaurids. The cortical bone records numerous growth zones composed of alternating lamellar and nonlamellar tissues occasionally with abundant primary osteons, especially in the lateral cortex. The medulla is completely occupied by cancellous bone, rather than forming a free, hollow cavity. Limb bones also show evidence of more rapid early growth, as large-bodied *Sphenacodon* and *Dimetrodon* tended to form large amounts of parallel-fibered and occasionally a woven-fibered matrix in juveniles (Huttenlocker et al. 2006, Huttenlocker and Rega 2012, Shelton et al. 2013). The numerous primary osteons are usually longitudinal and arranged in radial rows (Figure 28.1C), or sometimes more radially oriented in young individuals. Occasional fractures preserving pathologic woven bone have been documented, particularly in the neural spines (Enlow 1969, Huttenlocker et al. 2010, Rega et al. 2012). Some osseous lesions have been attributed to the oldest putative examples of osteomyelitis outside mammals (Moodie 1923).

Nonmammalian Therapsids

By the middle Permian (ca. 268 Ma), the diversity of basal synapsids was largely supplanted by a derived group of sphenacodontians called Therapsida (although some caseids and varanopids also survived into middle Permian times, but with low diversity and abundances). The clade Therapsida is defined as all synapsids more closely related to *Biarmosuchus* and mammals than to pelycosaurs such as *Dimetrodon* (Laurin and Reisz 1996). A considerable amount of research on therapsid histology has been published, particularly within the last decade (see Chinsamy-Turan 2012 for a detailed overview).

Basal Therapsids and Dinocephalians

Among the most basal therapsids, only the histology of biarmosuchians is known, based primarily on a representative sample from *Biarmosuchus* (Ricqles 1974b). Limb bone histology of *Biarmosuchus* demonstrates that, even at this early stage, therapsids already expressed more densely vascularized and haphazardly organized osseous tissues that resembled those of some mid- to large-bodied mammals. More recent reports on cranial ornamentation in the "horned" burnetiamorph biarmosuchians have shown rapid-growing osseous tissues in the skull, as well as pachyostosis and the fusion of cranial sutures (Sidor et al. 2017). The latter study has important implications for dimorphism in early therapsids and further bears on the taxonomic issues inherent in species with ontogenetically variable cranial adornments.

Dinocephalians were among the first therapsids to appear during the middle Permian. They were large, heavily built animals with some having pachyostotic skulls thought to have been used for head-butting (Barghusen 1975, Benoit et al. 2017). The group came to dominate the terrestrial landscape before disappearing during the end-Guadalupian mass extinction some 260 Ma (Kemp 2005, Atayman et al. 2015, Day et al. 2015). Relatively few researchers have examined dinocephalian bone histology because the group requires a comprehensive taxonomic revision. However, Ricqlès (1972) briefly examined several bones of the basal carnivorous brithopians and the omnivorous/herbivorous titanosuchians and found that highly vascularized fibrolamellar bone was also present in these basal eutherapsids. A more recent study by Shelton and Chinsamy (2016) confirmed the initial findings of Ricqlès (1972) and found that representatives of both groups display rapidly forming, densely vascularized bone tissues interrupted

VetBooks.ir

by cyclical growth marks during early to midontogeny, after which the deposition of lamellar-zonal bone indicates a switch to slower growth and eventually growth cessation (Shelton and Chinsamy 2016). The vascular canals are numerous and large, and primarily arranged in a laminar or plexiform pattern (Figure 28.1D, E). This differs from what Ricqlès (1972) observed in *Biarmosuchus*, which displays fewer, smaller, mostly longitudinally oriented primary osteons arranged in circular rows with some short, thin anastomoses. A laminar or plexiform arrangement is typical of large-bodied mammals (e.g., ruminants, Köhler et al. 2012, hippopotamus and elephant; Botha, personal observation) and sauropod dinosaurs (Sander 2000) and may result in stronger, stiffer bones that are better at resisting shear stress compared to other bone vascular patterns (Margerie et al. 2002, 2004). Given their large body sizes (basal skull lengths [BSLs] up to 80 cm; Kemp 2005), this type of bone tissue arrangement may have helped to strengthen dinocephalian bones, an important factor in supporting their considerable weight.

Anomodonts

In terms of diversity and abundance, the most successful Permo-Triassic therapsid group was the Anomodontia. Their highly specialized herbivorous masticatory apparatus likely helped them to diversify into a range of body sizes, ecological niches and geographical regions. Many of the derived forms underwent further adaptations in which their dentition was largely replaced by a rhamphotheca (a keratinized beak), and modifications to the jaw hinge and musculature allowed them to produce a particularly powerful bite (Kemp 2005). They appeared during the middle Permian and survived both the end-Guadalupian and Permo-Triassic mass extinctions before finally going extinct during the Late Triassic (Ruta et al. 2013, Day et al. 2015). The majority of anomodonts fall into a group known as the Dicynodontia, but there are a few basal nondicynodont anomodonts from South Africa and Russia. Little is known about the growth patterns of these basal taxa as only one specimen of the small-bodied anomodont *Galeops*, from the middle Permian of South Africa, has been sampled histologically (Botha-Brink and Angielczyk 2010). Although the presence of fibrolamellar bone in *Galeops* indicates that even the earliest anomodonts were capable of relatively rapid growth, the bone tissues are interrupted by wide regions of slow growing parallel-fibered bone (Figure 28.2A). The canals vary between small, narrow simple canals and longitudinally oriented primary osteons. These features differ from most other dicynodonts, which tend to have more complex vascular patterns in their limb cortices. The large-bodied basal dicynodont *Endothiodon* (BSL ~40 cm), and the relatively small *Diictodon* (Figure 28.2B) and closely related Emydopoidea (BSL ~7–24 cm), tend to have randomly distributed, longitudinally oriented primary osteons or reticular arrangements (Ray and Chinsamy 2004, Ray et al. 2009, Botha-Brink and Angielczyk 2010). Within the more recent Bidentalia, the Cryptodontia, which include both medium (BSL < 30 cm) and large-bodied (BSL > 40 cm) taxa, exhibit longitudinally oriented primary osteons, often in circumferential rows and plexiform arrangements appear in patches (Figure 28.2C, D). However, mammal-like plexiform and laminar vascular arrangements begin to dominate in later ontogenetic stages only in Dicynodontoidea (Figure 28.2D) among anomodonts (Gross 1934, Enlow and Brown 1957, Ricqlès 1972, Chinsamy and Rubidge 1993, Ray and Chinsamy 2004, Botha-Brink and Angielczyk 2010, Green et al. 2010, Ray et al. 2010). Although these arrangements tend to be present in the larger bodied taxa (BSL > 40 cm), the variation in vascular patterns may not be related to body size alone, as the basal dicynodont *Endothiodon* and the cryptodont *Rhachiocephalus* are large dicynodonts and do not show this pattern. It is likely that phylogeny also plays an important role in the selection of vascular patterns as plexiform and laminar bone tissues become increasingly prevalent in the Dicynodontoidea, even in the relatively smaller bodied Triassic *Lystrosaurus* species (Figure 28.2E) (although it should be noted that fully grown Triassic *Lystrosaurus* specimens have yet to be recovered and thus, even Triassic species may have been relatively large once skeletally mature; Botha-Brink et al. 2016).

Growth marks are present in all anomodonts studied to date, but they are especially prevalent in Permian taxa (Figure 28.2A–D), indicating that cyclical growth is a primitive feature of the clade as a whole. Many dicynodonts grew rapidly to the subadult stage and only exhibit growth marks relatively late in ontogeny (generally more than 50% of the maximum known size; Ray and Chinsamy 2004, Botha-Brink and Angielczyk 2010). Growth decreased during later ontogeny, forming a relatively avascular outer circumferential layer (indicating that growth had essentially ceased and skeletal maturity had been attained). Examples have been demonstrated in the Triassic kannemeyeriiforms *Kannemeyeria* and *Placerias* (Botha-Brink and Angielczyk 2010, Green et al. 2010), indicating that, like many other vertebrates, dicynodonts underwent asymptotic growth (*contra* Ray and Chinsamy 2004, Ray et al. 2005, Ray et al. 2010), and the absence of outer circumferential lamellae in specimens is more a reflection of the skeletal immaturity of the individual than an expression of an indeterminate growth strategy (Woodward et al. 2011, Lee et al. 2013). Haversian remodeling is present in the inner cortices of both small and large taxa, but it is more prevalent in larger bodied taxa. However, dense Haversian bone throughout the cortex has only been observed in adult Triassic kannemeyerids such as *Kannemeyeria* and *Placerias* (Botha-Brink and Angielczyk 2010, Green et al. 2010).

Another histomorphometric feature characteristic of dicynodonts is the small size or infilling of the medullary cavity. Dicynodont bones generally have relatively thick cortices with a medullary cavity infilled with trabeculae, which produces broad transition zones between compact and cancellous bone. When the medullary cavity is open and free of trabeculae (Figure 28.2C), it tends to be very small (Botha-Brink and Angielczyk 2010). Long bones of larger dicynodonts generally have a medullary cavity infilled with trabeculae, but exceptions do occur, such as the basal dicynodont *Endothiodon*, in which a small, but open, medullary cavity occurs. It has been hypothesized that the infilling of the medullary cavity in dicynodonts is the result of an aquatic lifestyle (Ray et al. 2005, Canoville and Laurin 2010) as many extant aquatic tetrapods

VetBooks.ir

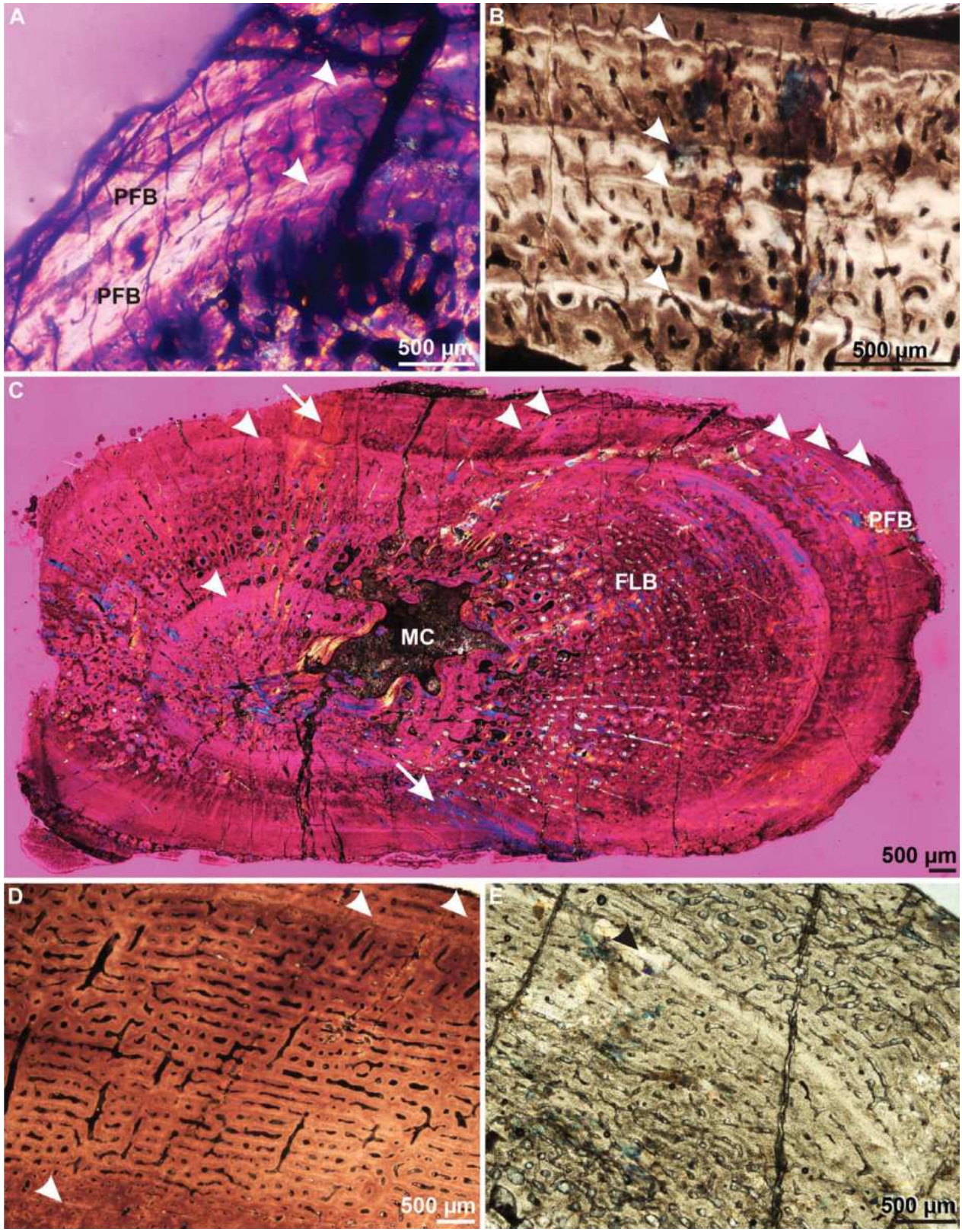


FIGURE 28.2 Anomodont osteohistology. A, Nondicynodont anomodont *Galeops* humerus SAM-PK-12261 showing wide regions of parallel-fibered bone, B, Dicynodont *Diictodon* fibula SAM-PK-K7725 showing zonal fibrolamellar bone. C, Dicynodont *Oudenodon* femur SAM-PK-4807 showing a thick compact cortex with highly vascularized fibrolamellar bone transitioning to less vascularized peripheral parallel-fibered bone. D, Dicynodont *Daptocephalus* humerus NMQR 3633 showing zonal fibrolamellar bone in a laminar vascular arrangement. E, Dicynodont *Lystrosaurus* humerus NMQR 1485 showing highly vascularized fibrolamellar bone interrupted by an annulus. Arrowheads indicate growth marks, and arrows indicate Sharpey's fibers (muscle insertions). Abbreviations: FLB, fibrolamellar bone; MC, medullary cavity; PFB, parallel-fibered bone.

VetBooks.ir

have this feature. However, this feature is also found in active, pelagic animals, in which the development of extensive spongiosae spreading into periosteal cortices results in decreasing the skeletal mass and consequently reducing the inertia of the moving body (Ricqlès and Buffrenil 2001, Kriloff et al. 2008, Houssaye 2012, Houssaye et al. 2016). To date, no morphological adaptations have been found in dicynodonts to suggest that any were aquatic, particularly not fully aquatic, active swimmers. The trabecular infilling of the medullary cavity is more likely to have resulted in increasing skeletal and body mass. Infilled medullary cavities and/or thick compact cortices might even have been associated with their dual-gate mode of locomotion where the hind limbs were held in a more parasagittal plane compared to the forelimb (Ray and Chinsamy 2003, Kemp 2005). The trabeculae in the medullary region likely provided a biomechanical advantage by acting as buttresses against the high bending loads present in the larger taxa. This feature would have aided smaller taxa as well. For example, *Lystrosaurus* is a medium-sized burrowing animal and its limb bones would have been susceptible to high bending and torsional loads during digging (Botha-Brink 2017). Notably thick cortices have also been reported for smaller dicynodonts such as *Diictodon* and *Cistecephalus*, both of which are considered to be fossorial (Ray and Chinsamy 2004, Nasterlack et al. 2012) and would have experienced similar biomechanical loads to *Lystrosaurus*.

Gorgonopsians

The most striking and iconic carnivorous therapsids of the late Permian were the gorgonopsians. They are commonly referred to as the "saber-toothed cats" of the Permian due to their greatly elongated canines, and they ranged in size from a small dog up to the size of the largest extant mammalian predators (Kemp 2005). They form part of a collective group known as the Theriodontia, which also include the mammal-like therocephalians and cynodonts. These theriodonts acquired increasingly mammalian features during their evolution, with improved locomotory and masticatory capacities. The extinction of the carnivorous dinocephalians during the end-Guadalupian mass extinction opened up a new niche for the gorgonopsians, allowing them to become the apex predators during the late Permian, preying on the herbivorous dicynodonts and smaller therocephalians and cynodonts. Very little of their osteohistology has been examined, mostly due to problems with the taxonomy of the clade (but see Gebauer 2007 and Kammerer 2016b for taxonomic reviews of some taxa), making it difficult to ensure positive generic identification of any thin sectioned material. However, a few brief descriptions have been made, beginning with Ricqlès (1969) who described some gorgonopsian material. Although generic identifications are problematic, it is clear that, similar to the biarmosuchians, dinocephalians and dicynodonts, a fibrolamellar complex dominates gorgonopsian limb bones (Figure 28.3A). More recent work on *Aelurognathus*, *Gorgonops* (previously *Scylacops*, Gebauer 2007) and *Cyonosaurus* (Figure 28.3B) have confirmed Ricqlès' initial observations of well-vascularized fibrolamellar bone tissues (Ray et al. 2004, Chinsamy-Turan and Ray 2012, Botha-Brink et al. 2016). The vascular patterns vary from reticular during early ontogeny to longitudinally oriented primary osteons with circumferential anastomoses during mid-to-late ontogeny. All three of these taxa contain regularly spaced growth marks (lines of arrested growth [LAGs] or annuli of lamellar bone) even during early ontogeny (Chinsamy-Turan and Ray 2012, Botha-Brink et al. 2016). This last feature differs from that of dicynodonts, which generally tend to exhibit growth marks only during mid to late ontogeny. However, much more work on gorgonopsian osteohistology is required before a general consensus of the growth patterns of this clade is reached.

Therocephalians

The Eutheriodontia include the therocephalians and cynodonts. The therocephalians first appeared as medium to large carnivores during the middle Permian and diverged into a variety of body sizes and ecological niches, evolving into highly specialized herbivorous forms during the Middle Triassic. They survived both the end-Guadalupian and Permo-Triassic mass extinctions and were important components of the recovery ecosystems after both events. Their osteohistology was briefly examined by Ricqlès (1969), Ray et al. (2004) and Chinsamy-Turan and Ray (2012) who identified fast-growing cyclical fibrolamellar bone in all taxa studied. More recent comprehensive studies have revealed important patterns in therocephalian life histories from the Permian to the Triassic (Huttenlocker and Botha-Brink 2013, 2014). Large-bodied Permian therocephalians (BSL ~25–40 cm) exhibited abundant vascular canals in a variety of motifs, ranging from plexiform, to radiating and reticular networks interspersed with longitudinally oriented primary osteons. The bones of smaller taxa tend to exhibit a predominance of longitudinally oriented primary osteons. The middle Permian predator *Lycosuchus* exhibits highly vascularized plexiform tissues in its limb bone cortices (Figure 28.3C). Some Permian therocephalians, however, showed unique tissue patterns with lower levels of vascularity and numerous, variably spaced growth marks, particularly the late Permian *Theriognathus* (Figure 28.3D). Regardless of body size, Permian therocephalians generally experienced multiyear growth to asymptotic size, and some taxa like *Theriognathus*, achieved skeletal maturity quite late based on delayed fusion of neurocentral sutures, even in large specimens (Huttenlocker and Botha-Brink 2014, Huttenlocker and Abdala 2015). At the Permian-Triassic boundary, the clade experienced a "Lilliput effect" in which large-bodied taxa disappeared during a global mass extinction (Huttenlocker and Botha-Brink 2013, Huttenlocker 2014). Even the large-bodied *Moschorhinus,* which is among the few known Permo-Triassic boundary-crossing therocephalians, experienced within-lineage dwarfing. Despite a decrease in body size, however, Triassic *Moschorhinus* grew more quickly than did its Permian counterpart, as evidenced by more densely vascularized bone tissues and fewer growth marks (Figure 28.3E, F) (Huttenlocker and Botha-Brink 2013). This is surprising because, within a given clade, large-bodied individuals tend to grow more quickly than their small-bodied relatives (Case 1978). The smaller Triassic survivors like *Tetracynodon* underwent relatively slower growth,

VetBooks.ir

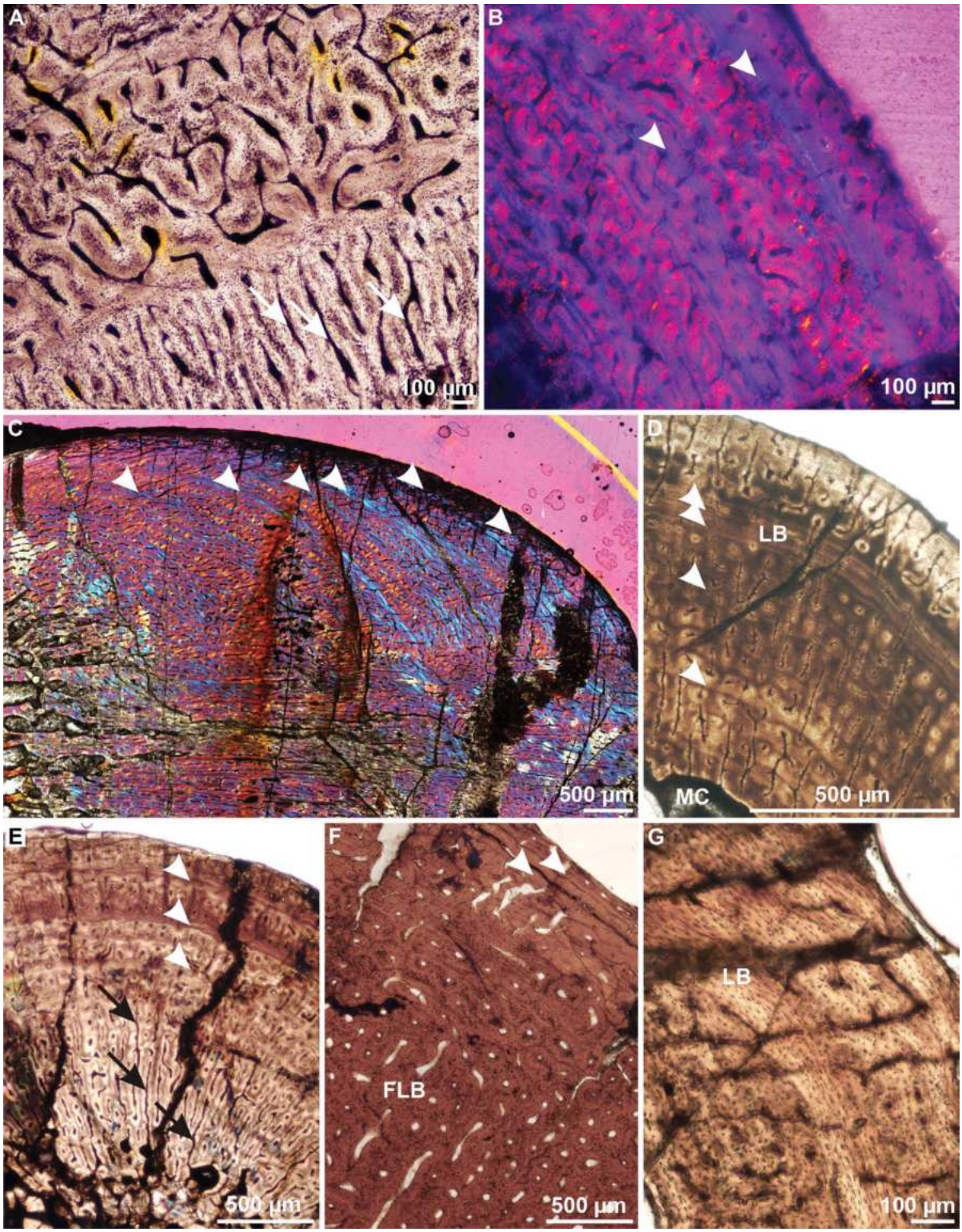


FIGURE 28.3 Gorgonopsian and therocephalian osteohistology. A, Gorgonopsian indet. limb bone SAM-PK-K10622 showing highly vascularized fibrolamellar bone with a change from inner cortical radial canals (bottom right) to a more reticular vascular arrangement (top left). B, *Cyonosaurus* ulna SAM-PK-K10428 showing zonal fibrolamellar bone. C, basal therocephalian *Lycosuchus* ulna SAM-PK-9084 showing rapidly deposited fibrolamellar bone interrupted by growth marks. D, Eutherocephalian *Theriognathus* femur NMQR 3375 showing growth marks. E, Permian eutherocephalian *Moschorhinus* humerus NMQR 3939 showing a mid- and outer cortex of rapidly forming fibrolamellar bone and three annuli. Note there is no growth deceleration at the subperiosteal surface, even after three growth cycles. F, Triassic eutherocephalian *Moschorhinus* humerus BP/1/4227 showing highly vascularized fibrolamellar bone, a midcortical annulus and two closely spaced annuli at the subperiosteal surface indicating growth deceleration. G, Baurioid eutherocephalian *Tetracynodon* humerus NMQR 3745 showing a wide region of lamellar bone. Arrowheads indicate growth marks, and arrows indicate radial vascular canals. Abbreviations: FLB, fibrolamellar bone; LB, lamellar bone; MC, medullary cavity.

VetBooks.ir

but all experienced shorter growth durations (Figure 28.3G). Increased aridity and unpredictable rainfall regimes during the Early Triassic (Smith and Botha-Brink 2014, MacLeod et al. 2017) resulted in elevated mortality rates and rapid attainment of skeletal (and presumably reproductive) maturity, which would have been advantageous in taxa with shortened life expectancies (Botha-Brink et al. 2016).

Nonmammaliaform Cynodonts

The most recent and mammal-like nonmammalian therapsids are the nonmammaliaform cynodonts. They appeared relatively later in the fossil record than other therapsid clades, with the first documented record from the late Permian (Botha et al. 2007, Kammerer 2016a). They were relatively rare components of Permian ecosystems, although this may reflect a poor preservation probability rather than a genuine rarity in their biological community as these early taxa are all relatively small (BSL ~5–14 cm; Abdala and Ribeiro 2010, Kammerer 2016a). After the Permo-Triassic mass extinction, however, they flourished, radiating into a speciose clade with an increasingly mammalian morphology before finally evolving into the first true mammals by the Early Jurassic. Consequently, there have been numerous osteohistological studies on nonmammaliaform cynodonts as they hold the key to understanding the origin and evolution of mammalian growth patterns (e.g., Ricqlès 1969, Botha and Chinsamy 2000, 2004, 2005, Ray et al. 2004, Chinsamy and Abdala 2008, Botha-Brink et al. 2012; in review, Veiga et al. 2018, Butler et al. 2018).

Rapidly forming fibrolamellar bone has been found throughout the clade, even in its most basal members such as the late Permian *Procynosuchus* (Ray et al. 2004). During the Early Triassic, nonmammaliaform cynodonts were still relatively small, reaching skeletal maturity within one to two years (Figure 28.4A). Two major lineages diverged at this time, the Cynognathia and Probainognathia. Within the Cynognathia, a group of large-bodied herbivorous taxa known as the Gomphodontia (named for their buccolingually expanded postcanines; Abdala and Ribeiro 2010) arose during the Middle Triassic. This clade includes the Traversodontidae, a family of diverse, globally distributed nonmammaliaform cynodonts that became highly abundant during the Late Triassic. The Gomphodontia exhibit high growth rates and multiyear growth to skeletal (and presumably reproductive) maturity, similar to large extant mammals. The bone tissues comprise rapidly forming fibrolamellar bone, with a variety of vascular arrangements, interrupted by narrow annuli and LAGs (Figure 28.4B, C) (Botha-Brink et al. 2012). Exceptions to this pattern are two basal traversodontids, *Andescynodon* and *Massetognathus*, where the dominant bone tissues are slower growing lamellar-zonal and parallel-fibered bone tissue, respectively (Chinsamy and Abdala 2008). These taxa are smaller than their more recent relatives (BSL approximately 13 and 20 cm, respectively; Chinsamy and Abdala 2008, Liu and Powell 2009), but other similar sized nonmammaliaform cynodonts, such as the Early Triassic *Thrinaxodon* and *Galesaurus*, exhibit faster growing bone tissues (in stressful conditions relating to a harsh, postextinction environment), thus factors other than body size are likely to have influenced the growth rates of these taxa. Chinsamy and Abdala (2008) proposed that there was an increase in growth rates within the traversodontids, as *Andescynodon* and *Massetognathus* exhibit slower growth rates than in more recent taxa such as *Exaeretodon*, *Gomphodontosuchus* and *Scalenodontoides* (Botha-Brink et al. 2012). This would imply a selection for slower growth rates in the basal traversodontids, as the more basal nontraversodontid gomphodontosuchines *Diademodon* and *Trirachodon* exhibit rapidly forming fibrolamellar bone during early and midontogeny (Botha-Brink et al. 2012).

The other major nonmammaliaform cynodont clade is the Probainognathia, which gave rise to the smaller bodied Prozostrodontia. The prozostrodontians exhibit increasingly mammalian characteristics such as more efficient locomotory and masticatory structures allowing for increased activity levels and energy assimilation, maxillary vibrissae indicating improved sensory capabilities and improved thermoregulatory and reproductive controls (implied from the loss of a pineal foramen) (Benoit et al. 2016a, b), as well as high growth rates (Figure 28.4D). They evolved into the tiny Mammaliaformes, which includes the crown group Mammalia, during the Late Triassic. The tritylodont and tritheledont prozostrodontians exhibit similar growth patterns to the Cynognathia, with highly vascularized, rapidly forming fibrolamellar bone being the dominant bone tissue type. Chinsamy and Hurum (2006) and Botha-Brink et al. (2012) suggested that the tritylodontid *Tritylodon* underwent sustained growth to skeletal maturity due to the presence of peripheral lamellar bone containing multiple LAGs in a radius and fibula. However, in the radius (Figure 28.4E), this region does not represent the outer circumferential lamellae, which indicates growth cessation because, although the LAGs are near the bone periphery, additional bone was deposited after these growth marks around most of the shaft, showing that the animal was still growing at the time of its death. The region containing the lamellar bone tissue is relatively wide and thus, could be mistaken for an outer circumferential layer. Multiple peripheral LAGs were also found in a fibula, but it is not known if this feature represents outer circumferential lamellae or just a temporary change in growth rate similar to the radius. Wide zones of slow-growing bone tissue have recently been found traversing the midcortex of the limb bones of a more basal prozostrodontian *Prozostrodon* (Figure 28.4D) and LAGs have been found in the tritheledontid *Irajatherium* (Botha-Brink et al. 2018). Therefore, without more material, it is difficult to determine whether *Tritylodon* underwent sustained or cyclical growth.

Recent work on the tiny brasilodontid prozostrodontian taxa *Brasilodon* and *Brasilitherium*, which are currently considered to be the sister taxa to Mammaliaformes, has shown that they grew relatively more slowly than the more basal nonmammaliaform cynodonts. The bones of these taxa contain a mixture of comparatively less vascularized fibrolamellar and parallel-fibered bone (Botha-Brink et al. 2018). This pattern is similar to those of the Early Jurassic mammaliaform *Morganucodon* and the Late Cretaceous multituberculate mammals *Kryptobaatar* and *Nemegtbaatar* (Chinsamy and Hurum 2006). The relatively slower growth rates in these brasilodontids compared to other nonmammaliaform cynodonts may be related to phylogeny and/or decreased body

VetBooks.ir

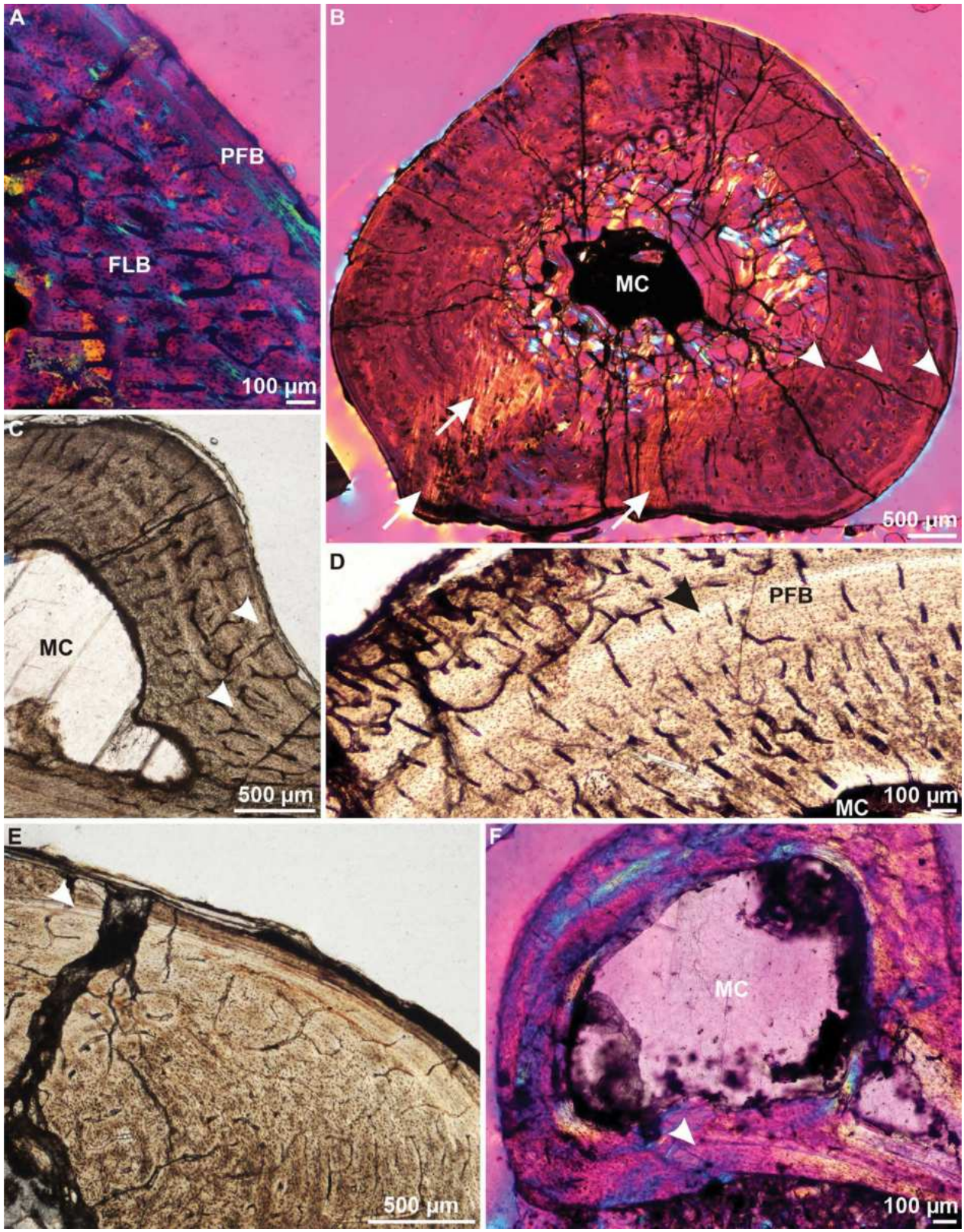


FIGURE 28.4 Nonmammaliaform cynodont osteohistology. A, Basal eucynodont *Thrinaxodon* humerus BP/1/5208 showing rapidly forming fibrolamellar bone and peripheral slower forming parallel-fibered bone. B, Gomphodontosuchine *Diademodon* fibula UCMZ T448 showing zonal fibrolamellar bone. C, Gomphodontosuchine *Trirachodon* showing zonal fibrolamellar bone. D, Prozostrodontian *Prozostrodon* femur UFRGS-PV-248T showing a wide region of parallel-fibered bone. E, Tritylodontid *Tritylodon* radius BP/1/5167 showing an outer cortical growth mark with continued peripheral growth. F, Brasilodontid *Brasilitherium* femur UFRGS-PV-1043T showing a midcortical growth mark. Arrowheads indicate growth marks, and arrows indicate Sharpey's fibers (muscle insertions). Abbreviations: FLB, fibrolamellar bone; MC, medullary cavity; PFB, parallel-fibered bone.

VetBooks.ir

sizes as all these taxa were very small (BSL ~3–4 cm). When compared with similar-sized extant mammals, they may have grown more slowly to adult size as their osteohistology shows they took more than one year for growth to attenuate (as shown by the presence of a midcortical growth mark prior to growth deceleration), thus taking more than one year for these animals to reach skeletal maturity (Figure 28.4F). Thus, although the Prozostrodontia exhibit increasingly mammalian characteristics, including rapid juvenile growth, the small derived nonmammalian prozostrodontians still exhibit an extended growth period compared to similar-sized extant mammals.

Summary of Nonmammalian Synapsid Histology

Despite a great deal of histovariation due to the effects of phylogeny, biomechanics, body size and lifestyle, there are some osteohistological features that distinguish the derived therapsids from the more basal nonmammalian synapsids. For example most of the pelycosaur bone tissues studied to date exhibit relatively slowly forming parallel-fibered and lamellar bone tissues. There are exceptions to this pattern such as *Ophiacodon* and some sphenacodontids.

The predominance of fibrolamellar bone in even the earliest, most basal therapsids indicates that rapid growth rates are plesiomorphic for the clade. The high frequency of densely vascularized bone tissues among them indicate that therapsids grew rapidly to at least reproductive maturity. The dominance of fibrolamellar bone throughout the skeleton indicates that therapsids grew faster than their pelycosaur-grade ancestors, in which fibrolamellar bone is absent or, if present, limited to certain elements in isolated regions in some eupelycosaurs (*Ophiacodon* and some sphenacodontids). The implication is that pelycosaurs generally exhibited a greater investment in individual growth spread out over their lifetimes, and possibly over a greater length of time than in similarly sized therapsids.

Therapsids for which the complete life history is known (i.e., osteohistology data from different ontogenetic stages is available) exhibit cyclical growth where growth decreased or ceased temporarily during the unfavorable season. Those for which growth marks have not been observed are represented by immature individuals, such as the nonmammaliaform cynodonts *Cynognathus* and *Scalenodontoides*, and thus, the occurrence of sustained growth to reproductive or skeletal maturity cannot be confirmed without the assessment of older individuals. However, the large size of the nonmammaliaform cynodont individuals studied (BSL 30 and 40 cm, respectively) indicates that they grew in a sustained manner to at least midontogeny (Botha-Brink et al. 2012). A few possible exceptions to this are Early Triassic eutheriodonts such as *Thrinaxodon*, which likely underwent rapid sustained growth to reproductive maturity (Botha-Brink et al. 2016). However, the presence of a single *annulus* in one bone of *Thrinaxodon* shows that the capacity to produce growth marks existed (Botha and Chinsamy 2004). The widespread occurrence of growth marks among the Therapsida, a clade that lived in a variety of environmental conditions (middle Permian to Early Jurassic climates) and geographical regions indicates that this feature represents an endogenous circadian rhythm and not merely a response to random or even seasonal environmental stresses (Huttenlocker et al. 2013, see also Chapter 31). Some therapsid taxa, however, expressed growth marks relatively late in ontogeny. This is particularly noticeable in the dicynodont and eutheriodont clades, indicating that a greater part of their growth (mainly early ontogeny) occurred in a sustained manner compared to other taxa.

Although it may be possible to trace endothermic-like physiology in some therapsid groups on the basis of growth rates, bone remodeling and bioapatite isotopic ratios, it remains unclear as to whether these instances pinpoint the origins of true mammalian endothermy, some type of intermediary or independent evolution of mammal-like thermophysiology. These questions remain open ended because some early mammaliaform cynodonts preserved attributes of ectothermy, and some modern monotremes have been suggested to be mainly ectothermic or intermediate (Grady et al. 2014). These can only be further resolved by better taxonomic sampling and implementation of phylogenetic comparative methods within a well-sampled evolutionary framework (e.g., Huttenlocker and Farmer 2017, Olivier et al. 2017). However, it is likely, considering the combined morphological and osteohistological evidence, that therapsids had higher metabolic rates than did their predecessors. The increasingly mammal-like features acquired during therapsid evolution (e.g., improved locomotory, masticatory and ventilatory capabilities necessary for increased energy assimilation) suggest that high standard metabolic rates were likely a feature of some therapsid groups, especially in the later cynodonts (see Chapter 37).

Acknowledgments

C. Shelton and P. M. Sander are gratefully acknowledged for providing the *Ophiacodon* image, and C. Shelton and A. Chinsamy for the anteosaurid and titanosuchid dinocephalian images. Thank you to M. Laurin and V. de Buffrénil for their helpful reviews. This research was funded by the National Research Foundation (UID 98819, 104688), DST/NRF Centre of Excellence in Palaeosciences and Palaeontological Scientific Trust (PAST), Johannesburg, South Africa, to JB; the National Science Foundation (DEB-1209018, DBI-1309040) and Bureau of Land Management National Conservation Lands (L17AC00064) to AH.

REFERENCES

Abdala, F., and A. M. Ribeiro. 2010. Distribution and diversity patterns of Triassic cynodonts (Therapsida, Cynodontia) in Gondwana. *Palaeogeogr. Palaeoclimatol. Palaeoecol.* 286: 202–217.

Angielczyk, K. D. 2009. *Dimetrodon* is not a dinosaur: using tree thinking to understand the ancient relatives of mammals and their evolution. *Evol. Educ. Outreach* 2: 257–271.

Atayman, S., et al. 2015. Taxonomic re-evaluation of tapinocephalid dinocephalians. *Palaeont. Afr.* 44: 87–90.

Barghusen, H. R. 1975. A review of fighting adaptations in dinocephalians (Reptilia, Therapsida). *Paleobiology* 1: 295–311.

VetBooks.ir

Bennett, A. F., and J. A. Ruben. 1986. The metabolic and thermoregulatory status of therapsids. In *The Ecology and Biology of Mammal-like Reptiles*, eds. N. Hotton, P. D. MacLean, J. J. Roth, and E. C. Roth, 207–218. Washington: Smithsonian Institution Press.

Benoit, J., et al. 2016a. Palaeoneurological clues to the evolution of defining mammalian soft tissue traits. *Sci. Rep.* 6: 25604.

Benoit, J., et al. 2016b. The sixth sense in mammalians forerunners: variability of the parietal foramen and the evolution of the pineal eye in South African Permo-Triassic eutheriodont therapsids. *Acta Palaeont. Pol.* 61: 777–789.

Benoit, J., et al. 2017. Synchrotron scanning reveals the palaeoneurology of the head-butting *Moschops capensis* (Therapsida, Dinocephalia). *PeerJ* 5: e3496.

Botha, J., and A. Chinsamy. 2000. Growth patterns deduced from the histology of the cynodonts *Diademodon* and *Cynognathus*. *J. Vertebr. Paleontol.* 20: 705–711.

Botha, J., and A. Chinsamy. 2004. Growth and life habits of the Triassic cynodont *Trirachodon,* inferred from bone histology. *Acta Palaeont. Pol.* 49: 619–627.

Botha, J., and A. Chinsamy. 2005. Growth patterns of *Thrinaxodon,* a non-mammalian cynodont from the Early Triassic of South Africa. *Palaeontology* 48: 385–394.

Botha, J., et al. 2007. The oldest cynodont: new clues on the origin and diversification of Cynodontia. *Zool. J. Linn. Soc.* 149: 477–492.

Botha-Brink, J. 2017. Burrowing in *Lystrosaurus*: preadaptation to a postextinction environment? *J. Vertebr. Paleont.* 37: e1365080.

Botha-Brink, J., and K. D. Angielczyk. 2010. Do extraordinarily high growth rates in Permo-Triassic dicynodonts (Therapsida, Anomodontia) explain their success before and after the end-Permian extinction? *Zool. J. Linn. Soc.* 160: 341–365.

Botha-Brink, J., et al. 2012. The radiation and osteohistology of non-mammaliaform cynodonts. In *The Forerunners of Mammals: Radiation, Histology and Biology*, ed. A. Chinsamy-Turan, 223–246. Bloomington: Indiana University Press.

Botha-Brink, J., et al. 2016. Breeding young as a survival strategy during Earth's greatest mass extinction. *Sci. Rep.* 6: 24053.

Botha-Brink, J., et al. 2018. Osteohistology of Late Triassic prozostrodontian cynodonts from Brazil. *PeerJ* 6: e5029.

Butler, E., et al. 2018. Postcranial anatomy of the Early Triassic non-mammaliaform cynodont *Galesaurus planiceps* (Owen, 1859) from the Karoo Basin, South Africa. *Palaeontology* 1–32.

Canoville, A., and M. Laurin. 2010. Evolution of humeral microanatomy and lifestyle in amniotes, and some comments on paleobiological inferences. *Biol. J. Linn. Soc.* 100: 384–406.

Case, T. J. 1978. Speculations on the growth rate and reproduction of some dinosaurs. *Paleobiology* 4: 320–328.

Chinsamy, A., and F. Abdala. 2008. Palaeobiological implications of the bone microstructure of South American traversodontids (Therapsida: Cynodontia). *South Afr. J. Sci.* 104: 225–230.

Chinsamy, A., and J. H. Hurum. 2006. Bone microstructure and growth patterns of early mammals. *Acta Palaeontol. Pol.* 51: 325–338.

Chinsamy, A., and B. S. Rubidge. 1993. Dicynodont (Therapsida) bone histology: phylogenetic and physiological implications. *Palaeontol. Afr.* 30: 97–102.

Chinsamy-Turan, A. ed. 2012. *The Forerunners of Mammals: Radiation, Histology and Biology*. Bloomington: Indiana.

Chinsamy-Turan, A., and S. Ray 2012. Bone histology of some therocephalians and gorgonopsians, and evidence of bone degradation by fungi. In *The Forerunners of Mammals: Radiation, Histology and Biology*, ed. A. Chinsamy-Turan, 199–222. Bloomington: Indiana University Press.

Codron, J., et al. 2017. Predator prey interactions among Permo-Triassic terrestrial vertebrates as a deterministic factor influencing faunal collapse and turnover. *J. Evol. Biol.* 30: 40–54.

Day, M. O., et al. 2015. When and how did the terrestrial mid-Permian mass extinction occur? Evidence from the tetrapod record of the Karoo Basin, South Africa. *Proc. R. Soc. B* 282: 20150834.

Didier, G., et al. 2017. Likelihood of tree topologies with fossils and diversification rate estimation. *Syst. Biol.* 66: 964–87.

Enlow, D. H. 1969. The bone of reptiles. In *Biology of the Reptilia Volume 1: Morphology A*, ed. C. Gans, A. Bellairs, and T. Parsons, 45–80. London: Academic Press.

Enlow, D. H., and S. O. Brown. 1957. A comparative histological study of fossil and recent bone tissues. Part II. *Texas J. Sci.* 9: 136–214.

Evans, D. C., et al. 2009. A re-evaluation of sphenacodontid synapsid material from the lower Permian fissure fills near Richards Spur, Oklahoma. *Palaeontology* 52: 219–227.

Felice, R. N., and K. D. Angielczyk. 2014. Was *Ophiacodon* (Synapsida, Eupelycosauria) a swimmer? A test using vertebral dimensions. In *Early Evolutionary History of the Synapsida*, eds. C. F. Kammerer, K. D. Angielczyk, and J. Fröbisch, 25–51. Dordrecht: Springer.

Gebauer, E. V. I. 2007. Phylogeny and evolution of the Gorgonopsia with a special reference to the skull and skeleton of GPIT/RE/7113 (*'Aelurognathus?' parringtoni*). PhD dissertation, Eberhard-Karls University of Tubingen.

Grady, J. M., et al. 2014. Evidence for mesothermy in dinosaurs. *Science* 344: 1268–1272.

Green, J. L., et al. 2010. Limb bone histology and growth in *Placerias hesternus* (Therapsida: Anomodontia) from the Upper Triassic of North America. *Palaeontology* 53: 347–364.

Gross, W. 1934. Die typen des mikroskopischen knochenbaues bei foslen stegocephalen und reptilien. *Zeitschr. Anat. Entwickl.* 103: 731–764.

Houssaye, A. 2012. Bone histology of aquatic reptiles: what does it tell us about secondary adaptation to an aquatic life? *Biol. J. Linn. Soc.* 108: 3–21.

Houssaye, A., et al. 2016. Adaptive patterns in aquatic amniote bone microanatomy-more complex than previously thought. *Int. Comp. Biol.* 56: 1349–1369.

Huttenlocker, A. 2014. Body size reductions in nonmammalian eutheriodont therapsids (Synapsida) during the End-Permian Mass Extinction. *PLoS One* 9: e87553.

Huttenlocker, A. K., and F. Abdala. 2015. Revision of the first therocephalian, *Theriognathus* Owen (Therapsida: Whaitsiidae), and implications for cranial ontogeny and allometry in non-mammaliaform eutheriodonts. *J. Paleontol.* 89: 645–664.

Huttenlocker, A. K., and J. Botha-Brink. 2013. Body size and growth patterns in the therocephalian *Moschorhinus kitchingi* (Therapsida: Eutheriodontia) before and after the end-Permian extinction in South Africa. *Paleobiology* 39: 253–277.

Huttenlocker, A. K., and J. Botha-Brink. 2014. Growth patterns and the evolution of bone microstructure in Permo-Triassic therocephalians (Amniota, Therapsida) of South Africa. *PeerJ* 2: e325.

Huttenlocker, A. K., and C. G. Farmer. 2017. Bone microvasculature tracks red blood cell size diminution in Triassic mammal and dinosaur forerunners. *Curr. Biol.* 27: 48–54.

Huttenlocker, A. K., and E. Rega. 2012. The paleobiology and bone microstructure of pelycosaurian-grade synapsids. In *The Forerunners of Mammals: Radiation, Histology and Biology*, ed. A. Chinsamy-Turan, 90–119. Bloomington: Indiana University Press.

Huttenlocker, A., et al. 2006. Osteohistology of *Sphenacodon* (Synapsida: Sphenacodontidae) and the hidden diversity of growth patterns in basal synapsids. *J. Vertebr. Paleontol.* 26(supplement): 79–80A.

Huttenlocker, A. K., et al. 2010. Comparative anatomy and osteohistology of hyperelongate neural spines in the sphenacodontids *Sphenacodon* and *Dimetrodon* (Amniota: Synapsida). *J. Morphol.* 271: 1407–1421.

Huttenlocker, A. K., et al. 2011. Comparative osteohistology of hyperelongate neural spines in the Edaphosauridae (Amniota: Synapsida). *Palaeontology* 54: 573–590.

Huttenlocker, A. K., et al. 2013. The biology of bone. In *Bone Histology of Fossil Tetrapods. Advancing Methods, Analysis, and Interpretation*, eds. K. Padian, and E-T. Lamm, 13–34. Berkeley: University of California Press.

Jasinoski, S. C. and A. Chinsamy-Turan, A. 2012. Biological inferences of the cranial microstructure of the dicynodonts *Oudenodon* and *Lystrosaurus*. In *The Forerunners of Mammals: Radiation, Histology and Biology*, A. Chinsamy-Turan ed., 148–176. Bloomington, IN: Indiana University Press.

Kammerer, C. R. 2016a. A new taxon of cynodont from the *Tropidostoma* Assemblage Zone (upper Permian) of South Africa, and the early evolution of Cynodontia. *Palaeontology* 2: 387–397.

Kammerer, C. R. 2016b. Systematics of the Rubidgeinae (Therapsida: Gorgonopsia). *PeerJ* 4: e1608.

Kemp, T. S. 1982. *Mammal-Like Reptiles and the Origin of Mammals*. London: Academic Press.

Kemp, T. S. 2005. *The Origin and Evolution of Mammals*. Oxford: Oxford University Press.

Kielan-Jaworowska, Z., et al. 2004. *Mammals from the Age of Dinosaurs: Origins, Evolution, and Structure*. New York: Columbia University Press.

Köhler, M., et al. 2012. Seasonal bone growth and physiology in endotherms shed light on dinosaur physiology. *Nature* 487: 358–361.

Kriloff, A., et al. 2008. Evolution of bone microanatomy of the tetrapod tibia and its use in palaeobiological inference. *J. Evol. Biol.* 21: 1–11.

Lambertz, M., et al. 2016. A caseian point for the evolution of a diaphragm homologue among the earliest synapsids. *Ann. N Y Acad. Sci.* 1385: 3–20.

Laurin, M. 2004. The evolution of body size, Cope's Rule and the origin of amniotes. *Syst. Biol.* 53: 594–622.

Laurin, M., and V. de Buffrénil. 2016. Microstructural features of the femur in early ophiacodontids: a reappraisal of ancestral habitat use and lifestyle of amniotes. *C. R. Palevol* 15: 115–127.

Laurin, M., and R. R. Reisz. 1996. The osteology and relationships of *Tetraceratops insignis*, the oldest known therapsid. *J. Vertebr. Paleontol.* 16: 95–102.

Lee, A. H., et al. 2013. The biology of bone. In *Bone Histology of Fossil Tetrapods. Advancing Methods, Analysis, and Interpretation*, eds. K. Padian, and E-T. Lamm, 217–252. Berkeley: University of California Press.

Liu, J., and J. Powell. 2009. Osteology of *Andescynodon* (Cynodontia: Traversodontidae) from the Middle Triassic of Argentina. *Am. Mus. Novit.* 3674: 1–19.

MacLeod, K. G., et al. 2017 Warming and increased aridity during the earliest Triassic in the Karoo Basin, South Africa. *Geology* 45: 483–486.

Mazierski, D. M., and R. R. Reisz. 2010. Description of a new specimen of *Ianthasaurus hardestiorum* (Eupelycosauria: Edaphosauridae) and a re-evaluation of edaphosaurid phylogeny. *Can. J. Earth Sci.* 47: 901–912.

Margerie, E de. 2002. Laminar bone as an adaptation to torsional loads in flapping flight. *J. Anat.* 201: 521–526.

Margerie, E. de, et al. 2004. Assessing a relationship between bone microstructure and growth rate: a fluorescent labelling study in the king penguin chick (*Aptenodytes patagonicus*). *J. Exp. Biol.* 207: 869–879.

Moodie, R. L. 1923. *Paleopathology. An Introduction to the Study of Ancient Evidence for Disease*. Urbana: University of Illinois Press.

Nasterlack, T., et al. 2012. New insights into the biology of the Permian genus *Cistecephalus* (Therapsida, Dicynodontia). *J. Vertebr. Paleontol.* 32: 1296–1410.

Olivier, C., et al. 2017. Fist palaeohistological inference of resting metabolic rate in an extinct synapsid, *Moghreberia nmachouensis* (Therapsida: Anomodontia). *Biol. J. Linn. Soc.* 121: 409–419.

Olson, E. C. 1968. The family Caseidae. *Fieldiana* 17: 225–349.

Ray, S., and A. Chinsamy. 2003. Functional aspects of the postcranial anatomy of the Permian dicynodont *Diictodon* and their ecological implications. *Palaeontology* 46: 151–183.

Ray, S., and A. Chinsamy. 2004. *Diictodon feliceps* (Therapsida, Dicynodontia): bone histology, growth, and biomechanics. *J. Vertebr. Paleontol.* 24: 180–194.

Ray, S., et al. 2004. Bone histology and growth patterns of some nonmammalian therapsids. *J. Vertebr. Paleontol.* 24: 634–648.

Ray, S., et al. 2005. *Lystrosaurus murrayi* (Therapsida, Dicynodonta): bone histology, growth and lifestyle adaptations. *Palaeontology* 48: 1169–1185.

Ray, S., et al. 2009. Growth patterns as deduced from bone microstructure of some selected neotherapsids with special emphasis on dicynodonts: phylogenetic implications. *Palaeoworld* 18: 53–66.

Ray, S., et al. 2010. Bone histology of a kannemeyeriid dicynodont *Wadiasaurus*: palaeobiological implications. In *New Aspects of Mesozoic Biodiversity*, ed. S. Bandyopadhyay, 73–89. Berlin: Springer-Verlag.

VetBooks.ir

Rega, E., et al. 2012. Healed fractures in the neural spines of an associated skeleton of *Dimetrodon*: Implications for dorsal sail morphology and function. *Fieldiana: Life Earth Sci.* 2012: 104–111.

Reisz, R. R. 2014. Pelycosaur-grade synapsids: introduction. In *The Early Evolutionary History of the Synapsida*, eds. C. F. Kammerer, K. D. Angielczyk, and J. Fröbisch, 289–304. Dordrecht: Springer.

Ricqlès, A. de. 1969. Recherches paléohistologiques sur les os longs des Tétrapodes. II, Quelques observations sur la structure des longs des Thériodontes. *Ann. Paléontol. (Vert.)* 55: 1–52.

Ricqlès, A. de. 1972. Recherches paléohistologiques sur les os longs des Tétrapodes. III - Titanosuchiens, Dinocéphales et Dicynodontes. *Ann. Paléontol. (Vert.)* 58: 17–60.

Ricqlès, A. de. 1974a. Evolution of endothermy: histological evidence. *Evol. Theor.* 1: 51–80.

Ricqlès, A. de. 1974b. Paleohistological research on the long bones of tetrapods IV: Eotheriodonts and pelycosaurs. *Ann. Paléontol.* 60: 3–39.

Ricqlès A. de. 1976. On bone histology of fossil and living reptiles, with comments on its functional and evolutionary significance. In *Morphology and Biology of Reptiles*, eds. A. d'A Bellairs, and C. Barry Cox, 123–151. London: Academic Press.

Ricqlès A, de, and V. Buffrènil. 2001. Bone histology, heterochronies and the return of tetrapods to life in water: where are we? In *Secondary Adaptation of Tetrapods to Life in Water*, eds. J. M. Mazin, and V. de Buffrènil, 289–310. München: Friedrich Pfeil Verlag.

Roopnarine, P. D., and K. D. Angielczyk. 2012. The evolutionary palaeoecology of species and the tragedy of the commons. *Biol. Lett.* 8: 147–150.

Roopnarine, P. D., and K. D. Angielczyk. 2015. Community stability and selective extinction during the Permo-Triassic mass extinction. *Science* 350: 90–93.

Roopnarine, P. D., and K. D. Angielczyk. 2016. The stability of ecological communities as an agent of evolutionary selection. Evidence from the Permian-Triassic Mass Extinction. In *Evolutionary Theory: A Hierarchical Perspective*, eds. N. Eldredge, T. Pievani, E. Serrelli, and I. Temkin, 307–333. Chicago: University of Chicago Press.

Ruta, M., et al. 2013. Decoupling of morphological disparity and taxic diversity during the adaptive radiation of anomodont therapsids. *Proc. R. Soc. B* 280: 20131071.

Sander, M. A. 2000. Longbone histology of the Tendaguru sauropods: implications for growth and biology. *Paleobiology* 26: 466–488.

Shelton, C. D. 2015. Origins of Endothermy in the Mammalian Lineage. PhD dissertation, Universitäts-und Landesbibliothek Bonn, 2015.

Shelton, C. D., and A. Chinsamy. 2016. Postcranial bone histology of dinocephalians (Therapsida) reveals periodic rapid rates of bone deposition and evidence of a pathology in a titanosuchid. *J. Vert. Paleontol., SVP Prog. Abstr. Book*, 2016: 223.

Shelton, C. D., and P. M. Sander. 2017. Long bone histology of *Ophiacodon* reveals the geologically earliest occurrence of fibrolamellar bone in the mammalian stem lineage. *C. R. Palevol* 16: 397–424.

Shelton, C. D., et al. 2013. Long bone histology indicates sympatric species of *Dimetrodon* (Lower Permian, Sphenacodontidae). *Earth Environ. Sci. Trans. R. Soc. Edinburgh* 103: 217–236.

Sidor, C. A. 2001. Simplification as a trend in synapsid cranial evolution. *Evolution* 55: 1419–1442.

Sidor, C. A., et al. 2017. Burnetiamorphs did it first: cranial adornment and rates of speciation in a Permian lineage of therapsids. *J. Vert. Paleontol., SVP Prog. Abstr. Book*, 2017: 194.

Smith, R. M. H., and J. Botha-Brink. 2014. Anatomy of an extinction: sedimentological and taphonomic evidence for drought-induced die-offs during the Permo-Triassic mass extinction in the main Karoo Basin, South Africa. *Palaeogeogr. Palaeoclimatol. Palaeoecol.* 396: 99–118.

Veiga, F. H., et al. 2018. Osteohistology of the non-mammaliaform traversodontids *Protuberum cabralense* and *Exaeretodon riograndensis* from southern Brazil. *Hist. Biol.* 31: 1231–1241.

Woodward, H. N., et al. 2011. Osteohistological evidence for determinate growth in the American alligator. *J. Herpetol.* 45: 339–342.

VetBooks.ir

29

Diversity of Bone Microstructure in Mammals

Vivian de Buffrénil, Christian de Muizon, Maïténa Dumont, Michel Laurin and Olivier Lambert

CONTENTS

Overview and Definitions 565
Origin and Mesozoic Mammals 565
Early Mammaliaforms 565
First Therians 566
Extant Mammalian Clades 567
Preliminary Remarks on Comparative Bone Histology in Mammals 569
Early (Mesozoic) Mammals 570
Morganucodon and the Allotheria (Multituberculates) 570
Prototheria (Monotremes and Stem Group) 571
Remark on Epiphyseal Structure in the Prototherians 571
Long Bone and Rib Microstructure 571
Skeletal Microstructures of the Metatheria 573
Epiphyseal Characteristics of Metatherian Long Bones 573
Microanatomy and Histology of Limb Long Bones 574
An Overview of Rib Structure 574
Long Bones and Ribs in the Eutheria 576
Preliminary Remarks 576
Limb Long Bones 576
Ribs 576
Histological Features of Long Bones in Early Eutherians 577
Observations of Pantodonts 577
Afrotheria (Sirenia, Proboscidea, Desmostylia and Tubulidentata) 579
Bone Microstructure in the Sirenia 579
Desmostylia 579
Proboscidea 581
Tubulidentata 581
Xenarthra 582
Terrestrial and Amphibious Cetartiodactyls 582
Aquatic Cetartiodactyls: The Cetaceans 584
Limb Bones 586
Ribs 586
Perissodactyls 588
Carnivores 590
Long Bones of the Pholidote *Phataginus tricuspis* 592
Histological Features of Long Bones and Ribs in the Lipotyphla 592
Chiroptera 594
Rodents 595
Lagomorphs 597
Primates 597

An Overview of Mammalian Vertebral Microstructures 599
Microanatomical Features 599
Histological Features 601
Remarks on Other Skeletal Elements: Osteoderms, Baculum and Antlers 601
Xenarthran Dermal Ossicles 601
Baculum 603
Antlers 604
Differentiation and Growth Process of the First Antlers 604
Antler Regeneration 605
Concluding Remarks 606
Acknowledgments 607
References 607

Overview and Definitions

Extant mammals constitute a highly successful clade of tetrapods, including more than 5000 species of placentals, about 340 of marsupials (pouched mammals) and five monotremes (egg-laying mammals). Because the diagnostic features of extant (crown group) mammals evolved in stepwise and often mosaic fashion, mammals have been defined in various ways, especially paleontologically, when extinct groups that possess some of these critical features have been considered. Here, the term Mammaliaformes will be used with an apomorphy-based definition: all synapsids (the sistertaxon to reptiles, including birds) that possess a squamosal-dentary joint. A series of other mammalian characters (e.g., presence of mammary glands, single bone in the lower jaw, endothermy, greatly enlarged brain, single bone housing the inner ear, diphyodont dental replacement and occlusion between lower and upper molars) were gradually acquired along this stem lineage (e.g., Rose 2006). Among mammaliaforms, Mammalia simply corresponds to the crown group, including the last common ancestor of monotremes, marsupials and placentals, and all its descendants. Finally, within Mammalia a stem and a crown group can also be defined for the three main lineages: stem monotremes and Monotremata, stem metatherians and Marsupialia, and stem eutherians and Placentalia, respectively (Kemp 2005, Zachos and Asher 2018, Martin 2018, Asher 2018a).

Origin and Mesozoic Mammals

Early Mammaliaforms

As mentioned above, mammaliaforms evolved from within a larger clade called synapsids. The latter diverged from other tetrapods (mainly Reptilia) during the Carboniferous, and non-mammalian synapsids include the grade "pelycosaurs" along with the clades therapsids and cynodonts (which are monophyletic when Mammalia are included in them; see Angielczyk and Kammerer 2018 and Chapter 28). The oldest known mammaliaforms (with a squamosal-dentary joint) are the Late Triassic *Morganucodon* and the Early Jurassic *Sinocodon* (Figure 29.1). Among these early mammaliaforms, morganucodonts were small, shrew-like animals, already characterized by diphyodonty and a one-to-one occlusion of molars. They had a worldwide distribution, and at least some of them had adaptations to feeding on hard-shelled insects. Haramiyidans reached a larger size (up to 350 g) and had an omnivorous to herbivorous diet. Some forms have been interpreted as specialized for life in the trees; among those, the Late Jurassic *Maiopatagium* possessed a gliding membrane (as in dermopterans), and a four-limbed suspending roosting behavior has been hypothesized (Meng et al. 2017). Evidence for the presence of fur covering the body, as well as a protective ankle spur similar to that of platypus, have been observed among haramiyidans. Docodonts appear in the fossil record during the Middle Jurassic. With their more complex molars able to crush and grind, they were somewhat more omnivorous. Adaptations to fossorial, arboreal and even semiaquatic lifestyles have been found in various docodonts. A remarkable example is the Late Jurassic *Castorocauda*, bearing a beaver-like tail and webbed feet, and reaching a body mass of 800 g (Ji et al. 2006).

The earliest members of the crown group Mammalia date from the Middle Jurassic. The separation between monotremes and placentals + marsupials occurred about 165 Ma ago (Martin 2018). Among the first relatives of monotremes (australosphenidans), the Middle Jurassic *Pseudotribos* already showed fossorial adaptations. The earliest crown monotreme is recorded from the Early Cretaceous of Australia (Archer et al. 1985). Among the stem group to Marsupialia and Placentalia (i.e., the Theria), eutriconodonts are characterized by the middle ear bones being detached from the mandible. They display a wide range of locomotor adaptations, from terrestrial to arboreal, with a gliding membrane, and from semiaquatic to fossorial, with diversified diets (insects, invertebrates, fish and even small tetrapods). Among eutriconodonts the Early Cretaceous *Repenomamus* stands out for its large size (body mass estimated at up to 14 kg); fossilized stomach contents revealed that it fed, at least occasionally, on small dinosaurs (Hu et al. 2005). Another Early Cretaceous form, *Spinolestes*, combined different types of hair with protective spines and dermal scutes (Martin et al. 2015). Multituberculata is another large group of nontherian mammals, ranging from the Late Jurassic to the Eocene. With their typical multicusped molars and premolars, enlarged lower incisor, and often arcuate P4, these rodent-like small to medium-sized animals (skull up to 70 mm long) had an herbivorous to omnivorous diet. Some multituberculates had fossorial and saltatorial adaptations. Ranging from the Middle Jurassic to the Late Cretaceous, dryolestids were nontherian insectivorous

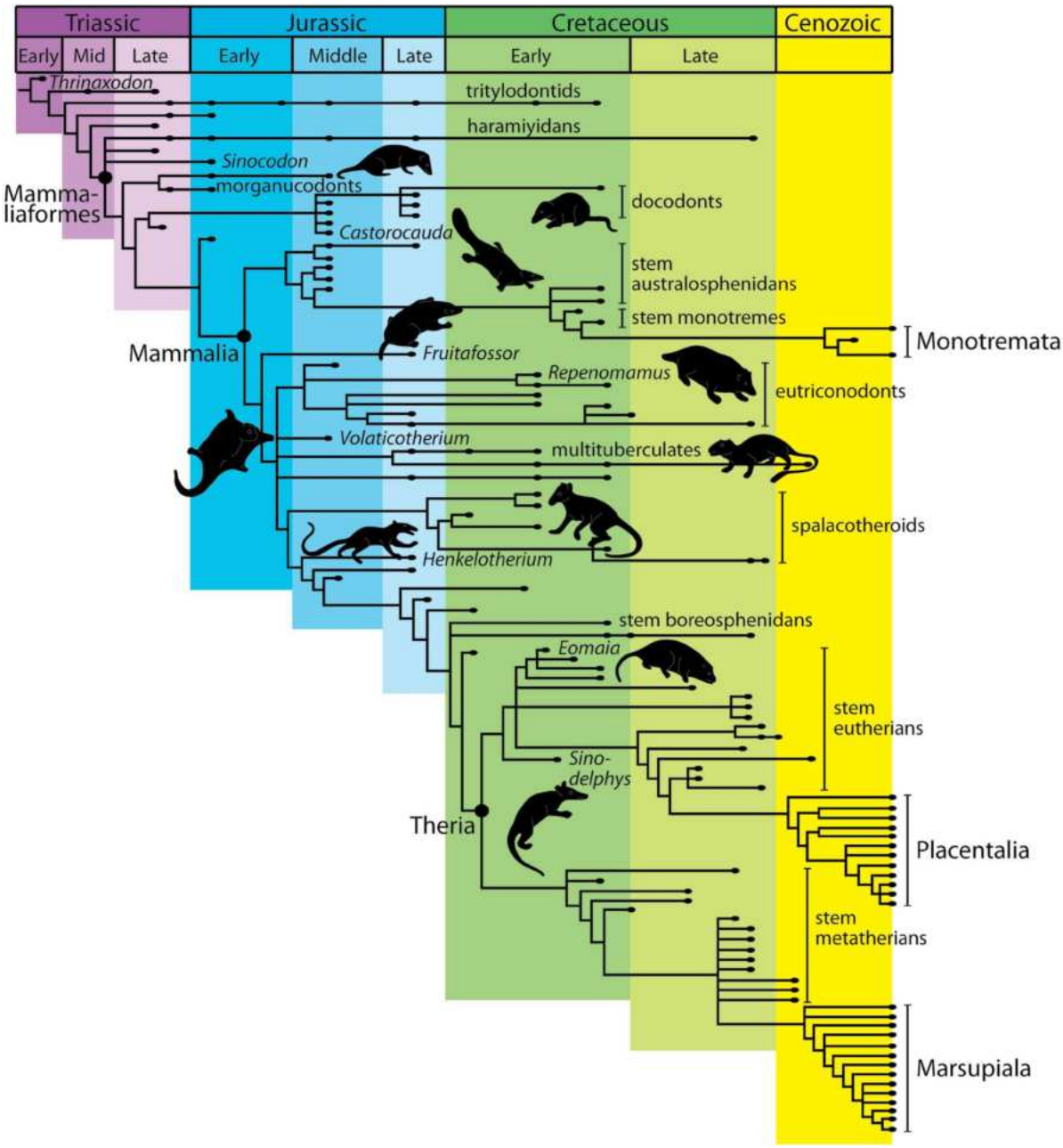


FIGURE 29.1 General phyletic tree of the Mammaliaformes, with their closest relatives within the Epicynodontia. (Tree based on Martin 2018, except for the modified position of *Sinodelphys*, following Bi et al. 2018.)

mammals characterized by an elongated and narrow snout. Among them, the small *Henkelotherium* (body length about 70 mm) had a gracile skeleton adapted to climbing and elongated caudals that may have been used for balancing and steering during leaps (Martin 2018). Well-suited for cutting and grinding, the tribosphenic molars of stem boreosphenids allowed these Cretaceous, Northern Hemisphere close relatives of the earliest therians to feed on tough plant material.

First Therians

Sinodelphys, from the Early Cretaceous of China, has long been considered the oldest known metatherian (Luo et al. 2003). However, a recent revision of this taxon included it in the Eutheria (Bi et al. 2018). Following this interpretation, the oldest known metatherians are now the so-called "Trinity therians", such as *Holoclemensia* and *Pappotherium*, from the Early Cretaceous (ca. 110 Ma) of western North America (Turnbull 1971), which are known only from isolated teeth. The crown group (Marsupialia) probably originated in the latest Cretaceous, and most Mesozoic metatherians are outside Marsupialia. However, because the fossil remains of metatherians in the Late Cretaceous and early Cenozoic are essentially isolated teeth and jaws, the taxonomic composition of the clade Marsupialia varies greatly according to different phylogenetic analyses, which are extremely labile.

Although the generalized dentition of most early metatherians suggests an insectivorous or omnivorous diet, some larger North American taxa (up to 2 kg) have dental specializations that suggest a carnivorous and durophagous diet (e.g., *Didelphodon*; Wilson et al. 2016). Another major radiation of carnivorous stem metatherians is known in South America from the early Paleocene to the late Pliocene; the Sparassodonta include a great variety of predaceous forms ranging from the size of a weasel to that of a large bear, and even including saber-toothed representatives (Muizon et al. 2019).

No crown placental mammal is currently known before the K-Pg boundary. The oldest stem eutherians are from the early Late Jurassic (*Juramaia*, Luo et al. 2011) and the Early Cretaceous of China (*Eomaia*, Ji et al. 2002; *Sinodelphys*, Luo et al. 2003; *Ambolestes*, Bi et al. 2018). Eutherians remain small through the Cretaceous, with long snouts and slender mandibles, and a predominantly insectivorous diet encountered, for instance, in the asiorychtitheres, a Late Cretaceous radiation of small eutherians in central Asia. Scansorial adaptations are found in both *Eomaia* and *Juramaia*, and facultative bipedal cursorial abilities have been inferred from limb bone features in zalambdalestids, as in extant elephant shrews (Kielan-Jaworowska 1978, Martin 2018).

Extant Mammalian Clades

Only a few mammalian lineages survived the end-Cretaceous mass extinction (Figure 29.2). This catastrophic event was followed by a major early Cenozoic radiation, during which all extant orders appeared (Kemp 2005, Asher 2018b).

The crown group Monotremata includes the duck-billed platypus (ornithorhynchids) and four species of echidna (tachyglossids). The geologically oldest ornithorhynchid is known from the Paleocene of Patagonia.

Marsupials can be split into two major geographic groups, comprising forms from the Americas and forms from Australasia. The Australasian group is monophyletic, but the American group collectively is not: the South American microbiotheres have been shown to be genetically closest to the Australian clade, so the American group is paraphyletic. Because the earliest known marsupials (didelphoids) are found in the Northern Hemisphere, it is inferred that the group migrated to South America and then across to Australia and southeast Asia during the Cretaceous. American marsupials include opossums (didelphids) and shrew opossums (caenolestids), whereas the Australian australidelphian clade includes dasyuromorphs (e.g., thylacines), notoryctids (marsupial moles), peramelians (e.g., bandicoot) and the most speciose clade, diprotodonts (e.g., wombats and kangaroos). The South American microbiotheres (e.g., extant "monito del monte", genus *Dromiciops*) are sometimes included in the australidelphians because of their sister-taxon relationship with them, but no microbiotheres are known from Australia. Whereas the oldest known marsupial is probably the North American polydolopimorphian genus *Glasbius*, most marsupial evolution took place in South America and Australia, in coexistence with several stem metatherian lineages. A major radiation of South American marsupials is represented by the primate- and/or rodent-like polydolopimorphians. In regard to their dental morphology, they are commonly regarded to have been adapted to frugivory and/or granivory (Goin et al. 2016). Polydolopimorphians disappeared at the end of the Paleogene and were ecologically replaced during the Neogene

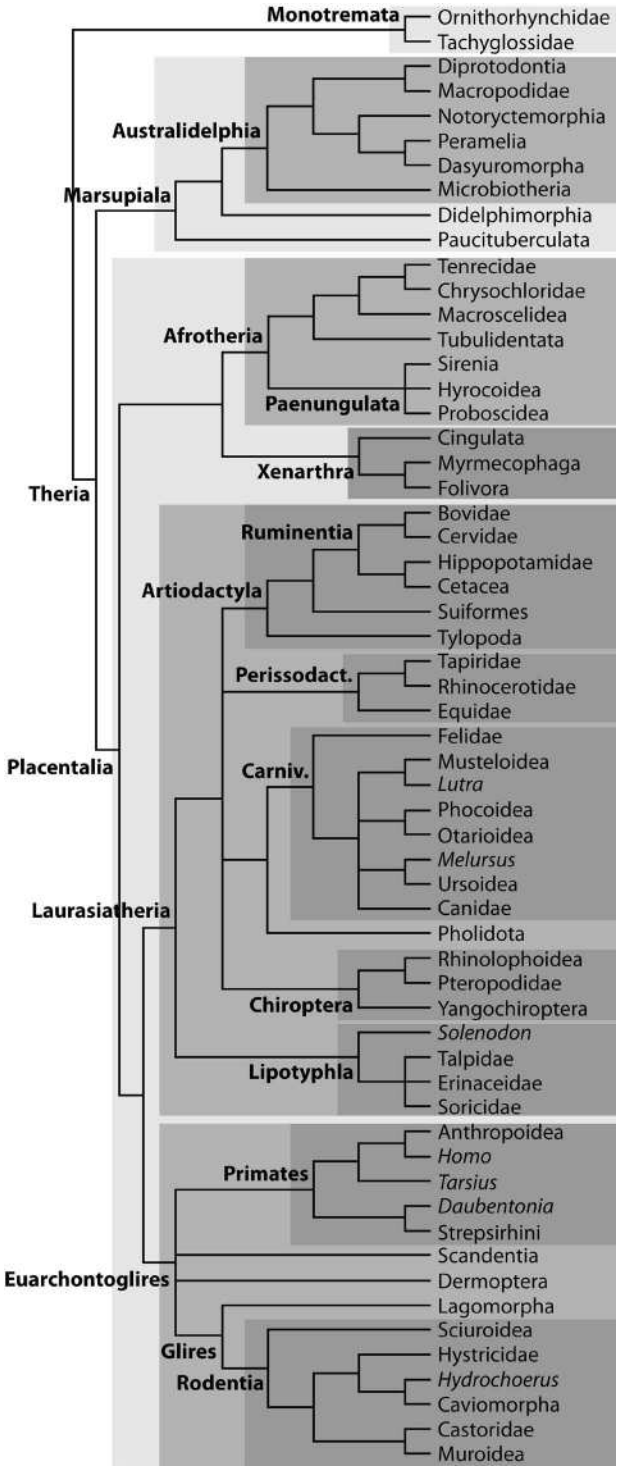


FIGURE 29.2 Basic phyletic structure of the clade Theria. The content of the main taxonomic divisions, along with the nomenclature applied to them, are used as a basic frame for organizing the present review. (Tree based on Asher 2018a.)

VetBooks.ir

by the caenolestoids. In Australia, the four extant groups of Australasian marsupials are well known as early as the late Oligocene, but earlier records of metatherians are restricted to the early Eocene Tingamarra (Southeastern Queensland) local fauna (Godthelp et al. 1992). The Tingamarra metatherian fauna includes two polydolopimorphian marsupials (*Thylacotinga* and *Chulpasia*) and two taxa of small insectivorous metatherians (*Archaeonothos* and *Djarthia*), which are not closely related to Marsupialia (Beck 2015).

About 18 extant orders of placentals are currently recognized and placed in four major groups: Xenarthra, Afrotheria, Laurasiatheria, and Euarchontoglires (see Asher 2018b).

Xenarthra includes vermilinguans (anteaters), folivorans (sloths and ground sloths) and cingulates (armadillos and glyptodonts). The earliest xenarthran record is represented by armadillo scutes and indeterminate xenarthran limb bones from the late Paleocene-early Eocene of Brazil. This is why the possession of osteoderms is considered plesiomorphic within Xenarthra (Hill 2006). This clade is also known for a particular design of vertebral articulation (e.g., Alves et al. 2017) and a low level of basal metabolism (Hayssen and Lacy 1985, but see also White and Seymour 2004). The most iconic extinct cingulates are glyptodonts, characterized by their thick and unarticulated carapace; they appeared during the middle Eocene and reached a size of more than 3 m during the Pleistocene. Although folivorans only appear in the fossil record of South America during the early Oligocene, their past diversity and disparity contrasts markedly with the arboreal, suspensory habitat of the two small extant genera. For example, giant ground sloths reached a weight of several tons (*Megatherium*) and a highly specialized aquatic sloth, *Thalassocnus*, has been described from marine deposits of the late Neogene of Peru and Chile (Muizon and McDonald 1995). The fossil record of vermilinguans is traced back to the early Miocene; these early forms already bore a long, edentulous snout and were most likely myrmecophages.

Afrotheria gathers proboscideans (elephants), sirenians (sea cows) and hyracoids (hyraxes), all three placed in the clade Paenungulata, with tubulidentates (including the fossorial aardvark), macroscelidids (elephant shrews), tenrecids (tenrecs) and chrysochlorids (golden moles). Apart from sirenians, the earliest known fossils from all these groups are found in Africa. Proboscideans appear in the fossil record during the Paleocene and were already diverse in size during the early Eocene (Gheerbrant et al. 2002). They gradually evolved key morphological features of extant elephants (e.g., anteriorly situated orbit, graviportal limbs, tusks, horizontal tooth replacement and lamellar enamel on cheek teeth), and entered Eurasia during the late Oligocene. All extant hyracoids (grouped in three genera) are small and constitute only a remnant of a much higher past diversity, including medium-sized to large herbivores from the middle to late Paleogene. Although extant sirenians only comprise two fully aquatic, tail-propelled genera, i.e., *Trichechus* spp. (the manatees) in the Atlantic and the dugong (*Dugong dugon*) in the Indian Ocean, their fossil record extends back to the Eocene. The earliest sirenians were quadrupedal forms, like the 2-m long *Pezosiren* in the Caribbean (Domning 2001), combining weight-bearing hind limbs with a series of aquatic adaptations (e.g., dorsal position of nostrils and dense ribs). The fully extinct group Desmostylia includes a few genera of large, hippo-like semiaquatic mammals, from late Oligocene and Miocene marine deposits of the northern Pacific. Desmostylians are either related to sirenians and proboscideans or to Euungulata (perissodactyls + artiodactyls). Other afrotheres (macroscelideans, tubulidentates, chrysochlorids, and tenrecids) have a relatively limited fossil record, mostly from Africa (apart from a few tubulidentates from the Oligocene of Europe).

Euarchontoglires contains primates, dermopterans (including the flying lemur) and scandentians (treeshrews), together with lagomorphs and rodents (the last two comprising the clade Glires). Several extinct euarchontoglire groups (e.g., carpolestids, pleasiadapids and micromomyids) have been placed on the stem leading to primates (e.g., Bloch and Boyer 2003), with the oldest being *Purgatorius*, from the early Paleocene of Montana and characterized by a highly flexible ankle joint. The earliest diverging primates include groups leading to lemurs, galagos, lorises and tarsiers, all retaining a relatively small brain and a long snout. They first appear in the earliest Eocene, before the radiation on northern continents of small, arboreal forms with insectivorous and frugivorous diets. Anthropoid primates, including monkeys and apes, have been proposed to appear in the fossil record during the Middle Eocene, with radiations recorded both in Asia and North Africa. The fossil record of both scandentians and dermopterans (the latter characterized by a gliding membrane) is sparse and traces back to the Eocene of Asia. Among Glires, taxa from the Paleocene of Asia (e.g., the eurymylid *Heomys* and the mimotonid *Mimotona*) have been placed on the stem to either rodents or lagomorphs. Species from the early Eocene already possess a single pair of enlarged, ever-growing central incisors on both the upper and lower jaws. With more than 2000 living species, rodents are the most diverse mammalian order. They underwent an explosive radiation phase during the late Eocene in North America, Eurasia and Africa, and reached South America as early as the middle Eocene (Antoine et al. 2012). There, caviomorphs invaded ecological niches contrasting with typical rodent niches (e.g., large, semiaquatic forms like the Late Miocene *Phoberomys*, up to 700 kg, see Sánchez-Villagra et al. 2003). The earliest lagomorphs come from middle Eocene deposits of North America.

Finally, Laurasiatheria includes lipotyphlans (e.g., hedgehogs, moles and shrews), chiropteres (bats), carnivorans (including pinnipeds), pholidotes (pangolins), perissodactyls and artiodactyls (the latter including cetaceans). Several other groups of laurasiatheres are exclusively fossil but have constituted an important element of the Cenozoic mammalian faunas (Muizon et al. 2015). For example, pantodonts and tillodonts, mainly distributed in North America and Eurasia during the Paleocene and Eocene (with a unique occurrence in South America; Muizon et al. 2015), were among the first large to very large mammals to evolve after the K/Pg extinction. They ranged from the size of a rabbit to that of a small rhinoceros and formed part of the megaherbivorous component of the early Paleogene faunas. Furthermore, several other groups of large herbivorous mammals are known during most of the Cenozoic in South America, but absent until the Pleistocene from North America. Among them, litopterns

VetBooks.ir

were equid-like cursorial mammals, whereas notoungulates were more diverse and ranged from the size and aspect of a hare to that of a large hornless cow. Both of them survived until the Holocene and have been regarded as forming the sister group of perissodactyls on the basis of molecular analyses (Welker et al. 2015). Others, such as pyrotheres and astrapotheres, were elephant-like and/or rhinoceros-like and survived until the Oligocene and Miocene, respectively.

Among lipotyphlans, whereas the earliest erinaceid and soricid are, respectively, from the Paleocene and Eocene of North America, the oldest talpid is found in late Eocene deposits of Europe. The earliest bats, including *Onychonycteris* from the early Eocene of Wyoming, already possessed the capability for powered flight (e.g., elongate manual digits, structures to support the patagium and gracile skeleton), together with probably more limited laryngeal echolocation abilities (Simmons et al. 2008). Virtually nothing is thus known about intermediary stages of the evolution of flight among early chiropteres.

Whereas stem Carnivora include a series of extinct groups (e.g., Nimravidae and Viverravidae) whose fossil records are traced back to the early Paleocene, the oldest crown carnivorans date from the late Eocene. The first felids (Oligocene and early Miocene of Europe) display robust limbs and retractile claws, suggesting an arboreal habitat. Other feliforms (viverrids, herpestids and hyaenids) also radiated during the Miocene, mostly in Eurasia and Africa. Canids and ursids appear in the fossil record of North America during the Middle and Late Eocene, respectively, whereas procyonids (raccoons) and mustelids (weasels, otters) are first found in Late Eocene-Early Oligocene deposits. Pinnipeds are a monophyletic group of arctoid carnivorans, either more closely related to ursids or to mustelids (Berta et al. 2018). The earliest stem pinnipeds date from the Late Oligocene of the North Pacific, and already possessed fore and hind limbs modified as flippers, indicating an amphibious lifestyle. The first members of the extant pinniped families Phocidae (true seals), Otariidae (fur seals and sea lions) and Odobenidae (walruses) are found in Early to Middle Miocene marine deposits from the North Atlantic (phocids) and North Pacific (otariids and odobenids).

Although pangolins are represented today by only eight species distributed in Africa and Asia, the fossil record of Pholidota starts during the Eocene, with a much broader distribution. The oldest forms are represented by finely preserved specimens from Messel (e.g., *Eomanis*, already displaying the typical overlapping horny scales of extant pangolins).

Perissodactyla contains few extant species (eight horses, five to six rhinos and four tapirs), contrasting with the considerable past diversity of this group of herbivorous mammals. Size range is especially noteworthy during the Paleogene, from tiny Early Eocene tapiroids to large, rhino-like Eocene brontotheres, and the giant, graviportal indricothere *Paraceratherium* (latest Eocene to Oligocene of Asia, up to 6 m tall). The oldest relatives of horses are found in the early Eocene of Europe and North America (e.g., *Hyracotherium*, *Pliolophus, Eohippus*), and were no larger than a small dog. A major equid radiation occurred during the Miocene in North America, with numerous grazing forms characterized by hypsodont teeth and gradual adaptation to cursoriality (McFadden 2005). Rhinocerotoids were far more diverse from the Eocene to the Miocene than now, including dog-sized browsers, hippo-like grazers, and the abovementioned giant indricotheres. From the Late Oligocene, true rhinos radiated in all northern continents as well as Africa. The greatest diversity of tapiroids is to be found during the Eocene of North America and Eurasia, with a series of browsers displaying a gradual development of the proboscis.

Artiodactyls are characterized by a highly distinctive ankle morphology (double-pulley astragalus and paraxonic foot), which allows tracing the group down to the early Eocene. Based on molecular and morphological evidence, cetaceans are nested within artiodactyls, as a sister group to hippos. The earliest known cetaceans (e.g., *Pakicetus*) date from the Early Eocene and were quadrupedal, with fore and hind limbs capable of bearing their weight on land (Gingerich et al. 2001, Thewissen et al. 2001). A gradual detachment of the pelvis from the sacrum occurred during the Middle Eocene among amphibious protocetids, before a strong reduction of the hind limb in more derived, tail-propelled forms (basilosaurids) (Gingerich et al. 1990). The latter gave rise to the two extant cetacean suborders (mysticetes, baleen whales and relatives and odontocetes, echolocating toothed whales) before the end of the Eocene (Marx et al. 2016a). Osteological correlates for an early form of sonar system are found in the geologically oldest odontocetes (Geisler et al. 2014). Contrastingly, the earliest mysticetes retained teeth and were devoid of baleen, the keratinous filtering devices characterizing all extant mysticetes. Some toothed mysticetes have been reconstructed as combining teeth with an early form of baleen, but such an interpretation remains debated (Deméré et al. 2008, Marx et al. 2016b). Although the fossil record of hippopotamids is restricted to the Miocene, a relationship with the extinct, Late Eocene to Oligocene anthracotheres has been proposed, partly filling the gap with the time of divergence from cetaceans (Lihoreau et al. 2015). Suids (pigs) appear in the Eurasian fossil record during the Oligocene, and radiated from the Miocene onward in the Old World, whereas tayassuids (peccaries) are first found in North America during the Miocene, before a dispersal to South America. Primarily appearing in North America, and present there since the Eocene, camelids were a major part of the large herbivore fauna during the Miocene. Today's camels in Eurasia and Africa and llamas in South America result from Late Miocene to Pliocene migrations. Other major artiodactyl groups are gathered in the clade Ruminantia (including giraffids, bovids and cervids). The earliest ruminants appear in North America and Eurasia during the late Eocene, and by the early Miocene in Africa, where bovids became dominant (Kemp 2005).

Preliminary Remarks on Comparative Bone Histology in Mammals

As mentioned in the historical introduction of this book, early (and now classic) comparative syntheses of bone histology broadly considered the features of mammals, as exemplified by Quekett (1849), Foote (1911, 1916), Amprino and Godina (1947) and Enlow and Brown (1958). These texts pointed out the diversity of diaphyseal and epiphyseal microstructures

VetBooks.ir

in this large clade. Mammals have an ambiguous position in comparative bone histology because they are the group that provided most of the fundamental knowledge on skeletal tissue biology, but since the great historical reviews quoted above have been the subjects of the fewest paleohistological studies (Kolb et al. 2015b). Several reasons may explain this situation. Extant mammals, though very diverse from taxonomic and adaptive points of view, differ little from the extinct forms to which they are phylogenetically close, at least for post-Eocene terrestrial taxa (aquatic forms show more pronounced differences). Therefore, the recourse to bone histology to infer the basic life history traits and physiological features of extinct mammals may seem less critical than in Paleozoic or Mesozoic amphibians, archosaurs or synapsids, which have no morphofunctional equivalents in extant faunas. Moreover, pre-Cenozoic mammalian faunas, for which important biological questions remain enigmatic, are often represented by taxa of small size, with poorly preserved specimens (numerous species are known only from teeth), too rare to be submitted to the destructive processing required by histology. In addition, because of the intense Haversian remodeling of cortical bone that occurs in most mammals, the histological structure of primary periosteal deposits is generally inaccessible in adults, at least in the deep cortical regions formed during the most active stage of skeletal growth. For the same reason, one of the most fruitful traits of bone histology from a biological perspective (i.e., the cyclical growth marks) are seldom preserved in adults; as a consequence, the occurrence of these marks has long been considered irregular and uneven in mammals and other endothermic animals, thus limiting the heuristic value of bone histology in these taxa.

Despite these limitations, the study of mammals ranks as one of the strongest and most reliable sources of information in comparative skeletal histology because it can directly benefit from the conceptual and technical progresses of biomedical research, which are mainly based on mammalian models. In the last decade or so, interest in mammals for comparative bone histology has been revived. This revival results, in part, from the increasing sophistication of histomorphometric methods, which allow meaningful comparisons among mammals (e.g., Amson 2021), and between mammals and other taxa more frequently considered in paleohistology, such as dinosaurs and other archosauromorphs (e.g., Sander and Andrassy 2006, Köhler et al. 2012). The renewed interest in the study of mammals also results from the observation that cyclical growth marks in this group are much more common and better preserved than previously thought, not only in dental tissues, a situation long known and used in a practical perspective (Perrin and Myrick 1980, Klevezal 1996), but also in primary cortical tissues of diverse skeletal sites (long bones, mandible, ribs, baculum, etc.) in taxa little studied hitherto from this perspective (Köhler and Moyá-Solà 2009, Marin-Moratalla et al. 2013, Amson et al. 2015).

Recent review articles have addressed this topic (see especially Kolb et al. 2015, b). This chapter is an additional attempt. To avoid redundancy, we focus here on subjects less developed hitherto in other reviews (microanatomical features of bones, structure of osteoderms, antlers and baculum). Mammalian bones show great structural diversity within a single skeleton. This raises the question of the most representative territory for comparative studies. Short bones must be discarded because their deep primary cortices are extensively resorbed and only the most recent cortical layers (representing late growth) remain accessible. Similarly, flat bones, whether in the cranium, mandible or limb girdles, are unsuitable for basic histological comparisons because they undergo extensive inner and outer remodeling (local morphogenetic work) during which most of the early primary cortex is removed. Consequently, the following account of the histological traits of mammalian bones will mainly, though not exclusively, focus on the midshaft regions of appendicular long bones and ribs, which constitute current standard sampling locations, allowing comparisons of homologous skeletal elements among taxa. The taxonomic frame of this chapter is limited to mammaliaforms proper; premammalian taxa (therocephalians and cynodonts) are described in Chapter 28 by J. Botha and A. Huttenlocker (see also Botha-Brink et al. 2012, Chinsamy-Turan 2012).

Early (Mesozoic) Mammals

Until the study by Chinsamy and Hurum (2006) (see also Hurum and Chinsamy-Turan 2012) few studies specifically dealt with bone microstructures in early mammals and Prototheria, which are scarce in both the fossil record and extant faunas. Histological descriptions of early mammal limb bones now include the zalambdalestids *Zalambdalestes* and *Barunlestes* and the multituberculates *Kryptobaatar* and *Nemegtbaatar*, along with *Morganucodon*, a taxon whose phylogenetic affinities with either more basal therapsids or therians remain unclear (Chinsamy and Hurum 2006, Hurum and Chinsamy-Turan 2012; see also Wilkinson 1999 for the debate about *Morganucodon* affinities). Additionally, the inner structure of a mandible from the Paleocene multituberculate *Ptilodus* was described by Enlow and Brown (1958).

Morganucodon and the Allotheria (Multituberculates)

The descriptions given below summarize the initial observations by Chinsamy and Hurum (2006), which remain hitherto the most detailed source of information and were summarized *verbatim* in the 2012 review of these authors (Hurum and Chinsamy-Turan 2012) and in Kolb et al. (2015a) .

In *Morganucodon*, the deep cortices of the ulna display woven-fibered tissue housing sparse longitudinal primary osteons and broad resorption bays. The bone represents a woven-parallel complex at this level, with evidence of inner resorption but no Haversian systems. In more peripheral cortical layers, bone structure turns into avascular parallel-fibered bone. The figure given by Chinsamy and Hurum (2006) suggests that the cross section they studied might have been located close to the metaphysis. The histological characteristics of the femur (a bone 1.5 mm in mean diameter at mid-diaphysis) of the same species could not be clearly settled due to severe diagenesis. Otherwise, this bone has a clear tubular organization, with a compact cortex void of inner resorption and a medullary cavity entirely free of trabeculae. Such an

VetBooks.ir

architecture suggests a terrestrial habitat (e.g., Quémeneur et al. 2013). The corticodiaphyseal index (CDI) of this bone, as measured from Chinsamy and Hurum's (2006) illustrations, has a medium value: 41% (a similar index, the *relative bone thickness* or RBT, calculated by Chinsamy and Hurum 2006 is only 26%). Perimedullary remodeling, creating a thick layer of endosteal lamellar tissue, spreads symmetrically.

Bone structure in multituberculate long bones is known from femoral cross sections sampled at midshaft (*Kryptobaatar dashzevegi*) and from a metaphysis (*Nemegtbaatar gobiensis*). At mid-diaphysis, *Kryptobaatar's* femur is a gracile tubular bone with a very low mean CDI of 18.6%. Histologically, the femoral cortex is described as "a mixture of parallel-fibered and woven textured type of bone tissue", housing some primary osteons at an incipient stage of formation (Chinsamy and Hurum 2006). This concise description calls for further investigation. The sections from the metaphysis of the *Nemegtbaatar* femur are difficult to interpret. As Chinsamy and Hurum (2006) noted, metaphyses are the site of complex inner and outer remodeling activities related to the growth in length of the bones (see also Chapters 9 and 11). Therefore, they are not representative of the basal histological type prevailing in the periosteal cortices of long bones. The important information from the *Nemegtbaatar* femur is that the outermost periosteal cortex is locally made of parallel-fibered bone with relatively sparse longitudinal or oblique simple vascular canals. Furthermore, the mandibular cortex of *Ptilodus* is apparently made of "lamellar" tissue displaying simple vascular canals arranged radially and longitudinally (Enlow and Brown 1958).

Prototheria (Monotremes and Stem Group)

Apart from the now classic study of the evolution of epiphyseal structure by Haines (1942), histological descriptions of prototherian long bone cortices were presented by Amprino and Godina (1947), Enlow and Brown (1958), Chinsamy and Hurum (2006), Hurum and Chinsamy-Turan (2012) and Kolb et al. (2015b). Furthermore, miscellaneous histomorphometrical measurements of limb bones, ribs and vertebrae were conducted in *Ornithorhynchus*, *Tachyglossus* and *Zaglossus* by Canoville and Laurin (2010), Quémeneur et al. (2013) and Canoville et al. (2016). At both microanatomical and histological levels, the few data published up to now are surprisingly discrepant (compare for example the observations of *Ornithorhynchus* by Enlow and Brown 1958 and Chinsamy and Hurum 2006), which suggests substantial intraspecific variation, especially for bone remodeling. For this reason, new first-hand observations are presented below on limb bones and ribs of two extant monotreme taxa: *Ornithorhynchus anatinus* and *Tachyglossus aculeatus*.

Remark on Epiphyseal Structure in the Prototherians

The detailed and extensive synthesis conducted by Haines (1941) remains the main first-hand description of the structural features of prototherian epiphyses (see also Ricqlès 1979). This study shows that long bone epiphyses in *Echidna* sp. [*sic*] consist of a cartilaginous mass in which a diffuse calcification field spreads during growth. This calcified volume is supplied with blood by vessels originating from the metaphysis and proliferating upward, in the form of a big ramified "pipe", to perforate the growth plate and reach the core of the epiphyseal cartilage. Several points of ossification then appear in the mineralized cartilage volume. As Haines (1942) pointed out, this epiphyseal structure is unparalleled in other mammals, and its evolutionary origin remains unknown.

Long Bone and Rib Microstructure

The radius, femur and tibia of *O. anatinus* are basically similar to each other in both their microanatomical and histological features. Though tubular, these bones have a small but well circumscribed medullary cavity void of spongy tissue (Figure 29.3A, B). The highest CDI is encountered in the radius (94.2%), and the lowest (63.4%) in the femur. Such compact bones are commonly encountered in amphibious and aquatic tetrapods (see below).

Histologically, the bones of *O. anatinus* comprise three strata (Figure 29.3A–C). The medullary cavity is surrounded by a very thick layer of endosteal parallel-fibered bone, occasionally housing sparse, simple radial vascular canals. This tissue is recognizable by the spindle-like morphology of its cell lacunae and their orientation parallel to the bone contour; otherwise, its birefringent properties are relatively poor. In ordinary light, it looks opaque, an aspect due to the great local development of canaliculi around the cell lacunae (Figure 29.3C, inset). The small diameter of the medullary cavity in this taxon seemingly results from a protracted or accelerated deposit (or both) of this secondary endosteal layer. The latter is limited by a reversion line and bordered by a stratum of variable thickness that occupies a median position in the cortex. In polarized light the median stratum shows a convoluted, irregular aspect, along with longitudinal primary osteons and traces of a relatively mild Haversian substitution (Figure 29.3B, C). In ordinary transmitted light, it is highly translucent and needs extended field depth to be seen. Due to resorption over the femoral shaft and off-centered growth, the median layer may locally outcrop at the surface of the cortex (Figure 29.3A–C). The third, more peripheral layer is also translucent; it consists of strongly birefringent lamellar bone of periosteal origin (Figure 29.3B), displaying faint and irregularly spaced annuli (Figure 29.3A, B). This layer is separated from the subjacent one by a reversion line (Figure 29.3B, C).

The three-stratum structure observed in *Ornithorhynchus* is common in mammals. It has already been mentioned by several authors (see e.g., Ricqlès' 1975 general synthesis) and was described and analyzed in detail by Enlow (1963) in his classic *Principles of Bone Remodeling*. In the course of this chapter, it will be encountered in many taxa. Deciphering the microstructure of *O. anatinus* bones in terms of growth pattern is relatively straightforward, with an exception for the median, well-vascularized stratum. The complex, convoluted geometry (especially obvious in the femur) of this layer is strongly reminiscent of the compacted, coarse cancellous bone that forms at the metaphyseal level (see Chapters 4 and 8). This indication is

VetBooks.ir

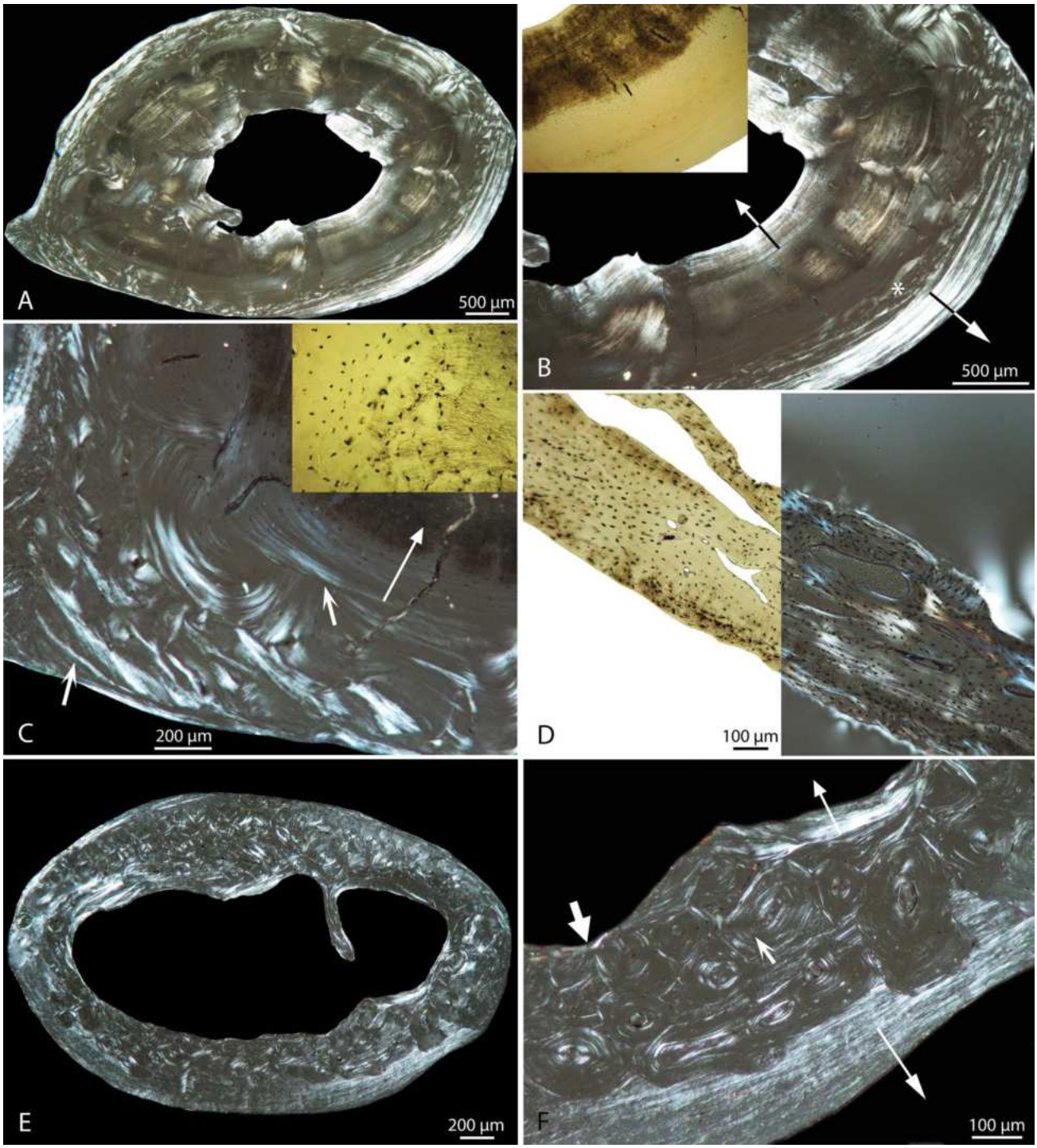


FIGURE 29.3 Long bone and rib microstructure in the Monotremata (Prototheria). A, Femur of an adult *Ornithorhynchus anatinus*. Mid-diaphyseal cross section viewed in transmitted polarized light. B, Detail of the section shown in A. Main frame: polarized light; inset: detail of the cortex in ordinary transmitted light. Inward directed arrow: perimedullary endosteal bone. Outward directed arrow: periosteal bone of the cortex. Asterisk: compacted coarse cancellous bone. C, Detail of the femur cortex showing the three-strata pattern in polarized light. The two small arrows point to reversion lines. The inset shows the difference in canaliculi of the cell lacunae between translucent and opaque layers. D, Partial view of the femur cortex of *Tachyglossus aculeatus*. Cross section at mid-diaphysis. Left half: ordinary transmitted light; right half: polarized light. E, Cross section in a rib of *T. aculeatus*. Polarized light. F, Detail of the rib cortex shown in E. Thick arrow: perimedullary resorption field. Long thin arrows: same meaning as in part B. The short arrow points to a secondary osteon (Haversian system) in the remodeled core of the cortex.

VetBooks.ir

consistent with the presence of a reversion line along its outer margin. However, another interpretation could be that this tissue forms locally, at the mid-diaphyseal level, through the compaction of a former perimedullary spongiosa. The resorption lines framing it below and above would then be due to inner (perimedullary) and outer (subperiosteal) remodeling of the bone related to morphogenetic processes. In the course of this chapter, it shall be observed that the presence in the middiaphyseal region of compacted coarse cancellous bone possibly originating from metaphyses can also be suspected in other taxa and could well be relatively frequent in mammals. This feature was recently shown in the aardvark *Orycteropus afer* by Legendre and Botha-Brink (2018), the armadillo *Dasypus novemcinctus* by Heck et al. (2019) and the rodent *Bathyergus suillus* (Montoya-Sanhueza and Chinsamy 2017). The question is further considered in the section relative to Tubulidentata.

Compared to the amphibious *Ornithorhynchus*, the terrestrial echidna *T. aculeatus* has lightly built bones. The femur available for study has compactness and CDI values (21% and 13.8%, respectively) well below those commonly encountered in mammals (see also Amson 2021). This feature might be an individual characteristic, but the humerus used by Canoville and Laurin (2010) was also very lightly built (compactness: 26%). Due to the huge development, through cortical resorption, of the medullary cavity of this bone, only the most peripheral layer of the cortex persists (Figure 29.3D). It is made of a vascularized tissue (longitudinal and oblique simple canals) showing characteristics intermediate between woven-fibered bone (multipolar osteocyte lacunae distributed randomly within the matrix) and parallel-fibered bone (gross, irregular birefringence). The base of the cortex is eroded and remodeled and turns into a spongiosa. No external fundamental system (EFS) appears in the studied femur. This overall structure is comparable to that described and illustrated for the same bone by Amprino and Godina (1947). *Tachyglossus* ribs are more robust (compactness = 64.3%, CDI = 42%, i.e., "normal" values for a terrestrial mammal; cf. Canoville et al. 2016) and their cortices basically display two strata (Figure 29.3E, F). The periphery of the medullary cavity is lined with a discontinuous layer of secondary lamellar bone, with obvious signs of local resorption related to the drift of the medullary cavity during growth. The rest of the cortex is a thick layer of lamellar tissue, intensely remodeled in its lower region where it turns into dense Haversian bone. The drift process affecting the medullary cavity also involved cortical growth. It resulted in the presence of an apposition surface on one side of the bone, combined with surficial resorption on the opposite side (Figure 29.3E). The cortices of the two *Tachyglossus* bones used here are void of cyclical growth marks.

Skeletal Microstructures of the Metatheria

Extant and extinct metatherian faunas are relatively diverse (340 extant species: Sanchez-Villagra 2013); however, studies of the inner structure of their bones, at a histological level, have concerned only a small number of recent taxa: the Didelphidae *Didelphis virginiana* (Foote 1911, Amprino and Godina 1947, Enlow and Brown 1958, Singh et al. 1974, Hamrick 1999, Hurum and Chinsamy-Turan 2012), *D. marsupialis* (Haines 1941), *D. albiventris*, *Lutreolina crassicaudata* (Kolb et al. 2015b) and the Macropodidae *Macropus rufus* (Amprino and Godina 1947, Hurum and Chinsamy-Turan 2012) and *M. fuliginosus* (Chinsamy and Warburton 2020; see this reference for further literature survey). In parallel with these histological studies, comparative investigations on the microanatomical features (inner compactness and architecture) conducted by Canoville and Laurin (2010) for the humerus, Quémeneur et al. (2013) for the femur, Canoville et al. (2016) for the ribs and Dumont et al. (2013) for the vertebrae, included four marsupial taxa within broad tetrapod samples: *D. virginiana*, *M. rufogriseus*, *Vombatus ursinus* and *Perameles nasuta*. To our knowledge, only one fossil bone of a marsupial, the femur of an undetermined Pleistocene *Vombatus* sp. (Walker et al. 2020) has been examined in a histological perspective. In the present review, additional first-hand histological observations dealing with *M. rufogriseus*, *V. ursinus* and *P. nasuta*, along with the small (squirrel-sized) extinct taxon *Pucadelphys andinus*, from the Early Paleocene of Bolivia (Muizon 1995), are presented.

Epiphyseal Characteristics of Metatherian Long Bones

Long bone epiphyses in large and small marsupials have a simple structure compared to that of eutherians, prototherians and even some large lizards (Varanidae). They consist of a thick cap of cartilage, in the core of which a relatively small volume becomes calcified and ultimately replaced by bone trabeculae. Haines' (1941) study showed that, opposite to the condition prevailing in prototherians and eutherians, marsupial epiphyses do not contain vascular canals, at least in the extant taxa studied hitherto (no information is available for fossil forms). The intraepiphyseal supply of osteoclast and osteoblast precursors involved in the local replacement of calcified cartilage by bone originates from the perichondrium. According to Haines (1941; see also Haines 1942, Ricqlès 1979), the absence of cartilage canals in marsupials appears to be a "primitive" character, likely to reflect the plesiomorphic condition of mammals. Therefore, the occurrence of canals in both the Prototheria and the Eutheria should represent two derived and convergent evolutionary acquisitions. The gross structure of marsupial epiphyses is shared with small eutherians, whatever their phylogenetic position, as exemplified by mice and other tiny rodents (Haines 1942). Moreover, data on the timing of growth plate activity in marsupials, along with its morphological consequences, were presented by Washburn (1946) and Hamrick (1999). These studies pointed out an important delay in epiphyseal fusion in opossum species compared to most of the eutherian taxa used for comparison. Shared with some rodents (rat, guinea pig), this feature is proposed to represent a primitive condition, like the relative acceleration in the ossification process that occurs in the anterior part of the postcranial skeleton of all marsupials (Weisbecker et al. 2008). Moreover, recent data by Chinsamy and Warburton (2020) show that the fusion of proximal epiphyses in *M. fuliginosus* limb bones is much delayed compared to distal epiphyses.

VetBooks.ir

Microanatomy and Histology of Limb Long Bones

Appendicular long bones in the species studied by Canoville and Laurin (2010), Quémeneur et al. (2013) or Chinsamy and Warburton (2020) have a typical tubular structure, whatever the size or locomotory adaptation of the taxa. CDIs for the femur are 28.4% in *D. virginiana*, 29.2% in *M. rufogriseus* and 52.6% in *V. ursinus*. The transition between the compact cortex and the hollow medullary region is sharp in *Didelphis* and *Macropus*, but more progressive in *Vombatus*. *Vombatus* bones are known to have particularly thick cortices (a feature possibly related to subterranean life: Walker et al. 2020), and one case of pathological hyperplasia of the humeral cortex has been described in this taxon (Slon et al. 2014). CDI values in the stylopod bones of *M. fuliginosus*, as computed from Chinsamy and Warburton's (2020) figures, seem to be variable (31.2% to 49.1% for the femur), but generally higher than the values observed in the *M. rufogriseus* femur measured here.

Published descriptions of bone microstructure in *Didelphis* species, which are all relatively small (the largest, *D. virginiana*, has a maximum body mass of 6 kg in males, e.g., Maunz and German 1997), show that limb bone cortices are mainly composed of parallel-fibered tissue displaying variable patterns of birefringence in cross section (Enlow and Brown 1958, Chinsamy and Hurum 2006, Hurum and Chinsamy-Turan (2012), Kolb et al. 2015b). Toward the depth of the cortex (approximately its deepest third), the bone matrix turns into the woven-fibered type (Kolb et al. 2015b). A thin EFS of parallel-fibered or lamellar bone occurs in adults. Although periosteal cortices are relatively thick, cyclical growth marks are considered rare in the long bone cortices of this taxon (see, e.g., Kolb et al. 2015b). Only Hurum and Chinsamy-Turan (2012) mentioned one single line of arrested growth (LAG) in an adult *D. virginiana*. Our own observations show the occurrence of two faint and interrupted LAGs in the femoral EFS of an adult *D. virginiana* (Figure 29.4A). Haversian remodeling, when present (the specimen described by Hurum and Chinsamy-Turan (2012) was void of Haversian systems), is mild and confined to the lower-most cortical layers (Amprino and Godina 1947, Enlow and Brown 1958, Kolb et al. 2015b). Vascularization is always present, in the form of either longitudinal primary osteons, oblique or radial simple vascular canals or a mixture of the three. Even the, perimedullary deposits of secondary (endosteal) bone tissue can show oblique to radial canals (Hurum and Chinsamy-Turan 2012). Quantitative data by Singh et al. (1974) indicate a vascular density of 3.2 canals per unit of surface (i.e., a standardized microscopic field area), a score relatively modest compared with that of, e.g., artiodactyls (score 6.3), Felidae (score 6) and Pongidae (score 7.5), but in the same range as, or somewhat higher than, that of small eutherians such as "insectivores" and mustelids (score 2), and lemurines (score 1).

Long bone cortices of larger species such as *V. ursinus* (body weight [BW] up to 39 kg), *M. rufogriseus* (up to 20 kg), *M. fuliginosus* (up to 70 kg) and *M. rufus* (up to 90 kg) share similarities with those of the *Didelphis* species (Hurum and Chinsamy-Turan 2012 and personal observations; see Figure 29.4B–G), but they also display differences. According to our observations, their vascularization consists of abundant primary osteons oriented longitudinally or obliquely (in a circular direction) in approximately the deep two-thirds of the cortex (Figure 29.4C, D). The simple canals occurring in the peripheral third (Figure 29.4C, E) are either longitudinal or radial. Canal density progressively decreases toward the bone periphery, to disappear entirely from superficial strata. In the thick-walled femur of *V. ursinus*, deep (early) cortical layers are preserved. They display a broad area of dense Haversian tissue in which primary periosteal deposits no longer exist (Figure 29.4B). Conversely, in the thinner-walled femur of *M. rufogriseus,* the deep cortical zone has been extensively resorbed (Figure 29.4C); its early histological features are inaccessible. Other cortical layers reflect later deposits, when growth rate had decreased. They are made of parallel-fibered tissue (Figure 29.4D) in which scattered primary osteons occur around the medullary cavity. The cortex of the *M. rufogriseus* femur studied here is devoid of secondary osteons. Both *Vombatus* and *M. rufogriseus* femora do not show a clear EFS but they display faint cyclical growth marks (Figure 29.4B), while short radial bundles of Sharpey's fibers are distributed throughout the cortex.

These observations basically agree with the histological description of Walker et al. (2020) on the humerus of *Vombatus* ursinus and *Vombatus* sp., and with the results of the study by Chinsamy and Warburton (2020) on a large sample of *M. fuliginosus*. In the humeral cortex of *Vombatus*, Walker et al. (2020) mention and illustrate the occurrence of "restricted areas of compacted coarse cancellous bone (CCCB)". In *M. fuliginosus*, the histological structure of bone in young specimens, and that encountered in the deep cortex of older individuals, consists of a woven-parallel tissue housing a variably oriented (but mainly reticular) canal network. Peripheral layers are generally of the parallel-fibered type. Cyclical growth marks, represented by zones and annuli in the deep cortex, and lines of arrested growth in more peripheral layers, regularly occur in this taxon. The full set of microstructural data available for *Didelphis*, *Vombatus* and *Macropus* finally suggests that marsupial long bones – beyond a comparable gross pattern that reveals the succession of two clear-cut growth phases, a phase of fast growth followed by a long-lasting phase of slow growth – nevertheless display some differences prompting further, more broadly documented investigations.

The femur of *P. andinus* has a very simple microstructure (Figure 29.4F). The primary periosteal cortex of this small but robust tubular bone (mean ICD = 55%) is entirely made of pure lamellar tissue with sparse simple vascular canals of small diameter. The canals are strongly oblique and oriented in a radial direction.

An Overview of Rib Structure

From a microanatomical point of view, the ribs of *D. virginiana, P. nasuta, V. ursinus* and *M. rufogriseus* call for few comments, because their gross inner architecture is comparable to that observed in most other terrestrial mammals (see Canoville et al. 2016). The ribs are oval in cross section and have a relatively thick cortex, especially in a small form like *Perameles* (CDI *ca*. 52%). In *M. rufogriseus*, ribs and femur differ in some of their histological features. Although the

VetBooks.ir

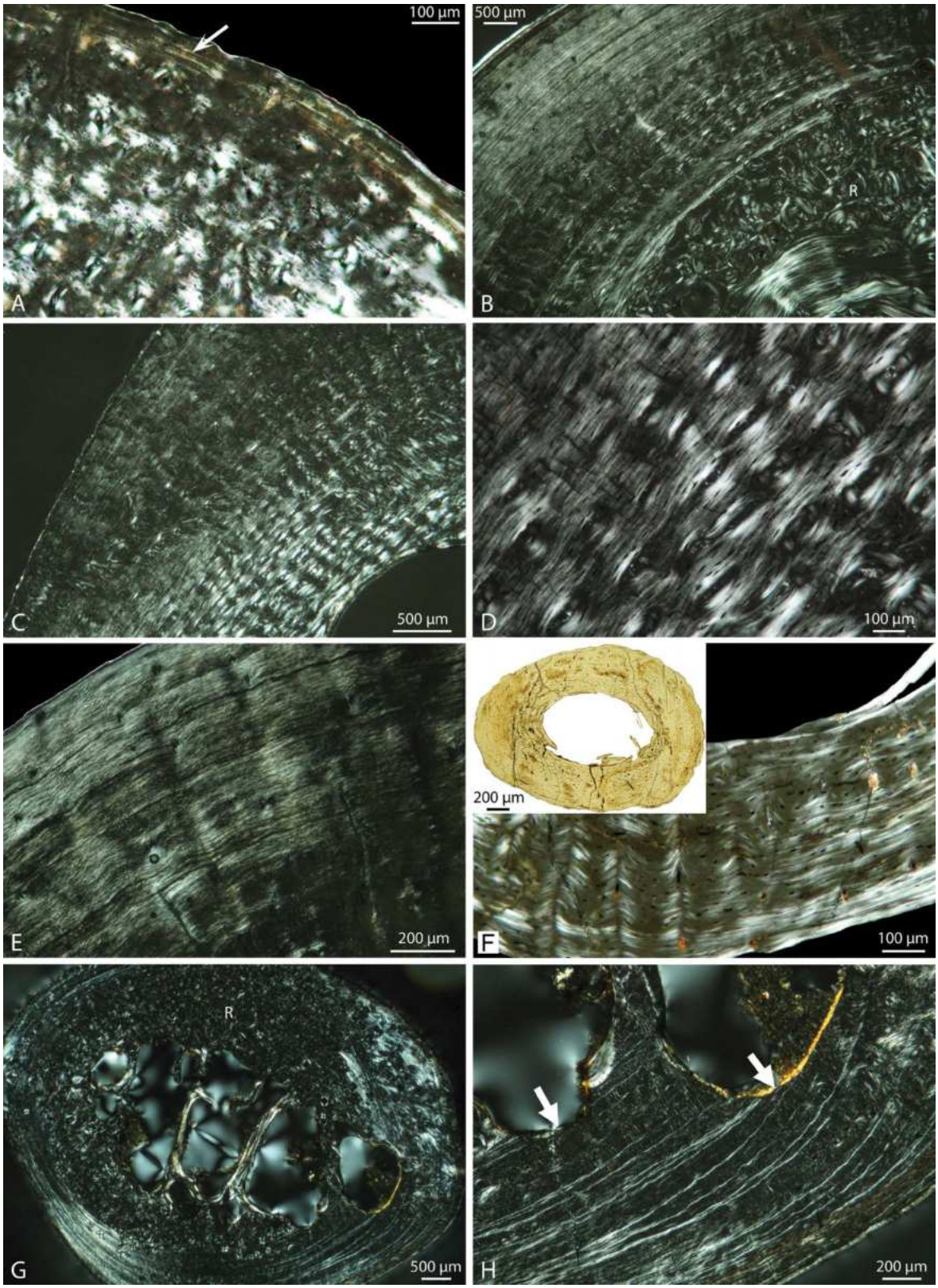


FIGURE 29.4 Long bone and rib microstructure in the Marsupials (Metatheria). A, Femur cortex of *Didelphis virginiana*. Polarized transmitted light. The arrow points to a line of arrested growth (LAG). B, Cortex of *Vombatus ursinus* femur at mid-diaphysis (polarized light). C, Cortex of *Macropus rufogriseus* femur at mid-diaphysis (polarized light). D, Detail of the femur cortex shown in C. E, Detail of the peripheral (outer) layer of the *V. ursinus* femur shown in B. Polarized light. F, Mid-diaphyseal cross section of *Pucadelphys andinus* femur. Inset: general aspect of the bone section in ordinary transmitted light. Main frame: detail of the cortex in polarized light. G, Cross section in a rib of *M. rufogriseus* viewed in polarized light. H, Detail of the rib cortex showing extensive resorption of the cortex (thick arrows) and the occurrence of sharp, but irregular, LAGs. In B and G, R designates Haversian remodeling.

intercellular matrix of both bones consists of parallel-fibered tissue, the ribs (Figure 29.4G, H) display broad areas of dense Haversian tissue extending up to the outer margin of the cortex, in addition to conspicuous (strongly birefringent in cross section) LAGs (Figure 29.4H). These lines are locally interrupted and their spacing is particularly odd. Their pattern suggests that they could be principally related to local growth and morphogenetic requirements rather than to a general and cyclical arrest in growth activity involving the organism as a whole.

Long Bones and Ribs in the Eutheria

Preliminary Remarks

The gross external morphology of eutherian long bones, and to a lesser extent their ribs, is broadly variable, consistent with habitat and locomotory adaptations (running, jumping, digging, climbing, swimming, flying, etc.). These adaptations also have an effect on inner bone architecture.

Limb Long Bones

As mentioned above, tiny eutherian forms such as small rodents share the relatively simple epiphyseal structure already described for metatherians. In larger forms, the thick cap of cartilage that covers long bone epiphyses calcifies and then ossifies (starting from a central area) to form a voluminous, secondary intraepiphyseal ossification center (see Chapter 4). During the stages of most active growth, cartilage canals originating from both the perichondrium and the metaphysis are locally abundant (Haines 1942, Ricqlès 1979). In the fossil record, epiphyseal structure is poorly documented in pre-Cenozoic taxa. All limb long bones in the small pantodont *Alcidedorbignya inopinata*, from the early Paleocene of the Santa Lucia Formation (Tiupampa, Bolivia), a site dated 65 Ma, already had voluminous, well-preserved secondary ossification centers (Muizon et al. 2015), identical to those of similar-sized extant eutherians.

The metaphyseal region of long bones, with its typical cone-like morphology relating the wide epiphysis to the narrower diaphysis, is generally well-differentiated in mammals. It comprises a core of spongy tissue surrounded by a compact cortex, the thickness of which progressively decreases toward the adjacent epiphysis. Metaphyses are subject to complex remodeling processes, combining outer cortical resorption and inner compaction of the spongy tissue, and related to the growth in length of the bones (a model initially developed by Lacroix 1945 and Enlow 1962, 1963). This characteristic remodeling pattern is particularly well illustrated by eutherians; however, in some very specialized bones, such as the humerus, radius and phalanges of extant cetaceans, this remodeling pattern becomes unnecessary because these bones have lost a differentiated diaphysis and are basically composed of two epimetaphyseal regions fused by their apices. The compliance of trabecular architecture with Wolff's law (see Chapter 4) is particularly well illustrated by mammalian metaphyses, even when the bones do not have to cope with gravitational constraints (e.g., cetacean humeri). Although steep differences in the global compactness of long bone shafts occur between taxa, as exposed in more detail below, metaphyses are very seldom affected. One of the most striking exceptions to this general situation is observed in some aquatic forms, such as the Miocene phocid seal *Nanophoca vitulinoides* (Dewaele et al. 2018), in which the metaphyses of all long bones, in addition to their diaphyses, are totally compact (i.e., osteosclerotic).

The microanatomical characteristics of the diaphyseal region of limb long bones (humerus, radius, femur, tibia) in extant eutherians have been considered in the context of broad comparative surveys (review in Laurin et al. 2011; see also Quémeneur et al. 2013, and Amson 2021). Data on basal Mesozoic forms are almost nonexistent. A variable but generally faint phylogenetic signal is contained in the microstructure of long bones of extant mammalian taxa; however, their inner architecture predominantly reflects habitats and locomotory adaptations (see Chapter 35). Observations conducted in large and diversified samples show that distantly related taxa sharing the same habitat and locomotory constraints have a similar bone structure; conversely, closely related taxa with distinct locomotory constraints may display different architectural characteristics.

In terrestrial and amphibious taxa, the pattern most frequently encountered in long bone shafts is the (likely) plesiomorphic tubular pattern, with a compact periosteal cortex surrounding a hollow medullary cavity. As in other tetrapods, the transition zone between the medulla and the cortex is either sharp (terrestrial forms) or progressive and variable (amphibious forms), and the relative cortical thickness, i.e., the CDI, ranges from 20 to 60% in most cases. It may, however, show some degree of discrepancy between taxa in relation to the morphology and diameter of bones, specific body sizes or peculiar ecological specializations (Laurin et al. 2011; see also Houssaye et al. 2016a). The inner architecture of appendicular long bones ceases to be tubular, or to display the current values of CDI and compactness, in nonterrestrial forms, be they fossorial (Legendre and Botha-Brink 2018), flying (e.g., data in Canoville and Laurin 2010) or secondarily adapted to a permanent aquatic habitat (e.g., Houssaye et al. 2016b). The broad subject of bone microanatomy and lifestyle is fully considered in Chapter 35.

Ribs

For obvious reasons, ribs are often more accessible than limb bones for histological preparations, especially in the fossil record. The histological message of these two kinds of bones may nevertheless differ for three main reasons. (1) Rib diameter, and consequently the rate of periosteal accretion on its cortex, are generally smaller than those of limb bones; therefore, ribs may display distinct histological features. (2) The functional role of ribs greatly differs from that of limb bones; their inner remodeling can thus diverge accordingly. (3) All mammalian ribs have a strong curvature, the creation and maintenance of which requires strongly off-centered growth, with slow growth and/or resorption on the medial side of the bone and faster accretion on the lateral side (see Chapter 9). This situation has clear consequences on the microanatomical and histological structures of ribs compared to other bones.

VetBooks.ir

Among extant mammals (data on early forms are too sparse to allow generalizations), the main microanatomical traits of ribs differ little among taxa, provided comparisons bear on animals that share similar size and habitat. For example, the compactness profile of a prototherian rib strongly resembles that of a rat, a shrew or a small primate. Conversely, spectacular discrepancies are observed between terrestrial and fully aquatic mammals (Canoville et al. 2016). Such differences are consistent with those of limb bones.

Histological Features of Long Bones in Early Eutherians

As for *Morganucodon* and the metatherians, most of the first-hand data available for one of the earliest eutherian clades, the Zalambdalestidae, are due to Chinsamy and Hurum (2006) and Hurum and Chinsamy-Turan (2012).

Limb bone shafts in *Zalambdalestes lechei*, a taxon from the Early Campanian, have a tubular architecture (Chinsamy and Hurum 2006), with a relatively low CDI value of 32.9% (17% for Chinsamy and Hurum's [2006]RBT). This general design is likely to be plesiomorphic within the Eutheria. Bone histological traits appear similar in all Zalambdalestidae: femur and rib cortices are basically composed of parallel-fibered bone. LAGs seem to be common, at least in the femur, but no differentiated EFS was observed. Vascularization in all bones is scarce. It consists of primary osteons with some isolated secondary osteons. It is noteworthy that, due to the broad expansion of the medullary cavity in the femoral shaft of Zalambdalestidae, the cortex remaining in adults represents only late stages of growth, when the apposition rate had already decreased. The bone layers corresponding to the most active phase of growth are missing. In the absence of growth series, this situation calls for some caution in the interpretation of cortical histology in terms of individual or specific growth rates.

Observations of Pantodonts

Very little information exists in the literature about bone structure in Paleocene mammals, and no precise histological observations have been published about pantodonts, a relatively diverse group known worldwide from the early Paleocene to the Middle Eocene (Kemp 2005). Pantodonts were an ecologically important component of terrestrial mammalian faunas (e.g., Morgan et al. 1995). The brief first-hand observations presented here deal with *Coryphodon oweni* and *A. inopinata*.

C. oweni was a bulky animal, the size of a cow (BW *ca.* 500 kg), that spent an amphibious life in the swamps and ponds of Europe and North America, from the Late Paleocene to the Middle Eocene (Uhen and Gingerich 1995). A *Coryphodon* rib was described very succinctly by Enlow and Brown (1958) as "composed predominantly of circumferential lamellae". Further observations about an unidentified fragmentary limb bone (this bone has a large average diameter: 29.7 mm) are given here.

Cross sections of this bone reveal a quasi-amedullary structure (Figure 29.5A): a large central third of the bone area comprises a dense spongiosa with short, convoluted trabeculae. The transition from the cancellous medulla to the compact cortex is very gradual and the cortex itself has a relatively low overall compactness due to the proliferation of numerous unachieved secondary osteons (Figure 29.5A, B); in the absence of an open medullary cavity, global compactness (86.4%) is nevertheless high. The histological structure of the *Coryphodon* bone is quite unusual for a terrestrial mammal of this size. The deepest cortex is made of an ill-characterized parallel-fibered bone: osteocyte lacunae are multipolar and randomly distributed, whereas the matrix displays a faint and irregular birefringence (Figure 29.5B). Most of the cortex, however, is made of parallel-fibered bone, with a clear birefringence (Figure 29.5C) and conspicuous annuli. Throughout the cortex, more than 30 annuli can be counted, although Haversian remodeling extensively erased the deepest growth marks. *Annulus* spacing (i.e., some 95 µm in the middle third of the cortex) decreases very gradually toward the bone periphery; however, the last four to six annuli are much more tightly spaced and thus form an EFS (Figure 29.5D). This feature shows that somatic growth had reached an end in the studied specimen and that it was most likely an adult. Bone structure suggests that *Coryphodon* had a relatively slow but regular and long-lasting somatic growth, a developmental pattern common in some large ectopoikilotherm reptiles, but quite unusual for a mammal of this size. To our knowledge, among large eutherians, the only equivalent to this growth pattern is represented by the Plio-Pleistocene bovid *Myotragus balearicus*, from the Balearic Islands (Köhler and Moyà-Solà 2009). This taxon is supposed to have had a low growth rate and a flexible, crocodile-like growth strategy adapted to environmental fluctuations. To some extent, this conclusion could be applied to *C. oweni*, with the restriction that its growth, though slow, was very constant and regular, possibly in relation to steady environmental resources.

A. inopinata was a relatively small terrestrial pantodont from the early Paleocene of Bolivia (detailed description in Muizon et al. 2015). It was a terrestrial herbivorous animal comparable in size to a rabbit. The bone sample available for observation is the distal third of a humerus, and the studied section is from the transition zone between the diaphysis and the metaphysis. At this level, the humerus presents a triangular shape in cross section (Figure 29.5E). The microstructural features of this bone differ steeply from those observed in *Coryphodon*: it has a tubular, though robust (compactness = 72.8%) diaphysis. Histologically, the cortex consists of a tissue intermediary between parallel-fibered bone and lamellar bone, meagerly vascularized by longitudinal primary osteons and simple canals of small (<15 µm) diameter. Osteons and simple canals are arranged in one or two circular rows (Figure 29.5F) in the middle of the cortex. Faint but regularly spaced annuli occur (Figure 29.5G). The outermost cortical layer consists of avascular lamellar tissue that might constitute an EFS. A small local formation showing the characteristics of CCCB, and separated from the rest (peripherally located) of the cortex by a reversion line, is wedged between the basal cortex and the secondary lamellar layer that coats the lateral wall of the medullary cavity (Figure 29.5H). Considering the level of the section, this tissue, bordered by two reversion lines, is likely to have been formed in the metaphysis, before being relocated during growth toward the diaphysis (Enlow's 1963 growth model). In general, the bone structure in the primary

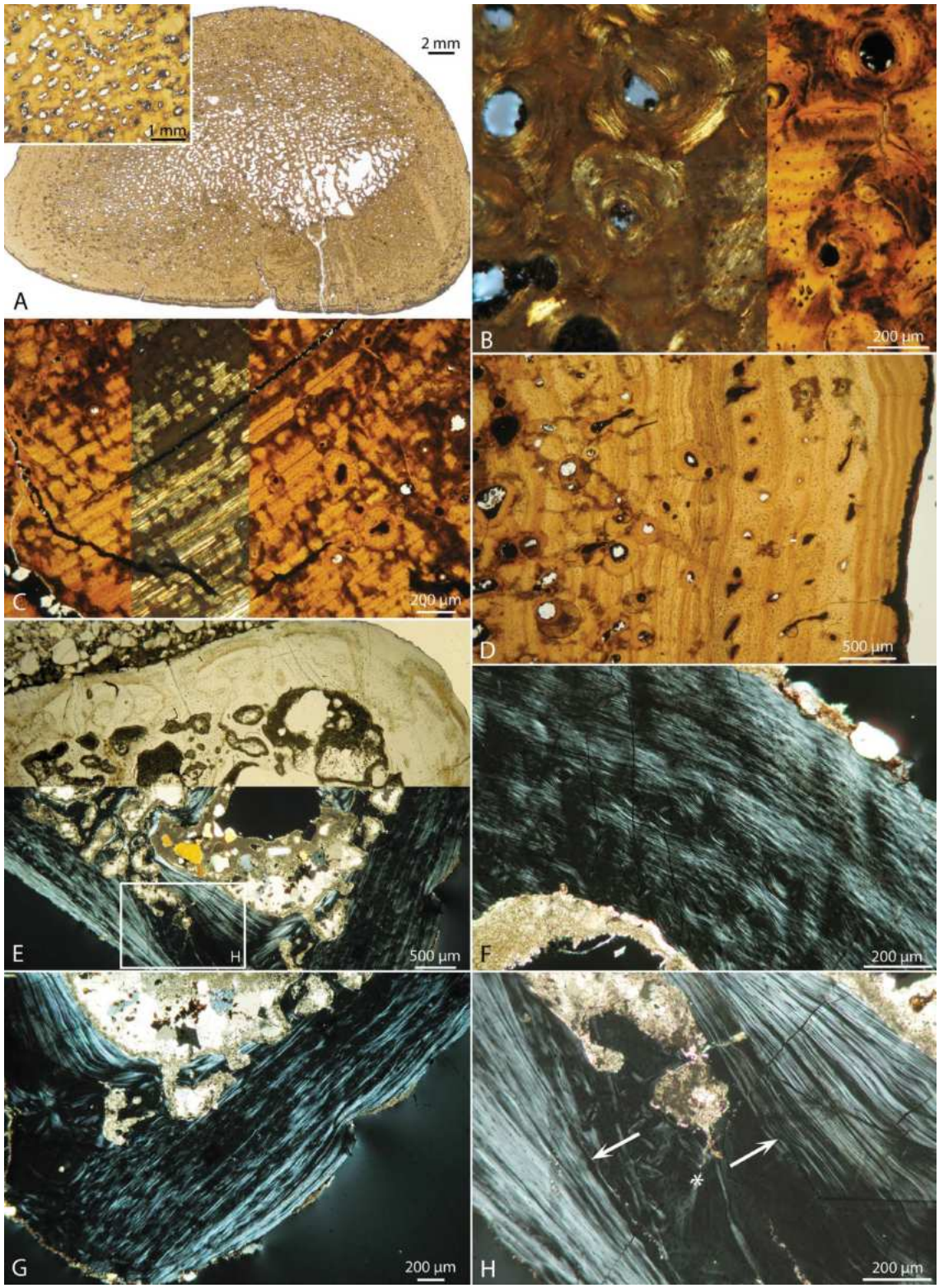


FIGURE 29.5 Long bone microstructure in the pantodonts *Coryphodon oweni* and *Alcidedorbignya inopinata*. A. Cross section in the diaphysis of an unidentified limb bone from *C. oweni*. Main frame: general view of the bone. Inset: detail of the cortex. B, Detail of the deep, remodeled cortex of the bone shown in A. Left field: polarized light. C, Detail of the peripheral cortex of the *C. oweni* bone, with very evenly spaced annuli. Central band: polarized light. D, External fundamental system in the peripheral-most cortical layer in the bone of *C. oweni*. E, General view of a cross section in the humerus of *A. inopinata*. Lower half: polarized light. The white frame indicates the field detailed in H. F, Detail of the parallel-fibered tissue with faint annuli in the cortex of the bone shown in E. G, Other cortical field in the same specimen, showing sharper and more numerous annuli. Polarized light. H, Detail of the three-strata structure of the cortex. The medial field (asterisk) possibly corresponds to a stratum of compacted coarse cancellous bone (CCCB), framed by two reversion lines (arrows).

VetBooks.ir

periosteal deposits of the *Alcidedorbignya* humerus suggests a modest absolute growth rate, with feebly pronounced cyclical episodes of slackening.

Afrotheria (Sirenia, Proboscidea, Desmostylia and Tubulidentata)

Beyond several short mentions of the histological structure of limb long bones and ribs in the Afrotheria (e.g., Aeby 1878, Nopcsa 1923, Nopcsa and Heidsieck 1934, Enlow and Brown 1958), the most significant early contributions in this field are from Lefeuvre (1909) and Fawcett (1942), who described in detail the histological peculiarities of the skeleton in, respectively, the Oligocene dugondid *Halitherium shinzii* and the extant Florida manatee, *Trichechus manatus* (see also Kaiser 1970, 1974 for microanatomical reviews). More recently, detailed comparative investigations were conducted on this question by e.g., Buffrénil and Schoevaert (1989), Ricqlès and de Buffrénil (1995) and Buffrénil et al. (2010) in sirenians, Curtin et al. (2012) in proboscideans, Hayashi et al. (2013) in desmostylians and Legendre and Botha-Brink (2018) in Tubulidentata.

Bone Microstructure in the Sirenia

The spectacular microanatomical peculiarities of sirenian ribs and (to a lesser extent) limb bones, i.e., a high compactness, the absence of a differentiated medullary cavity (osteosclerosis) and the frequent occurrence of swollen, hyperplasic cortices (pachyostosis), have been recorded since the second half of the 19th century (Aeby 1878), and have been the subject of several recent studies (e.g., Buffrénil et al. 2010, Houssaye et al. 2016a). In *D. dugon*, a taxon in which osteosclerosis is strong, but that does not present pachyostosis, the histological features of the humerus are basically identical to those of the ribs (Buffrénil and Schoevaert 1989). In the bones of young individuals, the medullary region is occupied by a very dense network of stout trabeculae forming a tight spongiosa (Figure 29.6A). At midshaft, the core of the trabeculae consists of hypertrophic calcified cartilage, while their surface is covered with thick layers of endosteal parallel-fibered or lamellar tissues. As a consequence, the thin intertrabecular spaces are reduced to less than 100 µm. On microradiographs, both tissues display clear differences in mineral rate; moreover, *globuli ossei* may occur throughout the medulla. This situation clearly reflects an interruption (or shortening) of the normal course of endochondral ossification. Primary trabeculae, formed just under the growth plate and comprising a core of calcified cartilage covered with thin endosteal bone layers (see Chapter 9), normally undergo repeated remodeling to be finally eliminated during the growth in length of the bones, and replaced by the medullary cavity. In the ribs and humerus of the dugong and all other sirenians since the earliest taxon attributed to this Order, *Pezosiren portelli* (a fully quadrupedal form from the early Middle Eocene of Jamaica), the remodeling process of the medullary region stops at the stage of the primary endosteoendochondral trabeculae (Buffrénil and Schoevaert 1989, Buffrénil et al. 2010), a condition interpreted by Ricqlès and Buffrénil (2001) as pedomorphic. The cortex surrounding the medullary region is made of a woven-parallel complex in the form of laminar, plexiform or reticular tissue types (Figure 29.6A). In later growth stages, woven-parallel complexes are progressively replaced by woven-fibered and parallel-fibered tissues containing variably oriented (but mainly longitudinal) simple vascular canals or primary osteons, along with conspicuous cyclical growth marks (annuli and LAGs: Figure 29.6B, C). At this stage, secondary osteons spread from the medullary region toward the cortex (Figure 29.6B). Haversian substitution is generally mild in sirenians, with the exception of the dugong in which it extends to most of the cortex in the adults; therefore, broad areas of primary cortices, along with remnants of primary endosteoendochondral trabeculae, can remain visible in adults, as exemplified by *Pezosiren*, *Protosiren* and *Halitherium* (Buffrénil et al. 2010). In contrast to the humerus and the ribs, the radius, ulna, metacarpals and phalanges of the dugong have a normal (or quasi-normal) tubular structure, though their medullary cavity can be occupied by some trabeculae. Their deep cortex is made of woven-fibered tissue containing simple vascular canals, and their outer cortex is of the parallel-fibered type with conspicuous cyclical growth marks.

No EFS could be clearly distinguished in the 15 sirenian taxa (mainly represented by ribs) observed for this review, although an annulus can occasionally be located against the margin of a bone. However, Amprino and Godina (1947) mentioned the occurrence of an EFS in an unidentified sirenian bone. The hyperplasia of sirenian rib cortices is supposed to be due to protracted apposition (Buffrénil et al. 2010), which could explain the absence of the signs of an abrupt collapse in local growth rate. Although osteosclerosis and pachyostosis are mainly restricted to the thoracic region in sirenians, they can also extend toward the rear part of the skull and involve the exoccipitals (Buffrénil and Schoevaert 1989).

Desmostylia

The reference descriptions of bone microstructures in desmostylians (Hayashi et al. 2013) are relative to the humerus, femur and ribs of the four known desmostylian genera: *Behemotops*, *Paleoparadoxia*, *Ashoroa* and *Desmostylus*. Additional observations were conducted for this review in the ribs of *Paleoparadoxia tabatai* and *Desmostylus* sp. Data from both sources are in close agreement, at least for the ribs of the two latter taxa.

The first three genera have very robust bones (Figure 29.6D, E), with compactness indices ranging from 85.9% (rib of *Behemotops*) to 99.1% (humerus of *Paleoparadoxia*). The medullary cavity is partly occluded by stout trabeculae framing small cavities. Hayashi et al. (2013) described the trabeculae as intensely remodeled, which also agrees with our own observations of the ribs (Figure 6D, inset). The microanatomical aspect of *Desmostylus* bones (Figure 29.6F) greatly differs from that prevailing in the bones of the other three taxa: *Desmostylus* ribs are lightly built, with thin cortices and an extensive medullary spongiosa (global compactness index 48% to 62%, according to Hayashi et al. 2013). However, their medullary cavity is not hollow; it contains a loose network of thin, intensely remodeled trabeculae. Similarly, the femur of

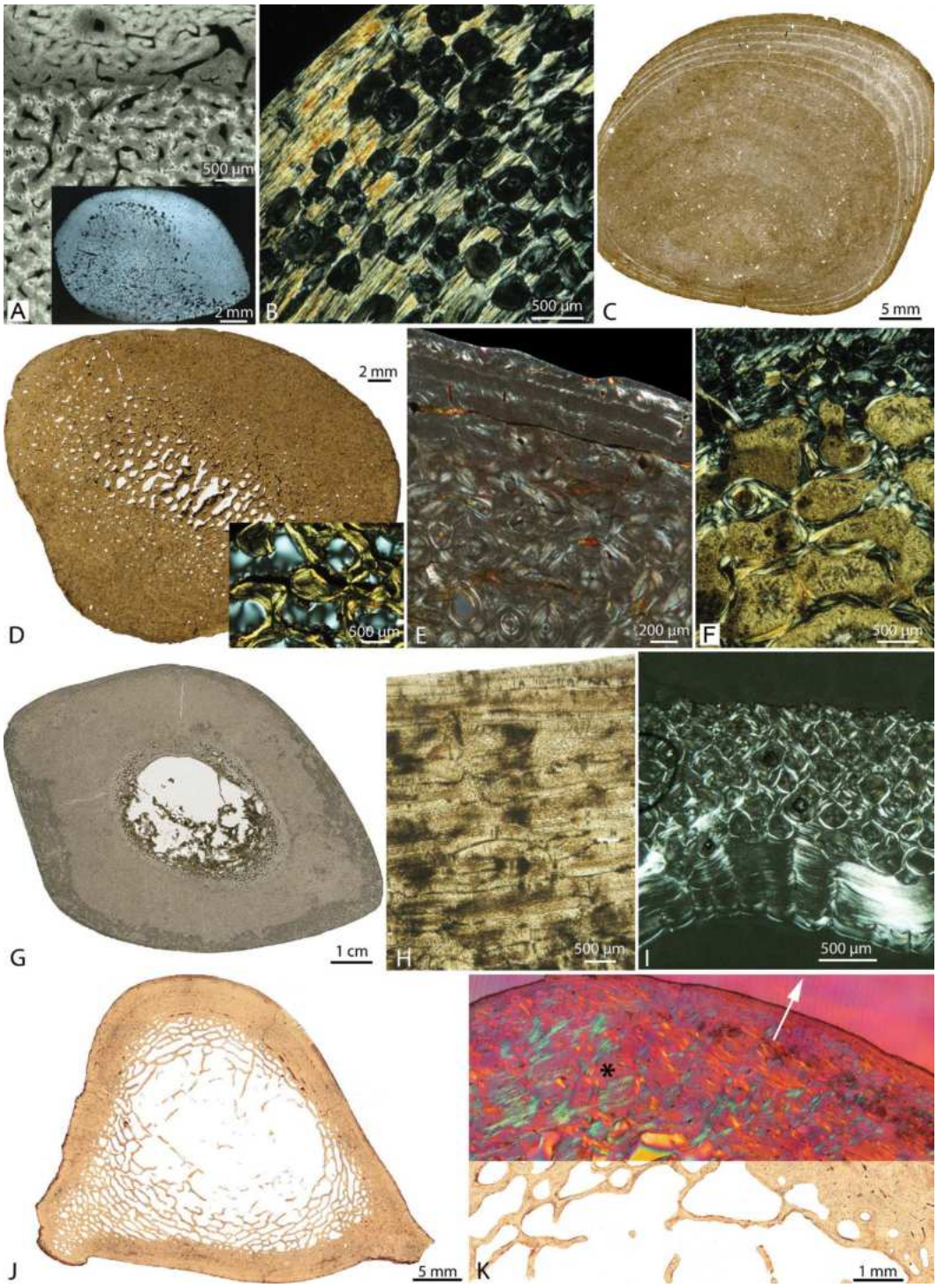


FIGURE 29.6 Microstructure of ribs and long bones in the Afrotheria. A, Main frame: detail of the medulla and basal cortex in a rib from a juvenile *Dugong dugon*. Microradiograph: The medulla is occupied by a network of massive primary trabeculae comprising a core of calcified cartilage (white areas). Thick deposits of endosteal bone fill intertrabecular spaces. The insert shows the microradiograph of a cross section in a subadult rib. Cortical vascularization is reticular to plexiform. B, Cross section of an adult Dugong rib viewed in polarized light. Haversian remodeling starts in the medulla and spreads to the base of the cortex. C, Cross section in a rib of a *Halitherium schinzii*. The bone is totally compact and very sharp annuli occur in the periosteal cortex. D, Cross section in a rib of the desmostylian *Paleoparadoxia tabatai*. Inset: trabeculae of the medullary region viewed in polarized light. E, Detail of *P. tabatai* rib cortex showing peripheral lines of arrested growth. F, Basal cortex and loose network of medullary trabeculae in a *Desmostylus* sp. rib. Polarized light. G, Cross section in the tibia of an elephant, *Loxodonta africana*. H, Plexiform to parallel-fibered tissue bordered by a quasi-avascular EFS in the outer cortex in the elephant tibia. I, Cortex of *E. maximus* rib showing Haversian remodeling outcropping at the bone surface, due to superficial resorption. J, General view of a mid-diaphyseal cross section in the femur of a Tubulidentata, the Cape aardvark, *Orycteropus afer.* K, Detail of the aardvark femur cortex showing CCCB (asterisk), separated from the periosteal cortex (arrow) by a reversion line. Upper half: polarized light. (Courtesy L. Legendre and J. Botha-Brink.)

VetBooks.ir

this taxon has a low compactness index (69% at most) compared to other desmostylians (Hayashi et al. 2013). The bone cortex in *Behemotops*, *Paleoparadoxia* and *Ashoroa* is of extreme compactness and consists mostly of dense Haversian tissue (Figure 29.6E), with secondary osteons strictly oriented in a longitudinal direction. Remnants of primary periosteal tissue spared by remodeling remain visible at the periphery of the bones. According to Hayashi et al. (2013), the primary cortex in all desmostylians is made of parallel-fibered bone containing LAGS. Our observations agree with this statement in the case of *Desmostylus*, a taxon displaying a thin, almost avascular layer of parallel-fibered bone crossed by abundant Sharpey's fibers (Figure 29.6F). In the rib of *Paleoparadoxia* that we could observe, the peripheral layer, devoid of secondary osteons, is made of a monorefringent tissue closer to the woven-fibered type than to parallel-fibered bone (Figure 29.6E). It contains sparse, simple vascular canals oriented longitudinally and two sharp LAGs. Whether this layer must be considered as the real EFS of a fully grown adult (despite the broad spacing of the LAGs), or reflects a mere decrease in growth rate in a subadult is an open question.

Proboscidea

The microstructure of proboscidean bones was briefly mentioned in the now classical syntheses by Foote (1911, 1916), Amprino and Godina (1947) and Enlow and Brown (1958); however, the most detailed first-hand study on this topic is by Curtin et al. (2012) (see also Sander and Andrassy 2006, Kolb et al. 2015b). This study, dealing with the femur and tibia, was conducted in four elephantid taxa: the extant *Elephas maximus* and *Loxodonta africana* and the extinct *Mammuthus columbi* and *M. exilis* (a dwarf insular species reaching some 150 cm at shoulder height: Herridge and Lister 2012). All the bone samples used by Curtin et al. (2012) are from late-term fetuses, newborn individuals and early juveniles. This material provides an interesting opportunity to have access to primary periosteal cortices deposited before the onset of extensive perimedullary resorption and Haversian remodeling, a situation relatively rare in comparative surveys. Additionally, midshaft sections from a tibia and a rib of, respectively, adult *L. africana* and *E. maximus* are also considered here (personal observations by VB) for documenting the ontogenetic modifications and final histological aspects of cortical bone in fully grown elephants.

Curtin et al.'s (2012) results show that the microanatomical features of limb long bones differ between, on the one hand, the two extant elephants and, on the other hand, the two mammoths: whatever the ontogenetic stage considered, the bones of the extant elephants have a hollow medullary cavity (though some trabeculae may locally occur in *Loxodonta*), whereas the medullary region is filled by a dense trabecular network in the mammoths. The tibia of the adult *L. africana* examined here (Figure 29.6G) has an open medullary cavity (CDI value: 62.5%); conversely the rib medulla comprises some thin trabeculae forming a loose spongiosa. Previous qualitative observations by Mahboubi et al. (2014) about *Numidotherium koholense*, an archaic proboscidean from the Early Eocene of Algeria, led to the conclusion that this taxon had tubular bones and was thus terrestrial. The illustrations given by the authors (cf. their figure 5) nevertheless suggest that the medullary cavity was densely occupied by trabeculae (as observed by Curtin et al. 2012), which would *a priori* suggest possible amphibious habits (see Chapter 35). This question, relative to the mode of life of early proboscideans, needs to be further documented with quantitative data.

Histologically, the osseous tissue that initially constitutes long bone cortices in young elephantids is a pure, well-characterized laminar woven-parallel complex, as already pointed out by Sander and Andrassy (2006). Foote (1916), followed by Enlow and Brown (1958), mention a "pattern of plexiform tissue" in the outer regions of bone cortices in *Elephas*. This tissue was not observed in *Loxodonta*. The walls of primary osteons are of parallel-fibered bone instead of the more commonly encountered lamellar tissue. Laminar thickness shows substantial but irregular variations in each bone. There is nevertheless a trend toward a gradual reduction of laminar thickness from deep to more superficial regions of the cortex. In newborn individuals, the boundary between prenatal and postnatal bone deposits seems to be marked by a local difference in the orientation of vascular canals. In the tibia of the adult *Loxodonta*, the laminar tissue remains visible in a thin peripheral-most layer (Figure 29.6H). It is bordered by an EFS (400–500 µm in thickness) containing two LAGs. Otherwise, most of the cortex is occupied by dense Haversian tissue, as already mentioned and illustrated by Ezra and Cook (1959). This extensive remodeling, along with the expansion of the medullary cavity, results in a quasi-complete disappearance of the periosteal deposits formed during the most active stage of individual growth. In the adult rib, only the dense Haversian tissue is visible (Figure 29.6I); moreover, secondary osteons, variably eroded by broad resorption fields developing on the medial and lateral surfaces of the bone, outcrop superficially. The wall of the medullary cavity in the adult tibia and rib is coated by a thick layer of secondary endosteal tissue (40% of total cortical thickness, for the rib shown in Figure 29.6I) locally varying in structure from the parallel-fibered to the lamellar types. In the tibia, this endosteal layer is crossed by radial simple vascular canals and contains some longitudinal secondary osteons.

Tubulidentata

To our knowledge, only one article deals with the bone structure of tubulidentates, i.e., the study of the aardvark (*O. afer*, a fossorial form) by Legendre and Botha-Brink (2018). This detailed work pointed out an unusual structure in the tubular stylopodial and zeugopodial elements of this taxon (Figure 29.6J): most of the cortex is composed of CCCB. This tissue normally occurs in metaphyses (its formation in the diaphyseal region is less frequent), and results from the compaction, through endosteal deposits, of the peripheral region of the local spongiosa. This process accompanies the outer resorption of the metaphyses and prepares their integration to the narrower diaphyseal territory during the growth in length of the bones (i.e., Enlow's 1963 classical model; see Chapter 9). CCCB is a transitory formation, soon erased by the enlargement of the medullary cavity; however, in the aardvark, it apparently remains in place. Beyond minor variations, the basic structure of limb bones in *O. afer* thus includes the

VetBooks.ir

following, from the periphery toward the core of the shaft (Figure 29.6K). (1) There is a thin and poorly vascularized layer of subperiosteal parallel-fibered tissue. (2) A thick ring of CCCB that may house abundant, and often reticular, vascular networks along with Sharpey's fibers is included. A resorption line occurs between the periosteal layer and the subjacent layer of CCCB. (3) In perimedullary position, an avascular stratum of secondary lamellar tissue is also bordered by a reversion line. Several additional resorption lines may be present within the outer periosteal tissue, depending on local morphogenetic processes. Haversian remodeling is uneven among the bones of a single skeleton or the sectors of a single cross section. It initially develops in the mass of the compacted coarse cancellous tissue and extends little to the cortex. Legendre and Botha-Brink (2018) tentatively interpret the peculiar structure of the aardvark long bones in light of two distinct (but possibly synergistic) causes: either the negative effect of the low metabolic activity that characterizes this taxon on subperiosteal accretion and cortical remodeling, or the influence of specific mechanical constraints related to a fossorial behavior.

Xenarthra

Owing to the recent comparative studies by Straehl et al. (2013), Amson et al. (2014) and Heck et al. (2019), the microstructure of xenarthran limb bones and ribs is now precisely documented. More general descriptions were previously given by, e.g., Foote (1911), Amprino and Godina (1947) and Enlow and Brown (1958). At a microanatomical level, limb bones and ribs of extant xenarthrans (all are terrestrial) have a gross tubular architecture. However, the occurrence of a free, totally hollow medullary cavity is an infrequent situation; most often, trabecular networks of variable spatial density occupy the medullary region (Figure 29.7A, B). Global bone compactness and the CDI of the Cingulata are comparable to the mean values currently observed in other terrestrial mammals; conversely, limb bones and ribs of the Pilosa tend to be more compact (Straehl et al. 2013, Amson et al. 2014). According to Straehl et al. (2013), the microstructural features of xenarthran bones are not significantly influenced by body size, phylogeny or locomotion pattern. This assertion does not include *Thalassocnus*, a semiaquatic taxon represented by five successive species, ranging from the late Miocene to the early Pliocene, in the Pisco Formation (Peru). In pace with the gradual adaptation of this genus to feeding on algae in shallow coastal waters (Muizon and McDonald 1995), the compactness of most of its bones (humerus, radius, femur, tibia and ribs) increased by about 20–22% during a period of 4 million years, at most (Figure 29.7C–E). The resulting condition in the most derived species, *Thalassocnus carolomartini* and *T. yaucensis*, consists of almost entirely compact bones, with compactness indices between 95.5 and 99% (Amson et al. 2014).

According to Straehl et al.'s (2013) descriptions, the histological features of xenarthran long bones are relatively diverse (a useful summary is presented in the table 2 of these authors). The long bones of adults in most taxa have an EFS made of avascular parallel-fibered or lamellar tissues that may have LAGs. The wall of the medullary cavity is coated by a thick layer of secondary, avascular lamellar bone. The structure of the osseous tissue between these two layers seems to be dominated by a great variability in the kinds and orientation of vascular canals: most taxa have a mixture of primary and secondary osteons with longitudinal, radial or circular orientations. Similarly, the tissue types between the canals apparently comprise an assemblage of various categories. The detailed study by Heck et al. (2019) of the femur and tibia of the cingulate *D. novemcinctus,* along with personal observations by VB on the humerus of *Zaedyus pichiy* (Figure 29.7B, F), suggest that in adults the core of the cortex consists of a thick layer of CCCB bordered on one side by perimedullary endosteal tissue and on the other by parallel-fibered periosteal bone forming an EFS. This structure prevails in the diaphyseal territory, at some distance from the metaphyses. In *Zaedyus*, a reversion line occurs between the peripheral periosteal deposit and the subjacent CCCB (Figure 29.7F). Such a histological pattern is therefore roughly comparable to that described above for the limb bones of e.g., *O. anatinus*, and mentioned below for several other mammals. In juvenile *D. novemcinctus*, the CCCB constitutes most of the cortex volume, and there is no outer layer of periosteal tissue. Xenarthran long bones are variably affected by Haversian remodeling. Most bones in the sample studied by Straehl et al. (2013) showed dense Haversian tissue with either longitudinal or "irregularly oriented" osteons. Intense remodeling is also encountered in all *Thalassocnus* bones, and involves both cancellous (Figure 29.7G) and compact (Figure 29.7H) tissues. It spreads to the whole cortex, sparing only the EFS (Figure 29.7I). Conversely, remodeling seems to be mild in the tibia and femur of *D. novemcinctus* (Heck et al. 2019). In *Z. pichiy*, Haversian substitution is active but spares the outermost cortical layers (Figure 29.7B, F).

Amson et al. (2014) have shed light on the mechanism that gradually differentiated during the evolution of *Thalassocnus* (from the condition in *T. natans* to that in *T. yaucensis*) to make the inner structure of bones compact. In the rib of a juvenile *T. littoralis* (Figure 29.7J), the cortex, though proportionally thick, is porous and displays numerous open resorption bays. Conversely, the rib of an adult of the same species has much fewer open bays; it consists of dense Haversian tissue and intertrabecular spaces in its medullary spongiosa are narrower or occluded (Figure 29.7K). These observations indicate that, during sustained remodeling, *Thalassocnus* rib and limb bones were made compact through imbalanced resorption and reconstruction: the volume of bone secondarily deposited by endosteal osteoblasts (reconstruction phase) exceeded the volume of the osseous tissue previously eroded *in situ* by the osteoclasts.

The peculiar case of xenarthran osteoderms is considered specifically below, in the part dealing with osteoderms, baculum and antlers.

Terrestrial and Amphibious Cetartiodactyls

Bone microstructure in terrestrial and amphibious artiodactyls is relatively well documented since the pioneer works by Foote (1911, 1916), Amprino and Godina (1947) and Enlow and Brown (1958), and seems to be relatively homogenous among extant and extinct taxa, beyond minor differences (Martiniaková et al. 2007). Conversely, the microanatomical

VetBooks.ir

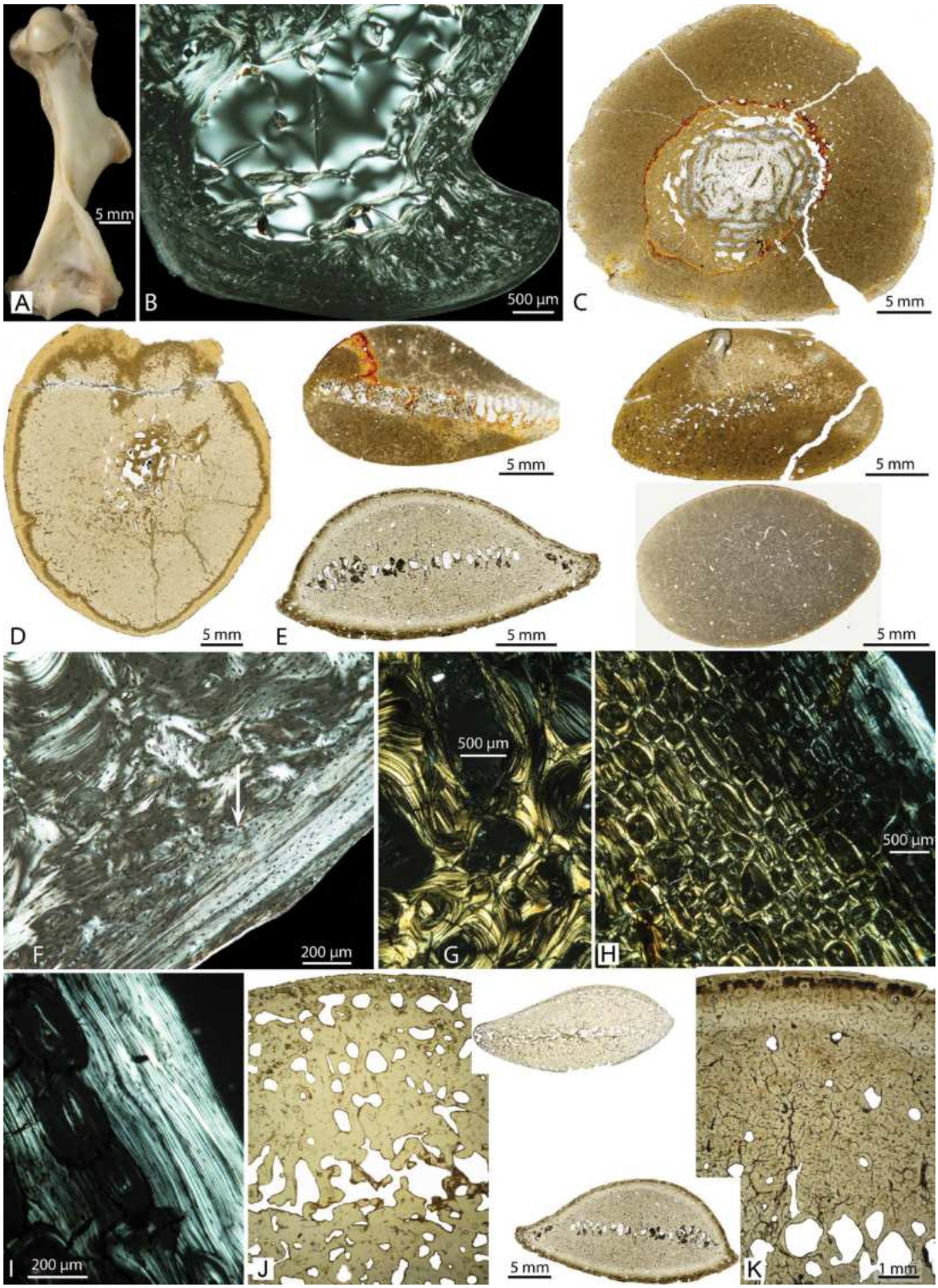


FIGURE 29.7 Microstructure of long bones and ribs in the Xenarthra. A, General view of *Zaedyus pichiy* humerus. B, Mid-diaphyseal cross section in the humerus of *Z. pichiy*. Polarized light. C, Midshaft cross section in the tibia of *Thalassocnus littoralis*. D, Mid-diaphyseal cross section in the tibia of *T. carolomartini*. E, Four subsequent stages of rib compaction among *Thalassocnus* species. Upper left: *T. natans* (7 Ma), lower left: *T. littoralis* (6 Ma), upper right: *T. carolomartini* (5 Ma) and lower right: *T.* cf. *yaucensis* (later than *ca*. 5 Ma). F, Detail of the tissues forming the humeral cortex of *Z. pichiy*. The arrow points to a reversion line between the median layer (likely compacted coarse cancellous bone) and the periosteal cortex. G, Detail of the remodeled trabeculae in the core spongiosa of *T. carolomartini* tibia. Polarized light. H, Dense Haversian bone in *T. littoralis* tibial cortex. Polarized light. I, Detail of the external fundamental system, with some cyclical growth marks, in *T. littoralis* tibia. Polarized light. J, Main frame: cross section in a rib from a juvenile *T. littoralis*. Cortical compactness is low. Upper lateral inset: general aspect of the rib section. K, Main frame: cross section in a rib from an adult *T. littoralis*. Cortical compactness is made high by the filling of intracortical cavities. Lower lateral inset: general aspect of the rib section.

VetBooks.ir

and histological features of the cetacean skeleton changed and diversified in pace with the adaptation of the members of this clade to a fully aquatic habitat (synthetic studies in Gray et al. 2007, Houssaye et al. 2015).

At a microanatomical level, limb bones in most noncetacean cetartiodactyls have a typical tubular architecture. Compactness values range from 40 to 80% (mean 60.8%) for the humerus, 70 to 80% (mean 79%) for the radius, 54 to 59% (mean 56%) for the femur, and 62 to 80% (mean 70.7%) for the tibia (Germain and Laurin 2005, Kriloff et al. 2008, Canoville and Laurin 2010, Quémeneur et al. 2013). As in other mammals, bone compactness tends to be higher in amphibious or incipiently aquatic forms. Aberrant or paradoxical situations may also exist: for example, the limb elements of an extinct Oligocene giraffid, *Lorancameryx pachyostoticus*, a terrestrial form, present unusually swollen cortices associated with a narrow medullary cavity (this cavity is devoid of trabeculae: Morales et al. 1993).

Histologically, the numerous taxa examined hitherto by several authors (recent reviews in Köhler et al. 2012, Marin-Moratalla et al. 2014 and Jordana et al. 2016) basically display similar characteristics, at comparable developmental stages, whatever their phylogenetic position (see in particular Kolb et al. 2015a, Marin-Moratalla et al. 2013, and Becker et al. 2020). Limb bone cortices at early stages of postnatal growth mainly consist of reticular to plexiform woven-parallel complexes, a structure clearly shown by Mori et al. (2003) and Jordana et al. (2016) in Bovidae and Cervidae. With decrease in growth rate, cortical tissue structure first turns into laminar and, at later stages, vascular orientation becomes preferentially longitudinal, while the spatial density of canals decreases. Fully grown adult bones generally have an EFS made of quasi-avascular woven-fibered, parallel-fibered or lamellar tissues. The enlargement of the medullary cavity erases early deposits, so that most of the cortex volume consists of laminar or plexiform tissues (Figure 29.8A–C). Even small forms such as the Pleistocene *Candiacervus ropalophorus* (Kolb et al. 2015a) and the European roe deer, *Capreolus capreolus*, basically display this histological structure. Up to now, the most radical exception to this general pattern is *Myotragus balearicus* (Köhler and S. Moya-Solà 2009), whose cortices display a "lamellar-zonal" structure more reminiscent of a crocodile than of a mammal. The basic features of bone laminae in artiodactyls correspond to what is commonly encountered in other tetrapods. Lamina density (number of laminae per length unit) can nevertheless strongly differ between taxa (Hofmann et al. 2014).

Laminar bone in terrestrial artiodactyls is generally very regular; however, some episodes of particularly fast or slow growth can be recorded in cortices in the form of rings in which the orientation of vascular canals differs from what prevails in the rest of the cortex. This situation was observed by Amson et al. (2015) in the Middle Miocene cervid *Dicrocerus elegans*, and by Kolb et al. (2015a) in *Candiacervus*, a Pleistocene dwarf deer. Figure 29.8C shows a similar condition in a cross section from the femur of an adult *C. capreolus*: a part (approximately one half to two thirds) of the cortex consists of homogeneous laminar tissue, whereas in other parts, thick layers of a woven-parallel complex with longitudinal and oblique primary osteons are wedged within the laminar tissue. In a more peripheral position, the cortex of this specimen comprises layers of another type of woven-parallel tissue with short, quadrangular laminae similar to those observed by Mori et al. (2003) in foals, and further described below in perissodactyls. The same pattern was observed in a red deer (personal observations: VB). Finally, the outermost cortical layer of the studied *Capreolus* specimen is made of compact woven-fibered bone housing a few longitudinal simple vascular canals.

Most of the bones from wild artiodactyls studied hitherto display annuli or LAGs (review in Köhler et al. 2012) sharp enough to allow age estimates (Figure 29.8D, E), although the first growth marks are generally erased by the expansion of the medullary cavity (Jordana et al. 2016). Skeletochronology is regularly applied now to artiodactyls (e.g. Marín-Moratalla et al. 2013, Calderón et al. 2019). The occurrence of perimedullary deposits of secondary lamellar tissue, as well as the development of Haversian remodeling, are two additional characteristics of artiodactyl long bone cortices (though highly plesiomorphic in amniotes). Compared to many other mammalian taxa, Haversian substitution is relatively mild, but variable, in artiodactyl limb bones. Secondary osteons, when present, are either scattered at relatively low density in the whole cortex (Figure 29.8F, G), or concentrated in some cortical areas (often muscular insertions), where they form dense Haversian tissue (Figure 29.8H).

The histological structure of ribs differs from that of long bones by two main features: the composition of their primary cortices and the intensity of the Haversian substitution that they undergo. Rib cortices are not necessarily made of plexiform or laminar woven-parallel tissues. In adults, most of the cortex spared by perimedullary resorption and Haversian remodeling often consists of woven-fibered or occasionally parallel-fibered tissue with longitudinal primary osteons or simple vascular canals. This tissue was observed in a species as large as the bison (*Bison bison*; Figure 29.8I). It often contains conspicuous annuli or LAGs (Figure 29.8I). It is likely that the deep primary cortices formed in early growth stages consist of more common woven-parallel tissues, but they are eroded by perimedullary resorption during growth. Haversian remodeling is much more extensive in ribs than in appendicular elements, and often reaches the outer margins of the bones (Figure 29.8J). With the pronounced lateral drift that characterizes rib growth, along with the resorption activities consistent with this process, the most peripheral secondary osteons often crop out at the bone surface and are themselves submitted to extensive surficial resorption (Figure 29.8J).

Aquatic Cetartiodactyls: The Cetaceans

Available comparative data converge to show that, in the course of the adaptation of cetaceans to a fully aquatic habitat, the microstructure of their long bones and ribs experienced two successive and partly opposite specializations compared to the theoretical plesiomorphic condition of artiodactyls. This condition can be briefly summarized as tubular bones with compact cortices made of woven-parallel tissues variably remodeled in adults.

VetBooks.ir

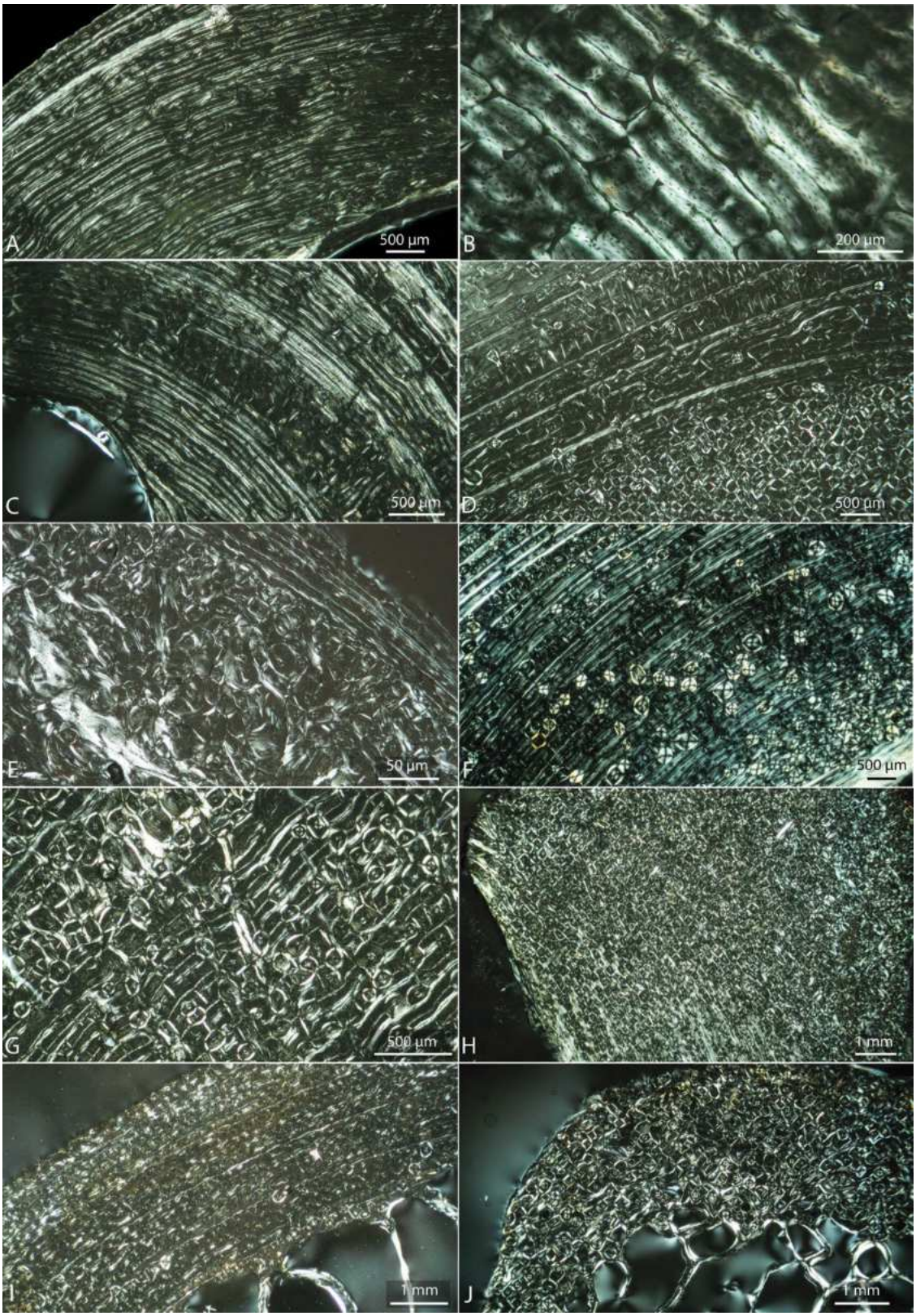


FIGURE 29.8 Microstructure of long bones and ribs in noncetacean artiodactyls (all photos in polarized light). A, Laminar bone in the femoral cortex of the cervid *Capreolus capreolus*. B, Close view at plexiform bone in the femur of *C. capreolus*. C, Irregular structure of the laminar bone tissue of the red deer *Cervus elaphus*. D, Annuli and lines of arrested growth (LAGs) in the tibia of *Boselaphus tragocamelus*. E, LAGs in the femur of *Cervus dama*. F, Perimedullary remodeling in the cortex of *Syncerus caffer* tibia. G, Mildly remodeled cortex in the tibia of *B. tragocamelus*. H, Intensely remodeled cortex under a muscular insertion in *B. tragocamelus*. I, *Bison bison* rib cortex, showing mild remodeling and LAGs. J, Strongly remodeled rib cortex in *Camelus bactrianus*.

VetBooks.ir

Limb Bones

In the archaeocetes, a paraphyletic group of early forms spanning the Eocene, limb elements (most archaeocetes retained four limbs) show diverse structural modifications that resulted in amedullary bones of variable, but generally high, compactness (specific reviews in Gray et al. 2007, Houssaye et al. 2015). During this evolutionary stage, cetacean locomotion changed from an initial drag-based swimming mode, as performed by the earliest taxa (Pakicetidae, Ambulocetidae, Remingtonocetidae and at least a part of the Protocetidae), toward the incipient lift-based propelling mode of the fully aquatic Basilosauridae. The eight archaeocete species studied by Houssaye et al. (2015) present an increase in bone mass through osteosclerosis in the femur. The humerus was similarly compacted, but only in the earliest and still quadrupedal taxa (Remingtonocetidae and Protocetidae in Houssaye et al.'s 2015 study). In the Basilosauridae, which were more adapted to fast swimming, this bone became cancellous, most of its volume being then occupied by spongy tissue. This structure still prevails in extant forms (Felts and Spurrell 1965, 1966, Buffrénil and Schoevaert 1988, Houssaye et al. 2015; see also Figure 9A–C). As pointed out by Gray et al. (2007), the specialized features of bone inner structure in the earliest (fully quadrupedal) forms of archaeocetes predate the modification of the outer morphology of the bones. Unfortunately, detailed descriptions at an appropriate histological level are not available for the limb bones of archaeocetes.

In the Neoceti (crown group cetaceans, including mysticetes and odontocetes), which rely on advanced lift-based swimming, a specialization opposite that of the archaeocetes was selected in most taxa: a reduction in skeletal mass resulting in decreased body inertia and improved speed and maneuverability (Webb and Buffrénil 1990). In the growth series of humeri from common dolphins (*Delphinus delphis*) studied by Buffrénil and Schoevaert (1988), initial periosteal deposits consist of compact woven-parallel bone housing variably oriented primary osteons (Figure 29.9A), which can be longitudinal or form a reticular or a subplexiform network. Haversian substitution soon develops in new periosteal layers to transform them into dense Haversian bone. Deeper within the cortex, this tissue is itself submitted to an extensive, imbalanced remodeling process that makes the compact layers cancellous (Figure 29.9B). In adult common dolphins, this process results in a complete replacement of the compact cortex by a secondary, intensely remodeled spongiosa extending to the whole shaft volume (Figure 29.9C). Comparative data by Felts and Spurrell (1965, 1966) show that this local growth pattern is likely to occur also in the humerus and (to a lesser extent) the radius of most other Neoceti, at least the Odontoceti.

Ribs

Rib histology of extant and extinct cetaceans is well known, especially through the comparative studies by Buffrénil et al. (1990) and Gray et al. (2007). The tissue structure of the compacted medullary region of archaeocetes is convergent with that observed in sirenians (see above) and differs from the generalized condition of terrestrial artiodactyls. In *Basilosaurus cetoides* and *Zygorhiza kochii* (Figure 29.9D, E), the trabeculae occupying the medullary region have the structure of primary endosteoendochondral trabeculae, i.e., remnants of calcified cartilage matrix, covered with endosteal lamellar layers. Conspicuous *globuli ossei* occur at this level (Figure 29.9E). Further remodeling normally involved in the differentiation of a medullary cavity did not occur due to inhibition of chondroclastic activity. As in sirenians, the course of endochondral ossification was characteristically truncated (Buffrénil et al. 1990, Ricqlès and Buffrénil 2001), while protracted endosteal deposits tended to fill intertrabecular spaces. Similar characteristics are likely to have been shared to various degrees by other archaeocetes (Gray et al. 2007). Medullary compaction in archaeocetes is often accompanied by cortical hyperplasia but these two features are not necessarily linked and developed to the same degree in a given taxon. For example, in the protocetid *Eocetus wardii* (Bartonian of Egypt), the medullary spongiosa is of medium compactness and contains only a few calcified cartilage remnants, whereas the cortex is strongly pachyostotic (Figure 29.9F).

Despite minor differences, the primary periosteal cortices of archaeocete ribs are histologically similar among most of the taxa sampled hitherto, and comparable to those of terrestrial artiodactyls. Deep cortical layers are of woven-parallel tissue and display a reticular, plexiform or laminar pattern. This tissue becomes poorly vascularized or avascular woven-fibered toward the bone periphery. Haversian remodeling is variable, but generally mild, and LAGs have been observed in several taxa (including *Ichthyolestes*, *Ambulocetus* and *Kutchicetus*: Gray et al. 2007). The situation is different in the swollen, pestle-like part of the ribs of some large forms such as *B. cetoides*. In this taxon, subperiosteal accretion created very thick deposits of woven-parallel tissue with variably oriented and incompletely formed (very broad central lumen and thin wall) primary osteons (Figure 29.9G). Such cortices, made of so-called "fine cancellous bone" (see Chapter 8), are less compact than rib cortices of other archaeocetes; moreover, the annuli that they exhibit result from a cyclic tightening of the bone texture.

At both microanatomical and histological levels, the rib structure of most Neoceti (at least the odontocetes) does not considerably differ from the common condition of terrestrial cetartiodactyls (Gray et al. 2007, Houssaye et al. 2015, Canoville et al. 2016). They display compact cortices and a differentiated, open medullary cavity (though it can accommodate some endosteal trabeculae), while their cortex shows extreme Haversian remodeling (Figure 29.9H). In adults, primary periosteal tissues are no longer visible, except by the faint remnants of an EFS made of parallel-fibered tissue (Figure 29.9I). Though comparative data are scarce, two particular and opposite conditions seem to occur in the mysticetes and in the ziphiids (highly specialized, deep diving odontocetes) along with some fossil platanistids (coastal forms). According to the data from Houssaye et al. (2015; see also Muizon et al. 2019), mysticete ribs tend to be more compact than the ribs of most odontocetes. This conclusion can also be applied to part of the Cetotheriidae (a mysticete clade known from the Miocene to the early Pleistocene) that seem to have expressed this trend to

VetBooks.ir

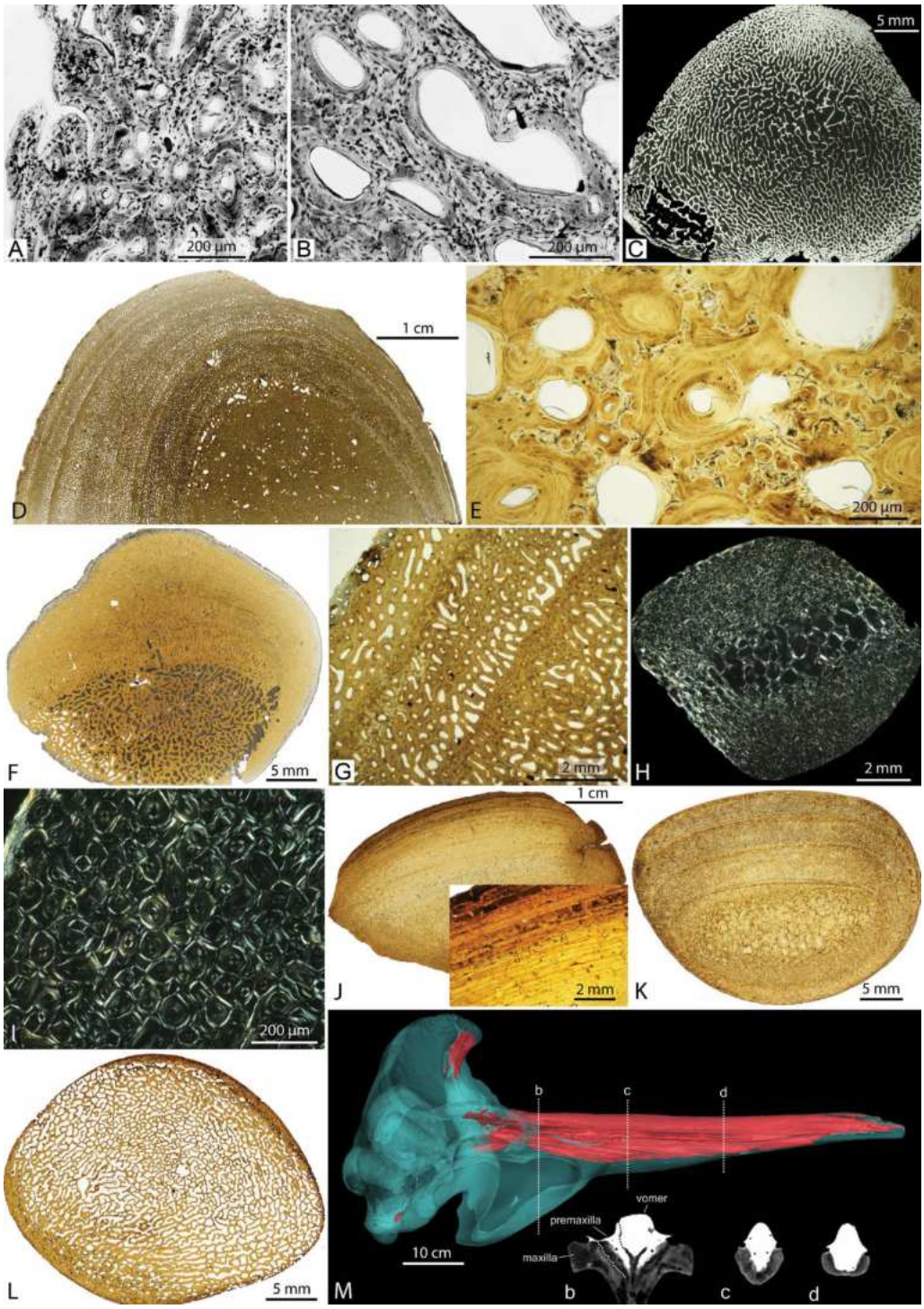


FIGURE 29.9 Microstructure of long bones and ribs in cetaceans. A, Semicompact cortical tissue initially deposited by the periosteum on the humeral shaft of the dolphin, *Delphinus delphis*. B, *D. delphis* humerus. The newly deposited cortex is made more cancellous through imbalanced remodeling and turns to a spongiosa. C, Typical structure of the humeral shaft in adult *D. delphis*. Microradiograph of a cross section. The bone has nearly no compact tissue. D, Half cross section in a rib of the archaeocete *Basilosaurus cetoides*. The cortex is hyperplasic and there is no medullary cavity. E, Preserved primary trabeculae in a rib of the archaeocete *Zygorhiza kochii*. F, Growth off-centering and hyperplasic cortex in a rib of *Eocetus wardii*. G. Fine cancellous bone in the cortex of *B. cetoides* rib. Cyclical growth marks are created by a periodic tightening of the bone structure. H, Cross section in the rib shaft of a common dolphin, *D. delphis*. Polarized light. I, densely remodeled cortex in a rib from *D. delphis*. The upper left margin of the bone represents a birefingent external fundamental system. J, Cross section of a completely compact rib of the extinct mysticete *Brandtocetus suessi*. Inset: Plexiform tissue with lines of arrested growth in the *Brandtocetus* rib. K, Fully compact rib of an unidentified cetothere (Mysticeti) from the Tortonian of Crimea. L, Cross section of a rib of the extinct *Zarachis flagellator*. As in several platanistids and ziphiids, the rib shaft is entirely cancellous. M, Scanner image of *Mesoplodon densirostris* (Ziphiidae) skull showing (red and white areas) the limits of the hyperdense and hypermineralized rostrum.

VetBooks.ir

an extreme degree: some of them have ribs with a compactness index close to 100% and a thick, pachyostotic cortex made of laminar to plexiform tissue with cyclical growth marks and nearly no Haversian remodeling (Figure 29.9J, K). Conversely, the ribs of the ziphiid *Mesoplodon densirostris* (and possibly other ziphiid taxa) and those of the platanistid *Zarhachis flagellator* (Early to Middle Miocene) are totally cancellous (Figure 29.9L). Most of the shaft volume is then occupied by a spongiosa with thin, highly remodeled trabeculae.

Among the many peculiarities of the cetacean skeleton, the occurrence of hyperdense and hypermineralized cranial elements ranks among the most spectacular. The rostral region of several extant and extinct Ziphiidae indeed includes bones (most often the maxillae, premaxillae and vomer: Lambert et al. 2011, Bakker and Post 2020) having a compactness of 100% (Figure 29.9M), a relative mineral content reaching 86% (vs 66% in normal bone), and a density close to 2.8 (Buffrénil and Casinos 1995, Zioupos et al. 1997, Li et al. 2013). The collagen meshwork of these bones is extremely regressed (Zylberberg et al. 1998) and their mineral component increased in proportion. As a consequence, the hardness and stiffness of these bones reach the highest values encountered in vertebrates (Zioupos et al. 1997). Moreover, these bones may develop bizarre excrescences with diverse shapes, as exemplified by the premaxillae of *Globicetus hiberus* (Bianucci et al. 2013, Dumont et al. 2016). The role of these uncommon protuberances, and the significance of local bone hyperdensity, remain unclear (see, e.g., MacLeod 2002). As suggested by Gol'din (2014), these compact and hard excrescences could form acoustic mirrors for intraspecific recognition, through echolocation, in total darkness at great depth.

Perissodactyls

The microanatomical and histological features of perissodactyl limb bones are mainly known through the study of various Equidae, including extant horses (in addition to the classical reviews, see also Stover et al. 1992, Mori et al. 2003, Nacarino-Meneses et al. 2016a and Nacarino-Meneses and Köhler 2018), and two fossil taxa, *Parahippus* (Enlow and Brown 1958), a gracile Miocene taxon morphologically close to extant equids, but the size of a pony, and *Hipparion* (Martinez-Maza et al. 2014, Orlandi-Oliveras et al. 2018), a slightly more recent taxon similar to extant horses, but in which some dwarf forms evolved in insular conditions. To our knowledge, no histological study specifically deals with limb bone histology in extant or extinct tapirids, rhinocerotids or titanotheres. Conversely, rib structure has been considered at a microanatomical level in *Equus*, *Tapirus*, *Rhinoceros* and *Ceratherium* among extant faunas (Canoville et al. 2016), and briefly described histologically in the extinct equids *Parahippus*, *Equus simplicidens* (a Pleistocene zebra formerly called *Plesippus shoshonensis*), as well as the Eocene tapirs *Heptodon* and *Hyrachyus*, and the Miocene rhinocerotid *Teleoceras* (Enlow and Brown 1958). To further document the issue, bone microstructure in the humerus, radius and a metapodial of the basal equid *Pliolophus quesnoyensis*, a very small (cat-sized), gracile form from the Early Eocene of Europe and North America (see, e.g., Bronnert et al. 2017), is described here.

Although perissodactyls are basically adapted to long and fast running, the architectural features of long bones in most of them do not significantly differ from those of most other terrestrial mammals. For example, the femur and tibia of *Hipparion* have CDI indices of *ca.* 39 and 45%, respectively (computed from Martinez-Maza et al.'s 2014 illustrations), two values close to those mentioned above for artiodactyls. Similarly, equid ribs are not significantly different from the ribs of other mammals of comparable size (Canoville et al. 2016). The main exception is represented by the Rhinocerotidae. These large perissodactyls (BW up to 2900 kg in adult male *Diceros bicornis*), adapted to a defense behavior based on the kinetic energy of heavy frontal blows, have thicker cortices and higher bone compactness than most other terrestrial mammals, as suggested by the compactness value of their ribs (85.7%: Buffrénil et al. 2010, Canoville et al. 2016).

In all equids after the Eocene, including in the Late Miocene dwarf *Hipparion* forms from Mediterranean islands described by Orlandi-Oliveras et al. (2018), the basic histological structure predominantly observed in the periosteal cortices of long bones consists of woven-parallel complexes,. In early growth stages, the latter display relatively irregular plexiform or laminar-like organizations. Bone structure subsequently turns into a simpler pattern comprising longitudinal primary osteons and, in terminal growth stages, a thin layer of poorly vascularized woven-fibered or parallel-fibered tissues is deposited. This broad histological pattern was observed, with some variation, in the humerus, femur, tibia and metapodials of *Parahippus* (Enlow and Brown 1958), *Hipparion* (Martinez-Maza et al. 2014) and several extant horse and ass species (e.g., Stover et al. 1992, Nacarino-Meneses and Köhler 2018, Nacarino-Meneses et al. 2016a). The detailed studies by Stover et al. (1992) and Mori et al. (2003) show that juvenile and subadult horses (foals) often display, at least in broad sectors of long bone cortices, a peculiar type of woven-parallel complex. Cortical structure is indeed roughly reminiscent of the laminar and plexiform tissues, but the thick concentric strata, which topographically correspond to "laminae", are subdivided into quadrangular subunits by radial septa. As a consequence, their organization, as viewed in cross sections (Figure 29.10A, B), does not consist of circular primary osteons but of roughly square compartments, arranged within the cortex in concentric rows around the bone axis; each compartment contains one longitudinal primary osteon of large diameter (*ca.* 300 µm). Stover et al. (1992) proposed the model of "saltatory primary osteonal formation" to explain this histological structure. The latter clearly diverges from typical laminar and plexiform tissues, although many intermediary forms exist between them (the "squares" may be more or less elongated to become rectangles; see, e.g., *Hipparion* tibia in Martinez-Maza et al. 2014). Comparative data show that the peculiar type of tissue commonly encountered in foals is neither exclusive to horses nor universal in this clade. This tissue type may indeed occur in artiodactyls, as observed and described above for deer femora (see also Cuijpers and Lauwerier 2008); moreover, it is not necessarily present in all long bones and all cortical regions of perissodactyls. However, this peculiar type of woven-parallel tissue is clearly much more frequent in perissodactyls than in artiodactyls.

VetBooks.ir

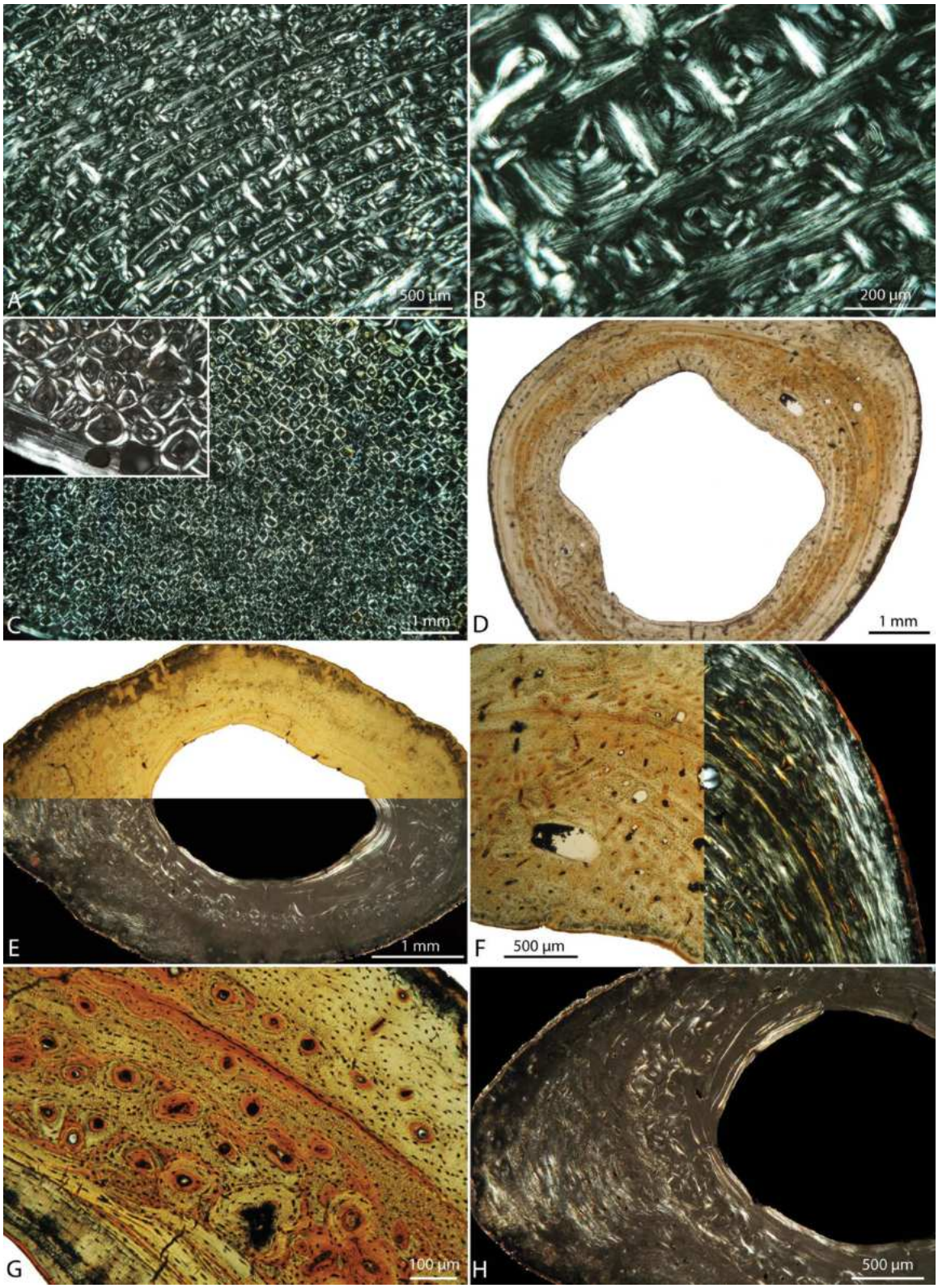


FIGURE 29.10 Microstructure of long bones and ribs in perissodactyls. A, General view of the special woven-parallel tissue created by the so-called *saltatory primary osteonal formation* in the tibial cortex of the equid *Equus quagga*. Polarized light. B, Closer view at the histological result of *saltatory primary osteonal formation*. C, Intensely and entirely remodeled rib cortex in *Rhinoceros sondaicus*. Inset: External fundamental system in the rib cortex of *R. sondaicus*. D, Cross section in the humerus of the extinct equid *Pliolophus quesnoyensis*. E, Cross section in the radius of *P. quesnoyensis*. F, Humeral cortex of *P. quesnoyensis*. The bone tissue is of a rough, atypical parallel-fibered type with lines of arrested growth. G, Closer view at *P. quesnoyensis* humeral cortex. Primary and secondary osteons occur in the cortex. H, Other field in *Pliolophus* radial cortex. Secondary osteons are concentrated in the base of the cortex.

VetBooks.ir

In most equids, primary cortices contain sharp cyclical growth marks (generally, LAGs) usable for age determination. In *Hipparion*, the best bone for growth mark counting is the third metapodial (Martinez-Maza et al. 2014, Orlandi-Oliveras et al. 2018), whereas it is the femur in the hemione (Nacarino-Meneses et al. 2016b). According to Nacarino-Meneses and Köhler (2018), long bones in early foals have a neonatal line, i.e., a sharp and bright line of arrested growth set in place just after birth, and functionally similar to the neonatal line described in many other tetrapods (e.g., Castanet et al. 1993; see also Chapter 31). Of course, this line disappears entirely through perimedullary resorption in later growth stages. Haversian remodeling is particularly intense and extensive in the limb bones and ribs of perissodactyls, which results in the formation of dense Haversian tissue in adults (Figure 29.10C). In a given cross-sectional plan, remodeling starts in the vicinity of the medullary cavity to spread into the whole cortex, sparing only a thin EFS of parallel-fibered tissue (Figure 29.10C, inset). In *Hipparion*, Haversian tissue is restricted to some cortical sectional sectors, which differ among the bones of a single skeleton and seem to present species-specific patterns (Martinez-Maza et al. 2014). Comparative data by Zedda et al. (2008) (see also Martiniakova et al. 2007) suggest that the relative extent of Haversian tissue in long bones is broader in horses than in cows, and that the secondary osteons of equids have a larger diameter, more lamellae and a wider Havers' canal than those of bovids. Haversian remodeling is also very dense in the ribs of equids, rhinocerotids and tapirids (Enlow and Brown 1958).

Long bone microstructure in the tiny basal equid *P. quesnoyensis* is completely different from that of later, more derived (and larger) perissodactyls. The humerus shaft of this taxon has a mean CDI value of 41%, and its medullary cavity is devoid of trabeculae; the radius, however, is more robustly built (CDI *ca*. 58%; see also Figure 29.10D, E). Histologically, long bone cortices, unlike those of most other terrestrial perissodactyls and cetartiodactyls (i.e., euungulates), contain no trace of laminar or plexiform tissues. In the humerus (Figure 29.10D, F, G), the greater part of the cortex is occupied by atypical parallel-fibered bone that houses variably oriented primary and secondary osteons (the main orientation is longitudinal, but oblique and short circular canals also occur). This tissue is birefringent, but it also contains an abundant population of variably oriented osteocyte lacunae, connected to each other by a dense network of canaliculi that the natural staining of bone during fossilization clearly reveals (Figure 29.10G). The peripheral region comprises a thick layer of more birefringent and poorly vascularized parallel-fibered tissue. Cell lacunae are fewer in this layer and lack canaliculi. Cyclical growth marks, in the form of annuli or LAGs, occur throughout the periosteal cortex (Figure 29.10D, F, G). The microstructure of the radius (Figure 29.10H) comprises a thick layer of perimedullary lamellar bone, a clearly delimited median layer of densely remodeled tissue, and a thick peripheral nonremodeled layer of parallel-fibered bone.

Carnivores

The microstructure of limb bones is remarkably consistent among extant and extinct terrestrial carnivores; conversely, it is more variable in amphibious and aquatic forms. At a microanatomical level, limb bones in most of the terrestrial taxa (canids, felids, ursids, mustelids, etc.) investigated hitherto are typically tubular, with a medullary cavity devoid of trabeculae (Figure 29.11A, E). Their mean compactness is generally close to 60% ± 10% for the humerus and the femur (Canoville and Laurin 2010, Quémeneur et al. 2013). Terrestrial mustelids tend to have more compact bones than other terrestrial carnivores, with indices between 65 and 75% for the humerus and the femur. Among extant carnivores, the most compact limb bones are those of the marine otter, *Enhydra lutris* (e.g., 93% for the humerus according to Nakajima and Endo 2013). A trend toward higher bone density in semiaquatic taxa is well established (e.g., Stein 1989, Fish and Stein 1991), not only in carnivores, but also in several other mammalian clades (see also Chapter 35). With compactness indices averaging 60–62% for, e.g., the humerus, the bones of most pinnipeds are not noticeably more compact than those of other carnivores (Nakajima and Endo 2013). Their morphology, variably triangular or ellipsoid in cross section, often gives them the architecture of a diploe; the core region is occupied by cancellous tissue.

Few data are currently available about the inner architecture of carnivores older than the Early Pliocene (later faunas do not greatly differ from extant taxa). One of the most intriguing observations deals with the generalized osteosclerosis and extreme compactness (*ca*. 100%) characterizing the whole postcranial skeleton (including all limb bones, ribs and vertebrae in the adults) of some Miocene seals from the North Sea and Paratethys region. This spectacular case is exemplified below (see, e.g., Figure 29.11H) by the small species *N. vitulinoides* (Dewaele et al. 2018; see also Koretsky and Rahmat 2017).

Histologically, limb bones are basically comparable among carnivores, provided the taxa share a similar size and mode of life (terrestrial or aquatic). The histological organization most frequently observed in adults, when remodeling spares primary tissues, consists of a three-stratum structure (Figure 29.11B, C). A thick layer of secondary lamellar tissue surrounds the medullary cavity, while the medium region of the cortex is occupied by a plexiform or reticular woven-parallel complex, in which longitudinal or oblique secondary osteons occur. In peripheral position, a thick layer of poorly vascularized or avascular parallel-fibered tissue, which may turn into lamellar bone to form an EFS, covers the bone cortex. This structure has been observed by several authors (from, e.g., Foote 1911 to Veitschegger et al. 2018) in diverse taxa. Our personal observations confirm its occurrence in small and large species such as *Mustela nivalis* (Figure 29.11B), M*artes martes* (Figure 29.11C), *Felis sylvestris*, *Meles meles*, *Canis lupus*, diverse seals and so forth. In a single bone section, however, whereas some sectors may strictly comply with the description quoted above, in neighboring sectors the cortex may comprise only one type of tissue. This situation is exemplified by the femur of *M. martes* shown in Figure 29.11D. Moreover, the femur of a river otter in Figure 29.11E and F exemplifies another situation closely reminiscent of that described above for the *Ornithorhynchus* femur or *Zaedyus* humerus: if the three-stratum structure is indeed present, the middle layer, however, displays the characteristics of compacted coarse cancellous tissue and is separated from the periosteal cortex by a clear

VetBooks.ir

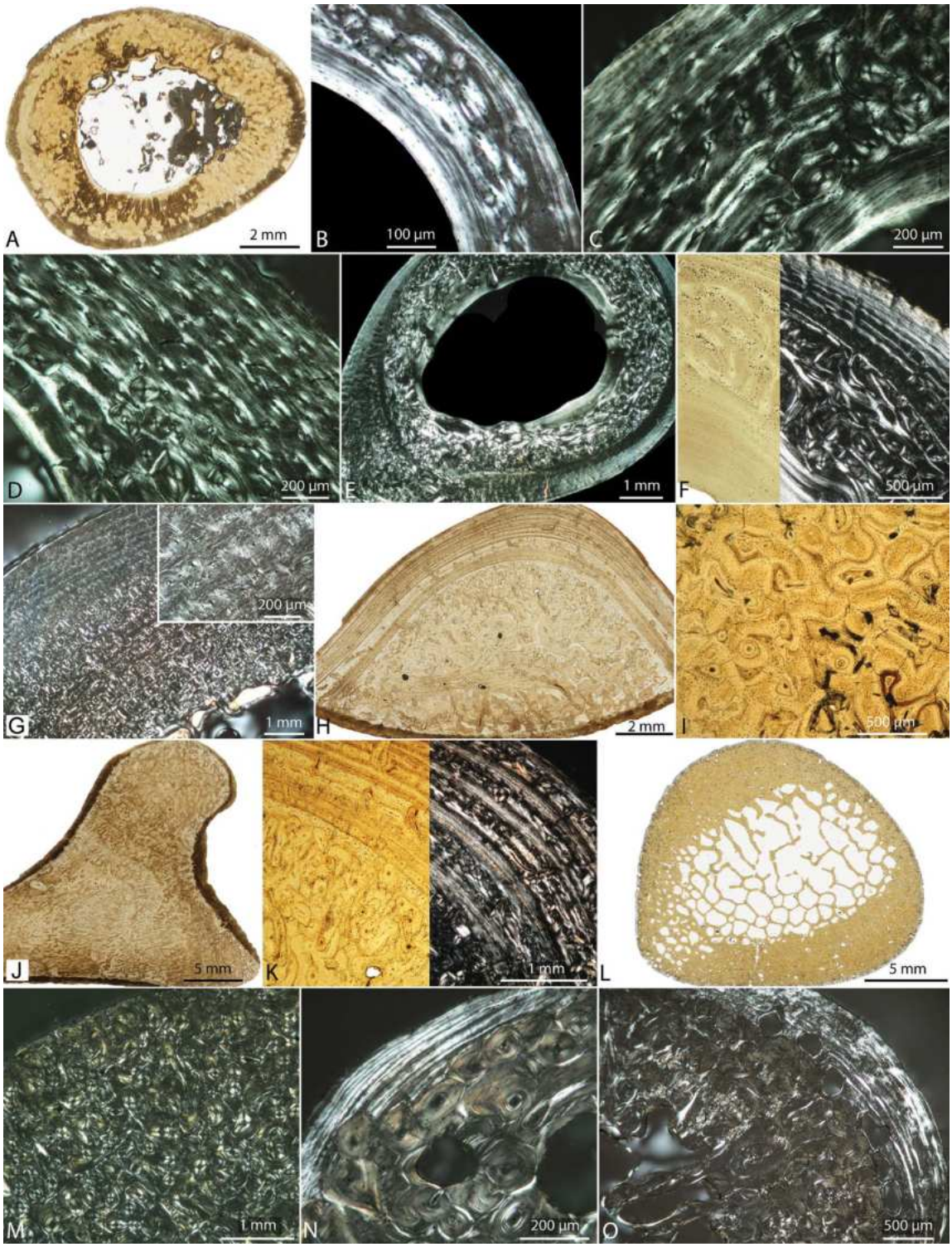


FIGURE 29.11 Microstructure of long bones and ribs in the Carnivora. A, Cross section at midshaft in the femur of *Potamotherium valletoni*, a Miocene mustelid. B, The three-strata structure in the femoral cortex of *Mustela nivalis*. Polarized light. C, Typical three-strata structure in the femoral cortex of the mustelid *Martes martes*. Polarized light. D, Other histological structure of *M. martes* femoral cortex in another field of the section shown in C. Polarized light. E, Cross section in the femoral shaft of a river otter, *Lutra lutra*. Polarized light. F, Detail of part E. Right half: polarized light. G, Detail of the femoral cortex of an adult lion, *Panthera leo*. Inset: Closer view of the woven-parallel complex with longitudinal primary osteons. H, Cross section in the humerus of the extinct phocid *Nanophoca vitulinoides* (Miocene of Belgium). I, Extreme remodeling resulting in totally compact bone tissue in the core of *N. vitulinoides* radius. J, Longitudinal section in the proximal epiphysis and metaphysis of *N. vitulinoides* femur. K, Annuli in the periosteal cortex in *N. vitulinoides* humerus. Right half: polarized light. L, Cross section in a rib from the extinct phocid *Callophoca obscura* (late Miocene – early Pliocene of Belgium). M, Detail of the remodeled rib cortex of the extant otariid *Otaria flavescens*. Polarized light. N, Rib cortex with annuli in a wild cat (*Felis silvestris*). Polarized light. O, Rib cortex with annuli in, *Enhydra lutris*. Polarized light.

VetBooks.ir

reversion line. In puppies, a reticular woven-parallel complex was observed throughout bone cortices by Enlow and Brown (1958). In the femur of adult lions (*Panthera leo*), most of the cortex spared by the expansion of the medullary cavity (the lion femur has a relatively modest CDI value: 38.2%) is composed of a woven-parallel complex with longitudinal primary osteons, regularly distributed in circular rows (Figure 29.11G). Its peripheral region consists of a thick layer of avascular woven-fibered tissue with conspicuous annuli. A narrow but very sharp EFS made of pure, highly birefringent lamellar tissue covers the outer surface of the shaft. The histological characteristics of the limb bones (humerus, femur, tibia) of the sabertooth felid *Smilodon fatalis* (Late Pleistocene of Peru), studied by Seymour et al. (2018) are basically comparable to those of the lion femur.

In the Carnivora, as in most other mammals, primary cortical tissues in long bones, whatever their histological type, generally produce conspicuous yearly growth marks in the form of annuli or LAGs (e.g., Figure 29.11F, H, K). In some taxa, like the extinct Pleistocene cave bear (*Ursus spelaeus*), such marks can be sharp and constant enough among individuals to allow demographic studies and population comparisons (Veitschegger et al. 2018). Haversian remodeling is active in carnivoran long bones but its distribution within the cortex is uneven. It starts in deep layers (where it results in dense Haversian bone) to spread outward with variable extent (Figure 29.11G). Enlow and Brown (1958) pointed out the similarity in bone structure between extant carnivores and the extinct *Oxyaena*, a cougar-sized, cat-like "creodont" from the Late Paleocene-Early Eocene of North America. "Creodonts" (not demonstrably a monophyletic group) were considered part of the Carnivora until the middle of the 20th century, but are now considered phyletically distinct from, though morphologically convergent with, the Carnivora proper (Lange-Badré 2006).

The long bones of *N. vitulinoides* and other Miocene seals from the southern margin of the Paratethys region, e.g., *Sarmatonectes*, *Pontophoca*, *Praepusa* and so forth, differ from this common histological pattern (Dewaele et al. 2018 and personal observations). In their compact medulla, intertrabecular spaces are completely filled by abundant endosteal deposits, intensely remodeled by Haversian substitution (Figure 29.11H). This remodeling process was seemingly imbalanced, with a characteristic excess in reconstructive tissue. Secondary deposits were so pronounced that they resulted in an occlusion of the Haversian canals (Figure 29.11I). Moreover, the secondary osteons themselves were submitted to further Haversian remodeling (see also Chapter 11). The diaphyseal, metaphyseal and epiphyseal regions of long bones, including ribs, were similarly affected by this process and transformed, at least in adults, into solid and compact osseous formations (Figure 29.11J). Primary periosteal cortices in *Nanophoca* consist of a woven-parallel tissue with longitudinal primary osteons. Toward the bone periphery, this tissue becomes a poorly vascularized formation of woven-fibered bone with annuli and LAGs (Figure 29.11K).

The inner structure of carnivore ribs does not deserve specific comments because it closely resembles that of many other mammals (e.g., cetartiodactyls) of comparable size. The medullary cavity contains a loose network of thin and intensely remodeled trabeculae (Figure 11L), while the whole cortex consists of dense Haversian tissue in adults (Figure 29.11M). An EFS made of parallel-fibered or lamellar bone with annuli or LAGs may locally persist (Figure 29.11N, O).

Long Bones of the Pholidote *Phataginus tricuspis*

To our knowledge, bone microstructure of pholidotes has not been described hitherto; therefore, subserial cross sections were made for this review in the shaft region of a *Phataginus tricuspis* (tree pangolin) femur. This bone (42 mm in length) belonged to a subadult and epiphyseal fusion was not entirely completed. At midshaft, *P. tricuspis* femur is a robust, oval-shaped tubular bone (Figure 29.12A) with a 62.5% mean CDI value. Its medullary cavity is surrounded by a ring of cancellous bone comprising short, convoluted, and oddly oriented trabeculae (Figure 29.12B, C). Histologically, the latter are made of highly remodeled lamellar tissue.

The basal, perimedullary part of the cortex is also remodeled by Haversian substitution. It displays a complex, disorganized aspect, with variably oriented coils of lamellar bone mixed with secondary osteons (Figure 29.12C, D). Again, such a structure can be interpreted as a compacted spongiosa, subsequently submitted to remodeling. More peripheral cortical regions consist of a tissue showing ambiguous histological features: it contains randomly oriented osteocyte lacunae with abundant canaliculi, but its matrix shows a faint and irregular birefringence (Figure 29.12D). In some sectors of the sections, whatever their location in the bone shaft, a reversion line separates this stratum from subjacent layers, and may even run through it. The actual meaning of this line cannot be settled with certainty; it most likely reflects local morphogenetic processes related to off-centered or twisted growth, because it does not occur all around the cortex and, where present, does not mark a clear-cut border between the periosteal cortex and the perimedullary compacted cancellous tissue. Therefore, this compacted cancellous tissue most likely results from a local process; the hypothesis of preserved metaphyseal CCCB seems irrelevant here. Vascular canals, when present in the cortex (the outermost layer is avascular), are longitudinal primary osteons. Moreover, numerous large erosion bays occur throughout the cortex, along with secondary osteons at various stages of completion. Cyclical growth marks, as LAGs, locally occur in the peripheral-most layer.

Histological Features of Long Bones and Ribs in the Lipotyphla

The shaft of long bones in the adults of small taxa such as, e.g., the European shrew, *Crocidura russula* (BW *ca*. 6-14 g), has a simple microanatomical structure: it is typically tubular with a broad medullary cavity devoid of trabeculae (Canoville and Laurin 2010). However, the inner architecture of the humerus in fully fossorial moles, the Talpini (in which this bone displays a complex outer morphology) is characterized by an elliptical medullary cavity, surrounded by a broad cancellous zone and a relatively thin peripheral compact cortex (Meier et al. 2013). Histologically, primary cortices in small lipotyphlans are made of poorly or non-vascularized parallel-fibered

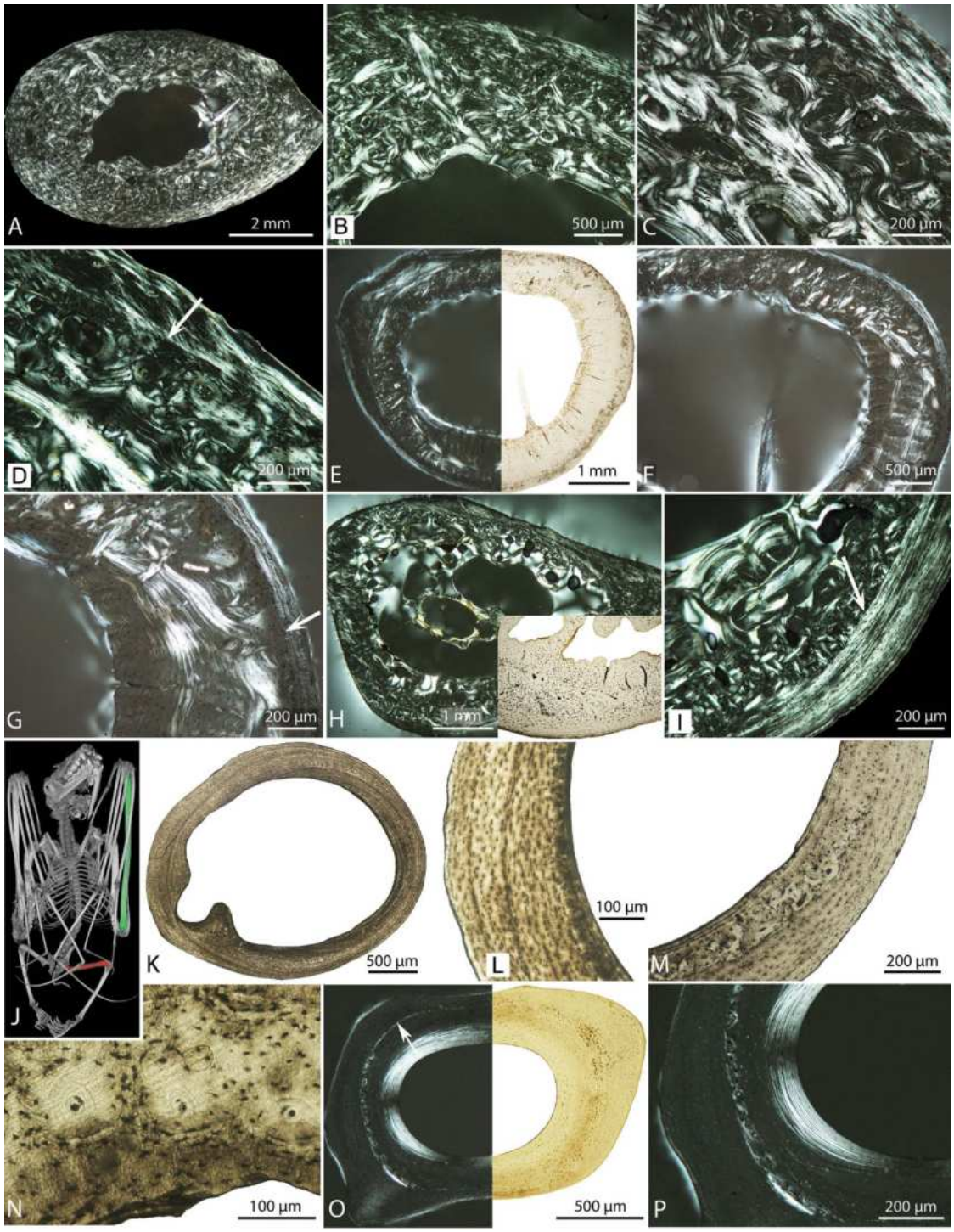


FIGURE 29.12 Microstructure of long bones in the Pholidota, Lipotyphla and Chiroptera. A, Mid-shaft cross section in the femur of the tree pangolin *Phataginus tricuspis* (Pholidota). Polarized light. B, Detail of the cortex structure in *P. tricuspis* femur. Polarized light. C, Other view of *P. tricuspis* femur showing the three-stratum structure in the cortex of this bone. D, Other view of *P. tricuspis* femoral cortex showing the reversion line (arrow) between the peripheral periosteal deposits and the median stratum. Polarized light. E, Cross section in the femur of the Hispaniolan solenodon, *Solenodon paradoxus* (Eulipotyphla). Left half: polarized light. F, Closer view of the cortex of *S. paradoxus* femur. Polarized light. G, Detail of the three-stratum structure of *S. paradoxus* femoral cortex. Polarized light. H, Cross section of the femur of the hedgehog *Erinaceus europaeus* (Eulipotyphla). Polarized light. The inset shows the aspect of the bone cortex in ordinary transmitted light. I, Close view of the three-stratum structure of *Erinaceus* femoral cortex. Arrow: reversion line between the median stratum and the outer periosteal cortex. Polarized light. J, Synchrotron image of the skeleton of the bat *Rousettus aegyptiacus*. The femur is coloured red and the radius green. K, Cross section of the femur. L, Detail of a cross section of the radius. M, Detail of the cortex structure with primary and secondary osteons in deep cortical layers. N, Closer view of the basal layer of the femur. O, Cross section of the radius of *Myotis* sp. Left half: polarized light. A LAG (arrow) occurs in the middle of the cortex. P, Detail of the cortical structure of the *Myotis* radius.

VetBooks.ir

tissue, with fibers having a mainly circular orientation (pronounced birefringence in cross sections observed in polarized light). The wall of the medullary cavity is coated with a thick layer of secondary endosteal lamellar tissue, and the outermost cortical stratum comprises an EFS also made of lamellar tissue (personal observation). Enlow and Brown (1958) described a similar, basic histological structure in the limb bones of the European mole (*Talpa europaea*), but with sparse simple vascular canals "entering the endosteal surface in a radial direction" in the tibia. Moreover, the periosteal cortices of the humerus and radius of this species was described as housing vascular canals oriented in multiple directions (oblique, radial, circumferential and longitudinal), deflecting the cortical strata and conferring to the cortex a "disorganized" appearance. The occurrence of osteoid tissue and the lack of an EFS in the specimen studied by Enlow and Brown (1958) suggest that it was an actively growing (likely juvenile) individual. Because the long bones of *Talpa* have a well-developed medullary cavity bordered by cancellous tissue, the tissue type described by Enlow and Brown (1958) is unlikely to remain visible in fully grown adults.

A comparable histological structure, partly colonized by secondary osteons, can also be observed (personal observations by VB) in a broad stratum located in the middle of the femoral cortex (in mid-diaphyseal sections) of two "large" extant lipothyphlans, the Hispaniolan solenodon *Solenodon paradoxus* (Figure 29.12E–G) and the hedgehog *Erinaceus europeus* (Figure 29.12H, I). This stratum, however, lies under a peripheral layer of parallel-fibered tissue, from which it is clearly separated by a sharp resorption line running all around the bone shaft (Fig. 12 G, I). This configuration suggests that the central stratum may consist of CCCB of metaphyseal origin, as otherwise indicated by its histological structure. In the extinct giant hedgehog *Deinogalerix*, long bone cortices as described by Kolb et al. (2015b) are made of parallel-fibered tissue framed by perimedullary and peripheral (EFS) lamellar layers. This tissue houses longitudinal simple vascular canals and primary osteons, along with cyclical LAGs and traces of a mild Haversian remodeling.

Chiroptera

Only a few descriptive microanatomic studies of bats have been published to date. Foote (1916) was the first to describe and sketch mid-diaphyseal cross sections of femora in 55 bat genera, a study later resumed by Amprino and Godina (1947) and Enlow and Brown (1958) in radii and humeri from undetermined chiropteran species. These authors pointed out that bat bones are characterized by a very thin cortex and a large medullary cavity devoid of trabeculae or cancellous bone. Such a structure parallels that of proximal wing elements of birds and pterosaurs, and it is interpreted as an adaptation to flight-induced torsion (Currey and Alexander 1985, Swartz et al. 1992, Swartz and Middleton 2008). It is hypothesized to maximize the polar moment of inertia of the bones (Swartz et al. 1992); however, bats were recently shown to have relatively thicker bone cortices than birds (Pratt et al. 2018). Most limb bone diaphyses are elliptical (in cross sections) in bats, but some appear planoconvex (Foote 1916), or have a quasi-rectangular shape in cross section, as exemplified by the radius of the Vespertilionidae, *Pipistrellus kuhlii* (Figure 29.12O).

Bone tissue in chiropteran limbs was described as mostly lamellar (Enlow and Brown 1958, Amprino and Godina 1947) with circumferential lamellae. However, recent studies (e.g., Lee and Simons 2015, Skedros and Doutré 2019), along with personal observations by MD and VB in *P. kuhlii*, *Rousettus aegyptiacus* and *Myotis* sp. rather find the occurrence of parallel-fibered tissue, with a lamellar component restricted to both the endocortical side and the periosteal margin of the cortex, where it may form an EFS (Figure 29.12J–P). Collagen fibers are oriented longitudinally within the bone cortex, which results in total darkness for cross sections observed in polarized light. Enlow and Brown (1958) also sampled mandibles from *Pteropus* (Pteropodidae) and *Artibeus* (Phyllostomidae), and noticed that they comprise a tissue similar to that of the shrew mandible (Soricidae), where the outer and inner compact regions are made of nonvascular circumferential lamellae and a series of small cavities in the deep (perimedullary) cortex. LAGs occur in chiropteran bones (Klevezal and Kleinenberg 1967) but they are relatively scarce, which is likely due to an early cessation of local skeletal growth. The radii of *P. kuhlii* and *Myotis* sp. studied here show one very sharp LAG, and several LAGs occur in the femur of *R. aegyptiacus*. The scarcity of cyclical growth marks makes the bone tissue of bats unsuitable for age determination.

Vascular canals are sparse or absent in bat bone cortices. Foote (1916) noticed that large-bodied taxa have poorly vascularized femora with longitudinal and occasionally radial simple canals, as exemplified by *Rousettus* (Figure 29.12K–M). In the radius of *Myotis* sp., a few longitudinal primary osteons of small diameter form a short circular file in the middle of the cortex (Figure 29.12 O, P). Small bats have avascular bones, a feature that, according to Lee and Simons (2015) and Pratt et al. (2018) questions Margerie's (2002) hypothesis that a laminar organization (bone having circumferential vascular canals; see Chapter 8) is a general adaptive feature in flying vertebrates.

Haversian remodeling has been observed, with variable frequency, in the deep cortex of *R. aegyptiacus* (Figure 29.12M, N) and other Pteropodidae (e.g., Bennett and Forwood 2010, Lee and Simons 2015, Skedros and Doutré 2019). For example, Bennett and Forwood (2010) observed secondary osteons in all the *Pteropus poliocephalus* (Pteropodidae) bones they studied, except the proximal phalanx V (see also Skedros and Doutré 2019 for the humeri and Metacarpal III of this species). Remodeling is proposed by these authors to begin early in development, when the animals start to fly; however, in the bones of *P. kuhlii*, intracortical remodeling does not occur. Skedros and Doutré (2019) suggested that the formation of secondary osteons in bats could depend on calcium demand during hibernation and lactation (e.g., Whalen et al. 1972, Doty and Nunez 1985 and Kwiecinski et al. 1987). Few studies specifically considered the effects of hibernation on mammalian bones (e.g., McGee-Lawrence et al. 2008, Fedorov et al. 2012, and Pineda et al. 2017), and especially in bats (e.g., Kunz et al. 1998). Cortical thinning and osteolysis (increase in osteoclastic activity) during hibernation were observed in the small form *Myotis lucifugus* (Vespertilionidae).

VetBooks.ir

Rodents

As Enlow and Brown (1958) pointed out, the microanatomical and histological features of rodent long bones are roughly comparable to those of several other mammals including monotremes, lipotyphlans, and carnivorans.

At a microanatomical level, these bones are tubular and have relatively high CDIs (45–80% for the femur), even in generalist terrestrial forms such as *Rattus rattus*, *Marmota marmota*, *Histrix cristata*, *Cavia porcellus* and the kha-nyou *Laonastes aenigmamus* (e.g., Canoville and Laurin 2010, Quémeneur et al. 2013 and personal observations by VB). In the adults of some semiaquatic taxa such as the Castoridae or the Myocastoridae, compactness and CDI in limb bones reach high values (80% or more for both indices in some bones; see Wall 1983, Stein 1989). The situation of fossorial rodents remains to be further documented. The detailed study by Montoya-Sanhueza and Chinsamy (2017) of the large bathyergid *Bathyergus suillus* shows that the cortex of most long bones in this taxon gradually increases in relative thickness during growth, which results in compactness and CDI values around 80% for zeugopodial elements of adults. This trend is also exemplified by the humerus of adult naked mole rats, *Heterocephalus glaber* (Montoya-Sanhuesa et al. 2021).

Histologically, long bones and ribs in the adults of small rodents (BW < 50 g) have a simple structure: their periosteal cortices are made of a parallel-fibered tissue with scarce longitudinal simple vascular canals (the marrow volume is nevertheless densely vascularized: Roche et al. 2012) that turns into avascular lamellar tissue toward the bone periphery (Figure 29.13A). In some taxa, the center of the cortex may consist, at least locally, of a layer of woven-fibered tissue. Thick endosteal deposits of lamellar bone coat the wall of the medullary cavity, and may substantially contribute to total cortical thickness (Montoya-Sanhuesa et al. 2021). In actively growing juveniles, cortices are made of either woven-fibered or parallel-fibered tissues, vascularized by longitudinal primary osteons (see, e.g., the study of two dormouse species by Garcia-Martinez et al. 2010). The development of the medullary cavity through the resorption of deep cortical regions generally results in the disappearance of this vascularized layer in adults (e.g., Sontag 1986, Orlandi-Oliveras 2016). In small rodents, cortices are most often devoid of cyclical growth marks and Haversian remodeling. This characteristic might be due to the short lifespan of these taxa, as suggested by the example of *H. glaber*, a long-living species (up to 7 years) in which limb bones have both LAGs and secondary osteons (Montoya-Sanhuesa et al. 2021). The histological structure observed (personal observation: VB) in the southern water vole *Arvicola sapidus* differs from this general model because the median part of the thick cortices of long bones, spared by resorption, shows a broad ring of a vascularized tissue displaying a convoluted structure and housing simple vascular canals with variable orientations (longitudinal, radial and oblique). This layer merges on its peripheral side with the parallel-fibered tissue of the outer cortex, but a reversion line can locally be inserted between them (Figure 29.13B; see also the description of Montoya-Sanhuesa et al. 2021 about *H. glaber*).

The basic three-stratum structure observed in *A. sapidus* is also encountered in most medium-sized and large rodents, from rats and guinea pigs to the largest extant form, the capybara *Hydrochoerus hydrochoeris* (BW up to 60 kg). Two examples of this structure in medium-sized taxa, *Laonastes aenigmamus* and *Cuniculus paca*, are given in Figure 29.13C, D (see also Kolb et al. 2015b for this structure in *Mikrotia* sp., a giant Late Miocene murine). Beyond rodents, a similar structure also occurs in terrestrial carnivores, as described above. The study of the mole rat *Bathyergus* by Montoya-Sanhueza and Chinsamy (2017), as well as the article by Garrone et al. (2019) on *Lagostomus maximus*, a Chinchillidae, showed the possible complexity of its mode of formation: the central layer may comprise fast-growing primary periosteal tissue, set in place at the beginning of postnatal growth, but it may also represent CCCB formed either locally or at the metaphyseal level, and maintained during growth to reach the diaphyseal territory (a possible situation already described above for several taxa). As shown in Figure 29.13B–D, G, this central stratum is bordered by reversion lines on both its sides, a situation that could substantiate the second hypothesis. In any case, the local morphogenesis of the shaft appears to be a complex process, in which more than one episode of peripheral resorption may occur, as exemplified by Figure 29.13C.

Peripheral primary periosteal deposits generally consist of parallel-fibered tissue. The tibia of *Myocastor coipus* nevertheless presents a tissue more akin to the woven-fibered type, abundantly vascularized by longitudinal primary osteons and simple radial canals (Figure 29.13E). A complex cortical structure is observed in the tibia of the largest extant rodent, the caviomorph capybara (*H. hydrochoeris*). In contrast to the femur, the tibia and the radius in this species have high global compactness (60 and 77%, respectively, vs 54% for the femur) and their small medullary cavity contains a strong network of thick trabeculae. From the center to the periphery of the tibial shaft, five histological territories can be observed (Figure 29.13F). Bone tissue on the walls of the medullary cavity and in the trabeculae protruding into it consists of actively remodeled endosteal lamellar tissue. The base of the cortex comprises a compacted spongiosa that shows a complex, convoluted and variable assemblage of lamellar bone. Scattered secondary osteons occur at this level. Peripheral to this formation is a thick layer of parallel-fibered bone displaying numerous longitudinal primary osteons. Toward the bone periphery, this tissue is abruptly replaced (the presence of a reversion line is much likely at this level, but cannot be ascertained) by a strong layer of an atypical tissue with a dominant radial structure. Finally, the shaft periphery is covered by a lamellar EFS, devoid of vascular canals and cyclical growth marks, and separated from the subjacent layer by a clear reversion line (Figure 29.13G). The histological complexity of the *Hydrochoerus* tibia is unique, not only among rodents, but also among mammals in general.

Differences among taxa mainly involve the type and density of vascular canals and the intensity of Haversian remodeling; whereas small forms have sparse simple canals, large forms have primary osteons with longitudinal, oblique or reticular orientations, as exemplified, among others, by the

VetBooks.ir

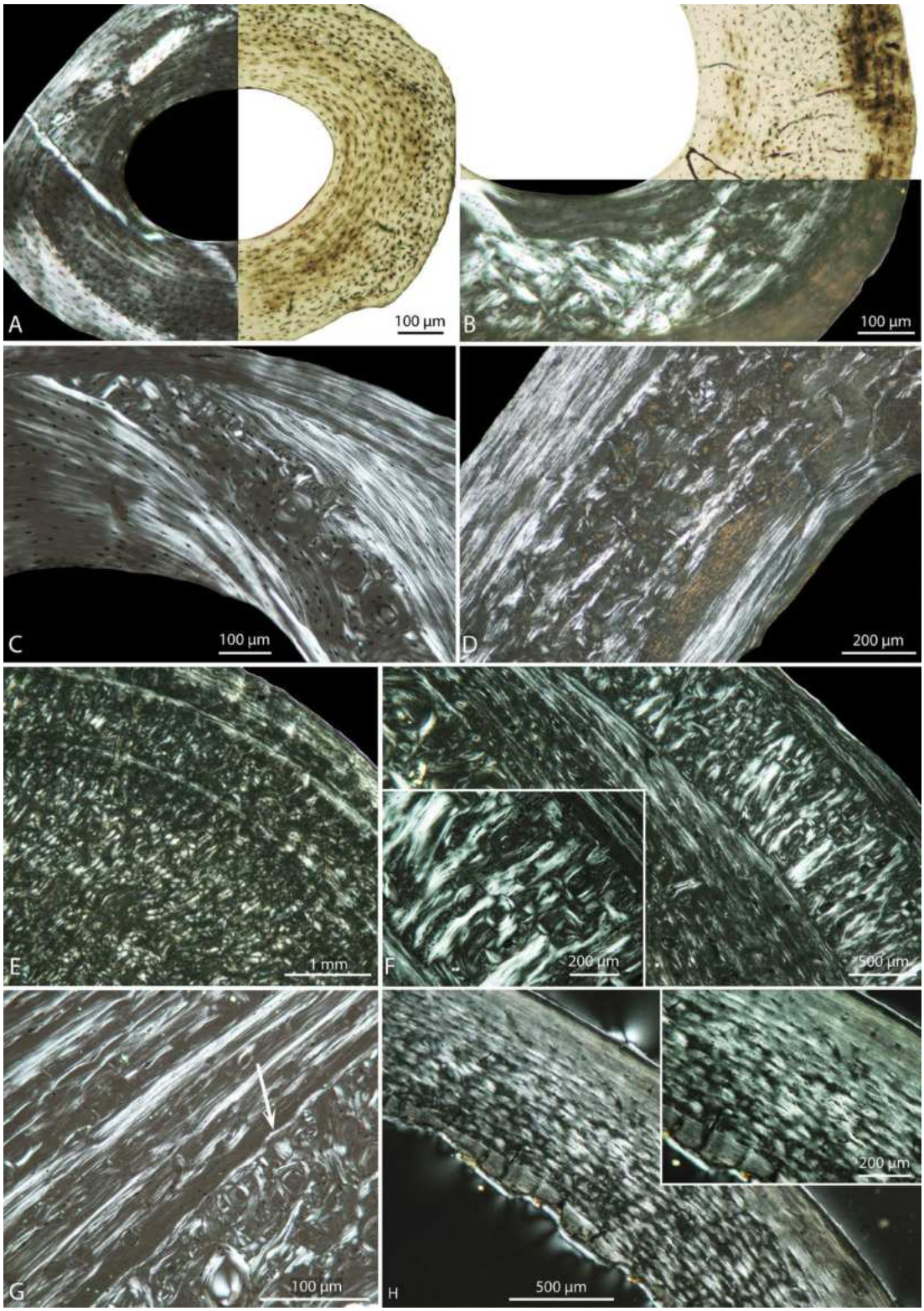


FIGURE 29.13 Microstructure of long bones in the Glires (rodents and lagomorphs). A, Mid-diaphyseal cross section of the tibia of a terrestrial vole, *Arvicola terrestris*. Left half: polarized light. B, Mid-diaphyseal cross section of the tibia of an aquatic vole, *A. sapidus*. Lower half: polarized light. C, Detail of the femur cortex of *Laonastes aenigmamus*, an Asiatic hystricognathe, viewed in polarized light. D, Detail of the tibia cortex of *Cuniculus* [*Agouti*] *paca*, a South American hystricognathe, viewed in polarized light. E, Lines of arrested growth and external fundamental system in the tibia of a coypu, *Myocastor coipus*. Polarized light. F, Detail view of the tibia cortex in a cabiai, *Hydrochoerus hydrochoeris*, showing the local variation in cortical structure. Inset: closer view of the convoluted, radial-like bone of the middle stratum. Polarized light. G, Reversion line (arrow) between the middle (lower right) and outer (upper left) bone strata in the tibial cortex of *H. hydrochoeris*. Polarized light. H, Cortical microstructure in the femur of the rabbit *Oryctolagus cuniculus*. Inset: closer view of the cortex. Polarized light.

VetBooks.ir

femur of some of the largest rodents that ever lived, the giant, cow-sized caviomorphs (possibly *Phoberomys* and *Dinomys*) from the Miocene of Venezuela studied by Geiger et al. (2013). In rats and other rodents weighing several hundred grams, Haversian substitution is mild, when it occurs. Data by Singh and Gunberg (1971) show that in rat long bones, secondary osteons progressively increase in spatial density with age, and their proportion compared to that of primary osteons changes. These parameters may affect age estimates. Secondary osteons are more numerous in large taxa such as Castorimorpha and Hystricognathi (see also Miszkievicz et al. 2019 for Murinae), but they are mainly confined to the central, well-vascularized stratum. Although the size of limb bones and ribs of some very large rodents is comparable to that of many artiodactyls or primates, these bones are never entirely remodeled (the bones of giant caviomorphs are not remodeled at all, and the giant dormouse *Hypnomys* displays only a few secondary osteons). Comparative data suggest that Haversian remodeling in rodents is a variable process that may reflect the strong and uneven influence of epigenetic factors and life history events. Outer cortical layers often display conspicuous annuli or LAGs (Figure 29.13E). More than 10 LAGs were counted by Orlandi-Oliveras et al. (2016) in the femoral EFS of *Hypnomys onicensis*.

Lagomorphs

Following the main descriptions by Foote (1911), Amprino and Godina (1947), Enlow and Brown (1958) and Kolb et al. (2015b) (see also Pazzaglia et al. 2015), along with personal observations by VB in *Lepus europaeus* and *Oryctolagus cuniculus*, bone structure in lagomorphs is basically similar to that of rodents of comparable size. However, periosteal cortices in limb bones and ribs of adult lagomorphs are thin because the enlargement of the medullary cavity still proceeds after the growth in diameter of the shaft has ceased. Quantitative data on this topic in *O. cuniculus* are given by Pazzaglia et al. (2015). As a consequence, the central, well-vascularized layer is reduced or may be absent in adults; the cortex is then made entirely of periosteal parallel-fibered bone, housing longitudinal simple canals, along with variable deposits of endosteal lamellar tissue around the medullary cavity (Figure 29.13H). Descriptions and illustrations by Pazzaglia et al. (2015) give detailed data on the development of long bone cortices in rabbits aged 1.5 month to 7.5 years. In early growth stages the bone cortex consists of a woven-parallel complex with longitudinal primary osteons. By the age of 6 months, the cortical matrix turns into the parallel-fibered type with simple vascular canals and longitudinal primary osteons, which tend to align in circular rows (a pattern incorrectly called "typical laminar" by Pazzaglia et al. op. cit.). In the course of growth, vascularization becomes scarcer, and the peripheral cortex of adults is made of a poorly vascularized or avascular parallel-fibered tissue, bordered by a thin layer of lamellar bone (EFS). Substantial Haversian remodeling occurs in the rabbit. It increases with age to form dense Haversian bone but, as in the rodents, it remains confined to the central, well-vascularized layer of the cortex. Cyclical growth marks can be sharp, as observed by Kolb et al. (2015b) in *Prolagus* specimens.

Primates

Though observations of several strepsirrhinians form part of large data sets on the geometry of limb long bones in primates (e.g., Schaffler and Burr 1984, Demes and Jungers 1993), precise histological studies of this clade are, to our knowledge, restricted to *Microcebus murinus*, a small (50–100 g) extant cheirogaleid from Madagascar (Castanet et al. 2004). Long bones in this species are tubular and lightly built, with a wide medullary cavity. A circular series of broad resorption cavities may occur in the deep cortex of some individuals (Figure 14A, C). Histologically, long bone cortices have the typical three-stratum pattern observed in many other therians. They include a perimedullary layer of lamellar tissue of variable thickness, a central stratum of parallel-fibered tissue containing longitudinal or slightly oblique vascular canals (simple canals and primary osteons) and a well-developed outer avascular layer of lamellar tissue presenting LAGs (Figure 29.14A, B). Measurements of accretion rates made by Castanet et al. (2004) yielded results extremely close to those obtained by Raman (1969) and Sontag (1986) in rats: a maximum accretion rate of 8–9 µm*day^{-1} in actively growing juveniles and a rate of 3–4 µm*day^{-1} by the end of somatic growth. A very slow residual subperiosteal growth (0.1 µm*day^{-1}) is subsequently maintained during 5–6 years, thus allowing long-term formation of LAGs and age recording. Haversian remodeling proper is limited, and the broad erosion cavities in the deep cortex are only partly reconstructed (Figure 29.14C).

In the Simiiformes, the microanatomical features of limb bones and ribs have been studied in detail in a great number of extant taxa of variable sizes, morphologies and locomotor adaptations (reviews in Ruff and Runestad 1992, Jerome and Petersen 2001). Long bones and ribs in these taxa are basically tubular (Figure 29.14D) and their main architectural characteristics (compactness, CDI and Bone Profiler parameters) fall within the average trends observed in other terrestrial mammals (reviews in Currey and Alexander 1985, Polk et al. 2000; see also Patel et al. 2013). Considerable attention has been paid to the relationship between the cross-sectional geometry of limb bones (the femur is currently taken as a reference) and the main locomotor adaptations of taxa (quadrupedality versus bipedality, terrestriality versus arboreality, walking versus leaping and so forth). Results obtained hitherto point to the complexity of this question that integrates several influences, including gender (e.g., Burgess et al. 2016), ontogenetic developmental stage (Ruff et al. 2013, Sarringhaus et al. 2016), nature of the bones considered (Shaw and Ryan 2012) and genetically determined individual peculiarities (Hansen et al. 2009). In the absence of aquatic taxa, osteosclerosis and pachyostosis are unknown in primates, with a major exception for *Homo erectus*, whose femur (along with several other bones) presents a high CDI value (63–74%), due to increased perimedullary endosteal deposits, along with a swollen, hyperplasic shaft cortex (Kennedy 1985, Verhaegen and Munro 2011). This unexpected peculiarity was initially supposed to be due to a difference in the phosphocalcic metabolism of early *Homo* species, compared to extant humans (Kennedy 1985); it is now tentatively considered to reflect an incipient aquatic adaptation in *H. erectus*, oriented to foraging on marine mollusks in shallow waters (Verhaegen and Munro 2011).

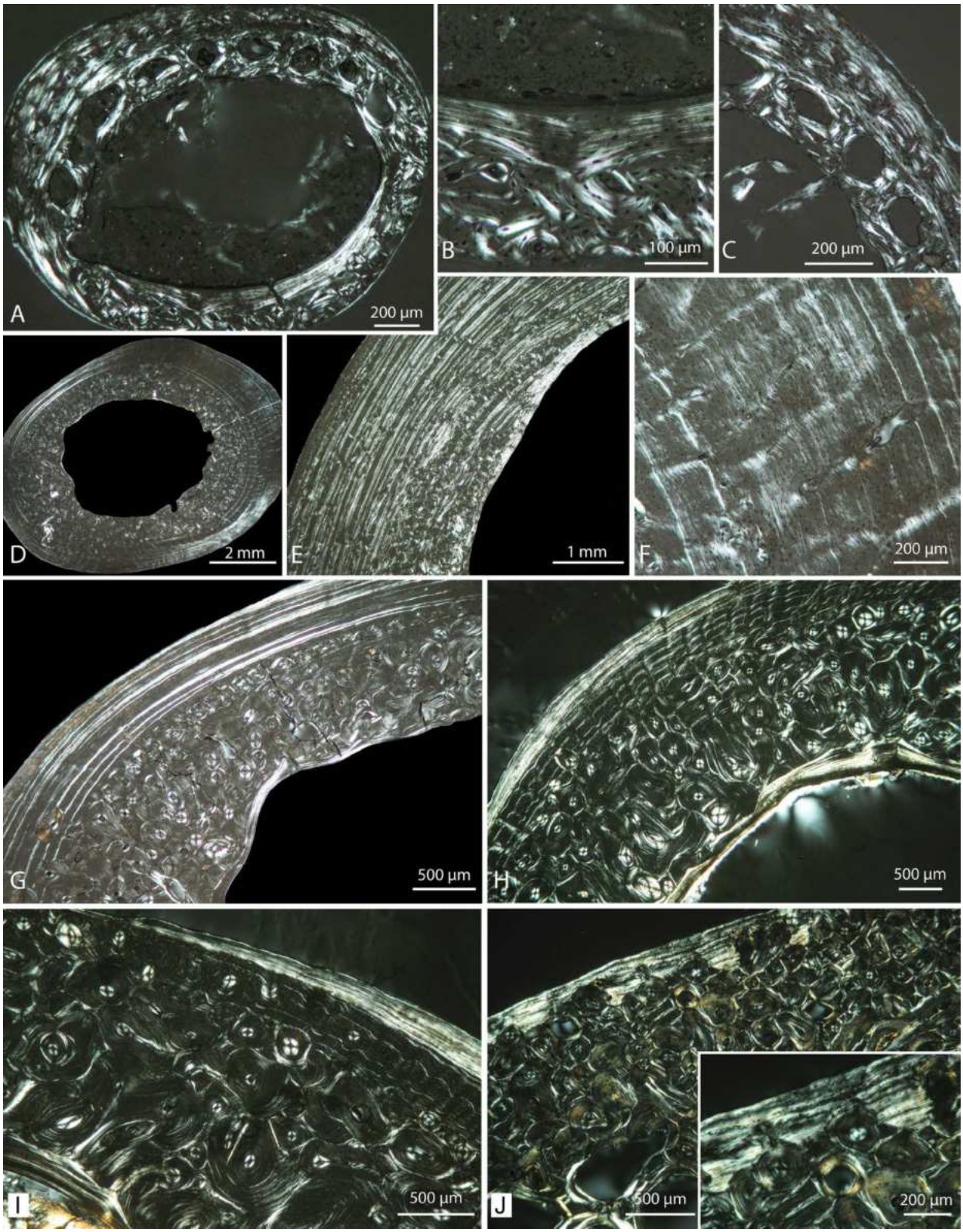


FIGURE 29.14 Microstructure of long bones and ribs in the Primates. A, Mid-diaphyseal cross section of the femur of *Microcebus murinus*. Polarized light. B and C, Details of the femoral cortex of *M. murinus* in two distinct fields. D, Mid-diaphyseal cross section of the tibia of *Macaca radiata*. Polarized light. E, Local occurrence of laminar bone tissue in the femur of *Hylobates* sp. Polarized light. F, Detail of the primary, parallel-fibered cortical tissue of *M. radiata* tibia. Polarized light. G, Conspicuous lines of arrested growth (LAGs) in another cortical sector of the *M. radiata* tibia. Polarized light. H, Conspicuous and regular LAGs in the nonremodeled part of *Hylobates* tibial cortex. Polarized light. I, Detail of the heavily remodeled cortex and external fundamental system (brightly birefringent outer layer) of *Hylobates* tibia. J, Cortex of a gorilla (*Gorilla gorilla*) rib showing intense remodeling, along with remnants of primary parallel-fibered tissue containing annuli (inset). Polarized light.

VetBooks.ir

At a histological level, the structure of long bones and ribs in medium- and large-sized Catarrhini is well documented by several comparative studies in Cercopithecidae, Hylobatidae and Hominidae, in addition of course to the ocean of studies dealing specifically with *Homo sapiens*. In general, bone histological traits, whether in a relatively small (3–5 kg) savannah dweller such as a grivet monkey (*Chlorocebus aethiops*), a chimpanzee (*Pan troglodytes*: 40–50 kg) or an extant human (60–90 kg), mainly differ in the extent and/or the chronology of Haversian remodeling. Moreover, these traits are fairly comparable to those described above for many other mammals of similar sizes, including carnivorans, rodents, terrestrial xenarthrans and so forth: clearly, primates, including *H. sapiens*, have no remarkable peculiarity, at least in the gross histological structure of their bones. Recent ontogenetic follow-up of bone structure in *C. aethiops*, the gibbon *Hylobates lar* and *P. troglodytes* (McFarlin et al. 2016), as well as *H. sapiens* (Goldman et al. 2009), suggest the synthetic reconstruction of long bone growth, as viewed in cross section, given below. In early postnatal growth (stage 2–4 years in *H. sapiens*), primary periosteal deposits in all taxa comprise a woven-parallel complex housing primary osteons and simple vascular canals with longitudinal, oblique or, more rarely, sublaminar orientations. At this stage, the wall of the medullary cavity can be devoid of endosteal, lamellar deposits (*C. aethiops*) or can present such deposits in the form of either a continuous layer (*Hylobates*) or remodeled trabeculae (*Pan* and *Homo*).

In the course of cortical growth, primary periosteal deposits first develop into a tissue type intermediate between woven-parallel and parallel-fibered bone (this tissue is called *transition fibrolamellar* [TFL], by Goldman et al. 2009 and McFarlin et al. 2016). It still contains longitudinal primary osteons, but the proportion of simple canals increases. In the smaller species (*C. aethiops*), this tissue may have one growth mark. Among the four taxa studied in detail, *P. troglodytes* is an exception, because the second tissue to be deposited, at least in some cortical regions, is another form of woven-parallel complex, laminar bone. Personal observations indicate that this tissue may also occur in broad portions of the cortical area in, e.g., *C. aethiops*, *M. fascicularis* and *M. radiata* (Figure 29.14E). In subsequent growth stages, the TFL tissue becomes parallel-fibered before becoming a lamellar tissue with scarce, simple longitudinal or radial canals (Figure 29.14F). In *Hylobates*, *Pan* and *Homo*, the parallel-fibered or lamellar layers are generally not pure and uniform; instead they display variably developed inclusions of another tissue that can be either parallel-fibered, within lamellar deposits, or TFL, within parallel-fibered strata. Conspicuous cyclical growth marks (LAGs) generally occur in cortices at this stage (Figure 29.14F–H). In the meantime, the medullary cavity develops to a variable extent, either symmetrically or asymmetrically, and tends to destroy early deposited cortical layers. Haversian remodeling also spreads within the cortex, starting from the initial woven-parallel layer. As a consequence, the proportion of primary to secondary osteons gradually decreases during ontogeny (Mulhern and Ubelaker 2003). This process is of limited extent in the femoral cortex of *C. aethiops*, but intense, extensive and always asymmetrical in the other three species (Figure 29.14H, I). Data by Schaffler and Burr (1984) on secondary osteon density and the proportion of dense Haversian tissue in the long bones of 20 primate species pointed out a significant influence of the locomotion mode on the degree of Haversian remodeling. Terrestrial bipedality (*H. sapiens*) is related to maximum Haversian remodeling, then comes suspensory locomotion, terrestrial quadrupedality and arboreal quadrupedality.

The quantitative area measurements presented by Goldman et al. (2009) and McFarlin et al. (2016) show that, in adult *Chlorocebus*, most of the cortex consists of lamellar tissue. In the other taxa, the nonremodeled parts of the adult cortex are also principally made of this tissue, mixed with variable (but generally small) inclusions of parallel-fibered or TFL bone. The observation presented above (frequency of laminar bone in primates) suggests that the lamellar tissue referred to in this case could be that of the primary osteons of laminar bone, rather than a thick consistent deposit of true lamellar bone, as occurs in, e.g., lizards and small mammals. The proportion of secondary tissue is an important feature that contributes to distinguishing human bones from bones belonging to perissodactyls or artiodactyls in archaeological sites (Cuijpers 2006, Hillier and Bell 2007). Dense Haversian tissue occupies about one-third of the cortical area in adult *Hylobates*, one-half in the cynomolgus monkey (*M. fascicularis*: Jerome and Petersen 2001), and two-thirds to three-quarters in *Pan* and *Homo*. Primate ribs are also heavily affected by Haversian remodeling (Figure 29.14J).

As exemplified by *H. sapiens* (Goldman et al. 2009), tangible intraspecific variability exists in the timing and location of the dynamic processes affecting bone deposits, including the shift from one tissue type to another, the extent and intensity of Haversian remodeling, or the off-centering of growth (see, e.g., Havill 2004 for variability in remodeling dynamics). Therefore, discrepancies may exist in the aspect of bone sections, even among genetically very close individuals; histological descriptions must properly cope with this variability.

An Overview of Mammalian Vertebral Microstructures

Microanatomical Features

Vertebral microanatomy in primates and, to a lesser extent, laboratory animals, has been described in great detail in a medical context (review in Hordon et al. 2000); conversely, few studies consider the problem in a broad comparative scope, with the aim of revealing possible adaptive patterns in vertebral architecture. Two such studies, based on samples reflecting mammalian diversity, and considering diverse structural parameters of vertebral centra, were presented by Dumont et al. (2013) and Houssaye et al. (2014). The mammalian vertebral centrum is a short endochondral bone comprising intraepiphyseal (secondary) ossification centers. Most of its volume is occupied by a spongiosa with trabeculae of both endosteal and periosteal origin, and by a compact periosteal cortex of variable thickness, resorbed in depth to contribute to the core spongiosa (Figure 29.15A). Two kinds of trabeculae, with distinct mechanical characteristics, exist in mammalian

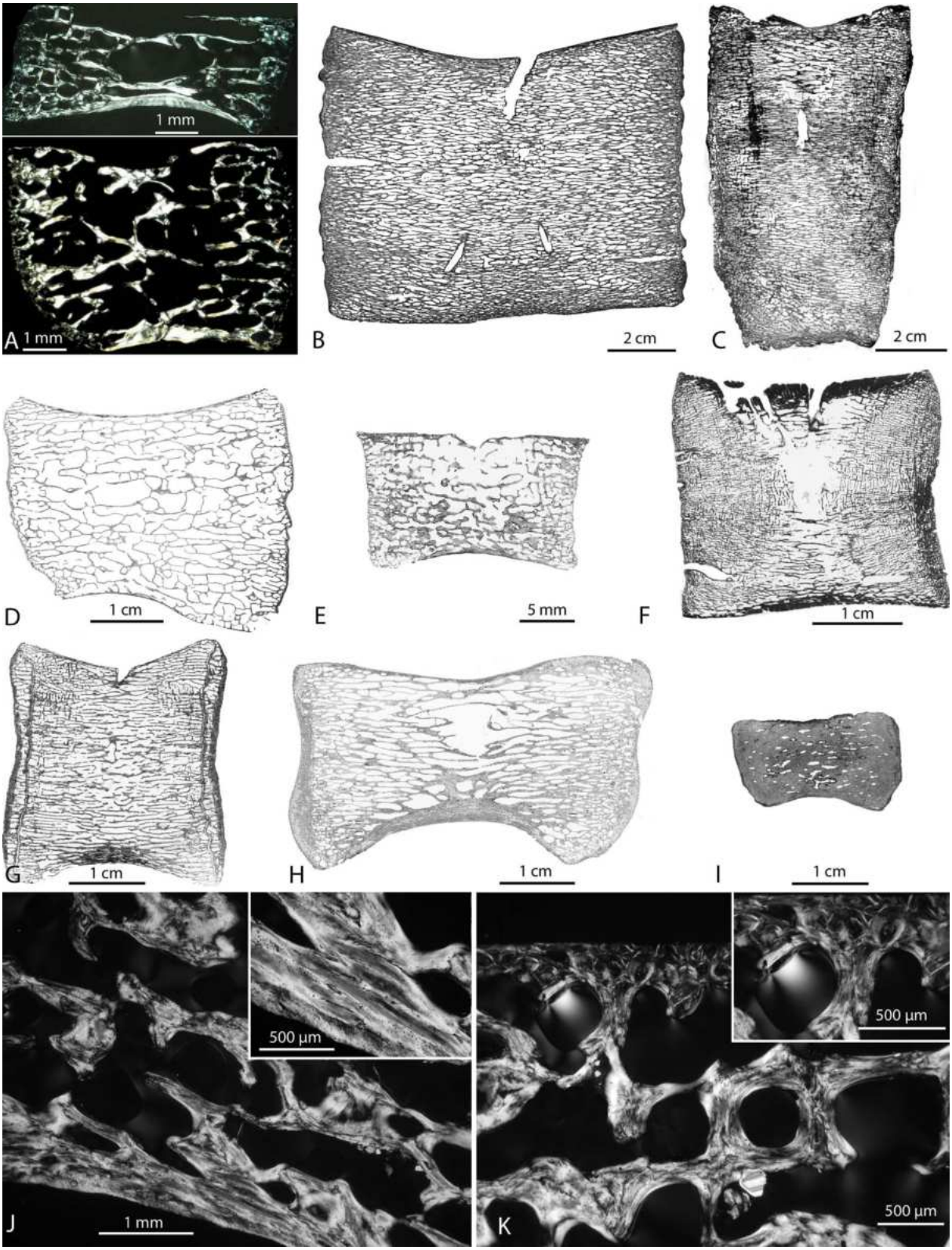


FIGURE 29.15 Comparative overview of mammalian vertebral microstructures. A, Architecture of the centrum in small mammals. Upper field: lumbar vertebra of the rodent *Sciurus vulgaris*. Lower field: dorsal vertebra of the lipotyphlan *Erinaceus europaeus*. Polarized light. B, Dorsal vertebra of the cetacean *Ziphius cavirostris*. C, Lumbar vertebra of the proboscidean *Elephas maximus*. D, Lumbar vertebra of the carnivoran (pinniped) *Cystophora cristata*. E, Lumbar vertebra of the primate *Hylobates* sp. F, Dorsal vertebra of the sirenian *Dugong dugon*. G, Dorsal vertebra of the cetacean *Delphinus delphis*. H, Lumbar vertebra of the artiodactyl *Cervus elaphus*. I, Lumbar vertebra of the carnivoran (pinniped) *Nanophoca vitulinoides*. J, Histology of the centrum in *Hylobates* sp. (ventral part). Inset: closer view of the nonremodeled periosteal cortex. Polarized light. K, Histology of the centrum in *Hylobates* sp. (dorsal part). Inset: closer view of the densely remodeled floor of the neural canal.

VetBooks.ir

vertebrae: rod-like and platelet-like trabeculae (Liu et al. 2009; see also above, Chapter 4). Global vertebral compactness (i.e., a two-dimensional [2D] proxy of the *trabecular bone volume* used in human medicine) is broadly variable in mammals and ranges, for example, from 27.9% in the eastern mole, *Scalopus aquaticus* (Houssaye et al. 2014), to 93.8% in the small Miocene seal *N. vitulinoides* (Dewaele et al. 2018). Similarly, most other parameters considered by Dumont et al. (2013), e.g., relative length of the trabecular network, mean width of the trabeculae, relative number of their intersections (*nodes*) or architectural polarization (i.e., the dominant orientation of the trabeculae as measured with Geraeat's 1998 method), show great discrepancies among mammals (Figure 29.15A–I). Diverse patterns, sharing no obvious consistency with taxonomic contexts, have thus been observed (Dumont et al. 2013, Houssaye et al. 2014). For example, in some primates (including *H. sapiens*) and in the sirenians, trabecular intersections are mainly orthogonal (Figure 29.15E, F), whereas, at the opposite extremity of the morphological spectrum, trabeculae mainly parallel to each other and to the sagittal axis of the centrum (extreme structural polarization) occur in diverse taxa such as the Irrawaddy dolphin, *Orcaella brevirostris* (Dumont et al. 2013), the common dolphin, *Delphinus delphis* (Fig. 15G), and the rodent *Castor fiber* (Houssaye et al. 2014). Between these two peculiar designs, most mammalian vertebral centra have a low architectural polarization and show substantial interindividual variability for this parameter (Figure 29.15D). In contrast to the situation in long bones, the relationships between the compactness of vertebral centra and the locomotory adaptations of the taxa are faint, though not absent. Quantitative microanatomical data converge to show that body size influences diverse parameters that reflect the relative development of trabecular networks. In other words, for a given centrum area (as measured in sagittal section), large species have proportionally longer trabecular networks, but their trabeculae are thinner. This general trend is especially pronounced in pelagic taxa that are propelled by oscillations of their caudal peduncle, a highly efficient lift-based propelling mode. Mean trabecular thickness and the relative number of nodes are also influenced, positively (nodes) or negatively (trabecular thickness), by body size. This is not the case for global bone compactness and architectural polarization. In aquatic mammalian taxa, vertebrae are generally untouched by the pachyostotic, osteosclerotic or osteoporotic-like processes that commonly occur in ribs or limb bones. Osteosclerotic vertebral centra are nevertheless documented (Figure 29.15I), as mentioned above, in the adults of the small extinct seal *N. vitulinoides*, and in the spectacularly pachyosteosclerotic vertebrae that characterize the odontocete *Pachyachanthus*, from the Middle Miocene of Central Europe (Kazár 2010).

Histological Features

Histologically, whatever the taxon considered, the core spongiosa of a mammalian centrum consists of densely remodeled trabeculae. The latter are thus made of complex assemblages of endosteal lamellar bone deposits, separated by reversion lines (Figure 29.15J, K). Remnants of primary periosteal tissue can nevertheless be seen in the core of the trabeculae newly formed by the patchy resorption of the deep cortical regions (Figure 29.15J). The histological structure of primary cortices has seldom been described. In a large sample of taxa varying in size from that of a shrew to that of a horse, the compact cortex of dorsal and lumbar vertebrae observed by one of us (VB) was exclusively made of lamellar (small species: Figure 29.15J, K) or parallel-fibered tissues in the adults (juveniles were not represented in the sample). Actually, only the peripheral-most layers of the cortex remain in adults; deeper layers are resorbed to be incorporated into the core spongiosa. Cortical structure in juveniles is likely to be more diversified. The ventral cortex of the vertebrae is generally devoid of secondary osteons (Figure 29.15J); whereas dense Haversian bone can occasionally be observed in the floor of the neural canal (Figure 29.15K).

Remarks on Other Skeletal Elements: Osteoderms, Baculum and Antlers

Xenarthran Dermal Ossicles

Cingulate osteoderms (Figure 29.16A), whether firmly sutured to form a rigid carapace (glyptodonts) or simply articulated one to the other (armadillos and, *pro parte*, pampatheres), have the typical architecture of a diploe. They display a cancellous core of variable compactness (compactness is higher in armadillos), framed, in peripheral and deep positions, by compact cortices (Figure 29.16B). This type of osteoderm has been studied in detail in several Cingulata by, e.g., Hill (2006), Chavez-Aponte et al. (2008), Krmpotic et al. (2009), Wolf et al. (2012) Asakura et al. (2017) and Ciancio et al. (2017). Recent data from Bergqvist et al. (2019) show, however, that the osteoderms of the oldest known xenarthran, *Riostegotherium yanei*, a cingulate dated late Paleocene to early Eocene (58–50 Ma), were somewhat different: they did not display the diploe structure but were quasi-compact, although well vascularized. Osteoderms in armadillos, pampatheres and glyptodonts basically display a roughly similar histological structure. Their cortices can be made of woven-fibered tissue (mostly in the superficial cortex) or parallel-fibered bone (deep cortex), but in both cases, the histological features of these tissues are relatively atypical because they also integrate numerous strong bundles of fibers originating from the surrounding dermis. *Riostegotherium* was no exception in this respect. Our observations of *Prozaedyus* (a Miocene Dasypodidae from South America) show that the basal cortex of osteoderms is made of well-characterized parallel-fibered tissue (Figure 29.16C) and that their superficial cortex, though principally composed of woven-fibered bone, is nevertheless covered by a thin (*ca.* 60-µm thick) layer of birefringent parallel-fibered tissue that may contain cyclical growth marks (Figure 29.16D). Beyond some discrepancies among authors about details of fiber orientation, the most common pattern arising from published data (and from first-hand observations conducted for this review in *Glyptatelus* and *Trachycalyptoides,* two Glyptodontidae, in addition to *Prozaedyus*) is the occurrence, in the deep (basal) cortex, of a system of "branching fiber bundles" (according to Hill's 2006 terminology) oriented parallel or slightly oblique

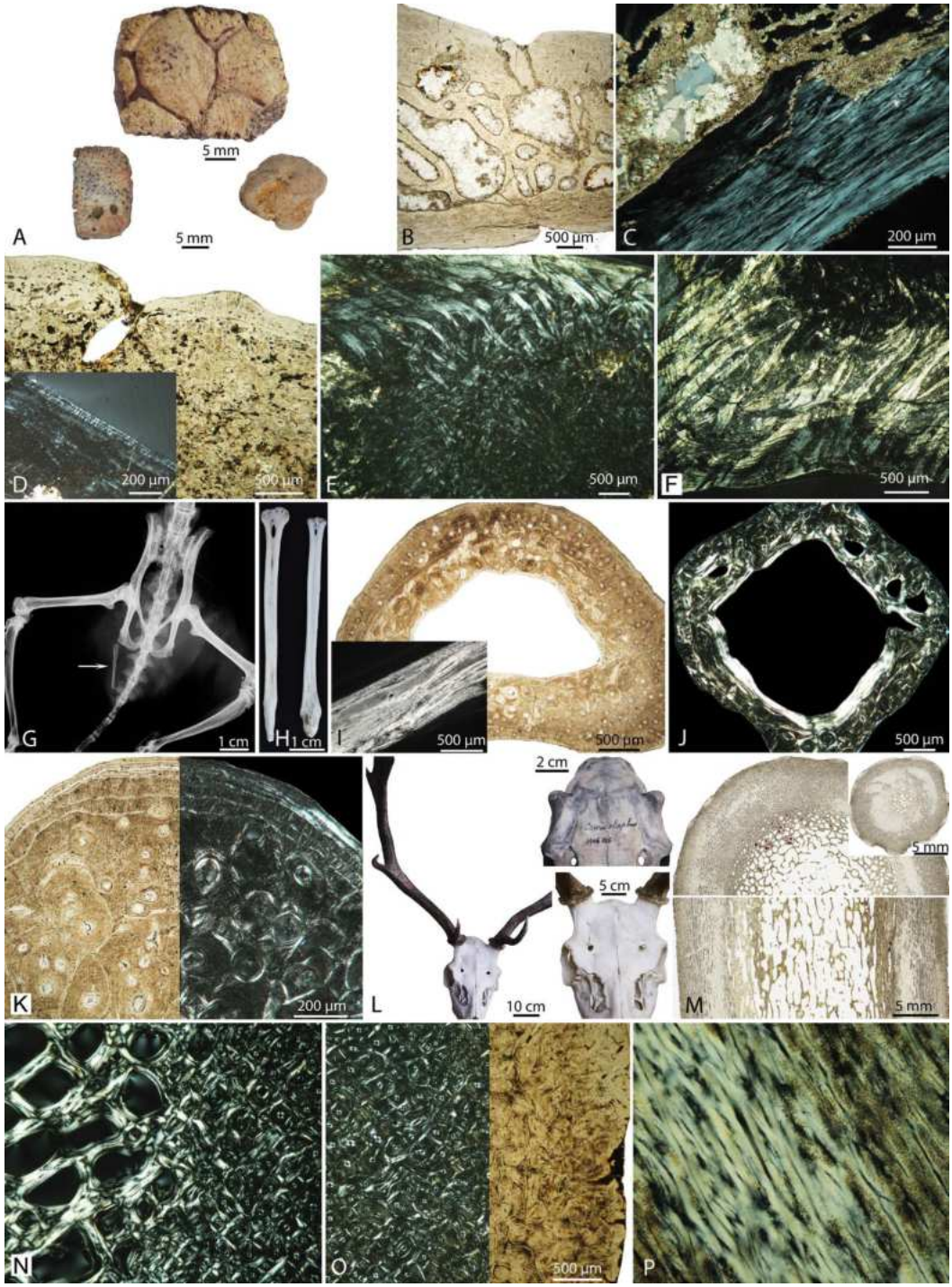


FIGURE 29.16 Microstructure of mammalian osteoderms, baculum and antlers. A, Morphology of xenarthran osteoderms. Upper field: in the cingulate *Glyptatelus* sp. Lower left: in the cingulate *Prozaedyus* sp. Lower right: in the pilosan *Glossotherium* sp. B, Diploe structure of *Prozaedyus* osteoderms. C, Parallel-fibered bone tissue in the basal cortex of *Prozaedyus* osteoderm. Polarized light. D, Histology of the superficial cortex of *Prozaedyus* osteoderms. Inset: peripheral-most layer polarized light. E and F, Strong bundles of "extrinsic" fibers in *Glossotherium* osteoderms. G, Pelvic region of *Laonastes aenigmamus* skeleton (X-ray proof). The arrow points to the baculum. H, Two *Meles meles* bacula. I, Main frame: cross section of *M. meles* baculum. Inset, longitudinal section. J, Strongly remodeled cortex in the distal extremity of *M. meles* baculum. K, LAGs and heavy remodeling of *M. meles* baculum at midshaft. Right half: polarized light. L, General view at the antlers of cervids. Left field: large antlers in a fallow deer (*Dama dama*). Lower right: antler pedicles in *D. dama*. Upper right: lateral frontal crests (at the origin of antler pedicles) in a juvenile red deer (*Cervus elaphus*). M, Cross and longitudinal sections of antlers. Upper main frame: cross section of the beam of a *C. elaphus* antler. Inset, cross section of the tip of a tine in the same species. Lower frame: sagittal section of the beam of a *C. elaphus* antler. N, Remodeled core spongiosa and Haversian systems in the deep cortex of a *C. elaphus* antler beam. O, Intensely remodeled outer cortex in the section described in N. Left half: polarized light. P. Longitudinal section of the beam of a *C. elaphus* antler. Polarized light.

VetBooks.ir

to the osteoderm surface and, in the superficial cortex, of a system of Sharpey's fibers quite variable in diameter, oriented perpendicular to the osteoderm surface and seemingly anchoring it to the surrounding dermis. The equatorial (articular) margin of the osteoderms contains thick bundles of long fibers running parallel to the deep and superficial faces.

Both cortices are vascularized by simple canals and primary osteons, with a greater vascular density in the superficial cortex. The trabeculae of the core spongiosa are intensely remodeled, but Haversian substitution in the superficial and deep cortex is variable and generally mild, if present at all (Figure 29.16B, C). The compact core region of *Riostegotherium* osteoderms was occupied by remodeled bone in which primary and secondary osteons occurred (Bergqvist et al. 2019).

Mylodontid osteoderms (Figure 29.16A) are entirely compact intradermal ossicles displaying an irregular ovoid morphology. Their gross histology is known from specimens of *Glossotherium chapadmalense* (Late Pliocene of Florida) described by Hill (2006). According to this author, mylodont osteoderms "consist mainly of mineralized fiber bundles with variable orientations". In the basal (deep) region, fibers are oriented irregularly in three orthogonal planes, whereas in the superficial region, fiber bundles have a prevalent orientation perpendicular to the osteoderm surface. LAGs may locally occur in peripheral layers. The core region is vascularized and remodeled by Haversian substitution. Our own observations of three *Glossotherium* sp. osteoderms agree with this description (Figure 29.16E, F).

The modalities of osteoderm formation in Cingulata (the question has not yet been considered in mylodontids) remain incompletely elucidated. Three main hypotheses are proposed in the recent literature. According to Hill (2006), xenarthran osteoderms result from a metaplastic process that locally transforms dermal tissues into bone through the calcification of fiber bundles and the differentiation of scleroblasts into osteocytes. Conversely, Vickaryous and Hall (2006) revealed the occurrence of osteoblasts secreting regular osteoid tissue during the early stages of osteoderm formation in the nine-banded armadillo, *D. novemcinctus*. Dermal ossicles would then result from normal membrane osteogenesis. A synthetic hypothesis was more recently proposed by Wolf et al. (2012) (see also Main et al. 2005): the involvement of an initial osteoblastic process, followed in later growth stages by the metaplastic incorporation and mineralization of dermal fibers, and by a final phase of osteoblastic osteogenesis, through which the layer of parallel-fibered tissue covering the superficial surface of the osteoderm is formed. This model could explain the composite nature of compact cortices frequently observed in the osteoderms of cingulates.

Baculum

In eight extant eutherian orders (Afrosoricida, Carnivora, Chiroptera, Erinaceomorpha, Lagomorpha, Primates, Pinnipedia, Rodentia and Soricomorpha), the males of some species display an inner bony reinforcement of the penis known as *os penis* or *baculum* (reviews in Burt 1960; see also Miller 2009 for marine mammals). An equivalent of this element in females is the tiny *os clitoridis*. The baculum is rare in the fossil record because its mineralization rate is lower than in other skeletal elements (Stockley 2012). As a consequence, the evolutionary history of this bone, which occurs only in mammals, is poorly known. The mammalian baculum displays extreme interspecific diversity in shape and size, along with marked intraspecific variability (e.g., Tasikas et al. 2009). It can be a slender, relatively long element (it reaches 18% of body length in the walrus, *Odobenus rosmarus*: Miller and Burton 2001; see also Ramm 2007), with a simple, subcylindrical morphology, as exemplified by many pinnipeds and mustelids (e.g., Baryshnikov et al. 2003; see also Figure 29.16G–H), or a short element that may display a flat shaft and large excrescences (e. g., bats and some rodents: Comelis et al. 2018, Stockley 2012). A sagittal groove housing the urethra may be present (e.g., in canids: Sharir et al. 2011) or not (most other taxa). Broad-scope comparative studies have failed to show a clear correlation between baculum size or shape, and the general morphological, behavioral and physiological characteristics of the taxa considered. The extensive statistical analysis by Schultz et al. (2016) resulted in a plausible explanation of the puzzling variability that characterizes the morphology and taxonomic distribution of the baculum: though very common, this bone may have evolved independently a minimum of nine times, and been lost at least ten times, during mammalian history; therefore, it is likely to represent a convergence rather than a homologous character among clades (see also Brindle and Opie 2016 on this topic).

The ontogenetic development of the baculum remains incompletely elucidated and seems to be a variable and complex process. This bone originates from mesenchymal condensations located along the urethra, in the territory of the genital tubercle (Murakami 1986, 1987, Murakami and Mizuno 1986). It mainly develops during postnatal life, through both membrane and endochondral ossifications (depending on the part of the bone considered), under the influence of androgens, bone morphogenetic proteins and other growth factors (Williams-Ashman and Reddi 1991, Izumi and Murakami 2000, Cohn 2011). The transient and local formation of chondroid bone has been suspected by Beresford (1981) to contribute to the early development of the baculum. The growth in length of the baculum is limited in time (in the phocid *Cystophora cristata*, for example, it stops at the age of 5 years), but its growth in diameter or thickness, and consequently in weight, can proceed throughout life, albeit at a low rate, as exemplified by most pinnipeds (Miller et al. 1999, Miller and Burton 2001).

Though many morphological descriptions of mammalian bacula are available because of their utility in taxonomy (e.g., Burt 1960, Dixson 1987, Patterson and Thaeler 1982), relatively few data on the inner microstructures of this element have been published. In canids, the cross section of this bone has the shape of a robust horseshoe (the groove is the urethral canal), the wall of which displays a cancellous core region (created by multiple large resorption bays), framed laterally and medially by compact cortices (Sharir et al. 2011). In the bat *Pipistrellus*, the baculum is Y-shaped and the core of its three branches is occupied by a relatively thin tunnel topographically comparable to a medullary cavity (Herdina et al. 2015). Personal observations by VB reveal a similar tubular structure in the baculum of the badger *M. meles* (Figure 29.16I, J).

VetBooks.ir

The CDI is 53–58% at midshaft in this bone, and decreases to *ca*. 40% toward the bone extremities (Fig. 16J). Illustrations in Stanley and Hillemann (1960) also show a roughly tubular structure in the baculum of the coypu (*Myocastor coypus*); conversely, the baculum of the black rat, *R. norvegicus*, is a solid rod, devoid of a central cavity but well vascularized (Kelly 2000).

Histological descriptions of the baculum cortex are particularly scarce. In dogs, Sharir et al. (2011) found two distinct regions in cross sections: an outer layer some 100 µm thick made of birefringent lamellar tissue, and a deep region completely remodeled by Haversian substitution. The nature of the primary periosteal tissue in this deep region was not described. In *M. meles* (personal observations), the remnants of local primary bone spared by remodeling are made of a parallel-fibered tissue that appears monorefringent in cross sections (Figure 29.16K) and irregularly birefringent in longitudinal sections (Figure 29.16I, inset). Cell lacunae have a roundish shape in cross sections, whereas they are spindle-like and aligned with the longitudinal direction of bone layers in sagittal sections. These features indicate that the collagenous meshwork of primary deposits is predominantly oriented in a longitudinal direction. In peripheral cortical layers, the bone tissue becomes a more typical parallel-fibered type, with conspicuous cyclical growth marks in the form of translucent (in ordinary light) and birefringent (in polarized light) LAGs (Figure 29.16K). In *M. meles*, the growth and remodeling patterns of the baculum strictly parallel those of an appendicular long bone: the cortex is intensely remodeled by Haversian substitution and shows densely packed secondary osteons at various stages of completion (dense Haversian tissue: Fig. 16K). Moreover, the diameter of the medullary cavity is enlarged through a classical (and slightly off-centered) process of peripheral resorption, followed by the accretion of reconstructive layers of secondary lamellar tissue (Figure 29.16J). Finally, most of the baculum volume in adult badgers consists of secondary lamellar bone. Sharpey's fibers are present but restricted for this reason to the most peripheral (less remodeled) layers of the cortex.

Antlers

Cephalic excrescences in the form of horns, crests, frills and so forth are common among tetrapods, but deciduous and repeatedly regenerated appendages, the antlers (Figure 29.16L), are encountered only in the Cervidae, an artiodactyl (Ruminentia) clade comprising some 44 species, all of which except one (*Hydropotes inermis*) have antlers (reviews in Chapman 1975, Crigel et al. 2001, Price et al. 2005, Rössner et al. 2021). With the exception of the reindeer (*Rangifer tarandus*), the full development of these excrescences is a typical characteristic of males. Antlers consist of a simple or ramified bilateral system of osseous "horns" comprising a major rod, the beam and minor shoots, the tines. In adult males, they actively develop during 3–4 months each year (midspring to end of summer) from two excrescences of the frontal bones, the pedicles. During their active growth, antlers are covered with soft tissues (skin and periosteum) forming the velvet. The shedding of the velvet in late summer or early autumn marks the end of the yearly growth of antlers. They nevertheless remain in place as bare, hard and mineralized elements used in various behaviors (defense against predators, intraspecific fights, etc.), until the beginning of the next spring. They then detach from the pedicle, leaving two scabs that heal in some weeks, before new antlers start developing. In the red deer (*Cervus elaphus*, the weight of a fully grown pair of antlers in large specimens can reach some 10 kg, i.e., 5% of total body mass (synthetic data are given by Lincoln 1992).

The presence of deciduous antlers is a major synapomorphy of the Cervidae. However, its origin and the evolutionary stages of its formation remain unknown (review in Davis et al. 2011). Heckenberg's (2017) comparative study shows that the oldest recognizable deer, *Procervulus* and *Ligeromeryx*, dated from the Early Miocene, are likely to have already had this type of appendage. In conclusion to a recent and broad comparative survey, Rössner et al. (2021) determined that cervid antlers, their basic structure and their general mode of development, have remained roughly unchanged throughout the evolution of the Cervidae. Many observational and experimental studies have been conducted since the middle of the 19th century about the intriguing questions of antler structure, growth, shedding and regeneration. The main aspects of this complex and still incompletely elucidated topic are summarized below.

In transverse section, the microanatomical structure of a dry antler beam is very comparable to that of a long bone in terms of compactness profile (Figure 29.16M). The beam comprises a compact cortex surrounding a broad, geometrically isotropic medullary spongiosa made of thin and short trabeculae (mean ICD 28–40%); a transition zone of intermediate compactness is wedged between them (Wislocki 1942, Rolf and Enderle 1999). To our knowledge, the only important divergence from this pattern occurs in *Elaphurus davidianus*, which has much more compact antlers (Ceacero et al. 2015).

Differentiation and Growth Process of the First Antlers

The initial differentiation process of antlers starts during fetal life in both males and females with the incipient formation of the pedicles, which become anatomically visible only some months after birth. The periosteum situated over the lateral crests of the frontals (i.e., protuberances located behind the orbits, close to the frontoparietal suture: Figure 29.16L) is different from that covering the other parts of the bone: it is thicker, and comprises mesenchymal cells supposed to be of direct neural crest origin (review in Kierdorf et al. 2007; see also Kierdorf and Kierdorf 2002). Cytologic studies conducted 50 years ago by Hartwig (1967, 1968) have established by cell culture and ectopic transplantations that these cells have the intrinsic properties to develop a pedicle structure wherever they are transplanted, in contrast to the cells from other periosteal sites. This capability justified the term *antlerogenic* applied to this cell population (Li and Suttie 1994, 1988, Li et al. 1995). Local antlerogenic cells function as osteoblasts and contribute, through ordinary subperiosteal accretion, to developing the pedicle in the form of a domelike local swelling, some millimeters high in the juvenile male red deer (Li and

VetBooks.ir

Suttie 1994). Up to this stage, this protuberance comprises in its apical region and, from outer to inner levels, an epidermis and a dermis of ordinary structure containing sebaceous glands and hair follicles, along with the fibrous (outer) membrane and the inner cambial cell layer of a periosteum. Still deeper, the osseous trabeculae produced by the osteogenic activity of the periosteum osteoblasts are oriented sagittally. In skull parts other than the pedicle, the periosteum is thinner because cambial cells are less numerous (Li and Suttie 1994). A medullary cavity partly filled with remodeled trabeculae occupies the core of the pedicle. The cortex and the medullary tissues are densely vascularized.

The sexual dimorphism of deer antlers appears at the onset of puberty. In males, an increase in the circulating testosterone level provokes the multiplication of the mesenchymal, osteoblast-like cambial cells located at the pedicle apex, and the latter further increases in height (up to 60 mm). This process does not occur in females. Experimental castration of young males impedes the activation of the apical "osteoblasts", whereas the injection of this hormone to young females triggers it (Kierdorf et al. 1995b). The key role of testosterone on antler development in preadults has been pointed out since Wislocki et al.'s (1947) study, and subsequently ascertained by different lines of evidence, including the direct localization of this hormone in the osteogenic tissues of growing antlers (Bubenik et al. 1974, see also Suttie et al. 1995). Once activated by testosterone, the cambial cells of the periosteum will behave differently whether they are at the apex or on the peripheral wall of the pedicle. On the peripheral wall, they constitute typical osteoblasts and secrete an osteoid tissue that mineralizes. In the apical region, the cambial layer of the periosteum becomes a perichondrium and its mesenchymal cells behave as chondroblasts (Kierdorf et al. 1995a, Kierdorf and Kierdorf 2002). This crucial process, seemingly akin to some form of metaplasia (see Chapter 12), was designated by Suttie et al. (1991) as *ossification pattern change* (OPC). Its histogenetic mechanisms remain unexplained, although recent data by Ma et al. (2019) shed some light on the complex interplay of the local signaling molecules and the transcription factors involved in this process. Apical chondroblasts actively proliferate (Matich et al. 2003) and the chondrocytes thus produced enter a maturation gradient resulting in hypertrophy. They nevertheless do not align in isogenic groups. They secrete, and are entrapped in, an atypical cartilaginous matrix that forms longitudinally oriented trabeculae (Frasier et al. 1975; see also Wislocki 1942, 1947). The matrix subsequently calcifies before being resorbed by chondroclasts and replaced by bone to form secondary trabeculae. This substitution is operated by typical bone cells; it is not a metaplastic process (Kierdorf et al. 1994, 1995a). Remnants of unresorbed calcified cartilage frequently remain in the core of the secondary trabeculae (Kierdorf and Kierdorf 2002). In the following growth stages, trabeculae are further remodeled to finally consist of brecciate lamellar bone. The growth in length of an antler therefore relies on a complex process comparable to endochondral ossification. Differences nevertheless exist between this process and the typical endochondral ossification that occurs in, e.g., limb bones (matrix composition, absence of isogenic groups in the antlers, etc.), justifying the expression *modified mammalian endochondral ossification* used by Banks (1974). Conversely, the growth in diameter of the beam and tines proceeds through a normal membrane ossification process operated by the periosteum as long as the velvet stays in place. In the meantime, the base of the cortex undergoes an extensive, patchy resorption that contributes to the enlargement of the core spongiosa. The primary cortical tissue consists of a woven-parallel complex comprising a loose scaffolding of woven-fibered tissue, filled by very quickly deposited primary osteons, the whole forming an irregular, convoluted reticular-like pattern. Haversian substitution is extensive, and soon after its accretion the cortex turns to a dense Haversian tissue, in which no trace of primary deposits persists (Figure 29.16N–P). Antler bone is remarkable for its low mineral content: 50–63% (Landete-Castillejos et al. 2007, Ceacero et al. 2015), which varies with both the taxa considered and the sampling location (beam base or tine shaft). As a consequence, it has a very low Young's modulus, 7.2 to 10.0 GPa, i.e., less than half that of a human femur (Currey 2002).

The blood supply to the osteogenic tissues of the apical and peripheral periosteum relies on a dense network of capillaries originating from both the dermis above the periosteum and the central medullary tissues. By the end of the growth of the first antler, local blood irrigation stops in the velvet through an ischemic process. The precise causes of this process remain incompletely understood, but long-term hormone samplings clearly reveal a steep peak in circulating testosterone by the time the velvet dries (Goss 1968, Arnett et al. 1989). As a consequence, the velvet is shed, and the antlers then display a bare, dry surface. Rolf and Enderle's (1999) observations show that blood supply in the antler core nevertheless persists "almost till the time the antlers cast". Finally, the base of the antlers, at the interface with the pedicles, is submitted to extensive osteoclastic resorption (e.g., Goss et al. 1992) that results in their cast and the local presence of a scab. This terminal stage occurs some 10–11 months after the start of antler growth.

Antler Regeneration

One or two months after antler shedding, by the end of spring, the healing of the scab is complete, and a new population of mesenchymal cells colonizes the apex of the pedicle. The regeneration of new antlers in adult specimens (more than 2 years in the European red deer) relies on the same osteogenic events and cell populations as the development of the first antler: it involves the periodic activation of stem cells located within the periosteum of the distal pedicle (Kierdorf et al. 2007). The main difference between these two stages is that most of the antler regeneration occurs during a phase (April to July) of low, though gradually increasing, plasma levels of testosterone (Bartoš et al. 2009), whereas higher initial testosterone levels occur at the onset of the first antler growth in preadults. The peak of circulating testosterone occurring during the rut period (September–October) provokes the shedding of the velvet and marks the end of the active growth of the antlers. The role of melatonin in this process, in synergy with testosterone, seems to be well established (Bubenik and Smith 1987, Yang et al. 2017). Several other hormonal factors, possibly interacting with sex steroids, have been proposed to influence the antler growth process (reviews in Chapman 1975,

VetBooks.ir

Lincoln 1992, Crigel et al. 2001, see also Bartoš et al. 2009); conversely, a direct, specific influence of insulin-like growth factor 1 (IGF1), once hypothesized by Suttie et al. (1985), has been questioned (Bartoš et al. 2009). Moreover, an important role is supposed to be played by the physical condition of individuals, social stimuli (Lincoln 1992) and environmental constraints, among which the seasonal fluctuations of light and food are of prominent importance (Chapman 1975, Landete-Castillejos et al. 2012, Melnycky et al. 2013).

The complete growth of antlers in adult deer requires 120–150 days, depending on the species. During that time, a considerable amount of bone weighing several kilograms can be created (not to speak of some extinct taxa such as *Megaloceros giganteus*, which could produce much larger antlers in absolute and relative terms: Gould 1973, Lincoln 1992). The length of red deer antlers is estimated to increase by 1 cm or more per day (Bartoš et al. 2009), an extraordinary rate that contributes to making the antlers unique in bone biology. The growth in diameter of beam and tine cortices is obviously much lower but, to our knowledge, no experimental measurement has been made hitherto on this topic. Gomez et al. (2013) observed accretion rates up to 2.15 µm*day^{-1} on the walls of primary osteons (centripetal deposits) in the antlers of *Cervus elaphus*.

Though antler mineral content is relatively low, these appendages constitute huge calcium reservoirs, and their development mobilizes considerable mineral resources. This is why their active growth coincides with a period of general resorption that creates a reversible osteoporotic state in many target sites of the skeleton, including, for example, stylopodial bones (Meister 1956), metapodials (Brockstedt-Rasmussen et al. (1987) and especially the ribs, which may lose up to 23% of their mass during the peak of antler growth (Hillman et al. 1973, Baxter et al. 1999). When antler development is completed, the resorption is balanced by secondary deposits. As mentioned above, antlers themselves are periodically submitted to intense and extensive Haversian substitution that creates dense Haversian tissue throughout their cortices (Fig. 16N).

Concluding Remarks

This review, like previous articles on the same topic, points out the broad histological diversity of long bone cortices in mammalian bones. However, beyond obvious discrepancies, and considering only terrestrial taxa (aquatic taxa form a distinct question), three main trends are discernible. In very small taxa, whatever their phylogenetic affinities (some rodents, Lipotyphla, bats, early tiny equids, etc.), primary cortical bone consists of avascular, or nearly avascular, parallel-fibered or lamellar tissues. In medium-sized taxa, from monotremes to primates, but with the exception of the euungulates, bone shaft cortices display the three-stratum pattern frequently described in this review, with (1) a perimedullary layer of endosteal lamellar tissue; (2) a median layer, variably and unevenly remodeled by Haversian substitution, that may originally consist of any type of osseous tissue with or without vascularization, including occasionally nonperiosteal CCCB and (3) a peripheral layer of mildly or nonremodeled parallel-fibered or lamellar periosteal bone that may form an EFS. This layer often contains cyclical growth marks (*annuli* or LAGs) as sharp as those encountered in poikilothermic vertebrates. In the euungulates, primary periosteal cortices are basically made of a homogenous formation of laminar and/or plexiform tissue, in which Haversian remodeling develops gradually but extensively.

The most striking difference between the bones of mammals and those of most other tetrapods is not related to the nature of the tissues encountered; there is no histological uniqueness for mammals and all the tissues observed in their skeleton also occur, with variable frequency, in other tetrapods. Rather, the structure of bone cortices in mammals, in terms of the nature and distribution of bone tissue types, is strongly (and perhaps predominantly) influenced by the cascade of local or general morphogenetic processes that occur during bone growth and result in relatively complex structural patterns. The situation seems much simpler in the long bone shafts of lissamphibians (e.g., Enlow and Brown 1957), sauropsids (e.g., Enlow 1969, Ricqlès 1976), and nonmammalian synapsids (see Chapter 28).

An important piece of information arising from this review is the frequency of CCCB in the shafts of mammalian bones. In some cases, this tissue may simply reflect local morphogenetic processes, especially growth drift. Most often, however, it forms through the compaction of the peripheral regions of metaphyseal spongiosae (endosteal intertrabecular deposits), according to the classical model (see Chapter 9) by Lacroix (1945) and Enlow (1963). This model implicitly postulates that the CCCB is a transitional tissue that is normally removed through perimedullary (inner) and superficial (outer) resorption processes when metaphyseal regions are relocated into the diaphysis (see, e.g., Legendre and Botha-Brink 2018 for discussion). The recent renewal of interest for mammalian bone histology, and the multiplication of detailed, precise and well-illustrated observations, show that this tissue is encountered in the diaphyseal region, at a distance from the metaphyses, much more frequently than previously suspected. In addition to the rodent *Bathyergus suillus* (Montoya-Sanhueza and Chinsamy 2017), the tubulidentate *O. afer* (Legendre and Botha-Brink 2018) and the xenarthran *D. novemcinctus* (Heck et al. 2019), it has been suspected in the present review to occur in the mid-diaphyseal region of long bones in several other taxa. CCCB should logically be absent in cross sections sampled exactly in the so-called neutral plane, where the ossification of a bone starts. However, the location of this plane in an adult mammal seldom corresponds to the middle of the bone shaft (see, e.g., Hughes 1952); as a consequence, precise bone sampling in the neutral plane proves uncertain in current histological practice. Most likely, diaphyseal sections containing CCCB are not sampled exactly in the neutral plane, but close to it. It nevertheless remains that CCCB may still occur at distance from the sites where it formed. The morphogenetic events that may result in the retention or disappearance of CCCB away from the metaphyseal region represent a complex question that remains to be considered for each bone and each taxon. It can nevertheless be admitted that a significant influence is exerted by several parameters, including (1) the shape of a bone, especially in the transition zone between metaphysis and diaphysis, (2) the thickness of the CCCB layer initially formed at the metaphyseal level, (3) the dynamics of medullary cavity enlargement and (4) the occurrence of asymmetric (growth in length of the bone) or off-centered (growth

VetBooks.ir

in width) developmental patterns. Moreover, considering the very special structure of CCCB (a geometrically complex and histologically composite tissue), the persistence of this tissue in a large fraction of the diaphyseal volume can be suspected to have serious biomechanical consequences (see discussion of this topic in Legendre and Botha-Brink 2018). Further studies should address this important issue through broad comparative surveys.

Acknowledgments

We are extremely grateful to all our colleagues who facilitated the documentation and editing of this review. In particular, Maitena Dumont would like to thank Prof. Yossi Yovel, from Tel Aviv University, for providing the samples of *R. aegypticus* and the Israel Science Foundation Grant # 0390452. Three-dimensional CT scans of *Rousettus* were downloaded from www.Morphosource.com, Duke University (http://www.morphosource.org/Detail/MediaDetail/Show/media_id/37407, Morphosource media number M37407-68609, collection number mmz:mammals:159353). The University of Michigan Museum of Zoology provided access to data on *R. aegypticus*, the collection of which was funded by oVert TCN; NSF DBI-1701714; NSF DBI-1701713. We also want to thank Prof. C. Lefevre and Mr. E. Pellé (Muséum National d'Histoire Naturelle, Paris), as well as Dr. E. Gheerbrant (CNRS, France) for their help in the collection of the comparative samples.

REFERENCES

Aeby, C. 1878. Das histologische Verhalten fossilen Knocken aun Zahngewebes. *Arch. Mikrosk. Anat.* 15: 371–382.

Alves, L. S., et al. 2017. Gross osteology, radiographic and computed tomographic morphology of the axial skeleton of the nine-banded armadillo (*Dasypus novemcinctus*). *Anat. Histol. Embryol.* 46: 167–177.

Amprino R. and G. Godina. 1947. La struttura delle ossa nei vertebrati. Ricerche comparative negli anfibi e negli amnioti. *Comment. Pontif. Acad. Scien.* 11(9): 329–462.

Amson, E., et al. 2014. Gradual adaptation of bone structure to aquatic lifestyle in fossil sloths from Peru. *Proc. Roy. Soc. B* 281: 1–6.

Amson, E., et al. 2015. Growth and life history of Middle Miocene deer (Mammalia, Cervidae) based on bone histology. *C. R. Palevol.* 14: 637–645.

Amson, E. 2021. Humeral diaphysis structure across mammals. *Evolution* 14. doi: 10.1111/evo.14170.

Angielczyk, K. D. and C. F. Kammerer. 2018. Non-Mammalian synapsids: the deep roots of the mammalian family tree. In *Handbook of zoology: Mammalia: mammalian evolution, diversity and systematics*, eds. Zachos F. E. and R. J. Asher, 117–198. Berlin, De Gruyter.

Antoine, P.-O., L. Marivaux, D. A. Croft, G. Billet et al. 2012. Middle Eocene rodents from Peruvian Amazonia reveal the pattern and timing of caviomorph origins and biogeography. *Proc. R. Soc. B: Biol. Sci.* 279: 1319–1326.

Archer, M., et al. 1985. First Mesozoic mammal from Australia—an Early Cretaceous monotreme. *Nature* 318: 363–366.

Arnett, T. R., et al. 1989. Studies with cells derived from growing deer antler. *Bone* 10: 143.

Asakura, Y., et al. 2017. Comparative paleohistology in osteoderms of Pleistocene *Panochthus* sp. Burmeister, 1886 and *Neuryurus* sp. Ameghino, 1889 (Xenarthra, Glyptodontidae). *C. R. Palevol* 16: 795–803.

Asher, R. J. 2018a. Diversity and relationships within crown Mammalia. In *Handbook of zoology: Mammalia: mammalian evolution, diversity and systematics*, Zachos F. E. and R. J. Asher eds, 301–352. Berlin, De Gruyter, Berlin.

Asher, R. J. 2018b Taxonomy, trees, and truth in historical mammalogy. In *Handbook of zoology: Mammalia: mammalian evolution, diversity and systematics*, eds. Zachos F. E. and R. J. Asher, 39–58. Berlin, De Gruyter.

Bakker, H. and K. Post. 2020. Records of beaked whales *Ziphirostrum* and *Aporotus* (Odontoceti, Ziphiidae) from the Miocene of the Netherlands. *Deinsea* 19: 17–26.

Banks, W. J. 1974. The ossification process of the developing antler in the white-tailed deer (*Odocoileus virginianus*). *Calcif. Tissue Res.* 14: 257–274.

Bartoš, L., et al. 2009. Testosterone, but not IGF-1, LH, prolactin or cortisol, may serve as antler-stimulating hormone in red deer stags (*Cervus elaphus*). *Bone* 44: 691–698.

Baryshnikov, G. F., et al. 2003. Morphological variability and evolution in the baculum (*os penis*) in Mustelidae (Carnivora). *J. Mammal.* 84: 673–690.

Baxter, B. J., et al. 1999. Bone turnover associated with antler growth in red deer (*Cervus elaphus*). *Anat. Rec.* 256: 14–19.

Becker, M., C. Witzel, U. Kierdorf, K. Frölich et al. 2020. Ontogenetic changes of tissue compartmentalization and bone type distribution in the humerus of Soay sheep. *J. Anat.* 237: 334–354.

Bennett, M. B. and M. R. Forwood. 2010. Histomorphometric changes in the wing bones of the fruit bat, *Pteropus poliocephalus*, (Megachiroptera: Pteropodidae) in relation to increased bone strain and the failure of a good (?) hypothesis. *Aust. Zool.* 35: 341–348.

Bergqvist, L. P., et al. 2019. Osteoderm microstructure of *Riostegotherium yanei*, the oldest Xenarthra. *An. Acad. Bras. Cienc.* 91 (suppl. 2): e20181290.

Berta, A., et al. 2018. The origin and evolutionary biology of pinnipeds: seals, sea lions, and walruses. *Ann. Rev. Earth Planet. Sci.* 46: 203–228.

Bi, S., et al. 2018. An Early Cretaceous eutherian and the placental–marsupial dichotomy. *Nature* 558: 390–395.

Bianucci, G., et al. 2013. Bizarre fossil beaked whales (Odontoceti, Ziphiidae) fished from the Atlantic Ocean floor off the Iberian Peninsula. *Geodiversitas* 35: 105–153.

Bloch, J. I. and D. M. Boyer. 2003. Grasping primate origins. *Science* 298: 1606–1610.

Botha-Brink, J., et al. 2012. The radiation and osteohistology of non-mammaliaform cynodonts. In *Forerunners of mammals*, ed. Chinsamy-Turan, A., 223–246. Bloomington, Indiana University Press.

Brindle, M. and C. Opie. 2016. Postcopulatory sexual selection influences baculum evolution in primates and carnivores. *Proc. R. Soc. B* 283: 20161736.

Brockstedt-Rasmussen, H., et al. 1987. The rhythmic relation between antler and bone porosity in Danish deer. *Bone* 8: 19–22.

Bronnert, C., et al. 2017. A primitive perissodactyl (Mammalia) from the Early Eocene of Le Quesnoy (MP7, France). *Hist. Biol*. 30: 237–250.

Bubenik, G. A. and P. S. Smith. 1987. Circadian and circannual rhythms of melatonin in plasma of male white tailed deer and the effect of oral administration of melatonin. *J. Exp. Zool*. 241: 81–89.

Bubenik, G. A., et al. 1974. Immunohistological localization if testosterone in the growing antler of the white-tailed deer (*Odocoileus virginianus*). *Calcif. Tissue Res*. 14: 121–130.

Buffrénil, V. de and A. Casinos. 1995. Observations histologiques sur le rostre de *Mesoplodon densirostris* (Mammalia, Cetacea, Ziphiidae): le tissu osseux le plus dense connu. *Ann. Sci. Nat., Zool*., 13 ème sér. 16: 21–32.

Buffrénil, V. de, and D. Schoevaert. 1988. On how the periosteal bone of the delphinid humerus becomes cancellous: ontogeny of a histological specialization. *J. Morphol*. 198: 149–164.

Buffrénil, V. de and D. Schoevaert. 1989. Données quantitatives et observations histologiques sur la pachyostose du squelette du dugong, *Dugong dugon* (Müller) (Sirenia: Dugongidae). *Can. J. Zool*. 67: 2107–2119.

Buffrénil, V. de, et al. 1990. Bone histology of the ribs of the archaeocetes (Mammalia: Cetacea). *J. Vert. Paleontol*. 10: 455–466.

Buffrénil, V. de, et al. 2010. Evolution of sirenian pachyosteosclerosis, a model-case for the study of bone structure in aquatic tetrapods. *J. Mammal. Evol*. 17: 101–120.

Burgess, L. M., et al. 2016. Ontogenetic scaling of fore limb and hind limb joint posture and limb bone cross-sectional geometry in vervets and baboons. *Am. J. Phys. Anthropol*. 161: 72–83.

Burt, W. H. 1960. Bacula of North American mammals. *Misc. Pub. Mus. Zool. Univ. Michigan* 113: 1–76.

Canoville, A. and M. Laurin. 2010. Evolution of the humeral microanatomy and lifestyle in amniotes, and some comments on palaeobiological inferences. *Biol. J. Linn. Soc*. 100: 384–406.

Canoville, A., et al. 2016. Microanatomical diversity of amniote ribs: an exploratory quantitative study. *Biol. J. Linn. Soc*. 118: 706–733.

Castanet, J., et al. 1993. Bone and individual aging. In *Bone, a Treatease*, Vol. 7, ed. Hall, B. K., 245–283. Boca Raton, FL, CRC Press.

Castanet, J., et al. 2004. Lines of arrested growth in bone and age determination in a small primate: *Microcebus murinus*. *J. Zool. Lond*. 263: 31–39.

Ceacero, F., et al. 2015. Inter-specific differences in the sculpture and mechanics but nor the chemical composition of antlers in three deer species. *Ann. Zool. Fennici* 52: 368–376.

Chapman, D. I. 1975. Antlers – bones of contention. *Mammal Rev*. 5: 121–172.

Chinsamy-Turan, A. 2012. The microstructure of bones and teeth of nonmammalian therapsids. In *Forerunners of mammals*, ed. Chinsamy-Turan, A., 65–90. Bloomington, IN, Indiana University Press.

Chinsamy, A. and J. H. Hurum. 2006. Bone microstructure and growth pattern of early mammals. *Acta Palaeontol. Pol*. 51: 325–338.

Chinsamy, A. and B. S. Rubidge. 1993. Dicynodont (Therapsida) bone histology: phylogenetic and physiological implications. *Palaeontol. Afr*. 30: 97–102.

Chinsamy, A. and N. M. Warburton. 2020. Ontogenetic growth and development of a unique fibrocartilage entheses in *Macropus fuliginosus*. *Zoology*. https://doi.org/10.1016/j.zool.2020.125860.

Cohn, M. J. 2011. Development of the external genitalia: conserved and divergent mechanisms of appendage patterning. *Dev. Dyn*. 240: 1108–1115.

Comelis, M. T., et al. 2018. Morphological and histological characters of penile organization in eleven species of molossid bats. *Zoology* 127: 70–83.

Crigel, M.-H., et al. 2001. Les bois du cerf: revue de littérature scientifique. *Ann. Méd. Vét*. 145: 25–38.

Cuijpers, A. G. F. M. 2006. Histological identification of bone fragments in archaeology: telling humans apart from horses and cattle. *Int. J. Osteoarchaeol*. 16: 465–480.

Cuijpers, S. and R. C. G. M. Lauwerier. 2008. Differentiating between bone fragments from horses and cattle: a histological identification method for archaeology. *Environ. Archaeol*. 13: 165–179.

Currey, J. D. 2002. *Bones. Structure and Mechanics*. Princeton, NJ and Oxford, Princeton University Press.

Currey, J. D. and R. McN. Alexander. 1985. The thickness of the walls of tubular bones. *J. Zool*.206: 453–468.

Curtin, A. J., et al. 2012. Noninvasive histological comparison of bone growth patterns among fossil and extant neonatal elephantids using synchrotron radiation X-ray microtomography. *J. Vert. Paleontol*. 32: 939–955.

Davis, E. B., et al. 2011. Evolution of ruminant headgear: a review. *Proc. R. Soc. B* 278: 2857–2865.

Deméré, T. A., et al. 2008. Morphological and molecular evidence for a stepwise evolutionary transition from teeth to baleen in mysticete whales. *Syst. Biol*. 57: 15–37.

Demes, B. and W. L. Jungers. 1993. Long bone cross-sectional dimensions, locomotor adaptations and body size in prosimian primates. *J. Hum. Evol*. 25: 57–74.

Dewaele, L., et al. 2018. Generalized osteosclerotic condition in the skeleton of *Nanophoca vitulinoides*, a dwarf seal from the Miocene of Belgium. *J. Mammal. Evol*. 26: 517–543. https://doi.org/10.1007/s10914-018-9438-9.

Dixson, A. F. 1987. Baculum length and copulatory behavior in primates. *Am. J. Primatol*. 13: 51–60.

Domning, D. P. 2001. The earliest known fully quadrupedal sirenian. *Nature* 413: 625–627.

Doty, S. B. and E. A. Nunez. 1985. Activation of osteoclasts and the repopulation of bone surfaces following hibernation in the bat, *Myotis lucifugus*. *Anat. Rec*. 213: 481–495.

Dumont, M., et al. 2013. Inner architecture of vertebral centra in terrestrial and aquatic mammals: a two-dimensional comparative study. *J. Morphol*. 274: 570–584.

Dumont, M., et al. 2016. Structure and growth pattern of the bizarre hemispheric prominence of the rostrum of the fossil beaked whale *Globicetus hiberus* (Mammalia, Cetacea, Ziphiidae). *J. Morphol*. 277: 1292–1308.

Enlow, D. H. 1962. A study of the post-natal growth and remodeling of bone. *Am. J. Anat*. 110: 79–101.

Enlow, D. H. 1963. *Principles of bone remodeling*. Springfield, IL, Charles C Thomas.

Enlow, D. H. 1969. The bone of Reptiles. In *Biology of the Reptilia*, 1, ed. Gans, C., 45–80; London, Academic press.

Enlow, D. H. and S. O. Brown.1957. A comparative study of fossil and recent bone tissues. Part II. Reptilian and bird bone tissues. *Tex. J. Sci*. 9: 186–214.

Enlow, D. H. and S. O. Brown. 1958. A comparative histological study of fossil and recent bone tissues. Part III. *Texas J. Sci.* 10: 187–230.

Ezra, H. C. and S. F. Cook. 1959. Histology of Mammoth bone. *Science* 129: 465–466.

Fawcett, D. W. 1942. The amedullary bones of the Florida manatee (*Trichechus latirostris*). *Am. J. Anat.* 71: 271–309.

Fedorov, V. B., et al. 2012. Preservation of bone mass and structure in hibernating black bears (*Ursus americanus*) through elevated expression of anabolic genes. *Funct. Integr. Genomics* 12: 357–365.

Felts, W. J. L. and F. A. Spurrell. 1965. Structural orientation and density in cetacean humeri. *Am. J. Anat.* 116: 171–204.

Felts, W. J. L. and F. A. Spurrell. 1966. Some structural and developmental characteristics of cetacean (Odontocete) radii. A study of adaptive osteogenesis. *Am. J. Anat.* 118: 103–134.

Fish, F. E. and B. R. Stein. 1991. Functional correlates of differences in bone density among terrestrial and aquatic genera of the family Mustelidae (Mammalia). *Zoomorphology* 110: 339–345.

Foote, J. S. 1911. The comparative histology of femoral bones. *Trans. Am. Microsc. Soc.* 30: 87–141.

Foote, J. S. 1916. *A contribution to the comparative histology of the femur.* Baltimore, MD, Lord Baltimore Press, Smithsonian Institute Washington

Frasier, M. B., et al. 1975. Characterization of developing antler cartilage matrix. 1. Selected histochemical and enzymatic assessment. *Calcif. Tissue Res.* 17: 273–288.

García-Martínez, R., et al. 2011. The ontogeny of bone growth in two species of dormice: reconstructing life history traits. *C. R. Palevol* 10: 489–498.

Garrone, M. C., et al. 2019. Ontogenetic variability in the limb bones histology of plain vizcacha (*Lagostomus maximus*, Chinchillidae, Rodentia): implications for life history reconstruction of fossil representatives. *Hist. Biol*. Doi.org/10.1080/08912963.2019.1648450.

Geiger, M., et al. 2013. Diversity and body size in giant caviomorphs (Rodentia) from the northern Neotropics – A study of femoral variation. *J. Vert. Paleontol.* 33: 1449–1456.

Geisler, J. H., et al. 2014. A new fossil species supports an early origin for toothed whale echolocation. *Nature* 508(7496): 383–386.

Gheerbrant, E., et al. 2002. A new large mammal from the Ypresian of Morocco: evidence of surprising diversity of early proboscideans. *Acta Palaeontol. Pol.* 47: 493–506.

Gingerich, P. D., et al. 1990. Hind limbs of Eocene *Basilosaurus*: evidence of feet in whales. *Science* 249: 154–157.

Gingerich, P. D., et al. 2001. Origin of whales from early artiodactyls: hands and feet of Eocene Protocetidae from Pakistan. *Science* 293: 2239–2242.

Godthelp, H., M. Archer, R. Cifelli, S. J. Hand, and C. F. Gilkeson. 1992. Earliest known Australian Tertiary mammal fauna. *Nature* 356: 514–516.

Goin F. J., M. O. Woodburne, A. N. Zimicz, G. M. Martin and L. Chronogubsky. 2016. *A Brief History of South American Metatherians. Evolutionary Contexts and Intercontinental Dispersals.* Dordrecht, Springer.

Gol'din, P. 2014. "Antlers inside": Are the skull structures of beaked whales (Cetacea: Ziphiidae) used for echoic imaging and visual display? *Biol. J. Linn. Soc.* 113: 510–515.

Goldman, H. M., et al. 2009. Ontogenetic patterning of cortical bone microstructure and geometry at the human mid-shaft femur. *Anat. Rec.* 292: 48–64.

Gomez, S., et al. 2013. Labeling studies on cortical bone formation in the antlers of red deer (*Cervus elaphus*). *Bone* 52: 506–515.

Goss, R. J. 1968. Inhibition of growth and shedding of antlers by sex hormones. *Nature* 220: 83–85.

Goss, R. J., et al. 1992. The mechanism of antler casting in the fallow dear. *J. Exp. Zool.* 264: 429–436.

Gould, S. J. 1973. Positive allometry of antlers in the "Irish elk" *Megaloceros giganteus*. *Nature* 244: 375–376.

Gray, N.-M., et al. 2007. Sink or swim? Bone density as a mechanism for buoyancy control in early cetaceans. *Anat. Rec.* 290: 638–653.

Haines, W. R. 1941. Epiphyseal structure in lizards and marsupials. *J. Anat. Lond.* 75: 282–294.

Haines, W. R. 1942. The evolution of epiphyses and of endochondral bone. *Biol. Rev.* 17: 267–292.

Hamrick, M. W. 1999. Development of epiphyseal structure and function in *Didelphis virginiana* (Marsupiala, Didelphidae). *J. Morphol.* 239: 283–296.

Hansen, H. L., et al. 2009. Cross-sectional geometry of the femoral midshaft in baboons is heritable. *Bone* 45: 892–897.

Hartwig, H. 1967. Experimentelle Untersuchungen zür Entwicklunsphysiologie de Stangenbildung beim Reh (*Capreolus c. capreolus* L. 1758). *Roux Arch. Entwicklungsmech.* 158: 358–384.

Hartwig, H. 1968. Durch Periostverlagerung experimentelle erzeugte, heterotope Stirnzapfenbildung beim Reh. *Z. Säugetier.* 33: 246–248.

Havill, L. M. 2004. Osteon remodeling dynamics in *Macaca mulatta*: normal variation with regard to Age, sex, and skeletal maturity. *Calcif. Tissue Int.* 74: 95–102.

Hayashi, S., et al. 2013. Bone inner structure suggests increasing aquatic adaptations in Desmostylia (Mammalia, Afrotheria). *PLoS One* 8(4): e59146. doi: 10.1371/journal.pone.0059146.

Hayssen, V. and R. C. Lacy. 1985. Basal metabolic rates in mammals: taxonomic differences in the allometry of BMR and body mass. *Comp. Biochem. Physiol.* 81A: 741–754.

Heck, C. T., et al. 2019. Ontogenetic changes in the long bone microstructure in the nine-banded armadillo (*Dasypus novemcinctus*). *PLoS One* 14(4): e0215655.

Heckenberg, N. S. 2017. Origination of antlerogenesis. *J. Morphol.* 278: 182–202.

Herdina, A. N., et al. 2015. Correlative 3D-imaging of *Pipistrellus* penis micromorphology: validating quantitative micro-CT images with undecalcified serial ground section histomorphometry. *J. Morphol.* 276: 695–706.

Herridge, V. L. and A. M. Lister. 2012. Extreme insular dwarfism evolved in a mammoth. *Proc. R. Soc. B* 279: 3193–3200.

Hill, R. V. 2006. Comparative anatomy and histology of xenarthran osteoderms. *J. Morphol.* 267: 1141–1460.

Hillier, M. L. and L. S. Bell. 2007. Differentiation human bone from animal bone: a review of histological methods. *J. Forensic Sci.* 52: 249–263.

Hillman, J. R., et al. 1973. Cyclic bone remodeling in deer. *Calcif. Tissue Res.* 12: 223–230.

Hofmann, R., et al. 2014. Constraints on the lamina density of laminar bone architecture of large-bodied dinosaurs and mammals. *Acta Paleontol. Pol.* 59: 287–294.

Hordon, L. D., et al. 2000. Trabecular architecture in women and men of similar bone mass with and without vertebral fracture: I. Two-dimensional histology. *Bone* 27: 271–276.

Houssaye, A., et al. 2014. Amniote vertebral microanatomy. What are the major trends? *Biol. J. Linn. Soc.* 112: 735–746.

Houssaye, A., et al. 2015. Transition of Eocene whales from land to sea: evidence from bone microstructure. *PLoS One* 10: e0118409. doi: 10.1371/journal.pone.0118409.

Houssaye, A., et al. 2016a. Adaptive patterns in aquatic amniote bone microanatomy – More complex than previously though. *Integr. Comp. Biol.* 56: 1349–1369.

Houssaye, A., et al. 2016b. Biomechanical evolution of solid bones in large mammals: a microanatomical investigation. *Biol. J. Linn. Soc.* 117: 350–371.

Hu, Y.-M., et al. 2005. Large Mesozoic mammals fed on young dinosaurs. *Nature* 433: 149–152.

Hughes, H. 1952. The factors determining the direction of the canal for the nutrient artery in the long bones of mammals and birds. *Acta Anat.* 15: 261–280.

Hurum, J. H. and A. Chinsamy-Turan. 2012.The radiation, bone histology and biology of early mammals. In *Forerunners of mammals*, ed. Chinsamy-Turan, A., 249–270. Bloomington, Indiana University Press.

Izumi, K. and Murakami 2000. Ultrastructure of the developing fibrocartilage of the *os penis* of rat. *J. Morphol.* 243: 187–191.

Jerome, C. P., and P. E. Peterson. 2001. Non-human primate models in skeletal research. *Bone* 29: 1–6.

Ji, Q., et al. 2002. The earliest known eutherian mammal. *Nature* 416: 816–822.

Ji, Q., et al. 2006. A swimming mammaliaform from the Middle Jurassic and ecomorphological diversification of early mammals. *Science* 311: 1123–1127.

Jordana, X., et al. 2016. Ontogenetic changes in the histological features of zonal bone tissues of ruminants: a quantitative approach. *C. R. Palevol* 15: 255–266.

Kaiser, H. E. 1970. *Das Abnorme in der Evolution*. Leiden, E. J. Brill.

Kaiser, H. E. 1974. *Morphology of the Sirenia. A macroscopic x-ray atlas of the morphology of recent species*. Basel, S. Karger.

Kazár, E. 2010. Revision of the genus Pachyacanthus Brandt, 1871 (Mammalia: Cetacea: Odontoceti). *Ann. Naturhist. Mus. Wien, Serie A* 112: 537–568.

Kelly, D. A. 2000. Anatomy of the baculum-corpus cavernosum interface in the Norway rat (Rattus norvegicus), and implications for force transfer during copulation. *J. Morphol.* 244: 69–77.

Kemp, T. S. 2005. *The origin and evolution of mammals*. pp. 331. New York, Oxford University Press.

Kennedy, G. E. 1985. Bone thickness in *Homo erectus*. *J. Hum. Evol.* 14: 699–708.

Kielan-Jaworowska, Z. 1978. Evolution of the therian mammals in the Late Cretaceous of Asia. Part III. Postcranial skeleton in Zalambdalestidae. *Palaeontol. Polonica* 38: 5–41.

Kierdorf, U. and H. Kierdorf. 2002. Pedicle and first antler formation in deer: anatomical, histological and developmental aspects. *Z. Jagdwiss.* 48: 22–34.

Kierdorf, H., et al. 1994. Light microscopic observations on the ossification process in the early developing pedicle of fallow deer (*Dama dama*). *Ann. Anat.* 176: 243–249.

Kierdorf, H., et al. 1995a. A light microscopic study of primary antler development in follow deer (*Dama dama*). *Ann. Anat.* 177: 525–532.

Kierdorf, U., et al. 1995b. Effects of castration on antler growth in fallow deer (*Dama dama* L.). *J. Exp. Zool.* 273: 33–43.

Kierdorf, U., et al. 2007. Deer antler regeneration: cells, concepts and controversies. *J. Morphol.* 268: 726–738.

Klevezal, G. A. 1996. *Recording structures of mammals: determination of age and reconstruction of life history*. London, Routledge.

Klevezal, G. A. and S.E. Kleinenberg. 1967. *Age determination of mammals by layered structures of teeth and bones*. Moscow, Nauka. Translated 1969 from Russian by Israel Progr. Sci. Transl. Jerusalem.

Köhler, M. 2010. Fast or slow? The evolution of life history traits associated with insular dwarfing. *Recerca (Instituto Menorqui d'Estudis)* 19: 261–280.

Köhler, M. and S. Moya-Solà. 2009. Physiological and life history strategies of a fossil large mammal in a resource-limited environment. *PNAS* 106: 20354–20358.

Köhler, M., et al. 2012. Seasonal bone growth and physiology in endotherms shed light on dinosaur physiology. *Nature* 487: 358–361.

Kolb, C., et al. 2015a. Growth in fossil and extant deer and implications for body size and life history evolution. *BMC Evol. Biol.* 15: 19.

Kolb, C., et al. 2015b. Mammalian bone paleohistology: a survey and new data with emphasis on island forms. *PeerJ* 3: e1358. doi: 10.7717/peerj.1358.

Koretsky, I. and S. J. Rahmat. 2017. Preliminary report of pachyosteosclerotic bones in seals. *OARA* 1: 0000501.

Krmpotic, C. M., et al. 2009. Osteoderm morphology in recent and fossil euphractine xenarthrans. *Acta Zool. (Stockholm)* 90: 339–351.

Kunz, T. H., et al. 1998. Changes in body mass and fat reserves in pre-hibernating little brown bats (*Myotis lucifugus*). *Écoscience* 5: 8–17.

Kwiecinski, G. G., et al. 1987. Annual skeletal changes in the little brown bat, *Myotis lucifugus lucifugus*, with particular reference to pregnancy and lactation. *Am. J. Anat.* 178: 410–420.

Lacroix, P. 1945. Remarques sur le mécanisme de l'allongement des os. *Arch. Biol.* 56: 185–197.

Lambert, O., et al. 2011. Hyperdense rostral bones of ziphiid whales: diverse processes for a similar pattern. *C. R. Palevol* 10: 453–468.

Landete-Castillejos, T., et al. 2007. Body weight, early growth and antler size influence antler bone mineral composition of Iberian red deer (*Cervus elaphus hispanicus*). *Bone* 40: 230–235.

Landete-Castillejos, T., et al. 2012. Does nutrition affect bone porosity and mineral tissue distribution in deer antlers? The relationship between histology, mechanical properties and mineral composition. *Bone* 50: 245–254.

Lange-Badré, B. 2006. Les mammifères créodontes dans les Annales de Paléontologie: conceptions anciennes et idées récentes. *Ann. Paléontol.* 92: 197–203.

Laurin, M., et al. 2011. Bone microanatomy and lifestyle: de descriptive approach. *C. R. Palevol* 10: 381–402.

Lee, A. H. and E. L. Simons. 2015. Wing bone laminarity is not an adaptation for torsional resistance in bats. *PeerJ* 3: e823.

Lefeuvre, D. 1909. *Structure histologique des os fossiles de l'Halitherium*. Paris, C. R. Congrès Soc. Savantes.

Legendre, L. J. and J. Botha-Brink. 2018. Digging the compromise: investigating the link between bone histology and fossoriality in the aardvark (*Orycteropus afer*). *PeerJ* 6: e5216. doi: 10.7717/peej.5216.

Li, C. and J. M. Suttie. 1994. Light microscopic studies of pedicle and early first antler development in red deer (*Cervus elaphus*). *Anat. Rec.* 239: 198–215.

Li, C. and J. M. Suttie. 1998. Electron microscopic studies of antlerogenic cells from five developmental stages during pedicle and early antler formation in red deer (*Cervus elaphus*). *Anat. Rec.* 252: 587–599.

Li, C. K. et al. 1995. Histogenesis of antlerogenic tissues cultivated in diffusion chambers in vivo in red deer (*Cervus elaphus*). *J. Exp. Zool.* 272: 345–355.

Li, Z., et al. 2013. Hypermineralized whale rostrum as the exemplar for bone mineral. *Connect. Tissue Res.* 54: 167–175.

Lihoreau, F., et al. 2015. Hippos stem from the longest sequence of terrestrial cetartiodactyl evolution in Africa. *Nat. Commun.* 6: 6264.

Lincoln, G. A. 1992. Biology of antlers. *J. Zool. Lond.* 226: 517–528.

Liu, X. S., et al. 2009. Micromechanical analyses of vertebral trabecular bone based on individual trabeculae segmentation of plates and rods. *J. Biomech.* 42: 249–256.

Luo, Z.-X., et al. 2003. An Early Cretaceous tribosphenic mammal and metatherian evolution. *Science* 302: 1934–1940.

Luo, Z.-X., et al. 2011. A Jurassic eutherian mammal and divergence of marsupials and placentals. *Nature* 476: 442–445.

Ma, L., et al. 2019. Crosstalk between activin A and Shh signaling contributes to the proliferation and differentiation of antler chondrocytes. *Bone* 123: 176–188.

MacLeod, C. D. 2002. Possible function of the ultradense bone in the rostrum of Blainville's beaked whale (*Mesoplodon densirostris*). *Can. J. Zool.* 80: 178–184.

Margerie, E. de. 2002. Laminar bone as an adaptation to torsional loads in flapping flight. *J. Anat.* 201: 521–526.

Mahboubi, S., et al. 2014. Was the Early Eocene proboscidean Numidotherium koholense semi-aquatic or terrestrial? Evidence from stable isotopes and bone histology. *C. R. Palevol* 13: 501–509.

Main, R. P., et al. 2005. The evolution and function of thyreophoran dinosaur scutes: implications for plate function in stegosaurs. *Paleobiology* 31: 291–314.

Marín-Moratalla, N., X. Jordana and M. Köhler. 2013. Bone histology as an approach to providing data on certain key life history traits in mammals: implications for conservation biology. *Mamm. Biol.* 78: 422–429.

Marin-Moratalla, N., et al. 2014. Correlation of quantitative bone histology data with life history and climate: a phylogenetic approach. *Biol. J. Linn. Soc.* 112: 678–687.

Martin, T. 2018. Mesozoic mammals - early mammalian diversity and ecomorphological adaptations. In *Handbook of zoology: Mammalia: mammalian evolution, diversity and systematics*, eds. Zachos F. E. and R. J. Asher, Berlin, De Gruyter, Berlin.

Martin, T., et al. 2015. A Cretaceous eutriconodont and integument evolution in early mammals. *Nature* 526: 380–384.

Martinez-Maza, C., et al. 2014. Life-history traits of the Miocene *Hipparion concudense* (Spain) inferred from bone histological structure. *Plos One* 9: e103708. doi: 10.1371/journal.pone.0103708.

Marx, F. G., et al. 2016a. *Cetacean paleobiology*. Chichester (UK), John Wiley and Sons.

Marx, F. G., et al. 2016b. Suction feeding preceded filtering in baleen whale evolution. *Mem. Mus. Victoria* 75: 71–82.

Matich, J., et al. 2003. Mitotic activity in the growing red deer antler. *Cell. Biol. Int.* 27: 625–632.

Martiniaková, M., et al. 2007. Histological study of compact bone tissue in some mammals: a method for species determination. *Int. J. Osteoarchaeol.* 17: 82–90.

Maunz, M. and R. Z. German. 1997. Ontogeny and limb bone scaling in two new world marsupials, *Monodelphis domestica* and *Didelphis virginiana*. *J. Morphol.* 231: 117–130.

McFadden, B. J. 2005. Fossil horses - evidence for evolution. *Science* 307: 1728–1730.

McFarlin, S. C., et al. 2016. Primary bone microanatomy records developmental aspects of life history in catarrhine primates. *J. Hum. Evol.* 92: 60–79.

McGee-Lawrence, M. E., et al. 2008. Mammalian hibernation as a model of disuse osteoporosis: the effects of physical inactivity on bone metabolism, structure, and strength. *Am. J. Physiol.* 295: R1999–R2014. doi:10.1152/ajpregu.90648.2008.

Meier, P. S., et al. 2013. Evolution of bone compactness in extant and extinct moles (Talpidae): exploring humeral microstructure in small fossorial mammals. *Evol. Biol.* 13: 55.

Meister, W. W. 1956. Changes in histological structure of the long bones of white-tailed deer (*Odocoileus virginianus*) during the growth of the antlers. *Anat. Rec.* 124: 709–721.

Melnycky, N. A., et al. 2013. Scaling of antler size in reindeer (*Rangifer tarandus*): sexual dimorphism and variability in resource allocation. *J. Mammal.* 94: 1371–1379.

Meng, Q.-J., et al. 2017. New gliding mammaliaforms from the Jurassic. *Nature* 548: 291–296.

Miller, E. H. 2009. Baculum. In *Encyclopaedia of marine mammals* (2nd ed.), eds.. Perrin, W. F., B. Würsig and J. G. M. Thewissen, 68–71. Burlington, MA, Academic Press.

Miller, E. H. and L. E. Burton. 2001. It's all relative: allometry and variation in the baculum (os penis) of the harp seal, *Pagophilus groenlandicus* (Carnivora: Phocidae). *Biol. J. Linn. Soc.* 72: 345–355.

Miller, E. H., et al. 1999. Baculum and testes of the hooded seal (*Cystophora cristata*): growth and size-scaling and their relationships to sexual selection. *Can. J. Zool.* 77: 470–479.

Miszkievicz, J. J., J. Louys and S. O'Connor. 2019. Microanatomical record of cortical bone remodeling and high vascularity in a fossil giant rat midshaft femur. *Anat. Rec.* 302: 1934–1940.

Montoya-Sanhueza, G. and A. Chinsamy. 2017. Long bone histology of the subterranean rodent *Bathyergus suillus* (Bathyergidae: ontogenetic pattern of cortical bone thickening. *J. Anat.* 230: 203–233.

Montoya-Sanhuesa, G., et al. 2021. Long bone histomorphogenesis of the naked mole-rat: histodiversity and intraspecific variation. *J. Anat.* Doi: 10.1111/joa.13381.

Morales, J., et al. 1993. Pachyostosis in a Lower Miocene giraffoid from Spain, *Lorancameryx pachyostoticus* nov. gen. nov. sp. and its bearing on the evolution of bony appendages in artiodactyls. *Geobios* 26: 207–230.

Morgan, M. E., et al. 1995. Comparative paleoecology of Paleogene and Neogene mammalian faunas: body-size structure. *Palaeogeogr. Palaeoclimatol. Palaeoecol.* 115: 287–317.

Mori, R., et al. 2003. Comparative histology of the laminar bone between young calves and foals. *Cells Tissues Organs* 175: 43–50.

Muizon, C. de (ed). 1995. Pucadelphys andinus *(Marsupialia, Mammalia) from the Early Paleocene of Bolivia*. Paris, Mémoires du Muséum National d'Histoire Naturelle.

Muizon, C. de and H. G. McDonald. 1995. An aquatic sloth from the Pliocene of Peru. *Nature* 375: 224–227.

Muizon, C. de, et al. 2015. *Alcidedorbignya inopinata*, a basal pantodont (Placentalia, Mammalia) from the early Paleocene of Bolivia: anatomy, phylogeny and palaeobiology. *Geodiversitas* 37: 397–642.

Muizon, C. de, et al. 2019. *Mystacodon selenensis*, the earliest known toothed mysticete (Cetacea, Mammalia) from the late Eocene of Peru: anatomy, phylogeny and feeding adaptations. *Geodiversitas* 41: 401–499.

Mulhern, D. M. and D. H. Ubelaker. 2003. Histologic examination of bone development in juvenile chimpanzees. *Am. J. Phys. Anthropol.* 122: 127–133.

Murakami, R. 1986. Development of the *os penis* in genital tubercles cultured beneath the renal capsule of adult rats. *J. Anat.* 149: 11–20.

Murakami, R. 1987. A histological study of the development of the penis of wild-type and androgen-insensitive mice. *J. Anat.* 153: 223–231.

Murakami, R. and T. Mizuno. 1986. Proximal-distal sequence of development of the skeletal tissues in the penis of rat and the inductive effect of epithelium. *J. Embryol. Exp. Morphol.* 92: 133–143.

Nacarino-Meneses, C., et al. 2016a. Histological variability in the limb bones of the Asiatic wild ass and its significance for life history inferences. *PeerJ* 4: e2580. doi : 10.7717/peej.2580.

Nacarino-Meneses, C., et al. 2016b. First approach to bone histology and skeletochronology of *Equus hemionus*. *C. R. Palevol* 15: 267–277.

Nacarino-Meneses, C. and M. Köhler. 2018. Limb bone histology records birth in mammals. *Plos One* 13: e0198511. http://doi.org/10.1371/journal.pone.0198511.

Nakajima, Y. and H. Endo. 2013. Comparative humeral microanatomy of terrestrial, semiaquatic and aquatic carnivorans using micro-focus CT scan. *Mammal Study* 38: 1–8.

Nopcsa, F. von. 1923. Vorläufige Notiz über die Pachyostose und Osteosklerose einiger Marine Wirbeltiere. *Anat. Anz.* 56: 353–359.

Nopcsa, F. von and E. Heidsieck. 1934. Uber eine pachyostotische Rippe aus der Kreide Rügens. *Acta Zool.* 14: 431–455.

Orlandi-Oliveras, G., et al. 2016. Bone histology of the giant fossil dormouse *Hypnomys onicensis* (Gliridae, Rodentia) from Balearic Islands. *C. R. Palevol* 15: 238–244.

Orlandi-Oliveras, G., et al. 2018. Bone histology provides insights into the life history mechanisms underlying dwarfing in hipparionins. *Sci. Rep.* 8: 17203. doi:10.1038/s41598-018-35347-x.

Patel, B. A., et al. 2013. Humeral cross-sectional shape in suspensory primates and sloths. *Anat. Rec.* 296: 545–556.

Patterson, B. D. and C. S. Thaeler Jr. 1982. The mammalian baculum: hypotheses on the nature of bacular variability. *J. Mammal.* 63: 1–15.

Pazzaglia, U. E., et al. 2015. Setup of a bone aging experimental model in the rabbit comparing changes in cortical and trabecular bone: morphological and morphometric study in the femur. *J. Morphol.* 276: 733–747.

Pineda, N., et al. 2017. Hibernating little pocket mice show few seasonal changes in bone properties. *Anat. Rec.* 300: 2175–2183.

Perrin, W. F. and Myrick Jr, A. C. 1980. Report of the workshop. In *Growth of odontocetes and sirenians: problems in age determination*, eds. Perrin, W. F. and A. C. Myrick, 1–50. Cambridge, UK, International Whaling Commission.

Polk, J. D., et al. 2000. A comparison of primate, carnivoran and rodent limb bone cross-sectional properties: are primates really unique? *J. Hum. Evol.* 39: 297–325.

Pratt, I.V., et al. 2018. Interpreting the three-dimensional orientation of vascular canals and cross-sectional geometry of cortical bone in birds and bats. *J. Anat.* 232: 931–942.

Price, J. S., et al. 2005. Deer antlers : a zoological curiosity or the key to understanding organ regeneration in mammals? *J. Anat.* 207: 603–618.

Quekett, J. T. 1849. On the intimate structure of bone as composing the skeleton in the four great classes of animals, viz., mammals, birds, reptiles, and fishes, with some remarks on the great value of the knowledge of such structure in determining the affinities of minute fragments of organic remains. *Trans. Microsc. Soc. Lond.* 2: 46–58.

Quémeneur, S., et al. 2013. Microanatomy of the amniote femur and inference of lifestyle in limbed vertebrates. *Biol. J. Linn. Soc.* 109: 644–655.

Raman, A. 1969. Appositional growth rate in rat bones using the tetracycline labelling method. *Acta Orthop. Scandinav.* 40: 193–197.

Ramm, S. A. 2007. Sexual selection and genital evolution in mammals: a phylogenetics analysis of baculum length. *Am. Nat.* 169: 360–369.

Ricqlès, A. 1972. Recherches paléohistologiques sur les os longs des tétrapodes. III. – Titanosuchiens, Dinocéphales et Dicynodontes. *Ann. Paléontol.* 58: 17–60.

Ricqlès, A. de. 1975. Recherches paléohistologiques sur les os longs des tétrapodes VII. – Sur la classification, la signification fonctionnelle et l'histoire des tissus osseux des tétrapodes. Première partie, structures. *Ann. Paléontol.* 61: 51–129.

Ricqlès, A. de. 1979. Quelques remarques sur l'histoire évolutive des tissus squelettiques chez les vertébrés et plus particulièrement chez les tétrapodes. *Ann. Biol.* 18: 1–35.

Ricqlès A. de. 1976. On bone histology of fossil and living reptiles, with comments on its functional and evolutionary significance. In *Morphology and biology of Reptiles*, eds. Bellairs, A. d'A. and C. Barry Cox, 123–151. *Lin. Soc. Symp. Ser.* N°3

Ricqlès, A. de. 1979. Quelques remarques sur l'histoire évolutive des tissus squelettiques chez les vertébrés et plus particulièrement chez les tétrapodes. *Ann. Biol.* 18: 1–35.

Ricqlès, A. de and V. de Buffrénil. 1995. Sur la présence de pachyostéosclérose chez la rhytine de Steller (*Rhytina* (*Hydrodamalis*) *gigas*), sirénien récent éteint. *Ann. Sci. Nat. Zool. Paris, 13ème série* 16: 47–53.

Ricqlès, A. de and V. de Buffrénil. 2001. Bone histology, heterochronies and the return of tetrapods to life in water: where are we? In *Secondary adaptation of tetrapods to life in water*, eds. Mazin, J.-M. and V. de Buffrénil, 289–310. München, Verlag Dr. Friedrich Pfeil.

Roche, B., et al. 2012. Structure and quantification of microvascularisation within mouse long bones: what and how should we measure? *Bone* 50: 390–399.

Rolf, H. J. and A. Enderle. 1999. Hard fallow deer antler: a living bone till antler casting? *Anat. Rec.* 255: 69–77.

Rose, K. D. 2006. *The beginning of the age of mammals*. Baltimore: MD, Johns Hopkins University Press.

Ruff, C. B. and J. A. Runestad. 1992. Primate limb bones structural adaptations. *Annu. Rev. Anthropol.* 21: 407–433.

Ruff, C. B., et al. 2013. Ontogenetic changes in limb bone structural proportions in mountain gorillas (*Gorilla beringei beringei*). *J. Hum. Evol.* 65: 693–703.

Sanchez-Villagra, M. 2013. Why are there fewer marsupials than placentals? On the relevance of geography and physiology to evolutionary patterns of mammalian diversity and disparity. *J. Mammal. Evol.* 20: 279–290.

Sánchez-Villagra, M. R., et al. 2003. The anatomy of the world's largest extinct rodent. *Science* 301: 1708–1710.

Sander, M. P. and P. Andrassy. 2006. Lines of arrested growth and long bone histology in Pleistocene large mammals from Germany: What do they tell us about dinosaur physiology? *Palaeontogr. Abt. A* 277: 143–159.

Sarringhaus, L. A., et al. 2016. Long bone cross-sectional properties reflect changes in locomotor behavior in developing chimpanzees. *Am. J. Phys. Anthropol.* 160: 16–29.

Schaffler, M. B. and D. B. Burr. 1984. Primate cortical bone microstructure: relationship to locomotion. *Am. J. Phys. Anthropol.* 65: 191–197.

Schultz, N. G., et al. 2016. The baculum was gained and lost multiple times during mammalian evolution. *Integr. Comp. Biol.* 56: 644–656.

Seymour, K. L., et al. 2018. *Smilodon fatalis* from Talara, Peru: sex, age, mass, and histology. In *Smilodon, the iconic sabertooth*, eds. Werdelin, L., H. G. McDonald and C. A. Shaw, 30–52. Baltimore, MD, John Hopkins University Press.

Sharir, A., et al. 2011. The canine baculum: the structure and mechanical properties of an unusual bone. *J. Struct. Biol.* 175: 451–456.

Shaw, C. N. and T. M. Ryan. 2012. Does skeletal anatomy reflect adaptation to locomotor patterns? Cortical and trabecular architecture in human and nonhuman anthropoids. *Am. J. Phys. Anthropol.* 147: 187–200.

Simmons, N. B., et al. 2008. Primitive Early Eocene bat from Wyoming and the evolution of flight and echolocation. *Nature* 451: 818–821.

Singh, I. J. and D. L. Gunberg. 1971. Quantitative histology of changes with age in rat bone cortex. *J. Morphol.* 133: 241–252.

Singh, I. J., et al. 1974. A comparative histological study of mammalian bone. *J. Morphol.* 144: 421–438.

Skedros, J. G. and M. S. Doutré. 2019. Collagen fiber orientation pattern osteon morphology and distribution and presence of laminar histology do not distinguish torsion from bending in bat and pigeon wing bones. *J. Anat.* 234: 748–763.

Slon, V., D. Stein, H. Cohen, B. Medlej et al. 2014. Hyperostotic bone disease in a wombat (*Vombatus ursinus*). *Res. Vet. Sci.* 97: 88–95.

Sontag, W. 1986. Quantitative measurements of periosteal and cortical-endosteal bone formation and resorption in the midshaft of female rat femur. *Bone* 7: 55–62.

Stanley, H. P. and H. H. Hillemann. 1960. Histology of the reproductive organs of nutria, *Myocastor coypus* (Molina). *J. Morphol.* 106: 277–279.

Stein, B. R. 1989. Bone density and adaptation in semiaquatic mammals. *J. Mammal.* 70: 467–476.

Stockley, P. 2012. The baculum. *Curr. Biol.* 22: R1032.

Stover, S. M., et al. 1992. Histological features of the dorsal cortex of the third metacarpal bone mid-diaphysis during postnatal growth in thoroughbred horses. *J. Anat.* 181: 455–469.

Straehl, F. R., et al. 2013. Evolutionary patterns of bone histology and bone compactness in Xenarthran mammal long bones. *PLoS One* 8(7): e69275. doi: 10.1371/journal.pone.0069275.

Suttie, J. M., et al. 1985. Insulin-like growth factor 1 (IGF-1) antler-stimulating hormone? *Endocrinology* 116: 846–848.

Suttie, J. M., et al. 1991. Temporal change in LH and testosterone and their relationship with the first antler in red deer (*Cervus elaphus*) stags from 3 to 15 months of age. *J. Endocrinol.* 131: 467–474.

Suttie, J. M., et al. 1995. Role of steroids in antler growth of red deer stags. *J. Exp. Zool.* 271: 120–130.

Swartz, S. M. and K. M. Middleton. 2008. Biomechanics of the bat limb skeleton: scaling, material properties and mechanics. *Cells Tissues Organs* 187: 59–84.

Swartz, S. M., et al. 1992 Wing bone stresses in free flying bats and the evolution of skeletal design for flight. *Nature* 359: 726–729.

Tasikas, D. E., et al. 2009. Baculum variation end allometry in the muskrat (*Ondatria zibethicus*): a case for sexual selection. *Evol. Ecol.* 23: 223–232.

Thewissen, J. G. M., E. Williams, L. Roe and S. Hussain. 2001. Skeletons of terrestrial cetaceans and the relationship of whales to artiodactyls. *Nature* 413: 277–281.

Turnbull, W. D. 1971. The Trinity therians: their bearing on evolution in marsupials and other therians. In *Dental morphology and evolution*, Dahlberg, A. A. ed., 151–179. Chicago, IL, University of Chicago Press.

Uhen, M. D. and P. D. Gingerich. 1995. Evolution of *Coryphodon* (Mammalia, Pantodonta) in the Late Paleocene and Early Eocene of Northwestern Wyoming. *Contr. Mus. Paleontol. Michigan* 29: 259–289.

Veitschegger, K., et al. 2018. Paleohistology and life history evolution in cave bears, *Ursus spelaeus* sensu lato. *PLoS One* 13 (11): e0206791. https://doi.org/10.1371/journal.pone.0206791.

Verhaegen, M. and S. Munro. 2011. Pachyosteosclerosis suggests archaic *Homo* frequently collected sessile littoral food. *Homo-J. Comp. Hum. Biol.* 62: 237–247.

Vickaryous, M. K. and B. K. Hall. 2006. Osteoderm morphology and development in the nine-banded armadillo, *Dasypus novemcinctus* (Mammalia, Xenathra, Cingulata). *J. Morphol.* 267: 1273–1283.

Walker, M. M., J. Louys, A. I. R. Herries, G. J. Price et al. 2020. Humerus midshaft histology in a modern and fossil wombat. *Aust. Mamm.* https://doi.org/10.1071/AM20005.

VetBooks.ir

Washburn, S. L. 1946. The sequence of epiphyseal union in the opossum. *Anat. Rec.* 95: 353–363.

Webb, P. and V. Buffrénil, V. de. 1990. Locomotion in the biology of large aquatic vertebrates. *Trans. Am. Fish. Soc.* 119: 629–641.

Weisbecker, V., et al. 2008. Ossification heterochrony in the therian postcranial skeleton and the marsupial-placental dichotomy. *Evolution* 62: 2027–2041.

Welker, F., M. J. Collins, J. A. Thomas, M. Wadsley, S. Brace, E. Cappellini, S. T. Turvey, M. Reguero, J. N. Gelfo and A. Kramarz. 2015. Ancient proteins resolve the evolutionary history of Darwin's South American ungulates. *Nature* 522: 81–84.

Whalen, J. P., et al. 1972. A radiographic and histologic study of bone in the active and hibernating bat (*Myotis lucifugus*). *Anat. Rec.* 172: 97–108.

White, G. R. and R. S. Seymour. 2004. Does basal metabolic rate contain a useful signal? Mammalian BMR allometry and correlation with a selection of physiological, ecological, and life-history variables. *Physiol. Biochem. Zool.* 77: 929–941.

Wilkinson, M. 1999. Choosing and interpreting a tree for the oldest mammal. *J. Vert. Paleontol.* 19: 187–190.

Williams-Ashman, H. G. and A. H. Reddi. 1991. Differentiation of mesenchymal tissues during phallic morphogenesis with emphasis on the *os penis*: roles of androgens and other regulatory agents. *J. Steroid Biochem. Mol. Biol.* 39: 873–881.

Wilson, G. P., et al. 2016. A large carnivorous mammal from the Late Cretaceous and the North American origin of marsupials. *Nat. Commun.* 7: 13734.

Wislocki, G. B. 1942. Studies on the growth of deer antlers. I. On the structure and histogenesis of the antlers of the Virginia dee (*Odocoileus virginianus borealis*). *Am. J. Anat.* 71: 371–415.

Wislocki, G. B., et al. 1947. Osteogenesis of antlers investigated by histological and histochemical methods. *Anat. Rec.* 99: 265–295.

Wolf, D., et al. 2012. Osteoderm histology of the Pampatheriidae (Cingulata, Xenarthra, Mammalia): implications for systematics, osteoderm growth, and biomechanical adaptation. *J. Morphol.* 273: 388–404.

Yang, F., et al. 2017. The regulatory mechanism of MLT/MLT1 signaling on the growth of antler mesenchymal cells. *Molecules* 22: 1793. doi:10.3390/molecules22101793.

Zachos, F. E. and R. J. Asher (eds). 2018. *Handbook of zoology: Mammalia: mammalian evolution, diversity and systematics*. Berlin: De Gruyter.

Zedda, M., et al. 2008. Comparative bone histology of adult horses (*Equus caballus*) and cows (*Bos taurus*). *Anat. Histol. Embryol.* 37: 442–445.

Zioupos, P., et al. 1997. Mechanical properties of the rostrum of the whale Mesoplodon densirostris, a remarkably dense bony tissue. *J. Zool. London* 241: 725–737.

Zylberberg, L., et al. 1998. Rostrum of a toothed whale: ultrastructural study of a very dense bone. *Bone* 23: 241–247.

VetBooks.ir

Section VI

Integrative Questions

VetBooks.ir

VetBooks.ir

30

Phylogenetic Signal in Bone Histology

Jorge Cubo, Lucas Legendre and Michel Laurin

CONTENTS

Introduction: What is a Phylogenetic Signal? 617
How to Detect a Phylogenetic Signal 618
Empirical Studies 620
When to Test for a Phylogenetic Signal 622
References 622

Introduction: What is a Phylogenetic Signal?

The potential utility of bone histology and bone microstructure in phylogenetic reconstruction and in taxonomic determinations of bone fragments has been discussed for over a century and a half. Some authors have proposed that variation in bone microstructural and histological traits contains a significant phylogenetic signal and diagnostic taxonomic information (Quekett 1849, Zavattari and Cellini 1956, Houde 1986, 1987, Dittmann 2003). Others have argued that bone microstructural characters are essentially the outcome of ontogenetic and functional factors, an opinion that does not necessarily exclude the presence of a phylogenetic signal (see Padian 2013). Among these factors, the most often discussed are Amprino's (1947) rule, according to which variation in the growth rate of bone tissue mainly determines variation in its structure (Castanet et al. 1996, 2000, Margerie et al. 2002a, 2004, Montes et al. 2010), and Wolff's (1892) law, which postulates that bone microstructure predominantly reflects adaptations to biomechanical constraints (Lanyon 1984, Currey and Alexander 1985, Thomason 1985, Carter et al. 1991, Margerie 2002b, 2005, Ruff et al. 2006, Cubo et al. 2015).

The debate between proponents of the presence of a phylogenetic signal and those who view bone tissue as highly plastic and reflecting functional and ecological constraints continues, because deciphering the influence of these various signals in bone histology is more difficult than it might seem at first glance. Functional adaptation to current conditions (autapomorphies) may mask a phylogenetic signal, complicating the task of systematic biologists interested in the reconstruction of phylogenetic patterns. Conversely, phylogenetic patterns may explain why organisms do not appear to have reached optimal adaptation to current conditions (Ackerly 2009; Pennell et al. 2014b), although such assumptions always require proper testing (Gerhold et al. 2015). Thus, detection and quantification of the phylogenetic signal carried by the variation of any osteohistological trait is relevant to discussing its adaptive significance (Cubo et al. 2008; Legendre et al. 2013). This chapter reviews the literature on quantifying the phylogenetic signal in bone histological and microanatomical traits in vertebrates. However, before analyzing relevant literature, it seems useful to discuss the meaning of the "phylogenetic signal" concept.

The concept of phylogenetic signal has two different meanings. In the field of systematics, it refers to strict synapomorphies, i.e., cases of secondary (historical) homology tested by phylogenetic analysis (Pinna 1991). In other words, a character state is considered to have an optimal phylogenetic signal when it is present in only one clade (Figure 30.1).

According to Pinna (1991), cladistic practitioners of parsimony use pattern-detecting analyses, in which primary homology (phenotypic similarity) becomes either a single statement of secondary homology (a strict synapomorphy) or multiple statements of secondary homology (convergent evolution). However, phylogenetic signal can also be assessed using other phylogenetic methods, such as maximum likelihood and Bayesian methods. Showing its occurrence is a prerequisite to phylogenetic (comparative) analyses of any data using any method. In phylogenetic inference, characters are often discrete, and when they show a continuous range of variation, they are typically categorized before analysis, which results in discarding data, although methods have been developed to

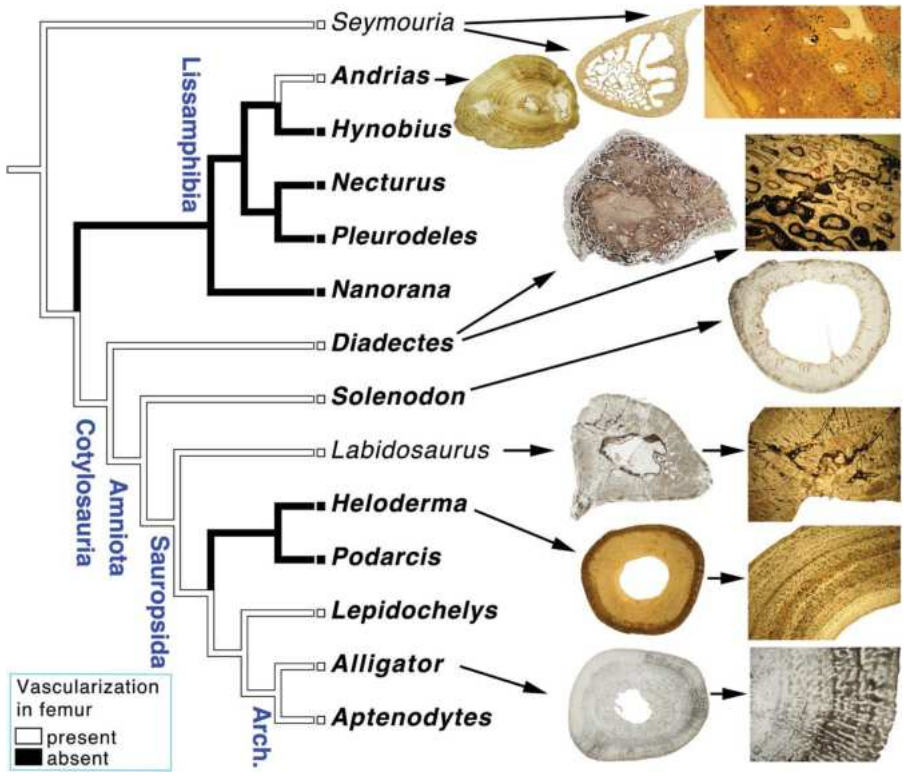


FIGURE 30.1 Evolutionary pattern of the character "presence/absence of vascular canals in the femur mid-shaft", optimized on a phylogeny of tetrapods (topology after Marjanović and Laurin 2019). Evolutionary patterns such as this one represent the "classical" definition of phylogenetic signal in systematics, i.e., secondary homology of discrete character states for one or several clades in the tree; a pattern with only one unambiguous synapomorphy for a given clade is considered to present a high phylogenetic signal. Here, the pattern is clearly homoplastic, with two independent losses of vascular canals (or vascularization): one near the base of Lissamphibia, and another one near the base of Squamata (here represented by *Heloderma* and *Podarcis*). In fact, this character displays even more homoplasy because some squamates (de Buffrénil and Castanet 2000) and anurans (Canoville et al. 2018) have vascular canals in their long bones, whereas some turtles lack them. Thus, there have been more losses of vascularization than shown here, and this character was reversed several times, as shown in *Andrias*. Nevertheless, the pattern shown represents the typical condition for several higher taxa, such as vascularization patterns in most stem-tetrapods (Steyer et al. 2004, Sanchez et al. 2008) and early amniotes (e.g., Laurin and de Buffrénil 2016). According to this definition of phylogenetic signal, most discrete histological features present a low signal in tetrapod phylogeny, and have traditionally been considered uninformative in this context. The use of quantitative histological features, however, as well as statistical procedures to estimate the amount of correlation between these features and a phylogeny, allow more precise estimation of the influence of evolutionary processes on histological data (see text).

bypass this step (Goloboff et al. 2006). It has been shown that the phylogenetic signal increases with the number of states (Rineau et al. 2018), and a continuous character can be considered the boundary case of a discrete character with an infinite number of states.

Thus far, only a few histological traits of vertebrate mineralized tissues have proved to be useful in phylogenetic reconstructions. For instance, perichondral bone may be a synapomorphy of the last common ancestor of Osteostraci and Gnathostomata (Nian-Zhong et al. 2005). This is also the case for endochondral bone, a synapomorphy of Osteichthyes (Janvier 1996a, b), and acellular bone, a synapomorphy of Acanthomorpha (Franz-Odendaal et al. 2006). More examples can be found in the tissues typically observed in odontodes, which have often been discussed by systematists (e.g., Burrow and Turner 1999).

In the field of phylogenetic comparative methods (PCMs), the phylogenetic signal has been defined as "a tendency for related species to resemble each other more than they resemble species drawn at random from the tree" (Blomberg and Garland 2002, p. 905). A character displaying a strong phylogenetic signal is also often described as presenting phylogenetic autocorrelation (Jombart et al. 2010b). PCMs mostly deal with continuously varying traits, and the presence of a significant phylogenetic signal can be tested using statistical methods.

How to Detect a Phylogenetic Signal

Two groups of methods for continuous data have been described. The first methods implemented to test for phylogenetic signal were simple autocorrelation tests, i.e., they inferred how much the value of a character of interest for a given organism is influenced by its phylogenetic position in the tree (Keck et al. 2016b). The first of these estimators was Moran's *I* (Gittleman and Kot 1990), based on patristic distances (i.e., branch lengths between pairs of terminal taxa) expressed as a phylogenetic weighting matrix (Pavoine et al. 2008, Münkemüller et al. 2012). This statistic parameter was

VetBooks.ir

then expanded into several other estimators, including various ways to express branch lengths in the weighting process, such as regressions on distance matrices based on a Mantel test (Legendre et al. 1994), or phylogenetic eigenvector regression (PVR; Diniz-Filho et al. 1998). All these estimators are based on simple regressions between a character and a phylogeny, without considering any evolutionary hypotheses. The inclusion of branch length information is thus facultative (though useful when available), or in some cases not possible (Münkemüller et al. 2012, Pavoine and Ricotta 2013). These methods can also be used to estimate a local signal for each individual species in the tree, which can give a good preliminary assessment of phylogenetic patterns for a given character (Figure 30.2).

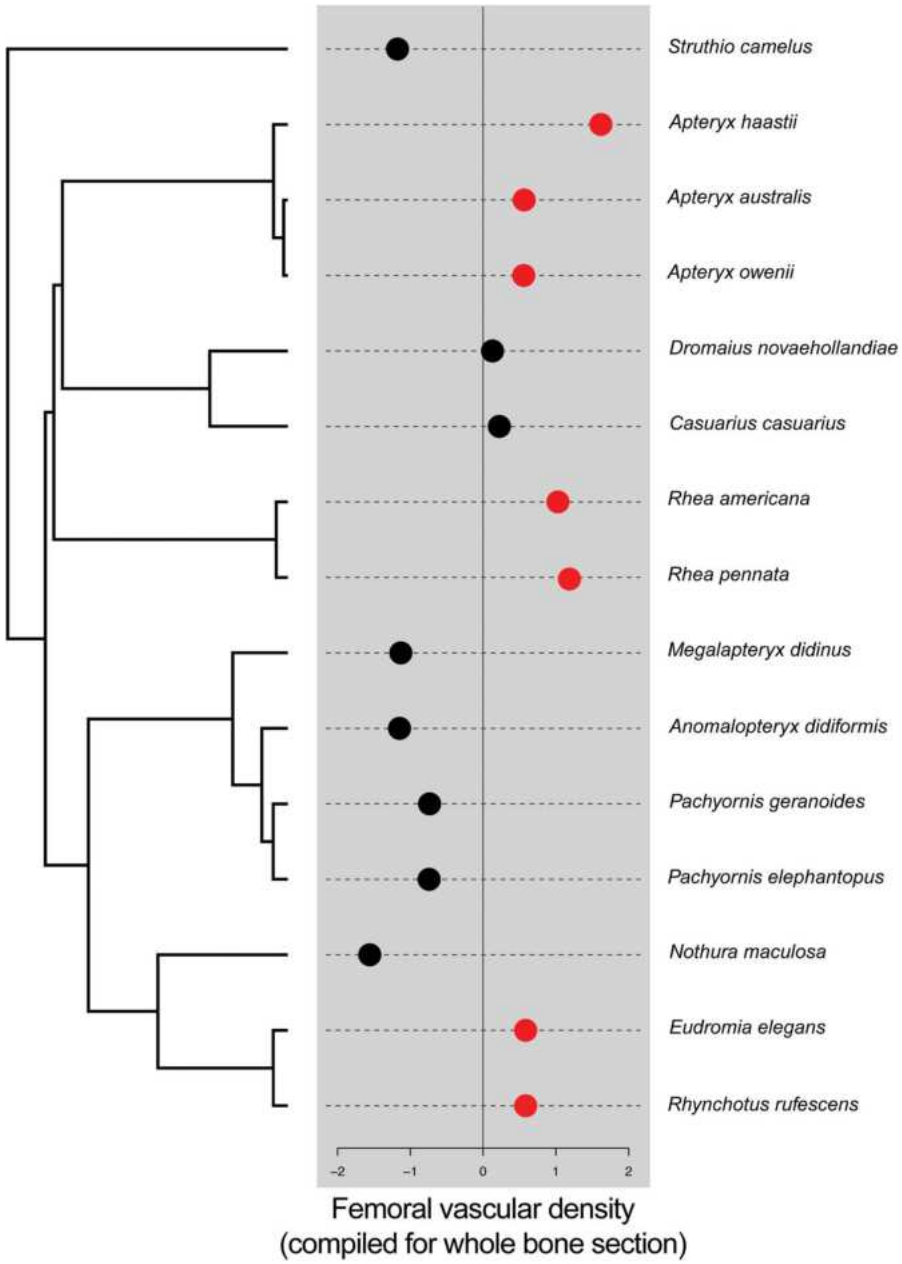


FIGURE 30.2 Estimates of local autocorrelation of femoral vascular density (measurements taken from Legendre et al. 2014) for each species in a phylogeny of extant paleognaths (taken from Haddrath and Baker 2012), as performed and plotted in the R package "phylosignal" (Keck et al. 2016b). This method estimates local hot spots of phylogenetic positive autocorrelation (here estimated as local Moran's *I*), i.e., clades in the tree for which phylogenetic signal is significantly greater than for their respective sister groups. In this example, we can see that some clades present significant differences in character value (highlighted in red): kiwis, rheas, and two tinamou species. It is thus, in some respect, a way to reconcile the "traditional" definition of phylogenetic signal in systematics (i.e., apomorphic character states visible on a tree) with that of the comparative approach (i.e., correlation between the structure of a character and that of a phylogeny). However, such shifts in values for some clades cannot be unambiguously interpreted as evolutionary shifts, because autocorrelation-based estimators of phylogenetic signal do not include an explicit evolutionary model (see text). This approach is thus an interesting preliminary look at potential constraints on the variation of vascular density, but this pattern needs further investigation using additional procedures before drawing conclusions about the underlying evolutionary processes.

VetBooks.ir

These diverse procedures have been criticized in recent literature because they do not assume an explicit evolutionary model (Adams and Church 2011, Freckleton et al. 2011). However, Diniz-Filho et al. (2012) found that PVR performs correctly with an appropriate phylogenetic eigenvector selection procedure, and Mantel tests have been shown to perform well when an evolutionary model is included (Debastiani and Duarte 2017). Additionally, when the character of interest follows a complex model of evolution, estimators that incorporate an evolutionary model (see below) can be more sensitive to its highly variable parameters. Autocorrelation methods such as Abouheif's C_{mean} (Abouheif 1999) might then adequately assess the presence of a phylogenetic signal, as shown by a case study using simulated data (Münkemüller et al. 2012). The use of autocorrelation estimators can, therefore, be a good way to assess general patterns in the variation of histological characters, but investigations of potential evolutionary processes underlying these patterns require the use of other statistical procedures.

On the contrary, several more recent methods assume an evolutionary model, which in most cases is a strict Brownian motion model, i.e., a model in which continuous traits evolve randomly over time along a branch, at a constant rate (Felsenstein 1973). Such estimators always rely on a calibrated phylogeny, and include the widely used Pagel's λ (Pagel 1999, Freckleton et al. 2002) and Blomberg's K (Blomberg et al. 2003). According to these last two methods, the variation of a phenotypic trait contains a high phylogenetic signal when it follows a Brownian motion model (values of Pagel's λ and Blomberg's K near 1), whereas the phylogenetic signal is low (values of Pagel's λ and Blomberg's K near 0) when the variation of the phenotypic trait does not follow a Brownian motion model because of the action of natural selection or other constraining factors (Münkemüller et al. 2012). Both types of methods have been the subject of many large-scale comparative reviews (Pavoine et al. 2008, 2010, Münkemüller et al. 2012, Keck et al. 2016a, b); overall, estimators based on an explicit evolutionary model tend to perform better than autocorrelation methods when branch length information is available and accurate, and vice versa (Münkemüller et al. 2012). It is important to mention that all estimators are strongly dependent on sample size, tree balance, and intraspecific variation (e.g., Ives et al. 2007).

Empirical Studies

Tests of phylogenetic signal are currently performed in most studies of variation in continuous bone histological traits. However, only three studies have been specifically devoted to the study of phylogenetic signal in the variation of bone histological traits. The first (Cubo et al. 2005) quantified and tested the presence of a phylogenetic signal in the vascular density, vascular orientation, index of Haversian remodeling, cortical thickness, and cross-sectional area of the femur in a sample of 35 amniote species, using both regressions on distance matrices based on Mantel tests and the amount of character change under squared-change parsimony, where statistical significance was assessed by randomized trees (Laurin 2004). This study concluded that phylogeny explains 81.8% of the variation of bone size (an anatomical trait), 86.2% of the variation of bone cortical thickness (a microanatomical trait) but only 18.7% of the variation of bone vascular density (a histological trait). Although all three tests were significant, Cubo et al. (2005) concluded that phylogenetic signal in histological traits is weak because the R^2 of the regression corresponding to bone vascular density is low (phylogeny explains less than 20% of its variation; see also Figure 30.3).

A few years later, Legendre et al. (2013) quantified the phylogenetic signal in a set of bone histological traits (vascular orientation, vascular density, cellular shape, cellular size and cellular density) observed in a sample of 25 species of amniotes (16 extant and 9 extinct taxa). Three methods were used: PVR, tree length distribution (using squared-change parsimony), and regressions on distance matrices. This study showed that most histological traits contain a significant phylogenetic signal (with the phylogeny often explaining 20–60% of their variation) and concluded that the presence of a phylogenetic signal is mostly influenced by sample size and the phylogenetic level of the clade under study (e.g., amniotes, diapsids, archosaurs, etc.). To further investigate these issues, Legendre et al. (2014) decided to perform exhaustive tests of phylogenetic signal in a set of 62 osteohistological features (the same traits as above, but quantified along four transects in each section) in an exhaustive sample of extant paleognathous birds, a clade having a long evolutionary history but containing a relatively low number of species, and for which many phylogenetic hypotheses have been proposed (e.g., Sackton et al. 2019). Four methods were employed to quantify the phylogenetic signal (Pagel's λ, Abouheif's C_{mean}, Blomberg's K, and Diniz-Filho's PVR) and four topologies were considered for the paleognathous phylogeny (see Legendre et al. 2014). They showed that roughly one half of the analyzed traits contain a significant phylogenetic signal, as revealed by one of the four methods (Figure 30.3). All methods showed high consistency for all topologies except one that was built using a much smaller sample, thus confirming that sample size has a much higher effect on the significance of phylogenetic signal than topology or branch length information, as was documented in previous simulation studies (see above). Furthermore, some of the cellular variables, which had previously been shown to exhibit a very weak phylogenetic signal in all previous studies compiled for whole bone sections, presented a much higher signal when compiled for specific transects (e.g., medial side of femoral transverse section).

In parallel, several other studies have assessed the presence (and sometimes the strength) of the phylogenetic signal in bone microanatomy. These studies typically relied on a sigmoidal compactness profile model and the software Bone Profiler (see Girondot and Laurin 2003, and Chapter 4 of this book on *Bone microanatomy*) to analyze mid-diaphyseal cross sections of long limb bones. Three methods were used to test the presence of a phylogenetic signal: regressions on distance matrices with permutations to test their significance (Legendre et al. 1994), PVR with variance partition (Desdevises et al. 2003), and comparison of the squared length of the reference tree to that of a population of random trees obtained by reshuffling the terminal taxa (Laurin 2004).

VetBooks.ir

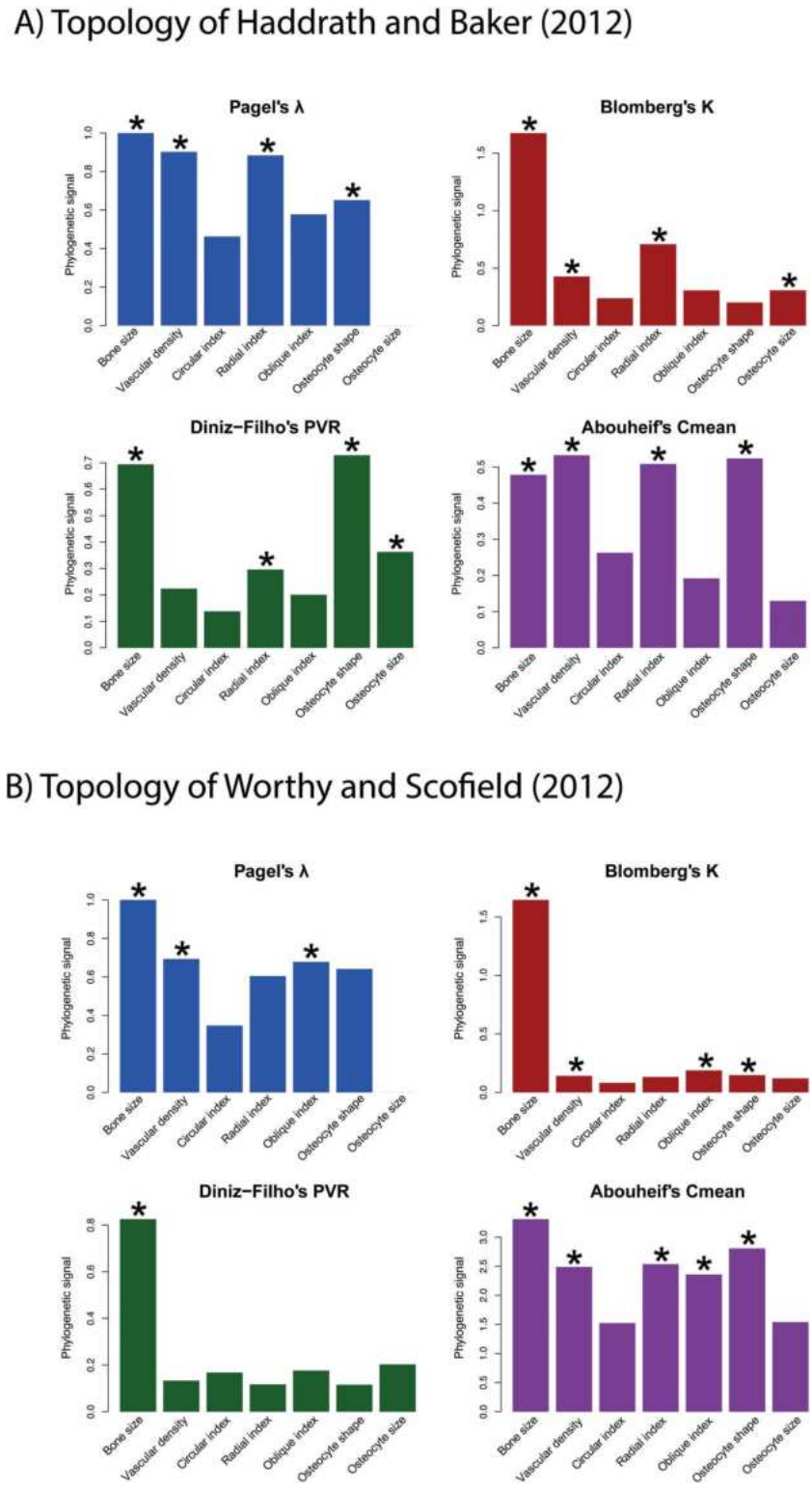


FIGURE 30.3 Bar plot showing the amount of phylogenetic signal for seven histological variables, measured using four different estimators – Pagel's λ, Blomberg's *K*, Diniz-Filho's PVR, and Abouheif's C_{mean} – using a data set taken from Legendre et al. (2014), for two paleognath phylogenies taken from Haddrath and Baker (2012) and Worthy and Scofield (2012), respectively. Significant signal for a given character is highlighted with an asterisk. Bone size shows a strong signal for both topologies and almost all estimators, whereas the signal for vascular indices and cellular variables is overall lower, as described by Cubo et al. (2005) and Legendre et al. (2013). In general, λ and C_{mean} show a greater consistency than the other two estimators, thus corroborating the results of Münkemüller et al. (2012), who identified them as the most reliable estimators under a Brownian motion model and for ultrametric trees in their respective categories. In contrast, PVR is the least consistent of all four estimators, and *K* shows a very high discrepancy between bone size and other characters, which might be due to its tendency to capture a very strong signal when the character of interest follows a strict Brownian motion model (Münkemüller et al. 2012.)

VetBooks.ir

These studies revealed that many but not all bone microanatomical characters display a phylogenetic signal, and that some characters display a signal more often than others. For instance, most studies found a phylogenetic signal in compactness parameter P, which reflects the relative size of the medullary region, but few showed such a signal in compactness parameter Max, i.e., compactness in the outermost cortex. Comparing these various studies shows that their results are influenced by the taxonomic composition of samples. For example, no signal was found in the lissamphibian femur for compactness profile parameter Min (i.e., compactness in the medulla) by Laurin et al. (2004), whereas such a signal could be found in the amniote radius and the tetrapod tibia (Germain and Laurin 2005, Kriloff et al. 2008). Similarly, no signal was found for compactness profile parameter S (width of the transition zone between medullary and cortical regions) in several studies, such as Quemeneur et al. (2013) on the amniote femur, but a signal was found in the amniote humerus (Canoville and Laurin 2010) and rib (Canoville et al. 2016). Microanatomical characters of trabeculae in mammalian vertebral centra also display a fairly strong phylogenetic signal (Dumont et al. 2013).

Among the studies on this topic, only three (Canoville and Laurin 2009, 2010, Laurin et al. 2009) have quantified the proportion of variance in bone microanatomical characters explained by the phylogeny. Results strongly depend on the variable considered, with some variables showing nonsignificant results (no phylogenetic signal), and others showing a strong signal, with up to 99.91% of the variance explained by the phylogeny. Such is the case, for example, in the radial estimate of parameter Min, based on the average of 60 compactness profiles, each of which was determined from a portion of the section representing only 6 degrees (Canoville and Laurin 2009: table 1). Results also differ sharply among studies: only one character displays such a signal in a sample of femora from 46 lissamphibian species studied by Laurin et al. (2009), whereas Canoville and Laurin (2009) found a signal for most characters in a sample of humeri from only 37 lissamphibian species. Such discrepancies may result from methodological biases, since Laurin et al. (2009) used a broken-stick model to select principal coordinates reflecting phylogeny, whereas Canoville and Laurin (2009) used both this method and a backward elimination procedure. The latter yielded far more positive results, a phenomenon also observed in the results on the amniote humerus, in which a broken-stick model yields a significant phylogenetic signal in fewer than half of the studied microanatomical characters, whereas a backward elimination procedure found a ubiquitous phylogenetic signal in these data.

When to Test for a Phylogenetic Signal

Since estimates of phylogenetic signal have become routinely used in quantitative bone histology over the last decade, many large-scale studies focusing on the link between bone microstructure and lifestyle have performed such estimates as a preliminary assessment of the influence of phylogeny on their data set, prior to using other phylogenetic modeling procedures such as phylogenetic regressions (e.g., Houssaye et al. 2013, 2014, 2016, Amson and Kolb 2016). However, all phylogenetic generalized linear models (e.g., phylogenetic analyses of variance, phylogenetic regressions) consider the phylogenetic signal of the data set in their correlation structure (e.g., in the error term of the regression), and not in individual variables (Freckleton 2009). For this reason, a strong phylogenetic signal in individual variables does not necessarily imply that any model built using these variables will itself present a strong signal, and vice versa.

Therefore, testing phylogenetic signal in individual variables is not a prerequisite for any phylogenetic modeling procedure, and using it as a preliminary test to choose between phylogenetic and nonphylogenetic regressions is incorrect (Revell 2010). To make this choice for a given data set, it is instead necessary to test for phylogenetic signal in the residuals of the regression, which can be expected to include such phylogenetic information (Mundry 2014); if that signal is significant, then the use of PCM is mandatory in further analyses (see Mitchell et al. 2017 for a case study of the use of PCM on bone histological features). Most R packages commonly used to perform PCM, such as *adephylo* (Jombart et al. 2010a), *ape* (Paradis et al. 2004; Paradis and Schliep 2019), *caper* (Orme et al. 2018), *geiger* (Harmon et al. 2008; Pennell et al. 2014a), *phylolm* (Ho and Ané 2014), *phylosignal* (Keck et al. 2016b), *phytools* (Revell 2012), and *picante* (Kembel et al. 2010), include several functions to test for phylogenetic signal in the context of such comparative analyses, using several of the estimators discussed above. *caper*, for example, allows one to perform a phylogenetic regression while simultaneously estimating Pagel's λ in its residuals, which is a powerful and fast approach to assessing the relevance of PCM for a data set.

In conclusion, the debate on the phylogenetic signal contained by the variation of bone histological traits remains open. Quantifications performed at a broad phylogenetic scale using sparse sampling (Cubo et al. 2005, Legendre et al. 2013), or on a narrow phylogenetic scale using an exhaustive sampling (Legendre et al. 2014), lead to similar conclusions: phylogenetic signal in osteohistological traits is moderate to low, which means that natural selection or other factors may act on these features and mask the signal. Legendre et al. (2014) nevertheless identified a strong signal for several histological features when large, dense samples of the clades of interest were used and when intraindividual variation was considered. This result advocates for a large-scale and integrative approach when dealing with phylogenetic signal in bone histology. More comprehensive data sets are required to assess the influence of phylogeny on bone microstructure in tetrapods as a whole and in amniotes. For bone microanatomy, the situation seems to be simpler because such features appear to present a strong phylogenetic signal, despite the fact that it also reflects selective constraints linked to adaptation to various lifestyles (see Chapter 35).

REFERENCES

Abouheif, E. 1999. A method for testing the assumption of phylogenetic independence in comparative data. *Evol. Ecol. Res.* 1: 895–909.

Ackerly, D. 2009. Conservatism and diversification of plant functional traits: evolutionary rates versus phylogenetic signal. *PNAS* 106: 19699–19706.

Adams, D. C. and J. O. Church. 2011. The evolution of large-scale body size clines in *Plethodon* salamanders: evidence of heat-balance or species-specific artifact? *Ecography* 34: 1067–1075.

Amprino, R. 1947. La structure du tissu osseux envisagée comme expression de différences dans la vitesse de l'accroissement. *Arch. Biol.* 58: 315–330.

Amson, E. and C. Kolb. 2016. Scaling effect on the mid-diaphysis properties of long bones – the case of the Cervidae (deer). *Sci. Nat.* 103: 1–10.

Blomberg, S. P. and T. Garland. 2002. Tempo and mode in evolution: phylogenetic inertia, adaptation and comparative methods. *J. Evol. Biol.* 15: 899–910.

Blomberg, S. P., et al. 2003. Testing for phylogenetic signal in comparative data: behavioral traits are more labile. *Evolution* 57: 717–745.

Burrow, C. J. and S. Turner. 1999. A review of placoderm scales, and their significance in placoderm phylogeny. *J. Vert. Paleontol.* 19: 204–219.

Canoville, A. and M. Laurin. 2009. Microanatomical diversity of the humerus and lifestyle in lissamphibians. *Acta Zool.* 90: 110–22.

Canoville, A. and M. Laurin. 2010. Evolution of humeral microanatomy and lifestyle in amniotes, and some comments on paleobiological inferences. *Biol. J. Linn. Soc.* 100: 384–406.

Canoville, A., et al. 2016. Microanatomical diversity of amniote ribs: an exploratory quantitative study. *Biol. J. Linn. Soc.* 118: 706–33.

Canoville, A., et al. 2018. Quantitative data on bone vascular supply in lissamphibians: comparative and phylogenetic aspects. *Zool. J. Linn. Soc.* 182(1): 107–28.

Carter, D. R., et al. 1991. Musculoskeletal ontogeny, phylogeny, and functional adaptation. *J. Biomech.* 24: 3–16.

Castanet, J., et al. 1996. Expression de la dynamique de croissance dans la structure de l'os périostique chez *Anas platyrhynchos*. *C. R. Acad. Sci. Paris III* 319: 301–308.

Castanet, J., et al. 2000. Periosteal bone growth rates in extant ratites (ostriche [sic] and emu). Implications for assessing growth in dinosaurs. *C. R. Acad. Sci. II*323: 543–550.

Cubo, J., et al. 2005. Phylogenetic signal in bone microstructure of sauropsids. *Syst. Biol.* 54: 562–574.

Cubo, J., et al. 2008. Phylogenetic, functional, and structural components of variation in bone growth rate of amniotes. *Evol. Dev.* 10: 217–227.

Cubo, J., et al. 2015. First reported cases of biomechanically adaptive bone modeling in non-avian dinosaurs. *PLoS One* 10: e0131131.

Currey, J. D. and R. M. Alexander. 1985. The thickness of the walls of tubular bones. *J. Zool.* 206: 453–468.

de Buffrénil, V. and J. Castanet. 2000. Age estimation by skeletochronology in the Nile monitor (*Varanus niloticus*), a highly exploited species. *J. Herpetol.* 34: 414–24.

Debastiani, V. J. and L. d. S. Duarte. 2017. Evolutionary models and phylogenetic signal assessment via Mantel test. *Evol. Biol.* 44: 135–143.

Desdevises, Y., et al. 2003. Quantifying phylogenetically structured environmental variation. *Evolution* 57: 2647–2652.

Diniz-Filho, J. A. F., et al. 1998. An eigenvector method for estimating phylogenetic inertia. *Evolution* 52: 1247–1262.

Diniz-Filho, J. A. F., et al. 2012. On the selection of phylogenetic eigenvectors for ecological analyses. *Ecography* 35: 239–249.

Dittmann, K. 2003. Histomorphometric analysis of primate and domesticated animal long bone microstructure. In *Decyphering ancient bones*, G. Grupe and J. Peters eds., 215–225. Rahden (Germany), VML Verlag Marie Leidorf GmbH.

Dumont, M., et al. 2013. Inner architecture of vertebral centra in terrestrial and aquatic mammals: a two-dimensional comparative study. *J. Morphol.* 274: 570–84.

Felsenstein, J. 1973. Maximum likelihood and minimum-steps methods for estimating evolutionary trees from data on discrete characters. *Syst. Zool.* 22: 240–249.

Franz-Odendaal, T. A., et al. 2006. Buried alive: how osteoblasts become osteocytes. *Dev. Dyn.* 235: 176–190.

Freckleton, R. P. 2009. The seven deadly sins of comparative analysis. *J. Evol. Biol.* 22: 1367–1375.

Freckleton, R. P., et al. 2002. Phylogenetic analysis and comparative data: a test and review of evidence. *Am. Nat.* 160: 712–726.

Freckleton, R. P., et al. 2011. Comparative methods as a statistical fix: the dangers of ignoring an evolutionary model. *Am. Nat.* 178: E10–E17.

Gerhold, P., et al. 2015. Phylogenetic patterns are not proxies of community assembly mechanisms (they are far better). *Funct. Ecol.* 29: 600–614.

Germain, D. and M. Laurin.2005. Microanatomy of the radius and lifestyle in amniotes (Vertebrata, Tetrapoda). *Zool. Scr.* 34: 335–350.

Girondot, M. and M. Laurin. 2003. Bone profiler: a tool to quantify, model and statistically compare bone section compactness profiles. *J. Vert. Paleontol.* 23: 458–461.

Gittleman, J. L. and M. Kot. 1990. Adaptation: statistics and a null model for estimating phylogenetic effects. *Syst. Zool.* 39: 227–241.

Goloboff, P. A., et al. 2006. Continuous characters analyzed as such. *Cladistics* 22: 589–601.

Haddrath, O. and A. J. Baker. 2012. Multiple nuclear genes and retroposons support vicariance and dispersal of the palaeognaths, and an Early Cretaceous origin of modern birds. *Proc. R. Soc. B: Biol. Sci.* 279: 4617–4625.

Harmon, L. J., et al.. 2008. GEIGER: investigating evolutionary radiations. *Bioinformatics* 24: 129–131.

Ho, L. S. T., Ané, C. 2014. A linear-time algorithm for Gaussian and non-Gaussian trait evolution models. *Syst. Biol.* 63: 397–408.

Houde, P. 1986. Ostrich ancestors found in the Northern Hemisphere suggest new hypothesis of ratite origin. *Nature* 324: 563–565.

Houde, P. 1987. Histological evidence for the systematic position of *Hesperornis* (Odontornithes: Hesperornithiformes). *Auk: Ornithol. Adv.* 104: 125–129.

Houssaye, A., et al. 2013. Microanatomical and histological features in the long bones of mosasaurine mosasaurs (Reptilia, Squamata) – Implications for aquatic adaptation and growth rates. *PLoS One* 8: e76741.

Houssaye, A., et al. 2014. Amniote vertebral microanatomy – What are the major trends? *Biol. J. Linn. Soc.* 112: 735–746.

Houssaye, A., et al. 2016. Biomechanical evolution of solid bones in large animals: a microanatomical investigation. *Biol. J. Linn. Soc.* 117: 350–371.

Ives, A. R., et al. 2007. Within-species variation and measurement error in phylogenetic comparative methods. *Syst. Biol.* 56: 252–270.

Janvier, P. 1996a. *Early vertebrates*. Oxford (UK), Oxford University Press.

Janvier, P. 1996b. The dawn of the vertebrates: characters versus common ascent in the rise of current vertebrate phylogenies. *Palaeontology* 39: 259–287.

Jombart, T., et al. 2010a. adephylo: new tools for investigating the phylogenetic signal in biological traits. *Bioinformatics* 26: 1907–1909.

Jombart, T., et al. 2010b. Putting phylogeny into the analysis of biological traits: a methodological approach. *J. Theor. Biol.* 264: 693–701.

Keck, F., et al. 2016a. Phylogenetic signal in diatom ecology: perspectives for aquatic ecosystems biomonitoring. *Ecol. Appl.* 26: 861–872.

Keck, F., et al. 2016b. Phylosignal: an R package to measure, test, and explore the phylogenetic signal. *Ecol. Evol.* 6: 2774–2780.

Kembel, S. W., et al. 2010. picante: R tools for integrating phylogenies and ecology. *Bioinformatics* 26: 1463–1464.

Kriloff, A., et al. 2008. Evolution of bone microanatomy of the tetrapod tibia and its use in palaeobiological inference. *J. Evol. Biol.* 21: 807–826.

Lanyon, L. E. 1984. Functional strain as a determinant for bone remodeling. *Calcif. Tissue Int.* 36: S56–S61.

Laurin, M. 2004. The evolution of body size, Cope's rule and the origin of amniotes. *Syst. Biol.* 53: 594–622.

Laurin, M. and V. de Buffrénil. 2016. Microstructural features of the femur in early ophiacodontids: a reappraisal of ancestral habitat use and lifestyle of amniotes. *C. R. Palevol* 15: 115–27.

Laurin, M., et al. 2004. The evolution of long bone microanatomy and lifestyle in lissamphibians. *Paleobiology* 30: 589–613.

Laurin, M., et al. 2009. Use of paleontological and molecular data in supertrees for comparative studies: the example of lissamphibian femoral microanatomy. *J. Anat.* 215: 110–123.

Legendre, L., et al. 2013. Phylogenetic signal in bone histology of amniotes revisited. *Zool. Scr.* 42: 44–53.

Legendre, L. J., et al. 2014. Bone histology, phylogeny and palaeognathous birds (Aves, Palaeognathae). *Biol. J. Linn. Soc.* 112: 688–700.

Legendre, P., et al. 1994. Modeling brain evolution from behavior: a permutational regression approach. *Evolution* 48: 1487–1499.

Margerie, E. de, et al. 2002a. Bone typology and growth rate: testing and quantifying "Amprino's rule" in the mallard (*Anasplatyrhynchos*). *C. R. Biol.* 325: 221–230.

Margerie, E. de. 2002b. Laminar bone as an adaptation to torsional loads in flapping flight. *J. Anat.* 201: 521–526.

Margerie, E. de, et al. 2004. Assessing a relationship between bone microstructure and growth rate: a fluorescent labelling study in the king penguin chick (*Aptenodytes patagonicus*). *J. Exp. Biol.* 207: 869–879.

Margerie, E. de, et al. 2005. Torsional resistance as a principal component of the structural design of long bones: comparative multivariate evidence in birds. *Anat. Rec.* 282A: 49–66.

Marjanović, D. and M. Laurin. 2019. Phylogeny of Paleozoic limbed vertebrates reassessed through revision and expansion of the largest published relevant data matrix. *PeerJ* 6: e5565.

Mitchell, J., et al. 2017. Bone histological correlates of soaring and high-frequency flapping flight in the furculae of birds. *Zoology* 122: 90–99.

Montes, L., et al. 2010. Relationship between bone growth rate and bone tissue organization in amniotes: first test of Amprino's rule in a phylogenetic context. *Anim. Biol.* 60: 25–41.

Mundry, R. 2014. Statistical issues and assumptions of phylogenetic generalized least squares. In *Modern phylogenetic comparative methods and their application in evolutionary biology*, L. Z. Garamszegi ed., 131–156. Berlin, Springer.

Münkemüller, T., et al. 2012. How to measure and test phylogenetic signal. *Meth. Ecol. Evol.* 3: 743–756.

Nian-Zhong, W., et al. 2005. Histology of the galeaspid dermoskeleton and endoskeleton, and the origin and early evolution of the vertebrate cranial endoskeleton. *J. Vert. Paleontol.* 25: 745–756.

Orme, D., et al. 2018. CAPER: comparative analyses of phylogenetics and evolution in R. https://cran.r-project.org/web/packages/caper/index.html

Padian, K. 2013. Why study the bone microstructure of fossil tetrapods? In *Bone Histology of Fossil Tetrapods: Advancing Methods, Analysis and Interpretation*. K. Padian, and E.-T. Lamm eds., 1–12. Berkeley, CA, University of California Press.

Pagel, M. 1999. Inferring the historical patterns of biological evolution. *Nature* 401: 877–884.

Paradis, E., et al. 2004. APE: analyses of phylogenetics and evolution in R language. *Bioinformatics* 20: 289–290.

Paradis, E., Schliep, K. 2019. ape 5.0: an environment for modern phylogenetics and evolutionary analyses in R. *Bioinformatics* 35: 526–528.

Pavoine, S., et al. 2010. Decomposition of trait diversity among the nodes of a phylogenetic tree. *Ecol. Monogr.* 80: 485–507.

Pavoine, S., et al. 2008. Testing for phylogenetic signal in phenotypic traits: new matrices of phylogenetic proximities. *Theor. Popul. Biol.* 73: 79–91.

Pavoine, S. and C. Ricotta. 2013. Testing for phylogenetic signal in biological traits: the ubiquity of cross-product statistics. *Evolution* 67: 828–840.

Pennell, M. W., et al. 2014a. geiger v2.0: an expanded suite of methods for fitting macroevolutionary models to phylogenetic trees. *Bioinformatics* 30: 2216–2218.

Pennell, M. W., et al. 2014b. Is there room for punctuated equilibrium in macroevolution? *Trends Ecol. Evol.* 29: 23–32.

Pinna, M. C. C. de. 1991. Concepts and tests of homology in the cladistic paradigm. *Cladistics* 7: 367–394.

Quekett, J. T. 1849. On the intimate structure of bone as composing the skeleton in the four great classes of animals viz., mammals, birds, reptiles and fishes, with some remarks on the great value of the knowledge of such structure in determining the affinities of minute fragments of organic remains. *Trans. R. Microsc. Soc.* 2: 46–58.

Quemeneur, S., et al. 2013. Microanatomy of the amniote femur and inference of lifestyle in limbed vertebrates. *Biol. J. Linn. Soc.* 109: 644–655.

Revell, L. J. 2010. Phylogenetic signal and linear regression on species data. *Meth. Ecol. Evol.* 1: 319–329.

Revell, L. J. 2012. Phytools: an R package for phylogenetic comparative biology (and other things). *Meth. Ecol. Evol.* 3: 217–223.

Rineau, V., et al. 2018. Impact of errors on cladistic inference: simulation-based comparison between parsimony and three-taxon analysis. *Contr. Zool.* 87:25–40.

Ruff, C., et al. 2006. Who's afraid of the big bad Wolff? "Wolff's law" and bone functional adaptation. *Am. J. Phys. Anthropol.* 129: 484–498.

VetBooks.ir

Sackton, T. B., et al. 2019. Convergent regulatory evolution and loss of flight in paleognathous birds. *Science* 364: 74–78.

Sanchez, S., et al. 2008. Salamander-like development in a seymouriamorph revealed by palaeohistology. *Biol. Lett.* 4: 411–14.

Steyer, J.-S., et al. 2004. First histological and skeletochronological data on temnospondyl growth: palaeoecological and palaeoclimatological implications. *Palaeogr. Palaeoclimatol. Palaeoecol.* 206: 193–201.

Thomason, J. J. 1985. The relation of trabecular architecture to inferred loading patterns in the third metacarpals of the extinct equids *Merychippus* and *Mesohippus*. *Paleobiology* 11: 323–335.

Wolff, J. 1892. *Das Gesetz der Transformation der Knochen*. A. Hirschwald Verlag, Berlin, Germany.

Worthy, T. H. and R. P. Scofield. 2012. Twenty-first century advances in knowledge of the biology of moa (Aves: Dinornithiformes): a new morphological analysis and moa diagnoses revised. *N. Z. J. Zool.* 39: 87–153.

Zavattari, E. and I. Cellini. 1956. La minuta architettura delle ossa degli uccelli e il suo valore nella sistematica dei grandi gruppi. *Monit. Zool. Ital.* 64: 189–200.

VetBooks.ir

31

Cyclical Growth and Skeletochronology

Vivian de Buffrénil, Alexandra Quilhac and Jacques Castanet

CONTENTS

Introduction 626
Biological Rhythms and Cyclical Growth 627
Tissue Sampling and Current Technical Processes in Skeletochronology 627
Basic Methodological Options 627
Tissue Sampling and Processing 629
Bone and Cementum 629
Dentin 629
Structural Characteristics of Yearly Growth Marks in Bone 630
General Interpretative Framework 630
Histology of SGMs 630
Structural Data on LAGs 630
Structure of the Annuli 632
Remarks on Zones 632
Neonatal Line 634
Spacing Pattern of SGMs 634
Eroded and Supernumerary SGMs 634
Remarks on LAGs in Secondary Bone 636
Periodicity and Duration of SGM Formation in Bone 636
Observing the Periodicity of SGMs 636
Duration of Age Recording by Bone SGMs 637
Structural Features of Skeletal Growth Marks in Dental Tissues 637
Diversity of Dental Tissues Containing Growth Marks 637
Structure and Periodicity of Dental Growth Marks 637
Dentinal GLGs 637
Cementum LAGs 639
A Central Tool in Biology and Paleobiology 639
References 640

Introduction

Accurate assessment of individual age is essential for numerous research fields, including developmental biology and population dynamics, as well as for taxonomic determinations. The need for an efficient aging (biochronological) method is particularly important in paleontology and evolutionary biology, because vertebrate fossils are often rare and fragmentary, and thus provide only limited information on individual growth stage, a parameter essential to infer the life history traits of a taxon and compare it to related forms. In this context, a method of age determination must comply with at least four main constraints to be of some use. (1) It must be based on resistant, nonperishable parts of the body so that it can be used in similar conditions in extant and extinct taxa. (2) It must not depend on the extrapolation of curves, because most extinct taxa (and numerous extant ones) are not represented by enough specimens. (3) The method must yield age determinations with an annual precision, at least. Below this threshold, estimates would not properly reflect chronological age, but rather broad developmental categories (e.g., adult, subadult or juvenile) that are of limited relevance to studies on, e.g., population structure or individual growth. (4) Age recording must be as long-lasting as possible during the animal's life span. However, if it stops before the death of the animal, this situation must be detectable so that significant underestimates of age can be avoided.

Altogether, these constraints tend to exclude from paleobiological studies most of the aging techniques used in extant taxa,

VetBooks.ir

such as tooth eruption and wear (Clarke et al. 1992, Kierdorf and Becher 1997), eye lens weight (Malcom and Brooks 1981, Pascal and Delattre 1981), body measurements and, to a lesser extent, the degree or pattern of epiphysis or suture fusion (Kvam 1983, Maisano 2002). For reviews of these methods, see Gibbons (1976), Pascal and Castanet (1978), Anthony (1988), Castanet et al. (1993) and Zug (1991). In the end, only one aging method can fulfill the conditions mentioned above: skeletochronology.

This term, created by Castanet (1982), refers to the use of cyclical growth marks of known (or postulated) periodicity, occurring in the calcified parts of the vertebrate skeleton. Such marks can be found in the core or on the surface of all skeletal elements, including bones, teeth, scales, fin rays and intradermal ossifications (review in Castanet et al. 1993). An increasing number of comparative studies shows that skeletal growth marks (SGMs) occur in all vertebrate taxa, although their morphological, physiological and ecological characteristics may broadly differ. Similar marks also exist in invertebrate exoskeletons (Clark 1974), as well as in some nonskeletal parts of the vertebrate body; e.g., fish otoliths (e.g., Brothers et al. 1976, Panfili and Loubens 1991), horny scales of tortoises (Germano and Bury 1998), nails and claws of some mammals and reptiles (Morris 1972, Thomas et al. 1997), and cetacean baleen and earplugs (Jonsgård 1969). The formation of SGMs is the expression of a highly plesiomorphic biochronological rhythmicity that can be traced back to the Silurian (Giles et al. 2013, see also Downs and Donoghue 2009, Keating and Donoghue 2016). In fossils, SGMs form under the same conditions as in extant taxa, and their preservation depends mainly on the resistance of extracellular matrices to diagenetic processes.

The practical use of these cyclical growth marks for age determination began in the early 20th century, with the pioneer works by Heincke (1908) and Cunningham (1905) on the skeletons of marine osteichthyans and chondrichthyans. Today, it is a central tool for all biological and ecological studies involving age, in extant and extinct lineages. Hundreds of articles refer to SGMs in most vertebrate taxa (Castanet et al. 1992; Schöne and Gillikin 2013), as do reviews and textbooks for the fundamental and applied dimensions of skeletochronology (e.g., Klevezal and Kleinenberg 1967, Perrin and Myrick 1980, Castanet 1985, 1987, Baglinière et al. 1992, and Klevezal 1996 for extant species, and Woodward et al. 2013 for fossils). A succinct historical account of the main steps of the development of this method is given by Castanet (1982) (see also Meunier 1988). In addition to its original role in age determination, skeletochronology is now the basis of a rich series of studies that attempt to model the growth rates and processes of fossil taxa (short synthesis in Erickson 2014 and Woodward et al. 2013). This is perhaps the most fruitful and intellectually challenging contribution of skeletochronology.

Biological Rhythms and Cyclical Growth

The processes responsible for the accretion of cyclical (circum-annual) growth marks in skeletal tissues are now relatively well defined and documented by both comparative and experimental data since the pioneering work of Pengelley and Kelly (1966) and Gwinner (1967). Growth marks in both skeletal and nonskeletal tissues reflect a seasonal decrease in the main physiological parameters of the animals, with the resulting onset of a diapause or hibernation episode. This process, observed in nearly all metazoans, is rooted in the deepest level of the evolution of plants and animals (Cloudsley-Thompson 1980). In vertebrates, whatever their phyletic position, metabolic activity levels periodically drop (Geiser 1988, Carey et al. 2003) and the blood levels of various hormones, nutrients and electrolytes decrease (Wang 1985, Hellgren 1998). As a consequence, growth is slowed or stopped (Oudet and Petrovic 1977, 1982, Steinberg et al. 1979). In a given species, this episode can be either strong and of general occurrence in populations (e.g., in the ground squirrel: Lyman 1984), or mild, facultative and unevenly distributed among conspecific individuals in relation to local, microclimatic events, as exemplified by monitor lizards (Cissé 1971, Christian et al. 1995) and tortoises (Nussear et al. 2007). In osteichthyans (Meunier and Pascal 1981, Meunier 1988), amphibians (Marangoni et al. 2009), nonavian reptiles (Castanet and Naulleau 1974, Gregory 1982), birds (Lawrence and Wolowyk 1988) and mammals (Lyman 1963, Steinberg et al. 1979, Boissin and Canguilhem 1988), independent lines of experimental evidence converge to indicate that this process results from endogenous causes, because it still occurs when the animals are naturally (e.g., deep sea fishes: Geistdoerfer 1982) or artificially (Mrosovsky 1990) maintained in stable environmental conditions (constancy of temperature, hygrometry, lighting and photoperiod, food supply, etc.). These endogenous rhythms are themselves controlled by central neuroendocrine mechanisms commonly called *biological clocks* (Paul et al. 2007). In the ground squirrel (*Spermophilus lateralis*), experimental results by Ruby et al. (1996) located this *time-giving* structure in the suprachiasmatic nuclei of the brain.

In natural conditions, endogenous rhythms are synchronous with various seasonal changes of the environment, designated as *synchronizers* (Castanet and Naulleau 1985, Saint Girons 1985). Synchronizers have been shown to be linked to seasonal variations of either temperature, water level, availability of prey species or pasture, migrations and so on. The duration of daylight, as detected by the epiphysis (a photosensitive organ), seems to be a major synchronizer, at least in terrestrial ecosystems (Cloudsley-Thompson 1980, Petermann and Gauthier 2018).

Tissue Sampling and Current Technical Processes in Skeletochronology

Basic Methodological Options

Nearly all skeletal tissues, including bone (from limbs, skull, mandible, ribs, tympanic bullae, osteoderms, scales, fin-rays etc.), dentin and cementum contain clear cyclical growth marks potentially useful for age determination (Fig. 31.1A–E). Enamel also displays cyclical marks, but these have a nonannual periodicity: the striae of Retzius represent an infradiel rhythm, while the cross striation of enamel prisms has a daily periodicity (e.g., Bromage 1991, Line 2000, Antoine et al.

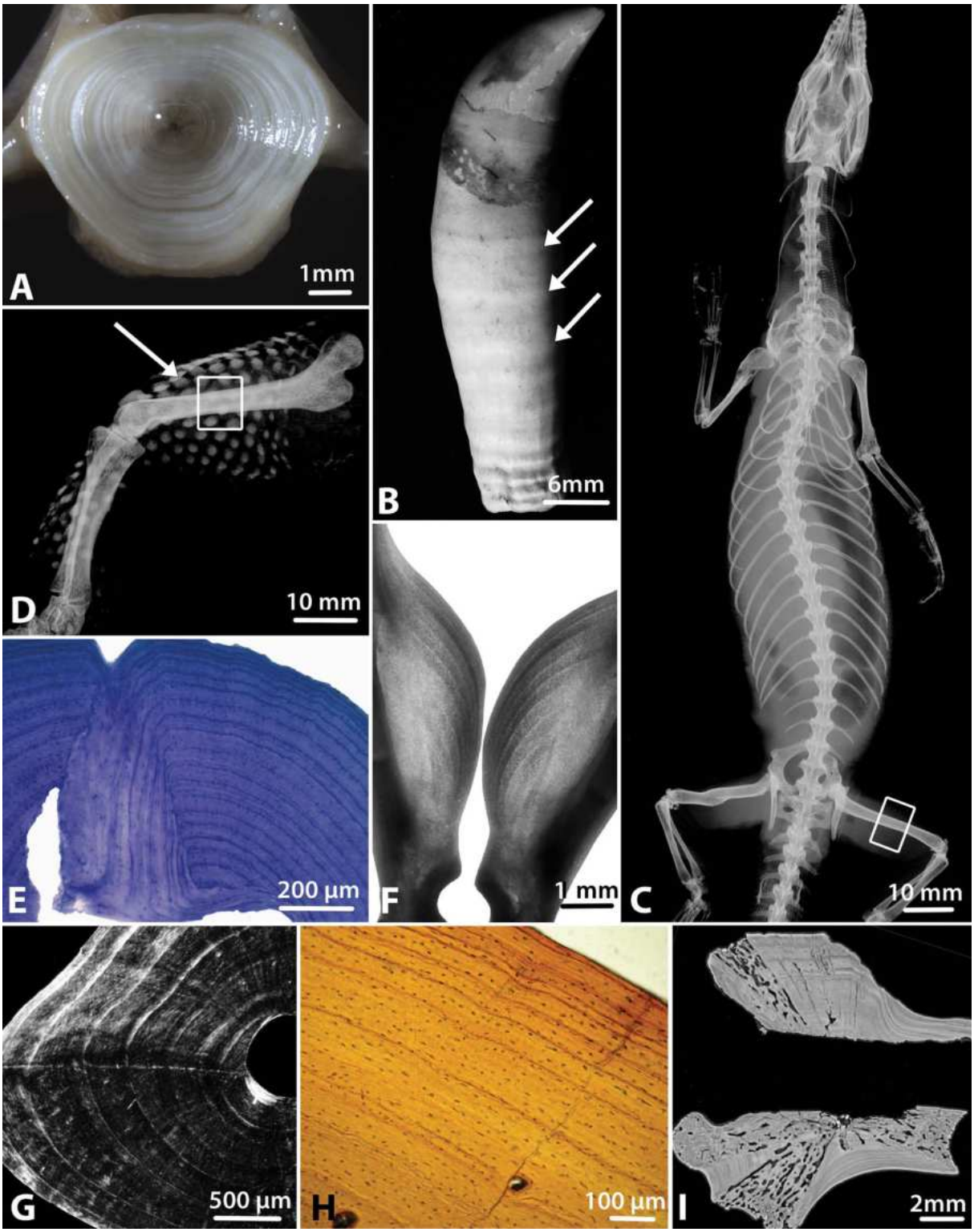


FIGURE 31.1 Technical overview. A, Centrum of the actinopterygian (Moridae) *Salilota australis*, showing superficial growth marks. B, Tooth of a Nile crocodile, *Crocodylus niloticus*, with superficial growth marks. C, X-ray proof of *Varanus pilbarensis* (Squamata, Varanidae). The best site for skeletochronology is indicated by the hollow rectangle. D, Rear leg of *Heloderma horridum* (Squamata, Helodermatidae) showing (1) the best location for sampling the femur (square) and (2) an osteoderm (arrow) in which skeletal growth marks may occur. E, Coloration of decalcified bone by Erlich's hematoxylin, i.e., the most common process for revealing lines of arrested growth (LAGs) in bone and cement. Femur of the lizard *Shenodon punctatus* (Rhynchocephalia, Sphenodontidae). F, Annuli seen by transparency (back-lighting of the bone) in a mandibular plate from *Vipera aspis* (Squamata, Viperidae). G, LAGs in a ground section from a fibula of *Varanus niloticus* (transmitted polarized light). H, LAGs in the femur of the fossil anuran Alytid *Latonia gigantea* (Middle Miocene). I, Virtual section (sagittally oriented) obtained by computed tomography (CT scan) in a vertebral centrum from the squamate *Pachyvaranus crassispondylus* (Upper Cretaceous).

VetBooks.ir

2009, Mahoney et al. 2018). Enamel marks are most useful for the study of tooth development; however, their formation is very limited in time; they are thus unsuited for long-term aging. Bone, dentin and cementum have respective advantages, disadvantages and constraints, depending on the taxa considered, and all require specific care. Tooth tissues can be used for age estimation at diverse time scales in mammals, but because teeth do not occur in extant birds, and because they are regularly replaced in non-mammalian taxa, they are of little use for skeletochronology in these clades. Conversely, growth marks in bone are useful in all vertebrates.

Growth marks may occur on the surface of bones and teeth, but they are better revealed by sections. In bones, superficial marks appear on the outer side of calcified cartilage as faint wavelets (Figure 31.1A). They have mainly been observed on the articular surfaces of vertebral centra and apophyses (Meunier 1992, Wintner and Cliff 1999, Erickson 2003). Such marks are seldom used because, in addition to their morphological variability, they are particularly sensible to *in vivo* wear, because calcified cartilage is a brittle material. Their distinctness is thus strongly influenced by the age of the animals. Moreover, such marks are rarely preserved or useful in fossils.

The so-called tide marks on tooth roots (Figure 31.1B) were initially considered for age determination in pinnipeds (Scheffer 1950), in which they can be fairly conspicuous, and in various other mammals (e.g., rodents: Goodwin et al. 2005). However, the presence of such marks is particularly inconstant in mammals, and they tend to be obscured by the accumulation of cementum layers with age (Scheffer and Myrick 1980). Their use is anecdotal today, and most skeletochronological studies rely on internal marks.

Tissue Sampling and Processing

Bone and Cementum

As far as possible, samples of bone intended for skeletochronological studies should be taken from long limb bones (including phalanges), which often have a simple, tubular morphology and symmetrical growth patterns. The samples must come from the diaphyseal region that presents the thickest cortex and thinnest medullary cavity (a region generally marked by the penetration of the nutrient canal in the bone shaft), where the growth record is likely to be most complete. Sometimes it is useful to identify the best site for sectioning by first taking an X-ray or another kind of transparent image (Figure 31.1C, D).

Growth marks in bone can occasionally be observed merely by shining a strong light (Figure 31.1F) through very thin, flat bones of small animals (one of the best examples is the counting of SGMs in the mandibular plate of snakes by Castanet 1974 and Castanet and Naulleau 1974), or the fin-rays of osteichthyans (Deelder and Willemse 1972; see also Schroeder and Baskett 1968 for similar observations of the pterygoid of *Rana catesbeiana*). However, the most frequent practice is to take thin sections of bone or teeth, and further discussion in this section is confined to these associated techniques.

An efficient and easy process commonly used to reveal growth marks in recent samples of bone or cementum is to stain decalcified sections (thickness 5–20 µm) with Erlich's hematoxylin (Figure 31.1E). Technical accounts of this technique are given by Castanet (1982), Klevezal (1996), and Perrin and Myrick (1980). The decalcification process can be conducted with various acids; the cheapest and quickest procedure is to use 3% or 5% nitric acid, with close monitoring of the process. When decalcified and thoroughly rinsed in tap water, the samples can be cut with either a classical microtome after paraffin embedding, or a freezing microtome. Slightly different techniques exist, like that based on the Jordet J-322 Dip-Quick stain procedure proposed by Rossell and Sheehan (1998), but their use is less current. Procedures for staining growth marks in nondecalcified tissue slices have also been described (e.g., Villanueva et al. 1986); they are generally more complex but no more efficient.

The use of mere ground sections of dry bone or cementum, without staining, is also broadly used for the observation of growth marks in recent (Figure 31.1G) and fossil (Figure 31.1H) bone tissue. Optimal section thickness should be about 100 µm ± 20 (excessive thinness or thickness decreases optical contrast), adjusted for their optimal use under polarized light, especially for recent tissues. The respective merits of colored sections versus ground sections were compared in turtles by Goshe et al. (2009). Colored sections have allowed a better discrimination of the closely packed peripheral marks. Of course, in fossils, only ground sections, made with classical procedures (e.g., Lamm 2013), can be used. As mentioned above, if the bone structure is not severely degraded by diagenesis, such sections generally give better results in fossils than in recent samples because the percolation of groundwater through tissues during fossilization tends to naturally stain them and make the growth marks more legible (see, e.g., Sanchez et al. 2010). Ground sections are also required when osseous or dental tissues are labeled *in vivo* with fluorescent markers for assessing the periodicity of growth marks (see below).

In favorable cases, high-resolution computed tomography (CT scanning) gives convincing images of growth marks (Figure 31.1I), provided the latter entail cyclical differences in the local mineralization of the tissues.

Dentin

Several procedures are used to reveal *growth layer groups* (GLGs, according to Perrin and Myrick's 1980 terminology) in dentin. The simplest is to cut the teeth along their sagittal plane of symmetry and polish the two sectional surfaces thus obtained. This technique is commonly used for the teeth of medium-sized to large odontocetes (Scheffer and Myrick 1980). It can be improved by mild acid-etching of the sectional surface, a process creating slight relief that enhances GLG contours (Pierce and Kajimura 1980). Ordinary ground sections 60- to 80-µm thick are routinely used for recent and fossil teeth (see Figure 31.5), and good results are also obtained from recent material with microradiography of tooth slices (Hohn 1980). Staining decalcified tooth sections for dentin growth marks is time-consuming and of little benefit.

The reading of growth marks, whether in bone, dentine or cementum, can be somewhat subjective, depending on the observer (e.g., Keay 1995). This is why the reading of each section by different observers is highly recommended.

VetBooks.ir

Moreover, uncertainties about the recognition of growth marks can be partly reduced by computer image treatment (as initially proposed by Lieberman et al. 1990). Several software programs, such as Software for Assisted Acquisition of Skeletochronological Data (SAASD) (Chauvelon et al. 1991) or CALCIF (Laval and Planes 1992), are specifically dedicated to skeletochronology.

Structural Characteristics of Yearly Growth Marks in Bone

General Interpretative Framework

A yearly growth cycle in bone is classically considered (see, e.g., Castanet et al. 1993) to be formed of three possible kinds of growth marks (Figure 31.2): the zones (a term first used by Peabody 1958, 1961), which reflect relatively rapid growth in periods of full activity, the annuli (Peabody 1958, 1961), which are deposited when growth activity decreases but still occurs, and the lines of arrested growth (LAGs), a term representing the English translation by Zug et al. (1986) of the French *lignes d'arrêt de croissance* (LACs) proposed by Castanet (1974). LAGs are set in place each year during a stage of physiological diapause that is severe enough to stop growth activity temporarily. For synonymy of skeletochronological terms, see Castanet (1982, 1987).

The yearly fluctuation of growth rate is a gradual process and, in consistency with Amprino's (1947) rule, the local structure of bone in primary periosteal cortices reflects the growth rate prevailing when the bone layer was deposited. Successive modifications of bone structure form a continuum, basically influenced by three main conditions. (1) The rate of growth during the stages of fast growth will determine the histological features of the zones, and consequently the remaining range of possibilities for subsequent modification of bone histology when growth decreases. For example, if the tissue in a zone is of the lamellar type (slowest bone deposit), no annulus can be formed, only a LAG. (2) The slope of the decrease in growth rate does or does not allow a progressive change in bone structure with a succession of the three kinds of growth marks mentioned above. If the drop in growth rate is steep, a LAG can be created but no annulus. (3) If the final, or slowest, rate of growth during the stage of diapause drops to zero, then a clear LAG will be formed. Conversely, if growth remains at a significant (though low) level, then an annulus will be formed, but no LAG will occur. Histologically, this annulus may display variable characteristics according to the initial level of local growth and the amplitude of its drop. The diversity of annulus characteristics is further discussed below.

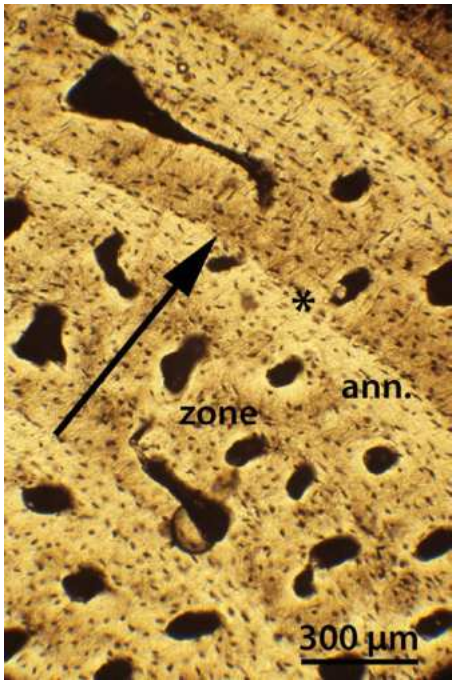


FIGURE 31.2 Typical succession, symbolized by an arrow, of cyclical growth marks in bone (here, the frontal bone of *Diplocynodon ratelii*, an alligatorid crocodilian from the Lower Miocene of France). In space as in time, a zone is followed by an *annulus* (ann.), and an *annulus* by a line of arrested growth (LAG: asterisk).

The histological organization of growth marks in a bone is thus contextual. The classical scheme of an annulus succeeding to a *zone*, and a LAG to an annulus (e.g., Castanet et al. 1993), is a theoretical view seldom observed in real bone sections. As described in the following paragraph, the histological aspect of LAGs is relatively clear and corresponds to a real and fairly constant structure; conversely, the histological condition of the annuli, and more so the zones, is obviously variable for the reasons explained above. This is why the notions of annulus and zone should be considered in a functional and contextual background, not in reference to strict, universal histological traits. Under normal conditions, growth rate decreases with age, or can vary according to local morphogenetic processes (e.g., differentiation of a crest, off-centered or drifting growth, etc.). Therefore, in a single bone section, the local contexts that prevail during the formation of growth marks may differ, as will the local characteristics of the marks themselves. Moreover, in numerous taxa, especially larger extant reptiles (e.g., crocodiles, varanids, tegus, iguanas), annual diapause episodes can be mild, variably pronounced or facultative, as mentioned above. In such cases, stochastic events (mainly related to climatic instability) may significantly interfere with biological cycles in various ways, thus modifying the form or distinctness of the marks and making their histological range of expression more complex (Buffrénil and Castanet 2000). These possible interferences must be kept in mind when interpreting cyclical growth marks in a bone, especially if it is a fossil.

Histology of SGMs

Structural Data on LAGs

On sections stained with hematoxylin, LAGs appear as concentric lines that are more chromophilous than the surrounding bone matrix (Figures 31.1E and 31.3A, B, I. Their color can vary from deep indigo blue to faint bluish gray, and their thickness from 5 to 10 µm. Thin LAGs tend to be more strongly stained than thicker ones. On ground sections, LAGs generally appear as thin, translucent lines in natural transmitted light,

VetBooks.ir

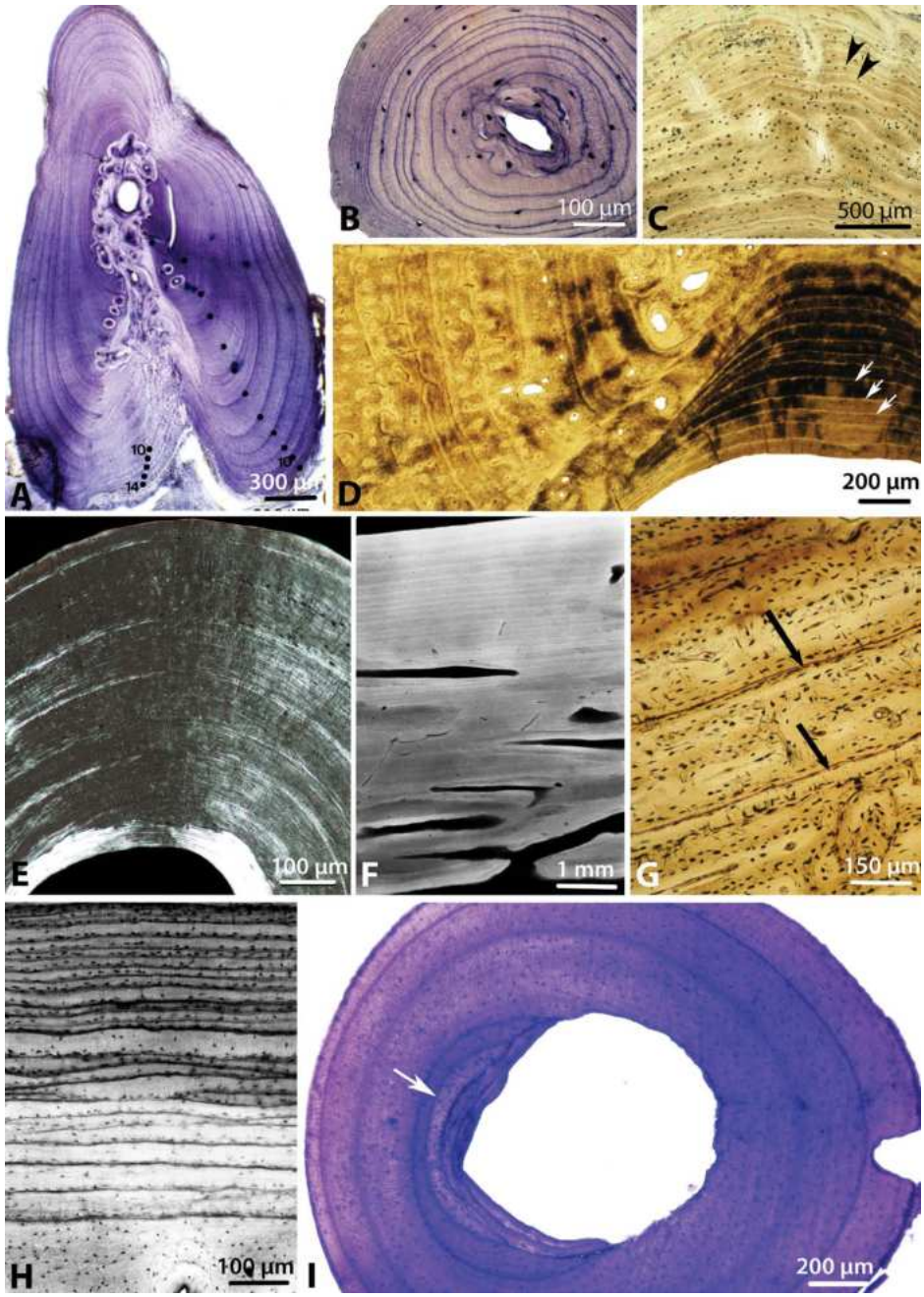


FIGURE 31.3 Structural features of skeletal growth marks: the lines of arrested growth (LAGs). A, Typical aspect of the LAGs stained with hematoxylin in a fin-ray of the osteichthyan *Lethrinus nebulosus*. Up to 14 LAGs can be counted. B, LAGs revealed by hematoxylin staining in the femur of *Euproctus sp.* (Salamandridae). C, Aspect of the LAGs (arrow heads) in ordinary transmitted light (cross section in the femur of an extant urodele, *Andrias japonicus*). D, Translucent LAGs (white arrows) in the frontal bone of a fossil crocodilian, *Diplocynodon ratelii*, from the Lower Miocene of France. E, LAGs in the in the femur of the anuran *Nanorana vicina* (Dicroglossidae). Ground section in transmitted polarized light. F, Hypermineralized LAGs in the femur of *Alligator mississippiensis*, as revealed by microradiography. G, Natural dark coloration of the LAGS (arrows) in fossils (humerus of the Miocene pinniped *Nanophoca vitulinoides*). H, Sharp LAGs in the mandible of the harbor porpoise, *Phocoena phocoena* (Phocoenidae). Hematoxylin staining. I, Neonatal line (arrow) in the femur of the lizard *Lacerta viridis*. Hematoxylin staining.

and as brilliantly birefringent lines in polarized light (Figure 3C–E), indicating a dominant circular (i.e., parallel to bone contour) orientation of their structure. Osteocyte lacunae, vascular canals and Sharpey's fibers do not occur in LAGs, although rare exceptions of radial canals crossing them can be observed. On X-ray proofs and tomographic documents, LAGs are slightly, but constantly, more opaque to X-rays than the surrounding matrix (Figure 31.3F). Differences ranging from 1% to 6% (in relative mineral volume) were measured by quantitative microradiography in diverse reptiles and amphibians (Castanet et al. 1970, Castanet 1979, 1982). Few studies have been conducted on the ultrastructure and histochemical

VetBooks.ir

characteristics of LAGs, and most of them involve reptiles (synthesis in Castanet 1982). Decalcified bone samples studied in transmission electron microscopy (TEM) show that these lines contain sparse collagen fibrils that are strongly opaque to electrons. They form a loose network with relatively broad interfibrillar spaces, a structure that could explain the high concentration of neutral mucopolysaccharides revealed in LAGs by the periodic acid Schiff (PAS) reaction (Castanet 1982). Such characteristics, like the general histological appearance of the LAGs in all kinds of preparations, are strongly reminiscent of reversion (i.e., cementing) lines (Frasca 1981, Castanet 1982); however, both result from distinct histogenetic processes. In routine histological observations, LAGs can be distinguished from reversion lines by two features: (1) they have a smooth contour, whereas reversion lines (as a result of previous local resorption) look scalloped at high magnification and (2) no discordant (i.e., geometrically or structurally uneven) bone deposits occur on the sides of LAGs, whereas such deposits are always associated with reversion lines (see Chapter 8).

In fossils, LAGs often appear as sharply defined black lines (e.g., Lee and O'Connor 2013). They can constitute a weak interface between adjacent bone layers, thus facilitating splitting between adjacent cortical layers. Percolation products then accumulate in these gaps and strongly mark the contour of LAGs (Figure 31.3G), rendering them easily legible.

LAGs have been described in all main extant and extinct vertebrate groups and in all categories of bone tissues. Their basic structure does not vary significantly, whether in osteichthyans (Figure 31.3A; see also Meunier et al. 1979, 2002), amphibians (Figure 31.3B, C, E; see also Castanet et al. 2003; Sanchez et al. 2010), nonavian reptiles (Figure 31.3D, I; see also Castanet 1974, Horner and Padian 2004), birds (Chinsamy et al. 1994, Turvey et al. 2005, Bourdon et al. 2009) or mammals (Figure 31.3G, H; see also Sander and Andrássy 2006, Kolb et al. 2015).

Structure of the Annuli

As mentioned above, the histological structure of annuli is much more variable than that of LAGs. According to a classical, widely acknowledged definition, a typical annulus comprises a layer of parallel-fibered or lamellar bone tissue (as defined in Chapter 8), poorly vascularized and broadly variable in thickness (Francillon-Vieillot et al. 1990, Castanet et al. 1993). It is generally considered to be wedged between either two zones (of diverse histological characteristics), or a zone, in medial position, and a LAG, in lateral position (LAGs are sometimes in the middle of annuli; cf. Lee and O'Connor 2013). This structural definition, already established by Peabody (1961), was subsequently developed on the basis of more detailed histological studies in extant lepidosaurs (Castanet 1974), crocodilians (Buffrénil 1980) and osteichthyans (Shirvell 1981, Lecomte 1990, Castanet et al. 1993, Meunier et al. 2002). The extension of skeletochronology to mammals and other large, supposedly tachymetabolic tetrapods (e.g., Horner et al. 2004; Woodward et al. 2013 for dinosaurs; Kolb et al. 2015, Köhler et al. 2012 for mammals) suggests a more comprehensive definition of the annuli: any cyclical modification of bone structure other than a LAG, and resulting from a decrease in bone accretion rate, should be considered an annulus. Such a definition is functional, not structural. Therefore, according to the local context of its occurrence, the structure of an annulus may comply with the original definition (Figures 31.2 and 31.4A, B), or sometimes be fairly different. For example, a mild cyclical drop in a very fast periosteal deposit such as, e.g., a radial fibrolamellar complex, may result in an annulus also made of a fibrolamellar complex, but with a different vascular orientation or a less dense vascular network (Figure 31.4C–E). Conversely, a similar decrease occurring in, e.g., laminar tissue can result in a classical annulus made of parallel-fibered bone, as shown by Woodward et al. (2013: figure 7.3). The actual structure of annuli is a continuum in which the modification of bone tissue characteristics due to growth decrease is basically gradual. An extreme illustration of this definition is given by the periosteal cortices of some aquatic tetrapods, such as ichthyosaurs and placodonts. In these taxa, primary cortices are deposited as fine cancellous tissue, the trabeculae of which have a dominant radial orientation. This general architecture is cyclically interrupted by circular layers (i.e., parallel to the contour of the bones) of compact bone, regularly spaced within the cortices, and often made of a different kind of osseous tissue (Buffrénil and Mazin 1990 1992; see also Chapter 29). A very similar situation occurs in, e.g., the pectoral spines of some teleosts (Figure 31.4F, H), as described by Meunier et al. (2002). LAGs can occur in the middle of such layers, which functionally represent genuine annuli. When present in well-preserved fossils, annuli are sharp and easily legible due to artifactual bone tissue impregnation by natural dyes.

The mineralization rate inside the annuli remains a puzzling question, and contradictory data have been presented. Castanet et al. (1977) recorded equal mineral contents in annuli and adjacent zones, whereas Buffrénil and Schoevaert (1989) illustrated clearly undermineralized annuli in a mammal, the sirenian *Dugong dugon* (Figure 31.4G). Moreover, annuli tend to be hypermineralized in osteichthyans (Figure 31.4H; see also Castanet et al. 1977, Meunier and Pascal 1980). Because parallel-fibered and lamellar bone tissues are slightly less mineralized than woven-fibered tissue (see Chapter 8), annuli should logically be less radiopaque than zones in most cases. This topic calls for further histological studies.

Remarks on Zones

Zones have no specific histological characteristics. They simply reflect the level of growth experienced by an animal during its annual period of activity. According to the size and general ecophysiological adaptation of a taxon, zones may consist of a fibrolamellar complex, as commonly encountered in large synapsids and diapsids (e.g., Figure 31.4B–E), but they can also consist of parallel-fibered (Figure 31.3E, I) or lamellar bone tissues, a situation quite common in small- to medium-sized ectotherms or in tiny, flat or thin bones of all taxa. The actual definition of zones is merely topographic: they are inserted between either two consecutive LAGs or annuli, or between a LAG and the annulus of the subsequent growth cycle.

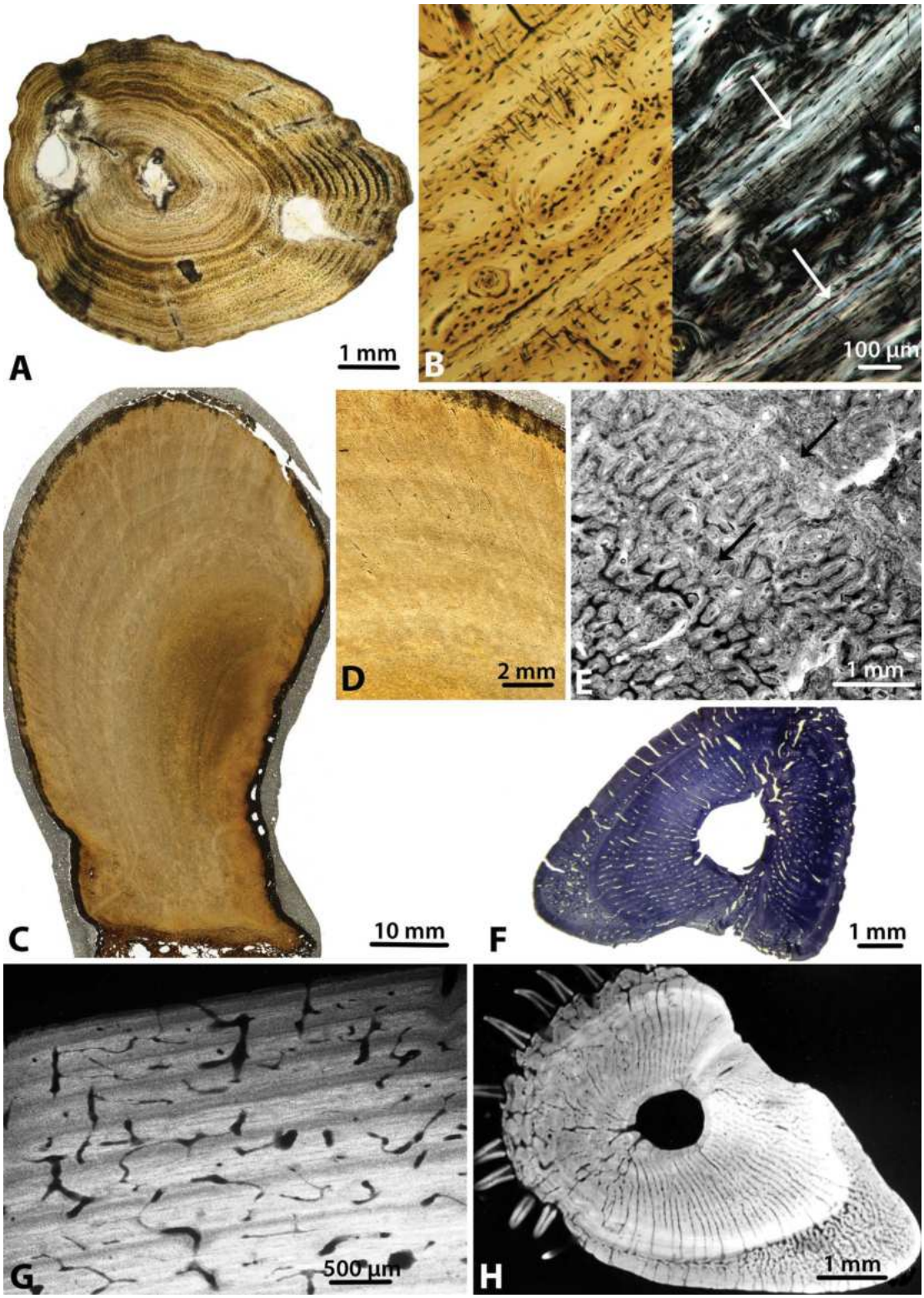


FIGURE 31.4 Structural features the annuli. A, Conspicuous series of annuli in the femur of a lissamphibian (Caudata) *Andrias japonicus*. Ground section in transmitted light. B, Frequent aspect of the annuli in the humerus of *Nanophoca vitulinoides*. Ground section in ordinary transmitted light (left) and in polarized light (right). C, Cross section in the premaxilla of a fossil beaked whale (Ziphiidae), *Aporotus recurvirostris*, showing faint cyclical growth marks in the form of annuli (broad, light bands) and zones (narrow darker bands). D, Closer view of *Aporotus* premaxillary SGMs. These marks are merely created by a slight, cyclical difference in the orientation of primary osteons. E, Same phenomenon as in D in the rib of the primitive Eocene cetacean (Basilosauridae) *Basilosaurus cetoides*. F, Annuli created by densification in bone texture in a spine of the siluriform *Hoplosternum littorale*. G, Hypomineralized annuli in the exoccipital of *Dugong dugon* (Mammalia, Sirenia). Microradiography. H, Hypermineralized annulus in the pectoral spine of *Hoplosternum littorale*.

VetBooks.ir

Neonatal Line

The neonatal line (also called *hatching line*) is the first SGM to be formed after birth, and it marks the beginning of postnatal cortical growth. It is basically a noncyclical line, since it is related to a unique event, birth, and it consists of a single or, sometimes, double LAG, separated from the medullary cavity by a layer of woven-fibered bone tissue (Figure 31.3I. The latter is laid down during the stage of fast embryonic growth. Up to now, neonatal lines have been mainly observed in the bones of squamates (e.g., Castanet 1987, Saint Girons et al. 1989, Buffrénil and Castanet 2000), but they are likely to occur also in numerous other tetrapod taxa, including mammals (Nacarino-Meneses and Köhler 2018). In a long bone, the enlargement of the medullary cavity during growth generally erases the neonatal line. This line is preserved only when the development of the medullary cavity is limited or strongly off-centered, a situation that maintains a part of the cortex free of resorption (e.g., Castanet 1987). Young specimens thus offer a much better chance to observe a neonatal line than older ones. There is little doubt (though formal evidence is still wanted) that the formation of the neonatal line is related to the physiological shock of the hatchling The frequent splitting of the line could reflect a close chronological proximity between birth and the first diapause (Saint Girons et al. 1989). To our knowledge, neonatal lines have not yet been reported in fossils, but this is a mere matter of opportunity. Two other kinds of noncyclical lines are known: the line of metamorphosis (e.g. Sinsch 2015), and the weaning line (Castanet et al. 2004). In their structure and functional meaning, these lines seem very comparable to the neonatal line (all are true LAGs, simply distinguished by the circumstances of their deposit), but they remain poorly documented.

Spacing Pattern of SGMs

The spacing pattern of successive LAGs or annuli is of special importance because, for a constant periodicity of SGM deposition, it tracks the global course of individual growth rate during ontogeny. In extinct taxa, the spacing between growth marks is a major, and sometimes unique, clue for assessing growth patterns. Substantial intraspecific variability, and individual irregularities, are frequent in SGM spacing (examples in Zug et al. 1986, Buffrénil and Castanet 2000, Hugi and Sanchez-Villagra 2012); however, four main patterns arise from the multitude of documented cases relative to specimens displaying long-lasting age records compared to their known specific longevity:

1. SGM spacing decreases gradually (Figure 31.5A), but remains significant, and visibly nonasymptotic, until the death of the animal (e.g., Hutton 1986; Castanet et al. 1988; Montori 1990). This condition occurs in taxa that appear to grow indefinitely, a condition that mainly reflects a combination of overall slow growth rates and the low survival rate of individuals to the stage of full skeletal maturity. Such taxa generally possess primitive epiphyses (*sensu* Haines 1942), but exceptions suggest that this condition is neither mandatory, as exemplified by *Sphenodon punctatus* (Castanet et al. 1988) and large varanids (Buffrénil et al. 2004), nor sufficient, as observed in alligator populations by Woodward et al. (2011).
2. In early growth stages, growth marks are widely spaced, and their spacing suddenly drops to remain relatively tight and constant afterward for long periods of time (Figure 31.5B). This pattern is encountered in taxa (numerous amphibians and reptiles) with "indefinite growth", in which a steep drop in growth rate occurs after the attainment of sexual maturity (Caetano 1990; Montori 1990).
3. Initial SGM spacing is wide, but abruptly drops close to the periosteal bone surface, where only some very tight growth cycles are visible (Figure 31.5C). These late cycles constitute the external fundamental system (EFS; also called *outer circumferential lamellae*: Ponton et al. 2004), a typical feature of taxa with definite, asymptotic growth (Lee and O'Connor 2013, Marin-Moratalla et al. 2013). This situation is general in animals with secondary, intraepiphyseal centers of ossification (e.g., Hugi and Sanchez-Villagra 2012), but occurs also frequently (e.g., in dinosaurs, including birds), or occasionally (e.g., in crocodylians) in taxa with primitive epiphyses (Sander and Klein 2005, Woodward et al. 2011; see also Laurin and Buffrénil 2016, and Chapter 27). An EFS tends to be more commonly seen in animals with relatively high growth rates, because proportionally more individuals survive to the stage of full skeletal growth.
4. Irrespective of their general, long-term spacing, growth marks in some taxa can be systematically split, thus indicating the occurrence of two diapause stages each year (Figure 31.5D). This peculiar situation is relatively frequent in newts (Caetano 1990, Montori 1990). It is further considered below (see the Section "Observing the Periodicity of SGMs").

In all taxa, SGM spacing is heavily influenced by local morphogenetic processes (such as, e.g., the formation of a crest), and records the successive shapes of a bone in the sectional plane. In most long bones that have a curved shaft (e.g., ribs), cortical accretion is faster, and SGM spacing broader, in the cortex of the convex side than in the cortex of the concave side (asymmetric growth: Figure 31.5E). In paleobiology, the study of SGM spacing pattern is, of course, the only method for documenting the evolutionary differentiation of local bone morphology in a phyletic series.

Eroded and Supernumerary SGMs

One of the main obstacles to using SGMs is the resorption or remodeling of bone cortices (dental marks do not have this problem). In long bones from middle- to large-sized taxa, whatever their phylogenetic position, the complete sequence of growth marks is rarely preserved because the expansion of the medullary cavity erodes the deepest cortical layers and erases the earliest marks, without which the age of the individual may be underestimated. Growth marks can be either partly

VetBooks.ir

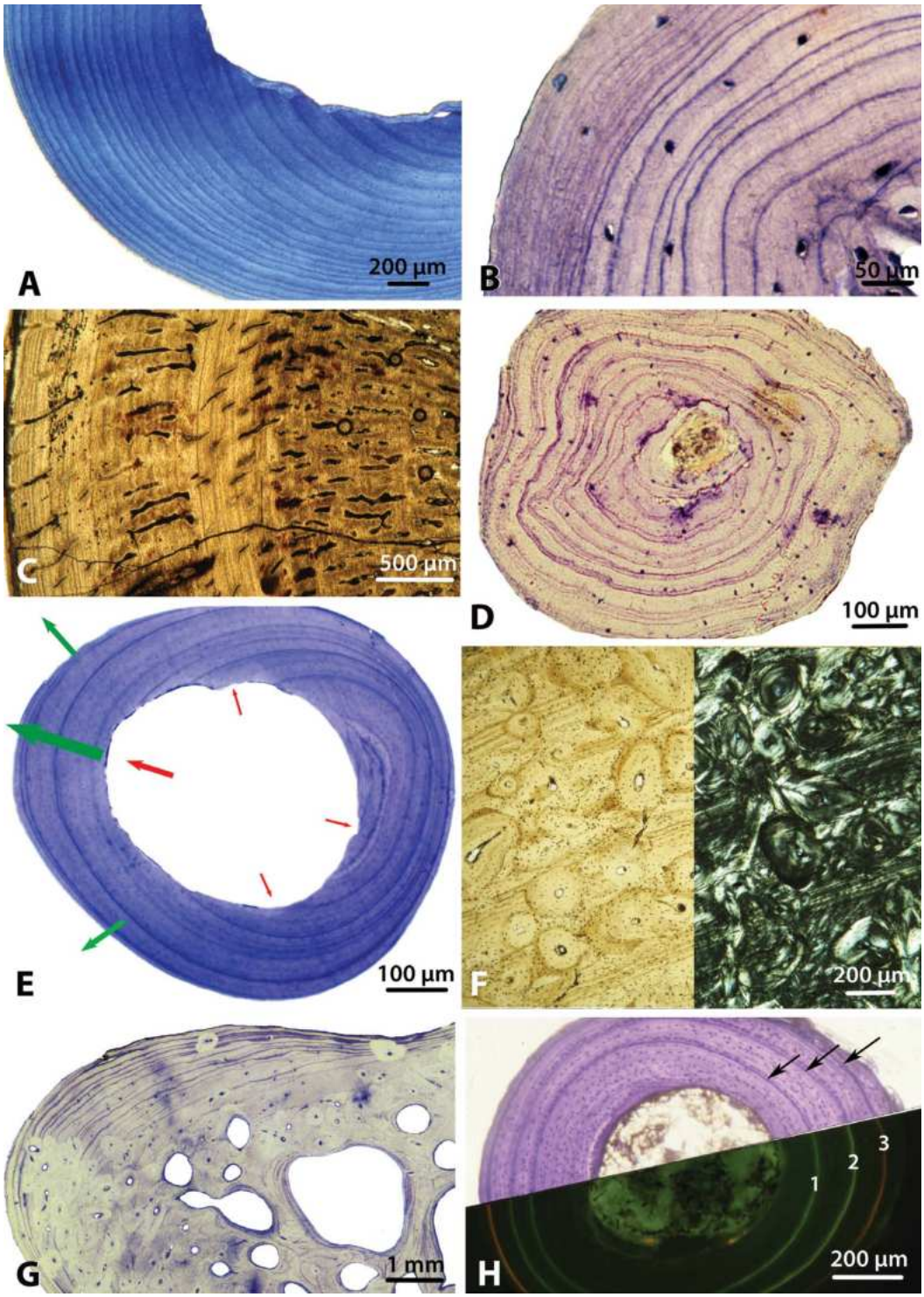


FIGURE 31.5 Skeletal growth mark (SGM) geometry in bone and labeling experiments. A, Regular, gradual decrease in the spacing of LAGs in the femoral cortex of *Sphenodon punctatus* (hematoxylin staining). B, Sudden decrease in LAG spacing, followed by long-lasting accretion of tightly spaced LAGs in the femur of the lissamphibian (Caudata) *Euproctus* sp. (hematoxylin staining). C, Sudden narrowing of LAG spacing, and formation of an EFS in the peripheral-most femoral cortex of *Ophiacodon insignis.* D, Split LAGs in the humerus of the urodele *Triturus alpestris* (hematoxylin staining). E, Strong off-centering of growth in the femur of *Lacerta muralis.* The green arrows indicate accretion, and the red arrows, resorption. F, Gradual destruction of the SGMs (here annuli) by Haversian remodeling in the femur cortex of the fossil (Early Pliocene) pinniped *Phocanella pumila*. Ground section in ordinary (left half) and polarized (right half) light. G, Merging LAGs in the mandible of primate (prosimian) *Microcebus murinus*. H, Labeling of bone growth with fluorescent markers in the femur of *Lacerta viridis* during three consecutive years. Two DCAF (numbers 1 and 2) and one xylenol orange (no. 3) injections were made at the epochs supposed to correspond to LAG (arrows) formation. The lower part of the picture corresponds to a ground section viewed in transmitted ultraviolet light; the upper part shows a hematoxylin-stained section sampled close to the location of the ground section.

VetBooks.ir

destroyed, if the expansion of the medullary cavity is asymmetrical (Figure 31.5E), or entirely destroyed, if it is symmetrical. In the former case, a reconstruction of the missing parts of the SGMs is possible through a simple graphic extrapolation of existing sectors (Castanet 1978, Lee and O'Connor 2013). In the latter case, a more complex correction is requested. If a growth series of the bone examined is available for the taxon under study, eroded marks can be restored using their contours recorded in the corresponding bones of smaller (supposedly younger) specimens (Chinsamy 1993). However, different individuals in a population do not grow uniformly, and size classes can be mistaken for age classes (Woodward et al. 2013, Ballard et al. 2015). Otherwise, an approximate solution can be found by fitting a curve based on either the length or the spacing of existing SGMs. Such curves can be drawn "by eye" (Hutton 1986) or involve modeling and calculations (Erickson and Tumanova 2000; Horner and Padian 2004).

In small osteichthyans and ectothermic tetrapods, Haversian remodeling is mild and limited. Conversely, it is more active in medium-sized to large taxa (crocodilians and chelonians), and very intense in tetrapods having, or supposed to have had, a tachymetabolic physiology (most synapsids, ornithodirans, etc.). Sparse secondary osteons can permit a reasonable reconstruction of growth marks and skeletochronology, but extensive Haversian remodeling (Figure 31.5F) precludes it. This is why, in mammals, reconstructions of age often rely more on the marks in cementum or dentine (though dentinal marks have other constraints; see below). In a single skeleton, the resorption of growth marks is highly variable from one bone to another, depending on local morphogenetic processes and biomechanical contexts.

The occurrence of supernumerary SGMs with unknown, nonannual periodicity is one of the major problems with interpreting skeletochronological results (e.g., Lewis 1979, Buffrénil and Pascal 1984). This situation can result from two main causes: stochastic events and local morphogenetic processes. In addition to the normal seasonal factors that synchronize SGM accretion, stochastic circumstances, primarily (but not exclusively) related to climatic events, may induce additional diapause stages in a year, and create supplementary marks. According to Klevezal (1996), a few weeks' cessation of somatic growth can provoke the formation of a LAG. This is how unusual excursions of weather patterns have been detected by abnormal spacing of growth marks in, for example, the bull snake, *Pituophis catenifer* (Peabody 1958), and the Amazonian manatee, *Trichechus manatus* (Best 1983).

Bones that have a complex shape (mandible, skull bones, etc.) have particular growth patterns that can involve slowing, stopping or acceleration of local accretion (Castanet 2006). These growth events generally result in local splitting, resorption or multiplication of growth marks (Figure 31.5G), and deeply interfere with the normal pattern of SGMs, making them illegible. Such a situation was described in the mandible of, e.g., the European adder *Vipera aspis* (Castanet and Naulleau 1974), and the mink *Mustela vison* (Buffrénil and Pascal 1984).

Remarks on LAGs in Secondary Bone

Typical LAGs may occasionally occur in secondary bone deposits, especially in the thick layers located on the walls of the medullary cavity. Though well-characterized and likely annual (Castanet 1982), these lines are useless for age determination. Indeed, the onset of the accretion of secondary deposits is unknown, but it is necessarily subsequent to the formation of primary cortices; moreover, the end of their accretion cannot be assessed. LAGs in secondary bone may nevertheless provide interesting information about the duration of local bone reconstruction.

Periodicity and Duration of SGM Formation in Bone

Observing the Periodicity of SGMs

Since the pioneer studies in skeletochronology of the early 1950s, the periodicity of osteological growth marks have been assessed by three methods that are still in use: individuals of known age (that may have been previously tagged if from a wild population), the observation of samples taken through time (e.g., each year) from the same individual, and single or multiple *in vivo* labeling of bone growth with tetracycline or other fluorescent markers. Synthetic accounts of amphibian, reptile and mammalian taxa in which SGM periodicity has been determined by at least one of these methods are given in Klevezal (1996; see also Castanet 1982). The first method, simple and applicable to all wild and captive vertebrates, yielded the earliest formal evidence of the annual periodicity of SGMs in bone (Schroeder and Baskett 1968, Tucker 1997). When practically feasible, this method has the advantage of introducing relatively little disturbance in the behavior of wild specimens because it involves few manipulations.

The principle of multiple sampling is to proceed to two GLG counts in the bones or teeth of a single animal with a time interval of one to several years. The number of additional SGMs formed between the first and second samplings indicates the periodicity of the marks. In wild, free-ranging animals, this method requires the capture, tagging, release and recapture of individuals. It has been broadly applied to amphibians (Hemelaar and van Gelder 1980, Hemelaar 1985; see also Castanet et al. 2003), in which the ablation of terminal phalanges is well tolerated (Ginnan et al. 2014).

In vivo labeling of bone tissue in captive or wild, free-ranging individuals is an experimental approach used since the pioneer studies by De Bont and van Coillie (1966) and Smirina (1972). Descriptions of its procedures are available in Meunier (1972, 1974) and Meunier and Boivin (1978) for fishes, Frazier (1985) and Castanet (1982) for amphibians and reptiles, and Perrin and Myrick (1980), Castanet (1982), and Klevezal (1996) for mammals. Whatever the chemical family to which they belong, tetracyclines and other fluorescent markers such as alizarine sulfate, DCAF-fluorescein (i.e. dicarboxymethyl-aminomethyl of fluorescein), and xylenol orange all bind with the calcium of apatite during the mineralization of newly deposited hard tissues. This process occurs within several days (depending on the metabolic level of the taxa) after the administration of the markers, and all mineralized tissues formed during this period contain a fluorescent line, clearly revealed in ground sections by transmitted ultraviolet light. According to the marker used, the marks display a red (alizarine), yellow-green (DCAF and tetracyclines) or orange color (Figure 31.5H). The date of the labeling is thus

VetBooks.ir

unambiguously inscribed in the bone or tooth tissue, and the number of SGMs formed between this date and the date of the tissue sampling gives the periodicity of SGM deposition. Multiple labeling operations, one each year or several at distinct seasons, are often made with different substances (e.g., DCAF + alizarin + xylenol orange), thus increasing the precision of the results (e.g., Castanet 1985, Hutton 1986).

In most studied taxa, whether osteichthyans, lissamphibians, reptiles or mammals (general syntheses in Klevezal 1996, Castanet et al. 1977, 1993), the three methods mentioned above revealed a basal annual periodicity for SGMs, whatever the tissue in which they appear (bone, dentin, cementum). Moreover, *in vivo* labeling confirmed that the zones are deposited during the stage of faster growth, whereas the annuli and LAGs are deposited in stages of slower or arrested growth, respectively (Castanet 1974, Hutton 1986). Nonannual periodicity, when observed, is most often due to supplementary SGMs. The latter can result from various stochastic events such as temporary deviations in weather patterns (Peabody 1958, Best 1983, Rogers and Harvey 1994) or pathological disorders (wound, illness, starvation, etc.), pronounced enough to provoke a drop in growth activity. Regular biannual growth cycles have been recorded in a few taxa, for example, in urodele populations (e.g., *Triturus marmoratus* or *Euproctus asper*) living at high altitude (Caetano et al. 1985, Montori 1990), or in osteichthyans (Lecomte et al. 1985). Such cases are explained by the occurrence of two diapause stages provoking the formation of two LAGs, one resulting from hibernation (winter diapause) and the other from estivation (summer diapause).

Duration of Age Recording by Bone SGMs

In extant taxa, when growth marks are laid down by centrifugal apposition on a free surface, the duration of growth can be estimated by the same approaches as those used for SGM periodicity i.e., the use of known-age individuals or *in vivo* labeling of skeletal growth. Other lines of evidence include the comparison of the morphometric data available for a specimen with growth curves known for its species, as well as the observation of other morphological or histological parameters such as epiphyseal fusion, suture occlusion or the presence of an external fundamental system. These suggest whether the specimen still had a significant capacity to grow, or had already reached the end of its somatic growth (Castanet et al. 2003). In the latter case, growth mark accretion is likely to have stopped; therefore, skeletochronological age might be underestimated. In fossil bones, compliance with this necessary precaution is uncertain because extinct taxa are seldom represented by samples broad enough to span the totality of postnatal growth.

In taxa with finite growth, the duration of cortical accretion generally differs among the bones of a single skeleton. For example, in numerous mammalian taxa, the mandible continues to grow in thickness (though at a low rate) and records age through LAG formation, long after most other bones (limb bones, ribs, vertebrae) have already stopped growing (e.g., Buffrénil 1982, Marmontel et al. 1996). Maximum age recorded by osseous skeletochronology in an amphibian is 23–24 years (23 LACs: Montori 1990). In reptiles, maximum skeletochronological ages are 35 years in *Sphenodon punctatus* (Castanet et al. 1988) and 64 years in *Crocodylus niloticus* (Hutton 1986). In mammals, longevity assessed by bone SGMs reaches some 22–26 years in the manatee *Trichechus manatus* (Marmontel et al. 1996) and 21–22 years in the harbor porpoise, *Phocoena phocoena* (Buffrénil 1982). However, maximum chronological age recorded for individuals is different from the age at which somatic growth essentially ceases.

Structural Features of Skeletal Growth Marks in Dental Tissues

Diversity of Dental Tissues Containing Growth Marks

Though present in all tooth-bearing vertebrates, dental growth marks are principally used for age assessment in mammals. The marks of bone cortices are of lesser interest because initial SGMs formed in rapidly growing mammalian bones are often erased by Haversian remodeling, whereas tooth marks remain permanently. In other taxa, the periodic and nearly constant replacement of teeth precludes the use of dental SGMs for age determination. A rich literature, including several broad comprehensive syntheses, describes the structure and practical use of tooth growth marks in terrestrial (Grue and Jensen 1979, Matson 1981, Klevezal 1996, Castanet 2006, Köhler et al. 2012) and aquatic mammals (e.g., Boyde 1980, Myrick 1980, Perrin and Myrick 1980).

Figure 31.6 shows the dental tissues likely to contain cyclical growth marks, in the simple case of a haplodont tooth such as the fang of a carnivoran. The striae of Retzius in enamel are deposited during the short period when the enamel cap is formed; they are thus unsuited for skeletochronology. Annual growth marks occur in three tissues: (1) acellular cementum, mainly located over the first third of the tooth root; (2) cellular cementum covering the rest of the tooth root, and especially the root apex (Grue and Jensen 1979, Lieberman and Meadow 1992) and (3) dentin, in the form of growth layer groups (GLGs).

Structure and Periodicity of Dental Growth Marks

Dentinal GLGs

In ground sections observed in transmitted light at low magnification, dentinal growth marks used for skeletochronology (dentin also contains other marks not used for skeletochronology) appear as an alternation of dark (i.e., opaque) broad layers and thinner light, translucent layers (Figures 31.6 and 31.7A, B). In reflected light, opaque layers become white, and translucent layers become dark (Perrin and Myrick 1980). The unit formed by one dark plus one light layer is a GLG. Like a zone plus an annulus or a LAG in bone, a dentinal GLG represents a complete growth cycle. The first growth mark observable in dentine is a thin, brightly birefringent line in polarized light called (like in bone) the neonatal line. It is separated from the base of the enamel layer by a thin stratum of prenatal monorefringent dentin (Perrin and Myrick 1980).

The structural reason for the difference in opacity between light and dark layers is not completely understood. Radiographic data, as well as electronic probes, show that light layers are

VetBooks.ir

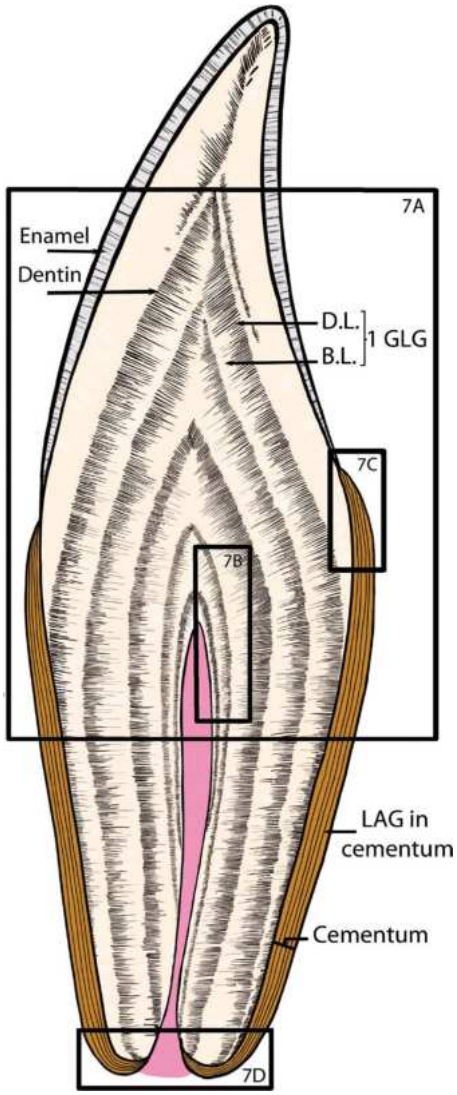


FIGURE 31.6 General distribution of cyclical growth marks in the tooth of a mammal. The sketch refers to a sagittal section viewed in ordinary transmitted light. Two tissues can display usable growth marks, the dentine with growth layer groups (GLGs) and the cementum, with typical lines of arrested growth (LAGs). The rectangles localize the fields shown in Figure 31.7. D.L., dark layer of dentin; B.L. bright layer of dentin.

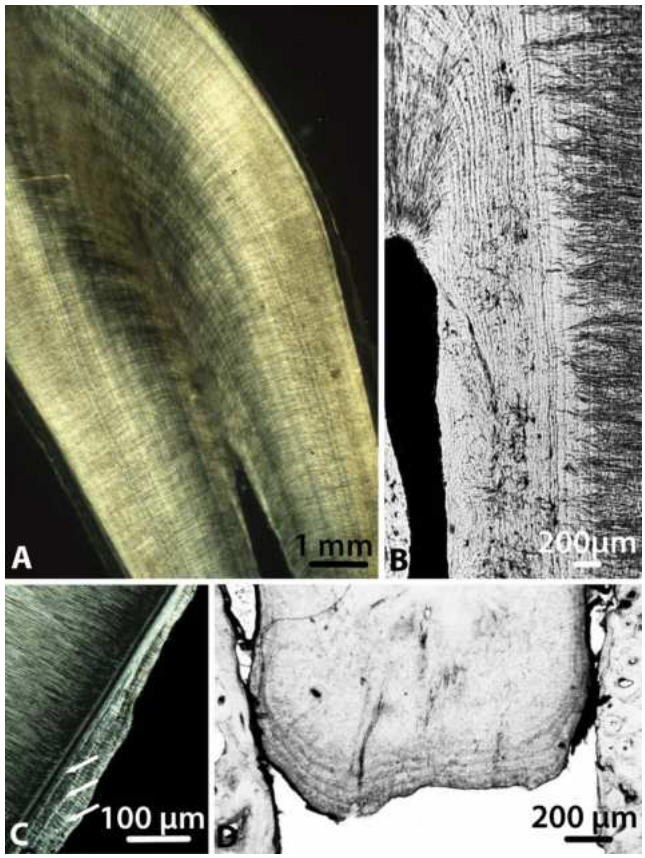


FIGURE 31.7 Gross histological aspect of growth marks in dentine and cementum, as seen in ordinary transmitted light. A, General aspect of growth layer groups in the orthodentin of a bottlenose dolphin (*Tursiops truncatus*). B, Growth marks in the slowly deposited dentine of the tooth of an old *Delphinus delphis* specimen. C, Three lines of arrested growth (LAGs; arrows) in the cementum of the upper part of tooth root in a *D. delphis* specimen. D, LAGs in the cementum layer of the root apex of a cat. Hematoxylin staining.

slightly more mineralized than dark ones (Klevezal 1996). In cetaceans, this difference is attributed to the combination of a relative deficit of calcospherite fusion in dark layers, thus resulting in a greater proportion of interglobular (hypomineralized) dentin, and a greater proportion of peritubular, hypermineralized dentin in light layers (Boyde 1980, see also Klevezal 1996). Histological observations of the sperm whale, *Physeter macrocephalus*, show that a clear, repetitive difference in the local orientation of Tomes fibers may exist between clear and dark layers (Boyde 1980). Within the GLGs, a minute subdivision into thinner strata is revealed by both simple microscopic observations and radiographic evidence (Myrick 1980, Klevezal 1996). These accessory marks (or sublayers) vary in number within the GLGs, which suggests that their periodicity is not constant, although it had initially been considered lunar (Scheffer 1970, Hui 1978). When particularly distinct, these sublayers can lead to errors in counting GLGs (e.g., Evans et al. 2002). A still more minute dentin stratification, composed of 20-µm-thick dark and light strata (40 µm for the combination of both) has been shown in various taxa (crocodiles, lagomorphs, carnivorans). Histological observations, fluorescent labeling, and electronic probes revealed that they result from a circadian rhythm of growth and mineralization of dentin, basically controlled by endogenous factors (Miani and Miani 1971, Rosenberg and Simmons 1980, Erickson 1996).

Experimental *in vivo* labeling of dental growth with tetracyclines or other fluorescent markers, like the observations of teeth from animals that died at known periods of the year, converge to indicate that the dark layers of GLGs (in transmitted light) are formed during yearly episodes of fast growth; they are thus functionally equivalent to zones in bone. Conversely, light layers, equivalent to annuli or LAGs, are deposited when growth activity is lower. Up to now, experimental data and tooth sections from known-aged specimens indicate a basic annual periodicity for GLGs (Klevezal 1980, 1996, Hohn et al. 1989, Rosas et al. 1993). When nonannual periodicity is observed, it is generally due to confusion between principal and accessory (nonannual) marks (Hui 1978), or to the

VetBooks.ir

accretion of two GLGs in a year. These situations result from populational (Klevezal 1980) or individual (Sergeant 1973) peculiarities.

The accretion of dentine layers by odontoblasts proceeds centripetally inside the pulp cavity, and it follows a simple geometric pattern (parallel lines, stacked cones, etc.; Figure 31.7A). The pulp cavity is progressively filled up, and dentin apposition finally stops when the lumen of the pulp cavity is occluded (Figure 31.7B). The age when this final stage occurs varies among taxa and individuals; however, the filling of the pulp cavity is generally completed long before skeletal growth ends. As a consequence, age determined from dentinal GLGs is often underestimated in old individuals and must be complemented by other skeletal recorders: bone, or cement. For example, dentin deposition stops after 7 cycles in *Berardius bairdi* (a beaked whale), whereas the longevity of this species is estimated up to 70 years based on cemental LAGs (Kasuya 1977). Similarly, the teeth of the harbor porpoise, *Phocoena phocoena*, display 13 GLGs, at most (Gaskin and Blair 1977), whereas the actual longevity of this species should be above 21 years based on mandibular growth marks (Buffrénil 1982). In herbivorous and omnivorous taxa, dentinal GLGs can be erased by wear in old individuals, but, in contrast to bone, they do not undergo inner resorption, except pathological cases (e.g., Scheffer and Myrick 1980). Finally, beyond the broad validation of SGMs for age determination, as shown in hundreds of articles, the uncertainties inherent to skeletochronology require the use of as many growth recording tissues as possible.

Cementum LAGs

Histologically, cemental LAGs (Figures 31.6 and 31.7C, D) are similar to bone LAGs, and they are evidenced by the same techniques (Klevezal 1996). Similarly, there is no significant difference in LAG structure between cellular and acellular cementum; however, according to Lieberman and Meadow (1992), these lines are less evenly spaced in cellular than in acellular cementum because the influence of mechanical stress is greater at the apex of the tooth root. Along the root apex, their deposition occurs as long as the tooth remains functional (Kasuya 1977, Stott et al. 1982) and, despite a tendency to become tightly packed with age, cementum LAGs remain easily discernible in old specimens (e.g., Kvam 1984, Debeljak 1996). This characteristic makes these marks reliable for age determination. Studies that compare age records in bone, dentin and cementum generally conclude that record clearly lasts longer in cementum than in the other two tissues (e.g., Garlich-Miller et al. 1993, Oosthuizen 1997).

The annual periodicity of cementum LAGs has been broadly evidenced, including in humans (Stott et al. 1982), by observations in known-aged specimens and experimental *in vivo* labeling. Special conditions may nevertheless occur, as exemplified by female northern elephant seals, *Mirounga angustirostris*, in which two LAGs are deposited annually until sexual maturity, and only one afterward (Klevezal and Stewart 1994). Comprehensive reviews of the use of cementum growth marks in skeletochronology are given by Grue and Jensen (1979), Matson (1981) and Klevezal (1996). According to Lieberman and Meadow (1992), LAGs in acellular cementum are laid down very regularly at the same period of the year in a given taxon. Conversely, in cellular cementum the period of LAG deposition, though basically annual, is chronologically more variable. In normal, nonpathological conditions, cementum layers are not submitted to inner Haversian remodeling.

A Central Tool in Biology and Paleobiology

Skeletochronology is now an essential tool for many studies related to life history traits, growth processes and population dynamics in extant, wild vertebrates. Assuming that basic parameters such as the periodicity of growth marks are clearly documented, this approach is potentially applicable to most taxa having either mildly remodeled cortices (poikilotherms) or a perennial dentition (mammals). Unfortunately, extant birds do not comply with these two basic prerequisites (e.g., Nelson and Bookhout 1980; for synthetic data on extinct birds, see Ricqlès et al. 2001).

In extinct taxa, the heuristic potential of skeletochronology is still greater than in extant taxa because no other methodology can reliably assess individual age and reconstruct growth curves. Since the early studies by Warren (1963), Reid (1981) and Ricqlès (1983), the role of skeletochronology in paleobiology has increased considerably (review in Woodward et al. 2013). Studies long remained concentrated on growth curve reconstruction in archosaurs (short review in Erickson 2014), but they recently diversified towards amphibians (e.g., Steyer et al. 2004, Gee et al. 2020) and mammals (e.g., Köhler et al. 2012, Martinez-Maza et al. 2014). A major consequence of the considerable effort devoted to archosaurs has been to reconsider the basic meaning of the accretion of SGMs. Formerly considered by Reid (1981) as evidence for a possible ectothermic regime in an undescribed sauropod from the Middle Jurassic, growth marks in dinosaurs were then supposed to indicate either "an imperfect mass homeothermy and incipient (mass) endothermy" (Ricqlès 1983), or a "failed endothermy" (Reid 1984, 1990), two close concepts converging to oppose the occurrence of cyclical growth marks to true tachymetabolic physiology (see also Padian and Horner 2004, Padian 2012). Comparative studies of endotherms that have SGMs in most of their bones (Castanet 2006, Sander and Andrássy 2006, Köhler et al. 2012) show that cyclical growth is an adaptive strategy, related to metabolic activity through complex and variable ecological compromises (see also Adolph and Porter 1993). Incidentally, this situation calls for some caution in the direct interpretation of paleoclimatic conditions from the occurrence of cyclical growth marks in fossils.

When applied to fossil taxa, age assessment through skeletochronology becomes increasingly difficult with distance in time and phylogenetic proximity. The periodicity (annual or biannual) of SGMs in fossils is assumed to be homologous by reference to the living phylogenetic bracket of all vertebrates (Witmer 1995). When supernumerary growth marks are suspected in a fossil specimen, it is sometimes difficult to assess whether they are true annual marks. Given the various factors that can disturb somatic growth over various seasons (e.g., pregnancy in females, territorial competition in males,

VetBooks.ir

long-lasting climatic deviations, etc.), the abnormal proximity of two or more growth marks is not robust evidence for a nonannual periodicity. In extant taxa, the question can be addressed by a comparative examination of individual growth patterns in a population. In fossils, this opportunity is rarely given and, in such circumstances, an age bracket should be considered (see Ballard et al. 2015). For the same reason, the problem of missing (eroded) marks is particularly acute in fossil specimens. As mentioned above, several authors have proposed methods for the retrocalculation of missing growth marks (Hutton 1986, Chinsamy 1993, Erickson and Tumanova 2000, Horner and Padian 2004, Woodward et al. 2013, Erickson 2014).

REFERENCES

Adolph, S. C. and W. Porter. 1993. Temperature, activity and lizard life history. *Am. Nat.* 142: 273–295.

Amprino, R. 1947. La structure du tissu osseux envisagée comme l'expression de différences dans la vitesse de l'accroissement. *Arch. Biol. (Liège)* 58: 315–330.

Anthony, E. L. P. 1988. Age determination in bats. In *Ecological and behavioral methods for the study of bats*, ed. Kunz, H., 47–58. Washington, Smithsonian Institute Press.

Antoine, D., et al. 2009. The developmental clock of the dental enamel: a test for the periodicity of prism cross striations and an evaluation of the likely sources of error in histological studies of this kind. *J. Anat.* 214: 45–55.

Baglinière, J. L., et al. (Eds.). 1992. *Tissus durs et âge individuel des vertébrés*. ORSTOM/INRA Colloques et Séminaires, Paris, France.

Ballard, H. W., et al. 2015. *Maiasaura*, a model organism for extinct vertebrate population biology: a large sample statistical assessment of growth dynamics and survivorship. *Paleobiology* 41: 503. doi:10.1017/pab.2015.19.

Best, R. C. 1983. Apparent dry season fasting in the Amazonian manatee (Mammalia: Sirenia). *Biotropica* 15: 61–64.

Boissin, J. and B. Canguilhem. 1988. Les rythmes circannuels chez les mammifères. *Arch. Int. Physiol. Biochem.* 96: 289–345.

Bourdon, E., et al. 2009. Bone growth marks reveal protracted growth in New Zealand kiwi (Aves, Apterygidae). *Biol. Lett.* 5: 639–642.

Boyde, A. 1980. Histological studies of dental tissues of odontocetes. In *Growth of odontocetes and sirenians: problems in age determination*, Perrin, W. F. and A. C. Myrick, 65–87. Cambridge, UK, International Whaling Commission.

Bromage, T. G. 1991. Enamel incremental periodicity in the pigtailed macaque: a polychrome fluorescent labeling study of dental hard tissues. *Am. J. Phys. Anthrop.* 86: 205–214.

Brothers, E. B., et al. 1976. Daily growth increments in otoliths from larval and adult fishes. *Fish. Bull. US* 74: 1–8.

Buffrénil, V. de 1980. Données préliminaires sur la structure des marques de croissance squelettiques chez les crocodiliens actuels et fossiles. *Bull. Soc. Zool. Fr.* 105: 355–361.

Buffrénil, V. de 1982. Données préliminaires sur la présence de lignes d'arrêt de croissance périostiques dans la mandibule du marsouin commun, *Phocoena* (L.) et leur utilisation comme indicateur de l'âge. *Can. J. Zool.* 60: 2557–2567.

Buffrénil, V. de and J. Castanet. 2000. Age estimation by skeletochronology in the Nile monitor (*Varanus niloticus*), a highly exploited species. *J. Herpetol.* 34: 414–424.

Buffrénil, V. de, et al. 2004. Comparative data on epiphyseal development in the family Varanidae. *J. Herpetol.* 39: 328–335.

Buffrénil, V. de and J.-M. Mazin. 1990. Bone histology of the ichthyosaurs: comparative data and functional interpretation. *Paleobiology* 16: 435–476.

Buffrénil, V. de and J.-M. Mazin. 1992. Contribution de l'histologie osseuse à l'interprétation paléobiologique du genre *Placodus* Agassiz, 1833 (Reptilia, Placodontia). *Rev. Paléobiol.* 11: 397–407.

Buffrénil, V. de and M. Pascal. 1984. Croissance et morphogenèse postnatales de la mandibule du vison (*Mustela vison* Schreiber): données sur la dynamique et l'interprétation fonctionnelle des dépôts osseux mandibulaires. *Can. J. Zool.* 62: 2026–2037.

Buffrénil, V. de and D. Schoevaert. 1989. Données quantitatives et observations histologiques sur la pachyostose du squelette du dugong, *Dugong dugon* (Müller) (Sirenia, Dugongidae). *Can. J. Zool.* 67: 2107–2119.

Caetano, M.-H. 1990. Use and results of skeletochronology in some urodeles (*Triturus marmoratus*, Latreille 1800 and *Triturus boscai*, Lataste 1879). *Ann. Sci. Nat. Zool. 13e Série* 11: 197–199.

Caetano, M.-H., et al. 1985. Détermination de l'âge de *Triturus marmoratus* (Latreille, 1800). *Amphibia-Reptilia* 6: 117–132.

Carey, H. V., et al. 2003. Mammalian hibernation: cellular and molecular responses to depressed metabolism and low temperature. *Phys. Rev.* 83: 1153–1181.

Castanet, J. 1974. Etude histologique des marques squelettiques de croissance chez *Vipera aspis* (L.) (Ophidia: Viperidae). *Zool. Scr.* 3: 137–151.

Castanet, J. 1978. Les marques de croissance osseuse comme indicateurs de l'âge chez les lézards. *Acta Zool. (Stockh.)* 59: 35–48.

Castanet, J. 1979. Données comparatives sur la minéralisation des marques de croissance squelettiques chez les vertébrés. Etude par microradiographie quantitative. *C. R. Acad. Sci. Paris* 289: 405–408.

Castanet, J. 1982. *Recherche sur la croissance du tissu osseux des reptiles. Application: la méthode squelettochronologique*. Thèse d'Etat, Paris, Université Paris VII.

Castanet, J. 1985. La squelettochronologie chez les reptiles. I – Résultats expérimentaux sur la signification des marques de croissance squelettiques chez les lézards et les tortues. *Ann. Sci. Nat. Paris* 7: 23–40.

Castanet, J. 1987. La squelettochronologie chez les reptiles. III – Application. *Ann. Sci. Nat. Paris* 8: 157–172.

Castanet, J. 2006. Time recording in bone microstructures of endothermic animals; functional relationships. *C. R. Palevol* 5: 629–636.

Castanet, J., et al. 1993. Bone and individual aging. In *Bone. Vol. 7: Bone growth B*, ed. Hall, B. K., 245–283. Boca Raton, CRC Press.

Castanet, J., et al. 2003. The skeletal histology of the Amphibia. In *Amphibian biology. Vol. 5. Osteology*, ed. Heatwole, H. and M. Davies, 1598–1683. Chipping Norton, Surrey Beatty & Sons.

Castanet, J., et al. 1970. Calcium et nature des zones de croissance cyclique dans l'os des vertébrés poïkilothermes. *C. R. Acad. Sci. Paris* 270: 2853–2856.

VetBooks.ir

Castanet, J., et al. 1977. L'enregistrement de la croissance cyclique par le tissu osseux chez les vertébrés poïkilothermes: données comparatives et essai de synthèse. *Bull. Biol. France Belgique* 111: 183–202.

Castanet, J., et al. 1992. Squelettochronologie à partir des os et des dents chez les vertébrés. In *Tissus durs et âge individuel des vertébrés*, eds. Baglinière, J. L., J. Castanet, F. Conand and F. Meunier, 257–280. Paris, ORSTOM/INRA Colloques et Séminaires.

Castanet, J. and G. Naulleau. 1974. Données expérimentales sur la valeur des marques squelettiques comme indicateur de l'âge chez *Vipera aspis* (L.) (Ophidia: Viperidae). *Zool. Scr.* 3: 201–208.

Castanet, J. and G. Naulleau. 1985. La squelettochronologie chez les reptiles. II – Résultats expérimentaux sur la signification des marques de croissance squelettiques utilisées comme critère d'âge chez les serpents. Remarques sur la croissance et la longévité de la vipère aspic. *Ann. Sci. Nat. Paris* 7: 41–62.

Castanet, J., et al. 1988. Skeletochronological data on the growth, age, and population structure of the Tuatara, *Sphenodon punctatus*, on Stephens and Lady Alice islands, New Zealand. *Herpetologica* 44: 25–37.

Castanet, J., et al. 2004. Lines of arrested growth in bone and age estimation in a small primate: *Microcebus murinus*. *J. Zool. Lond*. 263: 31–39.

Chauvelon, P., et al. 1991. LAADS: logiciel d'aide à l'acquisition de données en squelettochronologie. In *Tissus durs et âge individuel des vertébrés*, eds. Baglinière, J. L. et al., 423–432. Paris, ORSTOM/INRA Colloques et Séminaires.

Chinsamy, A. 1993. Bone histology and growth trajectory of the prosauropod dinosaur *Massospondylus carinatus*. *Mod. Geol.* 18: 319–329.

Chinsamy, A., et al. 1994. Growth rings in Mesozoic birds. *Nature* 368: 196–197.

Christian, K. A., et al. 1995. Seasonal activity and energetic of two species of varanid lizards in tropical Australia. *Oecologia* 103: 349–357.

Cissé, M. 1971. La diapause chex les varanidae du Sénégal. *Notes Afr.*131: 57–67.

Clark, G. R. 1974. Growth lines in invertebrate skeletons. *Ann. Rev. Earth Planet. Sci*. 2: 77–99.

Clarke, C. M. H., et al. 1992. A comparison of tooth eruption and wear and dental cementum techniques in age determination of New Zealand feral pigs. *Wildl. Res.* 19: 769–777.

Cloudsley-Thompson, J. L. 1980. *Biological clocks: their functions in nature*. London, Weidenfeld and Nicolson.

Cunningham, M. A. 1905. Zones of growth in the skeletal structures of Gadidae and Pleuronectidae. *Fish. Board Scotland Ann. Rep.* 23: 125–140.

Debeljak, I. 1996. A simple preparation technique of cave bear teeth for age determination by cementum increments. *Rev. Paléobiol*. 15: 105–108.

De Bont, A. F. and R. van Coillie. 1966. Scalimétrie à l'aide de tétracyclines. *Verh. Internat. Verein. Limnol*. 16: 1130–1134.

Deelder, C. L. and J. J. Willemse. 1972. Age determination in fresh-water teleost, based on annular structures in fin-rays. *Aquaculture* 1: 365–371.

Downs, J. P. and P. C. J. Donoghue. 2009. Skeletal histology of *Bothriolepis canadensis* (Placodermi, Antiarchi) and the evolution of the skeleton at the origin of jawed vertebrates. *J. Morphol.* 270: 1364–1380.

Erickson, G. M. 1996. Daily deposition of dentin in juvenile *Alligator* and assessment of tooth replacement rate using incremental line counts. *J. Morphol.* 228: 189–194.

Erickson, G. M. 2003. Using external vertebral growth rings to assess longevity in the Bengal monitor (*Varanus bengalensis*). *Copeia* 2003: 872–878.

Erickson, G. M. 2014. On dinosaur growth. *Ann. Rev. Earth Planet Sci*. 42: 675–697.

Erickson, G. M. and T. A. Tumanova. 2000. Growth curve of *Psittacosaurus mongoliensis* Osborn (Ceratopsia: Psittacosauridae) inferred from long bone histology. *Zool. Jour. Linn. Soc.* 130: 551–566.

Evans, K., et al. 2002. Factors affecting the precision of age determination of sperm whales (*Physeter macrocephalus*). *J. Cetac. Res. Manage.* 4: 193–201.

Francillon-Vieillot, H., et al. 1990. Microstructure and mineraliszation of vertebrate skeletal tissues. In *Skeletal biomineralization: patterns, processes and evolutionary trends*, Vol. 1, ed. J. G. Carter, 471–530. New York, Van Nostrand Reinhold.

Frasca, P. 1981. Scanning-electron microscopy studies of "ground substance" in the cement lines, resting lines, hypercalcified rings and reversal lines of human cortical bone. *Acta Anat.* 109: 115–121.

Frazier, J. 1985. A review of *in vivo* labels for studies of age determination and growth in amphibians and reptiles. *Herpetologica* 41: 222–227.

Garlich-Miller, J. L., et al. 1993. Comparison of mandibular with cenmental growth-layer counts for ageing Atlantic walrus (*Odobenus rosmarus rosmarus*). *Can. J. Zool*. 71: 163–167.

Gaskin, D. E. and B. A. Blair. 1977. Age determination of harbor porpoise, *Phocoena* (L.), in the western North Atlantic. *Can. J. Zool*. 55: 18–30.

Gee, B. M., et al. 2020. Histological skeletochronology indicates developmental plasticity in the early permian stem lissamphibian *Doleserpeton annectens*. Ecol. Evol. 10 : 2153–2169.

Geiser, F. 1988. Reduction of metabolism during hibernation and daily torpor in mammals and birds: temperature effect or physiological inhibition? *J. Comp. Physiol. B* 158: 25–37.

Geistdoerfer, P. 1982. Ryhtmes biologiques et croissance des poissons dans les grandes profondeurs marines. *Oceanis* 8: 599–609.

Germano, D. J. and R. B. Bury. 1998. Age determination in turtles: evidence of annual deposition of scute rings. *Chelonian Conserv. Biol*. 3: 123–132.

Gibbons, J. W. 1976. Aging phenomena in reptiles. In *Special review of experimental aging research*, eds. Elias, M. F., B. E. Eleftheriou and P. K. Elias. Bar Harbor, EAR, Inc.

Giles, S., et al. 2013. Histology of "Placoderm" dermal skeletons: implications for the nature of the ancestral gnathostomes. *J. Morphol.* 274: 627–644.

Ginnan, N. A., et al. 2014. Toe clipping does not affect the survival of leopard frogs (*Rana pipiens*) *Copeia* 2014: 630–653.

Goodwin, H. T., et al. 2005. Hibernation is recorded in lower incisors of recent and fossil ground squirrels (*Spermophilus*). *J. Mammal.* 86: 323–332.

Goshe, L. R., et al. 2009. An evaluation of histological techniques used in skeletochronological age estimation of sea turtles. *Chelonian Conserv. Biol.* 8: 217–222.

Gregory, P. T. 1982. Reptilian hibernation. In *Biology of the reptilia. Vol. 13. Physiology D: physiological ecology*, eds. Gans, C. and F. Pough eds., 53–154. New York, Academic Press.

Grue H. and B. Jensen. 1979. Review of the formation of incremental lines in tooth cementum of terrestrial mammals. *Dan. Rev. Game Biol.* 11: 1–48.

Gwinner, E. 1967. Circannuale Periodik der Mauser und der Zugunruhe bei einem Vogel. *Naturwissenschaften* 54: 447.

Haines, R. W. 1942. The evolution of epiphyses and of endochondral bone. *Biol. Rev.* 174: 267–291.

Heincke, F. 1908. Die Altersbestimmung de Fische. *Beteil. Deutsch. Int. Meeres Jahres* 4-5: 66–155.

Hellgren, E. C. 1998. Physiology of hibernation in bears. *Ursus* 10: 467–477.

Hemelaar, A. S. M. 1985. An improved method to estimate the number of year rings resorbed in phalanges of *Bufo bufo* (L.) and its application to populations from different latitudes and altitudes. *Amphibia-Reptilia* 6: 323–341.

Hemelaar, A. S. M. and J. J. van Gelder. 1980. Annual growth rings in phalanges of *Bufo bufo* (Anura, Amphibia) from the Netherlands and their use for age determination. *Netherl. J. Zool.* 30: 129–135.

Hohn, A. A. 1980. Analysis of growth layers in the teeth of *Tursiops truncatus*, using light microscopy, microradiography and SEM. In *Growth of odontocetes and sirenians: problems in age determination*, eds. Perrin, W. F. and A. C. Myrick, 155–160. Cambridge, UK, Int. Whaling Commission.

Hohn, A. A., et al. 1989. Growth layers in teeth from known-age, free-ranging bottlenose dolphins. *Mar. Mammal Sci.* 5: 315–342.

Horner, J. R. and K. Padian. 2004. Age and growth dynamics of *Tyrannosaurus rex*. *Proc. R. Soc. B* 271 (1551): 1875–1880.

Horner, J. R., et al. 2004. Variation in dinosaur skeletochronology indicators: implications for age assessment and physiology. *Paleobiology* 25: 295–304.

Hugi, J. and M. Sanchez-Villagra. 2012. Life history and skeletal adaptations in the Galapagos marine iguana (*Amblyrhynchus cristatus*) as reconstructed with bone histological data – a comparative study of iguanines. *J. Herpetol.* 46: 312–324.

Hui, C. A. 1978. Reliability of using dentin layers for age determination in *Tursiops truncatus*. U.S. Department of Commerce, PB-288 444.

Hutton, J. M. 1986. Age determination of living Nile crocodiles from the cortical stratification of bone. *Copeia* 1986: 332–341.

Jonsgård, Å. 1969. Age determination of marine mammals. In: *The biology of marine mammals*, ed. Andersen, H. T., 1–27. New York, Academic Press.

Keating, J. N. and P. Donoghue. 2016. Histology and affinity of anaspides, and the early evolution of the vertebrate dermal skeleton. *Proc. R. Soc. B* 283: 20152917.

Kasuya, T. 1977. Age determination and growth of the Baird's beaked whale with a comment on the fetal growth rate. *Sci. Rep. Whales Res. Inst.* 29: 1–20.

Keay, J. A. 1995. Accuracy of cementum age assignments for black bears. *Calif. Fish and Game* 81: 113–121.

Kierdorf, U. and J. Becher. 1997. Mineralization and wear of mandibular first molars in red deer (*Cervus elaphus*) of known age. *J. Zool. Lond.* 241: 135–143.

Klevezal, G. A. 1980. Layers in the hard tissues of mammals as a record of growth rhythms of individuals. In *Growth of odontocetes and sirenians: problems in age determination*, eds. Perrin, W. F. and A. C. Myrick, 89–94. Cambridge, UK, Int. Whaling Commission.

Klevezal, G. A. 1996. *Recording structures of mammals: determination of age and reconstruction of life history*. Brookfield, A. A. Balkema Publishers.

Klevezal, G. A. and S. E. Kleinenberg. 1967. Age determination of mammals from annual layers in teeth and bones. *Transl. Rus., Israel Prog. Sci. Transl.* IPST Cat. N 5433. Jerusalem.

Klevezal G. A. and B. S. Stewart. 1994. Patterns and calibration of layering in tooth cementum of female northern elephant seals, *Mirounga angustirostris*. *J. Mammal.* 75: 483–487.

Köhler, M., et al. 2012. Seasonal bone growth and physiology in endotherms shed light on dinosaur physiology. *Nature* 487: 358–361.

Kolb, C., et al. 2015. Growth in fossil and extant deer and implications for body size and life history evolution. *BMC Evol. Biol.* 15: 1–15.

Kvam, T. 1983. Age determination in European lynx *Lynx l. lynx (L.)* based on cranial development. *Fauna Norv. Ser. A* 4: 31–36.

Kvam, T. 1984. Age determination in European lynx *Lynx l. lynx* by incremental lines in tooth cementum. *Acta Zool. Fennica* 171: 221–223.

Lamm, E.-T. 2013. Preparation and sectioning of specimens. In *Bone histology of fossil tetrapods – advancing methods, analysis and interpretation*, eds. Padian, K. and E. Lamm, 55–160. Berkeley, University of California Press.

Laurin, M. and V. de Buffrénil 2016. Microstructural features of the femur in early ophiacodontids: a reappraisal of ancestral habitat use and lifestyle of amniotes. *C. R. Palevol* 15: 119–131.

Laval, P. and S. Planes. 1992. CALCIF: un logiciel de mesure des anneaux de croissance sur PC-AT. In *Tissus durs et âge individuel des vertébrés*, eds. Baglignière et al., 433–439. Paris, ORSTOM/INRA Colloques et Séminaires.

Lawrence, C. H. W. and M. W. Wolowyk. 1988. Torpor in mammals and birds. *Can. J. Zool.* 66: 133–137.

Lecomte, F. 1990. *Histologie osseuse et marques squelettiques de croissance chez quelques téléostéens guyanais d'intérêt aquacole: Ariidae (Siluriformes), Anostomidae et Serrasalmidae (Characoides)*. PhD thesis, Université Paris VII, 90-PA07-7207 (ANRT-Grenoble), p. 190.

Lecomte, F., et al. 1985. Mise en évidence d'un double cycle de croissance annuel chez un silure de Guyane, *Arius couma* (Val., 1839) (Teleostei, Siluriformes, Ariidae) à partir de l'étude squelettochronologique des épines de nageoires. *C.R. Acad. Sci. Paris* 300: 181–184.

Lee, A. H. and P. M. O'Connor. 2013. Bone histology confirms determinate growth and small body size in the Noasaurid theropode *Masiakasaurus knopfleri*. *J. Vert. Paleontol.* 33: 865–876.

Lewis, J. C. 1979. Periosteal layers do not indicate a1ges of sandhill cranes. *J. Wildl. Manage.* 43: 269–271.

Lieberman, D. E., et al. 1990. Computer image enhancement and analysis of cementum increments as applied to teeth of *Gazella*. *J. Archeol. Sci.* 17: 519–533.

Lieberman, D. E. and R. H. Meadow. 1992. The biology of cementum increments (with an archaeological application). *Mammal Rev.* 22: 57–77.

Line, S. R. P. 2000. Incremental markings of enamel in ectothermal vertebrates. *Arch. Oral Biol.* 45: 363–368.

Lyman, C. P. 1963. Hibernation in mammals and birds. *Am. Sci.* 51: 127–138.

Lyman, C. P. 1984. Pharmacological aspects of mammalian hibernation. *Pharmacol. Ther.* 25: 371–393.

Mahoney, P., et al. 2018. The biorhythm of human skeletal growth. *J. Anat.* 232: 26–38.

Maisano, J. A. 2002. Terminal fusion of skeletal elements as indicators of maturity in squamates. *J. Vert. Paleontol.* 22: 268–275.

Malcom, J. R. and R. J. Brooks 1981. Eye lens weight and body size as criteria of age in beaver (*Castor canadensis*). *Can. J. Zool.* 59: 1189–1192.

Marangoni, F., et al. 2009. Growth-mark formation and chronology of two neotropical anuran species. *J. Herpetol.* 43: 546–550.

Marin-Moratalla, N., et al. 2013. Bone histology a san approach to providing data on certain key life history traits in mammals: implications for conservation biology. *Mammal. Biol.* 78: 422–429.

Marmontel, M., et al. 1996. Age determination in manatees using growth-layer-groups counts in bone. *Mar. Mammal Sci.* 12: 54–88.

Martinez-Maza, C., et al. 2014. Life-history traits of the Miocene *Hipparion concudense* (Spain) inferred from bone histological structure. *Plos One* 9: e103708. Doi: 10.1371/journal.pone.0103708.

Matson, G. M. 1981. Workbook for cementum analysis. Matson's Milltown, Montana, p. 29.

Meunier, F. J. 1972. Marquages simples et multiples du tissu osseux de quelques téléostéens par des substances fluorescentes. *C. R. Acad. Sci. Paris* 275: 1685–1688.

Meunier, F. J. 1974. La technique de marquage vital des tissus squelettiques des poissons. *Bull. Fr. Pisc.* 255: 51–57.

Meunier, F. J. 1988. Détermination de l'âge individuel chez les osteichthyens à l'aide de la squelettochronologie: historique et méthodologie. *Acta Oecol.* 9: 299–329.

Meunier, F. J. 1992. L'estimation de l'âge individuel chez les chondrchthyens: revue bibliographique des problèmes méthodologiques. In *Tissus durs et âge individuel des vertébrés*, eds. Baglinière, J._L., J. Castanet, F. Conand and F. Meunier, 281–297. Paris, ORSTOM/INRA Colloques et Séminaires.

Meunier, F. J. and G. Boivin. 1978. Action de la fluorescéine, du bleu de calcéine et de diverses doses de tétracycline sur la croissance de la truite et de la carpe. *Ann. Biol. Anim. Biochim. Biophys.* 18: 1293–1308.

Meunier, F. J. and M. Pascal. 1980. Quelques données comparatives sur la croissance périodique des tissus squelettiques chez les osteichthyens. *Bull. Soc. Zool. Fr.* 105: 337–342.

Meunier, F. J. and M. Pascal. 1981. Etude expérimentale de la croissance cyclique des rayons de nageoire de la carpe (*Cyprinus carpio* L.). Résultats préliminaires. *Aquaculture* 26: 23–40.

Meunier, F. J., et al. 1979. Comparaison de methods squelettochronologiques et considérations fonctionnelles sur le tissu osseux acellulaire d'un osteichthyen du lagon Néo-Calédonien, *Lethrinus nebulosus* (Forskal, 1775). *Aquaculture* 17: 137–157.

Meunier, F. J., et al. 2002. Caractères histologiques des marques de croissance squeletiques chez l'Atipa, *Hoplosternum littorale* (Hancock, 1828) (Teleostei, Siluriformes) dans le marais de Kaw (Guyane française). *Bull. Fr. Pêche Piscic.* 364: 71–86.

Miani, A. and C. Miani. 1971. Circadian advancement rhythm of the calcification front in dog dentine. *Minerva Stomatol.*20: 169–178.

Montori, A. 1990. Skeletochronological results in the Pyrenean newt *Euproctus asper* (Dugès, 1852) from the pyrennean population. *Ann. Sci. Nat., Zool. 13ème Série* 11: 209–211.

Morris, P. 1972. A review of mammalian age determination methods. *Mammal. Rev.* 2: 69–104.

Mrosovsky, N. 1990. Circannual cycles in golden-mantled ground squirrels: fall and spring cold pulses. *J. Comp. Physiol. A* 167: 683–689.

Myrick, A. C. Jr. 1980. Examination of layered tissue of Odontocetes for age determination using polarized light microscopy. In *Growth of odontocetes and sirenians: problems in age determination*, eds. Perrin, W. F. and A. C. Myrick, 105–112. Cambridge, UK, Int. Whaling Commission.

Nacarino-Meneses, C. and M. Köhler. 2018. Limb bone histology records birth in mammals. *Plos One* 13: e0198511. Doi.org/10.1371/journal.pone.0198511

Nelson, R. C. and T. A. Bookhout. 1980. Counts of periosteal layers invalid for aging Canada Geese. *J. Wildl. Manage.* 44: 518–521.

Nussear, K. E., et al. 2007. Desert tortoise hibernation: temperatures, timing and environment. *Copeia* 2007: 378–386.

Oosthuizen, W. H. 1997. Evaluation of an effective method to estimate age of Cape fur seal using ground tooth sections. *Marine Mamm. Sci.* 13: 683–693.

Oudet, C. and A. Petrovic. 1977. Circannual growth variations of the mandibular condylar cartilage in the young rat. *J. Interdiscipl. Cycle Res.* 8: 338–340.

Oudet, C. and A. Petrovic. 1982. Daytime and seasons are sources of variations for cartilage and bone growth rate. In *Factors and mechanisms influencing bone growth*, eds. Oudet, C. and A. Petrovic, 481–498. New York, Alan R. Liss, Inc.

Padian, K. 2012. A bone for all seasons. *Nature* 487: 310–311.

Padian, K. and J. R. Horner. 2004. Dinosaur physiology. In *The dinosauria 2nd edn.*, eds. Weishampel, D. B., P. Dodson and H. Osmólska, 660–671. Berkeley, University of California Press.

Panfili, J. and G. Loubens. 1991. Mise en évidence des structures de croissance pour l'estimation de l'âge individuel des poissons. Exemple de *Prochilodus nigricans* (Prochilodidae, Characiforme). In *Tissus durs et âge individuel des vertébrés*, eds. Baglignière et al., 335–340. Paris, ORSTOM/INRA Colloques et Séminaires.

Pascal, M. and J. Castanet. 1978. Méthodes de détermination de l'âge chez le chat Haret des îles kerguelen.*Rev. Ecol. (Terre Vie)* 4: 529–555.

Pascal, M. and P. Delattre. 1981. Comparaison de différentes méthodes pour la détermination de l'âge individuel chez le vison (*Mustela vison* Schreiber). *Can. J. Zool.* 59: 202–211.

Paul, M. J., et al. 2007. Tracking the seasons: the internal calendar of vertebrates. *Philos. Trans. R. Soc. B* 363: 341–361.

Peabody, F. E. 1958. A Kansas drought recorded in growth zones of a bullsnake. *Copeia* 1958: 91–94.

Peabody, F. E. 1961. Annual growth zones in living and fossil vertebrates. *J. Morphol.* 108: 11–62.

Pengelley, E. T. and K. J. Kelly. 1966. A circannian rhythm in hibernating species of the genus *Citellus* with observations on their physiological evolution. *Comp. Biochem. Physiol.* 19: 603–617.

Perrin, W. F. and Myrick Jr, A. C. 1980. Report of the workshop. In *Growth of odontocetes and sirenians: problems in age determination*, eds. Perrin, W. F. and A. C. Myrick, 1–50. Cambridge, UK, International Whaling Commission.

Petermann, H. and J. A. Gauthier. 2018. Fingerprinting snakes: paleontological and paleoecological implications of zygantral growth rings in Serpentes. *PeerJ* 6: e-4819; doi 10.7717/peerj.4819.

Pierce, K. V. and H. Kajimura. 1980. Acid etching and highlighting for defining growth layers in cetacean teeth. In *Growth of odontocetes and sirenians: problems in age determination*, eds. Perrin, W. F. and A. C. Myrick, 99–104. Cambridge, UK, International Whaling Commission.

Ponton, F., et al. 2004. Variation of the outer circumferential layer in the limb bones of birds. *Acta Ornithol.* 39: 137–140.

Reid, R. E. H. 1981. Lamellar-zonal bone with zones and annuli in the pelvis of a sauropod dinosaur. *Nature* 292: 49–51.

Reid, R. E. H. 1984. Primary bone and dinosaurian physiology. *Geol. Mag.* 121: 589–598.

Reid, R. E. H. 1990. Zonal "growth rings" in dinosaurs. *Modern Geol.* 15: 19–48.

Ricqlès, A. de 1983. Cyclical growth in the long limb bones of a sauropod dinosaur. *Acta Palaeontol. Pol.* 28: 225–232.

Ricqlès, A. de, et al. 2001. The bone histology of basal birds in phylogenetic and ontogenetic perspectives. In *New perspectives on the origin and early evolution of birds: Proceedings of the International Symposium in Honor of John H. Ostrom*, eds. Gauthier, J. and I. F. Gall, 411–426. New Haven, Peabody Museum of Natural History, Yale University.

Rogers K. L. and L. Harvey. 1994. A skeletochronological assessment of fossil and recent *Bufo cognatus* from south-central Colorado. *J. Herpetol.* 28: 133–140.

Rosas, F. C. W., et al. 1993. Age and growth of the South Amarican sea lion, *Otaria flavescens* (Shaw, 1800), in Southern Brazil. *J. Mammal.* 74: 141–147.

Rosenberg, G. D. and D. J. Simmons. 1980. Rhythmic dentionogenesis in the rabbit incisor: circadian, ultradian, and infradian periods. *Calcif. Tissue Int.* 32: 29–44.

Rossell, C. R. and J. L. Sheehan. 1998. Comparison of histological staining procedures for skeletochronological studies. *Herpetol. Rev.* 29: 95.

Ruby, N. F., et al. 1996. Ablation of suprachiasmatic nucleus alters timing of hibernation in ground squirrels. *Proc. Natl. Acad. Sci. U S A* 93: 9864–9868.

Saint Girons, H. 1985. Influence des facteurs de l'environnement sur les cycles annuels et reproducteurs des reptiles. *Bull. Soc. Zool. Fr.* 110: 307–319.

Saint Girons, H., et al. 1989. Démographie compare de deux populations françaises de *Lacerta viridis* (Laurenti, 1768). *Rev. Ecol. (Terre Vie)* 44: 361–386.

Sanchez, S., et al. 2010. Paleoecological and paleoenvironmental influences revealed by long-bone paleohistology: the example of the Permian branchiosaurid *Apateon*. *Geol. Soc. Lond. Spec. Publ.* 339: 139–149.

Sander, P. M. and P. Andrássy. 2006. Lines of arrested growth and long bone histology in pleistocene large mammals from Germany: what do they tell us about dinosaur physiology? *Palaeontogr. Abt. A* 277: 143–159.

Sander, P. M. and N. Klein. 2005. Developmental plasticity in the life history of a prosauropod dinosaur. *Science* 310: 1800–1802.

Scheffer, V. B. 1950. Growth layers in the teeth of Pinnipedia as an indication of age. *Science* 112 (2907): 301–311.

Scheffer, V. B. 1970. Growth layers in a dugong tooth. *J. Mammal.* 51: 187–190.

Scheffer, V. B. and A. C. Myrick Jr. 1980. A review of studies to 1970 of growth layers in the teeth of marine mammals. In *Growth of odontocetes and sirenians: problems in age determination*, eds. Perrin, W. F. and A. C. Myrick, 51–63. Cambridge, UK, Int. Whaling Commission.

Schöne, B. R. and D. P. Gillikin. 2013. Unraveling environmental histories from skeletal diaries – advances in skeletochronology. *Palaeogeogr. Palaeoclimatol. Palaeoecol.* 373: 1–5.

Schroeder, E. E. and T. Baskett. 1968. Age estimation, growth rates and population structure in Missouri bullfrogs. *Copeia* 1968: 583–592.

Sergeant, D. E. 1973. Biology of white whales (*Delphinapterus leucas*) in western Hudson bays. *J. Fish. Board Can.* 30: 1065–1090.

Shirvell, C. S. 1981. Validity of fin-ray ageing for brown trout. *J. Fish Biol.* 18: 377–383.

Sinsch, U. 2015. Review: skeletochronological assessment of demographic life-history traits in amphibians. *Herpetol. J.* 25: 5–13.

Smirina, E. M. 1972. Annual layers in the bones of *Rana temporaria*. *Zool. Zh.* 51: 1529–1534.

Steinberg, B., et al. 1979. Changes observed in bone during hibernation using Procion red dye as a matrical marker. *J. Exp. Biol.* 210: 537–541.

Steyer, J.-S., et al. 2004. First histological and skeletochronological data on temnospondyl growth: palaeoecological and palaeoclimatological implications. *Palaeogeogr. Palaeoclimatol. Palaeoecol.* 206: 193–201.

Stott, G. G., et al. 1982. Cemental annulations as an age criterion in forensic dentistry. *J. Dent. Res.* 61: 814–817.

Thomas, R. B., et al. 1997. Estimation of age for *Trachemys scripta* and *Deirochelys reticularia* by counting annual growth layers in claws. *Copeia* 1997: 842–845.

Tucker, A. D. 1997. Validation of skeletochronology to determine age of freshwater crocodiles (*Crocodylus johnstoni*). *Mar. Freshwater Res.* 48: 343–351.

Turvey, S. T., et al. 2005. Cortical growth marks reveal extended juvenile development in New Zealand moa. *Nature* 435: 940–943.

Villanueva, A. R., et al. 1986. A new method for identification of cementum lines in undecalcified, plastic embedded sections of bone. *Stain Technol.* 61: 83–88.

Wang, L. C. H. 1985. Life at low temperature: mammalian hibernation. *Cryo-letters* 6: 257–274.

Warren, J. W. 1963. *Growth zones in the skeleton of recent and fossil vertebrates*. University Microfilms Inc., n 63-4544. University of California, Los Angeles.

Wintner, S. P. and G. Cliff. 1999. Age and growth determination of the white shark, *Carcharodon carcharias*, from the east coast of South Africa. *Fish. Bull.* 97: 153–169.

Witmer, L. M. 1995. The extant phylogenetic bracket and the importance of reconstructing soft tissue in fossils. In *Functional morphology and vertebrate paleontology*, ed. Thomason, J. J., 19–33. New York: Cambridge University Press.

Woodward, H. N., et al. 2011. Osteohistological evidence for determinate growth in the American alligator. *J. Herpetol.* 45: 339–342.

Woodward, H. N., et al. 2013. Skeletochronology. In *Bone histology of fossil tetrapods – advancing methods, analysis and interpretation*, eds. Padian, K. and E. T. Lamm, 195–215. Berkeley, University of California Press.

Zug, G. R. 1991. Age determination in turtles. *Society for the Study of Amphibians and Reptiles Herpetological circular,* 20, 1–28.

Zug, G. R., et al. 1986. Age determination of loggerhead sea turtles, *Caretta caretta*, by incremental growth marks in the skeleton. *Smithson. Contrib. Zool.* 427: 1–34.

VetBooks.ir

32

Aging and Senescence Processes in the Skeleton

Catherine Bergot and Vivian de Buffrénil

CONTENTS

Introduction 646
General Characteristics of Skeletal Aging Process 646
Brief Recapitulation of Bone Structure 646
Bone Senescence in a Macroanatomical Perspective 647
Cranial Sutures and Pubic Symphysis Reliefs 647
Age-Related Anatomical Modifications of the Spine 647
Intervertebral Disk Degeneration 647
The Vertebral Body in Conventional X-Ray Imaging 647
Age-Related Anatomical Modifications in Cancellous Formations of Limb Bones 648
Proximal Metaphysis of the Femur 648
Proximal Metaphysis of the Humerus 649
Calcaneum 649
Age-Related Anatomical Modifications in Cortical Bone 650
Aging of Bone at a Histomorphometric Scale 651
Age-Related Variations in Cancellous Bone 651
The Iliac Crest 651
The Vertebral Body 652
Age-Related Variations in Compact (Cortical) Bone 654
Porosity 654
Assessment of Age at Death 655
Aging of Bone at the Microscopic Scale 655
Advantages of X-Ray Microtomography 655
In Cancellous Bone 656
In Cortical Bone 656
Osteocyte Lacunae 656
Mineralization 657
Ash Weight and Aging 657
An Overview of Radiologic Approaches to Mineral Density 657
Evaluation of Bone Mineral Density In Vivo 657
Results of Quantitative Microradiography: Osteons vs Interstitial Bone 658
Frequent Structural and Mineralization Abnormalities in Aged Subjects 659
Trabecular Microcalli 659
Microcracks 659
Hypermineralized Zones 659
Occlusion of Osteocyte Lacunae 660
A Synthesis of Age-Related Bone Loss in Humans 660
Remarks on Age-Related Bone Loss in Nonhuman Taxa 660
An Overview of Skeletal Aging Processes in Nonhuman Mammals 660
Nonmammalian Taxa 661
Concluding Remarks 661
Assessing Bone Senescence in Wild and Fossil Specimens 661
Osteoporosis from a Genetic and Evolutionary Perspective 662
Acknowledgments 662
References 662

VetBooks.ir

Introduction

General Characteristics of Skeletal Aging Process

Aging is a universal phenomenon that affects nearly all beings. It consists of many transformations that affect an organism from birth to death, and involves three phases: growth, maturity, and senescence. In this chapter, we will consider only changes observed in the skeleton (bones and bone tissues) during the senescence phase, i.e., from the end of growth to death (growth processes proper are described in Chapter 9). The term senescence refers to the time-dependent degradation of the optimal structural-functional characteristics of the skeleton as they are defined at the onset of the *peak bone mass*, a broadly used concept that designates the condition of the skeleton just after the attainment of somatic maturity, when all parameters describing osseous structure (see below) are at their highest level (see, e.g., Weaver and Fuchs 2014 for the use of this term). Subsequent changes reflect long, gradual, irreversible, and most often degenerative processes, appearing as the result of both genetic and environmental factors (e.g., Almeida and O'Brian 2013, Galkin et al. 2019). Many review articles have been published about bone aging, including Dequeker (1975), Boskey and Coleman (2010), Wei and Sun (2018), Hoffman et al. (2019) and Almeida and Manolagas (2020).

Skeletal modifications due to aging have been studied extensively in humans, because of the fracture risk associated with them. Most of the current knowledge on this topic is derived from clinical observations and biomedical experiments. Miscellaneous data about nonhuman vertebrates nevertheless suggest that the observations made in *Homo sapiens* can be extended to other mammals, at least in their gross qualitative aspects. The main differences among taxa deal with the timing of the process and the skeletal regions most directly affected by aging. Therefore, although the synthetic information presented below mainly deals with humans, it is likely to constitute a basis for collecting and interpreting relevant observations about mammals in general. Conversely, senescence processes in reptiles, amphibians and finned vertebrates are too scarcely documented, and possibly too divergent from those of mammals, to allow reliable inferences based on human data.

Skeletal mass decreases with aging because bony tissue is gradually lost. When bone mass reduction is locally too important, the bones become unable to sustain their functional role, which results in many forms of fracture in humans, principally spinal compression, fracture of femoral neck and distal radius, with associated complications. Bone mass loss remains asymptotic until fracture occurs. This is why, from a medical perspective, attention has naturally focused on the mechanisms and extent of this osseous rarefaction to detect it preventively.

It is still difficult to clearly differentiate age-related modifications of the skeleton from some pathological processes broadly related to osteoporosis, because of their close link with sex steroid physiology and reproductive activity in general, especially in women (menopause) and other female tetrapods (e.g., Epstein et al. 1986, Wink and Elsey 1986, Lamberts et al. 1997, Zeni et al. 1999, Buffrénil and Francillon-Vieillot 2001). Natural skeletal senescence must also be distinguished from experimental and pathologic situations, such as immobilization, weightlessness, corticotherapy, amenorrhea and castration, although the latter may lead to similar consequences. The consequences of these situations for the skeleton can be modified or corrected by appropriate treatments. In contrast to skeletal aging, they are often transitory and reversible, but they can interfere with the aging process to enhance its symptoms.

Brief Recapitulation of Bone Structure

Osseous tissue is composed of a mineralized extracellular matrix, synthesized by the osteoblasts, and resorbed by the osteoclasts (see Parts II and III of this book). The combined actions of these cells result in a permanent remodeling of bones, a process that integrates global physiological status as well as local mechanical constraints. The overall functional competence of the skeleton is consequently maintained, through both a renewing of bone substance and a permanent adjustment of bone architecture (so-called adaptive remodeling). One of the most crucial characteristics of bone remodeling is to be balanced, with reconstruction compensating resorption, through most adult life. During the aging process, the balance impairment leads to bone loss.

In healthy adult humans, some 80% of the total mass of a dry skeleton is compact bone, and 20% is cancellous tissue (Eastell et al. 1989, Faulkner et al. 1991, Zebaze 2010). Statistical and comparative data show that substantial discrepancies in these proportions occur both within a single species, depending on skeletal sites, population and individual characteristics, and among tetrapod taxa in relation to habitat and locomotory mode (see Chapters 35 and 36). The surface available to exchanges between osseous and nonosseous tissues is considerably larger in cancellous formations, which represent about 80% of the total bone-to-marrow interface in a human skeleton. Because there are more surfaces available for resorption/formation mechanisms, remodeling is faster in cancellous than in compact bone (Frost 1964, Parfitt 2008, Seeman 2013). Because age-related alterations in bone structure are a direct consequence of the conditions in which remodeling occurs, it is therefore in spongiosae that the effect of senescence is most precocious and apparent.

In this chapter, modifications of skeletal mass and structure due to aging will be described and measured at all integration levels, from macroscopic anatomy to the cell level. Current methods vary with the skeletal site and the tissue parameters studied. They rely on a direct or indirect assessment of the amount of the bone tissue present. "Bone quality" is a frequently used, but rather informal, integrative concept that is often put in opposition to "bone quantity," which refers to the actual amount of bone tissue (parameters *B.Ar/T.Ar* or *BV/TV*; see Chapter 4). Bone quality involves internal microarchitecture (trabecular arrangement or intracortical porosity), as well as the characteristics of the osseous matrix, including its mineralization rate and homogeneity, its microhardness, and so on. Typical examples of the use of this expression are given by Dorr et al. (1993), Hanson and Bagi (2004), Larrue et al. (2011), Farlay et al. (2019) and Rolvien et al. (2019).

A rich set of methods and techniques is used to investigate age effects on bone. This involves *in vivo* and *in vitro*

techniques, including visual observations, and sophisticated imagery devices for microscopic investigations. Three main methodological approaches exist: gross morphometric methods (i.e., anatomy-based), histomorphometric quantification of the alteration of inner bone architecture, and densitometric methods for estimating the mass of mineralized osseous substance, principally through X-ray imaging (e.g. Allen and Krohn 2014). The vocabulary used for describing and analyzing the microstructural parameters of inner bone structure in two dimensions (2D) and three dimensions (3D) is now codified and precise (Parfitt et al. 1987, Dempster et al. 2013). The reader is referred to Chapter 4 on this topic.

Bone Senescence in a Macroanatomical Perspective

Assessing skeletal age through dental or osseous clues is relatively simple in young specimens, especially mammals; however, age-related skeletal modifications in adults are far less evident. They are based mostly on degenerative morphological features. They are nevertheless clear enough to have justified a strong research effort, dealing mainly, in addition to humans, with laboratory models represented by primates, rodents and lagomorphs. This effort aimed to define objective parameters through which quantification of aging modifications in diverse characteristic sites could be conducted. Several such sites were initially considered in adults, including, for example, teeth (Gustafson [1950] method and its variations), coxal bone (Rissech and Malgosa 2005) and sternocostal articular surfaces (Oettle and Steyn 2000). Information derived from them is approximate and refers to broad discrete categories. Age-related modifications in other skeletal sites are constant enough to give somewhat finer and more reproducible age classes. These sites are briefly presented below.

Cranial Sutures and Pubic Symphysis Reliefs

A synostotic process occurs in the cranial vault and face, gradually erasing sutures up to their total disappearance. This process shows strong interindividual variability (Nemeskeri et al. 1960, Acsàdi and Nemeskeri 1970, Masset 1982, 1989) but nevertheless allows, with some approximation, the assessment of an "osseous age", at least up to an age of about 40 years (Modi et al. 2015).

Time-dependent morphological modifications of the crests and grooves on the facets of the pubic symphysis were described and classified into several ontogenetic stages, thus defining age-estimation methods (Acsàdi and Nemeskeri 1970, Brooks and Suchey 1990, Iscan et al. 1992). These methods are of relatively poor accuracy and precision.

Age-Related Anatomical Modifications of the Spine

Spine alterations with age involve intervertebral disks and the vertebrae themselves. These alterations have specific characteristics in *H. sapiens*, related to the peculiar loading conditions created by permanent bipedality (Alexander 2001, Prakash et al. 2007).

Intervertebral Disk Degeneration

The degeneration of intervertebral disks results from both the dehydration of the core nucleus (*nucleus pulposus*), a distant remnant of the embryonic notochord (see Chapter 2), and a decrease in the proteoglycans content of the fibrocartilaginous matrix of the disks (review in Dowdell et al. 2017, Oichi et al. 2020). This degenerative process starts at about 40 years in humans, and alters the capability of the disks to act as shock or pressure absorbers, with the final consequence of degrading the mobility of the whole spine. Lumbar disk degeneration results in the disk space narrowing (Figure 32.1A–C), development of osteophytes. and end-plate sclerosis (Pye et al. 2007). Age is associated with higher osteophytes grades. Vertebral osteophytes often have a clawlike appearance, curved toward the adjacent disk (Wong et al. 2016). These phenomena bear many similarities to osteoarthritic formations (Rustenburg et al. 2018) observed in articular joints. Intervertebral sclerosis and osteophyte development also appear on articular surfaces of the vertebral arch, further contributing to overall spine disability.

The Vertebral Body in Conventional X-Ray Imaging

Standard radiographs reveal age-related bone loss through osseous condensations (osteophytes) and hypertransparency. Bone loss is made more obvious by increased radiolucency, a striated aspect due to the differential disappearance of horizontal trabeculae, and accentuation of the cortical outline (Figure 32.1D, E, H). Radiological signs of bone loss *in vivo* can be blurred or hidden by several factors degrading image contrast or sharpness; in consequence, this process cannot be visually detected on radiographs if less than at least 30%.

Vertebral body compression fractures occur when bone strength is not sufficient to absorb loadings, so they are common in the elderly. Osteoporotic compression fractures are exclusive of the dorsal and lumbar parts of the spine and are revealed on X-ray proofs by the characteristic deformations that they cause (Figure 32.1F–H). To assess fracture diagnosis and osteoporosis severity, semiquantitative techniques measuring vertebral body height on conventional lateral radiographs were developed. They allow the definition of typical qualitative compression patterns, each with several grades of severity: biconcave end plate (Figure 32.1F, H), when the middle vertebral height is decreased; wedge (cuneiform) fracture when the anterior wall collapses (Figure 32.1G, H) and crush (pancake-like) fracture patterns (Figure 32.1H) when the entire body is flattened (Meunier 1972, Genant 1993, see also Dewar 2015). Morphometric assessments are based on the calculation of ratios of the anterior, posterior and median heights of a vertebral body versus the corresponding normal reference values. A threshold of 15% loss for any of the height values characterizes the existence of a fracture (Melton et al. 1989, Eastell et al. 1991, McCloskey et al. 1993, Guglielmi and Diacinti 2003).

Vertebral deformations may also originate from degenerative or malignant pathologies, or in congenital malformations. However, although the actual meaning of these categories seems to be more related to osteoporotic processes of bone

VetBooks.ir

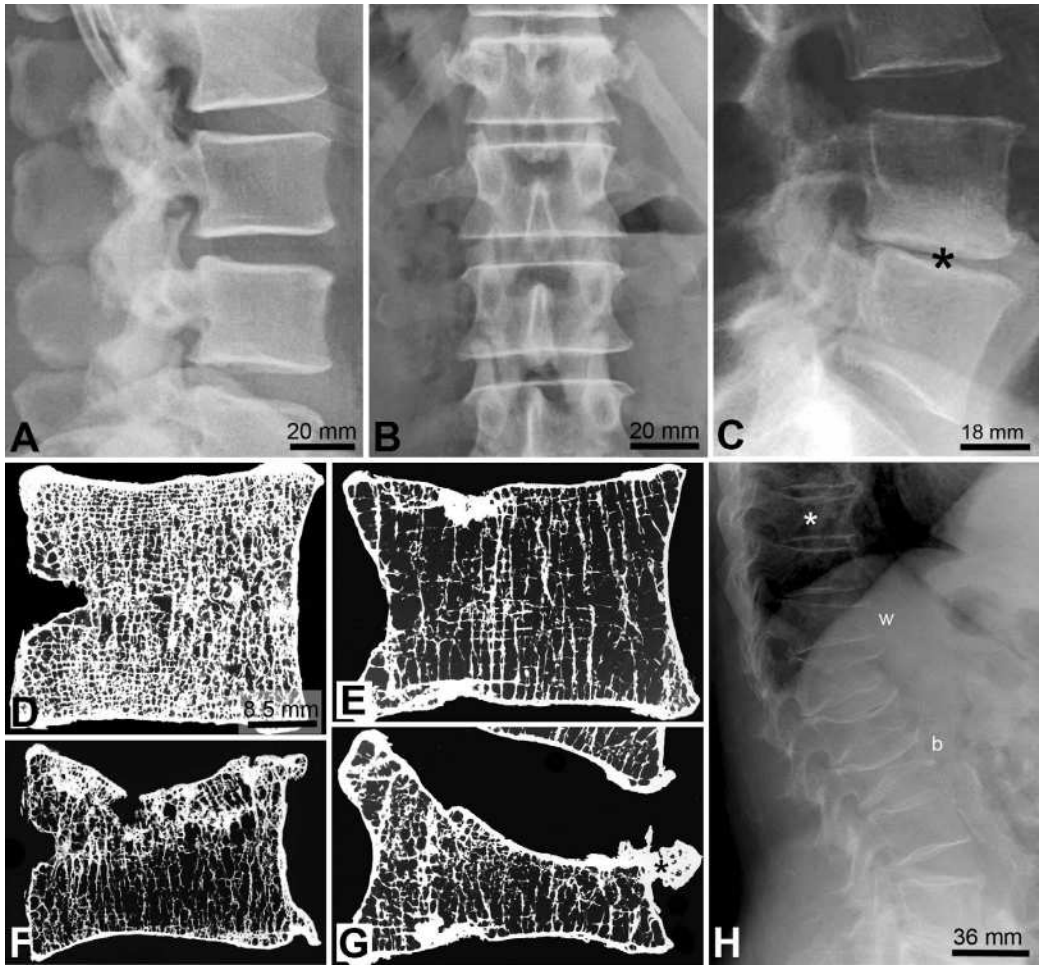


FIGURE 32.1 Age-related anatomical alterations of the human lumbar spine. A and B, Normal spacing of the vertebral bodies in a healthy spine in lateral (A) and anteroposterior (B) radiographic views. C, Pinching of a vertebral disk (asterisk). D–G, Microradiograph of sagittal slices of lumbar vertebral bodies (*ca*. 1 mm thick) showing the variations of the trabecular network. D, Healthy young subject. E, Osteoporotic vertebral body showing the rarefaction of the trabecular network. F, Fracture of the superior plateau leading to a biconcave aspect. G, Wedge fracture and conspicuous osteophyte (asterisk) in an osteoporotic vertebral body. Figures D–G are at the same scale. H, Spine of a subject combining several pathological traits, including osteoporosis, as revealed by the low radiopacity (asterisk) of the vertebral bodies, disk degeneration and two deformation patterns, i.e., biconcave (b) and wedge (w).

loss and bone fragility than to aging *sensu stricto*, the link to age is significant (Mégard et al. 1976, Melton et al. 1989, Old and Calvert 2004, McCarthy and Davis 2016).

The combination of vertebral fractures and disk degeneration (Figure 32.1H) leads to individual size decrease, and variably pronounced thoracic kyphosis and lumbar lordosis (McCarthy and Davis 2016). In paleoanthropological studies, the use of Meunier's or Genant's scores, or that of more precise quantitative indices, can be of prime utility for quickly assessing the degree of senescence and skeletal quality of fossil human remains, provided that reliable comparative populational data exist.

Age-Related Anatomical Modifications in Cancellous Formations of Limb Bones

In the cancellous formations of long and short bones of the appendicular skeleton, bone volume loss due to age leads to changes in the number, architecture and distribution of osseous trabeculae. Data from three characteristic sites of the human skeleton, the femur, the humerus and the calcaneum, are briefly presented below.

Proximal Metaphysis of the Femur

Osseous trabeculae in the proximal end of the femur, in humans and most other mammals, concentrate most of the mechanical stress, both in compression and tension, related to body weight and locomotion. According to Wolff's law (see Chapters 4 and 35), the orientation and distribution of metaphyseal (weight-bearing) trabeculae are permanently accommodated and optimized, through adaptive remodeling, to withstand the trajectory of dominant mechanical loads (reviews in Currey 2002, Allen and Burr 2014). In the femoral metaphysis (Figure 32.2A), osseous trabeculae are organized into two main formations: the cephalic bundle, oriented mostly vertically and designed to resist compression, and the arciform bundle that is oblique and adapted to tensile forces (Figure 32.2B, C). The crossing

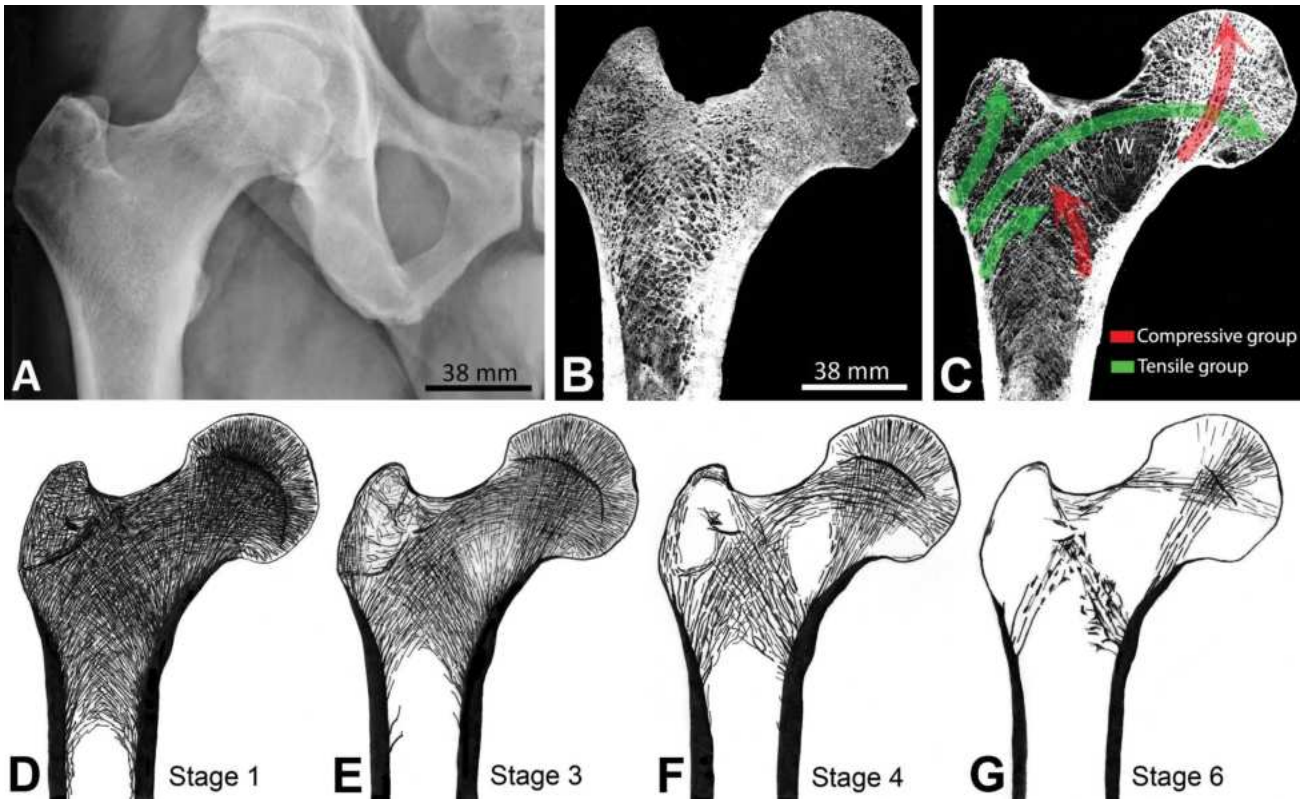


FIGURE 32.2 Trabecular network in the femoral head and its sequential degradation. A, Normal radiological aspect of the proximal femur in a male human subject (anteroposterior view). B, Polarized aspect of the trabecular network in the femoral head, viewed on the surface of a sagittal section of the bone (young subject). C, Indication of the trabecular bundles adapted to tension (in green) and compression (in red), clearly visible in an old subject. W, Ward's triangle. D–G, Four stages (i.e. grades) of the osteoporotic degradation of the trabecular network in the femoral head. (Derived from Nemeskeri et al.'s classification 1960.) The scales are identical for all images.

of these two main bundles (along with secondary ones) forms a dense ogival trabecular structure, which frames a looser triangular area (viewed in sagittal section) in the femoral neck, Ward's triangle (described in 1863). With age, the trabecular network loosens (Hall 1961), and Ward's triangle spreads to occupy most of the intracervical space; therefore, the apex of the ogive-like trabecular network is shifted above the level of the lesser trochanter. These gradual transformations are categorized into series of successive stages (Figure 32.2D–G and populational statistics in Figure 32.4A: one series, including six stages, is intended to contribute to the assessment of age at death (Nemeskeri et al. 1960); the other series, designated as *Singh's index* (Singh et al. 1970), describes seven grades, and is used as a clue for estimating bone mass and diagnosing osteoporosis radiographically (Hauschild et al. 2009, Bes et al. 2012).

The two grading methods are close to each other and clearly demonstrate bone loss due to aging, in a qualitative and descriptive perspective. However, the spreading degree of Ward's triangle is not a sufficient criterion to estimate age at death accurately. Grading based on radiographs strongly depends on both the quality of the X-ray proofs and the experience of the observer (Hauschild et al. 2009). Moreover, Singh's index is not or is only poorly correlated with vertebral bone mass as evaluated by densitometric methods; therefore, considered alone, it cannot be used as a fully reliable tool for diagnosing osteopenia (Sah et al. 2007, Klatte et al. 2015).

Proximal Metaphysis of the Humerus

Trabecular architecture in the proximal extremity of the human humerus (Figure 32.3A) is less complex and polarized than in the proximal femur, because this bone has no weight-bearing role and its shape is simpler. Trabeculae in the metaphysis are organized in bundles forming an ogive-like structure (Figure 32.3B) and, similar to the proximal femur, six stages of architectural degradation with age have been described (Nemeskeri et al. 1960). To our knowledge, no attempt to define a similar grading scheme was adapted by physicists or orthopedic surgeons to assess osteoporosis, although qualitative descriptions have been proposed (Hall and Rosser 1963).

A broad comparative study (421 complete skeletons of both genders) conducted by Bergot and Bocquet (1976) showed that the age-related degradations of trabecular architecture in humeral and femoral metaphyses (Figure 32.3C–H; see also Figure 32.4B) are similar, but somewhat steeper in females than in males, over 50 years of age. These results accord with trends of normative data for the amount of bone decrease with age in other skeletal sites.

Calcaneum

The broad cancellous formation that occupies most of the volume of the heel bone also displays a nonisotropic architecture

VetBooks.ir

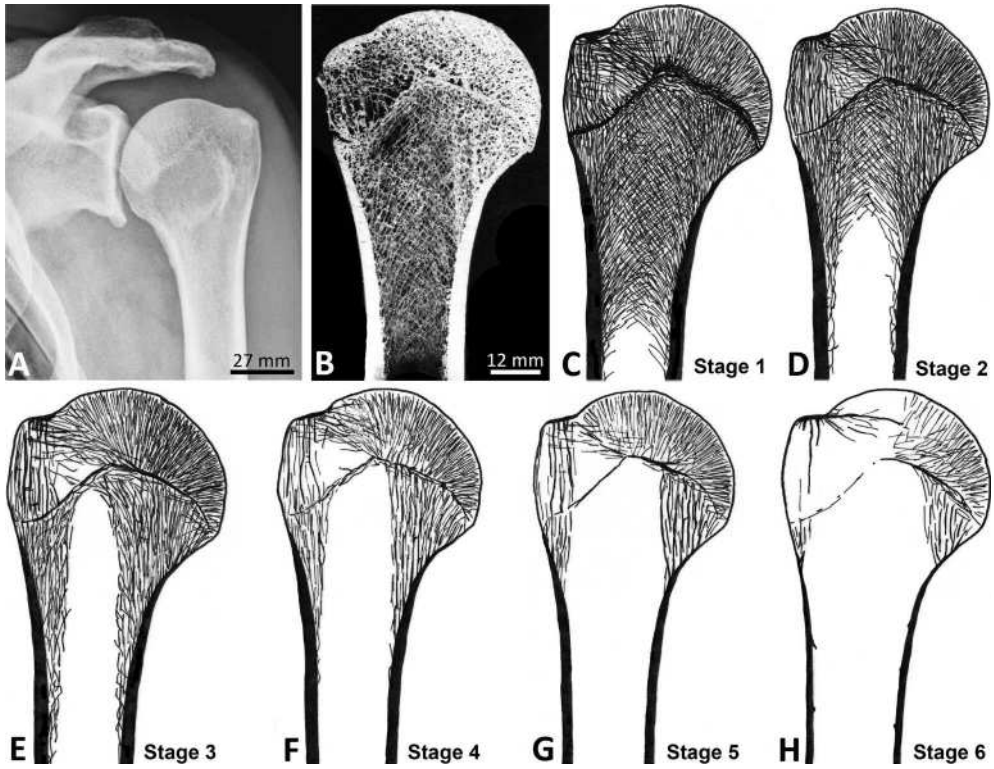


FIGURE 32.3 Trabecular network in the humeral head and its sequential degradation. A, Normal radiological aspect of the humeral head (anteroposterior view) in a male human specimen. B, Gross aspect of the trabecular network in the humeral head, as viewed on the surface of a sagittal section of the bone. C–H, The six identified stages (i.e. grades) of osteoporotic trabecular degradation in the human humerus. Same scales for B–H.

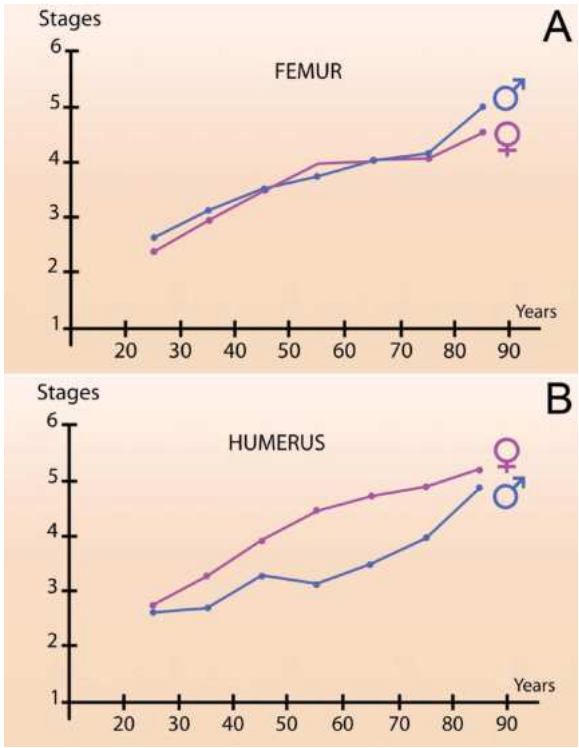


FIGURE 32.4 Average stage (among stages 1–6) of degradation of cancellous bone in the human femur and humerus in relation to age. Data are from a Portuguese population that lived in the Coimbra area in the late 19th and early 20th centuries (Bergot and Bocquet 1976.)

and some degree of trabecular polarization (Figure 32.5A, B) that reflects the main trajectory of local mechanical strains (Jhamaria 1983, Krause et al. 2013). Unlike the upper femur or the spine, with which it shares a relatively similar age-dependent transformational pattern, the human calcaneum is easily accessible to common imagery techniques, and it has been largely used in the qualitative and quantitative assessment of osteoporosis (Figure 32.5C; see also Laval-Jeantet et al. 1995a). A fractal approach to textural analysis based on X-ray images of cancellous bone was used in the calcaneum to reveal the quantity of the bone tissue present locally, its possible loss with age and the quality of trabecular networks in terms of functional polarity and architectural design (Benhamou et al. 1994, Pothuaud et al. 2000).

Age-Related Anatomical Modifications in Cortical Bone

The most striking aspect of bone loss with age in the diaphyseal region of long bones is a widening of the medullary canal and a thinning of the cortex. This is a gross alteration perceptible at a macroscopic level, and measurable on radiographs (anteroposterior incidence) in bones having a cylindrical diaphysis. It is a simple and reliable means to assess skeletal status from standard radiographs. The bones most commonly studied for this purpose in humans are the metacarpals, at the level where the medullary canal is narrowest, in the context of large population studies (e.g., Dequeker 1976, Garn 1980), the radius (Meema and Meema 1963), the femur, the humerus (Virtama and Helela 1969, Bergot and Bocquet 1976, Bocquet and Bergot 1977,

VetBooks.ir

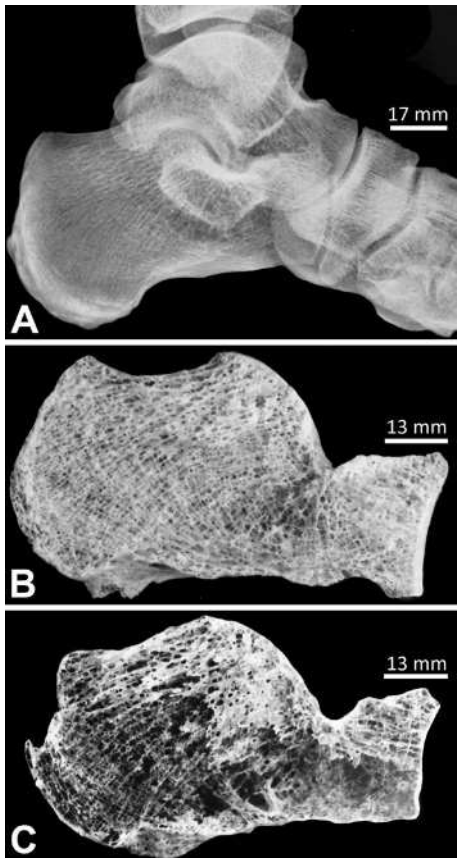


FIGURE 32.5 Trabecular network in the calcaneus and its age-related degradation. A, Normal radiological aspect of the calcaneus (lateral view) in a male human. B, Trabecular density and architecture as viewed on the surface of a sagittal section of the bone. C, Osteoporotic degradation of the trabecular network (same type of preparation as for B).

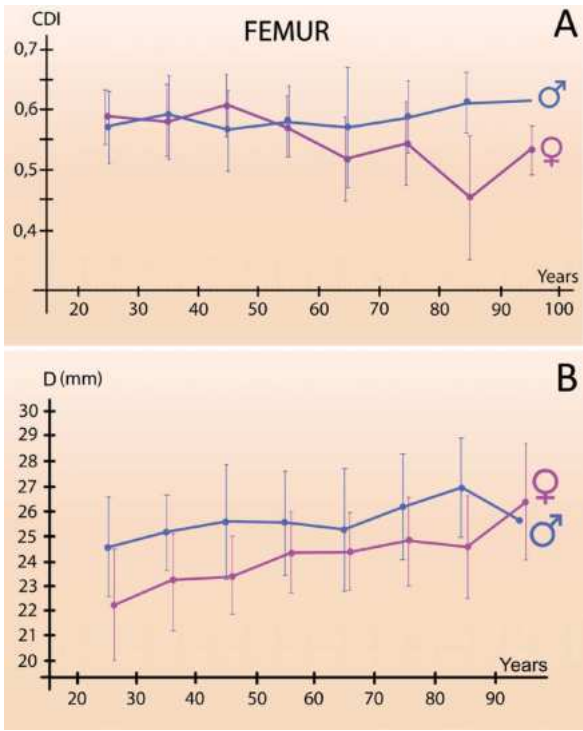


FIGURE 32.6 Age-related modification of the corticodiaphyseal index (A), and diameter (B) at the femoral midshaft in male and female humans. (data from Bergot and Bocquet 1976.)

Bloom and Laws 1970) and the tibia (Ruff and Hayes 1982). Cortical thickness measurements remain useful for clinical evaluation of bone mass and screening fracture risk in elderly populations (Tingart et al. 2003, Sah et al. 2007, Mather et al. 2013, Webber et al. 2015, Patterson et al. 2016, Teuling et al. 2017, He et al. 2018). Radiogrammetric measurements, aimed to calculate the corticodiaphyseal index of the bone (or CDI; see Chapter 4), are made directly on conventional radiographs or digitized images. Cortical thickness of long bones, as defined above, depends on the skeletal site considered, and on the gender, size and age of each individual. Values of CDI are, for example, more elevated in the femur and the metacarpals (CDI >0.5) than in the humerus (CDI *ca.* 0.3). A significant decrease of this index with age occurs in women, especially those older than 50 years (Figure 32.6A). This process is milder or absent in men (Meema and Meema 1963, Dequeker 1976, Noble et al. 1995, Nguyen et al. 2018). Ethnic variations are also documented (Virtama 1969, Nguyen et al. 2018). Such a gradual decrease of long bone CDI, especially in females, is widespread among tetrapods; it has been observed in mammals, as well as sauropsids (e.g., Wink et al. 1987 in *Alligator mississippiensis*, Buffrénil and Francillon-Vieillot 2001 in *Varanus niloticus*, etc.).

In pace with the age-related decrease of CDI value, a slight increase in diaphyseal diameter occurs through subperiosteal accretion (Figure 32.6B), especially in the shafts of the femur, tibia, humerus and metacarpals (Bocquet and Bergot 1977, Dequeker 1980, Garn 1980, Ruff and Hayes 1982), and in the femoral neck (Parfitt 1984, Robling et al. 2014). The bending strength of the femur can thus be maintained (Seeman 2008; for details, see chapters below on bone biomechanics).

Aging of Bone at a Histomorphometric Scale

Skeletal histomorphometry is mainly conducted in the context of human medicine, as well as in laboratory rodents and primates. Its aim is to quantify precisely (through the analysis of bone biopsies or tomographic virtual sections), the volume of bone in standard skeletal sites. Individual scores are then compared to reference population norms, so that a diagnostic for skeletal status can be determined. Bone histomorphometry typically deals with the microanatomical integration level. It considers structural details ranging in size from some tens to some hundreds of microns. Interindividual variation of such details is inaccessible to the naked eye and requires precise quantitative measurement.

Age-Related Variations in Cancellous Bone

The Iliac Crest

Early attempts to standardize the measurement of the proportion of mineralized osseous tissue in a given total volume of bone (including bone and cavities) were based on the iliac crest (Figure 32.7A) because this site, located superficially and at a

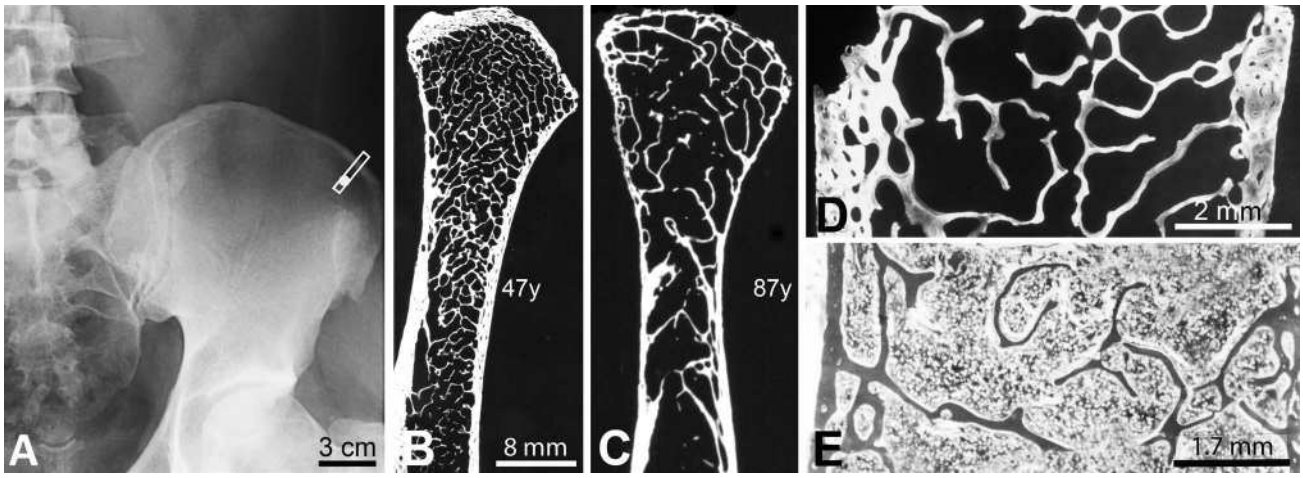


FIGURE 32.7 Age-related modification of trabecular bone volume with age at the iliac crest. A, Radiological aspect of the iliac crest (anteroposterior view) and sampling locations. The white disk indicates the location of the reference transiliac biopsy, and the rectangle shows the sampling site of the sections presented in B and C. B, Trabecular network in a normal (healthy) subject; C: Trabecular network in an osteoporotic subject (microradiographs of *ca*. 100-µm-thick sections). D and E, Transiliac biopsies in a healthy subject (D, microradiograph) and in an osteoporotic one (E, histological section).

distance from vital organs, is easy to access. A 7-mm transiliac biopsy is operated 2 cm below the anterosuperior iliac spine, and the bone sample (comprising the external and internal cortices along with the core spongiosa) is processed with classical methods for topographical histology (Meunier et al. 1968; Hernandez et al. 2008, Moreira-Kulak and Dempster 2010). Mineralized osseous tissue is thus sharply and unambiguously defined (Figure 32.7B–E). Current histomorphometric methods applied to such biopsies rely on computerized image analysis and yield precise ratios between bone tissue area and total area within selected regions of interest (ROIs). Though challenged by microcomputed tomography, a rapid noninvasive technique, biopsy analyses remain commonly used in histophysiological studies and therapeutic protocols because they give direct access to bone cells and several dynamic parameters related to the intensity of bone turnover (Frost 1983, Parfitt et al. 1987, Qiu et al. 2003, Mullender et al. 2005, Lindsay et al. 2006, Parfitt 2014).

The main parameter considered in iliac crest analyses is trabecular bone volume (TBV, a general expression that corresponds, in 2D, to *Tb.Ar/Tt.Ar* and, in 3D, to *Tb.V/Tt.V)*. This parameter has already been presented in Chapter 4. In brief, it expresses, most often in percentages, the proportion (in area or volume) of a cancellous bone sample actually occupied by mineralized osseous trabeculae (Parfitt et al. 1987, Parisien et al. 1997, Dempster 2013). TBV in the iliac crest significantly decreases in both genders (Courpron et al. 1973), but this drop is steeper in women, with an average TBV value of *ca*. 23% at the age of 40 years, and 16% at 80 years (Figure 32.7C, E and Figure 32.8); such a decrease is not observed in men (Mellish et al. 1987, Bergot et al. 1990). The 3D reconstructions of cancellous bone microanatomy reveal the existence of several patterns in the morphology of trabecular networks; the most common is the association of platelike elements, oriented parallel to strain lines, and rodlike elements connecting the plates (Parfitt's [1983] "plate and rod model"; see also Stauber and Müller 2006, Doube 2015, and Chapter 4). The imbalanced remodeling process induced by aging alters the plate to rod proportion, with preferential conservation of the plates. When rodlike elements become too sparse to maintain the cohesion of the plates, the mechanical competence of the spongiosa can be degraded up to reach the fracture threshold.

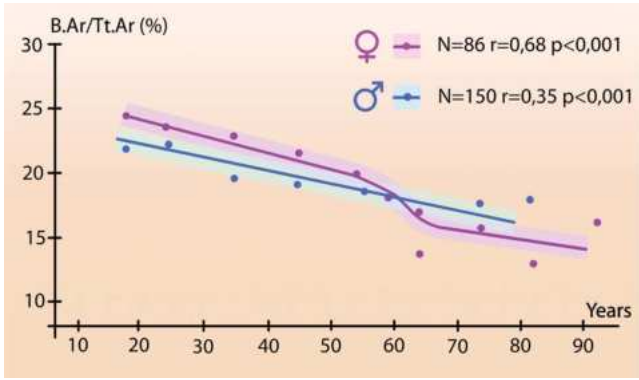


FIGURE 32.8 Decrease of bone area fraction (*B.Ar.f,* in percentage) in the iliac crest of male and female humans.

The Vertebral Body

Age-related degradation of cancellous bone, with a decrease in TBV and a preferential resorption of the transverse elements, has been shown in the body of the third lumbar vertebra in autopsy samples. Total bone loss in vertebral bodies reaches 60% in women and 45% in men in four decades. Age-related transformations of trabecular architecture in vertical (Figure 32.1D) and horizontal (Figure 32.9A, B) planes was demonstrated by the use of mathematical morphology techniques (Bergot et al. 1988). In the vertical plane, mean trabecular width decreases by 26% (172–128 µm) in women, and 20%

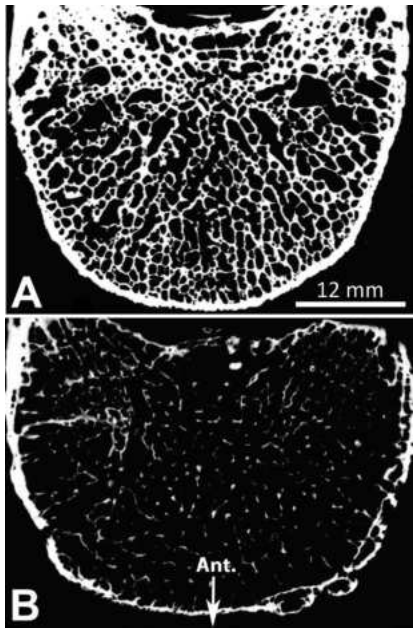


FIGURE 32.9 Loss of bone mass in vertebral body as viewed in the horizontal median plane. A: Young healthy vertebra. B: Steep decrease in trabecular area in the osteoporotic vertebra of an aged subject. X-ray proofs of *ca*. 500-µm-thick bone sections. Same scale for A and B.

in men (181–144 µm) between ages 40 and 80 years (Figure 32.10A, B). In the meantime, trabecular width, considered in the horizontal plane, remains roughly constant in men (114 µm), but decreases by 22% (144–112 µm) in women (Figure 32.10C, D). Intertrabecular spaces enlarge in pace with trabecular width decrease, but to a much larger extent than could be expected from the mere thinning of the trabeculae. Total bone loss thus results from a double process, i.e., the reduction of the width of the trabeculae, and the total disappearance of some of them, mainly horizontal trabeculae. In both genders and at all ages, mean trabecular width remains slightly above 100 µm (111 ± 26 µm). These early histomorphometrical results were later confirmed, with comparable quantitative results, by microtomographic approaches (e.g., Mosekilde et al. 2000, Gong et al. 2005, Liu et al. 2009, Fields et al. 2009, 2011).

Bone volume loss, whether related to age or to other circumstances, and whatever its form, is basically due to imbalanced remodeling: the volume of osseous tissue eroded away by osteoclasts is not compensated by equivalent secondary deposits. In the peculiar case of trabecular bone, imbalance and the consecutive thinning of the trabeculae exclusively result from an iterative deficit in reconstructive deposits through repeated remodeling cycles; conversely the width and extent of Howship's lacunae (i.e., the intensity of the resorption phase) remain constant (Lips et al. 1978, Seeman 2008). Moreover, the consequences of

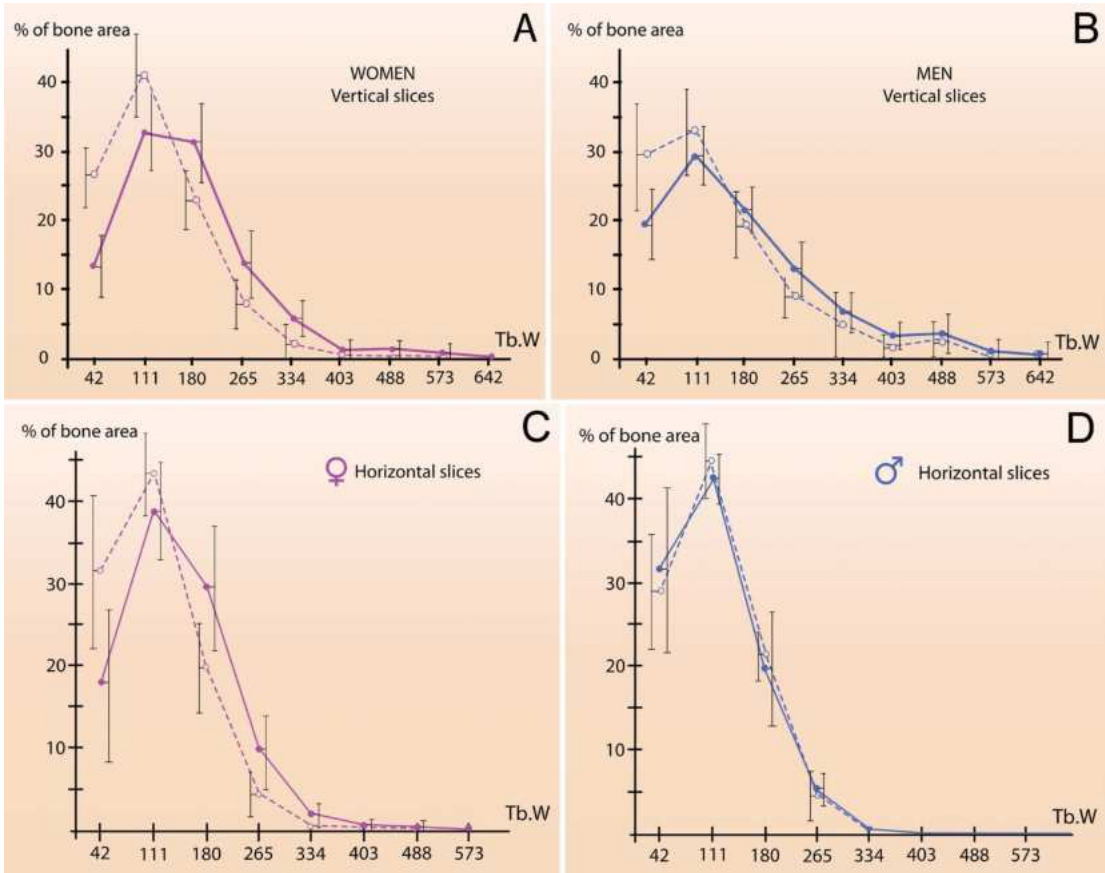


FIGURE 32.10 Contribution (in percentage) of the trabeculae to bone area in relation to their width (Tb.W) in the human third lumbar vertebra. A and B, In vertical sections in subjects aged 33–49 years (solid line), and 80–89 years (dotted line). C and D, Same measurements in horizontal sections (data from Bergot et al. 1988.)

imbalanced remodeling are enhanced by the rise in basic multicellular unit (BMU) activation frequency (see Chapter 11) caused by the estrogenic deficiency that follows menopause (Parfitt et al. 1983, Bjornerem 2018; see also Chapter 9).

Age-Related Variations in Compact (Cortical) Bone

Porosity

Age-related bone loss in compact cortices consists of a decrease in cortical thickness, accompanied or not by an increase in intracortical porosity. The latter parameter is defined as the relative area, or volume, occupied by cavities within a bone sample. It is measured on 2D images or 3D reconstructions and expressed as a direct ratio or a percentage. Bone porosity is complementary to another parameter, bone compactness (described in detail in Chapter 4): Porosity = [1 – Compactness], if presented as a simple ratio, or [100 – Compactness], in percentage. In long bones, cortical porosity is measured on transverse diaphyseal sections that can result from either true (material) processing of bone samples, microradiographs, or computed tomography (CT)-scan images, with or without 3D reconstructions. Cavities considered in porosity assessment are vascular canals (osteonal or Volkmann's canals) and resorption bays. Osteocyte lacunae and their canaliculi are not considered at this scale. In human biomedical research, relatively few studies specifically deal with cortical porosity compared to cancellous formations in the iliac crests and the vertebrae. Such studies mainly deal with long bone diaphyses, the iliac crest cortex and the femoral neck cortex. In comparative biology, bone compactness (or porosity) is commonly studied, but in relation to other problems than aging (see Chapter 35).

An increase in cortical porosity with age has long been observed in the femoral diaphysis (e.g., Jowsey 1960, Atkinson 1965, Martin et al. 1980). Increased levels reported in the literature vary broadly, from 2 to 5% to 30 to 40% or more, depending on the authors and the skeletal sites considered (e.g., Martin et al. 1980, McCalden et al. 1993, Bousson et al. 2001, Thomas et al. 2005). Beyond great interindividual variability, cortical porosity in long bones increases significantly with age in both genders (Figure 32.11A–E), a trend that some authors consider faster in women (Bousson et al. 2001, but see also McCalden et al. 1993). Cortical porosity is distributed unevenly within the cortex, especially in women, with a decreasing gradient from the endosteal margin to the outer subperiosteal region. It also varies with the sectors of diaphyseal circumference: in the femoral shaft, it is more pronounced in the anterior sector, where remodeling activity is high due to mechanical stress (Thomas et al. 2005), than in the medial and lateral ones, where remodeling activity is less.

Cortical porosity depends on both the number and the size of vascular canals. This question was studied in a population of 163 individuals of both genders and all ages, with microradiographs sampled transversely at mid-diaphysis in the femur,

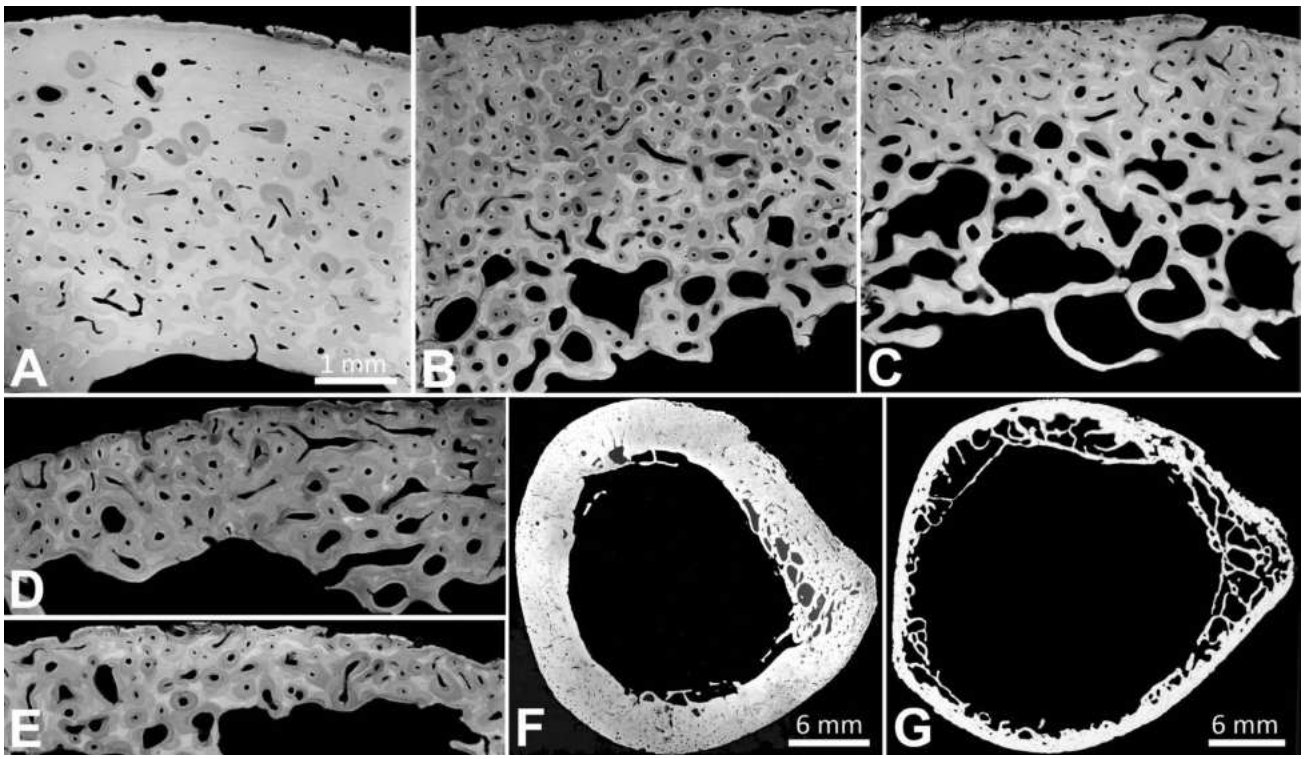


FIGURE 32.11 Microradiographs of 100-µm-thick sections. Age-related degradation of long bone cortices. A–E, Femoral mid-diaphysis. A, Normal porosity of the humeral cortex of a young healthy woman. B, Mild increase of cortical porosity, along with some thinning of the cortex and proliferation of secondary osteons. C, Increase in cortical porosity and thinning with age. D and E, Strong cortical thinning in old female subjects. F, General aspect of a cross section in the humeral shaft of a young, healthy adult. G, Result of the thinning process and inner imbalanced remodeling in the cortex of the humeral shaft of an old subject. Pictures A–E have the same scale.

VetBooks.ir

and studied with an automatic image analysis system (Bousson et al. 2001). There is a gradient, decreasing centrifugally, for the size and the mean number per square millimeter of canals. Up to 60 years, both parameters increase throughout the cortex. After 60 years, canal size continues to increase, but canal number decreases, which suggests that a coalescence of the canals occurs, related to bone loss. This age-dependent modification of cortical structure is even and homogeneous through the whole width of the male femoral cortex; in females, it prevails near the endosteal margin, and it results in marked cortical thinning with age (Figure 32.11C–E and Figure 32.12A). A similar age-dependent increase in cortical porosity also occurs in the femoral neck (Squillante and Williams 1993, Bousson et al. 2004), which reduces the mechanical capacities of this bone (McCalden et al. 1993; see also Currey and Shahar 2013 for nonhuman bones).

The same situation occurs in the humerus, a nonweight-bearing element of the skeleton in humans (Figure 32.11F, G and Figure 32.12B). In this bone, cortical porosity also increases with age and doubles in 40 years (between ages 40 and 80 years) in both genders. It is nevertheless more precocious in women than in men (Bergot et al. 1990). In general, a larger amount of bone is lost through cortical thinning than through mere cortical porosity.

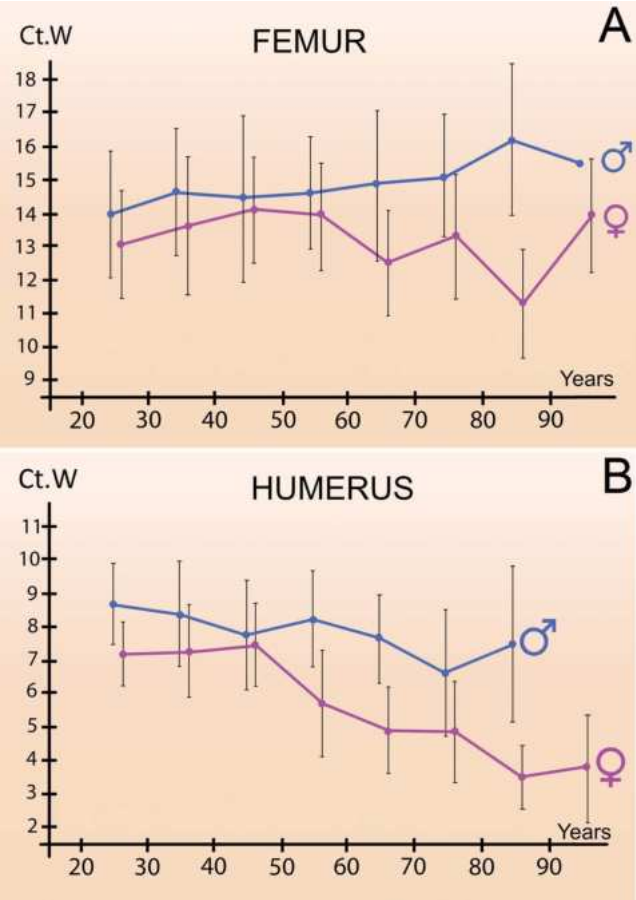


FIGURE 32.12 Statistics on the modification of cortical width in the femur (A) and the humerus (B) of male and female humans (data from Bocquet and Bergot 1977.)

Assessment of Age at Death

By the end of somatic growth, primary periosteal bone is proportionally the major component of cortices (Figure 32.11A). Subsequent Haversian remodeling gradually reduces this proportion through life-long iterative resorption and reconstruction cycles (Figure 32.11B–D) and the accumulation in cortices of several generations of secondary osteons that can be entire (recently formed osteons) or fragmentary (old osteons, themselves submitted to remodeling). So, in all vertebrates, osteonal distribution and appearance within compact cortices vary with age, a fundamental observation that has prompted several authors following Kerley (1965) and Kerley and Ubelaker 1978) to propose methods for the estimate of age at death from cortical samples in humans. Significant correlations were shown between, on the one hand, several parameters related to remodeling activity, i.e., the number of entire and fragmentary osteons, the proportion of interstitial (nonremodeled) tissue, the average number of lamellae per osteon, the average diameter of Haversian canals and, on the other hand, individual age (Singh and Gunberg 1970, Lynnerup et al. 2006, Martrille et al. 2009). No satisfactory equation for the calculation of individual age from osteonal population characteristics has yet been proposed. Based on the universality of secondary osteon accumulation with age, a similar use of quantitative data on Haversian substitution has been proposed in nonhuman tetrapods to assess developmental stages, including extinct taxa (e.g., Sander 2000, Klein and Sander 2008, Stein et al. 2010). Several methodological approaches have been used, differing by the skeletal sites considered (femur, tibia, humerus, radius, metacarpals, ribs, clavicles), the kind of technical preparations used (histological sections, microradiographs, tomographic images), the structural details considered (entire osteons only vs total osteonal remnants) and the sampling strategy adopted (size of investigated fields, integral vs sectorial, manual vs automatic counting of the osteons, etc.; see, e.g., Atkinson 1965, Jowsey 1966, Kurzawski 1983, Stein et al. 1999, Thomas et al. 2000, Bousson et al. 2001, Gosha and Agnew 2016). Moreover, bone remodeling proves to be a complex process influenced by many factors, including nutritional equilibrium, physical activity, hormonal status (menopause, thyroidian and parathyroidian activity, vitamin D level) and so forth (see above, chapter on *Bone remodeling*). All of them create substantial intra- and interindividual variability that inextricably interferes with the proper effect of aging.

Aging of Bone at the Microscopic Scale

Advantages of X-Ray Microtomography

X-ray microtomography is a nondestructive imaging technique operating with the same acquisition principles as conventional clinical CT scanners. More recent devices reach spatial resolutions below 100 µm and thus make internal bone architecture easily accessible. High-resolution µ-CT scanners (HR-pQCT) are used *in vivo* for peripheral skeletal site analysis (radius, tibial metaphyses) and desktop microscanners are used *in vitro* for imaging specimens at high resolution). The former have

clinical purposes, to evaluate volumetric mineral bone density as well as bone microarchitecture, in cortical and trabecular compartments separately; the latter explore the 3D structure of bone samples from humans and other animals, including fossils (reviews in Patsch et al. 2011, Nishiyama and Shane 2013). Reconstructions thus obtained give access to the real parameters of 3D structures. The most recent reconstruction methods can handle the entire volume of data (2D imagery proceeds slice by slice), thus avoiding the complex and potentially biased theoretical modeling derived from bidimensional images.

Histomorphometric parameters used in 3D analyses are derived from those used in 2D for the cancellous tissue of the iliac crest, i.e., TBV (3D equivalent of *Tb.Ar*), trabecular volumetric fraction, (*Tb.V.f*) (equivalent of *Tb.Ar.f*), number and size of the trabeculae and intertrabecular spaces, and so forth. A compendium of the 2D and 3D histomorphometric parameters most commonly used is presented in Dempster et al. (2013) (see also Parfitt et al. 1987, and Chapter 4) In addition, topological parameters frequently referred to include the degree of trabecular network anisotropy and the density of trabecular connections.

In Cancellous Bone

Three-dimensional investigations about age-dependent modifications of cancellous bone in vertebral bodies (Figure 32.13A, B) confirm the results obtained with 2D analyses: there is a significant global decrease in bone volume, associated with a diminution of trabecular number and connections, along with an increase in intertrabecular spaces (e.g., Arlot et al. 2008).

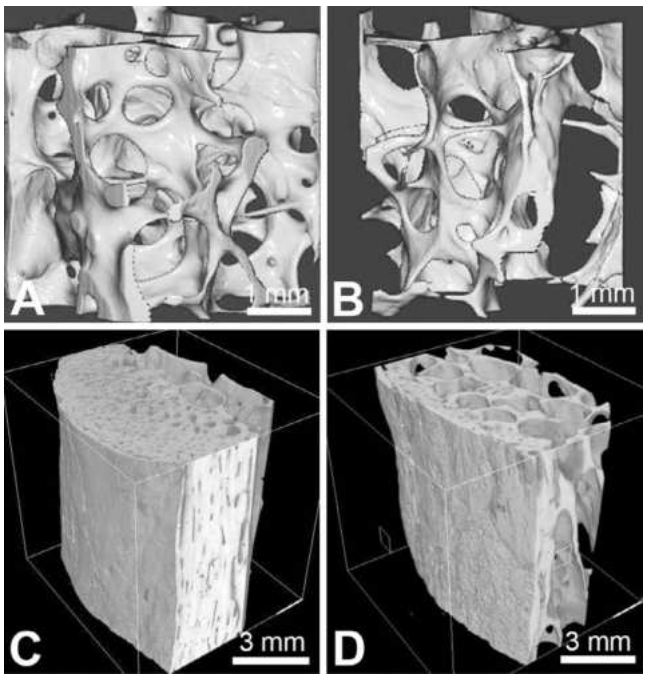


FIGURE 32.13 Synchrotron radiation µ-CT images: 3D aspects of trabecular and cortical age-related transformations (with permission of F. Peyrin, ESRF, Grenoble). A and B, Vertebral trabecular network in a young subject (A) and an old subject (B). C and D, Median cortex of the femoral neck in a healthy subject (C) and an elderly subject (D).

These phenomena are more pronounced in the center of the vertebral body, but the difference between center and periphery tends to decrease in older subjects (Chen et al. 2008).

In Cortical Bone

Great improvements in image resolution and segmentation result from the use of Synchrotron radiation (SR; Andronowski et al. 2018). Particularities of the synchrotron X-ray beam produce optimal contrast and signal-to-noise ratio, facilitating postprocessing calculations, particularly thresholding processes. They result in high quality images and more reliable quantitative analyses. It is particularly suitable for the study of cortical bone for which conventional µ-CT technology may be insufficient, with voxel sizes between 0.8 and 10 µm for acquisition fields 1–10 mm (Cooper et al. 2007, Ostertag et al. 2016). Haversian and Volkmann's canal networks are characterized by analogy with trabecular network in cancellous bone (Bousson et al. 2004, Chen et al. 2010, Chappard et al. 2013): the main parameters extracted are bone porosity, as well as the number, mean diameter, canal spacing and connectivity and so forth.

Three-dimensional analyses confirm that cortical porosity (canal diameter) increases with age, while the spaces between the canals decrease, especially in women, at least up to 60 years of age (Figure 32.13C, D). They also give additional information on the organization of canal networks within bone cortices and its variations with age: new branches appear and the merging of the widest canals explains the decrease in the number of canals measured on 2D images in older subjects (Thomas et al. 2000, Cooper et al. 2007). In the femoral neck cortex, Jordan et al. (2000) and Bell et al. (2001) described clusters of large remodeling osteons (named "super-osteons") that coalesce, leading to the "trabecularization" of the endosteal side of the cortex (Bell et al. 2001), so that the frontier is not clearly delineated between compact and trabecular tissue.

Osteocyte Lacunae

With resolutions of 1–2 µm, synchrotron imagery gives access to the 3D study of osteocyte lacunae and their canalicular networks (Carter et al. 2013b, Dong et al. 2014). Several 2D studies revealed a significant decrease in the spatial density of the lacunae with age or with osteoporosis, in both the cancellous bone of the iliac crest (Mullender et al. 1996, 2005) and the diaphyseal cortex of the femur (Busse et al. 2010). Conversely, Vashishth (2005) showed an age-related increase in cell lacuna density in the cancellous bone of the vertebral body in women but a decrease in the femoral cortex (Vashishth 2000). Recent studies also resulted in contrasted and variable data, depending on the authors and the sites investigated. Some tendency toward a decrease in cell lacunae with aging occurs in the anterior sector of the femoral diaphysis of women, but it does not seem to be statistically significant. Better evidence exists for a significant age-related reduction of the volume of osteocyte lacunae, i.e., old women present smaller and more rounded lacunae than younger ones (Carter et al. 2013a). A significant age-related decrease in lacunar density was shown in the cortex of the iliac crest, but only when both genders are mixed; conversely, a decrease in lacunar volume could not be shown in men or

VetBooks.ir

women (Bach-Gansmo 2016). In 13 samples from the femoral mid-diaphyseal region in two old women, Dong et al. (2014) showed that, beyond strong individual variability, lacunar density is significantly lower in highly cancellous regions (and *vice versa*). The synthetic study by Tiede-Lewis and Dallas (2019) confirmed these results. Moreover, the use of laser confocal microscopy after fluorescent labeling revealed a reduction of the lacunocanalicular networks in older women (70–86 years, n = 6) compared to younger subjects (20–23 years, n = 5). This alteration is predominantly due to canalicular rarefaction rather than to the decrease of cell lacuna density (Tiede-Lewis and Dallas 2019). It remains homogeneous in the whole cortex width, in contrast to canal porosity, which presents an increasing periosteal-endosteal gradient (Ashique et al. 2017).

Although 3D imagery allows us to collect more numerous and more realistic parameters than 2D imaging techniques, the sizes of the areas that it can analyze are restricted. As mentioned above, important differences in osteonal density, as well as in the number, size and shape of lacuna populations may exist in neighboring sectors of a single bone sample (Carter et al. 2013b, Gosha and Agnew 2016). For the present, general statements about the precise influence of aging on populations of osteocyte lacunae and their canaliculi cannot be drawn securely from available data. The local mechanical involvement of bones, especially their role in weight-bearing, are likely to be crucial elements, but their actual influence remains to be further deciphered (Gauthier et al. 2018).

Mineralization

An important approach to bone biology is the assessment of the total or local mineral content of the skeleton, i.e., the main element determining the mass of dry, defatted bone. First attempts conducted for this purpose relied on the measurement of ash weight, simply weighing the ash that remains after total calcination of a bone sample and expressing this weight in relation to the volume of the sample; bone mineral density (BMD) is thus expressed in grams per cubic centimeter. This parameter must not be confused with *bone mineral rate* (BMR), which is the relative weight (in percentage) of the ash compared to the total weight of the sample. Two main versions of the BMD parameter are commonly considered: it can refer to the total volume (bone substance + cavities: *V.Tt*) of a sample that can be a local fragment, an entire bone or the whole skeleton: this measurement is called *apparent mineral density*. Ash weight can also be expressed in reference to the volume of osseous tissue proper within a sample (*B.V*), all cavities (except cell lacunae) being excluded. This constitutes the *true mineral density*.

Ash Weight and Aging

Ash weight measurements indicate that, in the absence of any skeletal pathology (osteomalacia, osteopetrosis, etc.), true mineral density does not vary significantly with age, at least up to an age of 80 years in women. Its mean value is about 1.2 g/cm^3 in both genders (Laval-Jeantet et al. 1983, Boivin and Meunier 2002), but it tends to be lower (1.0 g/cm^3) in cancellous bone than in cortical (compact) bone. However, because apparent mineral density is based on the whole volume of the bone sample, its value depends on the amount of bone tissue present in the sample. This parameter, considered in the whole skeleton (Trotter and Hixon 1974) or a single bone, whether cancellous (Weaver and Chalmers 1966) or compact (Arnold 1960, Gong et al. 1964), decreases with age after the fourth decade (broad population studies in, e.g., Warming et al. 2002 and Kadam et al. 2018). Measuring true as well as apparent BMD is a destructive approach, but it is accurate and remains the reference technique for the validation of the diverse methods proposed for assessing bone mass.

An Overview of Radiologic Approaches to Mineral Density

A radiologic image is created by the differential attenuation of incident X photons in biological tissues, depending on their nature, quantity and mineralization rate (Beer-Lambert's law). X-ray imagery is of special interest because it gives a good contrast between bone and nonmineralized tissues, and it allows *in vivo* access to the inner structure of skeletal elements.

Evaluation of Bone Mineral Density In Vivo

Plain radiographs produce useful qualitative information on bone status. Simultaneous exposure of a reference aluminum or hydroxyapatite scale is used to calibrate gray values and quantify bone mineralization by photodensitometry: by referring the attenuation values of the scale with known density values, the mineral density of the bone can be determined. This technique is limited to the peripheral skeleton to avoid systematic errors due to variations in soft tissue thickness and composition. Measurements are frequently made in the second metacarpal or phalanges, with the scale inserted between the fingers. Photodensitometry is often combined with radiogrammetric measurements. Extensive data from population studies show a bone loss with aging in both genders (Maggio et al. 1997). But its interest for detecting bone deficit in other sites of the skeleton remains to be studied further.

Dual-energy X-ray absorptiometry (DXA) and quantitative CT (QCT) are the two major techniques available for evaluating bone mass *in vivo*. They were first developed for measuring sites of the skeleton where major osteoporosis fractures occur, i.e., lumbar spine and proximal femur, but they are also applied to peripheral skeletal sites (distal forearm, tibia, calcaneum). With DXA, bone mineral content is measured on 2D projection images integrating the totality of the bone sample through which the X-ray beam is propagated, and it is then expressed in grams per square centimeter. DXA BMD is an areal density. The measurement is thus size dependent and cannot distinguish between cortical and trabecular bone contributions.

With QCT, the measurements of BMD are expressed in grams per cubic centimeter, and they are not affected by shape or size of the bone; moreover, they are obtained for total volume of interest and for cortical and trabecular compartments separately. QCT BMD is an apparent BMD because the volume of interest considered is a mix of pure bone tissue and soft tissue (bone marrow, blood vessels, nerve endings). Devices dedicated to peripheral skeletal sites, i.e., pQCT, and mostly HR-pQCT,

permit a more precise segmentation of cortical and trabecular compartments of the appendicular skeleton. In clinical practice, results are compared to normal age-matched, sex-matched and ethnically matched reference databases (Prevrhal et al. 2003).

True BMD, at the bone tissue level, is only accessible with SR. Using specific calibration, the 3D distribution of the degree of mineralization can be evaluated within the sample (around 1.1 g/cm^3 in iliac crest samples; Nuzzo et al. 2002).

For further information about technical aspects, advantages and limitations of these methods, the reader is prompted to refer to Cann and Genant (1980), Cann (1988), Van Kuijk and van Rijn (2003), Link and Lang (2014), and Engelke (2017) on QCT; Lala et al. (2014) on pQCT and HR-pQCT; Adams (2003) and Jain and Vokes (2017) on DXA, and Nuzzo et al. (2002) on SR tomography.

Results of Quantitative Microradiography: Osteons vs Interstitial Bone

Gray level distribution in microradiographs clearly shows that bone mineralization differs in osteons and interstitial tissue, and may also vary within both of these compartments (Figure 32.14; see also Figure 32.11 and Chapter 11). Recent methods for image analysis and gray-level calibration allow us to complement morphological and microanatomical studies by quantifying the mineral content of a bone sample through the use of a reference aluminum scale exposed simultaneously with the osseous section. Results are expressed in gram of mineral per bone cubic centimeter (Boivin and Meunier 2002), or aluminum thickness equivalent (Bergot et al. 2009). In iliac crest samples, the mean degree of mineralization of bone (MDMB) is fairly constant and does not vary with age in the cortex or in bone trabeculae. Its mean value, *ca*. 1.1 g/cm^3, is close to that of true BMD obtained by ash weighing (Boivin and Meunier 2002). In midfemoral cortex (Figure 32.14), when osteonal bone is separated from interstitial bone through automatic segmentation, the variation with age of tissue mineralization in these two compartments can be compared. At all ages and in both genders, this parameter is lower in osteons than in interstitial bone, which agrees with visual observations of gray levels: secondary osteons are younger and thus less mature (less mineralized) than primary (interstitial) bone. In women, osteonal mineralization is maximal between 30 and 50 years, and minimal in the following decade, 50–59 years. In the oldest subjects, it is slightly higher in men than in women (Figure 32.15). The difference in mineralization between the two compartments tends to increase with age, especially in women (Bergot et al. 2009). Such increasing heterogeneity

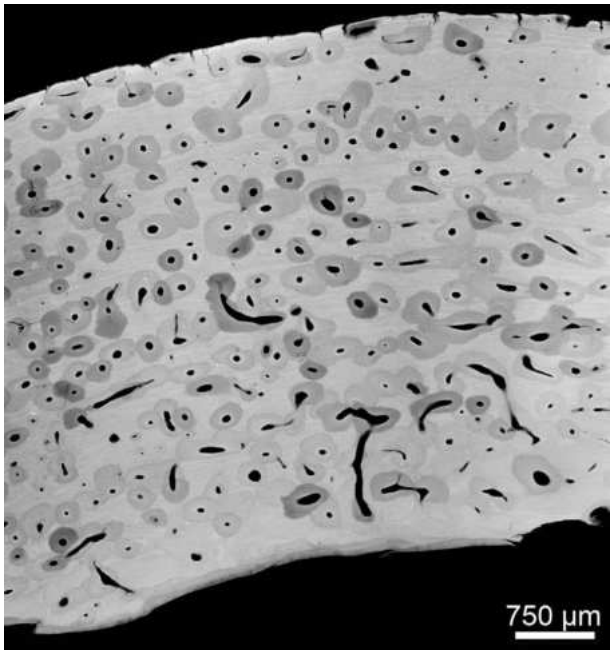


FIGURE 32.14 Microradiograph of 100-µm-thick section of femoral mid-diaphysis, mineral content of secondary osteons and interstitial tissue. Interstitial bone between the osteons has the lightest (whitish) gray values. According to the date of their formation, the secondary osteons display variable gray values (the youngest, poorly mineralized, are the darkest).

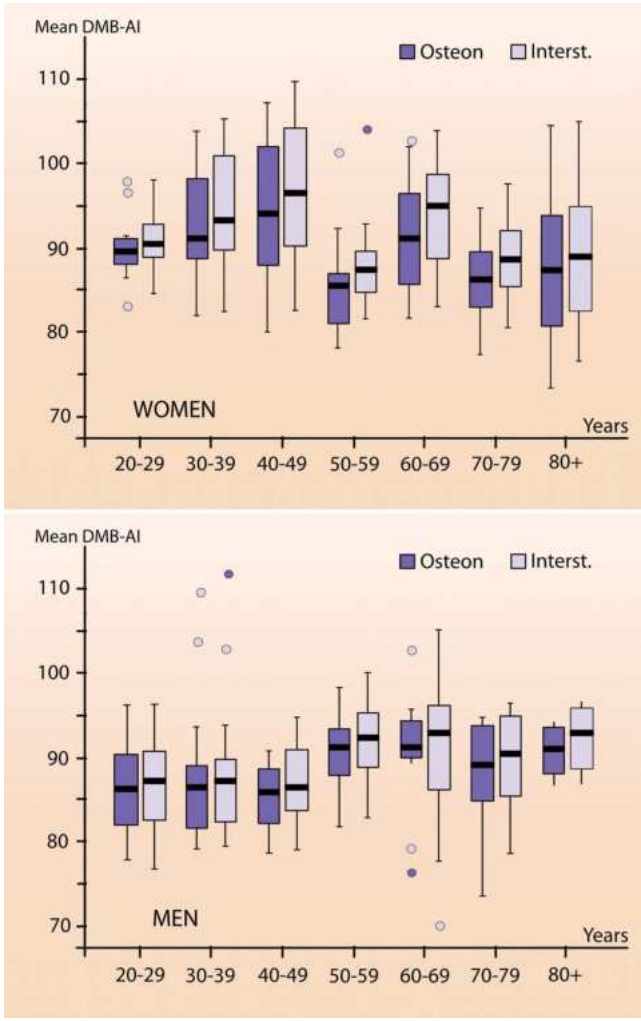


FIGURE 32.15 Whisker plots showing the variations of mineralization in osteons and interstitial (Insterst.) tissue separately, from femoral mid-shaft (cf. Figure 32.14). DMB-Al is an aluminum thickness equivalent constituting a relative expression of the degree of bone mineralization. In females (A), a sharp decrease of mineralization is observed between the fifth and sixth decades. Mean degree of mineralization in the elderly is higher in males (B) than in females, in both compartments.

VetBooks.ir

of mineralization in the whole cortical tissue, together with a decrease in bone volume, may contribute to bone fragility (brittleness), and to an increased fracture risk.

Frequent Structural and Mineralization Abnormalities in Aged Subjects

Several microanatomical and histological peculiarities are typically encountered in cancellous and compact osseous formations in elderly persons, as well as more diffuse, and lesser documented, possible alterations involving the organic and mineral phases of intercellular bone matrix (e.g., Milovanovic et al. 2018, Burr 2019). These degradations of skeletal quality are not exclusive of senescent processes, but their frequency proves to be low in young individuals, and very high in the elderly.

Trabecular Microcalli

As described above, bone trabeculae in cancellous formations become thinner with age and, consequently, they may break and be individually repaired through the transitory formation of a microcallus (Figure 32.16), which is subsequently resorbed through remodeling. Microcalli frequently occur in the vertically oriented trabeculae of human vertebral bodies, in the vicinity of the vertebral plateau, a region exposed to strong mechanical stress. They are a sign of fragility of the trabecular network (Hahn et al. 1995).

Microcracks

In pace with the general degradation of bone quality with age and the development of osteoporosis, fatigue microfractures proliferate in cancellous and compact bone tissues (e.g., Mori et al. 1997, Schaffler et al. 1995). Three-dimensional imagery also allows us to visualize microcracks in the bone matrix and follow their propagation with aging in cancellous (Arlot et al. 2008, Larrue et al. 2011) and compact (Vashishth et al. 2000)

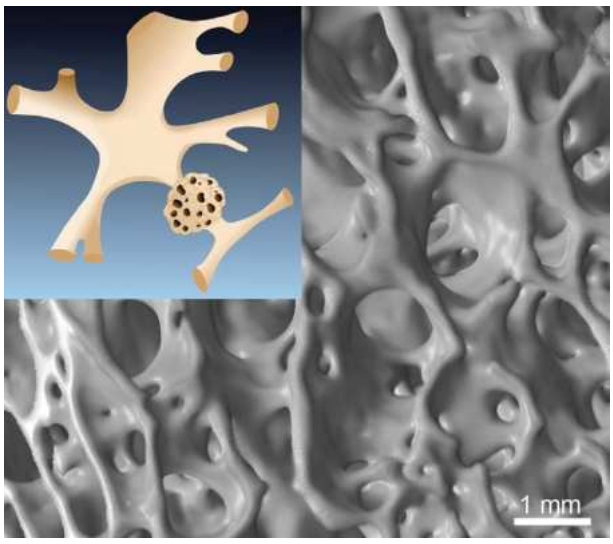


FIGURE 32.16 Trabecular network in the vertebral centrum of a young, healthy adult. The inset shows the aspect of trabecular microcalli that occur with the osteoporotic thinning of individual trabeculae.

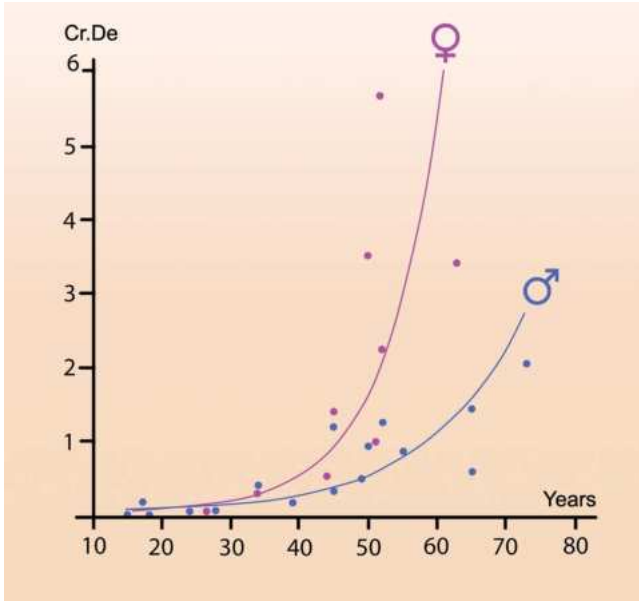


FIGURE 32.17 Exponential increase in the density of cortical microcracks (Cr. De, i.e. the number of cracks per square millimeter) with age in the cortex of the mid-diaphysis of the human femur (data from Schaffler et al. 1995.)

osseous formations. In cancellous bone, rodlike trabeculae are more susceptible to microcrack proliferation than platelike ones. Age-related microdamage also occurs in calcified cartilage. Microcracks are small fissures 40–100 µm in length and 5–6 µm in width (Wenzel et al. 1996) formed within the bone matrix by long-lasting iterative mechanical stresses. They are normally repaired through bone remodeling (according to Okazaki et al. 2014, microcalli could also be involved in this process in cancellous tissue), a restoration mechanism that progressively fails with aging. Schaffler et al.'s (1995) data show that microcrack density in compact bone (human rib cortex) increases exponentially with age (Figure 32.17), especially in females. In elderly persons, an important part of osteoporotic fractures affecting either individual trabeculae or broader osseous volumes result from the accumulation and coalescence of nonrepaired microfractures in cortical and cancellous tissues (e.g., Okazaki et al. 2014).

Hypermineralized Zones

In aged subjects, imagery techniques based on X-ray attenuation, (microradiography, SR) reveal clear and bright zones in the interstitial (extraosteonal) matrix, especially in the external-most region of the femoral neck cortex (Bousson et al. 2004) and in the femoral diaphysis. Because gray values are directly proportional to mineral content, such zones thus reflect local hypermineralization. They have also been observed through back-scatter electron microscopy (BSEM), at the periphery of the femoral neck and on the greater trochanter in the vicinity of tendinous or ligamentous insertions, in elder subjects (Vajda and Bloebaum 1999). The ultrastructural characteristics of these hypermineralized areas, as well as their origin and meaning, remain unclear.

VetBooks.ir

Occlusion of Osteocyte Lacunae

In addition to age-related decrease in the spatial density of osteocyte lacunae, a significant increase in the frequency of lacunar and canalicular occlusion by a hypermineralized substance (micropetrosis) was first observed by Frost (1960) in extra-Haversian bone of elderly subjects. Such hypermineralized lacunae were later reported and described in the femoral diaphyseal cortex in aged subjects of both genders (Busse et al. 2010). They were found to be less abundant in rodents than in humans, perhaps due to the short life span of rodents (Busse et al. 2010, Tiede-Lewis and Dallas 2019).

A Synthesis of Age-Related Bone Loss in Humans

Available data, obtained through numerous technical approaches and conducted at several levels of integration, from entire bones to cells, converge to indicate that aging and skeletal senescence mainly result in a decrease of the amount of bone (bone mass and inner bone volume), combined with alterations of matrix and cells. With aging, the osseous balance, i.e., the net result of bone accretion and bone resorption in each remodeling unit (the BMUs), becomes negative. Bone accretion then fails to compensate for bone resorption and, at local or general scales, bone mass decreases. The importance of bone loss varies with gender, the kind of bone considered (cancellous vs compact) and the skeletal site. Cancellous bone (mainly located in vertebral body and long bone metaphyses) is in contact with hematopoietic marrow through a very broad area, which enhances remodeling activity. This situation explains why bone loss in trabecular formations is proportionally more pronounced than in compact, cortical bone, although it may be less in absolute quantity.

In humans, the peak bone mass characteristic of fully grown young adults gradually decreases throughout life. In women, where the process is most pronounced, the normal curve of age-related bone loss, as measured through BMD in lumbar vertebrae, shows a plateau or a slight decrease up to the age of some 40 years, then a rapid drop until about 60 years (ages 40–60 years correspond to the perimenopausal stage), followed by a slow but steady involution until the end of life. Between 20 and 80 years a woman loses at least 30% of her peak bone mass, with substantial differences from one site to another. In men, age-related bone mass decrease is more gradual, slower and less pronounced throughout life than in women.

Significant BMD differences exist among Caucasian, African, Asian and Hispanic populations (Trotter 1960, Wang et al. 2009a, Nam et al. 2010, Zengin et al. 2016, Wang et al. 2019). Therefore, reference databases used in clinical practice to estimate age-related bone loss must be specific to skeletal sites, genders and main ethnic types. They are built with healthy subjects (i.e., subjects devoid of illness or medical treatment susceptible to affect bone metabolism) of all age classes for each gender and ethnic group. The reference mean values thus obtained nevertheless conceal substantial individual variability because BMD is influenced not only by genetic and ethnic characteristics, but also by nutritional (calcium intake), environmental (sunlight) and behavioral (physical activity) factors.

Age-related bone modifications represent a general phenomenon because they involve all individuals in a population and all bones in an individual skeleton. However, bone loss is not even and synchronous in all skeletal sites. Therefore, measurements performed in one site may prove irrelevant for another site or for the skeleton as a whole. Local or transient factors may have a positive or negative effect on bone mass. For example, pronounced asymmetry in bone mass exists between the right and left arms of regular tennis players: BMD level in the dominant arm is significantly higher than in nonplayers, especially in young subjects (Haapasalo et al. 1996). Conversely, immobilization or weightlessness provokes a rapid and severe bone loss, with a return to normal when such conditions cease (Spector et al. 2009). Pregnancy and breastfeeding also affect maternal skeletons, due to a rise in the recycling of bone calcium and phosphorus that they temporarily provoke. Such a process of calcium homeostasis does not seem to have a durable and marked effect on the maternal skeleton, at least in properly fed populations (review by Winter et al. 2020; but see also Sowers 1996).

Conversely, skeletal senescence and the gradual decrease in bone mass that occurs in adult life are irreversible, and are accompanied by anatomical and architectural modifications of the skeleton. Through remodeling, bone formations reorganize and modify their architecture to maintain and optimize their functional capabilities (same performance with less substance) for locomotion or soft tissue support.

Remarks on Age-Related Bone Loss in Nonhuman Taxa

Compared to the research effort devoted to humans, studies of bone aging in other species look particularly sparse, at least for wild populations in their natural habitat. Conversely, several laboratory animals, including rodents (mice and rats), lagomorphs (rabbit), canines (beagle), primates (rhesus macaque) and occasionally domestic artiodactyls (ewe, pig) and perissodactyls, are broadly used as models for experimental research on “aging”. Most of the studies thus conducted actually deal with physiological situations provoking bone loss such as ovariectomy or immobilization, or with experimental antiosteoporotic drug therapies (review in Barlet et al. 1994, Turner 2001). Studies in nonhuman taxa are seldom related to natural senescence.

Comparative data suggest that, because of the many (and sometimes stochastic) factors that may influence bone mass and bone remodeling, the problem proves to be species specific, and no animal model can be considered as a reliable proxy to human bone aging (Barlet et al. 1994). Some broad tendencies exist, at least among mammals for which knowledge is currently available.

An Overview of Skeletal Aging Processes in Nonhuman Mammals

All the typical expressions of skeletal aging and senescence observed in the human skeleton also occur, and in roughly similar conditions, in nonhuman eutherian species; however, they may not affect the same bones with comparable intensity. For example, some precise (statistically based) data about age-dependent

VetBooks.ir

decrease in BMD or bone volume fraction in the two most classical laboratory models are the following. In rats (*Rattus norvegicus*), between the ages of 3 and 27 months, BMD in cancellous bone decreases 49.7% in the vertebral centra, 58.4% in the femoral neck and 71.4 % in the proximal metaphysis of the tibia (Wang et al. 2001; see also Nyman 2018 for review and Sontag 1994 for contrasting data). In the rhesus macaque (*Macaca mulatta*), BMD modification in males between the ages of 10 (peak bone mass) and 34 years reaches 28% in the cancellous tissue of the distal radial metaphysis, and 58% in the compact bone of the lumbar spine (Colman et al. 1999). Comparable data, showing similar trends for both compact (porosity measurements) and cancellous bone, are available for numerous other mammals (e.g., Jowsey 1968), including rabbits (metaphyseal spongiosa and shaft cortex of the femur: Pazzaglia et al. 2015) and pigs (mandibular ramus: Willems et al. 2007).

The detailed reference BMD standards for the baboon (*Papio hamadryas*) presented by Havill et al. (2003) reveal a general age-related bone loss pattern similar to that of humans. Caution must nevertheless be paid to the interpretation of comparative data, because skeletal aging is, to a large extent, a species-specific and possibly a population-specific trait. The case of the albino rat (*R. norvegicus*) is important for this purpose: this species has basic biological differences from humans. First, the somatic growth of rats declines progressively but is continued after sexual maturity; the concept of peak skeletal mass is thus somewhat different for them than for larger animals (dogs, ewes, pigs and humans). Moreover, there is no well-characterized menopausal stage in this species, and cortical bone lacks Haversian osteons; in rodents, bone rarefaction does not lead to fractures. (see Barlet et al. 1994 and Turner 2001 for discussion on these issues). Bone mass, microarchitecture and level of remodeling are very different among existing strains of mice (e.g., Amblard et al. 2003). Mere comparative extrapolations from, or toward, this species and others are of questionable value.

In addition to BMD and other histomorphometric data, mammals may also show similar anatomical signs of skeletal senescence, such as compression of intervertebral disks and vertebral centra (e.g., Vincent et al. 2019 for mice), arthritic symptoms or microfracture accumulation (e.g., Frank et al. 2002). These easily detectable peculiarities constitute strong and fairly reliable indications of skeletal senility (although young individuals may display them rarely).

Nonmammalian Taxa

In nonmammalian vertebrates, homeotherms generally have a more active metabolism than poikilotherms, which results in more active bone remodeling. In birds, the skeleton is particularly involved in the formation of important calcium reserves for eggshell formation, a functional role endorsed by the formation and resorption, under hormonal control, of a special skeletal tissue, the medullary bone (e.g., Canoville et al. 2019; see Chapter 27). True (ordinary) cortical or cancellous bone formation is not significantly involved in this process; otherwise, the modalities of skeletal aging and senescence in birds are poorly known. In the adults of most species, only a thin cortical ring remains at the periphery of long bone shafts in somatically adult individuals. This bone, deposited at the end of somatic growth, may or may not be remodeled, but Haversian substitution, if present, is rapid and soon extends to the whole cortex. Despite the thinness of long bone cortices in most birds, age-induced osteopenia, through increased cortical porosity, has been observed in the ulna of one species at least, the rooster, *Gallus gallus* (Srinivasan et al. 2000).

In ectopoikilotherms, the rate of somatic growth is strongly influenced by environmental conditions (temperature, humidity and food availability), a situation that results in substantial size variability and cyclic growth. The annual formation of cyclic growth marks, taken by some authors (e.g., Castanet et al. 1993) as an "aging" phenomenon (in a strict reading of the term), is unrelated to senescence and excluded from the scope of this review (see Chapter 31). The existence of indefinite (lifelong) growth was considered a general characteristic in taxa possessing "primitive" epiphyses (i.e., epiphyses devoid of secondary ossification centers, according to Haines (1938) vocabulary), but this dogma is now questioned (see, e.g., Woodward et al. 2011 for the American alligator). Growth decline in large forms such as crocodilians and tortoises is very gradual and may spread over decades, at least at some skeletal sites. The concept of peak bone mass is then irrelevant, and the threshold marking the onset of senility very imprecise. Studies conducted on age-related alterations of the skeleton are particularly sparse (captive animals are inappropriate for such studies), and most of them fail to clearly separate the consequences of aging proper from the cumulative effect of repeated reproduction periods, or the effects of stochastic (mainly climatic) events on the physiology of the animals (see, e.g., Wink and Elsey 1986 for *A. mississippiensis*, and Buffrénil and Francillon-Vieillot 2001 for the Nile monitor, *V. niloticus*). One of the most robust results is that, in large forms such as crocodilians, turtles and a few varanids, the spatial density of secondary osteons, although relatively low, gradually increases with age (then given by yearly cyclic growth marks) in deep cortical layers.

Concluding Remarks

Assessing Bone Senescence in Wild and Fossil Specimens

In the absence of economic incitement or public health stakes, studies conducted on wild animals remain scarce, if not anecdotal. Skeletal aging processes in these taxa remain largely unknown. A double problem remains to be solved in wild taxa. On the one hand, statistically reliable reference data for assessing the degree of the deterioration of bone quality are lacking. On the other hand, the natural longevity of individuals living in natural conditions is relatively short, and most of them do not reach an age at which skeletal senescence processes begin. This is particularly true for game species, for which numerous specimens can be collected but, by definition, the latter are unlikely to have reached advanced ages. Beyond histomorphometric or histological clues, skeletal senescence can be reliably inferred in domestic or wild, extant or extinct taxa by the observation of external qualitative indices such as osteoarthritic symptoms, articular wear or exostoses.

VetBooks.ir

Osteoporosis from a Genetic and Evolutionary Perspective

Comparative data currently available show that age-dependent bone mass decreases and that osteoporosis affects all mammalian clades and probably all other tetrapods (and even vertebrates), beyond obvious differences in aging conditions, natural longevity and physiological characteristics among taxa at all phylogenetic ranks. These processes appear universal and most likely rely on highly plesiomorphic genetic controls that may show substantial intraspecific variability. Considerable research is dedicated to the genetics of osteoporosis in humans and laboratory animals. Experimental studies as well as clinical observations conclude that basic skeletal characteristics are highly heritable traits with between 70% (Rosen et al. 2000) and 85% (Ralston 1999) heritability for bone mass values and 50% for peak bone mass (Rosen 2000). Heritable skeletal features also characterize the course of skeletal growth. Significant, genetically controlled bone mass differences occur as early as the age of 10 years in humans (Duren et al. 2007), and numerous, well-documented familial and populational peculiarities in the severity, chronology and skeletal targets of osteoporotic processes have been published (e.g., Diaz et al. 1997, Barthe et al. 1998, Lau et al. 2005, Laine et al. 2007). As described above, the age-dependent decrease in bone mass basically results from imbalanced remodeling. Considering the complexity of bone remodeling and the diversity of cells, cell precursors, cell receptors, systemic, autocrine, paracrine factors and so forth involved in this process, imbalance can have many possible causes and reflect various genetic deficiencies (see, e.g., reviews by Blair et al. 2008, Zhu et al. 2018). The genetic studies (especially genome-wide association studies [GWAS]: see, e.g., Kung 2010) conducted in laboratory animals (e.g., Xiao et al. 2007, Duncan and Brown 2010, Alam et al. 2011, Youlten and Baldock 2019) and humans (e.g., Brown 2010) result in the identification of a considerable set of genes (further complexified by pleiotropic actions) likely involved in the etiology of osteoporosis. The recent review by Morris et al. (2019) lists as an atlas all possible genetic influences on this process (see also Trajanoska and Rivadeneira 2019).

The multiplicity of the factors involved in the regulation of bone mass, through balanced or imbalanced remodeling, necessarily creates great interindividual variability (a well-documented fact), because each of these factors may undergo mutations. In an evolutionary perspective, this variability can be a prominent target for selection, as far as the adaptation of a clade requires a modification of bone mass toward either a decrease or an increase, at a general or a local level in the skeleton. Such specific requirements characterize several adaptations, including the secondary adaptation of tetrapods to an aquatic life (e.g., ichthyosaurs, mosasaurs, sirenians, cetaceans, etc.). In this adaptive context, the tetrapod skeleton no longer retains its previous weight-bearing role. Therefore, depending on the precise adaptive requirements of the taxon, its mass may be increased to become a ballast for buoyancy and trim control, or eliminated as much as possible to reduce body inertia and improve agility and swimming speed. Comparative data show that these modifications rely on the selection of diverse patterns of alteration, degenerative or pathological in humans but adaptational in the taxa concerned, of remodeling balance, including osteoporotic-like processes. This particular issue is further considered in Chapter 36.

Acknowledgments

We are extremely grateful to our colleague Dr. Alexandra Quilhac (Sorbonne Université, UPMC, Paris, France) for her decisive help in the conception and realization of the figures of this chapter. We also thank Dr. Valérie Courpron for the generous authorization she gave us to use her synchrotron images in this article, and Caroline Hébert-Jacquier for her help in the presentation of the figures.

REFERENCES

Acsàdi, G. and J. Nemeskeri. 1970. *History of human life span and mortality*. Akademiai Kiado (Publ.), Budapest.

Adams, J. E. 2003. Dual-energy x-ray absorptiometry. In *Radiology of osteoporosis*, ed. Grampp, S., 87–100. Berlin Heidelberg, Springer-Verlag.

Alam, I., et al. 2011. Heterogenous stock rat: a unique animal model for mapping genes influencing bone fragility. *Bone* 48: 1169–1177.

Alexander, C. 2001. Idiopathic osteoporosis: an evolutional dysadaptation? *Ann. Rheum. Dis.* 60: 554–558.

Allen, M. R. and D. B. Burr. 2014. Bone modeling and remodeling. In *Basic and applied bone biology*, eds. D. B. Burr and M. R. Allen, 75–92. London, Academic Press.

Allen, M. R. and K. Krohn. 2014. Skeletal imaging. In *Basic and applied bone biology*, eds. Burr, D. B. and M. R. Allen, 93–113. London, Academic Press.

Almeida, M. and S. Manolagas. 2020. Aging and Bone. In *Principles of bone biology*, eds. Bilezikian, J.-P., T. L. Clemens, T. J. Martin and C. J. Rosen, 275–292. Cambridge, MA: Academic Press – Elsevier Inc.

Almeida, M. and C. A. O'Brien. 2013. Basic biology of skeletal aging: role of stress response pathways. *J. Gerontol. A Biol. Sci. Med. Sci.* 68: 1197–1208.

Amblard, D., et al. 2003. Lower bone cellular activities in male and female mature C3H/HeJ mice are associated with higher bone mass and different pyridinium crosslink profiles compared to C57BL/6J mice. *J. Bone Miner. Metab.* 21: 377–387.

Andronowski, J. M., et al. 2018. Recent advancements in the analysis of bone microstructure: new dimensions in forensic anthropology. *Forensic Sci. Res.* 3: 294–309.

Arlot, M. E., et al. 2008. Microarchitecture influences microdamage accumulation in human vertebral trabecular bone. *J. Bone Miner. Res.* 23: 1613–1618.

Arnold, J. S. 1960. Quantitation of mineralization of bone as an organ and tissue in osteoporosis. *Clin. Orthop. Rel. Res.* 17: 167–175.

Ashique, A. M., et al. 2017. Lacunar-canalicular network in femoral cortical bone is reduced in aged women and is predominantly due to a loss of canalicular porosity. *Bone Rep.* 7: 9–16.

Atkinson, P. J. 1965. Changes in resorption spaces in femoral cortical bone with age. *J. Pathol. Bacteriol.* 89: 173–178.

VetBooks.ir

Bach-Gansmo, F. L., et al. 2016. Osteocyte lacunar properties and cortical microstructure in human iliac crest as a function of age and sex. *Bone* 91: 11–19.

Barlet, J. P., et al. 1994. Modèles animaux d'ostéoporose postménopausique. *Reprod. Nutr. Dev.* 34: 221–236.

Barthe, N., et al. 1998. Measurement of bone mineral density in mother-daughter pairs for evaluating the family influence on bone mass acquisition: a GRIO survey. *Osteoporos. Int.* 8: 379–384.

Bell, K. L., et al. 2001. Super-osteons (remodeling clusters) in the cortex of the femoral shaft: influence of age and gender. *Anat. Rec.* 264: 378–386.

Benhamou, C. L., et al. 1994. Fractal organization of trabecular bone images on calcaneus radiographs. *J. Bone Miner. Res.* 9: 1909–1918.

Bergot, C. and J. P. Bocquet. 1976. Étude systématique en fonction de l'âge de l'os spongieux et de l'os cortical de l'humérus et du fémur. *Bull. Mém. Soc. Anthropol. Paris, Série XIII* 3: 215–242.

Bergot, C., et al. 1990. Variation du volume osseux et de la densité minérale au cours du vieillissement chez l'homme. *Rev. Rhumat.* 57: 791–798.

Bergot, C., et al. 1988. Measurement of anisotropic vertebral trabecular bone loss during aging by quantitative image analysis. *Calcif. Tissue Int.* 43: 143–149.

Bergot, C., et al. 2009. The degree and distribution of cortical bone mineralization in the human femoral shaft change with age and sex in a microradiographic study. *Bone* 45: 435–442.

Bes, C., et al. 2012. Can bone quality be predicted accurately by Singh index in patients with rheumatoid arthritis? *Clin. Rheumatol.* 31: 85–89.

Bjornerem, A., et al. 2018. Menopause-related appendicular bone loss is mainly cortical and results in increased cortical porosity. *J. Bone Miner. Res.* 33: 598–605.

Blair, H. C., et al. 2008. The developmental basis of skeletal cell differentiation and the molecular basis of major skeletal defects. *Biol. Rev.* 83: 401–415.

Bloom, R. A. and J. W. Laws. 1970. Humeral cortical thickness as an index of osteoporosis in women. *Br. J. Radiol.* 43: 522–527.

Bocquet, J. P. and C. Bergot. 1977. Évolution de l'os cortical de l'humérus en fonction de l'âge. *Bull. Mem. Soc. Anthropol. Paris, Série XIII* 4: 359–369.

Boivin, G. and P. J. Meunier. 2002. The degree of mineralization of bone tissue measured by computerized quantitative contact microradiography. *Calcif. Tissue Int.* 70: 503–511.

Boskey, A. L. and R. Coleman. 2010. Aging and bone. *J. Dent. Res.* 89: 1333–1348.

Bousson, V., et al. 2001. Distribution of intracortical porosity in human midfemoral cortex by age and gender. *J. Bone Miner. Res.* 16: 1308–1317.

Bousson, V., et al. 2004. Cortical bone in the human femoral neck; three-dimensional appearance and porosity using synchrotron radiation. *J. Bone Miner. Res.* 19: 794–801.

Brooks, S. and J. M. Suchey. 1990. Skeletal age determination based on the os pubis: a comparison of the Acsàdi-Nemeskeri and Suchey-Brooks methods. *Human Evol.* 5: 227–238.

Brown, M. 2010. Genomewide studies in osteoporosis. *Bone* 46: S9.

Buffrénil, V. de and H. Francillon-Vieillot. 2001. Ontogenetic changes in bone compactness in male and female Nile monitors. *J. Zool.* 254: 539–546.

Burr, D. B. 2019. Changes in bone matrix properties with aging. *Bone* 120: 85–93.

Busse, B., et al. 2010. Decrease in the osteocyte lacunar density accompanied by hypermineralized lacunar occlusion reveals failure and delay of remodeling in aged human bone. *Aging Cell* 9: 1065–1075.

Cann, C. E. 1988. Quantitative CT for determination of bone mineral density: a review. *Radiology* 166: 509–522.

Cann, C. E. and H. K. Genant. 1980. Precise measurements of vertebral mineral content using computed tomography. *J. Comput. Assist. Tomogr.* 4: 493–500.

Canoville, A., et al. 2019. Systemic distribution of medullary bone in the avian skeleton: ground truthing criteria for the identification of reproductive tissues in extinct avemetatarsalia. *BMC Evol. Biol.* 19: 71. doi.org/10.1186/s12862-019-1402-7.

Carter, Y., et al. 2013a. Femoral osteocyte lacunar density, volume and morphology in women across the lifespan. *J. Struct. Biol.* 183: 519–526.

Carter, Y., et al. 2013b. Variation in osteocyte lacunar morphology and density in the human femur: a synchrotron radiation μ-CT study. *Bone* 52: 126–132.

Castanet, J., et al. 1993. Bone and individual aging. In *Bone. Vol. 7: Bone growth B*, ed. Hall, B. K., 245–283. Boca Raton, CRC Press.

Chappard, C., et al. 2013. 3D characterization of pores in the cortical bone of human femur in the elderly at different locations as determined by synchrotron micro-computed tomography images. *Osteoporos. Int.* 24: 1023–1033.

Chen, H., et al. 2008. Regional variations of vertebral trabecular bone microstructure with age and gender. *Osteoporos. Int.* 19: 1473–1483.

Chen, H., et al. 2010. Age and gender dependent changes in three-dimensional microstructure of cortical and trabecular bone at the human femoral neck. *Osteoporos. Int.* 21: 627–636.

Colman, R. J., et al. 1999. Skeletal effects of aging in male rhesus monkeys. *Bone* 24: 17–23.

Cooper, D. M. L., et al. 2007. Age-dependent change in the 3D structure of cortical porosity at the human femoral midshaft. *Bone* 40: 957–965.

Courpron, P., et al. 1973. Données histologiques quantitatives sur le vieillissement osseux humain. *Rev. Rhum. Mal. Ostéoartic.* 40: 469–483.

Currey, J. D. 2002. *Bones. Structure and mechanics*. Princeton and Oxford, Princeton University Press.

Currey, J. D. and R. Shahar. 2013. Cavities in the compact bone in tetrapods and fish and their effect in mechanical properties. *J. Struct. Biol.* 183: 107–122.

Dempster, D. W., et al. 2013. Standardized nomenclature, symbols, and units for bone histomorphometry: a 2012 update of the report of the ASBMR Histomorphometry Nomenclature Committee. *J. Bone Miner. Res.* 28: 1–16.

Dequeker, J. 1975. Bone and ageing. *Ann. Rheumat. Dis.* 34: 100–115.

Dequeker, J. 1976. Quantitative radiology: radiogrammetry of cortical bone. *Br. J. Radiol.* 49: 912–920.

Dequeker, J. 1980. Measurement of bone mass and bone remodeling "in vivo." Value of the radiogrammetric approach. *Acta Rheumatol.* 4: 40–75.

Dewar, C. 2015. Diagnosis and treatment of vertebral compression fracture. *Radiol. Technol.* 86: 301–320.

Diaz, M. N., et al. 1997. The influence of family history of hip fracture on the risk of vertebral deformity in men and women: the European vertebral osteoporosis study. *Bone* 20: 145–149.

Dong, P., et al. 2014. 3D osteocyte lacunar morphometric properties and distributions in human femoral cortical bone using synchrotron radiation micro-CT images. *Bone* 60: 172–185

Dorr, L. D., et al. 1993. Structural and cellular assessment of bone quality of proximal femur. *Bone* 14: 231–242.

Doube, M. 2015. The ellipsoid factor for quantification of rods, plates, and intermediate forms in 3D geometries. *Front. Endocrinol.* 6: 1–5.

Dowdell, J., et al. 2017. Intervertebral disk degeneration and repair. *Neurosurgery* 80: S46–S54.

Duncan, E. L. and M. A. Brown. 2010. Mapping genes for osteoporosis – old dogs and new tricks. *Bone* 46: 1219–1225.

Duren, D. L., et al. 2007. Quantitative genetics of cortical bone mass in healthy 10-year-old children from the Fels longitudinal study. *Bone* 40: 464–470.

Eastell, R., et al. 1991. Classification of vertebral fractures. *J. Bone Miner. Res.* 6: 207–215.

Eastell, R., et al. 1989. Unequal decrease in bone density of the lumbar spine and ultradistal radius in Colles' and vertebral fracture syndromes. *J. Clin. Invest.* 83: 168–174.

Engelke, K. 2017. Quantitative computed tomography – current status and new developments. *J. Clin. Densitom.* 20: 309–321.

Epstein, S., et al. 1986. The influence of age on bone mineral regulating hormones. *Bone* 7: 421–425.

Farlay, D., et al. 2019. Bone remodeling and bone matrix quality before and after menopause in healthy women. *Bone* 128: 115030. doi.org/10.1016/j.bone.2019.08.003.

Faulkner, K. G., et al. 1991. Non-invasive measurements of bone mass, structure and strength: current methods and experimental techniques. *Am. J. Radiol.* 157:1229–1237.

Fields A. J., et al. 2009. Role of trabecular microarchitecture in whole-vertebral body mechanical behavior. *J. Bone Miner. Res.* 24: 1523–1530.

Fields, A. J., et al. 2011. Influence of vertebral trabeculae on the compressive strength of the human vertebra. *J. Bone Miner. Res.* 26: 263–269.

Frank, J. D., et al. 2002. Aging and accumulation of microdamage in canine bone. *Bone* 30: 201–206.

Frost, H. M. 1960. Micropetrosis. *J. Bone Joint Surg.* 42: 144–150.

Frost, H. M. 1964. Dynamics of bone remodeling. In *Bone biodynamics*, ed. Frost H. M., 315–334. Boston, Little Brown.

Frost, H. M. 1983. Bone histomorphomery: analysis of trabecular bone dynamics. In *Bone histomorphometry. Techniques and interpretation*, ed. Recker R., 109–131. Boca Raton, CRC Press.

Galkin, F., et al. 2019. Reversibility of irreversible aging. *Ageing Res. Rev.* 49: 104–114.

Garn, S. M. ed. 1980. *The earlier gain and the later loss of cortical bone*. Springfield, IL, Charles C Thomas.

Gauthier, R., et al. 2018. 3D microstructural analysis of human cortical bone in paired femoral diaphysis, femoral neck and radial diaphysis. *J. Struct. Biol.* 204: 182–190.

Genant, H. K., et al. 1993. Vertebral fracture assessment using a semi-quantitative technique. *J. Bone Miner. Res.* 8: 1137–1148.

Gong, H., et al. 2005. Regional variations in microstructural properties of vertebral trabeculae with aging. *J. Bone Miner. Res.* 23: 174–180.

Gong, J. R., et al. 1964. Composition of trabecular and cortical bone. *Anat. Rec.* 149: 325–332.

Gosha, T. P. and A. M. Agnew. 2016. Spatial variation in osteon population density at the human femoral midshaft: histomorphometric adaptations to habitual load environment. *J. Anat.* 228: 733–745.

Guglielmi, G. and D. Diacinti. 2003. Vertebral morphometry. In *Radiology of osteoporosis*, ed. Grampp, S., 101–110. Berlin, Heidelberg, Springer-Verlag.

Gustafson, G. 1950. Age determinations on teeth. *J. Am. Dent. Assoc.* 41: 45–54.

Haapasalo, H., et al. 1996. Dimensions and estimated mechanical characteristics of the humerus after long-term tennis loading. *J. Bone Miner. Res.* 11: 864–872.

Hahn, M., et al. 1995. Microcallus formations of the cancellous bone: a quantitative analysis of the human spine. *J. Bone Miner. Res.* 10: 1410–1416.

Haines, R. W. 1938. The primitive form of epiphyses in the long bones of tetrapods. *J. Anat. London* 72: 323–343.

Hall, M. C. 1961. The trabecular patterns of the neck of the femur with particular reference to changes in osteoporosis. *Can. Med. Assoc. J.* 85: 1141–1144.

Hall, M. C. and M. Rosser. 1963. The structure of the upper end of the humerus with reference to osteoporotic changes in senescence leading to fractures. *Can. Med. Assoc. J.* 88: 290–294.

Hanson, N. A. and C. M. Bagi. 2004. Alternative approach to assessment of bone quality using micro-computed tomography. *Bone* 35: 326–333.

Hauschild, O., et al. 2009. Evaluation of Singh index for assessment of osteoporosis using digital radiography. *Eur. J. Radiol.* 71: 152–158.

Havill, L. M., et al. 2003. Bone mineral density reference in adult baboons (*Papio hamadryas*) by sex and age. *Bone* 33: 877–888.

He, Q. F., et al. 2018. Radiographic predictors for bone mineral density: cortical thickness and index of the distal femur. *Bone Joint Res.* 7: 468–475.

Hernandez, J. D., et al. 2008. Technical approach to iliac crest biopsy. *Clin. J. Am. Soc. Nephrol.* 3: S164–S169.

Hoffman, C. M., et al. 2019. Impact of aging on bone, marrow and their interactions. *Bone* 119: 1–7.

Iscan M. Y., et al. 1992. Age assessment from the sternal end of the rib and pubis symphysis: a systemic comparison. *Anthropologie* 30: 41–44.

Jain, R.K. and T. Vokes. 2017. Dual-energy x-ray absorptiometry. *J. Clin. Densitom.* 20: 291–303.

Jhamaria, N. L., et al. 1983. The trabecular pattern of the calcaneum as an index of osteoporosis. *J. Bone Joint Surg. Br.* 65: 195–198.

Jordan, G.R., et al. 2000. Spatial clustering of remodeling osteons in the femoral neck cortex: a cause of weakness in hip fracture? *Bone* 26: 305–313.

Jowsey, J. 1960. Age changes in human bone. *Clin. Orthop.* 17: 210–218.

Jowsey, J. 1966. Studies of Haversian systems in man and some animals. *J. Anat.* 100: 857–864.

Jowsey, J. 1968. Symposium on equine bone and joint diseases. Age and species differences in bone. *Cornell Vet.* 58 (Suppl): 74–94.

Kadam, N. S., et al. 2018. Prevalence of osteoporosis in apparently healthy adults above 40 years of age in Pune City, India. *Indian J. Endocrinol. Metab.* 22: 67–73.

VetBooks.ir

Kerley, E. R. 1965. The microscopic determination of age in human bones. *Am. J. Phys. Anthropol.* 23: 149–164.

Kerley, E. R. and D. H. Ubelaker. 1978. Revisions in the microscopic method of estimating age at death in human cortical bone. *Am. J. Phys. Anthropol.* 49: 545–546.

Klatte, T. O., et al. 2015. The Singh index does not correlate with bone mineral density (BMD) measured with dual-energy x-ray absorptiometry (DXA) or peripheral quantitative computed tomography (pQCT). *Arch. Orthop. Trauma Surg.* 135: 645–650.

Klein, N. and P. M. Sander. 2008. Ontogenetic stages in the long bone histology of sauropod dinosaurs. *Paleobiology* 34: 247–263.

Krause, M., et al. 2013. Bone microarchitecture of the talus changes with aging. *Clin. Orthop. Relat. Res.* 471: 3663–3671.

Kung, A. W. C. 2010. Novel genetic loci associated with osteoporosis. *Bone* 47: S376–377.

Kurzawski, V. 1983. Mise au point sur les méthodes de détermination de l'âge par voie histologique osseuse. *Bull. Mém. Soc. Anthropol. Paris*, *Série XIII* 10: 413–423.

Laine, C. M., et al. 2007. A new autosomal dominant form of early onset primary osteoporosis in a 3-generation Finnish family. *Bone* 40: S58.

Lala, D., et al. 2014. Measuring apparent trabecular structure with pQCT: a comparison with HR-pQCT. *J. Clin. Densitom.* 17: 47–53.

Lamberts, S. W. J., et al. 1997. The endocrinology of aging. *Science* 278: 419–424.

Larrue, A., et al. 2011. Synchrotron radiation μ-CT at the micrometer scale for the analysis of the three-dimensional morphology of microcracks in human trabecular bone. *PLoS One* 6: e21297.

Lau, H. H. L., et al. 2005. Genetic and environment determinants of bone mineral density in Chinese women. *Bone* 36: 700–709.

Laval-Jeantet, A. M., et al. 1983. Cortical bone senescence and mineral bone density of the humerus. *Calcif. Tissue Int.* 35: 268–272.

Laval-Jeantet, A. M., et al. 1995a. Dual-energy x-ray absorptiometry of the calcaneus: comparison with vertebral dual-energy X-ray absorptiometry and quantitative computed tomography. *Calcif. Tissue Int.* 56: 14–18.

Laval-Jeantet, A. M., et al. 1995b. Quantitative imaging and absorptiometry of bone in aging. (Fr). *Ca. Anthropol. Biomét. Hum.* 13: 263–280.

Lindsay, R., et al. 2006. A novel tetracycline labeling schedule for longitudinal evaluation of the short-term effects of anabolic therapy with a single iliac crest bone biopsy: early action of teriparatide. *J. Bone Miner. Res.* 21: 366–373.

Link, T. M. and T. M. Lang. 2014. Axial QCT: Clinical applications and new developments. *J. Clin. Densitom.* 17: 438–448.

Lips, P., et al. 1978. Mean wall thickness of trabecular bone packets in the human iliac crest: changes with age. *Calcif. Tissue Res.* 10: 13–17.

Liu, X. S., et al. 2009. Micromechanical analyses of vertebral trabecular bone based on individual trabeculae segmentation of plates and rods. *J. Biomech.* 42: 249–256.

Lynnerup, N., et al. 2006. Assessment of age at death by microscopy: unbiased quantification of secondary osteons in femoral cross sections. *Forensic Sci. Int.* 159: S100–S103.

Maggio, D., et al. 1997. Age-related cortical bone loss at the metacarpal. *Calcif. Tissue Int.* 60:94–97.

Martin, R. B., et al. 1980. Studies of skeletal remodeling in aging men. *Clin. Orthop. Relat. Res.* 149: 268–282.

Martrille, L., et al. 2009. Age at death estimation in adults by computer-assisted histomorphometry of decalcified femur cortex. *J. Forensic Sci.* 54: 1231–1237.

Masset, C. 1982. *Estimation de l'âge au décès par les sutures crâniennes. Thèse de Doctorat d'État*, Université Paris VII, Paris, France.

Masset, C. 1989. Age estimation on the basis of cranial sutures. In *Age markers in the human skeleton*, ed. Iscan, M. Y., 71–103. Springfield, IL, Charles C Thomas.

Mather, J., et al. 2013. Proximal humerus cortical bone thickness correlates with bone mineral density and can clinically rule out osteoporosis. *J. Shoulder Elbow Surg.* 22: 732–738.

McCalden R. W., et al. 1993. Age-related changes in the tensile properties of cortical bone. *J. Bone Joint Surg. Am.* 75: 1193–1205.

McCarthy, J. and A. Davis. 2016. Diagnosis and management of vertebral compression fractures. *Am. Fam. Phys.* 94: 44–50.

McCloskey, E. V., et al. 1993. The assessment of vertebral deformity: a method for use in population studies and clinical trials. *Osteoporos. Int.* 3: 138–147.

Meema, H. E. and S. Meema. 1963. Measurable roentgenologic changes in some peripheral bones in senile osteoporosis. *J. Am. Geriat. Soc.* 11: 1170–1182.

Mégard, M., et al. 1976. Comparaison de l'indice des travées fémorales et de l'indice radiologique vertébral. *Lyon Méd.* 235: 85–93.

Mellish, R. W. E., et al. 1987. Iliac crest trabecular bone mass and structure in patients with non-steroid treated rheumatoid arthritis. *Ann. Rheumat. Dis.* 46: 830–836.

Melton, L. J. III, et al. 1989. Epidemiology of vertebral fractures in women. *Am. J. Epidemiol.* 129: 1000–1011.

Meunier, P. J., et al. 1968. La lecture quantitative de la biopsie osseuse. Moyen de diagnostic et d'étude des ostéoses décalcifiantes diffuses. *Rhumatologie* 20: 301–312.

Meunier, P. J., et al. 1972. Apport de la radiologie dans l'appréciation d'une déminéralisation rachidienne. *Cah. Med. Lyon.* 48: 4115–4122.

Milovanovic, P., et al. 2018. Bone tissue aging affects mineralization of cement lines. *Bone* 110: 187–193.

Modi, K., et al. 2015. Acsàdi-Nemeskeri scale based study on closure of skull sutures and its relation with age. *Int. J. Int. Med. Res.* 2: 40–44.

Moreira-Kulak, C. A. and D. W. Dempster. 2010. Bone histomorphometry: a concise review for endocrinologists and clinicians. *Arq. Bras. Endocrinol. Metab.* 54: 87–98.

Mori, S. et al. 1997. Trabecular bone volume and microdamage accumulation in the femoral heads of women with and without femoral head fractures. *Bone* 21: 521–526.

Morris, J. A., et al. 2019. An atlas of genetic influences on osteoporosis in humans and mice. *Nat. Genet.* 51: 258–266.

Mosekilde, L., et al. 2000. Trabecular bone structure and strength - remodelling and repair. *J. Musculoskel. Neuron. Interac.* 1: 25–30.

Mullender, M. G., et al. 1996. Osteocytes density changes in aging and osteoporosis. *Bone* 18: 109–113.

Mullender, M. G., et al. 2005. Differences in osteocyte density and bone histomorphometry between men and women and between healthy and osteoporotic subjects. *Calcif. Tissue Int.* 77: 291–296.

Nam, H.-S. et al. 2010. Race/ethnic differences in bone mineral densities in older men. *Osteoporos. Int.* 21: 2115–2123.

Nemeskeri, J., et al. 1960. Methoden zür Diagnose des Lebensalten von Skelettfunden. *Anthropol. Anz.* 24: 70–95.

Nguyen, B. N. T., et al. 2018. Cortical thickness index of the proximal femur: a radiographic parameter for preliminary assessment of bone mineral density and osteoporosis status in the age 50 years and over population. *Clin. Orthop. Surg.* 10: 149–156.

Nishiyama, K. K. and E. Shane 2013. Clinical imaging of bone microarchitecture with HR-pQCT. *Curr. Osteoporos. Rep.* 11:147–155.

Noble, P. C., et al. 1995. The effect of aging on the shape of the proximal femur. *Clin. Orthop. Relat. Res.* 316: 31–44.

Nuzzo, S., et al. 2002. Quantification of the degree of mineralization of bone in three dimensions using synchrotron radiation microtomography. *Med. Phys.* 29: 2672–2681.

Nyman, J. S. 2018. Age-related changes to bone structure and quality in rodent models. In *Conn's handbook of models for human aging*, eds. Ram, J. and P. M. Conn, 919–936. Cambridge, MA, Academic Press.

Oettle A. C. and M. Steyn 2000. Age estimation from sternal ends of ribs by phase analysis in healthy and osteoporotic women. *Osteoporos. Int.* 3: 1071–1079.

Oichi, T., et al. 2020. Pathomechanism of intervertebral disk degeneration. *JOR Spine* 3: e1076.

Okazaki, N., et al. 2014. Trabecular microfractures in the femoral head with osteoporosis: analysis of microcallus formations by synchrotron radiation micro-CT. *Bone* 64: 82–87.

Old, J. L. and M. Calvert, 2004. Vertebral compression fractures in the elderly. *Am. Fam. Phys.* 69: 111–116.

Ostertag, A., et al. 2016. Multiscale and multimodality computed tomography for cortical bone analysis. *Phys. Med. Biol.* 61: 8553–8576.

Parfitt, A. M. 1984. Age-related structural changes in trabecular and cortical bone: cellular mechanisms and biomechanical consequences. *Calcif. Tissue Int.* 36 (Suppl.1): S123–S128.

Parfitt, A. M. 2008. Skeletal heterogeneity and the purposes of bone remodeling: implications for the understanding of osteoporosis. In *Osteoporosis*, eds. Marcus, R., D. Feldman, D. A. Nelson and D. J. Rosen, 71–89. San Diego, CA, Academic Press.

Parfitt, A. M. 2014. A new approach to iliac bone histomorphometry: implication for biomechanics and cell biology. *J. Clin. Invest.* 124: 70–71.

Parfitt, A. M., et al. 1983. Relationships between surface, volume and thickness of iliac trabecular bone in aging and in osteoporosis. *J. Clin. Invest.* 72: 1396–1409.

Parfitt, A. M., et al. 1987. Bone histomorphometry: standardization of nomenclature, symbols and units. Report of the ASBMR Histomorphometry Nomenclature Committee. *J. Bone Miner. Res.* 2: 595–610.

Parisien, M., et al. 1997. Histomorphometric assessment of bone mass, structure, and remodeling: a comparison between healthy black and white premenopausal women. *J. Bone Miner. Res.* 12: 948–957.

Patsch, J. M., et al. 2011. Noninvasive imaging of bone microarchitecture. *Ann. NY Acad. Sci.* 1240: 77–87.

Patterson, J., et al. 2016. Cortical bone thickness of the distal part of the tibia predicts bone mineral density. *J. Bone Joint Surg. Am.* 98: 751–760.

Pazzaglia, U. E., et al. 2015. Setup of a bone aging experimental model in the rabbit comparing changes in cortical and trabecular bone: morphological and morphometric study in the femur. *J. Morphol.* 276: 733–747.

Pothuaud, L., et al. 2000. Fractal dimension of trabecular bone projection texture is related to three-dimensional microarchitecture. *J. Bone Miner. Res.* 15: 691–699.

Prakash, et al. 2007. Vertebral body integrity: a review of various anatomical factors involved in the lumbar region. *Osteoporos. Int.* 18: 891–903.

Prevrhal, S., et al. 2003. Peripheral quantitative computed tomography. In *Radiology of osteoporosis*, ed. Grampp, S., 115–129. Berlin-Heidelberg, Springer-Verlag.

Ralston, S. H. 1999. The genetics of osteoporosis. *Bone* 25: 85–86.

Pye, S. R., et al. 2007. Lumbar disk degeneration: association between osteophytes, end-plates sclerosis and disc space narrowing. *Ann. Rheum. Dis.* 66: 330–333.

Qiu, S., et al. 2003. Reduced iliac cancellous osteocyte density in patients with osteoporotic vertebral fracture. *J. Bone Miner. Res.* 18: 1657–1663.

Rissech C. and Malgosa A. 2005. Ilium growth study: applicability in sex and age diagnosis. *Forensic Sci. Int.* 147: 165–174.

Robling, A. G., et al. 2014. Mechanical adaptation. In *Basic and applied bone biology*, eds. Burr, D. B. and R. Allen, 175–204. Amsterdam, Elsevier-Academic Press.

Rolvien, T., et al. 2019. Recovery of bone mineralization and quality during asfotase alfa treatment in an adult patient with infantile-onset hypophosphatasia. *Bone* 127: 67–74.

Rosen, C. J. 2000. Pathogenesis of osteoporosis. *Baillière's Clin. Endocrinol. Metab.* 14: 181–193.

Rosen, C. J., et al. 2000. Mouse models in the genetics of osteoporosis. *Bone* 27: 3S.

Ruff, C. B. and W. C. Hayes. 1982. Subperiosteal expansion and cortical remodeling of the human femur and tibia with aging. *Science* 217: 945–948.

Rustenburg, C. M. E., et al. 2018. Osteoarthritis and intervertebral disk degeneration: quite different, quite similar. *JOR Spine* 1: e1033.

Sah, A. P., et al. 2007. Correlation of plain radiographs indices of the hip with quantitative bone mineral density. *Osteoporos. Int.* 18: 1119–1126.

Sander, M. 2000. Longbone histology of the Tendaguru sauropods: implications for growth and biology. *Paleobiology* 26: 466–488.

Schaffler, M. B., et al. 1995. Aging and matrix microdamage accumulation in human compact bone. *Bone* 17: 521–525.

Seeman, E. 2008. Bone quality: the material and structural basis of bone strength. *J. Bone Miner. Metab.* 26: 1–8.

Seeman, E. 2013. Age- and menopause-related bone loss compromise cortical and trabecular microstructure. *J. Gerontol. A Biol. Sci. Med. Sci.* 68: 1218–1225.

Singh, M. and D. L. Gunberg. 1970. Estimation of age at death in human males from quantitative histology of bone fragments. *Am. J. Phys. Anthropol.* 33: 373–382.

Singh, M., et al. 1970. Changes in trabecular pattern of the upper end of the femur as an index of osteoporosis. *J. Bone Joint Surg. Am.* 52: 457–467.

Sontag, W. 1994. Age-dependent morphometric change in the lumbar vertebrae of male and female rats: comparison with the femur. *Bone* 15: 593–601.

Sowers, M. 1996. Pregnancy and lactation as risk factors for subsequent bone loss and osteoporosis. *J. Bone Miner. Res.* 11: 1052–1060.

Spector, E. R., et al. 2009. Skeletal effects of long-duration head-down bed rest. *Aviat. Space Environ. Med.* 80 (5 Suppl): A23–A28.

Squillante, R. G. and J. L. Williams. 1993. Videodensitometry of osteons in females with femoral neck fractures. *Calcif. Tissue Int.* 52: 273–277.

Srinivasan, S., et al. 2000. Aging-induced osteopenia in avian cortical bone. *Bone* 26: 361–365.

Stauber, M. and R. Müller. 2006. Volumetric spatial decomposition of trabecular bone into rods ad plates – A new method for local bone morphometry. *Bone* 38: 475–484.

Stein, K., et al. 2010. Small body size and extreme cortical bone remodeling indicate phyletic dwarfism in *Magyarosaurus dacus* (Sauropoda: Titanosauria). *Proc. Natl. Acad. Sci. USA* 107: 9258–9263.

Stein, M. S., et al. 1999. An automated analysis of intracortical porosity in human femoral bone across age. *J. Bone Miner. Res.* 14: 624–632.

Teuling, J. W. A. M., et al. 2017. The influence of bone mineral density and cortical index on the complexity of fractures of the proximal humerus. *Bone Joint Res.* 6: 584–589.

Thomas, C. D., et al. 2000. Determination of age at death using combined morphology and histology of the femur. *J. Anat.* 196: 463–471.

Thomas, C. D., et al. 2005. Regional variation in intracortical porosity in the midshaft of the human femur: age and sex differences. *J. Anat.* 206: 115–125.

Tiede-Lewis, L. M. and S. L. Dallas. 2019. Changes in the osteocyte lacunocanalicular network with aging. *Bone* 122: 101–113.

Tingart, M. J., et al. 2003. The cortical thickness of the proximal humeral diaphysis predicts bone mineral density of the proximal humerus. *J. Bone Joint Surg. Br.* 85: 611–617.

Trajanoska, K. and F. Rivadeneira. 2019. The genetic architecture of osteoporosis and fracture risk. *Bone* 126: 2–10.

Trotter, M. and B. B. Hixon, 1974. Sequential changes in weight, density and percentage ash weight of human skeletons from an early fetal period through old age. *Anat. Rec.* 179: 1–18.

Trotter, M., et al. 1960. Densities of white and negro skeletons. *J. Bone Joint Surg. Am.* 42: 50–58.

Turner, A. S. 2001. Animal models of osteoporosis - necessity and limitations. *Eur. Cells Mater.* 1: 66–81.

Vajda, E. G. and R. D. Bloebaum. 1999. Age-related hypermineralization in the female proximal human femur. *Anat. Rec.* 255: 202–211.

Van Kuijk, C. and R. R. van Rijn. 2003. Spinal quantitative computed tomography. In *Radiology of osteoporosis*, ed. Grampp, S., 111–114. Berlin-Heidelberg, Springer-Verlag.

Vashishth, D., et al. 2000. Decline in osteocyte lacunar density in human cortical bone is associated with accumulation of microcracks with age. *Bone* 26: 375–380.

Vashishth, D., et al. 2005. Sexual dimorphism and age dependance of osteocyte lacunar density for human vertebral cancellous bone. *Anat. Rec. A* 282: 157–162.

Vincent, K., et al. 2019. Aging of mouse intervertebral disc and association with back pain. *Bone* 123: 246–259.

Virtama, P. and T. Helela. 1969. Radiographic measurements of cortical bone. *Acta Radiol.* Suppl. Stockholm 293.

Wang, L., et al. 2001. Male rodent model of age-related bone loss in man. *Bone* 29: 141–148.

Wang, X.-F., et al. 2009. Racial differences in macro and micro-architecture of the appendicular skeleton in young Chinese and Caucasian females. *Bone* 44: S18–555.

Wang, X.-F., et al. 2019. Dimorphism in axial and appendicular dimensions, cortical and trabecular microstructure and matrix mineral density in Chinese and Caucasian women. *Bone* 128. doi.org/10.1016/j.bone.20190115039.

Warming, L., et al. 2002. Changes in bone mineral density with age in men and women: a longitudinal study. *Osteoporos. Int.* 13: 105–112.

Weaver, C. M. and R. K. Fuchs. 2014. Skeletal growth and development. In *Basic and applied bone biology*, eds. Burr, D. B. and R. Allen, 245–260. Amsterdam, Elsevier-Academic Press.

Weaver, J. K. and J. Chalmers. 1966. Cancellous bone: its strength and changes with aging and an evaluation of some methods for measuring its mineral content. I. Age changes in cancellous bone. *J. Bone Joint Surg. Am.* 48: 289–299.

Webber, T., et al. 2015. Correlation between distal radial cortical thickness and bone mineral density. *J. Hand Surg. Am.* 40: 493–499.

Wei Y. and Sun Y. 2018. Aging of the bone. *Adv. Exp. Med. Biol.* 1086: 189–197.

Wenzel, T. E., et al. 1996. In vivo trabecular microcracks in human vertebral bone. *Bone* 19: 89–95.

Willems, N. M. B. K., et al. 2007. Age-related changes in micro-architecture and mineralization of cancellous bone in the porcine mandibular condyle. *J. Struct. Biol.* 158: 421–427.

Winter, E. M. 2020. Pregnancy and lactation, a challenge for the skeleton. *Endocr. Connect.* 9: R143–R157.

Wink, C. S. and R. M. Elsey. 1986. Changes in femoral morphology during egg-laying in *Alligator mississippiensis*. *J. Morphol.* 189: 183–188.

Wink, C. S., et al. 1987. Changes in femoral robusticity and porosity during the reproductive cycle in the female alligator (*Alligator mississippiensis*). *J. Morphol.* 193: 317–321.

Wong, S. H. J., et al. 2016. Review article: Osteophytes. *J. Orthop. Surg.* 24: 403–10.

Woodward, H. N., et al. 2011. Osteohistological evidence for determinate growth in the American Alligator. *J. Herpetol.* 45: 339–342.

Xiao, Y., et al. 2007. Gene expression profiling of bone marrow stromal cells from juvenile, adult, aged and osteoporotic rats: with an emphasis on osteoporosis. *Bone* 40: 700–715.

Youlten, S. E. and P. A. Baldock. 2019. Using mouse genetics to understand human skeletal disease. *Bone* 126: 27–36.

Zebaze, R. M., et al. 2010. Intracortical remodelling and porosity in the distal radius and post-mortem femurs of women: a cross-sectional study. *Lancet* 375(9727): 1729–1736.

Zengin, A. et al. 2016. Ethnic differences in bone geometry between White, Black and South Asian men in the UK. *Bone* 91: 180–185.

Zeni, S. N., et al. 1999. Bone mass changes during pregnancy and lactation in the rat. *Bone* 25: 681–685.

Zhu, S., et al. 2018. Coupling factors and exosomal packaging microRNAs involved in the regulation of bone remodeling. *Biol. Rev.* 93: 469–480.

VetBooks.ir

33

Basic Principles and Methodologies in Measuring Bone Biomechanics

Russell P. Main

CONTENTS

Introduction 668
The Hierarchical Organization of Bone Tissue, and Solid and Fluid Mechanics in the Vertebrate Skeleton 668
Measuring and Modeling *In Vivo* Skeletal Mechanics and Bone Tissue Properties 675
Modeling Musculoskeletal Biomechanics 677
Application of Biomechanical Analyses to Paleontological and Comparative Questions of Function 679
Biting Mechanics in Primates 679
Modeling Locomotion in Theropods 680
Conclusion 681
Acknowledgments 681
References 682

Introduction

The vertebrate skeleton serves many roles, including functional mechanical support and leverage for muscle action, a source for endocrine signals and a mineralized repository for assisting in ion homeostasis in the body. In extinct animals, for which we only have fossil remains, it is usually the mechanical functions of the bones and teeth that most capture our imagination and spark some of the greatest debate about species evolution, including the evolution of flight in birds and bipedal locomotion in primates. Similar functional debates date to some of the earliest examples of mineralized tissues in the fossil record, such as conodonts (Purnell 1993, Martínez-Pérez et al. 2014). Although the evolution of bizarre or unique bony structures has received considerable attention, these structures are often the most difficult to explain through defensible functional hypotheses. At the same time, an argument for the functional importance of highly conserved structures such as teeth, basic elements of the masticatory apparatus, and the proximal limb skeleton in sarcopterygians can be made given their conservation among a wide diversity of taxa. Furthermore, functional hypotheses for these conserved structures are less hampered by assumptions and better supported by phylogenetic analyses, which may include extant representatives with similar structures (Witmer 1995).

This chapter is focused on the multiscale mechanical forces experienced by the vertebrate skeleton. The specific objectives of this chapter are to discuss (1) the hierarchical organization of bone and the relevant mechanical forces experienced by the different skeletal components, (2) how skeletal function and its material properties are assessed experimentally, (3) the strengths and limitations in modeling skeletal mechanics, and (4) developing hypotheses and testing questions about skeletal biomechanics in extant and extinct species.

The Hierarchical Organization of Bone Tissue, and Solid and Fluid Mechanics in the Vertebrate Skeleton

When a limb bone is loaded during locomotion, when the dentary transmits the forces of masticatory muscles to food items or when a bovid horn sustains impact, stress develops in the bone and the bone tissue deforms. Compared to industrially manufactured structural materials such as steel, aluminum and glass, bone is incredibly heterogeneous in its composition and structure. This heterogeneity, in part, allows bone to sustain relatively high forces (e.g., strength) and to absorb a high amount of load energy (e.g., toughness) without fracturing (Figure 33.1). At the nanoscale, bone tissue matrix is a mineral-protein composite of (typically) aligned, amorphous, hydroxyapatite mineral and type I collagen. Many other proteins are present as well and are important for type I collagen fibrillogenesis, the cross-linking of collagen molecules and the mineralization of collagen (Burr and Akkus 2014). Interrupting the continuity of this tissue matrix are the osteocytes, bone cells embedded in the tissue matrix, which are present over a large range of densities (8000–79,000 cells/cm^3) that vary across bone elements, locations in the bone and phylogeny (Qiu et al. 2002, D'Emic and Benson 2013, Stein and Werner 2013, Buenzli and Sims 2015).

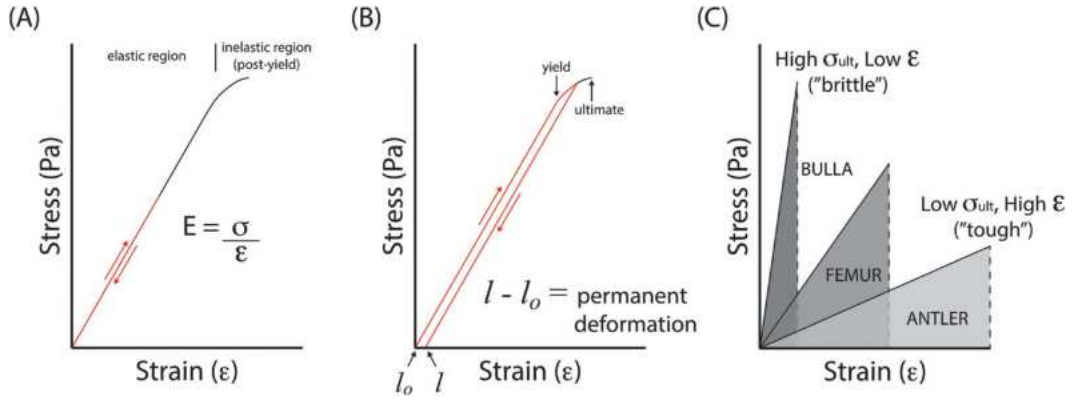


FIGURE 33.1 Stress-strain relationships for elastic and plastic deformation of a solid material (bone) with examples from different mammalian tissues. A, Elastic loading and unloading of tissue. B, Plastic deformation with loading beyond the linear elastic region. C, Examples of tissues with high mineral density (bulla) and low mineral density (antler). In (A), the material is loaded under increasing stress (σ) and strain (ε) before load is released and stress and strain return to zero. The relationship between applied stress and the resulting strain for linearly elastic materials is called the elastic (Young's) modulus (*E*). In (B), the material is loaded beyond the elastic limit, called the yield point, resulting in permanent deformation in the bone. When the load is released, the tissue stress returns to zero, but a permanent deformation remains ($l - l_o$). The unloading slope parallels the load slope. The bone sample would completely fracture on reaching the ultimate stress (or strain). In (C), the stress-strain curves for the whale bulla, deer antler and cow femur are presented. The bulla acts similar to a brittle material, like glass or ceramic, reaching a high ultimate stress (σ_{ult}) and absorbing little energy (area under the stress-strain curve) before fracturing. The antler is a tough material and absorbs more energy than the bulla or femur before breaking. (See Currey 1979 for more discussion.)

Many teleost fishes do not possess these cells. At a higher scale, the bone-cellular matrix is interrupted by vascular channels of varying density and organization (longitudinal, oblique, radial and circumferential vessels). Similar to engineered materials that bear load, bone is constantly experiencing dynamically changing loads that can cause fatigue damage to the bone tissue. However, unlike engineered materials that are devoid of living cells, this damage is constantly being remodeled by osteocytes, osteoclasts and osteoblasts to repair fatigue microdamage and, hypothetically, to align the mineral and collagen matrix with the prevailing loading conditions. The structural and histological consequence of this remodeling are secondary (Haversian) osteons. The bones of small animals and those with relatively thin cortices (e.g., birds, bats, small rodents) do not typically undergo intracortical remodeling, which places a greater importance on natural selection and adaptive plastic mechanisms for arriving at a viable bone morphology in these taxa.

All of these anatomical features contribute to what are defined as tissue-level material properties, such as bone mineral density (BMD, mg cm^{-3}) and elastic modulus. BMD is the density of the hydroxyapatite mineral present within a volume of bone tissue. With most radiation-based measurement tools (computed tomography [CT], X-ray), where the image resolution is greater than ~4 μm, this value also includes the lacunar-canalicular porosities, vascular pores and remodeling-induced resorption spaces. Micro-CT, nano-CT and synchrotron-based imaging modalities can identify some of these porosities, depending on the scan resolution. BMD relates directly to tissue elastic modulus (Carter and Hayes 1976, Currey 1999, Easley et al. 2010). Most of the experimentally determined values for elastic modulus have been derived from human bones or the bones of domesticated mammals (Table 33.1) (Currey 2002). The elastic modulus defines the physical relationship between stress and strain in the bone tissue. Stress is a normalized expression of force (axial tension or compression, bending or torque) relative to its distribution through an area of bone tissue, and strain is the resulting deformation of bone tissue in response to the applied stress (Figure 33.1A). In bone, the relationship between stress and strain is generally linear, until the yield point of the tissue is reached (Figure 33.1B). Within this region, the application of load (stress) will cause deformation as described by the linear relationship. As load is released, stress and strain (deformation) will decrease toward zero along this same relationship (Figure 33.1A). If a bone is loaded beyond its elastic region, surpassing the material yield point, induction of damage in the tissue will cause it to be permanently deformed on release of the load (Figure 33.1B). Permanent deformation is undesirable, and bone remodeling and adaptive modeling prevent it at the microstructural and gross levels. Loading beyond this yield point can cause the continued accumulation of damage in the tissue, which ultimately manifests as gross skeletal fracture.

While elastic modulus varies throughout the bone with local differences in BMD, it also varies across different anatomical axes. Anisotropy in tissue stiffness across different axes is due to differences in mineral, collagen and anatomical structure alignment across these axes. In long bones, the tissue is typically stiffest and strongest along the bone's long axis, coinciding with the predominant alignment of mineral and collagen along that axis. Cortical long bone tissue has been characterized as more compliant and weaker when tested in the radial and circumferential directions, where the radial direction is perpendicular to the periosteal and endosteal surfaces and the circumferential direction lies parallel to these surfaces. The bone is weaker in these directions because the applied forces can more easily separate crystals and collagen perpendicular to their long axes and across longitudinal vascular canals (Table 33.1) (Wainwright et al. 1982). Generally, bone is defined as transversely isotropic, maintaining similar mechanical characteristics across two axes, and possessing a third axis that differs from the other two (Bartel et al. 2006). Although the axial moduli are similar when

VetBooks.ir

TABLE 33.1

Elastic Moduli (GPa), Ultimate Strength (MPa), and Ultimate Strain (ε) for Adult Mammalian Cortical Bone

	Human		Bovine		
	Haversian		Haversian		Fibrolamellar
	Tension	Compression	Tension	Compression	Tension
Elastic Modulus					
E_3	17.7	18.2	23.1	22.3	26.5
$E_1 = E_2$	12.8	11.7	10.4	10.1	11.0
G	3.3		3.6		5.1
Ultimate Strength					
σ_3	133	205	150	272	167
σ_1	53	131	54	171	55
σ_2	53	131	39	190	30
τ	67		70		64
Ultimate Strain					
ε_3	0.031	0.019	0.020	0.016	0.033
ε_1	0.007	0.050	0.007	0.042	0.007
ε_2	0.007	0.050	0.007	0.072	0.002
γ^u	0.0087				

Notes: 1, 2, 3 = circumferential, radial, longitudinal.

$\sigma_1 = \sigma_2$ assumed for humans; $E_1 = E_2$ assumed for humans and bovine samples.

γ^u, shear yield strain is presented because no published values for ultimate torsional strain could be found.

A valuable summary of these values can be found in Tables 3.1 and 3.2 in Currey (2002). Values for a comparative list of samples for some of these properties are provided in table 4.3 in Currey (2002). A useful review of the relationships between these properties and bone material properties, in general, can be found in the appendices of Carter and Beaupré (2001).

Source: Values taken from Reilly et al. (1974), Reilly and Burstein (1975), and Mirzaali et al. (2016).

tested under tension or compression, the bone tissue is stronger in compression, and this depends on differences in bone fracture mechanics in tension versus compression (Currey 2002).

One final basic property of bone and other materials is Poisson's ratio, which defines the deformation across two material axes on loading in the third axis. This effect is common in all solids and describes how contraction (or expansion) can occur in two axes on the application of tension (or compression) in the third axis. A value of 0.3–0.4 is typically assigned to bone (Carter and Beaupré 2001).

Tissue-level properties are important for determining the strength and stiffness of a whole bone, and so is the structural distribution of that tissue. Important structural properties of bone tissue include the cross-sectional area (A, mm^2) and the second and polar moments of area (I and J, respectively, mm^4). In cancellous bone tissue, properties such as bone volume fraction (%), trabecular thickness (mm), trabecular number (1/mm), connectivity (1/mm^3), degree of anisotropy and structure model index (SMI) have been used to describe the mechanical competence (Bouxsein et al. 2010). For an axial load applied at the end of a long bone, the axial stress (σ_{ax}) that the load imparts is positively related to the magnitude of the applied force (F) and negatively related to the cross-sectional area over which that force is distributed (Figure 33.2A). Bending loads occur in bone due to off-axis load components directed perpendicular to the bone's long axis and/or bending loads that develop under the application of axial loads, due to bone curvature (Biewener 1983a, b, Bertram and Biewener 1988) (Figure 33.2B, C). These bending stresses (σ_b) are directly related to the magnitude of the bending moment applied to the bone ($F \times d$), where d is the moment arm of the applied force, or the distance between the point of load application and the location at which σ_b is calculated. Under pure bending loads, compressive stresses ($-\sigma_b$) develop in half of the bone's cortex and tensile stresses ($+\sigma_b$) in the other half. Bending stresses decrease toward the center of the bone, where there is a neutral axis of zero stress, and increases the greater the distance (y) from the neutral axis (Figure 33.2B). Bending stresses are resisted by increased second moments of area for a bone cross-section. The second moment of area describes the distribution of bone tissue about a given anatomical axis. The more bone tissue (A) distributed further away from the bending axis of interest (y), the greater the value is for I (Figure 33.3A), and the lower the induced stresses for a given applied bending moment. In the case of the cross-section of the goat radius, Iyy, which resists mediolateral bending, is three times greater than is Ixx, which resists craniocaudal bending (Figure 33.3B). The predominance of bone loading in bending and torsion among tetrapods may be one factor contributing to hollow bone centers, where stresses are very low (Figure 33.3C).

As the limb mechanics of a more diverse array of tetrapod taxa have been sampled, torsional loads have been described as the dominant loading mode in the long bones of salamanders, lizards, turtles, alligators, the forelimb and hindlimb bones of birds, and some mammals with less purely parasagittal gaits (Table 33.2) (Biewener and Dial 1995, Blob and Biewener 1999, Carrano and Biewener 1999, Main and Biewener 2007, Butcher et al. 2008, 2011, Sheffield and Blob 2011, Sheffield et al. 2011, Kawano et al. 2016). Torsional loads are applied about a bone's long axis and act to twist the bone, inducing shear stress (τ) and strain (γ) in the bone tissue. Governing the relationship

VetBooks.ir

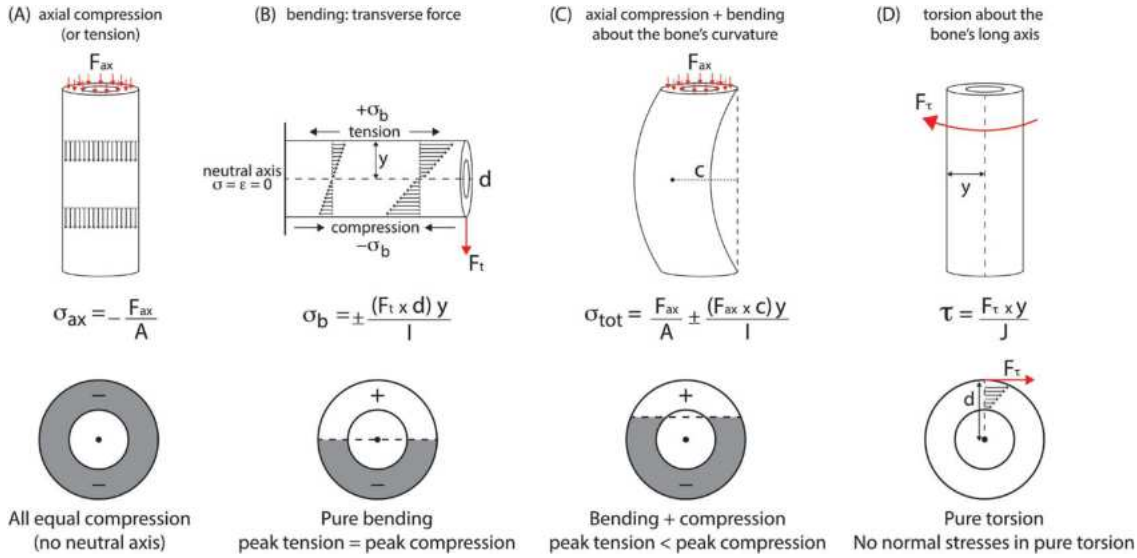


FIGURE 33.2 Different idealized loading modes for bone. A, A bone loaded in axial compression (F_{ax}) across its cross-sectional area (A). By definition, compressive stresses and strains are negative. Axial compression creates a uniform state of stress and strain within the tissue. The strain that develops from an applied stress depends on the elastic modulus for the material. Test bone samples loaded in the laboratory are often loaded in uniform axial tension or compression. B, A bone sample loaded in cantilever bending, as shown here, develops positive and negative stress ($+\sigma_b$, $-\sigma_b$) and strain that are uniform in pure bending. Stress and strain increase away from the neutral axis of bending to reach a maximum value at the bone sample's surface (y). The applied stress and strain are maximal at the end of the tissue (d) where the force (F_t) is applied and decreases toward the base ($d = 0$). Bending stress is countered by the distribution of bone tissue (second moment of area, I) around the bending axis. C, A sample is loaded in axial compression about the bone's radius of curvature (c). Both axial compression and bending stresses and strains develop in the bone. The convex surface experiences tension, as in pure bending, but this is overlain by axial compression, which shifts the neutral axis toward the convex surface. Both A and I are important in resisting these loads, meaning that the material area as well as its distribution about the axis of bending are important. D, A bone loaded in torsion about the bone's long axis. Torsional shear stresses (τ) increase with distance (y) from the centroid. Torsional loads are resisted by the polar moment of inertia (J), which is maximized when $I_{MAX} = I_{MIN}$ (e.g., circle).

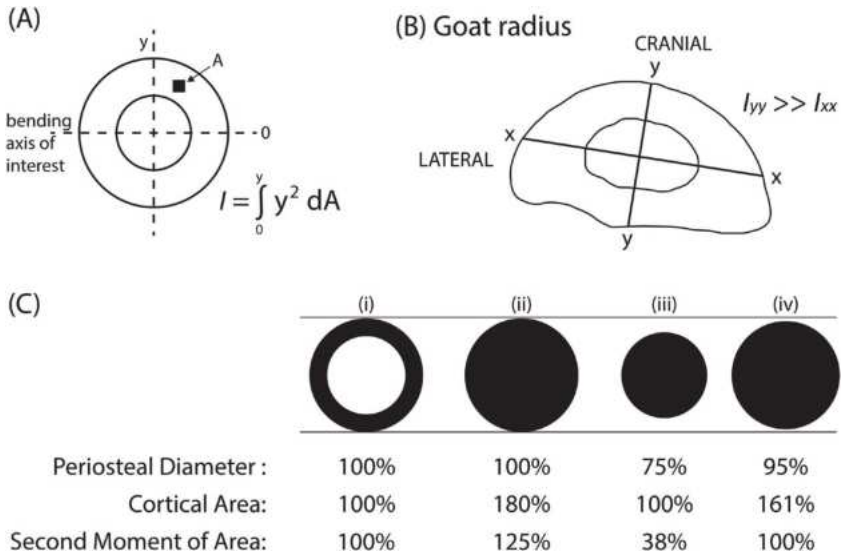


FIGURE 33.3 Second moment of area in resisting bending and torsional loads. A, The second moment of area (I, also called the moment of inertia) is highly influenced by the squared distance of each measurable bone unit away from the neutral axis (y^2). The more bone located at a distance from the neutral axis, the more resistant the structure is to bending (though local buckling may still be a concern) (Currey 2002). B, A transverse cross-section of the goat radius where I_{yy} ($= I_{MAX}$) and I_{xx} ($= I_{MIN}$) are based on structure alone, without information about *in vivo* bending regimes in the bone. In this case, I_{yy} is much greater than I_{xx}, suggesting greater resistance to mediolateral bending in an animal that swings its leg in a craniocaudal (parasagittal) direction. The selective forces shaping this bone may be constraining this bone's shape for the sake of load predictability, rather than minimizing craniocaudal stresses and strains (Bertram and Biewener 1988, Main and Biewener 2004). C, Relationships among periosteal diameter, cortical area, and the second moment of area. A wide, hollow bone maximizes both I and J, while minimizing weight (e.g., cortical area). Solid bones (ii, iv) that outperform or are similar to (i) in terms of I, are much heavier ($\gg A$), while solid bones with as much mass as (i) are much less resistant to bending and torsional loads (iii). (Based on van der Meulen et al. 2001.)

VetBooks.ir

TABLE 33.2

In Vivo Long Bone and Cranial Bone Strains Collected Using Axial or Rosette Strain Gauges*

Genus	Species	Bone Measured	Peak Principal (or Axial) Strain (με)	Peak Shear Strain (με)	Activity	Reference
LONG BONES						
Amphibia						
Lithobates	*catesbeiana*	Femur	470	475	Hopping	Blob et al. (2014)
Chaunus	*marinus*	Femur	208[a]		Hopping	Blob et al. (2014)
Reptilia (Including Aves)						
Pseudemys	*concinna*	Humerus	1398[a]	730	Walking	Young et al. (2017)
		Femur	–1701	2934	Walking	Butcher et al. (2008)
Trachemys	*scripta*	Femur	2000	1446	Walking	Young and Blob (2015)
Iguana	*iguana*	Femur	629	1121	Running	Blob and Biewener (1999)
		Tibia	1650[a]		Running	Blob and Biewener (1999)
Tupinambis	*merinae*	Femur	–238	278	Walking	Sheffield et al. (2011)
Alligator	*mississippiensis*	Humerus	–416	520	Walking	Blob et al. (2014)
		Femur	708	1027	Walking	Blob and Biewener (1999)
		Tibia	–880[a]	677	Walking	Blob and Biewener (1999)
Dromaius	*novaehollandiae*	Femur	1749	3405	Running	Main and Biewener (2007)
		Tibiotarsus	–1863	3583	Running	Main and Biewener (2007)
Gallus	*gallus*	Femur	856	224	Walking	Carrano and Biewener (1999)
		Tarsometatarsus	–900[a]	800	Walking	Loitz and Zernicke (1992)
		Tibiotarsus	–1870		Running	Biewener et al. (1986)
		Ulna	–2100		Flapping	Rubin and Lanyon (1982)
Meleagris	*gallopavo*	Tibiotarsus	–2350		Running	Rubin and Lanyon (1984a)
		Ulna	–1900		Flapping	Rubin and Lanyon (1984b), Fritton et al. (2000)
Anser	sp.	Humerus	–2800		Flying	Rubin and Lanyon (1984a)
Columba	*livia*	Humerus	–2330	1780	Vertical flight/level flight	Biewener and Dial (1995)
Mammalia						
Potoroo	*tridactylus*	Calcaneus	–1200		Hopping	Biewener et al. (1996)
Didelphis	*virginiana*	Femur	–713[a]	419	Running	Butcher et al. (2011)
Dasypus	*novemcinctus*	Femur	1226[a]	464	Running	Copploe et al. (2015)
Equus	*caballus*	Metacarpus	–1900		Trotting	Gross et al. (1992)
		Metacarpus	–4840		Galloping	Nunamaker et al. (1990)
		Metacarpus	–2430		Jumping	Biewener (1993)
		Metacarpus	–3000		Accelerating	Biewener (1993)
		Metatarsus	–1710		Galloping	Biewener (1993)
		Metatarsus	–4005		Jumping	Biewener (1993)
		Radius	–2800		Galloping	Rubin and Lanyon (1982)
		Radius	–3690		Jumping	Biewener (1993)
		Tibia	–3170		Galloping	Rubin and Lanyon (1982)
		Tibia	–5180		Jumping	Biewener (1993)
Ovis	*aries*	Calcaneus	–328	534	Trotting	Lanyon (1973)
		Femur	–700		Walking	Lanyon et al. (1981)
		Metatarsal	–1291		Trotting	Lieberman et al. (2004b)
		Radius	–1764		Walk	Lanyon et al. (1979)
		Tibia	–759		Trotting	Lieberman et al. (2004b)
		Tibia	–2100		Trotting	Lanyon and Bourn (1979)
		Vertebrae	270[a]		Trotting	Lanyon (1972)
Capra	*hircus*	Metacarpus (juvenile)	–1324[a]		Galloping	Moreno et al. (2008)
		Radius	–1850		Galloping	Biewener and Taylor (1986)
		Tibia	–1970		Galloping	Biewener and Taylor (1986)
Sus	*scrofa*	Radius	–2400		Trotting	Goodship et al. (1979)
Canis	*lupus*	Femur	–460		Walking	Manley et al. (1982)

VetBooks.ir

TABLE 33.2 (Continued)

Genus	Species	Bone Measured	Peak Principal (or Axial) Strain (με)	Peak Shear Strain (με)	Activity	Reference
		Radius	–2600		Galloping	Rubin and Lanyon (1982)
		Radius	400[a]	650	Walking	Carter et al. 1980
		Tibia	–2020		Galloping	Rubin and Lanyon (1982)
		Ulna	780[a]	740	Walking	Carter et al. (1980)
Mus	*musculus*	Tibia	600[a]		Walking	Sugiyama et al. (2012)
		Ulna	1676[a]		Trotting	Lee et al. (2002)
Rattus	*norvegicus*	Femur	–410	375	Walking	Keller and Spengler (1982, 1989)
		Tibia	740[a]		Walking	Rabkin et al. (2001)
		Ulna	–1200[a]		Running	Mosley et al. (1997)
Pteropus	*poliocephalus*	Humerus	–2004		Flying	Swartz et al. (1992)
		Radius	–2184		Flying	Swartz et al. (1992)
Hylobates	*lar*	Humerus	1492		Brachiating	Swartz et al. (1989)
		Radius	–1638		Brachiating	Swartz et al. (1989)
		Ulna	1421		Brachiating	Swartz et al. (1989)
Macaca	*mulatta*	Tibia	1272		Galloping	Demes et al. (2001)
		Ulna	1099		Galloping	Demes et al. (1998)
Homo	*sapiens*	Femur	1340		One-legged stand	Aamodt et al. (1997)
		Tibia	1675	5027	Running (17 km/h)	Milgrom et al. (2000)
CRANIAL BONES						
Osteichthyes						
Lepomis	*macrochirus*	Opercular	–1800		Prey strike	Lauder and Lanyon (1980)
Polypterus	*endlicheri*	Frontal	–174		Suction of prey	Markey et al. (2006)
Reptilia						
Anolis	*equestris*	Frontal	–1195	2036	Biting	Ross et al. (2018)
Gekko	*gekko*	Frontal	940	1774	Biting	Ross et al. (2018)
Iguana	*iguana*	Frontal	517	1008	Biting	Ross et al. (2018)
Uromastyx	*geyri*	Jugal	–1936	3195	Biting	Porro et al. (2014)
Salvator	*merianae*	Frontal	1004	1256	Biting	Ross et al. (2018)
Varanus	*exanthematicus*	Frontal	2000		Biting	Smith and Hylander (1985)
Alligator	*mississippiensis*	Angular	–273	430	Biting	Porro et al. (2013), Ross and Metzger (2004)
		Anterior root of zygoma		2316	Biting	Ross and Metzger (2004)
		Dentary	–2757	3683	Biting	Porro et al. (2013), Ross and Metzger (2004)
		Frontal	942	1269	Biting	Metzger et al. (2005)
		Jugal	–2286	3653	Biting	Metzger et al. (2005)
		Maxilla	2032	3943	Biting	Metzger et al. (2005)
		Prefrontal	–2085	3833	Biting	Metzger et al. (2005)
		Quadrate		644	Biting	Ross and Metzger (2004)
		Splenial	–2500	1373	Biting	Porro et al. (2013)
		Surangular		2162	Biting	Ross and Metzger (2004)
Mammalia						
Ovis	*aries*	Frontal	711	984	Chewing	Thomason et al. (2001)
Sus	*scrofa*	Frontal	136	76	Chewing	Sun et al. (2004), Ross and Metzger (2004)
		Mandible		213	Chewing	Ross and Metzger (2004)
		Maxilla		379	Chewing	Ross and Metzger (2004)
		Nasal		67	Chewing	Ross and Metzger (2004)
		Parietal	89	65	Chewing	Herring and Teng, (2000), Ross and Metzger (2004)
		Premaxilla		130	Chewing	Ross and Metzger (2004)
		Squamosal	984	1303	Chewing	Rafferty et al. (2000)

(Continued)

VetBooks.ir

TABLE 33.2 (Continued)

Genus	Species	Bone Measured	Peak Principal (or Axial) Strain (με)	Peak Shear Strain (με)	Activity	Reference
		Zygomatic	891	1729	Chewing	Rafferty et al. (2000), Herring et al. (2005)
Oryctolagus	*cuniculus*	Mandible	320		Chewing	Weijs and de Jongh (1977)
Procavia	*capensis*	Frontal	273	432	Chewing	Lieberman et al. (2004a)
		Mandible	–757	1093	Chewing	Lieberman et al. (2004a)
		Nasal	–113	156	Chewing	Lieberman et al. (2004a)
		Zygomatic arch	891	1729	Chewing	Lieberman et al. (2004a)
Macaca	*mulatta*	Mandible	–981	1941	Biting	Hylander and Bays (1979), Ross (2001)
		Orbital roof	54	111	Biting	Ross (2001), Ross and Metzger (2004)
		Orbital wall	95	265	Biting	Ross (2001)
		Zygomatic arch	169	1194	Biting	Ross (2001)
M.	*fascicularis*	Frontal	292	411	Biting	Hylander et al. (1991a, b)
		Mandible	–894	1602	Biting	Hylander (1979)
		Zygomatic arch	–1262	1970	Biting	Hylander and Johnson (1997)
Macaca	sp.	Postorbital bar		188	Chewing	Ross and Metzger (2004)
		Postorbital septum		48	Chewing	Ross and Metzger (2004)
Aotus	sp.	Mandible		1090	Biting	Ross (2001)
		Medial orbital wall		188	Biting	Ross (2001), Ross and Metzger (2004)
A.	*trivirgatus*	Frontal	–177	313	Chewing	Ross and Hylander (1996)
		Postorbital bar	690	532	Chewing	Ross and Hylander (1996), Ross and Metzger (2004)
		Postorbital septum	300	210	Chewing	Ross and Hylander (1996), Ross and Metzger (2004)
Otolemur	*garnetti*	Frontal	–383	745	Chewing	Ravosa et al. (2000a, b)
O.	*crassicaudatus*	Frontal	–315	642	Chewing	Ravosa et al. (2000a, b)
		Mandible	–1149	2004	Biting	Hylander (1979)
Otolemur	sp.	Mandible		1301	Chewing	Ross and Metzger (2004)
		Postorbital bar		398	Chewing	Ross and Metzger (2004)
		Medial orbital wall		346	Chewing	Ross and Metzger (2004)
Eulemur	sp.	Dorsal orbital		109	Chewing	Ross and Metzger (2004)
		Frontal	123	100	Chewing	Ross and Metzger (2004)
		Mandible		600	Chewing	Ross and Metzger (2004)
		Postorbital bar	464	284	Chewing	Ross and Metzger (2004)
		Zygomatic arch		530	Chewing	Ross and Metzger (2004)
Sapajus	sp.	Mandible	1272		Biting	Ross et al. (2016)
Papio	*anubis*	Frontal	167	212	Chewing	Hylander et al. (1991a, b)

Notes: [a] Indicates axial data collected using a single element strain gauge. All other strains presented are principal strains or shear strains derived from rosette strain gauges.

Many bone locations and different surfaces on a single bone have been sampled for some species. For each bone, the greatest mean peak strains recorded are presented (e.g., peak strains averaged over multiple individuals), regardless of which surface that principal or shear strain data may have originated. In some cases, peak principal and peak shear strains may have originated on different surfaces on the same bone.

[*] It is interesting to note that for the long bone data, all major vertebrate groups are represented, except fish. For the cranial bone strains, both reptiles and primates are well represented, and there are even some fish. However, no bone strains have ever been recorded from a bird skull *in vivo*. While 22 species have been added since the last comprehensive list of *in vivo* strain data (Fritton and Rubin 2001), there are some key groups that are in desperate need of greater sampling for both long bone and cranial bone strains.

between torsion-induced shear stress and strain is the shear modulus (G). Like bending stresses, torsional stresses are positively related to the torsional moment applied to the bone ($\tau = F \times y$), where y is the distance of the applied force from the axis of rotation (Figure 33.2D). The axis of rotation in the analysis of long bone cortical biomechanics is the centroid. The peak torsional moment is resisted by the polar moment of inertia (J), calculated as the sum of the maximum and minimum second moments of area (I_{MAX}, I_{MIN}). As for bending stresses, the more bone tissue that is located further from the axis of rotation, the greater is the value of J, and the lower the torsional stresses and strains.

VetBooks.ir

For a bone loaded in a combination of bending and axial compression or tension (Figure 33.2C), tissue-level stresses are distributed asymmetrically throughout the bone's cross-section, creating a stress or strain gradient in the direction of bending, with strain increasing from the medullary canal toward the periosteal bone surface (Figure 33.2C). It is important to note that the axis of bending during any activity (chewing, running, flying or swimming) can be constantly changing throughout the duty cycle, so a constant direction of bending in a bone should not be assumed (Rubin and Lanyon 1985, Blob and Biewener 1999, Main and Biewener 2004, 2006, Butcher et al. 2008). At the level of the living cells in the matrix, it is hypothesized that the strain gradients drive extracellular fluid through the osteocyte lacunar-canalicular system (OLCS). This fluid flow induces shear-based stress on the cell surface as well as drag-based stresses on the proteins in the glycocalyx anchoring the osteocytes and their processes to the boney matrix (Cowin et al. 1995, You et al. 2001, Wang et al. 2008, Fritton and Weinbaum 2009). Displacement of these tethering elements is transmitted to the cellular cytoskeleton by cell membrane integrins. Cytoskeletal deformation triggers physiological responses in the cell, stimulating anabolic bone signals to induce adaptive modeling in the loaded tissue, different from the signals that remove bone microdamage.

A high number of low-magnitude load cycles or a low number of high-magnitude load cycles (and combinations along this spectrum) can cause microcracks in the hydroxyapatite-collagen matrix that can coalesce into macroscopic cracks that may compromise the stiffness of the bone. Unlike acellular engineered materials, bone and other living tissues can dynamically repair this microscopic damage. These remodeling events are initiated, at least in part, by damage to the OLCS that results in the cellular production of proosteoclastic and provasculogenic factors (*RANKL*, *VEGF*) secreted by dying osteocytes near the crack (Burr et al. 1985, Kennedy et al. 2012). The results of these repair processes are the formation of secondary osteons in cortical tissues and hemiosteons in cancellous tissues. Once formed, the cement lines of secondary osteons can act as future growth arrestors that absorb crack elongation energy to blunt the progress of crack propagation during future loading events (Wainwright et al. 1982). The interface between the hydroxyapatite mineral and organic collagen phases in primary and secondary bone tissues have been hypothesized to act similarly. Primary bone is stiffer than completely remodeled bone in axial loading (Table 33.1) (Currey 2002) and has a fatigue life that is five times greater than secondary bone (Carter et al. 1976). The decrease in material properties that result from intracortical remodeling reflects the strength of selection on cellular mechanisms that remove microdamage in bone.

Measuring and Modeling *In Vivo* Skeletal Mechanics and Bone Tissue Properties

The best way to assess skeletal loading *in vivo* is to directly measure the tissue-level results of mechanical loading by surgically implanted strain gauges. However, this is not always possible to do even in extant taxa for a number of reasons, including ethical and practical concerns of working with humans or wild-caught animals, the minimum bone element size required for gauge implantation, and potentially poor locomotor or masticatory performance in a lab-based setting. When direct measures cannot be made, simplifying assumptions must be applied to estimate bone stress and strain using simple or computational models (Biewener 1983b, Rayfield 2007, Dumont et al. 2009, O'Higgins et al. 2012). There are also potential limitations in lab-based settings for locomotor studies because animals cannot typically achieve the entire range of behaviors in the lab that they would in the wild. Therefore, lab-based studies, although relatively easy to control for repeatable results, may not provide complete insight into the mechanical basis for the evolution of particular bone shapes and microstructures relative to *in vivo* mechanics in the wild.

Skeletal loading environments can be directly measured using implantable foil strain gauges. These strain gauges can be attached surgically to bone using self-catalyzing cyanoacrylate adhesive. *In vivo* strains from a wide variety of vertebrate taxa performing a vast array of locomotor and masticatory activities have been collected (Table 33.2). Rosette strain gauges are particularly helpful for determining principal strains at the measured location and the orientation of these strains relative to an anatomical axis of interest. Measures of shear strain induced by either eccentric or torsional bone loading may also be calculated from rosette strain gauges using standard equations (Carter et al. 1980, Biewener 1992, Biewener and Dial 1995, Carrano and Biewener 1999). One limitation of implantable strain gauges is that they only characterize strain at a single bone location that may not coincide with the location of peak strain in the bone. For long bones, it is generally difficult to assess how a bone is loaded without placing at least three rosette strain gauges around the circumference of the bone at the same anatomical level (e.g., mid-diaphysis). If this configuration is possible in the taxon of interest, rosette gauges will provide the direction of the principal and shear strains around the bone, while the longitudinal gauge readings can provide a cross-sectional analysis of the longitudinal distribution of normal strains at the anatomical location of gauge placement (Figure 33.4) (Biewener 1992).

Strain gauge analyses can be combined with kinematic, electromyographic (EMG) and/or force plate analyses to understand the contributions of limb positioning, muscle forces and ground reaction forces on local bone biomechanics (Reilly et al. 2005, Aiello et al. 2013). Strain gauge measures can be used as validation points for computational analyses, enabling the model to, with some confidence, project beyond the strict location of the gauges to other bony regions, such as cancellous bone tissues or the metaphysis (Porro et al. 2013, Yang et al. 2014, 2019, Panagiotopoulou et al. 2017). Combined force plate and kinematic (including X-ray cineradiographic) analyses to estimate bone loading can be conducted in absence of direct strain gauge data as well (Biewener 1983b).

A current limitation to both strain gauge and kinetic/kinematic data analyses is a lack of data collected in the field. Laboratory experiments only assess a subset of behaviors that may not include the greatest loads experienced by the skeleton in nature. Telemetry systems have been used in the past, but have required large battery packs and thus could only be

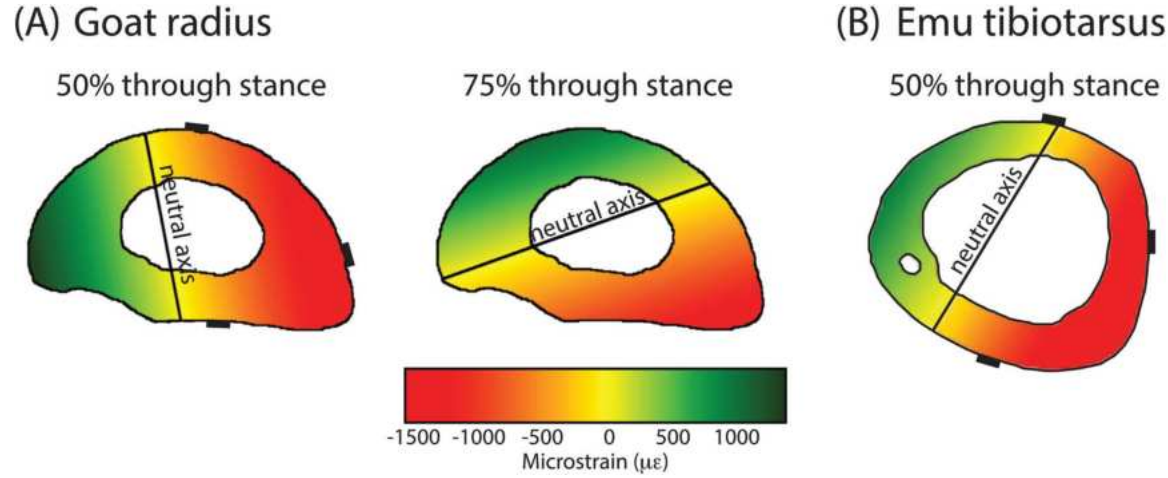


FIGURE 33.4 Normal (longitudinal) axial strain distributions for a goat radius and an emu tibiotarsus. A, The normal strain distribution in the goat radius shifts during the stance phase from mediolateral bending at 50% stance to nearly craniocaudal bending at 75% through stance, which is a shift of nearly 90° (Main and Biewener 2004). B, In contrast, the strain distribution in the emu tibiotarsus shows nearly mediolateral bending at midstance. Given the large amount of torsion present in this bone (Table 33.2), I_{MAX} and I_{MIN} are fairly similar, indicating a roughly circular bone (Main and Biewener 2007). Black rectangles on the bone surfaces indicate the position of the three strain gauges required to determine the normal strain distributions (Biewener 1992). The normal strain distributions are fairly independent of specific gauge positions (Verner et al. 2016), thus, it may be more useful to present the maximal predicted strains based on these normal strain models, rather than those measured from gauges located near the neutral axis.

carried by relatively large animals (Swartz et al. 1989, 1992). To assess bone strains in nature, miniaturized bridge amplifiers and data logging systems must be developed for the field of comparative biomechanics. This is the next critical step for advancing our understanding of the range of mechanical influences experienced by the skeleton in nature. Using such knowledge, we could begin to apply adaptive models, combining information about the range of strains experienced by the skeleton throughout a time period (days or weeks) and their frequency of occurrence over a given period of time (Fyhrie and Carter 1986, Beaupré et al. 1990, van der Meulen et al. 1993, Konieczynski et al. 1998, Fritton et al. 2000, Huiskes et al. 2000).

A number of methods can assess bone tissue mechanical properties at various levels of tissue organization. Whole bone strength (peak load, stress or strain) can be determined using a material testing system to load bones to yield or failure in uniaxial tension or compression, bending or torsion about a given axis. Because these loading modes are relatively simple, the peak stresses or strains engendered can be calculated using standard equations (Figure 33.2). Based on these biomechanical tests and measured or calculated *in vivo* bone loading, skeletal safety factors can be determined as:

$$\text{Safety factor} = \frac{\text{Peak } ex\ vivo \text{ stress (or strain)}}{\text{Peak } in\ vivo \text{ stress (or strain)}}$$

Safety factor provides some idea of how "overbuilt" a skeletal structure may be relative to the i*n vivo* forces experienced by the bone (Alexander 1981). The greater the safety factor, the less likely the bone is to fracture during a given mechanical activity. Cortical bone fails under compressive loading at ~20,000 με, but it begins to yield at 9800 με in compression and 8700 με in shear (Mirzaali et al. 2016, Morgan et al. 2018). Table 33.2 would indicate a wide range of potential safety factors, though many of them fall between 1.5 and 10 (Biewener 1993, Blob et al. 2014). All of the "standard" failure and yield strain values are from human or bovine bone (Table 33.1), establishing a clear need for axial and shear yield and failure properties from a broader comparative sample.

Whole bone strength depends on tissue-level material and structural properties. Tissue-level material properties can be determined for whole bone tests if the bone's structure or geometry can be properly measured or characterized. However, because whole bone structure is complex, involving nonuniform shapes and bone curvatures, strains calculated from *ex vivo* whole bone tests are approximate at best, which is why these tests are often conducted while directly collecting *ex vivo* strain gauge data (e.g., Blob and Biewener 1999, Blob et al. 2014).

Machining biological tissue samples of uniform and well-defined shape and size (e.g., prismatic rods or cubes) is the best way to experimentally measure bone tissue material properties at the meso- or microscale (e.g., Reilly and Burstein 1975, Lanyon et al. 1979). In these cases, the same load can be applied across a uniform structure where stress, strain, and elastic modulus can be accurately assessed. This approach represents an average of material characteristics over a heterogeneous material comprised of collagen, mineral, the OLCS, vasculature, and other porous spaces. However, this approach faithfully represents bone tissue as a functional unit that resists daily loading (Table 33.1). This type of approach has even been used to test individual secondary osteons by isolating them from the surrounding bone tissue to understand relationships between collagen fiber orientation and osteon strength and stiffness (Ascenzi and Bonucci 1967, 1968, Ascenzi et al. 1990, 1994).

VetBooks.ir

At a micro- and nanostructural level, bone tissue can vary in its mechanical properties in relation to bone material density (mineral crystals per volume of bone), protein composition and content, and the chemical interactions among collagen and other proteins. While changes in the mineral and proteins at this scale can affect whole bone material properties, such changes can be probed specifically using ultrasonography and micro- and nanoindentation instruments. Many biomedical rodent models have shown how aging, genetics, dietary alterations, and disease can cause changes in mineral and collagen composition that affect nano- and tissue-level material properties (Mehta et al. 1999, Vashishth et al. 2001, Reumann et al. 2011, Donnelly et al. 2012, Gharpure et al. 2016, Hunt et al. 2019).

Bone material properties can vary among taxa and in relation to functional demands (Biewener 1982, Currey 1987, 1988, 2002, Currey and Pond 1989, Brear and Currey 1990, Casinos and Cubo 2001, Erickson et al. 2002). Classic studies by John Currey showed the dependence of BMD and the associated differences in bone material properties to *in vivo* function for the whale tympanic bulla, the cow femur and the cervid antler (Currey 1979). This example demonstrates how BMD strongly influences bone material properties in relation to function. The highly mineralized whale bulla is very stiff and does not absorb much mechanical energy prior to fracture (i.e., brittle). The cervid antler is at the other end of the spectrum, having relatively low mineralization, but capable of absorbing a relatively high amount of mechanical energy prior to fracture (i.e., tough). For the whale bulla, the forces it has evolved to withstand are low magnitude vibrational energies, but they must be transmitted with little loss of energy for effective sensation, so toughness is sacrificed for stiffness (Figure 33.1C). In the antler, faithful transmission of force is less important than simply not breaking, so toughness through relatively low matrix mineralization is selected. The cow femur is intermediate between the two in mineralization, representing a selective compromise between toughness and stiffness. Thus, collagen composition, bone chemistry and BMD are important compositional features that can be favored evolutionarily. However, outside Currey's work, the breadth of vertebrate bone properties in relation to mechanical function is not well understood.

Modeling Musculoskeletal Biomechanics

The classic approach for modeling a structure under load is by conducting free body diagram (FBD) analysis on a static loading condition. The same can be done for dynamic musculoskeletal movements by analyzing a sequence of instantaneous "static" moments in time. To do this, the structure of the bone (or tooth, or other solid structure) being analyzed must be measured for the relevant lengths and dimensions (cross-sectional areas, lengths, radius of curvature, second moments of area), and the various forces acting on it must be evaluated. Development of an exhaustive accounting of the forces acting on the bone often requires a number of measures and assumptions.

First, the joint kinematics or position of the bone in three-dimensional (3D) space relative to external forces needs to be known to assess the orientations of the external forces relative to the bone (Figure 33.5). This can be done *in vivo* using high-speed video or cineradiography. This approach, even when used in natural settings, still requires idealized conditions and some control over the experimental setup (McGowan et al. 2005, Hedrick and Biewener 2007). When *in vivo* motion

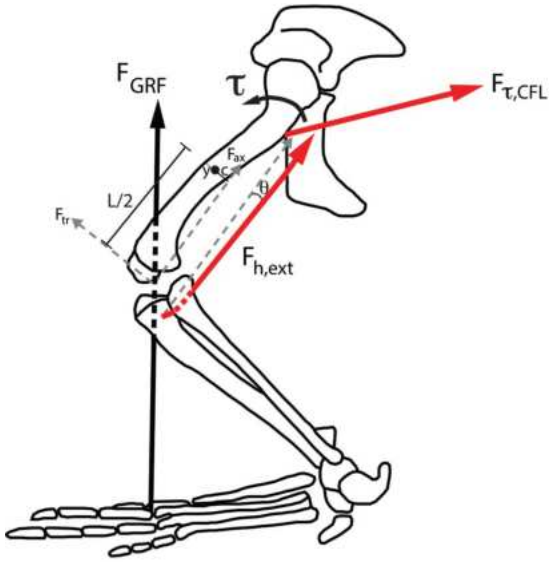


FIGURE 33.5 A simplified example of forces and moments to consider in a free body diagram (FBD) of the *Alligator* hindlimb. Limb kinematics were determined using X-ray cineradiographic video. The ground reaction force (F_{GRF}) was taken from published midstance values for *Alligator* (Blob and Biewener 1999, 2001). This example only considers flexion/extension moments on the femur caused by components of the F_{GRF} (F_{tr}, F_{ax}) and the hip extensor moment ($F_{h,ext}$). The torsional stress caused by the force of the *m. caudofemoralis longus* acting on the proximal femur is also shown. Not shown are the antagonistic knee extensors that counter the knee flexion caused by $F_{h,ext}$ or the torsional moment caused by F_{GRF} on the femur. All axial forces must act parallel to the femur. Therefore, a local coordinate system based on femoral position is established and muscle and GRF moments are resolved relative to that. In axial compression, the GRF component parallel to the long axis of the femur (F_{ax}) and the axial component of $F_{h,ext}$ are considered, where θ equals the angle between $F_{h,ext}$ and its component parallel to the femur's long axis. Bending stresses consider the transverse bending force of the GRF (F_{tr}) and the length at which this force is applied from the midshaft (*L*/2). Subtracted from this value are the bending moments induced by F_{ax} acting about the bone's curvature (*c*) and the component of $F_{h,ext}$ acting transverse to the bone's long axis [$F_{h,ext}$(sinθ)] (not shown). The midshaft torsional moment is calculated as the torsional force applied to the proximal femur ($F_{\tau,CFL}$) times the distance from the midshaft centroid to the midshaft bone surface (*y*), over the polar moment of inertia (*J*). (Complete details for this type of FBD reconstruction can be found in Biewener 1983b and Blob and Biewener 2001.)

VetBooks.ir

capture is not possible to collect, some estimation of the possible positions of the bones relative to external forces must be assumed. The possible position of the limbs can be constrained based on skeletal and soft tissue anatomy to determine realistic ranges of motion for the element of interest (Kambic et al. 2017, Manafzadeh and Padian 2018).

Following a measure or estimate of possible skeletal positions during the load cycle, the reaction forces on the skeletal element must be determined, whether this be the force exerted by a piece of food on the teeth/jaw, the force of the ground pushing back on the limb of a running animal, the aerodynamic forces acting on a wing during flight or the hydrodynamic forces acting on an appendage during swimming. This is best done directly using force plates for terrestrial locomotion, bite force sensors for feeding or wing-mounted pressure sensors and accelerometers or digital particle image velocimetry (DPIV) for flying or swimming animals. However, these approaches are not always accessible. In such cases, we must rely on biomechanical theory using, for example, the known or estimated body weight (BW) of the animal and the calculated forces required to keep the center of mass of that animal from falling to the earth, based on the kinematic position of the limb. This is more easily done if a definitive two-dimensional (2D) or 3D position of the limb is known. If not, the number of assumptions becomes compounded by having to estimate limb position, in addition to BW, and the various external mechanical forces that may act on the limb. In some cases, one could argue that the amount of speculation may outweigh the utility of the approach; though some examples presented later provide creative solutions to such cases.

Beyond the reaction forces applied to the skeletal element of interest, there are also muscles that exert force on or across a limb element. These muscles can apply tension directly to the area of interest on the bone itself, or apply force across the length and curvature of the bone, which can impose bending loads on the bone (Figure 33.5). It is possible to measure muscle forces directly in some unique anatomical conditions. For example, if a muscle or group of muscles inserts on the bone through a common tendon, strain gauge-based tendon buckle readings from that tendon can be calibrated to determine the muscle forces conveyed to the skeleton through that tendon (Biewener et al. 1988, Biewener 1992, Richards and Biewener 2007). These anatomical conditions are rare, however, and the vast majority of FBD analyses rely on indirect estimates of muscle force. Using the ground reaction forces exerted on the musculoskeletal system and anatomical limb position, the muscle forces required to maintain limb position are calculated about a joint (Figure 33.5). Often, several muscles spanning a joint may have a similar function; the composite force acting through these muscles can be calculated singly or as a group based on relative muscle mass. The stress attributed to vertebrate muscle during maximal power output is 300 kN m^{-2} (kPa; Close 1972) and is normalized to maximal muscle force based on the physiological cross-sectional area (PCSA) of the muscle. Typically, when both flexor and extensor muscles cross a joint, the muscles unlikely to contribute to the modeled function are ignored (for example, uniarticular hip flexors during the stance phase of running). However, many muscles are multiarticular and contribute forces across more than one joint. These muscles, even if not of interest to moment calculations about the joint of interest (e.g., extensor moment about the hip), must still be accounted for to calculate the forces present in the antagonistic muscles acting about the joint of interest (e.g., knee flexor action of a hip extensor being countered by a knee extensor during running to maintain a static knee). These estimates will increase the complexity of the musculoskeletal model. The presence of antagonistic muscle forces in these models would produce an infinite number of possible answers when trying to balance joint moments in an FBD analysis. This situation is typically avoided by minimizing the amount of force required by the muscles to balance the ground reaction force moment against the moments created by antagonistic muscles (Blob and Biewener 2001). However, it should be recognized that this approach may generate a minimum estimation of muscle-induced bone stress (or strain) within the limb.

Once the external and muscle forces have been validated, they can be applied about the bone with a known length, curvature, cross-sectional shape, and material properties to resolve the transverse (bending), longitudinal (axial) and torsional force components acting on a bone, which can then be used to calculate the axial, bending and shear stresses and strains that the bone experiences (Figure 33.5). It is obvious that the more assumptions that are made in the process, the more tenuous the calculated bone stresses and strains become.

FBD solutions are perfectly acceptable in many situations as long as proper boundary conditions can be applied and balanced. There are situations where the skeletal morphology or motions of interest are very complex and *in vivo* measures cannot be made to use for validation. In these cases, the best option is to use computational approaches. Finite element analyses (FEA) use 2D or 3D computational models to calculate estimates of the stresses and strains produced in a structure of interest. These computational techniques have been employed for decades in mechanical and biomedical engineering fields, but they have also been used in comparative mechanical studies for at least the last 30 years (Beaupré et al. 1990, Carter et al. 1991, Rensberger 1995). These analyses require the same 3D structural, material property, and external force inputs required by FBD analyses. However, by using this computational approach it is possible to extend the single-site analysis common in the FBD approach to the entire bone or structural unit of choice. Using these approaches, it would be possible to estimate stress or strain across an entire bone. Such knowledge can inform possible hypotheses about mechanical adaptations regarding the evolution of skeletal morphology relative to regions of low safety factor, which may indicate anatomical regions under increased selection relative to others. As with an FBD analysis, there are many assumptions that may go into FEA models, so a greater level of confidence can be placed in their conclusions if they are validated with direct mechanical measures of *in vivo* or *ex vivo* strain data (Porro et al. 2013, Yang et al. 2014, Panagiotopoulou et al. 2017). This additional validation provides greater confidence in the assumptions about other mechanical and material variables in the model, otherwise the entire model comes with the caveat that the resulting mechanical data may not be valid.

VetBooks.ir

In the last 10 to 15 years, advances in technical hardware, software and computational processing speed have allowed more advanced computational methods in developing musculoskeletal models. Detailed anatomical models of the skeletal system performing different mechanical functions can be developed using 3D X-ray cineradiography units (X-ray reconstruction of moving morphology [XROMM]) (Brainerd et al. 2010). These detailed kinematic models can be incorporated into complex musculoskeletal models for estimating muscle forces while reproducing realistic skeletal motions. Comparative reconstructions of muscular function have been increasingly examined using software for interactive musculoskeletal modeling (SIMM), OpenSim, or multidynamics analyses (MDA) (Delp and Loan 1995, Delp et al. 2007, Curtis et al. 2008). Integration of these models with data from experimental biomechanical sensors (EMG recordings, strain gauge and tendon buckle measures) increases the robusticity of these methods. Because invasive *in vivo* techniques are not available for many living taxa of interest or in paleontological studies, these computational approaches are being increasingly used in comparative biomechanical and paleontological studies as well (Hutchinson et al. 2005, 2015, Curtis et al. 2010, Rankin et al. 2018). Incorporating advanced imaging techniques such as CT and micro-CT, that can help to distinguish soft tissues such as cartilage, muscles, ligaments and tendons, could allow the development of complete, 3D musculoskeletal models from preserved museum specimens (Charles et al. 2016, Tsai et al. 2020). These combined anatomical and mechanical modeling approaches provide methodologies to test a broad array of functional musculoskeletal and evolutionary hypotheses, with a higher degree of confidence and sensitivity than ever before.

Ultimately, an integrated approach to *in vivo* musculoskeletal biomechanics would include an assessment of 3D motion of the skeletal limb elements with EMG measures of key muscles being used to inform SIMM or MDA musculoskeletal models overlying the skeletal reconstructions. Information gleaned from these models could be used as external force inputs for FEA models of the bone(s) of interest with the computational strains being validated by attaching strain gauges to the bones during skeletal movement. This would provide a truly integrated view of muscle and bone function during a variety of activities. However, there are few research labs capable of conducting this integrated approach, which speaks to the ever-increasing need for cross-disciplinary research among engineers, comparative biomechanists and paleontologists.

Application of Biomechanical Analyses to Paleontological and Comparative Questions of Function

Although no studies have accomplished all of the above *in vivo* and computational techniques in a single biomechanical study, many studies have used several *in vivo* mechanics and modeling sensitivity analyses to validate biting or locomotor musculoskeletal mechanics in living and extinct animals. Below are two examples, mastication in primates and theropod locomotor mechanics. These examples highlight some of the considerations necessary for collecting *in vivo* biomechanical data and appropriating that data, using the proper sensitivity analyses, to test functional hypotheses about living and fossil species.

Biting Mechanics in Primates

In reconstructing musculoskeletal biting mechanics in extant and fossil primates, it is necessary to account for musculoskeletal anatomy, EMG activity of the active masticatory muscles, material properties of the facial skeleton, and (if possible) *in vivo* bone strains collected from a number of different sites on the skull. Many of the *in vivo* EMG and bone strain data in the primate skull (macaques, humans) have been known for some time (e.g., Hylander 1977, Hylander et al. 1987, 1992, 1998, 2000, Hylander and Johnson 1997, Ross 2001, Ross et al. 2005, Smith et al. 2015a).

As computational FE modeling for quasi-static loading and biologists' interest in applying them to comparative biological systems grew, elastic properties were determined for the mandible and cranium of some primate species (Peterson and Dechow 2003, Wang and Dechow 2006, Davis et al. 2011, Gharpure et al. 2016). In addition to these data on bone properties, information on the muscle forces acting on the skull is also required. Estimation of peak force is relatively straightforward, and it has been approached with basic muscle anatomy and EMG activation data (Ross et al. 2005, Stansfield et al. 2018a). However, a more elegant approach is through using MDA, where both cranium and mandible can be modeled, muscles separated in distinct subsegments, wrapped around the cranium where needed, and made to act (computationally) as a functioning system to derive muscle forces and moments for input into FE models (Figure 33.6A) (Grosse et al. 2007, Curtis et al. 2008, Fitton et al. 2012, Liu et al. 2012, Shi et al. 2012). FE modeling of primate skulls was conducted with realistic input forces, material properties and bone strain validation data. To be sure, FE modeling is possible even if only the anatomy is known, but to be realistic and valid, these other mechanical factors should be incorporated as well. The groups conducting these studies have, in general, been very careful regarding sensitivity analyses and applying them to understand the effects of (for example) the distribution of material properties in the skull, the presence/absence and activity of different muscle groups, and the presence of cranial sutures on the resulting cranial stress and strain patterns (Ross et al. 2005, Strait et al. 2005, Kupczik et al. 2007, Fitton et al. 2012, Gröning et al. 2012, 2013, Stansfield et al. 2018a). More recently, the combination of sensitivity analyses and geometric morphometrics has arisen as a way of understanding how deformation in response to different loading conditions or variation within a population of animals might be important for interpreting analyses of extant and extinct species (Fitton et al. 2012, Smith et al. 2015a). By the time these same approaches were applied to *Australopithecus africanus* (*A. africanus*), *A. sediba*, *Paranthropus boisei* and ancient populations of *Homo*, there was already a wealth of data regarding sensitivity analyses and their effects on model outcomes in efforts to tests hypotheses about evolutionary changes relative to corresponding changes in cranial and mandibular morphology (Figure 33.6B) (Strait et al. 2009, Smith et al. 2015b, Ledogar et al. 2016, Stansfield et al. 2018b).

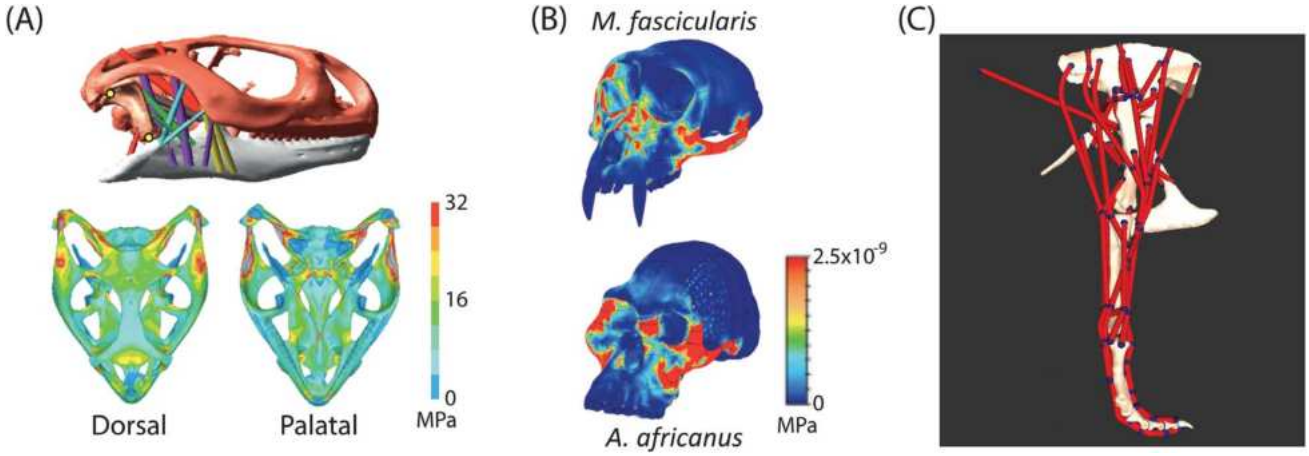


FIGURE 33.6 Computational biomechanical modeling applied to extant and extinct taxa. A, Multibody dynamics and finite element analysis (FEA) of *Uromastyx hardwickii*. The multidynamics analysis (MDA) models bilateral muscle activity of seven distinct pairs of muscle bellies on jaw adduction. Constraints on the system are two quadrate-based joints (yellow circles), a temporal ligament (in light blue), three fixed points on the occipital condyle, and material properties of the food particle. Food was bitten at the front of the mouth. Based on results from the MDA, boundary conditions (muscle forces, ligament forces, bite force and joint force) and bone and soft tissue properties were inputs for an FEA to determine the von Mises stress developed in the cranium during biting. The von Mises stress combines all the principal and shear stresses into a single number that is typically predictive of failure. B, FEA results for *Mulatta fascicularis* and *Australopithecus africanus* while biting with the postcanine teeth. Material properties for the cancellous and cortical bone and teeth were assigned. Four pairs of bilateral biting muscles were modeled. All of the postcanine teeth and articular eminences were constrained. Strain energy density is plotted here, which is similar to von Mises stress, and indicates a primarily distortional environment (as opposed to strains increasing the sample volume). C, A Software for Interactive Musculoskeletal Modeling (SIMM) model of a *Tyrannosaurus rex* hindlimb, showing the 37 unique muscle bellies modeled. Each muscle had a single origin and insertion point. Numerous muscles were subject to sensitivity analyses in regard to their muscle origins and wrapping surfaces around particular joints. Unrealistic net joint moments contrary to static standing were ruled out. The SIMM analysis used here suggests that *T. rex* had a mostly upright, but not columnar stance (hip flexion at 15°). (Figures were adapted from A, Moazen et al. 2008a, b; B, Strait et al. 2009; C Hutchinson et al. 2005.)

Other biting systems have been modeled in the bat, living and extinct crocodylomorphs and two lizards (*Uromastyx* and *Sphenodon*) (e.g., Dumont et al. 2005, Moazen et al. 2008a, b, Pierce et al. 2008, Curtis et al. 2010, 2011, Santana et al. 2012, Porro et al. 2013, 2014, Ballell et al. 2019). These papers all provide examples of the issues discussed above applied across a broad range of comparative species. A number of general reviews for the use of finite element models and geometric morphometrics, including their limitations and sensitivity considerations, have been published and are recommended for further review (Rayfield 2007, Dumont et al. 2009, O'Higgins et al. 2012, 2019, Panagiotopoulou et al. 2012, Polly et al. 2016).

Modeling Locomotion in Theropods

The examples provided above involve motion in the jaw and cranium during mastication. While efficiency and reduction of injury in eating are certainly important selective factors, the motion in itself can be reduced to a relatively simple rotational action controlled by relatively few constraints acting in the jaw. This is not nearly as complex as movement about the proximal joints of the limbs during locomotion where flexion/extension, abduction/adduction and long axis rotation are all valid for consideration in modeling limb motion in living and extinct taxa. Historically, limb motions were modeled only in flexion and extension and were largely confined to the study of mammals and terrestrial birds between 1970 and 1990. However, in the last 20 years, kinematic, bone strain and EMG data in nonmodel taxa have allowed consideration of a larger range of motion for tetrapod limbs.

Reconstructing the locomotion of theropods, and archosaurs in general, has been attractive as a means of studying locomotion in nonavian dinosaurs. The anatomy, kinematics and muscle activation data from crocodilian and bird species, as well as their importance in the evolution of birds, have been described (Gatesy 1991, 1997, 1999a, b, Gatesy and Biewener 1991, Gatesy and Dial 1996, Reilly and Elias 1998, Hutchinson 2001, 2002). Early musculoskeletal models were relatively simple, modeling the limb in flexion/extension and then abduction/adduction (Hutchinson and Garcia 2002, Hutchinson et al. 2005). Around this same time, *in vivo* femoral bone strains from extant archosaurs and lizards, including iguanas, alligators, chickens and emu, indicated that shear strains due to nonparasagittal long axis rotation is another important locomotor plane of motion to consider (Carrano and Biewener 1999, Blob and Biewener 1999, 2001, Main and Biewener 2007), even when avian archosaurs appear to be moving in a fairly parasagittal way (Hutchinson and Gatesy 2000, Kambic et al. 2017). A *Tyrannosaurus rex* musculoskeletal model in SIMM was used to run sensitivity analyses on muscle paths, origin and insertion centroids (where ambiguous), and muscle wrapping at the joints (Hutchinson et al. 2005) (Figure 33.6C). This locomotor simulation of *T. rex* used 3D scans of a museum sample to reconstruct a computational anatomical model, used assumptions about the scaling of muscle masses, and used basic tetrapod muscle physiological properties to determine optimum muscle moments generated by each of the 37 limb

VetBooks.ir

muscles when holding the limb at different positions. The results suggested that the greatest mechanical advantage for the muscles occurs over a limited period of limb excursion, which would make it unlikely that *T. rex* could generate the necessary muscle forces required to run with a typical bipedal aerial phase. This conclusion was confirmed using a different theropod limb flexion/extension, constraints-based exclusion approach to determine, using a number of anatomical, kinematic and kinetic constraints, that large theropods could only generate 1.0–1.5 BW of force in each limb, and not the ~2.0 BW required for bipedal running (Gatesy et al. 2009).

A recent 3D analysis of ostrich hindlimb biomechanics found that ostrich muscles do not actually operate at peak muscle force and moment efficiency during slow running, which prior theropod models had assumed (Hutchinson et al. 2015). This study also showed the importance of examining the hindlimb joints of animals in 3D planes and laid an important foundation to understand how the balance of muscle and external forces act in the hindlimb joints of birds. An impressive series of recent studies have combined SIMM models and FEA to predict the evolution of cancellous bone structure in the hindlimbs of avian and nonavian theropods. Boundary conditions for the FE models were based on both muscle forces and soft tissue constraints at the joints. Sensitivity analyses for variation in bone and soft tissue structures were not accounted for. However, given the complex analyses and scope of this work, simplifying assumptions such as these had to be made and are identified in the studies (Bishop et al., 2019a, b, c). Whereas these works represent a complex assessment of limb kinematics, ground reaction forces, anatomical anatomy and computational modeling, this is certainly not the entire hindlimb constraint space that could have been used. Noticeably missing from this model is some assessment of skeletal biomechanics. Mapping these limb motions and muscle reconstructions to an *in vivo* measure of skeletal mechanics provides one more validation constraint on the larger computational model.

Recent use of XROMM has addressed some of the problems of soft tissue constraints in archosaurs, where crocodilians and different avian taxa have been used to distinguish between *in vivo* range of motion, *ex vivo* soft tissue range of motion and *ex vivo* skeletal range of motion (Kambic et al. 2017, Manafzadeh and Padian 2018, Tsai et al. 2020). The most revealing of these examined guinea fowl moving through an XROMM imaging volume performing different functions compared to motions in the same joints in cadaveric birds (Kambic et al. 2017). This study showed that a very small portion (~30%) of the *ex vivo* 3D movement space is actually used *in vivo*. It also indicated that the limitation of constraining limb motion in paleontological and comparative studies is the lack of knowledge regarding the role of specific soft tissue constraints in limiting joint movement. More recently, crocodiles and quail have been examined to study the role of soft tissues, including ligaments, soft tissue bursae and cartilage caps in comparative skeletal range of motion analyses (Manafzadeh and Padian 2018, Tsai et al. 2020).

Nyakatura et al. (2019) recently reconstructed the gait of the Permian stem amniote *Orobates pabsti*. This novel study used kinematics and kinetics from a range of extant comparable taxa, 3D skeletonization of *Orobates* and an informed sensitivity and constraints-based gait exclusion approach to reconstruct the gait of *Orobates*, based on a known fossil trackway. This combination of approaches could serve as a model for further efforts to reconstruct locomotion in extinct taxa.

Conclusion

Bone is both a living organ and rigid support element. To the strength of the rigid support is added adaptive and reparative mechanisms that can sustain bone's strength and toughness through an animal's lifetime to the variety of functions the bone must serve. Bone is composed of both collagen and hydroxyapatite mineral that provides it strength in tensile, compressive and torsional loading. In addition, the density and distribution of these materials can provide different regions of the skeleton different mechanical attributes. Functional adaptation of the skeleton can modify these attributes and differentially alter a bone's safety factor during an animal's lifetime, preventing fatigue or catastrophic damage. The stresses and strains that the skeleton must withstand during life can be measured using a number of different techniques, each with its own strengths and limitations, to measure anatomical structures, motion of the skeleton, forces exerted by the skeleton, how those forces are transmitted to deformation of the skeleton, and the muscle activations responsible for skeletal and ground reaction force loading. These approaches can be combined with advanced measures of 3D skeletal movement (XROMM), FEA, MDA, and musculoskeletal SIMM modeling as a form of validation for these computational models that are often used to address more complex functional hypotheses in extant and extinct taxa.

Although we have an extraordinary array of measurement tools that allow us to learn more about musculoskeletal cell biology and mechanics, there are limitations in all of these approaches and we must be careful to validate our models and perform the necessary sensitivity analyses when applying these computational methods to new taxa. We must also realize that there is a vast amount of variation in biomechanical measurements because of differences in basic morphology, and not *all* questions require *all* kinematic, kinetic or material parameters to be known. For example, if similar taxa are being compared, perhaps similar material properties of biological tissues can be assumed. If the question asked is of a broad enough scope, perhaps some small detail about kinematics can be ignored. Regardless, in all cases, this must be rationalized and transparent to the reader. Otherwise, our ability to reproduce experimental results or use similar approaches to test related hypotheses is limited.

Acknowledgments

I give my deep thanks to Dr. Richard Blob for his critical comments on this manuscript and for providing references for Table 33.2. Dr. Callum Ross assisted with gathering references and clarifying data for Table 33.2. Dr. Corwin Sullivan provided the cineradiographic video to reproduce the *Alligator* kinematics for Figure 33.5. This work was supported in part by the National Science Foundation CMMI 1463523.

VetBooks.ir

REFERENCES

Aamodt, A., et al. 1997. *In vivo* measurements show tensile axial strain in the proximal lateral aspect of the human femur. *J. Orthop. Res.* 15: 927–931.

Aiello, B. R., et al. 2013. Correlation of muscle function and bone strain in the hindlimb of the river cooter turtle (*Pseudemys concinna*). *J. Morphol.* 274: 1060–1069.

Alexander, R. M. N. 1981. Factors of safety in the structure of animals. *Sci. Progr.* 67: 109–130.

Ascenzi, A. and E. Bonucci. 1967. The tensile properties of single osteons. *Anat. Rec.* 158: 375–386.

Ascenzi, A. and E. Bonucci. 1968. The compressive properties of single osteons. *Anat. Rec.*161: 377–391.

Ascenzi, A., et al. 1990. The bending properties of single osteons. *J. Biomech.* 23: 763–771.

Ascenzi, A., et al. 1994. The torsional properties of single selected osteons. *J. Biomech.* 27(7): 875–884.

Ballell, A., et al. 2019. Convergence and functional evolution of longirostry in crocodylomorphs. *Palaeontology* 62: 867–887.

Bartel, D. L., et al. 2006. *Orthopaedic biomechanics.* Upper Saddle River, NJ, Pearson Education.

Beaupré, G. S., et al. 1990. An approach for time-dependent bone modeling and remodeling - application: A preliminary remodeling simulation. *J. Orthop. Res.* 8: 651–661.

Bertram, J. E. A. and A. A. Biewener. 1988. Bone curvature: Sacrificing strength for load predictability? *J. Theor. Biol.* 131: 75–92.

Biewener, A. A. 1982. Bone strength in small mammals and bipedal birds: Do safety factors change with body size? *J. Exp. Biol.* 98: 289–301.

Biewener, A. A. 1983a. Allometry of quadrupedal locomotion: The scaling of duty factor, bone curvature and limb orientation to body size. *J. Exp. Biol.* 105: 147–171.

Biewener, A. A. 1983b. Locomotory stresses in the limb bones of two small mammals: The ground squirrel and chipmunk. *J. Exp. Biol.* 103: 131–154.

Biewener, A. A. 1992. *In vivo* measurement of bone strain and tendon force. In *Biomechanics: structures and systems. A practical approach*, 123–148. New York, Oxford University Press.

Biewener, A. A. 1993. Safety factors in bone strength. *Calcif. Tissue Int.* 53(Suppl 1): S68–S74.

Biewener, A. A. and K. P. Dial. 1995. *In vivo* strain in the humerus of pigeons (*Columba livia*) during flight. *J. Morphol.* 225: 61–75.

Biewener, A. A. and C. R. Taylor. 1986. Bone strain: A determinant of gait and speed? *J. Exp. Biol.* 123: 383–400.

Biewener, A. A., et al. 1988. Muscle forces during locomotion in kangaroo rats: Force platform and tendon buckle measurements compared. *J. Exp. Biol.* 137: 191–205.

Biewener, A. A., et al. 1996. Adaptive changes in trabecular architecture in relation to functional strain patterns and disuse. *Bone* 19: 1–8.

Biewener, A. A., et al. 1986. Bone modeling during growth: Dynamic strain equilibrium in the chick tibiotarsus. *Calcif. Tissue Int.* 39: 390–395.

Bishop, P. J., et al. 2019a. Cancellous bone and theropod dinosaur locomotion. Part I—an examination of cancellous bone architecture in the hindlimb bones of theropods. *PeerJ.* 6: e5778.

Bishop, P. J., et al. 2019b. Cancellous bone and theropod dinosaur locomotion. Part II—a new approach to inferring posture and locomotor biomechanics in extinct tetrapod vertebrates. *PeerJ.* 6: e5779.

Bishop, P. J., et al. 2019c. Cancellous bone and theropod dinosaur locomotion. Part III—Inferring posture and locomotor biomechanics in extinct theropods, and its evolution on the line to birds. *PeerJ*, 6: e5777.

Blob, R. W. and A. A. Biewener. 1999. *In vivo* locomotor strain in the hindlimb bones of *Alligator mississippiensis* and *Iguana*: Implications for the evolution of limb bone safety factor and non-sprawling limb posture. *J. Exp Biol.* 202: 1023–1046.

Blob, R. W. and A. A. Biewener. 2001. Mechanics of limb bone loading during terrestrial locomotion in the green iguana (*Iguana iguana*) and American alligator (*Alligator mississippiensis*). *J. Exp. Biol.* 204: 1099–1122.

Blob, R. W., et al. 2014. Diversity of limb-bone safety factors for locomotion in terrestrial vertebrates: Evolution and mixed chains. *Integr. Comp. Biol.* 54: 1058–1071.

Bouxsein, M., et al. 2010. Guidelines for assessment of bone microstructure in rodents using micro-X-ray reconstruction tomography. *J. Bone Miner. Res.* 25: 1468–1486.

Brainerd, E. L., et al. 2010. X-Ray reconstruction of moving morphology (XROMM): Precision, accuracy and applications in comparative biomechanics research. *J. Exp. Zool. A* 313: 262–279.

Brear, K. and J. D. Currey. 1990. Ontogenetic changes in the mechanical properties of the femur of the polar bear *Ursus maritimus*. *J. Zool. (Lond.) 222*: 49–58.

Buenzli, P. R. and N. A. Sims. 2015. Quantifying the osteocyte network in the human skeleton. *Bone* 75: 144–150.

Burr, D. B. and O. Akkus. 2014. Bone morphology and organization. In *Basic and applied bone biology*, eds. Burr, D. B. and M. R. Allen, 3–25. Amsterdam, Academic Press.

Burr, D. B., et al. 1985. Bone remodeling in response to *in vivo* fatigue microdamage. *J. Biomech.* 18: 189–200.

Butcher, M. T., et al. 2008. *In vivo* strains in the femur of river cooter turtles (*Pseudemys concinna*) during terrestrial locomotion: Tests of force-platform models of loading mechanics. *J. Exp. Biol.* 211: 2397–2407.

Butcher, M. T., et al. 2011. *In vivo* strains in the femur of the Virginia opossum (*Didelphis virginiana*) during terrestrial locomotion: Testing hypotheses of evolutionary shifts in mammalian bone loading and design. *J. Exp. Biol.* 214: 2631–2640.

Carrano, M. T. and A. A. Biewener. 1999. Experimental alteration of limb posture in the chicken (*Gallus gallus*) and its bearing on the use of birds as analogs for dinosaur locomotion. *J. Morphol.* 240: 237–249.

Carter, D. R. and G. S. Beaupré. 2001. *Skeletal function and form: Mechanobiology of skeletal development, aging, and regeneration*. Cambridge, UK, Cambridge University Press.

Carter, D. R. and W. C. Hayes. 1976. Bone compressive strength: The influence of density and strain rate. *Science* 194(4270): 1174–1211.

Carter, D. R., et al. 1976. Fatigue life of compact bone II. Effects of microstructure and density. *J. Biomech.* 9: 211–218.

Carter, D. R., et al. 1980. Measurement and analysis of *in vivo* bone strains on the canine radius and ulna. *J. Biomech.* 13: 27–38.

Carter, D. R., et al. 1991. Musculoskeletal ontogeny, phylogeny, and functional adaptation. *J. Biomech*. 24(Suppl. 1): 3–16.

Casinos, A. and J. Cubo. 2001. Avian long bones, flight and bipedalism. *Comp. Biochem. Physiol. A*131: 159–167.

Charles, J. P., et al. 2016. Muscle moment arms and sensitivity analysis of a mouse hindlimb musculoskeletal model. *J. Anat.* 229: 514–535.

Close, R. I. 1972. Dynamic mammalian properties of skeletal muscles. *Physiol. Rev.* 52: 129–197.

Copploe, J. V., et al. 2015. In vivo strains in the femur of the nine-banded armadillo (*Dasypus novemcinctus*). *J. Morphol*. 276: 889–899.

Cowin, S. C., et al. 1995. A case for bone canaliculi as the anatomical site of strain generated potentials. *J. Biomech*. 28: 1281–1297.

Currey, J. D. 1979. Mechanical properties of bone tissues with greatly differing functions. *J. Biomech*. 12: 313–319.

Currey, J. D. 1987. The evolution of the mechanical properties of amniote bone. *J. Biomech*. 20: 1035–1044.

Currey, J. D. 1988. The effect of porosity and mineral content on the Young's modulus of elasticity of compact bone. *J. Biomech*. 21: 131–139.

Currey, J. D. 1999. What determines the bending strength of compact bone? *J. Exp. Biol*. 202: 2495–2503.

Currey, J. D. 2002. *Bones: Structure and mechanics.* 1st ed. Princeton, NJ, Princeton University Press.

Currey, J. D. and C. M. Pond. 1989. Mechanical properties of very young bone in the axis deer (*Axis axis*) and humans. *J. Zool. (Lond.)* 218: 59–67.

Curtis, N., et al. 2008. Predicting skull loading: Applying multibody dynamics analysis to a macaque skull. *Anat. Rec.* 291: 491–501.

Curtis, N., et al. 2010. Comparison between *in vivo* and theoretical bite performance: Using multi-body modelling to predict muscle and bite forces in a reptile skull. *J. Biomech.* 43: 2804–2809.

Curtis, N., et al. 2011. Functional relationship between skull form and feeding mechanics in *Sphenodon*, and implications for diapsid skull development. *PLoS One* 6: 31–33. https://doi.org/10.1371/journal.pone.0029804

Davis, J. L., et al. 2011. An efficient method of modeling material properties using a thermal diffusion analogy: An example based on craniofacial bone. *PLoS One*, 6: e17004. https://doi.org/10.1371/journal.pone.0017004

Delp, S. L. and J. P. Loan. 1995. A graphics-based software system to develop and analyze models of musculoskeletal structures. *Computers in Biol. Med. 25*: 21–34.

Delp, S. L., et al. 2007. OpenSim: Open-source software to create and analyze dynamic simulations of movement. *IEEE Trans. Biomed. Eng.* 54: 1940–1950.

Demes, B., et al. 1998. Patterns of strain in the macaque ulna during functional activity. *Am. J. Phys. Anthropol.* 106: 87–100.

Demes, B., et al. 2001. Patterns of strain in the macaque tibia during functional activity. *Am. J. Phys. Anthropol.* 116: 257–265.

D'Emic, M. D. and R. B. J. Benson. 2013. Measurement, variation, and scaling of osteocyte lacunae: A case study in birds. *Bone* 57: 300–310.

Donnelly, E., et al. 2012. Reduced cortical bone compositional heterogeneity with bisphosphonate treatment in postmenopausal women with intertrochanteric and subtrochanteric fractures. *J. Bone Miner. Res*. 27: 672–678.

Dumont, E. R., et al. 2005. Finite-element analysis of biting behavior and bone stress in the facial skeletons of bats. *Anat. Rec. A*283: 319–330.

Dumont, E. R., et al. 2009. Requirements for comparing the performance of finite element models of biological structures. *J. Theor. Biol*. 256: 96–103.

Easley, S. K., et al. 2010. Contribution of the intra-specimen variations in tissue mineralization to PTH- and raloxifene-induced changes in stiffness of rat vertebrae. *Bone* 46: 1162–1169.

Erickson, G. M., et al. 2002. Evolution of the biomechanical material properties of the femur. *Anat. Rec.* 268: 115–124.

Fitton, L. C., et al. 2012. Masticatory loadings and cranial deformation in *Macaca fascicularis*: A finite element analysis sensitivity study. *J. Anat.* 221: 55–68.

Fritton, S. P. and C. T. Rubin. 2001. *In vivo* measurement of bone deformations using strain gauges. In *Bone mechanics handbook*, 2nd ed., ed. Cowin, S. C., 8–41. Boca Raton, FL, CRC Press.

Fritton, S. P. and S. Weinbaum. 2009. Fluid and solute transport in bone: Flow-induced mechanotransduction. *Ann. Rev. Fluid Mech*. 41: 347–374.

Fritton, S. P., et al. 2000. Quantifying the strain history of bone: Spatial uniformity and self-similarity of low-magnitude strains. *J. Biomech*. 33: 317–325.

Fyhrie, D. P. and D. R. Carter. 1986. A unifying principle relating stress to trabecular bone morphology. *J. Orthop. Res.* 4: 304–317.

Gatesy, S. M. 1991. Hind limb movements of the American alligator (*Alligator mississippiensis*) and postural grades. *J. Zool*. 224: 577–588.

Gatesy, S. M. 1997. An electromyographic analysis of hindlimb function in *Alligator* during terrestrial locomotion. *J. Morphol*. 234: 197–212.

Gatesy, S. M. 1999a. Guineafowl hind limb function. I: Cineradiographic analysis and speed effects. *J. Morphol*. 240: 115–125.

Gatesy, S. M. 1999b. Guineafowl hind limb function. II: Electromyographic analysis and motor pattern evolution. *J. Morphol*. 240: 127–142.

Gatesy, S. M. and A. A. Biewener. 1991. Bipedal locomotion: Effects of speed, size and limb posture in birds and humans. *J. Zool*. 224: 127–147.

Gatesy, S. M. and K. P. Dial. 1996. Locomotor modules and the evolution of avian flight. *Evolution* 50: 331.

Gatesy, S. M., et al. 2009. Constraint-based exclusion of limb poses for reconstructing theropod dinosaur locomotion. *J. Vert. Paleontol*. 29: 535–544.

Gharpure, P., et al. 2016. Elastic properties of chimpanzee craniofacial cortical bone. *Anat. Rec.* 299: 1718–1733.

Goodship, A. E., et al. 1979. Functional adaptation of bone to increased stress. *J. Bone Joint Surg.* 61A: 539–546.

Gröning, F., et al. 2012. Modeling the human mandible under masticatory loads: Which input variables are important? *Anat. Rec.* 295: 853–863.

Gröning, F., et al. 2013. The importance of accurate muscle modelling for biomechanical analyses: A case study with a lizard skull. *J. R. Soc. Interface* 10(84): 20130216. https://doi.org/10.1098/rsif.2013.0216

Gross, T. S., et al. 1992. Characterizing bone strain distribution *in vivo* using three triple rosette strain gages. *J. Biomech.* 25: 1081–1087.

Grosse, I. R., et al. 2007. Techniques for modeling muscle-induced forces in finite element models of skeletal structures. *Anat. Rec.* 290: 1069–1088.

Hedrick, T. L. and A. A. Biewener. 2007. Low speed maneuvering flight of the rose-breasted cockatoo (*Eolophus roseicapillus*). I. Kinematic and neuromuscular control of turning. *J. Exp. Biol.* 210: 1897–1911.

Herring, S. W. and S. Teng. 2000. Strain in the braincase and its sutures during function. *Am. J. Phys. Anthropol.* 112: 575–593.

Herring, S. W., et al. 2005. Ontogeny of bone strain: The zygomatic arch in pigs. *J. Exp. Biol.* 208: 4509–4521.

Huiskes, R., et al. 2000. Effects of mechanical forces on maintenance and adaptation of form in trabecular bone. *Nature*, 405(6787): 704–706.

Hunt, H. B., et al. 2019. Altered tissue composition, microarchitecture, and mechanical performance in cancellous bone from men with type 2 diabetes mellitus. *J Bone Miner. Res.* 34: 1191–1206. https://doi.org/10.1002/jbmr.3711

Hutchinson, J. R. 2001. The evolution of pelvic osteology and soft tissues on the line to extant birds (Neornithes). *Zool. J. Linn. Soc.* 131: 123–166.

Hutchinson, J. R. 2002. The evolution of hindlimb tendons and muscles on the line to crown-group birds. *Comp. Biochem. Physiol. A* 133: 1051–1086.

Hutchinson, J. R. and S. M. Gatesy. 2000. Adductors, abductors, and the evolution of archosaur locomotion. *Paleobiology* 26: 734–751.

Hutchinson, J. R. and M. Garcia. 2002. *Tyrannosaurus* was not a fast runner. *Nature* 415(6875): 1018–1021.

Hutchinson, J. R., et al. 2005. Analysis of hindlimb muscle moment arms in *Tyrannosaurus rex* using a three-dimensional musculoskeletal computer model: Implications for stance, gait, and speed. *Paleobiology* 31: 676–701.

Hutchinson, J. R., et al. 2015. Musculoskeletal modeling of an ostrich (*Struthio camelus*) pelvic limb: Influence of limb orientation on muscular capacity during locomotion. *PeerJ* 2015: 1–52.

Hylander, W. L. 1977. *In vivo* bone strain in the mandible of *Galago crassicaudatus*. *Am. J. Phys. Anthropol.* 46: 309–326.

Hylander, W. L. 1979. Mandibular function in *Galago crassicaudatus* and *Macaca fascicularis*: An *in vivo* approach to stress analysis of the mandible. *J. Morphol.*159: 253–296.

Hylander, W. L. and R. Bays. 1979. An *in vivo* strain-gauge analysis of the squamosal-dentary joint reaction force during mastication and incisal biting in *Macaca mulatta* and *Macaca fascicularis*. *Arch. Oral Biol.* 24: 689–697.

Hylander, W. L. and K. R. Johnson. 1997. *In vivo* bone strain patterns in the zygomatic arch of macaques and the significance of these patterns for functional interpretations of craniofacial form. *Am. J. Phys. Anthropol.* 102: 203–232.

Hylander, W. L., et al. 1987. Loading patterns and jaw movements during mastication in *Macaca fascicularis*: A bone-strain, electromyographic, and cineradiographic analysis. *Am. J. Phys. Anthropol.* 72: 287–314.

Hylander, W. L., et al. 1992. Muscle force recruitment and biomechanical modeling: An analysis of masseter muscle function during mastication in *Macaca fascicularis*. *Am. J. Phys. Anthropol.* 88: 365–387.

Hylander, W. L., et al. 1991a. Function of the supraorbital region of primates. *Arch. Oral Biol.* 36: 273–281.

Hylander, W. L., et al. 1991b. Masticatory-stress hypotheses and the supraorbital region of primates. *Am. J. Phys. Anthropol.* 86: 1–36.

Hylander, W. L., et al. 1998. Mandibular corpus strain in primates: Further evidence for a functional link between symphyseal fusion and jaw-adductor muscle force. *Am. J. Phys. Anthropol.* 107: 257–271.

Hylander, W. L., et al. 2000. Symphyseal fusion and jaw-adductor muscle force: An EMG study. *Am. J. Phys. Anthropol.* 112: 469–492.

Kambic, R. E., et al. 2017. 3-D range of motion envelopes reveal interacting degrees of freedom in avian hind limb joints. *J. Anat.* 231: 906–920.

Kawano, S. M., et al. 2016. Comparative limb bone loading in the humerus and femur of the tiger salamander: Testing the "mixed-chain" hypothesis for skeletal safety factors. *J. Exp. Biol.* 219: 341–353.

Keller, T. S. and D. M. Spengler. 1982. *In vivo* strain gage implantation in rats. *J. Biomech.* 15: 911–917.

Keller, T. S. and D. M. Spengler. 1989. Regulation of bone stress and strain in the immature and mature rat femur. *J. Biomech.* 22: 1115–1127.

Kennedy, O. D., et al. 2012. Activation of resorption in fatigue-loaded bone involves both apoptosis and active pro-osteoclastogenic signaling by distinct osteocyte populations. *Bone* 50: 1115–1122.

Konieczynski, D. D., et al. 1998. Evaluation of a bone's *in vivo* 24-hour loading history for physical exercise compared with background loading. *J. Orthop. Res.* 16: 29–37.

Kupczik, K., et al. 2007. Assessing mechanical function of the zygomatic region in macaques: Validation and sensitivity testing of finite element models. *J. Anat.* 210: 41–53.

Lanyon, L. E. 1972. *In vivo* bone strain recorded from thoracic vertebrae of sheep. *J. Biomech.* 5: 277–281.

Lanyon, L. E. 1973. Analysis of surface bone strain in the calcaneus of sheep during normal locomotion. Strain analysis of the calcaneus. *J. Biomech.* 6: 41–49.

Lanyon, L. E. and S. Bourn. 1979. The influence of mechanical function on the development and remodeling of the tibia. *J. Bone Joint Surg. A* 61: 262–273.

Lanyon, L. E., et al. 1979. The relationship of functional stress and strain to the processes of bone remodelling. An experimental study on the sheep radius. *J. Biomech.* 12: 593–600.

Lanyon, L. E., et al. 1981. *In vivo* strain measurements from bone and prosthesis following total hip replacement. An experimental study in sheep. *J. Bone Joint Surg. A* 63: 989–1001.

Lauder, G. V. and L. E. Lanyon. 1980. Functional anatomy of feeding in the bluegill sunfish, *Lepomis macrochirus*: *In vivo* measurement of bone strain. *J. Exp. Biol.* 84: 33–55.

Ledogar, J. A., et al. 2016. Mechanical evidence that *Australopithecus sediba* was limited in its ability to eat hard foods. *Nat. Comm.* 7: 1–9.

Lee, K. C. L., et al. 2002. Validation of a technique for studying functional adaptation of the mouse ulna in response to mechanical loading. *Bone* 31: 1–9.

Lieberman, D. E., et al. 2004a. Effects of food processing on masticatory strain and craniofacial growth in a retrognathic face. *J. Human Evol.* 46: 655–677.

Lieberman, D. E., et al. 2004b. Predicting long bone loading from cross-sectional geometry. *Am. J. Phys. Anthropol.* 123: 156–171.

VetBooks.ir

Liu, J., et al. 2012. The application of muscle wrapping to voxel-based finite element models of skeletal structures. *Biomech. Model. Mechanobiol.* 11: 35–47.

Loitz, B. J. and R. F. Zernicke. 1992. Strenuous exercise-induced remodelling of mature bone: Relationships between *in vivo* strains and bone mechanics. *J. Exp. Biol.* 170, 1–18.

Main, R. P. and A. A. Biewener. 2004. Ontogenetic patterns of limb loading, *in vivo* bone strains and growth in the goat radius. *J. Exp. Biol.* 207: 2577–2588.

Main, R. P. and A. A. Biewener. 2006. *In vivo* bone strain and ontogenetic growth patterns in relation to life-history strategies and performance in two vertebrate taxa: Goats and emu. *Physiol. Biochem. Zool.* 79: 57–72.

Main, R. P. and A. A. Biewener. 2007. Skeletal strain patterns and growth in the emu hindlimb during ontogeny. *J. Exp. Biol.* 210: 2676–2690.

Manafzadeh, A. R. and K. Padian. 2018. ROM mapping of ligamentous constraints on avian hip mobility: Implications for extinct ornithodirans. *Proc. R. Soc. B: Biol. Sci.* 285(1879): 20180727. https://doi.org/10.1098/rspb.2018.0727

Manley, P. A., et al. 1982. Evaluation of tension and compression forces in the canine femur *in vivo*. *Arch. Orthop. Trauma. Surg.* 99: 213–216.

Markey, M. J., et al. 2006. *In vivo* cranial suture function and suture morphology in the extant fish *Polypterus*: Implications for inferring skull function in living and fossil fish. *J. Exp. Biol.* 209: 2085–2102.

Martínez-Pérez, C., et al. 2014. Finite element, occlusal, microwear and microstructural analyses indicate that conodont microstructure is adapted to dental function. *Palaeontology* 57: 1059–1066.

McGowan, C. P., et al. 2005. The mechanics of jumping *versus* steady hopping in yellow-footed rock wallabies. *J. Exp. Biol.* 208: 2741–2751.

Mehta, S. S., et al. 1999. Bone material elasticity in a murine model of osteogenesis imperfecta. *Connect. Tissue Res.* 40: 189–198.

Metzger, K. A., et al. 2005. Comparison of beam theory and finite-element analysis with *in vivo* bone strain data from the alligator cranium. *Anat. Rec. A*283: 331–348.

Milgrom, C., et al. 2000. *In vivo* strain measurements to evaluate the strengthening potential of exercises on the tibial bone. *J. Bone Joint Surg. B* 82: 591–594.

Mirzaali, M. J., et al. 2016. Mechanical properties of cortical bone and their relationships with age, gender, composition and microindentation properties in the elderly. *Bone* 93: 196–211.

Moazen, M., et al. 2008a. Combined finite element and multibody dynamics analysis of biting in a *Uromastyx hardwickii* lizard skull. *J. Anat.* 213: 499–508.

Moazen, M., et al. 2008b. Rigid-body analysis of a lizard skull: Modelling the skull of *Uromastyx hardwickii*. *J. Biomech.* 41: 1274–1280.

Moreno, C. A., et al. 2008. Variability in forelimb bone strains during non-steady locomotor activities in goats. *J. Exp. Biol.* 211: 1148–1162.

Morgan, E. F., et al. 2018. Bone mechanical properties in healthy and diseased states. *Ann. Rev. Biomed. Eng.* 20: 119–143.

Mosley, J. R., et al. 1997. Strain magnitude related changes in whole bone architecture in growing rats. *Bone* 20: 191–198.

Nunamaker, D. M., et al. 1990. Fatigue fractures in thoroughbred racehorses: Relationships with age, peak bone strain, and training. *J. Orthop. Res.* 8: 604–611.

Nyakatura, J. A., et al. 2019. Reverse-engineering the locomotion of a stem amniote. *Nature* 565(7739): 351–355.

O'Higgins, P., et al. 2019. Geometric morphometrics and finite elements analysis: Assessing the functional implications of differences in craniofacial form in the hominin fossil record. *J Archaeol. Sci.* 101: 159–168.

O'Higgins, P., et al. 2012. Virtual functional morphology: Novel approaches to the study of craniofacial form and function. *Evol. Biol.* 39: 521–535.

Panagiotopoulou, O., et al. 2012. What makes an accurate and reliable subject-specific finite element model? A case study of an elephant femur. *J. R. Soc. Interface* 9: 351–361.

Panagiotopoulou, O., et al. 2017. *In vivo* bone strain and finite element modeling of a rhesus macaque mandible during mastication. *Zoology* 124: 13–29.

Peterson, J. and P. C. Dechow. 2003. Material properties of the human cranial vault and zygoma. *Anat. Rec. A*274: 785–797.

Pierce, S. E., et al. 2008. Patterns of morphospace occupation and mechanical performance in extant crocodilian skulls: A combined geometric morphometric and finite element modeling approach. *J. Morphol.* 269: 840–864.

Polly, P. D., et al. 2016. Combining geometric morphometrics and finite element analysis with evolutionary modeling: Towards a synthesis. *J. Vert. Paleontol.* 36(4): e1111225. https://doi.org/10.1080/02724634.2016.1111225

Porro, L. B., et al. 2013. *In vivo* bone strain and finite element modeling of the mandible of *Alligator mississippiensis*. *J. Anat.* 223: 195–227.

Porro, L. B., et al. 2014. *In vivo* cranial bone strain and bite force in the agamid lizard *Uromastyx geyri*. *J. Exp. Biol.* 217: 1983–1992.

Purnell, M. A. 1993. Feeding mechanisms in conodonts and the function of the earliest vertebrate hard tissues. *Geology* 21: 375–377.

Qiu, S., et al. 2002. Age and distance from the surface but not menopause reduce osteocyte density in human cancellous bone. *Bone* 31: 313–318.

Rabkin, B. A., et al. 2001. Long-term measurement of bone strain in vivo: The rat tibia. *J. Biomed. Mat. Res.* 58: 277–281.

Rafferty, K. L., et al. 2000. Three-dimensional loading and growth of the zygomatic arch. *J. Exp. Biol.* 203: 2093–2104.

Rankin, J. W., et al. 2018. Functional capacity of kangaroo rat hindlimbs: Adaptations for locomotor performance. *J. R. Soc. Interface* 15(144): 20180303. https://doi.org/10.1098/rsif.2018.0303

Ravosa, M. J., et al. 2000a. Masticatory stress, orbital orientation and the evolution of the primate postorbital bar. *J. Hum. Evol. 38*: 667–693.

Ravosa, M. J., et al. 2000b. Strain in the galago facial skull. *J. Morphol.* 245: 51–66.

Rayfield, E. J. 2007. Finite element analysis and understanding the biomechanics and evolution of living and fossil organisms. *Ann. Rev. Earth Planet. Sci.* 35: 541–576.

Reilly, D. T. and A. H. Burstein 1975. The elastic and ultimate properties of compact bone tissue. *J. Biomech. 8*: 393–405.

Reilly, S. M. and J. A. Elias. 1998. Locomotion in *Alligator mississippiensis*: Kinematic effects of speed and posture and their relevance to the sprawling-to-erect paradigm. *J. Exp. Biol*. 201: 2559–2574.

Reilly, D. T., et al. 1974. The elastic modulus for bone. *J. Biomech*. 7: 271–275.

Reilly, S. M., et al. 2005. Hindlimb function in the alligator: Integrating movements, motor patterns, ground reaction forces and bone strain of terrestrial locomotion. *J. Exp. Biol*. 208: 993–1009.

Rensberger, J. M. 1995. Determination of stresses in mammalian dental enamel and their relevance to the interpretation of feeding behaviors in extinct taxa. In *Functional morphology in vertebrate paleontology*, ed. Thomason J. J., 151–171. Cambridge, UK: Cambridge University Press.

Reumann, M. K., et al. 2011. Early growth response gene 1 regulates bone properties in mice. *Calcif. Tissue Int*. 89: 1–9.

Richards, C. T. and A. A. Biewener. 2007. Modulation of *in vivo* muscle power output during swimming in the African clawed frog (*Xenopus laevis*). *J. Exp. Biol*. 210: 3147–3159.

Ross, C. F. 2001. *In vivo* function of the craniofacial haft: The interorbital "pillar." *Am. J. Phys. Anthropol*. 116: 108–139.

Ross, C. F. and W. L. Hylander. 1996. *In vivo* and *in vitro* bone strain in the owl monkey circumorbital region and the function of the postorbital septum. *Am. J. Phys. Anthropol*. 101: 183–215.

Ross, C. F. and K. A. Metzger. 2004. Bone strain gradients and optimization in vertebrate skulls. *Ann. Anat*. 186: 387–396.

Ross, C. F., et al. 2005. Modeling masticatory muscle force in finite element analysis: Sensitivity analysis using principal coordinates analysis. *Anat. Rec. A*283: 288–299.

Ross, C. F., et al. 2016. *In vivo* bone strain in the mandibular corpus of *Sapajus* during a range of oral food processing behaviors. *J. Hum. Evol. 98*: 36–65.

Ross, C. F., et al. 2018. Bite force and cranial bone strain in four species of lizards. *J. Exp. Biol*. 221(Pt 23): jeb180240. https://doi.org/10.1242/jeb.180240

Rubin, C. T. and L. E. Lanyon. 1982. Limb mechanics as a function of speed and gait: A study of functional strains in the radius and tibia of horse and dog. *J. Exp. Biol*. 101: 187–211.

Rubin, C. T. and L. E. Lanyon. 1984a. Dynamic strain similarity in vertebrates; An alternative to allometric limb bone scaling. *J. Theor. Biol*. 107: 321–327.

Rubin, C. T. and L. E. Lanyon. 1984b. Regulation of bone formation by applied dynamic loads. *J. Bone Joint Surg. A* 66: 397–402.

Rubin, C. T. and L. E. Lanyon. 1985. Regulation of bone mass by mechanical strain magnitude. *Calcif. Tissue Int*. 37: 411–417.

Santana, S. E., et al. 2012. Dietary hardness, loading behavior, and the evolution of skull form in bats. *Evolution* 66: 2587–2598.

Sheffield, K. M. and R. W. Blob. 2011. Loading mechanics of the femur in tiger salamanders (*Ambystoma tigrinum*) during terrestrial locomotion. *J. Exp. Biol*. 214: 2603–2615.

Sheffield, K. M., et al. 2011. Locomotor loading mechanics in the hindlimbs of tegu lizards (*Tupinambis merianae*): Comparative and evolutionary implications. *J. Exp. Biol*. 214: 2616–2630.

Shi, J., et al. 2012. Developing a musculoskeletal model of the primate skull: Predicting muscle activations, bite force, and joint reaction forces using multibody dynamics analysis and advanced optimisation methods. *J. Theor. Biol*. 310: 21–30.

Smith, K. K. and W. L. Hylander, 1985. Strain gauge measurement of mesokinetic movement in the lizard *Varanus exanthematicus*. *J. Exp. Biol*. 114: 53–70.

Smith, A. L., et al. 2015a. Biomechanical implications of intraspecific shape variation in chimpanzee crania: Moving toward an integration of geometric morphometrics and finite element analysis. *Anat. Rec*. 298: 122–144.

Smith, A. L., et al. 2015b. The feeding biomechanics and dietary ecology of *Paranthropus boisei*. *Anat. Rec*. 298: 145–167.

Stansfield, E., et al. 2018a. A sensitivity study of human mandibular biting simulations using finite element analysis. *J. Archaeol. Sci. Rep*. 22: 420–432.

Stansfield, E., et al. 2018b. Can diet be inferred from the biomechanical response to simulated biting in modern and pre-historic human mandibles? *J. Archaeol. Sci.: Rep*. 22: 433–443.

Stein, K. W. H. and J. Werner. 2013. Preliminary analysis of osteocyte lacunar density in long bones of tetrapods: All measures are bigger in sauropod dinosaurs. *PLoS One*, 8: 1–9. https://doi.org/10.1371/journal.pone.0077109

Strait, D. S., et al. 2005. Modeling elastic properties in finite-element analysis: How much precision is needed to produce an accurate model? *Anat. Rec. A* 283: 275–287.

Strait, D. S., et al. 2009. The feeding biomechanics and dietary ecology of *Australopithecus africanus*. *Proc. Nat. Acad. Sci. U S A* 106: 2124–2129.

Sugiyama, T., et al. 2012. Bone's adaptive response to mechanical loading is essentially linear between the low strains associated with disuse and the high strains associated with the lamellar/woven bone transition. *J. Bone Miner. Res*. 27: 1784–1793.

Sun, Z., et al. 2004. Cranial sutures and bones: Growth and fusion in relation to masticatory strain. *Anat. Rec. A* 276: 150–161.

Swartz, S. M., et al. 1992. Wing bone stresses in free flying bats and the evolution of skeletal design for flight. *Nature* 359 (6397): 726–729.

Swartz, S. M., et al. 1989. Telemetered *in vivo* strain analysis of locomotor mechanics of brachiating gibbons. *Nature* 342(6247): 270–272.

Thomason, J. J., et al. 2001. *In vivo* surface strain and stereology of the frontal and maxillary bones of sheep: Implications for the structural design of the mammalian skull. *Anat. Rec*. 264: 325–338.

Tsai, H. P., et al. 2020. Contrast-enhanced XROMM reveals *in vivo* soft tissue interactions in the hip of *Alligator mississippiensis*. *J. Anat*. 236: 288–304.

van der Meulen, M. C. H., et al. 1993. Mechanobiologic influences in long-bone cross-sectional growth. *Bone* 14: 635–642.

van der Meulen, M. C. H., et al. 2001. Understanding bone strength: Size isn't everything. *Bone* 29: 101–104.

Vashishth, D., et al. 2001. Influence of nonenzymatic glycation on biomechanical properties of cortical bone. *Bone* 28: 195–201.

Verner, K. A., et al. 2016. Experimental tests of planar strain theory for predicting bone cross-sectional longitudinal and shear strains. *J. Exp. Biol*. 219: 3082–3090.

Wainwright, S. A., et al. 1982. *Mechanical design in organisms*. 2nd ed. Princeton, NJ, Princeton University Press.

Wang, Q. and P. C. Dechow. 2006. Elastic properties of external cortical bone in the craniofacial skeleton of the Rhesus monkey. *Am. J. Phys. Anthropol*. 131: 402–415.

VetBooks.ir

Wang, Y., et al. 2008. Strain amplification and integrin based signaling in osteocytes. *J. Musculoskel. Neuronal Interact*. 8: 332–334.

Weijs, W. A. and H. J. de Jongh. 1977. Strain in mandibular alveolar bone during mastication in the rabbit. *Arch. Oral Biol*. 22: 667–675.

Witmer, L. M. 1995. The extant phylogenetic bracket and the importance of reconstructing soft tissues in fossils. In *Functional morphology in vertebrate paleontology*, ed. Thomason, J. J., 19–33. Cambridge, UK, Cambridge University Press.

Yang, H., et al. 2014. Characterization of cancellous and cortical bone strain in the *in vivo* mouse tibial loading model using micro-CT-based finite element analysis. *Bone* 66: 131–139.

Yang, H., et al. 2019. Adaptive changes in micromechanical environments of cancellous and cortical bone in response to *in vivo* loading and disuse. *J. Biomech*. 89: 85–94.

You, L., et al. 2001. A model for strain amplification in the actin cytoskeleton of osteocytes due to fluid drag on pericellular matrix. *J. Biomech*. 34: 1375–1386.

Young, V. K. H. and R. W. Blob. 2015. Limb bone loading in swimming turtles: Changes in loading facilitate transitions from tubular to flipper-shaped limbs during aquatic invasions. *Biol. Lett*. 11: 20150110. https://doi.org/10.1098/rsbl.2015.0110

Young, V. K. H., et al. 2017. Humeral loads during swimming and walking in turtles: Implications for morphological change during aquatic reinvasions. *J. Exp. Biol*. 220: 3873–3877.

VetBooks.ir

34

Interpreting Mechanical Function in Extant and Fossil Long Bones

Russell P. Main, Erin L. R. Simons and Andrew H. Lee

CONTENTS

Mechanobiological Evolution and Plasticity in Bone Form 688
Bone Length 690
Curvature 692
Musculotendinous Entheses and Mechanical Function 694
Bone Cross-Sectional Shape 695
Primary Vascular Canal Orientation 701
Collagen Fiber Orientation 702
Intracortical Remodeling 705
Cancellous Bone 708
Integrative Studies of Limb Bone Biomechanics in Relation to Bone Shape and Histomorphology 712
Changes in Musculoskeletal Growth Allometries in Relation to Ontogenetic Biomechanics 712
Ontogenetic Changes in Bone Mechanics and Histomorphology in the Goat Radius 712
Ontogenetic Changes in Bone Mechanics and Histomorphology in the Emu Femur and Tibiotarsus 713
Using Limb Bone Morphology to Assess Gait in Living and Extinct Mammals and Dinosaurs 714
Summary 715
Acknowledgments 716
References 716

Mechanobiological Evolution and Plasticity in Bone Form

In every vertebrate taxon, the microstructure, growth rate, and distribution of tissue in each bone are the culmination of hundreds of millions of years of natural selection. The various selective influences on the skeleton are highlighted by its biomechanical function to protect the internal and sensory organs and support locomotor and masticatory functions. Other skeletal functions such as its role in hematopoiesis, endocrine function and mineral metabolism probably rely less on the exact distribution of marrow and of cortical and cancellous bone tissues, as long as these tissues and their resident cells are present. Thus, mechanics should be the primary influence for where and how bone tissue is distributed.

Mechanical loading-induced bone tissue strain, or some factor related to it (e.g., strain rate), has been recognized as a driving force in the mechanical adaptation of bone and a signal that bone cells sense. A description of the relationship between mechanical stress (or strain) and internal skeletal structures was first detailed in the mid-late 1800s by von Meyer, Culmann and Wolff (Wolff 1986, Roesler 1981). The culmination of their works can be summarized in the trajectorial theory of bone, which describes the alignment of cancellous bone tissues with principal stress trajectories in the bone. However, this theory does not necessarily distinguish between phylogenetic and ontogenetic adaptation. Roux added uniquely to this body of work the idea that functional adaptation during the ontogeny of the skeleton is a dynamic and self-regulating process, rather than supposing that bones always exist at some static optimum based on a predefined set point (Roux 1881).

In humans and biomedical animal models, the Mechanostat Theory has been popularized to characterize ontogenetic adaptation by describing a minimum effective strain (MES), above which bone mass will increase with loading or decrease with disuse (Frost 1982, 2003). However, it was also realized that each cortical or cancellous bone site has its own MES governing bone formation or resorption (Hsieh et al. 2001, Shulte et al. 2013). At about the same time the Mechanostat

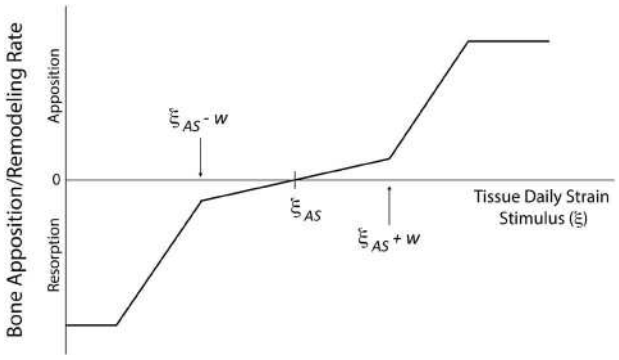


FIGURE 34.1 A theoretical mechanobiological model predicting the maintenance, apposition, and resorption of bone relative to tissue strain stimulus. The horizontal axis represents the cumulative daily strain stimulus (a combination of strain magnitude and number of loading cycles experienced per day). ξ_{AS} is the attractor stimulus, where no net bone formation or resorption occurs. A "lazy zone" is defined as $\xi_{AS} \pm w$, where w is the half-width of the range of strain stimuli experienced during normal daily activities. Within this range, only minor bone formation and resorption occur. Beyond these points ($\xi_{AS} \pm w$), changes in daily tissue strain stimulate significant bone formation and resorption, until the bone reaches a maximal limit for bone formation or resorption. Models similar to this one have been successfully used to predict plastic changes in both cortical and cancellous bone. (Based on Beaupré et al. 1990b and Carter and Beaupré 2001.)

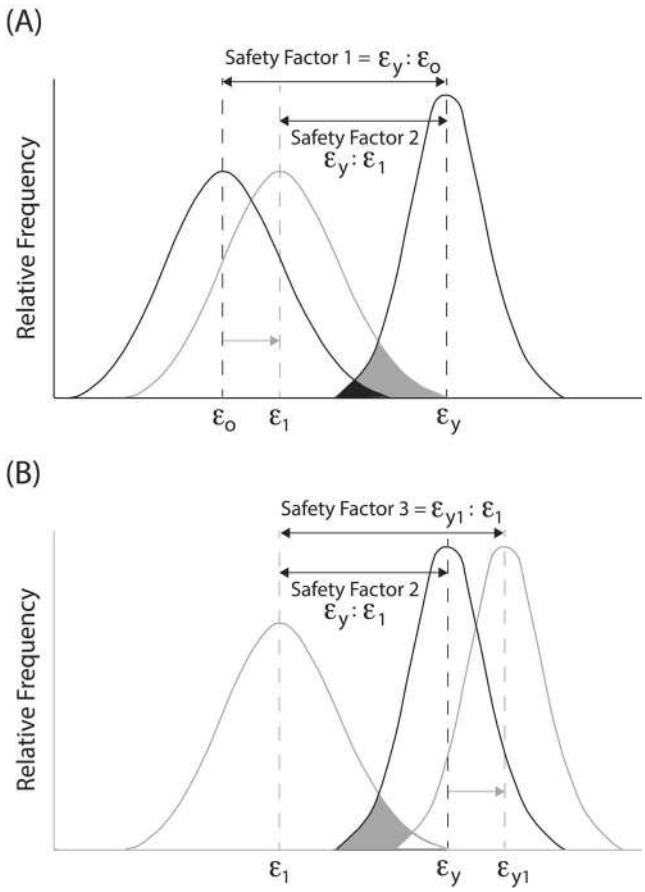


FIGURE 34.2 Adaptation of safety factors in biological tissues. A, A biological structure, in this case a bone, experiences a range of strains during daily activities within a population, with mean strain (ε_o). The bone itself also shows a distribution of inherent material properties within the population, with a mean yield or failure stress (ε_y). The ratio of $\varepsilon_y.\varepsilon_o$ is defined as the safety factor (Safety Factor 1). Where the curves overlap (black shaded area) represents those animals where the bone tissue fails and death could occur. If the population is subjected to a new physical challenge where bone tissue strains uniformly increase (ε_1), the safety factor for this structure decreases (Safety Factor 2), which causes a larger proportion of the population to be at risk for bone failure (black + gray shaded areas). B, By natural selection, future generations of animals develop an enhanced bone structure with an increased mean failure strain (ε_{y1}). This shift reestablishes the initial safety factor for the population (Safety Factor 3), with a smaller number of animals subject to bone failure (white shaded area). For the purposes used in this chapter, the adaptation described above at the population level is defined as evolutionary adaptation. It is also assumed that this can happen at an individual level, where the distributions represent the strains experienced by an animal over some period of time (ε_o) and the bone possesses a range of material properties throughout its structure (ε_y). This type of adaptation at the individual level would be ontogenetic adaptation, defined here as plasticity. (Modified from Alexander 1981 and Biewener 1993.)

was introduced for cortical bone, Carter and colleagues identified that the magnitude of the applied strains during loading and the number of loading cycles experienced by a bone act as a total strain stimulus associated with bone formation or resorption (Carter 1982, Beaupré et al. 1990a). This approach was subsequently applied in a number of adaptive finite element (FE) models that accurately reflect the regulation of bone formation and resorption in both cortical and cancellous bone tissues (Figure 34.1) (Fyhrie and Carter 1986, Beaupré et al. 1990b, van der Meulen et al. 1993; Levenston et al. 1998, Huiskes et al. 2000). This approach to studying ontogenetic adaptation does not rely on a single strain value, like the MES, to govern bone formation and resorption; it is more holistic in accounting for the overall strain experienced by a bone over the course of an entire day, a year or a lifetime.

Any particular bone within a population of animals experiences a range of strains throughout the population with a mean strain, ε_o (Figure 34.2A) (Alexander 1981, Biewener 1993). This distribution can be compared to the distribution of the inherent failure strain of the bone in the population (ε_y), and the ratio of the means of these curves represents the safety factor (ε_y:ε_o). Weaker bones within the population can experience strains that will cause them to critically fracture, and death could ensue (black shaded area, Figure 34.2A). If for some reason the mean strains encountered by this bone in a population increase (e.g., use of a new habitat), the daily strains experienced would increase (ε_1), as would the overall likelihood of fracture in the population (gray shaded area, Figure 34.2A). However, given the ontogenetic adaptive processes in bone that happen on an individual level, an accumulation of high-magnitude but noninjurious strains experienced by this bone in the population could cause the inherent strength of that bone to increase (ε_{y1}), decreasing the likelihood of fracture (white shaded area, Figure 34.2B), and maintaining a safety factor (ε_{y1}: ε_1). This type of plastic adaptation certainly happens at the level of the individual, and it can be characteristic of an entire population, allowing the bone to maintain its safety factor without any change in overall population genotype. In addition to the regulation of cancellous bone, as originally conceived by Wolff and his contemporaries, a number of skeletal

VetBooks.ir

features are subject to functional adaptation and include bone length (Losos et al. 2000), cortical bone geometry (Currey and Alexander 1985, Margerie et al. 2005), bone curvature (Pauwels 1980, Bertram and Biewener 1988), vascular canal (osteonal) orientation (Margerie 2002), collagen fiber orientation (CFO; Riggs et al. 1993, Skedros et al. 2009), and spatial control over intracortical bone remodeling (Martin 2000).

The evolution of skeletal structure and our interpretation of the effects of mechanobiology in this process depend not only on the mechanical forces that act on the adult skeleton, but on forces experienced throughout the lifetime of the animal and the inherent ability of the resident cells to sense (osteocytes) and adapt (osteoblasts, osteoclasts) to changes in mechanical loading to maintain skeletal safety factor. This adaptive plasticity inherent in the skeleton is influenced by natural selection just as much as the genetically defined initial bone shape, and variation in the sensitivity of these adaptive mechanisms may influence skeletal structure more in some taxa than in others. For example, the skeletons of animals with greater limb bone safety factors (amphibians and reptiles) may be more robustly built because they do not adapt as readily to changes in mechanical loading or repair bone microdamage as quickly as taxa with lower safety factors (mammals and birds) (Blob and Biewener 1999, Blob et al. 2014).

Adaptation is a loaded word that has the potential to cause confusion in this context. To the evolutionary biologist, adaptation means heritable, genotypic change to prevailing environmental or ecological conditions through the course of natural selection. To many, behavioral or structural adaptation acts over the course of an animal's lifetime (at the individual level, this is called *accommodation*) in response to more proximate changes in their environment. Like a weight lifter gaining muscle mass and then losing it in old age, these changes are plastic and are not heritable. However, they are still adaptive within their limited context. Plasticity can be a testing ground for evolution, because the genetic mechanisms for plasticity are heritable (West-Eberhard 1989, 2005, Levis et al. 2018). For example, if the diet of a local population of lizards changes so that their habitual soft-food diet changes to a hard-food source requiring larger muscles and more robust bones to process, only those lizards with greater plasticity will survive by phenotypic accommodation. Those incapable of adapting to this local dietary perturbation will be more likely to die. Other nearby populations of the same species feeding on their habitual soft-food diet will appear to be different morphologically, but not genetically. If at this stage the food source returns to normal, the morphology of the hard-food group would return to the overall population norm (*sensu* Herrel and Holanova 2008). If the diet change persists over many years, genetic differentiation could occur among these populations, leading to parapatric speciation. Thus, phenotypic adaptation can lead to genotypic evolution. For the purpose of this chapter, *plasticity* and *evolutionary* adaptation will be used to distinguish between short-term, reversible versus macroevolutionary modes of adaptation.

Consider that bone adaptation, whether it occurs on the scale of millions of years or over the course of a month, can act at multiple scales of tissue organization simultaneously. Within a bone, certain anatomical features may be more likely to be preferentially altered during plastic versus evolutionary adaptation, acting piecemeal to alter morphological and material features one by one, or perhaps all levels of organization are considered together as a functional conglomerate. Furthermore, how do these different features change during the course of an animal's lifetime? Different taxa have different growth trajectories and metabolisms, and the histological and gross anatomy that each individual animal or individual taxon presents with is a brief snapshot of the animal's ontogenetic maturation. This must be considered as well. One barely has to wade into the ontogenetic biomechanics literature to find clear examples of how bone shape and structure are altered by changing mechanical demands through an animal's life (Carrier 1983, Carrier and Leon 1990, Main 2007, Kuehn et al. 2019).

The goals of this chapter are to review the various structural and microstructural features in long bones and how they may, in theory, influence the skeleton's ability to withstand different types of biomechanical loading. First, potential relationships between structural and microarchitectural features and biomechanical function will be presented for laboratory settings where a clear and measurable alteration in mechanical environment has been used to assess changes (or lack thereof) in bone structure. Secondly, we will examine experimentally measured or observational changes in bone mechanics and their effects on skeletal structure. It is in these cases that the role of ontogeny might best be assessed. Lastly, paleohistological and comparative examples, with no direct information of mechanics, but with clear living correlates, will be presented. Ultimately, this chapter will address which skeletal and microstructural features may be most confidently used to develop hypotheses regarding long bone function and under which circumstances. We will also discuss which features may be more or less useful to comparative morphologists and paleontologists as a functional tool for mechanical inference.

Bone Length

Bone length is important in determining bending strains in a bone, as strains are directly proportional to the length of the bone and inversely related to the second moment of area (I). Ratios of bone length to bone dimeter or bone circumference (as a proxy for I) are often related to limb function or to body size. Much of the published discussion of bone length relates to locomotor classifications. Bone lengths for cursorial mammals and birds tend to scale with isometry relative to noncursors, which allows them to travel absolutely longer distances (Alexander et al. 1979, Maloiy et al. 1979, Biewener 1983a, Biewener 1989).

For the sake of this chapter, scaling relates to changes in anatomical measures to body mass or to another anatomical measure. The scaling of such dimensions is useful in predicting locomotor stresses, strains and overall performance with changes in body size. In isometric scaling, length measures scale with body mass (a volume, L^3) as $\propto M^{0.33}$ and relative to other length measures as $\propto L^{1.0}$. Length ratios (such as normalized curvature, length to diameter ratios), L_1/L_2 scale

VetBooks.ir

with $\propto M^0$. Area (*Ct.Ar*) would scale with $\propto M^{0.67}$. Second and polar moments of area (*I* and *J*, respectively) scale $\propto M^{1.33}$, but I_{MAX}/I_{MIN} (eccentricity) scales as $\propto M^0$. Scaling relationships with slopes greater or less than these values exhibit positive and negative allometry, respectively. For elastic similarity, structures scale $L \propto M^{0.25}$, $D \propto M^{0.375}$, $Ct.Ar \propto M^{0.75}$ and I and $J \propto M^{1.5}$ (*sensu* McMahon 1975), while for stress or strain similarity, $Ct.Ar \propto M^{1.0}$ and I and $J \propto M^{1.67}$.

Isometric scaling of bone length in mammals and birds would produce greater stresses in the muscles and bones of larger animals. However, among placental mammals and bird limb bones, peak limb bone stresses are fairly similar (Rubin and Lanyon 1984a, Biewener 1993), which suggests that this problem of isometry in bone length is solved by some other morphological feature. The effective mechanical advantage (EMA) of the limb is a relative measure of the muscle moment arm to the ground reaction force (GRF)-induced joint flexor moment and, in larger mammals and birds, is reduced by straightening the limb during stance. Straightening the limb reduces the moments exerted about each joint, as well as the muscle stresses and bending strains as the limb becomes straighter (Biewener 1983a, 1989). This evolutionary adaptation in mammals and terrestrial birds is typically associated with a decreased range of limb excursion and a decrease in the speed of travel relative to body size (Bertram and Biewener 1990, Gatesy and Biewener 1991, Iriarte-Díaz 2002). This pattern of decreased relative speed with greater limb length may not apply in some lizards where body mass may not change greatly relative to limb length or when sprint performance may be selectively linked to ecology (Losos 1990, Clemente et al. 2009). Coincident with longer limbs in larger mammals and birds, there tends to be a proximal to distal gradient in terms of segment length, where the autopodium is longer than the stylopodium. This limb gradient is likely related to locomotor energy expenditure and minimizing the moment of inertia of the distal limb segment (Fedak et al. 1982, Hildebrand 1995). Smaller mammals and terrestrial birds, on the other hand, tend to have limb segments with similar segment lengths compared to larger taxa. Interestingly, the forelimbs of volant birds show a pattern in which the different segments scale with slight positive allometry for length relative to body mass (Nudds 2007).

How can bone length be altered by plasticity? In applied loading models, compression is typically applied to one limb, while the contralateral limb represents a within-individual control (Main et al. 2020). The nonloaded control limb is generally unaffected in length or cross-sectional properties by loading on the contralateral limb (Sugiyama et al. 2010). While alterations of the growth plate by compression loading are not typically the focus of these studies, both mouse and rat axial compression loading models have shown decreased bone length in animals 6–8 weeks of age (Robling et al. 2001a, Main et al. 2014). In mice, when loading is started at older ages (10- to 16-week-old mice), compressive loading does not generally affect the attainment of adult bone length (Main et al. 2014), but adult rats show decreased bone length in the loaded limbs (27-weeks-old) (Robling et al. 2002). In these models, loading was applied along the long axis of the bone, causing compression of the growth plate, especially at younger ages. Similar to increased loading, neuropathy models have also shown that reduced load during growth decreased overall bone length as well (Lanyon 1980, Dysart et al. 1989, Biewener and Bertram 1994). Neuropathy experiments suggest that a lack of locomotor force decreases signaling in the neuropathic leg, except that both the neuropathic and contralateral limbs are shorter than in the age-matched control groups. The same pattern is also seen in hindlimb suspension experiments (Simske et al. 1992, Ehara and Yamaguchi 1996). The universal decrease in bone length in the hindlimb suspension and neuropathic models may be related to systemic neurological signals regulating bone growth (Sample et al. 2010).

Relatively mild, but highly repetitive treadmill, exercise-wheel running, and jumping exercises rarely affect bone lengths in growing or adult rodents (Honda et al. 2001, Kelly et al. 2006, Wallace et al. 2007, 2009, Nagasawa et al. 2008), though some treadmill studies of growing rats show increased length differences relative to control groups (Newhall et al. 1991, Iwamoto et al. 1999). As an exception to the typical rodent models, plastic adaptation of limb length was tested in juvenile anoles (*Anolis sagrei*) housed on "branches" (dowels) of two different-sized diameters for four months. At the end of the experiment, the lizards housed with the thin "branches" had shorter limbs than lizards housed with the large "branches". The shorter-limbed lizards still had longer limbs than taxa that live on thin-branched trees naturally, suggesting that plasticity has limits within the range of functional adaptation examined in this scenario (Losos et al. 2000). In just four months these lizards were able to alter their ontogenetic limb bone trajectories, whereas rodents undergoing different exercise regimes (treadmill, wheel running) did not show the same degree of plasticity. The epiphyseal and endochondral processes governing bone length are regulated differently in mammals than in reptiles, which may allow lizards more plasticity in the regulation of bone growth relative to age (Carter et al. 1998).

Lizards, birds and mammals have all been sampled; they show that the proportion of their limb segments or overall leg lengths can relate to speed or overall cursoriality. A number of lizard taxa show a positive relationship between longer overall limb lengths or *m. caudofemoralis* lengths and maximum sprint speed (Losos and Sinervo 1989, Losos 1990, Sinervo and Losos 1991, Bauwens et al. 1995, Bonine and Garland 1999, Losos and Irschick 1996, Zani 1996). The same is generally true for a survey of mammalian cursors (carnivores, ungulates) where total hindlimb length and, to a lesser degree, metatarsal to femur length (MT/F ratio) correlate positively with top speed (Garland and Janis 1993). Similarly, larger birds show a decreased ratio for femur to tarsometatarsal (TMT) length that is associated with increased overall speed, but restricts their limb range of motion – sacrificing mobility to specialize in high-speed running (Gatesy and Biewener 1991).

The distribution of limb segment lengths has been thoroughly studied in theropods by comparing the femur, tibiotarsal (TBT) and TMT lengths for avian and nonavian theropod skeletal and fossil samples (Gatesy and Middleton 1997). Most nonavian theropods make up a very small portion of the ternary morphospace, where the femur composes 30–45% of total limb length, the TBT 35–45% of total limb length and the

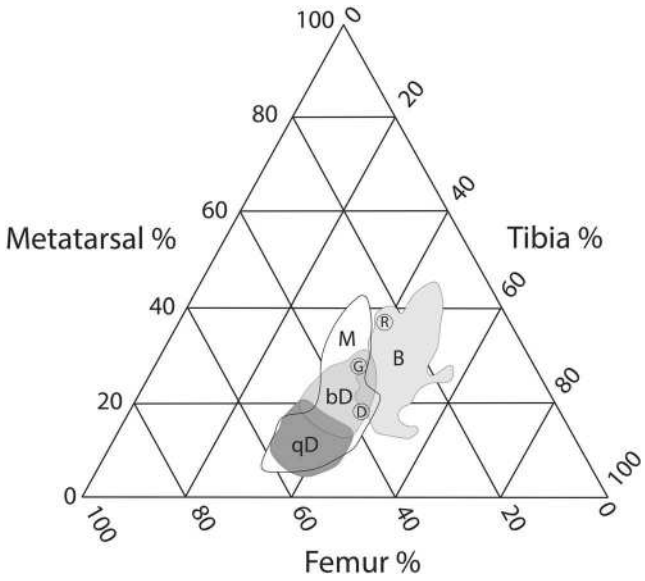


FIGURE 34.3 A ternary plot showing the segmental proportion of limb lengths made up by the femora, tibiae and metatarsals for mammals (M), birds (B), bipedal dinosaurs (bD) and quadrupedal dinosaurs (qD). Specific taxa are indicated for *Deinonychus* (D), *Gallimimus* (G) and ratites (R). As described in the text, mammals and birds maintain very little overlap in their ternary distributions. Both quadrupedal and bipedal dinosaurs overlap more closely with mammals than birds (avian bipedal dinosaurs). The low degree of overlap between dinosaurs and birds, except for the more "cursorial" bipedal dinosaurs, is surprising and indicates the diversification that has taken place in birds since their evolution. (Modified from Gatesy and Middleton 1997 and Carrano 1998.)

TMT 15–30% of total limb length (Figure 34.3). By comparison, bird limb morphospace is composed of hindlimbs where the femur made up between 10 and 45% of limb length, 35 and 55% TBT length and 10 and 45% TMT length. The percentage of the limb made up by the femur and TMT varied widely among birds, whereas nonavian theropods were more conservative in their relative segment lengths. The nonavian theropod morphospace made up about 24% of the entire theropod range, little of it overlapping with birds. In "cursorial" representatives (*Deinonychus*, ornithomimids and ratites), the TBT only varied by about 5% of total limb length between groups, whereas TMT length in *Deinonychus* (~20% limb length), *Gallimimus* (~27%) and ratites (~35%) became longer with increasingly specialized cursoriality. Femur length also changed among these three species from ~37% in *Deinonychus* at one end to ~25% in ratites.

Thus, in both extant and extinct taxa the ratio of proximal to distal bone lengths can typically distinguish between cursors and noncursors in a way that minimizes muscle and bone stresses and where overall limb length is related to overall *absolute* speed.

Curvature

Bone curvature increases bone strains and yet it persists as a defining characteristic among many tetrapod long bones. Bone curvature increases bending strains by providing a moment arm for the axial component of the GRF and the axially directed component of muscle forces to exert bending stresses about the bone (Biewener 1983a, b, Biewener 1989). Questions about the advantage of bone curvature have persisted for at least the last 40 years. Early on it was argued that plastic adaptation would act to reduce curvature during ontogeny as animals grew to minimize bending strains and maintain safety factors (Pauwels 1980). However, if bone curvature is so disadvantageous, why has natural selection not already removed it from tetrapod populations? Subsequent work quantifying curvature in mammals (mouse to horse) showed slight negative allometry relative to body mass ($\propto M^{-0.09}$), indicating some reduction in curvature at larger sizes (Biewener 1983a). However, it appears that bone curvature can only be altered so much because as animals increase in size their skeletons must adapt by aligning the limbs more parallel to the vertically oriented GRF, which increases the EMA and reduces bending about the bone (Biewener 1989).

Bone curvature has also been hypothesized to be helpful for two reasons. Although minimization of bone strain might seem reasonable for increasing the safety factor and decreasing the likelihood of fracture, perhaps strict minimization of locomotor-induced strain in the bone might actually be selected against. The osteocytes embedded in the bone tissue rely on fluid flow through their canaliculi to gain nutrients, exchange waste, and pass transcription factors and proteins to neighboring cells (Fritton and Weinbaum 2009). This fluid flow results from strain gradients produced by bending loads in the bone. Absolute resolution of the bending loads would actually be detrimental to the bones and should be selected against to a degree (Piekarski 1973, Lanyon 1980, Fritton and Weinbaum 2009). Secondly, it has been proposed that bone curvature predisposes the bone to be predictably bent in a certain direction during locomotion. A symmetrical cylindrical diaphysis would fare best for the minimization of bone material, but when experiencing diverse loading environments this shape could cause buckling of the bone in random directions (Rubin and Lanyon 1985, Bertram and Biewener 1988). Relatively straight, cylindrical bones are not common, but the straightest bones occur in large, graviportal animals (elephants, sauropods) that have a restricted range of limb motion and altered kinematics to promote high degrees of axial compressive loads (Biewener 1989).

The predisposition of a habitual bending direction provides a mechanism by which bone morphology can use evolutionary and/or plastic adaptation to withstand everyday loading with minimal risk of fracture. In many long bones, the GRF and muscle forces predispose peak bending about a particular axis, where muscle force is actively modulated to reduce bending stresses in response to the changes in GRF magnitude and orientation during stance (Main 2007). Therefore, loading about other possible bending axes can be resisted by other structural parameters, like bone eccentricity, to passively modulate bending loads in other directions (Bertram and Biewener 1988, Main and Biewener 2004, Main 2007, Willie et al. 2020). Most animals have bones with some degree of curvature, and the smallest animals often have relatively more

VetBooks.ir

curved bones among mammals and birds (Biewener 1983a, Carrano 2001, Brassey et al. 2013). Thus, in small mammals, limiting skeletal bending stresses due to bone curvature must not be as highly selected on as a detrimental source of absolute bending stresses as it is in larger taxa.

Bone curvature can be altered through plastic adaptation in response to changes in mechanical load (Currey 1968, Pauwels 1980). Subsequent osteotomy and controlled animal loading studies have described reductions in bone curvature to maintain safety factors in bone. Osteotomy of the ulna in both pigs and sheep showed that without the balancing influence of the ulna's presence to help support loads in the forelimb, the strains in the radius increased between about 1.1× in the sheep and 2× in the pig (Goodship et al. 1979, Lanyon et al. 1982). The increase in strain corresponded to a subsequent increase in cortical bone formation on the posterior periosteal surface of the radius with a concomitant increase in cross-sectional area and increased moments of inertia to compensate for the missing ulna. Thus, radial bone shape plastically adapted to the increased strains, reducing bone curvature, and returning the strains to normal levels after months of adaptation. Less extreme cases have been examined with the advent of rodent axial loading models. In growing rats, axial ulnar loading decreased the concave curvature of the ulna by 60% with loads that were about 1.7× the habitual loads (Mosley et al. 1997). With the removal of load from the limb during disuse, curvature decreases and this is likely due to the absence of normal mechanical feedback regulating bone shape. In both rat and chicken neuropathy studies in growing animals, the tibia (or TBT) had a greatly reduced radius of curvature compared to control animals (Lanyon 1980, Biewener and Bertram 1994). Collectively, these experimental loading studies have shown that skeletal overload can lead to a reduction in curvature to decrease strains and help maintain the safety factor while the protective effect of longitudinal curvature is not needed in the unloaded limbs of disuse models. The osteotomy and disuse models come with the caveat that the pathological effects of treatment may have disrupted normal growth and remodeling processes (Bertram and Swartz 1991), so further investigation into the plastic alteration of bone curvature may best be examined using controlled axial loading models or experimental manipulation of natural behaviors.

The scaling of curvature in mammals and birds has been examined in relation to body mass. In mammals ranging from 0.2 to 6000 kg, the radius of curvature in the femur and humerus normalized to the midshaft anteroposterior (AP) radius of each bone shows little change in relative bone curvature with size. The tibia and radius show strong negative allometry ($\propto M^{-0.13}$, $\propto M^{-0.16}$, respectively). However, a size-dependent breakpoint occurs at about 100 kg where the isometric scaling in smaller animals shifts to negative allometry above 100 kg (Bertram and Biewener 1992). This suggests that up to a given size, postural changes in the limb can act to help decrease bone stresses, but above this, selection acts to decrease curvature and alter the bone morphology to accommodate for increased body weight (Biewener 1989). Even some smaller taxa may have specific biomechanical circumstances for reducing curvature. The gibbon (*Hylobates lar*) is the only brachiating primate for which *in vivo* forelimb bone strains have been collected (Swartz et al. 1989). The humerus is loaded with high degrees of torsion, and it was argued that high torsional loading of a curved element would lead to particularly high shear strains, which is consistent with the gibbon having reduced humeral curvature relative to other anthropoid primates (Swartz 1990). It would be expected that other taxa with bones that are subjected to significant torsional loading may also possess low curvature. In volant avian taxa, curvature increased in the forelimb and hindlimb bones with increasing body mass (Cubo et al. 1999). It is intuitive to recognize that bone curvature should increase with body mass. However, these measures were not normalized by bone length or diameter (Biewener 1983a, Bertram and Biewener 1992), making it difficult relative to other studies to test for the role of curvature in avian functional hypotheses. For example, we know from a few studies, measuring *in vivo* bone strains, that torsional loading is a large component of loading in the ulna, humerus, femur and TBT (Rubin and Lanyon 1984a, Biewener et al. 1986, Carrano and Biewener 1999, Main and Biewener 2007). Overall a broader sample including normalized curvature values for both volant and terrestrial birds is needed for this analysis. *In vivo* strain measurements from both the humerus and femur of birds performing a diverse range of behaviors would also help in our interpretation of avian bone curvature. The greatest strains in bird wings (and perhaps legs) may take place when birds are landing or taking off (Biewener and Dial 1995), and it is most likely these behaviors that most strongly influence their bone design. To compare to an ontogenetic sample of emu, spanning 0.7–50 kg, both the femur and TBT showed negative allometry with increasing body mass (femur: $\propto M^{-0.20}$; TBT: $\propto M^{-0.19}$) for normalized craniocaudal bone curvature, corresponding to the hypothesis that increased torsion should result in decreased curvature (Swartz 1990, Main and Biewener 2007). Interestingly, ontogenetic curvature decreased here over a 70-kg range in body mass, while interspecific scaling in mammals did not show negative allometry until adult body size reached 100 kg; this suggests a possible difference in the regulation of bone curvature with increases in body mass during ontogeny versus interspecific scaling (Biewener 1983a, Bertram and Biewener 1992).

Bone curvature of the ungual bones in birds has been used to discern ecological niches because this anatomical unit plays such an important role in how the animal interacts with its environment and in food capture. Studies in living and extinct theropod dinosaurs found the terminal ungual on the third phalanx to be particularly diagnostic in distinguishing different lifestyles among birds and extinct theropods as ground dwelling, perching, predatory or scansorial (Birn-Jefferey et al. 2012, Cobb and Sellers 2020). Curvature in this bone was found to be independent of body mass and indicated different lifestyles with lower angles corresponding to terrestrial lifestyles, intermediate angles with predatory lifestyles and highly curved pedal bones with scansorial lifestyles. Based on known angular measures for extant taxa, extinct animals such as *Archaeopteryx* and *Microraptor* were placed in a scansorial group and *Confuciusornis* as a predator.

VetBooks.ir

Musculotendinous Entheses and Mechanical Function

Entheses have been a topic of research in relation to skeletal function for over 100 years (Lane 1887, 1888) as these are easily identifiable scars left on bone. Muscles attach to bone in two different ways. Fibrous connections insert directly onto the bone's diaphyseal surface through the periosteum, which pulls the muscles and tendons along as the bones grow. At maturity, the muscles then anchor directly to the bone (Perry and Prufrock 2018). Relatively little attention has been paid to fibrous entheses, even though some of the largest muscles in the body originate in this way. Fibrocartilaginous entheses occur close to the ends of the long bones and after death leave a pronounced scar on the bone where the transition from fibrocartilaginous tendon to calcified cartilage/bone occur (Villotte and Knüsel 2013). The remnants of these junctions often coincide with tubercles and boney processes.

Many properties of muscle can change in relation to plastic or evolutionary adaptation, including physiological cross-sectional area (PCSA), pennation angle, muscle fascicle length and muscle fiber type. In evolutionary biology, some of these characteristics can be reasonably interpreted through an extant phylogenetic bracket (EPB) (Witmer 1995), but there is always a level of uncertainty involving this method in the absence of closely related living relatives or extensive sensitivity analyses to test for the importance of the assumed variables. Furthermore, one must realize that each specimen is viewed through a snapshot where the ontogenetic stage becomes a relevant feature for the analysis of soft tissues, that do not leave much of a fossil trace except for entheseal scars that may be less well developed in younger animals than in adult or aged ones (Villotte and Knüsel 2013).

As muscles plastically adapt to increased physical challenges, PCSA increases to generate larger forces. Tendon cross-sectional area should increase as well to maintain the safety factor of the musculotendinous unit. Because tendon attaches directly to the bone, it stands to reason that larger forces should be produced to transmit the soft tissue stresses to the bone. With paleontological specimens, it is impossible to follow this adaptive mechanism back to the muscle because soft tissue is not preserved. In the last 15 years, new experimental models and analytical tests of morphology have emerged to examine the interplay between increased musculoskeletal stress and entheseal structure. In a study of adult female sheep exercised on a treadmill with a weighted backpack, 5 days/week for 90 days, there was a significant increase in muscle mass for the infraspinatus, biceps brachii and the quadriceps. Interestingly, no tendons increased in mass, except the origin of the gastrocnemius at the femur (Zumwalt 2006). Using a comprehensive characterization of entheseal morphology, including three-dimensional (3D) entheseal surface area and surface complexity across two planes (Zumwalt 2005), there was no significant change in entheseal morphology for those muscles that increased in mass and only a trend for the gastrocnemius ($p = 0.071$). A study of growing female CD-1 mice, given free access to either a running wheel (WHL) or a wire-mesh (CLB) tower for 78 days, relative to nonexercised control (CON) mice, examined the effect of these exercises on entheseal structures of the deltoid tuberosity, which serves as an attachment point for the protractors and retractors of the humerus (Rabey et al. 2015). At the completion of the study the CLB mice had the greatest muscle PCSA and the WHL group had the lowest PCSA, consistent with other endurance exercise studies (Swaddle and Biewener 2000). Despite these changes in muscle mass, the dimensions for their attachments to the deltoid tuberosity did not change. Fluorescent labels were administered to these mice, and exercise increased periosteal deposition in the CLB and WHL groups relative to the CON mice in the humerus, except in the deltoid tuberosity. A third study examined entheseal structure in 1-year old turkeys run on a downhill treadmill to examine the origin of the lateral gastrocnemius on the lateral epicondyle of the femur (Wallace et al. 2017). Similar to the previous mouse study, 10 weeks of downhill running caused an increase in cortical I_{MAX} of the femur; however, there was no change in the morphology of the entheseal site on the lateral epicondyle. The clear conclusion of these studies would seem to be that whereas exercise may increase muscle PCSA, tendon and muscle mass, and even bone mass, there are no effects on the entheseal structure caused by increased musculotendinous force magnitudes or the frequency of their use.

A recent set of studies examining historical human skeletal samples provided some novel insights for relating entheses to mechanical function. In a sample of post-pubertal young, middle-aged and older adults, all of whom were assumed to be subsistence farmers, hand entheses were analyzed. This analysis took a different approach than previous studies, analyzing groups of muscle entheses by principal component (PC) analyses, as opposed to direct comparisons between specific anatomical sites (Karakostis and Lorenzo 2016). PC1 was used to characterize overall size variation using a number of entheseal measures from digits I, II and V. PC1 was also able to differentiate between male and female samples. There was a great deal of variation in PC2, with positive values accounting for larger entheses, associated with powerful flexion, extension and abduction of digits I and V. Negative values on PC2 characterized entheses associated with the four intrinsic thenar muscles and two interossei of the first digit, corresponding to object manipulation between digits I and II. This approach was used again to examine a sample of hand entheses from 45 adult males from the mid-19th century for whom the occupations were known (Karakostis et al. 2017). From this sample, manual laborers could be distinguished from skilled laborers using the same metrics found in the previous study. Knowing the occupations of the people in the sample was helpful in drawing concrete morphofunctional associations.

This methodology has some limitations because it uses multivariate patterns to distinguish different groups. Not all fossil or archaeological samples are available with such abundance and are often known from limited scraps of bone. Returning to the turkey study discussed above, the authors sought to reanalyze the femur using the same multivariate PC analysis (Karakostis et al. 2019). While blinded to the identity of the animals, three entheseal structures including the origin of the medial gastrocnemius, the insertion of the gluteus primus and the medial supracondylar line, where the adductor magnus and

VetBooks.ir

part of the vastus medialis originate, were subjected to the multivariate analysis for entheseal shape. The authors were able to distinguish between control birds and uphill/downhill runners (Note: uphill runners were not included in the initial study). The analysis was also able to use features of the supracondylar line and the medial epicondyle to distinguish between uphill and downhill runners. When individual entheses were compared singularly among the three groups, there was no difference found, as was determined in the original paper (Wallace et al. 2017). It appears that this highly sensitive method can be used to analyze entheseal structures to distinguish subtle and short-term effects of applied muscle force in the skeleton.

It is unclear how useful this approach would be if based on lower sample sizes, more fragmentary material or samples with a high degree of taphonomic damage. Incorporation of cortical and cancellous characteristics might be incorporated to strengthen this approach in such situations. Traditional use of Sharpey's fibers to try to determine the direction of muscular tension in paleontological samples can only be used, at best, to understand the general direction of muscle action. Recreating bone and muscle mechanics based on software for interactive musculoskeletal modeling (SIMM), which does not typically use histology-based features such as Sharpey's fibers for orienting muscles, has produced some of the most successful biomechanical models to date (Hutchinson et al. 2005, Maidment et al. 2014). Continuing to develop multivariate entheseal relationships, based on *in vivo* experiments, would be valuable for incorporating entheseal analyses to comparative and fossil biomechanical hypotheses on a much broader scale.

Bone Cross-Sectional Shape

The ability of bone to resist different types of load *in vivo* is based to a large extent on its cross-sectional shape. Forces are not the same at all points along the diaphysis, so bones vary in shape along their lengths (Ruff and Hayes 1983). Cross-sectional shape can be measured relative to bone length or cross-sectional diameter to normalize measures of overall robusticity. However, here we will primarily discuss cross-sectional bone shape and eccentricity. Bones are typically loaded under a combination of three general types of load: axial, bending and torsion (Figure 33.2). To withstand axial compression and tension, any bone shape will do because the stresses that develop depend on the cross-sectional area of the bone. Bending loads require selection to optimize I across the bending axis ($I_{MAX} = I_{MIN}$). If the direction of bending is equally likely about all axes, a circle will result. If longitudinal bone curvature predisposes the bone to some type of bending, typically an ellipsoid bone shape may develop. If the bone is loaded in torsion, a circular bone maximizing J may be expected. Bones are rarely loaded under a singular type of load and often encounter combinations of two or three of these load types.

Mathematical simulation of cortical bone (re)modeling with detailed examples from extant taxa help us to understand how cross-sectional bone shapes might adapt during an animal's life (plastic adaptation) or over evolutionary time. In the case of pure torsional loading, there is strong selection away from a noncircular ellipsoidal shape to a more circular form (Figure 34.4A) (Levenston et al. 1998). Allowing this model to "optimize" results in a very thin-walled bone (e.g., like an "empty […] aluminium beer can," Currey and Alexander 1985), where the ratio of the radius of the bone (R) to cortical thickness (t) increases with increasing J. This shape is very similar to the adult emu femur where torsional loading predominates (Figure 34.4A). Because bending is also present in this bone a high J would also maximize I, enabling resistance to bending. In bones where bending in a single direction predominates, the optimal shape is an eccentric one where bone tissue is located as far from the neutral axis as possible. When starting with a circular bone shape, this shape is more or less achieved in simulation (Figure 34.4B) and mirrors the goat radius in which 87% of the axial strains are due to bending (Main and Biewener 2004). The eccentricity of this final shape of varying cortical thickness and widely varying I across different anatomical planes is typical of vertebrate bones where bending predominates. The interesting thing about the goat radius, and many other ungulate long bones, is that the zeugopodial and autopodial bones (in the forelimbs, at least) defy engineering logic in maintaining I_{MAX} transverse to the AP swing of the limbs (Figure 34.4B). The inherent strength in this eccentric structure is the primary resistance to withstanding mediolateral (ML) bending. Thus, the bone is structurally weaker in one direction, where loading can be controlled through neuromuscular feedback, while in the other plane of bending, the skeleton's structural resistance plays the dominant role.

Where equal amounts of bending and axial compression act in combination a shift in the neutral axis away from the centroid occurs. One surface is placed under greater compressive loads and a thicker cortex is predicted to form in this region of the bone. This example indicates bending in a single plane, but it represents well the plastic adaptation that occurs in the mouse tibia during applied axial compressive loads. Axial compression (–17 MPa), AP bending (±55 MPa) and ML bending (±20 MPa) all increase with load, and the bone is added to the posterolateral site of increased compression (Figure 34.4C) (Main et al. 2010, 2014). When torsion is added to the axial and bending loading environment, an eccentric ellipsoid is predicted (Figure 34.4D), which mirrors pretty well the juvenile emu femur at 20 weeks of age, where torsional shear and bending are fairly equal. Although the computational models appear to be accurate in predicting bone shape in a few specific cases, there has yet to be a thorough accounting of cross-sectional bone shape and eccentricity relative to *in vivo* loading modes. In birds, reptiles and even marsupial animals, where torsion-induced shear is fairly equal to axial bending, symmetrical circular bone shapes result (Biewener and Dial 1995, Blob and Biewener 1999, Butcher et al. 2008, 2011). More work needs to be done with ontogenetic and comparative bone strain data in relation to bone cross-sectional shapes relative to theoretical predictions. This work in extant taxa will be particularly valuable when applied accurately to functional hypotheses for fossil limb bones.

Plastic adaptation studies are classic ways to test hypotheses regarding cross-sectional bone shape in response to a known change in load. Osteotomy studies have shown that bone cross-sections increase in the posterior half of the radius in response to increased caudal bone strains on removal of the ulna to return

VetBooks.ir

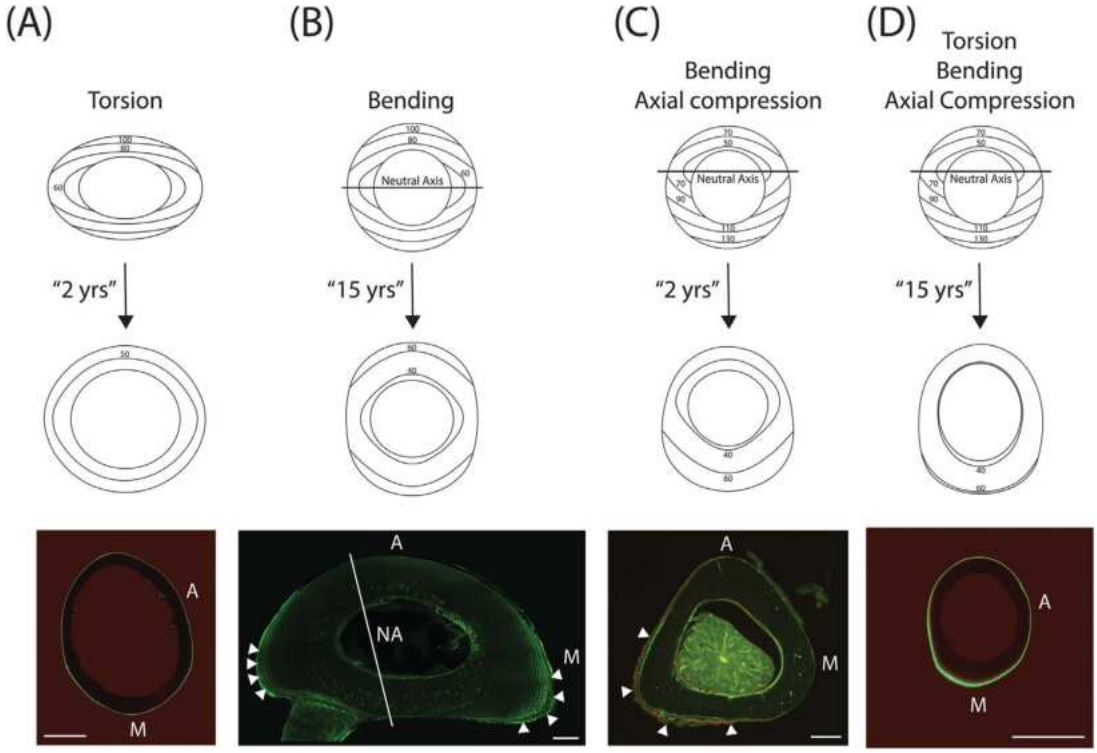


FIGURE 34.4 Theoretical cortical bone plasticity models. For each graphic (A–D), the preloaded structure is presented at the top. The "adapted" structure and the number of model iterations ("years") taken to arrive at that structure are presented in the middle. At the bottom are examples from our own research that indicate agreement with the adapted state in their overall shapes, the types of loads they experience *in vivo* and the patterns of growth, as indicated by the bone fluorescent labels administered. Please note the strain stimulus isoclines in the models are all greater at the initial stages than they are in the adapted stages. A, Torsional loading optimizes for a thin-walled circular shape to minimize torsional stresses. Optimization for *J* happens in only "2 years" from an elliptical starting point. A 49-week-old emu femur is shown at the bottom with a very thin-walled, rounded shape and uniform periosteal growth, consistent with the predominant torsion-induced shear strains experienced by this bone at this age (scale bar = 1 cm). B, In pure bending of a hollow cylinder, the neutral axis (NA) is positioned at the centroid of the bone. After "15 years" of adaptation, a more eccentric shape is reached to maximize I_{MAX} across the bending axis. In the growing juvenile goat, notice that most of the new bone growth occurs across the NA (white line) on the medial and lateral bone surfaces (solid arrowheads), with very little occurring on the anterior and posterior cortices (scale bar = 1 cm). C, When loading in a combination of axial compression and bending, the neutral axis shifts away from the centroid indicating the high degree of compression in the bone. After "2 years," the compressive cortex expanded to reduce the modeled strains to half their original values. A tibia from an experimental mouse loading study is shown at the bottom. This mouse received compressive loading at the knee that induced both bending and axial compression in the bone. Bone fluorescent labels indicate that the majority of bone added over the 2-week experiment coincided with expansion of the posterior and lateral surfaces of the tibia (solid arrowheads), which experience increased compressive loading (scale bar = 200 μm). D, When combining torsion, axial bending and compression, the adapted shape looks similar to (C), but it is more elliptical and thin walled as a result of the additional torsion. This model took "15 years" to reach the adapted state shown. A 20-week-old emu femur is shown at bottom. At this growth stage, the femur experiences a fairly even amount of torsion-induced shear and bending, thus, periosteal growth is enhanced on the posteromedial bone surface that experiences increased compression and the overall bone shape is fairly circular/elliptical (scale bar = 1 cm). The anterior (A) and medial (M) bone surfaces are indicated here and throughout the chapter. (Adaptation models are modified from Levenston et al. 1998.)

strains to a preoperative level (Goodship et al. 1979, Lanyon et al. 1982). However, there are clearly concerns by other biologists that the woven bone response is pathological (Burr et al. 1989, Bertram and Swartz 1991). To combat this issue, a turkey ulna loading model was introduced, representing the only applied avian loading model to date (Rubin and Lanyon 1984b). On isolating the ulna from all functional strains (e.g., disuse condition), no woven bone was detected in direct response to the surgery itself (Rubin and Lanyon 1984b, 1985); instead, when loaded in bending, a woven bone response was induced. Because the loads applied to the bone were physiological in magnitude, the woven bone response was likely due to inducing a plane of bending that was rotated about 90° from the *in vivo* bending direction (Lanyon and Rubin 1984, Rubin and Lanyon 1984b, Burr et al. 1989). In contrast, the mouse tibial loading model induces woven bone at about 9N of loading, corresponding to 2–3× normal strain levels in the bone (Souza et al. 2005, Sugiyama et al. 2012, Sun et al. 2018). The turkey loading model was also used to determine that eccentric bending, with as few as 36 loading cycles per day, was just as effective at forming new bone as 360 or 1800 cycles per day (Rubin and Lanyon 1984b). Using this model, it was determined that the circumferential, radial and longitudinal strain gradients accounted for 60% of the new bone formed on the periosteal surface (Gross et al. 1997).

Both rat ulnar and mouse ulnar and tibial loading models have been used to discover other important factors related to the stimulation of bone formation, including number of load cycles needed per day, number of loading days needed per week and load magnitudes required for bone (re)modeling (Mosley and Lanyon 1998, Robling et al. 2001a, b, 2002,

VetBooks.ir

Sugiyama et al. 2012, Yang et al. 2017, Sun et al. 2018). Subsequent studies have shown that osteocytic gene expression in these models is related to sites of greater compressive strains and load-induced bone formation (Robling et al. 2008, Moustafa et al. 2012, Holguin et al. 2016). An osteichthyan opercular adaptation model could lead to valuable insights in describing how fish without osteocytes (anosteocytic) and osteocytic teleosts may respond by plastic adaptation to applied load (Atkins et al. 2015). While osteocytes are thought to be key to bone's anabolic response to load in most vertebrates, it is unknown how bone's osteocyte lacunar-canalicular network architecture or the fluid flow that results from loading in this network might play in producing bone gain.

A number of exercise studies conducted primarily in chickens and rodents suggest minimal changes in bone geometry in response to mild exercise. With inconsistent results across studies, no clear summary of these experiments can be made. Treadmill exercise in rodents is difficult to characterize mechanically and results can vary based on the type of exercise, sex, age and the genetic strain of rodent used. Furthermore, the results of these studies take a phenomenological approach as the change in mechanics or overall strain (or stress) stimulus about a given bone is not typically quantified. As an example, in two treadmill studies conducted by the same research group, 11-week-old B6/129 male mice were exercised for 21 days on a treadmill. One study showed increased structural properties, postyield deformation and strain to failure (Wallace et al. 2007). The second study showed no structural differences (Wallace et al. 2009). Sometimes, even seemingly moderate changes in natural activity levels can have meaningful effects on bone structure if the loading mode is novel enough. Four-week-old female Balb/C mice restricted to traversing a twisting tunnel between their food and water for 8 weeks, compared with mice traversing a straight tunnel, had a slightly greater femoral I_y/I_x ratio, indicating that the habitual running in a "twisting" way for 8 weeks had induced a subtle increase in femoral resistance to ML bending (Carlson et al. 2007). Similar results were found in the humeri of female C57Bl/6J mice housed in the same twisting cages from 4 to 16 weeks of age, where humeral cortical area (*Ct.Ar*) increased by 11% (Wallace et al. 2013).

Genetic strain and age can both impact the results of exercise or loading experiments. This difference by mouse strain in these previous studies is interesting as the tibiae of C57Bl/6 and Balb/C are known to respond in slightly different fashions in tibial loading studies (Holguin et al. 2013). This is similar to other studies where the skeletons of Hsd:ICR mice respond to treadmill running but Crl:CD1 mice do not (Wallace et al. 2015) and C57Bl/6J and C3H/HeJ mice respond differently to jumping exercises (Kodama et al. 2000). This difference by genetic strain could potentially provide unique insights into the genetic regulation of skeletal mechanobiology during controlled loading studies, though very little has been achieved in this area (Robling and Turner 2002, Judex et al. 2004). Age is also a valid consideration when evaluating the results of these studies, as rodents and turkeys respond more readily to applied loading at younger ages (Rubin et al. 1992, Turner et al. 1995, Lynch et al. 2011, Willie et al. 2013, Main et al. 2014, Holguin et al. 2014, 2016). Of the animals in which skeletal plasticity during ontogeny has been examined, the juvenile skeleton may be the most "plastic" time to undergo morphological change in response to altered skeletal loading.

In contrast to exogenous mechanical loading studies, relatively more intense exercise, like jumping, is still within the realm of what might occur in a natural population and typically proves to be reliable in generating changes in bone mass in rodents (Honda et al. 2001, Umemura et al. 2002, Nagasawa et al. 2008, Ooi et al. 2009, Ju et al. 2014). Rat studies have shown that 10 jumps per day in growing rats (8-weeks-old) is enough to increase femoral periosteal and endosteal perimeters and *Ct.Ar* (Honda et al. 2001). One hundred jumps per day in rats leads to somewhat greater bone formation, but most of the formation is caused by going from 0 to 10 jumps per day (Nagasawa et al. 2008). It is not unreasonable to see how the initiation of some habitual activity requiring 10 more jumps per day above daily loading levels might result in plastic changes in the skeleton, even among natural populations.

Most work in this area has been conducted using traditional biomedical models because they are most tractable. However, some researchers have brought novel taxa into the lab to examine skeletal plasticity. A few controlled fish studies indicate that some mechanism for bone mechanotransduction is likely a plesiomorphic trait dating at least to the split between actinopterygian and sarcopterygian fish, hundreds of millions of years ago. Fish with osteocytic bone, including zebrafish exercised in a swim tunnel and *Polypterus* raised in a terrestrial habitat, showed significant changes in vertebral and pectoral girdle bones with increased swimming or terrestrial loading, respectively (Standen et al. 2014, Suniaga et al. 2018). In another study, when adult *Kryptolebias marmorata* were raised on land, stiffening of the acellular gill arches occurred within 7 days (Turko et al. 2017, Davesne et al. 2019). The changes in bone structure after 7 days is about how fast it takes for mice to form new bone after tibial compressive loading (Sun et al. 2018). The skeletons of fish with acellular bone undergo plastic (re)modeling in their pharynx when switched to a diet of increased hardness (cichlids) (Gunter et al. 2013) or by receiving external mechanical loads to the operculum (Atkins et al. 2015). Interestingly, the acellular bone in cichlids expresses genes in response to the altered load that are similar to those expressed in mammalian models during plastic skeletal adaptation to load (e.g., *alpl*, *runx2*, *osx*, *opg*, *cx43*, *bmp2*) (Mantila Roosa et al. 2011, Gunter et al. 2013, Holguin et al. 2016, Kelly et al. 2016). These gene-level responses suggest that osteocytes, which are critical for mammalian skeletal adaptation, are not necessary to mobilize osteoblasts for adaptive bone formation in all vertebrate taxa. And even some genes commonly associated with osteocytes (*opg* and *cx43*) are expressed in anosteocytic bone. Very little is known about the broader phylogenetic evolution of the cellular mechanisms regulating bone mechanotransduction, which deserves further attention.

Most of the comparative or paleontological cross-sectional geometry studies related to flight use extant analogues that are suspected to move in similar ways and where aspects of limb biomechanics or kinematics have previously been studied. For birds, the most complete set of *in vivo* forelimb strains, including torsion-induced shear strains, have been collected for pigeons performing different tasks (takeoff, steady flight, landing) (Biewener and Dial 1995). Some additional data were also

collected for axial strains from a goose humerus during flight and the ulnae of chickens and turkeys performing ground-based flapping (Rubin and Lanyon 1982, 1984b, Lanyon and Rubin 1984). In the latter three species, only the turkey had an associated cross-sectional strain distribution, but no shear strains were reported. Therefore, we only have torsional strains for the humerus of a single taxon, some information for the ulna but not during flight, and no information for other wing bones. The gray-headed flying fox (*Pteropus poliocephalus*) showed that the humerus and radius are loaded predominantly in longitudinal bending and torsion-induced shear (Swartz et al. 1992). Hindlimb bones are better represented, where analogous functional hypotheses can be based on two examples of femoral data (chicken, emu), three examples of TBT data (chicken, emu, turkey) and one example of TMT data (chicken), with the understanding that all of these birds are habitually terrestrial, limiting the number of behaviors for which biomechanical data exist (Rubin and Lanyon 1984b, Biewener et al. 1986, Loitz and Zernicke 1992, Biewener and Bertram 1994, Carrano and Biewener 1999, Main and Biewener 2007).

It was established earlier that symmetric, thin-walled bones (high ratio of *R/t* and I_{MAX}/I_{MIN} ratio ~1.0) are best suited for withstanding shear strains due to torsional bone loading. Relative to land mammals, birds and the forelimbs of bats have relatively high values for *R/t*, though flightless birds overlap with the mammalian range (Figure 34.5) (Currey and Alexander 1985, Swartz et al. 1992). Birds possess diverse morphologies across both the hindlimbs and forelimbs, but for the most part largely possess proximal limb bones that are mostly thin walled and circular, while diving birds have thicker cortices and/or more eccentric cortices (Cubo and Casinos 1998, Margerie et al. 2005, Habib and Ruff 2008). When extending the *in vivo* bird and bat biomechanical data to hypotheses of cross-sectional bone adaptation for different modes of flight (soaring, flapping, gliding), swimming birds or extinct fliers, the number of assumptions regarding the uniformity of flight biomechanics across different size ranges is an obvious limitation. This is especially true for intense activities such as takeoff, acceleration and swimming, and this continues to be a weakness in our comparative and paleontological studies of bone adaptation relative to the diversity of activities birds can conduct with their limbs (Gatesy and Dial 1996). Of course, it is impossible to expect bone strain data for all avian taxa, but the amount of light that would be shed on this dark corner of our biomechanical ignorance would be exceptional if strain data could be collected from hindlimb and forelimb bones of a few selectively chosen birds performing functions such as soaring or diving, that we currently have no record for.

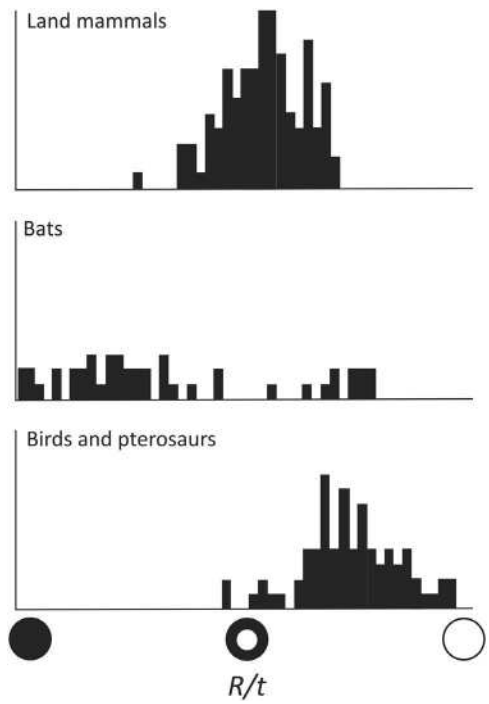


FIGURE 34.5 *R/t* values for mammals, bats, birds and pterosaurs. Low *R/t* values indicate a cortical thickness (*t*) similar to the bone's radius (*R*) (a solid bone), whereas high *R/t* values are consistent with thin-walled bones that maximize *J*. Birds and pterosaurs typically have thin-walled proximal forelimb and hindlimb bones. The forelimb bones of bats (humerus, radius) overlap the bird range. Mammals make up most of the middle range possessing thick-walled cortices of moderate *R* and have some overlap with the lower end of the avian distribution. (Modified from Currey and Alexander 1985 and Swartz et al. 1992.)

With the understanding that there is very little *in vivo* flight mechanics known from birds, there have been descriptions of the limb bones of extinct reptiles, including birds, that show skeletal selection for thin-walled wing bones of circular shape. A number of nonavian reptiles have low *R/t* values, indicating relatively thick cortices (Currey and Alexander 1985), but the bones are circular in cross-section, consistent with the long bone torsion present in these bones (Blob and Biewener 1999, Butcher et al. 2008, Sheffield et al. 2011, Hilliard Young and Blob 2015, Young et al. 2017). For pterosaurs, it is clear that despite a wealth of anatomical data (Padian 1983, Wilkinson 2008, Witton and Habib 2010) and even histological data (Ricqlès et al. 2000, Padian et al. 2004), the exploration of wing and leg cross-sectional geometry is lacking, in part due to a lack of specimens and (until recently) minimally destructive techniques that prevent destruction of the samples. Some of the only data that we have on this front is from Currey and Alexander (1985) and they only examined *R/t*. Recently, non-destructive synchrotron-based microtomography was used to characterize virtually reconstructed humeral cross sections of *Archaeopteryx* and two pterosaurs (*Rhamphorhynchus*, *Brasileodactylus*), showing thin-walled circular humeri typical for flying reptiles (Voeten et al. 2018). The long-tailed pterosaur, *Rhamphorhynchus*, aligns in a particularly unique place with a very low cortical area to total area (akin to high *R/t*) and a particularly high mass-normalized value for *J*, even relative to most birds. *Brasileodactylus* aligns with dinosaurs and most birds in regard to relative *Ct.Ar* values, but the mass-normalized *J* values are more in line with other archosaurs and a bit lower than extant specialized fliers that use continuous flapping, flap-gliding and soaring flight. Synchrotron-based microtomography is amazing in its ability to take virtual cross-sections without damaging the bone and allowing 3D reconstructions, but these devices are difficult to secure beam time on, so most taxa are represented by very small sample sizes that we assume to be representative of the broader population (Sanchez et al. 2012, 2014). Limited sample sizes and a lack of

VetBooks.ir

biomechanical data for flying vertebrates must be recognized as limiting factors in these studies of flying archosaurs, though this limitation is not often explicitly stated.

In the analyses of some nonhuman primates and humans, there are some behavioral correlates for differences in cross-sectional geometries among taxa, but the functional analyses have not typically been subjected to rigorous biomechanical analyses. Examining a group of four primate taxa, some arboreal and some terrestrial, the hindlimbs were found to be generally similar in their cross-sectional properties, but the forelimbs differed from each other based on habitat type, suggesting a rationale for analyzing both girdles in functional terms (Schaffler et al. 1985). However, the result of this limited sample size may be difficult to generalize because a sample of 71 primate, 30 carnivoran, and 59 rodent bones from species that are habitually terrestrial or arboreal found only minor differences in humeral properties between arboreal and terrestrial primates and carnivorans, suggesting that differences in habitat do not predict bone geometries (Polk et al. 2000), and that small sample sizes can lead to faulty conclusions.

The cross-sectional geometries of the femora and tibiae of Neanderthals, late Paleolithic, and recent humans have been examined in an attempt to provide insight into evolutionary changes in hindlimb use. Starting with a relatively recent population of extant humans, the Pecos Puebla Amerindians show essentially modern hindlimb morphology, in which the femora show a strong AP curvature and an I_{MAX}/I_{MIN} near 1.0 (1.38), suggesting roughly equal bending rigidity in the AP and ML planes. The tibia also shows very strong AP curvature and I_{MAX}/I_{MIN} ratios near 3.0, with the eccentricity acting to withstand AP bending. Incidentally, the mid-diaphyseal shape is quite similar to that of macaques, which experiences a mixture of AP and ML bending strains (Demes et al. 2001). Neanderthals had more robust lower limb bones with a more circular shape and greater relative cortical thickness. The Neanderthal femora are especially resistant to ML bending (Trinkaus et al. 1991, Trinkaus and Ruff 1999), and Lovejoy and Trinkaus (1980) found isolated Neanderthal tibiae to be nearly twice as resistant to torsion and bending in all directions compared to those of extant humans. The Neanderthal patterns mirror the general cross-sectional characteristics of a taxon with much more diverse (unpredictable) loading directions on the hindlimb bones. Much of the paleontological samples are based on very low sample sizes and are subject to taphonomic effects on the bone. With very few samples, there is very little idea of the variation that existed within and between populations. As has been shown previously with FE modeling of the hominid skull (Smith et al. 2015), the amount of variation in a population could surpass that between two different taxa. Recent studies have used principal components analyses of a more complete skeletal sample of mustelids to test for the morphological convergence of independently derived features associated with running and swimming (Botton-Divet et al. 2016, 2017). Another used a large phylogenetic range of mammals and diaphyseal cortical measures including R/t, $R_{MAX}t$, $R_{Mean}t$ and shape eccentricity (I_{MAX}/I_{MIN}) to show that *relative* two-dimensional (2D) and 3D measures of geometry are potentially important for identifying biomechanical influences in morphological evolution (Houssaye et al. 2018).

Unless dealing with a fossil species with a clear extant analogue from which biomechanical measures have been made (Hutchinson et al. 2005, 2015, Bishop et al. 2019a, b, c, Nyakatura et al. 2019), fossil bones rarely provide enough information to confidently form testable hypotheses. Ontogenetic studies may provide some of the best data for testing hypotheses about changes in locomotor mechanics in both extinct and extant taxa. There have been some successful examples within Dinosauria that used ontogenetic series of enough complete hindlimb skeletal elements to provide functional biomechanical assessments based on bone cross-sectional shape.

An ontogenetic series of femoral cross-sections in *Dysalotosaurus lettowvorbecki* (formerly known as *Dryosaurus*) (Dinosauria, Iguanodontid) were used to predict growth-related changes in posture (Figure 34.6) (Heinrich et al. 1993). Between the Small and Medium/Large classes there was an increase in *Ct.Ar* (~29%), as would be expected for growing animals. Bone eccentricity increased from the Small (1.27) to the Medium animals (1.44, $p = 0.072$), before decreasing back to the Small ratio in the Large group ($p = 0.053$). This ontogenetic pattern suggests an interesting hypothesis for *D. lettowvorbecki* regarding how ontogenetic postural changes might be predicted from fossils. The Small group began life as a quadruped and achieved bipedality in the Large group. The Medium stage was assumed to be transitory; placing the increasing mass of a newly acquired bipedal posture on the quadruped-type femora. The ontogenetic adaptation shown by the Medium class was an increased resistance to AP bending and an increase in I_{MAX} relative to I_{MIN}. The change in shape mirrors one where an axial compression-torsional environment is replaced by one selected for resistance to bending (Figure 34.4). Just as with applied exogenous loading (Rubin and Lanyon 1984b, Robling et al. 2001a, Main et al. 2014), an abrupt change in habitual loading can cause a rapid change in bone shape to adapt to the new mechanical challenge, in this case increased body mass and bipedality. Once the mechanical forces conveyed by this new posture are no longer perceived as a mechanobiological stimulus by the bone, (re)modeling continues to alter the bone until adult form is reached.

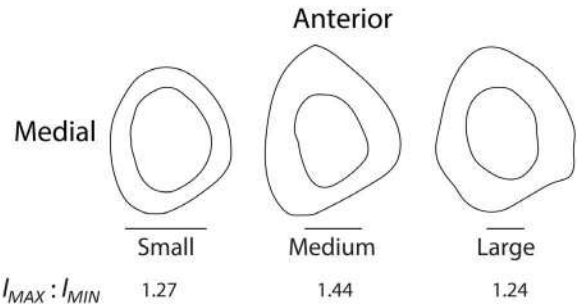


FIGURE 34.6 Three representative femoral cross-sections for *Dysalotosaurus lettowvorbecki* representing the three size classes discussed here. The mean values for I_{MAX}:I_{MIN} are shown below, indicating the increase in bone eccentricity during maturation from the Small to Medium group, expanding the bone to withstand AP bending. (Re)modeling eventually occurs in the Large group to reduce this ratio once the change to bipedal posture becomes habitual. Scale bar = 1 cm. (Modified from Heinrich et al. 1993.)

A similar ontogenetic analysis was conducted for *Maiasaura peeblesorum* using the scaling of morphometrics in a much larger sample, to track changes in limb bone mechanics during the transition from juvenile bipedality to adult quadrupedality (Dilkes 2001). Humeral I_x and I_y scaled with isometry relative to humeral length during growth, which makes an argument for an ontogenetic transition from bipedality to quadrupedality difficult. Positive allometry for humeral cortical thickness indicate medullary contraction, except on the cranial surface, which scaled with isometry. Thus, the humeri would become relatively stronger with size due to a relative increase in *Ct.Ar*, but *I* would not be substantially altered because bone mass was added uniformly around the endosteal surface. Based on this ontogenetic cross-sectional reconstruction, it remains difficult to ascertain a loading scenario in which the cranial surface might not scale similar to the other cortices. In denervated chick limbs and in the wing elements of growing emu, the lack of selective forces on unused bones can lead to increased morphological variation (Biewener and Bertram 1994, Kuehn et al. 2019). For adult *Maiasaura* femora, the relative cortical thickness becomes equally thick across all anatomical planes suggesting selection for increased resistance to torsional and axial compressive loads without any significant asymmetry to indicate a predominant loading direction. Interestingly, the tibia actually shows negative allometry in *I* relative to tibial length, suggesting that (1) relative weight support shifted toward the forelimbs, decreasing relative loading on the tibia; (2) the relative scaling of the fibula may have shown positive allometry suggesting that this bone accompanying the tibia took on more body mass as the *M. peeblesorum* grew or (3) a combination of these two factors. Usually negative allometry indicates a relative unloading of the limb bones relative to other limbs, and that is most likely the case here given the switch to quadrupedality (Carrier and Leon 1990).

A most unique study for *M. peeblesorum* reports two samples that essentially reconstruct the early osteotomy models (Goodship et al. 1979, Lanyon et al. 1982). Two tibiae with histologically identified exostoses appear to share a similar woven bone response with the early ulnar osteotomy studies in pigs and sheep (Figure 34.7) (Cubo et al. 2015). In reconstructions

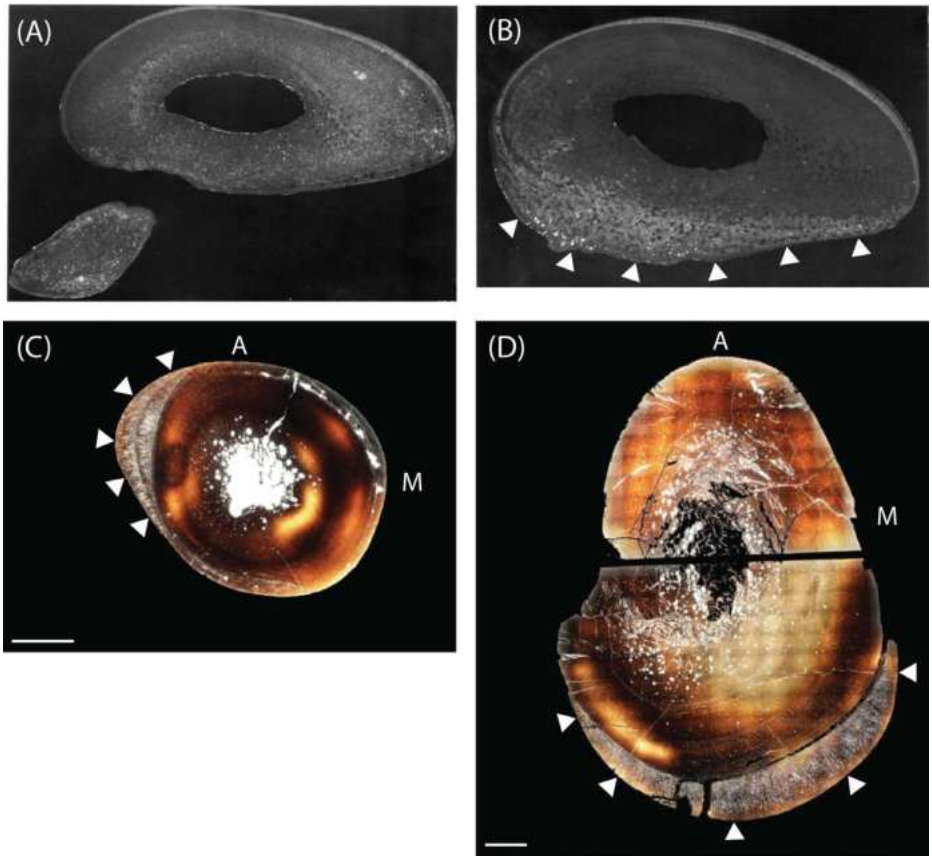


FIGURE 34.7 Pathological mechanical adaptation of cortical bone. A, Normal sheep radius and ulna. B, Sheep radius, 50 weeks following osteotomy of the ulna (same sheep, image reversed for comparison to the contralateral limb in A). Note the large posterior periosteal (re)modeling response to compensate for the missing ulna (arrowheads). Fifty weeks postosteotomy, anterior bone strains on the radius were slightly reduced in (B) relative to (A), showing the skeleton's ability to compensate for injury of nearby support elements. C, Tibial cross-section from a juvenile *Maiasaura peeblesorum*, showing a periosteal woven bone response (arrowheads) similar to the pathological response observed in (B). The location of the exostosis coincides with the position of the fibula in *M. peeblesorum*, suggesting a similar mechanism to compensate for an injured fibula. The tibia was found disparate of any fibula, so this hypothesis cannot be confirmed. D, Periosteal woven bone response from an adult *M. peeblesorum* (arrowheads) for which the position is difficult to reconcile without knowing more about *Maiasaura*'s zeugopodial mechanics. Scale bar: C and D = 1 cm. (A, B: Modified from Lanyon et al. 1982. Reprinted with permission from Elsevier. C, D: Adapted from Cubo et al. 2015.)

VetBooks.ir

of the adult posture of *M. peeblesorum* the fibula was placed anterolateral to the tibia. As with the sheep osteotomy study, if fibular support in the hindlimb is compromised, new bone would be formed on the tibia where the damaged fibula was located. This hypothesis is supported in the tibia from the smaller bipedal form of *M. peeblesorum* (Figure 34.7) with an apparent shift in I_{MAX} that may come close to the original orientation of I_{MAX} for the tibial-fibular complex – but this is difficult to validate without the fibula preserved *in situ*. The adult tibia is more difficult to reconcile because the woven bone response occurs on the posterior tibia. By this ontogenetic growth stage, the mechanics of the tibia would have shifted to support quadrupedality, and the tibia is likely bearing less relative load than in the smaller *M. peeblesorum*. However, the relative load-sharing between the tibia and fibula would likely have been unchanged. The only way that the described woven bone response could be produced is if the nature of the fibular fracture were partial so that it was weakened in withstanding AP bending or the tibia-fibular complex had shifted from resisting predominantly ML bending as a biped to resisting a more AP bending condition as an adult. The mechanistic explanation in this paper draws similarities between the juvenile bipedal and adult quadrupedal *M. peeblesorum* to humans and sheep, respectively, even though the anatomy and relative limb proportions of these comparative taxa are not likely reflective of *M. peeblesorum*. The interpretation of the position for the woven bone response in the adult tibia suggests that we do not know enough about adult *M. peeblesorum* tibial mechanics.

Over evolutionary time or in direct plastic response to altered loads, cortical bone (re)modeling is dependent on how the bone is loaded *in vivo* and the curvature of the bone, to indicate whether the bone is adapting to increase strain predictability (bending across I_{MIN}) or acting to increase bending resistance across I_{MAX}. Some bones have conflicting demands or multiple bending directions and will form new bone somewhere between the axes defining I_{MAX} and I_{MIN} (Demes et al. 1998, 2001, Lieberman et al. 2004, Main and Biewener 2004). Without knowing the *in vivo* loading mechanics, or how altered loading differs from habitual loading, predicting evolutionary or ontogenetically plastic changes in bone cross-sectional shape can be quite complicated. We do not yet have paired mechanical and morphological data from enough different taxa to make predictions about responses to alterations in load with age or in response to aberrant loading to extend this rationale to extinct animals.

Primary Vascular Canal Orientation

Biomechanical loads experienced during locomotion may influence microstructural features of long bones, in addition to the gross-level features discussed above. During bone modeling, primary osteons form around vascular canals, erecting an interconnected 3D network of channels that distribute blood vessels and nerves throughout cortical bone (Francillon-Vieillot et al. 1990, Ricqlès et al. 1991, Currey 2002). Through assessment of traditionally prepared histological slides or more recently high-resolution micro-CT (Pratt and Cooper 2017), these primary vascular canals can be classified based on their orientation relative to the periosteal bone surface (*circumferential* – parallel to periosteal surface, *radial* – orthogonal to periosteal surface, *longitudinal* – parallel to bone shaft and *oblique* – all others) (Ricqlès et al. 1991) (Figure 34.8). The

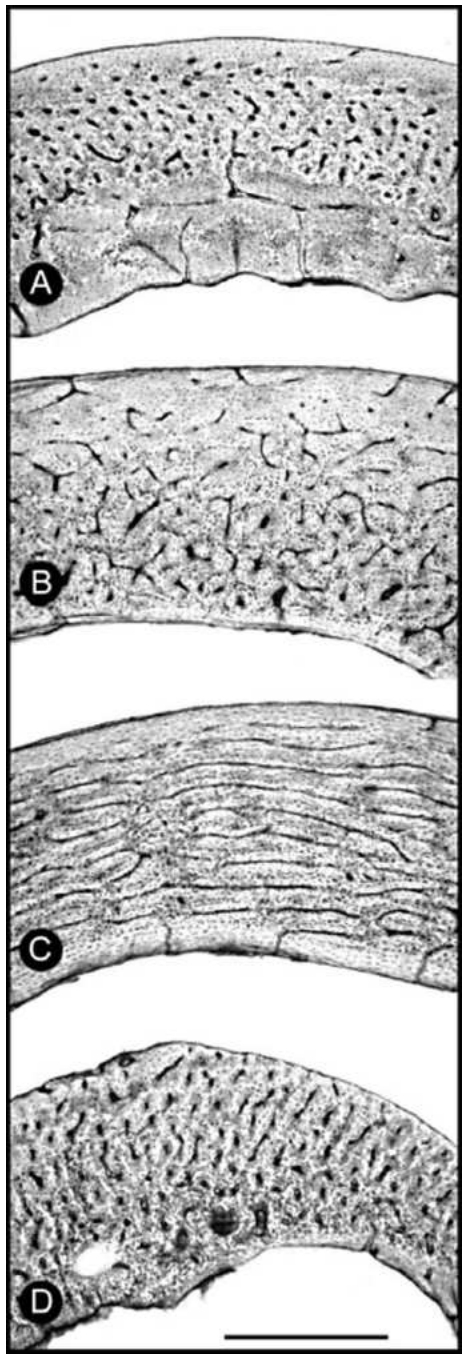


FIGURE 34.8 Primary vascular canals in cortical bone are classified based on orientation relative to the periosteal surface. Example histological sections of avian limb bones with a predominance of (A) longitudinal canals (parallel to the long axis of the bone shaft) (Common murre, tibiotarsus), (B) oblique canals (Great crested grebe, tibiotarsus), (C) circumferential canals (parallel to the periosteal surface) forming a laminar bone structure (Mallard, ulna) and (D) radial canals (orthogonal to the periosteal surface) (Razorbill, tarsometatarsus). (From Margerie et al. 2005.)

VetBooks.ir

specific organization of the primary vascular canal network in cortical bone has been hypothesized to correspond to differences in biomechanical load, growth rate and/or phylogenetic relationships (Padian 2013). Some animals retain the primary structure of long bones and only accumulate small amounts of remodeling (secondary/Haversian osteons) with age (Enlow and Brown 1956, 1957). The organization of the primary vascular canal network in these animals is a record of bone structure during ontogeny and can provide a unique opportunity to assess whether forces acting on bone during modeling affect microstructure.

Laboratory experiments investigating the direct effect of experimentally manipulated strain environments on primary vascular canal orientations are nearly nonexistent. Most studies examine the reorganization and orientation of secondary osteons formed by bone remodeling in response to load or lack of load (addressed later in the chapter). However, one study has shown that loading does indeed affect the organization of primary vascular canals. Britz et al. (2012) used sciatic neurectomy to immobilize the left tibiae of rats at 3 weeks of age for 27 weeks. There was a significant difference in orientation of primary vascular canals in the immobilized tibia when compared to those of age-matched control rats. The orientation of canals in the immobilized tibiae was significantly more radial, whereas the tibia of control rats possessed primarily longitudinal canal orientation. Thus, for the rat at least, the presence of load affects the primary vascular canal orientation in the tibia, but without directly measured strain it remains difficult to link canal orientation to a specific loading regime.

The idea that a specific orientation of primary vascular canals may reflect predominant biomechanical load has been around for some time. The majority of studies investigating this relationship have focused on birds, a large diverse group of animals that tend to retain primary bone structure. Margerie (2002) made the explicit hypothesis that laminar bone (bone dominated by a network of circumferential canals) was adapted to better resist torsional loads placed on avian wing bones during normal flapping flight. The 3D structure of the parallel concentric canals and the primary osteons surrounding them are thought to better resist the tissue-level shear strain that results from torsional loading (Margerie et al. 2004). In the mallard, bones expected to be experiencing predominantly torsional loads (humerus, ulna, and femur) did indeed exhibit a laminar bone microstructure (Margerie 2002). In a survey of additional avian species, the pattern for these elements tends to hold (Margerie et al. 2005). Additionally, birds with a broad wing shape (traditionally birds that use flapping or static soaring flight modes) have wing elements with a more laminar structure than birds with long narrow wings (classic dynamic soaring birds such as albatross) (Margerie et al. 2005, Simons and O'Connor 2012, Marelli and Simons 2014). Presumably, the longer secondary flight feathers of a broad wing may place more torsional loads on the ulna and humerus (Swartz et al. 1992, Biewener and Dial 1995). Although there seems to be a connection between laminar bone and torsional loads in birds, the relationship does not hold true for a few key taxa. Pigeons experience flight-induced torsional loads in the humerus (Biewener and Dial, 1995), yet laminarity in the humerus decreases during growth such that canal orientation is predominantly longitudinal in adults (McGuire et al., 2020). Humeri of bats also experience flight-induced torsional loads (Swartz et al. 1992), yet bat humeri are avascular in small species to poorly vascularized with predominantly longitudinal canals in larger bodied species (Lee and Simons 2015, Pratt et al. 2018, Skedros and Doutré 2019). Additionally, primary vascular canals take a predominantly longitudinal orientation in the femur of the alligator, an element also known to experience torsional load (Blob and Biewener 1999; Lee 2004). Thus, laminar bone is certainly not a universal adaptation to torsional loads and we must carefully consider other phylogenetic constraints on bone microstructure, such as slow somatic growth in bats, and other potential limitations of previous studies.

One such limitation is the paucity of directly measured strain data from avian limb elements. The biomechanical predictions that the humerus, ulna and femur of birds are predominantly loaded in torsion are based on measured strain from only a few species. Predominant torsional loads have been recorded in the pigeon humerus during flapping flight (Biewener and Dial 1995), the turkey ulna during wing flapping exercises (Rubin and Lanyon 1985) and the femur and tibiotarsus in the chicken and emu (Biewener et al. 1986; Carrano and Biewener 1999; Main and Biewener 2007). Collecting strain data from birds during natural behavior is certainly a challenging undertaking and may not be possible in many cases, but without which we are limited to the indirect comparison of vascular canal orientation in one species and biomechanics from another.

To confidently link specific vascular canal orientations to predominant biomechanical load, we must measure both strain and bone microstructure in the same individuals. This is the direction in which current studies are moving. As will be discussed in more detail below, a recent study measured primary vascular canal orientation and direct bone growth rates in hindlimb elements from an ontogenetic series of emu from which *in vivo* strain data had previously been recorded (Main and Biewener 2007; Kuehn et al. 2019). Results from the emu femur and TBT indicate that elevated bone laminarity was most strongly correlated with ontogenetic factors such as old age, large size, and slow growth rate. Shear strain from torsional loading was also positively correlated with laminarity, but had a weaker effect than the ontogenetic factors (Kuehn et al. 2019). Incorporating growth rate data in studies investigating primary vascular canal orientation is essential. Studies attempting to link vascular canal orientations to fast or slow bone growth have presented conflicting results, but it is clear that primary vascular canal structure changes throughout ontogeny (Castanet et al. 2000, Margerie et al. 2002, 2004, Skedros and Hunt 2004, Williams et al. 2004, Pratt and Cooper 2018). A great deal of work needs to be done to determine the role that periosteal bone growth versus biomechanical loading plays in the formation of the vascular canal network.

Collagen Fiber Orientation

Bone matrix consists of a mineral-fiber composite. The fibrous component consists mainly of collagen, which when preferentially aligned appears to confer specific mechanical properties to the tissue (e.g., Ascenzi and Bonucci 1967, 1968, 1972,

VetBooks.ir

Vincentelli and Evans 1971, Martin and Ishida 1989). Thus, visualization of preferred CFO in bone should provide insight into the mechanical environment of the bone in which these fibers formed when traditional mechanical tests are not practical (e.g., small animals, complex loading scenarios or extinct taxa).

There are many methods to observe CFO in bone. The methods differ in the type of probe used (e.g., visible light versus X-ray), resolution (e.g., millimeters versus nanometers), field of view (e.g., whole bone versus individual lamella) and degree to which visualization is 3D (e.g., traditional microscopy versus computed tomography). The intent of this chapter is not to compare those methods, which were reviewed recently by Georgiadis et al. (2016). Instead, we focus on polarized light microscopy (PLM), which has several advantages over other methods for visualizing CFO including accessibility, relative ease of specimen preparation, and wide field of view (e.g., Bromage et al. 2003, Spiesz et al. 2011, Georgiadis et al. 2016). For those reasons, PLM is still used by studies of comparative skeletal histology (including paleohistology).

The orientation of collagen fibers (and bioapatite crystallites) influences light transmission through a given histological section of bone (Figure 34.9A) (Boyde and Riggs 1990, Bromage et al. 2003, Georgiadis et al. 2016, e.g., Wolman 1975). When viewed with PLM, CFO is expressed as variation in hue and brightness (e.g., Warshaw et al. 2017). The pattern of hue is apparent with compensated PLM in which a bone histological slide and a full-wave compensator are inserted between crossed linear polarizers (Figure 34.9B). The compensator shifts the low-order white interference colors of bone collagen to different hues depending on CFO (Figure 34.9B). When the azimuthal or in-plane angle of collagen is aligned with the slow axis of the compensator (Z′), interference hue shifts to blue/green. When the azimuthal angle of collagen is perpendicular to Z′, the hue shifts to yellow/orange (Figure 34.9B, C). Note that in bones with collagen altered by diagenetic processes (e.g., heating or secondary mineral replacement), the interference hues of bioapatite dominate, resulting in a reversal of the color patterns described for collagen (Lee and O'Connor 2013). The "Maltese Cross" artifact (e.g., Bromage et al. 2003), however, affects compensated PLM (as it also does to linearly PLM). It is caused by the orientation of the crossed linear polarizers, which block light passing through in-plane collagen with an azimuth of 0°/180° or 90°/270° resulting in a magenta hue under full-wave compensation. A further complication is that the hue also appears increasingly magenta as collagen aligns perpendicular to the plane of section (i.e., as zenith angle approaches zero degrees). Consequently, the reduced directional specificity of compensated PLM limits its usefulness in the quantitative (or semiquantitative) assessment of CFO.

Elimination of the Maltese Cross artifact is possible with circularly PLM. The configuration of crossed linear polarizers, each bonded to a one-quarter wave compensator, transmits light passing through in-plane collagen fibers irrespective of their azimuthal angle (Bromage et al. 2003). When illuminated with monochromatic light (e.g., through a green bandpass filter) and imaged with a monochrome camera, bone collagen shows variation in gray scale brightness corresponding to out-of-plane or zenith angle (Figure 34.9D). Note that the use of monochromatic imaging eliminates interference hues and, consequently, precludes granular assessments of in-plane CFO. Therefore, use of monochromatic circularly PLM is best suited to test hypotheses framed in the context of relative out-of-plane CFO (e.g., relative distributions of longitudinal vs transverse CFO).

Several approaches can test hypotheses about the biomechanical function of CFO. These approaches involve comparison of CFO across one or more of the following: (1) cortical regions in a single element, (2) skeletal elements within individuals and across closely related species or (3) ontogenetic stages. For the sake of clarity, we present the major findings and limitations of these approaches in isolation with the understanding that the approaches are not mutually exclusive, and studies often use a mixture of two or more approaches.

Strain distribution across the bone cortex varies with the principal type of loading (Figure 33.2). Therefore, if CFO confers biomechanical properties to the bone cortex, then it should vary with loading type. Indeed, a number of studies report correlations between regional variation in CFO and inferred bending loads, which subject one side of the cortex to axial compressive strains and the opposing side to axial tensile strains (Figure 33.2B). CFO (based on measures using circularly PLM) is more oblique/transverse in cortical regions under compressive strains and more longitudinal in regions under tensile strains (e.g., Riggs et al. 1993, Kalmey and Lovejoy 2002, Lee 2004, Skedros and Hunt 2004, Skedros et al. 2007).

However, biomechanical interpretations of regional CFO are complicated by two major inconsistencies. First, regional CFO tends to skew toward longitudinal alignment, especially in primary bone tissues, irrespective of inferred or measured principal loading type (e.g., Riggs et al. 1993, McMahon et al. 1995, Lee 2004, Main 2007, Skedros et al. 2007, Warshaw et al. 2017, Skedros and Doutré, 2019). One explanation for the prevalence of longitudinal CFO is that small magnitudes of tensile strain are sufficient to induce osteoblasts to form longitudinal collagen fibers even in cortical regions subjected to large compressive or shear strain (McMahon et al. 1995, Warshaw et al. 2017). The implication is that longitudinal collagen confers resistance to tensile strains without compromising resistance to other strains. Preliminary data in the mouse femur supports this "tension-resistance priority" hypothesis (*sensu* McMahon et al. 1995) in that bone with longitudinal CFO is at least as strong in tension and compression than bone with a mixture of CFO (Ramasamy and Akkus 2007). Although further testing is warranted, regional CFO dominated by longitudinal alignment may reflect evolutionary selection to resist complex and unpredictable loading patterns. Alternatively, longitudinal CFO may simply be constrained by growth rates and/or tissue type (Warshaw et al. 2017). This interpretation is based on observations that longitudinal CFO is more prevalent in faster-growing bone tissue types (e.g., woven and parallel-fibered bone) than in slower-growing types (e.g., lamellar bone). Therefore, results from studies that do not account for covariation between CFO and tissue type must be interpreted with caution.

Second, regional CFO does not accurately reflect where peak strains occur in the cortex when detailed bone strain data are available. For example, in the goat radius, axial bone

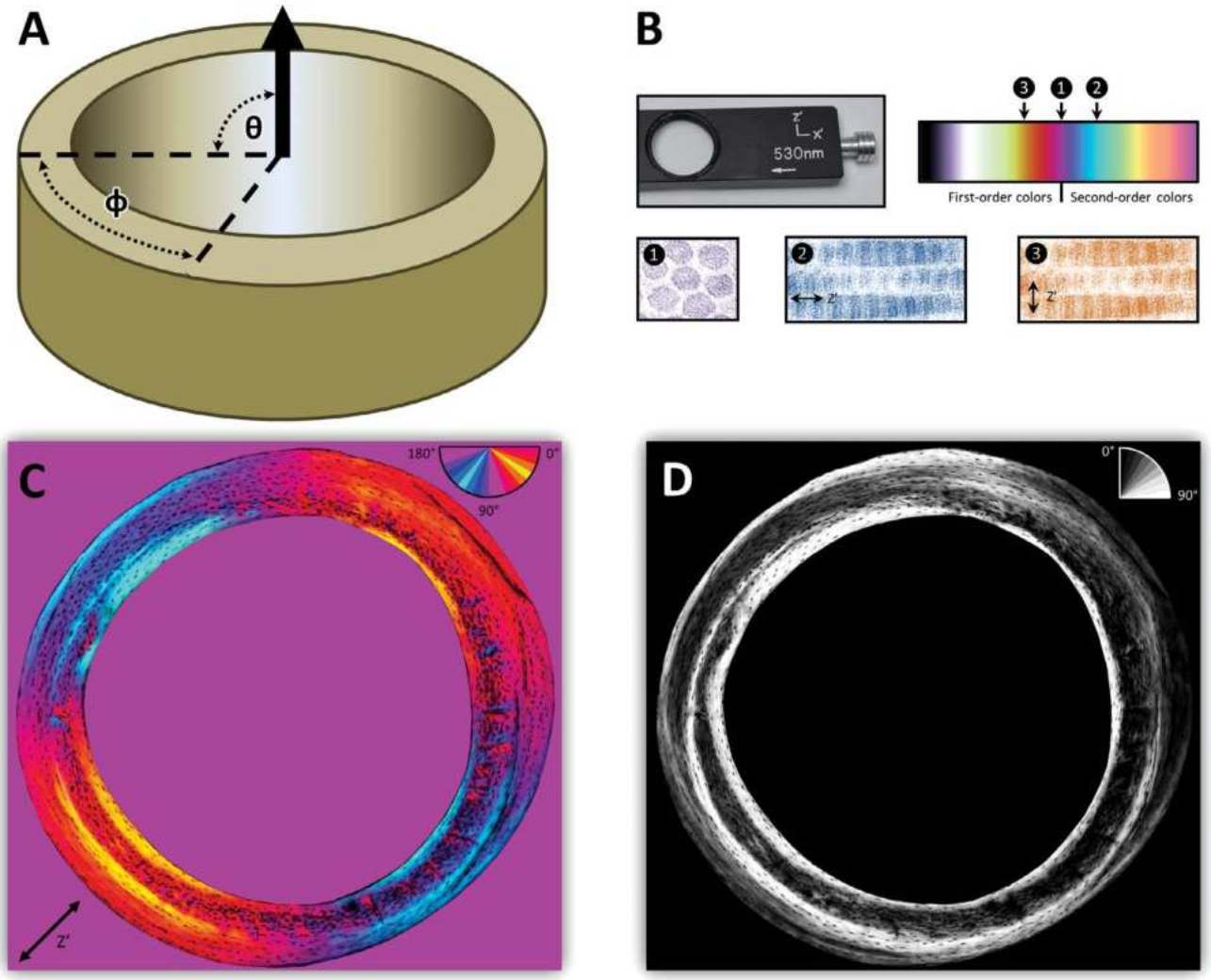


FIGURE 34.9 Orientation of bone collagen based on interference colors in compensated and circularly polarized light microscopy (PLM). A, A simplified portion of the midshaft of a bone illustrates two angles that describe the orientation of a given collagen fibril (or fiber). Zenith (θ) is the out-of-plane angle, and azimuth (φ) is the in-plane angle, following the convention in physics for the spherical coordinate system specified by ISO standard 80000-2:2019 (Item 2-17.3). Together, the zenith and azimuthal angles form coordinates that map the specific direction of the fibril in 3D space. B, Paleohistological imagery often uses light microscopy with crossed linear polarizers and a compensator to produce striking interference colors. These colors are produced by inserting a full-wave compensator into the optical path. The compensator shifts the natural interference colors of bone 530–550 nm. Note that the exact shift (530 nm) and the direction of the slow vibrational axis (Z′) are marked on the compensator. In a typical transverse section of bone, the compensator shifts the interference color of a fibril based on orientation [transmission emission microscopy views of fibrils based on Mescher (2018)]. B1, If a fibril is oriented parallel to the direction of light or perpendicularly either north-south or east-west, it appears magenta (optically extinct). B2, Perpendicularly oriented fibrils that are aligned with Z′ appear second-order blue/green, whereas (B3) those that are orthogonal to Z′ appear first-order yellow/orange. C, Compensated PLM is useful in showing the orientations of collagen fibers in the plane of section. For example, in a transverse undecalcified 100-μm section taken from the humerus of *Macrotus californicus*, in-plane collagen fibers parallel to the Z′-axis of the compensator appear light blue (i.e., φ = 135°/315°), whereas in-plane fibers perpendicular to the Z′- axis appear yellow (i.e., φ = 45°/225°). Note that compensated PLM suffers from the Maltese Cross artifact (Bromage et al. 2003) and requires rotation of the crossed polarizers and compensator to characterize in-plane fibers with azimuth angles of 0°/180° and 90°/270°. D, The Maltese Cross artifact is corrected under circularly PLM with gray scale conversion (see details in Bromage et al. 2003), but the interference colors now reflect the zenith (out-of-plane) angle. Together, both forms of PLM are needed to fully quantify the 3D orientation of bone collagen. (C and D are based on supplemental data from Lee and Simons 2015.)

strain calculated across the whole midshaft section during the entire galloping cycle showed that peak axial tension and compression occur in the lateral and medial cortices, respectively. However, those cortical regions contained predominantly longitudinal collagen and did not differ significantly in CFO (Main 2007). Regional CFO performs no better as a proxy for off-axis shear strain. Although the concentration of oblique/transverse collagen in the caudal cortex suggests a response to high shear strains, actual shear strains were similar to cortical regions dominated by longitudinal collagen (Main 2007). A plausible explanation for the weak specificity between regional CFO and bone strain relates to variability in the mechanical

VetBooks.ir

environment during locomotion such that all cortical regions experience some tension, compression and shear (e.g., McMahon et al. 1995, Main 2007, Skedros and Doutré 2019). Given the effect complex loading has on CFO, biomechanical interpretations of regional CFO are best reserved for special cases involving simple bending.

CFO varies among the long bones of an individual (or a species). Some of that variation may relate to biomechanical function. For example, a seminal study of the humerus, radius, ulna, femur and TBT in 22 avian species found that CFO covaries with geometric properties of bones that are associated with torsional rigidity (Margerie et al. 2005). Specifically, oblique/transverse CFO, circular cross-sectional shape, and relatively thin cortical walls occurred most frequently in the bones where there is some evidence of locomotor-induced torsional loading such as the humerus, femur and ulna (Rubin and Lanyon 1985, Biewener and Dial 1995, Carrano and Biewener 1999, Main and Biewener 2007). Conversely, longitudinal CFO, elliptical cross-sectional shape and relatively thick cortical walls occur in other bones that may be less "optimized" to torsional loading such as the radius and TBT (Margerie et al. 2005). Although the torsional-resistance hypothesis in the avian skeleton is persuasive, it may not be the most parsimonious hypothesis. Comparisons of the limb bones of approximately 19 nonhuman primate species (Warshaw et al. 2017) and one bat species (Skedros and Doutré 2019) revealed a proximodistal gradient in CFO. Specifically, CFO is slightly more oblique/transverse in proximal elements (e.g., humerus and femur) than in distal elements (e.g., radius, tibia and metacarpus). For both nonhuman primates and the bat, the variance in CFO among elements relates to tissue type such as proximal bones tend to have a greater concentration of bone types with oblique/transverse CFO such as lamellar, fibrolamellar and compacted coarse cancellous bone (Skedros and Doutré 2019, Warshaw et al. 2017). Whether bone type also contributes to biomechanical function is a reasonable question that is best tackled using an FE modeling approach in which the interaction among CFO, bone type and mechanical properties can be quantified.

Only a few studies have systematically assessed CFO across ontogeny, and fewer still have done so with corresponding biomechanical data. Without that data, it is difficult to place ontogenetic trends of CFO in the context of mechanical function. For example, a study on the calcaneus in a growth series of domestic sheep showed a nonlinear ontogenetic shift from relatively oblique to relatively longitudinal CFO (while still preserving regional differences) (Skedros et al. 2007). At face value, the CFO data suggest an ontogenetic shift from a calcaneus dominated by shear strains in juveniles to one dominated by axial strains in adults. The authors, however, note an ontogenetic increase in bone mineralization. Increased mineralization has a small but potentially impactful effect of dampening the luminance of bone collagen under circularly PLM (Boyde and Riggs 1990), thereby artificially inflating the appearance of (dark) longitudinal CFO. More importantly, the authors recognized the confounding influence of tissue type. A substantial amount of woven bone accounts for the relatively oblique CFO signal in juveniles. In adults, that woven bone is replaced by secondary osteons with more longitudinal CFO. Thus, without independent evidence of the mechanical environment, variation in tissue type is the most parsimonious explanation for the ontogenetic trend in CFO.

Even when bone strains and mineralization are known, ontogenetic trends in CFO are difficult to reconcile in the context of mechanical function. For example, in the radius of the goat, CFO is slightly more oblique/transverse in adults than in juveniles (Main 2007). Increased mineralization in the adult radius does not explain the oblique/transverse CFO because mineralization tends to dampen not enhance the birefringence under circularly PLM. In addition, axial compressive and shear strains stay relatively consistent during ontogeny, so oblique/transverse CFO in the adult radius does not constitute a response to those strains. Tissue-level examination, however, reveals that the oblique/transverse collagen of the adult radius mainly occurs in the circumferential lamellae of primary bone and especially in secondary osteons. Here in the radius of the goat, similar to other long bones of nonhuman primates (Warshaw et al. 2017), CFO is at least partially explained by tissue type.

Intracortical Remodeling

Remodeling in cortical bone can occur for at least two reasons: to replace mechanical damage and to access bone mineral for metabolic needs (Currey 2002, Martin 2002). The regionalization of remodeling for reasons other than damage repair has not been investigated explicitly (Parfitt 2002), and the general ontogenetic trend is for secondary remodeling to occur toward the endosteal surface in older bone tissue and to progress toward the periosteum over time (Francillon-Vieillot et al. 1990). This section will focus on the mechanical influences associated with bone remodeling.

Haversian bone is generally weaker than primary bone in tension and bending. However, the selective cost of relying on bone with accumulating microdamage is ultimately worse than the cost of creating porous spaces to remodel the damaged bone. Haversian systems act to stop crack propagation and repair the damage already present in the bone (Wainwright et al. 1982). Greater amounts of bone remodeling coincide with increased bone microdamage in bones experimentally subjected to increased strain frequencies and/or magnitudes (Burr et al. 1985). Three important papers outline the association between remodeling events with increased bending loads and the cellular expression of genes to initiate remodeling. Dog forelimbs loaded in three-point bending to create tissue strains equal to 1500 με and applied at 10,000 cycles per day showed increased microcracks in the radius and ulna, whereas dogs loaded to generate 625 με and either 10,000 or 1000 cycles did not show increased formation of microcracks. For context, principal strains as high as –2600 με have been measured from the canine radius *in vivo* (Rubin and Lanyon 1982), meaning that microdamage and remodeling to repair microdamage likely takes place on a regular basis during habitual loading. To quote Burr et al. (1985), "some mechanism of preferential microdamage repair must occur in regions with moderate microdamage accumulation. If this were true, we should expect to see the initiation of bone remodeling within a few days of the production of damage."

VetBooks.ir

This phenomenon was explored more closely in rats subjected to ulnar fatigue loading. A single ulna in adult rats was fatigue-loaded to a 30% reduction in stiffness and allowed 10 days of normal activity at which time the contralateral limb was loaded in the same way to examine the fresh induction of fatigue damage (Bentolila et al. 1998). The recovering ulna showed a 40% reduction in linear type microcracks within the 10-day period, but it also possessed more resorption spaces compared to the freshly fatigue-loaded (acute) ulna. In the acute fracture group all osteocytes appeared normal but were associated with fresh microdamage (Figure 34.10A), while in the recovering group, a lack of osteocytes or atypical osteocytes were present in association with areas of bone resorption (Figure 34.10B). Subsequent studies using the same rat ulnar fatigue model showed that relative to a nonloaded control limb, the fatigue-loaded limb showed increased caspace (a marker for cell death) expression in osteocytes within 200 µm of the induced microdamage within 3–7 days of loading (Figure 34.10C). Additionally, *RANKL* (proosteoclastic marker) and *VEGF* (provasculogenic marker) expression increased in cells away from the crack, and OPG (proosteoclast inhibition) expression decreased in osteocytes near the crack (Kennedy et al. 2012). Thus, damage of the bone leads to damage of the osteocytic processes, housed in the canaliculi, causing cell death, which initiates a molecular cascade to increase local osteoclastogenesis and vascularization to repair the microdamage. Similar cortical remodeling also occurs during disuse experiments, when osteocytes die due to a decrease in mechanical loading, which limits nutrient and waste exchange (Aguirre et al. 2006, Cabahug-Zuckerman et al. 2016).

In terrestrial vertebrates where remodeling occurs, the balance between bone formation and remodeling during ontogeny to maintain an adequate safety factor can be considered relative to the cost of swinging the limb during locomotion

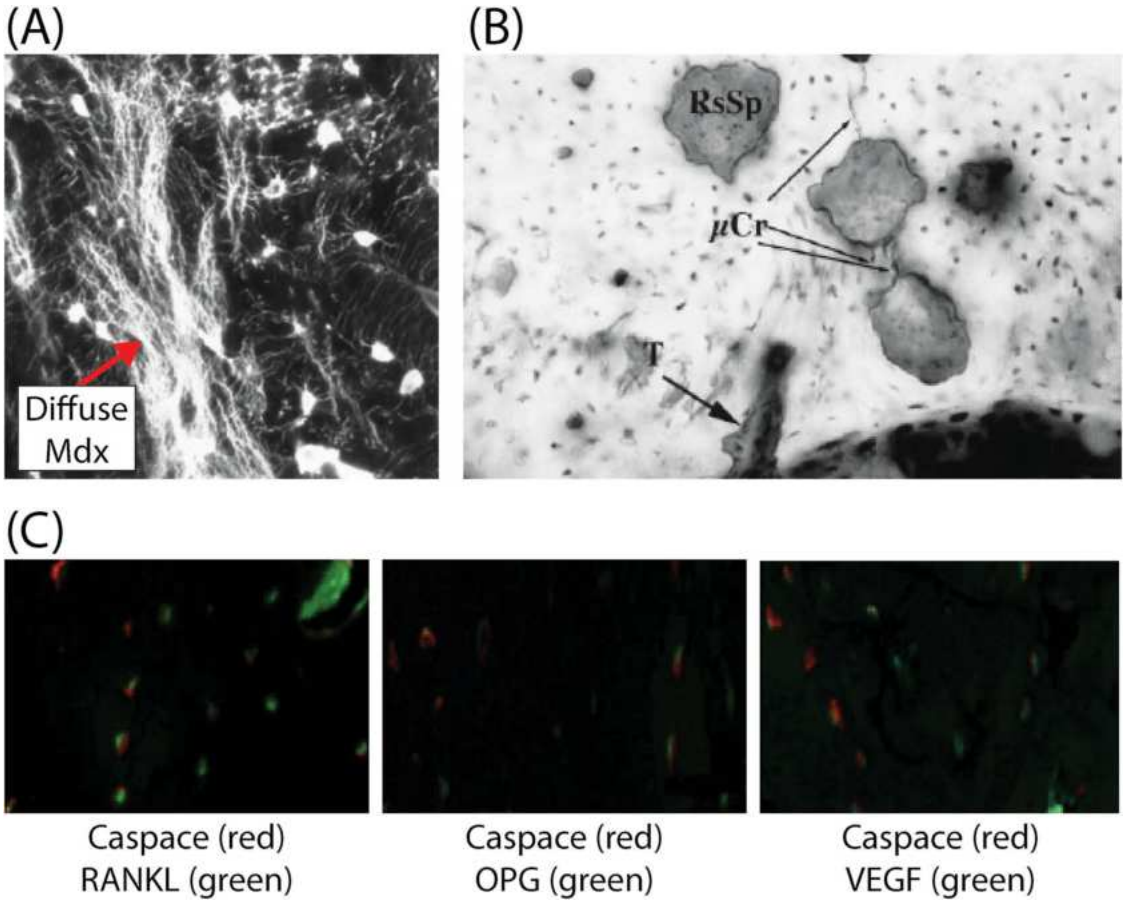


FIGURE 34.10 Microdamage and repair in cortical bone. A. Diffuse microdamage induced by axial compression in a rat ulna (Mdx). Osteocytes and canaliculi away from the Mdx appear normal. Lacunae and canaliculi close to the Mdx would be affected by the damage. B, Ten days later, microcracks (µCr) can be seen in the bone with accompanying resorption spaces (RsSp) interrupting the microcracks. Osteoclastic tunneling (T) from the endosteal surface can also be seen. In the areas just surrounding the resorption spaces, osteocytes are present at a lower density (or absent) compared to the primary lamellar bone. C, Immunohistochemical identification of the protein-level response by osteocytes to induced Mdx in the rat ulna. The Mdx is located in the lower left-hand corner of all images. The red caspace signal identifies dying osteocytes, most of which occur near the Mdx. *RANKL*, a proosteoclastogenic factor, and *VEGF*, a provasculogenic factor, are expressed by both dying and living cells away from the Mdx. Osteoprotegerin (*OPG*) is a proosteoclastogenic inhibitor and is expressed at a distance from the Mdx (far to the right). Osteocytes in proximity of the Mdx increase expression of factors for the invasion of osteoclasts and new blood vessels, while inhibiting *OPG* expression in osteocytes close to the Mdx. In A and B, the field widths are 260 and 560 µm, respectively. (Figures modified from Bentolila et al. 1998 and Kennedy et al. 2012. Reprinted with permission from Elsevier.)

VetBooks.ir

(Hildebrand 1995, Martin 2003). The primary hypothesis details a proposed proximodistal gradient between remodeling and periosteal growth in the limb elements (Lieberman et al. 2003). For example, the metatarsals may experience similar or higher strains than the femur and tibia and, at the cost of keeping distal bone mass to a minimum, would be accommodated through increased remodeling of damage. More proximal bones might instead show increased periosteal bone apposition to increase the overall strength of the bone, so that less microdamage occurs to begin with. In juvenile sheep, peak strains were 1.6× greater in the metatarsal than in the tibia. Following treadmill exercise, in which the sheep received 6000 additional cycles of loading per day, the juvenile limb skeleton adapted to the exercise treatment through increased periosteal expansion of the femur and tibia and no change in periosteal apposition in the metatarsal, relative to the nonexercised control group. Consistent with the original hypotheses, the tibia and metatarsal also showed increased intracortical remodeling in the exercise group, while the femur did not differ in secondary osteon density. It is interesting that the phylogenetic constraint to maintain relatively lightweight distal limbs would hold true in juveniles for intracortical remodeling, where one might think that a growing animal could rely on a modeling pathway, which is already active to dissipate strain. Additionally, the cortical sites showing increased remodeling did not necessarily coincide with the maximum strains in the bone. In the juvenile tibia, 98% of the added secondary osteons were in the anterior and medial compartments that did not coincide with the peak compressive strains in the caudal cortex. In the juvenile metatarsal, 52% of the added secondary osteons were in the anterior cortex, which did coincide with the peak compressive strains in the bone. While the exercise-induced remodeling was specific to certain anatomical regions, it was not associated with a common type of strain environment among the different bones.

Regional cortical differences in porosity and remodeling have been found in some vertebrate long bones. Although regional mechanical environments were not directly measured in the bones examined, using previously published data or mechanical models, areas of greater porosity in the turkey ulna were hypothesized to correspond to remodeling initiated by strain-induced mechanical microdamage (Skedros et al. 2003) and in the human femur to disuse osteoporosis at the expected position of the neutral axis (Thomas et al. 2005). While there are certainly differences between well-defined tensile versus compression cortices in some bones that have been well characterized (e.g., deer calcaneus), without known *in vivo* loads and the ontogenetic progression of these patterns, it is difficult to be too confident with the conclusions drawn between biomechanics and secondary remodeling (Skedros et al. 1994). Further review of regional patterns of intracortical bone remodeling can be found in McFarlin et al. (2008).

Small animals, the subject of most biomedical loading studies, do not typically display significant intracortical remodeling, except when microcracks are intentionally induced in the bones. Mammalian taxa below 2 kg do not typically display intracortical remodeling, suggesting that the repair of microcracks may not be a strong selective consideration for small animals that do not typically experience high bone strains (Keller and Spengler 1982, 1989, Mosley et al. 1997, Rabkin et al. 2001, Sugiyama et al. 2012). Among a large group of diverse mammals studied to examine the scaling of secondary osteons, no limb bones from mammals below 1.3 kg possessed intracortical remodeling (Felder et al. 2017). Of the 48 taxa examined between 1 and 15 kg, secondary osteons were absent in only 11 samples, and most of these were less than 9 kg. All mammals above 15 kg in this sample possessed secondary osteons.

Similar remodeling patterns are seen during ontogeny in birds as well. At a size of 3 kg, the emu (*Dromaius novaehollandiae*) TBT showed very little evidence of remodeling, and that was restricted to the anterolateral surface. Active remodeling in this bone is greatest between 16 and 27 kg, but still remains relatively sparse at 1–3 secondary osteons/mm^2 (Figure 34.11A) (Main 2006). The emu femur likely circumvents remodeling over a large size range (3–42 kg) with extensive endosteal resorption of older bone during ontogeny. Even up to full adult size, there is very little active remodeling in the femur (<1 secondary osteon/mm^2). The ontogenetic increase in J to resist torsion in the femur and clearing of the marrow canal for the proximal air sacs forces resorption of all older endosteal bone, leaving a very thin cortical shell in the adult, ranging from 2.5 to 4 mm (Figure 34.11B). Given the high strains experienced in the femur of these large birds (1800 με principal strains, 3400 με shear), it seems likely that some amount of damage must occur. Forelimb bones in emu (Figure 34.11C) and facultatively quadrupedal and bipedal dinosaurs (*Hypacrosaurus*, *Maiasaura*, *Tenontosaurus, Plateosaurus, Allosaurus*) tend to show a greater degree of remodeling than in the hindlimbs (Horner et al. 1999, 2000, Bybee et al. 2006, Klein and Sander 2008, Werning 2012). It is unlikely that large mechanical strains are causing the remodeling events in these secondarily used, and sometimes vestigial limb bones, especially relative to the hindlimbs that are supporting the majority of body weight. Perhaps in animals that show forelimb-hindlimb disparity in weight-bearing, the role for enhanced remodeling in the forelimb serves the metabolic needs of the animal, without removing bone from crucial weight-supporting elements (Padian et al. 2016). By comparison, the radius of 4 kg goats (*Capra hircus*) showed substantial secondary remodeling by 5 weeks of age, which more than doubled again by 12 weeks of age, consistent with the forelimbs bearing significant weight from birth (Figure 34.4B) (Main 2007).

The bones of some animals, such as large and small birds, bats and other small mammals and pterosaurs, do not perform the critical act of intracortical remodeling, calling into question its need for microdamage repair in tetrapods. This is reasonable to accept early in ontogeny as the bone is still expanding at the periosteum and older endosteal bone tissues are resorbed. But by adulthood, there should be some signs of remodeling given a lifetime of mechanical loading. Perhaps, in thin-walled bones, longitudinal intracortical resorption spaces would pose a mechanical risk to the extent that some amount of microdamage accumulation is acceptable. Or perhaps the remodeling of damaged bone in these animals takes place by another mechanism. The formation of microcracks may be coupled with the continual formation and remodeling

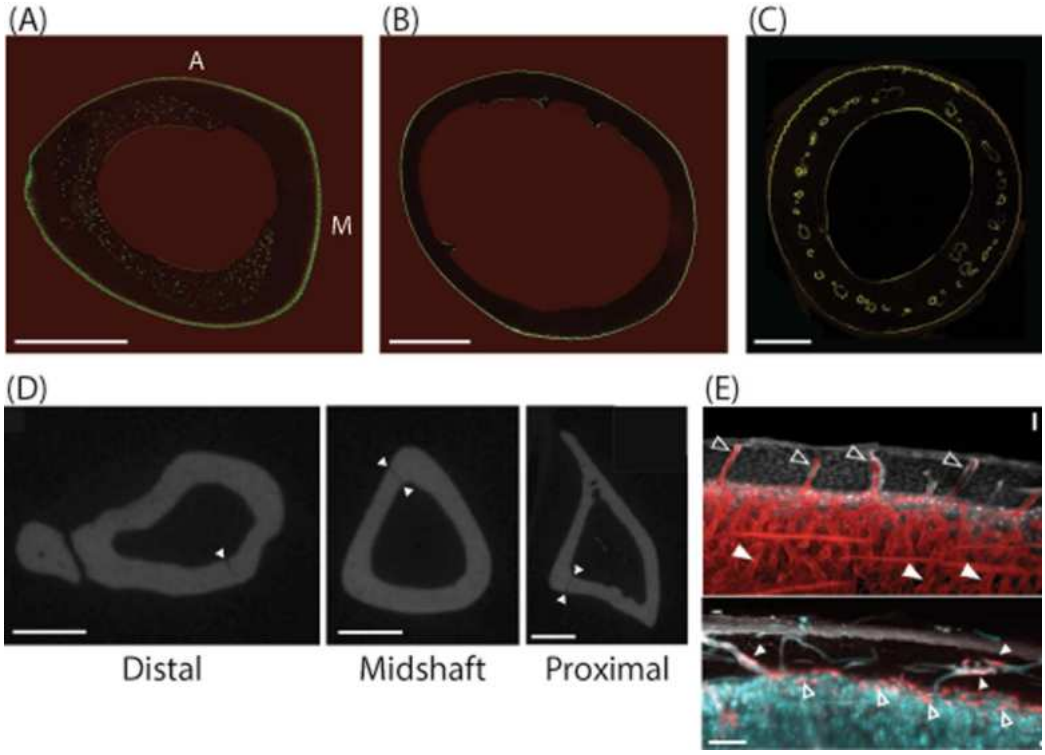


FIGURE 34.11 The constraints of intracortical remodeling in thin-walled bones. A, Cross-section of a TBT from a 20-week-old (12 kg) emu. Notice the extensive remodeling in this thick-walled bone (intracortical fluorescent dyes), particularly in the posterior and lateral cortices, and the uniform periosteal growth at this age (fluorescent dyes at the bone's surface). B, Cross-section of the femur of a 49-week-old (30 kg) emu. Very little to no active remodeling occurs in this bone. Periosteal growth is uniform around the circumference. C, Ulna from the same emu in (B) (scales are not the same). Notice the extensive remodeling present in this vestigial wing element. D, Micro-CT images from the tibia of a 16-week-old female mouse for the distal, midshaft and proximal diaphyses. The white arrowheads indicate small transcortical foramina (<15μm) that penetrate the entire cortex of the bone. These foramina are present along the entire diaphysis. Scan resolution is 10 μm. E, Upper panel: marrow sinusoids (closed arrows) and transcortical vessels (TCVs) traverse the transcortical foramina (open arrows) in a mouse tibia. Lower panel: osteoclasts (red) cluster along the endosteal surface (open arrows) and in the bone's cortex along the TCVs (closed arrows). The positioning of these cells near the endosteal surface and even within the cortical bone itself is beneficial for repairing local bone damage and remodeling of the transcortical foramina. Image captured by light sheet fluorescence microscopy. Scale bars: A and B = 1 cm; C = 1 mm; D = 500 μm; E: upper = 50 μm, lower = 100 μm. (E is modified from Grüneboom et al. 2019. Reprinted with permission from Springer Nature.)

of microscopic, transcortical foramina that repair the freshly damaged bone. By this mechanism, overall bone mass would be maintained for structural support. Mouse long bones have a prolific number of small intracortical, vessel-containing foramina throughout the length of their diaphyses, but show no evidence of longitudinal intracortical remodeling (Figure 34.11D, E). These foramina, which have been documented in both mice and humans, are commonly associated with large osteoclast populations (Figure 34.11E) (Grüneboom et al. 2019). While strains are not very high in mouse limbs, this might be a viable repair mechanism for removing old or damaged bone that occurs in taxa that experience high mechanical strains and possess thin-walled cortical bones. Higher metabolic rates in these animals would aid in achieving this process since bone turnover can occur more quickly without risking structural failure (Seymour et al. 2012). Osteocytes also have the ability to locally remodel their lacunae and the surrounding bone tissue through the partial resorption of mineral, but only up to about 10–20 μm^2 (Qing et al. 2012, Nango et al. 2016), which would not be enough to remove extensive microdamage.

Cancellous Bone

Cancellous bone plasticity is the foundation on which Wolff's theory of bone transformation was based. Wolff's theory focused on the proximal human femur, for which the stress and strain has been modeled extensively, as direct strain measures would be too invasive. Applying an adaptive continuum model approach to the proximal femur based on the rules defined in Figure 34.1, 2D iterative FE models were run. The virtual adaptation simulation began with isotropic bone tissue, homogeneously distributed at even density (Figure 34.12A). After 30 iterations, equivalent to 248 days of loading on the femoral head and greater trochanter, a very realistic distribution of cancellous and cortical bone density resulted, complete with dense cortical bone in the diaphysis, high-density compressive trabeculae beneath the femoral head and a low-density area consistent with Ward's Triangle in the middle of the femoral neck (Figure 34.12B, C) (Beaupré et al. 1990b, Carter and Beaupré 2001, van der Meulen et al. 2008). While this model did not

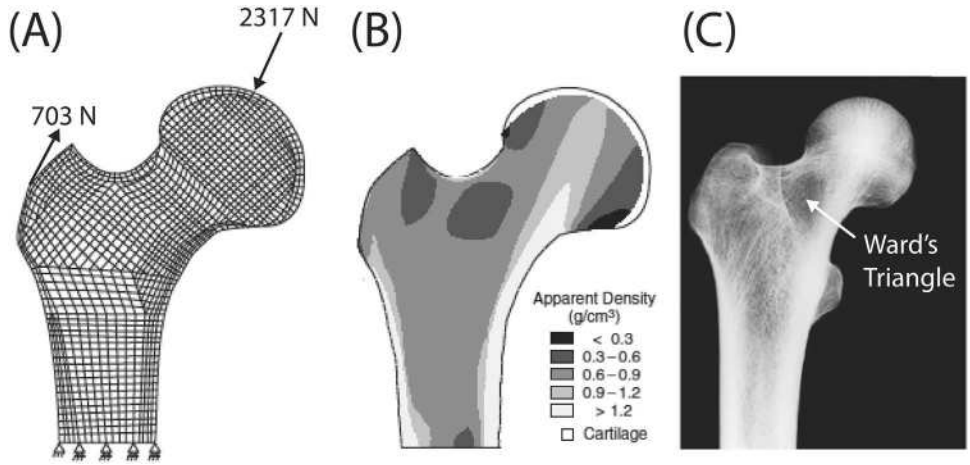


FIGURE 34.12 Computational adaptive models of the proximal human femur. A, Initial loading conditions for the finite element model. Material properties are isotropic and homogeneously distributed throughout the model. Forces are applied at the greater trochanter and the femoral head. Guiding principles for adaptation in this model are similar to those presented in Figure 34.1. B, Proximal femur model after "248 days" of (re)modeling in response to the two applied loads. The model compares very favorably to (C), showing the high-density primary compressive trabeculae corresponding to the application of load on the femoral head and the low-density region known as Ward's Triangle. (Modified from Beaupré et al. 1990b and van der Meulen et al. 2008.)

incorporate trabecular organization, Wolff reasoned that the trabeculae loaded in compression and tension should be orthogonal to each other, which would be stable for a static joint, but in a joint with multiple loading directions, it would expose the cancellous bone to very high shear stress (Pidaparti and Turner 1997). In fact, the primary angles among human femoral head trabeculae are often nonorthogonal, and lie near 60° to each other (Albright and Brand 1987). Examples of orthogonal organization of trabeculae exist in mammalian vertebrae and sheep and potoroo calcanei: these structures repeatedly experience a single type of compressive or bending loads (Lanyon 1973, Biewener et al. 1996, Silva and Gibson 1997, Huiskes et al. 2000, Harrison et al. 2008). These conclusions are based on evolutionary adaptation over millions of years.

Cancellous bone, like cortical bone, is highly plastic in response to applied loads and disuse. Much of this may be due to the large surface area, relative to cortical bone, available for osteoblasts and osteoclasts to remodel existing bone. Caudal vertebral tail compression studies used time-lapsed micro-CT images to construct baseline and postadaptation FE models, to determine where bone is formed and resorbed relative to local strain levels and how strains changed in the postadapted vertebrae. These morphological changes have even been linked to local changes in osteocyte gene expression (Christen et al. 2012, Lambers et al. 2013, Schulte et al. 2013). Using tibial loading and hindlimb suspension models in 16-week-old female C57Bl/6 mice, loading increased the proximal cancellous bone mass (bone volume fraction, BV/TV) by 18%. With this increase in cancellous bone mass, the frequency of cancellous strains in the –1500 to –2000 με decreased, while the frequency of strains between –400 and –1000 με increased. In contrast, and as expected, hindlimb suspension decreased cancellous BV/TV by 58% relative to the control mice, which increased the frequency of high magnitude cancellous strains between –3000 and –6000 με and decreased the frequency of low-magnitude strains between –500 and –2500 με (Yang et al. 2019). Similar changes with other overloading and disuse models are primarily modulated through changes in trabecular thickness (*Tb.Th*) and trabecular separation (*Tb.Sp*) (Jaworski and Uhthoff 1986, Sakata et al. 1999, Fritton et al. 2005, Lynch et al. 2010, Visigalli et al. 2010, Weatherholt et al. 2013, Willie et al. 2013). It is not only mammalian models that possess mechanosensitive cancellous bone. In adult turkeys run on a downhill treadmill over 10 weeks, cancellous bone mass increased by 21% relative to nonexercised controls, and this was primarily due to increased *Tb.Th* (Wallace et al. 2017).

During natural aging processes cancellous bone volume will often decrease in mammals, but the skeleton is still sensitive to mechanical stimuli. Ten-week-old and 26-week-old mice exposed to loads to induce +1200 με on the medial tibial midshaft showed a 95% and 0% increase in BV/TV, respectively (Lynch et al. 2011). However, when similar loads were applied to the two age groups, inducing strains in the cancellous bone of 26-week-old mice that were about twice those induced in the younger mice, BV/TV in the loaded limbs increased by 49% relative to the nonloaded control limbs. Thus, the older skeletal mechanobiological mechanism is still capable of inducing a significant change in cancellous bone; it just requires a greater strain stimulus. This phenomenon is true for cortical bone as well (Lynch et al. 2011, Razi et al. 2015a, b). However, these assessments do not describe changes in the orientation of the underlying bone. It is one thing to add new bone mass, which will undoubtedly make the cancellous bone stronger, but it is more efficient to remodel existing trabeculae to better align with the newly induced habitual mechanical forces, so that similar or greater cancellous strength might be achieved with minimal added bone mass. A case of trabecular bone loss proves this point. Using longitudinal *in vivo* micro-CT in rats, it was observed that ovariectomized rats quickly lose trabecular BV/TV in the proximal tibia over 54 weeks. In the face of this bone loss, the remaining metaphyseal and epiphyseal trabeculae (re)model to become thicker and align with each

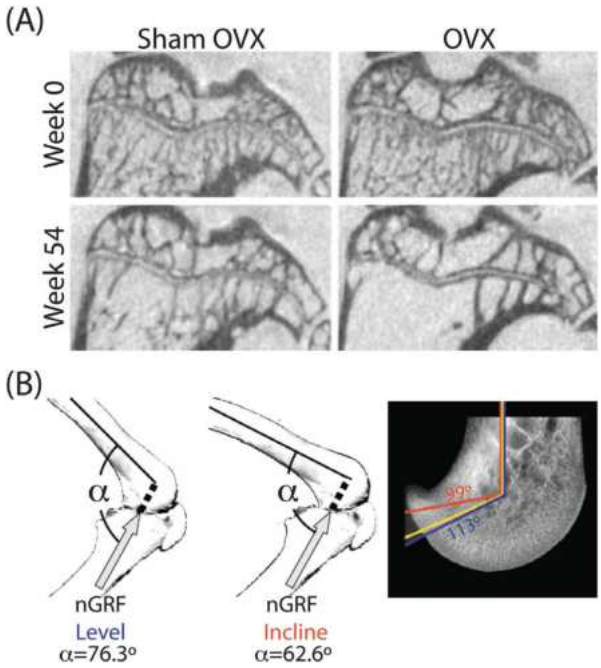


FIGURE 34.13 Plasticity in trabecular bone mass and orientation. A, Ovariectomy (OVX) induces bone loss in the epiphysis and metaphysis of the rat proximal tibia. During a 54-week study, both the sham and OVX groups lost trabecular bone, as is expected with aging. The OVX group lost bone more quickly and consolidated the remaining bone mass by (re)modeling the remaining trabeculae to align across the growth plate, maximizing efficient load transfer. The proximal tibia for the sham group appears to have begun this process by the end of the study. B, Two groups of guinea fowl were run on a level or an inclined treadmill (20°). Due to a change in inclined kinematics, the inclined normal ground reaction force (nGRF) was oriented more perpendicular to the long-axis of the femur (by ~14°) than the level running group. After 45 days of running under the two conditions, the inclined runners showed cancellous bone orientation that differed by 14° relative to the level runners. Given the alteration in nGRF orientation, these results show a highly sensitive response in cancellous bone plasticity relative to changes in external forces. (Modified from Waarsing et al. 2006 and Pontzer et al. 2006.)

other across the growth plate (Waarsing et al. 2006). Thus, an initially "random" array of trabeculae in the metaphysis and epiphysis appear to optimize load transfer between the bone regions as bone is lost (Figure 34.13A). Over the course of the 54-week study, even the sham OVX group (surgery but no ovary removal) lost cancellous bone, as many mammals do with age, but the strong trabecular remodeling was not (yet) present.

Alterations in trabecular alignment with mechanical changes in loading can occur in both young and adult animals. In one of the few examples where the ontogenetic accumulation of cancellous bone mass was related to trabecular orientation and mechanical stiffness, 6-week-old pigs initially showed an increase in isotropic cancellous bone in the vertebrae and tibial metaphyses (Tanck et al. 2001). By 56 weeks of age, BV/TV had increased to its peak in both bones, whereas peak anisotropy and stiffness occurred at 104 weeks of age once cancellous tissues had aligned with the long axis of the bone. The increase in sheer bone volume early in life has been detailed for fibrolamellar cortical bone tissues and is followed by subsequent infilling of aligned lamellar bone (Wainwright et al. 1982, Ricqlès et al. 1991, Margerie et al. 2004). In animals that primarily deposit only lamellar bone during postnatal development of the limbs, the early, disorganized endochondral bone is sandwiched between periosteal and endosteal layers of organized lamellar bone (Bach-Gansmo et al. 2015, Bortel et al. 2017).

Very little work has described plastic changes in trabecular alignment in relation to well-characterized changes in skeletal mechanics. Juvenile guinea fowl were exercised on a level treadmill or a treadmill inclined to a 20° angle. When running on the level versus the incline, the joint reaction forces changed by nearly 14°, and aligned more orthogonal to the long axis of the femur (Figure 34.13B). Consistent with the realignment of the joint reaction force, after 45 days of running, the orientation of the peak trabecular density in the inclined runners was oriented 99° relative to the long axis, while the level runners' trabeculae were aligned at 113° (Pontzer et al. 2006). It appears from these studies that both evolutionary and plastic adaptation may play a role throughout the ontogenetic adaptation of cancellous bone.

In a set of recent studies, cancellous bone orientation was used to validate musculoskeletal SIMM and FE models, first for extant birds and then for a pair of extinct theropods, *Daspletosaurus* and *Troodon* (Bishop et al. 2019a, b, c). Much of the methodology for the muscular mechanics are similar to the studies discussed in Chapter 33 for the ostrich and *Tyrannosaurus rex* (Hutchinson et al. 2005, 2015). Here, input forces from the SIMM models and an assumed GRF position were mapped to realistic skeletal anatomies converted to FE models to determine stresses in the femur and TBT. Instead of strain gauge measures for validation, the authors assumed that the mechanosensitive nature of cancellous bone could be used to validate the FE models. In the living birds examined, cancellous orientations in the femoral head, medial condyle, the cnemial crest and proximal TBT plateau aligned well with the principal stresses modeled at the joints, suggesting that the SIMM models are robust at the hip and knee. The cancellous bone in the proximal metaphysis and distal TBT had only minimal alignment with the modeled stresses. FE modeling in the TBT may be less accurate than in the femur, in general, because the modeled diaphyseal principal strains do not generally predict the large torsional strain component, which has been reported in birds (Biewener et al. 1986, Main and Biewener 2007). Nonetheless, this is an impressive set of studies that successfully used cancellous bone morphology to build on previous SIMM models for extinct theropods and should be refined and emulated in future musculoskeletal models of comparative and extinct taxa.

Two recent studies analyzed cancellous bone in the femoral head of nonhumanoid primates, recent humans and early fossil hominoids (*Australopithecus africanus*, *Paranthropus robustus*). The first study published a relatively large sample of nonhumanoid primates (*Papio*, *Pongo*, *Gorilla*, *Pan*), five recent populations of *Homo*, Pleistocene *Homo*, *A. africanus* and *P. roboustus*. This study hypothesized that *A. africanus* and *P. robustus* were habitually walking similar to humans and the femoral head of these taxa should show similar cancellous characteristics for BV/TV and a high degree of trabecular alignment, whereas the femoral heads of nonhumanoid primates would be more isotropic due to the more variable

use of their hindlimbs (Ryan et al. 2018). Analyzing cuboidal micro-CT segments from each femoral head, *A africanus* and *P. robustus* had cancellous anisotropy levels and material orientations similar to those of recent and Pleistocene *Homo*. This is distinct from *Pongo*, *Gorilla* and *Pan*, which had low anisotropy and highly varying material orientations (Figure 34.14A, B). However, recent and Pleistocene *Homo* have lower BV/TV than the nonhumanoid primates and the early hominids. Thus, even if the mechanics of early hominids had defined a particular direction for the femoral head trabeculae due to similar mechanics to those of recent *Homo*, their overall femoral bone mass was still ancestral. The second study compared two early hominids to *Pan*, *Pongo*, *Gorilla* and recent *Homo*, with one early hominid, StW 311, included

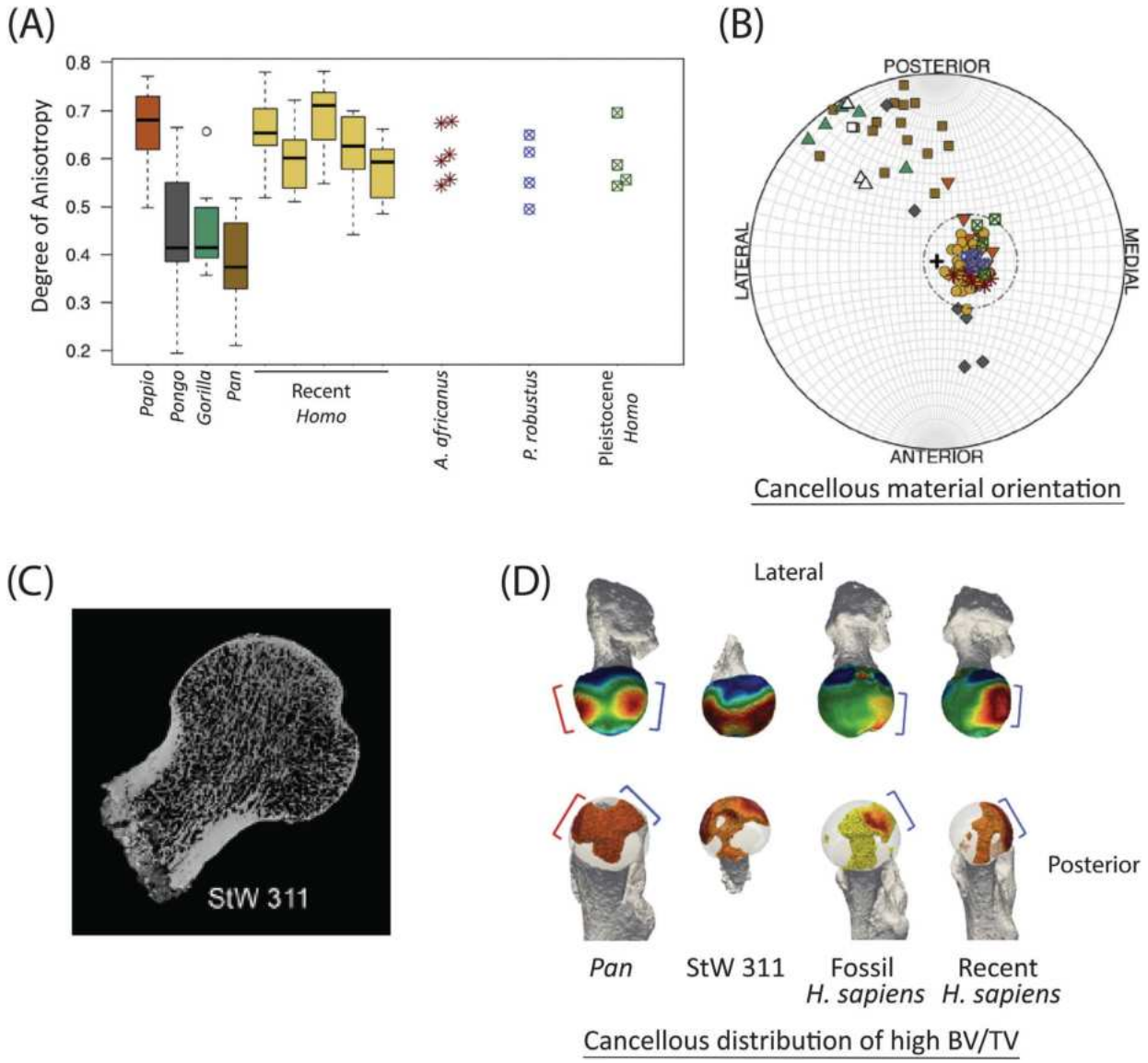


FIGURE 34.14 Developing hypotheses about locomotion in fossil hominids using femoral head cancellous bone. A, Most nonhumanoid primates (except *Papio*) have a low degree of anisotropy in their proximal femur given their varied hindlimb use. *Papio*, *Australopithecus africanus* and *Paranthropus robustus*, as well as other recent *Homo* populations, have a greater degree of anisotropy; the early fossil hominoids are not different from recent *Homo*. B, The overall cancellous orientation of the early fossil hominoids was also similar to that of *Homo*. In this figure, red stars: *A. africanus*; blue circle crosses: *P. robustus*; green crossed boxes: Pleistocene *Homo*; yellow circles: recent *Homo*; brown squares: *Pan*; green triangles: *Gorilla*; gray diamonds: *Pongo*; orange triangles: *Papio*. C, Two-dimensional micro-CT slice of the femoral head of StW 311. D, Primary distribution of cancellous BV/TV density measured in the entire femoral head (top), with BV/TV density increasing from blue to red. On the bottom are shown reconstructions of the densest regions of cancellous bone (80th percentile) in the femoral heads of *Pan*, StW 311, fossil *H. sapiens* and recent *H. sapiens*. The red brackets indicate the position of the hypothesized load transfer to the femoral head during arboreal habits, while the blue brackets indicate load transfer during terrestrial-based bipedal habits. Note that (D) is not examining the alignment or anisotropy of cancellous bone and is instead analyzing two hypotheses about the distribution for the densest concentrations of BV/TV in relation to suspected locomotion. (D) shows that *Pan* and StW 311 have similar distributions of dense BV/TV in the anterior and posterior regions of the femoral head, suggesting both arboreal and terrestrial bipedal activities, while *H. sapiens* shows a high-density BV/TV distribution consistent with bipedal walking. (Figures modified form Ryan et al. 2018 and Georgiou et al. 2020.)

VetBooks.ir

in both of these studies (Figure 34.14C). This second study took a different approach than the previous one and analyzed nearly the entire femoral head by micro-CT to examine the distribution of BV/TV density throughout the head (Georgiou et al. 2020). The authors suggest clear hypotheses for the distribution of cancellous bone, with predicted densities in the anterior and posterior femoral head for arboreal/terrestrial taxa and a high density in the superior/posterior region where the femoral head and acetabulum habitually meet in humans. One fossil specimen (StW 522) had a distribution that was very similar to that of recent *Homo*. The second (StW 311) had a distribution of densest trabeculae more similar to the nonhumanoid primates sampled (Figure 34.14D). Similar to the first study, the fossil samples possessed greater cancellous BV/TV than recent humans, while maintaining a level of anisotropy very similar to recent humans. If we consider these two studies to be complementary, StW 311 maintains a greater cancellous BV/TV that is not distributed through the femoral head as in extant humans, but the overall "grain" of the cancellous bone (high anisotropy) is more in line with humans than with nonhumanoid primates. We have seen throughout this section that cancellous bone alignment, not necessarily BV/TV, may be one of the most mechanosensitive indicators for joint reaction forces. Therefore, the cancellous anisotropy indicates that StW 311 may have been an early "human-like" walker, with retention of a broad distribution of dense cancellous bone. Further review of the use of cancellous bone as a biomechanical indicator in paleontological studies is in Kivell (2016a).

Integrative Studies of Limb Bone Biomechanics in Relation to Bone Shape and Histomorphology

In this chapter, we have discussed many features that could be tied to evolutionary or plastic adaptation. But few studies take an integrative approach trying to link more than one or two of these features to mechanical forces placed on the limb. Here we present four sets of studies that attempt to accomplish this.

Changes in Musculoskeletal Growth Allometries in Relation to Ontogenetic Biomechanics

Changes in size during ontogenetic growth can have important implications for performance in growing vertebrates when their musculoskeletal systems are highly responsive to adaptation and exposed to intense evolutionary selection. Two key studies established an early method for studying how musculoskeletal allometry and changing material properties in the limb bones during growth can affect locomotor performance at different ontogenetic stages (Carrier 1983, Carrier and Leon 1990). In the California gull (*Larus californicus*) hindlimb bones grew with negative allometry, which allowed juvenile bones with low mineralization to maintain similar stiffness as adults. In contrast, these altricial birds showed strong ontogenetic positive allometry in both wing bone length and wing bone *I*, corresponding to positive allometry in both pectoralis muscle mass and wing area (Carrier and Leon 1990). Thus, the limbs develop in concert with selection for each locomotor module in turn (Gatesy and Dial 1996). In the highly precocial jack rabbit (*Lepus californicus*), Carrier described a different ontogenetic strategy, in which metatarsal length scaled with positive allometry, while muscle mass, mechanical advantage of the gastrocnemius at the ankle and the second moment of area of the metatarsals scaled with negative allometry (Carrier 1983). From these scaling patterns, Carrier concluded that for their mass, younger rabbits could generate relatively larger propulsive forces at the ankle without risking damage to the metatarsals, which were still composed of weaker bone material than in adult rabbits. These concerted scaling patterns allowed the musculoskeletal systems of the young hares to produce large enough forces to achieve adult escape velocities early in ontogenetic growth. Similar ontogenetic relationships showing general negative allometry in the growing skeleton have been reported for a number of precocial and altricial taxa (Heinrich et al. 1999, Lammers and German 2002, Ruff 2003, Young 2005, Young et al. 2010).

Ontogenetic Changes in Bone Mechanics and Histomorphology in the Goat Radius

In addition to examining ontogenetic changes in musculoskeletal morphology and performance, *in vivo* mechanical measurements can provide further important insights into the development of the musculoskeletal system and ontogenetic changes in locomotor performance. As described previously in ontogenetic strain measures made for the chicken TBT (Biewener et al. 1986) it was hypothesized that relative measures of limb loading, scaling patterns in the goat radius and *in vivo* bone strains would not increase during ontogeny, which would allow young goats to perform safely at similar absolute speeds as adults (Main and Biewener 2004, 2006). Instead of the expected ontogenetic strain similarity, when traveling at the same absolute speed as adults, the less well-mineralized radii of juvenile goats experienced much lower strains than the radii of adult goats. Strong negative growth allometry in *Ct.Ar* ($\propto M^{0.53}$) and *I* ($I_{ML} \propto M^{1.03}$; $I_{AP} \propto M^{0.84}$) meant that the young goats had more robust radii for their size, giving them safety factors likely 3–6 times higher than adult goats during galloping (Main and Biewener 2006). The greater negative allometry for I_{AP} than for I_{ML} indicates that the radius grows to preferentially withstand ML bending relative to AP bending (Figure 34.15).

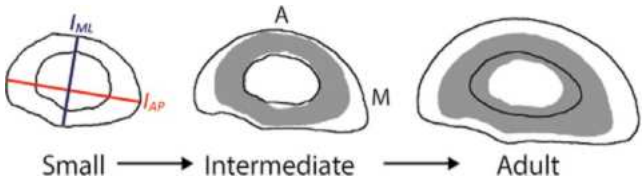


FIGURE 34.15 Ontogenetic development of radial eccentricity in goats. Small goats (3 weeks old) begin life with lower levels of eccentricity (I_{ML}:I_{AP} = 2.54). Eccentricity increases dramatically to 3.08 by 16 weeks of age in the Intermediate group. This increase coincides with a relative decrease in ML:AP bending strains from 1.27 in small goats to 1.09 in Intermediate goats. The eccentricity developed by 16 weeks is maintained into the Adult stage. (Modified from Main 2007.)

VetBooks.ir

To further investigate the *in vivo* limb mechanics in relation to this growth pattern and other changes in histological features in relation to limb biomechanics, we analyzed radial cross-sections for the small (3 weeks old) and intermediate (16 weeks old) goats from the 2004 study, with a sample of adult goat radii as well. The ontogenetic changes for regional patterns in peak tensile and compressive strains, strain ranges and the longitudinal, circumferential and radial strain gradients were related to periosteal and endosteal growth rates, porosity, secondary osteon density and CFO (Main 2007). As indicated in the prior study, periosteal growth was greater on the medial and lateral cortices, preferentially increasing their cortical thickness (Figure 34.4B, Figure 34.15). The mediolateral cortices are also where the greatest axial strains occurred. Thus, this growth asymmetry strengthened the bone in the cortices where it was needed most. Lower strains usually occurred in the thinner (anterior and posterior) cortices. This shape asymmetry along with the increasing AP curvature with age reinforce the hypothesis that strain predictability acts to maintain the greatest strains where the bone is most resistant to them, which in this case is the anatomical axis contrary to the direction of travel (Bertram and Biewener 1988). Regional changes in bone porosity and intracortical remodeling did not correlate with any regional patterns in the mechanical environment examined. Increased remodeling did correspond to the slowly growing, thin posterior cortex. Although this remodeling pattern did not correspond to any particular mechanical stimulus, the relative age of this tissue may have begun to accumulate fatigue microdamage, which would preferentially induce remodeling in this part of the bone. This posterior region was also associated with a predominance of transverse collagen fibers that did not associate with any mechanical signals. Shear strains have been linked to oblique/transverse collagen fibers (Evans and Vincentelli 1969, 1974), but shear strains on this posterior surface were not different than the cranial surface at all ages examined. Meanwhile the medial and lateral cortices were both dominated by longitudinal fibers, regardless of these cortices being exposed to the greatest compressive and tensile strains in the bone, respectively. Thus, in the goat radius, CFO does not correlate to habitual strain environments. In this study correlating *in vivo* bone strain during natural behaviors, cortical thickness and growth rate correspond closely to peak axial strains, but no other histological features align with bone mechanics.

Much of the prior comparative work drawing correlations between mechanics, histology and/or mechanical properties have typically used an inadequate number of strain gauges or a single time point during stance to accomplish reconstructions of bone strain environments (Lanyon et al. 1979, Riggs et al. 1993, Wallace et al. 2014). A number of histological comparisons are often made for one or more taxa by comparing analogous strain measures from a different taxon that may be at a different ontogenetic stage, which can affect histological interpretations of histology-based biomechanical hypotheses. Ultimately, until proven otherwise, we hold the position that mechanical and histological analyses must be conducted on the same experimental animals at the same developmental stages.

Ontogenetic Changes in Bone Mechanics and Histomorphology in the Emu Femur and Tibiotarsus

A pair of ontogenetic studies examined the role that limb bone scaling plays in the emu hindlimb skeleton that experiences significant torsion during growth and the effects that these loading patterns have on tissue microstructure in the femora and TBTs. Over a 4.4-fold increase in leg length and a 65-fold increase in body mass, peak bone strains in the femur and TBT increased with age and size (Main and Biewener 2007). In addition to a fair ML bending component, the predominant shear strains on the anterior and posterior surfaces of the femur and the posterior TBT indicate torsional loading, similar to previous avian hind limb studies (Biewener et al. 1986, Carrano and Biewener 1999). Bone mineralization increased from 49% to 72%, creating stiffer bone material to support loads. Bone curvature in both the AP and ML directions decreased for both bones. Due to an increasing torsional-induced shear component in these bones, that also increases with ontogeny, one would expect primarily circular bones. In the femur and TBT, both $Ct.Ar$ and I_{xx} ($\sim I_{AP}$) scaled with isometry. J ($\propto M^{1.41}$ for both bones) and I_{yy} ($\sim I_{ML}$) scaled with positive allometry. The 95% confidence intervals for I_{yy} overlaps the range for elastic similarity, for both bones, which indicates that resistance to torsional loads and ML bending are under strong selection. Not one of the geometric parameters met the expectations for strain similarity ($Ct.Ar \propto M^{1.0}$, I & $J \propto M^{1.67}$) explaining, in part, why the strains increased with age. Over the size range examined, shear strains in the femur were 2.5× those due to bending, while the ratio of cross-sectional I_{MAX}/I_{MIN} was 1.4, suggesting that a high ratio of shear to bending strains can be characterized by evolutionary selection for roughly circular bone shapes. In the TBT, the average ratio of I_{MAX}/I_{MIN} was 1.3, which is also consistent with selection for withstanding torsion-induced shear strains, which were 2.8× the strains due to bending. This pattern of bone growth contrasts the high eccentricity in the goat radius, where I_{MAX}/I_{MIN} was always greater than 2.5 throughout ontogeny reflecting resistance to ML bending loads, where the ratio of shear to bending strains was less than 0.80 at all ages.

Tracking mechanics and bone shape with growth can provide an understanding of changes in limb use during ontogeny. However, bone geometry is not the only factor determining structural strength, bone microarchitecture may contribute as well. In this particular case we ask, how does tissue microarchitecture reflect the consistent torsional loading during growth in the emu femur and TBT? A subset of the emu used in the study outlined above was subsequently used to examine correlations between laminar bone formation, growth and torsional loading. Laminar bone tissue, of all the bone tissue types, has been hypothesized to resist torsion-induced shear strains generated during flight and terrestrial locomotion in birds (Margerie 2002, Margerie et al. 2005). The emu humerus, radii and ulnae were also examined as negative controls for testing if laminarity could exist as a general phylogenetic signal in birds, even in the absence of any significant mechanical influences (Kuehn et al. 2019). Following a PC

VetBooks.ir

analysis relating age, mass, growth and laminarity for the two hindlimb bones, it was found that laminarity was most closely linked to adult growth characteristics such as decreased periosteal growth, increased body mass and age. When the analyses incorporated the shear strains measured on the caudal femur and caudal TBT, the patterns for laminarity were still dominated by adult growth characteristics: only 9% of the ontogenetic variation in primary vasculature was explained by shear strain measures. For the vestigial forelimb bones, no strain data were collected so mechanical data were not added to the PC models. In the forelimb bones, the PC analysis assigned only 20% of the variation in laminarity to growth stage characteristics. The remaining variability may be due to relaxed selection on the vestigial wing elements leading to increased anatomical variability (Maxwell and Larsson 2007).

A previous study reported high laminarity in the femur and TBT in emu at less than 2 months of age (Castanet et al. 2000). Our birds were two to three times heavier than the birds in the prior study at this age, and they may have been growing too fast for laminar bone to form. In addition to mechanics, variation in tissue microarchitecture may be related to environmental (dietary and rearing) conditions and genetic differences (Horner et al. 2000). Given the possible influences that these other factors have on primary tissue vasculature, as seen here for similarly aged birds, does not lend strong support for biomechanical hypotheses based on bone vasculature, because other influential factors are much more likely to vary during ontogeny than skeletal mechanics. A valuable study would be to alter dietary or rearing conditions among groups of birds and collect skeletal biomechanical and histological data to test for variability in histological factors typically used as predictors of limb bone mechanics. Additionally, projecting strain data from emu, chickens or pigeons to other taxa using different modes of locomotion will lead to misinterpretation for linking biomechanical and histological analyses (Biewener et al. 1986; Biewener and Dial 1995, Carrano and Biewener 1999, Main and Biewener 2007). Especially for birds, but really for any group of interest, studies examining a group of distantly related taxa at similar ontogenetic stages, either running on the treadmill or flying in a wind tunnel, would be one way to begin to solidify relationships among bird (and more widely tetrapod) tissue types in relation to limb mechanics. If this were coupled with neuropathy studies (Britz et al. 2012), limb disuse could be examined as well to further study bone formation during disuse, relative to normal limb functions.

Using Limb Bone Morphology to Assess Gait in Living and Extinct Mammals and Dinosaurs

An integrative set of studies examining bone lengths, diameters, eccentricities and curvatures measured over 1000 species of dinosaurs and nearly 500 mammalian species, combined with known bone mechanical data for mammals and birds to discuss the importance of changes in bone dimensions relative to locomotor habits (Carrano 1998, 1999, 2001).

Early dinosaurs show a combination of small body size and a generally cursorial hindlimb morphology (Sereno 1997). The transition to graviportal forms took place independently within ornithopods, ceratopsians, thyreophorans and prosauropods/sauropods. Only the coelurosaurs maintained cursorial features with large size, including tyrannosaurids and ornithomimids. As we have behavioral data to characterize living or recently extinct mammals as graviportal or cursorial, a PC analysis conducted for mammals showed that along one PC axis, taxa were characterized by shorter limb elements, longer lever arms, and shorter distal limbs (graviportal) at one end of the axis, while the other end was characterized by longer metatarsals, more slender limb elements, shorter femora, and muscle insertion points near the hip (cursoriality). A similar PC analysis showed that both ornithischian and saurischian dinosaurs follow this same general bauplan (Carrano 1999).

Carrano (2001) then measured secondary characteristics that have been characterized as evolutionarily plastic with regard to adapting to changes in mechanical demands with increasing body size – bone curvature and eccentricity. Eccentricity was measured as diametric ratios. Bone diameters for both dinosaurs and mammals showed negative allometry relative to bone length. The allometric decreases in diameter were generally similar across both the AP and ML axes, indicating an overall maintenance of bone shape with increased size. The only exception to this was the femoral ML diameter for dinosaurs, which scaled with positive allometry relative to the femoral AP diameter ($\propto FAP^{1.18}$), indicating greater resistance to ML bending loads with size; the same was true for emu during ontogenetic growth. Both mammals and dinosaurs show a decrease in bone curvature with size.

At the time, Carrano and Biewener (1999) reported predominantly torsional loading in the chicken femur, which was one of the few examples of torsion-induced shear strains in the long bones of terrestrial tetrapods. Mammals and dinosaurs have often been recognized as being subject to similar size-related constraints given their parasagittal limb posture. So what makes birds different in relation to their long bone loading? Mammals and most bipedal and quadrupedal dinosaurs are characterized by similar limb proportions (Figure 34.3). Mammals and nonavian dinosaurs have femora that comprise 30–60% of limb length, while the femora of birds only make up 10–35% of hind limb length. Consistent with this, birds have relatively longer TBTs as well. Relative to bone length, the femoral diameters of mammals and dinosaurs scale with very slight positive allometry ($\propto L^{1.06–1.09}$), while birds scale $\propto L^{1.36}$. Relative to their diameters, TBT lengths in birds scale closer to isometry than mammals and dinosaurs ($\propto L^{1.13}$ vs $\propto L^{1.25–1.27}$) (Carrano 1998). Relative to mammals and dinosaurs, bird bones become more robust and shorter, which would decrease the GRF-induced bending moments and increase resistance to torsion with increasing size (Gatesy 1991, Gatesy and Middleton 1997). Through these studies we find that dinosaurs and mammals are not identical in their limb bone scaling, but strong similarities exist in their scaling for bone shape that would indicate similar limitations on skeletal biomechanics with increasing body size. Birds, on the other hand, move their hindlimbs in unique ways among dinosaurs and have evolved novel morphologies to resist torsion-induced shear strains in their proximal hindlimb bones.

VetBooks.ir

Summary

This chapter has focused on outlining possible relationships between the gross morphology and histomorphology of limb bones and their mechanics, the strengths and shortcomings of these associations and future directions for advancing this area within the larger framework of comparative functional morphology. This section provides a summary of this discussion.

Limb length can often offer insight into general locomotor abilities relative to body size. Cursors typically have longer distal limb elements and relatively limited mobility and range of motion in their limbs, as a trade-off for their high degree of specialization. Limb lengths can be altered through exogenous loading experiments in rodent models, though less extreme exercise treatments rarely have such effects. Nonavian reptiles appear to have relatively more plastic growth plates than similarly sized mammals, allowing for some modulation of bone length, though this should be further characterized with a wider diversity of mammals and reptiles (including birds) relative to habitual changes in biomechanics.

Predicting limb bone mechanics using bone cross-sectional shape comes with a number of caveats. The prediction of the primary mode of loading seems possible given fairly clear differences in the cross-sectional shapes and cortical thickness in bones subjected to torsion versus bending. Bone curvature should also be considered when evaluating bone cross-sectional shape because it can obviously change the overall mechanics of the bone. Bone curvature and eccentricity seem to run contrary to one another, with greater curvatures occurring in the direction of leg swing while the greater width of eccentric bones tend to run orthogonal to this direction. It has been proposed here that neuromuscular control may regulate bending strains about the curvature while the wide dimension of an eccentric bone corresponds to a potential direction of bending without significant muscle to modulate the external forces acting on the bone. In a thick-walled bone where I_{MAX} and I_{MIN} are fairly similar, is the bone built to withstand bending loads about multiple directions or is the bone loaded in torsion? Future studies defining the relationships between bone curvature and eccentricity in relation to *in vivo* bone strains could shed light on how these features work together during ontogeny and in an evolutionary context to regulate bone strains.

Musculotendinous entheses may be gaining renewed relevance as new methods for analyzing these features are developed. However, these methods require multivariate information across multiple skeletal sites, though not necessarily different skeletal elements. This calls into question its use in paleontological studies where samples are sparse and can be affected by taphonomic processes that remove or degrade entheseal scars. Entheseal scars are often used in only a very general sense as muscle origin and insertion sites when reconstructing musculoskeletal models. Histological evidence of muscle orientation is not typically utilized in these studies.

Histomorphological features including intracortical remodeling, primary vascular canals and CFO require more information from biomechanical lab studies before solid conclusions can be drawn relating these features to limb mechanics. Intracortical remodeling is an established mechanism for repairing bone microdamage, which one might link to high-magnitude strain environments. Most studies that have tried to associate remodeling in the context of habitual biomechanics have not correlated well or have used taxa with thin-walled cortical bone, which are not typically remodeled extensively. Given patterns of cortical drift that occur in long bones, remodeling may simply coincide with old, but not particularly damaged, bone tissue. Cortical remodeling can also be found at high densities in vestigial skeletal elements, likely serving as mineral reservoirs. Primary vascular canals and CFOs have primarily been used as a proxy for torsional loading in comparative studies. However, they only appear to be useful on a taxon-by-taxon basis, even when torsional bone loading seems obvious, as they may also be highly sensitive to somatic growth rates and other environmental factors. Until there are more studies linking *in vivo* mechanics or validated musculoskeletal models to different behaviors in a larger variety of taxa, the utility of using these histological parameters to predict bone biomechanics remains tenuous.

Cancellous bone mass and orientation may provide one of the most sensitive morphological tools for testing hypotheses about limb posture and function in both plastic and evolutionary scenarios. For all ages examined thus far, cancellous bone can adapt to changes in applied loading to become stiffer and decrease (modeled) cancellous bone strains. However, a continued shortcoming in analyzing these tissues is the difficulty in empirically measuring stress and strains. If strain gauges can be attached to cortical bone in an analogous taxon or EPB-defined relatives of similar anatomy, subsequent FE models that match the *in vivo* cortical strains can be used to validate model-derived strains for cancellous bone.

Bone histomorphology is full of promise for comparative functional morphologists, but certain aspects have not been studied enough to realize their full potential. This is largely due to a lack of empirical biomechanical data for many of the extant taxa whose mechanics can be used to develop concrete functional hypotheses for limb use in extinct fossil species. The field needs to move away from using the limb mechanics of a singular extant taxon as representative for much larger clades that may exhibit habitual behaviors in their repertoire that were not measured in the singular representative taxon. Furthermore, our knowledge for how ontogeny affects bone morphology and histology is severely limited in relation to empirical biomechanical measures. The scaling of bone features or correlation of histological features that have been related to bone mechanics can convey a different significance when tracked through development. When attempting to take the small bits of correlative data that we already have to link long bone form and function, we need to be cautious about our conclusions as, for every example where bone histomorphology and function align, there are likely just as many examples where they do not. This does not mean that studies where we expect correlation and do not find it are failures, it simply means that we do not yet have enough empirical or mechanical modeling knowledge to understand the "rules" for functional correlation between bone histomorphology and limb bone mechanics.

VetBooks.ir

Acknowledgments

We thank Dr. Florian Witzmann for his help in classifying bone cellularity for the fishes discussed in this chapter and Dr. Emmanuel de Margerie for his comments on vascular canal organization. This work was supported in part by National Science Foundation CMMI 1463523 (RPM).

REFERENCES

Albright, J. A. and R. A. Brand. 1987. *The scientific basis of orthopaedics*. Norwalk, CT: Appleton and Lange.

Aguirre, J. I., et al. 2006. Osteocyte apoptosis is induced by weightlessness in mice and precedes osteoclast recruitment and bone loss. *J. Bone Miner. Res.* 21: 605–615.

Alexander, R. M. N. 1981. Factors of safety in the structure of animals. *Sci. Prog.* 67: 109–130.

Alexander, R. M. N., et al. 1979. Allometry of the limb bones of mammals from shrews (*Sorex*) to elephant (*Loxodonta*). *J. Zool.* 189: 305–314.

Ascenzi, A. and E. Bonucci. 1967. The tensile properties of single osteons. *Anat. Rec.* 158: 375–386.

Ascenzi, A. and E. Bonucci. 1968. The compressive properties of single osteons. *Anat. Rec.* 161: 377–391.

Ascenzi, A. and E. Bonucci. 1972. The shearing properties of single osteons. *Anat. Rec.* 172: 499–510.

Atkins, A., et al. 2015. The response of anosteocytic bone to controlled loading. *J. Exp. Biol.* 218: 3559–3569.

Bach-Gansmo, F. L., et al. 2015. Osteocyte lacunar properties in rat cortical bone: Differences between lamellar and central bone. *J. Struct. Biol.* 191: 59–67.

Bauwens, D., et al. 1995. Evolution of sprint speed in lacertid lizards: Morphological, physiological and behavioral covariation. *Evolution*. 49: 848–863.

Beaupré, G. S., et al. 1990a. An approach for time-dependent bone modeling and remodeling—theoretical development. *J. Orthop. Res.* 8: 651–661.

Beaupré, G. S., et al. 1990b. An approach for time-dependent bone modeling and remodeling - application: A preliminary remodeling simulation. *J. Orthop. Res.* 8: 662–670.

Bentolila, V., et al. 1998. Intracortical remodeling in adult rat long bones after fatigue loading. *Bone* 23: 275–281.

Bertram, J. E. A. and A. A. Biewener. 1988. Bone curvature: Sacrificing strength for load predictability? *J. Theor. Biol.* 131: 75–92.

Bertram, J. E. A. and A. A. Biewener. 1990. Differential scaling of the long bones in the terrestrial carnivora and other mammals. *J. Morphol.* 204: 157–169.

Bertram, J. E. A. and A. A. Biewener. 1992. Allometry and curvature in the long bones of quadrupedal mammals. *J. Zool.* 226: 455–467.

Bertram, J. E. A. and S. M. Swartz. 1991. The 'Law of Bone Transformation': A case of crying Wolff? *Biol. Rev.* 66: 245–273.

Biewener, A. A. 1983a. Allometry of quadrupedal locomotion: The scaling of duty factor, bone curvature and limb orientation to body size. *J. Exp. Biol.* 105: 147–171.

Biewener, A. A. 1983b. Locomotory stresses in the limb bones of two small mammals: The ground squirrel and chipmunk. *J. Exp. Biol.* 103: 131–154.

Biewener, A. A. 1989. Scaling of body support in mammals: Limb posture and muscle mechanics. *Science*. 245: 45–48.

Biewener, A. A. 1993. Safety factors in bone strength. *Calcif. Tissue Int.* 53(Suppl 1): S68–S74.

Biewener, A. A. and J. E. A. Bertram. 1994. Structural response of growing bone to exercise and disuse. *J. Appl. Physiol.* 76: 946–955.

Biewener, A. A. and K. P. Dial. 1995. *In vivo* strain in the humerus of pigeons (*Columba livia*) during flight. *J. Morphol.* 225: 61–75.

Biewener, A. A., et al. 1996. Adaptive changes in trabecular architecture in relation to functional strain patterns and disuse. *Bone* 19: 1–8.

Biewener, A. A., et al. 1986. Bone modeling during growth: Dynamic strain equilibrium in the chick tibiotarsus. *Calcif. Tissue Int.* 39: 390–395.

Birn-Jeffery, A. V., et al. 2012. Pedal claw curvature in birds, lizards and Mesozoic dinosaurs – Complicated categories and compensating for mass-specific and phylogenetic control. *PLoS One*. 7: e50555.

Bishop, P. J., et al. 2019a. Cancellous bone and theropod dinosaur locomotion. Part I-an examination of cancellous bone architecture in the hindlimb bones of theropods. *PeerJ*. 6: e5778.

Bishop, P. J., et al. 2019b. Cancellous bone and theropod dinosaur locomotion. Part II-a new approach to inferring posture and locomotor biomechanics in extinct tetrapod vertebrates. *PeerJ*. 6: e5779.

Bishop, P. J., et al. 2019c. Cancellous bone and theropod dinosaur locomotion. Part III-Inferring posture and locomotor biomechanics in extinct theropods, and its evolution on the line to birds. *PeerJ*, 6: e5777.

Blob, R. W. and A. A. Biewener. 1999. *In vivo* locomotor strain in the hindlimb bones of *Alligator mississippiensis* and *Iguana iguana*: Implications for the evolution of limb bone safety factor and non-sprawling limb posture. *J. Exp. Biol.* 202: 1023–1046.

Blob, R. W., et al. 2014. Diversity of limb-bone safety factors for locomotion in terrestrial vertebrates: Evolution and mixed chains. *Integr. Comp. Biol.* 54: 1058–1071.

Bonine, K. E. and T. Garland. 1999. Sprint performance of phrynosomatid lizards, measured on a high-speed treadmill, correlates with hindlimb length. *J. Zool.* 248: 255–265.

Bortel, E. L., et al. 2017. Combining coherent hard x-ray tomographies with phase retrieval to generate three-dimensional models of forming bone. *Front. Mater.* 4: 1–11.

Botton-Divet, L., et al. 2016. Morphological analysis of long bones in semi-aquatic mustelids and their terrestrial relatives. *Integr. Comp. Biol.* 56: 1298–1309.

Botton-Divet, L., et al. 2017. Swimming and running: A study of the convergence in long bone morphology among semi-aquatic mustelids (Carnivora: Mustelidae). *Biol. J. Linn. Soc.* 121: 38–49.

Boyde, A. and C. M. Riggs. 1990. The quantitative study of the orientation of collagen in compact bone slices. *Bone* 11: 35–40.

Brassey, C. A., et al. 2013. The role of cross-sectional geometry, curvature, and limb posture in maintaining equal safety factors: a computed tomography study. *Anat. Rec.* 296: 395–413.

Britz, H. B., et al. 2012. The effects of immobilization on vascular canal orientation in rat cortical bone. *J. Anat.* 220: 67–76.

VetBooks.ir

Bromage, T. G., et al. 2003. Circularly polarized light standards for investigations of collagen fiber orientation in bone. *Anat. Rec.* 274B: 157–168.

Burr, D. B., et al. 1985. Bone remodeling in response to *in vivo* fatigue microdamage. *J. Biomech.* 18: 189–200.

Burr, D. B., et al. 1989. Skeletal change in response to altered strain environments: Is woven bone a response to elevated strain? *Bone* 10: 223–233.

Butcher, M. T., et al. 2008. *In vivo* strains in the femur of river cooter turtles (*Pseudemys concinna*) during terrestrial locomotion: Tests of force-platform models of loading mechanics. *J. Exp. Biol.* 211: 2397–2407.

Butcher, M. T., et al. 2011. *In vivo* strains in the femur of the Virginia opossum (*Didelphis virginiana*) during terrestrial locomotion: testing hypotheses of evolutionary shifts in mammalian bone loading and design. *J. Exp. Biol.* 214: 2631–2640.

Bybee, P. J., et al. 2006. Sizing the Jurassic theropod dinosaur Allosaurus: Assessing growth strategy and evolution of ontogenetic scaling of limbs. *J. Morphol.* 267: 347–359.

Cabahug-Zuckerman, P., et al. 2016. Osteocyte apoptosis caused by hindlimb unloading is required to trigger osteocyte RANKL production and subsequent resorption of cortical and trabecular bone in mice femurs. *J. Bone Miner. Res.* 31: 1356–1365.

Carlson, K. J. and S. Judex 2007. Increased non-linear locomotion alters diaphyseal bone shape. *J. Exp. Biol.* 210: 3117–3125.

Carrano, M. T. 1998. Locomotion in non-avian dinosaurs: integrating data from hindlimb kinematics, *in vivo* strains, and bone morphology. *Paleobiology* 24: 450–469.

Carrano, M. T. 1999. What, if anything, is a cursor? Categories versus continua for determining locomotor habit in mammals and dinosaurs. *J. Zool.* 247: 29–42.

Carrano, M. T. 2001. Implications of limb bone scaling, curvature and eccentricity in mammals and non-avian dinosaurs. *J. Zool.* 254: 41–55.

Carrano, M. T. and A. A. Biewener 1999. Experimental alteration of limb posture in the chicken (*Gallus gallus*) and its bearing on the use of birds as analogs for dinosaur locomotion. *J. Morphol.* 240: 237–249.

Carrier, D. R. 1983. Postnatal ontogeny of the musculo-skeletal system in the Black-tailed jack rabbit (*Lepus californicus*). *J. Zool. Lond.* 201: 27–55.

Carrier, D. and L. R. Leon. 1990. Skeletal growth and function in the California gull (*Larus californicus*). *J. Zool.* 222: 375–389.

Carter, D. R. 1982. the relationship between *in vivo* strains and cortical bone remodeling. In *CRC critical reviews in bioengineering*, 8, Bourne J. R. ed., 1–28. Boca Raton, FL: CRC Press.

Carter, D. R. and G. S. Beaupré. 2001. *Skeletal function and form: mechanobiology of skeletal development, aging, and regeneration*. Cambridge, UK: Cambridge University Press.

Carter, D. R., et al. 1998. Epigenetic mechanical factors in the evolution of long bone epiphyses. *Zool. J. Linn. Soc.* 123: 163–178.

Castanet, J., et al. 2000. Periosteal bone growth rates in extant ratites (ostrich and emu). Implications for assessing growth in dinosaurs. *C. R. Acad. Sci.: Série III, Sciences de La Vie* 323: 543–550.

Christen, P., et al. 2012. Bone morphology allows estimation of loading history in a murine model of bone adaptation. *Biomech. Model. Mechanobiol.* 11: 483–492.

Clemente, C. J., et al. 2009. Evolutionary relationships of sprint speed in Australian varanid lizards. *J. Zool.* 278: 270–280.

Cobb, S. E. and W. I. Sellers. 2020. Inferring lifestyle for Aves and Theropoda: A model based on curvatures of extant avian ungual bones. *PLoS One*. 15: e0211173.

Cubo, J. and A. Casinos. 1998. The variation of the cross-sectional shape in the long bones of birds and mammals. *Ann. Sci. Nat. - Zool. Biol. Anim.* 19: 51–62.

Cubo, J., et al. 1999. Sagittal long bone curvature in birds. *Ann. Sci. Nat. - Zool. Biol. Anim.* 20: 153–159.

Cubo, J., et al. 2015. First reported cases of biomechanically adaptive bone modeling in non-avian dinosaurs. *PLoS One*. 10: e0131131.

Currey, J. D. 1968. The adaptation of bones to stress. *J. Theor. Biol.* 20: 91–106.

Currey, J. D. 2002. *Bones: structure and mechanics.* 1st ed. Princeton, NJ: Princeton University Press.

Currey, J. D. and R. M. N. Alexander. 1985. The thickness of the wall of tubular bones. *J. Zool.* 206: 453–468.

Davesne, D., et al. 2019. The phylogenetic origin and evolution of acellular bone in teleost fishes: insights into osteocyte function in bone metabolism. *Biol. Rev.* 94: 1338–1363.

Demes, B., et al. 2001. Patterns of strain in the macaque tibia during functional activity. *Am. J. Phys. Anthropol.* 116: 257–265.

Demes, B., et al. 1998. Patterns of strain in the macaque ulna during functional activity. *Am. J. Phys. Anthropol.* 106: 87–100.

Dilkes, D. W. 2001. An ontogenetic perspective on locomotion in the Late Cretaceous dinosaur *Maiasaura peeblesorum* (Ornithischia: Hadrosauridae). *Can. J. Earth Sci.* 38: 1205–1227.

Dysart, P. S., et al. 1989. Growth of the humerus after denervation. An experimental study in the rat. *J. Anat.* 167: 147–159.

Ehara, Y. and M. Yamaguchi. 1996. Histomorphological confirmation of bone loss in the femoral-metaphyseal tissues of rats with skeletal unloading. *Res. Exp. Med.* 196: 163–170.

Enlow, D. H. and S. O. Brown. 1956. A comparative histological study of fossil and recent bone tissues. Part I. *Tex. J. Sci.* 8: 405–443.

Enlow, D. H. and S. O. Brown. 1957. A comparative histological study of fossil and recent bone tissues. Part II. *Tex. J. Sci.* 9: 186–214.

Evans, F. G. and R. Vincentelli. 1969. Relation of collagen fiber orientation to some mechanical properties of human cortical bone. *J. Biomech.* 2: 63–71.

Evans, F. G. and R. Vincentelli. 1974. Relations of the compressive properties of human cortical bone to histological structure and calcification. *J. Biomech.* 7: 1–10.

Fedak, M. A., et al. 1982. Energetics and mechanics of terrestrial locomotion. II. Kinetic energy changes of the limbs and body as a function of speed and body size in birds and mammals. *J. Exp. Biol.* 97: 23–40.

Felder, A. A., et al. 2017. Secondary osteons scale allometrically in mammalian humerus and femur. *R. Soc. Open Sci.* 4: 170431.

Francillon-Vieillot, H., et al. 1990. Microstructure and mineralization of vertebrate skeletal tissues. In *Skeletal biomineralization: patterns, processes and evolutionary trends*, Vol 1, Carter, J. G., ed., 471–548. New York: Van Nostrand Reinhold.

Fritton, J. C., et al. 2005. Loading induces site-specific increases in mineral content assessed by microcomputed tomography of the mouse tibia. *Bone* 36: 1030–1038.

Fritton, S. P. and S. Weinbaum. 2009. Fluid and solute transport in bone: flow-induced mechanotransduction. *Ann. Rev. Fluid Mech*. 41: 347–374.

Frost, H. M. 1982. A determinant of bone architecture: The minimum effective strain. *Clin. Orthop. Rel. Res*. 175: 286–292.

Frost, H. M. 2003. Bone's mechanostat: A 2003 update. *Anat. Rec*. 275A: 1081–1101.

Fyhrie, D. P. and D. R. Carter. 1986. A unifying principle relating stress to trabecular bone morphology. *J. Orthop. Res*. 4: 304–317.

Garland, T. and C. M. Janis. 1993. Does metatarsal/femur ratio predict maximal running speed in cursorial mammals? *J. Zool*. 229: 133–151.

Gatesy, S. M. 1991. Hind limb scaling in birds and other theropods: Implications for terrestrial locomotion. *J. Morphol*. 209: 83–96.

Gatesy, S. M. and A. A. Biewener. 1991. Bipedal locomotion: effects of speed, size and limb posture in birds and humans. *J. Zool*. 224: 127–147.

Gatesy, S. M. and K. P. Dial. 1996. Locomotor modules and the evolution of avian flight. *Evolution*. 50: 331–340.

Gatesy, S. M. and K. M. Middleton. 1997. Bipedalism, flight, and the evolution of theropod locomotor diversity. *J. Vert. Paleontol*. 17: 308–329.

Georgiadis, M., et al. 2016. Techniques to assess bone ultrastructure organization: orientation and arrangement of mineralized collagen fibrils. *J. R. Soc. Interface* 13: 20160088.

Georgiou, L., et al. 2020. Evidence for habitual climbing in a Pleistocene hominin in South Africa. *PNAS* 117: 8416–8423.

Goodship, A. E., et al. 1979. Functional adaptation of bone to increased stress. *J. Bone Joint Surg*. 61A: 539–546.

Gross, T. S., et al. 1997. Strain gradients correlate with sites of periosteal bone formation. *J. Bone Miner. Res*. 12: 982–988.

Grüneboom, A., et al. 2019. A network of trans-cortical capillaries as mainstay for blood circulation in long bones. *Nat. Metab*. 1: 236–250.

Gunter, H. M., et al. 2013. Shaping development through mechanical strain: the transcriptional basis of diet-induced phenotypic plasticity in a cichlid fish. *Mol. Ecol*. 22: 4516–4531.

Habib, M. B. and C. B. Ruff. 2008. The effects of locomotion on the structural characteristics of avian limb bones. *Zool. J. Linn. Soc*. 153: 601–624.

Harrison, N. M., et al. 2008. Heterogeneous linear elastic trabecular bone modelling using micro-CT attenuation data and experimentally measured heterogeneous tissue properties. *J. Biomech*. 41: 2589–2596.

Heinrich, R. E., et al. 1999. Ontogenetic changes in mineralization and bone geometry in the femur of muskoxen (*Ovibos moschatus*). *J. Zool*. 247: 215–223.

Heinrich, R. E., et al. 1993. Femoral ontogeny and locomotor biomechanics of *Dryosaurus lettowvorbecki* (Dinosauria, Iguanodontia). *Zool. J. Linn. Soc*. 108: 179–196.

Herrel, A. and V. Holanova. 2008. Cranial morphology and bite force in Chamaeleolis lizards – Adaptations to molluscivory? *Zool*. 111: 467–475.

Hildebrand, M. 1995. *Analysis of vertebrate structure*. 4th ed. New York: John Wiley & Sons, Inc.

Hilliard Young, V. K. and R. W. Blob. 2015. Limb bone loading in swimming turtles: Changes in loading facilitate transitions from tubular to flipper-shaped limbs during aquatic invasions. *Biol. Lett*. 11: 20150110.

Holguin, N., et al. 2013. Adaptation of tibial structure and strength to axial compression depends on loading history in both C57BL/6 and BALB/c mice. *Calcif. Tissue Int*. 93: 211–221.

Holguin, N., et al. 2014. Aging diminishes lamellar and woven bone formation induced by tibial compression in adult C57BL/6. *Bone* 65: 83–91.

Holguin, N., et al. 2016. Activation of Wnt signaling by mechanical loading is impaired in the bone of old mice. *J. Bone Miner. Res*. 31: 2215–2226.

Honda, A., et al. 2001. Effect of high-impact and low-repetition training on bones in ovariectomized rats. *J. Bone Miner. Res*. 16: 1688–1693.

Horner, J. R., et al. 1999. Variation in dinosaur skeletochronology indicators: implications for age assessment and physiology. *Paleobiology* 25: 295–304.

Horner, J. R., et al. 2000. Long bone histology of the hadrosaurid dinosaur *Maiasaura peeblesorum*: Growth dynamics and physiology based on an ontogenetic series of skeletal elements. *J. Vert. Paleontol*. 20: 115–129.

Houssaye, A., et al. 2018. 3D quantitative comparative analysis of long bone diaphysis variations in microanatomy and cross-sectional geometry. *J. Anat*. 232: 836–849.

Hsieh, Y. F., et al. 2001. Mechanical loading of diaphyseal bone *in vivo*: The strain threshold for an osteogenic response varies with location. *J. Bone Miner. Res*. 16: 2291–2297.

Huiskes, R., et al. 2000. Effects of mechanical forces on maintenance and adaptation of form in trabecular bone. *Nature* 405: 704–706.

Hutchinson, J. R., et al. 2005. Analysis of hindlimb muscle moment arms in *Tyrannosaurus rex* using a three-dimensional musculoskeletal computer model: implications for stance, gait, and speed. *Paleobiology*. 31: 676–701.

Hutchinson, J. R., et al. 2015. Musculoskeletal modelling of an ostrich (*Struthio camelus*) pelvic limb: Influence of limb orientation on muscular capacity during locomotion. *PeerJ*. 3: e1001.

Iriarte-Díaz, J. 2002. Differential scaling of locomotor performance in small and large terrestrial mammals. *J. Exp. Biol*. 205: 2897–2908.

Iwamoto, J., et al. 1999. Differential effect of treadmill exercise on three cancellous bone sites in the young growing rat. *Bone* 24: 163–169.

Jaworski, Z. F. G. and H. K. Uhthoff. 1986. Reversibility of nontraumatic disuse osteoporosis during its active phase. *Bone* 7: 431–439.

Ju, Y. I., et al. 2014. Effects of different types of jump impact on trabecular bone mass and microarchitecture in growing rats. *PLoS One*. 9: e107593.

Judex, S., et al. 2004. Genetically linked site-specificity of disuse osteoporosis. *J. Bone Miner. Res*. 19: 607–613.

Kalmey, J. K. and C. O. Lovejoy. 2002. Collagen fiber orientation in the femoral necks of apes and humans: Do their histological structures reflect differences in locomotor loading? *Bone* 31: 327–332.

Karakostis, F. A., et al. 2017. Occupational manual activity is reflected on the patterns among hand entheses. *Am. J. Phys. Anthropol*. 164: 30–40.

VetBooks.ir

Karakostis, F. A. and C. Lorenzo. 2016. Morphometric patterns among the 3D surface areas of human hand entheses. *Am. J. Phys. Anthropol.* 160: 694–707.

Karakostis, F. A., et al. 2019. Experimental evidence that physical activity affects the multivariate associations among muscle attachments. *J. Exp. Biol.* 222: jeb213058.

Keller, T. S. and D. M. Spengler. 1982. *In vivo* strain gage implantation in rats. *J. Biomech.* 15: 911–917.

Keller, T. S. and D. M. Spengler. 1989. Regulation of bone stress and strain in the immature and mature rat femur. *J. Biomech.* 22: 1115–1127.

Kelly, N. H., et al. 2016. Transcriptional profiling of cortical versus cancellous bone from mechanically-loaded murine tibiae reveals differential gene expression. *Bone* 86: 22–29.

Kelly, S. A., et al. 2006. Experimental evolution and phenotypic plasticity of hindlimb bones in high-activity house mice. *J. Morphol.* 267: 360–374.

Kennedy, O. D., et al. 2012. Activation of resorption in fatigue-loaded bone involves both apoptosis and active pro-osteoclastogenic signaling by distinct osteocyte populations. *Bone* 50: 1115–1122.

Kivell, T. L. 2016. A review of trabecular bone functional adaptation: What have we learned from trabecular analyses in extant hominoids and what can we apply to fossils? *J. Anat.* 228: 569–594.

Klein, N. and M. Sander. 2008. Ontogenetic stages in the long bone histology of sauropod dinosaurs. *Paleobiology* 34: 247–263.

Kodama, Y., et al. 2000. Exercise and mechanical loading increase periosteal bone formation and whole bone strength in C57BL/6J mice but not in C3H/Hej mice. *Calcif. Tissue Int.* 66: 298–306.

Kuehn, A.L., et al. 2019. The effects of growth rate and biomechanical loading on bone laminarity within the emu skeleton. *PeerJ.* 7: e7616.

Lambers, F. M., et al. 2013. Trabecular bone adapts to long-term cyclic loading by increasing stiffness and normalization of dynamic morphometric rates. *Bone* 55: 325–334.

Lammers, A. R. and R. Z. German. 2002. Ontogenetic allometry in the locomotor skeleton of specialized half-bounding mammals. *J. Zool.* 258: 485–495.

Lane, W. A. 1887. A remarkable example of the manner in which pressure-changes in the skeleton may reveal the labour history of the individual. *J. Anat. Physiol.* 21: 385–406.

Lane, W. A. 1888. Anatomy and physiology of the shoemaker. *J. Anat. Physiol.* 22: 592–628.

Lanyon, L. E. 1973. Analysis of surface bone strain in the calcaneus of sheep during normal locomotion. Strain analysis of the calcaneus. *J. Biomech.* 6: 41–49.

Lanyon, L. E. 1980. The influence of function on the development of bone curvature. An experimental study on the rat tibia. *J. Zool.* 192: 457–466.

Lanyon, L. E., et al. 1982. Mechanically adaptive bone remodelling. *J. Biomech.* 15: 141–145.

Lanyon, L. E., et al. 1979. The relationship of functional stress and strain to the processes of bone remodelling. An experimental study on the sheep radius. *J. Biomech.* 12: 593–600.

Lanyon, L. E., and C. T. Rubin. 1984. Static *vs* dynamic loads as an influence on bone remodelling. *J. Biomech.* 17: 897–905.

Lee, A. H. 2004. Histological organization and its relationship to function in the femur of *Alligator mississippiensis*. *J. Anat.* 204: 197–207.

Lee, A. H. and P. M. O'Connor. 2013. Bone histology confirms determinate growth and small body size in the noasaurid theropod *Masiakasaurus knopfleri*. *J. Vert. Paleontol.* 33: 865–876

Lee, A. H. and E. L. R. Simons. 2015. Wing bone laminarity is not an adaptation for torsional loading in bats. *PeerJ.* 3: e823.

Levenston, M. E., et al. 1998. Loading mode interactions in simulations of long bone cross-sectional adaptation. *Comput. Method. Biomech. Biomed. Eng.* 1: 303–319.

Levis, N. A., et al. 2018. Morphological novelty emerges from pre-existing phenotypic plasticity. *Nat. Ecol. Evol.* 2: 1289–1297.

Lieberman, D. E., et al. 2003. Optimization of bone growth and remodeling in response to loading in tapered mammalian limbs. *J. Exp. Biol.* 206: 3125–3138

Lieberman, D. E., et al. 2004. Predicting long bone loading from cross-sectional geometry. *Am. J. Phys. Anthropol.* 123: 156–171.

Loitz, B. J. and R. F. Zernicke. 1992. Strenuous exercise-induced remodelling of mature bone: Relationships between *in vivo* strains and bone mechanics. *J. Exp. Biol.* 170: 1–18.

Losos, J. B. 1990. Morphology and locomotor performance. *Evolution* 44: 1189–1203.

Losos, J. B., et al. 2000. Evolutionary implications of phenotypic plasticity in the hindlimb of the lizard *Anolis sagrei*. *Evolution* 54: 301–305.

Losos, J. B. and D. J. Irschick. 1996. The effect of perch diameter on escape behaviour of Anolis lizards: Laboratory predictions and field tests. *Anim. Behav.* 51: 593–602.

Losos, J. B. and B. Sinervo. 1989. The effects of morphology and perch diameter on sprint performance of *Anolis* lizards. *J. Exp. Biol.* 145: 23–30.

Lovejoy, C. O. and E. Trinkaus. 1980. Strength and robusticity of the Neandertal tibia. *Am. J. Phys. Anthropol.* 53: 465–470.

Lynch, M. E., et al. 2010. Cancellous bone adaptation to tibial compression is not sex dependent in growing mice. *J. Appl. Physiol.* 109: 685–691.

Lynch, M.E., et al. 2011. Tibial compression is anabolic in the adult mouse skeleton despite reduced responsiveness with aging. *Bone* 49: 439–446.

Maidment, S. C. R., et al. 2014. Locomotion in ornithischian dinosaurs: an assessment using three-dimensional computational modelling. *Biol. Rev.* 89: 588–617.

Main, R. P. 2006. *Skeletal mechanics, bone histomorphology, and growth in tetrapods*. Cambridge, MA: Harvard University.

Main, R. P. 2007. Ontogenetic relationships between *in vivo* strain environment, bone histomorphometry and growth in the goat radius. *J. Anat.* 210: 272–293.

Main, R. P. and A. A. Biewener. 2004. Ontogenetic patterns of limb loading, *in vivo* bone strains and growth in the goat radius. *J. Exp. Biol.* 207: 2577–2588.

Main, R. P. and A. A. Biewener. 2006. *In vivo* bone strain and ontogenetic growth patterns in relation to life-history strategies and performance in two vertebrate taxa: goats and emu. *Physiol. Biochem. Zool.* 79: 57–72.

Main, R. P. and A. A. Biewener. 2007. Skeletal strain patterns and growth in the emu hindlimb during ontogeny. *J. Exp. Biol.* 210: 2676–2690.

Main, R. P., et al. 2010. *In vivo* tibial stiffness is maintained by whole bone morphology and cross-sectional geometry in growing female mice. *J. Biomech.* 43: 2689–2694.

Main, R. P., et al. 2014. Load-induced changes in bone stiffness and cancellous and cortical bone mass following tibial compression diminish with age in female mice. *J. Exp. Biol.* 217: 1775–1783.

Main, R. P., et al. 2020. Murine axial compression tibial loading model to study bone mechanobiology: Implementing the model and reporting results. *J. Orthop. Res.* 38: 233–252.

Maloiy, G. M. O., et al. 1979. Allometry of the legs of running birds. *J. Zool.* 187: 161–167.

Mantila Roosa, S. M., et al. 2011. Gene expression patterns in bone following mechanical loading. *J. Bone Miner. Res.* 26: 100–112.

Marelli, C. A. and E. L. R. Simons. 2014. Microstructure and cross-sectional shape of limb bones in Great Horned Owls and Red-tailed Hawks: How do these features relate to differences in flight and hunting behavior? *PLoS One* 9: e106094.

Margerie, E. de. 2002. Laminar bone as an adaptation to torsional loads in flapping flight. *J. Anat.* 201: 521–526.

Margerie, E. de, et al. 2002. Bone typology and growth rates: testing and quantifying 'Amprino's rule' in the mallard (*Anas platyrhynchos*). *C. R. Biol.* 325: 221–230.

Margerie, E. de, et al. 2004. Assessing a relationship between bone microstructure and growth rate: A fluorescent labelling study in the king penguin chick (*Aptenodytes patagonicus*). *J. Exp. Biol.* 207: 869–879.

Margerie E. de, et al. 2005. Torsional resistance as a principal component of the structural design of long bones: Comparative multivariate evidence in birds. *Anat. Rec. A.* 282: 49–66.

Martin, R. B. 2000. Toward a unifying theory of bone remodeling. *Bone* 26: 1–6.

Martin, R. B. 2002. Is all cortical bone remodeling initiated by microdamage? *Bone* 30: 8–13.

Martin, R. B. 2003. Fatigue microdamage as an essential element of bone mechanics and biology. *Calcif. Tissue Int.* 73: 101–107.

Martin, R. B. and J. Ishida. 1989. The relative effects of collagen fiber orientation, porosity, density, and mineralization on bone strength. *J. Biomech.* 22: 419–426.

Maxwell, E. E. and H. C. E. Larsson. 2007. Osteology and myology of the wing of the emu (*Dromaius novaehollandiae*), and its bearing on the evolution of vestigial structures. *J. Morphol.* 268: 423–441.

McFarlin, S. C., et al. 2008. Regional variability in secondary remodeling within long bone cortices of catarrhine primates: the influence of bone growth history. *J. Anat.* 213: 308–324.

McGuire, R. S., et al. 2020. Development of limb bone laminarity in the homing pigeon (*Columba livia*). *PeerJ.* 8: e9878.

McMahon, J. M., et al. 1995. Pattern of collagen fiber orientation in the ovine calcaneal shaft and its relation to locomotor-induced strain. *Anat. Rec.* 242: 147–158.

McMahon, T. A. 1975. Using body size to understand the structural design of animals: quadrupedal locomotion. *J. Appl. Physiol.* 39: 619–627.

Mescher, A. L. 2018. *Junqueira's basic histology text & atlas.* 15th ed. New York: McGraw-Hill Education.

Mosley, J. R. and L. E. Lanyon. 1998. Strain rate as a controlling influence on adaptive modeling in response to dynamic loading of the ulna in growing male rats. *Bone* 23: 313–318.

Mosley, J. R., et al. 1997. Strain magnitude related changes in whole bone architecture in growing rats. *Bone* 20: 191–198.

Moustafa, A., et al. 2012. Mechanical loading-related changes in osteocyte sclerostin expression in mice are more closely associated with the subsequent osteogenic response than the peak strains engendered. *Osteoporos. Int.* 23: 1225–1234.

Nagasawa, S., et al. 2008. Effects of low-repetition jump exercise on osteogenic response in rats. *J. Bone Miner. Metab.* 26: 226–230.

Nango, N., et al. 2016. Osteocyte-directed bone demineralization along canaliculi. *Bone* 84: 279–288.

Newhall, K., et al. 1991. Effects of voluntary exercise on bone mineral content in rats. *J. Bone Miner. Res.* 6: 289–296.

Nudds, R. L. 2007. Wing-bone length allometry in birds. *J. Avian Biol.* 38: 515–519.

Nyakatura, J. A., et al. 2019. Reverse-engineering the locomotion of a stem amniote. *Nature* 565: 351–355.

Ooi, F. K., et al. 2009. Minimum level of jumping exercise required to maintain exercise-induced bone gains in female rats. *Osteoporos. Int.* 20: 963–972.

Padian, K. 1983. A functional analysis of flying and walking in pterosaurs. *Paleobiology* 3: 218–239.

Padian, K. 2013. Why study the bone microstructure of fossil tetrapods? In *Bone histology of fossil tetrapods: advancing methods, analysis, and interpretation*, Padian, K., Lamm, E.-T., eds., 1–11. Berkeley, CA: University of California Press.

Padian, K., et al. 2004. Growth in small dinosaurs and pterosaurs: the evolution of archosaurian growth strategies. *J. Vert. Paleontol.* 24: 555–571.

Padian, K., et al. 2016. A hypothesis of differential secondary bone formation in dinosaurs. *C. R. Palevol* 15: 40–48.

Parfitt, A. M. 2002. Targeted and nontargeted bone remodeling: Relationship to basic multicellular unit origination and progression. *Bone* 30: 5–7.

Pauwels, F. 1980. *Biomechanics of the locomotor apparatus.* Berlin: Springer.

Perry, J. M. G. and K. A. Prufrock. 2018. Muscle functional morphology in paleobiology: The past, present, and future of "paleomyology." *Anat. Rec.* 301: 538–555.

Pidaparti, R. M. V. and C. H. Turner. 1997. Cancellous bone architecture: Advantages of nonorthogonal trabecular alignment under multidirectional joint loading. *J. Biomech.* 30: 979–983.

Piekarski, K. 1973. Analysis of bone as a composite material. *Int. J. Eng. Sci.* 11: 557–565.

Polk, J. D., et al. 2000. A comparison of primate, carnivoran and rodent limb bone cross-sectional properties: Are primates really unique? *J. Hum. Evol.* 39: 297–325.

Pontzer, H., et al. 2006. Trabecular bone in the bird knee responds with high sensitivity to changes in load orientation. *J. Exp. Biol.* 209: 57–65.

Pratt, I. V. and D. M. L. Cooper. 2017. A method for measuring the three-dimensional orientation of cortical canals with implications for comparative analysis of bone microstructure in vertebrates. *Micron* 92: 32–38.

Pratt, I. V. and D. M. L. Cooper. 2018. The effect of growth rate on the three-dimensional orientation of vascular canals in the cortical bone of broiler chickens. *J. Anat.* 233: 531–541.

Pratt, I. V., et al. 2018. Interpreting the three-dimensional orientation of vascular canals and cross-sectional geometry of cortical bone in birds and bats. *J. Anat.* 232: 931–942.

Qing, H., et al. 2012. Demonstration of osteocytic perilacunar/canalicular remodeling in mice during lactation. *J. Bone Miner. Res.* 27: 1018–1029.

Rabey, K. N., et al. 2015. Locomotor activity influences muscle architecture and bone growth but not muscle attachment site morphology. *J. Hum. Evol.* 78: 91–102.

Rabkin, B. A., et al. 2001. Long-term measurement of bone strain *in vivo*: The rat tibia. *J. Biomed. Mater. Res.* 58: 277–281.

Ramasamy, J. G. and O. Akkus. 2007. Local variations in the micromechanical properties of mouse femur: the involvement of collagen fiber orientation and mineralization. *J. Biomech.* 40: 910–918.

Razi, H., et al. 2015a. Aging leads to a dysregulation in mechanically driven bone formation and resorption. *J. Bone Miner. Res.* 30: 1864–1873.

Razi, H., et al. 2015b. Skeletal maturity leads to a reduction in the strain magnitudes induced within the bone: A murine tibia study. *Acta Biomater.* 13: 301–310.

Ricqlès, A. J. de, et al. 2000. Palaeohistology of the bones of pterosaurs (Reptilia: Archosauria): anatomy, ontogeny, and biomechanical implications. *Zool. J. Linn. Soc.* 129: 349–385.

Ricqlès, A. J. de, et al. 1991. Comparative microstructure of bone. In *Bone, volume 3: bone matrix and bone specific products*, Hall, B.K., ed., 1–78. Boca Raton, FL: CRC Press.

Riggs, C. M., et al. 1993. Functional associations between collagen fibre orientation and locomotor strain direction in cortical bone of the equine radius. *Anat. Embryol.* 187: 231–238.

Robling, A. G., et al. 2001a. Modulation of appositional and longitudinal bone growth in the rat ulna by applied static and dynamic force. *Bone* 29: 105–113.

Robling, A. G., et al. 2001b. Recovery periods restore mechanosensitivity to dynamically loaded bone. *J. Exp. Biol.* 204: 3389–3399.

Robling, A. G., et al. 2002. Improved bone structure and strength after long-term mechanical loading is greatest if loading is separated into short bouts. *J. Bone Miner. Res.* 17: 1545–1554.

Robling, A. G., et al. 2008. Mechanical stimulation of bone *in vivo* reduces osteocyte expression of Sost/sclerostin. *J. Biol. Chem.* 283: 5866–5875.

Robling, A. G. and C. H. Turner. 2002. Mechanotransduction in bone: Genetic effects on mechanosensitivity in mice. *Bone* 31: 562–569.

Roesler, H. 1981. Some historical remarks on the theory of cancellous bone structure (Wolff's Law). In *Mechanical properties of bone*, S. C. Cowin ed., 27–42. New York: The American Society of Mechanical Engineers.

Roux X. 1881. *Der Kampf der Teile im Organismus*. Leipzig, Germany: W. Engelmann.

Rubin, C. T., et al. 1992. Suppression of the osteogenic response in the aging skeleton. *Calcif. Tissue Int.* 50: 306–313.

Rubin, C. T. and L. E. Lanyon. 1982. Limb mechanics as a function of speed and gait: A study of functional strains in the radius and tibia of horse and dog. *J. Exp. Biol.* 101: 187–211.

Rubin, C. T. and L. E. Lanyon. 1984a. Dynamic strain similarity in vertebrates: an alternative to allometric limb bone scaling. *J. Theor. Biol.* 107: 321–327.

Rubin, C. T. and L. E. Lanyon. 1984b. Regulation of bone formation by applied dynamic loads. *J. Bone Joint Surg. A* 66A: 397–402.

Rubin, C. T. and L. E. Lanyon. 1985. Regulation of bone mass by mechanical strain magnitude. *Calcif. Tissue Int.* 37: 411–417.

Ruff, C. B. 2003. Growth in bone strength, body size, and muscle size in a juvenile longitudinal sample. *Bone* 33: 317–329.

Ruff, C. B. and W. C. Hayes. 1983. Cross-sectional geometry of Pecos Pueblo femora and tibiae—A biomechanical investigation: I. Method and general patterns of variation. *Am. J. Phys. Anthropol.* 60: 359–381.

Ryan, T. M., et al. 2018. Human-like hip joint loading in *Australopithecus africanus* and *Paranthropus robustus*. *J. Hum. Evol.* 121: 12–24.

Sakata, T., et al. 1999. Trabecular bone turnover and bone marrow cell development in tail-suspended mice. *J. Bone Miner. Res.* 14: 1596–1604.

Sample, S. J., et al. 2010. Systemic effects of ulna loading in male rats during functional adaptation. *J. Bone Miner. Res.* 25: 2016–2028.

Sanchez, S., et al. 2012. Three-dimensional synchrotron virtual paleohistology: A new insight into the world of fossil bone microstructures. *Microsc. Microanal.* 18: 1095–1105.

Sanchez, S., et al. 2014. The humerus of *Eusthenopteron*: a puzzling organization presaging the establishment of tetrapod limb bone marrow. *Proc. R. Soc. B: Biol. Sci.* 281: 20140299.

Schaffler, M. B., et al. 1985. Structural and mechanical indicators of limb specialization in primates. *Folia Primatol.* 45: 61–75.

Schulte, F. A., et al. 2013. Local mechanical stimuli regulate bone formation and resorption in mice at the tissue level. *PLoS One*, 8: e62172.

Sereno, P. C. 1997. The origin and evolution of dinosaurs. *Annu. Rev. Earth Planet. Sci.* 25: 435–489.

Seymour, R. S., et al. 2012. Blood flow to long bones indicates activity metabolism in mammals, reptiles and dinosaurs. *Proc. R. Soc. B: Biol. Sci.* 279: 451–456.

Sheffield, K. M., et al. 2011. Locomotor loading mechanics in the hindlimbs of tegu lizards (*Tupinambis merianae*): comparative and evolutionary implications. *J. Exp. Biol.* 214: 2616–2630.

Silva, M. J. and L. J. Gibson. 1997. Modeling the mechanical behavior of vertebral trabecular bone: Effects of age-related changes in microstructure. *Bone* 21: 191–199.

Simons, E. L. R. and P. M. O'Connor. 2012. Bone laminarity in the avian forelimb skeleton and its relationship to flight mode: Testing functional interpretations. *Anat. Rec.* 295: 386–396.

Simske, S. J., et al. 1992. The physical and mechanical effects of suspension-induced osteopenia on mouse long bones. *J. Biomech.* 25: 489–499.

Sinervo, B. and J. B. Losos. 1991. Walking the tight rope: Arboreal sprint performance among *Sceloporus occidentalis* lizard populations. *Ecology* 72: 1225–1233.

Skedros, J. G. and M. S. Doutré. 2019. Collagen fiber orientation pattern, osteon morphology and distribution, and presence of laminar histology do not distinguish torsion from bending in at and pigeon bones. *J. Anat.* 234: 748–763.

Skedros, J. G., et al. 1994. Differences in osteonal micromorphology between tensile and compressive cortices of a bending skeletal system: Indications of potential strain-specific differences in bone microstructure. *Anat. Rec.* 239: 405–413.

Skedros, J. G. and K. J. Hunt. 2004. Does the degree of laminarity correlate with site specific differences in collagen fibre orientation in primary bone? An evaluation in the turkey ulna diaphysis. *J. Anat.* 205: 121–134.

Skedros, J. G., et al. 2003. Ontogenetic and regional morphologic variations in the turkey ulna diaphysis: Implications for functional adaptation of cortical bone. *Anat. Rec.* 273: 609–629.

Skedros, J. G., et al. 2004. Relationships of loading history and structural and material characteristics of bone: Development of the mule deer calcaneus. *J. Morphol.* 259: 281–307.

Skedros, J. G., et al. 2009. Interpreting cortical bone adaptation and load history by quantifying osteon morphotypes in circularly polarized light images. *Bone* 44: 392–403.

Skedros, J. G., et al. 2007. Ontogenetic structural and material variations in ovine calcanei: a model for interpreting bone adaptation. *Anat. Rec.* 290: 284–300.

Smith, A. L., et al. 2015. The feeding biomechanics and dietary ecology of *Paranthropus boisei*. *Anat. Rec.* 298: 145–167.

Souza, R. L. de, et al. 2005. Non-invasive axial loading of mouse tibiae increases cortical bone formation and modifies trabecular organization: A new model to study cortical and cancellous compartments in a single loaded element. *Bone* 37: 810–818.

Spiesz, E. M., et al. 2011. A quantitative collagen fibers orientation assessment using birefringence measurements: Calibration and application to human osteons. *J. Struct. Biol.* 176: 302–306.

Standen, E. M., et al. 2014. Developmental plasticity and the origin of tetrapods. *Nature* 513: 54–58.

Sugiyama, T., et al. 2012. Bones' adaptive response to mechanical loading is essentially linear between the low strains associated with disuse and the high strains associated with the lamellar/woven bone transition. *J. Bone Miner. Res.* 27: 1784–1793.

Sugiyama, T., et al. 2010. Functional adaptation to mechanical loading in both cortical and cancellous bone is controlled locally and is confined to the loaded bones. *Bone* 46: 314–321.

Sun, D., et al. 2018. Evaluation of loading parameters for murine axial tibial loading: Stimulating cortical bone formation while reducing loading duration. *J. Orthop. Res.* 36: 682–691.

Suniaga, S., et al. 2018. Increased mechanical loading through controlled swimming exercise induces bone formation and mineralization in adult zebrafish. *Sci. Rep.* 8: 1–13.

Swaddle, J. P. and A. A. Biewener. 2000. Exercise and reduced muscle mass in starlings. *Nature* 406: 585–586.

Swartz, S. M. 1990. Curvature of the forelimb bones of anthropoid primates: Overall allometric patterns and specializations in suspensory species. *Am. J. Phys. Anthropol.* 83: 477–498.

Swartz, S. M., et al. 1992. Wing bone stresses in free flying bats and the evolution of skeletal design for flight. *Nature* 359: 726–729.

Swartz, S. M., et al. 1989. Telemetered *in vivo* strain analysis of locomotor mechanics of brachiating gibbons. *Nature* 342: 270–272.

Tanck, E., et al. 2001. Increase in bone volume fraction precedes architectural adaptation in growing bone. *Bone* 28: 650–654.

Thomas, C. D. L., et al. 2005. Regional variation of intracortical porosity in the midshaft of the human femur: age and sex differences. *J. Anat.* 206: 115–125.

Trinkaus, E., et al. 1991. Robusticity versus shape: The functional interpretation of Neanderthal appendicular morphology. *Anthropol. Sci.* 99: 257–278.

Trinkaus, E. and C. B. Ruff. 1999. Diaphyseal cross-sectional geometry of Near Eastern Middle Palaeolithic humans: The Femur. *J. Archaeol. Sci.* 26: 409–424.

Turko, A. J., et al. 2017. Skeletal stiffening in an amphibious fish out of water is a response to increased body weight. *J. Exp. Biol.* 220: 3621–3631.

Turner, C. H., et al. 1995. Aging changes mechanical loading thresholds for bone formation in rats. *J. Bone Miner. Res.* 10: 1544–1549.

Umemura, Y., et al. 2002. A time course of bone response to jump exercise in C57BL/6J mice. *J. Bone Miner. Metab.* 20: 209–215.

Van der Meulen, M. C. H., et al. 1993. Mechanobiologic influences in long-bone cross-sectional growth. *Bone* 14: 635–642.

Van der Meulen, M. C. H., et al. 2008. Skeletal development: Mechanical consequences of growth, aging, and disease. In *Osteoporosis, two-volume set*. 3rd ed. Amsterdam: Elsevier Inc.

Villotte, S. and C. J. Knüsel. 2013. Understanding entheseal changes: Definition and life course changes. *Int. J. Osteoarchaeol.* 23: 135–146.

Vincentelli, R. and F. G. Evans. 1971. Relations among mechanical properties, collagen fibers, and calcification in adult human cortical bone. *J. Biomech.* 4: 193–201.

Visigalli, D., et al. 2010. Hind limb unloading of mice modulates gene expression at the protein and mRNA level in mesenchymal bone cells. *BMC Musculoskel. Disord.* 11: 147.

Voeten, D. F. A. E., et al. 2018. Wing bone geometry reveals active flight in *Archaeopteryx*. *Nat. Commun.* 9: 923.

Waarsing, J. H., et al. 2006. Bone loss dynamics result in trabecular alignment in aging and ovariectomized rats. *J. Orthop. Res.* 24: 926–935.

Wainwright, S. A., et al. 1982. *Mechanical design in organisms*. 2nd ed. Princeton, NJ: Princeton University Press.

Wallace, I. J., et al. 2014. Exercise-induced bone formation is poorly linked to local strain magnitude in the sheep tibia. *PLoS One*. 9: e99108.

Wallace, I. J., et al. 2015. Effects of load-bearing exercise on skeletal structure and mechanics differ between outbred populations of mice. *Bone* 72: 1–8.

Wallace, I. J., et al. 2013. Physical activity engendering loads from diverse directions augments the growing skeleton. *J. Musculoskel. Neuronal. Interact.* 13: 283–288.

Wallace, I. J., et al. 2017. Physical activity alters limb bone structure but not entheseal morphology. *J. Hum. Evol.* 107: 14–18.

Wallace, J. M., et al. 2007. Exercise-induced changes in the cortical bone of growing mice are bone- and gender-specific. *Bone* 40: 1120–1127.

Wallace, J. M., et al. 2009. Short-term exercise in mice increases tibial post-yield mechanical properties while two weeks of latency following exercise increases tissue-level strength. *Calcif. Tissue Int.* 84: 297–304.

Warshaw, J., et al. 2017. Collagen fiber orientation in primate long bones. *Anat. Rec.* 300: 1189–1207.

Weatherholt, A. M., et al. 2013. Cortical and trabecular bone adaptation to incremental load magnitudes using the mouse tibial axial compression loading model. *Bone* 52: 372–379.

Werning, S. 2012. The ontogenetic osteohistology of *Tenontosaurus tilletti*. *PLoS One*. 7: e33539.

West-Eberhard, M. J. 1989. Phenotypic plasticity and the origins of diversity. *Ann. Rev. Ecol. Syst.* 20: 249–278.

West-Eberhard, M. J. 2005. Phenotypic accommodation: Adaptive innovation due to developmental plasticity. *J. Exp. Zool. B Mol. Dev. Evol.* 304B: 610–618.

Wilkinson, M. T. 2008. Three-dimensional geometry of a pterosaur wing skeleton, and its implications for aerial and terrestrial locomotion. *Zool. J. Linn. Soc.* 154: 27–69.

VetBooks.ir

Williams, B., et al. 2004. Bone strength during growth: influence of growth rate on cortical porosity and mineralization. *Calcif. Tissue Int*. 74: 236–245.

Willie, B. M., et al. 2013. Diminished response to *in vivo* mechanical loading in trabecular and not cortical bone in adulthood of female C57Bl/6 mice coincides with a reduction in deformation to load. *Bone* 55: 335–346.

Willie, B. M., et al. 2020. Bone adaptation: Safety factors and load predictability in shaping skeletal form. *Bone* 131: 1115114.

Witmer, L. M. 1995. The extant phylogenetic bracket and the importance of reconstructing soft tissues in fossils. In *Functional morphology in vertebrate paleontology.*1st ed., Thomasen, J. J. ed., 19–33. Cambridge, UK: Cambridge University Press.

Witton, M. P. and M. B. Habib. 2010. On the size and flight diversity of giant pterosaurs, the use of birds as pterosaur analogues and comments on pterosaur flightlessness. *PLoS One*. 5: e13982.

Wolff, J. 1986. *The law of bone remodelling*. Berlin: Springer-Verlag.

Wolman, M. 1975. Polarized light microscopy as a tool of diagnostic pathology. *J. Histochem. Cytochem*. 23: 21–50.

Yang, H., et al. 2017. Effects of loading duration and short rest insertion on cancellous and cortical bone adaptation in the mouse tibia. *PLoS One*. 12: e0169519.

Yang, H., et al. 2019. Adaptive changes in micromechanical environments of cancellous and cortical bone in response to *in vivo* loading and disuse. *J. Biomech*. 89: 85–94.

Young, J. W. 2005. Ontogeny of muscle mechanical advantage in capuchin monkeys (*Cebus albifrons* and *Cebus apella*). *J. Zool*. 267: 351–362.

Young, J. W., et al. 2010. Ontogeny of long bone geometry in capuchin monkeys (*Cebus albifrons* and *Cebus apella*): implications for locomotor development and life history. *Biol. Lett*. 6: 197–200.

Young, V. K. H., et al. 2017. Humeral loads during swimming and walking in turtles: implications for morphological change during aquatic reinvasions. *J. Exp. Biol*. 220: 3873–3877.

Zani, P. A. 1996. Patterns of caudal-autotomy evolution in lizards. *J. Zool*. 240: 201–220.

Zumwalt, A. C. 2005. A new method for quantifying the complexity of muscle attachment sites. *Anat. Rec. B*. 286: 21–28.

Zumwalt, A. 2006. The effect of endurance exercise on the morphology of muscle attachment sites. *J. Exp. Biol*. 209: 444–454.

VetBooks.ir

35

Bone Microanatomy and Lifestyle in Tetrapods

Aurore Canoville, Vivian de Buffrénil and Michel Laurin

CONTENTS

Water, Land and Bones 724
Methodological and Terminological Overview 726
Data Acquisition Processes and Nature of the Raw Data 726
Nature of the Samples, Location and Orientation of the Sampling Planes 727
Why Study a Single Bone Element at a Time? 727
How to Code Lifestyle in Comparative Analyses 728
Statistical Comparisons and the Interplay Between Function and Phylogeny 728
The Phylogenetic Signal 728
The Ecological Signal 729
Paleobiological Inferences 729
Reference Studies in Extant Taxa 730
Appendicular Skeleton 730
Some General Patterns 730
Specializations of Major Tetrapod Taxa 730
Remarks on Fossorial and Arboreal Forms 732
Axial Skeleton 733
Turtle Shell 735
Lifestyle Inferences Based on Bone Microanatomy: A Review 736
Conclusion 738
References 738

Water, Land and Bones

The story of land vertebrates, their rapid diversification and conquest of different ecological adaptive zones started sometime between the Late Devonian and the Late Carboniferous. Limbed vertebrates originated among fully aquatic sarcopterygians, the tetrapodomorphs, which include, among others, *Eusthenopteron* and *Panderichthys*. Tetrapodomorphs thrived in the seas of the Middle and Late Devonian (Ahlberg and Clack 2006). Fossil tracks suggest that the first limbed stem-tetrapods arose as early as the Middle Devonian (Stössel 1995, Niedźwiedzki et al. 2010, Narkiewicz and Narkiewicz 2015), yet the earliest known stegocephalian body fossils, such as *Ichthyostega* and *Acanthostega*, suggest that these animals were apparently still mostly aquatic by the end of the Devonian (Long and Gordon 2004). The fossil record reveals that the evolution of four limbs (with well-defined limb segments and digits) and the terrestrialization process of vertebrates were not simultaneous, but gradual, in a series of adaptive shifts (Ahlberg and Milner 1994, Long and Gordon 2004, Ahlberg and Clack 2006). Moreover, the evolution of a terrestrial lifestyle in tetrapods seems to have been a nonlinear process that may have happened several times independently (Laurin 2010a). Optimization of lifestyle on a tree suggests that fully terrestrial stem-tetrapods were already present by the Late Carboniferous, about 340 Mya (Laurin and Buffrénil 2016: fig. 6). Stegocephalian biodiversity during the Carboniferous was dominated by stem-tetrapods and stem-amphibians that started to diversify their body plans and ecology. For example, aïstopods (Lepospondyli) constitute the first limbless tetrapods and appeared in the fossil record during the Early Carboniferous (Germain 2008). However, their lifestyle remains controversial (Schoch 2014). Many Carboniferous stegocephalians were semi-aquatic or fully aquatic, but it is not clear whether these conditions were primary or secondary (Laurin 2010a). Some taxa, such as the temnospondyls, thrived during the Carboniferous, Permian and Triassic and comprised small to giant forms with fully aquatic to almost fully terrestrial taxa (Schoch 2014). Lepospondyls were much smaller and encompassed the same size range as lissamphibians; they also included

VetBooks.ir

aquatic, amphibious and terrestrial taxa. Lissamphibians probably originated among lepospondyls (Marjanović and Laurin 2019), although alternative hypotheses exist regarding their origin (Schoch 2014). Lissamphibians include more than 8273 extant nominal species (www.amphibiaweb.org, accessed on January 7, 2021), with terrestrial, amphibious and fully aquatic forms (Duellman and Trueb 1994).

The oldest amniote fossil is from the Upper Carboniferous (about 319 Ma, Middle Pennsylvanian; Carroll 1964), but Amniota probably appeared about 10 My earlier (Didier and Laurin 2020). The amniote egg enabled them to become the dominant land vertebrates and rapidly diversify in body size and morphology and to colonize yet unexplored ecological resource zones (Laurin 2004). Many amniote groups independently returned to a partly or fully aquatic lifestyle by the Early Permian (Vermeij and Motani 2018), starting with the mesosaurs (Carroll 1988, Canoville and Laurin 2010, Modesto 2010, Nuñez Demarco et al. 2018), followed by other taxa such as ichthyosaurs, sauropterygians, some crocodylomorphs, various clades of chelonians and squamates (e.g., mosasaurs, some snakes and iguanas), dinosaurs (e.g., possibly some spinosaurids, and several groups of ornithurine birds) and mammals (e.g., cetaceans, desmostylians, sirenians, pinnipeds).

Fossil remains also reveal that some dicynodonts and temnospondyls from the Late Paleozoic occupied burrows (e.g., Smith 1987, Hembree et al. 2004), thus suggesting that various groups of tetrapods independently evolved digging and/or fossorial adaptations (Hasiotis et al. 2007) as early as the Permian. Several clades of stegocephalians (often fossorial or aquatic forms) evolved partial or complete limblessness (e.g., aïstopods, adelogyrinids, caecilians, snakes), while others became bipedal. *Eudibamus*, a small bolosaurid parareptile from the Early Permian, may be the oldest known bipedal tetrapod (Berman et al. 2000). Finally, aerial locomotion appeared repeatedly in the evolutionary history of amniotes, with the first gliding reptile, *Coelurosauravus*, recovered from the Upper Permian of Madagascar, Germany and England (Frey et al. 1997). Pterosaurs were the first true flying vertebrates, in the Late Triassic (Barrett et al. 2008), followed from the Jurassic onward by multiple maniraptoran dinosaur taxa, including birds (Voeten et al. 2018), and later bats in the Early Eocene (Simmons et al. 2008).

All these distinct locomotor adaptations and associated lifestyles generally affect bone architecture through different mechanical constraints and loading patterns (e.g., Wainwright and Reilly 1994, Habib and Ruff 2008, Botton-Divet et al. 2016, 2017). Distantly related taxa adapted to a similar lifestyle often exhibit closely convergent morphologies (e.g., Kelley and Motani 2015, Houssaye and Fish 2016), as emblematically exemplified by marine amniote faunas (Kelley and Pyenson 2015). Likewise, true flying amniotes (pterosaurs, birds, bats) all exhibit modifications of the pectoral girdle and/or an extension of the distal forelimb compared to their terrestrial relatives (Padian 1985, Rayner 1988, Gatesy and Middleton 2007).

Several studies since the end of the 19th century pointed out that lifestyle and locomotion type also influence the inner architecture and compactness of skeletal elements, i.e., bone microanatomy. Kiprijanoff (1881–1883) was probably the first to describe the spongy architecture of the limb bones of ichthyosaurs and plesiosaurs. Later, Nopcsa (1923), followed by Nopcsa and Heidsieck (1934), Zangerl (1935), Fawcett (1942) and Ricqlès (1974a, b, 1977), among others, noticed characteristic differences in bone density or compactness between terrestrial amniotes and their aquatic relatives. In parallel, Meister (1962) and then Olson and Hasegawa (1979) reported comparable differences between flying and diving birds. These first studies also revealed that bone structure may reflect different adaptive strategies of the taxa, depending on the degree of their secondary adaptation to the aquatic realm or their peculiar ecological specialization (Zangerl 1935, Meister 1962, Taylor 1994, 2000, Ricqlès and Buffrénil 2001). In brief, broad perspectives were thus opened to infer the locomotion pattern of extinct taxa from the inner structure of their bones.

The first comparative studies specifically investigating the relationship between lifestyle and bone inner structure began in the early 1980s. Most of these works focused on differences in bone density or relative cortical thickness among aquatic, semiaquatic and terrestrial mammals (Wall 1983, Buffrénil et al. 1986, Stein 1989, Fish and Stein 1991). Lissamphibians were considered subsequently (Leclair et al. 1993, Castanet and Caetano 1995). The early study by Currey and Alexander (1985) was a milestone because it considered all main amniote clades (among mammals and sauropsids) and diverse lifestyles and locomotor adaptations (terrestrial, fossorial, flying, and aquatic). Moreover, it compared different limb bones and followed a quantitative approach based on a *k* parameter describing relative cortical thickness at midshaft (this parameter is equivalent to the more commonly used *corticodiaphyseal index*). This study showed that the various skeletal elements of a given taxon differ in relative cortical thickness, with distal elements usually having a thicker cortex than proximal ones in terrestrial mammals and flying birds. Moreover, most flying amniotes (e.g., the pterosaur *Pteranodon*, bats and flying birds) have lower cortical thickness values than terrestrial birds and mammals. Currey and Alexander (1985) also noticed, as previously pointed out by Felts and Spurrell (1965) in whales, that body size may influence cortical thickness in terrestrial amniotes. Further investigations increased the number of extant and extinct clades of known ecological adaptation and sometimes employed less destructive sampling methods, thus enabling the collection of larger data sets.

Sophisticated methods were used to model and compare bone microanatomy (e.g., 3D or 2D), through compactness profiles (rather than mere density or global compactness), along with increasingly sophisticated analyses based on phylogeny-informed comparative methods. Observed morpho-functional relationships can then be transposed to fossils to help decipher ambiguous or controversial lifestyle adaptations in extinct taxa. An ever-increasing number of Paleozoic vertebrates has been considered in this respect, such as the finned tetrapodomorph *Eusthenopteron* (Laurin et al. 2007, Meunier and Laurin 2012, Sanchez et al. 2016), the Devonian stem-tetrapod *Acanthostega* (Sanchez et al. 2016), numerous basal stegocephalians (Ricqlès 1981, Laurin et al. 2004, Kriloff et al. 2008) and relatively basal amniotes (Ricqlès 1974a, b, Laurin et al. 2004, Germain and Laurin 2005, Kriloff et al. 2008, Canoville and Laurin 2010, Laurin and Buffrénil 2016). This will hopefully help paleontologists to piece together the

very complex history of the conquest of land by vertebrates (Laurin 2010a). This source of information has also been used to understand the timing of adaptation of more recent, secondarily aquatic taxa, such as ichthyosaurs (Buffrénil and Mazin 1990, Nakajima et al. 2014a, Houssaye et al. 2014b, 2018b), mosasaurs (Houssaye et al. 2008, Houssaye et al. 2013b), sirenians (Buffrénil and Schoevaert 1989, Buffrénil et al. 2010), cetaceans (Buffrénil et al. 1990, Gray et al. 2007, Thewissen et al. 2007, Houssaye et al. 2015, Cooper et al. 2016) and some extinct sloths (Amson et al. 2014, 2018). Finally, a great deal of work involving bone microanatomy has been carried out to tackle fundamental questions regarding the evolution of turtles: the origin and evolution of the shell and whether this unique body plan appeared in an aquatic, terrestrial, or fossorial ancestor (Scheyer and Sander 2007, Scheyer et al. 2014, 2015, Cerda et al. 2016, Lyson et al. 2016).

This chapter is intended to summarize the most relevant data on the relationship between bone microanatomy and lifestyle adaptations in extant and extinct tetrapodomorphs. Special attention will be paid to methodological approaches and the critical assessment of the results.

Methodological and Terminological Overview

Data Acquisition Processes and Nature of the Raw Data

The inner architecture of bone, a concept that includes relative cortical thickness, global compactness, compactness profile and the geometry of trabecular networks, has been traditionally studied from thin sections. This involves a destructive sampling of the skeletal elements of interest and the making of thin sections following standard procedures used in comparative bone histology (see, for example, Lamm 2013). Depending on the problem considered, the size and degree of complexity of the sample, the resulting sections are either drawn with a camera lucida or directly digitized to be transformed in both cases into a binary document using a standard image editing software. One color (usually black; Figure 35.1) depicts bone tissue and the other one (usually white) represents all cavities (see, e.g., Laurin et al. 2007, 2011, Scheyer and Sander 2009, Buffrénil et al. 2010, Canoville and Laurin 2010, Houssaye et al. 2013b, Scheyer et al. 2015, Klein et al. 2016).

Today, nondestructive techniques are increasingly used for bone microanatomical investigations. Since the early 2000s, conventional and synchrotron X-ray microtomography have become more accessible to the biological and paleontological communities (Rossi et al. 2004, Tafforeau et al. 2006) and are now widely used to investigate the microanatomy of extant and extinct taxa (e.g., Amson et al. 2014, 2017, Houssaye et al. 2015, 2016a, b, Canoville et al. 2016). Nondestructive techniques provide two decisive advantages: they preserve specimen integrity, which allows the processing of larger samples and extensive comparative analyses, and with 3D data sets there is the potential to investigate bone microanatomy in different sectional planes (Houssaye et al. 2018a) and provide a better understanding of the overall adaptation of a given skeletal element to specific biomechanical constraints and ecology (Houssaye and Botton-Divet 2018).

Several programs are currently applied to digital sections (whatever their origin) to extract parameters describing bone microanatomy. Relative cortical thickness can be measured with image processing software (e.g., Castanet and Caetano 1995), whereas more complex sets of parameters depicting the overall organization of a bone, its global compactness or

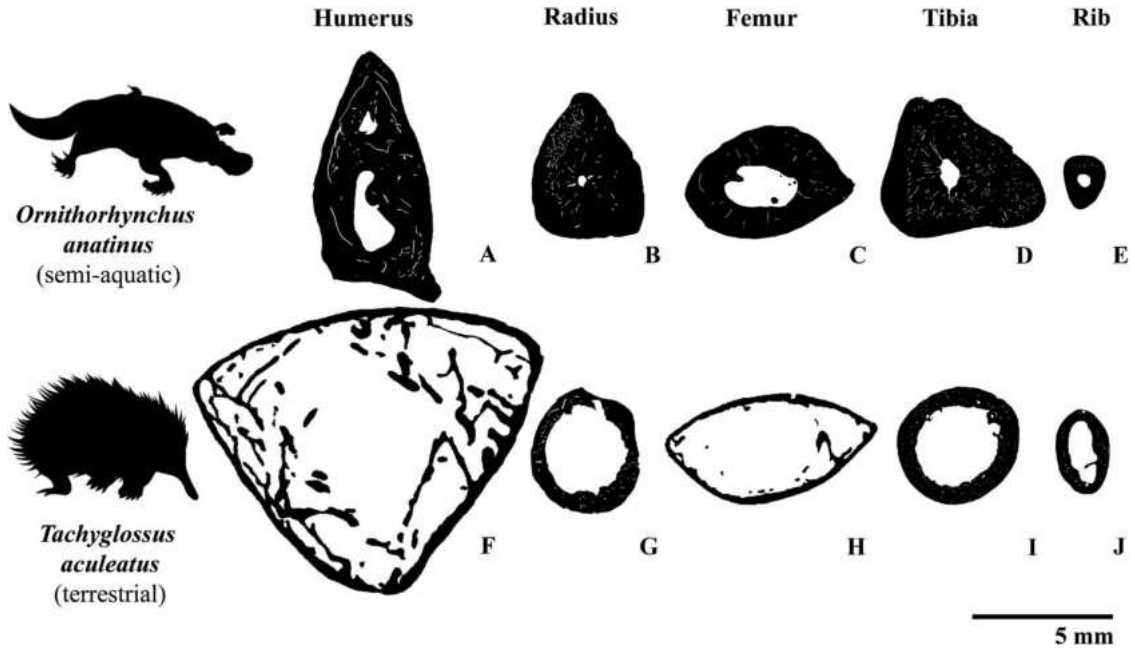


FIGURE 35.1 Mid-diaphyseal cross sections of various long bones in two closely related monotremes: the semiaquatic *Ornithorhynchus anatinus* (A–E) and the terrestrial *Tachyglossus aculeatus* (F–J). These sections were, respectively, published and analyzed in one or several of these articles: Germain and Laurin (2005), Kriloff et al. (2008), Canoville and Laurin (2010), Laurin et al. (2011), Quémeneur et al. (2013) and Canoville et al. (2016).

VetBooks.ir

the characteristics of its trabecular network can be obtained with software specifically designed for the study of bone tissues. Among them, Bone Profiler (Girondot and Laurin 2003) can extract several parameters that describe the distribution of bone tissue in a section, i.e., its compactness profile (technical details in Girondot and Laurin 2003). In brief, Bone Profiler models bone microanatomy using four main parameters, *P*, *S*, *Min*, and *Max*, and a few more that will not be presented here. Collectively, these parameters allow comparison of the amount and distribution of bone tissue in a section. In the compactness profile, the X-axis represents the position on the radius, 0 being the ontogenetic bone center and 1 its periphery. The Y-axis quantifies compactness. A sigmoid curve is created in which *P* is the position of the inflection point, which is also the location of the transition zone between medulla and cortex. Parameter *S* (i.e., the reciprocal of the slope at the inflexion point) is proportional to the width of the transition zone between medulla and cortex. *Min* and *Max* are the lower and upper asymptotes, respectively, and give indications about the compactness in the center and at the periphery of the bone, respectively. Bone Profiler has been and is still currently used in most quantitative studies of the relationship between bone microanatomy and lifestyle adaptations in extant and extinct sarcopterygians. Because this software is based on a sigmoid model, it is particularly well suited to skeletal elements (and sectional planes) in which a compact cortex is well differentiated from a less compact medullary region, regardless of the morphology of the bone. It has been most frequently used on cross-sections of long bones. Other software, especially ImageJ (Abramoff et al. 2004) and its plug-in BoneJ (Doube et al. 2010) are also commonly used to describe and quantify (in two or three dimensions) the characteristics of trabecular networks in long bone epiphyses (Amson et al. 2017, Mielke et al. 2018) and vertebrae (Dumont et al. 2013), and eventually quantify cortical compactness (Houssaye et al. 2008, Houssaye and Bardet 2012, Houssaye et al. 2013a, 2014a, b, Houssaye and Botton-Divet 2018, Montañez-Rivera et al. 2018).

Nature of the Samples, Location and Orientation of the Sampling Planes

The use of standardized samples is critical for comparative microanatomical studies. Hence, selected specimens should ideally all be adults. Ontogenetic change is known to affect bone microanatomy in several ways. Cortical thickness and compactness, as well as the relative size of the medullary cavity, are not constant throughout the growth of a given skeletal element, but they stabilize at somatic adulthood (Buffrénil and Francillon-Vieillot 2001, Montoya-Sanhueza and Chinsamy 2017). Moreover, several studies have highlighted the effects of senescence on bone microstructure, which is usually associated with a loss in bone volume and mass (Castanet et al. 1993, Castanet et al. 2001), so it is not advantageous to choose individuals that are very old adults. When possible, it is also recommended to favor wild individuals over animals that were kept in captivity. Captivity is often associated with limited locomotion and a different diet, which can affect the overall compactness and architecture of skeletal elements (e.g., Meers 2002). The reproductive status of an individual can also affect cortical thickness and trabecular volume, especially in females (e.g., Buffrénil and Francillon-Vieillot 2001, Montoya-Sanhueza and Chinsamy 2017). Female birds are unique among extant tetrapods in forming medullary bone, a sex-specific, estrogen-dependent tissue, during the egg-laying cycle (Dacke et al. 1993). This ephemeral osseous reserve is a key source of calcium for eggshell formation. It is deposited in the cavities of skeletal elements shortly before the onset of the laying cycle and partly or completely resorbed by the end of the cycle when eggshell calcifies (Dacke et al. 1993). The overall microanatomy of some skeletal elements is thus considerably affected during the reproductive cycle of female birds (e.g., Canoville et al. 2019).

By convention, bone microanatomy is commonly observed in cross section around the center of ossification included in the so-called *neutral plane* of long bones (which is not necessarily midway between both epiphyses), where the compact cortex is the thickest and where the diaphyseal tissue is free from metaphyseal remnants. Several studies have highlighted that cortical thickness and overall architecture can vary drastically along the shaft of these elements (Wall 1983, Nakajima and Endo 2013, Nakajima et al. 2014b, Canoville et al. 2016, Houssaye et al. 2018a). In long bones, the analysis of trabecular networks is generally restricted to epiphyses or metaphyses (e.g., Doube et al. 2011, Amson et al. 2017). The overall microanatomy of vertebrae can be studied either along their median sagittal or their neutral transverse sectional planes (Buffrénil et al. 2008, Houssaye et al. 2010, Dumont et al. 2013). Osteoderm microanatomy is usually observed in cross sections, orthogonal to the long axis of the element (e.g., Scheyer and Sander 2007).

Why Study a Single Bone Element at a Time?

Many of the comparative studies mentioned above focused on a single element that was compared across several taxa (e.g., Canoville and Laurin 2010 for the humerus; Canoville et al. 2016 for the ribs; Dumont et al. 2013 for the vertebrae). It is advantageous to study evolutionary patterns and produce paleobiological inference models. Comparing different elements in various taxa would be problematic because each element differs from the others in size, shape, position and orientation, among other factors. Thus, stylopodial elements (humerus and femur) of taxa with a sprawling posture may have a more or less horizontal orientation and experience much torsion during locomotion, whereas the zeugopodial elements may alternate between nearly horizontal and nearly vertical orientations during locomotion, and presumably experience more bending strain (Hildebrand and Goslow 2001). Also, stylopodial elements often have a greater diameter and a larger medullary cavity than zeugopodial elements, at least when the zeugopod is composed of two elements of similar sizes, which is the primitive condition for stegocephalians. Obviously, in such cases, the stylopodial element has to be about as strong as both zeugopodial elements combined, a requirement likely to explain much of the difference in robustness between elements of these two limb segments. However, even the humerus and the femur can be expected to differ in many taxa because they do not experience exactly the same mechanical loading, given

VetBooks.ir

that the proportion of the animal's weight that is supported by fore and hind limbs differs in most taxa. This discrepancy will be maximal in bipedal animals (in which the forelimbs are not weight-bearing), or those, like bats, that fly with their forelimbs only, but should apply also to various extents to nearly all taxa. For similar reasons, comparisons between long limb bones and vertebrae or ribs are even more problematic. Thus, it would be unadvisable to apply an inference model designed for one bone to another skeletal element, or to draw conclusions about the evolution of limb elements based on nonhomologous elements in various taxa.

Similarly, skeletal adaptations to various lifestyles may affect various parts of the skeleton differently. The sirenian *Dugong dugon*, for example, has some very compact bones (ribs, humerus), but other bones are not more compact than those of a terrestrial mammal such as, e.g., *Panthera leo* (Buffrénil and Schoevaert 1989). Therefore, skeletal adaptations must be studied in precise taxonomic and anatomical contexts.

How to Code Lifestyle in Comparative Analyses

Most data available in the literature about habitat use are qualitative observations unsuited to a quantification of lifestyles in terms of proportion of habitat use, proportion of foraging time or, for aquatic taxa, time spent at various depths and at the surface. When such data exist (e.g., Hays et al. 2002), they have not been compiled into comprehensive databases. For this reason, most studies have divided lifestyles into a variable number of categories (generally, two to four), from terrestrial to aquatic (or between ground-dwelling, arboreal, flying, etc.). However, detailed information on habitat for a large number of taxa should improve deciphering the diversity of microanatomical features. For taxa that swim mostly or exclusively at the surface and regularly return to land, there should be little or no evolutionary pressure to evolve pachyosteosclerosis. This might explain the lack of obvious microanatomical specialization to an amphibious lifestyle in amphibious rodents (Canoville and Laurin 2010). Conversely, in fully aquatic amniotes that come to the surface only to breathe, mean swimming depth and swimming speed are crucial. Sluggish swimmers in shallow waters, such as sirenians and the now-extinct aquatic sloths (Amson et al. 2014), typically evolve osteosclerosis or pachyostosis as a passive means for buoyancy and body trim control. In contrast, pelagic, deep, active divers such as most extant cetaceans have spongy bones, presumably because beyond a few tens of meters below the surface, lung volume is so reduced that it no longer generates significant buoyancy and that energy can be saved during locomotion by limiting inertia through a reduction of skeletal mass. Extant cetaceans display a fair amount of microanatomical variability (Canoville et al. 2016: figure 9), which might be explained to a large extent by a corresponding variability in habitat use. Hays et al. (2002) found that the mean swimming depth of *Chelonia mydas* populations differed substantially between sites. Thus, to get an accurate picture for a single species, much sampling effort is required. Of course, gathering such data for dozens of species will be far more time-consuming, although the technology required for this has been around for some time.

Statistical Comparisons and the Interplay Between Function and Phylogeny

The Phylogenetic Signal

In a comparative context, the statistical analysis of microanatomical and ecological data requires phylogeny-informed methods to detect and take into consideration the presence of a phylogenetic signal. This term refers to the similarity in character value or state due to phylogenetic relationships. In other words, closely related taxa tend to resemble each other more than distantly related taxa. This phenomenon seems intuitively obvious, especially at a large taxonomic scale (for instance, two vertebrate taxa resemble each other more than a vertebrate and an arthropod or mollusk), but its implications for statistical analyses were not fully grasped until Felsenstein (1985) developed the method of phylogenetic independent contrasts designed to cope with the statistical nonindependence of raw comparative data. Several other analytical approaches taking phylogeny into account were developed subsequently (Grafen 1989, Harvey and Pagel 1991, Legendre et al. 1994, Martins and Hansen 1997, Pagel 1997, Diniz-Filho et al. 1998, Desdevises et al. 2003) with the aim of replacing the usual data processing by phylogeny-informed analyses. Further theoretical arguments and simulations by Revell (2010) pointed out that phylogeny-informed analyses should be performed when a phylogenetic signal occurs in residuals of regression models rather than in the original variables derived from raw data.

Several methods have been proposed to test for the presence of a phylogenetic signal. These are reviewed in Chapter 30 and need not be presented again here. Instead, we provide a brief history of when and how phylogenetic signal was studied in bone histology or microanatomy. The first paper that assessed the presence of a phylogenetic signal in bone microanatomy was Laurin et al. (2004), in which this was achieved by regressing distance matrices of bone microanatomical characters against a phylogenetic distance matrix. Statistical significance was then assessed through random permutations, as originally proposed by Legendre et al. (1994), as well as through a new method developed by Laurin (2004). The latter consists of comparing the amount of change implied by a reference tree (which must be obtained independently of the data analyzed) with that of a population of random trees. For discrete characters, the random trees can be obtained in many ways, but for continuous data (as are most bone microanatomical and histological data), if squared-change parsimony is used (and this is better than linear parsimony), the length of random trees (expressed as the sum of their branch lengths) has to match that of the reference tree. The easiest way to achieve this is to randomly permutate the tips while keeping the tree shape and branch lengths constant. Laurin et al. (2004) concluded that some bone microanatomical characters contained a phylogenetic signal.

Soon thereafter, assessments of phylogenetic signal in bone microanatomical and histological data became increasingly frequent. Germain and Laurin (2005) used the same methods as Laurin et al. (2004) and similarly found a phylogenetic signal in several characters. The study by Cubo et al. (2005) was the first to be devoted exclusively to the study of a phylogenetic

VetBooks.ir

signal in bone histology and microanatomy. It used both the test based on squared-change parsimony described above and Mantel tests (regressions between distance matrices, with the significance assessed by randomly permuting the data) to reveal a phylogenetic signal in histological and microanatomical characters in various clades. This study found a signal in both kinds of characters for some clades (sauropsids, diapsids, archosaurs, and to a lesser extent, in lepidosaurs and neognaths) but not in others (never in turtles). This signal was more pervasive in bone microanatomy (cross-sectional area, as a proxy of size, and cortical thickness) than in histological characters. Among the latter, the signal was strong in vascular density, but not significant in vascular orientation and index of Haversian remodeling.

Not all subsequent studies that tackled phylogenetic signal in bone microanatomy and histology need to be covered here. It might be sufficient to mention that the one of the last study dedicated mainly to this issue found that all the investigated histological characters (no microanatomical feature was included) displayed a phylogenetic signal (Legendre et al. 2013). Furthermore, it showed that the phylogeny explained between 20 and 60% of the variance in these characters. It thus concluded that these data need to be analyzed through phylogeny-informed methods, and indeed, this is now the established practice.

The Ecological Signal

An ecological signal in bone microanatomy is the structural variation that reflects an adaptation to lifestyle. This topic was first investigated long ago (e.g., Nopcsa 1923, Nopcsa and Heidsieck 1934), but this chapter will focus on quantitative studies that included statistical tests of quantitative bone microanatomical data. Phylogeny-informed analytical methods were not used in the earliest studies: early quantitative analyses incorporated no phylogenetic data (Wall 1983, Fish and Stein 1991, Leclair et al. 1993, Castanet and Caetano 1995). The first studies to use a phylogeny-informed method were by Laurin (2004) and Germain and Laurin (2005), who used the method developed by Legendre et al. (1994); i.e., regressions of distance matrices in which the phylogeny was represented by a distance matrix, and permutations were used to test the significance of the relationship. However, regressions on distance matrices are conservative (Legendre 2000), so subsequent studies used other methods supposed to be more powerful. Kriloff et al. (2008) and Canoville and Laurin (2009) used variance partition with phylogenetic eigenvector regressions (PVR), previously developed by Desdevises et al. (2003), with reference to Diniz-Filho et al.'s (1998) principles. This method summarizes the distance matrix by a restricted number of phylogenetic axes that are obtained by principal coordinate analysis. It has the advantage of allowing classical linear regressions using the original variables, and a quantification of the proportion of the variance that can be explained by phylogeny (i.e., the phylogenetic signal), by other explanatory variables (here, the ecological signal) and by a covariance of both. However, simulations have shown that such methods yield unreliable probabilities (Purvis et al. 1994, Rohlf 2006, Laurin 2010b, Freckleton et al. 2011), and as such, they should not be used to assess the statistical significance of relationships between bone microanatomy and lifestyle. Subsequent studies (e.g., Laurin et al. 2009, Canoville and Laurin 2010) used phylogenetic independent contrasts, in addition to variance partition with PVR. Phylogeny-informed analyses are now currently used to investigate the relationship between bone microanatomy and lifestyle (e.g., Canoville et al. 2016, Zhou et al. 2018, Kilbourne and Hutchinson 2019).

Paleobiological Inferences

The aim of early studies by Nopcsa (1923) and Nopcsa and Heidsieck (1934) were more to document how bones adapt to an aquatic lifestyle than to infer lifestyles from bone microanatomy. Later studies looked at bone microanatomy both to assess how aquatic some taxa were, and to collect more precise data about which habitat they occupied. Explicit comparisons were made to extant taxa of known lifestyle, or with extinct taxa whose lifestyle seemed well documented by taphonomic or morphological data (e.g., Ricqlès 1974b: 35). However, lifestyle inferences still rested on a qualitative and hence somewhat subjective assessment of bone microanatomy and histology. Furthermore, the relevant comparative data on the other taxa were found in other papers, which were simply cited to support the interpretations. A quantitative approach to microanatomy-based lifestyle inference was inaugurated by Buffrénil and Rage (1993), who quantified the compactness of nine nominal genera of extant snakes and of the Cretaceous presumed stem-ophidian *Simoliophis* to infer the latter's lifestyle. For the first time, all the relevant information required to infer the lifestyle of an extinct taxon was found in a single study. In that case, it provided strong evidence that *Simoliophis* was a fairly aquatic taxon, because the aquatic snakes included in the comparative sample had a higher compactness than terrestrial snakes, and *Simoliophis* had a greater compactness than any sampled extant snake.

More recent studies have taken a statistical approach to first establish a reference relationship between bone microanatomy and lifestyle, and then use it for paleobiological inferences. The latter should ideally be restricted to clades in which a relationship has been previously shown. This last point was first made for discrete characters by Witmer (1995) and extended to quantitative data by Laurin et al. (2004). But body size must also be considered, given that it affects many attributes of organisms, including bone structure (e.g., Currey and Alexander 1985, Dumont et al. 2013). This is why the first quantitative, statistically supported paleobiological inference model (Laurin et al. 2004) applied inference models only to extinct taxa in the size range of the extant taxa comprising the reference data set. In brief, to be reliable, inferences should ideally be performed only within the morphospace that was explored in the taxa used to produce the model.

The first inference models (discussed above) did not take into consideration the systematic affinities of the extinct taxa whose lifestyle had to be inferred. However, given that the nature and strength of relationships between variables may differ between portions of the Tree of Life, it would be

VetBooks.ir

desirable to take affinities into consideration. The first paleobiological inference model based on bone histology that met this criterion was produced by Organ et al. (2007) to infer genome size in long-extinct organisms based on osteocyte lacuna size. Their method is based on a phylogenetic regression that takes into account the covariation expected on the basis of the phylogeny, and character mapping, which is analogous to optimization. More recently, Legendre et al. (2016) also produced a phylogeny-informed paleobiological inference model using the eigenvector map method (Guénard et al. 2013), which summarizes the phylogeny through a number of axes obtained through principal coordinate analysis, as in variance partition with PVR (see above). The model produced by Legendre et al. (2016) was designed to infer metabolic rate, but this method, used on microanatomical data, could be used to produce lifestyle inference models that take into consideration the systematics of extinct taxa to which the model is applied. Much progress remains to be done in the field of paleobiological inference in general, and lifestyle inference based on bone microanatomy in particular.

Reference Studies in Extant Taxa

So far, studies investigating the relationship between lifestyle adaptations and bone microanatomy have mainly dealt with the appendicular skeleton. Axial (vertebrae and ribs) and dermal (osteoderm, turtle shell) elements have been less frequently considered. Moreover, the majority of these studies focused on amniote clades, and only a few dealt with lissamphibians. Finally, the microanatomical adaptation of skeletal elements has been best documented in secondarily aquatic amniotes, and remains poorly studied in fossorial and arboreal tetrapods.

Appendicular Skeleton

In extant faunas, terrestrial tetrapods, whatever the zoological group to which they belong (except turtles), usually have tubular limb bones, with dense cortices and an open medullary cavity, mostly free of trabeculae (e.g., Laurin et al. 2011, Canoville and Laurin 2010). In amniotes at least, studies of bone microstructures and lifestyle have mainly focused on the divergence from this generalized condition induced by particular habitats and locomotory modes.

Some General Patterns

There is a progressive increase in limb bone compactness from terrestrial to semiaquatic and finally fully aquatic, shallow diving (coastal or continental) tetrapods (Stein 1989, Buffrénil 1990, Ricqlès and Buffrénil 2001; see also Figures 35.1 and 35.2). The evolution of high limb bone density in shallow-water dwellers is commonly recognized as an adaptation to counteract buoyancy and/or control body trim (Nopcsa 1923, Fawcett 1942, Kaiser 1960, Wall 1983, Taylor 2000, Ricqlès and Buffrénil 2001). Conversely, pelagic and deep diving forms, represented in extant faunas by most cetaceans and pinnipeds, show a distinct bone structure most often (but not necessarily) associated with local skeletal lightening. In limb long bones, this is manifested by an overall cancellous inner architecture, where most of the shaft consists of a trabecular network, with a small or nonexistent free medullary cavity and thin compact cortices (Felts and Spurrell 1965, 1966, Wall 1983, Buffrénil and Schoevaert 1988, Kriloff et al. 2008, Canoville and Laurin 2010, Laurin et al. 2011; see Figure 35.2A–C). When resulting in a decrease in bone mass, this peculiar organization is interpreted as providing enhanced acceleration and maneuverability performances under water, therefore, saving energy during locomotion (Zangerl 1935, Buffrénil et al. 1986, Ricqlès and Buffrénil 2001).

Specializations of Major Tetrapod Taxa

In mammals and most sauropsids, semiaquatic/amphibious species have higher limb bone compactness than their fully terrestrial relatives (Wall 1983, Stein 1989, Canoville and Laurin 2010, Laurin et al. 2011, Nakajima and Endo 2013, Houssaye and Botton-Divet 2018; see Figures 35.1 and 35.2D–I). They also often display a different inner architecture, with thicker cortices and a trabecular network colonizing the medullary cavity (Wall 1983, Stein 1989, Houssaye and Botton-Divet 2018). Some quantitative studies conducted hitherto failed to discriminate amphibious taxa from their terrestrial relatives (Stein 1989, Laurin et al. 2004), though others did (Germain and Laurin 2005, Canoville and Laurin 2010, Quémeneur et al. 2013). Amphibious taxa are not phenotypically intermediate between aquatic and terrestrial forms (Laurin et al. 2011). A series of studies conducted on different limb elements (humerus, radius, femur, tibia) have shown that amphibious and terrestrial taxa greatly overlap in their microanatomical features, though centroid position and dispersion around it generally differ between the two lifestyles (Germain and Laurin 2005, Kriloff et al. 2008, Canoville and Laurin 2010, Quémeneur et al. 2013).

The lack of a sharp separation between terrestrial and amphibious taxa might also reflect the great ecological and morphological heterogeneity of amphibious forms (Canoville 2010, Houssaye and Botton-Divet 2018). Some rodents and mustelids often swim at the surface of the water (Williams 1983, Fish 1984) and have long bone compactness similar to their terrestrial relatives: bone mass increase in this case would presumably be energetically disadvantageous. Others have a preferential subaquatic locomotion, such as some lutrines (Fish 1994, Pfeiffer and Culik 1998, Houssaye and Botton-Divet 2018), the common hippopotamus *Hippopotamus amphibius* (Wall 1983, Coughlin and Fish 2009, Houssaye et al. 2016b), the platypus *Ornithorhynchus anatinus* (Fish et al. 1997, 2001, Germain and Laurin 2005, Canoville 2010, Laurin et al. 2011; see Figure 35.1A–D), the marine iguana *Amblyrhynchus cristatus* (Canoville 2010, Hugi and Sánchez-Villagra 2012) and some crocodilians (Canoville 2010). These taxa tend to have thick cortices that act as a ballast in some or all limb bones. However, to our knowledge, this question has not been fully investigated for most amphibious taxa with detailed data about characteristic swimming depth (especially surface vs submerged). Land-dwelling graviportal animals such as elephants and rhinoceroses have higher global compactness

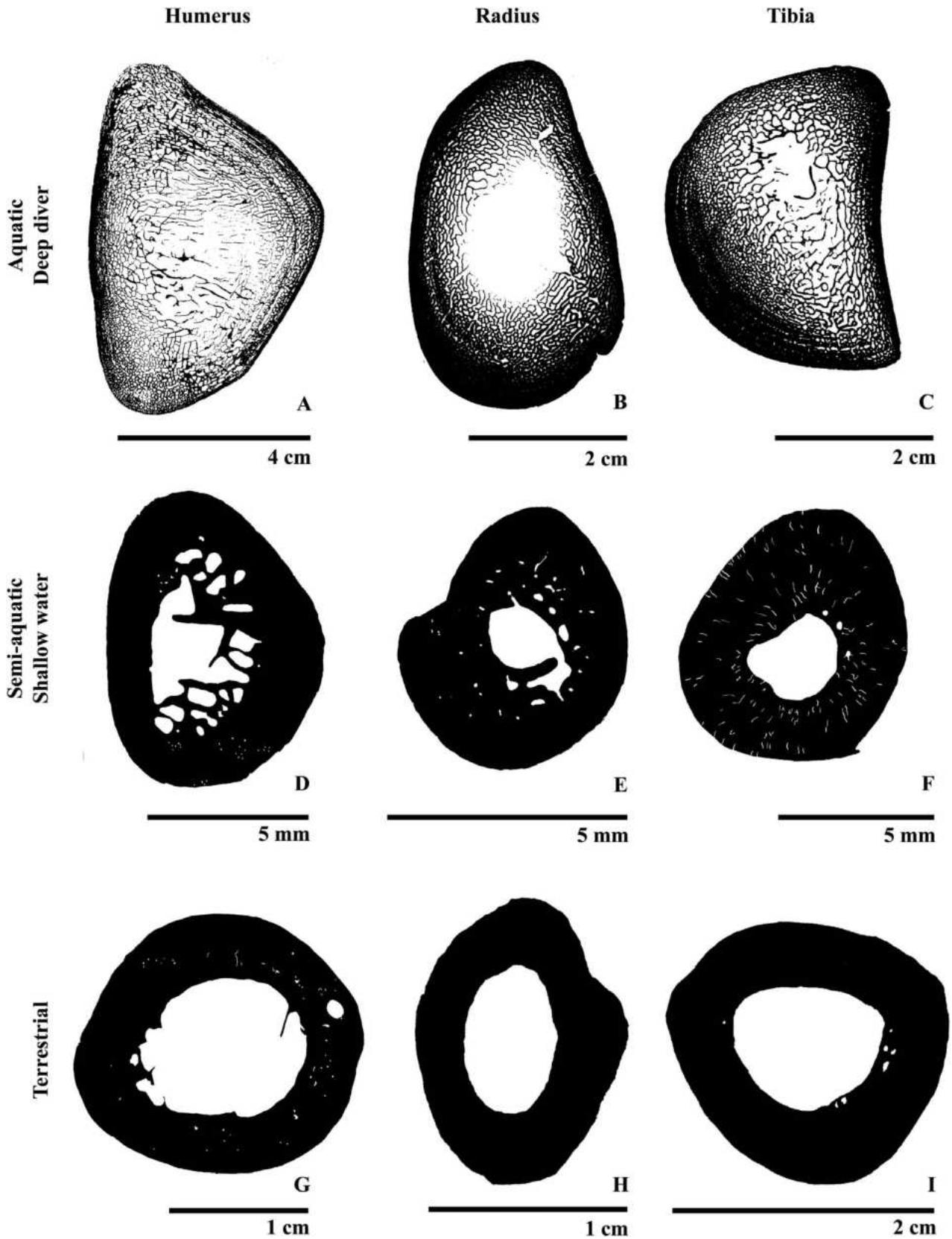


FIGURE 35.2 Mid-diaphyseal cross sections of various limb bones in three mammalian species with different lifestyles: the mostly aquatic, deep-diver *Mirounga Leonina* (A–C); the semiaquatic, shallow diver *Myocastor coypus* (D–F) and the terrestrial *Canis lupus* (G–I). These sections were published and analyzed in one or several of these articles: Germain and Laurin (2005), Kriloff et al. (2008), Canoville and Laurin (2010) and Laurin et al. (2011).

values in limb bones than their smaller relatives, along with thicker cortices and a relatively smaller medullary cavity filled by a spongiosa (Wall 1983, Alexander and Pond 1992, Houssaye et al. 2016b).

Although less investigated, several studies have documented the relationship between lifestyle and long bone microanatomy in birds. Flying birds generally have lightweight skeletons, with thinner cortices than their fully terrestrial or aquatic relatives (Habib and Ruff 2008). Semiaquatic birds seem to have intermediate bone compactness values between flying and flightless diving birds (Habib and Ruff 2008). Flightless diving birds encompass several distantly related clades (Pan-Alcidae, Spheniscidae, members of Phalacrocoracidae) and all show, by convergence, some degree of osteosclerosis in their limb bones (Meister 1962, Habib and Ruff 2008, Smith and Clarke 2014, Ksepka et al. 2015, Canoville and Buffrénil 2016).

Evidence suggests that long bone microanatomy is also affected by lifestyle in lissamphibians. Aquatic anurans and urodeles generally have osteosclerotic limb bones, with higher global compactness than related terrestrial forms (Laurin et al. 2004, 2011, Canoville and Laurin 2009). However, as in most other tetrapod groups, statistical analyses often fail to find a clear difference between semiaquatic and terrestrial taxa (Laurin et al. 2004, Kriloff et al. 2008, Canoville and Laurin 2009).

For all these tetrapod groups (mammals, lepidosaurs, crocodilians, birds, lissamphibians), various quantitative comparative studies (Laurin et al. 2004, Germain and Laurin 2005, Kriloff et al. 2008, Canoville and Laurin 2009, 2010, Quémeneur et al. 2013, Houssaye et al. 2016b) suggest that stylopodial elements contain a stronger ecological signal for all locomotion types than zeugopodial elements. This confirms previous reports of a decreasing proximodistal gradient of compactness along the limbs of some aquatic taxa, as exemplified by the dugong (Buffrénil and Schoevaert 1989) and the king penguin, *Aptenodytes patagonicus* (Canoville and Buffrénil 2016). The same situation occurs, but with an increasing compactness gradient, in flying birds (Currey and Alexander 1985, Margerie et al. 2005) and in dolphin flippers (Buffrénil et al. 1986).

Terrestrial turtles differ from other tetrapod groups: while most (semiaquatic or aquatic) freshwater forms show the expected osteosclerotic pattern of tetrapods living in shallow water, some terrestrial species surprisingly show the same peculiarity (Germain and Laurin 2005, Kriloff et al. 2008, Canoville 2010, Canoville and Laurin 2010, Queméneur et al. 2013, Nakajima et al. 2014b; see also Figure 35.3A–H). Moreover, terrestrial turtles lack the common limb bone tubular architecture and rather exhibit a reduced or absent free medullary cavity, filled with either a loose or a dense spongiosa (Laurin et al. 2011, Nakajima et al. 2014b; Figure 35.3A–D). As a result, terrestrial and freshwater turtles cannot be discriminated through long bone microanatomy alone (Germain and Laurin 2005, Kriloff et al. 2008, Canoville 2010, Canoville and Laurin 2010, Quémeneur et al. 2013, Nakajima et al. 2014b). However, open-sea (pelagic) turtles such as *Chelonia mydas*, *Dermochelys coriacea* and *Caretta caretta* all have lightly built limb bones, with an extensive spongiosa and relatively thin compact cortices throughout the shaft, as otherwise seen in, e.g., most extant cetaceans (Germain and Laurin 2005, Kriloff et al. 2008, Nakajima et al. 2014b; Figure 35.3I).

Remarks on Fossorial and Arboreal Forms

Among tetrapods, many clades have morphological specializations, evolved convergently, for scratch-digging and fossoriality. A few preliminary studies have investigated the limb bone microanatomy of semifossorial, fossorial and subterranean mammals and squamates considering either the global compactness at midshaft or the trabecular architecture of epiphyses. Independent studies have repeatedly reported higher compactness values in small fossorial mammals and squamates than in surface-dwelling terrestrial relatives of similar size, yet without investigating this relationship quantitatively and in large samples. This situation was observed in the dwarf armadillo, *Zaedyus pichiy* (Laurin et al. 2011), the mole rat *Heterocephalus glaber* (Nasterlack et al. 2012), the Cape dune mole rat, *Bathyergus suillus* (Montoya-Sanhueza and Chinsamy 2017, 2018), the aardvark *Orycteropus afer* (Legendre and Botha-Brink 2018) and diverse other mammals and squamates by Magwene (1993). However, Meier et al. (2013) failed to find an ecological signal related to the global compactness of the humerus in 11 extant talpid taxa with terrestrial, semiaquatic and fossorial lifestyles. They nevertheless noticed a significant difference in the width of the transition zone between the medullary cavity and the compact cortex (i.e., Bone Profiler parameter *S*); this zone is wider in fossorial than in nonfossorial talpids. The microanatomical consequences of digging may be uneven in distinct skeletal regions. In xenarthrans, bone compactness in fossorial taxa increases only in the humerus, the bone most involved in digging (Straehl et al. 2013), and fossoriality seems to affect the trabecular architecture of forelimb epiphyses (Amson et al. 2017).

Only a few studies have considered the possible relationship between arboreality and bone microanatomy. The so-called tree sloths are represented by two extant genera, *Bradypus* and *Choloepus*, and the crown-clade that contains them also includes giant ground sloths (Toledo et al. 2017). *Bradypus* and *Choloepus* are among the few fully arboreal mammalian taxa. Straehl et al. (2013) first compared the humeral and femoral global compactness of these taxa with other terrestrial and fossorial members of xenarthrans and found that the global compactness values of "tree sloths" are not significantly different from other nonarboreal xenarthrans. Montañez-Rivera et al. (2018) further investigated the limb bone microanatomy of xenarthrans and reported that tree sloths convergently evolved lower cortical compactness values than their relatives due to an active Haversian remodeling and the presence of numerous immature secondary osteons throughout the cortex. Montañez-Rivera et al. (2018) hypothesized that this difference is most likely related to their low metabolic rate, but it could also be associated with the functional demands of their suspensory and arboreal lifestyle (but it could also be related to the age of the specimens sampled). In Sciuromorpha (squirrels and their relatives), Mielke et al. (2018) investigated the effect of lifestyle (climbing, gliding, fossorial) on the trabecular structure of the femoral epiphyses and reported that some parameters describing epiphyseal trabecular networks in

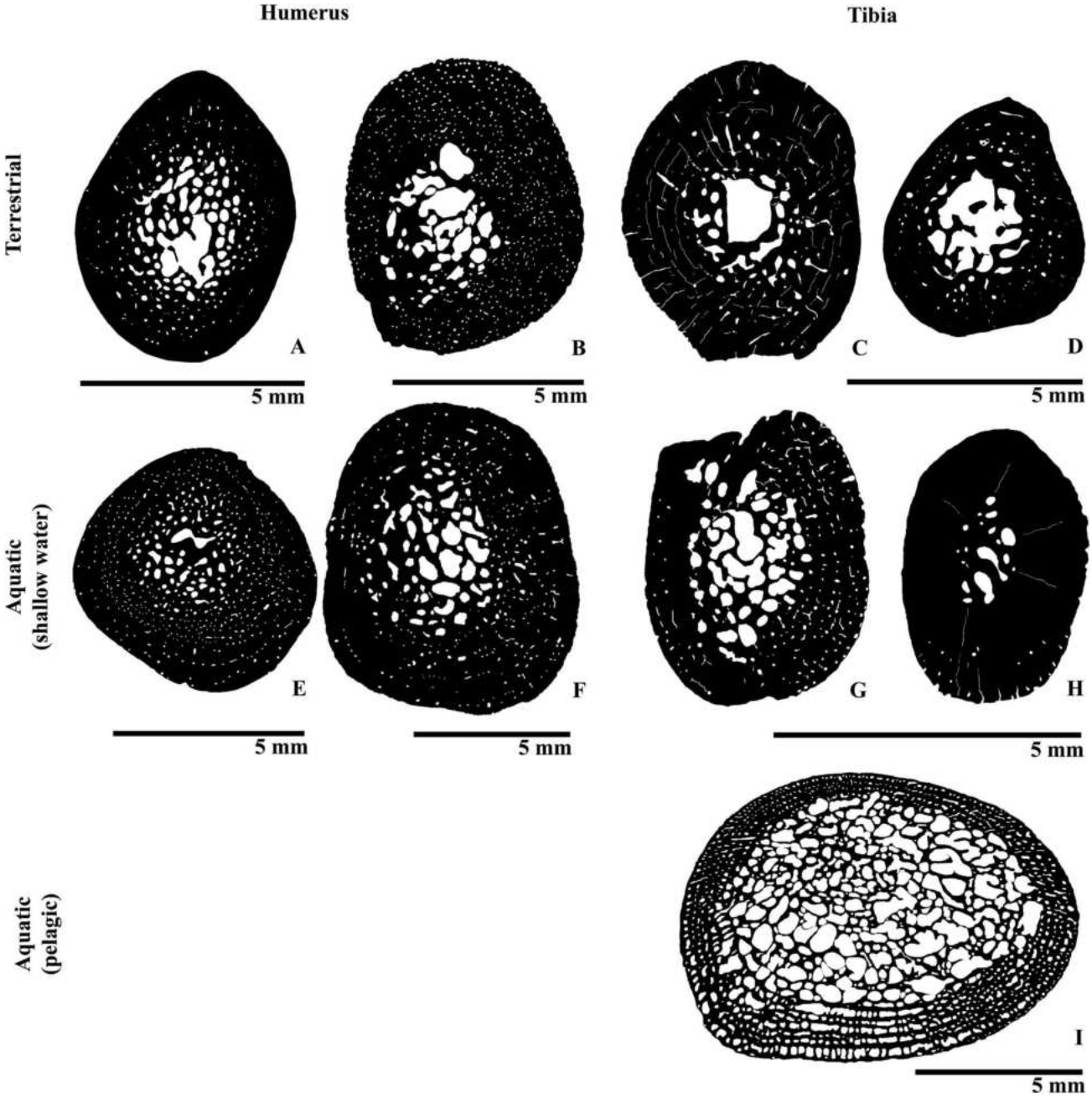


FIGURE 35.3 Mid-diaphyseal cross sections of the humerus (A, B, E, F) and tibia (C, D, G–I) of various turtle species with terrestrial (A–D), shallow-water, aquatic (E–H), and deep-sea, pelagic (I) lifestyles. A and D, *Testudo graeca*. B, *Chelonoidis carbonarius*. C, *Astrochelys radiata*. E, *Erymnochelys madagascariensis*. F, *Chelydra serpentina*. G, *Chelydra rossignonii*. H, *Chelus fimbriata*. I, *Dermochelys coriacea*. These sections were published and analyzed in one or several of these articles: Kriloff et al. (2008), Canoville and Laurin (2010) and Laurin et al. (2011).

epiphyses bear a functional and thus ecological signal. Hence, arboreal taxa appear to be statistically different from semifossorial ones based on the *trabecular separation* parameter (i.e., spacing of the trabeculae).

Axial Skeleton

Ribs and vertebrae represent an important portion of the total skeletal mass in tetrapods; they constitute a complex musculoskeletal unit highly subjected to biomechanical constraints linked to locomotion and body support, particularly in limbless tetrapods.

Many studies have investigated the relationship between lifestyle and rib or vertebral microanatomy. The broad comparative study by Canoville et al. (2016) highlighted a significant relationship among rib cortical thickness, global compactness and lifestyle (see, for example, the case of birds, Figure 35.4), although this relationship seems weaker than in limb bones, and weaker than the relationship between rib microanatomy and body size (i.e., body size greatly influences

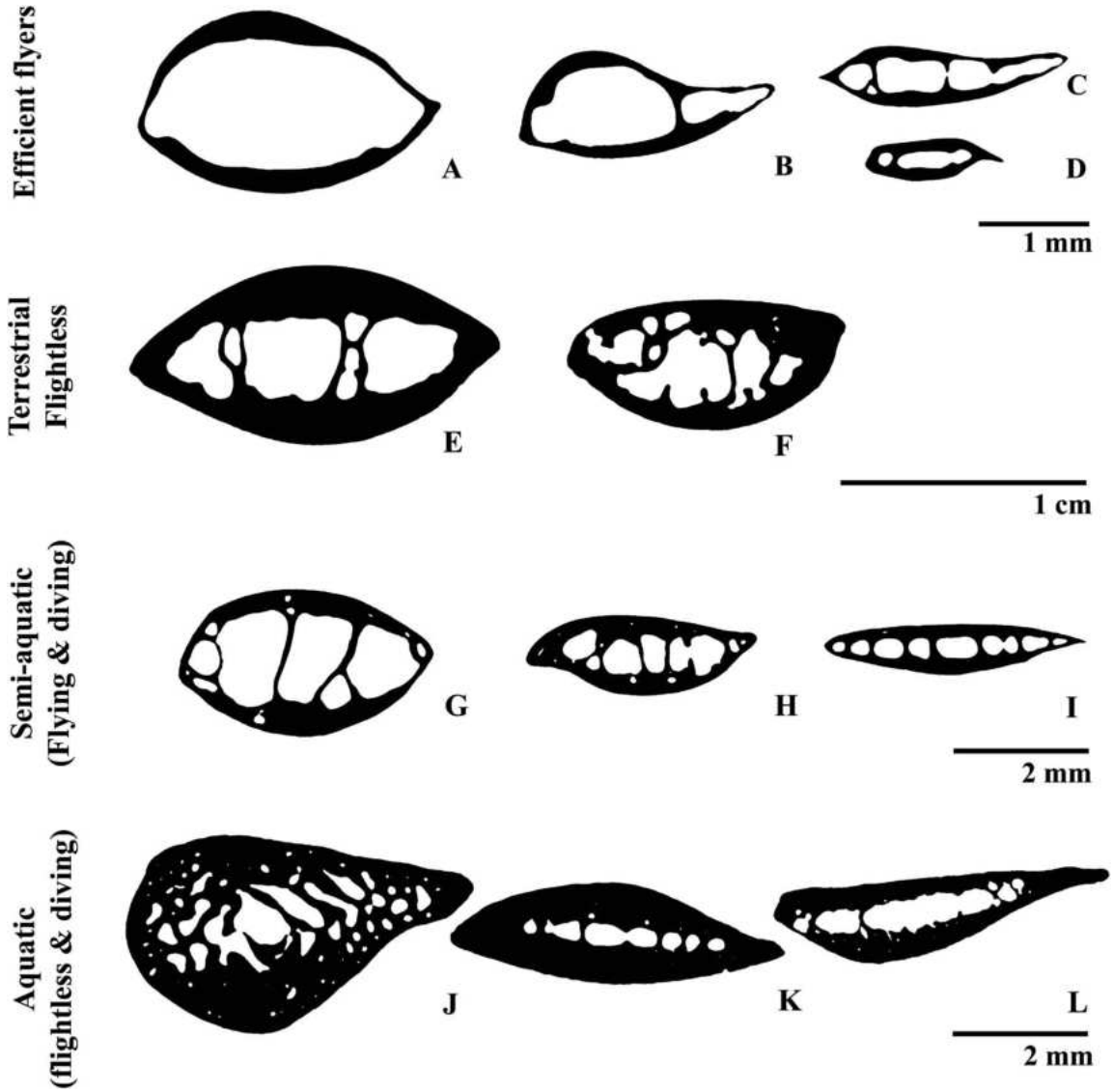


FIGURE 35.4 Mid-diaphyseal cross sections of the rib of various bird species, which are efficient flyers (A–D), flightless and terrestrial (E, F), semiaquatic (with flying and diving activities, G–I), or flightless divers (J–L). A, *Buteo buteo*. B, *Ardea cinerea*. C, *Corvus corone*. D, *Dendrocopos major*. E, *Struthio camelus*. F, *Casuarius casuarius*. G, *Morus bassanus*. H, *Phalacrocorax carbo*. I, *Melanitta nigra*. J, *Aptenodytes patagonicus*. K, *Eudyptes chrysocome*. L, *Spheniscus humboldti*. These sections were published and analyzed in Canoville et al. (2016).

the development of the medullary spongiosa in ribs, see Figure 35.5). As observed in limb bones, flying amniotes (bats and birds) have thinner compact cortices and lower global compactness values in their ribs than their nonflying relatives. Conversely, semiaquatic and fully aquatic amniotes living in shallow water usually have thicker cortices and higher compactness values than fully terrestrial species. Finally, the rib microanatomical patterns of some groups diverge from that observed in their long limb bones. Pelagic taxa, and in particular cetaceans, display a great variability in rib compactness: some species, e.g., the narwhal *Monodon monoceros*, have relatively thick compact cortices, whereas others, like Blainville's beaked whale *Mesoplodon densirostris*, have very lightly built, spongy ribs (Canoville et al. 2016). Therefore, in cetaceans, rib microanatomy is not merely influenced by lifestyle in the same manner as limb bones, as previously reported in the common dolphin *Delphinus delphis* (Buffrénil and Schoevaert 1988).

The influence of lifestyle adaptations on vertebral microanatomy has been mainly documented in mammals, lepidosaurs and to some extent archosaurs. As for the ribs, extant snakes have a simple, conservative vertebral microanatomy, regardless of lifestyle (semiaquatic vs terrestrial; Buffrénil and Rage 1993, Houssaye et al. 2013a). Broad comparative studies encompassing various mammalian clades (Dumont et al. 2013) or amniotes in general (Houssaye et al. 2014a) have shown that vertebral microanatomy varies to some extent among ecological groups. Whereas shallow-water dwellers and fossorial taxa generally show thicker cortices than pelagic and terrestrial ones, microanatomical differences mostly

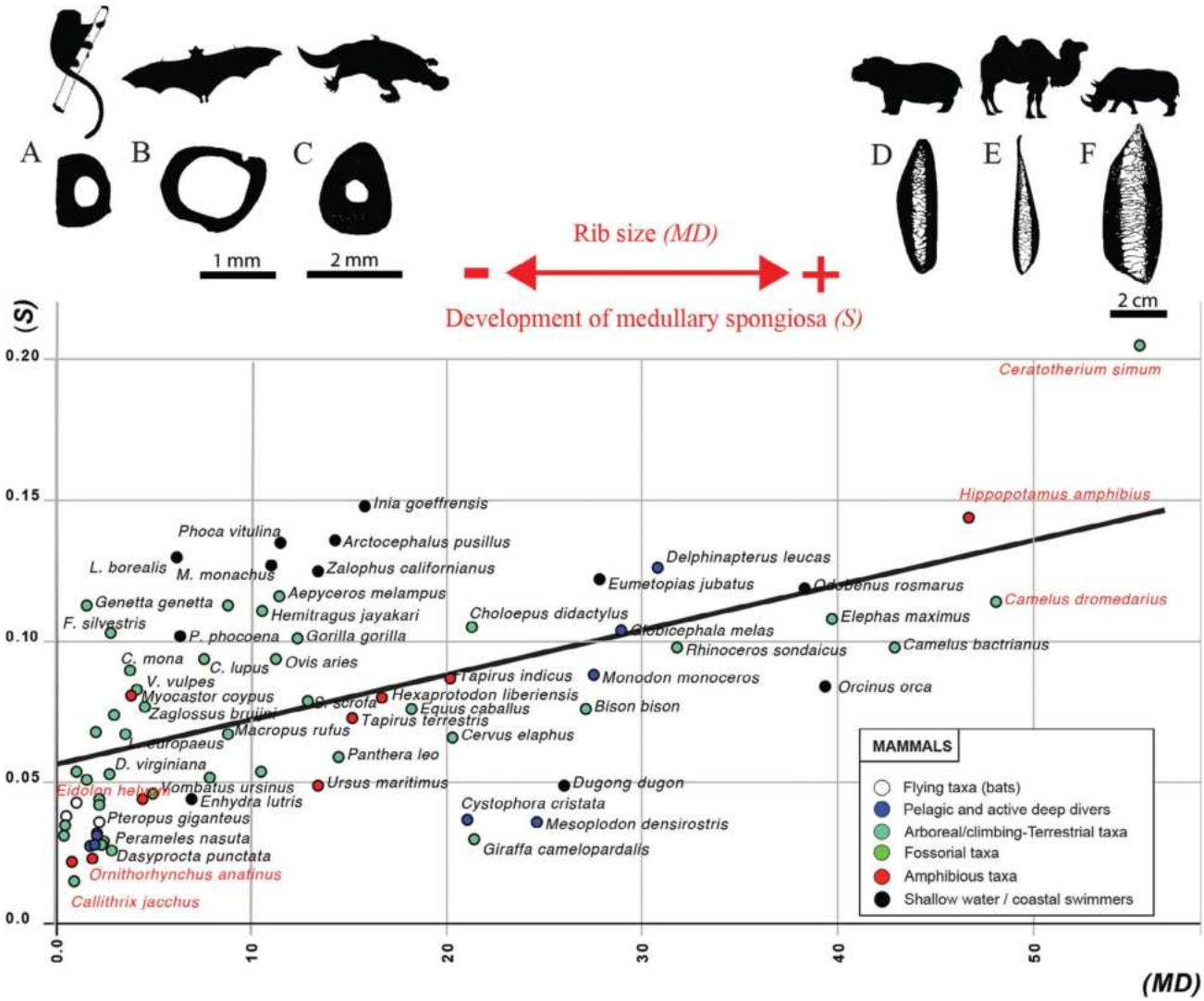


FIGURE 35.5 Linear regression of the relationship between maximal diameter of the rib (as a proxy of body size) and parameter *S* (representing the width of the transition zone between cortical compacta and medulla; this width often depends on the presence and width of a spongiosa in this transition zone). The slope of the simple, nonphylogenetic regression line is significantly different from zero ($P < 0.0001$). The rib cross sections of the species highlighted in red are represented in A–F. A, *Callithrix jacchus*. B, *Eidolon helvum*. C, *Ornithorhynchus anatinus*. D, *Hippopotamus amphibius*. E. *Camelus dromedarius*. F. *Ceratotherium simum*. These sections were published and analyzed in Canoville et al. (2016), from which this figure is modified.

concern the structure of the trabecular network. Fossorial, arboreal and flying taxa show relatively few, but thick trabeculae (Houssaye et al. 2014a). Conversely, aquatic animals possess a rather light vertebral organization, with numerous and relatively thin trabeculae (Dumont et al. 2013, Houssaye et al. 2014a). Interestingly, whereas the limb bones and ribs of some amphibious species and most shallow-water dwellers are (pachy-)osteosclerotic, the vertebrae of these animals are not. The global compactness of these forms is overall higher than their terrestrial, flying and pelagic relatives, but they preserve a generalized, predominantly spongy vertebral architecture (Dumont et al. 2013, Houssaye et al. 2014a). Finally, for most amniote groups the number and length of trabeculae greatly increase with specific size (Dumont et al. 2013).

Turtle Shell

With the exception of pelagic sea turtles, the appendicular skeleton of most testudines does not bear a clear ecological signal (Germain and Laurin 2005, Kriloff et al. 2008, Canoville 2010, Canoville and Laurin 2010, Quémeneur et al. 2013, Nakajima et al. 2014b). Several studies have hypothesized that this results from the unique body plan of turtles and that changes in skeletal density are primarily associated with modifications of the carapace's inner structure (Scheyer and Sander 2007, Kriloff et al. 2008). Subsequent comparative studies investigating the shell microanatomy of turtle taxa adapted to either aquatic or terrestrial ecologies showed that terrestrial forms usually exhibit a diploe shell structure, with well-developed, but poorly vascularized compact cortices,

VetBooks.ir

surrounding a dense spongiosa with thick trabeculae. Cortices are better vascularized in fully aquatic taxa (Scheyer 2007, Scheyer and Sánchez-Villagra 2007, Scheyer and Sander 2007). Coastal and shallow-water dwellers have a reduced inner cortical bone layer compared with their terrestrial relatives, but a relatively thickened external compacta. An overall lightening of the carapace structure occurs in pelagic species, with a reduction in thickness of both inner and outer cortices, leading to a homogeneous, spongy architecture of the shell (Scheyer et al. 2014).

Lifestyle Inferences Based on Bone Microanatomy: A Review

Several early studies inferred the lifestyle of extinct taxa from nonstatistical qualitative comparisons; however, this chapter covers only statistically validated inference models, with a focus on taxa whose lifestyles were poorly understood or could not safely be inferred based on other types of evidence (e.g., morphological or taphonomic). When results confirmed previous interpretations, these will be presented only briefly, whereas discordant results will be discussed more extensively.

The first quantitative model used to infer the lifestyle of early vertebrates (Laurin et al. 2004) mostly confirmed previous interpretations, with one notable exception. That model was binary (aquatic vs amphibious to terrestrial) and based on data from 41 individuals and 23 species of extant urodeles. It performed well with these taxa: cross-validation analyses indicated that 39 individuals and 21 species were inferred properly. Moreover, it yielded results congruent with previous interpretations on the lifestyle of the Early Permian temnospondyl *Doleserpeton* (a small dissorophoid temnospondyl), the coeval gymnarthrid amphibian *Cardiocephalus* and the Early Triassic procolophonid parareptile *Phaanthosaurus*. The lifestyles of these taxa are uncontroversial and need not be discussed extensively; their well-ossified skeletons and lack of lateral-line sulci (in the first two taxa; amniotes never display these) are good evidence of a terrestrial lifestyle. Ricqlès (1981, p. 149) had already suggested a terrestrial lifestyle for *Doleserpeton* based on a qualitative interpretation of its bone histology and microanatomy. *Cardiocephalus* occurs in the Fort Sill locality in Oklahoma, which is dominated by terrestrial taxa (Sullivan et al. 2000; Polley and Reisz 2011). As for *Phaanthosaurus*, this taxon is typically interpreted as terrestrial (Sennikov 1996), like procolophonids in general (e.g., Falconnet et al. 2012).

More surprising was the inference, according to the model, of *Chroniosaurus* as amphibious or terrestrial (Laurin et al. 2004). This reflects the moderately thick cortex surrounding a fairly large, well-defined medullary region existing in the long bones of this taxon. Golubev (1998) had interpreted C*hroniosaurus* as aquatic, an opinion congruent with the dominant position of chroniosuchians in stegocaphalian assemblages that he thought were aquatic. However, the structure of the dorsal armor, with overlap between successive plates, and ventral processes that interlock with the neural arches (Golubev 1998: figure 1), were interpreted by Laurin et al. (2004) as adaptations designed to better support the weight of the animal on land by stiffening the vertebral column, especially in the vertical plane. Indeed, among temnospondyls, similar dorsal armor is found among dissorophoids, which are thought to have been among the most terrestrial temnospondyls, and it has similarly been interpreted as trunk stiffening for terrestrial locomotion (Demar 1966). The absence of lateral-line sulci on the skull also supports a fairly terrestrial lifestyle in chroniosuchians. Both interpretations might be reconciled by the fact that the binary inference model does not discriminate between a terrestrial and an amphibious lifestyle. *Chroniosaurus* may have been active both on land and in water, which would explain its cooccurrence with more aquatic stegocephalians.

The lifestyle of several other Permo-Carboniferous stegocephalians was inferred using microanatomy-based models in subsequent studies, which we will now review in taxonomic order. The lifestyles of the temnospondyls *Eryops megacephalus, Trimerorhachis insignis* and *Acheloma dunni* were assessed by Quémeneur et al. (2013) using an inference model based on the femur of 155 extant amniote species. It would have been desirable to have included lissamphibians in that sample because temnospondyls fit well outside the extant phylogenetic bracket of amniotes, but lissamphibians are much smaller and do not overlap with the size range of the three studied temnospondyl taxa. *Acheloma*, which displays a thin compact cortex and a very loose medullary spongiosa, was inferred as terrestrial, which is uncontroversial (e.g., Gee et al. 2019).

The inferences of the two other taxa were more surprising. *Eryops*, with its very thin cortex merging gradually into an extensive medullary spongiosa, was inferred as aquatic, which may not be totally congruent with the other highly variable interpretations of its lifestyle found in the literature. Werneburg et al. (2010: 135) concluded that "Obviously, eryopids spent most of their time in water and only occasionally ventured on land in fluvial environments", which is congruent with its bone microanatomy. However, Pawley and Warren (2006) argued for a terrestrial lifestyle, based on several lines of evidence that are worth reviewing briefly here. Among these, the most convincing is the reduction of the dermal shoulder girdle and the relatively good ossification of the appendicular skeleton. However, in the latter, the femur obviously retained a large amount of cartilage in the distal condyles (Pawley and Warren 2006: figure 9), which is also compatible with a fairly aquatic lifestyle. Pawley and Warren (2006: 561) cite this following passage from Romer (1946, 1947: 134), who stated that *Eryops megacephalus* was "as well adapted for terrestrial life as many of its reptilian contemporaries". However, Romer clearly viewed many early amniotes (certainly the earliest ones) and their close relatives as fairly aquatic animals, and indeed, Romer (1946) compared *Eryops* to *Limnoscelis*, for which he argued a fairly aquatic lifestyle. Faunal associations also suggest a fairly aquatic lifestyle because as Pawley and Warren (2006: 561) recognized, in Texas, it is associated with aquatic taxa. Thus, several lines of evidence suggest that the aquatic lifestyle implied by bone microanatomy in *Eryops* is plausible.

The inference of *Trimerorhachis insignis* as amphibious is more problematic. The thick cortex merging gradually into an

VetBooks.ir

extensive medullary spongiosa looks typical of aquatic taxa, and several osteological characters, such as the retention of a great deal of cartilage in the appendicular skeleton (Pawley 2007), the small size of the limbs and the lateral-line sulci on the skull (Romer 1947), suggest likewise. The poor performance of the model in this case probably reflects the fact that only three aquatic taxa were included in the sample of Quémeneur et al. (2013), which suggests that only a small part of the morphospace occupied by aquatic amniotes had been sampled.

The Early Permian seymouriamorph *Discosauriscus* was long known only from its larvae, but more recent studies have documented its metamorphosis into apparently terrestrial adults (Klembara 1995). Following these discoveries, the adults of all seymouriamorphs have generally been considered terrestrial (Laurin 2000). Kriloff et al. (2008) confirmed this interpretation for *Discosauriscus*, based on a tibial section and two inference models (binary and ternary).

The lifestyle of several Permo-Carboniferous synapsids has long been debated. On the basis of a fragmentary radius, Ricqlès (1974b: 35) inferred an aquatic (or possibly amphibious) lifestyle for *Ophiacodon retroversus.* This inference was based explicitly on the gradual transition between cortex and spongiosa (which also occupied the medullary region) and dense cortical vascularization by primary longitudinal canals. At first, Germain and Laurin (2005), who analyzed the same radius section of *O. retroversus*, seemed to confirm its aquatic lifestyle. However, more recent studies cast doubt about this interpretation. Shelton and Sander (2017) attributed the fairly dense vascularization to a relatively high metabolic rate, whereas Laurin and Buffrénil (2016) showed that the femur of an *O. uniformis* specimen showed surprisingly little spongy bone. Furthermore, a femoral section from the early (Carboniferous) ophiacodontid *Clepsydrops* showed a fairly thin, compact and poorly vascularized cortex. All this suggests that ophiacodontids were primitively terrestrial. *Ophiacodon* may have returned to an amphibious lifestyle, which would be consistent with the fairly thick femoral cortex observed by Laurin and Buffrénil (2016). Bone microanatomy yields equivocal data on that taxon. It is plausible that the radius section examined by Ricqlès (1974b) and Germain and Laurin (2005) was not mid-diaphyseal but close to the metaphysis, thus explaining the extensive spongiosa.

Ricqlès (1974b) interpreted the other Permo-Carboniferous synapsids that he sampled (*Ennatosaurus tecton, Varanops brevirostris, Edaphosaurus boanerges* and *Dimetrodon*) as terrestrial. Subsequently, Kriloff et al. (2008) inferred a terrestrial lifestyle for *Dimetrodon* based on a tibial section. The lifestyles of the other taxa sampled by Ricqlès (1974b) have not yet been inferred using quantitative, statistical models.

For therapsids, inferences based on radial and tibial sections have yielded both expected and some surprising results. For the dicynodont therapsid *Lystrosaurus*, Germain and Laurin (2005) inferred an amphibious lifestyle based on a radius section and a linear discriminant model. They, however, pointed out that the position of that taxon, outside the distribution polygons of extant taxa in the morphospace, called for caution. Indeed, the lifestyle of *Lystrosaurus* has been controversial. Some workers have considered it aquatic, like Broom (1903), who based his argument on the shape of the shoulder girdle, and Watson (1913), who emphasized the large amount of unmineralized cartilage that must have been present, as well as the broad hands, which he thought characteristic of an aquatic adaptation. Watson (1913) suggested that the lifestyle of *Lystrosaurus* was similar to that of seals or sirenians. Camp (1956) also considered *Lystrosaurus* aquatic because of its poorly ossified limbs. Cluver (1971) thought that the snout of this taxon was adapted to feeding on low vegetation in water. Other authors doubted that *Lystrosaurus* was aquatic (King 1991) and considered it fossorial (King and Cluver 1991). The abundance of *Lystrosaurus* skeletal remains recovered in fossilized burrow structures from the Lower Triassic of South Africa supports the latter hypothesis of a fossorial lifestyle for this animal (Botha-Brink 2017). *Lystrosaurus'* unusual long bone microanatomy might thus be related to its burrowing activity. However, such a relationship between bone inner architecture and fossoriality remains to be tested in extant tetrapods (see above).

The bone microanatomy of a *Dicynodon* tibia was studied by Kriloff et al. (2008). This compact tibia, with a compact medullary spongiosa, implied a terrestrial lifestyle, which is a result congruent with the prevailing interpretation that most dicynodonts were terrestrial (King 1990). Kriloff et al. (2008) also assessed the lifestyle of an undetermined gorgonopsian, based on the microanatomy of its tibia that had been illustrated by Ricqlès (1969, Plate II). Not surprisingly, this bone with a moderately thick cortex yielded a terrestrial lifestyle, congruent with prevailing interpretations (Cruickshank 1973).

Among sauropsids, in addition to the work on *Phaanthosaurus* noted above, Kriloff et al. (2008) inferred an amphibious lifestyle for the parareptile *Pareiasaurus*. Their inference model, based on the tibia, implied an aquatic lifestyle, which is consistent with a fairly thick cortex that merges gradually into a medullary spongiosa and a very small medullary cavity. The fairly compact tibia (about 74% at mid-diaphysis) might possibly reflect graviportality, but Kriloff et al. (2008) suggested a lifestyle similar to that of a hippopotamus. Given the weight of other types of evidence, they concluded that *Pareiasaurus* was more likely amphibious. These other types of evidence include the reasonably well-ossified skeleton, which, along with trackways, strongly suggests that pareiasaurs were capable of terrestrial locomotion, even though their gross morphology has also been interpreted as suggesting fairly aquatic habits (Gubin et al. 2003). Based on limb morphology, Piveteau (1955: 358) suggested a lifestyle similar to that of the hippopotamus. The isotopic analyses by Canoville et al. (2014) suggest a terrestrial lifestyle, even though the possibility of diagenetic alteration and the multifactorial determination of isotopic ratios imply that this provides only moderately strong refutation of previous hypotheses about the lifestyle of pareiasaurs. Also, a possible explanation of their isotopic results could be that the pareiasaurs studied by Canoville et al. (2014) drank estuarine (brackish) water rather than the fresh water drunk by therapsids. Canoville et al. (2014: 270) dismissed this possibility because it is not consistent with the hypothesis that pareiasaurs inhabited freshwater bodies, but given the controversy

about the freshwater or marginal marine habitat of many Carboniferous and Permian stegocephalians (Schultze 2009; Laurin and Soler-Gijón 2010), this hypothesis should perhaps be examined more closely in the future. Besides, many extant amniotes inhabit oceans and seas, and the diversity of marine amniotes was even greater in the past, given that there were also coastal marine sloths (Amson et al. 2014).

Germain and Laurin (2005) inferred an amphibious lifestyle for the Triassic sauropterygian *Neusticosaurus*. This is a little surprising given its very compact bone (98%) and this may reflect the limited sample size of aquatic taxa included (seven). That taxon is usually considered fully aquatic (Carroll 1988), but it is possible that given its small size, it could crawl onto the shore, like seals and sea lions.

Conclusion

In recent decades, several studies that have taken advantage of progress in analytical methods and compilations of extensive comparative datasets have confirmed the presence of an ecological signal (strongest in the stylopod) in bone microanatomy. Statistically validated inference models were produced and have started yielding interesting clues about the lifestyles of long-extinct vertebrates. However, bone microanatomy has so far been sampled in only a small proportion of extant nominal species. Much progress can be expected in the future through more extensive sampling of this microanatomical diversity, more sophisticated phylogeny-informed inference methods (e.g., Legendre et al. 2016; Organ et al. 2007), and more accurate ecological characterizations of both extant taxa and extinct ones, permitted by non-destructive methods such as micro-CT-scanning.

REFERENCES

Abramoff, M. D., et al. 2004: Image processing with ImageJ. *Biophoton Inter.* 11: 36–42.

Ahlberg, P. E., and J. A. Clack. 2006. Palaeontology: a firm step from water to land. *Nature* 440: 747–749.

Ahlberg, P. E., and A. R. Milner. 1994. The origin and early diversification of tetrapods. *Nature* 368: 507–514.

Alexander, R. M., and C. M. Pond. 1992. Locomotion and bone strength of the white rhinoceros, *Ceratotherium simum*. *J. Zool*. 227: 63–69.

Amson, E., et al. 2014. Gradual adaptation of bone structure to aquatic lifestyle in extinct sloths from Peru. *Proc. R. Soc. B* 281: 20140192.

Amson, E., et al. 2017. Trabecular architecture in the forelimb epiphyses of extant xenarthrans (Mammalia). *Front. Zool.* 14: 52.

Amson, E., et al. 2018. Evolutionary adaptation to aquatic lifestyle in extinct sloths can lead to systemic alteration of bone structure. *Proc. R. Soc. B* 285: 20180270.

Barrett, P. M., et al. 2008. Pterosaur distribution in time and space: an atlas. *Zitteliana*28: 61–107.

Berman, D. S., et al. 2000. Early Permian bipedal reptile. *Science* 290: 969–972.

Botha-Brink, J. 2017. Burrowing in *Lystrosaurus:* preadaptation to a postextinction environment?. *J. Vertebr. Paleontol*. 37: e1365080.

Botton-Divet, L., et al. 2016. Morphological analysis of long bones in semi-aquatic mustelids and their terrestrial relatives. *Integr. Comp. Biol*. 56: 1298–1309.

Botton-Divet, L., et al. 2017. Swimming and running: a study of the convergence in long bone morphology among semi-aquatic mustelids (Carnivora: Mustelidae). *Biol. J. Linnean Soc.* 121: 38–49.

Broom, R. 1903. On the structure of the shoulder girdle in *Lystrosaurus*. *Ann. S. Afr. Mus.* 4: 139–41.

Buffrénil, V. D. 1990. Contribution à l'étude des spécialisations de la structure osseuse des mammifères marins. Doctoral dissertation, Paris 7.

Buffrénil, V. D., et al. 1986. Comparaison de la structure et du volume squelettiques entre un delphinidé (*Delphinus delphis* L.) et un mammifère terrestre (*Panthera leo* L.). *Can. J. Zool*. 64: 1750–1756.

Buffrénil, V. D., et al. 1990. L'histologie osseuse des champsosauridés: données descriptives et interprétation fonctionnelle. *Ann. Paléontol*. 76: 255–275.

Buffrénil, V. D., and J. C. Rage. 1993. La 'pachyostose' vertébrale de *Simoliophis* (Reptilia, Squamata): données comparatives et considérations fonctionnelles. *Ann. Paléontol*. 79: 315–335.

Buffrénil, V. de, and H. Francillon-Vieillot. 2001. Ontogenetic changes in bone compactness in male and female Nile monitors (*Varanus niloticus*). *J. Zool*. 254: 539–546.

Buffrénil, V. de, and J. M. Mazin. 1990. Bone histology of the ichthyosaurs: comparative data and functional interpretation. *Paleobiology* 16: 435–447.

Buffrenil, V. de, and D. Schoevaert. 1988. On how the periosteal bone of the delphinid humerus becomes cancellous: ontogeny of a histological specialization. *J. Morphol*. 198: 149–164.

Buffrénil, V. de, and D. Schoevaert. 1989. Données quantitatives et observations histologiques sur la pachyostose du squelette du dugong, *Dugong dugon* (Müller) (Sirenia, Dugongidae). *Can. J. Zool*. 67: 2107–2119.

Buffrenil, V. de, et al. 1990. Bone histology of the ribs of the archaeocetes (Mammalia: Cetacea). *J. Vertebr. Paleontol*. 10: 455–466.

Buffrénil, V. de, et al. 2008. Specialization of bone structure in *Pachyvaranus crassispondylus* Arambourg, 1952, an aquatic squamate from the Late Cretaceous of the southern Tethyan margin. *Lethaia* 41: 59–69.

Buffrénil, V. de, et al. 2010. Evolution of sirenian pachyosteosclerosis, a model-case for the study of bone structure in aquatic tetrapods. *J. Mammal. Evol*. 17: 101–120.

Camp, C. L. 1956. Triassic dicynodont reptiles, Part 2. Triassic dicynodonts compared. *Mem. Univ. Calif.* 13: 305–348.

Canoville, A. 2010. Diversité microanatomique et histologique des os longs chez les tétrapodes: inferences paléobiologiques.. PhD dissertation, Université Pierre et Marie Curie, Paris.

Canoville, A., and V. de Buffrénil. 2016. Ontogenetic development and intraspecific variability of bone microstructure in the king penguin *Aptenodytes patagonicus*: considerations for paleoecological inferences in Sphenisciformes. In ICVM11-2016 Program and Abstracts. *Anat. Rec.* 299: 270.

Canoville, A., and M. Laurin. 2009. Microanatomical diversity of the humerus and lifestyle in lissamphibians. *Acta Zool*. 90: 110–122.

Canoville, A., and M. Laurin. 2010. Evolution of humeral microanatomy and lifestyle in amniotes, and some comments on palaeobiological inferences. *Biol. J Linnean Soc.* 100: 384–406.

Canoville, A., et al. 2014. Insights into the habitat of Middle Permian Pareiasaurs (Parareptilia) from preliminary isotopic analyses. *Lethaia* 47: 266–274.

Canoville, A., et al. 2016. Microanatomical diversity of amniote ribs: an exploratory quantitative study. *Biol. J Linnean Soc.* 118: 706–733.

Canoville, A., et al. 2019. Systemic distribution of medullary bone in the avian skeleton: ground truthing criteria for the identification of reproductive tissues in extinct Avemetatarsalia. *BMC Evol. Biol.*19: 71.

Carroll, R. L. 1964. The earliest reptiles. *Zool. J Linnean Soc.* 45: 61–83.

Carroll R. L. 1988. *Vertebrate paleontology and evolution*. New York: WH Freeman and Company.

Castanet, J., and M. H. Caetano. 1995. Influence du mode de vie sur les caractéristiques pondérales et structurales du squelette chez les amphibiens anoures. *Can. J. Zool.* 73: 234–242.

Castanet, J., et al. 1993. *Bone and individual aging*. In: Hall BK, ed. London: CRC Press, 245–283.

Castanet, J., et al. 2001. Signification de l'histodiversité osseuse: le message de l'os. *Biosystema* 19: 133–147.

Cerda, I. A., et al. 2016. Bone shell microstructure of *Condorchelys antiqua* Sterli, 2008, a stem turtle from the Jurassic of Patagonia. *C. R. Palevol* 15: 128–141.

Cluver, M. A. 1971. The cranial morphology of the dicynodont genus *Lystrosaurus*. *Ann. S. Afr. Mus.* 56: 155–274.

Cooper, L. N., et al. 2016. Aquatic habits of cetacean ancestors: integrating bone microanatomy and stable isotopes. *Integr. Comp. Biol.* 56: 1370–1384.

Coughlin, B. L., and F. E. Fish. 2009. Hippopotamus underwater locomotion: reduced-gravity movements for a massive mammal. *J. Mammal.* 90: 675–679.

Cruickshank, A. R. I. 1973. The mode of life of gorgonopsians. *Palaeont. Afr.* 15: 65–67.

Cubo, J., et al. 2005. Phylogenetic signal in bone microstructure of sauropsids. *Syst. Biol.* 54: 562–574.

Currey, J. D., and R. M. Alexander. 1985. The thickness of the walls of tubular bones. *J. Zool.* 206: 453–468.

Dacke, C. G., et al. 1993. Medullary bone and avian calcium regulation. *J. Exp. Biol.* 184: 63–88.

Demar, R. E. 1966. The phylogenetic and functional implications of the armor of the Dissorophidae. *Fieldiana: Zool.* 16: 55–88.

Desdevises, Y., et al. 2003. Quantifying phylogenetically structured environmental variation. *Evolution* 57: 2647–2652.

Didier, G., and M. Laurin. 2020. Exact distribution of divergence times from fossil ages and tree topologies. *Systematic Biology* 69: 1068–1087.

Diniz-Filho, J. A. F., et al. 1998. An eigenvector method for estimating phylogenetic inertia. *Evolution* 52: 1247–1262.

Doube, M., et al. 2010. BoneJ: free and extensible bone image analysis in ImageJ. *Bone* 47: 1076–1079.

Doube, M., et al. 2011. Trabecular bone scales allometrically in mammals and birds. *Proc. R. Soc. Lond.* 20110069.

Duellman, W. E., and L. Trueb. 1994. *Biology of amphibians*. Baltimore: JHU Press.

Dumont, E. R. 2010. Bone density and the lightweight skeletons of birds. *Proc. R. Soc. B.* 20100117.

Dumont, M., et al. 2013. Inner architecture of vertebral centra in terrestrial and aquatic mammals: a two-dimensional comparative study. *J. Morphol.* 274: 570–584.

Falconnet, J., et al. 2012. First procolophonid (Reptilia, Parareptilia) from the Lower Triassic of Madagascar. *C. R. Palevol* 11: 357–369.

Fawcett, D. W. 1942. The amedullary bones of the Florida manatee (*Trichechus latirostris*). *Am. J. Anat.* 71: 271–309.

Felsenstein, J. 1985. Phylogenies and the comparative method. *Am. Nat.* 125: 1–15.

Felts, W. J., and F. A. Spurrell. 1965. Structural orientation and density in cetacean humeri. *Am. J. Anat.* 116: 171–203.

Felts, W. J., and F. A. Spurrell. 1966. Some structural and developmental characteristics of cetacean (Odontocete) radii. A study of adaptive osteogenesis. *Am. J. Anat.* 118: 103–134.

Fish, F. E. 1984. Mechanics, power output and efficiency of the swimming muskrat (*Ondatra zibethicus*). *J. Exp. Biol.* 110: 183–201.

Fish, F. E. 1994. Association of propulsive swimming mode with behavior in river otters (*Lutra canadensis*). *J. Mammal.* 75: 989–997.

Fish, F. E., and B. R. Stein. 1991. Functional correlates of differences in bone density among terrestrial and aquatic genera in the family Mustelidae (Mammalia). *Zoomorphology* 110: 339–345.

Fish, F. E., et al. 1997. Energetics of swimming by the platypus *Ornithorhynchus anatinus*: metabolic effort associated with rowing. *J. Exp. Biol.* 200: 2647–2652.

Fish, F. E., et al. 2001. Energetics of terrestrial locomotion of the platypus *Ornithorhynchus anatinus*. *J. Exp. Biol.* 204: 797–803.

Freckleton, R. P., et al. 2011. Comparative methods as a statistical fix: the dangers of ignoring an evolutionary model. *Am. Nat.* 178: E10–E17.

Frey, E., et al. 1997. Gliding mechanism in the Late Permian reptile *Coelurosauravus*. *Science* 275: 1450–1452.

Gatesy, S. M., and K. M. Middleton. 2007. Skeletal adaptations for flight. In: Hall BK, ed. *Fins into limbs: evolution, development, and transformation*. Chicago: University of Chicago Press, 269–283.

Gee, B. M., et al. 2019. A juvenile specimen of the Trematopid *Acheloma* from Richards Spur, Oklahoma and challenges of trematopid ontogeny. *Front. Earth Sci.* 7: 38. doi: 10.3389/feart.2019.00038.

Germain, D. 2008. A new Phlegethontiid specimen (Lepospondyli, Aistopoda) from the Late Carboniferous of Montceau-Les-Mines (Saône-Et-Loire, France). *Geodiversitas* 30: 669–680.

Germain, D., and M. Laurin. 2005. Microanatomy of the radius and lifestyle in amniotes (Vertebrata, Tetrapoda). *Zool. Scr.* 34: 335–350.

Girondot, M., and M. Laurin. 2003. Bone profiler: a tool to quantify, model, and statistically compare bone-section compactness profiles. *J. Vertebr. Paleontol.* 23: 458–461.

Golubev, V. K. 1998. Narrow-armored chroniosuchians (Amphibia, Anthracosauromorpha) from the Late Permian of Eastern Europe. *Paleont. J.* 32: 278–287.

Grafen, A. 1989. The phylogenetic regression. *Philos. Trans. R. Soc. B* 326: 119–157.

Gray, N. M., et al. 2007. Sink or swim? Bone density as a mechanism for buoyancy control in early cetaceans. *Anat. Rec.* 290: 638–653.

Gubin, Y. M., et al. 2003. Pareiasaurian tracks from the Upper Permian of Eastern Europe. *Paleont. J.* 37(5): 514–523.

Guénard, G., et al. 2013. Phylogenetic eigenvector maps: a framework to model and predict species traits. *Methods Ecol. Evol*. 4: 1120–1131.

Habib, M. B., and C. B. Ruff. 2008. The effects of locomotion on the structural characteristics of avian limb bones. *Zool. J. Linnean Soc.* 153: 601–624.

Harvey, P. H., and M. D. Pagel. 1991. *The comparative method in evolutionary biology.* Oxford, UK: Oxford University Press.

Hasiotis, S. T., et al. 2007. The trace-fossil record of vertebrates. In: *Trace fossils: concepts, problems, prospects.* Amsterdam: Elsevier, 196–218.

Hays, G. C., et al. 2002. Behavioural plasticity in a large marine herbivore: contrasting patterns of depth utilisation between two green turtle (*Chelonias mydas*) populations. *Mar. Biol.* 141: 985–990.

Hembree, D. I., et al. 2004. Amphibian burrows and ephemeral ponds of the Lower Permian Speiser Shale, Kansas: evidence for seasonality in the midcontinent. *Palaeogeogr. Palaeoclimatol. Palaeoecol.* 203: 127–152.

Hildebrand, M., and G. E. Goslow. 2001. *Analysis of vertebrate structure*. 5th ed. New York: Wiley.

Houssaye, A. 2013. Palaeoecological and morphofunctional interpretation of bone mass increase: an example in Late Cretaceous shallow marine squamates. *Biol. Rev.* 88: 117–139.

Houssaye, A., and N. Bardet. 2012. Rib and vertebral microanatomical characteristics of hydropelvic mosasauroids. *Lethaia* 45: 200–209.

Houssaye, A., and L. Botton-Divet. 2018. From land to water: evolutionary changes in long bone microanatomy of otters (Mammalia: Mustelidae). *Biol. J. Linnean Soc*. 125: 240–249.

Houssaye, A., and F. E. Fish. Functional (secondary) adaptation to an aquatic life in vertebrates: an introduction to the symposium. *Integr. Comp. Biol*. 56: 1266–1270.

Houssaye, A., et al. 2008. An analysis of vertebral 'pachyostosis' in *Carentonosaurus mineaui* (Mosasauroidea, Squamata) from the Cenomanian (early Late Cretaceous) of France, with comments on its phylogenetic and functional significance. *J. Vertebr. Paleontol.* 28: 685–691.

Houssaye, A., et al. 2010. Vertebral microanatomy in squamates: structure, growth and ecological correlates. *J. Anat*. 217: 715–727.

Houssaye, A., et al. 2013a. Jack-of-all-trades master of all? Snake vertebrae have a generalist inner organization. *Naturwissenschaften* 100: 997–1006.

Houssaye, A., et al. 2013b. Microanatomical and histological features in the long bones of mosasaurine mosasaurs (Reptilia, Squamata)–implications for aquatic adaptation and growth rates. *PLoS One* 8: e76741.

Houssaye, A., et al. 2014a. Amniote vertebral microanatomy–what are the major trends?. *Biol. J. Linnean Soc.* 112: 735–746.

Houssaye, A., et al. 2014b. A new look at ichthyosaur long bone microanatomy and histology: implications for their adaptation to an aquatic life. *PLoS One* 9: e95637.

Houssaye, A., et al. 2015. Transition of Eocene whales from land to sea: evidence from bone microstructure. *PLoS One* 10: e0118409.

Houssaye, A., et al. 2016a. Adaptive patterns in aquatic amniote bone microanatomy—more complex than previously thought. *Integr. Comp. Biol*. 56: 1349–1369.

Houssaye, A., et al. 2016b. Biomechanical evolution of solid bones in large animals: a microanatomical investigation. *Biol. J. Linnean Soc*. 117: 350–371.

Houssaye, A., et al. 2018a. 3D quantitative comparative analysis of long bone diaphysis variations in microanatomy and cross-sectional geometry. *J. Anat*. 232: 836–849.

Houssaye, A., et al. 2018b. Structural, functional, and physiological signals in ichthyosaur vertebral centrum microanatomy and histology. *Geodiversitas* 40: 161–170.

Hugi, J., and M. R. Sánchez-Villagra. 2012. Life history and skeletal adaptations in the Galapagos marine iguana (*Amblyrhynchus cristatus*) as reconstructed with bone histological data—a comparative study of iguanines. *J. Herpetol*. 46: 312–324.

Kaiser, H. E. 1960. Untersuchungen zur vergleichenden Osteologie der fossilen und rezenten Pachyostosen. *Palaeontograph A* 114: 113–196

Kelley, N. P., and R. Motani. 2015. Trophic convergence drives morphological convergence in marine tetrapods. *Biol. Lett.* 11: 20140709.

Kelley, N. P., and N. D. Pyenson. 2015. Evolutionary innovation and ecology in marine tetrapods from the Triassic to the Anthropocene. *Science* 348: aaa3716.

Kilbourne, B. M., and J. R. Hutchinson. 2019. Morphological diversification of biomechanical traits: mustelid locomotor specializations and the macroevolution of long bone cross-sectional morphology. *BMC Evol. Biol.*19: 37.

King, G. 1990. *The dicynodonts—a study in palaeobiology.* London: Chapman and Hall.

King, G. M. 1991. The aquatic *Lystrosaurus*: a palaeontological myth. *Hist. Biol.* 4: 285–321.

King, G. M., and M. A. Cluver. 1991. The aquatic *Lystrosaurus*: an alternative lifestyle. 4: 323–341.

Kiprijanoff, A. V. 1881–1883. Studien über die fossilen Reptilien Russlands. *Mém. Acad. Imp. Sci. Saint Petersbourg* 7: 1–144.

Klein, N., et al. 2016. Diverse aquatic adaptations in *Nothosaurus* spp. (Sauropterygia)—inferences from humeral histology and microanatomy. *PLoS One* 11: e0158448.

Klembara, J. 1995. The external gills and ornamentation of skull roof bones of the Lower Permian tetrapod *Discosauriscus* (Kuhn 1933) with remarks to its ontogeny. *Paläontol. Z*. 69: 265–281.

Kriloff, A., et al. 2008. Evolution of bone microanatomy of the tetrapod tibia and its use in palaeobiological inference. *J. Evol. Biol*. 21: 807–826.

Ksepka, D. T., et al. 2015. Bone histology in extant and fossil penguins (Aves: Sphenisciformes). *J. Anat*. 227: 611–630.

Lamm, E. T. 2013. Preparation and sectioning of specimens. In: Padian K, Lamm ET, eds. *Bone histology of fossil tetrapods.* Berkeley: University of California Press, 55–160.

Laurin, M. 2000 Seymouriamorphs. In *Amphibian biology*, Heatwole H. and R. L. Carroll, eds., 1064–1080. Chipping Norton: Surrey Beatty & Sons.

Laurin, M. 2004. The evolution of body size, cope's rule and the origin of amniotes. *Syst. Biol*. 53: 594–622.

Laurin, M. 2010a. *How vertebrates left the water.* Berkeley: Univ of California Press.

Laurin, M. 2010b. Assessment of the relative merits of a few methods to detect evolutionary trends. *Syst. Biol*. 59: 689–704.

Laurin, M., and V. de Buffrénil, V. 2016. Microstructural features of the femur in early ophiacodontids: a reappraisal of ancestral habitat use and lifestyle of amniotes. *C. R. Palevol* 15: 115–127.

Laurin, M., and R. Soler-Gijón. 2010 Osmotic tolerance and habitat of early stegocephalians: indirect evidence from parsimony, taphonomy, paleobiogeography, physiology and morphology. *Geological Society, London, Special Publications* 339: 151.

Laurin, M., et al. 2000. Early tetrapod evolution. *Trends Ecol. Evol*. 15: 118–123.

Laurin, M., et al. 2004. The evolution of long bone microstructure and lifestyle in lissamphibians. *Paleobiology* 30: 589–613.

Laurin, M., et al. 2007. A microanatomical and histological study of the paired fin skeleton of the Devonian sarcopterygian *Eusthenopteron foordi*. *J. Paleontol*. 81: 143–153.

Laurin, M., et al. 2009. Use of paleontological and molecular data in supertrees for comparative studies: the example of lissamphibian femoral microanatomy. *J. Anat*. 215: 110–123.

Laurin, M., et al. 2011. Bone microanatomy and lifestyle: a descriptive approach. *C. R. Palevol* 10: 381–402.

Leclair Jr, R., et al. 1993. Allométrie de la masse du squelette chez des amphibiens anoures. *Can. J. Zool*. 71: 352–357.

Legendre, L., et al. 2013. Phylogenetic signal in bone histology of amniotes revisited. *Zool. Scr.* 42: 44–53.

Legendre, L. J., and J. Botha-Brink. 2018. Digging the compromise: investigating the link between limb bone histology and fossoriality in the aardvark (*Orycteropus afer*). *PeerJ*. 6: e5216.

Legendre, L. J., et al. 2016. Palaeohistological evidence for ancestral high metabolic rate in archosaurs. *Syst. Biol.* 65: 989–996.

Legendre, P. 2000. Comparison of permutation methods for the partial correlation and partial Mantel tests. *J. Statist. Comput. Simul*. 67: 37–73.

Legendre, P., et al. 1994. Modeling brain evolution from behavior: a permutational regression approach. *Evolution* 48: 1487–1499.

Long, J. A., and M. S. Gordon. 2004. The greatest step in vertebrate history: a paleobiological review of the fish-tetrapod transition. *Physiol. Biochem. Zool*. 77: 700–719.

Lyson, T. R., et al. 2016. Fossorial origin of the turtle shell. *Curr. Biol*. 26: 1887–1894.

Magwene, P. M. 1993.What's bred in the bone: histology and cross-sectional geometry of mammallike reptile long bones. Evidence of changing physiological and biomechanical demands. M.Sc. dissertation, Harvard University, Cambridge, Massachusetts.

Margerie, E. de, et al. 2005. Torsional resistance as a principal component of the structural design of long bones: comparative multivariate evidence in birds. *Anat. Rec.* 282: 49–66.

Marjanović, D., and M. Laurin. 2019. Phylogeny of Paleozoic limbed vertebrates reassessed through revision and expansion of the largest published relevant data matrix. *PeerJ* 6: e5565.

Martins, E. P., and T. F. Hansen. 1997. Phylogenies and the comparative method: a general approach to incorporating phylogenetic information into the analysis of interspecific data. *Am. Nat.* 149: 646–667.

Meers, M. B. 2002. Cross-sectional geometric properties of the crocodylian humerus: an exception to Wolff's Law? *J. Zool*. 258: 405–418.

Meier, P. S., et al. 2013. Evolution of bone compactness in extant and extinct moles (Talpidae): exploring humeral microstructure in small fossorial mammals. *BMC Evol. Biol*. 13: 55.

Meister, W. 1962. Histological structure of the long bones of penguins. *Anat. Rec.* 143: 377–387.

Meunier, F. J., and M. Laurin. 2012. A microanatomical and histological study of the fin long bones of the Devonian sarcopterygian *Eusthenopteron foordi*. *Acta Zool*. 93: 88–97.

Mielke, M., et al. 2018. Trabecular architecture in the sciuromorph femoral head: allometry and functional adaptation. *Zool. Lett*. 4: 10.

Modesto, S. P. 2010. The postcranial skeleton of the aquatic parareptile *Mesosaurus tenuidens* from the Gondwanan Permian. *J. Vertebr. Paleontol*. 30: 1378–1395.

Montañez-Rivera, I., et al. 2018. Bone cortical compactness in 'tree sloths' reflects convergent evolution. *J. Anat*. 233: 580–591.

Montoya-Sanhueza, G., and A. Chinsamy. 2017. Long bone histology of the subterranean rodent *Bathyergus suillus* (Bathyergidae): ontogenetic pattern of cortical bone thickening. *J. Anat*. 230: 203–233.

Montoya-Sanhueza, G., and A. Chinsamy. 2018. Cortical bone adaptation and mineral mobilization in the subterranean mammal *Bathyergus suillus* (Rodentia: Bathyergidae): effects of age and sex. *PeerJ*. 6: e4944.

Nakajima, Y., and H. Endo. 2013. Comparative humeral microanatomy of terrestrial, semiaquatic, and aquatic carnivorans using micro-focus CT scan. *Mammal Study* 38: 1–8.

Nakajima, Y., et al. 2014a. Osteohistology of the Early Triassic ichthyopterygian reptile *Utatsusaurus hataii*: implications for early ichthyosaur biology. *Acta Palaeontol. Pol*. 59: 343–352.

Nakajima, Y., et al. 2014b. Turtle humeral microanatomy and its relationship to lifestyle. *Biol. J. Linnean Soc*. 112: 719–734.

Narkiewicz, K., and M. Narkiewicz. 2015. The age of the oldest tetrapod tracks from Zachełmie, *Poland*. *Lethaia* 48: 10–12.

Nasterlack, T., et al. 2012. New insights into the biology of the Permian genus *Cistecephalus* (Therapsida, Dicynodontia). *J. Vertebr. Paleontol*. 32: 1396–1410.

Niedźwiedzki, G., et al. 2010. Tetrapod trackways from the early Middle Devonian period of Poland. *Nature* 463: 43–48.

Nopcsa, F. B. 1923. Vorläufige Notiz über die Pachyostose und Osteosklerose einiger mariner Wirbeltiere. *Anat. Anz*. 56: 353–359.

Nopcsa, F. von, and E. Heidsieck.1934. Über eine pachyostotische Rippe aus der Kreide Rügens. *Acta Zool*. 15: 431–455.

Nuñez Demarco, P., et al. 2018. Was *Mesosaurus* a fully aquatic reptile? *Front. Ecol. Evol*. 6. http://doi.org/10.3389/fevo.2018.00109

Olson, S. L., and Y. Hasegawa. 1979. Fossil counterparts of giant penguins from the North Pacific. *Science* 206: 688–689.

Organ, C. L., et al. 2007. Origin of avian genome size and structure in non-avian dinosaurs. *Nature* 446: 180–184.

Padian, K. 1985. The origins and aerodynamics of flight in extinct vertebrates. *Palaeontology* 28: 413–433.

Pagel, M. 1997. Inferring evolutionary processes from phylogenies. *Zool. Scr.* 26: 331–348.

Pawley, K. 2007. The postcranial skeleton of *Trimerorhachis insignis* Cope, 1878 (Temnospondyli: Trimerorhachidae): a plesiomorphic temnospondyl from the Lower Permian of North America. *J. Paleont*. 81: 873–894.

Pawley, K., and A. Warren. 2006. The appendicular skeleton of *Eryops megacephalus* Cope, 1877 (Temnospondyli: Eryopidae) from the Lower Permian of North America. *J. Paleont*. 80: 561–580.

Pfeiffer, P., and B. M. Culik. 1998. Energy metabolism of underwater swimming in river-otters (*Lutra lutra* L.). *J. Comp. Physiol. B*. 168: 143–148.

Piveteau, J. 1955. Amphibiens, reptiles, oiseaux. In *Traité de paléontologie*, Vol. V, J. Piveteau, ed. Paris: Masson et Cie.

Polley, B., and R. R. Reisz. 2011. A new Lower Permian trematopid (Temnospondyli: Dissorophoidea) from Richards Spur, Oklahoma. *Zool. J. Linn. Soc.* 161: 789–815.

Purvis, A., et al. 1994. Truth or consequences: effects of phylogenetic accuracy on two comparative methods. *J. Theor. Biol.* 167: 293–300.

Quémeneur, S., et al. 2013. Microanatomy of the amniote femur and inference of lifestyle in limbed vertebrates. *Biol. J. Linnean Soc.* 109: 644–655.

Rayner, J. M. 1988. The evolution of vertebrate flight. *Biol. J. Linnean Soc.* 34: 269–287.

Revell, L. J. 2010. Phylogenetic signal and linear regression on species data. *Methods Ecol. Evol.* 1: 319–329.

Ricqlès, A. de. 1969. Recherches paléohistologiques sur les os longs des tétrapodes II. — Quelques observations sur la structure des os longs des thériodontes. *Ann. Paléont.* 55: 3–52.

Ricqlès, A. de. 1974a. Recherches paléohistologiques sur les os longs des tétrapodes. V. Cotylosaures et mésosaures. *Ann. Paléontol*. 60: 171–216.

Ricqlès, A. de. 1974b. Recherches paléohistologiques sur les os longs des tétrapodes. VI. Eothériodontes et pélycosaures. *Ann. Paléontol*. 60: 1–39.

Ricqlès, A. de. 1977. Recherches paléohistologiques sur les os longs des tétrapodes. VII. Sur la classification, la signification fonctionnelle et l'histoire des tissus osseux des tétrapodes. Deuxième partie, suite. *Ann. Paléontol*. 63: 33–56.

Ricqlès, A. de. 1981. Recherches paléohistologiques sur les os longs des tétrapodes. VI. Stégocéphales. *Ann. Paléontol*. 67: 141–160.

Ricqlès, A de, and V. de Buffrénil. 2001. Bone histology, heterochronies and the return of tetrapods to life in water: where are we? In *Secondary adaptation of tetrapods to life in water*, Mazin, J-M. and V. de Buffrénil eds, 289–310. Berlin: Verlag.

Rohlf, F. J. 2006. A comment on phylogenetic correction. *Evolution* 60: 1509–1515.

Romer, A. S. 1946. The primitive reptile *Limnoscelis* restudied. *Am. Jour. Sci*. 244: 149–188.

Romer, A. S. 1947. Review of the Labyrinthodontia. *Bull. Mus. Comp. Zool. Harv.* 99: 1–368.

Rossi, M., et al. 2004. MicroCT Scan in paleobiology: application to the study of dental tissues. *Nucl. Instr. Meth. Phys. Res. B* 213: 747–750.

Sanchez, S., et al. 2016. Life history of the stem tetrapod *Acanthostega* revealed by synchrotron microtomography. *Nature* 537: 408.

Scheyer, T. M. 2007. Comparative bone histology of the turtle shell (carapace and plastron): implications for turtle systematics, functional morphology and turtle origins. PhD thesis, University of Bonn.

Scheyer, T. M., and M. R. Sánchez-Villagra. 2007. Carapace bone histology in the giant pleurodiran turtle *Stupendemys geographicus*: phylogeny and function. *Acta Palaeontol. Pol.* 52: 137–154.

Scheyer, T. M., and P. M. Sander. 2007. Shell bone histology indicates terrestrial palaeoecology of basal turtles. *Proc. R. Soc. B* 274: 1885–1893.

Scheyer, T. M., and P. M. Sander. 2009. Bone microstructures and mode of skeletogenesis in osteoderms of three pareiasaur taxa from the Permian of South Africa. *J. Evol. Biol.* 22: 1153–1162.

Scheyer, T. M., et al. 2014. The shell bone histology of fossil and extant marine turtles revisited. *Biol. J. Linnean Soc.* 112: 701–718.

Scheyer, T. M., et al. 2015. Shell bone histology of solemydid turtles (stem Testudines): palaeoecological implications. *Org. Divers. Evol*. 15: 199–212.

Schoch, R. R. 2014. *Amphibian evolution: the life of early land vertebrates*. Chichester, UK: John Wiley & Sons.

Schultze, H.-P. 2009. Interpretation of marine and freshwater paleoenvironments in Permo–Carboniferous deposits. *Palaeogeogr. Palaeoclimatol. Palaeoecol*. 281: 126–136.

Sennikov, A. 1996. Evolution of the Permian and Triassic tetrapod communities of Eastern Europe. *Palaeogeogr. Palaeoclimatol. Palaeoecol.* 120: 331–351.

Shelton, C. D., and P. M. Sander. 2017. Long bone histology of *Ophiacodon* reveals the geologically earliest occurrence of fibrolamellar bone in the mammalian stem lineage. *C. R. Palevol* 16: 397–424.

Simmons, N. B., et al. 2008. Primitive Early Eocene bat from Wyoming and the evolution of flight and echolocation. *Nature* 451: 818–822.

Smith, N. A., and J. A. Clarke. 2014. Osteological histology of the Pan-Alcidae (Aves, Charadriiformes): correlates of wing-propelled diving and flightlessness. *Anat. Rec.* 297: 188–199.

Smith, R. M. 1987. Helical burrow casts of therapsid origin from the Beaufort Group (Permian) of South Africa. *Palaeogeogr. Palaeoclimatol. Palaeoecol*. 60: 155–169.

Stein, B. R. 1989. Bone density and adaptation in semiaquatic mammals. *J. Mammal*. 70: 467–476.

Stössel, I. 1995. The discovery of a new Devonian tetrapod trackway in SW Ireland. *J. Geol. Soc.* 152: 407–413.

Straehl, F. R., et al. 2013. Evolutionary patterns of bone histology and bone compactness in xenarthran mammal long bones. *PLoS One* 8: e69275.

Sullivan, C., et al. 2000. Large dissorophoid skeletal elements from the Lower Permian Richards Spur Fissures, Oklahoma, and their paleoecological implications. *J. Vertebr. Paleontol.* 20: 456–461.

Tafforeau, P., et al. 2006. Applications of Xray synchrotron microtomography for non-destructive 3D studies of paleontological specimens. *Appl. Phys. A* 83: 195–202.

VetBooks.ir

Taylor, M. A. 1994. Stone, bone or blubber? Buoyancy control strategies in aquatic tetrapods. In: Maddock, L., Q Bone and J. M. V. Rayner, eds. *Mechanics and physiology of animal swimming*. Cambridge, UK: Cambridge University Press, 151–161.

Taylor, M. A. 2000. Functional significance of bone ballast in in the evolution of buoyancy control strategies by aquatic tetrapods. *Hist. Biol*. 14: 15–31.

Thewissen, J. G., et al. 2007. Whales originated from aquatic artiodactyls in the Eocene epoch of India. *Nature* 450: 1190–1195.

Toledo, N., et al. 2017. Evolution of body size in anteaters and sloths (Xenarthra, Pilosa): phylogeny, metabolism, diet and substrate preferences. *Earth Environ. Sci. Trans. R. Soc. Edin.* 106: 289–301.

Vermeij, G. and R. Motani. 2018. Land to sea transition in vertebrates: the dynamics of colonization. *Paleobiology* 44: 1–14.

Voeten, D. F., et al. 2018. Wing bone geometry reveals active flight in *Archaeopteryx*. *Nature Commun*. 9: 923.

Wainwright, P. C., and S. M. Reilly. 1994. *Ecological morphology: integrative organismal biology*. Chicago: University of Chicago Press.

Wall, W. P. 1983. The correlation between high limb-bone density and aquatic habits in recent mammals. *J. Paleontol*. 57: 197–207.

Watson, D. 1913. V.—The Limbs of *Lystrosaurus*. *Geol. Mag.* 10: 256–258.

Werneburg, R., S. G. Lucas, J. W. Schneider, and L. F. Rinehart. 2010. First Pennsylvanian *Eryops* (Temnospondyli) and its Permian record from New Mexico. *New Mexico Museum of Natural History & Science Bulletin* 49:129–136.

Williams, T. M. 1983. Locomotion in the North American mink, a semi-aquatic mammal. I. Swimming energetics and body drag. *J. Exp. Biol*. 103: 155–168.

Witmer, L. M. 1995. The extant phylogenetic bracket and the importance of reconstructing soft tissues in fossils. In: Thomason J. J., ed. *Functional morphology in vertebrate paleontology*. New York: Cambridge University Press, 19–33.

Zangerl, R. 1935. *Pachypleurosaurus edwardsi*, Cornalia sp. Osteologie, Variationsbreite - Biologie. In: B. Peyer: Die Triasfauna der Tessiner Kalkalpen. *Abh. Schweiz. Pal. Ges.* 56: 1–80.

Zhou, X., et al. 2018. Molecular footprints of aquatic adaptation including bone mass changes in cetaceans. *Genome Biol. Evol*. 10: 967–975.

VetBooks.ir

36

Bone Histology and the Adaptation to Aquatic Life in Tetrapods

Alexandra Houssaye and Vivian de Buffrénil

CONTENTS

Introduction 744
Typical Osseous Microanatomical Specializations Linked to an Aquatic Lifestyle 744
General Remarks 744
High Variability of Patterns 745
Bone Mass Increase in a Microanatomical Perspective 746
Cancellous Organization 747
Parallels Among Lineages 747
Processes Possibly Involved in Bone Structure Specializations 747
Preliminary Considerations 747
Osteosclerosis 748
Pachyostosis 750
Cancellous Structure 750
Functional Considerations 753
Physiological Changes Associated with Adaptation to an Aquatic Lifestyle 753
References 754

Introduction

The amniotes are originally terrestrial, but they secondarily diversified to colonize different habitats, including aquatic ones. From the Early Permian, a return to an aquatic lifestyle occurred numerous times independently in distinct amniote lineages (review in Kelley and Pyenson 2015). Although exclusively aquatic amniotes are only represented today by sirenians, cetaceans and a few snakes, water-dwelling forms are more numerous and diverse in the fossil record. The ecological shift from land to sea is naturally associated with extensive changes in body shape and in many organismal systems, among which is the skeleton (Kelley and Motani 2015). Bones are often strongly affected in their outer morphology as well as their inner structure. The later changes are of two kinds: microanatomical and histological, and they express two levels of adaptation: functional (i.e., related to locomotion constraints) and physiological.

Determining an evolutionary shift in adaptation has to be done in reference to sister groups considered to reveal the plesiomorphic condition of a clade. Concerning adaptations to an aquatic life, interpretations and conclusions must be made in light of the condition observed in the terrestrial sister group. Ancestral forms are rather well known for some lineages (e.g., cetaceans, sirenians, sloths; Domning 2001; Uhen 2010; Amson et al. 2014), but they are much less documented for others such as plesiosaurs and ichthyosaurs (Sander et al. 1997; Liu et al. 2011). Moreover, in some clades, aquatic forms still very close to terrestrial ones are well known, as exemplified in mammals by the Early Eocene raoellid *Indohyus* and the pakicetid *Pakicetus* (reviews in Bajpai et al. 2009; Muizon 2009), as well as by the contemporaneous fully quadrupedal sirenian *Pezosiren portelli* (Domning 2001). However, the exclusively terrestrial sister groups of some of these clades remain debated or unknown (see, e.g., Caldwell and Palci 2007 for mosasaurs). When evidence is not sufficient, the reference comparative condition is assumed to be close to the general character state observed in terrestrial forms, such as a tubular-like organization of long bones.

Typical Osseous Microanatomical Specializations Linked to an Aquatic Lifestyle

General Remarks

Compared to the tubular architecture prevailing in the long bones of terrestrial forms (Figure 36.1), two main microanatomical specializations are encountered in most aquatic amniotes, whether extant or extinct: (1) an increase in bone mass due to high inner compactness, hyperplasic cortices,

VetBooks.ir

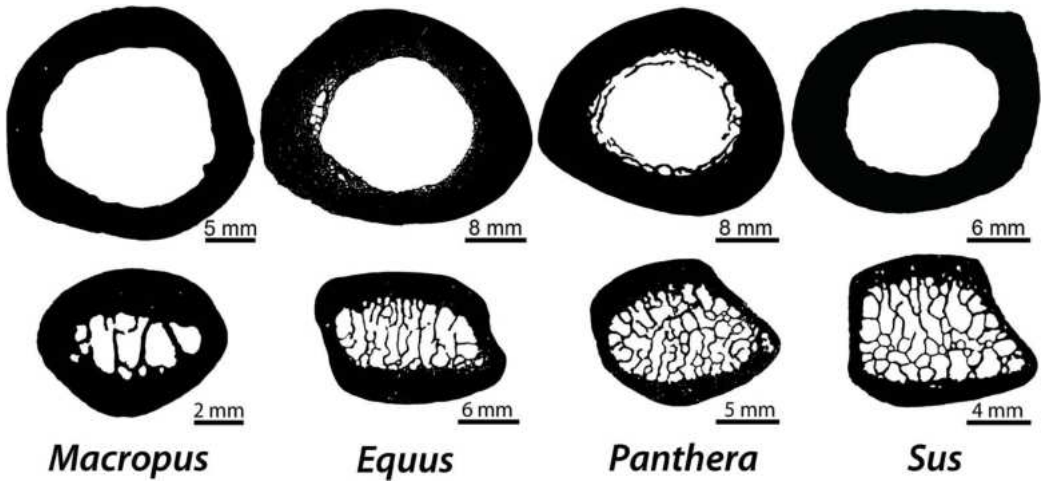


FIGURE 36.1 Reference tubular bones in a sample of terrestrial mammal femora (upper row) and ribs (lower row).

or both, or (2) a cancellous inner organization (often designated as "osteoporotic-like") extending to the entire bone volume, with no open medullary cavity. These specializations generally (but not exclusively) involve the appendicular and postcranial axial skeleton, and are essentially documented in ribs, vertebrae and stylopod bones (e.g., Houssaye et al. 2016). Cranial bones can also be affected (e.g., Buffrénil and Schoevaert 1989; Buffrénil and Casinos 1995) but less frequently and less extensively. Available comparative data suggest that bone mass increase is preferentially encountered in taxa incipiently readapting to life in water and poorly designed for fast swimming. Such forms live in shallow coastal zones and recur to hydrostatic means to control their buoyancy and body trim in water (Taylor 1994; Ricqlès and Buffrénil 2001). Conversely, a cancellous organization is observed in active swimmers (most of them use lift-based propulsion modes) requiring good maneuverability and acceleration abilities, and relying on a hydrodynamic control of buoyancy and trim (Webb and Buffrénil 1990; Ricqlès and Buffrénil 2001).

High Variability of Patterns

The basic bone specializations mentioned above display a strong diversity consisting of different degrees of bone mass increase, different distributions of the osseous tissue in the bone, different modes of geometrical structuration in the trabecular network of cancellous formations and so forth. There is also a high diversity in the distribution and combination of these specializations within a single skeleton (Houssaye et al. 2016) and some taxa can show a patchwork of local specializations. For example, ziphiid whales may display extremely cancellous ribs but also extraordinarily compact and mineralized skull regions (rostrum, tympanic bullae: Buffrénil and Casinos 1995; Lambert et al. 2011). Similarly, the mosasauroid *Dallasaurus*, which has altogether anatomically nonspecialized (terrestrial-like) limbs but no sacrum, has tubular (terrestrial-like) femora and ribs, and osteosclerotic humeri (Houssaye et al. 2013).

In reference to the frequency of bone structural specialization, skeletal regions may be ranked in the following order: the skull is seldom affected (Lambert et al. 2011) and vertebrae are affected to a limited extent, except in Cenomanian-Turonian marine ophidiomorph squamates (e.g., Buffrénil and Rage 1993; Houssaye 2013; see also Chapter 20 on lepidosaurs), Late Mesozoic and Paleocene champsosaurids (Choristodera; Buffrénil et al. 1990b) and some Middle Miocene marine mammals from the peritethyan and North Sea regions (e.g., Kazár 2010; Dewaele et al. 2019). Rib structure is frequently modified in aquatic taxa, but this situation is far from being general, and highly pelagic species such as most extant cetaceans and pinnipeds (e.g., Canoville et al. 2016), thalattosuchians (see Chapter 26), ichthyosaurs (Talevi and Fernández 2012) and plesiosaurs (Street and O'Keefe 2010) often have a nonspecialized rib structure. Among appendicular bones, the stylopod (humerus and femur) is frequently affected (review in Houssaye et al. 2016), whatever the degree of specialization to life in water. However, advanced streamlining often results in the regression and loss of the hind limbs; therefore, the humerus might well be the most frequent target of bone structural specialization in aquatic amniotes. The inner structure of this bone is almost never modified in terrestrial animals (with extremely rare exceptions such as the giraffoid *Lorancameryx pachyostoticus*; Morales et al. 1993), but is nearly always transformed, in one way or another, in aquatic or incipiently aquatic taxa. This qualitative remark agrees with the quantitative data presented by Canoville and Laurin (2010) (see also Laurin et al. 2011 and Chapter 35) showing a stronger ecological signal for the humerus than for the other skeletal elements in tetrapods. Variation along the diaphysis of a long bone can also be pronounced: the region around the growth center can be osteosclerotic, whereas the inner bone organization becomes mainly cancellous slightly away from this point (see Houssaye et al. 2015). Such variation within a single bone is rarely observed in terrestrial taxa but seems to be common in aquatic forms (Houssaye et al. 2014, 2016). In brief, the pronounced variability described above may create the risk that contradictory indications occur in the bones of a single skeleton, if considered separately. This is why the examination of several distinct skeletal elements must be recommended as far as possible. Moreover, the intraskeletal location of osteosclerosis, pachyostosis or cancellous states generally contains

VetBooks.ir

pachyostosis or cancellous states generally contains a strong ecological (adaptive) signal since it has direct and heavy consequences on the static and dynamic properties of the body in water.

The analysis of fossils in the evolutionary context of a return to an aquatic lifestyle does not only provide information about the ecology of fossil forms, thus enabling the reconstruction of the history of the adaptation of individual lineages (see, e.g., the xenarthran *Thalassocnus* in Amson et al. 2014), it also enables a better understanding of the types and extents of bone adaptation to specific locomotion requirements. Beyond the great diversity of the evolutionary trajectories of aquatic tetrapod clades, some general tendencies emerge from available comparative data. (1) Since the earliest stages of the "return" of a tetrapod clade to life in water, long bones (at least) have already lost their plesiomorphic tubular architecture, and even if the body shape is not yet modified, the inner structure of these bones is no longer typically tubular, as exemplified by the earliest sirenian *Pezosiren portelli* (Buffrénil et al. 2010) and the pakicetid *Ichthyolestes pinfoldi* (Thewissen et al. 2007). (2) The bones (at least in limited skeletal territories) of most amniote clades incipiently adapting to life in water are either osteosclerotic, pachyostotic or pachyosteosclerotic. (3) No clade incipiently readapting to life in water has cancellous bones (skeletal lightening); the initial skeletal adaptation appears to be mandatorily oriented toward bone mass increase.

Bone Mass Increase in a Microanatomical Perspective

Increase in bone mass consists in an augmentation of bone compactness, commonly named osteosclerosis (Figure 36.2A–D). In this context, this term is used to designate a physiological

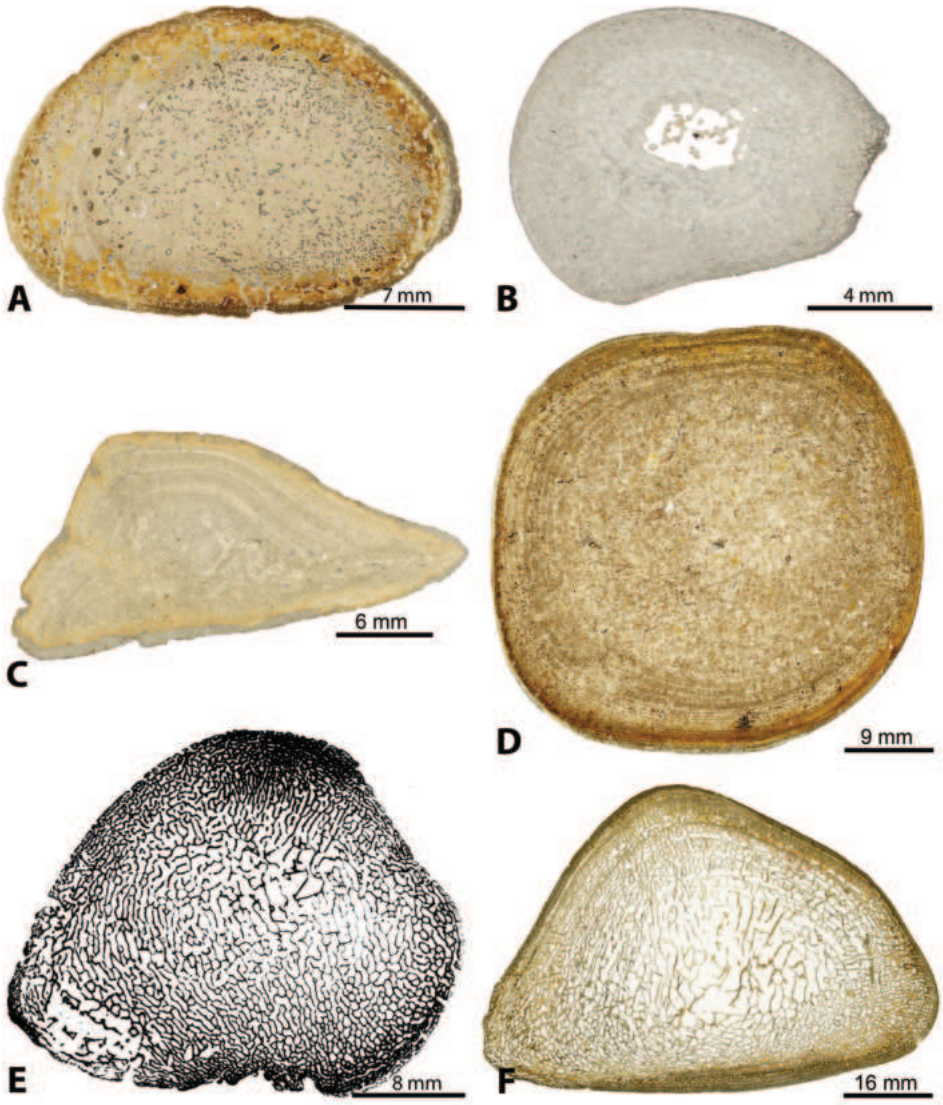


FIGURE 36.2 Modifications of bone inner structure and volume in aquatic tetrapods. A–C, Typical aspects of the condition designated as "osteosclerosis". A, Rib of the basal sirenian *Pezosiren portelli* (early Middle Eocene of Jamaica). B, Tibiotarsus of the extant sea bird *Aptenodytes patagonicus*. C, Humerus of the extinct seal *Cryptophoca maeotica* (Upper Miocene of Eastern Europe). D, Association of extreme osteosclerosis and pachyostosis in a rib of the extinct sirenian *Halitherium schinzii* (Early Oligocene of Europe). E, Cancellous organization of the humerus of the extant common dolphin, *Delphinus delphis*. F, Similar condition in the humerus of the extant elephant seal, *Mirounga leonina*.

VetBooks.ir

state, occurring in 100% of conspecific populations (or supposed so in fossils); it by no means refers to the multiple pathological processes resulting in entirely solid bones known in human and veterinary medicine (Tolar et al. 2004; Lamb and Jackson 2015). Osteosclerosis may occur conjointly with an increase in bone volume through additional deposits of cortical bone (Figure 36.2D), a distinct state called pachyostosis (see Ricqlès and Buffrénil 2001 for terminology). Bone mass increase can show various patterns and degrees. In long bones, osteosclerosis is illustrated by the occurrence of a very thick cortex and a correlative reduction of the medullary cavity (Figure 36.2B) that may be entirely missing. A characteristic example of this process found in the placodonts (Buffrénil and Mazin 1992; Klein et al. 2015; see also Chapter 21). Moreover, trabecular areas can also be much tighter with much reduced intertrabecular spaces (Houssaye 2013). In rare cases, the endosteoendochondral spongiosa in long bones or vertebral centra can be entirely occluded, as exemplified, respectively, by the limb bones of the seal *Nanophoca* (Dewaele et al. 2019) and of the sirenian *Sobrarbesiren* (Díaz-Berenguer et al. 2018), and the vertebrae of some Late Cretaceous marine squamates (Houssaye 2013; see also Figure 36.2C). Well-pronounced cases of bone mass increase can be easily identified, whereas feeble intensities are ambiguous. It remains complicated to determine a morphological feature, an index or a compactness threshold from which pachyostosis and osteosclerosis, respectively, could be diagnosed. This has been proposed for mammal ribs (Buffrénil et al. 2010), with a threshold for osteosclerosis around a compactness index (*BAr/TAr*; see Chapter 4) value of 82% and, for pachyostosis, a value of 0.18 or higher for an index expressing cortical development (mean rib circumference divided by rib length).

Cancellous Organization

At mid-diaphysis, stylopod bones of active, fast-swimming marine tetrapods are almost entirely cancellous, and made of a spongiosa of both endosteal and periosteal origins (Figure 2E, F). Compact periosteal tissue, when present, is restricted to cortical periphery. A cancellous organization can result from peculiar remodeling processes (see below), but it can also be of primary origin (e.g., in ichthyosaurs: Buffrénil et al. 1987; Houssaye et al. 2014, 2018). A spongy structure has long been associated with the idea of a lightened skeleton (Felts and Spurrell 1965; Buffrénil et al. 1986). However, when considered in reference to the global volume of a bone, or the totality of the skeleton, a local cancellous organization does not necessarily mean that bone mass is decreased. Similar compactness indices can indeed be observed in cancellous and tubular bones. A cancellous organization may result principally from a difference in the distribution of the osseous tissue rather than from a decrease in the net local amount of this tissue. This type of structural organization is observed in most if not all of the bones of efficient pelagic swimmers such as cetaceans (Buffrénil and Schoevaert 1988), hydropedal mosasauroids (Houssaye et al. 2013), sea turtles (Rhodin 1985) and ichthyosaurs (Buffrénil and Mazin 1990). Comparative analyses have shown that the trabecular network is tighter in large bones, with a relative increase in the number of trabeculae and a reduction of intertrabecular spaces; however, the trabeculae in such bones tend to be thinner, which reduces the effect of their multiplication on bone compactness (Houssaye and Bardet 2012; Dumont et al. 2013).

Parallels Among Lineages

In amniote evolutionary history, parallel shifts in microanatomical specialization have been observed in distinct lineages. Several of them have shifted from an initial condition of bone mass increase in the early stage(s) of their aquatic adaptation, when they inhabited shallow waters, retained a rather "terrestrial-like" morphology and were (or supposed to have been) poorly efficient swimmers relying on drag-based propulsion, to a cancellous organization of their bones, when they became active swimmers in open seas, with advanced body streamlining, flippers and a lift-based mode of propulsion. This evolutionary pattern closely fits mosasauroids and cetaceans. Plesiopedal and plesiopelvic mosasauroids show bone mass increase (Houssaye 2013), whereas hydropedal and hydropelvic mosasauroids show a cancellous organization (Houssaye and Bardet 2012; see also Chapter 20). The types of osseous specializations presented by the taxa prove to be independent from size, because juvenile hydropelvic mosasauroids show a cancellous organization, whereas larger adult plesiopelvic forms are osteosclerotic (Houssaye and Tafforeau 2012). Similarly, some early (Eocene) whales, the archaeocetes, show bone mass increase (pakicetids, remingtonocetids, protocetids, basilosaurids; Buffrénil et al. 1990a; Gray et al. 2007; Thewissen et al. 2007; Houssaye et al. 2015), whereas the same bones in extant cetaceans often have a cancellous organization (Buffrénil and Schoevaerts 1988).

Processes Possibly Involved in Bone Structure Specializations

Preliminary Considerations

Pointing out transitions from pachyosteosclerotic to cancellous patterns in the evolution of amniote lineages toward increasing swimming abilities, Nopcsa (1923) tentatively proposed an origin for the spongy organization observed in active swimmers. He suggested that, because of the irreversibility of evolution, transition from osteosclerosis to a less compact structure could not merely be a return to a structure with a well-developed marrow cavity, an organization optimal only in the context of high gravity (Currey 2003). From Nopcsa's point of view, lightening was thus accomplished by general resorption of the bone. Zangerl and Peyer (1935) also suggested that the cancellous microstructure observed in ichthyosaur and whale bones is "postpachyostotic" and that increased bone density is a transitory stage common to most secondarily marine amniotes. This idea was also developed by Felts and Spurrell (1965) who considered that the cetacean humerus structure resulted from "an evolutionary 'opening up' of the vascular spaces of a pachyostotic form in a manner selective for the conditions in the evolving flipper of the several cetacean forms".

VetBooks.ir

The recent multiplication of comparative data shows that the evolution of bone structure in the course of the adaptation of amniote taxa to an aquatic life is diverse. Following the historical contributions mentioned above, several authors (e.g., Ricqlès and Buffrénil 2001) further elaborated that some type of mandatory adaptive trajectory occurred in aquatic amniotes. (1) In an initial stage, when adaptation was incipient, peculiar developmental modalities leading to osteosclerotic or pachyosteosclerotic conditions must have been selected in response to the unavoidable physiological impact of the constraints of the aquatic environment (pressure, light, thermal conduction, apnea, diving etc. (2) In subsequent adaptational stages, a reversion of this condition oriented toward relative skeletal lightening occurred, when the taxa became anatomically and physiologically more closely specialized to life in water. Although this view can be supported by the evolution of, e.g., cetaceans and mosasaurs, other taxa do not comply with it. The sirenians, for example, considerably improved their morphological and physiological adaptations to life in water (reaching a degree of specialization comparable to, though different from, that of cetaceans), since the Early Eocene quadrupedal *Pezosiren portelli* (Domning 2001). However, far from reducing their initial pachyosteosclerotic condition, they increased it (Buffrénil et al. 2010). Several taxa showing an intermediate mode of life, like the pinnipeds, did not experience pronounced bone structural specialization, with some rare and puzzling exceptions further considered below. The recent discovery of Middle Miocene peri-Tethyan marine mammal faunas in Austria and Ukraine (see, e.g., the peculiar case of *Pachyacanthus suessii* in Kazár 2010) show that a late reversion from a (supposedly) cancellous condition toward a very heavy pachyostotic one, occurred in some cetacean clades, at least in a circumscribed geographic area. A comparable situation is also documented in several phocid species that inhabited the North Sea during the middle Miocene and experienced extreme osteosclerosis (Dewaele et al. 2019). Altogether, these comparative elements suggest that the development of osteosclerosis, pachyostosis, pachyosteosclerosis or, conversely, that of cancellous states, likely responds to circumstantial, and sometimes geographically circumscribed, adaptive requirements. However, elementary observations show that some pachyosteosclerotic and/or osteosclerotic amniotes are found together with nonaffected ones in the same outcrops (e.g., the pachyosteosclerotic *Pontosaurus kornhuberi* and the nonaffected *Aphanizocnemus*, both ophidiomorphs from the Cenomanian site of En Nammoura, northern Lebanon; Bardet et al. 2008, Houssaye 2013), which is evidence that bone structural specializations (here bone mass increase) in aquatic amniotes reflect species-specific adaptational options, and are by no means a direct, mandatory result of the peculiar properties of local environments.

Osteosclerosis

The general cause of osteosclerosis is a gross alteration of the bone remodeling process; however, distinct histological patterns occur, which suggests that diverse processes are involved. Some bones are characterized by a drastic inhibition of endochondral and periosteal resorption, which impedes the differentiation of a free medullary cavity in the long bones, and of a spongiosa in, e.g., the core of the vertebral centra. Both areas then display high compactness. This situation often results in the persistence, at large distance from the epiphyses, of large remnants of calcified cartilage matrix. The latter may either form a homogeneous mass occupying the medullary region of the bones (Figure 36.3A), as observed in, e.g., some regions of the skeleton in choristoderes (champsosaurs: Buffrénil et al. 1990a), and in mesosaurs (Klein et al. 2019a) and pachypleurosaurs (Hugi et al. 2011), or be present in the core of trabeculae, which then remain as primary endosteoendochondral trabeculae, as exemplified by stem ophidians, choristoderes (Figure 36.3B), sirenians, early cetaceans (Archaeoceti: Figure 36.3C) and so forth (Buffrénil and Schoevaert 1989; Buffrénil et al. 1990a; Houssaye et al. 2008). This condition seemingly occurs through an inhibition of the activity or recruitment pathway of chondroclast and osteoclast populations. However, some taxa, such as the placodont *Placodus*, have a fairly compact medullary core with only a residual medullary cavity, but do not exhibit calcified cartilage remains (Buffrénil and Mazin 1992); this suggests that inhibition of chondroclast activity in these forms was mild or occurred relatively late in ontogeny. In the same taxon, the broad resorption field due to osteoclast activity that normally enlarges the medullary cavity in long bones was severely inhibited. Another process consists of active but imbalanced remodeling with excessive secondary bone deposits that fill the intertrabecular spaces and provoke the occlusion of the medullary cavity. This situation has been observed in the Permian diapsid reptiles *Pachypleurosaurus* (Figure 36.3D) and *Claudiosaurus germaini* (Buffrénil and Mazin 1989; see also Figure 36.3E), in extant and extinct sirenians (Buffrénil et al. 2008b; see also Figure 36.3F) and in the middle Miocene seal *Nanophoca vitulinoides* (Dewaele et al. 2019; see also Figure 36.3G, H). This situation is obviously caused by an excess in the activity of endosteal osteoblasts during remodeling (see also Chapter 11).

Various hypotheses have been proposed since the beginning of the 20th century to explain the causes and processes from which osteosclerosis results. A first set of hypotheses involved endocrine disorders (Fawcett 1942; Cave and Aumonier 1967; Arnett et al. 2003; Gogakos et al. 2010). A depressed functioning of the thyroid gland has been invoked as a possible early consequence of the aquatic (especially marine) conditions the amniotes had to face in the initial stages of their readaptation to life in water: feeble lighting, hypoxia, increased pressure, lower ambient temperature and so forth. However, the occurrence of osteosclerosis in animals that have been adapted to an aquatic lifestyle for tens of millions of years (e.g., sirenians), and thus had a great deal of time to adapt to environmental factors possibly causing hypothyroidism, weakens this hypothesis. Moreover, the influence of these environmental constraints, notably feeble light and high pressure, should have been stronger for deep divers, but the latter do not show osteosclerosis. In addition, hypoxia is now well known to stimulate bone resorption and provoke bone loss (Arnett et al. 2003; Knowles 2015), not the opposite effect. Osteosclerosis rarely involves the skeleton as a whole but is restricted to a subset of bones; therefore, its main cause is unlikely to straightforwardly reflect systemic endocrine factors (Buffrénil and Schoevaert 1989; Buffrénil et al. 2010).

VetBooks.ir

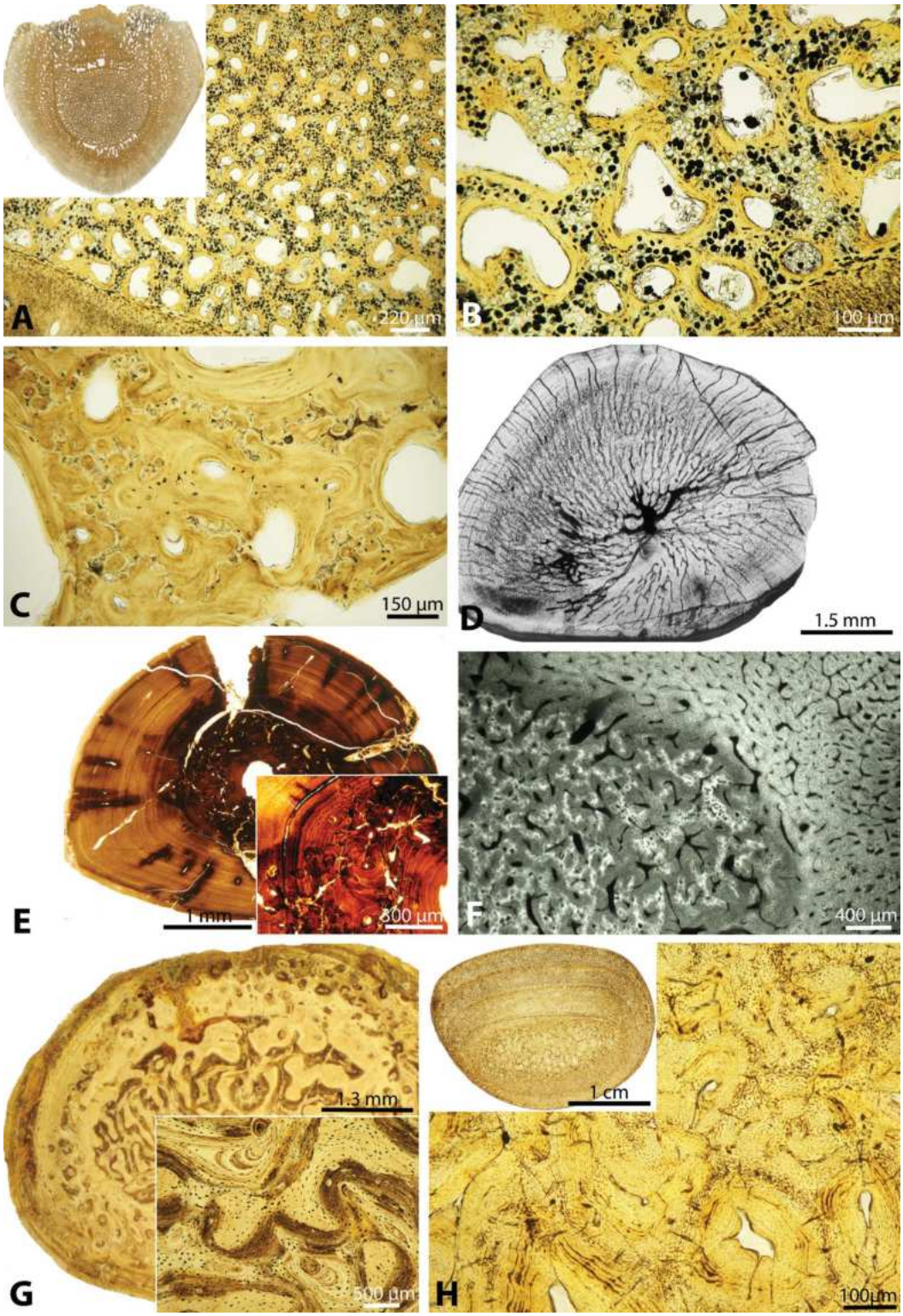


FIGURE 36.3 Histological aspects of osteosclerosis. A, Highly compact vertebra of the choristodere *Champsosaurus* sp. (Upper Paleocene of Western Europe). B, Primary trabeculae in the core of *Champsosaurus* vertebral centra. C, Detail of the dense spongiosa in the core of a rib of the archaeocete *Zygorhiza kochii* (Upper Eocene of North America). Broad remnants of calcified cartilage matrix are still present and display *globuli ossei*. D, Absence of perimedullary resorption in a rib of the Triassic nothosaur *Pachypleurosaurus*. E, Strong reduction of the medullary cavity through imbalanced remodeling in the humerus of the early diapsid *Claudiosaurus germaini* (Late Permian of Madagascar). The inset is an enlargement of the perimedullary region. F, Maintenance of calcified cartilage remnants and full filling of intertrabecular spaces by endosteal deposits in the humerus of the extant sirenian *Dugong dugon*. Microradiography. G, Compacted radius shaft in the extinct dwarf seal *Nanophoca vitulinoides*. The inset is an enlargement of the medullary region of the bone. H, Same process in a rib of an undetermined cetothere (Mammalia: Cetacea) from the Upper Miocene of Eastern Europe. The inset shows the general aspect, characterized by extreme compactness, of the bone section.

VetBooks.ir

A second set of hypotheses, logically related to the physiological considerations mentioned above, involve heterochronic processes through a reprogramming of the activity of the chondroclasts and osteoclasts (Ricqlès 1989; Ricqlès and Buffrénil 2001). Finally, the occurrence of mutations, grossly akin to those causing the so-called metabolic bone diseases, has been proposed (Buffrénil and Rage 1993; Dewaele et al. 2019). Ricqlès (1989) suggested that a primitive (i.e., plesiomorphic in amniotes) "functional complex" of structural and regulatory genes could control the temporal aspects of cellular differentiation and activities involved in the elaboration of the skeleton. These "complexes" would have been conserved, with minor variations, in all amniotes, but mutations could have changed the timing of some osteogenetic processes. However, heterochrony, if considered a process involving the organism as a whole, can hardly explain some of the patterns observed, like the association of non-(or partly) resorbed growth cartilages evoking pedomorphosis, with pachyostosis that rather evokes peramorphosis. With regard to the important variability (in, e.g., distribution and intensity) displayed by osteosclerosis in aquatic amniote taxa (see Houssaye et al. 2016), the scenario of a unique mutation seems very unlikely; rather, diverse mutations acting on the activity of the osteoclasts and osteoblasts could have affected various taxa and various regions of the skeleton, with a greatly localized effect, in these taxa. Bone modeling and remodeling are extremely complex, and still incompletely elucidated, processes (see Chapters 9 and 11), in which several cell lineages and a cascade of many endocrine, paracrine and autocrine factors and their specific receptors, in addition to gene expression regulators, are involved (review in Burr and Allen 2014; see also Giustina et al. 2008; Florencio-Silva et al. 2015). This cascade offers several possibilities for hereditary (i.e., genetic) interindividual variability to occur, with similar ultimate consequences: modifying, at a general or local level, the conditions and results of bone remodeling. The development of osteosclerosis is thus unlikely to result from a unique cause in all taxa; it would rather be an opportunistic process possibly due to the evolutionary selection of distinct causal processes among clades, but with a convergent morpho-functional result.

Genomic investigations of this topic remain incipient. The recent study by Zhou et al. (2018), comparing marine mammals (mainly cetaceans) with their terrestrial relatives, revealed a significant correlation between the level of inner bone compactness and the peculiarities that some genes, known to be involved in the control of bone structure and remodeling, present in marine mammals. Though deserving further substantiation by new studies, this contribution first suggested that the specialized structural features of the skeleton in aquatic amniotes result mainly from complex, genetically determined processes.

Pachyostosis

Pachyostosis is considered to rely on a unique process that is hyperplasia of the cortical bone deposits, which confers a bloated aspect to the bones (Figure 36.4A, B). However, in the absence of detailed growth series, it remains unclear whether this condition is caused by an increase in the speed or in the duration of local growth, or both. The swollen aspect of the premaxillae of the Miocene/Pliocene beaked whale *Aporotus recurvirostris* was seemingly due to a local increase in the rate of apposition that resulted in the occurrence of fibrolamellar bone with radial canals, as opposed to the laminar or plexiform tissues prevailing in the rest of the bone (Buffrénil and Lambert 2011). Such a process is also well illustrated by the ribs of two extinct cetaceans, the protocetid *Eocetus wardii* and an undetermined cetothere from the Miocene of Crimea (possibly *Brandtocetus*), where the development of a pachyostotic cortex mainly involved the lateral face of the ribs and was due to local acceleration of bone accretion (Figure 36.4C–F). This characteristically resulted in histological tissue types (either laminar or radial woven-parallel complexes) known to reflect higher accretion rates than the tissue (woven-parallel complex with longitudinal primary osteons) prevailing in cortical parts that were growing more slowly. In *Eocetus*, this acceleration occurred during a short period, restricted to early cortical growth, as shown by the position of the radial woven-parallel formation in the deep cortex (Figure 36.5F, G). Though a similar process has seldom been described in the comparative literature, it is likely to be the more frequent mechanism causing pachyostosis because protraction of the duration of local periosteal accretion would create a great diversity in the aspect of homologous conspecific bones, depending on individual ages, a situation that has not been mentioned (to our knowledge) in the literature, except in the snake *Eupodophis descouensi* where the degree of pachyostosis seems to vary with size: it is absent in the smallest, juvenile, specimen, and progressively increases with size in the three other specimens known to date (Rieppel and Head 2004, Houssaye 2013). Moreover, osteoblastic activity, like bone remodeling, is controlled by systemic hormones (growth hormone, insulin-like growth factor, sex steroids, etc.) and multiple local regulators, all liable to undergo heritable mutational modifications affecting the level or duration of their activity, as well as the interactions that they may have (see also Chapter 9). Therefore, the actual cause of pachyostosis and its structural results can be variable and of great complexity.

Cancellous Structure

Histological observations of the many aquatic amniotes presenting spongy bones suggest that two distinct developmental processes could have been selected during evolution for the replacement of compact cortical tissue by cancellous formations: (1) the maintenance of the fine cancellous tissue initially deposited by the periosteum in fast-growing (and possibly endotherm – homeotherm) taxa and (2) the transformation of initially compact cortices into cancellous ones through imbalanced remodeling. The first process (Figure 36.5A, B) has been mainly described in the probable ichthyosaurian *Omphalosaurus nisseri*, in typical ichthyosaurs (Buffrénil and Mazin 1990; Houssaye et al. 2018) and in the placodont *Placodus* (Buffrénil and Mazin 1992). It is likely to occur also in the limb bones of the extant seal *Mirounga leonina* (Figure 36.5C). Cortical bone is deposited as a scaffold of longitudinally and radially oriented trabeculae composed of woven-fibered tissue (Figure 36.5B) to form typical fine cancellous bone (see Chapter 8). In normal cortical development,

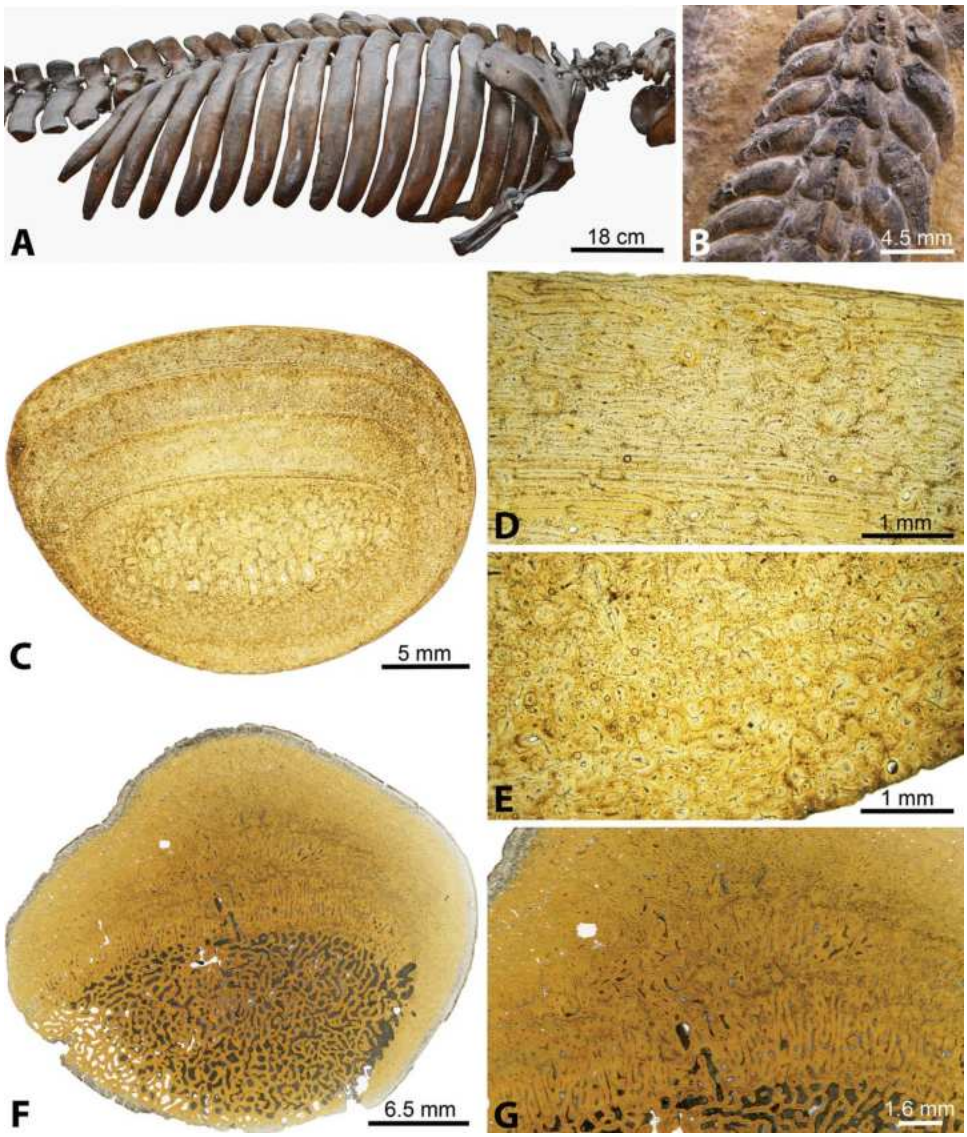


FIGURE 36.4 Morphological and histological aspects of pachyostosis. A and B, Typical morphology of pachyostotic bones, with a swollen, hyperplasic cortex. A, Thoracic region of the sirenian *Halitherium schinzii*, B, Partial view of the thorax of the Late Cretaceous marine squamate *Pachyophis woodwardi*. C, Creation of a thick cortex through asymmetrical acceleration of subperiosteal bone accretion in a rib of an undetermined Upper Miocene cetothere. Note the difference in growth mark spacing between the two faces of the bone. D and E, Histological aspects of the growth rate differences mentioned for C. On one face of the bone, fast-growing laminar woven-parallel bone is deposited (D), whereas woven-parallel bone tissue with longitudinal primary osteons is deposited on the other, slow-growing face (E). F and G, Similar processes in a rib of the Late Eocene cetacean *Eocetus wardii*. In this specimen, growth acceleration on one side of the bone occurred during a limited period and resulted in the deposit of radiating woven-parallel tissue. Subperiosteal growth rate then decreased. The other face of the bone was submitted to extensive resorption through which the deep (medullary) spongiosa was displaced toward the surface of the bone.

intertrabecular spaces in these formations are occluded by centripetal deposits of lamellar or parallel-fibered tissue creating primary osteons. The combination of these osteons and the primary trabeculae is characteristic of the broad category of woven-parallel (also called fibrolamellar) tissue types. In the aquatic tetrapods mentioned above, the formation of the osteons does not occur or stops at an early stage, thus leaving the cortices in a permanent spongy condition during ontogeny.

In the second situation, observed in Mesozoic marine crocodiles (Hua and Buffrenil 1996; see also Chapter 26), plesiosaurs (Wiffen et al. 1995; Wintrich et al. 2017), mosasaurs (Houssaye and Bardet 2012; Houssaye et al. 2013), Neoceti (Buffrénil and Schoevaert 1988) and, according to Buffrénil and Mazin (1990), in some advanced (Jurassic) ichthyosaurs (but see also Houssaye et al. 2014), osseous cortices are initially formed as compact bone, whatever their histological structure (parallel-fibered, woven-fibered or woven-parallel tissues). Extensive remodeling, initiated by the formation of large resorption lacunae, subsequently develops in the cortices and progresses in pace with subperiosteal accretion (Figure 36.5D–F). Characteristically, this remodeling activity is imbalanced.

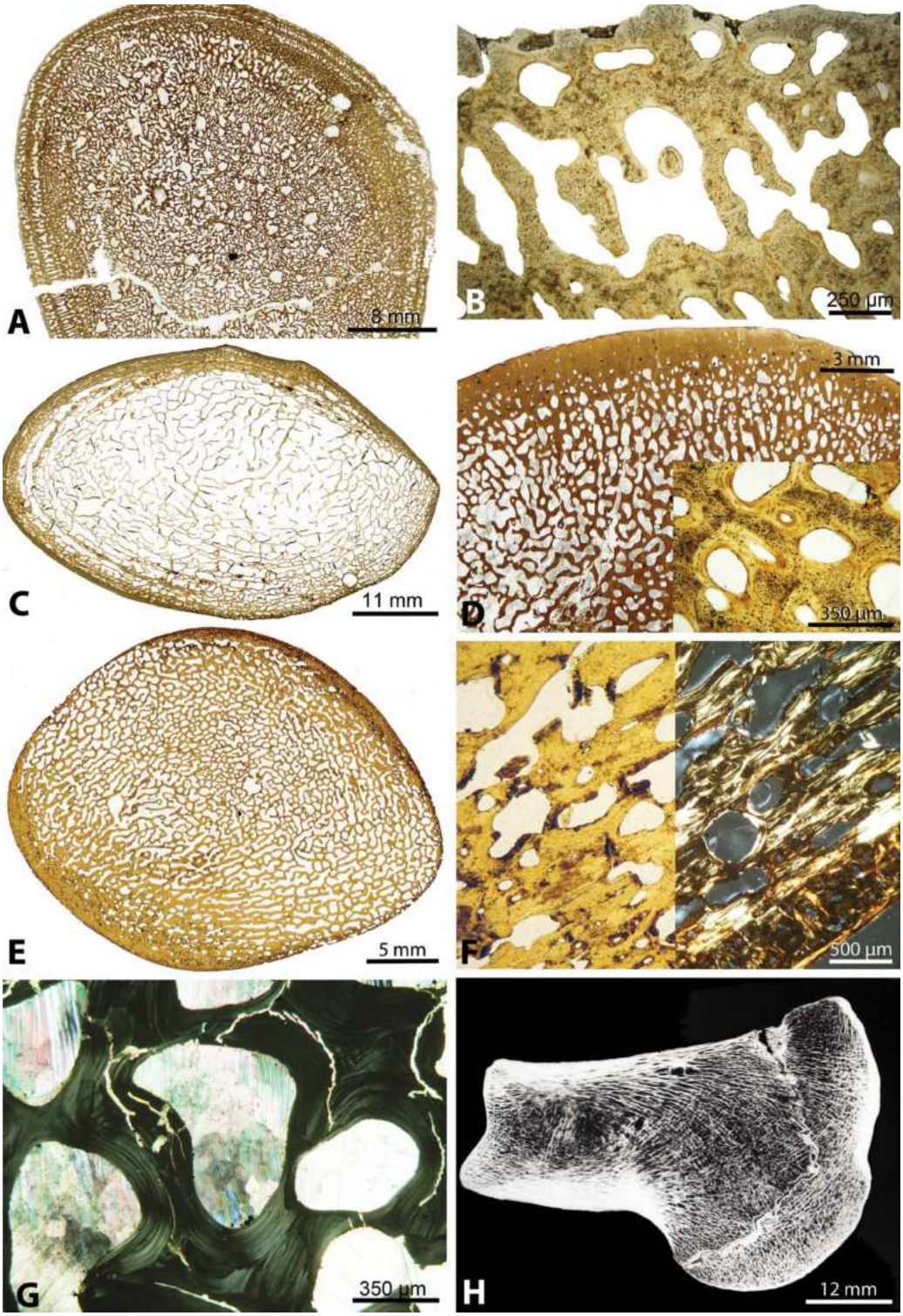


FIGURE 36.5 Histological aspects of cancellous long bones, and the basic mechanisms creating them. A, Maintenance of the so-called fine cancellous bone in the femur of the early ichthyosaur *Omphalosaurus nisseri*, from the Middle Triassic of Spitzberg. The primary osteons normally filling intertrabecular spaces do not develop. B, Aspect of the trabeculae in the fine cancellous bone of *Omphalosaurus* femur. They are made of woven-fibered tissue only. C–F, Creation of cancellous cortices through imbalanced remodeling. In this case, reconstructive deposits do not compensate for the volume of tissue previously eroded, and compact cortices become cancellous. Three cases are considered: a rib of the extant elephant seal (C); the femur of the Upper Jurassic ichthyosaur *Stenopterygius quadriscissus* (D) and a rib of *Zarhachis flagellator*, a platanistoid cetacean from the Miocene of the United States. (E). The inset in D is a closer view of the trabeculae shown in the main frame. F, Closer view of the eroded cortex of *Z. flagellator* rib. Right half: polarized light. G, Detail of the intensely remodeled trabeculae in the femur of *Stenopterygius*. Polarized light. H, Elaborated, and possibly adaptive, trabecular architecture in the humerus of the common dolphin. Microradiography of a sagittal section. Notice that trabecular architecture extends continuously in both the metaphyseal and epiphyseal (not yet fused) regions of the bone.

VetBooks.ir

Eroded bone volume is not, or is only partly, compensated by secondary, reconstructive deposits (Buffrénil and Schoevaert 1988), a situation basically comparable to that of the osteoporotic process commonly affecting aged individuals (see Chapter 32) and subjects confined to bed or living in weightless conditions for long periods (disuse osteoporosis). The reconstruction deficit can result from three possible causes, which may combine in diverse ways. 1) It can be space-dependent, i.e., the reconstructive activity occurs on a smaller area than the previous resorption. 2) It can be time-dependent, i.e., the reconstruction is too short in time to entirely compensate the resorption. 3) It can be speed-dependent, i.e., the reconstruction progresses much more slowly than the resorption, thus creating an accumulation of nonreconstructed volumes. The final result of these three processes is that the cortices gradually lose bone mass, but at the same time, a medullary cavity does not form. The trabeculae of the cancellous tissue thus created are subsequently submitted to repeated remodeling to the point where they may become entirely composed of secondary endosteal hemiosteons made of lamellar tissue (Figure 36.5G). Two main differences distinguish this general process from pathological osteoporosis. On the one hand, albeit imbalanced, it integrates the requirements of "adaptive remodeling" and maintains a definite trabecular architecture (Figure 36.5H). On the other hand, it starts in early stages of skeletal growth (Buffrénil and Schoevaert 1988), whereas pathological imbalanced remodeling is a characteristic of senile (or otherwise weakened) organisms, or is induced by a suspension of the weight-bearing role of the skeleton (disuse osteoporosis).

Functional Considerations

A passive, density-dependent control of buoyancy appears crucial for poorly efficient swimmers and divers, and enables them to passively reach neutral (i.e., when body density equals that of water) or negative (i.e., when body density is higher than that of water) buoyancy, at shallow depth (Domning and Buffrénil 1991; Taylor 1994). In addition, such a passive control of body trim saves a significant amount of energy, otherwise spent for maintaining the horizontal orientation of the body required for efficient swimming. In this context, individuals developing more pronounced, or more adequately located, bone mass increase might have been positively selected. Adaptive changes in inner bone structure seem to occur rather quickly in the evolutionary history of lineages readapting to an aquatic lifestyle. In cetaceans, sirenians, and mosasauroids, at least, they predate outer changes of the skeleton (Gray et al. 2007; Buffrénil et al. 2010; Houssaye 2013). The example of the Late Miocene xenarthran *Thalassocnus* (Amson et al. 2014) shows that a pronounced and extensive osteosclerotic state evolved over 3–4 million years.

Conversely, in taxa capable of fast swimming, and using a hydrodynamic control of buoyancy and body trim, heavy bones would decrease acceleration capacity and maneuverability. As a result, active swimmers, which are often adapted to pursuing and catching individual prey, evolved toward a loss of bone mass increase and even, for some of them, toward a true lightening of the skeleton. The latter process preferentially affects bones of limited mechanical involvement in water, such as the appendicular skeleton (Buffrénil et al. 1986; Robineau and Buffrénil 1993). This would enable a decrease in body inertia and an improvement of acceleration and maneuverability abilities. This shift would occur during the evolution of lineages through the selection of individuals showing a more pronounced tendency toward negatively imbalanced remodeling and a lighter, cancellous organization of bones. Moreover, this type of bone structure could possibly allow a more homogeneous distribution of stresses in a multidirectional stress environment (as opposed to monodirectional dominant gravity).

Physiological Changes Associated with Adaptation to an Aquatic Lifestyle

A relationship between bone histological features (notably collagenous weave and vascular networks) and accretion rate has long been highlighted (Amprino 1947; Margerie et al. 2002; see also Chapter 10). This relationship was later extended to the resting metabolic rate (e.g., Ricqlès 1992; Padian et al. 2001; Montes et al. 2007). Though the link between bone histology and metabolic rate is considered indirect (Reid 1987; Chinsamy-Turan 2005), reasonable inferences about thermal physiology from bone histological features can be suggested.

Changes in thermal physiology induced by the process of aquatic adaptation have been investigated in marine mammals (Lavigne et al. 1986; Seibel and Drazen 2007). However, mammals are all endotherms and changes in growth rate clear enough to suggest physiological transformations are difficult to evidence in their histological features. Conversely, most reptiles are supposed to be ectotherms and changes (notably increase) in their physiology should be more easily observable in their bone tissue. Terrestrial squamates generally display lamellar or parallel-fibered bone with no or limited vascularization (only in the largest forms; e.g., Buffrénil et al. 2008a), whereas crown crocodylians (Eusuchia) normally show well-vascularized parallel-fibered and lamellar bone, and can even form woven tissue for short periods (Woodward et al. 2014; see also Chapter 26).

A clear increase in the degree of vascularization is observed in marine reptiles compared to their closest terrestrial relatives. This is notable in the vertebrae of Late Cretaceous hindlimbed snakes and stem-ophidians, which display abundant radially oriented simple vascular canals with some anastomoses, whereas terrestrial squamates display no or only a few vascular canals (in the largest species; Buffrénil et al. 2008a). A similarly high vascularization is observed in pachypleurosaur vertebrae (Klein et al. 2019b). In *Dermochelys* and hydropedal mosasauroids, vascular canals essentially consist of longitudinally oriented primary osteons arranged in circumferential rows. In hydropedal mosasauroids, this high vascularization is associated with the occurrence of a peculiar type of parallel-fibered bone tissue housing large, variably shaped and randomly oriented osteocyte lacunae. This tissue is reminiscent of woven bone, but referred to as "atypical parallel-fibered bone"

VetBooks.ir

by Houssaye et al. (2013). True woven-fibered bone can even be present in places. Local occurrences of woven-fibered bone were also described in some sauropterygians such as nothosaurs (Klein 2010; Klein et al. 2016) and the pachypleurosaur *Anarosaurus* (Klein 2012). The latter taxa display incipient fibrolamellar bone, comprising "zones" (see Chapter 31) made of woven and parallel-fibered bone containing incompletely or fully developed primary osteons, alternating with annuli made of true parallel-fibered tissue (Klein 2010). Typical fibrolamellar bone with a dense plexiform vascular network (a tissue characteristic of endotherms in recent faunas) has been described in ichthyosaurs (Buffrénil and Mazin 1990; Kolb et al. 2011; Figure 36.5E, F), placodonts (Buffrénil and Mazin 1992; Klein et al. 2015; Figure 36.5G, H), and plesiosaurs (Wiffen et al. 1995; Wintrich et al. 2017).

Therefore, a general increase in growth rate seems to have evolved in marine reptiles. This conclusion, based on histological data, converges with the results of phylogenetic eigenvector maps (Fleischle et al. 2018), isotopic analyses (Bernard et al. 2010), and the recent discovery of preserved blubber in an ichthyosaur (Lindgren et al. 2018). The latter is supposed to have played an insulatory role (in addition to energy store and buoyancy functions) as in extant marine mammals. Altogether, these data suggest gigantothermy in hydropedal mosasauroids and *Dermochelys*, and endothermy in ichthyosaurs and plesiosaurs. Although all medium-sized and large endotherms display fibrolamellar tissue at least in stylopod bones, the reverse situation (i.e., this tissue is entirely lacking in ectotherms) is not necessarily true, and intermediary physiological conditions are likely to have existed. The ability to maintain an elevated body temperature through internally generated heat might have been a strong selective advantage for the evolutionary development of paraxial and thunniform swimming modes (Carey and Gibson 1983; Bushnell and Jones 1994), according to the "sustained locomotor activity/aerobic scope" hypothesis of endothermy origin (Bennett and Ruben 1979; Graham and Dickson 2000). It might also have been advantageous according to the "parental care hypothesis" of the origin of endothermy (Farmer 2000).

REFERENCES

Amprino, R. 1947. La Structure du tissu osseux envisagée comme expression de différences dans la vitesse de l'accroissement. *Arch. Biol.* 58: 315–330.

Amson, E., et al. 2014. Osteology and functional morphology of the forelimb of the marine sloth *Thalassocnus* (Mammalia, Tardigrada). *J. Mammal. Evol.* 22: 169–242.

Arnett, T. R., et al. 2003. Hypoxia is a major stimulator of osteoclast formation and bone resorption. *J. Cell. Physiol.* 196: 2–8.

Bajpai, S., et al. 2009. The origin and early evolution of whales: macroevolution documented on the Indian Subcontinent. *J. Biosci.* 34(5): 673–686.

Bardet, N., et al. 2008. The Cenomanian-Turonian (Late Cretaceous) radiation of marine squamates (Reptilia): the role of the Mediterranean Tethys. *Bull. Soc. Géol. France* 179: 605–622.

Bennett, A. F. and J. A. Ruben. 1979. Endothermy and activity in vertebrates. *Science* 206: 649–654.

Bernard, A., et al. 2010. Regulation of body temperature by some Mesozoic marine reptiles. *Science* 328: 1379–1382.

Buffrénil, V. de and A. Casinos. 1995. Observations histologiques sur le rostre de *Mesoplodon densirostris* (Mammalia, Cetacea, Ziphiidae): le tissu osseux le plus dense connu. *Ann. Sci. Nat. Zool.* 16: 21–32.

Buffrénil, V. and O. Lambert. 2011. Histology and growth pattern of the pachy-osteosclerotic premaxillae of the fossil beaked whale *Aporotus recurvirostris* (Mammalia, Cetacea, Odontoceti). *Geobios* 44: 45–56.

Buffrénil, V. de and J. M. Mazin. 1989. Bone histology of *Claudiosaurus germaini* (Reptilia, Claudiosauridae) and the problem of pachyostosis in aquatic tetrapods. *Hist. Biol.* 2: 311–322.

Buffrénil, V. de and J.-M. Mazin. 1990. Bone histology of the ichthyosaurs: comparative data and functional interpretation. *Paleobiol.* 16: 435–447.

Buffrénil, V. de and J. M. Mazin. 1992. Contribution de l'histologie osseuse à l'interprétation paléobiologique du genre *Placodus* Agassiz, 1833 (Reptilia, Placodontia). *Rev. Paléobiol.* 11: 397–407.

Buffrénil, V. de and J. C. Rage. 1993. La "pachyostose" vertébrale de *Simoliophis* (Reptilia, Squamata): données comparatives et considérations fonctionnelles. *Ann. Paléontol.* 79: 315–335.

Buffrénil, V. de and D. Schoevaert. 1988. On how the periosteal bone of the delphinid humerus becomes cancellous: ontogeny of a histological specialization. *J. Morphol.* 198: 149–164.

Buffrénil, V. de and D. Schoevaert. 1989. Données quantitatives et observations histologiques sur la pachyostose du squelette du dugong, *Dugong Dugon* (Müller) (Sirenia, Dugongidae). *Can. J. Zool.* 67: 2107–2119.

Buffrénil, V. de, et al. 1986. Comparaison de la structure et du volume squelettiques entre un delphinidé (*Delphinus delphis* L.) et un mammifère terrestre (*Panthera leo* L.). *Can. J. Zool.* 64: 1750–1756.

Buffrénil, V. de, et al. 1987. Caractères structuraux et mode de croissance du fémur d'*Omphalosaurus nisseri*, ichthyosaurien du Trias moyen du Spitsberg. *Ann. Paléontol. (Vert.)* 73: 195–216.

Buffrénil, V. de., et al. 1990a. Bone histology of the ribs of the archaeocetes (Mammalia: Cetacea). *J. Vert. Paleontol.* 10: 455–466.

Buffrénil, V. de, et al. 1990b. L'histologie osseuse des Champsosauridés: données descriptives et interprétation fonctionnelle. *Ann. Paléontol. (Vert.)* 76: 255–275.

Buffrénil, V. de, et al. 2008a. Bone vascular supply in monitor lizards (Squamata: Varanidae): Influence of size, growth, and phylogeny. *J. Morphol.* 269: 533–543.

Buffrénil, V. de, et al. 2008b. Variation in bone histology of middle Eocene sirenians from Western Europe. *Geodiversitas* 30: 425–432.

Buffrénil, V. de, et al. 2010. Evolution of sirenian pachyosteosclerosis, a model-case for the study of bone structure in aquatic tetrapods. *J. Mamm. Evol.* 17: 101–120.

Burr, D. B. and M. R. Allen. 2014. *Basic and Applied Bone Biology*. New York, Associated PressElsevier.

Bushnell, P. G. and D. R. Jones. 1994. Cardiovascular and respiratory physiology of tuna: adaptations for support of exceptionally high metabolic rates. *Environ. Biol. Fish.* 40: 303–318.

VetBooks.ir

Caldwell, M. W. and A. Palci. 2007. A new basal mosasauroid from the Cenomanian (U. Cretaceous) of Slovenia with a review of mosasauroid phylogeny and evolution. *J. Vert. Paleontol.* 27: 863–880.

Canoville, A. and M. Laurin. 2010. Evolution of humeral microanatomy and lifestyle in amniotes, and some comments on palaeobiological inferences. *Biol. J Linn. Soc.* 100: 384–406.

Canoville, A., et al. 2016. Microanatomical diversity of amniote ribs: an exploratory quantitative study. *Biol. J Linn. Soc.* 118: 706–733.

Carey, F. G. and Q. H. Gibson. 1983. Heat and oxygen exchange in the rete mirabile of the bluefin tuna, *Thunnus thynnus. Comp. Biochem. Phys. A* 74: 333–342.

Cave, A. J. E. and F. J. Aumonier. 1967. Observations on dugong histology. *J. Roy. Microsc. Soc.* 87: 113–121.

Chinsamy-Turan, A. 2005. *The Microstructure of Dinosaur Bone: Deciphering Biology with Fine-Scale Techniques.* Baltimore, Johns Hopkins University Press.

Currey, J. D. 2003. How well are bones designed to resist fracture? *J. Bone Miner. Res.* 18: 591–598.

Dewaele L., et al. 2019. Generalized osteosclerotic condition in the skeleton of *Nanophoca vitulinoides*, a dwarf seal from the Miocene of Belgium. *J. Mammal. Evol.* 26: 517–543.

Díaz-Berenguer, E., et al. 2018. First adequately-known quadrupedal sirenian from Eurasia (Eocene, Bay of Biscay, Huesca, northeastern Spain). *Sci Rep.* 8: 1–13.

Domning, D. P. 2001. The earliest known fully quadrupedal sirenian. *Nature* 413: 625–627.

Domning, D. P. and V. de Buffrénil. 1991. Hydrostasis in the Sirenia: quantitative data and functional interpretations. *Mar. Mammal Sci.* 7: 331–368.

Dumont, M., et al. 2013. Inner architecture of vertebral centra in terrestrial and aquatic mammals: a two-dimensional comparative study. *J. Morphol.* 274: 570–584.

Farmer, C. G. 2000. Parental care: the key to understanding endothermy and other convergent features in birds and mammals. *Am. Nat.* 155: 326–334.

Fawcett, D.W. 1942. The amedullary bones of the Florida manatee (*Trichechus latirostris*). *Am. J. Anat.* 70: 271–309.

Felts, W. J. L. and F. A. Spurrell. 1965. Structural orientation and density in cetacean humeri. *Am. J. Anat.* 116: 171–204.

Fleischle, C. V., et al. 2018. Quantitative histological models suggest endothermy in plesiosaurs. *PeerJ* 6: e4955.

Florencio-Silva, R., et al. 2015. Biology of bone tissue: structure, function, and factors that influence bone cells. *BioMed. Res. Int.* 2015: 421746.

Giustina, A., et al. 2008. Growth hormone, insulin-like growth factors, and the skeleton. *Endocr. Rev.* 29: 535–359.

Gogakos, A. I., et al. 2010. Thyroid and bone. *Arch. Biochem. Biophys.* 503: 129–136.

Graham, J. B. and K. A. Dickson. 2000. The evolution of thunniform locomotion and heat conservation in scombrid fishes: new insights based on the morphology of *Allothunnus fallai*. *Zool. J. Linn. Soc-Lond.* 129: 419–466.

Gray, N.-M., et al. 2007. Sink or swim? Bone density as a mechanism for buoyancy control in early cetaceans. *Anat. Rec.* 290: 638–653.

Houssaye, A. 2013. Palaeoecological and morphofunctional interpretation of bone mass increase: an example in late cretaceous shallow marine squamates. *Biol. Rev.* 88: 117–139.

Houssaye, A. and N. Bardet. 2012. Rib and vertebral micro-anatomical characteristics of hydropelvic mosasauroids. *Lethaia* 45: 200–209.

Houssaye, A. and P. Tafforeau. 2012. What vertebral microanatomy reveals about the ecology of juvenile mosasaurs (Reptilia, Squamata). *J. Vert. Paleontol.* 32: 1042–1048.

Houssaye, A., et al. 2008. An analysis of vertebral 'pachyostosis' in *Carentonosaurus mineaui* (Mosasauroidea, Squamata) from the Cenomanian (early Late Cretaceous) of France, with comments on its phylogenetic and functional significance. *J. Vert. Paleontol.* 28: 685–691.

Houssaye, A., et al. 2013. microanatomical and histological features in the long bones of mosasaurine mosasaurs (Reptilia, Squamata) -Implications for aquatic adaptation and growth rates. *PLoS One* 8: e76741.

Houssaye, A., et al. 2014. A new look at ichthyosaur long bone microanatomy and histology: implications for their adaptation to an aquatic life. *PLoS One*. 9: e95637.

Houssaye, A., et al. 2015. Transition of Eocene whales from land to sea: evidence from bone microstructure. *PLoS One* 10: e0118409.

Houssaye, A., et al. 2016. Adaptive patterns in aquatic amniote bone microanatomy—more complex than previously thought. *Integr. Comp. Biol.* 56: 1349–1369.

Houssaye, A., et al. 2018. Structural, functional, and physiological signals in ichthyosaur vertebral centrum microanatomy and histology. *Geodiversitas* 40: 161–170.

Hua, S. and V. de Buffrenil. 1996. Bone histology as a clue in the interpretation of functional adaptations in the thalattosuchia (Reptilia, Crocodylia). *J. Vert. Paleontol.* 16: 703–717.

Hugi, J., et al. 2011. Long bone microstructure gives new insights into the life of pachypleurosaurids from the Middle Triassic of Monte San Giorgio, Switzerland/Italy. *C.R. Palevol* 10: 413–426.

Kazár, E., 2010. Revision of the genus *Pachyacanthus* Brandt, 1871 (Mammalia: Cetacea: Odontoceti). *Ann. Naturhist. Mus. Wien, Serie A*. 112: 537–567.

Kelley, N. P. and N. D. Pyenson. 2015. Evolutionary innovation and ecology in marine tetrapods from the Triassic to the Anthropocene. *Science* 348: 3716–3716.

Kelley, N. P. and R. Motani. 2015. Trophic convergence drives morphological convergence in marine tetrapods. *Biol. Lett.* 11: 20140709.

Klein, N. 2010. Long bone histology of Sauropterygia from the Lower Muschelkalk of the Germanic Basin provides unexpected implications for phylogeny. *PLoS One* 5: e11613.

Klein, N., 2012. Postcranial morphology and growth of the pachypleurosaur *Anarosaurus heterodontus* (Sauropterygia) from the Lower Muschelkalk of Winterswijk, The Netherlands. *Paläontol. Z.*. 86: 389–408.

Klein, N., et al. 2015. Long bone histology and microanatomy of Placodontia (Diapsida: Sauropterygia). *Contrib. Zool.* 84: 59–84.

Klein, N., et al. 2016. Diverse aquatic adaptations in *Nothosaurus* spp. (Sauropterygia — inferences from humeral histology and microanatomy. *PLoS One* 11: e0158448.

Klein, N., et al. 2019a. Microanatomy and growth of the mesosaurs *Stereosternum tumidum* and *Brazilosaurus sanpauloensis* (Reptilia, Parareptilia). *Foss. Rec.* 22: 91–110.

Klein, N., et al. 2019b. Microstructure of vertebrae, ribs, and gastralia of Triassic sauropterygians—New insights into the microanatomical processes involved in aquatic adaptations of marine reptiles. *Anat Rec.* 302: 1770–1791

Knowles, H. J. 2015. Hypoxic regulation of osteoclast differentiation and bone resorption activity. *Hypoxia* 3: 73–82.

Kolb, C., et al. 2011. The palaeohistology of the basal ichthyosaur *Mixosaurus* (Ichthyopterygia, Mixosauridae) from the Middle Triassic: palaeobiological implications. *C. R. Palevol* 10: 403–411.

Laurin, M., et al. 2011. Bone microanatomy and lifestyle: a descriptive approach. *C. R. Palevol* 10: 381–402.

Lamb, F. and R. Jackson. 2015. Osteopetrosis (marble bone disease). *Am. J. Clin. Pathol.* 8: 255–272.

Lambert, O., et al. 2011. Rostral densification in beaked whales: diverse processes for a similar pattern. *C. R. Palevol* 10: 453–468.

Lavigne, D. M., et al. 1986. Metabolic rates of seals and whales. *Can. J. Zool.* 64: 279–284.

Lindgren, J., et al. 2018. Soft-tissue evidence for homeothermy and crypsis in a Jurassic ichthyosaur. *Nature*. 564: 359–365.

Liu, J., et al. 2011. New mixosaurid ichthyosaur specimen from the Middle Triassic of SW China: further evidence for the diapsid origin of ichthyosaurs. *J. Paleontol.* 85: 32–36.

Margerie, E. de, et al. 2002. Bone typology and growth rate: testing and quantifying "Amprino's Rule" in the mallard (*Anas platyrhynchos*). *C.R. Biol.* 325: 221–230.

Montes, L., et al. 2007. Relationships between bone growth rate, body mass and resting metabolic rate in growing amniotes: a phylogenetic approach. *Biol. J. Linn. Soc.* 92: 63–76.

Morales, J., et al. 1993. Pachyostosis in a Lower Miocene giraffoid from Spain, *Lorancameryx pachyostoticus* nov. gen. nov. sp. and its bearing on the evolution of bony appendages in artiodactyls. *Geobios* 26: 207–230.

Muizon, C. de. 2009. L'origine et l'histoire évolutive des Cétacés. *C. R. Palevol* 8: 295–309.

Nopcsa, F. 1923. Vorläufige Notiz über die Pachyostose und Osteosklerose einiger mariner Wirbeltiere. *Anat. Anz.*56: 352–359.

Padian, K., et al. 2001. Dinosaurian growth rates and bird origins. *Nature* 405–408.

Reid, R. E. H. 1987. Bone and dinosaurian "endothermy." *Mod Geol.*11: 133–54.

Rhodin, A. G. J. 1985. Comparative chondro-osseous development and growth of marine turtles. *Copeia* 3: 752–771.

Ricqlès, A. de. 1989. Les Mécanismes hétérochroniques dans le retour des tétrapodes au milieu aquatique. *Geobios Mémoire Spécial* 12: 337–348.

Ricqlès, A. de. 1992. Paleoherpetology now: a point of view. In *Herpetology: Current Research on the Biology of Amphibians and Reptiles*, Adler K. (ed.), 97–120. Society for the Study of Amphibians and Reptiles.

Ricqlès, A. de and V. de Buffrénil. 2001. Bone histology, heterochronies and the return of tetrapods to life in water: where are we? In *Secondary Adaptation of Tetrapods to Life in Water*, Mazin J.-M. and V. de Buffrénil (eds.), 289–310. München, Pfeil.

Rieppel, O. and Head, J. J. 2004. New specimens of the fossil snake genus *Eupodophis* Rage & Escuillié, from the Cenomanian (late Cretaceous) of Lebanon. *Mem. Soc. Ital. Sci. Nat. Mus. Civico Storia Milano* 32: 1–26.

Robineau, D. and V. de Buffrénil. 1993. Nouvelles données sur la masse du squelette chez les grands cétacés (Mammalia, Cetacea). *Can. J. Zool.* 71: 828–834.

Sander, P. M., et al. 1997. A new pistosaurid (Reptilia: Sauropterygia) from the Middle Triassic of Nevada and its implications for the origin of the plesiosaurs. *J. Vert. Paleontol.* 17: 526–533.

Seibel, B. A. and J. C. Drazen. 2007. The rate of metabolism in marine animals: environmental constraints, ecological demands and energetic opportunities. *Philos. Trans. R. Soc. B: Biol. Sci.* 362: 2061–2078.

Street, H. P. and F. R. O'Keefe. 2010. Evidence of pachyostosis in the cryptocleidoid plesiosaur *Tatenectes laramiensis* from the Sundance Formation of Wyoming. *J. Vert. Paleontol.* 30: 1279–1282.

Talevi, M. and M. S. Fernández. 2012. Unexpected skeletal histology of an ichthyosaur from the Middle Jurassic of Patagonia: implications for evolution of bone microstructure among secondary aquatic tetrapods. *Naturwissenschaften*. 99: 241–244.

Taylor, L. H. 1994. Stone, bone or blubber? Buoyancy control strategies in aquatic tetrapods. In *Mechanics and Physiology of Animal Swimming*, Maddock, L., Q. Bone, and J. M. V. Rayner (eds.), Vol. 11, 151–161. Cambridge, UK, Cambridge University Press.

Thewissen, J. G. M., et al. 2007. Whales originated from aquatic artiodactyls in the Eocene epoch of India. *Nature* 450(7173): 1190–1194.

Tolar, J., et al. 2004. Osteopetrosis. *N. Engl. J. Med.* 351: 2839–2849.

Uhen, M. D., 2010. The origin(s) of whales. *Ann. Rev. Earth Planet. Sci*. 38: 189–219.

Webb, P. and V. de Buffrénil. 1990. Locomotion in the biology of large aquatic vertebrates. *Trans. Am. Fish. Soc.* 119: 629–641.

Wiffen, J., et al. 1995. Ontogenetic evolution of bone structure in Late Cretaceous Plesiosauria from New Zealand. *Geobios* 28: 625–640.

Wintrich, T., et al. 2017. A Triassic plesiosaurian skeleton and bone histology inform on evolution of a unique body plan. *Sci. Adv.* 3: e1701144.

Woodward, H. N., et al. 2014. Quantification of intraskeletal histovariability in *Alligator mississippiensis* and implications for vertebrate osteohistology. *PeerJ* 2: e422.

Zangerl, R. and B. Peyer. 1935. Die Triasfauna Der Tessiner Kalkalpen. IX. Pachypleurosaurus Edwardsi, Cornalia Sp. *Abh. Schweiz. Pal. Ges.* 56: 1–80.

Zhou, X., et al. 2018. Molecular footprints of aquatic adaptation including bone mass changes in cetaceans. *Genome Biol. Evol.* 10: 967–975.

VetBooks.ir

37

Bone Histology and Thermal Physiology

Jorge Cubo, Adam Huttenlocker, Lucas J. Legendre, Chloé Olivier and Armand de Ricqlès

CONTENTS

Introduction 757
Basic Concepts and Their Historical Development 757
Homeotherms and Poikilotherms 758
Endotherms and Ectotherms 758
Paleophysiology: Early Thoughts 759
Paleophysiology: The 1970s Change of Paradigm 759
Physiological Basis of Endothermy 760
Bone Histology as a Clue to Physiology 761
Origin and Evolution of Endothermy in Synapsida 763
Basal Synapsids 763
Therapsids 764
Origin and Evolution of Endothermy in Diapsida 766
References 767

Introduction

Recent conceptual and methodological advances in bone paleohistology have allowed vertebrate paleontologists to gain insights into the physiology of extinct taxa. Among them, the origins and evolutionary courses of endothermy in amniotes have received great attention because they are major events in vertebrate evolution. They modified the energetic relationships between organisms and their environments (Walter and Seebacher 2009), and coincided with major changes in the respiratory and circulatory systems, as well as physiological, behavioral and ecological traits (Seymour et al. 2004).

Other aspects of the physiology of extinct vertebrates have received less attention. Two of them are fundamental to homeostasis in terrestrial vertebrates: (1) deciphering the role of bone tissue in regulating the acid–base balance related to excess blood carbon dioxide and/or lactic acidosis in early tetrapods and Pseudosuchia (Janis et al. 2020) and (2) understanding the role of bone tissue in calcium homeostasis. Although the role of Haversian remodeling in calcium homeostasis has been widely studied (Parfitt 1994), the contribution of medullary bone to this function is far from completely deciphered (Lee and Werning 2008, Pronvai 2017, Canoville et al. 2020). This chapter will focus on the origin and evolution of endothermy in amniotes, and especially archosaurs and synapsids. Bernard et al. (2010), Harrell et al. (2016) and Séon et al. (2020) inferred the thermometabolism of marine reptiles using a geochemical approach. With the exception of Fleischle et al. (2018), who inferred the thermometabolism of Sauropterygia, paleohistological studies on marine reptiles have been aimed at inferring lifestyle and growth dynamics: see for instance Buffrénil and Mazin (1990), Houssaye et al. (2014) and Anderson et al. (2019) for ichthyosaurs, Houssaye et al. (2013) for mosasaurs and Hua and Buffrénil (1996) for Thalattosuchia.

Basic Concepts and Their Historical Development

The concept of a distinction between warm- and cold-blooded animals goes back to Aristotle (384–322 BC). In the "Great Chain of Being," warm-blooded animals (mammals and birds) occupy the higher ladders, sharing this character with Man.

During the 19th and 20th centuries, the development of zoology and comparative physiology progressively blurred the deceptively simple distinction between cold- and warm-blooded species. Among "warm-blooded" animals, the hibernating mammals, the cyclical torpor of bats and hummingbirds and so forth offered examples of life history traits in which

VetBooks.ir

high, constant body temperatures are not sustained (e.g. Ruf and Geiser 2015). Among "cold-blooded" animals the situation has also proven paradoxical (Clarke and Pörtner, 2010; Legendre and Davesne, 2020). Some sharks, tunas and marine turtles are known to produce enough heat to raise their body temperature higher than that of the surrounding waters. Shivering in "brooding pythons" allows these snakes to produce enough heat to keep their eggs warm enough to develop. Actively foraging species of large lizards, notably varanids exemplified by the great Komodo dragon, "warm up" through protracted day locomotion and keep warm at night. Smaller heliothermic lizards can reach body temperatures as high as or higher than those of similar-sized mammals. Even among insects, shivering moths, during cold mornings, have to "warm up their engines" before being able to take off (Heinrich, 1993). Sphingid moths converge with hummingbirds to a great extent in their life history traits and physiology, with high body temperature, body insulation, "inflight refueling" and cyclical torpor.

Even considering the extant world only, the thermal physiology of animals is highly diverse (Prosser and Brown 1961, Whittow 1970) to the point that "the exception may be the rule" (Ricqlès 2002). This situation should always be kept in mind when venturing into the possible thermal physiologies of fossils from a remote past.

To better capture the significance of the various thermal situations observed among vertebrates, more precise concepts than the "cold-bloodedness versus warm-bloodedness" dichotomy have been devised.

Homeotherms and Poikilotherms

A homeothermic animal (from Greek *homoios*: equal, *thermos*: heat) is able to maintain a relatively constant body temperature by regulating its thermogenesis, and especially its thermolysis (Schocander 1955), so that its body temperature does not depart, under normal physiological conditions, from a narrow species-specific optimum. Typically, among extant animals, this optimum is high (more than 35°C) (Ostrom 1969a), and homeotherms effectively match the concept of warm-blooded animals, namely birds and mammals. This is why homeothermy is often (mistakenly) synonymized with warm-bloodedness.

Poikilothermy (from Greek *poikilos*: varied) is characterized by extensive variation in body temperature under normal environmental conditions. The fluctuations are generally multicyclical (daily, seasonally) and imposed by the environment. Among extant faunas, poikilothermy occurs in animals whose body temperature is rather low (10–35°C or less) and metabolism less active (Whittow 1970): poikilotherms grossly match the cold-blooded concept. However, strictly speaking, although there are no precise definitions for warm-blooded and cold-blooded animals, the terms refer to relatively high or low average body temperatures, respectively.

Endotherms and Ectotherms

To the classical concepts above, Cowles (1962) added a somewhat different terminology: an endothermic animal (from Greek *endon*: from within) produces by itself enough heat to sustain its optimal body temperature. Conversely, ectothermic animals (from Greek *ektos*: from without) must largely or mainly rely on external heat sources from the environment to reach their optimal functional body temperature (Rodbard 1953). Endotherms have to rely on an active metabolism, responsible for an intense thermogenesis (tachymetabolism: see King and Farner 1961 on birds; Jansky 1962 on mammals). This is not the case for ectotherms. Ectothermic metabolism may be eight to ten time less active than that of endothermic vertebrates (see Bogert 1953, Hughes 1963, Templeton 1970 and Bennett 1971 on reptiles and Brattstrom 1970 on amphibians).

It is clear that, among extant vertebrates, there is often a cooccurrence between homeo- and endothermy (mammals and birds) and poikilo- and ectothermy (other vertebrates). However, the actual situation may vary because different conditions can be dissociated and recombined: endotherms may also be poikilotherms and ectotherms can produce enough heat to raise their core temperature and so forth. This suggests how thermal physiologies may have been varied along evolutionary pathways.

Thermal physiology (Cowles 1962) also uses several other concepts: for instance stenotherms (from Greek *stenos*: narrow) are animals that tolerate only narrow variations of body temperature, whereas eurytherms (from Greek *eurys*: wide) tolerate much wider thermal variations, in both their environments and their internal body temperatures. Heliotherms are generally ectotherms that rely on basking to raise their body temperature. A distinction should also be made about the circumstances under which heat is produced. Basal metabolism is checked at rest under neutral thermic external circumstances (no thermogenesis or thermolysis needed). Measurements of exercise metabolism and related higher thermogenesis should take into account exercise being performed under aerobic or anaerobic conditions. Thermal physiology has to deal not only with physiology in the strictest sense, but also with ecological and behavioral factors. Because of the ratios between linear and volume increments, body size also plays a major, pervading role in thermal physiology.

It should be emphasized that the abovementioned classical definitions of comparative physiology (Whittow 1970) were first framed within nonevolutionary contexts, or within evolutionary contexts antedating phylogenetic methods (cladistics), a situation that can currently raise problems. Ectothermy is basically a plesiomorphic condition of thermal physiology, widespread among the animal kingdom. In contrast, endothermy supported by tachymetabolism is a relatively uncommon situation, apparently shared only by mammals and birds in the extant world. Is endothermy a synapomorphy, justifying a Class Homeothermia including birds and mammals? This has sometimes been considered (Schuh 1951, Inger 1957, Cowles 1958, Heath 1968, Gardiner 1982). However, phylogenetic analyses at morphological and molecular levels demonstrate that this physiological condition has evolved independently in the synapsid and archosaurian lineages, a case of convergent evolution (see below). In addition, other forms

VetBooks.ir

of endothermy also independently evolved among several groups, e.g. in teleosts (Portier 1903: thunnids, Wegner et al. 2015: *Lampris guttatus*) and sharks (*Carcharodon carcharias*, *Isurus oxyrinchus*; see Bernal et al., 2012). Accordingly, endothermy is polyphyletic in its general physiological sense, and it is autapomorphic in each lineage where it has evolved (Lovegrove 2017, Legendre and Davesne 2020).

Paleophysiology: Early Thoughts

The problem of thermal physiology of dinosaurs is probably as old as the concept of Dinosauria itself, devised by Owen (1841) and published in 1842. According to Desmond (1979, 1982, see also Sloan 1992), the "invention" of the dinosaur was part of Owen's strategy to counter the opinions of Robert Edmund Grant, who favored transformationist views akin to Lamarckism. Owen, when "designing" the dinosaur, focused on their "advanced" characteristics, especially regarding the locomotor system, almost putting them on par with Mammals. But because they are technically reptiles on osteological grounds, Owen reasoned, they should have shared all the usual reptilian characteristics regarding behavior and physiology, notably cold-bloodedness. Hence the advanced locomotory apparatus is explained away as a mere adaptation, without any major significance for physiology. Owen thus showcased Linnean systematics to downplay the Cuvierian analysis of connections between structures and functions (Padian 2004). Thus, following Owen, one must start by postulating that dinosaur growth processes, ecologies and behaviors were fundamentally those of extant reptiles. Not all specialists agreed: Huxley's (1868, 1870) views of dinosaurs as bird ancestors made him focus on the advanced or birdlike characteristics of dinosaurs, including warm-bloodedness and birdlike hearts and lungs (Desmond 1982, p. 127, Parsons 2001, p. 129). According to Farlow and Brett-Surman (1997, p. 349), E.D. Cope and R.S. Lull were also among the earliest to consider dinosaur endothermy. That the issue has been discussed ever since, even in low tones, is shown by Joleaud's (1921) remarks.

A similar story developed about the biological interpretation of pterosaurs (Padian 2004, Sloan 1992). Again, Owen (1841) explained away the advanced characteristics of pterosaurs as mere adaptations by linking *a priori* Linnean systematics to physiology, without considering evidence from functional anatomy. This way of thinking to interpret the biology of pterosaurs was vigorously opposed by Harry Govier Seeley, the Victorian specialist on pterosaurs (Seeley 1870) who, on the bases of comparative and functional anatomy, viewed them as warm-blooded animals (Seeley 1864, 1901).

Nevertheless, Owen's (1841) opinion that, because dinosaurs and pterosaurs are classified as reptiles, they should have had mostly reptilian characteristics in each and every regard, survived as the baseline to be challenged. This opinion, which was deemed to *a priori*, represent the "null hypothesis" to start with, prevailed up to the 1970s.

Regarding what we now call synapsids, it became progressively clear to Owen during the 1850s–1870s that a Permo-Triassic group of South African reptiles that he named Theriodontia in 1876 formed a transition between "lower" tetrapods and mammals, a position subsequently supported by Cope (1878, 1887) and Seeley (1889). Broom (1910) then specifically asked the question of the origins of endothermy, stating that, while it was linked to parasagittal locomotion, it evolved through bipedality among Sauropsids, but on "all fours" among "mammalian reptiles" at an undetermined stage of their evolution. Again, the notion of a primitive "reptilian" condition, expressed by the mammalian reptile concept for the Permo-Triassic synapsids, implicitly influenced for a long time the vision of these animals as ectotherms (Colbert 1958).

Paleophysiology: The 1970s Change of Paradigm

The 1960s and 1970s witnessed a burst of new interest in the issue of the origins of endothermy among birds and mammals, and the status of their forebears in the fossil record was raised in the "evolutionary" (precladistic) intellectual environment of the time.

A perennial argument since Owen's time has been the physiological significance of upright limbs, working along a parasagittal axis, compared to sprawling limbs, working through extensive lateral excursions (Schuh 1951). Among extant vertebrates, there is a good correlation between endothermy and parasagittal gait. The correlation is actually perfect for bipedal birds, but not so much for mammals, where several taxa apparently retain a more or less sprawling gait (Jenkins 1971). Physiological explanations of the correlation have diverged: for some authors, the *primum movens* has been the evolution toward parasagittal limbs among ectotherms (Heath 1968). Because erect, parasagittal limbs are biomechanically more efficient, they might have been selected and in turn allowed the evolution of endothermy, a metabolically costly regime, but one that permits the optimal use of the more efficient limbs for foraging and other behaviors. Others suggest that endothermy came first (Olson 1959, Reed 1960, Ostrom 1969 a, b, Jenkins 1971) and in turn favored a progressive evolution of the limbs toward more efficient and less costly locomotion, that, at the same time, allows the animal to exploit the environment more efficiently to cope with the extra costs of its elevated metabolism. A view of "reciprocal causation" may formally reconcile the two opposing approaches, but it would be interesting to devise an independent test to check if endothermy already evolved among sprawling tetrapods, or only among those with a fully parasagittal gait. Bone histology has played this role (Ricqlès 1969a, 1972a, b, 1974a). Early therapsids, dicynodonts and archosauriforms, all with sprawling gaits, already had fast-growing bone tissues similar to those of extant endotherms with rapid postnatal development, such as artiodactyls.

Following the discoveries of the individual age significance of "growth rings" in the bones of ectotherms (Bryuzgin 1939), Peabody (1961) suggested that the occurrence (or lack) of growth rings in fossil bones could bring evidence on the origin of endothermy. Peabody's work was influential on later histological works and it took some time to recognize that growth

VetBooks.ir

marks can also occur in the bones of extant endotherms, although most often following patterns different from those of ectotherms (Ricqlès 2000). Nevertheless, the value of this character for interpreting thermal physiologies among fossil animals was weakened.

Speculations on the origin of the epidermal structures we call hair and feathers and their relationships with the origin of endothermy among tetrapods began as early as the late 19th century and were summarized later by Broili (1941), Schuh (1951), and Brink (1956). Hypotheses on their role in thermoregulation were numerous. Cowles (1958, 1962) and Inger (1957) suggested that these structures are detrimental to ectotherms in any case and that the origin of tetrapods could have been followed soon by trends toward an elevation of metabolic levels.

In Synapsida, the occurrence of hairs, notably vibrissae, among advanced therapsids (cynodonts), as well as numerous anatomical and taphonomic data, together suggested to Brink (1956) that their behavior and physiology were at least partly mammalian: all their characteristics indicate an increase in metabolism (1955–1956). Those suggestions were accepted and elaborated by Olson (1959), Van Valen (1960), Jenkins (1971), Hopson (1973), and Bakker (1971a).

The case of pterosaurs has been perhaps less contentious. Following a stream of observations starting in the early 19th century about a hairy covering in pterosaurs (Broili 1941) and taking into account Seeley's (1901) anatomical deductions, Reed (1960), Heath (1968, p. 273), and Ostrom (1969a, p. 369) accepted the idea of their endothermy.

Much more contentious was the issue of the origin of the endothermy of birds, which were nested at the time somewhere within Sauropsida, without any agreement on which was the nonavian "sister group" of Aves.

First, common studies by ecophysiologists and paleontologists explored the thermal consequences of the body mass of dinosaurs (Bogert 1953, Colbert 1962, Colbert 1947). Extrapolating from extant crocodilians, they elaborated the "ectothermic-homeothermic" model for dinosaurs, the best of both worlds. Mass homeothermy resulting from the surface/volume ratios at large body sizes would have endowed dinosaurs with the benefits of homeothermy coupled with the low metabolic cost of ectothermy. This model of a mild warm-bloodedness of dinosaurs became very popular, keeping dinosaurs in the "good reptiles" realm. It continued to be supported by some authors. But could it account for everything, notably the thermal regime of small dinosaur species, or of small young growing dinosaurs?

Some paleophysiological works about dinosaurs were first driven by the issue of their extinction. Wieland (1942) suggested that environmental overheating at the end of the Cretaceous would have been fatal to the dinosaurs because they were already endothermic, but Russell (1965) claimed that endothermic dinosaurs, without insulating phaneras and unable to hibernate, were doomed by the lowering temperatures at the end of the Cretaceous.

Following earlier works by Ostrom (1969a), concluding that Mesozoic and Recent biogeography suggested that both extant reptiles and dinosaurs did not fit the classical "cold-blooded" picture, Robert T. Bakker became the major proponent of dinosaurian endothermy (e.g., Bakker 1971a, b, 1972), using a large amount of data from gross anatomy, paleoecology and histology. At about the same time, Ricqlès (1969b, 1972a, b, 1974b) arrived at rather similar conclusions based on bone histology.

Those interpretations were strongly countered by those who relied on the "good reptile model" of dinosaur physiology (e.g., Bennett and Dalzell 1973, Feduccia 1973, 1985, Spotila et al. 1973). The debate prompted a symposium at the American Association for Advancement of Sciences (AAAS) held in 1978 (Thomas and Olson 1980), which offered a baseline for further work.

In the meantime, the advance of phylogenetic analysis and its application to the problem of bird origins (Bakker and Galton 1974) gave growing support to the dinosaurian origin of birds, and more specifically to their sister group relationship with theropods, following Ostrom's (1969a) description of *Deinonychus* and its comparison with *Archaeopteryx*. Hence, endothermy could have been a plesiomorphy in birds, and an autapomorphy of a much wider clade including at least most archosaurs (Ricqlès 1978, 2000).

Since then, the story has been told several times (Desmond 1975, Parsons 2001, Padian 2004, Ricqlès 2011) and much elaborated on (Horner et al. 2000, Chinsamy-Turan 2005), and it has proved its heuristic value in the large amount of current research and new results.

Physiological Basis of Endothermy

Parsimony analyses suggest that mammalian and avian endothermy are convergent features: birds and mammals are two phylogenetically distant groups of tetrapods whose last common ancestor was probably ectothermic. This hypothesis is also supported by differences in several anatomical and metabolic features (e.g., circulatory and respiratory systems, body temperature and resting metabolic rate ranges). Mammals and birds are characterized by the presence of specific mechanisms of nonshivering thermogenesis underlying their more or less constant body temperature (Rowland et al. 2015). The energy released by the oxidation of carbohydrates, fatty acids and amino acids is used to pump protons across the inner membrane of mitochondria (from the lumen to the intermembrane space) generating a gradient. The energy released by the entrance of protons from the intermembrane space to the mitochondria lumen through the adenosine triphosphate (ATP) synthesizing enzyme is stored in the form of ATP molecules. Uncoupling protein 1 (UCP1) facilitates the flux of protons from the intermembrane space to the mitochondria lumen (proton leak), generating heat in the brown adipocytes of neonatal and hibernating eutherian mammals as well as in adult rodents (Walter and Seebacher 2009, Little and Seebacher 2014, Jastroch and Seebacher 2020). In contrast, birds lack both brown adipocytes and UCP1 (Newman, 2011).

During mammalian muscle contraction, neural stimulation produces a depolarization of the cytoplasmic membrane (sarcolemma), leading to the release of calcium ions (stocked in the sarcoplasmic reticulum) into the sarcoplasm,

VetBooks.ir

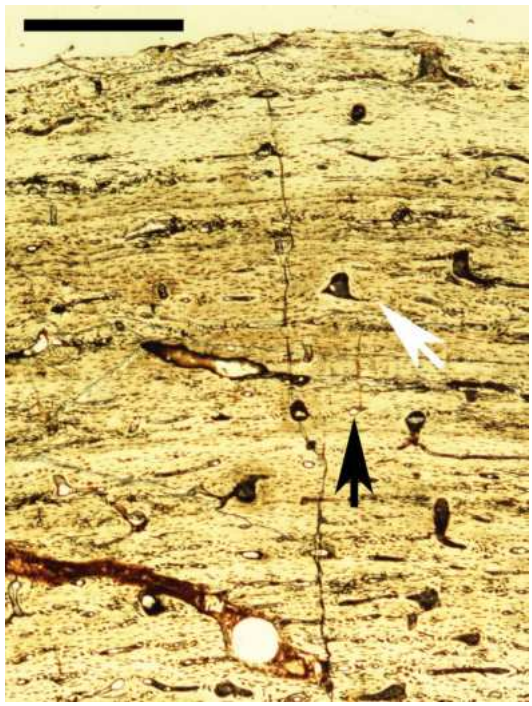
producing muscular fiber contraction through the activity of myosin ATPase, generating heat (Rowland et al. 2015). Sarcoendoplasmic reticulum calcium ATPase 1 (SERCA1) uses energy derived from ATP hydrolysis to transport Ca^{2+} from the sarcoplasm to the sarcoplasmic reticulum, facilitating muscular fiber relaxation, and generating heat (Rowland et al. 2015, Bal and Periasamy 2020). Mammals may share the capacity of generating heat in muscles without muscle contraction through the futile cycling of SERCA1. When bound to sarcolipin (SLN), SERCA1 undergoes the conformational changes without transporting Ca^{2+} but transforming the energy derived from ATP hydrolysis into heat (Rowland et al. 2015, Bal and Periasamy 2020; see Campbell and Dicke 2018 for an alternative point of view).

Walter and Seebacher (2009) suggested that adenine nucleotide translocase (ANT) may be involved in nonshivering thermogenesis in skeletal muscle in birds. However, the molecular mechanisms involved in this source of metabolic heat are not completely elucidated (review in Legendre and Davesne 2020). Bird endothermy is associated with high aerobic metabolism to fuel the energetic demands of heat production. This is possible through the presence of a feature that has long been considered unique to this group: patterns of unidirectional airflow through the lungs. Indeed, this feature allows the pulmonary epithelium to be supplied with oxygen-rich air at each inhalation (exhaled air transits through another path), whereas in mammalian bidirectional airflow, the pulmonary alveoli are supplied with oxygen-depleted air as a result of the mixing between new inhaled air and remaining air in the lungs after previous exhalations. Evidence for cervical and abdominal air-sac systems in the nonavian theropod dinosaur *Majungatholus atopus* suggests that patterns of unidirectional airflow through the lungs may have evolved at the more inclusive node of Neotheropoda (O'Connor and Claessens 2005). This is congruent with the paleohistological (Cubo et al. 2012) and geochemical (Amiot et al. 2006) data suggesting that at least some Mesozoic dinosaurs had high resting metabolic rates and an endothermic metabolism. Evidence for cervical and abdominal air-sac systems was also found in the Lower Cretaceous pterosaur *Anhanguera santanae* (Claessens et al. 2009), suggesting that patterns of unidirectional airflow through the lungs, and an endothermic metabolism, may have evolved by the last common ancestor of Ornithodira (pterosaurs and dinosaurs, including birds). The unexpected finding of patterns of unidirectional airflow through the lungs of extant alligators, using sophisticated physiological methods (Schachner et al. 2013, Farmer and Sanders 2010), suggests that the precursor to this respiratory system may have already been present in the last common ancestor of archosaurs (crocodiles, pterosaurs and dinosaurs including birds). Recent work on bone paleohistology in extinct archosauromorphs shows congruent conclusions: high resting metabolic rate and perhaps endothermy probably evolved as early as the Early Triassic Archosauromorpha (Legendre et al. 2016, Huttenlocker and Farmer 2017, Cubo and Jalil 2019). Because extant crocodylians are known to be ectotherms, this hypothesis implies a reversion within Pseudosuchia (taxa more closely related to crocodiles than to birds; Seymour et al. 2004). The discovery of patterns of unidirectional airflow through the lungs of *Varanus exanthematicus* (Schachner et al. 2014) and, more recently, in *Iguana* (Cieri et al. 2014) suggests that the basis of this respiratory system was also found in the closely related Mesozoic mosasaurs, facilitating the high aerobic metabolism that exists in active foragers, including in many endothermic animals.

Bone Histology as a Clue to Physiology

Paleobiological inferences of resting metabolic rates and thermometabolic regimes are based on two biological hypotheses: (1) "the types of tissue deposited in the bones of extinct animals are the most direct evidence of basal metabolic rates, because they directly reflect growth rates […]. The sustained deposition of fast-growing bone tissues, as displayed by mammals, birds and other dinosaurs, must reflect sustained high basal metabolic rates" (Padian and Horner 2002, p. 123) and (2) the null hypothesis to be tested is that the extinct tetrapod under analysis was ectothermic because phylogenetic optimization using parsimony suggests that the basal condition for Tetrapoda is the presence of ectothermy (Cubo and Jalil 2019). The first hypothesis is tested using regression analyses that take into account the phylogeny (phylogenetic generalized least-squares regressions [PGLS]; Grafen 1989). For instance, Cubo and Jalil (2019) tested whether a given bone histological variable (e.g., vascular density as shown in Figure 1) explains a significant fraction of the variation of resting metabolic rate (quantified through respirometry) using a sample of extant tetrapods. In cases where the histological variable explains a significant fraction of the variation of resting metabolic rate in extant taxa, the former can be used to infer the latter in extinct taxa. Such inferences have been recently performed in Archosauromorpha (Legendre et al. 2016, Cubo and Jalil 2019), synapsids (Olivier et al. 2017, Faure-Brac and Cubo 2020), Sauropterygia (Fleischle et al. 2018) and Pseudosuchia (Cubo et al. 2020) using phylogenetic eigenvector maps (PEMs) (Guénard et al. 2013). This last method tests once again whether the histological variable is useful in inferring resting metabolic rates of the extinct taxa under analysis, and performs such inferences (Legendre et al. 2016, Olivier et al. 2017, Fleischle et al. 2018, Cubo and Jalil 2019, Cubo et al. 2020, Faure-Brac and Cubo 2020). The resting metabolic rates inferred for extinct taxa using PEMs are then used to test the null hypothesis. In cases where the resting metabolic rate inferred for a given extinct taxon is higher than, and the corresponding confidence interval excludes, the highest value measured in extant ectotherms, then we conclude that this extinct taxon was endothermic because the null hypothesis of ectothermy has been rejected (FIGURE 37.1). Although these studies provide promising clues to the origin of endothermy in these major vertebrate clades, their inferences are generally limited to single bony elements (e.g., femur) assumed to represent similar ontogenetic stages to control for histovariation in tissue texture as much as possible.

VetBooks.ir



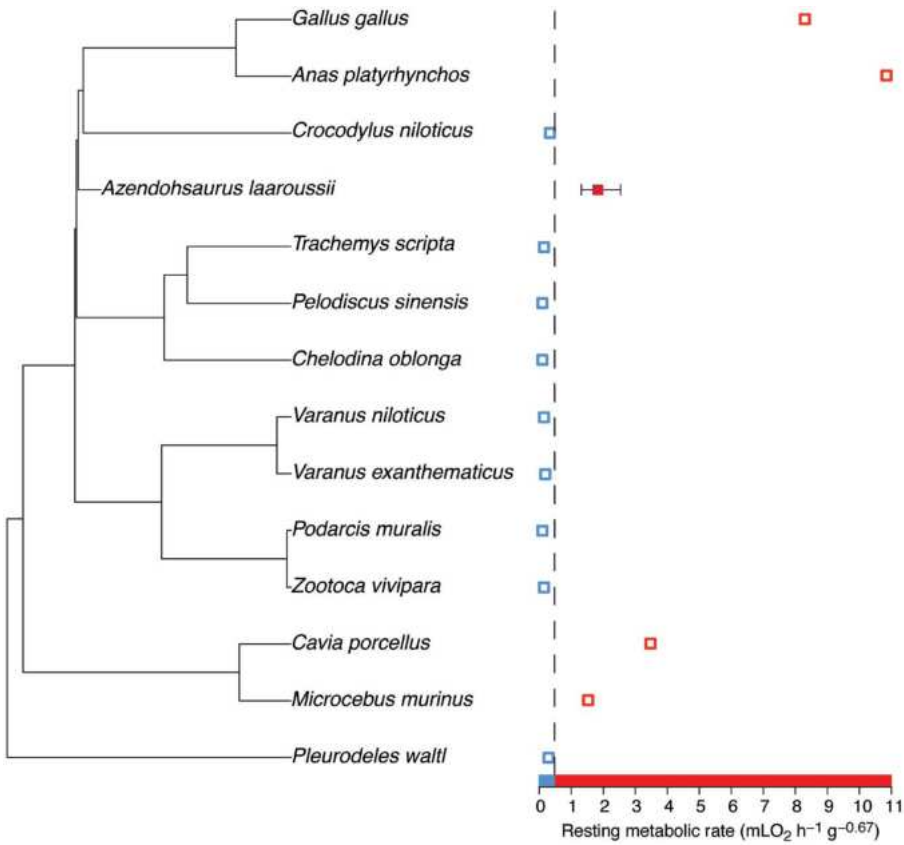


FIGURE 37.1 Vascular density (the number of vascular canals by square millimeter quantified in four orthogonal transects of femoral transverse sections) explains a significant fraction (73.3%) of the variation of resting metabolic rates in a sample of 13 species of extant tetrapods. Thus, vascular density can be used confidently as a proxy to infer the resting metabolic rate of extinct amniotes. We performed such inferences in *Azendohsaurus laaroussii*, an extinct archosauromorph, as a case study using phylogenetic eigenvector maps (PEMs) (Cubo and Jalil 2019). Top, medial cortex of a femoral transverse section of *A. laaroussii*. Two types of vascular canals can be observed: simple vascular canals (black arrow) and primary osteons (white arrow). Scale bar = 0.5 mm. Bottom, inference obtained using PEMs. Empty squares are resting metabolic rates quantified in extant tetrapods using respirometry; solid square and bar are the value inferred for *A. laaroussii* and the corresponding 95% confidence interval. Blue represents the ectothermic state and red represents the endothermic state.

VetBooks.ir

Origin and Evolution of Endothermy in Synapsida

Studies of nonmammalian synapsids have been influential in understanding the evolutionary origins of endothermy, because they record the oldest evidence of a major shift in thermometabolism and energetics, perhaps beginning as early as the middle Permian or even earlier (see Chapter 28). Their fossil record features several phases of life history innovations that have been linked to homeothermy and an elevated thermometabolic status: (1) evolution of large body size in basal synapsids that would have promoted mass homeothermy; (2) increased energetics in Permo-Triassic therapsids, manifested by postural, behavioral and bone microstructural evidence (including accelerated bone growth and intensified remodeling) and (3) increased aerobic capacities in Triassic cynodonts and perhaps other contemporary therapsids. Moreover, the early to middle Permian climatic transition was characterized by a shift from tropical environments, dominated by basal synapsids, to temperate, therapsid-dominated communities at higher paleolatitudes. Some researchers viewed this as an expansion of thermal niche permitted by increases in basal metabolism in therapsids (Kemp 2006a, b, 2007, Hopson 2012).

Basal Synapsids

By Early Permian times, basal (or "pelycosaur-grade") synapsids occupied a range of body sizes and dietary niches, from small predators (*Varanosaurus*) to large carnivores (*Dimetrodon*) and herbivores (*Edaphosaurus*) (Laurin 2004; Reisz and Fröbisch 2014). Although their fossils are best represented from tropical wetland habitats along a paleoequatorial belt, some were capable of inhabiting more upland environments, where they were less dependent on aquatic ecosystems for feeding or reproduction. The evolution of internal fertilization and the amniotic egg relaxed prior constraints on egg size, producing more precocial neonates with greater body mass (Carroll 1991, Laurin and Girondot 1999) and perhaps higher overall growth rates than in earlier stem-amniote groups that lacked this reproductive innovation (e.g., temnospondyls, microsaurs). The success of these early synapsids as terrestrial colonizers has been attributed, in part, to their large body sizes and inertial homeothermy, i.e., the passive maintenance of a relatively constant temperature due to body mass. Turner and Tracy (1986) argued that because seasonal variations in precipitation and temperature impact daily activities of small tetrapods, the ability to be active at suboptimal temperatures over a greater period (afforded by a low surface area to volume ratio) gave mid- to large-bodied synapsids a selective advantage. They argued that behavioral adjustments could be of lesser benefit if large size permitted sufficient thermal inertia to sustain foraging activities. Accessory appendages, such as the dorsal sail of *Dimetrodon*, were suggested to have augmented temperature regulation by absorbing or dissipating heat in a controlled manner, a function hypothesized first by Romer (1948, 1961) and further supported by the biophysical models of Bramwell and Fellgett (1973) and Tracy et al. (1986). Haack (1986), however, questioned the efficacy of the dorsal sail as a heat exchanger, estimating that it would have required up to 4 hours for a 250-kg *Dimetrodon* to reach its activity temperature. Microstructural studies on the neural spines demonstrate that they were moderately vascularized, but less so in edaphosaurids than in sphenacodontids, and their histological organization more likely reflects their growth and mechanics than any thermoregulatory role (Ricqlès 1974b, Huttenlocker et al. 2010, 2011, Rega et al. 2012).

Bone tissue texture and remodeling and, indirectly, the level of growth activity that these features suggest, have provided the strongest evidence for endothermy in extinct synapsids, particularly in the later therapsids. By the 1950s and 1960s, comparative surveys revealed a stark contrast in the histological organization of long bone cortices in basal synapsids and therapsids (Enlow and Brown 1957, Ricqlès 1969a 1974a, b). In contrast to the mammalian taxa then investigated, cortical bone tissues in basal (nontherapsid) synapsids generally recorded cyclic growth with regularly organized vascular motifs and a matrix resembling that of extant reptiles. However, some large-bodied carnivores (e.g., *Ophiacodon*, sphenacodontids) apparently incorporated more parallel-fibered and occasionally woven-fibered matrix during early ontogeny, with fewer cyclic growth marks in some cases (Huttenlocker et al. 2006, Huttenlocker and Rega 2012, Shelton et al. 2013, 2017). In contrast, the earliest therapsids presented richly vascularized cortices with large amounts of woven-fibered tissue as in the mammalian condition (Ricqlès 1974b). Moreover, some large-bodied therapsids may exhibit extensive cortical remodeling and Haversian bone formation (e.g., some large Triassic dicynodonts). Cortical remodeling in earlier synapsids was extremely limited and confined to the perimedullary regions as in many extant lizards (though greater remodeling has been observed anecdotally in exercised and fasted varanids; Owerkowicz and Crompton 1997). The paucity of woven-fibered tissues or any Haversian remodeling in basal synapsids suggested to Ricqlès (1974a, b) (see also Laurin and Buffrénil 2016) that these forms had a more reptile-like thermophysiology than later therapsids. This view holds that the deposition of "fibrolamellar" bone in therapsids was correlated with rapid somatic growth and its associated metabolic demands, whereas its rarity among basal synapsids reflects their presumably lower metabolic demands.

In addition to rapid growth to large body sizes, other traits probably reflect a transition in the bioenergetics of therapsids compared with their basal synapsid forebears, including reduced *caudofemoralis* muscle and overall tail mass, as well as parasagittal limbs consistent with increased efficiency in walking and running (thereby conserving body heat). Bennett and Ruben (1986) highlighted these features, among others, to propose two competing hypotheses for the origins of endothermy: the "thermoregulation first" and the "aerobic capacity first" hypotheses. The former posits that endothermy arose as a temperature regulating mechanism—i.e., that selection acted directly on increasing and maintaining body temperature through resting metabolic rate. Evidence for this view is wanting, because experimental models have failed to identify a mechanistic link between visceral heat production and resting metabolic rate in reptiles (e.g., *Varanus exanthematicus*; see Bennett et al. 2000). The aerobic capacity model, on the other hand, postulates that selection on maximal aerobic capacity

VetBooks.ir

raised resting metabolic rate due to a presumed linkage in the two states (Bennett and Ruben 1979, Hayes and Garland 1995). However, the mechanism linking resting metabolism, a product of leaky mitochondrial membranes in the visceral organs of mammals during basic cellular processes, to maximal aerobic metabolism (VO_{2max}), which is a result of energy use from skeletal muscle, has not been identified (Farmer 2001). Moreover, exercise conditioning in mammals that raises VO_{2max} has no significant effect on basal metabolic rates (Bullough et al. 1995), and neither may selection for greater VO_{2max} in some lab-raised mice (Konarzewski et al. 1997, Wone et al. 2015). Nevertheless, key transformations in skeletal organization in therapsids reflects changes in the locomotor system that almost certainly influenced athletic ability and understanding how these changes were associated with adjustments in thermometabolism remains an active area in synapsid research.

Recently, Hopson (2012) suggested that increased aerobic activity metabolism may have coincided with the origin of therapsids, thereby allowing wide-ranging foraging as in varanids, and argued that this first step was necessary to obtain the energy requirements that permitted incremental increases in basal metabolic rate for maintenance and thermal niche expansion (Kemp 2006a, b, 2007). The "foraging mode" hypothesis is supported by specializations for greater food-getting and food-processing abilities in therapsids. In an earlier version of this hypothesis, Hopson (1973) emphasized that positive selection bearing on aerobic activity metabolism promoted mammal-like reproduction in later therapsids (cynodonts), as better foraging capabilities circumvented constraints on provisioning for small, altricial young with short incubation times. Offering an alternative perspective on the origins of endothermy in mammals and birds, Farmer (2001) argued the opposite: selection of improved parental care resulted in a commitment to endothermy, i.e., the "parental care" hypothesis. This view is supported by the selective advantage of endothermy to the incubation of embryos, as well as hormonal feedback mechanisms that directly link thermogenesis to reproduction and, by extension, brood survival. Moreover, Tattersall et al. (2016) recently showed that modern tegus are capable of facultative endothermy while incubating their young, consistent with the parental care hypothesis and supporting the hypothesis that near mammalian levels of maximal aerobic metabolism are not necessary to sustain higher than ambient body temperatures. Conversely, however, greater aerobic scope could improve food-getting abilities and foraging range while providing for growing young.

Therapsids

Several proxies have been evaluated to test elevated metabolic rates and possibly endothermy within the derived nonmammalian Therapsida: respiratory turbinates (e.g., Hillenius 1992, 1994, Ruben et al. 1996, Crompton et al. 2015, 2017, Owerkowicz et al. 2015), qualitative histology (Ricqlès et al. 1991), paleobiological inference model based on quantitative histology (e.g., Legendre et al. 2016, Huttenlocker and Farmer 2017, Olivier et al. 2017, Fleischle et al. 2018, Faure-Brac and Cubo 2020), oxygen isotopes (Bernard et al. 2010, Rey et al. 2017, Séon et al. 2020) and, where present, fossilized evidence of hairs or hairlike integument (e.g., Ruben and Jones 2000, Ruben et al. 2012, Benoit et al. 2018).

Present in almost all extant mammals and birds, the nonsensory "respiratory" mucosa of the respiratory turbinates is important for a high metabolic rate because they reduce the desiccation and heat-loss rates when the warm humid air is expired from the lungs (Hillenius 1992, 1994). These anatomical structures may correlate with high ventilation rates, and, by extension, high metabolic rates (McNab 1978, Hillenius 1994, Ruben et al. 1996). Owerkowicz et al. (2015) identified a quantitative relationship between the anatomy of the respiratory turbinates and metabolic rates in mammals. The observation of turbinates in fossils remains complicated because they are so fragile; their presence is often interpreted from bony ridges or turbinate scars (Ruben et al. 2012). Maxillary ridges were originally argued to support respiratory turbinates in the late Permian therocephalian *Glanosuchus* and the Triassic cynodont *Massetognathus* (Hillenius 1994, 2000, Ruben et al. 2012). Structures resembling cartilaginous maxilloturbinals were reported in the nasal cavity of the Lower Triassic dicynodont *Lystrosaurus declivis* on the basis of computed tomography (Laaß et al. 2011). However, these interpretations have been disputed (Hopson 2012) and are unconfirmed in other closely allied Permo-Triassic therapsids that have been studied using computed tomography (Sigurdsen et al. 2012, Huttenlocker et al. 2018). Moreover, the respiratory turbinates would be sufficient to reduce the desiccation and heat-loss rates only if inhaled and exhaled air can bypass the oral cavity (Taylor 1977, Schmidt-Nielsen 1981, Biewener et al. 1985). No bony evidence exists of an intranarial larynx separating internal nares from the oral cavity prior to the cynodont (mammaliline) synapsids (Crompton et al. 2015).

Thus, Crompton et al. (2017) formed a hypothesis describing three evolutionary changes in the structure and function of the respiratory turbinates: (1) large respiratory cavity with cartilaginous respiratory turbinals for brain cooling by the time of the divergence of cynodonts from noncynodont synapsids, (2) evolution of pharyngeal muscles separating the internal nares from the oral cavity for efficient heat and water conservation in nonmammalian mammaliaforms and (3) ossified maxilloturbinates enhancing the efficiency for controlling heat and water loss in Mammalia.

According to Amprino's (1947) rule, bone tissue texture reflects growth rate. Fibrolamellar bone (FLB; i.e., primary osteons composed of lamellar bone enclosed within a woven-fibered bone matrix) indicates a high growth rate (Francillon-Vieillot et al. 1990, Ricqlès et al. 1991). Paleohistological analyses have shown the presence of FLB in nonmammalian cynodonts such as *Procynosuchus*, *Trucidocynodon* and *Langbergia* (Botha-Brink et al. 2012), *Thrinaxodon* (Ricqlès 1969b, Botha and Chinsamy 2005, Botha-Brink et al. 2012), *Cynognathus* and *Diademodon* (Botha and Chinsamy 2000, Botha-Brink and Angielczyk 2010), *Trirachodon* (Botha and Chinsamy 2004, Botha-Brink et al. 2012) and *Tritylodon* (Ricqlès 1969b, Ray et al. 2004, Chinsamy and Hurum 2006, Botha-Brink et al. 2012). FLB has also been described in some gorgonopsians (*Scylacops* and *Aelurognathus*) and therocephalians by Chinsamy-Turan and Ray (2012) and Huttenlocker

VetBooks.ir

and Botha-Brink (2014), respectively. The qualitative histology of the anomodonts has been intensively studied, especially within the Dicynodontia. The presence of FLB has been demonstrated in the dromasaur *Galeops* and the dicynodonts *Eodicynodon*, *Diictodon*, *Endothiodon*, *Cistecephalus*, *Dicynodontoides*, *Rhachiocephalus*, *Aulacephalodon*, *Tropidostoma*, *Oudenodon*, *Dicynodon*, *Kannemeyeria*, *Placerias*, *L. declivis*, *L. murrayi* and *L. maccaigi* (Ricqlès 1972c, Ray et al. 2005, Botha-Brink and Angielczyk 2010, Green et al. 2010), among others. Olivier et al. (2017) also reported the presence of "incipient fibrolamellar bone" (iFLB) in the stylopods of *Moghreberia nmachouensis*. Qualitative bone histological studies attest to a high growth rate that is consistent with a high resting metabolic rate in the majority of Permo-Triassic therapsids (see Chapter 28).

Relationships between resting metabolic rates, bone growth rates and phylogeny have been tested by Montes et al. (2007, 2010) and Cubo et al. (2008, 2012). Recently, these relationships have been used to perform quantitative inferences of the resting metabolic rates of fossil taxa using paleobiological models. Models were built using histological features (density, shape and area of the osteocyte lacunae and vascular density) within a phylogenetic context using the PEMs (Guénard et al. 2013). This method was used by Olivier et al. (2017) and Faure-Brac and Cubo (2020) to infer the origins and early evolution of endothermy in synapsids. The paleobiological inference models of Olivier et al. (2017), based on histological characteristics of the femur and humerus (density, shape and area of the osteocyte), suggest the presence of endothermy in three exemplary dicynodonts (*M. nmachouensis*, *Oudenodon baini* and *Lystrosaurus* sp.). Optimization of these inferences onto a phylogenetic tree of tetrapods using the parsimony method constrained the temporal (more than 260 My) and phylogenetic (Neotherapsida) frames of the acquisition of mammalian endothermy (Olivier et al. 2017). Faure-Brac and Cubo (2020) used a more comprehensive sample including basal synapsids and obtained congruent inferences. These results are congruent with the high growth rates inferred on the basis of Amprino's (1947) rule in the qualitative histological studies of *M. nmachouensis*, *O. baini* and *Lystrosaurus* sp.

Another approach was used by Rey et al. (2017) to understand the evolution of mammalian endothermy: the analysis of oxygen isotopic compositions in the bones and teeth of Permo-Triassic therapsids (dinocephalians [*Criocephalosaurus, Sinophoneus, Struthiocephalus*, *Anteosaurus* and a titanosuchid], dicynodonts [*Dicynodon*, *Diictodon, Oudenodon, Rhachiocephalus, Tropidostoma, Lystrosaurus, Shansiodon, Kannemeyeria, Parakannemeyeria, Moghreberia*], gorgonopsians [*Aelurosaurus* and *Cyonosaurus*], therocephalians [*Ictidosuchoides*, *Glanosuchus* and *Pristerognathus*] and cynodonts [*Cynognathus, Diademodon* and an undetermined eucynodont]). The isotopic ratio $\delta^{18}O/\delta^{16}O$ of vertebrate apatite phosphate reflects the isotopic composition of the animal's body water and its body temperature. The body temperature of the therapsid fossils was inferred from the calculated isotopic ratio $\delta^{18}O$. This ratio is related to their supposed lifestyle (terrestrial, semiaquatic and aquatic), their consumption of ambient and plant-based water (affected by climatic features such as air temperature, hygrometry and precipitation rate), paleolatitude and their phylogenetic relationships (Rey et al. 2017). The analyses of Rey et al. (2017) suggested an ectotherm-like thermoregulation in all Permian therapsids when Olivier et al. (2017) supposed a high metabolic rate in *Oudenodon*. However, both studies suggested a high metabolic rate and an endothermic metabolism in *Lystrosaurus* and *Moghreberia*. Rey et al. (2017) also suggested a dual acquisition of endotherm-like thermoregulation in a derived clade of dicynodonts (Lytrosauridae + Kannemeyeriiformes) and Eucynodontia contrary to the single, early appearance proposed by Olivier et al. (2017) and Faure-Brac and Cubo (2020). All these studies suggested the acquisition(s) of endothermy near or prior to the Permo-Triassic boundary.

Increased metabolic rates have been more confidently attributed to advanced therapsids, such as Triassic cynodonts and their contemporaries, mainly on the basis of their mammal-like feeding systems and other skeletal specializations that suggest a grossly mammal-like diaphragmatic functioning. McNab (1978) proposed that, as basal synapsids and therapsids became committed to inertial homeothermy, a selective pressure favored high mass-specific metabolic rates as body sizes decreased in some therapsid lineages, such as cynodonts and therocephalians during the Permian-Triassic transition. Both groups evolved secondary palates that separated the oral and nasal cavities and allowed simultaneous breathing and oral processing of food. This palatal structure is typical of the Triassic species that exhibited smaller adult body sizes (Huttenlocker 2014) and a shorter growth period, as supported by bone histological evidence (Huttenlocker and Botha-Brink 2014, Botha-Brink et al. 2016). Some of them also exhibited smaller vascular and cellular spaces with higher vascular densities, consistent with smaller red blood cells with greater O_2 diffusion capacity, and therefore improved ability for high aerobic activity (Huttenlocker and Farmer 2017). These important physiological and life history traits were likely influenced during the Permo-Triassic transition by changes in environmental conditions, such as atmospheric conditions, changes in daily activity and foraging patterns and transition to subterranean protective shelters such as burrows or dens. Similar applications of phylogenetic comparative methods (PCMs) have begun shedding light on how tissue texture and bone histometrics reflect thermometabolism across groups, and how the evolution of these traits might have shaped their success of synapsids (Faure-Brac and Cubo 2020).

Ultimately, the presence of insulating fur, usually recorded by soft tissue impressions in fossils, would indicate a high heat production and, at least, incipient endothermy (Ruben et al. 2012). Hairs and hair-related integument were described in *Castorocauda lutrasimilis*, a Chinese mammaliaform dated to the Middle Jurassic (Ji et al. 2002, 2006). A paleoneurological study of Benoit et al. (2016) concerned the evolution of cranial structures associated with the branches of the trigeminal nerve in Therapsida, especially the infraorbital nerve and vibrissae sensitivity. Supposing that the infraorbital and maxillary canals are homologous in mammals, the maxillary canal (or infraorbital canal) that is fully ossified, retracted and unbranched as observed in early probainognathians would provide passage of the infraorbital nerve and innervating tactile hairs at least by the Middle Triassic (Benoit et al. 2016).

VetBooks.ir

In addition, the disappearance of the parietal foramen and the development of the cerebellum in these early probainognathians would be related to a mutation of the gene *Msx2*, which also controls hair cycling and hair shaft differentiation (Ma et al. 2003, Benoit et al. 2016). The studies of Benoit et al. (2016, 2018) would support the hypothesis of Hillenius (2000), which supposed the existence of insulating fur at least by the Early Triassic, linked to changes in the septomaxilla and then in the function of the Harderian glands (notably responsible for preening the fur in mammals). However, the presence of vibrissae or hairlike structures in fossils does not allow a firm conclusion about the appearance of endothermy. They could originally have had a mechanosensory or protective function (Ruben and Jones 2000, Maderson 2003).

Origin and Evolution of Endothermy in Diapsida

Along with its synapsid sister group, diapsids have long been the subject of evolutionary hypotheses regarding the rise of endogenous heat production. Among extant sauropsids, only birds can sustain nonshivering thermogenesis. Although a few other taxa, such as tegu lizards (Tattersall et al. 2016) and the leatherback sea turtle (Wallace and Jones 2008), – have been described as potentially displaying endothermic abilities, the exact molecular mechanisms implied in heat production in those groups are currently unknown. In the fossil record, however, many diapsid groups, particularly among archosaurs, have been regarded as potential endotherms, and many different sources of evidence for and against their hypothesized high metabolism have been investigated in recent decades (e.g., Benton 1979, Reid 1987, Paladino et al. 1990, Seymour et al. 2004).

Historically, bone histology has always been an important source of paleophysiological hypotheses in archosaurs, although physiological inferences were hamstrung by a lack of corroborating quantitative studies and were likely biased by the individual bones available to those researchers (reflecting only instantaneous growth rates at a single point in ontogeny). In the early 1930s, for example, Gross (1934) suggested high apparent bone growth rates in several "reptiles" (then including both fossil synapsids and diapsids) based on the microstructure of available limb bones, most notably the archosauromorph *Erythrosuchus*. The definition of "Amprino's Rule", i.e., that variations in bone microstructure are determined by variation in bone growth rate (Amprino 1947), fueled many hypotheses about the potential link between physiology and bone microstructure in diapsids, with a focus on nonarchosaurian archosauromorphs and nonavian dinosaurs. Ricqlès (1978) was the first to describe the importance of an evolutionary context to hypothesize the ancestral condition inherited by all members of a given group, and suggested that many of the bone growth patterns observed in extinct reptiles indicated a high bone growth rate compatible with endothermy (see the "Introduction and Historical Overview" section above). At the time, this hypothesis was also supported by several indirect observations on macroanatomical features, such as the erect stance and limb proportions of nonavian dinosaurs being in several respects similar to those of extant mammals (Bakker 1971a). Several studies, however, showed that those features could not necessarily be linked functionally to high metabolism, and, as such, were not evidence for ancestral endothermy in dinosaurs (Benton 1979). Similarly, the dense vascular networks and Haversian remodeling in dinosaur bone supposedly linked to high metabolic rates can also be observed in extant ectotherms (e.g., Woodward et al. 2011, 2014), and cannot alone be considered a good proxy for endothermy (Bouvier 1977, McNab 1978). For this reason, the high growth rates of nonavian dinosaurs and other large archosauromorphs were considered to be linked with their large body size rather than nonshivering thermogenic abilities (Reid 1987), a feature labeled "gigantothermy" by Paladino et al. (1990).

In recent years, a resurgence of interest in nonavian dinosaur physiology has stimulated the identification of many key features originally considered autapomorphic to extant birds to have appeared at a much more inclusive level among archosaurs and closely related outgroups. These include feathers (Norell and Xu 2005), unidirectional pulmonary airflow (Cieri and Farmer 2016; also see the "Introduction and Historical Overview" section above), air sacs (e.g., Claessens et al. 2009), costovertebral joints and a furrowed thoracic ceiling of the lungs (Brocklehurst et al. 2018) and convoluted nasal turbinates (Bourke et al. 2014, 2018)—all of which have been identified in several species of nonavian dinosaurs. The evolution of these features can also be linked with the fact that the nonavian dinosaur/bird transition has been shown to be steplike, mosaic and progressive through time. Birds have evolved many developmental heterochronies over time compared to their nonavian relatives in morphological characters (e.g., Bhullar et al. 2012), and have experienced significant body size and genome size reduction that have been shown to be linked with the evolution of powered flight (Kapusta et al. 2017). However, these morphoecological changes have been shown to have arisen from continuing rapid rates of evolution originating in the deep adaptive radiation of nonavian dinosaurs (e.g., Benson et al. 2014). In this context, high metabolic rates could thus have occurred at a much more inclusive level than that of the clade Aves among Archosauria, which would have been facilitated by the earlier independent evolution of increased pulmonary airflow, body covering, and muscle hyperplasia (Newman et al. 2013, Lovegrove 2017). As such, diapsid/archosaurian endothermy might have appeared contingently, as an evolutionary byproduct of these earlier acquisitions (i.e., an evolutionary spandrel *sensu* Gould 1997). To achieve such high metabolic rates, nonavian dinosaurs would also have required a high hematocrit and a large four-chambered heart, as has been repeatedly hypothesized from the size of their nutrient foramina and presence of a highly specialized four-chambered heart in extant, ectothermic crocodilians (Seymour et al. 2004, Seymour 2016).

In that context, many recent paleohistological studies have attempted to find new approaches to detect a potential functional signal in bone microstructure that could be linked to high metabolism, other than the presence or absence of a given bone tissue type. Such studies have focused mostly on quantitative osteohistological features in a phylogenetic context, encouraged by the rise of cladistics in paleontology (Cracraft 1981), followed by that of PCMs and associated automated

VetBooks.ir

procedures and software to correlate and model quantitative traits in an evolutionary context (Paradis 2012, Garamszegi 2014). The identification of a strong phylogenetic signal in several histological traits (see Chapter 30), as well as a significant relationship between those variables and bone growth rate (Montes et al. 2007) led to the building of predictive models for bone growth rate based on phylogenetic regressions that used those traits as independent variables (Cubo et al. 2012, Legendre et al. 2013). These models identified several nonarchosaurian archosauromorphs, as well as nonavian dinosaurs and fossil pseudosuchians, as presenting high bone growth rates similar to those of extant mammals, and thus compatible with endothermy.

Estimates of bone growth rate based on counting the lines of arrested growth (LAGs) in sections of limb bones in nonavian dinosaurs, particularly theropods, have been used in a series of papers to estimate the body mass and maximum growth rate of these dinosaurs, by fitting various growth modeling functions (Erickson 2005, Erickson et al. 2007, Lee and Werning 2008, Griebeler et al. 2013). These studies have provided further evidence for high bone growth rates in several species of theropods and sauropodomorph dinosaurs compared to those of extant reptiles, but not as high as those of extant birds. These results prompted comparisons between dinosaurian growth curves and those of extant endotherms and ectotherms, with nonavian dinosaurs always recovered as presenting intermediate growth rates between those of ectotherms and endotherms (Werner and Griebeler 2014). For this reason, nonavian dinosaurs have been proposed as presenting a third heat production strategy, labeled "mesothermy", considered analogous to the "intermediate" metabolic rates of some extant vertebrates such as tuna, lamnid sharks and echidnas (Grady et al. 2014). However, these results and their interpretation are controversial. Myhrvold (2013, 2016) has shown some methodological inconsistencies in the reconstruction of growth curves from LAGs, such as conversion errors from annual to daily bone growth rates. Furthermore, several problems have been identified in the definition of taxonomic groups, branch length information, choice of variables, and modeling procedures. Replications of these results have shown an important overlap in values of resting metabolic rates estimated from bone growth rates using this methodology, as well as a low overall correlation between maximum growth rate and resting metabolic rate (Myhrvold 2015, 2016). More generally, the endothermy/ectothermy dichotomy – or trichotomy if including mesothermy as a third character state – has also been considered to represent a too strict and unrealistic simplification of the continuum of values of resting metabolic rate as observed in extant vertebrates, and inferred in extinct ones. Understanding the physiological strategy behind a given metabolic rate value is therefore better undertaken in discussing individual strategies of each taxon in a given sample, without trying to cluster those values in arbitrary categories that do not necessarily reflect the actual physiological processes underlying them (D'Emic 2015, Legendre et al. 2016, Legendre and Davesne 2020).

More recently, a study estimated the resting metabolic rates of several extinct archosauromorphs (Legendre et al. 2016) from a histological data set expanded from Montes et al. (2007) and Cubo et al. (2012), using phylogenetic predictive modeling procedures. This approach found high resting metabolic rate values for several nonarchosaur archosauromorphs, pseudosuchians and nonavian dinosaurs, and found an ancestral archosaurian metabolic rate value close to that of extant mammals, again suggesting that high metabolic rates were ancestral among archosaurs. The same methodology was also used to estimate high bone growth rates and resting metabolic rates in other archosauromorphs (Cubo and Jalil 2019), sauropterygians (Fleischle et al. 2018, 2019) and synapsids (Olivier et al. 2017, Faure-Brac and Cubo 2020), confirming previous hypotheses on plesiosaur (e.g., Wintrich et al. 2017) and Neotherapsida (e.g., Huttenlocker and Farmer 2017) metabolisms. It thus appears likely that nonshivering thermogenesis, or at least an analogous heat production strategy, appeared very early in the evolution of sauropsids, and may even have evolved several times independently. The methodology of Legendre et al. (2016), however, could be improved in several ways. First, as shown by Fleischle et al. (2018), the protocol used to measure histological variables on thin sections and compile them (e.g., as ratios) has a strong influence on the results of any given modeling procedure, and it needs to be standardized in all histological studies. Such a standardized protocol in paleohistology has yet to be defined (see Prondvai et al. 2018). Second, the predictive modeling procedure used here (PEMs; Guénard et al. 2013) is only one in a range of available PCMs dedicated to missing data estimation and ancestral state reconstruction, and more procedures (e.g., Penone et al. 2014) need to be included in future histological studies on this matter. Third, the very small sample of extant taxa used to build the models does not remotely encompass the diversity of extant tetrapods, and requires significant expansion. Finally, histological characters are not the only proxies that such models could use to reconstruct metabolic rates, and many other characters related to known diapsid innovations, such as nasal passages or lung structure (see above), could theoretically also be used to estimate the metabolism of extinct reptiles and reconstruct their evolution. The use of PCMs in paleophysiology has now become an entire field of research for paleontologists (Benton 2015, Bapst et al. 2016), and many more applications of these procedures to the ancestral diapsid metabolism controversy are likely to be developed in the next few years by a new generation of paleohistologists (Ricqlès 2011).

REFERENCES

Amiot, R., et al. 2006. Oxygen isotopes from biogenic apatites suggest widespread endothermy in Cretaceous dinosaurs. *Earth Planet. Sci. Lett.* 246: 41–54.

Amprino, R. 1947. La structure du tissu osseux envisagée comme expression de différences dans la vitesse de l'accroissement. *Arch. Biol.* 58: 315–330.

Anderson, K. L., et al. 2019. Skeletal microstructure of *Stenopterygius quadriscissus* (Reptilia, Ichthyosauria) from the Posidonienschiefer (Posidonia Shale, Lower Jurassic) of Germany. *Palaeontology* 62: 433–449.

Bakker R. T. 1971a. Dinosaur physiology and the origin of mammals. *Evolution* 25: 636–658.

Bakker, R. T. 1971b. Ecology of the Brontosaurs. *Nature* 229: 172–174.

Bakker R. T. 1972. Anatomical and ecological evidences of endothermy in Dinosaurs. *Nature* 238: 81–85.

Bakker R. T. and P. M. Galton. 1974. Dinosaurs monophyly and a new class of vertebrates. *Nature* 248: 168–172.

Bal, N. C. and M. Periasamy. 2020. Uncoupling of sarcoendoplasmic reticulum calcium ATPase pump activity by sarcolipin as the basis for muscle non-shivering thermogenesis. *Philos. Trans. R. Soc. B Biol. Sci.* 375: 20190135.

Bapst, D. W., et al. 2016. Topology, divergence dates, and macroevolutionary inferences vary between different tip-dating approaches applied to fossil theropods (Dinosauria). *Biol. Let.* 12: 20160237.

Bennett A. F. 1971. A comparison of activities of metabolic enzymes in lizards and rats. *Comp. Biochem. Physiol.* 42: 637–647.

Bennett A. F. and B. Dalzell. 1973. Dinosaure physiology: a critique. *Evolution* 27: 170–174.

Bennett, A. F. and J. A. Ruben. 1979. Endothermy and activity in vertebrates. *Science* 206: 649–654.

Bennett, A. F. and J. A. Ruben. 1986. The metabolic and thermoregulatory status of therapsids. In *The ecology and biology of mammal-like reptiles*, 207–218. Washington, DC, Smithsonian Institution Press.

Bennett, A. F., et al. 2000. An experimental test of the thermoregulatory hypothesis for the evolution of endothermy. *Evolution* 54: 1768–1773.

Benoit, J., et al. 2016. Palaeoneurological clues to the evolution of defining mammalian soft tissue traits. *Sci. Rep.* 6: 25604.

Benoit, J., et al. 2018. Evolution of facial innervation in anomodont therapsids (Synapsida): Insights from X-ray computerized microtomography. *J. Morphol.* 279: 673–701.

Benson, R. B. J., et al. 2014. Rates of dinosaur body mass evolution indicate 170 million years of sustained ecological innovation on the avian stem lineage. *PLoS Biol.* 12: e1001853.

Benton, M. J. 1979. Ectothermy and the success of dinosaurs. *Evolution* 33: 983–997.

Benton, M. J. 2015. Exploring macroevolution using modern and fossil data. *Proc. R. Soc. B* 282: 20150569.

Bernal, D., Carlson, J. K., Goldman, K. J., Lowe, C. G., 2012. Energetics, Metabolism, and Endothermy in Sharks and Rays, in: Biology of Sharks and Their Relatives. CRC Press, Boca Raton, pp. 211–237.

Bernard, A., et al. 2010. Regulation of body temperature by some Mesozoic marine reptiles. *Science* 328: 1379–1382.

Bhullar, B. A. S., et al. 2012. Birds have paedomorphic dinosaur skulls. *Nature* 487: 223–226.

Biewener, A. A., et al. 1985. Regulation of respiratory airflow during panting and feeding in the dog. *Respir. Physiol.* 61: 185–195.

Bogert, C. M. 1953. The temperature of the Tuatara under natural conditions. *Zoologica* 38: 63–64.

Botha, J. and A. Chinsamy. 2000. Growth patterns deduced from the bone histology of the cynodonts *Diademodon* and *Cynognathus*. *J. Verterbr. Paleontol.* 20: 705–711.

Botha, J. and A. Chinsamy. 2004. Growth and life habits of the Triassic cynodont Trirachodon, inferred from bone histology. *Acta Palaeontol. Pol.* 49: 619–627.

Botha, J. and A. Chinsamy. 2005. Growth patterns of *Thrinaxodon liorhinus*, a non-mammalian cynodont from the Lower Triassic of South Africa. *Palaeontology* 48: 385–394.

Botha-Brink, J. and K. D. Angielczyk. 2010. Do extraordinarily high growth rates in Permo-Triassic dicynodonts (Therapsida, Anomodontia) explain their success before and after the end-Permian extinction? *Zool. J. Linn. Soc.* 160: 341–365.

Botha-Brink, J., et al. 2012. The radiation and osteohistology of Nonmammaliaform cynodonts. In *Forerunners of mammals*, ed. A. Chinsamy-Turan, 223–248. Bloomington, Indiana University Press.

Botha-Brink, J., et al. 2016. Breeding young as a survival strategy during Earth's greatest mass extinction. *Sci. Rep.* 6: 24053.

Bourke, J. M., et al. 2014. Breathing life into dinosaurs: tackling challenges of soft-tissue restoration and nasal airflow in extinct species: dinosaur nasal airflow. *Anat. Rec.* 297: 2148–2186.

Bourke, J. M., et al. 2018. Convoluted nasal passages function as efficient heat exchangers in ankylosaurs (Dinosauria: Ornithischia: Thyreophora). *PLoS One* 13: e0207381.

Bouvier, M. 1977. Dinosaur Haversian bone and endothermy. *Evolution* 31: 449.

Bramwell, C. D. and P. B. Fellgett. 1973. Thermal regulation in sail lizards. *Nature* 242: 203.

Brattstrom B. 1970. Amphibia. In *Comparative physiology of thermoregulation*, vol. 1, ed. G. C. Whittow, 135–166. London and New York, Academic Press.

Brink A. S. 1956. Speculations on some advanced mammalian characteristics in the higher mammal-like reptiles. *Paleontol. Afr.* IV: 77–97.

Brocklehurst, R. J., et al. 2018. Vertebral morphometrics and lung structure in non-avian dinosaurs. *Open Sci.*5: 180983.

Broili F. 1941. Haare bei Reptilien. *Anat. Anz.* 92: 62–68.

Broom 1910. A comparison of the Permian reptiles of North America with those of South Africa. *Bull. Am. Mus. Nat. Hist.* 28: 197–234.

Bryuzgin V. 1939. A procedure for investigating age and growth in Reptilia. *Doklady Acad Sci USSR (New. Ser.)* 23: 403–405.

Buffrénil, V. de and J. Mazin. 1990. Bone-histology of the ichthyosaurs - comparative data and functional interpretation. *Paleobiology* 16: 435–447.

Bullough, R. C., et al. 1995. Interaction of acute changes in exercise energy expenditure and energy intake on resting metabolic rate. *Am. J. Clin. Nutr.* 61: 473–481.

Campbell, K. L. and A. A. Dicke. 2018: Sarcolipin makes heat, but is it adaptive thermogenesis? *Front. Physiol.* 9: 714.

Canoville A., M. H. Schweitzer and L. Zanno 2020 Identifying medullary bone in extinct avemetatarsalians: challenges, implications and perspectives.. *Philos. Trans. R. Soc. B Biol. Sci.* 375: 20190133

Carroll, R. L. 1991. The origins of reptiles. In *Origins of the higher groups of tetrapods: controversy and consensus*, ed. H. P. Schultze and L. Trueb, 331–353. Ithaca, Cornell University Press.

Chinsamy, A. and J. H. Hurum. 2006. Bone microstructure and growth patterns of early mammals. *Acta Palaeontol. Pol.* 51: 325–338.

Chinsamy-Turan A. 2005. The microstructure of dinosaur bone. In *Deciphering biology with fine-scale techniques*. Baltimore, John Hopkins University Press.

Chinsamy-Turan, A. and S. Ray. 2012. Bone histology of some Therocephalians and Gorgonopsians, and evidence of bone degradation by fungi. In *Forerunners of mammals*, ed. A. Chinsamy-Turan, 199–222. Bloomington, Indiana, University Press.

Cieri, R. L. and C. G. Farmer. 2016. Unidirectional pulmonary airflow in vertebrates: a review of structure, function, and evolution. *J. Comp. Physiol. B*. 186: 541–552.

Cieri, R. L., et al. 2014. New insight into the evolution of the vertebrate respiratory system and the discovery of unidirectional airflow in iguana lungs. *Proc. Natl. Acad. Sci. U S A* 111: 17218–17223.

Claessens, L. P. A. M., et al. 2009: Respiratory evolution facilitated the origin of pterosaur flight and aerial gigantism. *PLoS One* 4: e4497.

Clarke, A., Pörtner, H.-O., 2010. Temperature, metabolic power and the evolution of endothermy. *Biological Reviews* 85, 703–727. https://doi.org/10.1111/j.1469-185X.2010.00122.x

Colbert E. H. 1958. Morphology and behavior. In *Behavior and evolution*, ed. A. Roe and G. G. Simpson, 27–47. New Haven, Yale University Press.

Colbert E. H. 1962. The weight of dinosaurs. *Am. Mus. Novit.* 2076: 1–16.

Colbert E. H., et al. 1947. Rates of temperature increase in the dinosaurs. *Copeia* 2: 141–142.

Cope E. D. 1878. Descriptions of extinct Batrachia and Reptilia from the Permian formations of Texas. *Proc. Am. Philos. Soc*. 17: 505–530.

Cope E. D. 1887. *The origin of the fittest, Essays on Evolution*. New York, Appleton.

Cowles E. D. 1958. Possible origin of dermal temperature regulation. *Evolution* 12: 347–357; Additional note: id.: 419-421.

Cowles R. B. 1962. Semantics in biothermal studies. *Science* 135: 270.

Cracraft, J. 1981. Pattern and process in paleobiology: the role of cladistic analysis in systematic paleontology. *Paleobiology* 7: 456–468.

Crompton, A. W., et al. 2015. Evolution of the mammalian nose; pp. In *The great transformations in vertebrate evolution*, ed. E. L. Brainerd, K. Dial, and N. H. Shubin, 189–203. Chicago, University of Chicago Press.

Crompton, A. W., et al. 2017. Structure of the nasal region of non-mammalian cynodonts and mammaliaforms: Speculations on the evolution of mammalian endothermy. *J. Vertebr. Paleontol*. 37: e1269116.

Cubo, J. and N. E. Jalil. 2019. Bone histology of *Azendohsaurus laaroussii*: Implications for the evolution of thermometabolism in Archosauromorpha. *Paleobiology* 45: 317–330.

Cubo, J., et al. 2008. Phylogenetic, functional, and structural components of variation in bone growth rate of amniotes. *Evol. Dev.* 10: 217–227.

Cubo, J., et al. 2012. Paleohistological estimation of bone growth rate in extinct archosaurs. *Paleobiology* 38: 335–349.

Cubo, J., et al. 2020. Were Notosuchia (Pseudosuchia: Crocodylomorpha) warm-blooded? A palaeohistological analysis suggests ectothermy. *Biol. J. Linn. Soc.* 131: 154–162.

D'Emic, M. D. 2015. Comment on "Evidence for mesothermy in dinosaurs." *Science* 348: 982–982.

Desmond A. J. 1975. *The hot blooded dinosaur, a revolution in paleontology*. New York, Dial Press.

Desmond A. J. 1979. Designing the dinosaur: Richard Owen response to Robert Edmond Grant. *Isis* 70: 224–234.

Desmond A. J. 1982. *Archetypes and ancestors. Paleontology in Victorian London 1850-1875*. London, Blond and Briggs.

Enlow, D. H. and S. O. Brown. 1957. A comparative histological study of fossil and recent bone tissues, Part II. *Texas J. Sci.* 9: 186–214.

Erickson, G. M. 2005. Assessing dinosaur growth patterns: a microscopic revolution. *Trends Ecol. Evol.* 20: 677–684.

Erickson, G. M., et al. 2007. Growth patterns in brooding dinosaurs reveals the timing of sexual maturity in non-avian dinosaurs and genesis of the avian condition. *Biol. Lett.* 3: 558–561.

Farlow J. O. and M. K. Brett-Surman. 1997. *The complete dinosaur*. Bloomington, Indiana University Press.

Farmer, C. G. 2001. Parental care: a new perspective on the origin of endothermy. In *New perspectives on the origin and early evolution of birds. Proceedings of the International Symposium in Honor of John H. Ostrom*, eds. J. Gauthier and L. F. Gall, 389–412. New Haven, Connecticut, Peabody Museum of Natural History, Yale University.

Farmer, C. G. and K. Sanders. 2010. Unidirectional airflow in the lungs of alligators. *Science* 327: 338–340.

Faure-Brac, M. G. and J. Cubo. 2020. Were the synapsids primitively endotherms? A palaeohistological approach using phylogenetic eigenvector maps. *Philos. Trans. R. Soc. B Biol. Sci*. 375: 20190138.

Feduccia, A. 1973. Dinosaurs as reptiles. *Evolution* 27: 166–169.

Feduccia A. 1985. On why dinosaurs lacked feathers. In *The beginning of birds, Proceedings of the International Archaeopteryx Conference*, eds. M. K. Hecht, J. Ostrom, V. Viol and P. Wellnhofer, 75–79. Eichstatt, Freunde des Juramuseum.

Fleischle, C. V., et al. 2018. Quantitative histological models suggest endothermy in plesiosaurs. *PeerJ* 6: e4955.

Fleischle, C. V., et al. 2019. Hematological convergence between Mesozoic marine reptiles (Sauropterygia) and extant aquatic amniotes elucidates diving adaptations in plesiosaurs. *PeerJ* 7: e8022.

Francillon Vieillot, H., et al. 1990. Microstructure and mineralization of vertebrate skeletal tissues. In *Skeletal biomineralization: patterns, process and evolutionary trends*, ed. J. G. Carter, 471–530. New York, Van Nostrand Reinhold.

Garamszegi, L. Z. 2014. *Modern phylogenetic comparative methods and their application in evolutionary biology*. Berlin, Springer.

Gardiner, B. 1982. Tetrapod classification. *Zool. J. Linn. Soc.* 74: 207–232.

Gould, S. J. 1997. The exaptive excellence of spandrels as a term and prototype. *Proc. Natl. Acad. Sci. USA* 94: 10750–10755.

Grady, J. M., et al. 2014. Evidence for mesothermy in dinosaurs. *Science* 344: 1268–1272.

Grafen, A. 1989. The phylogenetic regression. *Philos. Trans. R. Soc. B Biol. Sci*. 326: 119–157.

Green, J. L., et al. 2010. Limb bone histology and growth in *Placerias hesternus* (Therapsida: Anomodontia) from the Upper Triassic of North America. *Palaeontology* 53: 347–364.

Griebeler, E. M., et al. 2013. Aging, maturation and growth of sauropodomorph dinosaurs as deduced from growth curves using long bone histological data: an assessment of methodological constraints and solutions. *PLoS One* 8: e67012.

Gross, W. 1934. Die Typen des mikroskopischen Knochenbaues bei fossilen Stegoccphalen und Reptilien. *Z. Anat. Entwicklungs* 103, 731–764.

Guénard, G., et al. 2013. Phylogenetic eigenvector maps: a framework to model and predict species traits. *Methods Ecol. Evol*. 4(12): 1120–1131.

Haack, S. C. 1986. A thermal model of the sailback pelycosaur. *Paleobiology*, 12(4): 450–458.

Harrell, T. L., et al., 2016. Endothermic mosasaurs? Possible thermoregulation of Late Cretaceous mosasaurs (Reptilia, Squamata) indicated by stable oxygen isotopes in fossil bioapatite in comparison with coeval marine fish and pelagic seabirds. *Palaeontology* 59, 351–363. https://doi.org/10.1111/pala.12240

Hayes, J. P. and T. Garland. 1995. The evolution of endothermy: testing the aerobic capacity model. *Evolution* 49(5): 836–847.

Heath J. E. 1968. The origins of thermoregulation. In *Evolution and environment*, ed. C.T. Drake, 259–278. New Haven, Yale University Press.

Heinrich, B., 1993. The Hot-Blooded Insects: Strategies and Mechanisms of Thermoregulation. Springer Berlin Heidelberg, Berlin, Heidelberg. https://doi.org/10.1007/978-3-662-10340-1

Hillenius, W. J. 1992. The evolution of nasal turbinates and mammalian endothermy. *Paleobiology* 18: 17–29.

Hillenius, W. J. 1994. Turbinates in therapsids: evidence for Late Permian origins of mammalian endothermy. *Evolution* 48: 207–229.

Hillenius, W. J. 2000. Septomaxilla of non-mammalian synapsids: soft-tissue correlates and a new functional interpretation. *J. Morphol.* 245: 29–50.

Hopson J. A. 1973. Endothermy, small size and the origin of mammalian reproduction. *Am. Nat.* 107: 446–452.

Hopson, J. A. 2012. The role of foraging mode in the origin of therapsids: implications for the origin of mammalian endothermy. *Fieldiana Life Earth Sci.* 5: 126–148.

Horner J. R., et al. 2000. The bone histology of the hadrosaurid dinosaur *Maiasaura peeblesorum*: growth dynamics and physiology based on an ontogenetic series of skeletal elements. *J. Vertebr. Paleontol.* 20(1): 109–123.

Houssaye, A., et al. 2013. Microanatomical and histological features in the long bones of mosasaurine mosasaurs (Reptilia, Squamata) – implications for aquatic adaptation and growth rates. *PLoS One* 8: e76741.

Houssaye, A., et al. 2014. A new look at ichthyosaur long bone microanatomy and histology: implications for their adaptation to an aquatic life. *PLoS One* 9: e95637.

Hua, S. and V. de Buffrénil. 1996. Bone histology as a clue in the interpretation of functional adaptations in the Thalattosuchia (Reptilia, Crocodylia). *J. Vertebr. Paleontol.* 16: 703–717.

Hughes, G. M. 1963. *Comparative physiology of vertebrate respiration*. Cambridge, Harvard University Press.

Huttenlocker, A., et al. 2006. Osteohistology of *Sphenacodon* (Synapsida: Sphenacodontidae) and the hidden diversity of growth patterns in basal synapsids. *J. Vertebr. Paleontol.* 26(3 supplement): 79–80A.

Huttenlocker, A. K. 2014. Body size reductions in non-mammalian eutheriodont therapsids (Synapsida) during the end-Permian mass extinction. *PLoS One 9*(2): e87553.

Huttenlocker, A. K. and J. Botha-Brink. 2014. Bone microstructure and the evolution of growth patterns in Permo-Triassic therocephalians (Amniota, Therapsida) of South Africa. *PeerJ* 2: e325.

Huttenlocker, A. K. and C. G. Farmer. 2017. Bone microvasculature tracks red blood cell size diminution in Triassic mammal and dinosaur forerunners. *Curr. Biol.* 27: 48–54.

Huttenlocker, A. K. and E. Rega. 2012. Chapter 4: The Paleobiology and Bone Microstructure of Pelycosaurian-Grade Synapsids. In *Forerunners of mammals*, ed. A. Chinsamy-Turan, 90–119. Bloomington, Indiana University Press.

Huttenlocker, A. K., et al. 2010. Comparative anatomy and osteohistology of hyperelongate neural spines in the sphenacodontids *Sphenacodon* and *Dimetrodon* (Amniota: Synapsida). *J. Morphol.* 271: 1407–1421.

Huttenlocker, A. K., et al. 2011. Comparative osteohistology of hyperelongate neural spines in the Edaphosauridae (Amniota: Synapsida). *Palaeontology* 54: 573–590.

Huttenlocker, A. K., et al. 2018. Late-surviving stem mammal links the lowermost Cretaceous of North America and Gondwana. *Nature 558*(7708): 108.

Huxley T. H. 1868. On the animals which are most intermediate between birds and reptiles. In *T.H. Huxley collected works 1898–1902, III*, eds. M. Foster and E. R. Lankester, 303–313. London, Macmillan and Co.

Huxley T. H. 1870. Further evidence of the affinity between dinosaurian reptiles and birds. In *T. H. Huxley collected works 1898–1902, III*, eds. M. Foster and E. R. Lankester, 465–486. London, Macmillan and Co.

Inger R. F. 1957. Ecological aspects of the origin of the tetrapods. *Evolution* 9: 373–376.

Janis C. M., J. G. Napoli and D. E. Warren 2020 Palaeophysiology of pH regulation in tetrapods. *Philos. Trans. R. Soc. B Biol. Sci.* 375: 20190131

Jansky L. 1962. Maximal metabolism and organ thermogenesis in mammals. In *Comparative physiology of temperature regulation*, 133–174, eds. J. P. Mason and E. Viereck. Alaska, Arctic Aeromedical Lab.

Jastroch M. and F. Seebacher. 2020. Importance of adipocyte browning in the evolution of endothermy. *Philos. Trans. R. Soc. B Biol. Sci.* 375: 20190134.

Jenkins F. A. 1971. The post cranial skeleton of African cynodonts. *Peabody Mus. Nat. Hist.* 36: 1–216.

Ji, Q., et al. 2002. The earliest known eutherian mammal. *Nature* 416: 816–822.

Ji, Q., et al. 2006. A swimming mammaliaform from the Middle Jurassic and ecomorphological diversification of early mammals. *Science* 311: 1123–1127.

Joleaud L. 1921. Les Reptiles fossiles. In *Conférence de l'Association Française pour l'Avancement des Sciences.* Paris, Secrétariat de l'Association pour l'avancement des Sciences.

Kapusta, A., A. Suh and C. Feschotte. 2017. Dynamics of genome size evolution in birds and mammals. *Proc. Natl. Acad. Sci. U S A* 114(8): E1460–E1469.

Kemp, T. S. 2006a. The origin and early radiation of the therapsid mammal-like reptiles: a palaeobiological hypothesis. *J. Evol. Biol* 19(4): 1231–1247.

Kemp, T. S. 2006b. The origin of mammalian endothermy: a paradigm for the evolution of complex biological structure. *Zool. J. Linn. Soc* 147(4): 473–488.

Kemp, T. S. 2007. The concept of correlated progression as the basis of a model for the evolutionary origin of major new taxa. *Proc. R. Soc. B* 274(1618): 1667–1673.

King J. R. and D. S. Farner. 1961. Energy metabolism, thermoregulation and body temperature. In *Biology and comparative physiology of birds*, ed. A.H. Marshall, 215–288. London and New York, Academic Press.

Konarzewski, M., et al. 1997. Metabolic correlates of selection for swim stress-induced analgesia in laboratory mice. *Am. J. Physiol. Regul. Integr. Comp. Physiol.* 273(1): R337–R343.

Laaß, M., et al. 2011. New insights into the respiration and metabolic physiology of *Lystrosaurus*. *Acta Zool. Stockh.* 92: 363–371.

Laurin, M. 2004. The evolution of body size, Cope's rule and the evolution of amniotes. *Syst. Biol.* 53: 594–622.

Laurin, M. and V de Buffrénil. 2016. Microstructural features of the femur in early ophiacodontids: A reappraisal of ancestral habitat use and lifestyle of Amniotes. *C. R. Palevol* 15: 119–131.

Laurin, M. and M. Girondot. 1999. Embryo retention in sarcopterygians, and the origin of the extra-embryonic membranes of the amniotic egg. *Ann. Sci. Nat., Zool.* 20: 99–104.

Lee, A. H. and S. Werning, S. 2008. Sexual maturity in growing dinosaurs does not fit reptilian growth models *Proc. Natl. Acad. Sci. U S A* 105(2): 582–587.

Legendre, L. J. and D. Davesne. 2020. The evolution of mechanisms involved in vertebrate endothermy. *Philos. Trans. R. Soc. B Biol. Sci.* 375: 20190136.

Legendre, L. J., et al. 2013. Evidence for high bone growth rate in Euparkeria obtained using a new paleohistological inference model for the humerus. *J. Vertebr. Paleontol. 33*(6): 1343–1350.

Legendre, L. J., et al. 2016. Palaeohistological evidence for ancestral high metabolic rate in archosaurs. *Syst. Biol.* 65(6): 989–996.

Legendre, L. J., Davesne, D., 2020. The evolution of mechanisms involved in vertebrate endothermy. Philosophical Transactions of the Royal Society B: *Biological Sciences* 375, 20190136. https://doi.org/10.1098/rstb.2019.0136

Little, A. G. and F. Seebacher. 2014. The evolution of endothermy is explained by thyroid hormone-mediated responses to cold in early vertebrates. *J. Exp. Biol.* 217: 1642–1648.

Lovegrove, B. G. 2017. A phenology of the evolution of endothermy in birds and mammals: Evolution of endothermy. *Biol. Rev.* 92(2): 1213–1240. https://doi.org/10.1111/brv.12280

Ma, L., et al. 2003. 'Cyclic alopecia' in Msx2 mutants: defects in hair cycling and hair shaft differentiation. *Development* 130: 379–389.

Maderson, P. F. A. 2003. Mammalian skin evolution: a reevaluation. *Exp. Dermatol.* 12: 233–236.

McNab, B. K. 1978. The evolution of endothermy in the phylogeny of mammals. *Am. Nat.* 112(983): 1–21.

Montes, L., et al. 2007. Relationships between bone growth rate, body mass and resting metabolic rate in growing amniotes: a phylogenetic approach. *Biol. J. Linn. Soc.* 92: 63–76.

Montes, L., et al. 2010. Relationship between bone growth rate and bone tissue organization in amniotes: first test of Amprino's rule in a phylogenetic context. *Anim. Biol.* 60: 25–41.

Myhrvold, N. P. 2013. Revisiting the estimation of dinosaur growth rates. *PLoS One*, 8(12): e81917.

Myhrvold, N. P. 2015. Comment on "evidence for mesothermy in dinosaurs." *Science* 348(6238): 982–982.

Myhrvold, N. P. 2016. Dinosaur metabolism and the allometry of maximum growth rate. *PLoS One*, 11(11): e0163205.

Newman, S. A., 2011. Thermogenesis, muscle hyperplasia, and the origin of birds. *BioEssays* 33, 653–656. https://doi.org/10.1002/bies.201100061

Newman, S. A., et al. 2013. Gene loss, thermogenesis, and the origin of birds. *Ann. N. Y. Acad. Sci.* 1289(1): 36–47.

Norell, M. A. and X. Xu. 2005. Feathered dinosaurs. *Annu. Rev. Earth Planet. Sci.* 33(1): 277–299.

O'Connor, P. M. and L. Claessens. 2005. Basic avian pulmonary design and flow-through ventilation in non-avian theropod dinosaurs. *Nature* 436: 253–256.

Olivier, C., et al. 2017. First palaeohistological inference of resting metabolic rate in an extinct synapsid, *Moghreberia nmachouensis* (Therapsida: Anomodontia). *Biol. J. Linn. Soc.* 121: 409–419.

Olson E. C. 1959. The evolution of mammalian characters. *Evolution* 13: 344–353.

Ostrom J. H. 1969a. Terrestrial vertebrates as indicators of Mesozoic climates. *Proc. North Am. Paleontol. Convention* D: 347–376.

Ostrom J. H. 1969b. Osteology of *Deinonychus antirrhopus,* an unusual theropod from the cretaceous of Montana. *Bull. Peabody Museum Nat. Hist.* 30: 1–165.

Owen R. 1841. Report on English fossil reptiles: Part II. *Br. Assoc. Adv. Sci. (Plymouth Meeting)*: 60–204.

Owerkowicz, T. and A. W. Crompton. 1997. Effects of exercise and diet on bone-building: a monitor case. *J. Morphol.* 232: 306.

Owerkowicz, T., et al. 2015. Respiratory turbinates and the evolution of endothermy in mammals and birds. In *The great transformations in vertebrate evolution*, eds. E. L. Brainerd, K. Dial and N. H. Shubin, 143–165. Chicago, University of Chicago Press.

Padian K. 2004. *De Darwin aux dinosaures: Essais sur l'idée d'Evolution*. Paris, Odile Jacob.

Padian, K. and J. R. Horner. 2002. Typology versus transformation in the origin of birds. *Trends Ecol. Evol.* 17: 120–124.

Padian, K., et al. 2004. Growth in small dinosaurs and pterosaurs: the evolution of archosaurian growth strategies. *J. Vertebr. Paleontol.* 24: 555–571.

Paladino F. V., M. P. O'Connor and J. R. Spotila. 1990 Metabolism of leatherback turtles, gigantothermy and thermoregulation of dinosaurs. *Nature* 344, 858–860.

Paradis, E. 2012. *Analysis of phylogenetics and evolution with R*.2nd edition. New York, Springer-Verlag.

Parfitt, A. M. 1994. Osteonal and hemi-osteonal remodeling: the spatial and temporal framework for signal traffic in adult human bone. *J. Cell Biochem.* 55: 273–286.

Parsons K. M. 2001. *Drawing out leviathan - dinosaurs and the science wars.* Bloomington and Indianapolis, Indiana University Press.

Peabody, F. E. 1961. Annual growth zones in living and fossil vertebrates. *J. Morphol.* 108(1): 11–62.

Penone, C., et al. 2014. Imputation of missing data in life-history trait datasets: which approach performs the best? *Methods Ecol. Evol.* 5: 961–970.

Portier, P. 1903. Sur la temperature de *Thynnus alalonga*. *Bull. Soc. Zool. France* 28: 79–81.

Prondvai, E., 2017. Medullary bone in fossils: function, evolution and significance in growth curve reconstructions of extinct vertebrates. *Journal of Evolutionary Biology* 30, 440–460. https://doi.org/10.1111/jeb.13019

Prondvai, E., et al. 2018. Intraskeletal histovariability, allometric growth patterns, and their functional implications in bird-like dinosaurs. *Sci. Rep.* 8(1): 258.

Prosser C. L. and F. A. Brown. 1961. *Comparative animal physiology.* Philadelphia, Saunders.

Ray, S., et al. 2004. Bone histology and growth patterns of some non-mammalian therapsids. *J. Vertebr. Paleontol.* 24: 634–648.

Ray, S., et al. 2005. *Lystrosaurus murrayi* (Therapsida, Dicynodontia): bone histology, growth and lifestyle adaptations. *Palaeontology* 48: 1169–1185.

Reed C. A. 1960. Polyphyletic or monophyletic ancestry of Mammals; or what is a class? *Evolution* 14: 314–322.

Rega, E., et al. 2012. Healed fractures in the neural spines of an associated skeleton of *Dimetrodon*: Implications for dorsal sail morphology and function. *Fieldiana: Life Earth Sci.* 2012: 104–111.

Reid, R. E. H. 1987. Bone and dinosaurian "endothermy." *Mod. Geol.* 11: 133–154.

Reisz, R. R. and J. Fröbisch. 2014. The oldest caseid synapsid from the Late Pennsylvanian of Kansas, and the evolution of herbivory in terrestrial vertebrates. *PLoS One* 9(4): e94518.

Rey, K., et al. 2017. Oxygen isotopes suggest elevated thermometabolism within multiple Permo-Triassic therapsid clades. *eLife* e28589.

Ricqlès A. de 1969a. L'histologie osseuse envisagée comme un indicateur de la physiologie thermique chez les tétrapodes fossiles. *C. R. Acad. Sci. Paris D* 268: 782–785.

Ricqlès, A. de 1969b. Recherches paléohistologiques sur les os longs des tétrapodes II: Quelques observations sur les os longs des Theriodontes. *Ann. de Paléontol.* 55: 1–72.

Ricqlès A. de. 1972a. Vers une histoire de la physiologie thermique. Les données histologiques et leur interprétation fonctionnelle. *C. R. Acad. Sci. Paris, D* 275: 1745–1749.

Ricqlès A. de 1972b. Vers une histoire de la physiologie thermique. L'apparition de l'endothermie et le concept de reptile. *C. R. Acad. Sci. Paris, D* 275: 1875–1878.

Ricqlès, A. de. 1972c. Recherches paléohistologiques sur les os longs des tétrapodes III: Titanosuchiens, Dinocéphales et Dicynodontes. *Ann. Paléontol.* 58: 17–60.

Ricqlès A. de 1974a. Evolution of endothermy: histological evidence. *Evol. Theory* 1: 51–80.

Ricqlès, A. de 1974b. Recherches paléohistologiques sur les os longs des tétrapodes IV: Eotheriodontes et pelycosaures. *Ann. Paléontol.* 60: 3–39.

Ricqlès A. de 1978. Recherches paléohistologiques sur les os longs des tétrapodes. VII - Sur la classification, la signification fonctionnelle et l'histoire des tissus osseux des tétrapodes. Third part: Evolution. *Ann. Paléontol.* 64: 85–111; 153–184.

Ricqlès A. de 2000. L'origine dinosaurienne des oiseaux et de l'endothermie avienne: les arguments histologiques. *Ann. Biol.* 39(2): 69–100.

Ricqlès A. de 2002. Dinosaur physiology: hot, cold or lukewarm? In *Dinosaurs; the science behind the story*, eds. J. G. Scotchmoore, D. A. Springer, B Breithaupt and A. R. Fiorillo, 79–88. Alexandria, Virginia, American Geosciences Institute.

Ricqlès A. de 2011. Vertebrate paleohistology: past and future. *C. R. Palevol* 10(5–6): 509–515.

Ricqlès, A., et al. 1991. Comparative microstructure of bone. *Bone* 3: 1–78.

Rodbard S. 1953. Warm bloodedness. *Sci. Month.* 77: 137–142.

Romer, A. S. 1948. Relative growth in pelycosaurian reptiles. *Special Publication of the Royal Society of South Africa, Robert Broom Commemorative Volume*: 45–55.

Romer, A. S. 1961. Synapsid evolution and dentition. *International Colloquium on the Evolution of Mammals* 1: 9–56.

Rowland, L. A., et al. 2015. The role of skeletal-muscle-based thermogenic mechanisms in vertebrate endothermy. *Biol. Rev.* 90: 1279–1297.

Ruben, J. A. and T. D. Jones. 2000. Selective factors associated with the origin of fur and feathers. *Integr. Comp. Biol.* 40: 585–596.

Ruben, J. A., et al. 1997. New insights into the metabolic physiology of dinosaurs. In *The complete dinosaur*, eds. J. O. Farlow and M. K. Brett-Surman. Bloomington, Indiana University Press.

Ruben, J. A., et al. 2012. The evolution of mammalian endothermy. In *Forerunners of mammals*, ed. A. Chinsamy-Turan, 273–286. Bloomington, Indiana University Press.

Ruf, T., Geiser, F., 2015. Daily torpor and hibernation in birds and mammals. *Biological Reviews* 90, 891–926. https://doi.org/10.1111/brv.12137

Russell L.S. 1965. Body temperature of dinosaurs and its relationship to their extinction. *J. Paleontol.* 39(3): 497–501.

Schachner, E. R., et al. 2013. Pulmonary anatomy in the Nile crocodile and the evolution of unidirectional airflow in Archosauria. *PeerJ* 1: e60.

Schachner, E. R., et al. 2014: Unidirectional pulmonary airflow patterns in the savannah monitor lizard. *Nature* 506: 367.

Schmidt-Nielsen, K. 1981. Countercurrent systems in animals. *Sci. Am.* 244: 118–128.

Schocander P. F. 1955. Evolution of climatic adaptation in homeotherms. *Evolution* 9(1): 15–26.

Schuh, F. 1951. Das warmblüter Problem in der Paläontologie. *Paläont. Zetschr.* 24: 194–200.

Seeley, H. G. 1864. On the Pterodactyle as evidence of a new subclass of Vertebrata (Saurornia). *Rep. Brit. Assoc. Adv. Science (Bath Meeting)*: 69.

Seeley, H. G. 1870. Remarks on Professor Owen's monograph on *Dimorphodon*. *Ann. Mag. Nat. Hist.* 6: 129–152.

Seeley, H. G. 1889. Some scientific results of a mission to South Africa. *Trans. South Afr. Philos. Soc.* 1–16.

Seeley, H. G. 1901 *Dragons of the air, an account of extinct flying reptiles*. London, Methuen & Co.

Séon, N., et al. 2020. Thermophysiologies of Jurassic marine crocodylomorphs inferred from the oxygen isotope composition of their tooth apatite. *Philos. Trans. R. Soc. B Biol. Sci.* 375: 20190139.

Seymour, R. S. 2016. Cardiovascular physiology of dinosaurs. *Physiology* 31(6): 430–441.

Seymour, R. S., et al. 2004. Evidence for endothermic ancestors of crocodiles at the stem of archosaur evolution. *Physiol. Biochem. Zool.* 77: 1051–1067.

Shelton, C. D., et al. 2013. Long bone histology indicates sympatric species of *Dimetrodon* (Lower Permian, Sphenacodontidae). *Earth Environ. Sci. Trans. R. Soc. Edinb.* 103(3–4): 217–236.

Shelton, C. D. and P. M. Sander. 2017. Long bone histology of *Ophiacodon* reveals the geologically earliest occurrence of fibrolamellar bone in the mammalian stem lineage. *C. R. Palevol* 16(4): 397–424.

Sigurdsen, T., et al. 2012. Reassessment of the morphology and paleobiology of the therocephalian *Tetracynodon darti* (Therapsida), and the phylogenetic relationships of Baurioidea. *J. Vertebr. Paleontol.* 32(5): 1113–1134.

Sloan P. R. 1992. *(Introduction and comments to) The Hunterian Lectures in Comparative Anatomy, May June 1837 by Richard Owen*. Chicago, The University of Chicago Press.

Spotila J. R., et al. 1973. A mathematical model for body temperature of large reptiles: implication for dinosaurs ecology. *Am. Nat.* 107(955): 391–404.

Tattersall, G. J., et al. 2016. Seasonal reproductive endothermy in tegu lizards. *Sci. Adv.* 2(1): e1500951.

VetBooks.ir

Taylor, C. R. 1977. Exercise and environmental heat loads: different mechanisms for solving different problems? *Int. Rev. Physiol*. 15: 119–146.

Templeton J. R. 1970. Reptiles. In *Comparative physiology of thermoregulation*, ed. G. Whittow, 167–221. London and New York, Academic Press.

Thomas R. D. K. and E. C. Olson. 1980. *A cold look at the warm-blooded dinosaur.* AAAS Symposium. Boulder, Westview Press.

Tracy, C. R., et al. 1986. A biophysical analysis of possible thermoregulatory adaptations in sailed pelycosaurs. In *The ecology and biology of mammal-like reptiles*, eds. N.H. Hotton, P.D. MacLean, J.J. Roth, and E.C. Roth, 195–206. Washington DC, Smithsonian Institution Press.

Turner, J. S. and C. R. Tracy. 1986. Body size, homeothermy and the control of heat exchange in mammal-like reptiles. In *The ecology and biology of mammal-like reptiles*, eds. N.H. Hotton, P.D. MacLean, J.J. Roth, and E.C. Roth, 185–194. Washington, DC, Smithsonian Institution Press.

Van Valen L. 1960. Therapsids as mammals. *Evolution* 14: 304–313.

Wallace, B. P. and T. T. Jones. 2008. What makes marine turtles go: a review of metabolic rates and their consequences. *J. Exp. Mar. Biol. Ecol*. 356(1–2): 8–24.

Walter, I. and F. Seebacher. 2009: Endothermy in birds: underlying molecular mechanisms. *J. Exp. Biol*. 212: 2328–2336.

Wegner, N. C., et al. 2015. Whole-body endothermy in a mesopelagic fish, *the opah, Lampris guttatus*. *Science* 348: 784–790.

Werner, J. and E. M. Griebeler. 2014. Allometries of maximum growth rate versus body mass at maximum growth indicate that non-avian dinosaurs had growth rates typical of fast growing ectothermic sauropsids. *PLoS One 9*(2): e88834.

Whittow G. C. 1970. *Comparative physiology of thermoregulation*. London and New York, Academic Press.

Wieland G. R. 1942. Too hot for the dinosaurs. *Science* 96: 359.

Wintrich, T., et al. 2017. A Triassic plesiosaurian skeleton and bone histology inform on evolution of a unique body plan. *Sci. Adv.* 3(12): e1701144.

Wone, B. W., et al. 2015. A strong response to selection on mass-independent maximal metabolic rate without a correlated response in basal metabolic rate. *Heredity* 114(4): 419–427.

Woodward, H. N., et al. 2011. Osteohistological evidence for determinate growth in the American alligator. *J. Herpetol. 45*(3): 339–342.

Woodward, H. N., et al. 2014. Quantification of intraskeletal histovariability in *Alligator mississippiensis* and implications for vertebrate osteohistology. *PeerJ* 2: e422.

VetBooks.ir

38

Bone Ornamentation: Deciphering the Functional Meaning of an Enigmatic Feature

François Clarac

CONTENTS

A Morphologically Variable and Homoplastic Feature 774
Local Growth Patterns Involved in the Differentiation of Bone Ornamentation 775
Possible Functions of Bone Ornamentation: The Example of Crocodylomorpha 776
Bone Ornamentation and Heat Transfer: An Adaptation to the Ectothermic Sit-and-Wait Predator Lifestyle in Crocodylomorpha 776
Possible Involvement of Bone Ornamentation in Blood Acidity Buffering 777
The Influence of Ornamentation on the Mechanical Resistance of Bones 777
Concluding Remarks 778
Acknowledgments 778
References 778

A Morphologically Variable and Homoplastic Feature

Bone ornamentation, also designated as "bone sculpture", is a recurrent feature observed on the external surface of dermal bones in diverse regions of the vertebrate skeleton, including skull roof, lateral mandibular sides, some elements of the shoulder girdle, osteoderms and ossified scales. This anatomical term encompasses a broad variety of sculptural patterns that all share one basic characteristic: they consist of superficial repetitive reliefs (positive or negative), distinct from simple vascular imprints.

The first occurrence of bone ornamentation in vertebrates traces back to some of the most ancient stem gnathostomes: the Ordovician arandaspids (Sansom et al. 2005; Young 2009; Figure 38.1A). In these early forms the superficial sculpture of dermal bones mainly consists of tubercles of dentine capped by an enameloid layer, the odontodes. In Silurian stem osteichthyans, these tubercules lose their apical enamel layer on facial bones and are always associated with a basal network of vascular canals, possibly involved in the resorption and replacement of the odontodes (*Andreolepis*; Chen et al. 2016). During the Silurian and Devonian periods, both the stem osteichthyans (*Achoania* and *Psarolepis*; Zhu et al. 2001; Qu et al. 2013, 2015, 2016) and the stem actinopterygians (*Meemannia*, *Cheirolepis*; Zhu et al. 2010; Giles et al. 2015; Lu et al. 2016) bear dentine tubercles on their dermal bones. The tubercles are capped by an enameloid layer and are associated with a system of pores and canals to form the histological complex called "cosmine" (Aldinger 1937; Schultze 2015). In some Devonian sarcopterygians, such as *Porolepis* and *Osteolepis*, the pore and canal system not only interconnects around the dentine tubercles but is also linked to an underneath spongiosa in which the odontodes can be buried (Mondéjar-Fernández and Clément 2012). This type of tissue organization has been hypothesized to be an apomorphic form of cosmine recently named "eucosmine" (Mondéjar-Fernández 2018). In Devonian tetrapods and their close relatives, the loss of odontogenic tissues on the skull roof, the lateral side of the mandibles, and the postcranial bony plates may be considered an evolutionary step to a type of ornamentation exclusively involving bone tissue (e.g., *Eusthenopteron*, Zylberberg et al. 2010; *Panderichthys*, Vorobyeva and Schultze 1991; *Elpistostege*, Schultze and Arsenault 1985; *Tiktaalik,* Daeschler et al. 2006; *Acanthostega,* Clack 2002). Although bone sculpture was lost in most crown-tetrapods, in which dermal bones are generally smooth, reversions of this character occurred during the Mesozoic in some taxa such as the soft-shelled turtles (e.g., Scheyer et al. 2007, 2012), the crocodylians (e.g., Iordansky 1973) and some lissamphibians (Rocek 2000) that show a bone sculpture morphologically similar to that of early tetrapods.

In contrast to the sarcopterygians, crown actinopterygians evolved several layers of enamel above the dentine tubercules, forming a ganoine complex. In extant forms that still have ganoid scales (polypterids and lepisosteids), the tubercles have regressed and the ganoine contacts the basal bony layer (Zylberberg et al. 1997). Like sarcopterygians, crown actinopterygians secondarily lost odontogenetic tissues associated with dermal bones in favor of a fully osseous ornamentation (Sire et al. 2009), as in the chondrosteans and Lepisosteiformes (Meunier and Brito 2004). Like crown tetrapods, most

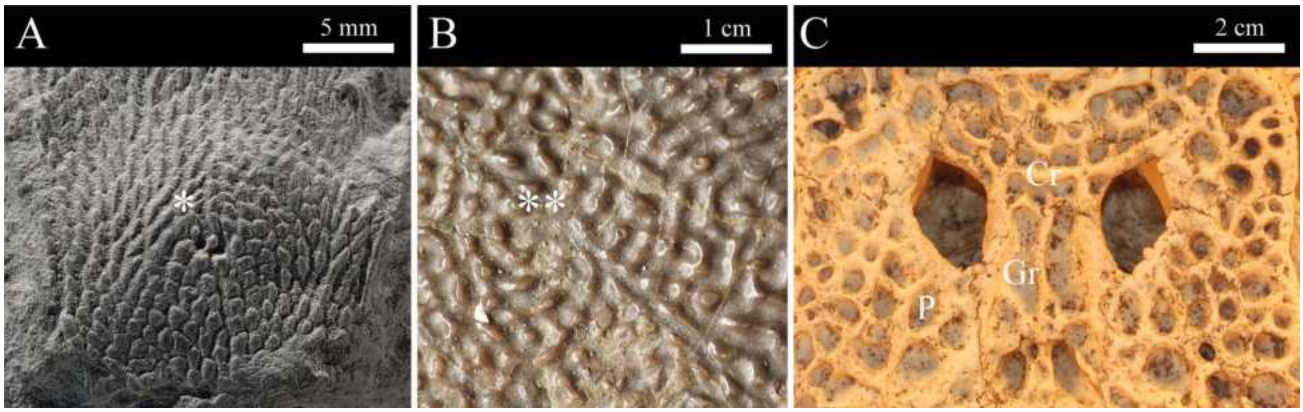


FIGURE 38.1 Diversity in vertebrate dermal bone ornamentation. A, Close-up of the pineal plate of *Sacabambaspis janvieri* (458–448 Ma "Caradoc", from Bolivia, cast specimen photographed by Alan Pradel at the Muséum National d'Histoire Naturelle paleontology collections). Asterisk, dentine tubercule. B, Close-up of the median thoracic plate of *Bothriolepis canadensis* (370 Ma, from Canada, Muséum National d'Histoire Naturelle paleontology collections). Asterisks, bony tubercule. C, Close-up of the skull table of a *Caiman yacare* (extant alligatorid from South America, Smithsonian National Museum of Natural History, vertebrate zoology collections, SMITH 281286). P, pit; Cr, crest; Gr, groove.

teleost species also lost bone ornamentation, with reversions in some Mesozoic and later taxa such as Osteoglossiformes and Siluriformes (Sire and Meunier 1993). In Placodermi (an enigmatic "armored-fish" group, which lived from the Early Silurian to the Late Devonian; Young 2010), the presence of odontogenic tissues in dermal plates varies depending on the taxa. The odontodes gave way to an apical ornamentation composed only of compact bone, as exemplified by *Bothriolepis canadensis* (Downs and Donoghue 2009; Giles et al. 2013). Several morphogenetic processes develop ornamentation in osseous tissues, which may be classified into three main categories. (1) The granular ornamentation (also called "tubercular" or "pustular") is a morphological pattern formed by the repetition of globular or ogival protuberances as observed on the dermal bones of some placoderms (Figure 38.1B), temnospondyls (Witzmann and Soler-Gijón 2010; Witzmann et al. 2010) and squamates (Hoffstetter 1955; Buffrénil et al. 2011). (2) The "vermicular" ornamentation, which is a network of shallow, sinuous, and interconnected grooves as observed on the osteoderms of some squamates (e.g., *Anguis fragilis*; Zylberberg and Castanet 1985). (3) The "pit-and-groove" ornamentation, a sculpture pattern produced by the juxtaposition of pits and grooves separated by a network of crests (Figure 38.1C). This pattern is observed in Devonian tetrapods such as *Acanthostega* (Clack 2002) and most temnospondyls (Schoch and Milner 2014). This is the most frequent ornamentation type, and it occurs in all major vertebrate clades, except birds and mammals: actinopterygians (Grande and Bemis 1998), early sarcopterygians (Janvier and Martin 1979), early tetrapods (Bystrow 1935; Piveteau and Deschaseaux 1955a, b; Laurin and Soler-Gijón 2006; Witzmann et al. 2010), crocodylians (Kälin 1955; Clarac et al. 2015), soft-shelled turtles (Scheyer et al. 2007, 2012) and lissamphibians (Rocek 2000; Laloy et al. 2013; Skutschas and Boitsova 2016). The shape and size of the pits vary during ontogeny, with a noticeable alignment of the main elongation axis along the bone radial growth. In this respect, two morphological traits have yet to be observed: the pits may be either elongated into grooves depending on the local growth activity of each individual bone, and within the limits of each bone (a general situation in temnospondyls; see, e.g., Bystrow 1935; Morkovin 2015), or can extend over an anatomical region irrespective of sutures and bone boundaries, as observed in the skulls of crocodylians (Buffrénil et al. 2015; Clarac et al. 2016).

Local Growth Patterns Involved in the Differentiation of Bone Ornamentation

The differentiation of bone ornamentation in gnathostomes relies on two main processes (review in Buffrénil et al. 2016). The first process is a preferential growth on top of the crests through local increase in the rate of subperiosteal accretion (Figure 38.2A). This mechanism seems to be the only one at work in placoderms and temnospondyls, as suggested by the illustrations of Downs and Donoghue (2009), Giles et al. (2013), Witzmann (2009) and Witzmann and Soler-Gijón (2010). The second process mainly relies on a spotty excavation of the bone surface through active (osteoclastic) bone resorption, followed by incomplete secondary reconstruction on the bottom of the pits (Figure 38.2B). This process, observed in several finned and limbed vertebrates, seems to be the only mechanism contributing to the differentiation of bone ornamentation in Pseudosuchia (crocodylomorphs and their close relatives; Buffrénil 1982; Buffrénil et al. 2015; Cerda et al. 2015). It is a flexible, dynamic, process through which the dimensions and positions of pits and ridges can be quickly adjusted to the overall size of the bones or to any other morphological requirement. Geometrically, this process is submitted to few constraints because of its capacity to erase existing reliefs (either by resorption of the crests or by complete filling of depressions) and replace them by new ones. Preferential apposition on ridges looks *a priori* more constrained in its potentialities because the transformation of bone ornamentation during growth must be based on the topography and geometry of preexisting reliefs.

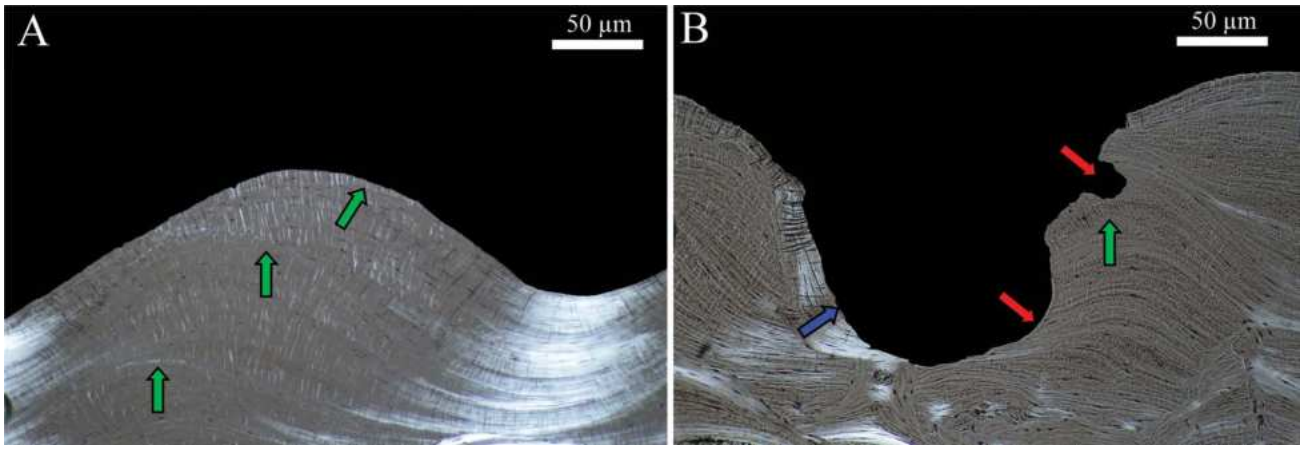


FIGURE 38.2 The osteogenesis of ornamentation on the opercular bone of *Arapaima gigas* (extant teleost from the Amazon basin, Muséum National d'Histoire Naturelle paleohistology collections, MNHN-AC/ET. 0034). A, Cyclic differential growth (green arrows). B, Cyclic resorption (red arrows) followed by secondary bone deposit (blue arrow). Ground sections in transmitted polarized light.

Unlike the situation prevailing in the pseudosuchians and temnospondyls, in which preferential accretion and remodeling occur exclusively, the differentiation of bone sculptural relief in most other vertebrates, e.g., actinopterygians (Figure 38.2), lissamphibians and turtles, involves a combination of these two processes (Buffrénil et al. 2016). In any case, the grooves and crests spread or are drifted under the influence of radial growth. Moreover, the bottom of the pits always houses the opening of at least one vascular canal, which connects the outer surface and the inner cancellous core of ornamented bones (Witzmann et al. 2010). These vascular canals may also be remodeled through resorption and reconstruction, whatever the mechanism that is chiefly responsible for the differentiation of the ornamental relief (Buffrénil et al. 2016).

Possible Functions of Bone Ornamentation: The Example of Crocodylomorpha

Bone Ornamentation and Heat Transfer: An Adaptation to the Ectothermic Sit-and-Wait Predator Lifestyle in Crocodylomorpha

The crocodylomorphs and their close relatives (Pseudosuchia) split from the avemetatarsalians (dinosaurs and pterosaurs) since the Early Triassic, some 250 million years ago (Nesbitt 2011). Several independent studies have concluded that they are derived from endothermic and terrestrial forms (Irmis et al. 2013; Legendre et al. 2016; see also Chapter 26 on Crocodylomorpha); the crocodylomorphs therefore secondarily became ectothermic and some of them became adapted to a semiaquatic lifestyle during the Triassic-Jurassic transition (200 Ma; Buffetaut 1982), such as neosuchians (which include living forms) and teleosaurids, which disappeared in the Cretaceous (Young et al. 2014). Qualitative histological studies of osseous cortices in the long bones of stem-archosauriforms (Ricqlès et al. 2003, 2008) suggested that these forms had a high metabolic rate, because their cortices are mainly fibrolamellar (although the presence of fibrolamellar bone can occasionally be observed in ectotherms, as exemplified by extant crocodylians; Tumarkin-Deratzian 2007). Further analyses based on histomorphometric data (size, shape and density of osteocyte lacunae in primary bone outside osteons, spatial density of vascular canals) have confirmed this previous interpretation, and there is quantitative evidence of a high metabolic rate in both early archosauromorphs and early pseudosuchians (Legendre et al. 2016). In addition to these assessments, some anatomical features of extant crocodylians, such as a four-chambered heart, with a quasi-complete separation of venous and arterial blood as in birds and mammals, also suggest an endothermic origin (Seymour et al. 2004). Unlike other ectothermic tetrapods, crocodylians have a full ventricular separation (Axelsson and Franklin 2001; Franklin and Axelsson 2000; Jensen et al. 2013), and the so-called cog-tooth valve connects the pulmonary artery to the aortic arches, thus reducing the systemic arterial blood pressure (a characteristic correlated with metabolic rate; Seymour et al. 2004). The study of both fossil and recent dry bones using a comparative methodological approach that combines three-dimensional (3D)-morphometry and quantitative phylogenetic analyses shows that the post-Triassic semiaquatic forms (neosuchians and teleosaurids) have a more pronounced bone ornamentation than both earlier crocodylomorph taxa and later terrestrial relatives (Clarac et al. 2017b; Figure 38.3). This suggests that bone ornamentation may have an adaptive value and therefore may have been positively selected during the transition of crocodylomorphs to an ectothermic, amphibious lifestyle in the Lower Jurassic. Histological observations of extant neosuchians reveal that the dermis that fills the ornamental pits on the osteoderm surface always houses a proliferation of blood vessels, whereas the surrounding dermis is mostly avascular (Clarac et al. 2018). These capillaries are mere diverticula of the vessels occupying the cores of ornamented bones (the latter have a "diploe" structure), and the whole network of vessels is connected to larger arteries and veins outside the basal (deep) cortex of both the osteoderms and the dermal skull bones. Seidel's (1979) model, further developed and experimentally supported by, e.g., Farlow et al. (2010) and Clarac and Quilhac (2019), gives

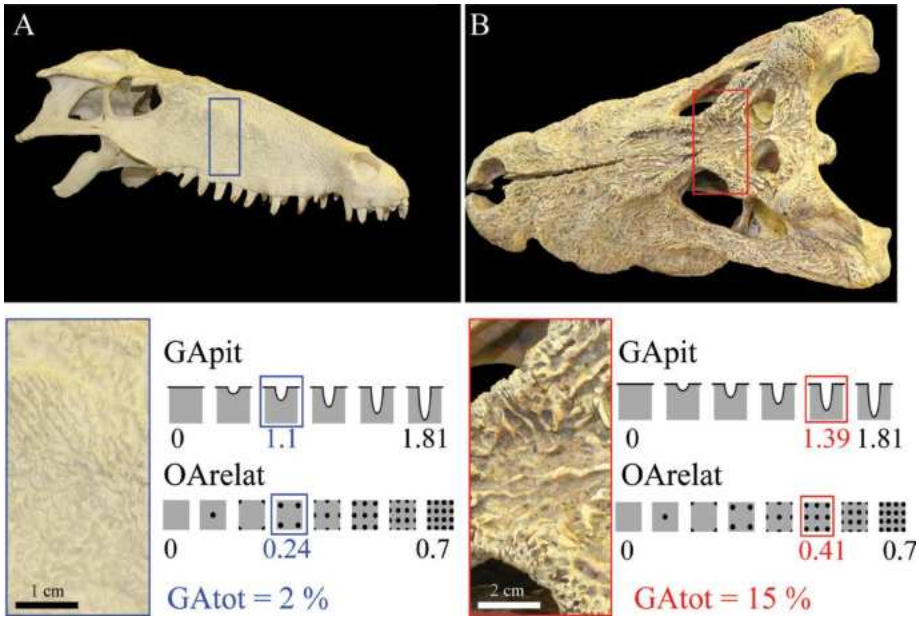


FIGURE 38.3 Variation of cranial ornamentation in relation to lifestyle in Crocodylomorpha. A, *Sebecus icaeorhinus* (Sebecidae, 56–48Ma, terrestrial lifestyle, South America, American Museum of Natural History paleontology collections, UA 8679). B, *Voay robustus* (Crocodylidae, 0.012–0.002Ma, semiaquatic lifestyle, Madagascar, American Museum of Natural History paleontology collections, AMNH-3101). GApit, local basic enlargement of bone area due to pit concavity (no unity); GAtot, gain in area on the total surface of a bone due to the ornamentation (in percentage); OArelat, the ratio of the area of the whole set of pits to the whole area of a bone (no unity; data after Clarac et al. 2017b).

peripheral vessels a role in heat exchanges during emerged and semiemerged basking periods. They capture solar heat on exposed skin surfaces and convey the warm blood, through the inner vessels of the skull bones or osteoderms, toward the core of the body, where it is distributed throughout the organism. Both heartbeat rate and vasodilation regulate this mechanism, depending on ambient temperature, to maintain the most vital organs at an optimal temperature (Seebacher 1999; Seebacher and Franklin 2004, 2007). The role of ornamentation in heat transfers is thus strictly related to the blood flow circulating in the vascular network housed in the pits; it does not depend on the bone morphology itself. A study using finite element methods has shown that neither the morphology of the ornamentation nor the presence of osteoderms themselves has a significant effect on global skin conduction (Clarac et al. 2017a).

Possible Involvement of Bone Ornamentation in Blood Acidity Buffering

Another line of functional hypothesis proposes that, during long submerged periods, the dermal bones enclosing blood vessels could contribute to buffer both respiratory acidosis, which is due to CO_2 increase in the blood plasma, and metabolic acidosis resulting from lactate accumulation (Clarac et al. 2020; Janis et al. 2020). This buffering action would basically rely on the release into the blood flow of mineral elements accumulated in bones, e.g., bicarbonates binding to the free protons dissolved in the blood plasma (due to respiratory acidosis: Janis et al. 2012), and calcium ions interacting with the lactate and thus inhibiting its acidity (in response to metabolic acidosis; Jackson et al. 2003; Jackson 2004). The latter process would occur in two stages within the bone blood vessels: (1) lactate release from the erythrocytes into the plasma and (2) formation of calcium cationic complexes with the final result of increasing plasma pH. In this regard, the bone resorption forming the ornamental pits actually releases bone calcium into the plasma and, additionally, liberates bone carbonates, which also increase plasma pH. The main opposition to this hypothesis is that the dynamics of such a mechanism should not be fast enough to fulfill immediate physiological needs. Therefore, the successive cycles of superficial resorption and secondary bone deposit resulting in the formation of the pseudosuchian ornamentation seem unlikely to be involved in acidosis buffering. The pathways that support exchanges between the blood plasma and the bone matrix nevertheless need to be further investigated. As discussed above, the pits that form the ornaments always house a cluster of blood vessels that remain close to the bone surface and thus extend the contact area between blood vessels and bone matrix, which could, therefore, increase the efficiency of a possible acidosis buffering process. In this regard, bone ornamentation might then be considered a potential adaptive function to anoxic conditions such as long-term apnea. Despite a probable absence of such a process, pit resorption itself undoubtedly contributes, like any other kind of bone remodeling, to phosphocalcic homeostasis (eggshelling, Dacke et al. 2015; diets).

The Influence of Ornamentation on the Mechanical Resistance of Bones

The potential mechanical function of bone ornamentation in crocodiles, a topic poorly documented up to now, was recently consolidated into one question: What are the positive or negative consequences that pits, grooves and crests may have on the response of bones to a local, sudden pressure stress?

VetBooks.ir

This question was considered through a finite-element analysis (FEA) (Clarac et al. 2019). The latter was performed on 3D models by comparing a set of "regular" (realistic) ornamented osteoderms with an equivalent set of nonornamented osteoderms in which the outer surface had virtually been smoothed at a level corresponding to the top of the crests (see Clarac et al. 2015 for methodology). When simulating an external predator attack, such as a claw or a tooth pressure on the outer surface, the presence of superficial pit and ridge sculpture actually tends to reduce the osteoderm resistance to pressure (*contra* Coldiron 1974). This increase in mechanical stress endured by the bone structure nevertheless remains very local (around the impact region) and has no influence on the global stress distribution within the whole osteoderm. This conclusion suggests that the presence of ornamentation does not result in improving the bone mechanical resistance, but slightly degrades it.

Concluding Remarks

Available data suggest that, if bone ornamentation has a functional role, whether related to thermoregulation or to acidosis buffering, it would rely on the presence of a dense superficial network of blood vessels, housed and protected by a system of repetitive relief. The main active element in this osteovascular device is likely to be the vessels themselves, and the price for their protection by osseous relief could then be a mild mechanical weakening of the bony elements. The crocodilian model cannot be straightforwardly exported to other taxa; however, considering the extreme morphological and microanatomical consistency of ornamental patterns in tetrapods (beyond discrepancies among the processes involved in the differentiation of this character), it seems likely that the conclusion derived from the study of crocodiles could also involve many other extant and extinct taxa, at least for the crucial role of the vascular bundles associated with bone sculpture.

Acknowledgments

I would like to send my friendly regards to Alan Pradel for providing a picture of *Sacabambaspis janvieri* as mentioned in the figure caption. I also want to address my most thankful regards to Vivian de Buffrénil for both his support and his supervision when I was a student.

REFERENCES

Aldinger, H. 1937. Permische Ganoidfische aus Ostgrönland. *Medd. Grønl.* 102: 5–392.

Axelsson, M., and C. E. Franklin. 2001. The calibre of the foramen of Panizza *in Crocodylus porosus* and under adrenergic control. *J. Comp. Physiol. B* 171: 341–346.

Buffetaut, E. 1982. Radiation évolutive, paléoécologie et biogéographie des crocodiliens mésosuchiens. *Mém. Soc. Géol. Fr.* 42: 1–88.

Buffrénil, V. de. 1982. Morphogenesis of bone ornamentation in extant and extinct crocodilians. *Zoomorphology* 99: 155–166.

Buffrénil, V. de, et al. 2011. An enamel-like tissue, osteodermine, on the osteoderms of a fossil anguid (Glyptosaurinae) lizard. *C. R. Palevol* 10: 427–438.

Buffrénil, V. de, et al. 2015. Differentiation and growth of bone ornamentation in vertebrates: a comparative histological study among the Crocodylomorpha. *J. Morphol.* 276: 425–445.

Buffrénil, V. de, et al. 2016. Comparative data on the differentiation and growth of bone ornamentation in gnathostomes (Chordata: Vertebrata). *J. Morphol.* 277: 634–670.

Bystrow, A. P. 1935. Morphologische Untersuchungen der Deckknochen des Schädels der Wirbeltiere. I. Mitteilung—Schädel der Stegocephalen. *Acta Zool. Stockholm* 16: 65–141.

Cerda, I. A, et al. 2015. Osteoderm histology of Proterochampsia and Doswelliidae (Reptilia: Archosauriformes) and their evolutionary and paleobiological implications. *J. Morphol.* 276: 385–402.

Chen, D., et al. 2016. The stem osteichthyan *Andreolepis* and the origin of tooth replacement. *Nature* 539: 237–241.

Clack, J. A. 2002. The dermal skull roof of *Acanthostega gunnari*, an early tetrapod from the Late Devonian. *Trans. R. Soc. Edinburgh Earth. Sci.* 93: 17–33.

Clarac, F. and A. Quilhac. 2019. The crocodylian skull and osteoderms: a functional adaptation to ectothermy? *Zoology* 132: 31–40.

Clarac, F., et al. 2015. A quantitative assessment of bone area increase due to ornamentation in the Crocodylia. *J. Morphol.* 276: 1183–1192.

Clarac, F., et al. 2016. Does skull morphology constrain bone ornamentation? A morphometric analysis in the Crocodylia. *J. Anat.* 229: 292–301.

Clarac, F., et al. 2017a. Do the ornamented osteoderms influence the heat conduction through the skin? A finite element analysis in Crocodylomorpha. *J. Therm. Biol.* 69: 39–53.

Clarac, F., et al. 2017b. The evolution of bone ornamentation in Pseudosuchia: morphological constraints versus ecological adaptation. *Biol. J. Linn. Soc.* 121: 395–408.

Clarac, F., et al. 2018. Vascularization in ornamented osteoderms: physiological implications in ectothermy and amphibious lifestyle in the crocodylomorphs? *Anat. Rec.* 301: 175–183.

Clarac, F., et al. 2019. The morpho-functional implication(s) of the crocodylomorph ornamented osteoderms: deciphering the role of the bone apical sculpture using finite element analyses. *Paleobiology* 45: 182–200.

Clarac, F., et al. 2020. The evolution of dermal shield vascularization in Testudinata and Pseudosuchia: phylogenetic constraints versus ecophysiological adaptations. *Philos. Trans. R. Soc. B* 375: 20190132.

Coldiron, R. W. 1974. Possible functions of ornament in the labyrinthodont amphibians. *Occ. Pap. Mus. Nat. Hist. Kansas* 33: 1–19.

Dacke, C. G., et al. 2015. Alligator osteoderms as a source of labile calcium for eggshell formation. *J. Zool.* 297: 255–264.

Daeschler, E. B., et al. 2006. A Devonian tetrapod-like fish and the evolution of the tetrapod body plan. *Nature* 440: 757–763.

Downs, J. P. and P. C. Donoghue. 2009. Skeletal histology of *Bothriolepis canadensis* (Placodermi, Antiarchi) and evolution of the skeleton at the origin of jawed vertebrates. *J. Morphol.* 270: 1364–1380.

Farlow, J. O., et al. 2010. Internal vascularity of the dermal plates of *Stegosaurus* (Ornithischia, Tyreophora). *Swiss J. Geosci.* 103: 173–185.

VetBooks.ir

Franklin, C. E. and M. Axelsson. 2000. An actively controlled heart valve. *Nature* 406: 847–848.

Giles, S., et al. 2013. Histology of "Placoderm" dermal skeletons: implication for the nature of the ancestral gnathostome. *J. Morphol*. 274: 627–644.

Giles, S., et al. 2015. Endoskeletal structure in *Cheirolepis* (Osteichthyes, Actinopterygii), an early ray-finned fish. *Palaeontology* 58: 849–870.

Grande, L. and W.E. Bemis. 1998. A comprehensive phylogenetic study of amiid fishes (Amiidae) based on comparative skeletal anatomy. An empirical search for interconnected patterns of natural history. *J. Vertebr. Paleontol*. 18(S1): 1–696.

Hoffstetter, R. 1955. Squamates de type moderne. In *Traité de Paléontologie*, vol. 5, J. Piveteau ed., 604–664. Paris, Masson et Cie.

Iordansky, N. N. 1973. The skull of the Crocodilia. In *Biology of the Reptilia*, vol. 4, Morphology, C. Gans ed., 201–262. London, Academic Press.

Irmis, R. B., et al. 2013. Early Crocodylomorpha. *Geol. Soc. London Spec. Publ*. 379: 275–302.

Jackson, D. C. 2004. Surviving extreme lactic acidosis: the role of calcium lactate formation in the anoxic turtle. *Resp. Physiol. Neurobiol*. 144: 173–178.

Jackson, D. C. et al. 2003. Lactate sequestration by osteoderms of the broad-nose caiman, *Caiman latirostris*, following capture and forced submergence. *J. Exp. Biol*. 206: 3601–3606.

Janis, C. M., et al.. 2012. Dermal bone in early tetrapods: a palaeophysiological hypothesis of adaptation for terrestrial acidosis. *Proc. Biol. Sci*. 279: 3035–3040.

Janis C. M., et al. 2020. Palaeophysiology of pH regulation in tetrapods. *Philos. Trans. R. Soc. B* 375: 20190131.

Janvier, P. and M. Martin. 1979. Les vertébrés Dévoniens de l'Iran central. II—Coelacanthiformes, Struniiformes, Ostéolépiformes. *Geobios* 12: 497–511.

Jensen, B., et al. 2013. Evolution and development of the building plan of the vertebrate heart. *Acta Biochim. Biophys.* 1833: 783–794.

Kälin, J. 1955. Crocodilia. In *Traité de Paléontologie*, vol. 5, J. Piveteau ed., 695–784. Paris, Masson et Cie.

Laloy, F., et al. 2013. A re-interpretation of the Eocene anuran *Thaumastosaurus* based on MicroCT examination of a 'Mummified' Specimen. *PLoS One* 8: e74874.

Laurin, M. and R. Soler-Gijón. 2006. The oldest known stegocephalian (Sarcopterygii: Temnospondyli) from Spain. *J. Vertebr. Paleontol*. 26: 284–299.

Legendre, L., et al. 2016. Palaeohistological evidence for ancestral high metabolic rate in archosaurs. *Syst. Biol*. 65: 989–996.

Lu, J., et al. 2016. The oldest actinopterygian highlights the cryptic early history of the hyperdiverse ray-finned fishes. *Curr. Biol*. 26: 1602–1608.

Meunier, F. and P. Brito. 2004. Histology and morphology of the scales in some teleosts *Cybium* 28: 225–235.

Mondéjar-Fernández, J. 2018. On cosmine: its origins, biology and implications for sarcopterygian interrelationships. *Cybium* 42: 41–65.

Mondéjar-Fernández, J. and G. Clément. 2012. Squamation and scale microstructure evolution in the Porolepiformes (Sarcopterygii, Dipnomorpha) based on *Heimeniaensis* from the Devonian of Spitsbergen. *J. Vertebr. Paleontol*. 32: 267–284.

Morkovin, B. I. 2015. On the development of surface ornamentation of skull bones in the ontogeny of Early Triassic benthosuchids (Amphibia, Temnospondyli). *Paleontol. J*. 49: 57–69.

Nesbitt, S. J. 2011. The early evolution of Archosaurs: relationships and the origin of major clades. *Bull. Am. Mus. Nat. Hist*. 352: 1–292.

Piveteau, J. and C. Deschaseaux. 1955a. Stereospondyli. In *Traité de Paléontologie, Amphibiens, Reptiles, Oiseaux 5*, J Piveteau ed., 136–172. Paris, Masson et Cie.

Piveteau, J. and C. Deschaseaux. 1955b. Trematosauria. In *Traité de Paléontologie, Amphibiens, Reptiles, Oiseaux 5*, J Piveteau ed., 126–135. Paris, Masson et Cie.

Qu, Q. M., et al. 2013. Scales and dermal skeletal histology of an early bony fish *Psarolepis romeri* and their bearing on the evolution of rhombic scales and hard tissues. *PLoS ONE* 8: e61485.

Qu, Q. M., et al. 2015. New genomic and fossil data illuminate the origin of enamel. *Nature* 526: 108–111.

Qu, Q. M., et al. 2016. The origin of novel features by changes in developmental mechanisms: ontogeny and three-dimensional microanatomy of polyodontode scales of two early osteichthyans. *Biol. Rev*. 92: 1189–1212.

Ricqlès, A. de, et al. 2003. On the bone histology of some Triassic pseudosuchian archosaurs and related taxa. *Ann. Paleontol*. 89: 67–101.

Ricqlès, A. de, et al. 2008. On the origin of high growth rates in archosaurs and their ancient relatives: complementary histological studies on Triassic archosauriforms and the problem of a 'phylogenetic signal' in bone histology. *Ann. Paleontol*. 94: 57–76.

Rocek, Z. 2000. Mesozoic anurans. In *Amphibian Biology*, vol. 5, H. Heatwole and M. Davies eds., 1598–1683. Chipping Norton, Surrey Beatty.

Sansom, I. J., et al. 2005. Histology and affinity of the earliest armoured vertebrate. *Biol. Lett*. 1: 446–449

Scheyer, T. M., et al. 2007. A plywood structure in the shell of fossil and living soft-shelled turtles (Trionychidae) and its evolutionary implications. *Org. Divers. Evol*. 7: 136–144.

Scheyer, T. M., et al. 2012. First record of softshelled turtles (Cryptodira, Tryonychidae) from the Late Cretaceous of Europe. *J. Vert. Paleontol*. 32: 1027–1032.

Schoch, R. R. and A. R. Milner. 2014. Temnospondyli. In *Handbook of Paleoherpetology*, Part 3A2, H. D. Sues ed. München, Verlag Dr. Friedrich Pfeil.

Schultze, H. P. 2015. Scales, enamel, cosmine, ganoine, and early osteichthyans. *C. R. Palevol*. 15: 83–102.

Schultze, H. P. and M. Arsenault. 1985. The panderichthyid fish Elpistostege: a close relative of tetrapods? *Palaeontology* 28: 293–309.

Seebacher, F. 1999. Behavioural postures and the rate of body temperature change in wild freshwater crocodiles *Crocodylus johnstoni*. *Physiol. Biochem. Zool*. 72: 57–63.

Seebacher, F. and C. E. Franklin. 2004. Integration of autonomic and local mechanisms in regulating cardiovascular responses to heating and cooling in a reptile (*Crocodylus porosus*). *J. Comp. Physiol. B* 174: 577–585.

Seebacher, F. and C. E. Franklin. 2007. Redistribution of blood within the body is important for thermoregulation in an ectothermic vertebrate (*Crocodylus porosus*). *J. Comp. Physiol. B* 177: 841–848.

Seidel, M. R. 1979. The osteoderms of the American alligator and their functional significance. *Herpetologica* 35: 375–380.

VetBooks.ir

Seymour, R. S., et al. 2004. Evidence for endothermic ancestors of crocodiles at the stem of archosaur evolution. *Physiol. Biochem. Zool.* 77: 1051–1067.

Sire, J.-Y. and F. J. Meunier. 1993. Ornementation superficielle et structure des plaques osseuses dermiques de quelques Siluriformes cuirassés (Loricariidae, Callichthyidae, Doradidae). *Ann. Sci. Nat. Zool. Paris* 14: 101–123.

Sire, J.-Y., et al. 2009. Origin and evolution of the integumentary skeleton in non-tetrapod vertebrates. *J. Anat.* 214: 409–440.

Skutschas, P. P. and E.A. Boitsova. 2016. Histology of sculptured cranial dermal bones of the stem salamander *Kokartus honorarius* (Amphibia: Caudata) from the Middle Jurassic of Kyrgyzstan. *Hist. Biol.* 29: 423–429

Tumarkin-Deratzian, A. R. 2007. Fibrolamellar bone in wild adult *Alligator mississippiensis*. *J. Herpetol.* 41: 341–345.

Vorobyeva, E. I. and H. P. Schultze. 1991. Description and systematics of panderichthyid fishes with comments on their relationship to tetrapods. In *Origins of Higher Groups of Tetrapods*, H. P. Schultze and L. Trueb eds., 68–109. Ithaca, NY, Comstock Publishing Associates.

Witzmann, F. 2009. Comparative histology of sculptured dermal bones in basal tetrapods, and the implications for the soft tissue dermis. *Paleobiodiversity* 2: 233–270.

Witzmann, F. and R. Soler-Gijón. 2010. The bone histology of osteoderms in temnospondyl amphibians and in the chroniosuchian Bystrowiella. *Acta Zool.* 91: 96–114.

Witzmann F., et al. 2010. Sculpture and vascularization of dermal bones, and the implications for the physiology of basal tetrapods. *Zool. J Linn. Soc.* 160: 302–340.

Young, G. C. 2009. An Ordovician vertebrate from western New South Wales, with comments on Cambro-Ordovician vertebrate distribution patterns. *Alcheringa* 33: 79–89.

Young, G. C. 2010. Placoderms (Armored fish): dominant vertebrates of the Devonian period. *Annu. Rev. Earth Planet. Sci.* 38: 523–550.

Young, M. T., et al. 2014. Re-description of a putative Early Cretaceous "teleosaurid" from France, with implications for the survival of metriorhynchids and teleosaurids across the Jurassic-Cretaceous Boundary. *Ann. Paleontol.* 100: 165–174.

Zhu, M., et al. 2001. A primitive sarcopterygian fish with an eyestalk. *Nature* 410: 81–84.

Zhu, M., et al. 2010. *Meemannia eos*, a basal sarcopterygian fish from the Lower Devonian of China – expanded description and significance. In *Morphology, Phylogeny and Paleobiogeography of Fossil Fishes*, D. K. Elliot, J. G. Maisey, X. Yu and D. Miao eds., 199–214. München, Verlag Dr. Friedrich Pfeil.

Zylberberg, L. and J. Castanet. 1985. New data on the structure and the growth of the osteoderms in the reptile *Anguis fragilis* L. (Anguidae, Squamata). *J. Morphol.* 186: 327–342.

Zylberberg, L., et al. 1997. Immunodetection of amelogenin-like proteins in the ganoine of experimentally regenerating scales of *Calamoichthys calabaricus*, a primitive actinopterygian fish. *Anat. Rec.* 249: 86–95.

Zylberberg, L., et al. 2010. A microanatomical and histological study of the postcranial dermal skeleton in the Devonian sarcopterygian *Eusthenopteron foordi*. *Acta Palaeont. Pol.* 55: 459–470.

VetBooks.ir

39

The Histology of Skeletal Tissues as a Tool in Paleoanthropological and Archaeological Investigations

Ariane Burke and Michelle S. M. Drapeau

CONTENTS

Introduction 781
Taxonomy 782
Histological Applications 782
Functional Analysis 784
Histological Applications 784
Pathology 785
Histological Applications 785
Age and Season of Death 786
Histological Applications 786
Taphonomy 788
Histological Applications 788
Conclusions 788
References 789

Introduction

Vertebrate remains are a rich source of information about individual organisms, the communities they formed and the environments they inhabited. Skeletal remains frequently preserve relatively well and form an abundant class of information in the paleontological and archaeological records. Furthermore, several events thought to have significantly affected the evolution of the human lineage are linked to human interactions with other animals, including the adoption of meat in the hominin diet, the evolution of hunting as a strategy for acquiring meat and the ability to target large prey species, and finally, animal domestication. As a result, osteological research is a key component of paleoanthropology and archeology, two closely allied, multidisciplinary fields that study the biological and cultural evolution of the human lineage.

Archaeology is the study of past human populations, their social structure, political and economic systems and their interactions with other populations and with the environment. Archaeological sites and the material culture they contain offer a means of reconstructing past human behaviors in chronological and environmental context. The faunal record contained in archaeological sites can be used to address a variety of questions about site-formation processes, the postdepositional history of a site and the chronology of human occupation. Faunal remains also provide valuable information about the environmental context of the occupations and the nature of some of the activities carried out by the site's inhabitants.

Paleoanthropology is an interdisciplinary field that has the objective of understanding human evolution. The archaeological record only begins 3.3 million years ago. Prior to that, our understanding of how our lineage evolved is based mainly on the analysis of fossil hominins themselves. Their habitat is reconstructed with the help of the faunal assemblages associated with hominin fossils. Functional anatomy is the study of how biological structure is related to function. Applied to bones or teeth, it focuses on the analysis of form and allows researchers to infer habitual activities of extinct hominins from their fossilized remains. It can be used to infer, for example, locomotion (e.g., the origins of bipedality), the types of habitat exploited (e.g., arboreal or terrestrial), the types of food consumed (e.g., meat, leaf, fruits), movements allowed (e.g., fine manipulation, throwing) and reproductive strategies (polygamy, monogamy). The analysis of dental wear patterns reveals the mechanical properties of the foodstuffs consumed. The chemical analysis of stable isotopes in tooth enamel allows the reconstruction of some aspects of the hominin diet (whether predominantly herbaceous or not), access to water and the general aridity of the landscape (Levin et al. 2006).

Osteological analyses are undertaken by paleoanthropologists and archaeologists with specialist training, alternatively designated as "bioarchaeologists", "archaeozoologists" or "zooarchaeologists", "physical anthropologists" or "human paleontologists". The term bioarchaeology was originally introduced by the British archaeologist Grahame Clark (Clark 1972)

VetBooks.ir

in reference to the analysis of faunal remains from archaeological sites, also known as archaeozoology (or zooarchaeology). The American physical anthropologist Jane Buikstra applied the term to the analysis of human remains (Buikstra 1977), and in the United States this narrow definition of the term is still common. In European countries, however, bioarchaeology has taken on a broader meaning and is applied to all forms of biological remains associated with human activity, including plant remains. Archaeozoology (or zooarchaeology) focuses on the analysis of animal bone assemblages from archaeological sites to the exclusion of human remains, which are studied by physical anthropologists. Human paleontology focuses on the analysis of human remains, including other hominins. All of these subfields are united by an interest in skeletal biology and use similar techniques to identify taxa, study their life history and reconstruct their communities, ultimately using the information gained to address the biocultural evolution of the human lineage. Skeletal histology contributes to this joint enterprise and has been applied to taxonomic identification, functional analyses, the identification of pathological conditions, the study of growth and aging processes, the identification of individual age and season of death and finally, taphonomic analysis.

Taxonomy

Paleoanthropological and archaeozoological analyses are primary focused on the taxonomic determination of vertebrate remains and the identification and quantification of skeletal elements. Faunal remains are paleoenvironmental proxies that help scientists reconstruct the climate conditions and vegetation cover that prevailed when humans, or their hominin ancestors, were present. Hominin fossils can be assigned to a broad chronostratigraphic time frame by association with extinct taxa, for example, and the chronology of occupation of an archaeological site can also be established using biostratigraphic information. Microvertebrates are sensitive to environmental conditions on relatively small temporal and spatial scales and provide a fine-grained record of environmental change over time. Macrovertebrates have broader environmental tolerances but can provide useful paleoenvironmental information on a regional scale. Archaeological assemblages, which tend to be dominated by macrovertebrates, potentially reflect human bias and must be interpreted carefully.

Archaeozoologists apply theoretical models to explore the implications of the statistical patterns of taxonomic and skeletal representation detected in faunal assemblages. The relative representation of different taxa, for example, can be interpreted in terms of human behavior such as prey selection and seasonal hunting strategies. The relative representation of skeletal elements in archaeological assemblages reveals the strategies humans used to acquire and transport animal carcasses, and the economic uses to which they were put (e.g., meat or marrow exploitation). The economic activities carried out at a given location can thus be identified, providing clues as to the function of a site within a broader pattern of land use.

Histological Applications

Taxonomic identification of skeletal remains relies on the presence of diagnostic, morphological landmarks. Faunal remains recovered from archaeological sites and paleontological contexts are often fragmentary due to human activities and postdepositional, diagenetic processes, making taxonomic identification difficult (Figure 39.1). Bone recovered from cultural contexts, including potential crime scenes, may have been exposed to fire, further complicating the task of taxonomic identification. Skeletal elements with distinctive features include teeth, which survive relatively well due to their compact shape and high mineral density, long bone epiphyses and some cranial elements. The degree of fragmentation and modification of an assemblage greatly affects the level of taxonomic identification that is possible on the basis of gross morphological landmarks. Unfortunately, the vast majority of faunal remains available for study consist of long bone shaft fragments that are relatively difficult, if not impossible, to identify macroscopically. As a result, scientists have explored other means of identifying bone fragments to taxon, including DNA analysis, collagen fingerprinting (zooarchaeology by mass spectroscopy [ZooMS]) and, of course, microstructure. The first two methods may be more precise than histological analysis, but in addition to being relatively costly they require good organic preservation, which limits their application in many paleontological and archaeological contexts.



FIGURE 39.1 A typical archaeozoological assemblage being sorted in the field prior to analysis. Photo courtesy of A. Trentacoste (with permission).

VetBooks.ir

Potential applications of bone histology as a tool for taxonomic identification include distinguishing between human bone and animal bone (of particular interest in forensic anthropology); discriminating between closely related species whose gross morphology is very similar or between wild and domestic populations of the same species, and identifying taxa exploited for the manufacture of bone tools or pottery. Nevertheless, histology is used sparingly as a tool for taxonomic identification in archaeology. Bone microstructure reflects phylogeny (Cubo et al. 2005, Legendre et al. 2013), habitat preference and biomechanical strain, and a strong functional signature may obscure phylogenetic signatures (Greenlee and Dunnell 2010). Bone preservation presents an additional challenge, since diagenetic processes such as microbial attack and mineral infiltration can transform or obscure histological structures.

Despite the challenges, qualitative and quantitative analyses of bone microstructure have proven useful for taxonomic identification of fragmentary bone in some archaeological and paleontological contexts. Different techniques have been applied, including observations of thin sections under bright-field microscopy or transmitted, polarized light; the preparation of ground sections for observation under scanning electron microscopy (SEM); and the observation of virtual thin sections using computed tomography (CT)-scanning technology. Forensic anthropology, a branch of physical anthropology that specializes in crime scene analyses, focuses on the identification of human bone, and forensic anthropologists have demonstrated that it is possible to distinguish between human and nonhuman bone fragments (Hillier and Bell 2007). Archaeologists also use bone histology to identify human remains in heavily fragmented or cremated assemblages (Cattaneo et al. 1999, Cuijpers 2006) because plexiform tissue (Figure 39.2), which occurs in several mammalian taxa, is not normally present in mature human bone (Cuijpers 2009). The presence of plexiform bone, therefore, can be used to classify bone fragments as nonhuman, whereas the presence of Haversian tissue cannot. This technique only works for mature bone, since plexiform tissue is sometimes present in immature human bone (Pfeiffer 2006, Cuijpers 2009). In the absence of plexiform bone, however, the pattern of osteon banding in Haversian bone may be useful for distinguishing between humans and other vertebrates, with human bone typically displaying a more random arrangement of osteons than bone from other mammalian taxa (Stout 2003, Mulhern and Ubelaker 2011).

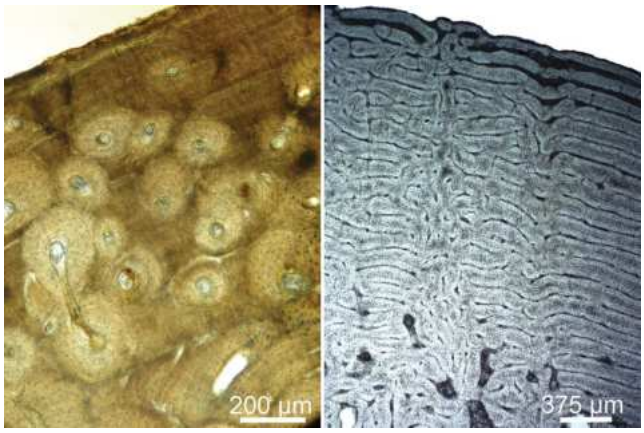


FIGURE 39.2 Taxonomic information: a comparison between cortical bone types in humans (Haversian tissue: left) and pigs (plexiform or reticular tissue: right). Photo courtesy of M. Drapeau and M. Zedda (with permission).

Other traits that have been investigated for taxonomic identification include the number and density of Haversian systems in mature bone, their size and shape, the diameter of Haversian canals and the number of interstitial lamellae. There is considerable overlap in the distribution of many of these traits across taxa (Mulhern and Ubelaker 2011), however, which limits their use. Furthermore, some of these attributes, such as osteon shape, are more likely to reflect biomechanical loading, rather than phylogeny. The strong link between mechanical loading and bone microstructure (explored more fully below) has led to the suggestion that cross-species comparisons should be restricted to the same element and possibly bone region (Zedda et al. 2017) which, in the case of bone fragments often lacking gross anatomical landmarks, is difficult to achieve.

The ability to distinguish between wild and domestic forms (e.g., sheep, goats, pigs or cattle) would be of immense benefit to archaeologists studying the origins of domestication in various world regions. The ability to separate sheep from goats, for example, is a long-standing problem in archaeozoology. The two taxa were among the first animals to be domesticated (aside from the dog) and formed the backbone of early Neolithic farming economies in Western Asia. Despite their morphological similarity, sheep and goats have different ecological requirements and reproductive characteristics; differentiating between them, therefore, sheds light on past husbandry practices (Halstead et al. 2002). There are gross anatomical differences between them, but the reliability of the diagnostic landmarks that have been proposed has been a subject of debate (Zeder and Lapham 2010) and the possibility that histology could be applied to this question was the impetus for early research into bone microstructure by archaeologists (Drew et al. 1971), although initial enthusiasm has since been tempered by caution (Zedda et al. 2017). Nevertheless, bone and tooth microstructure has been used to distinguish between various mammalian taxa (Martiniaková et al. 2007) and this information has been successfully applied to archaeological contexts (Greenlee and Dunnell 2010, Sawada et al. 2014).

A particularly interesting use of bone histology in archaeological research has been the identification of animal tissues in tool manufacturing. For example, bone has been identified as an ingredient in pottery making (Walter et al. 2004) using histological criteria. In a similar vein, histology can help establish whether a tool was made of bone or antler (Paral et al. 2007) and identify preferential selection of taxa by prehistoric toolmakers (Bradfield 2015, 2018). The taxonomic identification of bone used for toolmaking is not just interesting from a technological perspective, it also has potential for recognizing patterns of cultural transmission and the symbolic value of a taxon for a particular human community. The ethnological record, for example, demonstrates that the deliberate selection of specific animals for toolmaking may be ideologically motivated rather than a functional choice.

Histological analysis requires the production of thin sections and both methodological and taphonomic factors, such as

the diagenetic alteration of bone structure, can impede its use. Since archaeozoologists typically deal with tens of thousands of bone fragments and assemblages containing multiple taxa, bone histology has not been widely adopted for taxonomic identification. As we have seen above, however, in certain contexts (such as highly fragmentary assemblages or in the case of cremated remains) histology is a potentially powerful tool that can be used judiciously to enrich archaeological interpretation.

Functional Analysis

Functional analysis is used to infer past adaptations. In animals, functional analyses may be used to study patterns of locomotion, feeding habits or even patterns of human exploitation (such as the use of animals as mounts). When applied to anatomically modern humans, functional studies focus predominantly on traits that are plastic, i.e., traits that can be modified during the life of the individual in response to changes in their lifeways. For example, muscle attachment sites have long been observed to vary from smooth and featureless to very rugose with bone spurs and lytic lesions. The latter morphology is part of the normal aging process, but that process is known to be accelerated by the more forceful and regular contractions of the muscles, which, in turn, suggests various levels and types of activity (e.g., Hawkey and Merbs 1995, Villotte et al. 2010). Studies of the human skeleton, for example, have revealed that the distribution of bone tissue along the diaphysis of long bones is a plastic trait. During growth, bone tissue is deposited where the strains are largest. Thus, through cross-sectional analysis of long bones, it is possible to determine whether some individuals were more mobile or used their upper limbs more often than others (hunter-gatherers might be expected to be more mobile than farmers, for example) by comparing the robusticity of their upper and lower limbs (e.g., Ruff et al. 1984, Stock and Pfeiffer 2004).

Histological Applications

Haversian bone remodeling helps maintain mineral homeostasis, but it has also been shown to be a mechanism to maintain bone integrity by targeting remodeling at the sites of microcracks that develop in bone tissue that undergoes cycles of mechanical loading (Mori and Burr 1993, Burr 2002). Because of this function, it has been assumed that more loaded bones will undergo more remodeling events than less loaded bones, which is a hypothesis that has been verified experimentally in various taxa (O'Connor et al. 1982, Burr et al. 1985, Lieberman and Crompton 1998). In theory, Haversian remodeling could be used to infer loads experienced by the bones of individuals and, by extension, their activity types and level of activity. However, when comparing individuals, it is particularly difficult to tease apart the systemic remodeling influenced by factors such as diet, hormonal status, age, metabolic rate and so forth from that of targeted remodeling (Figure 39.3).

Since greater activity also raises the metabolism, a general increase of remodeling can be expected even in bones that are not mechanically loaded by the activity, further blurring the possibility to directly link remodeling rates to localized loading

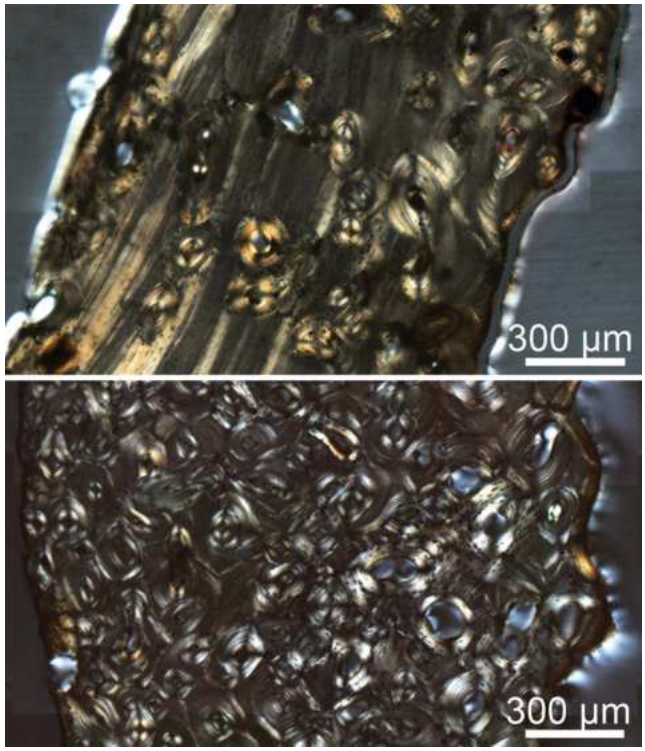


FIGURE 39.3 Functional histology: cross sections viewed through polarized light of the second metacarpal of a 36-year-old female (top) and a 50-year-old male (bottom) showing differences in Haversian remodeling in the cortex (Photo courtesy of M. Drapeau.)

events. In an attempt to control for these confounding factors, researchers have looked at loaded and unloaded bones from the same individuals; some found no evidence of direct effects (Pfeiffer et al. 2006; Raguin and Drapeau 2020) whereas others found that loading accelerates remodeling (Robling 1998, Robling and Stout 2003). Studies comparing right and left metacarpals of the same individuals have shown that greater loading on the dominant side does not result in greater remodeling (Drapeau et al. 2012, Borgel 2016). Given these inconsistent results and because of the necessity of using two bones from the same individuals to control for systemic effects, the use of remodeling in functional analyses remains limited for now. It has been suggested that variation in collagen fiber orientation provides information on whether the bone tissue was under tensile, compressive or shearing loads (Corando et al. 1989, Goldman et al. 2005, Skedros 2011, Skedros et al. 2006, 2011) and further research into how observed patterns can be translated into more specific loading history may eventually allow finer interpretation of individual behavior variation. Growth of long bones generally involves drift with one side growing while the other resorbs, processes that can be inferred from the distribution of primary bone and remodeled bone (Maggiano 2011). The study of the pattern of drift can inform about the direction of growth, on the development of bone torsion, and other factors that are at least partly determined by the intensity and direction of the mechanical loads (Maggiano 2011, Maggiano et al. 2015, 2016). Although none of these methods are very successful at the moment in inferring activity types or levels of activity, further documentation of human variation, including

VetBooks.ir

how these different variables interact and inform us about different aspects of the response of bone to load, is likely to lead to more straightforward interpretations.

Bone histology has also been used as a tool for functional analysis in archaeozoology, although it features less prominently than in paleontological research. Histological differences between wild and domestic animals, for example, such as the distribution and shape of secondary osteons in Haversian tissues, are attributable to different lifestyles (Zedda et al. 2019). This information is useful in the context of research into early animal domestication as discussed above. Economic patterns of animal exploitation may also be discernible histologically. Cattle are typically raised for meat and secondary products such as milk and hides, but they can also be used as draught animals, producing characteristic patterns of bone alteration and pathology (Bartosiewicz et al. 1997). Although patterns of bone and tooth alteration due to human exploitation are usually studied macroscopically, bone histology has been incorporated into archaeozoological practice.

Pathology

Bone pathologies are the result of a variety of factors including activity patterns, mechanical loading, the aging process, illness and injury. They can inform on the health status of the individuals and of the population in general and on the social inequalities and variation in status in human populations. Most pathologies are studied macroscopically, but histological analyses have been useful in identifying certain types of pathology, particularly in humans and allied species.

Histological Applications

Histology has been used to determine whether bone quality in past human populations was maintained through life, following patterns similar to those of modern human populations. In prehistorical and historical agricultural communities, as for current populations, older females have greater loss of bone mass than males (Martin and Armelagos 1985, Burr et al. 1990, Cho and Stout 2011). Some have shown that prehistoric populations, particularly women, have better bone maintenance in older age than modern populations of European descent, likely due to a more active lifestyle, and, for women, more numerous pregnancies and longer lactation events (Agarwal and Stuart-Macadam 2003, Cho and Stout 2011). Studies of populations with more intensive agriculture (Imperial Roman and Sudanese Nubians) also found that females of reproductive age tend to have lower bone maintenance due to greater bone turnover and loss, a condition interpreted as due to the stress of reproduction and lactation combined with a poor, grain-dominated diet (Martin and Armelagos 1985, Cho and Stout 2003, 2011). These examples underscore the large variation in bone quality and maintenance in past populations (Ericksen 1980, Curate 2014), likely reflecting the diverse conditions in which past populations lived.

Given that human remains recovered from archaeological contexts are often heavily fragmented, identification of specific pathologies can be a challenge. The possibility of identifying pathologies from small fragments using histology has been explored. For example, some types of remodeling hypothetically reflect pathological states. Type II osteons form within the confine of another, already formed osteon and are often assumed to be a result of mineral homeostasis related to metabolic stress (Streeter 2005) and possibly diet (Richman et al. 1979). Other osteon types, called zonal osteons, present a hypermineralized ring within the lamellae of the osteon and are hypothesized to be a microscopic manifestation of growth arrest, analogous to Harris lines (Stout and Simmons 1979). However, a recent study found no link between metabolic diseases and the incidence of zonal osteons, suggesting instead that they might be more a function of resorptive bay size (Raguin 2018).

Other research has identified microscopic characteristics of specific pathologies and even disease. Schultz, for example, provides a series of diagnostic characteristics for numerous disorders and underscores how light microscopy, used in conjunction with macroscopic observations, can be used to establish a diagnosis (Schultz 2001, 2011). More recently, D'Ortenzio et al. (2016) have identified histological markers of rickets in the enamel of teeth, allowing the diagnosis of this condition even if the individual recovered before death and their bones do not have any macroscopic traces of the disease (Figure 39.4).

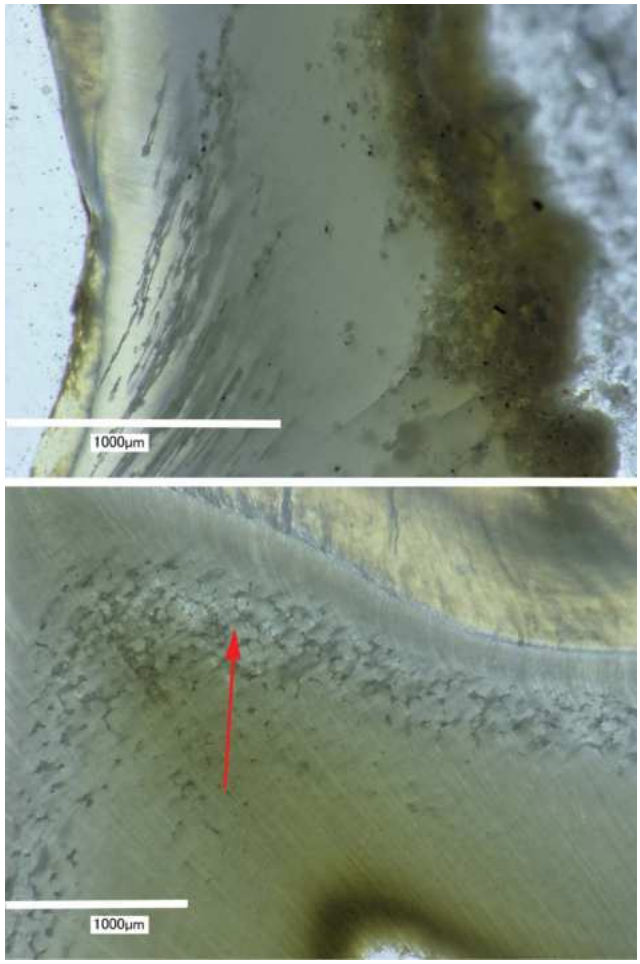


FIGURE 39.4 Rachitic tooth: decidual first upper molar (top) showing normal enamel development and a decidual second molar (bottom) showing a band of interglobular dentine (red arrow) indicative of vitamin D deficiency. Photo courtesy of R-A. Bigué (with permission).

VetBooks.ir

In addition, depending on which tooth the defect is observed, it is possible to determine the duration of the condition and the age at which the individual was affected (D'Ortenzio et al. 2016). Overall, histological analysis of archaeological samples can provide information on the health status of past populations and how it varies according to age and sex, providing information on social structure, subsistence patterns, diet, activity levels and so forth.

Age and Season of Death

Macroscopic analyses of hard tissues can be used to establish an individual's age and season of death. These include the degree of fusion of bone epiphyses and the pattern of eruption and wear of deciduous and adult teeth, all of which reflect an individual's age with more or less accuracy. This information is useful for the reconstruction of the age structure of taxa represented in archaeological assemblages which, in turn, provides valuable information about past human hunting strategies and patterns of prey selection as well as herd management strategies (Steele 2003). The presence of migratory animals provides clues as to the season of occupation of an archaeological site, but age profiles provide this information for a wider range of species – both migratory and nonmigratory – especially if very young individuals are present, since most wild animals have synchronous birthing seasons timed to coincide with favorable seasonal conditions. Shifts in herd structure also provide valuable clues as to the timing of the transition from hunting to herding (Zeder and Hesse 2000). In the case of domestic animals, herd management strategies linked to patterns of animal exploitation produce distinct population structures. For example, herds of sheep raised for meat, milk or wool have different age structures (Payne 1973), which archaeozoologists can use to reconstruct the economic strategies adopted by farmers in the past. The macroscopic tools used to establish age at death lack precision for all but the youngest age classes, however, and inferential arguments are often necessary to establish the season of death. The use of histological data, therefore, has been promoted as a more precise means of establishing individual age and season of death (Naji et al. 2015).

Histological Applications

Several techniques for establishing individual age and season of death rely on bone micromorphology. The study of microscopic wear patterns on the tooth surfaces of herbivores can be used to infer the type of fodder available, providing indirect information about seasonality that offers clues for the study of seasonal hunting strategies and herd management practices in the past (Henton 2012, Rivals and Deniaux 2005). Female birds form bone in the medullary cavities of their long bones during the breeding season as a means of storing calcium for egg production. In the wild, the breeding season is short and predictable, and the presence of medullary bone can be used to establish the season of death. In captivity, birds are induced to lay eggs for longer periods of time and archaeozoologists can use bone histology to study how domestic fowl were managed in the past. This technique is limited in application for obvious reasons, including the length of the breeding season and the absence of medullary bone in males. The study of histological structures using thin section microscopy holds the promise of providing more direct lines of evidence for establishing age and season of death. Various histological structures have been investigated, quantitatively and qualitatively, including the frequency and density of secondary osteons (which increases with age) and the presence of incremental growth structures.

The term skeletochronology (see above, Chapter 31) refers to the study of growth structures in hard tissues to establish an organism's age and, where possible, season of death. Incremental growth structures reflect annual growth rhythms, in addition to more stochastic life events such as weaning, episodic illness or starvation and injury (Klevezal and Kleinenberg 1967, Klevezal 1996). Growth increments form in periosteal bone and dental tissues, but the relatively high rate of bone turnover in adult mammals (contrary to reptiles and amphibians, who experience continuous growth) makes bone tissue much less suitable for skeletochronological analyses than dental tissues (Klevezal 1996). In addition, teeth preserve relatively well and are readily identifiable to species. As a result, dental tissues have been the focus of histological studies in paleontology and archaeology. Teeth are composed of three types of tissue: dentine, enamel and cementum (see Section IV). Dentine, which forms the core of the tooth surrounding the pulp cavity, may be resorbed after initial deposition, whereas enamel and cementum experience little or no turnover (cementum has been shown to resorb locally), thus preserving a continuous record of growth (Figure 39.5).

Skeletochronological analysis was first adopted by wildlife biologists as a tool for managing animal populations (McEwan 1963, Mitchell 1969, Grue and Jensen 1979) before being taken up by archaeologists as a tool for establishing the season of occupation of hunter-gatherer sites in the past (Gordon 1982). Archaeozoological analyses have been applied to a wide variety of taxa since then (e.g., Pike-Tay 1991, Lieberman and Meadow 1992, Burke 1995, Burke and Castanet 1995, Stutz 2002, Pike-Tay and Cosgrove 2002, Lam 2008, Munro et al. 2009,

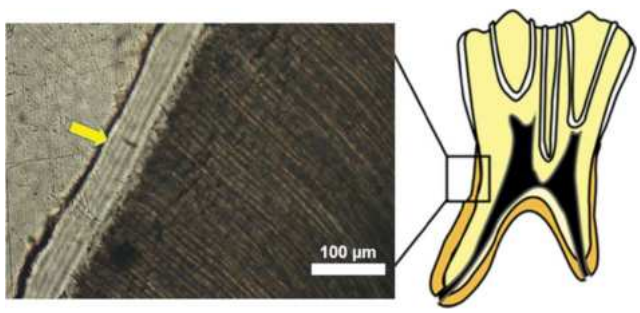


FIGURE 39.5 Skeletochronology: annual growth increments visible in the dental cementum of a cervid. Photo courtesy of W. Rendu (with permission).

VetBooks.ir

Kirillova and Shidlovskiy 2010, Pike-Tay and Ma 2011). Most of these studies use thin section microscopy and transmitted, polarized light to observe incremental structures, although a range of other techniques have been tested including the observation of polished, thick sections at low magnification and under SEM. As the use of skeletochronology in archaeological research matured and larger reference collections were compiled, evidence for intrapopulational growth asynchronies emerged (Lubinski and O'Brien 2001, O'Brien 2001). This resulted in a more realistic appraisal of the uncertainties involved, at least for the study of seasonality (Rendu et al. 2011).

Histological methods have been used to estimate age at death in humans for many decades, since it has applications in forensic anthropology and in bioarchaeology. The methods that have been developed are based on the principle that bone remodeling and the creation of new osteons is cumulative and should correlate with age. Although many variables have been measured, such as osteon size and Haversian canal size, it is usually the osteon population density (OPD), including fragments, and the quantity of remodeled bone that produce the most consistent results (Crowder et al. 2016). However, remodeling rates are influenced by a number of factors such as activity levels (see above), sex-linked hormones, health, dietary status, genetics and geographic origins. In addition, remodeling events are known to reach an asymptote at a certain age where osteon crowding results in new osteons erasing older ones. The age at which this OPD asymptote is reached varies from bone to bone and depends on the size of the bone and the quantity of cortical bone being remodeled. Furthermore, since bones drift during growth (i.e., one side of the cortex deposits bone while the other is resorbing) the actual age of bone tissue varies greatly from bone to bone (and to a lesser degree from individual to individual) once adulthood is reached, which influences the age at which the OPD asymptote is reached. This is important, because the asymptote determines the maximum age that can be inferred for an individual (Robling and Stout 2008). In the rib, for example, the OPD asymptote is reached at around 52 years of age in humans, beyond which the age of older individuals cannot be determined. Despite these limitations, several researchers have produced formulas for calculating age, with the most commonly used and validated being those of Kerley (1965) and Kerley and Ubelaker (1978) and Thompson (1979) for the femur and that of Stout (1986) and Stout and Paine (1992) for the rib. The precision of these formulas is often dependent on the age distribution of the reference sample used to derive them, with greater precision in the best represented age range in the sample (Crowder et al. 2016). Although limbs that have greater loadings appear to provide better estimates, the destructive nature of the method limits its application in forensic and archaeological contexts. Stout's method using the middle third of the sixth rib has the advantage of being easy to sample during autopsies and requires the sectioning of a relatively uninformative bone, particularly if many ribs of one individual are preserved.

Juveniles have higher but also more variable remodeling rates relative to adults (Robling and Stout 2008). In addition, their bones are growing and drifting, so histological methods developed using adult reference samples are not applicable (Robling and Stout 2008). Streeter (2005, 2011) developed a qualitative method to estimate broad age categories from cross sections of the sixth rib. A test of this method suggests that it tracks growth well, but it may not be accurate in populations with growth rates that are different from that of Streeter's reference sample (Agnew 2006).

Teeth are always useful in determining the age of individual humans. In juveniles, the pattern of mineralization and eruption of the teeth provides relatively precise ages. However, adults are much more difficult to age using dental patterns since all of the teeth are fully formed and erupted. Other aging methods have been developed from *in situ* or extracted teeth, but histological methods are more reliable (Soomer et al. 2003). Gustafson (1950) was the first to propose a comprehensive histological method based on subtle changes in the structure of the cement and the root. He used six criteria, five of which could be evaluated on longitudinal sections of the center of the tooth: attrition, secondary dentin formation, root transparency, cementum apposition and root resorption. Although it has been noted that many of these criteria are influenced by chewing habits and oral health (e.g., Chandler 2013), they remain widely used and have been modified, mostly by improving the standardization and measurement of each criterion.

Dental histology is used in paleoanthropology to establish and compare growth rates of different species. Compared with our closest relatives, the great apes, modern humans have very distinctive life histories, with relatively early weaning, a long childhood, late onset of reproduction, short interbirth intervals, a long life span and menopause. Since life cycles do not fossilize, the origin of this human pattern must be inferred from bones and teeth. To do so, it is important to be in a position to estimate the age at death of juveniles accurately to establish whether they followed an ape-like growth pattern or whether human-like characteristics had already evolved. Daily growth patterns in enamel are marked by laminations and birth leaves a very noticeable neonatal line, both of which can be observed either in thin section microscopy under transmitted light or using nondestructive synchrotron imagery. Counting the daily laminations accumulated on the crown starting from the neonatal line makes it possible to determine the stage of dental development at birth and accurately age individuals whose crowns are not fully formed (Beynon and Dean 1987). Studies have shown that *Australopithecus* and *Paranthropus* are characterized by faster growth rates than modern humans, and are similar to apes (Smith et al. 2015). Even *Homo erectus*, with its human-like body size, did not did not grow at the same pace or follow the same growth pattern as humans (Smith et al. 2010). Neandertal growth rates approach human values, but fossil *H. sapiens* from Middle Paleolithic contexts is the only other hominin that experiences a pattern of growth indistinguishable from that of modern humans (Smith et al. 2010). Extrapolation of dental growth rates to life history variables remains difficult to apply to fossil taxa, however, and these data need to be combined growth studies of other important systems such as the brain and skeletal system to achieve a comprehensive understanding of growth in extinct taxa and fossil populations (Guatelli-Steinberg 2009).

VetBooks.ir

Taphonomy

Taphonomy, a term coined by the paleontologist Ivan Efremov (Efremov 1940), is the study of the processes that affect bone prior to, during and after deposition, i.e., the transition from biosphere to lithosphere. Taphonomic analyses identify the agents responsible for creating faunal assemblages (including humans and other animals, or natural events such as flooding), and the postdepositional processes responsible for poor preservation, such as weathering, chemical alteration or water transport, which is a potential source of bias. Taphonomic analysis begins with the macroscopic identification of bone surface modifications, such as butchering marks, toothmarks or other modifications resulting from diagenetic processes (root etching, desquamation, etc.). Different agents and processes can produce alterations difficult to distinguish from one another on a macroscopic level, however, and histological analysis can help avoid the pitfalls of equifinality. For this reason, archaeozoologists have created a large body of experimental data that can be used to establish the identity of the various agents and processes known to affect the composition and conservation of faunal assemblages using macroscopic and microscopic observations (Denys and Patou-Mathis 2014, Fernandez-Jalvo and Andrews 2016, Brugal 2017). The taphonomic analysis of vertebrate remains contributes valuable information about site formation processes, such as the rate of accumulation of the archaeological deposits (how long bones were left exposed on the surface, for example) and the probability of postdepositional disturbances potentially affecting the integrity of the spatial relationships within occupation levels.

Histological Applications

Histology can be a useful tool for taphonomic analysis, helping to identify agents of bone modification and reconstructing the depositional and postdepositional history of vertebrate assemblages (Turner-Walker and Jans 2008). It is important to evaluate whether skeletal tissues have been affected by taphonomic processes before performing DNA, protein fingerprinting or isotopic analysis (Lee-Thorp and Sealy 2008) or using histological data to conduct functional analyses. Although this can be accomplished using macroscopic observation, a more precise assessment of the degree and impact of diagenetic changes can be produced using thin section microscopy and the Oxford Histological Index (OHI), which was developed as a tool for quantifying the degree to which histological structures are preserved. Several international workshops on bone and tooth diagenesis have been held to date, producing a large body of evidence identifying the different stages of bone alteration and diagenetic processes (Lee-Thorp and Sealy 2008) and numerous experimental studies (Smith et al. 2007, Fernández-Jalvo, Andrews et al. 2010).

Different diagenetic pathways interact, producing complex taphonomic patterns that can be hard to disentangle (Kendall et al. 2018). Well-preserved bone may experience some loss of organic material and alteration of mineral content (e.g., increased crystallinity and changes in apatite composition), but its OHI remains high. Subsequent alterations leading to poor preservation and low OHI include accelerated collagen hydrolysis (loss of the organic fraction, associated with abiotic factors), microbial attack (associated with biotic factors) and catastrophic mineral dissolution (Smith et al. 2007). Different types of alteration can be used to study changes in burial conditions over time, identify burials of different age within a cemetery or provide evidence of exhumation and reburial activities (Hollund et al. 2012). Booth and Madgwick (2016), for example, examined human burials from British Iron Age sites using thin section microcopy and determined that a diversity of mortuary rites was in use, an observation that has ideological and social ramifications extending beyond the study of funeral customs and touches on questions of identity and cultural diversity (Booth and Madgwick 2016).

Conclusions

In summary, bone and tooth microstructures are invaluable sources of information about individual organisms and the communities they lived in. Histological analyses are conducted by paleoanthropologists and archaeologists as a complement to macroscopic analyses and in some instances, to acquire information that could not be obtained otherwise. Bone microstructure helps distinguish human from nonhuman bone, for example, which is particularly useful when dealing with fragmentary and/or cremated assemblages, e.g., in funeral contexts or at suspected crime scenes. Histology has been successfully applied as a technique for taxonomic identification in archaeological contexts, but its use is relatively limited because of the uncertainties inherent in the method and the sampling effort that would be required. Faunal assemblages typically contain many thousands of fragments and the cost of production of thin sections for a significant proportion of these would be prohibitive; other techniques (e.g., ZooMS) are faster and less expensive, although they require good organic preservation, which limits their application.

Histological information can also be used to conduct functional analyses that contribute to our understanding of human evolution, both in the deep past and more recently. Applications in archaeozoology include the study of the origins of early farming and husbandry practices. The frequency and severity of pathological conditions, identified using bone and tooth histology, informs us about the health of past vertebrate populations. Skeletochronology has been used in paleoanthropology to study patterns of individual growth across hominin species, which highlight differences in adaptation. In archaeozoology, the age structure and season of death of prey populations are particularly useful for studying past human behavior, including hunting strategies and economic patterns of animal exploitation. Finally, histology is a technique used in taphonomic analysis to quantify the degree of conservation of microstructure and to identify depositional and postdepositional processes affecting vertebrate assemblages.

VetBooks.ir

Although histology is limited currently by the destructive nature of sample preparation techniques, attendant costs and the sheer number of specimens available, technological advances in scientific imagery are likely to lead to more widespread use in the near future, furthering our understanding of extinct species and past human and animal populations.

REFERENCES

Agarwal, S. C. and P. Stuart-Macadam. 2003. An evolutionary and biocultural approach to understanding the effects of reproductive factors on the female skeleton. In *Bone loss and osteoporosis: an anthropological perspective*, S. C. Agarwal and S. D. Stout eds., 105–119. New York: Kluwer Academic/Plenum Publishers.

Agnew, A. M. 2006. *Histomorphological aging of subadults: a test of Streeter's method on a medieval archaeological population*. M.A. thesis, Ohio State University.

Bartosiewicz, L., et al. 1997. *Draught cattle: their osteological identification and history*. Tervuren, Belgium: Musee Royal de l'Afrique Centrale.

Beynon, A. D. and M. C. Dean. 1987. Crown-formation time of a fossil hominid premolar tooth. *Arch. Oral Biol.* 32: 773–780.

Booth, T. J. and R. Madgwick. 2016. New evidence for diverse secondary burial practices in Iron Age Britain: a histological case study. *J. Archaeol. Sci.* 67: 14–24.

Borgel, S. 2016. *Manifestations microscopiques des charges biomécaniques sur le second métacarpe humain*. M. Sc. thesis, Université de Montréal.

Bradfield, J. 2015. Use-trace analysis of bone tools: a brief overview of four methodological approaches. *S. Afr. Archaeol. Bull.* 70: 3–14.

Bradfield, J. 2018. Identifying animal taxa used to manufacture bone tools during the Middle Stone Age at Sibudu, South Africa: results of a CT-rendered histological analysis. *PLoS One* 13: e0208319.

Brugal, J.-P., ed. 2017. Taphonomies. Paris: Editions des archives contemporaines.

Buikstra, J. E. 1977. Biocultural dimensions of archaeological study: a regional perspective. In *Biocultural adaptation in prehistoric America*, vol. 11, R. L. Blakely ed., 67–84. Athens, GA: Univ. of Georgia Press.

Burke, A. M. 1995. *Prey movements and settlement patterns during the Upper Palaeolithic in southwestern France*. Oxford: Tempus Reparatum.

Burke, A. and J. Castanet. 1995. Histological observations of cementum growth in horse teeth and their application to archaeology. *J. Archaeol. Sci.* 22: 479–493.

Burr, D. B. 2002. Targeted and nontargeted remodeling. *Bone* 30: 2–4.

Burr, D. B., et al. 1985. Bone remodeling in response to in vivo fatigue microdamage. *J. Biomech.* 18: 189–200.

Burr, D. B., et al. 1990. Patterns of skeletal histologic change through time: comparison of an archaic Native American population with modern populations. *Anat. Rec.* 226: 307–313.

Cattaneo, C., et al. 1999. Determining the human origin of fragments of burnt bone: a comparative study of histological, immunological and DNA techniques. *Forensic Sci. Int.* 102: 181–191.

Chandler, S. 2013. *A study to determine the accuracy of Gustafson's method of age estimation on adult teeth when applied to a sample of the population of the Western Cape*. M.Sc. thesis, University of the Western Cape.

Cho, H. and S. D. Stout. 2003. Bone remodeling and age-associated bone loss in the past: a histomorphometric analysis of the imperial roman skeletal population of Isola Sacra. In *Bone loss and osteoporosis: an anthropological perspective*, S. C. Agarwal and S. D. Stout eds., 207–228. New York: Kluwer Academic/Plenum Publishers.

Cho, H. and S. D. Stout 2011. Age-associated bone loss and intraskeletal variability in the Imperial Romans. *J. Anthropol. Sci.* 89: 109–125.

Clark, J. G. D. 1972. *Star Carr: a case study in bioarchaeology*. Reading, MA: Addison-Wesley.

Corando, S., et al. 1989. Orientation of collagen in human tibial and fibular shaft and possible correlation with mechanical properties. *Bone* 10: 139–142.

Crowder, C. M., et al. 2016. Histological age estimation. In *Handbook of forensic anthropology and archaeology*, S. Blau and D. H. Ubelaker eds., 293–307. New York: Routledge.

Cubo, J., et al. 2005. Phylogenetic signal in bone microstructure of sauropsids. *Syst. Biol.* 54: 562–574.

Cuijpers, A. G. F. M. 2006. Histological identification of bone fragments in archaeology: telling humans apart from horses and cattle. *Int. J. Osteoarchaeol.* 16: 465–480.

Cuijpers, S. 2009. Distinguishing between the bone fragments of medium-sized mammals and children. A histological identification method for archaeology. *Anthropol. Anz.* 67: 181–203.

Curate, F. 2014. Osteoporosis and paleopathology: a review. *J. Anthropol. Sci.* 92: 119–146.

D'Ortenzio, L., et al. 2016. The rachitic tooth: a histological examination. *J. Archaeol. Sci.* 74: 152–163.

Denys, C. and M. Patou-Mathis. 2014. *Manuel de taphonomie*. Arles, France: Errance.

Drapeau, M. S. M., et al. 2012. Remodeling in bones of the human hand and its relationship to loading. *Am. J. Phys. Anthropol.*, Supp. 54: 134 (Abstract).

Drew, I. M., et al. 1971. Prehistoric domestication of animals: effects on bone structure. *Science* 171(3968): 280–282.

Efremov, I. A. 1940. Taphonomy: a new branch of paleontology. *Pan-Am. Geol.* 74: 81–93.

Ericksen, M. F. 1980. Patterns of microscopic bone remodeling in three aboriginal American populations. In *Early Native Americans. Prehistoric demography, economy, and technology*, D. L. Browman ed., 239–270. The Hague: Mouton Publishers.

Fernandez-Jalvo, Y. and P. Andrews 2016. *Atlas of taphonomic identifications: 1001+ images of fossil and recent mammal bone modification*. New York: Springer.

Fernández-Jalvo, Y., et al. 2010. Early bone diagenesis in temperate environments: Part I: Surface features and histology. *Palaeogeogr. Palaeoclimatol. Palaeoecol.* 288: 62–81.

Goldman, H. M., et al. 2005. Relationships among microstructural properties of bone at the human midshaft femur. *J. Anat.* 206: 127–139.

Gordon, B. H. C. 1982. Tooth sectioning as an archaeological tool. National Museum of Man: *Archaeological Survey of Canada*. Canadian Studies Report, 14e:1–4.

Greenlee, D. M. and R. C. Dunnell. 2010. Identification of fragmentary bone from the Pacific. *J. Archaeol. Sci.* 37: 957–970.

Grue, H. and B. Jensen 1979. Review of the formation of incremental lines in tooth cementum of terrestrial mammals. *Danish Rev. Game Biol.* 11: 3–48.

Guatelli-Steinberg, D. 2009. Recent studies of dental development in Neandertals: implications for Neandertal life histories. *Evol. Anthropol.: Issues, News, Rev.* 18: 9-20.

Gustafson, G. 1950. Age determinations on teeth. *J. Am. Dent. Assoc.* 41: 45–54.

Halstead, P., et al. 2002. Sorting the sheep from the goats: morphological distinctions between the mandibles and mandibular teeth of adult *Ovis* and *Capra*. *J. Archaeol. Sci.* 29: 545–553.

Hawkey, D. E. and C. F. Merbs. 1995. Activity-induced musculoskeletal stress markers (MSM) and subsistence strategy changes among ancient Hudson Bay Eskimos. *Int. J. Osteoarchaeol.* 5: 324–338.

Henton, E. 2012. The combined use of oxygen isotopes and microwear in sheep teeth to elucidate seasonal management of domestic herds: the case study of Çatalhöyük, central Anatolia. *J. Archaeol. Sci.* 39: 3264–3276.

Hillier, M. L. and L. S. Bell 2007. Differentiating human bone from animal bone: a review of histological methods. *J. Forensic Sci.* 52: 249–263.

Hollund, H. I., et al. 2012. What happened here? Bone histology as a tool in decoding the postmortem histories of archaeological bone from Castricum, The Netherlands. *Int. J. Osteoarchaeol.* 22: 537–548.

Kendall, C., et al. 2018. Diagenesis of archaeological bone and tooth. *Palaeogeogr. Palaeoclimatol. Palaeoecol.* 491: 21–37.

Kerley, E. R. 1965. The microscopic determination of age in human bone. *Am. J. Phys. Anthropol.* 23: 149–164.

Kerley, E. R. and D. H. Ubelaker. 1978. Revision in the microscopic method of estimating age at death in human cortical bone. *Am. J. Phys. Anthropol.* 49: 545–546.

Kirillova, I. V. and F. K. Shidlovskiy. 2010. Estimation of individual age and season of death in woolly rhinoceros, *Coelodonta antiquitatis* (Blumenbach, 1799), from Sakha-Yakutia, Russia. *Q. Sci Rev.* 29: 3106–3114.

Klevezal, G. and S. Kleinenberg. 1967. *Age Determination of Mammals by Layered Structure in Teeth and Bone.* Foreign Languages Division, Department of the Secretary of State of Canada; Fisheries Research Board of Canada.

Klevezal, G. A. 1996. *Recording structures of mammals: determination of age and reconstruction of life history.* Rotterdam/Brookfield: A.A. Balkema.

Lam, Y. M. 2008. Variability in cementum deposition in springbok from the South African Cape. *J. Archaeol. Sci.* 35: 1062–1073.

Lee-Thorp, J. and J. Sealy. 2008. Beyond documenting diagenesis: the fifth international bone diagenesis workshop. *Palaeogeogr. Palaeoclimatol. Palaeoecol.* 266: 129–133.

Legendre, L., et al. 2013. Phylogenetic signal in bone histology of amniotes revisited. *Zool. Scr.* 42: 44–53.

Levin, N. E., et al. 2006. A stable isotope aridity index for terrestrial environments. *Proc. Nat. Acad. Sci. USA* 103: 11201–11205.

Lieberman, D. E. and A. W. Crompton. 1998. Responses of bone to stress: constraints on symmorphosis. In *Optimality in biological design: symmorphosis–fact or fancy*, E. Weibel, C. R. Taylor and L. Bolis eds., 78–86. Cambridge, UK: Cambridge University Press.

Lieberman, D. E. and R. H. Meadow. 1992. The biology of cementum increments (with an archaeological application). *Mamm. Rev.* 22: 1–21.

Lubinski, P. M. and C. J. O'Brien. 2001. Observations on seasonality and mortality from a recent catastrophic death assemblage. *J. Archaeol. Sci.* 28: 833–842.

Maggiano, C. M. 2011. Making the mold. A microstructural perspective on bone modeling during growth and mechanical adaptation. In *Bone histology. an anthropological perspective*. C. Crowder and S. Stout eds., 45–90. Boca Raton: CRC Press.

Maggiano, C. M., et al. 2016. Methods and theory in bone modeling drift: comparing spatial analyses of primary bone distributions in the human humerus. *J. Anat.* 228: 190–202.

Maggiano, I. S., et al. 2015. Drifting diaphyses: asymmetry in diametric growth and adaptation along the humeral and femoral length. *Anat. Rec.* 298: 1689–1699.

Martin, D. L. and G. J. Armelagos. 1985. Skeletal remodeling and mineralization as indicators of health: an example from prehistoric Sudanese Nubia. *J. Human Evol.* 14: 527–537.

Martiniaková, M., et al. 2007. Histological study of compact bone tissue in some mammals: a method for species determination. *Int. J. Osteoarchaeol.* 17: 82–90.

McEwan, E. H. 1963. Seasonal annuli in the cementum of the teeth of barren-ground caribou. *Can. J. Zool.* 41: 111–113.

Mitchell, B. 1969. Growth layers in dental cement for determining the age of red deer (*Cervus elapus* L.). *J. Anim. Ecol.* 36: 279–293.

Mori, S. and D. B. Burr. 1993. Increased intracortical remodeling following fatigue damage. *Bone* 14: 103–109.

Mulhern, D. M. and D. H. Ubelaker. 2011. Differentiating human from nonhuman bone microstructure. In *Bone histology. an anthropological perspective*, 109–134. C. Crowder and S. Stout eds., Boca Raton: CRC Press.

Munro, N. D., et al. 2009. Aging mountain gazelle (*Gazella gazella*): refining methods of tooth eruption and wear and bone fusion. *J. Archaeol. Sci.* 36: 752–763.

Naji, S., et al. 2015. La cémentochronologie. In *Message d'os. Archéométrie du squelette animal et humain*, eds M. Balasse et al., 217–240 Paris (France): Edition des Archives Contemporaines.

O'Brien, C. J. 2001. A re-evaluation of dental cementum increment formation in East African mammals: Implications for wildlife biology and archaeology. In *Innovations in assessing season of capture, age and sex of archaeofaunas*, A. P. Tay ed. Grenoble: Pensée Sauvage/Archaeozoologia.

O'Connor, J. A., et al. 1982. The influence of strain rate on adaptative bone remodelling. *J. Biomech.* 15: 767–781.

Paral, V., et al. 2007. Microscopic examination of ground sections – a simple method for distinguishing between bone and antler? *Int. J. Osteoarchaeol.* 17: 627–634.

Payne, S. 1973. Kill-off pattern in sheep and goats: the mandibles from Asvan Kale. *Anatolian St.* 23: 281–303.

Pfeiffer, S. 2006. Cortical bone histology in juveniles. *Doc. Archaeobiol.* 4: 15–28.

Pfeiffer, S., et al. 2006. Secondary osteon and Haversian canal dimensions as behavioral indicators. *Am. J. Phys. Anthropol.* 131: 460-468.

Pike-Tay, A. 1991. *Red deer hunting in the Upper Paleolithic of south-west France: a study in seasonality*. Oxford, UK: British Archaeological Reports Ltd.

Pike-Tay, A. and R. Cosgrove 2002. From reindeer to wallaby: Recovering patterns of seasonality, mobility, and prey selection in the Palaeolithic Old World. *J. Archaeol. Method Theory* 9: 101–146.

Pike-Tay, A. and X. Ma 2011. A pilot study in odontochronology for the pig domestication question in North-Central China. *Int. J. Osteoarchaeol.* 23: 590–599.

Raguin, E. 2018. *Histomorphometric assessment of double-zonal osteons in human cortical bone*. Ph.D. dissertation, Université de Montréal.

Raguin, E. and M. S. M. Drapeau. 2020. Relation between cross-sectional bone geometry and double zonal osteon frequency and morphology. *Am. J. Phys. Anthropol.* 171: 598–612.

Rendu, W., D. Armand, É. Pubert and M. Soressi. 2011. Approche taphonomique en cémentochronologie: réexamen du niveau 4 du Pech-de-l'Azé I (Carsac, Dordogne, France). *PALEO Revue Archéol. Préhist.* 21: 223–236.

Richman, E. A., et al. 1979. Differences in intracortical bone remodeling in three Aboriginal American populations: possible dietary factors. *Calcif. Tissue Int.* 28: 209–214.

Rivals, F. and B. Deniaux. 2005. Investigation of human hunting seasonality through dental microwear analysis of two Caprinae in late Pleistocene localities in Southern France. *J. Archaeol. Sci.* 32: 1603-1612.

Robling, A. G. 1998. *Histomorphometric assessment of mechanical loading history from human skeletal remains: the relation between micromorphology and macromorphology at the femoral midshaft*. Ph.D. dissertation, University of Missouri-Columbia.

Robling, A. G. and S. D. Stout 2003. *Histomorphology, geometry, and mechanical loading in past populations. In Bone loss and osteoporosis*. S. C. Agarwal and S. D. Stout eds., 189–205. New York: Kluwer Academic/Plenum Publishers.

Robling, A. G. and S. D. Stout. 2008. Histomorphometry of human cortical bone: applications to age estimation. In *Biological anthropology of the human skeleton.* 2nd Ed. M. A. Katzenberg and S. R. Saunders eds., 149–174. Hoboken, NJ: John Wiley & Sons, Inc.

Ruff, C. B., et al. 1984. Structural changes in the femur with the transition to agriculture on the Georgia coast. *Am. J. Phys Anthropol.* 64: 125–136.

Sawada, J., et al. 2014. Histomorphological species identification of tiny bone fragments from a Paleolithic site in the Northern Japanese Archipelago. *J. Archaeol. Sci.* 46: 270–280.

Schultz, M. 2001. Paleohistopathology of bone: a new approach to the study of ancient diseases. *Yearb. Phys. Anthropol.* 44: 106–147.

Schultz, M. 2011. Light microscopic analysis of macerated pathologically changed bones. In *Bone histology. an anthropological perspective*. C. Crowder and S. Stout eds., 253–296. Boca Raton: CRC Press.

Skedros, J. G. 2011. Interpreting load history in limb-bone diaphyses. Important considerations and their biomechanical foundations. In *Bone histology. an anthropological perspective*. C. Crowder and S. Stout eds. 153–220. Boca Raton: CRC Press.

Skedros, J. G., et al. 2006. The influence of collagen fiber orientation and other histocompositional characteristics on the mechanical properties of equine cortical bone. *J. Exp. Biol.* 209: 3025–3042.

Skedros, J. G., et al. 2011. A weighted osteon morphotypes scores outperforms regional osteon percent prevalence calculations for interpreting cortical bone adaptation. *Am. J. Phys. Anthropol.* 144: 41–50.

Smith, C. I., et al. 2007. Bone diagenesis in the European Holocene I: Patterns and mechanisms. *J. Archaeol. Sci.* 34: 1485–1493.

Smith, T. M., et al. 2010. Dental evidence for ontogenetic differences between modern humans and Neanderthals. *Proc. Natl. Acad. Sci.* 107: 20923–20928.

Smith, T. M., et al. 2015. Dental ontogeny in Pliocene and early Pleistocene hominins. *PLoS One* 10: e0118118.

Soomer, H., et al. 2003. Reliability and validity of eight dental age estimation methods for adults. *J. Forensic Sci.* 48: 1–4.

Steele, T. E. 2003. Using mortality profiles to infer behavior in the fossil record. *J. Mamm.* 84: 418–430.

Stock, J. T. and S. K. Pfeiffer. 2004. Long bone robusticity and subsistence behaviour among Later Stone Age foragers of the forest and fynbos biomes of South Africa. *J. Archaeol. Sci.* 31: 999–1013.

Stout, S. D. 1986. The use of bone histomorphometry in skeletal identification: the case of Francisco Pizarro. *J. Forensic Sci.* 31: 296–300.

Stout, S. D. 2003. Small bones of contention. Hard Evidence. In *Case studies in forensic anthropology.* D. W. Steadman ed., 234–244. Upper Saddle River, NJ: Prentice Hall.

Stout, S. D. and R. R. Paine. 1992. Brief communication: histological age estimation using rib and clavicle. *Am. J. Phys. Anthropol.* 87: 111–115.

Stout, S. D. and D. J. Simmons. 1979. Use of histology in ancient bone research. *Yearb. Phys. Anthropol.* 22: 228–249.

Streeter, M. 2011. Histological age-at-death estimation. In *Bone histology. an anthropological perspective*. C. Crowder and S. Stout ed., 135–152. Boca Raton: CRC Press.

Streeter, M. A. 2005. *Histomorphometric characteristics of the subadult rib cortex: normal patterns of dynamic bone modeling and remodeling during growth and development*. Ph.D. dissertation, University of Missouri-Columbia.

Stutz, A. J. 2002. *Pursuing past seasons: a re-evaluation of cementum increment analysis in paleolithic archaeology.* Ph.D. dissertation, University of Michigan.

Thompson, D. D. 1979. The core technique in the determination of age at death in skeletons. *J. Forensic Sci.* 24: 902–915.

Turner-Walker, G. and M. Jans. 2008. Reconstructing taphonomic histories using histological analysis. *Palaeogeogr. Palaeoclimatol. Palaeoecol.* 266: 227–235.

Villotte, S., et al. 2010. Subsistence activities and the sexual division of labor in the European Upper Paleolithic and Mesolithic: evidence from upper limb enthesopathies. *J. Human Evol.* 59: 35–43.

VetBooks.ir

Walter, T. L., et al. 2004. Histological examination of bone-tempered pottery from mission Espíritu Santo (41VT11), Victoria County. *Texas J. Archaeol. Sci.* 31: 393–398.

Zedda, M., et al. 2017. Differences in femoral morphology between sheep (*Ovis aries*) and goat (*Capra hircus*): macroscopic and microscopic observations. *Zoomorphology* 136: 145–158.

Zedda, M., et al. 2019. Distinguishing domestic pig femora and tibiae from wild boar through microscopic analyses. *Zoomorphology* 138: 159–170.

Zeder, M. and B. Hesse 2000. The initial domestication of goats (*Capra hircus*) in the Zagros Mountains 10,000 years ago. *Science* 287: 2254–2257.

Zeder, M. and H. Lapham. 2010. Assessing the reliability of criteria used to identify postcranial bones in sheep. *J. Archaeol. Sci.* 37: 2887–2905.

VetBooks.ir

40

A Methodological Renaissance to Advance Perennial Issues in Vertebrate Paleohistology

Alexandra Houssaye, Donald Davesne and Aurore Canoville

CONTENTS

Introduction 793
Controversial and Puzzling Tissue Types 793
Going Further in Paleoecology and Paleophysiology 794
What Molecules Can Reveal 795
Bone and Genome Size 795
Conclusion 796
References 796

Introduction

For over a century, microstructural studies of extant and fossilized skeletal tissues at various levels of integration have greatly improved our understanding of the growth, physiology, function, biomechanics, and evolution of hard tissues in most vertebrate taxa. The concurrent work of research teams all over the world has produced solid and consistent results that form the basis of our current knowledge of bone histology and paleohistology. It includes a good understanding of the diversity of bone tissues and of their growth processes in extant taxa, from which inferences can be drawn about extinct organisms. Until the new millennium, this knowledge had been acquired using fairly conventional and qualitative methods of analysis (photonic or electron microscopy), but methodological approaches in this field of research have been profoundly renewed and diversified over the last 20 years. Recent technical advances have revealed information previously thought inaccessible. Large-scale and quantitative comparative analyses carried out in a phylogenetic context have become more common and complemented qualitative descriptions. Recent technical progress, including the use of X-ray micro/nanotomography, synchrotron light sources, modeling (e.g., finite element analyses, phylogenetic comparative methods), paleogenomics, and molecular paleontology, has opened new avenues of investigation.

A wide range of research questions and approaches has become accessible as a result of these methodological and technical developments. Some old questions can now be further investigated by gathering complementary data to provide a better understanding of broad physiological and functional concepts, such as the link between vascularization and growth rate, tissue types and metabolism, the onset of bone remodeling, the mechanical properties of secondary osteons and so forth. The following section presents some of the current fields of investigation representing the foreseeable future of bone (paleo)histology.

Controversial and Puzzling Tissue Types

Despite solid knowledge about the structure and growth of skeletal tissues, various questions remain. For example, several studies, following Marotti et al. (1999) and Ferretti et al. (2002), established a clear distinction between two major types of primary bone accretion: static and dynamic osteogeneses. The former results in woven-fibered bone and the latter in either parallel-fibered or lamellar osseous tissues (see also Chapters 2 and 8 for details). According to this original model, further considered in a comparative perspective by Stein and Prondvai (2014) and Prondvai et al. (2014), the two tissue types are mutually exclusive because they originate from sharply distinct histogenetic and cytologic contexts, and the occurrence of intermediate organizational patterns is implicitly discarded. However, such ambiguous tissue types are occasionally observed and have been noted by several authors (e.g., Ricqlès 1975, Houssaye et al. 2013, Olivier et al. 2017). Most frequently, these intermediate tissue types have a matrix with a collagenous organization (indicated by birefringence) reminiscent of parallel-fibered bone, but with the large, unevenly

VetBooks.ir

sized and randomly distributed osteocyte lacunae generally encountered in woven-fibered bone. The existence of such tissues questions the fundamental binary structure of the model of static versus dynamic osteogenesis (Marotti et al. 1999). They also ask us to rethink the definition of fibrolamellar bone complexes (FLB), and the ongoing use of the imprecise term "incipient fibro-lamellar bone" (Klein 2010) naturally raises the need to better define these types of tissues, their relationship to growth rate and, indirectly, metabolism. Because these intermediate tissues (i.e., incipient fibrolamellar bone tissues) have so far been described mostly in marine squamates and sauropterygians, early archosaurs, and synapsids, they are at the heart of questions relevant to the origin of endothermy (Legendre et al. 2016, Wintrich et al. 2017).

Even well-defined tissues remain the subject of revolutionary discoveries. This is the case for endochondral bone, whose origin in osteichthyans after their divergence from chondrichthyans (Donoghue and Sansom 2002, Hirasawa and Kuratani 2015) has been debated for about 150 years. The question was essentially whether all osteoblasts involved in endochondral osteogenesis originate from osteoblast populations located outside cartilaginous anlages (in perichondral position) and invade the core of the anlages along the walls of the nutrient canal, or whether some of them also originate from hypertrophic chondrocytes through transdifferentiation (i.e., a change in cell identity) at the initial ossification center (Quilhac et al. 2014, Tsang et al. 2015). Recent lineage-tracing experiments have revealed that a subset of chondrocytes transdifferentiate into osteoblasts at the chondroosseous junction (Yang et al. 2014, Zhou et al. 2014). They thus raise the exciting question of the role of transdifferentiation in the emergence of endochondral ossification (Cervantes-Diaz et al. 2017).

Another tissue is currently the focus of active discussion: medullary bone. The microstructure and chemistry of this sex-specific tissue, produced by female birds during the egg-laying cycle and used as a labile reservoir of calcium for eggshells (Dacke et al. 1993), has been extensively studied but only in a few species related to the poultry industry. Conversely, the phylogenetic distribution and composition of medullary bone in other Neornithes are still incompletely known (Canoville et al. 2020). Although hypothesized to have arisen within Avemetatarsalia (bird-line archosaurs), and possibly outside Avialae (e.g., Chinsamy et al. 2009, Canoville et al. 2020), the numerous reports of medullary bone-like tissues in the fossil record are still dubious, because the current available diagnosis for medullary bone does not capture the extent of variability that exists in extant birds (Canoville et al. 2020; for further details, see Chapter 27 on Avemetatarsalia). Moreover, some avian pathological bone tissues share a set of criteria previously outlined as unique to medullary bone (Prondvai 2017, O'Connor et al. 2018, Canoville et al. 2020). Ongoing research aiming to characterize medullary bone in Neornithes should improve its identification in extinct avemetatarsalians. The unequivocal recognition of such a tissue in nonavian dinosaurs and related taxa would provide an objective means to identify sexually mature and gravid females and give access to a wealth of information on various aspects of their reproductive biology.

Chondroid bone is another intermediate tissue undergoing renewed interest (see Chapter 8). Distinct from cartilage and bone, chondroid bone contains chondrocyte-like cells partly assuming an osteoblastic activity and producing a woven bone-type extracellular matrix (Beresford 1981, Hall 2015). This tissue has been reported in skull elements of teleosts and in the cranial and postcranial bones of the embryo in other vertebrates (Hall 2015). Chondroid bone has also been described as a major constituent in diverse skeletal pathologies and is seen as an adaptation for high rates of osteogenesis (Hall 2015, Prondvai et al. 2020). Although known for over a century, chondroid bone seems to have been completely overlooked in extant vertebrates and is often misidentified (Beresford 1981, Prondvai et al. 2020). This tissue has also been largely underreported in extinct taxa (Bailleul et al. 2016). Hence, much remains to be done to better understand the evolution, physiology, function, prevalence, and microstructural diversity of this tissue. A recent study by Prondvai et al. (2020) challenged previous concepts on the periosteal development of limb bones in birds. Where the current literature would have described the formation of a rapidly deposited framework of woven bone (Shapiro and Wu 2019), Prondvai et al. (2020) observed the deposition of chondroid bone in the early post-hatching stages of duck limb bones. Future studies need to investigate the evolutionary significance of chondroid bone in the rapid skeletogenesis of birds and potentially other vertebrates.

A final tissue type that has remained enigmatic until relatively recently (Shahar and Dean 2013) is acellular (or, more accurately, anosteocytic) bone (considered in Chapter 8). This bone devoid of osteocytes is almost exclusively found in teleosts among extant vertebrates. A recent study clarified its precise phylogenetic distribution, confirming that osteocytes have been lost in the teleost subclade Euteleostei (Davesne et al. 2019). Despite the perceived key role of osteocytes in bone biology, results that have accumulated in the last decade strongly suggest that teleost acellular bone is structurally and mechanically equivalent to teleost cellular bone (Shahar and Dean 2013, Ofer et al. 2020), and that it is notably capable of extensive remodeling, including the occasional formation of secondary osteons (Witten and Huysseune 2009, Atkins et al. 2014). This polyvalence of acellular bone opens new questions and perspectives on the role and evolutionary origin of osteocytes in vertebrate bone, especially because the appearance of acellular bone predates that of cellular bone in the earliest skeletonizing vertebrates (Ørvig 1965, Keating et al. 2018). Within euteleosts, osteocytes seem to have reevolved independently in two so-called endothermic lineages (Davesne et al. 2018), suggesting an evolutionary pressure related to mineral metabolism. Further research on the developmental origin, growth, metabolism, and paleontological record of acellular bone should clarify these questions that are currently the focus of passionate discussions.

Going Further in Paleoecology and Paleophysiology

As presented in this book, the functional adaptation of bones to various habitats and lifestyles has been widely explored, even though areas of uncertainty remain. For instance, adaptation to fossoriality has been poorly studied and is currently a growing subject of research (Amson et al. 2017, Legendre

VetBooks.ir

and Botha-Brink 2018, Montoya-Sanhueza and Chinsamy 2018). In the context of paleoecology, technological developments also allow great advances in biomechanics. There are several levels at which bone can be studied from a biomechanical point of view. Combinations of X-ray diffraction and computed tomography or Raman spectroscopy have proven to be powerful and useful tools for studying the arrangement of bone matrix and the location of muscle attachments in paleontological samples (Sanchez et al. 2013, Dumont et al. 2016, Mürer et al. 2018). Microtomography, coupled or not with image processing and finite-element analyses, allows visualization and investigation of biomechanical adaptations of bone in three dimensions at different scales (from a small region of interest to the whole bone; MacNeil and Boyd 2008, Barak et al. 2013, Sanchez et al. 2013, Atkins et al. 2014, Bishop et al. 2018, Mielke et al. 2018). Much remains to be done to better understand how bone adapts to the functional constraints imposed on the skeleton and to improve paleoecological inferences; these methodological developments greatly expand the possibilities for research in this field.

Likewise, paleophysiology, and particularly the estimation of metabolic rates, has seen significant developments in the last decade through the boom of phylogenetic comparative methods. In addition to the classically studied nonavian dinosaurs (relevant to the origin of avian endothermy), the coupling of bone histology and phylogenetic comparative methods has enabled significant breakthroughs in reconstructing the paleophysiology of other groups such as early synapsids (Olivier et al. 2017, Faure-Brac and Cubo 2020), sauropterygians (Fleischle et al. 2018), early archosauromorphs (Legendre et al. 2016), and pseudosuchians (Cubo et al. 2020). These results corroborate that endothermy, or at least dedicated thermogenic strategies, evolved multiple times in vertebrates (Legendre and Davesne 2020). However, the fossil relatives of many taxa known today to exhibit a range of convergent thermogenic abilities have not yet been explored through the lens of paleohistology. For example, teleosts have been poorly studied in terms of comparative bone histology and paleohistology (Meunier 2011, Dean and Shahar 2012) despite their enormous diversity (about half of extant vertebrate species are teleosts). Several extant teleost clades have independently evolved so-called endothermy, and their fossil relatives would be ideal candidates for paleophysiological studies (Davesne et al. 2018).

What Molecules Can Reveal

Although not really touched upon in the present book, the field of molecular paleontology has been steadily developing for over two decades (e.g., Schweitzer 1995) and is currently booming thanks to a wealth of chemical protocols and new methodological advancements that can now be applied to fossil hard tissues (Schweitzer et al. 2008, Zylberberg and Laurin 2011, Pan et al. 2019). The new types of data collected using these diverse techniques are revolutionizing the field of paleontology and give us access to a world of information deemed inaccessible thus far. Numerous independent studies have now confirmed that endogenous organic structures and compounds can be preserved over millions of years in fossilized bone, teeth, and even eggshell. To cite a few, extracellular bone matrix and structures reminiscent of blood vessels, osteocytes, and chondrocytes have been retrieved from the demineralized skeletal fragments of various extinct tetrapods (e.g., Schweitzer et al. 2005, Cadena and Schweitzer 2012, Wiemann et al. 2018, Bailleul et al. 2020). Using different analytical methods, the preservation of original bone proteins (such as collagen) or of their breakdown products has also been repeatedly demonstrated in fossil specimens dating as far back as the Devonian (Schweitzer 1997, Zylberberg et al. 2010, Lindgren et al. 2011, Schroeter et al. 2017). Finally, studies have shown the presence of chemical markers of DNA in various bone and cartilage cells of nonavian dinosaurs, although this molecule was considered too unstable to be preserved over a few million years (Schweitzer et al. 2013, Bailleul et al. 2020). All these discoveries provide invaluable hints to the favored environmental conditions to preserve biomolecules, as well as on the chemical processes stabilizing these organic compounds during fossilization (Schweitzer et al. 2014, Wiemann et al. 2018, Boatman et al. 2019). In the future, the study of these fossilized biomolecules might allow us to improve our understanding of major evolutionary trends, such as the evolution of the reproductive biology and physiology of dinosaurs and other vertebrates (e.g., Schweitzer et al. 2016, Wiemann et al. 2020). It might also help us resolve some contentious parts of the tetrapod phylogeny (e.g., using ancient DNA; Mitchell et al. 2014; Delsuc et al. 2016).

Bone and Genome Size

Another approach, falling into the broad field of "paleogenomics" (Organ 2012), uses bone, and most specifically bone cell volumes, as proxies for the evolution of the vertebrate genome size. The correlation of genome size with the size of a variety of cells (including erythrocytes, neurons and land plant stomatal cells; Gregory 2001, Donoghue 2020) has been known for a long time. Applying this correlation to osteocyte lacunae to estimate genome sizes in extinct vertebrates was proposed as early as the 1970s (Thomson 1972). However, such an approach could not yield its full potential without comparative phylogenetic methods. The latter were first used in a study proposing that the relatively small size of extant bird genomes was a common feature shared by all theropod dinosaurs, having evolved considerably earlier than previously thought (Organ et al. 2007). Later studies proposed, for example, that pterosaurs independently evolved smaller genomes like those of birds and bats (Organ and Shedlock 2009), that amniotes ancestrally had a moderate genome size compared to lissamphibians (Organ et al. 2011), that the large genomes of urodeles appeared early in their evolutionary history (Laurin et al. 2016), and that no major change in genome size occurred at the tetrapod water-to-land transition (Organ et al. 2016). One important limitation of these paleogenomic studies is that using only thin sections, and thus two-dimensional (2D) measurements, may lead to misestimating the actual osteocyte lacuna volumes (D'Emic and Benson 2013). A way to circumvent this issue is to use three-dimensional (3D) data, and synchrotron microtomography now provides a sufficient resolution to measure accurately the volume of the lacunae, and also to collect significantly

larger data sets (Sanchez et al. 2013, Dong et al. 2014, Davesne et al. 2020). Synchrotron imaging of osteocyte lacunae in 3D, coupled with phylogenetic comparative methods, can therefore be seen as the next step in accurately reconstructing genome size through key evolutionary events that have the potential to be informed by the fossil record, such as vertebrate-specific and teleost-specific genome duplications (Donoghue 2020). Osteocytes are the main cell type to leave traces in fossilized bone; however, alternative approaches may also show some potential to estimate the size of fossil genomes. For example, it has recently been shown that the diameter of blood vessels correlates with erythrocyte size in Triassic synapsids and archosauromorphs (Huttenlocker and Farmer 2017), and thus might potentially be an indirect clue to genome size.

Conclusion

Vertebrate comparative bone histology and paleohistology are dynamic fields that are regaining strong interest with the current development of new approaches and techniques, as illustrated by the examples mentioned above. These recent developments highlight new possibilities that traditional histology could not offer. They have also tried to obtain more data while being as minimally invasive as possible, in particular through microtomography. As for inevitably destructive investigations, the creation of histological collections and repositories now makes it possible to avoid taking additional destructive samples when data are already available. In addition, the creation of a biannual International Symposium on Paleohistology has fostered stimulating exchanges among the different researchers in the fields (Cubo and Laurin 2011).

The future of this promising discipline should therefore be bright, exciting and very enlightening, pushing our knowledge of bone structure and function and of the biology of extinct vertebrates to previously inaccessible depths.

REFERENCES

Amson, E., et al.. 2017. Trabecular architecture in the forelimb epiphyses of extant xenarthrans (Mammalia). *Front. Zool.* 14: 52.

Atkins, A., M. et al. 2014. Remodeling in bone without osteocytes: billfish challenge bone structure–function paradigms. *Proc. Natl. Acad. Sci.* 111: 16047–16052.

Bailleul, A. M., et al. 2016. Chondroid bone in dinosaur embryos and nestlings (Ornithischia: Hadrosauridae): insights into the growth of the skull and the evolution of skeletal tissues. *C. R. Palevol* 15: 49–64.

Bailleul, A. M., et al. 2020. Evidence of proteins, chromosomes and chemical markers of DNA in exceptionally preserved dinosaur cartilage. *Natl. Sci. Rev.* 7: 815–822.

Barak, M. M., et al. 2013. Of mice, rats and men: trabecular bone architecture in mammals scales to body mass with negative allometry. *J. Struct. Biol.* 183: 123–131.

Beresford, W. A. 1981. Chondroid bone, secondary cartilage, and metaplasia. Baltimore, MD: Urban & Schwarzenberg, p. 405.

Bishop, P. J., et al. 2018. Cancellous bone and theropod dinosaur locomotion. Part I—an examination of cancellous bone architecture in the hindlimb bones of theropods. *PeerJ* 6: e5778.

Boatman, E. M., et al. 2019. Mechanisms of soft tissue and protein preservation in *Tyrannosaurus rex*. *Sci. Rep.* 9: 1–12.

Cadena, E. A., and M. H. Schweitzer. 2012. Variation in osteocytes morphology vs bone type in turtle shell and their exceptional preservation from the Jurassic to the present. *Bone* 51: 614–620.

Canoville, A., et al. 2020. Identifying medullary bone in extinct avemetatarsalians: challenges, implications and perspectives. *Philos. Trans. R. Soc. B* 375: 20190133.

Cervantes-Diaz, F., et al. 2017. Evolutionary origin of endochondral ossification: the transdifferentiation hypothesis. *Dev. Genes Evol.* 227: 121–127.

Chinsamy, A., et al. 2009. Palaeobiological implications of the bone histology of *Pterodaustro guinazui*. *Anat. Rec.* 292: 1462–1477.

Cubo, J., and M. Laurin. 2011. Perspectives on vertebrate evolution: topics and problems. *C. R. Palevol* 10: 285–292.

Cubo, J., et al. 2020. Were Notosuchia (Pseudosuchia: Crocodylomorpha) warm-blooded? A palaeohistological analysis suggests ectothermy. *Biol. J. Linn. Soc*131: 154–162.

Dacke, C. G., et al. 1993. Medullary bone and avian calcium regulation. *J. Exp. Biol.* 184: 63–88.

Davesne, D., et al. 2018. Histology of the endothermic opah (*Lampris* sp.) suggests a new structure–function relationship in teleost fish bone. *Biol. Lett.* 14: 20180270.

Davesne, D., et al. 2019. The phylogenetic origin and evolution of acellular bone in teleost fishes: insights into osteocyte function in bone metabolism. *Biol. Rev.* 94: 1338–1363.

Davesne, D., et al. 2020. Three-dimensional characterisation of osteocyte volumes at multiple scales, and its relationship with bone biology and genome evolution in ray-finned fishes. *J. Evol. Biol.*33: 808–830.

Dean, M. N., and R. Shahar. 2012. The structure-mechanics relationship and the response to load of the acellular bone of neoteleost fish: a review. *J. Appl. Ichthyol.* 28: 320–329.

Delsuc, F., et al. 2016. The phylogenetic affinities of the extinct glyptodonts. *Curr. Biol.* 26: R155–R156.

D'Emic, M. D., and R. B. J. Benson. 2013. Measurement, variation, and scaling of osteocyte lacunae: a case study in birds. *Bone* 57: 300–310.

Dong, P., et al. 2014. 3D osteocyte lacunar morphometric properties and distributions in human femoral cortical bone using synchrotron radiation micro-CT images. *Bone* 60: 172–185.

Donoghue, P. C., and I. J. Sansom. 2002. Origin and early evolution of vertebrate skeletonization. *Microsc. Res. Tech.* 59, 352–372.

Donoghue, P. C. J. 2020. Fossil cells. *Curr. Biol.* 30: R485–R490.

Dumont, M., et al. 2016. Structure and growth pattern of the bizarre hemispheric prominence on the rostrum of the fossil beaked whale *Globicetus hiberus* (Mammalia, Cetacea, Ziphiidae). *J. Morphol.* 277: 1292–1308.

Faure-Brac, M.G., and Cubo, J. 2020. Were the synapsids primitively endotherms? A palaeohistological approach using phylogenetic eigenvector maps. *Philos. Trans. R. Soc. B* 375: 20190138.

Ferretti, M., et al. 2002. Static and dynamic osteogenesis: two different types of bone formation. *Acta Embryol.* 206: 21–29.

Fleischle, C.V., et al. 2018. Quantitative histological models suggest endothermy in plesiosaurs. *PeerJ* 6: e4955.

Gregory, T. R. 2001. Coincidence, coevolution, or causation? DNA content, cell size, and the C-value enigma. *Biol. Rev.* 76: 65–101.

Hall, B. K. 2015. *Bones and Cartilage: Developmental and Evolutionary Skeletal Biology.* 2nd ed., p. 920. London: Elsevier.

Hirasawa, T., and S. Kuratani. 2015. Evolution of the vertebrate skeleton: morphology, embryology, and development. *Zool. Lett.* 1: 2.

Houssaye, A., et al. 2013. Microanatomical and histological features in the long bones of mosasaurine mosasaurs (Reptilia, Squamata) – Implications for aquatic adaptation and growth rates. *PLoS One* 8: e76741.

Huttenlocker, A. K., and C. G. Farmer. 2017. Bone microvasculature tracks red blood cell size diminution in Triassic mammal and dinosaur forerunners. *Curr. Biol.* 27: 48–54.

Keating, J. N., et al. 2018. The nature of aspidin and the evolutionary origin of bone. *Nat. Ecol. Evol.* 2: 1501–1506.

Klein, N., 2010. Long bone histology of Sauropterygia from the lower muschelkalk of the Germanic Basin provides unexpected implications for phylogeny. *PLoS One* 5: e11613.

Laurin, M., et al. 2016. Early genome size increase in urodeles. *C. R. Palevol* 15: 74–82.

Legendre, L. J., and J. Botha-Brink. 2018. Digging the compromise: investigating the link between limb bone histology and fossoriality in the aardvark (Orycteropus afer). *PeerJ* 6: e5216.

Legendre, L. J., and D. Davesne. 2020. The evolution of mechanisms involved in vertebrate endothermy. *Philos. Trans. R. Soc. B Biol. Sci.* 375: 20190136.

Legendre, L. J., et al. 2016. Palaeohistological evidence for ancestral high metabolic rate in archosaurs. *Syst. Biol.* 65: 989–996.

Lindgren, J., et al. 2011. Microspectroscopic evidence of Cretaceous bone proteins. *PLoS One* 6: e19445.

MacNeil, J.A., and S.K. Boyd. 2008. Bone strength at the distal radius can be estimated from high-resolution peripheral quantitative computed tomography and the finite element method. *Bone* 42: 1203–1213.

Marotti, G., et al. 1999. Static and dynamic bone formation and the mechanism of collagen fiber orientation. *Presented at the 5° Workshop on Osteobiology*, pp. 156–156.

Meunier, F. J. 2011. The Osteichthyes, from the Paleozoic to the extant time, through histology and palaeohistology of bony tissues. *C. R. Palevol* 10: 347–355.

Mielke, M., et al. 2018. Trabecular architecture in the sciuromorph femoral head: allometry and functional adaptation. *Zool. Lett.* 4: 10.

Mitchell, K. J., et al. 2014. Ancient DNA reveals elephant birds and kiwi are sister taxa and clarifies ratite bird evolution. *Science* 344: 898–900.

Montoya-Sanhueza, G., and A. Chinsamy. 2018. Cortical bone adaptation and mineral mobilization in the subterranean mammal *Bathyergus suillus* (Rodentia: Bathyergidae): effects of age and sex. *PeerJ*6: e4944.

Mürer, F.K., et al. 2018. 3D maps of mineral composition and hydroxyapatite orientation in fossil bone samples obtained by X-ray diffraction computed tomography. *Sci. Rep.* 8: 1–13.

O'Connor, J., et al. 2018. Medullary bone in an Early Cretaceous enantiornithine bird and discussion regarding its identification in fossils. *Nat. Commun.* 9: 1–8.

Ofer, L., et al. 2020. A comparison of the structure, composition and mechanical properties of anosteocytic vertebrae of medaka (*O. latipes*) and osteocytic vertebrae of zebrafish (*D. rerio*). *J. Fish Biol.* 2020 doi: 10.1111/jfb.14334.

Olivier, C., et al. 2017. First palaeohistological inference of resting metabolic rate in an extinct synapsid, *Moghreberia nmachouensis* (Therapsida: Anomodontia). *Biol. J. Linn. Soc.* 121: 409–419.

Organ, C. 2012. Genomics and the lost world: palaeontological insights into genome evolution. In *From Clone to Bone: The Synergy of Morphological and Molecular Tools in Palaeobiology*, eds. Asher, R. J. and Müller, J., pp. 387. Cambridge, UK: Cambridge University Press.

Organ, C. L., and A. M. Shedlock. 2009. Palaeogenomics of pterosaurs and the evolution of small genome size in flying vertebrates. *Biol. Lett.* 5: 47–50.

Organ, C. L., et al. 2007. Origin of avian genome size and structure in non-avian dinosaurs. *Nature* 446: 180–184.

Organ, C. L., et al. 2011. Paleogenomic data suggest mammal-like genome size in the ancestral amniote and derived large genome size in amphibians. *J. Evol. Biol.* 24: 372–380.

Organ, C., et al. 2016. Macroevolution of genome size in sarcopterygians during the water–land transition. *C. R. Palevol* 15: 65–73.

Ørvig, T. 1965. Palaeohistological notes — 2. Certain comments on the phyletic significance of acellular bone tissue in early lower vertebrates. *Ark. Zool.* 16: 551–556.

Pan, Y., et al. 2019. Applications of chemical imaging techniques in paleontology. *Natl. Sci. Rev.* 6: 1040–1053.

Prondvai, E. 2017. Medullary bone in fossils: function, evolution and significance in growth curve reconstructions of extinct vertebrates. *J. Evol. Biol.* 30: 440-460.

Prondvai, E., et al. 2014. Development-based revision of bone tissue classification: the importance of semantics for science. *Biol. J. Linn. Soc.* 112: 799–816.

Prondvai, E., et al. 2020. Extensive chondroid bone in juvenile duck limbs hints at accelerated growth mechanism in avian skeletogenesis. *J. Anat.* 236: 463–473.

Quilhac, A., et al. 2014. Globuli ossei in the long limb bones of Pleurodeles waltl (Amphibia, Urodela, Salamandridae). *J. Morphol.* 275: 1226–1237.

Ricqlès, A de. 1975. Recherches paléohistologiques sur les os longs des tétrapodes VII. – Sur la classification, la signification fonctionelle et l'histoire des tissus osseux des tétrapodes. Première partie. *Ann. Paléontol.* 61: 51–129.

Sanchez, S., et al. 2013. 3D microstructural architecture of muscle attachments in extant and fossil vertebrates revealed by synchrotron microtomography. *PLoS One* 8: e56992.

Schroeter, E. R., et al. 2017. Expansion for the *Brachylophosaurus canadensis* collagen I sequence and additional evidence of the preservation of Cretaceous protein. *J. Proteom Res.* 16: 920–932.

Schweitzer, M. H. 1995. Microstructural, elemental and biomolecular preservation of *Tyrannosaurus rex* cancellous tissues. Doctoral dissertation, Montana State University-Bozeman, College of Letters & Science.

Schweitzer, M. H., et al. 1997. Preservation of biomolecules in cancellous bone of *Tyrannosaurus rex*. *J. Vertebr. Paleontol.* 17: 349–359.

Schweitzer, M. H., et al. 2005. Soft-tissue vessels and cellular preservation in *Tyrannosaurus rex*. *Science* 307: 1952–1955.

VetBooks.ir

Schweitzer, M. H., et al. 2008. Microscopic, chemical and molecular methods for examining fossil preservation. *C.R. Palevol* 7: 159–184.

Schweitzer, M. H., et al. 2013. Molecular analyses of dinosaur osteocytes support the presence of endogenous molecules. *Bone* 52: 414–423.

Schweitzer, M. H., et al. 2014. A role for iron and oxygen chemistry in preserving soft tissues, cells and molecules from deep time. *Proc. R. Soc. B* 281: 20132741.

Schweitzer, M. H., et al. 2016. Chemistry supports the identification of gender-specific reproductive tissue in *Tyrannosaurus rex*. *Sci. Rep.* 6: 23099.

Shahar, R., and M. N. Dean. 2013. The enigmas of bone without osteocytes. *Bonekey Rep.* 2: 343.

Shapiro, F., and J. Y. Wu. 2019. Woven bone overview: structural classification based on its integral role in developmental, repair and pathological bone formation throughout vertebrate groups. *Eur. Cells Mater.* 38: 137.

Stein, K., and E. Prondvai. 2014. Rethinking the nature of fibrolamellar bone: an integrative biological revision of sauropod plexiform bone formation: rethinking the nature of fibrolamellar bone. *Biol. Rev.* 89: 24–47.

Tsang, K.Y., et al. 2015. Fate of growth plate hypertrophic chondrocytes: death or lineage extension? *Dev. Growth Differ.* 57: 179–192.

Thomson, K. S. 1972. An attempt to reconstruct evolutionary changes in the cellular DNA content of lungfish. *J. Exp. Zool.*180: 363–371.

Wiemann, J., et al. 2018. Fossilization transforms vertebrate hard tissue proteins into N-heterocyclic polymers. *Nat. Commun.* 9: 1–9.

Wiemann, J., et al. 2020. Phylogenetic and physiological signals in metazoan fossil biomolecules. *Sci. Adv.* 6: eaba6883.

Wintrich, T., et al. 2017. A Triassic plesiosaurian skeleton and bone histology inform on evolution of a unique body plan. *Sci Adv.* 3: e1701144.

Witten, P. E., and A. Huysseune. 2009. A comparative view on mechanisms and functions of skeletal remodeling in teleost fish, with special emphasis on osteoclasts and their functions. *Biol. Rev.* 84: 315–346.

Yang, L., et al. 2014. Hypertrophic chondrocytes can become osteoblasts and osteocytes in endochondral bone formation. *Proc. Natl. Acad. Sci. U.S.A.* 111: 12097–12102.

Zhou, X., et al. 2014. Chondrocytes transdifferentiate into osteoblasts in endochondral bone during development, postnatal growth and fracture healing in mice. *PLoS Genet.* 10: e1004820.

Zylberberg, L. and M. Laurin. 2011. Analysis of fossil bone organic matrix by transmission electron microscopy. *C. R. Palevol.* 10: 357–366.

Zylberberg, L., et al. 2010. A microanatomical and histological study of the postcranial dermal skeleton in the Devonian sarcopterygian *Eusthenopteron foordi*. *Acta Palaeontol. Pol.* 55: 459–470.

VetBooks.ir

Extended Table of Contents

The present book is organized more or less hierarchically, with respect to basic knowledge of tissue types and their characteristics, and phylogenetically, with respect to the taxa that they characterize. This is followed by a review of major questions and concepts. Therefore, instead of an index, we present an expanded Table of Contents so that readers can easily identify the types of tissues that interest them and, by reading those sections, the types of animals in which they appear as well as the overarching questions of the field.

Section I Introduction 1

1. Paleohistology: An Historical – Bibliographical Introduction 3
Armand J. de Ricqlès

Introduction 3

Early Microscopical Investigators 4

The "Early Vertebrates" Tradition 6

Tetrapods: Systematics or Functions – or Both? 9

Epiphyses and Endochondral Ossification 14

Concluding Remarks 16

Acknowledgments 16

References 16

Section II Morphology and Histology of The Skeleton 27

2. An Overview of the Embryonic Development of the Bony Skeleton 29
Vivian de Buffrénil and Alexandra Quilhac

Introduction 29

Late Gastrulation and the Tridermic Organization 29

The Inductive Role of the Chord 31

Skeletogenic Involvement of Neural Crests, Somites and Lateral Plates 31

Neural Crests and the Cephalic Domain 31

Somites and the Axial and Paraxial Skeleton 33

Lateral Plates and the Zono-Appendicular Skeleton 34

References 36

3. The Vertebrate Skeleton: A Brief Introduction 39
Michel Laurin, Alexandra Quilhac and Vivian de Buffrénil

Classifying Bones and Bone Groups 39

Homology and Analogy: Two Central Concepts in Anatomy 41

The Dermal Skeleton 41

The Endoskeleton 44

Accessory Skeletal Elements: Sesamoids and Calcified Tendons 49
Sesamoids 49
Calcified Tendons 51
The Shape of Bones 51
A Significant but General Criterion 51
Long Bones 51
Short Bones 52
Flat Bones 52
Remarks on the Mineralization of Skeletal Elements 52
Acknowledgments 52
References 52

Methodological Focus A: The New Scalpel: Basic Aspects of CT-Scan Imaging 55
Damien Germain and Sandrine Ladevèze
Introduction 55
Basic Principles of the Method 55
Two Examples of CT Scan Use in Anatomy 57
Mammalian Inner Ears and Species Ecology 57
Virtual Dissections in Paleontology: The Example of "Cuvier's Opossum" 58
References 58

4. Microanatomical Features of Bones and Their Basic Measurement 59
Vivian de Buffrénil, Eli Amson, Alexandra Quilhac, Dennis Voeten and Michel Laurin
An Intermediate Level of Integration: Microanatomy 59
Gross Microanatomical Structure of Long Bones 61
The Outer Envelopes of Bone 61
Diaphyseal Region 61
Metaphyses 64
Epiphyses 66
Microanatomy of Short Bones 68
Gross Microanatomy of Flat Bones 70
Remarks on Some Basic Concepts Used in Microanatomical Descriptions 71
Cortex versus Medulla 71
Compact versus Cancellous Bone 71
Tubular versus Diploe 71
Qualitative Classification of Cancellous Bone 72
An Overview of Vascular Canals in Bone 72
General Characteristics of Cortical Vascularization 72
Cartilage Canals 75
Remark on Dermal Bone Vascularization 75
Acknowledgments 76
References 76

VetBooks.ir

Methodological Focus B: Basic Aspects of 3D Histomorphometry 81
Eli Amson and Damien Germain

From 2D to 3D Histomorphometry 81
Indications of 3D Analyses and VOI Sampling 81
Characteristics of Usable 3D Files and VOIs 81
Basic 3D Parameters and Indices 82
References 83

5. Bone Cells and Organic Matrix 85
Louise Zylberberg

Bone as a Tissue 85
The Cells of Bone 86
The Lineage of Osteoblasts 86
From Preosteoblasts to Osteoblasts 86
The Osteoblast 86
Pathways of Osteoblast Differentiation 89
The Bone-Lining Cells 90
The Osteocytes 90
The Osteoclasts 92
Pathway of Osteoclast Formation 92
The Osteoclast 93
Bone Mineral Dissolution 96
Organic Dissolution 96
Osteoclast Regulation 96
Bone Matrix 97
The Organic Matrix 97
The Collagen Family 98
Collagens in the Bone Matrix 98
Noncollagenous Proteins 101
Proteoglycans 101
Glycoproteins 101
Osteonectin 102
Gla-Containing Proteins 102
RGD-Containing Proteins 102
Lipids 102
Other Components 102
The Mineral Phase 102
Mineral Matrix Relationships 103
Acknowledgments 103
References 103

VetBooks.ir

6. Current Concepts of the Mineralization of Type I Collagen in Vertebrate Tissues 109
William J. Landis, Ph.D., Tengteng Tang, Ph.D. and Robin DiFeo Childs, M.S.

Introduction 109
Collagen Basic Structure 109
Collagen Synthesis and Secretion 110
The Mineralization Process 110
The Normally Mineralizing Avian Leg Tendon Model 110
Type I Collagen Self-Assembly 111
Ultrastructural Appearance of Mineralized Type I Collagen 112
Intrafibrillar Mineralization of Type I Collagen 112
Interfibrillar Mineralization of Type I Collagen 117
Noncollagenous Proteins: Bone Sialoprotein 117
Noncollagenous Proteins: Osteopontin 118
Noncollagenous Proteins: Osteocalcin 118
Possible Temporal and Spatial Relationships Between Interfibrillar and Intrafibrillar Collagen Mineralization 119
Conclusions 119
Acknowledgments 120
References 120

7. An Overview of Cartilage Histology 123
Alexandra Quilhac

Introduction 123
An Ancient and Essential Tissue 123
Cartilage Location 124
The Main Types of Cartilage 124
Hyaline Cartilage 124
Cartilages of the Growth Plate, or Growth Cartilages 126
Articular Cartilage 126
Fibrocartilage 126
Elastic Cartilage 126
Calcified Cartilage 127
Chondrogenesis and Chondrocyte structure 128
Basic Aspects of Chondrogenesis 128
Chondrocyte Ultrastructure 129
Ultrastructure of the Extracellular Matrix 131
Collagen 131
Glycosaminoglycans 131
Proteoglycans 131
Noncollagenous Proteins 132
Water and Ions 132

VetBooks.ir

Cartilage Vascularization and Innervation 132
The Functions of Cartilage and Their Regulation 132
Modalities of Cartilage Growth 132
Function of Growth Plates 132
Mechanical Behavior 133
Repair 133
Cell Death, Degradation and Resorption of Cartilage 133
Cells 133
Matrix 134
References 135

Methodological Focus C: Virtual (Paleo-)Histology Through Synchrotron Imaging 139
Sophie Sanchez, Dennis F. A. E. Voeten, Damien Germain and Vincent Fernandez
Introduction 139
Principles of Synchrotron Radiation 139
Phase-Contrast Imaging 140
Principle 140
Applications to Virtual Histology 140
Facilities Available for Virtual Histology Using Phase-Contrast Imaging 141
(Micro-)Anatomy 141
Histology and Microstructure 144
Molecular Biology and Ultrastructure 144
Tomography Combined with Various Techniques 144
Principle 144
Applications to Virtual Histology 144
Facilities Available for Virtual Histology Through SAXS or XRD-CT 145
Prospects for The Field 145
Acknowledgments 145
References 145

8. Bone Tissue Types: A Brief Account of Currently Used Categories 147
Vivian de Buffrénil and Alexandra Quilhac
Introduction 148
Relevant Descriptors of Bone Microstructure 148
Global Topography and Origin of Bone Deposits 148
Cortical and Medullary Formations 148
Periosteal and Endosteal Tissues 150
Primary and Secondary Bone Tissues 150
Classifying Tissues in Static and Dynamic Osteogenesis 150
Microanatomical Description as a Prerequisite to Histological Analysis 151
Distinction of Osseous Tissues Based on Compactness 151

Coarse Cancellous Bone 152
Fine Cancellous Bone 152
Compact Bone Made Cancellous 152
Compacted Coarse Cancellous Bone (CCCB) 152
Vascular Canals in Cortices 152
Avascular Bone 154
Vascular Patterns in Bone Cortices 155
Types of Intercellular Matrix 155
Woven-Fibered Collagen Networks 155
The Parallel-Fibered Matrix 157
The Lamellar Matrix 157
Degraded Matrix of Hypermineralized Bone Tissue 158
Osteocytes and Their Diversity 158
Other Significant Features of Bone Matrices 159
Osteons 159
Primary Osteons in Compact Cortices 159
Secondary Osteons 159
Cyclical Growth Marks, Rest Lines and Reversion Lines 161
Annuli 161
Lines of Arrested Growth 161
Rest Lines 161
Reversal (Cementing or Resorption) Lines 163
Sharpey's Fibers 163
Current, Integrative Classification of Primary Compact Tissues 163
Woven-Fibered Tissue 163
Parallel-Fibered Bone Tissue 165
The Lamellar Tissue 165
Specialized Terminology Related to Lamellar or Parallel-Fibered Tissues 166
External and Internal Fundamental Systems 166
On Intermediate Tissue Types 166
Remarks on the "Lamellar-Zonal" Tissue 166
Some Peculiar Cases of Lamellar Bone in Basal Gnathostomes 168
Acellular Bone and Aspidin 168
Isopedin 168
Composite Tissues: The Woven-Parallel [Fibrolamellar] Complexes 169
Woven-Parallel Complexes With Longitudinal Osteons 171
Reticular Woven-Parallel Complex 171
Radial Woven-Parallel Complex 171
Laminar and Plexiform Woven-Parallel Complexes 171

Dense Haversian Bone: A Secondary Compact Tissue 172
Osseous Tissues in Cancellous Formations 172
Tissues Forming the Primary Trabeculae 172
The Tissues of Secondary, Endosteal Trabeculae 174
Trabeculae Resulting from Patchy Cortical Resorption 174
Remarks on Fine Cancellous Bone 174
Histological features of Compacted Coarse Cancellous Bone (CCCB) 174
Between bone and cartilage: chondroid bone 175
Acknowledgments 176
References 176

Methodological Focus D: FIB-SEM Dual-Beam Microscopy for Three-Dimensional Ultrastructural Imaging of Skeletal Tissues 183
Natalie Reznikov and Katya Rechav
Use of Dual-Beam FIB-SEM 3D Imaging in Skeletal Biology 183
Fundamental Principles and Practical use 184
General Geometry and Some Customized Geometries 184
Specimen Preparation 187
Imaging Parameters 187
3D Image Processing 188
Conclusion 189
Acknowledgments 189
References 189

Section III Dynamic Processes in Osseous Formations 191

9. Basic Processes in Bone Growth 193
Vivian de Buffrénil and Alexandra Quilhac
Interpreting Skeletal Growth 194
Initial Growth of Membrane Bones 194
From Mesenchymal Condensations to Bones 194
Remarks on Local Growth Controls 195
Basic Growth Pattern of Endochondral Bones 195
Ossification of the Cartilaginous Anlage 195
Basic Mechanisms of the Growth in Length of the Bones 197
Epiphyseal Structure and the Course of Growth 197
Subperiosteal Growth of Bone Cortices 199
Systemic Regulators of Skeletal Growth 199
Multiple Systemic Regulators 199
Action of GH, IGF-1 and the GH/IGF-1 Axis on Skeletal Growth 200
Molecular Structure and Secretion Context 200
Actions of GH and IGF-1 on Cartilage and Bone Cells 201

VetBooks.ir

VetBooks.ir

Thyroid Hormones 201
Nature and Secretion of Thyroid Hormones 201
Actions on the Growing Skeleton 202
Sex Steroids, Androgens and Estrogens 203
Secretion and Regulation of Sex Steroids 203
Action of Sex Steroids in Bone 205
Glucocorticoids (GCs) 205
Growth and Morphology of Bones 207
The Constraint of Rigidity 207
Basic Shaping Processes in the Growth of Bones 207
The Peculiar Growth Geometry of Some Flat Bones 207
Differentiation of Superficial Relief Through Accretion Rate, or Resorption 207
Morphogenetic Role of Heterochrony in Local Bone Deposits 207
Sequential Growth Remodeling in Appendicular Long Bones 209
Growth Off-Centering and Diaphyseal Curvature 210
Differential Contribution of Proximal and Distal Epiphyses 210
Brief Overview at the Problem 210
Chronology of Epiphyseal Fusion 210
The Quantitative Study of Epiphyseal Contribution to Growth 212
Integral Preservation of Endochondral Bone Formations 212
Interpreting Growth Patterns in the Cephalic Region 212
An Essential but Complex Issue 212
Cephalometry 213
Modeling of Facial Bone: The Histologic Mechanisms 214
References 215

10. Accretion Rate and Histological Features of Bone 221
Vivian de Buffrénil, Alexandra Quilhac and Jorge Cubo

A Keystone for Paleobiological Inferences 221
Quantifying Appositional Rate of Primary Periosteal Cortices 222
Histological Features and Apposition Rate: Comparative Results 223
Semiquantitative Approach 223
Recent Efforts Toward a Full Quantitative Approach 225
References 227

11. Bone Remodeling 229
Vivian de Buffrénil, Alexandra Quilhac

The Multiple Functional Involvements of Bone Remodeling 229
Basic Multicellular Unit and Bone Structure Unit, the Basic Units of Bone Remodeling 231
General Characteristics 231
Basic Structure and Functioning of the Haversian BMU 231

The Haversian BSU, i.e., the Secondary Osteon ... 233
Histological Structure of BMU and BSU in Trabecular Remodeling ... 236
The Multiple Regulation Processes of Bone Remodeling ... 237
Remodeling and Bone Damage Repair ... 237
Remarks on the Regulation of Adaptive Remodeling ... 237
Phosphocalcic Homeostasis and the Endocrine Regulation of Bone Remodeling ... 238
Contribution of Vitamin D to Phosphocalcic Homeostasis ... 238
Influence of the Central and Sympathetic Nervous Systems on Remodeling ... 239
The Message of Remodeling in Fossil Bones ... 239
A Basic Clue in Paleophysiology ... 240
Remark on the Histomorphometry of Bone Remodeling in Extant and Extinct Taxa ... 241
Remodeling Pattern as a Clue for the Estimation of Ontogenetic Age in Fossils ... 241
References ... 242

12. Remarks on Metaplastic Processes in the Skeleton ... 247
Vivian de Buffrénil and Louise Zylberberg
Definition and Development of Metaplastic "Osseous" Tissues ... 247
Osteoderms and Dermo-osseous Metaplasia ... 248
Calcified Tendons of Ornithodirans ... 251
References ... 254

Section IV Teeth ... 257

13. Histology of Dental Hard Tissues ... 259
Alan Boyde and Timothy G. Bromage
Tooth Germs and the Embryonic Origins of Dentine, Enamel and Cementum ... 260
Basics of Tooth Form ... 261
Dentine Histology ... 262
General Features ... 262
Mineralization and Mineralizing Front Morphology ... 262
Matrix Vesicles, Calcospherites, Interglobular Dentine and Secondary Nucleation ... 262
Periodic Growth Layer Lines in Dentine ... 264
Annual Growth Layers and Growth Layer Groups ... 264
Matrix Daily ... 264
Mineral Daily ... 264
Longer Interval Incremental Lines: A Few Too Many Days ... 264
Much Longer Aperiodic Growth Disturbance Lines: Neonatal Line ... 264
Calcospherites and Polarized Light Microscopy ... 264
Von Korff Fibers in Early Dentine Mineralization ... 265
Tubule-Centered Mineralization ... 266
Collagen Orientation in the Tubule Wall ... 266

Peritubular Dentine 266
Side Branches of Dentine Tubules 267
Postmortem Changes: Microbial and Fungal Bore Holes in Dentine 267
Dentine Resorption 268
Curvature of Dentine Tubules: Sinusoidal Oscillations and Decussations 268
Vasodentine and Osteodentine in Beaked Whales 268
Secondary, Tertiary and Responsive Reparative Dentine Phases 268
Calcified Dental Pulp 270
Pulp Stones 270
Enamel 270
Prisms and Packing Patterns 270
Prism Decussation 272
Relative Cell Movement Within the Ameloblast Layer 272
Rodent Incisor Inner-Enamel Decussation 272
Hunter-Schreger Bands 272
Periodic Growth Layer Lines in Enamel 272
Cross Striations or Varicosities: Circadian Rhythms 272
Regular-Period Striae of Retzius: Multidien Rhythms 277
Perikymata or Imbrication Lines at Tooth Surface: Prism-Free Layer 277
Growth Disturbance Lines: Hypoplasia 277
Daily, Ultradian Lines 277
Maturation and Surface Enamel Composition 277
Iron in Surface Enamel 277
Enamel Tubules and Spindles, Tufts and Lamellae 278
Enamel Tubules 278
Spindles 278
Tufts and Lamellae 278
Roots and Cementum: Crowns and Coronal Cementum 278
Primary Cementum 278
Secondary Cementum (See Also Dentine Resorption) 278
Coronal Cementum 278
The Cement-Dentine Junction Region in Murine Molars: Incorporation of Hertwig's Root Sheath 279
Cartilage Cementum 279
Annual Period of Cementum Deposition 279
Preparation Methods 279
Etching 279
Air Polishing and Air Abrasion 279
Replica Films for LM 281
TEM of Carbon Replicas 282

Replicas and 3D Resin Casts for Scanning Electron Microscopy 282
"Thin" Sections and Laser Ablation Microtomy (LAM) 282
Plastic Slides 282
Cyanoacrylate Glue 282
Imaging Methods 282
Reflected Light Confocal Microscopy 282
Reflected Light Metallurgical Microscope 284
Rotating Condenser Aperture 284
Polarized Light Microscopy (PLM) 284
Flatbed Scanner: 3D Images 284
BSE-SEM "at Bad Vacuum", High Chamber Pressure, No Coating and Instant Gratification SEM 285
Faxitron™ Point Projection Digital Microradiography 285
Scanning X-Ray Microscopy 285
X-Ray Microtomography (XMT or μCT) 285
Simultaneous-Inductively Coupled Plasma-Mass Spectrometry (si-LA-ICP-MS) 285
Summary 285
Acknowledgments 286
References 286

Section V Phylogenetic Diversity of Skeletal Tissues 289

14. Introduction 291
Michel Laurin
References 292

15. Finned Vertebrates 294
Jorge Mondéjar-Fernández and Philippe Janvier
Introduction 294
The Clades (Or Presumed Clades) 302
Myllokunmingiida 302
Euconodonta 302
Cyclostomi 302
Euphaneropida 302
Jamoytiida 303
Anaspida 304
Pteraspidomorphi 304
Thelodonti 307
Galeaspida 308
Osteostraci 309
Pituriaspida 311

Gnathostomata 311
Chondrichthyes 311
Acanthodii 311
Placodermi 313
Osteichthyes 315
Conclusion 318
References 319

16. Early Tetrapodomorphs 325
Sophie Sanchez, François Clarac, Michel Laurin and Armand de Ricqlès

Phylogenetic, Evolutionary and Biological Considerations 326
General Characteristics 326
Finned Stem-tetrapods 327
Limbed Stem-tetrapods 327
Temnospondyls 327
Embolomeres 328
Seymouriamorphs 328
Lepospondyls 328
Bone Microanatomy and Histology 328
Finned Stem-tetrapods 328
Tooth Microstructure 329
Postcranial Dermal Bone Microstructure (Scales and Rays) 329
Cosmine Evolution 329
Skull and Girdle Bone Microstructure 329
Fin Bone Microanatomy and Histology 329
General Conclusion 331
Limbed Stem-tetrapods 331
Tooth Microstructure 331
Postcranial Dermal Bone Microstructure (Scutes and Rays) 331
Skull and Girdle Bone Microstructure 332
Limb Bone Microanatomy and Histology 332
General Conclusion 332
Temnospondyls 333
Limb Bone Microanatomy and Histology 333
Skull Bone Microstructure 333
Scute and Osteoderm Microstructure 335
Vertebral Microstructure 335
Tooth Microstructure 335
General Conclusion 335
Embolomeres 336

Long Bone Microanatomy and Microstructure 336
Scute Microstructure 336
General Conclusion 336
Seymouriamorphs 336
Limb Bone Microanatomy and Histology 336
Skull Bone Microstructure 337
Vertebral Microstructure 338
Scute Microstructure 338
General Conclusion 338
Lepospondyls 338
Jawbone Histology 338
Skull Bone Microstructure 338
Vertebral Microstructure 339
Scute Microstructure 339
General Conclusion 339
Acknowledgments 339
References 339

17. Lissamphibia 345
Vivian de Buffrénil and Michel Laurin
Introduction 345
General Characteristics 345
Definition of Lissamphibians and General Phylogenetic Affinities 345
A Basic Trichotomy 346
Gymnophiona 346
Caudata 346
Anura 346
Microanatomical and Histological Features of Long Bones 347
Microanatomical Features in the Caudata 347
Bone Histology in Caudata 348
Microanatomical Features of Long Bones in the Anura 351
Histology of Anuran Long Bone Cortices 352
Remarks on Other Skeletal Elements 353
Cranial Bones 353
Gross Vertebral Organization in Lissamphibians 355
Anuran Osteoderms and Gymnophiona "Scales" 356
An Overview of Skeletal Neoteny 357
Some Concluding Remarks 359
References 359

18. Early Amniotes and Their Close Relatives 363
Aurore Canoville, Michel Laurin and Armand de Ricqlès

Introduction 363
Histological Survey and Paleobiological Inferences 364
Diadectomorphs 364
Skeletal Microstructure in *Diadectes* 364
Bone Microstructure in *Limnoscelis* 365
Mesosauria 365
Bone Microstructure in Mesosaurs 366
Dental Microstructure in Mesosaurs 368
Parareptiles 368
Bone Microstructure in Procolophonoids 368
Dental Microstructure in Procolophonoids 370
Dental Microstructure of Other Basal Parareptiles 370
Bone Microstructure in Pareiasaurs 370
Undetermined Small "Romeriid" Amniote (Protorothyrididae or Diapsida) 372
Captorhinids 372
Bone Microstructure in *Captorhinus* 372
Bone Microstructure in *Labidosaurus* 374
Bone Microstructure in *Moradisaurus* 374
Concluding Remarks 374
Dental Microstructure in *Captorhinus* 374
Dental Microstructure in *Moradisaurus* 376
Araeoscelidia 376
Bone Microstructure in *Dictybolos* 377
Bone Microstructure in *Araeoscelis* 377
Avicephala 377
Bone Microstructure in *Coelurosauravus* 377
Synthetic Remarks 379
Bone Histodiversity of Early Amniotes and Their Relatives 379
Dental Microstructure and Insertion in Early Amniotes 379
Early Amniote Paleobiology and the Permo-Triassic Crisis 379
References 381

19. Testudines 385
Torsten M. Scheyer and Ignacio A. Cerda

Introduction 385
Phylogenetic Position and Anatomical Peculiarities 385
Early Historical Studies 386
An Overview of Recent Histological Studies 386

VetBooks.ir

Skeletal Microstructures in Turtles ... 387
Endoskeletal Elements ... 387
Scleral Ossicles ... 389
Shell Bones and Osteoderms ... 389
Preliminary Remarks ... 389
The General Construction of Turtle Shell Bones ... 389
The Plywood-Like Pattern of Soft-Shelled Turtles ... 389
External Ornamentation of Shell Bones ... 393
Sutural Growth of Shell Bones ... 393
Ossicles of the Secondary Epithecal Shell of Dermochelyidae ... 393
Osteocytes and Osteocyte Lacunae ... 393
Accessory Osteoderms and Ossicles ... 394
Summary and Outlook ... 394
Institutional Abbreviations ... 394
Acknowledgments ... 394
References ... 394

20. Lepidosauria ... 399
Vivian de Buffrénil and Alexandra Houssaye

Introduction ... 399
Preliminary Remarks ... 399
An Overview of Studies of Skeletal Histology in Lepidosaurs ... 400
Squamates ... 400
"Lizards" and Snakes ... 400
Microanatomical and Histological Structure of Limb Long Bones in Lizards ... 400
Occurrence of Sesamoids ... 404
Vertebrae and Ribs in Lizards and Snakes ... 404
Remarks on Skull Bones and Teeth in Lizards and Snakes ... 406
Osteoderms ... 409
Aigialosaurs and Mosasaurs ... 410
General Features of Mosasauroidea ... 410
Microanatomy and Histology of Ribs ... 411
Microanatomy and Histology of Vertebrae ... 411
Microanatomy and Histology of Limb Long Bones ... 413
Cranial Bones and Teeth ... 415
Paleobiological and Paleoecological Inferences ... 415
The Strange Case of Marine Cenomanian Snakelike Forms ... 416
"Dolichosaurs" and Hind-Limbed Snakes ... 416
Structure of the Ribs and Vertebrae ... 417
A Note on the Inner Structure of Reduced Limbs ... 419
Paleobiological and Paleoecological Inferences ... 419

Rhynchocephalia 419
A Once Diverse Taxon 419
Overview of Rhynchocephalian Skeletal Structures 419
Acknowledgments 420
References 420

21. Sauropterygia: Placodontia 425
Torsten M. Scheyer and Nicole Klein
Introduction 425
Overview of Endoskeletal Element Studies 425
Overview of Studies of Dermal Armor Elements 426
New Data from *Cyamodus hildegardis* from the Besano Formation of Monte San Giorgio, Switzerland 430
Conclusions 430
Institutional Abbreviations 430
Acknowledgments 430
References 432

22. Sauropterygia: Nothosauria and Pachypleurosauria 435
Torsten M. Scheyer, Alexandra Houssaye and Nicole Klein
Introduction 435
Overview of Histological Studies 436
Conclusions and Outlook 441
Institutional Abbreviations 441
Acknowledgments 441
References 441

23. Sauropterygia: Histology of Plesiosauria 444
P. Martin Sander and Tanja Wintrich
Introduction 444
History of Research on Plesiosaur Histology 445
Descriptions by Skeletal Region 446
Skull: Dental Histology Only 446
Propodials 446
Vertebrae 449
Ribs and Gastralia 451
Girdle Bones 451
Limb Bones Other Than Propodials 452
Growth, Skeletochronology and Life History 452
Qualitative Indicators of Fast Growth 452
Ontogenetic Changes and Histologic Ontogenetic Stages 452
Histomorphometry 453
Growth Rates and Resting Metabolic Rates 453

Bone Density: Vertebrae and Propodials 454
Red Blood Cell Size 454
Paleobiological and Evolutionary Implications 454
Fast Growth and Endothermy 454
Aquatic Adaptation 455
Evolutionary Success 455
Conclusions 455
Acknowledgments 455
References 455

24. Ichthyosauria 458
P. Martin Sander

Introduction 458
On Ichthyosaurs 458
Ichthyosaur Evolution 458
History of Research on Ichthyosaur Histology 459
Descriptions by Skeletal Region 459
Skull 459
Axial Skeleton 461
Vertebrae 461
Ribs and Gastralia 461
Appendicular Skeleton 461
Girdle Bones 461
Propodials 462
Lower Limb Bones 463
Ontogenetic Changes 463
Growth, Skeletochronology and Life History 463
Histomorphometry 464
Paleobiological and Evolutionary Implications 464
Conclusions 464
Acknowledgments 465
References 465

25. Archosauromorpha: From Early Diapsids to Archosaurs 467
Armand de Ricqlès, Vivian de Buffrenil and Michel Laurin

Introduction 467
Historical Background 468
Choristodera 468
Champsosaurus and *Simoedosaurus* 469
Non-Archosauriform Archosauromorphs 469
The “Protorosauria” 469

Aenigmastropheus parringtoni 470
Tanystropheus and Macrocnemus (Tanystropheidae) 471
The Rhynchosauria 472
Stenaulorhynchus stockleyi 472
Hyperodapedon and *Teyumbaita sulcognathus* 472
The Allokotosauria 473
Trilophosaurus buettneri 473
Azendohsaurus laaroussii 473
Prolacerta broomi 474
The Archosauriformes 475
Proterosuchidae 475
Erythrosuchidae 476
The Proterochampsia 476
Doswelliidae 476
Proterochampsidae 476
The Euparkeriidae 476
Euparkeria 477
The Phytosaurs (Parasuchia) 477
Rutiodon 477
The Archosauria: Noncrocodylomorph Pseudosuchia 477
Ornithosuchidae 477
Erpetosuchidae 477
Aetosauria (Stagonolepididae) 477
Paracrocodylomorpha 480
Rauisuchidae 481
Discussion 481
Acknowledgments 483
References 483

26. Archosauromorpha: The Crocodylomorpha 486
Vivian de Buffrénil, Michel Laurin and Stéphane Jouve

The Crocodylian Family Tree 486
The Eusuchians 486
An Overview of Early Crocodylomorphs 487
The Crocodylomorph Skeleton in Histological Literature 489
Eusuchia and Related Forms 489
General Microanatomic Features of Long Bones and Ribs 489
Histology of Long Bones 492
Remarks on Ribs and Vertebrae 494
Skull Roof Elements and Osteoderms 496

Microanatomical Features ... 496
Histological Features ... 496
Remarks on *Susisuchus* and *Goniopholis* ... 496
The Tethysuchia: Dyrosaurs and *Sarcosuchus* ... 497
Thalattosuchians ... 499
Microanatomy of Thalattosuchian Skeletons ... 499
Histology of Thalattosuchian Bones ... 499
Notosuchia and Peirosaurids ... 501
Notosuchia ... 501
Peirosaurids ... 503
Basal Crocodylomorphs: The Sphenosuchians *Terrestrisuchus/Saltoposuchus* and *Hesperosuchus* ... 504
Concluding Remarks ... 505
References ... 505

27. Archosauromorpha: Avemetatarsalia – Dinosaurs and Their Relatives ... 511
Kevin Padian and Holly N. Woodward

Introduction ... 511
Nondinosaurian Avemetatarsalia ... 512
Introduction ... 512
Basal (Nondinosaur, Nonpterosauromorph) Avemetatarsalians ... 514
Ornithodira: Pterosauria ... 514
Ornithodira: Nondinosaurian Dinosauromorpha ... 518
Dinosauria ... 521
Basal Dinosauria ... 521
Dinosauria: Ornithischia ... 522
Heterodontosauridae ... 522
Thyreophora ... 522
Ceratopsia ... 525
Pachycephalosauria ... 526
Basal Ornithopoda ... 526
Hadrosaurids ... 528
Dinosauria: Saurischia ... 529
Basal Sauropodomorphs ... 529
Sauropoda ... 529
Theropoda: Nonavian Forms ... 531
Theropoda: Aves ... 533
The Transition from Basal Maniraptorans to the First Birds ... 533
History of the Question of the Evolution of Avian Growth Rates and Metabolism ... 534
Growth in Extant (Crown-Group) Birds ... 536
The Problem of Medullary Bone ... 538

Some Functional Questions about Nonavian Dinosaurs ... 539
Histological Problems in Dinosaurian Growth ... 539
Interindividual Differences in Body Size Versus Age ... 539
The Problem of Phyletic Dwarfism ... 540
What Explains the Distribution of Secondary Bone Tissue Among Elements in a Skeleton? ... 541
General Conclusions to the Paleohistological Consideration of the Ornithodira ... 542
References ... 543

28. Nonmammalian Synapsids ... 550
Jennifer Botha and Adam K. Huttenlocker
Introduction to Nonmammalian Synapsids ... 550
Nontherapsid Synapsids ... 551
Caseasauria ... 551
Eupelycosauria ... 551
Nonmammalian Therapsids ... 553
Basal Therapsids and Dinocephalians ... 553
Anomodonts ... 554
Gorgonopsians ... 556
Therocephalians ... 556
Nonmammaliaform Cynodonts ... 558
Summary of Nonmammalian Synapsid Histology ... 560
Acknowledgments ... 560
References ... 560

29. Diversity of Bone Microstructure in Mammals ... 564
Vivian de Buffrénil, Christian de Muizon, Maïténa Dumont, Michel Laurin and Olivier Lambert
Overview and Definitions ... 565
Origin and Mesozoic Mammals ... 565
Early Mammaliaforms ... 565
First Therians ... 566
Extant Mammalian Clades ... 567
Preliminary Remarks on Comparative Bone Histology in Mammals ... 569
Early (Mesozoic) Mammals ... 570
Morganucodon and the Allotheria (Multituberculates) ... 570
Prototheria (Monotremes and Stem Group) ... 571
Remark on Epiphyseal Structure in the Prototherians ... 571
Long Bone and Rib Microstructure ... 571
Skeletal Microstructures of the Metatheria ... 573
Epiphyseal Characteristics of Metatherian Long Bones ... 573

VetBooks.ir

Microanatomy and Histology of Limb Long Bones 574
An Overview of Rib Structure 574
Long Bones and Ribs in the Eutheria 576
Preliminary Remarks 576
Limb Long Bones 576
Ribs 576
Histological Features of Long Bones in Early Eutherians 577
Observations of Pantodonts 577
Afrotheria (Sirenia, Proboscidea, Desmostylia and Tubulidentata) 579
Bone Microstructure in the Sirenia 579
Desmostylia 579
Proboscidea 581
Tubulidentata 581
Xenarthra 582
Terrestrial and Amphibious Cetartiodactyls 582
Aquatic Cetartiodactyls: The Cetaceans 584
Limb Bones 586
Ribs 586
Perissodactyls 588
Carnivores 590
Long Bones of the Pholidote *Phataginus tricuspis* 592
Histological Features of Long Bones and Ribs in the Lipotyphla 592
Chiroptera 594
Rodents 595
Lagomorphs 597
Primates 597
An Overview of Mammalian Vertebral Microstructures 599
Microanatomical Features 599
Histological Features 601
Remarks on Other Skeletal Elements: Osteoderms, Baculum and Antlers 601
Xenarthran Dermal Ossicles 601
Baculum 603
Antlers 604
Differentiation and Growth Process of the First Antlers 604
Antler Regeneration 605
Concluding Remarks 606
Acknowledgments 607
References 607

VetBooks.ir

Section VI Integrative Questions 615

30. Phylogenetic Signal in Bone Histology 617
Jorge Cubo, Lucas J. Legendre and Michel Laurin

Introduction: What is a Phylogenetic Signal? 617
How to Detect a Phylogenetic Signal 618
Empirical Studies 620
When to Test for a Phylogenetic Signal 622
References 622

31. Cyclical Growth and Skeletochronology 626
Vivian de Buffrénil, Alexandra Quilhac and Jacques Castanet

Introduction 626
Biological Rhythms and Cyclical Growth 627
Tissue Sampling and Current Technical Processes in Skeletochronology 627
Basic Methodological Options 627
Tissue Sampling and Processing 629
Bone and Cementum 629
Dentin 629
Structural Characteristics of Yearly Growth Marks in Bone 630
General Interpretative Framework 630
Histology of SGMs 630
Structural Data on LAGs 630
Structure of the Annuli 632
Remarks on Zones 632
Neonatal Line 634
Spacing Pattern of SGMs 634
Eroded and Supernumerary SGMs 634
Remarks on LAGs in Secondary Bone 636
Periodicity and Duration of SGM Formation in Bone 636
Observing the Periodicity of SGMs 636
Duration of Age Recording by Bone SGMs 637
Structural Features of Skeletal Growth Marks in Dental Tissues 637
Diversity of Dental Tissues Containing Growth Marks 637
Structure and Periodicity of Dental Growth Marks 637
Dentinal GLGs 637
Cementum LAGs 639
A Central Tool in Biology and Paleobiology 639
References 640

32. Aging and senescence Processes in the Skeleton 645
Catherine Bergot and Vivian de Buffrénil

Introduction 646
General Characteristics of Skeletal Aging Process 646
Brief Recapitulation of Bone Structure 646
Bone Senescence in a Macroanatomical Perspective 647
Cranial Sutures and Pubic Symphysis Relief 647
Age-Related Anatomical Modifications of the Spine 647
Intervertebral Disk Degeneration 647
The Vertebral Body in Conventional X-Ray Imaging 647
Age-Related Anatomical Modifications in Cancellous Formations of Limb Bones 648
Proximal Metaphysis of the Femur 648
Proximal Metaphysis of the Humerus 649
Calcaneum 649
Age-Related Anatomical Modifications in Cortical Bone 650
Aging of Bone at a Histomorphometric Scale 651
Age-Related Variations in Cancellous Bone 651
The Iliac Crest 651
The Vertebral Body 652
Age-Related Variations in Compact (Cortical) Bone 654
Porosity 654
Assessment of Age at Death 655
Aging of Bone at the Microscopic Scale 655
Advantages of X-Ray Microtomography 655
In Cancellous Bone 656
In Cortical Bone 656
Osteocyte Lacunae 656
Mineralization 657
Ash Weight and Aging 657
An Overview of Radiologic Approaches to Mineral Density 657
Evaluation of Bone Mineral Density In Vivo 657
Results of Quantitative Microradiography: Osteons vs Interstitial Bone 658
Frequent Structural and Mineralization Abnormalities in Aged Subjects 659
Trabecular Microcalli 659
Microcracks 659
Hypermineralized Zones 659
Occlusion of Osteocyte Lacunae 660
A Synthesis of Age-Related Bone Loss in Humans 660
Remarks on Age-Related Bone Loss in Nonhuman Taxa 660

VetBooks.ir

An Overview of Skeletal Aging Processes in Nonhuman Mammals 660
Nonmammalian Taxa 661
Concluding Remarks 661
Assessing Bone Senescence in Wild and Fossil Specimens 661
Osteoporosis from a Genetic and Evolutionary Perspective 662
Acknowledgments 662
References 662

33. Basic Principles and Methodologies in Measuring Bone Biomechanics 668
Russell P. Main

Introduction 668
The Hierarchical Organization of Bone Tissue, and Solid and Fluid Mechanics in the Vertebrate Skeleton 668
Measuring and Modeling In Vivo Skeletal Mechanics and Bone Tissue Properties 675
Modeling Musculoskeletal Biomechanics 677
Application of Biomechanical Analyses to Paleontological and Comparative Questions of Function 679
Biting Mechanics in Primates 679
Modeling Locomotion in Theropods 680
Conclusion 681
Acknowledgments 681
References 682

34. Interpreting Mechanical Function in Extant and Fossil Long Bones 688
Russell P. Main, Erin L.R. Simons and Andrew H. Lee

Mechanobiological Evolution and Plasticity in Bone Form 688
Bone Length 690
Curvature 692
Musculotendinous Entheses and Mechanical Function 694
Bone Cross-Sectional Shape 695
Primary Vascular Canal Orientation 701
Collagen Fiber Orientation 702
Intracortical Remodeling 705
Cancellous Bone 708
Integrative Studies of Limb Bone Biomechanics in Relation to Bone Shape and Histomorphology 712
Changes in Musculoskeletal Growth Allometries in Relation to Ontogenetic Biomechanics 712
Ontogenetic Changes in Bone Mechanics and Histomorphology in the Goat Radius 712
Ontogenetic Changes in Bone Mechanics and Histomorphology in the Emu Femur and Tibiotarsus 713
Using Limb Bone Morphology to Assess Gait in Living and Extinct Mammals and Dinosaurs 714
Summary 715
Acknowledgments 716
References 716

VetBooks.ir

35. Bone Microanatomy and Lifestyle in Tetrapods 724
Aurore Canoville, Vivian de Buffrénil and Michel Laurin

Water, Land and Bones 724
Methodological and Terminological Overview 726
Data Acquisition Processes and Nature of the Raw Data 726
Nature of the Samples, Location and Orientation of the Sampling Planes 727
Why Study a Single Bone Element at a Time? 727
How to Code Lifestyle in Comparative Analyses 728
Statistical Comparisons and the Interplay Between Function and Phylogeny 728
The Phylogenetic Signal 728
The Ecological Signal 729
Paleobiological Inferences 729
Reference Studies in Extant Taxa 730
Appendicular Skeleton 730
Some General Patterns 730
Specializations of Major Tetrapod Taxa 730
Remarks on Fossorial and Arboreal Forms 732
Axial Skeleton 733
Turtle Shell 735
Lifestyle Inferences Based on Bone Microanatomy: A Review 736
References 738

36. Bone Histology and the Adaptation to Aquatic Life in Tetrapods 744
Alexandra Houssaye and Vivian de Buffrénil

Introduction 744
Typical Osseous Microanatomical Specializations Linked to an Aquatic Lifestyle 744
General Remarks 744
High Variability of Patterns 745
Bone Mass Increase in a Microanatomical Perspective 746
Cancellous Organization 747
Parallels Among Lineages 747
Processes Possibly Involved in Bone Structure Specializations 747
Preliminary Considerations 747
Osteosclerosis 748
Pachyostosis 750
Cancellous Bones 750
Functional Considerations 753
Physiological Changes Associated with Adaptation to an Aquatic Lifestyle 753
References 754

VetBooks.ir

37. Bone Histology and Thermal Physiology 757
Jorge Cubo, Adam Huttenlocker, Lucas J. Legendre, Chloé Olivier and Armand de Ricqlès

Introduction 757
Basic Concepts and their Historical Development 757
Homeotherms and Poikilotherms 758
Endotherms and Ectotherms 758
Paleophysiology: Early Thoughts 759
Paleophysiology: The 1970s Change of Paradigm 759
Physiological Basis of Endothermy 760
Bone Histology as a Clue to Physiology 761
Origin and Evolution of Endothermy in Synapsida 763
Basal Synapsids 763
Therapsids 764
Origin and Evolution of Endothermy in Diapsida 766
References 767

38. Bone Ornamentation: Deciphering the Functional Meaning of an Enigmatic Feature 774
François Clarac

A Morphologically Variable and Homoplastic Feature 774
Local Growth Patterns Involved in the Differentiation of Bone Ornamentation 775
Possible Functions of Bone Ornamentation: The Example of Crocodylomorpha 776
Bone Ornamentation and Heat Transfer: An Adaptation to the Ectothermic Sit-and-Wait Predator Lifestyle in Crocodylomorpha 776
Possible Involvement of Bone Ornamentation in Blood Acidity Buffering 777
The Influence of Ornamentation on the Mechanical Resistance of Bones 777
Concluding Remarks 778
Acknowledgments 778
References 778

39. The Histology of Skeletal Tissues as a Tool in Paleoanthropological and Archaeological Investigations 781
Ariane Burke and Michelle S. M. Drapeau

Introduction 781
Taxonomy 782
Histological Applications 782
Functional Analysis 784
Histological Applications 784
Pathology 785
Histological Applications 785
Age and Season of Death 786
Histological Applications 786

VetBooks.ir

VetBooks.ir

Taphonomy 788
Histological Applications 788
Conclusions 788
References 789

40. A Methodological Renaissance to Advance Perennial Issues in Vertebrate Paleohistology 793
Alexandra Houssaye, Donald Davesne and Aurore Canoville

Introduction 793
Controversial and Puzzling Tissue Types 793
Going Further in Paleoecology and Paleophysiology 794
What Molecules Can Reveal 795
Bone and Genome Size 795
Conclusion 796
References 796